COMPREHENSIVE ORGANOMETALLIC CHEMISTRY III

Editors-in-Chief
Robert H. Crabtree & D. Michael P. Mingos

Volume 12

APPLICATIONS III: FUNCTIONAL MATERIALS, ENVIRONMENTAL AND BIOLOGICAL APPLICATIONS

Volume Editor
Dermot O'Hare

COMPREHENSIVE ORGANOMETALLIC CHEMISTRY III

COMPREHENSIVE ORGANOMETALLIC CHEMISTRY III

Editors-in-Chief

D. Michael P. Mingos
University of Oxford, Oxford, UK

Robert H. Crabtree
Yale University, New Haven, CT, USA

Volume 12
APPLICATIONS III: FUNCTIONAL MATERIALS, ENVIRONMENTAL AND BIOLOGICAL APPLICATIONS

Volume Editor

Dermot O'Hare
University of Oxford, Oxford, UK

ELSEVIER

AMSTERDAM BOSTON HEIDELBERG LONDON NEW YORK OXFORD
PARIS SAN DIEGO SAN FRANCISCO SINGAPORE SYDNEY TOKYO

Elsevier Ltd.
The Boulevard, Langford Lane, Kidlington, Oxford OX5 1GB, UK

First edition 2007

The following article is a US Government work in the public domain and not subject to copyright:
5.12 TECHNETIUM ORGANOMETALLICS

The following material is reproduced with kind permission of Nature Publishing Group:
Figure 17 of 12.03 ORGANOMETALLIC DERIVED METALS, COLLOIDS AND NANOPARTICLES

British Library Cataloguing in Publication Data
A catalogue record for this book is available from the British Library

Library of Congress Catalog Number: 2006934994

ISBN–13: 978-0-0804-4590-8
ISBN–10: 0-08-044590-X

For information on all Elsevier publications
visit our website at books.elsevier.com

Printed and bound in Spain

06 07 08 09 10 10 9 8 7 6 5 4 3 2 1

Contents

Preface

The availability of remarkably efficient search engines has made the access to the relevant literature and specific facts remarkably quick and efficient, but the information retrieved is not always refereed, checked or placed in its appropriate context. As Henry Kissinger [1] has remarked: "The computer has solved the problem of storing knowledge and making a vast amount of data available. Simultaneously, it exacts the price of shrinking [one's] perspective". In this latest edition of Comprehensive Organometallic Chemistry we have tried to engage the best minds in the field to sift the literature in their area of expertise and distill it down to produce a readable summary of the essential material. We have instructed them to be comprehensive in their coverage and authoritative in their approach and thereby maintain the standard and reputation of the original Comprehensive Organometallic Chemistry published in 1982 and the Second Edition published in 1995. Both editions were edited by Professors Abel, Stone and Wilkinson. This Third Edition of Comprehensive Organometallic Chemistry (COMC-III) builds on the two previous collections and incorporates a vast amount of new knowledge published since 1993, and simultaneously interprets the developments by providing general and significant insights by leading experts in the field.

Those seeking a structured entry into the impressive field of organometallic chemistry will find, either the desired information itself, or at least a reference to the primary or secondary literature that covers the point at issue. In the COMC tradition, we hope that this work will be useful not only to experts, but also to workers in allied fields who need to turn to organometallic chemistry to solve some pressing problem. With this in mind we have devoted the first volume to fundamental principles in order to provide a helpful entry into this important field for graduate students and scientists whose primary expertise lies in other areas. We also hope that readers will dip into this work and develop numerous research ideas or encounter a myriad of surprising results. Indeed, the applications of organometallic chemistry continue to expand at a prodigious rate, hence the significant increase in the number of volumes devoted to applications in COMC-III (to organic synthesis, to functional materials, as well as environmental and biological applications). Organic chemists have edited the volumes on organometallic chemistry towards organic synthesis now organized by reaction type so as to be readily accessible to the organic community. The new volume on applications covers a wide range of topics from optoelectronics to clusters and nano-particles.

The forthcoming availability of the whole COMC (1982), COMC-II (1995) through to COMC-III series in a web format will further enhance the utility of the series, providing a truly comprehensive data source and an unparalleled depth of coverage. With these new features, we hope that the combined efforts of the volume editors and individual authors have not only expanded the database of the subject but also provided an expanding perspective for all who use it.

The authors of individual chapters, the editors of the volumes and the editorial staff at Elsevier have made a tremendous effort to produce such a monumental work on schedule. We should like to thank them all most sincerely for working so well together as a team and we are sure the readership will appreciate the mature perspective and insight which they have provided for them.

D. Michael P. Mingos
Robert H. Crabtree

[1] H. Kissinger, Does America Need a Foreign Policy?, Touchstone Press, NY, 2002.

Preface to Volume 12

Comprehensive Organometallic Chemistry III now contains an additional volume (Volume 12). It was decided that since organometallic compounds are now finding such a range of interesting and diverse applications outside the more traditional chemical ones that an additional volume was required. The volume focuses on the applications of compounds containing a metal-carbon bond in solid state synthesis and crystal engineering, molecular-based solids which might be of interest in the electronics industry, and the implications of organometallic compounds in medicine and the environment.

The material for Volume 12 is covered in 15 chapters which collectively encompass an amazingly diverse range of applications. It recognises that molecular organometallic chemistry has been extended to materials synthesis, and the magnetic, optical and electronic properties of molecular organometallic solids are of interest to a wider community. Contemporary organometallic chemistry is also making a major impact in the biological area and chapters devoted to sensors, and medicine have been included. The impact of organometallics on the environment has been addressed and green organometallic chemistry has been introduced as an alternative for the future.

The authors begin each of their chapters with a gentle introduction to their particular area of expertise for the non-specialist reader which they then develop into a comprehensively referenced review of the state-of-the-art in their discipline.

I would like to extend my warm thanks to the chapter authors for their efficient, helpful, cooperative and professional manner.

D. O'Hare

Editors-in-Chief

Michael Mingos has published more than 400 papers in inorganic, organometallic and theoretical chemistry. He has received numerous awards including the Corday-Morgan (1980) and Tilden (1988) Medals of the Royal Society of Chemistry, the Wilhelm Manchott Prize in 1995, the Michael Collins Award for Microwave Chemistry (1996) and was elected a Fellow of the Royal Society in 1992. He is perhaps best known for his contributions to the development of the polyhedral skeletal electron approach for inter-relating the structures of cluster compounds and their valence electron counts – commonly described as the Wade-Mingos Rules, but he has also developed a strong synthetic programme in cluster and supramolecular chemistry. He also pioneered the applications of microwave dielectric heating in organometallic and inorganic chemistry.

Currently Principal of St Edmund Hall and Professor of Inorganic Chemistry at the University of Oxford. He gained his B.Sc. at the University of Manchester (1965) and his D.Phil. at the University of Sussex (1968). He has subsequently received Honorary Degrees from both institutions. He became a Lecturer at Queen Mary College in 1971, before becoming a Fellow at Keble College, Oxford (1976–1992). In 1992 he moved to the Sir Edward Frankland BP Chair in Chemistry at Imperial College where he was elected Dean of the Royal College of Science in 1996.

His Editorial activities include a monograph on cluster chemistry, three undergraduate textbooks and many published reviews. He has also edited several books and served on the editorial boards of a number of international journals. He was Regional Editor of the Journal of Organometallic Chemistry from 1996 to 2006 and is Managing Editor of Structure and Bonding.

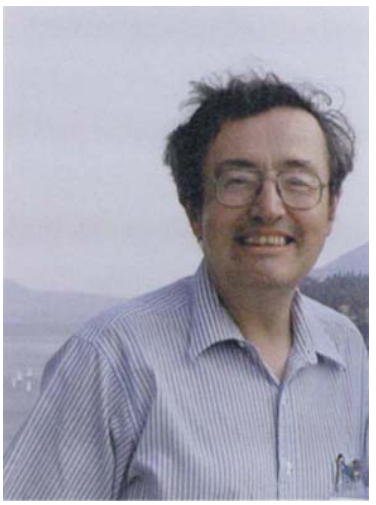

Robert Crabtree has published more than 400 papers in inorganic, organometallic and bioinorganic chemistry. He has received numerous awards including the Corday-Morgan (1984) Medal and Organometallic Chemistry Award (1991) of the Royal Society of Chemistry, the Organometallic Chemistry Award (1993) of the American Chemical Society, the Bailar Medal (U of Illinois, 2001), the Dow Lectureship (Berkeley, 2004) and the ISI Highly Cited Author Award (2000). He was chair of the inorganic chemistry division of the American Chemical Society (1998). He is known for the 'Crabtree catalyst' and contributions in alkane activation, sigma complexes, dihydrogen bonding, and molecular recognition in catalysis.

Currently Professor of Inorganic Chemistry at Yale University, he earned his B.A. at the University of Oxford (1970) and his D.Phil. at the University of Sussex (1973). He then became an Attaché de Recherche at the CNRS laboratory at Gif-sur-Yvette before moving to Yale in 1977.

His book, 'The Organometallic Chemistry of the Transition Metals' is now in its fourth edition (2005). He has also served on the editorial boards of a number of international journals. He was Regional Editor of the New Journal of Chemistry from 1998 to 2003 and is Editor-in-Chief of the 'Encyclopedia of Inorganic Chemistry'.

Editor of Volume 12

Dermot O'Hare was born in Newry, Co Down, and studied at Balliol College, Oxford University, where he obtained a B.Sc. in 1982 and his D.Phil in 1985 under the direction of Professor M.L.H Green. Subsequently, he was awarded a Royal Commission of 1851 Research Fellowship. He was a visiting research fellow at CR&D E.I. du Pont deNemours in Wilmington, Delaware in 1986/7 were he worked in the group lead by Prof J.S. Miller on molecular-based magnetic materials. In 1987 he returned to Oxford to a short term lectureship. In 1990 he was appointed to a permanent University position and a Septcentenary Tutorial Fellowship at Balliol College and in 1998 he became Professor. In 1996 he was honoured by the Institüt de France, Académie des Sciences as one of the top 50 leading scientists in Europe aged under 40. He was the Royal Society of Chemistry Sir Edward Frankland Fellow in 1996/67 and in 1997 he was awarded the Exxon European Chemical and Engineering Prize. His interests are wide ranging, and include exploratory synthetic organometallic chemistry, intercalation chemistry, time-resolved, in situ diffraction studies and the synthesis of meso- and microporous solids.

Contributors to Volume 12

A P Abbott
University of Leicester, Leicester, UK

S Barlow
Department of Chemistry, Georgia Institute of Technology, GA, USA

S Basharat
University College London, London, UK

J-M Basset
CNRS/CPE, Villeurbanne, France

S R Bayly
University of Oxford, Oxford, UK

P D Beer
University of Oxford, Oxford, UK

D Braga
Università degli Studi di Bologna, Bologna, Italy

D W Bruce
University of Exeter, Exeter, UK

J-P Candy
CNRS/CPE, Villeurbanne, France

C J Carmalt
University College London, London, UK

A E G Cass
Imperial College London, London, UK

B Chaudret
CNRS, Toulouse, France

C Copéret
CNRS/CPE, Villeurbanne, France

E Coronado
Universidad de Valencia, Valencia, Spain

P J Craig
De Montfort University, Leicester, UK

D L Davies
University of Leicester, Leicester, UK

R Deschenaux
Université de Neuchâtel, Neuchatel, Switzerland

P E Djurovich
Department of Chemistry, University of Southern California, CA, USA

B Donnio
Institut de Physique et Chimie des Matériaux de Strasbourg, Strasbourg, France

M Driess
Technical University Berlin, Berlin, Germany

P J Dyson
Institut des sciences et ingénierie chimiques, Lausanne, Switzerland

K A Francesconi
Karl-Franzens University Graz (Uni-Graz), Graz, Austria

J R Galán-Mascarós
Universidad de Valencia, Valencia, Spain

F Grepioni
Università degli Studi di Bologna, Bologna, Italy

D Guillon
Institut de Physique et Chimie des Matériaux de Strasbourg, Strasbourg, France

F Hapiot
Université d'Artois, Lens, France

C F Harrington
University of Leicester, Leicester, UK

E G Hope
University of Leicester, Leicester, UK

G Jaouen
CNRS UMR 7576, Paris, France

R O Jenkins
De Montfort University, Leicester, UK

J B Keister
University at Buffalo, Buffalo, NY, USA

N E Leadbeater
University of Connecticut, Storrs, CT, USA

L Maini
Università degli Studi di Bologna, Bologna, Italy

I Manners
University of Toronto, Toronto, ON, Canada

S Marder
Department of Chemistry, Georgia Institute of Technology, GA, USA

S Mathur
Leibniz-Institute of New Materials, Saarbrucken, Germany

Joel S Miller
University of Utah, Salt Lake City, UT, USA

E Monflier
Université d'Artois, Lens, France

D O'Hare
University of Oxford, Oxford, UK

K Philippot
CNRS, Toulouse, France

M Polito
Università degli Studi di Bologna, Bologna, Italy

G A Solan
University of Leicester, Leicester, UK

A M Stuart
University of Leicester, Leicester, UK

M E Thompson
Department of Chemistry, University of Southern California, CA, USA

Contents of All Volumes

VOLUME 1 FUNDAMENTALS

VOLUME 2 COMPOUNDS OF GROUPS 1 TO 2 AND 11 TO 12

VOLUME 3 COMPOUNDS OF GROUPS 13 TO 15

VOLUME 4 COMPOUNDS OF GROUPS 3 TO 4 AND THE F ELEMENTS

VOLUME 5 COMPOUNDS OF GROUPS 5 TO 7

VOLUME 6 COMPOUNDS OF GROUP 8

VOLUME 9 APPLICATIONS I: MAIN GROUP COMPOUNDS IN ORGANIC SYNTHESIS

VOLUME 10 APPLICATIONS II: TRANSITION METAL COMPOUNDS IN ORGANIC SYNTHESIS 1

VOLUME 13 CUMULATIVE SUBJECT INDEX

12.01
Precursors to Semiconducting Materials

C J Carmalt and S Basharat, University College London, London, UK

12.01.1 Introduction and Scope

This chapter deals with organometallic compounds that find application as precursors to semiconductors. Volatile organometallic compounds are being increasingly employed for the deposition of compound semiconductors from the vapor phase by a technique called metalloorganic chemical-vapor deposition (MOCVD). This technique for depositing semiconductor thin films now has several alternative names, including OMCVD (organometallic CVD). The abbreviations MOVPE or OMVPE, in which VPE is defined as vapor-phase epitaxy, are also used to highlight the deposition of homo- or heteroepitaxial layers. In this chapter, the original term MOCVD is adopted. The technique MOCVD involves vapor transport of the metal as a metalloorganic compound. For example, GaAs can be deposited from the pyrolysis of trimethylgallium in the presence of arsine (AsH_3) at 600–800 °C. Typically, the semiconductor alloy is deposited on single crystal wafer substrates such that each layer adopts the same crystalline orientation as the substrate. In order to control the composition of the semiconductor, the concentration of the precursors can be varied in the vapor phase. MOCVD is a complex process, which involves a series of gas-phase and surface reactions. However, the main steps involved are (i) evaporation and transport of the precursors, (ii) formation of the semiconductor alloy via pyrolysis of the precursors, and (iii) removal of decomposition products from the reactor zone. This technique allows precise control of purity, layer thickness, and doping concentrations, and can be used to grow large areas of semiconductor layers. Thus, it can be used to produce multilayer devices.

Aspects of the formation of semiconductors from organometallic compounds have been covered in reviews published since 1994 by Jones,[1] Cowley and Jones,[2] Neumayer and Ekerdt,[3] Gleizes,[4] O'Brien and co-workers,[5,6] Buhro,[7] Maury,[8] and Getman and Franklin.[9] Compound semiconductors have also been deposited using other techniques, such as chemical-beam epitaxy (CBE) and metalloorganic molecular-beam epitaxy (MOMBE). Some

of the precursors employed for the deposition of semiconductors have also been used for the formation of nanoparticles (see Section 12.01.3).

12.01.2 Organometallic Precursors for the Growth of III–V Semiconductors

12.01.2.1 Introduction—Conventional Precursors

Informative reviews of the growth techniques and structural, optical, and electrical properties and applications of III–V semiconductors have been published by Strite *et al.*,[10] Ambacher,[11] and Jones and O'Brien.[12] Some of the applications of III–V semiconductors are described in Table 1.

This section focuses on the use of organometallic complexes for the deposition of III–V thin films via dual-source routes using conventional precursors. The conventional approach to growing III–V materials is where separate group III and V precursors are combined (Table 2). The metalloorganic precursors traditionally employed are readily available commercially and have convenient vapor pressures. Manasevit first described the use of organometallic compounds to deposit semiconductor films in 1968.[13] These original precursors introduced by Manasevit are still favored today. The volatile group III trialkyls, trimethylgallium (Me_3Ga), trimethylaluminum (Me_3Al), and trimethylindium (Me_3In), in combination with the group V hydride gases (ammonia, phosphine, and arsine) result in III–V layers that contain relatively low levels of carbon contamination. This is due to the large quantity of "active" atomic hydrogen produced by the pyrolysis of the group V hydride gas and thus clean removal of carbon-containing fragments from the growth surface. The optical and electrical properties of semiconductor films grown by techniques such as MOCVD and CBE are critically dependent on the purity and nature of the metalloorganic precursor. For example, the decomposition characteristics heavily influence the incorporation of intrinsic impurities, such as carbon, in the film. Extrinsic impurities, for example, Zn, Si, and solvent, depend on the synthetic and purification routes. Significant developments in metalloorganic precursor technology have been reported in the past 10 years, as discussed below.

12.01.2.1.1 Group III nitrides

The conventional MOCVD of AlN, GaN, and InN involve the reaction of Me_3Al, Me_3Ga, or Me_3In with ammonia (NH_3).[14] The high thermal stability of NH_3 results in the need for high substrate temperatures (>1,000 °C) and high V/III ratios (e.g., 2,000 : 1) are required to inhibit nitrogen desorption. Therefore, due to the high temperatures, the choice of substrate material available is limited. Recent reports on the deposition of GaN from R_3Ga and NH_3 have attempted to overcome the large lattice and thermal mismatches between GaN and most commercially available substrates (e.g., sapphire). This mismatch makes the deposition of single crystal, defect-free materials difficult, as crack formation can occur when the thickness of the grown film exceeds a critical thickness.[15] This, in turn, may be responsible for weak light-emitting diode (LED) light output. However, high-quality GaN films have been obtained on (0001) sapphire substrates by exposing the substrates to Me_3Ga and NH_3, one at a time.[16,16a] The best films were obtained at 800–900 °C with a thin GaN buffer layer pre-deposited at 500 °C and a V/III ratio of 5,000. The formation of high-quality GaN films at relatively lower temperatures than conventional MOCVD has been attributed to the migration enhancement of the Ga adatoms on the grown surface and the easy access of cracked N–H radicals.[16,16a] Similarly, separate admittances of Me_3Al or Me_3Ga and NH_3 resulted in AlN and GaN films on Si(111) and Si(001)

Table 1 Applications of III–V semiconductors

III–V Semiconductor	*Applications*
GaN	Blue light-emitting diodes (LEDs)
GaP	Red LEDs, photocathodes
InP	Weather radar devices, Gunn diodes
GaAs	Solar cells, LEDs
Ga(AsP)	Red LEDs
AlGaAs	Heterostructure lasers, solar cells, field effect transistors (FETs)
InGaN	Green LEDs
InGaP/AlGaInP	Red laser pointers
GaSb/AlGaSb	Thermal imaging devices, environmental sensors
AlGaInP	Yellow/green LEDs

Table 2 MOCVD of III–V compounds

III–V Semiconductor	*Reactants*	*Growth temperature* (°C)
AlN	Me_3Al, NH_3	1,250
GaN	Me_3Ga, NH_3	925–975
GaP	Me_3Ga, PH_3	700–800
InP	Me_3In, PH_3	650
GaAs	Me_3Ga, AsH_3	600–750
Ga(AsP)	Me_3Ga, AsH_3, PH_3	700–725
AlGaAs	Me_3Al, Me_3Ga, AsH_3	650–800
AlAs	Me_3Al, AsH_3	700
InGaAs	Me_3In, Me_3Ga, AsH_3	650
InGaAlP	Me_3In, Me_3Al, Me_3Ga, PH_3	750
AlSb	Me_3Al, Me_3Sb	450
GaSb	Me_3Ga, Me_3Sb	500–550
InSb	Me_3In, Me_3Sb	470
AlGaSb	Me_3Al, Me_3Ga, Me_3Sb	450

substrates at 1,000 °C.[17] The use of buffer layers, including AlN and GaN, lead to a marked improvement in luminescence and electrical properties of GaN and crystalline quality. Thus, high-quality GaN films were achieved by using a high-temperature-grown AlN buffer.[18]

In order to grow GaN films with a lower defect density, silicon carbide (SiC) was chosen as an alternative substrate as it has a relatively small lattice mismatch with GaN. Single-crystalline hexagonal GaN films have been grown on 3C-SiC/Si(111) substrates using a number of buffer layers by MOCVD.[19] The use of buffer layers greatly improved the surface morphology and structural and optical qualities of the GaN film. Thus, well-orientated GaN growth along the *c*-axis with good surface morphology was achieved. Zirconium diboride, ZrB_2, layers provide an electrically conductive lattice-matched substrate for GaN growth.[20,21] The lattice mismatch between ZrB_2 and GaN on the basal plane is only about 0.6%, compared with 14.9% in the case of sapphire. GaN films were grown on metallic ZrB_2 by MOCVD using Me_3Ga and NH_3. Cross-sectional transmission electron microscopy (TEM) showed that when ZrB_2 is exposed to an ammonia atmosphere, cubic ZrB_xN_{1-x} is formed on the surface, which protects the nucleation of GaN. However, high-quality GaN growth was achieved by depositing a very thin AlN (from Me_3Al and NH_3) or GaN layer at low temperature.

Surface decomposition pathways for a number of precursors can provide information on reaction mechanisms. This is important as it can lead to more appropriate precursor design and optimized growth conditions. For example, the surface chemistry of two related Al precursors, Me_3Al and Me_2AlH, has been studied by high-resolution electron energy loss spectroscopy (HREELS). For both complexes, the dominant surface species at room temperature is based on intact methyl groups, such that Me_2Al is formed from either loss of a methyl group from Me_3Al or hydrogen from Me_2AlH.[22] A surface methylene group (CH_2) was identified at higher temperatures, which suggests that there is a competing decomposition pathway involving hydrogen abstraction from a surface methyl group (Figure 1).

Further information about the surface chemistry occurring during the MOCVD of AlN was provided by Fourier-transform infrared (FTIR) and X-ray photoelectron spectroscopy (XPS) studies on mixtures of Me_3Al

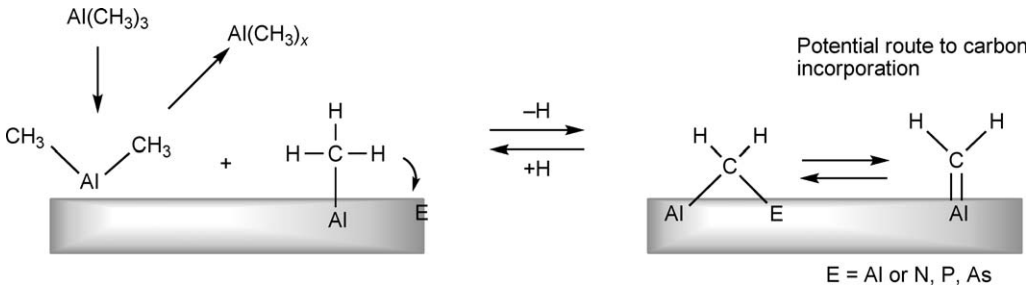

Figure 1 Mechanism for the proposed decomposition of Me_3Al on an AlE (E = N, P, or As) surface.

and NH_3 adsorbed on α-Al_2O_3.[23] These studies suggested that co-adsorption of Me_3Al and NH_3 at room temperature results in the surface adduct [Me_2AlNH_3] and adsorbed NH_3. Increasing the substrate temperature to 600 K and above resulted in the appearance of a vibrational band corresponding to AlN, which suggests the formation of extended (Al–N) networks on the surface. AlN is then formed by the elimination of H_2 at the surface from the $Al(NH_2)_2Al$ species (Scheme 1). This decomposition pathway is the potential route to carbon incorporation during epitaxial growth of III–V semiconductors. In general, greater carbon incorporation in Al-based alloys is observed in comparison to Ga-based alloys. The increased bond strength of Al–C (Al–CH_3 272 kJ mol^{-1}) compared with Ga–C (Ga–CH_3 247 kJ mol^{-1}) results in an increased number of methyl radicals strongly bound to an Al atom on the substrate surface.

The surface decomposition of Et_3Ga on GaAs(100) has been investigated due to its extensive use in the CVD growth of III–V films.[24] Deuterium labeling indicated that decomposition of the surface ethyl group proceeds exclusively via a β-hydride elimination mechanism (Figure 2). Thus, during hydride elimination, an alkyl group hydrogen is transferred to the surface. This transfer occurs above the temperature where hydrogen desorbs from Ga or As surface sites (480–510 K), and so the surface-bound hydrogen immediately desorbs dissociatively.

AlN and GaN films have been grown on sapphire by laser photochemical vapor deposition at temperatures 600–950 °C (1–5 torr).[25] The precursors Et_3Ga and NH_3 for GaN and Me_3Al and NH_3 were employed. Photochemical vapor deposition is a direct consequence of the ability of short wavelength radiation ($\lambda < \sim 300$ nm) to rupture the chemical bonds in many CVD precursors. Indeed, kinetic modeling of the growth rate dependence on laser pulse energy indicated that the NH_2 radical is the dominant species, photolytically produced. The growth of $(11\bar{2}0)$-orientated GaN films was achieved in the presence of 193 nm photons. Thus, the surface kinetics was being driven by photochemistry in the gas phase. Microwave plasma MOCVD has been used to deposit high-quality GaN thin films in a nitrogen–hydrogen microwave plasma.[26] Trimethylgallium was employed as the Ga precursor, and the primary N-atom precursors were speculated to be NH radicals. The deposit was identified as stoichiometric GaN using XPS and powder X-ray diffraction (XRD) and the material was highly orientated along the c-axis.

Molecular-beam epitaxy (MBE) is another technique that has been used to grow high-quality GaN thin films. Conventional MBE involves the employment of gaseous sources of the elements as precursors. However, a hybrid technique called MOMBE has been developed, which uses metalloorganic species for the group III elements combined with plasma-activated nitrogen or ammonia for the group V species.[27] MOMBE of GaN has been achieved using Me_3Ga or Et_3Ga combined with atomic nitrogen from a plasma source or ammonia. During the growth of GaN, these reactive nitrogen species can react with the decomposition products of the trialkylgallium to form volatile compounds, which effectively reduce the growth rate. The loss of active nitrogen has been suggested to be due to the formation of ammonia from a reaction between hydrogen and active nitrogen and the formation of hydrogen cyanide through a reaction between hydrogen, carbon, and nitrogen. The formation of

$$2Me_2AlNH_{3(ads)} \xrightarrow[300–600\,K]{} MeAl(NH_2)_2AlMe_{(ads)} + 2CH_{4(g)}$$

$$MeAl(NH_2)_2AlMe_{(ads)} \xrightarrow[600–1050\,K]{} Al(NH)_2Al_{(ads)} + 2CH_{4(g)}$$

$$Al(NH)_2Al_{(ads)} \xrightarrow[600–1050\,K]{} 2AlN_{(ads)} + H_{2(g)}$$

Scheme 1

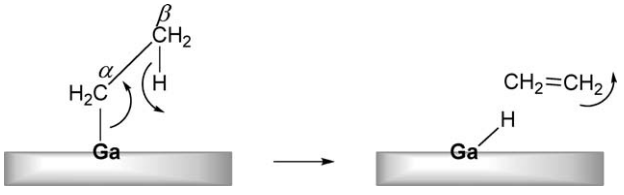

Figure 2 β-Hydride elimination from a coordinated ethyl group to give ethylene and surface-bound hydrogen.

ethenylamine via reaction of active nitrogen and ethyl radicals from Et_3Ga was observed when triethylgallium was employed as the Ga source. The above could also account for carbon incorporation during the growth of GaN. In the past 10 years, much effort has also been put toward the development of III–V materials technology grown from trialkylgroup III species and group V trihydrides, including violet-blue GaN LEDs,[28] InGaN/AlGaN double-heterostructure blue LEDs,[29,30] InGaN/GaN LEDs,[31,32,33] AlGaN[34] and AlGaN/GaN heterostructure field effect transistor (HFET).[35]

Single-source precursors, of the type $[Me_2MN(H)R]_n$, have been employed for the deposition of semiconductor films (Section 12.01.2.2.1). The successful formation of semiconductor films from these compounds resulted in the use of similar species formed *in situ* in the vapor phase prior to layer growth.[36] The aim of the method was to combine the advantages of low growth temperatures typical in the use of single-source precursors with the high growth rates associated with high vapor pressure reagents. Atmospheric pressure (AP)CVD of Me_3Al and the volatile primary alkylamines, Bu^tNH_2 and Pr^iNH_2, at 400–600 °C afforded AlN films with variable levels of residual carbon and oxygen present (4.7–17.0 at.% by auger electron spectroscopy (AES)). Post-growth oxidation of the amorphous AlN films was the cause of the oxygen contamination. However, the carbon impurities were attributed to the decomposition of surface-adsorbed methyl radicals derived from Me_3Al. The mechanism of AlN growth from Me_3Al and RNH_2 ($R = Bu^t$ or Pr^i) was proposed to proceed via the gas-phase formation of elimination products, such as $[Me_2AlN(H)R]_2$ (**1**, $R = Bu^t$; **2**, Pr^i), prior to film deposition (Scheme 2). The *t*-butyl and *i*-propyl group may be eliminated via β-hydride elimination when these complexes are pyrolyzed on or near the substrate. The result of this would be the formation of intramolecular Al–N bonds and growth of stoichiometric AlN. Support for this mechanism was obtained by the formation of AlN directly from compounds **1** and **2** (Section 12.01.2.2.1).[37] Interestingly, Bu^tNH_2 and R_3Ga ($R = Me$, Et) did not result in the formation of GaN and only droplets of Ga metal were formed.[38] This was attributed to the weaker Lewis acidity of R_3Ga in relation to Me_3Al, which in turn would result in the dissociation of any adducts rather than elimination reactions.[39,39a,39b]

In an attempt to reduce the carbon contamination in AlN films, Bu^tNH_2 was used in combination with $Bu^t{}_3Al$.[40] Atmospheric pressure MOCVD at 500–600 °C afforded AlN films, which on deposition of a protective Al overlayer by pyrolysis of $Bu^t{}_3Al$ at 400 °C, resulted in the prevention of post-growth oxidation of the films. AES indicated that the AlN films contained residual carbon (4.7–7.2 atom.%), and thus $Bu^t{}_3Al$ has no significant advantages over Me_3Al for growth of AlN from R_3Al/RNH_2 mixtures. These results suggest that the decomposition of the organic radical of RNH_2 may play an important role in carbon incorporation since high-purity Al films have been deposited from $Bu^t{}_3Al$.[41]

Trimethylsilylazide (Me_3SiN_3) has been utilized as an alternative nitrogen source for the formation of AlN films, when used in combination with Me_3Al.[42] AlN films were deposited by atmospheric pressure MOCVD at 300–450 °C, and notably no silicon was detected by AES. The proposed mechanism for the formation of AlN from Me_3SiN_3 and Me_3Al involved the formation of $[Me_2AlN_3]$ **3** in the gas phase with concomitant production of tetramethylsilane

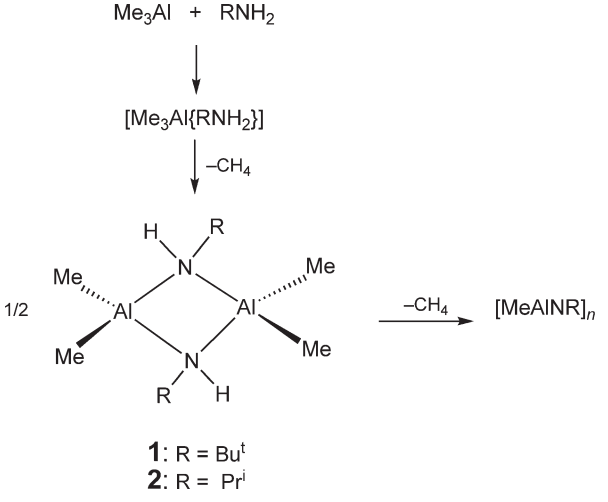

Scheme 2

(Me_4Si), according to Equation (1). Carbon was present at a level of 9.8%, probably due to the decomposition of Al–Me groups on or near the substrate.

$$Me_3Al + [Me_3SiN_3] \longrightarrow \underset{\mathbf{3}}{[Me_2AlN_3]_n} + Me_4Si \quad (1)$$

Tetramethylsilane is a relatively stable species, which would be unlikely to be pyrolyzed below 450 °C, and so Si would be transported effectively away from the growth zone. Support for the proposed mechanism was obtained from the *ex situ* reaction of Me_3SiN_3 and Me_3Al, which produced Me_4Si, as detected by mass spectroscopy.[42] Interestingly, the attempted formation of GaN from Me_3SiN_3 and Me_3Ga was unsuccessful. This is presumably due to the weaker Lewis acidity of Me_3Ga relative to Me_3Al. In contrast, epitaxial GaN films have been grown by low-pressure (LP) CVD (LPCVD) from hydrazoic acid (HN_3) and Et_3Ga.[43] This method of depositing epitaxial films is superior to the traditional routes (using trialkylgallium and NH_3) for two main reasons. First, the labile nitrogen source, HN_3, results in lower temperature deposition (600 vs. >800 °C). Second, the III/V ratios employed were 1 : 5, whereas growth techniques involving NH_3 require ratios of at least 1 : 2,000. The GaN films produced from Et_3Ga and HN_3 crystallized in the expected wurtzite structure and were slightly polycrystalline. However, due to the toxic and explosive nature of hydrazoic acid, this method has not found widespread application.

Dimethylhydrazine (Me_2NNH_2) was thought to be an attractive nitrogen source because it has a lower decomposition temperature (50% decomposition occurs at 550 °C) than ammonia, which is only 30% decomposed at 900 °C. Growing GaN by MOCVD from the reaction of Me_3Ga[44,45] or Et_3Ga[46,47] and Me_2NNH_2 was found to be similar to the growth of GaN using ammonia with respect to growth scheme and temperatures. For example, at temperatures above 900 °C, smooth epitaxial films could be obtained via a two-dimensional growth mode. At lower temperatures, GaN was deposited but growth proceeded in three dimensions resulting in rough surfaces. A similar growth pattern was observed when NH_3 was used as the group V source. The proposed film growth mechanism is depicted in Figure 3.[48] The first step involves the diffusion of Me_3Ga and $MeNNH_2$ molecules from the gas phase to the surface of the substrate. The adsorbed Me_3Ga and $MeNNH_2$ molecules on the surface sites are in equilibrium with their own native gaseous molecules and then reaction occurs to form GaN, probably via intermediate species of the type Me_2Ga, MeGa, NH_2, and NMe_2. Thus, the reaction of Me_2Ga and NH_2 was

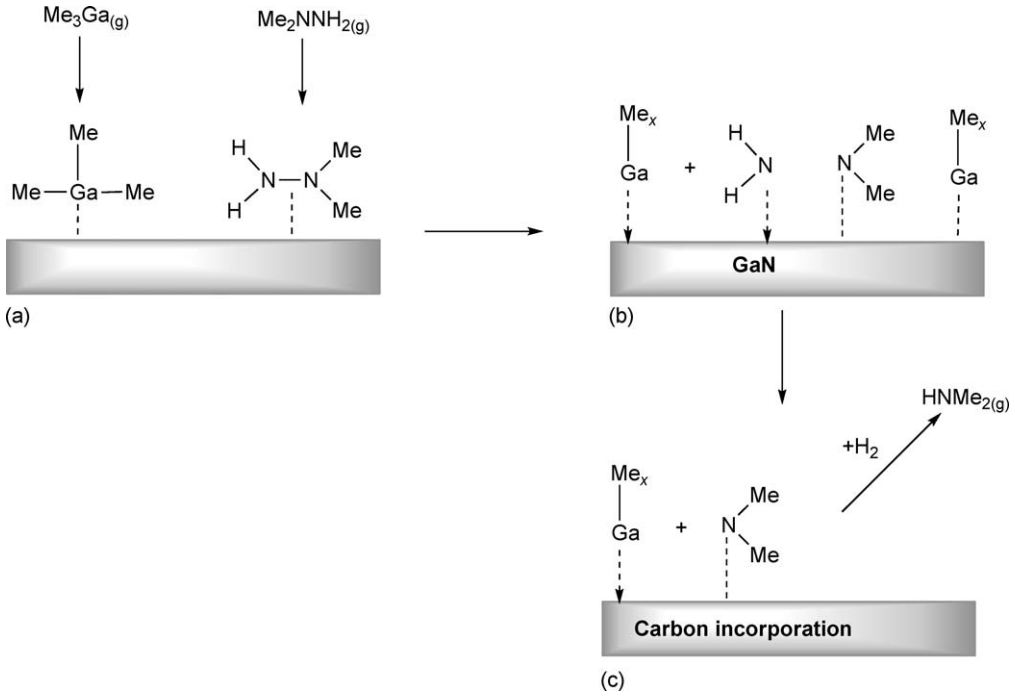

Figure 3 Proposed film-growth mechanism of GaN from Me_3Ga and Me_2NNH_2: (a) diffusion and surface adsorption; (b) surface reaction to form GaN; (c) carbon incorporation or reaction with H_2.

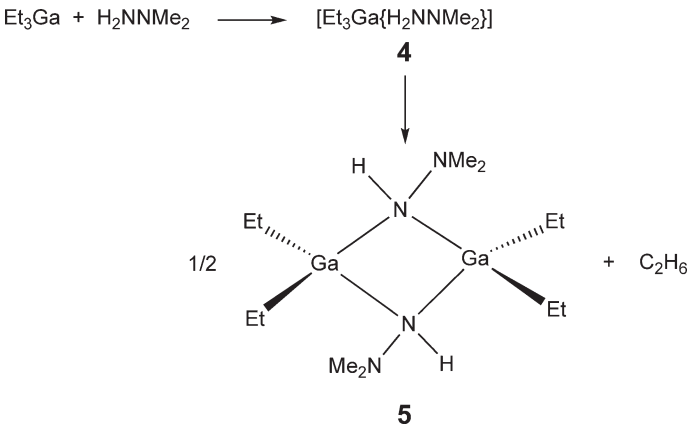

Scheme 3

proposed to be the main route for GaN growth due to smaller steric hindrance. Carbon incorporation in the films was assumed to be due to both MeGa and NMe_2. However, the introduction of H_2 would reduce carbon via reaction with NMe_2 to form stable species such as dimethylamine, which in turn could desorb away from the substrate surface.

Co-pyrolysis of Me_2NNH_2 and Et_3Ga in H_2 at ambient temperature indicated that an adduct and intermediate dimer are formed at low temperatures, as shown in Scheme 3.[49] The dimers began to decompose at 400 °C with the production of ammonia and the decomposition completed at 850 °C. Evidence for the formation of a similar adduct between Me_3Ga and Me_2NNH_2 was also obtained from pyrolysis studies.[50]

Epitaxial GaN layers were grown from Me_3Ga and Bu^tNNH_2 at 923–958 K by MOCVD.[51,52] Interestingly, films deposited using Bu^tNNH_2 have much less carbon content than those using $MeNNH_2$. This result is due to β-hydride elimination of the *t*-butyl ligand of Bu^tNNH_2 to form a stable hydrocarbon species.[53] Low-temperature atomic layer growth (ALG) of AlN has been achieved on Si(100) using $MeNNH_2$ and $[AlH_3\{NMe_2Et\}]$ **6**.[54] The technique of ALG involves flowing the source gases into the reactor in separate, sequential steps. Exposure temperatures of 660 K for $MeNNH_2$ and 420 K for compound **6** were selected. The growth was suggested to proceed through the dehydrogenation of AlH_xNH_y species generated during the ALG of AlN from $MeNNH_2$ and compound **6**.

1,1-Dimethylhydrazine has been used successfully as a liquid-phase nitrogen precursor for the growth of the cubic phase of GaN (from Me_3Ga and Me_2NNH_2) on GaAs (deposited from Me_3Ga and AsH_3[55,56] or Bu^tAsH_2).[57,58] In addition, the growth of a range of alloys at low temperature has been achieved using Me_2NNH_2, including GaN_xP_{1-x},[59] GaN_xAs_{1-x},[60,60a–60c,61] InN_xAs_{1-x},[62] GaInNAs,[63,63a–63c] and GaAsSbN.[64] Group III sources employed were Me_3Ga, Et_3Ga, or Me_3In and group V included Me_2NNH_2, PH_3, Bu^tAsH_2, AsH_3, Me_3Sb, and Et_3Sb, depending upon which alloy was grown. Gallium nitride passivation layers have also been grown *in situ* on near-surface $In_xGa_{1-x}As$/GaAs quantum wells from Me_3Ga, Me_3In, and Bu^tAsH_2 using Me_2NNH_2 as the nitrogen source.[65] However, the combustion or decomposition of dimethylhydrazine is strongly exothermic, causing a potential safety hazard and restricting its widespread use in MOCVD. Furthermore, nitrogen trifluoride and hydrazine have been shown to be more efficient nitrogen sources than unsymmetrical dimethylhydrazine for the growth of GaAsN and (In)GaAsN (from Et_3Ga or Me_3Ga, Me_3In, and AsH_3).[66]

Trialkylaluminum compounds, such as Et_3Al and Me_3Al, are the most commonly used metalloorganic Al sources. However, trialkylaluminum compounds are characterized by the presence of Al–C bonds which can lead to significant levels of trace carbon in the resulting semiconductor films. The carbon is thought to be the result of decomposition of methyl radicals (Figure 1) strongly bound to an Al atom on or adjacent to the growth surface.[67] Efforts to overcome this problem include the use of amine adducts of alane (AlH_3). Thus, the reaction of trimethylamine alane $[AlH_3\{NMe_3\}]$ **7** with NH_3 was shown to afford AlN at temperatures as low as 127 °C.[68] Annealing at temperatures above 900 °C resulted in greater AlN formation but with chemisorbed NH_2 remaining on the surface. However, the high reactivity and low decomposition temperature of compound **7** can lead to enhanced gas-phase reactions and particle formation, non-uniform deposition on the substrate, and reactant depletion.[69] In order to use alane adducts for the deposition of semiconductor films, techniques that minimize interaction of reactants in the gas phase must be utilized. One method is low-pressure MOCVD where the gas-phase interactions are limited at reduced pressure. An

alternative is the application of ALG and both techniques have been employed for the deposition of AlN films from compound **6** and NH_3. Using ALG, the Al precursor **6** and NH_3 were delivered to the growth surface in separate steps in order to promote film formation through a sequence of surface reactions.[70] AlN films were deposited on a range of substrates (Si(100), Si(111), Al_2O_3) at 250–450 °C and were found to have carbon and oxygen contamination at the surface and smaller concentrations in the bulk film. By XPS, the N(1s) data showed the presence of chemically bonded H in the films as NH_{3-x} ($x = 0$–2) species. The reaction of NH_3 with **6** was found to be incomplete at temperatures below 277 °C resulting in unreacted NH_x species, but above 327 °C, the NH_x concentration was lower.

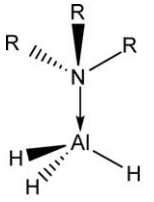

6: $NE_3 = NEt_3$
7: $NE_3 = NMe_2Et$

MOCVD of GaN commonly uses trialkylgallium and NH_3, with or without a H_2 carrier gas. In contrast, hydride vapor-phase epitaxy (HVPE) utilizes GaCl generated *in situ* via the reaction of liquid Ga with HCl in a hot zone. This technique has the advantages of high throughput and easy scaling to large wafer dimensions. However, slow gas-phase switching times have restricted the application of HVPE. Diethylgallium chloride, [Et_2GaCl], has been employed as the gallium precursor in the epitaxial growth of GaN, which produces a HVPE-like growth chemistry in an MOCVD system.[71] A two-step growth process was employed, which involved the deposition of a low-temperature GaN buffer layer from [Et_2GaCl] and NH_3, followed by high-temperature epitaxial growth of GaN. The growth rate decreased with increasing growth temperature, which has been attributed to a thermodynamic equilibrium limitation at the growth front. Additional reaction pathways are provided at the growth surface due to the presence of chlorine in the growth chemistry. The gas-phase reactions at the GaN growth front can be summarized, as shown in Scheme 4. The last reaction in Scheme 4 suggests an equilibrium between the steady-state concentrations of HCl and GaCl at the growth front. This reaction was thought to be the cause of the different surface morphology of the films formed from [Et_2GaCl] compared to those deposited from Et_3Ga. These reactions would provide reaction pathways for the removal of surface structure along with chemical defects and impurities.

12.01.2.1.2 Group III phosphides, arsenides, and antimonides

The conventional precursors employed for the deposition of group III phosphides and arsenides (Table 2) are the group III trialkyl species in combination with the group V hydride gases, arsine (AsH_3) and phosphine (PH_3). Although much of the research on the CVD reactions of R_3M and EH_3 has been published prior to 1994 (COMC (1995)), studies are still being conducted to understand the mechanism and surface chemistry of these reactions. A kinetic model based on the collision theory of chemical reactions has been proposed for the MOCVD of GaAs from Me_3Ga and AsH_3.[72] This model suggests that four heterogeneous deposition reactions occur: As-containing and Ga-containing species with As and Ga sites, as well as C-incorporation reactions. The surface reactions and kinetic phenomena of GaAs monomolecular layer growth using chemical adsorption of Me_3Ga and AsH_3 have been studied.[73] Molecular layer epitaxy (MLE) can produce single crystalline films, monolayer by monolayer, by injection of component gases of the materials, alternatively, onto the substrate in an ultrahigh vacuum (UHV) chamber. It was observed that the growth rate per cycle was greatly influenced by the surface stoichiometry of arsenic during growth.

$$(C_2H_5)_2GaCl \longrightarrow GaCl + 2C_2H_4 + H_2$$

$$GaCl + NH_3 \longrightarrow GaN + HCl + H_2$$

$$GaN + HCl \rightleftharpoons GaCl + 1/2\ N_2 + 1/2\ H_2$$

Scheme 4

The adsorption species was concluded to be $GaCH_3$ under monolayer growth conditions, as detected by a real time optical monitoring method.[74] A possible reaction of $GaCH_3$ with AsH_3 was proposed, as shown in Equation (2).

$$GaCH_{3(ad)} + AsH_3 \longrightarrow GaAs_{(ad)} + CH_4 + H_2 \quad (2)$$

Further information about the surface mechanisms was obtained from the *in situ* study of GaAs growth from Me_3Ga and Et_3Ga precursors by MOCVD. During growth with a constant AsH_3 partial pressure, three different phases were observed by reflectance anisotropy spectroscopy (RAS).[75,76] At high temperatures, all the processes on the surface are fast compared to the time for the growth of one monolayer. Kinetic limited growth was observed at low temperature where the surfaces are covered by adsorbates from undecomposed precursors. These prevent attachment and lower the growth rate causing increased carbon incorporation. At intermediate temperatures, the surfaces become Ga-rich during growth in the mass transport limited regime. Detailed studies into the dependence of carbon incorporation on growth conditions for group III arsenides grown with trimethylgroup III complexes and arsine have also been reported in the past 10 years.[77] To attempt to lower the carbon contamination, alternative group III sources have been explored, such as triisopropylgallium as the Ga source.[78] It was found that carbon-doping levels were at least two orders of magnitude lower than those in GaAs layers grown under similar conditions using Me_3Ga. In addition, the formation of heterostructures, such as InGaP/GaAs, using PH_3 and AsH_3 has been studied.[79] The growth of abrupt GaAs/InGaP/GaAs heterojunctions by MOCVD is difficult because of the intermixing of arsenic and phosphorus at the heterointerfaces.[80]

Much of the recent research has been aimed at developing safer liquid group V precursors for use in MOCVD of III–V materials. Both AsH_3 and PH_3 are extremely toxic gases and are generally stored in high-pressure cylinders such that there is a risk of toxic release during transport. To overcome transport problems, the use of on-site electrochemical generation of AsH_3 using a commercially available arsine generator has been investigated.[81] Epitaxial GaAs was deposited using Me_3Ga and the generated AsH_3. The AsH_3 is generated on-site and at-point-of-use from the electrolytic conversion of solid As source material, which substantially improves the safety of the MOCVD process in two ways. First, the AsH_3 is generated when needed, and second, only a small volume of AsH_3 is present. However, alternative group V precursors have been developed in an attempt to replace the group V hydride gases. A highly successful alternative to PH_3 is *t*-butylphosphine (Bu^tPH_2), although other primary alkyl phosphines (RPH_2) have been utilized.[82,83] High quality layers at significantly lower V/III ratios were deposited using Bu^tPH_2, and it is less hazardous than phosphine.[84,85] The thermal decomposition of a number of phosphines in the presence of Me_3In showed that the decomposition led to the formation of PH_3 and hydrocarbons either via a β-hydride or free-radical mechanism.[82] The onset of decomposition occurred at 350 °C for cyanoethylphosphine, 250 °C for benzylphosphine, and 300 °C for cyclopentylphosphine. However, premature reaction with Me_3In occurred with all of these phosphines at room temperature, resulting in the evolution of CH_4 and the deposition of an involatile liquid or solid. In contrast, Bu^tPH_2 does not pre-react with Me_3In and thus, has superior gas-phase chemistry for the deposition of III–V materials. The involatile product was proposed to comprise of polymers of generic formula $[MeInPR]_n$ (**11**, $R = CH_2CH_2CN$; **12**, $CH_2C_6H_5$; **13**, *c*-C_5H_9), which result via $[Me_2In(PHR)]_2$ **8–10**, from mixtures of Me_3In and RPH_2. A general mechanism for the proposed pre-reaction is presented in Scheme 5.

In contrast, Bu^tPH_2 is sufficiently bulky, due to the *t*-butyl group, to both shield and deactivate the In center in the species $[Me_2InP(H)R]$. Further attack by other Bu^tPH_2 molecules is inhibited, preventing chain propagation and polymer formation. Overall, Bu^tPH_2 is a suitable alternative to PH_3, can be stored in bubblers at room temperature, and mounted directly onto an MOCVD system. Furthermore, Bu^tPH_2 exhibits higher incorporation efficiency than PH_3, and so lower V/III ratios and substrate temperatures can be employed. A range of III/V phosphides have been deposited from the relevant trialkyl group III complex and Bu^tPH_2, including InP,[86,87] AlInP, AlInGaP,[88,88a,88b] InP/InGaAsP,[89,90] and GaAsP.[91] Interestingly, under self-limiting growth conditions, it was found that the carbon concentration in InP layer grown using Me_3In and Bu^tPH_2 was almost the same as using Et_3In and Bu^tPH_2.[92]

Cyclohexylphosphine (*c*-$C_6H_{11}PH_2$) has also been utilized as a group V source to InP.[93] Thus, LPCVD of Me_3In and *c*-$C_6H_{11}PH_2$ resulted in the formation of polycrystalline InP films on both Si and InP(100) substrates at temperatures above 580 °C. Pre-cracking of *c*-$C_6H_{11}PH_2$ at 800 °C causes the phosphine to decompose via a β-hydride elimination pathway to yield *in situ* PH_3 and cyclohexene. The V/III ratio precursor ratios were varied from 4.5 to 179.1 and improved surface morphology was observed for higher V/III ratios.

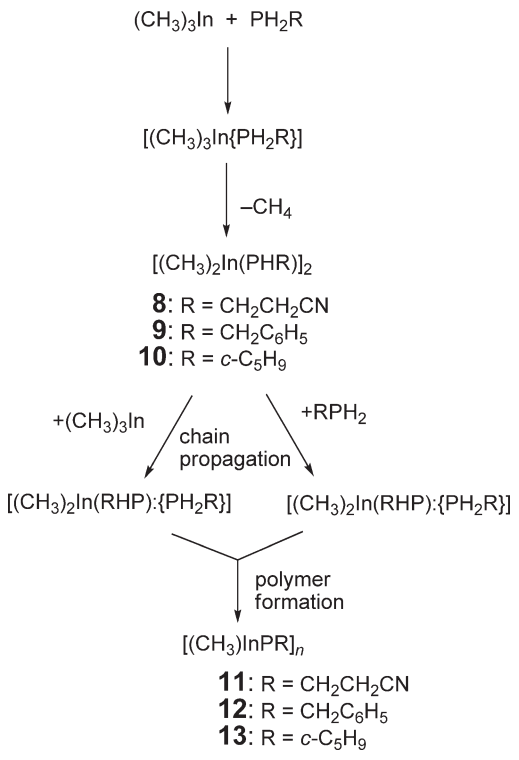

Scheme 5

A novel approach to InP films involved the reaction between the indium(I) precursor [In(C_5Me_5)] and white-P_4 by MOCVD.[94] The advantages of the reagents [In(C_5Me_5)] and P_4 include the following.

(i) Pre-reactions should be limited because In(I) derivatives have no tendency to form adducts with Lewis bases, such as phosphine.
(ii) Low-temperature (100–300 °C) epitaxial growth is possible, and so interdiffusion of epitaxial layer should not occur.
(iii) The high thermal stability of the pentamethylcyclopentadienyl group and the low reaction temperature should minimize the degradation of this organic substituent. Thus, the incorporation of carbon into the growing film should be prevented.

Epitaxial InP films were grown from [In(C_5Me_5)] and P_4 at 150–250 °C on InP substrates with a growth rate of 2–34 Åmin^{-1}. The low growth rate was attributed to either the low volatility of [In(C_5Me_5)] and/or the low dissociation rate of P_4. The growth rate was improved either by substituting white-P_4 for PH_3 or using a P_4-cracking furnace. Although [In(C_5Me_5)] has a low sublimation temperature (55 °C at 0.001 torr) and is non-pyrophoric, it is extremely reactive to oxygen and water, which would limit its widespread use in MOCVD.

Primary alkylarsines, $RAsH_2$, have been studied as potential replacements to AsH_3. Pyrolysis of hex-5-enylarsine, $CH_2{=}CH(CH_2)_4AsH_2$ **14** at 600 °C *in vacuo* resulted primarily in the formation of hex-1-ene, $CH_2{=}CH(CH_2)_3CH_3$.[95] The proposed mechanism for the decomposition of compound **14** involves the loss of H_2, as shown in Scheme 6. The next step consists of a bimolecular reaction between $CH_2{=}CH(CH_2)_4As$ and **14**,

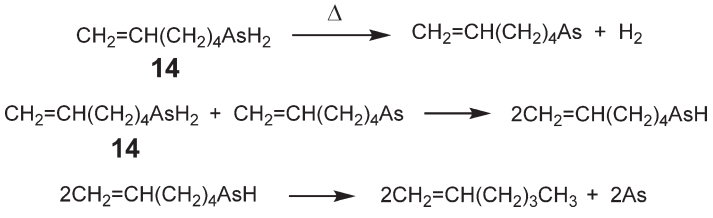

Scheme 6

resulting in the reductive elimination of hex-1-ene. In an H_2 atmosphere at room temperature, the reaction of Me_3Ga and compound **14** resulted in the elimination of CH_4 and the formation of a white solid, which was proposed to be $[Me_2GaAs((CH_2)_4CH{=}CH_2)H]_3$ **15**. However, above 350 °C, pyrolysis of Me_3Ga and $CH_2{=}CH(CH_2)_4AsH_2$ produced Me_2AsH, $MeAsH_2$, cyclohexane, and methylenecyclopentane, suggesting a stepwise free-radical decomposition mechanism. The mechanism shown in Scheme 6 does not account for the ability of $RAsH_2$ precursors to remove surface alkyl radicals and suggests that As atoms may be produced near or at the growth surface. This is in contrast to experimental data for GaAs growth using $RAsH_2$.

The most successful replacement for AsH_3 is tertiarybutylarsine (Bu^tAsH_2) as it is a liquid and has a convenient vapor pressure of 81 torr at 10 °C. Interestingly, experiments have shown a reduction in both O and C concentrations for GaAs and AlGaAs grown using Bu^tAsH_2 when compared to materials grown with AsH_3.[96] Thus, high-quality films of GaAs and AlGaAs have been grown from Me_3Ga, Me_3Al, and Bu^tAsH_2 by MOCVD at 640–700 °C.[97] It was observed that an increase in the V/III ratio caused a decrease in the growth rates of both GaAs and AlGaAs when using Bu^tAsH_2, which can be attributed to the excess group V species competing with group III atoms for group III surface sites. The carbon incorporation in AlGaAs films grown using Bu^tAsH_2 was found to be significantly lower than in layers deposited from arsine under higher V/III ratios and/or lower temperature conditions.[98] These studies indicate that the carbon originates from Me_3Ga and Me_3Al and not Bu^tAsH_2.[99] AlGaAs films have also been grown using CBE from triisopropylgallium (Pr^i_3Ga) and compound **7**. Trace quantities of diethyl ether in Pr^i_3Ga from the metalloorganic synthetic procedure can cause oxygen contamination, and by minimizing the concentration of diethyl ether, dramatic improvements in the AlGaAs purity were observed, particularly in terms of oxygen incorporation.[100] An alternative is to eliminate diethyl ether from the synthesis route, and adducts, of the type $[Pr^i_3Ga\{NR_3\}]$ (**16**, $NR_3 = NEt_3$; **17**, NMe_2Et), have been prepared from the reaction between gallium trihalide and Pr^iMgBr in trialkylamine solvent.[101] The use of compound **16** in combination with **7** leads to AlGaAs of improved purity.

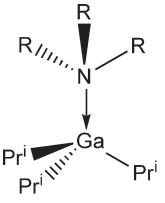

16: $NR_3 = NEt_3$
17: $NR_3 = NMe_2Et$

Atomic layer epitaxy (ALE) of GaAs has been achieved using the gallium precursors Me_3Ga, Et_3Ga, and trisneopentylgallium, $[\{(CH_3)_3CCH_2\}_3Ga]$, in combination with Bu^tAsH_2 at 470–550 °C.[102,103] Both Me_3Ga and $[\{(CH_3)_3CCH_2\}_3Ga]$ are self-limiting precursors due to the presence of methyl radicals during the growth process.[104] Differences in the surface structures were found between self-limiting and non-self-limiting conditions. In the former, well-defined terraces without droplets were observed. In contrast, the surface morphology of a non-self-limiting surface prepared from Et_3Ga showed the presence of droplets. For $[\{(CH_3)_3CCH_2\}_3Ga]$, the first step of the decomposition involves the pyrolytic fission of a Ga–neopentyl bond, and subsequent reactions of the molecule, including β-methyl elimination, result in a methyl radical attached to the surface. In contrast, Et_3Ga decomposes via β-hydride elimination, and a breakdown of self-limiting behavior occurs.

Tertiarybutylarsine has also been used for the growth of InAs/GaAs heterostructures,[105,106] InAs quantum dots,[107] InAs/InP single quantum well (QW) structures,[108] InGaAs/GaAs quantum dot lasers,[109] InGaAsP/InGaAs multiple step QW structure,[110,111] and InGaAsP/GaAs single QW laser diode structures.[112] In all cases, Bu^tAsH_2 was used in combination with the relevant trialkylgroup III species. CBE of AlAs with Me_3Al, Bu^tAsH_2, or $As(NMe_2)_3$ **18** at 750 °C showed significant differences in the resulting films.[113] Rough growth surfaces and films of poor crystal quality were obtained from growth with Bu^tAsH_2, whereas streaky patterns were observed with compound **18**. The growth rate was found to increase with increasing group V flux. Similarly, p-type GaAs films have been grown by CBE using compound **18** and Me_3Ga.[114] The use of **18** as the As source leads to a significant reduction in carbon contamination in GaAs and AlGaAs films grown by CBE, even in combination with methyl-based precursors.[115] The decomposition of compound **18** involves the formation of *N*-methylene imine and surface hydrogen via β-hydride elimination from $[N{-}CH_3]$ (Figure 4). Surface methyl radicals generated from the pyrolysis of Me_3Ga can be removed as the stable CH_4 molecule, which therefore reduces the carbon contamination in the resulting GaAs films.

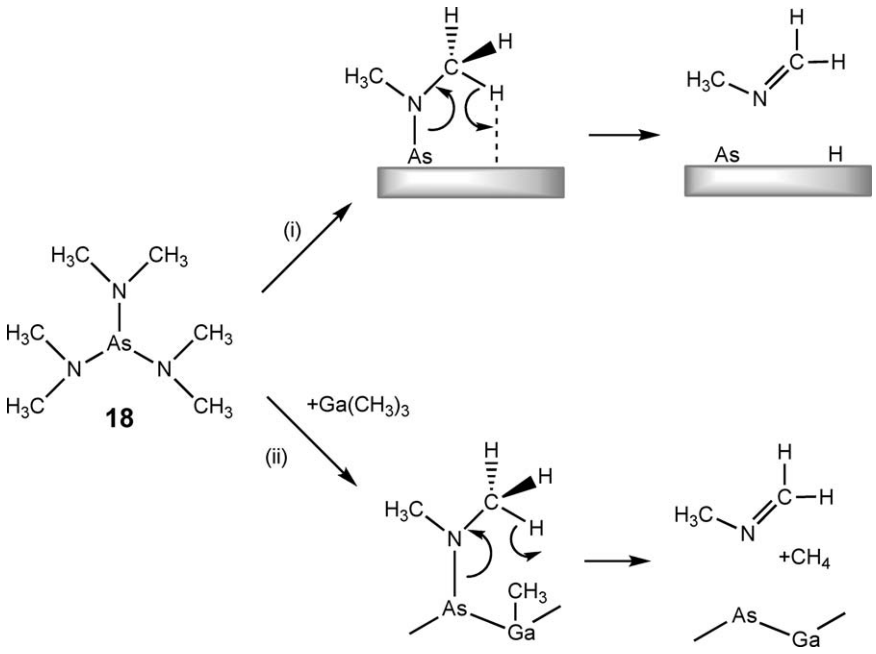

Figure 4 Decomposition mechanism of compound **18**: (i) β–hydride elimination from [N–CH_3]; (ii) removal of surface methyl radicals.

Diethyl-tertiarybutylarsine (Bu^tAsEt_2) and diethyl-isopropylarsine (Pr^iAsEt_2) are alternative precursors to AsH_3, which combine the advantages of the lower intrinsic toxicity associated with trialkylarsines with the use of β-hydride eliminating groups.[116] However, Bu^tAsEt_2 and Pr^iAsEt_2 have only low vapor pressures of 3.6 and 6.1 torr, respectively, at 25 °C. The use of Bu^tAsEt_2 and Pr^iAsEt_2 in combination with Me_3Ga or Et_3Ga resulted in p-type GaAs layers with 77 K mobilities in the range 3,500–4,100 $cm^2 V^{-1} s^{-1}$, indicating that these As sources do not provide sufficient active hydrogens to remove all the carbons during MOCVD. The incorporation of Ga and In into (GaIn)As grown by MOCVD used the group V precursors AsH_3, Bu^tAsH_2, and Bu^tAsEt_2.[117,118] Multilayer structures of (GaIn)As layers were grown alternately with AsH_3 and either Bu^tAsH_2 or Bu^tAsEt_2. It was found that the In/Ga ratio in the solid increased with decreasing number of As–H bonds in the group V precursor. These differences in In/Ga incorporation were attributed to increased binary growth rate of InAs in the alternatively grown (GaIn)As. The effect of increased In incorporation was greater when using Bu^tAsEt_2.

The vapor pressure of R_3Al compounds can be increased by replacing the methyl groups with bulky sterically hindered groups, such as *t*-butyl. These groups reduce the tendency of the R_3Al molecules to associate via bridging alkyl groups and $Bu^t{}_3Al$ is monomeric. Thus, the vapor pressure of $Bu^t{}_3Al$ is sufficient for MOCVD and high-quality AlGaAs layers have been grown from $Bu^t{}_3Al$, Et_3Ga, and AsH_3 at 650 °C.[119] Carbon was not detected in the resultant films, either by secondary ion mass spectroscopy (SIMS) or low-temperature (4 K) PL spectroscopy. The low levels of carbon in the AlGaAs layers grown using $Bu^t{}_3Al$, Et_3Ga, and AsH_3 are consistent with the high-quality Al films (C < 0.5 wt.%) grown from $Bu^t{}_3Al$.[120] The facile removal of the *t*-butyl radical from the substrate surface via β-hydride elimination affords Al films, which are carbon free (Figure 5).

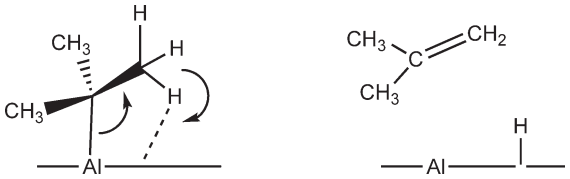

Figure 5 β-Hydride elimination from a coordinated *t*-butyl radical resulting in surface-bound hydrogen and isobutene.

A gallane–quinuclidine adduct (compound **19**) has been used as an alternative Ga source for the MOMBE growth of GaAs films.[121] The surface decomposition of compound **19** is similar to the related alane adduct, $[AlH_3\{NMe_3\}]$ **7**, and growth of GaAs is observed at much lower temperatures than those employed when Ga alkyl precursors are utilized.

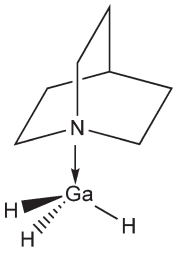

19

Unlike the other group V elements, antimony has no stable hydride at room temperature. Because of the lack of a stable hydride, most of the antimonide-based III–V semiconductors are grown using Me_3Sb.[122] This source is chosen because of its ready availability and its high vapor pressure. High-quality GaSb layers were grown by MOCVD using Me_3Ga and Me_3Sb at relatively high growth temperatures (~600 °C).[123,124] However, a range of alternative Sb precursors have been investigated in order to lower the growth temperature, which in turn should minimize interdiffusion between layers in heterostructures. Another problem with Me_3Ga and Me_3Sb is the possibility of carbon contamination due to methyl radicals. Epitaxial GaSb was deposited from Me_3Ga or Et_3Ga in combination with Me_3Sb, Et_3Sb, or $Sb(NMe_2)_3$ by LPCVD.[125,126] When using Me_3Ga as the Ga source, growth is kinetically limited in the temperature range 560–640 °C, whereas with Et_3Ga, it is mass transport limited in the range 525–640 °C. Pre-reaction between Et_3Ga and Et_3Sb or $Sb(NMe_2)_3$ resulted in surface defects; however, featureless morphology was obtained for GaSb layers deposited from Me_3Ga or Et_3Ga and Me_3Sb. The electrical properties of the resulting films were found to be optimal for layers grown with Et_3Ga and Me_3Sb or Et_3Sb, the most robust combination being Et_3Ga and Me_3Sb. Alternatively, Et_3Ga and Bu^tSbMe_2 were used to deposit GaSb films on GaAs substrates.[127] This combination provided more efficient growth and good island nucleation resulting in thick layers.

Tris(dimethylamino)stibine, $Sb(NMe_2)_3$, has been used, in combination with Me_3In, to grow high-quality InSb epitaxial layers at 275–425 °C.[128,129] It was suggested that the decomposition of Me_3In may be accelerated by $Sb(NMe_2)_3$ via a free-radical mechanism and the carbon contamination reduced by reaction of NMe_2 radicals with methyl radicals to give the stable volatile molecule NMe_3. However, a more complex mechanism, such as that described above for compound **18** and Me_3Ga (Figure 4), may occur. InSb films grown from Me_3In and Bu^tSbMe_2 were similar to those deposited from $Sb(NMe_2)_3$.[128] Epitaxial layers of ternary and quaternary alloys, such as GaAsSb,[130] GaInAsSb,[131] InAsSb,[132] and AlGaAsSb[135] have been grown by MOVPE using a range of group III and V sources. The Sb sources utilized include Me_3Sb, $Sb(NMe_2)_3$, and Bu^tSbMe_2, and the As source employed was Bu^tAsH_2. In general, the conventional trimethyl compounds of the group III elements were used to deposit the alloys, although for InAsSb, triisopropylindium was used.

The growth of AlSb and other AlSb-containing alloys has proved to be the most challenging of all the antimony-containing III–V semiconductors. This difficulty is primarily due to the lack of suitable sources for the growth of AlSb at low temperatures and the resulting incorporation of excess amounts of carbon. The strong Al–C bond and lack of active hydrogen species, necessary for the removal of methyl radicals, results in heavy carbon contamination. However, AlSb films have been grown at 500 °C and 76 torr using trimethylamine alane **7** and Et_3Sb.[133] The ternary alloy, AlGaSb, was grown from $Bu^t{}_3Al$ and either Me_3Sb or Et_3Sb by low-pressure MOCVD.[134] The carbon contamination in the resulting films was significantly lower than that observed in layers grown with Me_3Al,[135] due to the β-hydride elimination pathway.

12.01.2.2 Single-source Organometallic III–V Precursors

An alternative method for lowering the growth temperature of III–V semiconductors is to use single-source precursors, which already contain an M–E (M = Al, Ga, In; E = N, P, As, Sb) bond at the core of the molecule, with various other ligands attached to each of the elements. The desired reaction pathway involves adsorption of the

precursor without breaking the M–E bond but with loss of the ancillary ligands. Single-source precursors potentially display a range of advantages over conventional MOCVD precursors, including the following.

(i) Reduced toxicity (AsH_3, PH_3 are eliminated from the CVD process).
(ii) Low-temperature growth is possible.
(iii) Pre-reaction is limited as there is only one precursor.
(iv) Air and moisture stability is possible.

However, single-source precursors have yet to be commercialized for the growth of III–V semiconductors due to their disadvantages, including the following.

(i) Low volatility, which renders the use of established MOCVD equipment difficult.
(ii) Epitaxial growth may be prevented by the low surface mobility of polynuclear decomposition fragments.
(iii) The control of stoichiometry can be difficult using single-source precursors, particularly in the growth of ternary and quaternary materials, for example $In_xGa_{1-x}As_x$.

Single-source organometallic precursors for III–V semiconducting materials have been reported. Many of the precursors to GaAs and GaP were reported prior to 1994, as discussed in a number of reviews[2,7–9] and mentioned in chapter 11, volume 1 of COMC (1995).

12.01.2.2.1 Group III nitride precursors

The trimethylaluminum–ammonia adduct $[Me_3Al\{NH_3\}]$ **20** was prepared by bubbling NH_3 through a solution of Me_3Al in pentane.[136,137] The adduct **20** was investigated as a single-source precursor to AlN in an attempt to achieve low growth temperatures while retaining sufficient precursor volatility.[136] Compound **20** is monomeric and thus expected to have a high vapor pressure for use in MOCVD. Indeed, polycrystalline AlN films were deposited on Si(100) substrates from **20** at 400–800 °C. In contrast, epitaxial AlN layers, suitable for use as buffer layers, were deposited from **20** on sapphire(0001) substrates at 900 °C. The carbon contamination in the resulting AlN films was low (0.6–4.8 at.%), which was attributed to the efficient removal of CH_3 radicals by active hydrogen deriving from the adjacent NH_3 groups attached to the Al center. Although the mechanism for the growth of AlN from **20** has not been established, it is likely to proceed, as shown in Scheme 7, via $[Me_2AlNH_2]_3$ **21**. This mechanism is different to that proposed for the gas-phase chemistry of Me_3Al and NH_3 by FTIR and XPS studies (Section 1.2.1.1);[23] however, sequential elimination of alkane and the formation of amide (NH_2) species is common to both proposed mechanisms. MOCVD of related complexes, of the type $[Me_2AlN(H)R]_2$ (**1**, R = Bu^t; **2**, R = Pr^i), afforded AlN films between 700 and 800 K.[37] Carbon contamination was observed in the resulting films and was mainly attributed to the methyl groups bonded to the aluminum atoms using mass analysis experiments. The *t*-butyl group was found to be a superior substituent to isopropyl since the deposition temperature was lowered by 50 K, less carbon was incorporated, and higher nitrogen content was observed. This is probably due to the *β*-hydride elimination of the *t*-butyl group being more effective at removal of methyl radicals from the growth surface.

The molecular precursor cyclotrigallazane, $[H_2GaNH_2]_3$ **22**, has no organic substituents, and should therefore yield carbon-free GaN. Compound **22** was synthesized from the reaction of $[H_3Ga\{NMe_3\}]$ **23** and ammonia.[138] Wells and co-workers later published the formation of **22** from $LiGaH_4$ and NH_4X (X = Cl, Br).[139] The use of $LiGaH_4$ in place

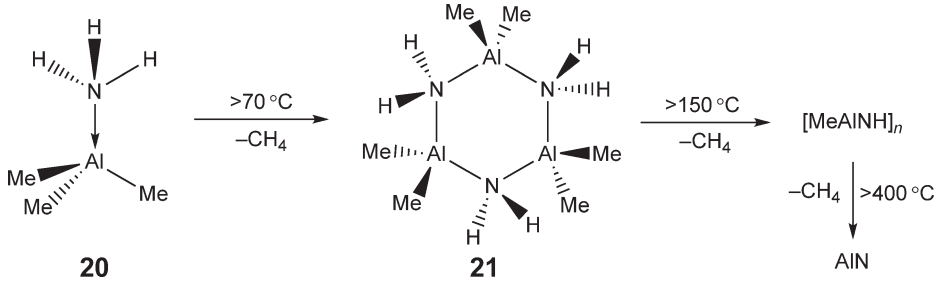

Scheme 7

of **23** eliminates one synthetic step as compound **23** is prepared from $LiGaH_4$. The structure of **22** consists of alternating H_2Ga and NH_2 units forming a six-membered $(GaN)_3$ ring which adopts a chair conformation.[140]

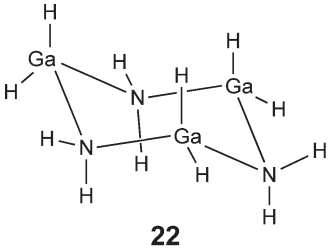

22

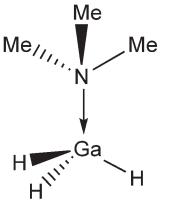

23

Pyrolysis of powdered samples of **22** under a range of conditions resulted in the formation of nanocrystalline GaN. The powder XRD data indicated that the nanocrystalline GaN had neither the pure wurtzite or pure zinc blende structure but a random arrangement of stacking planes with an equal amount of cubic and hexagonal planes.[138] Interestingly, changing the atmosphere of the pyrolysis from Ar to N_2 to NH_3 had no effect and the results obtained were the same. At 900 °C, the nanocrystalline GaN slowly converted into the known wurtzite phase. It was suggested that the formation of metastable GaN with such a high percentage of the cubic phase was a result of a topochemical reaction in which hydrogen elimination occurs along a reaction coordinate established by the structure of compound **22**. Thin films of polycrystalline GaN were also deposited on Si(100) using precursor **22**. Powder XRD showed that the polycrystalline GaN films had the wurtzite structure. Under ammonothermal conditions, **22** can be converted to nanocrystalline GaN.[141]

The trimeric compound $[Et_2GaNH_2]_3$ **24** has been prepared by the reaction of Et_3Ga with ammonia.[142] Crystalline GaN films have been grown by low-pressure MOCVD at 500–700 °C from compound **24**. The films deposited at 600 °C are crystalline without cracks but with not a very smooth surface. The relatively low carbon content (~2 at.%) in the resulting films is probably related to the facile evolution of ethylene via β-hydride elimination (Figure 2). The synthesis of the related dimeric compound $[Bu^t(H)Ga(NEt_2)]_2$ **25** was achieved by the addition of 4 equiv. of ^{t}BuLi to $[Cl_2GaNEt_2]_2$.[143] Compound **25** was found to be air stable, although it decomposes at elevated temperatures. Preliminary CVD studies using **25** showed that gallium-rich films are formed, as Et_2NH is a facile leaving group. These results suggest that it would be necessary to add an external nitrogen source, such as NH_3, in order to deposit GaN films from compound **25**.[143]

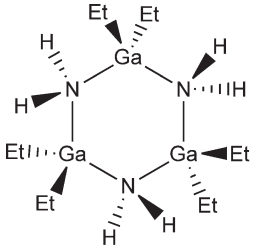

24

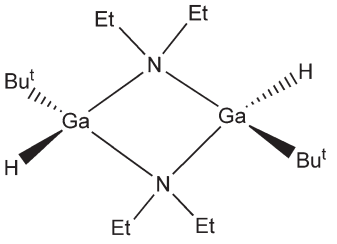

25

A series of precursors to group III nitrides that contain the azide (N_3) ligand have been characterized. The azide group contains a preformed strong Ga–N bond and reduces the number of Ga–C and N–C bonds, which potentially minimizes the possibility of carbon incorporation into the material during growth. A simple and stable molecular source for GaN is $[H_2GaN_3]$ **26**, which was prepared by the $LiGaH_4$ reduction of $[Br_2GaN_3]$.[144] The deuterated analog $[D_2GaN_3]$ **27** was synthesized in a similar manner from $LiGaD_4$ and $[Br_2GaN_3]$.[145] Mass spectral data indicate that both **26** and **27** are trimeric. These complexes are volatile at room temperature and can be distilled at 40 °C (0.20 torr) without decomposition. The decomposition pathway of compounds **26** and **27** represents one of the simplest chemical routes to GaN, as shown in Equation (3). Furthermore, only benign H_2 or D_2 and N_2 byproducts are formed.

$$[X_2GaN_3] \longrightarrow X_2 + N_2 + GaN \qquad (3)$$

26: X = H
27: X = D

The significant vapor pressure of compound **26** allowed rapid mass transport of the precursor at 22 °C and the facile decomposition pathway resulted in film growth at temperatures as low as 200 °C. Epitaxial GaN films were deposited from **26** at 650 °C via LPCVD.[146] The growth rate of the GaN films deposited was 800 Å min^{-1}. Despite these excellent growth properties, the high reactivity of **26** necessitates careful manipulation of the neat product, as a vigorous exothermic decomposition can result.

The perdeuterated derivative **27** is thermally more robust than **26** and thus easier to handle.[145] Gallium nitride films were grown from compound **27** on Si(111) substrates via AlN buffer layers using gas-source MBE. Monocrystalline wurtzitic GaN films were obtained at substrate temperatures as low as 275 °C. The high degree of crystallinity of GaN grown under these conditions is unusual at such low temperatures. Films grown at 400–500 °C from **27** were also monocrystalline and highly orientated. Depositions of compound **27** in the presence of atomic N at 650 °C resulted in epitaxial films of cubic and hexagonal structures. The related complex $[HClGaN_3]_n$ **28** comprises $[HClGaN_3]_3$ trimers in the vapor phase, which decompose readily at low temperatures by elimination of HCl and N_2 (Equation (4)).[147] GaN layers on sapphire and Si substrates were deposited from this compound. However, $[H_2GaN_3]$ is a superior precursor as no HCl is eliminated. The halide compound $[Cl_2GaN_3]$ was prepared from $[Cl_3Ga\{N_3SiMe_3\}]$ and has also been used to grow high-quality GaN films on Si.[148]

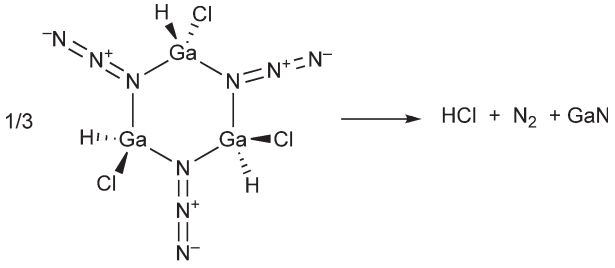

(4)

28

A range of dialkyl group 13 azides have been synthesized and employed as precursors to the respective nitrides. Polymeric $[Me_2GaN_3]_n$ **29** was synthesized by the reaction of $[Me_2GaCl]$ with NaN_3.[149] Thin polycrystalline GaN films with strong (0002) preferred orientation were deposited from compound **29** at 450–650 °C via LPCVD.[149] Films were deposited on GaAs(100), GaAs(111), sapphire(0001), and quartz. At higher temperatures, cracks were evident on the surface of the GaN films. The indium analog, $[Me_2InN_3]_2$ **30**, is dimeric, and was prepared from the reaction of Me_3In with HN_3.[150] InN thin films were deposited from **30** on Si(111) substrates at 350–450 °C by LPCVD. The films were shown to be nitrogen-deficient InN (In : N ≈ 1 : 0.6) by XPS with high surface impurity concentrations (C 20%, O 27%). Powder XRD showed that the films were polycrystalline with the expected hexagonal wurtzite structure. The related compounds $[R_2InN_3]_2$ (**31**, R = Pr^i; **32**, R = Bu^t) have been used to prepare InN fibers via thermolysis in reluxing diisopropylbenzene in the presence of H_2NNMe_2.[151]

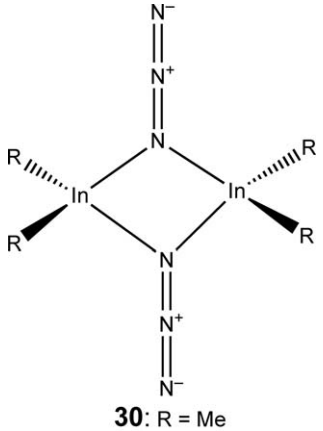

30: R = Me
31: R = Pr^i
32: R = Bu^t

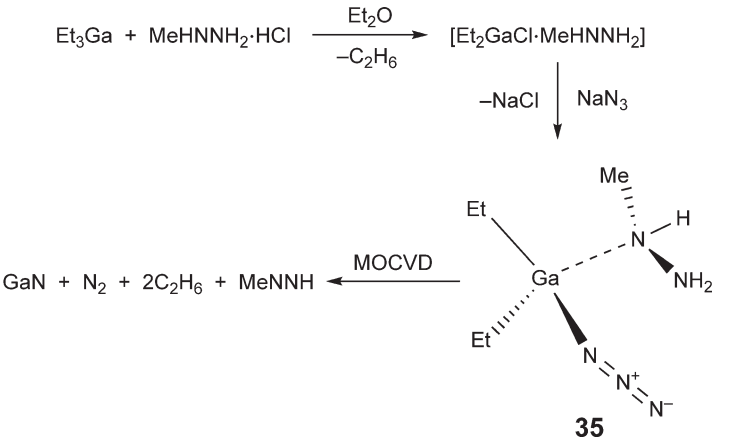

Scheme 8

Dibenzylaluminum and gallium azides, of the type $[(C_6H_5CH_2)_2MN_3(THF)]$ (**33**, M = Al; **34**, M = Ga), were investigated as precursors for the low-temperature synthesis of AlN and GaN.[152] However, pyrolysis studies indicated that both **33** and **34** decompose before becoming volatile and $C_6H_5CH_2$–$CH_2C_6H_5$ was produced. In contrast, epitaxial *h*-GaN films were grown on Si(111) substrates from $[Et_2GaN_3(Me(H)NNH_2)]$ **35** via high vacuum MOCVD at 400–800 °C.[153] Compound **35** was prepared as shown in Scheme 8. The atomic ratio of Ga : N in the resulting GaN films was found to be 1 : 0.94 by XPS with minimal carbon incorporation (~0.1 at.%). The gas-phase products of the MOCVD reaction were analyzed by gas chromatography-mass spectroscopy (GC-MS), which revealed the presence of N_2, C_2H_6, and MeNNH (Scheme 8). These results suggest that compound **35** undergoes protonation of the ethyl ligands by methylhydrazine to deposit GaN films. The related precursor $[Et_2GaN_3(Bu^tNH_2)]$ **36** also afforded crystalline GaN thin films on sapphire(0001) and GaAs(001) substrates at 500–800 °C via MBE.[154] Compound **36** was also used for the growth of GaMnN thin films.[154]

Dimethylhydrizodimethylgallium, $[Me_2GaN(H)NMe_2]_2$ **37**, was used to produce polycrystalline GaN thin films on GaAs(100) at 580 °C by LPCVD.[155,149] By scanning electron microscopy (SEM), the film had the appearance of precipitated particles, suggesting poor adhesion to the substrate. The poor morphology and film quality was attributed to Ga–N bond cleavage, which was observed to occur at 260 °C during pyrolysis studies. Thin films of AlN were grown on Si(100) and Si(111) substrates by LPCVD at 400–800 °C from $[R_2AlN(H)NMe_2]_2$ (**38**, R = Me; **39**, R = Et).[156] Polycrystalline AlN films were obtained on Si(111) using precursor **38** at 800 °C, whereas amorphous AlN films were afforded from **39** on Si(100) at lower temperatures.

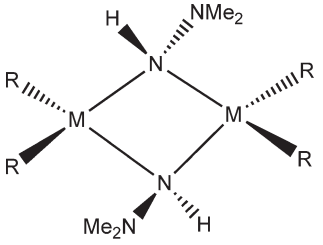

37: M = Ga; R = Me
38: M = Al; R = Me
39: M = Al; R = Et
40: M = Ga; R = H

Pyrolysis of the related precursor $[H_2GaN(H)NMe_2]_2$ **40** on a supported inert oxide film, HfO_2, has been studied recently.[157] Compound **40** combines the advantages of both hydrido and hydrazido ligands and exhibits remarkable stability and volatility compared to most gallium hydride compounds. Initial studies showed that compound **40** decomposed to gallium metal when heated in a hot wall LPCVD reactor.[158] However, temperature-programmed reaction (TPR), AES, and isothermal reaction spectroscopy (IRS) using a time-of-flight mass spectrometer indicated

$H_2GaNHNMe_{2(s)} \longrightarrow H_2GaNH_{(s)} + NMe_2^{\cdot}$

40

$H_2GaNHNMe_{2(s)} \longrightarrow HGaNH_{(s)} + HNMe_2$

$HGaNH_{(s)} \longrightarrow H_2 + GaN_{(s)}$

$H_2GaNH_{(s)} \longrightarrow 3/2\ H_2 + GaN_{(s)}$

Scheme 9

that the $[H_2GaN(H)NMe_2]_2$ dimers dissociate to monomers during dosing at 355 K and GaN starts to form at 550 K, with film-forming reaction becoming fast at 575 K.[157] Scheme 9 shows the proposed mechanism and the data is consistent with monomer N–N bond cleavage to form the hydrides $[H_2GaNH]$ and [HGaNH], which can eliminate hydrogen to produce GaN.

The MOCVD of AlN, GaN, and InN thin films using the single-source precursors $[(N_3)_2Ga(CH_2)_3NMe_2]$ **41**, $[(N_3)In\{(CH_2)_3NMe_2\}_2]$ **42**, $[(N_3)Al\{(CH_2)_3NMe_2\}_2]$ **43**, and $[Me_2AlN_3(^tBuNH_2)]$ **44** has been achieved.[159,160] Compounds **41–44** are non-pyrophoric and no additional nitrogen sources were used for the growth of the nitrides. Epitaxial AlN and GaN and polycrystalline InN[161] were deposited on sapphire or GaAs(100) substrates by low-pressure MOCVD using **41–44**. The polycrystalline films of InN were grown at 450 °C, whereas highly orientated, epitaxial films were obtained at 750 °C for GaN and 900 °C for AlN. It was suggested that the chelating *N,N*-3-dimethylaminopropyl group cleaves from the group III element center via *β*-hydride elimination to give $H_2C{=}CHCH_2NMe_2$, as shown by *in situ* mass spectroscopy.[159] Recently, pyrolysis of compound **41** was investigated by matrix-isolation FTIR spectroscopy.[162] These experiments showed that a *β*-hydrogen elimination had not occurred as no allyldimethylamine was detected. Thus, fragmentation of **41** probably occurs via homolysis of the M–C bond to afford a radical, of the type $Ga(N_3)_2$. These radicals are likely to trap H atoms to form $[HGa(N_3)_2]$, which can eliminate HN_3 to give $Ga(N_3)$. Both HN_3 and $Ga(N_3)$ were detected and these results suggest that gallium(I) azide is a key intermediate in the deposition of GaN.

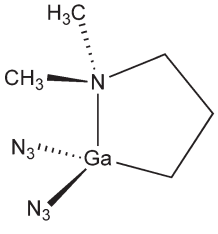

41

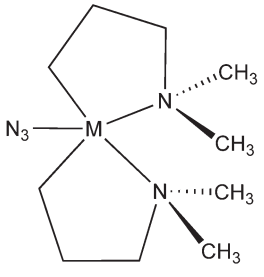

43: M = Al
45: M = Ga
42: M = In

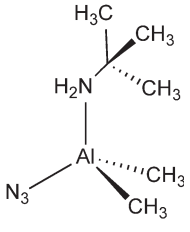

44

Further studies were reported on the azido complexes **41**,[163,164] $[(N_3)Ga\{(CH_2)_3NMe_2\}_2]$ **45**,[165] and **42**.[166] Epitaxial GaN films were deposited from compound **41** via low-pressure MOCVD in the absence of ammonia at temperatures above 700 °C.[164] Powder XRD of the resulting films showed that they were crystalline above 700 °C with epitaxial films obtained at 800 °C. Rutherford back scattering (RBS) analysis revealed a 1 : 1 ratio of Ga : N, which was also confirmed by electron probe microanalysis. Films of GaN were also grown from compound **45**;[165] however, those deposited using the gallium bisazide **41** were of higher quality suggesting that fewer Ga–C bonds and more Ga–N_3 moieties produce better films. Films of GaN were also deposited from **41** on sapphire substrates under low-pressure MOCVD conditions using NH_3 as a reactive gas.[167] Surprisingly, it was found that rather than the presence of ammonia, the substrate temperature is the dominant factor in the growth of highly orientated GaN films from **41**. Thus, no improvement of the structural quality of the resulting film was obtained with the

use of ammonia as a carrier gas. The related compound, $[(2,6\text{-}(Me_2NCH_2)_2C_6H_3)Ga(N_3)_2]$ **46**, was found to be very stable, and even at 600 °C no growth of GaN was observed, and the precursor was recovered unchanged.[168] The single-source precursor **42** produced dense crystalline InN thin films as described above.[169] However, InN nanowhiskers were deposited on sapphire substrates from **42** by employing a cold wall CVD reactor at 500 °C.[166]

The silyl and stannylamino group III complexes $[Cl_3Ga\{NH(SiMe_3)_2\}]$ **47**,[170] $[Cl_2Ga\{NH(SiMe_3)\}]_2$ **48**,[170,171] $[X_3M\{N(SnMe_3)_3\}]$ (**49**, M = Al, X = Cl; **50**, X = Br; **51**, M = Ga, X = Cl; **52**, X = Br; **53**, M = In, X = Cl; **54**, X = Br),[172] $[Et_2AlCl\{NH(SiMe_3)_2\}]$ **55**[173] have been synthesized and characterized. Pyrolysis of compounds **47–54** under inert conditions above 350 °C afforded polycrystalline powders of MN, with those prepared from the stannyl derivatives contaminated with metallic tin. The XRD patterns of the powders obtained at 550–650 °C from **48** were similar to the mixture of cubic and hexagonal GaN reported previously from the thermal decomposition of compound **22** (Figure 6).[170,138] Hexagonal GaN was isolated from the thermal decomposition of the precursor $[GaN(SiMe_3)_2(OSiMe_3)_2py]$ **56** via the elimination of $O(SiMe_3)_2$ and pyridine, as shown in Equation (5).[174]

$$\underset{\textbf{56}}{[GaN(SiMe_3)_2(OSiMe_3)_2py]} \xrightarrow{210\,^{\circ}C} GaN + 2O(SiMe_3)_2 + py \qquad (5)$$

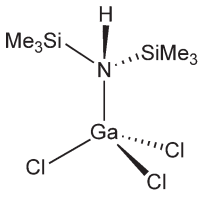

47

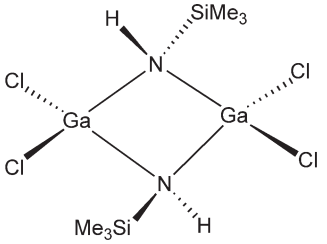

48

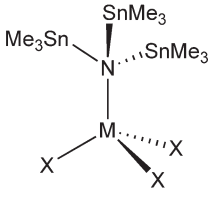

49: M = Al; X = Cl
50: M = Al; X = Br
51: M = Ga; X = Cl
52: M = Ga; X = Br
53: M = In; X = Cl
54: M = In; X = Br

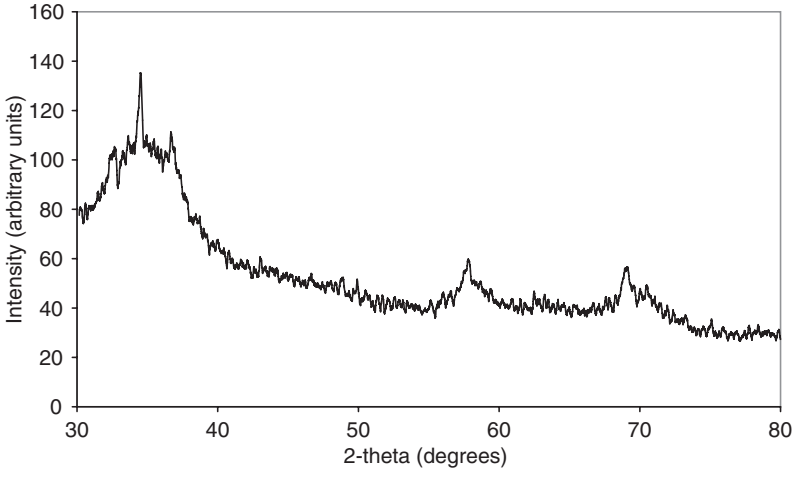

Figure 6 X-ray powder diffraction pattern of the yellow product obtained from the pyrolysis of compound **48** at 650 °C.

12.01.2.2.2 Group III phosphide, arsenide, and antimonide precursors

The chemistry of complexes involving a direct bond between group 13 and phosphorus, arsenic, or antimony was largely reported prior to 1994 (see COMC (1995)). More recent interest relating to their potential as precursors in the CVD of III–V semiconducting materials was mainly studied by Cowley and Jones,[2] Maury,[8] and Wells and co-workers.[175] Group III phosphide, arsenide, and antimonide precursors published since 1994 are discussed in this section.

The non-stoichiometric single-source precursor, $[Ga(AsBu^t_2)_3]$ **57**, has been employed for the growth of GaAs thin films.[176] The precursor was prepared by reacting Bu^t_2AsLi with $GaCl_3$ and was found to have a vapor pressure of 2×10^{-4} torr at 150 °C. Epitaxial GaAs films were grown from compound **57** at 415–590 °C in a CBE reactor at 8×10^{-6} torr. However, high levels of Si, O, and C impurities were detected by SIMS. Temperature-programmed desorption studies of **57** indicated that the Ga–As bond of the precursor was broken by 420 °C.

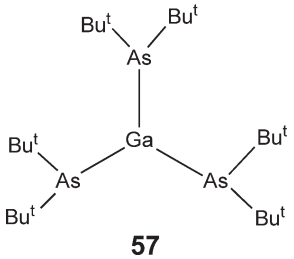

57

Dehalosilylation reaction of $[Bu^n_2MCl]$ with $P(SiMe_3)_3$ resulted in the isolation of $[Bu^n_2MP(SiMe_3)_2]_2$ (**58**, M = Ga; **59**, M = In).[177] Thermolysis of compound **58** at 400 °C produced GaP and Bu^nSiMe_3, as shown in Scheme 10. X-ray fluorescence analysis showed a 1:1 ratio of Ga:P and revealed a small impurity of silicon. These results show that **58** is a potential CVD precursor to GaP via a dealkylsilylation reaction mechanism. In contrast, thermolysis of the indium analog **59** gave a mixture of InP and metallic indium (Scheme 10). This suggests that a more facile β-hydrogen elimination pathway is occurring and butene was detected as a byproduct.

Thermolysis of $[Et_2GaP(SiMe_3)_2]_2$ **60** and the mixed-pnictogen compounds $[(Me_3Si)_2P\{\mu\text{-}GaEt_2\}_2As(SiMe_3)_2]$ **61** and $[(Me_3Si)_2P\{\mu\text{-}GaEt_2\}_2Sb(SiMe_3)_2]$ **62** resulted in the formation of crystalline GaP, GaP_xAs_{1-x}, and GaP_xSb_{1-x}, respectively.[178] Similarly, pyrolysis of $[Et_2GaAs(SiMe_3)_2]_2$ **63**, $[Et_2GaSb(SiMe_3)_2]_2$ **64**, and $[(Me_3Si)_2As\{\mu\text{-}GaEt_2\}_2Sb(SiMe_3)_2]$ **65** gave GaAs, GaSb, and $GaAs_xSb_{1-x}$, through a β-hydride elimination pathway.[179] Pyrolysis of the related complexes $[X_2GaP(SiMe_3)_2]_2$ (X = Cl, Br, I),[180] $[X_3GaP(SiMe_3)_3]$,[175] and $[Cl_3InE(SiMe_3)_3]$ (E = P or As)[181] afforded nanocrystalline ME materials. In addition, the compounds $[Me_2GaP(SiMe_3)_2]_2$ and $[Et_2InE(SiMe_3)_2]_2$ (E = P, As) have been prepared as potential precursors but no thermal decomposition or CVD studies have been reported.[182,183]

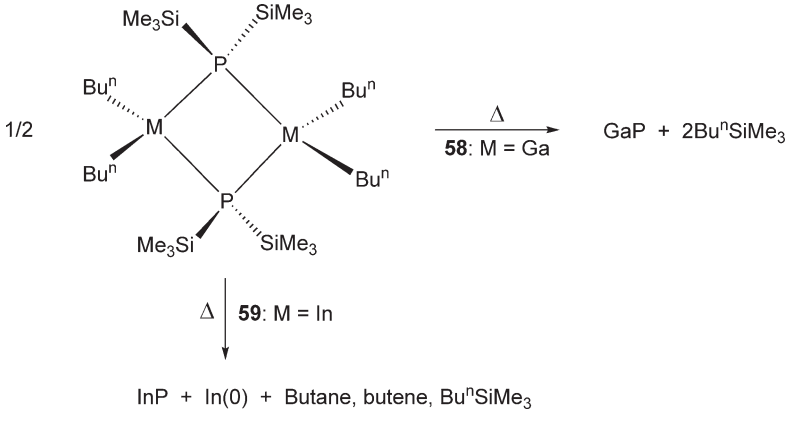

Scheme 10

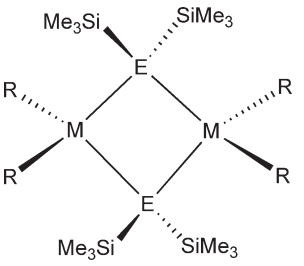

60: M = Ga; E = P; R =Et
63: M = Ga; E = As; R =Et
64: M = Ga; E = Sb; R =Et
68: M = Al; E = Sb; R =Et
69: M = Al; E = Sb; R =Bu^{i}

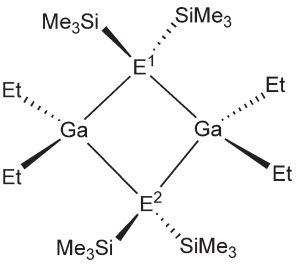

61: E^1 = P; E^2 = As
62: E^1 = P; E^2 = Sb
65: E^1 = As; E^2 = Sb

The phenylated compounds, [Ph_2GaEPh_2] (**66**, E = P; **67**, E = As), were synthesized from the reaction of Ph_3Ga with Ph_2EH.[184] Pyrolysis of **66** and **67** at 450 °C produced crystalline GaAs and GaP, which were characterized by powder XRD. Phenyl group migration was found to be the dominant reaction pathway to afford bulk GaAs and GaP.

Thin films of AlSb have been grown on polycrystalline Al_2O_3 and Si(100) from [$Et_2AlSb(SiMe_3)_2]_2$ **68** and [$Bu^{i}_2AlSb(SiMe_3)_2]_2$ **69** by high vacuum CVD in the temperature range 325–550 °C.[185] The best condition for high-quality AlSb films depended on the ligands attached to the Al center in the precursor. Thus, AlSb films with a 1 : 1 stoichiometry were deposited at 375–425 °C from compound **68**, whereas higher temperatures of 425–475 °C were required to obtain films of similar quality from **69**. Silicon impurities were observed at higher deposition temperatures, reaching 27.5% at 550 °C. The related compound [$Bu^{t}_2GaSbEt_2]_2$ **70**, has been employed as a precursor to GaSb thin films.[186] Crystalline GaSb films (sphalerite type) were deposited on Si(100) by high vacuum CVD at 350–550 °C. The Sb : Ga ratio ranges from 1.0 to 1.03, according to energy-dispersive X-ray analysis (EDXA); however, surface carbon contamination was observed by AES spectroscopy. Thermal decomposition of the Lewis acid–base adducts [$Bu^{t}_3Ga\{SbBu^{t}_3\}$] **71** and [$Bu^{t}_3Ga\{SbPr^{i}_3\}$] **72** at 275–450 °C resulted in the formation of crystalline GaSb particles.[187] Thermolysis of compound **71** gave crystalline, highly-orientated GaSb whiskers, which were not observed when **72** was employed as the precursor. Thermolysis of the trimeric compound [$Et_2InSb(SiMe_3)_2]_3$ resulted in the isolation of nanocrystalline InSb.[188]

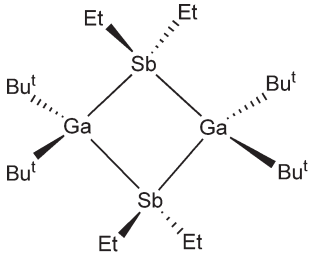

70

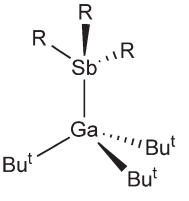

71: R = Bu^{t}
72: R = Pr^{i}

The reaction of $^{n}Bu_3In$ with pnictogen sulfides, As_2S_3, P_2S_5, and Sb_2S_5, resulted in the formation of the sulfur-bridged heterobinuclear complexes [$^{n}Bu_2In(SAs^{n}Bu)_3]_2S$ **73**, [$^{n}Bu_2InSP(S)^{n}Bu]_2S$ **74**, and [$^{n}Bu_2InSSb(S)^{n}Bu]_2S$ **75**, as shown in Equations (6)–(8).[189] Surprisingly, these compounds decomposed to give the corresponding indium pnictides InP, InAs, and InSb, by dip-dry pyrolysis at 500–600 °C. Little sulfur contamination of the resulting material was observed.

$$Bu^{n}_3In + As_2S_3 \longrightarrow Bu^{n}_2In\text{–}(SAsBu^{n})_6\text{–}SInBu^{n}_2 \quad (6)$$

73

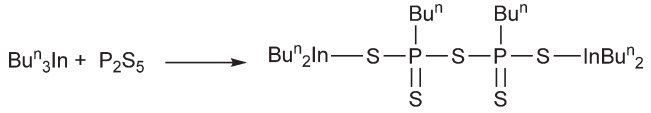

(7)

74

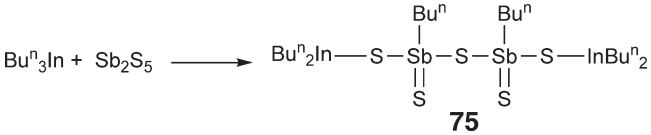

(8)

75

12.01.3 Organometallic Precursors for the Growth of II–VI Semiconductors

12.01.3.1 Introduction

The intermediate energy bandgaps of II–VI semiconductors have led to their use in a variety of devices.[190] For example, cadmium chalcogenides have applications in solid-state solar cells, sensors, and in FETs. The Zn- and Cd-based chalcogenides have been grown by both conventional MOCVD (Table 3) and using single-source precursors. Low-temperature growth is important because these II–VI materials interdiffuse and form defects at temperatures above ~500 °C.

12.01.3.2 Conventional and Single-source Approach to II–VI Materials

The growth of II–VI materials, such as ZnS/ZnSe or CdS/CdSe, is problematic using conventional precursors of the type R_2M (M = Zn or Cd), because these species pre-react in the gas phase with the group VI hydride gases (H_2S or H_2Se). This results in deposition of the II–VI material at the MOCVD reactor inlet. However, in the cases of ZnS and ZnSe, these problems have been overcome by the application of adducts, such as $[Me_2Zn\{NEt_3\}]$ **76** and $[Me_2Z\{NC_5H_5\}]$ **77**. These compounds prevent the pre-reaction between Me_2Zn and the group VI hydride by stabilization of intermediate elimination products, of the type [MeZnSeH], as shown in Figure 7.[191] The prevention of the pre-reaction allows transport of the Zn species into the growth zone. The pyridine adduct of [MeZn(S^{t}Bu)] has been isolated and characterized.[192,193] The X-ray structure determination showed that this compound exists as dimers, of the type $[MeZn(S^tBu)(NC_5H_5)]_2$ **78**, in the solid state, which provides some support to the mechanism proposed in Figure 7. Unfortunately, nitrogen or sulfur donors do not form strong enough complexes with Me_2Cd, as it is a weaker acceptor and so pre-reactions are not inhibited.[194]

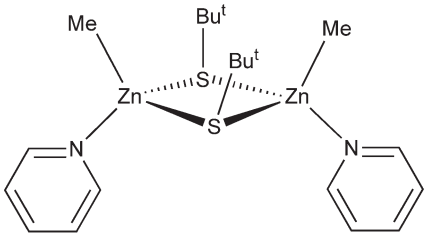

78

Table 3 MOCVD of II–VI compounds

II–VI Semiconductor	*Reactants*	*Growth temperature* (°C)
ZnS	Me_2Zn, H_2S	250–350
ZnSSe	Me_2Zn, H_2Se, H_2S	250–350
CdS	Me_2Cd, H_2S	300–400
CdSe	Me_2Cd, H_2Se	300–400
CdTe	Me_2Cd, Pr^i_2Te	350–400
CdHgTe	Me_2Cd, Pr^i_2Te, Hg	350–400

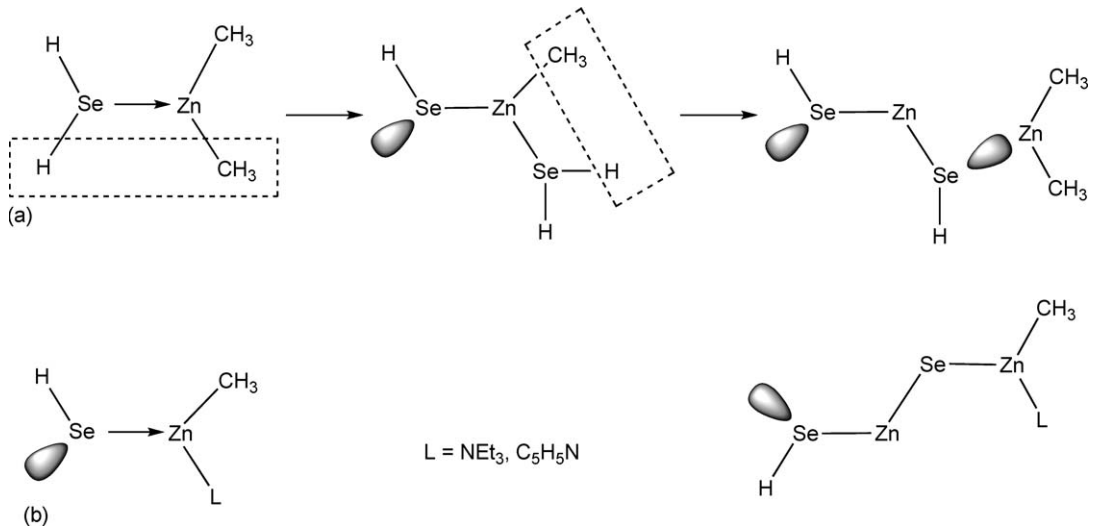

Figure 7 (a) Proposed mechanism for the pre-reaction between Me_2Zn and H_2Se; (b) possible mechanism for the prevention of the pre-reaction by nitrogen donors.

The growth of ZnS has been achieved from ^{t}BuSH and Me_2Zn or compound **76** at temperatures 325–400 °C, with little evidence of pre-reaction.[195] The optimum temperature was 405 °C, and the resulting ZnS films exhibited excellent surface morphology and good crystallinity.

The group VI precursors, R_2X_2 (R = Me or Et; X = S or Se), in combination with compound **76**, have enabled growth of ZnS, ZnSe, and ZnS_xSe_{1-x} below 400 °C via low-temperature pyrolytic MOCVD.[196,197] These temperatures are ~150 °C lower with respect to related MOCVD growth using alkyls of the type R_2X.[198] This was attributed to the lower thermal stability of R_2X_2 due to a weakening of the X–C bonds induced by the stronger X–X bond. In the case of R_2X, it was found that the use of light hydrocarbon species increases the thermal stability of the Se alkyl, such that $Bu^t{}_2Se$ allows growth at 300 °C, whereas Et_2Se and Me_2Se require temperatures of 450 °C.[199] For the Me_2Zn/$Bu^t{}_2Se$ system, the mass-transport limited growth occurred from 290–360 °C, whereas the compound **76**/$Bu^t{}_2Se$ combination moved to higher temperatures (320–380 °C).[200,201] The combination, Et_2Zn and $Bu^t{}_2Se$, has also been used to deposit ZnSe films.[202] Temperatures >480 °C are required when the group VI source is R_2X, to prevent layer interdiffusion. Therefore, the use of R_2X_2 allows low growth temperatures, and also reduced H incorporation is observed in the resulting films.

The introduction of nitrogen into ZnSe as an active p-type dopant is necessary for ZnSe-based semiconductor lasers. A number of nitrogen precursors have been employed, including $[Zn\{N(SiMe_3)_2\}_2]$, Me_3SiN_3, and triallylamine, in combination with $Bu^t{}_2Se$, $Pr^i{}_2Se$, and compound **76**, to grow ZnSe:N.[203] Trimethylsilylazide was found to be unsuitable as temperatures above 380 °C are required for the incorporation of nitrogen and it is not stable during storage. In addition, significant levels of electrically active nitrogen in the resulting ZnSe were not observed when $(allyl)_3N$ was employed. The most promising candidate is $[Zn\{N(SiMe_3)_2\}_2]$, since photoluminescence spectroscopy indicated that significant levels of nitrogen were incorporated in the ZnSe films when this precursor was used. However, possibly due to deactivation of electrically active nitrogen by hydrogen incorporation in the crystal lattice, the ZnSe layers remained n-type.

An alternative sulfur source, propylene sulfide $CH_3CH{=}CHS$, has a convenient vapor pressure (65 torr at 10 °C) and shows no pre-reaction with Me_2Cd.[204] High-quality CdS was deposited from Me_2Cd and $CH_3CH{=}CHS$ at 300–450 °C, and the growth rate was observed to increase with substrate temperature up to 400 °C. Above 450 °C, re-evaporation of CdS resulted in a reduction in the growth rate. However, the precursor $CH_3CH{=}CHS$ has a relatively high thermal stability, and fairly high VI/II ratios (14 : 1) are necessary.

Mixed alkyl/dithio- or diselenocarbamates are potential precursors to II–VI materials as they provide access to lower deposition temperatures. Zinc selenide, cadmium sulfide, and cadmium selenide thin films have been deposited from compounds of the type $[RM(E_2CNEt_2)]_2$ (**79**, M = Zn, E = S, R = Me; **80**, M = Cd, E = S, R = Me; **81**, M = Cd, E = Se, R = Me; **82**, M = Cd, E = S, R = CH_2CMe_3; **83**, M = Cd, E = Se, R = CH_2CMe_3).[205] The films were superior and higher growth rates were obtained as compared with those

grown from the parent thio- or selenocarbamates. Compounds **79–83** are dimeric in the solid state and obtained by the comproportionation of the metal dithio- or diselenocarbamate with the corresponding metal alkyl.[206] Compound **82** resulted in the deposition of CdS films on GaAs substrates by MOCVD at 425 °C. However, these complexes possess low vapor pressures, and the MOCVD must be carried out in high vacuum (10^{-2}–10^{-6} mbar), which may restrict their widespread application. The related alkyl diselenoimidodiphosphinato complex, $[MeCd\{(SePPr^{i}_{2})_{2}N\}]_{2}$ **84**, was prepared by the comproportionation reaction between Me_2Cd and $[Cd\{(SePPr^{i}_{2})_{2}N\}]$.[207] The structure of compound **84** is dimeric and similar to compound **83**. Hexagonal CdSe films were deposited from compound **84** by LP-MOCVD at 425–475 °C.

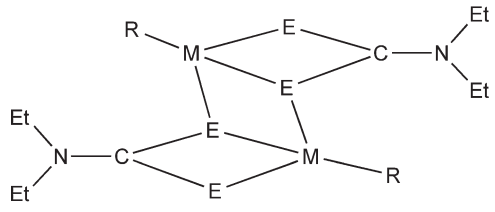

79: M = Zn; E = S; R = Me
80: M = Cd; E = S; R = Me
81: M = Cd; E = Se; R = Me
82: M = Cd; E = S; R = CH_2CMe_3
83: M = Cd; E = Se; R = CH_2CMe_3

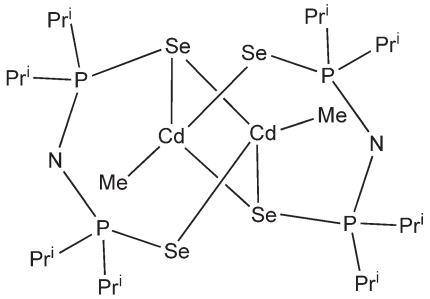

84

The mercury(II) analogs $[RHg\{(EP^{i}Pr_{2})_{2}N\}]$ (E = S: **85**, R = Me; **86**, R = Et; **87**, R = thienyl; **88**, R = 2-selenyl; **89**, R = Ph; E = Se: **90**, R = Me; **91**, R = Et; **92**, R = thienyl; **93**, R = 2-selenyl; **94**, R = Ph) have been synthesized from the reaction of the sodium salt of $NH(EP^{i}Pr_{2})_{2}$ with the appropriate alkyl/aryl mercury halide in methanol, according to Scheme 11.[208] Thermolytic decomposition of the aryl-substituted precursors resulted in the formation of HgE and therefore these complexes may be suitable CVD precursors.

A number of organic tellurides have been investigated as precursors.[209] Methyl(allyl) telluride (Me(allyl)Te) has previously been used as a precursor for the MOCVD growth of CdTe and HgTe. The decomposition of Me(allyl)Te alone and in combination with Me_2Cd and Hg in H_2 or He carrier gases has been studied using GC-MS.[210] The decomposition of Me(allyl)Te alone resulted in the formation of Me_2Te_2 as the major Te compound, with little Te deposited. Co-pyrolysis of Me(allyl)Te, Me_2Cd, and Hg in H_2 at 350 °C resulted in the formation of methane, 1-butene, 1,5-hexadiene, and Me_2Te. Evidence for the production of free radicals, such as ($Me^{\cdot}$) and ($MeCd^{\cdot}$), were also obtained. Due to the formation of Me_2Te, which is a poor precursor for telluride growth, Me(allyl)Te is not a

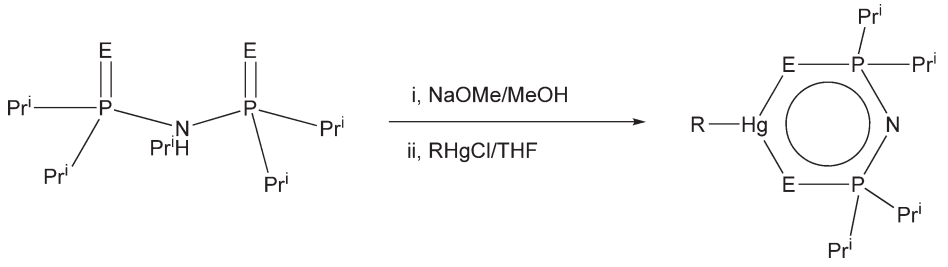

85: E = S; R = CH_3
86: E = S; R = CH_2CH_3
87: E = S; R = C_4H_4S
88: E = S; R = C_4H_4Se
89: E = S; R = C_6H_5
90: E = Se; R = CH_3
91: E = Se; R = CH_2CH_3
92: E = Se; R = C_4H_4S
93: E = Se; R = C_4H_4Se
94: E = Se; R = C_6H_5

Scheme 11

suitable precursor. In contrast, diisopropyltelluride has been shown to be a superior precursor for the deposition of tellurides, such as (Hg, Cd)Te, from Me_2Cd and Hg.[211]

12.01.4 Organometallic Precursors for the Growth of III–VI and IV–VI Semiconductors

12.01.4.1 Introduction

Access to unusual or metastable phases represents an area of great promise for single-source precursors. Such phases are possible either because of kinetic control of a metastable phase or because of entry into an unusual part of a phase diagram, since lower deposition temperatures are typically associated with single-source precursors. Controlling the deposited phase by the molecular design of the precursor has been investigated in the CVD of gallium and indium chalcogenides.[212] The III–VI compounds are semiconductors and are potential alternatives to II–VI materials in optoelectronic and photovoltaic devices.[213] In addition, they have a potential application as passivating layers for III–V devices and are related to ternary phases, such as $CuInE_2$ (E = S or Se) with uses in solar cells.[214] Tin sulfides have three main phases: (i) SnS_2, (ii) SnS, and (iii) Sn_2S_3, which is a mixed Sn(II)/Sn(IV) compound. The orthorhombic forms of tin sulfide (SnS) and tin selenide (SnSe) are narrow-bandgap semiconductors and have the potential to serve as efficient materials in photovoltaic applications.

12.01.4.2 Growth of III–VI semiconductors

Gallium sulfide can exist as a solid with several structural types and compositions. The wurtzite-type hexagonal structures, α-Ga_2S_3 and β-Ga_2S_3, as well as a monoclinic γ-Ga_2S_3 phase exist. The subvalent gallium sulfide (GaS) exists as a hexagonal layered structure. Thin films of α-Ga_2S_3 have been deposited by aerosol-assisted (AA)CVD from $[MeGa(SCOMe)_2(dmpy)]$ **95** (dmpy = 3,5-dimethylpyridine).[215] The decomposition of compound **95** shows two distinct steps of mass loss. The first step corresponds to the loss of dmpy and thioacetic acid and the second to the loss of acetone (Equation (9)). At relatively low temperatures of 275–310 °C, uniform crystalline Ga_2S_3 films were obtained from $[MeGa(SCOMe)_2(dmpy)]$ with no evidence of impurities from carbon or oxygen.

$$\underset{\mathbf{95}}{2[MeGa(SCOMe)_2(dmpy)]} \xrightarrow{\text{heat}} Ga_2S_3 + 2dmpy + 2Me_2C{=}O + MeC(O){-}S{-}C(O)Me \qquad (9)$$

Amine adducts of *tert*-butylthiolate gallium hydrides have been prepared as potential precursors to gallium sulfide; however, the compounds could not be readily isolated in high yield.[216] In contrast, the gallium cubane precursor $[Bu^tGaS]_4$ **96** has been used to deposit a novel metastable face-centered cubic phase of GaS, identified on the basis of electron and X-ray diffraction studies (Figure 8).[217] The formation of the metastable cubic phase in place of the thermodynamically favored hexagonal phase has been shown to be dependent on the stability of the precursor in the vapor phase. The Ga_4S_4 core of compound **96** was shown by mass spectroscopy to remain intact during the CVD process until surface initiation of film growth of the metastable cubic phase. Hence, the single-source precursor acts as a predesigned molecular motif to the solid-state phase. However, photolytic decomposition of **96** in the vapor phase produced thermodynamic hexagonal GaS.[218]

A series of related gallium chalcogenide cubanes, of the type $[RGaE]_4$ ($R = C_5Me_5$: **97**, E = S **98**, E = Se; **99**, E = Se, $R = C_5Me_4Et$), form Ga_2E_3 phases and not the metastable GaE phase.[219] This is indicative of core fragmentation during the deposition process, and the authors suggest that this is a result of the presence of the cyclopentadienyl ligand. This is supported by the formation of GaSe and GaTe films from the MOCVD of $[RGaE]_4$ (E = Se:**100**, $R = Bu^t$; **101**, $R = CEtMe_2$; **102**, $R = CEt_2Me$; E = Te: **103**, $R = Bu^t$; **104**, $R = CEtMe_2$; **105**, $R = CEt_2Me$).[220,221] Powder XRD of the films showed that the GaSe and GaTe films were polycrystalline hexagonal layered GaE structures.[222] The formation of these hexagonal structures was proposed to occur due to the fragmentation of the Ga_4E_4 cubane core during deposition to form trimeric "Ga_3E_3" building blocks. Mass spectral analysis of $[RGaSe]_4$ and $[RGaTe]_4$ shows prominent $[Ga_3E_3R_2]^+$ fragments, which were not observed for $[RGaS]_4$. It was proposed that while $[RGaS]_4$ decomposes via consecutive Ga–R bond cleavage, the decomposition of $[RGaSe]_4$ and $[RGaTe]_4$ involves loss of "RGaE" fragments (Equation (10)).

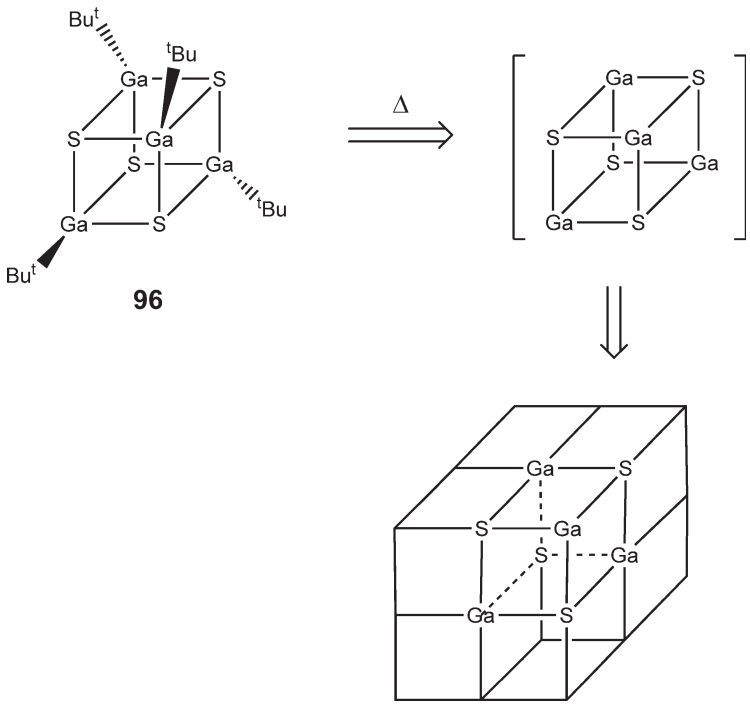

Figure 8 Proposed mechanism for the formation of cubic GaS from compound **96**.

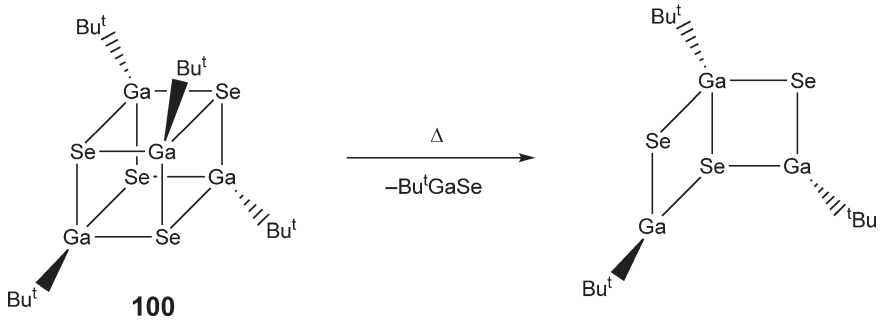

(10)

A facile chalcogenide exchange has been observed for the reaction between compound **103** and elemental sulfur or selenium, resulting in the stoichiometric formation of the appropriate cubane, $[Bu^tGaE]_4$ (compounds **96** and **100**), and metallic tellurium.[223] Hexagonal gallium sulfide (GaS) films have also been obtained using the silylated gallium–sulfur compounds $[R^1{}_2Ga(SSiR^2{}_3)]_2$ (**106**, $R^1 = Me$, $R^2 = Ph$; **107**, $R^1 = Me$, $R^2 = Pr^i$; **108**, $R^1 = Et$, $R^2 = Ph$; **109**, $R^1 = Et$, $R^2 = Pr^i$), as shown in Scheme 12.[224] The ethyl derivatives, **108** and **109**, were found to decompose initially via loss of ethylene, followed by a second unresolved step to give GaS. In contrast, the methylgallium compounds,

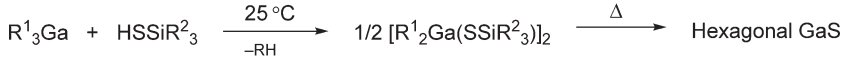

106: $R^1 = Me$; $R^2 = Ph$
107: $R^1 = Me$; $R^2 = Pr^i$
108: $R^1 = Et$; $R^2 = Ph$
109: $R^1 = Et$; $R^2 = Pr^i$

Scheme 12

106 and **107**, decomposed in a single uniform step to yield GaS. As expected, the precursors with isopropylsilyl groups were more volatile than those of triphenylsilyl ligands.

GaSe is a layered material with a hexagonal structure containing van der Waals interactions. In contrast, Ga_2Se_3 is cubic with a tetrahedral coordination in which every third metal position is vacant. Thin films of cubic Ga_2Se_3 have been grown from Me_3Ga in combination with H_2Se or $Bu^t{}_2Se$.[225] It was found that Me_3Ga pre-reacts with H_2Se in the gas phase to give films, which are only partially epitaxial. However, the use of $Bu^t{}_2Se$ yielded superior films of good crystal quality. LPCVD of $[(Me_2EtC)InSe]_4$ **110** and $[Bu^t{}_2In(SeBu^t)]_2$ **111** at 230–429 °C resulted in the deposition of indium selenide (InSe) films.[226] Films grown from compound **110** were stoichiometric InSe, whereas those deposited from **111** were indium rich. Interestingly, use of $[^tBuInSe]_4$ **112** as the precursor at 320–420 °C only resulted in indium metal films. No film growth was observed below 300 °C for **112**, and therefore this compound may be more susceptible to core cleavage at the high temperatures required. Cleavage of all In–Se bonds would result in the deposition of indium metal. Phase-pure InSe films were deposited from $[Me_2In(SeMe)]_2$ **113** at 270–320 °C.[227,228] Powder XRD of the films showed that they were single phased and polycrystalline with a hexagonal lattice.

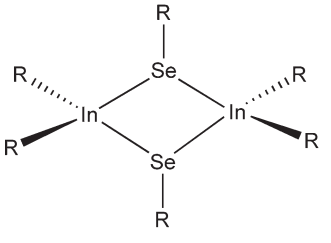

111: R = Bu^t
113: R = Me

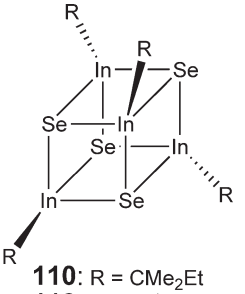

110: R = CMe_2Et
112: R = Bu^t

Mixed alkyl/dithio- or diselenocarbamates of gallium and indium can act as precursors to III–VI materials.[229,230] Compounds of general formula $[R^1{}_2M(S_2CNR^2{}_2)]$ (M = Ga: **114**, R^2 = Et, R^1 = Me; **115**, R^1 = Et; **116**, $R^1 = CH_2CMe_3$; **117**, $R^1 = Bu^t$, R^2 = Me; **118**, R^2 = Et; **119**, $R^2 = Pr^n$; M = In: **120**, R^2 = Et, R^1 = Me; **121**, R^1 = Et; **122**, $R^1 = CH_2CMe_3$) have been synthesized and characterized, and they range from liquids (M = Ga) to low-melting solids. Gallium sulfide (GaS) films have been grown by AP-MOCVD from compound **117** at 375–425 °C, whereas gallium-rich films were deposited from **118**. The indium compounds **120**–**122** deposited thin films of various phases of In_xS_y by LPCVD onto GaAs(100) substrates. Thus, the methyl derivative indium compound **120** gave orthorhombic InS and monoclinic In_6S_7 phases at 425 and 400 °C, while cubic β-In_2S_3 resulted at 325 °C.

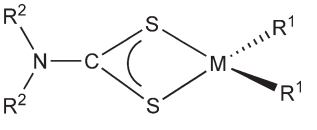

114: M = Ga; R^1 = Me; R^2 = Et,
115: M = Ga; R^1 = Et; R^2 = Et,
116: M = Ga; $R^1 = CH_2CMe_3$; R^2 = Et
117: M = Ga; $R^1 = Bu^t$; R^2 = Me,
118: M = Ga; $R^1 = Bu^t$; R^2 = Et,
119: M = Ga; $R^1 = Bu^t$; $R^2 = Pr^n$
120: M = In; R^1 = Me; R^2 = Et,
121: M = In; R^1 = Et; R^2 = Et,
122: M = In; $R^1 = CH_2CMe_3$; R^2 = Et

In contrast, the ethyl compound **121** afforded monophasic β-In_2S_3 at 400–325 °C and the neopentyl derivative **122** deposited In_6S_7 at 400 and 375 °C. Compound **121** is the only precursor that contains β-hydrogen atoms, which could be readily eliminated. This could in turn influence the film's composition, particularly determining the level of carbon incorporation. The monothiocarbamate complex, $[Et_2In(SOCNEt_2)]_n$ **123**, has also been used as a precursor to deposit β-In_2S_3 thin films on glass by LP-MOCVD.[231] Recently, a new class of single-source precursors based on the bidentate bis(diisopropylselenophosphoryl)amide ligand, $[NH(SePPr^i{}_2)_2]$, has been used to deposit III–VI materials.[232] The compounds $[R_2M(SePPr^i{}_2)_2N]$ (**124**, M = Ga, R = Me; **125**, M = In, R = Me; **126**, M = In, R = Et) were prepared via

the reaction of R_3M with $NH(SePPr^i_2)_2$. Thin films of cubic Ga_2Se_3 were grown from compound **124** by AACVD and LP-MOCVD. Similarly, thin films of hexagonal γ-In_2Se_3 were deposited from the methyl derivative **125**.

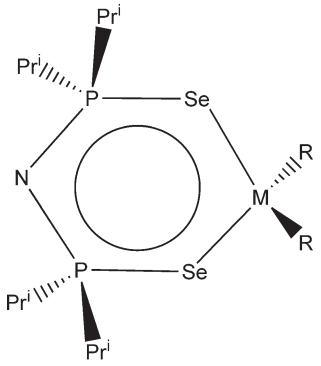

124: M = Ga; R = Me
125: M = In; R = Me
126: M = In; R = Et

12.01.4.3 Single-source Organometallic Precursors for IV–VI Materials

The benzyl-substituted tin chalcogenides $[(R_3Sn)_2S]$ **127**, $[R_2SnS]_3$ **128**, $[(R_3Sn)_2Se]$ **129**, and $[R_2SnSe]_3$ **130** ($R = CH_2C_6H_5$) have been synthesized and investigated as single-source precursors to tin sulfide or tin selenide.[233] Compounds **127–130** were prepared from the corresponding benzyltin chloride and anhydrous sodium chalcogenide, according to Scheme 13. Pyrolysis of compounds **127–130** at 450 °C yielded gray or black powders and bibenzyl as the major products. The powders produced from **127** and **129** were analyzed as SnS and SnSe with some contamination from elemental tin. In contrast, the solids obtained from pyrolysis of the cyclic compounds **128** and **130** were purer and only contained SnS and SnSe, respectively. Solid solutions, of the type $Sn(S_xSe_{1-x})$, were prepared by the

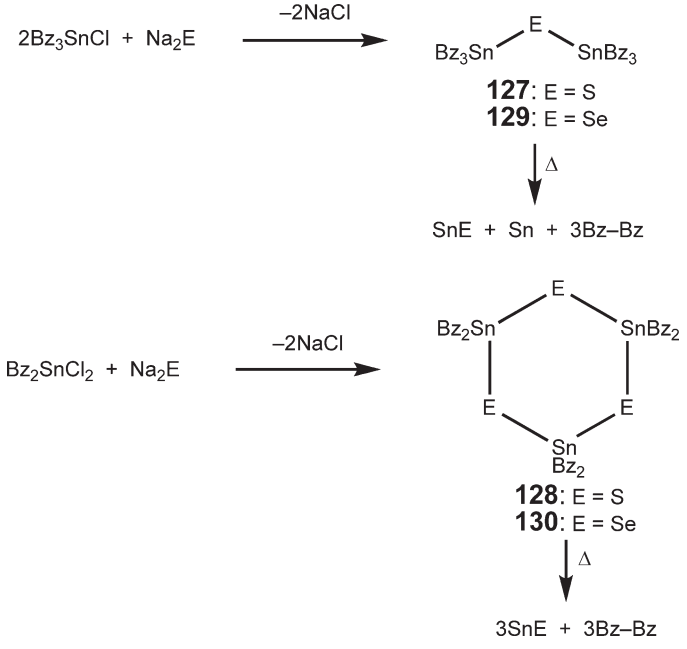

Scheme 13

co-pyrolysis of mixtures of **127** and **129**, and by varying the ratio of **127** : **128**, the value of *x* could be controlled. Solid solutions could also be synthesized by heating mixtures of compound **127** and elemental selenium.[234]

The phenyl analogs of **127–130** also resulted in the formation of tin chalcogenides, after pyrolysis.[235] The formation of tin chalcogenides from the perphenylated precursors proceeds by phenyl group migration to form stable volatile byproducts such as tetraphenyltin, diphenylsulfide, diphenyl selenide, or diphenyl telluride. The migration of the aryl group causes a reduction of the metal from Sn(IV) to Sn(II). Thin films of SnTe were deposited from $[\{(Me_3Si)_2CH\}_2Sn(\mu\text{-Te})]_2$ **131** by MOCVD at 400 °C.[236] The SnTe films were free of carbon contamination and crystalline. In contrast, the selenium analog $[\{(Me_3Si)_2CH\}_2Sn(\mu\text{-Se})]_2$ **132** was thermally stable and no deposition was observed.

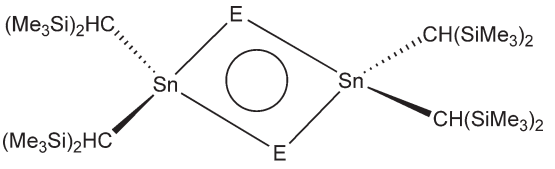

131: E = Te
132: E = Se

Thermal decomposition of $[Ph_2Sn(S_2CN(CH_2)_4)_2]$ **133** and $[Ph_3Sn(S_2CN(CH_2)_4)]$ **134** resulted in the formation of a mixture of γ-Sn_2S_3 and SnS, both orthorhombic phases.[237,238] Similarly, APCVD of $[Me_2Sn(S_2CN(C_4H_9)CH_3)]$ **135** and $[BuSn(S_2CN(C_4H_9)CH_3)_3]$ **136** at 350–550 °C, in the presence of H_2S, afforded SnS and Sn_2S_3 films on glass.[238] In an attempt to develop a mild, low-temperature route to the formation of SnS thin films, the APCVD reaction of $[^nBu_3SnO_2CCF_3]$ **137** with H_2S has been studied.[239] Tin(II) sulfide films were deposited at 350–600 °C under nitrogen, and no contamination from fluorine was observed in the resulting films. Compound **137** was thought to be reduced to tin(II) before the film was deposited, although the mechanism for film growth was not studied.

12.01.5 Organometallic Precursors for the Growth of Ternary Chalcogenide Semiconductors

12.01.5.1 Introduction

Single-source precursors have a potentially important role with regard to simplifying the production of ternary and higher-order materials. One possibility is to have three elements incorporated into one source and/or to have a second source deliver the fourth element. Single-source precursors for ternary or higher-order materials are rare, which may be partly due to the difficulty in obtaining heterometallic precursors with the elements in the proper ratio. However, this approach has been carried out for chalcogenide-containing materials.

12.01.5.2 Organometallic Precursors for Copper Indium Sulfide

Alkylindium thiolate complexes readily react with copper dithiocarbamate compounds to yield binuclear complexes, according to Scheme 14.[240] No structural data is available for these mixed metal complexes; however, they have been used to deposit thin films of copper indium sulfide. Thin films of chalcopyrite $CuInS_2$ and tetragonal $CuIn_5S_8$ were

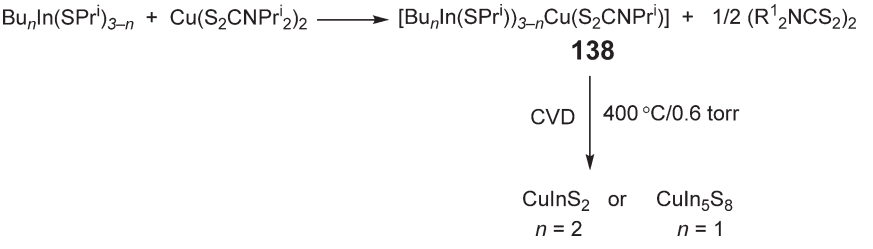

Scheme 14

grown from $[Bu_nIn(SPr^i)_{3-n}Cu(S_2CNPr^i_2)]$ **138** by LP-MOCVD. These ternary materials are potential candidates for terrestrial solar cells with high conversion efficiencies.

12.01.5.3 Organometallic Precursors for Cadmium Zinc Chalcogenides

A single-source precursor to the ternary material $Cd_{0.5}Zn_{0.5}Se$ has been developed by O'Brien and Nomura utilizing a comproportionative approach.[190] Thus, the reaction between Me_2Zn and $Cd(Se_2CNEt_2)_2$ results in the formation of $[Me_2CdZn(Se_2CNEt_2)_2]$ **139**, as shown in Equation (11). Compound **139** deposits polycrystalline $Cd_{0.5}Zn_{0.5}Se$ (at 450 °C, 0.2 torr), which has a bandgap energy estimated at 2.1 eV. In the crystal structure of **139**, the cadmium and zinc atoms were modeled as randomly occupying the metal sites. The related complex $[Me_3CCH_2Zn_{0.5}$-$Cd_{0.5}Se_2CNEt_2]$ **140** also decomposes to the corresponding ternary $Cd_{0.5}Zn_{0.5}Se$.[206]

$$(CH_3)_2Zn + Cd(Se_2CNEt_2)_2 \xrightarrow{450\,^\circ C} [(CH_3)_2CdZn(Se_2CNEt_2)_2] \quad (11)$$

References

1. Jones, A. C. *Chem. Soc. Rev.* **1997**, 101–110.
2. Cowley, A. H.; Jones, R. A. *Polyhedron* **1994**, *13*, 1149–1157.
3. Neumayer, D.; Ekerdt, J. G. *Chem. Mater.* **1996**, *8*, 9–25.
4. Gleizes, A. N. *Chem. Vap. Deposition* **2000**, *6*, 155–173.
5. O'Brien, P.; Pickett, N. L.; Otway, D. J. *Chem. Vap. Deposition* **2002**, *8*, 237–249.
6. O'Brien, P.; Malik, M. A.; Chunggaze, M.; Trindale, T.; Walsh, J. R.; Jones, A. C. *J. Cryst. Growth* **1997**, *170*, 23–29.
7. Buhro, W. E. *Polyhedron* **1994**, *13*, 1131–1148.
8. Maury, F. *Adv. Mater.* **1991**, *3*, 542–548.
9. Getman, T. D.; Franklin, G. W. *Comments Inorg. Chem.* **1995**, *17*, 79–94.
10. Strite, S.; Lin, M. E.; Morkoc, H. *Thin Solid Films* **1993**, *231*, 197–210.
11. Ambacher, O. *J. Phys. D: Appl. Phys.* **1998**, *31*, 2653–2710.
12. Jones, A. C.; O'Brien, P. *CVD of Compound Semiconductors: Precursor Synthesis, Development and Applications*; VCH: Weinheim, 1997.
13. Manasevit, H. M. *Appl. Phys. Lett.* **1968**, *12*, 156–159.
14. Nakamura, S. *Adv. Mater.* **1996**, *8*, 689–692.
15. Honda, Y.; Kuroiwa, Y.; Yamaguchi, M.; Sawaki, N. *J. Cryst. Growth* **2002**, *242*, 77–81.
16. Wang, H. Y.; Huang, S. C.; Yan, T. Y.; Gong, J. R.; Lin, T. Y.; Chen, Y. F. *Mat. Sci. Eng. B* **1999**, *57*, 218–223.

16a. Tsuchiya, H.; Akamatsu, M.; Ishida, M.; Hasegawa, F. *Jpn. J. Appl. Phys.* **1996**, *35*, L748–L750.

17. Gong, J.-R.; Yeh, M.-F.; Wang, C.-L. *J. Cryst. Growth* **2003**, *247*, 261–268.
18. Akasaki, I.; Amano, H. *J. Cryst. Growth* **1995**, *146*, 455–461.
19. Park, C. I.; Kang, J. H.; Kim, K. C.; Nahm, K. S.; Suh, E.-K.; Lim, K. Y. *Thin Solid Films* **2001**, *401*, 60–66.
20. Tomida, Y.; Nitta, S.; Kamiyama, S.; Amano, H.; Akasaki, I.; Otani, S.; Kinoshita, H.; Liu, R.; Bell, A.; Ponce, F. A. *Appl. Surf. Sci.* **2003**, *216*, 502–507.
21. Tolle, J.; Roucka, R.; Tsong, I. S.; Ritter, C.; Crozier, P. A.; Chizmeshya, A. V. G.; Kouetakis, J. *Appl. Phys. Lett.* **2003**, *82*, 2398–2400.
22. Hill, J. J.; Aquino, A. A.; Mulcahy, C. P. A.; Harwood, N.; Jones, A. C.; Jones, T. S. *Surf. Sci.* **1995**, *340*, 9–56.
23. Liu, H.; Bertolet, S. C.; Rogers, J. W. *Surf. Sci.* **1994**, *320*, 145–160.
24. Wong, K. C.; McEllistrem, M. T.; McBurnett, B. G.; Culp, R. D.; Cowley, A. H.; Ekerdt, J. G. *Surf. Sci.* **1998**, *396*, 260–265.
25. Alwan, J. J.; Eden, J. G. *Chem. Vap. Deposition* **1997**, *3*, 209–217.
26. Ihashi, N.; Itoh, K.; Matsumoto, O. *Plasma Chem. Plasma Process.* **1997**, *17*, 453–465.
27. Li, T.; Campion, R. P.; Foxon, C. T.; Rushworth, S. A.; Smith, L. M. *J. Cryst. Growth* **2003**, *251*, 499–504.
28. Khan, M. A.; Chen, Q.; Skogman, R. A.; Kuznia, J. N. *Appl. Phys. Lett.* **1995**, *66*, 2046–2047.
29. Nakamura, S.; Mukai, T.; Senoh, M. *Appl. Phys. Lett.* **1994**, *64*, 1687–1689.
30. Nakamura, S.; Senoh, M.; Iwasa, N.; Nagahama, S. *Appl. Phys. Lett.* **1995**, *64*, 1868–1870.
31. Yang, J. W.; Lunev, A.; Simin, G.; Chitnis, A.; Shatalov, M.; Khan, M. A.; Van Nostrund, J. E.; Gaska, R. *Appl. Phys. Lett.* **2000**, *76*, 273–275.
32. Poschenrieder, M.; Schulze, F.; Blasing, J.; Dadgar, A.; Diez, A.; Christen, J.; Krost, A. *Appl. Phys. Lett.* **2002**, *81*, 1591–1593.
33. Potin, V.; Hahn, E.; Rosenauer, A.; Gerthsen, D.; Kuhn, B.; Scholz, F.; Dussaigne, A.; Damilano, B.; Grandjean, N. *J. Cryst. Growth* **2004**, *262*, 145–150.
34. Chen, T.-C.; Johnson, M.; Poochinda, K.; Stoebe, T. G.; Ricker, N. L. *Opt. Mater.* **2004**, *26*, 417–420.
35. Khan, M. A.; Kuznia, J. N.; Olson, D. T.; Schaff, W. J.; Burm, J. W.; Shur, M. S. *Appl. Phys. Lett.* **1994**, *65*, 1121–1123.
36. Jones, A. C.; Auld, J.; Rushworth, S. A.; Williams, E. W.; Haycock, P. W.; Tang, C. C.; Critchlow, G. W. *Adv. Mater.* **1994**, *3*, 229–231.
37. Sung, M. M.; Jung, H. O.; Lee, J. K.; Kim, S. H.; Park, J. T.; Kim, Y. *Bull. Kor. Chem. Soc.* **1994**, *15*, 79–83.
38. Friedman, D. J.; Norman, A. G.; Geisz, J. F.; Kurtz, S. R. *J. Cryst. Growth* **2000**, *208*, 11–17.
39. Rushworth, S. A.; Brown, J. R.; Houlton, D. J.; Jones, A. C.; Roberts, V.; Roberts, J. S.; Crichlow, G. W. *Adv. Mater. Opt. Electron.* **1996**, *6*, 119–126.

39a. Beaumont, B.; Vaille, M.; Boufaden, T.; Jani, B. E.; Gibart, P. *J. Cryst. Growth* **1997**, *170*, 316–320.

39b. Liu, Z.; Lee, R. T.; Stringfellow, G. B. *J. Cryst. Growth* **1998**, *191*, 1–2.

40. Jones, A. C.; Auld, J.; Rushworth, S. A.; Houlton, D. J.; Critchlow, G. W. *J. Mater. Chem.* **1994**, *4*, 1591–1594.
41. Jones, A. C.; Auld, J.; Rushworth, S. A.; Critchlow, G. W. *J. Cryst. Growth* **1994**, *135*, 285–289.

42. Auld, J.; Houlton, D. J.; Jones, A. C.; Rushworth, S. A.; Critchlow, G. W. *J. Mater. Chem.* **1994**, *4*, 1245–1247.
43. Bu, Y.; Lin, M. C.; Fu, L. P.; Chtchekine, D. G.; Gilliland, G. D.; Chen, Y.; Ralph, S. E.; Stock, S. R. *Appl. Phys. Lett.* **1995**, *66*, 2433–2435.
44. Sato, H.; Takahashi, H.; Watanabe, A.; Ota, H. *Appl. Phys. Lett.* **1996**, *68*, 3617–3619.
45. Park, E.-H.; Park, J.-S.; Yoo, T.-K. *J. Cryst. Growth* **2004**, *272*, 426–431.
46. Bourret-Courchesne, E. D.; Ye, Q.; Yu, K.-M.; Ager, J. W., III. *J. Cryst. Growth* **2001**, *231*, 89–94.
47. Bourret-Courchesne, E. D.; Kin-Man, Y.; Irvine, S. J. C.; Stafford, A.; Rushworth, S. A.; Smith, L. M.; Kanjolia, R. *J. Cryst. Growth* **2000**, *221*, 246–250.
48. Hsu, Y. J.; Hong, L. S.; Huang, K. F.; Tsay, J. E. *Thin Solid Films* **2002**, *419*, 33–39.
49. Bourret-Courchesne, E. D.; Ye, Q.; Peters, D. W.; Arnold, J.; Ahmed, M.; Irvine, S. J. C.; Kanjolia, R.; Smith, L. M.; Rushworth, S. A. *J. Cryst. Growth* **2000**, *217*, 47–54.
50. Lee, R. T.; Stringfellow, G. B. *J. Electron. Mater.* **1999**, *28*, 963–969.
51. Hsu, Y. J.; Hong, L. S.; Jiang, J. C.; Chang, J. C. *J. Cryst. Growth* **2004**, *266*, 347–353.
52. Hsu, Y. J.; Hong, L. S.; Tsay, J. E. *J. Cryst. Growth* **2003**, *252*, 144–151.
53. Pohl, U. W.; Moller, C.; Knorr, K.; Richter, W.; Gottfriedsen, J.; Schumann, H.; Rademann, K.; Fielicke, A. *Mater. Sci. Eng. B* **1999**, *59*, 20–23.
54. Robinson, D. W.; Rogers, J. W., Jr., *Thin Solid Films* **2000**, *372*, 10–24.
55. Kuwano, N.; Kobayashi, K.; Oki, K.; Miyoshi, S.; Yaguchi, H.; Onabe, K.; Shiraki, Y. *Jpn. J. Appl. Phys.* **1994**, *33*, 3415–3416.
56. Kuwano, N.; Nagatomo, Y.; Kobayashi, K.; Oki, K.; Miyoshi, S.; Yaguchi, H.; Onabe, K.; Shiraki, Y. *Jpn. J. Appl. Phys.* **1994**, *33*, 18–22.
57. Sormunen, J.; Riikonen, J.; Sopanen, M.; Lipsanen, H. *J. Cryst. Growth* **2004**, *270*, 346–350.
58. Sormunen, J.; Toivonen, J.; Sopanen, M.; Lipsanen, H. *J. Cryst. Growth* **2004**, *222*, 286–292.
59. Geisz, J. F.; Reedy, R. C.; Keyes, B. M.; Metzger, W. K. *J. Cryst. Growth* **2003**, *259*, 223–231.
60. Ougazzaden, A.; Le Bellego, Y.; Rao, E. V. K.; Juhel, M.; Leprince, L.; Patriarche, G. *Appl. Phys. Lett.* **1997**, *70*, 2861–2863.

60a. Gupta, J. A.; McKinnon, W. R.; Noad, J.; Coulas, D.; Williams, R. L.; Driad, R.; McAlister, S. P. *J. Cryst. Growth* **2001**, *231*, 48–56.

60b. Moody, B. F.; Barletta, P. T.; El-Masry, N. A.; Roberts, J. C.; Aumer, M. E.; LeBoeuf, S. F.; Bedair, S. M. *Appl. Phys. Lett.* **2002**, *80*, 2475–2477.

60c. Beaudry, J.-N.; Masut, R. A.; Desjardins, P.; Wei, P.; Chicoine, M.; Bentoumi, G.; Leonelli, R.; Schiettekatte, F.; Guillon, S. *J. Vac. Sci. Technol., A* **2004**, *22*, 771–775.

61. Gao, Q.; Tan, H. H.; Tagadish, C.; Sun, B. Q.; Gal, M.; Ouyang, L.; Zou, J. *J. Cryst. Growth* **2004**, *264*, 92–97.
62. El-Emawy, A. A.; Cao, H.-J.; Zhmayev, E.; Lee, J.-H.; Zubia, D.; Osinshi, M. *Phys. Stat. Sol. (b)* **2001**, *228*, 263–267.
63. Pan, Z.; Miyamamoto, T.; Schlenker, D.; Sato, S.; Koyama, F.; Iga, K. *J. Appl. Phys.* **1998**, *84*, 6409–6411.

63a. Li, N. Y.; Hains, C. P.; Yang, K.; Lu, J.; Cheng, J.; Li, P. W. *Appl. Phys. Lett.* **1999**, *75*, 1051–1053.

63b. Baskar, K.; Sundgren, P.; Douheret, O.; Landgren, G. *J. Cryst. Growth* **2003**, *248*, 431–436.

63c. Miyamoto, T.; Kageyama, T.; Makino, S.; Schlenker, D.; Koyama, F.; Iga, K. *J. Cryst. Growth* **2000**, *209*, 339–344.

64. Peake, G. M.; Waldrip, K. E.; Hargett, T. W.; Madine, N. A.; Serkland, D. K. *J. Cryst. Growth* **2004**, *261*, 398–403.
65. Riikonen, J.; Sormunen, J.; Koskenvaara, H.; Mattila, M.; Sopanen, M.; Lipsanen, H. *J. Cryst. Growth* **2004**, *272*, 621–626.
66. Kurtz, S.; Reedy, R.; Keyes, B.; Barber, G. D.; Geisz, J. F.; Friedman, D. J.; McMahon, W. E.; Olson, J. M. *J. Cryst. Growth* **2002**, *234*, 323–326.
67. Jones, A. C.; Rushworth, S. A.; Auld, J. *J. Cryst. Growth* **1995**, *146*, 503–510.
68. Bertolet, D. C.; Lui, H.; Rogers, J. W., Jr. *J. Appl. Phys.* **1994**, *75*, 5385–5390.
69. Kidder, J. N., Jr.; Kuo, J. S.; Ludviksson, A.; Pearsall, T. P.; Rogers, J. W., Jr.; Grant, J. M.; Allen, L. R.; Hsu, S. T. *J. Vac. Sci. Technol., A* **1995**, *13*, 711–715.
70. Kidder, J. N., Jr.; Yun, H. K.; Rogers, J. W., Jr.; Pearsall, T. P. *Chem. Mater.* **1998**, *10*, 777–783.
71. Zhang, L.; Gu, S. L.; Kuech, T. F.; Boleslawski, M. P. *J. Cryst. Growth* **2000**, *213*, 1–9.
72. Tao, M. *J. Appl. Phys.* **2000**, *87*, 3554–3562.
73. Nishizawa, J.-I.; Kurabayashi, T. *Thin Solid Films* **1997**, *306*, 179–186.
74. Weyers, M.; Sato, M. *Jpn. J. Appl. Phys.* **1995**, *34*, 434–441.
75. Pristovsek, M.; Zorn, M.; Weyers, M. *J. Cryst. Growth* **2004**, *262*, 78–83.
76. Creighton, J. R.; Baucomm, K. *Surf. Sci.* **1998**, *409*, 372–383.
77. Fujii, K.; Satoh, M.; Kawamura, K.; Gotoh, H. *J. Cryst. Growth* **1999**, *204*, 10–18.
78. Zhang, R.; Tsui, R.; Shiralagi, K.; Tresek, J. *J. Electron. Mater.* **1998**, *27*, 446–450.
79. Sharma, T.; Arora, B. M.; Gokhale, M. R.; Rajgopalan, S. *J. Cryst. Growth* **2000**, *221*, 509–514.
80. Tsai, C. Y.; Moser, M.; Geng, C.; Haerle, V.; Forner, T.; Michler, P.; Hangleiter, A.; Scholz, F. *J. Cryst. Growth* **1994**, *145*, 786–791.
81. Van der Ziel, J. P.; Tang, X.; Johnson, R. *Appl. Phys. Lett.* **1997**, *71*, 791–793.
82. Abdul-Ridha, H. H.; Bateman, J. E.; Fan, G. H.; Pemble, M. E.; Povey, I. M. *J. Electrochem. Soc.* **1994**, *141*, 1886–1893.
83. Abdul-Ridha, H. H.; Bateman, J. E.; Crowte, R. C.; Hoye, P.; Jones, A. C.; Padda, R.; Patrikarakos, D. G.; Pemble, M. E. *J. Cryst. Growth* **1994**, *145*, 485–491.
84. Chen, G. Y.; Cheng, D.; Hicks, R. F.; Noori, A. M.; Hayashi, S. L.; Goorsky, M. S.; Kanjolia, R.; Odedra, R. *J. Cryst. Growth* **2004**, *270*, 322–328.
85. Shenai, D. V.; Timmons, M. L.; DiCarlo, R. L.; Marsman, C. J. *J. Cryst. Growth* **2004**, *272*, 603–608.
86. Beccard, R.; Lengeling, G.; Schmitz, D.; Gigase, Y.; Jürgensen, H. *J. Cryst. Growth* **1997**, *170*, 97–102.
87. Keiper, D.; Westphalen, R.; Landgren, G. *J. Cryst. Growth* **1999**, *204*, 256–262.
88. Rushworth, S. A.; Smith, L. M.; Ravetz, M. S.; Coward, K. M.; Odedra, R.; Kanjolia, R.; Bland, S. W.; Dimroth, F.; Bett, A. W. *J. Cryst. Growth* **2003**, *248*, 86–90.

88a. Stolz, W. *J. Cryst. Growth* **2000**, *209*, 272–278.

88b. Mashita, M.; Ishikawa, H.; Izumiya, T.; Hiraoka, Y. S. *Jpn. J. Appl. Phys.* **1997**, *36*, 4230–4234.

89. Skogen, E. J.; Barton, J. S.; Raring, J. W.; Coldren, L. A.; Denbaars, S. P. *J. Cryst. Growth* **2004**, *272*, 564–569.
90. Zimmermann, G.; Ougazzaden, A.; Gloukhian, A.; Rao, E. V. K.; Delprat, D.; Ramdane, A.; Mircea, A. *Mater. Sci. Eng. B* **1997**, *44*, 37–40.
91. Chen, G.; Cheng, D.; Hicks, R. F.; Noori, A. M.; Hayashi, S. L.; Goorsky, M. S.; Kanjolia, R.; Odedra, R. *J. Cryst. Growth* **2004**, *270*, 322–328.
92. Otsuka, N.; Nishizawa, J.; Kikuchi, H.; Oyama, Y. *J. Cryst. Growth* **2000**, *209*, 252–257.
93. Glass, J. A.; Spencer, J. T. *Thin Solid Films* **1998**, *315*, 86–93.

94. Haugan, H. J.; Yu, W.; Lee, S. T.; Petrou, A.; McCombe, B. D.; Brewer, K. S.; Lees, J. F.; Beachley, O. T., Jr. *J. Cryst. Growth* **2002**, *244*, 157–167.
95. Forster, D. F.; Glidewell, C.; Cole-Hamilton, D. J.; Povey, I. M.; Hoare, R. D.; Pemble, M. E. *J. Cryst. Growth* **1994**, *145*, 104–112.
96. Watkins, S. P.; Brake, D. M.; Haacke, G. *J. Appl. Phys.* **1994**, *75*, 2952–2956.
97. Biefeld, R. M.; Chui, H. C.; Hammons, B. E.; Breiland, W. G.; Brennan, T. M.; Jones, E. D.; Kim, M. H.; Grodzinski, P.; Chang, K. H.; Lee, H. C. *J. Cryst. Growth* **1996**, *163*, 212–219.
98. Mashita, M.; Ishikawa, H.; Izumiya, T. *J. Cryst. Growth* **1995**, *155*, 164–179.
99. Leu, S.; Höhnsdorf, F.; Stolz, W.; Becker, R.; Salzmann, A.; Greiling, A. *J. Cryst. Growth* **1998**, *195*, 98–104.
100. Freer, R. W.; Martin, T.; Lane, P. A.; Whitehouse, C. R.; Whitaker, T. J.; Houlton, M.; Calcott, P. D. J.; Lee, D.; Jones, A. C.; Rushworth, S. A. *J. Cryst. Growth* **1995**, *150*, 539–545.
101. Freer, R. W.; Whitaker, T. J.; Martin, T.; Calcott, P. D. J.; Houlton, M.; Lee, D.; Jones, A. C.; Rushworth, S. A. *Adv. Mater.* **1995**, *5*, 478–481.
102. Arès, R.; Watkins, S. P.; Yeo, P.; Horley, G. A.; O'Brien, P.; Jones, A. C. *J. Appl. Phys.* **1998**, *83*, 3390–3397.
103. Aït-Lhouss, M.; Castaño, J. L.; García, B. J.; Piqueras, J. *J. Appl. Phys.* **1995**, *78*, 5834–5836.
104. Yeo, P.; Arès, R.; Watkins, S. P.; Horley, G. A.; O'Brien, P.; Jones, A. C. *J. Electron. Mater.* **1997**, *26*, 1174–1177.
105. Gupta, J. A.; Woicik, J. C.; Watkins, S. P.; Miyano, K. E.; Pellegrino, J. G.; Crizier, E. D. *J. Cryst. Growth* **1998**, *195*, 34–40.
106. Arès, R.; Watkins, S. P.; Tran, C. A. I. *J. Cryst. Growth* **1997**, *170*, 574–578.
107. Huang, G. S.; Tang, X. H.; Zhang, B. L.; Zhang, Y. C.; Tjin, S. C. *J. Cryst. Growth* **2004**, *268*, 444–448.
108. Frankland, D.; Masut, R. A.; Leonelli, R. *J. Vac. Sci. Technol., A* **2002**, *20*, 1132–1134.
109. Kaiander, I. N.; Sellin, R. L.; Kettler, T.; Ledentsov, N. N.; Bimberg, D.; Zakharov, N. D.; Werner, P. *Appl. Phys. Lett.* **2004**, *84*, 2992–2994.
110. Zhao, J. H.; Tang, X. H.; Mei, T.; Zhang, B. L.; Huang, G. S. *J. Cryst. Growth* **2004**, *268*, 432–436.
111. Li, H.; Mei, T.; Lantz, K. P.; Karunasiri, G. *J. Appl. Phys.* **2004**, *96*, 6799–6802.
112. Zhang, B. L.; Tang, X. H.; Huang, G. S.; Zhu, J. Y. *J. Cryst. Growth* **2004**, *268*, 396–400.
113. Shi, B. Q.; Kondow, M.; Tu, C. W. *J. Cryst. Growth* **2000**, *216*, 80–86.
114. Lamare, B.; Benchimol, J. L.; Juhel, M.; Akamatsu, B.; Legay, P.; Alendra, G. *J. Cryst. Growth* **1994**, *141*, 347–351.
115. Bohling, D. A.; Abernathy, C. R.; Jensen, K. F. *J. Cryst. Growth* **1994**, *136*, 118–126.
116. Zimmermann, G.; Spika, Z.; Marschner, T.; Spill, B.; Stolz, W.; Göbel, E. O.; Gimmnich, P.; Lorbeth, J.; Gresling, A.; Stolzmann, A. *J. Cryst. Growth* **1994**, *145*, 512–519.
117. Kirpal, G.; Gerhardt, M.; Gottschalch, V.; Franzheld, R.; Semmelhack, H. C. *Thin Solid Films* **1999**, *342*, 113–118.
118. Kirpal, G.; Gerhardt, M.; Benndorf, G.; Shwabe, R.; Pietag, F.; Pietzonka, I.; Lippold, G.; Wagner, G.; Franzheld, R.; Gottschalch, V. *J. Cryst. Growth* **1997**, *170*, 167–172.
119. Wang, C. A.; Salim, S.; Jensen, K. F.; Jones, A. C. *J. Electron. Mater.* **1996**, *25*, 771–774.
120. Jones, A. C.; Auld, J.; Rushworth, S. A.; Critchlow, G. W. *J. Cryst. Growth* **1994**, *135*, 285–289.
121. Foord, J. S.; Whitaker, T. J.; O'Hare, D.; Jones, A. C. *J. Cryst. Growth* **1994**, *136*, 127–132.
122. Bielfeld, R. M. *Mater. Sci. Eng. R* **2002**, *36*, 105–142.
123. Roya, F.; Gianai, A.; Pascal-Delannoy, L.; Gouskov, L.; Malzac, J. P.; Camassel, J. *Mater. Sci. Eng. B* **1994**, *28*, 169–173.
124. Koljonen, T.; Sopanen, M.; Lipsanen, H.; Tuomi, T. *J. Electron. Mater.* **1995**, *24*, 1691–1696.
125. Wang, C. A.; Salim, S.; Jensen, K. F.; Jones, A. C. *J. Cryst. Growth* **1997**, *170*, 55–60.
126. Shin, J.; Verma, A.; Stringfellow, G. B.; Gedbridge, R. W., Jr. *J. Cryst. Growth* **1995**, *151*, 1–8.
127. Graham, R. M.; Jones, A. C.; Mason, N. J.; Rushworth, S.; Smith, L.; Walker, P. J. *J. Cryst. Growth* **1994**, *145*, 363–370.
128. Biefeld, R. M.; Baucom, K. C. *J. Cryst. Growth* **1994**, *135*, 401–408.
129. Shin, J.; Verma, A.; Stringfellow, G. B.; Gedbridge, R. W., Jr. *J. Cryst. Growth* **1994**, *143*, 15–21.
130. Shin, J.; Hsu, T. C.; Hsu, Y.; Stringfellow, G. B. *J. Cryst. Growth* **1997**, *179*, 1–9.
131. Wang, C. A. *J. Cryst. Growth* **1998**, *191*, 631–640.
132. Huang, K. T.; Hsu, Y.; Cohen, R. M.; Stringfellow, G. B. *J. Cryst. Growth* **1995**, *156*, 311–319.
133. Biefeld, R. M.; Allerman, A. A.; Pelczynski, M. W. *Appl. Phys. Lett.* **1996**, *68*, 932–934.
134. Wang, C. A.; Finn, M. C.; Salim, S.; Jensen, K. F.; Jones, A. C. *Appl. Phys. Lett.* **1995**, *67*, 1384–1386.
135. Koljonen, T.; Sopanen, M.; Lipsanen, H.; Tuomi, T. *J. Cryst. Growth* **1996**, *169*, 417–423.
136. Jones, A. C.; Rushworth, S. A.; Houlton, D. J.; Roberts, J. S.; Roberts, V.; Whitehouse, C. R.; Critchlow, G. W. *Chem. Vap. Deposition* **1996**, *2*, 5–8.
137. Jones, A. C.; Whitehouse, C. R.; Roberts, J. S. *Chem. Vap. Deposition* **1995**, *1*, 65–74.
138. Hwang, J.-W.; Campbell, J. P.; Kozubowski, J.; Hanson, S. A.; Evans, J. F.; Gladfelter, W. L. *Chem. Mater.* **1995**, *7*, 517–525.
139. Janik, J. F.; Wells, R. L. *Inorg. Chem.* **1997**, *36*, 4135–4137.
140. Campbell, J. P.; Hwang, J.-W.; Young, V. G., Jr.; Von Dreele, R. B.; Cramer, C. J.; Gladfelter, W. L. *J. Am. Chem. Soc.* **1998**, *120*, 521–531.
141. Jegier, J. A.; McKernan, S.; Purdy, A. P.; Gladfelter, W. L. *Chem. Mater.* **2000**, *12*, 1003–1010.
142. Park, H. S.; Waezsada, S. D.; Cowley, A. H.; Roesky, H. W. *Chem. Mater.* **1998**, *10*, 2251–2257.
143. Grocholl, L.; Cullison, S. A.; Wang, J.; Swenson, D. C.; Gillan, E. G. *Inorg. Chem.* **2002**, *41*, 2920–2927.
144. McMurran, J.; Dai, D.; Balasubramanian, K.; Steffek, C.; Kouvetakis, J.; Hubbard, J. K. *Inorg. Chem.* **1998**, *37*, 6638–6644.
145. Torrison, L.; Tolle, J.; Tsong, I. S. T.; Kouvetakis, J. *Thin Solid Films* **2003**, *434*, 106–111.
146. McMurran, J.; Smith, D. J.; Kouvetakis, J. *Appl. Phys. Lett.* **1999**, *74*, 883–885.
147. McMurran, J.; Kouvetakis, J.; Nesting, D. C.; Smith, D. J.; Hubbard, J. *J. Am. Chem. Soc.* **1998**, *120*, 5233–5237.
148. Kouvetakis, J.; McMurran, J.; Matsunaga, P.; O'Keeffe, M.; Hubard, J. L. *Inorg. Chem.* **1997**, *36*, 1792–1797.
149. Lakhotia, V.; Neumayer, D. A.; Cowley, A. H.; Jones, R. A.; Ekerdt, J. G. *Chem. Mater.* **1995**, *7*, 546–552.
150. Bae, B.-J.; Park, J. E.; Kim, B.; Park, J. T. *J. Organomet. Chem.* **2000**, *616*, 128–134.
151. Dingman, S. D.; Rath, N. P.; Markowitz, P. D.; Gibbons, P. C.; Buhro, W. E. *Angew. Chem., Int. Ed.* **2000**, *39*, 1470–1472.
152. Muñoz-Hernández, M.-Á.; Rutherford, D.; Tiainen, H.; Atwood, D. A. *J. Organomet. Chem.* **1999**, *582*, 103–107.
153. Sung, M. M.; Kim, C.; Yoo, S. H.; Kim, C. G.; Kim, Y. *Chem. Vap. Deposition* **2002**, *8*, 50–52.
154. Kim, K. H.; Lee, K. J.; Kang, H. S.; Yu, F. C.; Kim, J. A.; Kim, D. J.; Baik, K. H.; Yoo, S. H.; Kim, C. G.; Kim, Y. S., *et al. Phys. Stat. Sol. (b)* **2004**, *241*, 1458–1461.
155. Neumayer, D. A.; Cowley, A. H.; Decken, A.; Jones, R. A.; Lakhotia, V.; Ekerdt, J. G. *Inorg. Chem.* **1995**, *34*, 4698–4700.
156. Kim, Y.; Kim, J. H.; Park, J. E.; Bae, B. J.; Kim, B.; Kim, B.; Park, J. T.; Yu, K.-S.; Kim, Y. *Thin Solid Films* **1999**, *339*, 200–202.

157. Luo, B.; Lee, S. Y.; White, J. M. *Chem. Mater.* **2004**, *16*, 629–638.
158. Luo, B.; Gladfelter, W. L. *J. Chem. Soc., Chem. Commun.* **2000**, 825–826.
159. Fischer, R. A.; Miehr, A.; Ambacher, O.; Metzger, T.; Born, E. *J. Cryst. Growth* **1997**, *170*, 139–143.
160. Miehr, A.; Mattner, M. R.; Fischer, R. A. *Organometallics* **1996**, *15*, 2053–2059.
161. Fischer, R. A.; Miehr, A.; Metzger, T.; Born, E.; Ambacher, O.; Augerer, H.; Dimitrov, R. *Chem. Mater.* **1996**, *8*, 1356–1359.
162. Müller, J.; Bendix, S. *Chem. Commun.* **2001**, 911–912.
163. Winkler, H.; Devi, A.; Manz, A.; Wohlfart, A.; Rogge, W.; Fischer, R. A. *Phys. Stat. Sol. (a)* **2000**, *1777*, 27–35.
164. Devi, A.; Rogge, W.; Wohlfart, A.; Hipler, F.; Becker, H. W.; Fischer, R. A. *Chem. Vap. Deposition* **2000**, *6*, 245–252.
165. Devi, A.; Sussek, H.; Pritzkow, H.; Winter, M.; Fischer, R. A. *Eur. J. Inorg. Chem.* **1999**, 2127–2134.
166. Parala, H.; Devi, A.; Hipler, F.; Maile, E.; Birkner, A.; Becker, H. W.; Fischer, R. A. *J. Cryst. Growth* **2001**, *231*, 68–74.
167. Miehr, A.; Ambacher, O.; Rieger, W.; Metzger, T.; Born, E.; Fischer, R. A. *Chem. Vap. Deposition* **1996**, *2*, 51–55.
168. Cowley, A. H.; Gabbai, F. P.; Olbrich, F.; Corbelin, S.; Lagow, R. J. *J. Organomet. Chem.* **1995**, *487*, C5–C7.
169. Fischer, R. A.; Sussek, H.; Miehr, A.; Pritzkow, H.; Herdtweck, E. *J. Organomet. Chem.* **1997**, *548*, 73–82.
170. Carmalt, C. J.; Mileham, J. D.; White, A. J. P.; Williams, D. J. *Dalton Trans.* **2003**, 4255–4260.
171. Carmalt, C. J.; Mileham, J. D.; White, A. J. P.; Williams, D. J.; Steed, J. W. *Inorg. Chem.* **2001**, *40*, 6035–6038.
172. Cheng, Q. M.; Stark, O.; Stowasser, F.; Wohlfart, A.; Fischer, R. A. *J. Mater. Chem.* **2002**, *12*, 2470–2474.
173. Carmalt, C. J.; Mileham, J. D.; King, S. J.; Sabir, E.; Tocher, D. A. *Organometallics* **2004**, *23*, 2939–2943.
174. Barry, S. T.; Richeson, D. S. *Chem. Mater.* **1994**, *6*, 2220–2221.
175. Janik, J. F.; Baldwin, R. A.; Wells, R. L.; Pennington, W. T.; Schimek, G. L.; Rheingold, A. L.; Liablesands, L. M. *Organometallics* **1996**, *15*, 5385–5390.
176. Lakhotia, V.; Heitzinger, J. M.; Cowley, A. H.; Jones, R. A.; Ekerdt, J. G. *Chem. Mater.* **1994**, *6*, 871–874.
177. Barry, S. T.; Belhumeur, S.; Richeson, D. S. *Organometallics* **1997**, *16*, 3588–3592.
178. Jouet, R. J.; Wells, R. L.; Rheingold, A. L.; Incarvito, C. D. *J. Organomet. Chem.* **2000**, *601*, 191–198.
179. Foos, E. E.; Jouet, R. J.; Wells, R. L.; Rheingold, A. L.; Liable-Sands, L. M. *J. Organomet. Chem.* **1999**, *582*, 45–52.
180. Aubuchon, S. R.; McPhail, A. T.; Wells, R. L. *Chem. Mater.* **1994**, *6*, 82–86.
181. Wells, R. L.; Aubuchon, S. R.; Kher, S. S.; Lube, M. S. *Chem. Mater.* **1995**, *7*, 793–800.
182. Dillingham, M. D. B.; Burns, J. A.; Byers-Hill, J.; Gripper, K.; Pennington, W. T.; Robinson, G. H. *Inorg. Chim. Acta* **1994**, *216*, 267–269.
183. von Hänisch, C. *Z. Anorg. Allg. Chem.* **2001**, *627*, 68–72.
184. Pan, Y. L.; Boudjouk, P. *Main Group Chem.* **1995**, *1*, 61–67.
185. Park, H. S.; Schulz, S.; Wessel, H.; Roesky, H. W. *Chem. Vap. Deposition* **1999**, *5*, 179–184.
186. Schulz, S.; Fahrenholz, S.; Kuczkowski, A.; Assenmacher, W.; Seemayer, A.; Hommes, A.; Wandelt, K. *Chem. Mater.* **2005**, *17*, 1982–1989.
187. Kuczkowski, A.; Schulz, S.; Assenmacher, W. *J. Mater. Chem.* **2001**, *11*, 3241–3248.
188. Foos, E. E.; Jouet, R. J.; Wells, R. L.; White, P. S. *J. Organomet. Chem.* **2000**, *598*, 182–186.
189. Nomura, R.; Shimokawatoko, T.; Matsuda, H.; Baba, A. *J. Mater. Chem.* **1994**, *4*, 51–54.
190. O'Brien, P.; Nomura, R. *J. Mater. Chem.* **1995**, *5*, 1761–1773.
191. Jones, A. C. *Chem. Brit.* **1995**, *31*, 389–391.
192. Malik, M. A.; Motevalli, M.; Walsh, J. R.; O'Brien, P.; Jones, A. C. *J. Cryst. Growth* **1996**, *169*, 243–249.
193. Malik, M. A.; Motevalli, M.; Walsh, J. R.; O'Brien, P.; Jones, A. C. *J. Mater. Chem.* **1995**, *5*, 731–736.
194. Pickett, N. L.; Foster, D. F.; Cole-Hamilton, D. J. *J. Mater. Chem.* **1996**, *6*, 507–509.
195. Forster, D. F.; Patterson, I. L. J.; James, L. D.; Cole-Hamilton, D. J.; Armitage, D. N.; Yates, H. M.; Wright, A. C.; Williams, J. O. *Adv. Mat. Opt. Electron.* **1994**, *3*, 163–169.
196. Prete, P.; Lovergine, N.; Zanotti-Fregonara, C.; Mancini, A. M.; Smith, L. M.; Rushworth, S. A. *J. Cryst. Growth* **2000**, *209*, 279–285.
197. Prete, P.; Lovergine, N.; Cannoletta, D.; Mancini, A. M.; Mele, G.; Vasapollo, G. *J. Appl. Phys.* **1998**, *84*, 6460–6462.
198. Irvine, S. J. C.; Stafford, A.; Ahmed, M. U.; Brown, A.; Keyrandish, H. *J. Electron. Mater.* **1997**, *26*, 723–727.
199. Lovergine, N.; Prete, P.; Leo, G.; Calcagnile, L.; Cingolani, R.; Mancini, A. M.; Romanato, R.; Drigo, A. V. *Cryst. Res. Technol.* **1998**, *33*, 183–195.
200. Kuhn, W. S.; Helbing, R.; Qu'Hen, B.; Gorochov, O. *J. Cryst. Growth* **1995**, *146*, 580–586.
201. Kamata, A. *J. Cryst. Growth* **1994**, *145*, 557–561.
202. Taudt, W.; Wachtendorf, B.; Beccad, R.; Wahid, A.; Heuken, M.; Gurskii, A. L.; Vakarekska, K. *J. Cryst. Growth* **1994**, *145*, 582–588.
203. Taudt, W.; Lampe, S.; Sauerländer, F.; Söllner, J.; Hamadeh, H.; Heuken, M.; Jones, A. C.; Rushworth, S. A.; O'Brien, P.; Malik, M. A. *J. Cryst. Growth* **1996**, *169*, 243–249.
204. Almond, M. J.; Cockayne, B.; Cooke, S. A.; Rice, D. A.; Smith, P. C.; Wright, P. J. *J. Mater. Chem.* **1995**, *5*, 1351–1355.
205. Malik, M. A.; O'Brien, P. *Adv. Mater. Opt. Electron.* **1994**, *3*, 171–175.
206. Abrahams, I.; Malik, M. A.; Motevalli, M.; O'Brien, P. *J. Organomet. Chem.* **1994**, *465*, 73–77.
207. Malik, M. A.; Crouch, D.; Malik, M. A.; Motevalli, M.; O'Brien, P.; Park, J.-H. *J. Mater. Chem.* **2003**, *13*, 639–640.
208. Crouch, D. J.; Hatton, P. M.; Helliwell, M.; O'Brien, P.; Raftery, J. *Dalton Trans.* **2003**, 2761–2766.
209. Dumont, H.; Bourée, J.-E.; Marbeuf, A.; Gorochov, O. *Appl. Surf. Sci.* **1994**, *79/80*, 275–280.
210. Hails, J. E.; Cole-Hamilton, D. J.; Bell, W. *J. Cryst. Growth* **1994**, *145*, 596–601.
211. Hails, J. E. *Adv. Mat. Opt. Electron.* **1994**, *3*, 151–161.
212. Bochmann, M. *Chem. Vap. Deposition* **1996**, *2*, 85–96.
213. Lazell, M. R.; O'Brien, P.; Otway, D. J.; Park, J.-H. *J. Chem. Soc., Dalton Trans.* **2000**, 4479–4486.
214. Rees, W. S. Jr., Ed. *CVD of Nonmetals*; VCH: New York, 1996.
215. Shang, G.; Hampden-Smith, M. J.; Duesler, E. N. *Chem. Commun.* **1996**, 1733–1734.
216. Mîinea, L. A.; Hoffman, D. M. *Polyhedron* **2001**, *20*, 2425–2430.
217. Cleaver, W. M.; Spath, M.; Hnyk, D.; McMurdo, G.; Power, M. B.; Stuke, M.; Rankin, D. W. H.; Barron, A. R. *Organometallics* **1995**, *14*, 690–697.
218. Pernot, P.; Barron, A. R. *Chem. Vap. Deposition* **1995**, *1*, 75–78.
219. Schulz, S.; Gillan, E. G.; Ross, J. L.; Rogers, L. M.; Rogers, R. D.; Barron, A. R. *Organometallics* **1996**, *15*, 4880–4883.
220. Stoll, S. L.; Gillan, E. G.; Barron, A. R. *Chem. Vap. Deposition* **1996**, *2*, 182–184.
221. Gillan, E. G.; Barron, A. R. *Chem. Mater.* **1997**, *9*, 3037–3048.

222. Power, M. B.; Barron, A. R.; Hnyk, D.; Robertson, H. E.; Rankin, D. W. H. *Adv. Mat. Opt. Electron.* **1995**, *5*, 177–185.
223. Fahlman, B. D.; Barron, A. R. *Organometallics* **1998**, *17*, 5310–5314.
224. Medina, I.; Fink, M. J. *Mat. Sci. Eng. B* **2005**, *116*, 375–379.
225. Ng, T. L.; Maung, N.; Fan, G.; Poole, I. B.; Williams, J. O.; Wright, A. C.; Foster, D. F.; Cole-Hamilton, D. J. *Chem. Vap. Deposition* **1996**, *2*, 185–189.
226. Stoll, S. L.; Barron, A. R. *Chem. Mater.* **1998**, *10*, 650–657.
227. Choi, I.-H.; Yu, P. Y. *J. Appl. Phys.* **2003**, *93*, 4673–4677.
228. Cho, J. Y.; Jeong, H. C.; Kim, K. S.; Kang, D. H.; Kim, H. K.; Shim, I. W. *Bull. Kor. Chem. Soc.* **2003**, *24*, 645–646.
229. Haggata, S. W.; Malik, M. A.; Motevalli, M.; O'Brien, P.; Knowles, J. C. *Chem. Mater.* **1995**, *7*, 716–724.
230. Keys, A.; Bott, S. G.; Barron, A. R. *Chem. Mater.* **1999**, *11*, 3578–3587.
231. Horley, G. A.; Chunggaze, M.; O'Brien, P.; White, A. J. P.; Williams, D. J. *J. Chem. Soc., Dalton Trans.* **1998**, 4205–4210.
232. Park, J.-H.; Afzaal, M.; Helliwell, M.; Malik, M. A.; O'Brien, P.; Raftery, J. *Chem. Mater.* **2003**, *15*, 4205–4210.
233. Boudjouk, P.; Seidler, D. J.; Grier, D.; McCarthy, G. J. *Chem. Mater.* **1996**, *8*, 1189–1196.
234. Boudjouk, P.; Remington, M. P.; Seidler, D. J.; Jarabek, B. R.; Grier, D. G.; Very, B. E.; Jarabek, R. L.; McCarthy, G. J. *Mater. Res. Bull.* **1999**, *34*, 2327–2332.
235. Boudjouk, P.; Seidler, D. J.; Bahr, S. R.; McCarthy, G. J. *Chem. Mater.* **1994**, *6*, 2108–2112.
236. Chuprakov, I. S.; Dahmen, K.-H.; Schneider, J. J.; Hagen, J. *Chem. Mater.* **1998**, *10*, 3467–3470.
237. Menezes, D. C.; de Lima, G. M.; Porto, A. O.; Donnici, C. L.; Ardisson, J. D.; Doriguetto, A. C.; Ellena, J. *Polyhderon* **2004**, *23*, 2103–2109.
238. Kana, A. T.; Hibbert, T. G.; Mahon, M. F.; Molloy, K. C.; Parkin, I. P.; Price, L. S. *Polyhedron* **2001**, *20*, 2989–2995.
239. Price, L. S.; Parkin, I. P.; Field, M. N.; Hardy, A. M. E.; Clark, R. J. H.; Hibbert, T. G.; Molloy, K. C. *J. Mater. Chem.* **2000**, *10*, 527–530.
240. Nomura, R.; Matsuda, H. *Proc. 16th Int. Conf. Organomet. Chem.*; Royal Society of Chemistry, Brighton, **1994**, 138–143.

12.02
From Metal–Organic Precursors to Functional Ceramics and Related Nanoscale Materials

S Mathur, Leibniz-Institute of New Materials, Saarbrucken, Germany
M Driess, Technical University Berlin, Berlin, Germany

12.02.1 Introduction

The development of new materials is a fundamental cornerstone of modern chemical research. The operating regime of chemistry has traditionally been outside the domain of nanodimensional materials, encompassing at one end molecules and molecular clusters with sizes in angstrom range, and at the other end macroscopic crystals large enough for the coherent diffraction of X-rays. The synthesis of inorganic materials has been revolutionized by the impact of chemical approaches, which now allow synthesizing solid phases from the controlled assembly of atomic or molecular units. Chemical methods based on the transformation of molecular precursors to materials have not only contributed to the development of new materials but have also provided insight in the reaction mechanisms involved in the formation of solid phases, thereby offering a means for the logical synthesis and assembly of inorganic materials.[1–3] The indispensable strength of chemistry to manipulate matter at the atomic and molecular scale is evident in the novel forms of materials and compositions, which would not exist naturally.[1,1a–1d]

Metal–organic or organometallic compounds containing elements necessary for the formation of a particular solid-state phase (e.g., $Ti(OR)_4$ for TiO_2, $Ga(NR_2)_3$ for GaN) are termed "molecular precursors" and are finding increasing applications in the synthesis of nanodimensional materials.[4–27] Given the pre-existing metal–ligand interactions in

molecular clusters, such as metal–nitrogen for nitrides, the activation energy barrier for the nucleation of solid-state structure is lowered, which facilitates the growth at lower temperatures when compared to conventional synthesis procedures. The transformation of the molecular precursor is associated with the structural rearrangement and elimination of organic ligands as depicted in Figure 1.

To arrive at new materials and compositions, scientists are using innovative approaches based on the principles of coordination chemistry, organometallic chemistry, and last but not least, organic chemistry.[1,1a–1d] Recent advances in modern solid-state synthesis are largely attributed to the use of molecular building blocks in material synthesis, and the attention devoted to understand the chemistry of material processing and modification.[1,1a–3b] The simplicity of precursor-based methods was demonstrated by Bawendi and co-workers in the synthesis of high-quality CdE (E = S, Se, Te) semiconductor nanocrystallites.[28] The rapid injection of the organometallic precursors dimethylcadmium, $(CH_3)_2Cd$, and trimethylsilyl sulphide (selenide or telluride) into a hot coordinating solvent was the key to the chemically controlled reaction and crystal size. Conventional wet chemical synthesis generally consists of the reaction between Cd and S (Se, Te) compounds in the presence of appropriate capping reagents such as thioglycerol or tri-*n*-octylphosphine selenide (telluride).[29] However, the samples obtained are generally polydisperse in size and shape and exhibit poor crystallinity. Therefore, the strategy using molecular carriers for metal and ligand has several advantages such as size-selective synthesis, possibility to *in situ* coat the nanoparticles, and tune the morphology by addition of different surface active reagents.[1,1a–1d] The wide applicability of this simple approach is however limited by the health hazards associated with the use of $(CH_3)_2Cd$, which is especially toxic at high synthesis temperatures (>200 °C), given its low vapor pressure and reactivity toward atmospheric moisture. Interestingly, chemical precursors containing Cd–S (Se, Te) in a single molecule such as $Cd\{Se(C_2H_5)\}_2$[30,31] are benign and obviate the need of hazardous precursors. Thus, suitability of the material synthesis procedure is a trade-off among the precursor attributes (simplicity of synthesis, toxicity, ease of handling, cost, availability, etc.) and desired material properties. The fact that most of the potential chemical precursors to advanced ceramics are not commercial products, that is, the availability factor, outweighs the inherent advantages of molecular precursors as depicted in Figure 2, where the

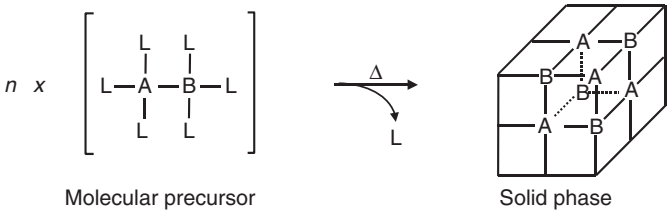

Figure 1 Conceptual representation of the molecule-to-material approach.

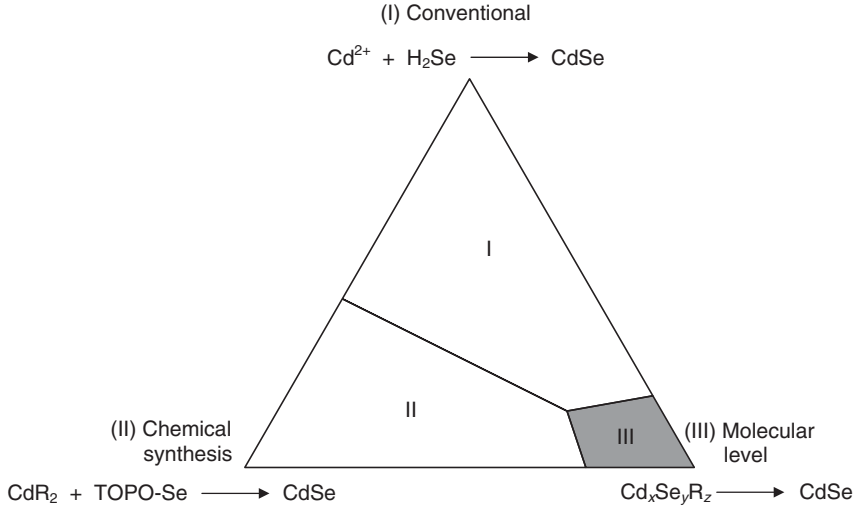

Figure 2 Chemical approaches for the synthesis of CdSe from different precursors.

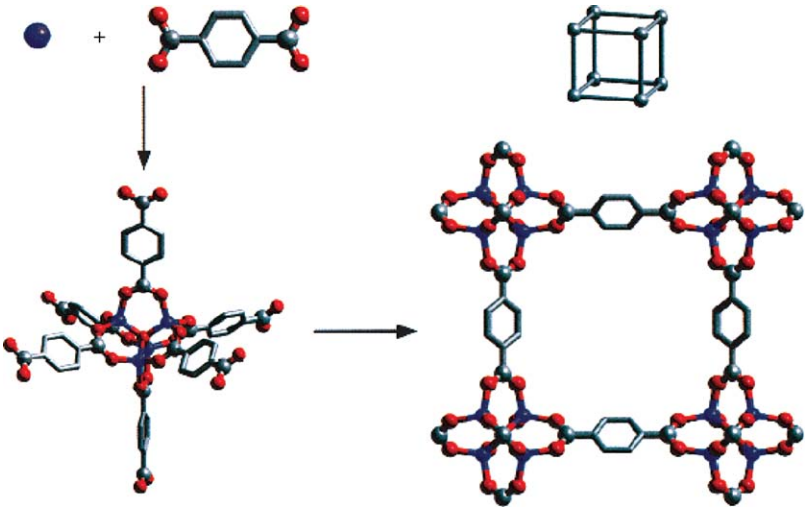

Figure 3 Representation of the molecular structure of MOF-5.[37]

surface area roughly relates to the amount of effort dedicated to the different types of chemical syntheses shown at the corners of the triangle.

The role of molecules and molecular interactions in assembling matter from the tiniest building blocks, has established "chemistry as the creative force" to explore the synthetic and structural space of functional nanostructures.[1,1a–1d] Insight gained in chemical transformations allows designing molecular reactants as well as reaction intermediates, which will decompose or (self-)assemble to form condensed inorganic phases or three-dimensional (3-D) networks. The versatility of designing solid-state architectures from well-defined building blocks and their impetus on the functional properties has recently been demonstrated for the class of metal–organic frameworks (MOFs).[32] Yaghi and co-workers have shown that MOFs offer various advantages such as ordered structures, high thermal stability, adjustable chemical functionality, extra-high porosity, which can be used for storage of hydrogen or carbon dioxide gases.[33–36] The representative of these metal salts, the MOF-5 derivative, obtained from 1,4-benzene dicarboxylic acid and zinc ions, is shown in Figure 3.[37] The as-formed structure is porous, without the need for structure directing agents, in which zinc oxide clusters are joined by benzene dicarboxylate linkers to give an extended cubic framework with porosity of 12 Å.

Given the implications of molecular level processing, the molecules-to-materials rationale has been successfully applied to various material compositions.[1,1a–3b] However, the viability of precursor design with respect to material composition is rather vulnerable because the correlation between the starting entities and the final products is poorly understood. Nevertheless, recent chemical approaches have yielded materials designed to have predetermined structures, compositions, and properties, providing proof-of-principle for new concepts. Therefore, this chapter mainly focuses on the conceptual advancements in synthesis and application of molecular precursors in the preparation of inorganic materials.

12.02.1.1 Material Synthesis: Top-down versus Bottom-up Approaches

The various possibilities of processing functional ceramics can be broadly divided into integrating (bottom-up) or disintegrating (top-down) transformation of the chemical precursor species. Whereas top-down processes are based on the structural decomposition, largely by mechanical methods, of bulk matter into ultrafine particles, the bottom-up methodologies rely on the synthesis of extended frameworks from single molecules or their aggregates. Nevertheless, the understanding of building solid-state phases from molecular building blocks demands a comprehensive and thorough analysis of the value chain "Synthesis–Processing–Microstructure–Property–Function" (Figure 4).

Traditional methods of synthesizing and processing inorganic materials were designed to overcome intrinsic energy barriers such as slow reaction states and large diffusion path lengths in the reaction mixture. The supply of energy is empirically optimized through several intermittent grinding (mechanical) and heating (thermal) steps. Although successful for bulk materials, the top-down methods have limited applications in the synthesis of nanosized materials,

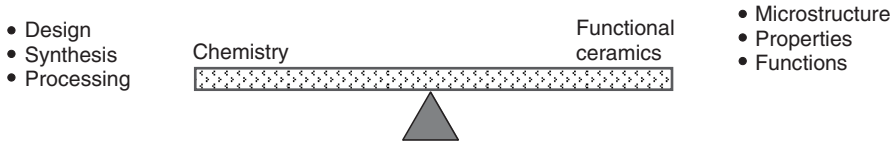

Figure 4 Chemistry-functional ceramics relationship.

which demand means to synthesize crystalline phases at lower temperatures. Conventional materials have grains varying in size anywhere from hundreds of microns (μm) to millimeters (mm), but they are also made of polyatomic or molecular assemblies of matter, where the distribution (ordered or statistical) and multiplicity of such building blocks are responsible for the familiar averaged properties of bulk materials. Because these macroscale properties effectively extend down to the microscale, traditional manufacturing techniques are experiencing a miniaturization trend for the fabrication of microstructures (e.g., in microelectronics) in a "top-down" approach. On the other hand, well-known mono-atomic or molecular units offer the ultimate building blocks for an atom-by-atom or molecule-by-molecule synthesis of nanostructures in a "bottom-up" fashion.

12.02.1.2 Metal–Organic Routes to Materials: Opportunities and Limitations

Organometallic and metal–organic precursors offer opportunities for the architectural design of novel ceramic materials on the atomic scale.[2,2a–2d] As a result, the composition, structure, and functional properties can be varied and controlled to a large extent. The vicinity and desired arrangement of phase-constituting elements in pre-ceramic compounds strongly influence the transformation of the molecular units into the ceramic solids. The idea behind the chemical synthesis of ceramics is to transform molecular precursors into materials under retention of the structural units, which are inherent to the precursor molecule and the target material. The functional goals of using molecular precursors in material synthesis include: (i) overcoming slow diffusion rates, (ii) reduction in reaction (crystallization) temperature, (iii) higher compositional and phase purity in target materials, (iv) access to thermodynamically labile phases, and (v) atomistic control over the evolution of matter on several length scales.

The degree of mixing in conventional synthesis is limited by diffusion rates, decomposition temperature, and initial particle size, whereas the phase-building elements are mixed at the atomic scale in the case of chemical methods, which translates into faster reaction kinetics and formation of crystalline phase at relatively lower reaction temperatures.

Further, the chemical techniques offer facile control over structure, morphology, and composition, either by the systematic variation of the reaction parameters (reaction time, temperature, concentration of reactants) or influenced by the addition of surface-active reagents (stabilizers).[38,39] The chemical interaction between the stabilizer molecules and the particle surface provides means to control the nucleation process because high stabilizer-to-reactant concentrations favor the formation of smaller nuclei whereas tight-binding molecules can check the growth due to higher steric hindrance. Use of organometallic compounds simplifies precursor delivery and allows controlling the reaction kinetics, which influences the particle size and size dispersion in the final material; for instance, ultrafine particles can be obtained by encouraging particle nucleation over particle growth.[1,1a,3b,39] Further, the nucleation process can be regulated by varying the amounts or ratios of the reactants or reaction time, for example, by massively exceeding the supersaturation ratio in precipitation reactions or by increasing the amount of water added in an alkoxide-based sol–gel process to drive hydrolysis at the expense of condensation reactions.

Traditional chemical synthesis procedures operate mostly in thermodynamic equilibrium because they are driven by the intrinsic chemical behaviors of the starting materials. For instance, the difference in the solubility of precursors or intermediates will result in a heterogeneous mixture, which would require subsequent grinding, calcination, and decomposition steps, typically associated with solid-state syntheses. Similarly, the difference in pH values necessary to induce precipitation of cations in a mixture of dissimilar metals poses barriers in obtaining chemically homogeneous mixed metal hydroxides. The entropy-driven tendency of demixing is unfavorable for synthesizing thermodynamically metastable compounds and phases. Applications of molecular precursors that are stable enough to carry forward characteristic structural units (e.g., metal–oxygen for forming oxides) epitomize the chemical control in the selective synthesis of metastable phases. For example, the molecule, $[(Bu^t)GaS]_4$, with a cubane structure produces a new cubic GaS phase in the chemical-vapor deposition (CVD) process due to the presence of appropriate structural element in the starting material[40] The cubic phase is not obtained by other routes and precursors, and it has been

shown that the formation of cubic GaS is a consequence of the retention of Ga_4S_4 core during the deposition and growth process (Figure 5). Interestingly, the dimeric compound $[(Bu^t)_2GaSBu^t]_2$ produces only the thermodynamically stable hexagonal GaS.[6,40] A comprehensive overview of precursor-based synthesis of semiconducting materials is presented in the Chapter 12.01.

Heterometal cubanes of general formula, $[M'_{4-x}M''_x(LH)_4](OAc)_{4-x}(ClO_4)_x$, have shown to be versatile single-source precursors to prepare metal-doped transition metal oxides.[13,41–42] The heterocubanes allow several combinations of constituting metals (M′ = Zn; M″ = Mn, Co, Ni), which have been used to tune the composition of the resulting material (Figure 6). An interesting outcome of the molecular level design was the mixing of two chemical species (ZnO and NiO), which normally would segregate into monometal phases.

In a similar approach, nanocrystalline zinc silicate can be synthesized via chemical-vapor synthesis (CVS) by using the *O*-silylated Zn_4O_4 cubane $[MeZn(OSiMe_3)]_4$.[43] Interestingly, the Zn : Si ratio in the latter single precursor

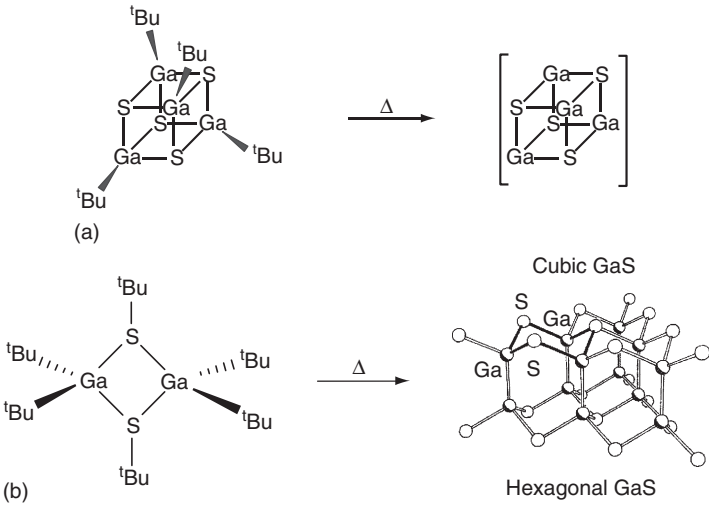

Figure 5 Formation of (a) cubic and (b) hexagonal GaS phases from different molecular precursors containing preformed Ga–S units.[6,39]

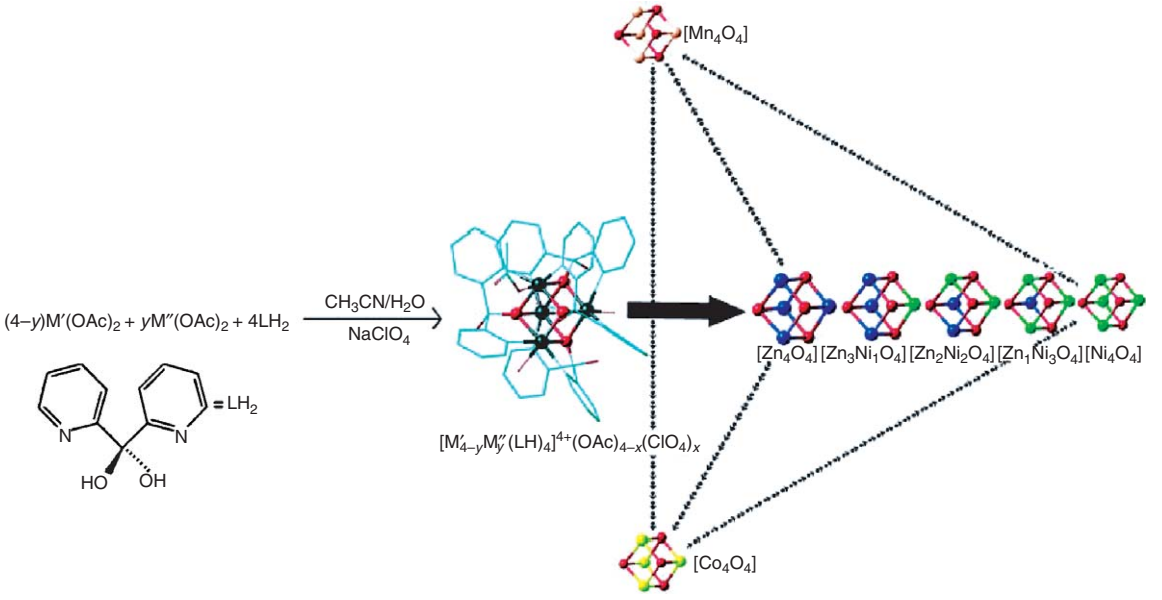

Figure 6 Possible metal combinations in heterocubanes of general formula $[M'_{4-x}M''_x(LH)_4](OAc)_{4-x}(ClO_4)_x$ illustrating the flexibility of precursor design.[13] Reproduced with permission from Wiley.

determines that at high temperature (900 °C), when sintering occurs, α-Zn_2SiO_4 is formed embedded in an amorphous SiO_2 matrix (Figure 7).

The advantage of metal–organic precursors is twofold: the metal combinations can be systematically varied and it is also possible to choose appropriate ligands and their combinations to judiciously tune the precursor properties (Figure 8). For example, three Mg–Al alkoxides, $[MgAl_2(OPr^i)_8]$, $[MgAl_2(OBu^t)_8]$, and $[MgAl_2(OBu^t)_4H_4]$, differing only in their organic periphery, have been examined as single molecular precursors for the gas-phase synthesis of $MgAl_2O_4$ films.[44–45] From the viewpoint of precursor concept, $[MgAl_2(OPr^i)_8]$, $[MgAl_2(OBu^t)_8]$, and

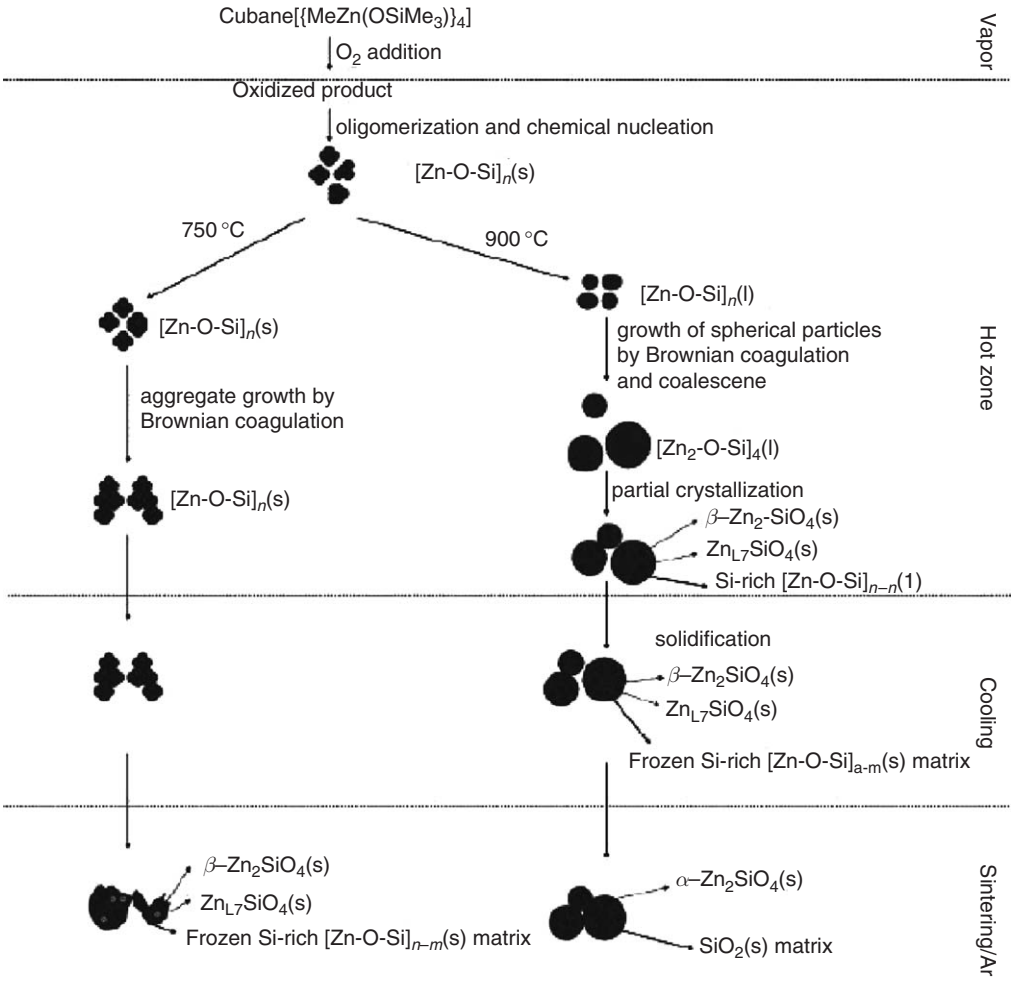

Figure 7 Formation of nanocrystalline α-Zn_2SiO_4 from oxidative decomposition of $[MeZn(OSiMe_3)]_4$ as single-source precursor.[41] Reproduced with permission from Wiley.

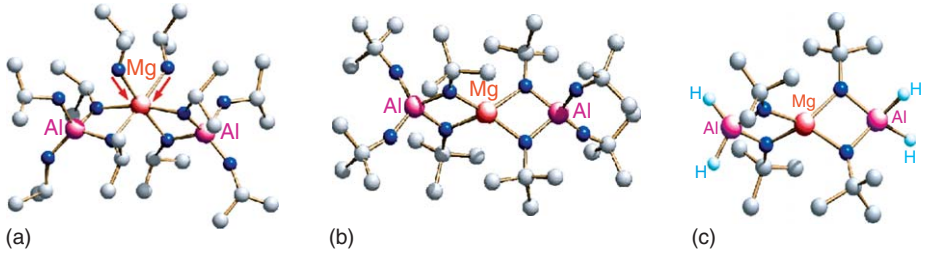

Figure 8 Molecular structure of different Mg–Al alkoxides used as precursors to $MgAl_2O_4$. (a) $[MgAl_2(OPr^i)_8]$, (b) $[MgAl_2(OBu^t)_8]$, and (c) $[MgAl_2(OBu^t)_4H_4]$.

Table 1 Chemical precursors used in the synthesis of nanomaterials

Nanomaterials	*Precursors*[a]
Hydrides/halides	MH_x, R_xMH_y, $M(BH_4)_x$ $MHal_x$(Hal = F, Cl, Br, I)
Nitrates	$M(NO_3)_x$, $M(NH_4)_x(NO_3)_y$, $M(NO_3)_x{\cdot}yH_2O$
Oxalates, acetates	$M(HOOCCOO)_x$, $M(CH_3COO)_x$
Alkyls	MR_x $MR_xR^1{}_y$
Carbonyls	$M(CO)_x$, $(CO)_x$ ML_y (L = donor ligand)
Cyclopentadienylides	$M(C_5H_5)_x$, $(C_5H_5)M(CO)_xR_y$, $(N_3)_xM(C_5H_5N)_y$
Amides	$MR_x(NH_2)_y$, $M(NR_2)_x$, $(N_3)_xM(RN)_y$
Silanes	R_xSiL_y (L = OR, halide)
Silazanes	$M\{N(SiR_3)_2\}_x$
β-Diketonates	$M(\beta\text{-dik})_x$ (β-dik = acac, dpm, tmhd, od, hfac, fod)
Alkoxides	$M(OR)_x$, $LM(OR)_x$ (L = R, O, OH, halide)
Siloxanes	$M(OSiR_x)$, $R_3Si\text{-}O\text{-}MR_x$, $M(R)_x(OSiR_3)_y$
Thiolates (selenolates, tellurates)	$M(ER)_x$ (E = S, Se, Te)
Thiocarbamates	$M(R_2NCOS)_x$

[a]M = Metal; R = Me, Et, ^{i}Pr, ^{t}Bu, ^{n}Bu, ^{i}Bu, Ph, and substituted alkyl or phenyl.

$[MgAl_2(OBu^t)_4H_4]$ are "chemically equivalent," because each of them contains similar MOFs and the right proportion of atomic constituents necessary to form the $MgAl_2O_4$ phase. However, the decomposition behavior in the gas phase, governed by the nature of the ligand(s), was found to be different for the three compounds. $[MgAl_2(OPr^i)_8]$ displays strong tendency to oligomerize upon aging to species such as $[MgAl_2(OPr^i)_8]_2$ and $[Mg_2Al_3(OPr^i)_{13}]$ that are less volatile.[46] In addition, the premature fragmentation of the precursor leads to films with non-ideal Mg : Al ratio. The molecular framework based on bulkier *tert*-butoxide ligands ($[MgAl_2(OBu^t)_8]$) was found to be thermally and structurally more stable, allowing intact transport of precursor in the gas phase and thus stoichiometric spinel films. The replacement of terminal alkoxide groups on Al centers by hydride ligands produced hydride-modified Mg–Al *tert*-butoxide precursor, $[MgAl_2(OBu^t)_4H_4]$, which possessed an enhanced volatility ($[MgAl_2(OBu^t)_8]$, 100 °C; $[MgAl_2Me_4(OBu^t)_4]$, 60 °C; $[MgAl_2H_4(OBu^t)_4]$, 45 °C) due to drastic reduction in the molecular weight; however, the higher vapor pressure resulted in rough films. Nevertheless, the combination of hydride and *tert*-butoxide ligands induced designed ligand elimination, based on the β-hydride elimination.[45]

A wide range of chemical precursors are available for the material synthesis, the most common of which are listed in Table 1. The specific selection criterion depends on the requirements of the target material, the processing technique, and (commercial) availability. In order to act as suitable chemical sources for high-purity nanomaterials, the metal–organic precursor should possess adequate stability of the molecular framework to survive different experimental conditions and importantly an element ratio appropriate for the target material.

12.02.1.3 Functional Ceramics: Chemical Composition, Function and Form

The common definition of ceramics refers to inorganic and non-metallic materials that may be amorphous or crystalline, extracted from natural raw materials, and heat treated to attain their characteristic (hard and brittle) physical properties. However, the advanced ceramics refers to compositions synthetically prepared and/or altered to meet the requirements of specific technical applications. The concept of high-performance ceramics is mainly used to distinguish them from generally traditional clay-based products such as floor tiles, pottery, and sanitary ware. The advanced ceramics are broadly divided into two categories: (i) structural or engineering ceramics representing materials capable of withstanding mechanical stresses, pressure, tensile strain, etc., and (ii) functional ceramics—compositions in which the inherent material properties (e.g., optical, electrical, or magnetic) play an active role in determining the final function. In addition, the technical ceramics are grouped under different categories based on their chemical composition such as oxides, silicates, and non-oxide ceramics (e.g., borides, carbides, nitrides). Nevertheless, an unambiguous categorization in different subgroups is not feasible due to the diversity of application and properties of ceramic materials, which justifies the presence of certain compositions. Figure 9 shows an arbitrary classification of the materials, which outlines the trend of applications of ceramic materials from simple structural applications to a combination of different properties in composite materials, which do not exist in nature. The multifunctionality of materials is desired to meet needs as different as human safety, comfort, and communication.

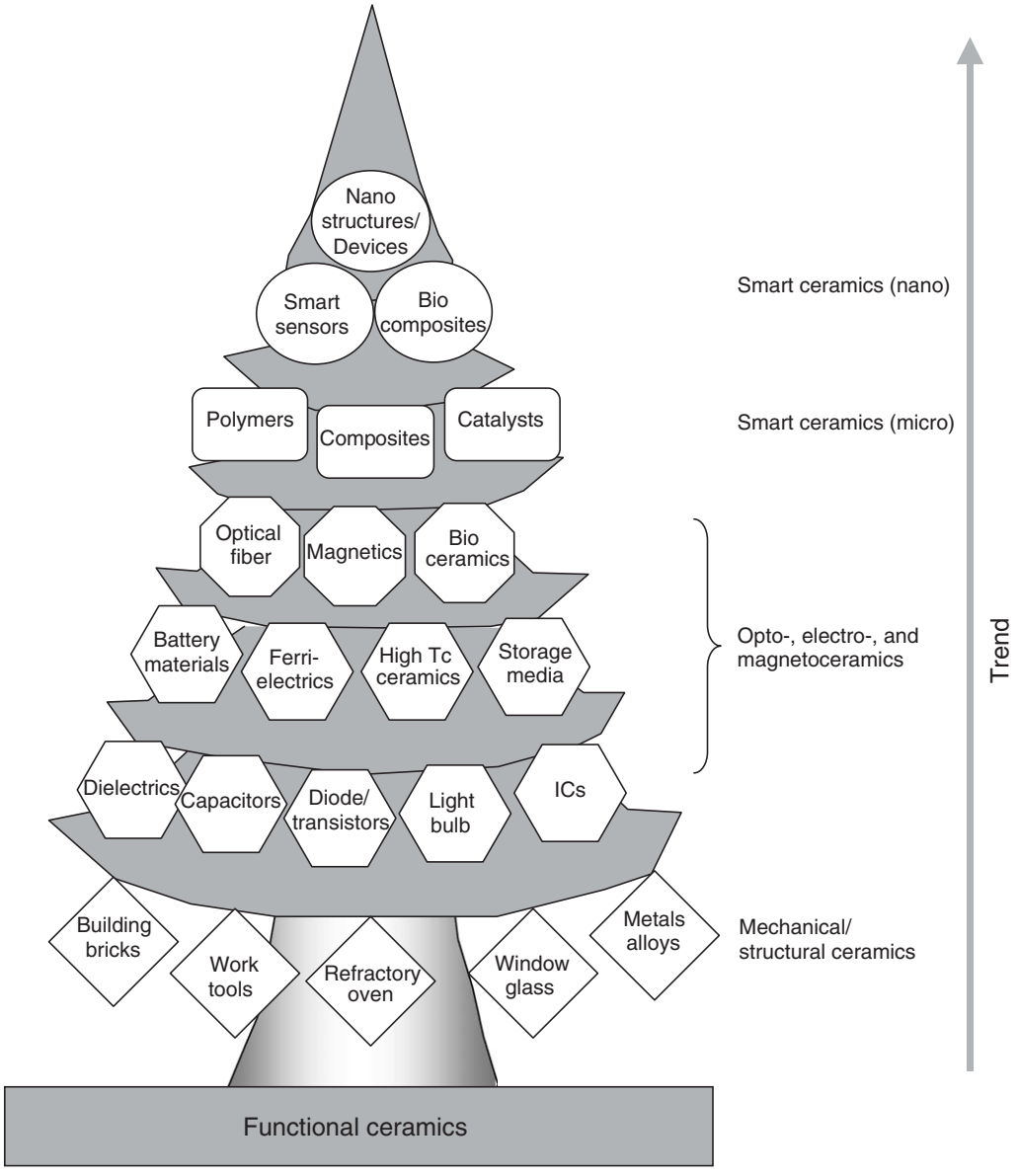

Figure 9 Trend of development in functional ceramics.

"Nanodimensional materials" are commonly defined as material structures assembled from layers or clusters of atoms in which at least one of the dimensions is in the order of nanometers (nm).[1,1a–1d,47] At this scale, atoms function in the fabled realm of quantum physics, so that characteristics inconceivable at micro- or macroscales can be experimentally demonstrated. A number of methods exist for the synthesis of nanostructured materials, including synthesis from atomic or molecular precursors (chemical- or physical-vapor deposition, gas condensation, chemical precipitation, aerosol reactions, biological templating, etc.), from processing of bulk precursors (mechanical attrition, crystallization from the amorphous state, phase separation, etc.), and from natural templates (e.g., biological systems).[3,3a,3b,48–52] New chemical approaches have enabled production of uniform nanostructures with different sizes (1–100 nm), shapes (spheres, triangles, cubes, bars, rods, wires, tubes), and compositions (metals, semiconductors, insulators, organic, inorganic–organic hybrids), which in most of the cases exhibit interesting physical effects due to dimensional confinement (Figure 10).[39]

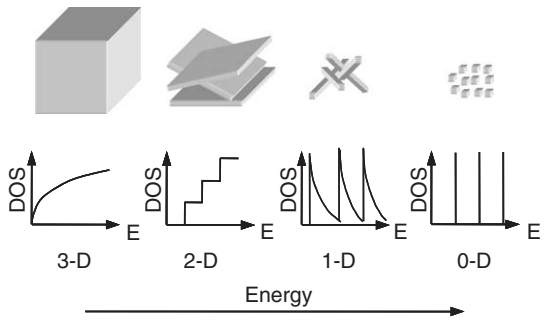

Figure 10 Forms and corresponding density of states (DOS) in materials.

12.02.2 Methods for Transformation of Molecular Precursors to Materials

The preparative methods for nanodimensional materials are decisive for their functional properties, because ceramics prepared through different routes exhibit different properties despite similar chemical composition. Molecular level homogeneity achieved in the chemical processing routes offers significant advantages, for example, easy and better composition control, feasibility to prepare metastable phases, low sintering temperatures, and improved consistency of the final material.[2,2a–2d] Chemical preparative techniques for the synthesis of nanomaterials involve reactions in "solid" (mechanical attrition, mechanochemical synthesis, sonochemical treatment), "liquid" (co-precipitation, hydrothermal synthesis, sol–gel, micro-emulsion, polymeric precursor methods), and "gas" (chemical vapor deposition, aerosol synthesis, atomic layer deposition) phases. This chapter primarily presents only a subset of the wide variety of chemical material syntheses procedures with examples selected to underscore the influence of precursor chemistry and highlight the fortification of the inherent advantages of chemical routes through the application of molecular precursors. The account is not comprehensive but wherever appropriate, underlying principles of the synthetic methodologies and theoretical consideration are given to provide the uninitiated reader an overall picture.

12.02.2.1 Co-precipitation

Chemical reactions inducing precipitation of sparingly soluble products fall under this category. Precipitation reactions can be initiated by altering reaction parameters (pH, temperature, concentration) or through chemical reactions (hydrolysis, complexation, oxidation, reduction). The target composition can directly form as a result of the reaction or an intermediate precursor may form first, which can be processed (drying, calcination, etc.) to the final product. The particle size and morphology of products obtained by precipitation reactions are governed by nucleation and growth processes; when precipitation begins, numerous small crystallites are initially formed (nucleation), which coalesce and aggregate to thermodynamically stable larger particles (growth). The degree of supersaturation is the key step to any precipitation processes, which depend on the equilibrium relationship between the products and its reactants, and is expressed as the solubility product constant.

Chemical reactions involving precipitation of elemental (metals) or binary phases (metal oxides, nitrides, chalcogenides, etc.) are relatively straightforward. The process becomes more complicated in the simultaneous precipitation of various components from the reaction mixture; this is especially challenging when several stable compositions exist in a multi-component system. The products of room-temperature precipitation reactions are usually amorphous, and calcination or annealing steps are inevitable to obtain a defined material. Since the nature of the amorphous intermediates is difficult to determine by experimental techniques, any inhomogeneity with respect to the elemental distribution shows up, in the form of constituent segregation and secondary products, in the final material.

Given the solubility considerations in aqueous solutions, metal precursors in co-precipitation reactions are commonly available salts and other inorganic compounds, and the application of molecular precursors is limited to few systems. For example, ferroelectric $BaTiO_3$ has been prepared by precipitating a mixed metal alkoxide precursor, $[BaTi(OOC(CH_3)_6CH_3)(OCH(CH_3)_2)_5]$ with hydrogen peroxide in diphenyl ether and using oleic acid as stabilizer.[53] The presence of Ba–O–Ti linkages was found to be advantageous for crystallization of the perovskite phase at relatively low temperature (100 °C). The advantages of chemical interactions between the phase-building elements have been employed in the synthesis of metal ferrites (MFe_2O_4; M = Mn, Fe, Co, Ni, or Zn), where metal chelate precursor, formed *in situ* by the reaction between metal chloride and diethylene glycol, was hydrolyzed to obtain a

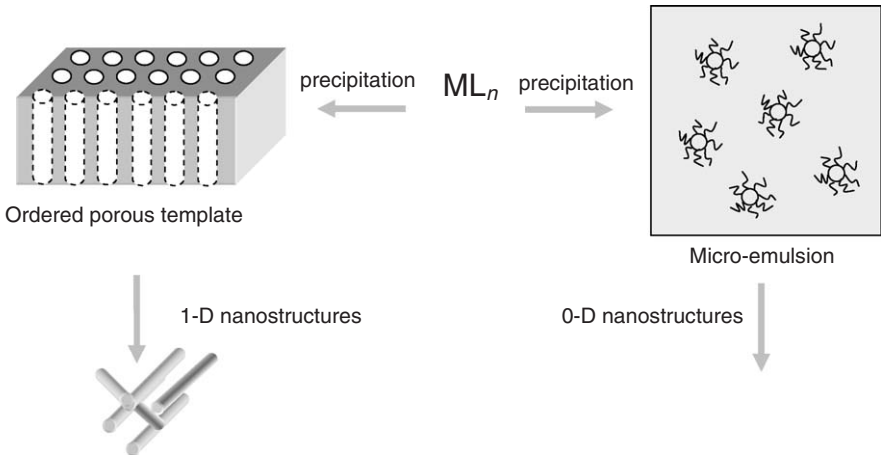

Figure 11 Templated precipitation of chemical precursors to form zero- and one-dimensional materials.

precipitate with homogeneous distribution of cations.[54] Precipitation in confined geometries, such as micro-emulsion and porous templates, has been successfully used to tune the morphology of the materials (Figure 11). For instance, molecular precursors of general formula $[MAl_2(OR)_8]$ (M(II) = Cu, Co, Ni; R = –Pr^i, –Bu^t) were hydrolyzed in water-in-oil emulsions to obtain mixed metal hydroxides, which produced crystalline spinel phases after short heat treatments.[55] Similarly, $CoFe_2O_4$ nanorods have been obtained by the precipitation of mixed metal oxalate $CoFe_2(C_2O_4)_3$ in micelles followed by its decomposition in air (720 °C).[56] A large number of reports are available on the synthesis of ultrafine oxide powders (Fe_3O_4,[57] ZrO_2,[58] $BaTiO_3$,[59] $NiTiO_3$,[60] $MnFe_2O_4$,[61] $ZnAl_2O_4$,[62] α,β-$Zn_2(SiO_4)$,[43] composites CeO_2/ZrO_2,[63] and biomaterial $Ca_5(PO_4)_3(OH)$[64]) by co-precipitation reactions.

Precipitative methods for metal sulphides were initially used by Brus and co-workers, in which they prepared CdS by reaction between cadmium sulphate and ammonium sulphide.[30] Meanwhile, co-precipitation approach has been successfully applied to the synthesis of various metal chalcogenide particles involving metathesis reactions between metal and chalcogenide ions that instantaneously produce precipitates of metal (Zn, Cd, Hg, Pb, Sb, In, Ga, etc.) chalcogenides (Equation (1)).[1,1a–1d,31]

$$\mathrm{MX} + \mathrm{E} \xrightarrow{\mathrm{S/L}} \mathrm{ME} \quad (1)$$

MX = metal precursor (halide, oxide, carboxylate)
E = chalcogen source (elemental or compound)
S = high boiling solvent
L = coordinating reagent (surfactant)

In addition to the reactions between ionic species in aqueous media, the reaction between metal and chalcogen-containing molecular carriers are readily kinetically controlled and allow better size- and shape-control of final material.[1,1a–1d,65–66]

The advantages of co-precipitation reactions are (i) homogeneity of components distribution, (ii) relatively low reaction temperature, (iii) fine and uniform particle size with weakly agglomerated particles, and (iv) low cost. However, these reactions are highly susceptible to the reaction conditions, and due to incomplete precipitation of the metal ions, a control over the stoichiometry of precursors is rather difficult. In addition, the co-precipitation reactions are not suited for certain oxides/hydroxides, for instance, in the case of amphoteric systems.

12.02.2.2 Sol–Gel Process

Traditionally, sol–gel technique refers to inorganic polymerization reactions based on the hydrolysis and polycondensation of metal–organic compounds, in particular metal alkoxides, carried out under controlled pH, amount of water, and precursor concentration.[67–71] The process essentially consists of four steps: (i) hydrolysis, (ii) condensation, (iii) drying, and (iv) heat treatment. Typically, homogeneous solution of metal alkoxide precursors ($M(OR)_x$ or $MM'(OR)_{x+y}$) is "activated" by controlled hydrolysis (stoichiometric amount of protic reagents) to initiate polymerization reactions that

produce homo- (M–O–M) or heterometal (M–O–M′) linkages.[67–71] The metal species bearing a terminal hydroxy group react with other species in the solution to form oligomeric structures linked by oxo or hydroxo ligands, which can be transformed into polymeric gels by aging. The polymerization reactions followed by drying and thermal treatments result in the elimination of water (oxolation) and alcohol (alcoholation), finally producing a solid material.

The fundamental reaction in the hydrolysis of metal alkoxides is a nucleophilic substitution (S_N2) that involves a nucleophilic addition of $OH^{-\delta}$ group onto the electrophilic metal center ($M^{+\delta}$). As a result, the coordination number (CN) of the metal atom is increased in the transition state, which leads to the migration of proton toward an alkoxy group, consequently knocking off the protonated ROH ligand (Figure 12). The chemical reactivity of metal alkoxides toward nucleophilic reactions mainly depends on the strength of the nucleophile, the electrophilic character of the metal atom, and its ability to increase the CN.

Subject to the alkoxide/water ratio, stoichiometric or complete replacement of alkoxy groups can be achieved (Equation (2)). The variation and control of the degree of hydrolysis ("n" in $M(OR)_{x-n}(OH)_n$) profoundly influences the morphology and structure of the resulting gels.[67]

$$M(OR)_x + nH_2O \longrightarrow M(OR)_{x-n}(OH)_n + n\text{ROH} \qquad (2)$$

Because hydroxide group is a marginally better departing group than the alkoxo moiety, the condensation process can be tailored to favor the formation of dimers, chains, or 3-D networks.[72] The kinetics of hydrolysis and condensation can also be tuned by chemical modification of the precursor compounds, for example, by incorporating less hydrolyzable or polymerizable groups.[73–75] For instance, hydrolysis and condensation of $Ti(OPr^i)_4$ produced nanoparticles of size 10–20 nm (Figure 13). Substitution of one of the isopropoxide ligands with a bidentate acetylacetonate (acac) group checked the hydrolysis rate owing to relatively higher stability of Ti–acac bonds toward nucleophilic attack. As a result, spherical nanoparticles with a smaller size (5 nm) were obtained. Incorporation of two acac units in the precursor led to the formation of polymeric chains, because the probability of cross-condensation reactions is checked in a particular direction due to the presence of acac ligands in the coordination sphere of Ti (Figure 13).[67]

The main advantages of sol–gel processing are an easy control over the microstructure of the material from the earliest stages of the processing, higher purity, low or high porosity, and a greater homogeneity. In addition, net-shape casting, extrusion, and coatings on large and complex surfaces are the major engineering applications.[71] On the other hand, costs of the precursors, large shrinkage, production of volatiles, and fragmentation of the green body due to internal stresses are some of the limitations associated with this technique.

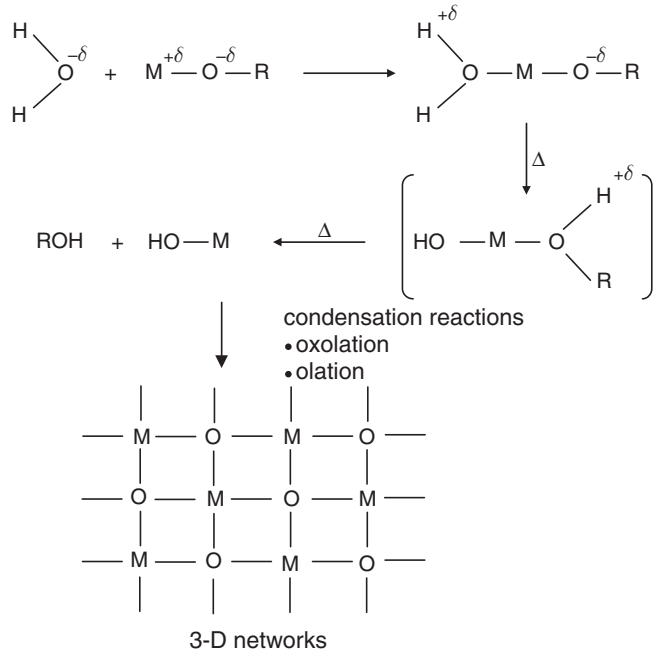

Figure 12 Nucleophilic attack by water molecule on metal alkoxide precursor.

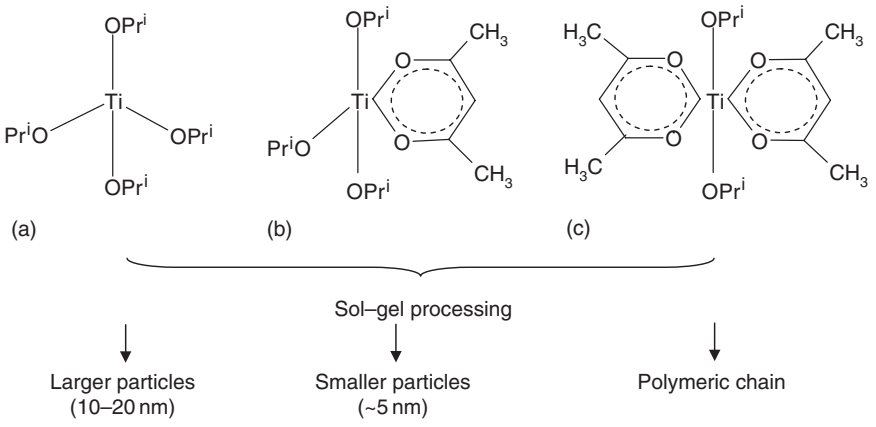

Figure 13 Tunable morphology of TiO_2 particles induced by different Ti–ligand coordinations.

12.02.2.3 Micro-emulsion Technique

Micro-emulsions, as noted originally by Schulman in 1943, are transparent, seemingly homogeneous solutions of water, oil, surfactant, and an alcohol- or amine-based co-surfactant.[76] These isotropic dispersions of two immiscible liquids such as oil and water are stabilized by the presence of emulsifier(s) (surfactant molecules that can be cationic, anionic, or neutral), which are located at the interfaces between oil and water domains.[77] The most common examples are the water-in-oil (W/O) and the oil-in-water (O/W) micro-emulsions. The use of micro-emulsions in the synthesis of materials allows size-selective growth of small particles in water droplets homogeneously entrapped in a hydrocarbon solvent. The important properties are governed mainly by the water-to-surfactant molar ratio.

The reverse micelle technique is suitable for tailoring small and uniform nanoparticles of discrete nanoscaled oxides or hydroxides with controlled size distribution (<10 nm).[55,59,78–88] The principle advantage of the method is that the concentration of metal–organic in the water droplets is very high, so the reaction easily forms particles that are gelled throughout. However, a controlled formation of oxide materials is subject to the reactivity of the starting material toward water and the reaction parameters, which actually determine the size and agglomeration effects in final powder. As a consequence, the results can be different for similar precursors. For example, micro-emulsion-based hydrolysis of titanium alkoxides caused uncontrolled aggregation and flocculation of particles,[89] whereas TiO_2 particles with diameter less than 10 nm were prepared by controlled hydrolysis of titanium isopropoxide in reverse micelles of sodium bis(2-ethylhexyl)sulfosuccinate–hexane–water.[90] Similarly, transition metal–aluminium hetero-metal alkoxides of general formula $MAl_2(OR)_8$ have been successfully used to perform a size-selective synthesis of nanocrystalline MAl_2O_4 spinels (Figure 14).

Microemulsion-based synthesis of nanodimensional materials provides a physical means to control particle size and shape while still exploiting the advantages of sol–gel processing. The principle limitation of emulsion methods is that

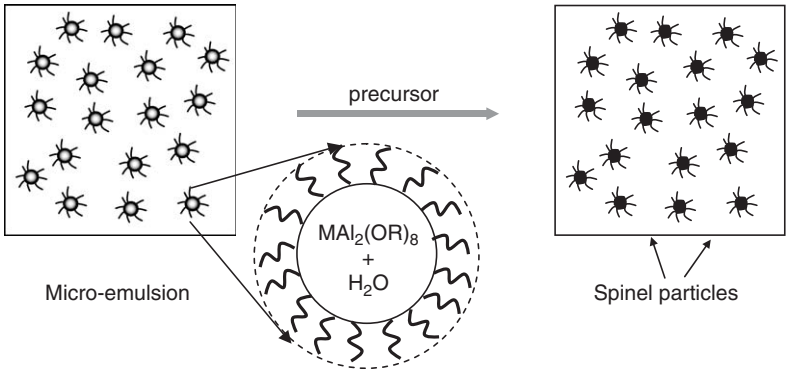

Figure 14 Molecule-based micro-emulsion technique for the size-selective synthesis of MAl_2O_4 spinels.

the emulsion structure is not at thermodynamic equilibrium and should be stabilized by the addition of surfactants that lowers the interfacial tension between the phases and decreases the rate at which the droplets coalesce. In addition, the surfactant should be chemically inert with respect to all other components, and the possible interference of the counterions of the cationic surfactants needs to be considered. Furthermore, the surfactant molecules have large molecular weights, and even a small amount of unremoved surfactant can lead to substantial organic residues in the final material.

12.02.2.4 Colloidal and Polymeric Routes

The chemical precursor approach, in which polymeric or molecular precursors are first processed in the desired shape and then decomposed to the final solid-state material with retention of the original shape, is an important route for producing advanced ceramics in a wide range of forms and sizes. Since the pioneering work of Yajima on the fabrication of ceramic fibers from polysilane,[91] the polymeric precursor routes for the synthesis of covalently bonded ceramics (e.g., Si_3N_4, AlN, BN, SiC) and composites (e.g., SiC–AlN, SiC–TiC) have been extensively investigated.[92–97] The major driving force was to transfer the chemical homogeneity achieved in the initial precursor mixture to the final processed material. Interrante and co-workers[92–97] prepared SiC–AlN ceramics by pyrolysis of organosilicon and organoaluminum compounds, which showed that the molecular level homogeneity attained in the precursor stage was maintained in the pyrolyzed products.

For the synthesis of multi-component oxide powders, Pechini-type methods are frequently employed, where the cations present in aqueous or non-aqueous solutions are complexed using organic ligands (e.g., citric acid, $HOC(CH_2COOH)_2$–COOH), to form polybasic chelates.[98–100] The polyhydroxy–metal complex, when treated with a polyfunctional alcohol (e.g., ethylene glycol, $HOCH_2CH_2OH$), undergoes esterification reaction with the concurrent formation of water and a mixed-cation precursor. This method works with readily available reagents such as oxides, carbonates, or nitrates as cation sources, with the added advantage that it requires no special apparatus or atmosphere control. The organic molecules used as complexing aids not only function as chelating agents and a resin vehicle but also provide combustion heat for calcinations; however, an excess of organic content can have a negative effect by raising the temperature too high during calcination. The structural information on intermediate species is difficult to obtain and the chemical bonding of the cations onto the polymer chains is generally assumed. Although these methods claim the advantages of molecular level mixing and the formation of mixed metal polymeric precursors, evidence is not always available. Nevertheless, this approach represents a low-temperature route to multi-component materials. For example, nanocrystalline yttrium aluminum garnet ($Y_3Al_5O_{12}$) could be obtained at 1,000 °C when compared to 1,600 °C required for the solid-state reaction.[101–103] In an another example, the refractory calcium aluminate ($CaAl_2O_4$) was prepared in high purity at 900 °C, whereas the solid-state reaction between calcia (CaO) or calcium carbonate ($CaCO_3$) requires temperatures in excess of 1,400 °C to complete the reaction, which still contains undesirable $CaAl_4O_7$, $Ca_{12}Al_{14}O_{33}$ phases, and undecomposed starting materials.[104]

12.02.2.5 Hydrothermal and Solvothermal Methods

Hydrothermal or solvothermal processes are characterized by chemical reactions or transformations under supercritical conditions, in water or organic solvent, respectively.[105–106] This methodology takes advantage of enhanced diffusion of chemical species and higher solubility of inorganic materials at elevated temperatures and pressures.[107] Several review articles devoted to these techniques have recently appeared.[108–109] Solvothermal processing allows many inorganic materials to be prepared at temperatures substantially below those required by solid-state reactions. Unlike the sol–gel and co-precipitation reactions, the as-formed products of solvothermal/hydrothermal processing are mostly crystalline. These processes are used to synthesize new materials (metastable phases) as well as to obtain functional materials in new morphologies, such as nanoparticles, nanowires, and nanotubes.[110–113] The first step of hydrothermal processing is similar to sol–gel or a co-precipitation reaction, whereby precursors (alkoxides, amides, nitrates, chlorides, sulfates, etc.) are dissolved in a suitable medium or water to form a homogeneous solution and heated in a sealed autoclave (steel bomb with Teflon lining) well beyond the boiling point of the solvent to create autogenous pressure. At the critical point (e.g., water, 374 °C and 218 atm), the fluid is said to be supercritical and is capable of dissolving chemical compounds that would otherwise exhibit low solubilities under ambient conditions. One of the peculiar advantages of the hydrothermal synthesis is that besides the synthesis of inorganic materials, it is also possible to synthesize new crystalline precursors that can be structurally characterized. For example, a new

hydroxo–stannate, $Sr_2Sn(OH)_8$, has been obtained from the hydrothermal studies on $SrO–SnO_2$ system. The compound acts as a single source to $SrSnO_3$ (<700 °C) and Sr_2SnO_4 (>900 °C),[114] subject to the thermal treatment.

Solvothermal methods offer a simple, direct, and low-temperature route to obtain nanometric particles with narrow size dispersions, and represent an alternative to calcinations for promoting crystallization under milder temperatures. Another feature of the hydrothermal treatment performed under near-supercritical conditions concerns the morphology of the materials that can be governed by monitoring temperature, pressure, reaction time, and nature of the solvent. The easy access to the shaping of materials (crystal growth, preparation of fine microcrystallites) and low crystallization temperatures make hydrothermal synthesis an attractive method for producing submicrometer particles with a narrow size distribution, avoiding the firing steps required in sol–gel processing. The drawbacks include the trial-and-error nature of the method to understand the chemical reactivity of supercritical fluids which governs the course of the hydrothermal synthesis and consequently the composition, structure, and morphology of the nanomaterial. Further, the observation of reaction is difficult due to the sealed reaction vessel, and it remains difficult to predict the outcome of new reactions.

12.02.2.6 Chemical Vapor Deposition

Chemical vapor deposition (CVD) refers to chemical reactions which transform gaseous precursor molecules by chemical reactions into a solid material (film or powder) by their decomposition on a hot substrate (Figure 15).[115–118] The film growth involves the partial or complete fragmentation of precursor molecules to produce reactive intermediates, which can adsorb onto the substrate and decompose to nucleate the solid phase.[119–120] Predominant decomposition in the gas phase leads to homogeneous nucleation, which results in the formation of particles (unfavorable); however, a heterogeneous nucleation is favorable to obtain a continuous film. Depending upon the interactions of the adatoms with the surface, the surface adsorption can be physical (essentially van der Waals interaction) or chemical (covalent linkage between the molecule and the surface) in nature. The adsorbed molecules may wander on the surface and react with other surface species to form the solid deposit. The mobility of surface species is largest on metallic and semiconducting surfaces, where bonding is not very directional. In the case of dielectrics, the highly directional covalent bonds tend to hold the chemisorbed molecules, thereby limiting the mobility. The volatile byproducts released in the gas-phase decomposition, collision, and surface reactions can be removed in vacuum and on line analyzed by infrared spectroscopy or mass spectrometry to control the decomposition process as well as to elucidate the thermal decomposition of the precursor molecule. In a simplified view of the surface, it is assumed that there are a fixed total number of reactive sites upon which an incoming atom (“adatom”) or molecule can adsorb. Once a site is occupied, a second molecule will not adsorb on it. This is equivalent to the assumption that the number of atoms adsorbing is equal to those desorbing, if no reaction is taking place. The number of atoms or molecules adsorbing on the surface is proportional to the concentration of the gas-phase species or, in other words, equivalent to the partial pressure. Besides the four important parameters, namely, temperature, deposition time, pressure, and surface specificity, the chemical nature of the precursor substance is of paramount importance in determining the quality of the film in terms of homogeneity, morphology, and contamination.

Since the conversion of an organometallic precursor to a useful thin film involves stripping most of the coordinated ligands, a well-understood decomposition chemistry is a prerequisite. The efficiency of the CVD process can be increased by choosing ligands that decompose through chemically productive pathways and with low activation barrier. The precursors based on ligands with complex concomitant fragmentation reactions usually lead to the incorporation of heteroatoms such as C, B, N, O, or Si.[115–118] Further, the intact vapor transport of the molecular precursor is highly essential to have a control over the process. Thermal instability or dissociative tendency of the precursor can initiate a cascade of reactions, leading to non-ideal geometry or undesirable deposits.[121–123]

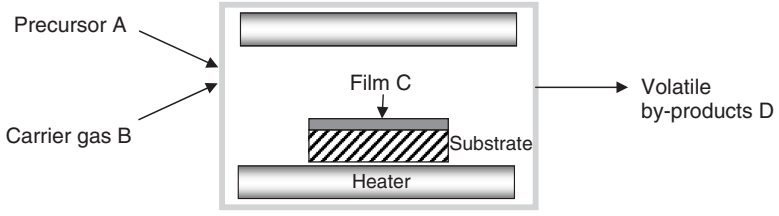

Figure 15 Schematic representation of a typical CVD reactor.

Another strategy to synthesize the particle from volatile organometallic precursors is achieved by promoting homogeneous gas-phase nucleation, the so-called chemical vapor synthesis (CVS).[124] In this case, the precursor is evaporated using a carrier gas and reacted with a co-substrate (e.g., O_2) to produce the desired material, which can be collected as powder. The typical experimental setup is assembled according to Figure 16.[124]

Transformation of the cubane-like precursor $[MeZn(OSiMe)]_4$ into ZnO particle films has been previously demonstrated.[124–125] Interestingly, it turned out that the same precursor is able to function as the source of both elemental zinc and zinc oxide, depending on the reaction conditions (Figure 17). While the formation of ZnO is the kinetic product, the generation of elemental Zn is due to thermodynamic control.

A reaction mechanism has been proposed to explain the formation of Zn, ethane, and cyclotetrasiloxane (Figure 18). According to this suggestion, the decomposition occurs in two steps where Zn_4 seeds are produced in an $(Me_2SiO)_4$ matrix, which then at higher temperature fuse to give $Zn_m(Me_2SiO)_{4n}$ droplets. Higher temperatures favor the formation of "free" Zn particles, which tend to form Zn whiskers after deposition onto the glass wall.

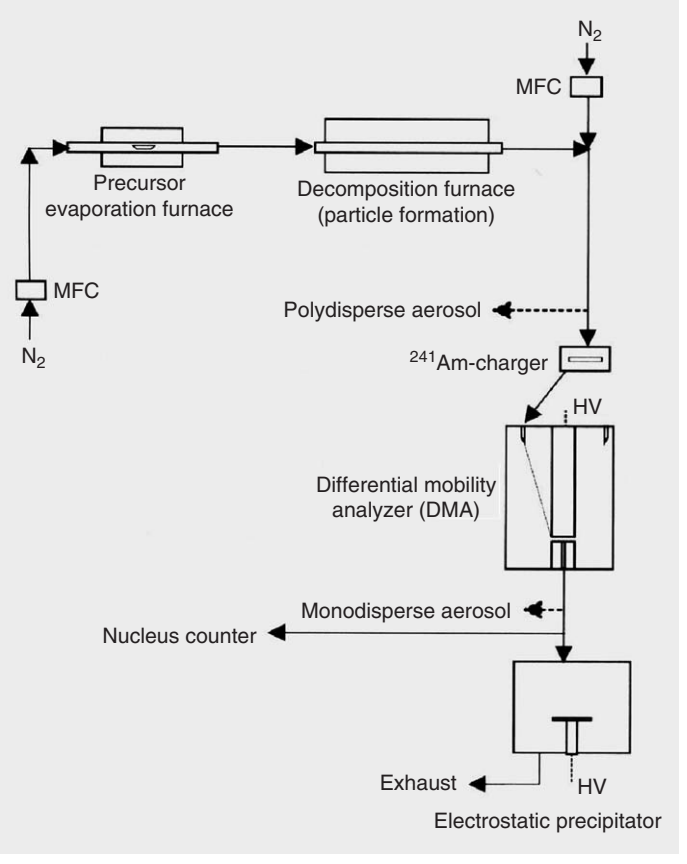

Figure 16 Experimental setup for chemical-vapor synthesis.[124] Reproduced with permission from Elsevier.

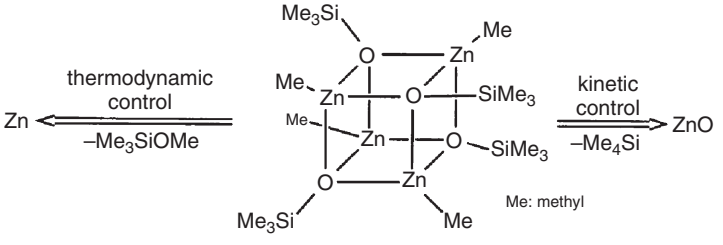

Figure 17 Decomposition pathways of $[MeZn(OSiMe_3)]_4$.[124]

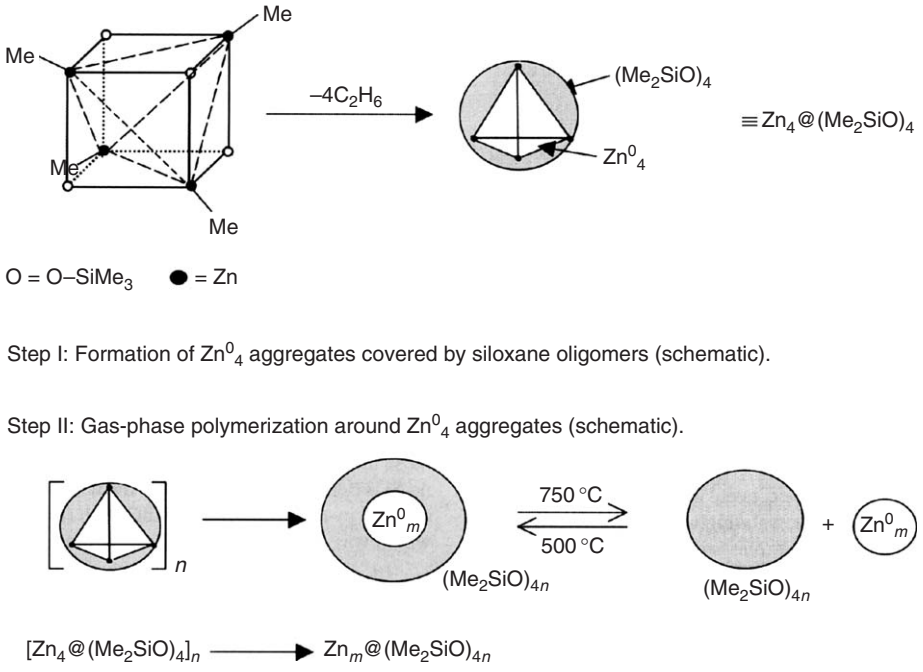

Figure 18 Proposed mechanism for the gas-phase decomposition of $[MeZn(OSiMe)]_4$.[124] Reproduced with permission from Elsevier.

12.02.3 Functional (Nano) Ceramics

Functional ceramics are usually polycrystalline materials with properties depending on chemical composition and microstructure (Figure 19). The major drawbacks in large-scale production of ceramics are the lack of chemical homogeneity and microstructure control that are related to processing parameters (time, temperature, medium) and chemical behavior of the reactants. Heterogeneity of chemical composition in ceramics results from slow reaction

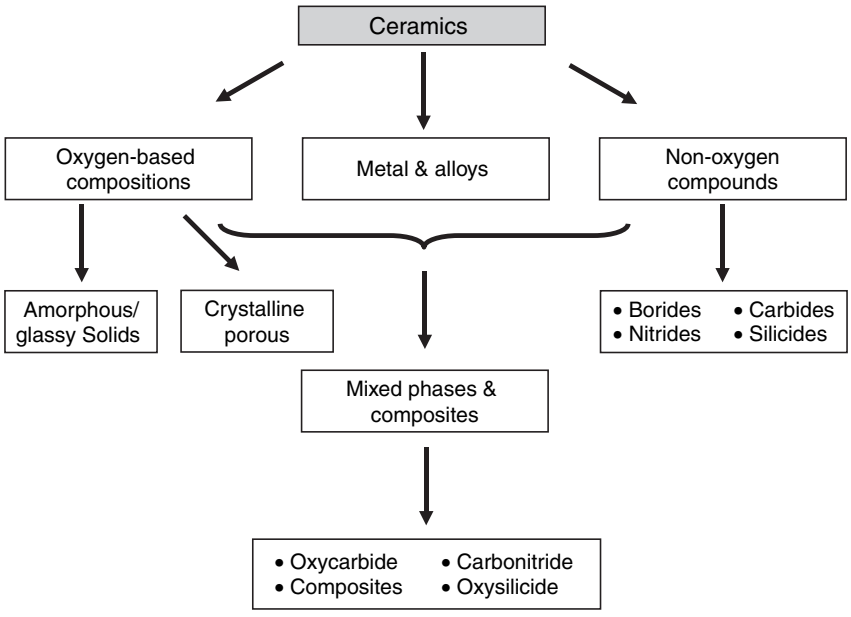

Figure 19 Classification of functional ceramics.

rates, incomplete decomposition of intermediates, secondary phases, and elemental segregation, which is one of the overriding problems and the factor responsible for the failure of high-performance ceramics in meeting the expected performance levels.[2,2a–2d] For example, polycrystalline ceramics such as thermistors and varistors rely on electrically active interfaces and grain boundaries for their unique operating characteristics, which can be inhibited by segregation effects. Similarly, the clustering of dopants in optical ceramics (e.g., Nd : YAG) can drastically reduce their useful optical properties.[126] Although knowledge base of microstructure evolution is scientifically sound and well established, the important aspects do not include the understanding of chemical reactions that occur at processing temperatures, and which can be tuned by changing the chemical precursors.[127] The precipitation of pre-ceramic precursors, from both aqueous and non-aqueous solutions, is less straightforward and understood than the precipitation of metals. This limitation is specifically genuine in the synthesis of multi-component ceramics, because it is extremely difficult to experimentally determine whether the as-prepared precursor is a single-phase solid solution or a homogeneous-appearing multi-phasic mixture of constituent species.

12.02.3.1 Binary Ceramics

A large number of binary ceramics such as carbides, nitrides, and oxides have been obtained by the decomposition of metal–organic precursors. The following text presents some selected examples to demonstrate the promises and limitations of molecular precursor approach. A complementary account of the synthesis of metal oxide nanoparticles from solution-based methods is given in Chapter 12.03.

12.02.3.1.1 Metal oxides

Binary metal oxides are finding extensive applications due to their extraordinary mechanical (e.g., Al_2O_3), dielectric (e.g., ZrO_2, HfO_2), semiconducting (e.g., SnO_2, Ga_2O_3), photocatalytic (e.g., TiO_2, CeO_2), optical (e.g., Eu_2O_3), biocidal (e.g., ZnO), and magnetic (e.g., Fe_3O_4) properties. Given the presence of metal–oxygen units, metal–organic compounds such as alkoxides, ß-diketonates, siloxides are highly favored as precursors to oxide materials both by hydrolytic (e.g., sol–gel) or thermolytic (e.g., CVD) procedures. In the context of liquid-phase processing, high-purity aluminum oxides, prepared by Yoldas from aluminum alkoxides (Equation (3)), represent one of the fundamental steps taken toward the processing of high-performance materials from molecular precursors.[128]

$$[Al(OR)_3]_n \xrightarrow{H_2O} Al(O)_x(OH)_y(OR)_{3-(x/2+y)} \xrightarrow{\Delta} Al_2O_3 \qquad (3)$$

Volatile metal alkoxides are increasingly being used as precursors for CVD because they are readily converted by thermolysis to pure metal oxides.[129] The first systematic study in this direction was reported by Bradley and Faktor,[130–131] who investigated the formation of ZrO_2 from $Zr(OBu^t)_4$ in a stoichiometric reaction (Equation (4)).

$$[Zr(OR)_4] \xrightarrow{CVD} ZrO_2 + 4alkene + 2H_2O \qquad (4)$$

It needs to be borne in mind that metal alkoxides do not invariably give rise to pure metal oxides, and the chemical composition of the product depends on the overall chemical configuration of the starting molecule. For example, $Al_2(OBu^t)_6$, $Mo_2(OBu^t)_6$, and $W_2(OBu^t)_6$ give rise to Al_2O_3, MoO_2, and WO_2, respectively, whereas the cyclohexyl derivatives behave differently, producing materials rich in carbon.[132]

Iron oxide films and nanoparticles are currently being extensively investigated due to their applications in catalysis, magnetic recording media, gas sensors, and anticorrosion protective paints.[133–136] The production of magnetic nanoparticles has been reported by different physical (e.g., molecular beam epitaxy,[137] reactive sputtering,[138] and pulsed laser deposition[139]) and chemical (e.g., sol–gel,[140] electrochemical synthesis,[141] ball milling,[142] aerosol synthesis,[143] and CVD[144] methods; however, the synthesis of iron oxide nanoparticles with controlled size and phase purity is still a challenging problem.[145–151]

Iron ethoxide $[Fe(OEt)_3]_n$ was used by Armelao and Artigliato[145] for the sol–gel synthesis of nanocrystalline and transparent hematite thin films. The iron sites were found to be octahedrally coordinated both in the crystalline and amorphous state, which showed the inherent advantage of using a single molecular source in achieving the bonding requirement of the solid phase.[145] Although iron ethoxide is an interesting precursor for solution methods, its application in gas-phase techniques is limited due to its poor volatility. The attempted volatilization (200 °C/10^{-2} torr) resulted in the formation of polynuclear iron cluster, $Fe_9O_3(OC_2H_5)_{21}(C_2H_5OH)$,

with low vapor pressure.[152] The molecular structure of this species revealed a cyclic arrangement of Fe–O rings based on different coordination of Fe(III) centers. The oxo–alkoxide species represent a molecular intermediate probably involved in the alkoxide-to-oxide conversion.[152]

The thermal instability of iron ethoxide is related to the degree of association of the ethoxide molecule in the solid state. It is known that the corresponding aluminum compound is an infusible solid due to the extensive polymerization of $Al(OEt)_3$ through alkoxy bridging. The bridging tendency in alkoxide species is governed by the propensity of the metal centers to increase their coordination state,[27,153–154] which can be tuned either by increasing the steric bulk of the alkoxide ligands or using chelating ligands.[155–156] Indeed, the *tert*-butoxide analog $[Fe(OBu^t)_3]_2$ (Figure 20) was found to be an excellent precursor for the deposition of different iron oxide phases.[149] Kiyomura and Gomi[157] have used iron(III) acac complex in a plasma-assisted CVD process to grow magnetite films on Si(111) with a uniform morphology at 400 °C; however, the carbon content in the deposited film was rather high (2–6 at.%) due to thermally robust nature of the precursor.

The technological potential of titanium oxide has tremendously increased due to enhancement in functional properties, when present in nanocrystalline form, and suitability for solar cell, photochemical, and optical applications. [158–161] The most widely reported precursors for the synthesis of TiO_2 particles and films are titanium halides (e.g., $TiCl_4$, TiI_4) and titanium tetraalkoxides ($Ti(OR)_4$; R = Et, Pr^i, Bu^t). The halides have the disadvantage of producing gaseous hydrogen halides as byproducts from the hydrolysis process, which makes alkoxides an attractive alternative because alkoxides contain enough oxygen to form TiO_2, without additional oxygen source; however, O_2 is generally required to minimize carbon incorporation into the deposited layers.

Solar energy conversion devices and chemical sensors make use of the anatase form of TiO_2, which is difficult to prepare in pure form and is generally accompanied by the rutile modification that dominates at high temperatures. For this reason, a control over the solid-state structure is highly desirable. The anatase phase can be selectively obtained when the material is formed under mild conditions; for example, Rambabu *et al.* have used titanium tetraisopropoxide, $Ti(OPr^i)_4$, as a single-source precursor to obtain nanocrystalline anatase (5–7 nm) at a temperature as low as 85 °C by the *in situ* conversion of titania sol.[162] Interestingly, $Ti(OPr^i)_4$, when used in a hydrothermal synthesis, produces rutile nanoparticles, indicating the role of high-temperature and high-pressure conditions on the structure of the resulting nanoparticles. Hydrolysis and condensation rates of alkoxide precursors can be tailored by addition of chelating ligands that slow down the hydrolysis process. Influence of the precursor structure on the physical properties of the resulting titania phase was demonstrated by Boyle *et al.*, who employed a series of structurally different carboxylic acid-modified titanium alkoxides[163] (Figure 21) in a sol–gel process to obtain TiO_2 films. The density of the films was found to vary for different precursors, which was related to the gel structure and the geometry of the basic unit (Figure 21), which is corroborated by the fact that metal–oxygen framework observed in the solid-state structures are maintained in solution.

ZnO is being regarded as one of the important metal oxide semiconductors for future applications. Since its chemical and physical properties are highly dependent on composition and shape (defects), reliable methods are necessary to ensure control over the latter. The heterocubane $(MeZnO^iPr)_4$ was shown to be a suitable organometallic precursor for gas-phase CVS and solid-state synthesis of nanoscaled ZnO.[41,164] Interestingly, highly defective nanocrystalline ZnO can be prepared at far from thermodynamic equilibrium, which contains three types of defects that are related to each other: microstructural strain, presence of impurities in the ZnO lattice, and oxygen vacancies.[164]

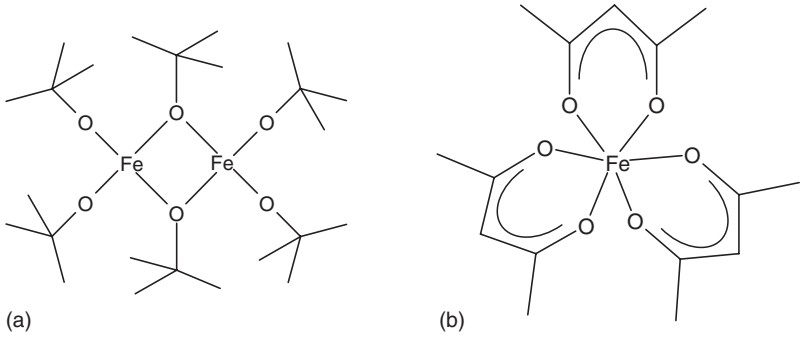

Figure 20 Schematic representation of the molecular structures of (a) $[Fe(OBu^t)_3]_2$ and (b) $Fe(acac)_3$.

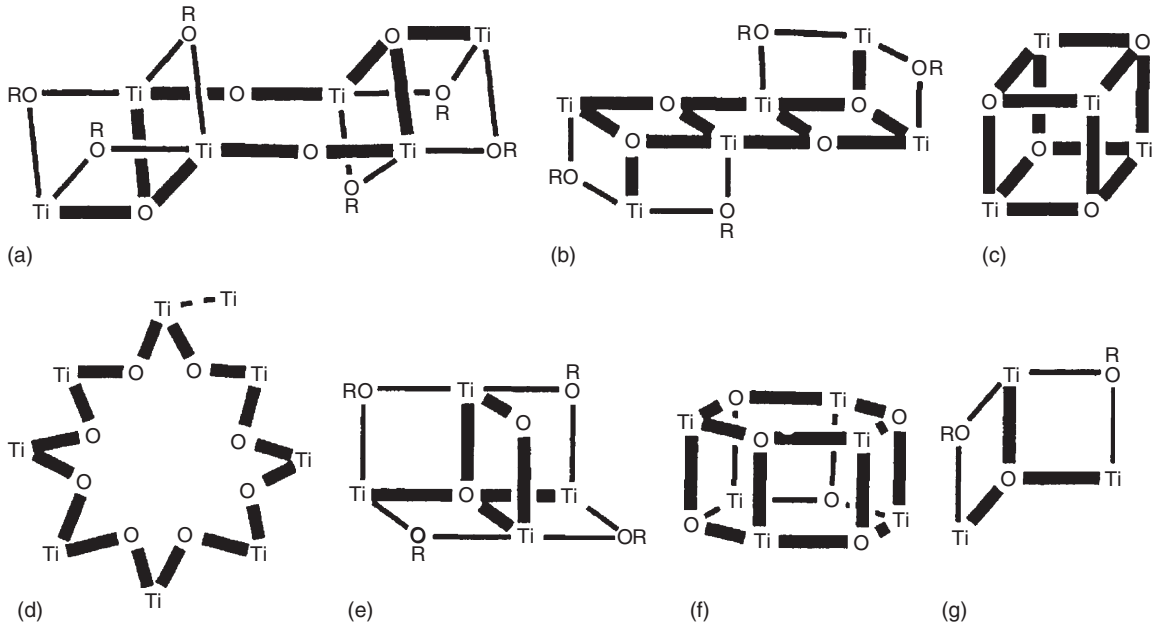

Figure 21 Structural motifs of the titanium–oxygen cores obtained in titanium alkoxides modified by carboxylate groups (redrawn after Ref: 162).

12.02.3.1.2 Metal chalcogenides, nitrides, pnictides

The observation of quantum-confinement effects as a function of crystal size is most remarkably manifested in semiconductor nanoparticles such as ZnS, CdS, CdSe, etc., which have generated substantial interest for their applications in device technology based on the novel optical and transport properties.[165–166] For example, the band gap in CdS can be tuned between 4.5 and 2.5 eV as the size is varied from the molecular regime to the macroscopic crystal, and the radiative lifetime allowed optical excitation ranges from tens of picoseconds to several nanoseconds.[39,167] The colloidal processing methods, based on controlled nucleation and rapid termination of growth, allow an easy access to large quantities of nanomaterials, but with relatively large dispersities (~10%). For a size-controlled synthesis, molecular precursors containing preformed metal–chalcogen bonds and existing as discrete molecular species are promising starting materials.[10,168] O'Brien *et al.* have studies the thermolysis of metal dithio- and diselenocarbamate complexes ($M\{E_2CNMe(C_6H_{13})\}_2$) (M = Cd, Zn, Pb; E = S, Se, Te) as single molecular precursors for a one-step synthesis of CdS, ZnS, CdSe, and ZnSe nanoparticles.[169,171] The fabrication of semiconductor nanocrystals from these molecular precursors (Figure 22) is a one-step process, typically performed in the temperature range 200–250 °C. This approach has been extended to the synthesis of PbS and PbSe from lead(II) alkyldithio- or alkyldiselenocarbamates, respectively.[169,172,173] Cadmium bis(diethylmonothiocarbamate), ($Cd(Et_2mtc)_2$), was shown to be a suitable source for the deposition of nanocrystalline and transparent CdS films at low temperatures (300–450 °C).[174] The different aspects of growing semiconducting materials from organometallic precursors are extensively reviewed in Chapter 12.01.

Farneth *et al.* have investigated the mechanism of the solid-state conversion of a series of II–VI precursors of general formula $(R_4N^+)_4[S_4M_{10}(SPh)_{16}]^{4-}$ (R = Me, Et; M = Cd, Zn) to the bulk metal sulphide structure.[5] The transformation, as followed by combined TGA and mass spectroscopy, proceeds in two discrete reaction steps. In the case of cadmium derivative, the loss of countercations around 200 °C produces a new molecular solid, which was characterized (X-ray) to be $Cd_{10}S_{16}Ph_{12}$. This intermediate composition gave a broad X-ray diffraction pattern that indicated very small (<25 Å) sphalerite-phase (cubic) crystals of CdS. The second decomposition reaction eliminates S_6Ph_{12} around 350 °C and produces phase-pure CdS (wurtzite) (Equation (5)).

$$(R_4N^+)_4[S_4M_{10}(SPh)_{16}]^{4-} \xrightarrow{200\,^\circ C} Cd_{10}S_{16}Ph_{12} + 4NMe_4SPh$$
$$\downarrow \; 350\,^\circ C,\ -S_6Ph_{12}$$
$$CdS \qquad (5)$$

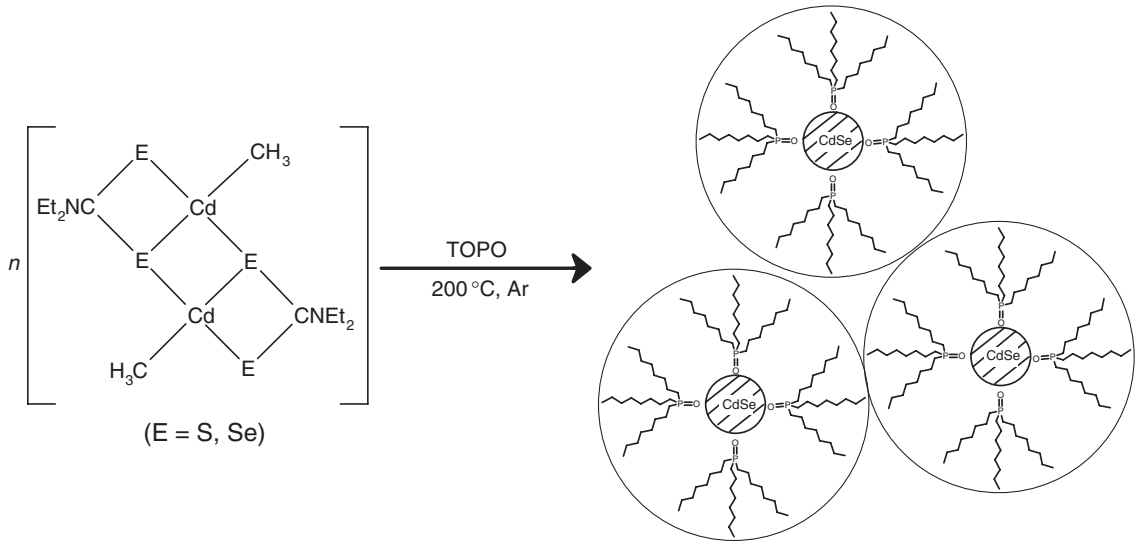

Figure 22 Single-source approach for preparing semiconductor nanocrystallites in tri-octyl phosphine oxide TOPO (redrawn after Ref: 10).

The main implication of this work is the formation of molecular clusters as tractable intermediates, which display the features of nanocrystalline solids. The molecular precursors $(R_4N^+)_4[S_4M_{10}(SPh)_{16}]^{4-}$ and the resulting nanocrystals have been intensively studied; however, the chemical reaction associated with the transformation of the molecular species to metal sulphides is poorly understood. The decomposition of selenium analog $(R_4N^+)4[Se_4M_{10}(SPh)_{16}]^{4-}$ to form MSe (M = Zn, Cd) was examined by Strouse *et al.*[168] The Cd : Se ratio in $[Se_4Cd_{10}(SPh)_{16}]^{4-}$ is significantly higher (2.5 : 1) than required for stoichiometric CdSe. Since the CdSe nanomaterial grown in hexadecylamine is strictly stoichiometric, unidentified Cd byproducts are required to balance the reaction stoichiometry; for instance, $Cd(SPh)_3^-$ has been suggested as a labile fragment that would yield a Cd : Se stoichiometry of 1.5 : 1 based on the Cd_6Se_4 core of the cluster. Several mechanisms for nucleation of CdSe have been put forward, such as the fragmentation of the M_{10} cluster into M^{2+} and Se^{2-} or $(CdSe)_n$ species that can reassemble to form the nucleus or the alternative possibility that the cluster remains intact acting as partial nuclei and that the nanomaterial growth proceeds by scavenging free M and Se atoms present in the solution. This work exemplifies the challenges associated with the development of molecule-to-material approach, which goes beyond the simple curiosity of identifying the precursor and the end product.

Among metal nitrides, gallium nitride (GaN) has attracted most attention due to its applications in high-efficiency blue light-emitting diodes and ultraviolet optoelectronic devices.[175] As a consequence, there is a growing interest in the synthesis of GaN nanocrystals and nanostructured films. The technical production of GaN by CVD utilizes high-temperature interaction of $(CH_3)_3Ga$, with NH_3. Given the lability of Ga–N bonds, a very large excess of ammonia is necessary to push the reaction to completion, and due to the high stability of N–H bonds in NH_3, high reaction temperatures (>1,000 °C) are mandatory, which severely limits the choice of substrate material. Chemical precursors containing direct Ga–N bonds and devoid of any strong N–H bonds offer significant improvements in the processing such as lower deposition temperatures, exclusion of NH_3 from the process, reduction in N vacancies, and elimination or drastic reduction of carbon impurities.[176–181] Several molecular precursors such as $[Ga(NH_2)_{3/2}]_n$ (450 °C),[182] $[H_2GaNH_2]_3$ (600 °C),[183] $[Ga\{N(CH_3)_2\}_3]_2$ (600 °C),[184] $[H_2GaN_3]$ (350 °C),[181] and $[Ga(N_3)_3]_n$ (280 °C)[185] have been used to prepare gallium nitride nanocrystals and films. Nearly all the precursors produced gallium nitride compositions; however, the temperature of crystallization and residual organic contamination depended on the organic content in the precursor framework. Precursor route has intrinsic limitations such as (low) volatility of precursors and carbon contamination in films, which emphasizes the need of precursor design and efficient decomposition pathways to produce the desired phase with minimum level of impurities and at lowest possible decomposition temperatures.

Detonation of gallium azides, (R_3N)-$Ga(N_3)_3$, was used by Fischer and Frank to obtain nanocrystals of hexagonal GaN.[178] Kouvetakis *et al.* have reported several related routes for GaN synthesis utilizing carbon- and hydrogen-free single-source precursor, Cl_2GaN_3, to grow thin oriented films of high-quality GaN on sapphire at 700 °C.

The extremely low vapor pressure of Cl_2GaN_3, an involatile polymeric solid, and the inherent loss of substantial quantities of $GaCl_3$ are the major limitations of this otherwise interesting approach (Equation (6)). To overcome this problem, a modified monohydride precursor $(HClGaN_3)_3$ was synthesized,[186–187] which was moderately volatile and decomposed easily at low temperatures by elimination of HCl and N_2 to produce GaN (Equation (7)).

$$(Cl_2GaN_3)_3 \longrightarrow GaN + GaCl_3 + N_2 \quad (6)$$

$$(HClGaN_3)_3 \longrightarrow GaN + HCl + N_2 \quad (7)$$

As expected, the dihydride analog $(H_2GaN_3)_3$ was found to be more volatile owing to its reduced molecular weight and increased covalent character. Indeed, $[H_2GaN_3]_3$ is volatile at room temperature and is an efficient CVD source[179] because it eliminates environmentally benign byproducts (H_2 and N_2) to yield stoichiometric GaN at temperatures as low as 150 °C (Equation (8)).

$$[H_2GaN_3]_3 \longrightarrow GaN + H_2 + N_2 \quad (8)$$

The high reactivity of $[H_2GaN_3]_3$, desirable for its transformation to GaN phase, makes this precursor susceptible to decomposition via exothermic reaction, which limits its viability due to different handling. Nevertheless, the pyrophoric nature of the azide precursors can be reduced by stabilizing metal center through intramolecular coordination.[180,188] Kim *et al.* have synthesized mononuclear Lewis acid–base adduct $[Et_2Ga(N_3)\cdot MeHNNH_2]$, which decomposes via loss of stable molecular species (Equation (9)), yielding high-quality GaN films with little contamination.[188]

$$[Et_2Ga(N_3)\cdot MeHNNH_2] \longrightarrow GaN + N_2 + C_2H_6 + MeNNH \quad (9)$$

Thermolysis of $[Et_2Ga(N_3)]_3$, $[(N_3)_3Ga\{NMe_2(CH_2)_3\}]$, and $[(Et_3N)Ga(N_3)_3]$ in triglyme has produced nanometric GaN particles (Figure 23),[181] For the solution-phase synthesis of GaN nanocrystals, Gladfelter *et al.* have used a cyclotrigallazane, prepared by the reaction of $[GaH_3(NMe_3)]$ in supercritical ammonia. This compound dehydrogenates in the solid state to form nanocrystalline gallium nitride.

Metal pnictides are best represented by the 13–15 compounds (e.g., GaAs), which are well known for their electronic and optoelectronic applications. Molecular precursor approach to the preparation of these materials has been investigated and reviewed by Maury[189] and Cowley,[190,190a] who have also actively contributed to the field.[191–200] The use of III–V adducts as substitutes for highly reactive group III alkyls by Benz *et al.*[201–202] was among the pioneering steps in this direction. Lewis acid–base adducts of formulas $ClR_2Ga \leftarrow ER'_3$ (E = As, P; R and R′ = Me or Et) were synthesized to overcome the problem of high reactivity and toxicity of conventional dual sources.[201,203] Films of GaP[204–205] and InP[205] were successfully grown from the cyclic trimers of general formula $[Et_2M–P(Et)_2]_3$ (M = Ga, In) with covalent metal–phosphorus bonds.[192,201] The thermal decomposition of two series of molecular precursors with general formulas $(C_6F_5)_{3-n}Me_nGa \leftarrow AsEt_3$ ($n = 0$ or 2) and $[ClR_2Ga \leftarrow AsEt_2]_2CH_2$ (R = Me, Et) were evaluated to test the relative stabilities of the central M–E bond with respect to peripheral M–ligand and E–ligand interactions. The strength of the Lewis acid–base dative bonds can be tuned by means of the more or less electron-donating nature of the alkyl groups, and varying the admixture of halogen (Cl) or pseudo-halogen (C_6F_5)

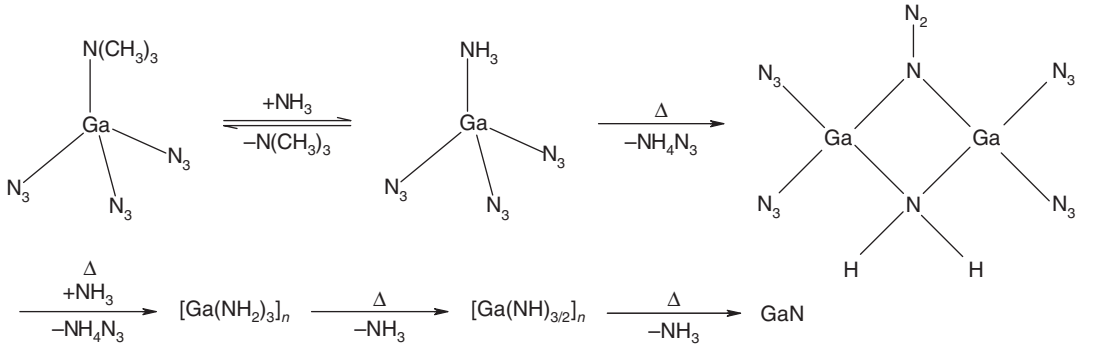

Figure 23 Decomposition steps involved in the synthesis of GaN from $[Ga(N_3)_3N(CH_3)_3]$ (redrawn after Ref: 181).

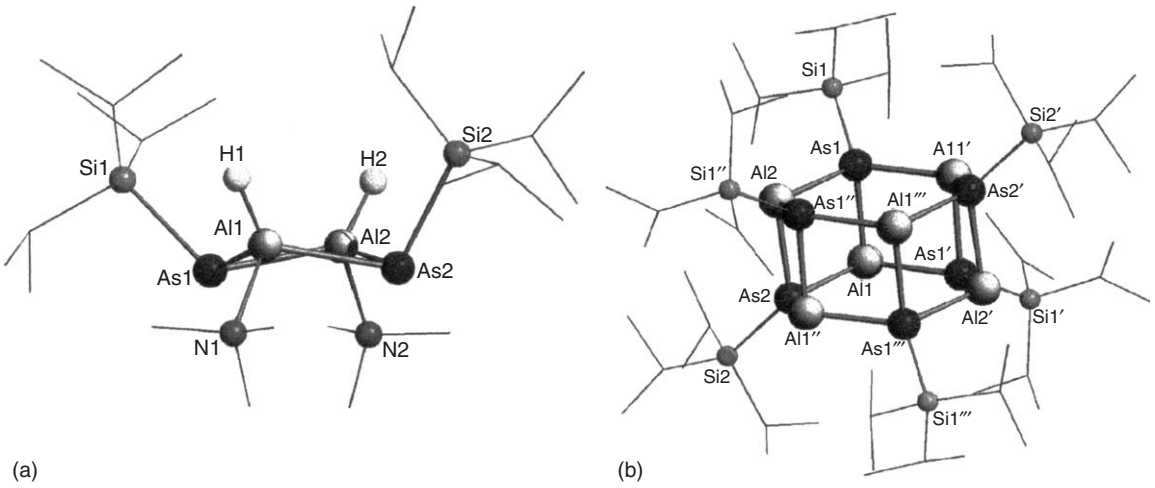

Figure 24 Molecular structure of (a) dimeric and (b) rexanmeric $[HAl\text{-}As(Si^{i}Pr_3)]_n$ aggregates as building blocks for AlAs.[189] Reproduced with permission from Wiley.

substituents, whereas the M–E bonds are fragile and cause loss in volatility and surface mobility.[206–208] Cowley and Jones have also used a variety of single-source organometallics that involve covalent M–E bonds between group III and group V elements such as $[Me_2Ga(\mu\text{-}AsBu^{t}_2)]_2$,[199–201,209–211] $[Me_2Ga(\mu\text{-}AsBu^{t}_2)]_2$,[4,201,212] and $[\{Ga(AsBu^{t}_2)\}_3]$.[201,211] The films deposited using the methyl derivative $[Me_2Ga(\mu\text{-}AsBu^{t}_2)]_2$ were arsenic deficient,[201,210] whereas $[Et_2Ga(\mu\text{-}AsBu^{t}_2)]_2$ produced epitaxial films, which showed low Hall mobilities due to the formation of gallium islands, apparently caused by the partial fragmentation of molecular precursor.

Antimonides of group 13 elements are useful for applications in optoelectronic devices due to their small band gaps ($E_g = 1.60$ (AlSb), 0.67 (GaSb), 0.16 eV (InSb)) and high electron mobility.[213] For instance, GaSb is used for the production of light-emitting and light-detecting devices operating in the 2 μm wavelength range, field-effect transistors, and infrared detectors.[213] CVD of group 13 nitrides, phosphides, and arsenides typically involves group 13 alkyls and group 15 hydrides as precursors; however, an analogous process is not possible for the preparation of group 15 antimonides because SbH_3 is thermally unstable (decomposes below –60 °C), which is also valid for primary ($RSbH_2$) and secondary stibines (R_2SbH). Further, an excess of stibine during film growth may lead to the formation of elemental Sb on the substrate, which has to be strictly avoided due to the low volatility of elemental Sb. An alternative pathway suggests the use of heterocycles $[R_2MER^{1}_2]_x$ or polycycles $(RMER^{1})_y$ that are attractive single-source precursors, especially due to the lower metal–carbon bond energies, when compared to pure group 13 and 15 alkyls (Figure 24).[189–190] A similar approach was demonstrated by Schulz *et al.* by using $Bu^{t}_3Ga\text{–}Sb(Bu^{t})_3$ and $Bu^{t}_3Ga\text{–}Sb(Pr^{i})_3$ as single-molecule precursors for the synthesis of carbon-free GaSb nanocrystals and whiskers.[214]

12.02.3.1.3 Nitride and carbide of silicon and boron

Silicon-containing ceramics (oxide, carbide, nitride, etc.) exhibit very high (~3,000 °C) melting points, low mobility of atoms, low plasticity, and high hardness, mainly due to the covalent character of the chemical bonds.[19] Therefore, these materials can substitute metals, alloys, and intermetallics in many high-temperature engineering, chemical, and electronic applications. Since the early investigations on the preparation of ceramics from organometallic oligomers and polymers in 1970s,[215] numerous new organometallic compounds have been developed as precursors to various ceramics like SiC, Si_3N_4, AlN, BN, B_4C, TiC, TiN.[216–218] The choice of organometallic molecules for use as molecular precursors has been largely an empirical process, with few guidelines relating to molecular structure of the precursor and chemical composition of the final material available. In the preparation of silicon pre-ceramic polymers, compounds containing Si–Si, Si–H, Si–N, Si–C, and Si–Cl bonds, derived from the reactions of different alkyl chlorosilanes, are used as precursor species (Figure 25).[219]

The facile chemical (cross-linking, dechlorination) reactions producing, sometimes by thermal treatments, tractable, soluble, and fusible precursor compounds makes this class of polyceramic precursors highly versatile. However, the stablity of the building units is subject to different chemical parameters; for example, the chorosilanes $SiHCl_3$, SiH_2Cl_2, and SiH_3Cl are stable compounds and do not split off HCl, whereas the corresponding aminosilane, $SiCl(NH_2)_3$, would decompose into NH_4Cl and solid diimide $Si(NH_2)_2$.

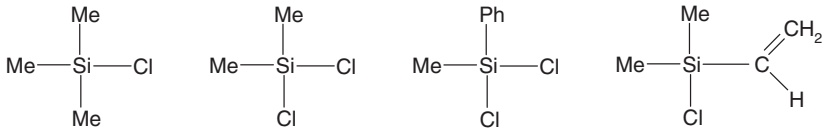

Figure 25 Alkyl chlorosilanes used as building blocks in the synthesis of organometallic precursors to non-oxide ceramics.

Polysilazanes are silicon compounds based on an alternating Si–N backbone that may or may not contain organic substitutes (Figure 26). Polysilazanes are prepared in a straightforward reaction of $(CH_3)_nSiCl_{4-n}$ with NH_2(H, R), whereby HCl is eliminated and a low-molecular compound is formed that can be polymerized by employing dehydrocoupling catalysts like KH, $Ru_3(CO)_{12}$, etc.[220] The amount of carbon present in the polymer is decisive for the composition of the ceramic material. Minimizing the amount of carbon results in a ceramic with the stoichiometry closer to Si_3N_4, whereas the Si_3N_4/SiC composite is formed in the case of carbon-rich precursors.[221] Single polymeric precursor for Si_3N_4 with the ideal atomic ratio Si : N : C = 3 : 4 : 0 cannot be directly prepared, but various polysilazanes have been shown to convert to pure Si_3N_4.[222–225] Depending on the chemistry of the polymer and pyrolysis conditions, a single polymeric polysilazane can transform either to pure Si_3N_4 or a combination of Si_3N_4 and SiC.[221]

Conventional CVD processes for SiC generally utilize separate Si (e.g., $SiCl_4$, SiH_4, $SiBr_4$) and C (e.g., CH_4, C_2H_2, C_3H_8) sources and require temperatures in excess of 1,000 °C for the phase formation. High temperatures cause significant deformation of substrate materials making SiC coating and control over microstructure a challenging issue.[226] Such limitations clearly illustrate the need of low-temperature alternatives. Lee and co-workers have obtained epitaxial cubic-SiC films using 1,3-disilabutane (Figure 27) as a single precursor at temperatures as low as 900 °C.[227] Polycrystalline SiC films using this precursor were obtained at 650 °C.

Given the expensive nature of 1,3 disilabutane, substituted derivatives [MeSi(H)-μ-$(CH_2)_2$Si(Me)CH_2SiH_2Me] (II) and $[Si(Me)HCH_2]_2$ (III) (Figure 28) have been used by Interrante *et al.* as precursors to SiC.[228–229] The results

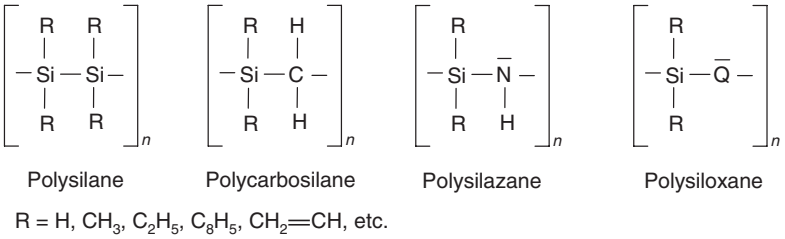

Figure 26 General representation of organometallic precursors to silicon-containing ceramics.

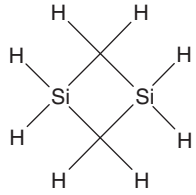

Figure 27 Schematic representation of 1,3-disilabutane.

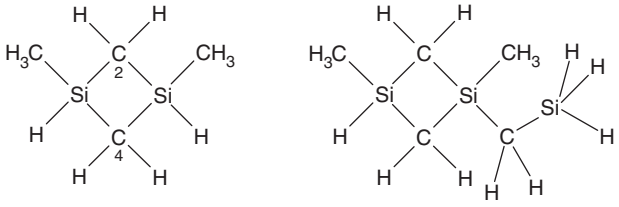

Figure 28 Two substituted derivatives of 1,3-disilabutane.

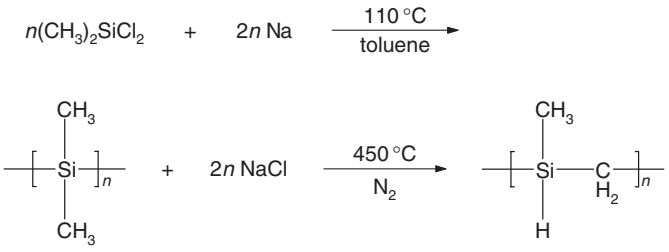

Figure 29 Reaction pathway to synthesize silicon carbide precursors.

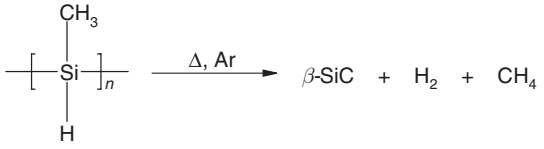

Figure 30 Conversation from PMS precursor to stoichiometric SiC.

indicated that the decomposition chemistry is complicated in the case of II and III due to molecular rearrangments that adversely affected the product purity.

In contrast to the sol–gel and other processing methods, synthetic organometallic polymers obtained from well-defined building units can be directly used in application such as coatings, fibers, or bulk shapes, and subsequently pyrolyzed to the desired ceramic. The repetition and/or combination of modular units shown in Figure 29 allows the fabrication of different organometallic precursors. Polycarbosilanes used as precursors to silicon carbide (SiC) can be synthesized with different alkyl groups according to the following equation.[230]

The polymeric precursor route to silicon-based ceramics was developed by Yajima *et al.* using polycarbosilane (–[MeHSiCH$_2$]$_x$–) as precursor to SiC.[231–234] One of the drawbacks of this method was the initial Si : C ratio of 1 : 2, which resulted in excess carbon in the final product and thus inferior mechanical properties.[235] To assure stoichiometric purity, pure and modified polymethylsilane (PMS) precursors with an Si : C ratio of 1 : 1 were successfully used by Laine *et al.* to obtain stoichiometric SiC (Figure 30).[236]

Boron nitride has received growing attention for technological applications due to its excellent material properties namely high hardness, chemical inertness, and dielectric behavior. Cubic boron nitride (c-BN) has a zinc blende structure with sp^3-bonding resembling diamond, whereas hexagonal boron nitride (h-BN) possesses a layered and sp^2-bonded structure similar to graphite. Significant efforts and progress have been made in the synthesis of c-BN by various physical and chemical methods;[237] however, the narrow phase-stability region, high compression stress, and problems in controlling boron and nitrogen ratio remain as problems to be solved.[238–239] To control the chemical composition, Boo *et al.* have used isopropyl amine and *tert*-butylamine complexes of triethylborane ((^{i}Pr)H$_2$NBEt$_3$, (^{t}Bu)H$_2$NBEt$_3$) as molecular precursors with desired B : N ratio (1 : 1) to grow crackfree h-BN film on Si(100) at 850 °C.[240]

Boron carbide (B$_4$C) is a highly refractory material of importance for both structural and electronic applications due to its high temperature stability and thermoelectric properties, respectively.[241–242] In comparison to high-temperature powder synthesis techniques, the development of polymer precursors to boron carbide ceramics is gaining increasing attention due to a number of potential advantages, such as (i) precise control over stoichiometry and the possibility to systematically vary the composition, (ii) ceramic formation under milder conditions due to low decomposition temperatures, and (iii) versatility in terms of net-shaped components. Mirabelli *et al.* reported that [2-(vinyl)pentaborane] (2-(H$_2$C═CH)B$_5$H$_8$) thermally polymerizes to vinylpentaborane oligomers, which can be converted to pure boron carbide (B$_4$C) with high yields under mild conditions.[243] Isao *et al.* reported that boric acid and 2-hydroxybenzyl alcohol (HBA) reacted to produce a phenolic resin–B$_2$O$_3$ hybrid, which could be easily pyrolyzed (1,500 °C) into B$_4$C fine powders upon heating.[244] Recently, Pender *et al.* reported a simple and efficient synthesis of aligned boron carbide nanofibers based on a new single-source precursor 6,6′-(CH$_2$)$_6$(B$_{10}$H$_{13}$)$_2$, which possesses B : C ratio (4 : 1.2) close to that required for boron carbide (4 : 1). The reaction involved in precursor-to-ceramic conversion is given in Equation (10), which yielded stoichiometric B$_4$C with high yield (84.6%) due to a clean ligand stripping in the precursor molecule.[241]

$$6,6'\text{-}(CH_2)_6(B_{10}H_{13})_2 \longrightarrow 5B_4C + CH_4 + 17H_2 \quad (10)$$

12.02.3.2 Ternary Ceramics

Ternary systems, containing three different chemical elements, demand suitable precursors with element ratios corresponding to the material of choice. Further, the stoichiometry control present in the molecular carrier should be preserved during the processing steps, which is not trivial given the ambiguity associated with the structure and composition of intermediate species. Nevertheless, various single precursors tested in the material synthesis provide the proof of principle for the application of molecules-to-materials approach in multi-component ceramics.

12.02.3.2.1 Oxides

A number of ternary oxide ceramics have been obtained following precursor concept.[44,265] For example, stoichiometric $MgAl_2O_4$ films were successfully prepared from magnesium–aluminum isopropoxide containing appropriate Mg : Al ratio (1 : 2).[245–247] Similarly, mixed metal acetates of general formula $M_3Fe_6(OOCCH_3)_{17}(O)_3(OH)\cdot 12$pyridine (M = Ni, Co, Mn) were employed to prepare stoichiometric ferrites.[248] The ideal cation stoichiometry present in the precursor is lost if the large number of pyridine molecules of crystallization are rapidly removed, which result in the segregation of cations. Moreover, high temperatures (800–1,000 °C) are required to transform the precursors into respective ferrites. $[Ni(H_2O)_6][FeCl(EDTA)H]_2\cdot 4H_2O$,[248] synthesized as a water-soluble complex by Apblett *et al.*, bears the appropriate Ni : Fe ratio desired for the formation of nickel ferrite ($NiFe_2O_4$); however, the pyrolysis of this compound leads to phase separation into Fe_2O_3 and $NiFe_2O_4$ compositions. Mathur *et al.*[249] have used heterobimetallic precursors of the type $[MM'_2(OR)_8]$ (M = Co, Cu, Zn; M′ = Al, Ga) for low-temperature synthesis of high-purity spinel particles by sol–gel and micro-emulsion methods.[149,250–251] For a comparative evaluation of the single- and multi-component approaches, $CoAl_2O_4$ spinel was synthesized from the single-source $[CoAl_2(OBu^t)_8]$, and using a stoichiometric mixture of $[Al(OPr^i)_3]_4$ and $Co(OR)_2$ ($R = -C(C_6H_5)_3$). The XRD studies revealed that the single-source synthesis yielded single-phase $CoAl_2O_4$, whereas minor phase separation occurred in the dual source system due to the differences in the hydrolysis behavior of individual metal sources.[129] The class of *spiro*-compounds with the general formula $MM'_2(OR)_8$ was extended by introducing divalent cobalt and trivalent iron in a molecular framework to obtain a single molecular precursor to cobalt ferrite, which is the first example of a Co–Fe mixed metal alkoxide.[252] The decomposition of the Co–Fe precursor in sol–gel or CVD process produced stoichiometric $CoFe_2O_4$ particles and films, respectively.

One of the major strengths of the molecule-based chemical methods is the ability to selectively synthesize metastable phases. The inherent limitations of conventional synthesis procedures are evident in the synthesis of orthoferrite $GdFeO_3$, which, according to the Gd_2O_3–Fe_2O_3 phase diagram, is thermodynamically less favored than the $Gd_3Fe_5O_{12}$ composition. As a result, garnet ($Gd_3Fe_5O_{12}$) phase is invariably formed in a mixture of Ln^{3+} and Fe^{3+} constituents.[253] The absence of chemical linkage between the cations favors the demixing, which results in the co-existence of undesired phases (e.g., $Ln_3Fe_5O_{12}$ and Fe_3O_4 in the synthesis of $LnFeO_3$) in the final ceramic material. Access to metastable rare earth iron perovskites of general formula $LnFeO_3$ (Ln = any lanthanide ion) was provided, for the first time, by a designed assembly of trivalent lanthanide and iron ions in a molecular framework (Figure 31).[254]

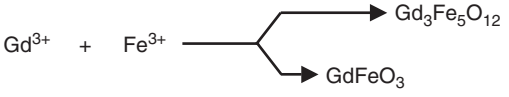

The appropriate Gd : Fe ratio and preformed Gd–O–Fe bonds facilitate the selective synthesis of orthoferrite films and particles.[254] Controlled hydrolysis of Gd–Fe heterometal alkoxide produced nanocrystalline $GdFeO_3$ at a much lower temperature (700 °C) than that required for the solid-state reaction using Gd_2O_3 and Fe_2O_3 powders (~1,800 °C). The contention that the chemical mixing of the ions is retained during the various stages of the processing is confirmed by the crystallization of $GdFeO_3$ directly from an amorphous precursor without the crystallization of any intermediate phases. It is noteworthy that synthesis of $LaFeO_3$ from a mixture of lanthanum and iron alkoxide did not result in the formation of monophasic material, and the product contained significant amounts of $LaCO_3OH$ as the secondary phase.[255] Pure $LaFeO_3$ and $SmFeO_3$ powders were obtained by the thermal decomposition of heteronuclear cyanide complexes $La\{Fe(CN)_6\}\cdot 5H_2O$ and $Sm\{Fe(CN)_6\}\cdot 4H_2O$, respectively.[256–257] Authors have also performed, for comparison's sake, a solid-state reaction between Sm_2O_3 and Fe_2O_3 powders. The XRD data of the two samples showed that

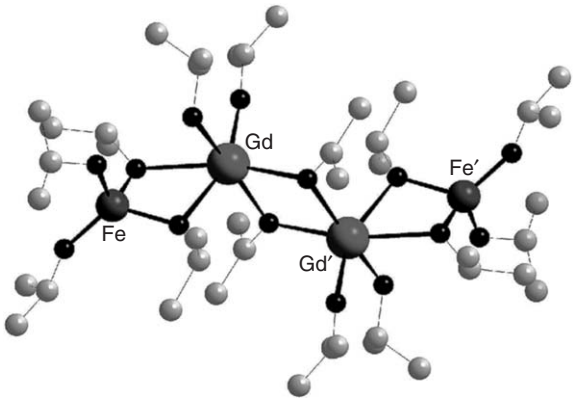

Figure 31 Molecular structure of $[\{GdFe(OPr^i)_6\}(HOPr^i)]_2$.[254] Reproduced with permission from Blackwell Publishing.

single-phase $SmFeO_3$ is present at 700 °C in the powder obtained from the Sm–Fe precursor while single metal oxides were present as the major phases till 1,000 °C, in the ball-milled sample (Figure 32).

Precursor-derived synthesis of perovskite (ABO_3) initiated by Mazdiyasani *et al.* was based on simultaneous hydrolytic decomposition of titanium and barium alkoxides;[258–260] however, a precise structure and composition of the precursor was not known in their studies. Plausible mechanisms put forward for the formation of perovskite phases involve (i) an acid–base-type reaction in which an anion of the formula $Ti(OH)_6^{2-}$ is initially formed during the hydrolysis of Ti alkoxide and later neutralized by the alkaline earth cations,[261] and (ii) the formation of negatively charged TiO_2 particles (due to the absorption of hydroxyl groups) in which the alkaline earth cations diffuse to counterbalance the negative charge. These models do not take into account the formation of heterometal species in the alkoxide or partially hydrolyzed solution, which is a prominent feature of alkoxide chemistry.[27,153,262–264]

The potential of heterometal alkoxide precursors to "preform" the ceramic on a molecular level has also been demonstrated for $BaTiO_3$ and $BaZrO_3$ oxides.[265] The improved homogeneity, phase purity, and lower crystallization

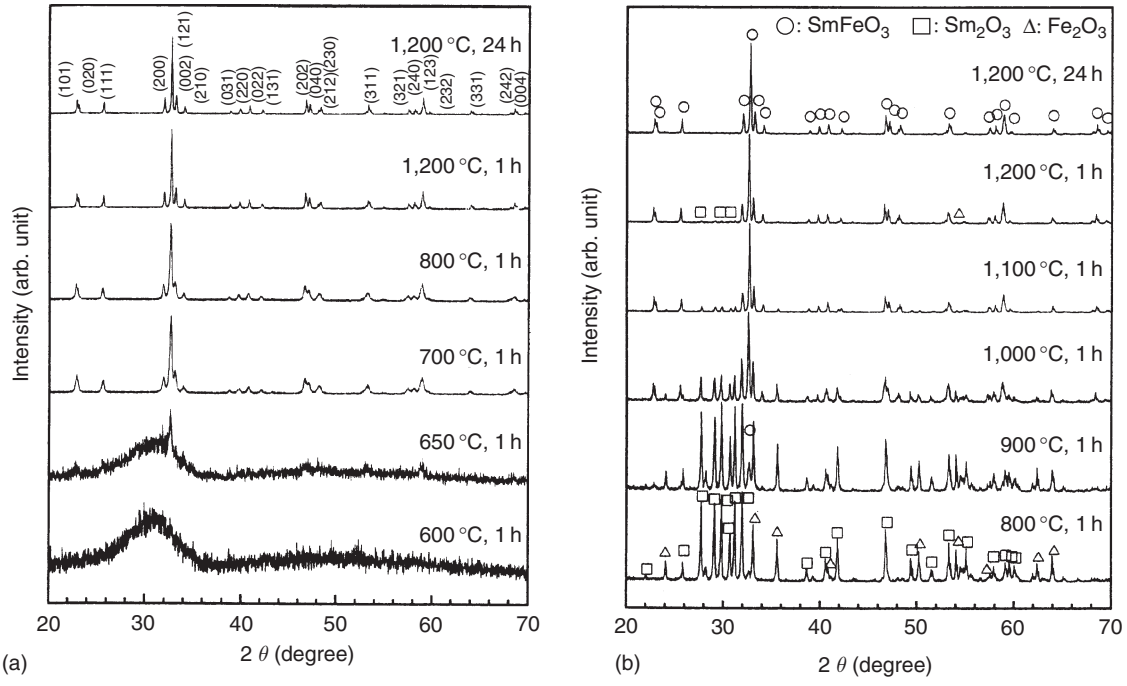

Figure 32 XRD profiles of (a) $Sm\{Fe(CN)_6\}\cdot 4H_2O$ complex decomposed at different temperatures and (b) the ball-milled mixture of Sm_2O_3 and Fe_2O_3 calcined at different temperatures.[256] Reproduced with permission from the Royal Society of Chemistry.

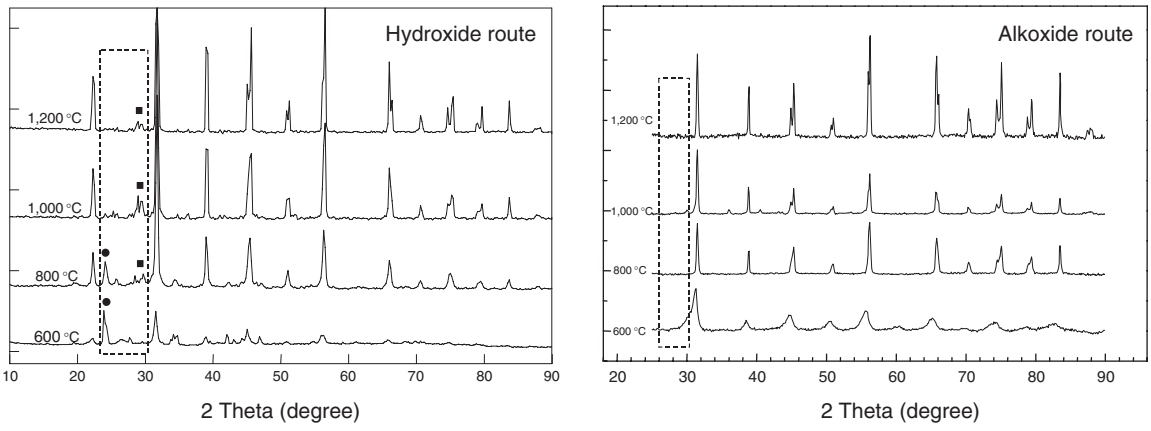

Figure 33 XRD patterns of $BaTiO_3$ particles obtained by hydroxide and alkoxide sol–gel methods ($BaCO_3$ (•) and Ba_2TiO_4(■)).[265] Reproduced with permission from the Materials Research Society.

temperatures for gel → oxide conversion are attributed to the use of mixed metal compounds containing preformed Ba–O–Ti and Ba–O–Zr bonds. The nature and chemical composition of intermediate species play a dominant role in deciding the purity and temperature of crystallization of the desired phase. For example, the formation of *ortho*-titanate or zirconate phase (Ba_2MO_4; M = Ti, Zr) in sols containing individual Ba and Ti(Zr) precursors require high (>1,000 °C) temperatures to decompose into $BaMO_3$.[265] The strict control over the metal ratios through stoichiometric clusters allows the crystallization of perovskite nanoparticles at low temperature. $BaTiO_3$ nanoparticles were also prepared using inorganic salts of individual elements in a classical sol–gel route. The X-ray powder diffractograms (Figure 33) revealed that the powder obtained from the conventional method was contaminated even at 1,200 °C by side-products like $BaCO_3$ and Ba_2TiO_4, whereas a single-phase material could be obtained using the mixed metal alkoxide precursor. In addition, the volume- and number-weighted size dispersion is significantly narrow for the perovskite powders obtained from alkoxide precursors (Figure 34), which is not the case for powders obtained by hydroxide route.

Appropriate cation in the molecular precursor with respect to the solid-state phase is an important prerequisite to have a chemical control over the phase formation. For example, the decomposition of Pb–Ti heterometal precursor, $[PbTi_2(O)_4(OOCCH_3)(OCH_2CH_3)_7]_2$,[266] based on the Pb : Ti ratio 1 : 2, produced a mixture of TiO_2, $PbTiO_3$, and $PbTi_3O_7$ phases, whereas the precursor $[Pb_2Ti_2(O)_4(OOCCH_3)_2(OCH_2CH_3)_8]_2$ (Pb : Ti = 1 : 1) with similar ligands but ideal cation ratio could be converted into single-phase $PbTiO_3$ at 600 °C.[267]

The reactions involved in alkoxide-to-oxide transformation were demonstrated by Gaskins and Lannutti, who prepared barium titanate at room temperature by reacting a barium titanium oxo alkoxide, $Ba_4Ti_4O_4(OPr^i)_{16}(Pr^iOH)_3$ (Figure 35), with acetone.[268] The transient oxo species formed in the transformation of the molecular cluster possess oxygen CNs for the metals that are necessarily less than those found for extended solid-state structure of $BaTiO_3$. As a consequence, the cluster grows (condenses) through oxygen supplied by the acetone molecules, a reaction called as aldol condensation.[129] The deficiency in oxygen coordination as the two alkoxide groups are replaced by an oxo unit provides a driving force for the cluster growth. A close look at the metal–oxygen core of the oxo–alkoxide molecule reveals a resemblance with a $BaTiO_3$ structural subunit (Figure 35). This structural similarity probably helps in lowering the barrier to a direct molecule-to-material conversion.

A single-source precursor is not always a guarantee for control over stoichiometry, and heterometallic precursors may become a disadvantage when they disproportionate during the gas-phase transport, as observed for $SrTa_2(OR)_{12}$ compounds, due to the large disparity in the vapor pressure of the parent alkoxides.[269,269a] Nevertheless, the replacement of simple (monoanionic) alkoxide ligands by chelating alkoxides (donor functionalized) offers a possibility to increase the strength of Sr–(O)R–Ta bridge. Jones *et al.* have used dimethyl aminoethanol (dmae) and bis(dimethylamino) isopropanol (bis-dmap) to obtain novel Sr–Ta heteroleptic alkoxides, $SrTa_2(OEt)_{10}(R)_2$ (R = dmae, bis(dmap)). It can be discerned from the solid-state structure of the dmap derivative that in contrast to $SrTa_2(OPr^i)_{12}(Pr^iOH)_2$, the Sr atom in $SrTa_2(OEt)_{10}$(bis-dmap)$_2$ is higher coordinated (CN = 8) (Figure 36). The use of $SrTa_2(OEt)_{10}$(dmae) in MOCVD has produced crystalline films of $SrTa_2O_6$.[269,269a]

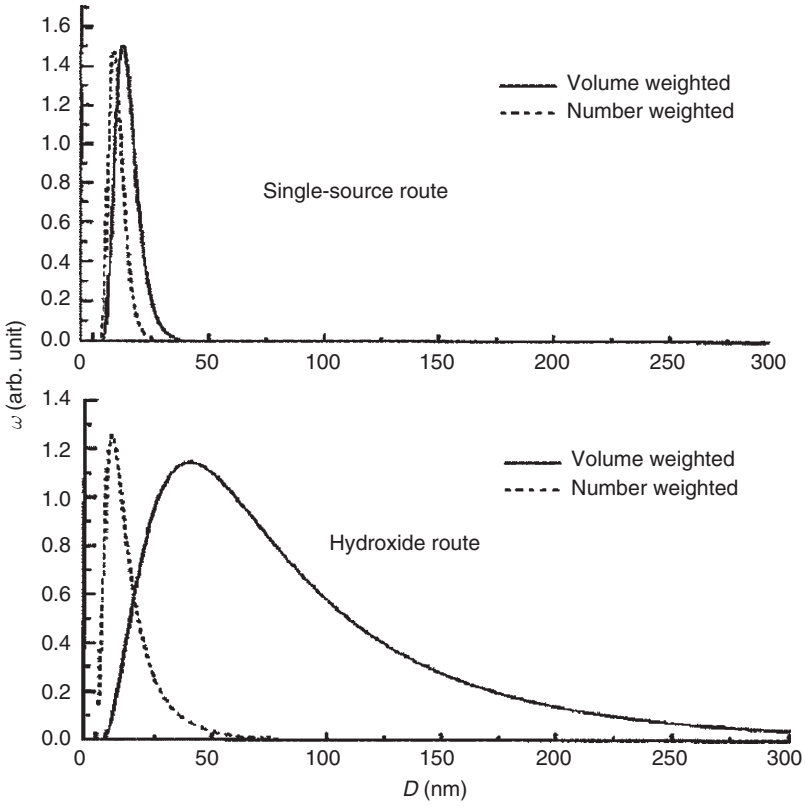

Figure 34 Particle size-distribution curves for $BaZrO_3$ powders obtained from the alkoxide single–source precursor (SSP) and conventional hydroxide routes.[265] Reproduced with permission from the Materials Research Society.

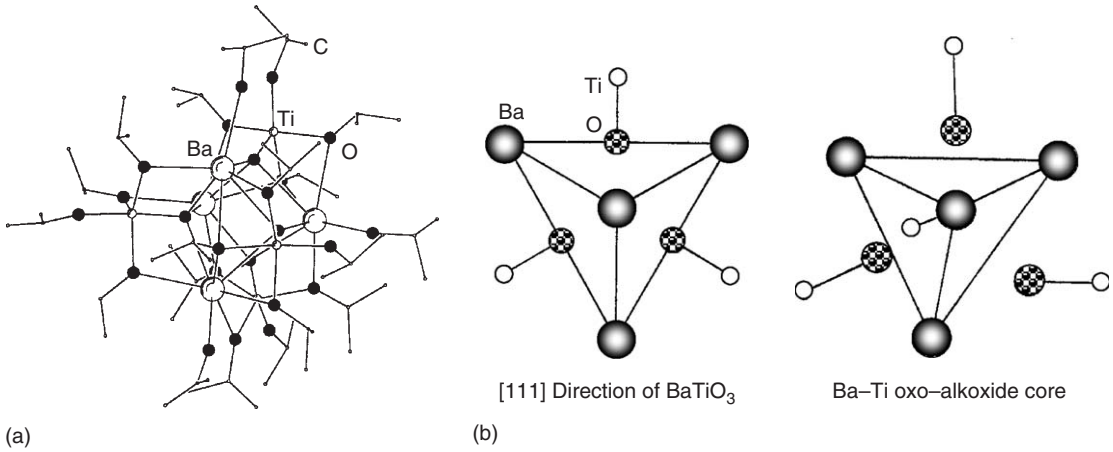

Figure 35 (a) Molecular structure of Ba–Ti oxo–alkoxide, reproduced with permission from the Royal Society of Chemistry. (b) Comparison of the core structure of monoclinic barium–titanium oxo–isopropoxide with the $BaTiO_3$ structure viewed along the [111] direction, reproduced with permission from Wiley.[268]

12.02.3.2.2 Heterometal chalcogenides

Ternary chalcopyrites ($CuInSe_2$, $CuInS_2$, $CuGaSe_2$, etc.), owing to their direct band gaps, are interesting materials for the absorption of solar spectrum and thus useful solar cell materials.[270] To achieve the deposition of these materials on polymeric substrates, low-temperature processes are desired. A step in this direction has been the use of ternary single-source

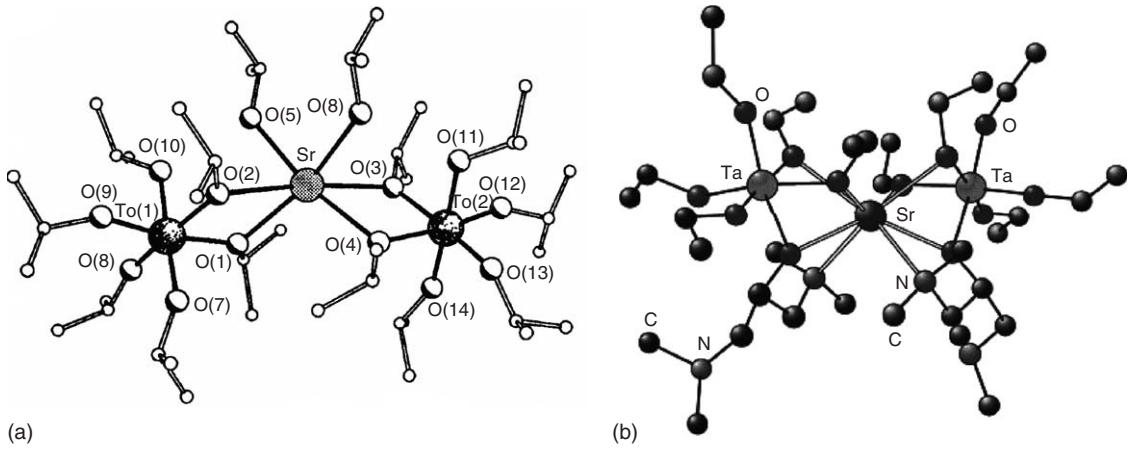

Figure 36 (a) Molecular structure of $Sr\{Ta(OPr^i)_6\}_2 \cdot Pr^iOH$ reproduced with permission from the Royal Society of Chemistry and (b) molecular structure of $[Sr\{Ta(OEt)_5(bis\text{-}dmap)\}_2]$.[268] reproduced with permission from Wiley.

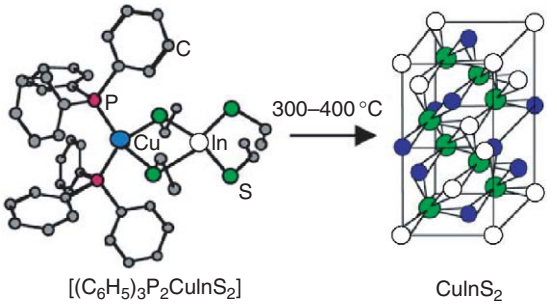

Figure 37 Precursor to copper indium diselenide.

precursors of general formula $[\{ER_3\}_2Cu(YR')_2In(YR')_2]$ (E = P, As, Sb; Y = S, Se; and R = alkyl, aryl) reported by Banger *et al.*[271] This class of precursors allows engineering the molecular architecture to modulate the precursor properties (liquid state, high volatility, thermal stability), for example, the phosphine-stabilized complexes $[\{P(Bu^n)_3\}_2Cu(SEt)_2In(SEt)_2]$ (A) and $[\{P(Bu^n)_3\}_2Cu(SPr^n)_2In(SPr^n)_2]$ (B) that represent the first liquid precursors for the deposition of $CuInS_2$ (Figure 37). $[\{PPh_3\}_2Cu(SEt)_2In(SEt)_2]$ was used to deposit well-adherent mirror-like films of $CuInS_2$ at 390 °C. No evidence of phosphorus or carbon contamination was obtained indicating a clean decomposition of the precursor.[272]

12.02.3.2.3 Ternary non-oxide ceramics

Among ternary non-oxide ceramics, the boron–carbon–nitrogen is gaining increasing attention due to the outstanding properties of boron carbonitride, BC_xN_y. These compounds are superhard, like diamond, and show remarkable stability against oxidation at elevated temperatures.[273] When compared to diamond that decomposes to carbon dioxide at 800 °C in air, cubic boron nitride (c-BN) is resistant toward oxidation till 1,600 °C. However, the application of c-BN is complicated due to high internal stresses in thin films. Boron carbonitride exhibits high hardness and oxidation resistance by low internal stresses; these properties make it an interesting alternative material. The starting materials pyridine borane ($C_5H_5N \cdot BH_3$) and triazaborabicyclodecane ($BN_3H_2(CH_2)_6$) containing boron, carbon, and nitrogen have been used as single-source precursors to deposit BC_xN_y on low-melting materials like aluminum and polymers.[274] Riedel *et al.* have made a comparative evaluation of the suitability of $C_5H_5N \cdot BH_3$ and $BN_3H_2(CH_2)_6$ in a plasma-assisted CVD process. They found that the atomic hydrogen produced by the decomposition of precursor in the plasma reduces the carbon content in the films. Since $BN_3H_2(CH_2)_6$ contains a higher amount of hydrogen, BC_xN_y films produced with this precursor revealed a lower carbon content. This example illustrates the role that auxiliary elements (ligands) can play in the final composition of the material.[275]

12.02.3.3 Quaternary Ceramics

Synthesis of multi-component single phases such as (Pb,Zr)TiO_3, InGaN, and $YBa_2Cu_3O_{7-\delta}$ by chemical methods is plagued by the unavailability of suitable precursors. The mismatch in the physicochemical behaviors (vapor pressure, decomposition temperature, and chemical properties) of individual components often leads to unwanted side-reactions, unfavorable for producing single-phase materials. For instance, the control of stoichiometry in the synthesis of strontium bismuth tantaliate (SBT), $SrBi_2Ta_2O_9$, is still a knotty problem because of the relatively high volatility of the bismuth components. Recently, attempts have been made to obtain SBT films and powders from a mixture of $SrTa_2(OEt)_{12}$ and $Bi(CH_3)_3$ or by mixing individual alkoxides, but none of these reports deals with a single-source SBT system,[276–277] Lee *et al.* have prepared a ternary alkoxide $[SrBi_2Ta_2(OCH_2CH_2OCH_3)_{18}]$ (Figure 38), which was characterized by solution NMR studies.[278] The intrinsic advantage of using a single chemical source was confirmed by the formation of single-phase SBT films. The common chemical routes to SBT employs a 20–30% excess of Bi component, which seems to be a must to compensate for the loss of Bi during the heat treatments.[278–279] The use of Sr–Bi–Ta methoxyethoxide, however, shows that excess Bi is not necessary for the formation of pure ferroelectric phase. The TGA analysis shows that the dried alkoxide precursor decomposes gradually and monotonously with no abrupt heat release, which would be the case for a heterogeneous mixture. The low-temperature (350 °C) synthesis of SBT films with a homogeneous and dense grain structure together with the TGA analysis suggests a chemical network of Sr, Bi, and Ta ions that is responsible for retarding the loss of the Bi component.

In contrast to quaternary oxides, the approach of synthesizing non-oxide ceramic materials from multi-component precursor molecules already containing the basic structure (coordination) and bonds desired in the final ceramic product has proved to be of great value.[11] The continuous quest to obtain materials with improved properties and the possibility of improving the compositional homogeneity and tailoring the composition through new organometallic molecular or polymeric precursors have led to investigations of new pre-ceramic precursors based on additional elements (e.g., Si–B–N–C systems). Jansen *et al.*[280] have prepared amorphous ceramics with the chemical composition $Si_3B_3N_7$ and $SiBN_3C$ by the pyrolysis of the single-source trichlorosilylamino–dichloroborane, $Cl_3Si–NH–BCl_2$, under ammonia and inert gas atmosphere, respectively. These ceramics possess optimized mechanical properties when compared to material prepared from modified polymers or by co-polymerization.[281] The borosilicon nitride, $Si_3B_3N_7$, and the borosilicon carbonitride, $SiBN_3C$, remain amorphous on heating in vacuum or N_2 atmosphere up to 1,800 and 1,900 °C, respectively, and no separation into thermodynamically stable crystalline phases was observed.

In addition, an extremely high resistance against oxidation up to 1,550 °C was observed for $SiBN_3C$, which is simply too high for a metastable nonoxide ceramic.[281] The exceptional properties of these amorphous compounds seem to have their origin in the precursor chemistry and pre-organized Si–N–B bonds. The atomic arrangement in the precursor (Figure 39) is an important condition for the homogeneous elemental distribution and it avoids regional inhomogeneity due to boron- or silicon-enriched clusters.[282] The Si–B–N–C ceramics prepared from other precursors show segregation into crystalline Si_3N_4 and turbostratic BN at temperatures over 1,400 °C,[283–284] which demonstrates the advantage of molecular precursors in achieving a high degree of connectivity in the amorphous ceramic that is responsible for the unusual material properties.

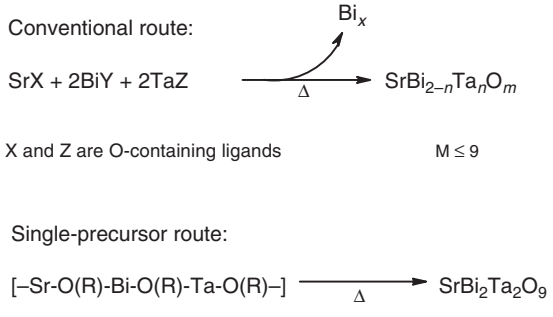

Figure 38 Different approaches to obtain Sr–Ba–Ta–O ceramics.

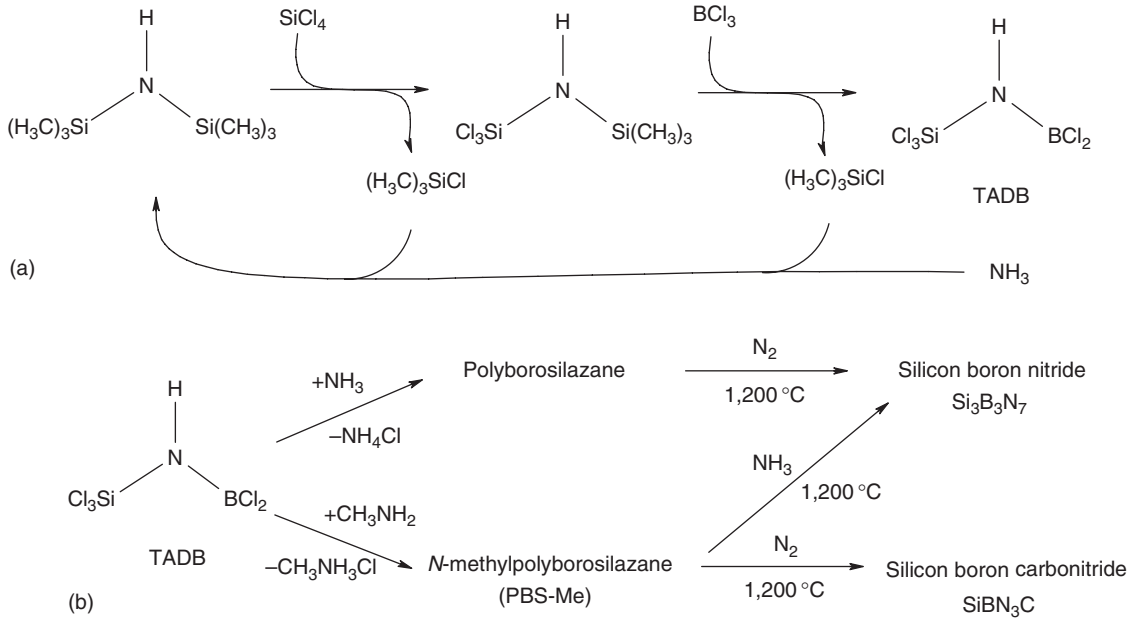

Figure 39 (a) Synthesis of the precursor molecule TADB and (b) pyrolysis and polymerization of TADB.

12.02.4 Conclusions and Outlook

Molecular compounds possessing the element combination and structural elements appropriate for the targeted solid phase are interesting scaffolds to perform chemically controlled synthesis of nanomaterials. Further properties of "tailor-made" precursors are subject to the nature and conditions of the processing methods. These specific criteria, for example, can be high vapor pressure, a large temperature window between evaporation and decomposition, and thermal lability for the gas-phase methods, whereas high solubility, stability in solution (no dissociations or rearrangements), and high reactivity are of interest for liquid-phase techniques. The specific precursor requirements are seldom met in a single molecular species, which is responsible for the quest for "ideal" precursor and the rapidly developing "chemistry–material science" interface (Figure 40).

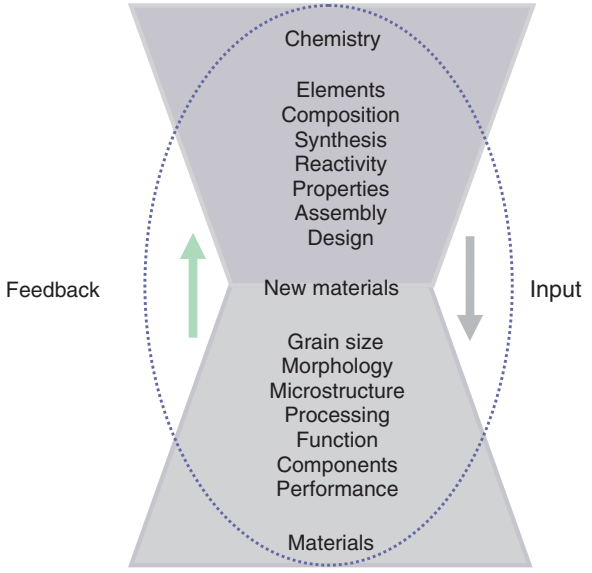

Figure 40 Road map of development of new functional ceramics based on the "chemistry-material science" interface.

Applications of molecular derivatives in various synthetic procedures (Section 12.02.2) illustrate that precursors with a predefined metal stoichiometry and reaction chemistry can enforce a molecular level homogeneity in the obtained materials, thereby enabling phase- and size-controlled synthesis. The success of chemical routes to nanomaterials is attributed to molecular precursors, which transform into solid phases at much lower temperatures than those required for conventional procedures. Although the field is still far from maturity, the continuing efforts of a large number of research groups are unfolding novel aspects of molecule-derived material synthesis.[1,1a–1d] However, it should be noted that a significant number of reports emerge from the material curiosity of a synthetic chemist, and a targeted development of experimental chemical methods, necessary to achieve inorganic nanostructures by controlled and/or self-organized growth, needs greater attention. A better understanding of the underlying principles of chemical synthesis and the process of molecule-to-material conversion requires:

- new strategies for chemically driven synthesis;
- combinatorial methods for exploration of possible kinetic and thermodynamic traps;
- general chemical principles for designing morphology and size in the final material;
- control of reaction intermediates to synthesize metastable phases;
- computational methods applicable to complex systems;
- validation of synthetic pathways to create a knowledge base; and
- proof-of-principle for the commercial viability of chemical strategies in material syntheses.

Acknowledgments

Authors would like to thank Dr. Hao Shen, Leibniz Institute of New Materials, Saarbruecken, Germany, for his help in the preparation of this manuscript.

References

1. Rao, C. N. R.; Müller, A.; Cheetham, A. K., Eds. *The Chemistry of Nanomaterials*; Wiley-VCH: Weinheim, 2004.
1a. Siegel, R. W. *Advanced Topics in Materials Science and Engineering*; Plenum: New York, 1993.
1b. Murray, C. B.; Kagan, C. R.; Bawendi, M. G. *Annu. Rev. Mater. Sci.* **2000**, *30*, 545.
1c. Fendler, J. H. *Nanoparticles and Nanostructured Films*; Wiley-VCH: Weinheim, 1998.
1d. Edelstein, A. S.; Cammarata, R. C. *Nanomaterials: Synthesis, Properties and Applications*; Institute of Physics Publishering: Bristol, 1996.
2. Burda, C.; Chen, X.; Narayanan, R.; El-Sayed, M. A. *Chem. Rev.* **2005**, *105*, 1025.
2a. Mathur, S.; Shen, H. In *Encyclopedia of Nanoscience and Nanotechnology*; Nalwa, H., Ed.; American Scientific Publisher: California, 2004; Vol. 4, p 131.
2b. Cushing, B. L.; Kolesnichenko, V. L.; O'Connor, C. J. *Chem. Rev.* **2004**, *104*, 3893.
2c. Alivisatos, A.; Barbara, P. F.; Castleman, A. W.; Chang, J.; Dixon, D. A.; Klein, M. L.; McLendon, G. L.; Miller, J. S.; Ratner, M. A.; Rossky, P. J.; Stupp, S. I., *et al. Adv. Mater.* **1998**, *10*, 1297.
2d. Day, P. *Pure Appl. Chem.* **1999**, *71*, 931.
3. Hsu, Y. J.; Lu, S. H.; Lin, Y. F. *Adv. Func. Mater.* **2005**, *15*, 1350.
3a. Hörz, M.; Zern, A.; Berger, F.; Hang, J.; Müller, K.; Aldinger, F.; Weinmann, M *J. Europ. Ceram. Soc.* **2005**, *25*, 99.
3b. de Groot, M. W.; Taylor, N. J.; Corrigan, J. F. *J. Mater. Chem.* **2004**, *14*, 654.
4. Cowley, A. H.; Jones, R. A. *Angew. Chem.* **1989**, *101*, 1235.
5. Farneth, W. E.; Herron, N.; Wang, Y. *Chem. Mater.* **1992**, *4*, 916.
6. MacInnes, A. N.; Power, M. B.; Barron, A. R. *Chem. Mater.* **1993**, *5*, 1344.
7. Cheon, J.; Arnold, J.; Yu, K. M.; Bourret, E. *Chem. Mater.* **1995**, *7*, 2273.
8. Holl, M. M. B.; Wolczanski, P. T.; Proserpio, D.; Bielecki, A.; Zax, D. B. *Chem. Mater.* **1996**, *8*, 2468.
9. Lazell, M.; O'Brien, P.; Otway, D. J.; Park, J.-H. *J. Chem. Soc., Dalton Trans.* **2000**, 4479.
10. Trindade, T.; O'Brien, P.; Pickett, N. L. *Chem. Mater.* **2000**, *13*, 3843.
11. Veith, M. *J. Chem. Soc., Dalton Trans.* **2002**, 2405.
12. Mathur, S.; Veith, M.; Shen, H.; Hüfner, S. *Mater. Sci. Forum* **2002**, *386–388*, 341.
13. Polarz, S.; Orlov, A. V.; van den Berg, M. W. E.; Driess, M. *Angew. Chem., Int. Ed.* **2005**, *44*, 7892.
14. Mathur, S.; Veith, M.; Shen, H.; Hüfner, S. *Ceram. Eng. Sci. Proc.* **2002**, *23*, 557.
15. Mathur, S. In *Chemical Physics of Thin Film Deposition Processes for Micro- and Nano-Technologies*; Pauleau, Y., Ed; Kluwer: Dordrecht, The Netherlands, p. 91, 2002.
16. Jones, A. C. *Chem. Soc. Rev.* **1997**, 101.
17. Devi, A.; Rogge, W.; Wohlfart, A.; Hipler, F.; Becker, H. W.; Fischer, R. A. *Chem. Vap. Deposition* **2000**, *6*, 245.
18. Fischer, R. A.; Sussek, H.; Miehr, A.; Pritzkow, H.; Herdtweck, E. *J. Organomet. Chem.* **1997**, *548*, 73.
19. Jansen, M. *Solid State Ionics* **1997**, *101–103*, 1.
20. Carpenter, J. P.; Lukehart, C. M.; Milne, S. B.; Stock, S. R.; Wittig, J. E.; Jones, B. D.; Glosser, R.; Zhu, J. G. *J. Organometal. Chem.* **1998**, *557*, 121.
21. Park, H. S.; Waezsada, S. D.; Cowley, A. H.; Roesky, H. W. *Chem. Mater.* **1998**, *10*, 2251.

22. Kessler, V. G.; Hubert-Pfalzgraf, L.-G.; Daniele, S. *Chem. Mater.* **1994**, *6*, 2336.
23. Caulton, K. G.; Hubert-Pfalzgraf, L.-G. *Chem. Rev.* **1990**, *90*, 969.
24. Chandler, C. D.; Roger, C.; Hampden-Smith, M.-J. *Chem. Rev.* **1993**, *93*, 1205.
25. Baxter, D. V.; Chisholm, M. H.; Gama, G. J.; Andrew, A. L.; Parkin, I. P. *Chem. Vap. Deposition* **1995**, *1*, 49.
26. Bradley, D. C. *Polyhedron* **1994**, *13*, 1111.
27. Mehrotra, R. C.; Singh, A. *Chem. Soc. Rev.* **1996**, 1.
28. Murray, C. B.; Norris, D. J.; Bawendi, M. G. *J. Am. Chem. Soc.* **1993**, *115*, 8706.
29. Brus, L. E. *Appl. Phys. A* **1991**, *53*, 465.
30. Brennan, J. G.; Siegrist, T.; Carrol, P. J.; Stuczynski, S. M.; Brus, L. E.; Steigerwald, M. *J. Am. Chem. Soc.* **1989**, *111*, 4141.
31. Trindade, T.; O'Brien, P. *Adv. Mater.* **1996**, *8*, 161.
32. Ockwig, N. W.; Delgado-Friedrichs, O.; O'Keeffe, M.; Yaghi, O. M. *Acc. Chem. Res.* **2005**, *38*, 176.
33. Li, H.; Eddaoudi, M.; O'Keeffe, M.; Yaghi, O. M. *Nature* **1999**, *402*, 276.
34. Eddaoudi, M.; Kim, J.; Rosi, N.; Vodak, D.; Wachter, J.; O'Keeffe, M.; Yaghi, O. M. *Science* **2002**, *295*, 469.
35. Chae, H. K.; Siberio-Pe'rez, D. Y.; Kim, J.; Go, Y. B.; Eddaoudi, M.; Matzger, A. J.; O'Keeffe, M.; Yaghi, O. M. *Nature* **2004**, *427*, 523.
36. Yaghi, O. M.; O'Keeffe, M.; Ockwig, N. W.; Chae, H. K.; Eddaoudi, M.; Kim, J. *Nature* **2003**, *423*, 705.
37. Eddaoudi, M.; Moler, D. B.; Li, H. L.; Chen, B. L.; Reineke, T. M.; O'Keeffe, M.; Yaghi, O. M. *Acc. Chem. Res.* **2001**, *34*, 319.
38. Xia, Y. N.; Yang, P. D.; Sun, Y. G.; Wu, Y. Y.; Mayers, B.; Gates, B.; Yin, Y. D.; Kim, F.; Yan, Y. Q. *Adv. Mater.* **2003**, *15*, 353.
39. Alivisatos, A. P. *Science* **1996**, *271*, 933.
40. Gillan, E. G.; Barron, A. R. *Chem. Mater.* **1997**, *9*, 3037.
41. Polarz, S.; Roy, A.; Merz, M.; Halm, S.; Schroder, D.; Schneider, L.; Bacher, G.; Kruis, F. E.; Driess, M. *Small* **2005**, *1*, 540.
42. Schroder, D.; Schwarz, H.; Polarz, S.; Driess, M. *Phys. Chem. Chem. Phys.* **2005**, *7*, 1049.
43. Roy, A.; Polarz, S.; Rabe, S.; Rellinghaus, B.; Zäheres, H.; Krüis, F. E.; Driess, M. *Chem. Eur. J.* **2004**, *10*, 1565.
44. Mathur, S.; Veith, M.; Ruegamer, T.; Hemmer, E.; Shen, H. *Chem. Mater.* **2004**, *16*, 1304.
45. Mathur, S.; Shen, H.; Hemmer, E.; Ruegamer, T.; Holzapfel, C. *Mater. Res. Soc. Symp. Proc.* **2005**, *848*, FF1.10.1.
46. Meese-Marktscheffel, J. A.; Fukuchi, R.; Kido, M.; Tachibana, G.; Jensen, C. M.; Gilje, J. W. *Chem. Mater.* **1993**, *5*, 755.
47. Gleiter, H. *Nanostruct. Mater.* **1992**, *1*, 1.
48. Schmid, G. *Nanoparticles: From Theory to Applications*; Wiley-VCH, Weinheim, 2003.
49. Liz-Marz, L. M.; Kamat, P. V. *Nanoscale Materials*; Kluwer: Boston, 2003.
50. Rosi, N. L.; Mirkin, C. A. *Chem. Rev.* **2005**, *105*, 1547.
51. Alvisatos, P. *Nat. Biotechnol.* **2004**, *22*, 47.
52. Niemeyer, C. M. *Angew. Chem., Int. Ed.* **2001**, *40*, 4128.
53. O'Brien, S.; Brus, L.; Murray, C. B. *J. Am. Chem. Soc.* **2001**, *123*, 12085.
54. Coruntu, D.; Remond, Y.; Chou, N. H.; Jun, M. J.; Coruntu, G.; He, J.; Goloverda, G.; O' Connor, C.; Kolesnichenko, V. *Inorg. Chem.* **2002**, *41*, 6137.
55. Meyer, F.; Hempelmann, R.; Mathur, S.; Veith, M. *J. Mater. Chem.* **1999**, *9*, 1755.
56. Zhang, Z.; Rondinone, A. J.; Ma, J.-X.; Shen, J.; Dai, S. *Adv. Mater.* **2005**, *17*, 1415.
57. Lee, J.; Isobe, T.; Senna, M. *Colloids Surf. A* **1996**, *109*, 121.
58. Dechamps, M.; Diuricic, B.; Pickering, S. J. *J. Am. Ceram. Soc.* **1995**, *78*, 2873.
59. Wang, J.; Fang, J.; Ng, S.-C.; Gan, L.-M.; Chew, C.-H.; Wang, X.; Shen, Z. *J. Am. Ceram. Soc.* **1999**, *82*, 873.
60. Hasegawa, M. *Ceram. Forum Int.* **1993**, *70*, 490.
61. Kodama, T.; Ookubo, M.; Miura, S.; Kitayama, Y. *Mater. Res. Bull.* **1996**, 1501.
62. Gang, J.; Feng, Y.; Mingqiang, L.; Jinhuai, L. *Sensors* **2002**, *2*, 71.
63. Lin, J.; Duh, J. *J. Am. Ceram. Soc.* **1997**, *80*, 92.
64. Wang, L.; Zhang, Y.; Muhammed, M. *J. Mater. Chem.* **1995**, *5*, 309.
65. Turner, E. A.; Huang, Y.; Corrigan, J. F. *Eur. J. Inorg. Chem.* **2005**, 4465.
66. Yosef, M.; Schaper, A. K.; Fröba, M.; Schlecht, S. *Inorg. Chem.* **2005**, *44*, 5890.
67. Brinker, C. J.; Scherer, G. W. *Sol-Gel Science: The Physics and Chemistry of Sol-Gel Processing*; Academic Press: San Diego, CA, 1990.
68. Pierre, A. C. *Introduction to Sol-Gel Processing*; Kluwer: Boston, 1998.
69. Wright, J. D.; Sommerdijk, N. A. *Sol-Gel Materials: Chemistry and Applications*; Taylor and Francis: London, 2001.
70. Sakka, S. *Sol-Gel Science and Technology: Topics in Fundamental Research and Applications*; Kluwer: Boston, 2002.
71. Hench, L. L.; West, J. K. *Chem. Rev.* **1990**, *90*, 33.
72. Brinker, C. J. *J. Non-Cryst. Solids* **1988**, *100*, 31.
73. Schubert, U. *J. Chem. Soc., Dalton Trans.* **1996**, 3343.
74. Sanchez, C.; Ribot, F.; Lebeau, B. *J. Mater. Chem.* **1999**, *9*, 35.
75. Livage, J. *J. Mater. Sci. Forum* **1994**, *152–153*, 43.
76. Hoar, T. P.; Schulman, J. H. *Nature* **1941**, *152*, 102.
77. Schulman, J. H.; Stockenius, W.; Prince, L. M. *J. Phys. Chem.* **1959**, *63*, 1977.
78. Steigerwald, M. L.; Alivisatos, A.; Gibson, J. M.; Harris, T. D.; Kortan, R.; Muller, A. J.; Thayer, A. M.; Duncan, T. M.; Douglass, D. C.; Brus, L. E. *J. Am. Ceram. Soc.* **1998**, *110*, 3046.
79. Moran, P. D.; Bartlett, J. R.; Bowmaker, G. A.; Woolfrey, J. L.; Cooney, R. P. *J. Sol-gel Sci. Tech.* **1999**, *15*, 251.
80. Lim, G. K.; Wang, J.; Ng, S. C.; Gan, L. M. *Langmuir* **1999**, *15*, 7472.
81. Maugey, M.; Bellocq, A.-M. *Langmuir* **1999**, *15*, 8602.
82. Moulik, S. P.; De, G. C.; Panda, A. K.; Bhowmik, B. B.; Das, A. R. *Langmuir* **1999**, *15*, 8361.
83. Lee, H. S.; Lee, W. C. *J. Appl. Phys.* **1999**, *85*, 5231.
84. Porcar, L.; Marignan, J. *J. Sol-gel Sci. Tech.* **1999**, *13*, 99.
85. Roth, M.; Hempelmann, R. *J. Mater. Chem.* **1999**, *9*, 493.
86. Li, M.; Schnablegger, H.; Mann, S. *Nature* **1999**, *402*, 393.
87. Fang, J.; Wang, J.; Ng, S. C.; Chew, C. H.; Gan, L. M. *J. Mater. Sci.* **1999**, *34*, 1943.
88. Ng, W. B.; Wang, J.; Ng, S. C.; Gan, L. M. *J. Am. Ceram. Soc.* **1999**, *82*, 529.

89. Osseo-Asare, K.; Arriagada, F. J. In *Better Ceramics Through Chemistry III*; Brinker, C. J., Clark, D. E., Ulrich, D. R., Eds.; Materials Research Society: Pittsburgh, 1988.
90. Moran, P. D.; Bartlett, J. R.; Woolfrey, J. L.; Bowmaker, G. A.; Cooney, R. P. *J. Sol-Gel Sci. Techn.* **1997**, *8*, 65.
91. Yajima, S.; Hayashi, J.; Omori, M. *Chem.Lett.* **1975**, 931.
92. Seyferth, D.; Wiseman, G. H. *J. Am. Ceram. Soc.* **1984**, *67*, C132.
93. Interrante, L. V.; Czekaj, C. L.; Hackney, M. L.; Sigel, G. A.; Shields, P. J.; Slack, G. A. *Mater. Res. Soc. Symp. Proc.* **1988**, *121*, 465.
94. Czekaj, C. L.; Hackney, M. L.; Hurley, W. J., Jr.; Interrante, L. V.; Sigel, G. A.; Shields, P. J.; Slack, G. A. *J. Am. Ceram. Soc.* **1990**, *73*, 352.
95. Löffelholz, J.; Jansen, M. *Adv. Mater.* **1995**, 7, 289.
96. Nakashima, H.; Koyama, S.; Kuorda, K.; Sugahara, Y. *J. Am. Ceram. Soc.* **2002**, *85*, 59.
97. Li, X.; Edirisinghe, M. J. *Chem. Mater.* **2004**, *16*, 1111.
98. Pechini, M. P. US Patent 3330694, 1967.
99. Lessing, P. A. *Ceram. Bull.* **1998**, *68*, 1002.
100. Eror, N. G.; Anderson, H. U. In *Better Ceramics Through Chemistry II*; Brinker, C. J., Clark, D. E., Ulrich, D. R., Eds.; Materials Research Society Symposia Proceedings; Materials Research Society: Pittsburgh, PA, 1996, p 571.
101. Veith, M.; Mathur, S.; Kareiva, A.; Jilavi, M.; Zimmer, M.; Huch, V. *J. Mater. Chem.* **1999**, *9*, 3069.
102. Ikesue, A.; Yoshida, K.; Kamata, K. *J. Am. Ceram. Soc.* **1996**, *79*, 507.
103. Yang, J. M.; Jeng, S. M.; Chang, S. *J. Am. Ceram. Soc.* **1996**, *79*, 1218.
104. Gülgün, M. A.; Popolla, O. O.; Kriven, W. M. *J. Am. Ceram. Soc.* **1994**, 77, 531.
105. Segal, D. *J. Mater. Chem.* **1997**, *7*, 1297.
106. Barb, D.; Diamandescu, L.; Rusi, A.; Tarabasani-Mihaila, D.; Morariu, M.; Teodorescu, V. *J. Mater. Sci.* **1986**, *21*, 1118.
107. Demazeau, G. *J. Mater. Chem.* **1999**, *9*, 15.
108. Yu, S.-H. *J. Ceram. Soc. Jpn.* **2001**, *109*, S65.
109. Rajamathi, M.; Seshadri, R. *Curr. Opin. Solid State Mater. Sci.* **2002**, *6*, 337.
110. Feng, Q.; Kanoh, H.; Miyai, Y.; Ooi, K. *Chem. Mater.* **1995**, 7, 1226.
111. Yanagisawa, K. *J. Mater. Sci. Lett.* **1993**, *12*, 1842.
112. Somiya, S., Ed. *Hydrothermal Preparation of Fine Powders, Advanced Ceramics III*; Elsevier: London, 1990.
113. Wang, A.; Capitain, F.; Monnier, V.; Matar, S.; Demazeau, G. *J. Mater. Synth. Proc.* **1997**, *5*, 235.
114. Wu, M.; Li, X.; Shen, G.; Li, J.; Xu, R.; Proseripos, D. M. *J. Solid Sate Chem.* **2000**, *151*, 56.
115. Stringfellow, G. B. *Organometallic Vapor-Phase Epitaxy: Theory and Practice*; Academic Press: New York, 1989.
116. Pierson, H. O. *Handbook of Chemical Vapour Deposition*; Noyes Publications: Park Ridge, 1992.
117. Rees, W. S., Jr. *CVD of Nonmetals*; Wiley: New York, 1996.
118. Kodas, T. T., Hampden-Smith, M. J., Eds. In *The Chemistry of Metal CVD*; VCH: Weinheim, 1994.
119. Hampden-Smith, M. J.; Kodas, T. T. *Chem. Vap. Deposition* **1995**, *1*, 10.
120. Hampden-Smith, M.-J.; Kodas, T. T. *Chem. Vap. Deposition* **1995**, *1*, 39.
121. Veith, M.; Mathur, S.; Lecerf, N.; Shen, H.; Hüfner, S. *Chem. Mater.* **1999**, *11*, 3103.
122. Kim, C. G.; Koh, W.; Ku, S. J.; Nah, E. J.; Yu, K. S.; Kim, Y. *J. Phys. IV* **1999**, *9*, Pr8–853.
123. Mathur, S.; Barth, S.; Shen, H. *Chem. Vap. Deposition* **2005**, *11*, 11.
124. Merz, K.; Schonen, R.; Driess, M. *J. Phys. IV France* **2001**, *11*, Pr3–467.
125. Driess, M.; Merz, K.; Schoenen, R.; Rabe, S.; Krüis, F. E.; Roy, A.; Birkner, A. *C. R. Chimie* **2003**, *6*, 273.
126. Ikesue, A.; Kinoshita, T.; Kamata, K.; Yoshida, K. *J. Am. Ceram. Soc.* **1995**, *78*, 1033.
127. Kolar, D. *Pure Appl. Chem.* **2000**, *72*, 1425.
128. Yoldas, B. E. *Am. Ceram. Soc. Bull.* **1975**, *54*, 286.
129. Bradley, D. C.; Mehrotra, R. C.; Rothwell, I.; Singh, A. *Alkoxo and Aryloxo Derivatives of Metals*; Academic Press: London, 2001.
130. Bradley, D. C.; Faktor, M. M. *J. Appl. Chem.* **1959**, *9*, 5425.
131. Bradley, D. C.; Faktor, M. M. *Trans. Faraday Soc.* **1959**, *55*, 2117.
132. Baxter, D. V.; Chisholm, M. H.; Distasi, V. F.; Klang, J. A. *Chem. Mater.* **1991**, *3*, 221.
133. Ao, B.; Kummerl, L.; Harrer, D. *Adv. Mater.* **1995**, *7*, 495.
134. Hibst, H. *J. Magn. Magn. Mater.* **1988**, *74*, 173.
135. Bradley, F. N. *Materials for Magnetic Functions*; Hayden: New York, 1976.
136. Sun, H.; Cantalini, C.; Faccio, M.; Pelino, M.; Catalano, M.; Tapfer, L *J. Am. Ceram. Soc.* **1996**, *79*, 927.
137. Pascal, C.; Pascal, J. L.; Favier, F.; Elidrissi Moubtassim, M. L.; Payen, C. *Chem. Mater.* **1999**, *11*, 141.
138. Matteazzi, P.; Le Caer, G. *Mat. Sci. Eng. A* **1991**, *149*, 135.
139. Tang, Z. X.; Nafis, S.; Sorensen, C. M.; Hadjipanayis, G. C.; Klabunde, K. J. *J. Magn. Magn. Mater.* **1989**, *80*, 285.
140. Dhara, S.; Rastogi, A. C.; Das, B. K. *Thin Solid Films* **1994**, *239*, 240.
141. Kandori, K.; Ohkasi, N.; Yasukawa, A.; Ishikawa, I. *J. Mater. Res.* **1998**, *13*, 1698.
142. Morales, M. P.; de Julien, C.; Gonzalez, J. M.; Serna, C. J. *J. Mater. Res.* **1994**, *9*, 135.
143. Morales, M. P.; Gonzalez, J. M.; Serna, C. J. *J. Mater. Res.* **1992**, 7, 2538.
144. Cabanas, M. V.; Vallet-Regi, M.; Labeau, M.; Gonzalez-Calbet, J. M. *J. Mater. Res.* **1993**, *8*, 2694.
145. Armelao, L.; Artigliato, A. *J. Mater. Res.* **1997**, *12*, 1441.
146. Cao, X.; Prozorov, R. Koltypin, Yu.; Kataby, G.; Felner, I.; Gedanken, A. *J. Mater. Res.* **1997**, *12*, 402.
147. Hashimoto, T.; Yamada, T.; Yoko, T. *J. Appl. Phys.* **1996**, *80*, 3184.
148. Kiyomura, T.; Gomi, M. *J. Phys. IV* **1997**, 7, C1–611.
149. Mathur, S.; Veith, M.; Sivakov, V.; Shen, H.; Huch, V.; Hartmann, U.; Gao, H. B. *Chem. Vap. Deposition* **2002**, *8*, 277.
150. Miller, J. S. *Adv. Mater.* **2002**, *14*, 1105.
151. Arunachalam, V. S.; Fleischer, E. L. *MRS Bull.* **2001**, *26*, 1020.
152. Veith, M.; Grätz, F.; Huch, V. *Eur. J. Inorg. Chem.* **2001**, 367.
153. Mehrotra, R. C.; Singh, A.; Sogani, S. *Chem. Soc. Rev.* **1994**, 215.
154. Mehrotra, R. C.; Singh, A.; Sogani, S. *Chem. Rev.* **1994**, *94*, 1643.
155. Mehrotra, R. C.; Singh, A.; Tripathi, U. M. *Chem. Rev.* **1991**, *91*, 1287.
156. Herrmann, W. A.; Egli, A.; Herdtweck, E.; Alberto, R.; Baumgärtner, F. *Angew. Chem.* **1996**, *108*, 486.

157. Kiyomura, T.; Gomi, M. *J. Phys. IV* **1997**, *7*, C1–611.
158. Regan, B. O.; Graetzel, M. *Nature* **1991**, *353*, 737.
159. Sopyan, I.; Watanabe, M.; Murasawa, S.; Hashimoto, K.; Fujishima, A. *Chem. Lett.* **1996**, 69.
160. Pawlewicz, W. T.; Exarhos, G. J.; Conaway, W. E. *Appl. Opt.* **1983**, *22*, 1837.
161. Malato, S.; Blanco, S.; Richter, C.; Maldonado, M. I. *Appl. Catal. B* **2000**, *25*, 31.
162. Gnanasekar, K. I.; Subramanian, V.; Robinson, J.; Jiang, J. C.; Posey, F. E.; Rambabu, B. *J. Mater. Res.* **2002**, *17*, 1507.
163. Boyle, T. J.; Tyner, R. P.; Alam, T. M.; Scott, B. L.; Ziller, Z. W.; Potter, B. G. *J. Am. Chem. Soc.* **1999**, *121*, 12104.
164. Ischenko, V.; Polarz, S.; Grote, D.; Stavarache, V.; Fink, K.; Driess, M. *Adv. Func. Mater.* **2005**, *15*, 1945.
165. Banyai, L.; Koch, S. W. *Semiconductor Quantum Dots*; World Scientific: Singapore, 1993.
166. Waggon, U. *Optical Properties of Semiconductor Quantum Dots*; Springer-Verlag: Berlin, 1997.
167. Vossmeyer, T.; Katsikas, L.; Giersig, M.; Popovic, I. G.; Diesner, K.; Chemseddine, A.; Eychmüller, A.; Weller, H *J. Phys. Chem.* **1994**, *98*, 7665.
168. Cumberland, S. L.; Hanif, K. M.; Javier, A.; Khitrov, G. A.; Strouse, G. F.; Woessner, S. M.; Yun, C. S. *Chem. Mater.* **2002**, *14*, 1576.
169. Trinidade, T.; O'Brien, P.; Zhang, X. *Chem. Mater.* **1997**, *9*, 523.
170. Lazell, M.; O'Brien, P. *Chem. Commun.* **1999**, 2041.
171. Ludolph, B.; Malik, M. A.; O'Brien, P.; Revaprasadu, N. *Chem. Commun.* **1998**, 1849.
172. Trindade, T.; Monteiro, O. C.; O'Brien, P.; Motevalli, M. *Polyhedron* **1999**, *18*, 1171.
173. Trindade, T.; O'Brien, P.; Zhang, X.; Motevalli, M. *J. Mater. Chem.* **1997**, *7*, 1011.
174. Chunggaze, M.; Malik, M. A.; O'Brien, P. *Adv. Mater. Opt. Electron.* **1998**, *7*, 311.
175. Nakamura, S.; Pearton, S.; Fasol, G. *The Blue Laser Diode: The Complete Story*; Springer: Berlin, 2000.
176. Neumayer, D. A.; Ekerdt, J. G. *Chem. Mater.* **1996**, *8*, 9.
177. Jones, A. C.; Whitehouse, C. R.; Robert, J. S. *Chem. Vap. Deposition* **1995**, *1*, 65.
178. Frank, A. C.; Fischer, R. A. *Adv. Mater.* **1998**, *10*, 961.
179. McMurran, J.; Kouvetakis, J.; Smith, D. J. *Appl. Phys. Lett.* **1999**, *74*, 883.
180. Müller, J.; Bendix, S. *Chem. Commun.* **2001**, 911.
181. Winkler, H.; Devi, A.; Manz, A.; Wohlfart, A.; Rogge, W.; Fischer, R. A. *Phys. Stat. Sol. A* **2000**, *177*, 27.
182. Janik, J. F.; Wells, R. L. *Chem. Mater.* **1996**, *8*, 2708.
183. Hwang, J.-W.; Compbell, J. P.; Kozubowski, J.; Hanson, S. A.; Evans, J. F.; Gladfelter, W. L. *Chem. Mater.* **1995**, 7, 517.
184. Gonsalves, K. E.; Carlson, G.; Rangarajan, S. P.; Benaissa, M.; Jose-Yacaman, M. J. *J. Mater. Chem.* **1996**, *6*, 1451.
185. Fischer, R. A.; Miehr, A.; Herdtweck, E.; Mattner, M. R.; Ambacher, O.; Metzger, T.; Born, E.; Weinkauf, S.; Pulham, C. R.; Parsons, S. *Chem. Eur. J.* **1996**, *2*, 1353.
186. McMurran, J.; Dai, D.; Balasubramanian, K.; Steffek, C.; Kouvetakis, J.; Hubbard, J. L. *Inorg. Chem.* **1998**, *37*, 6638.
187. McMurran, J.; Kouvetakis, J.; Nesting, D. C.; Smith, D. J.; Hubbard, J. L. *J. Am. Chem. Soc.* **1998**, *120*, 5233.
188. Sung, M. M.; Kim, C.; Yoo, S. H.; Kim, C. G.; Kim, Y. *Chem. Vap. Deposition* **2002**, *8*, 50.
189. Lin, J. L.; Petrovykh, D. Y.; Kirakosian, A.; Rauscher, H.; Himpsel, J. F.; Dowben, P. A. *Appl. Phys. Lett.* **2001**, *78*, 829.
190. Cowley, A. H.; Jones, R. A. *Polyhedron* **1994**, *13*, 1149.
190a. Driess, M.; Kuntz, K.; Merz, K.; Pritzkow, H. *Chem. Eur. J* **1998**, *4*, 1628.
191. Miller, J. E.; Mardones, M. A.; Nail, J. W.; Cowley, A. H.; Jones, R. A.; Ekerdt, J. G. *Chem. Mater.* **1992**, *4*, 447.
192. Maury, F.; Constant, G. *Polyhedron* **1984**, *3*, 581.
193. Maury, F.; Constant, G.; Fontaine, P.; Biberian, J. P. *J. Cryst. Growth* **1986**, *78*, 185.
194. Maury, F.; Constant, G. *J. Cryst. Growth* **1983**, *62*, 568.
195. Maury, F.; Hammadi, A. E.; Constant, G. *J. Cryst. Growth* **1984**, *68*, 88.
196. Hammadi, A. E.; Maury, F.; Muller, G.; Bensoam, J.; Constant, G. *Acad. Sci. Paris, Ser. II* **1984**, *299*, 1255.
197. Maury, F.; Hammadi, A. E. *J. Cryst. Growth* **1988**, *91*, 97.
198. Maury, F.; Hammadi, A. E. *J. Cryst. Growth* **1988**, *91*, 105.
199. Cowley, A. H.; Jones, R. A.; Mardones, M. A.; Nunn, C. M. *Organometallics* **1991**, *10*, 1635.
200. Miller, J. E.; Kidd, K. B.; Cowley, A. H.; Jones, A. C.; Ekerdt, J. G.; Gysling, H. J.; Wernberg, A. A.; Blanton, T. N. *Chem. Mater.* **1990**, *2*, 589.
201. Gleizes, A. N. *Chem. Vap. Deposition* **2000**, *6*, 155.
202. Benz, K. W.; Renz, H.; Weidlein, J.; Pilkuhn, M. H. *J. Electron. Mater.* **1981**, *10*, 185.
203. Zaouk, A.; Salvetat, E.; Sakaya, J.; Maury, F.; Constant, G. *J. Cryst. Growth* **1981**, *55*, 135.
204. Maury, F.; Combes, M.; Constant, G.; Carles, R.; Benucci, J. B. *J. Phys. C1* **1982**, 347.
205. Maury, F.; Combes, M.; Constant, G. In *Procedings of EUROCVD4*; Bloem, J., Verspui, G., Wolff, L. R., Eds.; Philips Centre for Manufacturing Technology: Eindhoven, 1983.
206. Zurcher, S.; Morstein, M.; Spencer, N. D.; Lemberger, M.; Bauer, A. *Chem. Vap. Deposition* **2002**, *8*, 171.
207. Maury, F. *Adv. Mater.* **1991**, *3*, 542.
208. Maury, F. In *Transformation of Organometallics into Common and Exotic Materials: Design and Activation*; Laine, R. M., Ed.; NATO ASI Series E, Martinus Nijhoff: Kluwer Academic, The Netherlands, 1988, p 195.
209. Cowley, A. H.; Benac, B. L.; Ekerdt, J. G.; Jones, A. C.; Kidd, K. B.; Lee, J. Y.; Miller, J. E. *J. Am. Chem. Soc.* **1988**, *110*, 6248.
210. Miller, J. E.; Ekerdt, J. G. *Chem. Mater.* **1992**, *4*, 7.
211. Ekerdt, J. G.; Sun, Y. M.; Jackson, M. S.; Lakhotia, V.; Pacheco, K. A.; Koschmieder, S. U.; Cowley, A. H.; Jones, A. C. *J. Cryst. Growth* **1992**, *124*, 158.
212. Cowley, A. H.; Jones, A. C.; Null, C. M.; Westmorland, D. L. *Chem. Mater.* **1990**, *2*, 221.
213. Berger, L. I. *Semiconductor Materials*; CRC Press: New York, 1996.
214. Park, H. S.; Schulz, S.; Wessel, H.; Roesky, H. W. *Chem. Vap. Deposition* **1999**, *5*, 179.
215. Rice, R. W. *Am. Ceram. Soc. Bull.* **1982**, *62*, 889.
216. Riedel, R.; Dressler, W. *Ceram. Int.* **1996**, *22*, 233.
217. Greil, P. *J. Europ. Ceram. Soc.* **1998**, *18*, 1905.
218. Corrin, R. J. P. *Angew. Chem., Int. Ed.* **2000**, *39*, 1376.
219. Peuckert, M.; Vaahs, T.; Brück, M. *Adv. Mater.* **1990**, *2*, 398.
220. Blum, Y. B.; Schwartz, K. B.; Laine, R. M. *J. Mater. Sci.* **1989**, *24*, 1707.

221. Schwartz, K. B.; Rowcliffe, D. J.; Blum, Y. D.; Laine, R. M. *Better Ceramics Through Chemistry II*; Brinker, C. J., Clark, D. E., Ulrich, D. R., Eds.; Materials Research Society Symposium Proceedings, Materials Research Society: Pittsburgh, 1986; Vol. 73, p 407.
222. Legrow, G. E.; Lim, T. F.; Lipowitz, J.; Reaoch, R. S. *Am. Ceram. Soc. Bull.* **1987**, *66*, 363.
223. Blanchard, C. R.; Schwab, S. T. *J. Am. Ceram. Soc.* **1994**, *77*, 1729.
224. Wynne, K. J.; Rice, R. W. *Annu. Mater. Sci.* **1984**, *14*, 297.
225. Arai, M.; Sakurada, S.; Isoda, T.; Tomizawa, T. *Polym. Prepr.* **1993**, *34*, 286.
226. Maseeh, F.; Senturia, S. D. *Sens. Actuators A* **1990**, *23*, 861.
227. Lee, K. W.; Yu, K. S.; Kim, Y. *J. Cryst. Growth* **1997**, *179*, 153.
228. Interrante, L. V.; Larkin, D. J.; Amato, C. *Mat. Res. Soc. Symp. Proc.* **1992**, *250*, 283.
229. Han, B.; Hudson, J. B. *Mat. Res. Soc. Symp. Proc.* **1993**, *282*, 457.
230. West, R. In *Ultrastructure Processing of Ceramics, Glasses and Composites*; Hench, L. L., Ulrich, D. R., Eds.; Wiley-Interscience: New York, 1984, p 235.
231. Yajima, S.; Okamura, K.; Hayashi, J.; Omori, M. *J. Am. Ceram. Soc.* **1975**, *59*, 324.
232. Yajima, S.; Hayashi, J.; Omori, M.; Okamura, K. *Nature* **1976**, *261*, 683.
233. Yajima, S.; Shishido, T.; Kayano, H. *Nature* **1978**, *73*, 525.
234. Yajima, S. *Am. Ceram. Soc. Bull.* **1983**, *62*, 893.
235. Zhang, Z. F.; Scotto, C. S.; Laine, R. M. *J. Mater. Chem.* **1998**, *8*, 2715.
236. Zhang, Z. F.; Babonneau, F.; Laine, R. M.; Mu, Y.; Harrod, J. F.; Rahn, J. A. *J. Am. Ceram. Soc.* **1990**, *74*, 670.
237. Saitoh, H.; Yarbrough, W. A. *Diamond Relat. Mater.* **1992**, *1*, 137.
238. Mishima, O.; Era, K.; Tanaka, J.; Yamaoka, S. *Appl. Phys. Lett.* **1988**, *53*, 962.
239. Comez-Aleixandre, C.; Essafti, A.; Fernandez, M.; Fierro, J. L. G.; Albella, J. M. *J. Phys. Chem.* **1996**, *100*, 2148.
240. Boo, J.-H.; Lee, S.-B.; Yu, K.-S.; Kim, Y.; Kim, Y.-S.; Park, J. T. *J. Korean Phys. Soc.* **1999**, *34*, 532.
241. Pender, M. J.; Sneddon, L. G. *Chem. Mater.* **2000**, *12*, 280.
242. Mondal, S.; Banthia, A. K. *J. Eur. Ceram. Soc.* **2005**, *25*, 287.
243. Mirabelli, M. G. L.; Lynch, A. T.; Sneddon, L. G. *Solid State Ionics* **1989**, *32–33*, 655.
244. Isao, H.; Yoshiaki, F.; Toshi, T.; Keiko, Y. *J. Mater. Sci. Lett.* **1999**, *18*, 1629.
245. Rocheleau, R. E.; Zhang, Z.; Gilje, J. W.; Meese-Marktscheffel, J. A. *Chem. Mater.* **1994**, *6*, 1615.
246. Jones, K.; Davies, T. J.; Emblem, H. G.; Parkes, P. *Mat. Res. Soc. Symp. Proc.* **1986**, *73*, 111.
247. Bichmore, C. R.; Waldner, K. F.; Laine, R. M. *J. Am. Ceram. Soc.* **1996**, *79*, 1419.
248. Apblett, A. W.; Cubano, L. A.; Georgieva, G. D.; Mague, J. T. *Chem. Mater.* **1996**, *8*, 650.
249. Meyer, F.; Dierstein, A.; Beck, C.; Hempelmann, R.; Mathur, S.; Veith, M. *Nanostruct. Mater.* **1999**, *12*, 71.
250. Mathur, S.; Veith, M.; Rapalaviciute, R.; Shen, H.; Goya, G. F.; Martins Filho, W. L.; Berquo, T. S. *Chem. Mater.* **2004**, *16*, 1906.
251. Mathur, S.; Shen, H.; Rapalaviciute, R.; Kareiva, A.; Donia, N. *J. Mater. Chem.* **2004**, *14*, 1.
252. Mathur, S.; Shen, H. *J. Phys. IV* **2002**, *12*, Pr4–1.
253. Music, S.; Popovic, S.; Czakonagy, I.; Gashi, F. *Mater. Sci. Lett.* **1993**, *12*, 869.
254. Mathur, S.; Shen, H.; Lecerf, N.; Fjellvag, H.; Goya, G. F. *Adv. Mater.* **2002**, *14*, 1405.
255. Kominami, H.; Inoue, H. *J. Am. Ceram. Soc.* **2002**, *85*, 2148.
256. Traversa, E.; Sakamoto, M.; Sadaoka, Y. *J. Am. Ceram. Soc.* **1996**, *79*, 1401.
257. Aono, H.; Sato, M.; Traversa, E.; Sakamoto, M.; Sadaoka, Y. *J. Am. Ceram. Soc.* **2001**, *84*, 341.
258. Diaz-Guemes, M. I.; Carreno, T. G.; Serna, C. J.; Palacios, J. M. *J. Mater. Sci.* **1989**, *24*, 1011.
259. Mazdiyasni, K. S.; Dolloff, R. T.; Smith, J. S., II. *J. Am. Ceram. Soc.* **1969**, *52*, 523.
260. Lemoine, C.; Gilbert, B.; Michaux, B.; Pirard, J.-P.; Lecloux, A. J. *J. Non-Cryst. Sol.* **1994**, *175*, 1.
261. Pastor, R. C. *Mater. Res. Bull.* **1986**, *21*, 761.
262. Caulton, K. G.; Hubert-Pfalzgraf, L. G. *Chem. Rev.* **1990**, *90*, 969.
263. Hubert-Pfalzgraf, L. G. *Polyhedron* **1994**, *13*, 1181.
264. Easom, K. A.; Klabunde, K. J.; Sorensen, C. M. *Polyhedron* **1994**, *13*, 1197.
265. Veith, M.; Mathur, S.; Lecerf, N.; Huch, V.; Decker, T. *J. Sol-Gel Sci. Techn.* **2000**, *15*, 145.
266. Chae, H. K.; Payne, D. A.; Xu, Z.; Ma, L. *Chem. Mater.* **1994**, *6*, 1589.
267. Hubert-Pfalzgraf, L. G.; Daniele, S.; Papiernik, R.; Massiani, M. C.; Septe, B.; Vaissermann, J.; Daran, J. C. *J. Mater. Chem.* **1997**, *7*, 753.
268. Gaskins, B. C.; Lannutti, J. J. *J. Mater. Res.* **1996**, *11*, 1953.
269. Jones, A. C.; Davies, H. O.; Leedham, T. J.; Wright, P. J.; Crobie, M. J.; Steiner, A.; Bickley, J. F.; O'Brien, P.; White, A. J. P.; Wiliams, D. J. *J. Mater. Chem.* **2001**, *11*, 544.
269a. Crosbie, M. J.; Wright, P. J.; Davies, H. O.; Jones, A. C.; Leedham, T. J.; O'Brien, P.; Critchlow, G. W. *Chem. Vap. Deposition* **1999**, *5*, 9.
270. de Groot, C. H.; Moodera, J. S. *J. Appl. Phys.* **2001**, *89*, 4336.
271. Banger, K. K.; Harris, J. D.; Cowen, J. E.; Hepp, A. F. *Thin Solid Films* **2002**, *403–404*, 390.
272. Banger, K. K.; Cowen, J.; Hepp, A. F. *Chem. Mater.* **2001**, *13*, 3827.
273. Vel, L.; Demazeau, G.; Etourneau, J. *Mater. Sci. Eng.* **1991**, *10*, 149.
274. Hegemann, D.; Riedel, R.; Dressler, W.; Oehr, C.; Schindler, B.; Brunner, H. *Chem. Vap. Deposition* **1997**, *3*, 257.
275. Iwamoto, Y.; Volger, W.; Kroke, E.; Riedel, R.; Saitou, T.; Matsunaga, K. *J. Am. Ceram. Soc.* **2001**, *84*, 2170.
276. Kadokura, H.; Okuhara, Y.; Mitsuya, M.; Funakubo, H. *Chem. Vap. Deposition* **2000**, *6*, 225.
277. Amanuma, K.; Hase, T.; Miyasaka, Y. *Appl. Phys. Lett.* **1995**, *66*, 221.
278. Kim, Y.; Chae, H. K.; Lee, K. S.; Lee, W. I. *J. Mater. Chem.* **1998**, *8*, 2317.
279. Chen, C. T.; Li, T.; Zhang, X.; Desu, S. B. *J. Mater. Res.* **1997**, *12*, 1569.
280. Baldus, H. P.; Jansen, M.; Wagner, O. *Key Eng. Mater.* **1994**, *88–91*, 75.
281. Baldus, H. P.; Jansen, M. *Angew. Chem.* **1997**, *109*, 338.
282. Jüngermann, H.; Jansen, M. *Materialwiss. Werkst.* **1998**, *29*, 573.
283. Jalowiecki, A.; Bill, J.; Aldinger, F.; Mayer, J. *Composites Part A* **1996**, *27A*, 717.
284. Mayer, J.; Szabo, D. V.; Rühle, M.; Seher, M.; Riedel, R. *J. Eur. Ceram. Soc.* **1995**, *15*, 717.

12.03 Organometallic Derived Metals, Colloids, and Nanoparticles

B Chaudret and K Philippot, CNRS, Toulouse, France

12.03.1 Introduction

The recent period has evidenced an ever increasing interest for chemical species of nanometric size.[1,1a–9] This size corresponds to proteins, to organic macromolecules such as polymers or dendrimers, or to relatively small molecules which self-organize into different sorts of objects such as micelles or vesicles. Inorganic molecular clusters[10] may also reach this size and display interesting physical properties.[11] Inorganic nanoparticles are in this respect of special interest due to the many properties of these objects which may be exploited for practical applications. Thus, metal, metal oxide, or various metal-based compounds (e.g., quantum dots) display optical, magnetic, electronic and catalytic properties, which find applications in topics as diverse as catalysis and other chemical processes, biology, microelectronics, or nanoelectronics.

Many methods to produce in solution particles of pure metal, metal oxides, or, more generally, chalcogenides have been reported in the literature, especially during the past few years.[1,1a] The interest in the physical and chemical properties of these objects raises a question concerning the control of the particle monodispersity. Thus, since the properties of these nano-objects are in general size dependent, it is essential to be able to find a means to control the particles' size and shape in order to reach a monodisperse assembly of particles having the desired property. This is, for example, crucial for the luminescence of the quantum dots. In addition, depending on the use of the particles, it is important to control organization in order to be able to address the particles in selected devices. Finally, a large

proportion of the atoms present in a nanoparticle are surface atoms; therefore, the chemical and physical properties of the nanoparticles will be strongly influenced by the nature of the surface species. It is then essential to first gain knowledge on the nature and amount of the chemical species present at their surface and to control these surface species. In this respect, the well-known reduction methods[12–15] display limitations due to their lack of variability. The use of reverse micelles as "nanoreactors" inside which salt reduction and particle growth occur has allowed to obtain monodisperse nano-objects which may display a defined shape (spheres, rods, wires) and which may self-assemble on various substrates.[16,17] In these processes, salt and water are always in contact with the surface of the particles, thus passivating them, modifying their reactivity, and, in some cases, leading to the production of oxides or hydroxides.

The use of an organometallic precursor, able to decompose either spontaneously or in the presence of a reducing gas, has appeared as a valuable alternative for the synthesis of nanosized objects.[18–20] Such organometallic precursors have been used as material precursors in high-temperature decomposition processes, for example, in chemical-vapor deposition (CVD) or deposition onto inorganic support to produce heterogeneous catalysts.[21,22]

Two main advantages can be foreseen when using organometallic precursors:

(i) The metal is pre-reduced, either in a low oxidation state (preferably zerovalent) or in a formal oxidation state, which nevertheless corresponds to a net reduction of the metal (e.g., linked to hydride or alkyl ligands).
(ii) The displacement of suitable organic ligands in mild conditions should afford a surface not containing contaminants detrimental for the chemical or physical properties of the resulting nano-objects.

The first point has led to consider carbonyl complexes as precursors for metal nanoparticles. Such compounds have been previously widely used as precursors of metals in MOCVD for the deposition of films or nanoparticles. They may be decomposed thermally in solution to produce fine powders or metal nanoparticles but generally at high temperature. They may also be decomposed by other techniques, namely, UV irradiation or sonolysis. In order to be able to obtain a better control of the size and size distribution of the particles as well as to obtain clean surfaces for undertaking a reproducible chemistry, an alternative approach may be developed, based on the use of organometallic precursors able to decompose in mild conditions, generally using a reducing gas. The ideal precursor is an organometallic complex containing ligands, preferentially alkyl groups, olefins, or polyolefins, able either to be hydrogenated to give a bare metal atom which would condense in the reaction medium or to be substituted by CO to give an unstable intermediate.

Both approaches have been developed in the recent years and both have led to interesting results. The thermolysis of carbonyl precursors has been largely employed for the preparation of nanoparticles of interest in physics and material science, whereas the use of somewhat more sophisticated precursors has interested mainly the field of catalysis.

We will hereafter separate these two approaches. The first section concerns the decomposition of carbonyl precursors for the synthesis of metal and metal oxide nanoparticles. In the second section, we will present results concerning the use of hydrocarbyl precursors, similarly for the synthesis of metal and metal oxide particles. We also mention in this chapter the preparation of other compounds of nanometric size (e.g., chalcogenides) using organometallics.

12.03.2 Synthesis of Nanoparticles from Carbonyl Metal Complexes

Metal carbonyls are commercially available and easily handled precursors which may be readily decomposed thermally. They have been used for a long time for the preparation of magnetic colloids of cobalt and iron and for the preparation of supported catalysts through various procedures, the thermolysis being the most common one. They have attracted a renewed interest, in particular following the search for new magnetic materials pertinent for information storage, which has stimulated the synthesis of magnetic nanoparticles displaying a large anisotropy and blocked at room temperature.

12.03.2.1 Synthesis through Thermolysis

12.03.2.1.1 Monometallic compounds

An early report by Hess and Parker in 1966 has demonstrated the possibility to obtain magnetic cobalt nanoparticles through refluxing $Co_2(CO)_8$ in a solvent, typically toluene, in the presence of various polymers (polyether, polyesters, etc.). Nanoparticles of size varying from 1 to 100 nm could be obtained in this way (Figure 1).[23] At the same time,

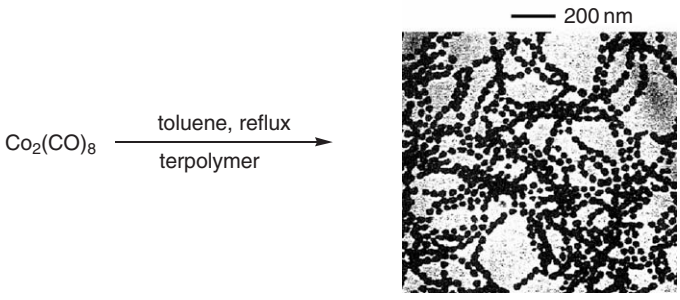

Figure 1 Schematic synthesis of Co nanoparticles from $Co_2(CO)_8$ in a polymer matrix. Reproduced with permission from Wiley.

Thomas reported a very similar study (decomposition of $Co_2(CO)_8$ in a hydrocarbon in the presence of a terpolymer), which resulted in the formation of nanoparticles of 2–30 nm according to the reaction conditions. The author was particularly interested in the modification of the magnetic properties due to dipolar couplings as a function of the separation of the particles.[24] Similar procedures are still used for the production of cobalt particles in organic matrices. For example, a recent paper reports thermolysis reactions of $Co_2(CO)_8$ in a block co-polymer, PS_{25300}-*b*-MMA_{25900}, hence producing cobalt nanoparticles embedded in the poly(methylmethacrylate) (PMMA) blocks.[25]

A comparable study was carried out in 1979 using $Fe(CO)_5$ as a precursor. The decomposition temperature was adjusted near 150 °C, and the polymers used vary from polybutadiene to various co-polymers. Iron nanoparticles of size between 5 and 20 nm were obtained according to the reaction conditions. The particles of mean diameter below 10 nm are well dispersed and superparamagnetic at room temperature, whereas the larger ones are agglomerated into chains of particles which are blocked at room temperature, hence indicating the presence of dipolar couplings between the particles. The particles were found very sensitive to oxidation when exposed to air or water.[26] A procedure also involving thermolysis of $Fe(CO)_5$ carried out in the presence of polymeric dispersants was recently used to prepare magnetic nanocomposites consisting of an iron core of 8–20 nm size and an organic shell of 1–4 nm thickness.[27]

A renewed interest for the use of carbonyl precursors has recently appeared with the search for self-assembled ferromagnetic nanomaterials usable in applications such as high-density information storage. For this purpose, a number of groups have adapted procedures and reaction media previously used for the synthesis of III–V or II–VI quantum dots (see Section 12.03.3.3.3) to prepare magnetic nanoparticles, in general of cobalt and iron–platinum alloy. Thus, thermolysis at 110 °C of $Co_2(CO)_8$ in a toluene solution, in the presence of trioctylphosphine oxide (TOPO), leads to cobalt nanoparticles adopting a new ε-cobalt phase resembling the β-phase of manganese. The nanoparticles adopting this new phase display a saturation magnetization close to that of bulk cobalt and transform into a fcc structure upon heating at 500 °C.[28] This cobalt phase was also obtained simultaneously by Sun and Murray using the inorganic precursor $CoCl_2$[29] and is related to the polytetrahedral phase previously described for small cobalt particles (*vide infra*). These studies induced a lot of research on the decomposition of carbonyl precursors through high-temperature processes for the preparation of magnetic particles. Rapid thermolysis at high temperature (181 °C) of $Co_2(CO)_8$ in the presence of various organic molecules containing long alkyl chains and able to act as surfactants or ligands, such as oleic acid and TOPO, allows the production of monodisperse spherical nanocrystals in the 3–17 nm range adopting the same ε-cobalt.[30] When a mixture of surfactants/ligands is employed, namely, oleic acid and TOPO, anisotropic nano-objects, initially thought to be in nanorods form,[31] were shown to consist of ferromagnetic nanodisks, which self-assemble in one dimension (Figure 2).[32] Interestingly, cobalt nanoparticles prepared in a very similar way from $Co_2(CO)_8$, oleic acid, and trioctylphosphine (TOP) in refluxing dioctylether were shown to be highly active catalysts for the Pauson–Khand reaction. Furthermore, the colloidal catalyst could be recycled five times without loss of activity.[33] Assembly of magnetically coupled cobalt nanoparticles into rings was achieved using a synthetic procedure involving the decomposition of $Co_2(CO)_8$ in the presence of resorcinarene tetraphosphonite.[34]

Similarly, the decomposition of $Fe(CO)_5$ by thermolysis produces metal nanoparticles, the size and shape of which may be controlled by the surrounding medium. For example, a fairly complex procedure was employed for the fabrication of nanorods. Small iron nanospheres are first prepared by thermolysis of $Fe(CO)_5$ in the presence of TOPO. Addition of this solution to excess $Fe(CO)_5$ in TOP at 320 °C leads to the production of nanorods

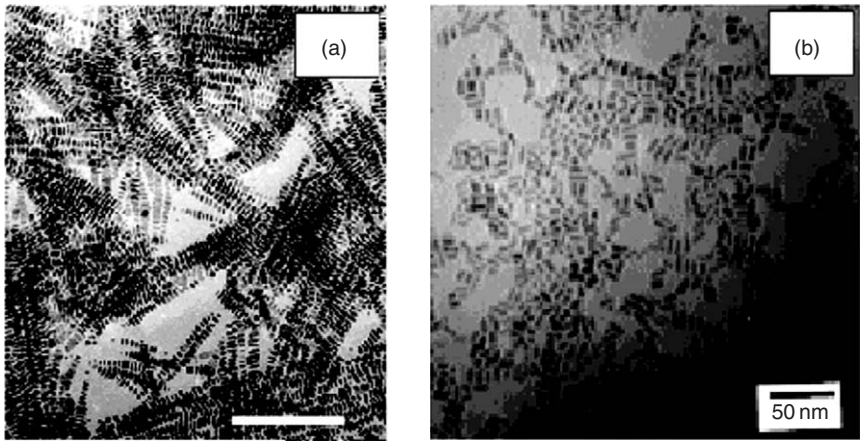

Figure 2 TEM micrographs of (a) hcp-Co self-assembled nanodisks (bar = 100 nm) and (b) Fe nanorods respectively obtained by thermolysis of cobalt and iron carbonyl complexes.[32,35] Reproduced with permission from ACS Publications.

(Figure 2(b)).[35] Fe nanoparticles were also prepared by decomposition of $Fe(CO)_5$ in the presence of surfactants (oleic acid and oleyl amine). The monodispersity of the particles was achieved in this case either using platinum acetylacetonate ($Pt(acac)_2$ with acac = $(CH_3CO)_2CH$)) as heterogeneous nucleation agent or a supersaturation of $Fe(CO)_5$.[36]

12.03.2.1.2 Bi- and trimetallic compounds

This procedure has recently been extended to the preparation of bi- and even trimetallic nanoparticles. Thus, nanoparticles of FePt were synthesized through reduction of $Pt(acac)_2$ in the presence of 1,2 hexadecanediol, followed by addition of $Fe(CO)_5$ in the presence of oleic acid and oleyl amine and reflux at 297 °C.[37] Exchange of ligands was performed on the as-synthesized product to give nanocrystal superlattices, which, after annealing at 560 °C, transformed into assemblies of ferromagnetic nanocrystals displaying the "hard" tetragonal phase, and on which recording studies could be carried out.[38] This work opened the door to an extensive search for nanoparticles of hard magnetic phases able at recording information and to the modification of these particles for various purposes. For example, the FePt particles were made water soluble through removal of the oleic acid and oleyl amine ligands and replacement by tetramethylammonium hydroxide, hence producing a new ferrofluid in aqueous solution.[39] Colloidal $CoPt_3$ nanoparticles were prepared from $Co_2(CO)_8$ and $Pt(acac)_2$. The control of the reaction conditions allows variation of the particles' mean size from 1.5 to 7.2 nm. Alloy-type and core-shell Co–Pt nanoparticles were obtained, respectively, upon mixing $Co_2(CO)_8$ and $Pt(hfacac)_2$, or upon decomposing first the cobalt precursor and adding the nanoparticles to the platinum complex.[40] A similar synthesis was used to produce $CoPt_3$ nanoparticles of size precisely controlled between 3 and 18 nm. This method uses $Co_2(CO)_8$ and $Pt(acac)_2$ as precursors and involves injection of the cobalt solution into a platinum solution preheated at a temperature varying from 140 to 220 °C in the presence of hexadecylamine and 1-adamantane carboxylic acid as stabilizers.[41] The authors conclude that the size control is of purely kinetic nature. The increase in stabilizers leads to an increase in the particle size as a result of the slower rate of nucleation. Whereas the small particles all display a spherical shape, the control on the reaction conditions also leads to a shape control, larger particles initially adopting a cubic shape.[42] Both Fe–Pt and Co–Pt nanoparticles were assembled into three-dimensional (3-D) superlattices by a technique of three-layer oversaturation derived from methods traditionally used for the crystallization of molecular species. In this case, the colloidal solution is separated from a non-solvent by a buffer layer. Slow diffusion of the different solutions leads to a reduced solubility of the nanoparticles, and hence slow crystallization. Faceted supercrystals were obtained in this way (Figure 3).[43,44]

Fe–Pd and Co–Pt nanoparticles were prepared by thermal decomposition of carbonyl precursors, $Co(NO)(CO)_3$ or $Fe(CO)_5$, in the presence of an acetylacetonate of, respectively, platinum and palladium, and using oleic acid and oleylamine as ligands. Only annealing after 3 h at 700 °C did the Co–Pt films, obtained after deposition of the particles on a silicon wafer, transform into the hard tetragonal phase. In the case of Fe–Pd, no such transformation occurred up to 700 °C.[45] Monodisperse Fe–Pd nanoparticles of size ranging from 11 to 16 nm were prepared through a similar procedure, but using adamantic tetracarboxylic acid and hexadecylamine as ligands. This illustrates the role of the ligand structure in the size and dispersity control.[46]

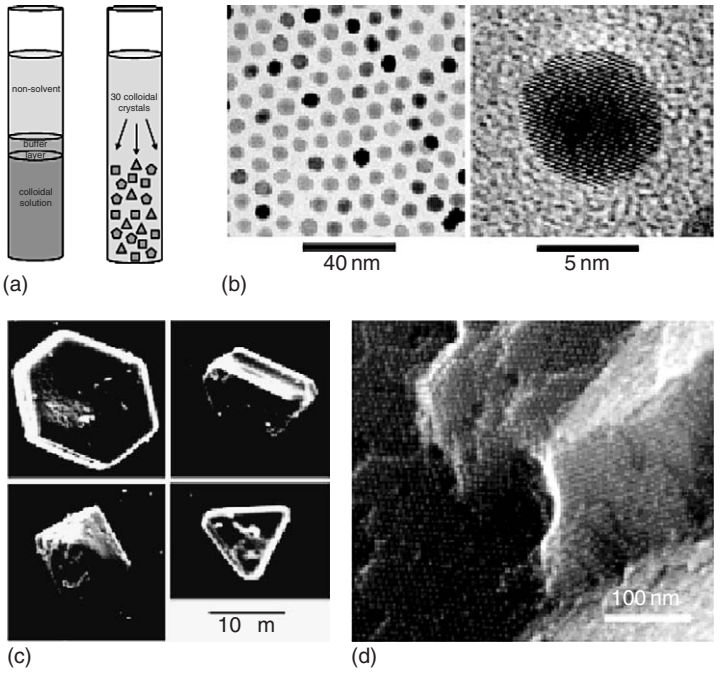

Figure 3 (a) Schematic illustration of the oversaturation technique followed for the crystallization of FePt and $CoPt_3$ nanoparticles, (b) TEM and HRTEM micrographs of 6.3 nm $CoPt_3$ nanoparticles prepared at 170 °C and annealed at 280 °C for 1 h, (c) SEM images of colloidal crystals of $CoPt_3$ nanoparticles illustrating the different shapes obtained, and (d) HRSEM image demonstrating the ordering of 6.3 nm $CoPt_3$ nanocrystals onto the surface of a colloidal crystal.[42,43] Reproduced with permission from Wiley.

Core-shell Co–Pt particles of low size dispersity were synthesized by a two-stage route upon decomposing $Co_2(CO)_8$ on preformed Pt nanoparticles. The thickness of the Co shell can be controlled by changing the amount of cobalt carbonyl.[47] The same authors obtained well-dispersed core-shell fcc Ag–Co particles upon decomposing $Co_2(CO)_8$ by $AgClO_4$ in toluene at 140 °C in the presence of oleic acid and tridodecylamine.[48]

More exotic magnetic phases could also be produced by similar procedures. For example, MnPt nanoparticles were obtained through decomposition of $Mn_2(CO)_{10}$ and $Pt(acac)_2$ in the presence of oleic acid and oleyl amine. The 3 nm particles adopt a crystalline fcc structure and display a ferromagnetic behavior up to room temperature.[49]

Trimetallic particles may also be obtained by this route. Thus Nikles reported the preparation of Fe–Co–Pt nanoparticles using a procedure similar to those used for the synthesis of Fe–Pt nanoparticles but upon mixing an additional cobalt precursor. Several compositions were obtained, and the particles were shown to self-assemble upon removal of the solvent (Figure 4).[50] In a similar way, Fe–Pt–Cu particles could be obtained starting upon adding

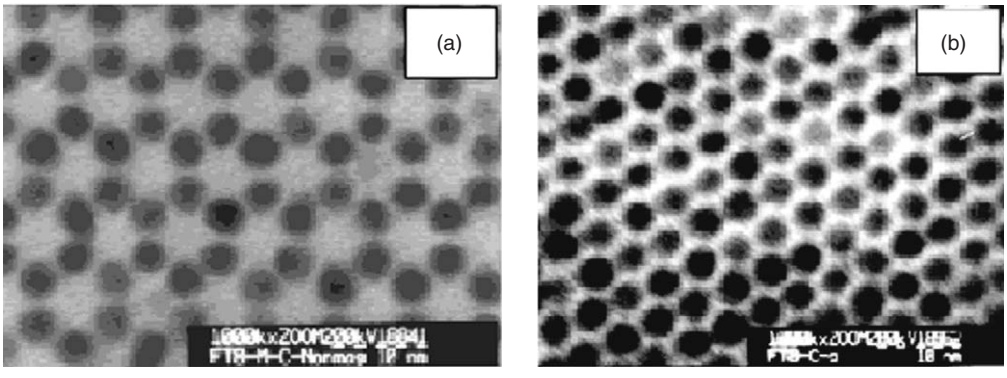

Figure 4 TEM images of (a) a thin film and (b) a thick film of self-assembled $Fe_{49}Co_7Pt_{44}$ nanoparticles.[50] Reproduced with permission from ACS Publications.

$Fe(CO)_5$ on a mixture of platinum and copper acetylacetonates in the presence of oleic acid and oleyl amine. The particles organize into both cubic close-packed and honeycomb superstructures.[51]

12.03.2.1.3 Metal oxide compounds

The use of carbonyl precursors may also lead to the preparation of oxides. Highly crystalline and monodisperse maghemite nanoparticles were hence obtained by a procedure totally similar to that employed for the preparation of Fe nanoparticles (high-temperature decomposition of $Fe(CO)_5$ in the presence of oleic acid and oleyl amine), but upon adding an organic oxidant: trimethylamine-*N*-oxide. Particles of different sizes (4, 7, and 13 nm) could be isolated depending upon the reaction conditions.[52] This procedure was extended to cobalt ferrite, $CoFe_2O_4$, using a bimetallic precursor, namely, $CpCoFe_2(CO)_9$. The particles adopt the expected cubic spinel structure and display sizes between 4 and 9 nm (Figure 5).[53] The kinetics of the various steps of formation of cobalt oxide nanoparticles in solution in the presence of PMMA, namely, nucleation, growth, and stabilization, were studied by Tannenbaum *et al*.[54] Finally, more unexpectedly, the same procedure allows the formation of tungsten oxide nanorods of length varying as a function of the reaction temperature upon decomposing $W(CO)_6$ in the presence of oleylamine and trimethylamine-*N*-oxide. Typical rod sizes were 4–5 nm diameter and between 25 and 130 nm length.[55] Heating a *tert*-amylalcohol solution of the complex $Mo(CO)_6$ at 120 °C leads to the synthesis of lamellar molybdenum oxide nanoparticles.[56]

12.03.2.1.4 Other metal compounds

Other compounds can be prepared in the same way. For example, iron phosphide nanorods and nanowires form in a reaction mixture at 300 °C containing both TOP and TOPO. The nanorods of Fe_2P display diameters of ca. 5 nm and aspect ratios may be higher than 200.[57]

12.03.2.2 Synthesis through Methods Other than Thermolysis

Other methods have been used for the decomposition of carbonyl precursors. For example, an early report on nickel particles' preparation through UV irradiation of $Ni(CO)_4$ was published by Tanner *et al*. Triangular particles of ca. 6 nm mean size were produced in this way.[58] Similarly, the irradiation of a solution of the carbonyl polyoxoanion rhodium complex $[Rh(CO)_2{\cdot}P_2W_{15}Nb_3O_{62}]^{8-}$ in the presence of H_2 and cyclohexene involves the formation of a black precipitate containing Rh(0) nanoclusters with a size in the range 1.0–4.0 nm.[59]

As another method, sonolysis has been developed by Suslick to decompose carbonyl metal complexes into nanopowders, nanostructured materials, and nanoparticles in solution.[60] Superparamagnetic iron nanoparticles stabilized by polyvinylpyrrolidone (PVP) or oleic acid were thus obtained upon sonochemical decomposition of

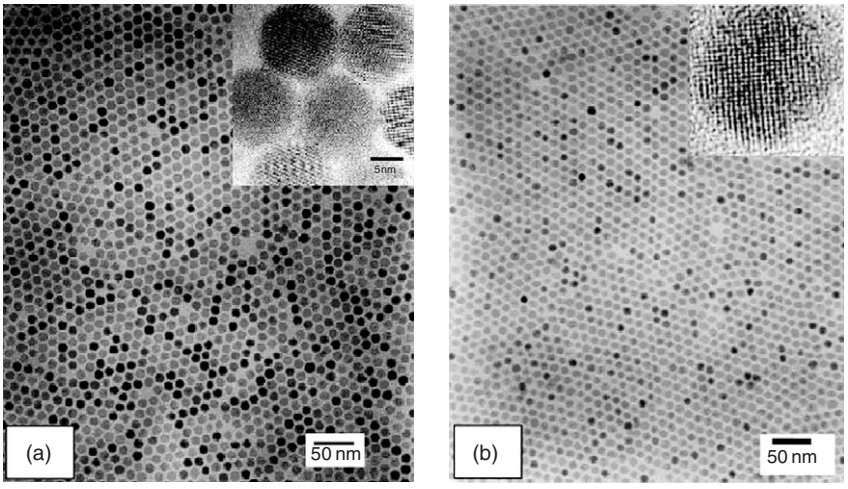

Figure 5 TEM images of 2-D hexagonal assemblies of (a) 11 nm γ-Fe_2O_3 and (b) 9 nm $CoFe_2O_4$ nanoparticles, with HRTEM images (inset).[52,53] Reproduced with permission from ACS Publications.

$Fe(CO)_5$.[61] Sonolysis was also used in our group to prepare iron nanoparticles stabilized by polydimethylphenylene oxide (PPO). The particles were found to be superparamagnetic and to adopt, depending on their size, the α (bcc) or the γ (fcc) structure.[62] This method was extended to other precursors such as $Co(NO)(CO)_3$, recently used by Gedanken to produce cobalt particles.[63]

Finally, laser pyrolysis of $Fe(CO)_5$ produces partially or fully oxidized Fe nanoparticles of 20 nm mean diameter using an infrared laser in mixtures containing SF_6.[64] A similar procedure carried out in isopropanol produced 5 nm nanoparticles of γ-Fe_2O_3.[65]

12.03.3 Synthesis of Metal Nanoparticles from Hydrocarbyl Complexes

Another organometallic approach has been developed in parallel for the past 15 years. It takes profit of the intrinsic reactivity of the metal complexes toward ligand displacement or ligand reduction.[18,19] In this case, the reactions may take place in very mild conditions (room temperature or below), and a rigorous control of the surface species may be achieved. The ideal precursor is an organometallic complex containing an olefinic or polyolefinic ligand, able either to be hydrogenated to give a bare metal atom which would condense in the reaction medium or to be substituted by CO to give an unstable intermediate. Prototypes of such complexes are $Ru(\eta^6\text{-}C_8H_{10})(\eta^4\text{-}C_8H_{12})$ and $Ni(\eta^4\text{-}C_8H_{12})_2$, which decompose satisfactorily under dihydrogen in mild conditions (Scheme 1). Complexes accommodating alkyl, allylic, or cyclopentadienyl groups may also decompose easily, for example, $PtMe_2(C_8H_{12})$, $Co(C_8H_{13})(C_8H_{12})$, $Rh(C_3H_5)_3CpCu^tBuNC$, or $CpIr(C_8H_{12})$. More complex structures may however be used when such olefinic precursors are not available or difficult to obtain. For example, $M(dba)_2$ (dba = dibenzylidene acetone; M = Pd, Pt) is a good precursor for the preparation of nanoparticles of Pd or Pt after treatment with dihydrogen or carbon monoxide. Mixed complexes such as $Rh(acac)(C_8H_{12})$ (acac = $(CH_3CO)_2CH$) also decompose in mild conditions but release potential ligands of the particles, namely, acacH or the corresponding diol, after hydrogenation, which may or may not perturb the surface.

For clarity, the results obtained on noble metals, magnetic metals, and other metals, and main group elements will be reported separately. The chosen examples will allow the presentation of the different stabilization modes that can be used with this method to get well-defined nanoparticles.

12.03.3.1 Organometallic Synthesis of Noble Metal Nanoparticles

12.03.3.1.1 Stabilization by polymers

$Ru(\eta^6\text{-}C_8H_{10})(\eta^4\text{-}C_8H_{12})$ reacts rapidly with dihydrogen (1–3 atm) at room temperature in a hydrocarbon solvent to give ruthenium particles and cyclooctane.[66] In the presence of a polymer (PVP; nitrocellulose, NC; cellulose acetate, CA), the reaction produces particles, the size of which depends upon the nature of the polymer and upon the relative concentration of the precursor in the polymer. In this way, monodisperse particles of 1 to 1.5 nm mean size have been

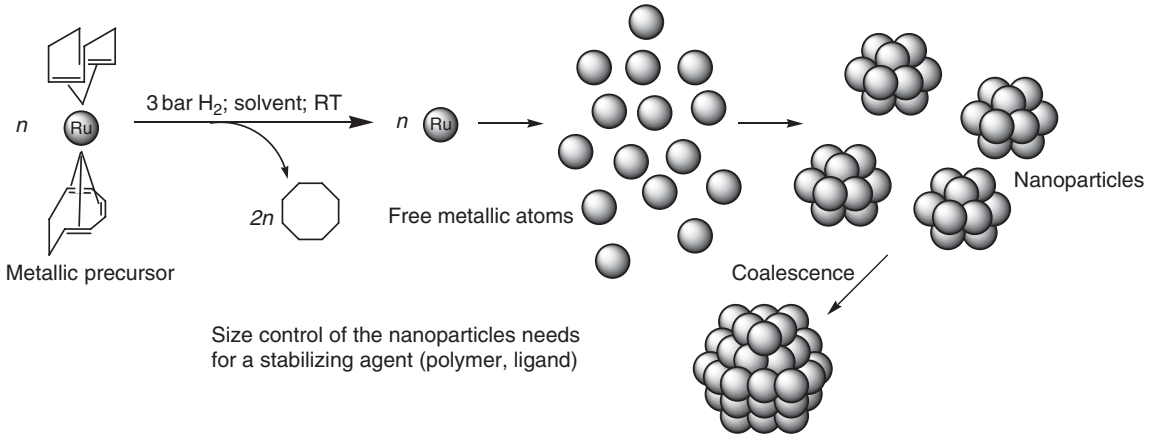

Scheme 1 Schematic representation of the organometallic approach for the synthesis of metal nanoparticles from $Ru(C_8H_{10})(C_8H_{12})$.

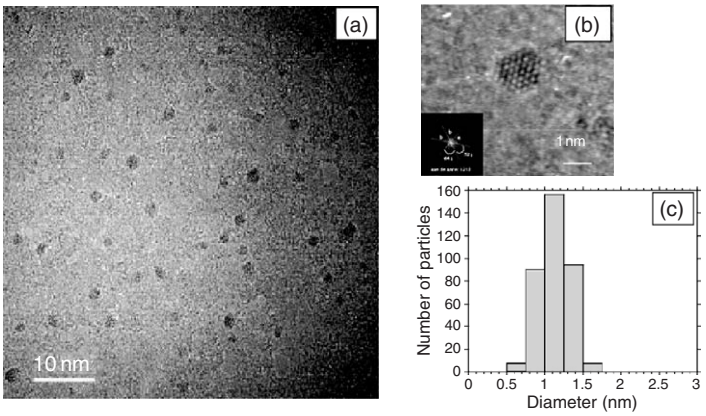

Figure 6 (a) TEM micrograph, (b) HREM micrograph showing a well-crystallized particle, and (c) size histogram (mean size ca. 1.1 nm) of Ru nanoparticles embedded in PVP. Reproduced with permission from ACS Publications.

prepared in PVP or NC. In both cases, the particles display very low size dispersity. In contrast, the reaction in CA produces larger particles, displaying a broader size dispersity, which evidences the influence of the nature of the polymer and of its coordination ability on the stabilization of the particles. The particles in PVP were analyzed by transmission electron microscopy (TEM) and HREM (Figures 6(a) and 6(b)) and WAXS.[67] The particles adopt the hcp structure of bulk ruthenium. An interesting effect of the size reduction on the crystal lattice has been evidenced. A contraction of 1.1% in the metal–metal distance (0.266 nm, 0.27058 in the bulk) is observed together with a relaxation of the *c* parameter (0.436 nm, 0.42811 in the bulk), which leads to a c/a ratio of 1.633, close to the ideal one, instead of 1.582 in bulk ruthenium.

Palladium nanoparticles can be easily prepared by displacement of the dba ligands by CO from $Pd(dba)_2$. An intermediate unstable carbonyl complex forms, which collapses into clusters. By this method, palladium nanoparticles of sizes in the range 2–5 nm could be obtained using PVP[68] or cellulose derivatives[69] as stabilizers. Such particles were recently used to probe the mechanism of the Heck reaction. A correlation between the initial reaction rate and the particle sizes was established. The small particles proved more active in agreement with the presence of more surface palladium atoms with low metal–metal coordination number.[70]

In a very similar way, platinum particles were prepared by displacement of dba by CO from $Pt(dba)_2$. In this case, if the reaction is carried out in THF, no stabilizer is necessary and stable particles of ca. 1.5 nm form in solution.[71]

The particles adopt the fcc structure of platinum, in the case of particles prepared in the presence of PVP, with a contraction of the Pt–Pt distance of 1.2% (0.274 nm) compared to the bulk. These lattice effects are similar to what may be observed in high vacuum and evidence the lack of stress experienced by the particles in these media.[72] The structure of the surface of such Pt particles was investigated by infrared spectroscopy of adsorbed CO (Figure 7).[73] The presence of vibrational couplings between CO groups attached to a face of the particles was evidenced. This experiment shows the similarity between the particles prepared in organic solutions and the clean metal surfaces in ultrahigh vacuum (UHV).[74] PVP-coated particles of this type were embedded into an amorphous microporous titania–silica mixed oxide by means of a modified sol–gel procedure. The resulting material was found to be more selective than both the PVP-coated nanoparticles in solution and platinum particles on the mixed oxide without polymer for the hydrogenation of 2-hexyne into *cis*-2-hexene.[75]

Co-decomposition of $Ru(\eta^6\text{-}C_8H_{10})(\eta^4\text{-}C_8H_{12})$ and $Pt(dba)_2$ leads to the formation of bimetallic Ru_x–Pt_{1-x} particles.[76] Platinum-rich particles are fcc, whereas ruthenium-rich ones are hcp. There is a critical composition Ru_3-Pt, for which most of the particles are twinned. In this case, the particles are monodisperse and very small (1.1 nm). This composition corresponds roughly to the limit of solubility of ruthenium in the platinum lattice for bulk alloys. The particles adopt a twinned fcc structure with the twinning wall lying in a (111) plane located in the middle of the particle. The homogeneity in the size and shape of the twinned particles suggests a well-defined atomic organization, namely, a twinned truncated octahedron for the particles which can also be described as well-defined clusters.

Palladium and platinum nanoparticles may be prepared in a block co-polymer. The complexes Pd[*endo*-2-(cyclopentadienylmethyl)norborn-5-ene](1-phenylallyl) and $PtMe_3$[*endo*-2-(cyclopentadienylmethyl)norborn-5-ene] are dispersed in the matrix by ring-opening metathesis polymerization using W or Mo alkylidene catalysts.

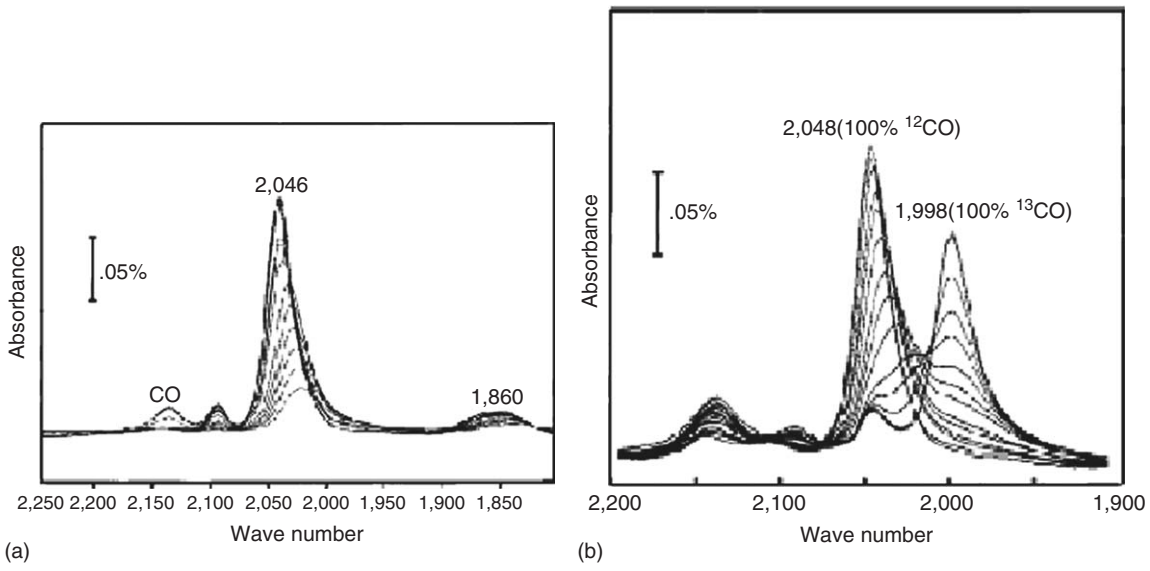

Figure 7 Infrared spectra of (a) CO and of (b) $^{13}CO/^{12}CO$ adsorbed on 1.5 nm Pt/PVP in dichloromethane.[74] Reproduced with permission from ACS Publications.

Subsequent reduction of the metal complexes in the solid polymer affords the metal particles. The result is the selective concentration of the nanoparticles in selected areas.[77]

These organometallic precursors may also be decomposed in harsher conditions. Thus, $Pd_2(dba)_2$ is transformed by ultrasound irradiation into agglomerated clusters of ca. 80 nm containing nanosized particles. This material was found catalytically active for Heck coupling reaction.[78]

12.03.3.1.2 Stabilization by ligands

The decomposition of $Ru(\eta^6\text{-}C_8H_{10})(\eta^4\text{-}C_8H_{12})$ by dihydrogen (1–3 atm) previously mentioned can occur in the presence of various ligands: long-chain thiols or amines, phosphines, oxazolines, alcohols, silanes. In the presence of thiols or amines,[67] hcp particles of 2–3 nm mean size form, which display a low size dispersity. The ^1H and ^{13}C NMR spectra of octanethiol-protected ruthenium particles point to the absence of exchange between free and coordinated ligands at the NMR timescale. In this case, it is possible to observe by ^{13}C NMR the carbon atoms of the alkyl chain of the coordinated ligand as broad peaks except for the carbons located in the α-and β-positions relative to sulfur which are too broad to be observed.

In the case of the particles accommodating amine ligands, a new phenomenon has been evidenced, namely, a dynamic exchange at the NMR timescale between free and coordinated amines. It has been correlated to the TEM and HREM results, which show that, at the early stage of the reaction, the particles display a spherical aspect and a small size (ca. 2–3 nm), and that after a few hours, the particles coalesce into elongated wormlike particles, still constituted of pure, unoxidized hcp ruthenium. This NMR observation is particularly interesting since it evidences for these particles a fluxionality similar to that of molecular clusters, which is well documented. The ruthenium nanoparticles contain coordinated mobile surface hydrides, as recently demonstrated by a combination of NMR techniques in solution, gas phase, and in the solid state.[79]

The nature of the stabilizing ligand can be very diverse; for example, heptanol and organosilane have recently been used for the stabilization of ruthenium particles. Thus, reaction of $Ru(\eta^6\text{-}C_8H_{10})(\eta^4\text{-}C_8H_{12})$ with H_2 in heptanol[80] leads to particles of low size dispersity (3 nm), well dispersed in the solvent and adopting the hcp structure of bulk ruthenium. Using octylsilane as stabilizer, the decomposition of $Ru(\eta^6\text{-}C_8H_{10})(\eta^4\text{-}C_8H_{12})$ under H_2 produces 2.3 nm Ru nanoparticles displaying a narrow size distribution. Infrared spectroscopy and both solution and solid NMR investigations could be successfully applied to characterize the alkysilane fragments grafted on the Ru nanoparticles.[81]

Pd nanoparticles were similarly prepared through decomposition of $Pd_2(dba)_3$ under H_2 in the presence of HDA or polyphosphines as stabilizers. The influence of the ligands on the particles' shape was established: good ligands like polyphosphines lead to stable spherical nanoparticles of small size (near 2 nm) while the HDA protective effect

depends on the ligand concentration as a result of the equilibria present at the surface of the particles and monitored by solution NMR spectroscopy.[82]

$Pt(dba)_2$ reacts with CO in THF to give a colloid containing fcc particles of 1.2 nm mean size and displaying a narrow size distribution. This colloid is relatively stable and can further be used as a starting material to prepare ligand-protected platinum nanoparticles. Addition of 0.2 equiv. PPh_3 to this reaction mixture or decomposition of $Pt(dba)_2$ in the same medium in the presence of phosphine leads to phosphine-protected particles, which adopt a non-periodic icosahedral structure. Interconversion between the two colloids is possible by addition of CO on one side or of PPh_3 on the other. These species are well defined and relatively robust.[83] It may therefore be interesting to emphasize their similarity with the molecular cluster, $Pd_{145}(CO)_{60}(PEt_3)_{30}$, recently characterized by Dahl. The size of the metal core of this cluster is estimated to be of the same order of magnitude as these platinum phosphine colloids, and it is noteworthy that this Pd_{145} cluster adopts a non-periodic structure.[84]

These experimental procedures are not specific of the phosphine ligands and may be employed using more classical ligands for nanoparticles such as octanethiol.[72] In this case, a very stable colloid is formed, which may be isolated from the reaction medium and redissolved for reactivity or spectroscopic studies. The colloid contains monodisperse fcc particles of 1.6 nm mean size. WAXS studies demonstrate the strong fixation of the ligands at the surface of the particles (Figure 8). This is corroborated by solution NMR studies that, as for ruthenium, evidence the absence of exchange between free and coordinated ligands at the NMR timescale.

The strong coordination of sulfur to platinum enables the construction of "supramolecular" networks incorporating the metal particles. Thus, platinum particles of 1.6 nm mean size can be prepared using as protecting ligands thiophenols substituted in the 4-position by a hydroxo, a carboxylate, or an amino group.[85] Self-assembly of the nanoparticles is observed for the colloids stabilized by 4-HO-C_6H_4-SH or 4-HOOC-C_6H_4-SH. If a mixture containing a 1 : 1 mixture of the 4-HO-C_6H_4-SH and 4-H_2N-C_6H_4-SH is used, the particles self-organize into very long nanotubes, the walls of which are constituted by a monolayer of platinum nanoparticles (Figure 9).

Fluorinated thiols (perfluorooctanethiol, $C_6F_{13}C_2H_4SH$) were also used by Korgel and Johnston to stabilize platinum and iridium nanoparticles prepared in supercritical carbon dioxide by hydrogenation of the organometallic precursors $PtMe_2(C_8H_{12})$ and $CpIr(C_8H_{12})$ at 80 °C and 276 bar.[86] Pt and Ir nanocrystals are obtained with a mean size between 2 and 12 nm as a function of predominantly the precursor concentration (higher concentrations giving rise to larger particles). The long-chain perfluoronated thiol ligands leads to a good solubility of the nanoparticles in the environmentally benign CO_2 solvent.

The synthetic method described above is very simple and can be in principle transposed to any metal/ligand combination. One of the most challenging problems regarding the use of nanoparticles in catalysis concerns asymmetric catalysis. Only a few examples of asymmetric heterogeneous catalysis have been reported, the most popular ones based on a platinum cinchonidine system.[87–89] Using the chiral xylofuranoside diphosphite ligand, Pd nanoparticles with a

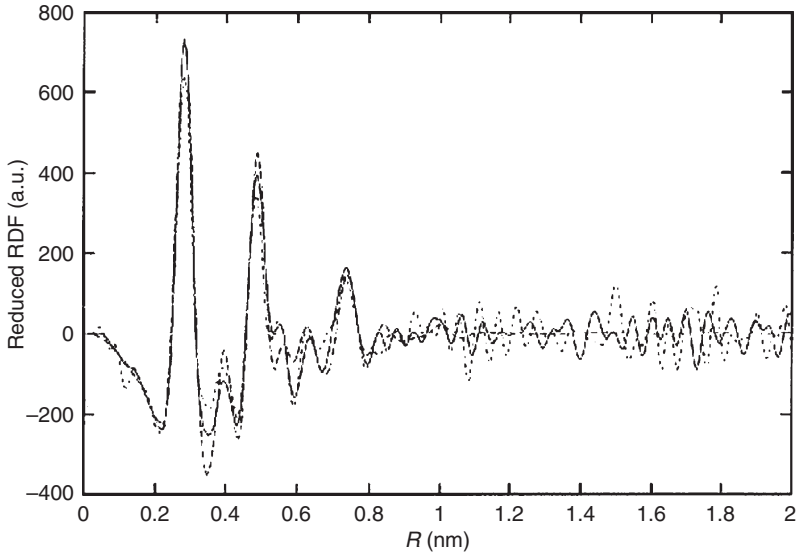

Figure 8 WAXS analysis of octanethiol-stabilized Pt colloid (solid line: experimental data; dotted line: cuboctahedral model). Reproduced with permission from the Royal Society of Chemistry.

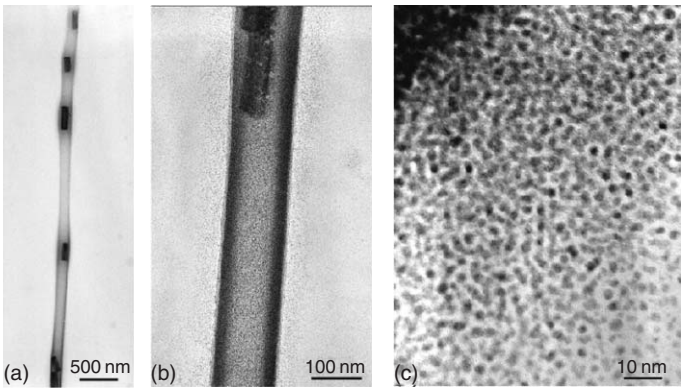

Figure 9 HREM micrographs of nanotubes resulting from the assembly of Pt nanoparticles stabilized by a 1 : 1 mixture of the 4-HO-C_6H_4-SH and 4-H_2N-C_6H_4-SH. Reproduced with permission from the Royal Society of Chemistry.

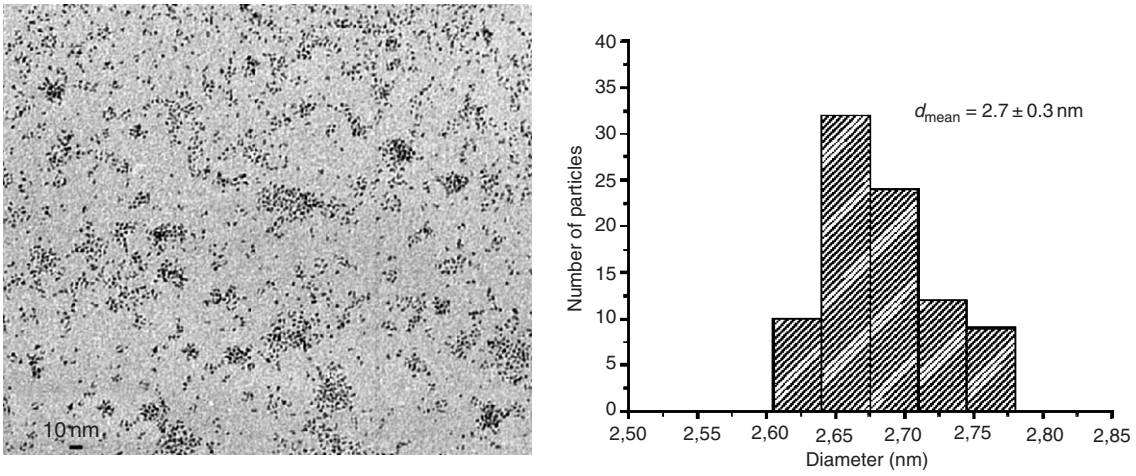

Figure 10 TEM image of oxazoline-stabilized ruthenium nanoparticles and corresponding size histogram (mean size = 2.7 nm). Reproduced with permission from the Royal Society of Chemistry.

mean size of 4 nm were synthesized which display a novel activity in enantioselective allylic alkylation of *rac*-3-acetoxy-1,3-diphenyl-1-propene with dimethylmalonate: the reaction proceeds with only one enantiomer of the substrate, hence demonstrating a very high degree of kinetic resolution.[90] Phosphine-stabilized palladium nanoparticles were also recently reported by Hyeon *et al.* through thermolysis of $Pd(acac)_2$. They compared the spectroscopic properties of the nanoparticles to those of molecular complexes prepared by substitution of dba on $Pd(dba)_2$.[91]

Asymmetric oxazolines or amino alcohols provide an excellent stabilization of platinum particles, which can be handled like molecular species. Self-organized superstructures adopting shapes of wires or of pseudo-crystals form spontaneously, probably due to ligand interactions through hydrogen bonding.[92] Very small ruthenium nanoparticles (Figure 10) containing the same ligands (1 to 2 nm according to the ligand) were used in catalytic reactions such as asymmetric hydrogenation or asymmetric hydrogen transfer, but so far lead only to poor enantioselectivity.[93]

12.03.3.1.3 Stabilization by polyoxoanions

Finke *et al.* have developed for the past 10 years an original method for nanoparticles' synthesis using organometallic cationic complexes attached to polyoxoanions as metal precursors.[94] A complete and detailed work has been performed to elucidate the mechanism of formation of the nanoclusters and to develop a general procedure to be able to distinguish "homogeneous" from "heterogeneous" catalysis. This research has been recently reviewed.[95]

Thus, iridium nanoparticles may be prepared through reduction by dihydrogen of an Ir(I) complex, $(Bu_4N)_5Na_3$-$[(1,5\text{-COD})Ir{\cdot}P_2W_{15}Nb_3O_{62}]$ (1,5-COD = 1,5-cyclooctadiene), in acetone solution and at room temperature.[96] This method allows the formation of nearly monodisperse Ir nanoclusters, which can be isolated as a powder and redissolved in acetone or acetonitrile to give a stable colloidal solution. TEM investigations revealed the presence of 3.0 ± 0.4 nm spherical nanoparticles, which were identified as cubic-close-packed (ccp) Ir(0) metal cores by EDX, whereas electrophoresis established the stabilizing role of the polyoxoanions by adsorption on the outer surface of the nanoclusters. The average chemical composition of $[Ir(0)_{\sim 900}(P_4W_{30}Nb_6O_{123}{}^{16-})_{\sim 60}](Bu_4N)_{\sim 660}Na_{\sim 300}$ has been determined.

Since Ir(0) nanoparticles had initially been observed during catalytic cyclohexene hydrogenation, the question was how to determine the exact role of these species during catalysis.[97] Extensive mechanistic studies were then performed in the catalytic conditions with $(Bu_4N)_5Na_3[(1,5\text{-COD})Ir{\cdot}P_2W_{15}Nb_3O_{62}]$ as pre-catalyst.

In order to elucidate the mechanism of the formation of the Ir(0) nanoclusters, and in particular to try to understand why the tendency is to form nanoclusters close to the well-known "magic" numbers (M_{13}, M_{55}, M_{147}, M_{309}, M_{561}, M_{923}, and M_{1415}), the authors carried out complete kinetic and mechanistic analyses of the $Ir(0)_{\sim 300}$ nanoclusters formation during cyclohexene hydrogenation.[98] The kinetic method consisted in monitoring the H_2 loss and, employing the concept of pseudo-elementary mechanistic steps, comparing the results with calculated curves according to the three following simple steps: nucleation, autocatalysis, and hydrogenation (Scheme 2).

The results have been compared to those obtained for the hydrogenation of the cyclooctadiene moiety linked to the metal precursor (a more direct way of following the Ir(0) nanoclusters formation), which gave rise to the same k_1 and k_2 rate constants. This result strongly suggests that these two experiments monitor the same process, namely $Ir(0)_n$ nanocluster formation. Finally, the proposed mechanism of the $Ir(0)_{\sim 300}$ nanoclusters formation corresponds to a slow nucleation process associated to a fast autocatalytic surface growth (Scheme 3). Ir(0) atoms are slowly and continuously generated via step II and undergo aggregation to the critical nucleus size, $Ir(0)_n$ (step III). The sum of steps I–III provides homogeneous nucleation. Each new Ir(0) atom is added to the surface of an existing $Ir(0)_n$ nanocluster (step IV), the key being that the $Ir(0)_{n+1}$ product of the reaction is also a catalyst for that reaction, thereby producing autocatalysis. The important consequence of autocatalytic surface growth is that it separates nucleation and growth in time-involving near-monodisperse ($\leq$15%) size distribution.

After verification of four important key points, namely: (i) the nanoclusters are "living metal polymers" and consequently increasing size nanoclusters can be synthesized by design; (ii) the ratio of rates of growth to nucleation, R ($= k_2$[nanocluster active sites]/k_1), should correlate with and should be useful to predict the size of new nanoclusters; (iii) the autocatalytic surface growth should tend to favor the so-called "magic number" size nanoclusters; and (iv) it should be possible to prepare a sequential series of nanoclusters centered about the transition metal magic number nanocluster sizes (M_{13}, M_{55}, M_{147}, M_{309}, M_{561}, M_{923}, etc.), the application of the mechanism-based principle

$$\text{Pre-catalyst} \xrightarrow{k_1} \text{Catalyst} \qquad \text{(a)}$$

$$\text{Pre-catalyst} + \text{Catalyst} \xrightarrow{k_2} 2\text{Catalyst} \qquad \text{(b)}$$

$$\text{Catalyst} + \text{Cyclohexene} + H_2 \xrightarrow{k_3} \text{Catalyst} + \text{Cyclohexane} \qquad \text{(c)}$$

Scheme 2 Pseudo-elementary steps of Ir nanoclusters' growth mechanism. Reproduced with permission from ACS Publications.

$$(1,5\text{-COD})Ir{\cdot}P_2W_{15}Nb_3O_{62}{}^{8-} + 2S\ (S = \text{acetone}) \rightleftharpoons Ir(1,5\text{-COD})S_x{}^{+} + P_2W_{15}Nb_3O_{62}{}^{9-} \qquad \text{(I)}$$

$$Ir(1,5\text{-COD})S_x{}^{+} + 2.5H_2 \longrightarrow C_8H_{16}\ (\text{cyclooctane}) + H^{+} + Ir(0) \qquad \text{(II)}$$

$$nIr(0) \longrightarrow Ir(0)_n \qquad \text{(III)}$$

$$(1,5\text{-COD})Ir{\cdot}P_2W_{15}Nb_3O_{62}{}^{8-} + 2.5H + Ir(0)_n \longrightarrow C_8H_{16} + Ir(0)_{n+1} + H^{+} + P_2W_{15}Nb_3O_{62}{}^{9-} \qquad \text{(IV)}$$

Scheme 3 Mechanism for the formation of Ir(0) nanoclusters: slow, continuous nucleation (steps I–III for the pseudo-elementary step A → B; rate constant k_1), followed by fast, autocatalytic surface growth (step IV; rate constant k_2).[98] Reproduced with permission from ACS Publications.

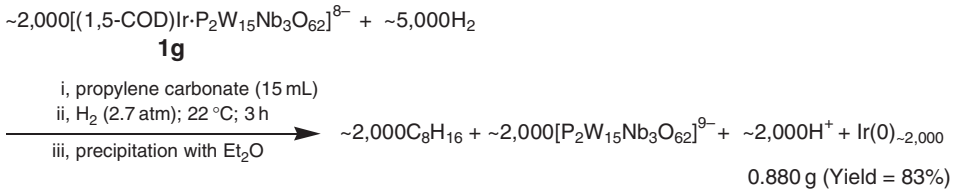

Scheme 4 Scaled-up synthesis of $Ir(0)_{\sim 2,000}$ nanoclusters (100). Reproduced with permission from ACS Publications.

of autocatalytic surface growth and the living metal polymer phenomenon has allowed the rational synthesis of a series of Ir(0) nanoclusters with average composition: $Ir(0)_{\sim 150}$, $Ir(0)_{\sim 300}$, $Ir(0)_{\sim 560}$, and $Ir(0)_{\sim 900}$.[99]

An optimized and reproducible synthesis in propylene carbonate as solvent and in the absence of olefin led to the isolation of ca. 880 mg of 3.8 ± 0.6 nm $Ir(0)_{\sim 2,000}$ nanoclusters determined as $[(Bu_4N)]_{\sim 11,000}Na_{\sim 5,000}Ir_{\sim 2,000}(P_4W_{30}Nb_6O_{123})_{\sim 1,000}(C_4H_6O_3)_{\sim 5,000}$ ($C_4H_6O_3$ = propylene carbonate; Scheme 4).[100]

The same methodology has been extended to the synthesis of Rh(0) nanoclusters from the analogous Rh(I) precursor, $(Bu_4N)_5Na_3[(1,5\text{-COD})Rh{\cdot}P_2W_{15}Nb_3O_{62}]$.[101,102] By this way, 4.0 ± 0.6 nm, that is, nanoparticles of average composition, $Rh(0)_{\sim 1,500}$ to $Rh(0)_{\sim 3,700}$ are formed and stabilized by tetrabutylammonium and polyoxoanions (Scheme 5). Hydrogen gas-uptake stoichiometry and quantitative kinetic studies evidenced that these nanoclusters grow through the same mechanism as the one reported for their Ir(0) congeners, namely, a slow nucleation, followed by a fast autocatalytic surface growth (living metal polymer).

A comparative study has been reported on the efficiency of different anionic ligands for the formation and stabilization of Ir(0) nanoclusters.[95] The investigated anions include the polyanions $P_2W_{15}Nb_3O_{62}{}^{9-}$, $SiW_9Nb_3O_{40}{}^{7-}$, $C_6H_5O_7{}^{3-}$ (citrate^{3-}), $[-CH_2\text{-}CH(CO_2{}^-)^-]_n{}^{n-}$, (polyacrylate^{n-}), and $P_3O_9{}^{3-}$ (trimetaphosphate), and the common monoanions Oac^-, Cl^-, and OH^-.[103–105] They have been evaluated according to five criteria: their ability (i) to provide a high level of kinetic control in the nanocluster synthesis (measured by the ratio k_2/k_1, i.e., the rate constants ratio of autocatalytic growth to continuous nucleation); (ii) to yield near-monodisperse nanoclusters; (iii) to allow isolable and redissolvable nanoclusters; (iv) to allow the highest catalytic activity of the redissolved nanoclusters in cyclohexene hydrogenation; and (v) to allow the longest catalytic lifetime (total turnovers). The following anion efficiency series for the stabilization of Ir(0) nanoclusters could be established: $P_2W_{15}Nb_3O_{62}{}^{9-} \sim SiW_9Nb_3O_{40}{}^{7-} > C_6H_5O_7{}^{3-} > P_3O_9{}^{3-} \sim OH^-$. In order to better understand the underlying factors that were behind this order of anion efficiency, molecular level factors such as basicity (σ-donor ligand ligating ability), hard/soft considerations, and geometry factors were considered. It appears that while basicity was expected as important (increased basicity, and thus increased σ-donation should lead to higher Ir–O bond energies), it needed to be associated with other factors. Thus, the match between the O–O distance in the coordinating anion and the surface Ir(0)–Ir(0) distance correlates rather well with the anion's ranking. The preferred tridentate oxoanion stabilizers of Ir(0) nanoclusters are those that have the best agreement between the ligand O–O and the Ir–Ir distances.

Solution catalytic lifetimes of polyoxoanion- and tetrabutylammonium-stabilized Rh(0) nanoclusters were compared with those of three well-known Rh catalysts ($RhCl(PPh_3)$, $[(1,5\text{-COD})Rh(CH_3CN)_2]BF_4$, and $5\%Rh/Al_2O_3$) for cyclohexene hydrogenation under identical conditions. Rh(0) nanoclusters exhibit catalytic lifetimes that are the

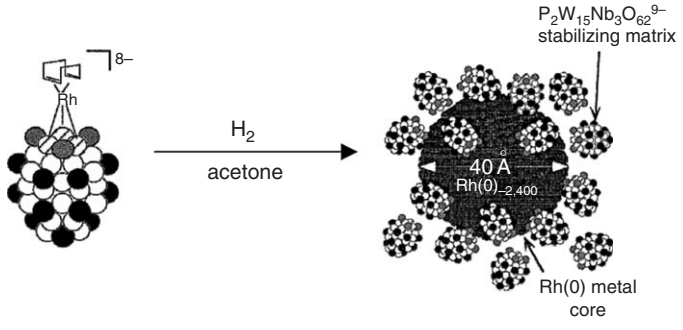

Scheme 5 Schematic synthesis of Rh nanoclusters from polyoxoanion precursor.[102] Reproduced with permission from ACS Publications.

longest ones reported for a transition metal nanocluster in solution for olefin hydrogenation (≥193,000 turnovers) and approached those of a solid-oxide-supported heterogeneous Rh(0) catalyst.[106]

A crucial point in catalysis is to know the true active species, and in metal particle catalysis to know the true number of catalytically active surface sites.[107] In this respect, polyoxoanion- and tetrabutylammonium-stabilized Rh(0) nanoclusters were compared with a commercial 5% Rh/Al_2O_3 catalyst. Both catalysts were examined under identical conditions while catalyzing cyclohexene hydrogenation. Finally, the CS_2 poisoning method was found to work as well with Rh(0) nanoclusters as it did with the 5% Rh/Al_2O_3 heterogeneous catalyst, allowing to determine the number of catalytic active sites.

The ability of Rh(0) nanoclusters to hydrogenate arenes has also been tested. Polyoxoanion- and tetrabutylammonium-stabilized Rh(0) nanoclusters were formed *in situ* by reducing $(Bu_4N)_5Na_3[(1,5\text{-COD})Rh{\cdot}P_2W_{15}Nb_3O_{62}]$ with H_2 in a monophasic propylene carbonate solution under mild conditions (22 °C, 3.7 atm H_2) and in the presence of anisole, the chosen substrate.[108,109] In these conditions, 5.3 (±1.0) nm non-agglomerated Rh(0) nanoclusters are formed containing an average Rh atoms number of ~5,700. Methoxycyclohexane is the major hydrogenation product, but a very interesting partial hydrogenation of anisole into 1-methoxycyclohexene is also observed with selectivity up to 30%. A combination of kinetics of hydrogenation and of nanocluster formation provided evidence for the true catalyst nature of the nanoclusters. The best results (2,600 total turnovers) show a lifetime slightly better than those generally found in the literature for hydrogenation nanocatalysts (2,000 TTOs).

Finally, Finke *et al.* evidenced through the use of various techniques (kinetic, Hg(0) poisoning, etc.) that the true catalyst in a benzene hydrogenation system beginning with $Ru(II)(\eta^6\text{-}C_6Me_6)(OAc)_2$ as the pre-catalyst is Ru metal. In fact, Ru nanoclusters formed during the hydrogenation have sufficient activity to account for all the observed activity.[110]

12.03.3.1.4 Stabilization by ionic liquids

A great attention is presently devoted to efficient catalytic systems that might combine the advantages of both homogeneous (catalyst modulation) and heterogeneous (catalyst recycling) catalysis. Ionic liquids appear as very interesting systems since they can be considered as non-polluting solvents and can also provide facile products' separation and catalysts' recycling. The group of Dupont has been developing from a few years the synthesis of transition metal nanoparticles in room-temperature ionic liquids as stabilizers with the objective to test them in hydrogenation or carbon–carbon coupling catalytic reactions. These authors use the same method as that developed by Chaudret and co-workers, that is, the hydrogenation of organometallic precursors like $Ru(\eta^4\text{-}C_8H_{12})(\eta^6\text{-}C_8H_{10})$, $Pt_2(dba)_3$, or $[Ir(C_8H_{12})Cl]_2$.

Thus, the use of imidazolium ionic liquids allowed the formation and the stabilization of iridium nanoparticles.[111] Treatment of the complex $[IrCl(C_8H_{12})_2]_2$ in 1-*n*-butyl-3-methylimidazoilium hexafluorophosphate ([BMI][PF6]) under dihydrogen (4 bar) at 75 °C affords the formation of a colloidal solution containing well-dispersed Ir nanoparticles with a mean size of 2.5 nm. This solution promoted biphasic hydrogenation of various olefins under mild reaction conditions. The olefin loss with time has been followed under a constant pressure of H_2: sigmoidal curves, which could be fitted to the $A \rightarrow B$, $A + B \rightarrow 2B$ autocatalytic mechanism, characteristic of nanocluster formation and growth, were obtained as previously observed by Finke *et al.* The products could be isolated almost quantitatively by simple decantation, and the isolated Ir nanoparticles maintained their efficiency for up to at least seven recycles. These Ir nanoparticles are also active for arenes[112] and ketones[113] hydrogenation.

The same methodology could be applied to platinum using $Pt_2(dba)_3$ and various room-temperature ionic liquids, and led to metallic Pt nanoparticles with a mean size near 2.0–2.5 nm (Scheme 6).[114] The isolated Pt(0) nanoparticles could be redispersed in the ionic liquid or in acetone or else used in solventless conditions for liquid–liquid biphasic,

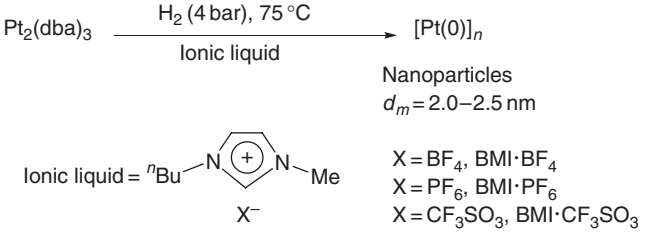

Scheme 6 Synthesis of Pt nanoparticles in ionic liquids. Reproduced with permission from ACS Publications.

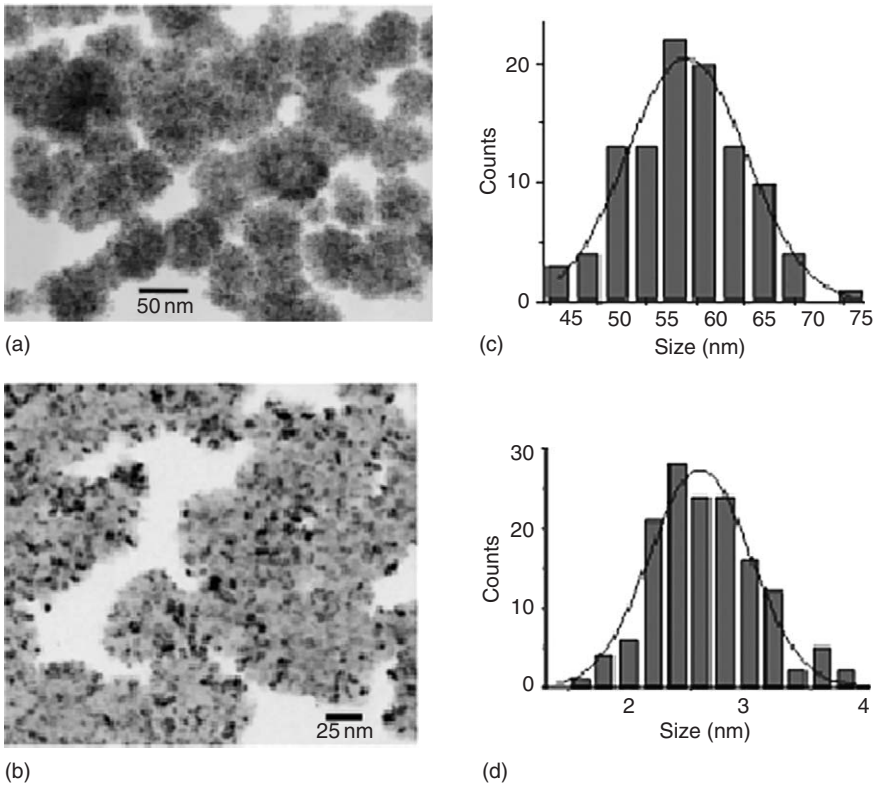

Figure 11 Images of the Ru nanoparticles prepared in BMI·PF_6, showing (a) the superstructures, (b) inside the spherical superstructures, and the corresponding histograms (c) and (d).[115] Reproduced with permission from Wiley.

homogeneous, or heterogeneous hydrogenation of alkenes and arenes under mild reaction conditions (75 °C, 4 bar H_2). Recycling experiments have also been performed.

The use of the complex Ru(η^6-C_8H_{10})(η^4-C_8H_{12}) for the formation of small Ru(0) nanoparticles (Figure 11) dispersed in 1-*n*-butyl-3-methylimidazolium hexafluorophosphate (BMI·PF_6), tetrafluoroborate (BMI·BF_4), or trifluoromethane sulfonate (BMI·CF_3SO_3) has also been described.[115] In this case, small nanoparticles with diameters of 2.6 ± 0.4 nm, which were agglomerated inside spherical superstructures (diameters ~57 nm), were obtained, giving rise to efficient multi-phase catalytic activity for alkenes and benzene hydrogenation under mild conditions (75 °C, 4 bar). When benzene was used as substrate, an interesting partial hydrogenation has been observed leading to the formation of cyclohexene with a selectivity of up to 39% at low benzene conversion.

Very recently, the same authors reported the synthesis of stable ligand-free Pd nanoparticles dispersed in the BMI·PF_6 ionic liquid and displaying an irregular shape with a monomodal particle size distribution centered at 1.7 ± 0.3 nm.[116] Their catalytic properties have been tested in the Heck coupling of aryl halides with *n*-butylacrylate at different temperatures with interesting results. However, TEM investigations revealed changes in shape and in size of colloidal Pd catalysts (mean size after catalysis: 6.01 ± 0.7 nm), and ICP-AS analysis showed significant metal leaching from the ionic phase to the organic one at low substrate conversion. The authors considered that these results were strong indications that Pd nanoparticles dispersed in the ionic liquid act as a reservoir of catalytically active Pd species.

12.03.3.1.5 Stabilization by the reaction medium

When using Ru(η^6-C_8H_{10})(η^4-C_8H_{12}), the decomposition by H_2 in neat THF or in non-coordinating solvents such as pentane leads to the precipitation of ill-defined ruthenium powder. However, when using alcohols as solvents, the reaction produces colloidal solution, containing ruthenium particles which are stable for over 1 year under argon but which precipitate upon exposure to air.[117] The particles prepared in neat methanol are very large, polycrystalline (76 nm), mesoporous, and display a relatively large specific area ($>40\ m^2\ g^{-1}$). In THF/methanol mixtures, the size of

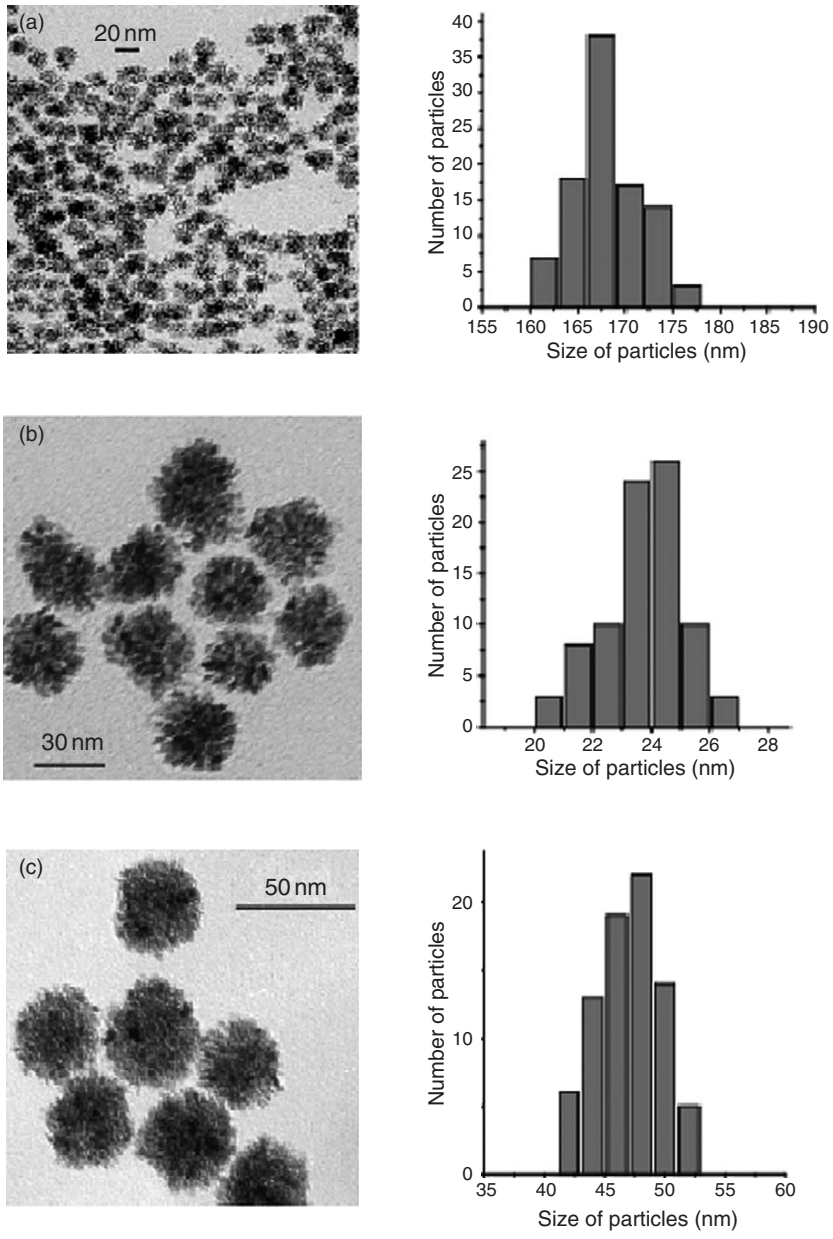

Figure 12 Micrographs and size histograms of Ru nanoparticles synthesized in MeOH/THF mixtures ((a): MeOH/THF = 5/95; (b): MeOH/THF = 25/75; (c): MeOH/THF = 50/50). Reproduced with permission from Wiley.

the polycrystalline particles was found to depend upon the reaction medium. It remains of the same order of magnitude as that observed in neat methanol up to a THF content of 25 vol.%, after which the size decreases linearly with the THF content: for a THF content in the solution of 50 vol.%, the size of the particles is 47 nm, for 90 vol.% 20 nm, and for 97.5 vol.% ca. 3–6 nm (Figure 12).[118] A similar trend, namely, size decrease, is observed upon changing MeOH for higher alcohols. The size of the particles is ca. 5 nm when the reaction is carried out in isopropanol and ca. 2.5 nm in pentanol. Finally, it was found for the reactions carried out in MeOH/THF mixtures that addition of cyclooctane leads to an increase in the size of the particles. These surprising results were attributed to phase separation in the solution between cyclooctane resulting from hydrogenation of the ligands of the ruthenium precursor and the alcohol. In this respect, the larger droplets would be formed in the most polar solvent systems and

hence the most segregated medium. This is in excellent agreement with the sizes of the particles measured in neat alcohols. The most lipophilic one (pentanol) gives rise to the smallest particles.

The hydrido complex $[(1,5\text{-}C_8H_{12})RhH]_4$ can be used as a source of small rhodium crystallites. Aromatic hydrocarbon solutions of this complex are unstable when exposed to dihydrogen, allowing the formation of 2 nm size, crystalline but agglomerated Rh nanoparticles, that show catalytic properties in aromatic hydrocarbures' hydrogenation.[119]

12.03.3.2 Organometallic Synthesis of Magnetic Metal Nanoparticles

12.03.3.2.1 Stabilization by polymers

In a way very similar to $Ru(\eta^6\text{-}C_8H_{10})(\eta^4\text{-}C_8H_{12})$, the complex $Co(\eta^3\text{-}C_8H_{13})(\eta^4\text{-}C_8H_{12})$ readily decomposes at room temperature in solution in the presence of a low pressure (generally 3 bar) of dihydrogen. When using PVP as a stabilizer, nanoparticles of 1.6 or 2.0 nm mean size were obtained as a function of the precursor concentration, whereas with PPO larger particles (4 nm) form.[120] The particles of small size (1.6 or 2 nm) adopt a non-periodic polytetrahedral structure, whereas the larger ones (4 nm) adopt the hcp structure of bulk cobalt.[121] Interestingly, and somewhat surprisingly, these particles were demonstrated to display the same magnetic properties as particles of same size prepared in ultrahigh vacuum in the gas phase by time-of-flight experiments.[122] Thus, the particles are superparamagnetic, with blocking temperatures near 10 K, and display an enhanced magnetization at saturation per cobalt atom compared to bulk cobalt.[123] Addition of O_2, pyridine, isocyanides, or CO leads to a dramatic decrease of the magnetic properties of the particles. This demonstrates (i) the absence or low contamination of the as-prepared particles and (ii) the presence of a relation between the π-accepting properties of the ligand and the magnetic properties of the nanomaterials.

Nickel particles can be prepared directly by decomposition of $Ni(\eta^4\text{-}C_8H_{12})_2$ in dichloromethane in the presence of PVP: 2 nm or 3 nm particles can be obtained depending on the concentration of the precursor.[124] The particles adsorb CO in solution in both bridged and linear geometries. Vibrational couplings between adsorbed CO molecules were detected, consistent with an ordered surface for the colloidal nickel particles.

Nickel particles may also be prepared by decomposition of the same precursor, $Ni(C_8H_{12})_2$, by H_2 in THF or a hydrocarbon solvent. The particles display a larger size (4–5 nm) and adopt the fcc structure of bulk nickel. These particles present the same magnetic properties as bulk nickel.[125] Coordination studies at their surface confirm the strong magnetization decrease in the presence of CO but also demonstrate that coordination of a pure σ-donor ligand such as amines has no effect on the magnetic properties of the particles.[126]

As for noble metal particles, this synthetic method can be adapted to the preparation of bimetallic nanoparticles. Thus Co–Pt, Co–Rh, and Co–Ru particles[127–129] of various compositions have been prepared by co-decomposition of $Co(\eta^3\text{-}C_8H_{13})(\eta^4\text{-}C_8H_{12})$ with $Pt(dba)_2$, $Rh(acac)(\eta^4\text{-}C_8H_{12})$, or $Ru(\eta^6\text{-}C_8H_{10})(\eta^4\text{-}C_8H_{12})$. As a general rule, nanoparticles of size found between 1.5 and 2.5 nm were obtained whatever the metals and the compositions. Platinum-rich nanoparticles adopt the structure of the corresponding metal, namely fcc and hcp, whereas cobalt-rich particles adopt the polytetrahedral structure of cobalt. For intermediate compositions, as-yet unknown non-periodic structures are observed. The bimetallic nanoparticles show an enhanced coercivity as compared to cobalt in agreement with an enhanced anisotropy, as also observed in bulk alloys.

12.03.3.2.2 Stabilization by ligands

The stabilization of magnetic nanoparticles can also be achieved by ligands or ligand mixtures. The decomposition of $Co(\eta^3\text{-}C_8H_{13})((\eta^4\text{-}C_8H_{12})$ in the presence of long-chain acid and/or amine ligands yields nanoparticles of controllable size, shape, and, therefore, magnetic properties.[130] Thus, decomposition of $Co(\eta^3\text{-}C_8H_{13})(\eta^4\text{-}C_8H_{12})$ in the presence of a mixture of oleic amine and oleic acid affords at room temperature spherical nanoparticles of ca. 4 nm mean size. However, at 150 °C in the presence of dihydrogen, these particles convert into regular nanorods. Changing the length of the hydrocarbyl chain of the amine surprisingly allows the control of the aspect ratio of the rods from ca. 1.5 for octylamine to ca. 25 for hexadecylamine (Figure 13).[131] Upon changing the shape and the aspect ratio of the nanoparticles, it is also possible to control the magnetic properties of the nano-objects from superparamagnetic to ferromagnetic at room temperature. An appropriate choice of a long alkyl-chain ligand mixture (hexadecylamine/stearic acid) leads to the formation of unprecedented hexagonal superlattices of nanorods resulting from crystallization in solution (Figure 14).[132]

The ratio of the different components of the ligand mixture also dramatically influences the shape of the particles. Thus, in the presence of oleic acid only, the reaction of decomposition of $Co(\eta^3\text{-}C_8H_{13})(\eta^4\text{-}C_8H_{12})$ produces very

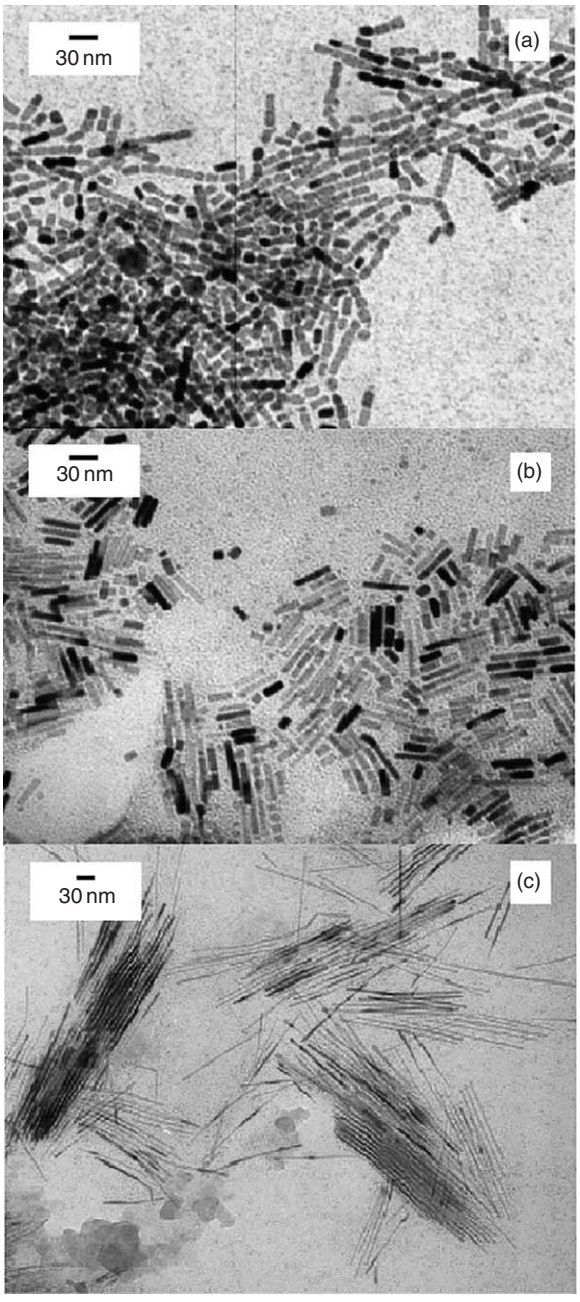

Figure 13 TEM micrographs of amine-stabilized cobalt nanoparticles ((a): C_8NH_2; (b): $C_{12}NH_2$; (c): $C_{16}NH_2$) showing the variation of the aspect ratio according to the length of the amine alkyl chain. Reproduced with permission from Wiley.

regular spherical nanoparticles, which form superlattices in two or three dimensions upon deposition over a carbon grid, whereas using a 2 : 1 mixture of oleic acid and oleylamine leads to the formation of very long Co nanowires of 4 nm mean diameter and exhibiting the same hcp structure as the nanorods and bulk cobalt. It has recently been possible using magnetic holography to measure the magnetic properties of one such nanowire (Figure 15). In all cases, the nano-objects display a magnetization at saturation per cobalt atom identical to that observed for bulk cobalt, hence demonstrating the absence of influence of pure σ-donor ligands such as amines and acids on their magnetic properties.[133]

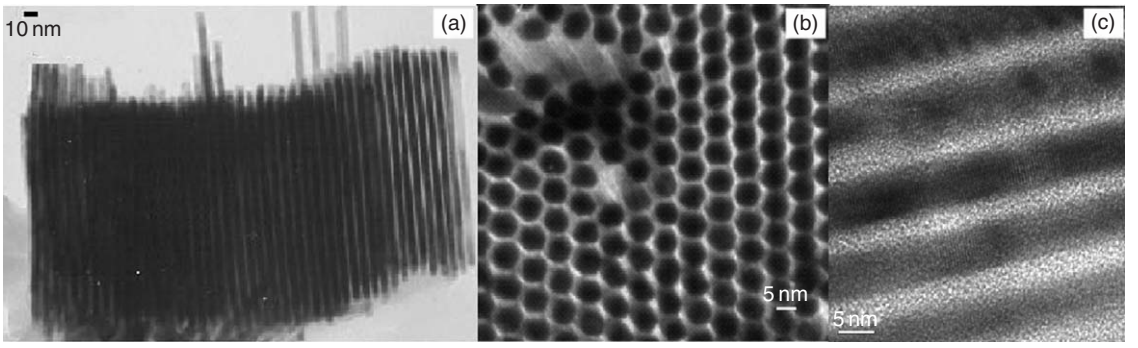

Figure 14 TEM ((a) and (b)) and HREM (c) micrographs of self-organized Co nanorods stabilized by a stearic acid/hexadecylamine mixture. Reproduced with permission from Wiley.

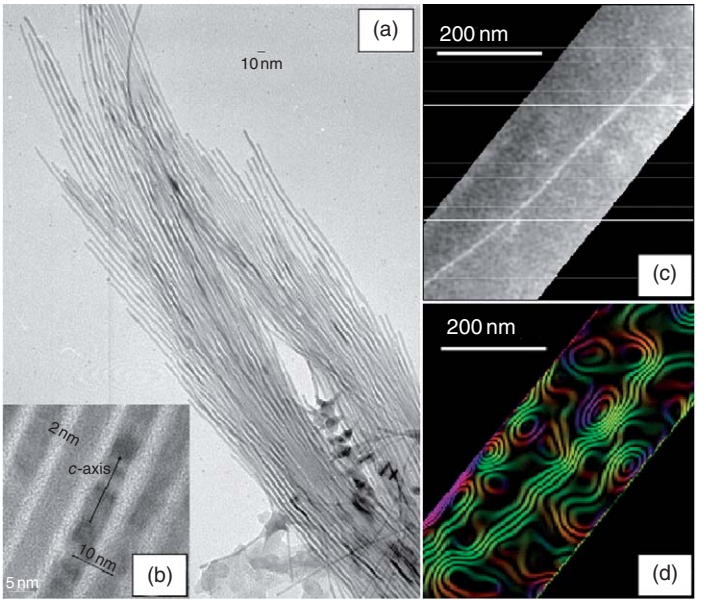

Figure 15 (a) TEM and (b) HREM and (c) and (d) holography images of Co nanowires. Reproduced with permission from the American Institute of Physics.

In the case of iron, the decomposition of the $Fe[N(SiMe_3)_2]_2$ complex in the presence of a long-chain acid and a long-chain amine mixture in various proportions produces monodisperse zerovalent iron nanoparticles displaying magnetic properties that match those of bulk iron. These nanoparticles adopt a cubic shape and are incorporated into extended crystalline superlattices containing nanocubes in close proximity and with their crystallographic axes aligned (Figure 16).[134]

Similar reactions were carried out with nickel using $Ni(\eta^4\text{-}C_8H_{12})_2$ as a precursor but in the presence of amines only. It was found that the relative concentrations of amine and nickel are decisive as far as the aspect ratio of the particles is concerned. For a low concentration of amine, spherical particles or double-arrow-shaped particles were obtained, whereas for 10 equiv. of amine relative to nickel, very regular nanorods of ca. 3 nm mean diameter were formed. Again, all these species display the same magnetization at saturation as bulk nickel. This contrasts with particles produced in the presence of TOPO as ligands, which show a reduced magnetization which was attributed to the π-accepting properties of the ligand.[135]

Bimetallic NiFe and CoFe nanoparticles were prepared by associating an olefinic complex, $Ni(\eta^4\text{-}C_8H_{12})_2$ or $Co(\eta^3\text{-}C_8H_{13})(\eta^4\text{-}C_8H_{12})$ to $Fe(CO)_5$. NiFe particles were synthesized in the presence of HDA in refluxing anisole. The particles are monodisperse, display a size of 3.3 nm, and organize into 2-D and 3-D superstructures on a carbon grid.[136] In similar conditions but in the presence of long-chain amines and long-chain acids, the reaction between

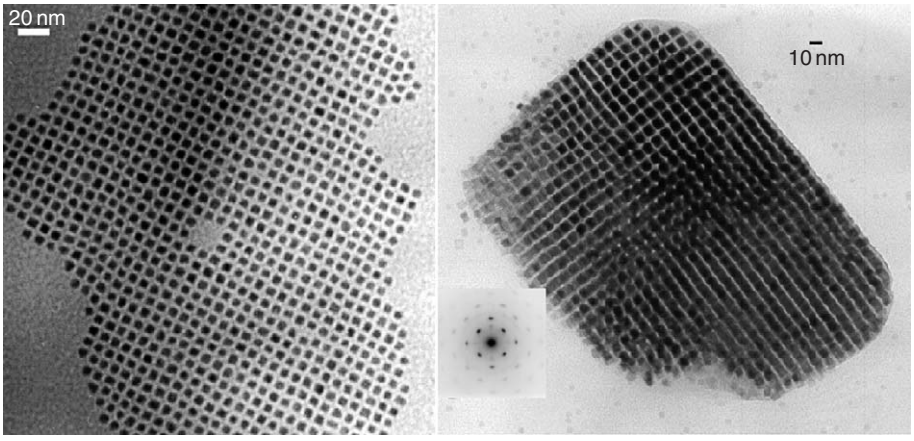

Figure 16 Cubic shape iron nanoparticles self-assembled into cubic extended crystalline superlattices.

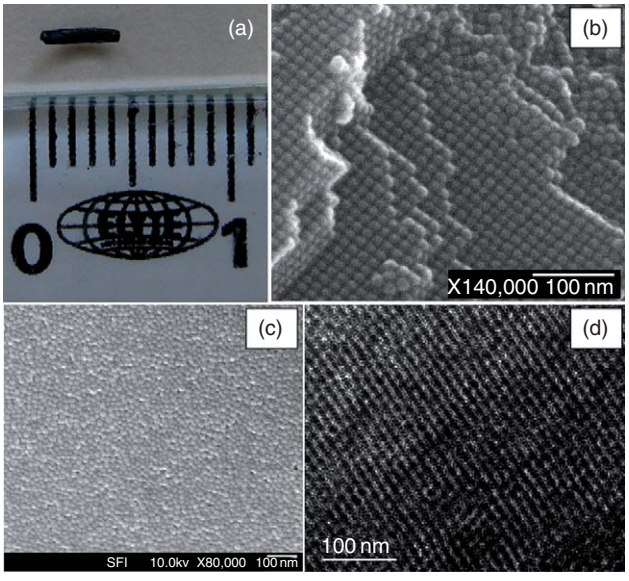

Figure 17 (a) Image of an FeCo supercrystal of the millimetric size; (b) SEM-FEG image of an FeCo supercrystal (c) SEM-FEG image of the surface of an FeCo supercrystal (d) TEM-FEG image after ultramicrotomy of an FeCo supercrystal. Reproduced with permission from Nature Publishing Group.

$Co(\eta^3\text{-}C_8H_{13})((\eta^4\text{-}C_8H_{12})$ and $Fe(CO)_5$ affords in excellent yield a black crystalline material which precipitates from the solution. As shown in Figure 17, the super-crystals of millimetric size are composed of monodisperse nanoparticles organized into a compact superlattice, shown on a broken supercrystal to be fcc. These particles display interesting soft magnetic properties but slowly oxidize in air. A thermal treatment of the supercrystals at 500 °C for 30 min allows the deposition of the surface of the individual particles of a thin graphite layer. Before annealing, the particles adopt a polytetrahedral structure, which transforms into bcc-like bulk Fe-Co after annealing.[137]

12.03.3.3 Organometallic Synthesis of Nanoparticles of Other Metals and Main Group Elements

12.03.3.3.1 Metals

The organometallic approach can be extended to d^{10}-metals and to main group elements. For example, CpCu(^{t}BuNC) is decomposed by CO at room temperature to give copper nanoparticles which may be stabilized by

polymers (PVP, PPO)[138] or by PPh_3.[139] Although not an organometallic complex *stricto sensu*, the alkoxide $Cu(OCH(Me)CH_2NMe_2)_2$, known to be a CVD precursor, can be used to produce copper nanoparticles upon thermolysis at 300 °C in HDA. The particles have a size of ca. 7.5 nm and a strong tendency to organize into 2-D super-lattices.[140]

The dialkyl $ZnCy_2$ complex (with $Cy = \eta^1\text{-}C_6H_{11}$) decomposes thermally at 130 °C in wet anisole to produce 6 nm Zn particles protected by a thin ZnO layer. Full oxidation of the particles at 600 °C leads to ZnO particles of similar size and geometry.[141] Upon mixing a dialkylzinc, namely $ZnEt_2$ and $Cu(OCH(Me)CH_2NMe_2)_2$ in HDA at 250 °C, it is possible to prepare bimetallic Cu/Zn particles of various relative compositions and of mean size between 5 and 10 nm. EDX and selected area electron diffraction (SAED) demonstrate the presence of the CuZn and $CuZn_2$ besides Cu, hence demonstrating the alloying of copper and zinc (Figure 18).[142]

The decomposition of CpIn, whether thermal or photochemical, rapidly produces In(0) nanoparticles.[143] When the reaction is carried out using PVP as a stabilizer, the presence of a small amount of water is required in order to obtain monodisperse indium nanoparticles. In the presence of the oxygen donor ligand TOPO, the decomposition of a toluene solution of CpIn produces rigorously monodisperse 5 nm. In particles which self-assemble into an hcp superlattice (Figures 19(a) and 19(b)). In the same conditions, but using HDA instead of TOPO, slightly elongated particles were obtained which did not show any sign of self-organization.[144] In this case, the rate of decomposition was also found important, since the same reaction carried out in the presence of UV light yields very long (mm)

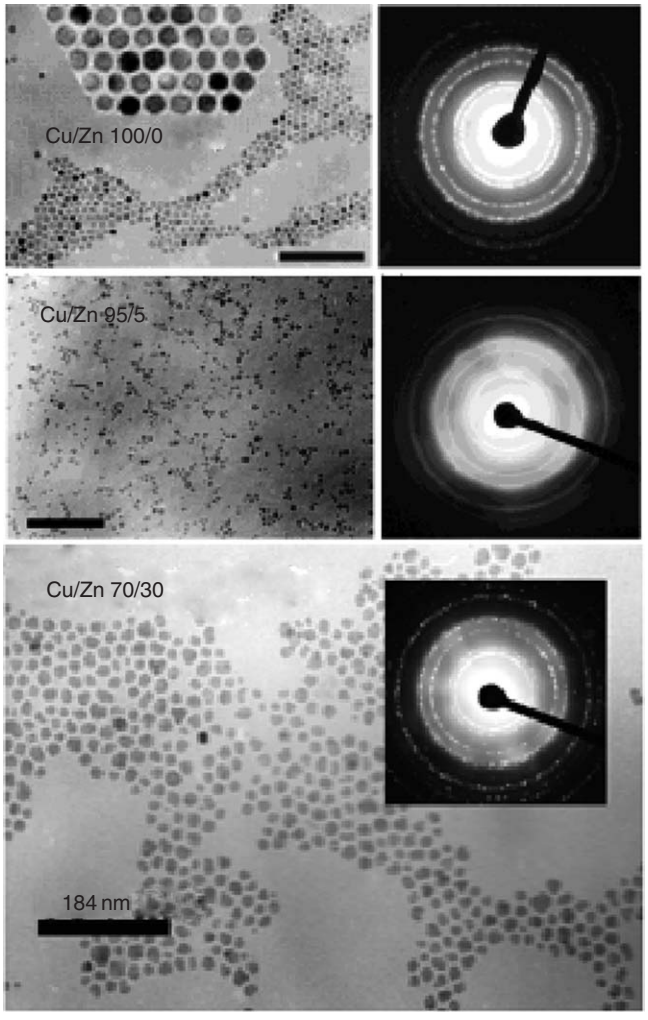

Figure 18 TEM images and selected area electron diffraction (SAED) of the toluene solutions of Cu/Zn 100/0, 95/5, and 70/30 systems stabilized in hexadecylamine.[142] Reproduced with permission from ACS Publications.

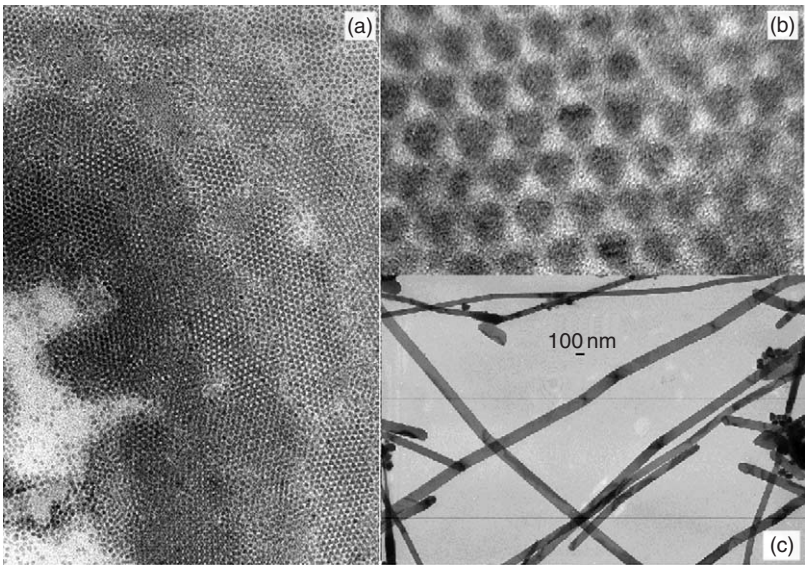

Figure 19 (a) TEM and (b) HRTEM images of self-organized TOPO-stabilized In nanoparticles synthesized by decomposition of InCp in toluene (individual mean size = 5 nm); (c) In_3Sn nanowires obtained by simultaneous decomposition of toluene solution of InCp and $[Sn(NMe_2)_2]_2$ under UV light in the presence of HDA with the ratio 1/1/0.5. Reproduced with permission from Wiley.

indium nanowires, the diameter of which can be adjusted to some extent by the concentration of HDA present in the solution. This procedure can be adapted to the production of In_3Sn nanoribbons upon using a mixture of CpIn and $[Sn(NMe_2)_2]_2$ as precursors (Figure 19(c)). Finally CpIn also decomposes spontaneously in methanol at room temperature to give aggregates of nanoparticles. The individual particles display a size of ca. 15 nm and are included in aggregates of ca. 400 nm. These particles may be used for the realization of gas sensors on a silicon chip.[145]

$[Sn(NMe_2)_2]_2$ decomposes in toluene under UV irradiation, in the presence of HDA and hexadecylammonium chloride (HDA,HCl) in a 3 : 1 ratio, to form a precipitate which consists of identical ovoid tin particles of 18×15 nm.[146] These particles display the tetragonal structure of bulk Sn and are arranged into a non-compact, probably monoclinic 3-D superlattice, inside which the atomic planes of individual particles are aligned. The decomposition of $[Sn(NMe_2)_2]_2$ can also be achieved thermally in wet anisole. The quantity of water is critical to control the size dispersity of the particles, the optimum being obtained for $[H_2O]/[Sn] = 0.5$. The particles can be oxidized in an oven at 600 °C into SnO_2 without changes in their size and shape.[147] They can also be deposited onto the silicon platform of a microelectronic device and oxidized in air using the integrated heater of the chip. In the latter case, the nanomaterial obtained can be used as the sensitive layer of a gas-sensing device.[148]

12.03.3.3.2 Metal oxides

Organometallic precursors may also be used for the direct preparation of metal oxide nanoparticles.

As a first example, and although it has been decided in this chapter not to deal with the vast domain of supported nanoparticles, the organometallic precursor bis(toluene) titanium gave interesting results. Thus, the impregnation of mesoporous alumina by a solution of bis(toluene) titanium leads to a black metallic deposit, which, after oxidation at 400 °C, leads to the growth of TiO_2 nanoparticles.[149] In organic solution bis(cyclooctatetraene)titanium complex ($Ti(C_8H_8)_2$) reacts with dry DMSO to yield a precipitate of amorphous TiO_2. In the presence of phosphorus ligands, namely, PBu_3, $OPBu_3$, and $OPOct_3$, crystalline nanoparticles in 3–25 nm range can be obtained, depending upon the ligands.[150]

Zinc alkyl derivatives have been widely used for the preparation of ZnO nanoparticles. Thus, decomposition of $ZnEt_2$ in the presence of O_2 at high temperature (200 °C) in TOPO produces TOPO-capped ZnO nanoparticles.[151]

The decomposition of the dialkylzinc precursor ($ZnCy_2$) can be carried out at room temperature in the presence of H_2O vapor and various ligands. In this case, crystalline and luminescent nanoparticles adopting the zincite phase are produced.[152] The size and shape of the particles can be modulated, depending upon the nature and concentration of the amine ligand used, from spherical particles in the 3–4 nm range to very long (>100 nm) nanorods of 4 nm diameter

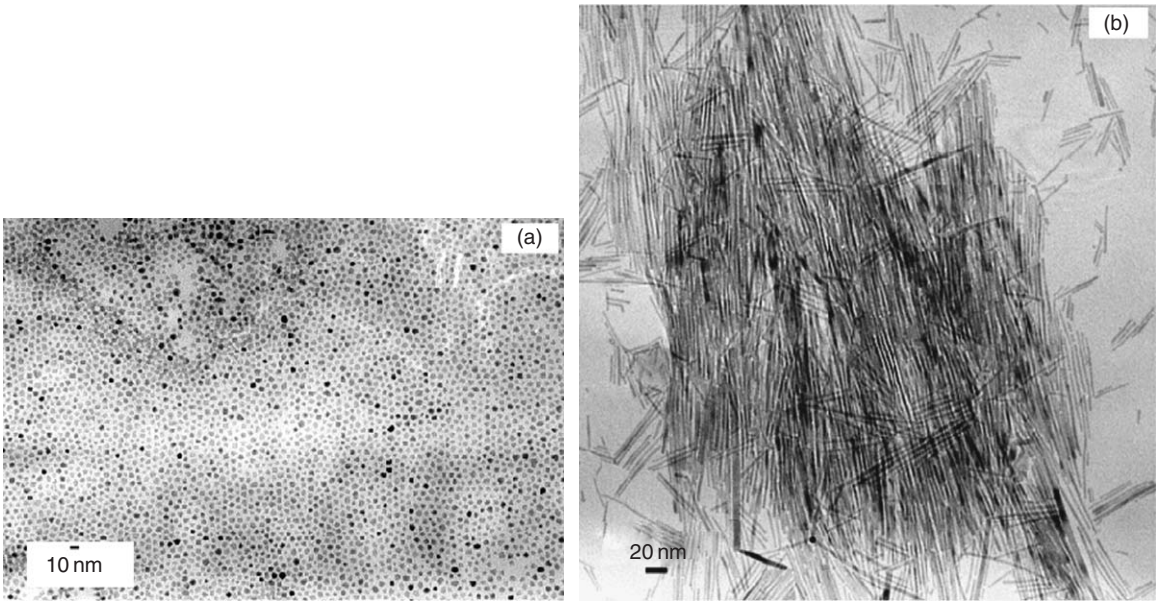

Figure 20 (a) TEM micrographs of ZnO nanodisks obtained by a slow oxidation/evaporation process from a THF solution of HDA and (b) ZnO nanowires grown in pure octylamine. Reproduced with permission from Wiley.

(Figure 20). It is demonstrated by NMR that the ligand coordinates on the zinc precursor as well as on the oxide nanoparticles, and therefore is probably present throughout the oxidation process.[153] The same reaction carried out using a mixture of long-chain amines and long-chain carboxylic acids as stabilizers produces monodisperse spherical nanoparticles in the 3–4 nm range, which self-organize into 2-D or 3-D superlattices, depending upon the nature of the ligands.[154] ZnO nanoparticles can also be produced by thermolysis of $EtZnO^iPr$ at 160 °C in TOPO without the need for any extra oxygen source. In this case, 3 nm crystalline hexagonal particles are obtained (Figure 21).[155]

12.03.3.3.3 Quantum dots; metal chalcogenides, phosphides, and arsenides

The quantum dots (II–VI semiconductor nanoparticles) represent one of the earliest use of solution organometallic chemistry to produce nanoparticles and the largest development to date. It is out of the scope of this chapter to deal with all applications of the quantum dots, since, according to Eychmüller, "the literature dealing with this topic is virtually unmanageable."[156] However, we will present the early results of organometallic synthesis and some recent developments.

The use of the organometallic precursor $CdMe_2$ was first reported by Steigerwald. Upon reaction with $Se(SiMe_3)_2$, a solid forms, which after annealing at 400 °C was identified as CdSe. A particle size was estimated in the order of 5–7.5 nm.[157] This procedure was improved upon in 1993 by Bawendi *et al.* They reported a high-temperature synthesis of CdE nanoparticles (E = S, Se, Te) using $CdMe_2$ and TOPSe, TOPTe, or $(TMS)_2E$ as the chalcogenide source. The originality of this preparation lies in the injection of a TOP solution of the reagents into hot TOPO. The result is a burst of homogeneous nucleation, and further heating at 230–260 °C allows the controlled growth of the particles. Particles ranging from 1.5 to 11.5 nm and displaying low size dispersity can be obtained in this way.[158] This method has proved to be very successful and has become very popular for the synthesis of quantum dots of various sizes. The precise size control obtained by this method allows the organization of the CdSe nanoparticles at a solid or liquid interface into 3-D quantum dots close-packed superlattices.[159] Interestingly, one nanoparticle of CdSe synthesized by this organometallic route has been used to make a single-electron transistor after deposition on a SiO_2-covered silicon substrate, between two gold electrodes.[160] The luminescence quantum yield of the dots can be improved up to 50% by growing on top of the particles a layer of another semiconductor displaying a large band gap. This can be achieved using diethylzinc as a precursor and a synthesis carried out near 200 °C. This can lead to CdSe/ZnSe[161] or CdSe/ZnS.[162] The latter particles display the best optical properties, and are robust giving then rise to interesting prospects for application in electroluminescent devices. Such core-shell CdSe/ZnS nanoparticles were recently tailored to exhibit a blue luminescence.[163] By changing the surfactants to a mixture of hexylphosphonic acid

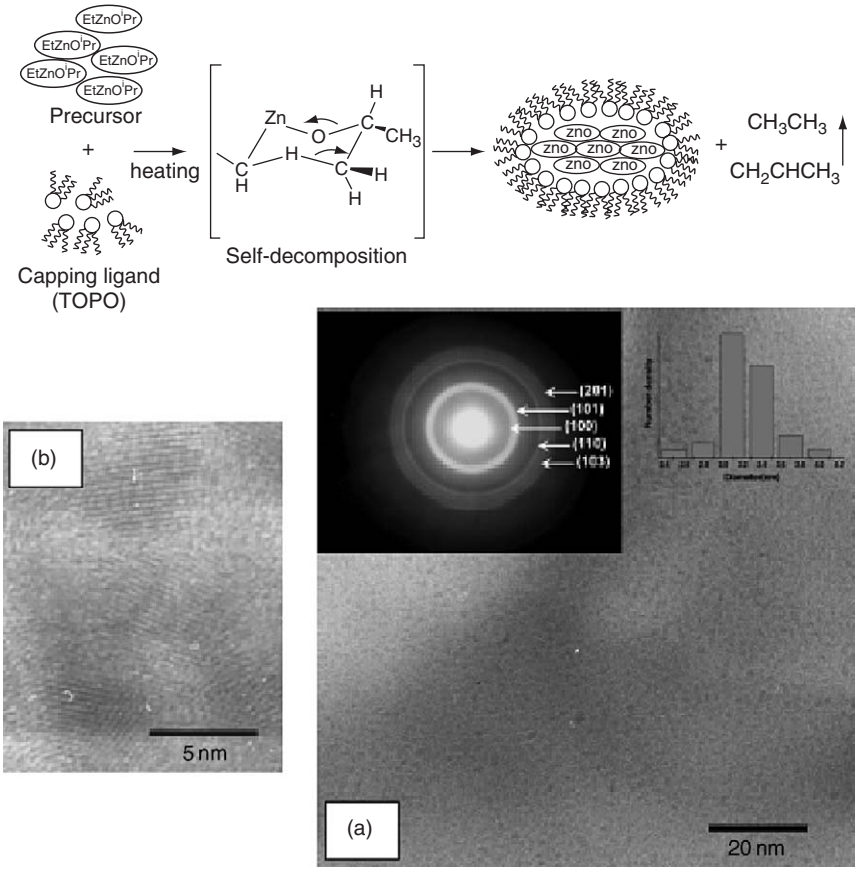

Figure 21 Schematic thermolysis of EtZnO^{i}Pr precursor in the presence of TOPO and (a) TEM and (b) HREM images of the so-obtained ZnO nanoparticles.[155] Reproduced with permission from the Royal Society of Chemistry.

and TOPO and controlling different parameters, namely ratio of surfactants, injection volume, and monomer concentration, it is possible to grow CdSe nanorods as well as tear-drop and tetrapod shapes (Figure 22).[164] These CdSe nanorods, like the spherical particles, can be covered by a shell of ZnS using $ZnMe_2$ as the zinc precursor (Figures 22(i)–22(k)).[165] Improvements of this method, which requires both a volatile toxic precursor and high reaction temperature, were searched for the past few years. Thus, the replacement of the highly volatile and toxic precursor dimethylcadmium ($CdMe_2$) by less volatile organometallic precursors has been investigated by Fischer, namely, dineopentylcadmium, bis(3-diethylaminopropyl) cadmium, and (2,2′-bipyridine)dimethylcadmium, that proved efficient as precursors for the preparation of TOPO-stabilized CdSe nanoparticles.[166] The substitution of dimethylcadmium by cadmium naphtenate allows CdSe nanorods' synthesis to be carried out at 160 °C. Nearly monodisperse nanorods of various sizes can be obtained in this way.[167] In order to investigate the collective properties of the quantum dots, a procedure apparented to molecular crystallization was set up by Weller's group. It consists in letting diffuse a non-solvent (methanol) into a toluene solution of TOPO-capped CdSe nanoparticles. The presence of a buffer layer of isopropanol allows a smooth diffusion and the formation of regular 3-D supercrystals of monodisperse nanoparticles (Figure 23).[168]

Doping of CdSe quantum dots with manganese has proved difficult and has necessitated the use of a specially designed organometallic precursor, $Mn_2(\mu\text{-SeMe})_2(CO)_8$.[169]

Organometallic precursors were also used for the preparation of III–V semiconductors. Buhro reported the use of a single-source precursor $\{Bu^t_2In[\mu\text{-}P(SiMe_3)_2]\}_2$, which upon methanolysis in toluene leads to a mixture of InP and In nanoparticles, which promote the growth of InP fibers through a solution–liquid–solid mechanism.[170]

Nanometric particles of InP were readily prepared by the decomposition of an indium phosphide complex, $In(PBu^t_2)_3$, at 167 °C in 4-ethylpyridine. The resulting material shows marked quantum confinement effects, and was investigated using optical absorption and photoluminescence spectroscopies, and TEM.[171] Similar precursors were used

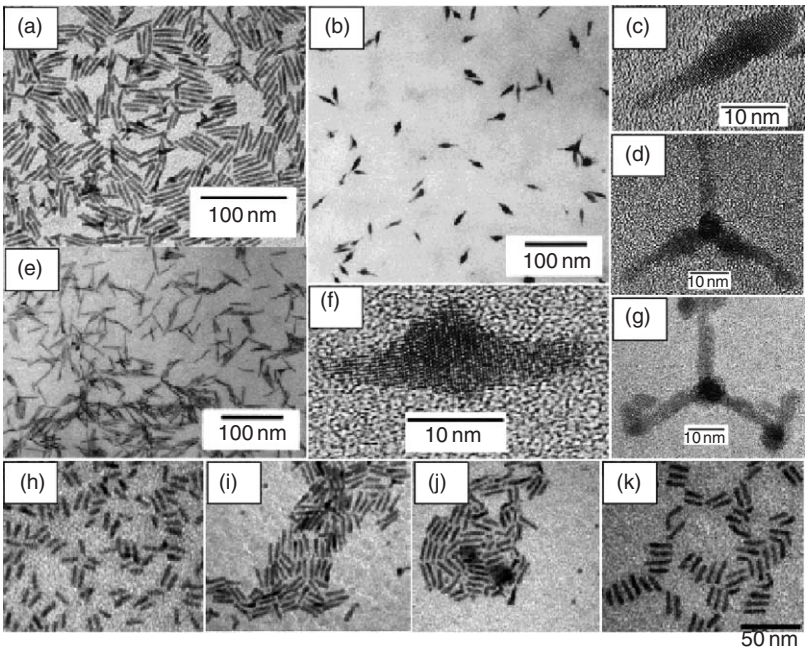

Figure 22 TEM images of (a) 34.5 ± 4.5 nm CdSe rods (10 : 1 aspect ratio); (b) teardrop-shaped CdSe nanocrystals; (c) and (f) HREM images of teardrop-shaped CadSe nanocrystals; (d) and (g) HREM images of tetrapod-shaped CdSe nanocrystals; (e) CdSe rods (11 : 1 aspect ratio); (h) CdSe rods (22×4 nm); (i)–(k) Cd-Se/ZnS core-shell nanorods grown from rods shown in (h).[164,165] Reproduced with permission from ACS Publications.

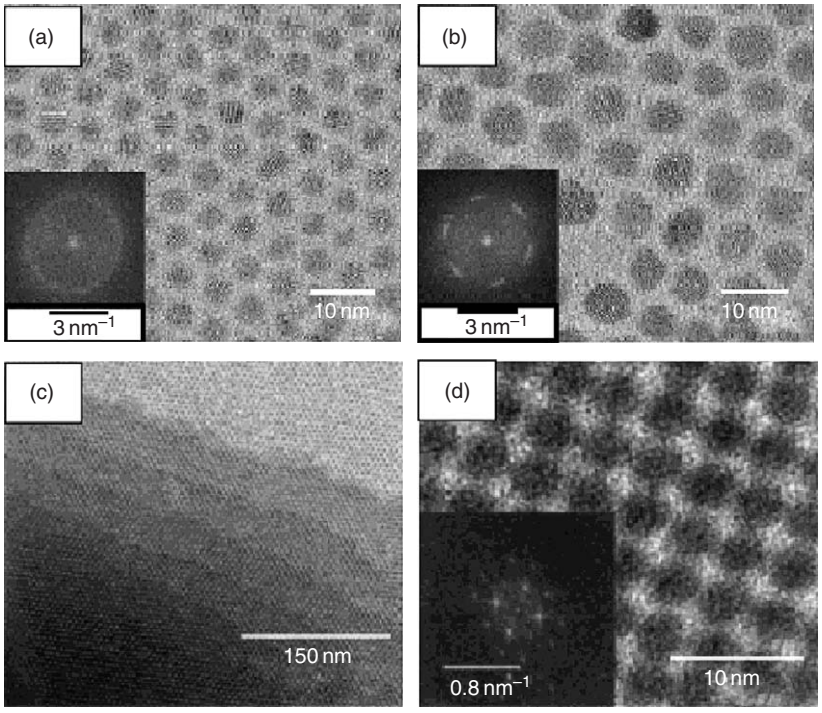

Figure 23 TEM images of (a) 3.5 nm and (b) 7 nm CdSe particles self-assembled in CdSe 2-D arrangements with corresponding FFT; TEM images of (c) 3.5 nm CdSe particles self-assembled in 3-D arrangement within (d) a (100) projection along the superlattice, with corresponding FFT.[166,167] Reproduced with permission from Wiley.

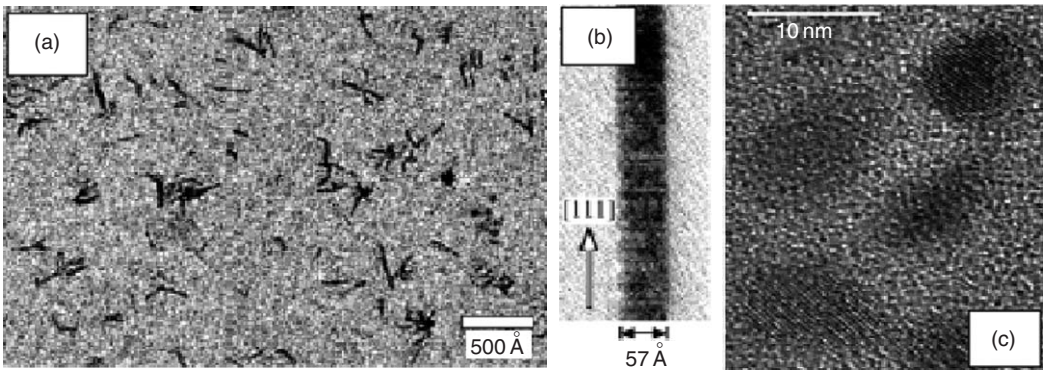

Figure 24 TEM images of (a) 3 nm InP nanorods, (b) isolated 5.7 nm InP nanorod, and (c) InAs quantum dots.[168,169] Reproduced with permission from the Royal Society of Chemistry.

for synthesizing InP nanorods of diameters in the range 3–30 nm and length of 10 to 100 nm (Figures 24(a) and 24(b)).[172] InAs quantum dots in the 8 nm range were produced by decomposition of $Bu^t_2AsInEt_2$ in molten HDA at 280 °C. The particles show a blue shift in their optical spectra compared to the parent bulk material (Figure 24(c)).[173]

Other compounds benefit from similar synthesis procedures. For example, luminescent zinc phosphide, Zn_3P_2, nanoparticles in the 5–10 nm size range were prepared by reacting $ZnMe_2$ with $HPBu^t_2$ in the presence of TOPO or 4-ethylpyridine.[174]

Finally, sulfides were also obtained through an organometallic approach for other purposes. For example, nanoparticles of MoS_2, an important compound for applications in catalysis and lubrification, of 10–30 nm mean diameter were synthesized through decomposition of $Mo(CO)_6$ at 140 °C in the presence of sulfur.[175]

12.03.4 Conclusion

In summary, the use of nano-objects for increasingly sophisticated applications has rapidly grown for the past few years. This concerns the fields of catalysis, energy conversion, micro- and nanoelectronics, magnetic and optical devices, sensors, biology, and more. These applications require in turn complex nanoparticles with size, shape, composition, outer layer, and surface species as well controlled as possible. The organometallic approach toward such materials seems perfectly adapted since it allows to play on the key synthesis parameters of these very difficult syntheses, namely, rate of nucleation, rate of growth, and control of the surface chemistry. In particular, the surface chemistry may allow both to build complex nanostructures through various associations of surface ligands and lead to a rich surface reactivity involving multiple or cascade reactions. Some spectacular results have been already obtained thanks to this approach, but, more generally, these elements suggest that there is a strong potential for organometallic chemists to play a key role in this field. This should also lead to an impressive development in surface organometallic chemistry in the future.

References

1. Schmid, G., Ed. *Clusters and Colloids: From Theory to Applications*; Wiley-VCH: Weinheim, 1994.
1a. Schmid, G., Ed. *Nanoparticles: From Theory to Applications*; Wiley-VCH: Weinheim, 2004.
2. de Jongh, L. G. *Physics and Chemistry of Metal Cluster Compounds*; Kluwer: Dordrecht, 1994.
3. Klabunde, K. J.; Cardenas-Trivino, G. In *Active Metals: Preparation, Characterization, Applications*; Fürstner, A., Ed.; Wiley-VCH: Weinheim, 1996; pp 237–277.
4. Lewis, L. N. In *Catalysis by Di-and Polynuclear Metal Cluster*; Adams, R. D., Cotton, F. A., Eds.; Wiley-VCH: New-York, Weinheim, 1998; pp 373–394.
5. Feldheim, D. L., Foss, C. A., Jr., Eds. *Metal Nanoparticles*; Marcel Dekker: New York, 2002.
6. El-Sayed, M. A. *Acc. Chem. Res.*, **2001**, *34*, 257–264.
7. Roucoux, A.; Schulz, J.; Patin, H. *Chem. Rev.* **2002**, *102*, 3757–3778.
8. Cushing, B. L.; Kolesnichenko, V. L.; O'Connor, C. J. *Chem. Rev.* **2004**, *104*, 3893–3946.
9. Katz, E.; Willner, I. *Angew. Chem., Int. Ed.* **2004**, *43*, 6042–6108.
10. Müller, A.; Beckmann, E.; Bögge, H.; Schmidtmann, M.; Dress, A. *Angew. Chem., Int. Ed.* **2002**, *41*, 1162–1167.
11. Marvaud, V.; Decroix, C.; Scuiller, A.; Tuyèras, F.; Guyard-Duhayon, C.; Vaissermann, J.; Marrot, J.; Gonnet, F.; Verdaguer, M. *Chem. Eur. J.* **2003**, *8*, 1692–1705.

12. Hirai, H. *J. Macromol. Sci. Chem.*, **1979**, *5*, 633–649.
13. Bönnemann, H.; Braun, G.; Brijoux, W.; Brinkmann, R.; Schulze Tilling, A.; Seevogel, K.; Siepen, K. *J. Organomet. Chem.* **1996**, *520*, 143–162.
14. Yu, W.; Liu, M.; Liu, H.; Ma, X.; Liu, Z. *J. Colloid Interface Sci.* **1998**, *208*, 439–444.
15. Liu, M.; Yu, W.; Liu, H. *J. Mol. Catal. A: Chemical* **1999**, *138*, 295–303.
16. Pileni, M. P. *J. Phys. Chem.* **1993**, *97*, 6961–6973.
17. Pileni, M. P. In *Metal Nanoparticles*; Feldheim, D. L., Foss, C. A., Jr., Eds.; Marcel Dekker: New York, 2002; chapter 9, pp 207–236.
18. Philippot, K.; Chaudret, B. *C.R. Chimie* **2003**, *6*, 1019–1034.
19. Chaudret, B. *C.R. Physique* **2005**, *6*, 117–131.
20. Green, M. *Chem. Commun.* **2005**, 3002–3011.
21. Teyssandier, F.; Dollet, A. In *Non-equilibrium Processing of Materials*; Suryanarayana, C., Ed.; Pergamon: Amsterdam, 1999; pp 257–285.
22. Kodas, T. T.; Hampden-Smith, H., Eds. *The Chemistry of Metal CVD*; Wiley-VCH: Weinheim, 1994.
23. Hess, P. H.; Parker, P. H., Jr., *J. Appl. Polym. Sci.* **1966**, *10*, 1915–1927.
24. Thomas, J. R. *J. Appl. Phys.* **1966**, *37*, 2914–2915.
25. Tadd, E. H.; Bradley, J.; Tannenbaum, R. *Langmuir* **2002**, *18*, 2378–2384.
26. Griffiths, C. H.; O'Horo, M. P.; Smith, T. W. *J. Appl. Phys.* **1979**, *50*, 7108–7115.
27. Burke, N. A. D.; Stöver, H. D. H.; Dawson, F. P. *Chem. Mater.* **2002**, *14*, 4752–4761.
28. Dinega, D. P.; Bawendi, M. G. *Angew. Chem., Int. Ed.* **1999**, *38*, 1788–1791.
29. Sun, S.; Murray, C. B. *J. Appl. Phys.* **1999**, *85*, 4325–4330.
30. Puntes, V. F.; Krishnan, K. M.; Alivisatos, P. *Appl. Phys. Lett.* **2001**, *78*, 2187–2189.
31. Puntes, V. F.; Krishnan, K. M.; Alivisatos, A. P. *Science* **2001**, *291*, 2115–2117.
32. Puntes, V. F.; Zanchet, D.; Erdonmez, C. K.; Alivisatos, P. *J. Am. Chem. Soc.* **2002**, *124*, 12874–12880.
33. Kim, S. W.; Son, S. U.; Lee, S. S.; Hyeon, T.; Chung, Y. K. *Chem. Commun.* **2001**, 2212–2213.
34. Tripp, S. L.; Pusztay, S. V.; Ribbe, A. E.; Wei, A. *J. Am. Chem. Soc.* **2002**, *124*, 7914–7915.
35. Park, S. J.; Kim, S.; Lee, S.; Khim, Z. G.; Char, K.; Hyeon, T. *J. Am. Chem. Soc.* **2000**, *122*, 8581–8582.
36. Farrell, D.; Majetich, S. A.; Wilcoxon, J. P. *J. Phys. Chem. B* **2003**, *107*, 11022–11030.
37. Sun, S.; Murray, C. B.; Weller, D.; Folks, L.; Moser, A. *Science* **2000**, *287*, 1989–1992.
38. Zeng, H.; Sun, S.; Vedantam, T. S.; Liu, J. P.; Dai, Z. R. *Appl. Phys. Lett.* **2002**, *14*, 2583–2585.
39. Salgeirino-Maceira, V.; Liz-Marsan, L. M.; Farle, M. *Langmuir* **2004**, *20*, 6946–6950.
40. Park, J. I.; Cheon, J. *J. Am. Chem. Soc.* **2001**, *123*, 5743–5746.
41. Shevchenko, E. V.; Talapin, D. V.; Rogach, A. L.; Kornowski, A.; Haase, M.; Weller, H. *J. Am. Chem. Soc.* **2002**, *124*, 11480–11485.
42. Shevchenko, E. V.; Talapin, D. V.; Kornowski, A.; Wiekhorst, F.; Klötzer, J.; Rogach, A. L.; Haase, M.; Weller, H. *J. Am. Chem. Soc.* **2003**, *125*, 9090–9101.
43. Rogach, A.; Talapin, D. V.; Shevchenko, E. V.; Kornowski, A.; Haase, M.; Weller, H. *Adv. Mater.* **2002**, *14*, 653–664.
44. Shevchenko, E. V.; Talapin, D. V.; Scnablegger, H.; Kornowski, A.; Festin, Ö.; Svedlinh, P.; Haase, M.; Weller, H. *Adv. Mater.* **2002**, *14*, 287–290.
45. Chen, M.; Nikles, D. E. *J. Appl. Phys.* **2002**, *91*, 8477–8479.
46. Hou, Y.; Kondoh, H.; Kogure, T.; Ohta, T. *Chem. Mat.* **2004**, *16*, 5149–5152.
47. Sobal, N. S.; Ebels, U.; Möhwald, H.; Giersig, M. *J. Phys. Chem. B* **2003**, *107*, 7351–7354.
48. Sobal, N. S.; Hilgendorff, M.; Möhwald, H.; Giersig, M.; Spasova, M.; Radetic, T.; Farle, M. *Nano Lett.* **2002**, *2*, 621–624.
49. Ono, K.; Okuda, R.; Ishii, Y.; Kaminura, S.; Oshima, M. *J. Phys. Chem. B* **2003**, *107*, 1941–1942.
50. Chen, M.; Nikles, D. E. *Nano Lett.* **2002**, *2*, 211–214.
51. Sun, X.; Harrell, J. W.; Nikles, D. E.; Sun, K.; Wang, L. M.; Li, J.; Wang, Z. L. *Mat. Res. Soc. Symp. Proc.* **2003**, *774*, P9.8.1.
52. Hyeon, T.; Lee, S. S.; Park, J.; Chung, Y.; Na, H. B. *J. Am. Chem. Soc.* **2001**, *123*, 12798–12801.
53. Hyeon, T.; Chung, Y.; Park, J.; Lee, S. S.; Kim, Y-W; Park, B. H. *J. Phys. Chem. B* **2002**, *106*, 6831–6833.
54. King, S.; Hyunh, K.; Tannenbaum, R. *J. Phys. Chem. B* **2003**, *107*, 12097–12104.
55. Lee, K.; Seo, W. S.; Park, J. T. *J. Am. Chem. Soc.* **2003**, *125*, 3408–3409.
56. Moreno, B.; Vidoni, O.; Ovalles, C.; Chaudret, B.; Urbina, C.; Krentzein, H. *J. Colloid and Interface Sci.* **1998**, *207*, 251–257.
57. Qian, C.; Kim, F.; Ma, L.; Tsui, F.; Yang, P.; Liu, J. *J. Am. Chem. Soc.* **2004**, *126*, 1195–1198.
58. Hoon, S. R.; Kilner, M.; Russel, G. J.; Tanner, B. K. *J. Mag. Mag. Mat.* **1983**, *39*, 107–110.
59. Nagata, T.; Pohl, M.; Weiner, H.; Finke, R. G. *Inorg. Chem.* **1997**, *36*, 1366–1377.
60. Suslick, K. S.; Price, G. J. *Annu. Rev. Mater. Sci.* **1999**, *29*, 295–326.
61. Suslick, K. S.; Fang, M.; Hyeon, T. *J. Am. Chem. Soc.* **1996**, *118*, 11960–11961.
62. de Caro, D.; Ould Ely, T.; Mari, A.; Chaudret, B.; Snoeck, E.; Respaud, M.; Broto, J.-M.; Fert, A. *Chem. Mater.* **1996**, *8*, 1987–1991.
63. Shafi, K. V. P. M.; Gedanken, A.; Prozorov, R. *Adv. Mater.* **1998**, *10*, 590–593.
64. Alexandrescu, R.; Morjan, I.; Cojacaru, S.; Petcu, S.; Teodorescu, V.; Huisken, F.; Kohn, B.; Ehbrecht, M. *Mater. Chem. Phys.* **1998**, *55*, 115–121.
65. Veintemillas-Verdaguer, S.; Morales, M. P.; Serna, C. J. *Mater. Lett.* **1998**, *35*, 227–231.
66. Duteil, A.; Quéau, R.; Chaudret, B.; Mazel, R.; Roucau, C. *Chem. Mater.* **1992**, *5*, 341–347.
67. Pan, C.; Pelzer, K.; Philippot, K.; Chaudret, B.; Dassenoy, F.; Lecante, P.; Casanove, M.-J. *J. Am. Chem. Soc.* **2001**, *123*, 7584–7593.
68. Bradley, J. S.; Hill, E. W.; Behal, S.; Klein, C.; Chaudret, B.; Duteil, A. *Chem. Mater.* **1992**, *4*, 1234–1239.
69. Duteil, A.; Quéau, R.; Chaudret, B.; Mazel, R.; Roucau, C.; Bradley, J. S. *Chem. Mater.* **1993**, *5*, 341–347.
70. Le Bars, J.; Specht, U.; Bradley, J. S.; Blackmond, D. G. *Langmuir* **1999**, *15*, 7621–7625.
71. Rodriguez, A.; Amiens, C.; Chaudret, B.; Casanove, M.-J.; Lecante, P.; Bradleu, J. S. *Chem. Mater.* **1996**, *8*, 1978–1986.
72. Dassenoy, F.; Philippot, K.; Ould Ely, T.; Amiens, C.; Lecante, P.; Snoeck, E.; Mosset, A.; Casanove, M.-J.; Chaudret, B. *New J. Chem.* **1998**, 703–711.
73. de Caro, D.; Bradley, J. S. *New J. Chem.* **1998**, 1267–1273.
74. de Caro, D.; Bradley, J. S. *Langmuir* **1998**, *14*, 245–247.
75. Lange, C.; De Caro, D.; Gamez, A.; Storck, S.; Bradley, J. S.; Maier, W. F. *Langmuir* **1999**, *15*, 5333–5338.

76. Pan, C.; Dassenoy, F.; Casanove, M.-J.; Philippot, K.; Amiens, C.; Lecante, P.; Mosset, A.; Chaudret, B. *J. Phys. Chem. B* **1999**, *103*, 10098–10101.
77. Chan, Y. N. C.; Craig, G. S. W.; Schrock, R. R.; Cohen, R. E. *Chem. Mater.* **1992**, *4*, 885–894.
78. Arul Dhas, N.; Cohen, H.; Gedanken, A. *J. Phys. Chem. B* **1997**, *101*, 6834–6838.
79. Pery, T.; Pelzer, K.; Buntkowsky, G.; Philippot, K.; Limbach, H.-H.; Chaudret, B. *Chem. Phys. Chem.* **2005**, *6*, 605–607.
80. Pelzer, K.; Philippot, K.; Chaudret, B. *Z. Phys. Chem.* **2003**, *217*, 1539–1547.
81. Pelzer, K.; Laleu, B.; Lefebvre, F.; Philippot, K.; Chaudret, B.; Candy, J.-P.; Basset, J.-M. *Chem. Mater.* **2004**, *16*, 4937–4941.
82. Ramirez, E.; Jansat, S.; Philippot, K.; Lecante, P.; Gomez, M.; Masdeu-Bulto, A.; Chaudret, B. *J. Organomet. Chem.* **2004**, *689*, 4601–4610.
83. de Caro, D.; Ould Ely, T.; Mari, A.; Chaudret, B.; Snoeck, E.; Respaud, M.; Broto, J.-M.; Fert, A. *Chem. Mater.* **1996**, *8*, 1987–1991.
84. Tran, N. T.; Powell, D. R.; Dahl, L. F. *Angew. Chem., Int. Ed.* **2000**, *39*, 4121–4125.
85. Gomez, S.; Erades, L.; Philippot, K.; Chaudret, B.; Collière, V.; Balmes, O.; Bovin, J.-O. *Chem. Commun.* **2001**, 1474–1475.
86. Shah, P. S.; Husain, S.; Johnston, K. P.; Korgel, B. A. *J. Phys. Chem. B* **2001**, *105*, 9433–9440.
87. Bönnemann, H.; Braun, G. A. *Angew. Chem., Int. Ed.* **1996**, *35*, 1992–1995.
88. Gamez, A.; Kohler, J.; Bradley, J. *Catal. Lett.* **1998**, *55*, 73–77.
89. Köhler, J. U.; Bradley, J. S. *Langmuir*, **1998**, *14*, 2730–2735.
90. Jansat, S.; Gómez, M.; Philippot, K.; Muller, G.; Guiu, E.; Claver, C.; Castillón, S.; Chaudret, B. *J. Am. Chem. Soc.* **2004**, *126*, 1592–1593.
91. Son, S. U.; Jang, Y.; Yoon, K. Y.; Kang, E.; Hyeon, T. *Nano lett.* **2004**, *4*, 1147–1151.
92. Gomez, M.; Philippot, K.; Collière, V.; Lecante, P.; Muller, G.; Chaudret, B. *New J. Chem.* **2003**, *27*, 114–120.
93. Jansat, S.; Picurelli, D.; Pelzer, K.; Philippot, K.; Gómez, M.; Muller, G.; Lecante, P.; Chaudret, B. *New J. Chem.* **2006**, *30*, 115–122.
94. Finke, R. G. In *Metal Nanoparticles*; Feldheim, D. L., Foss, C. A., Jr., Eds.; Marcel Dekker: New York, 2002; Chapter 2, pp 17–54.
95. Finke, R. G.; Özkar, S. *Coord. Chem. Rev.* **2004**, *248*, 135–146.
96. Lin, Y.; Finke, R. G. *J. Am. Chem. Soc.* **1994**, *116*, 8335–8353.
97. Lin, Y.; Finke, R. G. *Inorg. Chem.* **1994**, *33*, 4891–4910.
98. Watzky, M. A.; Finke, R. G. *J. Am. Chem. Soc.* **1997**, *119*, 10382–10400.
99. Watzky, M. A.; Finke, R. G. *Chem. Mater.* **1997**, *9*, 3083–3095.
100. Hornstein, B. J.; Finke, R. G. *Chem. Mater.* **2003**, *15*, 899–909.
101. Aiken, J. D., III; Finke, R. G. *J. Am. Chem. Soc.* **1998**, *120*, 9545–9554.
102. Aiken, J. D., III; Finke, R. G. *Chem. Mater.* **1999**, *11*, 1035–1047.
103. Özkar, S; Finke, R. G. *J. Am. Chem. Soc.* **2002**, *124*, 5796–5810.
104. Özkar, S; Finke, R. G. *Langmuir* **2002**, *18*, 7653–7662.
105. Özkar, S; Finke, R. G. *Langmuir* **2003**, *19*, 6247–6260.
106. Aiken, J. D., III; Finke, R. G. *J. Am. Chem. Soc.* **1999**, *121*, 8803–8810.
107. Widegren, J. A.; Finke, R. G. *J. Mol. Catal. A: Chemical* **2003**, *198*, 317–341.
108. Widegren, J. A.; Finke, R. G. *Inorg. Chem.* **2002**, *41*, 1558–1572.
109. Widegren, J. A.; Finke, R. G. *J. Mol. Catal. A: Chemical* **2003**, *191*, 187–207.
110. Widegren, J. A.; Bennett, M. A.; Finke, R. G. *J. Am. Chem. Soc.* **2003**, *125*, 10301–10310.
111. Dupont, J.; Fonseca, G. S.; Umpierre, A. P.; Fichtner, P. F. P.; Teixera, S. R. *J. Am. Chem. Soc.* **2002**, *124*, 4228–4229.
112. Fonseca, G. S.; Umpierre, A. P.; Fichtner, P. F. P.; Teixera, S. R.; Dupont, *J. Chem. Eur. J.* **2003**, *9*, 3263–3269.
113. Fonseca, G. S.; Scholten, J. D.; Dupont, J. *Synlett.* **2004**, *9*, 1525–1528.
114. Scheeren, C. W.; Machado, G.; Dupont, J.; Fichtner, P. F. P.; Texeira, S. R. *Inorg. Chem.* **2003**, *42*, 4738–4742.
115. Silveira, E. T.; Umpierre, A. P.; Rossi, L. M.; Machado, G.; Morais, J.; Soares, G. V.; Baumvol, I. J. R.; Teixeira, S. R.; Fichtner, P. F. P.; Dupont, J. *Chem. Eur. J.* **2004**, *10*, 3734–3740.
116. Cassol, C. C.; Umpierre, A. P.; Machado, G.; Wolke, S. I.; Dupont, J. *J. Am. Chem. Soc.* **2005**, *127*, 3298–3299.
117. Vidoni, O.; Philippot, K.; Amiens, C.; Chaudret, B.; Balmes, O.; Malm, J.-O.; Bovin, J.-O.; Senocq, F.; Casanove, M.-J. *Angew. Chem., Int. Ed.* **1999**, *38*, 3736–3738.
118. Pelzer, K.; Vidoni, O.; Philippot, K.; Chaudret, B.; Collière, V. *Adv. Funct. Mater.* **2003**, *13*, 118–126.
119. Duan, Z.; Hampden-Smith, M. J. *Chem. Mater.* **1992**, *4*, 1146–1148.
120. Osuna, J.; de Caro, D.; Amiens, C.; Chaudret, B.; Snoeck, E.; Respaud, M.; Broto, J.-M.; Fert, A. *J. Phys. Chem.* **1996**, *100*, 14571–14574.
121. Dassenoy, F.; Casanove, M.-J.; Lecante, P.; Verelst, M.; Snoeck, E.; Mosset, A.; Ould Ely, T.; Amiens, C.; Chaudret, B. *J. Chem. Phys.* **2000**, *112*, 8137–8145.
122. Billas, I. M. L.; Châtelain, A.; de Heer, W. A. *Science*, **1994**, *265*, 1682–1684.
123. Respaud, M.; Broto, J.-M.; Rakoto, H.; Fert, A. R.; Thomas, L.; Barbara, B.; Verelst, M.; Snoeck, E.; Lecante, P.; Mosset, A., *et al. Phys. Rev. B* **1998**, *57*, 2925–2935.
124. de Caro, D.; Bradley, J. S. *Langmuir* **1997**, *13*, 3067–3069.
125. Ould Ely, T.; Amiens, C.; Chaudret, B. *Chem. Mater.* **1999**, *11*, 526–529.
126. Cordente, N.; Amiens, C.; Chaudret, B.; Respaud, M.; Senocq, F.; Casanove, M.-J. *J. Appl. Phys.* **2003**, *94*, 6358–6365.
127. Ould Ely, T.; Pan, C.; Amiens, C.; Chaudret, B.; Dassenoy, F.; Lecante, P.; Casanove, M.-J.; Mosset, A.; Respaud, M.; Broto, J.-M. *J. Phys. Chem. B* **2000**, *104*, 695–702.
128. Zitoun, D.; Amiens, C.; Chaudret, B.; Fromen, M.-C.; Lecante, P.; Casanove, M.-J.; Respaud, M. *J. Phys. Chem. B.* **2003**, *107*, 6997–7005.
129. Zitoun, D.; Respaud, M.; Fromen, M.-C.; Lecante, P.; Casanove, M.-J.; Amiens, C.; Chaudret, B. *J. Magn. Magnet. Mater.* **2004**, *272–276*, 1536–1538.
130. Dumestre, F.; Chaudret, B.; Amiens, C.; Fromen, M.-C.; Casanove, M.-J.; Renaud, P.; Zurcher, P. *Angew. Chem., Int. Ed.* **2002**, *41*, 4286–4289.
131. Dumestre, F.; Chaudret, B.; Amiens, C.; Fromen, M.-C.; Casanove, M.-J.; Renaud, P.; Zurcher, P. *Angew. Chem., Int. Ed.* **2002**, *41*, 4286–4289.
132. Dumestre, F.; Chaudret, B.; Amiens, C.; Respaud, M.; Fejes, P.; Renaud, P.; Zurcher, P. *Angew. Chem., Int. Ed.* **2003**, *42*, 5213–5216.
133. Snoeck, E.; Dunin-Borkowski, R. E.; Dumestre, F.; Renaud, P.; Amiens, C.; Chaudret, B.; Zurcher, P. *Appl. Phys. Lett.* **2003**, *82*, 88–90.
134. Dumestre, F.; Chaudret, B.; Amiens, C.; Renaud, P.; Fejes, P. *Science* **2004**, *303*, 821–823.
135. Cordente, N.; Respaud, M.; Senocq, F.; Casanove, M.-J.; Amiens, C.; Chaudret, B. *Nano Lett.* **2001**, *1*, 565–568.

136. Dumestre, F.; Martinez, S.; Zitoun, D.; Fromen, M.-C.; Casanove, M.-J.; Lecante, P.; Respaud, M.; Serres, A.; Benfield, R., Amiens, C., *et al. Faraday Discussion* **2004**, *125*, 265–278.
137. Desvaux, C.; Amiens, C.; Fejes, P.; Renaud, P.; Respaud, M.; Lecante, P.; Snoeck, E.; Chaudret, B. *Nat. Mater.* **2005**, 1–4.
138. de Caro, D.; Agelou, V.; Duteil, A.; Chaudret, B.; Mazel, R.; Roucau, C.; Bradley, J. S. *New J. Chem.* **1995**, *19*, 1265–1274.
139. de Caro, D.; Wally, H.; Amiens, C.; Chaudret, B. *J. Chem. Soc. Chem. Commun.* **1994**, 1891–1892.
140. Hambrock, J.; Becker, R.; Birkner, A.; Weiss, J.; Fischer, R. A. *Chem. Commun.* **2002**, 68–69.
141. Rataboul, F.; Nayral, C.; Casanove, M.-J.; Maisonnat, A.; Chaudret, B. *J. Organomet. Chem.* **2002**, *643–644*, 307–312.
142. Hambrock, J.; Schröter, M. K.; Birkner, A.; Wöll, C.; Fischer, R. A. *Chem. Mater.* **2003**, *15*, 4217–4222.
143. Soulantica, K.; Maisonnat, A.; Fromen, M.-C.; Casanove, M.-J.; Lecante, P.; Chaudret, P. *Angew. Chem., Int. Ed.* **2001**, *40*, 448–451.
144. Soulantica, K.; Maisonnat, A.; Senocq, F.; Fromen, M.-C.; Casanove, M.-J.; Chaudret, P. *Angew. Chem., Int. Ed.* **2001**, *40*, 2983–2986.
145. Soulantica, K.; Erades, L.; Sauvan, M.; Senocq, F.; Maisonnat, A.; Chaudret, B. *Adv. Funct. Mater.* **2003**, *13*, 553–557.
146. Soulantica, K.; Maisonnat, A.; Fromen, M.-C.; Casanove, M.-J.; Chaudret, B. *Angew. Chem., Int. Ed.* **2003**, *42*, 1945–1949.
147. Nayral, C.; Viala, E.; Fau, P.; Senocq, F.; Jumas, J.-C.; Maisonnat, A.; Chaudret, B. *Chem. Eur. J.* **2000**, *6*, 4082–4090.
148. Fau, P.; Sauvan, M.; Trautweiler, S.; Nayral, C.; Erades, L.; Maisonnat, A.; Chaudret, B. *Sensor. Actuator. B* **2001**, *78*, 83–88.
149. Schneider, J. J.; Czap, N.; Hagen, J.; Ensling, J.; Gütlich, P.; Reinoehl, U.; Bertagnolli, H.; Luis, F.; de Jongh, L. J.; Wark, M.; Grubert, G.; Hornyak, G. L.; Zanoni, R. *Chem, Eur. J.* **2000**, *6*, 4305–4321.
150. Tang, J.; Redl, F.; Zhu, Y.; Siegrist, T.; Brus, L. E.; Steigerwald, M. L. *Nano. lett.* **2005**, *5*, 543–548.
151. Shim, M.; Guyot-Sionnest, P. *J. Am. Chem. Soc.* **2001**, *123*, 11651–11654.
152. Monge, M.; Kahn, M. L.; Maisonnat, A.; Chaudret, B. *Angew. Chem., Int. Ed.* **2003**, *42*, 5321–5324.
153. Kahn, M. L.; Monge, M.; Collière, V.; Senocq, F.; Maisonnat, A.; Chaudret, B. *Adv. Funct. Mater.* **2005**, *15*, 458–468.
154. Kahn, M. L.; Monge, M.; Snoeck, E.; Maisonnat, A.; Chaudret, B. *Small* **2005**, *1*, 221–224.
155. Kim, C. G.; Sung, K.; Chung, T. M.; Jung, D. Y.; Kim, Y. *Chem. Commun.* **2003**, 2068–2069.
156. Eychmüller, A. In *Nanoparticles: From Theory to Application*; Schmid, G., Ed.; Wiley-VCH: Weinheim, 2004; 50–79.
157. Stuczynski, S. M.; Brennan, J. G.; Steigerwald, M. L. *Inorg. Chem.* **1989**, *28*, 4431–4432.
158. Murray, C. B.; Norris, D. J.; Bawendi, M. G. *J. Am. Chem. Soc.* **1993**, *115*, 8706–8715.
159. Murray, C. B.; Kagan, C. R.; Bawendi, M. G. *Science* **1995**, *270*, 1335–1338.
160. Klein, D. L.; Roth, R.; Lim, A. K. L.; Alivisatos, A. P.; McEuen, P. L. *Nature* **1997**, *389*, 699–701.
161. Danek, M.; Jensen, K. F.; Murray, C. B.; Bawendi, M. G. *Chem. Mater.* **1996**, *8*, 173–180.
162. Dabbousi, B. O.; Rodriguez-Viejo, J.; Mikulec, F. V.; Heine, J. R.; Mattousi, H.; Ober, R.; Jensen, K. F.; Bawendi, M. G. *J. Phys. Chem. B* **1997**, *101*, 9463–9475.
163. Steckel, J. S.; Zimmer, J. P.; Coe-Sullivan, S.; Stott, N. E.; Bulovic, V.; Bawendi, M. G. *Angew. Chem. Int. Ed.* **2004**, *43*, 2154–2158.
164. Manna, L.; Scher, E. C.; Alivisatos, A. P. *J. Am. Chem. Soc.* **2000**, *122*, 12700–12706.
165. Mokari, T.; Banin, U. *Chem. Mat.* **2003**, *15*, 3955–3960.
166. Hambrock, J.; Birkner, A.; Fischer, R. A. *J. Mater. Chem.* **2001**, *11*, 3197–3201.
167. Nann, T.; Riegler, J. *Chem. Eur. J.* **2002**, *8*, 4791–4795.
168. Talapin, D. V.; Shevchenko, E. V.; Kornovski, A.; Gaponik, N.; Haase, M.; Rogach, A. L.; Weller, H. *Adv. Mater.* **2001**, *13*, 1868–1871.
169. Mikulec, F. V.; Kuno, M.; Bennati, M.; Hall, D. A.; Griffin, R. G.; Bawendi, M. G. *J. Am. Chem. Soc.* **2000**, *122*, 2532–2540.
170. Trantler, T. J.; Goel, S. C.; Hickmann, K. M.; Viano, A. M.; Chiang, M. Y.; Beatty, A. M.; Gibbons, P. C.; Buhro, W. E. *J. Am. Chem. Soc.* **1997**, *119*, 2172–2181.
171. Green, M.; O'Brien, P. *Chem. Commun.* **1998**, 2459–2460.
172. Ahrenkiel, S. P.; Micic, O. I.; Miedaner, A.; Curtis, C. J.; Nedeljkovic, J. M.; Nozik, A. J. *Nano lett.* **2003**, *3*, 833–837.
173. Malik, M. A.; O'Brien, P.; Helliwell, M. *J. Mater. Chem.* **2005**, *15*, 1463–1467.
174. Green, M.; O'Brien, P. *Chem. Mat.* **2001**, *13*, 4500–4505.
175. Duphil, D.; Bastide, S.; Lévy-Clément, C. *J. Mater. Chem.* **2002**, *12*, 2430–2432.

12.04 Organometallic Complexes for Optoelectronic Applications

M E Thompson and P E Djurovich, Department of Chemistry, University of Southern California, CA, USA
S Barlow and S Marder, Department of Chemistry, Georgia Institute of Technology, GA, USA

12.04.1 Non-linear Optical Properties of Organometallic Compounds

12.04.1.1 Introduction

Intense light, such as that of a laser beam, changes the optical properties of a non-linear optical (NLO) material; these changes, in turn, affect the properties of the light beam as it propagates through the material. NLO effects were first observed in 1961 by Franken and co-workers, when they illuminated a quartz crystal with a Ruby laser (the fundamental wavelength being 680 nm), and detected a weak ultraviolet emission at 340 nm.[1] This phenomenon is known as second harmonic generation (SHG) or frequency doubling. More generally, the NLO properties of materials can be used to control the phase, the state of polarization, or the frequency of light beams. For instance, they can be exploited to store and restore information optically, or to deflect light beams and route optical light beams between fiber optic channels. In emerging photonic technologies for use in areas such as telecommunications, light is used to carry information and optical waveguides including optical fibers are used to transport and modulate the light. For many applications, passive materials, in which the light does not alter the properties of the material, can be used to transport light. However, for other applications where modulation of the propagation characteristics of light is required, it is necessary to use active NLO materials. There is a strong technological demand for high-performance NLO materials that generally fall into two main categories:

- Second-order materials which exhibit quadratic effects such as SHG or electrooptic (EO) switching (in which the refractive indices of EO materials can be modulated by application of an electric static field). The materials must be non-centrosymmetric at both microscopic and macroscopic levels.
- Third-order materials which exhibit cubic effects such as third harmonic generation (THG) or four-wave mixing (FWM). These materials have no restrictions on their symmetry.

Loosely held electrons, typically in extended π-systems, can give rise to very large optical non-linearities in organic and organometallic molecules. The macroscopic non-linearities of organic and organometallic materials result mainly from the sum of contributions from the molecular constituents. Hence, although maximizing NLO properties requires high chromophore loadings (and orientation in the case of second-order materials), it is also necessary to understand the structure–property relations governing the non-linearities of molecular chromophores.

12.04.1.1.1 Linear and non-linear polarizations

Application of an electric field E to a system of positive and negative charges will result in a charge separation, that is, an induced dipole with an associated moment, μ. For small fields, the displacement of charges from their equilibrium positions in a molecule is approximately linearly proportional to the strength of the applied field and the associated induced dipole vector is given by the product of the field vector, E, and the linear polarizability α_{ij} (a second-rank tensor) such that the following (Equation (1)) holds good:

$$(\text{polarization})_i = \mu_i = \alpha_{ij} E_j \tag{1}$$

where i and j refer to components in the molecular frame. In bulk materials, the linear polarization per unit volume is given by an analogous equation (Equation (2)).

$$P_i = \chi_{ij} E_j \tag{2}$$

where χ_{ij} is the linear susceptibility tensor of the ensemble of molecules. If one assumes that the molecules that make up the optical material are independently polarized by light with no intermolecular coupling, χ_{ij} is related to the sum of all the individual polarizabilities, α_{ij}.

However, Equations (1) and (2) are approximations; generally, polarizability cannot be regarded as a constant and the induced polarization is a non-linear function of field strength. This non-linearity becomes increasingly important at very intense electric fields. The non-linear dependence of a dipole moment on field can be expressed as a Taylor series as shown in Equations (3) and (4)

$$\mu_i(E) = \mu_i(0) + \frac{\partial \mu_i}{\partial E_j}\bigg|_0 E_j + \frac{1}{2!}\frac{\partial^2 \mu_i}{\partial E_j \partial E_k}\bigg|_0 E_j E_k + \frac{1}{3!}\frac{\partial^3 \mu_i}{\partial E_j \partial E_k \partial E_l}\bigg|_0 E_j E_k E_l \ldots \tag{3}$$

$$\mu_i(E) = \mu_i(0) + \alpha_{ij}E_j + \frac{1}{2!}\beta_{ijk}E_j E_k + \frac{1}{3!}\gamma_{ijk}E_j E_k E_l \ldots \tag{4}$$

where the 0 subscript indicates evaluation of the differentials at $E = 0$ and i, j, ... refer to components in the molecular frame. The first term, $\mu_i(0)$, is the dipole moment of the molecule in the absence of any electric field. The second term is the linear polarization, equivalent to the linearly induced dipole moment of Equation (1). Just as the second-rank tensor α_{ij} is the linear polarizability, the higher-order terms β_{ijk} and γ_{ijkl} (Equation (4)) are called the first and second hyperpolarizabilities, respectively, and are third- and fourth-rank tensors, respectively. The terms beyond $\alpha_{ij}E_j$ are not linear in E and are, therefore, collectively referred to as non-linear polarization; it is these terms that give rise to NLO effects. Except in rather intense electric fields, $\alpha_{ij}E_j > 1/2\beta_{ijk}E_iE_k > 1/6\gamma_{ijkl}E_iE_kE_l$; thus, the observation of NLO effects was greatly aided by the availability of the intense light from laser with its associated large electric fields.

The observed bulk polarization density is given by an expression (Equation (5)) analogous to Equation (4):

$$P_i(E) = P_i(0) + \chi^{(1)}_{ij}E_j + \chi^{(2)}_{ijk}E_jE_k + \chi^{(3)}_{ijkl}E_jE_kE_l \ldots \tag{5}$$

where the $\chi^{(n)}$ are linear ($n = 1$) and non-linear ($n > 1$) susceptibilities and $P(0)$ is the intrinsic static dipole moment density of the sample.

Second-order (and other even-order) NLO effects create an asymmetric polarization (a field of E will lead to an induced polarization of $P(\text{ind}) = \chi^{(1)}E + \chi^{(2)}E^2 + \cdots$, while a field of $-E$ will lead to an inequivalent polarization of $P(\text{ind}) = -\chi^{(1)}\text{E} + \chi^{(2)}E^2 + \cdots$). Hence, only molecules that are non-centrosymmetric can have a non-zero β and only non-centrosymmetric materials can have non-zero $\chi^{(2)}$ (i.e., a centrosymmetric arrangement of non-centrosymmetric molecules will have zero $\chi^{(2)}$).

12.04.1.1.2 Second-order non-linear polarization of matter and second-order NLO effects

12.04.1.1.2.(i) Frequency doubling and sum frequency generation

The electronic charge displacement (polarization) induced by an oscillating electric field (e.g., light) can be viewed as a classical oscillating dipole that itself emits radiation at the oscillation frequency. If an intense light beam passes through a second-order NLO material, light at twice the input frequency will be produced as well as a DC electric field. The first process is known as SHG and the second as optical rectification. SHG is a form of three-wave mixing, since two photons with frequency ω have combined to generate a single photon with frequency 2ω. Since the oscillating dipole re-emits at all of its polarization frequencies, one observes light at both ω and 2ω. In a similar manner, this idea can be extended to third- and higher-order non-linear terms; by analogy, third-order processes involve interaction of three fields in a molecule to produce a fourth field (FWM). The general picture of second-order NLO effects involves the interaction of two distinct waves with electric fields E_1 and E_2 (potentially of different polarizations and frequencies), with the electrons of the NLO material. Suppose, for example, that two laser beams with different frequencies are used. With two interacting waves of amplitudes E_1 and E_2, the second-order term of Equation (5) becomes the following (Equation (6)):

$$\chi^{(2)}E_1\cos(\omega_1 t)E_2\cos(\omega_2 t) \tag{6}$$

which is equivalent to Equation (7) shown below.

$$\frac{1}{2}\chi^{(2)}E_1E_2\cos[(\omega_1 + \omega_2)t] + \frac{1}{2}\chi^{(2)}E_1E_2\cos[(\omega_1 - \omega_2)t] \tag{7}$$

From Equation (7) it can be seen that when two light beams of frequencies ω_1 and ω_2 interact in an NLO material, polarization and, therefore, re-emitted light occurs at sum $(\omega_1 + \omega_2)$ and difference $(\omega_1 - \omega_2)$ frequencies. The combination of frequencies is called sum (or difference) frequency generation (SFG). SHG is a special case of SFG where the two frequencies are equal; the sum is the second harmonic and the difference is the DC component.

12.04.1.1.2.(ii) Changing the propagation characteristics of light: the pockels effect

It is possible to change the amplitude, phase, or path of light at a given frequency by using a static DC electric field to polarize the material and modify the refractive indices. Consider the special case $\omega_2 = 0$ (Equation (7)) in which a DC electric field is applied to the material. The optical frequency polarization arising from the second-order susceptibility is shown in Equation (8)

$$P^{(2)}_{\text{opt}} = \chi^{(2)} E_1 E_2 (\cos \omega_1 t) \tag{8}$$

where E_2 is the magnitude of the electric field caused by a voltage applied to the non-linear material and the total optical polarization (ignoring χ^3 and higher terms) is shown in Equation (9).

$$P_{\text{opt}} = \chi^{(1)} E_1 (\cos \omega_1 t) + \chi^{(2)} E_1 E_2 (\cos \omega_1 t) = \left(\chi^{(1)} + \chi^{(2)} E_2\right) E_1 (\cos \omega_1 t) \tag{9}$$

Thus, the applied field, E_2, changes the "effective" linear susceptibility (i.e., the polarization dependent on the light field, E_1). Since the linear susceptibility is related to the refractive index, the refractive index of the material is also changed by the applied field. This is known as the linear electrooptic (LEO) or Pockels effect, and is used to modulate the polarization or phase of light by changing the applied voltage.

12.04.1.1.3 Third-order non-linear polarization of matter and third-order NLO effects

If we reconsider Equation (5) for the expansion of polarization of a molecule as a function of a single electric field with frequency ω and assume that the even-order terms are zero (e.g., if the molecule is centrosymmetric), we see the following (Equation (10)):

$$\mu = \mu(0) + \alpha E \cos(\omega t) + \frac{\gamma}{6} E^3 \cos^3(\omega t) \ldots \tag{10}$$

which, using the trigonometric identity (Equation (11))

$$\cos^3(\omega t) = \frac{3}{4}\cos(\omega t) + \frac{1}{4}\cos(3\omega t) \tag{11}$$

can be rewritten as (Equation (12)):

$$\mu = \mu(0) + \alpha E \cos(\omega t) + \frac{\gamma}{6} E^3 \frac{3}{4} \cos(\omega t) + \frac{\gamma}{6} E^3 \frac{1}{4} \cos(3\omega t) \ldots \tag{12}$$

or as (Equation (13)):

$$\mu = \mu(0) + \left(\alpha + \frac{\gamma}{6} E^2 \frac{3}{4}\right) E \cos(\omega t) + \frac{\gamma}{6} E^3 \frac{1}{4} \cos(3\omega t) + \cdots \tag{13}$$

Thus, the interaction of light with third-order NLO molecules creates a polarization component at its third harmonic. Similarly, the induced polarization for a bulk material would lead to THG through $\chi^{(3)}$, with the material susceptibility analogous to γ. In addition, there is a component at the fundamental, and we note that the $[\alpha + \gamma/6.E^2.3/4]$ term of Equation (13) is similar to the term responsible for the LEO effect. Similarly, it can be shown that the application of an intense light field or voltage will also induce a refractive index change in a third-order NLO material; these effects are known as the optical and the DC Kerr effects, respectively. The sign of $\chi^{(3)}$ will determine if the third-order contribution to the refractive index is positive or negative. Materials with positive $\chi^{(3)}$ have the property of self-focusing a laser and those with negative $\chi^{(3)}$ will be self-defocusing.

It should be noted that γ and $\chi^{(3)}$ are complex quantities; properties such as self-focusing depend on the refractive real part, γ_{real} and $\chi^{(3)}{}_{\text{real}}$, while frequency tripling depends on the moduli, $|\gamma_{\text{real}}|$ and $|\chi^{(3)}|$. One of the factors that can give rise to positive imaginary contributions, γ_{imag} and $\chi^{(3)}{}_{\text{imag}}$, is two-photon absorption, which corresponds to the excitation of a molecule by two photons, the sum of whose energies correspond to the energy difference between the two states in question. The design and synthesis of molecules with large two-photon absorption cross sections, δ (which should not be confused with the third hyperpolarizability), has gained increasing attention in recent years. Due to the potential for well-defined excitation in volumes of the order of the wavelength of light employed at depth in otherwise absorbing media, there are potential applications in 3D fluorescence imaging,[2,3] photodynamic therapy,[4]

NLO transmission,[5] and 3D microfabrication.[6–8] However, there have been rather few studies of organometallic compounds at this time, especially studies in which two-photon spectra have been determined.

12.04.1.1.4 Introduction to the design of second-order NLO chromophores

We have already noted that nonzero β is only found in non-centrosymmetric molecules; one structural motif that fulfills this symmetry requirement is a more or less linear π-system with donor and acceptor end groups, for example, *p*-nitroaniline, **1**, or 4-dimethylamino-4′-nitrostilbene, **3** (Figure 1). The sum-over-states approach describes how the hyperpolarizabilities depend on the properties of the excited states of the molecule. In simple donor–acceptor compounds, β can be well described as arising principally from the contributions of the ground state (g) and one low-lying CT state (e) strongly coupled to the ground state (often the first-excited state).[9] Using this two-state approximation, the static (zero-frequency) limit of β is given (using the Taylor series definition of β given in Equation 4) by Equation (14).

$$\beta_0 = \frac{6\mu_{ge}^2 \Delta\mu_{ge}}{(\hbar\omega_{ge})^2} \tag{14}$$

Equation (14) clearly indicates that molecules whose linear spectra show intense (i.e., large μ_{ge}) low-energy (i.e., low $E_{ge} = \hbar\omega_{ge}$) CT (i.e., large $\Delta\mu_{ge}$, either positive or negative, as indicated by solvatochromism or by Stark spectroscopy) transitions are good candidates for second-order NLO investigations.

Thus, β is determined by the interplay of the three parameters in Equation (14), each of which varies in a different way with the strengths of donor and acceptor, with the nature of the bridge, and with the nature of the environment (e.g., solvent polarity). In a two-state valance-bond analysis, both the ground- and the first-excited states can be viewed as linear combinations of the neutral and charge-separated (zwitterionic) limiting resonance forms, as shown for **1–3** in Figure 1, and the ground- and excited-state structures are determined by the relative contribution of each limiting resonance form, which, in turn, depend on the nature and size of the molecule (e.g., the aromaticity of the phenylene ring of **1** favors neutral contributions to the ground state), the donor and acceptor strengths (increased strengths favor the zwitterionic structure), and the environment (more polar solvents favor more zwitterionic contributions). When using this two-state model, it follows that if the neutral form dominates the ground state, the zwitterionic form will prevail in the excited state, leading to an increase of the dipole moment upon excitation ($\mu_g \cdot \Delta\mu_{ge} > 0$). Conversely, if the charge-separated form is the main contributor to the ground state, then the neutral form dominates the excited state so that the excited-state dipole moment is smaller than the ground-state dipole ($\mu_g \cdot \Delta\mu_{ge} < 0$). Therefore, a positive β_0 indicates a predominance of the neutral form in the ground state. On the other hand, a negative β_0 implies that the zwitterionic form prevails in the ground state. The case where both ground and excited states arise from equal mixing between the limiting resonance forms leads to vanishing quadratic hyperpolarizability ($\Delta\mu_{ge} = 0$). This has been confirmed by semi-empirical calculations perfomed on donor–acceptor polyenes which show β_0 can be correlated with a structural parameter, the bond-length alternation (BLA), between adjacent C–C bonds in the bridge.[10–12] The ground-state structure of the gas-phase molecule was artificially tuned from a neutral to a zwitterionic structure by varying an external static electric field F parallel to the acceptor–donor axis. It was shown that there is positive peak in α_0, β_0 vanishes and γ_0 peaks negatively at zero BLA (the "cyanine limit") independently of the nature of the push–pull molecule; the positions of peaks in β_0 and γ_0 are shown in Figure 2. While these results were derived for organic species, they are anticipated to apply equally well to organometallic systems that can be approximated as two-level systems and illustrate that donor and acceptor strengths must be carefully balanced to optimize the hyperpolarizability (β or γ) of interest.

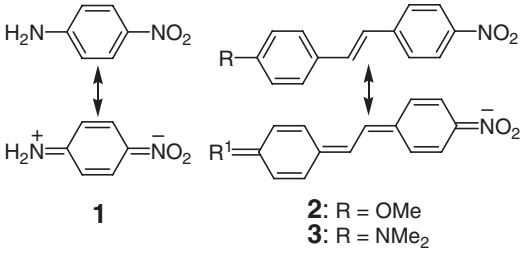

Figure 1 Neutral and zwitterionic resonance forms for simple organic donor–acceptor compounds.

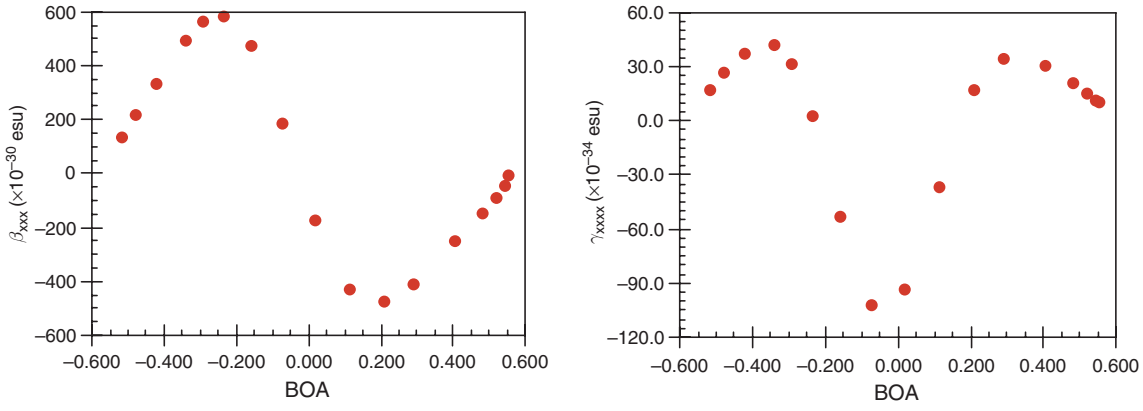

Figure 2 Dependence of the first and second hyperpolarizabilities on bond-order alternation (BOA) calculated for a donor–acceptor polyene under the influence of an external electric field. The left-hand side of each plot corresponds to a structure dominated by the neutral resonance structure, whereas the right-hand side corresponds to a zwitterionic structure. In a two-state model BOA = 0 corresponds to an equal mixture of the two resonance forms.

In addition to dipolar motifs, other non-centrosymmetric designs may give non-zero β; there has been considerable interest in octupolar organic, inorganic, and organometallic molecules.[13] Due to the lack of dipole moments in these species, it is anticipated that it may be easier to achieve non-centrosymmetry in crystals. However, studies have usually focused on determining β in solution using hyper-Raleigh scattering (HRS).[14] Here, dipolar terms, such as that of Equation (14), are not to be expected (although they have been reported in some systems where, despite a non-polar ground state, the excited state breaks symmetry to acquire a dipole moment[15]), but rather octupolar contributions to β. A sum-over-states expression for octupolar contributions analogous to Equation (14) has been derived, but involves three states, since excited-state/excited-state transition dipole moments, regarding which most chemists have little intuition, is less readily translated into design guidelines. Similar equations are available for γ;[16] again, there are both two-level and three-level terms and control of the latter requires an understanding of excited-state/excited-state transition dipoles.

12.04.1.1.5 Dispersion-enhanced versus static hyperpolarizabilities

If one measures β using light chosen such that the frequency of both the fundamental and the second harmonic (frequency-doubled) light are very far in energy from any frequency at which the molecule absorbs, the measured β will approach its static (or zero-frequency) value, β_0. However, in general, β is frequency dependent (as is γ), that is, it shows dispersion with frequency. Ideally, one would wish to know the dispersion spectrum of β (or γ) for a given compound over a range of frequencies; while this has been measured for a few compounds, typically values are only available at one or two conveniently accessible frequencies. Thus, many values of β in the literature are dispersion enhanced. Comparisons of β measurements made at different frequencies should be made with caution. While the value at a particular wavelength may be useful if one is interested in applications at that particular wavelength, for understanding structure–property relationships, it is important to be able to compare values from different studies at different frequencies and establish the extent to which trends are due to underlying trends in the static hyperpolarizability, rather than to differing dispersion effects. The two-level model proposed by Oudar[17] predicts that the dispersion enhancement of β (as determined by frequency-doubling phenomena) should be given by Equation (15).

$$\beta(-2\omega;\omega,\omega) = \beta_0 \frac{\omega_{ge}^4}{\left(\omega_{ge}^2-(2\omega)^2\right)\left(\omega_{ge}^2-\omega^2\right)} \tag{15}$$

Where ω is the fundamental frequency and ω_{ge} is the absorption maximum of the molecule. Analogous, but mathematically more complex, expressions have been applied to γ (with different dispersion dependencies expected

for different third-order NLO effects). Equation (14) has been widely used to estimate static β_0 from single-frequency measurements of β. However, this expression is really only applicable when

(i) $\omega_{ge} >> 2\omega_{ge}$, that is, in the so-called non-resonant régime,
(ii) one excited state dominates the non-linearity, and
(iii) one tensor component dominates the NLO response.

The third condition is more or less met in many dipolar chromophores, but Equation (15) has often been applied where the first two conditions are not met, that is, where ω_{ge} is close to 2ω (and where damping terms are required to avoid $\beta_0 \rightarrow 0$), or where more than one excited state contributes significantly to β (as is the case for some classes of organometallic compounds). In some cases, however, there is some evidence that, due to cancelation of opposing effects, reasonable estimates can sometimes be obtained from this equation even when not all the conditions are not met.[18] In any case, the values of β_0 given in this chapter are those given in the original publications; inevitably, the reliability of these values varies from compound to compound. Similar caveats apply to the interpretation of reported $\chi^{(2)}{}_0$, $\chi^{(3)}{}_0$, and γ_0 values.

12.04.1.1.6 Techniques for measuring hyperpolarizabilities

SHG efficiencies of crystalline powders, measured using the so-called Kurtz–Perry technique,[19] have typically been reported relative to those of well-known acentric crystals, such as urea. Complications can be observed due to SHG at acentric surface defect or surface sites; for example, SHG similar to that of urea has been measured for an organoruthenium species, despite its crystals belonging to a centrosymmetric space group.[20] However, SHG gives us only limited insight into molecular structure–property relations since it is dependent on the vagaries of crystal packing; moreover, many high-β chromophores tend to have rather high dipole moments that tend to align antiparallel. For applications, interest has shifted to poled polymer systems: here, a dipolar chromophore mixed with (or covalently bound to) a polymer host is aligned in an electric field above the glass transition temperature of the polymer; when the material is cooled below T_g and the field removed, the acentric order remains "frozen in." The efficiency of different materials in films can be compared by measuring $\chi^{(2)}$ (or the related parameter, d_{33}) by SHG or by measuring the EO coefficient, r_{33}. These latter quantities can be used to deduce β if one can also make a reasonable estimate of the degree of alignment of the molecules.

Molecular first hyperpolarizabilities, β, have generally been measured in solution by either electric-field-induced second harmonic generation (EFISH) or HRS. The former technique[21,22] involves measuring second harmonic efficiencies from a solution of a neutral dipolar molecule in a strong electric field, which induces the acentric order necessary for the observation of second-order properties. The quantity measured is the scalar product of the vectorial part of β and the dipole moment, μ. An advantage of this technique is that $\mu\beta$ is a useful figure of merit for poled polymer systems (except for high-dipole-moment molecules at high loadings, where dipole–dipole repulsions become important). A disadvantage is that one only obtains the component of β along the dipole moment axis, although in many dipolar, more-or-less linear π-systems, the principal component of β often does lie more or less along the axis of μ. Moreover, EFISH is also unsuitable for ionic and non-dipolar chromophores (as is electric-field poling). In contrast, HRS is suitable for all types of chromophores; however, HRS relies on incoherent frequency doubling arising from the locally asymmetric environments of molecules in isotropic solution, and so the signals measured are typically rather weak, requiring great care to be taken in correcting for a variety of other processes, especially two-photon fluorescence.[23–26] In some cases, β has been estimated from the two-level model: values of μ_{ge} and ω_{ge} from the optical spectrum, along with $\Delta\mu_{ge}$ determined using solvatochromic data or Stark spectroscopy, are input into Equation (14). This method is clearly only valid for dipolar chromophores. Techniques for second-order NLO effects have been compared in more detail elswhere.[27]

Commonly employed techniques for third-order materials are THG, degenerate four-wave mixing (DFWM), and z-scan. These techniques have been thoroughly compared elsewhere.[28]

A variety of quantum chemical computational methods have also been used to compute β and γ;[29–45] these will be not be discussed in detail in this chapter. However, it is worth noting that comparison between experimental and computational methods should be made with caution: the latter typically apply to the gas phase where it has been shown that β can be significantly smaller than in condensed phases.[46,47] Moreover, confusion may also arise due to the choice of conventions defining the experimental and computational hyperpolarizabilities (see below).

12.04.1.1.7 Caveat lector: conventions defining hyperpolarizabilities

Confusingly, several alternative conventions are used for the definition of the non-linear polarizabilities β, γ, etc. For example, a common alternative form of Equation (4), popular with experimentalists, omits the factors of $1/n!$ before each E^n term; that is, the nth order polarizabilities are equated to $(1/n!) \times (\partial^n \mu / \partial E^n)$, rather than simply to the differential. The sum-over-states expressions for β and γ are consequently also different; thus, the two-level expressions for β may differ from Equation (14) in the numerical constants. Values of β and γ vary by factors of up to 6 depending on the convention employed. Unfortunately, there is considerable confusion in the literature regarding these conventions; many studies do not explicitly indicate which convention is being used, complicating comparisons of hyperpolarizabilities between different studies, and in several studies comparison has been made, apparently unwittingly, between experimental and computational values defined with different conventions. Due to the considerable confusion, the authors have not attempted to standardize the literature and use one single convention in this chapter. Thus, when comparing values between different chromophores, the reader should take care to compare "like with like." A detailed comparison of the alternative conventions is given in Ref: 48. The reader should also note that γ is sometimes quoted as an orientational average or as the principal component along the long axis of the molecule.

12.04.1.1.8 Units in non-linear optics

Although the bulk SHG and EO coefficients, d_{33} and r_{33}, are frequently quoted in pmV^{-1} and two-photon absorption is usually quoted in GM ($1\,GM = 10^{-50}\,cm^4 s(photon)^{-1}$), most NLO quantities (and most of those discussed in this chapter) are typically expressed in cgs units. These are not usually stated explicitly, but "esu" is used to denote that the units are the appropriate "electrostatic units" for that quantity in the cgs system; the authors have followed this practice in this chapter. Some important conversions from esu to SI are given in Table 1.

12.04.1.2 *d*-Block Metal Compounds with η^2–η^7 Ligands

12.04.1.2.1 Group 8 metallocenes

12.04.1.2.1.(i) Second-order NLO properties of metallocene donor–acceptor compounds

Ferrocene is one of the most widely studied organometallic components of second-order NLO chromophores. The reasons for this are not difficult to discern. For many organometallic chemists, ferrocene is one of the first species that springs to mind as a strong donor group; it is reasonably stable, at least by the standards of much of organometallic chemistry, and its well-developed functionalization chemistry allows for its facile incorporation into various conjugated systems. Moreover, an early report of a powder SHG efficiency 62× that of urea in *Z*-*p*-nitrostyrylferrocene (at 1064 nm), **4** (Figure 3),[49] created much interest,[49] as evidenced by its being cited over 250 times. Many similar experiments have been conducted on ferrocene derivatives.[50–64] Molecular structures of three of the most efficient examples studied, **5** ($SHG_{1064} = 123 \times$ urea),[50] **6** ($SHG_{1064} = 200 \times$ urea),[51] and **7** ($SHG_{1064} = 140 \times$ urea),[59] are shown in Figure 3.

Although metallocene-based species were among those that sparked widespread interest in organometallic nonlinear optics, understanding the structure–property relationships governing their NLO properties is not particularly straightforward.[65] It might be assumed that the low ionization potential of ferrocene (6.86–6.89 eV[66,67]) would make the ferrocenyl group a better donor than 4-(dimethylamino)phenyl (IP of $Me_2NPh = 7.14$–7.6 eV[68,69]) and be comparable to the 4-(diphenylamino)phenyl (IP of $Ph_3N = 6.86$ eV[70]) groups (even within amine donors, ionization

Table 1 Conversions for some properties important in non-linear optics[a]

Quantity	*SI units*	*Conversion from esu*[b]
Dipole moment, μ	C m	$\mu_{SI} = (1/3) \times 10^{-11} \times \mu_{esu}$[c]
β	$C\,m^3\,V^{-2}$	$\beta_{SI} = (1/3)^3 \times 10^{-19} \times \beta_{esu}$
$\mu\beta$	$C^2\,m^4\,V^{-2}$	$\mu\beta_{SI} = (1/3)^4 \times 10^{-30} \times \mu\beta_{esu}$
$\chi^{(2)}$	$m\,V^{-1}$	$\chi^{(2)}{}_{SI} = (4\pi/3) \times 10^{-4} \times \chi^{(2)}{}_{esu}$
γ	$C^2\,m^4\,V^{-3}$	$\gamma_{SI} = (1/3)^4 \times 10^{-23} \times \gamma_{esu}$
$\chi^{(3)}$	$m^2\,V^{-2}$	$\chi^{(3)}{}_{SI} = (4\pi/3)^2 \times 10^{-8} \times \chi^{(3)}{}_{esu}$

[a]Adapted from a more extensive table in Ref: 27.
[b]The subscripts "SI" and "esu" denote the quantity in question expressed in those unit conventions.
[c]$1\,D = 10^{-18}$ esu.

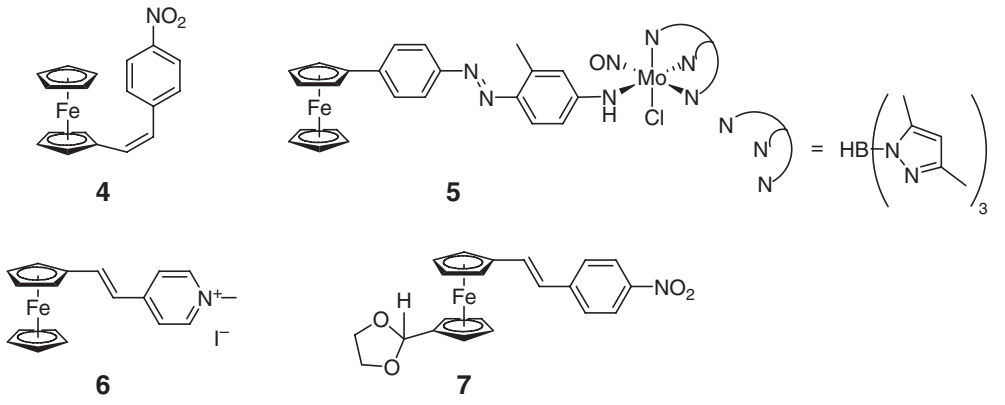

Figure 3 Structures of some ferrocene-based chromophores with high powder SHG efficiencies.

potential is a poor guide to π-donor strength: 4-(dialkylamino) phenyl is a stronger p-donor than 4-(diphenylamino)-phenyl).[71,71a,71b] However, the three highest orbitals of ferrocene are essentially 3D metal with rather little cyclopentadienyl character. Thus, the frontier orbitals of ferrocene do not couple so strongly to those of attached π-systems as those of organics (Outside the area of NLO this can be seen, for example, by comparing the electronic coupling between redox centres as determined by Hush theory for the mixed-valence $[FcCH–CHFc]^{+}$[72,72a] and $[FcCCFc]^{+}$[72b] cations with those for their 4-(di-p-anisylamino) phenyl-terminated analogs.)[72,72c,72d,] Thus, the π-donor abilities of ferrocene do not mirror its abilities to act as a donor in electron-transfer reactions.[65] According to photoelectron spectroscopy, it is the HOMO–3 of ferrocene which is principally located on the cyclopentadienyl rings that couples strongly to the π-system.[73]

The UV–VIS–NIR spectra of ferrocene donor–acceptor species show two low-energy solvatochromic bands, whereas those of corresponding all-organic species typically show only one such band. Several origins for the spectra have been proposed: in one model the low-energy bands are regarded as *d–d* transitions with little contribution to the NLO response, whereas the higher-energy band is a metal-to-acceptor transition;[29] in another model, the low-energy band is regarded as metal to acceptor in character and the higher-energy band as a charge transfer (CT) from the highest orbital arising from the coupling of cyclopentadienyl and bridge orbitals to the acceptor.[73] In the case of relatively weak acceptors, as in the case of **4** and its *E*-isomer, **8**, the lower energy of these two bands is considerably weaker. For **10**, it is estimated that the LE transition is responsible for only ca. 37% of the two-level contributions to β_0 (E_{ge} and μ_{ge} from spectra; $\Delta\mu_{ge}$ from Stark spectra).[73] In species with longer polyene bridges or with considerably stronger acceptors, these two bands are closer in energy and oscillator strength, and the two-level contributions of the lower-energy state to β_0 grow in relative importance; in **11** (Figure 4) the LE state is responsible for ca. 75% of the two-level contributions.

In species with short π-systems and relatively weak acceptors, ferrocene compounds exhibit similar $\mu\beta$ and β values to all-organic analogs with *p*-methoxyphenyl donors; using EFISH at 1,907 nm, $\mu\beta$ values of 140 and 153×10^{-48} esu and β values of 31 and 34×10^{-30} esu were measured for **8**[74] and its *p*-methoxyphenyl-donor analog, **2**,[75] respectively, with considerably greater values determined for its *p*-dimethylaminophenyl-donor analog, **3**. The ferrocene species also has a somewhat inferior transparency than the organic species due to the presence of the low-energy transition. In longer species with strong acceptors, some of the properties of ferrocene-donor species begin to approach those of amine analogs; for example, **16** and **17** (Figure 4) show similar $\mu\beta$ (and estimated $\mu\beta_0$) values of 4,600 (3,300), and 5,500 (3,200) $\times 10^{-48}$ esu, respectively, (EFISH, 1,907 nm) and, in this case, the ferrocene species does not show inferior transparency to its all-organic analog.[76] The highest reported $\mu\beta$ we are aware of for a metallocene derivative is $11{,}200 \times 10^{-48}$ esu for **15** (Figure 4; EFISH, 1,907 nm).[77] The largest β values reported are highly resonantly enhanced values for a polyene with a ferrocene donor and an organochromium acceptor, and are discussed in more detail in Section 12.04.1.3.1.(ii).[78] A rather large, though also presumably considerably dispersion enhanced, value of 970×10^{-30} esu was also measured for **18** (Figure 4) using HRS at 1,000 nm;[45] it was shown that, for this compound and similar species, calculated or measured (HRS) β-values could be correlated with experimental (X-ray) BLAs in accordance with the ideas described in Section 12.04.1.1.4.[45]

Ruthenocenes have been much less widely explored than ferrocene; presumably, this can, at least in part, be attributed to the greater expense involved and to the more limited functionalization chemistry. Ruthenocene species typically show rather smaller non-linearities relative to their ferrocene analogs, although they do show superior

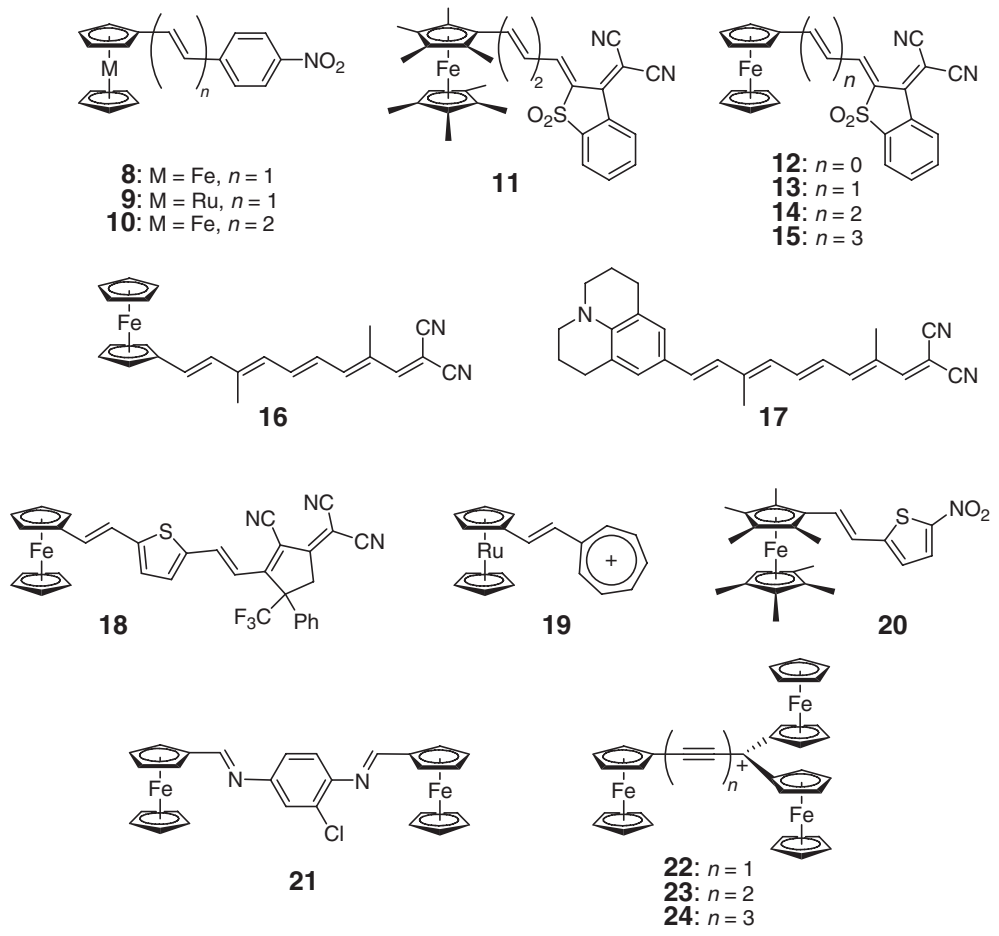

Figure 4 Structures of some group 8 metallocene compounds studied as second-order chromophores and discussed in Section 12.04.1.2.1.(i) along with that of an all-organic analog.

transparency owing to their higher-lying low-energy transitions.[74,77] For example, $\mu\beta$ and β values for **9** are around half the magnitude of the respective values for **8**; low-energy absorption maxima of **8** and **9** are 496 and 390 nm, respectively.[74] Some of the largest non-linearities reported for ruthenocenes are reported for species with the tropylium ion as acceptor; values of $\beta = 649 \times 10^{-30}$ esu and $\beta_0 = 120 \times 10^{-30}$ esu were reported for **19** (Figure 4) using HRS at 1,064 nm.[79] Osmocene has barely been investigated at all in this context, the cost and limited functionalization chemistry being even more serious deterrents than in the case of ruthenocene; although the synthesis and optical spectra of the osmium analog of **4**, and its *E*-isomer, have been reported,[73] no NLO measurements have been published.

In addition to solution measurements, several bulk measurements have been made on ferrocene chromophores incorporated into poled polymer films.[45,80–84] These measurements have shown that there are no special problems associated with poling ferrocene chromophores. The best bulk performance achieved for a ferrocene-based polymer material was an EO coefficient, r_{33}, of 25 pm V^{-1} (1,300 nm) for a film of **18** incorporated at 20 wt.% into amorphous polycarbonate;[45] this is not, however, competitive with the performance of state-of-the-art all-organic poled polymer systems. In some cases, the chromophores have been covalently linked to the polymer chain.[80] Bulk SHG measurements have also been made on self-assembled Langmuir–Blodgett films incorporating ionic ferrocene-based chromophores,[85–90] and on self-assembled monolayers of thiol-functionalized ferrocenyl chromophores on Au.[91]

Since ferrocene derivatives may also be readily and reversibly oxidized to ferrocenium ions, this has been proposed and demonstrated as a means of electrochemically "switching" NLO responses.[91–94] Generally, the oxidized species is found to have a considerably lower hyperpolarizability, consistent with ferrocenium being a much poorer donor than ferrocene; for example, HRS has been used to measure the second-order properties of a solution of **20** (Figure 4) through multiple redox cycles, the NLO response varying by a factor of >6 between **20** and $[\mathbf{20}]^+$.

Large hyperpolarizabilities have been reported for CT complexes formed between ferrocene imines and acceptors such as tetracyanoethylene (TCNE), 7,7,8,8-tetracyanoquinodimethane (TCNQ), and *p*-chloranil (CA);[95,96] for example, compound **21** shows $\beta = 33 \times 10^{-30}$ esu (HRS, 1,064 nm), but complexes with TCNE, TCNQ, and CA show values of 126, 204, and 279×10^{-30} esu (β_0 is estimated to be enhanced from 5.5 to 33–53 $\times 10^{-30}$ esu). Presumably, the NLO active states are associated with the intermolecular CT in these complexes.

Metallocene donors have been linked though a variety of π-bridges to a very wide variety of acceptors: organic groups of widely varying acceptor strengths,[97–107] including some with open-shell organic radical centers,[94,108] fullerenes,[109] other transition metal organometallics,[36,55,56,78,102,104,110–114] transition metal coordination complexes,[92,106,115] and main group "metal" acceptors.[116,117] The species incorporating other organometallic groups are discussed in other sections of this chapter. Another type of acceptor group that is rather unusual is found in compounds **22–24** (Figure 4) and can be described as a carbocation stabilized by additional ferrocene donors; β_0 values of 135, 171, and 228×10^{-30} esu have been estimated for $n = 1$, 2, and 3 species, respectively, from HRS data.[118] Other species have incorporated ferrocene donors with other organometallic groups in the bridge in place of all-organic conjugation; these are also discussed in detail in other sections (Casalboni, 2000 #2523).[119–121] Ferrocene has also been incorporated into octupolar chromophores for which β values as high as 500×10^{-30} esu have been measured using HRS at 1,907 nm.[122]

12.04.1.2.1.(ii) Third-order NLO properties of metallocene compounds

Several studies have also focused on the third-order NLO properties of ferrocene-based conjugated species. A range of species were studied using DFWM at 602 nm (ps pulses); values of $\gamma = 1{,}550$, 504, 925, and 270×10^{-36} esu were measured for **25**, **26**, **27**, and **28**, respectively (Figure 5).[123] A range of other styryl-substituted ferrocenes related to **28** have been studied using *z*-scan at 800 nm, with values of γ_{real} as high as 840×10^{-36} esu (this study also gave a value of $\gamma_{real} = 640 \times 10^{-36}$ esu for **26**).[60] A series of chromophores based on ferrocenyl donors with a molybdenum coordination complex as acceptor have been studied using THG; γ_{real} was found to be generally negative and the largest value, $-3{,}450 \times 10^{-36}$ esu, was found for **30** (1,907 nm, ns pulses).[84,124] Structure **5** on the other hand was found to show

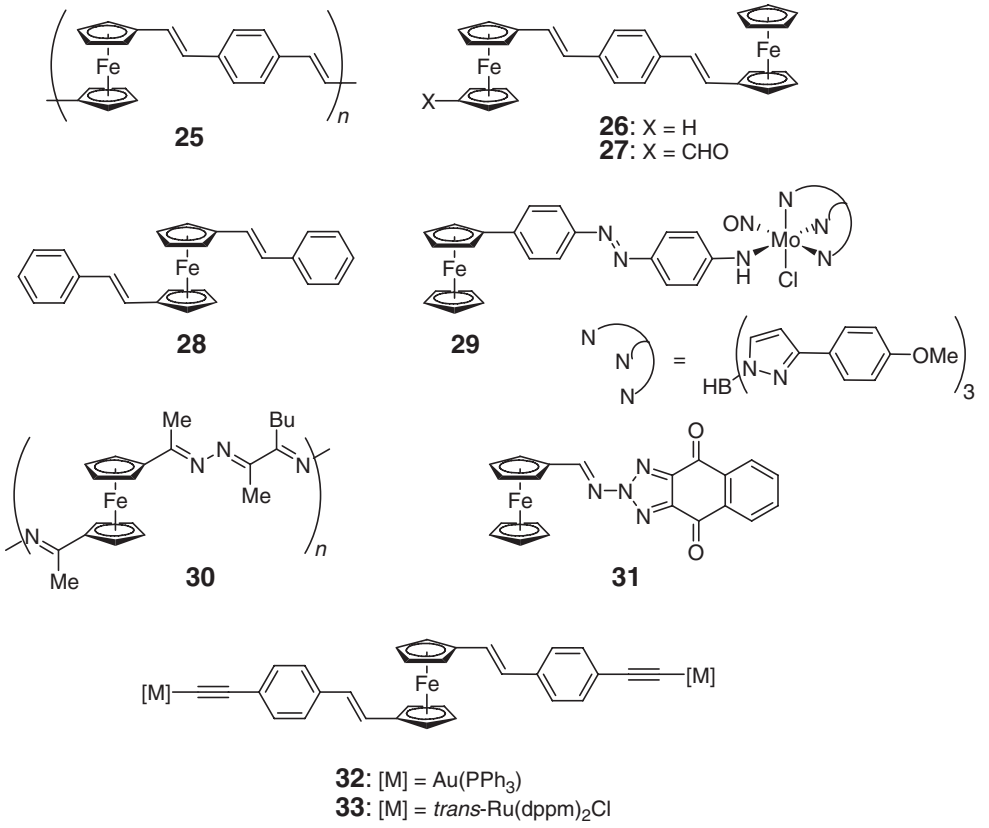

Figure 5 Structures of some group 8 ferrocenes studied as third-order chromophores and discussed in Section 12.04.1.2.1.(ii).

$\gamma_{real} = +605 \times 10^{-36}$ esu. Large positive imaginary γ, corresponding to some sort of absorption process, were also measured ($3{,}450 \times 10^{-36}$ esu for **30**, 860×10^{-36} esu for **5**). THG (1,064 and 1,907 nm) was used to measure $\chi^{(3)}$ of films in PMMA; a film containing **30** showed $|\chi^{(3)}|$ of 0.40 and 0.90×10^{-12} esu at 1,064 and 1,907 nm, respectively (0.20 and 0.08×10^{-12} esu for **5**), the differences being attributed to dispersion effects. Value of $\chi^{(3)}$ for polymer **31** is also wavelength dependent as measured by THG, varying from 9.4 to 21×10^{-12} esu (1,050 and 1,950 nm, respectively).[125] The dispersion of **37** has been measured by *z*-scan in the vicinity of the low-energy transitions.[126] Large (up to 3.1×10^{-28} esu) values of γ (*z*-scan, 523 nm) have been reported for complexes between silver, mercury, or cadmium ions and pyridine-based ligands incorporating ferrocene;[127,128] however, these values are likely to be resonantly enhanced and, due to the ns pulses employed, may also be due to effects that are not purely electronic in nature. Poly(ferrocenylacetylene) has been shown to be have lower $\chi^{(3)}$ than poly(phenylacetylene).[129] Ferrocene-substituted phthalocyanines have also been studied.[106]

Ferrocene has also been used as a bridging group between two conjugated units substituted with other organometallic groups;[130] two examples, **33** and **34**, are shown in Figure 5 and have been studied using *z*-scan at 800 nm. Both γ_{real} ($-1{,}100$ and $-7{,}100 \times 10^{-36}$ esu, respectively) and γ_{imag} (300 and $10{,}600 \times 10^{-36}$ esu, respectively) are rather large; the large γ_{imag} are attributed to moderate-to-large two-photon cross-sections (70 and 2,500 GM, respectively) at 800 nm and the large values of γ_{real} are presumably due in part to two-photon dispersion effects. Similar Ru and Au species not incorporating ferrocene are discussed in Section 12.04.1.3.2.

12.04.1.2.2 Other sandwich compounds

12.04.1.2.2.(i) Group 4

Small powder SHG efficiencies have been reported for $Cp_2ZrCl(XAr)$ where X = O or S and Ar = aryl; the largest value obtained was 4.5× that of KH_2PO_4, where X = S, Ar = 2,3,5,6-tetrafluorophenyl.[131,132] The third-order properties of group 4 metallocene derivatives have been investigated by solution THG measurements at 1,907 nm.[133,134] The metallocene dihalides all show small signals ($\gamma < 5 \times 10^{-36}$ esu), but some species with extended organic conjugation from the metal show larger γ than might be anticipated from the sum of the hyperpolarizabilities of constituent organometallic and organic fragments: γ-values of 92 and 154×10^{-36} esu were found for **35** and **38**, respectively (Figure 6). Hyperpolarizabilities were found to decrease in the order Ti > Zr > Hf ($\gamma = 58$ and 51×10^{-36} esu for **36** and **37**, respectively). These species are transparent in the visible and the measured values are, therefore, expected to be close to the static values, γ_0.

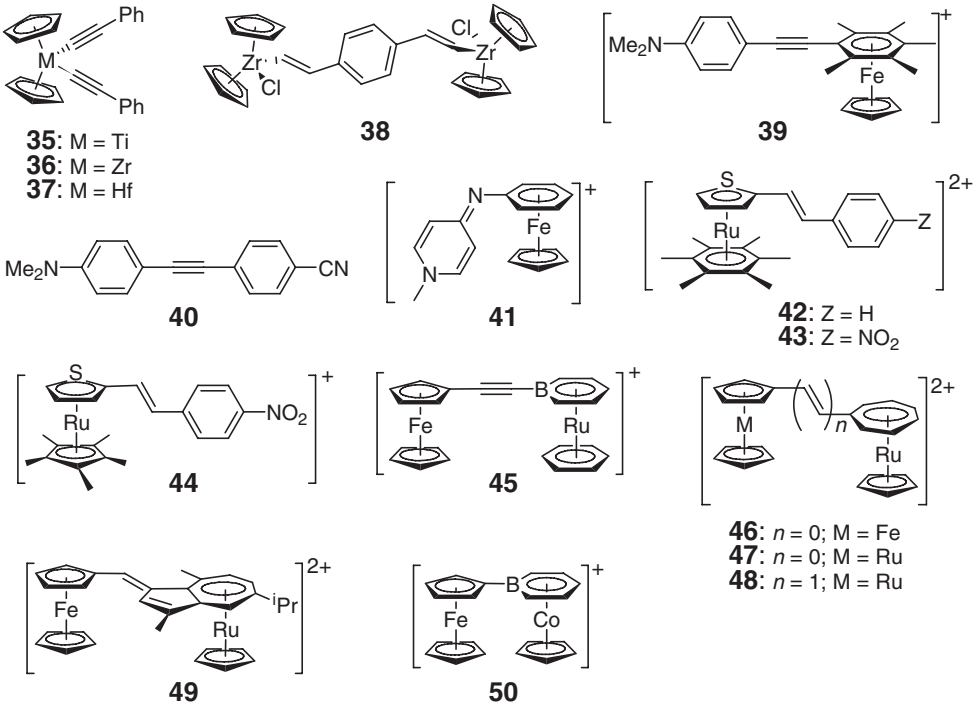

Figure 6 Structures of some sandwich compounds discussed in Section 12.04.1.2.2.(i) along with that of an all-organic analog.

12.04.1.2.2.(ii) Group 6

Bis(η^6-arene)metal^0 complexes of group 6 are isoelectronic with the group 8 metallocenes and rather better electron donors, at least in an electron-transfer sense. However, there have been very few studies of their incorporation into conjugated systems, presumably since their synthesis, functionalization, and handling is more difficult than that for the metallocenes. NLO data are limited to z-scan measurements of $\chi^{(3)}{}_{\text{real}}$ performed at 1,064 nm for films of oligomers formed by the reaction of Cr(η^6-arene)$_2$ {arene = benzene and a $C_6Et_nH_{6-n}$ mixture} with acrylonitrile. Some of the Cr species are believed to undergo aerial oxidation, with the hydroxide counterion initiating some cyclization in the acrylonitrile chains, while other samples were intentionally oxidized with tetracyanoethylene. Rather large values of Re($\chi^{(3)}$) were obtained, with a value of -1.7×10^{-10} esu obtained from a polymer/organometallic oligomer composite.[135] A range of complexes of the type $[Cp_2M(SPh)(L)]^+[PF_6]^-$ (M = Mo, W) where L is a benzonitrile derivative have been examined by powder SHG, but with only weak effects observed.[136] An inclusion complex of Cp_2WH_2 with thiourea tested negative for SHG.[137]

12.04.1.2.2.(iii) Group 8

The (η^6-arene)(η^5-cyclopentadienyl)Fe^{II} cationic group has been shown to be a reasonably effective acceptor; β for **39** (HRS, 1,064 nm) is reported to be 318×10^{-36} esu. β_0 is estimated at 168×10^{-36} esu, which, when allowing for the different conventions used in defining β, is similar to that for 4-dimethylamino-4′-cyanotolane, **40**,[138] suggesting that the organometallic group has similar acceptor properties to a *p*-cyanophenyl group.[139] Structure **41** shows negligible β; a crystal structure confirms that this is due to substantial ground-state CT leading to a cyanine-like low BLA in the bridging group.[139] An analog of **39** without arene methylation could not be studied due to its light sensitivity; indeed, (arene)CpFe salts have been used as photoinitiators,[140] suggesting that these compounds may be of limited use for optical applications requiring exposure to visible or UV light. Salts of (η^6-C_6H_6)CpFe$^+$ with nickel dithiolene counterions have been studied using DFWM, but the results suggested that the Ni moieties, rather than the organometallic cations, dominate the observed non-linearity.[141]

The (η^6-arene)(η^5-thiophene)Ru^{II} dicationic group has been substituted through the 2-position of the thiophene with styrene groups bearing a range of donors and acceptors.[142] Two such examples are included in Figure 6: the lowest-energy band in the spectrum shows a blue shift (386 to 410 nm) on replacing the *p*-hydrogen of **42** with the NO_2 group of **43** and the value of β (HRS, 1,064 nm) increases from 66 to 226×10^{-30} esu (β_0 estimated at 27 and 78×10^{-30} esu; for comparison, the free 2-(4-nitrostyryl)thiophene ligand shows $\lambda_{max} = 383$ nm, $\beta = 54 \times 10^{-30}$ esu, $\beta_0 = 23 \times 10^{-30}$ esu), suggesting that the sandwich compound principally plays a donor role, despite its formal double positive charge. TD-DFT calculations suggest that the optical transitions in these species have rather complex origins, with considerable configuration interaction, with the metal playing both a donor and acceptor role in the principal low-energy transition of **44**. Replacement of the (C_6H_6)Ru^{2+} fragment of **44** with Cp*Ru$^+$ group (**45**, Figure 6) leads to increased β (389×10^{-30} esu) and β_0 (137×10^{-30} esu), although there is little change in the absorption maximum.

The (η^6-boratobenzene)(η^6-C_6H_6)Ru$^+$ moiety has been linked to a ferrocene donor by way of the boron atom (**45**, Figure 6); however, the visible spectrum shows no low-energy CT absorption and HRS at 1,064 nm gave no observable signal.[114] As in other donor–acceptor systems[110,114] and in mixed valence systems,[143] coupling through the boron atom of boratobenzene ligands appears rather weak.

The CpRu$^+$ fragment has also been coordinated to tropylium ion in donor–acceptor species in the hope of increasing its acceptor strength (**46–48**, Figure 6).[144] HRS measurements at 1,064 nm afford values of $\beta = 125$, 264, and 358×10^{-30} esu for **46–48**, respectively; the absorption maxima for the corresponding ruthenocenyl tropylium species (for $n = 1$, **19**) without the CpRu$^+$ group are, however, red shifted relative to **47** and **48**, and show greater β-values of 378 and 649×10^{-30} esu for $n = 0$ and $n = 1$, respectively. Once attempts are made to correct for dispersion, the net effect of the CpRu$^+$ fragment on the acceptor properties of the tropylium ring is unclear: β_0 values of 35 and 17×10^{-30} esu were estimated for **47** and **48**, respectively, with 4 and 120×10^{-30} esu for their CpRu$^+$-free analogs.[144] The seven-membered ring of a donor-substituted azulenylium cation has also been coordinated to the CpRu$^+$ fragment to give **49** (Figure 6);[104] in this system, coordination of the CpRu$^+$ fragment leads to a small blue shift of the absorption bands (724 to 698 nm), but a small increase in β (220 to 326×10^{-30} esu) and the estimate of β_0 (101 to 134×10^{-30} esu).

12.04.1.2.2.(iv) Group 9

Group 9 boratobenzene sandwich compounds have also been used as acceptors. Analogs of **45** (Figure 6) where the (η^6-C_6H_6)Ru$^+$ fragment is replaced by the isoelectronic Cp*Rh$^+$ or Cp*Ir$^+$ fragments have been studied using HRS

at 1,064 nm, and rather small values of $\beta = 59$ and 46×10^{-30} esu, respectively, found.[114] In the less extended Co(III) species, **50** (Figure 6), there is a more conspicuous lower-energy CT band (585–650 nm depending on solvent) than in the Rh or Ir species; the HRS-determined (1,064 nm) value of β (90×10^{-30} esu) is also somewhat larger, although this is presumably resonantly enhanced.[110] Inclusion complexes of (η^4-1,3-hexadiene)MCp (M = Co, Rh) with thiourea tested negative for SHG.[137]

12.04.1.2.3 Half-sandwich compounds with η^7- or η^6-rings

The tropylium ion, attached to the ferrocenyl donor, directly or through C≡C or CH=CH bridges, has been coordinated to $Cr(CO)_3$ and the resulting complexes have been studied using HRS at 1,064 nm; the measured β-value for **51** (Figure 7) was 320×10^{-30} esu and β_0 was estimated at 113×10^{-30} esu.[145,146] Chromophores have also been studied in which the (η^7-tropylium)$Cr(CO)_3$ moiety is connected to a cymantrene donor[147] and are discussed in Section 12.04.1.2.4.(i).

Simple (η^6-arene)$Cr(CO)_3$ were studied using powder SHG, with unremarkable results.[148] Inclusion compounds of (η^6-arene)$Cr(CO)_3$ with thiourea and tris-*o*-thymotide have also been studied using powder SHG (1,064 nm);[137,149] the highest efficiency, 2.3 × that of urea, was found for a 3 : 1 complex thiourea/(η^6-C_6H_6)$Cr(CO)_3$ and results from the combination of small hyperpolarizabilities (-0.8×10^{-30} esu according to EFISH at 1,907 nm[150]) and a crystal structure in which all the organometallic guests are aligned with their Cr–arene vectors oriented in the same direction.

The (η^6-arene)$Cr(CO)_2L$ (L = CO, PPh_3) moiety has also been linked to π-donor and acceptor systems through alkyne and alkene bridges connected to the arene;[36,111,151] some examples studied are shown in Figure 7. Müller *et al.* showed the (η^6-arene)$Cr(CO)_2L$ group can act as a donor with acceptor-substituted π-systems: the low-energy absorption of these species is assigned to a metal-to-ligand charge transfer (MLCT) and is red shifted relative to species with electron-rich π-systems.[36] The value β for **52** (HRS, 1,500 nm) was found to be 15×10^{-30} esu, with β_0 estimated to be 12×10^{-30} esu; comparison with *E*-4-dimethylamino-4′-nitrostilbene, **3** (according to EFISH at 1,907 nm, $\beta = 73 \times 10^{-30}$ esu, $\beta_0 = 55 \times 10^{-30}$ esu, Figure 1),[75,152] and *E*-4-nitrostyrylferrocene, **8** (Figure 4, according to EFISH at 1,907 nm, $\beta = 31 \times 10^{-30}$ esu),[74] suggests that the (η^6-arene)$Cr(CO)_3$ is a relatively weak donor compared to 4-(dimethylamino)phenyl or ferrocenyl. As in many other systems, smaller values of β are found for alkyne-bridged species than their alkene analogs ($\beta = 10 \times 10^{-30}$; $\beta_0 = 8 \times 10^{-30}$ esu for **57**; HRS, 1,500 nm), and β increases with the increase of the conjugation length ($\beta = 44 \times 10^{-30}$; $\beta_0 = 31 \times 10^{-30}$ esu for **54**; HRS, 1,500 nm). Donor strength is significantly increased if one of the carbonyl ligands is replaced with a phosphine; indeed, $\beta = 52 \times 10^{-30}$ and $\beta_0 = 41 \times 10^{-30}$ esu (HRS, 1,500 nm) for **60**. The (η^6-arene)$Cr(CO)_3$ can also act as an acceptor; in species such as **61** the MLCT is blue shifted relative to that in **57** and a higher-energy transition assigned to an intraligand CT is red shifted. Comparison of **55** ($\beta = 20 \times 10^{-30}$; $\beta_0 = 14 \times 10^{-30}$ esu; HRS, 1,500 nm) with **3** shows that the

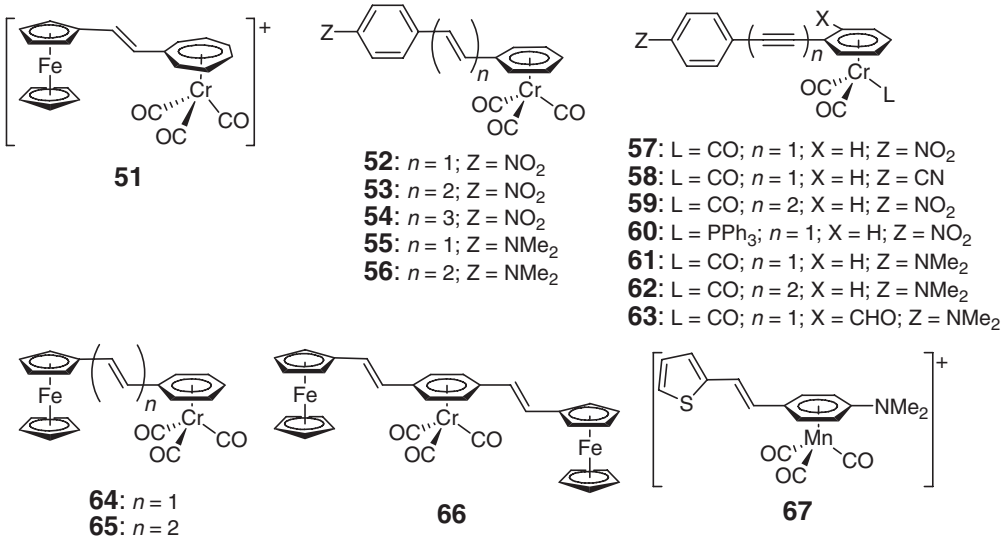

Figure 7 Structures of some tropylium and arene half-sandwich compounds of chromium and manganese discussed in Section 12.04.1.2.3.

(η^6-phenyl)$Cr(CO)_3$ group is a poorer π-acceptor than 4-nitrophenyl. The largest value is obtained when the arene coordinated to the Cr is substituted with an additional acceptor group; $\beta = 52 \times 10^{-30}$, $\beta_0 = 39 \times 10^{-30}$ esu for **63** (HRS, 1,500 nm).[36]

Garcia *et al.*[151] found a value of β of 28×10^{-30} esu (HRS, 1,064 nm) for the benzonitrile derivative **58** and larger values for some related species with thiophene–nitrile-based acceptors; in all three cases this value increased significantly on coordination of the nitrile group to $CpRu(dppe)^+$ or, to an even greater extent, in the case of coordinating $CpFe(dppe)^+$. However, these values are presumably significantly resonantly enhanced. Moreover, there appear to be at least three low-energy CT bands in these heterobimetallics: two MLCT transitions associated with the Cr^0 and group 8 M(II) centers, and an intraligand CT transition, and so the structure–property relationships in this class of compounds are likely to be rather complex.

The (η^6-arene)$Cr(CO)_3$ moiety has also been combined with the ferrocenyl donor: values of $\beta = 193$ and 300×10^{-30} esu (HRS, 1,064 nm) have been reported for **64** and **65** (Figure 7) respectively. Estimated β_0 values of 119 and 164×10^{-30} esu, respectively, suggest, comparing with **52**, that the (η^6-arene)$Cr(CO)_3$ group has similar acceptor properties to the isoelectronic (η^7-tropylium)$Cr(CO)_3$ group,[111] although the multiple transitions observed in this type of molecule mean than it is difficult to reliably correct for dispersion.

The third-order properties of **66** were studied using z-scan at 800 nm; values of γ_{real} and γ_{imag} were found to be 850 and 95×10^{-36} esu, respectively, both somewhat larger than for the analogous Cr-free compound, **26** (640 and 30×10^{-36} esu).[60] Powder SHG at 1,300 nm revealed only very weak solid-state second-order activity.

A value of $\beta = 377 \times 10^{-30}$ was measured for **67** (Figure 7) using HRS at 1,064 nm and a value of $\beta_0 = 67 \times 10^{-30}$ esu estimated.[56]

12.04.1.2.4 Half-sandwich compounds with η^5-rings

12.04.1.2.4.(i) Groups 6 and 7

Inclusion complexes of a variety of (η^5-ligand)$M(CO)_3$ compounds including (η^5-thiophene)$Cr(CO)_3$ and $CpM(CO)_3$ (M = Mn, Re) with thiourea have been tested using powder SHG, but all showed SHG efficiencies lower than that of urea.[137] The cymantrenyl group has also been incorporated into donor–acceptor compounds; some examples studied by HRS (1064 nm) are shown in Figure 8.[147,153] Moving from **68** to **69** to **70** or from **71** to **72** to **73** shows an increasing red shift of the low-energy visible band, consistent with the donor strength of the auxiliary ligand L increasing in the order $CO < P(OMe)_3 < PPh_3$. The effects on β are less straightforwardly determined due to the near-resonant situation for some of these compounds and strong solvent dependence; however, values of β of 94, 151, and 73×10^{-30} esu were found in dichloromethane for **71**–**73**, respectively.[153] Similarly, the effect of $Cr(CO)_3$ complexation is unclear: $\beta = 240$ and 77×10^{-30} esu for **71** and **74**, respectively, but estimates of β_0 were 15 and 19×10^{-30} esu, respectively.[147] The β_0 value estimated for **75** is somewhat larger (58×10^{-30} esu),[147] although about half of that for the analogous compound with a ferrocenyl donor.[145]

The (η^5-thiophene)$Mn(CO)_3^+$ moiety has been linked to various donors and acceptors and the resulting species studied used HRS at 1,064 nm; for the three examples **76**–**78** shown in Figure 8, β was found to be 252, 413, and 613×10^{-30} esu, respectively.[56] In all cases, however, the measured hyperpolarizabilities were strongly resonance enhanced, this in part accounting for the high β-values. Correction for this dispersion is problematic especially if, as in the isoelectronic (η^6-arene)$Cr(CO)_3$ examples, more than one excited state contributes significantly to β; however, β_0 values of 84, 165, and 229×10^{-30} respectively have been reported, suggesting that this moiety acts principally as a

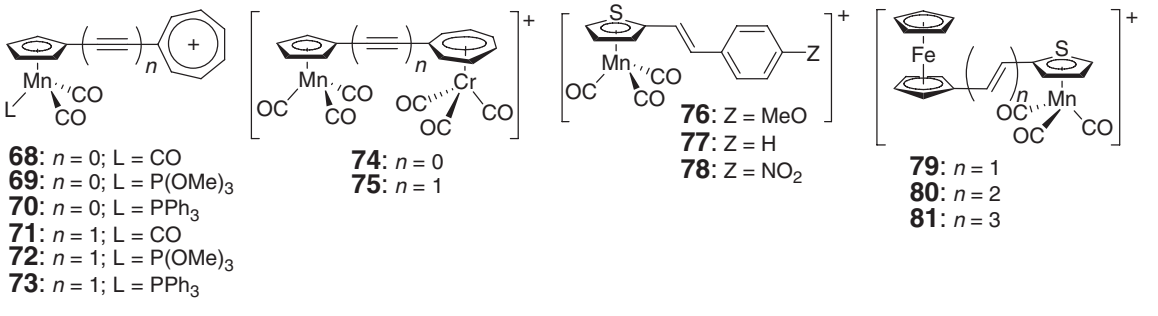

Figure 8 Structures of some cyclopentadienyl and thiophene complexes of manganese discussed in Section 12.04.1.2.4.(i).

donor. In the case of **78**, β and β_0 were also reported for the corresponding free ligand (326 and 137×10^{-30} esu, respectively) and suggest that coordination of $Mn(CO)_3^+$ enhances the donor strength of thiophenes. Species with a ferrocene donor linked to the (η^5-thiophene)$Mn(CO)_3^+$ group (**79–81**, Figure 8) all show high β(260–771×10^{-30} esu); however, this is thought to be due to the closeness of the lowest-energy absorption to the wavelength of the frequency-doubled radiation and estimated β_0 are all small (-34 to 13×10^{-30} esu.).

Several metal–sulfide clusters incorporating group 6 CpM fragments have been investigated as third-order materials.[154] For example, a γ of over 10^{-30} esu was reported for $(Cp^*W)_2S_6Au_2$ (DFWM, 532 nm); however, the authors acknowledge that this value is unlikely to be purely electronic in origin, with excited-state processes also contributing.[154,155] Moreover, any electronic component is likely to be strongly dispersion enhanced. Similar values are obtained for γ for other purely inorganic metal–sulfide clusters, indicating that the Cp^* group does not play a significant role.

12.04.1.2.4.(ii) Group 8

Group 8 CpM fragments have been linked to donor or acceptor groups in a number of ways. First, we will discuss those examples where the CpM group is linked to an extended π-system through η^1-coordination of a terminal acetylide or alkylidene group to the metal center. Second, we will discuss examples where the CpM group is bridged to another functionality by the nitrogen atom of a nitrile, or through a cyanide ion. Finally, we will consider complexes containing two linked CpFe centers that are derived from $Fe_2Cp_2(CO)_2(\mu\text{-}CO)(\mu\text{-}CMe)^+$.

Second-order NLO properties have been measured for a number of systems with the $Cp'M^{II}L_2C{\equiv}C$-type ($Cp' = Cp$, Cp^*, η^5-indenyl; L = phosphine, CO) moieties in the cases for Fe,[156–159] Ru,[159–163] and Os.[159] The parent compound, $CpRu(PPh_3)_2Cl$, has negligible non-linearity,[163] and small values (Table 2) are found for $Cp'M^{II}L_2C{\equiv}CPh$ species. Since these metal groups act primarily as donor groups, enhanced non-linearities are obtained when acceptor groups such as nitrophenyl are introduced: some representative examples are shown in Figure 9 and their NLO properties are tabulated in Table 2. Species with extended conjugation (**94** is shown as an example) show red-shifted absorptions, and enhanced β (at 1,064 nm), but no enhancement in static β_0. Apparently the best acceptors used so far in conjugation with $Cp'M^{II}L_2C{\equiv}C$–donors from the point of view of β_0 are 4-cyanophenyl coordinated to $M(CO)_5$ (M = Cr, W; data for the more non-linear W example, **95**, are given in Table 2).[162] Comparison of **82–84** suggest that β and β_0 increase in the order Fe < Ru < Os;[159] however, comparison of **86** and **87** suggests that Fe is a better donor than Ru.[158] Not surprisingly, CpM(dppe) (M = Fe, Ru) acts as a considerably stronger donor than the $CpM(CO)_2$ group (**91** and **92** vs. **82** and **83**).[159] Comparison of the hyperpolarizabilities of the 4-nitrophenyl substituted species **82–84**, **86–87**, **90–92** with that for 4-dimethylamino-4′-nitrotolane ($\mu\beta = 280 \times 10^{-48}$ esu, and $\beta = 46 \times 10^{-30}$ esu, EFISH at 1,907 nm)[138,164] appears to suggest that $CpML_2$ groups

Table 2 Linear and second-order non-linear (HRS, 1,064 nm or EFISH, 1,907 nm) properties of selected $CpML_n$ acetylides

Compound	λ_{max} (nm)	$\mu\beta(\times10^{-48})$ (esu)	$\mu\beta_0(\times10^{-48})$ (esu)	$\beta(\times10^{-30})$ (esu)	$\beta_0(\times10^{-30})$ (esu)	*Method*	*References*
82[a]	498			665	64	HRS	159
	504			1,160		HRS	157
83	447			664	161	HRS	159
84	461			929	181	HRS	159
85	348			52	24	HRS	156
86	595	2,100	1,155	169	93	EFISH	158
86$^+$	650	1	1	0.04	>0.02	EFISH	158
87	500	690	465	58	39	EFISH	158
88	476			746	119	HRS	162
89	310			16	10	HRS	163
90	460			468	96	HRS	163
91	370			49	22	HRS	159
92	364			58	27	HRS	159
93	506			2,135		HRS	157
94	507			1,257	89	HRS	162
95	456			700	150	HRS	162
96	351			175	87	HRS	156
96^{3+}	662			53		HRS	156

[a]The two sets of data given were recorded in different solvents.

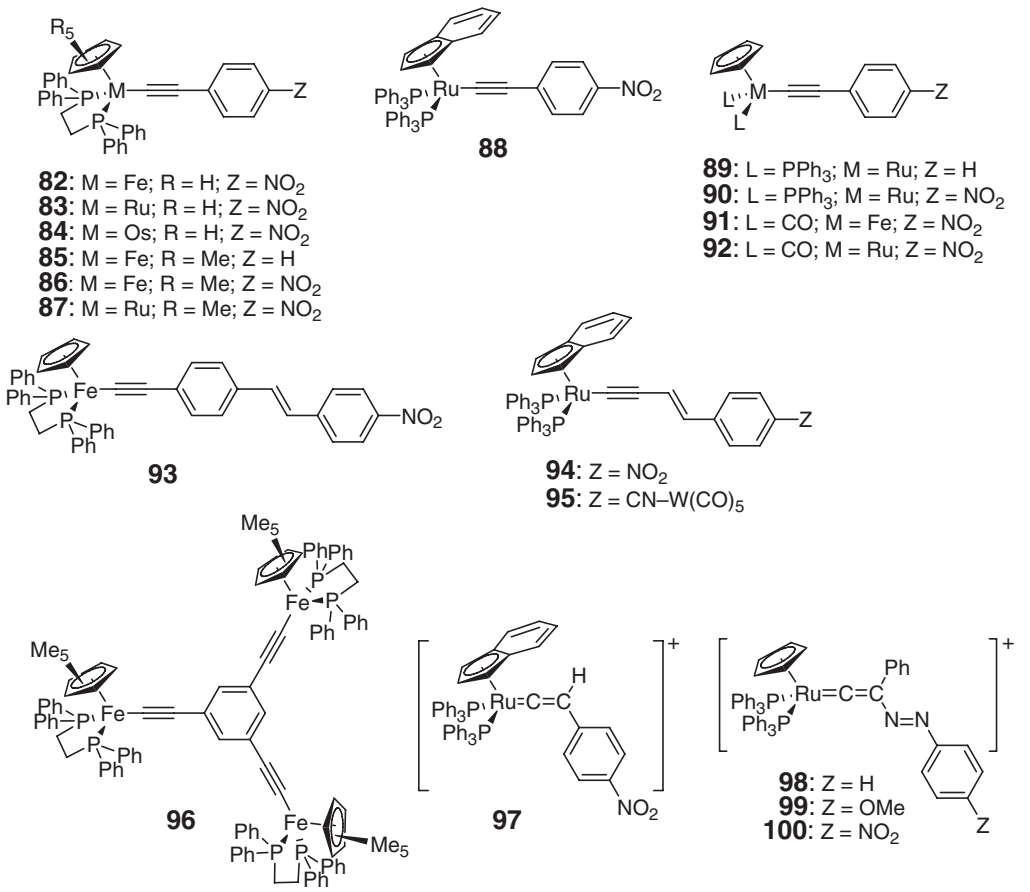

Figure 9 Structures of some half-sandwich alkynyl and alkylidene derivatives of group 8 metals discussed in Section 12.04.1.2.4.(ii).

are generally better donors than 4-(dimethylamino)phenyl. Switching of the second-order properties of Fe species on oxidation to the corresponding Fe(III) species has been demonstrated for species with dipolar, quadrupolar, and octupolar structural motifs;[156,158] the most dramatic changes being seen in compounds such as **86**. An analog of **90** in which the nitrophenyl acceptor is replaced with a tropylium derivative has also been studied, but shows a considerably lower β (120×10^{-30} esu) and β_0 (120×10^{-30} esu), possibly due to too much contribution from the alternative cumulene resonance form to the ground-state structure.[165]

Third-order properties have also been investigated for several dipolar members of this class using z-scan at 800 nm;[157,163,166] in the case of **90**, DFWM at 800 nm was also used ($\gamma_{real} = 260 \times 10^{-36}$ and 210×10^{-36} esu from DFWM and z-scan, respectively).[163] While small positive values of γ_{real} were found for $CpRu(PR_3)_2Cl$,[163] the $Cp'M^{II}L_2C{\equiv}C$ derivatives studied showed negative values of γ_{real} at 800 nm. These values are likely to be far from the static values due to resonant enhancement from a two-photon state; significantly, the most negative value ($-2{,}200 \times 10^{-36}$ esu) is found for **93**, one of the redder-absorbing species studied ($\lambda_{max} = 499$ nm),[157] and the example showing the highest value of γ_{imag}, attributed to two-photon absorption, at 800 nm (1200×10^{-36} esu). Compound **97** (Figure 9) can be regarded as a protonated version of compound **88** and is an intermediate in its synthesis.[162] Both its absorption maximum (379 nm) and its first hyperpolarizability (β and β_0 are 116 and 50×10^{-36} esu, respectively, according to HRS at 1,064 nm) suggest, not surprisingly, that the $Ind(PPh_3)_2Ru^+ =$ moiety is a poorer donor than the $Ind(PPh_3)_2Ru$–group. Chromophores based on the $CpRu(PPh_3)_2{}^+ =$ group have also been studied by HRS (1,064 nm); value of β (β_0) of 14 (6.6), 26 (12), and 150 (48) $\times 10^{-36}$ esu were reported for **98–100**, respectively.[167] The $BF_4{}^-$ salt of **99** shows an SHG efficiency similar to urea, despite a centrosymmetric crystal structure; this was attributed to crystal defects.[20]

The $Cp'L_2M^+$–N≡C–group is isoelectronic with the $Cp'L_2M$-C≡C–group. A number of compounds of this class have been studied. Early work focused on powder SHG measurements:[168,169]

$[Cp\{(+)\text{-DIOP}\}Fe(p\text{-}NCC_6H_4NO_2)]^+[PF_6]^-$ {(+)-DIOP = (2*S*,3*S*)-1,4-bis(diphenylphosphine)-2,3-*O*-isopropylidene-2,3-butanediol} was found to have an efficiency 38× that of urea.[168] More recent studies have employed HRS (1,064 nm) to investigate the molecular first hyperpolarizabilities. Despite its formal positive charge, the metal center in this type of complex seems to act principally as a donor, rather than acceptor. The Fe compound **101** (Figure 10) shows a β of 395×10^{-30} esu (β_0 estimated at 115×10^{-30} esu),[170] which is higher than that for its Ru analog **103** ($126–138 \times 10^{-30}$ esu):[171] these numbers can also be compared to date for the isoelectronic neutral acetylide analogs, **82** and **83**, shown in Table 2. Interestingly, replacement of the dppe ligand of **101** with the (*R*)-prophos ligand **102** leads to a significant increase in β to 545×10^{-30} esu; this has been attributed to a combination of the direct effect of a slightly stronger donor on β_0 and increased near-resonance enhancement associated with the slight red shift of the lowest-energy transition.[172] The hexafluorophosphate salt of the **102** cation can be crystallized in the space group *P*1 with one molecule per cell, that is, with perfect alignment of all the chromophores; this, combined with the HRS-derived β, suggests that these crystals could have high $\chi^{(2)}$, perhaps several times larger than that of the well-known organic crystal DAST (4-dimethylamino-*N*-methyl-4-stilbazolium *p*-toluenesulfonate). The highest value of β so far reported for this class of donor was for the extended compound **107** (570×10^{-30} esu, although β_0 is estimated to be very similar to that for **101**.[170]

The $CpRu(PPh_3)_2^+$ and $CpFe(CO)_2^+$ fragments have also been coordinated to the nitrile group of a benzonitrile linked to a ferrocene donor to give **109** and **110** (Figure 10), respectively.[102] The values of β determined (HRS, 1,064 nm) for solutions of the hexafluorophosphate salts of **109** (171×10^{-30} esu with β_0 estimated to be 28×10^{-30} esu) and **110** (186×10^{-30} esu, $\beta_0 = 25 \times 10^{-30}$ esu) are somewhat lower than those of the parent *E*-*p*-cyanostyrylferrocene (203×10^{-30} esu, $\beta_0 = 34 \times 10^{-30}$ esu), consistent with the $CpML_2^+$ groups acting as π-donors rather than π-acceptors in this type of complex. A larger value of β determined for the tetrafluoroborate salt of **110** (325×10^{-30} esu, $\beta_0 = 44 \times 10^{-30}$ esu) has been attributed to contributions from the non-centrosymmetric counterion. $CpFe(dppe)^+$ and $CpRu(dppe)^+$ groups have also been coordinated to nitriles on π-systems attached to the (η^6-phenyl)$Cr(CO)_3$ group;[151] these species are discussed in Section 12.04.1.2.3.

The third-order NLO properties of some Ru species based on benzonitriles, including **103**, **104**, **106**, and **108** (Figure 10) have been investigated in PMMA matrices using the Maker fringe THG technique; **106** exhibited the highest value of $\gamma(2280 \times 10^{-36}$ esu, presumably resonantly enhanced, with a $\chi^{(3)}$ value for the film of 0.76×10^{-12} esu).[173]

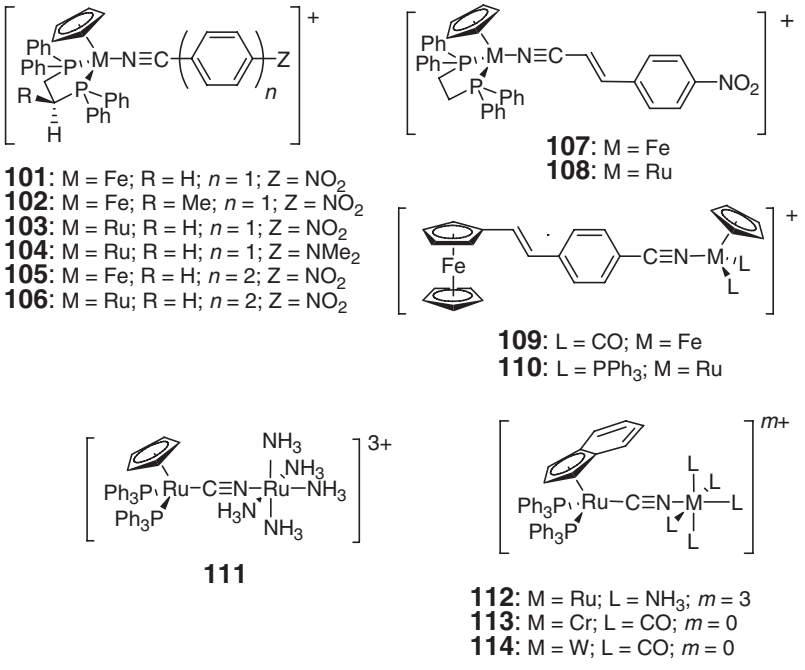

Figure 10 Structures of some group 8 half-sandwich compounds linked to donors or acceptors through nitrile groups or through a cyanide ion and discussed in Section 12.04.1.2.4.(ii).

The CN of the $Cp'L_2M^+$–N≡C–group can also be a cyanide ion that bridges to another metal center, as in the bimetallics, **111–114** (Figure 10); species such as **111** and **112**, which contain formal Ru(II) and Ru(III) centers, can be considered as unsymmetric mixed valence compound with the Ru(II) center acting a donor and the Ru^{III} center acting as an acceptor. Initially, a value of $\beta = 1080 \times 10^{-30}$ esu (HRS, 1064 nm) was reported for **111**.[174] However, this value was found to be too high, due to complications in calibrating the measurement with a value for the solvent that was subsequently found to be in error, and was revised to 157×10^{-30} esu.[25,175] A comparable value ($\beta = 108 \times 10^{-30}$ esu) was obtained for **112**, while only small β values of 25 and 40×10^{-30} esu were found for **113** and **114**, respectively.[162]

Species containing either the $Fe_2Cp_2(CO)_2(\mu\text{-CO})(\mu\text{-C}=)$ donor group[104,176] or the $Fe_2Cp_2(CO)_2(\mu\text{-CO})(\mu\text{-C}-)^+$ acceptor moiety[104,113] can be obtained from $Fe_2Cp_2(CO)_2(\mu\text{-CO})(\mu\text{-CMe})^+$.[177,178] Compounds **115–117** (Figure 11) exhibit strong low-energy positively solvatochromic bands ($\lambda_{max} = 474$, 564, 646 nm, respectively); these transitions are only slightly higher in energy than those off analogs with amine donors **118–120**. Values of $\mu\beta$ of 170, 1,100, and $3{,}100 \times 10^{-30}$ esu were determined for **115–117**, respectively, using EFISH at 1,907 nm; these values and the corresponding estimated $\mu\beta_0$ values (120, 660, and $1{,}500 \times 10^{-48}$ esu) can be compared to $\mu\beta$ values of −340, 462, and $2{,}730 \times 10^{-48}$ esu for **118–120**, respectively ($\mu\beta_0 = -229$, 249, and $1{,}092 \times 10^{-30}$ esu). Other examples of neutral chromophores with diiron donors and organic acceptors, **121** and **122**, have been studied using HRS at 1,500 nm; β-values were found to be 156 and 227×10^{-30} esu, respectively, with β_0-values of 68 and 84×10^{-30} esu, respectively.[104]

The $Fe_2Cp_2(CO)_2(\mu\text{-CO})(\mu\text{-C}-)^+$ acceptor group has been linked to organic[104,113,179] and organometallic (ferrocenyl)[104,113] donors using a variety of π-bridges; some examples are shown in Figure 11. For the organic

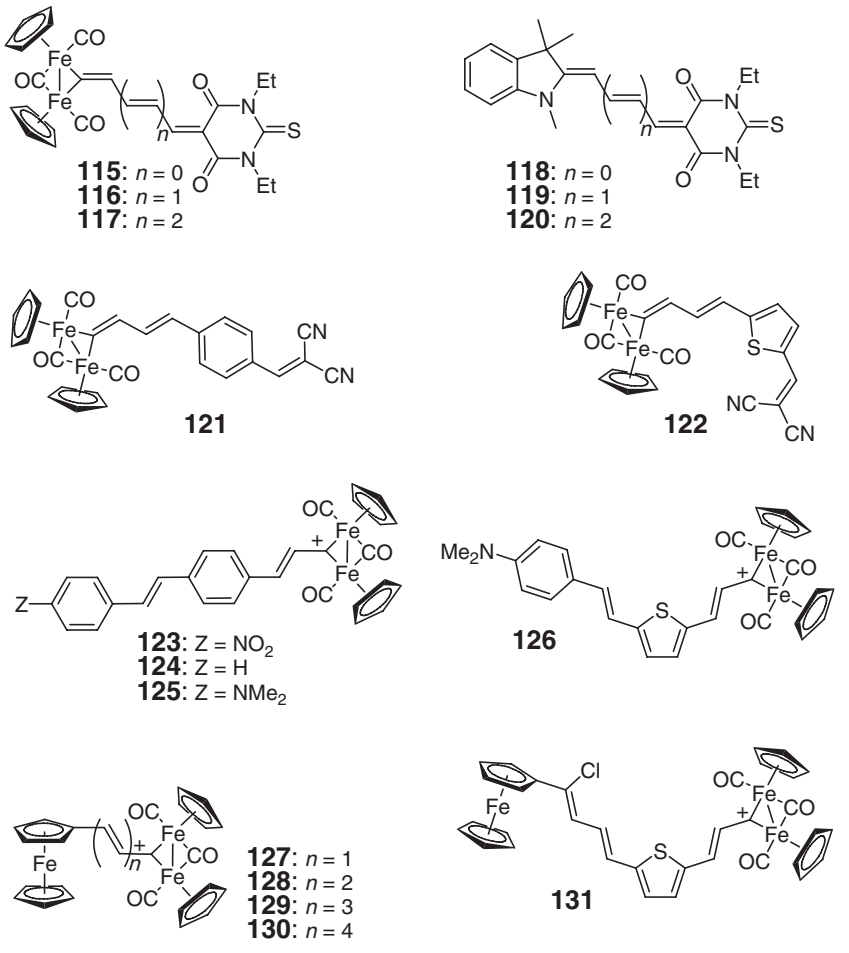

Figure 11 Structures of chromophores discussed in Section 12.04.1.2.4.(ii) that are derived from $Fe_2Cp_2(CO)_2(\mu\text{-CO})(\mu\text{-CMe})^+$, along with those of some all-organic analogs.

species, the absorption maximum is red shifted as the organic group is changed from acceptor to donor (463, 513, and 553 nm in CH_2Cl_2 for **123–125**, respectively), confirming the idea that the cation iron moiety acts as an acceptor group; β also increases from 346 to 792×10^{-30} esu between **123** and **124** (no value reported for **125**; β_0 estimated at 68 and 43×10^{-30} esu for **123** and **124**, respectively). Structure **126** shows a rather large β, but measurements were complicated by fluorescence effects. The largest β-value of the ferrocene species, $1{,}424 \times 10^{-30}$ esu, was measured for **131** using HRS at 1,064 nm.[104] Values of β_0 for **127–131** were estimated using the energy of the lowest-energy transition; however, all the compounds exhibit solvatochromic CT-type transitions, as expected for ferrocenyl species (see above) and so these values (674×10^{-30} esu for **131**) may be overestimates.

12.04.1.2.4.(iii) Groups 9 and 10

Replacement of the $CpFe(dppe)^+$ group of **101** (Figure 10) with the isoelectronic $CpCo(dppe)^{2+}$ fragment in **132** (Figure 12) leads to considerably lower first hyperpolarizability (ca. 45×10^{-30} esu) consistent with Co(III) acting as a weaker donor than its isoelectronic Fe(II) analog.[171] The Co(III) center does not act as a particularly effective acceptor either; **133** also shows a low β ($<40 \times 10^{-30}$ esu).[171]

Several donor–acceptor species incorporating the $CpNi(PPh_3)C{\equiv}C-$ donor have been studied using HRS at 1,064 nm and z-scan at 800 nm; examples are included in Figure 12.[180] The first hyperpolarizabilities of **134–136** were found to be 221, 326, and 445×10^{-30} esu, respectively, with corresponding estimated β_0 values of 59, 120, and 106×10^{-30} esu. Comparison of non-linear and linear ($\lambda_{max} = 439$ nm) optical data for **134** with group 8 analogs in Table 2 suggests that most group 8 $Cp'M(PR_3)_2$ groups act as stronger donors than $CpNi(PPh_3)$. Third-order properties at 800 nm qualitatively resemble those of $Cp'ML_2$ species in that γ_{real} is negative and γ_{imag} is positive (the largest values, -640 and 720×10^{-36} esu, respectively, being found for **135**), both features being attributed to two-photon absorption at 800 nm.

Several complexes between the $CpNi(PR_3)^+$ unit and benzonitrile have been studied using HRS at 1,064 nm; the largest β-values are obtained with acceptor-substituted benzonitriles (93 and 14×10^{-30} esu for **137** and **138**, respectively, cf. 18.5 and 4.4×10^{-30} esu for the corresponding free benznoitrile ligands), suggesting that the Ni center acts as a weak donor in this situation and that it is somewhat less effective than the group 8 $CpM(dppe)^+$ centers.[171,181] Maker fringe THG measurements (1,064 nm) have also been performed for several species of this type, including **138**; however, only very small signals were observed, indicating small values of γ.[181]

12.04.1.2.5 Miscellaneous compounds with η^2–η^4 ligands

η^2-Complexes of various donor-substituted alkynes, such as FcCH═CHC≡CPh with WTp^*COI {Fc = ferrocenyl; Tp^* = hydridotris(3,5-dimethylpyrazolyl)borate}, have been studied using powder SHG at 1,064 nm, but efficiencies were considerably less than that of urea; the molecular NLO properties have not been studied.[55] The isomers of $(dppe)(\eta^2\text{-}C_{60})M(CO)_3$ (M = Cr, Mo) show complex z-scan (532, ns pulses) behavior which is not only due to electronic effects, but also due to excited-state processes.[182,183] The inclusion complexes formed by several $(\eta^4\text{-ligand})Fe(CO)_4$ species with thiourea were subjected to the Kurtz–Perry powder technique, but none exceeded

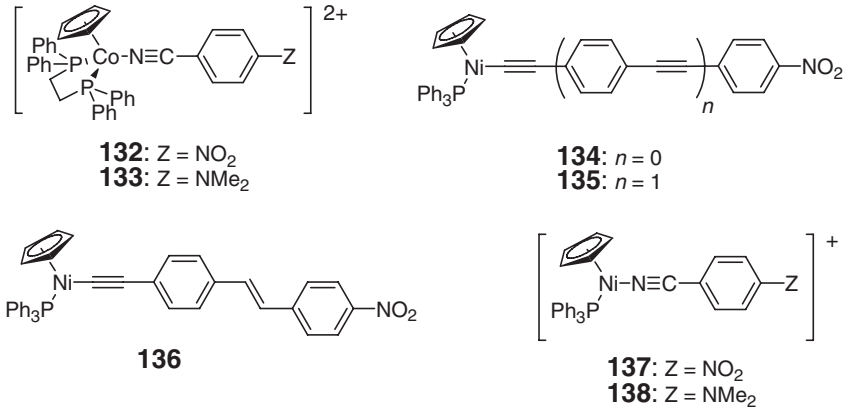

132: Z = NO_2
133: Z = NMe_2

134: $n = 0$
135: $n = 1$

136

137: Z = NO_2
138: Z = NMe_2

Figure 12 Structures of some group 9 and 10 half-sandwich chromophores discussed in Section 12.04.1.2.4.(iii).

urea in SHG efficiency. The $(\eta^2{:}\eta^2\text{-COD})_2$RhCl and $(\eta^2\text{-cyclooctene})_2$IrCl groups have been coordinated to donor-susbtituted pyridines; their impact on the linear and NLO properties is similar to that of the corresponding $M(CO)_2Cl$ groups (see below), although the olefin complexes seem in general to be slightly weaker acceptors, as one might expect.[184]

12.04.1.3 *d*-Block Metal Compounds with η^1-Carbon Ligands

12.04.1.3.1 Alkylidene compounds

12.04.1.3.1.(i) Group 6

Fischer carbenes have been used as electron acceptors in a variety of donor–acceptor architectures. Values of $\beta = 16$ and 34×10^{-30} esu were reported for **139** and **140** (Figure 13), respectively.[185] A number of species with amino rather than alkoxy susbtitution on the carbene carbon have also been studied; the highest value of β (350×10^{-30} esu; $\beta_0 = 154 \times 10^{-30}$ esu) was obtained for **141** (Figure 13).[186] Compounds **142–148** (Figure 13) have been studied by HRS at 1,064 nm.[78] Although spectroscopic and structural data suggest limited charge transfer in the ground state, the β-values have been found to be strongly solvent dependent. For example, values for **148** vary from 780×10^{-30} esu in hexane to $2{,}420 \times 10^{-30}$ esu in acetonitrile. For a given chain length and solvent, Cr and W species show β with similar magnitude; β increases with chain length. It should be pointed out that these values are likely to be strongly resonantly enhanced; correction for this is difficult due to the presence of two overlapping transitions close to the frequency of the frequency-doubled radiation.

Cumulene-type carbene complexes of $M(CO)_5$ have been studied, including **149** and **150** (Figure 13).[187] In fact, their negative solvatochromism suggests that their structures are better represented by zwitterionic σ-alkyne resonance structures (Figure 13). As with the carbenes **142–148**, Cr and W species show similar non-linearities: for example, **149** and **150** show β (β_0) values of 100 (31) $\times 10^{-30}$ esu and 102 (31) $\times 10^{-30}$ esu, respectively (HRS, 1,064 nm).

12.04.1.3.1.(ii) Group 8

Compounds of the type ClRu(dppm)═C═CHR$^+$ (dppm = bis(diphenylphosphino)methane) are precursors to ClRu(dppm)–C≡CR compounds (Section 12.04.1.4.2.(i)), the former being protonated forms of the latter. Several studies have used HRS (1,064 nm) and z-scan (800 nm) measurements to compare the NLO properties of the two

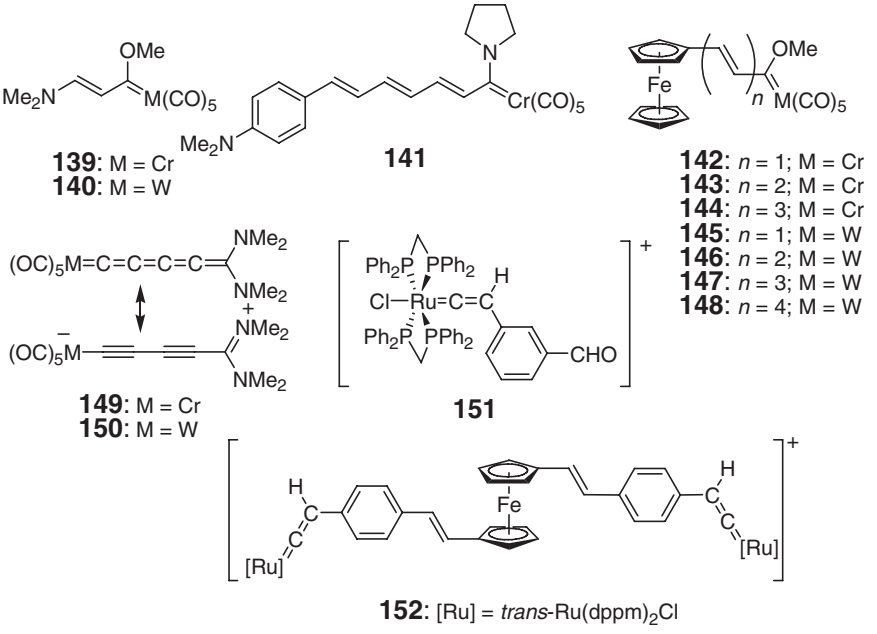

Figure 13 Structures of some alkylidene-based chromophores discussed in Section 12.04.1.3.1.(i).

classes of compounds.[130,188,189] Compound **151** shows a similar absorption maximum (320 nm), $\beta(45 \times 10^{-30}$ esu), β_0 (26×10^{-30} esu), γ_{real} (200×10^{-36} esu), and γ_{imag} (0×10^{-36} esu) values to its protonated alkynyl analog (321 nm, 58×10^{-30} esu, 34×10^{-30} esu, 150×10^{-36} esu, 0×10^{-36} esu, respectively).[188] Alkyne and alkylidene show similar λ_{max} and β-values for various dipolar and octupolar structures, although $\gamma(800)$ is much more variable, presumably due to how close the two-photon absorption peaks of the molecules lie to 800 nm.[189] Compound **152** also shows a similar absorption maximum (383 nm) to its alkynyl analog **33** (396 nm, Figure 5), but both $\gamma_{real}(800)$ and $\gamma_{imag}(800)$ have much smaller magnitudes (−3000 vs. -7100×10^{-36} and 2300 vs. 10600×10^{-36} esu, respectively).[130]

12.04.1.3.2 σ-Alkynyl compounds

Species that may be described as zwitterionic σ-alkynyl complexes of $M(CO)_5$ (M = Cr, W) complexes[187] are classified elsewhere (Section 12.04.1.4.1.(i)) as alkylidene complexes, since their structures can also be written in this way.

12.04.1.3.2.(i) Group 8

Species of the form RC≡CRu(P^P)$_2$X, where P^P represents a chelating bis(phosphine), R can be a variety of π-systems, and X can be a halide or another acetylide ligand, have been incorporated into a wide range of dipolar,[159,190–193] quadrupolar,[194] and octupolar[159,195–197] architectures. Selected NLO data for some of these compounds are summarized in Table 3 and some dipolar and quadrupolar structures are shown in Figure 14, with octupolar species in Figure 15.

Electrochemical and spectroscopic data confirm that the Ru center acts as a donor in these systems. Accordingly, there is a red shift of λ_{max} and an increase of β and β_0 on addition of the nitro acceptor when moving from **153** to **156** or from **154** to **157**. The nitro-substituted species, **156** and **157**, show both red-shifted absorption maxima and larger β-values than 4-dimethylamino-4′-nitrotolane,[138] suggesting that the *trans*-Ru(dppm)$_2$Cl and *trans*-Ru(dppe)$_2$Cl groups act as stronger donors than 4-(dimethylamino)phenyl. The variation with metal (**158** vs. **159** vs. **160**) has parallels with that seen in the group 8 metallocenes: although electrochemical and λ_{max} data suggest that the Fe donor orbitals in **158** are higher in energy than those of their Ru analog, **159**, the lowest-energy transition is more

Table 3 Linear, second-order non-linear (HRS, 1,064 nm), and third-order NLO (*z*-scan, 800 nm) properties of selected ruthenium acetylides

Compound	λ_{max} (nm)	β ($\times 10^{-30}$) (esu)	β_0 ($\times 10^{-30}$) (esu)	γ_{real} ($\times 10^{-36}$) (esu)	γ_{imag} ($\times 10^{-36}$) (esu)	$\lvert\gamma\rvert$ ($\times 10^{-36}$) (esu)	δ (800 nm) (GM)	*References*
153	308	20	12	<120	0	<120	0	159,193
153$^+$	833			1,300	−2,200	2,600		159
154	319	6	3	−170	71	180		193
155	388			−100	450	460	110	159
155$^+$	893			2,900	−1,200	3,100		159
156	473	767	129	170	230	290		193
157	476	351	55	320	<50	320		193
158	543	440	−14					190
159	467	530	97					190
160	490	620	74					190
161	464	833	161	−160	160	230		193
162	439	1,379	365	−920	970	1,300		193
163	490	1,964	235	200	1,100	1,100		193
164	489	2,676	342	40	<100	40		193
165	481	2,795	406					190
166	583	1,649	232					191
167	645	417	124					192
168	354			−3,200	1,400	3,500		194
169	438			−4,000	12,000	13,000		194
170	413	94		−330	2,200	2,200	530	195
170^{3+}	893			13,500	−4,700	14,000		159,196
171	411	151		−600	2,900	3,000	700	195
172	402			−5,050	20,100	20,700	4,800	197
175	383			−670	1,300	1,500		195

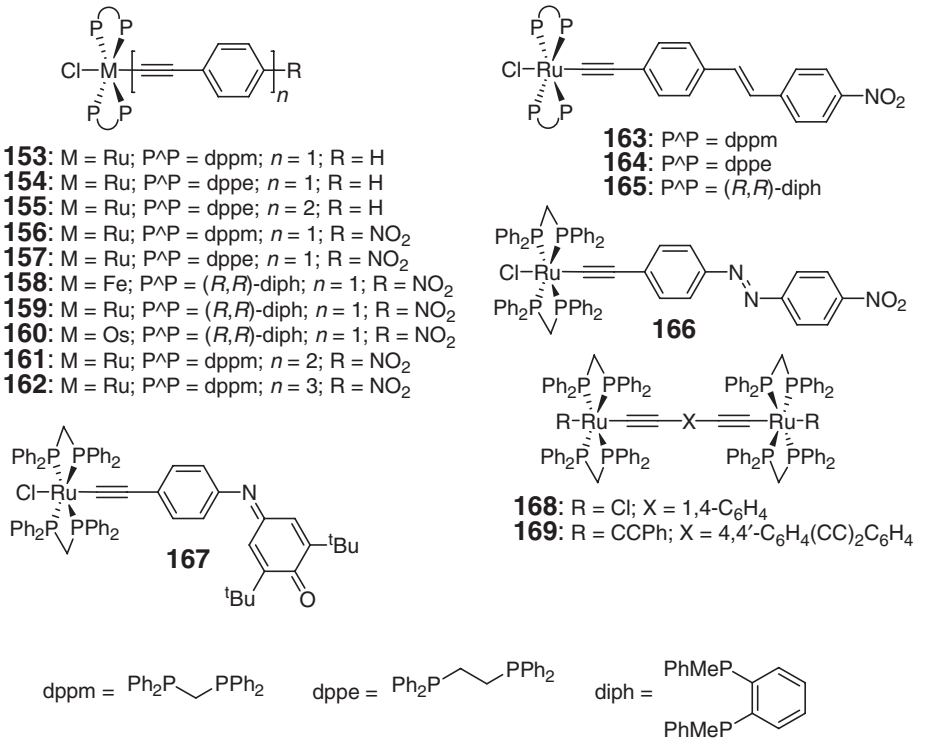

Figure 14 Structures of some dipolar and quadrupolar group 8 alkynyl chromophores discussed in Section 12.04.1.3.2.(i).

intense and β (and especially β_0, although the authors note that application of the two-level model may not be correct here) is larger for the Ru species.[190]

Increase of the conjugation length separating donor and acceptor (**156**, **161**, **162**) leads to increased β, although the much greater magnitude of the shift in β between **161** and **162** relative to that between **156** and **161** is unusual. Moreover, the increase in β with conjugation length is accompanied by a blue shift in λ_{max}, suggesting rather poor ground-state donor–acceptor coupling through the phenylene–ethynylene bridge. Replacement of one of the triple bonds of **161** with a double bond **163** leads to both a red shift of λ_{max} and to increased β, as has been seen for other second-order NLO systems. No consistent trend is seen on varying the bidentate bis(phosphine) ligands (**156** vs. **157**; **163** vs. **164**). Structure–property relations for γ are harder to discern due to large experimental uncertainties. "Switching" of third-order properties can be clearly seen to occur on one-electron oxidation of these species;[159] oxidation leads to large positive γ_{real} and large negative γ_{imag}, the latter being attributed to saturable absorption (the one-photon absorbance of the Ru(III) species is high at 800 nm). The effect is shown even more clearly in the octupolar molecule, **170** (Figure 15);[196] in this case, additional DFWM and transient absorption measurements have been performed to support the z-scan results.[159] Protonation to give Ru═C═CH cationic species (see Section 12.04.1.3.1.2) has also been suggested[130] as a strategy for "switching" NLO properties in this class of compounds. Examples of quadrupolar species are shown in Figure 14, with NLO data in Table 3; a ferrocene-bridged quadrupolar species[130] has already been described in Section 12.04.1.2.1.(ii).

Some octupolar species are shown in Figure 15 and data are also included in Table 3. When β-values are normalized for the number of ruthenium centers in the molecule, it can be seen that the octupolar species **171** has a non-linearity equivalent to that from three **175** chromophores acting essentially independently of each other.[195] However, this does not seem to be general; in another triruthenium octupolar system, **174**, β is only slightly larger than for the model "single-arm" chromophore, **176**.[198] The trends in γ are even less clear (e.g., in the comparison of **171**,[195] **175**,[195] and **172**[197]). The positive values of γ_{imag} are attributed to two-photon absorption and comparisons of cross-sections at a given wavelength do not provide particularly insightful structure–property relationships, since the two-photon maxima of the different species could well occur at different wavelengths. The γ_{real} values may, therefore, be considerably enhanced by two-photon dispersion effects and may not necessarily represent trends in γ_0. Indeed, the dispersion of γ_{real} and γ_{imag} for a related dendrimer, **173**, has been measured using variable-frequency z-scan and shows both real

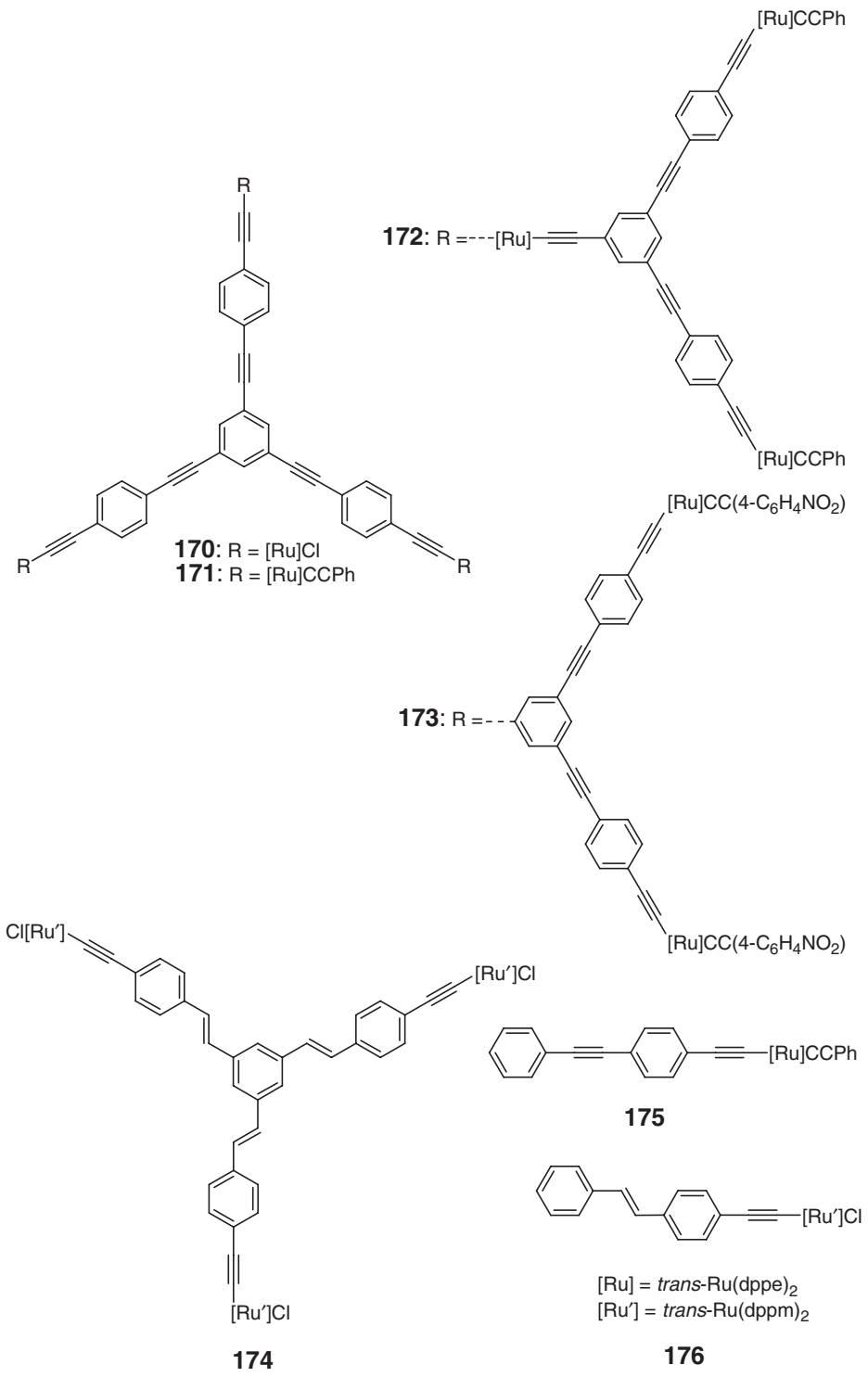

Figure 15 Structures of some octupolar ruthenium alkynyl chromophores discussed in Section 12.04.1.3.2.(i).

and imaginary parts of the second hyperpolarizability to be strongly frequency dependent.[159] It is worth noting that the cross-section, δ, derived for the dendrimer **172** is rather large compared to many of the high organic values in the literature, but it should be borne in mind that **172** has a rather high molecular weight (for examples of an organic octupolar species with high δ_{max}, see Ref: 199) and that this does not necessarily represent the peak of the two-photon

spectrum. Some osmium analogs of the above compounds have also been synthesized, but NLO data have not been published.[200]

12.04.1.3.2.(ii) Group 10

Platinum bis(alkynyl) species have been used as π-bridging groups in donor–acceptor chromophores,[201–203] some examples of which are shown in Figure 16. Structures **177** and **178** were studied using EFISH (1,064 nm);[201] the reported $\mu\beta$ ($\mu\beta_0$) were 670 (290) and 310 (130) $\times 10^{-48}$ esu, respectively, and the β (β_0) values were 126 (62) and 55 (26) $\times 10^{-30}$ esu, respectively. These results suggest that the Pt center is a reasonably effective bridge in mediating the donor–acceptor interaction; β and $\mu\beta$ values are enhanced relative to tolane analogs and, compared to 1,4-bis(phenylethynyl)benzene) analogs, β values are similar but $\mu\beta$ values lower. Poled PMMA films of various Pt-bridged species including **179** and **180** have been studied using SHG: the β-values deduced from the d_{33} measurements were 12 and 16 $\times 10^{-30}$ esu, respectively.[202]

However, most studies of alkynyl group 10 systems have been concerned with the third-order properties.[203–211] In general, these materials show reasonably large γ. Values of $\gamma_{real} = 11$ and 88 $\times 10^{-36}$ esu were determined for **182** and **183**, respectively, and were measured at 1,064 nm using the optical Kerr gate technique. The corresponding polymers, **183** and **184**, show values of 37 and 90–121 $\times 10^{-36}$ esu, respectively.[206] Large γ_{imag} at 532 nm was also

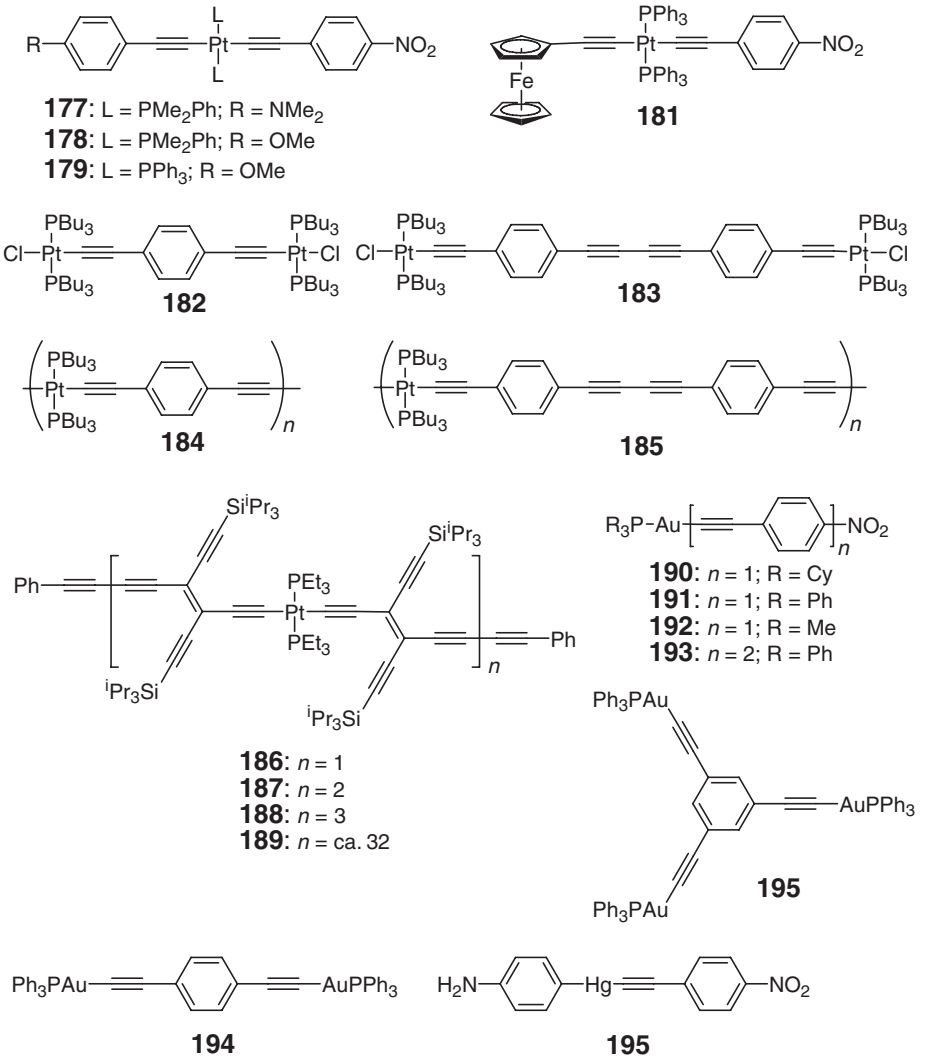

Figure 16 Structures of some group 10, 11, and 12 alkynyl chromophores discussed in Sections 12.04.1.3.2.(ii)–12.04.1.3.2.(iv), respectively.

measured for these compounds.[206] Lower magnitudes, but negative values of γ_{real} were measured using DFWM at 1,064 nm for other group 10 acetylide monomers and polymers;[205,208,210] for example, a value of $\gamma_{real} = -0.07 \times 10^{-36}$ esu was measured for the Ni analog of **183**.[210] In these types of materials, it generally appears that second hyperpolarizabilities decrease in the order Ni > Pd > Pt,[205] although this does not apply to all the Pd and Pt systems in Ref. 206. Pd–Pd-bonded groups have also been incorporated into acetylide-based polymers.[210] For the Pt-containing oligomers **186–189** absorption maxima were found to be more-or-less independent of n and γ (solution THG at 1,097 nm) and increased in a more-or-less linear fashion with n indicating that the Pt centers act as more-or-less insulating linkers between the organic groups (200×10^{-36} esu for **186**); in contrast, a superlinear increase was observed in related all-organic species.[209] Moreover, comparison of the value for **186** with that for an organic molecule similar to one of the ligands indicates that the non-linearity of these species is primarily due to the organic tetraethynylethene moieties.

12.04.1.3.2.(iii) Group 11

A number of dipolar,[194,212,213] quadrupolar,[194] and octupolar[214] species incorporating the $R^1C{\equiv}CAuPR_3$ group (Figure 16) have been investigated for second- and third-order NLO properties using HRS (1,064 nm) and z-scan (800 nm), respectively. The absorption maxima for dipolar species with nitrophenyl acceptors, **190–194** (Figure 16),[213] are blue shifted relative to their analogs with *trans*-ClRu(P^P)$_2$ donors[193] and the values measured for $\beta(\leq 59 \times 10^{-36}$ esu) and β_0 ($\leq 28 \times 10^{-36}$ esu) are considerably lower; γ-values are of similar magnitude to those of structurally similar *trans*-ClRu(P^P)$_2$Ru species. In some cases, values of γ_{real} for the gold-containing species are smaller for analogous Ru species, for example, **190–193** ($100–150 \times 10^{-36}$ esu)[213] versus **156** and **157**,[193] but if **193** ($1{,}300 \times 10^{-36}$ esu)[213] is compared to **161**,[193] the Au species has the higher value; however, it is worth noting that dispersion effects are probably important here and that it is, therefore, difficult to generalize about the relative effectiveness of Au and Ru in enhancing γ_0. Similarly, it is difficult to generalize on two-photon structure–property relationships since only single-wavelength data are available, but none of the gold species shows a particularly large cross-section at 800 nm. The octupolar **195** (Figure 16) shows a rather small β and β_0 (6×10^{-30} and 4×10^{-30} esu, respectively).[214] Ferrocene-bridged quadrupolar species[130] are described in Section 12.04.1.2.1.(ii).

The third-order properties of $(AgC{\equiv}CPh)_n$, $(AgC{\equiv}CPh{\cdot}AgS^tBu)_n$, and $(Ph_3PAgC{\equiv}CPh)_4$ have been probed using optically heterodyned optical Kerr effect measurements (fs, 647 nm);[215] very large γ-values (ca. $100{,}000 \times 10^{-36}$ esu and $70{,}000 \times 10^{-36}$ esu in 1 : 1 DMSO/$CHCl_3$), much larger than poly(phenylacetylene) under the same conditions ($5{,}200 \times 10^{-36}$ esu), were reported for the first two species, while the phosphine complex gave a negligible response. The large values were attributed to the incorporation of polarizable d^{10}-ions into extended oligomerized systems, but the exact mechanism leading to such large measured values is unclear at this time. These species are also highly transparent ($\lambda_{max} \leq 270$ nm). Oddly, γ-values of similar magnitudes but opposite signs were reported when the solvent polarity was changed.

12.04.1.3.2.(iv) Group 12

Mercury has also been inserted into the bridge of donor–acceptor chromophores and affords increased transparency relative to comparable all-organic bridges; thus, a β-value of 26×10^{-30} esu has been reported for **195** (Figure 16), compared to values of 24 and 28×10^{-30} esu for corresponding tolane (compound **195** minus the Hg) and bis(phenyl)-butadiyne analogs, respectively, while the absorption maxima are 307 nm for **195** and 379–384 nm for the all-organic analogs.[132,216,217]

12.04.1.3.3 Miscellaneous compounds with η^1-hydrocarbon ligands

Here we briefly mention a few compounds in which the only organometallic character arises from η^1-hydrocarbon ligands apart from alkylidenes (section 12.04.1.3.1) and alkynyl (section 12.04.1.3.2) ligands. A weak SHG signal was measured for an inclusion complex of (*p*-cyanobenzoyl)$Mn(CO)_5$.[137] The third-order properties, including two-photon absorption at 532 nm, of an usual alkyliridapyrrole have been studied.[218] Group 10 *trans*-$XM(PR_3)Ar$ species (X = Br, I; M = Pd, Pt; Ar = *p*-acceptor-substituted phenyl) have been investigated as second-order materials, but show rather small β ($\leq 3.8 \times 10^{-30}$ esu).[150,219] *E*-4′-*trans*-$PdBr(PR_3)_2$-4-stilbazole species tested negative for SHG in the solid state, but were expected to have reasonable β-values from the characteristics of their optical spectra.[220] Aryl–Pd linkages, as cyclometallated moieties, have also been used in second-order chromophore polymer composites.[221,222] Group 10 aryl linkages also feature in species such as [*trans*-$Ni(PBu_3)_2$(2,5-thienylene)]$_n$; γ_{real} for this species is larger (1.2×10^{-36} esu) than for several other group 10 acetylide polymers and for all-organic polythiophenes.[208]

12.04.1.3.4 Carbonyl complexes

In this section we consider species in which the only organometallic component is the inclusion of an $M(CO)_n$ unit (or units).

12.04.1.3.4.(i) Group 6

Some of the earliest studies of non-linear optics in organometallic compounds involved testing a large number $LM(CO)_5$ and $LL'M(CO)_4$ complexes, where L and L′ are substituted pyridines or phosphines for SHG at 1,064 nm.[148] Many examples gave no detectable SHG response; the best example, {4-(4-chlorobenzoyl)pyridine}$W(CO)_5$, had an efficiency close to that of ammonium dihydrogen phosphate. Small β-values (comparable to or less than that of **1**) have also been determined for pyridine, 4-butylpyridine, and 4-acetylpyrdine complexes of $W(CO)_5$.[150] Powder SHG measurements have also been carried out for inclusion complexes formed by several $LW(CO)_5$ species (L = pyridine, 4-picoline, 4-aminopyridine, 4-ethylpyridine) with tris-*o*-thymotide, but no signal was detected.[137] Several other studies have been concerned with the determination of β for extended donor-substituted pyridines coordinated through the nitrogen of the pyridine to $M(CO)_5$ fragments. Two groups have studied the effect of coordinating $M(CO)_5$ to **196** (Figure 17) using HRS at 1,064 nm; both agree that coordination increases β, rather different values were obtained. Lee *et al.* reported values of 185, 282, and 242×10^{-30} esu for **196**,[112] **198**, and **200**, whereas Mata *et al.* reported 21, 63, 95, and 101×10^{-30} esu for **196**, **198**, **199**, and **200**, respectively.[111] Both sets of values are likely to be strongly enhanced by dispersion enhancement: indeed, Mata *et al.* estimate β_0-values of 4, 23, 12, and 12 for $\times 10^{-30}$ esu for **196**, **198**, **199**, and **200**, respectively, although it should be borne in mind that correction for dispersion is especially problematic for ferrocenyl species. Similar effects are obtained in the homologs with an additional styryl group in the π-bridge: values of 146, 369, 448, and 535×10^{-30} esu were determined for **197** and **201–203**, respectively.[223] Mata *et al.* also found (using HRS, 1,064 nm) that coordination of the nitrogen of the donor-substituted benzonitrile, *E*-(*p*-cyanostyryl)ferrocene, to $M(CO)_5$ enhances β (estimated β_0) from 203 (34) $\times 10^{-30}$ esu to 271 (39) or 375 (48) $\times 10^{-30}$ esu for M = Cr and W, respectively.[111]

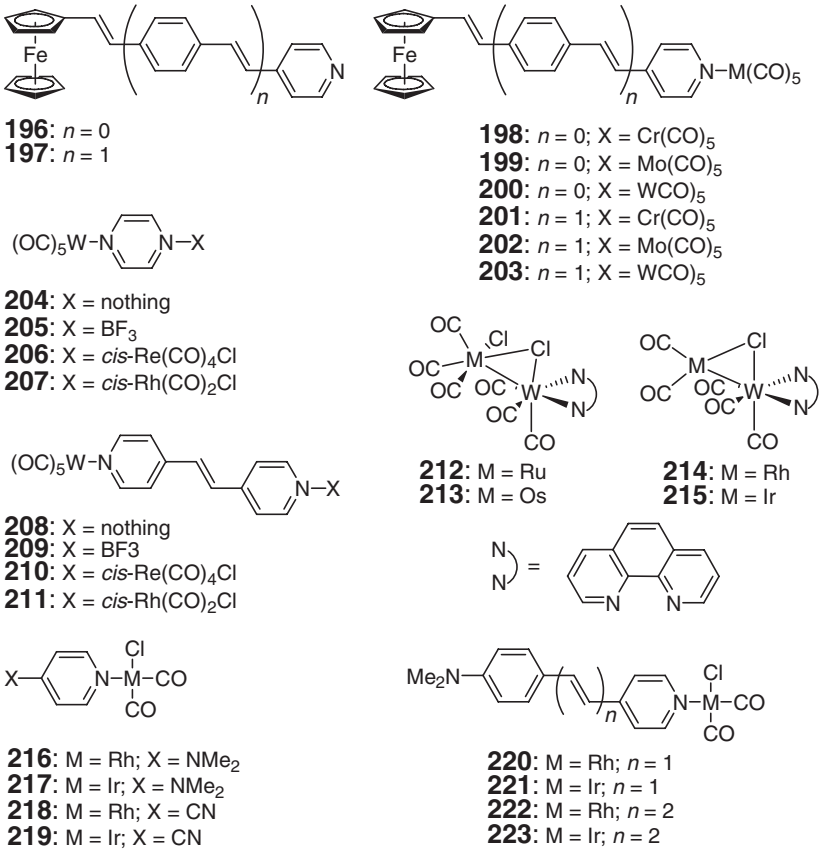

Figure 17 Structures of metal carbonyl compounds discussed in Section 12.04.1.3.4.

The $W(CO)_5$ moiety has also been incorporated in the compounds **204–211** (Figure 17), where possible β was measured using EFISH at 1,907 nm and estimated from solvatochromic data.[224] In these species the relevant excited state is believed to be a rather localized $W \rightarrow \pi^*$ CT transition; the effects of the rest of the molecule on this transition are not particularly straightforward. The highest values of β were measured for the two heterobimetallics with the longer bridging ligand (-52 and -41×10^{-30} esu for **210** and **211**, respectively; β_0 was estimated to be -39 and -31×10^{-30} esu, respectively).

In addition, β (EFISH, 1,907 nm) has been measured (and estimated from solvatochromic data) for several heterobimetallics containing $(phen)W(CO)_3$ {phen = phenathroline} fragments.[225] These values for the species **212–215** (Figure 17) are enhanced (up to -76×10^{-30} esu for **214** and **215**) β relative to $(phen)W(CO)_4$ (-13×10^{-30} esu). The lowest-energy band is assigned to a $W \rightarrow$ phen π^* transition in all cases; estimates based on solvatochromic data suggest that this excited state makes more or less the same contribution in **214** and **215** as in the parent $(phen)W(CO)_4$ and that a higher-lying CT state is responsible for the increased values seen in the heterobimetallic compounds.

12.04.1.3.4.(ii) Groups 7 and 8

The use of the $Re(CO)_4Cl$ group bridged by bidentate nitrogen ligands to $W(CO)_5$[224] has been discussed above (Section 12.04.1.3.4.(i)). Complexes of **196** (Figure 17) and the $Mn(CO)_5^+$ and $Re(CO)_5^+$ fragments both show larger β-values (602 and 712×10^{-30}, respectively, HRS, 1064 nm) than their isoelectronic neutral Cr and W analogs, **198** and **200** (Section 12.04.1.3.4.(i)),[112] although resonant enhancement no doubt plays an important role and these trends might not necessarily reflect those in β_0 (λ_{max} for the Re species is 532 nm).

Heterobimetallics where Ru or Os are linked to W through a Cl-bridged metal–metal bond[225] are discussed above (Section 12.04.1.3.4.(i)). The *fac*-$Os(CO)_3Cl_2$ fragment has also been coordinated to a variety of pyridines; like the isolobal group 9 $M(CO)_2Cl$ (see Section 12.04.1.3.4.(iii)) fragment, this species can act as both donor or acceptor, depending on the substitution on the pyridine.[184] Absorption maxima and values of $\mu\beta$ and β suggest that, for donor-substituted pyridines, this moiety has a similar acceptor strength to the group 9 $M(CO)_2Cl$ moieties; however, it appears to be a less effective donor when the ligand is 4-cyanopyridine.

12.04.1.3.4.(iii) Group 9

The use of the $Rh(CO)_2Cl$ group bridged by bidentate nitrogen ligands to $W(CO)_5$[224] has been discussed above (Section 12.04.1.3.4.(i)), as have heterobimetallics where Rh or Ir are linked to W through a Cl-bridged metal–metal bond.[225] The *cis*-$M(CO)_2Cl$ {M = Rh, Ir} groups have been coordinated to a variety of substituted pyridines and studied by EFISH.[184] It was found that, depending on the nature of the substitution, the organometallic group could either, when the pyridine is acceptor substituted, act as a donor, with an MLCT dominant, or, where the pyridine is donor substituted, as an acceptor, red shifting the intraligand CT band. The biggest enhancements on metal coordination occur with simple pyridines such as those shown in Figure 17: values of $\mu\beta$ for **216** and **217** (1,064 nm) are 51 and 58×10^{-48} esu, respectively, whereas for the parent pyridine the value is 0.25×10^{-48} esu; the corresponding β values are 0.07, 8.7, and 9×10^{-30} esu. For **218** and **219** the values are -12 and -31×10^{-48} esu, respectively, with a value of 0.36×10^{-48} calculated theoretically for the parent pyridine. Much larger values are attainable with extended conjugation, but the enhancement of $\mu\beta$ and β relative to the parent pyridine is substantially less dramatic. For example, for **223**, β (1,340 nm) is found to be 135×10^{-30} esu, whereas the value for the corresponding pyridine is 80×10^{-30} esu. The estimated $\mu\beta_0$ values are 580 and 211×10^{-48} esu for free ligand and Ir complex, respectively.

12.04.1.4 *p*-Block Metal Compounds

12.04.1.4.1 Group 13

Organometallic group 13 species investigated for non-linear optics are essentially limited to derivatives of the metalloid element, boron. A number of different organoboron systems have been used in NLO chromophores.[226] We have described the use of η^6-boratobenzene transition metal derivatives as acceptors in Section 12.04.1.2.2.(iii) and 12.04.1.2.2.(iv). In this section, we will discuss three-coordinate boranes, four-coordinate borates, and finally carboranes.

12.04.1.4.1.(i) Three-coordinate boranes

The B(mes)$_2$ {mes = 2,4,6-trimethylphenyl} fragment has been attached to π-systems through the boron atom and investigated as a potential acceptor in both dipolar[116,227–231] and quadrupolar[232] chromophores; the NLO properties of B(mes)$_2$-substituted compounds have been reviewed fairly recently.[233] An important difference noted between this group and the more traditional type of acceptor such as NO_2 is that, although B(mes)$_2$ is a π-electron acceptor, it is not a strong σ-acceptor and may even be a σ-donor; consequently, the dipole moments of donor–acceptor species incorporating B(mes)$_2$ are rather low compared to traditional donor–acceptor species. In some examples of these compounds, B(mes)$_2$ appears to be a stronger acceptor than NO_2,[229] and in others somewhere between CN and NO_2.[233] For example, β for **224** (Figure 18, EFISH at 1,907 nm) is measured at 45×10^{-30} esu,[233] whereas the analogs with nitro (**3**, Figure 1) and cyano acceptors show β of 73 and 36×10^{-30} esu by the same technique;[75,152] however, the dipole moments for **3** and the cyano species are 6.6 and 5.7 D, respectively, whereas that for **224** is only 3.0 D, suggesting **3** would be considerably more useful than **224** in poled polymer applications, something that one might not anticipate from the β-values alone.

The highest value of γ found in a study of quadrupolar examples (THG at 1,907 nm) was 229×10^{-36} esu for **225**, which was the longest system studied.[232] The third-order susceptibility, $\chi^{(3)}$ (DFWM, 532 nm), for the polymer, **226**, was found to be over 1,000 times that of *all-trans* polyacetylene, although this value is presumably dispersion enhanced and very far from the static value.[234]

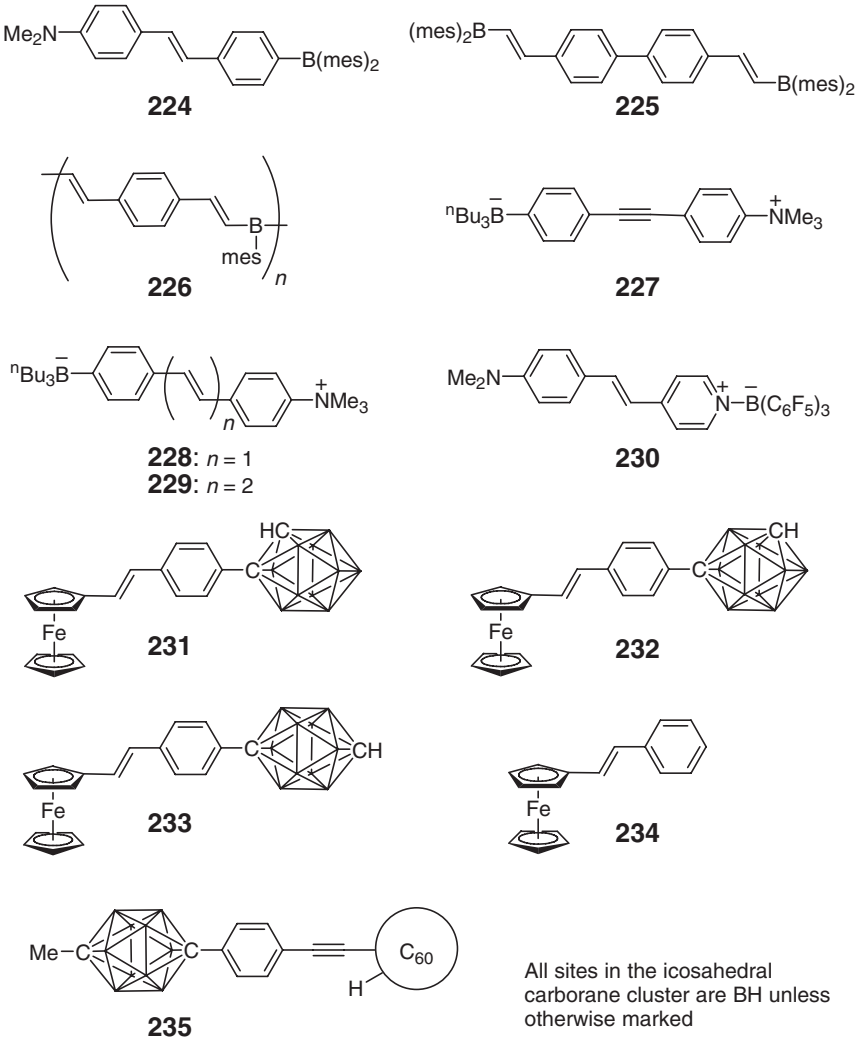

Figure 18 Structures of boron-containing compounds discussed in Section 12.04.1.4.1.

12.04.1.4.1.(ii) Four-coordinate borates

Organoborates have also been used as donors in conjunction with ammonium acceptors; these strong σ-donors and acceptors significantly polarize the π-bridging groups so that the lowest energy transition shows strong negative solvatochromism. The $\beta(\beta_0)$ values of 38 (19), 84 (38), and 153 (69) $\times 10^{-30}$ esu have been measured (estimated) using HRS at 1,064 nm for compounds **227–229**, respectively (Figure 18).[139] *E*-4-Dimethylamino-4′-nitrostilbene, **3** (Figure 1), a stilbene with more conventional π-donor and π-acceptors, can be usefully compared to **228**:[75,152] β and β_0 values are of similar order of magnitude (73 and 34×10^{-30} esu, respectively for **3** using EFISH at 1,907 nm), but **228** shows improved transparency ($\lambda_{max} = 302$ and 430 nm for **228** and **3**, respectively), and much larger $\mu\beta_0$ (3,250 and 363×10^{-48} esu for **228** and **3**, respectively).

The strong organoboron Lewis acid, $B(C_6F_5)_3$, has been coordinated to donor-substituted pyridines:[235] as with coordination of metal carbonyl moieties (see Section 12.04.1.3.4), this increases the acceptor ability of the pyridine group and accordingly increases $\mu\beta$, β, and β_0 (there is relatively little change in the ground-state dipole moment in these systems). For example, for **230** (Figure 18) EFISH (1,340 nm) gave $\mu\beta = 450 \times 10^{-48}$ esu, $\beta = 155 \times 10^{-30}$ esu, and an estimate of $\beta_0 = 73 \times 10^{-30}$ esu, whereas the corresponding values for the parent pyridine before coordinating to boron are $\mu\beta = 150 \times 10^{-48}$ esu, $\beta = 45 \times 10^{-30}$ esu, and $\beta_0 = 29 \times 10^{-30}$ esu. The effects induced by coordination of $B(C_6F_5)_3$ are similar to those of coordinating the inorganic boron Lewis acid, BF_3.

We also note that organoborate anions, in particular BPh_4^-, have also been used as counterions for cationic second-order NLO dyes (e.g., see Refs: 51, 236). In principle, non-dipolar contributions to β are possible with non-centrosymmetric species such as this; such contributions in the inorganic BF_4^- ion have been proposed as responsible for the different values of β determined for BF_4^- and PF_6^- salts.[102]

12.04.1.4.1.(iii) Carboranes

Carboranes have also been studied as components of second-order NLO chromophores and a brief survey of some of this work has recently appeared.[237] Simple aryl carboranes have been studied using powder SHG and EFISH; although only small non-linearities were obtained (SHG < urea; $\mu\beta = \leq 25 \times 10^{-30}$ esu; $\beta = \leq 6.3 \times 10^{-30}$ esu), the highest values of $\mu\beta$ and β were obtained with donor-substituted aryl groups, suggesting that the carborane acts as an acceptor.[238] The linear and non-linear (HRS at 1,064 nm) properties of compounds in which ferrocenyl groups are linked to various isomers of dicarbodecaborane, including compounds **231–233** (Figure 18), have been compared to **8** (Figure 4) and to styryl ferrocene **234**. The low-energy absorption maxima of **231–234** occur at an energy similar to one another, but at higher energy than **8**. The values of β were 114, 111, 131, 103, and 152×10^{-30} esu for **231–234** and **8**, respectively.[117] The data suggest that the carborane acts a weak acceptor in these compounds.

Despite expectations that both groups should act as acceptors and that β should be rather small, high non-linearities were reported for dyads where carboranes are linked to fullerenes; the highest value reported was $\beta = 1{,}189 \times 10^{-30}$ esu (with only small resonance enhancement) for **235** (Figure 18).[239,240]

12.04.1.4.2 Group 14

12.04.1.4.2.(i) Second-order materials

Four-coordinate organosilicon groups, such as Me_3Si–, are neither strong donors nor acceptors in dipolar chromophores; for example, β values (EFISH, 1,064 nm) of 3.8 and 12×10^{-30} esu were reported for **236** and **237** (Figure 19), respectively,[241] and can be compared to a value 32×10^{-30} esu for **238** (EFISH, 1,907 nm).[75] A series of five-coordinate species have also been studied: structure–property relationships are not straightforward, but comparison of λ_{max} and β (HRS, 1,064 nm) for **239** (257 nm, 10×10^{-30} esu) and **240** (320 nm, 13×10^{-30} esu) suggests that this group acts as a weak donor.[242]

Various silicon-based groups have also been used as bridges in dipolar donor–acceptor species.[119–121,241,243,244] Silane bridges can weakly transmit donor–acceptor interactions. Although β-values in these species are typically rather small, chromophores show better transparency than analogs with conjugated organic bridges. Replacement of an $–SiMe_2–$ bridge in **241** (Figure 19) with $–SiMe_2SiMe_2–$ **242** leads to an increase of β from 16×10^{-30} esu (approximately the sum expected from the independent effects of the left- and right-hand sides of the molecule) to 22×10^{-30} esu; β is larger still (38×10^{-30} esu) in the $–(SiMe_2)_6–$ species **243**. However, in systems with ferrocenyl donors, the opposite trend has been observed: β_0 values of 57 and 7×10^{-30} esu have been estimated from EFISH data for **244**[121] and **245**,[119] respectively. Chromophores with a cyclohexasilane bridge, such as **246**, have been reported to show larger β than analogs with open-chain bridges.[120]

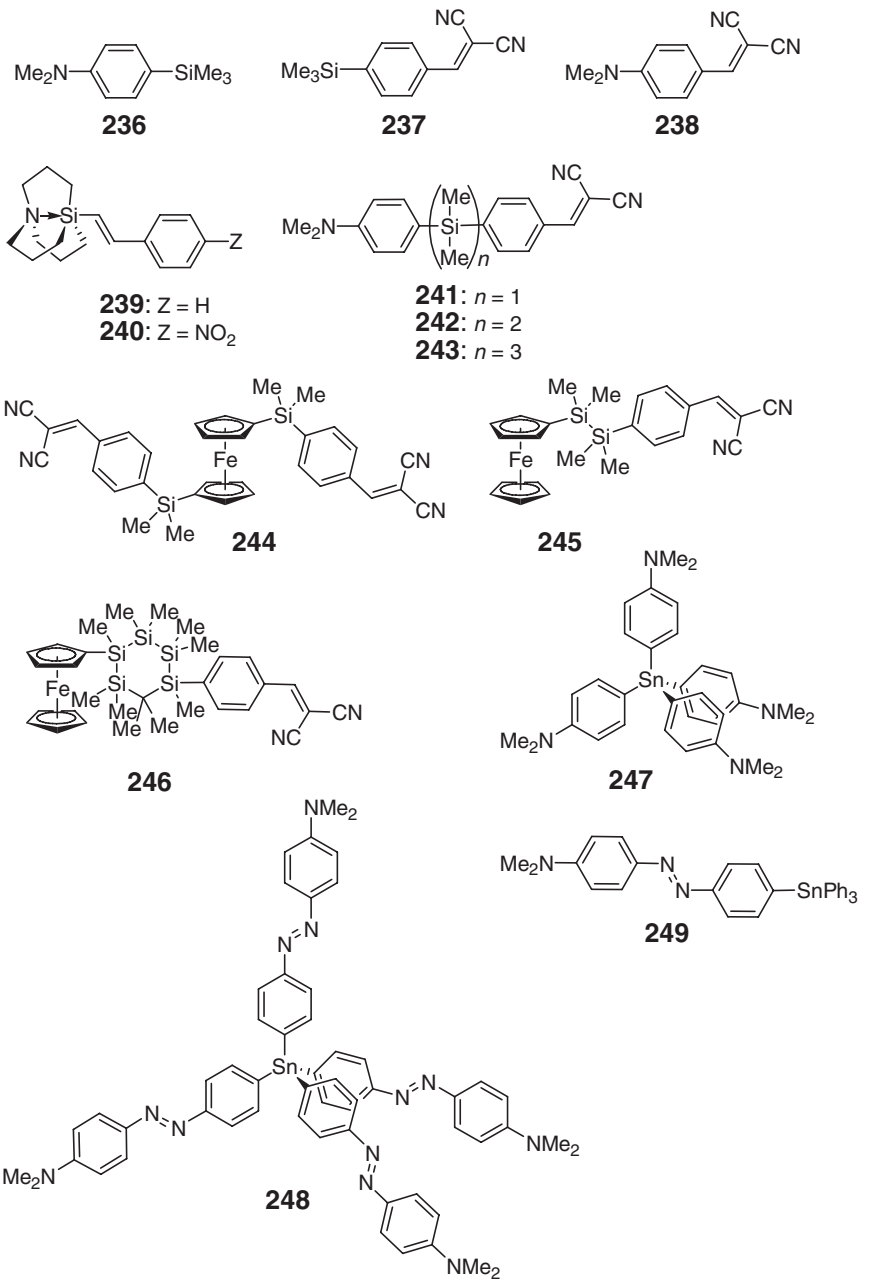

Figure 19 Structures of second-order chromophores containing group 14 elements and discussed in Section 12.04.1.4.2.(i), along with an all-organic analog.

Tin has been used a tetrahedral center for non-dipolar non-centrosymmetric chromophores. Two examples, **247**[245] and **248**,[246] are shown in Figure 19; HRS (1,064 nm) has been used to measure values of β of 13 and 159×10^{-30} esu, respectively. The value for **248** and the corresponding β_0 value (48×10^{-30} esu), arising from octupolar contributions, are interestingly close to the dipolar value obtained for a chromophore resembling one of its arms, **249** ($\beta = 181 \times 10^{-30}$ esu; $\beta_0 = 57 \times 10^{-30}$ esu).

12.04.1.4.2.(ii) Third-order properties of polysilanes, germanes, and stannanes

The third-order non-linearities of polysilanes, $[SiRR^1]_n$,[247] are among the highest for materials that are transparent throughout the visible and near-IR with values of $\chi^{(3)}$ for films exceeding 10^{-12} esu. These polymers have been the

subject of a large number of studies and only representative examples are referred to here. A large number of studies have been performed using THG,[248,249] the Kerr effect,[250] DFWM,[250] and computational methods.[251,252] These high hyperpolarizabilities have been attributed to σ- and σ^*-delocalization along the polysilane chain. Aryl silanes tend to show higher $\chi^{(3)}$ which is attributed to the interaction between phenyl π-orbitals and the σ- and σ^*-orbitals of the polymer; however, aryl species also show a red-shifted low-energy absorption and so the enhanced $\chi^{(3)}$ may be due to dispersion effects as well as to enhanced $\chi^{(3)}{}_0$.[253] Other factors found to influence $\chi^{(3)}$ include conformation and molecular weight.[252,254] The dispersion of $|\chi^{(3)}|$ has been well studied over a wide wavelength range[255] and maxima in $|\chi^{(3)}|$ have been correlated with peaks in two-photon absorption spectra.[256] We also note in passing that polysilanes have been used as components of $\chi^{(2)}$ polymers (e.g., see Ref: 257), but that in these cases the NLO activity is associated with organic chromophore side chains, rather than the polysilane itself.

Polygermanes have also received some attention: for films of poly(di-*n*-hexylsilane) and poly(di-*n*-hexylgermane), $\chi^{(3)}$ values of 7.2 and 3.3×10^{-12} esu, respectively, were obtained at room temperature using THG with 1,064 nm radiation (in which case the third harmonic lies close to λ_{max}) and 1.3 and 1.1×10^{-12} esu, respectively using 1,907 nm.[249]

Poly(di-*n*-butylstannane) has been studied in solution using *z*-scan and DFWM at 532 nm; extrapolation to concentrations anticipated in films suggests a solid-state $\chi^{(3)}$ of 500×10^{-12} esu.[258] This rather large value is presumably somewhat dispersion enhanced, but suggests that poly(stannanes) might warrant more investigation.

12.04.1.4.2.(iii) Other silicon-containing polymers

High third-order non-linearities (for many solutions, $|\chi^{(3)}{}_{real}| > 10^{-12}$ esu) have been reported for a range of conjugated organic polymers incorporating four-, five-, and six-coordinate silicon centers into the backbone of conjugated organic polymers.[135,259–263] Some of the structures investigated are shown in Figure 20. The best response for a film is for a sol–gel composite containing 14 wt.% of **253** which showed a $\chi^{(3)}{}_{real}$ of -95×10^{-12} esu (ps *z*-scan at 1,064 nm).[135]

12.04.1.5 NLO Conclusions

The NLO properties of organometallic compounds have now been studied for over 20 years. As speculated in early papers, a wide range of organotransition metal centers have been found to be capable of acting as strong donors and acceptors in extended conjugated molecules. High non-linearities have been obtained in several systems; however, no second-order materials based on an organometallic chromophore have yet been demonstrated to be competitive with the best all-organic materials in non-linearity. Moreover, the thermal and photostability of organometallic chromophores have been, in general, much less well studied than those of their organic counterparts. Although electrochemical switching of second-order non-linearities has been demonstrated for several organometallic chromophores, (electrochemical switching is, in principle, possible in organic chromophores exhibiting reversible electrochemistry. However, the potential, required for oxidation of triarylamine donors will typically be more oxidizing than those employed to switch some of the organometallics that have been studied), this switching has yet to be exploited in a functional device. Turning to third-order materials, polymeric materials based on the group 14 metalloid elements, particularly polysilanes and polygermanes, have some of the highest non-linearities known for materials that are transparent in the visible part of the spectrum. In addition, they can be readily processed into optical quality films.

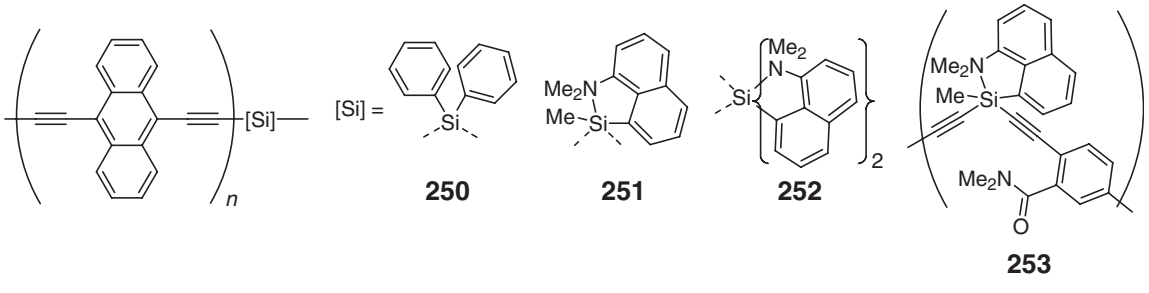

Figure 20 Structures of silicon-containing polymers discussed in Section 12.04.1.4.2.(iii).

12.04.2 Organic Light-Emitting Diodes

A light-emitting diode (LED) is a solid-state semiconductor device, the most common types of which are built from inorganic materials such as $In_xGa_{1-x}As$, GaN, etc.[264] The term organic light-emitting diode (OLED) refers to any LED that is composed of either molecular or polymeric materials. OLEDs use exclusively organic materials or a mixture of organic materials and metal complexes/polymers with organic ligands, thus the term OLED encompasses all the devices that are relevant here. The basic mechanism of electroluminescence (EL) in both inorganic LEDs and OLEDs is the same, that is, carrier recombination leads to the formation of an exciton, which radiatively relaxes to give the observed EL. In an inorganic semiconductor, an exciton is a correlated electron/hole pair. While the definition of an exciton in a molecular system is the same, it typically refers to the molecule in its excited state. Both inorganic and organic LEDs are composed of distinct carrier transporting and emitting regions of the device, sandwiched between the anode and cathode. Beyond these very basic similarities, however, the two types of LEDs are very different. Inorganic LEDs clearly fall outside the topic area intended for this series and will not be discussed.

The future holds tremendous opportunity for the low cost and high performance offered by organic LEDs. Full color displays that use OLEDs may eventually replace liquid-crystal displays (LCDs) in a range of mobile applications, ranging from cellular phones to laptop computers. The low power dissipation and high brightness of OLEDs make them ideal for such portable applications. OLED displays can be deposited on flexible plastic or metal foils, eliminating the fragile and heavy glass substrates used in LCDs and other flat panel displays. Moreover, OLED displays emit light without the pronounced directionality inherent in LCD viewing, all with efficiencies significantly higher than can be obtained with incandescent light bulbs. It is possible that portable and lightweight roll-up OLED displays will someday cover our walls, replacing the bulky and power-hungry cathode ray tube (CRT) that has been the standard device to view television for over 50 years. Another important application for OLEDs is in illumination. The high efficiencies and excellent color qualities for white OLEDs make them promising candidates for replacing conventional incandescent light sources.

This section focuses on the principles of EL in OLEDs, with particular attention to how organometallic complexes have been used to enhance the efficiencies of OLEDs. The role that organometallic complexes play in forming high efficiency, multicolored OLEDs is then discussed. The methods that are used to control the photophysical properties of the complexes, as well as the performance of organometallic OLEDs, are also covered. The goal of this discussion is to give the reader a working knowledge of how OLEDs operate and a picture of the progress in the field to date.

12.04.2.1 Mechanism of EL

12.04.2.1.1 Photophysical properties of organic and metal–organic materials

At the most basic level, an OLED electrically promotes molecular or polymeric chromophores into their excited state. These excited species can relax to the ground state by emitting light, whereby they are then available to be electrically excited again. While understanding this process of electrical excitation is important, we will first consider the photophysics of these materials since this will form a good platform to understand the nature of the excited states. The relationship of ground- and excited-state energies is easy to visualize with a Jablonski diagram, shown in Figure 21.[265–267] The ground state, S_0, is represented by a long horizontal bar and its vibrational sublevels by the ladder of energies above it and to the left. Absorption of a photon promotes the system from S_0 to the lowest-energy

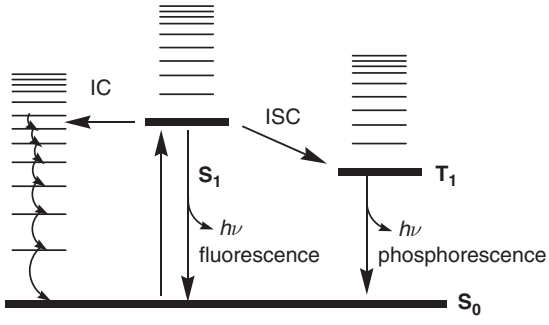

Figure 21 Jablonski diagram.

singlet excited state, S_1, which can decay through several different pathways. The S_1 state can radiatively relax (fluorescence), undergo internal conversion (IC) to the S_0 state (thermal deactivation), or intersystem cross (ISC) to the triplet state, T_1. Direct relaxation from the T_1 state to S_0 is symmetry forbidden, and thus a low probability event. Emission from the T_1 state (phosphorescence) is weak for most materials, often giving luminescent lifetimes of seconds to minutes, as opposed to nanoseconds for fluorescent transitions.[265] On the other hand, phosphorescence from organometallic complexes with heavy metals such as Ir, Pt, and Os can undergo fast radiative decay, often $<100\,\mu s$,[268] which leads to high emission efficiencies and provides the basis for high-efficiency EL discussed in detail below. While higher-energy singlet (S_n) and triplet (T_n) excited states are accessible by optical excitation, they are generally not assumed to be formed in the electroluminescent process and will not be considered here.

With few exceptions, the excited state formed in the EL process (either singlet or triplet) is the same one that could be formed by photoexcitation of the chromophore. Thus, photoluminescence (PL) is a very useful tool for screening materials in terms of the color and potential efficiency for emission in an OLED. The PL efficiency sets an upper limit on the EL efficiency since the excited state for emission is the same in both processes. However, solution PL measurements are not an ideal measure to use to estimate potential EL efficiency. In order to use the PL efficiency as a measure of the potential EL efficiency, the emitting material must be analyzed under identical conditions in both PL and EL experiments. Since OLEDs are solid-state devices, this requires that the PL efficiency be measured in the solid state in thin film form if the value is to be used to estimate the potential EL efficiency. PL measurements are typically carried out on fluid solutions of the emitting material and are susceptible to dynamic quenching processes that are not present in the solid state. Therefore, compounds with low-solution PL efficiencies may still be effective for use in high-efficiency OLEDs.

12.04.2.1.2 Basic steps in EL

An OLED is composed of one or more layers of organic material, totaling no more than 2,000 Å in thickness, sandwiched between an anode and a cathode (see Figure 22). One of the two electrodes is supported on a glass, metal, or plastic substrate. The organic materials are typically amorphous glasses, so that they can be deposited as smooth thin films, without the need for epitaxial growth to maintain uniformity over large areas. When an electric field is applied to the device, molecules at or near the anode/organic interface are oxidized. These oxidized molecules are referred to as holes since they lack an electron, that is, there is a "hole" in the filled molecular orbitals. At the

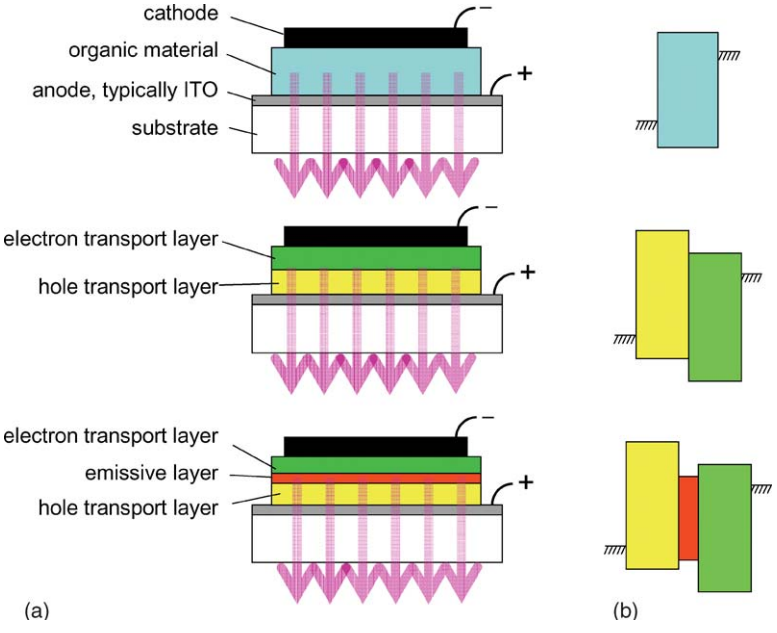

Figure 22 (a) Cross-sectional schematic diagrams of OLED structures (side view) (top) single layer, (middle) single heterostructure and (bottom) double heterostructure. ITO = indium–tin–oxide. The electrodes are typically 1,000–2,000 Å thick. The sum of the organic layer thicknesses are $<2{,}000$ Å. (b) Ideal energy level diagrams for each of the device structures.

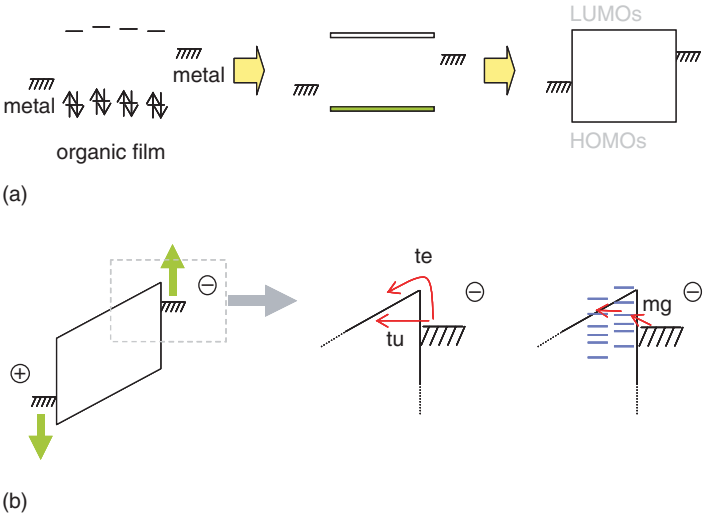

Figure 23 Energy level diagrams for OLED materials. Only the frontier orbitals are considered. (a) Transition from the molecular orbital energies to narrow bands in the solid state to the parallelogram image of the HOMO and LUMO energies are shown. (b) The effect of an applied bias on the energy levels (left). The red arrows illustrate carrier injection via tunneling (tu), thermionic emission (te), or midgap states (mg). The midgap states are shown in blue.

cathode a related process occurs, wherein molecules are reduced at or near the cathode/organic interface. These reduced molecules are referred to as electrons, since they carry an extra electron over the number associated with the molecules or polymers used to fabricate the device. The mechanism of EL can be broken down into four steps. First, carrier injection occurs from the electrodes to provide holes from the anode and electrons from the cathode. The carriers then migrate through the molecular or polymeric materials toward the center of the organic film. Subsequent recombination of a hole and an electron leads to the formation of either the S_1 or T_1 state, which finally relaxes to give the observed EL. Thus, the four steps involve (i) injection, (ii) migration, (iii) recombination, and (iv) emission.

It is important to be able to visualize the hole and electron energies for each of the materials used to make the OLED in order to understand the EL process. Only the frontier orbitals (HOMO and LUMO) need be considered for the description of holes, electrons, and excitons in these materials. The molecules form narrow valence and conduction bands (illustrated as green and gray rectangles in Figure 23) due to the relatively weak intermolecular interactions in most organic materials. The vertical axis in this scheme is energy and the horizontal axis is distance from base electrode. When an electric field is applied to the device, the rectangle is converted into a parallelogram, whose base is the HOMO band and the top is the LUMO band, as shown in Figure 23. The positive charge at the anode stabilizes both filled and vacant orbitals, while the negative charge at the cathode destabilizes the molecular orbitals (MOs). The vertical lines of the parallelogram have no meaning and are simply a guide for the eye. The HOMO and LUMO energies for these materials are typically determined from either direct methods, such as UV–photoelectron spectroscopy (UPS) of thin films for HOMO energies,[269] or inverse photoemission spectroscopy (IPES) for LUMO energies.[270–273] The HOMO and/or LUMO energies can also be estimated by indirect methods, such as electrochemistry,[274,275] and gas-phase ionization and electron affinity measurements,[276] or they can be predicted from theoretical calculations.[277] While these indirect methods can be precise, they ultimately need to be referenced back to the thin film values for effective modeling of OLED energetics. This picture is a significant oversimplification of the energetics of the device since it completely ignores interfacial interactions at the organic/organic and metal/organic interfaces.[278–280] However, the model is at a sufficient level needed to discuss the mechanism of EL in this chapter. The four steps leading to EL are discussed below.

12.04.2.1.3 Carrier injection

The first step in the electroluminescent process is carrier injection. Electrode materials are typically chosen to match the orbital energies of the organic materials as closely as possible. The anode materials are typically metal oxides, such as indium–tin–oxide (ITO), with work functions that are close to the HOMO energies of the materials they

contact. The cathode materials are typically metals with low work functions such as Li, Ca, or Al that are a close match to the LUMO energies of the materials that need to be reduced.

In the scheme shown in Figure 23, the energy difference between the electrode and the relevant MO is small enough that the carrier can be injected thermally (thermionic emission) or can tunnel from the electrode into the organic material.[280] Both processes have been described for OLEDs; however, an additional process involves carrier injection though midgap states.[281] During deposition of the metal onto organic materials, it is not uncommon for reaction and/or damage to occur at the surface of the organic film. Depth-profiling measurements show that the metal may penetrate 50 Å or more into the organic film.[282] The metal–organic reaction is expected to be most severe for reactive metals that are commonly used as cathode materials for OLEDs. The interaction between the deposited metal and the organic molecules ranges from minor "solvation" type effects, to electron transfer forming a reduced organic species, to bond rupture and molecular decomposition.[283] These metal–organic interactions lead to the formation of new species, with energy levels different from those of the pristine organic material, shown in blue in Figure 23.[281] These new states may fall between those of the cathode and the pristine organic material, and thus form midgap states. Injection of carriers into these midgap states will be more facile than into the pristine organic. In this case, the injection process involves injection into the midgap state first, followed by electron transfer from the defected region into the pristine organic material. Such a mechanism is thought to be common for electron injection in OLEDs.

12.04.2.1.4 Carrier migration and device heterostructure

The migration of holes or electrons though molecular materials occurs in response to the applied electric field. Holes migrate away from the positively charged anode and electrons away from the negatively charged cathode, with both carriers directed toward the interior of the organic film. The efficiency of carrier migration in a given material is described by the carrier mobility, in units of $cm^2 V^{-1} s^{-1}$. For most organic materials, intermolecular electron transfer to an adjacent molecule leads to the migration of hole or electron carriers through the solid thin film by a hopping-type mechanism. Chemists have studied electron-transfer processes of this type for many years, that is, outer-sphere self-exchange reactions.[284] While the self-exchange reaction provides a good description of the bimolecular electron- (or hole-) transfer process, specific models have also been developed to characterize and understand bulk carrier migration in amorphous molecular and polymeric solids. The most widely used models for carrier conduction in amorphous organic materials are the polaron[285] and disorder[286–288] models. In both of these models, the carrier traverses between molecules in the thin film by a thermally activated hopping process that is promoted by the applied electric field. The barrier to the individual hopping events limits the carrier mobility and the way this barrier originates is what differentiates the two models. The polaron model considers the principal barriers to carrier hopping as synonymous with those used to describe outer-sphere electron transfer. In this model, the carrier is effectively trapped by molecular distortions.[289–292] The presence of a charge on a molecule leads to a significant change in structure and this ion, along with the associated molecular distortion, is referred to as a polaron. In order for intermolecular charge transfer to occur (carrier migration) the two sites must distort to a common intermediate structure, that is, both the polaron and the neutral molecule must approach equal geometric structures. Marcus theory describes the situation for such self-exchange reactions, predicting that the large polaron distortion will lead to a large barrier to the electron transfer (due to the high reorganization energy for both the polaron and neutral molecule).[293–295]

The disorder model considers carrier migration through a lattice composed of a random distribution of molecular dipoles.[286–288,296,297] Each molecule in the lattice sees a different local field as a result of the orientation and spacing of the surrounding molecules. Some molecules will have neighboring molecules (dipoles) oriented in such a way that they stabilize the carrier in that region of the film, leading to a trapping site, while others will have the surrounding molecules oriented in a way that destabilizes the carrier, thus forming an antitrap. The statistics of van der Waals interactions among randomly positioned anisotropic molecules leads to a distribution of permanent dipoles. This distribution of dipoles generates a random electrostatic potential that adds to the local variations of the potential energy surface with the material. Therefore, films composed of molecules with a permanent dipole moment will distort the energy landscape experienced by a carrier executing random walk.[296,297,298–300] Consequently, the carrier mobility for doped films utilizing non-polar hosts is consistently higher than that observed in films with polar host materials.[296,297] Often, both the polaron and disorder models are required to fully explain the carrier conduction in organic solids.

Most materials will conduct one type of carrier, holes, or electrons, more efficiently than the other. Even though some molecular and polymeric materials are good conductors for both types, there is still a preference for one carrier to have a higher mobility than the other. If an OLED is fabricated with only a single organic layer, as shown in

Figure 22, most of the current passing through the device will simply involve transport of one type of charge from one electrode to the other. This situation leads to very little EL since EL recombination requires balanced amounts of holes and electrons within the organic material. The solution to this problem is to use multiple organic layers, such that both the holes and electrons are trapped within the organic thin film. Thus, a device with a separate hole-transporting layer (HTL) and electron-transporting layer (ETL) can give well-balanced hole and electron currents at or near the organic interface. This type of device architecture, referred to as a single heterostructure, is shown schematically in Figure 22. The HOMO and LUMO energy levels for the two materials are chosen such that there is an energetic barrier to holes migrating from the HTL into the ETL, as well as a barrier for electron migration from the ETL into the HTL (Figure 22(b)). The first such heterostructured organic LED was reported by Tang and Vaslyke in 1987.[301] Their device used a triarylamine as the HTL material and an aluminum coordination complex as both the ETL and emitting material. Alternatively, a separate emissive layer (EML) may also be inserted, such that the device structure consists of anode/HTL/EML/ETL/cathode, in an architecture referred to as a double heterostructure (Figure 22). A double heterostructure effectively confines both carriers in the emissive region and consequently enables devices to have higher efficiencies than those with single heterostructures.

The most common hole transporting materials in OLEDs are triarylamine derivatives, such as NPD (Figure 24). Triarylamine compounds are good examples of how molecules can be designed to maximize carrier mobility. The triarylamine group is nearly isostructural in its neutral and cationic forms,[139] which lowers the barrier to intermolecular energy transfer due to reorganization energies (polaron model of conductivity),[292,303] and also has a very low dipole moment, which minimizes dipole trapping (as described by the disorder model). The hole mobility of NPD ($10^{-4}\,cm^2\,V\,s^{-1}$)[303,304] is one of the highest values reported for an amorphous solid. Other common hole transporters with good hole mobilities include fluorene[305,306] and anthracene derivatives,[307–309] as well as a number of polymeric materials (Figure 24).[310,311] A paper also describes the use of organocobalt(III) complexes as hole transporting materials in OLEDs.[313] In this report, two different tris-cyclometallated complexes (see Figure 24) were used in both single and double heterostructure devices. While both complexes led to efficient EL, neither material gave

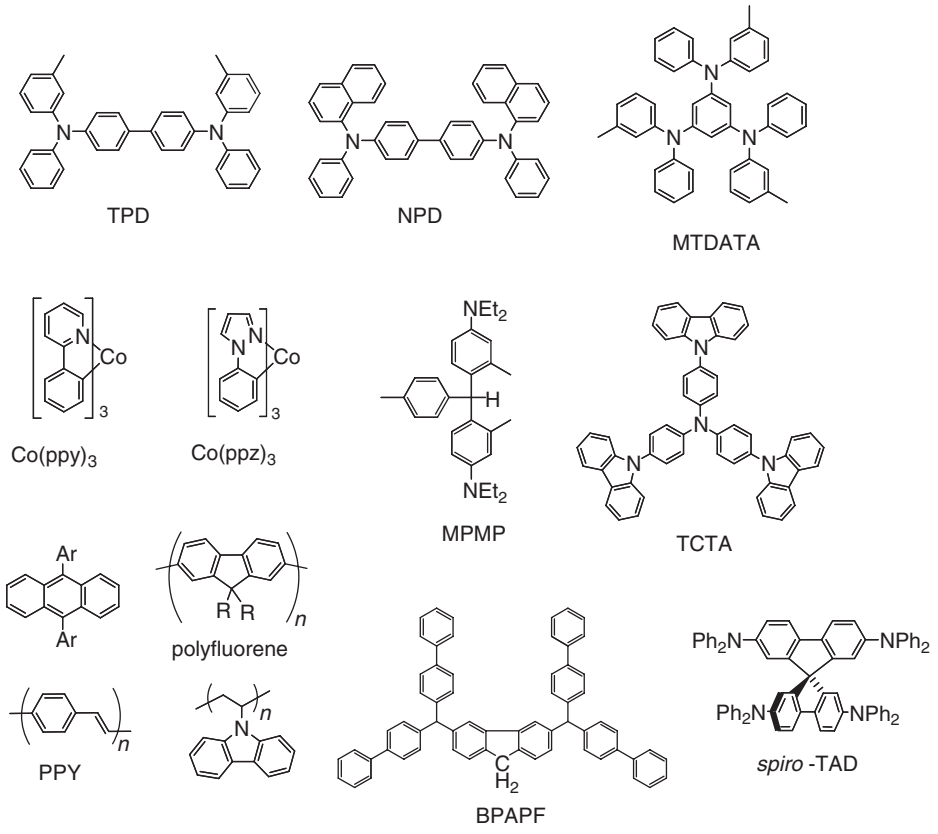

Figure 24 Representative materials used as hole transporters in OLEDs.

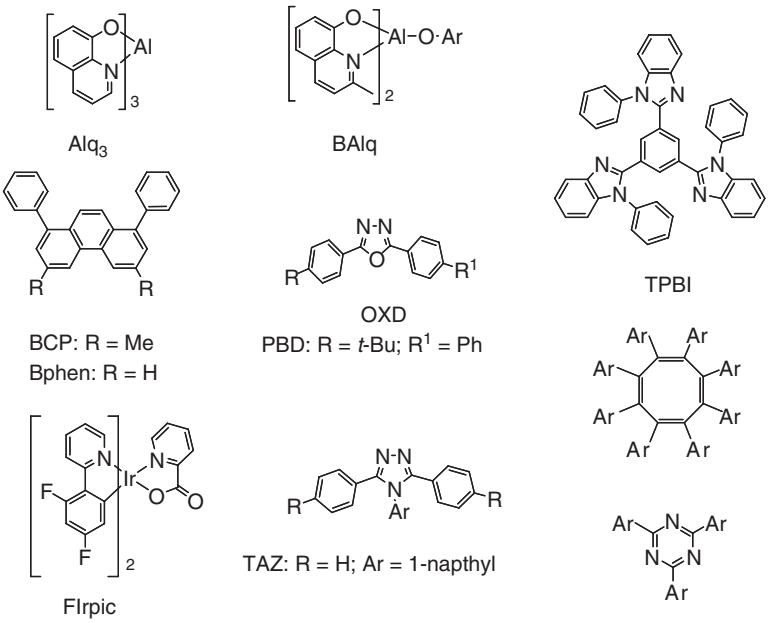

Figure 25 Representative materials used as electron transporters in OLEDs.

stable devices and light output diminished after only a few minutes of operation. The complexes were thought to degrade during use to cationic Co(II) complexes via reductive elimination from their oxidized forms (i.e., the hole), thereby inhibiting the device performance.

Most common electron transporters are derived from heterocyclic aromatic compounds, either as pure organic materials or as metal coordination complexes. Pure organic molecules such as phenanthrolines, oxidiazoles, and triazoles can have high electron mobilities (Figure 25).[310] Some of the highest carrier mobilities for amorphous molecular materials have been reported for oligofluorenes (10^{-3}–10^{-2} $cm^2 V^{-1} s^{-1}$),[305,313] however, inefficient carrier injection into these materials can often lead to relatively poor OLED performance. A wide range of carrier-conducting polymers have also been reported, some of which conduct charges through pendant groups[311] and others through main-chain conjugation pathways.[310] One of the most well-studied electron transporters is aluminum(8-hydroxyquinolate)$_3$, Alq_3.[314] This material has a field-dependent electron mobility of roughly 10^{-5}–10^{-6} $cm^2 V^{-1} s^{-1}$.[315,316] An electron-transporting organometallic complex, FIrpic, has also been reported (Figure 25). FIrpic was first used a blue phosphor in OLEDs,[317] but has also been employed as an efficient electron transporter in double heterostructure devices.[318] Unfortunately, neither the carrier mobilities nor conductivities of this complex have been reported, so direct comparison to other electron transporters cannot be made.

Although both hole- and electron-transporting organometallic complexes have been described, the application of organometallic complexes for this purpose has been little studied and it is expected that other complexes could also be used as carrier transport materials.

12.04.2.1.5 Carrier recombination

When the hole and electron migrate to positions such that they are residing on closely spaced or adjacent molecules, hole–electron recombination can occur, leading to the formation of an exciton and a molecule in its ground state, as shown in Figure 26. Two different electron-transfer processes are possible. One involves transfer of the valence electron of the anion to the LUMO of the hole, forming an excited state on the molecule that was formerly a cation. Alternatively, a lower-energy electron could be transferred from the anion to the hole, forming the excited state in the molecule that was formerly an anion. In principle, the electron could also be transferred directly from the higher-energy orbital of the electron to the half-filled level in the hole, leading to both molecules in their ground states. Fortunately, this last process is not usually observed since the high exergonicity (>2 eV) does not allow it to compete effectively with the rate of the nearly equienergetic processes leading to the formation of the exciton.[319] Once formed, the exciton can then relax radiatively to give the observed luminescence. The excited state formed in this

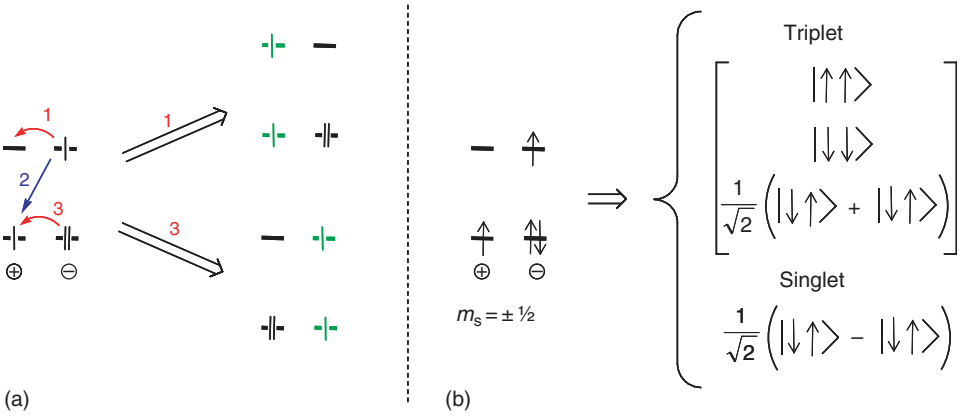

Figure 26 Hole/electron recombination pathways. (a) Electron transfer from the electron to the hole can occur via pathways 1 and 3, giving the exciton (shown in green). Pathway 2 is not typically observed. (b) The spins of the unpaired electrons in the hole and electron have a random Initial picture with no arrowheads on the electrons.

way is analogous to the one formed on absorption of a photon at the HOMO–LUMO energy, and the emission identical to that produced in a photoluminescent transition for the same material. However, the electrically created exciton is not formed under the same selection rules that usually apply to optically generated excited states.

For simplicity, the electrons illustrated in Figure 26 were intentionally drawn to not show their relative spins. A complete picture that accounts for the hole and electron must reflect the fact that the spins of each species have equal populations of $m_s = +1/2$ and $-1/2$. Thus, it is possible that the hole and electron in a pair of molecules undergoing recombination could have either identical or opposite spin. The result is that the exciton formed during recombination could be in either a singlet or a triplet state. Based on simple spin statistics, the ratio of singlets to triplets formed on recombination is 1 : 3, for a random mixture of $m_s = \pm 1/2$ in the hole and electron (Figure 26).[320,321] This splitting of the exciton into singlet and triplet fractions has a significant impact on the efficiency of EL. Fluorescence from many organic materials ($S_1 \rightarrow S_0$) can be very efficient, whereas phosphorescence ($T_1 \rightarrow S_0$) is often very inefficient and not typically observed at room temperature. Thus, if only the fluorescent-excited states are considered, the upper limit on OLED efficiency is 25%, even before losses due to low luminance efficiency or poor carrier balance are taken into account. This 25% efficiency limitation can be circumvented by designing systems that emit from the T_1 state at room temperature, allowing all of the excited states formed on recombination to be used effectively. This approach will be discussed in Section 12.04.2.3.1.

The picture given above for the mechanism of EL was described for molecular systems. The mechanism for OLEDs based on non-conjugated polymer is identical; carrier injection, transport, and recombination will have the same basic mechanism as that described above. OLEDs made with conjugated polymers will also behave in basically the same manner, although carrier migration in conjugated polymers is somewhat different in that very high carrier mobilities can occur through the polymer backbone. However, since the overall mobility is typically governed by the rate of interchain hopping, the same considerations apply as those given above for molecular systems. The issue of intra- versus interchain recombination is still an open issue and both processes may occur simultaneously. Nevertheless, while there is some debate as to whether the singlet to triplet ratio is 1 : 3 for conjugated polymer OLEDs,[322,323] it is clear that the polymer-based devices give a substantial number of triplet excitons on recombination,[324] thereby leading to severe restrictions on OLED efficiency.

12.04.2.2 OLED Efficiency and Chromaticity: Units

Literature reports describing OLED performance use several different, and sometimes contradictory, methods for measuring efficiency and color quality or chromaticity. A brief description of these various parameters used to characterize OLEDs will be covered here. For more detail, the reader is referred to other sources.[325] There are two prevailing methodologies that are followed in characterizing OLEDs. The first is an engineering approach that treats the OLED as a display device, and thus utilizes standard instruments and performance metrics/units developed to characterize other, more technologically evolved displays such as CRTs or LCDs. While this approach allows for straightforward comparison of OLED performance with other technologies, it tends to obscure important underlying

differences in device physics and offers little help in understanding how best to develop rational design criteria for improved materials and device structures. The second approach uses physical measurement techniques that are perhaps less routine, but give a clearer picture of the absolute device performance, independent of the emission energy.

An important distinction to be made is between the definitions of external and internal quantum efficiency. For display applications, the commonly accepted definition for the "external quantum efficiency" (η_{ext}) is the ratio of the number of photons emitted by the OLED into the viewing direction to the number of electrons injected (indicated by the block arrow in Figure 22). In contrast, the "internal quantum efficiency" (η_{int}) is the ratio of the total number of photons generated within the structure to the number of electrons injected.[326] While the external quantum efficiency could also be defined as the ratio of the total number of photons emitted from the device (to all directions) to the number of electrons injected, this definition is not as useful for display devices and is markedly more difficult to measure accurately than η_{ext}. A large fraction of the light can be waveguided by the substrate (typically glass or plastic) and by the organic layers comprising the organic heterostructure, ultimately emerging out of the edge of the substrate.[327,328] Thus, the total amount of light emitted from the device (surface and edges) is much higher than the light emitted in the viewing direction, leading to an efficiency based on the total light emitted which can be up to four times larger than η_{ext}.[328]

The primary complication introduced by treating the OLED as a display device is that the eye response, described by the "photopic" (light-adapted) luminous efficacy, must be taken into account. This corrects for the photosensitivity of a "standard" human eye (Figure 27). Thus, the % efficiencies (η_{ext} and η_{int}) discussed above must be modified to take into account the energy of each photon as well as the eye's sensitivity at that energy. The eye response-weighted equivalents (i.e., the photometric equivalents) of the radiometric quantities[329,330] of radiance [$W\,sr^{-1}\,m^{-2}$], radiant efficiency [$W\,sr^{-1}\,A^{-1}$], and power (or "wall plug") efficiency [$W_{optical}/W_{electrical}$] are then luminance (in $cd\,m^{-2}$), luminous efficiency [$cd\,A^{-1}$], and luminous power efficiency or luminosity (in $lm\,W^{-1}$). For a Lambertian source emitting into the half-plane, typical for an OLED, $1\,lm = \pi\cdot(1\,cd)$.

The luminous efficiency, η_L, in $cd\,A^{-1}$ is convenient for quantifying the properties of an OLED for display applications. In many respects, η_L is equivalent to η_{ext}, with the exception that η_L weights all incident photons according to the photopic response of the eye. While η_{ext} weights all photons equally, if emitted in the invisible spectral regions they would not contribute to η_L. A problem arises, however, when these photometric efficiencies are

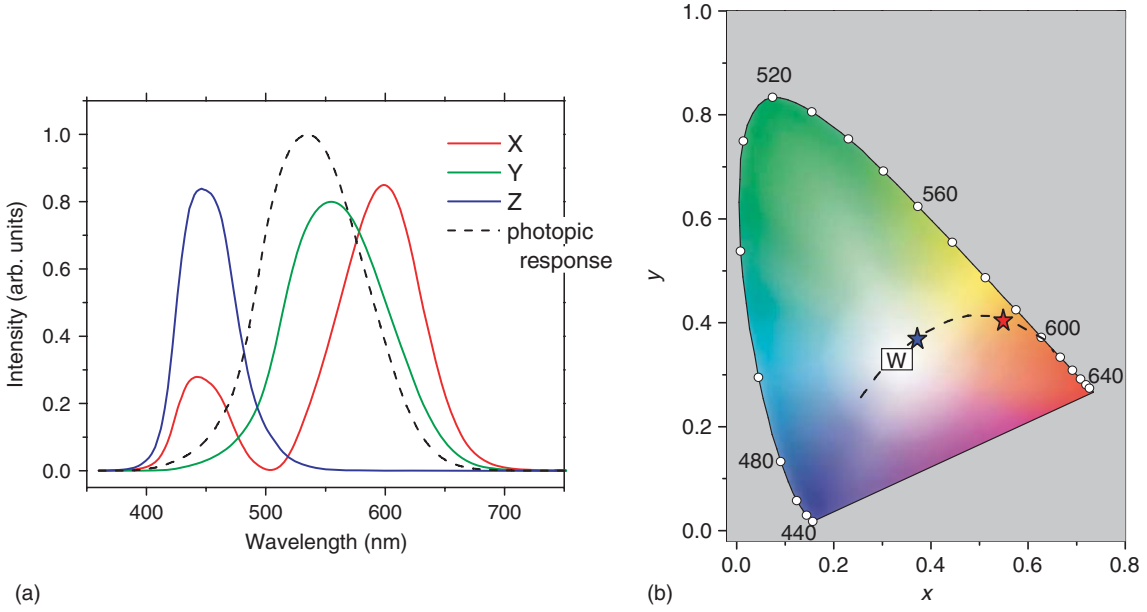

Figure 27 (a) Photopic response function (peak value: $683\,lm\,W^{-1}$ at $\lambda = 555\,nm$[330,687]) and the normalized tristimulus values are shown. (b) The CIE diagram shows the black body locus as a dashed line. The numbers on the periphery are the points corresponding to monochromatic light of that wavelength (nm). The equal energy (white point) is indicated by the square W. The red star is the CIE value of sunlight at sunrise (1,800 K). The blue star shows the CIE coordinates for sunlight at noon (4,900 K).

used to compare OLEDs with different emission spectra. Since the photometric values are strongly affected by the emission spectrum (favoring devices with emission in the green-to-orange part of the spectrum), it is impossible to compare device efficiencies without correcting for the spectral differences in the two devices. Thus, while photometric units are useful in a display application, efficiencies in % (photons/electrons) are more useful in scientific or engineering studies, since these units allow for direct comparison of devices, without requiring any spectral correction.

The system that is commonly used to describe and quantify the colors of OLEDs (as well as CRTs and other emissive displays) is the CIE system (CIE = Commission Internationale l'Eclairage).[331] There are three different types of cone cells in the eye, responsible for color discrimination, with their absorption maxima centered at 419, 531, and 558 nm,[332] represented by a set of three tristimulus functions (X, Y, and Z) (Figure 27). In order to represent the tristimulus values on a two-dimensional plot, X, Y, and Z are converted to their fractional contributions (i.e., $x = X/(X+Y+Z)$, $y = Y/(X+Y+Z)$). A plot of x versus y is used to visualize how the colors are organized by the CIE system. This plot is termed the CIE chromaticity diagram, and is shown in Figure 27. Monochromatic colors fall on the perimeter of the horseshoe-shaped curve starting with blue in the lower left, running through the colors of the spectrum in a clockwise direction, to red in the lower right. The circles on the periphery of the CIE plot are placed at 10 nm intervals, starting at 440 nm. The colors along the line at the bottom are not pure colors, but can be made by color mixing (e.g., purple is a mixture of blue and red). White or the neutral point is found at the center of the diagram, labeled W. As a given point is moved toward the white point from the perimeter the color remains constant, but becomes progressively more unsaturated. Mixing any two colors generates a new color, whose CIE coordinates fall on the line connecting the CIE coordinates of the two mixed colors. Similarly, three emissive colors can be combined to generate any color whose CIE coordinates fall within a triangle defined by the CIE coordinates of the three colors being used. This color-mixing scheme is the basis for all RGB displays.

12.04.2.3 Emissive Dopants for Increased OLED Efficiency

The emission spectrum produced by the OLED is controlled by the choice of the material used to form the emissive region in the single or double heterostructured device. A wide range of materials have been reported which efficiently produce EL throughout the visible spectrum.[310,333] The color of light emission can readily be controlled by altering the material(s) comprising the emissive region. Unfortunately, the use of a luminescent material in the form of a neat emitting layer leads to a limitation on device efficiency beyond that caused by the singlet : triplet exciton ratio discussed above. Most fluorescent materials show significant self-quenching in the solid state, reducing the maximum OLED efficiency to values even less than the 25% possible due to fraction of singlets formed. One solution to the problem of self-quenching involves doping a luminescent material into the emissive region of the OLED. The dopant can be added to either the HTL or ETL in a single heterostructure device, or into the emissive region of a double heterostructure OLED (Figure 22). The dopant in this device is chosen to have an excited-state energy lower than that of the material it is doped into, such that the dopant will trap the exciton formed in the OLED and subsequently emit. Alternatively, the dopant may trap holes and/or electrons in the emissive layer, and act as the site of carrier recombination. In many OLEDs, both exciton and carrier trapping are involved in localizing the exciton at the emissive dopant. If the dopant is co-deposited with a well-matched material, the EL output from this device will come exclusively from the dye dopant, even at very low dye loading levels.[334,335] The doping technique has been used to fabricate fluorescence-based OLEDs with colors that span the entire visible spectrum.[336]

The use of emissive dopants, as opposed to emission from the neat HTL or ETL, is an effective method of color tuning, but more importantly, this approach also significantly improves the device efficiency. The increase in efficiency can be attributed to the improved luminescence quantum efficiency of a dilute dopant relative to that of a neat ETL or HTL material. An additional improvement in OLED performance comes about from the trapping of both charge and excitons within the emissive layer.[56,337] Dye doping confers another benefit in that the EL output from doped devices is often significantly narrower than EL spectra from devices using neat emitting layers. This last point is highly desirable in full color display applications where a mixture of red, green, and blue light from individual pixels is used to generate the various colors of the visible spectrum. In order to create saturated colors, it is important for the individual red, green, and blue emission spectra to be as narrow as possible since, if the spectra are broad, the colors will be substantially unsaturated or washed out. The EL spectrum from a doped OLED typically resembles the narrow PL spectrum of the same dopant in dilute fluid solution because a doped film is a solid solution where the matrix material acts as a rigid "solvent." Taking this analogy further, the solvation of the dopant by the matrix is expected to affect the emission energy of the dopant. For example, the color of OLED emission from the fluorescent

dopant DCM2 has been tuned over a wide range using a solid-state solvation effect that relied only on variation in the polarity of the materials comprising the emissive layer within the device.[338,339]

12.04.2.3.1 Phosphorescent materials as emitters in OLEDs

The use of fluorescent dopants does not alter the 25% limitation on OLED efficiency that the 1 : 3 singlet–triplet ratio imposes on excitons formed during electron–hole recombination. Therefore, a solution to this problem is to use dopants that emit from triplet states (phosphorescent emitters) in order to harvest all of the triplet excitons formed in the recombination process. Attempts along these lines have been made with limited success using either lanthanide coordination complexes[340–349] or organic phosphors (benzophenone[350,351] and chrysene[352]). While these compounds phosphoresce, they have long radiative lifetimes (milliseconds for lanthanide complexes and seconds for organic materials) that allow the excited state to decay from competing non-radiative processes. Moreover, the long radiative lifetimes for the lanthanide complexes and organic compounds are not well matched to the electrical characteristics of OLEDs. The time it takes for the device carrier injection, conduction, and recombination to come to steady state, such that the rate of formation of excitons within the device reaches equilibrium, is called the RC time constant. Typically, OLEDs have RC time constants of 200–500 ns. While this time interval can be adjusted somewhat by device design, the value will stay in the range of hundreds of nanoseconds. The result is that phosphorescent dopants with long lifetimes will be promoted into their excited states faster than they can relax.[353–355] In the meantime, the OLED will continue to generate triplet excitons, which will not be effectively trapped by the excited dopant. The net result is that these dopants are inefficient at trapping triplet excitons and do not markedly increase the OLED efficiency over the level achievable with fluorescence dopants. Only in the best cases (lanthanide complexes) are high efficiencies achieved,[356–358] whereas in other cases no light output is observed at room temperature (organic phosphors).[350–352]

The key to efficiently utilize all the triplet excitons formed in the electroluminescent process is to employ phosphorescent dopants that have both comparatively short radiative lifetimes and high luminance efficiencies in the solid state when doped in an appropriate host material. The first triplet emitter used in OLEDs that satisfied these criteria was platinum octaethylporphyrin (PtOEP).[359] The strong spin-orbit coupling of the central Pt atom promotes significant mixing between singlet and triplet states, which facilitates intersystem crossing and leads to efficient phosphorescence at room temperature. The phosphorescence quantum yield of PtOEP is 0.5 at room temperature (>0.9 at 77 K) with a lifetime of 90 μs (131 μs at 77 K).[360] The high ISC rate of PtOEP also provides an added benefit since any singlet exciton trapped by the dopant will be converted rapidly to a triplet, thus giving rise to only one type of emission, that is, phosphorescence. Otherwise, concurrent luminescence from both singlet and triplet excitons in the device would lead to significant line broadening and unsaturated emission.

The highest efficiencies for PtOEP-doped OLEDs are achieved when the host material has a triplet energy (E_T) that is significantly higher than that of the PtOEP triplet (650 nm, $E_T = 1.91$ eV). For example, when 4,4′-di(*N*-carbazolyl)biphenyl (CBP, $E_T = 2.60$ eV)[361] is used as the host matrix, the external quantum efficiency (photon/electron) of a PtOEP-doped device is more than 6%.[362] If the host material has a triplet energy close to that of PtOEP, such as Alq_3 ($E_T = 1.90$ eV),[363,364] exciton trapping by the dopant is ineffective and the device efficiency declines to ca. 3%.[362] Similarly, devices made with host materials such as conjugated polymers, which also have low triplet energies,[365,366] have even lower EL efficiencies, often less than 3%.[367–369] By optimizing the host material and device architecture, OLEDs incorporating PtOEP dopants have been reported with external efficiencies as high as 9%.[370] It is important to recognize that the values of external quantum efficiency given above represent only a small fraction of the light produced within the OLED structure (see Section 12.04.2.2). The internal efficiencies of the PtOEP-based devices are actually three to five times higher than the measured external values. Therefore, PtOEP devices with a CBP host have internal efficiencies of 30%, and those with an Alq_3 host have internal efficiencies of more than 20%. The luminance efficiencies determined for PtOEP doped into each of these host materials shows that these internal efficiencies are close to the theoretical limits, that is, >90% of the excitons are being trapped at the dopant, and the EL efficiency is only limited by the PL efficiency of PtOEP.[359]

12.04.2.3.2 Confining carriers and triplet excitons in phosphor-doped OLEDs

While OLEDs with phosphorescent dopants can have significantly enhanced quantum efficiencies, they also require more complex device architectures than fluorescence-based devices. Singlet excitons have short diffusion lengths, on the order of 10–100 Å, whereas triplet states can diffuse >1000 Å due to their long lifetimes.[359,362] Thus, it is essential to use device configurations that confine the excitons within the luminescent layer. Triplet exciton confinement in a three layer, double heterostructure is possible if the HTL and ETL have higher optical energy gaps than the exciton

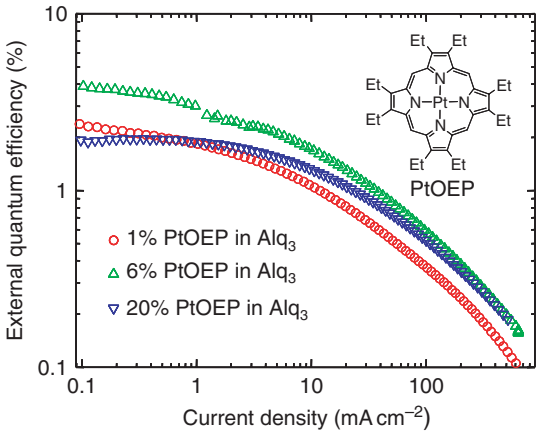

Figure 28 EQE (%) vs. J (mA cm^{-2}) for a range of PtOEP-doping concentrations. OLED structure: ITO/NPD/Alq_3-PtOEP/Alq_3/Mg–Ag.

binding energy, but this is not always achieved with common OLED materials. A good example is seen in devices made with PtOEP doped into CBP.[362] A single heterostructure device (ITO/NPD/CBP : PtOEP/Alq_3/Mg–Ag) gave an external efficiency of 4.2%. Although it is energetically unfavorable for the PtOEP excitons to diffuse into the adjacent HTL (NPD $E_T = 2.55$ eV),[371] that is not the case for diffusion into the ETL, where the excitons can undergo non-radiative recombination with Alq_3. A simple solution to this problem of exciton leakage involves inserting a material with a high triplet energy, such as BCP ($E_T = 2.5$ eV)[44] between the doped CBP and the Alq_3 electron-transporting layers (i.e., ITO/NPD/CBP : PtOEP/BCP/Alq_3/Mg–Ag, BCP = bathocuproine; Figure 28).[362] The result is a marked improvement in the device performance, from an external efficiency of 4.2% for the device without BCP to 5.6% with BCP.[362] Not only is the BCP layer effective at blocking migration of PtOEP excitons into the Alq_3 layer, but another benefit also comes from the deep HOMO level of BCP (6.5 eV),[372] which prevents holes in the luminescent layer from diffusing into the Alq_3 layer. Thus, the BCP forms a combined hole/exciton blocking layer. The effect of the BCP-blocking layer can also be seen in the EL spectra. Hole leakage into the ETL leads to a significant Alq_3 contribution in the EL spectrum of the unblocked device, whereas the BCP-blocked device displays a spectrum with only PtOEP emission.

For a compound to act as an ideal hole-blocking material, it must have a HOMO level deeper than that of the dopant and host material, and also have a triplet energy high enough to efficiently prevent triplet excitons from migrating out of the luminescent layer (Figure 28). The two most common hole-blocking materials are BCP[373–376] and BAlq (4-biphenyloxolato aluminum(III)bis(2-methyl-8-quinolinato)4-phenylphenolate) (see Figure 25).[317,377,378] A number of other organic materials have also been used as hole-blocking materials, for example, fluorinated phenylenes,[379] oxadiazole- and triazole-containing molecules (TPBI, PBD, TAZ),[380,381] 1,8-naphthalimides,[382] polyquinolines,[383] and carbon nanotubes doped into PPV.[384]

While the discussion in this section has focused on the need to control (prevent) carrier (hole) and exciton diffusion from the emissive layer to the ETL, the same issues are relevant at the interface between the HTL and the emissive layer. If the HTL material has a LUMO energy that is lower than that of the emissive layer, or a triplet energy that is too low, an electron-exciton-blocking layer may be needed to prevent carrier and exciton loss at that interface. A description of the best materials to act as electron-exciton-blocking materials for this interface will be considered in a later section (see Section 12.04.2.1.4).

12.04.2.3.3 Organometallic complexes as phosphorescent emitters in OLEDs

Although PtOEP is a good model compound to demonstrate the utility of triplet-emitting dopants, OLEDs that use PtOEP have several limitations. One is that the luminescent color of PtOEP is deep red, which is too low for most display applications, and the emission energy cannot be shifted to higher values through synthetic modification. Another is that while the PL efficiency of PtOEP is high in some host matrices, it is lower when doped into standard OLED materials. A third problem with PtOEP can be seen in the plots of external quantum efficiency versus current density, shown in Figure 28, for three different doping levels of PtOEP in Alq_3, 1, 6, and 20%. The 6% doped device

is the most efficient, with an external quantum efficiency of 4% at low current levels. Note that all three devices show the same trend of decreasing quantum efficiencies with increasing current. One origin of this roll-off in efficiency is a process well known to occur with triplet excitons, triplet–triplet (T–T) annihilation,[265] and is a consequence to the long radiative lifetime of PtOEP. During the T–T annihilation process, two molecules in the triplet state combine to form a singlet- and a ground-state molecule, $T_1 + T_1 \rightarrow S_1 + S_0$. The S_1 state of PtOEP formed in this process undergoes rapid intersystem crossing to the triplet, so the net result is that one of the two molecules in the triplet state is quenched. The annihilation process is a second-order quenching process that is expected to be enhanced as the population of triplets is increased, which occurs at high current density in a device.[355] The relatively long radiative lifetime of PtOEP thus enables the T–T annihilation process to become competitive with radiative decay.

A phosphorescent dopant with a higher luminance efficiency than PtOEP would increase the device efficiency markedly, however, the effects of T–T annihilation would still prevent such a device from giving high EL efficiency at high brightness. One obvious solution to this problem is to increase the PL efficiency and decrease the radiative lifetime at the same time. The shorter lifetime enables the triplet excitons to radiatively relax prior to diffusing into contact with each other, and thereby decreases the likelihood that the excitons will undergo self-annihilation. The first example of a phosphorescent dopant with a comparatively short radiative lifetime and high luminance efficiency used in OLEDs was a cyclometallated Ir complex, *facial*-tris(2-phenylpyridinato,N,$C^{2'}$)iridium(III), *fac*-Ir(ppy)$_3$, Scheme 1. This compound, first reported in 1985,[385] has a green emission ($\lambda_{max} = 520$ nm, $E_T = 2.48$ eV), high PL efficiency ($\Phi = 0.4$), and a short radiative lifetime ($\tau_{rad} = 5\,\mu s$) in fluid solution at room temperature. The PL efficiency is similar to PtOEP, whereas the radiative lifetime is nearly two orders of magnitude shorter. OLEDs that incorporated this Ir dopant at an optimal doping level of 6% gave external efficiencies close to 9% (internal efficiency >40%) when used in the same structure as that for the PtOEP device (ITO/NPD/CBP : Ir(ppy)$_3$/BCP/Alq$_3$/MgAg)[373] (see Figure 29). The roll-off in efficiency at high current densities is very low when compared to the PtOEP-based devices, as would be expected from the short radiative lifetime of Ir(ppy)$_3$. When the CBP host material was replaced with an electron-transporting triazole host material, TAZ, the external EL efficiency increased

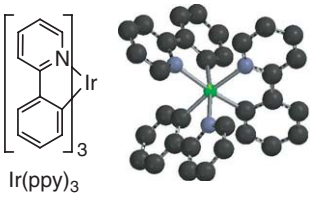

Scheme 1

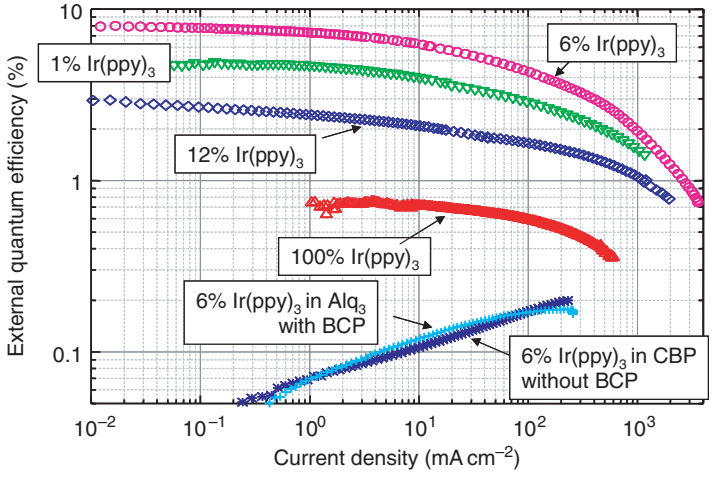

Figure 29 EQE (%) vs. J (mA cm^{-2}) for Ir(ppy)$_3$ devices (ITO/NPD/CBP-X% Ir(ppy)$_3$/BCP/Alq$_3$/Mg–Ag). The lines shown in dark blue and turquoise are for devices without the BCP HBL and with Alq$_3$ in place of CBP, respectively.

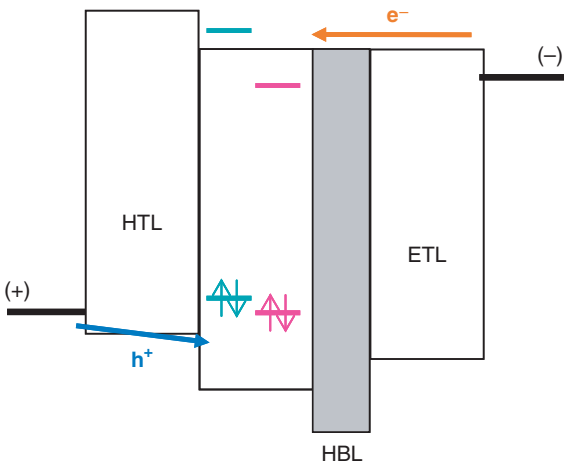

Figure 30 Energy level diagrams for double heterostructure OLED with a hole-blocking layer. The approximate energies of the HOMO and LUMO levels for $Ir(ppy)_3$ and PtOEP are shown in green and purple, respectively.

to >15%, corresponding to an internal efficiency of >75%.[374] In contrast, use of an electron-transporting host with a low triplet energy, that is, Alq_3, led to a marked decrease in efficiency (0.2%), (Figure 29).

It is worth revisiting the issue of hole confinement in the $Ir(ppy)_3$-doped devices discussed above. The need for exciton- and hole-blocking layers is also seen in $Ir(ppy)_3$-based OLEDs. The ordering of triplet energies for the materials is CBP > NPD > BCP > $Ir(ppy)_3$ > > Alq_3. The triplet excitons on $Ir(ppy)_3$ will not diffuse into the NPD layer, but can be readily transferred into the Alq_3 layer if the BCP-blocking layer is absent. Thus, when a BCP layer is omitted, the device efficiency drops to only 0.2% (see Figure 29). In addition to blocking the diffusion of excitons, the BCP layer also prevents holes in the doped CBP : $Ir(ppy)_3$ layer from migrating into the ETL. The explanation given earlier for using a BCP-blocking layer is that both holes and excitons must be confined within the emissive layer. While the energetic argument for exciton confinement is clear, the issue of hole blocking is not so obvious. The HOMO levels of all of the materials are illustrated in Figure 30 for both $Ir(ppy)_3$- and PtOEP-based devices.

The HOMO level for $Ir(ppy)_3$ lies above all of the materials used in the OLED, and as such is expected to be an efficient hole trap. Considering the fact that the $Ir(ppy)_3$ and PtOEP HOMO energies are significantly higher than the HOMO energies of either the host or Alq_3, hole blocking is not as important as exciton blocking in these cases. In fact, the BCP layer may not be acting as a hole blocker in this device at all since there is a 0.4 eV barrier for hole migration from $Ir(ppy)_3$ to Alq_3. The ability of $Ir(ppy)_3$ to act as a hole trap implies that the electroluminescent process may involve hole–electron recombination at the dopant itself. In this case, an exciton is formed from a hole on the Ir dopant that recombines with an electron on the CBP host (or an adjacent dopant). Thus, the triplet exciton is not transferred from the host, but formed directly on the dopant. This process has a significant advantage over recombination on the host material and subsequent energy transfer to the dopant, since the energy-transfer process is a potential loss channel. The direct recombination mechanism, though given for hole trapping at the dopant, can be equally applied for electron trapping at the dopant as well. A similar carrier recombination process involving a hole in the host or adjacent dopant is observed for many blue emissive organometallic phosphor-doped devices, as discussed below. In nearly all cases, carrier recombination at the dopant contributes to the high efficiencies observed for phosphorescence-based OLEDs that utilize organometallic emitters.

12.04.2.4 Cyclometallated Complexes for OLEDs

12.04.2.4.1 Synthesis of cyclometallated Ir and Pt complexes

The successful application of $Ir(ppy)_3$ as a phosphorescent dopant has led to a number of synthetic modifications of the parent complex. Most of the new derivatives were prepared in order to alter the luminescent properties (color, efficiency, stability, etc.) or to further characterize the excited-state properties of these materials. Tris-cyclometallated Ir complexes can be prepared using two general methods, either by direct formation in a one-step reaction or with a two-step synthesis that uses a μ-dichloro-bridged dimeric complex as an isolated intermediate. The first efficient direct synthesis to be reported involved the reaction of $Ir(acac)_3$ (acac = acetylacetonate) with an excess of

desired cyclometallating ligand (HC^N), (Equation (16)).[387] An alternative direct synthesis involves treating $IrCl_3 \cdot nH_2O$ with silver(I) salts and uses the desired cyclometallating ligand as a solvent, (Equation (17)).[387] Both of these procedures are carried out at high temperature (>180 °C) and are intolerant of many potential cyclometallating ligands. Prior to these reports, Nonoyama described the efficient cyclometallation of benzo[*h*]quinoline (bzq) by $IrCl_3 \cdot nH_2O$ at lower temperature (130 °C), which gave a μ-chloride-bridged dimer, $[(C^N)_2IrCl]_2$, in good yield (Equation (18)).[388] This type of reaction can be used to prepare a larger variety of cyclometallated complexes through reactions using Equations (16) or (17).[389,390] These dimer complexes can then serve as precursors for the synthesis of tris-cyclometallated complexes by several routes. Silver ion can be used to abstract the bridging chlorides in the presence of a cyclometallating ligand to give the desired tris-complex (Equation (19)).[391] However, it has also been shown that silver ion is not required and good yields of tris-complexes can be realized using a simple inorganic base in place of silver (Equation (20)).[392] Another synthetic method involves the conversion of the chloride-bridged dimer into a mononuclear species by replacing the μ-chloride ligands with the labile acac ligand, Equation (21a), followed by thermolysis of the $(C^N)_2Ir(acac)$ complex in the presence of excess cyclometallating ligand (Equation (21b)).[392]

$$Ir(acac)_3 + 3HC^N \rightarrow Ir(C^N)_3 + acacH \tag{16}$$

$$IrCl_3 \cdot nH_2O + 3Ag^+X^- + 3HC^N \rightarrow Ir(C^N)_3 + 3AgCl + 3HX \tag{17}$$

$$IrCl_3 \cdot nH_2O + 2HC^N \rightarrow (C^N)_2Ir(\mu\text{–}Cl)_2Ir(C^N)_2 \tag{18}$$

$$1/2(C^N)_2Ir(\mu\text{-}Cl)_2Ir(C^N)_2 + Ag^+X^- + HC^N \rightarrow Ir(C^N)_3 + AgCl + HX \tag{19}$$

$$1/2(C^N)_2Ir(\mu\text{-}Cl)_2Ir(C^N)_2 + K_2CO_3 + HC^N \rightarrow Ir(C^N)_3 + KHCO_3 + KCl \tag{20}$$

$$1/2(C^N)_2Ir(\mu\text{-}Cl)_2Ir(C^N)_2 + acacH + base \rightarrow (C^N)_2Ir(acac) + Cl^- \tag{21a}$$

$$(C^N)_2Ir(acac) + HC^N \rightarrow Ir(C^N)_3 + acacH \tag{21b}$$

While the syntheses shown here form homoleptic tris-complexes, the third cyclometallating ligand added when using Equations (19) and (20) need not be the same as that used to form the chloride-bridged dimer, thus enabling the formation of heteroleptic complexes, that is, $(C^N)_2Ir(C^N')$, by this synthetic route.[393–396] A large number of bis-cyclometallated Ir heteroleptic complexes have also been prepared which are have a third, non-cyclometallated chelate ligand. An example of such a complex is $(C^N)_2Ir(acac)$, shown in Equation (21b). The advantage of these mixed heteroleptic complexes is that they can be formed in high yield from $IrCl_3 \cdot nH_2O$ (via the chloride-bridged dimer), and often have photophysical properties nearly identical to their tris-organometallic analogs.[390] In this case, the non-organometallic ligand is an ancillary ligand and will be described generally by the abbreviation L^X. A wide variety of different ancillary ligands have been used to form $(C^N)_2Ir(L^X)$ complexes by reactions analogous to the one shown in Equation (21a).[113,390,397–405]

A given synthesis of tris-cyclometallated complexes will typically form either the *facial*- or the *meridonal*-isomer of $Ir(C^N)_3$ as the major product (Scheme 2). For example, the syntheses outlined in Equations (16) and (17) give complexes that are >90% the *facial*-form.[392] The chloride-bridged dimer has a "*meridioal*-like" disposition of ligands, with the *N*-coordinated heterocyclic rings in a *trans*-relationship (Scheme 2). It would be expected that simple replacement of the chloride with a chelating C^N ligand would give a *meridonal*-isomer; however, only *facial*-isomers are isolated from syntheses using Equation (19). The reason for this preponderance of *facial*-isomers is that the reactions are typically run at high temperatures (ca. 200 °C) and the thermodynamically more stable *facial*-form is thus favored over the kinetic (*mer*-) product. However, if the synthesis outlined in Equation (20) is carried out at lower temperature (< 130 °C), the *meridonal*-isomer can be prepared as the only isomer.[392] The isolated *meridonal*-isomer can then be converted to the *facial*-form by either thermal or photochemical routes.[392,396,406]

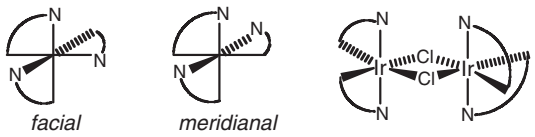

Scheme 2

The complexes that have been discussed to this point have all been neutral. Monomeric complexes containing the "$(C^N)_2Ir$" fragment have also been reported as cationic species, for example, $(C^N)_2IrL_2^+$. The syntheses of these cationic complexes parallel those of the neutral $(C^N)_2Ir(L^X)$ complexes. If the chloride-bridged dimer is treated with neutral ligand(s), the chlorides are displaced and the cationic complex is formed in good yield (Equation (22)).[407] Some of the first complexes prepared this way utilized a 2,2′-bipyridine ligand, for example, $(ppy)_2Ir(bpy)^+$.[408] As with the $(C^N)_2Ir(L^X)$ complexes, this procedure allows the preparation of a wide range of possible complexes through systematic variation of either the C^N^- or L_2 ligands, and several of these types of derivatives have been used in light-emitting electrochemical devices.

$$1/2(C^N)_2Ir(\mu\text{-}Cl)_2Ir(C^N)_2 + L_2 \rightarrow (C^N)_2IrL_2^+ + Cl^- \tag{22}$$

Organometallic platinum complexes with cyclometallating ligands have also been used as emissive centers in OLEDs. The syntheses of these complexes are related to those described for the Ir complexes above. The first step in the synthesis often involves the formation of a cyclometallated complex, for example, Equations (23a)[409] and (24).[410–412] The product of the reaction given in Equation (23a) was originally formulated as a chloride-bridged dimer ($(C^N)Pt(\mu\text{-}Cl)_2Pt(C^N)$), but has been recently shown to be a complex with one cyclometallated ligand and a second unmetallated ligand coordinated with a simple dative bond.[413] Subsequent treatment of the organometallic Pt complex with the ancillary ligand, for example, acacH and base affords the monomeric Pt complex, $(C^N)Pt(L^X)$, Equations (23b).[49] Bis-cyclometallated Pt complexes can be prepared in one step from a reaction between a Pt thioether precursor and the appropriate ortholithiated ligand, Equation (24).[411,412,414] Platinum alkynyl complexes have also been studied in OLEDs, and were prepared by treating either an $(N^C^N)PtCl$ or diimine–$PtCl_2$ complex with the free alkynyl complex in the presence of base and a Cu(I) catalyst (Equations (25a) and (25b)).[415,416] An alternative synthesis of diimine Pt alkynyl complexes involves ligand displacement from a cyclooctadiene (COD) precursor complex (Equation (26)).[125] A similar displacement reaction can also be used to prepare diimine Pt diaryl complexes (Equation (27)).[417]

$$K_2PtCl_4 + 2HC^N + \text{base} \rightarrow (C^N)Pt(Cl)N^CH + KCl \tag{23a}$$

$$(C^N)Pt(Cl)N^CH + \text{acacH} + \text{base} \rightarrow (C^N)Pt(L^X) + Cl^- \tag{23b}$$

$$Pt(SEt_2)_2Cl_2 + 2LiC^N \rightarrow Pt(C^N)_2 + 2SEt_2 + 2LiCl \tag{24}$$

$$(C^N^N)Pt(Cl) + HC{\equiv}CR + \text{base} \rightarrow (C^N^N)PtC{\equiv}CR + Cl^- \tag{25a}$$

$$(N^N)Pt(Cl) + 2HC{\equiv}CR + \text{base} \rightarrow (N^N)Pt(C{\equiv}CR)_2 + Cl^- \tag{25b}$$

$$(COD)Pt(C{\equiv}CR)_2 + N^N + \text{base} \rightarrow (N^N)Pt(C{\equiv}CR)_2 \tag{26}$$

$$(COD)Pt(Ar)_2 + N^N + \text{base} \rightarrow (N^N)Pt(Ar)_2 \tag{27}$$

The $Pt(C^N)_2$, $(C^N)Pt(L^X)$, and diimine Pt alkynyl and aryl complexes have been used as emissive dopants in OLEDs. All of the complexes nominally have square-planar structures, however, steric interactions between adjacent ligands in the $Pt(C^N)_2$ and $(N^N)Pt(Ar)_2$ complexes can cause significant deviations from planarity in these species.[414,417] In contrast, the L^X and alkynyl ligands show less steric crowding and have simple square-planar structures.[415,416]

OLEDs have also been fabricated with organometallic complexes of metal other than Ir and Pt, for example, Re, Os, and Au. These OLEDs are discussed in Section 12.04.2.5.1; however, the number of OLEDs that have been reported with these metals is relatively small compared to those made with Ir and Pt complexes. Considering the fact that only these materials represent a limited number of devices, and that they are not described for any general syntheses, we will not discuss them here.

12.04.2.4.2 Excited states in cyclometallated complexes

Several research groups using high resolution spectroscopy have studied the excited-state properties of cyclometallated transition metal complexes. This work has established that luminescence from these complexes originates from the lowest-excited state, that is, ligand-centered triplet (^{3}LC) with singlet metal-to-ligand charge transfer (^{1}MLCT) character mixed in through spin-orbit coupling.[418–423] A schematic representation of the energy level mixing in $4d^6$

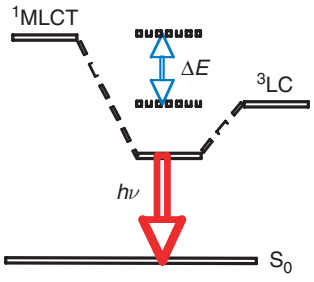

Scheme 3

and $5d^6$ complexes is shown in Scheme 3.[424–426] Mixing between ^{1}MLCT and ^{3}LC states can be treated by application of first-order perturbation theory. The formula shown in Equation (28) is used to define the lowest-energy excited state.

$$\Psi_{T_1} = \sqrt{1-\alpha^2}|^3\mathrm{LC}\rangle + \alpha|^1\mathrm{MLCT}\rangle \tag{28}$$

where Ψ_{T_1} is the wave function of the lowest-excited state and α is a coefficient that gives an estimate of the degree of singlet character mixed into the unperturbed triplet state (^{3}LC).[419,424] The value of α can be approximated with the formula given in Equation (29).

$$\alpha = \frac{\langle ^3\mathrm{LC}|H_{SO}|^1\mathrm{MLCT}\rangle}{\Delta E} \tag{29}$$

where $\langle ^3\mathrm{LC}|H_{SO}|^1\mathrm{MLCT}\rangle$ is the spin-orbital coupling matrix element, characterizing the strength of spin-orbital coupling between ^{3}LC and ^{1}MLCT, and ΔE is the energy difference between the ^{3}LC and ^{1}MLCT transitions.[424] Equations (28) and (29) have been used to correlate α-values with the luminescent properties of diimine and cyclometalated Rh(III) and Ir(III) complexes.[424] The mixing of ^{1}MLCT character into what is principally a ^{3}LC state has dramatic effects on the optical properties of those complexes.[418] The ^{3}LC oscillator strength and radiative decay rate in luminescent metal complexes are significantly increased when a small amount of ^{1}MLCT character is mixed into the lowest-excited state. Consequently, a large decrease in the luminescence lifetimes and concomitant increase in phosphorescence efficiency occurs.[423,424] For example, Güdel and co-workers estimated that the strongly luminescent complexes $[(ppy)_2Ir(bpy)]^+$ and $[(2\text{-thienylpyridyl})_2Ir(bpy)]^+$ have α-values of 0.085 and 0.053, respectively.[424] Other phosphorescent metal complexes have smaller α-values, such as $(ppy)Re(CO)_4$ (0.017) and $[(ppy)_2Rh(bpy)]^+$ (0.016). Considering the comparatively low values of α for these complexes, the excited states are still essentially triplets, even though they have singlet character mixed in. Strong spin-orbit coupling in any metal complex with a heavy atom such as Os, Ir, Pt, etc., will lead to α-values sufficiently large to effect efficient intersystem crossing to the triplet manifold. The strong σ-donation from C^- in a formally anionic cyclometallating ligand also stabilizes the ^{1}MLCT state and decreases the energy separation to the ^{3}LC state. This leads to a smaller ΔE term in the denominator in Equation (29) that further increases the value of α. Therefore, organometallic complexes with ligands cyclometallated onto heavy atoms are ideally suited to serve as phosphorescent dopants in OLEDs.

The model presented above for the electronic structure of heavy metal complexes (i.e., those with strong spin-orbit coupling) suggests a simple method for controlling the emission color. The emission energy is intimately related to the ^{3}LC energy of the C^N ligands in a cyclometallated complex. Since the lowest-excited state is ^{3}LC-dominant, the excited-state energy can be varied over a wide spectral range by employing different cyclometallating ligands in the complexes. For example, if the ppy ligands of $Ir(ppy)_3$ are replaced with other cyclometallating ligands with a triplet energy higher or lower than ppy, the triplet energy for the metal complex, and thus the emission color, will shift in response to the ligand change. However, before providing examples of changes in photophysical properties caused by individual ligand variations, it is helpful to describe the electronic structure of $Ir(ppy)_3$ and related complexes in more detail. MO calculations have been carried out on $Ir(ppy)_3$ and reliable results are obtained using density functional theory (DFT) at a B3LYP level with 6-31G(*d*, *p*) basis sets with an effective core potential used for the heavy atom.[427] The optimized molecular geometry accurately reproduces the structural features determined from X-ray

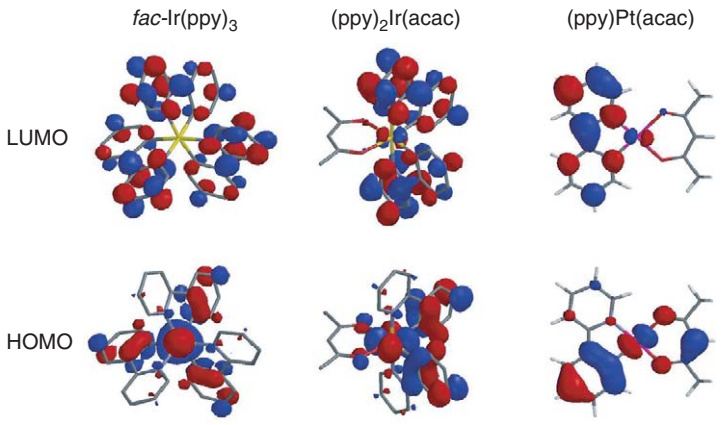

Figure 31 HOMO and LUMO plots for *fac*-Ir(ppy)$_3$, (ppy)$_2$Ir(acac), and (ppy)Pt(acac).

crystallography. The HOMO and LUMO orbitals for *fac*-Ir(ppy)$_3$, (ppy)$_2$Ir(acac), and (ppy)Pt(acac) are shown in Figure 31. The two iridium complexes have similar orbital compositions. There is roughly 50% metal character in the HOMO (d_{z^2} for Ir(ppy)$_3$ and d_{xy} for (ppy)$_2$Ir(acac)).[401,427] The LUMO is localized on the ppy ligand and has little metal character. The HOMO and LUMO orbitals of (ppy)Pt(acac) are similar to those of the Ir complexes, although there is additional acac character in the HOMO of the Pt complex.[409] The triplet states calculated for these three molecules show spin density that is localized on the C^N ligand and metal orbitals. The presence of multiple C^N ligands in the Ir complexes allows the triplet to delocalize to a greater spatial extent than possible in the Pt complex.[425]

To a first approximation, the amount of C^N ligand and metal character in the HOMO and LUMO is indicative of the amount of ^{1}MLCT/^{3}LC mixing in the excited state. Thus, (ppy)Pt(acac) is expected to have less MLCT character than that in either Ir(ppy)$_3$ or (ppy)$_2$Ir(acac) since there is a significant amount of electron density on the acac ligand in the HOMO of the Pt complex. The experimental spectra are consistent with this analysis. The PL spectrum of (ppy)Pt(acac) is markedly blue shifted from both Ir(ppy)$_3$ and (ppy)$_2$Ir(acac) (Figure 32), as expected for an excited state that has greater ^{3}LC character. The degree of vibronic structure in the emission spectrum of (ppy)Pt(acac) is significantly greater than the two iridium complexes. Emission originating from MLCT states typically has a Gaussian profile, while LC-based emission often shows vibronic fine structure. Thus, the higher level of fine structure in the (ppy)Pt(acac) spectrum is also consistent with less MLCT character for the Pt complex than for the two Ir complexes.

Although the discussion above was restricted to complexes with ppy ligands, a similar MO description is found for other Ir and Pt complexes with related cyclometallating ligands; the HOMO is comprised principally of orbitals on the metal–aryl linkage, whereas the LUMO is ligand localized.[398,400,403,428–430]

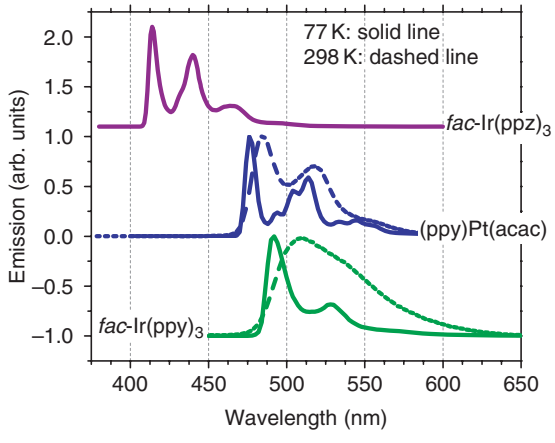

Figure 32 Photoluminescence spectra of (ppy)Pt(acac), *fac*-Ir(ppy)$_3$, *fac*-Ir(ppz)$_3$, and (ppy)$_2$Ir(acac) at 77 K and RT.

12.04.2.4.3 Tuning emission energy in cyclometallated complexes

The discussion of emission energy given here will focus on PL spectra since it typically matches the EL spectra of the same complexes. A good correlation exists between the PL and EL spectra, unless aggregation effects lead to red-shifted emission. The effect of aggregation has on emission color is most pronounced in Pt complexes and will be discussed separately in Section 12.04.2.6. The PL quantum efficiency also provides an important performance parameter. However, as discussed in Section 12.04.2.1.1, the PL efficiency can be used to set an upper limit on the ultimate EL efficiency only if the values are obtained under conditions similar to that found in the OLED structure. Thus, we will not discuss PL efficiencies extensively in this section, but will rather focus on emission energies. PL spectra are typically reported in one of the three different states; neat solid (thin film or powder), dilute fluid solution at room temperature, or frozen solutions at 77 K. Samples analyzed in fluid solution and the solid state at room temperature show broader line shapes than do low-temperature spectra. Luminescence spectra recorded at 77 K usually display highly structured vibronic features and the value of highest-energy peak corresponds to the triplet energy.[265] A red shift in emission upon going from 77 K to room temperature is attributed to a rigidochromic effect.[108,401,431] For the comparisons given below we have presented the data in as many different states as possible, but will generally try to compare data from samples measured at 77 K.

The emission energies of organometallic complexes can be effectively controlled by ligand modifications. These effects are readily observed in the PL spectra from a series of (C^N)Pt(β-diketonate) complexes (Table 4, Figure 33). The complexes in Table 4 have either acac or dipivolylmethane (dpm) as the β-diketonate ligand. Substituents on the ppy ligand can be used to vary the energy of the emissive state over a wide range. Alkyl substitution of the phenyl ring has little effect since the (ppy)Pt(acac) and (tpy)Pt(acac) complexes have the same emission energy ($\lambda_{max} = 480$ nm). Incorporating an electronegative atom such as fluorine onto the phenyl ring causes a hypsochromic shift in the emission spectrum. A single fluoride substituent in the 6′-position leads to a 12 nm blue shift in the emission of (6′Fppy)Pt(dpm) ($\lambda_{max} = 468$ nm), relative to (ppy)Pt(dpm). Difluoro substitution at the 4′,6′-positions on the phenyl ring gives a more pronounced blue shift in (4′6′F_2ppy)Pt(dpm) ($\lambda_{max} = 458$ nm). However, difluoro substitution at the 4′,5′-positions causes a much smaller shift in (4′5′F_2ppy)Pt(acac) ($\lambda_{max} = 476$ nm). On the basis on the DFT calculations, electron density in the HOMO is centered at the 5′-position of the phenyl ring and nodes exist at the 4′- and 6′-positions. Therefore, for (4′5′F_2ppy)Pt(acac), weak π-donation into this molecular orbital from the 5′-fluoro group raises the HOMO level and offsets the electron-withdrawing effect from the 4′-fluoro group. Similarly, substitution with a strong electron-donating methoxy group in the 5′-position lowers the HOMO energy and causes a pronounced red shift in (5′MeOppy)Pt(dpm) ($\lambda_{max} = 525$ nm) relative to the 4′-position in (4′MeOppy)Pt(dpm) ($\lambda_{max} = 480$ nm). On the other hand, the emission energy increases when electron-donating groups were incorporated onto the pyridyl ring since substitution on this ring increases the LUMO energy and

Table 4 Photophysical properties of (C^N)Pt(acac) complexes

(C^N)Pt(LX)		*Emission* λ_{max} (nm)	
C^N	*LX*	*77 K*	*298 K*
ppy	dpm	477	486
p-tpy	acac	480	485
o-tpy	acac	480	
6′fppy	dpm	468	476
4′6′F_2ppy	dpm	458	466
4′6′F_2ppy	acac	458	
4′5′F_2ppy	acac	476	484
4′6′F_2-4Meppy	dpm	456	
4′6′F_2-4MeOppy	dpm	438	456
4′6′F_2-4dmappy	dpm	440	447
4′MeOppy	dpm	480	490
5′MeOppy	dpm	525	
bt	dpm	530	
pq	dpm	555	
btp	acac	600	
thpy	dpm	550	575
pyrpy	dpm	580	603

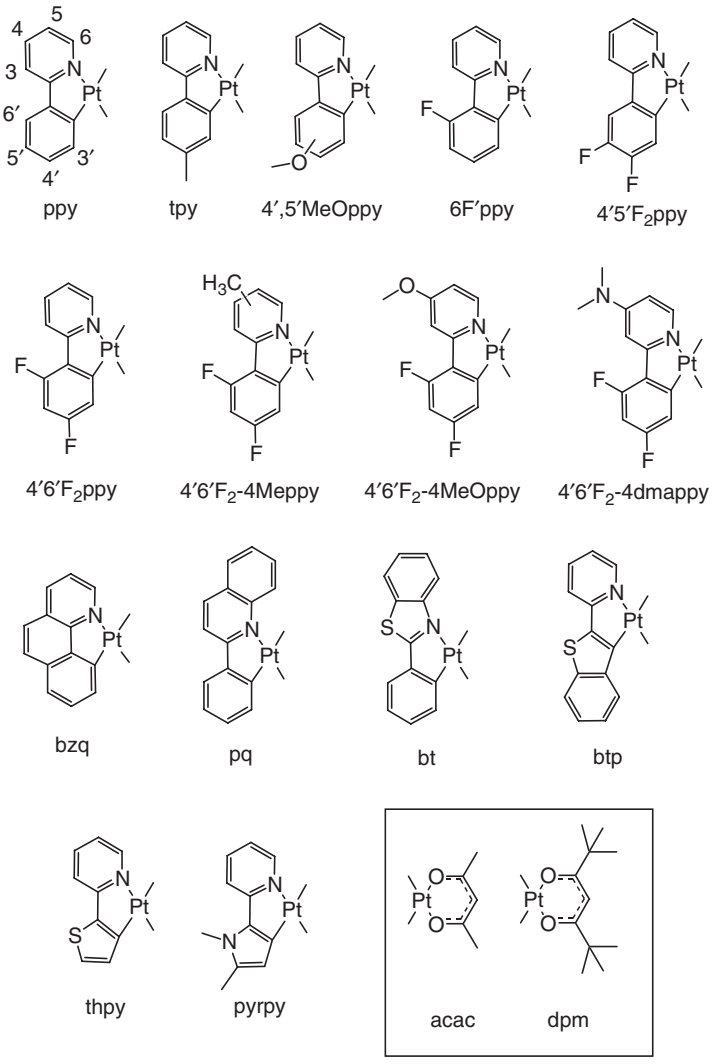

Figure 33 Structures of the (C^N)Pt(O^O) complexes used in the discussion of ligand-based emission color tuning.

consequently, the HOMO–LUMO gap. Consistent with this argument, a weak σ-donating methyl group in the 4-position on the pyridyl ring results in a slight blue shift [(4′6′F_2-4Meppy)Pt(dpm), $\lambda_{max} = 456$ nm], while a strong dimethylamino donor imparts a more substantial shift [(4′6′F_2-4dmappy)Pt(dpm), $\lambda_{max} = 440$ nm].

Changes in the nature of the C^N ring system can also have profound effects on the emission energy. Ligands with softer, more polarizable atoms such as sulfur and nitrogen incorporated in the ring system significantly lower the ^{3}LC energies of the complexes. For example, (thpy)Pt(dpm) and (pyrpy)Pt(dpm) complexes display orange-red emission with λ_{max} values of 550 and 580 nm, respectively. Extending the size of the conjugated π-system for C^N ligands also decreases the energy of the ^{3}LC transition relative to the ppy ligand, and thus of the Pt complex as well. For example, replacing the pyridyl group with a quinolyl, (pq)Pt(dpm), or benzothiazolyl, (bt)Pt(dpm), leads to a red-shifted emission. Replacing the phenyl group of ppy with a benzothiophene, (btp)Pt(acac), also leads to a marked bathochromic shift in emission energy.

The substituent effects that are observed in the emission spectra of the (C^N)Pt(β-diketonate) complexes are seen in Ir complexes coordinated with the same C^N ligands. The sensitivity of transition energy to the substitution position on 2-phenylpyridyl ligands has also been observed in related tris-cyclometallated iridium complexes.[386,387,392,432] Alkyl substituents have a comparatively small effect on the emission energy, giving shifts of only 3–10 nm. Likewise, fluorine substituents on the phenyl ring give rise to blue-shifted emission. Similarly, electron donors on the phenyl ring give bathochromic shift to the emission, whereas donors on the pyridyl group give hypsochromic shifts.

Extending the π-conjugation in the C^N ligand has also been used to red shift the emission spectra of Ir complexes. For these comparisons, we focus on three basic families of bis-cyclometallated complexes presented in Table 5; C^N = phenyl–pyridyl, phenyl–benzimidazolyl, and methylvinyl–pyridyl. In all cases, the expansion of the π-system leads to a marked bathochromic shift, the magnitude of which is dependent on the specific ligand used. The presence of fused rings, such as replacing pyridyl with quinolyl or phenyl with naphthyl, gives rise to a red shift on the order of 80–100 nm (compare entries 1 to 2, 3, 4, or 8 to 9, 10 in Table 5). Extending the π-system with additional fused rings leads to a further red shift, but the effect is less pronounced than that caused by the initial ligand modification. This is illustrated in comparing 4 to 6 and 10 to 11, where the initial fused ring gives a 100 nm shift as opposed to the 40 nm shift imparted by the additional ring. Likewise, replacing the methyl group in 12 with a phenyl

Table 5 Ligand structures and emission energies for (C^N)(acac) compounds

Entry	*C^N*	*PL* λ_{max} (nm)	*References*
1	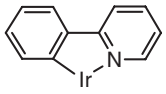	515	390
2	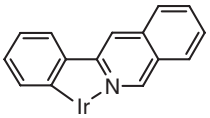	562	515
3	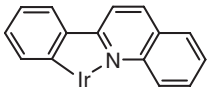	597	376
4	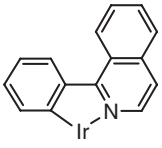	622	516
5	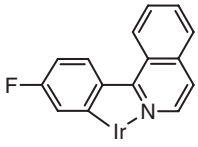	600	516
6	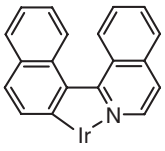	664	517
7	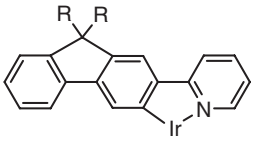	545	518
8	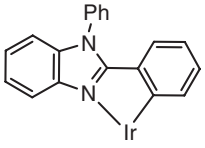	523	514

(*Continued*)

Table 5 (Continued)

Entry	*C^N*	*PL* λ_{max} (nm)	*References*
9	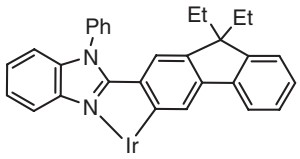	563	514
10	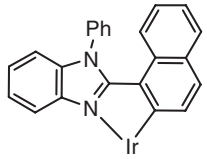	604	514
11	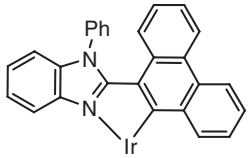	651	514
12	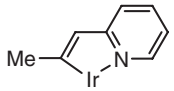	536	434
13	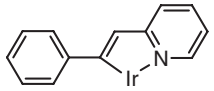	616	434
14	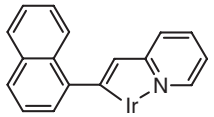	617	434
15	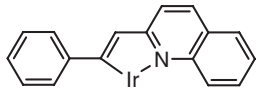	638	519

group, that is, 13, also causes a red shift (Table 5), whereas additional fused rings have a relatively minor effect on the emission energy (compare 13 to 14 and 15). The relative position of the fused ring can also significantly impact the emission energy as seen for 2, 3, and 4 in Table 5, where different regioisomers of the quinolyl moiety lead to 60 nm variations in the emission energy. The energy shifts observed as a consequence of extending the π-system of C^N ligands in $(C^N)_2Ir(acac)$ complexes are all consistent with the expected trends in the triplet energies for the C^N ligands themselves. Similar red shifts are observed in other Ir complexes with the same ligands. For example, a *facial*-iridium tris-cyclometallated complex with the same phenyl isoquinolyl ligand used in 4 gives a PL λ_{max} of 595 nm. Likewise, substituents shift the emission spectra of extended π-system C^N ligands in the same manner that occurs with the ppy ligand. Thus, the fluoro substituent in 5 gives a similar blue shift (compared to 4) as the same substitution does in complexes with a ppy ligand.

12.04.2.4.4 Blue luminescent cyclometallated complexes

The emission energies of Ir complexes with cyclometallated ppy ligands cannot be raised into the deep blue and near-UV part of the spectrum (λ_{max} <450 nm) through the use of electron-withdrawing and -donating substituents.

This is because the emission energy of the complex is inherently limited by the ^{3}LC energy of the ppy moiety (ppyH; $E_T = 430$ nm, 2.88 eV).[433] One approach pursued in order to shift the emission to higher energy was to decrease the size of the C^N π-system by replacing the phenyl ring with a vinyl group. Note, however, that this modification leads to a marked shift to lower emission energy relative to complexes with ppy ligands (see 12 in Table 5).[434] The decrease in emission energy in this case is understandable when one considers that the electron–electron repulsion in the triplet state increases with reduction in the size of the π-system, thereby lowering the triplet energy through increased singlet–triplet splitting (greater exchange energy).[265] For example, the triplet energies of vinyl-substituted benzene derivatives are ca. 5 kcal mol^{-1} (0.2 eV)[149,435] lower than that of biphenyl ($E_{0-0} = 436$ nm, 2.84 eV).[436]

Although stabilizing the HOMO of cyclometallated Ir complexes by adding electron-withdrawing fluoro substituents to the phenyl moiety leads to a blue shift in the emission energy, an alternate way to increase the emission energy is to destabilize the LUMO. This is a method that works with electron-donating substituents; however, the magnitude of the shift is limited to ca. 40 nm. A more effective approach is to replace the pyridyl functionality with other heterocyclic groups that have reduction potentials that are significantly higher than that of pyridine. One such modification involves replacing the pyridyl group of ppy with a pyrazolyl (i.e., Ir(ppz)$_3$). The emission energy of *fac*-Ir(ppz)$_3$ ($\lambda_{max} = 414$ nm, 77 K) is significantly greater than that of *fac*-Ir(ppy)$_3$ ($\lambda_{max} = 494$ nm, 77 K; Figure 32). The shift occurs because the photophysical properties of the Ir complexes mirror those of the ligands themselves. The triplet energy of the ppzH ligand (380 nm, 3.26 eV)[437] is much higher than that of ppyH (see above). Unfortunately, no detectable emission from *fac*-Ir(ppz)$_3$ is observed in fluid or solid solutions at room temperature.[392,438] The PL efficiency of *fac*-Ir(ppz)$_3$ is strongly temperature dependent, whereas the PL efficiency of *fac*-Ir(ppy)$_3$ is invariant with temperature when dispersed in a solid matrix.[439,440] Weak emission from *fac*-Ir(ppz)$_3$ is only observed in fluid solution at low temperature (<230 K), whereas intense emission occurs at 77 K. Evidently, emission from *fac*-Ir(ppz)$_3$ is prevented at room temperature by thermal population of a higher-lying excited state, which decays non-radiatively.

Considerable work has been carried out to understand the thermally activated decay processes in luminescent transition metal complexes.[441–443] In particular, Ru(II) and Os(II) tris-diimine have been extensively studied in this regard, since the photophysical properties of these materials exhibit strong temperature-dependent behavior. It has been found that the temperature-dependent luminescence in Ru(II) diimine complexes is characteristic of thermal population to ligand field (dissociative) states, whereas the Os(II) analogs have kinetic parameters more consistent with deactivation through higher-energy MLCT states.[444] The cyclometallated Ir(III) complexes reported here are isoelectronic with the Ru(II) and Os(II) tris-diimine materials, and are expected to mimic the photophysics of their Os(II) counterparts.[407] Thus, the *fac*-Ir(ppz)$_3$ complex could decay non-radiatively through higher-energy MLCT states.[428] However, the triplet energy of *fac*-Ir(ppz)$_3$ is very high ($E_T = 3.0$ eV, 70 kcal mol^{-1}) and comparable to the Ir–phenyl bond strength.[445] Therefore, thermal population to accessible ligand field states can also be considered as a possible non-radiative luminescent decay mechanism.

To achieve efficient luminescence from cyclometallated ppz-based Ir complexes at room temperature, it is necessary to retard or eliminate non-radiative processes that thermally deactivate the excited state. This can be accomplished by replacing the phenyl ring of the ppz ligand with the extended π-system of a fluorenyl group (i.e., *fac*-Ir(flz)$_3$). The fluorenyl substituent lowers the ^{3}LC energy of the complex, shifting it away from the non-radiative decay states that deactivate Ir(ppz)$_3$. The *fac*-Ir(flz)$_3$ complex displays an intense, structured emission in solution at 77 K ($\lambda_{max} = 480$ nm).[446] The well-defined vibronic fine structure in the emission spectrum of *fac*-Ir(flz)$_3$ is indicative of a predominant ^{3}LC character in the excited state. The PL efficiency of *fac*-Ir(flz)$_3$ at room temperature is high ($\Phi = 0.38$) and the measured lifetime is 37 µs. The radiative (k_r) and non-radiative (k_{nr}) decay rates estimated from the lifetime and PL efficiency are 1.0×10^4 s^{-1} and 2.0×10^4 s^{-1}, respectively. These rates are an order of magnitude lower than those reported for ppy-based tris-cyclometallated Ir complexes.[392,439,447] The low radiative rate for *fac*-Ir(flz)$_3$ is consistent with a low level of ^{1}MLCT character in the emissive excited state, and is due to the large separation between the ^{1}MLCT and ligand triplet energies.

While fluorenyl substitution leads to efficient emission at room temperature for the *fac*-Ir(flz)$_3$ complex, it largely negates the blue shift caused by the pyrazole moiety. Therefore, instead of bathochromically shifting the energy of the emitting state away from the non-radiative or deactivating states, an alternate approach to prevent excited-state deactivation is to use ligands that raise the energy of the non-radiative states, thereby retaining the high triplet energy of the complex. If the non-radiative or deactivating state is a metal-localized, ligand field state, strengthening the metal–ligand bonds will raise its energy since that state is comprised of antibonding counterparts to the metal–ligand bonding orbitals. This second approach is demonstrated in a family of cyclometallated *N*-heterocyclic carbene (NHC) complexes.[446] The NHC ligands form very strong bonds to transition metals,[448] which will shift the metal–carbene antibonding orbitals to high energy, thereby decreasing or eliminating decay through the ligand field state. Specifically, the two NHC ligands used are 1-phenyl-3-methyl-imidazolin-2-ylidene (pmi) and 1-phenyl-3-methyl-benzimidazolin-2-ylidene (pmb) (see Scheme 4). The photophysical and OLED properties of related carbene

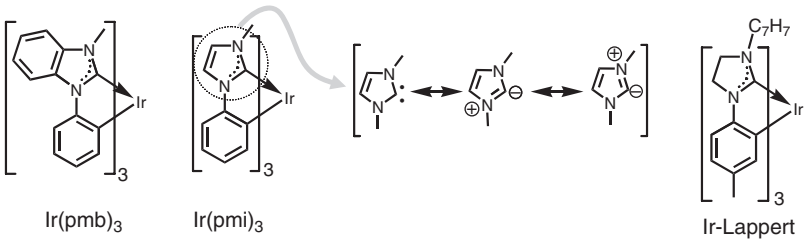

Scheme 4

complexes have been reported.[449] The carbene moiety is a neutral, two-electron donor, which makes the cyclometallated ligand a bidentate monoanionic ligand (C^C: used here as a general abbreviation for a cyclometallated carbene ligand). An early example of a tris-cyclometallated carbene complex, $Ir(C^C:)_3$, was reported in 1980 by Lappert *et al*., (see Ir-Lappert in Scheme 4).[450] While an X-ray structure was given for this complex, no spectroscopic or photophysical data were reported.

The $Ir(pmi)_3$ and $Ir(pmb)_3$ complexes display electrochemical and absorption characteristics comparable to those of *fac*-$Ir(ppz)_3$. The data are consistent with the $Ir(C^C:)_3$ complexes with both low HOMO and high LUMO energies. The *fac*-isomers undergo reversible oxidation (*fac*-$Ir(pmi)_3$, $E_{1/2}{}^{ox} = 0.22$ V; *fac*-$Ir(pmb)_3$, $E_{1/2}{}^{ox} = 0.48$ V) and no observable reduction within the accessible solvent window, similar to the values reported for *fac*-$Ir(ppz)_3$. An interesting feature of *fac*-$Ir(pmi)_3$ and *fac*-$Ir(pmb)_3$ complexes is the small difference in their MLCT absorption energies. This similarity is surprising in view of the large decrease in the MLCT absorption energy (ca. 0.3 eV) that occurs when the π-system of the pyridyl ring in $(ppy)_2Ir(acac)$ is expanded by adding a fused phenyl ring to form $(pq)_2Ir(acac)$.[376,390] Apparently, the minor variance of the MLCT energy upon extending the π-system of the imidazolyl–carbene moiety is due to poor conjugation of the phenyl and benzimidazolyl fragments, such that the phenyl and carbene moieties behave as independent chromophores.

The excited-state properties of the $Ir(C^C:)_3$ complexes are related to the $Ir(C^N)_3$ analogs in that both types of species emit from perturbed ^{3}LC states. The $Ir(C^C:)_3$ complexes display intense emission at 77 K in the near-UV and also luminesce at room temperature in fluid solution ($\lambda_{max} = 390$ nm). The emission spectra at 77 K are highly structured and have luminescent lifetimes between 2 to 7 μs. The PL efficiencies at room temperature for the $Ir(C^C:)_3$ complexes are low (0.002–0.05), but nevertheless higher than their pyrazolyl counterparts.

12.04.2.4.5 Using ancillary ligands to modify the excited-state properties

The excited-state properties of the complexes given above are dictated primarily by the ^{3}LC properties of the C^N ligand. Any variation in the photophysical properties required modification of the C^N ligand, particularly in the case for homoleptic derivatives. The ancillary ligand in heteroleptic complexes offers an alternate approach to modify the excited-state properties. One way ancillary ligands can be used for this purpose is suggested by the state-mixing interactions depicted in Figure 34, which shows that the energy of the emissive excited state is dependent on the relative energies of the ^{3}LC and ^{1}MLCT states. The approach takes advantage of the ability to independently vary the energies of the two states, which is possible in heteroleptic complexes. This can be illustrated with $(C^N)_2Ir(L^X)$ complexes, where the cyclometallating ligand is either 4′Meppy (tpy) or 4′6′F_2ppy, and the ancillary ligand is chosen to be "non-chromophoric," that is, to have sufficiently high singlet and triplet energies such that the excited-state properties are dominated by the "$(C^N)_2Ir$" fragment (see Figure 35). The energy of the ^{3}LC state is expected to be relatively constant for a related series of $(C^N)_2Ir(L^X)$ complexes while the energy of ^{1}MLCT states can be altered by varying the electron withdrawing/-donating effects of the ancillary ligand. A set of four ancillary ligands will be considered here (L^X = acac, $(pz)_2H$, $(pz)_4B$, P_2B), but a significantly more extensive series has been considered elsewhere.[401]

The absorption and emission spectra of the $(C^N)_2Ir(L^X)$ complexes progressively shift to higher energy with the ancillary ligand in the sequence acac < $(pz)_2H$ < $(pz)_4B$ < P_2B. Molecular orbital calculations on these complexes suggest that the nature of the frontier orbitals is not affected by the ancillary ligand.[401] The HOMO remains a mixture of metal and phenyl orbitals and the LUMO is predominantly localized on the pyridyl group, as illustrated in Figure 30. The ancillary ligand thus alters the ground-state energies by direct interaction with the metal center. This role for the ancillary ligand is confirmed by electrochemical measurements, which show that the oxidation potential is shifted by the choice of ancillary ligand, whereas the reduction potentials are relatively unperturbed.[401] The oxidation potentials of

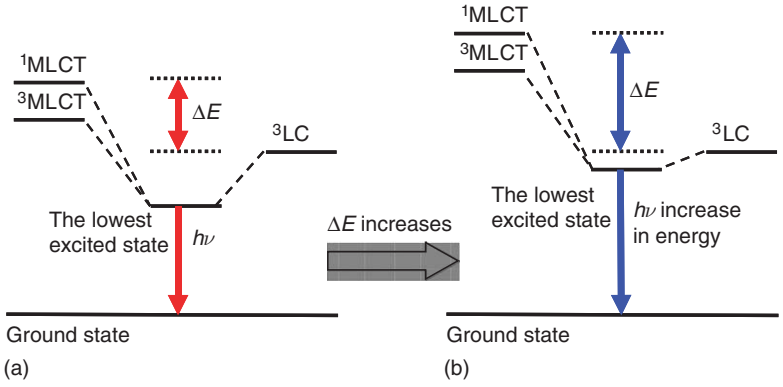

Figure 34 Schematic energy level diagram for state mixing in cyclometallated Ir(III) complexes with differing ΔE: (a) small ΔE, large admixture of ^{1}MLCT into the triplet states (principally ^{3}LC), low emission energy; (b) large ΔE, small admixture of ^{1}MLCT and triplet states, high emission energy.

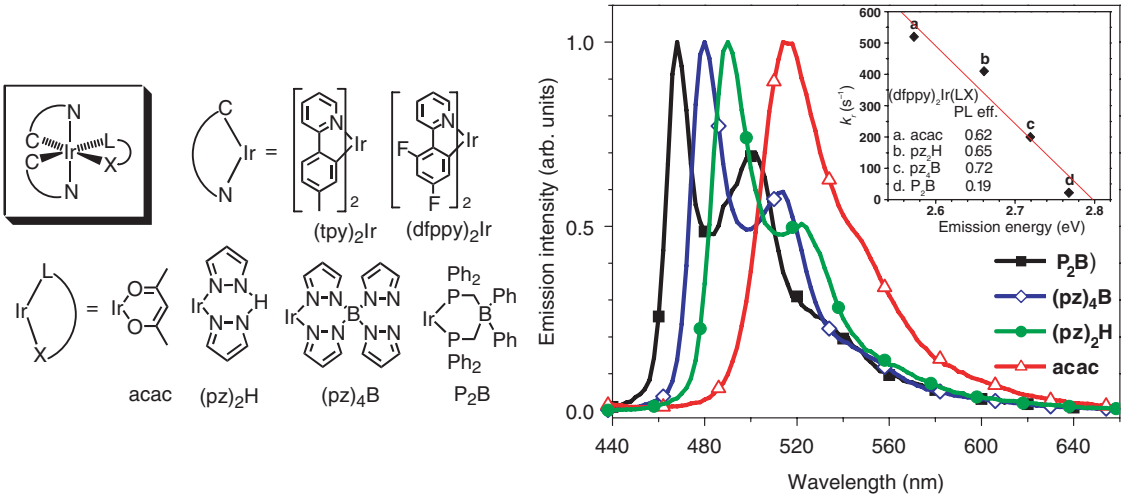

Figure 35 Molecular structures for the $(C^N)_2Ir(L^X)$ complexes considered here. The room temperature emission spectra and a plot of the radiative rate versus triplet energy for $(F_2ppy)_2Ir(L^X)$ complexes (inset) are also shown.

the $(4'Meppy)_2Ir(L^X)$ complexes are: L^X = acac (0.41 V), $(pz)_2H$ (0.55 V), $(pz)_4B$ (0.72 V), and P_2B (0.81 V) (vs. ferrocenium/ferrocene). In contrast, the reduction potentials for the same complexes fall between −2.62 and −2.68 V. Thus, the shift in absorption and emission energy is caused by changes in the HOMO energy, while the LUMO energy is relatively constant. Stabilizing the HOMO energy leads to an increase in the MLCT energy, which decreases the amount of MLCT character mixed into the lowest-excited state. As the MLCT energy increases, the energy of the excited state approaches that of the ^{3}LC state. The question that then occurs is at what point does the amount of MLCT character in the excited state get too low for efficient triplet emission?

The radiative rates for these complexes were determined from the PL quantum yields (inset of Figure 35) and the measured lifetimes (Figure 35 shows the data for the $4'6'F_2$ppy complexes). As the energy of emission increases, the radiative rate of emission decreases. This trend is not surprising when one considers the energy level diagram of Scheme 3. The increase in energy in this system is due to a decrease in the amount of MLCT character in the excited state. Since the principal source of efficient triplet emission is the mixing of MLCT character into the lowest-excited state, a decreasing amount of singlet MLCT character is expected to lower the radiative decay rate. This decrease in radiative decay rate is also accompanied by a decrease in the non-radiative decay rate. As the energy of the excited state increases, the coupling to the vibrational states that are the common source of non-radiative decay decreases, leading to a lower non-radiative decay rate.[444] For the complexes with acac, $(pz)_2$, and $(pz)_4B$ ligands, the decrease in

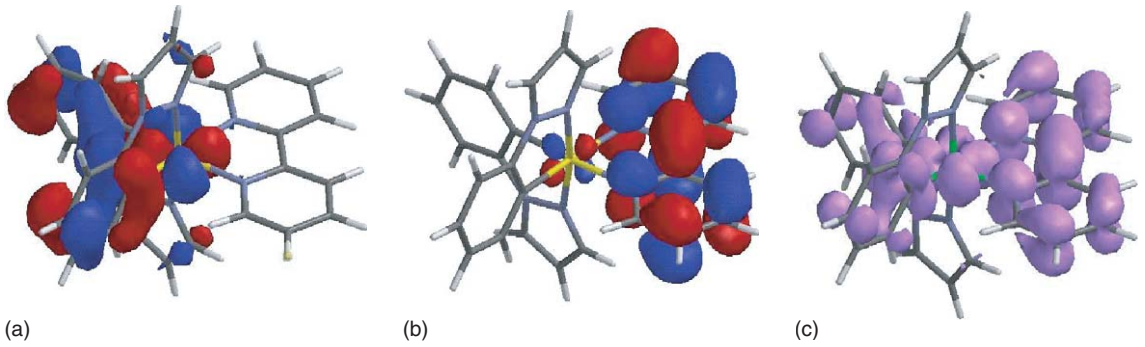

Figure 36 The singlet HOMO, LUMO, and triplet spin density surfaces of $(ppz)_2Ir(bpy)^+$ are shown.

non-radiative decay rate is greater than the decrease in radiative decay and the PL efficiency increases. In contrast, the decrease in the radiative rate for the derivative with P_2B is greater than the non-radiative rate, due to the marked reduction in MLCT character in the excited state. The low radiative rate for the complex with the P_2B ligand leads to a significant decrease in the luminance efficiency. From this study, it can be concluded that emission from $(4'6'F_2ppy)_2Ir(L\text{^}X)$ complexes cannot be shifted to energies greater than what is observed for $(4'6'F_2ppy)_2Ir(pz_4B)$ ($\lambda_{max} = 450$ nm) without adversely affecting the PL efficiency.

If the ancillary ligand has a triplet energy that is lower than the cyclometallated moiety, the ligand becomes directly involved in the emission process. When this ancillary ligand is another cyclometallating ligand, the emission is as intense as that from a homoleptic complex.[393,395,396] However, if the ancillary ligand is a β-diketonate[376] or N^O chelate (N^O = picolinate, quinolinate)[400,405] the emission is broad and can be relatively weak. Emission from the ancillary ligand is identified most clearly in Ir complexes that have cyclometallated ppz ligands. The high triplet energy of the $(ppz)_2Ir$ fragment makes it likely that the ancillary ligand will be the moiety with the lowest triplet energy. Emission from an ancillary ligand can be easily demonstrated in a series of cationic Ir complexes with diimine ligands. Several of these types of materials have been used to make light-emitting devices (see Section 12.04.2.5.2).[451] DFT calculations give some insight into the electronic structure of these heteroleptic derivatives. The discussion here will focus on the results for $(ppz)_2Ir(bpy)^+$; however, other $(C\text{^}N)_2Ir(N\text{^}N)^+$ complexes gave a similar picture for the HOMO and LUMO surfaces. The singlet HOMO, LUMO, and triplet spin density surfaces of $(ppz)_2Ir(bpy)^+$ are illustrated in Figure 36. The HOMO surface is similar in appearance to that seen in $(ppy)_2Ir(acac)$ (Figure 31), being principally composed of a mixture of Ir-d and phenyl-π orbitals distributed equally between the two phenylpyrazolyl ligands. On the other hand, the LUMO is predominantly localized on the bipyridyl ligand. The HOMO and LUMO orbitals are orthogonal to each other and thus, there is little electronic overlap between them. The spin density surface shares the same spatial extent as the singlet HOMO and LUMO surfaces, which leads to a description of the lowest-energy excited state as having metal–ligand-to-ligand charge-transfer (MLLCT) character.

The Ir complexes all display broad, featureless emission spectra in fluid solution or neat solid at room temperature, with maxima ranging from 485 to 630 nm. Emission energies for a number of organometallic diimine complexes are given in Figure 37. The emission spectra exhibit large Stokes′ shifts (ca. 4,000–6,000 cm^{-1}) from the lowest-energy absorption bands. The emission properties at room temperature are consistent with luminescence originating from a triplet MLLCT state. All the complexes undergo large rigidochromic blue shifts upon cooling solutions to 77 K. For example, the emission maximum of $(ph\text{–}ppz)_2Ir(dtb\text{–}bpy)^+$ in 2-MeTHF at room temperature is 570 nm, while at 77 K the maximum is centered at 480 nm, (Figure 37). The hypsochromic shifts are due to solvent reorganization in fluid solution at room temperature, which stabilize the CT states prior to emission. This process is significantly impeded in a rigid matrix at 77 K, and thus emission occurs at higher energy.

12.04.2.5 Monochromatic OLED Fabrication

A typical definition that is often made when describing OLEDs is to categorize them as either small molecule or polymer-based devices. However, this distinction is somewhat misleading since small molecule- and polymer-based OLEDs do not markedly differ in their operating principles. The mechanistic discussions given Section 12.04.2.1 apply equally well to both types of devices. A more logical way to differentiate OLEDs is by the fabrication method. Molecular materials (typically referred to as small molecules) can be distilled or sublimed at reduced pressure, and are

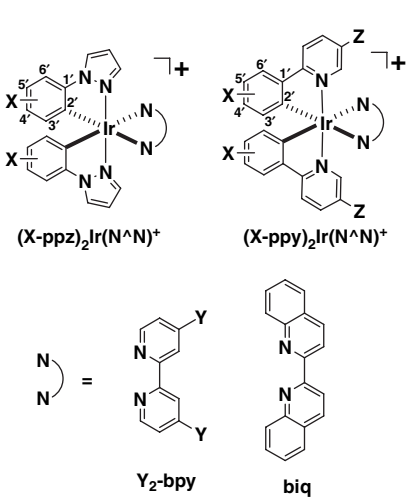

C^N	X, Z	N^N	Y	PL λ_{max} RT, soln.	PL λ_{max} 77K, soln.
ppy	H, H	bpy	H	581	532
F-mppy	4′-F, CH_3	dtb-bpy	*t*-butyl	543	-
ppz	H	bpy	H	565	487
ppz	H	dtb-bpy	*t*-butyl	550	465
ppz	H	MeO-bpy	OCH_3	550	440
ppz	H	CO-bpy	CO_2Et	625	545
ppz	H	biq	-	614	585
tb-ppz	5′-*t*-butyl	biq	-	622	592
MeO-ppz	4′-methoxy	dtb-bpy	*t*-butyl	615	522
ph-ppz	4′-phenyl	dtb-bpy	*t*-butyl	570	480
F_2ppz	4′,6′-	dtb-bpy	*t*-butyl	493	433

Figure 37 Representative organometallic diimine complexes and their photoluminescence energies.

thus readily deposited onto the substrate/electrode from the vapor phase. OLEDs can also be made using small molecules deposited from solution, but fabrication from the vapor phase is preferred in order to maintain high purity levels (i.e., no solvent or solvent born impurities are present in vapor-deposited film) and to enable formation of heterostructured devices. In contrast, since most polymers will decompose prior to vaporization these materials must be deposited from solution. OLEDs made with small molecules can also be prepared using a technique called organic vapor phase deposition (OVPD), a process that is intermediate between vacuum and organic solvent-based processes.[452–455] Using OVPD, a molecular material is either sublimed or distilled into a hot carrier gas stream where it is then transported until it condenses onto a cooled substrate. In this case, the high purity nitrogen or argon carrier gas acts as a solvent, thereby preventing any "solvent" born impurities from being incorporated into the thin film.

A significant challenge in the fabrication of large-area, high-definition OLED displays is the patterning of the individual red, green, and blue (RGB) pixels. A method commonly used for this task with OLEDs prepared from the vapor phase involves the use of a metal "shadow" mask. The shadow mask is inserted between the evaporation source and the substrate and physically blocks the deposition of the organic material over select areas on the substrate. The mask can be moved and used repeatedly for the RGB pixels. While patterning with a shadow mask is conceptually simple, it becomes very difficult to implement for large-area devices (displays larger than 30–40 cm). Solution-based methods for OLED fabrication such as ink-jet printing[456–458] and solvent-based conventional printing techniques[459,460] are more amenable to RGB patterning and are being explored for use in large-area display production. Another method for OLED fabrication involves the use of stamping.[461–465] This process is similar to conventional offset printing, whereby a material is coated on die or stamp and transferred onto a substrate by mechanical pressure, and has been used to deposit both organic and metal layers onto an ITO-coated substrate. RGB OLEDs could be fabricated onto a single substrate using any of these techniques.

12.04.2.5.1 OLEDs utilizing organometallic emitters

Tables 6–9 give the device structures and performance metrics for monochromatic OLEDs that utilize organometallic emitters. Figures 38–42 show the molecular structures for the various materials used in these devices. White OLEDs have also been prepared with these materials, but these will be discussed in a later section. Light-emitting electrochemical cells are treated in a separate section as well, since the finished devices have different operating characteristics than either of the other solution or vapor processed devices. Table 6 lists devices made solely with discrete molecular materials, while Table 7 gives data for devices made using polymeric materials. The only exception to the use of discrete molecular materials in Table 6 is for devices that use a conducting polymer, poly(3,4-ethylenedioxythiophene polystyrene sulfonate) (PEDOT), as a material to enhance the efficiency for hole injection into the organic layer. The mode of preparation for a given device is listed with the device parameters in the

Table 6 OLED performance parameters for devices utilizing molecular organoiridium compounds

Entry	*Emitter*[a] $Ir(C^N)_3$, $(C^N)_2Ir(L^X)$	*Method*[b]	*Device structure*[c] *ITO anode, metal cathode*	*EL* λ_{max} (nm)	*CIE*	*EQE* (%)	cd A^{-1}	lm W^{-1}	*References*
1	$Ir(pmb)_3$	vap	NPD/TCTA/UGH2 : Ir/BCP	389	0.17, 0.06	2.6	–	0.5	520
2	*mer*-$Ir(pmb)_3$	vap	NPD/TCTA/UGH2 : Ir/BCP	395	0.17, 0.06	5.8	–	1.7	520
3	$Ir(ppz)_3$	vap	NPD/mCP : Ir/BCP/Alq_3	450	0.16, 0.14	0.4	0.23	–	438
4	$(4'6'F_2ppy)_2Ir(pz_4B)$	vap	NPD/mCP/UGH2 : Ir/BCP/Alq_3	457	–	9.1	–	–	521
5	$(4'6'F_2ppy)_2Ir(pz_4B)$	vap	NPD/mCP/UGH2 : Ir/BCP	457	0.16, 0.26	11.6	–	13.9	522
6	$(4'6'F_2ppy)_2Ir(ttrzpyr)$	vap	NPD/SimCP : Ir/TBPI	462	0.15, 0.24	9.4	–	7.2	404
7	$(4tBu\text{-}4'6'F_2ppy)_2Ir(pic)$	vap	CFx/NPD/CBP : Ir/BCP/Alq_3	468	0.17, 0.30	1.0	2.0	–	523
8	$(4'6'F_2MeOppy)_2Ir(acac)$	vap	CFx/NPD/CBP : Ir/BCP/Alq_3	–	0.19, 0.31	0.4	0.7	–	523
9	$(4'6'F_2ppy)_2Ir(pic)$	vap	NPD/CBP : Ir/Balq	470	0.16, 0.29	5.7	–	6.3	317
10	$(4'6'F_2ppy)_2Ir(pic)$	vap	NPD/mCP : Ir/BAlq	472	–	7.5	–	8.9	524
11	$(4'6'F_2ppy)_2Ir(pic)$	vap	CFx/NPD/CBP : Ir/BCP/Alq_3	472	0.16, 0.32	3.3	5.8	–	523
12	$(4'6'F_2ppy)_2Ir(pic)$	vap	PEDOT/NPD/CDBP : Ir/BAlq	472	0.17, 0.34	10.4	20.4	10.5	525
13	$(4'6'F_2ppy)_2Ir(pic)$	vap	NPD/SimCP : Ir/TBPI	472	0.15, 0.28	14.4	–	11.9	404
14	$(4'6'F_2ppy)_2Ir(pic)$	vap	NPD/DCB : Ir/BPhen	472	0.17, 0.34	5.8	9.8	–	526
15	$(4'6'F_2ppy)_2Ir(pic)$	vap	NPD/DCB : Ir/BPhen	472	0.15, 0.30	5.1[d]	8.7	–	527
16	$(4'6'F_2ppy)_2Ir(pic)$	vap	NPD/DCB : Ir/BPhen	500	0.17, 0.40	9.1[d]	15.4	–	527
17	$(4MeO\text{-}4'6'F_2ppy)_2Ir(acac)$	vap	NPD/mCP : Ir/BCP/Alq_3	472	0.17, 0.30	1.9[d]	1.63	0.88	528
18	$Ir(G1\text{-}dend\text{-}4'6'F_2ppy)_3$	sol/vap	mCP : Ir/TBPI	473	0.17, 0.34	10.8	–	11	118
19	$Ir(flzr)_3$	vap	NPD/$Ir(ppz)_3$/mCP : Ir/BCP	480	0.26, 0.56	6.1	–	11.3	529
20	$(3'5'F_2Phimazpy)_2Ir(acac)$	vap	NPD/CBP : Ir/BCP/Alq_3	500	0.28, 0.41	1.2	3.2	1.4	532
21	$Ir(6'Fppy)_3$	vap	MPMP/neat-Ir/BCP/Alq_3	506	–	1.4[d]	3.8	–	387
22	*mer*-$Ir(4Meppy)_3$	vap	NPD/CBP : Ir/BCP/Alq_3	508	0.31, 0.59	5.4[d]	21.6	6.9	531
23	$Ir(pppy)_3$	vap	NPD/CBP : Ir/BCP/Alq_3	509	–	2.6[d]	10.2	–	532
24	$Ir(ppy)_3$	vap	NPD/CBP : Ir/BCP/Alq_3	510	0.27, 0.63	8.0	28	31	373
25	$Ir(ppy)_3$	sol/vap	TPD : CBP : Ir/BCP	510	0.26, 0.65	16.9	–	20.9	533
26	$Ir(ppy)_3$	vap	NPD/TCTA : Ir/CF–X/Alq_3	511	–	19.2	73	70	379
27	$Ir(ppy)_3$	vap	F_4TCNQ : MTDATA/NPD/CBP : Ir/BPhen/BPhen : Li	511	–	4.08	14.3	–	534
28	$Ir(ppy)_3$	vap	CuPc/F_4TCNQ : MTDATA/$Ir(ppz)_3$/CBP : Ir/BPhen/BPhen : Li	510	–	7.6	–	23	535
29	$Ir(ppy)_3$	vap	F_4TCNQ : MTDATA/$Ir(ppz)_3$/TCTA : Ir/BPhen : Ir/BPhen	510	–	9.5	–	29	536
30	$Ir(ppy)_3$	vap	F_4TCNQ : MTDATA/NPD/TCTA : Ir/BPhen : Ir/BPhen	510	–	12.6	44.3	–	537
31	$Ir(ppy)_3$	vap	F_4TCNQ : MeO-TPD/Spiro-TAD/TCTA : Ir/BPhen/BPhen : Cs	510	–	13.7	–	53	538
32	$Ir(ppy)_3$	vap	F_4TCNQ : MeO-TPD/Spiro-TAD/TCTA : Ir/TAZ : Ir/BPhen/BPhen : Cs	510	–	19.5	–	77	512
33	$Ir(ppy)_3$	vap	TPD/TRZ2 : Ir/BCP/Alq_3	512	–	10.2	–	14.0	539
			TPD/TRZ2 : Ir/Alq_3	510		10.0		15.9	
			TPD/CBP : Ir/TRZ2/Alq_3	510		9.2		9.5	

(*Continued*)

Table 6 (Continued)

Entry	*Emitter*[a] Ir(C^N)$_3$, (C^N)$_2$Ir(L^X)	*Method*[b]	*Device structure*[c] *ITO anode, metal cathode*	*EL* λ_{max} (nm)	*CIE*	*EQE* (%)	cd A^{-1}	lm W^{-1}	*References*
34	Ir(ppy)$_3$	vap	NPD/Cz2 : Ir/BCP/Alq$_3$	510	–	7.5[d]	30	–	540
			NPD/Cz3 : Ir/BCP/Alq$_3$			4.2[d]	17		
35	Ir(ppy)$_3$	vap	NPD/CBP : Ir/BCP/Alq$_3$	510	–	8	–	–	541
			TPD/CBP : Ir/BCP/Alq$_3$			12			
			TAPC/CBP : Ir/BCP/Alq$_3$			14			
36	Ir(ppy)$_3$	vap	CuPc/NPD/CBP : Ir/BAlq/Alq$_3$	510	0.30, 0.63	5.6	19.0	–	378
			CuPc/NPD/CBP : Ir/TBPI/Alq$_3$			7.5	25.3		
			CuPc/NPD/CBP : Ir/SAlq/Alq$_3$			4.7	15.6		
			CuPc/NPD/CBP : Ir/PAlq/Alq$_3$			5.3	18.0		
37	Ir(ppy)$_3$	vap	TPD/CBP : Ir/diazafluor/bpySibpy	510	0.27, 0.61	18	65	45	513
			TPD/CBP : Ir/diazafluor		0.28, 0.64	12[d]	45		
			TPD/CBP : Ir/diazafluor/Alq$_3$		0.29, 0.51	12[d]	45		
			TPD/CBP : Ir/BCP		0.24, 0.66	11[d]	40		
38	Ir(ppy)$_3$	vap	CuPc/NPD : Alq$_3$/CBP : Ir/Alq$_3$: NPD	515	–	4.4	–	12.7	542
39	Ir(ppy)$_3$	vap	NPD/CBP : Ir/BCP/Alq$_3$	515	0.30, 0.64	14.9	–	43.4	543
40	Ir(ppy)$_3$	vap	NPD/CBP : Ir/BCP/Alq$_3$	515	–	13.7	–	38.3	544
41	Ir(ppy)$_3$	vap	HMTPD/TAZ : Ir/Alq$_3$	515	–	15.4	–	40.2	374
42	Ir(ppy)$_3$	vap	PEDOT/TCTA/DFC : Ir/BCP/Alq$_3$	515	–	10.5	–	25	545
43	Ir(ppy)$_3$	vap	NPD/CBP : Ir/BCP/Alq$_3$	516	–	6.0	–	–	432
44	Ir(ppy)$_3$	vap	NPD/CBP : Ir/BCP/Alq$_3$	516	0.35, 0.60	7.7[d]	24.9	8.1	531
45	Ir(ppy)$_3$	vap	NPD/neat-Ir/BCP/Alq$_3$	520	–	0.8	–	–	373
46	Ir(ppy)$_3$	vap	MPMP/neat-Ir/BCP	522	–	0.9[d]	3.8	–	387
47	(4′Brppy)$_2$Ir(acac)	sol	PEDOT/neat-Ir	510	–	0.012	–	–	61
48	Ir(4Meppy)$_3$	vap	NPD/CBP : Ir/BCP/Alq$_3$	511	0.31, 0.62	5.4[d]	22.0	7.3	531
49	Ir(4′-4Me$_2$ppy)$_3$	vap	NPD/CBP : Ir/BCP/Alq$_3$	512	–	11.0	–	–	432
50	(5′-(C$_6$F$_5$)ppy)$_2$Ir(acac)	vap	NPD/CBP : Ir/BCP/Alq$_3$	513	–	11.2	45	19	546
51	Ir(4′Fppy)$_3$	vap	MPMP/neat-Ir/BCP/Alq$_3$	514	–	7.6[d]	1.9	–	387
52	Ir(G1-cbz-ppy)$_3$	sol	PEDOT/neat-Ir	515	–	0.15	–	–	547
				600					
53	Ir(G1-cbz-ppy)$_3$	sol	PEDOT/OXD7 : Ir	515	–	5.2	–	–	547
54	Ir(G2-cbz-ppy)$_3$	sol	PEDOT/neat-Ir	515	–	0.2	–	–	547
				600					
55	Ir(G2-cbz-ppy)$_3$	sol	PEDOT/OXD7 : Ir	515	–	7.6	–	–	547
56	Ir(5′CF$_3$ppy)$_3$	vap	MPMP/neat-Ir/BCP/Alq$_3$	517	–	0.6[d]	2	–	387
57	(tbi)$_2$Ir(acac)	vap	BPAPF/CBP : Ir/BCP/Alq$_3$	518	0.27, 0.59	4.0	13	5.0	514
58	Ir(G1-dend-ppy)$_3$	sol	neat-Ir	518	–	0.2	–	–	548
59	Ir(G1-dend-ppy)$_3$	sol/vap	neat-Ir/TBPI	518	–	4.6	–	10	549
60	Ir(G1-dend-ppy)$_3$	sol	CBP : Ir	518	–	8.1	28	6.9	548
61	Ir(G1-dend-ppy)$_3$	sol	CBP : TPBI : Ir	518	–	10.4	35	12.8	550

62	Ir(G1-dend-ppy)$_3$	sol/vap	CBP : Ir/TBPI	518	–	7.6[d]	31	18	551
63	Ir(G1-dend-ppy)$_3$	sol/vap	CBP : Ir/TBPI	518	0.31, 0.63	9.8	33	21	552
64	Ir(G1-dend-ppy)$_3$	sol/vap	TCTA : Ir/TBPI	518	0.31.0.63	17.0[d]	55	40	553
65	Ir(G2-dend-ppy)$_3$	sol	neat-Ir	518	–	2.1	–	–	548
66	Ir(G2-dend-ppy)$_3$	sol/vap	neat-Ir/TBPI	518	–	8.5	–	21	549
67	Ir(G2-dend-ppy)$_3$	sol/vap	CBP : Ir/TBPI	518	0.31, 0.63	10.4	34.3	27	552
68	(ppy)$_2$Ir(acac)	vap	HMTPD/TAZ : Ir/Alq$_3$	520	–	19	–	60	511
69	(ppy)$_2$Ir(acac)	vap	NPD/CBP : Ir/BCP/Alq$_3$	520	–	13.2	–	37	397
70	(ppy)$_2$Ir(acac)	vap	NPD/CBP : Ir/BCP/Alq$_3$	522	–	10.8	42	23	546
71	(ppy)$_2$Ir(acac)	vap	NPD/CBP : Ir/BCP/Alq$_3$	524	0.33, 0.60	5.5[d]	22.0	7.9	531
72	(ppy)$_2$Ir(acac)	vap	NPD/CBP : Ir/BCP/Alq$_3$	525	0.31, 0.64	12.3	50	38	376
73	Ir(4′CF$_3$O-5CF$_3$ppy)$_3$	vap	MPMP/neat-Ir/BCP/Alq$_3$	520	–	1.5[d]	5	–	387
74	Ir(5′CF$_3$-5NO$_2$ppy)$_3$	vap	MPMP/neat-Ir/BCP/Alq$_3$	521	–	0.01[d]	0.013	–	387
75	(ppy)$_2$Ir(Et$_2$dtc)	vap	NPD/CBP : Ir/BCP/Alq$_3$	523	–	0.9[d]	2.9	–	402
76	Ir(4′F-5CF$_3$ppy)$_3$	vap	MPMP/neat-Ir/BPhen/Alq$_3$	525	–	7.4[d]	30	–	371
77	Ir(4′F-5CF$_3$ppy)$_3$	vap	MPMP/neat-Ir/BPhen	525	–	4.9[d]	20	–	554
78	Ir(4′F-5CF$_3$ppy)$_3$	vap	MPMP/neat-Ir/BPhen	525	–	4.9[d]	20	–	387
79	Ir(6′F-5CF$_3$ppy)$_3$	vap	MPMP/neat-Ir/BCP/Alq$_3$	525	–	0.5[d]	2.1	–	387
80	Ir(5′CF$_3$-5CF$_3$ppy)$_3$	vap	MPMP/neat-Ir/BCP	525	–	2.8[d]	9.5	–	387
81	Ir(4′F-5CF$_3$ppyrm)$_3$	vap	MPMP/neat-Ir/BCP	525	–	2.8[d]	9.5	–	387
82	Ir(4′MeO-5CF$_3$ppy)$_3$	vap	MPMP/neat-Ir/BCP/Alq$_3$	530	–	0.5[d]	1.8	–	387
83	(4′6′F$_2$bt)$_2$Ir(acac)	vap	NPD/CBP : Ir/BCP/Alq$_3$	530	0.37, 0.60	11.2	45.0	13.9	555
84	(4′6′F$_2$bt-F)$_2$Ir(acac)	vap	NPD/CBP : Ir/BCP/Alq$_3$	530	0.37, 0.61	12.4	50.3	16.0	555
85	(cbi)$_2$Ir(acac)	vap	BPAPF/CBP : Ir/BCP/Alq$_3$	530	0.35, 0.61	12.1	44	13	514
86	(pbi)$_2$Ir(acac)	vap	BPAPF/CBP : Ir/BCP/Alq$_3$	530	0.36, 0.60	16.7	61	20	514
87	(4′-(Ph$_2$N)ppy)$_2$Ir(acac)	vap	NPD/CBP : Ir/BCP/Alq$_3$	531	0.38, 0.61	11.8	–	23.7	556
88	(PP)$_2$Ir(acac)	vap	NPD/CCP : Ir/BCP/Alq$_3$	534	0.36, 0.61	10.6	43.9	25.2	434
89	Ir(5′-4Me$_2$ppy)$_3$	vap	NPD/CBP : Ir/BCP/Alq$_3$	534	–	10.9	–	–	432
90	Ir(G1p-dend-ppy)$_3$	sol/vap	neat-Ir/TBPI	535	–	3.8	–	7	549
91	Ir(G1p-dend-ppy)$_3$	sol/vap	CBP : Ir/TBPI	535	0.42, 0.56	8.8	30.1	16.3	552
92	Ir(Ph$_5$ppy)$_3$	sol	CBP : Ir	535	–	2.9	9.3	1.9	557
93	Ir(4′-5Me$_2$ppy)$_3$	vap	NPD/CBP : Ir/BCP/Alq$_3$	536	–	8.6	–	–	432
94	(3′5′F$_2$-3piq)$_2$Ir(acac)	vap	NPD/CBP : Ir/BCP/Alq$_3$	540	0.36, 0.59	1.05	1.68	0.57	515
95	(4′CF$_3$-3piq)$_2$Ir(acac)	vap	NPD/CBP : Ir/BCP/Alq$_3$	542	0.46, 0.53	3.98	14.6	6.27	515
96	(4′-(C$_6$F$_5$)ppy)$_2$Ir(acac)	vap	NPD/CBP : Ir/BCP/Alq$_3$	544	–	12.3	41	20	546
97	Ir(5CF$_3$ppy)$_3$	vap	MPMP/neat-Ir/BCP/Alq$_3$	545	–	1.0[d]	4	–	387
98	(ppy-FH)$_2$Ir(acac)	sol	PEDOT/neat-Ir	545	–	0.030	–	–	61
99	Ir(DPF)$_3$	sol	PEDOT/neat-Ir	545	–	0.1	0.1	–	518
100	Ir(DPPF)$_3$	sol	PEDOT/neat-Ir	550	–	0.1	0.04	–	518
101	(ppy-FOFH)$_2$Ir(acac)	sol	PEDOT/neat-Ir	550	–	0.110	–	–	61
102	(ppy-FO$_2$FH)$_2$Ir(acac)	sol	PEDOT/neat-Ir	550	–	0.115	–	–	61

(*Continued*)

Table 6 (Continued)

Entry	*Emitter*[a] Ir(C^N)$_3$, (C^N)$_2$Ir(L^X)	*Method*[b]	*Device structure*[c] *ITO anode, metal cathode*	*EL* λ_{max} (nm)	*CIE*	*EQE* (%)	cd A^{-1}	lm W^{-1}	*References*
103	(ppyFO$_{10}$)$_2$Ir(acac)	sol	PEDOT/neat-Ir	550	–	0.045	–	–	61
104	(ppy-FO$_{30}$)$_2$Ir(acac)	sol	PEDOT/neat-Ir	550	–	0.070	–	–	61
105	Ir((G1-dend)$_2$-ppy)$_3$	sol/vap	neat-Ir/TBPI	550	–	13.6	47	30	558
106	(5-(C$_6$F$_5$)ppy)$_2$Ir(acac)	vap	NPD/CBP : Ir/BCP/Alq$_3$	559	–	14.9	47	29	546
107	(bt)$_2$Ir(acac)	vap	NPD/CBP : Ir/BCP/Alq$_3$	560	0.47, 0.52	9.28	34.0	11.4	555
108	(bt)$_2$Ir(acac)	vap	NPD/CBP : Ir/BCP/Alq$_3$	564	0.49, 0.48	2.21	9.6	4.6	539
109	(bt)$_2$Ir(acac)	vap	NPD/CBP : Ir/BCP/Alq$_3$	565	0.51, 0.49	11.9	–	–	376
110	Ir(3′F-5CF$_3$ppy)$_3$	vap	MPMP/neat-Ir/BCP/Alq$_3$	560	–	0.5[d]	2.2	–	387
111	(3piq)$_2$Ir(acac)	vap	NPD/CBP : Ir/BCP/Alq$_3$	562	0.49, 0.51	7.17	23.9	9.38	515
112	*mer*-Ir(ppy)$_3$	vap	NPD/CBP : Ir/BCP/Alq$_3$	564	0.42, 0.50	3.7[d]	15.3	5.3	531
113	(4′CF$_3$bt)$_2$Ir(acac)	vap	NPD/CBP : Ir/BCP/Alq$_3$	568	0.53, 0.47	2.60	10.8	4.6	559
114	(fbi)$_2$Ir(acac)	vap	BPAPF/CBP : Ir/BCP/Alq$_3$	568	0.51, 0.48	10.4	30	7.8	514
115	Ir(3Cl-5CF$_3$ppy)$_3$	vap	MPMP/neat-Ir/BCP/Alq$_3$	575	–	0.83[d]	3.3	–	387
116	(MDPP)$_2$Ir(acac)	vap	NPD/CBP : Ir/BCP/Alq$_3$	576	0.52, 0.48	6.02	–	9.89	560
117	(4-(C$_6$F$_5$)ppy)$_2$Ir(acac)	vap	NPD/NPD : Ir/BCP/Alq$_3$	578	–	16.9	43	28	546
118	(NEP)$_2$Ir(acac)	vap	NPD/CBP : Ir/BCP/Alq$_3$	580	0.49, 0.48	5.6	16.9	8.8	434
119	Ir(PQ)$_3$	vap	CuPc/NPD/CBP : Ir/BAlq/Alq3	589	0.56, 0.43	11	33.4	11.7	561
120	Ir(3′MeO-5CF$_3$ppy)$_3$	vap	MPMP/neat-Ir/Bphen	595	–	0.42[d]	1.4	–	387
121	(3′-(Ph$_2$N)ppy)$_2$Ir(acac)	vap	NPD/CBP : Ir/BCP/Alq$_3$	595	0.56, 0.44	7.6	–	7.4	556
122	Ir(HFP)$_3$	sol	PEDOT/neat-Ir	595	–	0.1	0.07	–	518
123	(PEP)$_2$Ir(acac)	vap	TCTA/CBP : Ir/BCP/Alq$_3$	596	0.57, 0.43	4.0	9.7	4.5	434
124	(PQ)$_2$Ir(acac)	vap	CuPc/NPD/CBP : Ir/BAlq/Alq$_3$	597	0.61, 0.38	10.3	17.6	–	378
125	(4′FPPQ)$_2$Ir(acac)	vap	NPD/CBP : Ir/BCP/Alq$_3$	598	0.61, 0.39	6.7	13.7	7.1	562
126	(G1-dend-ppy)$_2$Ir(btp)	sol/vap	CBP : Ir/TBPI	600	–	2.2[d]	7	4	551
127	(G1-dend-ppy)$_2$Ir(btp)	sol/vap	CBP : Ir/TBPI	602	0.64, 0.36	5.7	–	4.5	563
128	(PETP)$_2$Ir(acac)	vap	NPD/CCP : Ir/BCP/Alq$_3$	602	0.59, 0.40	7.4	16.6	7.8	434
129	(3′5′F$_2$piq)$_2$Ir(acac)	vap	NPD/CBP : Ir/BCP/Alq$_3$	606	0.62, 0.38	5.31	8.75	2.61	515
130	Ir(4′F-5Mepiq)$_3$	vap	NPD/CBP : Ir/BPhen	607	0.66, 0.34	15.5	–	12.4	564
131	(nbi)$_2$Ir(acac)	vap	BPAPF/CBP : Ir/BCP/Alq$_3$	608	0.63, 0.35	4.8	6.1	1.7	514
132	(4′MeOPPQ)$_2$Ir(acac)	vap	NPD/CBP : Ir/BCP/Alq$_3$	608	0.61, 0.38	2.8	3.9	1.7	562
133	(4′5F$_2$piq)$_2$Ir(acac)	vap	NPD/CBP : Ir/BCP/Alq$_3$	609	0.60, 0.36	7.41	13.4	5.78	515
134	(DBQ)$_2$Ir(acac)	vap	NPD/CBP : Ir/BCP/Alq$_3$	610	0.62, 0.38	11.9	23.3	7.9	565
135	(MDQ)$_2$Ir(acac)	vap	NPD/CBP : Ir/TBPI/Alq$_3$	610	0.60, 0.39	12.4	26.2	13.7	565
136	(5′MeObt)$_2$Ir(acac)	vap	NPD/CBP : Ir/BCP/Alq$_3$	610	0.63, 0.37	6.5	11.0	4.3	555
137	(4′Fpiq)$_2$Ir(acac)	vap	NPD/CBP : Ir/BCP/Alq$_3$	610	0.61, 0.36	8.67	13.7	4.7	516
138	(pqxn)$_2$Ir(CF$_3$pzpy)	vap	NPD/CBP : Ir/BCP/Alq$_3$	610	0.63, 0.37	8.8	14.5	5.0	566
139	Ir(4′Fpiq)$_3$	vap	NPD/CBP : Ir/BCP/Alq$_3$	610	0.61, 0.38	5.81	10.4	3.8	516
140	(4′MeOpiq)$_2$Ir(acac)	vap	NPD/CBP : Ir/BCP/Alq$_3$	611	0.65, 0.33	4.9[d]	12.8	6.58	567
141	(PPQ)$_2$Ir(acac)	vap	NPD/CBP : Ir/BCP/Alq$_3$	613	0.65, 0.35	10.4	15.2	7.5	562

142	$(4'PhPPQ)_2Ir(acac)$	vap	NPD/CBP : Ir/BCP/Alq_3	613	0.66, 0.34	6.0	9.1	4.9	562
143	$(4'-(Ph_2N)PPQ)_2Ir(acac)$	vap	NPD/CBP : Ir/BCP/Alq_3	616	0.67, 0.33	9.0	12.2	7.5	562
144	$(btp)_2Ir(acac)$	vap	NPD/CBP : Ir/BCP/Alq_3	616	0.68, 0.32	7.0	–	4.6	375
145	$(btp)_2Ir(acac)$	vap	NPD/CBP : Ir/BCP/Alq_3	617	0.68, 0.33	6.5	–	2.2	376
146	$(btp)_2Ir(acac)$	vap	PEDOT/TCTA/DFC : Ir/BCP/Alq_3	620	–	9	–	4	545
147	$(btp)_2Ir(acac)$	vap	PEDOT/TCTA/SSS : Ir/BCP/Alq_3	620	–	8.6	–	4.0	45
			PEDOT/TCTA/TST : Ir/BCP/Alq_3			10		4.0	
148	$(3'5'F_2\text{-}5Fpiq)_2Ir(acac)$	vap	NPD/CBP : Ir/BCP/Alq_3	617	0.66, 0.33	5.48	7.55	2.63	515
149	$(pqxn)_2Ir(tBupzpy)$	vap	NPD/CBP : Ir/BCP/Alq_3	618	0.62, 0.34	8.1	13.0	4.1	566
150	$(MPEQ)_2Ir(acac)$	vap	TNATA/NPD/CCP : Ir/BCP/Alq_3	620	0.65, 0.34	4.96	6.93	2.49	519
151	$(4Mepiq)_2Ir(acac)$	vap	NPD/CBP : Ir/BCP/Alq_3	620	0.66, 0.33	5.8[d]	12.3	6.44	567
152	$(4'\text{-}5Me_2piq)_2Ir(acac)$	vap	NPD/CBP : Ir/BCP/Alq_3	620	0.67, 0.33	10.3[d]	21.96	11.5	568
153	$Ir(piq)_3$	vap	NPD/CBP : Ir/BPhen	620	0.68, 0.32	10.3	–	8.0	108
154	$Ir(piq)_3$	vap	NPD/TCTA : Ir/BCP : Ir/Alq_3	628	–	3.6[d]	6.0	–	569
155	$(4'\text{-}7Me_2piq)_2Ir(acac)$	vap	NPD/CBP : Ir/BCP/Alq_3	621	0.66, 0.33	9.4[d]	19.91	10.42	568
156	$(7Mepiq)_2Ir(acac)$	vap	NPD/CBP : Ir/BCP/Alq_3	622	0.64, 0.35	5.6[d]	11.87	6.21	568
157	$(piq)_2Ir(acac)$	vap	NPD/CBP : Ir/BCP/Alq_3	624	0.68, 0.32	3.78	7.83	–	517
158	$(piq)_2Ir(acac)$	vap	NPD/CBP : Ir/BCP/Alq_3	630	0.68, 0.32	9.21	8.22	2.34	516
159	$(5Mepiq)_2Ir(acac)$	vap	NPD/CBP : Ir/BCP/Alq_3	622	0.67, 0.33	4.6[d]	9.84	5.15	567
160	$(5Mepiq)_2Ir(acac)$	vap	NPD/CBP : Ir/BCP/Alq_3	624	0.68, 0.32	4.19	8.91	–	517
161	$(PEQ)_2Ir(acac)$	vap	TCTA/CPB : Ir/BCP/Alq_3	624	0.66, 0.33	7.23	9.21	3.67	519
162	$(4'Fpbq)_2Ir(acac)$	vap	NPD/CBP : Ir/BCP/Alq_3	631	0.65, 0.33	5.63	4.20	1.5	516
163	$(5Fpiq)_2Ir(acac)$	vap	NPD/CBP : Ir/BCP/Alq_3	632	0.68, 0.31	10.2	9.39	4.15	515
164	$(2\text{-}niq)_2Ir(acac)$	vap	NPD/CBP : Ir/BCP/Alq_3	633	0.70, 0.30	2.27	3.79	–	517
165	$(3'5'F_2phqn)_2Ir(acac)$	vap	NPD/CBP : Ir/BCP/Alq_3	634	0.68, 0.32	2.42	2.24	0.83	570
166	$Ir(G1p\text{-}dend\text{-}btp)_3$	sol/vap	CBP : Ir/TBPI	634	0.67, 0.30	4.25	–	1	563
167	$(5Br\text{-}btp)_2Ir(acac)$	sol	PEDOT/neat-Ir	635	–	0.002	–	–	61
168	$(4'6'F_2phqn)_2Ir(acac)$	vap	NPD/CBP : Ir/BCP/Alq_3	638	0.68, 0.32	2.04	1.70	0.60	570
169	$(4'Mepiq)_2Ir(acac)$	vap	NPD/CBP : Ir/BCP/Alq_3	638	0.67, 0.30	3.1[d]	3.96	2.07	567
170	$(NPPQ)_2Ir(acac)$	vap	NPD/CBP : Ir/BCP/Alq_3	642	0.71, 0.29	2.1	1.6	0.60	562
171	$(4'Fphqn)_2Ir(acac)$	vap	NPD/CBP : Ir/BCP/Alq_3	650	0.69, 0.31	1.93	1.07	0.47	570
172	$(PEIQ)_2Ir(acac)$	vap	NPD/CBP : Ir/BCP/Alq_3	652	0.67, 0.30	3.16	1.69	0.85	519
173	$(phqn)_2Ir(acac)$	vap	NPD/CBP : Ir/BCP/Alq_3	668	0.70, 0.30	1.89	0.58	0.26	570
174	$(btp\text{-}FO_5)_2Ir(acac)$	sol	PEDOT/neat-Ir	670	–	0.150	–	–	61
175	$(btp\text{-}FO_{10})_2Ir(acac)$	sol	PEDOT/neat-Ir	670	–	0.200	–	–	61
176	$(btp\text{-}FO_{20})_2Ir(acac)$	sol	PEDOT/neat-Ir	670	–	0.450	–	–	61
177	$(btp\text{-}FO_{40})_2Ir(acac)$	sol	PEDOT/neat-Ir	670	–	1.500	–	–	61
178	$(1\text{-}niq)_2Ir(acac)$	vap	NPD/CBP : Ir/BCP/Alq_3	680	0.70, 0.27	0.38	0.24		517

[a]Structures for the materials are given in Figure 38. Unless otherwise stated all $Ir(C\hat{}N)_3$ complexes are facial isomers.
[b]OLED preparation method: vapor deposited = vap, solution deposited = sol.
[c]Definitions of the acronyms used here are given in Figure 39.
[d]The quantum efficiency was only given in cd A^{-1} units. The % efficiency listed here was estimated by approximating the EL spectrum as a Gaussian lineshape with a 70 nm full width at half maximum intensity centered at the reported λ_{max}.

Table 7 OLED performance parameters for polymer-based devices, utilizing organoiridium emitters

Entry	*Emitter*[a] $Ir(C^N)_3$, $(C^N)_2Ir(L^X)$	*Method*[b]	*Device structure*[c] *ITO anode, metal cathode*	*EL* λ_{max} (nm)	*CIE*	*EQE* (%)	cd A^{-1}	lm W^{-1}	*References*
1	$Ir(dpbic)_3$	sol/vap	PEDOT/PMMA : Ir/BCP	400	0.16, 0.06	1.5	–	–	449
2	$(ppy)_2Ir(P(n\text{-}Bu)_3)CN$	sol/vap	PEDOT/PVK : Ir/BCP/Alq_3	467	0.22, 0.40	1.4	–	1.0	571
3	$(4'6'F_2ppy)_2Ir(pic)$	sol/vap	PEDOT/PVK : Ir/BCP	474	0.18, 0.36	0.96	–	0.69	493
4	$(4'6'F_2ppy)_2Ir(pic)$	sol	PEDOT/PVK : OXD7 : Ir	475	0.16, 0.37	5.9	–	6.4	572
5	$(4'6'F_2ppy)_2Ir(pic)$	sol	PEDOT/PVK : OXD7 : Ir	497	0.17, 0.30	6.4[d]	14	–	573
6	$(4'6'F_2ppy)_2Ir(pic\text{-}styryl)$	sol/vap	PEDOT/co-PVK : OXD7 : co-Ir/BAlq	475	–	6.6	5.5	–	574
7	$(4'6'F_2ppy)_2Ir(pic\text{-}styryl)$	sol/vap	PEDOT/co-PVK : OXD7 : co-Ir/BAlq	475	–	3.5	4.1	–	575
8	$(4'6'F_2ppy)_2Ir(pic\text{-}styryl)$	sol/vap	PEDOT/co-PVK : OXD7 : co-Ir/BAlq	475	0.18, 0.38	6.5	–	9.1	576
9	$Ir(4'5'F_2ppy)_3$	sol/vap	PVK : PBD : Ir/Alq_3	510	–	2.8	8.5	–	577
10	$Ir(pppy)_3$	sol	PEDOT/PVK : PBD : Ir	510	–	11.2[d]	30.4	13.7	578
11	$Ir(ppy)_3$	sol	PEDOT/PVK : OXD7 : Ir	514	0.31, 0.60	10.5[d]	31	–	573
12	$Ir(ppy)_3$	sol/vap	PEDOT/PVK : Ir/TAZ/Alq_3	510	–	1.9	–	2	579
13	$Ir(ppy)_3$	sol/vap	PEDOT/PVK : Ir/TAZ/Alq_3	510	–	1.9	–	2	580
14	$Ir(ppy)_3$	sol/vap	PVK : OXD7 : Ir/BCP/Alq_3	515	–	7.5	–	5.8	581
15	$Ir(ppy)_3$	sol	PEDOT/co-Cbz–oxadiazole : Ir	515	–	7.8[d]	23	–	582
16	$Ir(ppy)_3$	sol	PEDOT/PVK : Ir	515	–	10.5	37.3	–	583
17	$Ir(ppy)_3$	sol	PEDOT/TDAPB : PBD : Ir	515	–	8.2	29	17.3	584
18	$Ir(ppy)_3$	sol	PEDOT/PVK : Ir/TAZ/Alq_3	515	–	6	–	–	585
			PEDOT/PFHP : Ir/TAZ/Alq_3			0.4			
19	$Ir(ppy)_3$	sol/vap	API : Ir/Alq_3	515	–	7	–	–	586
20	$Ir(ppy)_3$	sol	PEDOT/PVK/PF : Ir	515	–	0.90	3.9	–	587
21	$Ir(ppy)_3$	sol/vap	PVK : PBD : Ir/TBPI/Alq_3	515	–	8.5	30.1		588
22	$Ir(ppy)_3$	sol	PVK/CNPPP : Ir	515	0.33, 0.58	2.7	6.5		589
23	$Ir(ppy)_3$	sol/vap	PEDOT/PVK : Ir/BAlq	516	–	10.1	34.1	7.3	590
24	$Ir(ppy)_3$	sol	PEDOT/PVK : PBD : Ir	516	–	4.0[d]	12.7	–	591
			PEDOT/PF : Ir	520		1.2[d]	3.9		
25	$Ir(ppy)_3$	sol/vap	PEDOT/PVK : Ir/BCP	517	0.32, 0.61	4.9	–	6.3	493
26	$Ir(ppy)_3$	sol/vap	PEDOT/PVK : PBD : Ir/BCPac/Alq_3	520	–	8.0	28.1	6.0	592
27	$Ir(ppy)_3$	sol/vap	PEDOT/PVK : PBD : Ir/TBPI	520	–	3.9[d]	12.5	–	593
28	$Ir(ppy)_3$	sol/vap	PEDOT/PVK : Ir/TBPI	520	–	6.1	22.1	–	594
29	$(ppy)_2Ir(4'vinylppy)$	sol	co-PVK : co-Ir	512	–	4.4	–	5.0	595
30	$Ir(4'Meppy)_3$	sol	PEDOT/PVK : PBD : TPD : Ir	515	–	10.7	38	24	596
31	$Ir(4'Meppy)_3$	sol	PEDOT/PVK : PBD : Ir	515	–	7.6	27	14.1	597
32	$Ir(4'n\text{-}butylppy)_3$	sol	PVK/CNPPP : Ir	515	0.33, 0.58	5.1	12		589
33	$Ir(4'n\text{-}octylppy)_3$	sol	PEDOT/PVK : PBD : Ir	518	–	5.0[d]	16.0	–	591
34	$Ir(4'n\text{-}octylppy)_3$	sol	PEDOT/PF : Ir	518	–	1.9[d]	6.2	–	591
35	$(ppy)_2Ir(acac)$	sol	PEDOT/PVK : PBD : Ir	516	–	4.1[d]	13.0	–	591
36	$(ppy)_2Ir(acac)$	sol/vap	PVK : PBD : Ir/BCP/Alq3	516	0.28, 0.65	4.2	15.4	–	598

37	$(ppy)_2Ir(acac)$	sol	PEDOT/PVK/PF–Ir	515	–	0.95	4.1	–	591
			PEDOT/PF : Ir	526		1.1[d]	4.1		
38	(ppy)-Ir(acac-styryl)	sol/vap	PEDOT/co-PVK : OXD7 : co-Ir/BAlq	523	–	11	40.3	–	574
39	$(ppy)_2Ir$(acac-styryl)	sol/vap	PEDOT/co-PVK : OXD7 : co-Ir/BAlq	523	–	9	30	–	575
40	$(ppy)_2Ir$(acac-vinyl)	sol	PEDOT/co-TPD : co-PBD : co-Ir	527	–	11.8	–	38.6	91
41	$Ir(BHPP\text{-}ppy)_3$	sol	PVK/PBD : Ir	520	–	1.5	3.6	–	599
42	$Ir(DPPP\text{-}ppy)_3$	sol	PVK/PBD : Ir	520	–	0.4	0.7	–	599
43	$(ppy)_2Ir(Ac)$	sol/vap	PVK : TPD : Ir/BCP/Alq_3	530	–	4.5[d]	16.5	8.3	600
44	$Ir(PDPP)_3$	sol/vap	PEDOT/PVK : BlueJ : Ir/BCP	530	–	8.9	32	–	601
45	$Ir(CNPP\text{-}ppy)_3$	sol	PVK/PBD : Ir	530	–	0.7	1.6	–	599
46	$Ir(5\text{-}(Ph_2N)ppy)_3$	sol	PEDOT/PVK : TBPI : NPD : Ir	530	–	6.8[d]	25.2	4.7	602
47	$(4'\text{-}(p\text{-}tBuPh_2N)ppy)_2Ir(acac)$	sol	PEDOT/PVK : PBD : Ir	533	–	10.4	17.1	–	603
48	$Ir(DPF)_3$	sol	PEDOT/PVK : PBD : Ir	546	–	3.3[d]	12[e]	–	604
49	$Ir(DPF)_3$	sol	PEDOT/PVK : PBD : Ir	550	–	3.3[d]	12[e]	–	605
50	$(bzq)_2Ir(acac)$	sol	PVK : PBD : Ir	548	0.41, 0.57	1.9	6.9	–	598
51	$(pbiH)_2Ir(acac)$	sol/vap	PVK : Ir/BCP/Alq_3	548	–	5.8	21.5	–	606
52	$Ir(DPPF)_3$	sol	PEDOT/PVK : PBD : Ir	550	–	2.7[d]	9.6[e]	–	607
53	$Ir(DPPF)_3$	sol	PEDOT/PVK : PBD : Ir	550	–	8	29	–	604
54	$Ir(DPPF)_3$	sol	PEDOT/PVK : PBD : Ir	550	–	8	29	3.3	608
55	$(bt)_2Ir(acac)$	sol	PEDOT/PVK/PF-Ir	556	–	1.0	3.0	–	587
56	$(bt)_2Ir(acac)$	sol/vap	PVK : PBD : Ir/BCP/Alq_3	557	0.50, 0.49	3.2	9.5	–	598
57	$(bt)_2Ir(acac)$	sol/vap	PEDOT/PMOT : Ir/PBD	560	–	0.2	–	–	609
58	$(bt)_2Ir(acac)$	sol/vap	PEDOT/PMOT : Ir/PBD	560	–	0.7	–	–	610
59	$(bt)_2Ir(acac)$	sol	PEDOT/PVK : PBD : Ir	560	–	1.8[d]	8.0	–	591
			PEDOT/PF : Ir	560		0.7[d]	3.0		
60	$(bt)_2Ir(acac)$	sol/vap	PEDOT/PVK : Ir/BCP	565	0.50, 0.47	1.5	–	1.1	493
61	$(ppy)_2Ir(bpy)$	sol/vap	PEDOT/PVK : PBD : Ir/TBPI	560	–	5.2[d]	22.5	–	593
62	$(4'CF_3bt)_2Ir(acac)$	sol/vap	PEDOT/PVK : Ir/Alq_3	576	0.53, 0.46	0.8[d]	3.3	–	611
63	$(napy)_2Ir(CF_3acacCz)$	sol	PEDOT/PBD : co-PF–co-Cz–co-Ir	580	–	1.1	1.2	–	612
64	$(PQ)_2Ir(CF_3acacCz)$	sol	PEDOT/PBD : co-PF–co-Cz–co-Ir	580	–	2.8	3.1	–	612
65	$(CNPP\text{-}tpy)_2Ir(acac)$	sol	PVK/PBD : Ir	580	–	1.3	1.5	–	599
66	$(Fnapy)_2Ir(acac)$	sol	PVK/CNPPP : Ir	590	–	0.45	–	–	613
67	$(napy)_2Ir(acac)$	sol	PVK/CNPPP : Ir	590	–	1.24	–	–	613
68	$(ppy)_2Ir(bpyOAE)$	sol	PEDOT/PVK : PBD : Ir	593	–	0.012	–	–	614
69	$[(ppy)_2Ir]_2(bpy_2Ph_4)$	sol	PEDOT/PVK : Ir	595	–	0.07[d]	0.23	–	593
70	$Ir(HFP)_3$	sol	PEDOT/PVK : PBD : Ir	600	–	1.9[d]	2.4[e]	–	604
71	$Ir(HFP)_3$	sol	PEDOT/PFO : Ir	600	–	1.5[d]	2.1[e]	–	604
72	$Ir(HFP)_3$	sol	PEDOT/PF3CNP1 : Ir	600	–	1.5	3	–	615
73	$Ir(HFP)_3$	sol	PEDOT/PVK : PBD : Ir	600	–	1.7[d]	2.4[e]	–	616
74	$(BSN)_2Ir(acac)$	sol/vap	PVK : PBD : Ir/BCP/Alq_3	606	0.62, 0.34	1.5	2.1	–	598
75	$(PPQ)_2Ir(acac)$	sol/vap	PEDOT/PVK : PBD : Ir/TBPI	606	0.61, 0.37	6.1	11.6	–	617

(*Continued*)

Table 7 (Continued)

Entry	*Emitter*[a] Ir(C^N)$_3$, (C^N)$_2$Ir(L^X)	*Method*[b]	*Device structure*[c] *ITO anode, metal cathode*	*EL* λ_{max} (nm)	*CIE*	*EQE* (%)	cd A^{-1}	lm W^{-1}	*References*
76	(PPQ)$_2$Ir(acac)	sol/vap	PEDOT/PVK : PBD : Ir	610	–	3.2[d]	8.5	–	619
77	(piq)$_2$Ir(acac)	sol	PVK/CNPPP : Ir	610	–	0.07	–	–	613
78	(piq)$_2$Ir(acac)	sol	PEDOT/PVK/PFO(poss) : PBD : Ir	624	0.67, 0.33	2.4	1.04	–	619
79	(piq)$_2$Ir(CF$_3$acacCz)	sol	PEDOT/PBD : co-PF–co-Cz–co-Ir	610	–	4.9	4.0	–	612
80	(btp)$_2$Ir(acac)	sol/vap	PVK : PBD : Ir/BCP/Alq$_3$	612	0.66, 0.33	2.8	3.5	–	598
81	(btp)$_2$Ir(acac)	sol	PEDOT/PVK/PF : Ir	614	–	2.0	1.9	–	587
82	(btp)$_2$Ir(acac)	sol	PEDOT/PVK : PBD : Ir	614	–	1.0[d]	2.6	–	591
			PEDOT/PF : Ir	614		0.7[d]	1.9		
83	(btp)$_2$Ir(acac)	sol	PEDOT/PVK : PBD : Ir	614	0.66, 0.33	3.3	–	–	620
			PEDOT/PVK/PF : Ir			2.4			
84	(btp)$_2$Ir(acac)	sol	BDOHPF : LiOTf : Ir	616	–	0.2[d]	0.42	0.38	621
85	(btp)$_2$Ir(acac)	sol	PEDOT/PVK : OXD7 : Ir	619	0.66, 0.33	2.0[d]	4.3	–	573
86	(btp)$_2$Ir(acac)	sol	PEDOT/PVK : Ir	620	–	3.1	2.6	–	583
87	(btp)$_2$Ir(acac)	sol	PEDOT/PVK : OXD7 : Ir	621	0.69, 0.31	5.2	–	1.9	572
88	(btp)$_2$Ir(acac)	sol/vap	PEDOT/PVK : Ir/BCP	623	0.67, 0.31	2.2	–	0.60	493
89	(btp)$_2$Ir(acac-vinyl)	sol/vap	PEDOT/co-PVK : OXD7 : co-Ir/BAlq	620	–	6.9	14.5	–	574
90	(btp)$_2$Ir(acac-vinyl)	sol/vap	PEDOT/co-PVK : OXD7 : co-Ir/BAlq	620	–	5.5	7.1	–	575
91	(btp)$_2$Ir(acac-vinyl)	sol/vap	PEDOT/co-PVK : OXD7 : co-Ir/BAlq	620	0.68, 0.32	6.9	–	2.9	576
92	(btp)$_2$Ir(acac(CH$_2$)$_{10}$PF)	sol	PEDOT/CzPFR–co-Ir	620	–	1.3[d]	2.8	–	622
93	(CF$_3$napm)$_2$Ir(tBupzpy)	sol	BTPD–Si–PFCB/PF–TPA–OXD : Ir/TBPI	620	0.65, 0.34	7.9	–	3.3	623
94	(FPPQ)$_2$Ir(acac)	sol/vap	PEDOT/PVK : PBD/TBPI	627	0.68, 0.32	10.3	11.0	–	617
95	Ir(piq)$_3$	sol	PEDOT/PVK : TDAPB : PBD	630	0.65, 0.34	6.3	–	3.0	624
96	(Phqnx)$_2$Ir(CF$_3$pzpy)	sol/vap	PEDOT/PVK : PBD/TBPI	640	0.64, 0.31	3.15	–	–	625

[a]Structures for the materials are given in Figure 38. All Ir(C^N)$_3$ complexes are facial isomers.
[b]OLED preparation method: vapor deposited = vap, solution deposited = sol.
[c]Definitions of the acronyms used here are given in Figures 39 and 40.
[d]The quantum efficiency was only given in cd A^{-1} units. The % efficiency listed here was estimated by approximating the EL spectrum as a Gaussian lineshape with a 70 nm full width at half maximum intensity centered at the reported λ_{max}.
[e]The authors used an integrating sphere to measure the external efficiencies based on the total light emitted. A correction factor of 3 is applied to make the values comparable to the other external efficiencies listed here (see Section 12.04.2.2).

Table 8 OLED performance parameters for devices utilizing organoplatinum compounds

Entry	*Emitter*[a]	*Method*[b]	*Device structure*[c] *ITO anode, metal cathode*	*EL* λ_{max} (nm)	*CIE*	*EQE* (%)	cd A^{-1}	lm W^{-1}	*References*
1	(N^C^N)PtCl	vap	TNATA/BDTAPC/CBP:Pt/BCP	510	0.31, 0.63	11.2	40.2	–	626
2	(BPhen)Pt($C_6F_4CF_3$)$_2$	vap	NPD/CBP:Pt/BCP/Alq_3	516	0.30, 0.51	0.82	–	–	417
3	(BPhen)Pt(C_6F_5)$_2$	vap	NPD/CBP:Pt/BCP/Alq_3	519	0.33, 0.55	2.1	–	2.4	417
4	(BCP)Pt(C_6F_5)$_2$	vap	NPD/CBP:Pt/BCP/Alq_3	523	0.33, 0.51	0.91	–	–	417
5	(N^C^N)Pt(OPh)	vap	TNATA/BDTAPC/CBP:Pt/BCP	530	0.35, 0.63	16.5	67.1	–	626
6	(5,5-Me_2bpy))Pt(CCPh)$_2$	sol/vap	PVK:Pt/PBD	530	–	–	–	1.33	416
7	(ppy-OXD-TPA)Pt(acac)	vap	CuPc/neat-Pt	538	0.52.0.47	0.3[d]	1.2	–	627
8	(4′6′F_2ppy-CF_3)Pt(dpm)	vap	MPMP/neat-Pt/BPhen/Alq_3	540	–	0.3[d]	1.2	–	628
9	(Meppy(CF_3)$_2$)Pt(Ph_2P^O)	vap	MPMP/neat-Pt/BPhen/Alq_3	540	–	1.4[d]	6	–	628
10	(^{t}$Bu_2N_2O_2$)Pt	vap	NPD/$Bepp_2$:Pt	540	0.33, 0.47	–	–	1.44	629
11	(^{t}Bu_2C^N^N)Pt(CCC_6F_5)	vap	NPD/CBP:Pt/BCP/Alq_3	545	0.42, 0.53	0.2	1.9	–	415
12	(C^N^N)Pt(CCC_6F_5)	vap	NPD/CBP:Pt/BCP/Alq_3	548	0.44, 0.51	1.1	3.2	–	415
13	(salen)Pt-coPFO	sol	PEDOT/PF2-6:Pt	550	–	1.4[d]	6	–	103
14	(Me_4schiff)Pt	vap	NPD/CBP:Pt/BCP/Alq_3	550	0.48.0.52	11	31	14	630
15	(schiff)Pt	vap	NPD/$Bepp_2$:Pt	552	0.33, 0.35	–	–	10.79	630
16	(Prtmen)Pt	vap	NPD/CBP:Pt/BCP/Alq_3	560	0.51, 0.47	4.9	13.1	5.9	631
17	(Meppy(CF_3)$_2$)Pt(^{t}Bu_2P^O)	vap	MPMP/neat-Pt/BPhen/Alq_3	560	–	0.03[d]	0.15	–	628
18	(O^N^N)PtCl	vap	NPD/CBP:Pt/BCP/Alq_3	564	0.48, 0.50	0.7[d]	2.9	–	632
19	(O^N^N-^{t}Bu_2)PtCl	vap	NPD/CBP:Pt/BCP/Alq_3	564	0.50, 0.49	3.0[d]	13	–	632
20	(C^N^N)Pt(CCPh)	vap	NPD/CBP:Pt/BCP/Alq_3	564	0.48, 0.48	1.6	4.2	–	415
21	(C^N^N)Pt(CCPh)	vap	NPD/CBP:Pt/BCP/Alq_3	564	–	1.0[d]	4.2	–	633
22	(O^N^N-Me_2)PtCl	vap	NPD/CBP:Pt/BCP/Alq_3	565	0.51, 0.48	2.3[d]	9.7	–	632
23	(F-O^N^N-^{t}Bu_2)PtCl	vap	NPD/CBP:Pt/BCP/Alq_3	566	0.48, 0.51	1.9[d]	7.8	–	632
24	(C^N^N)Pt(CC^{t}Bu)	vap	NPD/CBP:Pt/BCP/Alq_3	567	0.48, 0.47	0.6	1.4	–	415
25	(PhOXD)$_2$Pt	sol	PEDOT/PVK/PVK:PBD:Pt	568	–	2.3	3.8	–	634
26	(F-O^N^N)PtCl	vap	NPD/CBP:Pt/BCP/Alq_3	572	0.53, 0.46	1.8[d]	7.3	–	632
27	(C^N^N)Pt(CCtol)	vap	NPD/CBP:Pt/BCP/Alq_3	574	–	0.3[d]	1.4	–	633
29	(C^N^N)Pt(CCtol)	vap	NPD/CBP:Pt/BCP/Alq_3	580	0.51, 0.47	0.6	1.4	–	415
28	(F-bt)Pt(acac)	vap	NPD/CBP:Pt/BCP/Alq_3	575	0.48, 0.51	6.6	16.0	6.6	635
30	Pt(thpy)$_2$	sol/vap	PVK:PBD:Pt/Alq_3	580	–	2.2	6.0	–	577
31	Pt(thpy)$_2$	sol/vap	PC:TPD:Pt/PBD	580	0.58, 0.42	5.4	–	–	636
32	(bt)Pt(acac)	vap	NPD/CBP:Pt/BCP/Alq_3	584	0.49, 0.50	5.5	14.3	5.7	635
33	(^{t}$Bu_2N_2O_2$)Pt	vap	NPD/$Bepp_2$:Pt	588	–	–	–	0.26	629
34	(^{t}Bu_2bpy)Pt(CCArCCH)$_2$	sol	PEDOT/PVK:Pt	590	–	0.29	0.65	–	637
35	[(^{t}Bu_2bpy)Pt(CCArCC)]$_4$	sol	PEDOT/PVK:Pt	590	–	0.46	0.93	–	637
36	Pt(thpy-$SiMe_3$)$_2$	sol/vap	PC:TPD:Pt/PBD	590	0.60, 0.39	11.5	–	–	636
37	(BIP)Pt(pyr)	sol/vap	PVK:Pt/PBD	592	0.35, 0.54	0.09[d]	0.31	–	638
38	(S^N^N)Pt(CCPh)	vap	NPD/CBP:Pt/BCP/Alq_3	608	–	0.3[d]	0.7	–	633
39	(S^N^N)Pt(CCPh)	vap	NPD/CBP:Pt/BCP/Alq_3	608	0.55, 0.33	0.6	0.7	–	415
40	(btp)Pt(acac)	vap	HMTPD/TBPI:Pt/Alq_3	610	0.67, 0.33	5.2	–	1.3	375
41	(S^N^N)Pt(CCtol)	vap	NPD/CBP:Pt/BCP/Alq_3	612	0.55, 0.31	0.8	1.0	–	415
42	(S^N^N)Pt(CCtol)	vap	NPD/CBP:Pt/BCP/Alq_3	612	0.59, 0.34	0.4[d]	1.0	–	633
43	Pt(iqdz)$_2$	vap	NPD/CBP:Pt/BCP/Alq_3	612	0.62, 0.37	12.8	19.8	12.4	639
44	(Pren)Pt	vap	NPD/CBP:Pt/BCP/Alq_3	620	0.65, 0.35	6.5	9.0	4.0	631
45	[(ppy)Pt(Spyr)]$_2$	vap	CuPc/NPD/neat-Pt/BAlq/Alq_3	670	0.65, 0.35	3.4	1.8	–	640
46	(4′6′F_2ppy)Pt(acac)	vap	PEDOT/NPD/neat-Pt/BCP	678	0.62, 0.36	2.7	1.7	1.8	641

[a]Structures for the materials used are given in Figure 41.
[b]OLED preparation method: vapor deposited = vap, solution deposited = sol.
[c]Definitions of the acronyms used here are given in Figures 39 and 40.
[d]The quantum efficiency was only given in cd A^{-1} units. The % efficiency listed here was estimated by approximating the EL spectrum as a Gaussian lineshape with a 70 nm full width at half maximum intensity centered at the reported λ_{max}.

Table 9 OLED performance parameters for devices utilizing organometallic emitting materials which do not contain either Ir or Pt

Entry	*Emitter*[a]	*Method*[b]	*Device structure*[c] *ITO anode, metal cathode*	*EL* λ_{max} (nm)	*CIE*	*EQE* (%)	cd A^{-1}	lm W^{-1}	*References*
	Al, Au								
1	Au(C^N^C)(CCPh-(NPh_2))	vap	TPD/CBP : Au/TPBI	515	–	5.5	17.6	14.5	642
2	Au(C^N^C)(CCPh)	vap	TPD/neat-Au/Alq_3	585	–	–	–	–	642
	B, Be, Cu								
3	BPh_2(F_2pyr-indole)	vap	NPD/neat-B	502	–	0.4[d]	0.82	–	643
4	BPh_2(pyr-aza)	vap	NPD/Cbz2/neat-B/Alq_3	490	0.20, 0.33	1.4[d]	2.34	–	644
5	BPh_2(pyr-aza)	vap	NPD/Cbz2/neat-B/Alq_3	490	0.20, 0.33	1.4[d]	2.34	–	645
6	BPh_2(pyr-aza)	vap	NPD/neat-B/Alq_3	515	0.28, 0.46	0.2[d]	0.57	–	644
7	BPh_2(pyr-aza)	vap	NPD/neat-B/Alq_3	515	0.28, 0.46	0.2[d]	0.57	–	645
8	Be(pyr-indole)$_2$	vap	NPD/neat-Be	515	0.31, 0.50	0.3[d]	1.06	–	644
9	$[CuN(SiMe_2)_2]_4$	vap	TPD/neat-Cu/OXD7	493	–	0.2	–	–	646
10	Cu_4(CCPh)$_2$(P^P)$_2$	sol/vap	PVK : Cu_4/TAZ	516	–	0.1	–	–	647
11	Cu_4(CCPh)$_2$(P^P)$_2$	sol	PVK : PBD : Cu_4	517	–	–	–	–	648
	Os								
12	Os(fptz)$_2$(PPh_2Me)$_2$	vap	BPAPF/CBP : Os/BCP/Alq_3	618	0.64, 0.35	15.3	21.3	6.3	649
13	Os(fppz)$_2$(PPh_2Me)$_2$	sol/vap	PEDOT/PFA-OXD : Os/TPBI	623	0.65, 0.34	9.3	12.65	–	650
14	Os(fppz)$_2$(PPh_2Me)$_2$	sol/vap	PVK : Os/F-TBB/Alq_3	626	0.65, 0.35	3.8[d]	7.0	–	651
15	Os(fppz)$_2$(PPh_2Me)$_2$	sol/vap	PVK : Os/PBD	626	–	2.4[d]	4.0	–	652
16	Os(fppz)$_2$($PPhMe_2$)$_2$	vap	PVK : Os/PBD	640	–	2.4[d]	3.0	–	652
17	Os(fppz)$_2$($PPhMe_2$)$_2$	sol/vap	PVK : Os/F-TBB/Alq_3	640	0.68, 0.32	2.8[d]	3.5	–	651
18	Os(fppz)$_2$($PPhMe_2$)$_2$	sol/vap	PS-TPD-TFV/PF-TPA-OXD : Os/TBPI	640	0.67, 0.33	12.8	8.4	2.7	653
19	Os(bptz)$_2$(PPh_2Me)$_2$	sol/vap	PVK : Os/PBD	658	–	1.6[d]	1.0	–	652
20	Os(bptz)$_2$(PPh_2Me)$_2$	sol/vap	PVK : Os/F-TBB/Alq_3	660	0.70, 0.30	1.9[d]	1.2	–	651
	Re								
21	$Re(CO)_3$(btpz)(bpy)	vap	NPD/CBP/TBPI : Re/TBPI	532	–	0.82	–	0.72	654
			NPD/CBP : Re/TBPI	530	0.32, 0.52	0.6	1.76	0.74	
22	$Re(CO)_3Cl$(bimpyr)	vap	TPD/neat-Re	600	–	0.09	–	0.9	655
23	$Re(CO)_3Cl$(bpy-TPA-OXD)	sol	PC : Re	675	–	0.1	–	–	656
24	$Re(CO)_3Cl$(co-phen)	sol	neat-(co-Re : co-PPV)	570	–	0.2	–	–	657
25	$Re(CO)_3Cl$(dmbpy)	vap	NPD/CBP : Re/BCP	557	0.36, 0.43	1.2[d]	5.1	–	658
26	$Re(CO)_3Cl$(dmfbpy)	vap	NPD/CBP : Re/BCP	608	–	0.5[d]	1.3	–	659
	$Re(CO)_3Cl$(dbufbpy)			608		0.4[d]	1.1		
27	$Re(CO)_3Cl$(dppz)	sol/vap	PEDOT/PVK : TPD : PBD : Re/PBD	580	–	0.03[d]	0.12	–	660
28	$Re(CO)_3Cl$(dppzCl_2)	sol/vap	PEDOT/PVK : TPD : PBD : Re/PBD	592	–	0.03[d]	0.12	–	660
29	$Re(CO)_3Cl$(dppzMe_2)	sol/vap	PEDOT/PVK : TPD : PBD : Re/PBD	570	–	0.03[d]	0.12	–	660
30	$Re(CO)_3Cl$(Me_2phen)	vap	NPD/CBP : Re/BCP	560	–	1.6[d]	7.15		661
31	$Re(CO)_3Cl$(phen)	vap	NPD/CBP : Re/BCP	560	–	1.5[d]	6.67		661
32	$Re(CO)_3Cl$(stilbene)	sol/vap	PVK : Re/BCP	630	–	0.5[d]	0.75	–	662
	Ru								
33	Ru(ifpz)$_2$(PPh_2Me)$_2$	vap	NPD/CBP : Ru/BCP/Alq_3	628	0.67, 0.33	4.44	5.08	2.36	663

[a]Structures for the materials used are given in Figure 42.
[b]OLED preparation method: vapor deposited = vap, solution deposited = sol.
[c]Definitions of the acronyms used here are given in Figures 39 and 40.
[d]The quantum efficiency was only given in cd A^{-1} units. The % efficiency listed here was estimated by approximating the EL spectrum as a Gaussian lineshape with a 70 nm full width at half maximum intensity, centered at the reported λ_{max}.

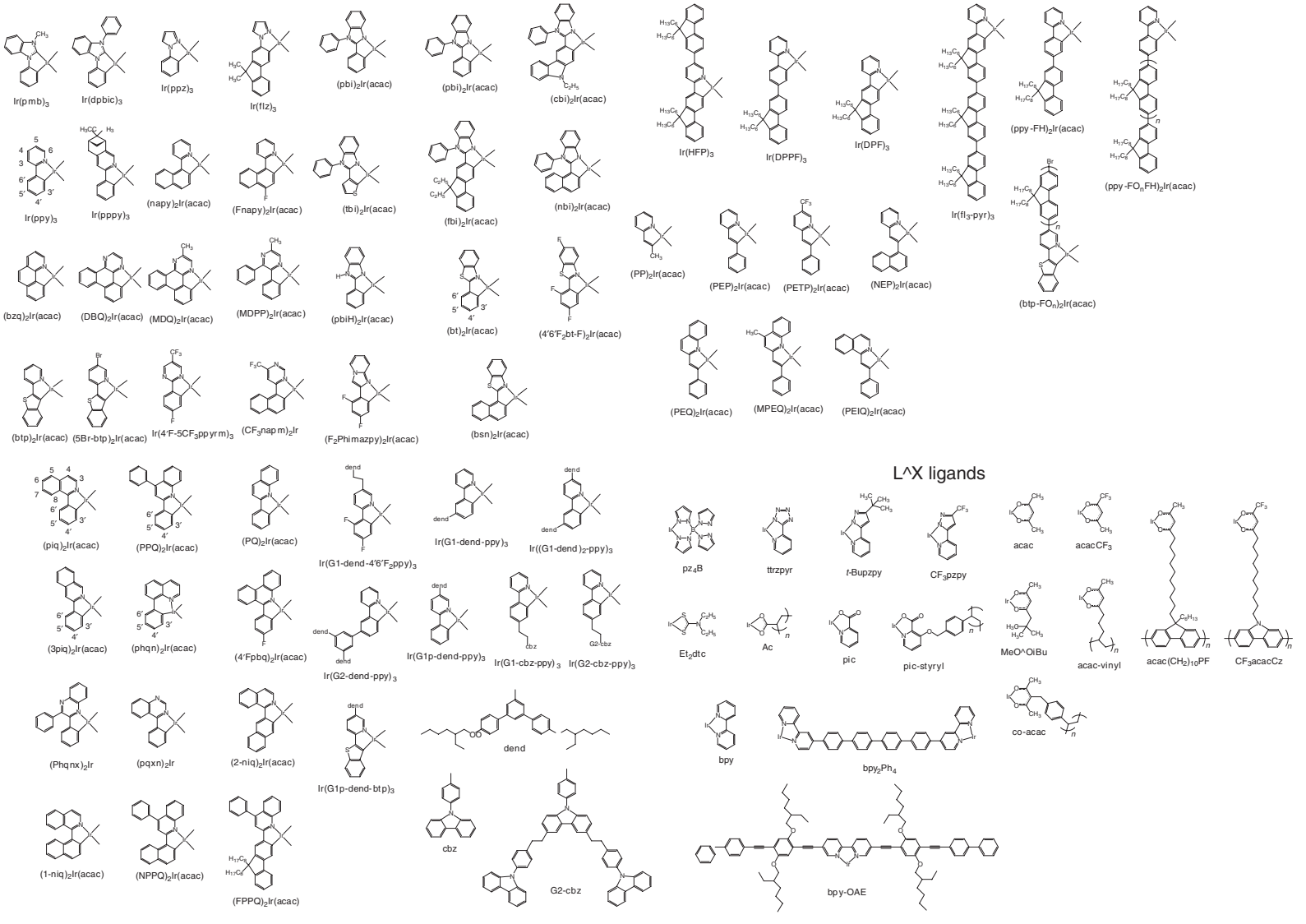

Figure 38 Ir complexes used in Tables 6 and 7.

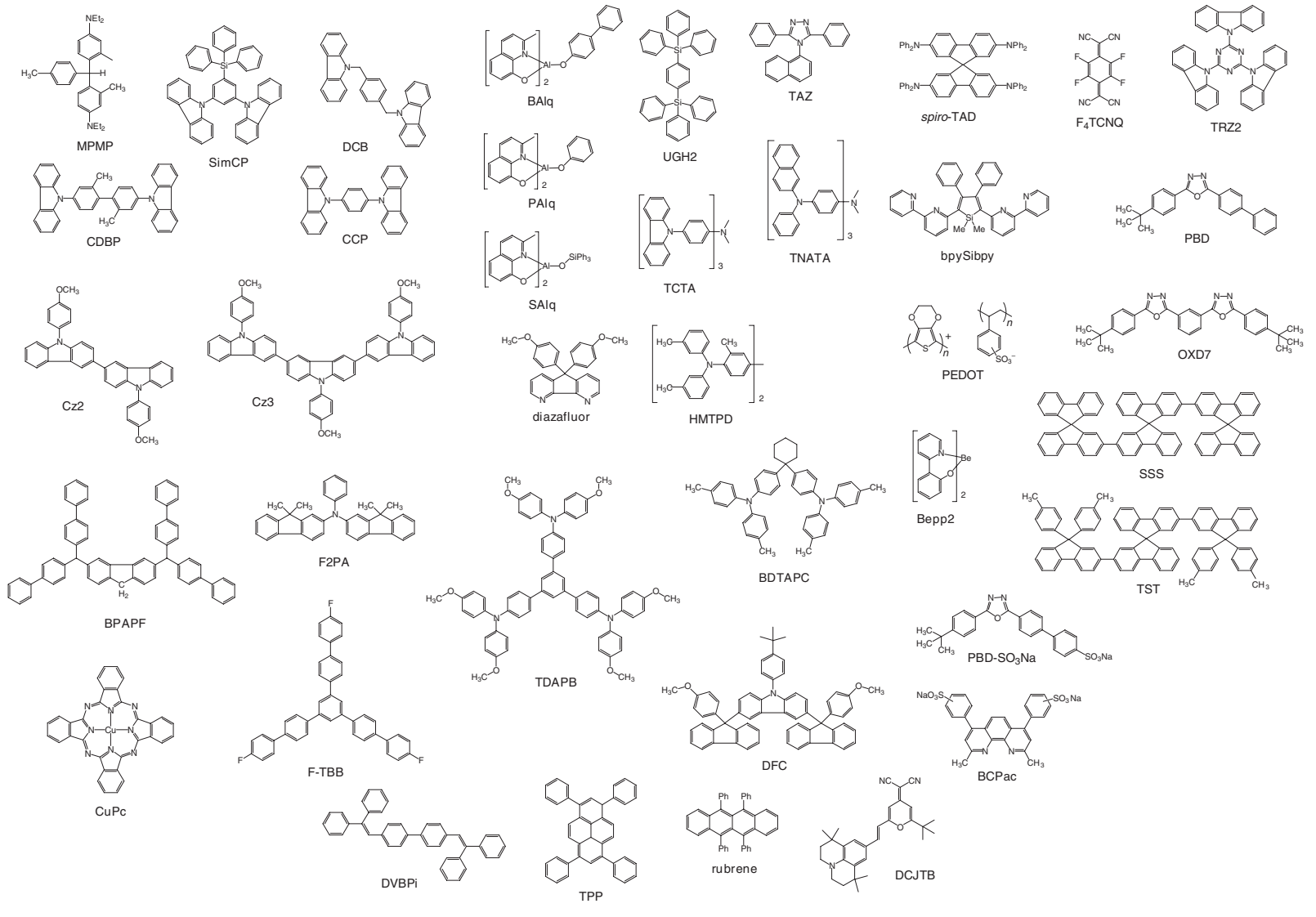

Figure 39 Molecular host materials used for electrophosphorescent devices.

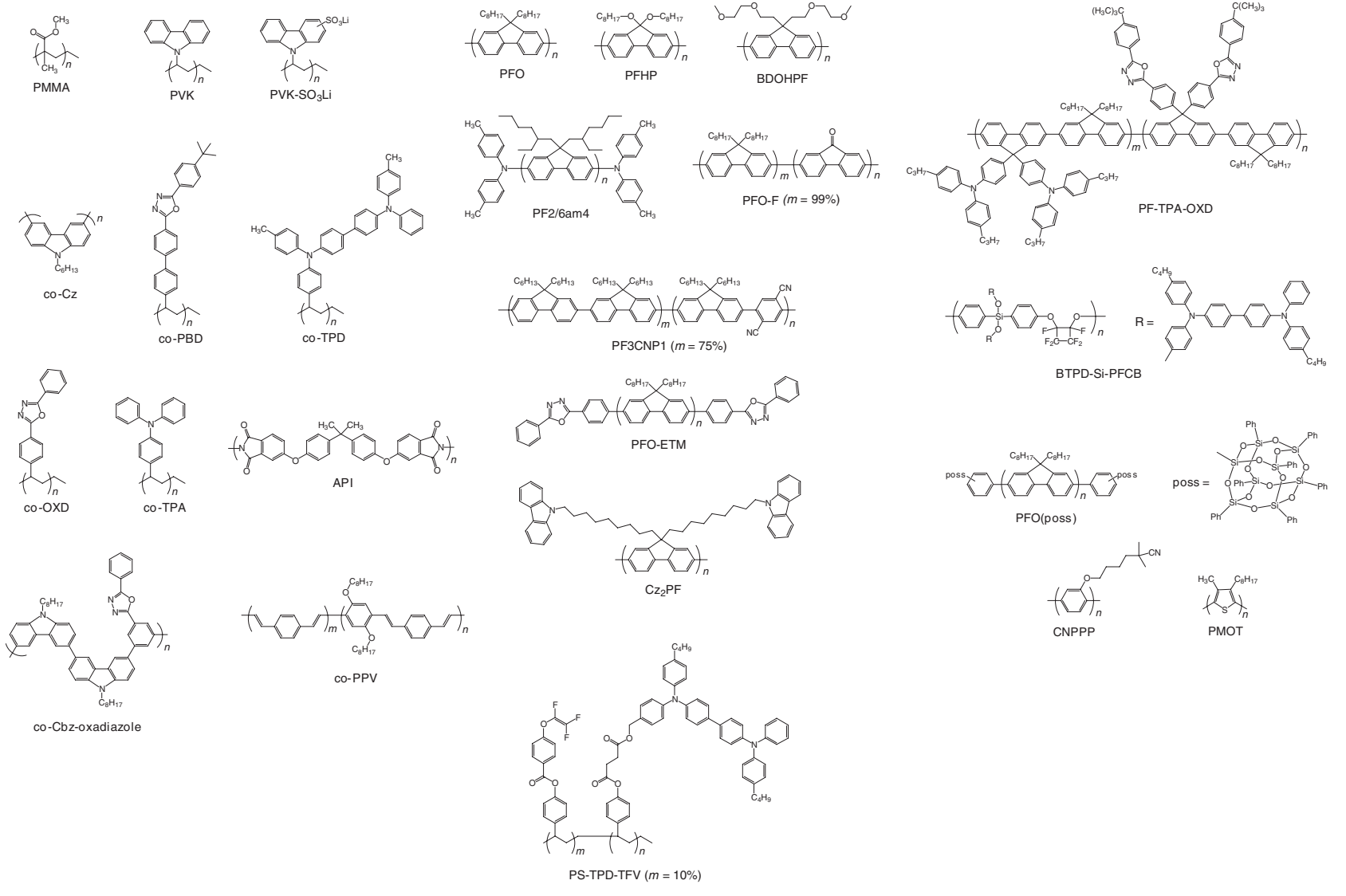

Figure 40 Polymeric host materials used in OLED devices.

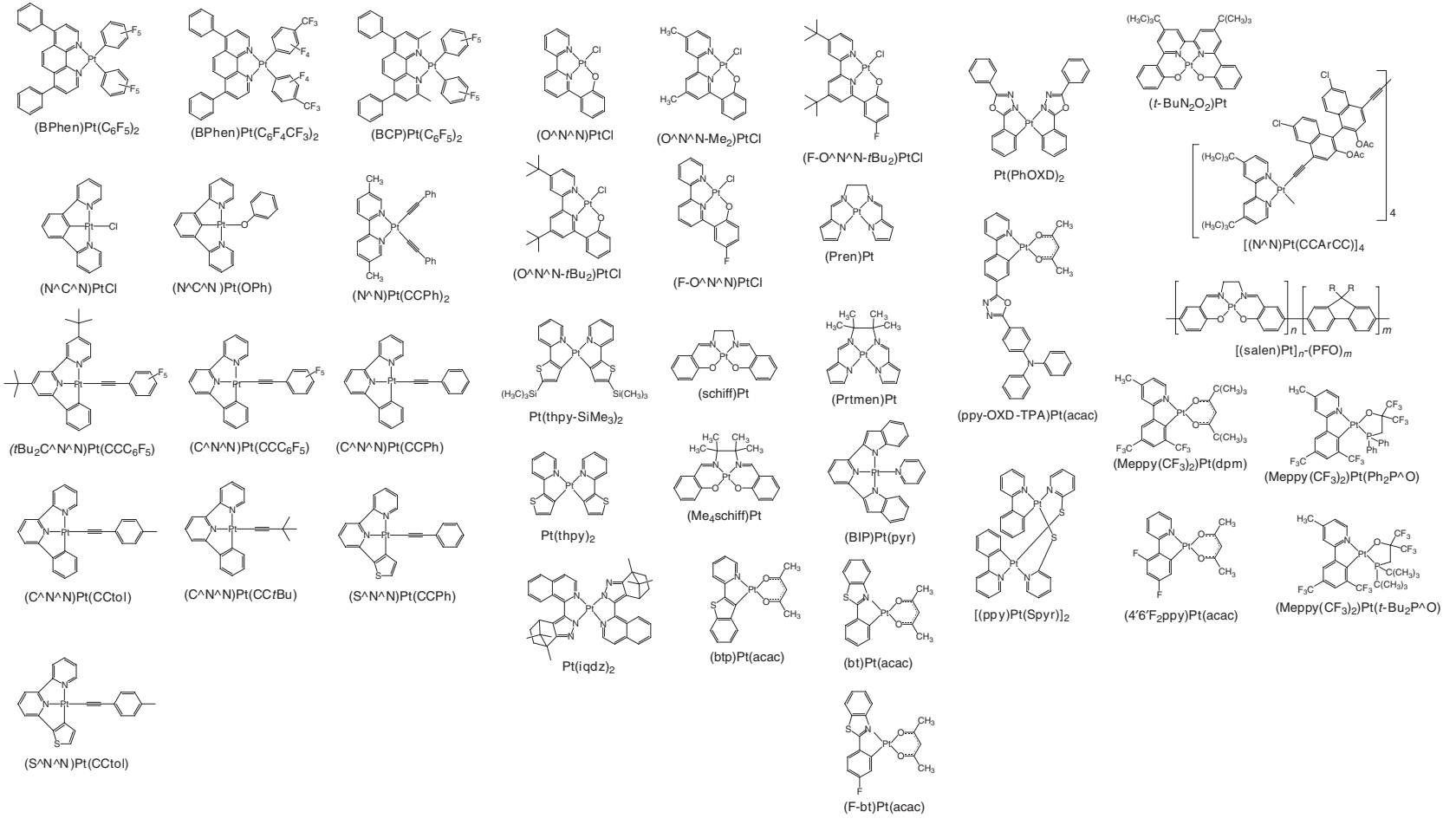

Figure 41 Pt complexes used in Table 8.

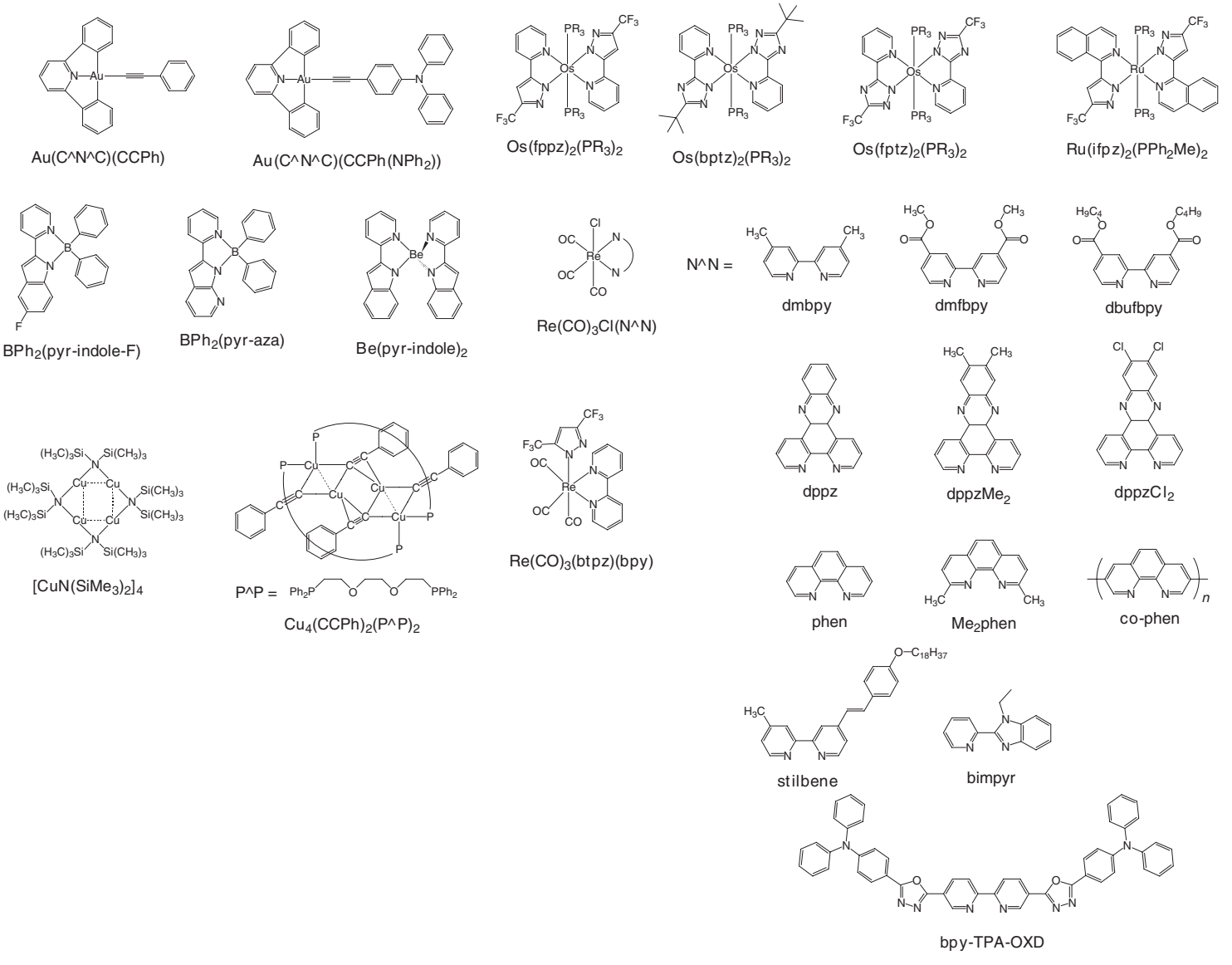

Figure 42 Organometallic complexes used in Table 9.

tables below. Tables 8 and 9 cover Pt and other metals, respectively, with both small molecule and polymer-based devices listed together. The device structures listed in the Tables 6–9 do not give the anode and cathode materials but typically employ ITO for the anode and either a co-deposited Mg–Ag alloy or LiF/Al as cathodes. The devices in the tables have been sorted on the basis of the peak wavelength for EL. Several different research groups have made OLEDs that use the same metal complex in a variety of different device configurations. For example, there are 42 devices in Tables 6 and 7 that use $Ir(ppy)_3$ as the emissive dopant. All of the data from devices with the same dopant, regardless of any difference in their emission λ_{max} values, have table 8 entries listed together for ease of comparison. The data used to create Tables 6–9 were taken only from literature reports, no devices from patents are included, and the literature reference for each device given in the last column of the table.

The first thing to note from the data in Tables 6–9 is that OLEDs with high quantum efficiency can be fabricated in nearly any visible color. The highest efficiencies are usually observed for devices using Ir complexes as dopants, likely due to the higher phosphorescence efficiency inherent for these species. For example, three devices have been reported that give nearly 100% internal quantum efficiency (entries 26, 32, and 67). High-efficiency devices have been reported for both small molecule- and polymer-based devices; however, the efficiencies are generally higher for the small molecule-based devices. It is also noteworthy that the majority of the devices have emission energies between 500 and 650 nm. The small number of OLEDs with blue to violet emission reflect the limited number of phosphorescent materials that emit at high energy, whereas few devices have emission wavelengths greater than 650 nm due to the paucity of complexes that emit strongly in the near-infrared.

The majority of the devices in Tables 6–9 have the emitter doped into a host matrix material. The various host matrix materials are shown in Figure 41. Devices with doped EMLs typically give higher efficiencies than comparable devices with EMLs composed of the neat emitter since the latter tends to lead to severe self-quenching. This effect is illustrated in $Ir(ppy)_3$-based devices in Section 12.04.2.3.3. The effect is further illustrated for a family of homoleptic emissive Ir complexes (Table 6, entries 21, 46, 51, 56, 73, 74, 76–82, 97, 110, 115, and 120). However, the inefficiencies caused by self-quenching can be ameliorated by using a neat emissive layer composed of an Ir complex that has cyclometallating ligands with a dendrimer-type structure. These complexes are comprised of an $Ir(ppy)_3$-type core and have branched aromatic dendrons on the periphery, as illustrated in Scheme 5. As the dendrons are made larger, they effectively isolate adjacent $Ir(ppy)_3$ molecules and inhibit self-quenching. This effect is clearly seen in comparing the devices given in Table 6 (entries 58, 60, and 65) to a related device made with a neat $Ir(ppy)_3$ emissive layer (Table 6, entry 45). The devices made with neat $Ir(ppy)_3$ and a neat complex with G1 dendrons give very similar efficiencies of 0.2%. An OLED made using a neat Ir complex with G2 dendrons, however, gives a 10-fold higher efficiency (2.1%) than the G1 analog. The steric shielding of the G2 dendrons markedly decreases self-quenching, thereby increasing device efficiency. The device with the G1 dendron Ir complex doped into CBP has the highest efficiency, similar to the efficiency in the analogous OLED doped with $Ir(ppy)_3$ (entry 24). A similar phenomenon is observed for the other complexes with dendrimer-type ligands (Table 6, entries 18, 52–55, 58–67, 90–92, 105, 126, 127, and 166).

Several of the devices listed in Table 6 give very high $lm\,W^{-1}$ values (entries 27–32), at EQE values similar to other devices in the table. The reason for this is that these devices have been designed to run at much lower operating

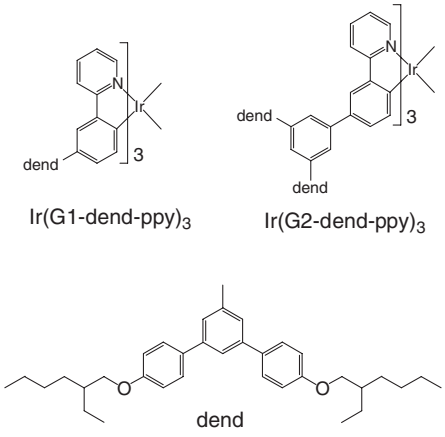

Scheme 5

voltages. The $\mathrm{lm\,W^{-1}}$ value reflects the drive voltage, such that a low drive voltage leads to a high $\mathrm{lm\,W^{-1}}$ value. In these devices the carrier transporting layers are doped with oxidizing (for HTL) and reducing (for ETL) agents to increase the number of charge carriers in these layers. The higher carrier population leads to a marked increase in the conductivity of the layer and thus, a lower voltage is required to pass a given current. More details about these doping effects can be found elsewhere.[466,467]

Performance data for monochromatic OLEDs where a luminescent Ir dopant is incorporated into polymer are given in Table 7. Polymer-based phosphorescent OLEDs have been reported with emission wavelengths that cover the entire visible spectrum, similar to the range observed for small molecule Ir-based OLEDs. In most electrophosphorescent polymer devices, the inert or carrier transporting polymer is doped with molecular materials that are chosen to show efficient emission and/or carrier transport. The best efficiencies are reported for devices with molecular emitters in non-conjugated polymers, where the Ir complex is either dispersed in the polymer matrix or covalently bound to the polymer chain. Whereas the small molecule devices are typically separated into well-defined HTL, EML, and ETL regions in heterostructure devices, the transporting and emissive materials are often mixed together into a single organic layer. For devices made with hole-transporting polymers, electron-transporting molecules such as oxidiazoles PBD or OXD7 are often dispersed in the polymer matrix along with the emissive dopant in order to achieve good carrier balance. The highest efficiencies, however, are still obtained from heterostructure devices with a separate ETL inserted between the polymer film and the cathode. Thus, a common device structure is ITO/(polymer + dopant + electron transporter)/ETL/cathode.

One of the most commonly used polymers in electrophosphorescent polymer OLEDs is poly(vinylcarbazole) (PVK). This material has excellent film-forming properties, a high glass transition temperature, good hole mobility ($10^{-5}\,\mathrm{cm^2\,V^{-1}\,s^{-1}}$)[468] and most importantly, high singlet and triplet energies. The high singlet and triplet energy for PVK are critical in achieving high efficiency. While conjugated polymers, such as poly(fluorenes) and poly(phenylenevinylenes), have been used extensively for fluorescence-based devices, they are not as useful for phosphorescence-based devices because they characteristically have low triplet energies. The triplet levels of most conjugated polymers are in the red to near-IR spectral region, and thus efficiently quench phosphorescence from dopants designed to emit in the visible part of the spectrum.[470]

A number of OLEDs have been reported which utilize platinum organometallic emitters, Table 8. While high-efficiency devices have been reported, the efficiencies of the Pt-based devices tend to be lower than their Ir-based counterparts. This is due to a number of factors. The Pt complexes tend to have lower PL efficiencies, limiting overall OLED efficiency. The Pt complexes also tend to have longer radiative lifetimes than their Ir counterparts, and are thus expected to experience higher levels of T–T annihilation. Moreover, the Pt complexes used to date are all square-planar complexes, which tend to aggregate in doped films. This effect has been used to make broadband emitters (discussed in the section on white OLEDs); however, the aggregation may enhance self-quenching at the doping levels required to make an efficient OLED.

The only metals other than Ir and Pt that have been used to fabricate high-efficiency OLEDs ($\eta_{ext} > 5\%$) are Ru, Au, and Os. While this table represents a significant number of devices, there has not been a systematic approach to studying devices with metals other than Ir or Pt. The efficiencies of these devices are directly related to their high phosphorescence efficiencies. The trends seen above carry into these devices as well; the highest efficiencies are observed for devices with good carrier balance (heterostructured device) and high dopant luminance efficiency.

12.04.2.5.2 Light-emitting electrochemical cells

A light-emitting electrochemical cell (LEC) is similar to an OLED; however, the method of fabrication of the single heterostructure device and its mode of action is somewhat different. The first example of a solid-state LEC utilized a spin-cast polymer blend sandwiched between two electrodes.[215,216] The polymer blend was comprised of a mixture of a semiconducting luminescent polymer and a salt ($Li^+CF_3SO_3^-$) dissolved in an ion-conducting polymer, polyethylene oxide (PEO). When an external bias is applied, the polymer is both oxidized (p-type doping) at the anode and reduced at the cathode (n-type doping). The ions redistribute within the organic film to compensate for the charge build-up due to polymer doping; Li^+ cations concentrate near the cathode and $CF_3SO_3^-$ anions near the anode. The function of the PEO is to facilitate the transport of charge-compensating ions to the p- and n-doped regions. Thus, once the ion redistribution is complete, a device is formed that can be described as anode/HTL/ETL/cathode, very similar to a simple single heterostructure OLED. This slow ion redistribution leads to a significant time delay between when a bias is applied and light emission is observed, since electron–hole recombination only occurs at the newly formed p–n junction. This process is reversible, such that when the bias is removed, the p- and n-doping is

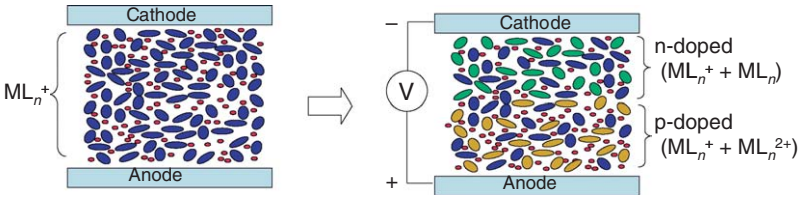

Figure 43 Schematic representation of p-n junction formation in an LEC.

lost and the ions return to a homogeneous distribution within the film. Luminance values of 200 cd m^{-2} at 4 V and external quantum efficiencies as high as 2% have been reported for this system.[215,216,470,471]

Tris-chelate complexes made with either Ru(II) or Os(II) and diimine ligands have been used as active materials in solid-state LECs.[472–484] Organometallic complexes derived from $(ppy)_2Ir(diimine)^+$ and a number of $(ppz)_2Ir(diimine)^+$ complexes (see Figure 36) have also been used to make LECs. The Ir complexes are more versatile in terms of color tunability[90,113,397,485,486] and device efficiency,[487,488] than the Ru and Os species. The LECs made with these cationic complexes have several advantages over devices made with semiconducting polymers. The metal complexes can be synthesized and purified with relative ease, show excellent electrochemical, photochemical, and thermal stability, have good charge transport properties, and often possess high photoluminescence efficiencies. The positive charges on the complexes are typically compensated by negatively charged counterions such as PF_6^- or ClO_4^-. Therefore, LECs based on these metal complexes do not require the presence of an added electrolyte or an ion-conducting polymer, which makes the device architecture simpler than LECs using conjugated polymers. A schematic representation of the process involved in the formation of a p–n junction in the LEC is shown in Figure 43. During operation, the anions migrate into the p-doped region, similar to what occurs in polymer-based LECs. However, the n-doping process occurs by reduction of the metal complex, and hence cation migration into the n-doped region is not required. This simplified redistribution process results in a short turn-on time in these devices, which ranges from several seconds to minutes.[472–484]

Table 10 gives LEC performance data for devices using the organometallic complexes described in Figure 37. Comparative data is also given for devices made with Os and Ru diimine complexes. The devices that use the $Ru(bpy)_3$ cation have a range of compositions of the metal salt layer and cathode materials (Table 10, entries 2–4). These factors affect the EL spectra, turn-on times, and the ultimate EQE values of the devices. The efficiencies given for these Ru complexes are good, but fall within the range accessible with fluorescent dopants. The identity of the counterion strongly affects the turn-on time, with the shortest times being observed for the smallest ions (Table 10, entry 4). This result is consistent with the picture presented above, which requires anion redistribution to occur for LECs to function efficiently.

Organometallic LECs are listed in entries 5–11 in Table 10, and all use $(C\hat{}N)_2Ir(N\hat{}N)^+PF_6^-$ complexes. The anode for all of these devices was ITO-coated glass, while the cathode is a vacuum-deposited metal. The LECs reported with organometallic complexes $(C\hat{}N)_2Ir(N\hat{}N)^+$ have a simple structure, with a single organometallic layer (ITO/PEDOT/organometallic cation salt/cathode). The PEDOT layer serves two functions in these devices; the first being to act as an efficient hole-injecting electrode, whereas the second is to make the surface less hydrophilic, and thus retard crystallization of the organometallic salt on spin coating. If the organometallic salt film is prepared without the PEDOT layer, the crystallized film leads to the formation of unstable devices.

The EL spectra of LECs closely match the PL spectra of the same materials, as neat thin films. The EL and PL spectra of three different LECs are shown in Figure 44. ITO makes a better anode than cathode in LECs, evidenced by the improved efficiency when the device is run in forward bias (entries 5 and 6 in Table 10). The identity of the metal cathode material also affects the device properties and turn-on times. Cs–Al gives shorter turn-on times and higher efficiencies than devices prepared with Au cathodes (entries 7 and 8 in Table 10). Lastly, through systematic changes in the C^N and N^N ligands, it is possible to tune the EL emission between blue and red (entries 9–11 in Table 10). While the efficiencies for organometallic LECs can be quite high (e.g., entries 9 and 10 in Table 10), their lifetimes are comparatively short. LEC lifetimes typically range from minutes to hours,[475,489] whereas small molecule-based electrophosphorescent OLEDs can have lifetimes $>10^6$ hours.[490] The details of the LEC degradation are not well known, although it has been shown that a principal source of decay is the formation of quenching sites within the emissive material of the film, a process that is accelerated by the presence of residual solvent.[478,491]

Table 10 LEC performance parameters

	Compound[a]		*Note*	λ_{max} (nm)	*CIE coord.* (x, y)	*Turn-on time*[b] (min)	*Peak EQE* (%)	*References*
1	$[Os(bpy)_2L]2$		Au as cathode	610	0.59, 0.41	3@6 V 90@3 V	1.1@6 V	483
2	$[Ru(bpy)_3]2$		–	609	NG	NG	0.5@3 V	484
3	$[Ru(bpy)_3]2$		blended with PMMA	630	NG	0.05@5 V	5.5@5 V	474
4	$[Ru(bpy)_3]$ $Y_2Y = BF_4^-$, ClO_4^-, PF_6^-, AsF_6^-		Ga-In cathode	660	NG	0.001–0.25	2.5@3 V	481
	$(C^\wedge N)_2Ir(N^\wedge N)X$							
	C^N	N^N						
5	ppy	dtb-bpy	Forward bias[c]	560	0.43, 0.55	120@3 V ~30@6 V	5@3 V	488
6	ppy	dtb-bpy	Reverse bias	580	0.49, 0.50	NG	<5@3 V[d]	488
7	F-mppy	dtb-bpy	Au cathode	542	0.37, 0.58	240@−3 V	0.15@3 V 1.1@−3 V	487
8	F-mppy	btb-bpy	Cs/Al cathode	542	0.37, 0.58	40@3 V	1.8@3 V	487
9	ppz	btb-bpy	Al Cathode	542	0.37, 0.59	35@3 V	6.9@e3 V	451
10	ppz	biq	Al Cathode	635	0.67, 0.32	32@3 V	7.4@3 V	451
11	$4,6F_2$ppz	btb-bpy	Al Cathode	492	0.20, 0.41	30@3 V	4.6@3 V	451

[a]Abbreviations given for the C^N and N^N ligands are given in Figure 41, X = PF_6^-, L = *cis*-1,2-bis(diphenylphosphino)-ethylene, NG = not given in the publication.
[b]The definitions for turn-on time varied between different labs, but it is basically the time before light emission is detected, ca. 1 Cd m^{-2}.
[c]Forward bias is defined as ITO = anode.
[d]The efficiency was not given for this device; however, the authors stated that the device efficiency was less than that observed in forward bias.

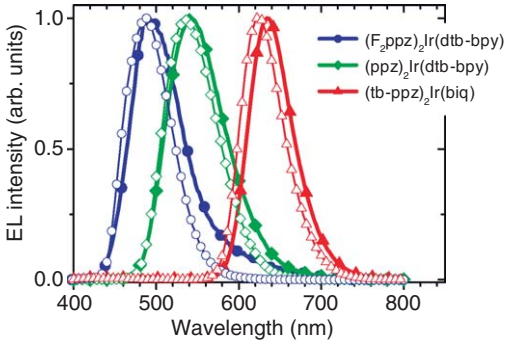

Figure 44 PL and EL spectra of $(ppz)_2Ir(diimine)^+$ complexes.

12.04.2.6 White OLEDs

Another potential application for LEDs is in illumination. The requirements for devices that serve as illumination sources are somewhat different than the monochromatic OLEDs described above. OLEDs targeted for RGB displays have to give electroluminescent spectra with a relatively narrow line shape centered on the peak wavelength. On the other hand, an illumination source is meant to approximate the blackbody solar spectrum and needs to have a broad line shape with roughly equal intensity across the entire visible spectrum. Therefore, in order to attain complete coverage across the visible spectrum, an OLED used for illumination purposes typically employs multiple emitters are that are either co-deposited into a single emissive layer or distributed into different layers or regions of the device. A number of the different device architectures have been reported to achieve efficient white EL and are discussed below.

Table 11 White OLED structures and best case performance of each

Architecture	η_{ext} (%)[a]	η_p (lm/W)[b]	*CIE*[c]	*CRI*	*References*
Phosphorescent triple-doped emissive layer	12	26, 42	(0.43, 0.45)	80	664
Multilayer phosphorescent	12	10, 17	(0.35, 0.36)	≤60	665
Phosphorescent excimer/aggregate	6.4	12.2, 21	(0.36, 0.44)	67	503
Multi-emissive phosphor doped layers	5.2	6.4, 11	(0.37, 0.40)	83	500
Interlayer sequential energy transfer	0.5	0.35, 0.6	(0.33, 0.33)	≤70	666
Hybrid polymer/inorganic	1.9	0.63, 1.1	(0.34, 0.29)	≤70	667
Three neat emissive layers	0.7	0.5, 0.9	(0.31, 0.41)	≤80	247

[a]Maximum reported forward viewing external quantum efficiency.
[b]Maximum reported forward viewing external power efficiency is the first number. The second is the total external power efficiency. Where not reported, it is the maximum forward viewing external power efficiency multiplied by 1.7 that assumes a small area contact (see text).
[c]Commission Internationale de l'Eclairage coordinates at 100 cd m^{-2}.

The important performance parameters used in assessing an OLED as an illumination source include its CIE coordinates and power efficiency in lum/W. These are the standard industry metrics used to characterize illumination sources ranging from incandescent light bulb to fluorescent tube sources. In addition to these two parameters, the color-rendering index (CRI) is also an important quality used for characterizing white light sources. The CRI is a measure of how well the light source approximates sunlight.[492] A score of 100 is a perfect match to the solar spectrum, although a value of 80 or above is considered a good quality illumination source that will be nearly indistinguishable from sunlight.

Most white organic LEDs (WOLEDs) utilize luminescence from several different colored emitters such that the combined output covers the visible spectrum uniformly. While WOLEDs with less than three distinct emitters have been reported, the most common approach in WOLEDs is to use all three, that is, blue, green, and red. One of the simplest device architectures involves mixing blue, green, and red dopants into a single emissive layer, such that the sum of the three emission spectra covers the visible spectrum.[493–495] The use of phosphorescent emitters in a triple doped emissive layer can then lead to highly efficient devices (Table 11). However, using three dopants in a single layer is problematic because energy readily transfers from the higher-energy blue dopant to the green dopant and from the green dopant to the red dopant. Therefore, careful adjustment of the concentration of each dopant is required to achieve a well-balanced emission color, with doping levels in the ratio blue > green >> red. In order to get well-balanced white emission, the doping level of the red dopant typically needs to be well below 1%.

One solution to the interdopant energy-transfer problem is to segregate the dyes into different layers. Efficient WOLEDs have been prepared using this stacked concept with either fluorescent[380,496–499] or phosphorescent emitters.[500] More simplified structures have also been described that use dual component fluorescent blue and orange emitters doped into separate layers.[380,501] While stacking the emitters in separate layers eliminates these energy-transfer problems, the device architecture can become significantly more complicated due to difficulties in achieving balanced carrier recombination and exciton localization within each of the emitting layers.

An alternate approach to the design of a WOLED takes advantage of the unique photophysics of organometallic platinum complexes, combining monomer and excimer/aggregate phosphorescence in a single emissive layer.[502,503] This dual emitting layer is formed spontaneously in a doped thin film, due to the range of dopant–dopant distances in the amorphous doped film. At low doping levels, only single molecule emission is observed, with the expected vibronic fine structure. As the concentration is increased, a new, strongly red-shifted band appears at roughly 580 nm (Figure 45). The new band displays a Gaussian-shaped peak, as expected for excimer or aggregate emission. Excimers involve the formation of excited state dimers.[504–508] An excimer is only bound in the excited state, and rapidly dissociates to two discrete molecules after relaxation to the ground state. In contrast, aggregates are bound in the ground state, typically through the formation of weak Pt···Pt bonds. Aggregates of this type have been observed both in solution[504–506,508–510] and in the solid state.[509] The aggregate structures seen in crystallographic studies can range in length from dimers to continuous chains.[510] Emission from these aggregate structures is attributed to a $^3[\pi^* \rightarrow d\sigma^*]$ (MMLCT: metal–metal to ligand charge transfer) transition. The emission spectra observed from both excimer and oligomer states are typically broad and unstructured, falling at lower energy than emission from the monomeric species. Unfortunately, differentiating between excimer and aggregate excited states in solution or doped

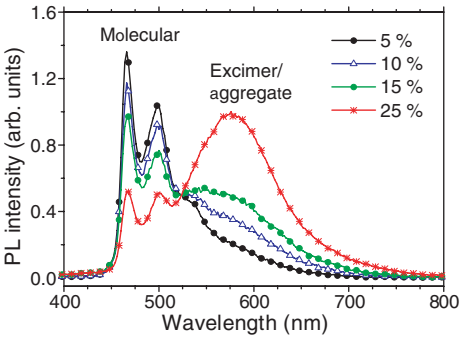

Figure 45 PL of (4′6′F_2ppy)Pt(acac) doped mCP films as a function of concentration. The weight percentage of (4′6′F_2ppy)Pt(acac) ranged from 5 to 25%, as indicated in the graph legend.

thin films is problematic, thus, the description of the low-energy species in the doped films is referred to as an excimer/aggregate.

A broadband emission profile can be observed from simultaneous emission by both monomer and aggregate species if the concentration of the Pt complex is properly adjusted. One benefit of this approach is that the breadth of the excimer/aggregate spectrum makes it possible to achieve good CIE and CRI values for a device with only two emitting centers, monomer and excimer. An intermediate doping level (3–5 wt.%) is a good value to use for white OLEDs, as both monomer and aggregate emission are then observed from a single doped film (Figure 45). The ratio of molecular to excimer/aggregate emission at a given doping level is also markedly affected by the steric bulk of the alkyl groups on the β-diketonate ligand.[503] The greater the steric bulk of the β-diketonate, the higher the doping level needs to be to get the proper ratio of monomer/aggregate in order to achieve balanced white emission.

An additional feature needs to be discussed with regard to WOLEDs (Table 12). Devices with a general structure ITO/NPD/CBP:dopant/BCP/Alq_3/LiF/Al have proved to be very effective for monochromatic phosphorescent OLEDs. The hole-blocking layer (BCP) used to confine both carriers and excitons to the luminescent layer prevents hole and exciton leakage into the electron-transporting layer (Alq_3), as discussed in Section 12.04.2.3.2. OLEDs of the general structure ITO/NPD/CBP : (4′6′F_2ppy)Pt(L^X)/ BCP/Alq_3/LiF/Al have been shown to emit white light from a single dopant luminescent layer.[502] Unfortunately, while these devices give the desired white emission (CIE = 0.33 0.31; CRI = 86), the EL spectra have a significant contribution from NPD emission (see Figure 46). The NPD emission is voltage dependent, which is indicative of poor charge confinement, and leads to decreased WOLED efficiency. The cause of this NPD emission is leakage of either electrons or excitons from the luminescent layer into the NPD layer. Blue phosphorescent dopants tend to have high LUMO energies that are comparable to those of the transport and host materials, shown in Figure 46. If the dopant and NPD have comparable LUMO energies, electrons can leak into the NPD layer. Likewise, exciton leakage into the HTL layer can occur when the emission energy of the dopant approaches the absorption energy of NPD. Eliminating electron/exciton leakage into the HTL should improve both the WOLED efficiency and color stability. Therefore, introduction of an electron/exciton-blocking layer (EBL) between the HTL and luminescent layer was deemed necessary to improve device characteristics. The cyclometallated complex, *fac-tris*(1-phenylpyrazolato-$N,C^{2'}$)iridium(III) [Ir(ppz)$_3$], makes an excellent EBL in these WOLED structures. The spectra of a single dopant WOLED, with an Ir(ppz)$_3$ EBL, shows no NPD emission. The quantum efficiency of the device with an EBL was 3.3%, a factor of 2 higher than the same device structure without the Ir(ppz)$_3$ EBL (peak efficiency = 1.9%).[502]

The use of the mCP host in place of CBP significantly improves the performance of WOLEDs. The efficiency, current–voltage characteristics, and spectra of a device are shown in Figure 46. High doping concentrations and improved energy transfer from mCP to the dopant lead to a maximum quantum efficiency of $6.4 \pm 0.6\%$ ($12.2 \pm 1.4\,\mathrm{lm\,W^{-1}}$, $17.0\,\mathrm{cd\,A^{-1}}$) at low brightness levels ($1\,\mathrm{cd\,m^{-2}}$) and $4.3 \pm 0.5\,\%$ ($8.1 \pm 0.6\,\mathrm{lm\,W^{-1}}$, $11.3\,\mathrm{cd\,A^{-1}}$) at $500\,\mathrm{cd\,m^{-2}}$. The quantum efficiency decreases with increasing current density, as observed for other devices;[361] however, the decrease is less severe than most other electrophosphorescent devices. If the Ir(ppz)$_3$ EBL is omitted (i.e., NPD/mCP : **1**/BCP/Alq_3), the EL spectrum again has a significant contribution from NPD and quantum efficiency of the devices drops by roughly a factor of 2. Overall, the Ir(ppz)$_3$ EBL increases the OLED efficiency, removes NPD emission from the spectra, and makes the spectrum independent of voltage.

Table 12 White OLED performance for organoiridium- and organoplatinum-based devices

Entry	*Emitter*[a]	*Method*[b]	*Device structure*[c] *ITO anode, metal cathode*	*EL* λ_{max} (nm)	*CIE*	*CRI*	*EQE*	lm W^{-1}	*References*
1	$Ir(ppy)_3$ DVBPi rubrene	vap	NPD/DVBPi/CBP:rubrene:Ir/BCP/Alq_3	460 510 560	0.30, 0.37	–	9.2 cd A^{-1}		668
2	$Ir(piq)_3$ TPP	vap	NPD/TCTA:TPP/BCP:Ir/Alq_3	464 628	0.34, 0.26	–	2.68 cd A^{-1}	–	669
3	$(4'6'F_2ppy)_2Ir(pic)$ DCJTB	vap	NPD/DCB:DCJTB:Ir/BPhen	472 580	0.33, 0.36	–	8.2 cd A^{-1}	–	670
4	$Ir(ppy)_3$ DCJTB	vap	NPD/CBP:DCJTB:Ir/BCP/Alq_3	520 568	0.33, 0.32	–	8.6 cd A^{-1}	–	671
5	$(4'6'F_2ppy)_2Ir(pz_4B)$ $Ir(ppy)_3$ $(PQ)_2Ir(acac)$	vap	NPD/TCTA/UGH2:Ir/TBPI	460 510 600	0.43, 0.45	80	12%	26	664
6	$(3'5'-(CF_3)_2ppy)_2Ir(pic)$ $(btp)_2Ir(acac)$	vap	PEDOT/NPD/CDBP:Ir/BAlq/CDBP:Ir/BAlq	472 620	0.35, 0.36	–	12%	10	665
7	$Ir(ppy)_3$ DCJTB	vap	NPD/CBP:DCJTB:Ir/BCP/Alq_3	436 520 568	0.43, 0.41	–	6.8 cd A^{-1}	–	674
8	$Ir(ppy)_3$ DCJTB	vap	NPD/CBP:DCJTB:Ir/BCP/Alq_3	436 520 568	0.34, 0.33	–	7.5 cd A^{-1}	–	673
9	$Ir(ppy)_3$ $(piq)_2Ir(acac)$	vap	MTDATA/NPD/TBPI:Ir/Alq_3	440 512 620	0.44, 0.44	–	15.3 cd A^{-1}	10.7	674
10	$(4'6'F_2ppy)_2Ir(pic)$ $(bt)_2Ir(acac)$ $(btp)_2Ir(acac)$	sol/vap	PEDOT/PVK:Ir/BCP	474 565 623	0.33, 0.41	77	2.1%	1.4	493
11	$(4'6'F_2ppy)_2Ir(pic)$ $(btp)_2Ir(acac)$	vap	PEDOT/NPD/CBP:Ir/BCP/CBP:Ir/BCP	472 620	0.35, 0.36	50	3.8%	3.6	500
12	$(4'6'F_2ppy)_2Ir(pic)$ $(bt)_2Ir(acac)$ $(btp)_2Ir(acac)$	vap	PEDOT/NPD/CBP:Ir/BCP	472 563 620	0.37, 0.40	83	5.2%	6.4	500
13	$Ir(4\text{-}tBuppy)_3$ $(piq)_2Ir(acacCF_3)$	sol	PEDOT/PVK/PFO(poss):Ir	424 510 610	0,33, 0.33		9 cd A^{-1}	5.5	675
14	$Ir(fl_3\text{-}pyr)_3$ PF2-6am4	sol	PEDOT/PF2-6am4:Ir	420 568	0.44, 0.46		2.6%		676
15	$(4'6'F_2ppy)_2Ir(pic\text{-}styryl)$ $(btp)_2Ir(acac\text{-}vinyl)$	sol/vap	PEDOT/co-PVK:OXD7:co-Ir/BAlq	475 620	0.34, 0.36		6.1%	5.2	576
16	$(4'6'F_2ppy)_2Ir(pic)$ $(btp)_2Ir(acac)$	sol	PEDOT/PVK:OXD7:Ir	475 621	0.33, 0.36	–	5.0%	3.3	574

17	$Ir(HFP)_3$ PFO	sol	PEDOT/PFO:Ir	420 600	0.33, 0.32	92	4.3 cd A^{-1}	1	677
18	$Ir(HFP)_3$ PFO PFO-F	sol	PEDOT/PFO:PFO-F:Ir	420 530 600	0.35, 0.39	86	3 cd A^{-1}	1	677
19	$Ir(HFP)_3$ PFO PFO-F	sol	PEDOT/PFO:PFO-F:Ir	420 530 600	0.35, 0.39	86	3 cd A^{-1}	1	678
20	$Ir(HFP)_3$ PFO-ETM	sol	PEDOT/PVK-SO_3Li/PFO-ETM:Ir/PBD-SO_3Na	420 600	0.33, 0.33	92	10.4 cd A^{-1}	3	679
21	$Ir(HFP)_3$ PFO-ETM PFO-F	sol	PEDOT/PVK-SO_3Li/PFO-ETM:PFO-F:Ir/PBD-SO_3Na	420 530 600	0.38, 0.40	86	7.2 cd A^{-1}	1.5	679
22	$Ir(ppy)_3$ DCM2	vap	TPD/CBP:DCM2/CBP:Ir/BCP/Alq_3	590	–	–	3.3%	–	680
23	$Ir(ppy)_3$ DCM2	vap	TPD/CBP:DCM2:Ir/BCP/Alq_3	600	–	–	9%	17	681
24	$(ppy)_2Ir(acac)$ Nile red	sol	PEDOT/PVK:PBD:Ir:Nile red	600	–	–	2.1%	–	682
25	$Ir(ppy)_3$ DCJTB	vap	NPD/TBPI:DCJTB:Ir/BCP/Alq_3	600	0.53, 0.45	–	8.1 cd/A	–	683
26	$Ir(ppy)_3$ $(btp)_2Ir(acac)$	sol/vap	PEDOT/PVK:Ir/BCP	623	0.66, 0.33	–	3.3%	1.2	493
27	$(4'6'F_2ppy)Pt(acac)$	vap	NPD/Irppz/mCP:Pt/BCP/Alq_3	468, 580	0.32, 0.40	6.4	17.0%	12.2	503
26	$(4'6'F_2ppy)Pt(acac)$	vap	F4-TCNQ:MTDATA/$Ir(ppz)_3$/mCP:Pt/BPhen/Bpen:Li	470, 580	0.35, 0.43	5.2	–	11	684
27	$(4'6'F_2ppy)Pt(acac)$ $(4'6'F_2ppy)_2Ir(pic)$	vap	PEDOT/NPD/CBP:Pt/BCP	468, 580	0.40.0.44	4.0	9.2%	4.4	502
28	$(4'6F_2ppy)Pt(MeO\text{^}OiBu)$	vap	PEDOT/NPD/CBP:Pt/BCP	468, 580	0.34, 0.35	1.9	–	2.5	502
29	$(4'6'F_2ppy)Pt(MeO\text{^}OiBu)$	vap	NPD/$Ir(ppz)_3$/CBP:Pt/BCP/Alq_3	468, 580	0.36, 0.44	3.3	–	7.3	503
30	$(4'6'F_2ppy)Pt(co\text{-}acac)$	sol/vap	PEDOT/co-TPA:co-OXD:co-Pt/BCP/Alq_3	500, 550	0.33.0.50	4.6	–	–	685

[a]Structures for the materials used are given in Figures 38 and 41. All the $Ir(C\text{^}N)_3$ complexes are facial isomers.
[b]OLED preparation method: vapor deposited = vap, solution deposited = sol.
[c]Definitions of the acronyms used here are given in Figures 39 and 40.

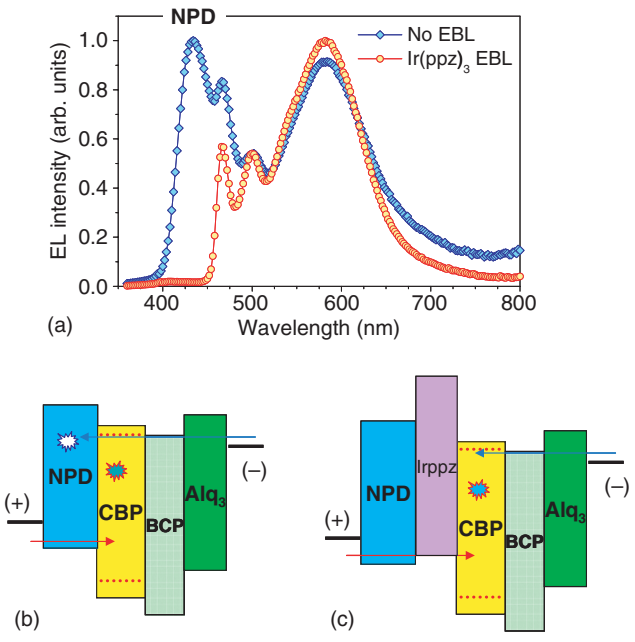

Figure 46 (a) Spectra for (4′6′F$_2$ppy)Pt(acac)-based OLEDs, with and without EBL (b) the electronic structures for the devices without and (c) with an EBL are shown below the spectra.

12.04.2.7 Conclusion

The advances made in the development of organic LEDs have been impressive since the initial report of a heterostructure device with an efficiency of 1%[301] to achieving an external efficiency of nearly 20% or higher.[379,511–513] This external efficiency corresponds to an internal efficiency of close to 100%. The key to achieving high efficiencies in these OLEDs is the organometallic dopant, which is the ultimate source of emission in these devices. The dopants that have been used to demonstrate high efficiency have phosphorescence efficiencies of nearly 100% in the solid state. This allows for efficient harvesting of both the singlet and triplet excitons that are generated in the electroluminescent process. Organometallic complexes are ideal candidates for this application, since many phosphoresce efficiently (particularly complexes of Ir) and ligand modifications can be used to tune the emission color to span a range from the near-UV to the near-IR. The highest efficiencies have been achieved for green emissive devices, but there is no reason that similar efficiencies could not be achieved for OLEDs of other colors. The future for organometallic complexes in organic LEDs is very bright. In addition to extending the ultrahigh efficiencies demonstrated for green devices to other colors, they will be key components in white emissive devices as well, where the emission energy and the spectral linewidth are both critical components in achieving both high efficiency and white color balance. Another area that organometallic complexes could play a significant role in OLEDs is as carrier-transporting materials. Very little work has been done to evaluate the stability and transporting properties of organometallic complexes in these devices. Overall, the field of EL is an excellent opportunity for the application of organometallic chemistry and materials to enhance efficiencies and stability of the devices.

References

1. Franken, P. A.; Hill, A. E.; Peters, C. W.; Weinreich, G. *Phys. Rev. Lett.* **1961**, *7*, 119.
2. Denk, W.; Strickler, J. H.; Webb, W. W. *Science* **1990**, *248*, 73.
3. So, P. T. C.; Dong, C. Y.; Masters, B. R.; Berland, K. M. *Ann. Rev. Biomed. Eng.* **2000**, *2*, 399.
4. Fisher, W. G. Partridge., W. P.; Dees, C.; Wachter, E. A. *Photochem. Photobiol.* **1997**, *66*, 141.
5. Spangler, C. W. *J. Mater. Chem.* **1999**, *9*, 2013.
6. Strickler, J. H.; Webb, W. W. *Proc. SPIE* **1990**, *1398*, 107.
7. Maruo, S.; Nakamura, O.; Kawata, S. *Opt. Lett.* **1997**, *22*, 132.

8. Cumpston, B. H.; Ananthavel, S. P.; Barlow, S.; Dyer, D. L.; Ehrlich, J. E.; Erskine, L. L.; Heikal, A. A.; Kuebler, S. M.; Lee, I.-Y. S.; McCord-Maughon, D.; Qin, J.; Röckel, H.; Rumi, M.; Wu, X.-L.; Marder, S. R.; Perry, J. W. *Nature* **1999**, *398*, 51.
9. Oudar, J. L. *J. Chem. Phys.* **1977**, *67*, 446.
10. Marder, S. R.; Perry, J. W.; Bourhill, G.; Gorman, C. B.; Tiemann, B. G.; Mansour, K. *Science* **1993**, *261*, 186.
11. Gorman, C. B.; Marder, S. R. *Proc. Natl. Acad. Sci. USA* **1993**, *90*, 11297.
12. Marder, S. R.; Gorman, C. B.; Meyers, F.; Perry, J. W.; Bourhill, G.; Brédas, J.-L.; Pierce, B. M. *Science* **1994**, *265*, 632.
13. Verbiest, T.; Houbrechts, S.; Kauranen, M.; Clays, K.; Persoons, A. *J. Mater. Chem.* **1997**, *7*, 2175.
14. Zyss, J.; Dhenaut, C.; Chauvan, T.; Ledoux, I. *Chem. Phys. Lett.* **1993**, *206*, 409.
15. Vance, F. W.; Williams, R. D.; Hupp, J. T. *Int. Rev. Phys. Chem.* **1998**, *17*, 302.
16. Kuzyk, M. G.; Dirk, C. W. *Phys. Rev. B* **1990**, *41*, 5098.
17. Oudar, J. L.; Chemla, D. S. *J. Chem. Phys.* **1977**, *66*, 2664.
18. Di Bella, S. *New J. Chem.* **2002**, *26*, 495.
19. Kurtz, S. K.; Perry, T. T. *J. Appl. Phys.* **1968**, *39*, 3798.
20. Whittall, I. R.; Cifuentes, M. P.; Costigan, M. J.; Humphrey, M. G.; Goh, S. C.; Skelton, B. W.; White, A. H. *J. Organomet. Chem.* **1994**, *471*, 193.
21. Chemla, D. S.; Oudar, J. L.; Jerphagnon, J. *Phys. Rev. B* **1975**, *12*, 4534.
22. Bethea, C. G. *Appl. Opt.* **1975**, *14*, 1447.
23. Hendrickx, E.; Clays, K.; Persoons, A. *Acc. Chem. Res.* **1988**, *31*, 675.
24. Clays, K.; Persoons, A. *Phys. Rev. Lett.* **1991**, *66*, 2980.
25. Morrison, I. D.; Denning, R. G.; Laidlaw, W. M.; Stammers, M. *Rev. Sci. Instrum.* **1996**, *67*, 1445.
26. Clays, K.; Wostyn, K.; Persoons, A. *Adv. Funct. Mater.* **2002**, *12*, 557.
27. Whittall, I. R.; McDonagh, A. M.; Humphrey, M. G.; Samoc, M. *Adv. Organomet. Chem.* **1998**, *42*, 291.
28. Whittall, I. R.; McDonagh, A. M.; Humphrey, M. G.; Samoc, M. *Adv. Organomet. Chem.* **1998**, *43*, 349.
29. Kanis, D. R.; Ratner, M. A.; Marks, T. J. *J. Am. Chem. Soc.* **1990**, *112*, 8203.
30. Kanis, D. R.; Ratner, M. A.; Marks, T. J. *J. Am. Chem. Soc.* **1992**, *114*, 10338.
31. Kanis, D. R.; Ratner, M. A.; Marks, T. J. *Chem. Rev.* **1994**, *94*, 195.
32. Hinchliffe, A.; Soscun, M. H. J. *Theochem* **1995**, *331*, 109.
33. van Hutten, P. F.; Hadziioannou, G.; Bursi, R.; Feil, D. *J. Phys. Chem.* **1996**, *100*, 85.
34. Matsuzaki, Y.; Nakano, M.; Yamaguchi, K.; Tanaka, K.; Yamabe, T. *Chem. Phys. Lett.* **1996**, *263*, 119.
35. McDonagh, A. M.; Whittall, I. R.; Humphrey, M. G.; Hockless, D. C. R.; Skelton, B. W.; White, A. H. *J. Organomet. Chem.* **1996**, *523*, 33.
36. Shigemoto, I.; Nakano, M.; Yamada, S.; Kiribayashi, S.; Yamanaka, S.; Yamaguchi, K. *Synth. Met.* **1997**, *86*, 2241.
37. Abe, J.; Nemoto, N.; Nagase, Y.; Shirai, Y.; Iyoda, T. *Inorg. Chem.* **1998**, *37*, 172.
38. Müller, T. J. J.; Netz, A.; Ansorge, M.; Schmälzlin, E.; Bräuchle, C.; Meerholz, K. *Organometallics* **1999**, *18*, 5066.
39. Raptis, S. G.; Papadopoulos, M. G.; Sadlej, A. J. *Phys. Chem. Chem. Phys.* **2000**, *2*, 3393.
40. Allis, D. G.; Spencer, J. T. *Inorg. Chem.* **2001**, *40*, 3373.
41. Cho, M.; An, S.-Y.; Lee, H.; Ledoux, I.; Zyss, J. *J. Chem. Phys.* **2002**, 9165.
42. Amatatsu, Y.; Ohara, Y. *Chem. Phys. Lett.* **2003**, *373*, 245.
43. Liyanage, P. S.; de Silva, R. M.; de Silva, K. M. N. *Theochem* **2003**, *639*, 195.
44. Alparone, A.; Millefiori, A.; Millefiori, S. *Chem. Phys.* **2004**, *298*, 75.
45. Ohnishi, S.; Gu, F. L.; Naka, K.; Imamura, A.; Kirtman, B.; Aoki, Y. *J. Phys. Chem. A* **2004**, *108*, 8478.
46. Mang, C.; Wu, K.; Zhang, M.; Hong, T.; Wei, Y. *Theochem* **2004**, *674*, 77.
47. Liao, Y.; Eichinger, B. E.; Firestone, K. A.; Haller, M.; Luo, J.; Kaminsky, W.; Benedict, J. B.; Reid, P. J.; Jen, A. K.-Y.; Dalton, L. R.; Robinson, B. H. *J. Am. Chem. Soc.* **2005**, *127*, 2759.
48. Kaatz, P.; Shelton, D. P. *J. Chem. Phys.* **1996**, *105*, 3918.
49. Kaatz, P.; Donley, E. A.; Shelton, D. P. *J. Chem. Phys.* **1998**, *108*, 849.
50. Willetts, A.; Rice, J. E.; Burland, D. M.; Shelton, D. P. *J. Chem. Phys.* **1992**, *97*, 7590.
51. Green, M. L. H.; Marder, S. R.; Thompson, M. E.; Bandy, J. A.; Bloor, D.; Kolinsky, P. V.; Jones, R. J. *Nature* **1987**, *330*, 360.
52. Coe, B. J.; Jones, C. J.; McCleverty, J. A.; Bloor, D.; Kolinsky, P. V.; Jones, R. J. *J. Chem. Soc., Chem. Commun.* **1989**, 1485.
53. Marder, S. R.; Perry, J. W.; Schaefer, W. P.; Tiemann, B. G. *Organometallics* **1991**, *10*, 1896.
54. Bunting, H. E.; Green, M. L. H.; Marder, S. R.; Thompson, M. E.; Bloor, D.; Kolinsky, P. V.; Jones, R. J. *Polyhedron* **1992**, *11*, 1489.
55. Benito, A.; Cano, J.; Martínez-Máñez, R.; Payá, J.; Soto, J.; JuIve, M.; Lloret, F.; Marcos, M. D.; Sinn, E. *J. Chem. Soc., Dalton Trans.* **1993**, 1999.
56. Coe, B. J.; Hamor, T. A.; Jones, C. J.; McCleverty, J. A.; Bloor, D.; Cross, G. H.; Axon, T. L. *J. Chem. Soc., Dalton Trans.* **1995**, 673.
57. O′Reilly, S. A.; White, P. S.; Templeton, J. L. *Chem. Mater.* **1996**, *8*, 93.
58. Lee, I. S.; Chung, Y. K.; Mun, J.; Yoon, C. S. *Organometallics* **1999**, *18*, 5080.
59. Balavoine, G. G. A.; Daran, J.-C.; Iftime, G.; Lacroix, P. G.; Manoury, E.; Delaire, J. A.; Maltey-Fanton, I.; Nakatani, K.; Bella, S. D. *Organometallics* **1999**, *18*, 21.
60. Iftime, G.; Balavoine, G. G. A.; Daran, J.-C.; Lacroix, P. G. Manoury, É. *C. R. Acad. Sci. Paris, Série IIc* **2000**, *3*, 139.
61. Chiffre, J.; Averseng, F.; Balavoine, G. G. A.; Daran, J.-C.; Iftime, G.; Lacroix, P. G.; Manoury, E.; Nakatani, K. *Eur. J. Inorg. Chem.* **2001**, 2221.
62. Mata, J. A.; Peris, E.; Llusar, R.; Uriel, S.; Cifuentes, M. P.; Humphrey, M. G.; Samoc, M.; Luther-Davies, B. *Eur. J. Inorg. Chem.* **2001**, 2113.
63. Davies, D. A.; Silver, J.; Cross, G.; Thomas, P. *J. Organomet. Chem.* **2001**, *631*, 59.
64. Roque, K.; Barangé, F.; Balavoine, G. G. A.; Daran, J.-C.; Lacroix, P. G.; Manoury, E. *J. Organomet. Chem.* **2001**, *637–639*, 531.
65. Huang, G.-S.; Liang, Y.-M.; Wu, X.-L.; Liu, W.-M.; Ma, Y.-X. *Appl. Organomet. Chem.* **2003**, *17*, 706.
66. Shin, D. M.; Lee, I. S.; Chung, Y. K. *Eur. J. Inorg. Chem.* **2003**, 2311.
67. Barlow, S.; Marder, S. R. *Chem. Commun.* **2000**, 1555.
68. Evans, S.; Green, M. L. H.; Jewitt, B.; Orchard, A. F.; Pygall, C. F. *J. Chem. Soc., Faraday Trans. 2* **1972**, *68*, 1847.
69. Cauletti, C.; Green, J. C.; Kelly, M. R.; Robbins, J.; Smart, J. C. *J. Electron Spectrosc. Relat. Phenom.* **1980**, *19*, 327.
70. Vilesov, F. I.; Terenin, A. N. *Dokl. Akad. Nauk. SSSR* **1957**, *115*, 744.

71. Schäfer, W.; Schweig, A. *Angew. Chem., Intl. Ed. Engl.* **1972**, *11*, 836.
72. Terenin, A.; Vilessov, F. *Adv. Photochem.* **1964**, *2*, 385.
73. Floris, B.; Tagliatesta, P. *J. Chem. Res. S* **1993**, 42.
74. Ribou, A. C.; Launay, J.-P.; Sachtleben, M. L.; Li, H.; Spangler, C. W. *Inorg. Chem.* **1996**, *35*, 3735.
75. LeVanda, C.; Bechgaard, K.; Cowan, D. O. *J. Org. Chem.* **1976**, *41*, 2700.
76. Lambert, C.; Nöll, G. *J. Am. Chem. Soc.* **1999**, *121*, 8434.
77. Barlow, S.; Risko, C.; Coropceanu, V.; Tucker, N. M.; Jones, S. C.; Levi, Z.; Khrustalev, V. N.; Antipin, M. Y.; Kinnibrugh, T. L.; Timofeeva, T.; Marder, S. R.; Brédas, J. L. *Chem. Commun.* **2005**, 764.
78. Barlow, S.; Bunting, H. E.; Ringham, C.; Green, J. C.; Bublitz, G. U.; Boxer, S. G.; Perry, J. W.; Marder, S. R. *J. Am. Chem. Soc.* **1999**, *121*, 3715.
79. Wang, X.-M.; Zhou, Y.-F.; Yu, W.-T.; Wang, C.; Fang, Q.; Jiang, M.-H.; Lei, H.; Wang, H.-Z. *J. Mater. Chem.* **2000**, *10*, 2698.
80. Staub, K.; Levina, G. A.; Barlow, S.; Kowalczyk, T. C.; Lackritz, H. S.; Barzoukas, M.; Fort, A.; Marder, S. R. *J. Mater. Chem.* **2003**, *13*, 825.
81. Cho, B. R.; Son, K. H.; Lee, S. H.; Song, Y.-S.; Lee, Y.-K.; Jeon, S.-J.; Choi, J. H.; Lee, H.; Cho, M. *J. Am. Chem. Soc.* **2001**, *123*, 10039.
82. Calabrese, J. C.; Cheng, L.-T.; Green, J. C.; Marder, S. R.; Tam, W. *J. Am. Chem. Soc.* **1991**, *113*, 7227.
83. Cheng, L.-T.; Tam, W.; Stevenson, S. H.; Meredith, G. R.; Rikken, G.; Marder, S. R. *J. Phys. Chem.* **1991**, *95*, 10631.
84. Blanchard-Desce, M.; Runser, C.; Fort, A.; Barzoukas, M.; Lehn, J.-M.; Bloy, V.; Alain, V. *Chem. Phys.* **1995**, *199*, 253.
85. Alain, V.; Blanchard-Desce, M.; Chen, C. T.; Marder, S. R.; Fort, A.; Barzoukas, M. *Synth. Met.* **1996**, *81*, 133.
86. Jayaprakash, K. N.; Ray, P. C.; Matsuoka, I.; Bhadbhade, M. M.; Puranik, V. G.; Das, P. K.; Nishihara, H.; Sarkar, A. *Organometallics* **1999**, *18*, 3851.
87. Wong, H.; Meyer-Friedrichsen, T.; Farrell, T.; Mecker, C.; Heck, J. *Eur. J. Inorg. Chem.* **2000**, *2000*, 631.
88. Wright, M. E.; Toplikar, E. G.; Kubin, R. F.; Seltzer, M. D. *Macromolecules* **1992**, *25*, 1838.
89. Wright, M. E.; Toplikar, E. G.; Lackritz, H. S.; Kerney, J. T. *Macromolecules* **1994**, *27*, 3016.
90. Alain, V.; Fort, A.; Barzoukas, M.; Chen, C. T.; Blanchard-Desce, M.; Marder, S. R.; Perry, J. W. *Inorg. Chim. Acta* **1996**, *242*, 43.
91. López-Garabito, C.; Campo, J. A.; Heras, J. V.; Cano, M.; Rojo, G.; Agulló-López, F. *J. Phys. Chem. B* **1998**, *102*, 10698.
92. Campo, J. A.; Cano, M.; Heras, J. V.; López-Garabito, C.; Pinilla, E.; Torres, R.; Rojoc, G.; Agulló-López, F. *J. Mater. Chem.* **1999**, *9*, 899.
93. Rojo, G.; Agulló-López, F.; Campo, J. A.; Cano, M.; Lagunas, M. C.; Heras, J. V. *Synth. Met.* **2001**, *124*, 201.
94. Kehzi, W.; Chunhui, H.; Guangxian, X.; Xinsheng, Z.; Xiaoming, X.; Lingge, X. L.Tiankai. *Thin Solid Films* **1994**, *247*, 1.
95. Wang, K. Z.; Huang, C. H.; Xu, G. X.; Zhao, X. S.; Xie, X. M.; Xu, L. G.; Li, T. K. *Thin Solid Films* **1994**, *179*, 1.
96. Gao, L.-H.; Wang, K.-Z.; Huang, C.-H.; Zhao, X.-S.; Xia, X.-H.; XU, J.-M.; LI, T.-K. *Chem. Lett.* **1995**, 1049.
97. Wang, K. Z.; Huang, C. H.; Zhou, D. J.; Xu, G. X.; Xu, Y.; Liu, Y. Q.; Zhu, D. B.; Zhao, X. S.; Xie, X. M. *Solid State Commun.* **1995**, *93*, 189.
98. Cao, Y.-W.; Chai, X.-D.; Yang, W.-S.; Lu, R.; Jiang, Y.-S.; Li, T.-J.; Blanchard-Desce, M.; Lehn, J.-M. *Thin Solid Films* **1996**, *284–285*, 859.
99. Chai, X. D.; Yang, W. S.; Lu, R.; Cao, Y. W.; Lu, N.; Jiang, Y. S.; Bai, Y. B.; Li, T. J. *Supramol. Sci.* **1998**, *5*, 679.
100. Kondo, T.; Horiuchi, S.; Yagi, I.; Ye, S.; Uosaki, K. *J. Am. Chem. Soc.* **1999**, *121*, 391.
101. Malaun, M.; Kowallick, R.; McDonagh, A. M.; Marcaccio, M.; Paul, R. L.; Asselberghs, I.; Clays, K.; Persoons, A.; Bildstein, B.; Fiorini, C.; Nunzi, J.-M.; Ward, M. D.; McCleverty, J. A. *J. Chem. Soc., Dalton Trans.* **2001**, 3025.
102. Asselberghs, I.; Clays, K.; Persoons, A.; McDonagh, A. M.; Ward, M. D.; McCleverty, J. A. *Chem. Phys. Lett.* **2003**, *368*, 408.
103. Sporer, C.; Ratera, I.; Ruiz-Molina, D.; Zhao, Y.; Vidal-Gancedo, J.; Wurst, K.; Jaitner, P.; Clays, K.; Persoons, A.; Rovira, C.; Veciana, J. *Angew. Chem. Int. Ed.* **2004**, *43*, 5266.
104. Alagesan, K.; Chandra-Ray, P.; Kumar-Das, P.; Samuleson, A. G. *Curr. Sci.* **1996**, *70*, 69.
105. Pal, S. K.; Krishnan, A.; Das, P. K.; Samuelson, A. G. *J. Organomet. Chem.* **2000**, *604*, 248.
106. Herrmann, R.; Pedersen, B.; Wagner, G.; Youn, J.-H. *J. Organomet. Chem.* **1998**, *571*, 261.
107. Mendez-Rojas, M. A.; Bodige, S. G.; Watson, W. H. *J. Chem. Crystallogr.* **1999**, *29*, 1225.
108. Naskar, D.; Das, S. K.; Giribabu, L.; Maiya, B. G.; Roy, S. *Organometallics* **2000**, *19*, 1464.
109. Mata, J. A.; Peris, E.; Asselberghs, I.; Van Boxel, R.; Persoons, A. *New J. Chem.* **2001**, *25*, 299.
110. Stankovic, E.; Toma, S. Van_Boxel, R.; Asselberghs, I.; Persoons, A. *J. Organomet. Chem.* **2001**, *637–639*, 426.
111. Mata, J. A.; Peris, E.; Uriel, S.; Llusar, R.; Asselberghs, I.; Persoons, A. *Polyhedron* **2001**, *20*, 2083.
112. Krishnan, A.; Pal, S. K.; Nanadakumar, P.; Samuelson, A. G.; Das, P. K. *Chem. Phys.* **2001**, *265*, 313.
113. Farrell, T.; Meyer-Friedrichson, T.; Malessa, M.; Hasse, D.; Saak, W.; Asselberghs, I.; Wostyn, K.; Clays, K.; Persoons, A.; Heck, J.; Manning, A. R. *J. Chem. Soc., Dalton Trans.* **2001**, 29.
114. Janowska, I.; Zakrzewski, J.; Nakatani, K.; Delaire, J. A.; Palusiak, M.; Walak, M.; Scholl, H. *J. Organomet. Chem.* **2003**, *675*, 35.
115. González-Cabello, A.; Claessens, C. G.; Martin-fuch, G.; Ledoux-Rack, I.; Vázquez, P.; Zyss, J.; Agulló-López, F.; Torres, T. *Synth. Met.* **2003**, *137*, 1487.
116. Peris, E. *Coord. Chem. Rev.* **2004**, *248*, 279.
117. Ratera, I.; Ruiz-Molina, D.; Sánchez, C.; Acalá, R.; Rovira, C.; Veciana, J. *Synth. Met.* **2001**, *121*, 1834.
118. Tsuboya, N.; Hamasaki, R.; Ito, M.; Mitsuishi, M.; Miyashitab, T.; Yamamoto, Y. *J. Mater. Chem.* **2003**, *13*, 511.
119. Hagenau, U.; Heck, J.; Hendrickx, E.; Persoons, A.; Schuld, T.; Wong, H. *Inorg. Chem.* **1996**, *35*, 7863.
120. Mata, J.; Uriel, S.; Peris, E.; Llusar, R.; Houbrechts, S.; Persoons, A. *J. Organomet. Chem.* **1998**, *562*, 197.
121. Lee, I. S.; Lee, S. S. Y.K.Chung; Kim, D.; Song, N. W. *Inorg. Chim. Acta* **1998**, *279*, 243.
122. Lee, I. S.; Seo, H.; Chung, Y. K. *Organometallics* **1999**, *18*, 1091.
123. Hudson, R. D. A.; Asselberghs, I.; Clays, K.; Cuffe, L. P.; Gallagher, J. F.; Manning, A. R.; Persoons, A.; Wostyn, K. *J. Organomet. Chem.* **2001**, *637–639*, 435.
124. Farrell, T.; Manning, A. R.; Murphy, T. C.; Meyer-Friedrichsen, T.; Heck, J.; Asselberghs, I.; Persoons, A. *Eur. J. Inorg. Chem.* **2001**, 2365.
125. Behrens, U.; Meyer-Friedrichsen, T.; Heck, J. *Z. Anorg. Allg. Chem.* **2003**, *629*, 1421.
126. Loucif-Saïbi, R.; Delaire, J. A.; Bonazzola, L.; Doisneau, G.; Balavoine, G.; Fillebeen-Khan, T.; Ledoux, I.; Puccetti, G. *Chem. Phys.* **1992**, *167*, 369.
127. Yuan, Z.; Taylor, N. J.; Sun, Y.; Marder, T. B.; Williams, I. D.; Cheng, L.-T. *J. Organomet. Chem.* **1993**, *449*, 27.
128. Tsuboya, N.; Lamrani, M.; Hamasaki, R.; Ito, M.; Mitsuishi, M.; Miyashita, T.; Yamamoto, Y. *J. Mater. Chem.* **2002**, *12*, 2701.
129. Bildstein, B. *Coord. Chem. Rev.* **2000**, *206–207*, 369.
130. Casalboni, M.; Sarcinelli, F.; Pizzoferrato, R.; D'Amato, R.; Furlani, A.; Russo, M. V. *Chem. Phys. Lett.* **2000**, *319*, 107.
131. Sharma, H. K.; Pannell, K. H.; Ledoux, I.; Zyss, J.; Ceccanti, A.; Zanello, P. *Organometallics* **2000**, *19*, 770.

132. Grogger, C.; Rautz, H.; Stüger, H. *Monatsh. Chem.* **2001**, *132*, 453.
133. Zhao, X.; Sharma, H. K.; Cervantes-Lee, F.; Pannell, K. H.; Long, G. J.; Shahin, A. M. *J. Organomet. Chem.* **2003**, *686*, 235.
134. Mamane, V.; Ledoux-Rak, I.; Deveau, S.; Zyss, J.; Riant, O. *Synthesis* **2003**, 455.
135. Ghosal, S.; Samoc, M.; Prasad, P. N.; Tufariello, J. T. *J. Phys. Chem.* **1990**, *94*, 2847.
136. Rojo, G.; Agulló-López, F.; Campo, J. A.; Heras, J. V.; Cano, M. *J. Phys. Chem. B* **1999**, *103*, 11016.
137. Nalwa, H. S. *Mater. Lett.* **1997**, *33*, 23.
138. Rangel-Rojo, R.; Kimura, K.; Matsuda, H.; Mendez-Rojas, M. A.; Watson, W. H. *Optics Commun.* **2003**, *228*, 181.
139. Li, G.; Song, Y.; Hou, H.; Li, L.; Fan, Y.; Zhu, Y.; Meng, X.; Mi, L. *Inorg. Chem.* **2003**, *42*, 913.
140. Hou, H.; Li, G.; Song, Y.; Fan, Y.; Zhu, Y.; Zhu, L. *Eur. J. Inorg. Chem.* **2003**, 2325.
141. Dhanalakshmi, K.; Sundararajan, G. *J. Organomet. Chem.* **2002**, *645*, 27.
142. Hurst, S. K.; Humphrey, M. G.; Morrall, J. P.; Cifuentes, M. P.; Samoc, M.; Luther-Davies, B.; Heath, G. A.; Willis, A. C. *J. Organomet. Chem.* **2003**, *670*, 56.
143. Qin, J.; Liao, J.; Dai, C.; Liu, D.; Wu, B.; Chen, C. *Chin. J. Org. Chem.* **1993**, *13*, 136.
144. Qin, J.; Liu, D.; Dai, C.; Chen, C.; Wu, B.; Yang, C.; Zhan, C. *Coord. Chem. Rev.* **1999**, *188*, 23.
145. Myers, L. K.; Langhoff, C.; Thompson, M. E. *J. Am. Chem. Soc.* **1992**, *114*, 7560.
146. Myers, L. K.; Ho, D. M.; Thompson, M. E.; Langhoff, C. *Polyhedron* **1995**, *14*, 57.
147. Afanas′ev, A. V.; Zinoviev, A. P.; Antipov, O. L.; Bushuk, B. A.; Bushuk, S. B.; Rubinov, A. N.; Fominih, J. Y.; Klapshina, L. G.; Domrachev, G. A.; Douglas, W. E. *Optics Commun.* **2002**, *201*, 207.
148. Carrondo, M. A. A. F. d. C. T.; Dias, A. R.; Garcia, M. H.; Matas, P. M.; Robalo, M. P.; Green, M. L. H.; Higgins, J.; Yang, Y. Y. *J. Organomet. Chem.* **1990**, *395*, 279.
149. Tam, W.; Eaton, D. F.; Calabrese, J. C.; Williams, I. D.; Wang, Y.; Anderson, A. G. *Chem. Mater.* **1989**, *1*, 128.
150. Stiegman, A. E.; Graham, E. M.; Perry, K. J.; Khundkar, L. R.; Cheng, L.-T.; Perry, J. W. *J. Am. Chem. Soc.* **1991**, *113*, 7658.
151. Lambert, C.; Gaschler, W.; Zabel, M.; Matschiner, R.; Wortmann, R. *J. Organomet. Chem.* **1999**, *592*, 109.
152. Bowser, R.; Davidson, R. S. **1994**. *77* , 269.
153. Yang, C.; Qin, J.; Si, J.; Wang, Y.; Ye, P.; Li, Y. *Synth. Met.* **1999**, *102*, 1578.
154. Lee, I. S.; Choi, D. S.; Shin, D. M.; Chung, Y. K.; Choi, C. H. *Organometallics* **2004**, *23*, 1875.
155. Hascall, T.; Beck, V.; Barlow, S.; Cowley, A. R.; O′Hare, D. *Organometallics* **2004**, *23*, 3808.
156. Heck, J.; Dabek, S.; Meyer-Friedrichsen, T.; Wong, H. *Coord. Chem. Rev.* **1999**, *190–192*, 1217.
157. Behrens, U.; Brussaard, H.; Hagenau, U.; Heck, J.; Hendrickx, E.; Körnich, J.; van der Linden, J. G. M.; Persoons, A.; Spek, A. L.; Veldman, N.; Voss, B.; Wong, H. *Chem. Eur. J.* **1996**, *2*, 98.
158. Heck, J.; Dabek, S.; Meyer-Friedrichsen, T.; Wong, H. *Coord. Chem. Rev.* **1999**, *190–192*, 1217.
159. Tamm, M.; Bannenberg, T.; Baum, K.; Fröhlich, R.; Steiner, T.; Meyer-Friedrichsen, T.; Heck, J. *Eur. J. Inorg. Chem.* **2000**, *116*, 1161.
160. Frazier, C. C.; Harvey, M. A.; Cockerham, M. P.; Hand, H. M.; Chauchard, E. A.; Lee, C. H. *J. Phys. Chem.* **1986**, *90*, 5703.
161. Eaton, D. F.; Anderson, A. G.; Tam, W.; Wang, Y. *J. Am. Chem. Soc.* **1987**, *109*, 1886.
162. Cheng, L.-T.; Tam, W.; Meredith, G. R.; Marder, S. R. *Mol. Cryst. Liq. Cryst.* **1990**, *189*, 137.
163. Garcia, M. H.; Royer, S.; Robalo, M. P.; Dias, A. R.; Tranchier, J.-P.; Chavignon, R.; Prim, D.; Auffrant, A.; Rose-Munch, F.; Rose, E.; Vaissermann, J.; Persoons, A.; Asselberghs, I. *Eur. J. Inorg. Chem.* **2003**, 3895.
164. Marder, S. R.; Cheng, L.-T.; Tiemann, B. G.; Friedli, A. C.; Blanchard-Desce, M.; Perry, J. W.; Skindhøj, J. *Science* **1994**, *263*, 511.
165. Tamm, M.; Grzegorzewski, A.; Steiner, T.; Jentzsch, T.; Werncke, W. *Organometallics* **1996**, *15*, 4984.
166. Lang, J.-P.; Yu, H.; Jia, S.-J.; Sun, Z.-R. *Phys. Chem. Chem. Phys.* **2003**, *5*, 5127.
167. Lang, J.-P.; Sun, Z.-R.; Xu, Q.-F.; Yu, H.; Tatsumi, K. *Mater. Chem. Phys.* **2003**, *82*, 493.
168. Weyland, T.; Ledoux, I.; Brasselet, S.; Zyss, J.; Lapinte, C. *Organometallics* **2000**, *19*, 5235.
169. Garcia, M. H.; Robalo, M. P.; Dias, A. R. M. Teresa Duarte; Wenseleers, W.; Aerts, G.; Goovaerts, E.; Cifuentes, M. P.; Hurst, S.; Humphrey, M. G.; Samoc, M.; Luther-Davies, B. *Organometallics* **2002**, *21*, 2107.
170. Paul, F.; Costuas, K.; Ledoux, I.; Deveau, S.; Zyss, J.; Halet, J.-F.; Lapinte, C. *Organometallics* **2002**, *21*, 5229.
171. Powell, C. E.; Cifuentes, M. P.; McDonagh, A. M.; Hurst, S. K.; Lucas, N. T.; Delfs, C. D.; Stranger, R.; Humphrey, M. G.; Houbrechts, S.; Asselberghs, I.; Persoons, A.; Hockless, D. C. R. *Inorg. Chim. Acta* **2003**, *352*, 9.
172. Whittall, I. R.; Humphrey, M. G.; Hockless, D. C. R.; Skelton, B. W.; White, A. H. *Organometallics* **1995**, *14*, 3970.
173. Whittall, I. R.; Humphrey, M. G.; Persoons, A.; Houbrechts, S. *Organometallics* **1996**, *15*, 1935.
174. Houbrechts, S.; Clays, K.; Persoons, A.; Cadierno, V.; Gamasa, M. P.; Gimeno, J. *Organometallics* **1996**, *15*, 5266.
175. Whittall, I. R.; Cifuentes, M. P.; Humphrey, M. G.; Luther-Davies, B.; Samoc, M.; Houbrechts, S.; Persoons, A.; Heath, G. A.; Hockless, D. C. R. *J. Organomet. Chem.* **1997**, *549*, 127.
176. Cheng, L.-T.; Tam, W.; Marder, S. R.; Stiegman, A. E.; Rikken, G.; Spangler, C. W. *J. Phys. Chem.* **1991**, *95*, 10643.
177. Tamm, M.; Jentzsch, T.; Werncke, W. *Organometallics* **1997**, *16*, 1418.
178. Whittall, I. R.; Humphrey, M. G.; Samoc, M.; Swiatkiewicz, J.; Luther-Davies, B. *Organometallics* **1995**, *14*, 5493.
179. Cifuentes, M. P.; Driver, J.; Humphrey, M. G.; Asselberghs, I.; Persoons, A.; Samoc, M.; Luther-Davies, B. *J. Organomet. Chem.* **2000**, *607*, 72.
180. Dias, A. R.; Garcia, M. H.; Robalo, M. P.; Green, M. L. H.; Lai, K. K.; Pulham, A. J.; Kuebler, S. M.; Balvoine, G. *J. Organomet. Chem.* **1993**, *453*, 241.
181. Dias, A. R.; Garcia, M. H.; Rodrigues, J. C.; Green, M. L. H.; Kuebler, S. M. *J. Organomet. Chem.* **1994**, *475*, 241.
182. Garcia, M. H.; Robalo, M. P.; Dias, A. R.; Piedade, M. F. M.; Galvão, A.; Wenseleers, W.; Goovaerts, E. *J. Organomet. Chem.* **2001**, *619*, 252.
183. Wenseleers, W.; Gerbrandij, A. W.; Goovaerts, E.; Garcia, M. H.; Robalo, M. P.; Mendes, P. J.; Rodrigues, J. C.; Dias, A. R. *J. Mater. Chem.* **1998**, *8*, 925.
184. Wenseleers, W.; Goovaerts, E.; Hepp, P.; Garcia, M. H.; Robalo, M. P.; Dias, A. R.; Piedade, M. F. M.; Duarte, M. T. *Chem. Phys. Lett.* **2003**, *367*, 390.
185. Dias, A. R.; Garcia, M.-H.; Rodrigues, J. C.; Petersen, J. C. T.Bjørnholm; Geisler, T. *J. Mater. Chem.* **1995**, *5*, 1861.
186. Laidlaw, W. M.; Denning, R. G.; Verbiest, T.; Chauchard, E.; Persoons, A. *Nature* **1993**, *363*, 58.
187. Laidlaw, W. M.; Denning, R. G.; Verbiest, T.; Chauchard, E.; Persoons, A. *Proc. S.P.I.E., Int. Soc. Opt. Eng.* **1994**, *2143*, 14.
188. Wu, Z.; Ortiz, R.; Fort, A.; Barzoukas, M.; Marder, S. R. *J. Organomet. Chem.* **1996**, *528*, 217.
189. Farrell, T.; Meyer-Friedrichsen, T.; Malessa, M.; Wittenburg, C.; Heck, J.; Manning, A. R. *J. Organomet. Chem.* **2001**, *625*, 32.

190. Hudson, R. D. A.; Manning, A. R.; Gallagher, J. F.; Garcia, M. H.; Lopes, N.; Asselberghs, I.; Van Boxel, R.; Persoons, A.; Lough, A. J. *J. Organomet. Chem.* **2002**, *655*, 70.
191. Nitay, M.; Priester, W.; Rosenblum, M. *J. Am. Chem. Soc.* **1978**, *100*, 3620.
192. Casey, C. P.; Konings, M. S.; Marder, S. R. *J. Organomet. Chem.* **1988**, *345*, 125.
193. Bandy, J. A.; Bunting, H. E.; Garcia, M.-H.; Green, M. L. H.; Marder, S. R.; Thompson, M. E.; Bloor, D.; Kolinsky, P. V.; Jones, R. J.; Perry, J. W. *Polyhedron* **1992**, *11*, 1429.
194. Farrell, T.; Meyer-Friedrichsen, T.; Heck, J.; Manning, A. R. *Organometallics* **2000**, *19*, 3410.
195. Whittall, I. R.; Cifuentes, M. P.; Humphrey, M. G.; Luther-Davies, B.; Samoc, M.; Houbrechts, S.; Persoons, A.; Heath, G. A.; Bogsányi, D. *Organometallics* **1997**, *16*, 2631.
196. Dias, A. R.; Garcia, M. H.; Mendes, P.; Piedade, M. F. M.; Duarte, M. T.; Calhorda, M. J.; Mealli, C.; Wenseleers, W.; Gerbrandij, A. W.; Goovaerts, E. *J. Organomet. Chem.* **1998**, *553*, 115.
197. Song, Y.; Fang, G.; Wang, Y.; Liu, S.; Li, C.; Song, L.; Zhu, Y.; Hu, Q. *Appl. Phys. Lett.* **1999**, *74*, 332.
198. Fang, G.; Mo, Y.; Song, Y.; Wang, Y.; Li, C.; Song, L. *Optics Commun.* **2002**, *205*, 337.
199. Roberto, D.; Ugo, R.; Bruni, S.; Cariati, E.; Franco Cariati; Fantucci, P.; Invernizzi, I.; Quici, S.; Ledoux, I.; Zyss, J. *Organometallics* **2000**, *19*, 1775.
200. Maiorana, S.; Papagni, A.; Licandro, E.; Persoons, A.; Clays, K.; Houbrechts, S.; Porzio, W. *Gazz. Chim. It.* **1995**, *125*, 377.
201. Licandro, E.; Maiorana, S.; Papagni, A.; Hellier, P.; Capella, L.; Persoons, A.; Houbrechts, S. *J. Organomet. Chem.* **1999**, *583*, 111.
202. Roth, G.; Fischer, H.; Meyer-Friedrichsen, T.; Heck, J.; Houbrechts, S.; Persoons, A. *Organometallics* **1998**, *17*, 1511.
203. Hurst, S. K.; Lucas, N. T.; Cifuentes, M. P.; Humphrey, M. G.; Samoc, M.; Luther-Davies, B.; Asselberghs, I.; Van Boxel, R.; Persoons, A. *J. Organomet. Chem.* **2001**, *633*, 114.
204. Hurst, S. K.; Lucas, N. T.; Humphrey, M. G.; Isoshima, T.; Wostyn, K.; Asselberghs, I.; Clays, K.; Persoons, A.; Samoc, M.; Luther-Davies, B. *Inorg. Chim. Acta* **2003**, *350*, 62.
205. McDonagh, A. M.; Cifuentes, M. P.; Humphrey, M. G.; Houbrechts, S.; Maes, J.; Persoons, A.; Samoc, M.; Luther-Davies, B. *J. Organomet. Chem.* **2000**, *610*, 71.
206. McDonagh, A. M.; Lucas, N. T.; Cifuentes, M. P.; Humphrey, M. G.; Houbrechts, S.; Persoons, A. *J. Organomet. Chem.* **2000**, *605*, 184.
207. McDonagh, A. M.; Cifuentes, M. P.; Lucas, N. T.; Humphrey, M. G.; Houbrechts, S.; Persoons, A. *J. Organomet. Chem.* **2000**, *205*, 193.
208. Hurst, S. K.; Cifuentes, M. P.; Morrall, J. P. L.; Nigel, T.; Lucas; Whittall, I. R.; Humphrey, M. G.; Asselberghs, I.; Persoons, A.; Samoc, M.; Luther-Davies, B.; Willis, A. C. *Organometallics* **2001**, *20*, 4664.
209. Powell, C. E.; Cifuentes, M. P.; Morrall, J. P.; Robert Stranger; Humphrey, M. G.; Samoc, M.; Luther-Davies, B.; Heath, G. A. *J. Am. Chem. Soc.* **2003**, *125*, 602.
210. Hurst, S. K.; Cifuentes, M. P.; McDonagh, A. M.; Humphrey, M. G.; Samoc, M.; Luther-Davies, B.; Asselberghs, I.; Persoons, A. *J. Organomet. Chem.* **2002**, *642*, 259.
211. McDonagh, A. M.; Humphrey, M. G.; Samoc, M.; Luther-Davies, B.; Houbrechts, S.; Wada, T.; Sasabe, H.; Persoons, A. *J. Am. Chem. Soc.* **1999**, *121*, 1405.
212. Cifuentes, M. P.; Powell, C. E.; Humphrey, M. G.; Heath, G. A.; Samoc, M.; Luther-Davies, B. *J. Phys. Chem. A* **2001**, *105*, 9625.
213. McDonagh, A. M.; Humphrey, M. G.; Samoc, M.; Luther-Davies, B. *Organometallics* **1999**, *18*, 5195.
214. Powell, C. E.; Morrall, J. P.; Ward, S. A.; Cifuentes, M. P.; Notaras, E. G. A.; Humphrey, M. G. *J. Am. Chem. Soc.* **2004**, *126*, 12234.
215. Hurst, S. K.; Humphrey, M. G.; Isoshima, T.; Wostyn, K.; Asselberghs, I.; Clays, K.; Persoons, A.; Samoc, M.; Luther-Davies, B. *Organometallics* **2002**, *21*, 2024.
216. Yoo, J.; Yang, S. K.; Jeong, M.-Y.; Ahn, H. C.; Jeon, S.-J. *Org. Lett.* **2003**, *5*, 645.
217. Morrall, J. P.; Powell, C. E.; Stranger, R.; Cifuentes, M. P.; Humphrey, M. G.; Heath, G. A. *J. Organomet. Chem.* **2003**, *670*, 248.
218. Nguyen, P.; Lesley, G.; Marder, T. B.; Ledoux, I.; Zyss, J. *Chem. Mater.* **1997**, *9*, 406.
219. D'Amato, R.; Furlani, A.; Colapietro, M.; Portalone, G.; Casalboni, M.; Falconieri, M.; Russo, M. V. *J. Organomet. Chem.* **2001**, *627*, 13.
220. Frazier, C. C.; Guha, S.; Chen, W. P.; Cockerham, M. P.; Porter, P. L.; Chauchard, E. A.; Lee, C. H. *Polymer* **1987**, *28*, 553.
221. Blau, W. J.; Byrne, H. J.; Cardin, D. J.; Davey, A. P. *J. Mater. Chem.* **1991**, *1*, 245.
222. Porter, P. L.; Guha, S.; Kang, K.; Frazier, C. C. *Polymer* **1991**, *32*, 1756.
223. Guha, S.; Kang, K.; Porter, P.; Roach, J. F.; Remy, D. E.; Aranda, F. J.; Rao, D. V. G. L. N. *Opt. Lett.* **1992**, *17*, 264.
224. Davey, A. P.; Page, H.; Blau, W.; Byrne, H. J.; Cardin, D. J. *Synth. Met.* **1993**, *55–57*, 3980.
225. Siemsen, P.; Gubler, U.; Bosshard, C.; Wada, S.; Diederich, F. *Chem. Eur. J.* **2001**, *7*, 1333.
226. Page, H.; Blau, W.; Davey, A. P.; Lou, X.; Cardin, D. J. *Synth. Met.* **1994**, *63*, 179.
227. Gubler, U.; Concilio, S.; Bosshard, C.; Biaggio, I.; Günter, P.; Martin, R. E.; Edelmann, M. J.; Wytko, J. A.; Diederich, F. *Appl. Phys. Lett.* **2002**, *81*, 2322.
228. Whittall, I. R.; Humphrey, M. G.; Houbrechts, S.; Persoon, A.; Hockless, D. C. R. *Organometallics* **1996**, *15*, 5738.
229. Whittall, I. R.; Humphrey, M. G.; Samoc, M.; Luther-Davies, B. *Angew. Chem. Int. Ed. Engl.* **1997**, *36*, 370.
230. Whittall, I. R.; Humphrey, M. G.; Houbrechts, S.; Maes, J.; Persoons, A.; Schmid, S.; Hockless, D. C. R. *J. Organomet. Chem.* **1997**, *544*, 277.
231. Teo, B. K.; Xu, Y. H.; Zhong, B. Y.; He, Y. K.; Chen, H. Y.; Qian, W.; Deng, Y. J.; Zou, Y. H. *Inorg. Chem.* **2001**, *40*, 6794.
232. Zhang, X.; Wu, X.; Qin, J.; Liu, D. *Acta Chim. Sin.* **1996**, *54*, 734.
233. Zhang, X.; Wu, X.; Qin, J.; Liu, D. *Chem. J. Chin. Univ.* **1995**, *16*, 79.
234. Hernández, F. E.; Marcano-, O. A.; Alvarado, Y.; Biondi, A.; Maillotte, H. *Optics Commun.* **1998**, *152*, 77.
235. Tam, W.; Calabrese, J. C. *Chem. Phys. Lett.* **1988**, *144*, 79.
236. Burdeniuk, J.; Milstein, D. *J. Organomet. Chem.* **1993**, *451*, 213.
237. Caruso, U.; Matola, A. D.; Panunzi, B.; Roviello, A.; Sirigu, A. *Polymer* **2001**, *42*, 3973.
238. Aiello, I.; Caruso, U.; Ghedini, M.; Panunzi, B.; Quatela, A.; Roviello, A.; Sarcinelli, F. *Polymer* **2003**, *44*, 7635.
239. Mata, J. A.; Peris, E.; Asselberghs, I.; Van Boxel, R.; Persoons, A. *New J. Chem.* **2001**, *25*, 1043.
240. Pizzotti, M.; Ugo, R.; Roberto, D.; Bruni, S.; Fantucci, P.; Rovizzi, C. *Organometallics* **2002**, *21*, 5830.
241. Pizzotti, M.; Ugo, R.; Dragonetti, C.; Annoni, E.; Demartin, F.; Mussini, P. *Organometallics* **2003**, *22*, 4001.
242. Entwistle, C. D.; Marder, T. B. *Angew. Chem. Int. Ed.* **2002**, *41*, 2927.
243. Yuan, Z.; Taylor, N. J.; Marder, T. B.; Williams, I. D.; Kurtz, S. K.; Cheng, L.-T. *J. Chem. Soc., Chem. Commun.* **1990**, 1489.
244. Lequan, M.; Lequan, R. M.; Ching, K. C. *J. Mater. Chem.* **1991**, *1*, 997.

245. Lequan, M.; Lequan, M.; Lequan, R. M.; Ching, K. C.; Barzoukas, M.; Fort, A.; Lahoucine, H.; Bravic, G.; Chasseau, D.; Gaultier, J. *J. Mater. Chem.* **1992**, *2*, 719.
246. Branger, C.; Lequan, M.; Lequan, R. M.; Barzoukas, M.; Fort, A. *J. Mater. Chem.* **1996**, *6*, 555.
247. Branger, C.; Lequan, M.; Lequan, R. M.; Large, M.; Kajzar, F. *Chem. Phys. Lett.* **1997**, 265.
248. Yuan, Z.; Taylor, N. J.; Ramachandran, R.; Marder, T. B. *Appl. Organomet. Chem.* **1996**, *10*, 305.
249. Yuan, Z.; Collings, J. C.; Taylor, N. J.; Marder, T. B.; Jardin, C.; Halet, J.-F. *J. Solid State Chem.* **2000**, *154*, 5.
250. Matsumi, N.; Chujo, Y. In *Contemporary Boron Chemistry, Spec. Publ. No. 253*; Davidson, M. G., Hughes, A. K., Marder, T. B., Wade, K., Eds.;, Roy. Soc. of Chem.: Cambridge, 2000.
251. Lambert, C. H.; Stadler, S.; Bourhill, G.; Bräuchle, C. *Angew. Chem. Int. Ed.* **1996**, *35*, 644.
252. Lesley, M. J. G.; Woodward, A.; Taylor, N. J.; Marder, T. B.; Cazenobe, I.; Ledoux, I.; Zyss, J.; Thornton, A.; Bruce, D. W.; Kakkar, A. K. *Chem. Mater.* **1998**, *10*, 1355.
253. Choi, D. H.; Song, S. Y.; Lim, S. J.; Park, S. Y.; Kim, N. *Synth. Met.* **1995**, *71*, 1731.
254. Grimes, R. N. *J. Chem. Ed.* **2004**, *81*, 657.
255. Murphy, D. M.; Mingos, D. M. P.; Forward, J. M. *J. Mater. Chem.* **1993**, *3*, 67.
256. Lamrani, M.; Hamasaki, R.; Mitsuishi, M.; Miyashita, T.; Yamamoto, Y. *Chem. Commun.* **2000**, 1595.
257. Hamasaki, R.; Ito, M.; Lamrani, M.; Mitsuishi, M.; Miyashita, T.; Yamamoto, Y. *J. Mater. Chem.* **2003**, *13*, 21.
258. Mignani, G.; Barzoukas, M.; Zyss, J.; Soula, G.; Balegroune, F.; Grandjean, D.; Josse, D. *Organometallics* **1991**, *10*, 3660.
259. Pedersen, B.; Wagner, G.; Herrmann, R.; Scherer, W.; Meerholz, K.; Schmälzlin, E.; Bräuchle, C. *J. Organomet. Chem.* **1999**, *590*, 129.
260. Mignani, G.; Krämer, A.; Puccetti, G.; Ledoux, I.; Soula, G.; Zyss, J.; Meyrueix, R. *Organometallics* **1990**, *9*, 2640.
261. Hissink, D.; van Hutten, P. F.; Hadziionnou, G.; van Bolhuis, F. *J. Organomet. Chem.* **1993**, *454*, 25.
262. Lequan, M.; Branger, C.; Simon, J.; Thami, T.; Chauchard, E.; Persoons, A. *Chem. Phys. Lett.* **1994**, *229*, 101.
263. Lequan, M.; Branger, C.; Simon, J.; Thami, T.; Chauchard, E.; Persoons, A. *Adv. Mater.* **1994**, *6*, 851.
264. Miller, R. D.; Michl, J. *Chem.Rev.* **1989**, *89*, 1359.
265. Kajzar, F.; Messier, J.; Rosilio, C. *J. Appl. Phys.* **1986**, *60*, 3040.
266. Baumert, J.-C.; Bjorklund, G. C.; Jundt, D. H.; Jurich, M. C.; Looser, H.; Miller, R. D.; Raboit, J.; Sooriyakumaran, R.; Swalen, J. D.; Twieg, R. J. *Appl. Phys. Lett.* **1988**, *53*, 1147.
267. Yang, L.; Wang, Q. Z.; Ho, P. P.; Dorsinville, R.; Alfano, R. R. *Appl. Phys. Lett.* **1988**, *53*, 1245.
268. Champagne, B.; Perpète, E. A.; André, J.-M. *Int. J. Quantum. Chem.* **1998**, *70*, 751.
269. Hamada, T. *J. Chem. Soc., Faraday Trans.* **1998**, *94*, 509.
270. Callender, C. L.; Carere, C. A.; Albert, J.; Zhou, L.-L.; Worsfold, D. J. *J. Opt. Soc. Am. B* **1992**, *9*, 518.
271. Hasegawa, T.; Iwasa, Y.; Koda, T.; Kishida, H.; Tokura, Y.; Wada, S.; Tashiro, H.; Tachibana, H.; Matsumoto, M.; Miller, R. D. *Synth. Met.* **1995**, *71*, 1679.
272. Hasegawa, T.; Iwasa, Y.; Sunamura, H.; Koda, T.; Tokura, Y.; Tachibana, H.; Matsumoto, M.; Aba, S. *Phys. Rev. Lett.* **1992**, *69*, 668.
273. Hasegawa, T.; Iwasa, Y.; Kishida, H.; Koda, T.; Tokura, Y.; Tachibana, H.; Kawabata, Y. *Phys. Rev. B* **1992**, *45*, 6317.
274. Tang, H.; Luo, J.; Qin, J.; Kang, H.; Ye, C. *Macromol. Rapid Commun.* **2000**, *21*, 1125.
275. Priestley, R.; Walser, A. D.; Dorsinville, R.; Zou, W. K.; Xu, D. Y.; Yang, N.-L. *Optics Commun.* **1996**, *131*, 347.
276. Douglas, W. E.; Guy, D. M. H.; Kar, A. K.; Wang, C. *Chem. Commun.* **1998**, 2125.
277. Antipov, O. L.; Domrachev, G. A.; Douglas, W. E.; Guy, D. M. H.; Klapshina, L. G.; Koritin, A. I.; Kuzhelev, A. S.; Semenov, V. V. *Appl. Organomet. Chem.* **2000**, *14*, 640.
278. Douglas, W. E.; Benfield, R. E.; Antipov, O. L.; Klapshina, L. G.; Kuzhelev, A. S.; Guy, D. M. H.; Jones, R. G.; Mustafa, A.; Domrachev, G. A. *Phys. Chem. Chem. Phys.* **2000**, *2*, 3195.
279. Afanas'ev, A. V.; Antipov, O. L.; Benfield, R. E.; Bushuk, B. A.; Bushuk, S. B.; Domrachev, G. A.; Douglas, W. E.; Fominikh, Z.; Jones, R. G.; Klapshina, L. G.; Kuzhelev, A. S.; Lopatina, T. I.; Mustafa, A.; Rubinov, A. N.; Semenov, V. V.; Yurasova, I. V.; Zinoviev, A. P. *Silicon Chem.* **2002**, *1*, 145.
280. Bushuka, S.; Douglas, W.; Kalvinkovskaya, Y.; Klapshina, L.; Rubinov, A.; Bushuk, B.; Stupak, A. *J. Luminesc.* **2003**, *105*, 81.
281. Schubert, E. F. *Light-Emitting Diodes*; Cambridge University Press: Cambridge, UK, 2003.
282. Turro, N. J. *Modern Molecular Photochemistry*; Benjamin/Cummings: Menlo Park, CA, 1978.
282a. Murov, S. L.; Carmichael, I.; Hug, G. L. *Handbook of Photochemistry*, 2nd ed.; Marcel Dekker: New York, 1993.
282b. Gilbert, A.; Baggott, J. *Essentials of molecular photochemistry*; CRC Press: Boca Raton, Fl, 1991.
283. Lees, A. J. *Chemical Reviews* **1987**, *87*, 711–743.
284. Hill, I. G.; Milliron, D.; Schwartz, J.; Kahn, A. *Applied Surface Science* **2000**, *166*, 354–362.
284a Frank, K. H.; Yannoulis, P.; Dudde, R.; Koch, E. E. *Journal Of Chemical Physics* **1988**, *89*, 7569–7576.
284b. Zhan, X. W.; Risko, C.; Amy, F.; Chan, C.; Zhao, W.; Barlow, S.; Kahn, A.; Bredas, J. L.; Marder, S. R. *Journal Of The American Chemical Society* **2005**, *127*, 9021–9029.
284c. Yoshida, H.; Tsutsumi, K.; Sato, N. *Journal Of Electron Spectroscopy And Related Phenomena* **2001**, *121*, 83–91.
284d. Sato, N.; Yoshida, H.; Tsutsumi, K. *Journal Of Materials Chemistry* **2000**, *10*, 85–89.
285. D'Andrade, B. W.; Datta, S.; Forrest, S. R.; Djurovich, P.; Polikarpov, E.; Thompson, M. E. *Organic Electronics* **2005**, *6*, 11–20.
286. Chen, E. S.; Chen, E. C. M.; Sane, N.; Talley, L.; Kozanecki, N.; Shulze, S. *Journal Of Chemical Physics* **1999**, *110*, 9319–9329.
287. Ruoff, R. S.; Kadish, K. M.; Boulas, P.; Chen, E. C. M. *Journal Of Physical Chemistry* **1995**, *99*, 8843–8850.
288. Rienstra-Kiracofe, J. C.; Tschumper, G. S.; Schaefer, H. F.; Nandi, S.; Ellison, G. B. *Chemical Reviews* **2002**, *102*, 231–282.
288a. Cahen, D.; Kahn, A. *Advanced Materials* **2003**, *15*, 271–277.
289. Ishii, H.; Sugiyama, K.; Ito, E.; Seki, K. *Advanced Materials* **1999**, *11*, 605–+.
290. Scott, J. C. *Journal Of Vacuum Science & Technology A* **2003**, *21*, 521–531.
291. Parthasarathy, G.; Burrows, P. E.; Khalfin, V.; Kozlov, V. G.; Forrest, S. R. *Applied Physics Letters* **1998**, *72*, 2138–2140.
292. Turak, A.; Grozea, D.; Feng, X. D.; Lu, Z. H.; Aziz, H.; Hor, A. M. *Applied Physics Letters* **2002**, *81*, 766–768.
293. Choong, V. E.; Mason, M. G.; Tang, C. W.; Gao, Y. *Applied Physics Letters* **1998**, *72*, 2689–2691.
294. Marcus, R. A. *Angewandte Chemie International Edition in English* **1993**, *32*, 1111–1121.
295. Wu, C. C.; Hung, W. Y.; Liu, T. L.; Zhang, L. Z.; Luh, T. Y. *Journal Of Applied Physics* **2003**, *93*, 5465–5471.
296. Hertel, D.; Bassler, H.; Scherf, U.; Horhold, H. H. *Journal Of Chemical Physics* **1999**, *110*, 9214–9222.
296a. Bassler, H. *Physica Status Solidi B-Basic Research* **1993**, *175*, 15–56.

296b. Heun, S.; Borsenberger, P. M. *Chemical Physics* **1995**, *200*, 245–255.
297. Shluger, A. L.; Stoneham, A. M. *Journal Of Physics-Condensed Matter* **1993**, *5*, 3049–3086.
297a. Song, K. S.; Williams, R. T. *Self Trapped Excitons*; Springer-Verlag: Berlin, 1993.
297b. Sakanoue, K.; Motoda, M.; Sugimoto, M.; Sakaki, S. *Journal Of Physical Chemistry A* **1999**, *103*, 5551–5556.
297c. Van Ginhoven, R. M.; Jonsson, H.; Peterson, K. A.; Dupuis, M.; Corrales, L. R. *Journal Of Chemical Physics* **2003**, *118*, 6582–6593.
298. Marcus, R. A. *Journal of Chemical Physics* **1956**, *24*, 966.
298a. Newton, M. D.; Sutin, N. *Annual Review Of Physical Chemistry* **1984**, *35*, 437–480.
298b. Marcus, R. A.; Sutin, N. *Biochimica Et Biophysica Acta* **1985**, *811*, 265–322.
299. Borsenberger, P. M.; Bassler, H. *Journal Of Chemical Physics* **1991**, *95*, 5327–5331.
299a. Borsenberger, P. M.; Bassler, H. *Physica Status Solidi B-Basic Research* **1992**, *170*, 291–302.
300. Heun, S.; Borsenberger, P. M. *Physica B* **1995**, *216*, 43–52.
300a. Borsenberger, P. M.; Magin, E. H.; Heun, S. *Macromolecular Symposia* **1997**, *116*, 51–58.
300b. Heun, S.; Borsenberger, P. M. *Journal Of Imaging Science And Technology* **1999**, *43*, 206–212.
301. Tang, C. W.; Vanslyke, S. A. *Applied Physics Letters* **1987**, *51*, 913–915.
302. Low, P. J.; Paterson, M. A. J.; Puschmann, H.; Goeta, A. E.; Howard, J. A. K.; Lambert, C.; Cherryman, J. C.; Tackley, D. R.; Leeming, S.; Brown, B. *Chem.-Eur. J.* **2004**, *10*, 83–91.
303. Naka, S.; Okada, H.; Onnagawa, H.; Yamaguchi, Y.; Tsutsui, T. *Synthetic Metals* **2000**, *111*, 331–333.
304. Deng, Z. B.; Lee, S. T.; Webb, D. P.; Chan, Y. C.; Gambling, W. A. *Synthetic Metals* **1999**, *107*, 107–109.
305. Wu, C. C.; Liu, T. L.; Hung, W. Y.; Lin, Y. T.; Wong, K. T.; Chen, R. T.; Chen, Y. M.; Chien, Y. Y. *Journal Of The American Chemical Society* **2003**, *125*, 3710–3711.
306. Era, M.; Kakiyama, N.; Noto, M.; Lee, S. H.; Tsutsui, T. *Molecular Crystals And Liquid Crystals* **2001**, *371*, 191–194.
307. Lee, M. T.; Liao, C. H.; Tsai, C. H.; Chen, C. H. *Advanced Materials* **2005**, *17*, 2493–+.
308. Tao, S. L.; Hong, Z. R.; Peng, Z. K.; Ju, W. G.; Zhang, X. H.; Wang, P. F.; Wu, S. K.; Lee, S. T. *Chemical Physics Letters* **2004**, *397*, 1–4.
309. Li, Y. Q.; Fung, M. K.; Xie, Z. Y.; Lee, S. T.; Hung, L. S.; Shi, J. M. *Advanced Materials* **2002**, *14*, 1317–+.
310. Mitschke, U.; Bauerle, P. *Journal Of Materials Chemistry* **2000**, *10*, 1471–1507.
311. Shirota, Y. *Journal Of Materials Chemistry* **2000**, *10*, 1–25.
312. Ren, X. F.; Alleyne, B. D.; Djurovich, P. I.; Adachi, C.; Tsyba, I.; Bau, R.; Thompson, M. E. *Inorganic Chemistry* **2004**, *43*, 1697–1707.
313. Wu, C. C.; Liu, T. L.; Lin, Y. T.; Hung, W. Y.; Ke, T. H.; Wong, K. T.; Chao, T. C. *Applied Physics Letters* **2004**, *85*, 1172–1174.
314. Colle, M.; Brutting, W. *Physica Status Solidi A-Applied Research* **2004**, *201*, 1095–1115.
315. Barth, S.; Muller, P.; Riel, H.; Seidler, P. F.; Riess, W.; Vestweber, H.; Bassler, H. *Journal Of Applied Physics* **2001**, *89*, 3711–3719.
316. Ma, D. G.; Wang, G.; Hu, Y. F.; Zhang, Y. G.; Wang, L. X.; Jing, X. B.; Wang, F. S.; Lee, C. S.; Lee, S. T. *Applied Physics Letters* **2003**, *82*, 1296–1298.
317. Adachi, C.; Kwong, R. C.; Djurovich, P.; Adamovich, V.; Baldo, M. A.; Thompson, M. E.; Forrest, S. R. *Applied Physics Letters* **2001**, *79*, 2082–2084.
318. Adamovich, V. I.; Cordero, S. R.; Djurovich, P. I.; Tamayo, A.; Thompson, M. E.; D'Andrade, B. W.; Forrest, S. R. *Organic Electronics* **2003**, *4*, 77–87.
319. Marcus, R. A. *The Journal of Chemical Physics* **1965**, *43*, 2654–2657.
320. Friend, R. H.; Gymer, R. W.; Holmes, A. B.; Burroughes, J. H.; Marks, R. N.; Taliani, C.; Bradley, D. D. C.; Dos Santos, D. A.; Bredas, J. L.; Logdlund, M.; Salaneck, W. R. *Nature* **1999**, *397*, 121–128.
321. Baldo, M. A.; O'Brien, D. F.; Thompson, M. E.; Forrest, S. R. *Physical Review B* **1999**, *60*, 14422–14428.
322. Wohlgenannt, M.; Tandon, K.; Mazumdar, S.; Ramasesha, S.; Vardeny, Z. V. *Nature* **2001**, *409*, 494–497.
323. Wilson, J. S.; Dhoot, A. S.; Seeley, A.; Khan, M. S.; Kohler, A.; Friend, R. H. *Nature* **2001**, *413*, 828–831.
324. Segal, M.; Baldo, M. A.; Holmes, R. J.; Forrest, S. R.; Soos, Z. G. *Physical Review B* **2003**, *68*.
325. Forrest, S. R.; Bradley, D. D. C.; Thompson, M. E. *Advanced Materials* **2003**, *15*, 1043–1048.
326. Sze, S. M. *Physics of Semiconductor Devices*, 2nd ed.; John Wiley: New York, 1981.
327. Kim, J. S.; Ho, P. K. H.; Greenham, N. C.; Friend, R. H. *Journal Of Applied Physics* **2000**, *88*, 1073–1081.
328. Bulovic, V.; Khalfin, V. B.; Gu, G.; Burrows, P. E.; Garbuzov, D. Z.; Forrest, S. R. *Phys. Rev. B* **1998**, *58*, 3730–3740.
329. Wolfe, W. L. *Introduction to Radiometry*; SPIE Optical Engineering Press: Bellingham, WA, 1998.
330. Ryer, A. *Light Measurement Handbook*; International Light, Inc.: Newburyport, MA, 1997.
331. Dartnall, H. J. A.; Bowmaker, J. K.; Mollon, J. D. *Proceedings Of The Royal Society Of London Series B-Biological Sciences* **1983**, *220*, 115–130.
332. Zollinger, H. *Color Chemistry*; Wiley-VCH: Weinheim, FDR, 1991.
333. Hung, L. S.; Chen, C. H. *Materials Science & Engineering R-Reports* **2002**, *39*, 143–222.
334. Shoustikov, A.; You, Y. J.; Burrows, P. E.; Thompson, M. E.; Forrest, S. R. *Synthetic Metals* **1997**, *91*, 217–221.
335. Suzuki, H.; Hoshino, S. *Journal Of Applied Physics* **1996**, *79*, 8816–8822.
336. Sibley, S. P.; Thompson, M. E.; Burrows, P. E.; Forrest, S. R. In *Optoelectronic Properties of Inorganic Compounds*; Roundhill, D. M., Fackler, J., Eds.;, Plenum: New York, 2000.
337. Chen, J.; Ma, D. *Journal of Applied Physics* **2004**, *95*, 5778–5781.
337a. Shaheen, S. E.; Kippelen, B.; Peyghambarian, N.; Wang, J. F.; Anderson, J. D.; Mash, E. A.; Lee, P. A.; Armstrong, N. R.; Kawabe, Y. *J. Appl. Phys.* **1999**, *85*, 7939–7945.
338. Bulovic, V.; Deshpande, R.; Thompson, M. E.; Forrest, S. R. *Chemical Physics Letters* **1999**, *308*, 317–322.
339. Bulovic, V.; Shoustikov, A.; Baldo, M. A.; Bose, E.; Kozlov, V. G.; Thompson, M. E.; Forrest, S. R. *Chemical Physics Letters* **1998**, *287*, 455–460.
340. Kido, J.; Nagai, K.; Ohashi, Y. *Chemistry Letters* **1990**, 657–660.
341. Kido, J.; Nagai, K.; Okamoto, Y.; Skotheim, T. *Chemistry Letters* **1991**, 1267–1270.
342. Kido, J.; Hayase, H.; Hongawa, K.; Nagai, K.; Okuyama, K. *Applied Physics Letters* **1994**, *65*, 2124–2126.
343. Sano, T.; Fujita, M.; Fujii, T.; Hamada, Y.; Shibata, K.; Kuroki, K. *Japanese Journal Of Applied Physics Part 1-Regular Papers Short Notes & Review Papers* **1995**, *34*, 1883–1887.
344. Jabbour, G. E.; Wang, J. F.; Kippelen, B.; Peyghambarian, N. *Japanese Journal Of Applied Physics Part 2-Letters* **1999**, *38*, L1553–L1555.
345. McGehee, M. D.; Bergstedt, T.; Zhang, C.; Saab, A. P.; O'Regan, M. B.; Bazan, G. C.; Srdanov, V. I.; Heeger, A. J. *Advanced Materials* **1999**, *11*, 1349–1354.

346. Hu, W. P.; Matsumura, M.; Wang, M. Z.; Jin, L. P. *Applied Physics Letters* **2000**, *77*, 4271–4273.
347. Yu, G.; Liu, Y. Q.; Wu, X.; Zhu, D. B.; Li, H. Y.; Jin, L. P.; Wang, M. Z. *Chemistry Of Materials* **2000**, *12*, 2537–2541.
348. Hong, Z. R.; Liang, C. J.; Li, R. G.; Li, W. L.; Zhao, D.; Fan, D.; Wang, D. Y.; Chu, B.; Zang, F. X.; Hong, L. S.; Lee, S. T. *Advanced Materials* **2001**, *13*, 1241–1245.
349. Xin, H.; Li, F. Y.; Shi, M.; Bian, Z. Q. A.; Huang, C. H. *Journal Of The American Chemical Society* **2003**, *125*, 7166–7167.
350. Hoshino, S.; Suzuki, H. *Molecular Crystals And Liquid Crystals Science And Technology Section A-Molecular Crystals And Liquid Crystals* **1997**, *294*, 313–316.
351. Hoshino, S.; Suzuki, H. *Applied Physics Letters* **1996**, *69*, 224–226.
352. Blumstengel, S.; Dorsinville, R. *Japanese Journal Of Applied Physics Part 2-Letters* **1999**, *38*, L403–L405.
353. Kwong, R. C.; Sibley, S.; Dubovoy, T.; Baldo, M.; Forrest, S. R.; Thompson, M. E. *Chemistry Of Materials* **1999**, *11*, 3709–3713.
354. Kwong, R. C.; Lamansky, S.; Thompson, M. E. *Advanced Materials* **2000**, *12*, 1134–1138.
355. Baldo, M. A.; Adachi, C.; Forrest, S. R. *Physical Review B* **2000**, *62*, 10967–10977.
356. Sun, P. P.; Duan, J. P.; Shih, H. T.; Cheng, C. H. *Applied Physics Letters* **2002**, *81*, 792–794.
357. Fang, J. F.; You, H.; Gao, H.; Ma, D. G. *Chemical Physics Letters* **2004**, *392*, 11–16.
358. Fang, J. F.; Ma, D. G. *Applied Physics Letters* **2003**, *83*, 4041–4043.
359. Baldo, M. A.; O'Brien, D. F.; You, Y.; Shoustikov, A.; Sibley, S.; Thompson, M. E.; Forrest, S. R. *Nature* **1998**, *395*, 151–154.
360. Papkovsky, D. B. *Sensors And Actuators B-Chemical* **1995**, *29*, 213–218.
361. Baldo, M. A.; Forrest, S. R. *Physical Review B* **2000**, *62*, 10958–10966.
362. O'Brien, D. F.; Baldo, M. A.; Thompson, M. E.; Forrest, S. R. *Applied Physics Letters* **1999**, *74*, 442–444.
363. Colle, M.; Garditz, C.; Braun, M. *Journal Of Applied Physics* **2004**, *96*, 6133–6141.
364. Burrows, H. D.; Fernandes, M.; de Melo, J. S.; Monkman, A. P.; Navaratnam, S. *Journal Of The American Chemical Society* **2003**, *125*, 15310–15311.
365. Romanovskii, Y. V.; Gerhard, A.; Schweitzer, B.; Scherf, U.; Personov, R. I.; Bassler, H. *Physical Review Letters* **2000**, *84*, 1027–1030.
366. Hertel, D.; Setayesh, S.; Nothofer, H. G.; Scherf, U.; Mullen, K.; Bassler, H. *Advanced Materials* **2001**, *13*, 65–70.
367. Higgins, R. W. T.; Monkman, A. P.; Nothofer, H. G.; Scherf, U. *Journal Of Applied Physics* **2002**, *91*, 99–105.
368. Cleave, V.; Yahioglu, G.; Le Barny, P.; Hwang, D. H.; Holmes, A. B.; Friend, R. H.; Tessler, N. *Advanced Materials* **2001**, *13*, 44–47.
369. Yang, X. H.; Neher, D.; Scherf, U.; Bagnich, S. A.; Bassler, H. *Journal Of Applied Physics* **2003**, *93*, 4413–4419.
370. Jabbour, G. E.; Wang, J. F.; Peyghambarian, N. *Applied Physics Letters* **2002**, *80*, 2026–2028.
371. Wang, Y. *Applied Physics Letters* **2004**, *85*, 4848–4850.
372. Gu, G.; Parthasarathy, G.; Burrows, P. E.; Tian, P.; Hill, I. G.; Kahn, A.; Forrest, S. R. *Journal Of Applied Physics* **1999**, *86*, 4067–4075.
373. Baldo, M. A.; Lamansky, S.; Burrows, P. E.; Thompson, M. E.; Forrest, S. R. *Applied Physics Letters* **1999**, *75*, 4–6.
374. Adachi, C.; Baldo, M. A.; Forrest, S. R.; Thompson, M. E. *Applied Physics Letters* **2000**, *77*, 904–906.
375. Adachi, C.; Baldo, M. A.; Forrest, S. R.; Lamansky, S.; Thompson, M. E.; Kwong, R. C. *Applied Physics Letters* **2001**, *78*, 1622–1624.
376. Lamansky, S.; Djurovich, P.; Murphy, D.; Abdel-Razzaq, F.; Lee, H. E.; Adachi, C.; Burrows, P. E.; Forrest, S. R.; Thompson, M. E. *Journal Of The American Chemical Society* **2001**, *123*, 4304–4312.
377. Watanabe, T.; Nakamura, E.; Kawami, S.; Fukuda, Y.; Tsuji, T.; Wakimoto, T.; Miyaguchi, S. *Proceedings of SPIE* **2001**, *4105*, 175.
378. Kwong, R. C.; Nugent, M. R.; Michalski, L.; Ngo, T.; Rajan, K.; Tung, Y. J.; Weaver, M. S.; Zhou, T. X.; Hack, M.; Thompson, M. E.; Forrest, S. R.; Brown, J. J. *Applied Physics Letters* **2002**, *81*, 162–164.
379. Ikai, M.; Tokito, S.; Sakamoto, Y.; Suzuki, T.; Taga, Y. *Applied Physics Letters* **2001**, *79*, 156–158.
380. Jiang, X. Y.; Zhang, Z. L.; Zhao, W. M.; Zhu, W. Q.; Zhang, B. X.; Xu, S. H. *Journal Of Physics D-Applied Physics* **2000**, *33*, 473–476.
381. Wang, C. S.; Jung, G. Y.; Hua, Y. L.; Pearson, C.; Bryce, M. R.; Petty, M. C.; Batsanov, A. S.; Goeta, A. E.; Howard, J. A. K. *Chemistry Of Materials* **2001**, *13*, 1167–1173.
382. Kolosov, D.; Adamovich, V.; Djurovich, P.; Thompson, M. E.; Adachi, C. *Journal Of The American Chemical Society* **2002**, *124*, 9945–9954.
383. Kim, J. L.; Kim, J. K.; Cho, H. N.; Kim, D. Y.; Kim, C. Y.; Hong, S. I. *Macromolecules* **2000**, *33*, 5880–5885.
384. Woo, H. S.; Czerw, R.; Webster, S.; Carroll, D. L.; Ballato, J.; Strevens, A. E.; O'Brien, D.; Blau, W. J. *Applied Physics Letters* **2000**, *77*, 1393–1395.
385. King, K. A.; Spellane, P. J.; Watts, R. J. *Journal Of The American Chemical Society* **1985**, *107*, 1431–1432.
386. Dedeian, K.; Djurovich, P. I.; Garces, F. O.; Carlson, G.; Watts, R. J. *Inorganic Chemistry* **1991**, *30*, 1685–1687.
387. Grushin, V. V.; Herron, N.; LeCloux, D. D.; Marshall, W. J.; Petrov, V. A.; Wang, Y. *Chemical Communications* **2001**, 1494–1495.
388. Nonoyama, M. *Bulletin of the Chemical Society of Japan* **1974**, *47*, 767–768.
389. Carlson, G. A.; Djurovich, P. I.; Watts, R. J. *Inorganic Chemistry* **1993**, *32*, 4483–4484.
390. Lamansky, S.; Djurovich, P.; Murphy, D.; Abdel-Razzaq, F.; Kwong, R.; Tsyba, I.; Bortz, M.; Mui, B.; Bau, R.; Thompson, M. E. *Inorganic Chemistry* **2001**, *40*, 1704–1711.
390a. Lowry, M. S.; Hudson, W. R.; Pascal, R. A.; Bernhard, S. *J. Am. Chem. Soc.* **2004**, *126*, 14129–14135.
391. Colombo, M. G.; Brunold, T. C.; Riedener, T.; Gudel, H. U.; Fortsch, M.; Burgi, H. B. *Inorganic Chemistry* **1994**, *33*, 545–550.
392. Tamayo, A. B.; Alleyne, B. D.; Djurovich, P. I.; Lamansky, S.; Tsyba, I.; Ho, N. N.; Bau, R.; Thompson, M. E. *Journal Of The American Chemical Society* **2003**, *125*, 7377–7387.
393. Beeby, A.; Bettington, S.; Samuel, I. D. W.; Wang, Z. J. *Journal Of Materials Chemistry* **2003**, *13*, 80–83.
394. DeRosa, M. C.; Mosher, P. J.; Yap, G. P. A.; Focsaneanu, K. S.; Crutchley, R. J.; Evans, C. E. B. *Inorganic Chemistry* **2003**, *42*, 4864–4872.
395. Frampton, M. J.; Namdas, E. B.; Lo, S. C.; Burn, P. L.; Samuel, I. D. W. *Journal Of Materials Chemistry* **2004**, *14*, 2881–2888.
396. Dedeian, K.; Shi, J. M.; Shepherd, N.; Forsythe, E.; Morton, D. C. *Inorganic Chemistry* **2005**, *44*, 4445–4447.
397. Nazeeruddin, M. K.; Humphry-Baker, R.; Berner, D.; Rivier, S.; Zuppiroli, L.; Graetzel, M. *Journal Of The American Chemical Society* **2003**, *125*, 8790–8797.
398. Coppo, P.; Plummer, E. A.; De Cola, L. *Chemical Communications* **2004**, 1774–1775.
399. Li, J.; Djurovich, P. I.; Alleyne, B. D.; Tsyba, I.; Ho, N. N.; Bau, R.; Thompson, M. E. *Polyhedron* **2004**, *23*, 419–428.
400. Kwon, T. H.; Cho, H. S.; Kim, M. K.; Kim, J. W.; Kim, J. J.; Lee, K. H.; Park, S. J.; Shin, I. S.; Kim, H.; Shin, D. M.; Chung, Y. K.; Hong, J. I. *Organometallics* **2005**, *24*, 1578–1585.
401. Li, J.; Djurovich, P. I.; Alleyne, B. D.; Yousufuddin, M.; Ho, N. N.; Thomas, J. C.; Peters, J. C.; Bau, R.; Thompson, M. E. *Inorganic Chemistry* **2005**, *44*, 1713–1727.
402. Chen, L.; Yang, C.; Qin, J.; Gao, J.; Ma, D. *Synthetic Metals* **2005**, *152*, 225–228.

403. Yang, C.-H.; Li, S.-W.; Chi, Y.; Cheng, Y.-M.; Yeh, Y.-S.; Chou, P.-T.; Lee, G.-H.; Wang, C.-H.; Shu, C.-F. *Inorganic Chemistry* **2005**, *44*, 7770–7780.
404. Yeh, S. J.; Wu, M. F.; Chen, C. T.; Song, Y. H.; Chi, Y.; Ho, M. H.; Hsu, S. F.; Chen, C. H. *Advanced Materials* **2005**, *17*, 285–289.
405. You, Y. M.; Park, S. Y. *Journal Of The American Chemical Society* **2005**, *127*, 12438–12439.
406. Karatsu, T.; Nakamura, T.; Yagai, S.; Kitamura, A.; Yamaguchi, K.; Matsushima, Y.; Iwata, T.; Hori, Y.; Hagiwara, T. *Chemistry Letters* **2003**, *32*, 886–887.
407. Dixon, I. M.; Collin, J. P.; Sauvage, J. P.; Flamigni, L.; Encinas, S.; Barigelletti, F. *Chemical Society Reviews* **2000**, *29*, 385–391.
408. Ohsawa, Y.; Sprouse, S.; King, K. A.; Dearmond, M. K.; Hanck, K. W.; Watts, R. J. *Journal Of Physical Chemistry* **1987**, *91*, 1047–1054.
409. Brooks, J.; Babayan, Y.; Lamansky, S.; Djurovich, P. I.; Tsyba, I.; Bau, R.; Thompson, M. E. *Inorganic Chemistry* **2002**, *41*, 3055–3066.
410. Chassot, L.; Von Zelewsky, A. *Helvetica Chimica Acta* **1983**, *66*, 2443–2444.
411. Chassot, L.; Muller, E.; Von Zelewsky, A. *Inorganic Chemistry* **1984**, *23*, 4249–4253.
412. Chassot, L.; Von Zelewsky, A. *Inorganic Chemistry* **1987**, *26*, 2814–2818.
413. Cho, J. Y.; Suponitsky, K. Y.; Li, J.; Timofeeva, T. V.; Barlow, S.; Marder, S. R. *Journal Of Organometallic Chemistry* **2005**, *690*, 4090–4093.
414. Jolliet, P.; Gianini, M.; von Zelewsky, A.; Bernardinelli, G.; Stoeckli-Evans, H. *Inorg. Chem.* **1996**, *35*, 4883–4888.
415. Lu, W.; Mi, B. X.; Chan, M. C. W.; Hui, Z.; Che, C. M.; Zhu, N. Y.; Lee, S. T. *Journal Of The American Chemical Society* **2004**, *126*, 4958–4971.
416. Chan, S. C.; Chan, M. C. W.; Wang, Y.; Che, C. M.; Cheung, K. K.; Zhu, N. Y. *Chemistry-A European Journal* **2001**, *7*, 4180–4190.
417. Nishida, J.; Maruyama, A.; Iwata, T.; Yamashita, Y. *Chemistry Letters* **2005**, *34*, 592–593.
418. Colombo, M. G.; Gudel, H. U. *Inorganic Chemistry* **1993**, *32*, 3081–3087.
419. Strouse, G. F.; Gudel, H. U.; Bertolasi, V.; Ferretti, V. *Inorganic Chemistry* **1995**, *34*, 5578–5587.
420. Lever, A. P. B. *Inorganic Electronic Spectroscopy*, 2nd ed.; Elsevier: New York, 1984.
421. Wiedenhofer, H.; Schutzenmeier, S.; Von Zelewsky, A.; Yersin, H. *Journal Of Physical Chemistry* **1995**, *99*, 13385–13391.
422. Schmidt, J.; Wiedenhofer, H.; Von Zelewsky, A.; Yersin, H. *Journal Of Physical Chemistry* **1995**, *99*, 226–229.
423. Yersin, H.; Donges, D. *Top. Curr. Chem.* **2001**, *214*, 81–186.
424. Vanhelmont, F. W. M.; Gudel, H. U.; Fortsch, M.; Burgi, H. B. *Inorganic Chemistry* **1997**, *36*, 5512–5517.
425. Yersin, H.; Humbs, W. *Inorganic Chemistry* **1999**, *38*, 5820–5831.
426. Komada, Y.; Yamauchi, S.; Hirota, N. *Journal Of Physical Chemistry* **1986**, *90*, 6425–6430.
427. Hay, P. J. *Journal Of Physical Chemistry A* **2002**, *106*, 1634–1641.
428. Choi, G. C.; Lee, J. E.; Park, N. G.; Kim, Y. S. *Molecular Crystals And Liquid Crystals* **2004**, *424*, 173–+.
429. Polson, M.; Ravaglia, M.; Fracasso, S.; Garavelli, M.; Scandola, F. *Inorganic Chemistry* **2005**, *44*, 1282–1289.
430. Sotoyama, W.; Satoh, T.; Sato, H.; Matsuura, A.; Sawatari, N. *Journal of Physical Chemistry A* **2005**, *109*, 9760–9766.
431. Lees, A. J. *Comments On Inorganic Chemistry* **1995**, *17*, 319–346.
431a. Tsuboyama, A.; Iwawaki, H.; Furugori, M.; Mukaide, T.; Kamatani, J.; Igawa, S.; Moriyama, T.; Miura, S.; Takiguchi, T.; Okada, S.; Hoshino, M.; Ueno, K. *J. Am. Chem. Soc.* **2003**, *125*, 12971–12979.
432. Jung, S. G.; Kang, Y. J.; Kim, H. S.; Kim, Y. H.; Lee, C. L.; Kim, J. J.; Lee, S. K.; Kwon, S. K. *European Journal Of Inorganic Chemistry* **2004**, 3415–3423.
433. Maestri, M.; Sandrini, D.; Balzani, V.; Maeder, U.; Von Zelewsky, A. *Inorganic Chemistry* **1987**, *26*, 1323–1327.
434. Paulose, B.; Rayabarapu, D. K.; Duan, J. P.; Cheng, C. H. *Advanced Materials* **2004**, *16*, 2003–2007.
435. Ni, T.; Caldwell, R. A.; Melton, L. A. *Journal Of The American Chemical Society* **1989**, *111*, 457–464.
435a. Ramamurthy, V.; Caspar, J. V.; Eaton, D. F.; Kuo, E. W.; Corbin, D. R. *J. Am. Chem. Soc.* **1992**, *114*, 3882–3892.
436. Taylor, H. V.; Allred, A. L.; Hoffman, B. M. *Journal of the American Chemical Society* **1973**, *95*, 3215–3219.
437. Pavlik, J. W.; Connors, R. E.; Burns, D. S.; Kurzweil, E. M. *Journal Of The American Chemical Society* **1993**, *115*, 7645–7652.
438. Nam, E. J.; Kim, J. H.; Kim, B. O.; Kim, S. M.; Park, N. G.; Kim, Y. S.; Kim, Y. K.; Ha, Y. *Bulletin Of The Chemical Society Of Japan* **2004**, *77*, 751–755.
439. Kawamura, Y.; Sasabe, H.; Adachi, C. *Japanese Journal Of Applied Physics Part 1-Regular Papers Short Notes & Review Papers* **2004**, *43*, 7729–7730.
440. Kawamura, Y.; Goushi, K.; Brooks, J.; Brown, J. J.; Sasabe, H.; Adachi, C. *Applied Physics Letters* **2005**, *86*, 071104.
441. Forster, L. S. *Coordination Chemistry Reviews* **2002**, *227*, 59–92.
442. Brennaman, M. K.; Meyer, T. J.; Papanikolas, J. M. *Journal Of Physical Chemistry A* **2004**, *108*, 9938–9944.
443. Wang, X. Y.; Del Guerzo, A.; Schmehl, R. H. *Journal Of Photochemistry And Photobiology C-Photochemistry Reviews* **2004**, *5*, 55–77.
444. Lumpkin, R. S.; Kober, E. M.; Worl, L. A.; Murtaza, Z.; Meyer, T. J. *Journal Of Physical Chemistry* **1990**, *94*, 239–243.
445. Nolan, S. P.; Hoff, C. D.; Stoutland, P. O.; Newman, L. J.; Buchanan, J. M.; Bergman, R. G.; Yang, G. K.; Peters, K. S. *Journal Of The American Chemical Society* **1987**, *109*, 3143–3145.
446. Sajoto, T.; Djurovich, P. I.; Tamayo, A.; Yousufuddin, M.; Bau, R.; Thompson, M. E.; Holmes, R. J.; Forrest, S. R. *Inorg. Chem.* **2005**, *44*, 7992–8003.
447. Finkenzeller, W. J.; Yersin, H. *Chemical Physics Letters* **2004**, *377*, 299–305.
448. Nemcsok, D.; Wichmann, K.; Frenking, G. *Organometallics* **2004**, *23*, 3640–3646.
449. Schildknecht, C.; Ginev, G.; Kammoun, A.; Riedl, T.; Kowalsky, W.; Johannes, H. H.; Lennartz, C.; Kahle, K.; Egen, M.; Gessner, T.; Bold, M.; Nord, S.; Erk, P. In *Organic Light-Emitting Materials and Devices IX*; *;* San Diego, CA: USA, 2005, p 59370E.
450. Hitchcock, P. B.; Lappert, M. F.; Terreros, P. *Journal Of Organometallic Chemistry* **1982**, *239*, C26–C30.
451. Tamayo, A. B.; Garon, S.; Sajoto, T.; Djurovich, P. I.; Tsyba, I. M.; Bau, R.; Thompson, M. E. *Inorg. Chem.* **2005**, *44*, 8723–8732.
452. Baldo, M.; Deutsch, M.; Burrows, P.; Gossenberger, H.; Gerstenberg, M.; Ban, V.; Forrest, S. *Advanced Materials* **1998**, *10*, 1505–+.
453. Baldo, M. A.; Kozlov, V. G.; Burrows, P. E.; Forrest, S. R.; Ban, V. S.; Koene, B.; Thompson, M. E. *Applied Physics Letters* **1997**, *71*, 3033–3035.
454. Shtein, M.; Gossenberger, H. F.; Benziger, J. B.; Forrest, S. R. *Journal Of Applied Physics* **2001**, *89*, 1470–1476.
455. Sun, Y. R.; Shtein, M.; Forrest, S. R. *Applied Physics Letters* **2005**, *86*.
456. Chang, S. C.; Liu, J.; Bharathan, J.; Yang, Y.; Onohara, J.; Kido, J. *Advanced Materials* **1999**, *11*, 734–737.
457. Hebner, T. R.; Wu, C. C.; Marcy, D.; Lu, M. H.; Sturm, J. C. *Applied Physics Letters* **1998**, *72*, 519–521.
458. Bharathan, J.; Yang, Y. *Applied Physics Letters* **1998**, *72*, 2660–2662.
459. Jabbour, G. E.; Radspinner, R.; Peyghambarian, N. *Ieee Journal Of Selected Topics In Quantum Electronics* **2001**, *7*, 769–773.
460. Pardo, D. A.; Jabbour, G. E.; Peyghambarian, N. *Advanced Materials* **2000**, *12*, 1249–+.

461. Choi, J. H.; Kim, D.; Yoo, P. J.; Lee, H. H. *Advanced Materials* **2005**, *17*, 166–+.
462. Lee, T. W.; Zaumseil, J.; Bao, Z. N.; Hsu, J. W. P.; Rogers, J. A. *Proceedings Of The National Academy Of Sciences Of The United States Of America* **2004**, *101*, 429–433.
463. Kim, C.; Forrest, S. R. *Advanced Materials* **2003**, *15*, 541–545.
464. Rhee, J.; Lee, H. H. *Applied Physics Letters* **2002**, *81*, 4165–4167.
465. Kim, C.; Burrows, P. E.; Forrest, S. R. *Science* **2000**, *288*, 831–833.
466. Gao, W. Y.; Kahn, A. *Journal Of Physics-Condensed Matter* **2003**, *15*, S2757–S2770.
467. Gao, W. Y.; Kahn, A. *Journal Of Applied Physics* **2003**, *94*, 359–366.
468. Gill, W. D. *Journal of Applied Physics* **1972**, *43*, 5033–5040.
469. Sudhakar, M.; Djurovich, P. I.; Hogen-Esch, T. E.; Thompson, M. E. *Journal Of The American Chemical Society* **2003**, *125*, 7796–7797.
470. Pei, Q. B.; Yu, G.; Zhang, C.; Yang, Y.; Heeger, A. J. *Science* **1995**, *269*, 1086–1088.
470a. Pei, Q. B.; Yang, Y.; Yu, G.; Zhang, C.; Heeger, A. J. *J. Am. Chem. Soc.* **1996**, *118*, 3922–3929.
471. Pei, Q. B.; Yang, Y. *Synthetic Metals* **1996**, *80*, 131–136.
471a. Pei, Q.; Yang, Y.; Yu, G.; Cao, Y.; Heeger, A. J. *Synthetic Metals* **1997**, *85*, 1229–1232.
472. Rudmann, H.; Shimada, S.; Rubner, M. F. *Journal Of Applied Physics* **2003**, *94*, 115–122.
473. Rudmann, H.; Shimada, S.; Rubner, M. F.; Oblas, D. W.; Whitten, J. E. *Journal Of Applied Physics* **2002**, *92*, 1576–1581.
474. Rudmann, H.; Shimada, S.; Rubner, M. F. *Journal Of The American Chemical Society* **2002**, *124*, 4918–4921.
475. Rudmann, H.; Rubner, M. F. *Journal Of Applied Physics* **2001**, *90*, 4338–4345.
476. Handy, E. S.; Pal, A. J.; Rubner, M. F. *Journal Of The American Chemical Society* **1999**, *121*, 3525–3528.
477. Lee, J. K.; Yoo, D.; Rubner, M. F. *Chemistry Of Materials* **1997**, *9*, 1710–1712.
478. Kalyuzhny, G.; Buda, M.; McNeill, J.; Barbara, P.; Bard, A. J. *Journal Of The American Chemical Society* **2003**, *125*, 6272–6283.
479. Fan, F. R. F.; Bard, A. J. *Journal Of Physical Chemistry B* **2003**, *107*, 1781–1787.
480. Gao, F. G.; Bard, A. J. *Chemistry Of Materials* **2002**, *14*, 3465–3470.
481. Buda, M.; Kalyuzhny, G.; Bard, A. J. *Journal Of The American Chemical Society* **2002**, *124*, 6090–6098.
482. Gao, F. G.; Bard, A. J. *Journal Of The American Chemical Society* **2000**, *122*, 7426–7427.
483. Bernhard, S.; Gao, X. C.; Malliaras, G. G.; Abruna, H. D. *Advanced Materials* **2002**, *14*, 433–436.
484. Bernhard, S.; Barron, J. A.; Houston, P. L.; Abruna, H. D.; Ruglovksy, J. L.; Gao, X. C.; Malliaras, G. G. *Journal Of The American Chemical Society* **2002**, *124*, 13624–13628.
485. Lo, K. K. W.; Chan, J. S. W.; Lui, L. H.; Chung, C. K. *Organometallics* **2004**, *23*, 3108–3116.
485a. Lowry, M. S.; Hudson, W. R.; Pascal, R. A.; Bernhard, S. *J. Am. Chem. Soc.* **2004**, *126*, 14129–14135.
485b. Lepeltier, M.; Lee, T. K. M.; Lo, K. K. W.; Toupet, L.; Le Bozec, H.; Guerchais, W. *Eur. J. Inorg. Chem.* **2005**, 110–117.
486. Lo, K. K. W.; Chung, C. K.; Lee, T. K. M.; Lui, L. H.; Tsang, K. H. K.; Zhu, N. Y. *Inorganic Chemistry* **2003**, *42*, 6886–6897.
487. Slinker, J. D.; Koh, C. Y.; Malliaras, G. G.; Lowry, M. S.; Bernhard, S. *Applied Physics Letters* **2005**, *86*, 173506.
488. Slinker, J. D.; Gorodetsky, A. A.; Lowry, M. S.; Wang, J. J.; Parker, S.; Rohl, R.; Bernhard, S.; Malliaras, G. G. *Journal Of The American Chemical Society* **2004**, *126*, 2763–2767.
489. Slinker, J.; Bernards, D.; Houston, P. L.; Abruna, H. D.; Bernhard, S.; Malliaras, G. G. *Chemical Communications* **2003**, 2392–2399.
490. Burrows, P. E.; Forrest, S. R.; Zhou, T. X.; Michalski, L. *Applied Physics Letters* **2000**, *76*, 2493–2495.
491. Zhao, W.; Liu, C. Y.; Wang, Q.; White, J. M.; Bard, A. J. *Chem. Mater.* **2005**, *17*, 6403–6406.
492. Wyszecki, G.; Stiles, W. S. *Color Science: Concepts and Methods, Quantitative Data and Formulas*; John Wiley & Sons: New York, 1967.
493. Kawamura, Y.; Yanagida, S.; Forrest, S. R. *Journal Of Applied Physics* **2002**, *92*, 87–93.
494. Tasch, S.; List, E. J. W.; Ekstrom, O.; Graupner, W.; Leising, G.; Schlichting, P.; Rohr, U.; Geerts, Y.; Scherf, U.; Mullen, K. *Applied Physics Letters* **1997**, *71*, 2883–2885.
495. Kido, J.; Shionoya, H.; Nagai, K. *Applied Physics Letters* **1995**, *67*, 2281–2283.
496. Huang, L.; Wang, K. Z.; Huang, C. H.; Gao, D. Q.; Jin, L. P. *Synthetic Metals* **2002**, *128*, 241–245.
497. Ko, C. W.; Tao, Y. T. *Applied Physics Letters* **2001**, *79*, 4234–4236.
498. Liu, S. Y.; Huang, J. S.; Xie, Z. Y.; Wang, Y.; Chen, B. J. *Thin Solid Films* **2000**, *363*, 294–297.
499. Kido, J.; Kimura, M.; Nagai, K. *Science* **1995**, *267*, 1332–1334.
500. D′Andrade, B. W.; Thompson, M. E.; Forrest, S. R. *Advanced Materials* **2002**, *14*, 147–151.
501. Yang, J. P.; Jin, Y. D.; Heremans, P. L.; Hoefnagels, R.; Dieltiens, P.; Blockhuys, F.; Geise, H. J.; Van der Auweraer, M.; Borghs, G. *Chemical Physics Letters* **2000**, *325*, 251–256.
502. D′Andrade, B. W.; Brooks, J.; Adamovich, V.; Thompson, M. E.; Forrest, S. R. *Advanced Materials* **2002**, *14*, 1032–1036.
503. Adamovich, V.; Brooks, J.; Tamayo, A.; Alexander, A. M.; Djurovich, P. I.; D′Andrade, B. W.; Adachi, C.; Forrest, S. R.; Thompson, M. E. *New Journal Of Chemistry* **2002**, *26*, 1171–1178.
504. Lu, W.; Zhu, N. Y.; Che, C. M. *Chemical Communications* **2002**, 900–901.
505. Lai, S. W.; Lam, H. W.; Lu, W.; Cheung, K. K.; Che, C. M. *Organometallics* **2002**, *21*, 226–234.
506. Buchner, R.; Cunningham, C. T.; Field, J. S.; Haines, R. J.; McMillin, D. R.; Summerton, G. C. *Journal Of The Chemical Society-Dalton Transactions* **1999**, 711–717.
507. Zheng, G. Y.; Rillema, D. P. *Inorganic Chemistry* **1998**, *37*, 1392–1397.
508. Cheung, T. C.; Cheung, K. K.; Peng, S. M.; Che, C. M. *Journal Of The Chemical Society-Dalton Transactions* **1996**, 1645–1651.
509. Charmant, J. P. H.; Fornies, J.; Gomez, J.; Lalinde, E.; Merino, R. I.; Moreno, M. T.; Orpen, A. C. *Organometallics* **1999**, *18*, 3353–3358.
510. Connick, W. B.; Marsh, R. E.; Schaefer, W. P.; Gray, H. B. *Inorganic Chemistry* **1997**, *36*, 913–922.
511. Adachi, C.; Baldo, M. A.; Thompson, M. E.; Forrest, S. R. *Journal Of Applied Physics* **2001**, *90*, 5048–5051.
512. He, G. F.; Pfeiffer, M.; Leo, K.; Hofmann, M.; Birnstock, J.; Pudzich, R.; Salbeck, J. *Applied Physics Letters* **2004**, *85*, 3911–3913.
513. Ono, K.; Yanase, T.; Ohkita, M.; Saito, K. *Chemistry Letters* **2004**, *33*, 276–277.
514. Huang, W. S.; Lin, J. T.; Chien, C. H.; Tao, Y. T.; Sun, S. S.; Wen, Y. S. *Chemistry Of Materials* **2004**, *16*, 2480–2488.
515. Li, C. L.; Su, Y. J.; Tao, Y. T.; Chou, P. T.; Chien, C. H.; Cheng, C. C.; Liu, R. S. *Advanced Functional Materials* **2005**, *15*, 387–395.
516. Su, Y. J.; Huang, H. L.; Li, C. L.; Chien, C. H.; Tao, Y. T.; Chou, P. T.; Datta, S.; Liu, R. S. *Advanced Materials* **2003**, *15*, 884–888.
517. Yang, C. H.; Tai, C. C.; Sun, I. W. *Journal Of Materials Chemistry* **2004**, *14*, 947–950.
518. Ostrowski, J. C.; Robinson, M. R.; Heeger, A. J.; Bazan, G. C. *Chemical Communications* **2002**, 784–785.
519. Rayabarapu, D. K.; Paulose, B.; Duan, J. P.; Cheng, C. H. *Advanced Materials* **2005**, *17*, 349–353.

520. Holmes, R. J.; Forrest, S. R.; Sajoto, T.; Tamayo, A.; Djurovich, P. I.; Thompson, M. E.; Brooks, J.; Tung, Y.-J.; D'Andrade, B. W.; Weaver, M. S.; Kwong, R. C.; Brown, J. J. *Applied Physics Letters* **2005**.
521. Ren, X. F.; Li, J.; Holmes, R. J.; Djurovich, P. I.; Forrest, S. R.; Thompson, M. E. *Chemistry Of Materials* **2004**, *16*, 4743–4747.
522. Holmes, R. J.; D'Andrade, B. W.; Forrest, S. R.; Ren, X.; Li, J.; Thompson, M. E. *Applied Physics Letters* **2003**, *83*, 3818–3820.
523. Laskar, I. R.; Hsu, S.-F.; Chen, T.-M. *Polyhedron* **2006**, *25*, 1167–1176.
524. Holmes, R. J.; Forrest, S. R.; Tung, Y. J.; Kwong, R. C.; Brown, J. J.; Garon, S.; Thompson, M. E. *Applied Physics Letters* **2003**, *82*, 2422–2424.
525. Tokito, S.; Iijima, T.; Suzuri, Y.; Kita, H.; Tsuzuki, T.; Sato, F. *Applied Physics Letters* **2003**, *83*, 569–571.
526. Lei, G. T.; Wang, L. D.; Duan, L.; Wang, J. H.; Qiu, Y. *Synthetic Metals* **2004**, *144*, 249–252.
527. Lei, G. T.; Wang, L. D.; Yong, Q. *Japanese Journal Of Applied Physics Part 2-Letters & Express Letters* **2004**, *43*, L1226–L1228.
528. Laskar, I. R.; Hsu, S. F.; Chen, T. M. *Polyhedron* **2005**, *24*, 189–200.
528a. Lo, S. C.; Richards, G. J.; Markham, J. P. J.; Namdas, E. B.; Sharma, S.; Burn, P. L.; Samuel, I. D. W. *Adv. Funct. Mater.* **2005**, *15*, 1451–1458.
529. Holmes, R. J.; Forrest, S. R.; Sajoto, T.; Tamayo, A.; Djurovich, P. I.; Thompson, M. E. *Org. Electron.* **2006**, *7*, 163–172.
530. Takizawa, S.; Nishida, J.; Tsuzuki, T.; Tokito, S.; Yamashita, Y. *Chemistry Letters* **2005**, *34*, 1222–1223.
531. Yang, C. H.; Fang, K. H.; Chen, C. H.; Sun, I. W. *Chemical Communications* **2004**, 2232–2233.
532. Xie, H. Z.; Liu, M. W.; Wang, O. Y.; Zhang, X. H.; Lee, C. S.; Hung, L. S.; Lee, S. T.; Teng, P. F.; Kwong, H. L.; Zheng, H.; Che, C. M. *Advanced Materials* **2001**, *13*, 1245–1248.
533. Echigo, T.; Naka, S.; Okada, H.; Onnagawa, H. *Japanese Journal of Applied Physics, Part 1: Regular Papers, Short Notes & Review Papers* **2005**, *44*, 626–629.
534. Zhou, X.; Blochwitz-Nimoth, J.; Pfeiffer, M.; Maennig, B.; Drechsel, J.; Werner, A.; Leo, K. *Synthetic Metals* **2003**, *137*, 1063–1064.
535. Pfeiffer, M.; Forrest, S. R.; Zhou, X.; Leo, K. *Organic Electronics* **2003**, *4*, 21–26.
536. Pfeiffer, M.; Forrest, S. R.; Leo, K.; Thompson, M. E. *Advanced Materials* **2002**, *14*, 1633–1636.
537. Zhou, X.; Qin, D. S.; Pfeiffer, M.; Blochwitz-Nimoth, J.; Werner, A.; Drechsel, J.; Maennig, B.; Leo, K.; Bold, M.; Erk, P.; Hartmann, H. *Applied Physics Letters* **2002**, *81*, 4070–4072.
538. He, G. F.; Schneider, O.; Qin, D. S.; Zhou, X.; Pfeiffer, M.; Leo, K. *Journal Of Applied Physics* **2004**, *95*, 5773–5777.
539. Inomata, H.; Goushi, K.; Masuko, T.; Konno, T.; Imai, T.; Sasabe, H.; Brown, J. J.; Adachi, C. *Chemistry Of Materials* **2004**, *16*, 1285–1291.
540. Brunner, K.; van Dijken, A.; Borner, H.; Bastiaansen, J.; Kiggen, N. M. M.; Langeveld, B. M. W. *Journal Of The American Chemical Society* **2004**, *126*, 6035–6042.
541. Goushi, K.; Kwong, R.; Brown, J. J.; Sasabe, H.; Adachi, C. *Journal Of Applied Physics* **2004**, *95*, 7798–7802.
542. Chwang, A. B.; Kwong, R. C.; Brown, J. J. *Applied Physics Letters* **2002**, *80*, 725–727.
543. Watanabe, T.; Nakamura, E.; Kawami, S.; Fukuda, Y.; Tsuji, T.; Wakimoto, T.; Miyaguchi, S.; Yahiro, M.; Yang, M. J.; Tsutsui, T. *Synthetic Metals* **2001**, *122*, 203–207.
544. Tsutsui, T.; Yang, M. J.; Yahiro, M.; Nakamura, K.; Watanabe, T.; Tsuji, T.; Fukuda, Y.; Wakimoto, T.; Miyaguchi, S. *Japanese Journal Of Applied Physics Part 2-Letters* **1999**, *38*, L1502–L1504.
545. Wong, K. T.; Chen, Y. M.; Lin, Y. T.; Su, H. C.; Wu, C. C. *Org. Lett.* **2005**, *7*, 5361–5364.
546. Tsuzuki, T.; Shirasawa, N.; Suzuki, T.; Tokito, S. *Advanced Materials* **2003**, *15*, 1455–1458.
547. Tsuzuki, T.; Shirasawa, N.; Suzuki, T.; Tokito, S. *Japanese Journal Of Applied Physics Part 1-Regular Papers Short Notes & Review Papers* **2005**, *44*, 4151–4154.
548. Markham, J. P. J.; Lo, S. C.; Magennis, S. W.; Burn, P. L.; Samuel, I. D. W. *Applied Physics Letters* **2002**, *80*, 2645–2647.
549. Markham, J. P. J.; Samuel, I. D. W.; Lo, S. C.; Burn, P. L.; Weiter, M.; Bassler, H. *Journal Of Applied Physics* **2004**, *95*, 438–445.
550. Anthopoulos, T. D.; Markham, J. P. J.; Namdas, E. B.; Samuel, I. D. W.; Lo, S. C.; Burn, P. L. *Applied Physics Letters* **2003**, *82*, 4824–4826.
551. Namdas, E. B.; Anthopoulos, T. D.; Samuel, I. D. W.; Frampton, M. J.; Lo, S.-C.; Burn, P. L. *Applied Physics Letters* **2005**, *86*, 161104.
552. Anthopoulos, T. D.; Markham, J. P. J.; Namdas, E. B.; Lawrence, J. R.; Samuel, I. D. W.; Lo, S. C.; Burn, P. L. *Organic Electronics* **2003**, *4*, 71–76.
553. Lo, S. C.; Male, N. A. H.; Markham, J. P. J.; Magennis, S. W.; Burn, P. L.; Salata, O. V.; Samuel, I. D. W. *Advanced Materials* **2002**, *14*, 975–979.
554. Wang, Y.; Herron, N.; Grushin, V. V.; LeCloux, D.; Petrov, V. *Applied Physics Letters* **2001**, *79*, 449–451.
555. Chang, W. C.; Hu, A. T.; Duan, J. P.; Rayabarapu, D. K.; Cheng, C. H. *Journal Of Organometallic Chemistry* **2004**, *689*, 4882–4888.
556. Nishida, J.-i.; Echizen, H.; Iwata, T.; Yamashita, Y. *Chemistry Letters* **2005**, *34*, 1378–1379.
557. Cumpstey, N.; Bera, R. N.; Burn, P. L.; Samuel, I. D. W. *Macromolecules* **2005**, *38*, 9564–9570.
557a. Sandee, A. J.; Williams, C. K.; Evans, N. R.; Davies, J. E.; Boothby, C. E.; Kohler, A.; Friend, R. H.; Holmes, A. B. *J. Am. Chem. Soc.* **2004**, *126*, 7041–7048.
558. Lo, S. C.; Anthopoulos, T. D.; Namdas, E. B.; Burn, P. L.; Samuel, I. D. W. *Advanced Materials* **2005**, *17*, 1945–1948.
559. Laskar, I. R.; Chen, T. M. *Chemistry Of Materials* **2004**, *16*, 111–117.
560. Zhang, G. L.; Guo, H. Q.; Chuai, Y.; Zou, D. C. *Materials Letters* **2005**, *59*, 3002–3006.
561. Saito, K.; Matsusue, N.; Kanno, H.; Hamada, Y.; Takahashi, H.; Matsumura, T. *Japanese Journal Of Applied Physics Part 1-Regular Papers Short Notes & Review Papers* **2004**, *43*, 2733–2734.
562. Ding, J.; Gao, J.; Fu, Q.; Cheng, Y.; Ma, D.; Wang, L. *Synth. Met.* **2005**, *155*, 539–548.
563. Anthopoulos, T. D.; Frampton, M. J.; Namdas, E. B.; Burn, P. L.; Samuel, I. D. W. *Advanced Materials* **2004**, *16*, 557–560.
564. Okada, S.; Okinaka, K.; Iwawaki, H.; Furugori, M.; Hashimoto, M.; Mukaide, T.; Kamatani, J.; Igawa, S.; Tsuboyama, A.; Takiguchi, T.; Ueno, K. *Dalton Transactions* **2005**, 1583–1590.
565. Duan, J. P.; Sun, P. P.; Cheng, C. H. *Advanced Materials* **2003**, *15*, 224–228.
566. Song, Y. H.; Yeh, S. J.; Chen, C. T.; Chi, Y.; Liu, C. S.; Yu, J. K.; Hu, Y. H.; Chou, P. T.; Peng, S. M.; Lee, G. H. *Advanced Functional Materials* **2004**, *14*, 1221–1226.
567. Fang, K.-H.; Wu, L.-L.; Huang, Y.-T.; Yang, C.-H.; Sun, I. W. *Inorg. Chim. Acta* **2006**, *359*, 441–450.
568. Huang, Y. T.; Chuang, T. H.; Shu, Y. L.; Kuo, Y. C.; Wu, P. L.; Yang, C. H.; Sun, I. W. *Organometallics* **2005**, *24*, 6230–6238.
569. Qin, D. S.; Tao, Y. *J. Appl. Phys.* **2005**, *97*, 044505.
570. Li, H. C.; Chou, P. T.; Hu, Y. H.; Cheng, Y. M.; Liu, R. S. *Organometallics* **2005**, *24*, 1329–1335.
571. Lee, C. L.; Das, R. R.; Kim, J. J. *Chemistry Of Materials* **2004**, *16*, 4642–4646.
572. Tanaka, I.; Suzuki, M.; Tokito, S. *Japanese Journal Of Applied Physics Part 1-Regular Papers Short Notes & Review Papers* **2003**, *42*, 2737–2740.

573. Nakamura, A.; Tada, T.; Mizukami, M.; Yagyu, S. *Applied Physics Letters* **2004**, *84*, 130–132.
574. Tokito, S.; Suzuki, M.; Sato, F. *Thin Solid Films* **2003**, *445*, 353–357.
575. Tokito, S.; Suzuki, M.; Sato, F.; Kamachi, M.; Shirane, K. *Organic Electronics* **2003**, *4*, 105–111.
576. Suzuki, M.; Hatakeyama, T.; Tokito, S.; Sato, F. *Ieee Journal Of Selected Topics In Quantum Electronics* **2004**, *10*, 115–120.
577. Lamansky, S.; Kwong, R. C.; Nugent, M.; Djurovich, P. I.; Thompson, M. E. *Organic Electronics* **2001**, *2*, 53–62.
578. Liu, H.-M.; He, J.; Wang, P.-F.; Xie, H.-Z.; Zhang, X.-H.; Lee, C.-S.; Sun, B.-Q.; Xia, Y.-J. *Applied Physics Letters* **2005**, *87*, 221103.
579. Lee, C. L.; Lee, K. B.; Kim, J. J. *Materials Science And Engineering B-Solid State Materials For Advanced Technology* **2001**, *85*, 228–231.
580. Lee, C. L.; Lee, K. B.; Kim, J. J. *Applied Physics Letters* **2000**, *77*, 2280–2282.
581. Yang, M. J.; Tsutsui, T. *Japanese Journal Of Applied Physics Part 2-Letters* **2000**, *39*, L828–L829.
582. van Dijken, A.; Bastiaansen, J.; Kiggen, N. M. M.; Langeveld, B. M. W.; Rothe, C.; Monkman, A.; Bach, I.; Stossel, P.; Brunner, K. *Journal Of The American Chemical Society* **2004**, *126*, 7718–7727.
583. Vaeth, K. M.; DiCillo, J. *Synthetic Metals* **2004**, *143*, 75–79.
584. Hino, Y.; Kajii, H.; Ohmori, Y. *Organic Electronics* **2004**, *5*, 265–270.
585. Noh, Y. Y.; Lee, C. L.; Kim, J. J.; Yase, K. *Journal Of Chemical Physics* **2003**, *118*, 2853–2864.
586. Li, H. R.; Zhang, F. J.; Zheng, D. S. *Semiconductor Science And Technology* **2003**, *18*, 278–283.
587. Chen, F. C.; He, G. F.; Yang, Y. *Applied Physics Letters* **2003**, *82*, 1006–1008.
588. Vaeth, K. M.; Tang, C. W. *Journal Of Applied Physics* **2002**, *92*, 3447–3453.
589. Zhu, W. G.; Mo, Y. Q.; Yuan, M.; Yang, W.; Cao, Y. *Applied Physics Letters* **2002**, *80*, 2045–2047.
590. Qiu, C. F.; Xie, Z. L.; Chen, H. Y.; Tang, B. Z.; Wong, M.; Kwok, H. S. *Ieee Journal Of Selected Topics In Quantum Electronics* **2004**, *10*, 101–106.
591. Chen, F. C.; Chang, S. C.; He, G. F.; Pyo, S.; Yang, Y.; Kurotaki, M.; Kido, J. *Journal Of Polymer Science Part B-Polymer Physics* **2003**, *41*, 2681–2690.
592. Hino, Y.; Yamazaki, M.; Kajii, H.; Ohmori, Y. *Japanese Journal Of Applied Physics Part 1-Regular Papers Short Notes & Review Papers* **2004**, *43*, 2315–2319.
593. Plummer, E. A.; van Dijken, A.; Hofstraat, H. W.; De Cola, L.; Brunner, K. *Advanced Functional Materials* **2005**, *15*, 281–289.
594. Vaeth, K. M.; Dicillo, J. *Journal Of Polymer Science Part B-Polymer Physics* **2003**, *41*, 2715–2725.
595. Lee, C. L.; Kang, N. G.; Cho, Y. S.; Lee, J. S.; Kim, J. J. *Optical Materials* **2003**, *21*, 119–123.
596. Yang, X. H.; Neher, D. *Applied Physics Letters* **2004**, *84*, 2476–2478.
597. Yang, X. H.; Neher, D.; Hertel, D.; Daubler, T. K. *Advanced Materials* **2004**, *16*, 161–166.
598. Lamansky, S.; Djurovich, P. I.; Abdel-Razzaq, F.; Garon, S.; Murphy, D. L.; Thompson, M. E. *Journal Of Applied Physics* **2002**, *92*, 1570–1575.
599. Yang, W.; Zhen, H. Y.; Jiang, C. Y.; Su, L. J.; Jiang, J. X.; Shi, H. H.; Cao, Y. *Synthetic Metals* **2005**, *153*, 189–192.
600. Wang, X. D.; Ogino, K.; Tanaka, K.; Usui, H. *Ieee Journal Of Selected Topics In Quantum Electronics* **2004**, *10*, 121–126.
601. Kim, T. H.; Yoo, D. H.; Park, J. H.; Park, O. O.; Yu, J. W.; Kim, J. K. *Applied Physics Letters* **2005**, *86*, 171108.
602. Gao, J.; You, H.; Qin, Z. P.; Fang, J. F.; Ma, D. G.; Zhu, X. H.; Huang, W. *Semiconductor Science And Technology* **2005**, *20*, 805–808.
603. Zhu, M. X.; Wu, Z. L.; Jiang, C. Y.; Liu, J.; Li, J. R.; Xing, K. Q.; Yang, Y. P.; Gan, Q.; Cao, Y.; Zhu, W. G. *Chinese Physics Letters* **2005**, *22*, 1793–1796.
604. Gong, X.; Ostrowski, J. C.; Moses, D.; Bazan, G. C.; Heeger, A. J. *Journal Of Polymer Science Part B-Polymer Physics* **2003**, *41*, 2691–2705.
605. Gong, X.; Robinson, M. R.; Ostrowski, J. C.; Moses, D.; Bazan, G. C.; Heeger, A. J. *Advanced Materials* **2002**, *14*, 581–585.
606. Wang, J. H.; Duan, L.; Wang, L. D.; Qiu, Y. *Chinese Physics Letters* **2003**, *20*, 1141–1143.
607. Gong, X.; Lim, S. H.; Ostrowski, J. C.; Moses, D.; Bardeen, C. J.; Bazan, G. C. *Journal Of Applied Physics* **2004**, *95*, 948–953.
608. Gong, X.; Ostrowski, J. C.; Moses, D.; Bazan, G. C.; Heeger, A. J. *Advanced Functional Materials* **2003**, *13*, 439–444.
609. Wang, X. J.; Andersson, M. R.; Thompson, M. E.; Ingandas, O. *Thin Solid Films* **2004**, *468*, 226–233.
610. Wang, X. J.; Andersson, M.; Thompson, M. E.; Inganas, O. *Synthetic Metals* **2003**, *137*, 1019–1020.
611. Laskar, I. R.; Liu, H. W.; Huang, C. P.; Cheng, J. A.; Chen, T. M. *Japanese Journal Of Applied Physics Part 2-Letters & Express Letters* **2005**, *44*, L727–L730.
612. Jiang, J. X.; Jiang, C. Y.; Yang, W.; Zhen, H. G.; Huang, F.; Cao, Y. *Macromolecules* **2005**, *38*, 4072–4080.
613. Zhu, W. G.; Ke, Y.; Wang, F.; Liu, C. Z.; Yuan, M.; Cao, Y. *Synthetic Metals* **2003**, *137*, 1079–1080.
614. Cunningham, G. B.; Li, Y. T.; Liu, S. X.; Schanze, K. S. *Journal Of Physical Chemistry B* **2003**, *107*, 12569–12572.
615. Gong, X.; Ostrowski, J. C.; Bazan, G. C.; Moses, D.; Heeger, A. J.; Liu, M. S.; Jen, A. K. Y. *Advanced Materials* **2003**, *15*, 45–49.
616. Gong, X.; Ostrowski, J. C.; Bazan, G. C.; Moses, D.; Heeger, A. J. *Applied Physics Letters* **2002**, *81*, 3711–3713.
617. Wu, F. I.; Su, H. J.; Shu, C. F.; Luo, L. Y.; Diau, W. G.; Cheng, C. H.; Duan, J. P.; Lee, G. H. *Journal Of Materials Chemistry* **2005**, *15*, 1035–1042.
618. Chang, C.-Y.; Hsieh, S.-N.; Wen, T.-C.; Guo, T.-F.; Cheng, C.-H. *Chemical Physics Letters* **2005**, *418*, 50–53.
619. Jiang, C. Y.; Yang, W.; Peng, J. B.; Xiao, S.; Cao, Y. *Advanced Materials* **2004**, *16*, 537–541.
620. Chen, F. C.; Yang, Y.; Thompson, M. E.; Kido, J. *Applied Physics Letters* **2002**, *80*, 2308–2310.
621. Chen, F. C.; Yang, Y.; Pei, Q. *Applied Physics Letters* **2002**, *81*, 4278–4280.
622. Chen, X. W.; Liao, J. L.; Liang, Y. M.; Ahmed, M. O.; Tseng, H. E.; Chen, S. A. *Journal Of The American Chemical Society* **2003**, *125*, 636–637.
623. Niu, Y. H.; Chen, B. Q.; Liu, S.; Yip, H.; Bardecker, J.; Jen, A. K. Y.; Kavitha, J.; Chi, Y.; Shu, C. F.; Tseng, Y. H.; Chien, C. H. *Applied Physics Letters* **2004**, *85*, 1619–1621.
624. Hino, Y.; Kajii, H.; Ohmori, Y. *Japanese Journal Of Applied Physics Part 1-Regular Papers Short Notes & Review Papers* **2005**, *44*, 2790–2794.
625. Hwang, F. M.; Chen, H. Y.; Chen, P. S.; Liu, C. S.; Chi, Y.; Shu, C. F.; Wu, F. L.; Chou, P. T.; Peng, S. M.; Lee, G. H. *Inorganic Chemistry* **2005**, *44*, 1344–1353.
626. Sotoyama, W.; Satoh, T.; Sawatari, N.; Inoue, H. *Applied Physics Letters* **2005**, *86*, 153505.
627. Wong, W. Y.; He, Z.; So, S. K.; Tong, K. L.; Lin, Z. Y. *Organometallics* **2005**, *24*, 4079–4082.
628. Ionkin, A. S.; Marshall, W. J.; Wang, Y. *Organometallics* **2005**, *24*, 619–627.
629. Lin, Y. Y.; Chan, S. C.; Chan, M. C. W.; Hou, Y. J.; Zhu, N. Y.; Che, C. M.; Liu, Y.; Wang, Y. *Chemistry-A European Journal* **2003**, *9*, 1263–1272.
630. Che, C. M.; Chan, S. C.; Xiang, H. F.; Chan, M. C. W.; Liu, Y.; Wang, Y. *Chemical Communications* **2004**, 1484–1485.
631. Xiang, H. F.; Chan, S. C.; Wu, K. K. Y.; Che, C. M.; Lai, P. T. *Chemical Communications* **2005**, 1408–1410.

632. Kwok, C. C.; Ngai, H. M. Y.; Chan, S. C.; Sham, I. H. T.; Che, C. M.; Zhu, N. Y. *Inorganic Chemistry* **2005**, *44*, 4442–4444.
633. Lu, W.; Mi, B. X.; Chan, M. C. W.; Hui, Z.; Zhu, N. Y.; Lee, S. T.; Che, C. M. *Chemical Communications* **2002**, 206–207.
634. Liu, J.; Zhu, M. X.; Jiang, C. Y.; Liu, Y.; Wu, Z. L.; Li, J. R.; Xing, K. Q.; Cao, Y.; Zhu, W. G. *Chinese Physics Letters* **2005**, *22*, 723–726.
635. Laskar, I. R.; Hsu, S. F.; Chen, T. M. *Polyhedron* **2005**, *24*, 881–888.
636. Cocchi, M.; Virgili, D.; Sabatini, C.; Fattori, V.; Di Marco, P.; Maestri, M.; Kalinowski, J. *Synthetic Metals* **2004**, *147*, 253–256.
637. Zhang, L.; Niu, Y. H.; Jen, A. K. Y.; Lin, W. B. *Chemical Communications* **2005**, 1002–1004.
638. Liu, Q. D.; Thorne, L.; Kozin, I.; Song, D. T.; Seward, C.; D'Iorio, M.; Tao, Y.; Wang, S. N. *Journal Of The Chemical Society-Dalton Transactions* **2002**, 3234–3240.
639. Kavitha, J.; Chang, S. Y.; Chi, Y.; Yu, J. K.; Hu, Y. H.; Chou, P. T.; Peng, S. M.; Lee, G. H.; Tao, Y. T.; Chien, C. H.; Carty, A. J. *Advanced Functional Materials* **2005**, *15*, 223–229.
640. Saito, K.; Hamada, Y.; Takahashi, H.; Koshiyama, T.; Kato, M. *Japanese Journal Of Applied Physics Part 2-Letters & Express Letters* **2005**, *44*, L500–L501.
641. D'Andrade, B.; Forrest, S. R. *Chemical Physics* **2003**, *286*, 321–335.
642. Wong, K. M. C.; Zhu, X. L.; Hung, L. L.; Zhu, N. Y.; Yam, V. W. W.; Kwok, H. S. *Chemical Communications* **2005**, 2906–2908.
643. Liu, Q. D.; Mudadu, M. S.; Schmider, H.; Thummel, R.; Tao, Y.; Wang, S. I. *Organometallics* **2002**, *21*, 4743–4749.
644. Wang, S. N. *Coordination Chemistry Reviews* **2001**, *215*, 79–98.
645. Liu, S. F.; Wu, Q. G.; Schmider, H. L.; Aziz, H.; Hu, N. X.; Popovic, Z.; Wang, S. N. *Journal Of The American Chemical Society* **2000**, *122*, 3671–3678.
646. Noto, M.; Goto, Y.; Era, M. *Chemistry Letters* **2003**, *32*, 32–33.
647. Ma, Y. G.; Che, C. M.; Chao, H. Y.; Zhou, X. M.; Chan, W. H.; Shen, J. C. *Advanced Materials* **1999**, *11*, 852–857.
648. Zhang, J. Y.; Kan, S. D.; Ma, Y. G.; Shen, J. C.; Chan, W. H.; Che, C. M. *Synthetic Metals* **2001**, *121*, 1723–1724.
649. Tung, Y. L.; Lee, S. W.; Chi, Y.; Tao, Y. T.; Chien, C. H.; Cheng, Y. M.; Chou, P. T.; Peng, S. M.; Liu, C. S. *Journal Of Materials Chemistry* **2005**, *15*, 460–464.
650. Wu, F. I.; Shih, P. I.; Shu, C. F.; Tung, Y. L.; Chi, Y. *Macromolecules* **2005**, *38*, 9028–9036.
651. Lu, J.; Tao, Y.; Chi, Y.; Tung, Y. *Synthetic Metals* **2005**, *155*, 56–62.
652. Tung, Y. L.; Wu, P. C.; Liu, C. S.; Chi, Y.; Yu, J. K.; Hu, Y. H.; Chou, P. T.; Peng, S. M.; Lee, G. H.; Tao, Y.; Carty, A. J.; Shu, C. F.; Wu, F. I. *Organometallics* **2004**, *23*, 3745–3748.
653. Niu, Y. H.; Tung, Y. L.; Chi, Y.; Shu, C. F.; Kim, J. H.; Chen, B. Q.; Luo, J. D.; Carty, A. J.; Jen, A. K. Y. *Chemistry Of Materials* **2005**, *17*, 3532–3536.
654. Ranjan, S.; Lin, S. Y.; Hwang, K. C.; Chi, Y.; Ching, W. L.; Liu, C. S.; Tao, Y. T.; Chien, C. H.; Peng, S. M.; Lee, G. H. *Inorganic Chemistry* **2003**, *42*, 1248–1255.
655. Wang, K. Z.; Huang, L.; Gao, L. H.; Jin, L. P.; Huang, C. H. *Inorganic Chemistry* **2002**, *41*, 3353–3358.
656. Gong, X.; Ng, P. K.; Chan, W. K. *Advanced Materials* **1998**, *10*, 1337–1340.
657. Ng, P. K.; Gong, X.; Chan, S. H.; Lam, L. S. M.; Chan, W. K. *Chemistry-A European Journal* **2001**, *7*, 4358–4367.
658. Li, F.; Cheng, G.; Zhao, Y.; Feng, J.; Liu, S. Y.; Zhang, M.; Ma, Y. G.; Shen, J. C. *Applied Physics Letters* **2003**, *83*, 4716–4718.
659. Li, F.; Zhang, M.; Feng, J.; Cheng, G.; Wu, Z. J.; Ma, Y. G.; Liu, S. Y.; Sheng, J. C.; Lee, S. T. *Applied Physics Letters* **2003**, *83*, 365–367.
660. David, G.; Walsh, P. J.; Gordon, K. C. *Chemical Physics Letters* **2004**, *383*, 292–296.
661. Li, F.; Zhang, M.; Cheng, G.; Feng, J.; Zhao, Y.; Ma, Y. G.; Liu, S. Y.; Shen, J. C. *Applied Physics Letters* **2004**, *84*, 148–150.
662. Li, B.; Li, M. T.; Hong, Z. R.; Li, W. L.; Yu, T. Z.; Wei, H. Z. *Applied Physics Letters* **2004**, *85*, 4786–4788.
663. Tung, Y. L.; Lee, S. W.; Chi, Y.; Chen, L. S.; Shu, C. F.; Wu, F. I.; Carty, A. J.; Chou, P. T.; Peng, S. M.; Lee, G. M. *Advanced Materials* **2005**, *17*, 1059–1064.
664. D'Andrade, B. W.; Holmes, R. J.; Forrest, S. R. *Advanced Materials* **2004**, *16*, 624–628.
665. Tokito, S.; Iijima, T.; Tsuzuki, T.; Sato, F. *Applied Physics Letters* **2003**, *83*, 2459–2461.
666. Deshpande, R. S.; Bulovic, V.; Forrest, S. R. *Applied Physics Letters* **1999**, *75*, 888–890.
667. Hide, F.; Kozodoy, P.; DenBaars, S. P.; Heeger, A. J. *Applied Physics Letters* **1997**, *70*, 2664–2666.
668. Zhang, Y. F.; Cheng, G.; Zhao, Y.; Hou, J. Y.; Liu, S. Y. *Applied Physics Letters* **2005**, *86*, 011112.
669. Qin, D. S.; Tao, Y. *Applied Physics Letters* **2005**, *86*, 113507.
670. Lei, G. T.; Wang, L. D.; Qiu, Y. *Applied Physics Letters* **2004**, *85*, 5403–5405.
671. Cheng, G.; Zaho, Y.; Xie, W.; Ma, Y.; Liu, S. *Optical And Quantum Electronics* **2004**, *36*, 659–664.
672. Cheng, G.; Li, F.; Duan, Y.; Feng, J.; Liu, S. Y.; Qiu, S.; Lin, D.; Ma, Y. G.; Lee, S. T. *Applied Physics Letters* **2003**, *82*, 4224–4226.
673. Cheng, G.; Qiu, S.; Zhao, Y.; Ma, Y. G.; Liu, S. Y. *Chinese Physics Letters* **2003**, *20*, 1607–1609.
674. Xie, W. F.; Zhao, Y.; Li, C. N.; Liu, S. Y. *Semiconductor Science And Technology* **2005**, *20*, 326–329.
675. Xu, Y.; Peng, J.; Jiang, J.; Xu, W.; Yang, W.; Cao, Y. *Applied Physics Letters* **2005**, *87*, 193502.
676. Al Attar, H. A.; Monkman, A. P.; Tavasli, M.; Bettington, S.; Bryce, M. R. *Applied Physics Letters* **2005**, *86*, 121101.
677. Gong, X.; Ma, W. L.; Ostrowski, J. C.; Bazan, G. C.; Moses, D.; Heeger, A. J. *Advanced Materials* **2004**, *16*, 615–619.
678. Gong, X.; Moses, D.; Heeger, A. J.; Xiao, S. *Journal Of Physical Chemistry B* **2004**, *108*, 8601–8605.
679. Gong, X.; Wang, S.; Moses, D.; Bazan, G. C.; Heeger, A. J. *Advanced Materials* **2005**, *17*, 2053–2058.
680. Baldo, M. A.; Thompson, M. E.; Forrest, S. R. *Nature* **2000**, *403*, 750–753.
681. D'Andrade, B. W.; Baldo, M. A.; Adachi, C.; Brooks, J.; Thompson, M. E.; Forrest, S. R. *Applied Physics Letters* **2001**, *79*, 1045–1047.
682. He, G. F.; Chang, S. C.; Chen, F. C.; Li, Y. F.; Yang, Y. *Applied Physics Letters* **2002**, *81*, 1509–1511.
683. Liu, S. Y.; Feng, J.; Zhao, Y. *Japanese Journal Of Applied Physics Part 1–Regular Papers Short Notes & Review Papers* **2004**, *43*, 2320–2322.
684. D'Andrade, B. W.; Forrest, S. R. *Journal Of Applied Physics* **2003**, *94*, 3101–3109.
685. Furuta, P. T.; Deng, L.; Garon, S.; Thompson, M. E.; Frechet, J. M. J. *Journal Of The American Chemical Society* **2004**, *126*, 15388–15389.
686. Halsted, C. P. *Information Display* **1993**.
687. Jordan, R. H.; Dodabalapur, A.; Strukelj, M.; Miller, T. M. *Applied Physics Letters* **1996**, *68*, 1192–1194.

12.05 Metallomesogens

D W Bruce, University of York, York, UK
R Deschenaux, Université de Neuchâtel, Neuchâtel, Switzerland
B Donnio and D Guillon, Institut de Physique et Chimie des Matériaux de Strasbourg, Strasbourg, France

12.05.1 Preamble

The purpose of this chapter is to give an account of the types of metal complexes that form liquid-crystal mesophases and to describe the way these complexes are organized within the phases as well as the nature of their physical properties. Since its rapid development in the mid-1980s, this subject has been covered by several reviews[1,1a–1q] and a book,[2] and these will inevitably provide the interested reader with different and, in many cases, more detailed perspectives. However, the aim of this chapter is to provide a self-contained introduction to the area of organometallic metallomesogens so that the first-time reader may gain a useful grasp of the subject and then be able to pursue it in more detail through the references given.

The subject matter in this review is organized according to groups from the periodic table. This complements an earlier review that contained organometallic systems[3] in which the material was arranged first by liquid-crystal phase behavior and then by ligand type. It is hoped that the interested reader will cross-reference these two sources to enhance their appreciation of the subject.

The chapter starts with a discussion of the basics of liquid-crystal phase behavior, the types of mesophase that are formed, and methods for their characterization; those requiring more detail and/or breadth are directed to the volumes of Ref: 4. This chapter does not cover liquid crystals that might be considered to be somehow "inorganic" in origin,

and so, for example, polymeric systems are largely omitted as there has been only modest development in the field since the publication of earlier reviews.[5,5a]

12.05.2 General Introduction

Matter is often considered as existing in one of three forms—solid, liquid, and gas. Yet, there exists a state of matter between the solid and liquid states that possesses properties reminiscent of each, so that like a solid it has order, while like a liquid it is fluid. This true state of matter is the liquid-crystal state and is generated in one of two ways. When a compound passes between the solid, liquid, and liquid-crystal state as a primary function of temperature and in the absence of solvent, the liquid-crystal behavior is termed "thermotropic." When the phase transitions are driven by the concentration of the liquid crystal in a solvent, the behavior is termed "lyotropic."

The recognition of the liquid-crystal state is usually attributed to the work of Reinitzer,[6] who, in 1888, published the apparent two melting points of cholesteryl esters (Figure 1), although there is evidence of the recognition of what we now know to be liquid-crystal properties in nerve myelin in the 1850s[7,7a] and also in the behavior of magnesium soaps at about the same time.[8] Another important event in the development of understanding of this new state of matter was the publication in 1922 by Friedel of '*Les états mésomorphes de la matière*',[9] a seminal report that was the very first classification of the various liquid-crystalline mesophases based on the order and symmetry of different molecular arrangements.

Since these initial discoveries, liquid crystals have become a major, multidisciplinary field of research that has made a significant impact on society following the discovery of the cyanobiphenyl liquid crystals by Gray in the early 1970s[10] and their utilization in the twisted nematic mode display device[11] that led to the birth of the liquid-crystal-display (LCD) industry, now worth >€45 billion/annum and ever increasing. The multidisciplinary nature of this field is evidenced by the pervasive nature of liquid-crystal science, extending from biology (the materials in cell membranes are liquid crystals), through chemistry to physics, mathematics, and electronic engineering.[†] Liquid crystal research is a constantly expanding field with new applications challenging the synthetic chemist and new phase types prompting physicists to ascertain how they may be harnessed. Thus, despite being regarded as a "mature" discipline, liquid-crystal research has probably never been so vibrant, and one of the significant developments in the last 15 years or so has been that of metallomesogens—a term coined in the first review of the subject by Giroud-Godquin and Maitlis.[1]

Before proceeding further, it will be of use to introduce some of the terminology commonly associated with liquid crystals. A material which has liquid-crystal properties is referred to as a "mesogen" and is said to exhibit "mesomorphism"; a material which is "liquid-crystal-like" is known as mesogenic, although something mesogenic is not necessarily mesomorphic. To avoid ambiguity, the (conventional) liquid state is referred to as the isotropic state. The temperature at which a material passes from the solid state into a mesophase is referred to as the melting point, while the temperature at which the mesophase transforms into an isotropic fluid is called the clearing point.

12.05.3 Thermotropic Liquid Crystals

Thermotropic liquid crystals can be divided into three principal types through the mesophases they form, two of which will be introduced at this stage. This classification is based on the essential shape of the molecules and while,

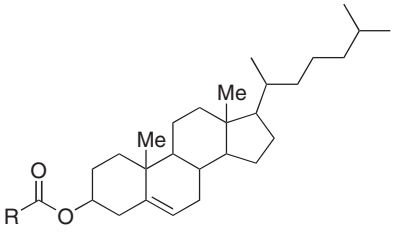

Figure 1 Reinitzer's cholesteryl liquid-crystalline esters.

[†]Since the completion of this review, the following volume has appeared, which gives a timely overview of non-display aspects of LC materials: *New Directions in Liquid Crystals*, ed D. W. Bruce, H. J. Coles, J. W. Goodby and J. R. Sambles, *Phil. Trans. Royal Soc. A*, 2006, **364**, 2565–2843.

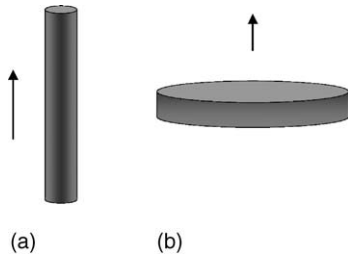

Figure 2 (a) The rod-like motif of calamitic mesogens; (b) the disk-like motif of discotic mesogens.

as will become evident, this taxonomy does not address all issues of physical properties and phase behavior, it does provide a framework by which we may begin to make sense of the observed behavior. The two types are the rod-like (calamitic) and the disk-like (discotic) liquid crystals.

As mentioned above, the liquid-crystal state exists between the solid and liquid states and is stabilized by the presence of intermolecular, anisotropic dispersion forces that result from the anisotropic nature of the molecules that form the phases. Thus, rod-like molecules are much longer than they are broad and, hence, possess one unique, long axis. Similarly, disk-like molecules are rather flat and, hence, possess one, unique short axis (Figure 2).

12.05.3.1 Calamitic Mesogens

A general structure of calamitic mesogens is often that given in Figure 3, which follows a design offered by Toyne.[12] If the figure is taken as indicative rather than prescriptive, then it forms a useful basis for the molecular design of calamitic mesogens.

What the model describes in general is an anisotropic molecule, normally, but by no means exclusively, composed of aromatic (or heteroaromatic) rings linked together in some way so that the overall anisotropy is maintained. In many cases, there will be three or more rings and the linking group(s) (B) may preserve the conjugation of the system, although this is not necessary (e.g., –CH═CH–, –C≡C–, –CH═N–, –N═N–, $–CO_2–$). The two terminal groups (A and C) can be the same or different, but in almost all cases, at least one will be an alkyl (or alkyloxy) group that enhances the anisotropy of the molecule and reduces the melting point. Where the terminal groups are not the same, in addition to an alkyl chain, there will often be a small, dipolar group (e.g., –CN, $–NO_2$, –OMe). There are many thousands of liquid-crystal molecules known and examples may be sought in Vill's remarkable database.[13] Occasionally, the molecule will possess a lateral group (D). In general, calamitic mesogens are not very tolerant of such lateral groups as they reduce the structural anisotropy. However, used cleverly they can have profound and beneficial effects, the best example of which is the inclusion of lateral fluoro substituents.[14]

Some examples of "typical" calamitic mesogens are given in Figure 4. Cyanobiphenyls are included in this list due to their special position in the development of LCDs, but it should be noted that in many ways they are not typical as their liquid-crystal mesophases arise from antiparallel molecular correlations.

While such a general model is quite appropriate to describe many known liquid-crystal species, it is increasingly inadequate, not because it is inaccurate, but rather because developments in the synthetic chemistry of liquid crystals have been such that, in reality, the usefulness of such general models might be called into question.[15] For example, a new and significant area of research concerns on so-called bent-core (or banana) liquid crystals where the structural anisotropy "rules" given above simply do not hold and a 120° bend in the molecule is effectively a requirement.[16] Some other developments may be found elsewhere.[17,17a,17b]

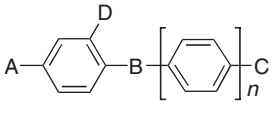

Figure 3 A general molecular structure for calamitic mesogens.

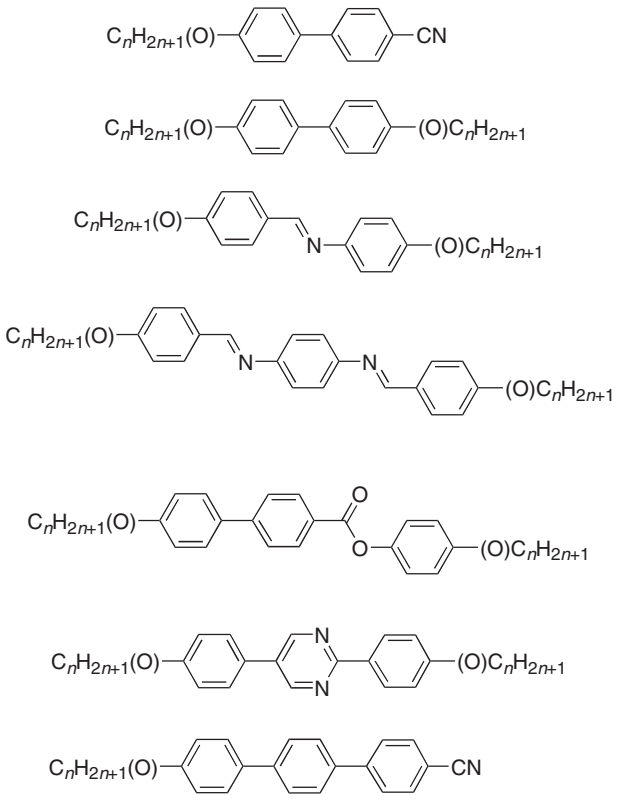

Figure 4 Some typical calamitic mesogens.

12.05.3.2 Mesophases of Calamitic Mesogens

The true liquid-crystal mesophases of calamitic mesogens are divided into two classes—the nematic and smectic phases and these will be described in turn. There is, in addition, a series of crystal smectic phases that are not really liquid-crystal phases but which for many years were classified as such; these will be mentioned briefly below.

12.05.3.2.1 The nematic phase

The nematic phase, abbreviated as N, has the simplest structure of all of the mesophases, is very fluid, and is also the least ordered mesophase. The word nematic comes from the Greek *nematos* meaning thread-like—this arises from the observed optical texture of the phase between crossed polarizers (*vide infra*). The nematic phase is characterized by one-dimensional orientational order of the molecules by virtue of correlations of the long molecular axes, although the orientational order is not polar. There is no translational order within the nematic phase. A schematic diagram of the nematic phase is shown in Figure 5.

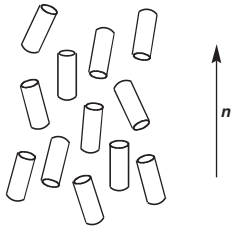

Figure 5 Schematic representation of the molecular arrangement in the nematic phase.

The parameter known as the "director" ($\boldsymbol{n}$) defines the average orientation of the molecules within the phase, while the degree of order within the phase is given by an order parameter, S, given by Equation (1):

$$S = \frac{1}{2}\langle 3\cos^2\theta - 1\rangle \tag{1}$$

Here, θ represents the angle between an individual molecule and the director, and this is summed over all molecules. Typically, for a nematic phase, $0.7 > S > 0.4$; note that the transition from the isotropic liquid to the nematic phase is discontinuous and so at the transition, S will jump from a value of zero to about 0.3–0.4. While beyond the scope of this chapter, it is important to note that it is the nematic phase of liquid crystals that is the basis for almost all display applications.

12.05.3.2.2 The chiral nematic phase

There exists a chiral version of the nematic phase, with the abbreviation N^*, that is found when a nematic phase is shown by a pure enantiomer, or by a mixture of enantiomers with one in excess, or by a racemic or non-chiral compound doped with a chiral material at, say, 5–10%. This was the phase seen in cholesteryl benzoate by Reinitzer and so for many years (and still occasionally today) it was known as the cholesteric phase, although the term "chiral nematic" is much preferred. A compound will possess either a nematic phase or a chiral nematic phase, but only in the most exceptional circumstances of pitch inversion will it show both. Due to the packing constraints imposed by the chiral nature of the materials, the molecules cannot simply align side-by-side in the phase and the long axis of one molecule will be slightly offset with respect to that of its neighbor. The net effect is for the director to precess through the phase (Figure 6), describing a helix that may be left- or right-handed depending on both the sense of the chirality and its position in the molecule;[18] two enantiomers of the same material will describe opposite twist senses for the helix.

The pitch (p) of the helical twist is often of the order of the wavelength of visible light and is very sensitive to temperature. Coupled with the fact that the chiral nematic phase exhibits selective Bragg reflection of light of the wavelength equal to np (where n is the average refractive index of the material), then N^* materials appear to change color with temperature, making them useful as non-invasive thermometers. A more extensive description of the properties and applications of N^* materials may be found elsewhere.[19]

12.05.3.2.3 The true smectic phases

The true smectic phases[20] are more highly ordered than the nematic phase and are characterized by partial translational ordering of the molecules into layers, in addition to orientational correlations. The simplest smectic phase is the smectic A (SmA) phase which is represented schematically in Figure 7(a). As in the nematic phase, the

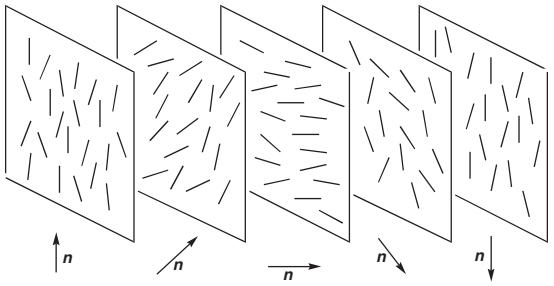

Figure 6 Schematic diagram of the chiral nematic phase.

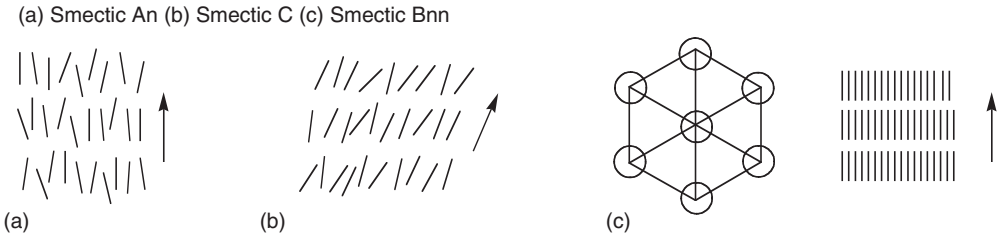

Figure 7 Schematic representation of the (a) SmA, (b) SmC and (c) SmB phases (viewed from above and from the side).

long axes of the molecules are oriented on average in the same direction, but the molecules are also loosely associated into layers, with the orientational direction perpendicular to the layer normal; diffusion between the layers occurs readily and the phase is fluid. In fact, this is a very idealized scheme and the layers in this (and the following phases) are much less well defined; a more precise description of the structure of the smectic phases may be found elsewhere.[20,21] If the SmA phase is modified slightly by tilting the molecules within the layer plane, then the smectic C phase (SmC) is obtained which is similarly fluid (Figure 7(b)).

Alternatively, the SmA may be modified by introducing hexagonal symmetry into the layer and increasing the order slightly so that the molecules sit at sites that describe a hexagonal net; this is the smectic B (SmB) phase (Figure 7(c)). As with all smectic phases, the SmB is fluid and interlayer diffusion of the molecules is facile, although rotation about the molecular long axes is concerted.

Two other smectic phases are obtained as tilted variations of the SmB, although both are more fluid. Thus, the smectic I (SmI) phase may be regarded as an SmB phase which is tilted toward a vertex of the hexagonal net, while the smectic F (SmF) phase may be regarded as an SmB phase which is tilted toward the edge of the hexagonal net (Figure 8).

These five phases are true smectic phases and in normal phase sequences would be expected to be found in the order shown in Scheme 1; the nematic and isotropic (I) phases are included for completeness.

In addition, the SmC, SmI, and SmF phases may exist as chiral modifications (SmC*, SmI,* and SmF*) either by doping with a chiral additive or by resolving a racemic material that shows one or more of the phases. Because of the low (C_2) symmetry in these phases, the molecular dipoles align within the layers that are then ferroelectric. However, the chirality also requires that the direction of the ferroelectricity precesses through space from one layer to the next and so in the bulk sample, the ferroelectricity is lost unless the helix is unwound by the use of surface anchoring and thin cells.

12.05.3.2.4 The crystal smectic phases

In addition to the true smectic phases, there is another class of mesophases, formerly also called smectic phases, which do possess extra positional order and which are derived from the true smectics and referred to as crystal smectic phases.[21] These phases are characterized by the appearance of interlayer correlations and, in some cases, by the loss of molecular rotational freedom. Thus, the (crystal) B, G, and J phases are SmB, SmF, and SmI phases, respectively, with interlayer correlations, whereas the E, H, and K phases are B, G, and J phases which have lost rotational freedom (note that, confusingly, there are both smectic and crystal B phases). These phases possess considerable disorder and are, therefore, properly intermediate between the solid and liquid states.

12.05.3.2.5 Polymorphism

The nature and number of any mesophases that are formed by a given material, and the temperatures at which they exist must be determined experimentally. This requires recourse to a selection of physical techniques, some of which are described below. However, it is helpful to know that, in most cases, the thermodynamic ordering of the various (fluid) mesophases maintains a fairly constant order that is given in Scheme 1 (although note that out-of-sequence or "re-entrant" phases are known).[22] It is rather unlikely that a single material will show all of these phases and it is found empirically that certain combinations are more likely than others.[20]

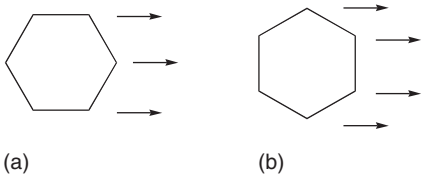

Figure 8 Schematic representation of the (a) SmI and (b) SmF mesophases showing the directions of tilt.

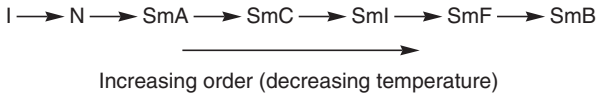

Scheme 1 Normal thermodynamic ordering of liquid-crystal mesophases.

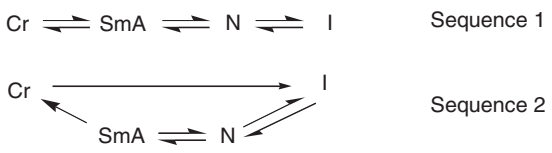

Scheme 2 Phase sequences illustrating enantiotropic (sequence 1) and monotropic (sequence 2) mesomorphism.

In most cases, the observed mesophases are found on both heating and cooling a material, so sequence 1 in Scheme 2 is fully reversible; such mesophases are termed "enantiotropic." However, in some cases a particular mesophase may only appear on cooling a material and is therefore metastable (sequence 2, Scheme 2); such phases are termed "monotropic."

12.05.3.3 Discotic Mesogens

Discotic liquid crystals came to prominence in the late 1970s when Chandrasekhar, Sadashiva, and Suresh reported the discovery of this new class of liquid-crystalline molecules, which were found to form columnar phases.[23] The first of these, a hexaalkanoate of benzene, is shown in Figure 9. There then followed a rather unfortunate confusion of nomenclature in which the phases formed by discotic molecules were themselves referred to as "discotic," carrying the abbreviation D. A liquid-crystal phase must be characterized by its symmetry and organization and not the shape of the molecules of which it is composed; this is particularly important in columnar systems as many non-discotic molecules exhibit columnar phases. Indeed, columnar mesophases have been recognized for many years and studies date back to at least the 1960s with the work of Skoulios with various metal soaps.[24] Therefore, columnar phases take the abbreviation Col followed by some descriptor that describes the symmetry of the phase.

The important feature of discotic mesogens is that now, the anisotropy is generated by the presence of a unique, "short" axis for, as their name suggests, the molecules are disk like. Within reason, design of such mesogens is almost akin to choosing your favorite disk-like molecule and grafting at least six peripheral alkyl chains onto it. Importantly, this disk-like core does not need to be totally planar and, for example, hexaaza crown ethers have been shown to form columnar mesophases. Some examples of discotic mesogens are shown in Figure 10.

12.05.3.4 Mesophases of Disk-like Mesogens

In contrast to calamitic materials, with discotic molecules,[25] it is the short axis that correlates and the simplest phase formed is a nematic phase. This is usually abbreviated as N_D and referred to as the discotic nematic phase, although for the reasons outlined above, this is somewhat unsatisfactory. In this nematic phase, there is again only orientational order as illustrated schematically in Figure 11(a). Materials showing this phase are relatively rare.

More common are the various columnar phases that are characterized by the symmetry of the side-to-side molecular arrangement of columns formed by the stacking of the disk-like molecules. Figure 11(b) shows a side-on view of the columnar hexagonal phase (Col_h) in which the molecules are arranged in columns which are further organized into a hexagonal array; within the columns there is some degree of liquid-like order. The common lattices of the columnar phases, namely hexagonal (a), oblique (b), and rectangular (c) and (d) are represented in Figure 12 as "aerial" views showing projections of the columns onto a two-dimensional plane; circles represent disks which are

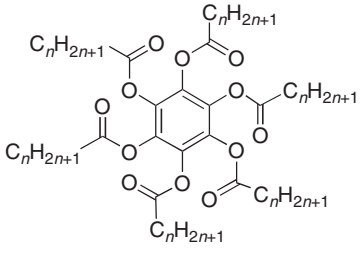

Figure 9 Discotic hexaalkanoates of benzene.

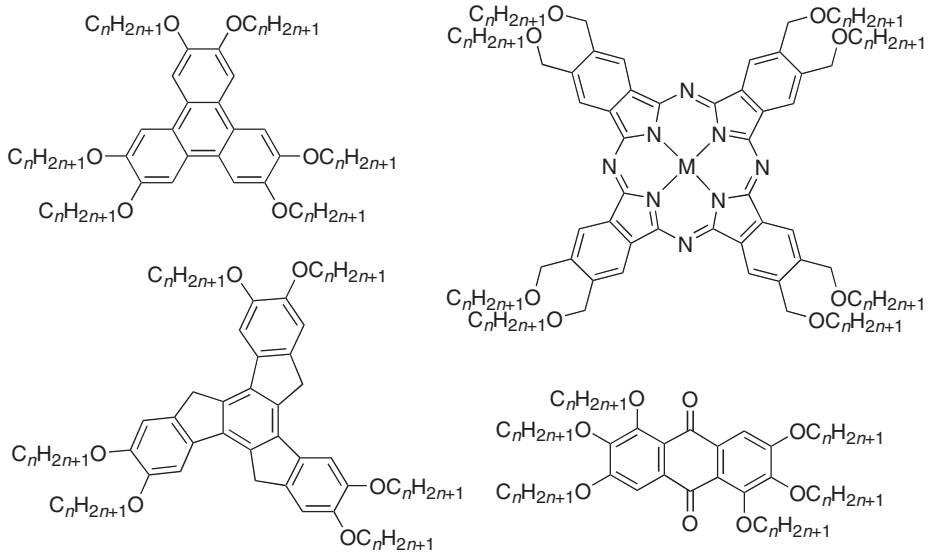

Figure 10 Representative examples of discotic materials.

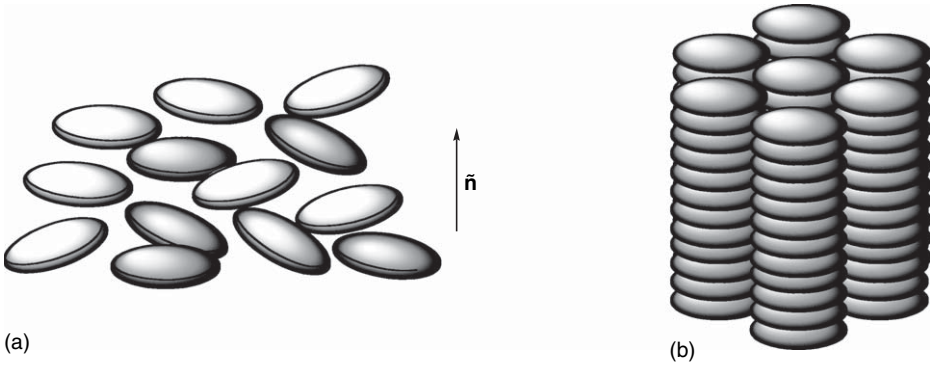

Figure 11 Schematic structure of the (a) N_D phase and (b) Col_h phase.

orthogonal within the columns, whereas ellipses represent disks which are tilted. Examples of the so-called columnar nematic phases have been described by Praefcke[26] and by Ringsdorf;[27] these are nematic arrays of columnar stacks.

12.05.3.5 Polycatenar Liquid Crystals

While it is in discotic liquid crystals that the formation of columnar phases is most readily recognized (*vide supra*), there exists a family of non-disk-like mesogens, the "polycatenar" liquid crystals, where these mesophases are also formed extensively. As will be seen from their shape, this observation is of some interest, but it is the fact that certain polycatenar materials can, within a homologous series, show mesomorphism characteristic of both rod-like and disk-like mesogens that makes them particularly interesting.

Polycatenar mesogens[28,29] are based on a calamitic motif (Figure 13), with a rather extended, central core that terminates in several alkoxy chains, hence giving rise to the name polycatenar (literally many-tailed). As a rule of thumb, it is said that there needs to be at least as many chains as rings if mesomorphism is to result. The nomenclature of polycatenar systems depends on the number of terminal chains, so that those with four chains are termed "tetracatenar," those with six chains "hexacatenar" and so on. Another aspect of the structure of polycatenar systems is that there can be more than one possible arrangement for a given number of chains. For example types A and B in Figure 13 show two different ways in which three terminal chains may be arranged, whereas types C–E show three possible arrangements for two terminal chains. The nomenclature associated with this indicates that a tetracatenar mesogen where each terminal ring was of type D in Figure 13 would be designated tetracatenar

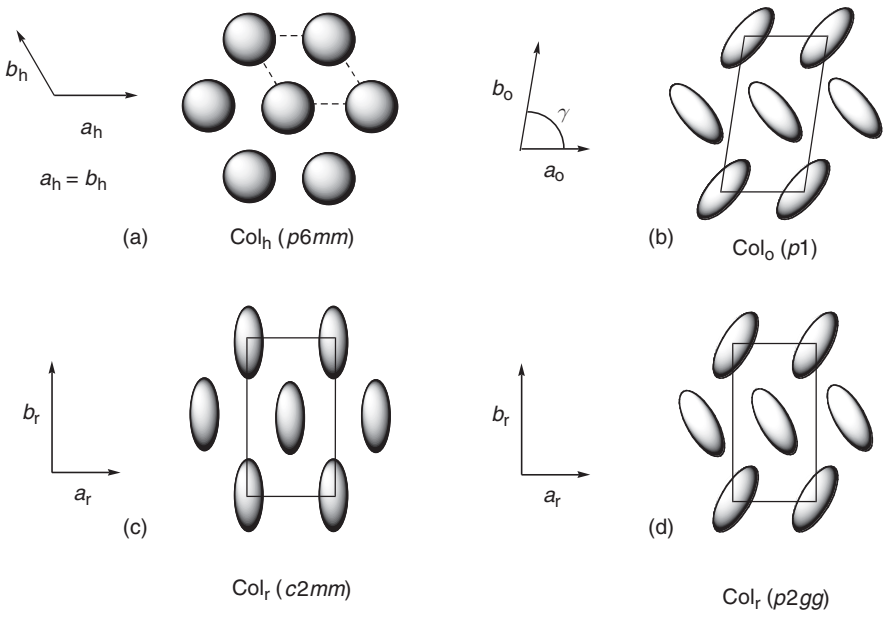

Figure 12 Representations of the lattices of the (a) hexagonal, (b) oblique, and (c) and (d) rectangular columnar phases.

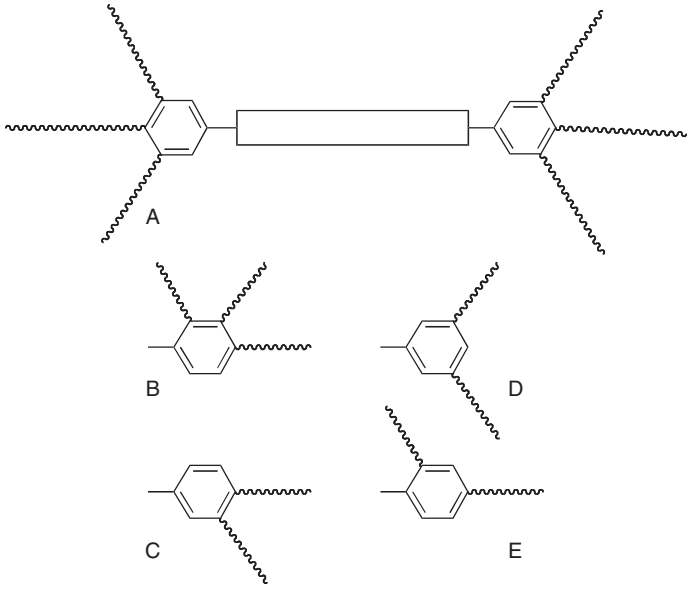

Figure 13 Schematic representation of polycatenar mesogens showing different substitution patterns of flexible chains on the terminal rings.

(2*mm*) + (2*mm*) (*o*, *m*, and *p* here refer to the *ortho*-, *meta*-, and *para*-positions of the terminal phenyl ring). Of course, terminal substitution patterns need not be symmetric, so that a tetracatenar (2*mm*) + (2*mp*) mesogen would have terminal functions C and D in Figure 13.

The number and arrangement of the chains has a profound effect on the mesomorphism, and, while it is not the intention here to describe this in too much detail, some explanation is required. The mesomorphism of most isomers is, in fact, rather straightforward as they form columnar phases. This is true for hexa-, penta-, and tetracatenar (2*mm*) + (2*mm*) systems, and the phases observed are normally either of hexagonal and/or rectangular (e.g., *c2mm* or *p2gg*) symmetry. Tricatenar (2*mp*) + (*p*) species tend to form smectic (usually SmC) and nematic phases, whereas

tricatenar (3*mpm*) mesogens often form cubic phases. However, the most interesting by far are the tetracatenar (2*mp*) + (2*mp*) mesogens and their mesomorphism will be described in a little more detail.

The reason for the interest is that in these systems, short-chain length homologs show nematic and/or SmC phases, whereas longer-chain homologs show columnar phases, in other words, the mesomorphism of rods and disks is combined into a single homologous series. When the chain length is short, the materials resemble calamitic materials and so N or smectic phases are expected. With these systems, however, it is always the tilted SmC phase that is observed, due to the fact that at the interface between the rigid core and the chains, the cross-sectional area of the chains is greater than that of the core and so to fill space efficiently, the cores must tilt (Figure 14).[30]

As the chains grow in length and/or as the temperature increases, the chains begin to occupy a greater volume and, in order to accommodate this additional volume requirement, the cores tilt even further. However, this can only go so far and eventually, the smectic layers can no longer hold together and they break up, leading to the formation of a columnar phase (Figure 15). Passage from the SmC to the columnar phase normally takes place gradually (e.g., one or

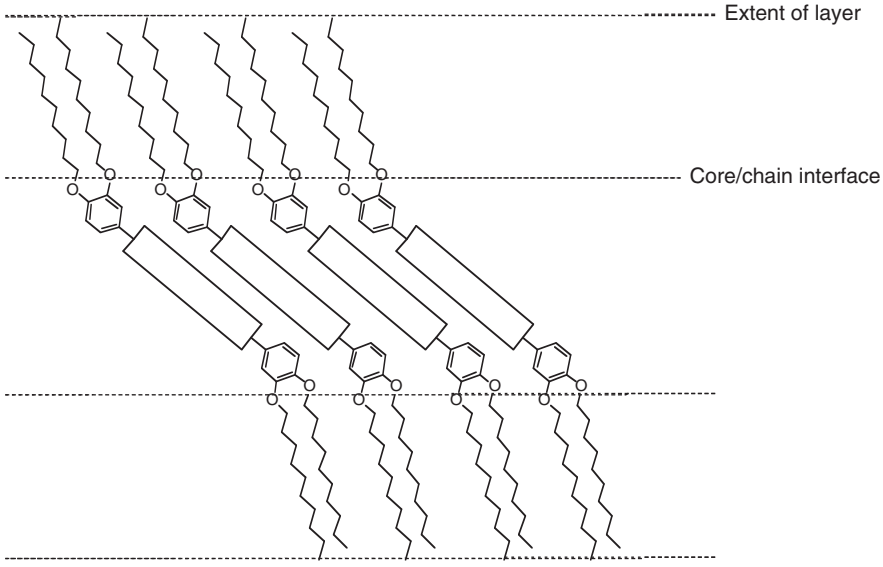

Figure 14 SmC phase of tetracatenar mesogens.

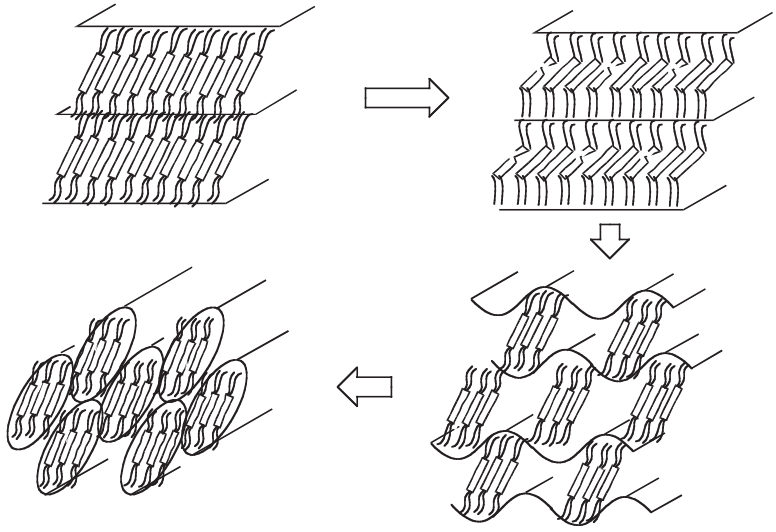

Figure 15 Schematic representation of the transition from SmC to columnar phase.

two compounds showing both phases) or via the intermediacy of another phase, often, but not always, of cubic symmetry.[31] As Figure 15 suggests, experimental data infer that the repeat unit in the columnar phases of these, and in fact other, polycatenar mesogens is constituted of more than one molecule, typically three or four. A general model for the arrangement of the molecules in these phases has been proposed recently.[32]

12.05.4 Lyotropic Liquid Crystals

If a surfactant molecule, such as cetyltrimethylammonium bromide (CTAB), is dissolved in water, at some specific concentration (known as the "critical micelle concentration" or cmc), the molecules will organize and form micelles.[33,33a] This formation of micelles (Figure 16) is caused by the hydrophobic effect,[34] which is driven entropically. Thus, in solutions of surfactant monomers, the hydrophobic chains are not molten and are surrounded by an organized layer of water; when the micelle forms, the water layer returns to the bulk and the chains become molten, greatly increasing the disorder in the system. Micelles may be formed by cationic (e.g., CTAB), anionic (e.g., $C_{12}H_{25}OSO_3Na$), or non-ionic (e.g., $C_{12}H_{25}(OCH_2CH_2)_6OH$) surfactants, and solvents are not limited to water.

If more surfactant is added above the cmc, the concentration of micelles increases (rather than the concentration of free surfactant) until the micelle concentration becomes so high that they themselves organize to form ordered arrays of lyotropic liquid-crystal phase. There are several well-characterized lyotropic liquid-crystal phases and a host of so-called intermediate phases whose characterization is not unequivocal. While cmc values are typically found in the range 10^{-5}–10^{-3} mol dm^{-3}, formation of lyotropic mesophases typically starts at around 20 wt.% of the surfactant in water.

As it is the aggregation of micelles that leads to the formation of lyotropic mesophases, then it is held to be true that the first mesophases formed is based on the micelles from which it is derived.[35] For example, spherical micelles give rise to micellar I_1 cubic phases that may be regarded as cubic arrays of spherical micelles. (Note that subscript "1" refers to a so-called normal or oil-in-water phase, i.e., it is composed of micelles that have the hydrophobic chains on the interior and the polar headgroups on the surface. There are also type "2" phases which are inverse or water-in-oil phases where this arrangement is reversed; such phases tend to happen at rather high surfactant concentrations.) Rod micelles give rise to hexagonal mesophases (termed H_1), which consist of a hexagonal array of the rods, while disk micelles give rise to a lamellar phase (L_α), which is a solvent-separated bilayer phase.

A theoretical phase diagram for a lyotropic system is shown in Figure 17 and reveals, in addition, the V_1 and V_2 phases which are bicontinuous cubic phases (normal and reversed, respectively)[36] whose structure can be described by models involving interpenetrating rods[37] or periodic minimal surfaces.[38,38a,39] Note also that each pair of phases is separated, at least in principle, by a cubic phase (a, b, c, d in Figure 17), and with a biphasic interface (two phases coexisting).

In addition to those formed by surfactant amphiphiles, two other types of lyotropic mesophases are generally recognized, neither of which exhibits a cmc. The first of these are lyotropic phases of rigid-rod polymers that can form mesophases in both aqueous and non-aqueous solvents;[40] these mesophases are of the nematic or hexagonal type. Examples include polymeric metal acetylide complexes[5] and DNA.[41] The other type is usually formed from flat and largely aromatic molecules which stack to give lyotropic columnar phases, also referred to as chromonic phases.[42,43] This latter class is formed from systems with ionic or strongly hydrophilic peripheral functions, and forms mesophases

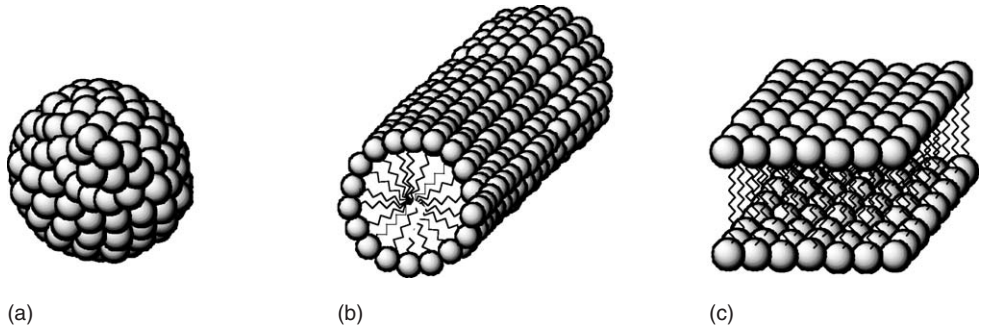

Figure 16 Schematic representation of: (a) a "normal" spherical micelle, (b) a "normal" cylindrical micelle, and (c) part of a plate-like micelle.

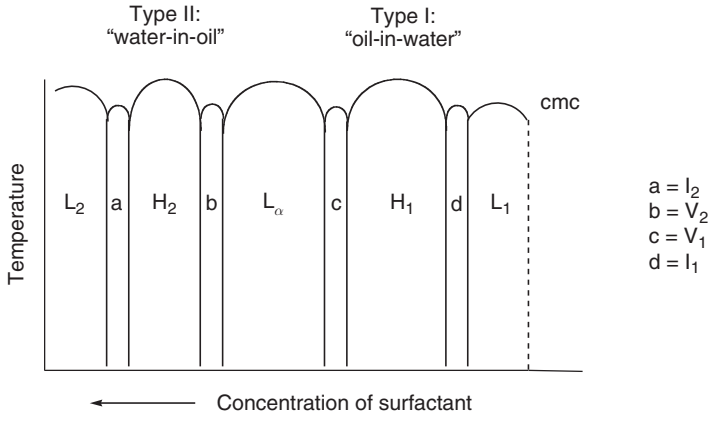

Figure 17 Idealized, theoretical phase diagram for a binary surfactant/water system (L_1 is a solution of micelles, L_2 is a solution of reversed micelles).

in water, or by much more thermotropic-like systems which are surrounded by apolar alkyl chains, and which form mesophases in apolar solvents such as alkanes.[44] Here, the stacks of molecules constitute the mesogenic unit which is known to organize into either a nematic phase where the stacks are well separated by water, or a hexagonal phase.

12.05.5 Physical Properties of Liquid Crystals

Probably, the single most important characteristic of liquid-crystal phases is that as fluids they are anisotropic;[45,45a] this means that their physical properties are likewise anisotropic, and it is this feature which is the basis for the widespread application of the materials and also, in many cases, of their characterization.

Consider, for example, the refractive indices of a nematic phase (Figure 18). In the figure, it is assumed that the molecules have a greater polarizability along their long axis than along either of their two short axes, so that in the case A, the electric vector of the light is coincident with the direction of greatest polarizability and so the light is retarded. However, in case B, the electric vector of the light is coincident with the direction of least polarizability and so the light is retarded only a little. The consequence is that the material has two refractive indices, $n_{\parallel}$ (case A) and $n_{\perp}$ (case B), and the difference between these ($\Delta n = n_{\parallel} - n_{\perp}$) is termed the birefringence. (Note that as the nematic phase has $D_{\infty h}$ symmetry, the two short axes are effectively equivalent and so the two possible $n_{\perp}$ reduce to only one.) Birefringence can either be positive ($\Delta n > 0$) or negative ($\Delta n < 0$).

This anisotropy, illustrated by refractive index, extends to other properties, and common properties of interest would be the anisotropy in linear polarizability ($\Delta\alpha$), dielectric permittivity ($\Delta\varepsilon$), and diamagnetism ($\Delta\chi$). In the nematic phase, these properties are quite strongly temperature dependent; the order parameter, S, increases as samples cool away from the N–I transition. This is illustrated in Figure 19 where it is also seen that the parallel component has the stronger temperature dependence as it is the orientational correlations that increase on cooling.

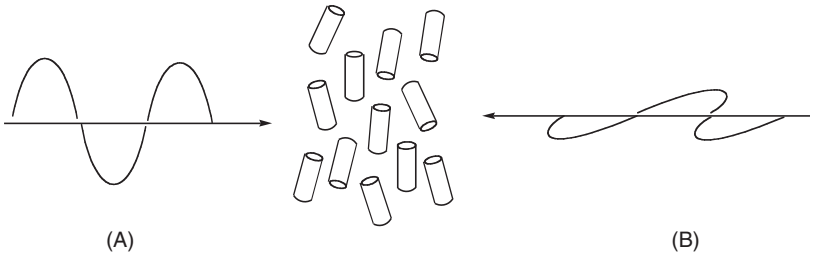

Figure 18 The interaction of polarized light with a nematic phase.

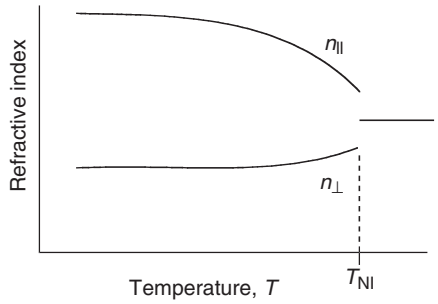

Figure 19 Variation of physical parameters in the nematic phase of liquid crystals.

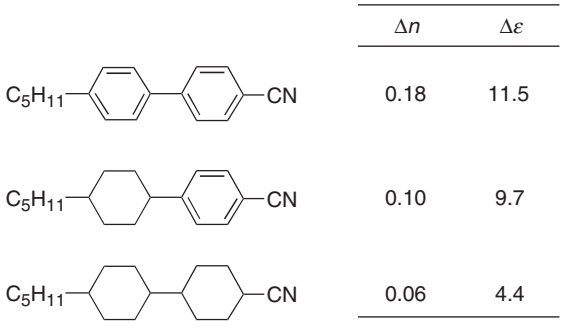

Figure 20 Birefringence and dielectric anisotropy as a function of molecular composition. Sage, I. Materials Requirements for Nematic and Chiral Nematic Electrooptical Displays. In *Thermotropic Liquid Crystals*; Gray, G. W., Ed.; Wiley: Chichester, 1987; Chapter 3, pp 64–98.

Note that at the transition to the isotropic phase, there is a discontinuity as there is only a single component of each parameter in the isotropic state.

Such properties are determined primarily by molecular features and as such can be tuned at the molecular level. The values for the birefringence and dielectric anisotropy of two-ringed cyano nematogens shown in Figure 20 illustrate this well; both quantities decrease as the polarizability of the materials decrease.[46]

12.05.6 Mesophase Characterization

Once a material is synthesized, it is necessary to establish which mesophases it forms and at what temperatures the transitions occur. Two techniques are used routinely in all laboratories for this purpose, namely polarized optical microscopy and differential scanning calorimetry, and it is important that these are used in conjunction with one another. In addition, the technique of X-ray scattering is often used to give unequivocal phase identification when microscopy cannot do so, and also to provide additional insights into the structures adopted. These three primary techniques will now be described in more detail.

12.05.6.1 Polarized Optical Microscopy

Polarized optical microscopy is usually the first technique used to characterize the mesomorphism of a new material and is a relatively rapid way of gaining information. The microscope is arranged so that plane-polarized light impinges on the sample (ca. 1 mg between microscope cover slips) whose temperature may be controlled. The light which passes through then encounters another piece of polaroid (the analyzer) which is set with its polarization director at 90° to the first polarizer; light which passes through the analyzer is then observed (Figure 21).

When viewed through such a microscope, an isotropic liquid would appear black as the plane-polarized light would pass through unaffected and be absorbed by the analyzer. However, liquid crystals are anisotropic fluids and their birefringence causes the plane polarization to be lost; the light becomes elliptically polarized instead (i.e., there are

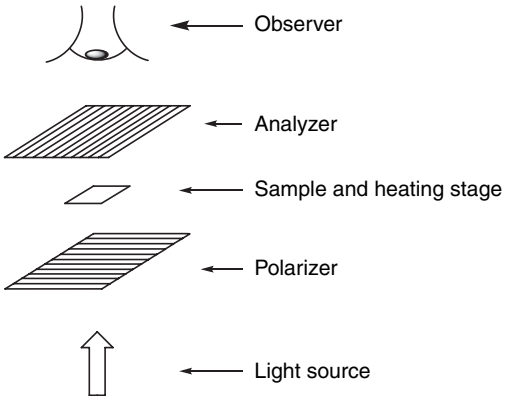

Figure 21 Schematic view of a polarizing, hot-stage microscope.

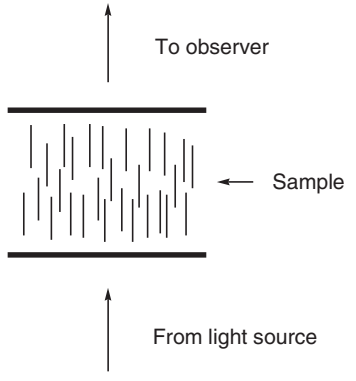

Figure 22 Idealized figure showing the homeotropic alignment of a nematic phase.

two refracted rays). The observer then views an interference pattern (texture) whose appearance is determined by the symmetry of the mesophase and, hence, the phase can be identified. Occasionally, however, the molecules in certain mesophases (N, SmA, SmB, Col_h) can arrange themselves so that the viewing of the sample is down its optic axis (Figure 22). In this case, the plane-polarized light experiences only one refractive index and so passes through the sample unchanged to appear black—this is the homeotropic texture. Textures are always best obtained on cooling a sample, the most diagnostic textures (the so-called "natural textures"[21]) being obtained on cooling either directly from the isotropic liquid or from the homeotropic texture of a preceding phase.

Miscibility is a very useful method often used in conjunction with microscopy. The simplest use of the technique is to bring two materials together on the cover slip in their mesophases in a contact preparation; the identity of the mesophase of one of the materials should already be known. If the two materials are co-miscible, then both have the same mesophase (at the temperature in question) and this can then be a useful method of phase identification. Unfortunately, if the two materials are immiscible then no information is obtained as two materials in the same phase are not necessarily miscible (e.g., water and chloroform which are both isotropic).

12.05.6.2 Differential Scanning Calorimetry

Transitions between a solid and a mesophase, or between two mesophases, or between a mesophase and an isotropic liquid, are thermodynamic events and are classified as either first or second order. In liquid crystals, transitions between phases are usually thought of as being weakly first order, although second-order transitions are not uncommon; the melting transition is, however, first order.

Thermodynamically, the term "first order" relates to the behavior of the free energy, G, with temperature. Thus, Equation (2) shows that the change in free energy with respect to temperature gives a measure of the entropy and it is

the behavior of this function through a phase transition that determines its order. Thus, if the function shows a discontinuity through the phase transition, then that transition is first order. At the transition, it is assumed that $\Delta G = 0$ and so there is an enthalpy of transition which is given by $\Delta H = T\Delta S$:

$$\left(\frac{\partial G}{\partial T}\right)_p = -S \tag{2}$$

However, it is also possible that there is no change in entropy (and, hence, enthalpy) during the transition; instead there is a discontinuity in the "second" derivative of the free energy with respect to temperature (the heat capacity—Equation (3)). Such transitions are termed "second order":

$$\left(\frac{\partial^2 G}{\partial T^2}\right)_p = -\frac{C_p}{T} \tag{3}$$

Typical enthalpy changes between successive liquid-crystal phases or between a liquid-crystal phase and an isotropic liquid are usually small at around $1\,\mathrm{kJ\,mol^{-1}}$, while transitions between a crystal and a liquid-crystal phase are strongly first order and often in the range of 30–50 $\mathrm{kJ\,mol^{-1}}$. Transitions between phases of the same symmetry are always first order and, while all liquid crystal transitions can be first order, the SmC–SmA and SmA–N transitions are often second order.

In the differential scanning calorimetry (DSC) experiment, the change in heat capacity as a function of temperature is recorded, leading to a measure of the enthalpy change (and, hence, the entropy change) accompanying a phase transition. Information about the phase transition may, therefore, be derived from the relative magnitudes of the transition enthalpies, so that melting enthalpies are (obviously) much larger than those found for an N–I transition. While such information is informative, it does not allow generalizations to be made and the corresponding entropy changes are often considered more useful.

The technique needs to be regarded as strictly complementary to optical microscopy, as all changes in optical texture do not necessarily correspond to a change in mesophase type, while all phase changes do not always lead to an easily identifiable change in texture. Thus, DSC traces should always be compared with the results of the optical study to be sure of proper correspondence.

12.05.6.3 Small-angle X-ray Diffraction

Small-angle X-ray diffraction provides, in general, a definitive way to determine the structure of a liquid-crystalline phase, and has played a major role in the identification of mesomorphic phases and in the study of their transitions. Based on the Bragg law, $2d\sin\theta = n\lambda$, which states that X-rays are reflected from adjacent planes separated by a distance when the path difference between them is an integer multiple of the wavelength used. X-ray diffraction experiments provide information not only about the interplanar distance, but also about the relative orientation and spatial orientational order of different sets of planes. Typically, layer thickness in smectic phases or intercolumnar distances in columnar mesophases are determined, along with the molecular organization within each layer or column, respectively.

X-ray diffraction experiments on liquid crystals are much more difficult to perform than conventional experiments on single crystals, because of the small number of reflections obtained, and because of other, special requirements such as temperature control and sample alignment. The latter is normally accomplished with the help of an external field, which is typically magnetic. Thus, on account of the diamagnetic anisotropy of the phase, calamitic mesogens are free to reorient in the nematic phase under the torque produced by the magnetic field and aligned, monodomain samples may be realized. By cooling down in the presence of the field, the orientation may then be kept in any subsequent smectic phases. For columnar mesophases, obtaining oriented samples is much more difficult to achieve, mainly because of the higher viscosity of the phases compared with those arising from calamitic materials. However, single domains of columnar mesophases can be obtained through a surface orientation process.[47] A typical X-ray diffraction experimental setup is shown in Figure 23.

The experiment consists of a source of X-rays (S), a monochromator (M), a sample chamber (C) (where the temperature may be controlled), and a detector (D). The most common source of X-rays is a generator using a sealed tube, and the monochromator, made, for example, from a quartz crystal, is used to select a single wavelength from the polychromatic beam emerging from the source. The sample is placed in a chamber equipped with temperature control and facilities for alignment with a magnetic field. As for the detector, different choices can be made

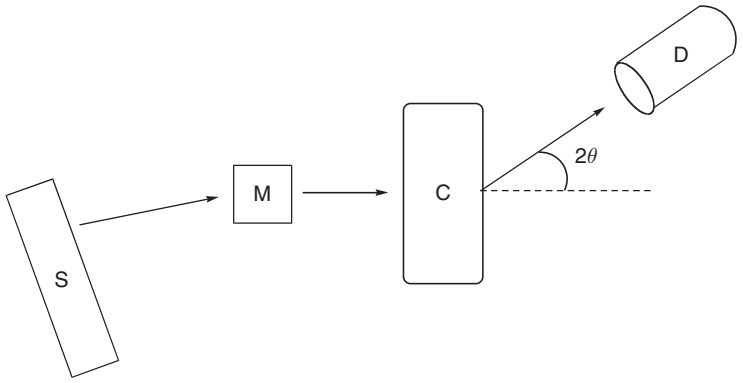

Figure 23 Schematic of X-ray diffraction experimental setup. S is the source of X-rays, M the monochromator, C the sample chamber, and D the detector; θ is the angle of diffraction.

depending on the type of information sought. To obtain an overview of the diffraction pattern, a two-dimensional detector or an image plate (or even photographic film) are suitable. For quantitative information, a scintillation counter or a linear position sensitive detector is essential.

Typical X-ray patterns of aligned liquid-crystalline phases are shown in Figure 24. In the case of the nematic phase, the calamitic molecules are oriented parallel to the magnetic field and consequently, a liquid-like peak (broad signal) corresponding to the length of the molecule appears along the direction of the field in the small-angle region (central part of the pattern). The diffuse peak arising from intermolecular distances is found in the perpendicular direction in the wide-angle region (side part of the pattern). In the SmA phase, the diffuse peaks observed at small angles in the magnetically aligned nematic phase condense into sharp Bragg spots (the mesogens remain aligned in the magnetic field); in the wide-angle region, the diffuse peaks remain similar as in the nematic phase owing to the two-dimensional-like arrangement of the molecules within each smectic layer. As for the SmC phase, the molecules are tilted with respect to the layers. In this case, when the molecules are still oriented parallel to the magnetic field, the layers become tilted with respect to this direction, and the diffraction corresponding to the smectic layers gives rise to two pairs of reflections at small angles; the angle between these pairs is twice the molecular tilt angle. In the case of the columnar mesophase, the orientation is obtained using a preparation technique by which a small drop of the sample is heated on a cleaned glass plate up to the isotropic state and cooled down slowly to the temperature of investigation. Using this method, well-aligned monodomains are obtained by surface interaction. The incident X-ray beam is parallel to the glass plate and the scattered intensity is collected on a two-dimensional detector. The example given below clearly shows the two-dimensional hexagonal symmetry of the columnar phase. In circumstances where aligned samples cannot be obtained, the information content is reduced and the spots "smear out" into rings that provide the same information on spacings, but a little less on properties such as tilt angles.

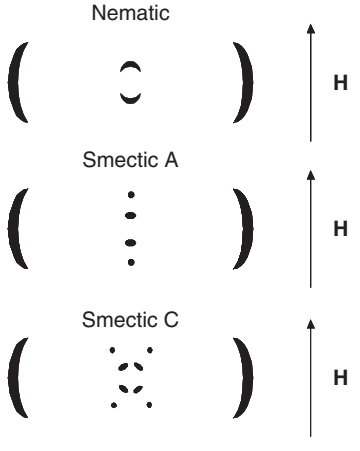

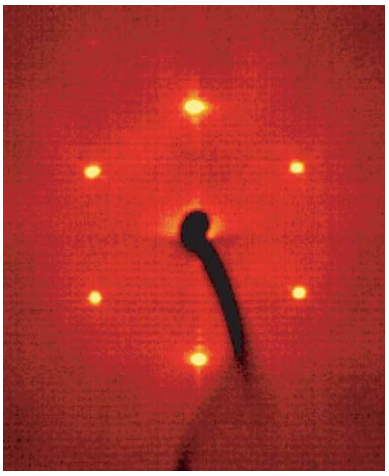

Figure 24 Typical X-ray diffraction patterns of aligned samples of the nematic, smectic A, smectic C, and columnar hexagonal mesophases.

12.05.7 Organometallic Liquid Crystals of the Main Group Elements

Organometallic liquid crystals of main group elements are extremely rare and the only significant study was of trimethylelement compounds of group 14, shown below as **1**.[48] Provided that the molecular aspect ratio was large enough, the bulky trimethyl substituents fixed at the termini of the organic moiety did not preclude mesophase formation in germanium and tin; in contrast, the Pb(IV) and the Si(IV) complexes were not mesomorphic. The complexes (**1**: M = Ge(IV), Sn(IV)) exhibited two, unidentified smectic phases above 160 °C over narrow temperature ranges at the expense of the broad temperature range nematic phase exhibited by the Schiff bases, substituted simply by alkoxy groups instead.

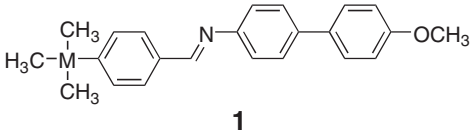

1

12.05.8 Organometallic Liquid Crystals of the Group 6 Elements

Invariably, the organometallic liquid crystals of group 6 elements have contained the "$M(CO)_3$" unit, bound in most cases η^6 to an arene. For example, a series of (η^6-hexaalkoxytriphenylene)tricarbonylchromium(0) complexes **2** were obtained by reacting the triphenylene, well known as a mesogen forming columnar phases,[4] with $[Cr(CO)_6]$ under reflux.[49] The chromium tricarbonyl moiety attached exclusively to one of the peripheral, disubstituted rings as deduced from spectroscopic data (**2**: $n = 5$–10). Upon complexation, the columnar stacking was severely disturbed by the bulky metallic fragment, and mesomorphism was either suppressed (**2**: $n = 5$–8), unidentified (**2**: $n = 10$), or modified (**2**: $n = 9$). Thus, the authors claimed observation of a nematic phase for the related chromium complex (Cr 37 N_D 58 I) with nonyloxy chains. The non-mesomorphic complexes melted at temperatures close to that of the free triphenylenes, with a stronger destabilization of their crystalline phase on increasing chain length with respect to the corresponding free triphenylenes.

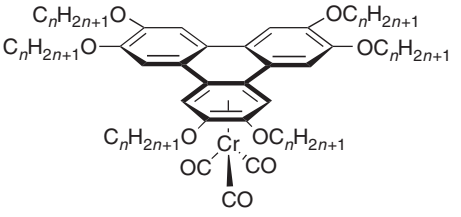

2

The (η^6-arene)tricarbonylchromium(0) complexes **3** were reported by Campillos *et al.*[50] and the uncomplexed ligands showed a mesomorphism typical of polycatenar mesogens (see Section 12.05.3.5.), progressing from N and SmC phases at shorter chain lengths to Col_o and Col_h phases at longer chain lengths. Upon complexation, the columnar mesophase was suppressed entirely, the nematic range was extended for the first two derivatives, and the SmC phase was now present for all homologs (Table 1). An important observation was the rather rapid decrease in the mesophase temperature range as the alkoxy chain length was increased; this was essentially due to a huge reduction in the clearing temperature of the complexes, the melting point being almost invariant (ca. 90 °C). Compared to the structurally related halotricarbonylrhenium(I), **7** and **8**, and the butadienetricarbonyliron(0) complexes **14** (*vide infra*), the disappearance of the columnar mesophases was rather surprising. X-ray studies showed that the SmC spacings were smaller for the free ligand than for the complexes and this was interpreted in terms of a variation in the ligand conformation. However, this observation is entirely consistent with the "core" of the complex possessing a larger cross section at the aliphatic–aromatic interface than the free ligand, reducing the mismatch with the two terminal chains leading to a much smaller tilt. This would, in turn, greatly reduce the driving force for columnar phase formation.

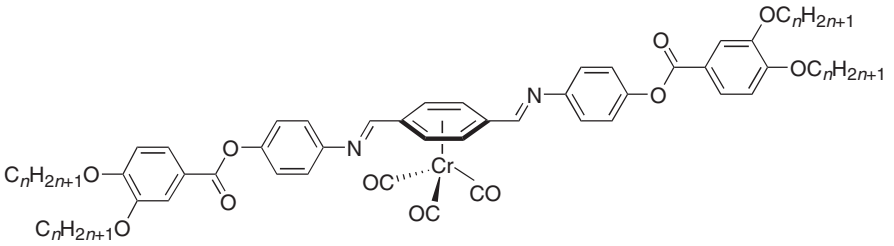

3

A series of tricarbonylchromium(0) complexes derived from cholesteryl 4-alkoxybenzoate (**4**: R = OC_nH_{2n+1}, n = 1–12) ligands has been reported to show broad temperature range chiral nematic phases (≈40–100 °C).[51] The complexes are unsymmetrical, and due to the bulkiness of the metallic fragments, an important decrease in both the melting (ca. 100 °C) and clearing (150–200 °C) temperatures was observed as compared to the metal-free ligand. The complete disappearance of the smectic phase present in the free ligand was also observed.

Table 1 Mesomorphism of polycatenar complexes of Cr^0, **3**

n	*Ligand*	*Complex*
8	Cr 137 SmC 198.5 N 206.5 I	Cr 95 SmC 102 N 140 I
10	Cr 125 SmC 185 I	Cr 94 SmC 110 N 131 I
12	Cr 127.5 SmC 128.5 Col_o 161 Col_h 186 I	Cr 92 SmC 118 I
14	Cr 123 Col_h 176 I	Cr 95 SmC 99 I

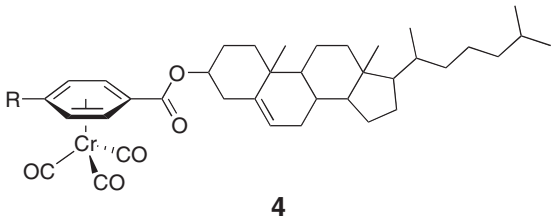

4

Lattermann and co-workers studied a series of mesomorphic metal complexes, **5**, with flexible, saturated tridentate ligands such as the non-mesogenic 1,4,7-tri-(3′,4′-didodecyloxy)benzyl-1,4,7-triazacyclononane. Due to the small diameter of the trisubstituted [9]aneN_3 ring, only monofacial coordination was possible. Upon complexation by metal complex fragments such as the group 6 tricarbonyls (**5**: $ML_3 = Cr(CO)_3$, $Mo(CO)_3$, and $W(CO)_3$)[52], the octahedral complexes were found to be mesomorphic giving an enantiotropic Col_r mesophase over a broad temperature range with no signs of decomposition observed in the isotropic liquid (Figure 25). While the melting points remained almost the same for the three complexes (ca. 60 °C), the clearing temperatures increased steeply from chromium to tungsten. When coordinated to the metal, the triazacyclononane ring lost its flexibility and the inner part of the complex adopted the shape of a cone or pyramid. The formation of the columnar mesophase then presumably resulted from the stacking of such cones on top of one another, with a net polarization expected in each column.

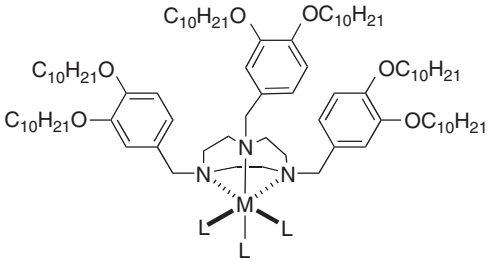

5

The case of an octahedral iron compound (**5**: $ML_3 = FeCl_3$; discussed here for completeness) was more complicated.[53] It displayed two apparently columnar mesophases, M1 and M2. The lower temperature phase, M1, was observed during the first heating cycle only, and M2 was observed above 70 °C but only after heating to 140 °C. Mössbauer and UV spectroscopy revealed that the peculiar thermal behavior of the iron complex was due to the existence of various octahedrally coordinated monomeric and dimeric species, as well as to reversible redox reactions.

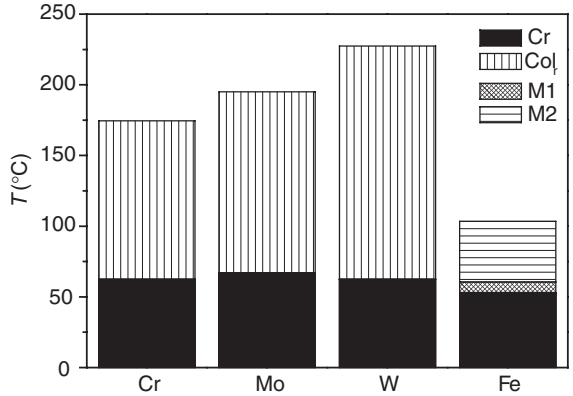

5

Figure 25 Mesomorphic properties of the 1,4,7-tri-(3′,4′-didecyloxy) benzyl-1,4,7-triazacyclononane metal complexes **5**: $[M(CO)_3L]$ for M = Cr, Mo and W, and $[FeCl_3L]$.

12.05.9 Organometallic Liquid Crystals of the Group 7 Elements

Organometallic liquid crystals of group 7 elements can be divided into three families, namely those based on halotricarbonylrhenium(I) complexes of α-diimines, tetracarbonylrhenium(I) amidines, and *ortho*-metallated complexes of imine mesogens.

12.05.9.1 Complexes of Bipyridines and Phenanthrolines

The use of properly extended 2,2′-bipyridine ligands[54] led to the metallomesogens shown as **6**.[55,56] These complexes (**6**: X = Y = H and X = F, Y = H) showed N and SmC phases well above 200 °C, with clearing temperatures ranging between 300 and 360 °C.

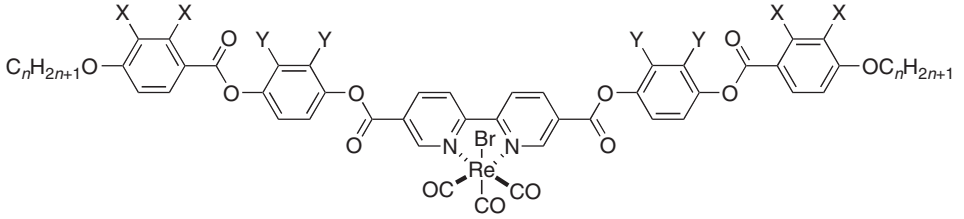

6

The study was extended to polycatenar derivatives **7** and the phase diagram for the behavior of the 3,4-tetracatenar materials (**7**: R = H) is shown in Figure 26.[57] Thus, the addition of the $ReBr(CO)_4$ moiety has suppressed the SmC phase and, due to the increase in the core volume, has ensured that the columnar phases (and now a cubic phase, too, with $Ia\bar{3}d$ symmetry[58]) occurred to longer chain length. In common with many other systems,[28,29] it is assumed that the phase indicated Col is, in fact, Col_h, while that indicated Col′ is one of the Col_r phases. All complexes of the hexacatenar derivative (**7**: R = OC_nH_{2n+1}) showed a columnar phase.

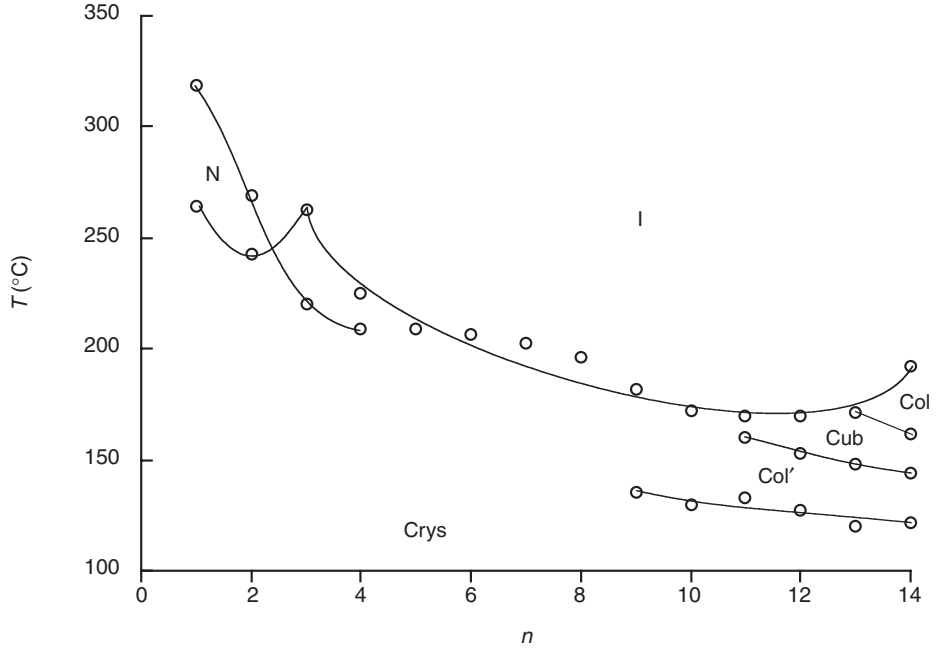

Figure 26 Phase behavior of the 3,4-tetracatenar Re(I) bipyridine complexes **7** (R = H).

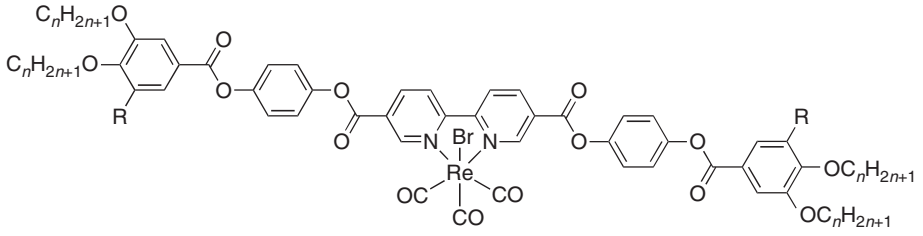

7

Polycatenar Re(I) complexes derived from 1,10-phenanthroline ligands were also reported **8**.[1q] At longer chain lengths ($n = 14$, 16), both the ligand and the complex exhibited a Col_h phase that showed a greater range and more stability for the complex. At shorter chain lengths ($n = 10$), the SmC phase of the ligand was suppressed and the complex was not mesomorphic, paralleling the behavior observed for the tetracatenar bipyridine complexes **7** above.

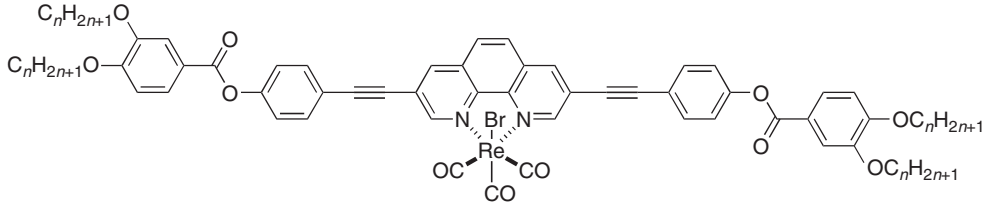

8

12.05.9.2 Complexes of Diazabutadienes

A few *N,N′*-bis(4″-(4′-alkoxybenzoyloxy)phenyl)-1,4-diaza-1,3-butadiene ligands were complexed to various [ReX(CO)$_5$] fragments to give new, mesomorphic, octahedral halotricarbonylrhenium(I) complexes (**9**: X = Cl, Br, I, CF_3SO_3; $n = 8$, 10, 12).[59,60] The parent ligands showed large-temperature-range SmC and nematic phases from ca. 130 °C, with decomposition occurring systematically in the nematic phase (above 200 °C), making assignment of the clearing point difficult.

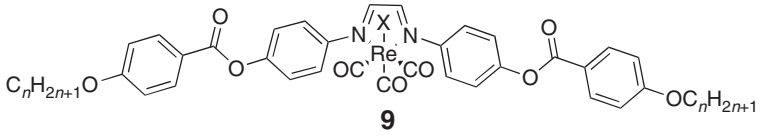

9

On complexation to many different metal fragments, i.e., [Mo(CO)$_4$], [MnBr(CO)$_3$], $PdCl_2$, CuCl, CuBr, and CuCN, mesomorphism was not observed. The exception was when the ligands were bound to [ReX(CO)$_3$] (**9**: X = Cl, Br, I, CF_3SO_3), when materials with a nematic, and in two compounds with dodecyloxy chains (X = Cl, Br), an additional SmC phase, no mesomorphism was detected for compounds with the bulkier triflate group. Clearing points were found to decrease in the order Cl > Br > I > CF_3SO_3, and with increasing n (Figure 27).

12.05.9.3 Complexes of Amidines

A couple of examples of mesomorphic amidine complexes prepared by reaction of the free ligand with [ReMe(CO)$_5$][1q] have been reported **10**. For $n = 10$ and 12, the ligands are mesomorphic showing a Col_h phase (roughly between 140 and 170 °C) and this phase is retained on complexation although the mesomorphic range is much shorter (ca. 10 °C) and the melting points were reduced to around 110–120 °C.

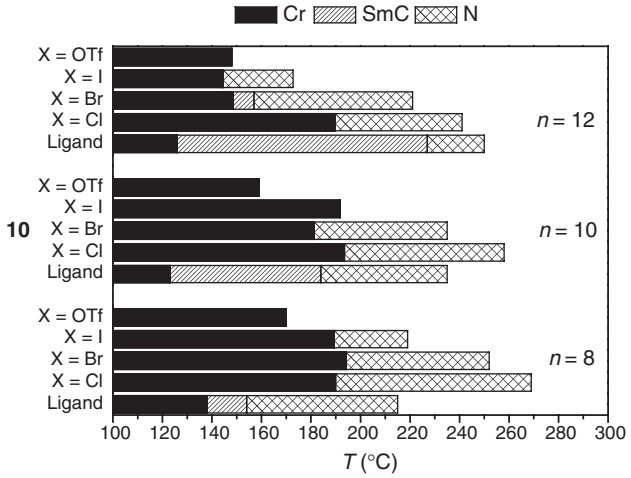

Figure 27 Mesomorphism of halotricarbonylrhenium(I) complexes **9**.

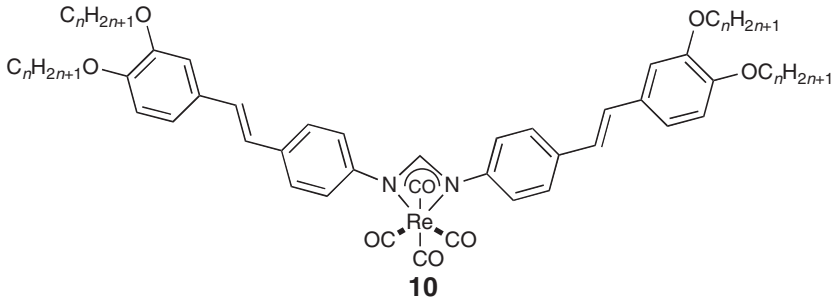

10

12.05.9.4 *Ortho*-metallated Complexes

Bruce and co-workers demonstrated mesomorphism in benzylideneaniline complexes bound to octahedral Mn(I) and Re(I), providing that the imine ligand was sufficiently anisotropic; these complexes were the first simple octahedral complexes to show N and lamellar phases.[61] They were formed by the *ortho*-metallation reaction of the imine with $[MMe(CO)_5]$ (M = Mn, Re). The parent ligands showed smectic and nematic phases at temperatures up to 300 °C, whereas on complexation to Mn(I), only a nematic phase was seen for **11** (**11**: M = Mn, $n = 5, 7$) and **12** (**12**: M = Mn; X = Y = H; $n = m = 8$) which cleared below 190 °C with decomposition.[62] The related Re(I) complexes yielded materials with very similar transition temperatures and enhanced thermal stability, so that decomposition was not observed at the clearing point.[63] Therefore, in the following part of this study, only rhenium complexes were studied.

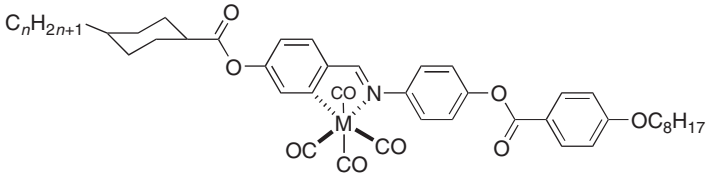

11

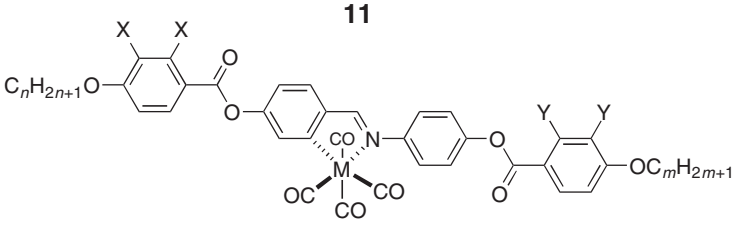

12

Both terminal chain-lengths were varied in a systematic way;[64] lateral ligand fluorination was employed[65] and the mesomorphism of the resulting complexes compared. In broad terms, the mesomorphism of the rhenium complexes was the same and not influenced to a great extent by the chain length, melting into the nematic phase between ca. 130 and 155 °C, and clearing between 140 and 200 °C. Fluorination, however, had a more dramatic effect on the mesophase stability (**12**: M = Re, X; Y = H, F). Thus, while the phase remained unchanged as nematic, its mesophase stability reduced considerably with increasing fluorine substitution (Table 2). This systematic study further revealed that complexes based on two-ring ligands were not mesomorphic, whereas monotropic nematic phases were observed for complexes of three-ring ligands, thus showing the need for ligands of sufficient anisotropy to generate mesomorphic systems with octahedral metal centers.[66]

The effect of the nature of the terminal group and the position of the imine link has also been investigated. Thus, when hexyl chains are substituted at each end of a rhenium complex with the same motif as **12**, a nematic phase was observed (Cr 129 N 167 I). Moreover, when one of the two hexyl chains were replaced by one (Figure 28) or two perfluorinated chains, the mesophase was changed to SmA phase, and occurred at higher temperatures, with decomposition taking place in the mesophase.[67,68]

Similar structural modifications using chiral aliphatic chains (citronellyloxy and its hydrogenated analog) were performed,[69] and these yielded complexes with a chiral nematic phase, though when 'both' terminal chains were chiral, mesomorphism was suppressed. The phases typically occurred between 120 and 160 °C. Siting the bulky rhenium fragment in one extremity of the molecule resulted in the destabilization of the mesomorphism, but not its suppression.

Four- and five-ring systems diimine ligands and their corresponding dinuclear rhenium complexes (Figure 29) were also prepared.[70] However, while the diimines exhibited smectic and nematic phases between 100 and 400 °C, none of the dirhenium complexes was mesomorphic.

Table 2 Mesomorphism of octahedral complexes **11** and **12**

	Complex	*Transition temperatures*
11	$n = 5$	M = Mn: Cr 135 N 184 dec.
		M = Re: Cr 147 N 177 I
	$n = 7$	M = Mn: Cr 122 N 180 dec.
		M = Re: Cr 129 N 171 I
12	X = Y = H, $n = m = 8$	M = Mn: Cr 154 N 190 dec.
		M = Re: Cr 154 N 176 I
	X = Y = H, $n = 12$, $m = 8$	M = Re: Cr 130 N 164 I
	X = Y = H, $n = m = 12$	M = Re: Cr 131 N 145 I
	X = F, Y = H, $n = m = 8$	M = Re: Cr 153 N 164 I
	X = F, Y = H, $n = 12$, $m = 8$	M = Re: Cr 143 N 149 I
	X = F, Y = H, $n = m = 12$	M = Re: Cr 141 I
	X = Y = F, $n = m = 8$	M = Re: Cr 137 N 160 I
	X = Y = F, $n = 12$, $m = 8$	M = Re: Cr 125 N 138 I
	X = Y = F, $n = m = 12$	M = Re: Cr 131 (N 125) I

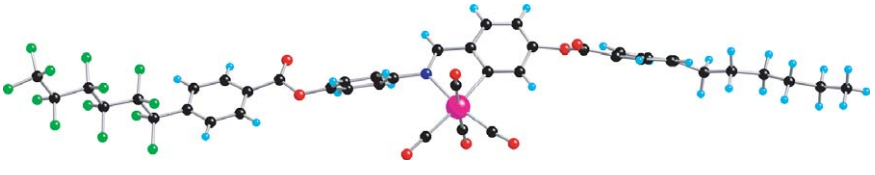

Figure 28 Single-crystal structure of a Re complex bearing an imine with one hydrocarbon and one fluorocarbon chain.

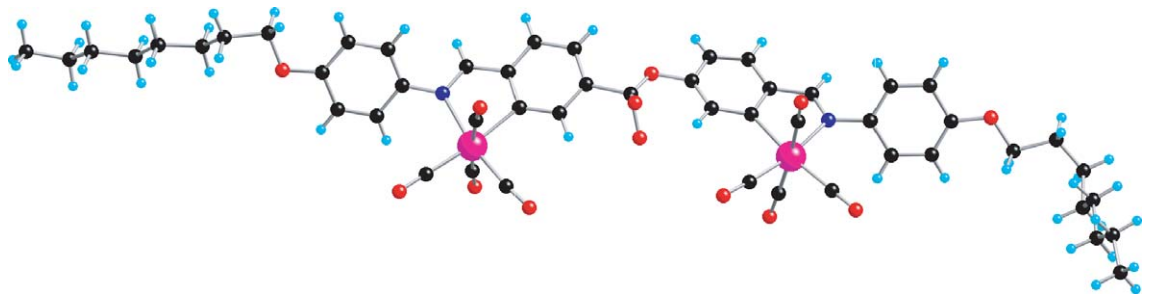

Figure 29 Single-crystal structure of a non-mesomorphic dirhenium complex.

12.05.10 Organometallic Liquid Crystals of the Group 8 Elements

A particular feature of the mesogens of group 8 elements is the extensive liquid-crystal chemistry of ferrocene and its derivatives, and as such this subject is given its own subsection below.

12.05.10.1 Complexes of Iron Carbonyls

A most interesting group of complexes are the mesomorphic η^4-butadienetricarbonyliron(0) materials, **13**, reported by Malthête and co-workers.[71,72]

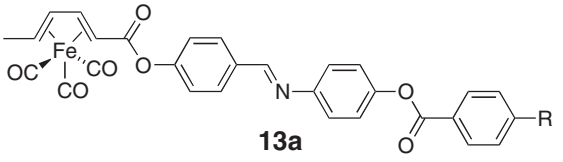

13a

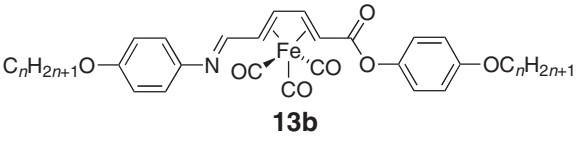

13b

All of the terminally substituted complexes (**13a**: R = C_7H_{15}, C_8H_{17}, $OC_{12}H_{25}$) showed wide-range nematic phases (range >100 °C, between 120 and 220–250 °C), while the disubstituted complexes (**13b**) displayed a nematic phase at short-to-medium chain lengths (n = 6–10) and a SmA phase as the chains grew longer (n = 9–12), though over narrow temperature ranges (<10 °C, below 100 °C). These compounds are interesting in that they possess a potentially chiral rigid unit (planar chirality if substituted unsymmetrically) with a rather large transverse dipole, making them good candidates as new ferroelectric liquid crystals. The resolution of the racemic mixture was successfully achieved, and the pure (−)-enantiomer exhibited SmA and N* phases (**13b**: n = 10, Cr 84 SmA 92 N* 97 I).

Other metallomesogens containing the optically active butadienetricarbonyliron(0) moiety, incorporated into promesogenic chiral nematic ligands derived from cholesteryl, have been reported.[73,74] Both the diastereoisomers exhibited a chiral nematic phase and a monotropic smectic phase, the chiral nematic phase being monotropic for the (+)-isomer (Cr 193 (S 93 N* 131) I), and enantiotropic for the (−)-isomer (Cr 117 (S 99) N* 133 I).

The results reported above clearly indicate that the butadiene iron tricarbonyl moiety can be inserted into mesogenic structures, to give, ferroelectric properties when designed suitably.

Related polycatenar complexes **14** were also reported[72] and, as might be expected for polycatenar complexes, nematic (**14**: n = 6, 10, 11), SmC (**14**: n = 10, 11), and Col_h (**14**: n = 12–16) phases were obtained (Table 3). The melting temperatures first decreased from 100 °C (**14**: n = 6) to ca. 60 °C (**14**: n = 12–14), then rose again to 85 °C

Table 3 Mesomorphism of polycatenar complexes of Fe^0, **14**

n	*Racemates* (±)	*Enantiomers*[a]
6	Cr 101.5 N 144.5 I	Cr 84 N* 139 I
10	Cr 72 SmC 104.5 N 124 I	Cr 73.5 SmC* 109 N* 127 I
12	Cr 59 Col_h 110 I	Cr 60.5 Col_h 112.5 I
16	Cr 85 Col_h 111 I	Cr 89.5 Col_h 103.5 I

[a](+) for n = 6, (−) for n = 7–16.

(**14**: $n \geq 15$). The clearing temperatures decreased almost linearly with n (144–100 °C). Resolution of the pure enantiomers gave rise to the corresponding chiral mesophases for the short-chain homologs (N^* and SmC^*), although it was not clear whether the Col_h phase was chiral. Some small temperature changes were observed, though a sort of odd–even effect could be observed for the clearing temperatures. Small spontaneous polarizations were also measured.

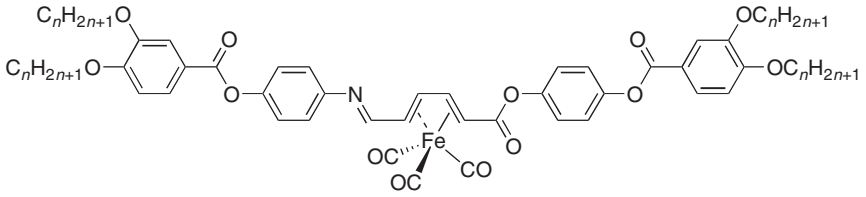

14

A series of materials was synthesized in which isonitriles were complexed to tetracarbonyliron(0) (**15**: $n = 6$, 8, 10, 12).[75] The free ligands from which complexes **15a** and **15b** were obtained showed a nematic phase at short chain length and the SmA phase as the chain grew longer, always decomposing on passing to the isotropic liquid. The free isonitriles used to form **15c** simply decomposed in the solid state before melting. However, all of the complexes melted at ca. 70–90 °C to show a SmC phase, although once more, decomposition was observed on clearing at 120 °C. The mesophase range was found to increase in the order **15c** < **15a** < **15b** (Figure 30).

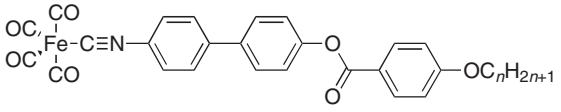

15a

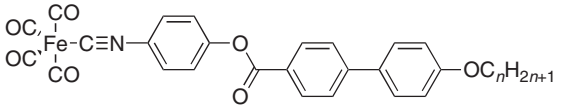

15b

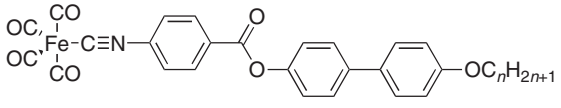

15c

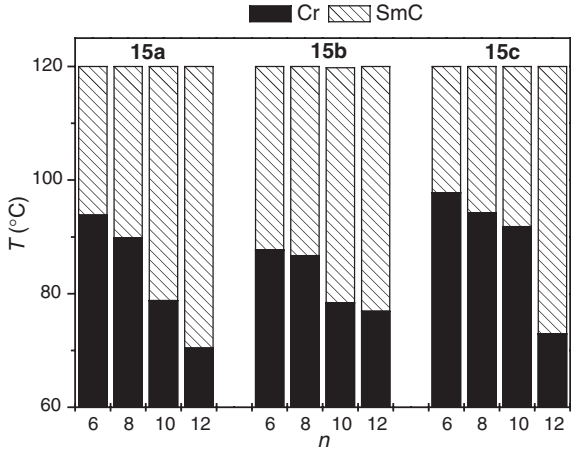

Figure 30 Mesomorphism of complexes **15**.

12.05.10.2 Ruthenium Carboxylate Complexes

Dimeric, ruthenium "saw-horse" complexes **16** were reported by Deschenaux *et al.*[76] A range of $[Ru_2(CO)_4(\mu^2,\eta^2\text{-}O_2CR)_2L_2]$ complexes were synthesized with differing R groups (**16**: R = H–, CF_3–, C_6H_5–, 4-MeO-C_6H_4–, 4-Me-C_6H_4–) and different values of *n* (**16**: *n* = 6, 10, 12, 14, 16). Despite the bulky central unit, induction of mesomorphism was achieved by introducing anisotropic pyridine-based ligands in the axial positions; all complexes were nematic, typically in the range 150–200 °C. The stability of the mesophase was found to be dependent upon the type of carboxylato bridges (decreasing order of stability: $C_6H_5 > C_6H_4$–$CH_3 > H$, C_6H_4–OCH_3). This class of metallomesogens represents a rare example of mesomorphic compounds containing covalent bonds between two metal atoms, and is of considerable interest due to its structure, electronic properties, and its potential catalytic reactivity.[77]

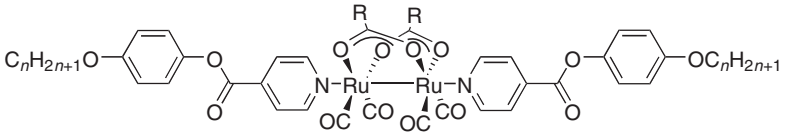

16

Another octahedral metallomesogen, **17**, containing a bulky ruthenium fragment and an elongated phenyl benzoate ligand was found to display a SmC phase above 225 °C.[78] However, on reaching the isotropic liquid, the complex started to sublime, and, thus, did not give rise to reproducible thermal behavior.

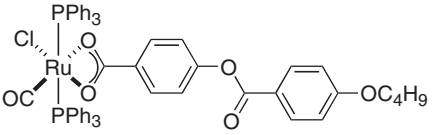

17

12.05.10.3 Ruthenium Arene Complexes

Interestingly, Choi *et al.*[79] reported an example of mesophase stabilization through the formation of a rod-coil ruthenium complex, **18**. Whereas the organic moiety exhibited an SmB phase between 120 and 123 °C, the ruthenium species displayed the same SmB phase, but over a much wider temperature range, i.e., between 44 and 108 °C.

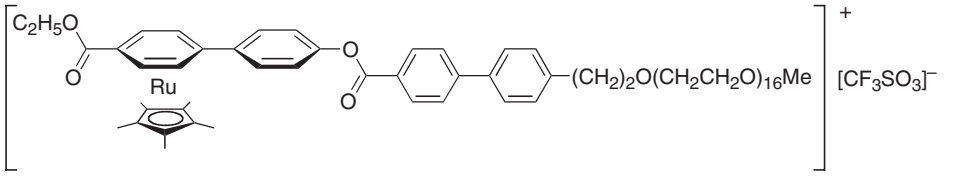

18

12.05.10.4 Ferrocene-containing Liquid Crystals

12.05.10.4.1 Introduction

Ferrocene (Fc) possesses a rich synthetic chemistry, a three-dimensional structure which allows the preparation of many derivatives, high thermal stability, and good solubility in common organic solvents.[80] These characteristics allow the synthesis of a great variety of liquid-crystalline materials. Furthermore, its unique electrochemical properties (fast and reversible one-electron transfer process) make Fc a valuable building block for the elaboration of redox-active supramolecular switches. In 30 years (1976–2006), liquid-crystalline ferrocenes have been established as a versatile class of metallomesogens.[1h] The aim of this chapter is to highlight the main results obtained for

ferrocene-containing liquid crystals, and give readers a view of the evolution of the structures that have been synthesized. Note that ferrocene-containing liquid-crystalline polymers will not be presented here.

12.05.10.4.2 Monosubstituted ferrocenes

The first ferrocene-containing thermotropic liquid crystals, compounds **19** to **21**, were reported by Malthête and Billard in 1976.[81] Enantiotropic, **19**, or monotropic, **20** and **21**, N phases were observed. Compounds **19–21** were designed to undertake Mössbauer studies in mesomorphic media. Ferrocenyl Schiff bases **19–21** represent the first well-characterized organotransition metallomesogens.

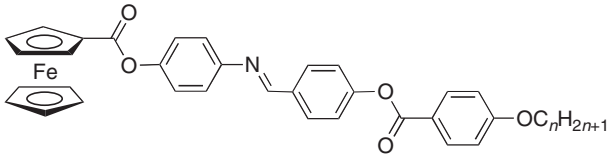

n = 8 Cr 153 N 167 I
n = 10 Cr 143 N 159 I

19

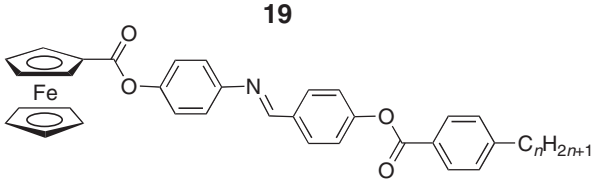

n = 5 Cr 182 (N 155) I
n = 6 Cr 164 (N 143) I
n = 8 Cr 152 (N 135) I

20

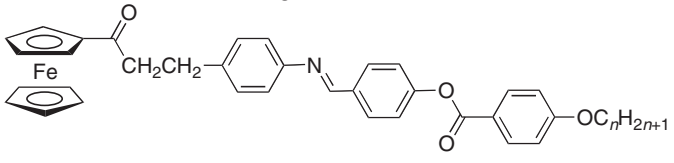

n = 8 Cr 137 (N 112) I
n = 10 Cr 135 (N 107) I

21

Since the results published by Malthête and Billard, many monosubstituted Fc derivatives have been prepared. They have been reviewed by Imrie *et al.*[82,82a] Nakamura *et al.* functionalized Fc with cholesteryl derivatives (e.g., **22**(*n*)).[83,83a–83m] These compounds gave rise to quite a complex phase sequence, which prevented identification of the mesophases. However, structural determination[83c–83e] of several derivatives and investigation of dynamic viscoelastic properties[83l] indicated that the materials displayed SmC phases. As cholesterol is an optically active chemical, the mesophase should be denoted as SmC*. Compound **23**, in which the cholesterol moiety is linked to Fc without a flexible spacer, gave a N* phase.[84] Therefore, the formation of disordered smectic phases seems to require a flexible bridge between cholesterol and Fc. A monosubstituted Fc derivative in which cholesterol is directly attached to the organometallic core was found to be non-mesomorphic, whereas the 1,1′-disubstituted Fc derivative exhibited a crystal SmB phase from 265 to 276 °C.[85]

The nematogenic behavior of monosubstituted Fc derivatives was attributed to steric effects induced by the Fc unit: the organic rod located on Fc compensates only poorly for the influence of the bulky organometallic. As a consequence, the latter prevents strong interactions between the molecules from taking place. Imrie *et al.* reported monosubstituted ferrocenes in which structural parameters (e.g., length of aromatic core, length of terminal chain, and number and position of lateral substituents) were systematically varied.[86,86a] It was found that a minimum of three phenyl rings in the core is required to stabilize the N phase. The stability of the latter phase increased markedly with the number of aromatic rings. For example, a nematic range as broad as 100 °C was obtained for **24**, which contains four aromatic rings. Lateral fluorination lowered the transition temperatures and suppressed smectic phases.

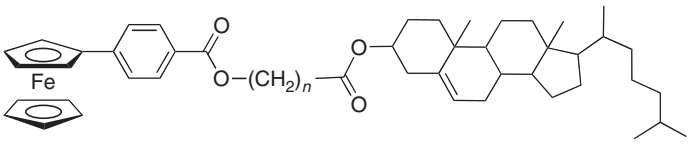

$n = 6$ g 24 SmC 51 I
$n = 8$ g 21 SmC 53 I

22

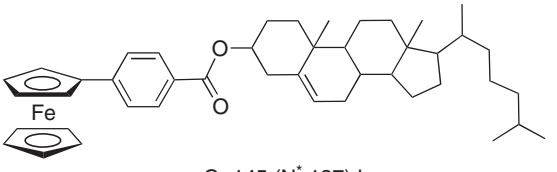

Cr 145 (N^* 137) I

23

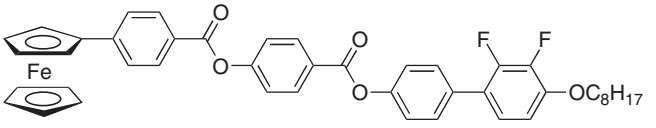

Cr 152 N 252 I

24

Heterobimetallic metallomesogens were reported by Galyametdinov *et al.*[87,87a–87c] These were prepared by complexing monosubstituted, mesomorphic Fc derivative **25a** with metals such as Cu(II), Pd(II), Ni(II), VO(IV), and $Fe^{II}Cl$. Heterobimetallic compounds **25b** (M = Cu(II), Pd(II), VO(IV)) and **26** gave rise to a nematic phase, whereas **25b** (M = Ni(II)) was not mesomorphic, and **25b** (M = $Fe^{II}Cl$) showed a smectic phase. The variation in mesomorphic behavior was attributed to different complexation geometries. The oxo-bridged hexa-iron complex, **26**, exhibited a nematic phase with a broad temperature range.

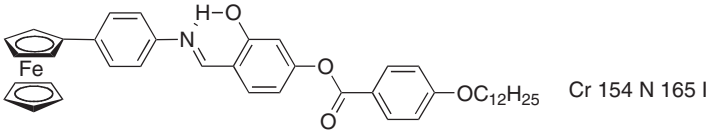

Cr 154 N 165 I

25a

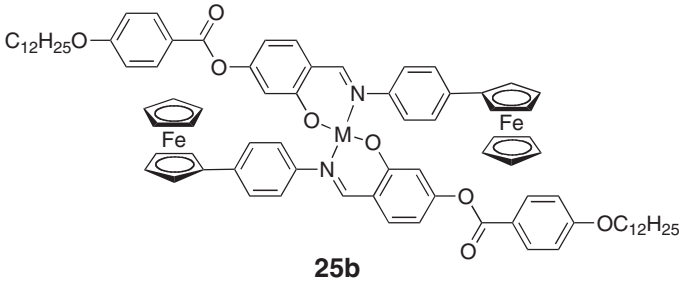

M = Cu	Cr 214 N 223 I
M = Pd	Cr 271 N 275 I
M = Ni	Cr 245 dec.
M = VO	Cr 243 (N 240) I
M = Fe–Cl	Cr 195 S 205 I

25b

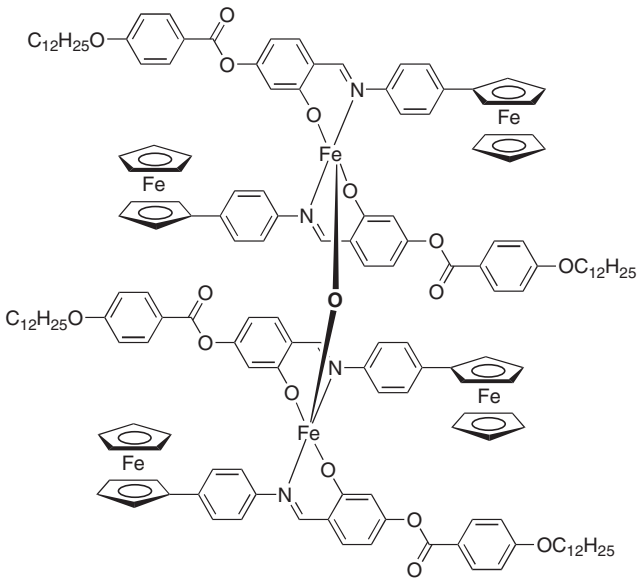

Cr 155 N 232 I

26

Related heteropolynuclear complexes **27**, based on a non-mesomorphic Fc enaminoketone ligand, were also prepared (**27**: M = Cu, Pd),[88,88a] but displayed only monotropic phases: Cr 144 (N 122) I for the copper complex and Cr 205 (SmC 195 N 198) I for the palladium analog (M = Pd).

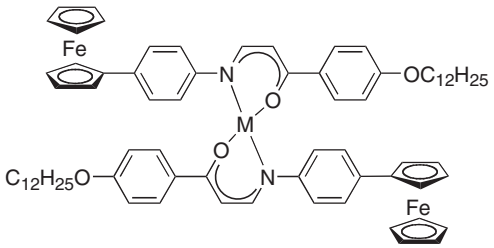

27

Enantiotropic SmA mesophases were obtained in mixed heteropolynuclear complexes containing enaminoketone and *ortho*-palladated imine groups **28**; transition temperatures and temperature ranges depended strongly on the nature of the enaminoketone derivative.[89] The trinuclear bis(imine) and the tetranuclear chloro-bridged precursory complexes were also mesomorphic, showing an unidentified smectic phase (Cr 118 S 131 I) and a SmA phase (Cr 238 SmA 248 I) respectively.

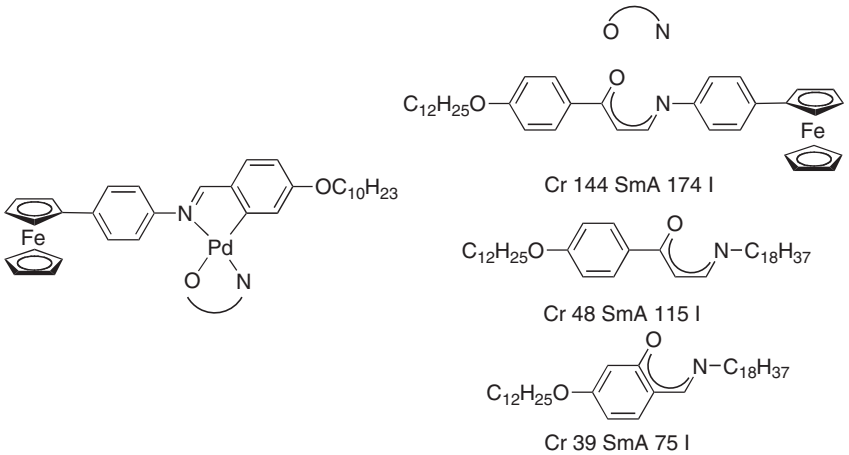

Cr 144 SmA 174 I

Cr 48 SmA 115 I

Cr 39 SmA 75 I

28

The formation of liquid crystals is not restricted to materials with a linear organic rod. Monosubstituted Fc derivatives carrying bidentate *N*-benzoyl-*N*′-arylthiourea ligands **29** (*n*) were shown to give rise to nematogenic properties.[90] Compounds **29** (*n*) could be used as a platform to prepare heterobimetallic metallomesogens.

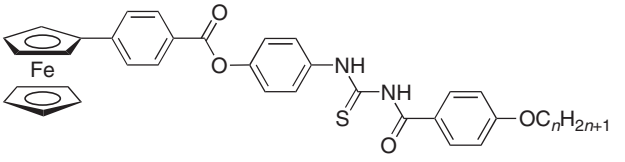

n = 8 Cr 160 N 176 I
n = 12 Cr 144 N 157 I
n = 16 Cr 126 N 146 I
n = 18 Cr 116 N 139 I

29

The peralkylated ferrocenes **30** and **31** were synthesized with a view to design switchable liquid crystals based on the ferrocene–ferrocenium redox couple.[91,91a] The peralkylated Fc moiety was selected as the redox-active center in order to utilize the ease of oxidation of this unit in comparison with less alkylated ferrocenes. Compounds **30** and **31** were readily oxidized with silver tosylate into the corresponding ferrocenium derivatives **32** and **33**, respectively. Compounds **30** and **31** did not display mesomorphism. As in the case of other monosubstituted ferrocenes, the organic part used here could not thwart the size of the organometallic core, and only isotropic fluids formed when the samples melted. However, the ferrocenium derivatives **32** and **33** exhibited liquid-crystalline behavior: a monotropic SmA phase was observed for **32** and a monotropic Col_r phase was obtained for **33**. The fact that the oxidized species gave rise to mesomorphism is an indication that the formation of liquid-crystalline phases depends on structural factors and ionic interactions.

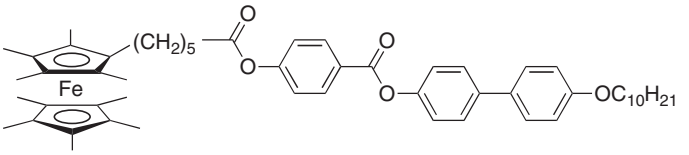

Cr 154 I

30

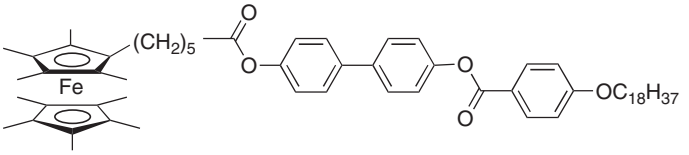

Cr 134 I

31

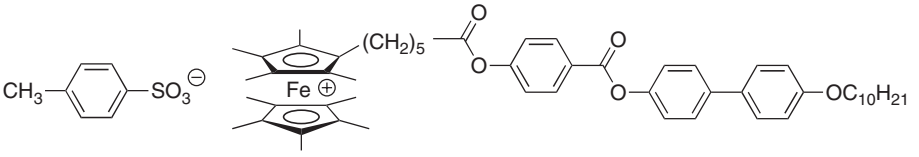

Cr 132 (SmA 83) I

32

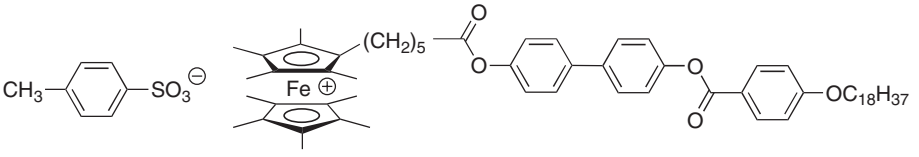

Cr 123 (Col_r 101) I

33

The SmA (monomolecular organization) nature of the mesophase displayed by **32** is due to the head-to-tail orientation of the molecules within the mesophase. The columnar phase obtained for **33** was found to have a centered rectangular symmetry. The discrepancy between the molecular volume of the flexible tail and that of the rigid rod is responsible for the formation of the columnar phase.

A detailed understanding of the influence of the structure, charge, and counterion on the thermal and mesomorphic properties requires the preparation and further study of ferrocenium materials. The above-reported results prove that liquid-crystalline switches should, in principle, be available by the incorporation of ferrocene/ferrocenium into mesomorphic materials.

Optically active liquid crystals were obtained by functionalization of Fc with a chiral organic motif. Compound **34** (source of chirality: (*S*)-ethyl lactate) showed a SmC^* phase,[92] and compound **35** (source of chirality: (*S*)-2-methylbutan-1-ol) exhibited five mesophases, including SmC^*, SmA, TGBA, BP, and N^* phases.[93] (The TGBA, or twist-grain boundary A phase (a TGBC phase also exists), is found in highly chiral materials and is a variant of the SmA phase; blue phases, BPI, BPII, and BPIII, also found in highly chiral systems, are cubic in organization; both are discussed by Goodby in Ref: 4, chapter V, vol. I. In liquid crystals, the term "highly chiral" would apply to compounds with a very high ability to induce a helical twist in a liquid-crystal solvent, or one that had a very short pitch as a pure material.) This example demonstrates that careful functionalization of Fc with appropriate chiral substituents can lead to any kind of chiral liquid-crystalline phase.

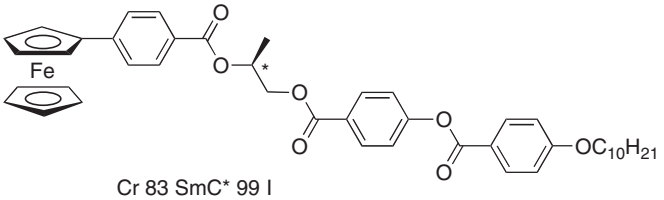

Cr 83 SmC^* 99 I

34

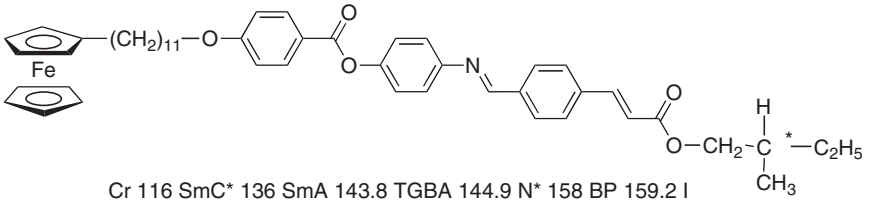

Cr 116 SmC^* 136 SmA 143.8 TGBA 144.9 N^* 158 BP 159.2 I

35

Finally, functionalization of a phthalocyanine with Fc gave rise to **36**, which exhibited a Col_h phase.[94] The ferrocene-free analog presented Col_r and Col_h phases. The loss of the Col_r phase was attributed to the bulky Fc unit.

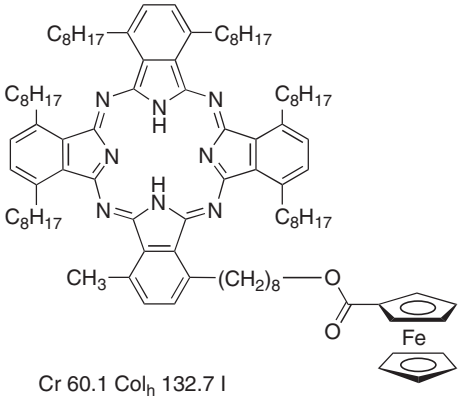

Cr 60.1 Col_h 132.7 I

36

12.05.10.4.3 1,1′-, 1,3-, and 1,2-disubstituted ferrocenes

Ferrocenes substituted at the 1,1′-positions attracted considerable attention as they exhibited enhanced mesomorphic tendency compared to monosubstituted derivatives. Indeed, the two substituents located on the organometallic core generate stronger intermolecular interactions than monofunctionalized systems. Various organic rods and functional groups were attached to Fc, as illustrated by compounds **37**–**42**. Ferrocenes **37** ($n = 5$, 6, 11)[95,95a] gave rise to monotropic smectic phases (Table 4). The other members of the series, **37** ($n = 4$, 7, 8, 9, 10), were found to be non-mesomorphic. Complexes **38** ($n = 3$, 4, 6, 8) were not mesomorphic and **38** ($n = 10$) seemed to give rise to an smectic phase (unidentified) between 85 and 88 °C during the second heating cycle.[96,96a] When **39** ($n = 7$) was cooled from the isotropic melt, a liquid-crystalline texture was observed (transition temperatures and liquid-crystalline range not given), that, according to the authors, was indicative of an smectic phase (unidentified).[97] Derivative **39** ($n = 10$) formed a nematic phase from 78 to 79 °C, but the latter did not reform when the sample was cooled from the isotropic fluid. All Schiff-base derivatives **40** (n) exhibited mesomorphic behavior (Table 4).[98] The first members of the series, **40** ($n = 4$–6), gave rise to enantiotropic N phases, and the long chain derivatives, **40** ($n = 10$–12), displayed enantiotropic SmA phases. The intermediate-chain-length derivatives, **40** ($n = 7$–9), exhibited monotropic N or SmA phases. Other di-1,1′-substituted Fc derivatives with pendant groups, such as **22**, exhibited complicated phase sequences which depend on the thermal history.[99,99a,99b] Derivatives with azido link between the Fc and the mesogen were found to exhibit a single N phase between 152–208 °C (melting temperatures) and 180–236 °C (clearing temperatures) with decreasing chain length.[100, 100a–100d]

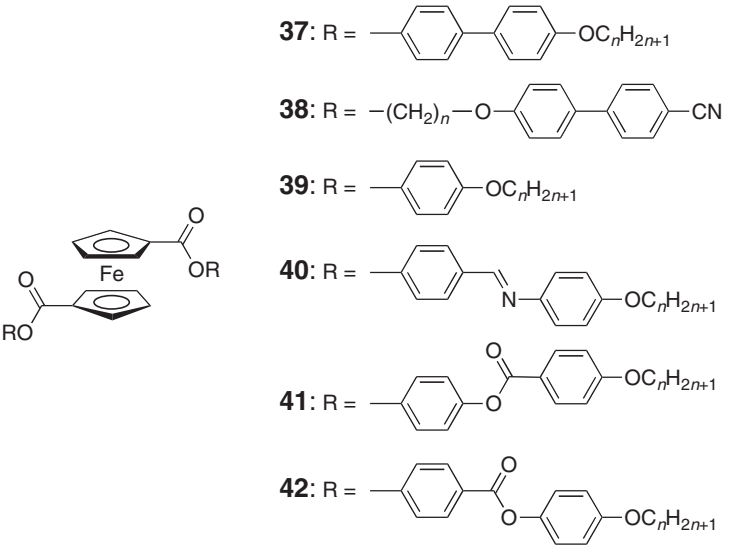

Isomeric families **41** (n) and **42** (n) differ in the orientation of the external ester functions.[101] Ferrocene derivatives **41** ($n = 1$–14, 16, 17) showed limited liquid-crystalline properties (Table 4). Only the first members of the series **41** ($n = 1$–6) exhibited monotropic N phases. More interesting mesomorphic properties resulted from series **42** ($n = 2$–12, 14, 16) (Table 4). The derivatives with short alkyl chains **42** ($n = 2$–4) gave rise to monotropic N phases. Compound **42** ($n = 5$) showed a short range (2 °C) enantiotropic N phase during the first heating run. The derivatives **42** ($n = 6$–8) exhibited monotropic N and/or SmA phases, and the long chain derivatives **42** ($n \geq 9$) showed enantiotropic SmA phases. The results observed for **41** (n) and **42** (n) showed the influence of the orientation of the ester function on the mesomorphic properties. An explanation of this influence was attempted on the basis of stereoelectronic factors. In **41** (n), electron delocalization occurs from the *O*-atom of the alkoxy chain to the ester function. In **42** (n), electron delocalization takes place in the opposite direction. Consequently, the *O*-atom of the ether group is more polar in **41** (n) than in **42** (n). The difference in polarity of the organic substituents is responsible for the different mesomorphic properties between **41** (n) and **42** (n). Related ruthenocene complexes derived from **42** were also reported ($n = 8$–12, 14).[102] They all showed a SmA phase, monotropic for $n = 8$, 9, and enantiotropic for the longer-chain-length homologs. Both melting and clearing temperatures were

Table 4 Phase transition temperatures of 1,1′-disubstituted ferrocenes **37** (*n*), **40** (*n*), **41** (*n*), and **42** (*n*)

Type	*n*	*Mesomorphism*
37	5	I 140 SmC 129
	6	I 139 SmC 132
	11	I 141 SmA 132
	4,7,8,9,10 are not mesomorphic	
40	4	Cr 180 N 191 I
	5	Cr 160 N 174 I
	6	Cr 168 N 177 I
	7	Cr 157 (N 146) I
	8	Cr 163 (SmA 149) I
	9	Cr 155 (SmA 151) I
	10	Cr 143 SmA 168 I
	11	Cr 141 SmA 162 I
	12	Cr 136 SmA 160 I
41	1	Cr 238 (N 187) I
	2	Cr 226 (N 203) I
	3	Cr 217 (N 176) I
	4	Cr 210 (N 176) I
	5	Cr 178 (N 159) I
	6	Cr 172 (N 153) I
	7–14, 16, 18 are not mesomorphic	
42	2	Cr 186 (N 177) I
	3	Cr 182 (N 144) I
	4	Cr 164 (N 157) I
	5	Cr 154 N 156 I
	6	Cr 167 (SmA 148 161 N) I
	7	Cr 165 (SmA 154) I
	8	Cr 164 (SmA 157) I
		Cr 173 (SmA 161) I[a]
	9	Cr 160 SmA 163 I
		Cr 169 (SmA 164) I[a]
	10	Cr 156 SmA 165 I
		Cr 167 SmA 169 I[a]
	11	Cr 155 SmA 167 I
		Cr 166 SmA 170 I[a]
	12	Cr 155 SmA 169 I
		Cr 165 SmA 173 I[a]
	14	Cr 153 SmA 169 I
		Cr 161 SmA 174 I[a]
	16	Cr 152 SmA 166 I
	18	Cr 150 SmA 163 I

[a]Ruthenocene derivatives analogous to **42**.

increased (by about 10 °C and 5 °C, respectively) with respect to those of the Fc compounds, leading to slightly smaller mesomorphic temperature ranges.

Unsymmetrically 1,1′-disubstituted ferrocenes **43** ($n = 11$–16)[103] were synthesized by combining the organic substituents used to prepare **41** (*n*) and **42** (*n*). Introduction of dissymmetry had two effects on the thermal and mesomorphic properties. First, a depression in the melting points was observed. Second, the smectogenic character of the materials was enhanced. Indeed, with the exception of **43** ($n = 11$), which showed only a SmA phase, all the members of the series showed both SmC and SmA phases. In view of the mesomorphic properties obtained for **43** (*n*) in comparison with those of **41** (*n*) and **42** (*n*), one can anticipate that the combination of very different substituents (e.g., chiral with non-chiral moieties, hydrocarbon with fluorocarbon motifs) should lead to ferrocenes showing rich mesomorphism.

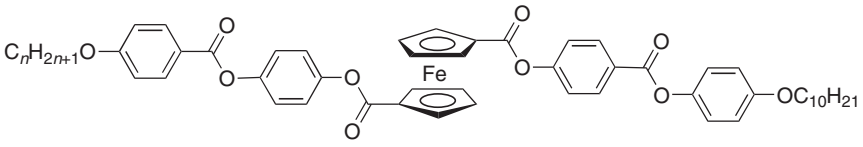

n = 11 Cr 144 SmA 149 I
n = 12 Cr 143 (SmC 138) SmA 150 I
n = 13 Cr 140 SmC 144 SmA 151 I
n = 14 Cr 135 SmC 142 SmA 152 I
n = 15 Cr 132 SmC 145 SmA 151 I
n = 16 Cr 132 SmC 148 SmA 153 I

43

Ferrocene was functionalized at the 1,1′-positions by a sugar moiety (1-amino-1-deoxy-D-sorbitol) and a long alkyl chain **44** in order to obtain lyotropic properties.[104] The substituents, in particular the sugar framework, were selected in view of successful investigations performed with organic-type amphiphilic carbohydrate surfactants. Compound **44** showed both thermotropic and lyotropic mesophases. In the bulk, a SmA phase formed from 98 to 137 °C. When **44** was mixed with an excess of water, a fluid L_α phase was obtained. For the thermotropic SmA phase, a *d*-layer spacing of 37.7 Å was determined. For the lyotropic lamellar phase, a *d*-layer spacing of 50 Å was found. Therefore, a 12.3 Å difference in layer thickness was obtained between the thermotropic and lyotropic mesophases. This increase in layer thickness was attributed to the incorporation of water molecules between the layers of **44** in the thermotropic phase.

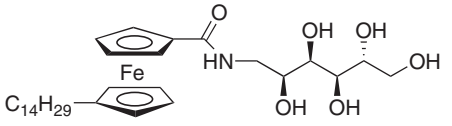

Thermotropic behavior: Cr 98 SmA 137 I
Lyotropic behavior: Lα at 60 °C (excess of water)

44

To enhance the mesomorphic character of disubstituted ferrocenes, the substituents were introduced into the 1,3-positions. From molecular modeling, it was clear that such a substitution pattern would enhance the molecular anisotropy (with respect to the 1,2-substitution pattern), and, therefore, strongly favor the formation of mesophases. Two families of 1,3-disubstituted Fc derivatives, **45** *n* = 1–14, 16, 18[105,105a] and **46** *n* = 5–8, 10, 12, 14, 16, 18,[106] were synthesized. All members of series **45** (*n*) and **46** (*n*) gave enantiotropic mesomorphic behavior (Table 5). In a few cases, additional monotropic mesophases were obtained. Interestingly, whereas N and SmC phases were observed for **45** (*n*), N and SmA phases were predominantly obtained for **46** (*n*). This difference has the same explanation as that for **41** (*n*) and **42** (*n*) (see above). Indeed, compounds **45** (*n*) and **46** (*n*) were built with the same organic substituents as those used to construct **41** (*n*) and **42** (*n*). Therefore, similar stereoelectronic effects should be encountered for **45** (*n*) and **46** (*n*). This reasoning is further supported by the fact that **42** (*n*) and **46** (*n*), which are positional isomers, preferentially display SmA phases. Four aromatic rings are required for mesomorphism to occur in disubstituted ferrocenes. Two[105b] or three[107] aromatic rings did not give rise to liquid-crystalline properties. This result shows again that Fc has to be considered as a bulky non-mesogenic unit. Unsymmetrically 1,3-disubstituted ferrocenes (structures not shown here) were prepared from the organic fragments that were used to synthesize **45** (*n*) and **46** (*n*).[108] The non-symmetrical materials gave mostly SmC and SmA phases (the N phase was obtained for two derivatives).

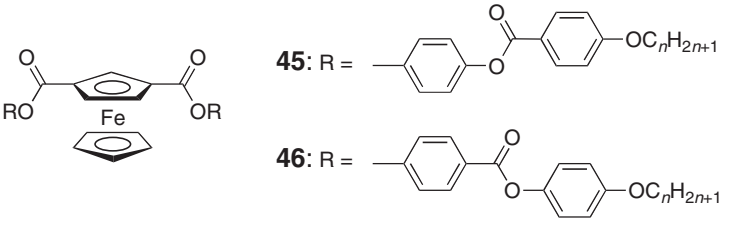

Table 5 Phase transition temperatures of 1,3-disubstituted ferrocenes **45** (*n*) and **46** (*n*)

Type	*n*	*Mesomorphism*
45	1	Cr 246 N 318 I
	2	Cr 253 N 316 I
	3	Cr 254 N 291 I
	4	Cr 246 N 281 I
	5	Cr 214 N 261 I
	6	Cr 184 N 247 I
	7	Cr 182 N 234 I
	8	Cr 178 N 225 I
	9	Cr 182 N 212 I
	10	Cr 182 N 208 I
	11	Cr 173 N 201 I
	12	Cr 166 (SmC 159) N 195 I
	13	Cr 166 SmC 169 N 191 I
	14	Cr 165 SmC 175 N 188 I
	16	Cr 162 SmC 179 N 181 I
	18	Cr 159 SmC 179 I
46	5	Cr 186 (SmA 178) N 248 I
	6	Cr 191 SmA 219 N 239 I
	7	Cr 190 SmA 228 N 233 I
	8	Cr 190 SmA 228 I
	10	Cr 185 SmA 227 I
	12	Cr 178 SmA 223 I
	14	Cr 174 SmA 219 I
	16	Cr 171 SmA 213 I
	18	Cr 168 (SmC 163) SmA 208 I

Unsymmetrically 1,3-disubstituted ferrocenes are planar chiral materials. Ferrocene (*S*)-**47** was obtained with an enantiomeric excess of 98%.[109] The absolute configuration of the Fc was determined on the basis of circular dichroism spectra,[110] and was assigned by applying the planar nomenclature.[111] Smectic C^* and SmA phases were observed for (*S*)-**47**. The spontaneous polarization of (*S*)-**47** was determined and a value of 2.8 nC cm^{-2} was obtained. This low value is in agreement with the structure of (*S*)-**47** that carries two organic fragments that differentiate only by the length of the terminal alkyl chains and the orientation of the external ester functions. Planar chirality is of interest as the chiral center is located at the Fc itself. Such structures might help to better our understanding regarding the role of Fc on the formation, nature, and stability of liquid-crystalline phases. Also, as most of the studies on chiral liquid crystals are developed with compounds having central chirality, planar chirality is an alternative way to obtain optically active materials.

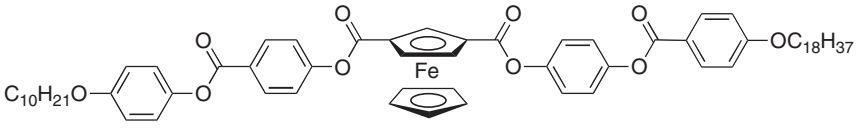

Cr 170 SmC* 198 SmA 202 I

(S)-**47**

Several 1,2-disubstituted Fc derivatives **48** ($n = 6$, 12) were prepared, but none of the compounds showed liquid-crystalline properties.[1h] From our systematic investigations on disubstituted ferrocenes, we could clearly establish the following liquid-crystal tendency: 1,3- > 1,1′- > 1,2-isomeric structures. This sequence can be explained in terms of structural features: (i) the 1,3-disubstituted ferrocenes possess the highest molecular anisotropy among the isomeric structures, (ii) the substituents located at the 1,1′-positions generate a step in the structure (S- or U-shape), which results in a reduction of the molecular anisotropy and a loss of colinearity of the mesogenic substituents, and (iii) the substituents located at the 1,2-positions give rise to a hairpin structure which lacks molecular anisotropy.

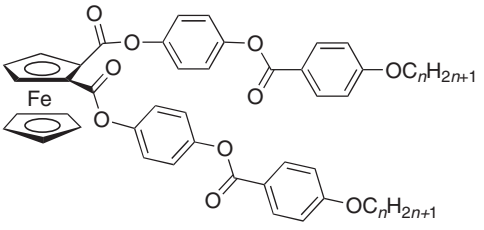

$n = 6$ Cr 149 I
$n = 12$ Cr 113 I

48

[3]Ferrocenophanes **49** and **50** carrying mesogenic groups at the 2,2′- or 3,3′-positions were prepared.[112] The 3,3′-isomer **50** displayed SmC and N phases, and the 2,2′-isomer **49** was found to be non-mesomorphic. Because of the bridge between the Cp rings, ferrocenophanes cannot give rise to conformations at the Fc level (as opposed to 1,1′-disubstituted ferrocenes). Therefore, **50** adopts a U-shape, and confirms that this conformation can produce mesomorphism for ferrocenes in which rotation around the Cp rings is allowed. Obviously, from these results, we cannot exclude the possibility, that the S-shape for 1,1′-disubstituted ferrocenes is not the one that is formed within the mesomorphic state. For materials where rotation is permitted, several conformations should be present within the mesomorphic state among the S and U ones. The non-mesomorphic behavior of **49** is the consequence of a lack of structural anisotropy.

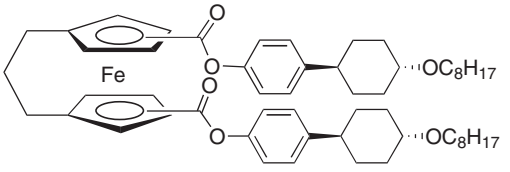

49: 2,2′-disubstituted Cr 135.5 I
50: 3,3′-disubstituted Cr 100 SmC 139.5 N 158 I

12.05.10.4.4 Influence of Fc on thermal and mesomorphic properties

For the design of ferrocene-based liquid crystals, the main structural feature that has to be taken into account is the three-dimensional structure of Fc. Interestingly, depending on the groups that are located on Fc, the latter unit can either reduce or enhance the stability of the liquid-crystalline state (see below).

We already mentioned that among the disubstituted Fc derivatives, the 1,3-disubstitution pattern is the one that induces the highest mesomorphic tendency, but because of the bulkiness of Fc, four rings are required for mesomorphism to occur. This observation confirms that Fc tends to decrease the liquid-crystalline tendency of the materials onto which it is included.

These results were confirmed by Thompson *et al.*,[1] who investigated the thermal and mesomorphic behavior of Fc materials and those of analogous compounds in which Fc was replaced by a benzene or a cyclohexane ring (see, for example, **51–53**).[113] They observed that Fc destabilizes the liquid-crystalline state. Indeed, whereas **51** and **52** show enantiotropic SmC and SmA or SmC and N phases, respectively, **53** displays only a monotropic N phase. This behavior indicates that Fc plays the role of a bulky unit, again as a consequence of its three-dimensional structure.

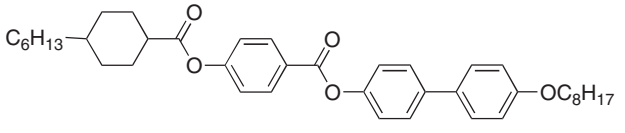

Cr 98 SmC 180 SmA 283 I

51

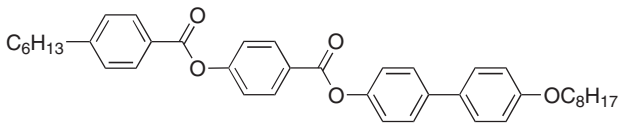

Cr 138 SmC 176 N 280 I

52

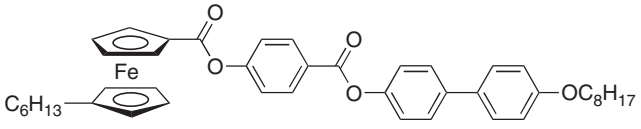

Cr 107 (N 63) I

53

Twin liquid crystals containing either Fc **54** and **55** or terephthalate **56** and **57** as the connecting unit between mesomorphic rods were reported by Tschierske *et al.*[114] Comparison of their thermal and liquid-crystalline properties revealed that the ferrocene-based materials have comparable or higher clearing temperatures and lower melting points than the structurally related terephthalates. Thus, broader liquid-crystalline domains are obtained for Fc materials. The stabilization of the liquid-crystalline state when Fc is used as the linking group was unexpected in view of literature data (see above). The authors explained this behavior as follows: the rotational flexibility of Fc could lead to an improved arrangement of the individual molecules within the layers, which results in a greater stability of the mesophases.

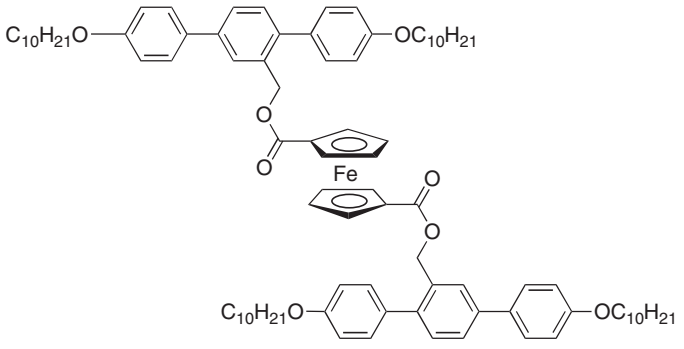

Cr 86 SmA 102 I

54

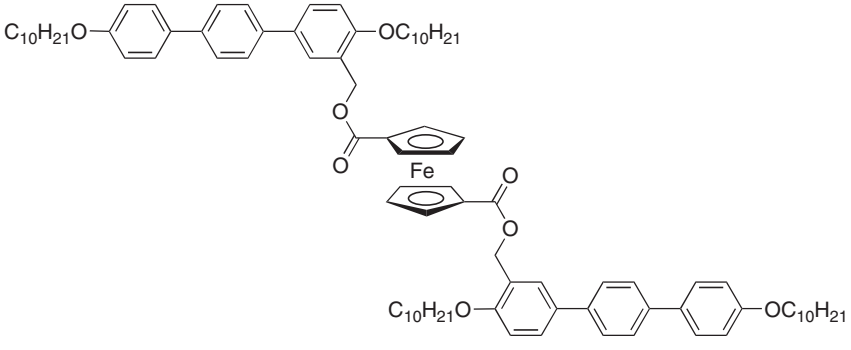

Cr 120 SmA 153 I

55

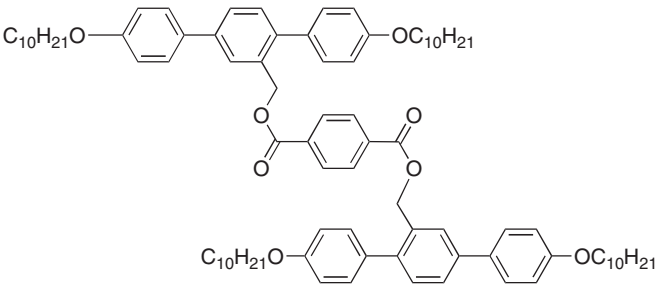

Cr 132 (SmA 94) I

56

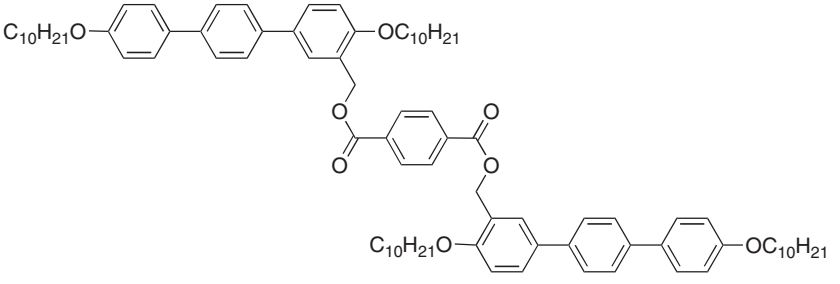

Cr 144 SmA 149 I

57

12.05.10.4.5 1,1′,3-Trisubstituted Fc derivatives

Trisubstituted ferrocenes **58** ($n = 12$, 14, 16, 18) and **59** were prepared to further explore the influence of the three-dimensional structure of Fc on the stability of mesophases.[107] Compounds **58** (n) showed monotropic SmA and/or SmC phases despite the presence of three aromatic rings on Fc. On the other hand, compound **59**, which was substituted by three mesogenic rods containing two aromatic rings each, led to enantiotropic SmC and SmA phases with a broad liquid-crystalline range (93 °C).

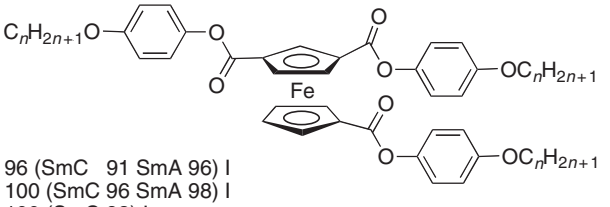

$n = 12$ Cr 96 (SmC 91 SmA 96) I
$n = 14$ Cr 100 (SmC 96 SmA 98) I
$n = 16$ Cr 100 (SmC 93) I
$n = 18$ Cr 102 (SmC 89) I

58

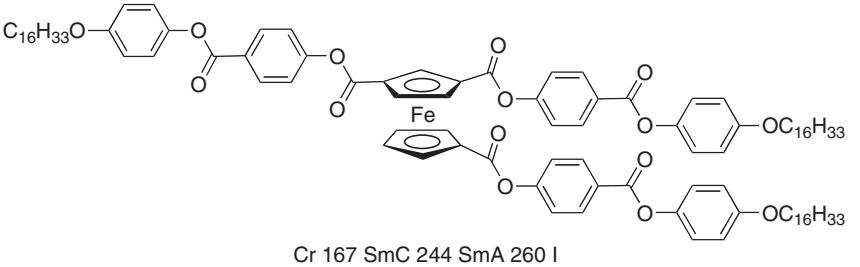

Cr 167 SmC 244 SmA 260 I

59

The data obtained for **58** (*n*) and **59** further emphasize the influence of the substitution pattern on mesomorphic properties. Whereas a two-aromatic ring system (plus the Cp nucleus) was found to be non-mesomorphic for 1,3-disubstitution,[105,105a] introduction of an additional substituent on the second Cp ring gave monotropic liquid crystals **58** (*n*). This result indicated that the repulsive interactions induced by the Fc core are compensated, at least in part, by the third substituent. This allows both substituted Cp rings to interact favorably, which results in mesomorphism promotion. In a structure such as **59**, the depth (bulkiness) of Fc (about 3.3 Å) is, in a way, hidden by the substituents anchored on the two Cp nuclei. Therefore, the 1,1′-3-trisubstitution pattern is a stronger mesomorphic promoter than the 1,3-disubstitution one (for identical substituents). This is supported by the fact that **46** ($n = 16$), the 1,3-disubstituted counterpart of **59**, gave a much narrower liquid-crystalline range (42 °C) than **59**.

Therefore, for Fc systems, mesomorphism strength varies according to the following series: 1,1′,3-trisubstitution > disubstitution > monosubstitution and for disubstituted Fc derivatives, liquid-crystal tendency varies in accordance with the following series: 1,3- > 1,1′- > 1,2-disubstitution.

12.05.10.4.6 Polycatenar ferrocenes

The tetracatenar derivative **60** gave rise to a Col_h phase from 52 to 84 °C.[115] With respect to polycatenar materials reported in the literature, **60** has a structural particularity as the alkyl chains are not grafted on phenyl rings, but are attached directly on Fc. Hexacatenar derivatives **61** (*n*) have a quite extended structure.[116] Compounds **61** ($n = 8$, 10) gave rise to $Ia\bar{3}d$ cubic phases, and higher homologs **61** ($n = 12$, 14, 16, 18) showed Col_h phases (Table 6). The shortest ($n = 6$) and longest ($n = 20$) chain derivatives of **61** were found to be non-mesomorphic.

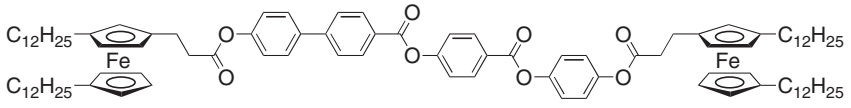

Cr 52 Col_h 84 I

60

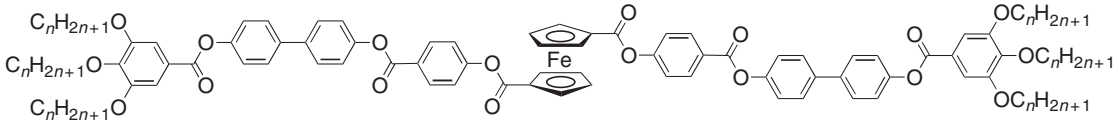

61

12.05.10.4.7 Hydrogen-bonded Fc derivatives

Hydrogen bonding was used to prepare supramolecular ferrocene-containing liquid crystals. The latter were obtained by associating an Fc derivative carrying a carboxylic acid function with either 4,4′-bipyridine **62**[115] or stilbazole derivatives **63** (*m*, *n*).[117] Tetracatenar derivative **62** gave rise to a Col_h phase from 66 to 72 °C. The

Table 6 Phase transition temperatures of hexacatenar ferrocenes **61** (*n*)

n	*Mesomorphism*
8	Cr 162.9 $Ia\bar{3}d$ 172.9 I
10	Cr 126.5 $Ia\bar{3}d$ 174.6 I
12	Cr 117.1 Col_h 172.3 I
14	Cr 112.6 Col_h 170.7 I
16	Cr 120.4 Col_h 171.9 I
18	Cr 120.9 Col_h 172.9 I
6, 20 are not mesomorphic	

Table 7 Phase transition temperatures of hydrogen-bonded ferrocenes **63** (*m*, *n*)

m	*n*	*Mesomorphism*
6	8	Cr 55 SmC 73 SmA 101 I
6	10	Cr 20 $Ia\bar{3}d$ 76 (SmC 72) SmA 89 I
6	12	Cr 65 $Ia\bar{3}d$ 78 SmA 90–95 I
10	8	Cr 61 $Ia\bar{3}d$ 88 I
10	10	Cr 69 $Ia\bar{3}d$ 87 I
10	12	Cr 76 $Ia\bar{3}d$ 88 I

formation of the Col_h phase for **62** was expected considering the behavior observed for the covalent-type tetracatenar Fc **60**. Among the tricatenar derivatives, the shortest chain Fc **63** ($m = 6$, $n = 8$) gave enantiotropic SmC and SmA phases (Table 7). The higher homologs **63** ($m = 6$, $n = 10$) and **63** ($m = 6$, $n = 12$) showed enantiotropic SmA and $Ia\bar{3}d$ cubic phases. An additional monotropic SmC phase was obtained for **63** ($m = 6$, $n = 10$). Complexes **63** ($m = 10$, $n = 8$, 10, 12) gave enantiotropic $Ia\bar{3}d$ cubic phases. It is remarkable that a slight modification of the length of the alkyl chains had such a pronounced influence on the mesomorphic behavior of compounds **63** (*m*, *n*). A subtle balance between the volume occupied by the central core and the flexible chains, as well as the surface between both parts, are responsible for the formation of the $Ia\bar{3}d$ cubic phases. A hydrogen bond is a valuable alternative to a covalent bond for the preparation of ferrocene-containing liquid crystals.

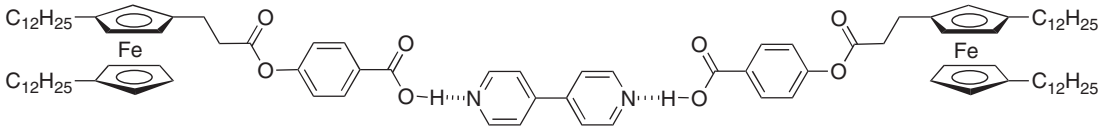

Cr 66 Col_h 72 I

62

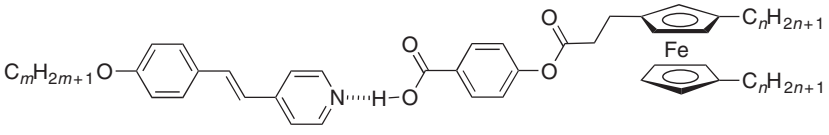

63

12.05.10.4.8 Ferrocene-containing liquid-crystalline dendrimers

Dendrimers represent a class of materials that combine unique features (well-defined macromolecular structure, monodispersity, and low viscosity) with remarkable properties such as encapsulation, catalysis, and chiroptical properties. Functionalized dendrimers are considered to be new materials with high potential applications.

The interest in liquid crystals motivated the design of liquid-crystalline dendrimers functionalized with Fc and fullerene (C_{60}). Dendrimers **64–66** were prepared by applying a convergent and iterative synthetic methodology. Monodisperse macromolecules were thus obtained.

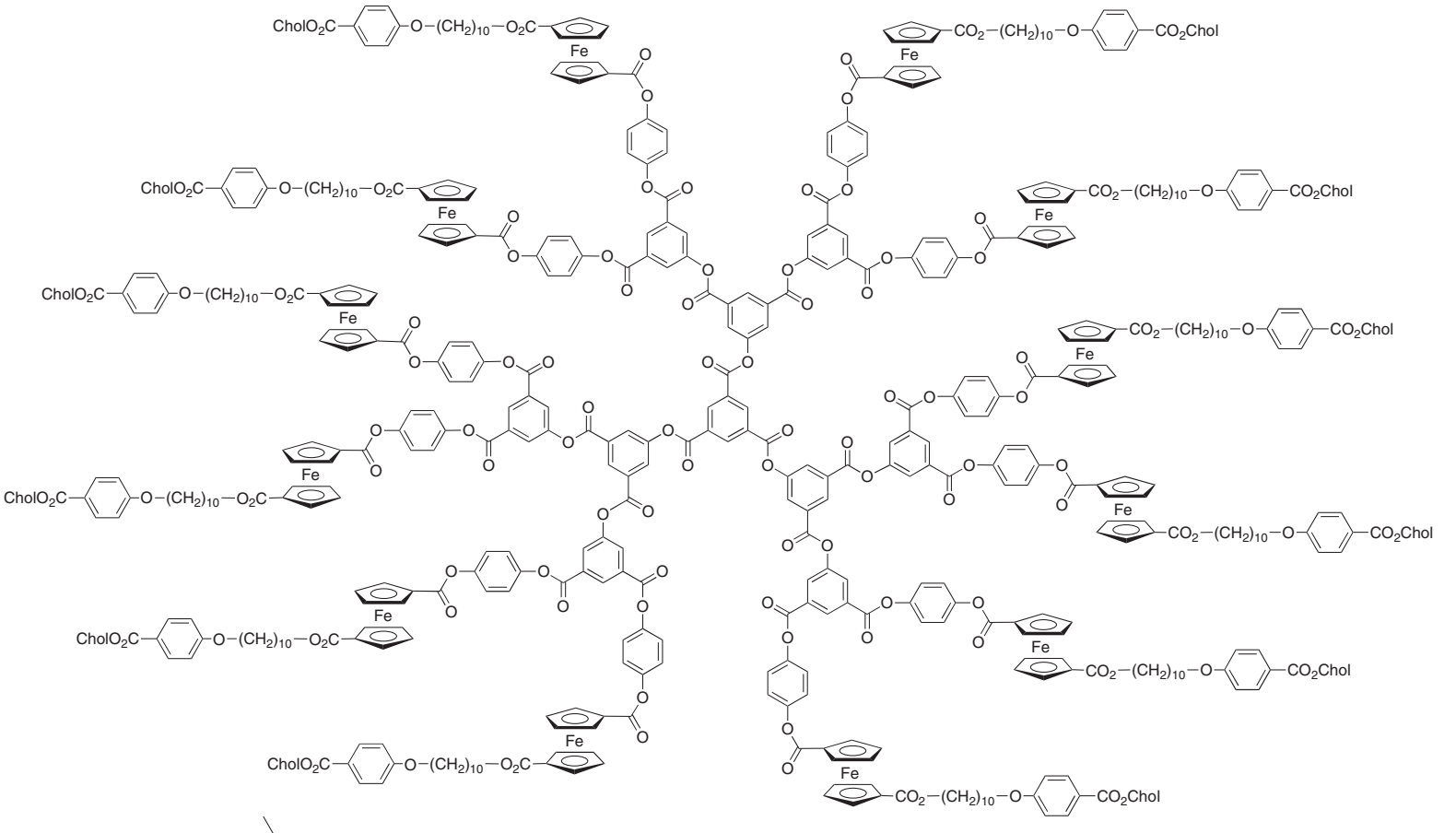

g 52 SmA 169 I

64

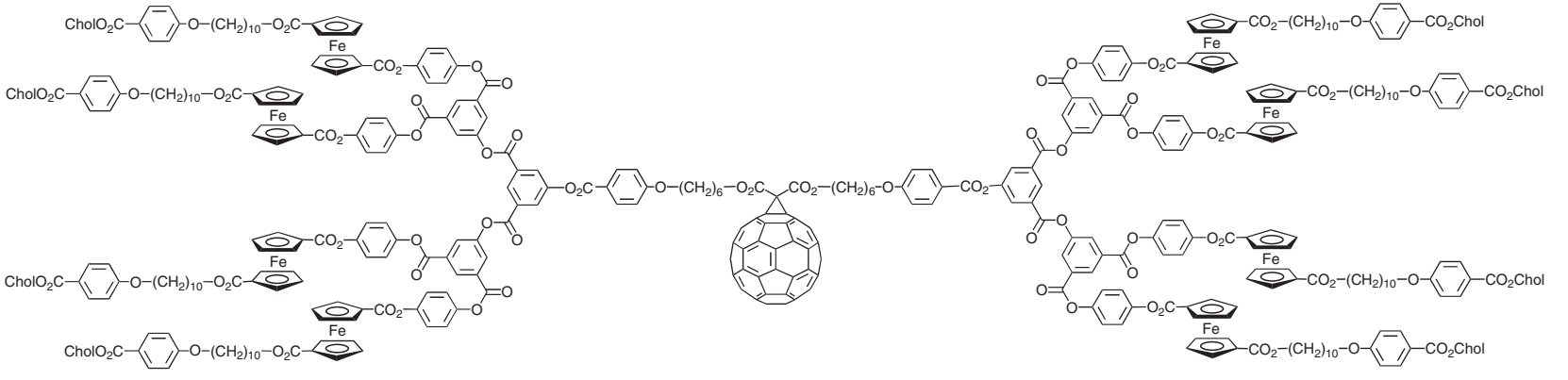

SmA 157 I

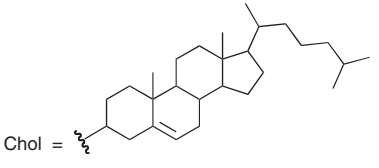

Chol =

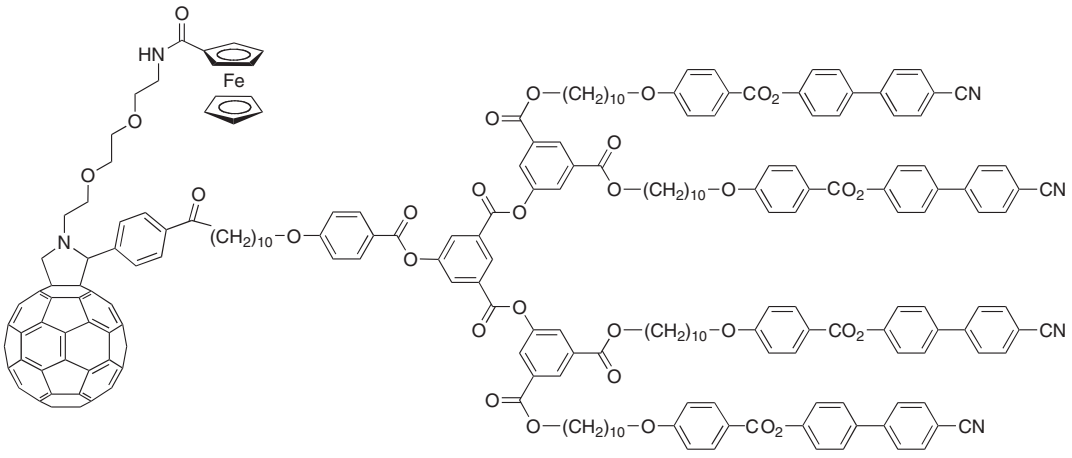

g 40 SmA 135 I

66

Second-generation dendrimer **64** gave rise to a SmA phase from 52 to 169 °C;[118] the first-generation dendrimer with six terminal Fc-cholesteryl units also gave rise to a SmA phase between 47 and 150 °C.[119] Methanofullerene **65** of second generation showed a SmA phase which cleared at 157 °C (the glass transition temperature was not detected);[120] the zeroth generation was also mesomorphic (SmA 118 **I**)[121] and exhibited interesting electrochemical[122] as well as photoinduced electron-transfer[123] properties. Second-generation fulleropyrrolidine **66** showed a SmA phase between 40 and 135 °C.[124] For **66**, photoinduced electron transfer was observed (through space mechanism) with a lifetime of the charge-separated state of 560 ns in tetrahydrofuran (THF). The association of Fc and C_{60} within a liquid-crystalline architecture could be an interesting way for the elaboration of supramolecular switches. Finally, **64–66** are thermally stable and soluble in common organic solvents.

12.05.10.4.9 Conclusions

Ferrocene has generated a great variety of liquid-crystalline materials that display rich mesomorphism. This is mainly due to the versatile synthetic chemistry that can be carried out with this compound. Furthermore, Fc gives rise to thermally stable derivatives. This is an important prerequisite for the design of liquid crystals. After 30 years of research devoted mainly to understanding the "structure-supramolecular organization" relationship, increased attention should be devoted to applications of ferrocene-containing liquid crystals. Considering the possibility of using the redox properties of Fc to generate mesomorphism, and the fact that Fc can be incorporated into well-defined macromolecular architectures such as dendrimers, this goal could lead to novel and unexpected results.

12.05.11 Organometallic Liquid Crystals of the Group 9 Elements

12.05.11.1 Complexes of β-Diketonates

Trzaska and Swager reported the mesomorphic behavior of two series of diketonato complexes of dicarbonylrhodium(I) and dicarbonyliridium(I) (**67**: M = Ir, Rh; $R = R^1 = R^2 = R^3 = R^4 = OC_nH_{2n+1}$; $n = 4$, 6, 8, 10, 12, 14, 16, 18).[125] All the complexes exhibited a Col_h phase over large temperature ranges, and they were well characterized by X-ray diffraction. The mesophase stability (Table 8) was found to be dependent on the length of the chains and increasing chain length was correlated with a smooth decrease in the clearing temperature (129–73 °C for M = Rh; 143–93 °C for M = Ir). The melting temperatures were high for the first homolog ($n = 4$), then room-temperature mesophases were observed from the hexyloxy to the decyloxy homologs. For longer-chain complexes, the melting temperatures rose again and resulted in the narrowing of the mesomorphic range (Figure 31). X-ray diffraction data suggested that the complexes stacked into columns in an antiparallel arrangement, consistent with the preferential antiparallel alignment of dipoles associated with the carbonyl groups. The data also suggested the

Table 8 Mesomorphism of complexes **67**

M	*Substitution pattern*	*Mesomorphism*
Rh	$R = OC_8H_{17}$; $R^1 = R^2 = R^3 = R^4 = H$	Not LC[a]
Rh	$R = R^1 = R^2 = OC_nH_{2n+1}$; $R^3 = R^4 = H$	Not LC
Ir	$R = R^1 = R^2 = OC_nH_{2n+1}$; $R^3 = R^4 = H$	Not LC
Rh	$R = R^1 = R^2 = R^3 = R^4 = OC_nH_{2n+1}$	Col_h
Ir	$R = R^1 = R^2 = R^3 = R^4 = OC_nH_{2n+1}$	Col_h

[a]LC = liquid crystalline.

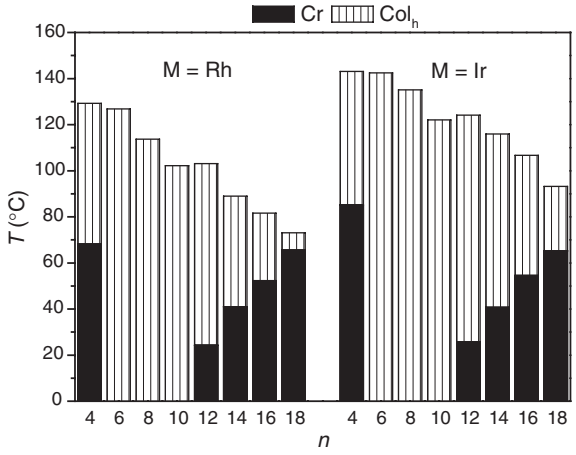

Figure 31 Mesomorphism of Rh(I) and Ir(I) complexes **67** ($R = R^1 = R^2 = R^3 = R^4 = OC_nH_{2n+1}$; $n = 4, 6, 8, 10, 12, 14, 16, 18$).

strong steric effects of the chains that would favor a dimeric, disk-shaped unit. Reducing the number of lateral chains led to non-mesomorphic compounds.[125,126]

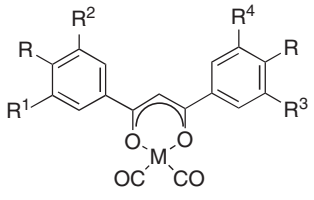

67

Elongated α-substituted-β-diketone ligands also form dicarbonylrhodium(I) and dicarbonyliridium(I) complexes, which, when properly elaborated, can yield new metallomesogens. Thus, **68** exhibited a N phase between 84 and 132.5 °C,[127] whereas the existence of the mesomorphic properties in complexes **69** appeared to depend on the linking group. Wan *et al*. claimed SmC and N phases for the rhodium complexes **69a** (M = Rh; $n = 7$–12, 14)[128,129] between 150 and 170 °C; the N phase was monotropic and occurred for the dodecyloxy compound, all the other derivatives showed the SmC phase. However, contradictory results were reported by Barberá *et al*.,[130] who did not observe mesomorphism for **69a** (M = Rh, Ir, $n = 10$, m.p. 145 and 128 °C respectively) and **69c** (M = Rh, Ir, $n = 10$, m.p. 111 and 116 °C respectively), but found a monotropic SmA phase for **69b** (M = Rh, $n = 10$, Cr 101 (SmA 93) I; M = Ir, $n = 10$, Cr 128 (SmA 96) I).

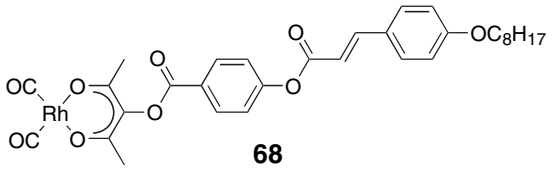

68

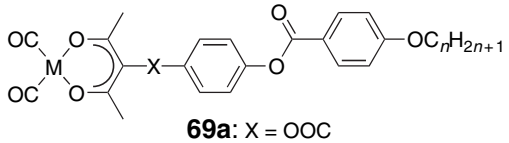

69a: X = OOC
69b: X = COO
69c: X = CH_2

Related materials **70** were prepared by Han *et al.*[131] All of the ligands showed monotropic phases, except for **70e**, where the phases were enantiotropic. All showed a N phase with a SmC phase seen for **70b** and **70e**. On complexation, mesomorphism was suppressed in **70d** and **70e**, while **70a** and **70c** showed a N phase (Cr 101.5 N 142.4 I and Cr 114.6 N 130.2 I) and **70b** showed a SmA phase (Cr 118.4 SmA 128.5 I). Clearing points for the mesomorphic complexes were rather similar (between 128 and 142 °C), whereas for the free ligands the difference was greater (between 53 and 185 °C).

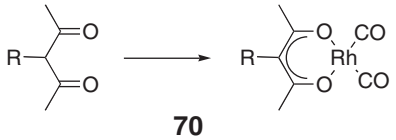

70

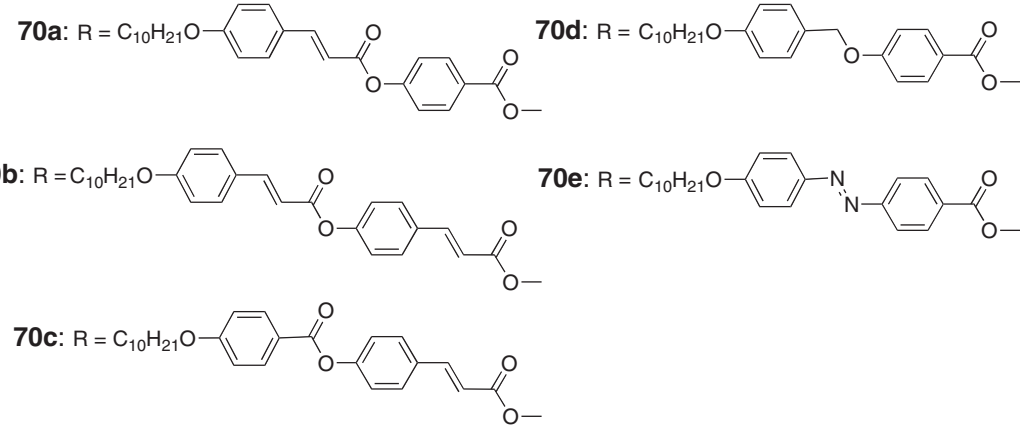

12.05.11.2 Complexes of Stilbazoles and Related Ligands

Reaction of the stilbazoles with $[M_2(\mu\text{-Cl})_2(COD)_2]$ (M = Rh, Ir; COD = 1,5-cyclooctadiene)[132] under CO led to a series of complexes (**71**: M = Rh, Ir).

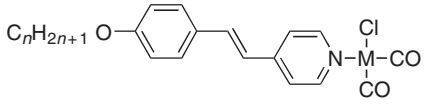

71

The rhodium(I) complexes were yellow/orange in the solid state, which is characteristic of mononuclear Rh(I), whereas the iridium(I) complexes were burgundy in the solid state and yellow in isotropic solution or in the melt. Infrared spectra suggested that the iridium complexes were associated in some way in the solid state, possibly in a

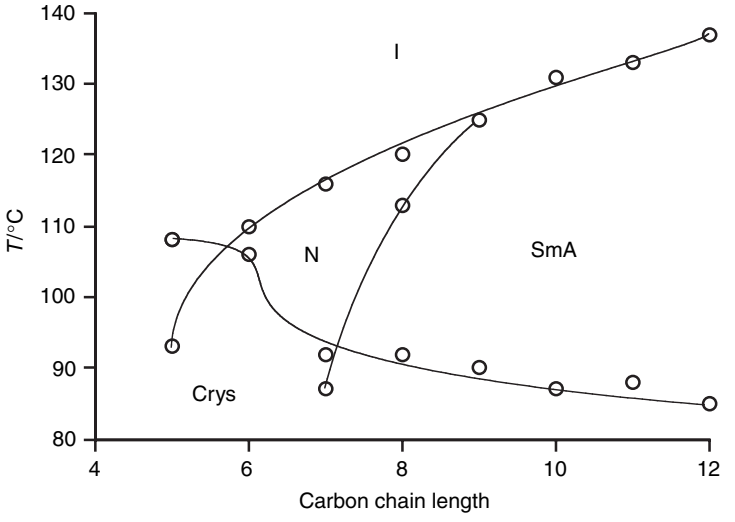

Figure 32 Phase diagram for the complexes **71** (M = Ir).

stacking arrangement as found in [IrCl(CO)$_2$(py)].[133] The phase diagram for the iridium complexes is shown in Figure 32.

The behavior is typical of relatively simple dipolar materials where a N phase was found at short chain lengths, giving way to a SmA phase in higher homologs. While the iridium complexes could be cycled in and out of the isotropic phase with few problems of decomposition, the rhodium complexes began to decompose rapidly on melting in air. Lateral fluorination of *cis*-iridium stilbazole complexes strongly destabilized the mesophase: the 2-fluorinated 4-alkoxystilbazole systems exhibited only monotropic N and SmA phases, whereas the structural isomeric 3-fluorinated compounds were not mesomorphic.[134]

These complexes also formed stable Langmuir films, which could be transferred onto a range of various substrates to yield Langmuir–Blodgett (LB) films.[135,136] A pyroelectric effect was observed in alternate layers incorporating an iridium complex,[137] and the electronic hyperpolarizability of some chiral derivatives was measured.[138]

Complexes related to these were previously synthesized by Esteruelas *et al.*[139,140] The mesomorphism of these complexes was less extensive than in related complexes with stilbazole ligands. Enantiotropic mesophases (N and SmA) were only established at the octyloxy homolog for both metals. Reaction of the rhodium derivatives with Me_3NO and an equivalent of ligand led to the *trans*-disubstituted derivatives, *trans*-[MCl(CO)(*n*-OPhIPy)$_2$] **72**, which curiously enough were non-mesomorphic, decomposing above 300 °C.

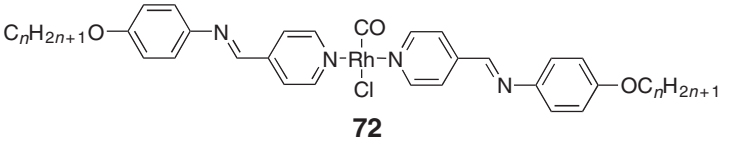

72

Dimeric stilbazole complexes of Ir(I) **73** were reported[141] and a very strong odd–even effect was noticed such that mesophases were observed when n = odd, but not when n = even.

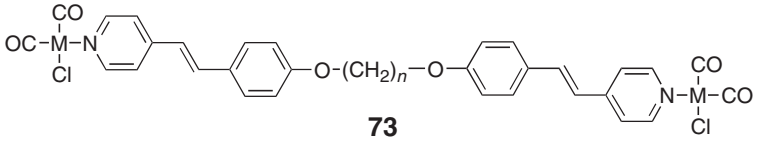

73

12.05.11.3 Carbonyl Complexes of Salicylaldimine Ligands

Appropriately designed salicylaldimine ligands can form mesomorphic complexes when bound to a metal center. For example, **74** shows a dicarbonylrhodium(I) moiety bound to a salicylaldimine where SmA and N phases were observed (Cr 112 SmA 116.5 N 122 I).[142]

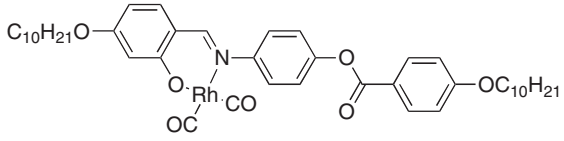

74

Berdagué *et al.* reported mesomorphic bimetallic systems resulting from the complexation of dicarbonylrhodium(I) and dicarbonyliridium(I) to a dimeric salicylaldimine bridged by a 1,4-diaminocyclohexyl unit (**75**: M = Rh, Ir).[143] Both complexes showed a SmA phase, although that of the iridium (Cr 142 SmA 169 **I**) compound had a higher mesophase stability than the rhodium congener (Cr 141 SmA 145 **I**).

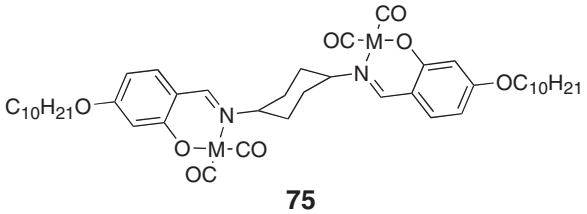

75

12.05.11.4 Acetylene Complexes

Mesomorphic, octahedral rhodium(III) complexes with a bulky central part[144] **76** were reported to exhibit smectic (unidentified) and nematic phases up to the decomposition points, at ca. 200 °C (Table 9).

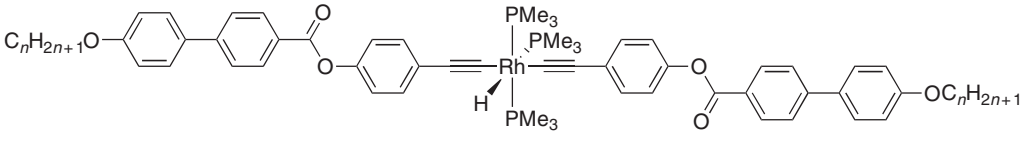

76

Table 9 Transition temperatures of some derivatives of **76**

n	*Transition temperatures*
8	Cr 136 S 174 N 203 dec.
10	Cr 142 S 172 N 202 dec.

12.05.12 Organometallic Liquid Crystals of the Group 10 Elements

In group 10 we find probably the largest collection of metallomesogens, mainly due to the large collection of *ortho*-metallated complexes of palladium(II), which have been exploited by several scientists.

12.05.12.1 Complexes of Monodentate Ligands

12.05.12.1.1 Complexes of isonitrile ligands

Some of the simplest systems reported raise a possible point of semantics as to whether these systems are, in fact, polycatenar in nature or perhaps ought to be described as discotic. The first of these **77** was based simply on the coordination of 3,4,5-trialkoxybenzonitriles to Pd(II),[145] following a motif for the formation of simple, calamitic systems[146] described some years earlier. Only two compounds with different chain lengths were studied ($n = 10$, 18). The ligands were themselves not mesomorphic, but on complexation, a Col_h phase was observed over small temperature ranges, i.e., 73–91 °C for the complex with six tridecyloxy chains, and between 58 and 80 °C for that with six octadecyloxy chains.

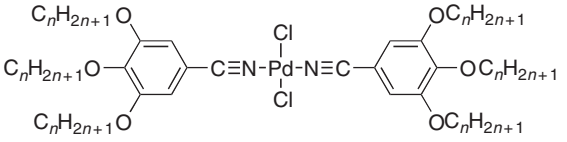

77

This structural motif was then used by Espinet and co-workers for the synthesis of a series of isonitrile complexes of Pd(II) and Pt(II)[147] (**78a**: M = Pd, Pt; X = Cl, Br; $n = 4$, 6, 8, 10 and **78b**: M = Pd, Pt; $n = 4$, 6, 8, 10). Again, none of the free isonitriles was found to be mesomorphic, but columnar mesophases were induced for the corresponding organometallic complexes.

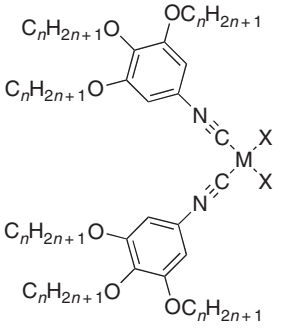

78a

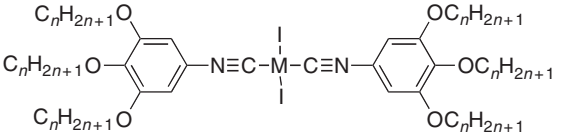

78b

Most of the complexes **78a** and **78b** exhibited Col_h phase, somewhere from the ambient temperature up to those greater than 200 °C. The mesophase stability was found to depend predominantly on the type of halide groups and chain length: the clearing temperatures decreased in the order Cl > Br > I with increasing n. On average, the transition temperatures, particularly those of the Col_h-to-I transitions, of the platinum complexes were higher than those of their palladium congeners (Table 10). All the chlorides and bromides showed wide-range, enantiotropic Col_h phases, whereas the iodides with butyloxy were not mesomorphic, and those with longer chain length displayed both monotropic (**78b**: M = Pd, $n = 6$, 8, 10; M = Pt, $n = 6$) and enantiotropic Col_h phases (**78b**: M = Pt, $n = 8$, 10). None of these complexes crystallized on cooling, and the Col_h phase was found to be stable in further heat-cool cycles. Interestingly, the chloro- and bromo-palladium and platinum complexes **78a** were obtained as *cis*-isomers, and thus

Table 10 Mesomorphism of complexes **78a** (*cis*) and **78b** (*trans*)

X	*n*	*Pd*	*Pt*
Cl	4	Cr 70 Col_h 220 I	Cr 73 Col_h 248 I
Cl	8	Col_h 184 I	Col_h 170 I
Br	4	Cr 77 Col_h 147 I	Cr 67 Col_h 220 I
Br	8	Cr 42 Col_h 143 I	Col_h 200 I
I	4	Cr 138 I	Cr 133 I
I	8	Cr 45 (Col_h 27) I	Cr 32 Col_h 41 I

exhibited a net dipole moment, whereas the iodides were all *trans*-compounds, and therefore apolar. This can explain the poorest tendency of the iodo complexes to give large mesomorphic domains and stable mesophases. By means of X-ray investigation, it was deduced that the columnar phase results from the antiparallel arrangement of the *cis*-isomers with the energetically favorable dipole–dipole interactions, and orthogonal stacking for the *trans*-derivatives. Note that the mesophase stability was greatly enhanced in the isonitrile palladium complexes **78** compared to the benzonitrile isomeric coordination compounds **77**.

Two homologs of **78a** (M = Pt, X = Cl, $n = 4, 6$) were investigated in the formation of LB films.[148] It was found that better films were obtained with the homolog that was mesomorphic at room temperature ($n = 6$). In the absence of more data, it is difficult to know how strongly this is correlated with the ambient liquid-crystal behavior of the material, or whether it results from a much lower degree of amphipathy due to the shorter chains. For example, well-ordered LB films of Ir(I) stilbazoles (**71**, see Section X.11.2) have been formed where the mesophase of the complex is found above 85 °C.

Takahashi *et al.*[149,150] studied the dihalo-palladium(II) and -platinum(II) systems (**79–80**: M = Pd, Pt; X = Cl, Br, I), some of which (**80**) are directly analogous to the nitrile complexes reported initially by Bruce and co-workers.[151] All the free alkoxy isonitrile ligands were mesomorphic (N and SmA phases below 85 °C). For M = Pd, both the bromo and iodo complexes were *trans* and gave mesomorphic complexes, whereas for M = Pt, only the iodo complexes behaved in this way; the other *cis*-complexes were not mesomorphic. In general, the complexes melted at temperatures between 120 and 200 °C giving either N or SmC phases, depending on the particular ligand; clearing points were between 200 and 300 °C. Whereas, in this case, the melting and clearing points were *very* similar for the same combination of metal, halogen, and ligand, it is interesting to compare this with the corresponding *nitrile* complexes mentioned above where significant differences were found between the behavior of the palladium and platinum systems. This is attributed to the difference in the strength of the interaction between the ligands and the metal, with the weaker Pd-nitrile interactions leading to deviations from predicted behavior (Table 11).

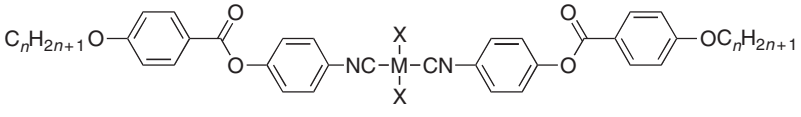

79a

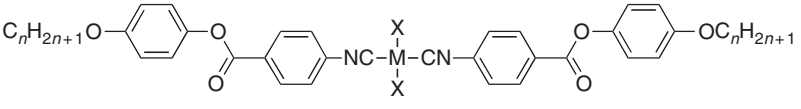

79b

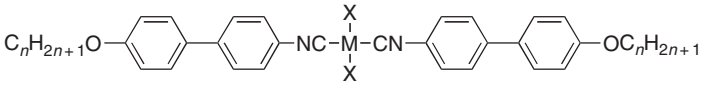

80

Table 11 Mesomorphism and transition temperatures of some derivatives of **79** and **80**

M, *X*	*79a*	*79b*	80
M = Pt	$n = 8$	$n = 8$	$n = 8$
X = I	Cr 163 N 230 I	Cr 196 SmC 222 N 265 I	Cr 154 N 228 I
	$n = 12$	$n = 12$	$n = 12$
	Cr 150 N 200 I	Cr 185 SmC 246 I	Cr 125 SmC 150 N 199 I
M = Pd	$n = 8$	$n = 8$	
X = I	Cr 157 N 241 I	Cr 186 SmC 218 N 266 I	
	$n = 12$		$n = 12$
	Cr 147 N 207 I		Cr 134 SmC 143 N 205 I
M = Pd			$n = 12$
X = Br			Cr 153 SmC 200 N 205 I

Chiral derivatives were reported by Omenat *et al.*[152] based on *trans*-PdI_2 complexes of some of the esters **79b** and **81**; the chirality was introduced via the terminal chain. For the chiral derivative, **79b**, SmC^* and N^* phases were observed at temperatures that were slightly lower than those of the non-chiral homologs: Cr 133.7 (SmC^* 109.5 N^* 127.3) I, Cr 176.4 SmC^* 188.9 N^* 246.7 I, and Cr 100.9 (N^* 92.7) I, for OR = $-OC^*HMeC_6H_{13}$, $-O(CH_2)_3$-$C^*HMeC_2H_5$, and $OC^*HMeCO_2C_4H_9$, respectively. For **81**, only the SmC^* phase was observed (Cr 155.3 SmC^* 288 dec.). Modest values for the spontaneous polarization between about 60 and 90 nC m^{-2} were found.

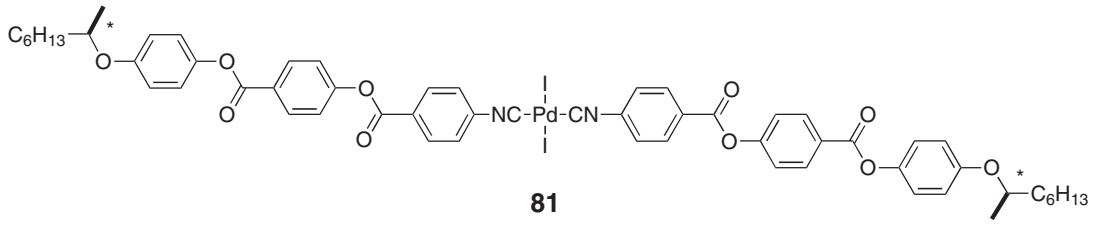

81

Wang *et al.*[153] described some Pd and Pt iodide complexes of laterally substituted isonitrile ligands (**82**: M = Pd, Pd; R = Me, $CHMe_2$) and while the ligands themselves were non-mesomorphic, the complexes (R = Me) gave nematic phases at shorter-chain lengths and SmC phases as the chains extended, with little difference on the transition temperatures between the palladium and platinum complexes. Typically, the complexes melted at temperatures between 150 and 260 °C and clearing points were between 270 and 300 °C. With the bulkier isopropyl side group ($R = CHMe_2$), the mesomorphism was totally suppressed, and the clearing temperatures depressed considerably.

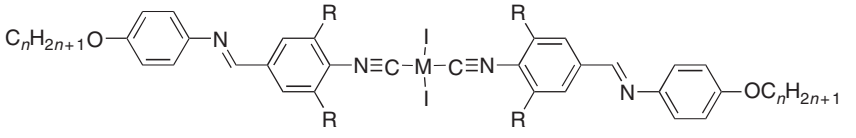

82

The same group later reported the chiral derivatives **83** in which the ligand is modified to include an acetylene linking group.[154] With the exception of the complexes with $R = R^1 = Me$ that showed a SmA phase, all the other materials showed a N^* phase with a pitch length, *p*, in the range 350–470 nm. Interestingly, the clearing points of the materials were highest when R = Me, R^1 = H and lowest when $R = R^1$ = H (Table 12).

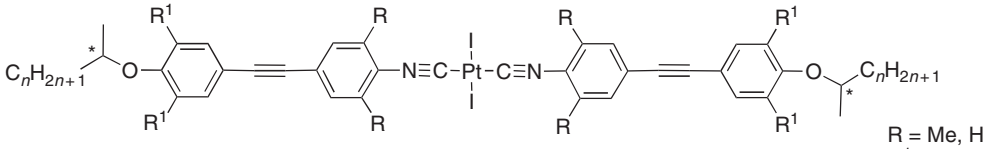

83

R = Me, H
R^1 = Me, H
n = 3–6

Espinet *et al.*[155] reported a rather nice series of 2,6-dipicolinate derivatives **84** whose structure is reminiscent of pincer-type complexes.[156,157] The first thing to note is that none of the Pd complexes of dipicolinate (**84a**: X = O) was found to be mesomorphic. However, in the case of complexes derived from 2,6-bis(thiocarboxylato)pyridine

Table 12 Mesomorphism of some derivatives of complexes **83** (*n* = 6)

R	R^1	(*S*)	(*R*)
Me	H	Cr 151 N^* 215 I	Cr 152 N^* 214 I
H	H	Cr 130 N^* 136 I	Cr 129 N^* 135 I
Me	Me		Cr 180 SmA 200 I

(84: X = S), a different pattern emerged. Thus, when complexed to ligand **a** ($m = 1$), no liquid-crystal properties were observed, whereas for ligand **a** ($m = 2$) the complexes exhibited mesomorphism showing predominantly SmC phases and, occasionally, a N phase. Melting points in the approximate range 140–200 °C were found with ligand **a** ($m = 2$). Moreover, when the pincer was substituted by thioalkyl chains (84: Y = S), instead of alkoxy chains (84: Y = O), the mesomorphic range was substantially enlarged, essentially due to an important reduction of the melting temperature. Chiral derivatives using ligands **b** and **c** were prepared with $n = 12$ and Y = O—none were mesomorphic.[157] However, when the chirality was introduced through the pincer using (*R*)-2-butyloxy and (*R*)-2-octyloxy chains, SmC* phases were observed.

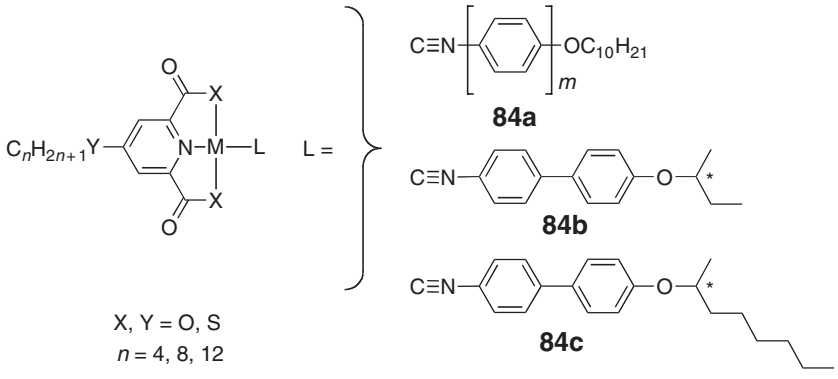

Nickel complexes of the thio pincer ligands (M = Ni; X = S) are also mesomorphic for ligand **a** ($m = 2$), and for both alkoxy (Y = O) and alkylthio (Y = S) chains on the pincer, showing (mainly) SmC and (occasionally) N phases.[157]

12.05.12.1.2 Acetylide complexes

The platinum(II) complexes **85** were found to be mesomorphic provided that the rigid core contained at least three aromatic rings.[158,159] The non-symmetrical compounds **85a** (R = Me) exhibited a N phase, in addition to a SmA phase for the complexes with $m + n \geq 22$. Melting points were typically around 170 °C (for $m + n \geq 12$), and the clearing temperatures in the range 180–220 °C. This shows that the relative bulk of the two trimethylphosphine groups in the center of the complex does not have an adverse effect on the overall structural anisotropy of the complex, and the high melting and clearing points suggest that the system may, in fact, tolerate slightly larger groups. This was shown to be the case when related, mesomorphic complexes bearing triethylphosphine ligands were synthesized (**85a–85d**: R = Et).[160] All the compounds exhibited solely a nematic phase, monotropic for **85a** (R = Et), and enantiotropic for **85b–85d** (R = Et). Increasing the molecular structural anisotropy thus stabilized the nematic phase, and the enlargement of the side group contributed to a substantial depression of the transition temperatures (Table 13).

Table 13 Transition temperatures of some derivatives of **85**

Complexes	*n (m)*	*R*	*Transition temperatures*
85a	8 (8)	Me	Cr 173.5 N 205.5 I
85a	8 (8)	Et	Cr 93 (N 62) I
85b	8	Me	Cr ~200 N > dec.
85b	8	Et	Cr 134 N 156 I
85c	8	Et	Cr 124 N 142 I
85d	8	Et	Cr 114 N 156 I

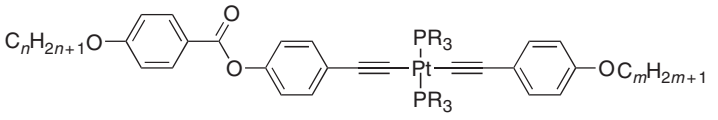

85a

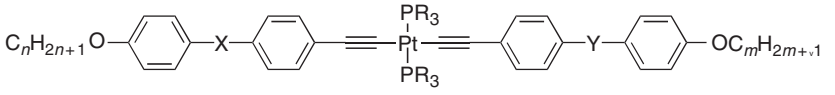

85b: X = COO, Y = OOC
85c: X = OOC , Y = COO
85d: X COO, Y = COO

However, a later study with more anisotropic-elongated acetylenes[161] (**86**: M = Pt, Pd, R = Me, Et, Pr) indicated that larger phosphines were not well tolerated as mesomorphism was lost on the introduction of tripropylphosphine (Table 14).[162] Increasing the size of the phosphine substituents considerably reduced the melting transition temperatures. Mesomorphism was absent in the analogous palladium complexes, decomposing rapidly above 100 °C due to their lower thermal stability compared to their platinum congeners.

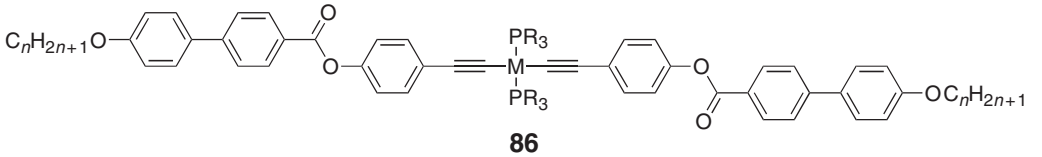

86

12.05.12.1.3 Carbene complexes

An unsymmetrically substituted bis(carbene)platinum(II) complex **87** was obtained by consecutive nucleophilic attack of propanol and then propylamine onto *trans*-diiodo(bis-isocyanide)platinum(II) complex.[163] The stable complex gave rise to a N phase (Cr 142 N 173 I).

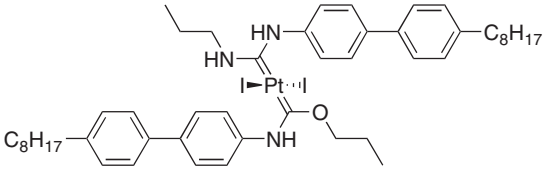

87

Smectic mesophases have been claimed for palladium(II) **88a** and **88b**[164] carbene complexes based on 1,3-dialkylbenzimidazol-2-ylidene and 1,3-dialkylimidazol-2-ylidene. However, examination of the X-ray diffraction data in combination with the large clearing enthalpies suggest that these materials are highly ordered and may be better described as crystals.

Table 14 Transition temperatures of some derivatives of **86**

n	*R*	*Transition temperatures*
8	Me	Cr 265 N 320 dec.
10	Me	Cr 258 N 320 dec.
8	Et	Cr 179 N 292 I
10	Et	Cr 165 N 266 I
8	Pr	Cr 111 I
10	Pr	Cr 105 I

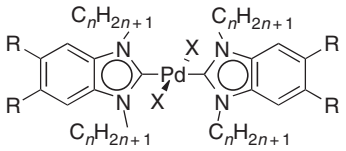

88a

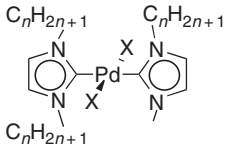

88b

12.05.12.1.4 Complexes of stilbazoles

Derivatives were also obtained (89) where one of the stilbazoles was replaced with an alkene.[165,166] These materials now showed much reduced melting and clearing points and SmA phases were seen between 50 and 100 °C for most derivatives synthesized. It was also noted that, in general, the materials were non-mesomorphic when $n+m \geq 8$, showed monotropic mesomorphism when $8 \leq n+m \leq 13$, and gave enantiotropic mesophases for $n+m \geq 14$. The simultaneous increase of both m and n resulted in the decrease of the stability of the crystal phase (reflected by the low melting point) and in the increase of the clearing temperature, thereby enhancing the temperature range of the SmA phase. Some of the complexes with $m=0$ were also mesomorphic ($n \geq 8$), showing SmA phases, although at higher temperatures. Mixture of some of these complexes was also carried out, and resulted in the enhancement of the SmA phase stability, essentially due to the depression of the melting points.

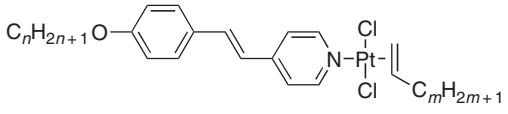

89

The acetylide complexes 90 were synthesized on Pt rather than on Pd, due to the lability of the latter metal that precluded isolation of such species other than Pt. These species were accessed as neutral analogs of related Ag(I) complexes in order to try to delineate the effect on the mesomorphism of the charge on the silver complexes and how this might relate to the stability of the cubic phase seen extensively in the silver complexes.[167] The Pt-acetylide complexes turned out[168] to be predominantly nematic in their phase behavior and the consequences in relation to cubic phase behavior were discussed. Curiously, however, the complexes did, in addition, show a SmC phase. It is almost universally true that liquid crystals bearing lateral chains show only nematic phases,[169] and so this aspect of the behavior of Pt complexes still requires explanation.

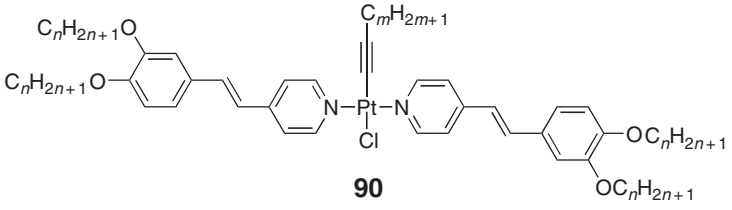

90

12.05.12.2 Complexes of *ortho*-metallated Palladium(II) and Platinum(II)

12.05.12.2.1 *ortho*-Metallated azo complexes

One of the earlier contributions to the revival of metal-containing liquid crystal systems was the synthesis of the *ortho*-metallated palladium complexes of mesogenic azobenzenes 91, 92 by Ghedini and co-workers, which represented the first systematic attempt to coordinate metals to known liquid-crystal systems.[170]

Initial studies[171] investigated the dipalladium complexes (**91**: M = Pd, X = Cl, R = OEt, $R^1 = C_4H_9CO_2$, $C_6H_{13}CO_2$, $CH_2{=}CH(CH_2)_8CO_2$) and the related mononuclear complexes (**92**: X = Cl, L = PPh_3, pyridine, quinoline, and aniline). All of the dinuclear complexes showed an enantiotropic nematic phase with melting points in the range 165–210 °C and clearing points between 185 and 215 °C; the free ligands typically melted in the range 65–80 °C and cleared between 105 and 125 °C. The role of the bridging halogen in these systems was also investigated (**91**: M = Pd; X = Br, I; R = OEt; $R^1 = C_6H_{13}CO_2$),[172] and it was found that the melting point increased in the order Cl < Br < I and that the temperature at which the nematic phase first appeared increased in the same order. Clearing points, however, followed a different trend, namely Br > I > Cl (X = Cl: Cr 190 N 205 I; X = Br: Cr 210 (SmB 205) SmA 215 N 250 I; X = I: Cr 220 SmA 225 N 230 I). The reasons for these various changes are unclear. While none of the related mononuclear complexes with triphenylphosphine or aniline was mesomorphic, those with L = py and quinoline gave materials with nematic and smectic phases. For the pyridine (*N,N-cis*) complex, the nematic phase stability was similar to that found in the parent dinuclear systems (Cr 180 SmB 198 N 235 I), while for the quinoline (*N,N-trans*) complex, melting points and clearing points were somewhat reduced (Cr 136 SmA 151 N 180 I).

The fact that complexation of such systems enhances mesophase stability was further demonstrated in the azopalladium(II) complexes with 4-alkyl-4′-alkoxyazobenzenes for which induction and/or mesophase stabilization were observed (**91**: M = Pd; R = H, CH_3, C_2H_5, C_3H_7; $R^1 = OC_nH_{2n+1}$; n = 1, 2, 7, 12, 18).[173–175] All the complexes were found to exist as equimolar mixtures of *cis*- and *trans*-isomers. Enantiotropic nematic phases, with, in some cases, additional smectic phases (SmA and SmC), were obtained; for short-chain-length complexes (n = 1, m = 1, 2, 7), mesomorphism occurred above 200 °C, whereas for the derivatives with long alkoxy chains (n = 1, m = 12, 18; m = 12, n = 2, 3), mesophases appeared between melting points in the range 130–180 and clearing points around 160–200 °C. Molecular and macroscopic biaxiality have been claimed for these materials on the basis of order parameter measurements made by infrared techniques, calorimetry, and optical microscopy.[176] Later investigations by neutron scattering and small-angle diffraction studies[177,178] suggested that the phases were uniaxial, although it is difficult to see how techniques that monitor rather short-range order could validate such a conclusion.

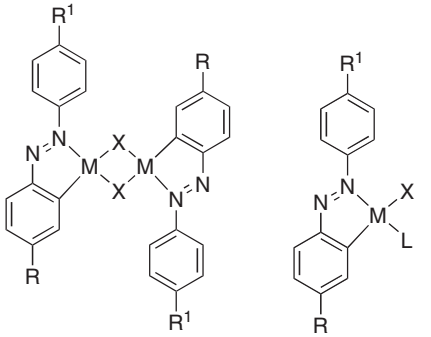

91 **92**

Several azopalladium(II) complexes of 4,4′-dialkoxyazobenzenes were also prepared. In one study, *ortho*-palladation of the 4,4′-di(tetradecyloxy)azobenzene (**91**: M = Pd, R = $R^1 = OC_{14}H_{29}$) led to the formation of enantiotropic smectic phases: SmC for the acetato-bridged complex (Cr 92 SmC 104.5 I), and SmB for the chloro-bridged analog (Cr 150 SmB 180).[179] Moreover, the use of a chiral acetate bridge (CH_3ClC^*HCOO) gave rise to a ferroelectric smectic phase (Cr 67 SmC^* 84 SmA 91 I). Other means of inducing ferroelectric mesophases consisted of incorporating chiral alkoxy substituents such as (*R*)-(−)-2-octanol and (*S*)-(−)-β-citronellol chains (**91**: M = Pd; X = Cl, I; $R = OC_nH_{2n+1}$; n = 7, 10, 12, 14; $R^1 = OCH_2CH_2CH_2C^*HMeCH_2CH_2CH{=}CMe_2$, $OC^*HMeC_6H_{13}$).[180] Again, both benzene rings of the ligands underwent *ortho*-palladation, and thus all the complexes existed as mixtures of isomers in various proportions. SmC^* and SmA phases were indeed induced (the free ligands with a citronellol chain exhibited N^* and/or SmA phases, whereas, they were not mesomorphic with 2-octanol).

The series of cyclopalladated dimers obtained from the nematogen 4,4′-di(hexyloxy)azobenzene (Cr 108 N 116 I), with various bridging systems (**91**: M = Pd; R = $R^1 = OC_6H_{13}$; X = Cl, Br, I, N_3, SCN, OAc; **93**), has been prepared, and the effectiveness of the bridging group in promoting mesophases evaluated.[181,182] From crystalline structures of homologous compounds, all complexes except the acetato bridged ones are planar and in their *trans* conformation; the latter possess a sort of "roof-shape," and exist as a *cis*:*trans* mixture.[183] This study revealed that mesomorphism was favored for chloro, bromo, azido, and oxalato complexes **93**, but not for the iodo, thiocyanato, or acetato derivatives (Table 15). The presence of the nematic phase below the more ordered smectic phases is rather surprising. While

Table 15 Thermal behavior of dinuclear complexes **91** (M = Pd, R = R^1 = OC_6H_{13}) and **93**

Type	*Mesomorphism*
91, X = Cl	Cr 213 N 221 E 235 dec.
91, X = Br	Cr 215 (N 196) I
91, X = I	Cr 211 I
91, X = N_3	Cr 186 SmA 190 dec.
91, X = SCN	Cr 220 I
91, X = OAc	Cr 140 I
93	Cr 238 N 246 SmA 290 dec.

such re-entrant behavior is known and possible, the authors tentatively explained this observation by the dissociation of molecular pairs into single molecular species of different mesomorphism. In the case of the oxalato complex, the nematic phase was transient and never reappeared on successive heating-cooling runs; the extensive decomposition of the chloride did not allow such an experiment to be carried out.

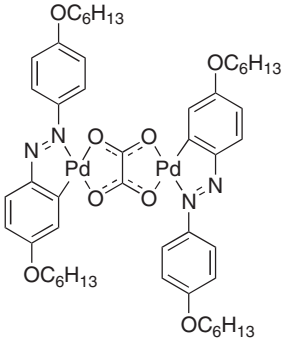

93

In order to obtain low-melting metallomesogens, several unsymmetric, mononuclear, *ortho*-metallated complexes combining 4,4′-bis(alkoxy)azobenzene and various types of simple chelating ligands, have been prepared. Such dinuclear, chloro-bridged complexes may be reacted with anionic chelating ligand, and converted to a stable, mononuclear species. Thus, complexes **94** (M = Pd, $n = m = 6$) with chelating ligand X–Y such as the *O,O*-monoanionic acetyle acetonate (acac) 1,1,1,5,5,5-hexafluoro-2,4-pentanedionato anion (hfac), and tropolonate, the *N,O* 2-aminophenate and 2-amino-2-methyl-1-propanoate,[184] as well as cyclopentadienyl[185] ligands were prepared, but none of them was mesomorphic, probably due to the bulkiness of the co-ligands relative to the small anisotropy of the complex. Note that luminescence was induced by cyclopalladation.[186] Low-temperature N^* and SmA phases were nevertheless observed at longer chain lengths in some related, chiral, palladium (II) complexes with an acac co-ligand Y–X (**94**: M = Pd; $n = 7$, 10, 12, 14, OC_mH_{2m+1} = (*R*)-(−)-2-octanol, (*S*)-(−)-β-citronellol).[187]

Other heteroligand palladium complexes **94** with Y–X being either a non-chiral *N*-[4′-(dodecyloxy)resorcylidene]-4-alkylaniline or a chiral *N*-[4′-(dodecyloxy)resorcylidene]-4-alkoxyanilines (**94**: M = Pd; $n = 14$, OC_mH_{2m+1} = (*R*)-(−)-2-octanol, (*S*)-(−)-β-citronellol) were prepared. They showed chiral mesophases over narrow temperature ranges.[188]

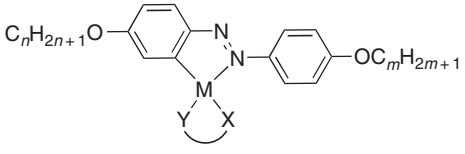

94

In order to obtain reliable thermal behavior and improve the mesomorphic properties of cyclometallated azobenzene complexes, the overall anisotropy of the complexes was enhanced by using elongated azobenzenes. Thus, Ghedini and co-workers prepared mesomorphic three- and four-ring azobenzene ligands and the corresponding *ortho*-metallated dinuclear and mononuclear complexes containing cyclopentadienyl,[185,189] acac,[190] tropolonate, and quinolate[191] ligands. Most of these new organometallic species were found to show mainly nematic phases with clearing temperatures lower than those of the parent ligands, except the chloro-bridged complexes (structures **95** and **97**) for which mesophases occur at elevated temperatures (Table 16). Some are the first examples of mesomorphic complexes of octahedral Pt(IV) and were obtained from the oxidative addition to the square-planar platinum(II) complexes by I_2 and MeI.

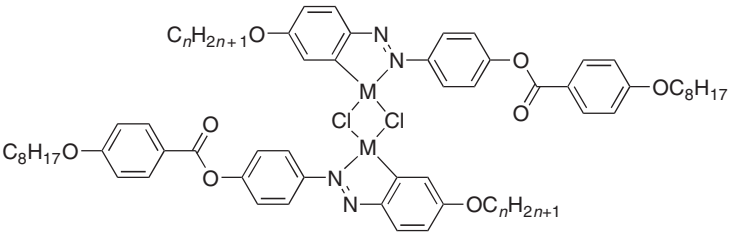

95

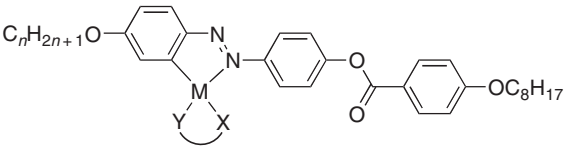

96

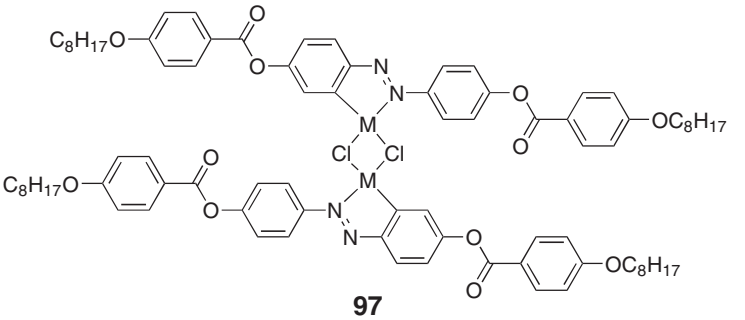

97

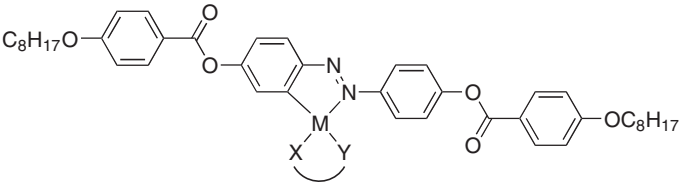

98

Note that an early example of such *ortho*-metallated complexes with elongated azobenzenes was reported by Hoshino *et al.* (**99**: $n = 1$–10, 12, 14, 16, 18).[192] In common with the parent ligands, the complexes were nematic, although melting and clearing points were raised by 60 and 102 °C, respectively, on complexation, giving the complexes a much wider nematic range. Variable-temperature ^{1}H NMR experiments using the $n = 4$ derivative in isotropic solution in $CDCl_3$ confirmed the presence of dynamic processes which were interpreted on the basis of a model where the lateral chain was, in fact, sitting in the central cleft of the molecule.

Table 16 Thermotropic behavior of the *ortho*-metallated complexes **95–98**

Type	*M*	*n*	*X-Y*	*Transition temperatures*
95	Pt	10		Cr 206 SmC 253 N 275 dec.
96	Pd	6	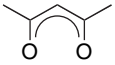	Cr 119 N 264 I
	Pd	6	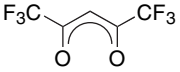	Cr 110 N 167 I
	Pd	6	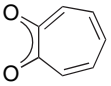	Cr 103 N 170 I
	Pd	6		Cr 117 N 144 I
	Pd	10		Cr 72.5 N 128.5 I
	Pt	10	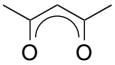	Cr 131 N 196 I
	PtI_2	10	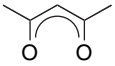	Cr 125 (E 60) I
	$PtMe_2$	10	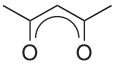	Cr 108 N 230 dec.
97	Pd			Cr 250 SmC 331 dec.
	Pt			Cr 263 SmC 342 dec.
98	Pd			Cr 143 N 226 I
	Pt			Cr 160 N 250 dec.
	Pt		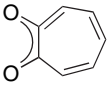	Cr 174 N 264 I
	PtI_2		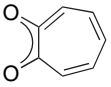	Cr 210 (N 209) I
	PtIMe		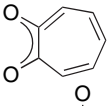	Cr 142 SmC 146 dec.
	Pt		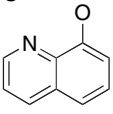	Cr 162 SmA 189 N 280 dec.
	PtI_2		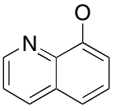	Cr 211 SmC 218 N 255 dec.
	PtIMe		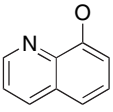	Cr 147 SmC 154 dec.
	Pt		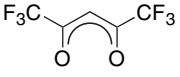	Cr 165 N 209 dec.
	PtI_2		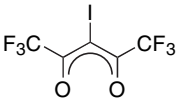	Cr 250 SmC 259 N 289 dec.

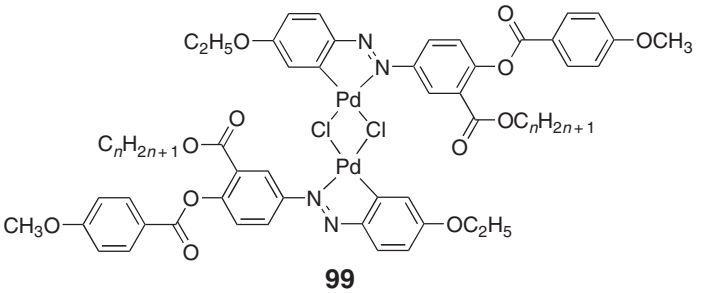

99

Two unsymmetrical cyclopalladated complexes **100** (Cr 100 I)[193,193a] and **101** (Cr 67.1 SmC* 76.7 N* 82.6 I)[194,194a] were investigated as photorefractive[195] materials. Substantial photorefractive responses were measured in both doped and undoped samples, as pure materials and as materials dispersed within polymers.

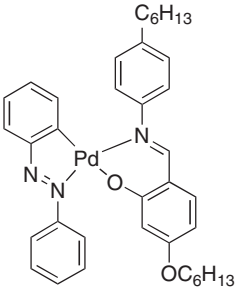

100

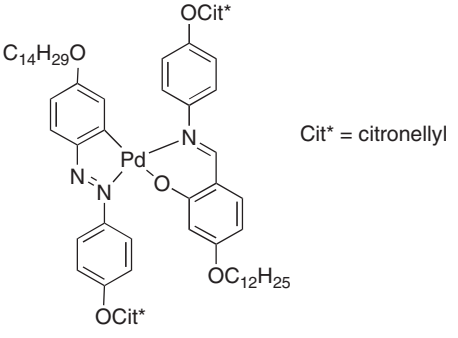

101

12.05.12.2.2 *ortho*-Metallated azoxy complexes

The mononuclear, *ortho*-palladated 4,4′-bis-hexyloxyazoxybenzene acac, **102**, showed a N phase between 90 and 105 °C,[196] with temperatures very comparable to that of the free azoxy ligand (Cr 80 N 126 I). This complex, dubbed Azpac, has been subjected to a vast number of studies in order to analyze some specific properties such as electric[197–201] and dielectric[202–206] properties, conductivity,[207] viscoelasticity,[208] and dynamics.[209–211]

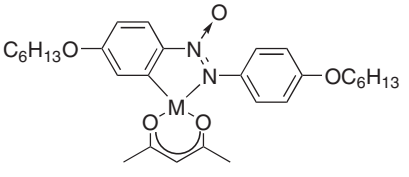

102

Other mixed-ligand, mononuclear *ortho*-palladated complexes whose molecular structure consists of two different ligands, namely 4,4′-dihexyloxyazoxybenzene with 2-hydroxy-4-alkoxy-4′-alkylazobenzene (**103**: $n = 1$–4, 6, 8),[212,213] and *N*-(4-dodecyloxysalicylidene)-4′-alkylaniline (**104a**: $n = 0$–4, 6, 8)[214], as well as the chiral alkoxy analogs (**104b**: R* = (*S*)-(−)-*β*-citronellyl, (*R*)-(−)-2-octyl)[215] were studied. In the complexes of the series **103**, obtained as single *trans*-isomers only, monotropic nematic phases were most commonly observed. However, smectic behavior seemed promoted in series **104a** and **104b**. For **104a**, obtained as an isomeric mixture of *N,N-trans/N,N-cis* in a 5 : 1 ratio, both SmA and N phases were observed: monotropic for $n = 0$, 2, 4 and enantiotropic for $n = 1$, 3, 6, 8. In most cases, the mesophases occurred between 125 and 145 °C.

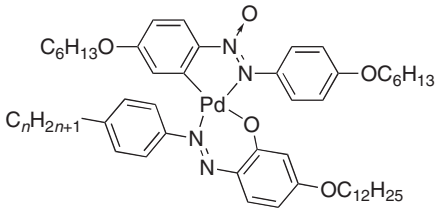

103

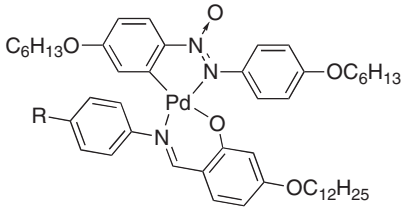

104a: R = C_nH_{2n+1}
104b: R = OR*

Incorporation of a chiral chain in the Schiff-base ligand led to the formation of a chiral crystal H^* phase, Cr 107.2 H^* 148.9 I and Cr 113 H^* 132.3 I, for both complexes **104b** bearing the citronellol or the 2-octanol chain (**104b**: R = OR^*), respectively; recall that both imine ligands exhibited a SmC^* phase (Cr 50.4 SmC^* 77.3 I and Cr 47 SmC^* 48 I). In this case, the *N,N-trans*/*N,N-cis* ratio was 9 : 1. Ligands and complexes with bulky chiral chains like (−)-*cis*-myrtanol or (−)-menthol were not liquid crystalline.

12.05.12.2.3 *ortho*-Metallated imine complexes

Similar to the *ortho*-metallated azo compounds just described, broad systematic studies have also been carried out on imines and their corresponding mono- and dinuclear complexes.

Dinuclear *ortho*-palladated complexes based on three imine ligands, and various bridging groups, were initially investigated; these were **105a** (X = OAc, Cl, Br, SCN; R = $C_{10}H_{21}$, $OC_{10}H_{21}$; R′ = $OC_{10}H_{21}$) and **105b** (X = OAc, Cl, Br, SCN; R = $C_{10}H_{21}$; R^1 = $OC_{10}H_{21}$).[216] Similar to their azo analogs, mixtures of *cis-trans*-complexes have to be considered for imines. While the acetato- and halo-bridged systems were found to exist as single *trans*-compounds, the thiocyanato compounds exist as a mixture of several isomers due to the different possibilities of coordination of the two unsymmetric thiocyanato groups.[217] In general, the OAc bridge was found to be ineffective in promoting mesomorphism in these systems and the non-planar complex of only one ligand showed any mesomorphism (monotropic SmA). For the other bridging ligands, SmA phases were commonly observed along with a SmC phase for two examples where X = Cl. Mesomorphic ranges were typically 80–100 °C for X = Cl or Br, with clearing temperatures all above 200 °C. For X = SCN, 30 °C was the maximum range for the SmA phase, but the mesophase occurred at much higher temperatures than that of the halo-bridged complexes. Interestingly, the lateral methyl group did not lead to any significant effects in the complexes even though it suppressed mesomorphism in the parent ligand.

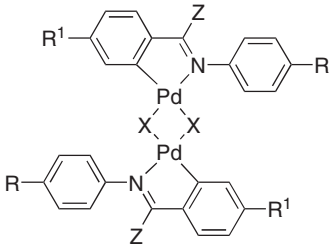

105a: Z = H
105b: Z = Me

Two parallel systematic studies were later undertaken in order to determine the role of both the chain length and chain type, in addition to the nature of the bridging group in determining mesomorphism. In one study concentrating on the effect of the chain length (**105a**: X = Cl; R = R^1 = OC_nH_{2n+1}; n = 2, 4, 6, 8, 10), results confirmed the absence of mesomorphism in the acetato-bridged complexes; previous mesophase assignments made on the chloro-bridged derivatives (SmA for all n, N for n = 2, and SmC for n = 8, 10) were also confirmed.[218] Note that Zhang *et al*. reported contradictory findings;[179] they observed monotropic SmC for long-chain acetato-bridged palladated systems, and only the SmC phase for the chloro-bridged analogs (**105a**: R = R^1 = OC_nH_{2n+1}; n = 6–12, 14).

The overall trends concerning the influence of the nature of the chains and bridges (**105a**: X = Cl, Br; R/R^1 = C_nH_{2n+1}/OC_mH_{2m+1}; n = 1, 2, 6, 10, m = 2, 6, 10) can be summarized as follows:[219] the longer the terminal chains, the lower the melting points and the more ordered the mesophases (smectic phase in place of the nematic phase). The complexes with solely alkoxy chains have more stable mesophases than those with both alkyl and alkoxy chains. Whereas SmC and SmA phases were seen for the chloro-bridged derivatives, those with bromine exhibited a SmA phase (and N for a few homologs), with the complete absence of any SmC phase. Finally, the mesophases existed at higher temperatures in the latter case (X = Br), compared to the former (X = Cl).

Studies of chloro- and acetato-bridged complexes derived from benzylidene ligands bearing polar groups either in the *para* position of the aldehyde ring (**105a**: R = C_8H_{17}, OC_8H_{17}; R^1 = H, F, Cl, Br, CN, NO_2, Me, OMe, CF_3, OCOMe, $OCOC_6H_5$, CO_2Me),[220] or aniline ring (**105a**: R^1 = OC_8H_{17}; R = H, Cl, CN, NO_2, Me, OMe[221] and **105a**: R = C_4H_9; R^1 = OMe) were undertaken.[222] None of the acetato-bridged complexes was mesomorphic, whereas all but one (R = H) of the chloro-bridged derivatives exhibited a SmA phase above 140 °C, at which temperature most of them started to decompose; this behavior was observed regardless of the location of the polar group. Interestingly, those with a cyano group or with the shortest chain were the only complexes to show a nematic phase.

The introduction of one or two chiral 2-octanol chains[223] in the benzylidene ligand led to new chloro-bridged *ortho*-palladated complexes exhibiting a ferroelectric SmC^* phase[224] along with a SmA phase. The two chiral chain systems (**105a**: X = Cl, R = OC_nH_{2n+1}; n = 6, 8, 10, 14; R^1 = $OC^*HMeC_6H_{13}$) and the isomeric analog (**105a**: X = Cl, R = $OC^*HMeC_6H_{13}$, R^1 = OC_8H_{17}) exhibited both mesophases typically between 100 and 220–230 °C; the mesomorphic temperature range of the SmC^* increased with elongation of the alkoxy chain. Interestingly, the SmC^* was more stable by 20 °C when the chiral chain was attached to the aniline ring. The mesophase stability of the SmC^* phase was reduced considerably in the complex containing four chiral chains (**105a**: X = Cl, R = R^1 = $OC^*HMeC_6H_{13}$): Cr 114 (SmC 88) SmA 121 **I**).

Treatment of the chloro-bridged dimeric species with potassium 2-chloropropionate,[225] or, alternatively, the acetato-bridged analogs with 2-bromopropionic acid[218] led to new carboxylato-bridged dimers (**105a**: X = $CH_3CHClCO_2$, $CH_3CHBrCO_2$, R = R^1 = OC_nH_{2n+1}) which were, against all expectations, mesomorphic, showing a broad-temperature-range SmA phase (ca. 100–150 °C); some dimers were stable up to nearly 250 °C. Only small differences were observed in the transition temperatures between the chloro- and bromo-propionate derivatives, probably due to the existence of the complexes as rich isomeric mixtures. Indeed, due to the chiral carboxylate group, in addition to the *cis*- and *trans*-isomers resulting from the arrangement of the two imines in the dimer, the chirality of the *trans* led to two enantiomers, Δ and Λ, the *cis* not being chiral. For both series, the thermal behavior was slightly complicated, and most of the complexes exhibited double clearing (or melting) behavior, that is the phase sequences Cr–SmA-I′–SmA-I or Cr-SmA-Cr′–SmA–I, respectively, were observed systematically. One dipalladium complex with tetradecyloxy chains and a bulkier carboxylate bridge ($Me_2CHCH_2C^*HClCO_2$) was reported to show a SmC^* between 106 and 147 °C.[179]

Another interesting part of this work concerned the study of dinuclear cyclopalladated complexes with mixed bridges **106a** and **106b**.[226] Indeed, the reaction of the dichloro-bridged complexes **106a** with silver thiolate ($AgSC_mH_{2m+1}$) led to dinuclear derivatives with mixed bridges μ-Cl/μ-SC_mH_{2m+1}, **106a** (n = 6, 8, 10; m = 6, 8, 10, 18). Likewise, treatment of the di-μ-acetato complexes with thiols (HSC_mH_{2m+1}) or, alternatively, dinuclear **106a** with silver acetate, afforded the mixed-bridge complexes μ-OAc/μ-SC_mH_{2m+1}, **106b** (n = 6, 8, 10; m = 6, 8, 10, 18). It is worth noting that in addition to their mesomorphism, such mixed-bridge complexes adopted a *cis*-geometry, as confirmed by NMR and X-ray studies. All the complexes **106a** displayed both SmC and SmA phases at lower temperatures than their dichloro predecessors, that is, between 100 and 200 °C, with little influence of the chain length; the SmA phase existed over most of this temperature range. As for complexes **106b**, the predominant phase was the SmA (N phase for n = 6 only); the transition temperatures were also reduced, decreasing with m (from 160 to 70 °C for the melting point, and 170 to 140 °C for the clearing point). Recall that such mixed-bridge complexes were obtained initially by the reaction of alkylthiols to a chloropropionate-bridge dinuclear complex (**106a**: n = 6; X = $MeCHClCO_2$; m = 6: Cr 140 N^* 157 I; m = 10: Cr 109.5 SmA 115 N^* 138 I; m = 18: Cr 92 SmA 128 N^* 132 I), to yield the first metallomesogens to show a chiral nematic phase.[225] Later, another such complex (**106a**: n = 2, X = $MeCHClCO_2$, m = 18) was found to exhibit a monotropic blue phase (BPI) along with a N^* phase.[227] Compound **106c** exhibited a broad SmA phase above 150 °C.

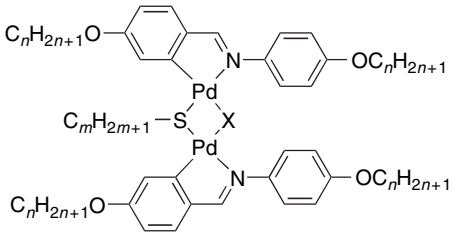

a: X = Cl
b: X = OAc
c: X = SC_mH_{2m+1}

Serrano and co-workers[228] reported some isomerically related dinuclear complexes with chiral 2-octanol chains **107**. The parent ligand of **107a** and **107b** showed a SmA, SmC^*, and a monotropic antiferroelectric SmC^* phase (SmC^*_A), whereas the parent ligand of **107c** and **107d** showed, in addition, a monotropic, antiferroelectric SmI^* phase (SmI^*_A). On complexation, both μ-acetato complexes, **107a** and **107c**, showed only a SmA phase in which the complex decomposed close to 200 °C. The μ-Cl complexes, **107b** and **107d**, also retained the SmA phase of the ligand, but, in addition, showed a monotropic SmC^* phase **107b** or an enantiotropic SmC^*_A phase **107d**. Both complexes decomposed in their SmA phases between 240 and 250 °C. The spontaneous polarization of **107d** was measured to be 15 nC cm^{-2} at 35 V μm^{-1} in the SmC^*_A phase.

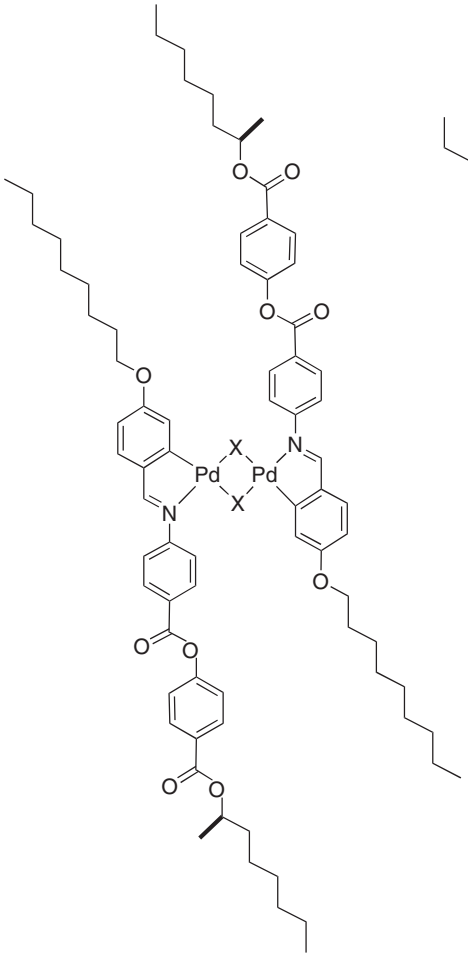

107a: X = OAc
107b: X = Cl

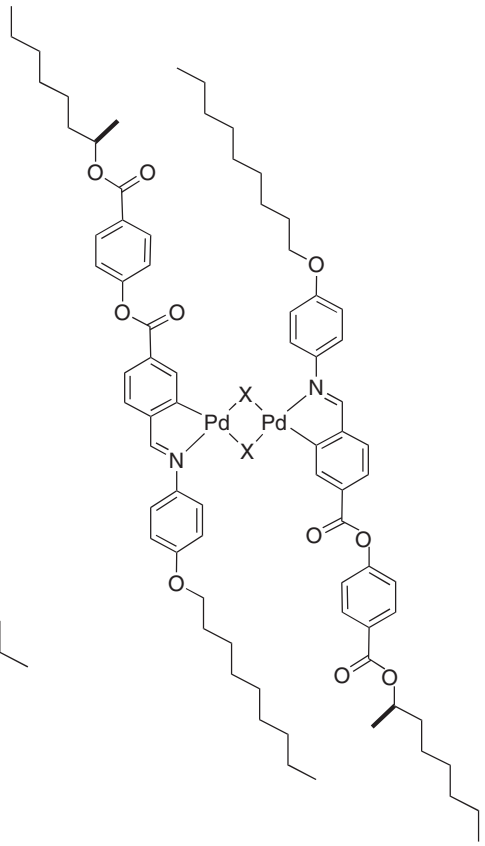

107c: X = OAc
107d: X = Cl

The reactivity of di-μ-hydroxo complexes of *ortho*-palladated imines, obtained by the treatment of the di-μ-acetato complexes (**105a**: X = OAc) with NaOH, has been exploited to extend the range of dinuclear complexes with double or mixed bridges, as well as produce some mononuclear examples. Thus, thermotropic, air-stable, μ-amido-μ-hydroxo **108a**, μ-anilido-μ-hydroxo **108b**, bis-μ-amido **108c**, μ-amido-μ-thiolato **108d**, and μ-amido-μ-carboxylato **108e** complexes, as well as the mononuclear complexes with mixed imine and *N*,*N*-dialkyldithiocarbamate ligands **108f**, were prepared (Figure 33).[229] Most of the complexes **108a** were liquid crystals, showing a N phase at short chain length at elevated temperatures ($n = 2$; $m = 14$, 18), and a SmA phase at longer chain lengths ($n = 6$, 10; $m = 1$, 6, 10, 14, 18) from 60–120 °C up to 160–180 °C where they decomposed. Complexes **108b** behaved similar to **108a** (slight increase in the transition temperatures), with a N phase for $n = 2$ and a SmA phase for $n = 6$, 10. Replacement of the hydroxo bridge by an alkylthiol led to complexes **108d**, which showed mainly a SmA phase for $n = 6$, 10 above 100 °C on average, but decomposing at the clearing point. Only a monotropic SmA phase was observed for the compounds with long amido and thiolato chains (m, $q \geq 10$), and none of the complexes with $n = 2$ was mesomorphic. The replacement of the μ-OH by μ-carboxylato gave slightly better results, and a stable SmA phase was seen between 76 and 107.5 °C for **108e** with $n = 10$. The complexes **108c** could not be studied because of their insolubility

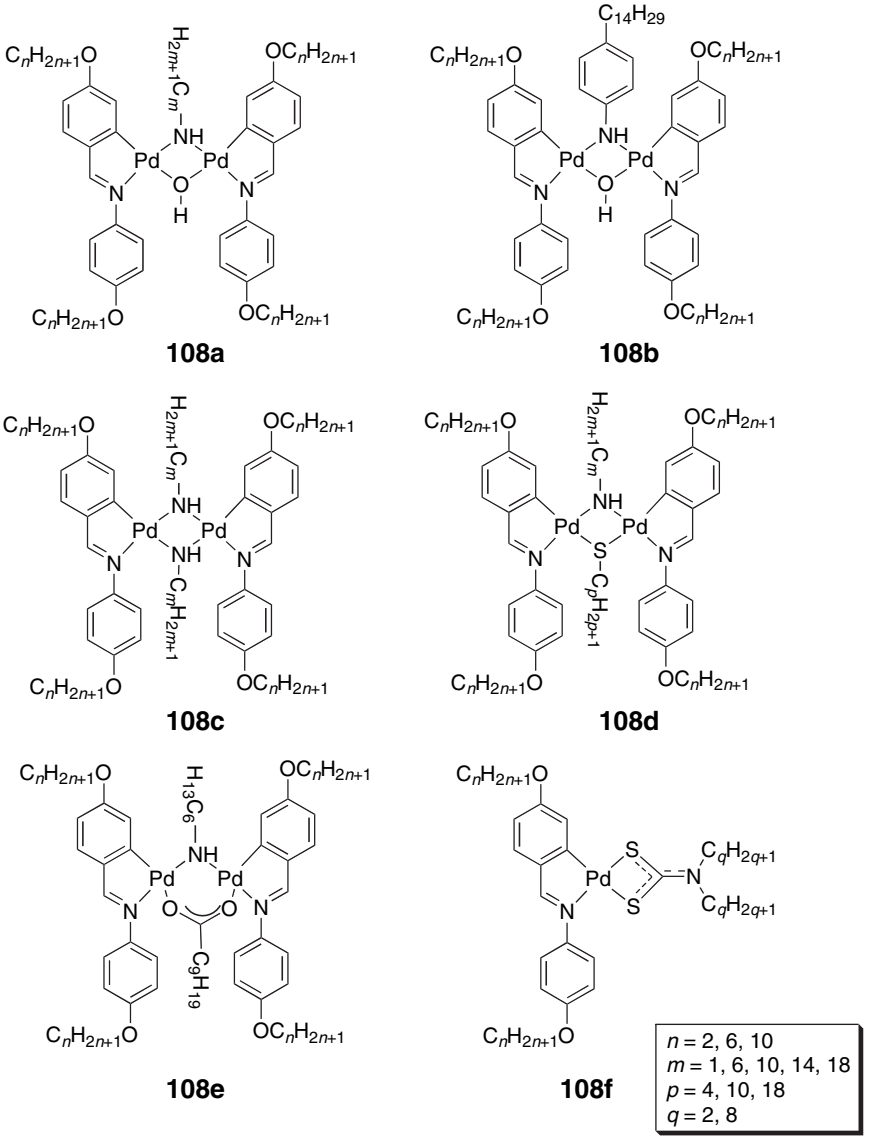

Figure 33 Structures of the various mixed dinuclear complexes **108a–e**, and of the mononuclear complex **108f**.

in organic solvents, and, consequently, it was impossible to isolate them as pure materials. Reaction of the μ-dihydroxo complex with dialkylamine in CS_2 led to the mononuclear species **108f**, which showed an enantiotropic SmA at very low temperatures for the derivatives with $n = 10$, and $q = 2$ (Cr 84 SmA 99.5 I) and 8 (Cr 56 SmA 73 I).

Starting from the binuclear μ-hydroxo complex, Espinet and co-workers synthesized an extensive and systematic range of complexes **109** of various bridging ligands (Figure 34).[230]

Complex **109a** showed a SmA phase at high temperature (>230 °C) for both values of n. However, when replaced by an alkylcarboxylate bridge **109b**, strong substituent dependence was observed so that for $n = 6$, only long chain bridging ligands ($m \geq 11$) led to mesomorphism (SmA and N below 120 °C), whereas for $n = 10$, only the μ-acetato ($m = 1$) complex did not show a mesophase; the others showed SmA (mainly) and SmC phases monotropically except for $m = 5$, 7 where mesomorphism was enantiotropic. In complex **109c**, for both $n = 6$, 10 and for $p = 1$, 2, an enantiotropic SmA phase was seen that in most cases had a wide range (ca. 50 °C), clearing between 103 and 145 °C. Use of the bridging alkoxybenzoate ligand **109d** was not very productive, and neither $n = 6$ nor $r = 4$, 10 was mesomorphic, whereas for $n = 10$, the complex with $r = 4$ gave enantiotropic SmC and SmA phases, and for

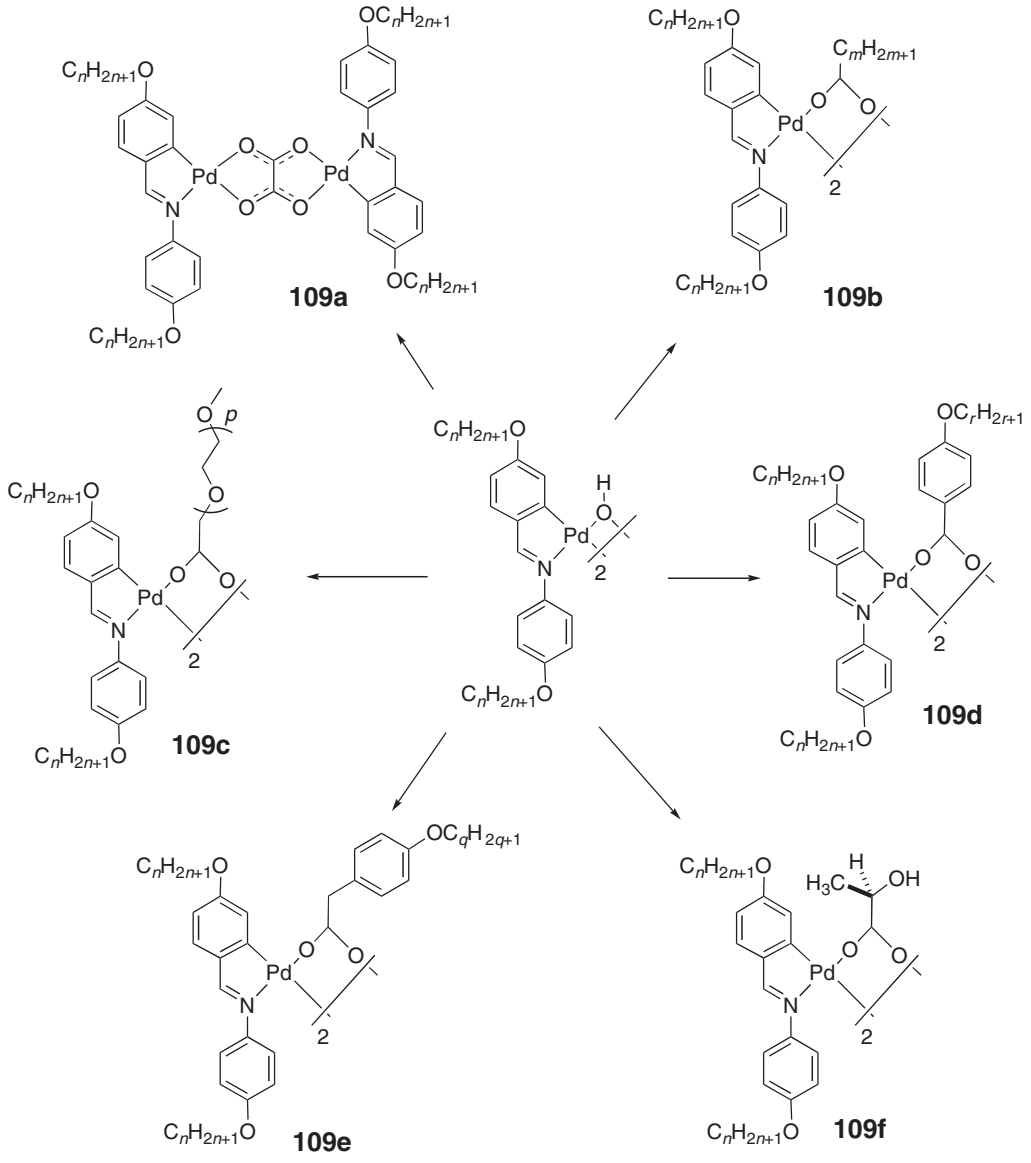

Figure 34 Structures of the various dinuclear complexes, **109** ($n = 6$, 10).

$r = 10$, a monotropic SmA phase was found. When the bridging ligand was the alkoxyphenylacetate (**109e**: $n = 6$, 10, $q = 2$, 4, 6, 8, 10, 12), all but two homologs ($n = 6$, $q = 2$, 4) showed both a SmA and SmC phase with a total mesomorphic range of around 40 °C in most cases. Both complexes ($n = 6$, 10) with the bridging lactate group **109f** showed a SmA phase.

Cleavage of the dinuclear $(\mu\text{-Cl})_2$ complexes (**105a**: X = Cl) with β-diketones or β-enaminoketones also led to various series of mononuclear derivatives **110**. Thus, the new complexes with acac co-ligand[218,231] (**110a**: R = Me, $n = m = 2$, 4, 6, 8, 10 and $n = 10$ and $m = 2$, 6) were mesomorphic at much lower temperatures than their dichlorodipalladium predecessors, but more interestingly, the mesophases were more accessible and stable in comparison to the parent complexes. A monotropic nematic phase was observed for the short-chain length compounds, both enantiotropic SmA and N phases at intermediate-chain length, and only the SmA phase for the derivative with two decyloxy chains. Therefore, lowering the symmetry of the complex appeared to be an excellent strategy for reducing the transition temperatures and simultaneously preserving a large mesomorphic range. However, some caution must be exercised in such an interpretation, as the mesophase stability of these complexes was found to be very sensitive to small, structural changes. The nematic phase became destabilized when the β-diketone used was trifluoroacetylacetonate (**110a**: R = CF_3), probably due to the steric hindrance introduced by the CF_3 group, and the existence of an equimolar mixture of isomers.[232,233] The use of aliphatic diketones (**110a**: R = $C_{10}H_{21}$, $n = m = 10$) was correlated with a strong reduction in mesomorphic character.[234]

The mononuclear complexes with β-aminoenonate (**110b**: $n = m = 2$, 4, 6, 8, 10), obtained as the *N,N-trans* isomer only, also yielded an accessible nematic phase (and a SmA for longer chains) over slightly narrower temperature ranges than in the acac derivatives.[218] Moreover, when the chain attached onto the fixed benzaldehyde ring was chiral (e.g., 2-octanol), the complex **110b** ($m = 8$) exhibited monotropic BPII, BPI, and N^* phases at reasonably low temperatures.[227] Using a similar approach, a SmC^* phase (**110c**: R = Me, $n = m = 14$, Cr 81.5 SmC^* 174 I) and a broad SmA phase (**110c**: R = $C_6H_5CH_2$, Me_2CH, Me_2CHCH_2, $n = m = 14$) were obtained in related mixed complexes with chiral amino acids, again at very accessible temperatures.[235]

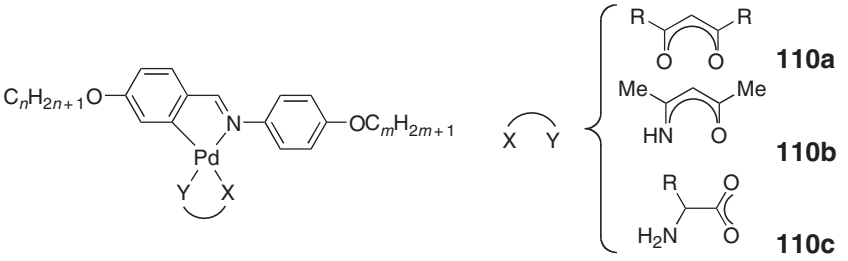

Espinet and co-workers investigated in detail the chiral derivatives of mononuclear *ortho*-palladated complexes incorporating a dialkoxybenzylidene and a di-4,4′-alkoxyphenyl-β-diketonato ligand[236] obtained from the cleavage of the dinuclear bridge by the thallium complex of the β-diketonate (**111**: $R^1 = OC^*HMeC_6H_{13}$, $R^2 = OC_{10}H_{21}$, $OC_{14}H_{29}$, R^3, $R^4 = OC_{10}H_{21}$). In both cases, monotropic SmC^* was observed. In an earlier publication, they described a material with a spontaneous polarization of 206 nC cm^{-2}, the highest value recorded for a metal-based system.[223] In this case, although the P_s value was lower than recorded above (−22 to −29 nC cm^{-2}), the switching time was now in the millisecond time regime—three orders of magnitude faster than the time reported for some dinuclear azine derivatives.[237]

With a view to optimizing the system and finding an enantiotropic SmC^* phase, the effects of the position and number of chiral chains on the ferroelectric behavior of this system were investigated, and a series of 12 new materials was prepared (**111**: R^1, R^2, R^3, $R^4 = OC^*HMeC_6H_{13}/OC_{10}H_{21}$).[238] Recall that the compounds with unsymmetrical diketone exist as a *cis-/trans*-isomeric mixture. The thermal behavior of these compounds is reported in Table 17, and several interesting observations were made. As the number of chiral chains increased, the transition temperatures decreased, and compounds with a chiral chain on the imine ligand exhibited monotropic behavior, whereas when this chain was on the diketone, the behavior was enantiotropic. All the compounds with two chiral chains exhibited only monotropic phases; the complex with two chiral chains on the β-diketonate ligand was devoid of mesomorphism.

Table 17 Mesomorphism of complexes **111**

R^1	R^2	R^3	R^4	*Transition temperatures*
$OC_{10}H_{21}$	$OC_{10}H_{21}$	$OC_{10}H_{21}$	$OC_{10}H_{21}$	Cr 80 SmC 150 SmA 154 N 155 I
$OC^*HMeC_6H_{13}$	$OC_{10}H_{21}$	$OC_{10}H_{21}$	$OC_{10}H_{21}$	Cr 118 (SmC* 109 SmA 117) I
$OC_{10}H_{21}$	$OC^*HMeC_6H_{13}$	$OC_{10}H_{21}$	$OC_{10}H_{21}$	Cr 118 (SmC* 114) I
$OC_{10}H_{21}$	$OC_{10}H_{21}$	$OC^*HMeC_6H_{13}$	$OC_{10}H_{21}$	Cr 63 SmC* 104 N* 115 I
$OC^*HMeC_6H_{13}$	$OC^*HMeC_6H_{13}$	$OC_{10}H_{21}$	$OC_{10}H_{21}$	Cr 72 (SmC* 60) I
$OC^*HMeC_6H_{13}$	$OC_{10}H_{21}$	$OC^*HMeC_6H_{13}$	$OC_{10}H_{21}$	Cr 85 (SmA 77) I
$OC_{10}H_{21}$	$OC^*HMeC_6H_{13}$	$OC^*HMeC_6H_{13}$	$OC_{10}H_{21}$	Cr 93 (SmX* 60 SmB 64) I
$OC_{10}H_{21}$	$OC_{10}H_{21}$	$OC^*HMeC_6H_{13}$	$OC^*HMeC_6H_{13}$	Cr 67 I
$OC^*HMeC_6H_{13}$	$OC^*HMeC_6H_{13}$	$OC^*HMeC_6H_{13}$	$OC_{10}H_{21}$	I
$OC^*HMeC_6H_{13}$	$OC_{10}H_{21}$	$OC^*HMeC_6H_{13}$	$OC^*HMeC_6H_{13}$	I
$OC_{10}H_{21}$	$OC^*HMeC_6H_{13}$	$OC^*HMeC_6H_{13}$	$OC^*HMeC_6H_{13}$	Cr 77 I
$OC^*HMeC_6H_{13}$	$OC^*HMeC_6H_{13}$	$OC^*HMeC_6H_{13}$	$OC^*HMeC_6H_{13}$	I

SmX*: Unidentified ordered smectic phase (SmX* = SmI*, SmF*).

None of the complexes with three and four chiral chains was liquid crystalline. In addition, the number and position of these chains drastically influenced the ferroelectric properties, particularly spontaneous polarization, as well as the non-linear optical responses.[239]

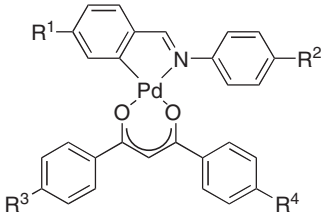

111

A similar, systematic study was also carried out with the platinum derivatives, and dinuclear cycloplatinated complexes of 4,4′-dialkoxybenzylidene with symmetric bridges di(μ-chloro) (**105a**: X = Cl), di(μ-acetato) (**105a**: X = OAc), di(μ-thiolato) (**106c**), di(μ-chloropropionato) (derived from **109b**) or unsymmetric bridges μ-chloro μ-thiolato **106a**, μ-acetato μ-thiolato **106b**, and μ-chloropropionato μ-thiolato (derived from **106b**).[240,241] Mononuclear species with acac and β-substituted-phenyldiketonate[242,243] co-ligands were also prepared. All the platinum complexes were mesomorphic, except the acetato-bridged material. They exhibited, in general, more ordered mesophases than their palladium analogs (e.g., a SmA phase was induced in place of the nematic phases), and overall, the transition temperatures, particularly the clearing temperatures, were slightly higher for Pt than Pd. Note that in the platinum complexes existing as isomeric mixtures, the composition was different to that in the palladium congeners, explaining some discrepancy between the two series. The substitution of palladium by platinum thus resulted in an overall increase in the mesophase stability.

Such metallomesogens possessing mixed bridges and non-centrosymmetric structures could represent interesting candidates for new molecular materials with non-linear optical properties, since they can easily be derivatized by the introduction of donor and acceptor groups.[244]

Some of the chloro-bridged palladium **105a** (R = C_nH_{2n+1}, $R^1 = OC_mH_{2m+1}$), a mixed-bridged μ-acetato μ-thiolato **106b** ($n = m = 6$), and a mononuclear complex **111** (R^1, R^2, R^3, $R^4 = OC_{10}H_{21}$) discussed above were also found to exhibit additional lyotropic mesophases in contact with apolar organic solvents such as linear alkanes (octane, decane, dodecane, and pentadecane), cycloocta-1,5-diene, and the chiral limonene.[245,246] A lyotropic lamellar phase was induced for the dichloro complexes with symmetrical chain length ($n = m = 6$, 10) in linear alkanes; the transition temperatures were found to decrease from pentadecane to octane.

Contact preparations of complexes **106b** and **111** with alkanes revealed the induction of a nematic phase with the complete destabilization of the thermotropic smectic phases. For both complexes, mixing with solvents resulted in the substantial depression of both melting and clearing temperatures. In the case of **106b**, the nematic range

increased concomitantly with the length of the solvent chain. While mixtures with cyclooctadiene did not yield a mesophase, mixtures with the limonene gave unexpected results, depending strongly on the metal complexes. Mesomorphism was suppressed or destabilized for complexes **105a**, and a chiral nematic phase was induced for **106b** and **111** over a large temperature range (Cr 93 N^* 147 I; Cr 65 N^* 136 I). This is the first case of chiral induction in binary systems between calamitic complexes and a chiral, apolar solvent.

Espinet and co-workers[247] also undertook an extensive investigation of the effect of oligo(ethyleneoxide) terminal chains in a series of complexes designated **112** (Figure 35), in each case retaining the same overall chain length in the two, related series (**112-i** to **112-iv** and **112-vi** to **112-viii**). In addition, one tetranuclear complex, **113**, was prepared.

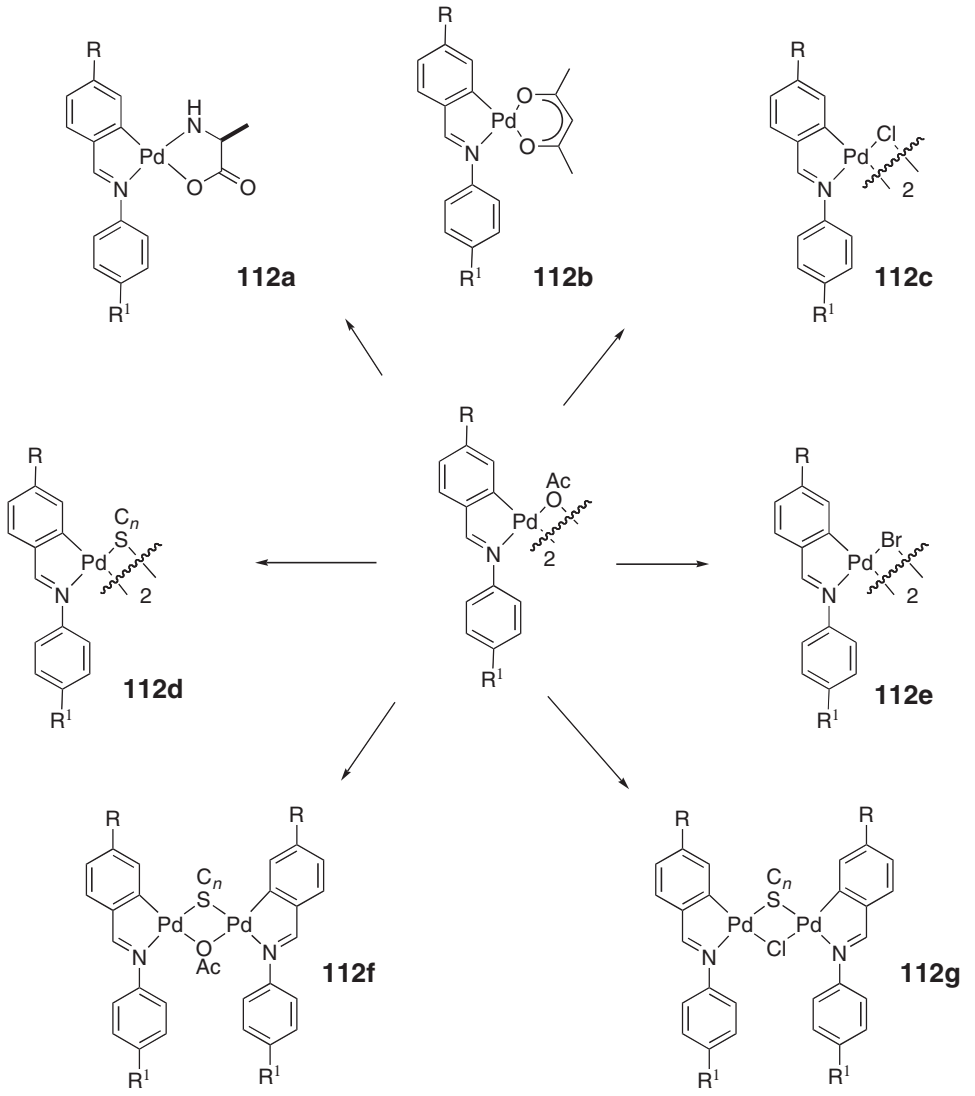

Figure 35 Structure of the Pd complexes **112**.

None of the precursor imine ligands containing ethylene oxide groups was mesomorphic, and neither was any of the parent μ-acetato dimers **112**. However, the μ-Cl and μ-Br dimers did show liquid-crystalline properties, with all the chloro complexes **112c-i** to **112c-viii** showing enantiotropic SmC and SmA phases, while for the longer-chain-bromo complexes studied **112e-v** to **112e-viii**, both phases were again seen, although the SmC phase was monotropic in the two unsymmetric derivatives (**vi**) and (**vii**). In general, the clearing points of the unsymmetrically substituted complexes were similar to one another and lower than those of the symmetric alkoxy materials **112-i**, while the materials substituted symmetrically with ethylene oxide chains were much lower again. This effect was more pronounced in the longer-chain complexes **112-v** to **112-viii** and also in bromo rather than chloro complexes (Figure 36).

Using octylthiolate chains, **112d-iv** was examined and found to melt directly to the isotropic liquid—use of chiral 2-thiooctyl led to a monotropic SmC* phase. In the μ-thiol-μ-acetato system, **112f-i** showed a SmA phase, **112f-iv** a monotropic SmC phase, while use of chiral thiolate in the latter derivative suppressed mesomorphism totally. Similarly, complexes **112g-iv** exhibited a monotropic SmC (with octylthiolate), or an enantiotropic SmC* phase (with an chiral 2-thiooctyl thiolate chain).

A complete series of the mononuclear β-diketonato derivatives **112b** was prepared and it was found that **112b-i** to **112b-iii** showed both SmA and N phases, while **112b-iv** gave only a monotropic N phase; clearing points dropped from ca. 125 °C in **112b-i** to ca. 21 °C in **112b-iv**. In the longer-chain derivatives, **112b-v** showed a nematic phase (monotropic) while **112b-vi** and **112b-vii** showed a SmA phase, the latter having a melting point below ambient temperature; **112b-viii** was isotropic at room temperature. The transition from N to SmA phases here suggests a degree of phase separation induced by the long ethylene oxide chains. Neither of the alanine complexes **112a** was mesomorphic, nor was the tetranuclear complex **113**.

In attempting to take further advantage of the ethylene oxide chains, experiments were undertaken to see if potassium picrate could usefully be extracted from aqueous medium by these complexes. Some transport was observed, but the extraction was rather modest.

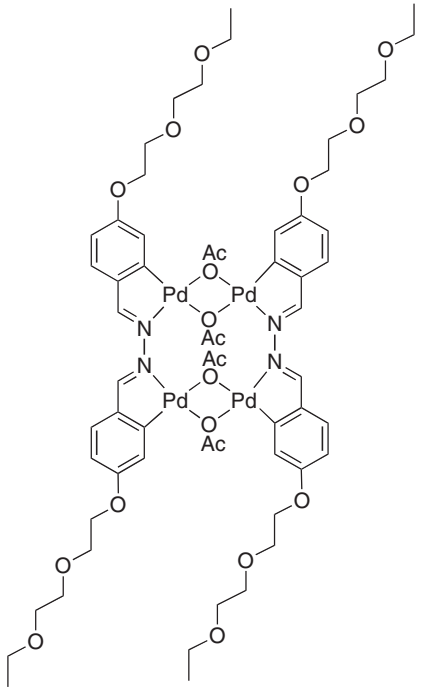

113

Rourke and co-workers demonstrated some years ago that cyclopalladated 4-alkoxy-*N*-(4′-alkoxybiphenyl)benzylidenes with various types of co-ligand, such as cyclopentadienyl (**114a**: (n, m) = (4, 4), (4, 7), (7, 4), (7, 7)),[248] β-diketones (**114b**: (n, m) = (4, 4), (4, 7), (7, 4), (7, 7); p, q = 1, 4, 6, 8),[249] and amino acids (**114c**: (n, m) = (4, 4), (4, 7),

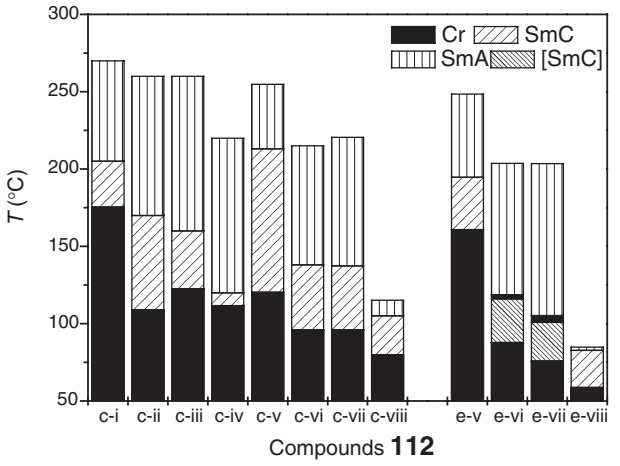

Figure 36 Graphical representation of the mesomorphism of the μ–Cl and μ–Br derivatives of **112**.

(7, 7), (10, 10); R = Me (alanine), ^{i}Pr (valine), ^{i}Bu (leucine), ^{s}Bu (isoleucine))[250] led to several new series of mononuclear, *ortho*-palladated mesogens. The free ligands displayed SmF, SmC, and nematic phases between 150 and 250 °C; the nematic phase occurred at ca. 200 °C. The derivatives containing the cyclopentadienyl ring, **114a**, exhibited mainly a nematic phase, while that with the longer chain (7, 7) showed an additional SmA phase. In this series, an important depression in transition temperatures with respect to free ligands was obtained, with the mesophases occurring between ca. 100 °C and 180 °C, above which temperature they decomposed. In the series with the amino acids, **114c**, the SmA phase was the only mesophase observed, but at temperatures greater than 200 °C, extensive decomposition took place. The thermal behavior of the β-diketonates **114b** was intermediate between that of **114a** and **114c**. All the complexes were mesomorphic, the majority showing both SmA and nematic phases typically in the range 70–250 °C depending on the chain lengths n, m, p, and q. The transition temperatures of the acac derivatives (**114b**: $p = q = 1$) perfectly mirrored those of the free ligands. The derivatives with $n = m = 4$, except for the acetylacetonates, all showed similar melting points at ca. 130 °C, and the chain length of the imine ligand had little influence on the mesomorphic temperature ranges. The nematic phase disappeared at the expense of the SmA phase when both p and q increased.

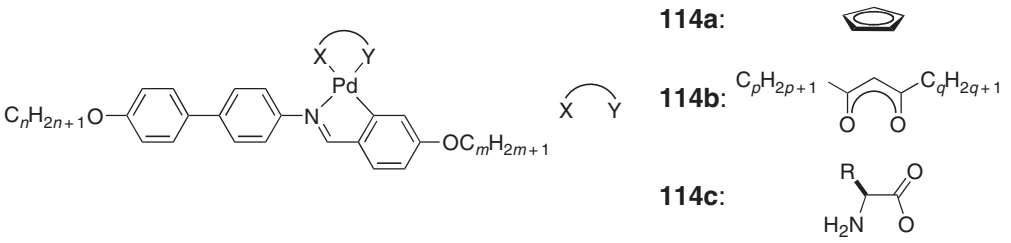

Di-cyclopalladation of ligands containing two imine groups, followed by the reaction with some β-diketones, led to a novel family of dinuclear complexes, showing a nematic phase.[251] For the acac derivatives (**115**: R = Me, n = 4–8), the transition temperatures were too high (greater than 200 °C), and the complexes decomposed in the mesophase or in the isotropic liquid, except for the decyloxy homolog (Cr 187 N 246 I). However, a great reduction in transition temperatures was achieved by increasing the lateral chain length (**115**: $n = 8$; R = butyl, hexyl) so that a nematic phase was seen between 100 and 150 °C; the nematic phase became monotropic or was suppressed totally when R was longer (**115**: $n = 8$, R = octyl) or bulkier (**115**: $n = 8$, R = Bu^{t}), respectively.

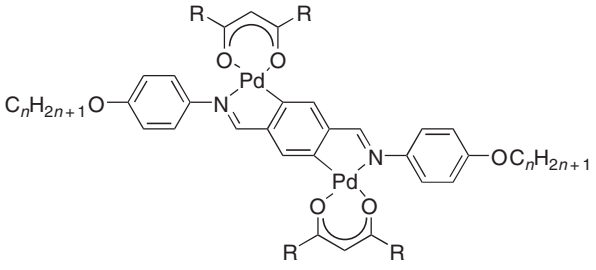

115

Praefcke and co-workers reported a series of disk-shaped, dinuclear *ortho*-palladated benzalimine complexes, **116**, which were the first example of organometallic complexes showing the nematic phase of disk-like molecules, N_D.[252]

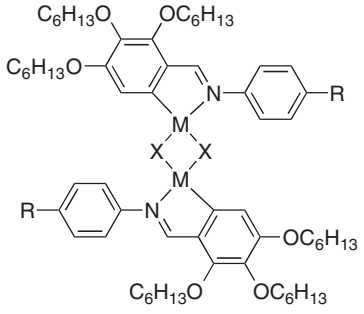

116

The chloro-bridged palladium complex was prepared by reacting the imine ligand with palladium acetate, followed by treatment with HCl, and the other complexes by ion-exchange reactions with KBr, KI, and KSCN. The flat, dinuclear halogeno- and thiocyanato-bridged complexes (**116**: M = Pd; X = Cl, Br, I, SCN; R = C_6H_{13}) exhibited a monotropic N_D phase, whereas the acetato-bridged complex (X = OAc) was not mesomorphic as a consequence of its open-book structure (Table 18). The peculiar clearing process of the thiocyanato complex was caused by the composition of the nematogen, in that the thiocyanate moiety can be bridged parallel or antiparallel to one other, leading to two structural isomers in the ratio 17 : 83. The structurally related chloro-bridged platinum complex (**116**: M = Pt; X = Cl; R = C_6H_{13}), prepared by the reaction of the amine with di-μ-chloro-bis[(η^3-2-methylallyl)platinum], also showed the N_D phase on cooling, although, it melted at a much higher temperature than the palladium congener.[253] The thiocyanato-bridged[254] platinum complex (**116**: M = Pt; X = SCN; R = C_6H_{13}) was not mesomorphic and the bromo and iodo derivatives were not prepared.[255] Interestingly, unlike the chloro-bridged palladium

Table 18 Mesomorphism of **116**

Metal	*R*	*X*	**116**	**116**/*TNF*
Pd	C_6H_{13}	Cl	Cr 79 (N_D 43.5) I	Cr 94 Col_h 188 I (50 mol%)
		Br	Cr 73 (N_D 28) I	Cr 99 Col_h 142.5 I (50 mol%)
		I	Cr 97 (N_D 27) I	Cr 85 Col_h 96 I (35 mol%)
				Cr 84 (N_D 73) I (50 mol%)
		OAc	Cr 56 I	No mesophase induction
		SCN	Cr 96 (N_D 50) I	Cr 85 N_D 112 I (50 mol%)
Pt	C_6H_{13}	Cl	Cr 92 (N_D 54.5) I	Col_h 195 I
		SCN	Cr 86 I	N_D 98 I
Pd	(*S*)-β-citronellol	Cl	Cr 65 I	Col_h 145 I
	(*S*)-β-citronellol	Br	Cr 67 I	Col_h 86 I
	(*S*)-β-citronellol	SCN	Cr 99 I	N^* + N 79 I
Pt	(*S*)-2-methylbutyloxy	Cl	Cr 90 (N^* 72) I	Col_h 189 I

complexes, the platinum complex existed as an isomeric mixture *syn*/*anti* (in the ratio 17 : 83) in solution, and attempts to separate the two isomers were unsuccessful because of decomposition processes; the thiocyanato platinum complex was obtained as a single antiparallel isomer. The molecular geometry and the number of peripheral chains thus appeared crucial in determining the type of mesophase observed, since the related *ortho*-metallated imine complexes with four alkoxy chains exhibited exclusively calamitic mesomorphism, mostly SmA phases (*vide supra*).

All these compounds also formed charge-transfer complexes when doped with strong electron acceptors such as 2,4,7-trinitro-9-fluorenone (TNF) as indicated by a change of color.[256,257] The bridging group was found to strongly influence the type of induced mesophases (Table 18). Thus, enantiotropic Col_h phases were induced in the binary mixtures of chloro- and bromo-bridged complexes with TNF respectively, with the suppression of the N_D phase above 10% of TNF. The iodo-bridged palladium complex showed both the Col_h and N_D phases but at various TNF concentrations, that is, above 45 mol% TNF, a monotropic N_D was induced. The N_D phase became stabilized for the thiocyanato-bridged complex and once again, the acetato-bridged complex did not show an induced mesophase in such mixtures. Contact preparations of the chloro-bridged platinum complex with TNF also resulted in an induced Col_h phase, with a higher thermal stability than its palladium analog, and an induced N_D phase for the thiocyanato compound (Table 18). The structures of the different mesophases were characterized by X-ray methods, and confirmed intercalation of TNF molecules between successive planar complexes in the columnar phases, while no such stacking was evidenced in the case of the nematic phase. The differences in the mesomorphism observed for the pure compounds and in the binary mixtures were explained from unequal core dimensions caused by the bridging groups, as well as space-filling (steric) and electronic effects.

Four chiral homologous complexes were also prepared.[258] None of the palladium complexes showed mesomorphic properties, whereas a monotropic chiral discotic nematic phase was observed for the platinum complex (Table 18). The absence of mesomorphism for the dinuclear palladium complexes may be due to the type of chiral chain used, which differed from that used for the platinum system. All of the complexes form charge-transfer complexes with TNF. A Col_h phase was induced for the two halo-bridged palladium complexes and for the platinum complex, as was observed for their non-chiral analogs. However, the chiral nematic phase of the platinum compound was suppressed. At low TNF content, a chiral N_D^* phase was stabilized for the thiocyanato-bridged compound along with a non-chiral N_D phase at higher concentration.

The dipalladium organyl **117**, derived from **118** (X = Cl) by ligand-exchange reaction between the bridging group and acac, was neither mesomorphic in its pure state nor in binary mixtures with pure alkanes. However, it formed a charge-transfer complex with TNF as indicated by a change in color. This association was found to induce a thermotropic mesophase, with a two-dimensional arrangement of columns and a maximum clearing temperature at ca. 60 mol% of TNF. Moreover, contact preparation with heptane, pentadecane, eicosane, and with eicosane/pentadecane mixtures (molar ratios 1 : 1, 2 : 1, and 1 : 2)[259] revealed induced lyotropic behavior for the charge-transfer complex. Several compositions were investigated with different donor–acceptor ratios (70 : 30 mol% to 30 : 70 mol%) and two columnar phases with hexagonal and nematic symmetry were induced. The N_{Col} phase was monotropic in mixtures of up to 50 mol% of TNF, and above this concentration became enantiotropic.

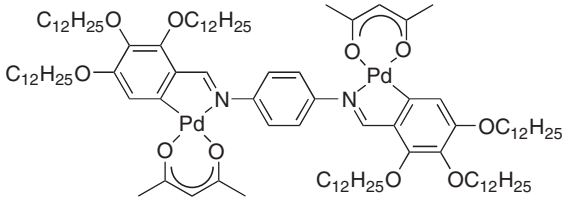

117

Praefcke and co-workers have carried out important research on macroheterocyclic tetrapalladium[44,260,261,261a] and tetraplatinum[262,263] organyls **118** and **119**, derived from polycatenar bis(imine)phenylene, and the nematogenic[264] bis(imine)-stilbenylene ligands. These $[M_4(\mu^2\text{-}X)_4L_2]$ complexes were prepared by *ortho*-metallation of the appropriate diimine with palladium acetate or di-μ-chloro-bis-[(η^3-2-methylallyl)platinum], followed by an acidic treatment to form the chloro-bridged compounds. The other complexes were obtained by ion-exchange reactions with KBr, KI, and

KSCN. The final structure of the complexes was confirmed by osmometry, single-crystal X-ray structure (**118**: M = Pd, Pt; X = OAc, Cl, Br, I, SCN, N_3 and **119**: X = Cl, Br, I, OAc, SCN), in addition to classic spectroscopic techniques. These large tetrametallaorganyls, with 12 alkoxy chains in the 2-, 3-, and 4-positions of each terminal ring, were thermotropic mesogens showing large-temperature-range columnar mesophases with either a rectangular or oblique lattice (Table 19).[265,266] The nature of the bridging group had some influence on these properties, as did the chain length and the length of the rigid spacer (phenylene, **118**, or stilbenylene, **119**, groups), whereas the metal ion, Pd(II) or Pt(II), appeared to have only minor effects. In the case of the benzylidene derivatives **118**, the number of chains was reduced to eight by substitution in positions 2 and 3 ($n = 12$, 18), or 2 and 4 ($n = 12$).[265] No change in the mesomorphism was detected and only changes in the transition temperature were observed (Cr 106 Col_r-*c2mm* 180 Col_r-*p2gg* 295 I, Cr 94 Col_r-*c2mm* 180 Col_r-*p2gg* 254 I, and Cr 93 Col_r-*c2mm* 257 I, respectively). The phase transformation between the two rectangular phases was not clearly defined, and both mesophases could coexist over several degrees.

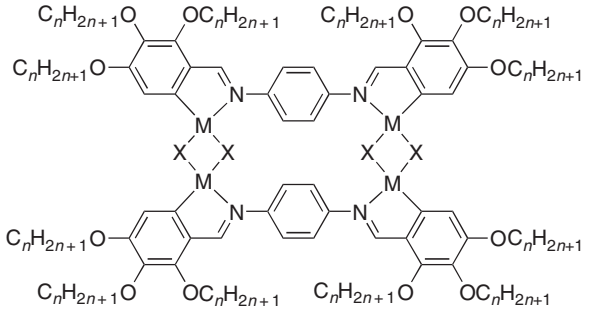

118

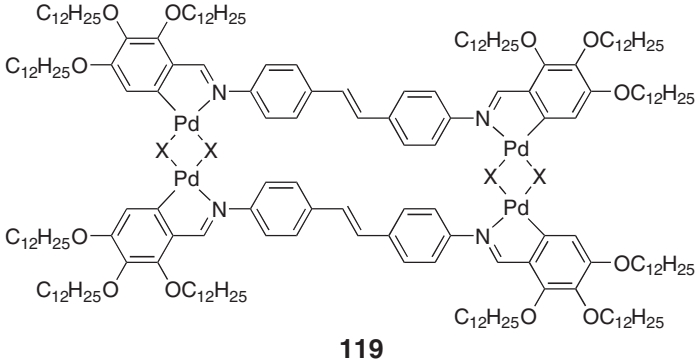

119

In addition to this thermotropic mesomorphism, the complexes formed lyotropic mesophases when dissolved in linear, lipophilic solvents such alkanes, and in chloroform, benzene, octanol, octadecanol, and stearic acid.[259,267–269] In alkanes, the mesophases were stable over wide ranges of temperature and concentration. In general, at high complex concentration, a columnar phase was observed, while at lower concentration, a nematic phase was usually induced. Here again, the mesophase behavior depended strongly on some intrinsic structural parameters, such as the type of bridges and the nature of the metal ions. Thus, while mesophases were not induced or stabilized in any of the μ-acetato complexes, the metal appeared to have more influence on the lyotropic properties. For example, the columnar phase was retained and two nematic phases were induced for the bromopalladium complexes (**118**: X = Br, M = Pd, $n = 12$)/pentadecane mixture, while the analogous mixture with the platinum analog was not mesomorphic.

Similarly, a nematic phase (along with a columnar phase) was induced for the iodoplatinum complex (**118**: X = I, M = Pt, $n = 12$) in pentadecane, while the palladium congener displayed only a columnar phase. The length of the rigid spacer, and, consequently, the dimensions of the complex also played an important role in the nature of the lyomesophase (Tables 19 and 20). Particularly for the phenylene complexes with chloride and bromide bridges, an unexpected transition, reversible with temperature, between two lyotropic nematic phases was detected on the basis of abrupt textural changes. In addition to the columnar phase, a single nematic phase was induced for the thiocyanato-bridged complex **118**, but not for the iodo- and azido-bridged members (**118**: M = Pd, X = I, N_3). The extension of the rigid spacer clearly diminished the tendency for nematic phase induction (no thermotropic nematic phase for **119**), and totally suppressed the nematic polymorphism (only one lyotropic nematic phase for some complexes

Table 19 Mesomorphic properties of the tetrametallo-organyls **118**

M	*n*	*X*	*Thermotropic phase*	*Lyotropic phase*
Pd	6	Cl	Cr 101 Col_r(*c2mm*) 329 dec.	Col_h, N in heptane, pentadecane, eicosane
		Br	Cr 103 Col_o 306 dec.	Col_h, N in heptane, pentadecane, eicosane
		I	Cr 123 Col_o 306 dec.	Col_h, N in heptane, pentadecane, eicosane
	8	Cl	Cr 76 Col_r (*c2mm*) 320 dec.	No information
	10	Cl	Cr 55 Col_o 220 M_1 316 I	Col_h, N_2 in pentane, hexane, nonane Col_h, N_2, (N_1) in decane Col_h, N_2, N_1 in dodecane, tridecane, pentadecane, heptadecane
	12	Cl	Cr 70 Col_r (*c2mm*) 298 dec.	Col_h, N_2 in pentane, hexane, nonane, decane Col_h, N_2, (N_1) in dodecane Col_h, N_2, N_1 in pentadecane, heptadecane
		Br	Cr 69 Col_o 279 dec.	Col_h, N_1, N_2 in pentadecane, eicosane
		I	Cr 62 Col_o 265 dec.	Col_h in pentadecane, no N
		OAc	Cr 71 M_2 114 M_3 230 dec	No mesophase in alkane
		SCN	Cr 50 Col_o 290 dec.	Col_h, N in pentadecane
		N_3	Cr 60 M_2 87 Col_r 150 dec.	Col_h in pentadecane, no N
	14	Cl	Cr 74 Col_r (*c2mm*) 200 Col_r (*p2gg*) 277 I	Col_h, N_2 in pentane, hexane, nonane, decane, dodecane Col_h, N_2, (N_1) in pentadecane Col_h, N_2, N_1 in heptadecane
	16	Cl	Cr 81 Col_r (*c2mm*) 265 I	No information
	18	Cl	Cr 95 Col_r (*c2mm*) 200 Col_r (*p2gg*) 249 I	No information
Pt	6	Cl	Cr 100 Col_o 357 dec.	Col_h, (N) in pentane, hexane, heptane
		Br	Cr 111 Col_o 341 dec.	Col, N in alkane
		I	Cr 107 Col_o 328 dec.	Col, N in alkane
		SCN	Cr 69 M_1 308 dec.	No information
	12	Cl	Cr 70 Col_o 280 dec.	Col_h, N_2, (N_1) in dodecane Col_h, N_1, N_2 in pentadecane, octadecane
		Br	Cr 68 Col_o 292 dec.	No mesophase in alkane
		I	Cr 55 Col_o 297 dec.	Col_h, N_1 in pentadecane
		SCN	Cr 17 Col_o 286 dec.	No information

M_1, M_2, M_3: unidentified mesophases.
(N) and (N_1) represent monotropic nematic phases.

of **119**). The transition between two nematic phases, being a unique case, was investigated thoroughly, and particularly in complexes **118** (M = Pd, X = Cl, n = 6, 10, 12, 14) in various alkanes. While the high-temperature nematic phase, N_2, was present in all mixtures, the appearance of the low-temperature nematic phase, N_1, seemed to be dependent on the chain length of the alkane solvent and that of the complex's terminal chains. Indeed, this study revealed that N_1 occurred enantiotropically for long-chain alkane solvent, monotropically for equal length of alkane and alkoxy groups, but did not form for short-chain paraffins. Evidence for the two nematic phases was also provided by measurement of the birefringence, which showed a substantial fall at the transition (e.g., **118** with M = Pd, X = Cl,

Table 20 Mesomorphic properties of the tetrapalladium organyls **119**

X	*Thermotropic phase*	*Lyotropic phase in pentadecane*
Cl	Cr 126 Col_o 248 M_3 270 dec.	Col_h, N
Br	Cr 126 Col_o 252 dec.	Col_h, no N
I	Cr 98 Col_o 244 dec.	Col_h, N
OAc	Cr 44 M_2 75 M_3 143 dec.	No mesophase
SCN	Cr 54 M_2 240 dec.	Col_h, M_1, no N

M_1, M_2, M_3: unidentified mesophases.

$n = 14$ in 40 wt.% of heptadecane, $\Delta n = 0.012$ in N_1 at 58 °C and 0.007 in N_2 at 60 °C), and by the investigation of some orientational properties. When the transition between these two nematic phases took place, in most cases both the mesophases coexisted in a biphasic region, therefore suggesting a first-order transition, although DSC did not confirm this as enthalpy changes were not detected.

A model for these two nematic phases has been proposed.[270] On the basis of UV/VIS spectroscopy and small-angle X-ray diffraction, the columnar nature of both nematic phases was confirmed with the solvent located between columnar aggregates rather than between the complexes. Due to swelling, the columns were arranged with only weak intercolumnar order. The correlation length of the columns was not given, but there was no long-range, intramolecular ordering. The large, flat metallaorganyls were stacked on top of each other, and arranged perpendicular to the axis of the columns forming the N_2 phase. In the N_1 phase, however, the complexes were tilted with respect to the columnar axis. If such a model were true, the N_1 phase would be a further example of a lyotropic biaxial nematic phase;[271] the only case reported so far was found in the ternary phase diagram constituted by potassium laurate/decanol/D_2O.[272]

Thus, the extension of the aliphatic crown in these discotic metallomesogens by the incorporation of apolar aliphatic solvents enhanced the mesomorphic range by stabilizing the existing columnar phase and favored the formation of more disordered mesophases such as the N_{Col} phase. The dependence of the mesomorphic properties on a combination of complex chain length and solvent chain length generated the idea of "internal" (i.e., complex chains) and "external" solvent (i.e., solvent chains),[44] and represents an interesting way of thinking about mesophase formation.

Formation of inclusion complexes caused by intercalation of small, electron-acceptor molecules, such as TNF and 2′-(2,4,5,7-tetranitro-9-fluorenylideneaminooxy)-propionic acid TAPA, between large, flat, electron-donor molecules has proved to be an original and effective means for mesophase induction, stabilization, and modification.[273] The stability of such charge-transfer complexes was connected to strong π–π interactions between the donor and acceptor molecules, and has been shown to stabilize smectic phases by enhancing lateral interactions in calamitic systems and columnar phases by improving columnar stacking in disk-like molecules. The tetrametallated organyls **118** and **119** discussed above, except those with an acetato bridge, also formed charge-transfer complexes with TNF, and gave rise to a viscous type of columnar phase on heating. X-ray studies revealed a change from oblique/rectangular symmetry to a hexagonal lattice. The nematic lyomesophase stability was enhanced (higher clearing temperatures) in all systems, compared to the behavior of the pure complexes in pentadecane. One exception was found (**119**: X = SCN) which showed the same phase sequence as that observed in pentadecane in the absence of TNF. The columnar phase was still present in all cases.

The structure of the different mesophases was characterized by X-ray diffraction, and confirmed the intercalation of TNF molecules in the columns formed by the planar complexes in both columnar phases. Induction of a chiral lyotropic nematic phase in a binary system composed of equimolar amounts of **118** and the chiral π-electron acceptor, TAPA, in heptane, pentadecane, and eicosane, has been demonstrated.[274] As for non-chiral systems, the temperature range of the chiral nematic phase was found to increase concomitantly with the chain length of the solvent. Three different regions were separated: on decreasing the concentration of pentadecane, a biphasic N/I region was seen in dilute conditions, followed by a N^*/N biphasic region, and then a N^* phase at lower solvent content. The chiral nematic phase existed over a large temperature range. Note that the helical pitch increased with increasing pentadecane content. This case study showed that charge-transfer interactions with chiral electron acceptors is an efficient way to introduce chirality in lyotropic systems and opens new prospects for producing chiral nematic phase in disk-like compounds.

12.05.12.2.4 *ortho*-Palladated azine complexes

Several series of dinuclear *ortho*-palladated complexes of symmetric azines were prepared with various bridges, and the mesomorphism analyzed accordingly (**120**: X = OAc, Cl, Br, SCN, $n = 10$).[275] In the complexes where X = Cl and Br, only the *trans*-isomer was observed (^{1}H NMR spectroscopy), while for X = SCN, two isomers were observed in a 60 : 40 ratio and it was assumed that these were *cis* and *trans*.[276] In each of these examples, the complex was assumed to be planar by comparing with related structures in the literature. However, where X = OAc, the situation was more complex and *trans*- and *cis*-isomers in the ratio 3 : 1 were produced consistently. ^{1}H NMR studies showed that the *trans*-isomer was optically active and hence the structure had to be that of an "open book" (Figure 37, R^1 = Me), although in the synthesis a racemic mixture was produced.

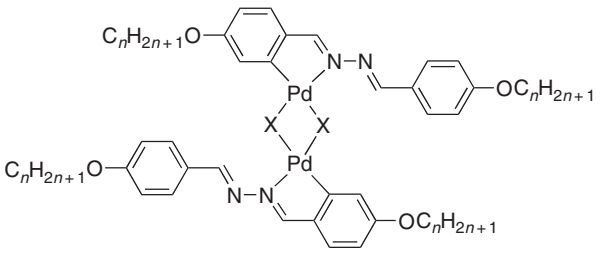

120

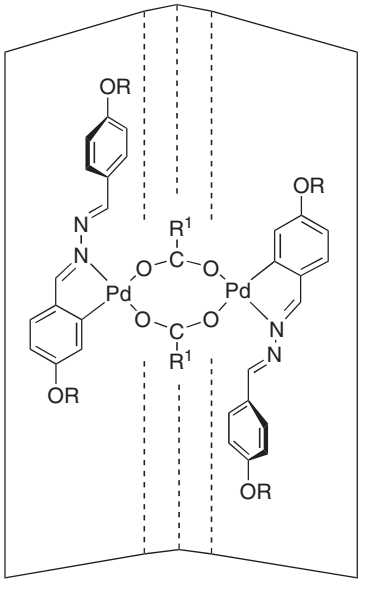

Figure 37 Schematic structure of the chiral *trans*-isomer of the μ-carboxylato palladium azines.

For the non-acetato-bridged dimers, the only mesophase seen was SmC which was typically in the range 100–250 °C (for $n = 10$) whereas for the acetato-bridged complexes, a nematic phase was seen for $6 \leq n \leq 8$ and for $n \geq 7$, a SmC phase was also seen (between ca. 100 and 160 °C). Mesophase ranges were very much larger in the planar materials.

Using the fact that the *trans*-isomer was chiral, a derivative was synthesized where the bridging carboxylate group was the optically pure (*R*)-2-chloropropionate (**120**: X = CHMeClCOO, $n = 10$).[237] Synthesized from the μ-Cl_2 species by reaction with the sodium salt of the acid, a mixture was produced which was shown by ^{1}H NMR spectroscopy to have the following composition: *trans*-$\Lambda R,R$ (34%), *trans*-$\Delta R,R$ (34%), *cis*-*R,R* (32%). Thus, while the *trans*-components described a pair of diastereoisomers, the *cis*-isomer was optically pure by virtue of the chiral acid groups. The mixture thus produced had the phase sequence Cr 102 SmC* 119 SmA 149 I and physical measurements showed that the SmC* phase was ferroelectric, with a rise time of around 330 ms at a square wave voltage of ±17 V and 0.5 Hz, and a cell thickness of 11 μm. Such response times were some three orders of magnitude longer than those found in calamitic SmC* phases, which was probably due to the greater viscosity of the palladium SmC* phase which, in turn, resulted from the molecular shape. The full series of (*S*)-chloropropionate from $n = 6$ to 16, was later published by another group, and revealed an important mesophase stabilization, essentially due to the depression of the melting point.[179,277] One complex with the larger, chiral carboxylate (X = (*S*)-$Me_2CHCH_2CHClCOO$, $n = 14$) also yielded a SmC* phase but at much lower temperatures (between 45 and 58 °C).

The effect of the length of the bridging carboxylate was also studied (**120**: X = $OOCC_mH_{2m+1}$, m = 0–11, 13,15,17, n = 10).[278,279] Thus, the shortest (m = 0–3) and longest ($m \geq 10$) carboxylates gave rise to a SmC phase that was enantiotropic only for m = 0–2, whereas the nematic phase seen for $m \geq 3$, was both enantiotropic ($2 \leq m \leq 6$, and m = 10, 13, 17) and monotropic ($7 \leq n \leq 9$, and m = 11, 15). The mesomorphic range decreased rapidly as the chain length was increased, dropping from ca. 40 °C to almost nothing, although transition temperatures stabilized at around 100 °C, revealing the important perturbation brought to the lateral molecular packing by the carboxylate.

12.05.12.2.5 *ortho*-Metallated pyrimidine complexes

Other work in this area by Ghedini considered the products of the cyclopalladation of the well-known liquid crystals, the 2-phenylpyrimidines.[280] Initially, dimeric products were obtained and then they were further reacted with species able to cleave the (μ-Cl)$_2$ bridge to give a series of mononuclear derivatives **121**.

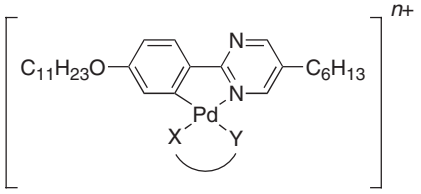

121

For X–Y = 8-hydroxyquinolato (n = 0) and X–Y = 1,10-phenanthroline (n = 1), the complexes were non-mesomorphic. However, when X–Y = *acac* (n = 0), a material with a monotropic SmA phase resulted (Cr 83 (SmA 68) I) and when X–Y = 2,2′-bipyridine (n = 1 $[BF_4]^-$ counterion), a material with an enantiotropic nematic phase was produced (Cr 146 N 158 I); related complexes with PF_6 or SbF_6 anions were non-mesomorphic. These are further, rare examples of ionic materials showing a thermotropic nematic phase.

Similarly, other mononuclear *ortho*-palladated phenylpyrimidines were obtained with β-diketonate ligands (**126**, **127**, **128** and **130** *vide infra*)[281] or imines **122**.[215]

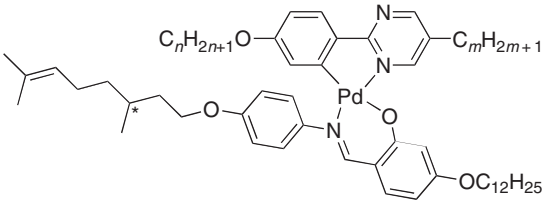

122

Chiral complexes **122** with various combinations of chains on the phenylpyrimidine ligand (**122**: (n, m) = (1, 6), (1, 9), (11, 6), (9, 9)) all exhibited a SmA phase, between ca. 100 and 130 °C, losing the SmC* of the free ligand (see **104b**). In solution, only the *N,N-trans* complexes (as depicted) were formed.

Further studies of the same system looked at the dimeric precursors to such monomeric species and considered the *trans*-dinuclear complexes **123** (X = Cl, Br, I, OAc).[282]

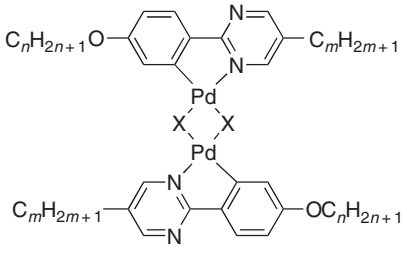

123

Four series of complexes were studied with the ligands (m, n) = (6, 1), (9, 1), (6, 11), (9, 9). None of the complexes with X = OAc and no derivatives with (m, n) = (6, 1) was mesomorphic; other non-mesomorphic combinations were (m, n) = (9, 1) with X = I, and (m, n) = (9, 9) with X = Cl. Of the remaining materials, all had a broad SmA phase (the parent ligands showed a nematic phase only) typically between 100 and 200 °C, while two materials ((m, n) = (9,1) with X = Cl and (m, n) = (9,9) with X = I) were reported to have another smectic phase (SmX) above the SmA phase. Later studies[283] showed that what had been identified as SmX was, in fact, SmA, while the phase identified as SmA was actually an ordered smectic phase.

Related derivatives were later reported by Guang *et al.*[284] in which the ligand had one end fixed (n = 6) and the bridging group was varied (X = O_2C–Me, O_2C–CH_2Cl, O_2C–CH_2Br, O_2C–$CHBrCH_3$, and O_2C–CH_2CH_2Br). For m = 6, the μ-acetato complex was reported as non-mesomorphic, while all other derivatives showed a SmC phase, with the μ-chloroacetato complex showing a SmA phase, too. Clearing points varied widely, but the bromo-substituted bridges consistently gave the lowest values. For the μ-chloro- and bromo-acetate complexes, several derivatives were prepared by varying m (from 6 to 12). As stated already, the chloroacetate with m = 6 gave SmC and SmA, but then the SmC phase was suppressed at longer chain length, reappearing for m = 11, 12. For the bromo-acetates, there was a marked odd–even effect so that for m = 7, 9, 11, only SmA was seen, while for m = 8, 10, 12, both SmC and SmA were observed; m = 6 gave only SmC.

Mesophase stabilization and induction were observed by the cyclopalladation of the macrocyclic 2-phenylpyrimidine derivatives. Indeed, enantiotropic SmA and N phases were observed in the dipalladium complex (**124**: X = Y = O, Cr 168 SmA 208 N 226 I), whereas the other dinuclear complex exhibited a nematic phase only (**124**: X = Y = CH_2O, Cr 118 (SmA 91) I).[285]

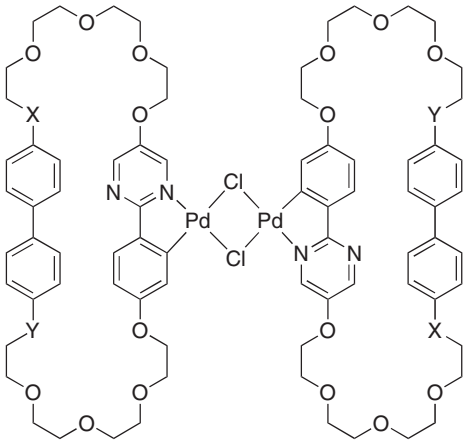

124

In order to create novel types of metallomesogens with unusual molecular shapes, Tschierske *et al.*[286] synthesized novel macrocyclic molecules combining two different molecular architectures, namely rod-like *para*-cyclophanes with two, half-disk-like 1,3-β-diketonate units fused together by *ortho*-palladation (**125**: R^1, R^2 = H or $OC_{10}H_{21}$; x, y = 1, 2, 3). The macrocyclic cyclophane containing two phenylpyrimidine units were prepared using a standard high-dilution, template-cyclization reaction. *ortho*-Palladation resulted in the formation of polymers, which were reacted with the appropriate Tl^I 1,3-β-diketonate to yield the final dinuclear complexes. The complexes were mesomorphic, with a smectic-to-columnar phase cross-over observed on increasing the chain number concomitantly with an important decrease of the transition temperatures (Table 21). The paracyclophane units themselves were mesomorphic, but showed only monotropic mesophases below 150–160 °C. The four-chain compound exhibited a SmA phase over a narrow temperature range, whereas those with 12 chains displayed an enantiotropic Col_h phase, regardless of the length of the polyether chains connecting the two central phenyl-pyrimidine moieties. While in this series the melting points were not changed, differences in the mesophase stability were observed as a function of the polyether chain length, particularly between the two isomeric compounds. Surprisingly, however, the compound with eight side chains was not mesomorphic. The two halves of the molecules were assumed to be planar, although due to the flexible connectors, they can also adopt several conformations. The number of chains thus influenced the nature of the mesophase, while micro-segregation between the central polar cores and the aliphatic chains helped in stabilizing this arrangement (rather high transition temperatures) provided the required number of side chains was present.

Table 21 Mesomorphic properties of **125**

R^1	R^2	x	y	*Phase transitions*
H	H	3	1	Cr 197 SmA 207 I
$OC_{10}H_{21}$	H	3	1	Cr 137 I
$OC_{10}H_{21}$	$OC_{10}H_{21}$	3	1	Cr 110 Col_h 178 I
$OC_{10}H_{21}$	$OC_{10}H_{21}$	1	2	Cr 108 Col_h 211 I
$OC_{10}H_{21}$	$OC_{10}H_{21}$	1	3	Cr 110 Col_h 208 I

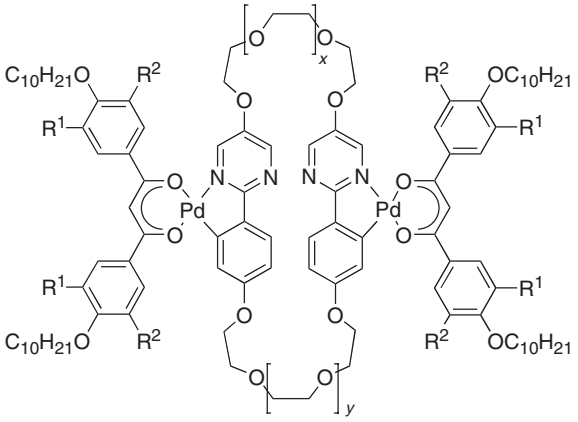

125

Hegmann *et al*. described an interesting concept for controlling the mesophase structure of novel molecules close to the calamitic/discotic cross-over point by combining a calamitic sub-unit, namely disubstituted 2-phenylpyrimidine and an half-discotic moiety, that is, substituted 1,3-diketonate, via *ortho*-palladation. The number of side chains on the diketonate fragment was increased step-by-step so that the overall molecular structure changed stepwise to a disk-like molecular shape. This type of study is important because with such molecular structures, mesophase transformations may occur through several intermediate mesophases including SmC, SmA, Cub, lamello-columnar (L_{Col}), Col_r, and Col_h phases, allowing for a better understanding of the intimate relationships between these different mesophases. This led to a novel series of liquid-crystalline, mononuclear *ortho*-palladated complexes (**126**: R^1, R^2, R^3, $R^4 = H$ or $OC_{10}H_{21}$)[287,288] for which a discontinuous change from smectic to columnar mesophases was witnessed with an increasing number of chains (Table 22). Thus, the first compound of the series with a total number of four chains showed both SmC and SmA phases. Increasing the number of chains to five led to the destabilization of the mesophase and monotropic behavior, whereas with six chains, the mesomorphism was totally suppressed. Mesomorphism was then regenerated with the further increase in the number of chains, and Col_h phases were formed. Moreover, the mesophase stability was enhanced on increasing the number of chains from seven to eight. The decrease in the mesophase stability of both the unsymmetric compounds (five- and seven-chained compounds) relative to the corresponding symmetrical analogs (four- and eight-chained compounds) was attributed to the fact that the former were obtained as *cis*/*trans*-isomeric mixtures with respect to the pyrimidine ring, and in a 1 : 1 ratio as deduced from NMR. The reasons for the absence of mesomorphism in the six-chained compound are not yet understood. Interestingly, a binary phase diagram between the two unsymmetrical compounds revealed the induction of another birefringent mesophase at the contact region with the destabilization of both mesophases of the pure compounds.

The existence of the biaxial SmA phase (SmA_b),[281] also known as the McMillan phase, has been demonstrated in some charge-transfer complexes (CT complexes) formed with the metallomesogens **126** and TNF by textural observations and X-ray investigations. (Like the biaxial nematic phase mentioned earlier, the SmA_b phase has additional long-range order in a direction perpendicular to the principal director, ***n*** (Figure 7)). Two novel

Table 22 Transitions temperatures of **126**

R^1	R^3	R^4	R^2	*Pure compounds*	*CT complexes*
H	H	H	H	Cr 113 SmC 117 SmA 133 I	SmA_b 178 Col 210 I
$OC_{10}H_{21}$	H	H	H	Cr 117 (SmA 99 N 101) I	SmA_b 162 Col 179 I
$OC_{10}H_{21}$	H	$OC_{10}H_{21}$	H	Cr 115 I	SmA_b 128 Col 165 I
$OC_{10}H_{21}$	$OC_{10}H_{21}$	H	H	Cr 59 Col_h 76 I[a]	
$OC_{10}H_{21}$	$OC_{10}H_{21}$	$OC_{10}H_{21}$	H	Cr 72 Col_h 134 I[a]	–
$OC_{10}H_{21}$	$OC_{10}H_{21}$	$OC_{10}H_{21}$	$OC_{10}H_{21}$	Cr 79 Col_h 163 I	–

[a]1 : 1 Mixture of stereoisomers.

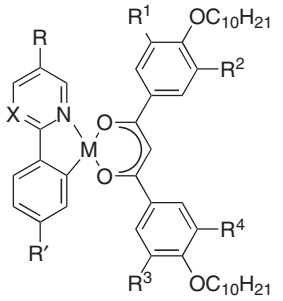

126: X = N; M = Pd; R = C_7H_{15}–; R′ = $C_{10}H_{21}O$–
127: X = N; M = Pd; R = $C_{10}H_{21}$–; R′ = $C_8H_{17}O$–
128: X = N; M = Pd; R = $C_5H_{11}O$–Ph–; R′ = C_9H_{19}–
129: X = CH; M = Pd; R = $C_8H_{17}O$– ; R′ = $C_{10}H_{21}O$–
130: X = N; M = Pt; R = C_7H_{15} –; R′ = $C_{10}H_{21}O$–
131: X = CH; M = Pt; R = $C_8H_{17}O$–; R′ = $C_{10}H_{21}O$–

Figure 38 Structures of the related complexes **126–131**.

mesophases were induced systematically (Table 22). At low TNF concentration, an ill-defined mesophase with a structure different to that of the pure compound was formed. This mesophase remained stable at high temperature and up to high concentration of TNF (ca. 60 mol%). X-ray diffraction and optical textures suggested a columnar type of mesophase. At higher concentrations of TNF, that is, upwards from 20 mol%, the three charge-transfer complexes formed the SmA_b phase. By X-ray diffraction, the charge-transfer complexes self-organized into layers, with the flat molecules arranged parallel to each other and orthogonal to the layers, with a long-range face-to-face organization, and short side-by-side correlations. This face-to-face interaction considerably hindered the molecular rotation around the long axis reducing the symmetry; hence, the phase is biaxial.

The study of **126** was later followed up by reports of the behavior of the related Pd(II) and Pt(II) complexes **127–131**,[288] in which the authors set out to investigate the transition from the behavior associated with calamitic materials to that associated with more disk-like materials (Figure 38). The results, summarized in Table 23, show that it is both the number and distribution of chains on the β-diketonate that determine the transition to disk-like behavior. Interestingly, none of the complexes show behavior characteristic of "both" rods and disks as found in polycatenar systems[28,29] (see 12.05.3.5).

12.05.12.2.6 Other *ortho*-metallated complexes

New, mesomorphic mono- (**132**: R = Me, Bu, n = 4–10) and di-cyclopalladated (**133**: R = Me, Bu, n = 4–10) pyridazine complexes have been reported.[289] They were obtained by the mono- and di-cyclopalladation of elongated pyridazines, followed by the reaction with various β-diketones. The mononuclear complexes **132** exhibited a single SmA phase between 180 and ca. 300 °C for R = Me, except the first homolog of the series (n = 4) which showed an additional SmB phase (Cr 156 SmB 183 SmA 276). For those with the bulkier ketonate (**132**: R = Bu), a significant depression in clearing temperatures of about 100 °C was observed, and a stable SmA phase was seen for all the homologs between 100 and 150 °C up to 190 °C. Amongst the dinuclear complexes, only the *cis*-di-cyclopalladated acac derivatives (**133**: R = Me) showed a SmA phase well above 200 °C for the short-chain-length homologs with extensive decomposition. Note that these dimetallated complexes have a sterically induced twist in the molecule that renders them chiral. The related platinum species could not be isolated as their acac derivatives.[290]

Table 23 Summary of the mesomorphism of complexes **126–131**[a]

				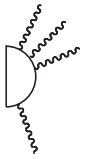	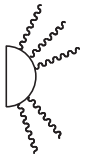	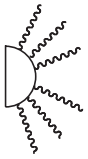
126	SmC, SmA	(SmA, N)	[c]	$Col_h(2)$	Col_h	Col_h
127	SmA	(SmA, N)	[c]	$Col_h(2)$, N_{Col}	Col_h	Col_h
128	SmA	SmC, SmA, N	(SmC, SmA)	$Col_h(2)$	Col_x, $Col_h(2)$	Col_h
129	[c]	[c]	[c]	[c]	[c]	Col_h
130	SmA	(SmA, N)	[c]	$Col_h(2)$	Col_h	Col_h
131	[c]	[c]		[b]	[b]	[b]

[a]$Col_h(2)$ represents a columnar hexagonal phase in which a repeat unit consists of two molecules of complex, Col_x is an unidentified columnar phase, and N_{Col} is a nematic columnar phase.
[b]Complex not synthesized.
[c]Complex not mesomorphic.
Monotropic phases are in parentheses.

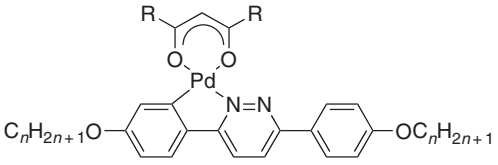

132

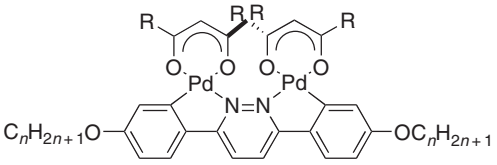

133

Other *ortho*-metallated pyridazine complexes (**134**, where R = –Me, $–CH_2Cl_2$) were reported by Guang *et al.*[284] For $n = m = 10$, the free ligand showed a SmA phase (Cr 79 SmA 102 I), as did the μ-Cl precursor complex (Cr 163 SmA 212 I) and the chloro- and bromoacetates (Cr 160 SmA 185 I and Cr 160 SmA 174 I, respectively); the simple μ-acetato complex was non-mesomorphic at all chain lengths reported. The lower symmetry complexes ($n = 6$, $m = 10$) were mesomorphic for the chloro- but not the bromoacetate, and a more extensive series where n was fixed as 10 and m was varied from 6 to 12 showed enantiotropic SmA phases for all except that with $m = 6$.

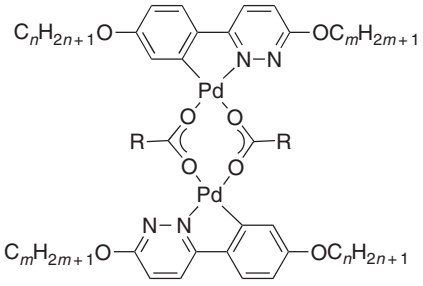

134

The dinuclear *ortho*-palladated complexes derived from (*S*)-2-(2′-hydroxyaryl)oxazoline Schiff's-base ligands (**135**: X = Cl; $x = 1$: R = $CHMe_2$; $x = 1$, 2: R = $C^*HCH_3CH_2CH_3$) showed a broad SmA phase.[291] In the planar, chloro-bridged complexes (*cis* : *trans* mixture 1 : 2), the phase existed from 50 to 170 °C, and up to 250 °C for the biphenyl derivative; as far as the non-planar acetato-bridged complexes (only *trans*-isomer) was concerned, only the biphenyl derivative was mesomorphic (**135**: X = OAc; $x = 2$: R = $C^*HCH_3CH_2CH_3$; Cr 179 SmA 232 I). Used as chiral dopants (ca. 10 mol%), a chiral nematic phase was induced systematically in both the chloro- and acetato-bridged series, with the suppression of the SmA phase in the chloro-bridged systems ($x = 1$).

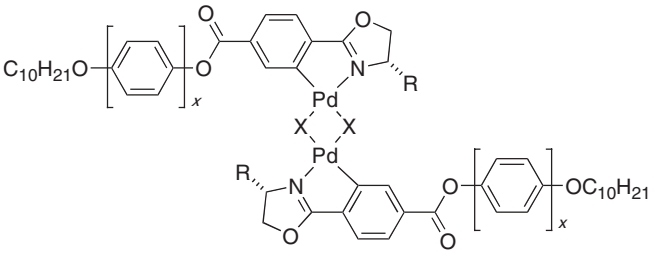

135

Serrano and co-workers have reported the synthesis of two interesting series of chiral, hexacatenar metal complexes, that is, mono- and dinuclear, derived from chiral oxazoline-based ligands.[292] None of the pure dinuclear compounds (**136**: X = OAc, Cl) was mesomorphic and most were room-temperature oils or glassy materials. This is likely due to the sterically demanding central chiral unit preventing molecular stacking and, hence, mesophase formation.

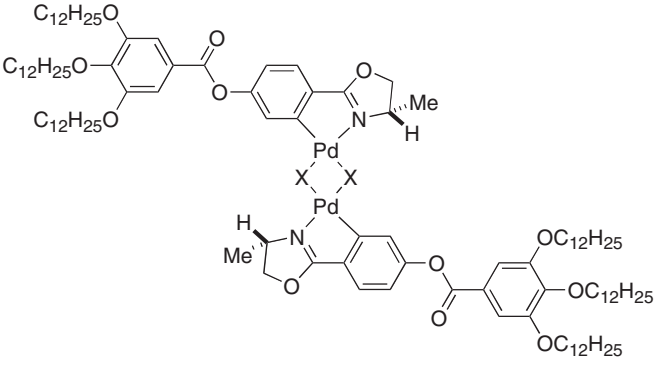

136

However, when mixed with TNF, they all formed charge-transfer complexes. At high TNF concentration (>66%), demixing of the two components occurred, whereas below this concentration, a mesophase was induced and, surprisingly, despite the six peripheral chains, a SmA phase was identified. At lower TNF concentrations, the more sterically demanding materials exhibited SmA glasses on cooling, although in general, the clearing temperatures increased with the TNF content. X-ray investigations revealed that the structure of the mesophase consisted of the face-to-face arrangement of the complexes and TNF into layers, with an additional side-by-side organization, resembling the model proposed for the McMillan phase. These compounds have also been shown to act as chiral dopants with nematic hosts and N^* phases have been induced.

Another example reported by El-ghayoury *et al.* concerned some *ortho*-palladated quinolines coordinated to non-mesomorphic, 5,5′-disubstituted-2,2′-bipyridines (**137**: X = BF_4, $C_{12}H_{25}OSO_3$).[293] Both complexes exhibited liquid crystallinity, but the thermal stability was much greater in the dodecylsulfate (DOS) salt compared to the tetrafluoroborate salt that degraded rapidly on heating at high temperature. Two different liquid-crystalline mesophases were found for the DOS salt: Cr 131 Col_r 168 SmA 216 I. At low temperature, the Col_r phase was identified by X-ray diffraction, and resulted from the stacking of the nearly flat aromatic cores on top of each other. However, the columns were not completely surrounded by aliphatic chains; hence, the polar centers of the columns were in lateral contact which one another, forming layers which are separated by layers of molten chains. The second mesophase was identified as SmA but with some local order of the columns still remaining.

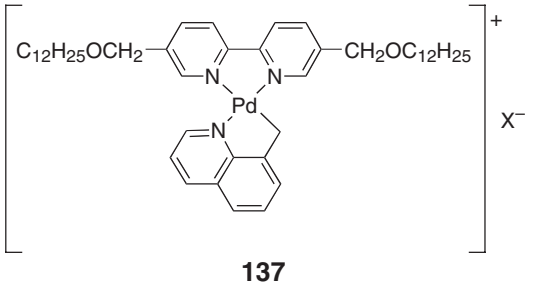

137

Some elaborated 6′-phenyl-2,2′-bipyridine ligands and the corresponding *C,N,N′*-cyclometallated chloropalladium(II) complexes, **138**, were found to be mesomorphic.[294] The ligands showed a nematic phase between 140 and 170 °C for short chain lengths, and between 130 and 140 °C for the dodecyloxy homolog. The complexes, however, exhibited very high temperature monotropic mesophases, namely a nematic for the short-chain-length complexes, replaced by a SmA for $n = 12$ (**138**: $n = 6, 8, 12$).[295] These high temperatures result from the rather elongated anisometric part, but shorter ligand anisotropy led to materials deprived from mesomorphism. The interest in such compounds arises from their photophysical properties, particularly their electroluminescent properties.[296] Reaction of the same ligands with an iridium dimer, followed by counterion exchange afforded a new series of cationic orthometallated iridium(III) complexes, unfortunately devoid of mesomorphism.[297]

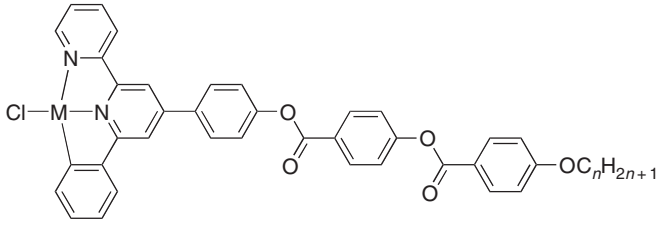

138

12.05.12.3 Allyl Complexes of Palladium(II)

Allylpalladium(II) complexes were realized[298] using salicylaldimine ligands and only a monotropic nematic phase was observed (**139a**: R = H: Cr 89.5 I, R = Me: Cr 94 (N 40) I; **139b**: R = H: Cr 138 (N 114.5) I, R = Me: Cr 148 (N 142.5) I).

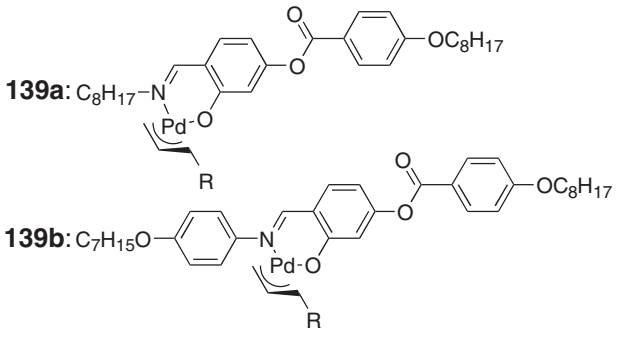

139

Other π-allyl complexes **140** containing 3,5-disubstituted pyrazole ligands ($4 \leq n \leq 18$) were reported by Torralba *et al.*,[299] and a single-crystal structure was determined for the complex with $n = 12$. The mesomorphism of the ligands was dominated by the formation of a SmC phase, with a SmA seen for $n \leq 10$. All of the complexes with $n \geq 10$ showed monotropic mesomorphism with a SmA seen for $n = 10$, SmA and SmC for $n = 12$, and all higher homologs showing only SmC phases. Clearing points varied from 107.5 °C ($n = 10$) to 95.5 °C ($n = 18$).

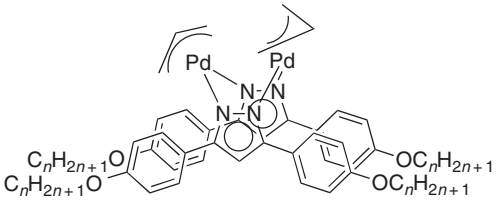

140

12.05.13 Organometallic Liquid Crystals of the Group 11 Elements

The majority of the organometallic liquid crystals of the group 11 elements contain an isonitrile ligand in one of three main types, namely (i) bound to a metal halide fragment, (ii) as a homoleptic, monocationic complex and (iii) in conjunction with σ-bound organic ligands such as acetylenes or aromatic groups. These will now be discussed.

12.05.13.1 Complexes of Isonitriles

12.05.13.1.1 Isonitrile metal halide complexes

Takahashi reported the first halogold(I) isonitrile systems (**141**: R = H, OC_mH_{2m+1}). Depending on the chain length, the ligands with R = H showed nematic and SmA mesophases, between ca. 70 and 85 °C, while the complex showed SmA and SmC phases at elevated temperatures (170–270 °C).[300] In order to perturb the strong intermolecular interactions and depress the transition temperatures, systems with lateral chains were then prepared (**141**: $R = OC_mH_{2m+1}$). The complexes showed nematic and SmA phases at reduced temperatures depending on n and m (90–190 °C) despite the non-mesomorphic nature of the ligands. However, increasing the size of the lateral substituent destabilized the mesophase. A chiral chlorogold(I) species, bearing a similar (R = H) but a chiral ligand ($OC^*HMeC_6H_{13}$), was also made and SmC^* phases were observed (Cr 152 SmC^* 185 SmA 285 dec.),[152] although the spontaneous polarization could not be evaluated due to the inherent conductivity of the complex preparations.

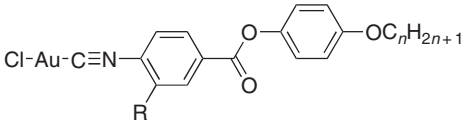

141

Alkoxyphenyl (**142a**: X = Cl, Br, I, n = 2, 4, 6, 8, 10, 12)[301] and alkoxybiphenyl (**142b**: X = Cl, Br, I, n = 4, 6, 8, 10, 12)[302] isonitrile ligands were also complexed to halogold(I) moieties to form thermally stable complexes. All the complexes **142a** formed SmA phases between 120 and 170 °C for X = Cl, and 100 and 150 °C for X = Br, with the exception of the iodo derivatives where the SmA phase was found to be monotropic only for n = 12. Thus, the widest mesomorphic temperature range followed the trend Cl > Br > I (Figure 39).

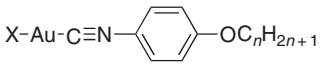

142a

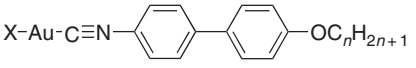

142b

Biphenylisonitrile derivatives **142b** were also mesomorphic and, this time, the iodo complexes also showed a SmA phase and transition temperatures were, in general, much higher in these materials (mesomorphic range between 120 and 300 °C, Figure 39). A nematic phase was also observed for the short-chain-length chloro- and bromogold(I) (n = 4). The trend in melting points of these materials (Cl < Br < I), which is the opposite of what was observed for **142a**, was interpreted according to polarizability arguments.[303] Lateral monofluorination of complexes **142a**, in the *ortho*-(3-F) or *meta*-(2-F) position relative to the alkoxy chain, was also investigated.[304] The 3-fluoro derivatives were mesomorphic, showing a SmA phase, although at much higher temperatures than in the non-fluorinated systems; the clearing temperatures of the former coincide with the melting temperatures of the latter. The 2-fluoro derivatives were very weakly mesomorphic in comparison, but a narrow nematic range was seen for the hexyloxy homolog and a SmA phase for the other members. The transition temperatures were found to decrease in the order 3–F > 2–F and in the order Cl > Br > I, the latter in accordance with the decrease in polarity of the Au–X bond, as seen above for complexes **142a**. Complexes with pseudohalides were synthesized (**142a** and **142b**: X = CN, SCN, n = 4, 6, 8, 10, 12) with a number of simple ligands,[305] some of which were monofluorinated. In each case, it was observed that lower transition temperatures resulted when thiocyanate was incorporated, rather than cyanide (Figure 39).

Mixture studies between various derivatives of **142** were unremarkable, showing a linear dependence of the SmA clearing point with composition and eutectic behavior in the melting point.[306]

Note that chlorocopper(I) derivatives **143b** which showed SmA and SmC phases (for n = 10, 12) between 100 and 200 °C, without apparent decomposition, were later reported.[307] Thus, compared to the analogous gold complexes, the mesomorphic ranges were reduced considerably in the copper complexes, in fact, by almost 100 °C. Complexation

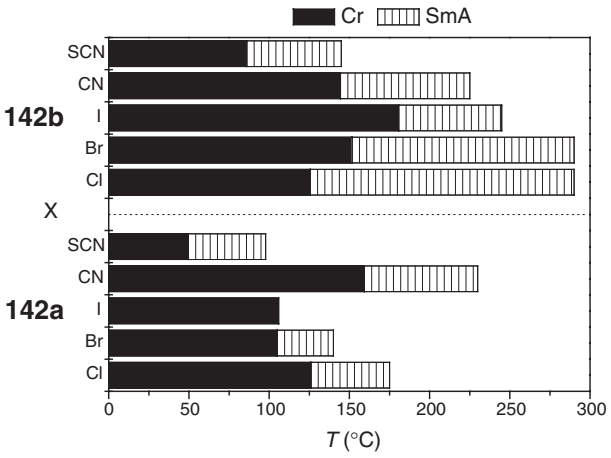

Figure 39 Influence of the halogen or pseudo halogen X on the mesophases stability of the complexes **142a** (bottom) and **142b** (top) for $n = 8$.

to "CuCl" of isonitrile ligand based on phenyl benzoates considerably enhanced the mesophase stability, with mesophase temperatures well in excess of 200 °C, without decomposition.

143a **143b**

The chlorocopper(I) complex **143a** was not found to be mesomorphic, but was later used in mixture studies with the gold(I) complex **142a** ($n = 12$). Above 50% of **143a** in the gold complex destabilized the SmA phase of the latter and there were significant biphasic areas in the binary phase diagram.[306]

The trialkoxyphenylisocyanatogold(I) complexes (**144**: M = Au, X = Cl, $n = 4$, 6, 8, 10; X = Br, I, CN, SCN, $n = 10$) were mesomorphic, forming a Col_h phase at room temperature despite being derived from non-mesomorphic ligands.[304,305]

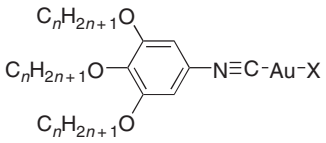

144

In the halogold series, the clearing temperatures (Figure 40) decreased in accordance with the increasing size of the halide group, and X-ray diffraction revealed an intra-columnar separation of only 4 Å, supporting the existence of a basic dimeric arrangement arising from two molecules disposed in an antiparallel fashion. These dimers would then stack on top of each other, probably rotated by, on average, 90° from one to the next to generate an overall circular columnar core in agreement with the hexagonal symmetry. The greater the size of the halide, the more perturbed was the stacking into columns, and the lower the clearing temperature.

This situation was slightly different for the cyano and the thiocyanato complexes, where the mesophase stability increased considerably compared to the halo compounds. In fact, X-ray diffraction suggested rather strong interactions between gold atoms (6.5 Å), in addition to a smaller stacking period of 3.3 Å, particularly for the SCN complex. Thus, the columnar structure remained basically the same, but was "tighter," consistent with greater mesophase stability.

Related chloro(isocyanato)copper(I) complexes **145** have also been studied, and again, mesomorphic complexes were found even though the ligand was non-mesomorphic.[305] Two series were prepared, and most of the di-3,4- (**145**: R = H, $n = 4$, 6, 8, 10,12) and tri-3,4,5-alkoxyphenylisocyanatocopper(I) complexes (**145**: R = OC_nH_{2n+1}, $n = 4$, 6, 8, 10, 12) exhibited Col_h phase, some of them at or near room temperature. Among the two-chained systems, the first two homologs of the series ($n = 4$, 6) were not mesomorphic, clearing at ca. 80 °C. The other derivatives exhibited a Col_h phase with little influence of the chain length on the melting temperatures, ca. 80–85 °C, but with an increase in

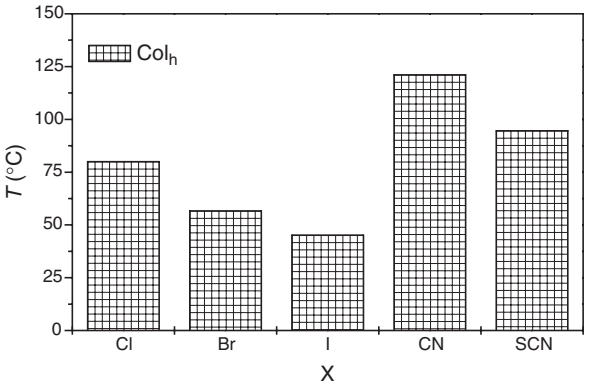

Figure 40 Mesomorphism of gold(I) complexes **144**, $n = 10$.

the mesophase stability on lengthening the chains, and clearing temperatures of 96.5, 115, and 124 °C for $n = 8$, 10, and 12, respectively. Except for the butyloxy derivative that was not mesomorphic (Cr 99 I), all the other tri-alkoxy complexes displayed a Col$_h$ phase from room temperature. The mesophase temperature range was substantially enhanced with respect to the dialkoxy compounds but with lower clearing temperatures, falling from 105 to 75 °C and then rising again to 94 °C for the dodecyloxy homolog.

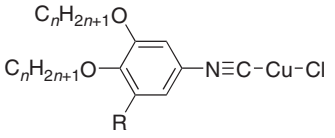

145

Espinet *et al.* also reported binuclear mesogenic copper(I) isocyanide complexes[308] **146** consisting of two tetrahedral [CuX$_2$(CNR)$_2$] units sharing an edge that contains the two bridging halogens. With such a structure, the four coordination positions for the isocyanide ligands are co-planar and, as such, mesomorphism might be anticipated. None of the complexes of the first series with the biphenylisocyanide ligands was mesomorphic (**146a**: X = Cl, Br, I) and all melted above 165 °C. However, with the other elongated isocyanide ligand (**146b**: X = Cl; $n = 4$, 6, 8, 10, 12 and X = Br, I; $n = 4$, 12), the complexes showed a SmA phase, though at rather elevated temperatures (melting above 180 °C up to the point of decomposition). While the melting temperatures were kept constant, the clearing or decomposition temperatures decreased with increasing chain length or on substitution of Cl by Br or I, thus narrowing the range of the SmA phase. The complexes with 3,4,5-trialkoxyphenylisocyanides (**146c**: X = Cl; $n = 4$, 6, 8, 10, 12 and X = Br, I; $n = 4$, 12) displayed mainly a Col$_h$ phase from room temperature up to 70–80 °C (Figure 41). The clearing temperature decreased in the order I > Br > Cl and those with short-chain lengths displayed a monotropic Col$_h$ phase, with a mean stacking period of ca. 5 Å.

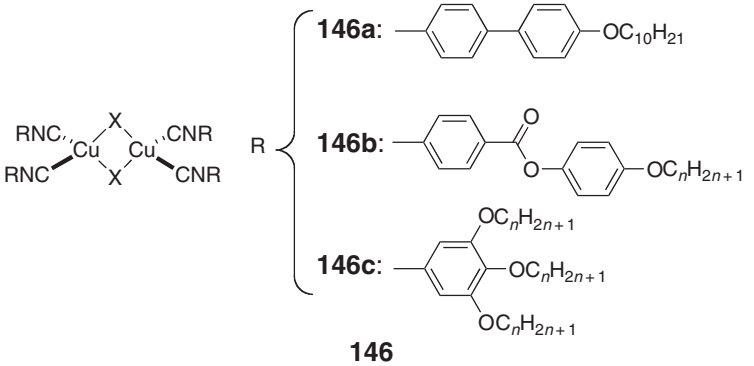

146

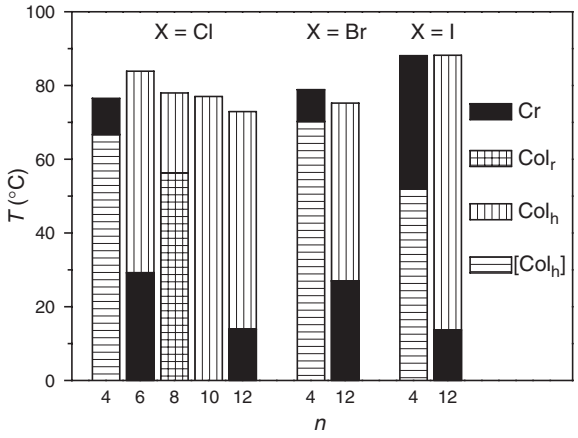

Figure 41 Mesomorphism of dicopper complexes **146c**.

12.05.13.1.2 Ionic bis(isonitrile) complexes

Gold and silver isonitriles complexes have been investigated (**147**: M = Au, Ag; X = NO_3, PF_6, BF_4; n = 4, 8, 12).[309] In general, the phenyl and biphenyl gold derivatives showed a SmA phase, whereas the analogous silver complexes displayed an additional SmC phase (Figure 42). Electrostatic interactions thus seem to favor and stabilize lamellar arrangements, since phenyl isocyanides yield mesomorphic materials upon complexation to silver or gold. Elongation of the aromatic parts enhanced the mesophase stability and that of the crystalline phase to a small degree. Irrespective of the isocyanide, the general trend of melting temperatures for the gold complexes is $[PF_6]^- > [BF_4]^-$ and is opposite for the clearing temperatures. Note that the behavior of **147b** is markedly different to that of **81** for which a nematic phase was observed, but no SmA phase.

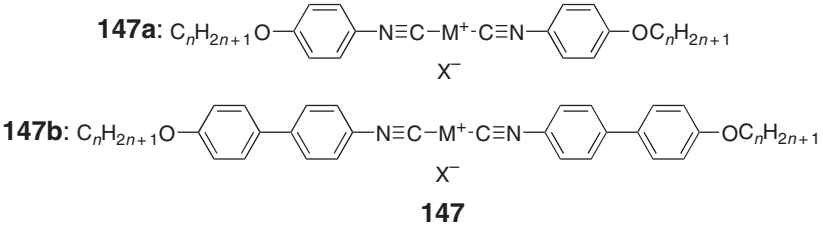

147

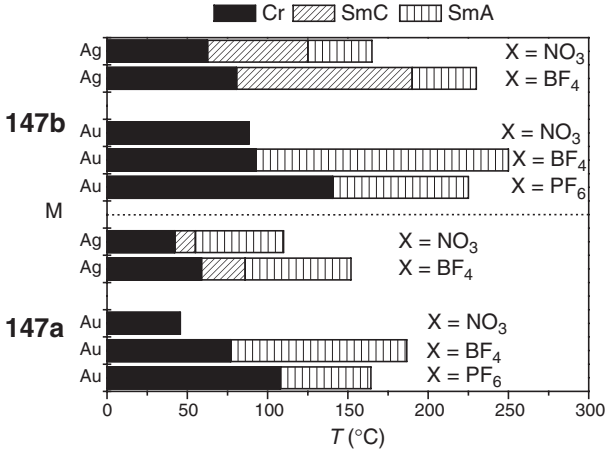

Figure 42 Influence of the metal and counter-anion on the mesophase stability of **147a** (bottom) and **147b** (top) for n = 8.

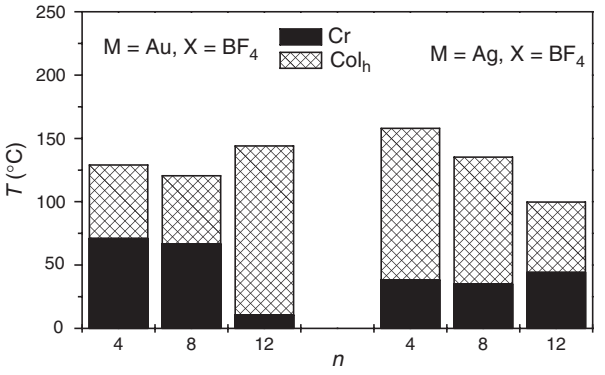

Figure 43 Mesomorphism of complexes **148**.

In a similar way, the mesomorphism of complexes **148** (M = Au, X = PF_6, BF_4, NO_3; n = 4, 8, 12 and M = Ag, X = BF_4, NO_3; n = 4, 8, 12) depended upon the nature of the anion (X) and, of course, the metal.[309] Thus, with gold, for n = 8, 12, the PF_6^- salts gave room temperature Col_h phases which cleared just above 100 °C; only the butyloxy homolog was not mesomorphic. However, with BF_4^- as counteranion, homologs with n = 4, 8, 12 were all mesomorphic showing a Col_h phase: the melting points dropped from 71 to 10 °C with increasing chain length, and the clearing temperatures similarly fell from 200 to 154 °C. The related nitrates (n = 8) were, however, thermally unstable and decomposition was observed in the columnar phase at about 50 °C. For the silver compounds, the PF_6^- salts were not reported but both the BF_4^- and NO_3^- salts were mesomorphic forming Col_h phases, the latter now showing greater thermal stability and clearing around 110–120 °C, albeit with decomposition. The nitrates melted at temperatures similar to their BF_4 analog, on average around 30–40 °C, except for the first member of the series which melted at 87.5 °C. The clearing points of the tetrafluoroborate salts fell from 196 to 144 °C with increasing n. Thus, in both silver and gold complexes, the tetrafluoroborate gave the widest range of mesophase (120–160 °C). The influence of the metals on the properties is not dramatic, as can be seen from the phase diagram (Figure 43) representing the thermal behavior of both the gold and silver tetrafluoroborate salts.

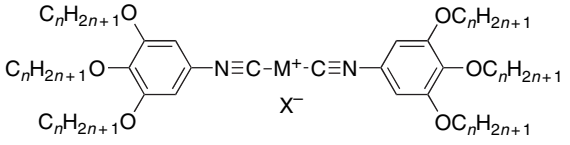

148

12.05.13.1.3 Mixed isonitrile acetylide complexes

Espinet and co-workers reported the gold complexes **149** (**149**: R = H, OC_nH_{2n+1}; n = 2, 4, 6, 8, 10; m = 6, 8, 10, 12) in which both an isonitrile and a substituted phenyl acetylene were bound across the gold(I) center.[310] Despite the non-mesomorphic nature of both ligands, the complexes consistently gave rise to SmA phases, usually between 100 and 200 °C depending on both chain lengths (n and m), although decomposition was a problem at high temperature; only the phenyl isonitrile derivatives (R = H) with chain length $n \leq 10$ carbons on the acetylide side were not mesomorphic. Interestingly, the melting points were found to systematically decrease as the length of the acetylide ligands (m) increased, at the expense of the chain length (n) of the isonitrile.

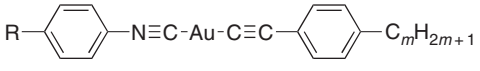

149

Takahashi and co-workers[311] carried out an interesting systematic study of related liquid-crystalline isonitrile gold(I) acetylide complexes in order to lower transition temperatures and avoid the decomposition processes usually

associated with such compounds. When both the ligands contained at least one aromatic ring such as **150** (**150**: Y = OCO, R = H), the complex was mesomorphic, showing mainly a SmA phase at 165 °C, with extensive decomposition. Introduction of a small lateral group (**150**: Y = COO, R = OEt) resulted in the lowering of the melting of the crystal to the SmA (Cr 142 SmA dec.), but still with some decomposition. However, when a larger lateral side chain was introduced (**150**: Y = COO, R = OC_6H_{13}), a nematic phase was induced instead (Cr 87.5 N 130 I); this time, no decomposition was detected. Complexes resulting from either an aromatic isonitrile and an aliphatic acetylene, **151**, or an aliphatic isonitrile and an aromatic acetylene, **152**, were also prepared. Compounds **151** appeared thermally unstable compared to complexes **150**, and showed SmA and N phases at low temperatures (below 130 °C). The type of phase and the mesophase stability were found to depend on the length of both the terminal and side chains. Thus, **151a** with R = OMe decomposed without showing a phase, whereas it showed an enantiotropic SmA phase for about 10 °C (**151a**: R = OEt; $n = 4, 5$), which changed to a small temperature range (less than 4 °C) nematic phase for larger side groups (**151a**: R = OPr; $n = 4, 5$); when both the terminal and lateral chains were elongated (**151a**: R = OPr, $n = 6$), the mesomorphism became metastable. Compound **151b** showed only a nematic phase, which was enantiotropic with a methoxy side group (Cr 78 N 108 I). Compounds **152** with linear terminal and octyl isonitrile chains showed enantiotropic nematic phases between 110 and 160 °C. Important reductions in clearing points (<100 °C), and to some extent in melting points (~80–100 °C), were obtained when the octyl isonitrile chain was branched; in these cases, the nematic phase stability was also reduced (Table 24). The complexes were thermally more stable than **151** and decomposition was observed less systematically.

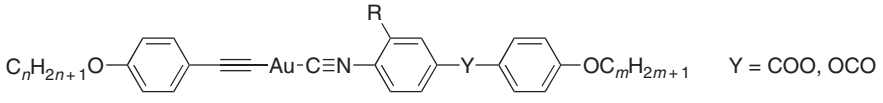

150

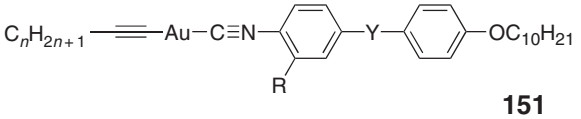

151a: Y = COO; R = OMe, OEt, OPr; n = 4–6
151b: Y = OOC; R = Et, OMe, OEt; n = 4

151

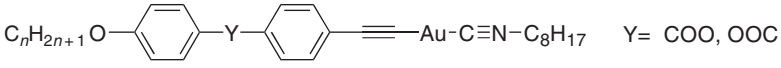

152

Other structural variations such as the introduction of a lateral chlorine atom on one ring of the phenyl benzoate moiety or the use of a branched terminal chain led to the depression of the transition temperatures concomitantly with the diminution of the nematic phase temperature range.

12.05.13.1.4 Mixed isonitrile phenyl complexes

The thermally, stable, liquid-crystalline perhalophenylgold(I) isocyanide complexes **153** have been thoroughly investigated by Espinet and co-workers.[312] Gold complexes (**153a–c**) (Figure 44) all showed a nematic phase at short chain lengths, N and SmA phases for intermediate chain length, and only a SmA phase for longer chain

Table 24 Influence of the ester group orientation and structure of the octyl isonitrile chain on the behavior of **152** ($n = 12$)

Y	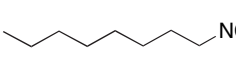	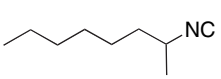	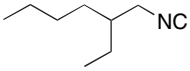
	Cr 110 N 156 dec.	Cr 101 (N 69) I	Cr 87 N 116 I
	Cr 133 N 163 dec.	Cr 77 (N 48) I	Cr 101 N 109 I

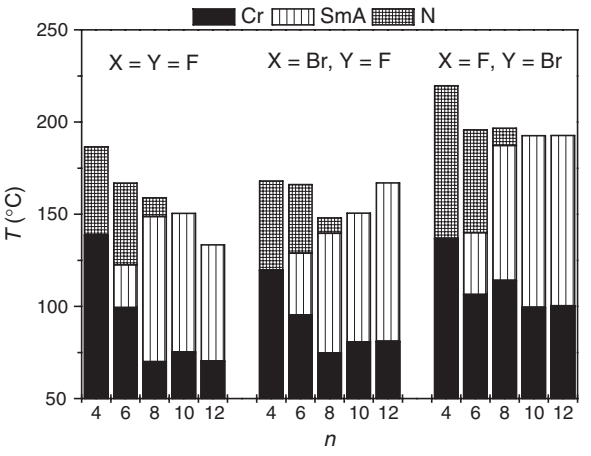

Figure 44 Mesomorphism of complexes **153a–153c**.

lengths. As observed by the authors, the variation in the thermal properties is regular, that is, both the melting and clearing transition temperatures decreased with increasing chain length to $n \geq 8$ where they are roughly constant. Moreover, the decrease in the transition temperatures with increasing n is small for **153c**, greater for **153b**, and very strong for **153a**. As a consequence, a change is produced in the sequence of melting and clearing temperature in the order **153c** > **153a** > **153b** for $n \leq 6$ and **153c** > **153b** > **153a** for $n \geq 8$ (Figure 44); these variations were explained in terms of polarization and polarizability arguments. The transition temperatures have been lowered, the mesomorphic range diminished, and the nematic phase enhanced when compared to the mesomorphic properties of the halogold complexes **142**. The mononuclear gold(III) compounds **153d** were thermally unstable and not investigated further. The use of a chiral chain affected mesomorphism quite drastically in compounds **153** (X = F, Y = Y, OC_nH_{2n+1} = O-(R)-2-butyl, OC_2H_5, $OC_{10}H_{21}$).[313] With one chiral chain in the *para*-position of the phenylene group, a broad N^* and monotropic TGBA and SmA ($n = 2$), or only an enantiotropic SmA ($n = 10$) mesophase was induced. Similarly, with one chiral chain attached on the isonitrile ligand, a broad N^* and monotropic SmA ($n = 2$) or only a enantiotropic SmA ($n = 10$) mesophase was formed, and the mesophase stability was slightly reduced. However, when both terminal chains were chiral, the three blue phases BPI, BPII, and BPIII were observed on cooling between the isotropic liquid and the N^* phase.

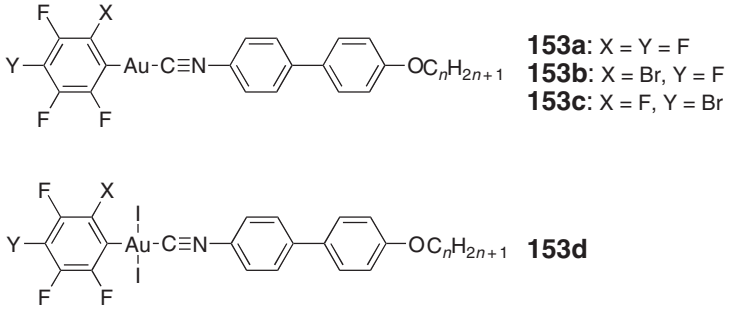

153

The related complexes **154**[314] and **155**[315] were also reported by Espinet and co-workers. Nine derivatives of **154**, whose mesomorphism was broadly similar, were prepared. Thus, for $m = 4$ and $n = 4$, 6, the complexes showed both SmA and nematic phases, while for $m = 4$ and $n = 8$, 10, the nematic phase disappeared and so only SmA was seen. For all complexes with $m = 8$ ($n = 4$, 6, 8, 10, 12), both SmC and SmA phases were seen. With one exception, the clearing points were above 200 °C, and overall mesomorphic ranges of up to 100 °C were found.

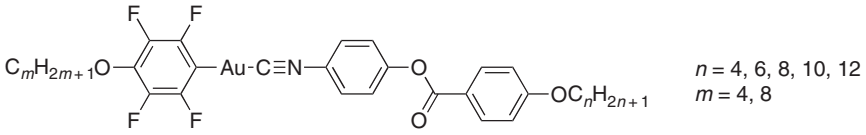

154

Five examples of **155** whose mesomorphism was dominated by the formation of the SmA phase with a N phase seen for one homolog and a SmC phase seen in three others were reported; clearing points were again above 200 °C. Short F···F interactions (2.66 Å) were found in the X-ray single-crystal structure of one homolog ($n = 4$, $m = 2$). The complexes were found to be fluorescent in the solid state and in solution, and to exhibit phosphorescence in the solid state and in frozen solution. The emission was also seen in the mesophase, although the intensity decreased with increasing temperature.

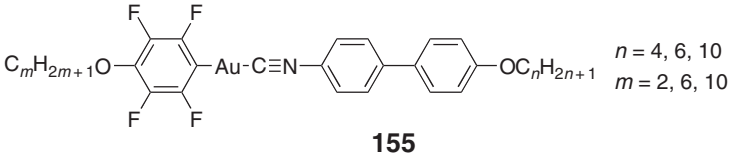

155

Complexes **156** were found[306] to show SmC and SmA phases; in binary mixtures with each other they were continuously miscible across the entire composition range and formed a solid solution on crystallization.

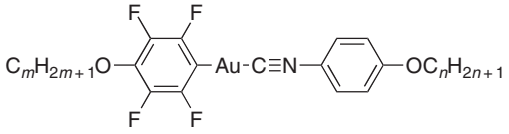

156a: $n = 6$, $m = 10$
156b: $n = 10$, $m = 6$

The dinuclear complexes **157a** and **157b**[312] all displayed a single nematic phase at high temperatures (Figure 45). This is attributed to the symmetric nature of these digold complexes, which means that the lateral, dipolar interactions (which normally stabilize smectic phases) cancel, favoring the nematic phase. As in the case of **153d**, the dinuclear gold(III) species **157c** and **157d** (**157c**: X = Br, I, $y = 1$; **157d**: X = Br, I, $y = 2$) decomposed upon thermal treatment to give the corresponding halogold(I) isocyanide complexes.

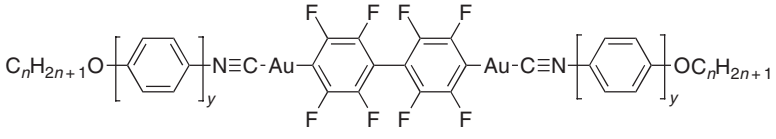

157a: $y = 1$
157b: $y = 2$

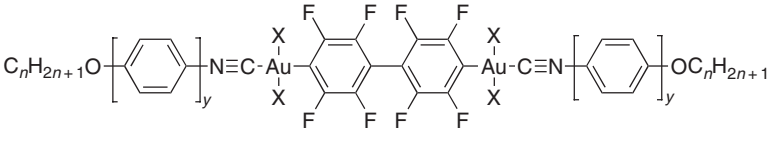

157c: $y = 1$
157d: $y = 2$

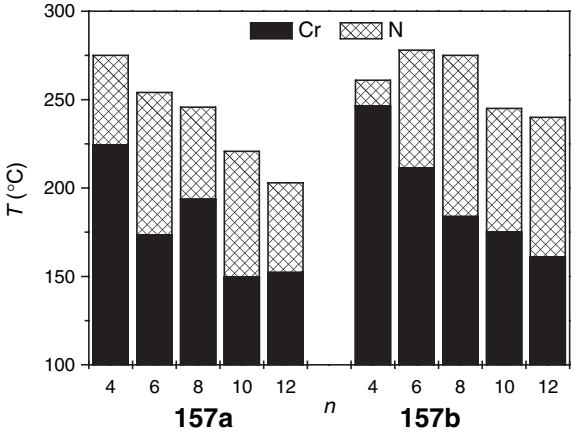

Figure 45 Thermal behavior of dinuclear complexes **157a** (left) and **157b** (right). Temperature varies with chain length.

12.05.13.2 Carbene Complexes

Takahashi and co-workers exploited the reactivity of bound isonitriles with aliphatic alcohol (ethanol, propanol, butanol, pentanol) and amines by synthesizing various gold(I) carbene complexes **158**.[316,317] The complexes existed as one of two geometric isomers which were separated in some cases, and which interconverted in solution. Somewhat in common with the gold systems bearing lateral alkoxy chains (see above), these new carbenes also showed reduced transition temperatures (110–160 °C) with little difference between the two isomers. The mesomorphism was again dominated by the SmA phase over a range of only around 15 °C. Within the series of carbene complexes having amino side groups, only those with a primary amine were mesomorphic (R = H, R^1 = Pr, Bu), showing a SmA phase before decomposition. Note also the interesting case of a dinuclear gold–carbene complex, where the two carbene species are linked via a hexyl diamine bridge, which was mesomorphic but decomposed below its clearing temperature (Cr 211 S dec.).

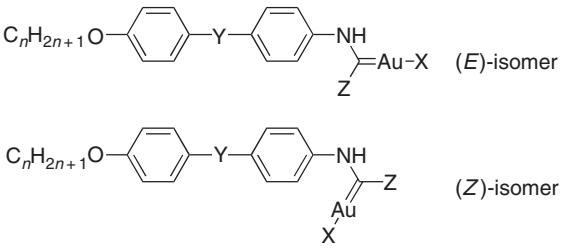

X = Cl, I; Y = OOC, COO, C≡C
Z = OC_mH_{2m+1}, NRR^1

158

Smectic mesophases have been claimed for other gold(I) **159**[318] carbene complexes based on 1,3-dialkylbenzimidazol-2-ylidene and 1,3-dialkylimidazol-2-ylidene. However, examination of the X-ray diffraction data in combination with the large clearing enthalpies suggest that these materials are highly ordered and may be better described as crystals. Related Pd(II) complexes have been described **88**.[164]

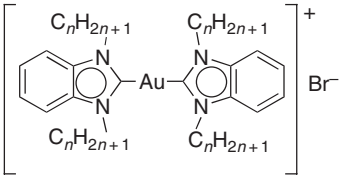

159

12.05.14 Organometallic Liquid Crystals of the Group 12 Elements

12.05.14.1 Diphenylmercury(II) Complexes

It is commonly accepted that one of the first publications on metallomesogens was by Vorländer,[319] who reported a number of mercury-based mesomorphic materials,[320] such as the symmetrical Schiff-base complexes of diarylmercury(II) (**160a**: R = H, NO_2, Me, OMe, OEt) and the related, asymmetric, monoaryl mercury chloride complexes **160b**. Both series of organometallic compounds exhibited high-temperature smectic phases.

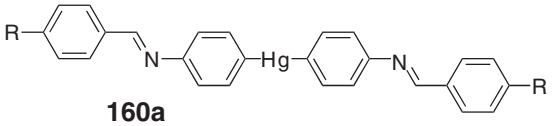

160a

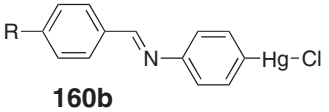

160b

Organophenylene mercury complexes, such as bis(4-hexyloxy-4′-phenyl)mercury(II)[321] and some bis(4-alkoxy-4″-biphenyl)mercury(II)[322] (**161**: $x = 1, 2$) were also reported to be mesomorphic. The former ($x = 1$) exhibited a monotropic SmA phase, as confirmed by an X-ray diffraction study (Cr 119 (SmA 97) I), whereas the strong thermal instability of the latter ($x = 2$) complexes at elevated temperature hampered an accurate characterization of the mesomorphism.

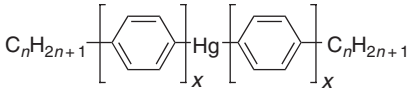

161

12.05.14.2 *ortho*-Metallated Complexes

Using azoxy ligands bearing chiral groups, Ghedini reported the formation of *ortho*-metallated complexes of mercury(II) (**162**: $n = 6, 10$), and demonstrated materials with a room-temperature SmC^* phase.[323] These complexes existed as an equimolar mixture of two isomers due to the non-selective metallation. Prior to the metallation both ligands were room-temperature liquid crystals: N^* 34 I and Cr 24.5 SmC^* 37 N^* 47 I for $n = 6$ and 10, respectively. The mesophase stability was enhanced upon complexation, and both complexes exhibited a single SmC^* up to 56 and 63.5 °C, respectively.

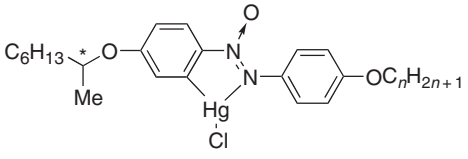

162

Strangely, closely related *ortho*-mercurated derivatives of dialkyl and dialkoxy azobenzene mesogens[324,325] complexes were not mesomorphic.

12.05.14.3 Diacetylide Complexes of Mercury(II)

Simple mercury(II) acetylide complexes were reported by Yang and Wen **163**,[326] and showed N and/or SmA phases between 70 and 90 °C up to ca. 120 °C.

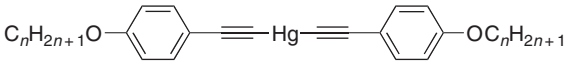

163

Yelamaggad *et al.*[327] reported the more elaborate acetylide complexes **164** ($n = 3, 4, 5, 7$), all of which showed a chiral nematic phase due to the presence of the chiral cholesteryl moiety. For all complexes, decomposition occurred somewhere above 200 °C—the lowest melting point was seen for the complexes with the two heptamethylene spacers.

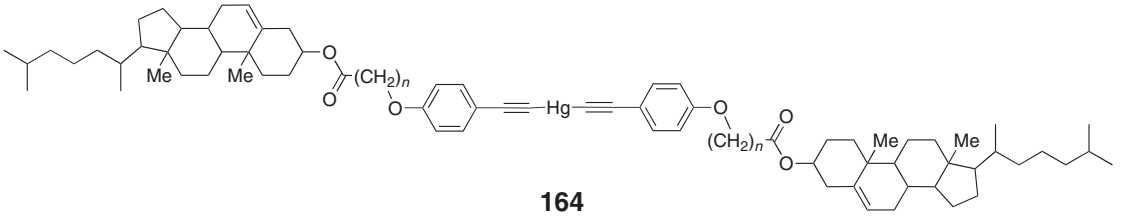

164

Two mesomorphic tetracatenar and one hexacatenar Hg(II) acetylides were reported (**165**: R = H or C_nH_{2n+1}).[328] The two tetracatenar complexes ($n = 5, 12$) exhibited a columnar phase, between 73 and 125 °C for the short-chain-length compound, and from room temperature up to 106 °C for the longer-chain derivative. The hexacatenar material ($n = 5$) displayed an unidentified phase between 70 and 122 °C that was probably columnar due to the structural similarity with the previous compounds. These mesophase assignments were performed by microscopy only, and exact phase symmetry was not determined.

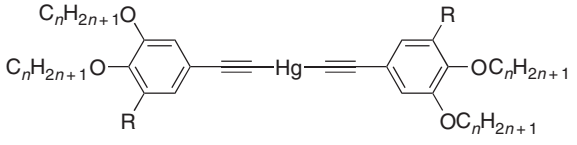

165

The synthesis of discotic, mercury-bridged, triphenylene dimers (**166**: R = OC_5H_{11}, $O(CH_2)_2CHMe(CH_2)_3CHMe_2$) was reported by Kumar *et al.*[329] The bis(2,3,6,7,10-pentapentyloxy-triphenylene-11-ethynyl)mercury(II) complex exhibited a highly viscous mesophase between 150 and 210 °C, and extensive decomposition precluded its identification. One of the pentyloxy chains was then replaced by the branched citronellyl chain, in the hope of reducing the transition temperatures. This new complex cleared into the isotropic liquid at 186 °C, but on cooling, a monotropic mesophase appeared at 185 °C, which transformed into a crystalline phase at 180 °C. On the basis of its "schlieren" texture, the mesophase was identified as N_D, although, curiously, the phase was not assigned as chiral despite the presence of the asymmetric citronellyl chains.

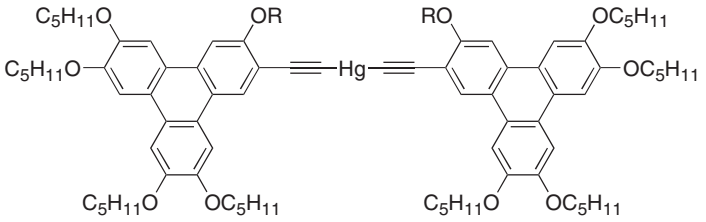

166

12.05.15 Concluding Comments

The literature of organometallic liquid crystals is somewhat more limited than that of liquid-crystalline coordination compounds and is dominated by a relatively small number of general motifs—most spectacularly by *ortho*-metallated complexes of palladium(II). One reason for this is no doubt related to the fact that while transition metal–carbon bonds are generally stronger than those of their main group counterparts (where there are precious few examples of liquid crystals), they are kinetically somewhat more labile and so stability to temperature, air, and moisture can be a significant issue. Nonetheless, ligand design has been most imaginative and some rather fascinating collections of liquid-crystal properties have been assembled.

References

1. Giroud-Godquin, A.-M.; Maitlis, P. M. *Angew. Chem., Int. Ed. Engl.* **1991**, *30*, 375–402.
1a. Ohta, K.; Yamamoto, I. *J. Synth. Org. Chem.* **1991**, *49*, 486–496.
1b. Espinet, P.; Esteruelas, M. A.; Oro, L. A.; Serrano, J.-L.; Sola, E. *Coord. Chem. Rev.* **1992**, *117*, 215–274.
1c. Bruce, D. W. Metal-containing Liquid Crystals. In *Inorganic Materials*, 1st ed.; Bruce, D. W., O'Hare, D., Eds.; Wiley: Chichester, 1992; Chapter 8, pp 405–490.
1d. Bruce, D. W. Metal-containing Liquid Crystals. In *Inorganic Materials*, 2nd ed.; Bruce, D. W., O'Hare, D., Eds.; Wiley: Chichester, 1996; Chapter 8, pp 429–522.
1e. Hudson, S. A.; Maitlis, P. M. *Chem. Rev.* **1993**, *93*, 861–885.
1f. Polishchuk, A.; Timofeeva, T. V. *Russ. Chem. Rev.* **1993**, *62*, 291–321.
1g. Bruce, D. W. *J. Chem. Soc., Dalton Trans.* **1993**, 2983–2989.
1h. Deschenaux, R.; Goodby, J. W. In *Ferrocenes: Homogeneous Catalysis, Organic Synthesis, Materials Sciences*; Togni, A., Hayashi, T., Eds.; VCH: Weinheim, 1995; Chapter 9, pp 471–495.
1i. Zhang, L. F.; Huang, S. D. *Huaxue Tonghao* **1995**, *2*, 7–16.
1j. Neve, F. *Adv. Mater.* **1996**, *8*, 277–289.
1k. Giroud-Godquin, A.-M. Metal-containing Liquid Crystals. In *Handbook of Liquid Crystals*; Demus, D., Goodby, J., Gray, G. W., Spiess, H.-W., Vill, V., Eds.; Wiley-VCH: Weinheim, 1998; Chapter XIV, pp 901–932.
1l. Donnio, B.; Bruce, D. W. *Struct. Bond.* **1999**, *95*, 193–247.
1m. Collinson, S. R.; Bruce, D. W. Metallomesogens-supramolecular Organization of Metal Complexes in Fluid Phases. In *Transition Metals in Supramolecular Chemistry*; Sauvage, J. P., Ed. Wiley: Chichester, 1999; Chapter 7, pp 285–369.
1n. Molochko, V. A.; Rukk, N. S. *Russ. J. Coord. Chem.* **2000**, *26*, 829–846.
1o. Binnemans, K.; Görller-Walrand, C. *Chem. Rev.* **2002**, *102*, 2303–2345.
1p. Donnio, B. *Curr. Opin. Colloid Interface Sci.* **2002**, *7*, 371–394.
1q. Date, R. W.; Fernandez Iglesias, E.; Rowe, K. E.; Elliott, J. M.; Bruce, D. W. *Dalton Trans.* **2003**, 1914–1931.
2. Serrano, J. L., Ed. *Metallomesogens: Synthesis, Properties and Applications*; VCH: Weinheim, 1995.
3. Donnio, B.; Guillon, D.; Deschenaux, R.; Bruce, D. W. In *Comprehensive Coordination Chemistry II*; McCleverty, J. A., Meyer, T. J., Eds.; Elsevier: Oxford, UK, 2003, Vol. 7, Chapter 7.9, pp 357–627.
4. Demus, D., Goodby, J., Gray, G. W., Spiess, H.-W., Vill, V., Eds.; *Handbook of Liquid Crystals*; Wiley-VCH: Weinheim, 1998.
5. Oriol, L.; Serrano, J.-L. *Adv. Mater.* **1995**, *7*, 348–369.
5a. Oriol, L.; Piñol, M.; Serrano, J.-L. *Prog. Polym. Sci.* **1997**, *22*, 873–911.
6. Reinitzer, F. *Monatsch. Chem.* **1888**, *9*, 421–441.
7. Virchow, R. *Virchows Arch.* **1854**, *6*, 571.
7a. Vill, V. *Mol. Cryst., Liq. Cryst.* **1992**, *213*, 67–71.
8. Heintz, W. *J. Prakt. Chem.* **1855**, *66*, 1–51.
9. Friedel, G. *Ann. Phys.* **1922**, *18*, 273–505.
10. Coates, D.; Gray, G. W. *Microsc.* **1976**, *24*, 117–150.
11. Schadt, M.; Helfrich, W. *Appl. Phys. Lett.* **1971**, *18*, 127–128.
12. Toyne, K. J. Liquid Crystal Behavior in Relation to Molecular Structure. In *Thermotropic Liquid Crystals*; Gray, G. W., Ed.; Wiley: Chichester, 1987; Chapter 2, pp 28–63.
13. Vill, V. *Liqcryst 2.0 - Database of Liquid Crystalline Compounds*, LCI: Hamburg (see also: http://liqcryst.chemie.uni-hamburg.de/).
14. Hird, M.; Toyne, K. J. *Mol. Cryst., Liq. Cryst.* **1998**, *323*, 1–67.
15. Demus, D. *Liq. Cryst.* **1989**, *5*, 75–110.
16. Peltz, G.; Diele, S.; Weissflog, W. *Adv. Mater.* **1999**, *11*, 707–724.
17. Tschierske, C. *J. Mater. Chem.* **1998**, *8*, 1485–1508.
17a. Tschierske, C. *J. Mater. Chem.* **2001**, *11*, 2647–2671.
17b. Tschierske, C. *Annu. Rep. Prog. Chem., Sect. C* **2001**, *97*, 191–267.
18. Goodby, J. W. *Science* **1986**, *231*, 350–355.
19. McDonnell, D. G. Thermochromic Cholesteric Liquid Crystals. In *Thermotropic Liquid Crystals*; Gray, G. W., Ed.; Wiley: Chichester, 1987; Chapter 5, pp 120–144.
20. Leadbetter, A. J. Structural Classification of Liquid Crystals. This classification was proposed in *Thermotropic Liquid Crystals*; Gray, G. W., Ed.; Wiley: Chichester, 1987; Chapter 1, pp 1–27.
21. Gray, G. W.; Goodby, J. W. *Smectic Liquid Crystals*; *Textures and Structures*; Leonard Hill: Glasgow, 1984.
22. Cladis, P. E. In *Handbook of Liquid Crystals*; Demus, D., Goodby, J., Gray, G. W., Spiess, H.-W., Vill, V., Eds.; Wiley-VCH: Weinheim, 1998, Vol. 1, Chapter VII, pp 391–405.
23. Chandrasekhar, S.; Sadashiva, B. K.; Suresh, K. A. *Pramana* **1977**, *9*, 471–480.
24. Skoulios, A. *Adv. Colloid. Interface Sci.* **1967**, *1*, 79–110.
25. Levelut, A. M. *J. Chim. Phys.* **1983**, *80*, 149–161.
26. Praefcke, K.; Singer, D.; Kohne, B.; Ebert, M.; Liebmann, M.; Wendorff, J. H. *Liq. Cryst.* **1991**, *10*, 147–159.
27. Bengs, H.; Karthaus, O.; Ringsdorf, H.; Baehr, C.; Ebert, M.; Wendorff, J. H. *Liq. Cryst.* **1991**, *10*, 161–168.
28. Malthête, J.; Nguyen, H.-T.; Destrade, C. *Liq. Cryst.* **1993**, *13*, 171–187.
29. Nguyen, H. T.; Destrade, C.; Malthête, J. *Adv. Mater.* **1997**, *9*, 375–388.
30. Guillon, D.; Heinrich, B.; Ribeiro, A. C.; Cruz, C.; Nguyen, H.-T. *Mol. Cryst. Liq. Cryst.* **1998**, *317*, 51–64.
31. Fazio, D.; Mongin, C.; Donnio, B.; Galerne, Y.; Guillon, D.; Bruce, D. W. *J. Mater. Chem.* **2001**, *11*, 2852–2863.
32. Donnio, B.; Heinrich, B.; Allouchi, H.; Kain, J.; Diele, S.; Guillon, D.; Bruce, D. W. *J. Am. Chem. Soc.* **2004**, *126*, 15258–15268.
33. Tiddy, G. J. T. In *Modern Trends of Colloid Science in Chemistry and Biology*; Birkhauser Verlag: Basel, 1985, p 148.
33a. Tiddy, G. J. T. *Phys. Rep.* **1980**, *57*, 1–46.
34. Tanford, C. *The Hydrophobic Effect*, 2nd ed.; Wiley: New York, 1980.
35. Israelachvili, J. N.; Mitchell, D. J.; Ninham, B. W. *J. Chem. Soc., Faraday Trans. II* **1976**, *72*, 1525–1568.

36. Seddon, J. M.; Templer, R. H. *Philos. Trans. R. Soc. London, Ser. A* **1993**, *344*, 377–401.
37. Luzzati, V.; Spegt, P. A. *Nature* **1967**, *215*, 701–703.
38. Charvolin, J.; Sadoc, J.-F. *J. Phys.* **1988**, *49*, 521–526.
38a. Charvolin, J.; Sadoc, J.-F. *Philos. Trans. R. Soc. London, Ser. A* **1996**, *354*, 2173–2192.
39. Hyde, S. T. Identification of Lyotropic Liquid Crystalline Mesophases. In *Handbook of Applied Surface and Colloid Chemistry*; Holmberg, K., Ed.; Wiley: Chichester UK, 2002; Chapter 16, pp 299–332.
40. See for example: Valenti, R.; Sartirania, M. L. *Il Nuovo. Cim. D* **1984**, *3*, 104.
41. Livolant, F.; Leforestier, A. *Prog. Polym. Sci.* **1996**, *21*, 1115–1164.
42. Attwood, T. K.; Lydon, J. E.; Hall, C.; Tiddy, G. J. T. *Liq. Cryst.* **1990**, *7*, 657–668.
43. Lydon, J. Chromonics. In *Handbook of Liquid Crystals*; Demus, D., Goodby, J., Gray, G. W., Spiess, H.-W., Vill, V., Eds.; Wiley-VCH: Weinheim, 1998; Chapter XVIII, pp 981–1007.
44. Praefcke, K.; Holbrey, J. D.; Usol'tseva, N. *Mol. Cryst. Liq. Cryst.* **1996**, *288*, 189–200.
45. De Gennes, P. G. *The Physics of Liquid Crystals*; Oxford University Press: Oxford, 1974.
45a. De Gennes, P. G.; Prost, J. *The Physics of Liquid Crystals*; Clarendon Press: Oxford, 1993.
46. Sage, I. Materials Requirements for Nematic and Chiral Nematic Electrooptical Displays. In *Thermotropic Liquid Crystals*; Gray, G. W., Ed.; Wiley: Chichester, 1987; Chapter 3, pp 64–98.
47. Diele, S.; Grande, S.; Kain, J.; Pelzl, G.; Weissflog, W. *Mol. Cryst. Liq. Cryst.* **2001**, *362*, 111–132.
48. Young, W. R.; Haller, I.; Green, D. C. *Mol. Cryst. Liq. Cryst.* **1971**, *13*, 305–321.
49. Schulte, J. L.; Laschat, S.; Schulte-Ladbeck, R.; von Armin, V.; Schneider, A.; Finkelmann, H. *J. Organomet. Chem.* **1998**, *552*, 171–176.
50. Campillos, E.; Deschenaux, R.; Levelut, A. M.; Ziessel, R. *J. Chem. Soc., Dalton Trans.* **1996**, 2533–2536.
51. Yang, J.; Huang, D.; Ding, F.; Zhao, W.; Zhang, L. *Mol. Cryst. Liq. Cryst.* **1996**, *281*, 51–56.
52. Schmidt, S.; Lattermann, G.; Kleppinger, R.; Wendorff, J. H. *Liq. Cryst.* **1994**, *16*, 693–702.
53. Walf, G. H.; Benda, R.; Litterst, F. J.; Stebani, U.; Schmidt, S.; Lattermann, G. *Chem. Eur. J.* **1998**, *4*, 93–99.
54. Rowe, K. E.; Bruce, D. W. *J. Mater. Chem.* **1998**, *8*, 331–341.
55. Rowe, K. E.; Bruce, D. W. *J. Chem. Soc., Dalton Trans.* **1996**, 3913–3915.
56. Rowe, K. E.; Bruce, D. W. *Mol. Cryst. Liq. Cryst.* **1999**, *326*, 15–40.
57. Rowe, K. E. PhD Thesis, University of Sheffield, 1996.
58. Willis, K. E.; Ungar, G. unpublished observations.
59. Morrone, S.; Harrison, G.; Bruce, D. W. *Adv. Mater.* **1995**, *7*, 665–667.
60. Morrone, S.; Guillon, D.; Bruce, D. W. *Inorg. Chem.* **1996**, *35*, 7041–7048.
61. Bruce, D. W. *Adv. Mater.* **1994**, *6*, 699–701.
62. Bruce, D. W.; Liu, X. H. *J. Chem. Soc., Chem. Commun.* **1994**, 729–730.
63. Bruce, D. W.; Liu, X. H. *Liq. Cryst.* **1995**, *18*, 165–166.
64. Liu, X. H.; Heinrich, B.; Manners, I.; Guillon, D.; Bruce, D. W. *J. Mater. Chem.* **2000**, *10*, 637–644.
65. Liu, X. H.; Manners, I.; Bruce, D. W. *J. Mater. Chem.* **1998**, *8*, 1555–1560.
66. Liu, X. H.; Abser, M. N.; Bruce, D. W. *J. Organomet. Chem.* **1998**, *551*, 271–280.
66a. Liu, X. H.; Abser, M. N.; Bruce, D. W. *J. Organomet. Chem. Publisher's erratum* **1999**, *577*, 150–152.
67. Guillevic, M. A.; Bruce, D. W. *Liq. Cryst.* **2000**, *27*, 153–156.
68. Guillevic, M. A.; Gelbrich, T.; Hursthouse, M. B.; Bruce, D. W. *Mol. Cryst. Liq. Cryst.* **2001**, *362*, 147–170.
69. Guillevic, M. A.; Danks, M. J.; Harries, S. K.; Collinson, S. R.; Pidwell, A. D.; Bruce, D. W. *Polyhedron* **2000**, *19*, 249–257.
70. Guillevic, M. A.; Light, M. E.; Coles, S. J.; Gelbrich, T.; Hursthouse, M. B.; Bruce, D. W. *J. Chem. Soc., Dalton Trans.* **2000**, 1437–1445.
71. Ziminski, L.; Malthête, J. *J. Chem. Soc., Chem. Commun.* **1990**, 1495–1496.
72. Jacq, P.; Malthête, J. *Liq. Cryst.* **1996**, *21*, 291–293.
73. Huang, D. J.; Yang, J.; Zhang, L. F.; Liu, Y.; Xiang, S. P. *Hecheng Huaxue* **1994**, *2*, 1–3.
74. Huang, D.; Yang, J.; Wan, W.; Ding, F.; Zhang, L. *Mol. Cryst. Liq. Cryst.* **1996**, *281*, 43–49.
75. Coco, S.; Espinet, P.; Marcos, E. *J. Mater. Chem.* **2000**, *10*, 1297–1302.
76. Deschenaux, R.; Donnio, B.; Rheinwald, G.; Stauffer, F.; Suss-Fink, G.; Velker, J. *J. Chem. Soc., Dalton Trans.* **1997**, 4351–4355.
77. Bruneau, C.; Dixneuf, P. H. *Chem. Commun.* **1997**, 507–512.
78. Barral, M. C.; Jiménez-Aparicio, R.; Priego, J. L.; Royer, E. C.; Torres, M. R.; Urbanos, F. A. *Inorg. Chem. Commun.* **1999**, *2*, 153–155.
79. Kim, D. J.; Oh, N. K.; Lee, M.; Choi, M. G. *Mol. Cryst. Liq. Cryst.* **1996**, *280*, 129–134.
80. Togni, A., Hayashi, T., Eds.; *Ferrocenes: Homogeneous Catalysis, Organic Synthesis, Materials Science*, VCH: Weinheim, 1995.
81. Malthête, J.; Billard, J. *Mol. Cryst. Liq. Cryst.* **1976**, *34*, 117–121.
82. Imrie, C.; Engelbrecht, P.; Loubser, C.; McCleland, C. W. *Appl. Organomet. Chem.* **2001**, *15*, 1–15.
82a. Imrie, C.; Loubser, C.; Engelbrecht, P.; McCleland, C. W.; Zheng, Y. *J. Organomet. Chem.* **2003**, *665*, 48–64.
83. Nakamura, N.; Hanasaki, T.; Onoi, H.; Oida, T. *Chem. Express* **1993**, *8*, 467–470.
83a. Nakamura, N.; Hanasaki, T.; Onoi, H. *Mol. Cryst. Liq. Cryst.* **1993**, *225*, 269–277.
83b. Hanasaki, T.; Ueda, M.; Nakamura, N. *Mol. Cryst. Liq. Cryst.* **1993**, *237*, 329–336.
83c. Nakamura, N.; Onoi, H.; Oida, T.; Hanasaki, T. *Mol. Cryst. Liq. Cryst.* **1994**, *257*, 43–48.
83d. Nakamura, N.; Oida, T.; Shonago, M.; Onoi, H.; Hanasaki, T. *Mol. Cryst. Liq. Cryst.* **1995**, *265*, 1–8.
83e. Nakamura, N.; Takayama, T. *Mol. Cryst. Liq. Cryst.* **1997**, *307*, 145–154.
83f. Nakamura, N.; Setodoi, S. *Mol. Cryst. Liq. Cryst.* **1998**, *312*, 253–261.
83g. Nakamura, N.; Setodoi, S. *Mol. Cryst. Liq. Cryst.* **1998**, *319*, 173–181.
83h. Nakamura, N.; Oida, T. *Mol. Cryst. Liq. Cryst.* **1999**, *326*, 55–64.
83i. Nakamura, N.; Setodoi, S. *Mol. Cryst. Liq. Cryst.* **1999**, *326*, 177–187.
83j. Nakamura, N.; Setodoi, S. *Mol. Cryst. Liq. Cryst.* **1999**, *333*, 151–163.
83k. Nakamura, N.; Setodoi, S.; Hanasaki, T. *Mol. Cryst. Liq. Cryst.* **2000**, *350*, 93–101.
83l. Nakamura, N.; Maekawahara, H.; Hanasaki, T.; Yamaguchi, T. *Mol. Cryst. Liq. Cryst.* **2000**, *352*, 125–132.
83m. Nakamura, N.; Takahashi, T.; Uno, K.; Hanasaki, T. *Mol. Cryst. Liq. Cryst.* **2002**, *383*, 27–35.
84. Zhao, K.-Q.; Hu, P.; Xu, H.-B.; Wan, W.; Zhou, Z.-Y.; Zhang, L.-F. *Mol. Cryst. Liq. Cryst.* **2001**, *364*, 759–768.
85. Deschenaux, R.; Marendaz, J.-L.; Santiago, J.; Goodby, J. W. *Helv. Chim. Acta* **1995**, *78*, 1215–1218.

86. Loubser, C.; Imrie, C. *Adv. Mater.* **1993**, *5*, 45–47.
86a. Loubser, C.; Imrie, C. *J. Chem. Soc., Perkin Trans. 2* **1997**, 399–409.
87. Galyametdinov, Yu. G.; Kadkin, O. N.; Ovchinnikov, I. V. *Bull. Acad. Sci. USSR, Div. Chem. Sci.* **1992**, *41*, 316–321.
87a. Galyametdinov, Yu. G.; Kadkin, O. N.; Ovchinnikov, I. V. *Izv. Akad. Nauk. SSSR, Ser. Khim.* **1992**, 402–407.
87b. Galyametdinov, Yu. G.; Kadkin, O. N.; Prosvirin, A. V. *Russ. Chem. Bull.* **1994**, *43*, 887–891.
87c. Galyametdinov, Yu. G.; Kadkin, O. N.; Prosvirin, A. V. *Izv. Akad. Nauk. Ser. Khim.* **1994**, 941–945.
88. Kadkin, O. N.; Galyametdinov, Yu. G.; Rakhmatullin, A. I.; Mavrin, V. Yu. *Russ. Chem. Bull.* **1999**, *48*, 379–381.
88a. Kadkin, O. N.; Galyametdinov, Yu. G.; Rakhmatullin, A. I.; Mavrin, V. Yu. *Izv. Akad. Nauk., Ser. Khim.* **1999**, 381–383.
89. Kadkin, O.; Galyametdinov, Y.; Rakhmatullin, A. *Mol. Cryst. Liq. Cryst.* **1999**, *332*, 109–118.
90. Seshadri, T.; Haupt, H.-J. *J. Mater. Chem.* **1998**, *8*, 1345–1350.
91. Deschenaux, R.; Schweissguth, M.; Levelut, A.-M. *Chem. Commun.* **1996**, 1275–1276.
91a. Deschenaux, R.; Schweissguth, M.; Vilches, M.-T.; Levelut, A.-M.; Hautot, D.; Long, G. J.; Luneau, D. *Organometallics* **1999**, *18*, 5553–5559.
92. Imrie, C.; Loubser, C. *J. Chem. Soc., Chem. Commun.* **1994**, 2159–2160.
93. Seshadri, T.; Haupt, H.-J. *Chem. Commun.* **1998**, 735–736.
94. Cook, M. J.; Cooke, G.; Jafari-Fini, A. *J. Chem. Soc., Chem. Commun.* **1995**, 1715–1716.
95. Bhatt, J.; Fung, B. M.; Nicholas, K. M.; Poon, C.-D. *J. Chem. Soc., Chem. Commun.* **1988**, 1439.
95a. Khan, M. A.; Bhatt, J. C.; Fung, B. M.; Nicholas, K. M. *Liq. Cryst.* **1989**, *5*, 285–290.
96. Bhatt, J.; Fung, B. M.; Nicholas, K. M. *J. Organomet. Chem.* **1991**, *413*, 263–268.
96a. Bhatt, J.; Fung, B. M.; Nicholas, K. M. *Liq. Cryst.* **1992**, *12*, 263–272.
97. Singh, P.; Rausch, M. D.; Lenz, R. W. *Liq. Cryst.* **1991**, *9*, 19–26.
98. Reddy, K. P.; Brown, T. L. *Liq. Cryst.* **1992**, *12*, 369–376.
99. Hanasaki, T.; Ueda, M.; Nakamura, N. *Mol. Cryst. Liq. Cryst.* **1994**, *250*, 257–267.
99a. Nakamura, N.; Mizoguchi, R.; Ueda, M.; Hanasaki, T. *Mol. Cryst. Liq. Cryst.* **1998**, *312*, 127–136.
99b. Hanasaki, T.; Matsushita, K.; Wanatabe, T.; Enomoto, S.; Sato, Y. *Mol. Cryst. Liq. Cryst.* **2000**, *351*, 103–110.
100. Polishchuk, A. P.; Timofeeva, T. V.; Antipin, M. Yu.; Struchkov, Yu. T.; Galyametdinov, Yu. G.; Ovchinnikov, I. V. *Sov. Phys. Crystallogr.* **1992**, *37*, 371–375.
100a. Polishchuk, A. P.; Timofeeva, T. V.; Antipin, M. Yu.; Struchkov, Yu. T.; Galyametdinov, Yu. G.; Ovchinnikov, I. V. *Kristallografiya* **1992**, *37*, 705–711.
100b. Galyametdinov, Yu. G.; Kadkin, O. N.; Gavrilov, V. I.; Tinchurina, L. M. *Russ. Chem. Bull.* **1995**, *44*, 350–353.
100c. Galyametdinov, Yu. G.; Kadkin, O. N.; Gavrilov, V. I.; Tinchurina, L. M. *Izv. Akad. Nauk., Ser. Khim.* **1995**, 358–361.
100d. Rochev, V. Ya; Bekesev, V. G. *J. Radioanalyt. Nucl. Chem.* **1995**, *190*, 333–340.
101. Deschenaux, R.; Marendaz, J.-L.; Santiago, J. *Helv. Chim. Acta* **1993**, *76*, 865–876.
102. Deschenaux, R.; Santiago, J. *J. Mater. Chem.* **1993**, *3*, 219–220.
103. Deschenaux, R.; Rama, M.; Santiago, J. *Tetrahedron Lett.* **1993**, *34*, 3293–3296.
104. Donnio, B.; Seddon, J. M.; Deschenaux, R. *Organometallics* **2000**, *19*, 3077–3081.
105. Deschenaux, R.; Marendaz, J.-L. *J. Chem. Soc., Chem. Commun.* **1991**, 909–910.
105a. Deschenaux, R.; Kosztics, I.; Marendaz, J.-L.; Stoeckli-Evans, H. *Chimia* **1993**, *47*, 206–210.
106. Deschenaux, R.; Santiago, J.; Guillon, D.; Heinrich, B. *J. Mater. Chem.* **1994**, *4*, 679–682.
107. Deschenaux, R.; Kosztics, I.; Nicolet, B. *J. Mater. Chem.* **1995**, *5*, 2291–2295.
108. Deschenaux, R.; Santiago, J. *Tetrahedron Lett.* **1994**, *35*, 2169–2172.
109. Chuard, T.; Cowling, S. J.; Fernandez-Ciurleo, M.; Jauslin, I.; Goodby, J. W.; Deschenaux, R. *Chem. Commun.* **2000**, 2109–2110.
110. Brettar, J.; Bürgi, T.; Donnio, B.; Guillon, D.; Klappert, R.; Scharf, T.; Deschenaux, R. *Adv. Funct. Mater.* **2006**, *16*, 260–267.
111. Wagner, G.; Herrmann, R. In *Ferrocenes: Homogeneous Catalysis, Organic Synthesis, Materials Science*; Togni, A., Hayashi, T., Eds.; VCH: Weinheim; 1995; pp 173–218.
112. Werner, A.; Friedrichsen, W. *J. Chem. Soc., Chem. Commun.* **1994**, 365–366.
113. Thompson, N. J.; Goodby, J. W.; Toyne, K. J. *Liq. Cryst.* **1993**, *13*, 381–402.
114. Andersch, J.; Diele, S.; Tschierske, C. *J. Mater. Chem.* **1996**, *6*, 1465–1468.
115. Deschenaux, R.; Monnet, F.; Serrano, E.; Turpin, F.; Levelut, A.-M. *Helv. Chim. Acta* **1998**, *81*, 2072–2077.
116. Seo, J.-S.; Yoo, Y.-S.; Choi, M.-G. *J. Mater. Chem.* **2001**, *11*, 1332–1338.
117. Massiot, P.; Impéror-Clerc, M.; Veber, M.; Deschenaux, R. *Chem. Mater.* **2005**, *17*, 1946–1951.
118. Chuard, T.; Deschenaux, R. *Chimia* **2003**, *57*, 597–600.
119. Deschenaux, R.; Serrano, E.; Levelut, A.-M. *Chem. Commun.* **1997**, 1577–1578.
120. Dardel, B.; Deschenaux, R.; Even, M.; Serrano, E. *Macromolecules* **1999**, *32*, 5193–5198.
121. Deschenaux, R.; Even, M.; Guillon, D. *Chem. Commun.* **1998**, 537–538.
122. Carano, M.; Chuard, T.; Deschenaux, R.; Even, M.; Marcaccio, M.; Paolucci, F.; Prato, M.; Roffia, S. *J. Mater. Chem.* **2002**, *12*, 829–833.
123. Even, M.; Heinrich, B.; Guillon, D.; Guldi, D. M.; Prato, M.; Deschenaux, R. *Chem. Eur. J.* **2001**, *7*, 2595–2604.
124. Campidelli, S.; Vázquez, E.; Milic, D.; Prato, M.; Barberá, J.; Guldi, D. M.; Marcaccio, M.; Paolucci, D.; Paolucci, F.; Deschenaux, R. *J. Mater. Chem.* **2004**, *14*, 1266–1272.
125. Trzaska, S. T.; Swager, T. M. *Chem. Mater.* **1998**, *10*, 438–443.
126. Poelsma, N. S.; Maitlis, P. M. *J. Organomet. Chem.* **1993**, *451*, 15–17.
127. Wan, W.; Zhao, K.; Guan, W.; Wang, C.; Zhang, L. *Chin. J. Appl. Chem.* **1997**, *14*, 81–83.
128. Wan, W.; Zhao, K. Q.; Guan, W. J.; Yang, L. M.; Zhang, L. F. *Acta. Chim. Sinica* **1998**, *56*, 278–283.
129. Wan, W.; Guan, W. J.; Zhao, K. Q.; Zheng, W. Z.; Zhang, L. F. *J. Organomet. Chem.* **1998**, *557*, 157–161.
130. Barberá, J.; Elduque, A.; Giménez, R.; Lahoz, F. J.; López, J. A.; Oro, L. A.; Serrano, J. L.; Villacampa, B.; Villalba, J. *Inorg. Chem.* **1999**, *38*, 3085–3092.
131. Han, J.; Fu Zhang, L.; Wan, W. *J. Organomet. Chem.* **2003**, *672*, 86–93.
132. Bruce, D. W.; Dunmur, D. A.; Esteruelas, M. A.; Hunt, S. E.; Le Lagadec, R.; Maitlis, P. M.; Marsden, J. R.; Sola, E.; Stacey, J. M. *J. Mater. Chem.* **1991**, *1*, 251–254.
133. Jeter, D. Y.; Fleischer, E. B. *J. Coord. Chem.* **1974**, *4*, 107–111.

134. Adams, H.; Bailey, N. A.; Bruce, D. W.; Hudson, S. A.; Marsden, J. R. *Liq. Cryst.* **1994**, *16*, 643–653.
135. Richardson, T.; Topaçli, A.; Majid, W. H. A.; Greenwood, M. B.; Bruce, D. W.; Thornton, A.; Marsden, J. R. *Adv. Mater. Opt. Electron.* **1994**, *4*, 243–251.
136. Greenwood, M. B.; Richardson, T.; Bruce, D. W.; Taylor, D. M.; Lacey, D.; Yarwood, J. *Thin Solid Films* **1996**, *284–285*, 46–48.
137. Wong, J. E.; Bruce, D. W.; Richardson, T. H. *Synth. Metals* **2005**, *148*, 11–14.
138. Bruce, D. W.; Thornton, A. *Mol. Cryst. Liq. Cryst.* **1993**, *231*, 253–256.
139. Esteruelas, M. A.; Sola, E.; Oro, L. A.; Ros, M. B.; Serrano, J. L. *J. Chem. Soc., Chem. Commun.* **1989**, 55–56.
140. Esteruelas, M. A.; Sola, E.; Oro, L. A.; Ros, M. B.; Marcos, M.; Serrano, J. L. *J. Organomet. Chem.* **1990**, *387*, 103–111.
141. Bruce, D. W.; Hall, M. D. *Mol. Cryst., Liq. Cryst.* **1994**, *250*, 373–375.
142. Oriol, L.; Piñol, M.; Poelsma, S.; Serrano, J. L.; Viñuales, A. *J. Polym. Sci. A, Polym. Chem.* **2000**, *38*, 4466–4477.
143. Berdagué, P.; Courtieu, J.; Maitlis, P. M. *J. Chem. Soc., Chem. Commun.* **1994**, 1313–1314.
144. Rourke, J. P.; Bruce, D. W.; Marder, T. B. *J. Chem. Soc., Dalton Trans.* **1995**, 317–318.
145. Lee, M.; Yoo, Y. S.; Choi, M. G. *Bull. Kor. Chem. Soc.* **1997**, *18*, 1067–1070.
146. Bruce, D. W.; Lalinde, E.; Styring, P.; Dunmur, D. A.; Maitlis, P. M. *J. Chem. Soc., Chem. Commun.* **1986**, 581–582.
147. Coco, S.; Díez-Expósito, F.; Espinet, P.; Fernández-Mayordomo, C.; Martín-Alvarez, J. M.; Levelut, A. M. *Chem. Mater.* **1998**, *10*, 3666–3671.
148. Parra, V.; del Caño, T.; Coco, S.; Rodríguez-Méndez, M. L.; de Saja, J. A. *Surf. Sci.* **2004**, *550*, 106–118.
149. Kaharu, T.; Takahashi, S. *Chem. Lett.* **1992**, 1515–1516.
150. Kaharu, T.; Tanaka, T.; Sawada, M.; Takahashi, S. *J. Mater. Chem.* **1994**, *4*, 859–865.
151. Adams, H.; Bailey, N. A.; Bruce, D. W.; Dunmur, D. A.; Lalinde, E.; Marcos, M.; Ridgway, C.; Smith, A. J.; Stryring, P.; Maitlis, P. M. *Liq. Cryst.* **1987**, *2*, 381–393.
152. Omenat, A.; Serrano, J. L.; Sierra, T.; Amabilino, D. B.; Minguet, M.; Ramos, E.; Veciana, J. *J. Mater. Chem.* **1999**, *9*, 2301–2305.
153. Wang, S.; Mayr, A.; Cheung, K. K. *J. Mater. Chem.* **1998**, *8*, 1561–1565.
154. Mayr, A.; Wang, S.; Cheung, K.-K.; Hong, M. *J. Organomet. Chem.* **2003**, *684*, 287–299.
155. Espinet, P.; Garcia-Orodea, E.; Miguel, J. *Inorg. Chem.* **2000**, *39*, 3645–3651.
156. Espinet, P.; Miguel, J. A.; García-Granda, S.; Miguel, D. *Inorg. Chem.* **1996**, *35*, 2287–2291.
157. Espinet, P.; García-Orodea, E.; Miguel, J. A. *Chem. Mater.* **2004**, *16*, 551–558.
158. Kaharu, T.; Matsubara, H.; Takahashi, S. *J. Mater. Chem.* **1991**, *1*, 145–146.
159. Kaharu, T.; Matsubara, H.; Takahashi, S. *J. Mater. Chem.* **1992**, *2*, 43–47.
160. Kaharu, T.; Matsubara, H.; Takahashi, S. *Mol. Cryst. Liq. Cryst.* **1992**, *220*, 191–199.
161. Bruce, D. W.; Lea, M. S.; Marsden, J. R.; Rourke, J. P.; Tajbakhsh, A. R. *J. Mater. Chem.* **1994**, *4*, 1017–1020.
162. Bruce, D. W.; Lea, M. S.; Marsden, J. R. *Mol. Cryst. Liq. Cryst.* **1996**, *275*, 183–194.
163. Zhang, S. W.; Motoori, F.; Takahashi, S. *J. Organomet. Chem.* **1999**, *574*, 163–170.
164. Lee, C. K.; Chen, J. C. C.; Lee, K. M.; Liu, C. W.; Lin, I. J. B. *Chem. Mater.* **1999**, *11*, 1237–1242.
165. Rourke, J. P.; Fanizzi, F. P.; Salt, N. J. S.; Bruce, D. W.; Dunmur, D. A.; Maitlis, P. M. *J. Chem. Soc., Chem. Commun.* **1990**, 229–231.
166. Rourke, J. P.; Fanizzi, F. P.; Bruce, D. W.; Dunmur, D. A.; Maitlis, P. M. *J. Chem. Soc., Dalton Trans.* **1992**, 3009–3014.
167. Donnio, B.; Rowe, K. E.; Roll, C.; Bruce, D. W. *Mol. Cryst. Liq. Cryst.* **1999**, *332*, 383–390.
168. Mongin, C.; Donnio, B.; Bruce, D. W. *J. Am. Chem. Soc.* **2001**, *123*, 8426–8427.
169. Weissflog, W. In *Handbook of Liquid Crystals*; Demus, D., Goodby, J., Gray, G. W., Spiess, H.-W., Vill, V., Eds.; Wiley-VCH: Weinheim, 1998, Vol. 2B, Chapter XI.
170. Ghedini, M.; Armentano, S.; Bartolino, R.; Rustichelli, F.; Torquati, G.; Kirov, N.; Petrov, M. *Mol. Cryst. Liq. Cryst.* **1987**, *151*, 75–91.
171. Ghedini, M.; Longeri, M.; Bartolino, R. *Mol. Cryst. Liq. Cryst.* **1982**, *84*, 207–211.
172. Ghedini, M.; Licoccia, S.; Armentano, S.; Bartolino, R. *Mol. Cryst. Liq. Cryst.* **1984**, *108*, 269–275.
173. Ghedini, M.; Armentano, S.; Neve, F. *Inorg Chim Acta* **1987**, *134*, 23–24.
174. Ghedini, M.; Armentano, S.; Neve, F. *J. Chem. Soc., Dalton Trans.* **1988**, 1565–1567.
175. Levelut, A.; Veber, M.; Francescangeli, O.; Melone, S.; Ghedini, M.; Neve, F.; Nicoletta, F. P.; Bartolino, R. *Liq. Cryst.* **1995**, *19*, 241–249.
176. Versace, C. C.; Bartolino, R.; Ghedini, M.; Neve, F.; Armentano, S.; Petrov, M.; Kirov, N. *Liq. Cryst.* **1990**, *8*, 481–487.
177. Bartolino, R.; Coddens, G.; Rustichelli, F.; Pagnotta, M. C.; Versace, C.; Ghedini, M.; Neve, F. *Mol. Cryst. Liq. Cryst.* **1992**, *221*, 101–108.
178. Formoso, V.; Pagnotta, M. C.; Mariani, P.; Ghedini, M.; Neve, F.; Bartolino, R.; More, M.; Pépy, G. *Liq. Cryst.* **1992**, *11*, 639–654.
179. Zhang, L.; Huang, D.; Xiong, N.; Yang, J.; Li, G.; Shu, N. *Mol. Cryst. Liq. Cryst.* **1993**, *237*, 285–297.
180. Ghedini, M.; Pucci, D.; Cesarotti, E.; Antogniazza, P.; Francescangeli, O.; Bartolino, R. *Chem. Mater.* **1993**, *5*, 883–890.
181. Crispini, A.; Ghedini, M.; Morrone, S.; Pucci, D.; Francescangeli, O. *Liq. Cryst.* **1996**, *20*, 67–76.
182. Ghedini, M.; Pucci, D.; Crispini, A.; Aiello, I.; Barigelletti, F.; Gessi, A.; Francescangeli, O. *Appl. Organomet. Chem.* **1999**, *13*, 565–581.
183. Ghedini, M.; Crispini, A. *Comments Inorg. Chem.* **1999**, *21*, 53–68.
184. Ghedini, M.; Morrone, S.; Neve, F.; Pucci, D. *Gazz. Chim. It.* **1996**, *126*, 511–515.
185. Ghedini, M.; Pucci, D.; Neve, F. *Chem. Commun.* **1996**, 137–138.
186. Ghedini, M.; Pucci, D.; Calogero, G.; Barigelletti, F. *Chem. Phys. Lett.* **1997**, *267*, 341–344.
187. Ghedini, M.; Pucci, D.; Cesarotti, E.; Francescangeli, O.; Bartolino, R. *Liq. Cryst.* **1994**, *16*, 373–380.
188. Pucci, D.; Francescangeli, O.; Ghedini, M. *Mol. Cryst. Liq. Cryst.* **2001**, *372*, 51–68.
189. Ghedini, M.; Neve, F.; Pucci, D. *Eur. J. Inorg. Chem.* **1998**, 501–504.
190. Ghedini, M.; Pucci, D.; Crispini, A.; Barberio, G. *Organometallics* **1999**, *18*, 2116–2124.
191. Ghedini, M.; Pucci, D.; Barberio, G. *Liq. Cryst.* **2000**, *27*, 1277–1283.
192. Hoshino, N.; Hasegawa, H.; Matsunaga, Y. *Liq. Cryst.* **1991**, *9*, 267–276.
193. Aiello, I.; Crispini, A.; Ghedini, M.; La Deda, M.; Barigelletti, F. *Inorg. Chim. Acta* **2000**, *308*, 121–128.
193a. Aiello, I.; Dattilo, D.; Ghedini, M.; Golemme, A. *J. Am. Chem. Soc.* **2001**, *123*, 5598–5599.
194. Talarico, M.; Barberio, G.; Pucci, D.; Ghedini, M.; Golemme, A. *Adv. Mater.* **2003**, *15*, 1374–1377.
194a. Talarico, M.; Termine, R.; Berberio, G.; Pucci, D.; Ghedini, M.; Golemme, A. *Appl. Phys. Lett.* **2004**, *84*, 1034–1036.
195. For an introduction and overview of molecular photorefractive materials, see:Ostroverkhova, O.; Moerner, W. E. *Chem. Rev.* **2004**, *104*, 3267–3314.
196. Ghedini, M.; Pucci, D.; Armentano, S.; Bartolino, R.; Versace, C.; Cipparrone, G.; Scaramuzza, N. It. Patent VE92,000,003, 1992.

197. Cipparrone, G.; Versace, C.; Duca, D.; Pucci, D.; Ghedini, M.; Umeton, C. *Mol. Cryst. Liq. Cryst.* **1992**, *212*, 217–224.
198. Versace, C.; Cipparrone, G.; Lucchetta, D.; Pucci, D.; Ghedini, M. *Mol. Cryst. Liq. Cryst.* **1992**, *212*, 313–318.
199. Scaramuzza, N.; Pagnotta, M. C. *Mol. Cryst. Liq. Cryst.* **1994**, *239*, 263–267.
200. Petrov, A. G.; Ionescu, A. T.; Versace, C.; Scaramuzza, N. *Liq. Cryst.* **1995**, *19*, 169–178.
201. Scaramuzza, N.; Pagnotta, M. C.; Pucci, D. *Mol. Cryst. Liq. Cryst.* **1994**, *239*, 195–202.
202. Beica, T.; Alexe-Ionescu, A. L.; Ionescu, A. T.; Miraldi, E.; Pucci, D.; Rajteri, M. *Mol. Cryst. Liq. Cryst.* **1995**, *270*, 91–100.
203. Ionescu, A. T.; Scaramuzza, N.; Versace, C. *J. Phys. Chem. B* **1997**, *101*, 8438–8442.
204. Ionescu, A. T.; Pucci, D.; Scaramuzza, N.; Versace, C.; Petrov, A. G.; Bartolino, R. *J. Chem. Phys.* **1995**, *103*, 5144–5148.
205. Scaramuzza, N.; Pagnotta, M. C.; Lucchetta, D. E.; Strangi, G.; Versace, C.; Ionescu, A. T. *Mol. Cryst. Liq. Cryst.* **2000**, *339*, 83–94.
206. Francescangeli, O.; Ferrero, C.; Pucci, D.; Ghedini, M. *Mol. Cryst. Liq. Cryst.* **2002**, *378*, 77–88.
207. Amoddeo, A.; Bartolino, R.; Caputi, L. S.; Colavita, E.; Formoso, V.; Ghedini, M.; Oliva, A.; Pucci, D.; Verscace, C. *Mol. Cryst. Liq. Cryst.* **1992**, *221*, 93–99.
208. Versace, C.; Formoso, V.; Lucchetta, D.; Pucci, D.; Ferrero, C.; Ghedini, M.; Bartolino, R. *J. Chem. Phys.* **1993**, *98*, 8507–8513.
209. Calucci, L.; Catalano, D.; Ghedini, M.; Jones, N. L.; Pucci, D.; Veracini, C. A *Mol. Cryst. Liq. Cryst.* **1996**, *290*, 87–98.
210. Calucci, L.; Forte, C.; Geppi, M.; Veracini, C. A. Z. *Naturforsch. A* **1998**, *53*, 427–435.
211. Dong, R. Y.; Morcombe, C. R.; Calucci, L.; Geppi, M.; Veracini, C. A. *Phys. Rev. E* **2000**, *61*, 1559–1566.
212. Ghedini, M.; Morrone, S.; Francescangeli, O.; Bartolino, R. *Chem. Mater.* **1994**, *6*, 1971–1977.
213. Ghedini, M.; Morrone, S.; De Munno, G.; Crispini, A. *J. Organomet. Chem.* **1991**, *415*, 281–291.
214. Ghedini, M.; Morrone, S.; Francescangeli, O.; Bartolino, R. *Chem. Mater.* **1992**, *4*, 1119–1123.
215. Ghedini, M.; Pucci, D.; Cesarotti, E.; Francescangeli, O.; Bartolino, R. *Liq. Cryst.* **1993**, *15*, 331–344.
216. Barberá, J.; Espinet, P.; Lalinde, E.; Marcos, M.; Serrano, J. L. *Liq. Cryst.* **1987**, *2*, 833–842.
217. Ciriano, M. A.; Espinet, P.; Lalinde, E.; Ros, M. B.; Serrano, J. L. *J. Mol. Struct.* **1989**, *196*, 327–341.
218. Buey, J.; Espinet, P. *J. Organomet. Chem.* **1996**, *507*, 137–145.
219. Baena, M. J.; Espinet, P.; Ros, M. B.; Serrano, J. L. *J. Mater. Chem.* **1996**, *6*, 1291–1296.
220. Marcos, M.; Ros, M. B.; Serrano, J. L. *Liq. Cryst.* **1988**, *3*, 1129–1136.
221. Ros, M. B.; Ruiz, N.; Serrano, J. L.; Espinet, P. *Liq. Cryst.* **1991**, *9*, 77–86.
222. Ghedini, M.; Armentano, S.; De Munno, G.; Crispini, A.; Neve, F. *Liq. Cryst.* **1990**, *8*, 739–744.
223. Barberá, J.; Espinet, P.; Ezcurra, A.; Ros, M. B.; Serrano, J. L. *J. Am. Chem. Soc.* **1994**, *116*, 1899–1906.
224. Castro, M.; De La Fuente, M. R.; Ros, B.; Perez Jubindo, M. A.; Serrano, J. L.; Puertolas, J. A. *Mol. Cryst. Liq. Cryst.* **1995**, *265*, 521–525.
225. Baena, M. J.; Buey, J.; Espinet, P.; Kitzerow, H. S.; Heppke, G. *Angew. Chem., Int. Ed. Engl.* **1993**, *32*, 1201–1203.
226. Buey, J.; Diez, G. A.; Espinet, P.; García-Granda, S.; Pérez-Carreño, E. *Eur. J. Inorg. Chem.* **1998**, 1235–1241.
227. Buey, J.; Espinet, P.; Kitzerow, H. S.; Strauss, J. *Chem. Commun.* **1999**, 441–442.
228. López de Murillas, D.; Piñol, R.; Ros, M. B.; Serrano, J.-L.; Sierra, T.; de la Fuente, M. R. *J. Mater. Chem.* **2004**, *14*, 1117–1127.
229. Díez, L.; Espinet, P.; Miguel, J. A. *J. Chem. Soc., Dalton Trans.* **2001**, 1189–1195.
230. Díez, L.; Espinet, P.; Miguel, J. A.; Rodriguez-Medina, M. P. *J. Organomet. Chem.* **2005**, *690*, 261–268.
231. Baena, M. J.; Espinet, P.; Ros, M. B.; Serrano, J. L. *Angew. Chem., Int. Ed. Engl.* **1991**, *30*, 711–712.
232. Omnès, L.; Timimi, B. A.; Gelbrich, T.; Hursthouse, M. B.; Luckhurst, G. R.; Bruce, D. W. *Chem. Commun.* **2001**, 2248–2249.
233. Bruce, D. W. *Chem. Rec.* **2004**, *4*, 10–22.
234. Thompson, N. J.; Iglesias, R.; Serrano, J. L.; Baena, M. J.; Espinet, P. *J. Mater. Chem.* **1996**, *6*, 1741–1744.
235. Huang, D. J.; Xiong, N. Y.; Yang, J.; Wang, S. M.; Li, G. N.; Zhang, L. F. *Mol. Cryst. Liq. Cryst.* **1993**, *231*, 191–198.
236. Baena, M. J.; Espinet, P.; Ros, M. B.; Serrano, J. L.; Ezcurra, A. *Angew. Chem., Int. Ed. Engl.* **1993**, *32*, 1203–1205.
237. Espinet, P.; Etxebarria, J.; Marcos, M.; Pérez, J.; Remon, A.; Serrano, J. L. *Angew. Chem., Int. Ed. Engl.* **1989**, *28*, 1065–1066.
238. Thompson, N. J.; Serrano, J. L.; Baena, M. J.; Espinet, P. *Chem. Eur. J.* **1996**, *2*, 214–220.
239. Espinet, P.; Etxebarría, J.; Folcia, C. L.; Ortega, J.; Ros, M. B.; Serrano, J. L. *Adv. Mater.* **1996**, *8*, 745–748.
240. Buey, J.; Díez, L.; Espinet, P.; Kitzerow, H. S.; Miguel, J. A. *Appl. Phys. B* **1998**, *66*, 355–358.
241. Buey, J.; Díez, L.; Espinet, P.; Kitzerow, H. S.; Miguel, J. A. *Chem. Mater.* **1996**, *8*, 2375–2381.
242. Ortega, J.; Folcia, C. L.; Etxebarria, J.; Ros, M. B.; Miguel, J. A. *Liq. Cryst.* **1997**, *23*, 285–291.
243. Díez, L.; Espinet, P.; Miguel, J. A.; Ros, M. B. *J. Mater. Chem.* **2002**, *12*, 3694–3698.
244. Buey, J.; Coco, S.; Díez, L.; Espinet, P.; Martín-Alvarez, J. M.; Miguel, J. A.; García-Granda, S.; Tesouro, A.; Ledoux, I.; Zyss, J. *Organometallics* **1998**, *17*, 1750–1755.
245. Usol'tseva, N.; Espinet, P.; Buey, J.; Serrano, J. L. *J. Mater. Chem.* **1997**, *7*, 215–219.
246. Usol'tseva, N.; Espinet, P.; Buey, J.; Praefcke, K.; Blunk, D. *Mol. Cryst. Liq. Cryst.* **1997**, *299*, 457–465.
247. Baena, M. J.; Buey, J.; Espinet, P.; García-Prieto, C. E. *J. Organomet. Chem.* **2005**, *690*, 998–1010.
248. Lydon, D. P.; Cave, G. W. V.; Rourke, J. P. *J. Mater. Chem.* **1997**, *7*, 403–406.
249. Cave, G. W. V.; Lydon, D. P.; Rourke, J. P. *J. Organomet. Chem.* **1998**, *555*, 81–88.
250. Saccomando, D. J.; Black, C.; Cave, G. W. V.; Lydon, D. P.; Rourke, J. P. *J. Organomet. Chem.* **2000**, *601*, 305–310.
251. Lydon, D. P.; Rourke, J. P. *Chem. Commun.* **1997**, 1741–1742.
252. Praefcke, K.; Singer, D.; Gündo ğan, B. *Mol. Cryst. Liq. Cryst.* **1992**, *223*, 181–195.
253. Praefcke, K.; Bilgin, B.; Pickardt, J.; Borowski, M. *Chem. Ber.* **1994**, *127*, 1543–1545.
254. Bilgin-Eran, B.; Singer, D.; Pickardt, J.; Praefcke, K. *J. Organomet. Chem.* **2001**, *620*, 249–255.
255. Praefcke, K.; Bilgin, B.; Pickardt, J.; Borowski, M. *J. Organomet. Chem.* **1999**, *592*, 155–161.
256. Singer, D.; Liebmann, A.; Praefcke, K.; Wendorff, J. H. *Liq. Cryst.* **1993**, *14*, 785–794.
257. Praefcke, K.; Singer, D. *Mol. Mater* **1994**, *3*, 265–270.
258. Bilgin Eran, B.; Singer, D.; Praefcke, K: *Eur. J. Inorg. Chem.* **2001**, 111–116.
259. Usolt'seva, N.; Praefcke, K.; Singer, D.; Gündo ğan, B. *Mol. Mater* **1994**, *4*, 253–263.
260. Praefcke, K.; Singer, D.; Gündo ğan, B. *Mol. Cryst. Liq. Cryst.* **1992**, *223*, 181–195.
261. Praefcke, K.; Singer, D.; Gündo ğan, B.; Gutbier, K.; Langner, M. *Ber. Bunsen-Ges. Phys. Chem.* **1994**, *98*, 118–121.
261a. Praefcke, K.; Singer, D.; Gündo ğan, B.; Gutbier, K.; Langner, M. *Ber. Bunsen-Ges. Phys. Chem.* **1993**, *97*, 1358–1361.
262. Praefcke, K.; Bilgin, B.; Usolt'seva, N.; Heinrich, B.; Guillon, D. *J. Mater. Chem.* **1995**, *5*, 2257–2264.
263. Bilgin-Eran, B.; Singer, D.; Pickardt, J.; Praefcke, K. *J. Organomet. Chem.* **2001**, *620*, 249–255.

264. Gündo ğan, B.; Praefcke, K. *Chem. Ber.* **1993**, *126*, 1253–1255.
265. Heinrich, B.; Praefcke, K.; Guillon, D. *J. Mater. Chem.* **1997**, 7, 1363–1372.
266. Praefcke, K.; Diele, S.; Pickardt, J.; Gündo ğan, B.; Nütz, U.; Singer, D. *Liq. Cryst.* **1995**, *18*, 857–865.
267. Usolt'seva, N.; Praefcke, K.; Singer, D.; Gündo ğan, B. *Liq. Cryst.* **1994**, *16*, 601–616.
268. Praefcke, K.; Holbrey, J. D.; Usolt'seva, N.; Blunk, D. *Mol. Cryst. Liq. Cryst.* **1997**, *292*, 123–139.
269. Nesrullajev, A.; Bilgin-Eran, B.; Kazanci, N. *Mat. Chem. Phys.* **2002**, *76*, 7–14.
270. Usolt'seva, N.; Hauck, G.; Koswig, H. D.; Praefcke, K.; Heinrich, B. *Liq. Cryst.* **1996**, *20*, 731–739.
271. Galerne, Y. *Mol. Cryst. Liq. Cryst.* **1988**, *165*, 131–149.
272. Yu, L. J.; Saupe, A. *Phys. Rev. Lett.* **1980**, *45*, 1000–1003.
273. Praefcke, K.; Holbrey, J. D. *J. Inclusion Phenom. Mol. Recognit. Chem.* **1996**, *24*, 19–41.
274. Usolt'seva, N.; Praefcke, K.; Singer, D.; Gündo ğan, B. *Liq. Cryst.* **1994**, *16*, 617–623.
275. Espinet, P.; Lalinde, E.; Marcos, M.; Perez, J.; Serrano, J. L. *Organometallics* **1990**, *9*, 555–560.
276. Elder, R. C.; Cruea, R. D. P.; Morrison, R. F. *Inorg. Chem.* **1976**, *15*, 1623–1626.
277. Zhang, L.; Huang, D.; Xiong, N.; Li, G. *Chin. Chem. Lett.* **1992**, *3*, 805–806.
278. Espinet, P.; Perez, J.; Marcos, M.; Ros, M. B.; Serrano, J. L.; Barberá, J.; Levelut, A. M. *Organometallics* **1990**, *9*, 2028–2033.
279. Levelut, A. M. *Mol. Cryst. Liq. Cryst.* **1992**, *215*, 31–46.
280. Ghedini, M.; Pucci, D. *J. Organomet. Chem.* **1990**, *395*, 105–112.
281. Hegmann, T.; Kain, J.; Diele, S.; Pelzl, G.; Tschierske, C. *Angew. Chem., Int. Ed.* **2001**, *40*, 887–890.
282. Ghedini, M.; Pucci, D.; De Munno, G.; Viterbo, D.; Neve, F.; Armentano, S. *Chem. Mater.* **1991**, *3*, 65–72.
283. Ghedini, M.; Pucci, D.; Bartolino, R.; Francescangeli, O. *Liq. Cryst.* **1993**, *13*, 255–263.
284. Guang, W.; Han, J.; Wan, W.; Zhao, K.; Zhang, L. *Liq. Cryst.* **2003**, *30*, 1259–1265.
285. Neumann, B.; Hegmann, T.; Wolf, R.; Tschierske, C. *Chem. Commun.* **1998**, 105–106.
286. Hegmann, T.; Neumann, B.; Kain, J.; Diele, S.; Tschierske, C. *J. Mater. Chem.* **2000**, *10*, 2244–2248.
287. Hegmann, T.; Peidis, F.; Diele, S.; Tschierske, C. *Liq. Cryst.* **2000**, *27*, 1261–1265.
288. Hegmann, T.; Kain, J.; Diele, S.; Schubert, B.; Bögel, H.; Tschierske, C. *J. Mater. Chem.* **2003**, *13*, 991–1003.
289. Slater, J. W.; Lydon, D. P.; Rourke, J. P. *J. Organomet. Chem.* **2002**, *645*, 246–255.
290. Slater, J. W.; Lydon, D. P.; Alcock, N. W.; Rourke, J. P. *Organometallics* **2001**, *20*, 4418–4423.
291. Lehmann, M.; Marcos, M.; Serrano, J. L.; Sierra, T.; Bolm, C.; Weickhardt, K.; Magnus, A.; Moll, G. *Chem. Mater.* **2001**, *13*, 4374–4381.
292. Lehmann, M.; Sierra, T.; Barberá, J.; Serrano, J. L.; Parker, R. *J. Mater. Chem.* **2002**, *12*, 1342–1350.
293. El-ghayoury, A.; Douce, L.; Skoulios, A.; Ziessel, R. *Angew. Chem., Int. Ed.* **1998**, *37*, 1255–1258.
294. Neve, F.; Ghedini, M.; Crispini, A. *Chem. Commun.* **1996**, 2463–2464.
295. Neve, F.; Ghedini, M.; Francescangeli, O.; Campagna, S. *Liq. Cryst.* **1998**, *24*, 673–680.
296. Neve, F.; Crispini, A.; Campagna, S. *Inorg. Chem.* **1997**, *36*, 6150–6156.
297. Neve, F.; Crespini, A. *Eur. J. Inorg. Chem.* **2000**, 1039–1043.
298. Ghedini, M.; Panunzi, B.; Roviello, A. *Liq. Cryst.* **1998**, *25*, 225–233.
299. Torralba, M. C.; Cano, M.; Gómez, S.; Campo, J. A.; Heras, J. V.; Perles, J.; Ruiz-Valero, C. *J. Organomet. Chem.* **2003**, *682*, 26–34.
300. Kaharu, T.; Ishii, R.; Takahashi, S. *J. Chem. Soc., Chem. Commun.* **1994**, 1349–1350.
301. Coco, S.; Espinet, P.; Falagán, S.; Martin-Alvarez, J. M. *New J. Chem.* **1995**, *19*, 959–964.
302. Benouazzane, M.; Coco, S.; Espinet, P.; Martin-Alvarez, J. M. *J. Mater. Chem.* **1995**, *5*, 441–445.
303. Espinet, P. *Gold Bull.* **1999**, *32*, 127–134.
304. Coco, S.; Espinet, P.; Martin-Alvarez, J. M.; Levelut, A. M. *J. Mater. Chem.* **1997**, *7*, 19–23.
305. Benouazzane, M.; Coco, S.; Espinet, P.; Martin-Alvarez, J. M. *J. Mater. Chem.* **1999**, *9*, 2327–2332.
306. Ballesteros, B.; Coco, S.; Espinet, P. *Chem. Mater.* **2004**, *16*, 2062–2067.
307. Benouazzane, M.; Coco, S.; Espinet, P.; Barbera, J. *J. Mater. Chem.* **2001**, *11*, 1740–1744.
308. Benouazzane, M.; Coco, S.; Espinet, P.; Barberá, J. *Inorg. Chem.* **2002**, *41*, 5754–5759.
309. Benouazzane, M.; Coco, S.; Espinet, P.; Martín-Alvarez, J. M.; Barberá, J. *J. Mater. Chem.* **2002**, *12*, 691–696.
310. Alejos, P.; Coco, S.; Espinet, P. *New J. Chem.* **1995**, *19*, 799–805.
311. Kaharu, T.; Ishii, R.; Adachi, T.; Yoshida, T.; Takahashi, S. *J. Mater. Chem.* **1995**, *5*, 687–692.
312. Bayón, R.; Coco, S.; Espinet, P.; Fernandez-Mayordomo, C.; Martin-Alvarez, J. *Inorg. Chem.* **1997**, *36*, 2329–2334.
313. Bayón, R.; Coco, S.; Espinet, P. *Chem. Mater.* **2002**, *14*, 3515–3518.
314. Coco, S.; Fernández-Mayordomo, C.; Falagán, S.; Espinet, P. *Inorg. Chim. Acta.* **2003**, *350*, 366–370.
315. Bayón, R.; Coco, S.; Espinet, P. *Chem. Eur. J.* **2005**, *11*, 1079–1085.
316. Ishii, R.; Kaharu, T; Pirio, N.; Zhang, S. W.; Takahashi, S. *J. Chem. Soc., Chem. Commun.* **1995**, 1215–1216.
317. Zhang, S. W.; Ishii, R.; Takahashi, S. *Organometallics* **1997**, *16*, 20–26.
318. Lee, K. M.; Lee, C. K.; Lin, I. J. B. *Angew. Chem., Int. Ed. Engl.* **1997**, *36*, 1850–1852.
319. Vorländer, D. *Z. Phys. Chem.* **1923**, *105*, 211–254.
320. Bruce, D. W.; Heyns, K.; Vill, V. *Liq. Cryst.* **1997**, *23*, 813–819.
321. Krigbaum, W. R.; Poirier, J. C.; Costello, M. J. *Mol. Cryst. Liq. Cryst.* **1973**, *20*, 133–163.
322. Chandrasekhar, S. *Curr. Sci.* **1978**, *47*, 523–525.
323. Omenat, A.; Ghedini, M. *J. Chem. Soc., Chem. Commun.* **1994**, 1309–1310.
324. Vicente, J.; Bermúdez, M. D.; Carrión, F. J.; Martínez-Nicolás, G. *J. Organomet. Chem.* **1994**, *480*, 103–109.
325. Barigelletti, F.; Ghedini, M.; Pucci, D.; La Deda, M. *Chem. Lett.* **1999**, 297–298.
326. Yang, Y. G.; Wen, J. X. *Liq. Cryst.* **1998**, *25*, 765–766.
327. Yelamaggad, C. V.; Anitha Nagamani, S.; Fujita, T.; Iyi, N. *Liq. Cryst.* **2002**, *29*, 1393–1399.
328. Varshney, S. K.; Shankar Rao, D. S.; Kumar, S. *Mol. Cryst. Liq. Cryst.* **2001**, *357*, 55–65.
329. Kumar, S.; Varshney, S. K. *Liq. Cryst.* **2001**, *28*, 161–163.

12.06
Organometallic Macromolecular Materials

I Manners, University of Toronto, Toronto, ON, Canada

12.06.1 Introduction

12.06.1.1 Organometallic Polymers

The remarkable growth in the applications of organic polymers in the latter half of the twentieth century can mainly be attributed to their ease of preparation, and the useful mechanical properties and unique propensity for fabrication that are characteristic of long-chain macromolecules. Analogous materials containing inorganic elements have been much slower to develop. Nevertheless, polymers with backbones based on non-metallic main group elements such as polysiloxanes **1**, polyphosphazenes **2**, and polysilanes **3** are well known as are a range of new systems that have gathered much attention as a result of their unique properties.[1–8] Polymers containing metallic elements offer a range of novel characteristics and provide potential access to new processible functional polymeric materials. In this chapter, "organometallic polymers" are discussed; the subset of this class of materials in which the metal is bound to the polymer via M–C bonds. For more general reviews of the flourishing field of metal-containing polymers which include metals bound by M–N, M–O, M–P, etc. bonds, the reader is referred to a number of recent texts and reviews.[9–15] Polymers exhibit a range of architectures and unique properties, the study of which represents a major

core area of polymer science. For detailed background material, the reader is referred to the many excellent introductory and advanced books on polymer science and the recent literature cited in this section.[16–22]

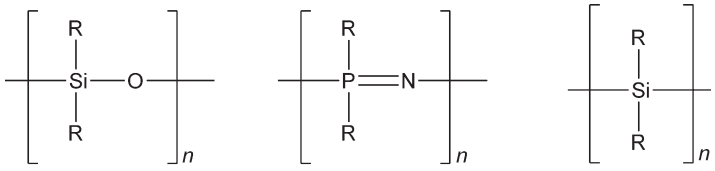

12.06.1.2 Structural Types

Organometallic complexes are well studied, and the presence of metal centers has been shown to give rise to a diverse range of interesting and often useful redox, magnetic, optical, electrical, and catalytic properties. In addition, metal centers have been shown to play a pivotal role with respect to both the structure and function of many biopolymers such as metalloproteins. The incorporation of transition metals into the structure of synthetic polymers, therefore, clearly offers considerable potential for the preparation of processable materials with properties that differ significantly from those of conventional organic polymers. For this reason, the development of organometallic polymers should create exciting new dimensions for polymer materials science and, from an applied angle, significant applications for some of these unique new materials are also to be expected.

Several different possible types of metal-containing polymer structures exist depending on where the metal atoms are incorporated and the nature of the linkages between them. A major subdivision of linear polymers involves a consideration of the location of the metallocenters. For example, the metal can be in the side-group structure (**I**) or directly in the main chain (**II**) (see Figure 1). We will use this general subdivision although we note that these situations represent extremes. For example, a situation that lies in between these two cases is one in which the

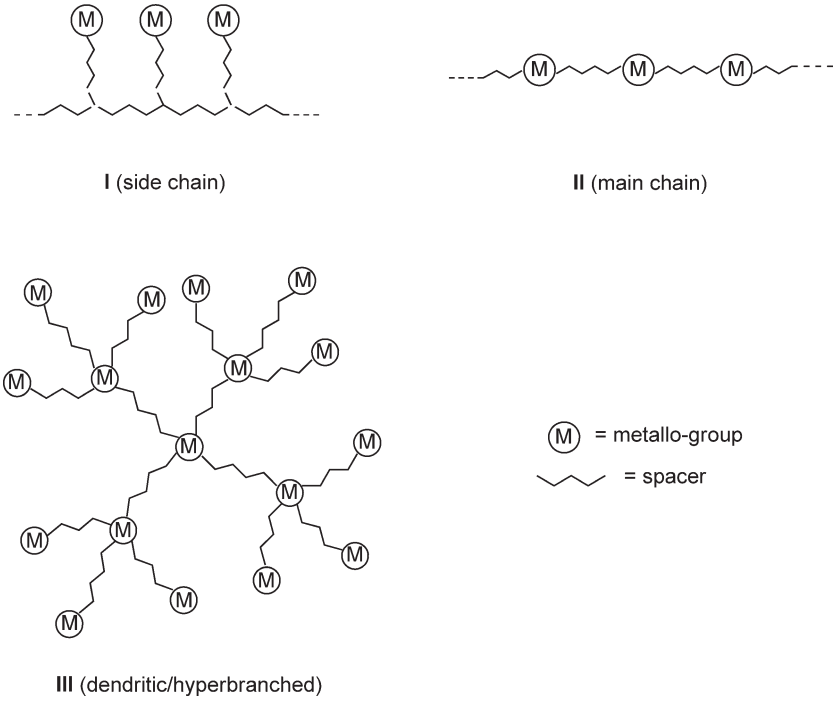

Figure 1 Structural classes of metal-containing polymers.

metal-containing moiety can be removed from, but electronically coupled, to the polymer backbone. In addition, it is possible to prepare materials with metals in both the side-group structure and the main chain. Dendrimers and hyperbranched polymers (**III**) represent another structural class of growing interest. In this case, the metallocenters can be located throughout the structure or, alternatively, in the core or at the periphery.

The linkages or "spacers" between the metallocenters can either possess conjugated structures (involving delocalization of σ- or π-electrons) or essentially localized electrons. Again, these situations represent extremes, and partial conjugation is often possible. Studies of how the electronic structure of the linker can be changed to control interactions between the metals are an important area of research and have important implications for the physical properties (e.g., conductivity, magnetic properties) and applications of the materials.

It is useful to consider the types of characteristics expected for metal-containing polymers that provide a key motivation for making the materials. Some of the main reasons for the incorporation of metals into polymer structures are now outlined.

12.06.1.3 Motivations for the Study of Organometallic Polymers

12.06.1.3.1 Conformational, mechanical, and morphological characteristics

Carbon is a small atom and is limited to coordination numbers ≤ 4, and is generally restricted to three geometries – linear, trigonal planar, and tetrahedral. The properties of organic polymers depend acutely on the nature of the polymer chain and the side-groups. By contrast, metal atoms cover an enormous range of size and can exhibit a broad array of coordination numbers; values up to 12 are well known and up to 8 are common.[23] In addition, a wealth of geometries is known for metal centers. For example, in contrast to carbon, four-coordinate metal complexes can possess either tetrahedral or square-planar geometries. The flexible bonding characteristics of transition metals can also give rise to structures that are completely unprecedented for carbon chemistry. For example, metal–metal quadruple bonds are well-known, and metallocenes and cyclobutadiene complexes exhibit a totally different type of geometry to that found in organic molecules. In ferrocene, the prototypical metallocene, rotation around the iron–cyclopentadienyl bond is virtually free.

12.06.1.3.2 Ceramic precursors

The possibility of using polymers, which can be processed easily into shapes, films, or fibers, as precursors to ceramics, has attracted intense recent interest.[24–29] Ceramics generally possess many desirable physical properties, such as hardness and useful electronic or magnetic properties, but their processability is generally poor. Polycarbosilanes have been successfully used to prepare silicon carbide monoliths and fibers via a pyrolysis technique, and a similar process that utilizes polyacrylonitrile has been used to make carbon fibers. For example, polycarbosilane **4** (Equation (1)) can be spun into fibers, which can then be heated in air to create a coating of SiO_2 that prevents melting. Subsequent thermal treatment at 800 °C yields amorphous SiC fibers and at higher temperatures, these are increasingly reinforced and strengthened by the presence of β-SiC crystallites.[8,28] The key to the success of this process is to use a polymer that, when pyrolyzed, forms the desired ceramic product in high yield, and allows the shape of the precursor polymer to be retained.

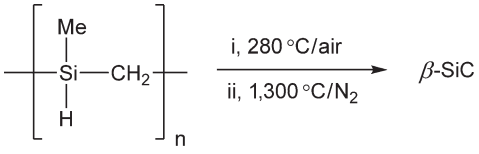

4 (1)

Transition metal-based polymers might also be expected to function as convenient precursors to metal-containing ceramic films, fibers, and coatings that would have high stability, and desirable/useful electronic or magnetic properties following thermal or photochemical treatment or exposure to ionizing radiation or plasmas. This provides a further motivation for making and studying metal-containing polymeric materials.

12.06.1.3.3 Magnetic, redox, electronic, and photophysical properties

Carbon atoms strongly prefer a spin-paired, singlet ground state and, as a consequence, the vast majority of organic compounds are diamagnetic. In contrast, transition metals routinely form stable ions in which unpaired electrons are present. Indeed, the existence of cooperative interactions that allows the alignment of the magnetic moments of transition metal ions in the solid state forms the basis of the vast array of magnetic materials, in applications from computer disks to video tapes. The possibility of accessing polymers that possess magnetic moment alignment, and thereby ferromagnetic, ferrimagnetic, or superparamagnetic properties in the solid state, provides an additional reason for interest in metal-based polymers.[30–31b] Clearly, processable materials of this type would be of considerable interest for many applications. However, the design would have to be intricate. In addition to the presence of cooperative interactions along a linear polymer chain, cooperative intermolecular interactions in three dimensions (3-D) between the chains would also need to be present. In the absence of an ordering mechanism, the materials would be paramagnetic and of less interest. Moreover, if the alignment were antiparallel, even less useful antiferromagnetic materials would result.[30]

As a consequence of their electronic structure, metal atoms (especially those of transition elements) generally exist in a variety of oxidation states. This can be expected to facilitate access to redox-active materials. In addition, the low electronegativity of transition metal atoms should promote electron mobility and access to interesting charge transport properties. The presence of transition metal centers can also impart interesting photophysical properties.[31,31a,31b] Due to spin–orbit coupling effects, phosphorescence and photoinduced charge transfer are well-established phenomena and, in fact, form the basis for many explorations of the photocatalytic properties of transition metal complexes. Areas such as non-linear optics and photonics, which require access to processable materials with electron delocalization and polarizability or high refractive indices, may also benefit from the incorporation of metals into polymer structures.[31,31a,31b]

12.06.1.3.4 Catalysis and bioactivity

The ability of transition metals to bind and activate organic molecules, and to release the transformed organic product with turnover, forms the basis of the vast catalytic chemistry of transition metal complexes.[32] In addition, metal atoms play a key role at the catalytic center of many enzymes.[33] For example, metalloenzymes play key roles in hydrolysis, oxidation, reduction, electron-transfer chemistry, and many other remarkable processes such as nitrogen fixation. The long-term development of synthetic polymers that perform catalytic chemistry in a manner analogous to enzymes, is a goal of profound interest.

12.06.1.3.5 Supramolecular materials and the development of hierarchical structures

Studies of biological systems have revealed that functional structures in nature generally display hierarchical order in that they are organized over a variety of length scales. A challenge of considerable interest for the future is to learn how to apply self-assembly principles that involve the use of non-covalent interactions to the generation of new synthetic materials with hierarchical order.[34] Significantly, the incorporation of transition elements into self-organizing motifs provides additional possibilities for supramolecular chemistry and the properties of the resulting assemblies. For example, metallic elements permit new types of "weak" interactions to exist that supplement the well-known hydrogen bonds, which play such a key role in the determination of the 3-D conformational structures of biopolymers such as nucleic acids. For example, unconventional hydrogen (or "hydride–proton") bonds ($H^{\delta-}\cdots H^{\delta+}$) involving electron-rich (e.g., metal hydride) and electron-poor hydrogen substituents have been used to generate novel materials with extended structures in the solid state.[35,35a] Interactions between gold atoms (Au···Au) or "aurophilic bonds" have approximately the same strength as conventional hydrogen bonds, and are a consequence of the relativistic effects that are significant for heavy metal elements. These have also been used in order to facilitate the formation of remarkable chain and catenane structures.[36–38] In addition, weak coordination bonds between vanadyl groups (V═O···V═O) have been used to generate liquid crystalline ordering.[39]

12.06.1.4 Historical Development of Organometallic Polymers

One of the key challenges in the area of organometallic polymers has been the development of truly high molecular weight materials. The main reasons for the widespread use of polymers are their excellent mechanical properties such as strength, deformability, and elasticity. Typically, chains must be 100 chain atoms for such connections to be possible. For a monomer of molecular weight 100, this corresponds to M_n = ca. 10,000, where M_n = number-average

molecular weight. The need for high molecular weights in order to obtain useful mechanical properties is neatly illustrated by a comparison of straight chain hydrocarbons. It is easy to appreciate the difference between a birthday candle (a mixture of C_{25}–C_{50} alkanes, i.e., M_n = ca. 500), which is a brittle material and breaks easily, and a polyethylene washbottle tip (chains of >1,000 carbon atoms, i.e., $M_n > 15{,}000$), which can be repeatedly bent.[18] Until around the last decade or two of the twentieth century, most organometallic polymers were of low molecular weight, insoluble, or poorly characterized. The rapid growth and bright future for the subject arise from a combination of key synthetic breakthroughs and the resulting developments in terms of the properties of the materials.

The first soluble metal-containing polymer, poly(vinylferrocene) **5**, was prepared by radical polymerization in 1955.[40] With the growing interest in new polymeric materials with novel properties, the 1960s and early 1970s were a time of much activity in the area of metal-containing polymer science. However, very few, well-characterized, soluble, high molecular weight materials were actually reported during this period. The first well-characterized organometallic polymer of appreciable molecular weight with metal atoms in the main chain, a polyferrocene–siloxane material **6**, was prepared by Pittmann in 1974 via a polycondensation strategy.[41] A noteworthy work by Neuse later in the same decade led to well-characterized but rather low molecular weight polyferrocenylenes **7**.[42] Also in the late 1970s, the first reports of members of the important class of rigid-rod polymetallayne polymers containing Pd and Pt **8** were made by Hagihara and co-workers.[43]

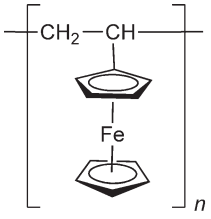

5

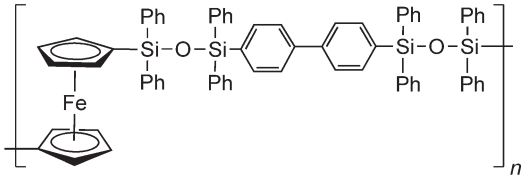

6

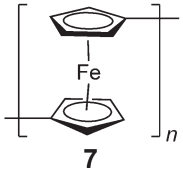

7

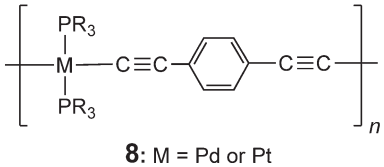

8: M = Pd or Pt

A series of important developments in the area of organometallic polymers occurred in the 1990s as a consequence of a range of key synthetic breakthroughs. For example, ring-opening polymerization (ROP) routes and ROP-related processes have provided access to polymetallocenes such as polyferrocenylsilanes (PFSs) **9** and analogs with, for example, disulfido spacers **10**.[44,45] Also included are main chain metal-containing polymeric materials with controlled architectures such as block co-polymers.[46] In the early 1990s, homopolymers and block co-polymers with metal-containing side-groups were also made available by the technique of ring-opening metathesis polymerization (ROMP).[47] In 1993, transition metal-catalyzed polycondensation strategies yielded the first polystannanes **11**, with main chains consisting of tin atoms.[48] Star and dendritic materials containing metal atoms either at the periphery, or distributed throughout the structure, were also described at around the same time.[49] Self-assembled and hierarchical structures based on organometallic polymers, such as liquid crystals, self-assembled block co-polymer micelles, and phase-separated thin films, are also starting to attract intense attention and this area is set to expand rapidly during the twenty-first century.[12]

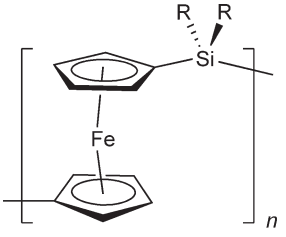

9

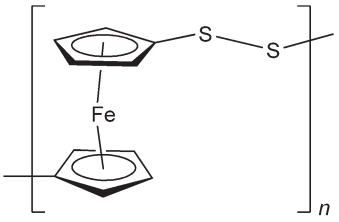

10

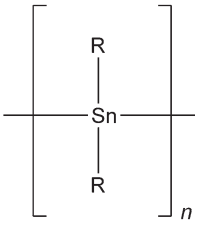

11

12.06.2 Side-Chain Organometallic Polymers

12.06.2.1 Introduction

Organometallic polymers with metal-containing groups in the side-chain structure have the longest history of any of the various classes of metal-containing macromolecules. As mentioned above, the first example, poly(vinylferrocene) (PVFc), was briefly described in 1955.[40] Since that time, a variety of side-chain polymeric materials have been prepared containing either main group metals or transition elements. This section surveys the synthesis and properties of some of the most interesting, well-characterized materials. In addition, possible applications of the side-chain organometallic polymers as electrode mediators, liquid crystalline materials, charge-transport materials, and as components of electronic devices such as diodes and sensors are discussed.

12.06.2.2 Side-chain Polymetallocene Homopolymers and Block Co-polymers

12.06.2.2.1 Organic polymers with metallocene side-groups

12.06.2.2.1.(i) Poly(vinylferrocene)

Since the discovery and elucidation of the structure of ferrocene **12** in the early 1950s,[50] this fascinating species has been a continual source of intrigue for chemists.[51,51a,52] In addition to possessing a vast organic chemistry (involving, e.g., electrophilic substitution reactions), this prototypical, amber-colored 18-electron metallocene also undergoes reversible one-electron oxidation to the 17-electron blue ferrocenium ion **13** (Equation (2)). Importantly, ferrocene is easy to prepare, cheap, commercially available, and air, moisture, and thermally stable.[51,51a] Based on these considerations, it is not surprising that the possibility of obtaining ferrocene-based polymeric materials where the unique physical and chemical features of this organometallic species are combined with the facile processability of high molecular weight polymers has attracted intense interest.[1,53]

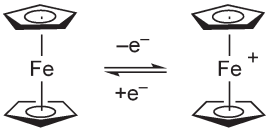

12 **13** (2)

Radical-initiated polymerization of vinylferrocene[40] **14** to give PVFc **15** was first conducted shortly after the discovery of ferrocene, and this method has been reinvestigated many times in subsequent years (Equation (3)).[54–59] Detailed characterization of this material was first reported in 1970.[60] The initiator normally used to prepare PVFc is azobis(isobutyronitrile) (AIBN), as peroxide initiators tend to oxidize the Fe center in the monomer. Molecular weights are typically less than 10,000 but the synthesis of polymers with $M_w > 10^5$ (PDI > 1.3) using this route have been reported where M_w = weight-average molecular weight. However, these higher molecular weight samples often possess a multimodal weight distribution.[57] It has been reported that the molecular weight of PVFc does not increase with a decrease in initiator concentration.[57] This was attributed to the high tendency for chain transfer with vinylferrocene in comparison to other vinyl monomers such as styrene.[57] Vinylferrocene can be co-polymerized with other vinyl monomers such as styrene, methyl methacrylate, and acrylonitrile, and the relative reactivity ratios for the monomers in these systems have been determined.[54–56]

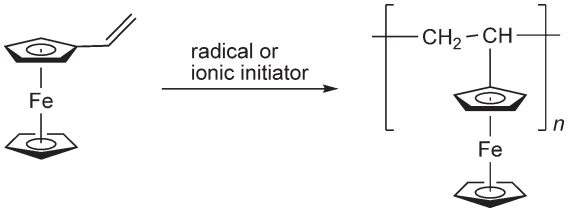

14 **15** (3)

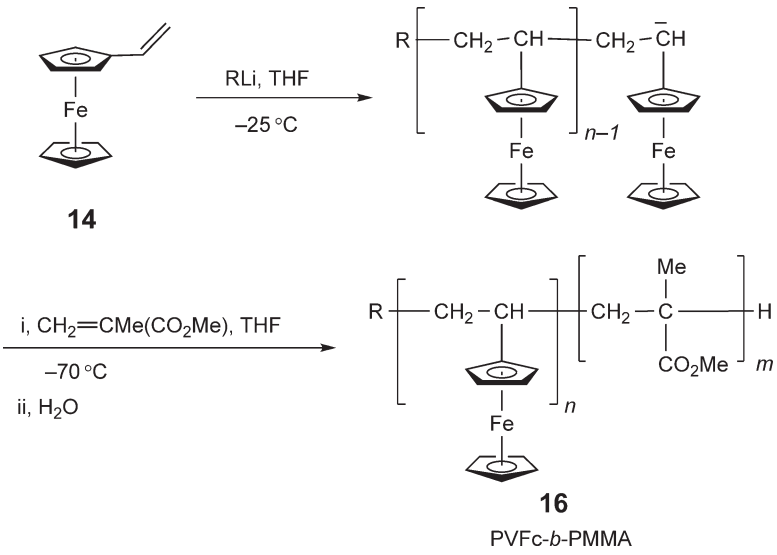

Scheme 1

Cationic initiation and Ziegler–Natta methods have also been employed successfully in order to obtain poly-(vinylferrocene) PVFc.[61] Due to the electron-donating nature of a ferrocene substituent, it was initially believed that anionic initators would not be able to induce the polymerization of vinylferrocene. However, in the early 1990s, living anionic polymerization of vinylferrocene in solution was achieved at low temperatures (−30 to −70 °C) in tetrahydrofuran (THF) using alkyllithium initiators.[62,62a,62b] Block co-polymers of poly(vinylferrocene) with poly(methyl methacrylate), PVFc-*b*-PMMA **16**, or polystyrene, PVFc-*b*-PS, as co-blocks were also briefly reported (Scheme 1; where Fc is the ferrocenyl group –(η^5-C_5H_4)Fe(η^5-C_5H_5)).[62,62a,62b]

Considerable effort has been invested in studies of the properties of PVFc, a yellow powder that is stable in air in the solid state. The material is also soluble in most common, moderately polar, organic solvents and the resulting solutions are stable to air. PVFc has been studied in solution and THF was found to be a good solvent for this material and benzene a marginal one.[57] However, in chlorinated solvents, the polymer is reported to be unstable, and a green precipitate is formed after a few weeks in air. The precipitate was believed to be ionic in nature and to contain ferrocenium units. Of probable relevance to this observation is the report that the photolysis of a CCl_4 solution of PVFc leads to oxidation of the ferrocene groups as shown in Equation (4).[57]

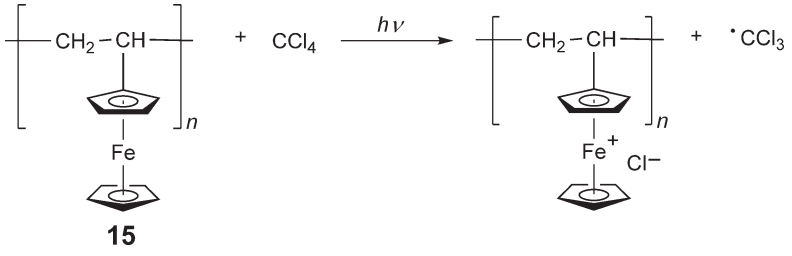

(4)

The λ_{max} for the low-energy *d*–*d* transition in PVFc in the visible region (in CH_2Cl_2) occurs at 440 nm, as determined by UV–VIS spectroscopy, a wavelength similar to that observed for unsubstituted ferrocene itself. The IR spectrum of PVFc shows peaks consistent with a monoalkyl ferrocene and the ^{57}Fe Mössbauer spectrum exhibits a doublet with an isomer shift of 0.78 mm s^{-1} and a quadrupole splitting of 2.44 mm s^{-1}.[57,60] The glass transition temperature has been assigned as 190 °C by differential scanning calorimetry (DSC)[57,60] and a melting point of ca. 280 °C has been reported,[40] but other studies of the microstructure and morphology of this material indicate that the polymer is amorphous.[63] More extensive investigations of the physical properties of PVFc report the T_g as 222 °C for higher molecular weight samples.[59,62,62a,62b]

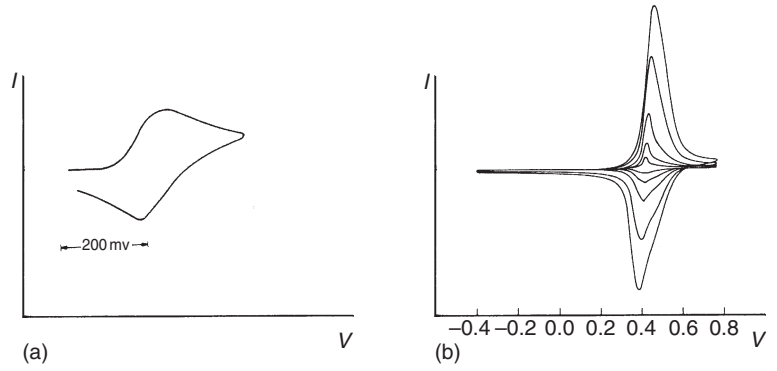

Figure 2 Cyclic voltammograms for poly(vinylferrocene) (a) in dimethylformamide (initial potential 250 mV vs. Ag wire), (b) as a thin film on Pt (various scan rates). Potentials are versus standard calomel electrode. ((a) Adapted with permission of Wiley, USA from Smith, T. W. *et al*., *J. Polym. Sci. Polym. Chem. Ed.*, **1976**, *14*, 2433. (b) Adapted with permission of The Electrochemic Society from Diaz, A. *et al*., *J. Electrochem. Soc.* **1990**, *137*, 503.)

Much of the interest in PVFc arises from the presence of redox-active iron sites attached to the polymer chain. Cyclic voltammetry experiments[64,65,65a] have revealed that the iron sites are non-interacting, as a single reversible oxidation wave is observed as the iron centers interconvert between Fe(II) and Fe(III) states (Figure 2). The intensity of the current per molecule is directly proportional to the molecular weight of the polymer sample.[65,65a] The observation of a single cyclic voltammetric wave in low dielectric constant solvents is in contrast to the situation for polymers where the ferrocene units are in close proximity in the polymer backbone, such as PFSs (see Section 3.4). For the latter materials, evidence for communication between iron centers is provided by the presence of "two" reversible oxidation waves. This has been explained in terms of the oxidation of one Fe center making the neighboring Fe centers more difficult to oxidize.

PVFc is an insulator in its pristine state (i.e., when all iron centers are present as Fe(II)) with a conductivity in the region of 10^{-14} S cm^{-1}.[66,67] Oxidation with, for example, I_2, quinones, or 7,7,8,8-tetracyanoquinodimethane (TCNQ), yields mixed-valent systems in which both Fe(II) and Fe(III) sites are present. These materials display much higher conductivities with values in the semiconductor range (10^{-8}–10^{-6} S cm^{-1}) that were found to be relatively independent of the counteranion present. The maximum conductivities were reached at ca. 50% oxidation of the ferrocene sites as would be expected for a hole-hopping model. Photoconductivity was not detected for the partially oxidized materials.[67] Based on studies of ferrocenium and mixed-valent biferrocene compounds[68,69] as well as Mössbauer spectroscopic analyses of vinylferrocene-containing co-polymers,[60,70] charge has been found to be localized mainly on iron. An electron-hopping (or more accurately hole-hopping) model has been suggested as the mode for electron transfer, as the all-carbon backbone of the polymer is insulating.[67]

The redox behavior of PVFc $(VFc^{0/+})_n$ has been utilized in the construction of a microelectrochemical diode along with a redox-active viologen-based *N,N′*-dibenzyl-4,4′-bipyridinium-based polymer $(BPQ^{2+/+})_n$.[71] The polymers were coated upon microelectrodes and current was found to pass when the negative lead was attached to the $(BPQ^{2+/+})_n$ electrode and the positive lead was connected to the $(VFc^{+/0})_n$ electrode. Thus, as the applied potential approached the difference in redox potentials of the two polymers, current flowed as shown in Equation (5a), and is favorable by ≈0.9 V. However, current does not flow if the applied potential is in the opposite sense as seen in Equation (5b), as it is disfavored by ≈0.9 V. The switching time of this diode, which is controlled by the time required to oxidize or reduce the polymers, was long in comparison with that of the solid-state diodes.[71]

$$BPQ^{+} + Fc^{+} \longrightarrow BPQ^{2+} + Fc^{0} \quad (5a)$$

$$BPQ^{2+} + Fc^{0} \longrightarrow BPQ^{+} + Fc^{+} \quad (5b)$$

12.06.2.2.1.(ii) Other organic polymers with metallocene-containing side-groups

A variety of other organic polymers with metallocene-containing side-groups have been synthesized. However, very few of the materials have been as well studied as PVFc. Crystalline organometallic complexes containing ferrocene

have been shown to possess interesting non-linear optical (NLO) properties[72] and this has led to an interest in the preparation of processable polymeric analogs. For example, a random co-polymer **17** of methyl methacrylate (95 mol%) and a ferrocene-containing methacrylate (5 mol%) have been synthesized using free-radical polymerization in order to evaluate the second-order NLO properties of the material.[73] The molecular weight of **17** was $M_n = 3.0 \times 10^4$ by gel-permeation chromatography (GPC) relative to PS standards and the thermal behaviour of the material was nearly identical to that of poly(methyl methacrylate). After poling, the material was analyzed for second-order NLO properties and was found to possess a second harmonic generation efficiency approximately 4 times that of a quartz standard.[73]

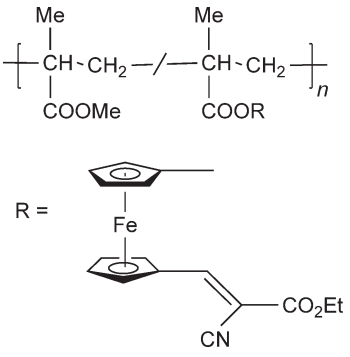

17

A series of very well-characterized polyacrylates, polymethacrylates, and related materials bearing ferrocene side-groups ultimately derived from ferrocenylethanol as starting material has been prepared via AIBN-initiated radical polymerization.[74] The absolute molecular weights were found to be in the range $M_w = 2.9 \times 10^4$–8.7×10^5 by light-scattering measurements.

ROMP of norbornenes with ferrocene side-groups using molybdenum alkylidene initiators has provided a controlled route to organic polymers with metallocene-containing side-groups such as **18** (Equation (6)). Molecular weights for homopolymer **18** were in the range of $M_n = 5{,}090$–$9{,}030$ with PDI values of 1.2 or less. Due to the living nature of the polymerization using the Mo catalysts, block co-polymers could also be prepared (Scheme 2).[75,76] For example, ROMP of norbornene to afford the living polynorbornene **19** followed by addition of the ferrocenyl-norbornene monomer yielded the living diblock co-polymer **20**. Subsequent end-capping with an aldehyde led to the isolated block co-polymers **21** with $M_n = 10{,}460$–$16{,}190$ and PDI values of 1.05–1.07.

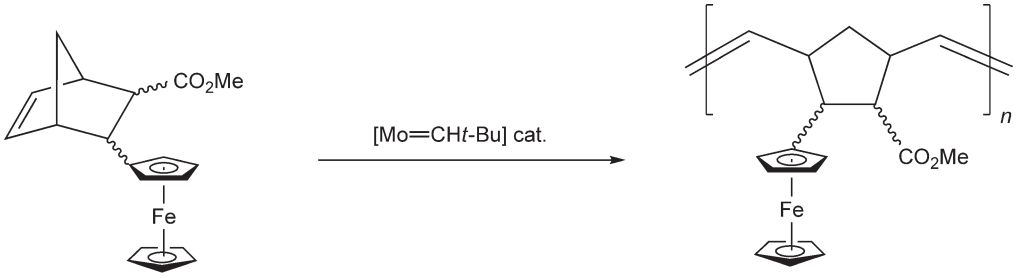

(6)

18

DSC measurements on the block co-polymers revealed two T_g's with values close to those of the individual homopolymers. This thermal behavior is consistent with a block rather than a random co-polymer structure. As was found for PVFc, cyclic voltammetry measurements showed the presence of one reversible oxidation wave, consistent with the existence of non-interacting redox sites. The living chain end of the polyferrocenylnorbornenes could also be capped with pyrene. The presence of the neighboring ferrocene moieties led to the emission of the pyrene unit being quenched by a factor of 30 compared to emission from 1-vinylpyrene.[76] The quenching mechanism might involve electron transfer from the ferrocene group, or energy transfer as the ferrocene *d–d* absorption band and the pyrene emission spectrum partially overlap.

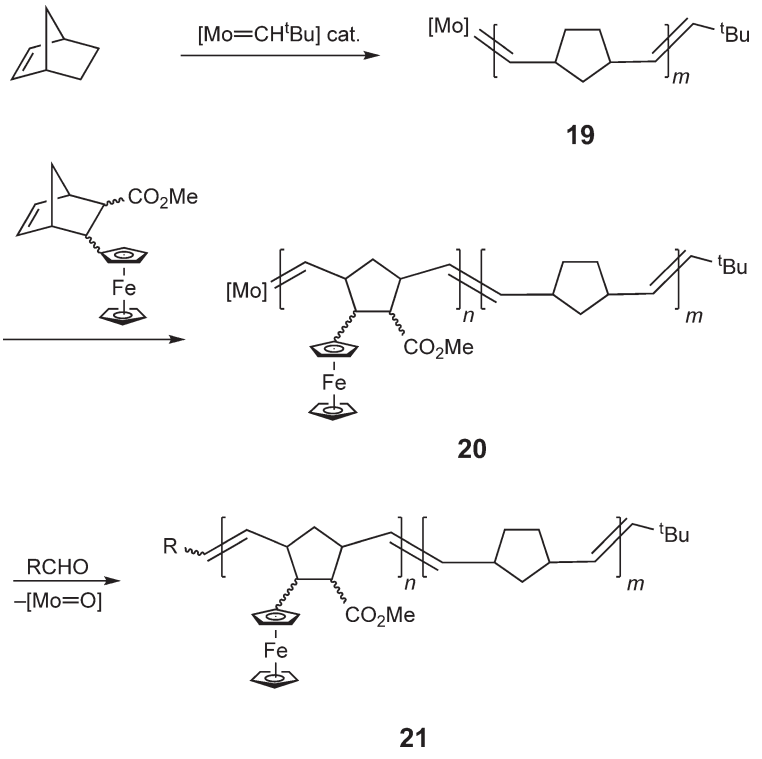

Scheme 2

The synthesis of poly(ethynylferrocene) (**22**, M = Fe) has been studied by a number of different research groups.[77–80] In 1995, well-defined materials with controlled molecular weights up to 1.4×10^4 (M_n) with fairly narrow polydispersities (<1.3) (values determined by GPC using a light-scattering detector) were prepared by living polymerization using an Mo alkylidene initiator. In addition, examples of the analogous poly(ethynylruthenocene) (**22**, M = Ru; $M_n = 6.7 \times 10^3$–1.6×10^4, PDI = 1.14–1.24) were also prepared.[81] The living polymers could be terminated with pyridine carboxaldehyde and the tertiary nitrogen subsequently quaternized with methyl iodide. The charged systems were found to exhibit a more intense, red-shifted absorption in the UV–VIS spectrum than the corresponding uncharged systems.

Polypyrroles and polythiophenes with pendant ferrocene groups (e.g., **23**) have also been prepared using electropolymerization techniques.[82] Studies of these materials using *in situ* conductivity measurements revealed that the redox conduction, due to hole hopping between the ferrocene units, was enhanced by a decrease of the Fc–backbone distance and by conjugation of the organometallic group with the polymer backbone (as in polymer **23** which possesses a redox conductivity of ca. 8×10^{-3} S cm^{-1}).

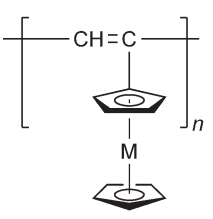

M = Fe or Ru

22

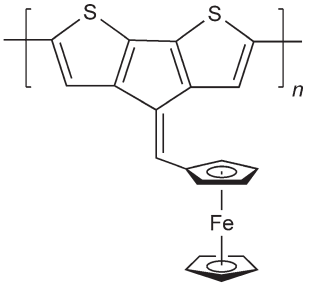

23

Ferrocene side-groups have also been introduced at low loadings into side-chain liquid crystalline polymers, with the aim of exploring the effect of redox activity on the properties of the materials. For example, the redox-active co-polymers **24** undergo reversible oxidation with Cu(II) salts or *p*-benzoquinone to generate the liquid crystalline ionomers **25** (Equation (7)).[83] Introduction of the neutral ferrocene moiety has only a minor influence on the liquid crystalline properties. However, after oxidation, significant effects on mesophase stability were noted. Thus, small-angle X-ray scattering (SAXS) and dynamic mechanical analysis showed that the ferrocenium groups and counteranions form ionic clusters which physically cross-link the material and give rise to elastomeric properties.

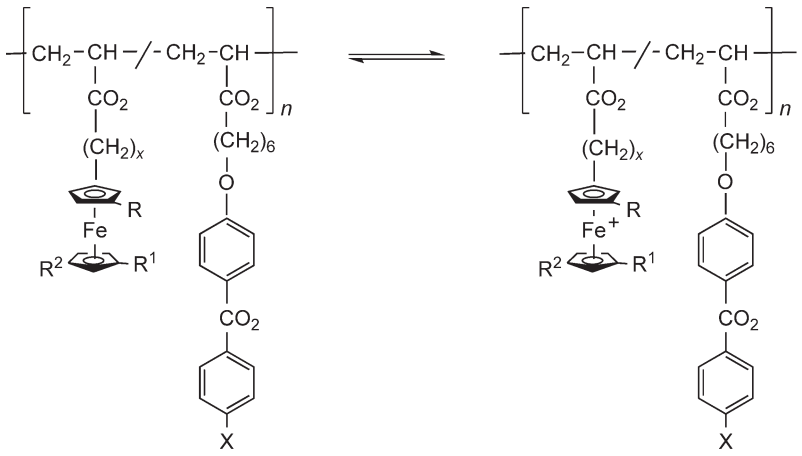

X = CN or OMe

24 **25**

(7)

This type of approach has been extended to main-chain liquid crystalline polymers **26** with low loadings of ferrocene groups in the side-group structure. In some cases, changes in liquid crystalline morphology from nematic to smectic were observed upon oxidation, as the formation of ionic domains facilitates the generation of layered structures (Figure 3).[84,84a]

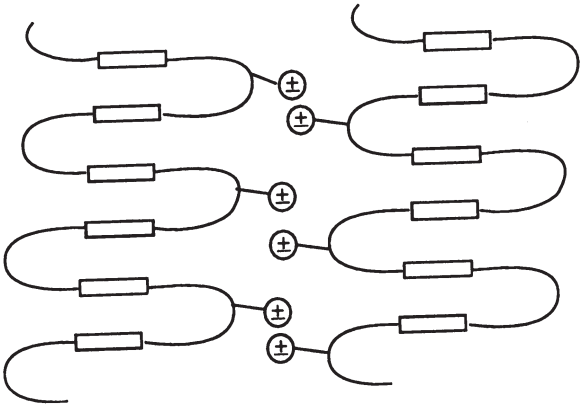

Figure 3 Formation of layered structures induced by oxidation of ferrocene groups in polymers **26** and the consequent formation of ionic clusters of cations and counteranions. The rigid group consists of a mixture of nitroxide isomers. (Reproduced with permission of Wiley-VCH from Wilbert, G. *et al.*, *Macromol. Chem. Phys.* **1997**, *198*, 3769.)

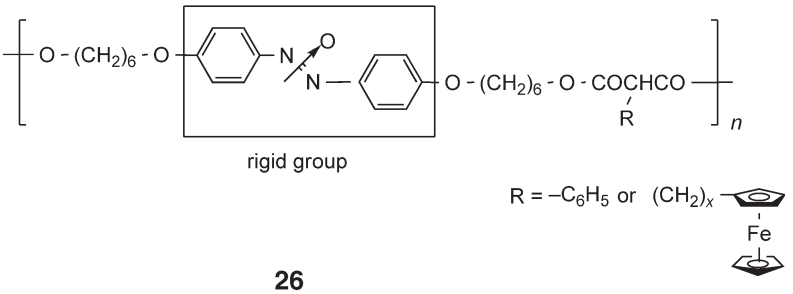

26

Ferrocene-containing polymers are also of interest for biomedical applications. For example, polypeptides with ferrocene side-groups have attracted attention as a range of water-soluble ferrocenium salts have been found to possess significant antiproliferative activity against various tumors. The water-soluble polymers **27** and analogs also show similar activity.[85] In addition, the cationic ferrocene polymers **28**, derived from a poly(allyl amine), have been used in multilayer biosensor devices.[86] Sequential layer-by-layer deposition of **28** and anionic glucose oxidase can be used to prepare alternating cationic–anionic polymer multilayer structures on alkane thiol-modified gold electrodes. Catalysis of the oxidation of glucose was detected and indicates that the ferrocene groups mediate electron transfer between reduced glucose oxidase and the gold electrode. In the absence of such electrode mediators, electron transfer is extremely slow as a thin insulating protein sheath surrounds the redox center in the enzyme. Analogous results have been reported for related systems based on ferrocene-modified organic polymers (e.g., the conjugated ferrocenyl-substituted polyaniline **29**).[87,88] Several examples of other redox metallopolymers which function in this manner are discussed in Section 2.3.2.

In general, much less work has been reported on side-chain polymers containing metallocenes other than ferrocene. For example, ruthenium and osmium analogs of PVFc have been described, but their characterization has been fairly limited.[63,89,90] Poly(vinylruthenocene) is reported to be a light yellow solid with a T_g of >250 °C and the preparation of samples with molecular weights of up to $M_w = 1.2 \times 10^5$ with broad molecular weight distributions (PDI = ca. 6) has been reported via the free-radical polymerization of vinylruthenocenes in benzene with AIBN as the initiator.[90] The polymers were proposed to possess a branched structure as a result of chain transfer to polymer. Co-polymers with other organic vinyl monomers have also been prepared.[90] Poly(vinylruthenocene) and poly(vinylosmocene) have been tested as preheat shields for targets in inertial confinement nuclear fusion.[89]

Organic polymers have also been used as supports for catalytically active early transition metal metallocenes as well as a broad range of other metal-based catalytic species (see Section 2.3.3). Macroporous PS beads, which are cross-linked with 1% or 2% divinylbenzene, have been particularly popular as a support. Generally, the beads are used in a swollen state, which is achieved by immersion in a suitable solvent, so that substrates can access the reactive sites. As an example, beads containing the organotitanium units **30**, derived from poly(chloromethylstyrene) (Equation (8)), were studied in the 1970s, and excellent activity for the hydrogenation of 1-hexene was demonstrated.[91–93] Analogous systems containing zirconocene units have also been studied for the polymerization of olefins and exhibit significant promise.[94,95]

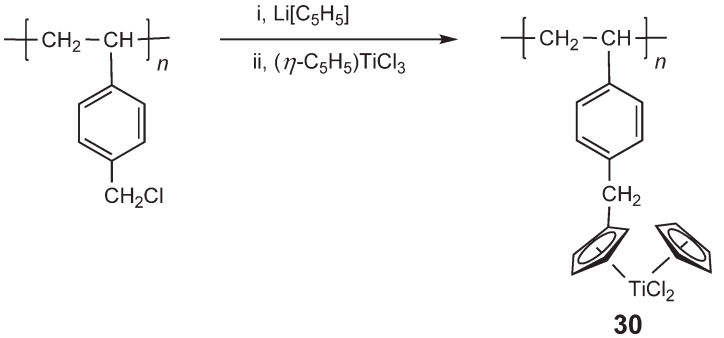

(8)

30

12.06.2.2.2 Inorganic polymers with metallocene side-groups

Many examples of "inorganic" polymers with metallocene-containing side-groups also exist. Most of the polymers prepared have been based on main chains of polyphosphazenes, polysilanes, polysiloxanes, and polycarbosilanes. These materials are surveyed in the following sections.

12.06.2.2.2.(i) Polyphosphazenes with ferrocene- or ruthenocene-containing side-groups

The earliest and most well-developed route to polyphosphazenes involves the thermal ROP of cyclic phosphazenes bearing halogen substituents at phosphorus. Use of this method and subsequent halogen replacement with alkoxides has led to the synthesis of ferrocene- and ruthenocene-containing polyphosphazenes **31** and **32** with molecular weights (M_w) in excess of 2×10^6.[96,97]

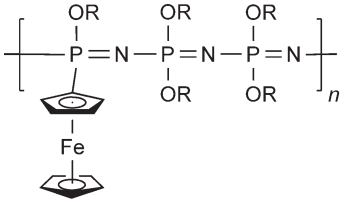

31

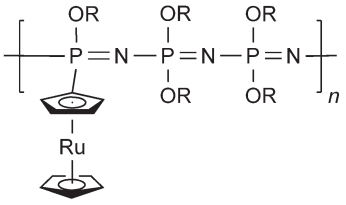

32

In general, cyclotriphosphazenes with less than three halogen substituents do not undergo thermal ROP. However, a range of cyclic phosphazenes without any halogen side-groups **33** have been found to polymerize, provided that transannular ferrocenyl substituents are present. ROP of **33** yields polymer **34** (Equation (9)) with molecular weights as high as $M_w = 1.8 \times 10^6$ (PDI = 6.2).[98,99] In most cases, the presence of a small amount of an initiator such as $[NPCl_2]_3$ is necessary for polymerization to occur. X-ray crystallographic studies of several of these strained ferrocenyl organocyclotriphosphazene monomers **33** have shown that the phosphazene ring is forced into a high energy, non-planar conformation.[100] By contrast, in most cyclotriphosphazenes, the phosphorus–nitrogen ring is virtually planar.

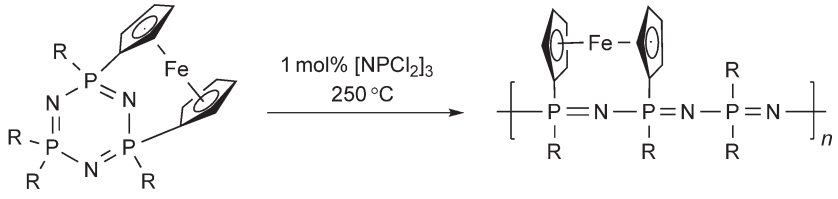

(9)

33 **34**

R = non-halogen substituent

Polymers **31** and **34** (as well as co-polymers bearing both ferrocene and ruthenocene moieties) have been partially oxidized with iodine, resulting in weakly semiconducting materials. These materials have also been deposited on electrode surfaces where the polymers act as electrode mediator coatings that aid electron transfer between the electrode and redox-active species in solution.[101]

Polyphosphazenes with ferrocenyl substituents **35** have also been synthesized via the functionalization of poly(methylphenylphosphazene) and related polymers by means of a deprotonation–electrophilic addition strategy (e.g., see Equation (10)).[102,103] This versatile reaction sequence has yielded materials with, for example, degrees of substitution of 45% and 36% for polymers **35** (R = H and Me), respectively. The molecular weights of the polymers were $M_w = 2.0 \times 10^5$ and 1.5×10^5 for **35** (R = H and Me), respectively (with PDI values of 1.4–2.0). The glass transition temperatures increased in comparison with the unsubstituted polymer ($T_g = 37\,^\circ C$) for **35** with values of 92 °C (R = H) and 87 °C (R = Me).

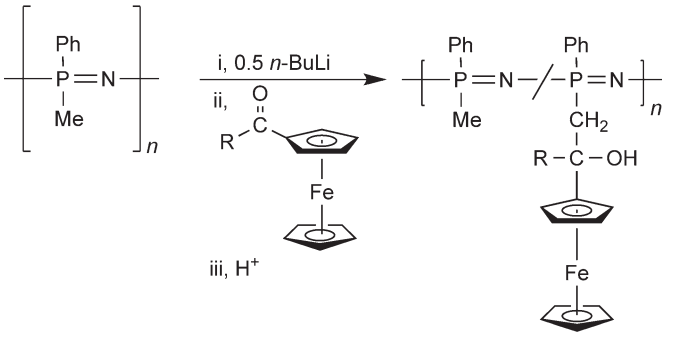

(10)

35

12.06.2.2.2.(ii) Polysilanes, polysiloxanes, and polycarbosilanes with metallocene side-groups

The synthesis of polysilanes bearing low loadings of ferrocene substituents **36** has been reported via Wurtz coupling (Equation (11)).[104] Random co-polymers with weights (M_w) up to 3.9×10^5 were isolated from mixtures of high and low molecular weight fractions. The ratio of methylphenylsilane to methylferrocenylsilane segments ranged from 6 : 1 to 27 : 1. In common with other polysilanes, these materials were photosensitive and depolymerized upon exposure to UV light. However, interestingly, the co-polymers displayed significantly greater stability than a corresponding sample of poly(methylphenylsilane), indicating that ferrocene moieties bound to the polymer chain provided a degree of stabilization for the polysilane backbone toward photodegradation. Cyclic voltammetry experiments[65a] revealed two oxidation waves for the co-polymers. The first wave, due to oxidation of iron sites, was reversible, whereas the second, irreversible oxidation at higher potential was assigned to oxidation of the polysilane backbone. No electrochemical interaction was observed between neighboring iron sites or between iron sites and the polymer backbone.

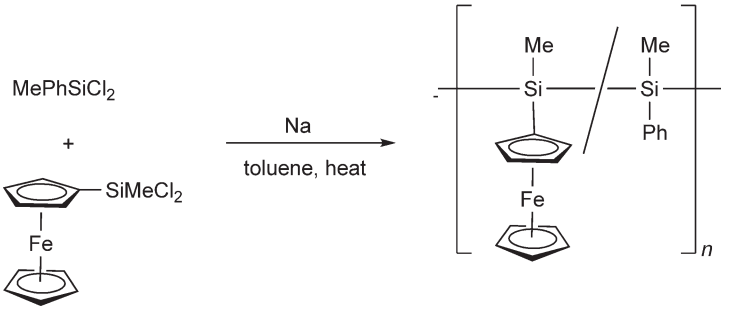

(11)

36

Polysiloxane random co-polymers (with molecular weights of 5,000–10,000) with pendant ferrocene groups have recently been synthesized **37** via hydrosilylation of vinylferrocene or 9-ferrocenyl-1-nonene with a poly(methylhydrosiloxane)-*r*-poly(dimethylsiloxane) random co-polymer (Equation (12)). These materials were used as amperometric biosensors for the detection of glucose.[105] In this case, the polymers effectively mediated electron transfer between reduced glucose oxidase and a conventional carbon paste electrode. The response of the sensor to glucose was dependent upon the nature of the polymeric backbone. The optimal response was achieved by finding a compromise between increased polymer flexibility and decreased spacing between individual relay (i.e., ferrocene) sites.

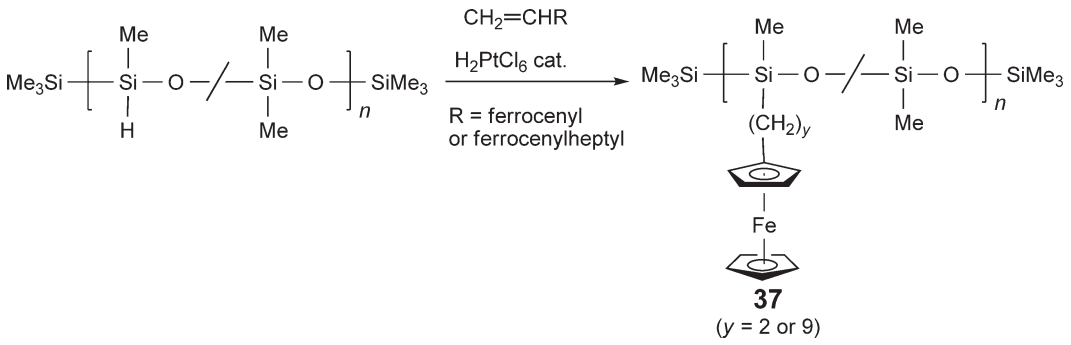

(12)

The hydrosilylation strategy has also been used to prepare well-characterized side-chain liquid crystalline polymers containing ferrocene.[106] Grafting of vinyl-terminated mesogens onto poly(methylhydrosiloxane-*r*-dimethylsiloxane) **38** yielded materials with 1,1′- **38a** and 1,3-disubstituted **38b** ferrocene units (Equation (13)). The molecular weights were in the range $M_w = 2.5 \times 10^3$–3.1×10^3 and the PDI values were 1.4–1.6. The liquid crystalline nature of the resulting polymers was investigated by polarizing optical microscopy, DSC, and X-ray diffraction. The materials were found to display "layered" type smectic A and/or smectic A and smectic C phases, depending specifically on the length of the flexible chains connected to the ferrocene unit.[106] For example, polysiloxane **38a** with $m = 6$ and $n = 12$ showed a $T_{lc} = 136\,^{\circ}C$ where the material melted to form a smectic C phase. At 140 °C, this transformed into a smectic A phase, and at the clearing temperature $T_{cl} = 183\,^{\circ}C$ an isotropic melt was formed. The proposed supramolecular organization of the smectic C phases is shown in Figure 4.

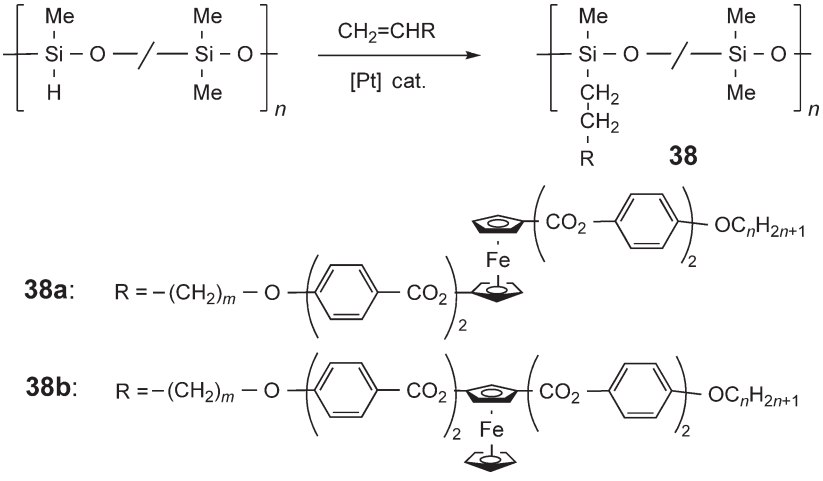

(13)

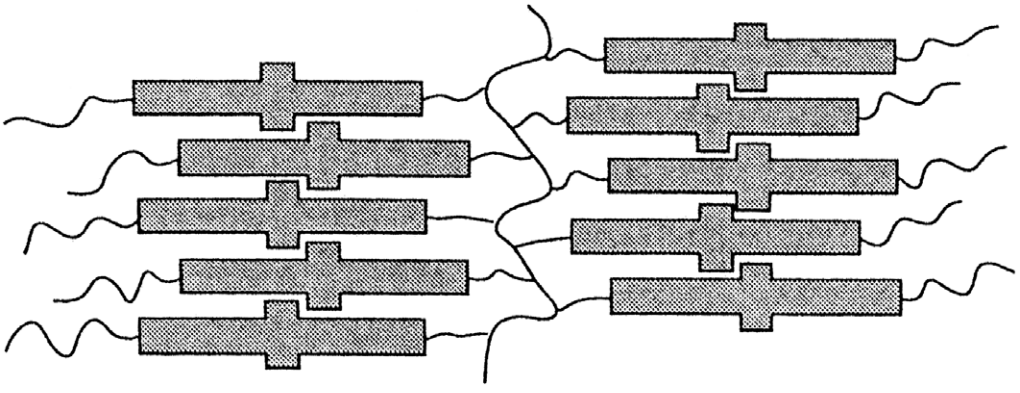

Figure 4 The proposed supramolecular organization of the ferrocene-containing side-groups in the smectic C phases of polymers **38**. (Reproduced with permission of The American Chemical Society from Deschenaux *et al.*, *Macromolecules*, **1998**, *31*, 5647.)

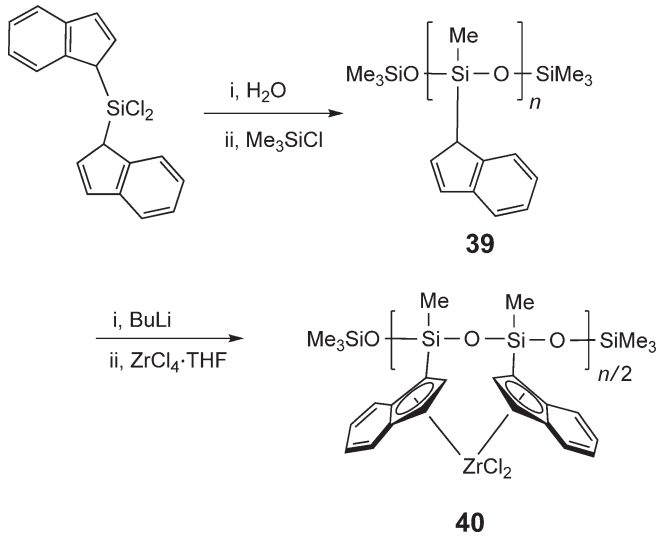

Scheme 3

Polysiloxanes with pendant zirconocene units have also been explored as olefin polymerization catalysts. For example, polysiloxanes **39** containing indenyl groups have been synthesized via hydrolytic condensation of the corresponding dichloroorganosilanes.[107] Treatment with BuLi followed by the metal halide was claimed to yield materials with idealized structure (**40**; Scheme 3). However, no structural characterization of the products was reported apart from their low molecular weights according to GPC measurements ($M_w = 700$–$3{,}600$). It seems likely that chain cleavage reactions occur in the BuLi deprotonation step and cross-linking processes on addition of the Zr halide are highly likely. Nevertheless, appreciable activities for the polymerization of ethylene and propylene were detected for **39** and analogous species in the presence of methylalumoxane.[107]

As an alternative approach, polycarbosilanes **42** bearing pendant zirconocene moieties have also been prepared by the ROP of the spirocyclic monomer **41** (Equation (14)).[108] In this case, the materials were structurally characterized but the soluble fraction was of low molecular weight ($M_w <$ ca. 3,000) and the high molecular weight fraction was insoluble in organic solvents. In the presence of activators, both fractions functioned as ethylene polymerization catalysts with moderate activity.[108]

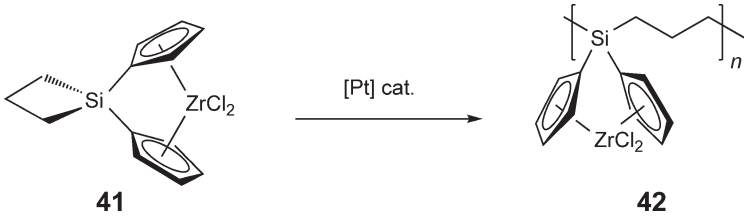

(14)

12.06.2.3 Other Side-chain Metallopolymers

12.06.2.3.1 Polymers with π-coordinated metals

The radical polymerization of various other organometallic vinyl monomers has been well studied. For example, in 1978, it was shown that vinylcymantrene **43** undergoes radical homopolymerization in the presence of AIBN as initiator at 50–80 °C in organic solvents such as benzene to yield poly(vinylcymantrene) **44** (Equation (15)).[109] Molecular weights varied from $M_w = 5 \times 10^3$ to 3.6×10^5 with broad PDI values in the range 3.2–8.9.

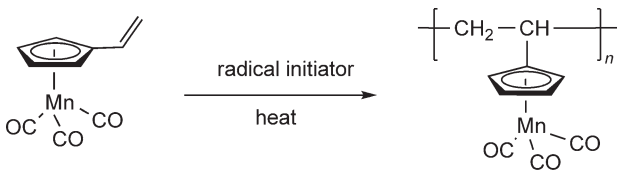

43 44 (15)

On photolysis, co-polymers of vinyl(methylcymantrene) with octyl methacrylate have been shown to lose CO and generate polymers **45** possessing 16-electron Mn centers, which coordinate to N_2 to yield **46** (Equation (16)). The coordination is reversible and can be used to prepare membranes that exhibit facilitated transport of this gas.[110] Comparison of the diffusion coefficient for normal "Henry-mode" diffusion and the facilitated "Langmuir-mode" diffusion, due to the mediation of the manganese centers which function as N_2 carriers, showed that the latter mechanism contributes substantially. Moreover, as expected for this interpretation, the contribution from the facilitated transport mode increased as the loading of the Mn sites became higher.

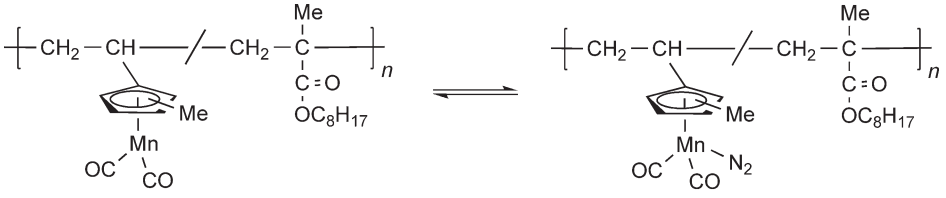

45 46 (16)

The attachment of cymantrene groups to polymers has attracted interest for other reasons. Studies have shown, for example, that adherent, abrasion-resistant coatings are formed on metals when thin films of the Mn-containing polymer are subjected to irradiation with UV light.[111] The polymerization of styrene tricarbonylchromium **47** has also been studied.[112] This species is available from the reaction of styrene with $Cr(CO)_3(NH_3)_3$. Although the Cr monomer **47** resisted attempts at homopolymerization, co-polymerizations with styrene, methyl acrylate, as well as with **41** to yield bimetallic polymers **48** were possible (Equation (17)). In addition, co-polymerization with vinylferrocene afforded co-polymers of low molecular weight (M_n = ca. 4,000). A variety of other organometallic vinyl momomers **49** has been successfully polymerized to yield polymers **50** that contain pendant Cr, W, and Ir carbonyl moieties (Equation (18)).[113]

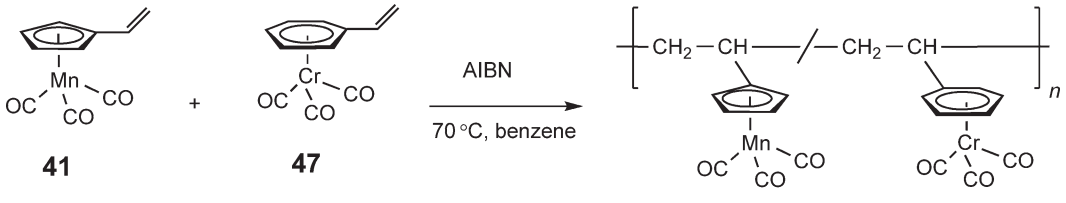

41 47 48 (17)

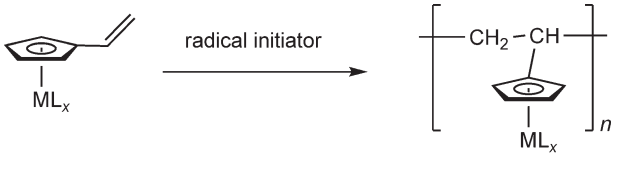

49 50 (18)

ML_x = $Cr(NO)(CO)_2$, $W(CO)_3Me$, or $Ir(CO)_2Cp$

12.06.2.3.2 Polymers with other pendant metal-containing units including the area of polymer-supported catalysts

Many other metal-containing groups have been attached to organic polymers. Polymers **51** containing Pd–C σ-bond linkages have been successfully prepared by the radical polymerization of *p*-substituted styrene derivatives (Equation (19)).[114] Substituents bearing main group metals have been appended to vinyl polymer backbones. For example, polymethacrylates with $SnBu_3$ substituents can be prepared via free-radical co-polymerization of the respective monomers or treatment of poly(methyl methacrylate)-*r*-poly(methacrylic acid) with $(Bu_3Sn)_2O$.[115] These materials have been explored as antifouling paints on ships and offshore oil platforms. Oxotitanium clusters have been similarly incorporated to generate novel inorganic–organic hybrid materials.[116] Polyaminophosphazenes with coordinated $PtCl_2$ units are of interest as tumor-inhibiting materials.[117] In addition, ROMP of norbornenes bearing pendant cationic organoiron substituents bound through arene–metal bonds has yielded redox-active organoiron polymers such as **52** (Equation (20)). These materials show reversible one-electron reduction waves at −50 °C by cyclic voltammetry, whereas the electron-transfer process to generate 19-electron neutral iron sites was irreversible at room temperature.[118]

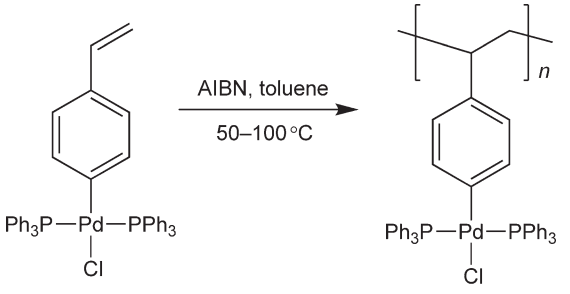

(19)

51

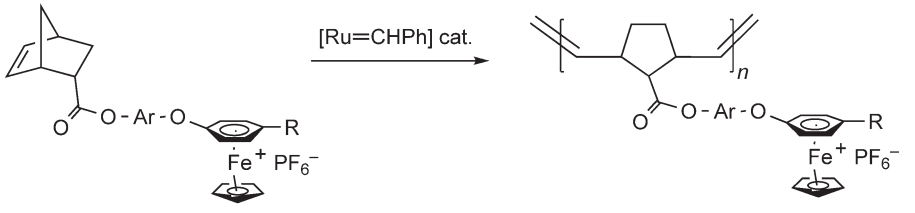

(20)

Ar = *p*-C_6H_4, R = Me

52

Of particular significance is the large number of catalytically active metal complexes that has been bound to polymer supports (such as cross-linked PS) by various methods.[119,119a–119c] Much of the work has been stimulated by the discovery of solid-phase peptide synthesis introduced by Merrifield in 1963 that culminated in his award of the Nobel Prize for chemistry in 1984. This area is of considerable interest for the preparation of polymers and also, and more generally, in organic synthesis, as separation of the products from the catalyst is, in principle, achieved cleanly and easily. Such systems are of particular interest for combinatorial chemistry as they generally offer the possibility of rapid combinatorial screening of libraries of catalysts. However, it should be noted that polymer-supported organic reactions can show significant differences with respect to substrate selectivity, rate, product distribution, and product stereochemistry for particular reactions.[119,119a–119c] In addition, leaching of the metal complex from the polymeric support over time is a common problem.

The vast area of polymer-supported catalysts is too broad to cover systematically in this chapter and readers are referred to Chapter 12.14. In addition, as the loadings of metal ions on the polymers are generally very low, the cited reviews are a more appropriate source of information.[119,119a–119c] We have already discussed supported catalytically active metallocene complexes in Section 2.1. Some illustrative examples of the types of transformations that have been achieved are shown in Table 1.

12.06.2.3.3 Block co-polymers with pendant metal-containing groups

Block co-polymers exhibit outstanding potential for a variety of applications as a result of their self-assembly into supramolecular structures (see Section 1.2.4). However, the exploration of organometallic multi-block materials was only begun in the early 1990s. Block co-polymers derived from the living anionic polymerization of vinylferrocene have been already briefly mentioned in Section 12.06.2.2.1.(i). In this section, side-chain metal-containing block co-polymers are surveyed. Examples of block co-polymers with metals in the main chain are discussed in Section 3.X.

Table 1 Representative reactions with polymer-supported catalysts

Catalytic metal	*Polymer support*	*Catalytic reaction*	*References*
Ru, Rh	Phosphinated polystyrene	Olefin isomerization	89
Rh	Phosphinated polystyrene	Olefin hydroformylation	90
Rh	Phosphinated polystyrene	Pyridine synthesis	91
Pd	Cyanomethylated polybenzimidazole	Alkene oxidation	92
Ni	P/O ligand on polystyrene	Ethylene polymerization	93
Cu	Nitroxide-functionalized polystyrene	Oxidation of alcohols	94

12.06.2.3.3.(i) Approaches using ROMP

ROMP provided the first examples of block co-polymers with pendant metal-containing groups. As discussed earlier, ROMP of substituted norbornenes has been used to prepare block copolymers with ferrocene side groups (see Section 12.06.2.2.1.(ii)). The technique of using norbornenes with pendant metal-containing groups is very versatile and also allows the preparation of block co-polymers that contain Sn, Pb, Zn, Pd, or Pt in the side-group structure.[47,120,121] The procedure for the case of Sn is illustrated in Schemes 2–5.[120] Addition of the Sn-containing norbornene derivative to living polynorbornene generated with a tungsten alkylidene catalyst, followed by capping with 1,3-pentadiene, which is unreactive toward the Sn sites but reactive with the chain end, afforded diblock co-polymer **53**. Thin films of the air sensitive metal-containing block co-polymers were characterized by transmission electron microscopy (TEM) and showed the presence of phase-separated microdomains in which the metal was confined to the domains derived from the metal-containing block.

Phase-separated metal-containing block co-polymers formed by ROMP offer interesting possibilities for the controlled formation of semiconductor and metal nanoclusters, which are of intense interest as a result of their size-dependent electronic and optical properties, as well as their catalytic behavior. Zinc-containing block co-polymers generated by ROMP have been shown to form ZnS nanoclusters within the phase-separated organozinc domains upon treatment with gaseous H_2S.[47] The cluster sizes generated were up to 30 Å and their small size led to quantum size effects. For example, a band gap of 5.7 eV was measured for the roughly spherical 30 Å clusters, which is substantially larger than that for bulk ZnS (3.5 eV). Similarly the Pt- or Pd-containing materials **54** were prepared by sequential ROMP of a metal-containing norbornene and methyltetracyclodecene.[121] Subsequent treatment of the Pt-containing materials with molecular H_2 led to the formation of Pt nanoclusters within the microphase-separated domains. TEM images for the Pd-containing materials, which possess a lamellar morphology before and after H_2 treatment, are shown in Figure 5.

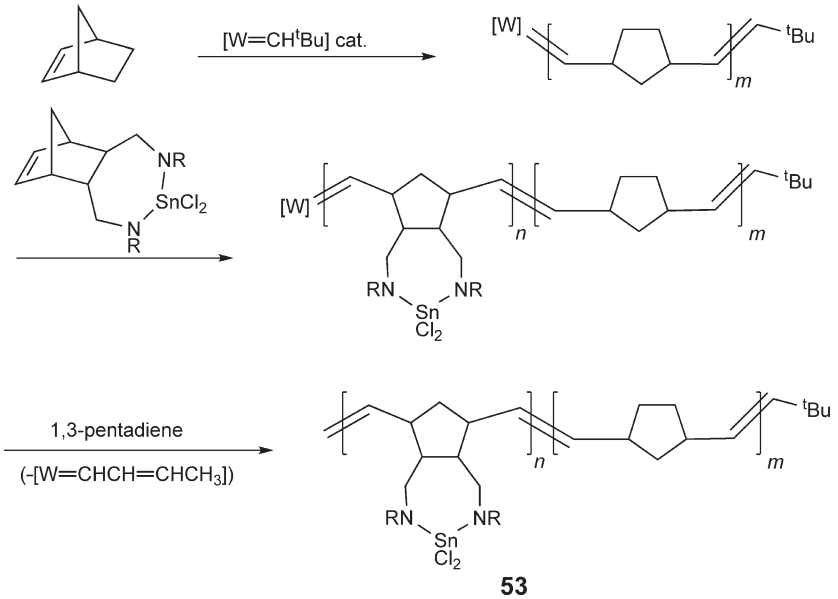

53

Scheme 4

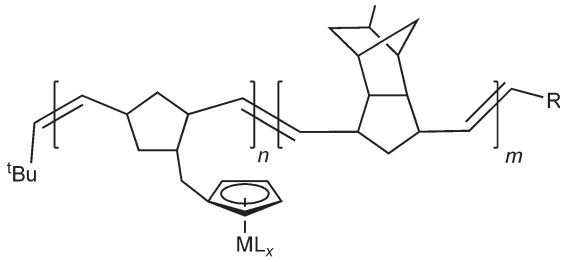

54

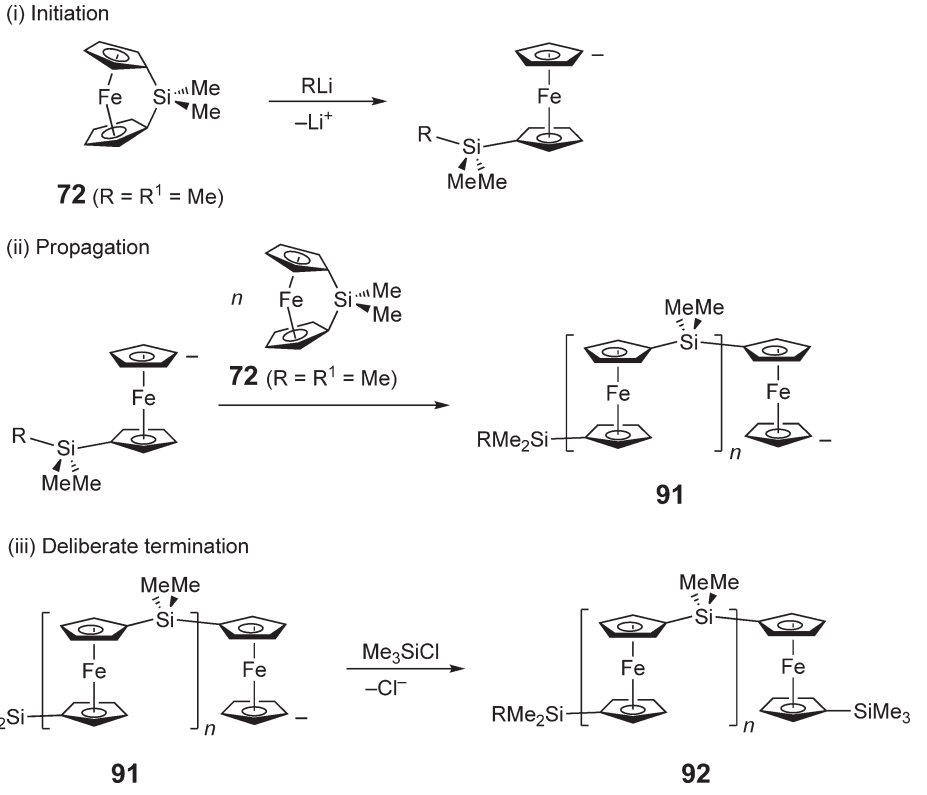

Scheme 5

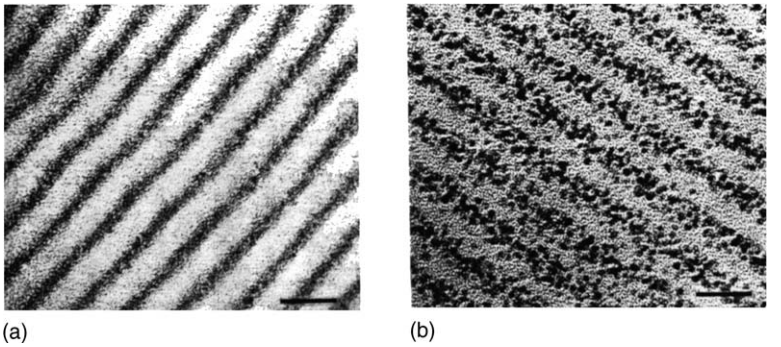

Figure 5 TEM images of thin films of a block co-polymer **54** (M = Pd) showing a lamellar morphology (a) before and (b) after treatment with H_2 showing the growth of Pd nanoclusters in the phase-separated Pd-containing domains. Regions containing Pd are dark as a result of the efficient electron scattering by this element. (Scale bar represents 2.5 nm.) (Reproduced with permission of The American Chemical Society from Chan, Y. N. C. *et al.*, *Chem. Mater.*, **1992**, *4*, 885.)

12.06.2.3.3.(ii) Coordination to olefinic substituents in preformed blocks

The coordination of metals to various other pendant sites present in block co-polymers has also been explored. For example, metal coordination to the olefinic groups present in the polybutadiene (PB) blocks of polystyrene-*b*-polybutadiene (PS-*b*-PB) diblock and PS-*b*-PB-*b*-PS triblock copolymers has been reported.[122] This was achieved by the reaction of PS-*b*-PB with various metal complexes such as $Fe_3(CO)_{12}$, $[Rh(\mu\text{-}Cl)(CO)_2]_2$, $PdCl_2(NCMe)_2$, and $PtCl_2(NCMe)_2$ to afford materials with Fe-, Rh-, Pd-, and Pt-containing blocks. Intermolecular cross-linking was possible but solubility in organic solvents was maintained and micellization was observed in most cases. However, on solvent removal and drying, many of the polymers became insoluble.

12.06.3 Main-Chain Polymetallocenes with Short Spacer Groups

12.06.3.1 Introduction

For many applications, side-chain metal-containing polymers are sufficient. However, to access the most profound alterations in polymer properties that arise from the presence of metal atoms in a polymer structure, incorporation in the main chain is required. Potential advantages of including metals in the backbone of a polymer rather than the side-group structure include the following:

(i) The influence of the varied geometries of transition metal centers on the conformational and thermophysical properties would be more significant.
(ii) The development of materials with properties that depend on the ability of the metal atoms to interact with one another in a controlled manner would be facilitated, as smaller changes accompany backbone motions compared with those of side-groups.
(iii) Access to interesting charge-transport properties and other characteristics that depend on delocalization effects would be favored as the metal could potentially be placed directly in the conjugation pathway.
(iv) Leaching of the metal from the polymer would be expected to be less problematic and this might be significant for catalytic or preceramic applications.

Although the first polymers with metals in the side chains were prepared as early as the mid-1950s, the development of main-chain metal-containing polymers has been much slower. This is particularly the case where the metal atoms are linked together by short spacers and their close spatial proximity might be expected to give rise to interesting properties due to the presence of metal–metal interactions. This section focuses on materials of this type, which contain metallocene units in the main chain, as polymers possessing the π-coordinated metallocene units dominate this particular area. Analogous materials with longer spacers, defined as >3 atoms between the π-coordinated metal centers, are structurally much more diverse but less well studied, and are discussed in Section 12.06.4.4.

As with the case of side-chain metal-containing polymers (Section 12.06.2), the development of main-chain polymers that incorporate metallocene units has represented a major area of research. Since the discovery and structural elucidation of ferrocene, the prototypical metallocene, a vast organic chemistry for this species has been demonstrated, and the reversible one-electron oxidation to the blue ferrocenium ion has been much exploited.[50,51,123,124] The exciting possibilities for polyferrocenes with short spacers between the metal-containing units are illustrated by the results of detailed studies of dimeric species. Thus, oxidation of biferrocenes and biferrocenylenes has provided access to mixed-valent species such as **55** and **56**, respectively, where the unpaired electrons are delocalized on a variety of timescales depending on the substituent, counterion, and solid-state environmental effects.[125,126] Many of the other properties of molecular ferrocenes also make their incorporation into polymer structures highly desirable. For example, liquid crystalline ferrocenes have been prepared and ferrocene-based charge-transfer materials such as **57** have attracted considerable attention with respect to their cooperative magnetic properties[127,52] (see Chapter 12.05 on the topic of organometallic mesogens and Chapter 12.07 on the topic of organometallic magnetic compounds). Equally encouraging are the facts that ferrocene is easy to prepare, cheap and commercially available, and air, moisture, and thermally stable.

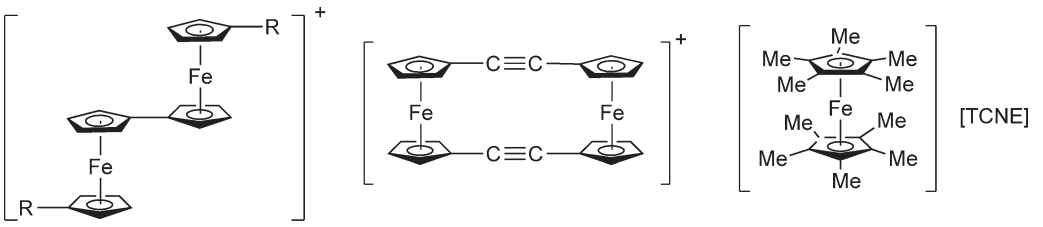

55 56 57

As described in Section 12.06.2, attempts to incorporate ferrocene into the side-chain structure of polymers have been very successful. In this case, a variety of high molecular weight materials have been prepared with either organic or inorganic main chains by subtle modifications of existing synthetic methodologies. The incorporation of ferrocene into the main chain of polymers where the organometallic groups are joined by long spacers (i.e., with ca. >3 atoms) has also been productive, as discussed in Section 12.06.4.4. In such cases, advantage can be taken of the facile derivatization of ferrocene to access well-defined difunctional monomers, which can then be productively used in step-growth polycondensation reactions. High molecular weight polymeric materials result, provided that the coupling methodology is compatible with the presence of the organometallic nucleus. In contrast to the situation with side-chain polymers and main-chain materials with long spacer groups, until the early 1990s the synthesis of main-chain polymers that contain ferrocene units in close proximity to one another had met with very limited success. The problem involving the synthesis of such materials arises from the fact that suitable, well-defined difunctional monomers are difficult to prepare in a high degree of purity. Under such conditions, step-growth polycondensation reactions are prone to yield low molecular weight oligomeric products. The discovery of ROP routes to such materials in 1992 represented a key solution to this problem (see Sections 3.3. and 3.4).[128] Such polymerizations proceed via a chain growth route, which tends to yield high molecular weight polymers without the stringent stoichiometry and conversion requirements characteristic of step-growth polycondensations (ref. IM book).

Despite these breakthroughs, it is very apparent that the incorporation of metallocenes other than ferrocene into polymer structures has been developed to a much lesser extent, and for the twenty-first century, this still remains a substantial synthetic challenge. This is despite the fact that many other metallocenes are readily accessible, stable and also exhibit interesting physical, redox, and catalytic properties.[123,125,129] The lesser ease of derivatization of most other metallocenes compared to ferrocene and, in some cases (e.g., that of ruthenocene), the problem of relative expense have clearly been important factors which have held back synthetic developments in this area. Nevertheless, it is anticipated that the development of main-chain polymers based on other metallocenes is likely to be very fertile ground for future research (for some very promising recent results, see Tamm and Braunschweig).

Excellent, critical reviews of the general field of main-chain metallocene-based polymers were published as early as 1970.[53] At this time, the authors were more than aware of the limitations in the characterization of the vast majority of the materials reported until then. Indeed, the authors stated that many of the structures assigned to the polymers in the article were "hypothetical and need rigorous analytical verification, and the description of experimental procedures and polymer properties more often than not has been superficial or has been lacking altogether".[130] Although the earlier, pioneering work in the area will be mentioned, this section focuses on the more recent developments, as many of the materials reported earlier were of low molecular weight, poor solubility, and were inadequately characterized.

12.06.3.2 Polymetallocenylenes and Polymetallocenes with Short Spacers via Condensation Routes

12.06.3.2.1 Polymetallocenylenes

The earliest routes to polyferrocenylene involved a range of poorly defined free-radical recombination processes (Equation (21)). The yields of soluble material of idealized structure 58 were generally low as were the molecular weights (<7,000). In several cases, more recent investigations have shown that the isolated materials possess structures much more complex than assumed.

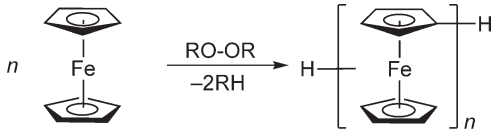

(21)

58

The most impressive early results on polyferrocenylenes in terms of product yield, molecular weight, and purity were obtained in 1979 using the step-growth polycoupling reaction of equimolecular amounts of dilithioferrocene·TMEDA (where TMEDA = *N,N,N′,N′*-tetramethylethylenediamine) with diiodoferrocene at temperatures not exceeding 25 °C (Equation (22)).[42] Thus, a total yield of 85% of light tan, soluble, spectroscopically well-defined (all heteroannular), amorphous, and diamagnetic polyferrocenylene **59** was produced with $M_n < 4{,}000$ (determined by vapor-pressure osmometry, VPO). Subsequent fractionation yielded small quantities of samples with M_n values of up to ca. 10,000.

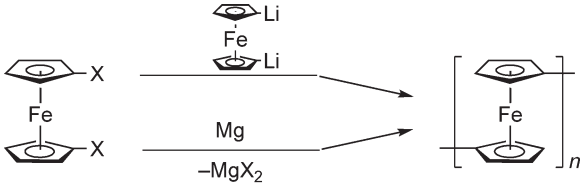

(22)

59

Following this development, dehalogenation of dihaloferrocenes with magnesium produced semicrystalline polyferrocenylene **59** in good yield (Equation (22)).[131,132] When a benzene-insoluble fraction of the product ($M_n = 4{,}600$) was partially oxidized with 7,7,8,8-tetracyanoquinodimethane (TCNQ), the electrical conductivity of the resulting material ($\sigma \sim 10^{-2}\,S\,cm^{-1}$) was found to be higher than that observed previously for the amorphous polyferrocenylene,[132] presumably as a consequence of an appreciable degree of crystallinity detected in the former.[133] Rapid electron transfer between the Fe(II) and Fe(III) sites was also detected for these TCNQ-doped crystalline materials on the Mössbauer spectroscopic timescale (ca. 10^{-7} s) at room temperature.[132] This is illustrated in Figure 6 where the individual quadrupolar doublets for the Fe(II) and the Fe(III) environments, which are still resolved at −196 °C, merge at 28 °C. On the other hand, analogous studies of I_2-oxidized materials indicated hole localization on the Mössbauer timescale and lower conductivities (σ = ca. $10^{-4}\,S\,cm^{-1}$). This was attributed to the amorphous nature of the materials as indicated by powder X-ray diffraction (PXRD) studies. These observations were supported by electrochemical studies of polyferrocenylene-modified electrodes in which the presence of multiple or broad peaks was interpreted in terms of some degree of hole delocalization among iron atoms on the cyclic voltammetric timescale.[134] Further detailed studies on the electronic structure of polyferrocenylene **59** by UV photoelectron spectroscopy (UPS) suggested that the appreciable rather than high conductivity for these polymers is a consequence of limited hole mobility.[135,135a] As expected, the doping of polyferrocenylene was predicted to be facile, based on the low ionization threshold energies. However, the band dispersion (or bandwidth) was only estimated to be roughly 0.6 eV. This value is rather small compared with the 2–4 eV typical of conjugated organic polymers such as poly(*p*-phenylene) and polyacetylene. Thus, the narrow bands would be expected to result in a relatively limited degree of hole delocalization, and this led to the description of the system as having intermediate delocalization between that of π-conjugated conducting polymers such as polyacetylene and σ-localized insulating polymers such as polyethylene. It should be noted that, although the hole delocalization is limited in polyferrocenylene **59**, as discussed above, it can become apparent using "slow" techniques with relatively long timescales, such as Mössbauer spectroscopy (ca. -10^{-7} s).

In 1996, an alternative synthetic methodology was developed which permits the synthesis of more soluble *n*-hexyl-substituted polyferrocenylenes. This involved the reaction of the dihexylfulvalene dianion with $[FeCl_2(THF)_2]$ (Equation (23)).[136,136a] Although this step-growth polycondensation method does not generate high molecular weight materials in large quantities, a fraction of poly(1,1′-dihexylferrocenylene) **60** with $M_n \sim 5{,}000$ and PDI = 1.2 was formed in very low yield. In addition, when oxidized with TCNQ or tetracyanoethylene (TCNE), this material exhibited photoconductivity and acted as a p-type semiconductor. The electrochemistry of both the polymer and individual oligomers is consistent with presence of substantial metal–metal interactions.[136,136a]

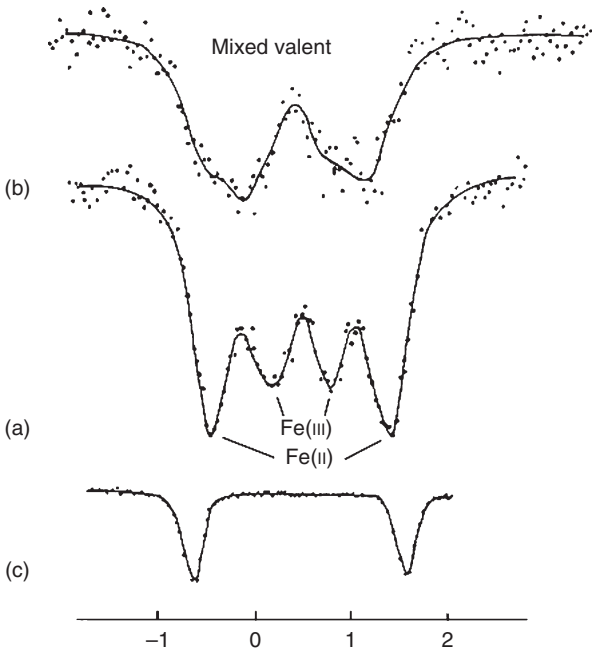

Figure 6 The Mössbauer spectra of polyferrocenylene **59** and its adduct with 0.81 equiv. of TCNQ showing that the quadrupolar doublets for the Fe(II) and Fe(III) environments, which (a) are still resolved at −196 °C; (b) merge at 28 °C due to hole delocalization on the timescale of the experiment (ca. 10^{-7} s); (c) the Mössbauer spectrum of polyferrocenylene at room temperature is shown for comparison and posesses a single Fe(II) quadrupolar doublet. (Adapted with permission of Elsevier Ltd, from Yamamoto, T. *et al*., *Inorg. Chim. Acta*, **1983**, *73*, 75.)

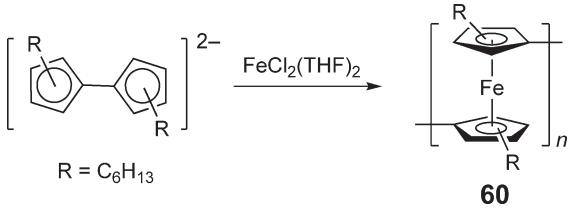

(23)

Copper-mediated polycondensations of diiodoferrocenes and bis(stannyl)ferrocenes at 150–180 °C were also used to prepare, in fairly low molecular weights, well-characterized polyferrocenylenes with substituents on the Cp rings (Equation (24)).[137] Yellow-orange to tan-colored polyferrocenylenes **61** with solubilizing groups such as methyl or trimethylsilyl substituents were prepared. These polymers possess molecular weights in the range of $M_n \sim 1{,}500$–$3{,}600$ (PDI ∼ 1.5–3.0). Electrochemical studies using cyclic voltammetry showed two waves with a very large redox coupling (460–485 mV) that is indicative of the presence of substantial metal–metal interactions (Figure 7), with the first wave representing initial oxidation at alternating iron sites (see Section 3.3.2.3 for a more detailed discussion on related systems). However, although the TCNE adducts of **61** showed broad intervalence electron-transfer bands in the near-IR (NIR) region, their Mössbauer spectra were consistent with a trapped valence state (i.e., discrete Fe(II) and Fe(III) sites) on the timescale for this technique (ca. 10^{-7} s).[137]

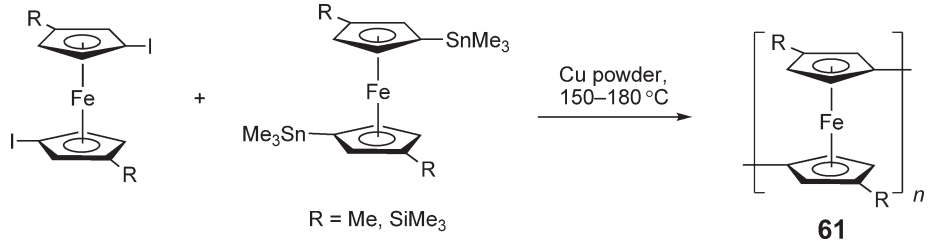

(24)

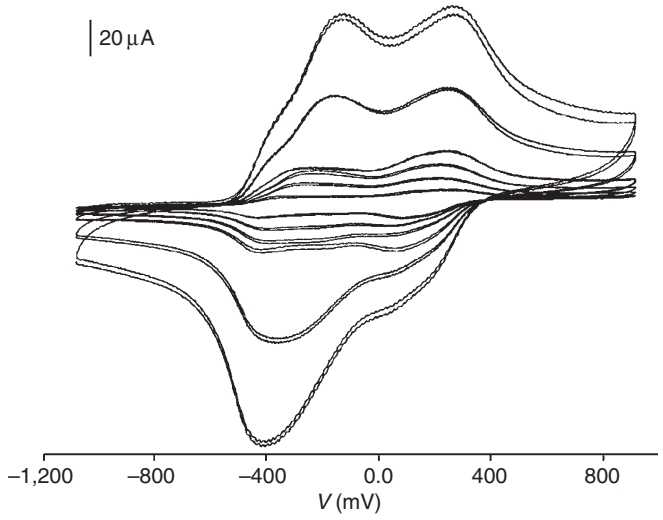

Figure 7 Cyclic voltammograms of polyferrocenylene **61** at various scan rates in CH_2Cl_2 (0.1 M of $[Bu_4N][PF_6]$ in CH_2Cl_2) that show two reversible oxidation waves separated by a redox coupling $\Delta E_{1/2}$ of ca. 0.47 V. (Adapted with permission of The American Chemical Society from Park, P. *et al*., *Macromolecules*, **2002**, *35*, 3810.)

Apart from the case of polyferrocenylenes, very little work has been reported on analogous materials containing directly linked metallocene units. The synthesis of very low molecular weight polyruthenocenylenes **62** (M_n = ca. 1,400) using, for example, Ullman coupling have been briefly described (Equation (25)). The few results on oligomeric materials in this area are summarized in an excellent review that covers work on polymetallocenylenes prior to 1981.[138]

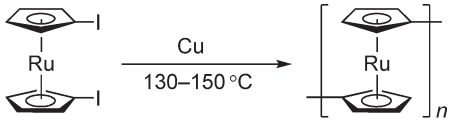

(25)

62

12.06.3.2.2 Other polymetallocenes with short spacers via polycondensation routes

Polymetallocenes with single carbon spacers (i.e., **63**) have been the focus of numerous investigations. Polycondensation routes developed in the 1960s involved the reaction of aldehydes with the corresponding metallocenes (M = Fe, Ru) as well as the cationic polymerization of carbinols. These and related routes have been critically reviewed in detail.[53] Both methods were carried out using Lewis or protic acid catalysts and yielded similar products. The materials obtained were oligomeric and consisted of a mixture of heteroannular (1,1′-) and homoannular (1,2- and 1,3-) metallocene units. Cross-linking was also noted at high temperatures and resulted in an increase in the number of methylene bridges per repeat unit.

A similar route was reported in the mid-1960s for the synthesis of polyferrocenes with phosphorus spacers **64**, **65**.[139,140] Reaction of ferrocene with $PPhCl_2$, $P(O)PhCl_2$, or $P(S)PhCl_2$ in the presence of a Lewis acid catalyst such as $ZnCl_2$ in melt or in solution at 80–170 °C yielded low molecular weight materials (M_n < 6,000 by VPO and generally <3,500). The composition of the materials depended on the reaction conditions. Again, this work has been reviewed in detail.[53]

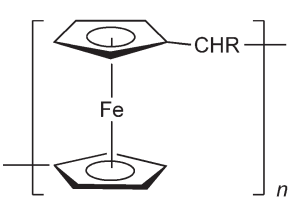

R = H, CH_3, C_6H_5

63

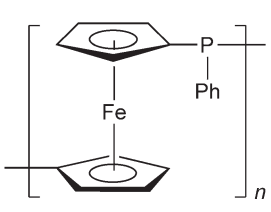

64

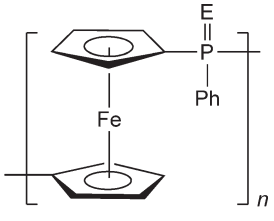

E = O, S

65

In 1982, well-defined materials of structure **64** were obtained from the reported polycondensation reaction of 1,1′-dilithioferrocene.TMEDA with $PPhCl_2$.[141] The molecular weights of the polyferrocenylphosphine (PFP) products were found to depend on the reaction conditions. For example, products with $M_w = 8{,}900$ (by light scattering) were reported when the reaction was performed in dimethoxyethane at 25 °C, while high molecular weights ($M_w = 131{,}000$–$161{,}000$) were obtained in diethyl ether at 25 °C or in dimethoxyethane at −40 °C. The high molecular weights in the latter cases are highly unexpected as dilithioferrocene is highly reactive and difficult to purify, and polycondensation reactions require exact reaction stoichiometries in order to achieve appreciable chain lengths.[15] Significantly, more recent work in the mid-1990s has shown that these high molecular weight products probably arise from a chain-growth reaction, rather than from a polycondensation, which involves the anionic ROP of a phosphorus-bridged [1]ferrocenophane generated *in situ* (see Section 12.06.3.3.3).[142]

The air and thermally stable (to >350 °C) polyferrocenylphenylphosphine **64** was shown to react with low concentrations of $Co_2(CO)_8$ to lead to products containing chelated cobalt centers.[143] According to IR and ^{31}P NMR data, three Co–P bonds are present per metal atom and the cobalt environments possess a pseudo-trigonal-bipyramidal geometry. The catalytic potential of the materials in the hydroformylation of 1-hexene was studied and was shown to be similar to that of the complex $HCo(CO)_3PPh_3$.

PFSs **66** of very low molecular weight were first described in two patents by Rosenberg in the 1960s.[144,145] The polymers were prepared from dilithioferrocene by a reported polycondensation reaction with the appropriate dihaloorganosilanes (Me_2SiCl_2 or Ph_2SiCl_2) in polar solvent mixtures at 0–25 °C. The resulting materials were described as black or chocolate-brown in colour. Although clearly impure, the partially soluble polymers were reported to be reasonably thermally stable (to >250 °C). VPO gave molecular weights M_n of 1,700–3,400 (R = Me) and 2,400–7,000 (R = Ph), which corresponded to ca. 5–19 repeat units.[145]

This work was preceded by an investigation of the alternative route which involved the condensation of $FeCl_2$ with $Li_2[Cp_2SiMe_2]$, which afforded even lower molecular weight samples of **66** (R = Me) that should be termed oligo(ferrocenyldimethylsilanes).[144] Recently, slightly higher molecular weight materials with M_n up to 4,100 have been reported using this route.[146] The low values for M_n obtained are to be expected for step-growth polycondensation processes involving dilithio reagents, which are difficult to obtain in a high degree of purity (see Section 1.4). The synthesis of low molecular weight polyferrocenylstannanes **67** with M_w up to 4,600 was reported using an analogous reaction pathway.[147,148]

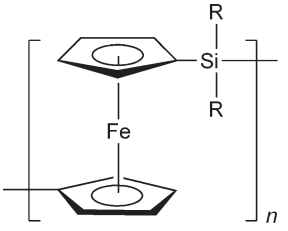

R = Me, Ph

66

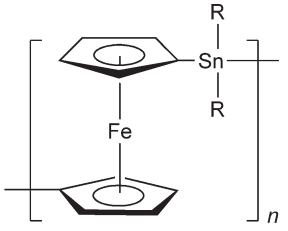

R = Me, Et, *n*-Bu, Ph

67

Poly(ferrocenylene vinylene) derivatives **68** with M_n values of 3,000–10,000 and polydispersities of ca. 2.2–2.8 (determined by GPC) were synthesized in 1995 in high yields via a titanium-induced McMurry coupling reaction of the corresponding alkylferrocenyl carbaldehyde monomers (Equation (26)).[149] Characterization of these soluble polymers by NMR and IR revealed the presence of *trans*-vinylene units. The UV–VIS spectra of the polymers are similar to those of the monomers and this indicates a fairly localized electronic structure in the former. The relatively limited electron localization is also reflected in the electrical and optical properties. For example, the values for iodine-doped conductivity ($\sigma = 10^{-2}\,S\,cm^{-1}$) and non-linear third-order optical susceptibility ($\chi^{(3)} = 1$–4×10^{-12} esu) are lower than those of linear conjugated polymers such as poly(1,4-phenylene–vinylene) ($\sigma = 2.5 \times 10^{3}\,S\,cm^{-1}$, $\chi^{(3)} = 8 \times 10^{-12}$ esu).

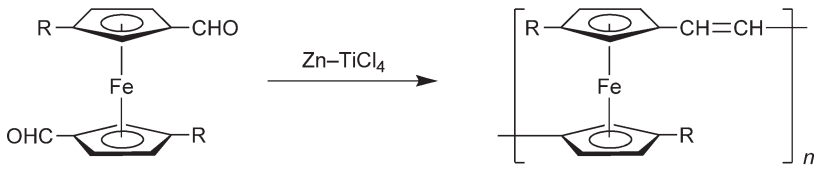

(26)

3.15

R = C_2H_5, C_6H_{13}, $C_{12}H_{25}$

68

Ferrocene–acetylene polymers **69** with the metallocene units linked through 1,3-positions have been prepared by a Pd-catalyzed polycondensation process and their properties have been investigated in some detail (Equation (27)).[150,151] Fractions of **69** (R = CH_2NMe_2) with molecular weights of up to $M_n \sim 4{,}300$ and PDI ~ 1.7 were successfully prepared. UV–VIS spectroscopy provided evidence for significant electron delocalization in these interesting 1,3-substituted materials. More detailed studies were conducted on polymers **69** (R = CH_2OMe) with proposed molecular weights of ca. 10,000. The relationship between λ_{max} for the ferrocene *d–d* band transition versus $1/n$ (n = number of ferrocene acetylene repeat units) was found to be linear with a limiting value of λ_{max} of 472 nm for $n = \infty$. In addition, electrochemical studies indicated the presence of redox couplings (ca. 0.15 V) that provided further evidence for substantial electronic communication between the metallocene units.[151]

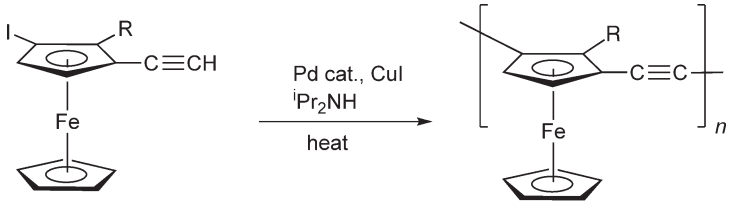

(27)

69

R = CH_2OMe or CH_2NMe_2

Disulfide-bridged oligoferrocenes **71** ($M_w < 3{,}500$) were prepared in an attempt to co-polymerize ferrocenedithiol with norbornadiene in the presence of AIBN in toluene.[62,152] Rather than the expected radical-induced polyaddition[153] to give **70** (Equation (28)), condensation of the ferrocene monomer was observed with norbornene and nortricyclane units as end groups (Equation (29)). The isolated oligomers **71** were characterized by NMR spectroscopy and field-desorption mass spectrometry, and possessed a chain length of 2–12 repeat units as determined by GPC.

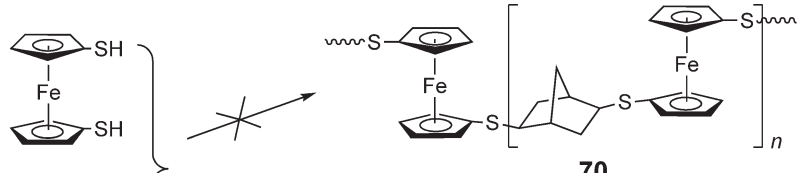

(28)

70

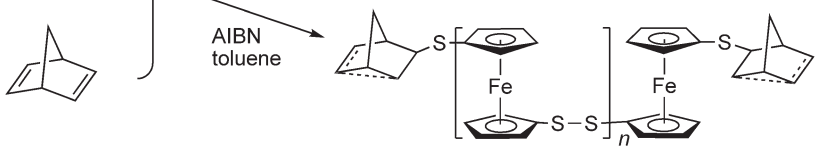

(29)

71

n = 1–11

12.06.3.3 ROP of Strained Metallocenophanes

12.06.3.3.1 Thermal ROP of silicon-bridged [1]ferrocenophanes

ROP reactions generally occur via a chain-growth mechanism[15] and therefore represent a particularly desirable route for the preparation of high molecular weight polyferrocenes. As is clear from the polymers described so far in Sections 12.06.3.1 and 12.06.3.2, such materials are very rare, particularly if the ferrocene groups are in close proximity to one another so as to permit substantial metal–metal interactions. The first syntheses of polymetallocenes via ROP methods were reported in early 1992. A novel atom-abstraction-induced ROP process for [3]trithiaferrocenophanes was described early in that year, and these results are discussed in Section 12.06.4.3.5.[154] Thermal ROP of strained metallocenophanes, which is discussed in this section, was reported a few months thereafter.[155]

A key general requirement for most ROP processes is a strained cyclic monomer. Ferrocenophanes, in which a single atom bridges the two cyclopentadienyl ligands (i.e., [1]ferrocenophanes), have been known since 1975 and fit this requirement.[156,156a] In contrast to the situation in ferrocene where the planes of the cyclopentadienyl (Cp) ligands are parallel to one another, in these species the Cp ligands are forced into a tilted higher-energy arrangement by the presence of a single bridging atom. However, although stoichiometric ring-opening reactions were described for silicon-bridged [1]ferrocenophanes in the late 1970s,[157] no successful ROP reactions for these species were reported until 1992.

The first examples of the use of ROP of strained metallocenophanes to prepare high molecular weight polymetallocenes ($M_n > 10^5$) involved silicon-bridged [1]ferrocenophane monomers.[155] Specifically, PFSs **73** (R, R^1 = Me or Ph) were prepared via the thermal ROP of strained, ring-tilted silicon-bridged [1]ferrocenophanes **72** (R, R^1 = Me or Ph) in the melt at 130–220 °C in evacuated Pyrex glass tubes (Equation (30)). These monomers have tilt angles of 16°–21° between the planes of the Cp ligands and possess strain energies of ca. 70–80 kJ mol^{-1} according to DSC measurements.[158,159] The strain present is illustrated by the Cp ring-tilted molecular structure of **72**, as determined by single crystal X-ray diffraction (Figure 8).[158]

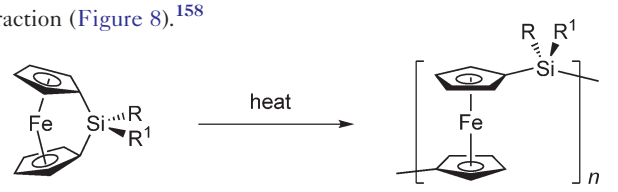

(30)

72 **73**

The thermal ROP route is very general and a wide range of semicrystalline and amorphous PFSs have thus been prepared with different substituents at silicon and/or on the Cp rings.[160] These thermally ring-opened materials have been fully characterized using a wide range of spectroscopic and analytical methods. Also, their molecular weights have been established by absolute methods, such as static light scattering to be in the range of $M_w = 10^5$–10^6. Detailed studies of the properties of these materials are described in Section 12.06.3.3.6.

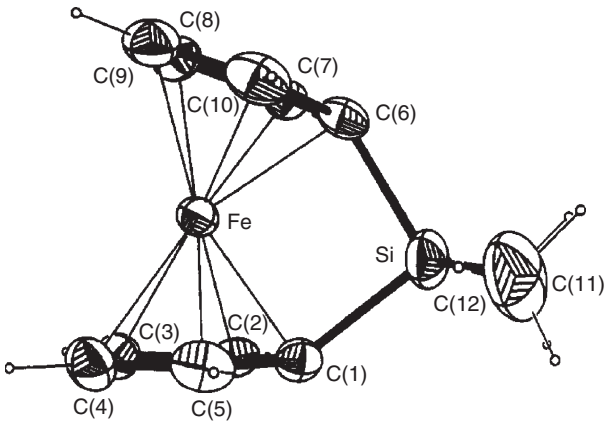

Figure 8 Molecular structure of silicon-bridged [1]ferrocenophane **72** (R = R^1 = Me) as determined by single crystal X-ray diffraction; the planes of the Cp ligands are tilted by 20.8°. (Reproduced with permission of The American Chemical Society from Finckh, W. *et al.*, *Organometallics*, **1993**, *12*, 823.)

Spirocyclic [1]ferrocenophanes have also been shown to thermally polymerize and these species function as cross-linking agents that allow access to PFSs with controlled cross-link densities.[161] Amber, solvent-swellable gels are available via this route (see Section 12.06.3.3.2). The [1]dichlorosilaferrocenophane **74** provides a very useful precursor to [1]ferrocenophanes **75** with alkoxy (or amino) substituents and subsequent ROP allows access to, for example, polyferrocenylalkoxysilanes **76** (Equation (31)).[162] In addition, polymers with Si–H or Si–Cl groups have been prepared and these provide opportunities for post-polymerization modification via hydrosilylation and nucleophilic subsitution, respectively.[160]

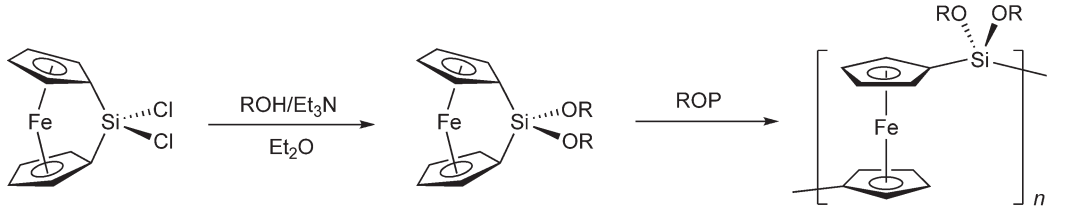

74 **75** **76** (31)

The mechanism of the thermal ROP of silicon-bridged [1]ferrocenophanes is not yet known in definitive detail. However, studies of the polymerization of monomers with unsymmetrically substituted Cp ligands indicate that ROP proceeds via cleavage of the Cp–Si bond.[163] It is possible that traces of nucleophilic impurities initiate the polymerization, although a mechanistic process involving radicals cannot be completely ruled out.[164]

The thermal ROP of silicon-bridged [1]ferrocenophanes requires moderately high temperatures (100–250 °C) and there is little or no molecular weight control. As a result, the molecular weight distributions are quite broad ($M_w/M_n \sim 1.5$–2.5). This polymerization method has now been superseded in many ways by ambient-temperature ROP methods that involve the use of anionic initiators (see Section 12.06.3.3.4) or transition metal catalysts (see Section 3.3.4).

12.06.3.3.2 Thermal ROP of other strained metallocenophanes

The thermal ROP methodology established for silicon-bridged [1]ferrocenophanes has been extended to many other strained metallocenophanes, which allows access to high molecular weight polyferrocenes with different spacer groups. As discussed later (see Section 12.06.3.3.6), this permits modification of the properties of the polymer, such as the extent of the metal–metal interactions.

Thermal ROP of germanium-bridged [1]ferrocenophanes **77** was reported shortly after that of the silicon-bridged analogs and high molecular weight polyferrocenylgermanes **78** ($M_w = 10^5$–10^6) were obtained at ca. 120 °C or higher temperatures (Equation (32)).[165]

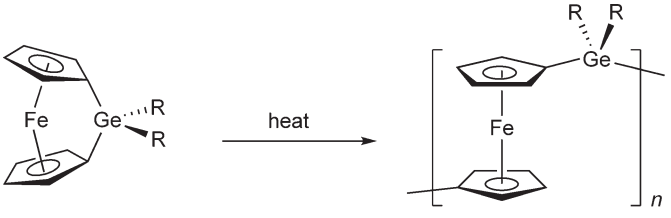

77 **78** (32)

Polyferrocenylphenylphosphines **80**, analogous to those previously synthesized from polycondensation routes (Section 12.06.3.2.2), have also been prepared via thermal ROP of phosphorus-bridged [1]ferrocenophanes **79** (Equation (33)).[166] Solubility of the materials was observed to increase when the cyclopentadienyl rings were substituted with *n*-butyl or trimethylsilyl groups. Sulfurization was carried out in order to facilitate their characterization by GPC as the PFP precursors **80** were found to adsorb to the porous material (styragel) generally used in GPC columns. Polymers with trimethylsilyl substituents on the cyclopentadienyl rings, however, could be analyzed by GPC without the need for sulfurization. A comparison between analogous unsulfurized (**80**; $R^1 = SiMe_3$; R = Ph) and sulfurized (**81**; $R^1 = SiMe_3$; R = Ph) polymer samples revealed that these materials possess essentially the same molecular weight, which indicated that chain cleavage does not occur during the sulfurization step.

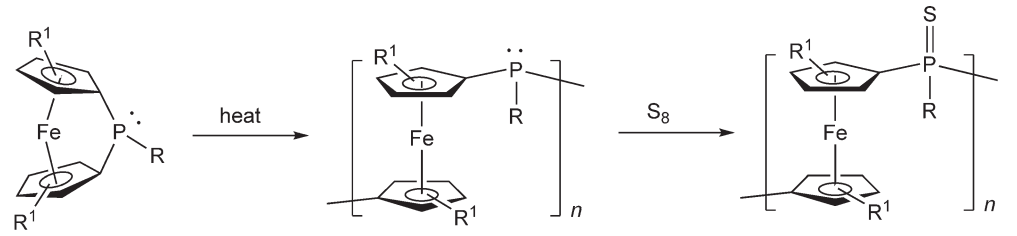

79 80 81

(33)

R^1 = H, *n*-Bu, $SiMe_3$

Thermal ROP of highly strained sulfur-bridged [1]ferrocenophanes **82**, which possess tilt angles between the planes of the Cp rings of ca. 31°, has been shown to yield the polyferrocenylsulfides **83**.[167] The unsubstituted polymer **83** (R = H) is insoluble in organic solvents, but random methylation of the Cp rings affords soluble materials **83** (R = Me).[167] First-row element-bridged [1]boraferrocenophanes **84** have also been reported. These highly strained species possess very large tilt angles (ca. 32°) and undergo ROP to give polyferrocenylboranes **85**.[168] The synthesis of [1]stannaferrocenophanes with bulky substituents at tin follwed by thermal ROP at 150 °C has led to high molecular weight polyferrocenylstannanes **86** ($M_w > 10^5$, PDI = ca. 1.5), a new class of bimetallic polymers.[169]

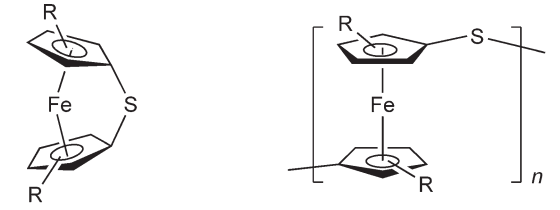

R = H or Me
82

R = H or Me
83

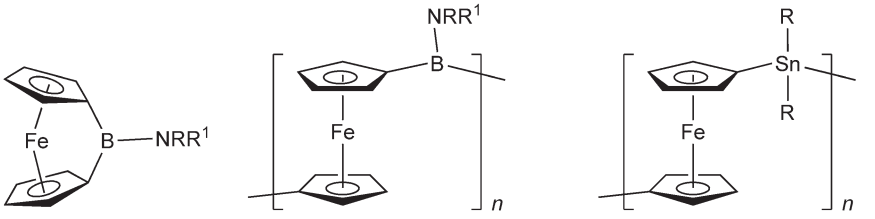

84 **85**

NRR^1 = $N(SiMe_3)_2$, N(*t*-Bu)$SiMe_3$, or $N(i\text{-Pr})_2$

R, R^1 = *t*-Bu, Mes
86

Strained [2]metallocenophanes can also function as ROP precursors. For example, hydrocarbon-bridged [2]ferrocenophanes **87** (M = Fe; $E_1 = E_2 = CH_2$) were found to undergo ROP at 300 °C, providing access to polyferrocenylethylenes **88** (M = Fe; $E_1 = E_2 = CH_2$) (Equation (34)).[170] The ferrocenylethylene polymers **88** were insoluble if R = H, but were readily soluble in the case where R = Me. In the latter case, a bimodal molecular weight distribution was detected, with both an oligomeric fraction (M_w = 4,800) and a high molecular weight fraction ($M_w = 9.6 \times 10^4$) present. Analogous strained monomers that contain ruthenium instead of iron, [2]ruthenocenophanes **87** (M = Ru; $E_1 = E_2 = CH_2$), possess ring tilt angles of ca. 30°, significantly larger than that present in the [2]ferrocenophanes **87** (M = Fe; $E_1 = E_2 = CMe_2$; 23°). Not surprisingly, they have been found to undergo ROP at lower temperatures (220 °C) to yield polyruthenocenylethylenes **88** (M = Ru; $E_1 = E_2 = CH_2$; R = H or Me).[171] The thermal ROP of [2]ferrocenophanes with C–P and C–S bridges has also been reported; however, analogous monomers with C–Si bridges are resistant to thermal ROP due to insufficient ring strain.[172]

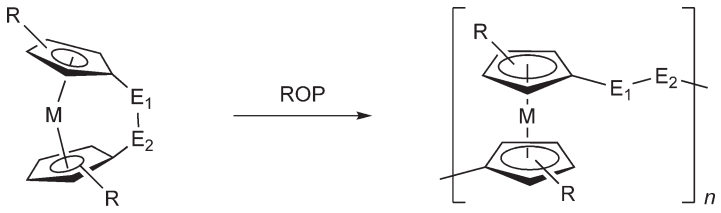

(34)

87 **88**

M = Fe or Ru
R = H or Me
$E_1 = E_2 = CH_2$ or CMe_2

The use of thermal ROP also allows access to a range of random co-polymers. For example, polyferrocenylsilane-*co*-polysilane materials **89** (Equation (35)) were prepared by the thermal ring-opening co-polymerization of silicon-bridged [1]ferrocenophanes with cyclic tetrasilanes.[173] These co-polymers are particularly interesting since they contain ferrocene moieties linked by σ-delocalized oligosilane segments. It is noteworthy that these photosensitive materials are inaccessible via thermal ROP of ferrocenophanes with oligosilane bridges due to insufficient ring strain.[158]

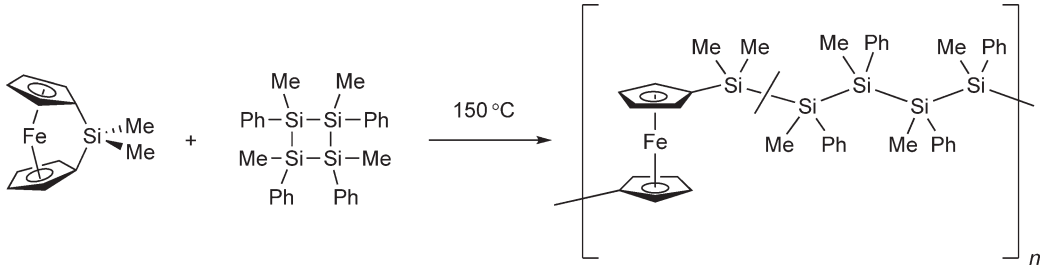

(35)

89

Thermal co-polymerization of different [1]ferrocenophanes has also been reported to give PFS random co-polymers.[174] In addition, random co-polymers **90** derived from [1]ferrocenophanes and silicon-bridged bis(benzene)chromium complexes have been synthesized (Equation (36)).[175]

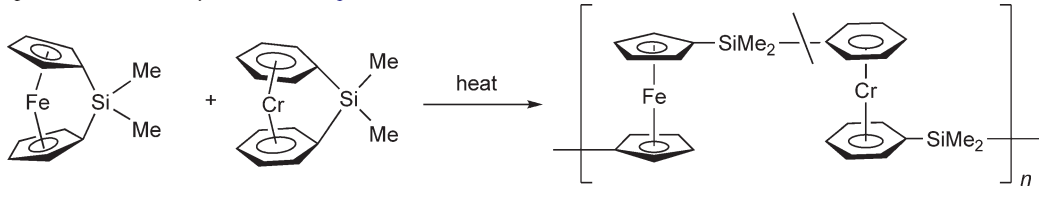

(36)

90

12.06.3.3.3 Living anionic ROP of strained metallocenophanes

Anionic ROP reactions of metallocenophanes were first reported in 1994.[176,176a] Silicon-bridged [1]ferrocenophanes **72** ($R = R^1 = Me$) were shown to undergo polymerization in the presence of an anionic initiator such as lithioferrocene.[176,176a] When extremely pure monomer and solvents were used, the living anionic ROP of **72** ($R = R^1 = Me$) could be achieved.[46,176,176a] The reaction involves the formation of an anionic polymer **91** whose living end can be subsequently terminated with various capping agents to afford PFSs **92** ($R = R^1 = Me$; Scheme 5). Since the initiation process is rapid and no chain transfer or uncontrolled termination occurs, PFSs with very narrow polydispersities (PDI < 1.10) are accessible. The molecular weights of the resulting polymers (M_n up to ca. 120,000) depend on the monomer-to-initiator ratio, as this governs the number of propagating sites (Figure 9).[46,176,176a] The living anionic ROP process appears to be very general for silicon-bridged [1]ferrocenophanes and has been extended to a range of different monomers.[177]

Although early attempts to induce the anionic ROP of phosphorus-bridged [1]ferrocenophanes only generated a mixture of oligomers,[141] living anionic ROP has been achieved when highly purified monomers are used.[142] Thus, PFPs, **64** with

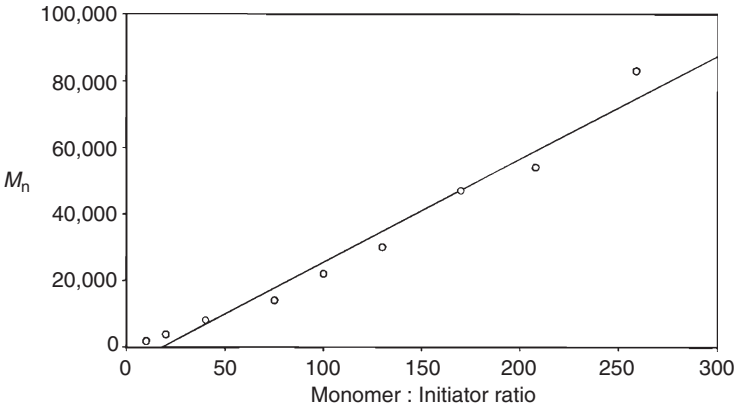

Figure 9 Plot of M_n versus monomer : initiator ratio for the living anionic ROP of silicon-bridged [1]ferrocenophane **72** (R = R^1 = Me). (Reproduced with permission of The American Chemical Society from Ni, Y. Z. *et al.*, *J. Am. Chem. Soc.*, **1996**, *118*, 4102.)

controlled molecular weights (up to $M_w \sim 36{,}000$) and narrow polydispersities (PDI = 1.08–1.25) have been prepared using organolithium initiators. It was reported in the early 1980s that high molecular weight PFPs **64** were generated under certain conditions in a polycondensation reaction of dilithioferrocene·TMEDA and $PhPCl_2$.[141] The results from studies of the anionic ROP of phosphorus-bridged [1]ferrocenophanes suggest, however, that the high polymers **64** generated in these cases are almost certainly formed via a chain-growth route, namely, the anionic ROP of a [1]ferrocenophane generated *in situ* under the reaction conditions (Equation (37)).[142,178] It is plausible that similar anionic ROP reactions occur, at least to some extent, in the condensation routes to PFSs described in patents in the 1960s.[142,178,179]

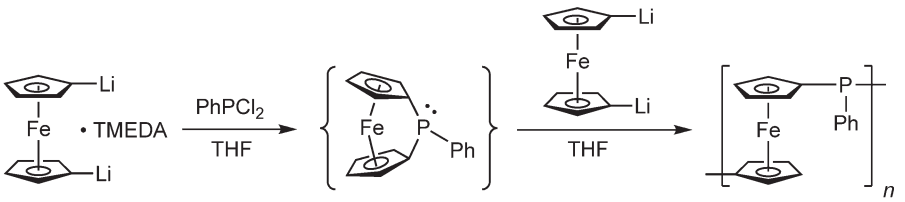

(37)

Highly purified monomer and solvents are necessary for living anionic ROP since the concentration of highly reactive propagation sites is extremely low. However, living polymerizations are exceptionally useful as they allow the preparation of well-defined homopolymers with controlled molecular weights and narrow molecular weight distributions (PDI < 1.2). Even more significantly, they allow the synthesis of block co-polymers via, for example, the addition of another monomer to the living anionic polyferrocene chain ends. The use of this technique to prepare polyferrocene block co-polymers and a discussion of the properties of these materials is given in Section 12.06.3.3.8.

12.06.3.3.4 Transition metal-catalyzed ROP of strained metallocenophanes

A very convenient, transition metal-catalyzed ROP route to polymetallocenes from strained metallocenophanes was reported in 1995.[180,181] A series of Rh(I), Pd(II), Pd(0), Pt(II), and Pt(0) complexes was found to catalyze the ROP of [1]silaferrocenophanes in solution at room temperature to yield high molecular weight PFSs ($M_n \sim 10^5$) (Equation (38)). A major advantage of these transition metal-catalyzed processes is that, in contrast to the anionic polymerization, ambient-temperature polymerization can be achieved without the need for extremely pure monomers and solvents. Co-polymerization of silicon-bridged [1]ferrocenophanes with other monomers is also possible. For example, transition metal-catalyzed ROP of silicon- and germanium-bridged [1]ferrocenophanes afforded random co-polymers with both silicon and germanium atoms in the main chain,[181,182] whereas reactions of silicon-bridged [1]ferrocenophanes with cyclocarbosilanes yielded polyferrocenylsilane-*r*-polycarbosilane random co-polymers.[183] The use of the mild, transition metal-catalyzed ROP route is especially advantageous in the case of [1]ferrocenophanes with halogen substitutents at the bridging silicon. Unlike the alkyl- or aryl-substituted [1]ferrocenophanes,

which typically undergo thermal ROP at 120–150 °C, the halogen-substituted analogs thermally polymerize at a much higher temperature (>250 °C). However, in the presence of a transition metal catalyst, these monomers undergo facile ROP at room temperature to give the corresponding polymers in high yields.[184]

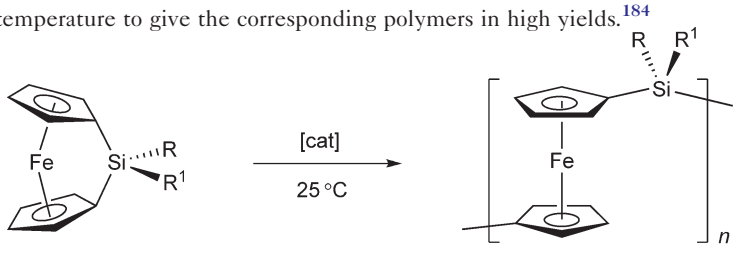

(38)

72 **73**

Studies have shown that unsymmetrical [1]ferrocenophanes in which only one of the cyclopentadienyl rings is methyl-substituted yield regioregular PFSs via transition metal-catalyzed ROP, whereas thermal ROP of the same monomers yields regioirregular materials.[163,183]

In the absence of additives, transition metal-catalyzed ROP of silicon-bridged [1]ferrocenophanes yields high molecular weight materials with no appreciable control over molecular weight. However, addition of hydrosilanes such as Et_3SiH permits molecular weight control and the polymers thus obtained **93** have been shown to possess an M_n value of ca. 10^3–10^4 with polydispersities typically in the range of 1.3–1.6 (Figure 10).[183] Characterization of the low molecular weight polymers by NMR and IR spectroscopy confirmed the nature of the end groups. Similarly, the use of poly(methylhydrosiloxane) as the source of Si–H bonds yields novel graft co-polymers **94**.[90] This methodology can also be extended to the preparation of star and block structures, including water-soluble materials.[183,185,186]

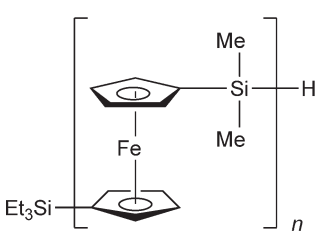

93

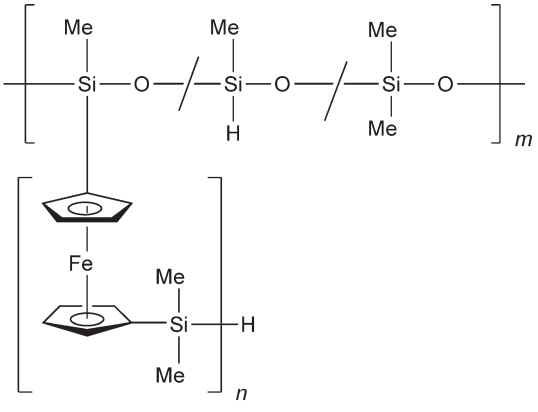

94

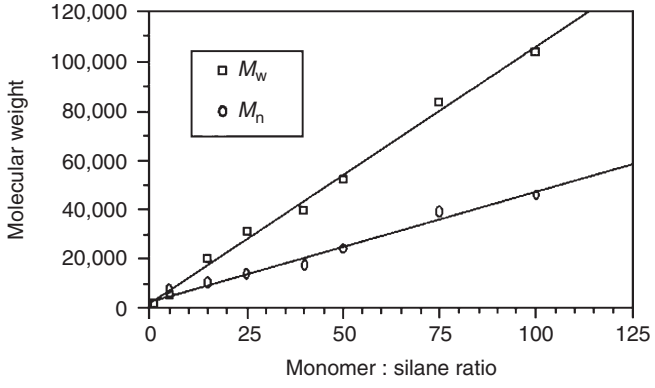

Figure 10 Plot of molecular weight versus the ratio of monomer : Et_3SiH for the Pt-catalyzed ROP of silicon-bridged [1]ferrocenophane **71** in the presence of Et_3SiH. (Reproduced with permission of The American Chemical Society from Gómez-Elipe, P. *et al.*, *J. Am. Chem. Soc.*, **1998**, *120*, 8348.)

Research has also focused on understanding the mechanism of the transition metal-catalyzed ROP reactions for [1]ferrocenophanes. A logical first step in the polymerization is insertion of the transition metal into the strained Cp-carbon-bridging element bond in the ferrocenophane. Polymers **93** formed in the presence of hydrosilanes are believed to result from competitive oxidative addition between the Si–H bond of the hydrosilane and the strained Cp–Si bond of the ferrocenophane at the catalytic center followed by reductive elimination. Detailed work has indicated that colloidal metal is the likely catalyst in the ROP reactions.[187]

Metal-catalyzed ROP has also been reported for a [2]ferrocenophane with a Ge–Ge bridge, whereas the analogous species with an Si–Si bridge resists polymerization.[188] The presence of weak Cp–Ge bonds may be important in the successful ROP observed in the former case.

12.06.3.3.5 Other ROP methods for strained metallocenophanes

Cationic ROP has been demonstrated for highly reactive [1]stannaferrocenophanes[189] and [2]ferrocenophanes with a C–S bridge.[172] [1]Stannaferrocenophanes have also been shown to undergo ROP in the presence of nucleophiles such as pyridine at room temperature.[189] Photochemically induced ROP of phosphorus-bridged [1]ferrocenophane **79** (R = Ph; R^1 = H) has also been reported and, after subsequent sulfurization of the resulting PFP **80**, poly(ferrocenylphenylphosphinesulfide) **81** with $M_n = 1.9 \times 10^3$ and PDI = 1.72 was isolated.[190] In addition, this reaction has been reported to occur when transition metal fragments are coordinated to the bridging phosphorus. For the tungsten species **95** ($ML_x = W(CO)_5$), polymer **96** ($ML_x = W(CO)_5$) with $M_n = 1.8 \times 10^4$ and PDI = 1.67 was isolated; for the manganese species **95** ($ML_x = Mn(CO)_2Cp$), polymer **96** ($ML_x = Mn(CO)_2Cp$) was obtained with $M_n = 1.1 \times 10^4$ and PDI = 2.0 (Equation (39)). Silicon-bridged [1]ferrocenophanes have been reported to undergo ^{60}Co γ-ray-induced ROP in the solid state and this allows access to stereoregular PFSs.[191]

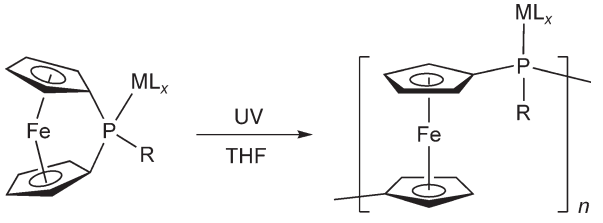

95 **96** (39)

12.06.3.3.6 Properties of polyferrocenylsilanes

ROP methods have allowed access to a wide variety of high molecular weight polyferrocenes of which the PFSs present the prototypical example. Studies of the latter materials have provided an excellent opportunity for the systematic and detailed examination of a class of main-chain metal-containing macromolecules; representative examples are included in Table 2. This section surveys some of the properties of these interesting polymers.

12.06.3.3.6.(i) Polyferrocenylsilanes in solution

The vast majority of PFSs are soluble in common organic solvents and GPC has proved to be useful in the determination of the molecular weights and molecular weight distributions of these metal-containing polymers. However, the determination of absolute values of M_w by static light-scattering methods has shown that the use of GPC with PS calibration standard significantly underestimates the molecular weight of these polymers. For example, detailed solution studies on a series of well-defined poly(ferrocenyldimethylsilane)s **73** (R = R^1 = Me) with PDIs < 1.2 that span a molecular weight range of 10,000–100,000 g mol^{-1} have been performed.[192] Using a gel permeation chromatograph equipped with refractive index, viscometry, and light-scattering detectors, it was shown that in THF poly(ferrocenyldimethylsilane) possesses a more compact random-coil conformation than PS of the same molecular weight in the same solvent. This explains the 30% underestimation of the true molecular weight of PFSs by conventional GPC methods using PS standards as the latter technique separates molecules on the basis of hydrodynamic size. Thus, Mark–Houwink parameters were also established for PFS **73** (R = R^1 = Me) and the a value of 0.62 is typical for flexible chains in a fairly poor solvent. In contrast, the value for PS in THF is larger (0.72). In this study, a universal calibration curve in THF was also established.[192]

Table 2 Thermal transition and GPC molecular weight data for selected polyferrocenylsilanes **73**

R	R^1	T_g (T_m) °C	M_n	*PDI*
H	H	16 (165)	[e]	[e]
Me	Me	33 (122–145)	3.4×10^5	1.5
Et	Et	22 (108)	4.8×10^5	1.5
n-Pr	*n*-Pr	24 (98)	8.5×10^4	2.7
n-Bu	*n*-Bu	3 (116, 129)	3.4×10^5	2.6
n-Pen	*n*-Pen	−11 (80–105)	3.0×10^5	1.6
n-Hex	*n*-Hex	−26	7.6×10^4	1.6
Me	H	9 (87,102)	4.2×10^5	2.0
Me	$CH_2CH_2CF_3$	59	8.1×10^5	3.3
Me	$CH{=}CH_2$	28	7.7×10^4	2.1
Me	*n*-$C_{18}H_{37}$	1 (16)	5.6×10^5	2.5
Me	Ph	90	1.5×10^5	2.0
Me	Fc[d]	99	7.1×10^4	2.3
Me	5-Norbornyl	81	1.1×10^5	1.5
OMe	OMe	19 (Tm = ?)	1.5×10^5	2.0
OEt	OEt	0	3.8×10^5	2.1
OCH_2F_3	OCH_2CF_3	16	2.2×10^5	1.2
OBu	OBu	−43	3.9×10^5	2.1
OHex	OHex	−51	0.9×10^5	2.6
$O(CH_2)_{11}CH_3$	$O(CH_2)_{11}CH_3$	(−30)	1.9×10^5	2.5
$O(CH_2)_{17}CH_3$	$O(CH_2)_{17}CH_3$	(32)	2.3×10^5	2.1
OC_6H_5	OC_6H_5	54	2.3×10^5	2.0
OC_6H_4-*p*-^{t}Bu	OC_6H_4-*p*-^{t}Bu	89	1.9×10^5	1.9
OC_6H_4-*p*-Ph	OC_6H_4-*p*-Ph	97	5.4×10^4	2.0
Me[f]	Me[f]	93	2.8×10^5	1.5
Me[g]	Me[g]	116	2.3×10^5	1.4

[a]Obtained from analysis of THF polymer solutions using polystyrene standards.
[b]DSC data collected at a heating rate of at 10 °C/min.$^{-1}$
[c]PDI = M_w/M_n.
[d]Fc = (□-C_5H_4)Fe(□-C_5H_5).
[e]Insoluble polymer.
[f]One Me group on each Cp ligand.
[g]One C_5Me_4 ligand and one C_5H_4 ligand.

Solution characterization by NMR proves to be an invaluable tool as these polymers possess ^{1}H, ^{13}C, and ^{29}Si NMR active nuclei in the polymer backbone. In several cases, high resolution NMR has been used to investigate the tacticity of PFSs.[184]

12.06.3.3.6.(ii) Polyferrocenylsilanes in the solid state: thermal transition behavior, morphology, and conformational properties

Glass transitions for poly(ferrocenylalkyl/arylsilanes) **73** determined by DSC cover a wide range of temperatures (ca. −51 to 150 °C) (Table 2). As expected, long flexible subsituents on silicon lead to lowest T_g values, whereas the replacement of hydrogen on the Cp ligands by groups such as Me or $SiMe_3$ leads to a very significant increase in T_g. Symmetrically substituted PFSs (R = R^1) often show a propensity to crystallize and several examples have been studied in detail by a range of techniques which include DSC, wide angle X-ray scattering (WAXS), atomic force microscopy (AFM), X-ray, and electron diffraction techniques on fibers and films.[160] Like many semicrystalline polymers, the morphology of many of these materials shows a dependence on thermal history. Their crystallinity has been observed to increase over time, especially when samples are annealed above the T_g. On the other hand, PFSs, which are unsymmetrically substituted at silicon, are generally amorphous, presumably as a consequence of their atactic stereostructure.

PFSs can be fabricated into films, shapes, and fibers using conventional polymer-processing techniques. The dimethylderivative **73** (R = R^1 = Me), which has been studied in the most detail, is an amber, film-forming thermoplastic (Figure 11), which possesses a T_g at 33 °C and melt transitions (T_m) in the range of 122–150 °C. The multiple melt transitions arise from the presence of crystallites of different sizes which melt at slightly different

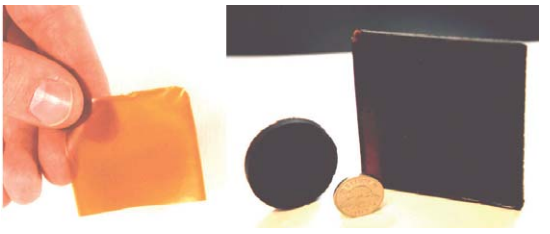

Figure 11 Polyferrocenyldimethylsilane **73** (R = R^1 = Me) as (a) a solvent-cast film and (b) melt-extruded shapes.

temperatures.[159,193] Poly(ferrocenyldimethylsilane) **73** (R = R^1 = Me) can be melt-processed above 150 °C (Figure 11) and can be used to prepare crystalline, nanoscale fibers (diameter 100 nm–1 μm) by electrospinning. In this method an electric potential is used to produce an ejected jet from a solution of the polymer in THF, which subsequently stretches, splays, and dries. The nanofibers of different thickness show different colors due to interference effects similar to those in soap bubbles.[194] As with the dimethyl material, other symmetrically substituted PFSs **73** (R = R^1) with short (C_2–C_5) alkyl chains at silicon also crystallize and similar melting behavior is observed (Table 2).[160] In contrast, the *n*-hexyl analog **73** (R = R^1 = *n*-hexyl) is an amber, amorphous gum with a T_g of −26 °C. Apparently, regular packing of PFS chains is no longer possible once the length of the alkyl chains on silicon exceeds five carbon atoms.

The possible conformations of PFS chains in the solid state have attracted significant interest from several research groups and much work has also focused on the prototypical material, poly(ferrocenyldimethylsilane) **73** (R = R^1 = Me). One contribution toward the understanding of conformations adopted by poly(ferrocenyldimethylsilane) chains involved X-ray structural studies of well-defined oligomers. In particular, a model pentamer **97** was successfully characterized by single crystal X-ray diffraction.[195,195a] The pentamer molecules possess a *trans*-planar zigzag conformation in which the end ferrocenes are twisted out of the plane (Figure 12). Interestingly, the powder diffractogram of the pentamer is similar to that of the analogous high polymer and this suggests a similar structure in the crystalline domains in the solid state of the latter, with an intense diffraction peak at d = 6.37 Å. The planes giving rise to this peak in the pentamer, the (011) planes, are shown in Figure 12. Further important insight has been provided by means of a molecular mechanics study of oligomeric models of PFSs.[196] The calculations showed that the molecules are conformationally flexible and in the lowest energy conformations, there is an electrostatic attraction between the positively charged iron atoms and the negatively charged Cp ligands that are in close proximity. As expected, for the isolated molecules, the conformations were found to be governed by intramolecular interactions, whereas, in the solid state, intermolecular interactions were predicted to be more important. Significantly, although it was concluded that a *trans*-planar structure analogous to the central portion of the pentamer is possible for the PFSs (Figure 12), twisting of some of the ferrocene units out of the plane in a manner similar to the end groups in the pentamer was also viewed as being favorable as a result of interchain iron–Cp interactions.

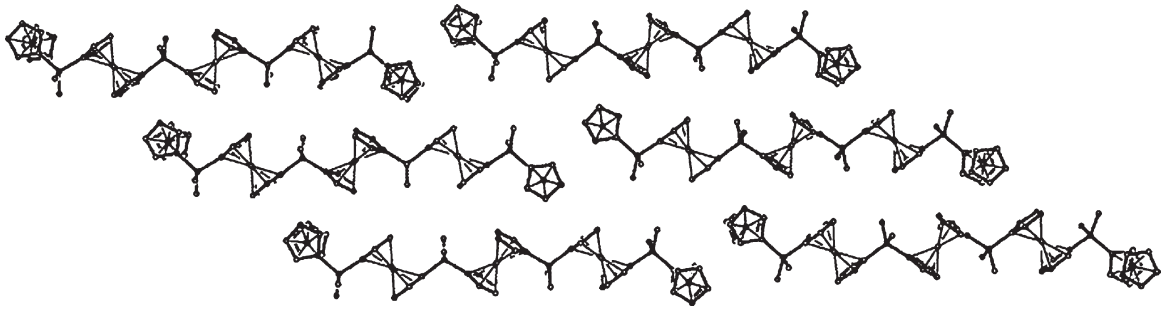

Figure 12 View of the crystal packing arrangement of pentamer molecules **97** parallel to the [011] plane showing three pairs of molecules. The terminal ferrocenyl groups are twisted in opposite directions perpendicular to the interior, *trans*-planar, zigzag units. (Reproduced with permission of The American Chemical Society from Rulkens, R. *et al.*, *J. Am. Chem. Soc.*, **1996**, *118*, 12683.)

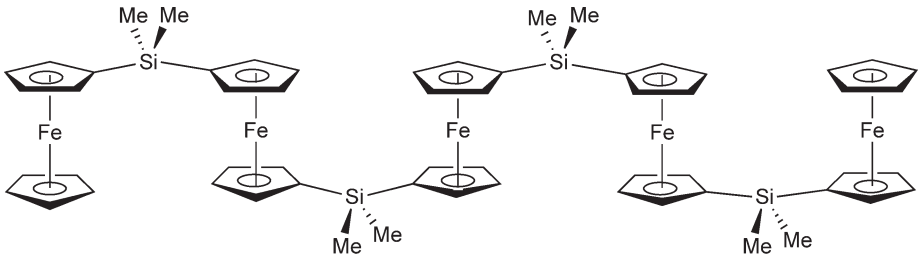

97

Detailed work on the morphology of PFS **73** (R = R^1 = Me) using X-ray diffraction techniques on films and fibers has revealed the coexistence of a 3-D monoclinic crystalline polymer phase and a 2-D mesophase with hexagonal or tetragonal packing of the macromolecules.[197] It is suggested that the coexistence of these phases is most likely a result of the close energies of the various conformations of the polymer backbone. The results for the 3-D monoclinic phase also support earlier suggestions that the linear polymer chains possess a *trans*-planar zigzag conformation in the solid state, as found for the low molecular weight pentamer analog **97** (see Figure 10). Studies on electrospun nanofibers (diameter 100–1,000 nm) of **73** (R = R^1 = Me) using single fiber electron diffraction techniques were also consistent with the assignment of a monoclinic unit cell.[194]

Alkoxy-substituted PFSs **76** are generally amorphous and T_g values as low as −51 °C have been detected when R = *n*-hexyloxy groups. PFSs symmetrically substituted with long alkoxy side chains (**76**, R = *n*-octadecyloxy) have been found to crystallize and form lamellar structures with interdigitated side-groups.[162] As noted above, PFSs with unsymmetrical substitution groups on the bridging silicon (**73**, R ≠ R^1) possess tacticity and offer the possibility of stereoregular polymer structures. The materials prepared by either thermal or transition metal-catalyzed ROP studied to date are, nevertheless, atactic. Interestingly however, ^{60}Co γ-irradiation of single crystals of the monomer **72** (R = Me; R^1 = Ph) yields a poly(ferrocenylmethylphenylsilane) **73** (R = Me; R^1 = Ph), which clearly exhibits appreciable stereoregularity by NMR and is probably syndiotactic.[191]

Hydrosilylation reactions have been performed with PFSs containing Si–H functionalities to attach mesogenic azobenzene groups. This has allowed the preparation of calamitic thermotropic side-chain liquid crystalline materials that display a nematic mesophase between ca. 53 and 250 °C.[198,198a]

The T_g values of PFSs, which can reach as low as ca. −50 °C, are remarkably low for a polymer structure with a bulky unit such as ferrocene in the main chain. Even when the influence of side-groups is small, the T_g values are still close to ambient temperature (e.g., for **73** (R = R^1 = H), T_g = 19 °C). By contrast, the T_g of PVFc is reported to be high (185 or 233 °C; Section 4.2.2.1.(i)). The ability of the iron atom in each ferrocene unit to act as a freely rotating "molecular ball-bearing"[199] probably plays a key role in generating the observed conformation flexibility in PFSs. This aspect has been explored by means of variable-temperature solid-state ^{2}H NMR studies of PFS **73** that were specifically deuterated either on the Cp rings or in the side-groups.[200]

12.06.3.3.6.(iii) Electrochemical and electronic properties

A key characteristic of PFSs is the presence of "two" reversible oxidation waves for Fe^{II}/Fe^{III} redox processes in the cyclic voltammograms of these materials in polar organic solvents, as illustrated for the case of PFS **73** (R = R^1 = Me) in Figure 13.[44,201,202] This is in contrast with the situation for ferrocene and side-chain polymers such as polyvinylferrocene where a single oxidation wave is detected (see Figure 2, Section 4.2.2.1.(i)). The proposed explanation for PFSs invokes initial oxidation at alternating iron sites as a consequence of significant interactions between the iron atoms. Thus, as one iron center is oxidized at potential $E_{1/2}(1)$, the neighboring sites become more difficult to oxidize and therefore do so at a higher potential $E_{1/2}(2)$. As a consequence, two oxidation waves with a redox coupling $\Delta E_{1/2} = E_{1/2}(2) - E_{1/2}(1)$ result. This process is depicted in Scheme 6.

Detailed electrochemical studies on model oligoferrocenylsilanes that possess two to nine ferrocene units fully support this explanation.[195] The peak separations for the different polymers, which provide a useful estimate of the degree of interaction between the metal centers, are generally in the range of $\Delta E_{1/2} = 0.20$–0.25 V in CH_2Cl_2 with some dependence on the substituents present at silicon. This corresponds to a comproportionation constant K_c of ca. 10^4 which is consistent with class II mixed-valence behavior. Class I materials have $K_c = 0$ and no signs of electron transfer, whereas class III materials generally have $K_c > 10^5$ and the valence electrons are completely

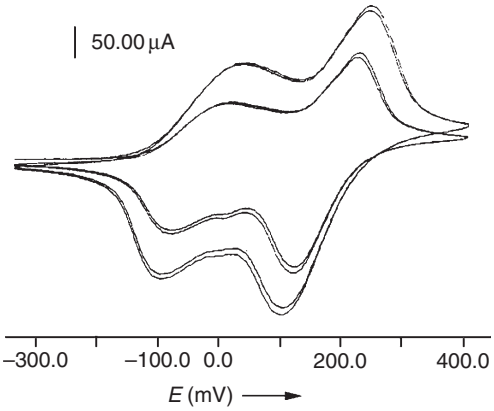

Figure 13 Cyclic voltammogram of polyferrocenyldimethylsilane **73** (R = R^1 = Me) in CH_2Cl_2 (0.1 M of $[Bu_4N][PF_6]$ in CH_2Cl_2) at scan rates of 500 and 1,000 mV s^{-1} showing two reversible oxidation waves separated by a redox coupling $\Delta E_{1/2}$ of ca. 0.24 V.

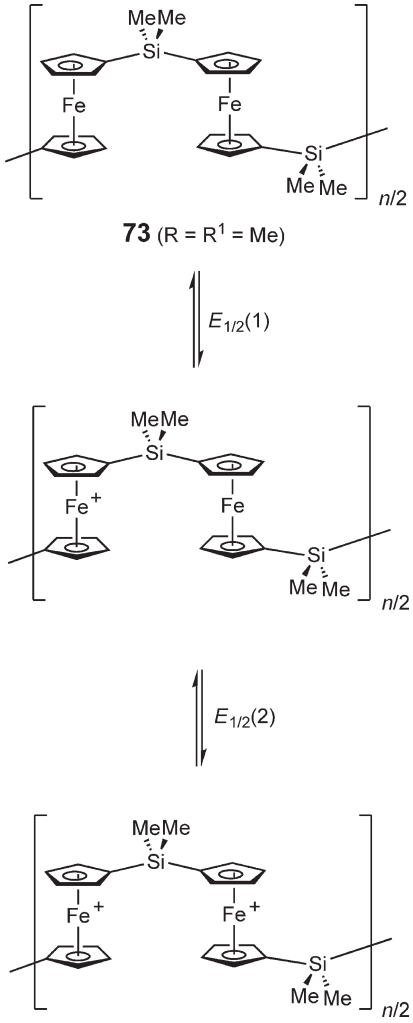

Scheme 6

delocalized. Oxidation of oligo- and polyferrocenylsilanes yields mixed-valence materials which display an intervalence electron-transfer band of significant intensity at ca. 1,300 nm due to hopping of electrons (or more correctly holes) between the Fe(II) and Fe(III) centers.[195] The valence electrons in these materials are localized on the Mössbauer timescale (ca. 10^{-7} s), which shows resolved Fe(II) and Fe(III) sites. These results are also consistent with class II behavior.[203,204]

The nature of the interaction between the iron centers in PFSs is an important question which has sparked significant attention. It does not appear to be simply an electrostatic or Coulombic effect of a positive charge on one iron center that influences the ease of electron removal on another in close proximity. Indeed, studies of linear and cyclic oligomers (and corresponding high polymers, *vide infra*) show that there is a strong dependence of $\Delta E_{1/2}$ on the nature of the bridging elements as well as the distance between the iron sites.[169] Although d–π–σ-conjugation through the Fe–Cp–Si orbitals is in principle possible, the degree of ground-state electron delocalization of this type in PFSs appears rather low. Thus, in contrast to π-conjugated polymers such as polyacetylenes and σ-conjugated polymers such as polysilanes and polystannanes, which show a decrease in band gap with increased chain length, as the HOMO–LUMO transition moves to lower energy, an analogous effect for PFSs has not been detected by UV–VIS spectroscopy.[169] Thus, the λ_{max} and extinction coefficient for the linear dimer $FcSiMe_2Fc$, the cyclic dimer $[fcSiMe_2]_2$, and the high polymer **73** (R = R^1 = Me) are very similar (where fc is the ferrocenylene group –(η^5-C_5H_4)Fe(η^5-C_5H_4)–). An explanation has been advocated that the variation of the metal–metal interactions depends on the nature of the bridging group which influences the "molecular-scale dielectric constant" of the medium between the iron centers.[205] As the dielectric constant of the medium determines the interactions detected, more polarizable atoms would be expected to lead to increased redox coupling, which has in fact been observed in practice.

When PFSs are oxidized, they undergo a color change from amber to blue. This interesting, reversible, electrochromic behavior has been studied in some detail for several polymers.[203,206] Pristine high molecular weight PFSs are insulating ($\sigma = 10^{-14}$ S cm^{-1}) and when partially oxidized or "p-doped" by I_2, the amorphous samples exhibit conductivities in the weak semiconductor range ($\sigma = 10^{-8}$–10^{-7} S cm^{-1}), whereas for the oriented crystalline samples (**73**, R = R^1 = *n*-Bu), the conductivities are in the semiconductor range (up to ca. 2×10^{-4} S cm^{-1}).[173] Detailed studies have indicated that iodine doping is partially reversible and, at high I_2 concentration, an $[I_5]^-$ species forms which may play a role in mediating metal–metal interactions and charge transport.[204,207]

The semiconductive nature of some PFSs makes them excellent candidates for applications where some conductivity is needed but high values are not desirable due to the associated effects of magnetic fields. For example, amorphous PFSs such as **73** (R = Me; R^1 = Ph) possess appreciable hole mobilities (ca. 10^{-5} cm^2 V^{-1} s^{-1})[173] and appear promising as charge dissipation materials with potential applications as protective coatings for dielectrics.[208] Thus, on exposure to low-energy electrons (20 keV), an apparent combination of electron scattering by the iron atoms and some degree of electron conductivity in the polymer film prevents appreciable charge buildup. In contrast, for insulating organic polymers such as Mylar, poly(ethylene terephthalate), an accumulation of the negative charge in the material leads to arcing which will inevitably result in material breakdown.

The magnetic properties of TCNE-oxidized, low molecular weight PFSs ($M_w \sim 1{,}500$) have been investigated. These studies indicated the presence of electron delocalization and, in some cases, the presence of ferromagnetic ordering at low temperature.[209] Attempts to reproduce this behavior with a variety of high molecular weight samples were reported to be unsuccessful.[210] Photo-oxidation of PFS in the presence of chloroform has also been demonstrated and the resultant oxidized materials are photoconducting.[211]

12.06.3.3.6.(iv) Redox-active polyferrocenylsilane gels

The incorporation of transition metals into cross-linked polymer networks leads to gels with interesting properties. Ultimately, such materials represent possibilities for the formation of electrochemical actuators or switches. Controlled cross-linking of PFSs has been achieved to yield redox-active gels that swell in solvents.[212] A cross-linked network **99** ($x + y : z = 1 : 0.02$–0.15) can be obtained and the degree of cross-linking can be controlled by using appropriate amounts of the spirocyclic [1]ferrocenophane **98** in the thermal polymerization mixtures (Equation (40)). From the measurement of the swelling response in various solvents, the solubility parameter (δ) for the linear poly(ferrocenyldimethylsilane) **73** (R = R^1 = Me) was estimated to be 18.7(7) MPa$^{1/2}$.[212]

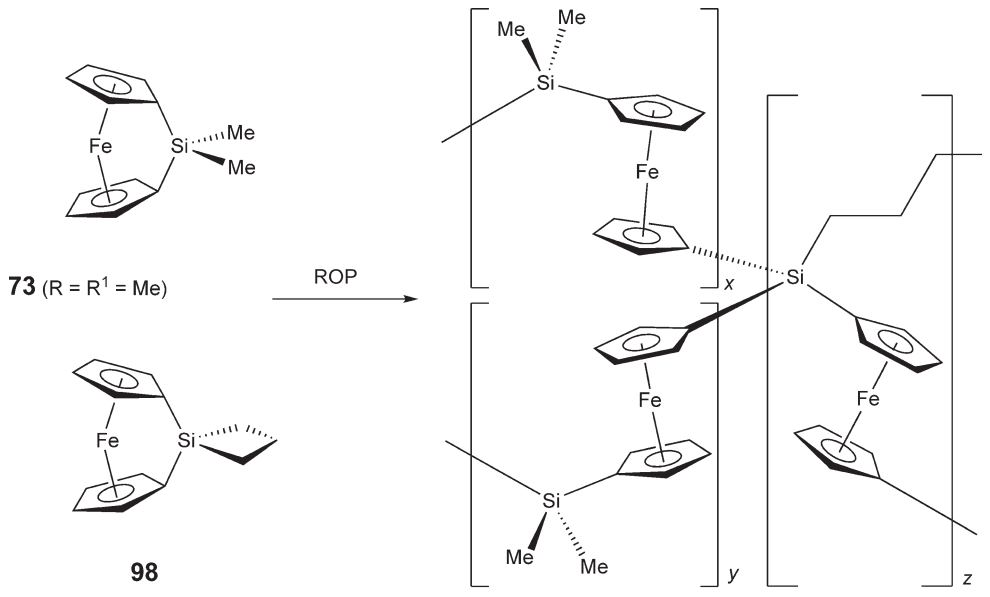

(40)

The metal–metal interactions in the polymer network were investigated by controlled potential electrolysis with the aid of an optically transparent thin-layer electrochemistry (OTTLE) cell. The visible–NIR spectrum of the fully reduced deep red-orange gel shows the lowest energy visible band assigned to a *d*–*d* transition. Upon oxidation, two new absorption peaks emerge: one at 640 nm is due to a ligand-to-metal charge transfer (LMCT) of the ferrocenium moiety, whereas the other peak, a broad absorption band centered at 1,300 nm, is assigned to an intervalence electron transfer (IVCT). The colour of the gel was observed to darken to a deep blue with increasing oxidation. The reversibility of the process was demonstrated by reversing the potential and allowing the gel to return to the fully reduced state, as indicated by the original deep red-orange colour of the gel and the disappearance of the LMCT and IVCT bands of the oxidized polymer.[212]

The swelling of the PFS gel in an organic solvent depends on the degree of oxidation of the iron sites. This has allowed the development of planar colloidal photonic crystal devices in which silica microspheres are arrayed in a matrix of cross-linked PFS.[213] The optical Bragg diffraction peak (stop-band) position, width, and intensity could then be tuned through reversible redox processes or change of solvents over a broad wavelength range by an anisotropic expansion of the photonic lattice. The optical response of the material was exceptionally fast, and attained its fully swollen state from the dry shrunken state on a sub-second timescale.

Through use of an alternative hydrolytic approach, poly(ferrocenylalkoxysilanes) have also been incorporated into gels and oxide matrices by means of sol–gel chemistry. For example, poly(ferrocenylalkoxysilanes) **76** ($R = R^1 = OMe$, O^iPr, or OCH_2Ph) were hydrolyzed in water using fluoride catalysts to afford orange, insoluble solids in which the electrochemical properties of the ferrocene units were conserved.[214]

12.06.3.3.6.(v) Thermal stability and conversion to nanostructured magnetic ceramics

The use of processable polymeric ceramic precursors is an attractive way of circumventing the difficulty inherent in the processing of ceramic materials into desired shapes (see Section 12.06.1.3.2). Ceramics obtained as films, coatings, fibers, or bulk shapes are especially appealing for practical applications. Polymers are of interest as precursors to ceramic monoliths, films, and fibers provided that the yield on pyrolysis is high. PFSs such as **73** ($R = R^1 = Me$) are thermally stable up to 350–400 °C. Above 500 °C, magnetic ceramic composites are formed which consist of iron particles in an essentially amorphous SiC/C matrix.[215] However, the ceramic yields are low (only 35–40% at 1,000 °C). The insoluble, semicrystalline poly(ferrocenyldihydrosilane) **73** ($R = R^1 = H$) and materials with acetylenic side-groups (e.g., **73**; ($R = Me$; $R^1 = C{\equiv}CPh$) give the highest ceramic yields with weight retentions of 63% and 81% at 1,000 and 900 °C, respectively.[174,216]

The use of highly cross-linked PFS networks **99** ($x = y = 0$) leads to much improved ceramic yields (ca. 90%), and the pyrolytic formation of shaped, magnetic ceramics is efficient. The cross-linked network can be formed by heating the [1]silaferrocenophane, **98**, in a mold (7 h at 150 °C and then 16 h at 180 °C). The resulting cross-linked network **99** ($x = y = 0$) resembles the mold used, such as a pentagon (Figure 14).

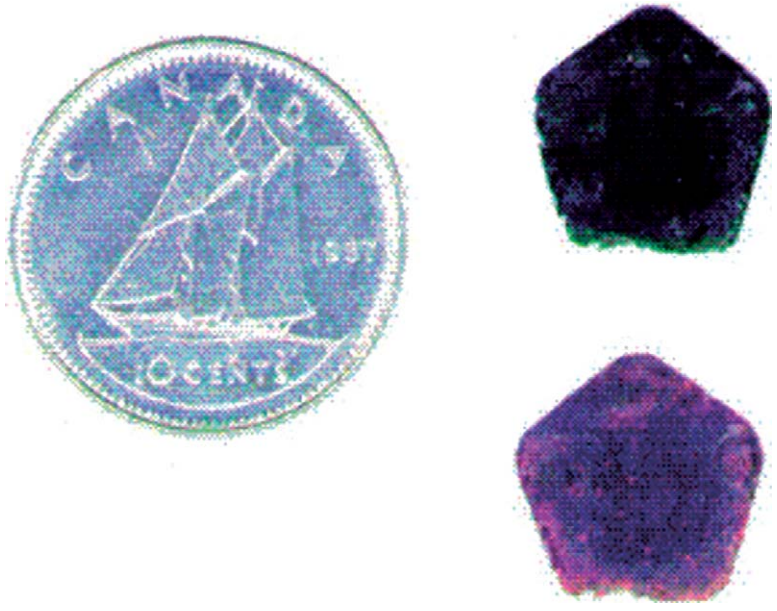

Figure 14 Photograph of the bulk organometallic polymer cast in a pentagonal Teflon mold before (bottom) and after (top) pyrolysis at 600 °C. The ceramic retains the shape of the precursor polymer and shows only a small contraction after pyrolysis (pyrolysis was not performed in a mold). (Reproduced with permission of The American Chemical Society from Ginzburg, M. *et al*., *J. Am. Chem. Soc.*, **2002**, *124*, 2625.)

Pyrolysis of molded samples of **99** ($x = y = 0$) above 500 °C leads to ceramics with a very small associated weight loss and contraction (<10%), which allows retention of the overall shape (Figure 14).[217,218] Furthermore, at 600 °C, the formation of small iron clusters dispersed within an amorphous "carbosilane" matrix is apparent. As the pyrolysis temperature is further raised to 1,000 °C, an increase in iron particle size is detected by PXRD and TEM. Magnetization measurements for ceramics formed at 650 and 850 °C show evidence for smaller, superparamagnetic Fe_n clusters, while for those formed at higher temperatures (1,000 °C), the size of the Fe_n clusters is large enough to display ferromagnetic behavior. Flexible films could also be formed from **99** ($x = y = 0$), and subsequent pyrolysis at 600 °C provides a route to rigid, superparamagnetic ceramic films.

The polymer-precursor approach can also be used in conjuction with soft-lithography techniques to permit the formation of micron-scale magnetic patterns.[218] For example, micromolding of monomer **98** within anisotropically etched channels in a silicon wafer followed by thermal ROP yielded patterned PFS films, and subsequent pyrolysis yielded a patterned magnetic ceramic film with 10% feature size contraction. Honeycomb-like cross-linked PFS inverse opal structures have been prepared by the thermal ROP of spirocyclic [1]silaferrocenophanes such as **98** confined within the interstitial void spaces of sacrificial colloidal crystal silica templates. These organometallic polymer inverse opals were converted in high yield to honeycomb-like magnetic ceramic replicas through pyrolysis at 900 °C.[219] Such approaches may allow the formation of shaped ceramic structures of interest for photonics applications or magnetically actuated components of microelectromechanical systems (MEMSs).

The pyrolysis of PFSs within the channels of the mesoporous silica MCM-41 and the creation of nanostructured magnetic ceramic nanocomposite materials has been achieved.[220] In addition, use of a sacrificial porous alumina yields organometallic and magnetic ceramic nanofibers.[221] Hyperbranched PFSs have also been synthesized and pyrolysis of these interesting materials has been found to lead to superparamagnetic ceramics.[222] Furthermore, pyrolysis of PFSs with pendant Co clusters yields ceramics containing hybrid Fe/Co nanoparticles.[223]

12.06.3.3.6.(vi) Charge-tunable and pre-ceramic microspheres

Microspheres based on metal-containing polymers should exhibit interesting redox, semiconductive, magnetic, and photonic properties intrinsic to the polymeric materials, and may prove useful for a variety of applications. The most common methods for microsphere preparation involve the use of steric stabilizers, which may adversely affect the properties of the resultant materials. This problem can be avoided by the use of a precipitation polymerization methodology, which allows for the autostabilization of the polymer microspheres without addition of stabilizers. This

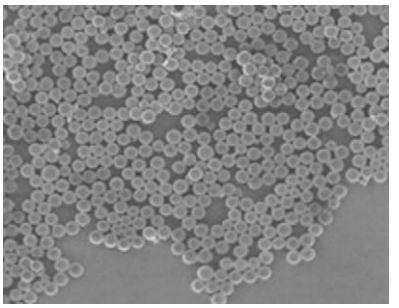

Figure 15 SEM micrograph of polyferrocenylsilane microspheres formed from precipitation polymerization methods with average particle diameters of 2.1 μm (Reproduced with permission of The American Chemical Society from Kulbaba, K. *et al.*, *J. Am. Chem. Soc.*, **2002**, *124*, 12522.)

approach, which has been used for the formation of cross-linked PS microspheres, has been adapted to allow the preparation of microspheres comprised of PFS.[224]

PFS microspheres can be formed by the addition of monomers **72** (R = R^1 = Me) and **98** in a 1 : 1 ratio to a mixture of xylenes and decane with a Pt(0) catalyst at 60 °C. Under gentle agitation, over a period of 18 h, polymer microspheres with diameters of ca. 2 μm are formed with a reasonably narrow size dispersity (Figure 15). Chemical oxidation of the resulting microspheres with iodine leads to positively charged particles, which electrostatically self-assemble with negatively charged silica nanospheres (diameter ca. 0.4 μm). SEM revealed the formation of composite superstructures in which the larger PFS core was surrounded by the smaller, negatively charged silica particles.

The development of magnetic particles is of intense interest for theoretical studies as well as potential applications in recording media and imaging. The cross-linked PFS microspheres can be used as precursors to spherical magnetic ceramic particles. Upon pyrolysis at either 600 or 900 °C, there is a contraction of the microspheres from 2 to 1.7 μm in diameter. Furthermore, the magnetic properties of the microspheres were found to be dependent on pyrolysis conditions. As with the bulk cross-linked material **99** ($x + y : z = 1 : 1$), at lower temperatures (600 °C) smaller, superparamagnetic Fe clusters are formed, while at higher temperatures (900 °C) the resulting clusters are larger and display room-temperature ferromagnetic behavior. As a result of the magnetic properties associated with the particles, their assembly into well-ordered arrays by interaction with an applied magnetic field becomes feasible.[224]

12.06.3.3.6.(vii) Water-soluble polyferrocenylsilanes: layer-by layer assembly applications

Water-soluble organic polymers are of considerable commercial importance, whereas few examples of water-soluble metal-containing polymers have been reported. Both cationic and anionic water-soluble PFs have been prepared by a variety of different synthetic methodologies.[225–231] These materials are of potential interest as electrode materials and as redox-active polymeric electrolytes whose ionic conductivity might be tuned by oxidation of the iron centers. Based on the potential formation of micellar aggregates, these materials may also prove useful as redox-active encapsulation agents.[232,232a,232b] Furthermore, various water-soluble ferrocenium salts have been shown to display anticancer activity.[233]

A typical water-soluble PFS polyelectrolyte, the cationic PFS **101**, can be prepared by thermal ROP of monomer **100**, followed by subsequent quaternization of the resulting polymer with Me_2SO_4 (Equation (41)).[226]

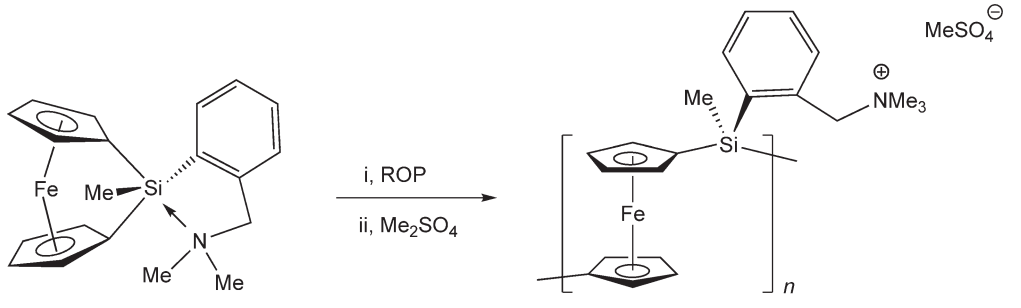

100 **101** (41)

A key application for these materials involves the creation of electrostatic superlattices through layer-by-layer assembly.[228–231] The technique involves the sequential adsorption of polycationic and polyanionic monolayers from aqueous solutions to form nanoscale multilayer polymer films of controlled thickness. Such film architectures can be manipulated to achieve unique tunable physical properties, and orchestrated for the construction of a range of devices. For example, well-characterized organic–organometallic polymer electrostatic superlattices have been prepared via alternate adsorption of anionic poly(styrenesulphonate) (PSS) and cationic PFS **101** on Si and Au substrates.[228] The wettability of the film surface is dependent on the outermost layer of the multilayer assembly, as shown by the advancing contact angle measurements. All-organometallic superlattices constructed from cationic and anionic PFS polyelectrolytes have also been prepared,[230,230a,231] and a cross-section of the film can be visualized by TEM after the film surface is sputtered with a layer of Au.[230,230a] In addition, superlattices on negatively charged silica microspheres can be prepared. Subsequent etching away of the silica with HF yields hollow organometallic microspheres.[230,230a]

12.06.3.3.6.(viii) Applications as variable refractive index sensors and as NLO materials

PFSs are promising materials as coatings for optical fiber gas sensors.[234] These devices function on the principle that environmentally induced changes in the refractive index of a thin (ca. 0.4 μm) PFS coating leads to changes in the power transmitted through the optical fiber. An example of NH_3-sensing by a device that uses a PFS coating (**73**; R = Me; R^1 = Ph) is shown in Figure 16. The sensor also works well for CO_2 but not N_2O. In addition, Langmuir–Blodgett films of PFSs have been studied and are of potential interest as chemomechanical sensors where changes in mechanical properties are induced by analytes.[235] Potential applications as second-order NLO materials have been investigated also.[236]

12.06.3.3.7 Properties of other ring-opened polymetallocenes and related materials

Similar ROP methods to those described for silicon-bridged [1]ferrocenophanes have been successfully used for germanium-bridged [1]ferrocenophanes.[182,237] The resulting high molecular weight polyferrocenylgermanes **78** are amber materials that exhibit similar electrochemical and thermal transition behavior to PFSs but with slightly lower T_g values.[182,237] Polyferrocenylgermanes that are symmetrically substituted on germanium also tend to crystallize, as in the case of PFS analogs. Random co-polymers of polyferrocenylgermanes and PFSs have been prepared from mixtures of [1]germa- and [1]silaferrocenophanes using either thermal or transition metal-catalyzed ROP.[181,182]

Tin-bridged [1]ferrocenophanes have also been successfully prepared by the use of sterically bulky subsituents at the bridging element, and undergo ROP to yield polyferrocenylstannanes **86**.[169,238] PFPs, polyferrocenylphosphine-sulfides, and polyelectrolytes derived from the ROP of phosphonium-bridged [1]ferrocenophanes have also been studied.[142,166,239,240] The polyferrocenes with organophosphorus spacers appear amorphous, presumably due to their

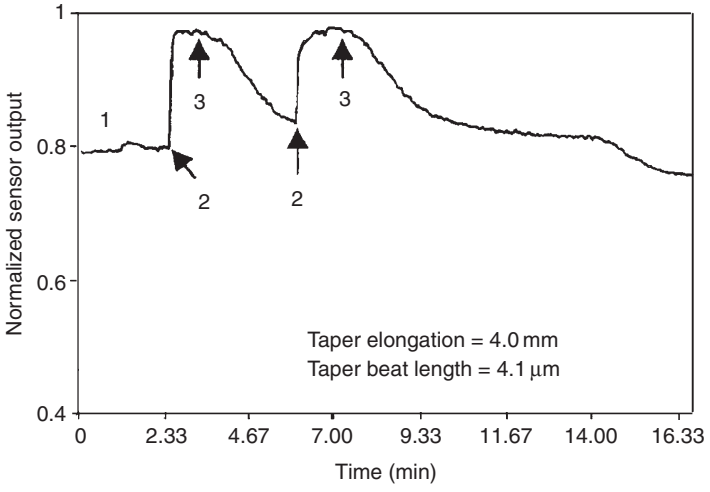

Figure 16 Response of sensor to NH_3. Point 1 is response under vacuum, point 2 is where NH_3 was introduced, and point 3 is where re-evacuation was initiated. (Reproduced with permission of Springer from Espada, L. I. *et al*., *J. Inorg. Organomet. Polym.*, **2000**, *10*, 169.)

atactic nature. The redox properties of the PFPs seem in some cases to be more complex than those of the corresponding polymers with group 14 element spacers. This appears to be a consequence of possible electron removal from the lone pair at phosphorus in addition to that from the ferrocene moieties.[241] PFPs with narrow polydispersities have been prepared via living anionic ROP of [1]phosphaferrocenophanes and have also been studied.[239]

Polyferrocenylsulfides **83** have been prepared from the ROP of highly strained sulfur-bridged [1]ferrocenophanes and appear to possess more substantial metal–metal interactions (redox coupling $\Delta E_{1/2} > 0.30$ V) than the analogous PFSs based on electrochemical measurements.[167] Polyferrocenylboranes **85** are sensitive to moisture which has hindered detailed studies of their properties.[168]

Disilane-bridged [2]ferrocenophanes are insufficiently strained to undergo ROP.[158] However, random polymers **89** with ferrocenylsilane and oligosilane units in the main chain have been prepared by the thermal co-polymerization of silicon-bridged [1]ferrocenophanes and cyclic tetrasilanes. The resulting co-polymers show interesting properties. For example, the Si–Si bonds in these materials can be photochemically cleaved by UV light and the conjugation in the backbone only appears to involve the σ-delocalized oligosilane segments. The random co-polymers also possess appreciable hole mobilities.[173]

ROP of hydrocarbon-bridged [2]ferrocenophanes yields polyferrocenylethylenes **88** ($E_1 = E_2 = CH_2$; R = H or Me). Due to the more insulating hydrocarbon bridge in these materials, only slight communication between the iron centers is observed by cyclic voltammetry (redox coupling of $\Delta E_{1/2} = 90$ mV). Nevertheless, cooperative magnetic behavior has been reported in TCNE-oxidized materials at low temperature.[242]

12.06.3.3.8 Polyferrocenylsilane block co-polymers

12.06.3.3.8.(i) Synthetic scope

Living anionic ROP of strained silicon-bridged [1]ferrocenophanes (Section 12.06.3.3.3) provides an excellent route to PFS block co-polymers with controlled block lengths and narrow polydispersities (PDI < 1.1).[82–84] Diblock, triblock, and more complex architectures are now known for a wide variety of organic, inorganic, or even other polyferrocene co-blocks. The prototypical materials prepared in the mid-1990s were the diblock co-polymers polyferrocenylsilane-*b*-polydimethylsiloxane (PFS-*b*-PDMS) **103** and polystyrene-*b*-polyferrocenylsilane (PS-*b*-PFS) **105**.[46] As shown in Scheme 7, initial anionic polymerization of monomer **72** gives a living polyferrocenyl lithium species **102**, which can be subsequently used to initiate the ROP of a co-monomer such as a cyclic siloxane to prepare **103** (Scheme 7).

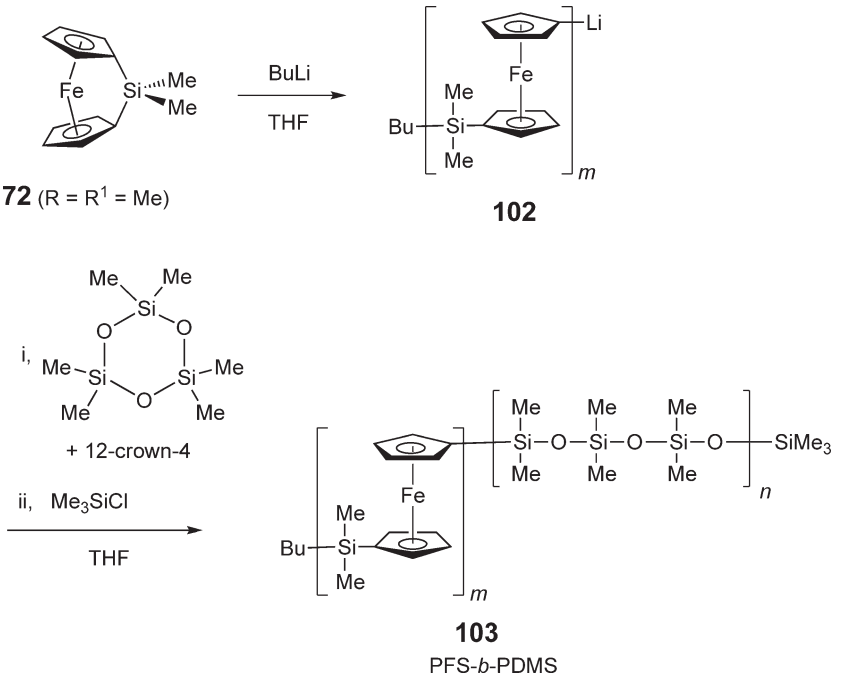

Scheme 7

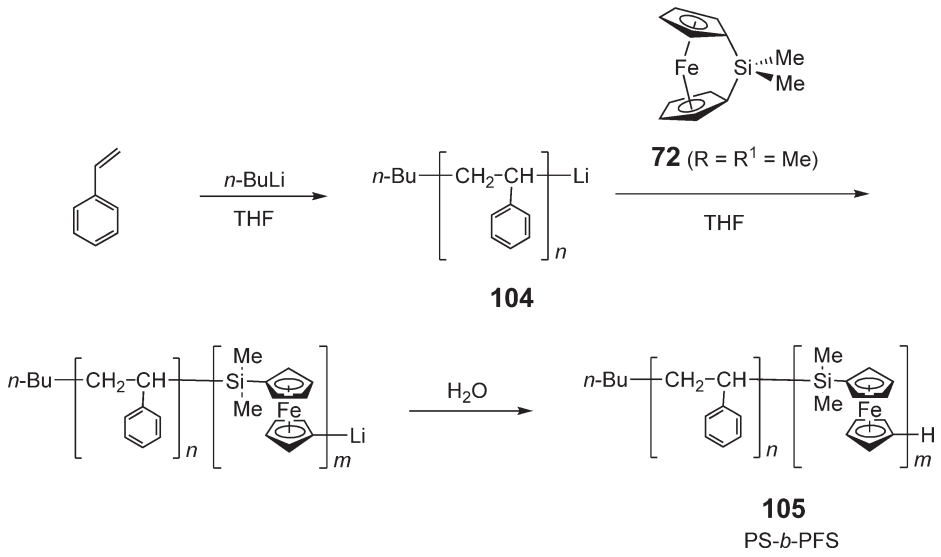

Scheme 8

The ROP of ferrocenophane **72** can also occur in the presence of the living anions of a preformed block. For example, co-polymer PS-*b*-PFS **105** can be prepared from anionic polymerization of styrene followed by ROP of **72**, initiated by the PS lithium species **104** (Scheme 8).

Moreover, PFS block co-polymers can be accessed via transition metal-catalyzed ROP of silicon-bridged [1]ferrocenophanes (Section 12.06.3.3.4) in the presence of a polymer terminated with a reactive Si–H bond.[183] This technique has been used successfully for the synthesis of both diblock and triblock co-polymers. For example, water-soluble PFS-*b*-PEO **106** (PEO = poly(ethylene oxide)) has been prepared from monomer **72** and commercially available poly(ethylene glycol) modified at the end group (Scheme 9).[185] In such cases, the polydispersity of the PFS blocks is higher than that obtained from anionic ROP (typically, PDI = 1.4) and the polydispersity of the co-block is determined by that of the original Si–H functionalized material. Nevertheless, block co-polymer syntheses that use the transition metal-catalyzed approach are very convenient, as the stringent purification and experimental requirements for living anionic polymerizations are unnecessary.

12.06.3.3.8.(ii) Self-assembly in block-selective solvents

Based on the studies of organic block co-polymers, PFS block co-polymers should self-assemble in solvents, which are selective for one of the blocks. In the case of organic block co-polymers, most studies have led to the identification of spherical structures where the less-soluble block constitutes the core within a corona formed by the more-soluble block. Only since the mid-1990s have non-spherical structures become more commonly reported.[243]

Initial studies on the solution micellization of PFS block co-polymers involved investigations of the aggregation of PFS-*b*-PDMS block co-polymers **103** in a selective solvent for the PDMS block.[244] Interesting cylindrical micellar architectures can be generated by simply dissolving the amber, tacky block co-polymer in *n*-hexane at room temperature (Figure 17). Novel wormlike micelles were obtained in the case of a material with a PFS : PDMS block ratio of 1 : 6. These structures maintain their integrity after solvent evaporation and the iron-rich cores can be readily visualized by TEM (Figure 18(a)). When the micelles are heated above the T_m of the poly(ferrocenyldimethylsilane) block (ca. 120–145 °C), spherical aggregates are formed. The spherical structures are also generated when an amorphous poly(ferrocenylmethylphenylsilane) or poly(ferrocenylmethylethylsilane) block is used in the co-polymer. These results suggest that the crystallization of the core polymer is the driving force for the unexpected formation of wormlike micelles below T_m.[245] In the case of even longer corona-forming PDMS blocks, cylindrical structures that possess an appreciably hollow cavity are formed (e.g., for a PFS : PDMS ratio of 1 : 13).[246]

The lengths of the cylindrical structures can be increased to over 10 μm by controlling the preparation technique. The cylinders show considerable stability in solution and are unchanged in size after heating to 80 °C. However, ultrasonication of samples of the cylindrical micelles leads to a shortening of their length as indicated by light-scattering and TEM studies.

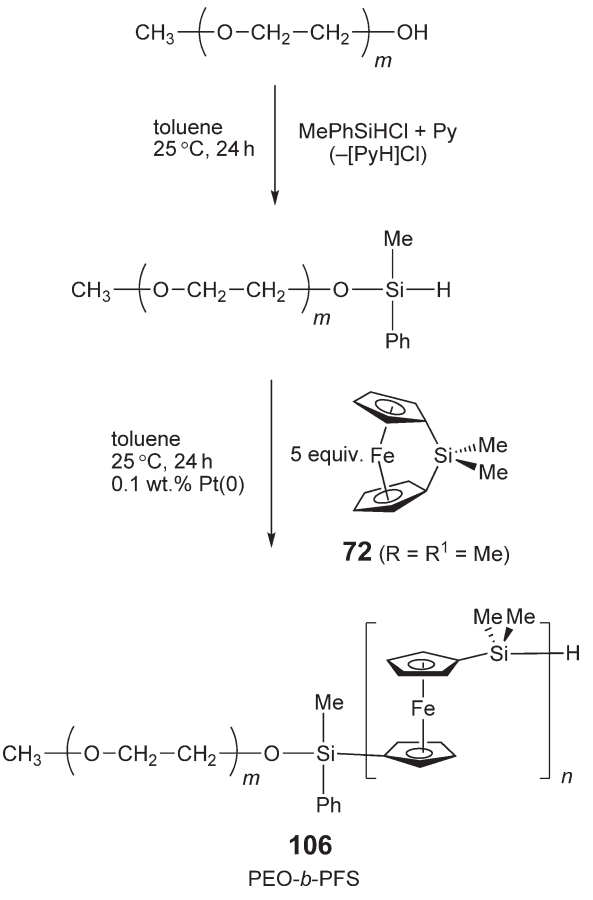

Scheme 9

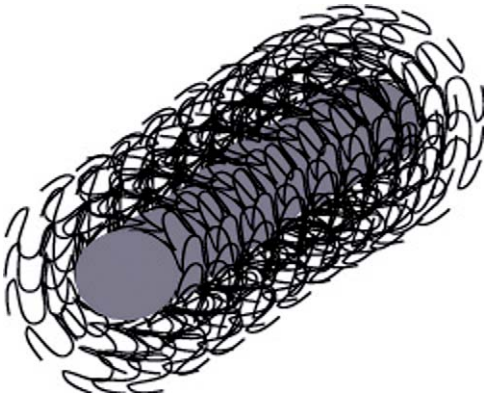

Figure 17 Schematic cross-sectional diagram of PFS-*b*-PDMS **103** cylindrical micelles showing the polyferrocenylsilane core and a poly(dimethylsiloxane) corona.

Cylindrical and tape-like morphologies have been identified in the case of PI-*b*-PFS (PI = polyisoprene) where the PFS block crystallizes.[247] Water-soluble polyferrocenyldimethylsilane-*b*-poly(aminoalkylmethacrylate) co-polymers of narrow polydispersity have also been prepared and cylindrical micelles have been identified.[248] Block co-polymers generated by transition metal-catalyzed ROP, such as PFS-*b*-PDMS-*b*-PFS triblock materials, have been shown to self-assemble in hexanes to yield a variety of remarkable architectures that include flower-like assemblies where the

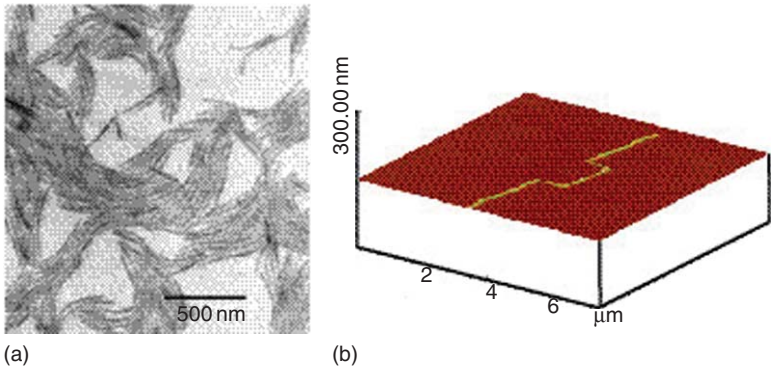

Figure 18 (a) Transmission electron micrograph of cylindrical micelles of PFS-*b*-PDMS **103** ($M_n = 35{,}100$, PDI = 1.1) aerosol-sprayed from *n*-hexane solution onto mica. The cylinders have an average contour length of 440 nm and an average diameter of 20 nm. The micrograph shows a region where the cylinders are starting to pack and form a 2-D film and regions where there are isolated cylinders. No staining of the sample is required as the PFS cores are readily observable due to high electron density contrast. (b) Scanning force micrograph after the oriented deposition of PFS-*b*-PDMS diblock co-polymer cylinders along pre-patterned grooves on a resist film, lift-off with acetone, followed by hydrogen plasma treatment. This process leads to aligned nanoscopic lines with a height of approximately 4 nm, composed of cylindrical clusters of Fe, Si, O, and C. (Reproduced with permission of The American Chemical Society from Massey, J. A. *et al*., *J. Am. Chem. Soc.*, **2002**, *124*, 12522 and **1998**, *120*, 9533.)

PFS block is semicrystalline.[249] In several systems, morphologies such as vesicles and compound micelles in addition to spheres and cylinders have been identified.

The cylindrical micelles consist of a wire-like core of PFS surrounded by a sheath or corona of insulating poly(dimethylsiloxane) and are of interest as semiconducting nanowires as well as precursors to magnetic wire-like ceramic structures. These structures are sufficiently stable to permit fabrication by spin- or dip-coating onto substrates. The cylindrical micelles have been positioned on the surface of a GaAs resist by capillary forces along grooves which were previously formed from electron-beam etching of the surface.[250] After reactive ion etching (RIE) of the micelles with hydrogen plasma, connected ceramic lines of reduced sizes, with potentially interesting conductive and magnetic properties, were generated (Figure 18(b)). In some cases, such a technique allows the formation of lines that have widths less than 10 nm and lengths greater than 500 nm through a combined "top-down/bottom-up" approach.[251] It should be noted that structures with such small dimensions are difficult to fabricate using other techniques. Furthermore, these well-defined aggregates may be of use as etching resists for semiconducting substrates such as GaAs or Si, and offer potential access to magnetic or semiconducting nanoscopic patterns on various substrates. As the accessibility of smaller and smaller width scales by lithographic techniques becomes limited, the use of such methods becomes necessary. For example, the formation of etch resists for use in the production of 2-D quantum wires with large aspect ratios in semiconducting substrates becomes possible.

12.06.3.3.8.(iii) Self-assembly in the solid state

PFS block co-polymers in which the blocks are immiscible (which is generally the case) would be expected to self-assemble to form phase-separated organometallic domains in the solid state. Based on the classical behavior of organic block co-polymers, thin films of polyferrocene diblock co-polymers would be expected to form domains such as spheres, cylinders (or their anti-structures), double diamonds (or gyroids), or lamellae (Section 1.2.5). The preferred domain structure would be expected to be controlled by the ratio of the blocks, their degree of immiscibility (as defined by the Flory–Huggins interaction parameter χ), and the overall molecular weight of the block co-polymer.[252]

The first studies of PFS block co-polymer films were reported in 1996 and utilized DSC and TEM to analyze the phase separation in the materials.[46] In the case of PS-*b*-PFS **105** and PFS-*b*-PDMS **103**, it was demonstrated that the electron-rich Fe atoms of the PFS block allow sufficient electron scattering to provide contrast with the organic or inorganic co-blocks and that selective staining of one of the blocks, which is generally required for all-organic materials, was unnecessary.[46,244] Detailed systematic studies confirm that spherical, cylindrical, and lamellar domains are formed by using the expected block ratio variations.[253–256] A detailed analysis of the thermodynamic interactions in PS-*b*-PFS **105** using birefringence, SAXS, and neutron-scattering techniques has also been performed.[257] The phase-separation can be influenced by the crystallization of the polyferrocenyldimethylsilane block, and analogous materials, with amorphous PFS blocks that order more readily without the need to anneal above T_m, have also therefore been studied.[177]

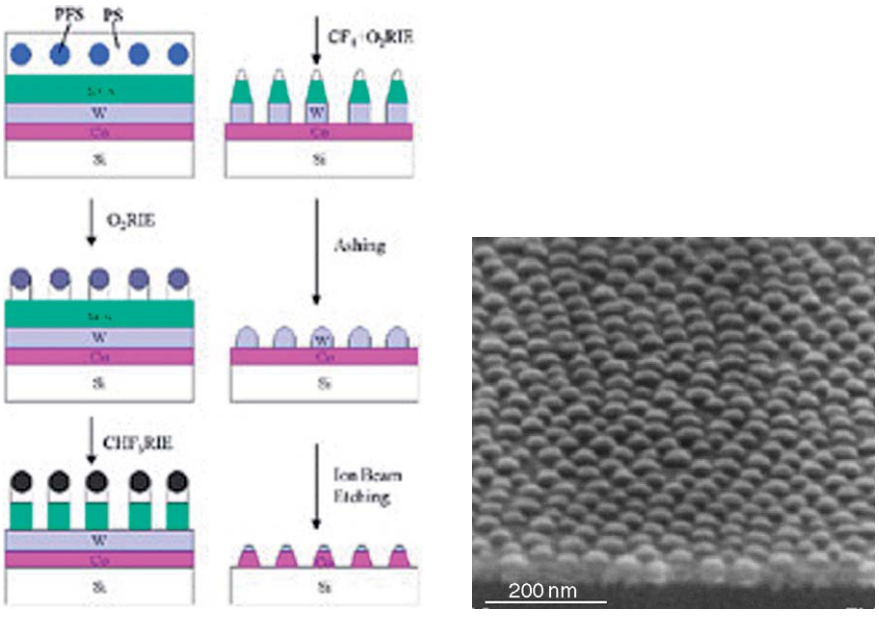

Figure 19 (a) Single-domain cobalt dot arrays with high magnetic particle density, patterned over large areas (e.g., 10 cm diameter wafers) using self-assembled block co-polymer lithography with PS-*b*-PFS **105** as a template. A thin film consisting of spheres of PFS in a matrix of PS is cast on a multilayer of silica, tungsten, and cobalt. The exposed PS is removed by O_2 reactive ion etching (RIE), while the silica is patterned using a CHF_3 RIE. The tungsten is patterned using a $CF_4 + O_2$ RIE, and the silica and residual polymer is removed by high pressure CHF_3 RIE. The cobalt dots are formed by ion beam etching. (b) A typical array of Co dots with tungsten caps obtained via this procedure. (Reproduced with permission of Wiley-VCH from Cheng, J. Y. *et al.*, *Adv. Mater.*, **2001**, *13*, 1174.)

The difference in etch resistance between the blocks in a co-polymer can be used to pattern surfaces on the nanometer scale via the exposure of phase-separated thin films to etching plasmas.[258] Such processes are particularly efficient if one of the blocks contains inorganic elements.[259] Block-selective ablation of thin films of phase-separated PFS block co-polymers would therefore be expected to be useful for the nanopatterning of surfaces.[254] An example that elegantly illustrates this approach utilizes PS-*b*-PFS materials **105**, which provide a spherical PFS morphology within a matrix of PS.[260] The high relative etching resistance of the PFS block compared to the PS block has allowed for the production of lithographic templates from such films upon etching. Subsequent use of the template in patterning substrates such as cobalt metal has generated arrays of magnetic cobalt nanodots with potential applications in data storage (Figure 19(a)). The nanopattern of Co dots formed is shown in Figure 19(b).

Pyrolysis of phase-separated PFS block co-polymer films also allows the formation of metal-rich nanostructures. For example, pyrolysis of a thin film of PS-*b*-PFS with cylinders of the amorphous PFS block perpendicular to the substrate and in a cross-linked PS matrix at 600 °C yields iron oxide-containing dots on a substrate.[261]

12.06.3.3.9 Polyferrocenylphosphine block co-polymers

It is also possible to form block co-polymers via the living anionic ROP of the phosphorus-bridged ferrocenophanes (Section 12.06.3.3.3).[142,239] Diblock co-polymers such as PI-*b*-PFP **108** can be prepared by the sequential anionic polymerization of isoprene and ferrocenophane **107** (Scheme 10). These materials yield spherical micelles in *n*-hexanes with an amorphous PFP core and a PI corona. The PI corona can be cross-linked via radical reactions to yield a permanently cross-linked shell, which retains its integrity even in good solvents for both blocks.[262] With PFP block co-polymers the possibility of the coordination of various catalytically active transition metal moieties to the phosphorus centers may prove useful for catalysis and for materials science applications.

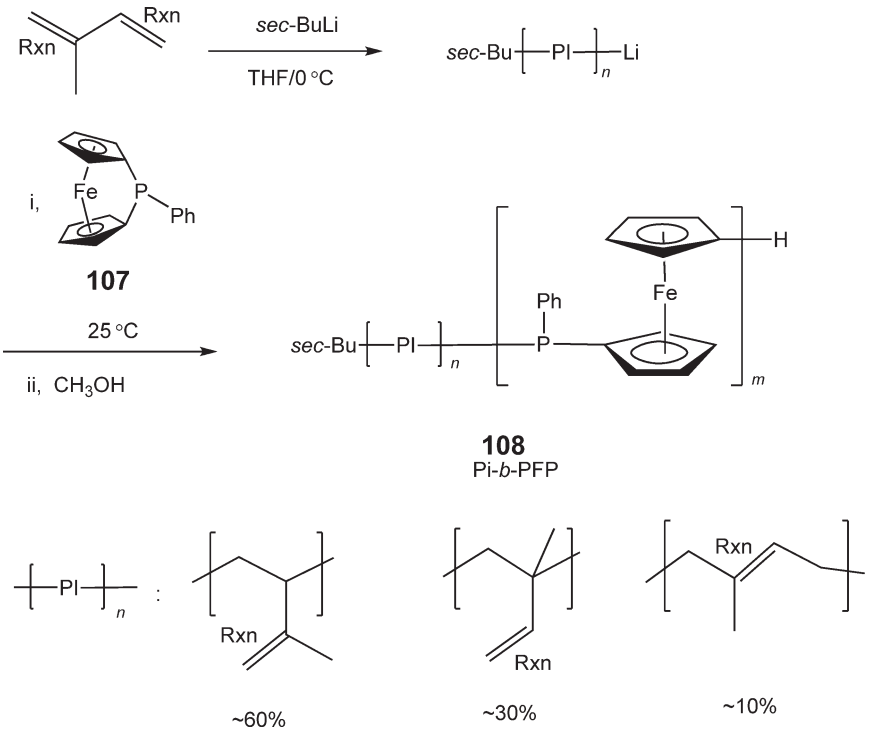

Scheme 10

12.06.3.4 Transition Metal-catalyzed ROMP of Metallocenophanes

The synthesis of poly(ferrocenylene–vinylene) via ROMP of the vinylene-bridged [2]ferrocenophane **109** was reported in 1997.[263] The monomer was obtained from the McMurry coupling of 1,1′-ferrocenedicarbaldehyde. In the presence of a molybdenum ROMP catalyst, **109** was found to undergo polymerization (Scheme 11) to give an insoluble orange powder **110**, which exhibited a conductivity of 10^{-3} S cm^{-1} after iodine doping. Partially soluble block co-polymers **111** were also

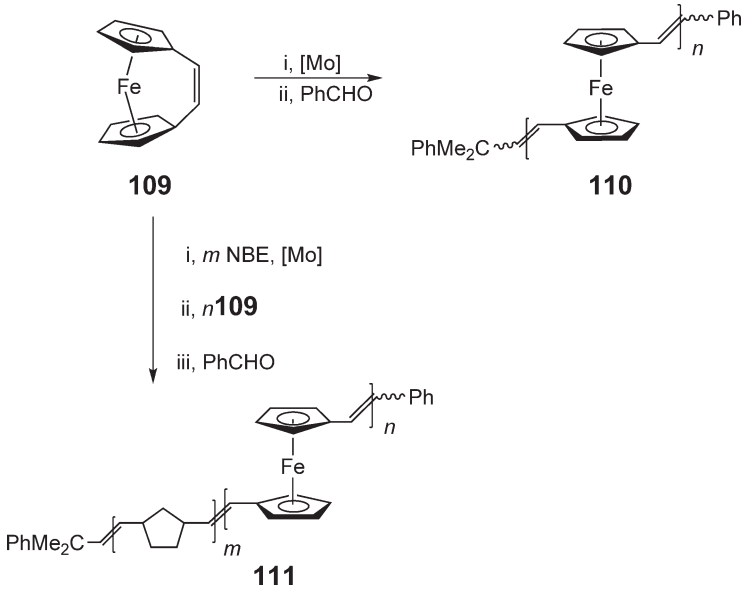

Scheme 11

obtained from ferrocenophane **109** and norbornene via the ROMP route (Scheme 11). When a ratio of [Mo]-catalyst : norbornene : **109** = 1 : 10 : 10 was used, the reaction gave a red gel with an M_w value of 1,710 determined by GPC analysis (vs. PS standards) and a slightly higher M_w of 3,000 by end-group analysis. Similar material generated from a reaction mixture with a catalyst : norbornene : **109** ratio of 1 : 50 : 10 gave considerably higher M_w of 21,000 by GPC. The cyclic voltammograms of **111** showed two reversible redox waves with a separation of 0.25 mV, which is similar to that of PFSs **73** ($\Delta E_{1/2} = 0.20$–0.25 V), and indicate a significant degree of interactions between the Fe centers.[263]

ROMP of [4]ferrocenophanes **112** (R = H) with unsaturated –C═C–C═C– bridges (Equation (42)) has also been used to obtain related polyferrocenylenedivinylenes **113** (R = H) with a π-conjugated structure.[264] These materials are rather insoluble but co-polymerization with *sec*-butylcyclooctatetraene yields more soluble materials with molecular weights up to $M_w = 24{,}400$ (PDI = 2.1). ROMP has also been used to prepare soluble, high molecular weight materials **113** (R = *t*-Bu) ($M_n > 300{,}000$) from substituted [4]ferrocenophane **112** with a solubilizing *t*-butyl group.[265]

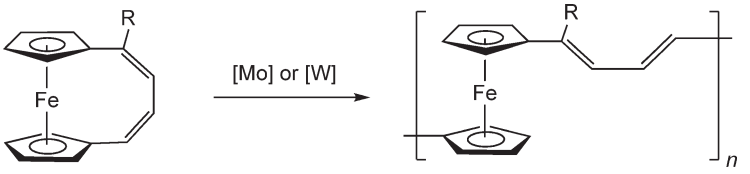

(42)

112
R = H or *t*-Bu

113

12.06.3.5 Atom-abstraction-induced ROP of Chalcogenido-bridged Metallocenophanes

In early 1992, a novel atom-abstraction-induced ROP process was described.[45] The synthesis of well-defined poly(ferrocenylene persulfides) **115** was achieved via the desulfurization of [3]trithiaferrocenophane **114** with PBu_3 (Equation (43)) and the resultant yellow materials were only soluble when ferrocene was substituted with alkyl groups. The rate of the desulfurization reaction and the nature of the resultant polymers have been reported to be solvent dependent.[266–268] The molecular weights have been determined to be in the range of $M_w = 12{,}000$–$359{,}000$ for **115** (R = *n*-Bu; R^1 = H) and 25,000 in the case of a less-soluble co-polymer between monomers **114** with (R = R^1 = H) : (R = ^{n}Bu; R^1 = H) = 53 : 47.[266,268] Polymerization of mono- and disubstituted *t*-Bu derivatives yielded highly soluble polymers **115** with M_w values of up to 26,000 (R = *t*-Bu; R^1 = H) and high polydispersities (PDI = 1.9–7.9).[267] These polymers have been fully characterized and exhibit very interesting properties. The materials are air stable in the solid state but are photosensitive in solution. The persulfide bond can be reductively cleaved with $Li[BEt_3H]$ and subsequently regenerated upon oxidation with I_2.[267] Electrochemical studies of **115** (R = R^1 = *t*-Bu) showed two reversible oxidation waves, as observed for PFSs, that can be attributed to oxidation of alternating iron sites along the polymer chain.[267,268] A wave separation of $\Delta E_{1/2} \sim 0.29$ V suggests that the interaction between iron sites is slightly greater than that observed in PFSs (Figure 20).[201]

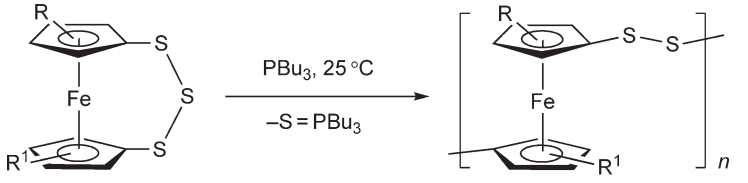

(43)

114

115

R = R^1 = H, *t*-Bu
R = *n*-Bu, *t*-Bu; R^1 = H

This atom-abstraction route was also used for the preparation of polymeric networks from alkylated [3,3′]bis-(trithia)ferrocenophanes.[266] A bimodal molecular weight distribution, with maxima at $M_n \sim 5{,}000$ and 5×10^5, was obtained by GPC for the material from which a polymer fraction was isolated ($M_n = 8.5 \times 10^5$). Low molecular weight poly(ferrocenylene perselenides) have also been prepared from the selenium analog of **114**. These materials also undergo photodegradation upon exposure to UV light in air.[268]

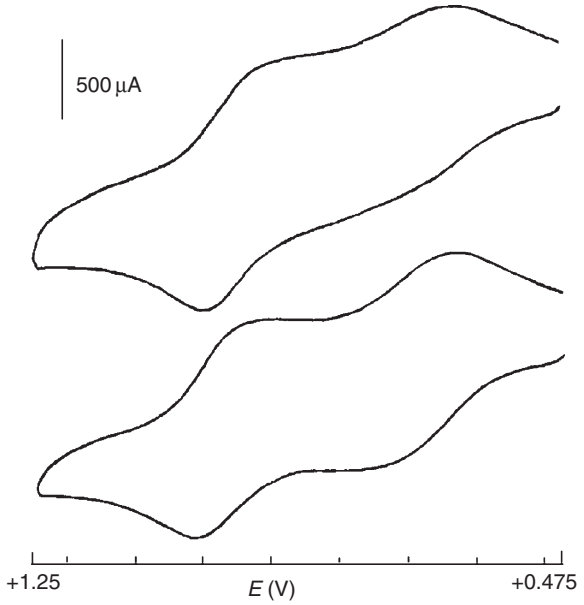

Figure 20 Cyclic voltammogram of poly(ferrocenylene persulfides) **115** (top: R = R^1 = *t*-Bu; bottom: R = *t*-Bu, R^1 = H) showing two reversible oxidation waves separated by a redox coupling $\Delta E_{1/2}$ of ca. 0.29 V for both polymers (in 0.1 M $[Bu_4N][PF_6]$ in CH_2Cl_2). (Reproduced with permission of The American Chemical Society from Compton, D. L. and Rauchfuss, T. S., *Organometallics*, **1994**, *13*, 4367.)

12.06.3.6 Face-to-face Polymetallocenes via Condensation Routes

Multi-decker sandwich structures, apart from those in which stacking takes place upon crystallization, are of considerable interest. Several attempts have been made to synthesize these types of polymeric structures, but in most cases dimer complexes, or double- or triple-decker structures, were produced. A synthesis of novel polymeric metallocenes held face to face by naphthalene or binaphthyl spacer groups has been developed. The condensation route involves palladium-catalyzed cross-coupling of chlorozinc ferrocenes or ruthenocenes with 1,8-diiodonaphthalene.[269,270] Since the ferrocene reagent is very reactive and cannot be prepared in pure form, it is difficult to achieve the exact stoichiometry of reactants required for a high degree of polymerization. Also, the rigidity of the polymer framework makes these materials relatively insoluble and, consequently, only materials with M_n up to 4,000 have been prepared. Crystallographic studies on a trimetal oligomer, as a model for a segment of the polymer, showed a cisoid arrangement for the naphthalene rings. Extrapolation would suggest a helical structure for the polymer.[271] An alternative, more successful route, in which a ferrocene monomer **116** is polymerized by treatment with sodium bis(trimethylsilyl)amide and $FeCl_2$ at room temperature (Equation (44)), has been reported by the same group.[272] The introduction of long hydrocarbon chains as substituents in the momoner unit clearly improves the solubility; thus, polymers **117** with values of M_n up to 18,000 can be easily prepared and, in some cases, components of higher molecular weight were also detected.

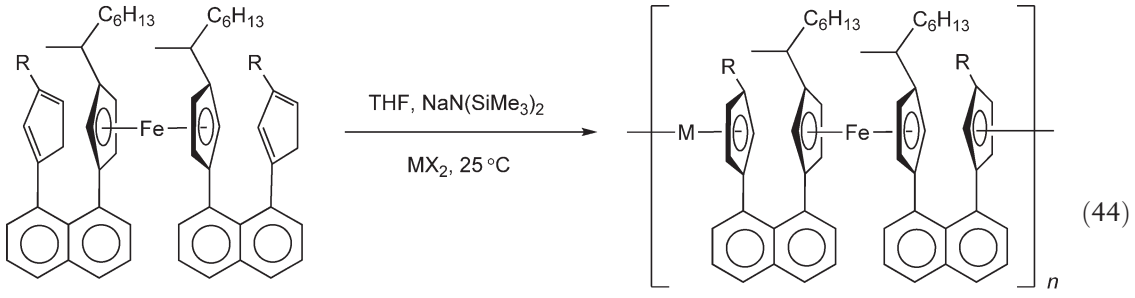

(44)

116

117

M = Fe, Co; X = Cl
M = Ni; X = CH_3COO
R = H, 2-octyl

This is a more general route to these materials and allows access to polynickelocenes from the reaction of alkylated bis(cyclopentadienyl)naphthalene with a nickel(II) reagent. Mixed nickel– or cobalt–iron structures can be also prepared in a similar fashion from **116** and the corresponding metal salts. However, to date, only low molecular weight products ($M_n < 4{,}000$ for nickelocene polymers and $<2{,}000$ for heterometallic materials) have been described.[273] The electrical and magnetic properties for these polymers were investigated. When the iron-based polymers were partially oxidized with I_2, an increase in the electrical conductivity from less than $10^{-12}\,S\,cm^{-1}$ to $6.7 \times 10^{-3}\,S\,cm^{-1}$ was detected, reflecting semiconductor behavior. This value is almost two orders of magnitude lower than that for the analogous crystalline poly(1,1′-ferrocenylene) (Section 12.06.3.2.1). The electrochemistry of oligomers reflects some degree of electronic interaction and charge delocalization between the metal centers of the partially oxidized species ($\Delta E_{1/2} = 100$–$200\,mV$ at $50\,mV\,s^{-1}$). The corresponding I_2-doped polymers appear to be weakly interacting mixed-valent systems by Mössbauer spectroscopy. The bulk magnetic susceptibility was determined for the paramagnetic nickelocene polymer and heterometallic co-polymers. In all of the polymers, the values were greater than those for the corresponding nickelocene or cobaltocene, which was interpreted in terms of cooperative magnetic behavior.[273]

Tetradecker sandwich oligomeric complexes **118** containing carborane C_2B_3 rings have been synthesized via successive deprotonation of the reactive C_2B_3 end rings followed by metathesis reactions with the appropriate metal salts (Scheme 12).[274] Oligomers having 5–17 metal atoms have been synthesized via this route. Cyclic voltammetry studies of these compounds suggested little intersandwich electronic communication, but good evidence for electronic delocalization within the individual tetradecker stacks.[275]

Among recent attempts to obtain polymers where the successive metal–ring bonding is laterally displaced, is the interesting synthesis of materials of structure **119**.[276] The synthesis of soluble helical cobaltocenium oligomers (**119**, up to six units) was achieved in high yields from the elaborate synthesis of [9]helicene hydrocarbon dianions, after treatment with $CoBr_2$·DME and anion metathesis. These are the first examples in which metallocenes are joined by fused conjugated aromatic systems. Electrochemical studies on their properties showed a weak interaction between the metals ($\Delta E_{1/2} = 130\,mV$), similar to the face-to-face polymers described already, and a high optical activity.

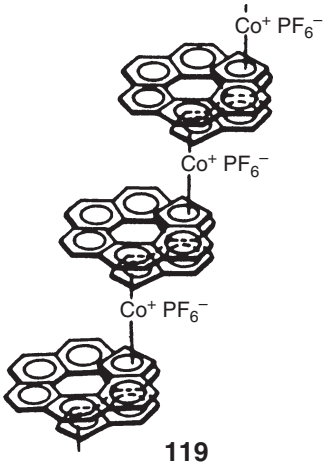

119

12.06.4 Main-Chain Metallopolymers Containing π-Coordinated Metals and Long Spacer Groups

12.06.4.1 Introduction

Polymers with main-chain metal-containing units in close spatial proximity (i.e., the spacer groups comprise three atoms or less), where the metal atoms can interact, are dominated by metallocene-based materials and this area was the focus of the previous section. Macromolecules where longer spacer groups are present between the metallocene units have also been well explored. The diversity of chemistry that has been successfully used to prepare metal-containing polymers with long spacers is much greater and a variety of π-hydrocarbon ligands other than

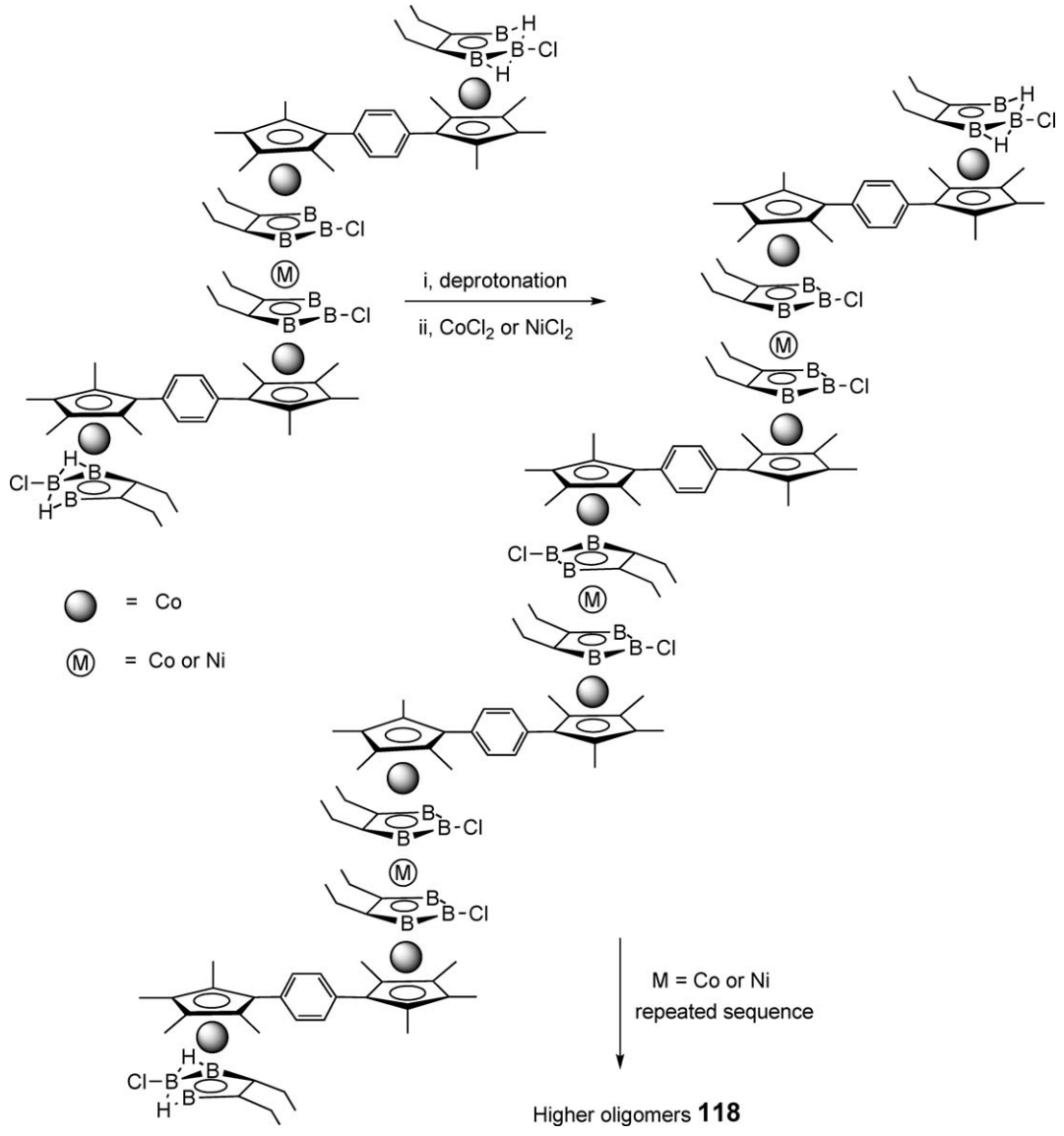

Scheme 12

cyclopentadienyl groups has been productively utilized. Nevertheless, apart from a few impressive exceptions, the studies reported to date have been, in general, less in-depth, and relatively few applications have been investigated in detail. This section surveys work in this general area.

12.06.4.2 Polymetallocenes with Long Insulating Spacer Groups

12.06.4.2.1 Organic spacers

The thermal stability and interesting physical properties of ferrocene provided the initial motivation for the inclusion of ferrocene moieties into polymer chains.[51,52] In the 1960s, numerous attempts to produce ferrocene-containing organic polymers, which included polyketones, polyesters, polyamines, polyamides, polyurethanes, polyureas, and materials with heterocyclic groups, were reported.[53] The synthetic methodologies that were used involved polycondensation methods at high temperatures, and frequently involved side-reactions that led to impure materials or cross-linking. In general, the resulting polymers were very poorly characterized and were of low molecular weight

($M_n < 6{,}000$). Often, no analytical data or structural characterization was provided. Room-temperature interfacial polycondensation methods were also investigated as a convenient alternative to classical polycondensations. Such methods were first reported for the preparation of polyamides and polyesters from the reaction of 1,1′-ferrocenyldicarbonyl chloride with several diamines and diols.[277] The synthesis of polyurethanes using this technique was also reported and involved the condensation of 1,1′-ferrocenedimethanol and 1,1′-bis(dihydroxyethyl)ferrocene with diisocyanates. Once again, however, these polymers possessed low molecular weights.[278] The early research in these areas has been summarized and critically reviewed and will not be discussed further here.[53]

In the 1980s, the successful synthesis of elastomeric polyamides **120** of high molecular weight ($M_n = 10{,}000$–18,000) was reported from the polycondensation of 1,1′-bis(β-aminoethyl)ferrocene with diacid chlorides (Scheme 13).[279] Also, polyureas **121** were prepared from the same ferrocene monomer and diisocyanates, and polyesters and polyurethanes were prepared from 1,1′-bis(β-hydroxyethyl)ferrocene. However, the latter materials had much lower molecular weights and were characterized only by scanning electron microscopy, X-ray, and IR analyses. The introduction of ferrocenes in which the functional groups are separated from the cyclopentadienyl ring by at least two methylene units was crucial in order to reduce steric effects and to avoid the instability found previously in polymers of α-functionalized ferrocene due to the α-ferrocenyl carbonium ion stability.[280]

The same type of methodology was also used to prepare ferrocene-containing arylidene polyesters **122** in good yields from dicarboxyl ferrocenes and organic diols. These materials were characterized by elemental analysis, IR spectroscopy, viscometry, and WAXS.[281] The polymers were found to be semicrystalline but were soluble in polar organic solvents. Conductivity studies showed an n-type semiconductor behavior ($\sigma = 3 \times 10^{-10}\,S\,cm^{-1}$ at room temperature) that followed a one-term Arrhenius-type equation with increasing conductivity over the range 25–220 °C.

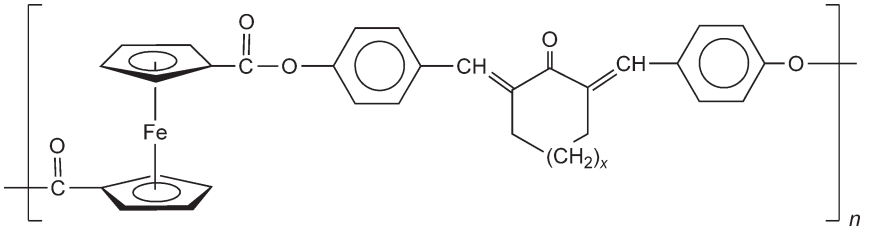

122

x = 0, 1, 2

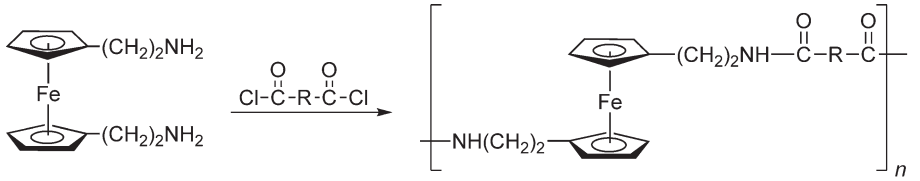

120

R = Ar, $(CH_2)_4$, $(CH_2)_8$

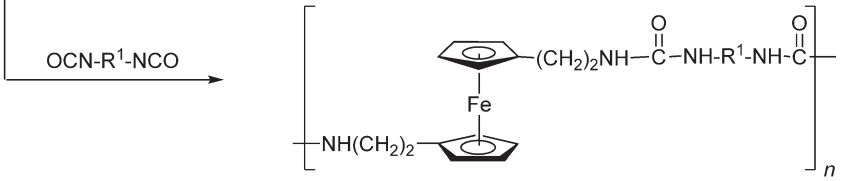

121

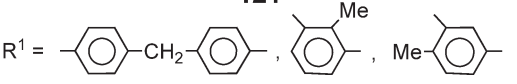

Scheme 13

Ferrocene-containing polymers with long spacers have been prepared as new NLO materials for SHG applications (e.g., frequency doubling).[282] The use of ferrocene derivatives in this area is attractive as a result of their demonstrated large hyperpolarizability values combined with their thermal and photochemical stability.[283] These factors make polyferrocenes desirable candidates for use as processable NLO materials. The polyurethane co-polymer **123** was synthesized using a functional ferrocene monomer (Equation (45)) and was well characterized; the molecular weight was estimated by GPC to be $M_n = 7{,}600$. The two possible orientations of the ferrocene NLO chromophore monomer unit that correspond to opposite dipole orientations were both present in the main chain.

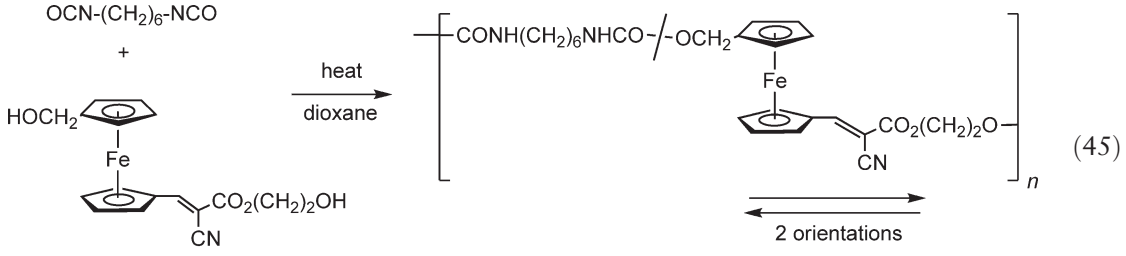

(45)

123

Contrary to previous results that involved related materials with a single orientation of the ferrocene-based NLO chromophores in the main chain,[284] co-polymer **123** displays SHG activity after corona poling at 150 °C with reasonable stability for the SHG signal. This suggests that the chain packing in the solid state that cancels dipole additive effects in the former materials does not operate for the latter polymers which leads to a positive response to poling.

A range of well-characterized ferrocene-containing co-polyesters, such as **124** were prepared via $Ti(O^iPr)_4$-catalyzed melt polycondensations at 140–170 °C.[285] The polymers had molecular weights in the range 9,000–30,300 (by capillary viscometry) and were analyzed by NMR, IR, and DSC. When ferrocene groups were incorporated into the main chain of the polyesters, an increase in the oxidation potential by ≈40 mV was seen, presumably due to a charge-transfer through-space interaction between the electron-poor ester group and the ferrocene unit as the separation was four to six σ-bonds. The first study of the rheological consequences of the incorporation of ferrocene groups into the main chain of a polymer was performed using dynamical mechanical analysis (DMA). Comparison with analogous iron-free polyesters demonstrated the strong influence of the ferrocene unit on the rheological properties, with unusual, rubber-like behavior observed. A tentative explanation was proposed in terms of the metallocene functioning as a large but highly flexible unit, which lowers the critical entanglement molecular weight.

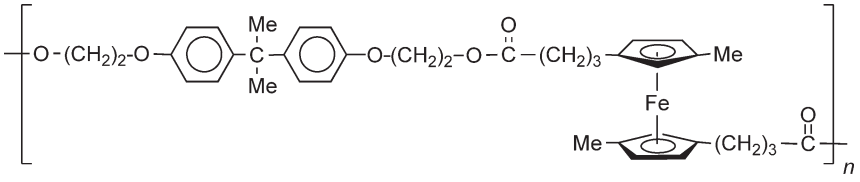

124

A wide variety of group 4 (Ti, Zr, Hf) metallocene-containing polyethers, polythioethers, polyesters, polyamines, polyoximes, and polyamidoximes has also been reported.[286,287] Their synthesis, which is based on the polycondensation (with HCl elimination) of Cp_2MCl_2 with difunctional organic species such as diols, dithiols, etc. (Scheme 14), was carried out either in aqueous solution or using interfacial condensation techniques, based upon the solubility of the difunctional base.[288–291b] The materials range in colour from yellow to orange for titanium and white to light grey for zirconium and hafnium. Molecular weights ranged from a range characteristic of oligomers up to ca. 10^6, although the solubility of the polymers was generally low. Characterization was often limited to IR, which showed characteristic bands for both the metallocene and organic fragments. This allowed an estimation of metal content since, in most cases, elemental analysis for carbon was inconsistent with expected values, possibly due to the high stability of thermal degradation products.

An interesting variant of the polycondensation approach involved the use of fluorescent dyes as the difunctional organic monomers.[292,293] Thus, soluble, high molecular weight titanium polydyes (e.g., $M_w = 5.3 \times 10^5$ by light-scattering measurements for the titanium polymer derived from the diphenol monomer bromophenol blue) were synthesized in yields that depended on the reaction conditions and the dye used. Structural characterization was

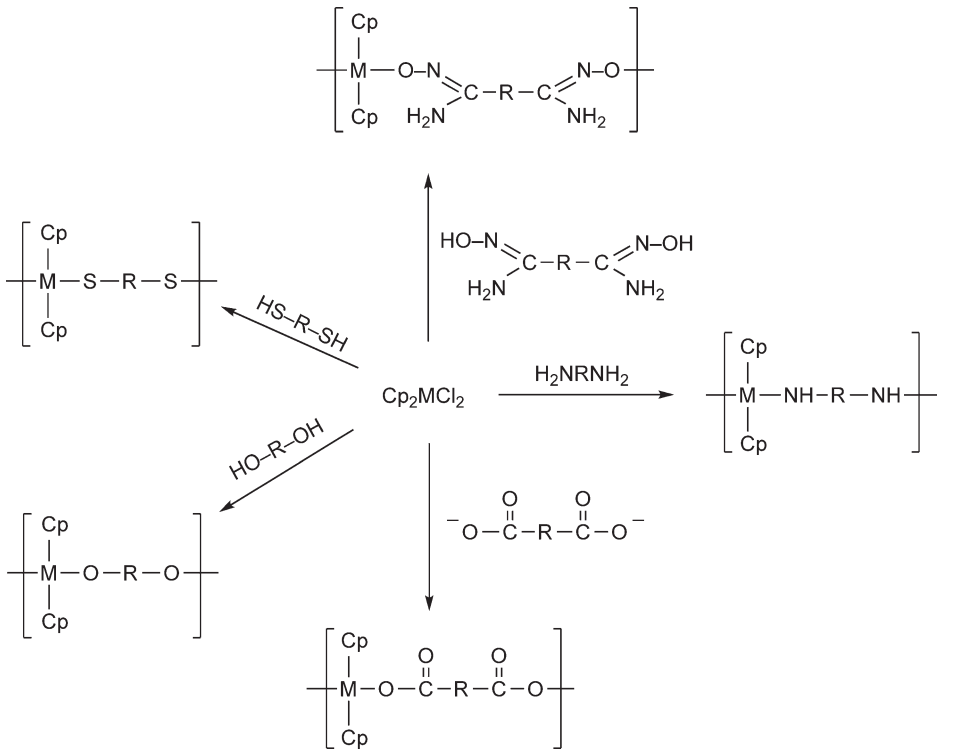

Scheme 14

achieved by IR and in some cases by elemental analysis. Their claimed advantage over monomeric dyes and dye/polymer dispersions was their potential permanent, non-leaching nature. These metallopolymeric dyes are fluorescent and, when used as coloring or doping agents in paper, cloth, paint, and plastic, they provided access to materials in which this property was retained.[292,293]

The synthesis of polymers containing main-chain cobaltocenium units has also been studied as this 18-electron organometallic moiety is isoelectronic with ferrocene. The synthesis of partially soluble polyesters (**125**; E = O; R = $(CH_2)_4$, $CH_2C_6H_4CH_2$) was reported using solution polymerization techniques, and the soluble fractions were of low molecular weight (M_n = ca. 2,500–4,000, with some material up to 8,000) (Equation (46)).[294–296] The products contained mixtures of $[PF_6]^-$ and Cl^- ions and were characterized by IR spectroscopy. Thermally induced polycondensations at 175–200 °C were also performed but failed to lead to the formation of soluble materials with substantially higher molecular weights (extensive decomposition was noted). Similar results were obtained when attempts were made to extend the synthetic routes to the formation of the analogous polyamides **125** (E = NH).[296]

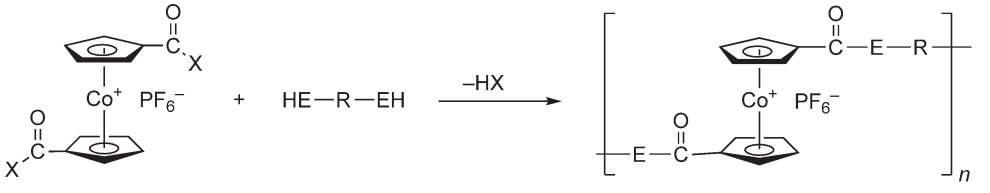

(46)

125

X = OH, Cl, OMe

E = O
E = NH

E = O ; R = $(CH_2)_4$, $CH_2C_6H_4CH_2$, Cp_2Ti, Cp_2Zr, R_2Sn, R_3Sb

E = NH ; R = C_6H_4, $C_6H_4CH_2C_6H_4$, $C_6H_4CH_2C_6H_4$

Attempts to achieve the formation of soluble high molecular weight polyesters via the polycondensation co-polymerization of cobaltocenium 1,1′-dicarboxylic acid with titanocene, zirconocene, tin, and antimony dihalides (**125**;

E = O; R = Cp_2Ti, Cp_2Zr, R_2Sn, R_3Sb) were reported in the 1970s.[296] These materials were isolated in 30–80% yields and were characterized by IR, TGA, and DSC but showed limited solubility in organic solvents or water. Nevertheless, molecular weights (by intrinsic viscosity in 2-chloroethanol) of approximately 80,000 (for R = Cp_2Ti or Cp_2Zr,) and 5,000 (for R = R_2Sn and R_3Sb) were determined.[296–300] Thermogravimetric analysis (TGA) indicated a temperature for 10% weight loss (T_{10}) around 350 °C for the Co/Ti and Co/Zr and around 250 °C for the lower molecular weight Co/Sn and Co/Sb materials. Hydrolytic instability of all of the polymers was noted on stirring with aqueous salt solutions.[296]

Well-characterized cobaltocenium polyamides **125** (E = NH), on the other hand, have been successfully prepared via the reaction of aromatic diamines with 1,1′-dicarboxylcobaltocenium chloride in molten antimony trichloride at 150–175 °C.[301] The products were isolated as $[PF_6]^-$ salts upon treatment with $[NH_4][PF_6]$, and were characterized by IR, ^{1}H NMR, and elemental analysis, all of which supported the assigned linear polyamide structure. Unfortunately, although the materials were soluble in dimethylsulfoxide (DMSO) and acids, and were slightly soluble in water and ethanol, viscosity and VPO measurements proved inconclusive due to polydissociation in solution. The authors based the determination of polymeric nature on their film-forming properties and the low concentration of the carboxyl end group with respect to the NH groups as detected by IR.[301]

Well-characterized polymers with ferrocene units joined by sulfur-containing moeities other than disulfide (see Section 1.3) have also been reported by introducing an alkyl spacer between the ferrocene and the thiol groups.[302] Thus, polyaddition of 1,1′-bis(2-mercaptopropylthio)ferrocene to divinylsulfone afforded a soluble, orange, low molecular weight ($M_n \sim 3{,}000$) material in 90% yield that was characterized by NMR and elemental analysis. A series of sulfur-containing ferrocene polymers was prepared from either 1,1′-bis(2-mercaptoethyl)ferrocene or 1,1′-dimercaptoferrocene by base-catalyzed polyaddition to activated diolefins containing electron-withdrawing substituents (e.g., **126**) and by interfacial condensation with acid dichlorides for the synthesis of poly(thioesters) (e.g., **127**). This afforded yellow, soluble polymers with low molecular weights ($M_n < 5{,}000$ by GPC; PDI = ca. 1.6–5.0) that were characterized by several analytical and spectroscopic methods.

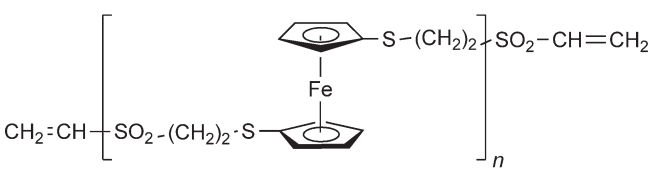

126

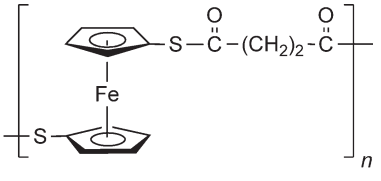

127

12.06.4.2.2 Organosilicon spacers

Structural modification of polysiloxanes (silicones) has also been an important area of interest and ferrocene has been introduced into organosilicon polymers that include siloxanes and carbosilanes. The first approaches to such siloxanes were made in the 1960s by means of the controlled hydrolysis of diethoxysilyl- or chlorosiloxanylsilyl-ferrocene derivatives,[303,304] but the products were oils with very low molecular weights due in part (in the former case) to intramolecular condensation side-reactions.[53] The first examples of well-characterized, high molecular weight polyferrocenylsiloxanes **128** were reported in 1974 from the condensation reaction in melt or solution, at 100–110 °C of 1,1′-bis(dimethylaminodimethylsilyl)ferrocene with three different disilanols.[41] Molecular weights (M_n) were in the range of 9,000–20,000 (by GPC) with melt polymerization giving the highest molecular weights and narrowest distributions. Intramolecular cyclization is favored over intermolecular condensation when using diphenylsilanediol. DSC studies revealed sharp melt transitions between 40–80 °C for these soluble, fibrous polymers. The polymer **128b** was found to be as thermally stable (up to 400 °C) and as stable to hydrolysis (in THF/H_2O) as the corresponding arylene polysiloxane without ferrocene moieties in the backbone.

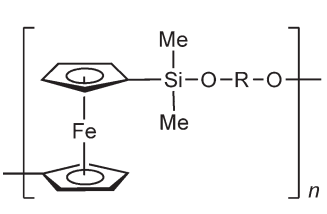

128

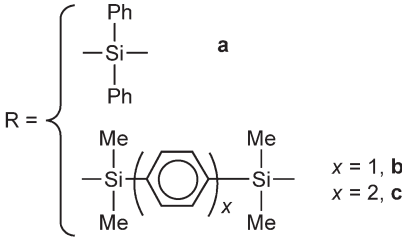

The use of Diels–Alder and platinum-catalyzed polyaddition reactions of vinylferrocene derivatives to prepare ferrocene-containing polycarbosilanes has also been described.[304–306] These reactions were also used to prepare materials with additional functional groups that led to ferrocene and silicon-containing polyesters, polyamides, and polyurethanes. Molecular weights varied in the range of 3,800–6,000 and products were liquids or elastomers.

Novel organometallic accordion-type[307] co-polymers were prepared in 1992 through the Knoevenagel polycondensation of a bis(ferrocene aldehyde)silane with several bis(cyanoacetates).[308] The reaction produced soluble co-polymers **129** that consisted of biferrocenylsilane units with long organic spacers in isomeric (*E*/*Z*) mixtures. They were fully characterized by spectroscopic and analytical methods and possesed significantly high molecular weights ($M_n = 9{,}100$–$26{,}600$).

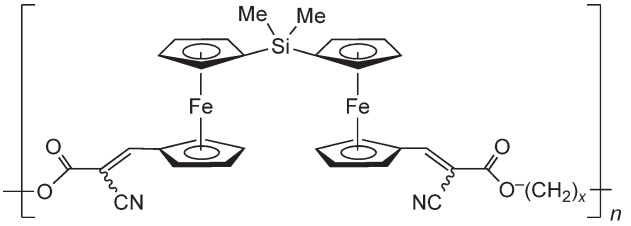

129

$x = 4, 6, 8$

An efficient and versatile approach to yellow-orange, film-forming ferrocene- and silicon-containing polyamides such as **130** and **131** has been developed.[309] Solution or interfacial polycondensation reactions at room or low temperature, between difunctional ferrocene acid chlorides and diaminosiloxanes or between ferrocene diamines and difunctional arenesiloxane acid chlorides, yielded materials for which molecular weights (M_n) of 10,600–12,500 were determined by VPO. These polymers were very well characterized structurally by a range of techniques including NMR and IR. The iron centers are non-interacting, as shown by a single reversible oxidation wave seen by cyclic voltammetry (Figure 21). The polymers are of interest for the chemical modification of electrodes; evaporatively deposited films on different electrodes (Pt, glassy carbon) exhibited the characteristic behavior of surface-confined redox couples.

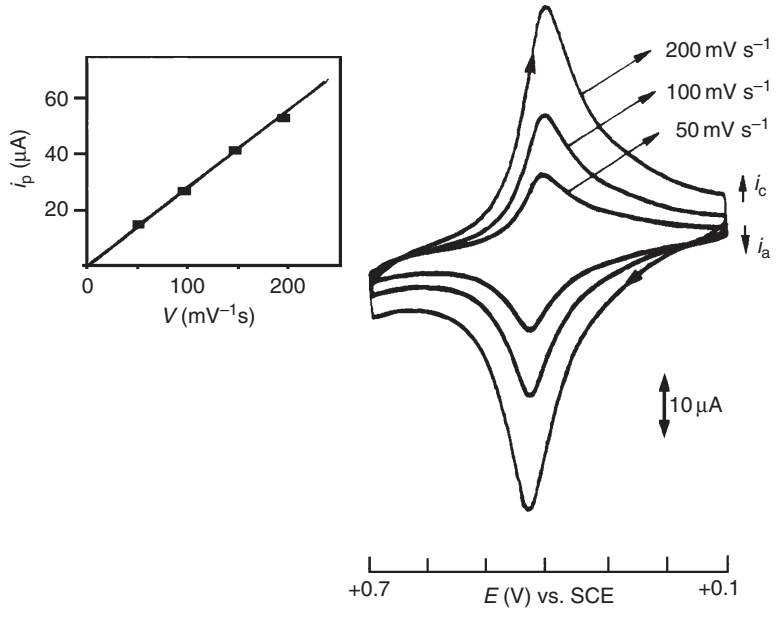

Figure 21 Cyclic voltammogram of a film of ferrocene-containing polyamide **130**, evaporatively deposited on a Pt-disk electrode measured in CH_3CN/0.1 M $[Bu_4N][PF_6]$. Inset shows a plot of current versus scan rate. (Adapted with permission of The American Chemical Society from Casado, C. M., *et al.*, *Inorg. Chem.*, **1995**, *34*, 1669.)

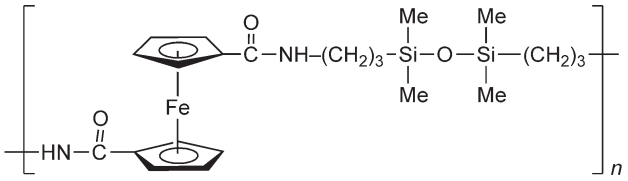

130

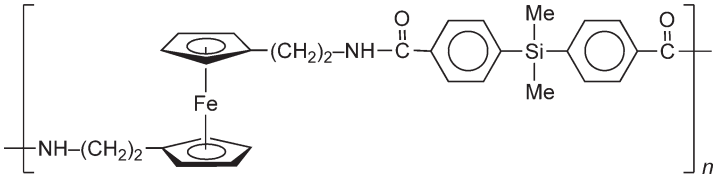

131

An interesting Rh- and Ru-catalyed dehydrocoupling approach to polyferrocenes has also been reported.[310] The reaction involved treatment of ferrocenedithiol with diarylsilanes (Equation (47)) and the resultant polymers **132** possessed M_n values of 2,700–4,600 and PDI values of 1.4–1.6.

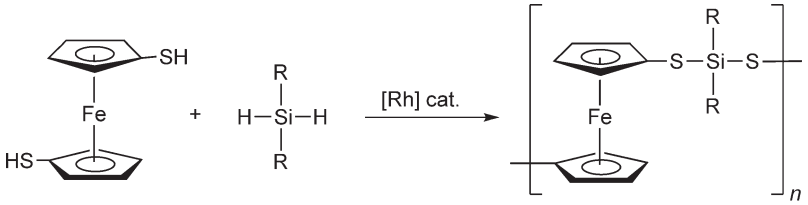

(47)

132

R = $C_6H_4R^1$-*p*
R^1 = M, OMe, F

12.06.4.2.3 Siloxane spacers

The synthesis of polymetallosiloxanes by controlled hydrolytic condensation of Cp_2MX_2 (M = Ti, Zr, Hf; X = Cl or OR) with dichloro- or dialkoxysiloxanes has been investigated based on the possible improvements in heat resistance that might be realized with the introduction of the metal moiety into the polysiloxane backbone. The results obtained in the area were critically reviewed since partial cleavage of the metal–ring bond occurred in all the cases and viscous, putty-like products were very poorly characterized, with virtually no data provided.[311] Only in the case where $Cp_2Ti(SH)_2$ and dichlorosiloxanes were used as reagents in the presence of triethylamine were linear oligomers (**133**, $n = 6$) formed with minimal M–Cp bond cleavage. Even in this case, the materials were hydrolytically sensitive.[312]

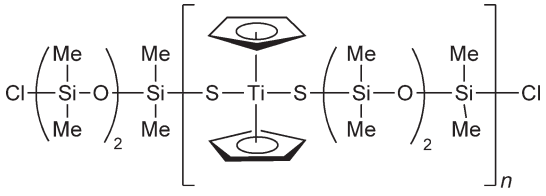

133

An interesting new approach in this area has been reported with the synthesis of novel polymeric zirconocene–silsesquioxanes **134**.[313,314] The condensation of zirconocene derivatives with polyhedral silsesquioxanes led to

amorphous polymers in high yields (≈90%) that were characterized by NMR spectroscopy and elemental analysis. These high molecular weight ($M_n = 14{,}000$) materials exhibited high thermal stability (to ca. 474–515 °C) and, surprisingly, **134a** is stable to both air and hydrolysis.

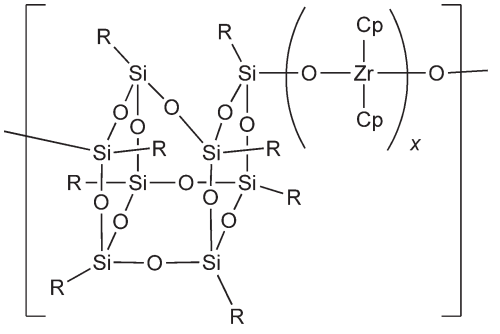

134a: $x = 1$
134b: $x = 2$

12.06.4.3 Polymetallocenes with Long Conjugated Spacer Groups

Polyferrocenylene exhibits significant electrical conductivity when doped (see Section 12.06.3.2.1) and, thus, the introduction of ferrocene units into the main chain of polymers with σ-, σ–π-, or π-conjugation in the backbone is a potentially appealing research objective. Studies of materials with short spacers were provided in Section 12.06.3; here we focus on polymers with spacers longer than three atoms.

Conjugated organic polymers such as polyacetylene, poly(*p*-phenylene), or poly(*p*-phenylene–vinylene) are typically insoluble and rigid materials that are difficult to process. Several attempts have been made to introduce skeletal ferrocene units into the main chain of these materials where they might be expected to increase both the flexibility and solubility.[315,315a–321] Unfortunately, most of the materials reported still had low molecular weights ($M_w < 5{,}000$) and poor solubility. An important development has involved the successful use of metal-catalyzed polycondensations to make such materials. For example, the successful use of a Pd-catalyzed coupling procedure has been reported to prepare high molecular weight, soluble polyferrocenes with *p*-oligophenylene spacers such as **135** (Equation (48)) with molecular weights (M_w) up to 35,500 as determined by light scattering.[321] Such studies revealed that the presence of the ferrocene unit adds significant chain flexibility relative to the rigid-rod organic polymer analog poly(*p*-phenylene). It was suggested that the presence of the ferrocene units introduces kink angles of at least 60° into the polymer backbone. DSC and polarizing microscopy studies of **135** indicated that the materials were semicrystalline, and TGA curves showed that they possess improved thermal stability to weight loss when compared to their poly(*p*-phenylene) analogs.

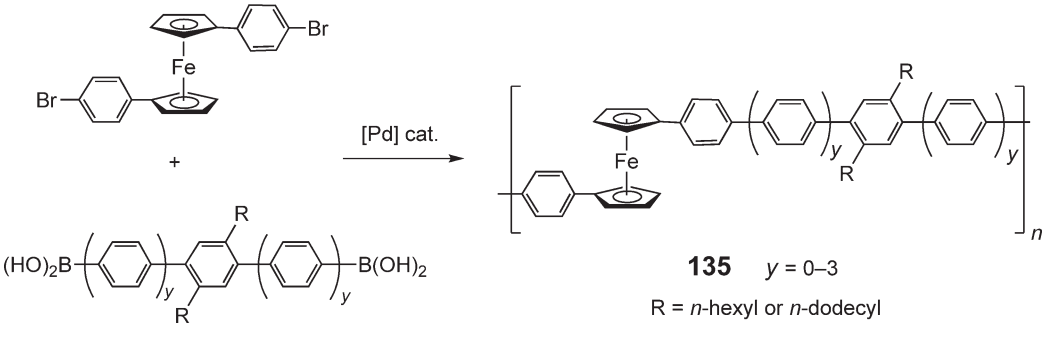

135 $y = 0$–3
R = *n*-hexyl or *n*-dodecyl

(48)

A wide range of analogous polymers (e.g., **136**) with acetylenic spacers has been prepared via the Pd-catalyzed polycondensation reactions between diiodoferrocenes and diethynyl arenes and has been very well characterized. [322,322a,322b] While polymer **136** (R = H) was found to be only partly soluble in organic solvents, the

alkyl-substituted analog **136** ($R = C_{12}H_{25}$) and related species with diethynylthiophene spacers were reported to be completely soluble. An analogous material with a diethynylpyridine spacer was found to be partly soluble in organic solvents, but dissolved completely in formic acid. Structural characterization was achieved by NMR and IR spectroscopy. Light-scattering analysis of the soluble fraction of **136** in $CHCl_3$ gave an M_w value of 1.5×10^3, and for **136** ($R = C_{12}H_{25}$) GPC gave an M_w value of 6.9×10^3 with a PDI = 1.47 relative to PS standards. The highest molecular weight values were found for the materials with diethynylthiophene and diethynylpyridine spacers (M_w up to 3.4×10^4 by light scattering). TGA showed that polymers **136** (R = H or $C_{12}H_{25}$) are stable to weight loss up to ca. 400 °C under nitrogen. Cyclic voltammetry showed single, broad oxidation waves at 0.23–0.25 V versus ferrocene/ferrocenium. The authors attributed the broadening of the CV peak to an exchange of electrons (ca. 1 s on the CV timescale) between metal centers through the π-conjugated chain. However, Mössbauer spectra of an I_2-oxidized sample of polymer **136** (R = H) showed no coalescence of the Fe(II) and Fe(III) quadrupolar doublets at ca. 0 °C, and indicated only slow exchange of electrons between the Fe(II) and Fe(III) sites on the timescale of this experiment (10^{-7} s). The unoxidized samples of polymers **136** (R = H) were found to be insulating ($\sigma = 1.0 \times 10^{-12}\,S\,cm^{-1}$); however, upon oxidation with I_2, the electrical (presumably p-type) conductivity increased to $1.3 \times 10^{-4}\,S\,cm^{-1}$. Interestingly, an Na-doped sample of the analogous polymer with a diethynylpyridine possessed an electrical conductivity of $1.2 \times 10^{-5}\,S\,cm^{-1}$, which suggested n-type behavior.

The red-orange polymer **137** and analogous materials were also prepared via Pd-catalyzed polycondensation reactions, and analysis by cyclic voltammetry showed the presence of only weak metal–metal coupling ($\Delta E_{1/2} = 70$–120 mV) between the widely spaced iron centers.[320] Low molecular weight ferrocene polymers **138** with fluorinated arene ligand spacers have also been prepared and, intriguingly, possess no detectable metal–metal communication.[323,324] Low molecular weight metal-containing polycarbosilanes **139** ($M_w < 4{,}000$) with ferrocene moieties in the main chain have been prepared in high yield via polycondensation routes that involve the use of the di-Grignard reagent of diacetylene and 1,1′-bis(chlorodiorganosilyl)ferrocenes as difunctional monomers.[325,325a] These materials were characterized by NMR spectroscopy, IR, and elemental analysis. Pyrolysis of the ferrocene-containing polycarbosilanes **139** at 1,350 °C under argon affords complex multiphase $Fe_xSi_yC_z$ ceramics in high yield (75–85%). Such high yields suggest that excellent shape retention would occur in the cases where shaped polymer samples, such as fibers or films, were used. The high ceramic yields were attributed to a facile thermally induced cross-linking via the acetylenic groups.[325,325a]

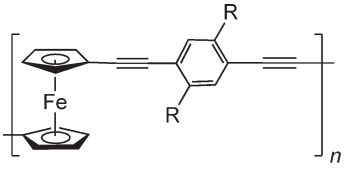

136

R = H or $C_{12}H_{25}$

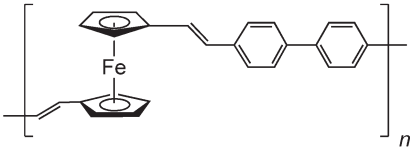

137

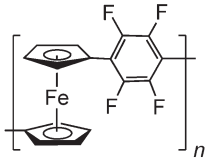

138

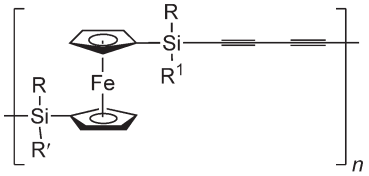

139

R = R^1 = Me, Ph

R = Me; R^1 = Ph

Polyferrocenes with hexasilane spacers **140** have also been synthesized in an attempt to obtain polymers where ferrocenes are joined to σ-delocalized polysilane segments in a regular alternating structure.[326] The condensation of dilithioferrocene and 1,6-dichlorodecamethylhexasilane gave a soluble, well-characterized polymer that showed a monomodal molecular weight distribution by GPC with a maximum at $M_w \approx 3{,}500$. After doping, conductivity values ($\sigma = 3 \times 10^{-5}\,S\,cm^{-1}$) were three orders of magnitude higher than that of octadecasilane. This suggested that conjugation between ferrocene and the hexasilanediyl linker contributes to the conductivity, although the values observed were lower than those for the corresponding polyferrocenylenes.[327]

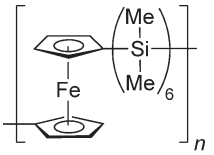

140

Thiophene units have also been employed in order to bridge ferrocenes and obtain conjugated polymers.[209] The reaction of a dizinc ferrocene derivative with dibromothiophene afforded a polyferrocenylene thienylene **141** with moderate molecular weight ($M_n \approx 4{,}500$) that was characterized by NMR spectrometry and elemental analysis. Studies on doped materials with $[SbCl_6]^-$, $[BF_4]^-$, and $[TCNQ]^-$ counteranions showed the presence of weak antiferromagnetic interactions.

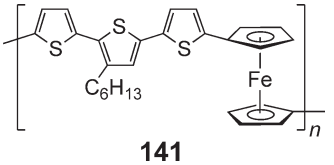

141

Condensation routes to well-characterized polyferrocenes with arene **142** and thiophene **143** spacers have been developed (Equations (49) and (50)).[205,328] These materials are soluble, with molecular weights (M_w) of 42,000–52,000 and broad polydispersities (PDI = 10–15).

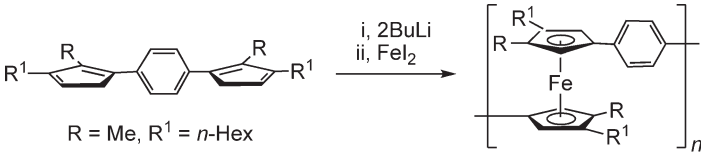

(49)

142

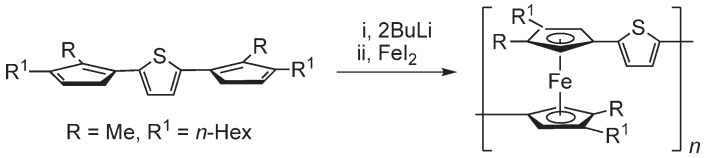

(50)

143

The magnetic properties of oxidized materials have been studied and were interpreted in terms of the temperature dependence of the magnetic moment of ferrocene units. Cyclic voltammetry studies of **142** (Figure 22) and **143**

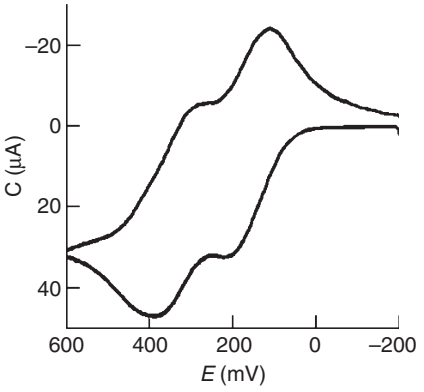

Figure 22 Cyclic voltammogram of a solution of polyferrocene **142** in CH_2Cl_2 that contains 0.1 M $[Bu_4N][PF_6]$ at a scan rate of 100 mV s^{-1}. (Adapted with permission of The American Chemical Society from Southard, G. E. and Curtis, M. D., *Organometallics*, **2001**, *20*, 508.)

showed the presence of two reversible oxidation waves with redox couplings ΔE of 0.17 and 0.19 V, respectively. This is consistent with the presence of moderate Fe···Fe interactions.

The nature of the metal–metal interactions in **142** and **143**, and in related polymeric materials, was analyzed in terms of a published theoretical analysis.[205] The conclusion reached was that the bridging groups affect the molecular-scale dielectric constant between the metal sites that in turn mediates the essentially through-space interaction. Based on this concept, more polarizable atoms would be expected to lead to stronger metal–metal coupling and this has been observed. For example, the less polarizable fluorinated arene groups in **138** lead to no detectable Fe···Fe interaction using cyclic voltammetry, whereas polarizable atoms such as sulfur (see Section 3.3.6) lead to large Fe···Fe ΔE values.

12.06.4.4 Other Metal-containing Polymers with π-Coordinated Metals and Long Insulating Spacer Groups

12.06.4.4.1 π-Cyclobutadiene ligands

Cyclobutadiene ligands in the main chain provide a useful methodology for the attachment of metals to polymeric structures. For example, a variety of well-characterized rigid-rod organocobalt polymers **156a** with complexed cyclobutadiene units in the main chain has been prepared by Pd-catalyzed Heck coupling (Equation (51)) and M_w values of 7,400–65,000 and PDIs of ca. 1.7–5.0 (by GPC) were observed.[329,329a] These materials were isolated as yellow solids and were found to exhibit interesting thermotropic liquid crystal behavior (Figure 23).[329,329a]

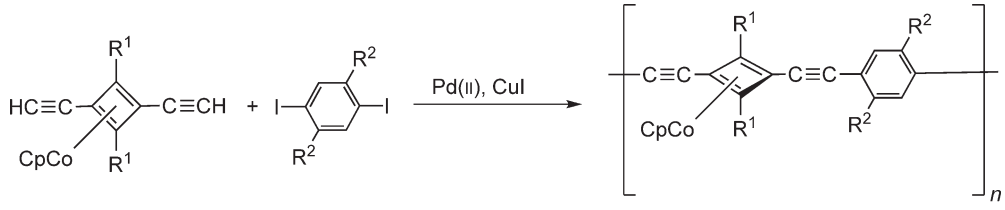

(51)

144a

R^1 = H, $SiMe_3$; R^2 = H, hexyl, dodecyl

The use of acyclic diene metathesis (ADIMET) provides an alternative synthetic approach to analogous Co polymers of type **144b** with M_w values of 1.3×10^5–3.1×10^5 (PDI = 2.9–3.7) (Equation (52)). These materials

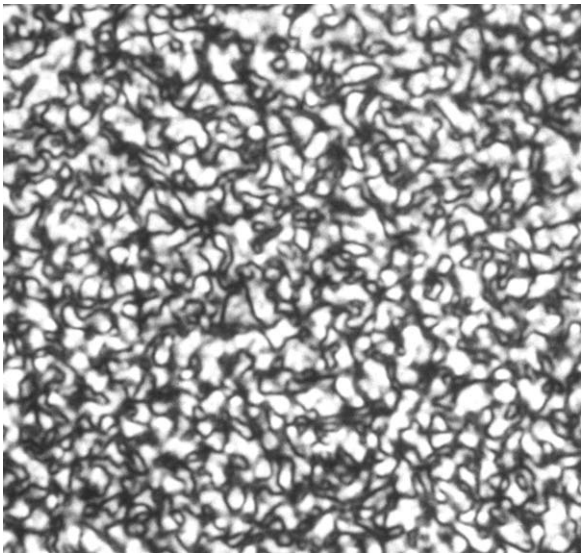

Figure 23 Schlieren texture of a film of polymer **144a** (R^2 = hexyl; R^1 = $SiMe_3$) at 165 °C under a polarizing microscope. (Adapted with permission of Wiley-VCH from Altmann, M. and Bunz, U. H. F., *Angew. Chem. Int. Ed. Engl.*, **1995**, *34*, 569.)

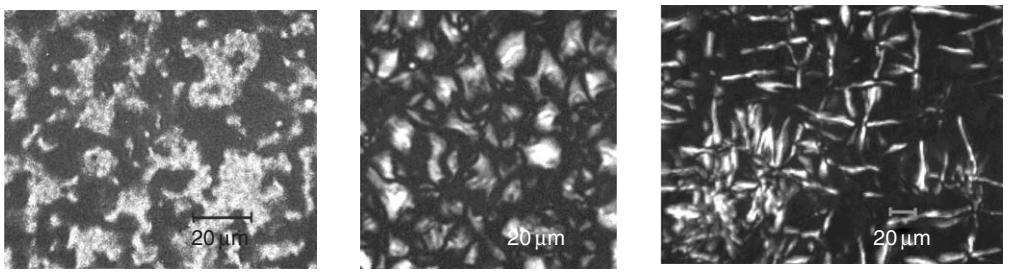

Figure 24 Schlieren textures of the frozen lyotropic phase of (a) polymer **144b** (R^2 = 2-ethylhexyl; $R^1 = SiMe_3$) (b) polymer **144b** (R^2 = (*S*)-3,7-dimethyloctyl; $R^1 = SiMe_3$) under cross-polarizers. The baton texture of polymer **144a** (R^2 = (*S*)-3,7-dimethyloctyl; $R^1 = SiMe_3$) shown in (c) is indicative of a higher, lamellar order structure. (Adapted with permission of Wiley-VCH from Steffen, W. *et al*., *Chem. Eur. J.*, **2001**, *7*, 117.)

show lyotropic liquid crystalline phases and chiroptical properties as a result of aggregation in poor solvents; TEM and polarizing microscopy studies indicate the formation of lamellar or irregular honeycomb-shaped morphologies (Figure 24). The results indicate that the presence of the organocobalt substituents leads to fundamentally different behavior from that of the parent poly(*p*-phenylenes).[329,329a]

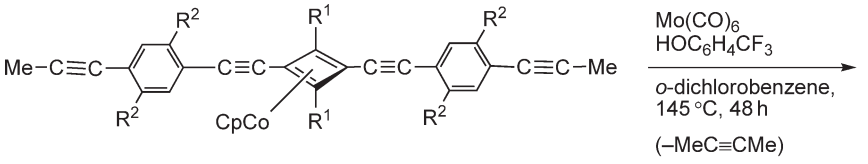

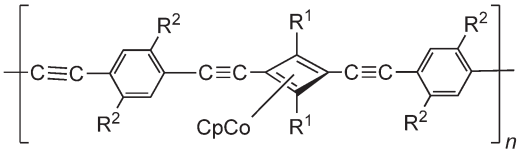

(52)

144b

$R^1 = SiMe_3$; R^2 = hexyl, 2-ethylhexyl, (*S*)-3,7dimethyloctyl, dodecyl

Analogous ochre-yellow polymers **145** that contain thiophene in the main chain (M_w = 11,300–35,300, PDI = 1.5–2.7) have also been prepared.[330] Upon slow concentration of their solutions in chlorinated solvents, such as chloroform, lyotropic nematic liquid crystalline phases form. In one case, a lyotropic smectic state was formed.

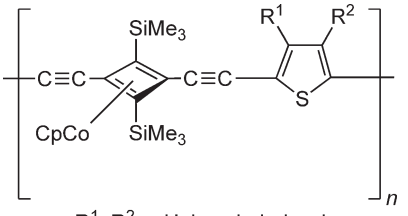

R^1, R^2 = H, hexyl, dodecyl

145

Materials with butadiyne bridging units in the main chain **146** and with $DP_n > 17$ have been reported using Hay's oxidative coupling of monomers that contain diterminal alkynes.[331–333] Organocobalt polymers **146** possess a conjugated backbone, as shown by the decrease in wavelength of one of the lowest energy visible absorption peaks relative to small molecule analogs. Thus, studies of the optical properties of linear model oligomers **146** (n = 2–7) showed a bathochromic shift in the UV–VIS absorption with concomitant increase in peak intensity as chain length

increased.[333] The effective conjugation length appeared to be achieved at $n = 7$ (heptamer), since its UV–VIS spectrum is almost superimposable with that of **146** ($n = 8$ or 9) and polymeric **146**. The optical properties of the polymers **146** have been studied in detail and the involvement of the metal in the electronic transitions has been elucidated.[334,335]

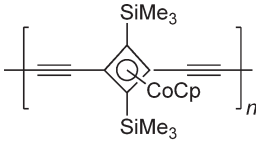

146

Polymers **148** that contain cyclobutadiene units in the main chain have also been reported via the rearrangement of main-chain metallocyclopentadiene units of polymers **147** (see Section 12.06.5.3; Equation (53)).[336–341] The similarity of molecular weights found for **147** and **148** indicated that no significant chain cleavage or side-reactions occur during this process.[337] Moreover, UV–VIS data indicated that the presence of conjugated spacers R leads to a long wavelength shift in the polymers relative to model compounds. This indicates that electron delocalization is present in the main chain.[338]

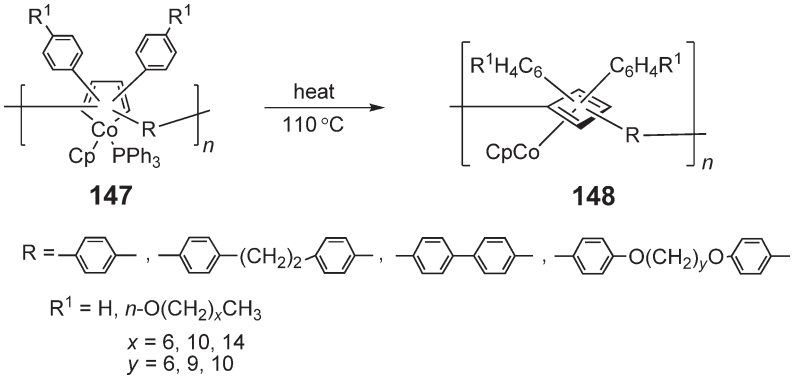

147 **148** (53)

The thermal reaction of cobalt polymers **148** with isocyanates at 120 °C leads to 2-pyridone-containing polymers **149**.[339] Well-characterized, yellow polyesters **150** that contain skeletal (cyclobutadiene)cobalt moieties in the main chain have been prepared via interfacial polycondensation approaches.[342] The use of solubilizing alkoxy substituents R afforded materials with $M_n = 10{,}700$–$22{,}500$ (PDI = 1.7–5.4). Thermotropic liquid crystallinity was detected by polarizing microscopy with, in some cases, mesophases stable over the range ca. 110 to >250 °C. Materials analogous to **150** with 1,3-disposition of the main-chain substituents on the cyclobutadiene ligands have also been studied.[342,343]

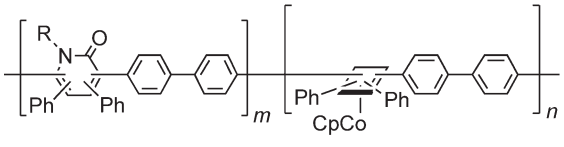

149

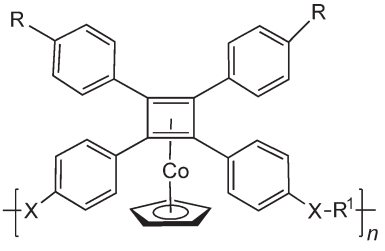

X = O, CO_2
$R^1 = (CH_2)_x$ (x = 5, 10, etc.), C_6H_4, C_6H_4-C_6H_4, etc.

150

An analogous synthetic approach that uses Ni(0)-catalyzed dehalogenative polycondensation.[344,345] yielded, for example, yellow polymers **151** with $M_n = 8{,}000$–$13{,}600$ and PDI = 1.3–2.1 by GPC (Equation (54)).[345] Comparison of the UV–VIS spectrum for the polymer with that for the model dimer was consistent with the presence of a

π-conjugated structure. Polarizing microscopy and PXRD studies suggested that a nematic mesophase was formed. For example, polymer **151** (R = *n*-dodecyl) formed a mesophase in the 146–184 °C range.[345]

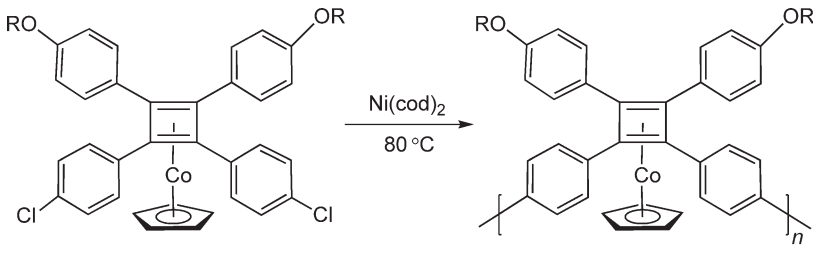

151

R = C_6, $C_{12–16}$ *n*-alkyl chains

(54)

12.06.4.4.2 π-Cyclopentadienyl ligands

Cymantrene-containing organometallic polymers **152** have been prepared by Suzuki coupling reactions (Equation (55)). These materials were unstable in the atmosphere and had molecular weights (M_n) of ca. 1.1×10^4 and broad polydispersities of ca. 6.[346] Analogous 1,2-substituted oligomeric **153** and polymeric **154** materials with butadiyne bridging units in the main chain have been reported using Hay's oxidative coupling of monomers containing diterminal alkynes.[347] The brown, film-forming polymers **154** were unstable in the atmosphere and possessed an M_w value of 15,200 and a PDI of 1.58 by GPC (relative to PS standards).

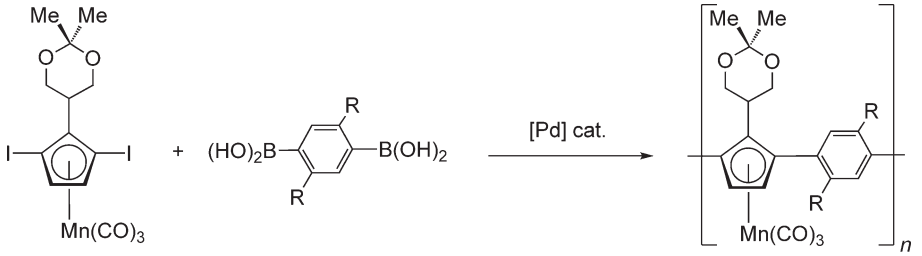

152

R = H or *n*-hexyl

(55)

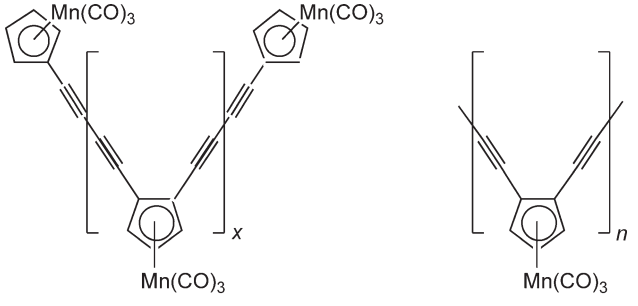

153 **154**

Analogous materials with cyclopentadienyliron units coordinated to cyclopentadienyl ligands in the main chain, but with shorter C_2 spacers, were described in Section 12.06.3.2.2. Polymers with cyclopentadienyl cobalt groups in the main chain have been reported via the treatment of precursor materials that contain cyclopentadienylcobalt groups (e.g., **147**) with *t*-butyl isocyanide followed by MeI.[348]

12.06.4.5 π-Arene ligands

Soluble π-complexed aromatic polyamides **155** have been prepared via polycondensation of (p-phenylenediamine)$Cr(CO)_3$ with terephthaloyl chloride in *N*,*N*-dimethylacetamide (Equation (56)).[349] The highly viscous solution of **155** exhibited lyotropic liquid crystalline behavior with a nematic texture visible by polarizing optical microscopy. The intrinsic viscosity for **155** in *N*,*N*-dimethylacetamide was determined to be 4.52 dl g^{-1} and GPC analysis using a viscosity detector gave an absolute molecular weight (M_w) of 78,000 (polydispersity = 1.7). The analogous polymer in which only half of the diamines were complexed to $Cr(CO)_3$ was also reported. The trimethylphosphine derivative **156** was prepared similarly via polycondensation of (p-phenylenediamine)$Cr(CO)_2PMe_3$ with terephthaloyl chloride. These materials are of importance, as the coordination solubilizes poly(p-phenyleneteraphthalamide) (used for making Kevlar fibers for bullet-proof vests, etc.) in common organic solvents but still allows for the formation of ordered, liquid crystalline solutions.

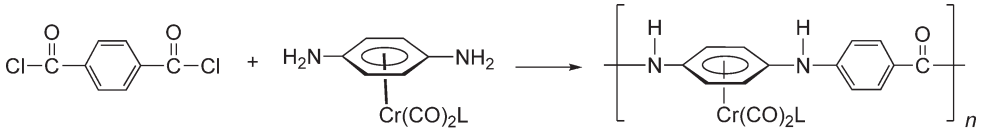

(56)

155: L = CO

156: L = PMe_3

Soluble π-complexed aromatic polyamides **157** have also been prepared with (η^5-C_5Me_5)Ru moieties (Equation (57)).[350] A variety of polymers with Fe(η^5-C_5H_5) groups attached to arene groups in the polymer main chain have been reported. These include polyethers, polythioethers, and polyamines.[351–354] In addition to linear materials, star-shaped polymers such as **158** have been reported.[355] These materials are redox-active as a result of the cationic ArFe(η^5-C_5H_5) moieties that undergo reversible reduction at −40 °C. The materials are photochemically labile and exposure to 200 nm UV light results in decomplexation to afford the corresponding organic polymers.

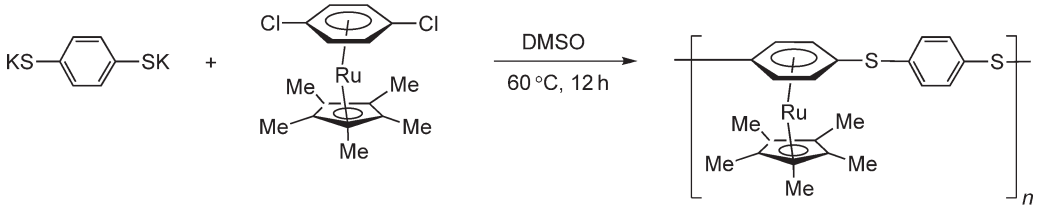

(57)

157

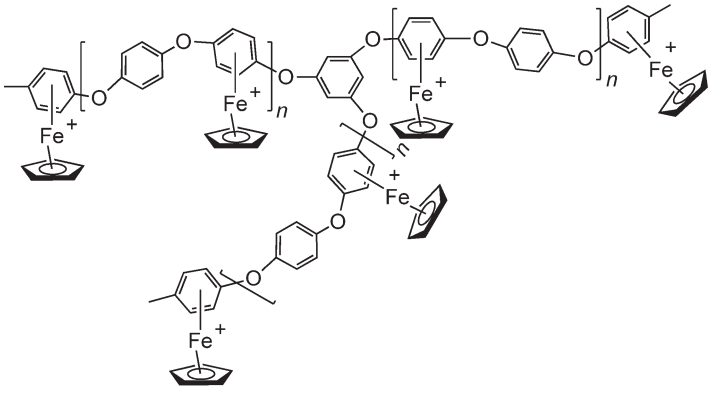

158: n = 2, 3, or 4

Polymers **159**, which contain cationic (arene)Fe(η^5-C_5H_5) units in the main chain together with azo dyes in the side-group structure, have also been developed (Scheme 15).[356] Photolysis in the presence of H_2O_2 led to photobleaching.

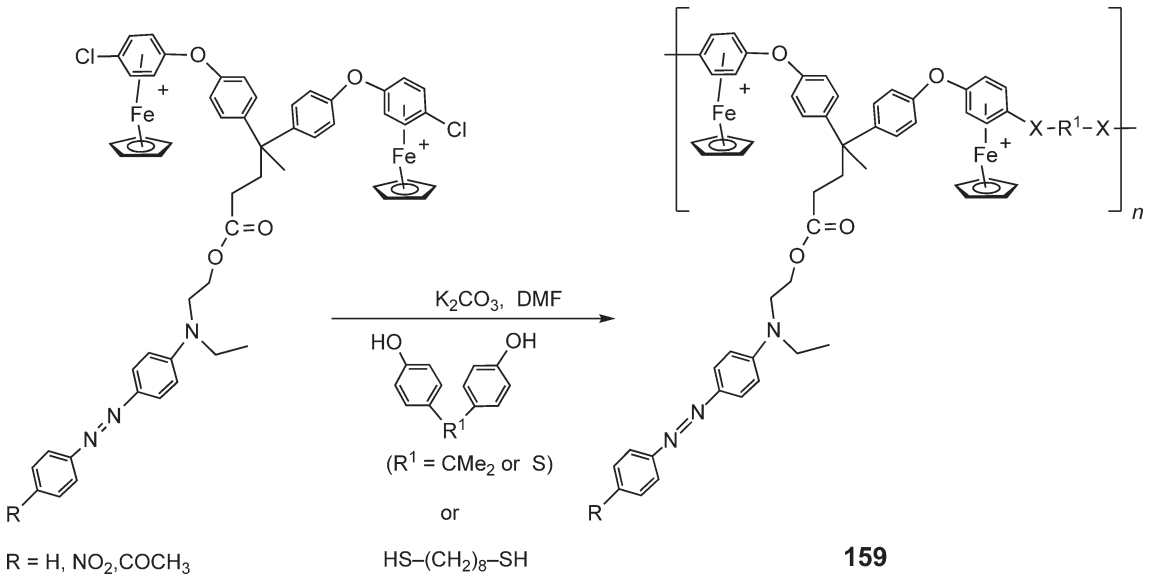

Scheme 15

The complexation of Fe(η^5-C_5H_5) groups to ca. 60% of the main-chain arene moieties in low molecular weight samples ($M_n = 1{,}700$) of poly(*n*-hexylphenylene) to yield **160** has also been reported.[357] Interchain cross-linking appears to be induced by electrochemical reduction to result in the formation of an insoluble polymer film on the electrode. Attachment of the FeCp group also leads to a modification of the photoluminescence intensity and emission wavelength.

Similar polymers with around 20% of the main-chain arene groups complexed by $Mo(CO)_3$ **161** have also been reported.[358] The quenching of photoluminescence detected for **160** and **161** results from the presence of the metal-based LUMO between the valence and conduction bands of the conjugated polymer chain. This leads to a pathway for non-radiative decay after photoexcitation that involves electron transfer to the 3*d* LUMO on the metal, which occurs before recombination with holes.[357,359]

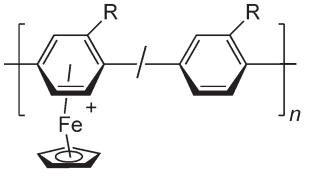

R = *n*-hexyl

160

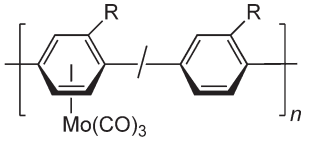

R = *n*-hexyl

161

An analogous polymer, **162**, with diethynyldiphenylene spacers that possesses 100% complexation of arene groups to $Cr(CO)_3$ moieties has been prepared.[360] The solubility was low, although molecular weights (M_n) of ca. 7,800 were estimated. In this case, the synthesis involved a cross-coupling reaction of the *p*-dichloroarene complex with the bis(trimethylstannyl)dialkyne.[360] Similar materials with diethynylthiophene spacers have also been described.[361]

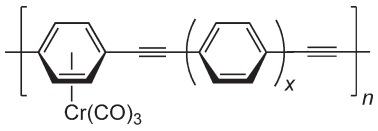

162: *x* = 1 or 2

12.06.4.5.1 π-Alkyne ligands

Soluble π-complexed polymers have also been prepared by means of coordination to alkyne groups in a polymer main chain. Both non-conjugated (e.g., alkynylsiloxanes[362]) and conjugated materials have been studied.

Treatment of π-conjugated poly(phenylene diacetylene) with controlled amounts of $Pt(C_2H_4)(PPh_3)_2$ led to the formation of polymers **163** with 20–50% complexation of the main-chain alkyne groups.[363] Subsequent pyrolysis at 600 °C led to the formation of conducting glassy carbon matrices containing coalescence-stable Pt nanoclusters which function as catalysts for H^+ and O_2 reduction.[363–366] Complexation of alkyne units of conjugated polymers to platinum can also lead to cross-linked materials **164**.[367–369] These networks can possess substantially increased charge carrier mobilities in comparison to the all-organic conjugated polymer precursor and may lead to improved semiconductor devices.[369]

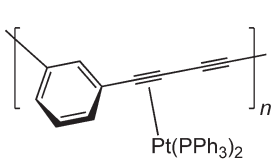

163

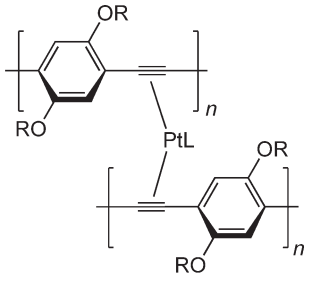

164

12.06.5 Organometallic Polymers with Metal–Carbon σ-Bonds in the Main Chain

12.06.5.1 Introduction

Polymers with metal–carbon bonds in the main chain represent one of the most extensive, interesting, and broad classes of metal-containing polymers. Rigid-rod transition metal–acetylide polymers or polymetallynes represent the most extensively studied subgroup of this class of metallopolymers. Although initial developments were reported in this area in the 1960s, it was not until the late 1970s that a series of well-characterized, soluble, high molecular weight materials that contained Pd and Pt was described. The key to this success was the discovery of efficient catalytic, step-growth polycondensation processes that involved difunctional monomers which were available in high purity and that proceeded to high conversion. This enabled the strict stoichiometry and conversion requirements necessary for the formation of high molecular weight materials via step-growth polycondensations to be successfully satisfied.[15] In the 1980s and early 1990s, the diversity of polymetallynes has been extended to include other metals, and a series of materials with metallocyclopentadiene units, that contain Co and Zr, in the main chain was also described. Various other polymers with metal–carbon single and multiple bonds in the main chain that involve sp^3- and sp^2-hybridized carbon centers, respectively, were also reported over the same period. A feature of the work on virtually all of these materials is the excellent structural characterization of the polymers by means of a wide variety of spectroscopic and analytical techniques. However, although absolute methods have been used in a number of cases, molecular weight characterization has often relied on the convenient but relative method, which involves the use of GPC, with PS standards for column calibration.[15] In the case of the rigid structures common for many of the polymers discussed in this chapter, appreciable differences in hydrodynamic behavior from that of PS would be anticipated. It is important, therefore, to bear in mind that the molecular weight data reported for many of the polymers is likely to be inaccurate.

12.06.5.2 Rigid-rod Transition Metal–Acetylide Polymers

12.06.5.2.1 Polymer synthesis

An array of versatile and efficient step-growth polycondensation methodologies has been developed for the synthesis of transition metal–acetylide polymers. In this section, a representative review of the types of routes available and materials accessible is given.

Polymeric Cu- and Hg-acetylides **165** (M = Cu or Hg; L = no substituent, where L = neutral two-electron donor ligand) were briefly reported in the 1960s via the use of oxidative coupling of diyne precursors (Scheme 16, Equation (58)). These

(a) Oxidative coupling

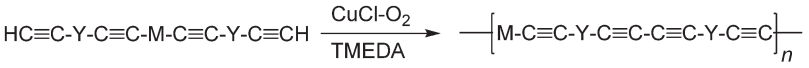

(58)

(b) Dehydrohalogenation

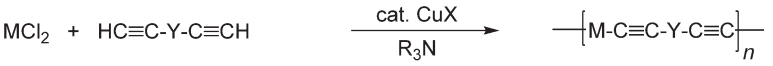

(59)

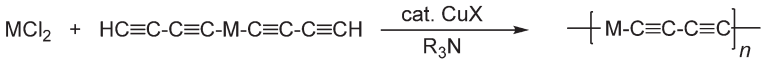

(60)

(c) Alkynyl ligand exchange

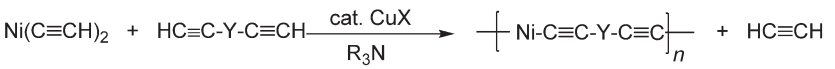

(61)

M = *trans*-Pt$(PR_3)_2$, *trans*-Pd$(PR_3)_2$
Ni = *trans*-Ni$(PR_3)_2$

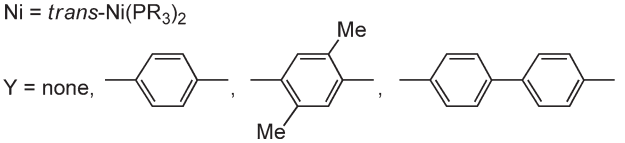

Scheme 16

materials were proposed to have a linear geometry; however, they were generally found to be intractable, which precluded their purification and definitive characterization.[370,371] In the mid- to late 1970s, the first soluble polymetallynes **165** (M = Pt) and **166** (M = Pd) that contained metal atoms in the main chain were reported by means of a similar route. Subsequent work resulted in the general development of this and other routes to group 10 metal-containing polyynes. From 1990 onward, a variety of new routes that allow the incorporation of metals from groups 8, 9, and 10 into the polymer backbone were described.

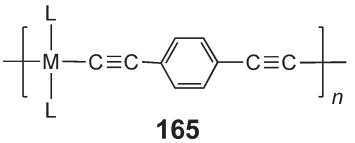

165

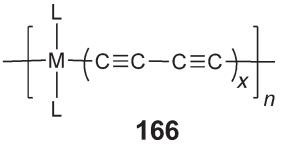

166

The first soluble transition metal polyyne oligomers **165** and **166** were reported in 1975 and consisted of $Pd(P^nBu_3)_2$ and $Pt(P^nBu_3)_2$ moieties in the main chain connected by butadiyne and diethynylbenzene bridging units. These were isolated as air stable, orange-yellow solids with average molecular weights (M_n) determined by vapor-pressure osmometry to be 5,700 and 7,300, respectively.[372] These materials were prepared by the oxidative coupling method shown in Scheme 16(a). Subsequent work, reported in 1977, showed that group 10 metal–acetylide polymers with improved molecular weights ($M_w > 10^5$) could be prepared through the use of three main approaches: oxidative coupling, dehydrohalogenation, and alkynyl ligand exchange (see Schemes 16(a)–(c)).[43,373–380]

12.06.5.2.2 Approaches to the preparation of high molecular weight group 10 metal–acetylide polymers

The first method involves oxidative homocoupling of bis(terminal alkynyl) complexes in the presence of a catalytic amount of cuprous halides and O_2 as the oxidizing agent (Scheme 16, Equation (58)).[378] The use of this catalyst system in organic synthesis is extensive and is better known as Hay's coupling reaction.[379] Extension of this methodology to organometallic synthesis was demonstrated by the conversion of

trans-bis-acetylide monomers into polymeric complexes. It is worth noting that this method is dependent only on one monomer type; thus, stoichiometric balance is already present and, so, high degrees of polymerization are usually obtained.

The second method involves a polycondensation reaction between metal halides and diterminal alkynes via a cuprous halide-catalyzed dehydrohalogenation process (Scheme 16, Equations (59) and (60)).[43, 372–377] The reactions are typically performed in amine solvents, such as diethylamine or piperidine under reflux conditions, to afford high molecular weight polymers. In cases of gaseous acetylenes such as acetylene or butadiyne, the polymers are most conveniently obtained via condensation of the corresponding mononuclear metal bis(alkynyl) complexes and metal halides. The degree of polymerization achieved through use of the dehydrohalogenation approach is dependent upon the exact ratio of the difunctional monomer pairs involved.

The aforementioned two methods work well for a majority of cases, particularly for platinum, and afford high molecular weight macromolecules, as estimated by GPC, with $M_w = 60{,}000$–$160{,}000$ based on the nature of the bridging alkynes. In the case of palladium, significantly lower molecular weights (M_w values up to 26,000) were obtained.[378] However, neither of these two methods is applicable to nickel due to the inherent instability of dihalonickel complexes in amine solvents and dialkynylnickel complexes in oxidizing media. Thus, the analogous Ni-containing acetylide polymers (with $M_n = 10{,}000$–$13{,}000$ by GPC) were prepared by means of an alkynyl ligand exchange process, which is catalyzed by CuI in amine solvents (Scheme 16, Equation (61)).[380]

Synthetic routes similar to those described in Scheme 16 have also been used to prepare the analogous polymeric species **167** and **168**, which contain mixed alkynyl ligands and/or mixed metals in the main chain.[374,376]

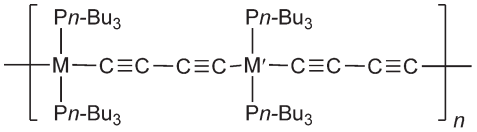

167

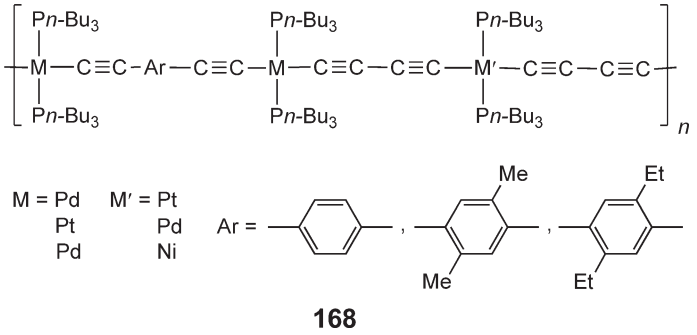

168

Although the aforementioned methods are generally applicable for the incorporation of group 10 metals into metal–acetylide polymers, these approaches could not be extended to metals from groups 8 and 9 due to the instability of the starting complexes in amine solvents. Research efforts into the molecular chemistry of hydrido–acetylide complexes of rhodium have resulted in a facile route to group 9 polymers **169** and **170**.[381–384] This method involves the direct oxidative addition of terminal alkynes to L_4RhMe with loss of methane (Equations (62) and (63)). The reaction, which resembles an earlier report on the synthesis of $Co(PMe_3)_4(C{\equiv}CPh)$,[385] proceeds rapidly at ambient temperature to produce soluble polymers when $L = P^nBu_3$, and an insoluble white solid was obtained when $L = PMe_3$. The authors did not report the molecular weight for the soluble polymer. However, the formation of free-standing films of the material upon evaporation of THF solvent suggested that the product was macromolecular in nature.

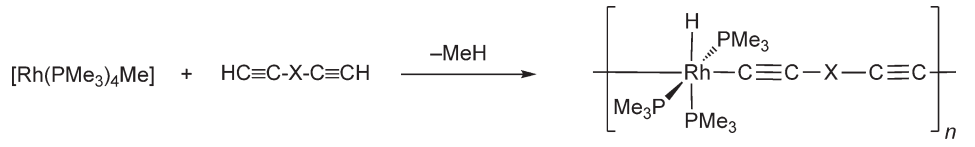

(62)

169

X = -*p*-C_6H_4-, -*p*-C_6H_4-C_6H_4-*p*-

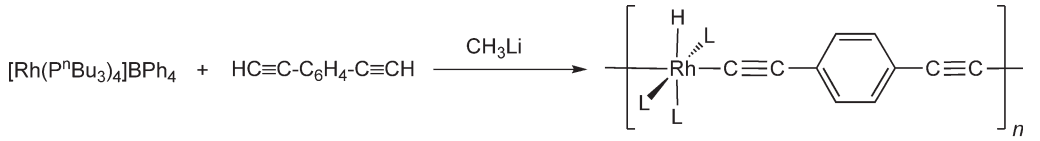

(63)

170

L= P^nBu_3

A convenient metathesis reaction that involves trimethyltin reagents[386] has been used to prepare polyynes that contain group 8 (Fe, Ru, Os),[387–390a] group 9 (Co, Rh),[391,392] and group 10 (Ni, Pd, Pt)[391–394] metals. The polymers were prepared through reaction of equimolar amounts of bis-trimethylstannyl acetylides and the appropriate metal halide complexes in the presence of CuI as a catalyst (Scheme 17, Equations (64)–(66)). This method is quite general and is reported to produce platinum polymers **171** (M = Pt; L = EBu_3; E = P or As) with slightly higher average molecular weights determined by GPC relative to PS (M_w = 82,000–210,000). The analogous Ni and Pd polymeric complexes were obtained with much lower molecular weights (M_w = 20,000–30,000). For rhodium, the polymer **173** was found to be a white, insoluble solid similar to the polymer **169** observed by the aforementioned method.[382]

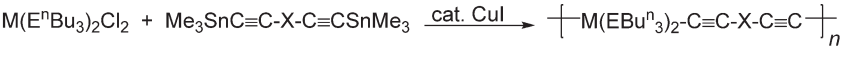

(64)

171

M = Ni, Pd, Pt
E = P, As (Pt only)

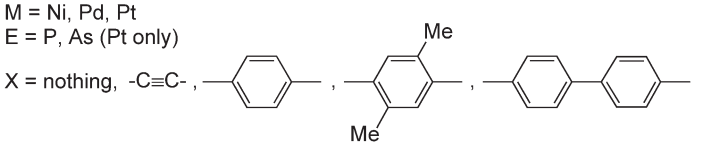

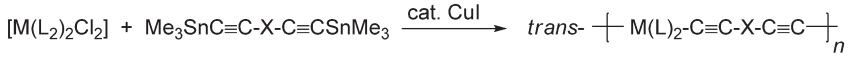

(65)

172

M = Fe, Ru; L = PMe_3, L_2 = depe, dppe
M = Os; L = dppm

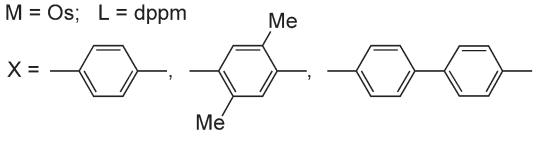

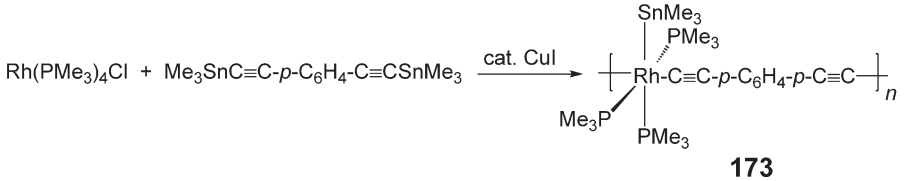

(66)

173

Scheme 17 Preparation of group 8, 9, and 10 polyynes through use of trimethyltin reagents.

Insoluble polymeric materials were also reported for Ru coordinated with trimethylphosphine (PMe_3) and for Os with diphenylphosphinomethane (dppm) and bis(ethynyl)biphenyl ligands **172**.

Recently, an extension of the dehydrohalogenation process to the synthesis of a new class of heterobimetallic polyyne materials **174** which contain mixed metals with alternating $Ru(dppe)_2$ and $Pd(P^nBu_3)_2$ moieties (dppe = bis(diphenylphosphino)ethane) in the polymer backbone has been reported (Equation (67)), with $M_w = 14{,}000$ (by GPC measurements).[395] The incorporation of ferrocene units into the polymer main chain and alternation between either $Ni(PBu_3)_2$ **175** or $Pd(PBu_3)_2$ **176** moieties has also been achieved (Equation (68)) and the molecular weights of the resulting polymers were $M_w = 26{,}100$ and 21,400, respectively.[395,396]

trans-[Ru(dppe)$_2$(C≡C-C$_6$H$_4$C≡CH)$_2$] + $(PBu^n_3)_2PdCl_2$ $\xrightarrow[Et_2NH]{\text{cat. CuI}}$

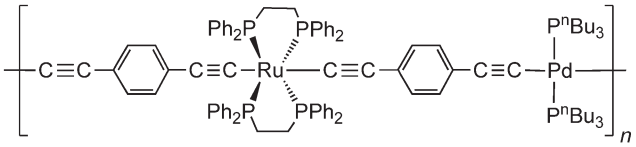

(67)

174

1,1′-((η-C$_5$H$_4$)$_2$Fe)(C≡C-C$_6$H$_4$-C≡CH)$_2$ $\xrightarrow[\text{cat. CuI, } Et_2NH]{(PBu^n_3)_2PdCl_2 \text{ or } (PBu^n_3)_2Ni(C{\equiv}CH)_2}$

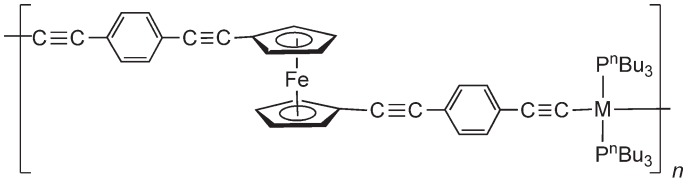

(68)

175: M = Ni

176: M = Pd

Gold(I)-containing polyynes **177–179**, with diphosphine and diacetylide spacers, have been prepared either by reaction of $[AuC{\equiv}CR]_x$ with the corresponding diphosphines or from the reactions of $[AuCl(SMe_2)]$ with the appropriate diethynylarene in the presence of a base.[397] The resultant oligomers were found to be insoluble in most organic solvents, but were partially soluble in THF, dichloromethane, and chloroform, with average molecular weights of 15,000–18,000 as estimated by GPC (relative to PS standards).

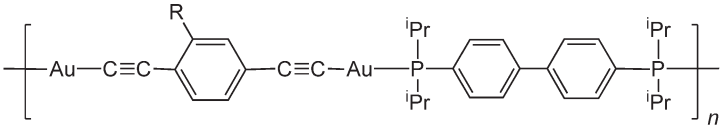

177: R = H

178: R = Me

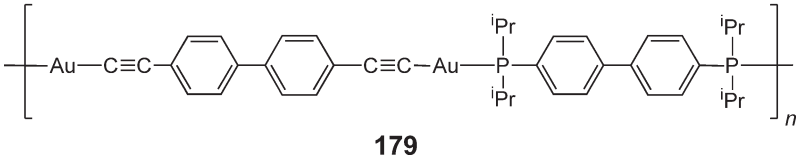

179

The synthesis of rigid-rod oligomeric Au(I) complexes **180** and **181**, with (isocyanoaryl)acetylide bridging ligands, has been achieved via elimination of $^tBuC{\equiv}CH$ from the precursor $^tBuC{\equiv}C$-Au-C≡N-Ar-C-Ar-C≡CH.[398,399] However, direct molecular weight determinations of the resultant oligomers were not possible due to insolubility. Similarly, the synthesis of the insoluble polymeric materials **182** with Au(I) centers bridged by diisocyanides and diacetylides has also been described.[400,401]

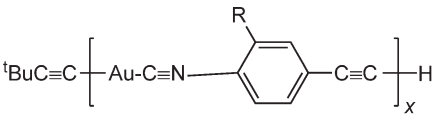

180: R = H
181: R = Me

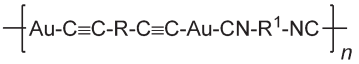

R = C_6H_4, C_6H_4-C_6H_4, $C_6H_2Me_2$, CH_2O-C_6H_4-CMe_2-C_6H_4-OCH_2
R^1 = C_6H_4, C_6H_3Me, $C_6H_2Me_2$, C_6Me_4, $C_6H_2{}^tBu_2$, $C_6H_2Me_2$-$C_6H_2Me_2$

182

A novel route to polymer chains **183** that contain metal moieties as terminal groups was reported and involved multiple (up to 100) insertions of arylisocyanides into the Pd–C bond of the heterodinuclear μ-acetylide complex $[Cl(PR_3)_2Pd\text{-}C{\equiv}C\text{-}Pt(PR_3)_2Cl]$.[402] Cross-linked Pt-containing polymers were obtained by reacting 1,3,5-triethynylbenzene with the *trans*-dihalo complexes via the dehydrohalogenation route. The 2-D polyhexagonal graphite-like polymers **184** and **185** were found to have very low solubility.[403]

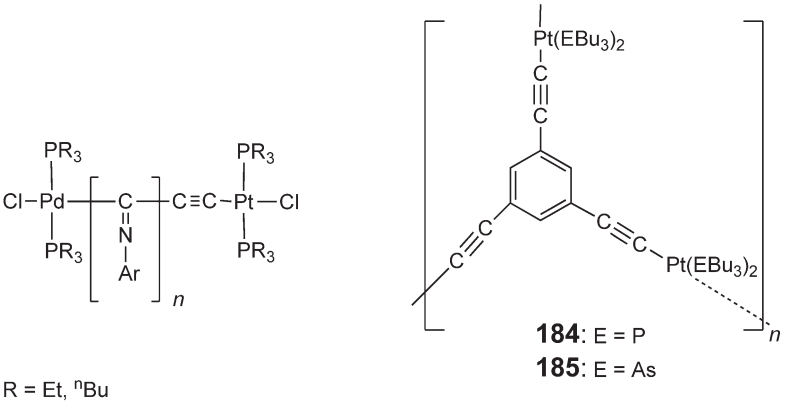

184: E = P
185: E = As

R = Et, ^{n}Bu
Ar = C_6H_4, C_6H_4-C_4H_9-*p*, C_6H_4-C_8H_{17}-*p*, C_6H_4-NO_2-*p*, C_6H_4-CH_3-*p*

183

Improved solubility was achieved by preparing polymer **186** through use of co-monomer mixtures of 1,3,5-triethynylbenzene and 2,5-diethynyl-*p*-xylene in various molar ratios (1 : 10, 1 : 50, 1 : 100) with *trans*-dichloro(tri-*n*-butylphosphine)platinum. The high degree of cross-linking for the 1 : 10 mixture resulted in an insoluble material, whereas soluble co-polymers were obtained for the other two mixtures with $M_w = 58{,}000$ and 27,000 (by GPC relative to PS) for the 1 : 50 and 1 : 100 molar ratio, respectively.[403]

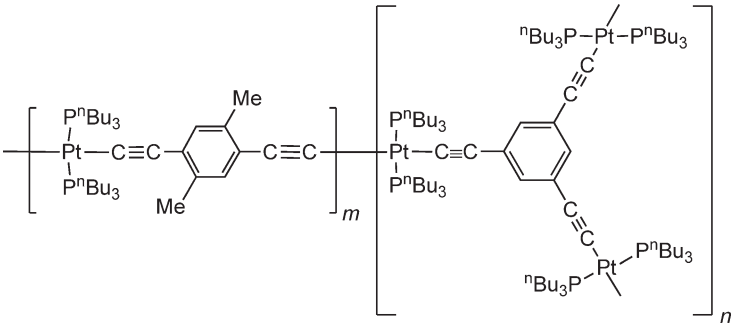

186

An interesting class of cationic polyyne polymers **187** was prepared by reaction of the bimetallic complex, μ-butadiynediyl-bis[*trans*-chlorobis(tri-*n*-butylphosphine)palladium], with an equimolar amount of 4,4′-bipyridyl in

the presence of excess $K[PF_6]$. The resultant polyelectrolyte **187** possessed alternating butadiyne and pyridyl spacer units in the main chain (Equation (69)). Other analogous polyelectrolytes were obtained similarly by use of the appropriate dihalide complex and bypyridyl derivatives.[404]

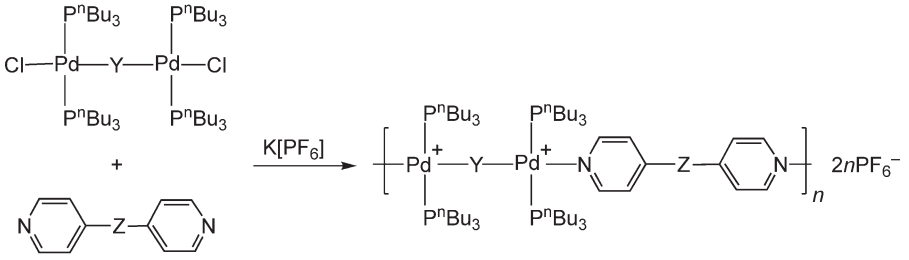

187

(69)

Y = -C≡C-C≡C-; Z = no substituent
Y = -C≡C-C≡C-; Z = CH_2CH_2
Y = -C≡C-C≡C-; Z = CH=CH

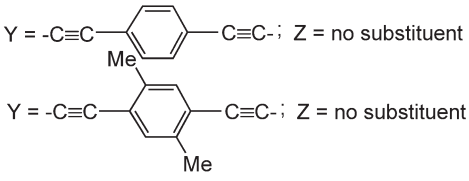

The synthesis of platinum polyynes with heteroaromatic organic spacer groups has also been readily accomplished, for example, species **188** with skeletal pyridyl units that make use of the dehydrohalogenation method (Scheme 16(a)) or an Me_3SnCl elimination procedure analogous to that in Equation (64) (Scheme 17).[405] The resultant polymers could be quaternized at nitrogen with methyl iodide and triflate. Materials such as **189** with a bithiazole spacer have also been prepared by the dehydrohalogenation method.[406]

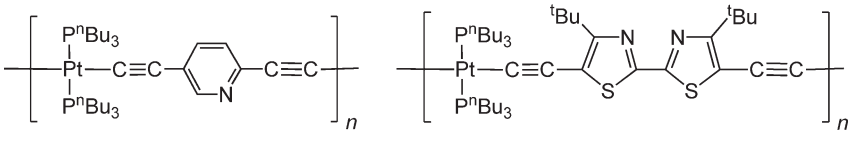

188 **189**

Electropolymerization has also been used to generate polymetallynes on an electrode surface. For example, the transition metal–polythiophene hybrid material **190** (Equation (70)) has been prepared using this approach, which appears to be highly promising for the creation of a broad range of intriguing materials.[407,408]

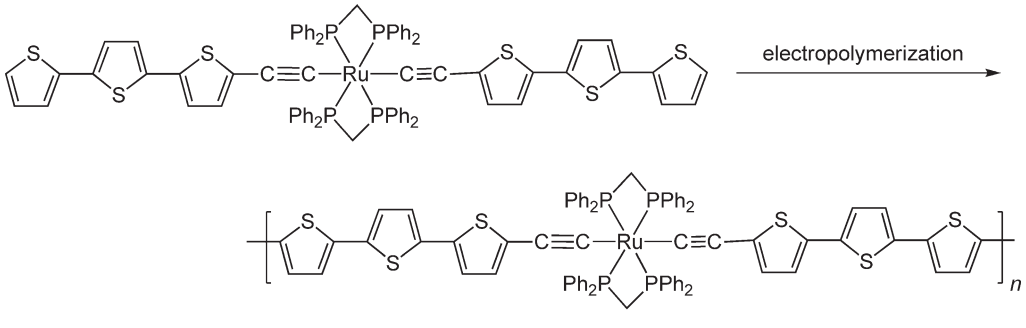

(70)

190

12.06.5.2.3 Structural and theoretical studies of polymers and model oligomers

Retention of the *trans*-configuration around the metal centers in the aforementioned Pt polymers was evident by spectroscopic analysis of model compounds that contain from one to six Pt centers as well as single crystal X-ray diffraction studies of representative species.[372,373,409] For example, a detailed study of the molecular structures and crystal packing arrangements for a series of symmetric and unsymmetric bis(acetylide) complexes, $[Pt(PMe_2Ph)_2(C{\equiv}CC_6H_4\text{-}p\text{-}R)(C{\equiv}CC_6H_4\text{-}p\text{-}R^1)]$ (R, R^1 = MeO, MeS, NH_2, NMe_2, CN, NO_2), and the analogous bis(butadiyne) complex has been described.[384] X-ray diffraction provided conclusive proof of the *trans*-configuration at the Pt center. The *trans*-disposition of the acetylide units has also been established for Ni and Pd analogs, as well as for group 8 and 9 complexes such as octahedral *trans*-$[Ru(dppe)_2(C{\equiv}CC_6H_5)_2]$ and *mer*,*trans*-$[Rh(PMe_3)_3(H)(C{\equiv}CC_6H_5)_2]$, respectively.[409–411] The binuclear Rh(I) complex $[Rh(PMe_3)_4(C{\equiv}C\text{–}C_6H_4\text{-}C{\equiv}C)Rh(PMe_3)_4]$ has also been characterized crystallographically.[382] Model compounds with organic heteroatomic spacers have also been studied.[406,412–414]

The ^{31}P NMR spectral data has also provided an exceptional tool for the determination of the configuration at the metal centers in polymers as well as oligomers.[43,372–375,378] For example, the *trans*-configuration of phosphine ligands in Pt–bis-acetylide complexes gives rise to a ^{31}P signal at 3.0–5.0 ppm, whereas the *cis*-configuration gives rise to a signal at −2.0 to −4.0 ppm (referenced to 85% phosphoric acid). In the Pt-containing polymers **165** and **166** and analogs, as well as the Pd and Ni analogs, no resonances were detected in the region assigned to the *cis*-configuration. Thus, these polymers are believed to possess a rod-like structure with an all-*trans*-configuration at the square-planar metal centers. Additional IR spectral analysis was also consistent with the above assignment.[373]

In a multinuclear solid-state NMR study carried out on the platinum complex *trans*-$[ClPt(P^nBu_3)_2\text{-}C{\equiv}C\text{-}p\text{-}C_6H_4\text{-}C{\equiv}C\text{-}Pt(P^nBu_3)_2Cl]$ and the corresponding polymers **165** (M = M′ = Pt; L = E^nBu_3; E = P or As), strong evidence for a *trans*-geometry at the Pt metal centers was provided by a ^{31}P NMR study which gave a chemical shift of 4.5 ppm, and ^{31}P–^{195}Pt coupling constants of 2,440 Hz (dimer) and 2,450 Hz (polymer) for the case where L = P^nBu_3 ligand.[415] Selected area electron diffraction and low-dose, high resolution TEM imaging techniques have also been employed to obtain structural information for the Pt polyyne, $[Pt(AsBu_3)_2\text{-}C{\equiv}C\text{-}p\text{-}C_6H_4\text{-}C{\equiv}C]_n$ of structural type **165**.[416,417] The results show detailed arrangement of the molecular chains into crystallites (ca. 50 nm in diameter) with grain and dislocation defects. The proposed monoclinic unit cell has measured parameters: $a = 2.08$ nm, $c = 1.20$ nm, $90° \leq \beta \leq 93°$, and calculated $b = 1.9$ nm.[416,417] The authors attributed the variation in β to the openness of the packing and the tendency of the polymer chains to align upon extension.

Many studies have been directed at an understanding of the degree of conjugation and electron delocalization in the main chain of polymetallaynes, with the aim of controlling the band gap (E_g) and bandwidth, and hence the electronic properties and applications of these interesting materials. Studies of the bonding in metal alkynyl, butadiynyl, and bis(alkynyl) complexes, by means of photoelectron spectroscopic studies and/or molecular orbital calculations,[418–420] have provided much useful information, and support previous calculational findings[421] that indicate that there is considerable mixing of the filled metal *d*-orbitals with the filled π-system of the alkynyl moiety. The energy mismatch between the metal *d*-levels and alkynyl π^*-levels, at least in cases in which there are no strong π-acceptor substituents in conjugation with the alkynyl moiety, leads to a lack of significant π-backbonding. However, the perturbation of the filled metal *d*-levels by the π-donor character of the alkynyl groups leads to low-lying metal–ligand charge-transfer (MLCT) absorptions. An in-depth compilation and analysis of data, obtained primarily from X-ray diffraction, electronic, and vibrational studies, that aims at probing the nature of bonding in metal–alkynyl complexes has been reported.[409]

Extended Hückel band calculations[422] on metal polyyne polymers have indicated that in $[L_nM\text{-}C{\equiv}C\text{-}Ar\text{-}C{\equiv}C\text{-}]_x$ systems, the highest occupied crystal orbital (HOCO, which is roughly analogous to the HOMO in a molecular system) is predominantly metal-*d* in character and is delocalized along the chain through the ML_n groups for $n = 2$ (square-planar) and $n = 4$ (octahedral) geometries. The calculations indicated that the lowest unoccupied crystal orbital (LUCO) is predominantly alkynyl-π^* in character. It was suggested, based on these studies, that the electrical conductivity of polymetallaynes can be improved through alteration of the character of the HOCO and the LUCO. The nature of the metal is expected to play a significant role in affecting the HOCO energy level in such a way that, the higher the energy and the more diffuse the *d*-orbitals, the higher the HOCO level will be. On the other hand, extending the π-conjugation length in the alkynyl spacer groups would be expected to lower the optical (HOCO–LUCO) band gap in metal polyyne systems, predominantly by lowering the energy of the LUCO. These calculations indicated that electrical conductivity is favored for polymetallaynes containing four-coordinate d^8-square-planar metals over those with six-coordinate octahedral metals, due mainly to the greater conduction bandwith in the former case (ca. 0.4 eV). Others have reported similar extended Hückel calculations on Pt-containing polymers and concluded that the Pt centers do contribute to some electronic delocalization along the polymer chain.[423] In addition, a

vibrational spectroscopic study of these Pt polyynes, of type **165** and **166**, in the solid state has suggested that the alkyne spacer units still possess their essentially acetylenic character and that π-conjugation is reduced in the presence of phenylene rings in the polymer main chain.[424]

Overall, although many details are still open to question, both theory and experiment (see Section 3.1) support the assertion that a significant degree of electron delocalization is present in the polymetallyne main chain. Furthermore, as shown below, the structure can be successfully tuned to influence the electronic properties. However, a key challenge for the future is the development of materials in which electron delocalization is even further enhanced.

12.06.5.2.4 Polymer properties

A wide variety of high molecular weight polymetallaynes have been reported that possess mainly d^8-square-planar metals (Ni, Pd, Pt) or six-coordinate d^6-octahedral metals such as Ru. Many of these materials have been very well characterized and, as a group, they provide fascinating insight into the role that main-chain metal atoms can play in influencing polymer properties.

12.06.5.2.4.(i) Thermal and atmospheric stability

Group 10 metal polyyne polymers of type **165** and **166** generally show good stability in air in the solid state.[373] The thermal stability of samples of these and related materials with M_w in the range 1.0×10^4–1.2×10^5 has been investigated by means of TGA, and the results indicated that the platinum-containing polymers are considerably more stable that their palladium and nickel analogs (Table 3). In air, the polymers decompose explosively with a weight loss of ca. 35–60%.[373] The Pt materials are also significantly more stable than the Pd and Ni analogs in solution. Even the Pt materials tend to lose small amounts of the ligands (e.g., phosphine) at the metal center and association in solution, through complexation of alkyne functionalities on neighboring chains has been proposed based on viscosity measurements.[373] Little has been reported on polymers that contain metals from groups 8 and 9 with regard to thermal and environmental stability.

12.06.5.2.4.(ii) Solution properties

The high solubility of many metal polyynes in common organic solvents, such as benzene, toluene, THF and methylene chloride, is attributed to the presence of organic substituents on the ancillary ligands attached to the metal or organic spacer unit which promotes good solvent–polymer chain segment interactions. As noted earlier, molecular weight measurements have generally involved the use of GPC with PS standards for column calibration. This relative technique generally provides only approximate estimates of the molecular weight as it is assumed that the hydrodynamic size of the polymers under study is similar to that of the calibration standard (generally PS) of the same molecular weight. This is clearly unrealistic for polymers with rigid backbones. However, the sedimentation equilibrium method has been used to provide absolute measurements of the molecular weight of several platinum polyynes and these clearly established the macromolecular nature of these materials. For example, samples of the representative polymer, **166** (M = $Pt(P^nBu_3)_2$; $x = 2$), were found to possess a molecular weight $M_w > 10^5$ by the sedimentation method.[43,375] The intrinsic viscosities of this and related polymers, $[\eta] = 1.19$–1.25, were found to be independent of the nature of the solvent and the solubility parameter δ was found to be in the range of 6.6–9.7 $(\text{cal ml}^{-1})^{1/2}$.[373,375] In addition, the α-value in the Mark–Houwink equation (ca. 1.7) was determined, and this indicated that this type of polymer has a stiff rod-like structure in

Table 3 Thermal stability of group 10 metal polyyne polymers (measured by TGA at heating rate of 5 °C min^{-1})

Polymer	$M_w \times 10^3$	*Decomposition temp.* (°C)	
		In air	*In* N_2
$[Pt(P^nBu_3)_2\text{-}C{\equiv}C\text{–}C{\equiv}C]_n$	120	270	350
$[Pd(P^nBu_3)_2\text{-}C{\equiv}C\text{–}C{\equiv}C]_n$	24	150	200
$[Ni(P^nBu_3)_2\text{-}C{\equiv}C\text{–}C{\equiv}C]_n$	10	150	165
$[Pt(P^nBu_3)_2\text{-}C{\equiv}C\text{–}C_6H_4\text{-}C{\equiv}C]_n$	72	230	300
$[Pd(P^nBu_3)_2\text{-}C{\equiv}C\text{–}C_6H_4\text{-}C{\equiv}C]_n$	25	145	170
$[Ni(P^nBu_3)_2\text{-}C{\equiv}C\text{–}C_6H_4\text{-}C{\equiv}C]_n$	13	135	140
$[Pt(P^nBu_3)_2(\text{-}C{\equiv}C\text{–}C{\equiv}C\text{-})2]_n$	30	210	210
$[Pd(P^nBu_3)_2(\text{-}C{\equiv}C\text{–}C_6H_4\text{-}C{\equiv}C\text{-})2]_n$	120	250	250
$[Pt(P^nBu_3)_2(\text{-}C{\equiv}C\text{–}C{\equiv}C\text{-})\text{-}Pt(P^nBu_3)_2(\text{-}C{\equiv}C\text{–}C_6H_4\text{-}C{\equiv}C\text{-})]_n$	34	–	330

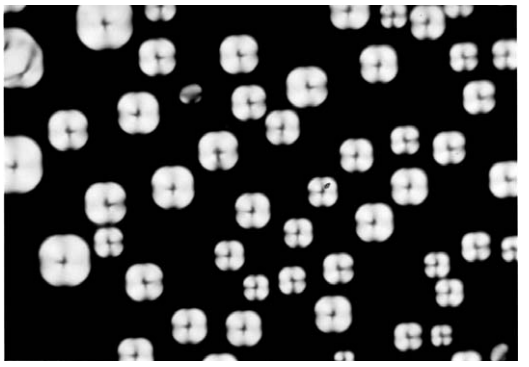

Figure 25 Liquid crystals of polymetallyne **167** (M = Pd; M′ = Pt; L = P^nBu_3) observed between cross-polarizers in trichloroethylene (200 × magnification). (Reproduced with permission of Springer from Hagihara, N. *et al.*, *Adv. Polym. Sci.*, **1981**, *41*, 149.)

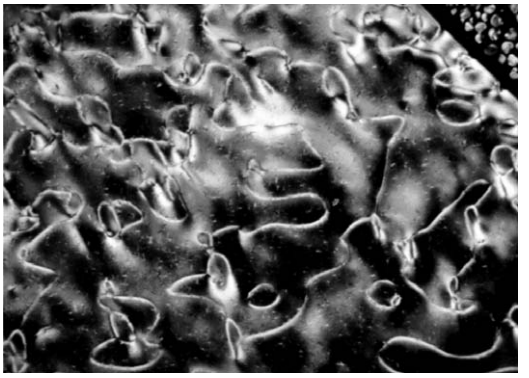

Figure 26 Nematic liquid crystals of polymetallyne **166** (M = Pt; L = P^nBu_3; $x = 2$; $n \sim 100$) observed between cross-polarizers in trichloroethylene at 25 °C. (Reproduced with permission of The American Chemical Society from Takahashi, S. *et al.*, *Macromolecules*, **1979**, *12*, 1016.)

solution.[373,375] It is noteworthy, however, that subsequent studies on the same polymer have led to the suggestion that the polymer chain is more flexible and can be represented by a worm-like model.[425,426]

The generally rigid, extended nature of metal polyynes is also evident in their tendency to form lyotropic liquid crystalline phases[373,427,428] (see also Chapter 12.05 on the topic of organometallic mesogens). Homometallic polymers, as well as mixed metal systems, that contain Pt, Ni, and Pd, have all been shown to exhibit liquid crystalline phases in trichloroethylene (Figure 25).[427,428] The formation of a nematic phase, observed between crossed polarizers, was reported for the platinum polyyne **166** (M = Pt(P^nBu_3)$_2$; $x = 2$) (Figure 26).[427] The lyotropic liquid crystalline phases formed by these polymers have also been detected by high resolution ^{31}P NMR spectroscopy.[429,430] The orientation of the polymer chain exhibits a strong response to the magnetic and electric perturbations and leads to either parallel or perpendicular alignment with respect to the applied magnetic field. It was established that the preferred direction of the liquid crystal molecule with respect to the magnetic field is determined by the magnetic anisotropy of the polymer and its structure.[429,430]

12.06.5.2.4.(iii) Optical properties

Metal-to-alkyne ligand charge-transfer (MLCT) transitions are a common spectral feature in all of the linear rigid-rod metal polyynes. Their optical absorption and emission properties have been examined in some detail.[396,393,416,431,432] The optical band gap that corresponds to the lowest energy transition between the valence band and conduction band varies depending upon the metal centers and their coordination geometry, the ancillary ligands, and the nature of the alkyne bridging units.[393,431,432] This transition was investigated as a function of chain length for a series of [R-(Pt(P^nBu_3)$_2$-C≡C-*p*-C_6H_4-*p*-C≡C)$_{n-1}$-Pt(P^nBu_3)$_2$-R] ($n = 2$–5; R = C≡CC_6H_5).[372] It was found that the low-energy band undergoes a red shift as n increases, but the magnitude of the shifts rapidly decreases with increasing n value (Table 4). However, no further significant bathochromic shift was observed in going from the

Table 4 Values of λ_{max} (nm) for the lowest optical absorption band for a series of oligo- and polyplatinaynes

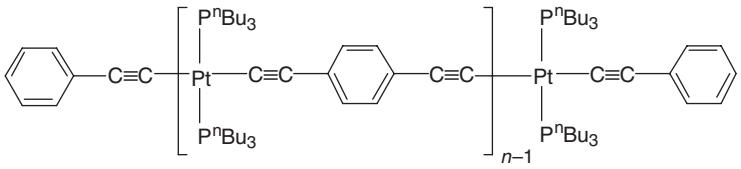

n	λ_{max} (nm)
2	363
3	371
4	376
5	378
131	380

hexamer ($\lambda_{max} = 378$ nm) to the high polymer ($\lambda_{max} = 380$ nm).[372,375] It was also found that the optical transitions for the polymers occur at lower energies than for the free alkyne ligands. These observations both suggest that appreciable π-conjugation occurs through the metal centers.[432] Further extension of the π-conjugation within the alkyne spacer has a significant effect on the lowest energy optical transitions as illustrated in Table 5. It is apparent that the triacetylenic bridge ($m = 1$) exhibits a lower optical gap than the diacetylenic analog ($m = 0$) ($E_g = 3.12$ vs. 3.23 eV),[394] and Similarly the band gap excitation for the more extended bis(arylene-ethynyl)benzene[432] is red-shifted in comparison with the comparable diethynylbenzene material[394,431] ($E_g = 3.13$ vs. 3.26 eV). The more extended anthracene spacer, which contains three fused benzene rings, is most effective in promoting the delocalization of π-electrons along the polymer backbone.[432] Thiophene and oligothiophene spacer units were also found to be more effective than arene spacers, whereas silyl spacers (SiR_2) were found to reduce delocalization.[432–434a]

Most polymetallaynes have band gaps of ca. 2.4–3.2 eV but the value can be reduced substantially to ca. 1.7 eV by the use of alternating donor (bis(phosphine)platinum acetylide) and acceptor (electron-deficient thienopyrazine) units in the backbone as in polymer **191**.[435] Similarly, donor–acceptor interactions appear to be important in polymer **192**, which possesses a ferrocenylfluorenyl spacer that has a band gap of 2.1 eV. In the absence of the donor metallocene group, the analogous polymer has a substantially wider gap ($E_g = 2.9$ eV).[436]

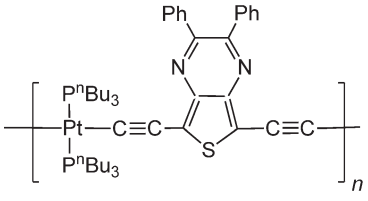

191

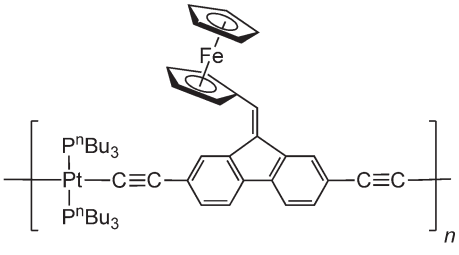

192

The π-conjugated organic polymers are of widespread interest with respect to their light-emissive properties, which permit applications in, for example, lasers, photocells, and light-emitting diodes (LEDs).[437–439] Light emission is possible from excited singlet states but is spin-forbidden from excited triplet states. The presence of transition metals in the π-conjugated framework of polymetallaynes introduces sufficient spin–orbit coupling for emission from excited triplet states to also be significant.[413] For example, the polymers shown in Table 5 exhibit photoluminescence at room temperature, and, for the lower three polymers in the table, the emission quantum yields (4–8%) were found to be ca. one-tenth of those for the free ligands (30–60%).[432] The lower quantum yields detected for the Pt polymers was attributed to the population of long-lived triplet states that were easily quenched under the conditions of the experiment. Performance of photoluminescence experiments at liquid helium temperatures allows for the observation of the emission from the triplet states. For example, the photoluminescence spectra of thin films of the polymetallayne **193** at 10 and 300 K are shown in Figure 27.[413] The high-energy emission at 450–600 nm is assigned

Table 5 Lowest optical transition measurements as a function of the alkynyl ligand spacer

Compound	E_g (eV)
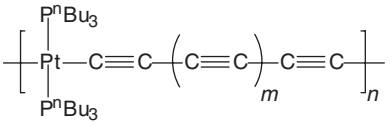	3.23 ($m = 0$) 3.12 ($m = 1$)
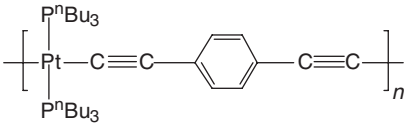	3.26
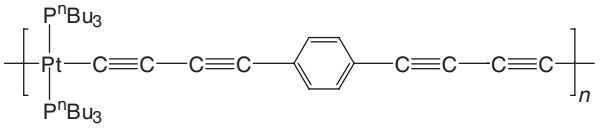	3.13
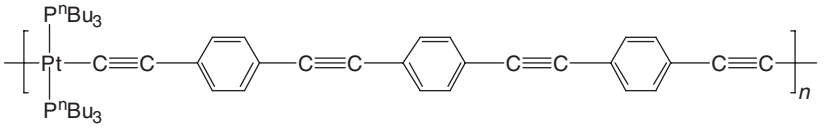	3.11
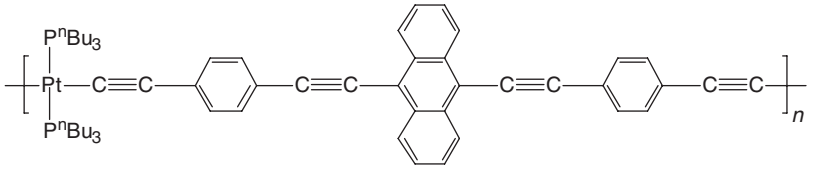	2.48
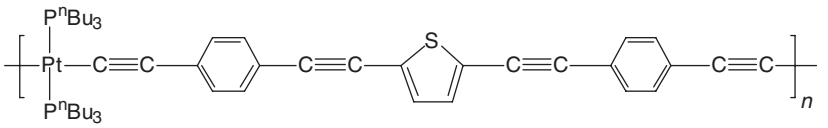	2.70

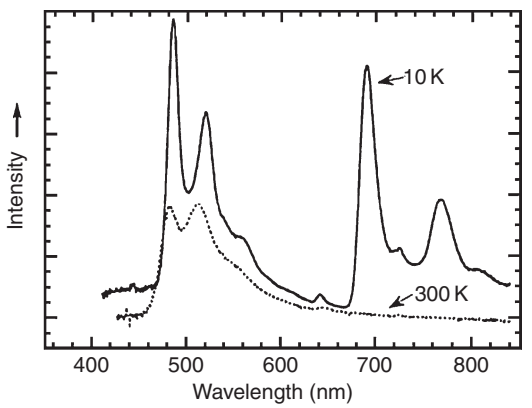

Figure 27 Photoluminescence spectra of a thin film of polyplatinayne **193** at 10 and 300 K. The excitation wavelength was 334–364 nm. (Adapted with permission of The Royal Society of Chemistry from Khan, M. S. *et al*., *J. Chem. Soc. Dalton Trans.*, **2002**, 2441.)

to fluorescence from the excited S_1 state and the low-energy band at 670–850 nm, which is only detected at 10 K, was assigned to phosphorescence from the excited triplet state T_1.

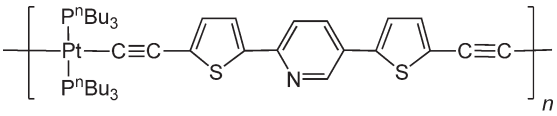

193

Detailed studies have been performed on the photophysics of a range of Pt polyynes,[433,440–442] and the energy gap law for triplet states in a series of platinum polyynes has been established.[443,443a] Convincing evidence for π-conjugation between metal sites in the main chain has been provided by some of the experiments.[440] The photophysics of polymers with fluorene and carbazole spacers has also been investigated in depth, and the studies indicate that the singlet state extends over more than one repeat unit whereas the triplet state is strongly localized.[444]

Studies of polymetallaynes that contain metals other than Pt are much more rare. However, the photophysical properties of rigid-rod, conjugated gold(I) polymers **180–182** have been investigated, and these materials were found to exhibit weak luminescence in the solid state at ca. 585 and 600 nm at room temperature when excited with UV light.[401]

12.06.5.2.4.(iv) Non-linear optical properties

The ability to manipulate light is critical to the creation of new photonic devices (see Chapter 12.04). Materials that exhibit NLO effects offer potential applications in many areas such as switching and frequency doubling or tripling.[31] It is well known that extended π-electron delocalized systems such as conjugated organic polymers exhibit appreciable third-order NLO susceptibilities. Significantly, the absence of a center of symmetry is not a structural requirement for third-order NLO materials; this provides a significant advantage over second-order NLO materials.[31] Thus, metal polyyne polymers, which possess low oxidation state transition metals with highly polarizable *d*-electrons in the conjugated backbone, should show enhanced hyperpolarizability. Indeed, studies of the third-order NLO properties[445–451] of a series of platinum polyynes have shown that these polymers exhibit large hyperpolarizabilities, comparable to inorganic semiconductors such as InSb ($1{,}700 \times 10^{-36}$ esu) and Ge ($2\ 300 \times 10^{-36}$ esu).[448] This suggests that these materials are potentially of interest for the construction of NLO devices [448].

12.06.5.2.4.(v) Electrical and photoconductive properties

The electrical conductivity and photoconductivity of metal polyynes have been studied in some detail.[452] For instance, it has been demonstrated that in the unoxidized state **166** (M = Cu) is an insulator ($\sigma = 10^{-9}$ S cm^{-1}) and, upon doping with I_2, the conductivity is increased to 10^2 S cm^{-1}.[453] Polyynes such as **165** (M = Ni, Pd, Pt; L = E^{n}Bu$_3$; E = P or As) can either be oxidized with nitric acid or doped with I_2.[416] Measurements on undoped films showed low conductivity values of ca. 10^{-7} S cm^{-1}, which improved to ca. 10^{-6} S cm^{-1} in the I_2-doped samples.[416] The Pt–acetylide pyridine polymers **188** showed conductivities of 2.5×10^{-3} S cm^{-1} upon doping with iodine. Quaternization followed by iodine doping gave a similar value (3.4×10^{-3} S cm^{-1}). These values appear to be the highest reported for soluble polymetallaynes.[405]

Electrochemical studies of several polymetallaynes have also been reported.[435,436,444] Reduction of organic spacer groups can be achieved and the oxidation of substituents (e.g., ferrocene) can be reversible. However, electrochemical oxidation of the platinum centers in polymetallaynes appears to occur in two irreversible redox steps (presumably involving Pt^{II}/Pt^{III} and Pt^{III}/Pt^{IV} couples). This observation suggests that the chemical doping experiments that were used to increase the electrical conductivities of the polymers described above are not simple processes.

The photoconductivity of platinum polyynes has been examined, and photocells have been fabricated using the materials **194** ($M_w = 2.8 \times 10^4$, PDI = 1.71) and **195** ($M_w = 1.9 \times 10^4$, PDI = 2.14). The quantum efficiencies detected were ca. 0.01%, a common value for single layer devices. The photocurrent was found to increase with an increase in bias voltage.[444] Similar studies of Pt polyynes **196** and **197** ($M_w = 8.3 \times 10^4$–1.8×10^5, PDI = 1.2–3.2) with thiophene and oligothiophene spacers, respectively, have also been reported and quantum efficiencies were around 0.04%.[433] In analogous work, the most promising photocurrent quantum yield of ca. 1% has been reported for the donor–acceptor polymer **191**. This value is unusually high for a single layer device.[435]

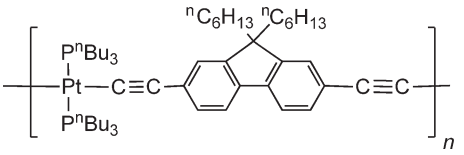

194

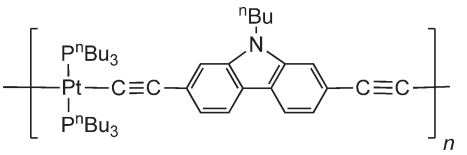

195

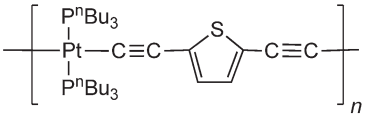

196

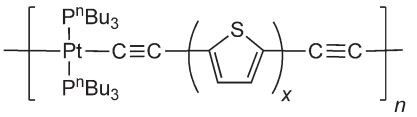

197

x = 2 or 3

12.06.5.3 Polymers with Skeletal Metallocyclopentadiene Units

The first members of an interesting new class of organometallic π-conjugated polymers that contain metallacyclopentadiene units in the main chain were reported in 1993.[336,454] Double addition of acetylenes to $CpCo(PPh_3)_2$ allowed polymers **198** to be prepared (Equation (71)). These materials were found to be intractable in common organic solvents and IR was used to estimate their degree of polymerization (ca. 20).[336]

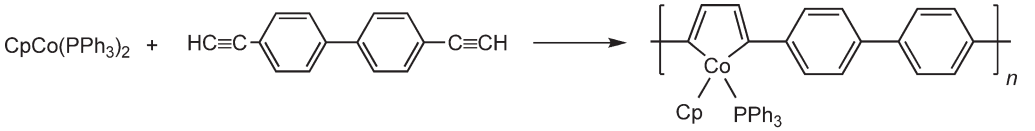

(71)

198

A similar synthetic approach was used to prepare Co polymers **199** (Equation (72)), which possessed improved solubility as a result of the presence of flexible aliphatic spacers in the main chain.[454]

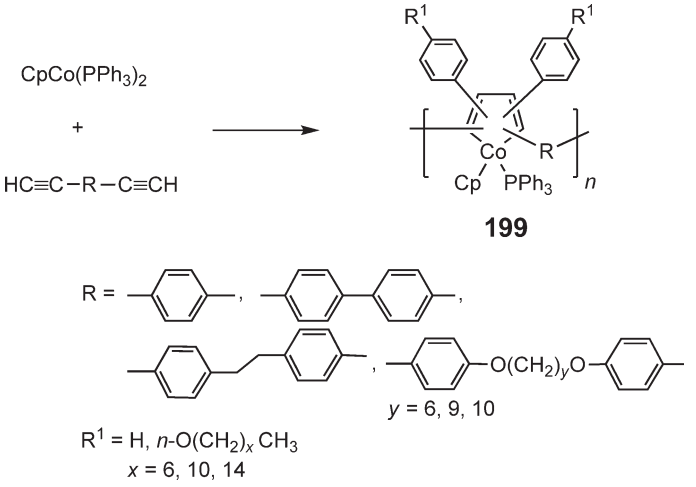

(72)

199

y = 6, 9, 10

R^1 = H, n-$O(CH_2)_x CH_3$

x = 6, 10, 14

Molecular weights for the soluble, orange-brown polymers **199** were determined by GPC (vs. PS standards) to be ca. $M_w = 9{,}000$–$16{,}000$ with PDI values in the range of 1.3–1.5.[341] Solubility can also be enhanced via the attachment of n-hexyl groups to the Cp ligands.[455] Regioregular polycobaltacyclopentadienes **200** have been prepared via a nickel-catalyzed route (Equation (73)) and these materials possess molecular weights up to $M_w = 5.6 \times 10^5$, PDI = 2.8.[456]

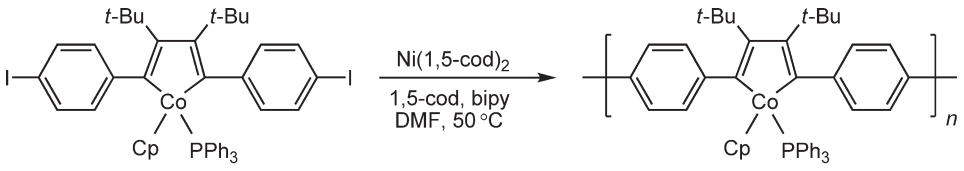

(73)

200

The polycobaltacyclopentadienes of type **198–200** are of interest as metal-containing analogs of π-conjugated organic polymers such as polythiophene and polypyrrole. This has led to substantial interest in their physical properties.[341,455–459] UV–VIS studies show that there is a shift in the lowest energy absorption band with an increased degree of polymerization, which is indicative of a significant degree of π-conjugation in the polymer main chain.[341,455] Band gaps of ca. 2.1–2.3 eV have been determined by measurement of the absorption edge of UV–VIS spectra and these are comparable to the value of 2.0 eV for polythiophene.[455] In the dark, polycobaltacyclopentadienes show low conductivity (σ = ca. 10^{-12} S cm^{-1}). However, upon irradiation with white light, a very substantial photoconductivity effect has been demonstrated.[455] Cyclic voltammograms of the polymers show quasi-reversible oxidations and irreversible reductions. Electrochemical studies of **200** revealed weak metal–metal interactions with $\Delta E_{1/2}$ values around 20% of those in poly(1,1′di(*n*-hexyl)ferrocenylene). The relatively weak interactions were attributed to an energy mismatch between the Co *d*-orbitals and the phenylene π-orbitals or the lack of coplanarity for the cobaltacyclopentadiene and arene units.[456] Cobaltacyclopentadiene polymers undergo thermal rearrangement to the more stable (η^4-cyclobutadiene)cobalt derivatives, and reaction with isocyanates afforded new polymers containing 2-pyridone moieties in the polymer backbone (for details, see Section 12.06.4.1).[337,339,340]

A novel extension of the metal-induced coupling of diynes involves the preparation of the red, moisture sensitive zirconocene-containing polymer **201** (Equation (74)) with M_w = 37,000 (PDI = 2.1) by GPC (relative to PS).[460] Related organosilicon polymers and macrocycles derived from the zirconocene coupling of $CH_3C{\equiv}CSiMe_2C_6H_4SiMe_2C{\equiv}CCH_3$ were also reported.[461,462]

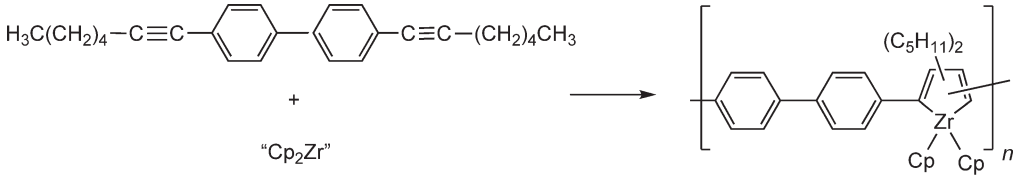

(74)

201

The Zr polymers **201** are not just of intrinsic interest but they also permit chemical modification reactions in which the Zr atom is replaced.[460,462,463] This allows for the introduction of diene, thiophene, phosphole, and aromatic functionalities, to yield novel π-conjugated organic polymers **202–205** with controlled structures and electronic properties (Scheme 18).

12.06.5.4 Other Polymers with M–C σ-Bonds in the Main Chain

A step-growth polycondensation route has been succesfully devised to prepare novel nickel polymers **207** with arene spacer groups. The procedure involved the polycondensation of the fluorinated dilithiated species **206** and an Ni(II) complex (Equation (75)).[464] The rod-like structure of these polymers was established by dilute-solution viscosity measurements, and the results were similar to those reported for the related platinum polyyne polymers **166** (M = Pt(P^{n}Bu$_3$)$_2$; *x* = 2) (Section 12.06.5.2.3).

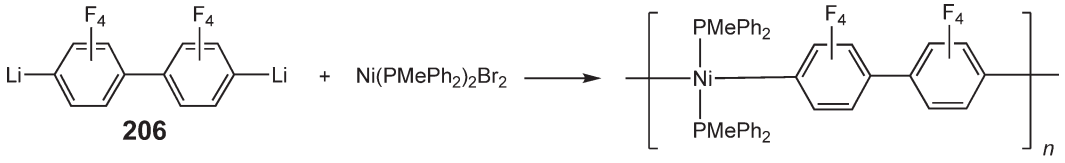

(75)

206 **207**

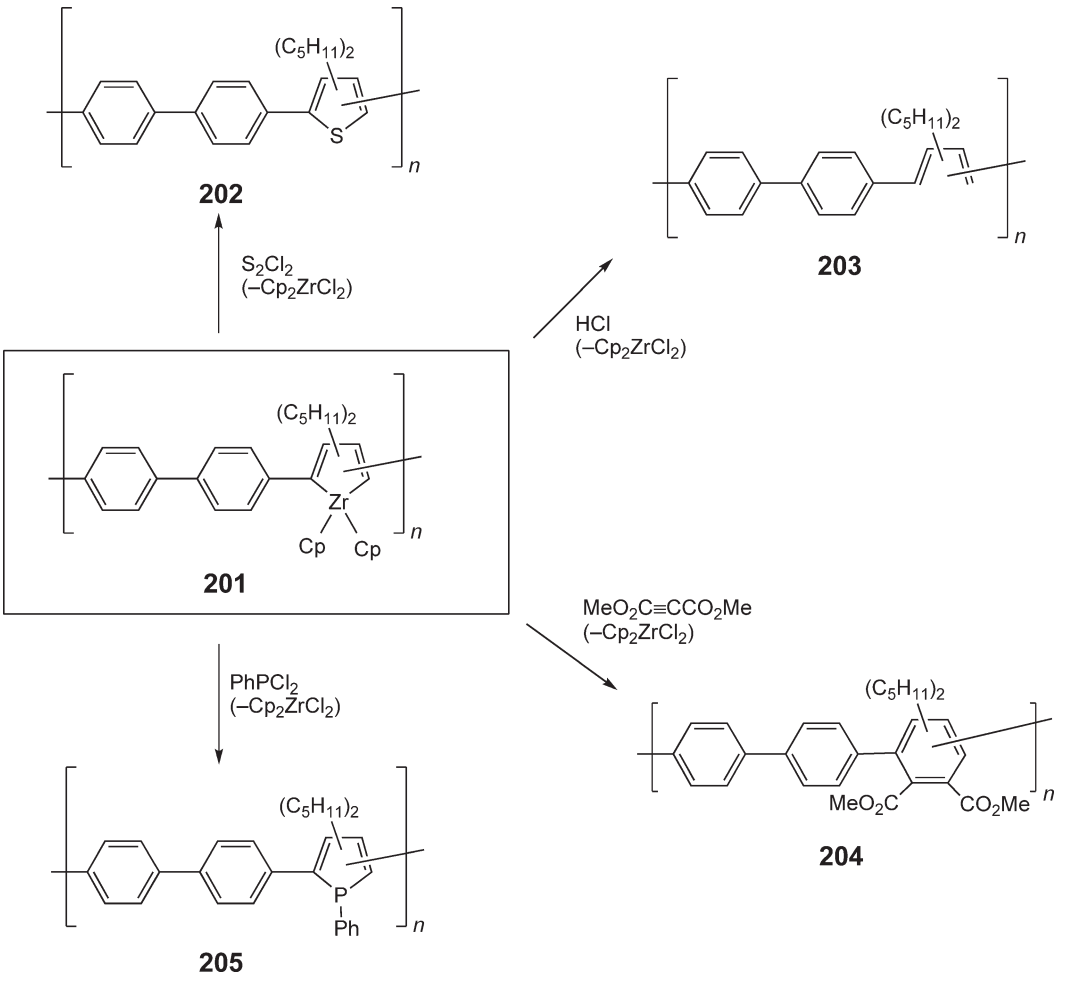

Scheme 18

The absolute molecular weights of these materials have been established by GPC by means of the universal calibration technique that involves the acquisition of intrinsic viscosity data. As with the aforementioned platinum polyyne polymers **166** (M = Pt(P^nBu_3)$_2$; $x = 2$), the intrinsic viscosities were found to be independent of the nature of the solvent and a Mark–Houwink α-value of 1.5 was determined, which is indicative of a rod-like structure. Interestingly, it was found that in this case, GPC, using PS standards, "underestimates" the true molecular weight of the polymers. This was attributed to the high molar mass of a repeat unit in the Ni polymer **207** compared to PS, which overcompensates for the effect of the rigid-rod structure that would be expected to lead to the opposite situation. Absolute values of M_w of up to ca. 1×10^5 were determined for the polymer samples.[465]

Polymers with M–C bonds in the main chain where the carbon atom is sp^3-hybridized are rare. Such materials have been successfully prepared via acyclic diene metathesis (ADMET) polymerization, which has been used to prepare polycarbostannanes **209** with molecular weights (M_w) up to 36,000 (PDI = 2.1) and ethylene as the byproduct (Equation (76)). The reaction is unusual in that the divinyl stannane **208** can function as both the monomer and the co-catalyst in the case of the W-catalyzed reaction.[466]

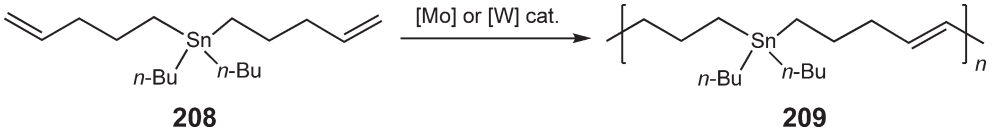

208 209 (76)

As another interesting variant on materials with M–C linkages, formally conjugated polymers **210** and **211** have been prepared via polycondensation routes and have been characterized in the solid state.[467–469] In the case of the intriguing metal–carbyne polymers **211**, the materials are fluorescent at room temperature,[468] unlike monomeric species such as $(RO)_3W{\equiv}CR$ (R = alkyl or aryl). Polymers such as **210** and **211** and analogs[469] represent very exciting targets for future study.

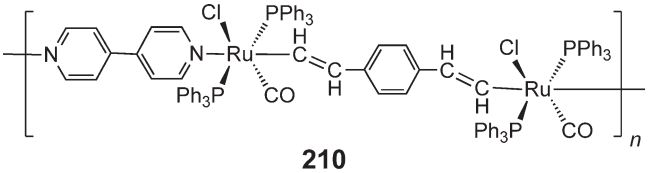

210

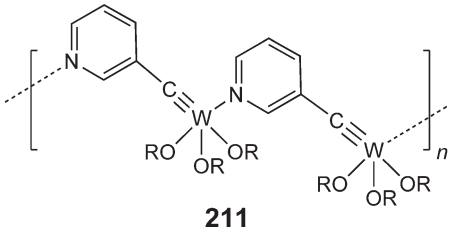

211

12.06.6 Polymers with Metal–Metal Bonds in the Main Chain

12.06.6.1 Introduction

The remarkable properties of high molecular weight polysilanes **212** and polygermanes **213**, which were first prepared in the late 1970s and early 1980s by Wurtz coupling procedures (Equation (77)), have led to considerable interest in the development of polymer chains based on the heavier group 14 element, tin, as well as other metals.[470–473] To appreciate the reasons for the interest in polymers containing metal–metal bonds in the backbone, it is very useful to first consider some of the unique features of polysilanes that have now been thoroughly studied.

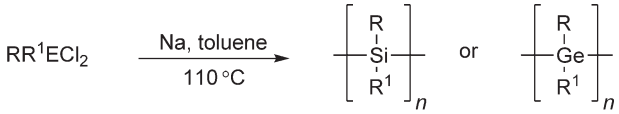

E = Si or Ge **212** **213** (77)

One of the most novel characteristics of the all-silicon backbone in polysilanes is that it possesses delocalized σ-electrons, a phenomenon that is virtually unknown in carbon chemistry.[472,474–477] This can be understood in terms of the nature of the molecular orbitals associated with the Si–Si σ-bonds. These are more diffuse than those associated with C–C σ-bonds as they are constructed from higher-energy 3*s*- and 3*p*-atomic orbitals and silicon is less electronegative than carbon. This leads to significant interactions between the adjacent Si–Si σ-bonds along a polysilane chain, a situation analogous to that for the π-bonds in π-delocalized polymers such as polyacetylene. Thus, a band model, rather than a localized model, is more appropriate for these catenated structures.[472,477] As a consequence of the delocalization of σ-electrons, the σ–σ^* transition that occurs at 220 nm in Me_3Si–$SiMe_3$ moves to lower energy as the number of silicon atoms in the chain increases. In the high polymers, the σ–σ^* band gap transitions occur in the near-UV region, at ca. 300–400 nm.[471,472,477,478] The electron delocalization also leads to appreciable electrical conductivity upon doping. For example, conductivities of up to 0.5 S cm^{-1} have been reported after doping with AsF_5.[477] In addition, many of the polymers are thermochromic, as the conformations adopted by the polymer change with temperature and consequently alter the degree of σ-delocalization along the main chain. Due to their low-energy, σ–σ^* transitions, polysilanes are photosensitive and have attracted considerable attention as photoresist materials in microlithography.[472,477] Polygermanes **213** appear to possess even more extensive σ-delocalization

than polysilanes and the σ–σ^* band gap transition for the high polymers is significantly red-shifted, by ca. 20 nm, in comparison to the silicon analogs.[479–481]

12.06.6.2 Polystannanes

12.06.6.2.1 Oligostannanes

The preparation of cyclic and linear catenated structures based on tin atoms has attracted significant attention in the literature, and prior to 1990, a range of cyclic and linear oligomers and remarkable clusters were reported.[482,483] Because of the lower electronegativity of Sn compared to Si and Ge, polystannanes would be expected to possess even more σ-delocalized structures and have therefore been regarded as a very desirable synthetic target.[482–484] Important work that underlined the potential significance of high polymeric polystannanes was carried in 1987.[482] These workers successfully prepared linear oligostannanes **214**, with 3–6 catenated tin atoms, via a salt elimination procedure (Equation (78)).

(78)

214

x = 3–6

Each of the discrete oligomers was characterized by single crystal X-ray diffraction and the structures are shown in Figure 28. The Sn–Sn bond lengths varied from 2.30 to 2.97 Å, and each oligomer was shown to possess a *trans*-planar conformation. Most interestingly, studies of the discrete oligomers by U–VIS spectroscopy showed that the σ–σ^* transition moves dramatically to lower energy as the chain length is increased (Figure 29). Indeed, whereas the trimer **214** ($x = 3$) is colorless, the linear hexamer **214** ($x = 6$) is yellow. The spectroscopic evidence for the formation of a band structure, in a manner similar to the well-known decrease in HOMO–LUMO gap with increasing chain length for π-conjugated materials, led to the proposed term "molecular metals" for these oligomers and prospective high molecular weight analogs.[482]

12.06.6.2.2 High molecular weight polystannanes

Attempts before the early 1990s to generate high molecular weight polystannanes via Wurtz coupling were unsuccessful and yielded only low molecular weight oligomers and reduction products. The lack of success compared with the corresponding silicon and germanium polymers was attributed to the relative ease of reduction of Sn(IV) and weakness of the Sn–Sn bond. The key breakthrough in this area was reported in 1993 when it was shown that transition metal-catalyzed dehydrogenative coupling reactions, which had been extensively applied to the synthesis of polysilanes, could be applied to secondary stannanes R_2SnH_2 (Equation (79)).[485] Yellow poly(dialkylstannanes) **215** (e.g., R = *n*-butyl, *n*-hexyl, or *n*-octyl) of substantial molecular weight (up to M_n = ca. 22,000) were prepared by means of various zirconium catalysts. These materials indeed possess σ-electrons that are extensively delocalized as illustrated by the band gap σ–σ^*-transition that occurs at 384–388 nm (in THF). In addition, exposure of thin films of the polymers to the oxidant AsF_5 leads to significant electronic conductivities of ca. 0.01–0.3 S cm^{-1}.[48]

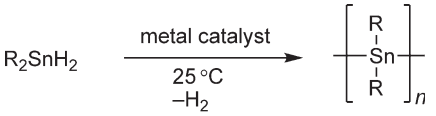

(79)

215

Even smaller band gaps are present in polystannanes with aryl substituents at tin[486,487] For example, dehydropolymerization of R_2SnH_2 (R = *p*-^{t}BuC$_6$H$_4$ or *p*-^{n}HexC$_6$H$_4$) afforded linear polymers (contaminated with some cyclics) with M_n values up to 20,000. The materials, which are yellow in color, possess λ_{max} values for the Sn σ–σ^* transition of 423–436 nm, that is red-shifted by 30–40 nm compared to those for poly(dialkylstannanes) and suggest that significant σ–π-conjugation that involves the Sn backbone and the aryl substituents is present.

The proposed mechanism for the formation of the polystannanes involves σ-bond metathesis and is analogous to that believed to operate for the dehydrocoupling route to polysilanes from primary silanes $RSiH_3$ by means of

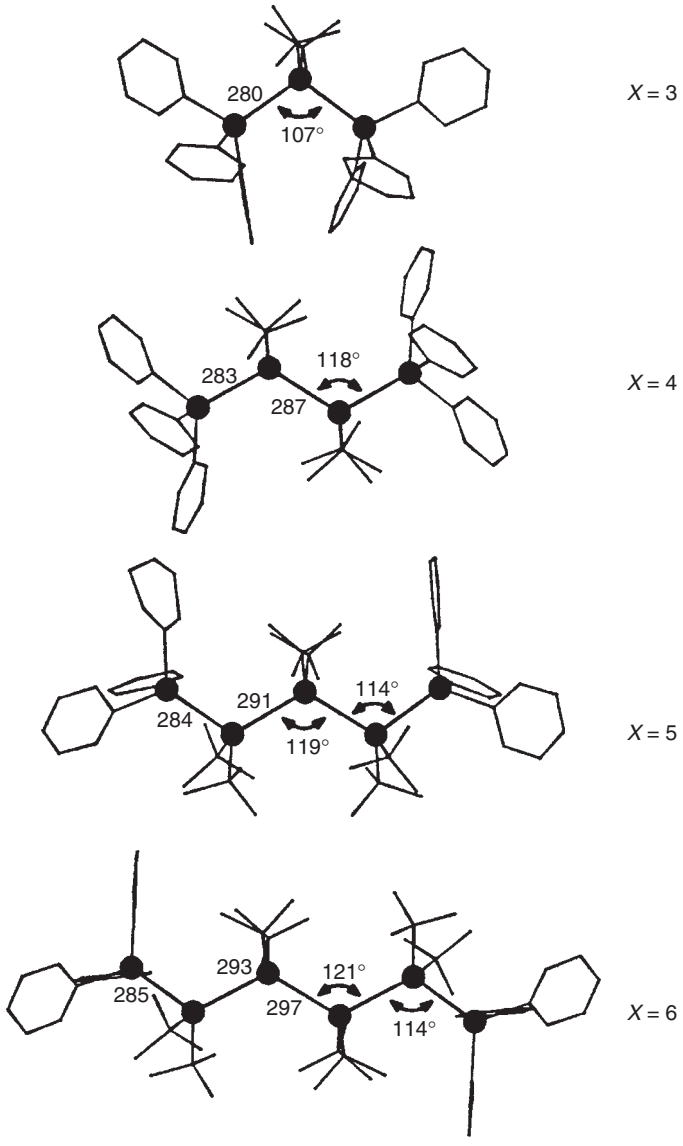

Figure 28 X-ray structures of oligostannanes **214** with $x = 3$–6. Bond lengths (pm) and angles (°) are indicated. (Adapted with permission of Wiley-VCH from Adans, S. and Drager, M., *Angew. Chem. Int. Ed. Engl.*, **1987**, *26*, 1255.)

Zr catalysts. The Zr pre-catalyst is believed to generate a metal hydride species that participates in a step growth process which involves 4-centered transition states (Scheme 19).[48]

Highly branched polystannane materials have been prepared via a dehydropolymerization/rearrangement process.[488] Whereas Ti and Zr metallocene pre-catalysts afford linear polystannanes via dehydropolymerization of $^{n}Bu_2SnH_2$, the Rh(I) complex $RhH(CO)(PPh_3)_3$ was found to react to afford either cyclic oligomers or branched polymers, depending upon the reaction conditions. The dark yellow gummy polymer formed **215**; R = ^{n}Bu; $M_n = 3.5 \times 10^4$, PDI = 1.4) was shown to possess a branched structure by ^{119}Sn NMR and by analysis of the cleavage products, after treatment with I_2 followed by PhMgBr, that included $BuSnPh_3$ as well as Bu_2SnPh_2. As a result of the branching, the λ_{max} in the UV–VIS spectrum of the material (in pentane) was 394 nm, slightly but significantly red-shifted from that of linear poly(di-*n*-butylstannane) (λ_{max} = 378–380 nm in the same solvent). The branched material was reported to possess greater stability to air oxidation and light in the solid state than the linear polymer. A representative list of selected polystannanes prepared by means of dehydrocoupling procedures is compiled in Table 6.

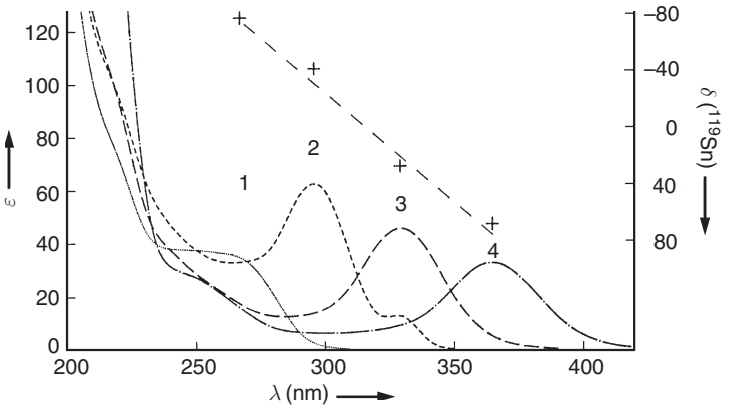

Figure 29 UV–VIS spectra of oligostannanes **214** with $x = 3$–6. (Adapted with permission of Wiley-VCH from Adans, S. and Drager, M., *Angew. Chem. Int. Ed. Engl.*, **1987**, *26*, 1255.)

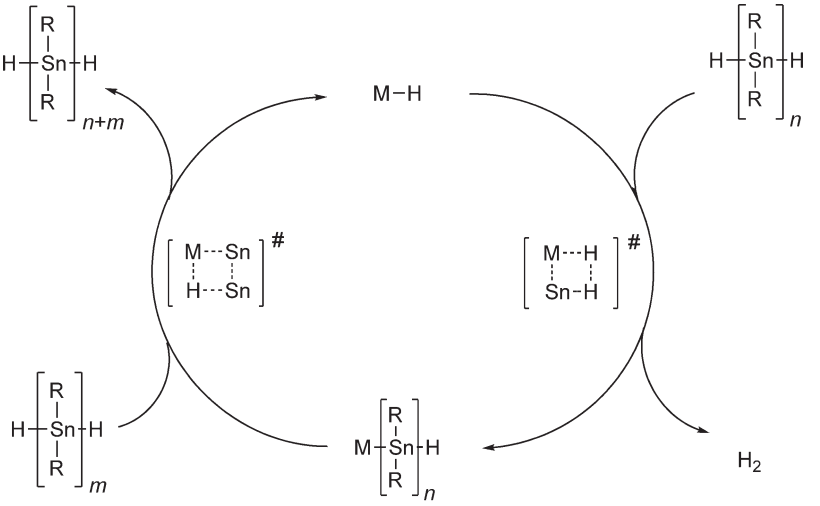

Scheme 19

Careful reinvestigations of Wurtz coupling procedures have now also successfully led to the isolation of high molecular weight polystannanes. The first detailed report of the preparation of polystannanes via Wurtz coupling in a refereed journal was published in 1996.[489,489a,48,485] Poly(di-*n*-butylstannane) was prepared from the reaction of Bu_2SnCl_2 with a sodium dispersion in toluene, in the presence of 15-crown-5, at 60 °C, in the dark (Equation (80)). The maximum yield of polymer was reached after 4 h and very high molecular weight material was formed ($M_n > 10^6$). Prolonged reaction times gave rise to chain scission. The spectroscopic data were consistent with the earlier reports for the same polymer formed by means of the dehydrocoupling route. Electrochemical reduction of dialkyldichlorostannanes $^nBu_2SnCl_2$ and $^nOct_2SnCl_2$ has also been reported and affords low molecular weight polystannanes **215** (R = ^{n}Bu or ^{n}Oct) with $M_n = 3.5 \times 10^3$–5.6×10^3 (PDI = 1.3–2.6).[490]

$$R_2SnCl_2 \xrightarrow[60\,^\circ C]{\text{Na, 15-crown-15}} \left[\begin{array}{c} R \\ | \\ -Sn- \\ | \\ R \end{array}\right]_n \qquad (80)$$

215

Table 6 UV/VIS and GPC molecular weight data for selected polystannanes **215** (R = alkyl or aryl) formed by means of dehydrocoupling

R	*Dehydrocoupling precatalyst*[a]	λ_{max} (nm, 25 °C)[b]	M_n[c]	*PDI*[c]	*References*
^{n}Bu	$Me_2CCp'Cp''ZrMe(Si(SiMe_3)_3$	384 (THF)	2.0×10^4	3.3	17
^{n}Bu	Cp_2ZrMe_2		1.4×10^4	3.3	17
^{n}Bu	$CpCp^*ZrMe_2$		1.3×10^4	5.6	17
^{n}Bu	$CpCp^*ZrMe(Si(SiMe_3)_3)$		7.8×10^3	2.2	17
^{n}Bu	$RhH(CO)(PPh_3)_3$	394 (pentane)[d]	3.5×10^3	1.4	20
^{n}Hex	$CpCp^*ZrMe(Si(SiMe_3)_3)$	384 (THF)	1.5×10^4	2.4	17
^{n}Oct	$CpCp^*ZrMe(Si(SiMe_3)_3)$		1.4×10^4	6.7	17
^{n}Oct	Cp_2ZrMe_2	388 (THF)	2.1×10^4	4.3	17
p-^{t}BuC$_6$H$_4$	Cp_2ZrMe_2	432 (THF)	1.5×10^4	1.35	18
p-^{n}HexC$_6$H$_4$	Cp_2ZrMe_2	436 (THF)	2.0×10^4	2.4	18

[a]Cp = (η-C_5H_5), Cp* = (η-C_5Me_5), Cp′ = (η-C_5H_4), Cp″ = (η-C_5Me_4), reaction conditions vary; consult reference for details.
[b]Limiting values for polymers with $M_n > 1 \times 10^4$.
[c]Obtained from GPC analysis of polymer in THF relative to polystyrene standards; PDI = M_w/M_n.
[d]Branched polymer.

The σ-delocalization in polystannanes has attracted significant theoretical interest.[484,491] Recent synthetic methods have permitted access to oligostannanes **216** with 3–15 catenated tin atoms.[491,492] The Sandorfy C model, which regards the polystannane backbone as a linear chain of interacting sp^3-hybrid orbitals, allows for an excellent degree of correlation between the experimental and calculated σ–σ^*-transition energies with changes in chain length.[491]

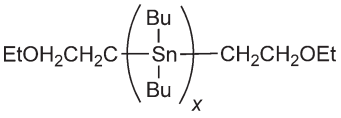

216
x = 3–15

Band structure calculations have also been reported for hypothetical polystannanes **213** (R = R^1 = H), and the results have been compared to analogous polysilanes and polygermanes.[484] The band gap (E_g) was calculated to decrease in the order Si > Ge > Sn for the *trans*-planar and *gauche*-helical structure (Table 7, Figure 30). The degree of delocalization was calculated to be much greater in the *trans*-planar configuration compared with the *gauche*-helical conformation. This is illustrated in Figure 31 which shows the calculated band structures in each case. The band dispersion (or bandwidth) is noticeably less in the case of the *gauche*-helical structures. Direct band gaps exist in the

Table 7 Calculated band parameters for polystannane $[SnH_2]_n$ **215** and analogous group 14 polymers $[SiH_2]_n$ **212**, and $[GeH_2]_n$ **213**

Polymer	*Conformation*	*Band gap* E_g (eV)	*Effective hole mass at valence band edge* m^*_h ([a])	*Effective electron mass at conduction band edge* m^*_e ([a])	*References*
$[CH_2]_n$	*trans*-Planar		0.21		2
$[CH{=}CH]_n$	*trans*-Planar		0.12		2
$[SiH_2]_n$	*trans*-Planar	3.89[b]	0.14	0.10	15
	gauche-Helical	5.94[c]	7.84	0.88	15
$[GeH_2]_n$	*trans*-Planar	3.31[b]	0.13	0.10	15
	gauche-Helical	5.13[c]	5.39	0.57	15
$[SnH_2]_n$	*trans*-Planar	2.80[b]	0.12	0.09	15
	gauche-Helical	4.65[c]	9.66	2.32	15

[a]Units are in mass of a free electron m_e.
[b]Direct band gap.
[c]Indirect band gap.

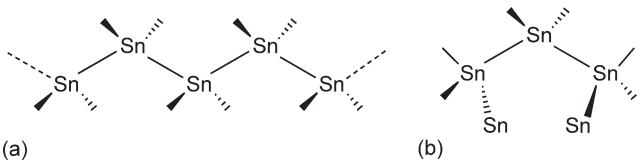

Figure 30 Polystannane conformations: (a) *trans*-planar and (b) *gauche*-helical.

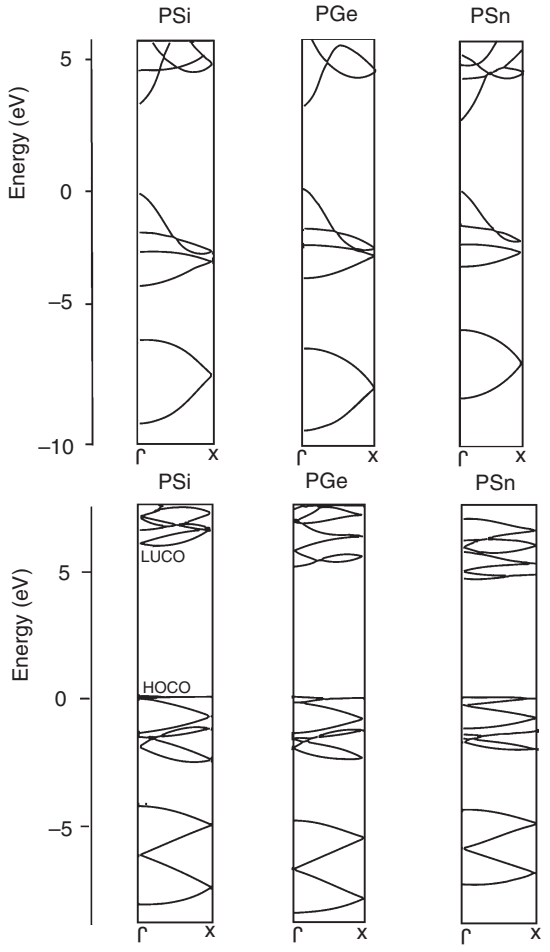

Figure 31 Band structures for polysilanes, polygermanes, and polystannanes (top, *trans*-planar conformation; below, *gauche*-helical conformation). (Adapted with permission of Elsevier Ltd. from Takeda, K. and Shikaishi K., *Chem. Phys. Lett.* **1992**, *195*, 121.)

cases of all of the polymers in the *trans*-planar conformation. Based on further calculations, the intriguing possibility of access to a metallic state for polystannanes appears to exist, in which the valence band and conduction band overlap if, for example, pressure is used to widen the bond angles to greater than ca. 150° along the polymer main chain. This bond angle is significantly greater than the value found in linear hexamers such as **214** ($x = 6$) for which the skeletal Sn–Sn–Sn angles are 114° and 121°.

A significant drawback for the practical application of polystannanes is their air and moisture sensitivity. This is not so significant in the solid state but the materials are appreciably sensitive in solution. Nevertheless, the properties of these fascinating materials are under detailed scrutiny.[493] The polymers are reasonably thermally stable up to ca. 270 °C, and polystannane **215** (R = *p*-^{t}BuC$_6$H$_4$) yields tin metal, when heated under nitrogen to 400 °C, and tin oxides in air, with a decomposition onset at around 225 °C. Polystannanes are highly photosensitive and exhibit

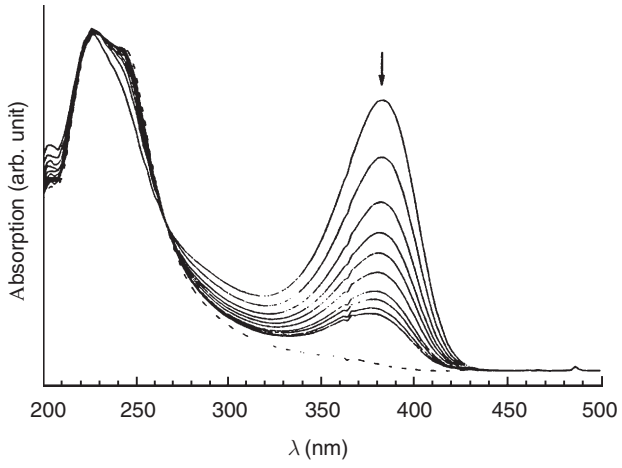

Figure 32 Photobleaching of polystannanes **215**. (Adapted with permission of The Royal Society of Chemistry from Imori, T. and Tilley, T. D., *Chem. Commun.*, **1993**, 1607.)

photobleaching behavior and, upon UV irradiation, depolymerize to yield cyclic oligomers (Figure 32). Green fluorescence has also been reported for polystannane **215** (R = ^{n}Bu) after UV excitation.[485] The dependence of the degree of σ-conjugation on conformation is expected to be significant, based on the work on polysilanes, and it is likely that the smallest band gaps for these materials have yet to be achieved.

12.06.6.3 Polymers that Contain Main-chain Metal–Metal Bonds that Involve Transition Elements

Polymers that contain metal–metal bonds in the polymer backbone might be expected to possess novel conductive and photochemical properties. This is an area in which considerable synthetic challenges must be overcome if progress is to be made. In general, comparatively little work has been carried out so far, but the area is so intriguing that the efforts made so far are of particular note.

In 1989, polycondensation routes to polyurethanes that contain Mo–Mo bonds (**217**, R = urethane linkage) or Fe-(μ-CO)$_2$Fe units **218** in the polymer backbone were reported (Equation (81)).[494–497] Polyurea and polyamide analogs and poly(ether urethane) co-polymers with Mo–Mo and Fe–Fe bonds in the polymer backbone were also reported by the same group.[498–500] These materials were generally of low molecular weight with M_n values usually less than 10,000. For example, different samples of the red, powdery material **217** possessed M_n = 4,800–6,000 (by vapor-pressure osmometry) which corresponds to ca. 6–8 repeat units, whereas **218**, a red-brown powder, possessed an M_n value of only 1,500 which corresponds to 2–3 repeat units.[496] Despite the low molecular weights, the polymers are of interest as photoreactive materials, as the metal–metal bonds can be cleaved photochemically by visible light. In contrast, conventional polymers generally require UV light for photodegradation.

As mentioned above, the M–M-bonded polymers are of interest as photochemically labile materials (Scheme 20). The quantum yields for the photodegradation of these polymers and model complexes decreased as the chain lengths increased. This effect has been observed in other polymer systems, and several explanations are possible. One invokes the theory that radiationless decay is faster in molecules with more vibrational modes and would thus make the quantum yield for the formation of requisite radical cage pair lower as the chains get longer.[500,501]

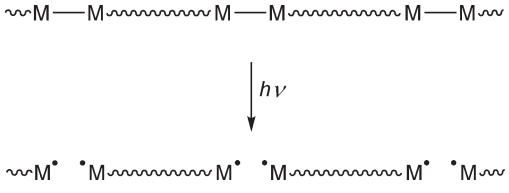

Scheme 20

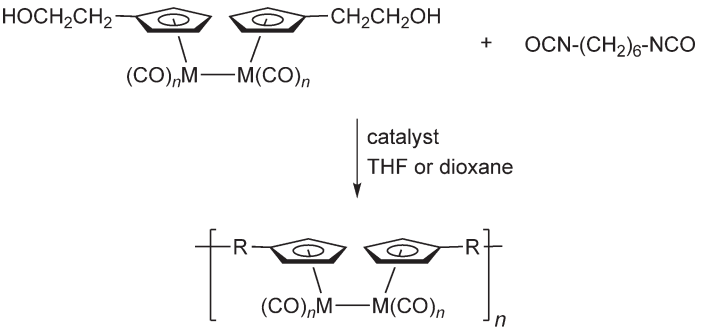

(81)

217: $(CO)_nM\text{-}M(CO)_n$ = $(CO)_3Mo—Mo(CO)_3$

218: $(CO)_nM\text{-}M(CO)_n$ = 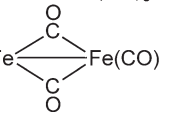

Studies of a series of polyamides that contain Mo–Mo bonds showed that both light and oxygen were necessary for degradation to take place in the solid state.[496–499] Oxygen reacted with the metal radicals produced by irradiation; otherwise, the M–M bonds re-formed via radical recombination. Studies of materials **219** with chlorine atoms that can act as "built-in" radical traps showed that photochemical degradation occurs over 5 days upon irradiation under nitrogen, and IR spectroscopy revealed the appearance of bands characteristic of $CpMo(CO)_3Cl$ units.[499] Nevertheless, the photodegradation was still found to be faster in air, presumably due to the higher concentration of radical trap present.

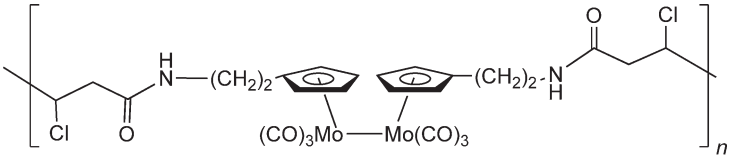

219

The synthesis of a further class of polymers with cyclopentadienylirondicarbonyl dimer units in the backbone has been described.[502] These materials possess organosiloxane spacers and were prepared via condensation reactions that are illustrated for the case of **220** (Equation (82)).

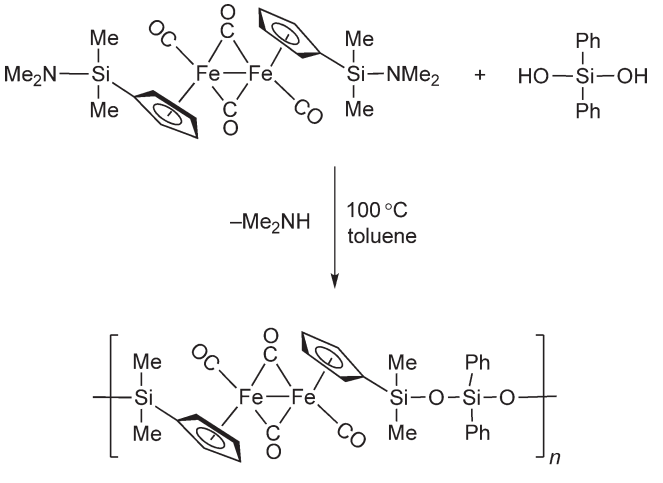

(82)

220

The materials were of low to medium molecular weight ($M_n = 4{,}000$–$13{,}500$) and showed very interesting electrochemical behavior. Studies of model compounds show that on reduction or oxidation the Fe–Fe bond is cleaved. The polymers, on the other hand, show reversible two-electron oxidation processes in THF/$[^nBu_4N][BF_4]$ at fast scan rates, as the Fe–Fe bonds reform after cleavage due to the fact that Fe atoms are held in close proximity by the bridging organosiloxane units.

Polymers with Pt–Pt bonds as part of the polymer main chain have also been reported (Equation (83)).[503,504] These yellow materials (e.g., **221**) are particularly interesting as they possess conjugated rigid-rod structures but are essentially insoluble or are only sparingly soluble in organic solvents; studies to date have been comparatively limited in scope. Analogs of **221** with diphosphine spacers as well as neutral analogs with acetylide spacers were also prepared and found to be insoluble in common solvents.[504]

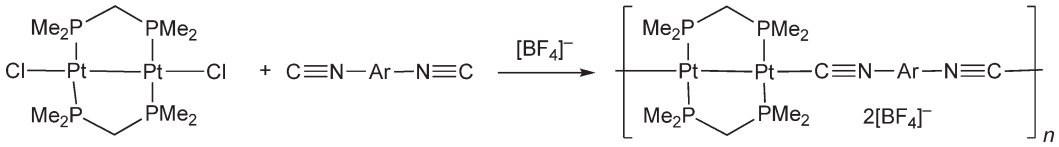

(83)

221

Polymers that contain bonds between main group metals and transition elements represent an area that is at a very early stage of development, and the challenges associated with the synthesis of high polymeric materials are substantial. Nevertheless, glimpses of the possibilities can be found in some linear and cyclic oligomers that have been prepared as model systems for prospective high polymeric analogs. For example, the hexametallic dimer **222** has been synthesized (Equation (84)) as a model for analogous high polymers.[505]

$$Na_2[(\eta\text{-}C_5H_5)(CO)_2Fe\text{-}CH_2\text{-}Fe(CO)_2(\eta\text{-}C_5H_5)] \quad + \quad 2(\eta\text{-}C_5H_5)(CO)_2Fe\text{-}SnPh_2Cl$$

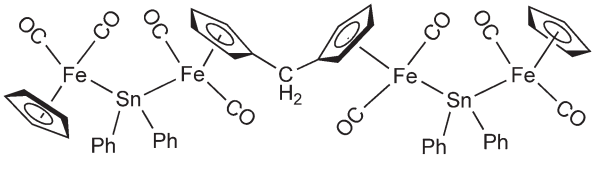

(84)

222

Attempts to prepare analogous polymers **223** have been briefly reported and have led to CH_2Cl_2-soluble materials with $M_n = 8{,}500$ when osmometry was used for molecular weight measurements (Equation (85)).[506]

$$Na_2[(\eta\text{-}C_5H_5)(CO)_2Fe\text{-}\{CH(NMe_2)\}_2\text{-}Fe(CO)_2(\eta\text{-}C_5H_5)] \quad + \quad Ph_2SnCl_2$$

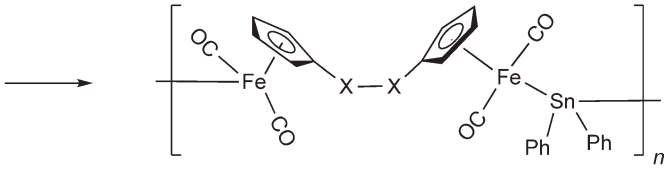

(85)

223: X = $CH(NMe_2)$

12.06.6.4 Polymers that Contain Metal Clusters in the Main Chain

Metal cluster complexes exhibit many useful catalytic, optical, and other potentially useful properties for materials science applications, and many impressive advances have been made with respect to their synthesis.[507–509] The incorporation of these remarkable metal-containing units into the main chain of polymer structures clearly offers exciting possibilities,[362,510,510a] but this area is, in general, poorly developed. The following three examples of linear

structures illustrate the growing interest and broad potential of this area. Dendritic structures that contain metal clusters are discussed in Section 12.06.7.

In 2000, the dark brown cluster polymer **224**, from the polycondensation of the hexanuclear ruthenium carbido species $Ru_6C(CO)_{15}$ with the diphosphinoalkyne $PhP_2C{\equiv}CPPh_2$ in refluxing THF, was reported.[511] The structure was assigned based on IR, NMR, and elemental analysis, and an estimated degree of polymerization of up to 1,000 was reported based on electron microscopy techniques. Polymer **224** has been shown to be electron-beam sensitive, and this allows the creation of Ru-based nanoparticle chains and, subsequently, conducting wires.[512,513]

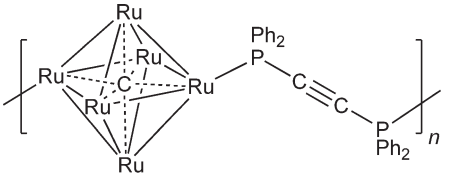

Ru = $Ru(CO)_x$

224

The first step is proposed to remove the sheath of carbonyl ligands and the second step involves fusion of the particles into larger clusters. Through use of films of **224** and a finely focused electron beam, wires with widths as small as 100 nm were accessible.

In 2001, an efficient step-growth polycondensation approach, reminiscent of that used to prepare metal–metal-bonded polymers **217** and **218**, was successfully developed to yield polyurethanes **225** with Mo_2Ir_2 clusters in the backbone.[514] Well-characterized polymers with molecular weights of up to $M_w = 136{,}000$ (PDI = 3.1), which correspond to a number average of around 30 clusters per polymer chain, were obtained by means of this method. It involved treatment of a diol of the Mo_2Ir_2 cluster with the diisocyanate OCN–R–NCO (R = aliphatic or aromatic spacer) in the presence of a tin catalyst. The unusual optical properties of organometallic clusters will drive applications-oriented work on these materials.[514]

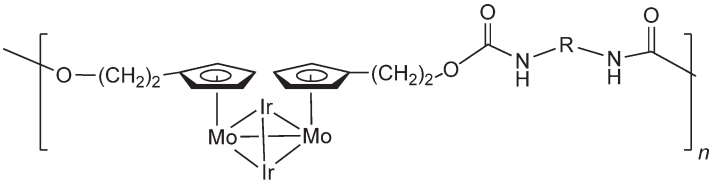

Mo_2Ir_2 = $Mo_2Ir_2(CO)_{10}$

225

12.06.7 Organometallic Dendrimers

12.06.7.1 Introduction

Since their discovery in the late 1970s to early 1980s,[515–517] scientific interest in dendrimers – well-defined, highly branched, and regularly repeating 3D macromolecular architectures – has been the subject of a large amount of attention.[518–522a] Different synthetic approaches that involve either "divergent"[515–518] or "convergent"[523–526] strategies are possible, and structures that involve a core and various numbers of layers or "generations" can thereby be constructed.[518–522a] The introduction of metals into such structures to create "metallodendrimers" offers many additional possibilities for applications as functional materials. For example, structures with metal-containing cores are of interest as models of biological systems such as metalloenzymes, surface-metallized architectures have potential for sensing and catalytic applications, and materials with metals distributed throughout the structure can exhibit antenna effects and have possible light-harvesting applications. Metallodendrimers can be subdivided on the basis of the location of the metallic moiety, which can be present in the core, on the surface, or throughout the structure.

Since the first examples were described in the early 1990s, a vast range of metallodendritic materials has been reported.[49,527–530] In keeping with the philosophy of other sections, the survey here is not intended to be rigorously

exhaustive in terms of listing every metallodendrimer reported in the literature but instead aims to illustrate the most important structural classes of these materials. Moreover, where possible, attention is focused on examples where studies of properties and potential functions have been performed.

As a result of their ease of solubility, characterization of dendritic materials can be readily achieved by means of standard polymer characterization techniques, such as NMR and GPC. However, despite the excellent characterization that pervades the materials discussed in this chapter, it should be noted that with the widespread introduction of mass spectrometric techniques which can characterize such macromolecules, the structural perfection assumed in many depictions of dendrimers have been shown to be highly idealized. Indeed, spectrometric analysis of many samples has revealed that imperfections and defects are, in fact, very common. In this section, organometallic dendrimers, a subset of metallodendrimers, are discussed.

12.06.7.2 Metallodendrimers with Metals at the Surface

A broad range of dendrimers containing metal centers at the periphery has been reported. Ni-containing dendrimers **226** up to the second generation have been synthesized (Equation (86)) and have been shown to function as homogeneous catalysts for the Kharasch addition of perhalogenated alkanes across the C═C bond of olefins.[531–533] Metallodendrimers **226** were found to be less active than a small molecular analog; however, a potential advantage of the dendritic catalyst was the ability to separate the catalyst from the products, which offers the possibility of recycling.

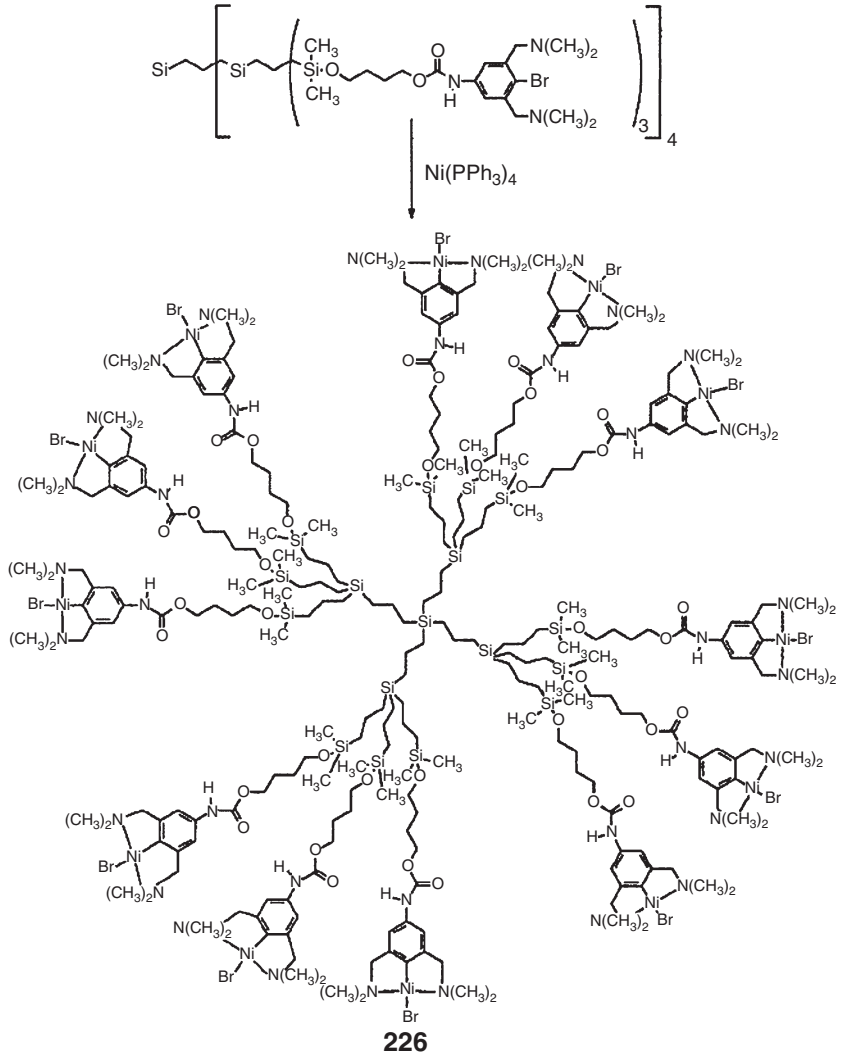

(86)

226

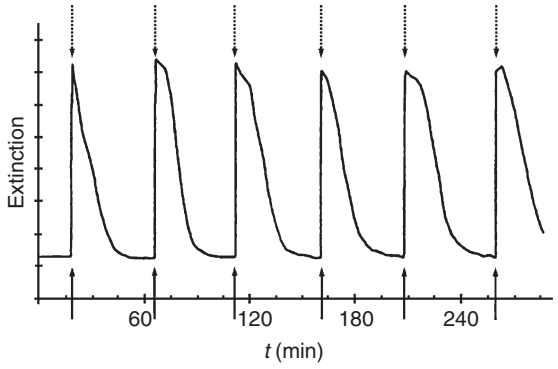

Figure 33 Repeated SO_2 adsorption and desorption cycles with platinum metallodendrimers **227**. The arrows mark saturation of the solution with SO_2 (solid) and with air (dashed). (Reproduced with permission of Wiley-VCH from Albrecht, M. and van Koten, G., *Adv. Mater.*, **1999**, *11*, 171.)

In another interesting application, a series of analogous platinum dendrimers have been found to function as useful sensors for SO_2.[534,535] For example, coordination of SO_2 to dendrimer **227** leads to the derivative **228**; a process that gives rise to an easily monitored color change from colorless to bright orange (Equation (87)). The coordination is reversible and repeated SO_2 adsorption/desorption cycles are shown for one of the metallodendrimers in Figure 33. The sensing is selective for SO_2 and the sensors show promising resistance to acids and water.

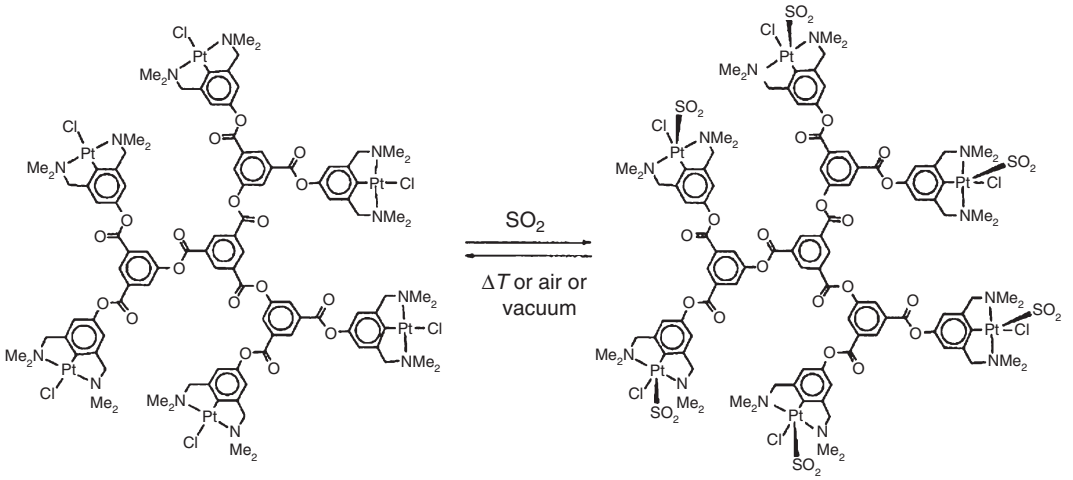

(87)

Metallodendrimers that contain peripheral ferrocene groups have been prepared by means of a variety of different methodologies.[536,537] From tetraallylsilane as the initiator core, novel silane dendrimers (e.g., **229**), in which reactive Si–Cl end groups are present, were constructed. The reaction with lithioferrocene or β-aminoethylferrocene afforded the corresponding tetraferrocenyl dendrimers **230** and **231** that represented the first examples of well-defined and well-characterized, redox-active macromolecules of this type (Scheme 21).[536]

A similar synthetic approach has also been used to synthesize the corresponding octaferrocenyl derivatives.[536] A series of remarkable ferrocenyl dendritic macromolecules based on flexible poly(propylene-imine) dendrimer cores containing 4, 8, 16, 32, or 64 peripheral ferrocenyl moieties has been prepared via condensation reactions of ferrocene carbonylchloride with the first-, second-, third-, fourth-, and fifth-generation diaminobutane-based

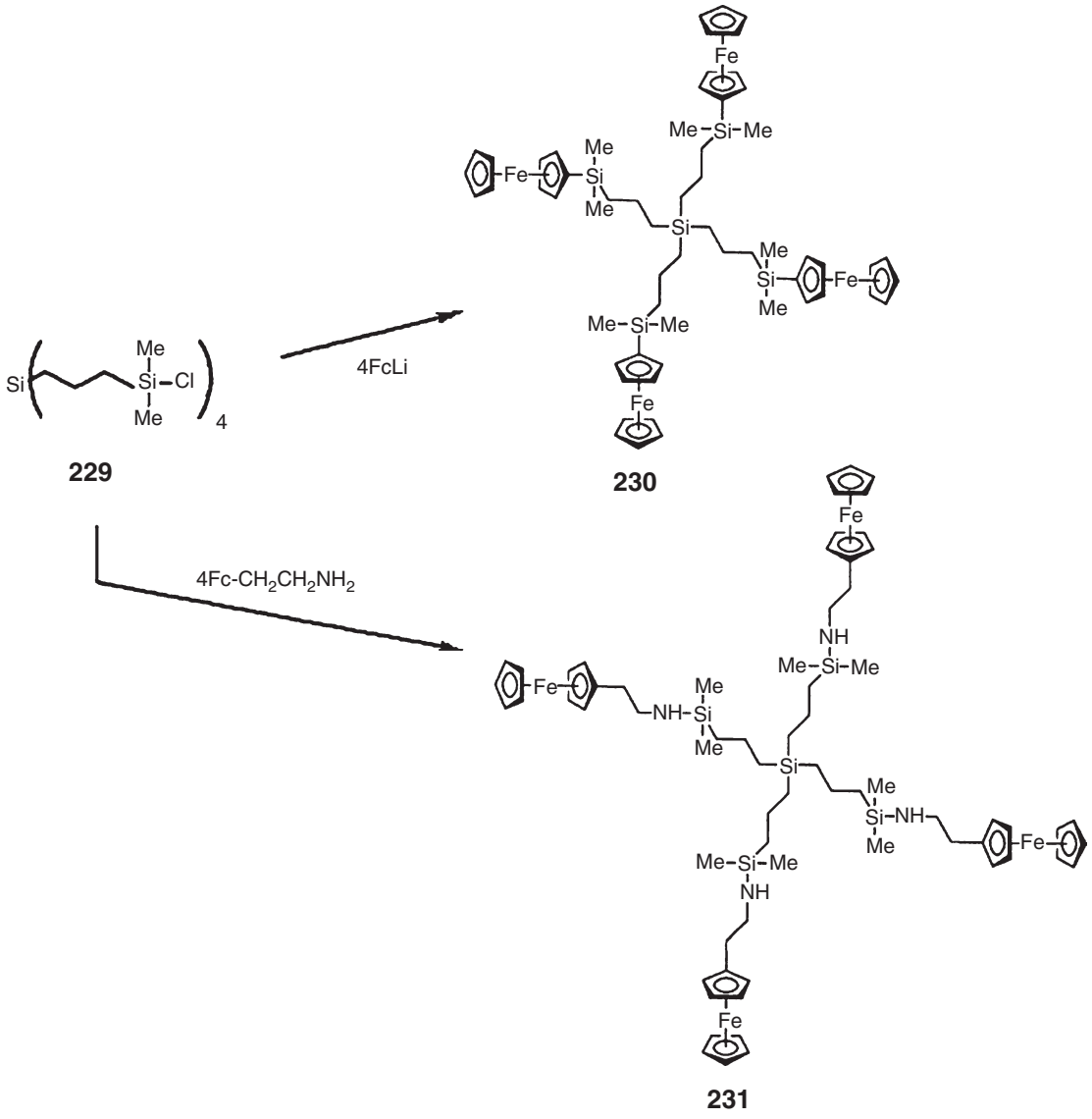

Scheme 21 Adapted from 35.

poly(propylene-imine) dendrimers functionalized with terminal NH_2 groups.[537] Examples with 8, 32, and 64 ferrocene units are illustrated as **232**, **233**, and **234**, respectively.

Cyclic voltammetric studies of these metallodendrimers showed one reversible oxidation wave characteristic of independent, non-interacting redox centers. Also, the use of these materials for modification of electrode surfaces was explored.[538–540] The researchers found that platinum, glass, and carbon-disk electrodes modified by electrodeposited films of these dendrimers are extremely durable and reproducible with no detected loss of electroactivity, even after their use in different electrolyte solutions or after standing for long periods in air. Studies on the thermodynamics and kinetics of adsorption of these redox-active dendrimers onto Pt electrodes by means of electrochemical and electrochemical quartz crystal microbalance techniques were conducted. These showed the adsorption processes to be activation controlled rather than diffusion controlled as well as dependent on the nature of the dendrimer but not the concentration. The adsorption free energies were found to decrease in the order **234** > **233** > **232**.[540] Dendrimers of type **232**–**234** and the cobaltocenium analog **235** have also been explored as guest systems for inclusion complexation by cyclodextrin (β-CD) hosts.[541–543]

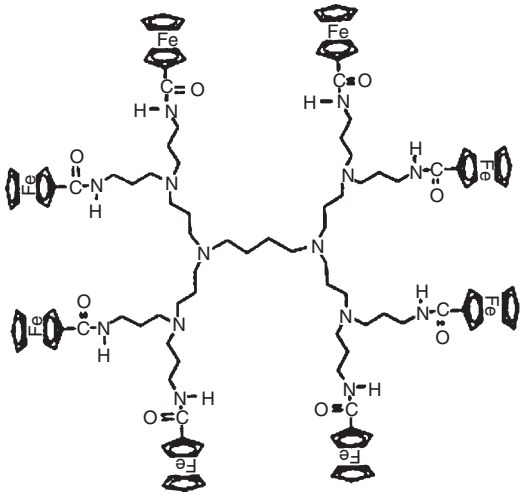

232

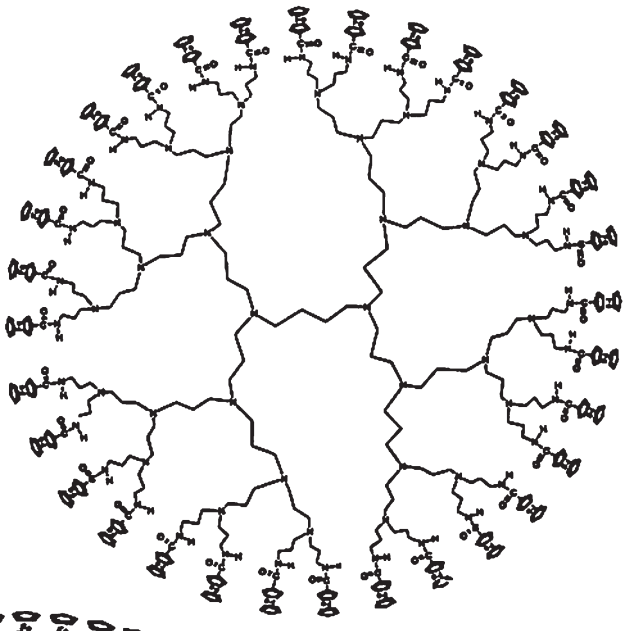

233

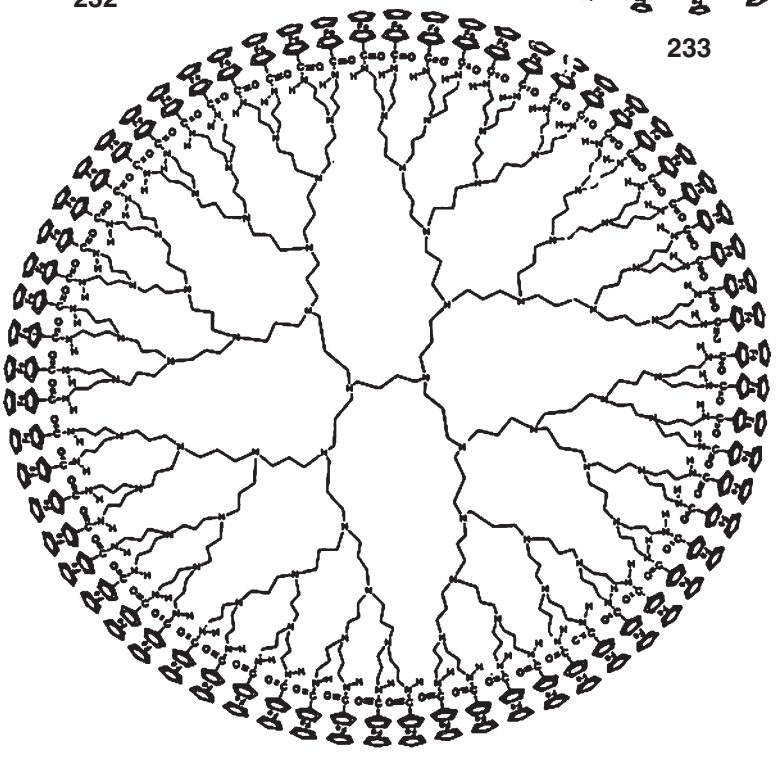

234

Amido–ferrocene dendrimers containing 3, 9, and 18 ferrocene moieties **236–238** have been prepared from the reaction of ferrocene carbonylchloride and the corresponding poly-NH_2 dendrimers. These materials were found to rapidly and reversibly bind small inorganic anions such as $[H_2PO_4]^{2-}$, $[HSO_4]^-$, Cl^-, Br^-, $[NO_3]^-$, as monitored by cyclic voltammetry. A dendritic effect was demonstrated; the sensing and recognition of the anions was found to improve as the number of generations was increased.[544] Analogous dendritic effects have also been observed for amidoferrocenyl dendrimers constructed by means of hydrogen bonding.[545]

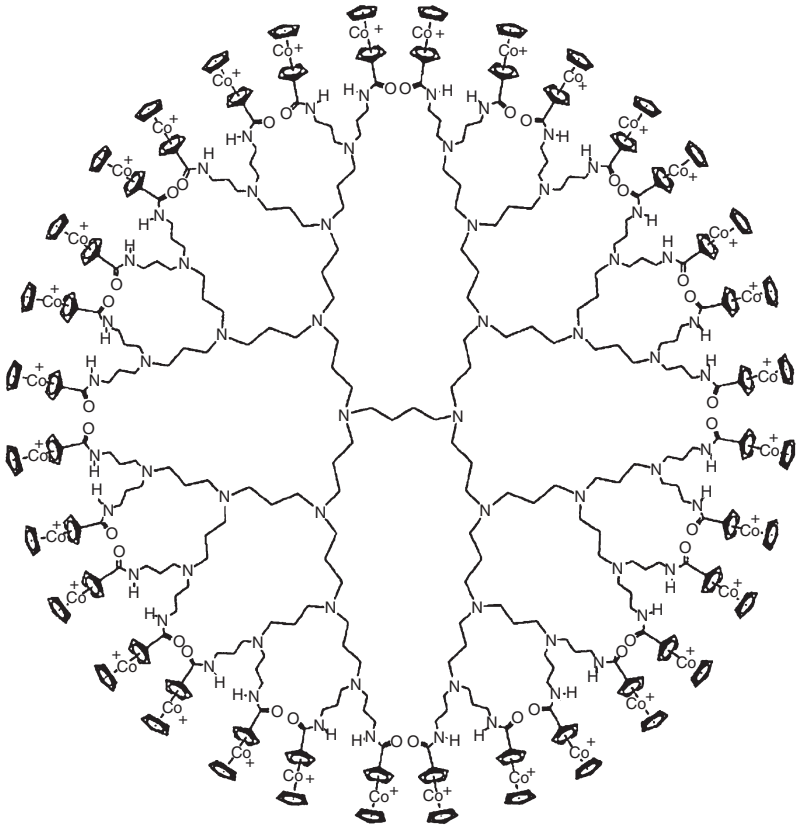

235

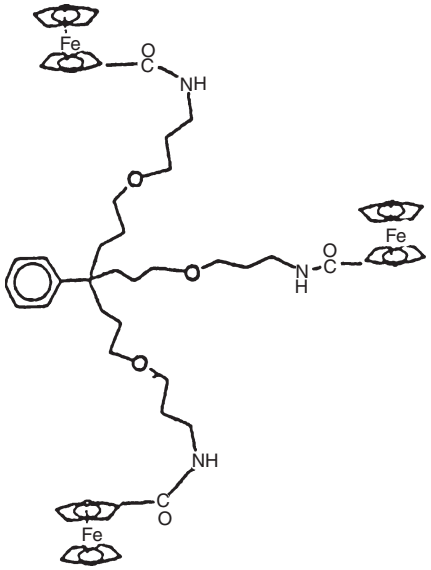

236

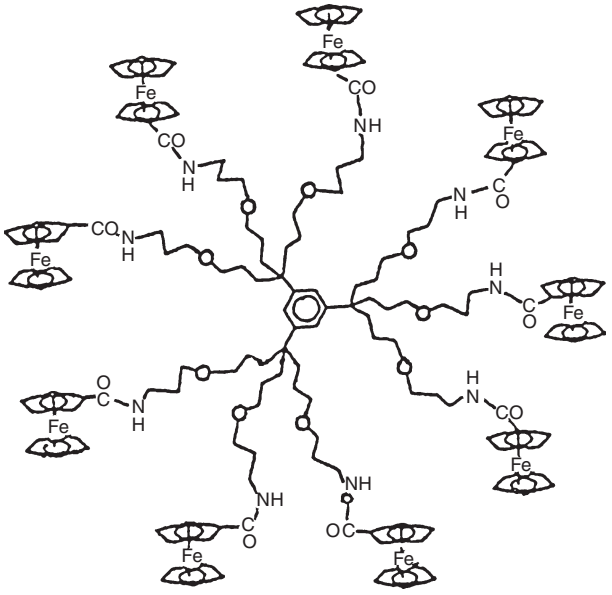

237

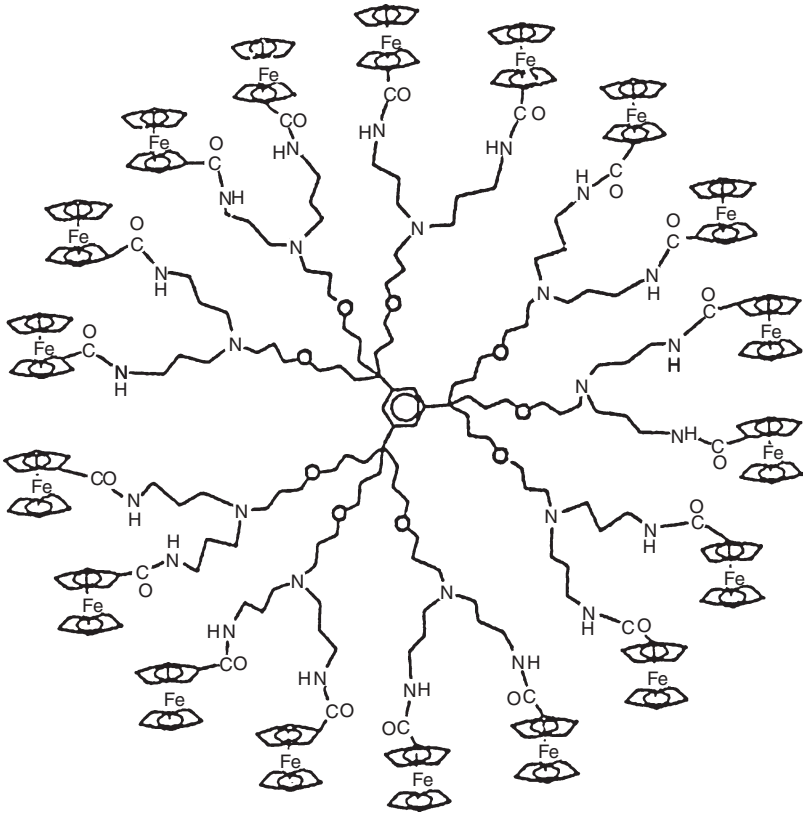

238

A convergent synthesis of novel dendrimers **239** and **240**, which possess interacting ferrocenyl units, via hydrosilylation reactions of the Si–H polyfunctionalized cores has been described.[546,546a] Cyclic voltammograms of these dendrimers exhibit two distinct oxidation waves separated by 190 and ~160 mV for **239** (see Figure 34) and **240**, respectively. This electrochemical behavior is consistent with the existence of significant communication between two ferrocenyl moieties linked together by a bridging Si atom. Similar cyclic voltammetric behavior is observed for linear oligomeric and polymeric analogs (see Section 12.06.3.3.6).

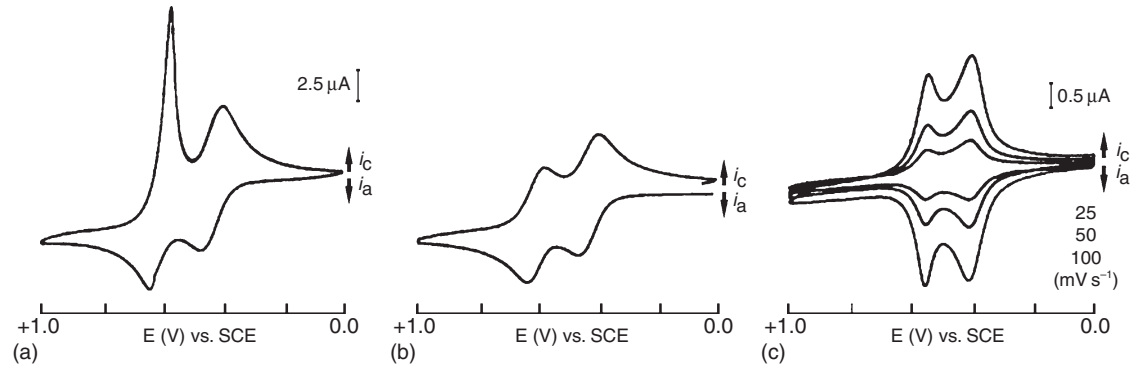

Figure 34 Cyclic voltammograms for ferrocene dendrimer **239** in (a) CH_2Cl_2 (b) CH_2Cl_2/MeCN 5 : 1, and (c) as a film on a Pt electrode. Supporting electrolyte: 0.1 M $[Bu_4N][PF_6]$; scan rate: 100 mV s^{-1}. (Reproduced with permission of The American Chemical Society from Cuadrado, C. M. *et al.*, *J. Am. Chem. Soc.*, **1997**, *119*, 7613.)

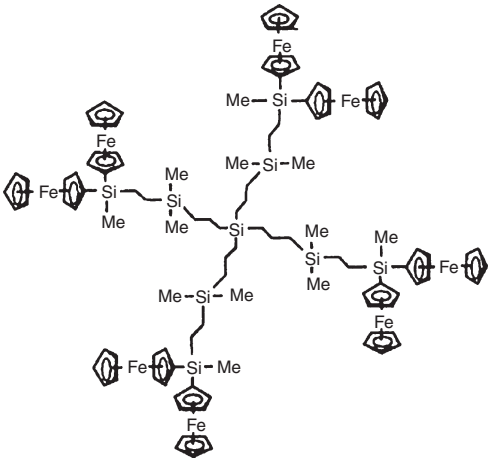

239

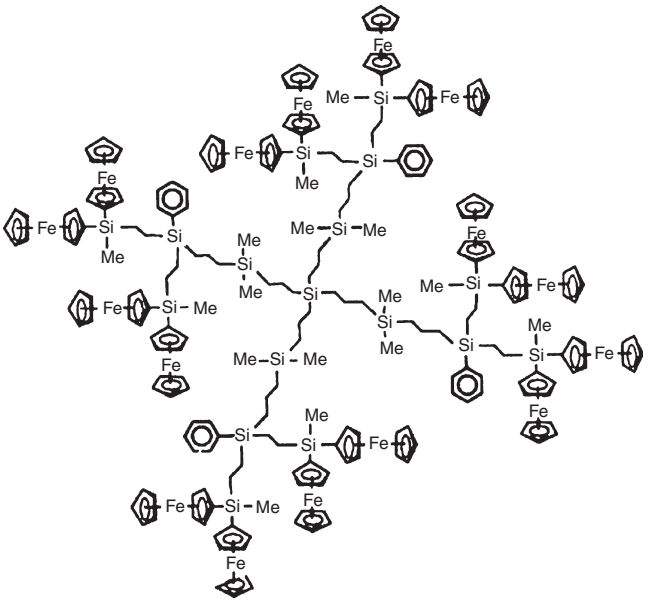

240

Another interesting class of ferrocene dendrimers **241** possesses electrochemical properties which can be tuned by *N*-methylation or protonation of the nitrogen sites. For example, a shift in *E* of 100–200 mV for the ferrocene groups is effected on protonation of the adjacent nitrogen centres.[547]

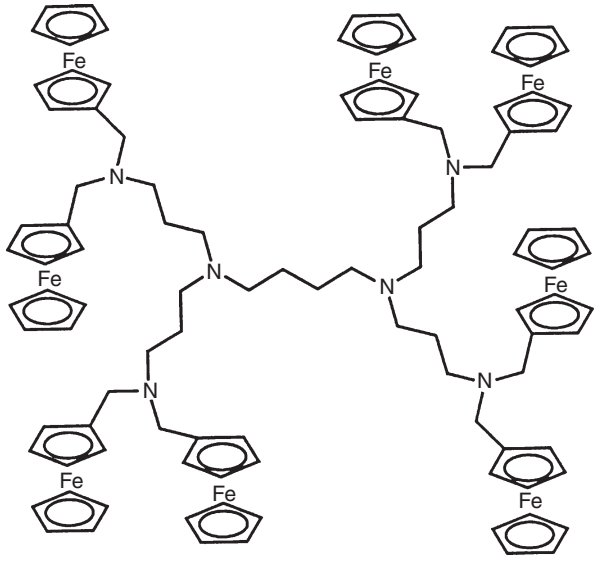

241

Ferrocene dendrimers are also of interest for reasons other than their redox activity. For example, metallodendrimer **242** possesses planar chiral ferrocene units that make the bidentate phosphine ligation sites of potential interest for applications in asymmetric catalysis. Indeed, asymmetric hydrogenations of dimethyl itaconate catalyzed by Rh complexes of **242** showed impressive ee values of 98%.[548]

Representative examples of other metallodendrimers with metal atoms at the surface are the ruthenium materials **243**[549–551] and the organometallic dendrimers **244**,[552] which possess peripheral cobalt clusters that were prepared by treatment of an alkyne-functionalized dendrimer precursor with $Co_2(CO)_8$ (Equation (88)). Dendrimers with 16 Au_2Ru_6 carbonyl clusters on the periphery have also been prepared and have been successfully imaged by high resolution TEM.[553]

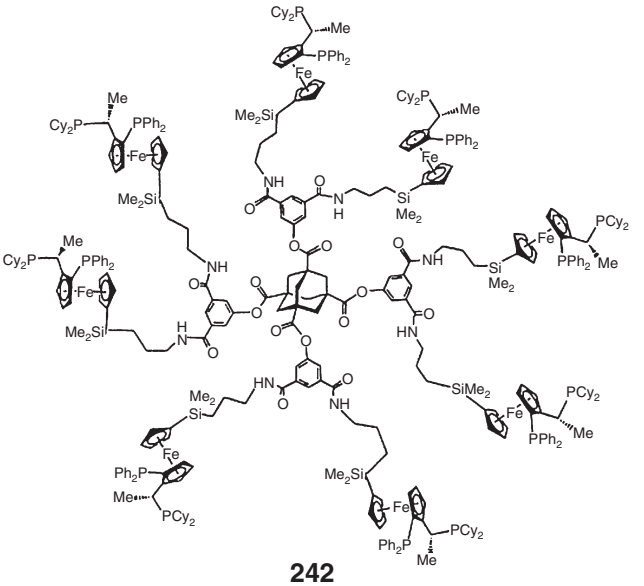

242

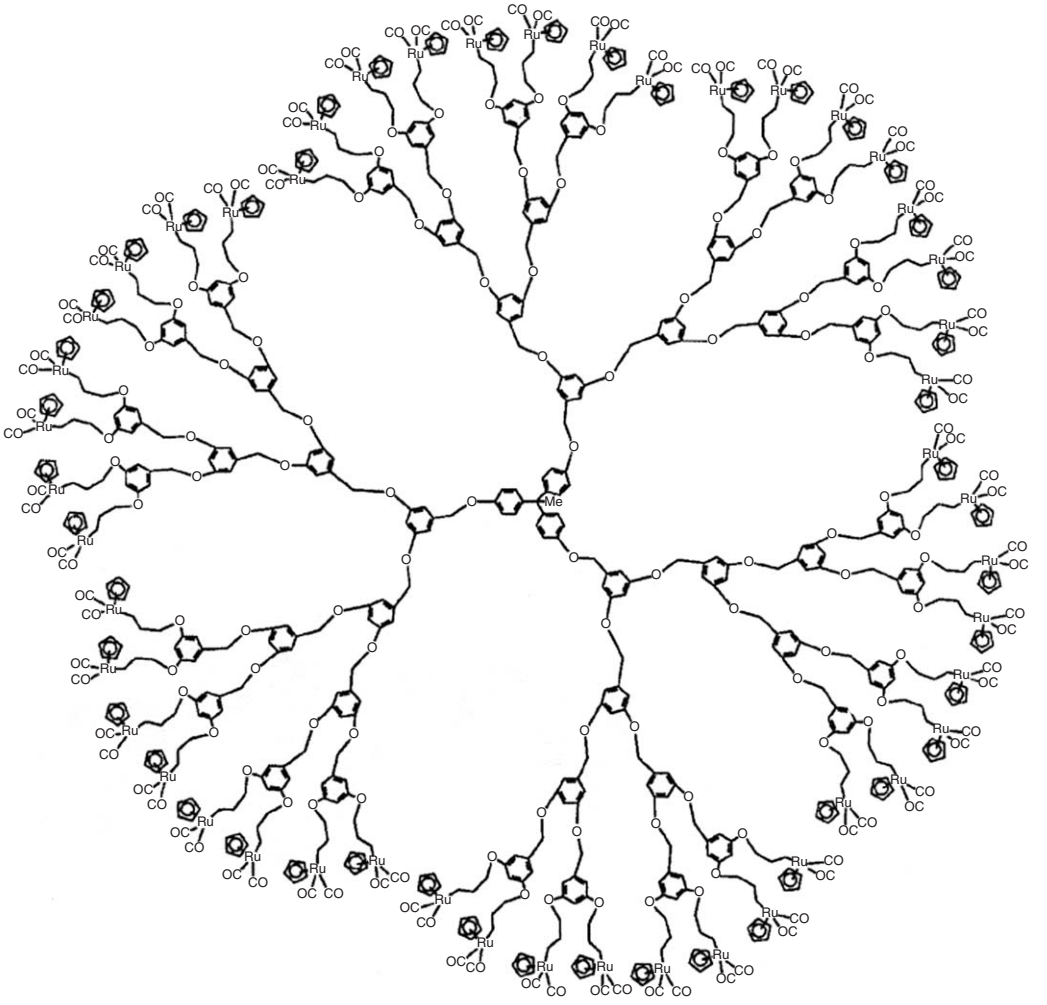

243

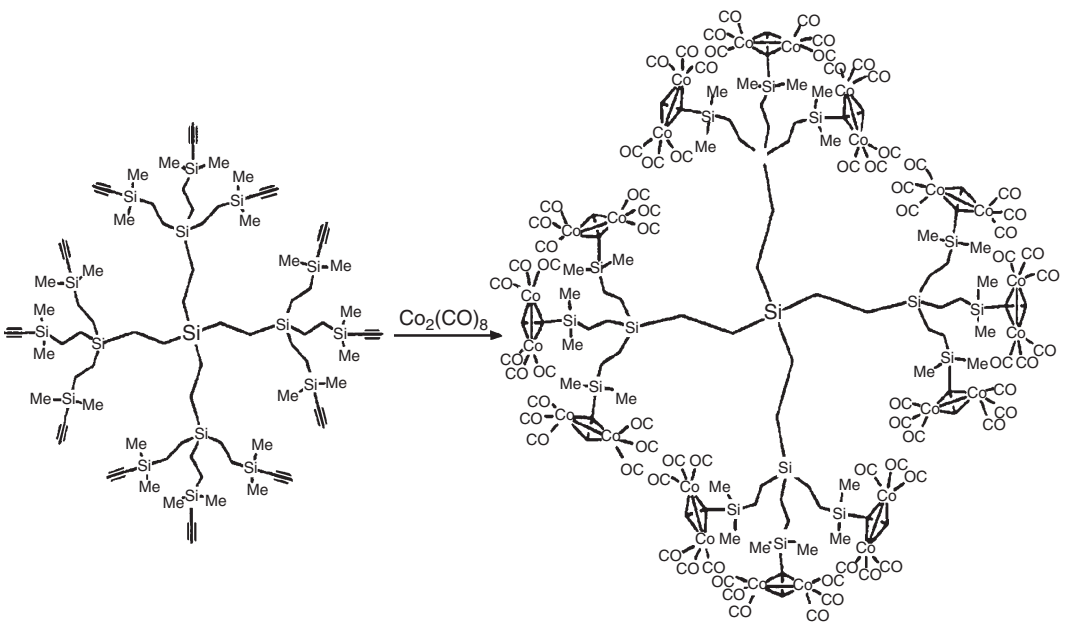

(88)

244

12.06.7.3 Metallodendrimers with Metals at Interior Sites

Metallodendrimers may also have metal-containing units placed within the interior of the structure in addition to, or instead of, in the core and at the periphery. Metal polypyridyl complexes have been particularly popular for the construction of metallodendrimers as a result of their ease of functionalization and the corresponding utilization of standard synthetic organic transformations.

Ferrocene units have also proved popular for the construction of dendrimers with metal atoms throughout the structure. An example of the materials prepared is the polyferrocene dendrimer **245**, which was synthesized by means of a hydrosilylation approach (Equation (89)).[554] Cyclic voltammetric studies of **245** showed that the central and surrounding ferrocene units oxidize reversibly but at different potentials. Cyclopentadienyliron arene cations also provide broad possibilities as cores for dendrimer contruction, and dendrimers with electrocatalytic functions have been reported.[555,555a,556]

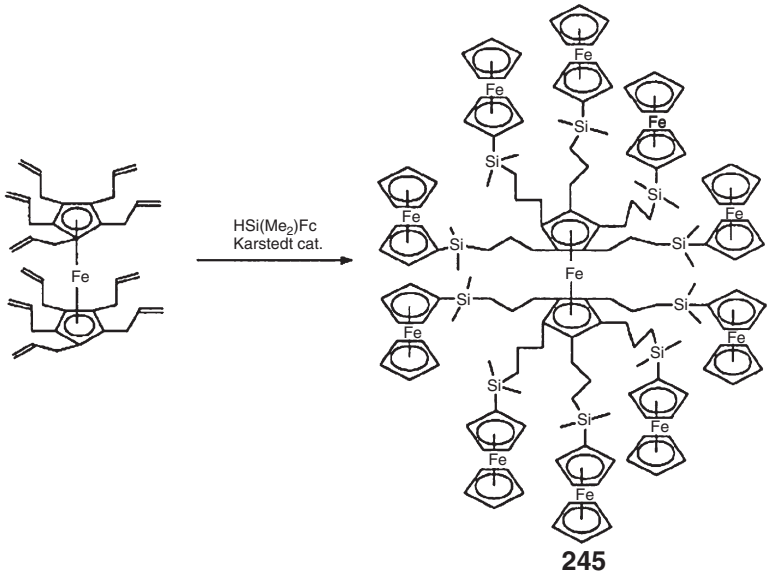

(89)

245

A variety of other strategies have been used to create metallodendritic architectures. Combinations of coordination chemistry and hydrogen bonding have allowed for the synthesis of remarkable "rosette-"type structures such as **246**

(Equation (90)).[557,558] Oxidative addition chemistry involving Pd(II) and Pt(II) centers and C–Br bonds has allowed for the convergent synthesis of novel metallodendrimers **247** (Equation (91)).[559–564] Metallodendrimers with $[Re_6Se_8]^{2+}$ units in the core and periphery have been prepared.[565] In another interesting development, Cu^{2+} ions can be coordinated to polyamidoamine dendrimers, and following reduction with aqueous hydrazine, dendrimer-stabilized metal colloids are formed.[566–568]

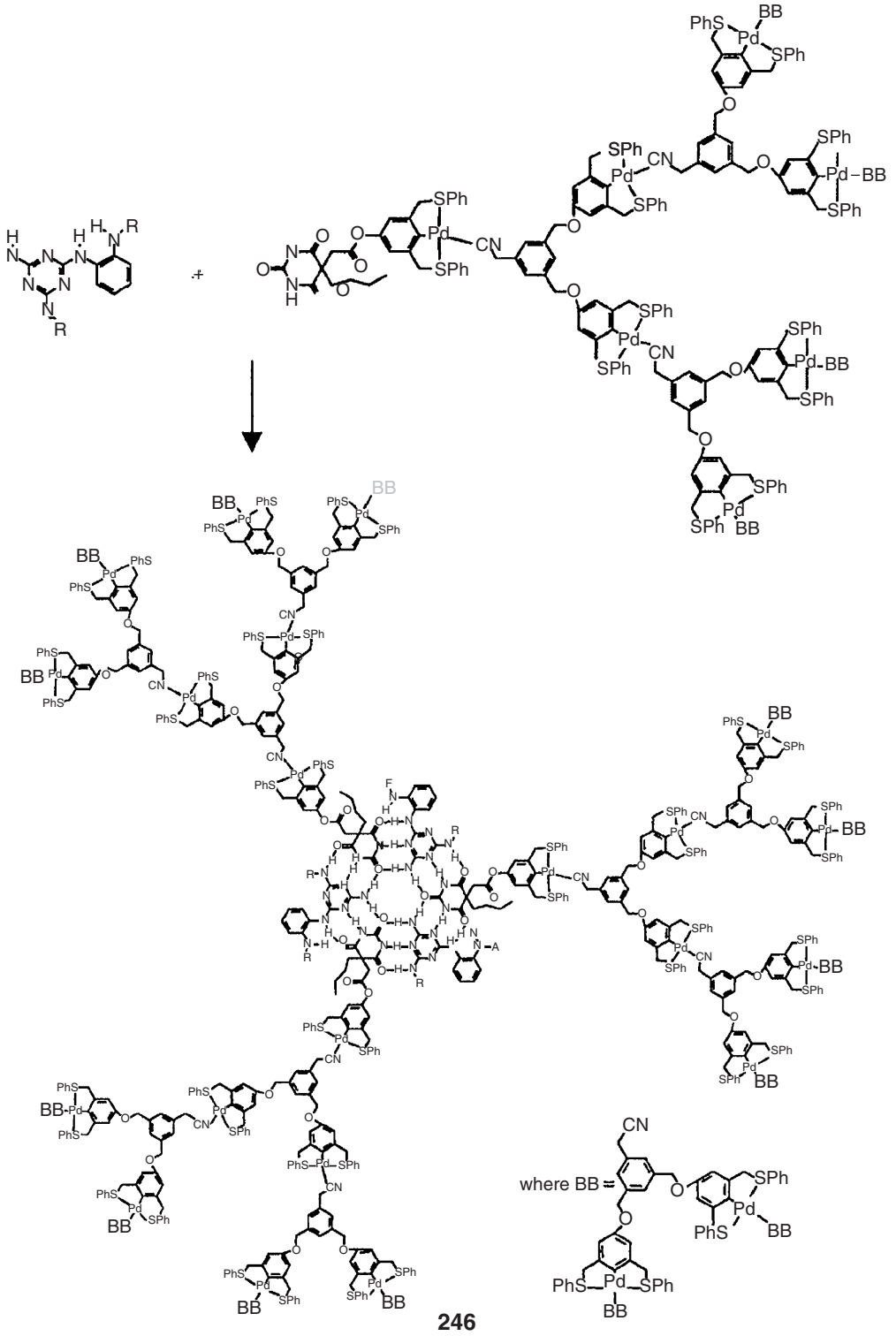

(90)

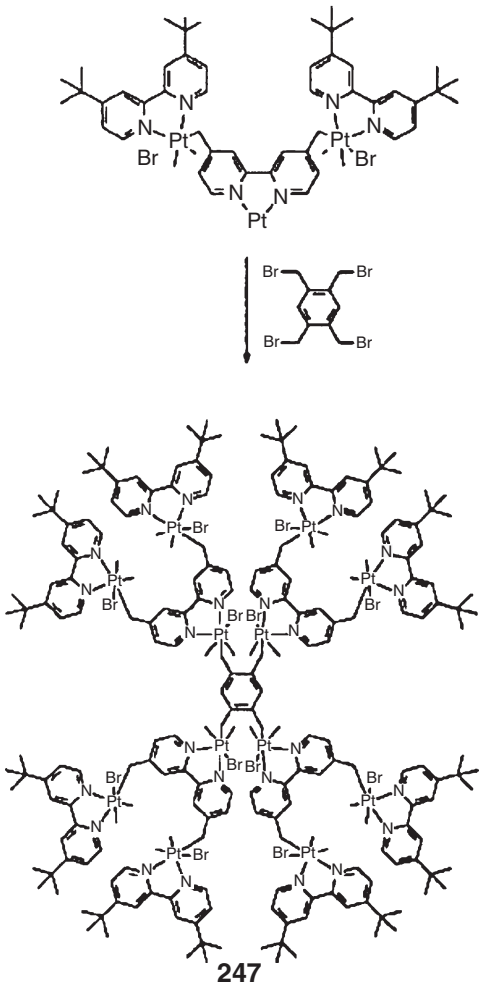

247 (91)

Platinum polyynes represent one of the most interesting and well-studied classes of linear metallopolymers. Dendritic analogs of these materials have been prepared via a variety of methodologies.[569–571] One example is the nonametallic dendrimer **248** that was prepared via a convergent route as illustrated in Equation (92).[569] Dendrimers based on ruthenium polyyne architectures have also been prepared and promising NLO properties have been identified.[572,573]

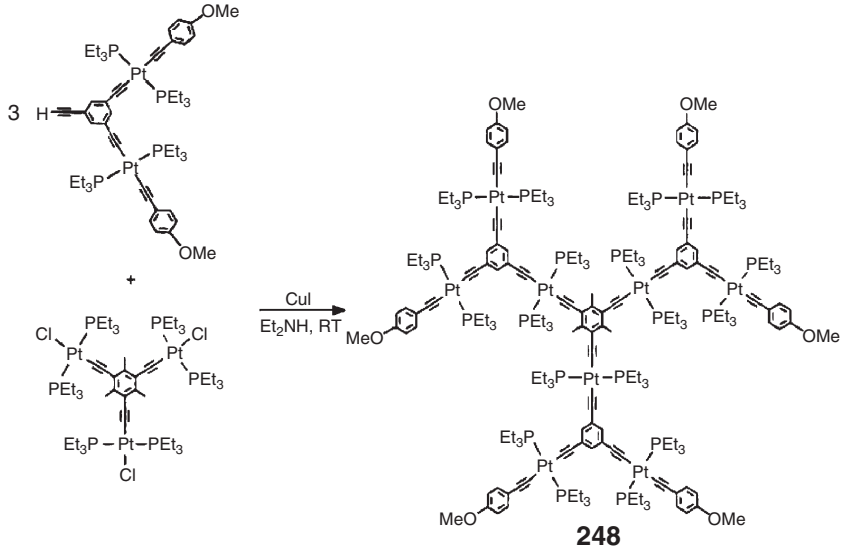

248 (92)

Incorporation of entities such as fullerenes into dendritic structures, in combination with metal centers, has begun to be explored as a method for the preparation of a range of exciting materials.[574,575] For example, remarkable dendrimers such as **249** with a C_{60} core and eight ferrocene units throughout the structure were prepared via a convergent synthetic approach. Dendrimer **249** was readily soluble in organic solvents, showed good thermal stability, and displayed a liquid crystalline smectic A phase under ambient temperature, which was identified by polarizing microscopy. The clearing temperature was found to be 157 °C.[575]

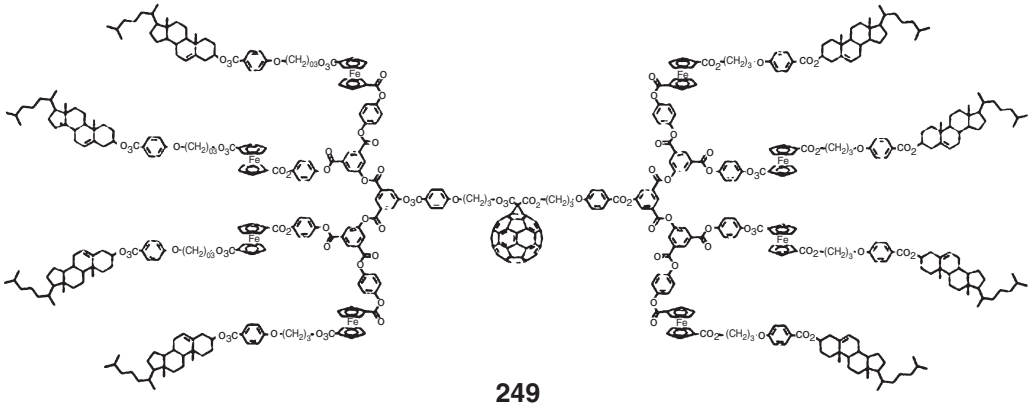

249

Abbreviations

E_g	band gap energy
K_c	comproportionation constant
M_n	number-average molecular weight
M_w	weight-average molecular weight
T_c	crystallization temperature
T_{cl}	clearing temperature
T_g	glass transition temperature
T_{lc}	melting temperature to give a mesophase
T_m	melting temperature
$\Delta E_{1/2}$	redox coupling
$[\eta]$	intrinsic viscosity
η_{sp}	specific viscosity
λ	wavelength
σ	electrical conductivity (in $S\,cm^{-1}$)

References

1. Manners, I. *Angew. Chem., Int. Ed.* **1996**, *35*, 1602.
2. Mark, J. E.; Allcock, H. R.; West, R. *Inorganic Polymers*; Prentice-Hall: Englewood Cliffs, 1992.
3. Clarson, S. J., Semlyen, J. A., Eds. *Siloxane Polymers*; Prentice-Hall: Englewood Cliffs, 1993.
4. Allcock, H. R. *Adv. Mater.* **1994**, *6*, 106.
5. Neilson, R. H.; Wisian-Neilson, P. *Chem. Rev.* **1988**, *88*, 541.
6. De Jaeger, R.; Gleria, M. *Prog. Polym. Sci.* **1998**, *23*, 179.
7. West, R. *J. Organomet. Chem.* **1986**, *300*, 327.
8. Miller, R. D.; Michl, J. *Chem. Rev.* **1989**, *89*, 1359.
9. Nguyen, P.; Gómez-Elipe, P.; Manners, I. *Chem. Rev.* **1999**, *99*, 1515.
10. Kingsborough, R. P.; Swager, T. M. *Prog. Inorg. Chem.* **1999**, *48*, 123.
11. Archer, R. D. *Inorganic and Organometallic Polymers*; Wiley-VCH: Weinheim, 2001.
12. Manners, I. *Science* **2001**, *294*, 1664.
13. Schubert, U. S.; Eschbaumer, C. *Angew. Chem., Int. Ed.* **2002**, *41*, 2892–2926.
14. Abd-El-Aziz, A. S. *Macromol. Rapid Commun.* **2002**, *23*, 995–1031.
15. Manners, I. *Synthetic Metal-containing Polymers*; Wiley-VCH: Weinheim, 2004.
16. Rosen, S. L. *Fundamental Principles of Polymeric Materials*; Wiley Interscience: New York, 1993.
17. Painter, P. C.; Coleman, M. M. *Principles of Polymer Science*, 2nd ed.; Technomic: Lancaster, 1997.

18. Sperling, L. H. *Introduction to Physical Polymer Science*; Wiley: New York, 2001.
19. Young, R. J.; Lovell, P. A. *Introduction to Polymers*, 2nd ed.; Chapman and Hall: New York, 1991.
20. Allcock, H. R.; Lampe, F. W. *Contemporary Polymer Chemistry*; Prentice-Hall: Englewood Cliffs, 1990.
21. Campbell, I. M. *Introduction to Synthetic Polymers*; Oxford University Press: New York, 2000.
22. Woodward, E. *Understanding Polymer Morphology*; Hanser: New York, 1995.
23. Cotton, F. A.; Wilkinson, G.; Murillo, C. A.; Bochman, M. *Advanced Inorganic Chemistry*, 6th ed.; Wiley Interscience: Toronto, 1999.
24. Baldus, H.-P.; Jansen, M. *Angew. Chem., Int. Ed.* **1997**, *36*, 328.
25. Bill, J.; Aldinger, F. *Adv. Mater.* **1995**, *7*, 775.
26. Segal, D. *Chemical Synthesis of Advanced Ceramic Materials*; Cambridge University Press: New York, 1991.
27. Peuckert, M.; Vaahs, T.; Brück, M. *Adv. Mater.* **1990**, *2*, 398.
28. Laine, R. M.; Babonneau, F. *Chem. Mater.* **1993**, *5*, 260.
29. Liu, Q.; Shi, W.; Babonneau, F.; Interrante, L. V. *Chem. Mater.* **1997**, *9*, 2434.
30. Leslie-Pelecky, D. L.; Rieke, R. D. *Chem. Mater.* **1996**, *8*, 1770.
31. Long, N. J. *Angew. Chem., Int. Ed.* **1995**, *34*, 21.

31a. Whittall, I. R.; McDonagh, A. M.; Humphrey, M. G.; Samoc, M. *Adv. Organomet. Chem.* **1998**, *42*, 291.

31b. Whittall, I. R.; McDonagh, A. M.; Humphrey, M. G.; Samoc, M. *Adv. Organomet. Chem.* **1998**, *43*, 349.

32. Crabtree, R. H. *The Organometallic Chemistry of the Transition Metals*, 3rd ed.; Wiley: New York, 2001.
33. Lippard, S. J.; Berg, J. M. *Principles of Bioinorganic Chemistry*; University Science Books: Mill Valley, 1994.
34. Antonietti, M.; Göltner, C. *Angew. Chem., Int. Ed.* **1997**, *36*, 910.

34a. Förster, S.; Antonietti, M. *Adv. Mater.* **1998**, *10*, 195.

35. Abdur-Rashid, K.; Gusev, D. G.; Landau, S. E.; Lough, A. J.; Morris, R. H. *J. Am. Chem. Soc.* **1998**, *120*, 11826.

35a. Crabtree, R. H.; Siegbahn, P. E. M.; Eisenstein, O.; Rheingold, A. L.; Koetzle, T. F. *Acc. Chem. Res.* **1996**, *29*, 348.

36. McArdle, C. P.; Vittal, J. J.; Puddephatt, R. J. *Angew. Chem., Int. Ed.* **2000**, *39*, 3819.
37. Bachman, R. E.; Fioritto, M. S.; Fetics, S. K.; Cocker, T. M. *J. Am. Chem. Soc.* **2001**, *123*, 5376.
38. Olmstead, M. M.; Jiang, F.; Attar, S.; Balch, A. L. *J. Am. Chem. Soc.* **2001**, *123*, 3260.
39. Zheng, H.; Lai, C. K.; Swager, T. M. *Chem. Mater.* **1995**, *7*, 2067.
40. Arimoto, F. S.; Haven, A. C. *J. Am. Chem. Soc.* **1955**, *77*, 6295.
41. Patterson, W. J.; McManus, S. P.; Pittman, C. U., Jr., *J. Polym. Sci., Polym. Chem.* **1974**, *12*, 837.
42. Neuse, E. W.; Bednarik, L. *Macromolecules* **1979**, *12*, 187.
43. Sonogashira, K.; Takahashi, S.; Hagihara, N. *Macromolecules* **1977**, *10*, 879.
44. Foucher, D. A.; Tang, B. Z.; Manners, I. *J. Am. Chem. Soc.* **1992**, *114*, 6246.
45. Brandt, P. F.; Rauchfuss, T. B. *J. Am. Chem. Soc.* **1992**, *114*, 1926.
46. Ni, Y. Z.; Rulkens, R.; Manners, I. *J. Am. Chem. Soc.* **1996**, *118*, 4102.
47. Sankaran, V.; Yue, J.; Cohen, R. E.; Schrock, R. R.; Silbey, R. J. *Chem. Mater.* **1993**, *5*, 1133.
48. Imori, T.; Lu, V.; Cai, H.; Tilley, T. D. *J. Am. Chem. Soc.* **1995**, *117*, 9931.
49. Newkome, G. R.; He, E.; Moorefield, C. N. *Chem. Rev.* **1999**, *99*, 1689.
50. Wilkinson, G. *J. Organomet. Chem.* **1975**, *100*, 273.
51. Togni, A.; Hayashi, T., Eds. *Ferrocenes*; VCH: New York, 1995.

51a. Long, N. J. *Metallocenes*; Blackwell: Oxford, 1998.

52. Bruce, D. W.; O'Hare, D., Eds. *Inorganic Materials*; Wiley: Toronto, 1992.
53. Neuse, E. W.; Rosenberg, H. *J. Macromol. Sci., Revs. Macromol. Chem.* **1970**, *C4*, 1.
54. Pittman, C. U., Jr.; Voges, R. L.; Elder, J. *Polym. Lett.* **1971**, *9*, 191.
55. Pittman, C. U., Jr. *J. Polym. Sci. Part A-1* **1971**, *9*, 3175.
56. Lai, J. C.; Rounsefell, T.; Pittman, C. U., Jr. *J. Polym. Sci. Part A-1* **1971**, *9*, 651.
57. Sasaki, Y.; Walker, L. L.; Hurst, E. L.; Pittman, C. U., Jr. *J. Polym. Sci., Polym. Chem. Ed.* **1973**, *11*, 1213.
58. George, M. H.; Hayes, G. F. *J. Polym. Sci., Polym. Chem. Ed.* **1975**, *13*, 1049.
59. George, M. H.; Hayes, G. F. *J. Polym. Sci., Polym. Chem. Ed.* **1976**, *14*, 475.
60. Pittman, C. U., Jr.; Lai, J. C.; Vanderpool, D. P.; Good, M.; Prados, R. *Macromolecules* **1970**, *3*, 746.
61. Aso, C.; Kunitake, T.; Nakashima, T. *Makromol. Chem.* **1969**, *124*, 232.
62. Nuyken, O.; Burkhardt, V.; Pöhlmann, T.; Herberhold, M. *Makromol. Chem., Macromol. Symp.* **1991**, *44*, 195.

62a. Nuyken, O.; Burkhardt, V.; Hübsch, C. *Macromol. Chem. Phys.* **1997**, *198*, 3353.

62b. Nuyken, O.; Burkhardt, V.; Pöhlmann, T.; Herberhold, M.; Litterest, F. J.; Hübsch, C. In *Macromolecular Systems: Microscopic Interactions and Macroscopic Properties*; Hoffmann, H., Schwoerer, M., Vogtmann, T., Eds.; Wiley: Weinheim, 2000; pp 305–324.

63. Swarup, S.; Nigam, A. N. *Polym. Commun.* **1989**, *30*, 190.
64. Smith, T. W.; Kuder, J. E.; Wychick, D. *J. Polym. Sci., Polym. Chem. Ed.* **1976**, *14*, 2433.
65. Flanagan, J. B.; Margel, S.; Bard, A. J.; Anson, F. C. *J. Am. Chem. Soc.* **1978**, *100*, 4248.

65a. Diaz, A.; Seymour, M.; Pannell, K. H.; Rozell, J. M. *J. Electrochem. Soc.* **1990**, *137*, 503.

66. Cowan, D. O.; Park, J.; Pittman, C. U., Jr.; Sasaki, Y.; Mukherjee, T. K.; Diamond, N. A. *J. Am. Chem. Soc.* **1972**, *94*, 5110.
67. Pittman, C. U., Jr.; Surynarayanan, B.; Sasaki, Y. In *Inorganic Compounds with Unusual Properties*; Advances in Chemistry Series; 1976; Vol. 150, p 46.
68. Cowan, D. O.; Kaufman, F. *J. Am. Chem. Soc.* **1970**, *92*, 219.
69. Cowan, D. O.; Kaufman, F. *J. Am. Chem. Soc.* **1970**, *92*, 6198.
70. Pittman, C. U., Jr.; Lai, J. C.; Vanderpool, D. P.; Good, M.; Prados, R. In *Polymer Characterization: Interdisciplinary Approaches*; Craver, C. D., Ed.; Plenum: New York, 1971; pp 97–124.
71. Kittlesen, G. P.; White, H. S.; Wrighton, M. S. *J. Am. Chem. Soc.* **1985**, *107*, 7373.
72. Green, M. L. H.; Marder, S. R.; Thompson, M. E.; Bandy, J. A.; Bloor, D.; Kolinsky, P. V.; Jones, R. J. *Nature* **1987**, *330*, 360.
73. Wright, M. E.; Toplikar, E. G.; Kubin, R. F.; Seltzer, M. D. *Macromolecules* **1992**, *25*, 1838.
74. Yang, Y.; Xie, Z.; Wu, C. *Macromolecules* **2002**, *35*, 3426.
75. Albagli, D.; Bazan, G.; Wrighton, M. S.; Schrock, R. R. *J. Am. Chem. Soc.* **1992**, *114*, 4150.
76. Albagli, D.; Bazan, G. C.; Schrock, R. R.; Wrighton, M. S. *J. Phys. Chem.* **1993**, *97*, 10211.

77. Nakashima, T.; Kunitake, T. *Makromol. Chem.* **1972**, *157*, 73.
78. Pittman, C. U., Jr.; Sasaki, Y.; Grube, P. L. *J. Macromol. Sci., Chem.* **1974**, *A8(5)*, 923.
79. Simionescu, C.; Lixandru, T.; Negulescu, I.; Mazilu, I.; Tataru, L. *Makromol. Chem.* **1973**, *163*, 59.
80. Simionescu, C.; Lixandru, T.; Mazilu, I.; Tataru, L. *Makromol. Chem.* **1971**, *147*, 69.
81. Buchmeiser, M.; Schrock, R. R. *Macromolecules* **1995**, *28*, 6642.
82. Zotti, G.; Zecchin, S.; Schiavon, G.; Berlin, A.; Pagani, G.; Canavesi, A. *Chem. Mater.* **1995**, 7, 2309.
83. Weisemann, A.; Zentel, R.; Lieser, G. *Acta Polym.* **1995**, *46*, 25.
84. Wilbert, G.; Traud, S.; Zentel, R. *Macromol. Chem. Phys.* **1997**, *198*, 3769.
84a. For related work see: Turpin, F.; Guillon, D.; Deschenaux, R. *Mol. Cryst. Liq. Cryst.* **2001**, *362*, 171.
85. Caldwell, G.; Meirim, M. G.; Neuse, E. W.; van Rensburg, C. E. J. *Appl. Organomet. Chem.* **1998**, *12*, 793.
86. Hodak, J.; Etchenique, R.; Calvo, E. J.; Singhal, K.; Bartlett, P. N. *Langmuir* **1997**, *13*, 2708.
87. Wang, C.-L.; Mulcandani, A. *Anal. Chem.* **1995**, *67*, 1109.
88. Hou, S.-F.; Fang, H.-Q.; Chen, H.-Y. *Anal. Lett.* **1997**, *30*, 1631.
89. Sheats, J. E.; Hessel, F.; Tsarouhas, L.; Podejko, K. G.; Porter, T.; Kool, L. B.; Nolan, R. L. Jr. In *Metal-containing Polymer Systems*; Sheats, J. E., Carraher, C. E., Jr., Pittman, C. U.; Jr., Eds.; Plenum: New York, 1985; pp 83–98.
90. Willis, C. T.; Sheats, J. E. *J. Polym. Sci., Polym. Chem.* **1984**, *22*, 1077.
91. Grubbs, R. H.; Gibbons, G.; Kroll, L. C.; Bonds, W. D.; Brubaker, C. H. *J. Am. Chem. Soc.* **1973**, *95*, 2373.
92. Bonds, W. D.; Brubaker, C. H.; Chandrasekaran, E. S.; Gibbons, C.; Grubbs, R. H.; Kroll, L. C. *J. Am. Chem. Soc.* **1975**, *97*, 2128.
93. Grubbs, R. H.; Lau, C. P.; Cukier, R.; Brubaker, C. H. *J. Am. Chem. Soc.* **1977**, *99*, 4517.
94. Barrett, A. G. M.; de Miguel, Y. R. *Chem. Commun.* **1998**, 2079.
95. Roscoe, S. B.; Fréchet, J. M. J.; Walzer, J. F.; Dias, A. J. *Science* **1998**, *280*, 270.
96. Allcock, H. R.; Lavin, K. D.; Riding, G. H. *Macromolecules* **1985**, *18*, 1340.
97. Allcock, H. R.; Riding, G. H.; Lavin, K. D. *Macromolecules* **1987**, *20*, 6.
98. Manners, I.; Riding, G. H.; Dodge, J. A.; Allcock, H. R. *J. Am. Chem. Soc.* **1989**, *111*, 3067.
99. Allcock, H. R.; Dodge, J. A.; Manners, I.; Riding, G. H. *J. Am. Chem. Soc.* **1991**, *113*, 9596.
100. Allcock, H. R.; Dodge, J. A.; Manners, I.; Parvez, M.; Riding, G. H.; Visscher, K. B. *Organometallics* **1991**, *10*, 3098.
101. Saraceno, R. A.; Riding, G. H.; Allcock, H. R.; Ewing, A. G. *J. Am. Chem. Soc.* **1988**, *110*, 7254.
102. Wisian-Neilson, P.; Ford, R. R. *Macromolecules* **1989**, *22*, 72.
103. Wisian-Neilson, P.; Zhang, C. P.; Koch, K. A. *Macromolecules* **1998**, *31*, 1808.
104. Pannell, K. H.; Rozell, J. M.; Ziegler, J. M. *Macromolecules* **1988**, *21*, 276.
105. Hale, P. D.; Boguslavsky, L. I.; Inagaki, T.; Karan, H. I.; Lee, H. S.; Skotheim, T. A. *Anal. Chem.* **1991**, *63*, 677.
106. Deschenaux, R.; Jauslin, I.; Scholten, U.; Turpin, F.; Guillon, D.; Heinrich, B. *Macromolecules* **1998**, *31*, 5647.
107. Arai, T.; Ban, H. T.; Uozumi, T.; Soga, K. *J. Polym. Sci., Polym. Chem.* **1998**, *36*, 421.
108. Peckham, T. J.; Nguyen, P.; Bourke, S. C.; Wang, Q.; Harrison, D. G.; Zoricak, P.; Russell, C.; Liable-Sands, L. M.; Rheingold, A.; Lough, A. J., *et al. Organometallics* **2001**, *20*, 3035.
109. Pittman, C. U., Jr.; Lin, C.-C.; Rounsefell, T. D. *Macromolecules* **1978**, *11*, 1022.
110. Nishide, H.; Kawakami, H.; Kurimura, Y.; Tsuchida, E. *J. Am. Chem. Soc.* **1989**, *111*, 7175.
111. McCormick, F. B.; Wright, B. B.; Williams J. W. In *Metal-containing Polymeric Materials*; Pittman, C. U., Jr., Carraher, C. E., Jr., Zeldin, M., Sheats, J. E., Culbertson, B. M., Eds.; Plenum: New York, 1996; p 177.
112. Pittman, C. U., Jr.; Grube, P. L.; Ayers, O. E.; McManus, S. P.; Rausch, M. D.; Moser, G. A. *J. Polymer. Sci. Part A-1* **1972**, *10*, 379.
113. Pittman, C. U., Jr.; Carraher, C. E., Jr.; Reynolds, J. R. In *Encyclopedia of Polymer Science and Engineering*; Kroschwitz, J. I., Ed.; Wiley Interscience: New York, 1987; Vol. 10, pp 564–578.
114. Fujita, N.; Sonogashira, K. *J. Polym. Sci., Polym. Chem.* **1974**, *12*, 2845.
115. Bellama, J. M.; Manders, W. F. In *Inorganic and Organometallic Polymers*; Zeldin, M., Wynne, K. J., Allcock, H. R., Eds.; ACS Symposium Series; American Chemical Society: Washington, DC, 1988; Vol. 360, p 483.
116. Moraru, B.; Hüsing, N.; Kickelbick, G.; Schubert, U.; Frazl, P.; Peterlik, H. *Chem. Mater.* **2002**, *14*, 2732.
117. Allcock, H. R.; Allen, R. W.; O'Brien, J. P. *J. Am. Chem. Soc.* **1977**, *99*, 3984.
118. Abd-El-Aziz, A. S.; May, L. J.; Hurd, J. A.; Okasha, R. M. *J. Polym. Sci. A Polym. Chem.* **2001**, *39*, 2716.
119. Hodge, P. *Chem. Soc. Rev.* **1997**, *26*, 417.
119a. Pittman, C. U., Jr. In *Comprehensive Organometallic Chemistry I*; Wilkinson, G., Stone, F. G. A., Abel, E. W., Eds.; Pergamon: Oxford, 1982; Vol. 8, p 553.
119b. Gates, B. C.; Lieto, J. In *Encyclopedia of Polymer Science and Engineering;* Kroschwitz, J. I., Ed.; 1985; Vol. 2, p 708.
119c. Pomogailo, A. D. *Catalysis by Polymer-immobilized Metal Complexes*; Gordon and Breach, 1998.
120. Cummins, C. C.; Beachy, M. D.; Schrock, R. R.; Vale, M. G.; Sankaran, V.; Cohen, R. E. *Chem. Mater.* **1991**, *3*, 1153.
121. Chan, Y. N. C.; Craig, G. S. W.; Schrock, R. R.; Cohen, R. E. *Chem. Mater.* **1992**, *4*, 885.
122. Bronstein, L. D.; Seregina, M. V.; Platonova, O. A.; Kabachii, Y. A.; Chernyshov, D. M.; Ezernitskaya, M. G.; Dubrovina, L. V.; Braginba, T. P.; Valetsky, P. M. *Macromol. Chem. Phys.* **1998**, *199*, 1357.
123. Long, N. J. *Metallocenes: An Introduction to Sandwich Complexes*; Blackwell: Oxford, 1998.
124. Togni, A. In *Ferrocenes*; Togni, A., Hayashi, T., Eds.; VCH: New York, 1995; pp 433–469.
125. Barlow, S.; O'Hare, D. *Chem. Rev.* **1997**, *97*, 637.
126. Kramer, J. A.; Hendrickson, D. N. *Inorg. Chem.* **1980**, *19*, 3330.
127. Deschenaux, R.; Goodby, J. W. In *Ferrocenes*; Togni, A., Hayashi, T., Eds.; VCH: New York, 1995; pp 471–495.
128. For an overview see: Manners, I. *Chem. Br.* **1996**, *32*, 46.
129. For interesting work on metallocene oligomers based on V, Cr, Co, and Ni, see: Atzkern, H.; Bergerat, P.; Beruda, H.; Fritz, M.; Hiermeier, J.; Hudeczek, P.; Kahn, O.; Köhler, F. H.; Paul, M.; Weber, B. *J. Am. Chem. Soc.* **1995**, *117*, 997.
130. Neuse, E. W.; Rosenberg, H. *J. Macromol. Sci., Revs. Macromol. Chem.* **1970**, *C4*, 130.
131. Sanechika, K.; Yamamoto, T.; Yamamoto, A. *Polym. J.* **1981**, *13*, 255.
132. Yamamoto, T.; Sanechika, K.; Yamamoto, A.; Katada, M.; Motoyama, I.; Sano, H. *Inorg. Chim. Acta* **1983**, *73*, 75.
133. Meier, H. *Organic Semiconductors*; Verlag Chemie: Weinheim, 1974.
134. Oyama, N.; Takizawa, Y.; Matsuda, H.; Yamamoto, T.; Sanechika, K. *Denki Kagaku oyubi Kogyo Butsuri Kagaku* **1988**, *56*, 781.

135. Seki, K.; Tanaka, H.; Ohta, T.; Sanechika, K.; Yamamoto, T. *Chem. Phys. Lett.* **1991**, *178*, 311.
135a. For theoretical calculations see: Böhm, M. C. *J. Chem. Phys.* **1984**, *80*, 2704.
136. Hirao, T.; Kurashina, M.; Aramaki, K.; Nishihara, H. *Dalton Trans.* **1996**, 2929.
136a. Nishihara, H.; Hirao, T.; Aramaki, K.; Aoki, K. *Synth. Met.* **1997**, *84*, 935.
137. Park, P.; Lough, A. J.; Foucher, D. A. *Macromolecules* **2002**, *35*, 3810.
138. Neuse, E. W. *J. Macromol. Sci., Chem.* **1981**, *A16*, 3.
139. Neuse, E. W.; Chris, G. J. *J. Macromol. Sci., Chem.* **1967**, *A1*, 371.
140. Pittman, C. U., Jr. *J. Polym. Sci., Polym. Chem. Ed.* **1967**, *5*, 2927.
141. Withers, H. P., Jr.; Seyferth, D.; Fellmann, J. D.; Garrou, P. E.; Martin, S. *Organometallics* **1982**, *1*, 1283.
142. Honeyman, C. H.; Peckham, T. J.; Massey, J. A.; Manners, I. *J. Chem. Soc., Chem. Commun.* **1996**, 2589.
143. Fellmann, J. D.; Garrou, P. E.; Withers, H. P.; Seyferth, D.; Traficante, D. D. *Organometallics* **1983**, *2*, 818.
144. Rosenberg, H.; Rausch, M. D. U.S. Patent 3060215, 1962.
145. Rosenberg, H. U.S. Patent 3426053, 1969.
146. Park, J.; Seo, Y.; Cho, S.; Whang, D.; Kim, K.; Chang, T. *J. Organomet. Chem.* **1995**, *489*, 23.
147. Osborne, A. G.; Whiteley, R. H.; Meads, R. E. *J. Organomet. Chem.* **1980**, *193*, 345.
148. Seyferth, D.; Withers, H. P. *Organometallics* **1982**, *1*, 1275.
149. Itoh, T.; Saitoh, H.; Iwatsuki, S. *J. Polym. Sci., Polym. Chem.* **1995**, *33*, 1589.
150. Plenio, H.; Hermann, J.; Leukel, J. *Eur. J. Inorg. Chem.* **1998**, 2063.
151. Plenio, H.; Hermann, J.; Sehring, A. *Chem. Eur. J.* **2000**, *6*, 1820.
152. Herberhold, M.; Brendel, H. D.; Nuyken, O.; Pöhlmann, T. *J. Organomet. Chem.* **1991**, *413*, 65.
153. Nuyken, O.; Pöhlmann, T.; Herberhold, M. *Macromol. Rep.* **1992**, *A29*, 211.
154. Brandt, P. F.; Rauchfuss, T. B. *J. Am. Chem. Soc.* **1992**, *114*, 1926.
155. Foucher, D. A.; Tang, B. Z.; Manners, I. *J. Am. Chem. Soc.* **1992**, *114*, 6246.
156. Osborne, A. G.; Whiteley, R. H. *J. Organomet. Chem.* **1975**, *101*, C27.
156a. Herberhold, M. *Angew. Chem., Int. Ed. Engl.* **1995**, *34*, 1837.
157. Fischer, A. B.; Kinney, J. B.; Staley, R. H.; Wrighton, M. S. *J. Am. Chem. Soc.* **1979**, *101*, 6501.
158. Finckh, W.; Tang, B. Z.; Foucher, D. A.; Zamble, D. B.; Ziembinski, R.; Lough, A.; Manners, I. *Organometallics* **1993**, *12*, 823.
159. Manners, I. *Adv. Organomet. Chem.* **1995**, *37*, 131.
160. Review: Kulbaba, K.; Manners, I. *Macromol. Rapid Commun.* **2001**, *22*, 711.
161. MacLachlan, M. J.; Lough, A. J.; Manners, I. *Macromolecules* **1996**, *29*, 8562.
162. Nguyen, P.; Stojcevic, G.; Kulbaba, K.; MacLachlan, M. J.; Liu, X.-H.; Lough, A. J.; Manners, I. *Macromolecules* **1998**, *31*, 5977.
163. Pudelski, J. K.; Manners, I. *J. Am. Chem. Soc.* **1995**, *117*, 7265.
164. Jäkle, F.; Rulkens, R.; Zech, G.; Massey, J. A.; Manners, I. *J. Am. Chem. Soc.* **2000**, *122*, 4231.
165. Foucher, D. A.; Edwards, M.; Burrow, R. A.; Lough, A. J.; Manners, I. *Organometallics* **1994**, *13*, 4959.
166. Honeyman, C. H.; Foucher, D. A.; Dahmen, F. Y.; Rulkens, R.; Lough, A. J.; Manners, I. *Organometallics* **1995**, *14*, 5503.
167. Rulkens, R.; Gates, D. P.; Balaishis, D.; Pudelski, J. K.; McIntosh, D. F.; Lough, A. J.; Manners, I. *J. Am. Chem. Soc.* **1997**, *119*, 10976.
168. Berenbaum, A.; Braunschweig, H.; Dirk, R.; Englert, U.; Green, J. C.; Jäkle, F.; Lough, A. J.; Manners, I. *J. Am. Chem. Soc.* **2000**, *122*, 5765.
169. Jäkle, F.; Rulkens, R.; Zech, G.; Foucher, D. A.; Lough, A. J.; Manners, I. *Chem. Eur. J.* **1998**, *4*, 2117.
170. Nelson, J. M.; Rengel, H.; Manners, I. *J. Am. Chem. Soc.* **1993**, *115*, 7035.
171. Nelson, J. M.; Lough, A. J.; Manners, I. *Angew. Chem., Int. Ed. Engl.* **1994**, *33*, 989.
172. Resendes, R.; Nelson, J. M.; Fischer, A.; Jäkle, F.; Bartole, A.; Lough, A. J.; Manners, I. *J. Am. Chem. Soc.* **2001**, *123*, 2116.
173. Rulkens, R.; Resendes, R.; Verma, A.; Manners, I.; Murti, K.; Fossum, E.; Miller, P.; Matyjaszewski, K. *Macromolecules* **1997**, *30*, 8165.
174. Pudelski, J. K.; Rulkens, R.; Foucher, D. A.; Lough, A. J.; Macdonald, P. M.; Manners, I. *Macromolecules* **1995**, *28*, 7301.
175. Hultzsch, K. C.; Nelson, J. M.; Lough, A. J.; Manners, I. *Organometallics* **1995**, *14*, 5496.
176. Rulkens, R.; Lough, A. J.; Manners, I. *J. Am. Chem. Soc.* **1994**, *116*, 797.
176a. Rulkens, R.; Ni, Y. Z.; Manners, I. *J. Am. Chem. Soc.* **1994**, *116*, 12121.
177. Temple, K.; Massey, J. A.; Chen, Z.; Vaidya, N.; Berenbaum, A.; Foster, M. D.; Manners, I. *J. Inorg. Organomet. Polym.* **1999**, *9*, 189.
178. Manners, I. *Polyhedron* **1996**, *15*, 4311.
179. Pannell, K. H.; Sharma, H. K. *Organometallics* **1997**, *16*, 3077.
180. Ni, Y. Z.; Rulkens, R.; Pudelski, J. K.; Manners, I. *Macromol. Rapid Commun.* **1995**, *16*, 637.
181. Reddy, N. P.; Yamashita, H.; Tanaka, M. *J. Chem. Soc., Chem. Commun.* **1995**, 2263.
182. Peckham, T. J.; Massey, J. A.; Edwards, M.; Manners, I.; Foucher, D. A. *Macromolecules* **1996**, *29*, 2396.
183. Gómez-Elipe, P.; Resendes, R.; Macdonald, P. M.; Manners, I. *J. Am. Chem. Soc.* **1998**, *120*, 8348.
184. Zechel, D. L.; Hultzsch, K. C.; Rulkens, R.; Balaishis, D.; Ni, Y. Z.; Pudelski, J. K.; Lough, A. J.; Manners, I.; Foucher, D. A. *Organometallics* **1996**, *15*, 1972.
185. Resendes, R.; Massey, J.; Dorn, H.; Winnik, M. A.; Manners, I. *Macromolecules* **2000**, *33*, 8.
186. Power-Billard, K. N.; Manners, I. *Macromol. Rapid Commun.* **2002**, *23*, 607.
187. Temple, K.; Jäkle, F.; Sheridan, J. B.; Manners, I. *J. Am. Chem. Soc.* **2001**, *123*, 1355.
188. Mochida, K.; Shibayama, N.; Goto, M. *Chem. Lett.* **1998**, 339.
189. Baumgartner, T.; Jäkle, F.; Rulkens, R.; Zech, G.; Lough, A. J.; Manners, I. *J. Am. Chem. Soc.* **2002**, *124*, 10062.
190. Mizuta, T.; Onishi, M.; Miyoshi, K. *Organometallics* **2000**, *19*, 5005.
191. Rasburn, J.; Foucher, D. A.; Reynolds, W. F.; Manners, I.; Vancso, G. J. *Chem. Commun.* **1998**, 843.
192. Massey, J. A.; Kulbaba, K.; Winnik, M. A.; Manners, I. *J. Polym. Sci., Polym. Phys.* **2000**, *28*, 3032.
193. Lammertink, R. G. H.; Hempenius, M. A.; Manners, I.; Vancso, G. J. *Macromolecules* **1998**, *31*, 795.
194. Chen, Z.; Foster, M. D.; Zhou, W.; Fong, H.; Reneker, D. H.; Resendes, R.; Manners, I. *Macromolecules* **2001**, *34*, 6156.
195. Rulkens, R.; Lough, A. J.; Manners, I.; Lovelace, S. R.; Grant, C.; Geiger, W. E. *J. Am. Chem. Soc.* **1996**, *118*, 12683.
195a. Nishihara, H. *Adv. Inorg. Chem.* **2002**, *53*, 41.
196. Barlow, S.; Rohl, A. L.; Shi, S.; Freeman, C. M.; O'Hare, D. *J. Am. Chem. Soc.* **1996**, *118*, 7578.
197. Papkov, V. S.; Gerasimov, M. V.; Dubovik, I. I.; Sharma, S.; Dementiev, V. V.; Pannell, K. H. *Macromolecules* **2000**, *33*, 7107.
198. Liu, X.-H.; Bruce, D. W.; Manners, I. *J. Chem. Soc., Chem. Commun.* **1997**, 289.

198a. Liu, X.-H.; Bruce, D. W.; Manners, I. *J. Organomet. Chem.* **1997**, *548*, 49.
199. Medina, J. C.; Li, C.; Bott, S. G.; Atwood, J. L.; Gokel, G. W. *J. Am. Chem. Soc.* **1991**, *113*, 366.
200. Kulbaba, K.; Manners, I.; Macdonald, P. M. *Macromolecules* **2002**, *35*, 10014.
201. Foucher, D. A.; Honeyman, C. H.; Nelson, J. M.; Tang, B. Z.; Manners, I. *Angew. Chem., Int. Ed. Engl.* **1993**, *32*, 1709.
202. Nguyen, M. T.; Diaz, A. F.; Dement'ev, V. V.; Pannell, K. H. *Chem. Mater.* **1993**, *5*, 1389.
203. Foucher, D. A.; Ziembinski, R.; Rulkens, R.; Nelson, J. M.; Manners, I. In *Inorganic and Organometallic Polymers II: Advanced Materials and Intermediates*; Wisian-Neilson, P., Allcock, H. R., Wynne, K. J., Eds.; ACS Symposium Series 572; American Chemical Society: Washington, DC, 1994, p 442.
204. Espada, L.; Pannell, K. H.; Papkov, V.; Leites, L.; Bukalov, S.; Suzdalev, I.; Tanaka, M.; Hayashi, T. *Organometallics* **2002**, *21*, 3758.
205. Southard, G. E.; Curtis, M. D. *Organometallics* **2001**, *20*, 508.
206. Nguyen, M. T.; Diaz, A. F.; Dement′ev, V. V.; Pannell, K. H. *Chem. Mater.* **1994**, *6*, 952.
207. Bakueva, L.; Sargent, E. H.; Resendes, R.; Bartole, A.; Manners, I. *J. Mater. Sci., Mater. Electron.* **2001**, *12*, 21.
208. Resendes, R.; Berenbaum, A.; Stojevic, G.; Jäkle, F.; Bartole, A.; Zamanian, F.; Dubois, G.; Hersom, C.; Balmain, K.; Manners, I. *Adv. Mater.* **2000**, *12*, 327.
209. Hmyene, M.; Yassar, A.; Escorne, M.; Percheron-Guegan, A.; Garnier, F. *Adv. Mater.* **1994**, *6*, 564.
210. Pudelski, J. K.; Foucher, D. A.; Honeyman, C. H.; Macdonald, P. M.; Manners, I.; Barlow, S.; O'Hare, D. *Macromolecules* **1996**, *29*, 1894.
211. Cyr, P.; Tzolov, M.; Manners, I.; Sargent, E. H. *Macromol. Chem. Phys.* **2003**, *204*, 915.
212. Kulbaba, K.; MacLachlan, M. J.; Evans, C. E. B.; Manners, I. *Macromol. Chem. Phys.* **2001**, *202*, 1768.
213. Arsenault, A. C.; Miguez, H.; Kitaev, V.; Ozin, G. A.; Manners, I. *Adv. Mater.* **2003**, *15*, 503.
214. Calléja, G.; Cerveau, G.; Corriu, R. J. P. *J. Organomet. Chem.* **2001**, *621*, 46.
215. Petersen, R.; Foucher, D. A.; Tang, B.-Z.; Lough, A.; Raju, N. P.; Greedan, J. E.; Manners, I. *Chem. Mater.* **1995**, *7*, 2045.
216. Berenbaum, A.; Lough, A. J.; Manners, I. *Organometallics* **2002**, *21*, 4415.
217. MacLachlan, M. J.; Ginzburg, M.; Coombs, N.; Coyle, T. W.; Raju, N. P.; Greedan, J. E.; Ozin, G. A.; Manners, I. *Science* **2000**, *287*, 1460.
218. Ginzburg, M.; MacLachlan, M. J.; Yang, S. M.; Coombs, N.; Coyle, T. W.; Raju, N. P.; Greedan, J. E.; Herber, R. H.; Ozin, G. A.; Manners, I. *J. Am. Chem. Soc.* **2002**, *124*, 2625.
219. Galloro, J.; Ginzburg, M.; Míguez, H.; Yang, S. M.; Coombs, N.; Safa-Sefat, A.; Greedan, J. E.; Manners, I.; Ozin, G. A. *Adv. Funct. Mater.* **2002**, *12*, 382.
220. MacLachlan, M. J.; Ginzburg, M.; Coombs, N.; Raju, N. P.; Greedan, J. E.; Ozin, G. A.; Manners, I. *J. Am. Chem. Soc.* **2000**, *122*, 3878.
221. Ginzburg-Margau, M.; Fournier-Bidoz, S.; Coombs, N.; Ozin, G. A.; Manners, I. *Chem. Comm.* **2002**, 3022.
222. Sun, Q.; Lam, J. W. Y.; Xu, K.; Xu, H.; Cha, J. A. K.; Wong, P. C. L.; Wen, G.; Zhang, X.; Jing, X.; Wang, F.; Tang, B. Z. *Chem. Mater.* **2000**, *12*, 2617.
223. Berenbaum, A.; Ginzburg, M.; Coombs, N.; Lough, A. J.; Safa-Sefat, A.; Greedan, J. E.; Ozin, G. A.; Manners, I. *Adv. Mater.* **2003**, *15*, 51.
224. Kulbaba, K.; Cheng, A.; Bartole, A.; Greenberg, S.; Resendes, R.; Coombs, N.; Safa-Sefat, A.; Greedan, J. E.; Stöver, H. D. H.; Ozin, G. A.; Manners, *J. Am. Chem. Soc.* **2002**, *124*, 12522.
225. Power-Billard, K. N.; Manners, I. *Macromolecules* **2000**, *33*, 26.
226. Jäkle, F.; Wang, Z.; Manners, I. *Macromol. Rapid Commun.* **2001**, *21*, 1291.
227. Wang, Z.; Lough, A. J.; Manners, I. *Macromolecules* **2002**, *35*, 7669.
228. Ginzburg, M.; Galloro, J.; Jäkle, F.; Power-Billard, K. N.; Yang, S.; Sokolov, I.; Lam, C. N. C.; Neumann, A. W.; Manners, I.; Ozin, G. A. *Langmuir* **2000**, *16*, 9609.
229. Hempenius, M. A.; Robins, N. S.; Lammertink, R. G. H.; Vancso, G. J. *Macromol. Rapid Commun.* **2001**, *22*, 30.
230. Halfyard, J.; Galloro, J.; Ginzburg, M.; Wang, Z.; Coombs, N.; Manners, I.; Ozin, G. A. *Chem. Comm.* **2002**, 1746.
230a. Halfyard, J.; Ginzburg, M.; Galloro, J.; Manners, I.; Ozin, G. A. unpublished results.
231. Hempenius, M. A.; Péter, M.; Robins, N. S.; Kooij, E. S.; Vancso, G. J. *Langmuir* **2002**, *18*, 7629.
232. Medina, J. C.; Gay, I.; Chen, Z.; Echegoyen, L.; Gokel, G. W. *J. Am. Chem. Soc.* **1991**, *113*, 365.
232a. Saji, T.; Hoshino, K.; Ishii, Y.; Goto, M. *J. Am. Chem. Soc.* **1991**, *113*, 450.
232b. Kakizawa, Y.; Sakai, H.; Yamaguchi, A.; Kondo, Y.; Yoshino, N.; Abe, M. *Langmuir* **2001**, *17*, 8044.
233. Koepf-Maier, P.; Koepf, H.; Neuse, E. W. *Angew. Chem., Int. Ed. Engl.* **1984**, *96*, 456.
234. Espada, L. I.; Shadaram, M.; Robillard, J.; Pannell, K. H. *J. Inorg. Organomet. Polym.* **2000**, *10*, 169.
235. Yim, H.; Foster, M. D.; Balaishis, D.; Manners, I. *Langmuir* **1998**, *14*, 3921.
236. Liu, Y. Y.; Zhang, X.; Tang, H. D.; Wang, T. J.; Qin, J. G.; Liu, D. Y.; Li, S. J.; Ye, C. *Chin. J. Chem.* **2002**, *20*, 1199.
237. Castruita, M.; Cervantes-Lee, F.; Mahmoud, J. S.; Zhang, Y.; Pannell, K. H. *J. Organomet. Chem.* **2001**, *637*, 664.
238. Sharma, H. K.; Cervantes-Lee, F.; Mahmoud, J. S.; Pannell, K. H. *Organometallics* **1999**, *18*, 399.
239. Peckham, T. J.; Massey, J. A.; Honeyman, C. H.; Manners, I. *Macromolecules* **1999**, *32*, 2830.
240. Peckham, T. J.; Lough, A. J.; Manners, I. *Organometallics* **1999**, *18*, 1030.
241. Durfey, D. A.; Kirss, R. U.; Frommen, C.; Feighery, W. *Inorg. Chem.* **2000**, *39*, 3506.
242. Nelson, J. M.; Nguyen, P.; Petersen, R.; Rengel, H.; Macdonald, P. M.; Lough, A. J.; Manners, I.; Raju, N. P.; Greedan, J. E., Barlow, S., *et al. Chem. Eur. J.* **1997**, *3*, 573.
243. Zhang, L.; Eisenberg, A. *J. Am. Chem. Soc.* **1996**, *118*, 3168.
244. Massey, J. A.; Power, K. N.; Manners, I.; Winnik, M. A. *J. Am. Chem. Soc.* **1998**, *120*, 9533.
245. Massey, J. A.; Temple, K.; Cao, L.; Rharbi, Y.; Raez, J.; Winnik, M. A.; Manners, I. *J. Am. Chem. Soc.* **2000**, *122*, 11577.
246. Raez, J.; Manners, I.; Winnik, M. A. *J. Am. Chem. Soc.* **2002**, *124*, 10381.
247. Cao, L.; Manners, I.; Winnik, M. A. *Macromolecules* **2002**, *35*, 8258.
248. Wang, X.-S.; Winnik, M. A.; Manners, I. *Macromol. Rapid Commun.* **2002**, *23*, 210.
249. Resendes, R.; Massey, J. A.; Temple, K.; Cao, L.; Power-Billard, K. N.; Winnik, M. A.; Manners, I. *Chem. Eur. J.* **2001**, *7*, 2414.
250. Massey, J. A.; Winnik, M. A.; Manners, I.; Chan, V. Z.-H.; Ostermann, J. M.; Enchelmaier, R.; Spatz, J. P.; Möller, M. *J. Am. Chem. Soc.* **2001**, *123*, 3147.
251. Cao, L.; Massey, J. A.; Winnik, M. A.; Manners, I.; Chan, V. Z.-H.; Spatz, J. P.; Ostermann, J. M.; Enchelmaier, R.; Möller, M. *Adv. Funct. Mater.* **2003**, *13*, 271.
252. Bates, F. S. *Science* **1991**, *251*, 898.
253. Massey, J. A.; Power, K. N.; Winnik, M. A.; Manners, I. *Adv. Mater.* **1998**, *10*, 1559.

254. Manners, I. *Chem. Comm.* **1999**, 857.
255. Lammertink, R. G. H.; Hempenius, M. A.; Thomas, E. L.; Vancso, G. J. *J. Polym. Sci., Polym. Phys.* **1999**, *37*, 1009.
256. Li, W.; Sheller, N.; Foster, M. D.; Balaishis, D.; Manners, I.; Annis, B.; Lin, J.-S. *Polymer* **2000**, *41*, 719.
257. Eitouni, H. B.; Balsara, N. P.; Hahn, H.; Pople, J. A.; Hempenius, M. A. *Macromolecules* **2002**, *35*, 7765.
258. Park, M.; Harrison, C.; Chaikin, P. M.; Register, R. A.; Adamson, D. H. *Science* **1997**, *276*, 1401.
259. Chan, V. Z.-H.; Hoffman, J.; Lee, V. Y.; Latrou, H.; Avgeropoulos, A.; Hadjichristidis, N.; Miller, R. D.; Thomas, E. L. *Science* **1999**, *286*, 1716.
260. Cheng, J. Y.; Ross, C. A.; Chan, V. Z.-H.; Thomas, E. L.; Lammertink, R. G. H.; Vancso, G. J. *Adv. Mater.* **2001**, *13*, 1174.
261. Temple, K.; Kulbaba, K.; Power-Billard, K. N.; Manners, I.; Leach, A.; Xu, T.; Russell, T. P.; Hawker, C. J. *Adv. Mater.* **2003**, *15*, 297.
262. Cao, L.; Manners, I.; Winnik, M. A. *Macromolecules* **2001**, *34*, 3353.
263. Buretea, M. A.; Tilley, T. D. *Organometallics* **1997**, *16*, 1507.
264. Stanton, C. E.; Lee, T. R.; Grubbs, R. H.; Lewis, N. S.; Pudelski, J. K.; Callstrom, M. R.; Erickson, M. S.; McLaughlin, M. L. *Macromolecules* **1995**, *28*, 8713.
265. Heo, R. W.; Somoza, F. B.; Lee, T. R. *J. Am. Chem. Soc.* **1998**, *120*, 1621.
266. Galloway, C. P.; Rauchfuss, T. B. *Angew. Chem., Int. Ed. Engl.* **1993**, *32*, 1319.
267. Compton, D. L.; Rauchfuss, T. B. *Organometallics* **1994**, *13*, 4367.
268. Compton, D. L.; Brandt, P. F.; Rauchfuss, T. B.; Rosenbaum, D. F.; Zukoski, C. F. *Chem. Mater.* **1995**, *7*, 2342.
269. Arnold, R.; Matchett, S. A.; Rosenblum, M. *Organometallics* **1988**, *7*, 2261.
270. Foxman, B. M.; Rosenblum, M. *Organometallics* **1993**, *12*, 4805.
271. Foxman, B. M.; Gronbeck, D. A.; Rosenblum, M. *J. Organomet. Chem.* **1991**, *413*, 287.
272. Nugent, H. M.; Rosenblum, M. *J. Am. Chem. Soc.* **1993**, *115*, 3848.
273. Rosenblum, M.; Nugent, H. M.; Jang, K.-S.; Labes, M. M.; Cahalane, W.; Klemarczyk, P.; Reiff, W. M. *Macromolecules* **1995**, *28*, 6330.
274. Meng, X.; Sabat, M.; Grimes, R. N. *J. Am. Chem. Soc.* **1993**, *115*, 6143.
275. Pipal, J. R.; Grimes, R. N. *Organometallics* **1993**, *12*, 4459.
276. Katz, T. J.; Sudhakar, A.; Teasley, M. F.; Gilbert, A. M.; Geiger, W. E.; Robben, M. P.; Wuensch, M.; Wards, M. D. *J. Am. Chem. Soc.* **1993**, *115*, 3182.
277. Knobloch, F.; Rauscher, W. *J. Polym. Sci., Part. A-1* **1961**, *54*, 651.
278. Okawara, M.; Takemoto, Y.; Kitaoka, H.; Haruki, E.; Imoto, E. *Kogyo Kagazu Zasshi* **1962**, *65*, 685.
279. Gonsalves, K.; Zhan-ru, L.; Rausch, M. D. *J. Am. Chem. Soc.* **1984**, *106*, 3862.
280. Pittman, C. U.; Rausch, M. D. *Pure Appl. Chem.* **1986**, *58*, 617.
281. Abd-Alla, M. M.; El-Zohry, M. F.; Aly, K. I.; Abd-El-Wahab, M. M. *J. Appl. Polym. Sci.* **1993**, *47*, 323.
282. Wright, M. E.; Toplikar, E. G.; Lackritz, H. S.; Kerney, J. T. *Macromolecules* **1994**, *27*, 3016.
283. Marder, S. R.; Perry, J. W.; Tiemann, B. G.; Schaefer, W. P. *Organometallics* **1991**, *10*, 1896.
284. Wright, M. E.; Toplikar, E. G. *Macromolecules* **1992**, *25*, 6050.
285. Wilbert, G.; Wiesemann, A.; Zentel, R. *Makromol. Chem.* **1995**, *196*, 3771.
286. Carraher, C. E. Jr.; Sheats, J. E.; Pittman, C. U., Jr., Eds. *Organometallic Polymers*; Academic Press: New York, 1978; p 79.
287. Sheats, E.; Carraher, C. E., Jr., Pittman, C. U. Jr., Eds. *Metal-Containing Polymeric Systems*; Plenum: New York, 1985; p 1.
288. Millich, F.; Carraher, C. E., Jr.; Eds. *Interfacial Synthesis,* Dekker: New York, 1977; Vol. II, p 367.
289. Carraher, C. E., Jr.; Bahaj, S. T. *Polym. J.* **1973**, *14*, 42.
290. Carraher, C. E., Jr.; Bahaj, S. T. *Polymer* **1974**, *15*, 9.
291. Carraher, C. E., Jr.; Preston, J., Eds. *Interfacial Synthesis,* Dekker: New York, 1982; Vol. III, p 77.
291a. Carraher, C. E., Jr.; Christensen, M. J. *Angew. Makromol. Chem.* **1978**, *69*, 61.
291b. Carraher, C. E., Jr.; Lee, J. *J. Macromol. Sci.* **1975**, *A-9*, 19.
292. Carraher, C. E., Jr.; Preston, J., Eds. *Interfacial Synthesis,* Dekker: New York, 1982; Vol. III, p 93.
293. Carraher, C. E., Jr.; Schwarz, R. A.; Schroeder, J. A.; Schwarz, M.; Molloy, H. M. *Am. Chem. Soc. Div. Org. Coat. Plast. Chem.* **1980**, *43*, 798.
294. Pittman, C. U., Jr.; Ayers, O. E.; McManus, S. P.; Sheats, J. E.; Whitten, C. *Macromolecules* **1971**, *4*, 360.
295. Pittman, C. U., Jr.; Ayers, O. E.; Suryanarayanan, B.; McManus, S. P.; Sheats, J. E. *Makromol. Chem.* **1974**, *175*, 1427.
296. Carraher, C. E., Jr.; Sheats, J. E.; Pittman, C. U., Jr., Eds. *Organometallic Polymers;* Academic Press: New York, 1978; p 87.
297. Carraher, C. E., Jr.; Sheats, J. E. *Makromol. Chem.* **1973**, *166*, 23.
298. Carraher, C. E., Jr. *Macromolecules* **1971**, *4*, 263.
299. Carraher, C. E., Jr.; Peterson, G. F.; Sheats, J. E.; Kirsch, T. *Makromol. Chem.* **1974**, *175*, 3089.
300. Sheats, J. E.; Carraher, C. E., Jr.; Bruyer, D.; Cole, M. *Am. Chem. Soc. Div. Org. Coat. Plast. Chem.* **1974**, *34*, 474.
301. Carraher, C. E.; Jr. Sheats, J. E.; Pittman, C. U., Jr., Eds. *Organometallic Polymers;* Academic Press: New York, 1978; p 95.
302. Nuyken, O.; Pöhlmann, T.; Herberhold, M. *Macromol. Chem. Phys.* **1996**, *197*, 3343.
303. Schaaf, R. L.; Kan, P. T.; Lenk, C. T. *J. Org. Chem.* **1961**, *26*, 1790.
304. Greber, G.; Hallensleben, M. L. *Makromol. Chem.* **1966**, *92*, 137.
305. Greber, G.; Hallensleben, M. L. *Makromol. Chem.* **1967**, *104*, 90.
306. Greber, G.; Hallensleben, M. L. *Makromol. Chem.* **1965**, *83*, 148.
307. Moore, J. S.; Stupp, S. I. *Macromolecules* **1990**, *23*, 65.
308. Wright, M. E.; Sigman, M. S. *Macromolecules* **1992**, *25*, 6055.
309. Casado, C. M.; Morán, M.; Losada, J.; Cuadrado, I. *Inorg. Chem.* **1995**, *34*, 1668.
310. Yamaguchi, I.; Ishii, H.; Sakano, T.; Osakada, K.; Yamamoto, T. *Appl. Organomet. Chem.* **2001**, *15*, 197.
311. Neuse, E. W.; Rosenberg, H. J. *J. Macromol. Sci., Revs. Macromol. Chem.* **1970**, *C4*, 119.
312. Neuse, E. W.; Rosenberg, H. *J. Macromol. Sci. Revs. Macromol. Chem.* **1970**, *C4*, 121.
313. Lichtenhan, J. D. *Comments Inorg. Chem.* **1995**, *17*, 115.
314. Haddad, T. S.; Lichtenhan, J. D. *J. Inorg. Organomet. Polym.* **1995**, *5*, 237.
315. Kasahara, A.; Izumi, T. *Chem. Lett.* **1978**, 21.
315a. Gooding, R.; Lillya, C. P.; Chien, C. W. *Chem. Commun.* **1983**, 151.
316. Gamble, S.; Pattin, J. T.; Boncella, J. M. *Makromol. Chem., Rapid Commun.* **1992**, *13*, 109.
317. Bayer, R.; Pöhlman, T.; Nuyken, O. *Makromol. Chem., Rapid Commun.* **1993**, *14*, 359.

318. Knapp, R.; Rehahn, M. *Makromol. Chem., Rapid Commun.* **1993**, *14*, 451.
319. Ingham, S. L.; Khan, M. S.; Lewis, J.; Long, N. J.; Raithby, P. R. *J. Organomet. Chem.* **1994**, *470*, 153.
320. Bochmann, M.; Lu, J.; Cannon, R. D. *J. Organomet. Chem.* **1996**, *518*, 97.
321. Knapp, R.; Velten, U.; Rehahn, M. *Polymer* **1998**, *39*, 5827.
322. Yamamoto, T.; Morikita, T.; Maruyama, T.; Kubota, K.; Katada, M. *Macromolecules* **1997**, *30*, 5390.
322a. Morikita, T.; Maruyama, T.; Yamamoto, T.; Kubota, K.; Katada, M. *Inorg. Chim. Acta* **1998**, *269*, 310.
322b. Morikita, T.; Yamamoto, T. *J. Organomet. Chem.* **2001**, *637–639*, 809.
323. Hollandsworth, B.; Hollis, W. G. Jr.; Slebodnick, C.; Deck, P. A. *Organometallics* **1999**, *18*, 3610.
324. Deck, P. A.; Lane, M. J.; Montgomery, J. L.; Slebodnick, C. *Organometallics* **2000**, *19*, 1013.
325. Corriu, R. J. P.; Devylder, N.; Guerin, C.; Henner, B.; Jean, A. *Organometallics* **1994**, *13*, 3194.
325a. Corriu, R. J. P.; Devylder, N.; Guerin, C.; Henner, B.; Jean, A. *J. Organomet. Chem.* **1996**, *509*, 249.
326. Tanaka, M.; Hayashi, T. *Bull. Chem. Soc. Jpn.* **1993**, *66*, 334.
327. Yakamoto, T.; Sanechika, K.; Yakamoto, A.; Katado, M.; Motoyama, I.; Sano, H. *Inorg. Chim. Acta* **1983**, *73*, 75.
328. Southard, G. E.; Curtis, M. D. *Organometallics* **1997**, *16*, 5618.
329. Altmann, M.; Bunz, U. H. F. *Angew. Chem., Int. Ed. Engl.* **1995**, *34*, 569.
329a. Steffen, W.; Köhler, B.; Altmann, M.; Sherf, U.; Stitzer, K.; zur Loye, H.-C.; Bunz, U. H. F. *Chem. Eur. J.* **2001**, *7*, 117.
330. Altmann, M.; Enkelmann, V.; Lieser, G.; Bunz, U. H. F. *Adv. Mater.* **1995**, *7*, 726.
331. Bunz, U. H. F. *Pure Appl. Chem.* **1996**, *68*, 309.
332. Altmann, M.; Bunz, U. H. F. *Makromol. Chem., Rapid Commun.* **1994**, *15*, 785.
333. Altmann, M.; Enkelmann, V.; Beer, F.; Bunz, U. H. F. *Organometallics* **1996**, *15*, 394.
334. Harrison, C.; Seminario, J. M.; Bunz, U. H. F.; Myrick, M. L. *J. Phys. Chem. A* **2000**, *104*, 5937.
335. Rengel, H.; Altmann, M.; Neher, D.; Harrison, B. C.; Myrick, M. L.; Bunz, U. H. F. *J. Phys. Chem. B* **1999**, *103*, 10335.
336. Ohkubo, A.; Aramaki, K.; Nishihara, H. *Chem. Lett.* **1993**, 271.
337. Tomita, I.; Nishio, A.; Endo, T. *Macromolecules* **1994**, *27*, 7009.
338. Lee, J. C.; Nishio, A.; Tomita, I.; Endo, T. *Macromolecules* **1997**, *30*, 5205.
339. Tomita, I.; Nishio, A.; Endo, T. *Macromolecules* **1995**, *28*, 3042.
340. Tomita, I.; Nishio, A.; Endo, T. *Appl. Organomet. Chem.* **1998**, *12*, 735.
341. Rozhanskii, L.; Tomita, I.; Endo, T. *Macromolecules* **1996**, *29*, 1934.
342. Rozhanskii, L.; Tomita, I.; Endo, T. *Polymer* **1998**, *40*, 1581.
343. Rozhanskii, L.; Tomita, I.; Endo, T. *Macromolecules* **1997**, *30*, 1222.
344. Rozhanskii, L.; Tomita, I.; Endo, T. *Chem. Lett.* **1997**, 477.
345. Sawada, Y.; Tomita, I.; Endo, T. *Macromol. Chem. Phys.* **2000**, *201*, 510.
346. Setayesh, S.; Bunz, U. H. F. *Organometallics* **1996**, *15*, 5470.
347. Bunz, U. H. F.; Enkelmann, V.; Beer, F. *Organometallics* **1995**, *14*, 2490.
348. Tomita, I.; Lee, J. C.; Endo, T. *J. Organomet. Chem.* **2000**, *611*, 570.
349. Dembek, A.; Burch, R. R.; Feiring, A. E. *J. Am. Chem. Soc.* **1993**, *115*, 2087.
350. Dembek, A.; Fagan, P. J.; Marsi, M. *Macromolecules* **1993**, *26*, 2992.
351. Abd-El-Aziz, S.; Epp, K. M.; de Denus, C. R.; Fisher-Smith, G. *Organometallics* **1994**, *13*, 2299.
352. Abd-El-Aziz, S.; de Denus, C. R.; Zaworotko, M. J.; MacGillivray, L. R. *J. Chem. Soc., Dalton Trans.* **1995**, 3375.
353. Abd-El-Aziz, S.; de Denus, C. R.; Todd, E. K.; Bernardin, S. A. *Macromolecules* **2000**, *33*, 5000.
354. Abd-El-Aziz, S.; Todd, E. K.; Ma, G. Z. *J. Polym. Sci., Polym. Chem.* **2001**, *39*, 1216.
355. Abd-El-Aziz, S.; Todd, E. K.; Afifi, T. H. *Macromol. Rapid Commun.* **2002**, *23*, 113.
356. Abd-El-Aziz, S.; Afifi, T. H.; Budakowski, W. R.; Friesen, K. J.; Todd, E. K. *Macromolecules* **2002**, *35*, 8929.
357. Funaki, H.; Aramaki, K.; Nishihara, H. *Synth. Met.* **1995**, *74*, 59.
358. Funaki, H.; Aramaki, K.; Nishihara, H. *Chem. Lett.* **1992**, 2065.
359. Matsuda, J.; Aramaki, K.; Nishihara, H. *J. Chem. Soc., Faraday Trans.* **1995**, *91*, 1477.
360. Wright, M. E. *Macromolecules* **1989**, *22*, 3256.
361. Morisaki, Y.; Chem, H.; Chujo, Y. *Polym. Bull.* **2002**, *48*, 243.
362. Kuhnen, T.; Stradiotto, M.; Ruffolo, R.; Ulbrich, D.; McGlinchey, M. J.; Brook, M. A. *Organometallics* **1997**, *16*, 5048.
363. Pocard, N. L.; Alsmeyer, D. C.; McCreery, R. L.; Neenan, T. X.; Callstrom, M. R. *J. Am. Chem. Soc.* **1992**, *114*, 769.
364. Schueller, O. J. A.; Pocard, N. L.; Huston, M. E.; Spontak, R. J.; Neenan, T. X.; Callstrom, M. R. *Chem. Mater.* **1993**, *5*, 11.
365. Hutton, H. D.; Pocard, N. L.; Alsmeyer, D. C.; Schueller, O. J. A.; Spontak, R. J.; Huston, M. E.; Huang, W. H.; McCreery, R. L.; Neenan, T. X.; Callstrom, M. R. *Chem. Mater.* **1993**, *5*, 1727.
366. Neenan, T. X.; Callstrom, M. R.; Schueller, O. J. A. *Macromol. Symp.* **1994**, *80*, 315.
367. Huber, C.; Bangerter, F.; Caseri, W. R.; Weder, C. *J. Am. Chem. Soc.* **2001**, *123*, 3857.
368. Kokil, A.; Huber, C.; Caseri, W. R.; Weder, C. *Macromol. Chem. Phys.* **2003**, *204*, 40.
369. Kokil, A.; Shiyanovskaya, I.; Singer, K. D.; Weder, C. *J. Am. Chem. Soc.* **2002**, *124*, 9978.
370. Korshak, V. V.; Sladkov, A. M.; Kurdryavtsev, Y. P. *Vysokomol. Soedin.* **1960**, *2*, 1824.
371. Hay, A. S. *J. Polym. Sci. A* **1969**, *7*, 1625.
372. Fujikura, Y.; Sonogashira, K.; Hagihara, N. *Chem. Lett.* **1975**, 1067.
373. Hagihara, N.; Sonogashira, K.; Takahashi, S. *Adv. Polym. Sci.* **1981**, *41*, 149.
374. Sonogashira, K.; Kataoka, S.; Takahashi, S.; Hagihara, N. *J. Organomet. Chem.* **1978**, *160*, 319.
375. Takahashi, S.; Kariya, M.; Yatake, T.; Sonogashira, K.; Hagihara, N. *Macromolecules* **1978**, *11*, 1063.
376. Takahashi, S.; Ohyama, Y.; Murata, E.; Sonogashira, K.; Hagihara, N. *J. Polym. Sci., Polym. Chem. Ed.* **1980**, *18*, 349.
377. Takahashi, S.; Morimoto, H.; Murata, E.; Kataoka, S.; Sonogashira, K.; Hagihara, N. *J. Polym. Sci., Polym. Chem. Ed.* **1982**, *20*, 565.
378. Takahashi, S.; Murata, E.; Sonogashira, K.; Hagihara, N. *J. Polym. Sci., Polym. Chem. Ed.* **1980**, *18*, 661.
379. Hay, A. S. *J. Org. Chem.* **1962**, *27*, 3320 and references therein.
380. Sonogashira, K.; Ohga, K.; Takahashi, S.; Hagihara, N. *J. Organomet. Chem.* **1980**, *188*, 237.
381. Fyfe, H. B.; Mlekuz, M.; Zargarian, D.; Marder, T. B. In *Organic Materials for Non-linear Optics II*; Hahn, R. A., Bloor, D., Eds.; The Royal Society of Chemistry: Cambridge, 1991; p 204.

382. Fyfe, H. B.; Mlekuz, M.; Zargarian, D.; Taylor, N. J.; Marder, T. B. *Chem. Commun.* **1991**, 188.
383. Fyfe, H. B.; Mlekuz, M.; Stringer, G.; Taylor, N. J.; Marder, T. B. In *Inorganic and Organometallic Polymers with Special Properties*; Laine, R. M., Ed. NATO ASI Series E, Vol. 206, p 331.
384. Marder, T. B.; Lesley, G.; Yuan, Z.; Fyfe, H. B.; Chow, P.; Stringer, G.; Jobe, I. R.; Taylor, N. J.; Williams, I. D.; Kurtz, S. K. In *Materials for Nonlinear Optics: Chemical Perspectives*; Stucky, G. D., Marder, T. B., Sohn, J., Eds.; American Chemical Society Symposium Series 455; American Chemical Society: Washington, DC, 1991, p 605.
385. Klein, H.-F.; Karsch, H. H. *Chem. Ber.* **1975**, *108*, 944.
386. Cardin, J.; Cardin, D. J.; Lappert, M. F. *J. Chem. Soc. Dalton Trans.* **1977**, 767.
387. Davies, J.; Johnson, B. F. G.; Lewis, J.; Raithby, P. *J. Organomet. Chem.* **1991**, *414*, C51.
388. Johnson, B. F. G.; Kakkar, A. K.; Khan, M. S.; Lewis, J.; Raithby, P. *J. Organomet. Chem.* **1991**, *409*, C12.
389. Khan, M. S.; Kakkar, A. K.; Ingham, S. L.; Raithby, P. R.; Lewis, J.; Spencer, B.; Wittman, F.; Friend, R. H. *J. Organomet. Chem.* **1994**, *472*, 247.
390. Faulkner, C. W.; Ingham, S. L.; Khan, M. S.; Lewis, J.; Long, N. J.; Raithby, P. R. *J. Organomet. Chem.* **1994**, *482*, 139.
390a. Atherton, Z.; Faulkner, C. W.; Ingham, S. L.; Kakkar, A. K.; Khan, M. S.; Lewis, J.; Long, N. J.; Raithby, P. R. *J. Organomet. Chem.* **1993**, *462*, 265.
391. Davies, J.; Johnson, B. F. G.; Khan, M. S.; Lewis, J. J. *Chem. Commun.* **1991**, 187.
392. Khan, M. S.; Davies, S. J.; Kakkar, A. K.; Schwartz, D.; Lin, B.; Johnson, B. F. G.; Lewis, J. *J. Organomet. Chem.* **1992**, *424*, 87.
393. Johnson, B. F. G.; Kakkar, A. K.; Khan, M. S.; Lewis, J.; Dray, A. E.; Friend, R. H.; Wittman, F. *J. Mater. Chem.* **1991**, *1*, 485.
394. Lewis, J.; Khan, M. S.; Kakkar, A. K.; Johnson, B. F. G.; Marder, T. B.; Fyfe, H. B.; Wittman, F.; Friend, R. H.; Dray, A. E. *J. Organomet. Chem.* **1992**, *425*, 165.
395. Lavastre, O.; Even, M.; Dixneuf, P. H.; Pacreau, A.; Vairon, J.-P. *Organometallics* **1996**, *15*, 1530.
396. Lavastre, O.; Even, M.; Dixneuf, P. H.; Pacreau, A.; Vairon, J.-P. *Organometallics* **1997**, *16*, 184.
397. Jia, G.; Puddephatt, R. J.; Scott, J. D.; Vittal, J. J. *Organometallics* **1993**, *12*, 3565.
398. Jia, G.; Puddephatt, R. J.; Vittal, J. J.; Payne, N. C. *Organometallics* **1993**, *12*, 263.
399. Jia, G.; Payne, N. C.; Vittal, J. J.; Puddephatt, R. J. *Organometallics* **1993**, *12*, 4771.
400. Irwin, M. J.; Jia, G.; Payne, N. C.; Puddephatt, R. J. *Organometallics* **1996**, *15*, 51.
401. Irwin, M. J.; Vittal, J. J.; Puddephatt, R. J. *Organometallics* **1997**, *16*, 3541.
402. Onitsuka, K.; Joh, T.; Takahashi, S. *Angew. Chem., Int. Ed. Engl.* **1992**, *31*, 851.
403. Khan, M. S.; Schwartz, D. J.; Pasha, N. A.; Kakkar, A. K.; Lin, B.; Raithby, P. R.; Lewis, J. Z. *Anorg. Allg. Chem.* **1992**, *616*, 121.
404. Onitsuka, K.; Ogawa, H.; Joh, T.; Takahashi, S. *Chem. Lett.* **1988**, 1855.
405. Bunten, K. A.; Kakkar, A. K. *Macromolecules* **1996**, *29*, 2885.
406. Wong, W. Y.; Chan, S. M.; Choi, K. H.; Cheah, K. W.; Chan, W. K. *Macromol. Rapid Commun.* **2000**, *21*, 453.
407. Wolf, M. O. *Adv. Mater.* **2001**, *13*, 545.
408. Zhu, Y.; Millet, D. B.; Wolf, M. O.; Rettig, S. J. *Organometallics* **1999**, *18*, 1930.
409. Manna, J.; John, K. D.; Hopkins, M. D. *Adv. Organomet. Chem.* **1995**, *38*, 79.
410. Atherton, Z.; Faulkner, C. W.; Ingham, S. L.; Kakkar, A. K.; Khan, M. S.; Lewis, J.; Long, N. J.; Raithby, P. R. *J. Organomet. Chem.* **1993**, *462*, 265.
411. Chow, P.; Zargarian, D.; Taylor, N. J.; Marder, T. B. *Chem. Commun.* **1989**, 1545.
412. Wong, W. Y.; Lu, G. L.; Choi, K. H.; Lin, Z. Y. *J. Chem. Soc., Dalton Trans.* **2001**, 3250.
413. Khan, M. S.; Al-Mandhary, M. R. A.; Al-Suti, M. K.; Feeder, N.; Nahar, S.; Köhler, A.; Friend, R. H.; Wilson, P. J.; Raithby, P. R. *J. Chem. Soc., Dalton Trans.* **2002**, 2441.
414. Khan, M. S.; Al-Mandhary, M. R. A.; Al-Suti, M. K.; Hisahm, A. K.; Raithby, P. R.; Ahrens, B.; Mahon, M. F.; Male, L.; Marseglia, E. A., Tedesco, E., *et al. J. Chem. Soc., Dalton Trans.* **2002**, 1358.
415. Duer, M. J.; Khan, M. S.; Kakkar, A. K. *Solid State Nucl. Magn. Reson.* **1992**, *1*, 13.
416. Dray, E.; Wittmann, F.; Friend, R. H.; Donald, A. M.; Khan, M. S.; Lewis, J.; Johnson, B. F. G. *Synth. Met.* **1991**, *41–43*, 871.
417. Dray, E.; Rachel, R.; Saxton, W. O.; Lewis, J.; Khan, M. S.; Donald, A. M.; Friend, R. H. *Macromolecules* **1992**, *25*, 3473.
418. Lichtenberger, D. L.; Renshaw, S. K.; Wong, A.; Tagge, C. D. *Organometallics* **1993**, *12*, 3522.
419. Lichtenberger, D. L.; Renshaw, S. K.; Bullock, R. M. *J. Am. Chem. Soc.* **1993**, *115*, 3276.
420. Louwen, J. N.; Hengelmolen, R.; Grove, D. M.; Oskam, A.; DeKock, R. L. *Organometallics* **1984**, *3*, 908.
421. Kostic, N. M.; Fenske, R. F. *Organometallics* **1982**, *1*, 974.
422. Frapper, G.; Kertesz, M. *Inorg. Chem.* **1993**, *32*, 732.
423. Lhost, O.; Toussaint, J. M.; Bredas, J. L.; Wittmann, H. F.; Fuhrmann, K.; Friend, R. H.; Khan, M. S.; Lewis, J. *Synth. Met.* **1993**, *55–57*, 4525.
424. Markwell, R. D.; Butler, I. S.; Kakkar, A. K.; Khan, M. S.; Al-Zakwani, Z. H.; Lewis, J. *Organometallics* **1996**, *15*, 2331.
425. Motowoka, M.; Norisuye, T.; Teramoto, A.; Fujita, H. *Polym. J.* **1979**, *11*, 665.
426. Abe, A.; Kimura, N.; Tabata, S. *Macromolecules* **1991**, *24*, 6238.
427. Takahashi, S.; Murata, E.; Kariya, M.; Sonogashira, K.; Hagihara, N. *Macromolecules* **1979**, *12*, 1016.
428. Takahashi, S.; Morimoto, H.; Takai, Y.; Sonogashira, K.; Hagihara, N. *Mol. Cryst. Liq. Cryst.* **1981**, *72*, 101.
429. Takahashi, S.; Takai, Y.; Morimoto, H.; Sonogashira, K.; Hagihara, N. *Mol. Cryst. Liq. Cryst.* **1982**, *82*, 139.
430. Takahashi, S.; Takai, Y.; Morimoto, H.; Sonogashira, K. *Chem. Commun.* **1984**, 3.
431. Wittman, F.; Fuhrmann, K.; Friend, R. H.; Khan, M. S.; Lewis, J. *Synth. Met.* **1993**, *55–57*, 56.
432. Khan, M. S.; Kakkar, A. K.; Long, N. J.; Lewis, J.; Raithby, P.; Nguyen, P.; Marder, T. B.; Wittmann, F.; Friend, R. H. *J. Mater. Chem.* **1994**, *4*, 1227.
433. Chawdbury, N.; Köhler, A.; Friend, R. H.; Wong, W. Y.; Lewis, J.; Younus, M.; Raithby, P. R.; Corcoran, T. C.; Al-Mandhary, M. R. A.; Khan, M. S. *J. Chem. Phys.* **1999**, *110*, 4963.
434. Wong, W. Y.; Wong, C. K.; Lu, G. L.; Cheah, K. W.; Shi, J. X.; Lin, Z. *J. Chem. Soc., Dalton Trans.* **2002**, *24*, 4587.
434a. Wong, W. Y.; Wong, C. K.; Lu, G. L.; Lee, A. W. M.; Cheah, K. W.; Shi, J. X. *Macromolecules* **2003**, *36*, 983.
435. Younus, M.; Köhler, A.; Cron, S.; Chawdhury, N.; Al-Mandhary, M. R. A.; Khan, M. S.; Lewis, J.; Long, N. J.; Friend, R. H.; Raithby, P. R. *Angew. Chem., Int. Ed. Engl.* **1998**, *37*, 3036.
436. Wong, W. Y.; Wong, W. K.; Raithby, P. R. *J. Chem. Soc., Dalton Trans.* **1998**, 2761.
437. Tessler, N.; Denton, G. J.; Friend, R. H. *Nature* **1996**, *382*, 695.
438. Yu, G.; Gao, J.; Hummelen, J. C.; Wudl, F.; Heeger, A. J. *Science* **1995**, *270*, 1741.
439. Kraft, A.; Grimsdale, A. C.; Holmes, A. B. *Angew. Chem., Int. Ed.* **1998**, *37*, 402.

440. Belijonne, D.; Wittmann, H. F.; Köhler, A.; Graham, S.; Younus, M.; Lewis, J.; Raithby, P. R.; Khan, M. S.; Friend, R. H.; Brédas, J. L. *J. Chem. Phys.* **1996**, *105*, 3868.
441. Wilson, J. S.; Köhler, A.; Friend, R. H.; Al-Suti, M. K.; Al-Mandhary, M. R. A.; Khan, M. S.; Raithby, P. R. *J. Chem. Phys.* **2000**, *113*, 7627.
442. Chawdhury, N.; Köhler, A.; Friend, R. H.; Younus, M.; Long, N. J.; Raithby, P. R.; Lewis, J. *Macromolecules* **1998**, *31*, 722.
443. Wilson, J. S.; Chawdhury, N.; Al-Mandhary, M. R. A.; Younus, M.; Khan, M. S.; Raithby, P. R.; Köhler, A.; Friend, R. H. *J. Am. Chem. Soc.* **2001**, *123*, 9412.
443a. Köhler, A.; Wilson, J. S.; Friend, R. H. *J. Chem. Phys.* **2002**, *116*, 9457.
444. Wong, W. Y.; Lu, G. L.; Choi, K. H.; Shi, J. X. *Macromolecules* **2002**, *35*, 3506.
445. Frazier, C.; Guha, S.; Chen, W. P.; Cockerham, P. M.; Porter, P. L.; Chauchard, E. A.; Lee, C. H. *Polymer* **1987**, *28*, 553.
446. *Nonlinear Optical Properties of Organic Materials*, Proc. SPIE No. 971; The International Society for Optical Engineering: Washington DC, 1988; p 186.
447. Frazier, C.; Chauchard, E. A.; Cockerham, P. M.; Porter, P. L. *Mat. Res. Soc. Symp. Proc.* **1988**, *109*, 323.
448. Guha, S.; Frazier, C. C.; Porter, P. L.; Kang, K.; Finberg, S. *Opt. Lett.* **1989**, *14*, 952.
449. Messier, J., Kajzar, F., Prasad, P., Eds.; *Organic Molecules for Nonlinear Optics and Photonics*; NATO ASI Series E; Kluwer: Dordrecht, 1991, Vol. 194, p 391.
450. Blau, W. J.; Byrne, H. J.; Cardin, D. J.; Davey, A. P. *J. Mater. Chem.* **1991**, *1*, 245.
451. Davey, P.; Page, H.; Blau, W. J.; Byrne, H. J.; Cardin, D. J. *Synt. Met.* **1993**, *55–57*, 3980.
452. Nishihara, H. In *Handbook of Organic Conductive Molecules and Polymers*, *Conductive polymers: Synthesis and Electrical Properties*; Nalwa, H. S., Ed.; Wiley: New York, 1997; Vol. 2, p 799.
453. Matsuda, H.; Nakanishi, H.; Kato, M. *J. Polym. Sci., Polym. Lett.* **1984**, *22*, 107.
454. Tomita, I.; Nishio, A.; Igarashi, T.; Endo, T. *Polym. Bull.* **1993**, *30*, 179.
455. Shimura, T.; Ohkubo, A.; Matsuda, N.; Matsuoka, I.; Aramaki, K.; Nishihara, H. *Chem. Mater.* **1996**, *8*, 1307.
456. Matsuoka, I.; Aramaki, K.; Nishihara, H. *J. Chem. Soc., Dalton Trans.* **1998**, 147.
457. Murata, M.; Hoshi, T.; Matsuoka, I.; Nankawa, T.; Kurihara, M.; Nishihara, H. *J. Inorg. Organomet. Polym.* **2000**, *10*, 209.
458. Matsuoka, I.; Yoshikawa, H.; Kurihars, M.; Nishihara, H. *Synth. Met.* **1999**, *102*, 1519.
459. Matsuoka, I.; Aramaki, H. K.; Nishihara, H. *Mol. Cryst. Liq. Cryst.* **1996**, *285*, 199.
460. Mao, S. S. H.; Tilley, T. D. *Macromolecules* **1997**, *30*, 5566.
461. Mao, S. S. H.; Tilley, T. D. *J. Am. Chem. Soc.* **1995**, *117*, 5365.
462. Mao, S. S. H.; Tilley, T. D. *J. Organomet. Chem.* **1996**, *521*, 425.
463. Lucht, B. L.; Mao, S. S. H.; Tilley, T. D. *J. Am. Chem. Soc.* **1998**, *120*, 4354.
464. Sturge, K. C.; Hunter, A. D.; McDonald, R.; Santarsiero, B. D. *Organometallics* **1992**, *11*, 3056.
465. Guo, X. A.; Sturge, K. C.; Hunter, A. D.; Williams, M. C. *Macromolecules* **1994**, *27*, 7825.
466. Wolfe, P. S.; Gomez, F. J.; Wagener, K. B. *Macromolecules* **1997**, *30*, 714.
467. Jia, G.; Wu, W. F.; Yeung, R. C. Y.; Xia, H. P. *J. Organomet. Chem.* **1997**, *539*, 53.
468. Pollagi, T. P.; Geib, S. J.; Hopkins, M. D. *J. Am. Chem. Soc.* **1994**, *116*, 6051.
469. John, K. D.; Hopkins, M. D. *Chem. Commun.* **1999**, 589.
470. Mazdyasni, K. S.; West, R.; David, D. L. *J. Am. Ceram. Soc.* **1978**, *61*, 504.
471. West, R. *J. Organomet. Chem.* **1986**, *300*, 327.
472. Miller, R. D.; Michl, J. *Chem. Rev.* **1989**, *89*, 1359.
473. Matyjaszewski, K. *J. Inorg. Organomet. Polym.* **1991**, *1*, 463.
474. Teramae, H.; Takeda, K. *J. Am. Chem. Soc.* **1989**, *111*, 1281.
475. Nelson, J.; Pietro, W. J. *J. Phys. Chem.* **1988**, *92*, 1365.
476. Savin, A.; Jepsen, O.; Flad, J.; Andersen, O. K.; Preuss, H.; von Schnering, H. G. *Angew. Chem., Int. Ed. Engl.* **1992**, *31*, 187.
477. Mark, J. E.; Allcock, H. R.; West, R. *Inorganic Polymers*; Prentice-Hall Englewood Cliffs, 1992; pp 186–236.
478. The lowest absorption bands of polysilanes have also been assigned to excitonic rather than interband transitions, see: Tachibana, H.; Matsumoto, M.; Tokura, Y.; Moritomo, Y.; Yamaguchi, A.; Koshihara, S.; Miller, R. D.; Abe, S. *Phys. Rev. B* **1993**, *47*, 4363.
479. Trefonas, P. III; West, R. *J. Polym. Sci., Polym. Chem. Ed.* **1985**, *23*, 2099.
480. Miller, R. D.; Sooriyakumaran, R. *J. Polym. Sci., Polym. Chem. Ed.* **1987**, *25*, 111.
481. Mark, J. E.; Allcock, H. R.; West, R. *Inorganic Polymers*; Prentice-Hall: Englewood Cliffs, 1992; p 243.
482. Adams, S.; Dräger, M. *Angew. Chem., Int. Ed.* **1987**, *26*, 1255.
483. Sita, L. R. *Acc. Chem. Res.* **1994**, *27*, 191.
484. Takeda, K.; Shiraishi, K. *Chem. Phys. Lett.* **1992**, *195*, 121.
485. Imori, T.; Tilley, T. D. *Chem. Commun.* **1993**, 1607.
486. Lu, V.; Tilley, T. D. *Macromolecules* **1996**, *29*, 5763.
487. Lu, V. Y.; Tilley, T. D. *Macromolecules* **2000**, *33*, 2403.
488. Babcock, J. R.; Sita, L. R. *J. Am. Chem. Soc.* **1996**, *118*, 12481.
489. Devylder, N.; Hill, M.; Molloy, K. C.; Price, G. J. *Chem. Commun.* **1996**, 711.
489a. An earlier report of the synthesis of polystannanes via Wurtz coupling was published as a conference proceeding but the spectroscopic data reported for the claimed polymers do not match the data found subsequently, see: Zhou, W. K.; Wang, N. L. *Polym. Prepr. (Am. Chem. Soc., Div. Polym. Chem.)* **1992**, *33*, 188.
490. Okano, M.; Matsumoto, N.; Arakawa, M.; Tsuruta, T.; Hamano, H. *Chem. Commun.* **1998**, 1799.
491. Sita, L. R.; Terry, K. W.; Shibata, K. *J. Am. Chem. Soc.* **1995**, *117*, 8049 and references cited therein.
492. Shibata, K.; Weinert, C. S.; Sita, L. R. *Organometallics* **1998**, *17*, 2241.
493. Bukalov, S. S.; Leites, L. A.; Lu, V. *Macromolecules* **2002**, *35*, 1757.
494. Tenhaeff, S. C.; Tyler, D. R. *Chem. Commun.* **1989**, 1459.
495. Tenhaeff, S. C.; Tyler, D. R. *Organometallics* **1991**, *10*, 473.
496. Tenhaeff, S. C.; Tyler, D. R. *Organometallics* **1991**, *10*, 1116.
497. Tenhaeff, S. C.; Tyler, D. R *Organometallics* **1992**, *11*, 1466.
498. Nieckarz, G. F.; Tyler, D. R. *Inorg. Chim. Acta* **1996**, *242*, 303.
499. Nieckarz, G. F.; Litty, J. J.; Tyler, D. R. *J. Organomet. Chem.* **1998**, *554*, 19.

500. Male, J. L.; Lindfors, B. E.; Covert, K. J.; Tyler, D. R. *Macromolecules* **1997**, *30*, 6404.
501. Male, J. L.; Lindfors, B. E.; Covert, K. J.; Tyler, D. R. *J. Am. Chem. Soc.* **1998**, *120*, 13176.
502. Morán, M.; Pascual, M. C.; Cuadrado, I.; Losada, J. *Organometallics* **1993**, *12*, 811.
503. Irwin, M. J.; Jia, G.; Vittal, J. J.; Puddephatt, R. J. *Organometallics* **1996**, *15*, 5321.
504. Puddephatt, R. J. *Chem. Commun.* **1998**, 1055.
505. McArdle, P.; O'Neill, L.; Cunningham, D. *Inorg. Chim. Acta* **1999**, *291*, 252.
506. McArdle, P.; O'Neill, L.; Cunningham, D.; Manning, A. R. *J. Organomet. Chem.* **1996**, *524*, 289.
507. Whittall, I. R.; McDonagh, A. M.; Humphrey, M. G.; Samoc, M. *Adv. Organomet. Chem.* **1999**, *43*, 349.
508. Johnson, B. F. G. *Coord. Chem. Rev.* **1999**, *190–192*, 1269.
509. Feliz, M.; Garriga, J. M.; Llusar, R.; Uriel, S.; Humphrey, M. G.; Lucas, N. T.; Samoc, M.; Luther-Davies, B. *Inorg. Chem.* **2001**, *40*, 6132.
510. Jordan, M. R.; White, P. S.; Schauer, C. K.; Mosley, M. A. *J. Am. Chem. Soc.* **1995**, *117*, 5403.
510a. Kuhnen, T.; Stradiotto, M.; Ruffolo, R.; Ulbrich, D.; McGlinchey, M. J.; Brook, M. A. *Organometallics* **1997**, *16*, 5048.
511. Johnson, B. F. G.; Sanderson, K. M.; Shephard, D. S.; Ozkaya, D.; Zhou, W.; Ahmed, H.; Thomas, M. D. R.; Gladden, L.; Mantle, M. *Chem. Commun.* **2000**, 1317.
512. Thomas, M. D. R.; Ahmed, H.; Sanderson, K. M.; Shephard, D. S.; Johnson, B. F. G.; Zhou, W. *Appl. Phys. Lett.* **2000**, *76*, 1773.
513. Thomas, M. D. R.; Ahmed, H.; Sanderson, K. M.; Shephard, D. S.; Johnson, B. F. G.; Ozkaya, D.; Sharma, N.; Humphreys, C. *J. Appl. Phys.* **2001**, *90*, 947.
514. Lucas, N. T.; Humphrey, M. G.; Rae, A. D. *Macromolecules* **2001**, *34*, 6188.
515. Newkome, G. R.; Moorefield, C. N.; Vogtle, F. *Dendritic Molecules: Concepts, Syntheses, Perspective*; VCH: Weinheim, 1996.
515a. Newkome, G. R.; Moorefield, C. N.; Vögtle, F. *Dendrimers and Dendrons: Concepts, Syntheses, Applications*; Wiley-VCH: Weinheim, 2001.
516. Buhleier, E.; Wehner, W.; Vogtle, F. *Synthesis* **1978**, 155.
517. Tomalia, D. A.; Baker, H.; Dewald, J. R.; Hall, M.; Kallos, G.; Martin, S.; Roeck, J.; Ryder, J.; Smith, P. A. *Polym. J. (Tokyo)* **1985**, *17*, 117.
518. Tomalia, D. A.; Naylor, A. M.; Goddard, W. A. III *Angew. Chem., Int. Ed. Engl.* **1990**, *29*, 138.
519. Tomalia, D. A. *Sci. Am.* **1995**, *May*, 62.
520. Schluter, A. D.; Rabe, J. P. *Angew. Chem., Int. Ed. Engl.* **2000**, *39*, 864.
521. Fischer, M.; Vögtle, F. *Angew. Chem., Int. Ed. Engl.* **1999**, *38*, 884.
522. Bosman, A. W.; Janssen, H. M.; Meijer, E. W. *Chem. Rev.* **1999**, *99*, 1665.
522a. Majoral, J.-P.; Caminade, A.-M. *Chem. Rev.* **1999**, *99*, 845.
523. Miller, T. M.; Neenan, T. X. *Chem. Mater.* **1990**, *2*, 346.
524. Miller, T. M.; Neenan, T. X.; Zayas, R.; Bair, H. E. *J. Am. Chem. Soc.* **1992**, *114*, 1018.
525. Hawker, C.; Fréchet, J. M. J. *Chem. Commun.* **1990**, 1010.
526. Hawker, C. J.; Fréchet, J. M. J. *J. Am. Chem. Soc.* **1990**, *112*, 7638.
527. Astruc, D.; Chardac, F. *Chem. Rev.* **2001**, *101*, 2991.
528. Hearshaw, M. A.; Moss, J. R. *Chem. Commun.* **1999**, 1.
529. Cuadrado, I.; Morán, M.; Casado, C. M.; Alonso, B.; Losada, J. *Coord. Chem. Rev.* **1999**, *193–195*, 395.
530. Gorman, C. B. *Adv. Mater.* **1998**, *10*, 295.
531. Knapen, J. W. J.; van der Made, A. W.; de Wilde, J. C.; van Leeuwen, P. W. W. N. M.; Wijkens, P.; Grove, D. M.; van Koten, G. *Nature* **1994**, *372*, 659.
532. van Koten, G.; Grove, D. M. *Am. Chem. Soc. Div. Polym. Mater. Sci. Eng.* **1995**, *73*, 228.
533. Gossage, R. A.; de Kuil, L. A.; van Koten, G. *Acc. Chem. Res.* **1998**, *31*, 423.
534. Albrecht, M.; van Koten, G. *Adv. Mater.* **1999**, *11*, 171.
535. Albrecht, M.; Gossage, R. A.; Lutz, M.; Spek, A. L.; van Koten, G. *Chem. Eur. J.* **2000**, *6*, 1431.
536. Alonso, B.; Cuadrado, I.; Moran, M.; Losada, J. *J. Chem. Soc., Chem. Commun.* **1994**, 2575.
537. Cuadrado, I.; Moran, M.; Casado, C. M.; Alonso, B.; Lobete, F.; Garcia, B.; Ibisate, M.; Losada, J. *Organometallics* **1996**, *15*, 5278.
538. Alonso, B.; Moran, M.; Casado, C. M.; Lobette, F.; Losada, J.; Cuadrado, I. *Chem. Mater.* **1995**, *7*, 1440.
539. Losada, J.; Cuadrado, I.; Moran, M.; Casado, C. M.; Alonso, B.; Barranco, M. *Anal. Chim. Acta* **1997**, *338*, 191.
540. Takada, K.; Diaz, D. J.; Abruna, H. D.; Cuadrado, I.; Casado, C.; Alonso, B.; Moran, M.; Losada, J. *J. Am. Chem. Soc.* **1997**, *119*, 10763.
541. Gonzalez, B.; Casado, C. M.; Alonso, B.; Cuadrado, I.; Moran, M.; Wang, Y.; Kaifer, A. E. *Chem. Commun.* **1998**, 2569.
542. Castro, R.; Cuadrado, I.; Alonso, B.; Casado, C. M.; Moran, M.; Kaifer, A. E. *J. Am. Chem. Soc.* **1997**, *119*, 5760.
543. Kaifer, A. E. *Acc. Chem. Res.* **1999**, *32*, 62.
544. Valerio, C.; Fillaut, J.-L.; Ruiz, J.; Guittard, J.; Blais, J.-C.; Astruc, D. *J. Am. Chem. Soc.* **1997**, *119*, 2588.
545. Daniel, M. C.; Ruiz, J.; Astruc, D. *J. Am. Chem. Soc.* **2003**, *125*, 1150.
546. Cuadrado, I.; Casado, C. M.; Alonso, B.; Moran, M.; Losada, J.; Belsky, V. *J. Am. Chem. Soc.* **1997**, *119*, 7613.
546a. Alonso, B.; González, B.; García, B.; Ramírez-Oliva, E.; Zamora, M.; Casado, C. M.; Cuadrado, I. *J. Organomet. Chem.* **2001**, *637–639*, 642.
547. Alvarez, J.; Ren, T.; Kaifer, A. E. *Organometallics* **2001**, *20*, 3543.
548. Köllner, C.; Pugin, B.; Togni, A. *J. Am. Chem. Soc.* **1998**, *120*, 10274.
549. Liao, Y.-H.; Moss, J. R. *J. Chem. Soc. Chem. Commun.* **1993**, 1774.
550. Liao, Y.-H.; Moss, J. R. *Organometallics* **1995**, *14*, 2130.
551. Liao, Y.-H.; Moss, J. R. *Organometallics* **1996**, *15*, 4307.
552. Seyferth, D.; Kugita, T.; Rheingold, A. L.; Yap, G. P. A. *Organometallics* **1995**, *14*, 5362.
553. Feeder, N.; Geng, J. F.; Goh, P. G.; Johnson, B. F. G.; Martin, C. M.; Shephard, D. S.; Zhou, W. Z. *Angew. Chem., Int. Ed.* **2000**, *39*, 1661.
554. Jutzi, P.; Batz, C.; Neumann, B.; Stammler, H.-G. *Angew. Chem., Int. Ed. Engl.* **1996**, *35*, 2118.
555. Moulines, F.; Djakovitch, L.; Boese, R.; Gloaguen, B.; Theil, W.; Fillaut, J.-L.; Delville, M.-H.; Astruc, D. *Angew. Chem., Int. Ed. Engl.* **1993**, *32*, 1075.
555a. Marvaud, V.; Astruc, D. *Chem. Commun.* **1997**, 773.
556. Rigaut, S.; Delville, H. M.; Astruc, D. *J. Am. Chem. Soc.* **1997**, *119*, 11132.
557. Huck, W. T. S.; Hulst, R.; Timmerman, P.; van Veggel, F. C. J. M.; Reinhoudt, D. N. *Angew. Chem., Int. Ed. Engl.* **1997**, *36*, 1006.
558. van Manen, H. J.; van Veggel, F. C. J. M.; Reinhoudt, D. N. *Top. Curr. Chem.* **2001**, *217*, 121.
559. Achar, S.; Puddephatt, R. J. *Angew. Chem., Int. Ed. Engl.* **1994**, *33*, 847.
560. Achar, S.; Vittal, J.; Puddephatt, R. J. *Organometallics* **1996**, *15*, 43.

561. Achar, S.; Vittal, J.; Puddephatt, R. J. *Chem. Commun.* **1994**, 1895.
562. Achar, S.; Puddephatt, R. J. *Organometallics* **1995**, *14*, 1681.
563. Liu, G.-X.; Puddephatt, R. J. *Inorg. Chim. Acta* **1996**, *251*, 319.
564. Liu, G.-X.; Puddephatt, R. J. *Organometallics* **1996**, *15*, 5257.
565. Roland, B. K.; Carter, C.; Zheng, Z. *J. Am. Chem. Soc.* **2002**, *124*, 6234.
566. Zhao, M.; Sun, L.; Crooks, R. M. *J. Am. Chem. Soc.* **1998**, *120*, 4877.
567. Balogh, L.; Tomalia, D. A. *J. Am. Chem. Soc.* **1998**, *120*, 7355.
568. Zhao, M.; Crooks, R. M. *Angew. Chem., Int. Ed.* **1999**, *38*, 364.
569. Onitsuka, K.; Fujimoto, M.; Ohshiro, N.; Takahashi, S. *Angew. Chem., Int. Ed.* **1999**, *38*, 689.
570. Onitsuka, K.; Kitajima, H.; Fujimoto, M.; Iuchi, A.; Takahashi, S. *Chem. Commun.* **2002**, 2576.
571. Onitsuka, K.; Iuchi, A.; Fujimoto, M.; Takahashi, S. *Chem. Commun.* **2002**, *8*, 741.
572. McDonagh, A. M.; Humphrey, M. G.; Samoc, M.; Luther-Davies, B. *Organometallics* **1999**, *18*, 5195.
573. Hurst, S. K.; Cifuentes, M. P.; Humphrey, M. G. *Organometallics* **2002**, *21*, 2353.
574. Deschenaux, R.; Serrano, E.; Levelut, A. M. *Chem. Commun.* **1997**, 1577.
575. Dardel, B.; Deschenaux, R.; Even, M.; Serrano, E. *Macromolecules* **1999**, *32*, 5193.

12.07
Organometallic Magnetic Materials

E Coronado and J R Galán-Mascarós, Universidad de Valencia, Valencia, Spain
J S Miller, University of Utah, Salt Lake City, UT, USA

12.07.1 Introduction

Molecule-based materials exhibiting cooperative physical properties constitute one of the most active areas of interest in contemporary materials chemistry and science. An attractive chemical feature of these materials is the synthetic versatility provided by molecular chemistry. From the point of view of the physical properties, molecule-based materials can exhibit the properties of interest usually associated with the inorganic network solids,[1] as for example, high DC metal-like electrical conductivity and superconductivity,[2] ferromagnetism,[3–25] and non-linear optical responses.[26,27]

While the first molecule-based magnet was reported in 1967 with the synthesis of $[Fe(S_2CNEt_2)_2Cl]$, the field did not gain momentum until the first organic-based magnet, an organometallic-based magnet, $[Fe^{III}Cp^*_2]^{\cdot+}[TCNE]^{\cdot-}$ (*vide infra*), was reported in 1985.[28–30] The former material exhibits ferromagnetism below $T_c = 2.43$ K,[31] while the latter is a magnet at 4.8 K.[28] Since then, many other molecule-based ferromagnets have been prepared, with some of them exhibiting critical temperatures above room temperature. Besides the perennial pursuit to develop new molecule-based magnets, a current trend is to develop so-called multifunctional magnetic materials (i.e., materials that combine magnetism with a second property of interest, such as conductivity[32–35] or optical activity).[36–38] Another trend is to develop nanomagnets (i.e., uniform molecules of nanometer size that behave as magnets or as so-called single molecule magnets).[39,40]

Organometallic chemistry provides remarkable examples of molecule-based magnets, and more recently of multifunctional magnetic materials. These magnets fall into two major categories, namely, molecule-based magnets possessing M–C bonds and those derived from reactions involving, typically breaking, M–C bonds. This review focuses on the former class of magnetically ordered materials, which are predominately based on metallocenes. Prussian blue, $Fe^{III}_4[Fe^{II}(CN)_6]_3$, arguably can be considered as organometallic due to its Fe–C bonds, as is iron carbonyl,[41] and is the prototype of a large family of molecule-based magnets. Nonetheless, the Prussian blue family of magnets are not discussed, but several reviews are available.[42–45] Likewise, this review does not focus on molecule-based magnets prepared from organometallic

species, as typified by the reaction of either bis(benezene)vanadium(0), $V^{\circ}(C_6H_6)_2$,[46,47] or vanadium carbonyl, $V^{\circ}(CO)_6$,[48,49] and tetracyanoethylene, TCNE. The reactions form the room-temperature $V(TCNE)_x \cdot y(CH_2Cl_2)$ magnet.[50] Reactions with other electron acceptors, for example, 1,2,4,5-tetracyanopyrazine[51] with $V^{\circ}(CO)_6$, also form magnetically ordered materials, but with reduced ordering temperatures.[52–54]

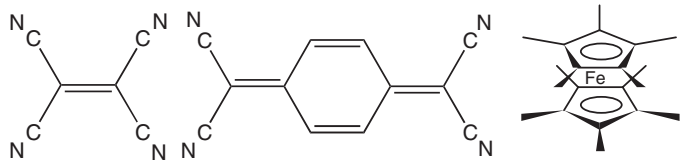

12.07.2 Magnetic Charge-Transfer Salts Based on Metallocenes

While targeting to make a new molecule-based conductor from the reaction of TCNQ (TCNQ = 7,7,8,-tetracyano-*p*-quinodimethane) and decamethylferrocene, $Fe^{II}(C_5Me_5)_2$, $[Fe^{III}(C_5Me_5)_2]^{\cdot+}[TCNQ]^{\cdot-}$ was prepared and characterized to magnetically order as a metamagnet; that is, it had an antiferromagnetic ground state, which above a critical field, H_c, of 1.3 kOe, had a transition to a high-moment ferromagnetic-like state.[55,56] This unexpected and unusual observation of magnetic ordering, albeit to an antiferromagnetic state that had a low-lying ferromagnetic-like state,[29,57] led to a new paradigm for the stabilization of the ferromagnetic ground state. As magnetic ordering requires spin coupling in the bulk, the use of a smaller radical anion acceptor should provide stronger spin coupling. $[TCNE]^{-}$ was selected as it has the identical spin ($S = 1/2$), but as it is delocalized over fewer atoms and is one-half the size, it would nominally have twice the spin density, and being smaller should lead to enhanced spin coupling and stabilization of the ferromagnetic with respect to the antiferromagnetic ground state. Hence, $[Fe^{III}(C_5Me_5)_2]^{+}[TCNE]^{-}$ was designed, synthesized, and subsequently characterized to be a bulk ferromagnet with an ordering temperature, T_c, of 4.8 K, and a coercivity, H_{cr}, of 1 kOe at 2 K.[28,58–60]

With the discovery of $[Fe^{III}(C_5Me_5)_2]^{+}[TCNE]^{-}$ as the first organic-based magnet in addition to its detailed characterization of its physical and magnetic properties, many related materials were synthesized. These new materials were based on substitution of pendant groups on the cyclopentadienyl ring, expansion of the ring, substitution of iron with other metal ions, and replacement of the TCNE with alternative electron acceptors. Aspects of these studies are summarized elsewhere.[61–63] Due to the availability of several reviews covering different aspects of the magnetic behavior of metallocenium-based molecule-based magnets, this review covers specific aspects that have recently been reported.

Electron-transfer salts of metallocenes and strong electron acceptors have provided numerous magnetically interesting materials. This is, in part, a consequence of formation of metallocenium cations that are paramagnetic. Table 1 lists the physical properties of metallocenes and decamethylmetallocenes as well as their cations. While $Co^{II}Cp_2$ and $Co^{II}Cp^{*}_2$ (Cp = cyclopentadienide; Cp^{*} = decamethylcyclopentadienide) have an $S = 1/2$ ground state, and could form a donor–acceptor complex with, for example, a neutral organic radical (e.g., a nitronyl nitroxide), and might have sufficient spin coupling to magnetically order, such materials have not been reported. The $[Co^{III}Cp_2]^{+}$ and $[Co^{III}Cp^{*}_2]^{+}$ cations can easily form electron-transfer salts with electron acceptors, for example, TCNE, but these cations are diamagnetic and form only paramagnetic electron-transfer salts. Ferrocene and TCNE react via Equation (1) to form a diamagnetic charge-transfer complex of $[Fe^{II}Cp_2]^{\circ}[TCNE]^{\circ}$ composition.[64–68] In contrast, $FeCp^{*}_2$, as occurs for all methyl-substituted metallocenes, is easier to oxidize by ~0.05 V/Me group; hence, it is ~0.50 V easier to oxidize than $Fe^{II}Cp_2$ and reacts with TCNE to form the paramagnetic electron-transfer salt of $[Fe^{III}Cp^{*}_2]^{+}[TCNE]^{-}$ composition[58] (Equation (2)).

$$FeCp_2 + TCNE \rightarrow [Fe^{II}Cp_2]^{\circ}[TCNE]^{\circ} \text{ (light green)} \quad (1)$$

$$FeCp^{*}_2 + TCNE \rightarrow [Fe^{III}Cp^{*}_2]^{\cdot+}[TCNE]^{\cdot-} \text{ (dark green)} \quad (2)$$

The original report of the preparation of $[Fe^{II}Cp_2]^{\circ}[TCNE]^{\circ}$ described that it exhibited ferromagnetic behavior. A subsequent reinvestigation revealed the presence of Fe(III) via ^{57}Fe Mössbauer spectroscopy, and that decomposition induced from the grinding synthesis undoubtedly was the source of the magnetic impurity.[64]

Table 1 Electronic structure and ground-state as well as Landé *g* values and reduction potentials (vs. SCE) of metallocenes and decamethylmetallocenes as well as their cations, $[MCp_2]^{z+}$[69]

M	*Cp*	*z*	*S*	*State*	*Electronic structure*	$g_{\|}$	$g_{\perp}$	g_x	g_y	<*g*>	*Ip* (eV)	$E_o^{+/o}$ (V)
Co	Cp_2	0	1/2	$^2E_{1g}$	$e_{2g}^4a_{1g}^2e_{1g}^1$	1.638		1.637	1.627	1.634	5.55	−0.91
Co	Cp_2	+	0	$^1A_{1g}$	$e_{2g}^4a_{1g}^2$							
Co	Cp^*_2	0	1/2	$^2E_{1g}$	$e_{2g}^4a_{1g}^2e_{1g}^1$	1.754		1.693	1.733	1.727	4.705	−1.47
Co	Cp^*_2	+	0	$^1A_{1g}$	$e_{2g}^4a_{1g}^2$							
Cr	Cp_2	0	1	$^3E_{2g}$	$e_{2g}^3a_{1g}^1$						5.7	−0.55
Cr	Cp_2	+	3/2	$^4A_{2g}$	$e_{2g}^2a_{1g}^1$	2.002	1.977			1.985		
Cr	Cp^*_2	0	1	$^3E_{2g}$	$e_{2g}^3a_{1g}^1$						4.93	−1.04
Cr	Cp^*_2	+	3/2	$^4A_{2g}$	$e_{2g}^2a_{1g}^1$	1.99	2.01			2		
Fe	Cp_2	0	0	$^1A_{1g}$	$e_{2g}^4a_{1g}^2$						6.86	0.41
Fe	Cp_2	+	1/2	$^2E_{2g}$	$e_{2g}^3a_{1g}^2$	4.35	1.26			2.29		
Fe	Cp^*_2	0	0	$^1A_{1g}$	$e_{2g}^4a_{1g}^2$						5.88	−0.12
Fe	Cp^*_2	+	1/2	$^2E_{2g}$	$e_{2g}^3a_{1g}^2$	4.433	1.35			2.378		
Mn	Cp_2	0	5/2	$^6A_{1g}$	$e_{2g}^1a_{1g}^1e_{1g}^2$	3.53	1.14			1.94	6.26	
Mn	Cp_2	+	1	$^3E_{2g}$	$e_{2g}^3a_{1g}^1e_{1g}^1$							
Mn	Cp^*_2	0	1/2	$^2E_{2g}$	$e_{2g}^3a_{1g}^2$	3.33	1.64			2.2	5.33	−0.56
Mn	Cp^*_2	+	1	$^3E_{2g}$	$e_{2g}^3a_{1g}^1$							
Ni	Cp_2	0	1	$^3A_{1g}$	$e_{2g}^4a_{1g}^2e_{1g}^2$						6.5	−0.09
Ni	Cp_2	+	1/2	$^2E_{1g}$	$e_{2g}^4a_{1g}^2e_{1g}^1$	1.75		1.83	1.87	1.82		
Ni	Cp^*_2	0	1	$^3A_{2g}$	$e_{2g}^4a_{1g}^2e_{1g}^2$						5.82	−0.65
Ni	Cp^*_2	+	1/2	$^2E_{1g}$	$e_{2g}^4a_{1g}^2e_{1g}$	1.831		1.973	2.014	1.939		
Os	Cp_2	0	0	$^1A_{1g}$	$e_{2g}^4a_{1g}^2$							0.84
Os	Cp_2	+	1/2									
Os	Cp^*_2	0	0	$^1A_{1g}$	$e_{2g}^4a_{1g}^2$							
Os	Cp^*_2	+	1/2	$^2A_{1g}$	$e_{2g}^4a_{1g}^1$	5.26	2.06			3.1		0.22
Re	Cp^*_2	0	1/2	$^2E_2$		5.08	0.34					
Ru	Cp_2	0	0	$^1A_{1g}$	$e_{2g}^4a_{1g}^2$						7.45	0.96
Ru	Cp^*_2	0	0	$^1A_{1g}$	$e_{2g}^4a_{1g}^2$							0.55
Ru	Cp^*_2	+	1/2			2.059	2.008			2.025		
V	Cp_2	0	3/2	$^4A_{2g}$	$e_{2g}^2a_{1g}^1$	1.988	2.001			1.997	6.81	−0.55
V	Cp^*_2	0	3/2	$^4A_{2g}$	$e_{2g}^2a_{1g}^1$	2.005	1.996			1.999	5.85	

Over the past two decades several magnetically ordered materials have been made from first-row MCp^*_2 (M = Cr, Mn, Fe), but neither from MCp_2 nor second-row metal ions.[61–63] The failure to report MCp_2-based magnets most likely arises from the lack of trying. Nonetheless, as MCp_2 are smaller than MCp^*_2, they should enable shorter separations between spin sites, which in turn should lead to stronger spin couplings, and higher magnetic ordering temperatures. Electron-transfer salts based on $Mn^{II}Cp_2$ will be challenging to prepare due to it being less stable with respect to $Mn^{II}Cp^*_2$.

The most thoroughly studied magnetically ordered systems are $[MCp^*_2][TCNE]$ and $[MCp^*_2][TCNQ]$ (M = Cr, Mn, Fe), which all order as ferromagnets (Table 2,[56,73–79] Figure 1). Of these, the best studied is $[FeCp^*_2][TCNE]$.[61–63] The properties of $[MCp^*_2][TCNQ]$ follow the same trends as observed for $[MCp^*_2][TCNE]$, the T_c's increase as Mn > Fe > Cr, but TCNE-based magnets all have higher T_c's. The genesis of this trend is unknown, as it does not obey the mean-field prediction of $T_c \propto S$ (as $S_{Cr} > S_{Mn} > S_{Fe}$). This trend is also evident for the $[MCp^*_2]^+[C_2(CN)_3OAc]^-$ (M = Cr, Mn, Fe) family, albeit they exhibit more complex magnetic behaviors.[70] Furthermore, two polymorphs of $[FeCp^*_2][TCNQ]$ have been reported: one that has a metamagnetic ground state ($T_c \sim 2.6$ K),[55,56,71] and the other has a ferromagnetic ground state ($T_c \sim 3.0$ K).[56,72]

12.07.2.1 Structure of Magnetically Ordered $[MCp^*_2]$[acceptor]

All magnetically ordering electron-transfer salts possess one-dimensional (1-D) chains of alternating $[MCp^*_2]^+$ and $[acceptor]^-$, as typified by $[FeCp^*_2][TCNE]$, (Figure 2). This motif is observed for $[FeCp^*_2][TCNE]$, which has been extensively studied, and $[FeCp^*_2][TCNE]\cdot MeCN$, and the former and latter have Fe···Fe separations of 10.621 and 10.415 Å, respectively. Furthermore, the MeCN solvent in the latter forms sheets separating layers of 1-D chains (Figure 3(b)). This reduces the spin coupling across the sheets thereby reducing T_c, as observed (*vide infra*).

Table 2 Summary of the magnetic properties of magnetically ordered [MCp*$_2$][TCNE] and [MCp*$_2$][TCNQ]

$[MCp^*_2]^+$, M^{III}	*Fe*	*Mn*[73]	*Cr*[74–76,d]	*Cr*[77d]	*Fe*[56d]	*Fe*[56,72d]	*Mn*[78]	*Cr*[79]
Acceptor	TCNE	TCNE	TCNE	TCNE	TCNQ	TCNQ	TCNQ	TCNQ
S	1/2	1	3/2	3/2	1/2	1/2	1	3/2
θ, K	16.9[c]	22.6	22.1	12.6	3.8	10	10.5	11.6
T_c, K	4.8	8.8	3.65	2.1	3.0	2.6	6.2	3.1
H_{coer},[c] Oe	1000	1200	[a]	[b]	15		3600	[b]
H_c,[c] Oe						1300		
M_s, emu Oe mol^{-1}	16 300	20 000	24 000	19 000	16 650	13 400	16 700	22 500
M, emu Oe mol^{-1}	16 000	6800	[a]	[b]	2000	[a]	13 700	[b]

[a]None.
[b]Not reported.
[c]2 K.
[d]One of two polymorphs.
[e]$\theta_{\|} = 30$ K.

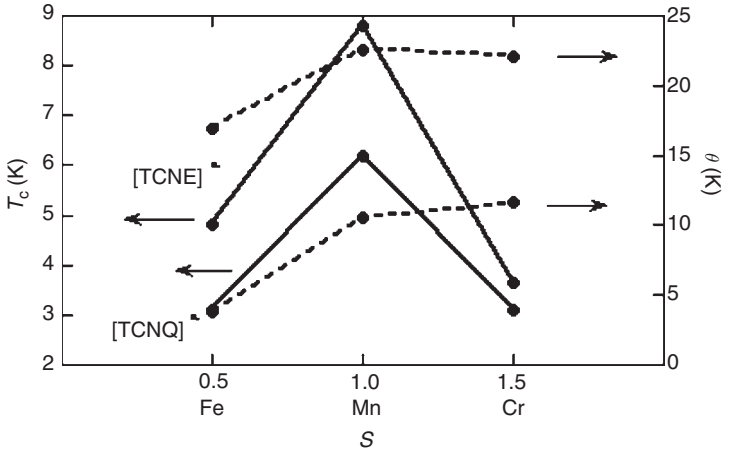

Figure 1 The T_c and θ dependencies as a function of S for [MCp*$_2$][TCNE] and [MCp*$_2$][TCNQ] (M = Cr, Mn, Fe).

Figure 2 Structure of a segment of a 1-D chain of [FeCp*$_2$][TCNE] with alternating [FeCp*$_2$]$^+$ and [TCNE]$^-$ observed for both [FeCp*$_2$][TCNE]·MeCN and [FeCp*$_2$][TCNE].[59]

The intra- and interchain interactions can be schematically summarized in Figure 4. From a simplistic nearest-neighbor model, there is one intrachain interaction, J_z, and three interchain interactions arising between two acceptors (A), J_{AA}, two metallocenium cations (D), J_{DD}, or between a cation and acceptor, J_{DA}. These interactions can have different magnitudes and either be ferromagnetic ($J > 0$) or antiferromagnetic coupling ($J < 0$). The

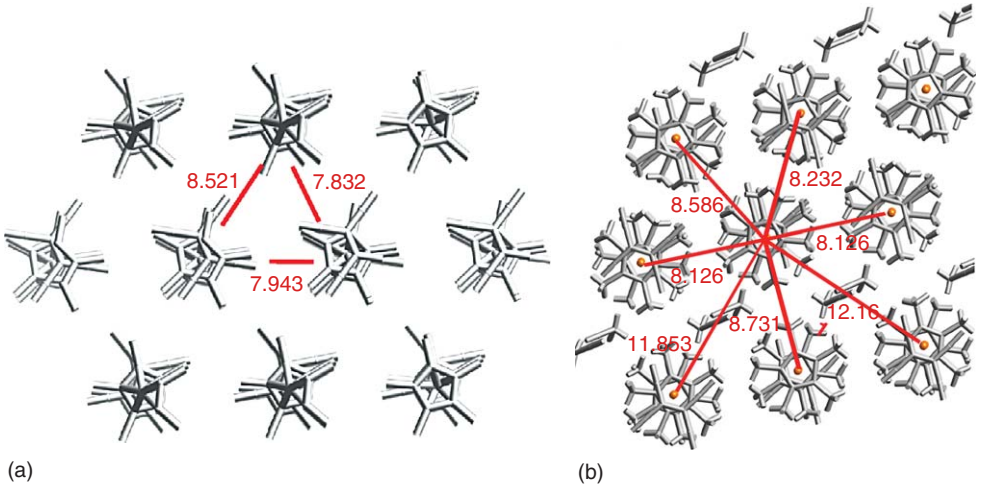

Figure 3 Structure of the parallel 1-D chains of [FeCp*$_2$][TCNE] for (a) [FeCp*$_2$][TCNE] (Me groups excluded), and (b) [FeCp*$_2$][TCNE]·MeCN showing the intrachain separations.[59]

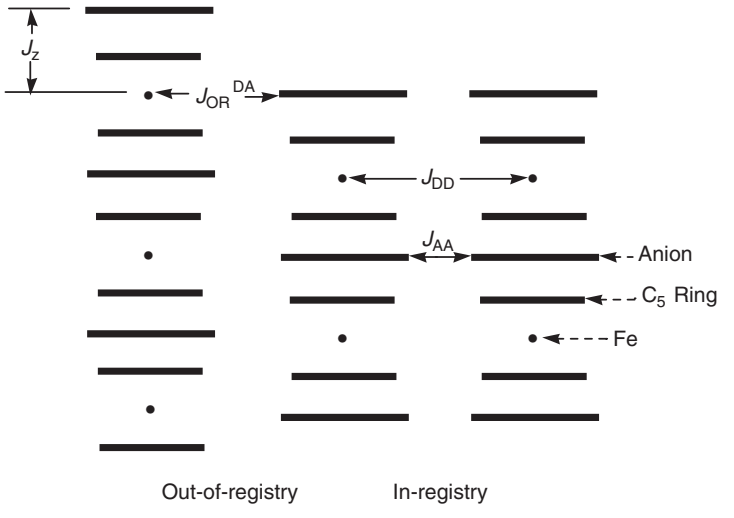

Figure 4 Schematic illustration of intra- and in-registry and out-of-registry interchain interaction present for magnetically ordered [MCp*$_2$][anion].[80] Reprinted with permission from the copyright owner (in process of obtaining).

observed magnetic behavior is the consequence of summation of all of these interactions in the lattice, and even small changes can lead to different behaviors.[80] For example, [FeCp*$_2$][TCNQ] forms three different polymorphs: having metamagnetic, ferromagnetic, or paramagnetic ground state. Their intrachain interactions for the ferromagnetic and metamagnetic polymorphs are shown in Figure 5, and while qualitatively all the inter- and intrachain interactions are similar, differences in their distances and relative orientations lead to different magnetic ground states.

12.07.2.2 TCNQ-based Magnets

As noted above, several polymorphs of [FeCp*$_2$][TCNQ] composition have been isolated. [FeCp*$_2$]$_2$[TCNQ]$_2$ forms a herringbone arrangement that has diamagnetic [TCNQ]$_2^{2-}$ dimers flanked by $S = 1/2$ [FeCp*$_2$]$^+$ cations, and is the paramagnetic phase.[71] The two other phases are different packings of the typical 1-D chain of alternating $S = 1/2$ [FeCp*$_2$]$^+$ cations $S = 1/2$ [TCNQ]$^-$ anions (Figures 2 and 5).[71,72] The arrangement on the left of Figure 5 has an antiferromagnetic ground state, and above a critical field of 1300 Oe has a ferromagnetic-like state.[56] Hence, it is a metamagnet (Figure 6). In contrast, the structural arrangement on the right of Figure 5 has a ferromagnetic ground

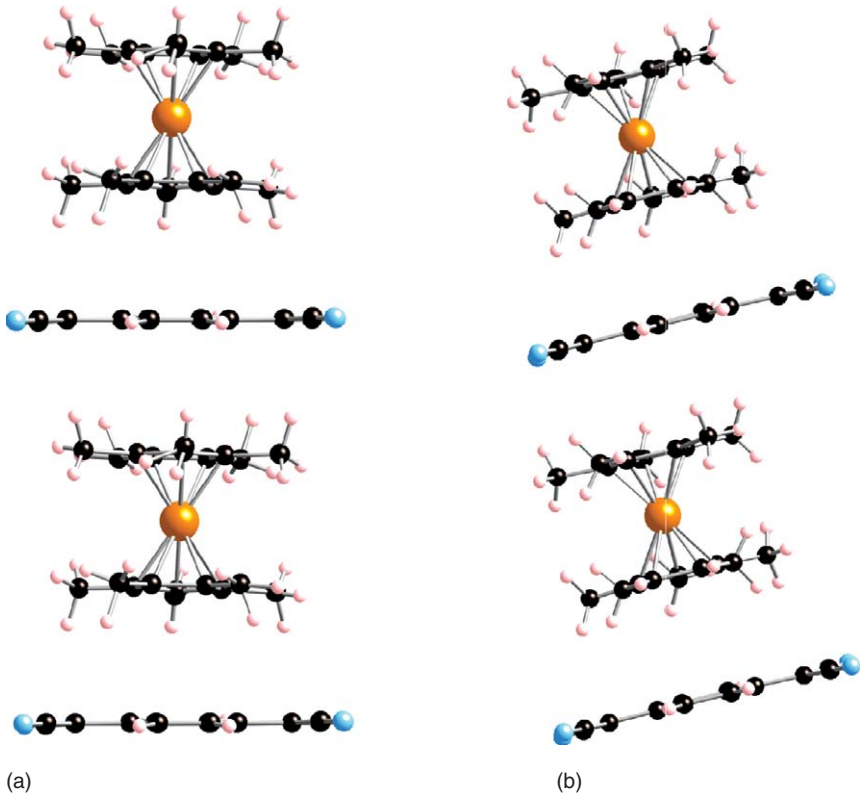

Figure 5 Segment of 1-D chain looking edgewise at the TCNQ for (a) metamagnetic[71] and ferromagnetic[72] polymorphs of [FeCp*$_2$][TCNQ]. The Fe···Fe separations are 10.550 and 10.837 Å, respectively.

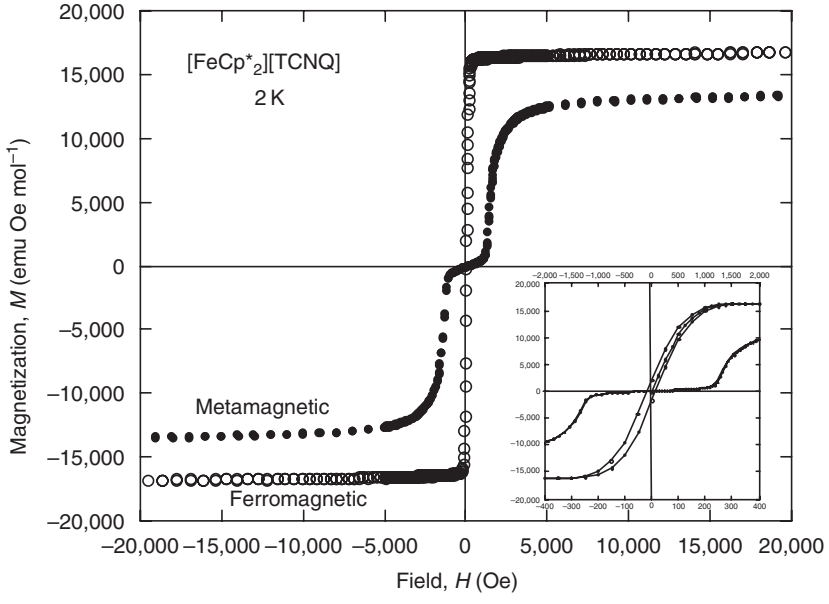

Figure 6 *M*(*H*) data for both the ferro- and metamagnetic phases of [FeCp*$_2$][TCNQ].[56]

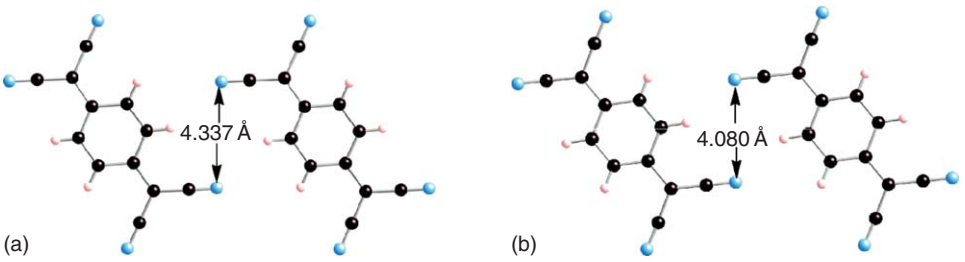

Figure 7 In-registry $[TCNQ]^{\cdot-}\cdots[TCNQ]^{\cdot-}$ interactions for (a) ferromagnetic and (b) metamagnetic polymorphs of $[FeCp^*_2][TCNQ]$.[71,72]

state below 3 K, (Figure 6). The most obvious structural difference between the meta- and ferromagnetic phases lies in the shorter 4.080 Å $[TCNQ]^{\cdot-}\cdots[TCNQ]^{\cdot-}$ interaction for the metamagnetic phase with respect to the longer 4.337 Å separation for the ferromagnetic phase (Figure 7). This interaction should be antiferromagnetic and the shorter separation would favor an antiferromagnetic ground state, as observed.

12.07.2.3 Electron Acceptors that Stabilize Magnetic Ordering

In addition to $[TCNE]^{\cdot-}$ and $[TCNQ]^{\cdot-}$ electron-transfer salts of decamethylmetallocenes stabilizing magnetically ordered ground states, others have been successfully used.[61–63] These include dimethyl and diethyl dicyanofumarate $\{[R(O)OC(CN)]_2$ (R = Me, Et)}, tricyanoethylenecarboxylate $\{[C_2(CN)_3OAc]^-\}$, 2,3-dihalo-5,6-dicyanoquinone (DCX_2Q; X = Cl, Br, I), 2,3-dicyano-1,4-naphthoquinone (DCNQ) 2,5-dimethyl-*N*,*N*′-dicyanoquinodiimine (Me_2DCNQI), 1,4,9,10-anthracenetetrone (ATO), bis(ethylenedithiolate)nickelate(III) $\{Ni(S_2C_2H_2)_2]^{\cdot-}\}$, bis-(benzenedithiolate)nickelate(III) $\{Ni(S_2C_6H_4)_2]^{\cdot-}\}$, bis(toluenedithiolate)nickelate(III) $\{[Ni(S_2C_6H_3Me)_2]^{\cdot-}\}$, and bis(2-thioxo-1,3-dithiole-4,5-dithiolate)nickelate(III), $\{[Ni(dmit)_2]\cdot^-\}$. Two types of magnetic states are stabilized, namely, ferromagnetic and metamagnetic states (Table 3). The ditholate-based magnetic materials have also been reviewed.[61,81] This means that in general they are comparable in energy and subtle changes in the intra- and interchain couplings can alter their ferro- or antiferromagnetic ground state. This is evident as application of a relatively small applied field [<10 000 Oe (~1 K, ~0.7 kcal mol^{-1})] switches the antiferromagnetic into a ferromagnetic-like state.

Table 3 Summary of the Weiss constants, θ, and critical temperatures, T_c, of magnetically ordered $[M^{III}Cp^*_2]^+$-based magnets

Magnet	θ (K)	T_c (K)	*Type*[e]	H_{coer},[b] Oe (*T*, K)	H_c,[c] kOe (*T*, K)	*References*
$[CrCp^*_2][DCNQ]$	6	4	M		~0 (1.8)	90
$[CrCp^*_2][Et(O)OC(CN)]_2$	*22*	5.4	M		~0[a]	90
$[CrCp^*_2][Me(O)OC(CN)]_2$	*23*	5.7	F	<50 (1.8)		91
$[CrCp^*_2][TCNE]$	*22.2*	3.65	F	~0 (2)		74
$[CrCp^*_2][TCNE]$	12.2	2.1	F	~0[a]		77
$[CrCp^*_2][TCNQ]$	12.8	3.1	F	~0[a]		79
$[FeCp^*_2][ATO]$	10	3	F	1000 (1.8)		92
$[FeCp^*_2][DCNQ]$	4.0	4.0	M	1200 (1.8)	3 (1.8)	85
$[FeCp^{\#}_2]$[f][DCNQ]	6.8	4.1	M		*2* (1.8)	87
$[FeCp^*_2][Me_2DCNQI]$	3.1	3.9	M		5.5 (1.7)	93
$[FeCp^*_2][Ni(S_2C_2H_2)_2]$	−9.8	3.2	M		4 (2)	94,95
$[FeCp^*_2][TCNE]$	16.9	4.8	F	1000 (2)		58
$[FeCp^*_2][TCNQ]$	3.8	3	F	15 (2)		56,72
$[FeCp^*_2][TCNQ]$	12.3	2.55	M		1.3 (2)	55,56,71
$[FeCp^*_2]_{0.855}[CoCp^*_2]_{0.145}[TCNE]$	[a]	0.75	F	[a]		96,97
$[FeCp^*_2]_{0.915}[CoCp^*_2]_{0.085}[TCNE]$	[a]	2.75	F	[a]		96
$[FeCp^*_2]_{0.923}[CoCp^*_2]_{0.077}[TCNE]$	[a]	3.8	F	[a]		96
$[FeCp^*_2]_{0.955}[CoCp^*_2]_{0.045}[TCNE]$	[a]	4.4	F	[a]		96

(*Continued*)

Table 3 (Continued)

Magnet	θ (K)	T_c (K)	*Type*[e]	H_{coer},[b] Oe (T, K)	H_c,[c] kOe (T, K)	*References*
$[FeCp^*_2][C_2(CN)_3OAc]$	18	5.7	M		0.25 (2)	70
$[MnCp^*_2][DBrDQ]$	20	[a]	M		[a]	52
$[MnCp^*_2][DClDQ]$	26.8	8.5	M		5 (2.3)	98,99
$[MnCp^*_2][DCNQ]$	11	8.0	M		3 (1.8)	86
$[MnCp^*_2][Et(O)OC(CN)]_2$	15.5	12	M		10 (1.8)	100
$[MnCp^*_2][DIDQ]$	19	[a]	M		[a]	56
$[MnCp^*_2][Me(O)OC(CN)]_2$	16	10.6	F	7000 (1.8)		100
$[MnCp^*_2][Ni(S_2C_6H_4)_2]$	[a,d]	2.3	M		0.2 (2)	94
$[MnCp^*_2][Ni(S_2C_6H_3Me)_2]$	24.6	2.1	M		0.06 (2)	101
$[MnCp^*_2][TCNE]$	22.6	8.8	F	1.2 (2)		73
$[MnCp^*_2][C_2(CN)_3OAc]$	3	7	M		5.8 (1.8)	70
$[MnCp^*_2][TCNQ]$	10.5	6.5[c]	F	3.6 (3)		78
$[MnCp^*_2]\{Ni[dmit]_2\}$	[a]	2.5	F	[a]		102
$[MnCp^*_2]\{Ni[S_2C_2(CF_3)_2]_2\}$	2.6	2.4	M		0.8 (1.85)	103
$[MnCp^*_2]\{Pd[S_2C_2(CF_3)_2]_2\}$	3.7	2.8	M		0.8 (1.85)	103
$[MnCp^*_2]\{Pt[S_2C_2(CF_3)_2]_2\}$	1.9	2.3	M		0.8 (1.85)	103

[a]Not reported.
[b]H_{coer} = coercive field.
[c]H_c = critical field.
[d]Does not obey Curie–Weiss law.
[e]F = ferromagnet; M = metamagnet.
[f]$Cp^{\#} = Fe(1,2,3\text{-}Me_3C_9H_4)_2$.

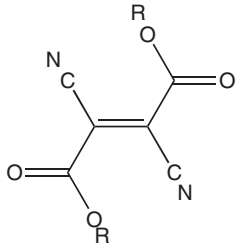

$[R(O)OC(CN)]_2$(R = Me, Et)

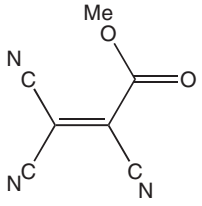

$C_2(CN)_3OAc$

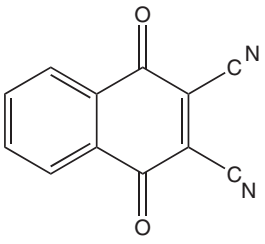

DCNQ

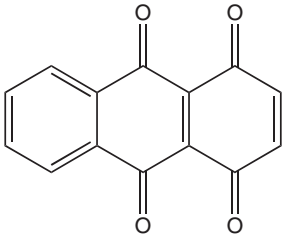

ATO

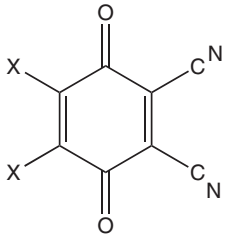

(DCX_2Q; X = Cl, Br, I)

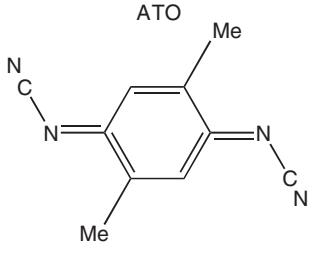

Me_2DCNQI

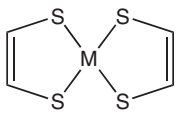

$[M(S_2C_2H_2)_2]^{\bullet-}$(M = Ni)

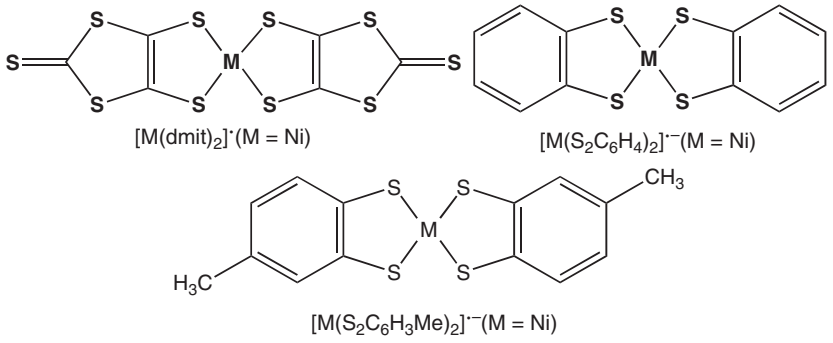

12.07.2.4 TCNE-based Magnets

$[FeCp^*_2][TCNE]$ was originally synthesized from acetonitrile as long green-reflecting needle crystals and it was these crystals that were extensively studied. These crystals did not diffract, they were a solvate of $[FeCp^*_2][TCNE]\cdot MeCN$ composition, but the solvent was easily lost, and desolvated $[FeCp^*_2][TCNE]$ was studied. The structure of $[FeCp^*_2]$-$[TCNE]\cdot MeCN$ was ultimately determined (Figure 3(b)). The structure of desolvated $[FeCp^*_2][TCNE]\cdot MeCN$, that is $[FeCp^*_2][TCNE]$, has been elusive due to $[TCNE]^{\cdot-}$ disorder; nonetheless, the major features, which are similar to that reported for $[FeCp^*_2][TCNE]\cdot MeCN$, were observed (Figure 3(a)).[58] Key differences included a 2% longer intrachain Fe···Fe separation for $[FeCp^*_2][TCNE]$ with respect to $[FeCp^*_2][TCNE]\cdot MeCN$, and two shorter interchain separations and no longer through-solvent interchain separations for $[FeCp^*_2][TCNE]$ with respect to $[FeCp^*_2][TCNE]\cdot MeCN$. The longer Fe···Fe intrachain separation suggests weaker couplings and a reduced T_c, while the shorter interchain separations suggest the opposite. In any event, the magnetic properties of $[FeCp^*_2][TCNE]\cdot MeCN$ were not reported.

Recently, using sealed tubes of $[FeCp^*_2][TCNE]\cdot MeCN$ in equilibrium with MeCN enabled the study of their magnetic properties.[82] Using the maximum in the 10 Hz AC $\chi'(T)$ data as the blocking temperature, T_f, the magnetic behavior of $[FeCp^*_2][TCNE]\cdot MeCN$ was determined. The T_f of $[FeCp^*_2][TCNE]$ was previously determined to be 5.1 K,[84] a little greater than its T_c of 4.8 K.

The in-phase $\chi'(T)$ and out-of-phase $\chi''(T)$ components of the AC susceptibility for $[FeCp^*_2][TCNE]$ and $[FeCp^*_2][TCNE]\cdot MeCN$ are identical (Figure 8) with a T_f of 4.96 K. This verifies that the loss of MeCN converts the monoclinic $[FeCp^*_2][TCNE]\cdot MeCN$ unit cell into the orthorhombic $[FeCp^*_2][TCNE]$ unit cell.[59] Both exhibit essentially no, or a minimal, frequency dependence, as ϕ, a figure-of-merit of glassiness,[83] is less than 0.01.

The $\chi'(T)$ and $\chi'''(T)$ of solvated $[FeCp^*_2][TCNE]\cdot MeCN$, however, differs significantly from that observed for $[FeCp^*_2][TCNE]$ (Figure 9). The T_f is substantially reduced by 40% to 2.87 K, and ϕ increase over 30-fold indicating extensive disorder and a glassy behavior. Similar results are observed for solvated $[FeCp^*_2][TCNE]\cdot S$ (S = EtCN, PrCN, PhCN, 1,2-$C_6H_4Cl_2$, NCC_4H_8CN).[82]

As a control, S = THF was studied. Crystals of $[FeCp^*_2][TCNE]$ prepared from THF did not have THF within the unit cell;[59] hence, no solvent effect was expected. Nonetheless, T_f unexpectedly increased by 11% to 5.50 K (Figure 10). This was ultimately attributed to pressure induced by the THF solvent that does not occur for the nitrile-based solvents. The T_f for $[FeCp^*_2][TCNE]$ is pressure dependent and increases by $\sim 0.22\,K\,kbar^{-1}$ ($P < 14$ kbar) (Figure 11).[84] Hence, the THF solvent exerts a pressure of ~2.5 kbar.

The decease in T_f for $[FeCp^*_2][TCNE]\cdot S$ is attributed to solvent in the lattice that increases the spin coupling paths, thereby reducing the ordering temperature. This is illustrated in Figure 3(b) with respect to Figure 3(a). Furthermore, the solvent in the lattice contributes to greater disorder, which manifests itself in a glass behavior as denoted by the increase in ϕ, for magnetic glassiness.

12.07.2.5 DCNQ-based Magnets

$[FeCp^*_2][DCNQ]$ orders at ~4 K as a metamagnet with a critical field (H_c) of 3 kOe at 1.8 K. As is typical for a metamagnet, it exhibits a small amount of hysteresis with a coercive field, H_{cr}, of 1.2 kOe as well as a remanence of

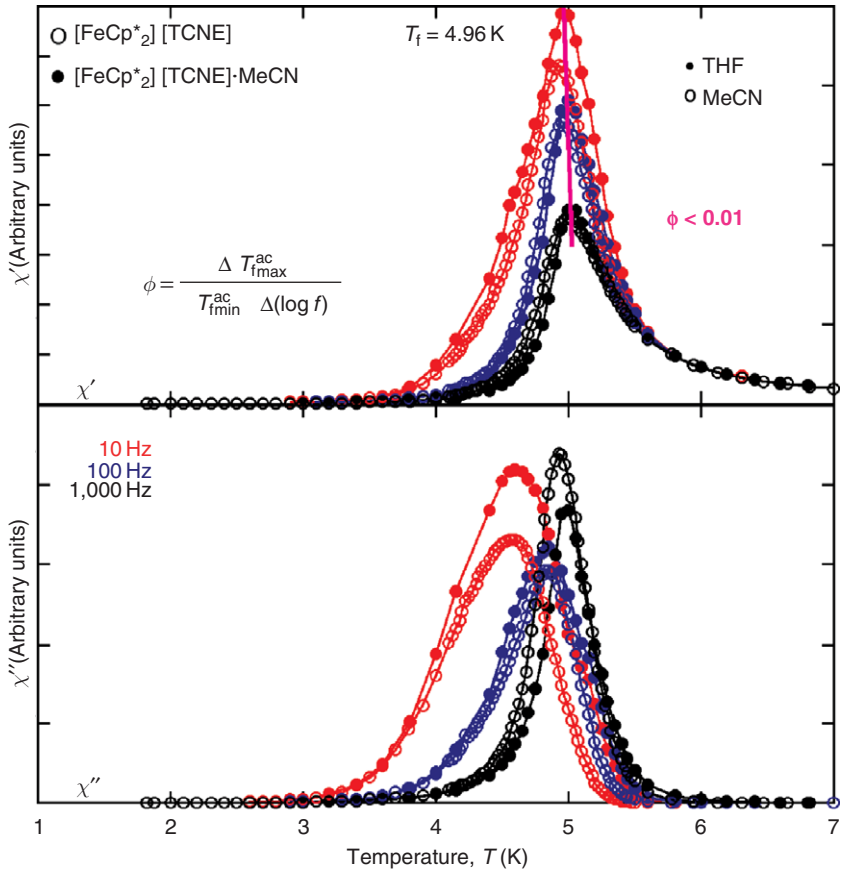

Figure 8 The temperature dependencies of the in-phase (χ') and out-of-phase (χ'') components of the AC susceptibility for [FeCp*$_2$][TCNE] (o) and [FeCp*$_2$][TCNE]·MeCN (·). Note that the lines are guide for the eyes.

500 emu Oe mol^{-1}, which is attributed to canting of the moments.[85] Application of hydrostatic pressure ($\leq$5 kbar) leads to an increase in the ordering temperature by $\sim$0.33 K kbar^{-1} as well as an increase in H_c of 1400 Oe kbar^{-1}.[29,86] Hence, the antiferromagnetic coupling increases, as pressure is applied.

The metallocenium-based magnets discussed above possess D_5-symmetry and are decamethylmetallocenium salts. Recently, the DCNQ electron-transfer salt of bis(1,2,3-trimethylindenyl)iron(II), Fe^{II}Cp$^{\#}_2$, has been reported to order as a metamagnet with an antiferromagnetic ground state and a T_c of 4.1 K and critical field, H_c, of 2000 Oe at 1.8 K.[87] The antiferromagnetic ground state is clearly evident, as while there is a absorption in $\chi'(T)$, there is no $\chi''(T)$ signal, as expected for an antiferromagnet.

The lower symmetry of the [Fe^{III}Cp$^{\#}_2$]$^+$ cation lifts the orbital degeneracies adding suspicion to the applicability of a McConnell model, which has been used to model sign of the magnetic coupling in the ground state.[88,89] Nonetheless, this model may be valid if accidental orbital degeneracies occur, or if other charge-transfer excited states mix via configurational interaction (CI) with the ground state to stabilize a high-spin ground state. Detailed computational studies are required to evaluate the importance of these alternatives. It is also curious that while the expected 1-D alternating cation and anion chain occurs for [FeCp$^{\#}_2$]$^+$[DCNQ]$^{\cdot-}$, it does not form a uniform chain, as the indenyl$\cdots$DCNQ planes alternate from 3.42 and 3.64 Å. Nonetheless, the magnetic ordering of [FeCp$^{\#}_2$]$^+$[DCNQ]$^{\cdot-}$ expands the design criteria for new molecule-based magnets based on metallocenes, as lower symmetry may suffice, whereas in the past has not been fruitful, and a uniform chain is not necessary.

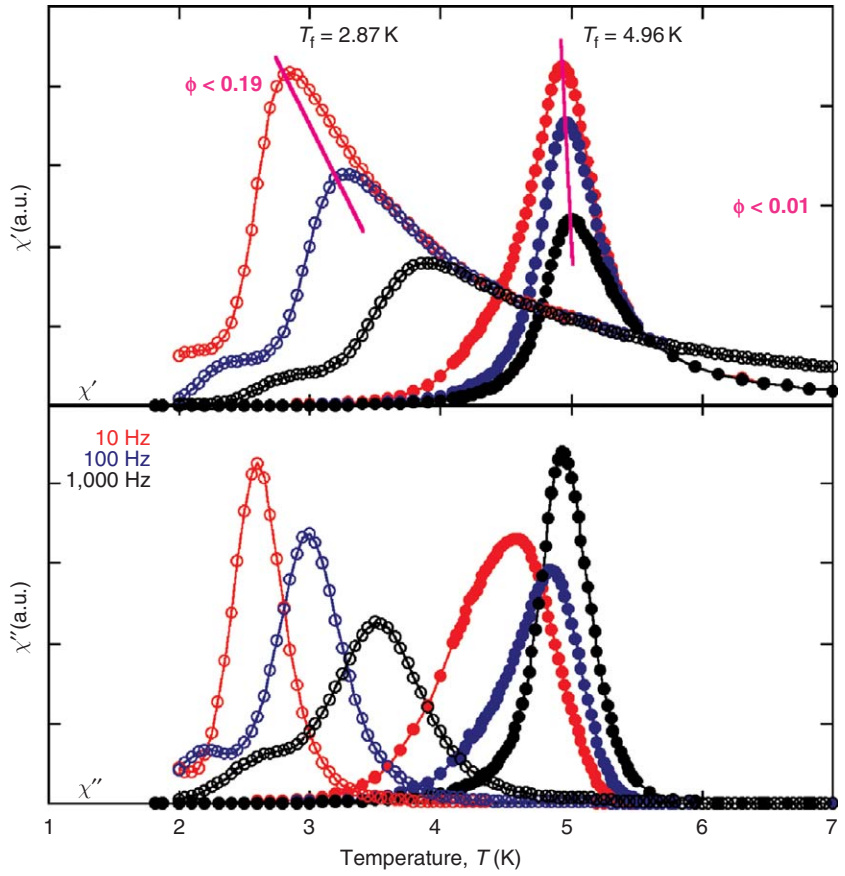

Figure 9 The temperature dependencies of the in-phase (χ') and out-of-phase (χ'') components of the AC susceptibility for [FeCp*$_2$][TCNE] (·), and solvated [FeCp*$_2$][TCNE]·MeCN (o). Note that the lines are guide for the eyes.

Bis (1,2,3-trimethylindenyl) iron(II), FeCp#$_2$

12.07.2.6 Electron-transfer Salts Based on Metallocenes and Inorganic Polyoxometalates

In addition to reacting organic aceptors with electron-donating metallocenes, inorganic polyoxometalates can be used as electron acceptors. These anions are discrete fragments of metal–oxide structures of unrivaled electronic versatility and structural variation that impact many fields of science and technology, such as chemistry, catalysis, materials science, biology, and medicine.[104] Several polyoxometalates have been combined with the $S = 1/2$

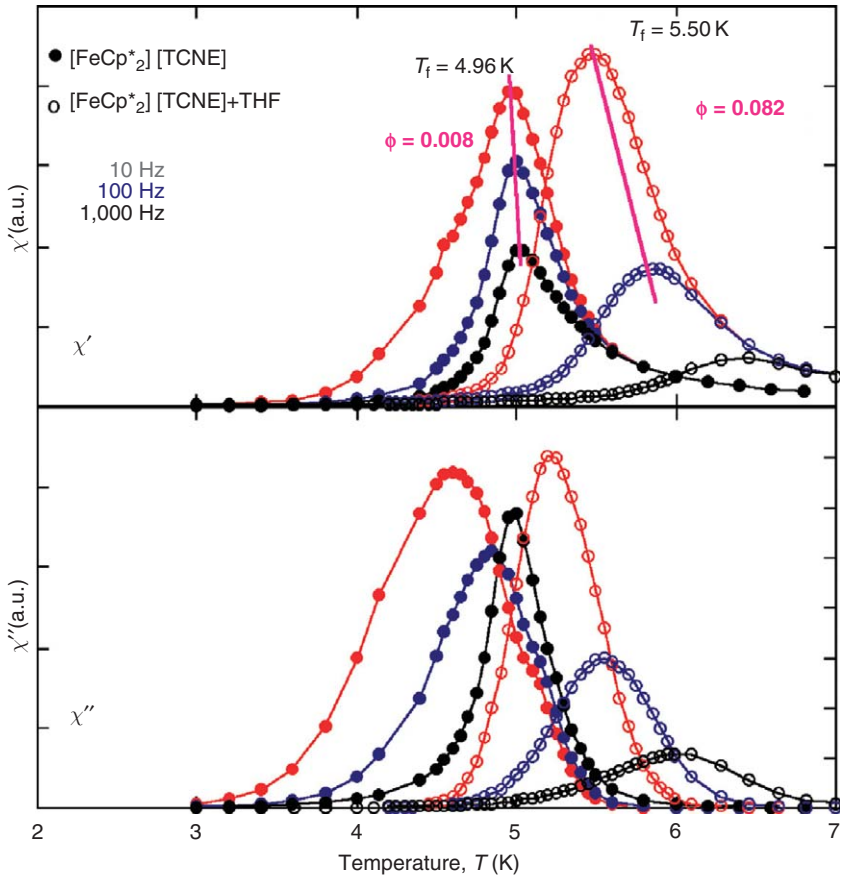

Figure 10 The temperature dependencies of the in-phase (χ') and out-of-phase (χ'') components of the AC susceptibility for [FeCp*$_2$][TCNE] (·) and [FeCp*$_2$][TCNE] in equilibrium with THF (o). Note that the lines are guide for the eyes.

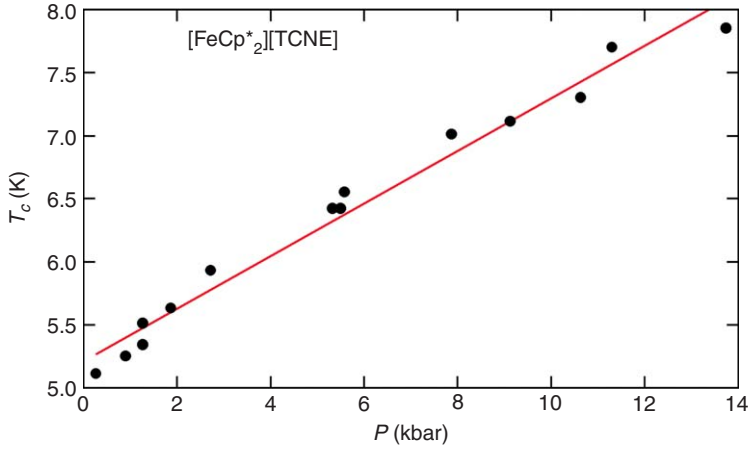

Figure 11 Pressure dependence of the T_f for [FeCp*$_2$][TCNE].[84]

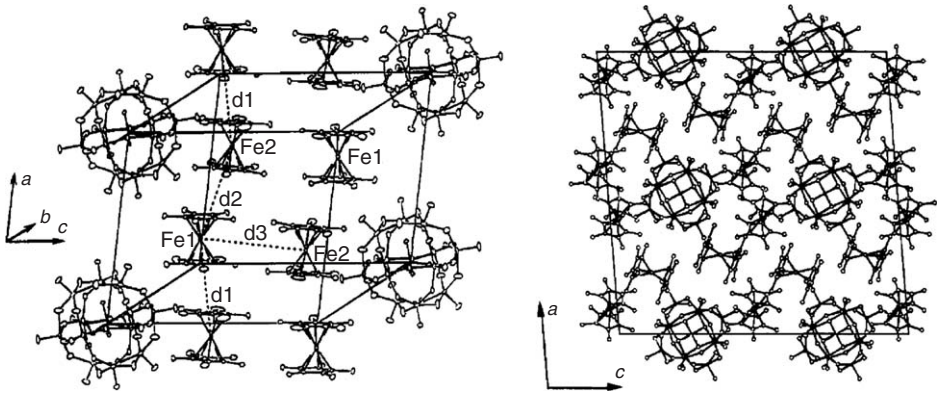

Figure 12 View of the crystal packing of the salts (a) $[FeCp^*_2]_4[SiMo^{VI}_{12}O_{40}]$ and (b) $[FeCp^*_2]_4[HFeW^{VI}_{12}O_{40}]$.[105]

decamethylferrocenium cation. The first report[105] used the Keggin anions to afford the salts $[FeCp^*_2]_4[Keggin(S)_n]$ with Keggin = $[SiMo^{VI}_{12}O_{40}]^{4-}$, $[SiW^{VI}_{12}O_{40}]^{4-}$, $[PMo^{V}Mo^{VI}_{11}O_{40}]^{4-}$ and $[HFeW^{VI}_{12}O_{40}]^{4-}$, and S = H_2O, DMF, or MeCN. The three former salts are isostructural and contain a 1-D decamethylferrocenium chain. These chains create hexagonal channels that incorporate columns of polyanions (Figure 12(a)). In turn, the Fe(III) dodecatungstate derivative exhibits a 3-D structure in which the organometallic cations form a large cuboctahedron that contains within its cavity the Keggin anion (Figure 12(b)). Despite the magnetic character of the two later polyanions (the reduced phosphomolybdate contains a delocalized spin $S = 1/2$, and the Fe(III) dodecatungstate contains a localized spin $S = 5/2$ on the iron), no magnetic interactions have been detected down to 2 K, as expected in view of the weak anion–cation contacts and large distances. This family shows the structural role played by the polyoxometalates in the stabilization of 1-D or 3-D packings for the organometallic cation. The synthesis of tertiary phases incorporating the organic acceptor TCNE has been proposed[105] to be a promising research for new molecule-based ferromagnets with increasing critical temperatures, although to date the attempts to obtain such materials have been unsuccessful.

The polyanions are diamagnetic or just contain one paramagnetic center in the above family of compounds. To increase the magnetic character of the polyanion the ferromagnetically coupled cluster $[Co_4(H_2O)_2(PW_9O_{34})_2]^{10-}$ was used.[106] A salt containing one polyoxometalate anion, two decamethylferrocenium, and eight K^+ cations in the unit cell has been obtained. In this structure the two decamethylferrocenium moieties are related by an inversion center located in the centrosymmetric tetrametallic unit Co_4O_{16} of the polyanion. An interesting structural feature of this salt, which contrasts with the K^+ salt, is that all the polyanions have the same orientation. Such a feature will enable in the future to study in detail the magnetic anisotropy of the Co_4O_{16} cluster. The magnetic properties of this hybrid salt indicate that down to 2 K the two magnetic sublattices behave independently. In fact, the maximum in χT at 9 K, characteristic of the ferromagnetic cobalt cluster, is maintained when potassium cations are changed by the organometallic magnetic cations. Thus, these magnetic cations seem to have no significant intercluster interactions.

12.07.3 Hybrid Magnets Containing Metallocenes

Oxalate-based bimetallic complexes have been used very successfully for the construction of molecule-based magnets since the beginning of the 1990s, when Okawa *et al.* reported the "templating" effect of bulky organic monocations to construct polymeric oxalate-bridged 2-D honeycomb networks (Figure 13). The general formula is $[cat^+][M^{II}M^{III}(ox)_3]$, where cat^+ represents the organic cation $[XR_4]^+$ (X = N, P), which is inserted between the extended hexagonal honeycomb anionic layers.[107] Depending on the choice of metal ions, these materials order magnetically as ferro-,[108–110] ferri-,[111–113] or weak ferromagnets,[113,114] with critical temperatures ranging from 5 up to 44 K. The formation of these magnets is controlled by the presence of the bulky cation, that also determines the interlayer separation. This interlayer separation has no significant effect in the magnetic properties.

It was also found that octahedral tris-chelated complexes of the type $[Z(bpy)_3]^{2+/3+}$ (Z = Ru^{II}, Fe^{II}, Co^{II}, Ni^{II}...; bpy = 2,2′-bipyridine) are able to induce the formation of 3-D cubic chiral 3-connected 10-gon (10,3) networks of general formula $[Z(bpy)_3][M^{II}_2(ox)_3]$ or $[Z(bpy)_3][A^{I}M^{II}(ox)_3]$ (Figure 13).[115,116] Magnetically, these compounds

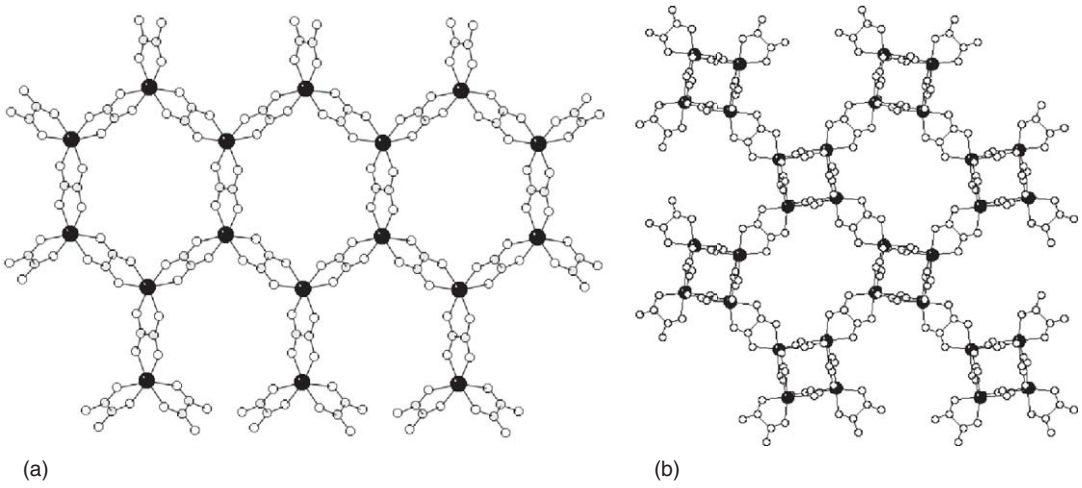

Figure 13 Scheme of (a) 2-D and (b) 3D polymeric anionic structures from oxalate bimetallic complexes of general formula $[M^{II}M^{III}(ox)_3]^-$.

presented paramagnetic behavior in most cases, with few exceptions showing weak ferromagnetism.[117] For the preparation of the analogous bimetallic 3-D networks, an extra anion is needed for electroneutrality of the network that occupies the holes left in the structure. The series $[Z(bpy)_3][ClO_4][M^{II}M^{III}(ox)_3]$ was found to behave magnetically in a similar fashion to the 2-D counterparts, but with weaker magnetic interactions.[118,119] This can be explained by the slightly longer metal-to-metal distances in these 3-D networks, and by the different relative orientation of the magnetic orbitals, due to the chirality of the materials. While in the 2-D systems adjacent metals ions always possess the opposite chirality, the 3-D systems are enantiopure.

In addition to these two major families of magnets, other types of cations, with different geometries, shapes, and charges also stabilize different extended bimetallic oxalate complexes of controlled and increased dimensionality, such as dimers,[120–122] trimers,[123–127] tetramers,[128,129] 1-D chains,[130] and 3-D extended networks from "templating" organic radicals.[131]

All these examples are based on electronically "innocent" cations. In the search for multifunctional magnets, electroactive cations were also introduced to impose a given structural type, and incorporate a second property to the solid. The most interesting results in this regard are a series of ferromagnetic molecule-based metals,[34,132–134] incorporating organic radicals, such as tetrathiafulvalene (TTF) derivatives, and a series of photoactive magnets,[135,136] by insertion of photoswitchable and NLO (non-linear optical properties) active organic cations in between the oxalate honeycomb networks (Figure 13(a)).

Following the same strategy, decamethylmetallocenium, $[MCp^*_2]^+$, has also been shown to stabilize bimetallic oxalate complexes of the 2-D honeycomb type, as in the family of organometallic-inorganic magnets of $[Z^{III}Cp^*_2][M^{II}M^{III}(ox)_3]$ ($Z(III) = Fe$, Co) composition. The most interesting feature of this family comes from the hybrid character of these materials: ferro- or ferrimagnetic layers of $[M^{II}M^{III}(ox)_3]^-$ alternate with layers of diamagnetic or paramagnetic species. In fact, this family represents the first series of chemically designed magnetic multilayers, giving the opportunity to study how the magnetic properties are affected by the mutual interactions between the two networks.

All $[Z^{III}Cp^*_2][M^{II}M^{III}(ox)_3]$ are isostructural, as determined by X-ray powder analysis. The crystal structure was solved for a single crystal of the $[FeCp^*_2][MnFe(ox)_3]$.[137] It consists of anionic layers of the well-known hexagonal honeycomb bimetallic oxalate-bridged network, formed by planar six-membered rings where each M(II) ion is connected by an oxalate bridge to three M(III) centers, and vice versa, exhibiting alternating chirality, what allows for the growth of the planar structure.

The decamethylferrocenium cations appear intercalated in between the anionic layers (Figure 14), located at the center of the hexagonal rings, and exhibit the staggered configuration with local D_{5d}-symmetry. These cations are tilted with respect to the anionic layer by 32.68° defined by the fivefold symmetry axis of the cation and the bimetallic plane. The $[FeCp^*_2]^+$ are pointing toward the center of the hexagons of two adjacent layers (Figure 14).

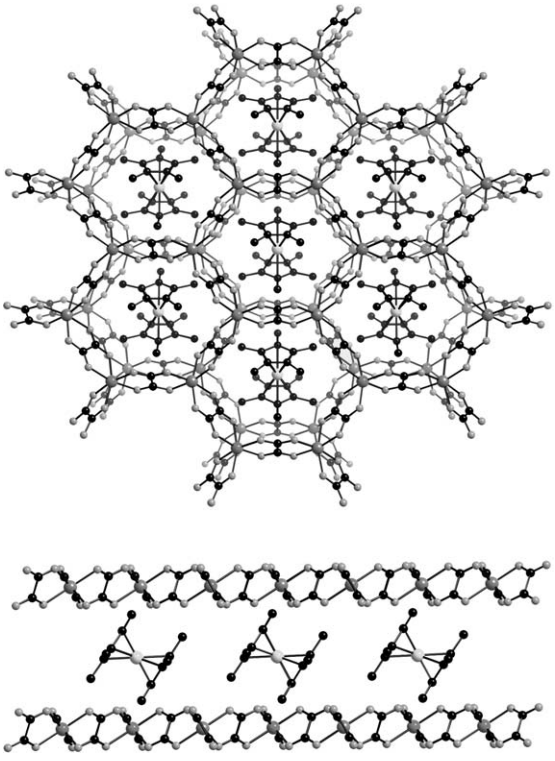

Figure 14 Top and edge views of the crystal structure of the series $[Z^{III}Cp^*_2][M^{II}M^{III}(ox)_3]$.

The interlayer separation of 9.2 Å is similar to that found in previous compounds of the 2-D phases, and there is no evidence of hydrogen bond interactions between the cations and the layers (the minimum H···O distance is 2.58 Å).

The most striking feature of this structure, in comparison with most of the $[XR_4]^+$ derivatives, is related to the stacking of the anionic layers. In this case, all the bimetallic layers are of the same type and are eclipsed with respect to each other creating hexagonal channels running along the *c*-axis, instead of a staggered arrangement. In general, these derivatives have a much better crystallinity, since the graphite-like arrangement favors the presence of stacking faults.[138] A second distinctive feature of this structure with respect to the other structurally known 2-D phases is that the cations do not penetrate into the honeycomb net (the minimum distance of the cation to this plane is 0.88 Å: the distance from the mean plane defined by the metals to the closest hydrogen from a methyl group).

As mentioned before, the layered and segregated structure of these materials make them solution-obtained examples of magnetic multilayers, and therefore with much lower presence of defects when compared with those built by physical methods. In this case, using different metallocenes one can construct magnetic multilayers where ferromagnetic layers are intercalated with paramagnetic or diamagnetic layers by the use of the paramagnetic ($S = 1/2$) or diamagnetic decamethylcobaltocenium. The combined magnetic study of these two isostructural families, where the only difference is the presence of spin carriers in between the layers, allowed us to reach many important conclusions regarding these hybrid quasi-2-D magnets. The magnetic features of these compounds are summarized in Table 4.

12.07.3.1 Magnets Formed by Bimetallic M(II) Cr(III) Oxalates and Metallocenes

The magnetic behavior of the $[CoCp^*_2][M^{(II)}Cr(ox)_3]$ (M(II) = Mn, Fe, Co, Ni, Cu) series[143] closely resembles that of the corresponding $[XR_4]^+$ salts. These compounds show ferromagnetic interactions between neighboring Cr(III) and M(II) ions (Table 4). The magnetic exchange promoted by the oxalate bridge in these materials is dominated by the electronic configuration of the given metal centers, and can be predicted by considering only the singly occupied molecular orbitals (SOMOs) of the interacting magnetic centers. The exchange parameter J can be expressed by the

Table 4 Magnetic properties of the $[A][M^{II}M^{III}(ox)_3]$-layered hybrid magnets

[A]	$M^{II}M^{III}$	*Ordering*	T_c (K)	H_{coer} at 2(Oe)K	*References*
$[NBu_4]^+$	VCr	Ferro	<2	-	139
	CrCr	Ferri	<2	-	140
	MnCr	Ferro	6	20	108
	FeCr	Ferro	12	320	108
	CoCr	Ferro	10	80	108
	NiCr	Ferro	14	160	108
	MnFe	Weak ferro	27	-	113
	FeFe	Ferri	44	-	113
	MnV	Ferro	<2	-	139
	VV	Ferri	11	1640	139
	FeMn	Weak ferro	21	150	141
	CoMn	Ferri	13	420	141
	NiMn	Ferri	21	830	141
$[FeCp^*_2]^+$	MnCr	Ferro	5.3	10	143
	FeCr	Ferro	13.0	330	143
	CoCr	Ferro	9.0	50	143
	NiCr	Ferro	15.0		142
	CuCr	Ferro	7.0	40	143
	MnFe	Weak ferro	28.4	40	143
	FeFe	Ferri	43.3	1240	143
	MnRu	Ferro	<2	-	154
	FeRu	Ferro	13.8	2210	154
	CoRu	Ferro	3.1	-	154
	CuRu	Ferro	<2	-	154
$[CoCp^*_2]^+$	MnCr	Ferro	5.1	40	143
	FeCr	Ferro	12.7	1940	143
	CoCr	Ferro	8.2	250	143
	CuCr	Ferro	6.7	200	143
	MnFe	Weak ferro	25.4	150	143
	FeFe	Ferri	44.0	100	143
	MnRu	Ferro	<2	-	154
	FeRu	Ferro	12.8	3200	154
	CoRu	Ferro	2.8	-	154
	CuRu	Ferro	<2	-	154
$[CpFe–C_5H_4–CH_2NR_3]^+$					149
$R = CH_2H_5$	MnCr	Ferro	5.5	-	149
	NiCr	Ferro	16.3	2100	149
$R = n\text{-}C_3H_7$	MnCr	Ferro	6.2	-	149
	NiCr	Ferro	16.6	2100	149
$R = n\text{-}C_4H_9$	MnCr	Ferro	5.3	-	149
	NiCr	Ferro	17.1	2000	149
$[1\text{-}CH_3–2\text{-}CH_2NBu_3–C_5H_3–Fe–Cp]^+$	MnCr	Ferro	5.3	-	149
	NiCr	Ferro	17.0	2200	149
$(Sp)\text{-}[1\text{-}CH_2N\text{-}(n\text{-}C_3H_7)_3\text{-}2\text{-}CH_3–C_5H_3FeCp]^+$	MnCr	Ferro	5.4	-	150

average of the individual interactions of the SOMOs (J_{ij}), taking into account that orthogonality of the interacting SOMOs favors ferromagnetic interactions. Thus, in the Ni derivative, all possible contributions to the magnetic exchange are ferromagnetic because of the orthogonality of the SOMOs of the Cr(III) ions (t_{2g}) and those of the Ni^{II} ions (e_g). In the other derivatives, there are SOMOs of t_{2g}-symmetry that are not orthogonal to those of the Cr(III) ion and represent an antiferromagnetic contribution to the magnetic exchange. Experimentally, all these compounds still show a net ferromagnetic exchange, although weaker than that of the Ni^{II} derivative. This derivative, though, showed a slightly different X-ray powder pattern, indicating that it is not isostructural to the rest of the series, however, the structure still remains unknown.

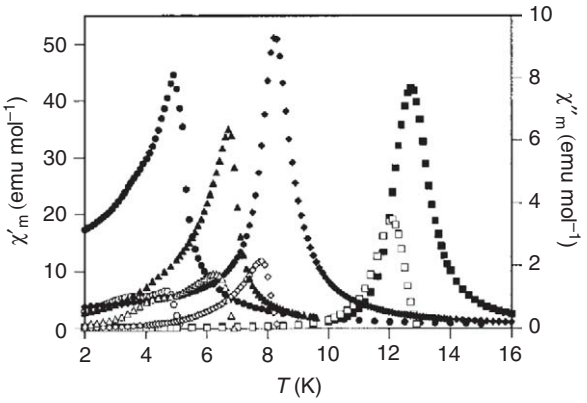

Figure 15 In-phase (χ'_m) and out-of-phase (χ''_m) AC magnetic susceptibilities for the $[CoCp^*_2][M^{II}Cr(ox)_3]$ (M^{II} = Mn, ●; Fe, ■; Co, ◆; Cu, ▲) series.

The ordering temperatures, determined by AC magnetic susceptibility measurements (Figure 15), are also analogous to those of the corresponding $[XR_4]^+$ salts (Table 4). It is well known that structural changes in these magnets, such as increasing the interlayer separation, have little effect on the magnetic properties, suggesting that the magnetic ordering is quasi-2-D. Ferromagnetic ordering was confirmed by the field dependence of the magnetization, which at high applied fields approaches values just slightly lower to those expected for parallel alignment of the spins. The reduced values are a consequence of spin canting in the ferromagnetic state, as already reported for the corresponding $[XR_4]^+$ salts. The coercive loops at 2 K reported for the decamethylcobaltocenium derivatives are larger in all cases: from four times in the case of Mn (from 10 to 40 Oe), up to more than six times in the Fe(II) derivative (from 330 to 1960 Oe). This difference in coercivity must be due to the different arrangement of the magnetic layers in the crystal structure, since it necessarily must be related to the domain wall movement between layers.

As expected, the $[FeCp^*_2][M^{II}Cr(ox)_3]$ (M(II) = Mn, Fe, Co, Ni, Cu) show a very similar thermal behavior for the magnetic susceptibility, with ferromagnetic near-neighbor interactions, and overall ferromagnetic ordering, with similar critical temperatures (Table 4). Again, the biggest difference when compared with the analogous magnets is the magnetic hysteretic behavior of the ferromagnetic state. In this case, the coercive fields are much lower than those of the corresponding $[CoCp^*_2]^+$ salts, and very close to those of the $[XR_4]^+$ salts. This indicates that the presence of paramagnetic units in between the ferromagnetic layers actually decreases the coercivity, facilitating the domain wall movement. Thus, the structural changes increasing the coercivity when passing from the graphite-like to the eclipsed stacking are cancelled by the electronic changes when a paramagnetic layer is intercalated in between the ferromagnetic layers.

Specific heat measurements have also been performed for these materials.[144] All of them show typical λ-peaks confirming the onset of a ferromagnetically ordered state below T_c (Figure 16). These data are in very good

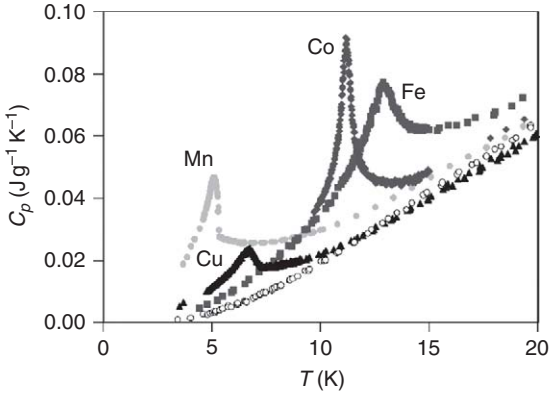

Figure 16 Specific heat measurements for the series $[FeCp^*_2][M^{II}Cr(ox)_3]$.[143]

agreement with the magnetic data, except for the Co(II) derivatives. $[FeCp^*_2][CoCr(ox)_3]$ has a λ-peak at 11.1 K instead of 9 K, the temperature at which the AC magnetic susceptibility shows the appearance of an out-of-phase signal (Table 4). At 9 K the specific heat shows only a second small bump. The peak at 11.1 K in the specific heat disappears for the $[CoCp^*_2]^+$ counterpart, suggesting that the $[FeCp^*_2]^+$ cations are related to the appearance of this feature.

ESR spectra studies[143] were also performed with the aim to study the Zeeman splitting of the paramagnetic $[FeCp^*_2]^+$ ($S = 1/2$) produced by the ferromagnetic ordering, thus acting as a probe to estimate the internal magnetic field generated by the inorganic layers. The typical spectrum of $[FeCp^*_2]^+$ can only be observed at low temperatures (below 50 K) and shows an anisotropic signal with $g = 4.45$ and $g = 1.02$.[143] The best candidates to monitor the Zeeman splitting are those where the bimetallic oxalate layer is ESR silent. The ESR spectrum of the salt $[FeCp^*_2][FeCr(ox)_3]$ (Figure 17) is very similar to the typical $[FeCp^*_2]^+$ spectrum. Below the ferromagnetic transition (13 K) g moves monotonically toward lower magnetic fields (from 8000 G at 15 K to 3500–4000 G at 4.3 K), with the signal becoming less anisotropic in the process. This g shift demonstrates that below T_c $[FeCp^*_2]^+$ probes the internal magnetic field of the ferromagnet, which is added to the applied magnetic field decreasing the resonance field; therefore, the internal magnetic field generated by the oxalate layers can be estimated about 4,000 G. A similar effect was observed for the $[FeCp^*_2][MnCr(ox)_3]$ derivative. In the other magnets, the lines from the oxalate layers do not allow for a good resolution of the $[FeCp^*_2]^+$ spectrum.

The presence of Fe centers in some of these magnets allowed for the use of ^{57}Fe Mössbauer spectroscopy for a more detailed characterization, since this technique gives valuable information on the electronic, magnetic, and lattice-dynamic properties. It was already used to study the iron-containing $[XR_4]^+$ derivatives.[145,146] However in this case, the insertion of $[FeCp^*_2]^+$ in between the magnetic layers adds versatility to these magnets. The characteristic spectrum of $[FeCp^*_2]^+$ shows a broad asymmetric band centered at 0.46 mm s^{-1}. When $[FeCp^*_2]^+$ is inserted into the ferromagnetic layers, the characteristic resonance line associated with $[FeCp^*_2]^+$ is observed above T_c. Below T_c this band becomes weaker and broadens (Figure 18). This corresponds to the spectrum of a Zeeman split nuclear spin $I = 3/2$ due to fast relaxation processes, and the fluctuation in the electronic hybrid spin $S = 1/2$ between $M_S = +1/2$ and $M_S = -1/2$ is faster than the Mössbauer time scale ($>10^{-7}$ s), as the time-averaged magnetic field "seen" by the nucleus is zero. At very low temperatures (1.8 K) the spectra are more complicated, as the relaxation processes become slower, but even at these temperatures the magnetic hyperfine spectra are not resolved. Therefore, although the $[FeCp^*_2]^+$ is polarized by the internal magnetic field generated by the bimetallic layers below T_c, fast relaxation processes prevent clear observation of the corresponding sextet. This was attributed to two factors, namely, the relatively low T_c in these materials, and the screening provided by the pentamethylcyclopentadienyl ligands. For $[FeCp^*_2][FeCr(ox)_3]$, in addition to the resonance of the $[FeCp^*_2]^+$, there is a second signal provided by the Fe^{II} ions in the bimetallic network, as a quadrupolar doublet with typical parameters of a high-spin Fe^{II} center. below T_c the

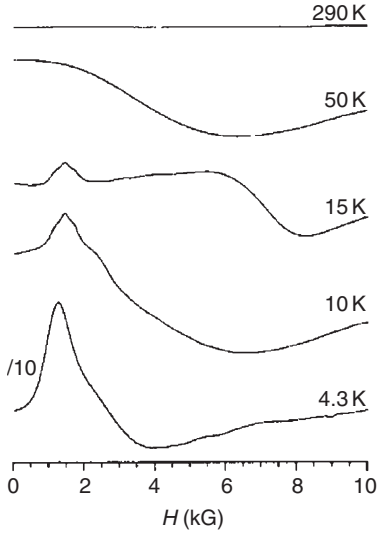

Figure 17 ESR spectra as a function of temperature for $[FeCp^*_2][FeCr(ox)_3]$.[143]

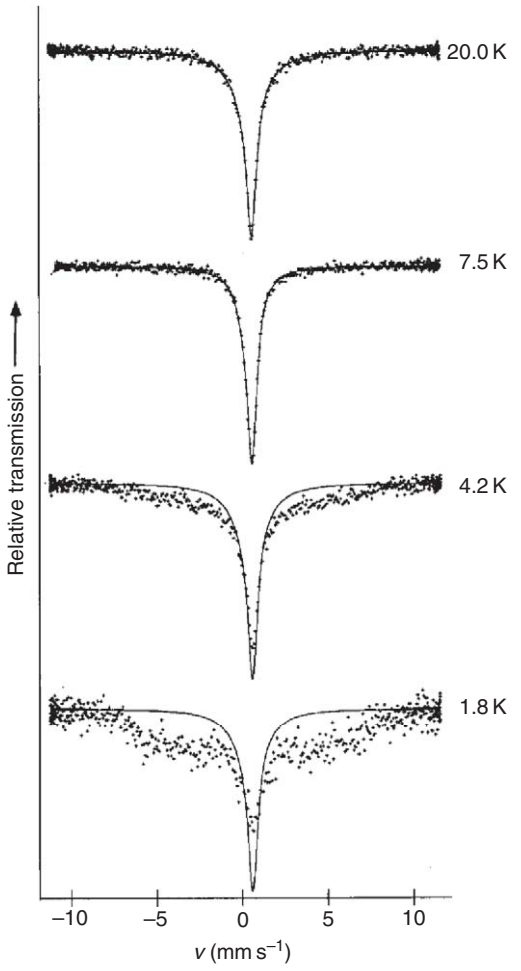

Figure 18 Mössbauer spectra as a function of temperature for the compound $[FeCp^*_2][CoCr(ox)_3]$.[143]

presence of an internal magnetic field leads to a splitting of this doublet into a doublet and a triplet ($H_{int} = 65$ kG at 4.2 K), which is the typical multiplet expected for a high-spin Fe^{II} ion; and the $[FeCp^*_2]^+$ band shows a relaxation spectrum similar to the previous case.[143]

These magnets have also been studied by muon spin resonance (μ^+SR), a technique that provides information on the magnitude, distribution, and dynamics of the local magnetic fields in magnetic materials.[147] Usually, the complexity of molecule-based magnets prevents the use of this technique. However, in this case quantitative results on the internal magnetic fields "seen" by the muons have been obtained. Accurate T_c values were derived for $[FeCp^*_2][MnCr(ox)_3]$,[148] that shows precession signals below the transition temperature at three different sites (Figure 19) with magnetic fields of ~1730(7), ~1200(1), and ~790(1) G. These values for the internal magnetic fields generated by the magnetic ordering are of the same order of magnitude as those estimated by ESR (3000–4000 G for the decamethylferrocenium site). Calculations indicated that all the observed resonance sites may be found approximately 1 Å above the extended oxalate layer in the vicinity of the oxygen atoms, although the possibility for the muon to stop in the Cp^* moieties cannot be ruled out completely.

The ferrocenium cation is too small to stabilize this type of 2-D networks, but it has also been reported that functionalized ferrocenium cations[149] such as $[CpFeC_5H_4CH_2NR_3]^+$ and even optically active derivatives[150] such as (*Rp*)- and (*Sp*)-$[1\text{-}CH_2N(n\text{-}C_3H_7)_3\text{-}2\text{-}CH_3\text{–}C_5H_3Fe\text{-}C_5H_5]^+$ can be used for the preparation of the $Mn^{II}Cr^{III}$ and $Ni^{II}Cr^{III}$ 2-D oxalate-based magnets, the latter being one of the few examples of this 2-D organometallic-inorganic magnets exhibiting optical activity in addition to ferromagnetic ordering, although both properties appear independent from each other. The magnetic properties for this series (Table 4) are essentially identical to the other analogs,

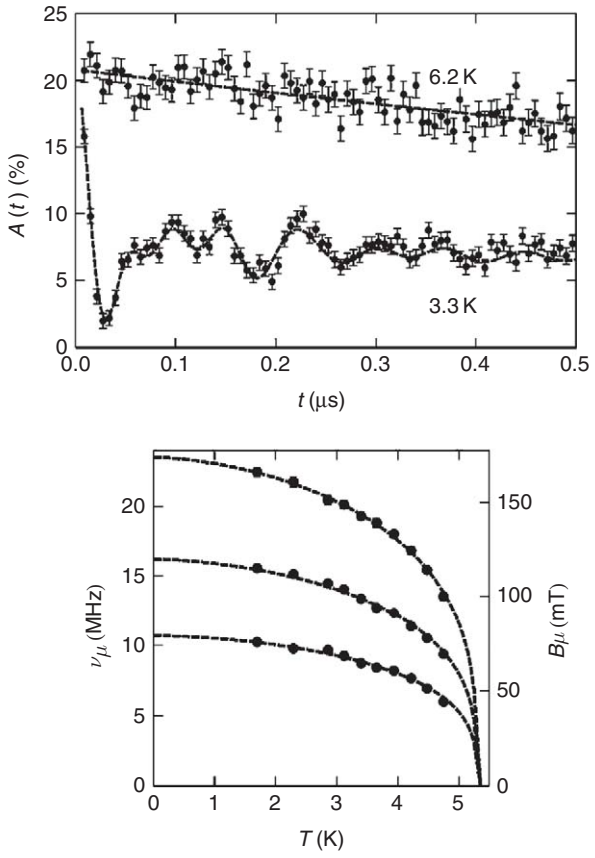

Figure 19 Asymmetry spectra for $[FeCp^*_2][MnCr(ox)_3]$ (a) measured above and below T_c and (b) temperature evolution of the precession frequencies.[148]

although unusually high coercivity was found for $Ni^{II}Cr^{III}$ derivatives. The lack of structural information makes difficult to derive any conclusions from this observation.

12.07.3.2 Magnets Formed by Bimetallic $M^{II}Fe^{III}$ Oxalates and Metallocenes

An analogous series was obtained for both $[CoCp^*_2][M^{II}Fe(ox)_3]$ and $[FeCp^*_2][M^{II}Fe(ox)_3]$ (M(II) = Mn, Fe). In this case, however, fewer derivatives were prepared, because $[Fe(ox)_3]^{3-}$ is less stable with respect to $[Cr(ox)_3]^{3-}$ (Table 4).

Magnetically, the exchange coupling promoted by the oxalate bis-chelating bridge is antiferromagnetic. This is understood since all d-orbitals of high spin Fe(III) are SOMOs, and all contributions from the magnetic exchange are antiferromagnetic. In addition, the exchange interaction is also much stronger; thus, the onset of long-range order occurs at higher temperatures. The $Mn^{II}Fe^{III}$ derivatives show a broad maximum in near 50 K, indicating the presence of low-dimensional antiferromagnetism, and then order as weak ferromagnets below 25 K, due to the spin canting present in the network built exclusively by spins $S = 5/2$ (Figure 20). The $Fe^{II}Fe^{III}$ derivatives show also antiferromagnetic exchange, and order ferrimagnetically, due to the antiparallel alignment of non-compensating $S = 5/2$ and $S = 2$ spins. Accordingly, a peak appears in the χ_m versus T plot at the critical temperature (≈44 K) and then χ_m continues to decrease steadily, becoming negative (Figure 20). This extraordinary behavior is rare among molecule-based materials.[151,152] Examples have been known in ferrites and garnets, and it is typical of type-N ferrimagnets, according to Néel classification,[153] where the magnetization of the two magnetic sublattices varies with temperature in such a way that they cancel at the compensation temperature. In this particular case, and as it was already observed for some of the $[XR_4]^+$ analogous salts,[113] the Fe(III) ground state is orbitally non-degenerate. Thus, the

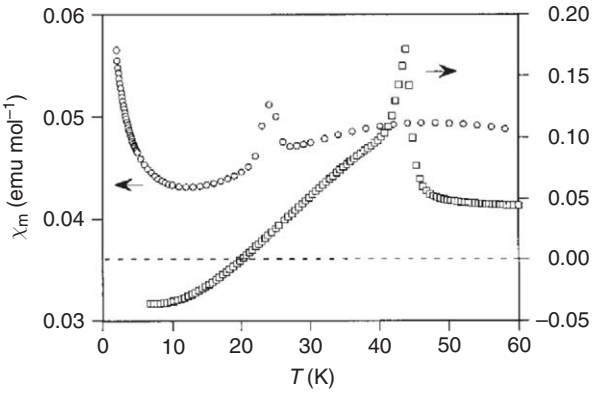

Figure 20 DC magnetic susceptibility for the series $[CoCp^*_2][M^{II}Fe(ox)_3]$ (M(II) = Mn, ○; Fe, □).[143]

magnetization of the Fe(III) sublattice should follow a Brillouin curve in the molecular field approximation, but that of the Fe(II) will not, as it has an orbitally degenerate ground state. The compensation temperature varies from 20 to 27 K by substitution of $[CoCp^*_2]^+$ by $[FeCp^*_2]^+$, indicating that the presence of the paramagnetic ions between the ferrimagnetic layers affects the magnetically ordered state in these materials.

ESR studies also gave important information about the magnetic ordering occurring for $[FeCp^*_2][MnFe(ox)_3]$ (Figure 21). The ESR signal associated with the bimetallic anionic network is an isotropic band centered at $g = 2.0$, which decreases in intensity upon cooling in agreement with the antiferromagnetic coupling between the two interacting $S = 5/2$ spins. Below 20 K, this signal becomes very weak and the paramagnetic signal from $[FeCp^*_2]^+$ dominates, which facilitates the study of its thermal evolution. As in the Cr(III) series, in the ordered phase (below 25 K), g moves toward lower magnetic fields upon cooling. However, in this instance the shift is smaller. Thus, at 4.2 K the g signal is centered around 6000 G, while in the previous two cases it was centered over the range 3500–4000 G, resulting in an estimated internal field of around 2000 G. This difference is attributed to $[FeCp^*_2][MnFe(ox)_3]$ being a weak ferromagnet; thus, the internal magnetic field generated by this magnet is smaller than those produced by the ferromagnets.

In this series, the Mössbauer spectra are more complex than in the Cr(III) series because of the presence of Fe(III) centers in the oxalate layers. The $Fe^{II}Fe^{III}$ compound contains three different iron sites. At high temperatures, a singlet and two doublets are observed (Figure 22). The singlet is characteristic of $[FeCp^*_2]^+$. One of the doublets is

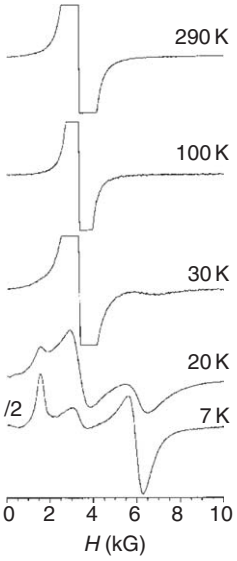

Figure 21 ESR spectra as a function of temperature for $[FeCp^*_2][MnFe(ox)_3]$.[143]

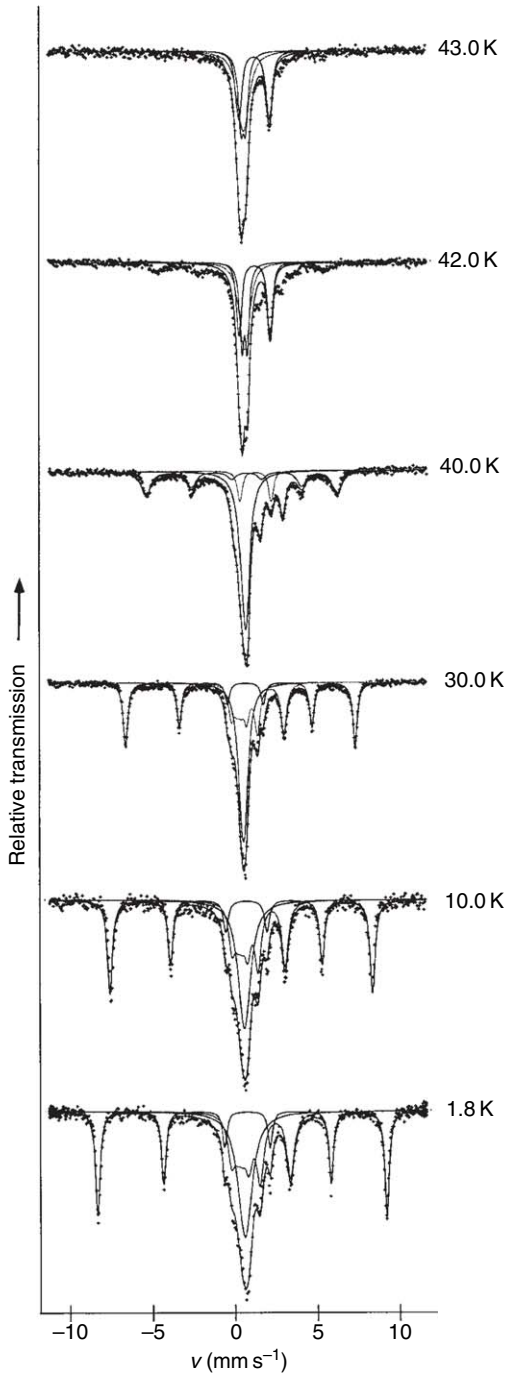

Figure 22 Mössbauer spectra at different temperatures for $[FeCp^*_2][FeFe(ox)_3]$.[143]

very similar to that found in $Fe^{II}Cr^{III}$; thus, it is assigned to high-spin Fe(II). The other doublet exhibits a smaller isomer shift and quadrupolar splitting, and can be assigned to high-spin Fe(III). Observation of these two signals indicates that the Fe^{II}/Fe^{III} network is a "trapped valence system" where the electron-transfer rate between the two iron species is less than the Mössbauer timescale ($<10^7\ s^{-1}$). Just below T_c (44 K), the shape of the spectrum becomes more complicated and the bands are broadened. The evolution of this spectrum as a function of the temperature is complex because the two Fe ions of the anionic layer behave differently. Thus, at 40 K, all the high-spin Fe(III) ions

show a nuclear Zeeman splitting, and no trace of the original doublet is observed. In contrast, at this temperature only some of the high-spin Fe(II) ions (70%) show a nuclear Zeeman splitting, and only at 30 K does the original doublet disappear completely. This is direct proof that in the $Fe^{II}Fe^{III}$ oxalate-based anionic layer the magnetization for the Fe(II) sublattice increases faster than that for the Fe(III) sublattice, and the origin for the appearance of negative magnetization. Although in this case T_c is much higher than in the Cr(III) derivatives, the same relaxation behavior is found for the signal from $[FeCp^*_2]^+$. Even at very low temperatures the relaxation is too fast to observe the hyperfine magnetic splitting. Thus, the presence of a fast spin flip for the electronic spin of decamethylferrocenium may suggest that the magnetic ordering in these materials has strong 2-D character.

12.07.3.3 Magnets Formed by Bimetallic $M^{II}Ru^{III}$ Oxalates and Metallocenes

Organometallic monocations were also used in the preparation of bimetallic oxalate magnets based on $[Ru(ox)_3]^{3-}$.[154] The $[XR_4]^+$ analogs had already been prepared, but some opposite conclusions about the ferro- or antiferromagnetic nature of the magnetic exchange observed had been reached,[155] due to the high orbital anisotropy of the Ru(III) ($S = 1/2$) centers.

$[CoCp^*_2][M^{II}Ru(ox)_3]$ and $[FeCp^*_2]$ $[M^{II}Ru(ox)_3]$ (M(II) = Mn, Fe, Co, Cu, Zn) are isostructural to the rest of the series of identical stoichiometry (Table 4). In these cases, the Zn derivative is particularly relevant, because it allows for the study of the magnetic behavior of the Ru(III) centers in the oxalate-bridged bimetallic network in the absence of magnetic exchange. Indeed, the data can be fitted to a Curie–Weiss law with a negative Weiss constant ($\theta = -5.3$ K). This behavior was explained by an incomplete quenching of the orbital contribution to the magnetic moment, from the orbitally degenerate ground state of low-spin Ru(III).

The magnetically condensed compounds showed much weaker magnetic exchange when compared to the Cr and Fe derivatives, probably due to the poorer orbital energy matching between the first-row transition metals with those of Ru. Indeed the $\chi_m T$ versus T plots show small decreases from room temperature for the Mn(II), Co(II), and Cu(II) derivatives, as expected for antiferromagnetic interactions. At lower temperatures, $\chi_m T$ reaches a minimum and then $\chi_m T$ increases. This apparent ferrimagnetic behavior was ruled out, and assigned to the anisotropy of the Ru(III) centers that dominates the magnetic behavior at high temperatures. Thus, weak ferromagnetic interactions were proposed in these three cases, with only the Co(II) compound exhibiting ferromagnetic ordering above 2 K. Ferromagnetic interactions were found to be stronger in the Fe^{II} compound, with a much higher-ordering temperature with $T_c = 14$ K observed in this case. A small frequency dependence of the AC magnetic susceptibility was observed, indicating glassy behavior for this system (Figure 23).

Mössbauer spectra of $[CoCp^*_2][FeRu(ox)_3]$ were also reported,[154] and showed a quadrupole doublet with similar parameters of those of $[CoCp^*_2][FeCr(ox)_3]$. Below 14 K, in agreement with magnetic measurements, long-range magnetic ordering of the Fe(II) is established. Very similar features were observed in the Mössbauer spectra of $[FeCp^*_2][FeRu(ox)_3]$ (Figure 24), in addition to the contribution of $[FeCp^*_2]^+$. As in the rest of the series, resolution of this line in the ordered state was not achieved.

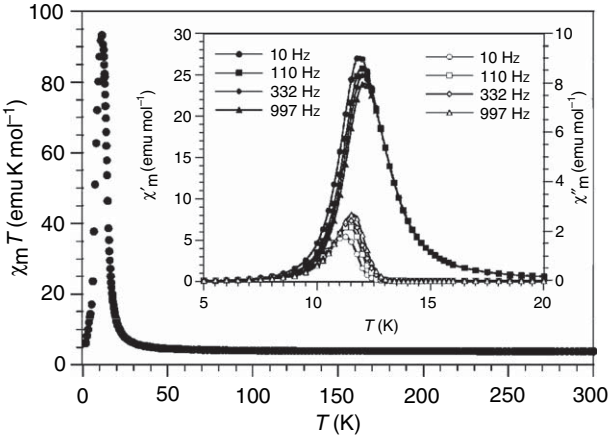

Figure 23 AC magnetic susceptibility for $[CoCp^*_2][FeRu(ox)_3]$.[154]

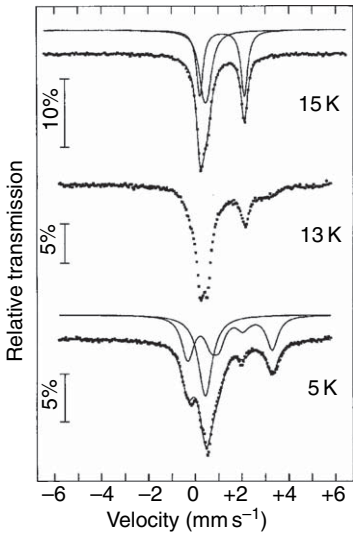

Figure 24 Mössbauer spectra at different temperatures for $[FeCp^*_2][FeRu(ox)_3]$.[154]

12.07.3.4 Magnets Formed by Trimetallic Oxalates and Metallocenes

One aspect that shows the versatility of these hybrid materials with respect to magnetism concerns the possibility of changing the chemical composition of the extended magnetic network. Thus, by making small changes in this inorganic sublattice the physical properties of the resulting solid solution can be tuned. With the $[XR_4]^+$ salts, it was shown that since the $M^{II}Cr^{III}$ pairwise interactions are ferromagnetic, while the $M^{II}Fe^{III}$ interactions are antiferromagnetic, a solid solution of $M^{II}[Cr^{III}_xFe^{III}_{1-x}]$ $(0 < x < 1)$ enables the study of analogous materials with the presence of competing interactions.[156] Importantly, these compounds proved that the critical temperatures can be tuned depending on the Cr/Fe ratio, and spin glass-like behavior accompanied by a huge increase in the coercive fields is observed for intermediate values. The hysteretic behavior can be easily tuned by altering the chemical composition of the material. Since the preparation of the decamethylcobaltocenium derivatives already showed a huge increase in the coercivity, the same strategy was applied in this case, with striking results. For example, values as high as 16.7 kOe (1.67 T) have been reached with $[CoCp^*_2][Fe^{II}(Cr^{III}_{0.5}Fe^{III}_{0.5})(ox)_3]$ (Table 5). The introduction in this type of solid solutions[157] of the highly anisotropic Ru(III) ion,[158] that also favors ferromagnetic interactions, instead of Cr(III), has made it possible to prepare solid solutions with coercive fields as high as 2.2 T (Figure 25), in the material $[CoCp^*_2][Fe^{II}(Ru^{III}_{0.5}Fe^{III}_{0.5})(ox)_3]$. Furthermore, in this compound the magnetization is not saturated at the maximum available field (50 kOe), as the hysteresis loop only closes at that field. This is clear evidence for the strong anisotropic field in these hard magnets, and indicates that the coercive fields will be even larger if the samples are

Table 5 Critical temperature (T_c) and coercive field at 2 K (H_{coer}) for the series $[CoCp^*_2][Fe^{II}M^{III}_xFe^{III}_{1-x}(ox)_3]$

M^{III}	x	T_c (K)	H_{coer} (Oe)	*References*
Cr(III)	0.00	44.0	100	143
	0.20	33.7	1150	142
	0.33	27.1	13 440	142
	0.50	21.4	16 750	156
	0.66	14.4	5650	142
	0.80	12.5	3340	142
	1.00	12.7	1940	143
Ru(III)	0.00	44.0	100	158
	0.30	37.0	400	158
	0.53	30.0	22 000	158
	0.73	21.0	14 000	158
	1.00	12.8	3200	158

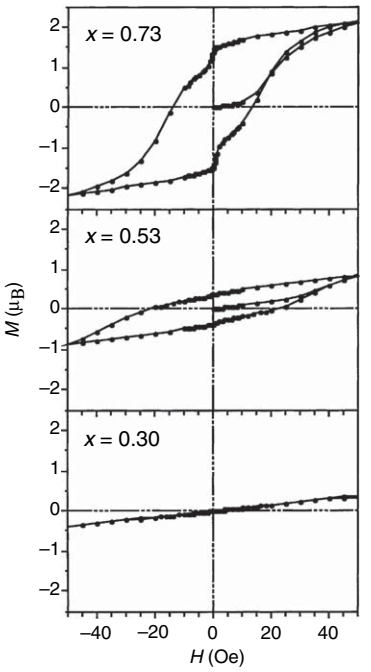

Figure 25 Hysteresis loops at 2 k for the series $[CoCp^*_2][Fe^{II}(Ru^{III}_{0.5}Fe^{III}_{0.5})(ox)_3]$.[158]

magnetized by higher magnetic fields. These values for coercivity are among the highest ever found in molecule-based magnets, as in the dicyanamide series,[159–163] in porphyrin-based molecular magnets,[164,165] and in cyanide bimetallic magnets,[166] and comparable to those of hard magnets.[167]

The increased coercivity found in these solid-state solutions can be explained in terms of mixing hard and soft magnets. The $Fe^{II}Fe^{III}$ ferrimagnets are very hard, and large magnetic fields are required to magnetize the material. When a soft magnet is incorporated into this material, a softening of the material occur, and upon application of the maximum field available (50 kOe in the reported cases), a larger magnetization of the material is achieved, which gives rise to an enhancement of the hysteresis properties. Finally, it is noted that the disorder that occurs in the two types of solid solutions (Cr^{III}/Fe^{III} and Ru^{III}/Fe^{III} mixtures) is purely magnetic and connected to chemical composition. In fact, these materials can be viewed as "crystalline magnetic solid-state solutions," the simplest disordered spin systems, where there is no structural disorder at all. The structure of the pure Cr(III) and Fe(III) derivatives is maintained and also the particle size, which is homogeneous and around 1 μm. Therefore, structural defects are not expected to play a significant role in the magnetic hardness of these materials.

12.07.3.5 Other Hybrid Magnetic Materials

There are other examples from analogous strategies, by changing either the organometallic cation or the coordination framework.

For the oxalate-based magnets, the diamagnetic organometallic cation $[Ru(bpy)_2ppy]^+$ (ppy = $NC_5H_4C_6H_4$) is also able to act as "templating" cation for the growth of a chiral 3-D network, as described above. The salts $[Ru(bpy)_2ppy][M(II)Cr(ox)_3]$ (M(II) = Mn, Ni)[119] exhibit ferromagnetic interactions between spin carries reaching ferromagnetic ordering at 5.8 and 11.0 K, respectively.

The successful approach with oxalate complexes has also been applied to other building blocks for coordination magnetic materials. Decamethylmetallocenium cations were used as "templating" agents for the preparation of dicyanamide-based magnetic materials. Binary compounds of dicyanamide with paramagnetic metals afforded several molecule-based magnets with striking magnetic properties.[159–162] With the incorporation of the metallocenium cations, the structure of these coordination polymers changes to cubic, and the magnetic exchange through the ligand becomes weaker, due to the different bridging mode adopted. The family $[Cp^*_2Z][M[N(CN)_2]_3]$[168,169] (Z = Co, Fe; M = Mn, Fe, Co, Ni) shows weak antiferromagnetic interactions, and no magnetic ordering above 2 K.

12.07.4 Polynuclear Magnetic Molecules Based on Metallocenes

Metallocenes have also been used to construct high-spin paramagnetic molecules, since they are good intramolecular spin couplers between organic radicals, for example, between two organic radicals connected by a 1,1′-metallocenylene bridge.[170] Depending on the nature of the organic radicals, different types of magnetic properties have been found. In the case of perchlorotriphenylmethyl radicals (Figure 26), a non-negligible spin density on the ferrocenium moiety is the origin for ferromagnetic exchange.[171] When nitronyl nitroxide radicals are used instead, more complex behavior has been reported[172,173] with small variations, structural or electronic, having important effects on the magnetic properties. A very detailed investigation on the simplest nitronyl nitroxide diradical (Figure 26), including structural, magnetic, NMR data along DFT calculations concluded that the magnetic interaction promoted by the ferrocene bridge is antiferromagnetic,[174] demonstrating that metallocene is not a robust magnetic coupler, since small distortions, even those induced by hydrogen bonding in the solid state, may change the sign and magnitude of the interaction.

Metallocenes functionalized with organic radicals have also been used as ligands toward other paramagnetic metal centers, yielding molecular species with unusual magnetic properties, such as spin frustration,[175] due to the topology of such species, where competing antiferromagnetic interactions arise from the fact that the metals and radicals act at the same time as spin carriers and as magnetic couplers. This type of combination has also yielded magnetic chiral coordination polymers that spontaneously resolve from solution.[176]

Worth of noticing is the one-way photoinduced self-assembly process shown by a polychlorotriphenylmethyl radical linked to a ferrocenyl group through an imino bridge. The *trans*-isomer of this metal–organic radical derivative is converted, both thermally or with light irradiation (Figure 27), in to the *cis*-form, which aggregates in solution through the formation of two hydrogen bonds to give thermodynamically stable diradical dimers showing strong antiferromagnetic interactions. This molecular system represents the unique known example of a photoinduced supramolecular phenomenon in which a doublet species is converted into a singlet one.[177,178]

A similar metal–organic radical derivative, but with an CH═CH bridge, that permits a more effective electronic coupling between the radical subunit and the ferrocenyl one, shows in solid state a reversible valence tautomerism phenomenon (Figure 28), as demonstrated by magnetic measurements and Mössbauer experiments in the temperature range of 293 and 4 K. This novel valence tautomeric example combining an organic radical as an acceptor unit,

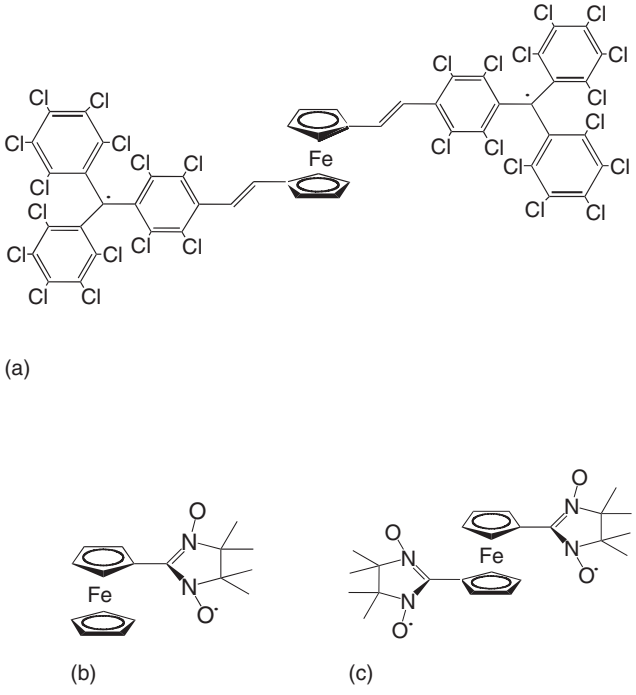

Figure 26 Scheme for the functionalized ferrocene moieties with organic radicals as dimers or trimers: (a) perchlorotriphenylmethyl, (b) and (c) nitronyl nitroxide.

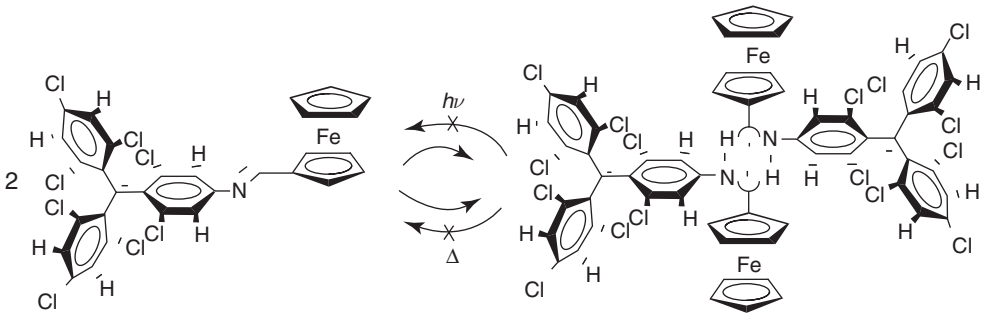

Figure 27 Thermal and light-induced isometization of an imino-bridged polychlorotriphenyl radical-ferrocenyl unit.

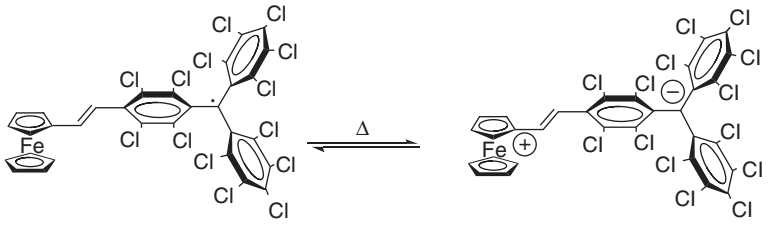

Figure 28 Valence tautomerism in a ferrocene – organic radical dimer.

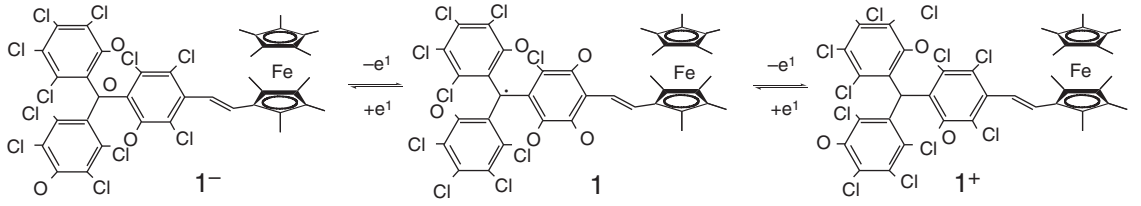

Figure 29 The three redox states of a molecule – based switch from a ferrocene – organic radical dimer.

and a ferocene unit as the donor group should be useful in designing novel multifunctional switchable molecular systems that can be used as information-storage devices at the nanoscopic scale.[179]

One remarkable development on this regard has been the preparation of molecule-based switches, taking advantage of the multifunctional redox properties of a molecular array involving simultaneous changes of three different outputs (linear optical, NLO, and magnetic properties) of a dimer formed by a ferrocene unit and a perchlorotriphenylmethyl radical linked by a CH═CH bridge (Figure 26) that exists in three redox states (Figure 29).[180] Magnetically, the compound goes from diamagnetic, in its monoanionic form, to paramagnetic increasing its magnetic moment from neutral (1.7 μ_B) to monocationic (2.5 μ_B). The magnetic exchange of the latter, where both radical and ferrocenium moieties possess unpaired spins, was very weak. The three species could be interconverted by chemical reagents or electrical stimuli, and the cyclic switching redox properties of this molecule were easily monitored by UV–VIS spectroscopy.

12.07.5 Conclusions and Perspectives

Although most organometallic complexes are diamagnetic, some of them have been very important in the design and development of novel magnetic materials. Metallocenes have been of particular interest in this context. This class of metal complexes has always been involved in the major developments occurred in molecule-based magnets.

Thus, the first organic-based magnet was in fact an organometallic-based magnet formed by decamethylferrocenium $[Fe^{III}Cp^*_2]^{\cdot+}$ and the tetracyanoethylene anion, $[TCNE]^{\cdot-}$, reported in 1985. Such a discovery played a key

role in the field of the molecule-based magnets. Many families of structurally and electronically related compounds have been produced since then, which allow to better understand the magnetic phenomena. At the same time, this provides an opportunity to investigate the unique features of these molecular compounds, for example, the mechanism of the intrachain magnetic coupling in these electron-transfer salts, the nature – ferromagnetic or antiferromagnetic – of the interchain magnetic coupling, or the chemical control on the crystal structure and magnetic properties.

More recently, in 1997, and in the context of multifunctional molecule-based materials, organometallic complexes were also used in the design of hybrid magnetic materials built up from two magnetic networks. Thus, the first example of layered magnets, where paramagnetic metal complexes are inserted in between ferromagnetic layers, is formed by decamethylmetallocenes and extended layers of bimetallic tris(oxalato) complexes. This extensive series of compounds provided a remarkable example of molecule-based magnetic multilayers where the magnetic properties can be chemically tuned by changing the metal composition of either the bimetallic layers or the metallocene complex. Thus, a variety of magnetic materials ranging from very soft to very hard ferromagnets and ferrimagnets, as well as weak ferromagnets and glassy magnets with tunable critical temperatures, has been designed.

Finally, in the search for novel magnetic molecules useful in molecular electronics, metallocenes were used as intramolecular magnetic couplers between pure organic radicals with the aim of tuning the magnetic properties of the molecule by playing with the redox properties of these organometallic couplers.

Acknowledgments

EC and JRGM thank the support of the European Union (Network of Excellence MagMaNEt). JSM gratefully acknowledges the data obtained by M. L. Taliaferro, and the continued partial support from the U. S. DOE (No. DE FG 03-93ER45504) and the AFOSR (No. F49620-03-1-0175). They also thank J. Veciana for helpful discussion.

References

1. Miller, J. S. *Adv.Mater.* **1990**, *2*, 98.
2. Williams, J. M.; Ferraro, J. R.; Thorn, R. J.; Carlson, K. D.; Geiser, U.; Wang, H. H.; Kini, A. M.; Wangbo, M. H. *Organic Superconductors. Synthesis, Structure, Properties and Theory*; Grimes, R. N., Ed.; Prentice Hall: Englewood Cliffs, 1992.
3. Coronado, E., Delhaes, P., Gatteschi, D., Miller, J. S., Eds.; *Molecular Magnetism: From Molecular Assemblies to the Devices*; Kluwer: Dordrecht, 1995; Vol. E321.
4. Blundell, S. J.; Pratt, F. L. *J. Phys.: Condens. Matter.* **2004**, *16*, R771.
5. Ovcharenko, V. I.; Sagdeev, R. Z. *Russ. Chem. Rev.* **1999**, *68*, 345.
6. Kinoshita, M. *Phil. Trans. Roy. Soc. London(A)* **1999**, *357*, 2855.
7. Miller, J. S.; Epstein, A. J. *Chem. Commun.* **1998**, 1319.
8. Plass, W. *Chem. unserpv Zeit.* **1998**, *32*, 323.
9. Day, P. *J. Chem. Soc., Dalton Trans.* **1997**, 701.
10. Miller, J. S.; Epstein, A. J. *Chem. Eng. News* **1995**, *73*(#40), 30.
11. Miller, J. S.; Epstein, A. J. *Adv. Chem. Ser.* **1995**, *245*, 161.
12. Miller, J. S.; Epstein, A. J. *Angew. Chem., Int. Ed. Engl.* **1994**, *33*, 385.
13. Kahn, O. *Adv. Inorg. Chem.* **1995**, *43*, 179.
14. Kinoshita, M. *Jap. J. Appl. Phys.* **1994**, *33*, 5718.
15. Gatteschi, D. *Adv. Mater.* **1994**, *6*, 635.
16. Kahn, O. *Molecular Magnetism*; VCH: New York, 1993.
17. Caneschi, A.; Gatteschi, D.; Rey, P. *Prog. Inorg. Chem.* **1991**, *39*, 331.
18. Buchachenko, A. L. *Russ. Chem. Rev.* **1990**, *59*, 307.
19. Caneschi, A.; Gatteschi, D.; Sessoli, R.; Rey, P. *Acc. Chem. Res.* **1989**, *22*, 392.
20. Miller, J. S.; Epstein, A. J. *New Aspects of Organic Chemistry*; Yoshida, Z., Shiba, T., Oshiro, Y., Eds.; VCH: New York, 1989.
21. Miller, J. S.; Epstein, A. J.; Reiff, W. M. *Acc. Chem. Res.* **1988**, *21*, 114.
22. Miller, J. S.; Epstein, A. J.; Reiff, W. M. *Science* **1988**, *240*, 40.
23. Miller, J. S.; Epstein, A. J.; Reiff, W. M. *Chem. Rev.* **1988**, *88*, 201.
24. Kahn, O. *Struct. Bond.* **1987**, *68*, 89.
25. Crayson, J. A.; Devine, J. N.; Walton, J. C. *Tetrahedron* **2000**, *56*, 7829.
26. Evans, O. R.; Lin, W. B. *Acc. Chem. Res.* **2002**, *37*, 511.
27. Zyss, J., Ed. *Molecular Nonlinear Optics*; Elsevier: Boston, MA, 1993.
28. Miller, J. S.; Epstein, A. J.; Reiff, W. M. *Mol. Cryst., Liq. Cryst.* **1985**, *120*, 27.
29. Miller, J. S. *Adv. Mater.* **2002**, *14*, 1105.
30. Day, P. *Notes Rec. Roy. Soc. London* **2002**, *56*, 95.
31. Wickman, H. H.; Trozzolo, A. M.; Williams, H. J.; Hull, G. W.; Merritt, F. R. *Phys Rev B* **1967**, *155*, 563.
32. Coronado, E.; Galán.Mascarós, J. R. *J. Mater. Chem.* **2005**, *15*, 66.
33. Coronado, E.; Day, P. *Chem. Rev.* **2004**, *104*, 5419.
34. Coronado, E.; Galán-Mascarós, J. R.; Gómez-García, C. J.; Laukhin, V. *Nature* **2000**, *408*, 447.

35. Albeola, A.; Galán-Mascarós, J. R.; Giménez-Saiz, C.; Gómez-García, C. J. *J. Am. Chem. Soc.* **2003**, *125*, 10774.
36. Imai, H.; Inoue, K.; Kikuchi, K.; Yoshida, Y.; Ito, M.; Sunahara, T.; Onaka, S. *Angew. Chem., Int. Ed.* **2004**, *43*, 5618.
37. Minguet, M.; Luneau, D.; Lhotel, E.; Villar, V.; Paulsen, C.; Amabilino, D. B.; Veciana, J. *Angew. Chem., Int. Ed.* **2002**, *41*, 586.
38. Coronado, E.; Galán-Mascarós, J. R.; Gómez-García, C. J.; Martínez-Ferrero, E.; Almeida, M.; Waerenborgh, J. C. *Eur. J. Inorg. Chem.* **2005**, 2064.
39. Gatteschi, D.; Sessoli, R. *Angew. Chem., Int. Ed.* **2003**, *42*, 268.
40. Christou, G.; Gatteschi, D.; Hendrickson, D. N.; Sessoli, R. *MRS Bull.* **2000**, *25*, 66.
41. Miller, J. S. *Chem. Eng. News* **2005**, *83*(#24), 4.
42. Verdaguer, M.; Girolami, G. S. *Magnetism - Molecules to Materials*; Miller, J. S., Drillon, M., Eds.; Wiley-VCH: Mannheim, 2004; Vol. 5, p 283.
43. Hashimoto, K.; Ohkoshi, S.-I. *Phil. Trans. Roy. Soc. London A* **1999**, *357*, 2977.
44. Verdaguer, M.; Bluezen, A.; Train, C.; Garde, R.; Fabrizi de Biani, F.; Desplanches, C. *Phil. Trans. Roy. Soc. London* **1999**, *357*, 2959.
45. Verdaguer, M.; Bluezen, A.; Marvaud, V.; Vaissermann, J.; Seuleiman, M.; Desplanches, C.; Scuiller, A.; Train, C.; Garde, R., Gelly, G., *et al. Coord. Chem. Rev.* **1999**, *190–192*, 1023.
46. Manriquez, J. M.; Yee, G. T.; McLean, R. S.; Epstein, A. J.; Miller, J. S. *Science* **1991**, *252*, 1415–1417.
47. Miller, J. S.; Yee, G. T.; Manriquez, J. M.; Epstein, A. J. *Conjugated Polymers and Related Materials: The Interconnection of Chemical and Electronic Structure*; *(Proceedings of Nobel Symposium #NS-81)*; Salaneck, W. R., Lundstom, I., Ranby, B., Eds.; Oxford University Press: Oxford, 1993; pp 461–474.
48. Zhang, J.; Zhou, P.; Brinckerhoff, W. B.; Epstein, A. J.; Vazquez, C.; McLean, R. S.; Miller, J. S. *A. C. S. Symp. Ser.* **1996**, *644*, 311.
49. Pokhodnya, K. I.; Epstein, A. J.; Miller, J. S. *Adv. Mater.* **2000**, *12*, 410.
50. Miller, J. S.; Epstein, A. J. *J. Chem. Soc., Chem. Commun.* **1998**, 1319.
51. Vickers, E. B.; Selby, T. D.; Miller, J. S. *J. Am. Chem. Soc.* **2004**, *126*, 3716.
52. Fitzgerald, J. P.; Kaul, B. B.; Yee, G. T. *Chem. Commun.* **2000**, 49.
53. Kaul, B. B.; Yee, G. T. *Inorg. Chim. Acta* **2001**, *326*, 9.
54. Vickers, E. B.; Selby, T. D.; Thorum, M. S.; Taliaferro, M. L.; Miller, J. S. *Inorg. Chem.* **2004**, *43*, 6414.
55. Candela, G. A.; Swartzendruber, L. J.; Miller, J. S.; Rice, M. J. *J. Am. Chem. Soc.* **1979**, *101*, 2755.
56. Taliaferro, M. L.; Palacio, F.; Miller, J. S. *J. Mater. Chem.* **2006**, *16*, 2677.
57. Miller, J. S. *Inorg. Chem.* **2000**, *39*, 4392.
58. Miller, J. S.; Calabrese, J. C.; Epstein, A. J.; Bigelow, R. W.; Zhang, J. H.; Reiff, W. M. *J. Chem. Soc. Chem. Commun.* **1986**, 1026.
59. Miller, J. S.; Calabrese, J. C.; Rommelmann, H.; Chittipeddi, S.; Epstein, A. J.; Zhang, J. H.; Reiff, W. M. *J. Am. Chem. Soc.* **1987**, *109*, 769.
60. Chittipeddi, S.; Cromack, K. R.; Miller, J. S.; Epstein, A. J. *Phys. Rev. Lett.* **1987**, *58*, 2695.
61. Yee, G. T.; Miller, J. S. *Magnetism - Molecules to Materials*; Miller, J. S., Drillon, M., Eds.; Wiley-VCH: Mannheim, 2004; Vol. 5, p 223.
62. Miller, J. S.; Epstein, A. J. *Angew. Chem., Int. Ed.* **1994**, *106*, 399.
63. Miller, J. S.; Epstein, A. J. *Research Fontiers in Magnetochemistry*; O'Connor, C. J., Ed.; World Scientific: New Jersey, 1993; p 283.
64. Webster, O. W.; Mahler, W.; Benson, R. E. *J. Am. Chem. Soc.* **1962**, *84*, 3678.
65. Rosenblum, M.; Fish, R. W.; Bennett, C. *J. Am. Chem. Soc.* **1964**, *86*, 5166.
66. Brandon, R. L.; Osipcki, J. H.; Ottenberg, A. *J. Org. Chem.* **1966**, *31*, 1214.
67. Adman, E.; Rosenblum, M.; Sullivan, S.; Margulis, T. N. *J. Am. Chem. Soc.* **1967**, *89*, 4540.
68. Sullivan, B. W.; Foxman, B. *Organometallics* **1983**, *2*, 187.
69. Robbins, J. L.; Edelstein, N.; Spencer, B.; Smart, J. C. *J. Am. Chem. Soc.* **1982**, *104*, 1882.
70. Wang, G.; Slebodnick, C.; Butcher, R. J.; Tam, M. C.; Craword, T. D.; Yee, G. T. *J. Am. Chem. Soc.* **2004**, *126*, 16890.
71. Miller, J. S.; Zhang, J. H.; Reiff, W. M.; Preston, L. D.; Reis, A. H., Jr.; Gerbert, E.; Extine, M.; Troup, J.; Ward, M. D. *J. Phys. Chem.* **1987**, *91*, 4344.
72. Broderick, W. E.; Eichorn, D. M.; Liu, X.; Toscano, P. J.; Owens, S. M.; Hoffman, B. M. *J. Am. Chem. Soc.* **1995**, *117*, 3641.
73. Yee, G. T.; Manriquez, J. M.; Dixon, D. A.; McLean, R. S.; Groski, D. M.; Flippen, R. B.; Narayan, K. S.; Epstein, A. J.; Miller, J. S. *Adv. Mater.* **1991**, *3*, 309.
74. Zuo, F.; Zane, S.; Zhou, P.; Epstein, A. J.; McLean, R. S.; Miller, J. S. *J. Appl. Phys.* **1993**, *73*, 5476.
75. Miller, J. S.; McLean, R. S.; Vazquez, C.; Calabrese, J. C.; Zuo, F.; Epstein, A. J. *J. Mater. Chem.* **1993**, *3*, 215.
76. Zhou, P.; Makivic, M.; Zuo, F.; Miller, J. S.; Epstein, A. J. *Phys. Rev. B* **1994**, *49*, 4364.
77. Eichhorn, D. M.; Skee, D. C.; Broderick, W. E.; Hoffman, B. M. *Inorg. Chem.* **1993**, *32*, 491.
78. Broderick, W. E.; Thompson, J. A.; Day, E. P.; Hoffman, B. M. *Science* **1990**, *249*, 401.
79. Broderick, W. E.; Hoffman, B. M. *J. Am. Chem. Soc.* **1991**, *113*, 6334.
80. Dixon, D. A.; Suna, A.; Miller, J. S.; Epstein, A. J. *NATO ARW Molecular Magnetic Materials*; Kahn, O., Gatteschi, D., Miller, J. S., Palacio, F., Eds.; 1991; Vol. E198, 171.
81. Gama, V.; Duarte, M. T. *Magnetism - Molecules to Materials*; Miller, J. S., Drillon, M., Eds.; Wiley-VCH: Mannheim, 2004; Vol. 5, 1.
82. Taliaferro, M. L.; Selby, T. D.; Miller, J. S. *Chem. Mater.* **2003**, *15*, 3602.
83. Mydosh, J. *Spin Glasses*; Francis and Taylor, 1993, p 64.
84. Huang, Z. J.; Cheng, F.; Ren, Y. T.; Xue, Y. Y.; Chu, C. W.; Miller, J. S. *J. Appl. Phys.* **1993**, *73*, 6563.
85. Yee, G. T.; Whitton, M. J.; Sommer, R. D.; Frommen, C. M.; Reiff, W. M. *Inorg. Chem.* **2000**, *39*, 1874.
86. Hamlin, J. J.; Brekett, B. R.; Tomita, T.; Shilling, J. S.; Tyree, W. S.; Yee, G. T. *Polyhedron* **2003**, *22*, 2249.
87. Crisp, J. A.; Meredith, M. B.; Hanus, T. P.; Wang, G.; Brennessel, W. W.; Yee, G. T. *Inorg. Chem.* **2005**, *44*, 172.
88. McConnell, H. M. *Proc. R. A. Welch Found. Conf. Chem. Res.* **1967**, *11*, 144.
89. Miller, J. S.; Epstein, A. J. *J. Am. Chem. Soc.* **1987**, *109*, 3850.
90. Yee, G. T.; Kaul, B. B. *J. Solid State Chem.* **2001**, *159*, 420.
91. Kaul, B. B.; Sommer, R. D.; Noll, B. C.; Yee, G. T. *Inorg. Chem.* **2000**, *39*, 865.
92. Kaul, B. B.; Yee, G. T. *Polyhedron* **2001**, *20*, 1757.
93. Rabaça, S.; Meira, R.; Pereira, L. C. J.; Duarte, M. T.; da Gama, V. *J. Organomet. Chem.* **2001**, *632*, 67.
94. de Gama, V.; Belo, D.; Santos, I. C.; Henriques, R. T. *Mol. Cryst. Liq. Cryst.* **1997**, *306*, 17.
95. de Gama, V.; Belo, D.; Rabaça, S.; Santos, I. C.; Alves, H.; Waerenborgh, J. C.; Duarte, M. T.; Henriques, R. T. *Eur. J. Inorg. Chem.* **2000**, 2101.
96. Narayan, K. S.; Kai, K. M.; Epstein, A. J.; Miller, J. S. *J. Appl. Phys.* **1991**, *69*, 5953.
97. Narayan, K. S.; Morin, B. G.; Miller, J. S.; Epstein, A. J. *Phys. Rev. B* **1992**, *46*, 6195.
98. Narayan, K. S.; Heres, O.; Epstein, A. J.; Miller, J. S. *J. Magn. Magn. Mater.* **1992**, *110*, L6.
99. Miller, J. S.; McLean, R. S.; Vazquez, C.; Yee, G. T.; Narayan, K. S.; Epstein, A. J. *J. Mater. Chem.* **1991**, *1*, 479.

100. Kaul, B. B.; Durfee, W. S.; Yee, G. T. *J. Am. Chem. Soc.* **1999**, *121*, 6862.
101. de Gama, V.; Rabaça, S.; Ramos, C.; Belo, D.; Santos, I. C.; Duarte, M. T. *Mol. Cryst, Liq. Cryst.* **1999**, *335*, 81.
102. Faulmann, C.; Pullen, A. E.; Riviere, E.; Journaux, Y.; Retailleau, L.; Cassoux, P. *Synth. Met.* **1999**, *103*, 2296.
103. Broderick, W. E.; Thompson, J. A.; Hoffman, B. M. *Inorg. Chem.* **1991**, *30*, 2958.
104. Borrás, J. J., Coronado, E., Müller, A., Pope, M. T., Eds.; *Polyoxometalate Molecular Science*; NATO ASI Series: Kluwer, 2003; Vol. 98.
105. Le Maguerès, P.; Ouahab, L.; Golhen, S.; Grandjean, D.; Peña, O.; Jegaden, J. C.; Gómez-García, C. J.; Delhaes, P. *Inorg. Chem.* **1994**, *33*, 5180.
106. Clemente-León, M.; Coronado, E.; Galán-Mascarós, J. R.; Gómez-García, C. J. to be published.
107. Pelleaux, R.; Schmalle, H. W.; Huner, R.; Fisher, P.; Hauss, T.; Ouladdiaf, B.; Decurtins, S. *Inorg. Chem.* **1997**, *36*, 2301.
108. Tamaki, H.; Zhong, Z. J.; Matsumoto, N.; Kida, S.; Koikawa, M.; Achiwa, N.; Hashimoto, Y.; Okawa, H. *J. Am. Chem. Soc.* **1992**, *114*, 6974.
109. Zhong, Z.-J.; Matsumoto, N.; Okawa, H.; Kida, S. *Chem. Lett.* **1990**, 87.
110. Ohba, M.; Tamaki, H.; Matsumoto, N.; Okawa, H.; Kida, S. *Chem. Lett.* **1991**, 1157.
111. Tamaki, H.; Mitsumi, M.; Nakamura, K.; Matsumoto, N.; Kida, S.; Okawa, H.; Iijima, S. *Chem. Lett.* **1992**, 1975.
112. Okawa, H.; Matsumoto, N.; Tamaki, H.; Ohba, M. *Mol. Cryst. Liq. Cryst.* **1993**, *233*, 257.
113. Mathonière, C.; Nuttall, J.; Carling, S. G.; Day, P. *Inorg. Chem.* **1996**, *35*, 1201.
114. Mathonière, C.; Carling, S. G.; Yusheng, D.; Day, P. *J. Chem. Soc., Chem. Commun.* **1994**, 1551.
115. Decurtins, S.; Schmalle, H. W.; Schnewly, P.; Ensling, J.; Gütlich, P. *J. Am. Chem. Soc.* **1994**, *116*, 9521.
116. Pointillart, F.; Train, C.; Gruselle, M.; Villain, F.; Schmalle, H. W.; Talbot, D.; Gredin, P.; Decurtins, S.; Verdaguer, M. *Chem. Mater.* **2004**, *16*, 832.
117. Hernández-Molina, M.; Lloret, F.; Ruiz-Pérez, C.; Julve, M. *Inorg. Chem.* **1998**, *37*, 4131.
118. Coronado, E.; Galán-Mascarós, J. R.; Gómez-García, C. J.; Martínez-Agudo, J. M. *Inorg. Chem.* **2001**, *40*, 113.
119. Andres, R.; Brisard, M.; Gruselle, M.; Train, C.; Vaissermann, J.; Malezieux, B.; Jamet, J. P.; Verdaguer, M. *Inorg. Chem.* **2001**, *40*, 4633.
120. Triki, S.; Berezovsky, F.; Pala, J. S.; Coronado, E.; Gómez-García, C. J.; Clemente, J. M.; Riou, A.; Molinie, P. *Inorg. Chem.* **2000**, *39*, 3771.
121. Coronado, E.; Galán-Mascarós, J. R.; Gómez-García, C. J. *Dalton Trans.* **2000**, 205.
122. Rashid, S.; Turner, S. S.; Day, P.; Light, M. E.; Hursthouse, M. B. *Inorg. Chem.*, **2000**, *39*, 2426.
123. Coronado, E.; Galán-Mascarós, J. R.; Giménez-Saiz, C.; Gómez-García, C. J.; Ruiz-Pérez, C. *Eur. J. Inorg. Chem.* **2003**, 2290.
124. Coronado, E.; Galán-Mascarós, J. R.; Giménez-Saiz, C.; Gómez-García, C. J.; Ruiz-Pérez, C.; Triki, S. *Adv. Mater.* **1996**, *8*, 737.
125. Rochon, F. D.; Melanson, R.; Andruh, M. *Inorg. Chem.* **1996**, *35*, 6086.
126. Stanica, N.; Stager, C. V.; Cimpoesu, M.; Andruh, M. *Polyhedron* **1998**, *17*, 1787.
127. Andruh, M.; Melanson, R.; Stager, C. V.; Rochon, F. D. *Inorg. Chim. Acta* **1996**, 309.
128. Coronado, E.; Giménez, M. C.; Gómez-García, C. J.; Romero, F. M. *Polyhedron* **2003**, *22*, 3115.
129. Marinescu, G.; Andruh, M.; Lescouëzec, R.; Muñoz, M. C.; Cano, J.; Lloret, F.; Julve, M. *New J. Chem.* **2000**, *24*, 527.
130. Coronado, E.; Galán-Mascarós, J. R.; Gómez-García, C. J.; Martí-Gastaldo, C. *Inorg. Chem.* **2005**, *44*, 6197.
131. Alberola, A.; Coronado, E.; Giménez-Saiz, C.; Gómez-García, C. J.; Romero, F. M.; Tarazón, A. *Eur. J. Inorg. Chem.* **2005**, 389.
132. Alberola, A.; Coronado, E.; Galán-Mascarós, J. R.; Giménez-Saiz, C.; Gómez-García, C. J. *J. Am. Chem. Soc.* **2003**, *125*, 10774.
133. Alberola, A.; Coronado, E.; Galán-Mascarós, J. R.; Giménez-Saiz, C.; Gómez-García, C. J.; Martínez-Ferrero, E.; Murcia-Martínez, A. *Synth. Met.* **2003**, *135–136*, 687.
134. Coronado, E.; Galán-Mascarós, J. R.; Gómez-García, C. J.; Martínez-Ferrero, E.; van Smaalen, S. *Inorg. Chem.* **2004**, *43*, 4808.
135. Bénard, S.; Yu, P.; Audière, J. P.; Rivière, E.; Clèment, R.; Ghilhem, J.; Tchertanov, L.; Nakatani, K. *J. Am. Chem. Soc.* **2000**, *122*, 9444.
136. Bénard, S.; Rivière, E.; Yu, P.; Nakatani, K.; Delouis, J. F. *Chem. Mater.* **2001**, *13*, 159.
137. Clemente-León, M.; Coronado, E.; Galán-Mascarós, J. R.; Gómez-García, C. J. *Chem. Commun.* **1997**, 1727.
138. Nutall, C. J.; Day, P. *J. Solid State Chem.* **1999**, *147*, 3.
139. Min, K. S.; Rhinegold, A. L.; Miller, J. S. *Inorg. Chem.* **2005**, *44*, 8344. Min, K.; Miller, J. S. *J. Chem. Soc. Dalton*, **2006**, 2463.
140. Nuttall, C. J.; Bellitto, C.; Day, P. *J. Chem. Soc. Chem. Commun.* **1995**, 1513.
141. Coronado, E.; Galán-Mascarós, J. R.; Martí-Gastaldo, C. *J. Mater. Chem.* **2006**, *16*, 2685.
142. Galán-Mascaros, J. R. PhD dissertation, Universidad de Valencia, 1999.
143. Coronado, E.; Galán-Mascarós, J. R.; Gómez-García, C. J.; Ensling, J.; Gütlich, P. *Chem. Eur. J.* **2000**, *6*, 552.
144. Coronado, E.; Galán-Mascarós, J. R.; Gómez-García, C. J.; Burriel, R. *J. Magn. Magn. Mater.* **1999**, *196–197*, 558.
145. Iijima, S.; Mizutani, F. *Mol. Cryst. Liq. Cryst.* **1997**, *306*, 227.
146. Iijima, S.; Mizutani, F.; Mitsunmi, M.; Matsumoto, N.; Okawa, H. *Inorg. Chim. Acta* **1996**, *253*, 47.
147. Blundell, S. J. *Contemp. Phys.* **1999**, *40*, 175.
148. Lancaster, T.; Blundell, S. J.; Pratt, F. L.; Coronado, E.; Galán-Mascarós, J. R. *J. Mater. Chem.* **2004**, *14*, 1518.
149. Malézieux, B.; Andrés, R.; Brissard, M.; Grusselle, M.; Train, C.; Herson, P.; Troitskaya, L. L.; Sokolov, V. I.; Ovseenko, S. T., Demeschik, T. V., *et al. J. Organomet. Chem.* **2001**, *637–639*, 1201.
150. Gruselle, M.; Thouvenot, R.; Malézieux, B.; Train, C.; Gredin, P.; Demeschik, T. V.; Troitskaya, L. L.; Sokolov, V. I. *Chem. Eur. J.* **2004**, *10*, 4763.
151. Zhou, P.; Morin, B. G.; Epstein, A. J.; McLean, R. S.; Miller, J. S. *J. Appl. Phys.* **1993**, *73*, 6569.
152. Buschmann, W. E.; Paulson, S. C.; Wynn, C. M.; Girtu, M.; Epstein, A. J.; White, H. S.; Miller, J. S. *Chem. Mater.* **1998**, *10*, 1386.
153. Néel, L. *Ann. Phys.* **1948**, *3*, 137.
154. Coronado, E.; Galán-Mascarós, J. R.; Gónez-García, C. J.; Martínez-Agudo, J. M.; Martínez-Ferrero, E.; Waerenborgh, J. C.; Almeida, M. *J. Solid State Chem.* **2001**, *159*, 391.
155. Larionova, J.; Mombelli, B.; Sanchiz, J.; Kahn, O. *Inorg. Chem.*, **1998**, *37*, 679.
156. Coronado, E.; Galán-Mascarós, J. R.; Gómez-García, C. J.; Martínez-Agudo, J. M. *Adv. Mater.* **1999**, *11*, 558.
157. Narayan, K. S.; Morin, B. G.; Miller, J. S.; Epstein, A. J. *Phys. Rev. B* **1992**, *46*, 6195.
158. Coronado, E.; Galán-Mascarós, J. R.; Gómez-García, C. J.; Martínez-Agudo, J. M. *Synth. Met.* **2001**, *122*, 501.
159. Kurmoo, M.; Kepert, C. J. *New J. Chem.* **1998**, *22*, 1515.
160. Manson, J. L.; Kmety, C. R.; Huang, Q. Z.; Lynn, J. W.; Bendele, G. M.; Pagola, S.; Stephens, P. W.; Liable-Sands, L. M.; Rheingold, A. L.; Epstein, A. J., *et al. Chem. Mater.* **1998**, *10*, 2552.
161. Batten, S. R.; Murray, K. S. *Coord. Chem. Rev.* **2003**, *246*, 103.
162. Batten, S. R.; Jensen, P.; Moubaraki, B.; Murray, K. S.; Robson, R. *Chem. Commun.* **1998**, 430.
163. Manson, J. L. *Magnetism - Molecules to Materials*; Miller, J. S., Drillon, M., Eds.; Wiley-VCH: Mannheim, 2004; Vol. 5, p 71.

164. Etzkorn, S. J.; Hibbs, W.; Miller, J. S.; Epstein, A. J. *Phys. Rev. B* **2004**, *70*, 134419.
165. Hibbs, W.; Rittenberg, D. K.; Sugiura, K.; Burkhart, B. M.; Morin, B. G.; Arif, A. M.; Liable-Sands, L.; Rheingold, A. L.; Sundaralingam, M.; Epstein, A. J., *et al. Inorg. Chem.* **2001**, *40*, 1915.
166. Vos, T. E.; Miller, J. S. *Angew. Chem., Int. Ed.* **2005**, *44*, 2416.
167. McCurrie, R. A. *Ferromagnetic Materials. Structure and Properties*; Academic Press: London, 1994.
168. Van de Werff, P. M.; Martínez-Ferrero, E.; Batten, S. R.; Jensen, P.; Ruiz-Pérez, C.; Almeida, M.; Warenborgh, J. C.; Cashion, J. D.; Moubaraki, B., Galán-Mascarós, J. R., *et al. Dalton Trans.* **2005**, 285.
169. Raebiger, J. W.; Manson, J. L.; Sommer, R. D.; Geiser, U.; Rheingold, A. L.; Miller, J. S. *Inorg. Chem.* **2001**, *40*, 2578.
170. Elsner, O.; Ruiz-Molina, D.; Ratera, I.; Vidal-Gancedo, J.; Rovira, C.; Veciana, J. *J. Organomet. Chem.* **2001**, *637*, 251.
171. Elsner, O.; Ruiz-Molina, D.; Vidal-Gancedo, J.; Rovira, C.; Veciana, J. *Chem. Commun.*, **1999**, 579.
172. Jürgens, O.; Vidal-Gancedo, J.; Rovira, C.; Wurst, K.; Sporer, C.; Bildstein, B.; Schottenberger, H.; Jaitner, P.; Veciana, J. *Inorg. Chem.* **1998**, *37*, 4547.
173. Nakamura, Y.; Koga, N.; Iwamura, H. *Chem. Lett.* **1991**, 69.
174. Sporer, C.; Heise, H.; Wurst, K.; Ruiz-Molina, D.; Kopacka, H.; Jaitner, P.; Köhler, F.; Novoa, J. J.; Veciana, J. *Chem. Eur. J.* **2004**, *10*, 1355.
175. Ruiz-Molina, D.; Sporer, C.; Wurst, K.; Jaitner, P.; Veciana, J. *Angew. Chem., Int. Ed.* **2000**, *39*, 3688.
176. Sporer, C.; Wurst, K.; Amabilino, D. B.; Ruiz-Molina, D.; Kopacka, H.; Jaitner, P.; Veciana, J. *Chem. Commun.* **2002**, 2342.
177. Ratera, I.; Ruiz-Molina, D.; Vidal-Gancedo, J.; Wurst, K.; Daro, N.; Letard, J.-F.; Rovira, C.; Veciana, J. *Angew. Chem., Int. Ed.* **2001**, *40*, 919.
178. Ratera, I.; Ruiz-Molina, D.; Vidal-Gancedo, J.; Novoa, J. J.; Wurst, K.; Letard, J.-F.; Rovira, C.; Veciana, J. *Chem. Eur. J.* **2004**, *10*, 603.
179. Ratera, I.; Ruiz-Molina, D.; Renz, F.; Ensling, J.; Wurst, K.; Rovira, C.; Gütlich, P.; Veciana, J. *J. Am. Chem. Soc.* **2003**, *125*, 1462.
180. Sporer, C.; Ratera, I.; Ruiz-Molina, D.; Zhao, Y.; Vidal-Gancedo, J.; Wurst, K.; Jaitner, P.; Clays, K.; Persoons, A., Rovira, C., *et al. Angew. Chem., Int. Ed.* **2004**, *43*, 5266.

12.08
Medicinal Organometallic Chemistry

G Jaouen, CNRS UMR 7576, Paris, France
P J Dyson, Institut des sciences et ingénierie chimiques, Lausanne, Switzerland

12.08.1 Introduction

The medicinal properties of inorganic (coordination) compounds have been extensively reviewed[1,1a–1h] as there is no doubt of their clinical success, notably that of cisplatin and other platinum compounds. Organometallic compounds have also had clinical applications for a long time, a prominent example being the antisyphilis drug Salvarsan® introduced into clinical use in 1910,[2] and recently found to comprise a mixture of mostly small ring compounds.[3] Metallocene-type complexes based on Ti, Fe, V, Mo, Re, Nb, and Hf were evaluated as anticancer compounds shortly after the discovery of cisplatin,[4,4a–4d] and titanocene dichloride has been extensively studied, but clinical trials were recently discontinued principally due to formulation problems.[5,5a] The last decade has witnessed many promising developments in the field of medicinal organometallic chemistry, with organometallic compounds displaying anticancer activity, finding applications as antibiotics and antiviral agents as well as in other areas. The role of organometallic compounds in medicine, with an emphasis on the work published in the last 10 years, constitutes the subject of this chapter. Organometallic diagnostic and imaging agents and radiopharmaceuticals are described elsewhere.[6]

12.08.2 Anticancer Compounds

Metal-based drugs have probably had most impact in the area of cancer therapy, with cisplatin still used to treat approximately 70% of all cancer patients. Cisplatin is particularly useful for treatment of testicular, ovarian, oropharyngeal, bronchogenic, cervical, and bladder carcinomas, lymphoma, osteosarcoma, melanoma, and neuroblastoma.[7,7a] Metallocene-type compounds were the first organometallic compounds to be evaluated in cancer therapy, and until recently, $Ti(\eta^5\text{-}C_5H_5)_2Cl_2$ was undergoing clinical trials (see above). Despite this setback to the field,

many new potential organometallic anticancer compounds continue to be developed, and two main classes can be defined – those with known therapeutic action (e.g., selective estrogen receptor modulators (SERMs), see Section 12.08.2.1), and compounds with comparatively simple ligands, used, for example, to provide appropriate solubility properties, prepared without a specific type of cancer in mind.

12.08.2.1 Selective Estrogen Receptor Modulators (SERMs)

Two-thirds of breast cancer tumors contain the alpha form of the estrogen receptor (ER) and therefore growth is stimulated by estrogens. The mechanism of action of the estrogens in these tumors is due to the specific interaction of the hormone with this receptor, and binding of the hormone to its receptor is followed by a sequence of events, which causes the expression of a large number of specific genes responsible for a number of processes including cellular growth.[8,8a] Adjuvant treatment of these hormone-dependent cancers includes administration of antiestrogens also known as SERMs and recently antiaromatases.[9] The standard antiestrogen for the past 20 years has been hydroxytamoxifen (OH-Tam), which, for reasons of bioavailability, is administered in its non-hydroxylated form, tamoxifen (Figure 1).

Unfortunately, a third of hormone-dependent tumors do not respond to tamoxifen and another third acquire resistance. In order to overcome these deficiencies, several platinum complexes derived from estradiol, estrone, or the synthetic estrogen hexestrol were prepared as estradiol receptors.[10,10a–10f] These compounds proved to be similar in activity to those observed in the presence of the corresponding platinum complexes alone, and thus seem to be fundamentally linked to the cytotoxicity of these complexes, and were therefore not studied further. Tamoxifen has also been coupled to platinum, but again, it is only slightly cytotoxic toward hormone-dependent breast cancers,[11] and therefore the inorganic complexes of platinum still do not appear suitable for coupling to a hormonal delivery system. However, a number of organometallic-derivatized tamoxifen compounds have been prepared that show considerable promise.

A titanocene-type derivative of tamoxifen, in which the aromatic β-ring of tamoxifen is substituted by a Cp_2TiCl_2 entity, has been prepared according to the route shown in Scheme 1.[12] This synthesis starts with a McMurry coupling

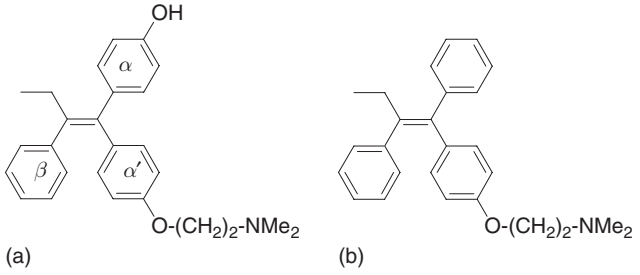

Figure 1 (a) Hydroxytamoxifen (left) and (b) tamoxifen (right).

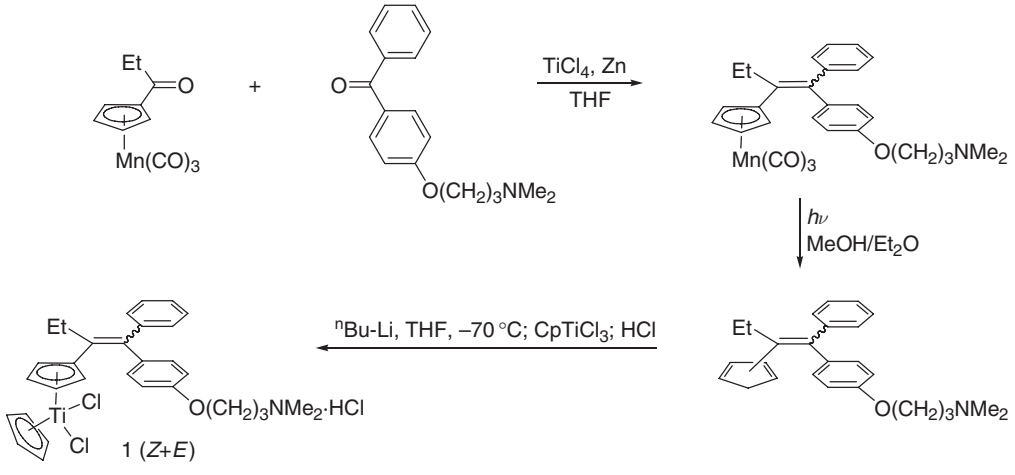

Scheme 1 Synthesis of the Cp_2TiCl_2 derivative of tamoxifen, **1**.

reaction between propionylcyclopentadienylmanganese tricarbonyl and the appropriate ketone, affording the diphenylethylene complex which is converted into a cyclopentadiene via photochemical decomplexation, and immediately recomplexed in the presence of $CpTiCl_3$ to give the target compound, **1**.

This complex still has a marked affinity for the estradiol receptor (relative binding affinity (RBA) = 8.5%) and it exhibits estrogenic effects on hormone-dependent breast cancer cells (MCF7) *in vitro* – comparable effects to those of estradiol. This estrogenic activity is observed at extremely low molarities (10 nM and 0.1 μM) and is also found for the Cp_2TiCl_2 entity alone, suggesting that it is effectively linked to that molecule. In fact, the hydrolysis of Cp_2TiCl_2 is a complex phenomenon that has been the subject of several studies.[13,13a] Hydrolysis is strongly dependent on the experimental conditions, but in biological media, a recent study showed that loss of the Cp ligands as well as the chloride ligands takes place.[14] Although titanium has not yet been studied as a SERM, some metal ions have been studied in this context. For example, treatment of the receptor with Cd^{2+} at very low concentration (ca. 1 nM) results in coordination of this metal at the level of the ER ligand-binding domain.[15,15a,15b] The complex formed with this exogeneous metal activates ER alpha in an analogous fashion to estradiol. Specifically, the cadmium ion is able to coordinate with cysteins 381 and 447, glutamic acid 523, histidine 524, and aspartic acid 538 of the receptor ligand-binding domain. The idea is that this type of coordination may cause the receptor to act in the same way as the natural ligand, by shutting the trap between the two helices H4 and H12 and causing activation of the transcriptional machinery and proliferation of the hormone-dependent breast cancer cells. This hypothesis could also apply to the case of Ti(IV) and would provide an explanation for the estrogenic effect observed for Cp_2TiCl_2.

The $CpRe(CO)_3$ moiety has been incorporated into the tamoxifen framework[16,16a] via a related strategy used for the preparation of **1** according to the synthesis shown in Scheme 2. Complexes bearing side chains of varying lengths (n = 2–5 and 8, viz. **2a–e**) were prepared, as it was thought that the $CpRe(CO)_3$ unit would lead to changes inside the

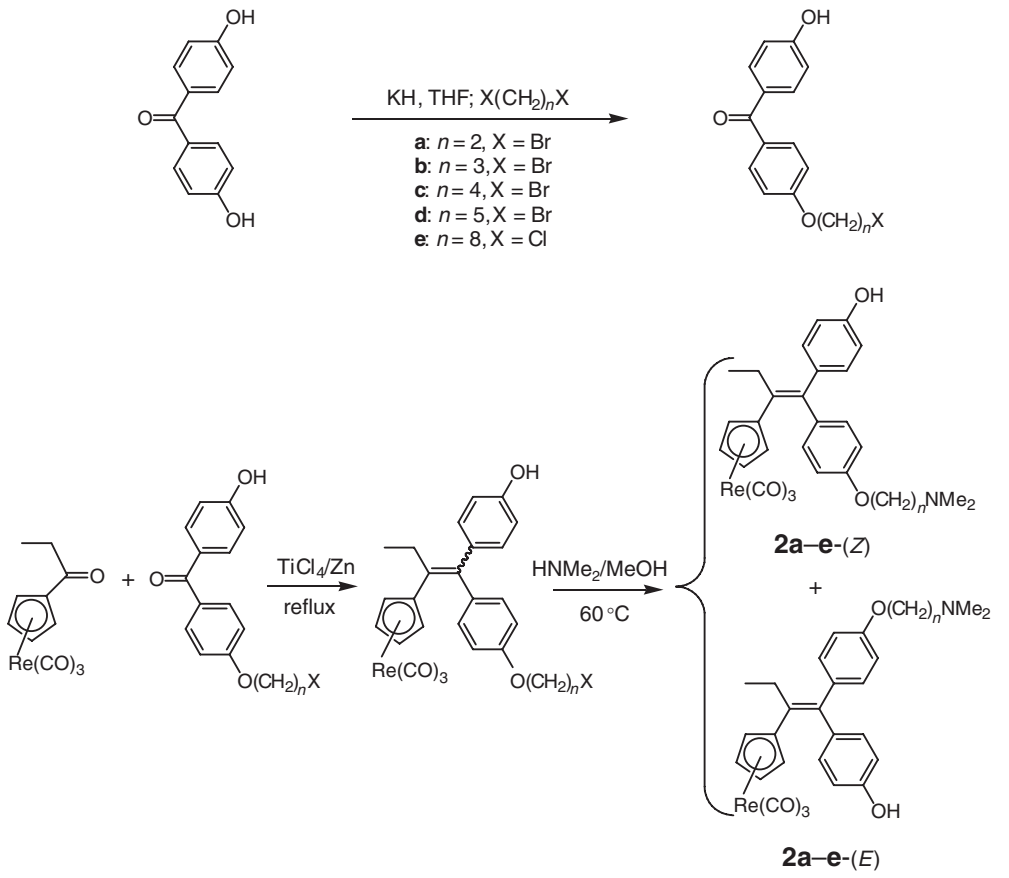

Scheme 2 Synthesis of the cyclopentadienylrhenium tricarbonyl derivatives of OH-tamoxifen **2a–e** by McMurry cross-coupling.

active receptor site with respect to the interactions of the dimethyl amino side chain, known to be responsible for the antiestrogenic effect of tamoxifen.

McMurry coupling of the appropriate ketones gave the alkenes which are converted into amines by treatment with dimethylamine at 60 °C. The McMurry coupling reaction gives a mixture of (*Z*) and (*E*)-isomers that can be separated by semipreparative HPLC.

There is a net decrease in RBA value for **2a–e** (38.5 and 6.4, respectively for (*Z* + *E*)-OH-Tam and (*Z* + *E*)-**2a**), and the value decreases steadily as the side chain is lengthened, so that for $n = 5$, for example, the RBA value is 2%. However the RBA values do not seem to be a determining factor in the anti-proliferative effect of these complexes. On MCF7 breast cancer cells, the observed anti-proliferative effect is very similar for any length of chain ($n = 2$ or 5) or either isomer (*Z* or *E*). The effect is slightly higher than that observed with OH-Tam, the standard antiestrogen. On hormone-independent breast cancer cells (MDA-MB231), that is, those without the alpha form of the ER, estradiol and OH-Tam have no effect, and the rhenium complexes have only a marginal effect. Overall, the rhenium complexes have an antiestrogenic effect very close to that of OH-Tam, an effect that is not influenced by the length of the side chain or by the isomeric form.

The β-phenyl ring of OH-Tam has also been substituted by a ferrocenyl group to give complexes **3a–e**, called ferrocifens (see Figure 2). The synthesis of these complexes employs McMurry coupling reactions,[17,17a–17c] similar to those described previously. The complexes are obtained in the form of a mixture of the isomers (*Z* + *E*), which can be separated by HPLC, but rapidly isomerize in protic solution; thus, most of the biological studies were performed on mixtures of the two isomers.

The complexes with the shortest dimethyl amino side chains ($n = 2$, 3, or 4) retain the best affinity for the two forms of the estradiol receptor. On MCF7 hormone-dependent breast cancer cells, the anti-proliferative effect of these complexes at molarities of 1 μM is slightly stronger than that of OH-Tam for complexes where $n = 3$ and 5 **3b** and **3d**, and this effect is not completely suppressed by addition of estradiol. This seems to indicate that the observed anti-proliferative effect is the combination of an antihormonal effect linked to the tamoxifen skeleton and mediated by the estradiol receptor, and a cytotoxic effect induced by the presence of the ferrocenyl substituent. In fact, the cytotoxic properties of the ferricinium cation ($Fc^{+\cdot}$), which is easily formed by oxidation in biological media, are well known.[18,18a] It should however be noted that ferrocene alone has no effect despite being able to enter cells without difficulty.

Ferrocifens exhibit a strong cytotoxic effect on MDA-MB231 cells (hormone-independent breast cancer cells). In cells without ERα, OH-Tam has no effect, while ferrocifens **3b** and **3d** have a remarkable anti-proliferative effect ($IC_{50} = 0.5$ μM). It has been shown that derivatives of estradiol bearing a ferrocenyl substituent in position 17α, **4** and **5** (Figure 3), have an estrogenic effect *in vitro*, but are devoid of any cytotoxic effect either on hormone-dependent or hormone-independent cells. Simply delivering an estrogenic molecule bearing a ferrocenyl substituent payload into

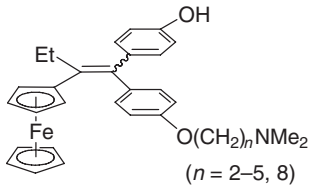

3a–e-(*Z*+*E*)

Figure 2 Structure of hydroxy ferrocifens **3a–e**.

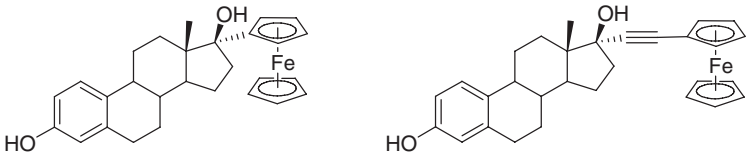

4 **5**

Figure 3 Ferrocenyl estrogen derivatives **4** and **5**.

the interior of a target cell is not sufficient to obtain a cytotoxic effect. The production of this effect seems to be linked to a specific structure that allows the ferrocenyl—double bond—phenol pattern to come into play.

The mechanism of action of ferrocifens in the cell remains elusive. However, molecular modeling studies have revealed that ferrocifens such as (*Z*)-**3b** may be inserted into the antagonist configuration of the active site of the ER. The interior of the active site is sufficiently large to accommodate the ferrocenyl group, and interactions between His524 and the ferrocenyl group, and between Asp351 and the nitrogen of the basic chain, provide correct positioning of the organometallic hormone and particularly of the dimethyl amino side chain, which is known to be the source of the antihormonal effect, also explaining why the antiestrogenic effect is comparable to that of OH-Tam. As far as the cytotoxic effect of these molecules is concerned, this is clearly linked to the presence of a ferrocenyl substituent which may be reversibly oxidized under certain conditions. The cascade of events that presumably begins with the oxidation of the ferrocene and leads finally to apoptosis of the cells has not yet been elucidated, and the molecular targets remain unknown. Is it perhaps linked to the presence of ERβ, the second form of the receptor which seems to play a role in oxidation phenomena in the cell,[19,19a] or could involve the regulation of particular enzymes or other proteins implicated in the cellular cycle.

The ruthenium analogs of the ferrocifens **3a–d**, that is, ruthenocifens **6a–d** have been isolated as a mixture of the two isomers ($Z+E$) which cannot be separated by HPLC, presumably because interconversion is too rapid.[20] The complexes for which $n=2$ (**6b**) and 3 (**6c**) have very high RBA values for ERα (85% and 53%, respectively), significantly higher than that of OH-Tam (RBA = 38.5). *In vitro*, complexes **6b** and **6c** have an anti-proliferative effect slightly higher than that of OH-Tam on hormone-dependent MCF7 cells and no effect on hormone-independent MDA-MB231 cells. Unlike ferrocifens, the ruthenium complexes behave as antiestrogens. It is conceivable that this difference is due to the irreversible oxidation of the ruthenocenyl moiety (demonstrated electrochemically) that leads to rapid decomposition of the organometallic entity compared to the ferrocenyl species which undergo reversible oxidation.[21]

12.08.2.2 Ferricenium and Ferrocene Polymer Compounds

A number of non-SERM ferrocene-based compounds have been evaluated as anticancer agents for a range of cancers. In the simplest cases, ferricenium salts such as ferricenium picrate and ferricenium trichloroacetate were shown to display reasonable anti-proliferative activity compared to ferrocene itself.[22] The ferricenium salts are more water soluble than ferrocene, and their superior activity was proposed to be due to their possession of an appropriate lipophilicity/hydrophilicity balance to permeate cell membranes. Accordingly, ferrocenes with functional groups that might help to impart similar properties have been prepared and studied, notably with polyaspartamide groups, some examples of which are illustrated in Figure 4.[23,23a]

These ferrocene-containing polymers act as pro-drugs in that the amino group being protonated at physiological pH could facilitate cellular uptake. They are particularly effective *in vitro* against the Colo 320 DM cell line, an important finding as cancers of the intestinal system are known to resist chemotherapeutic treatment. A number of other polymer-ferrocene systems have been investigated as anticancer agents and they have been reviewed in detail very recently.[24]

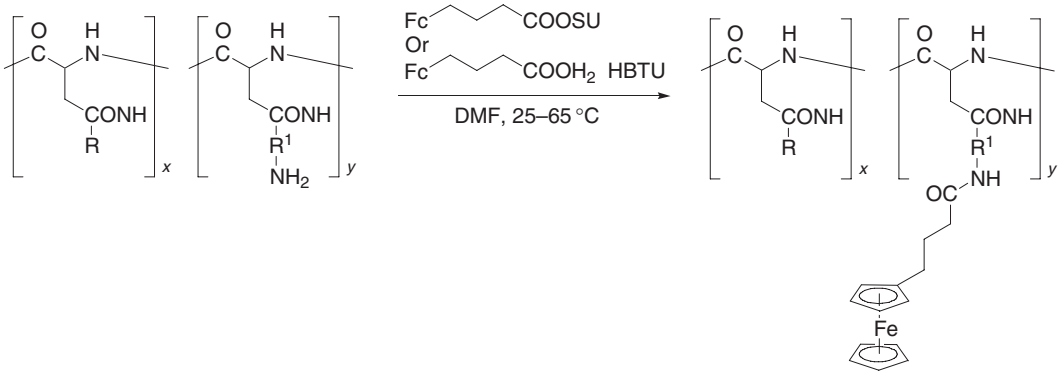

Figure 4 Polyaspartamide-ferrocene anticancer compounds, nine examples where R and R^1 correspond to, for example, $-(CH_2)_3NMe_2$, $-(CH_2)_3CH_3$, $-(CH_2)_2OH$, $-(CH_2)_2NH(CH_2)_2CH_3$, etc.

Anti-proliferation agents based on an 11-vertex ferratricarbaborane have been demonstrated.[25] These complexes may be viewed as ferrocene analogs, but they are more resistant to degradation and possibly exhibit lower toxicity. Similar broad anti-proliferation activity is demonstrated by $M(C_5H_5)(MeC_3B_7H_9)$ complexes.[147]

12.08.2.3 Titanocenes and Molybdenocenes

As mentioned in the introduction, metallocene-type complexes based on the early transition metals were evaluated as anticancer compounds shortly after the discovery of cisplatin. While the biological activity of each of the metallocene dihalides is unique,[26] titanocene dichloride **7** has been the subject of a number of studies and even entered clinical evaluation, although evaluation was discontinued (not due to its anti-proliferative properties), principally due to formulation problems, despite showing superior activity to certain cancers than other established drugs.[27] This class of compound continues to be modified and studied for anticancer activity, for example, the titanocene-type derivative of tamoxifen **1**, described above, and other developments described below.

In order to improve the poor water solubility of $Ti(\eta^5\text{-}C_5H_5)_2Cl_2$ **7**, the chloride ligands have been substituted by other ligands (including weakly coordinating liands) such as I^-, $CF_3SO_3^-$, $[FeCl_4]^-$, and $[AsF_6]^-$ as well as neutral ligands including MeCN, phenanthroline, 6-thioguanine, glycine, and L-alanine affording mono- and dicationic salts.[28,28a] While water solubility improved, the activity of these salts was found to be lower than that of their neutral precursor **7**. An alternative approach to overcome the poor water solubility of **7** was to encapsulate it in β-cyclodextrin which provides a water-soluble inclusion complex with potential as an orally administered drug;[29] a similar strategy has also been applied to the molybdenum analog.[30] The presence of hydrogen bonding groups also improves water solubility, and such groups have been attached to the cyclopentadienyl rings in titanium compounds, although the main motivation for this development was to increase the cytotoxicity via increased interactions with DNA (i.e., combining coordination and H-bonding).[31] The compounds were prepared according to the route shown in Scheme 3 from the reaction of $TiCl_2{\cdot}2THF$ and 2-furylfulvene, 2-thiophenylfulvene, or 1-methyl-2-pyrrolylfulvene. The activity of **8a–c** *in vitro* against pig kidney carcinoma cells (LLC-PK) was found to be considerably greater than that of **7**.

Other approaches to improve the anti-proliferative properties of titanocene compounds have been to coordinate known organic anticancer drugs to the titanium center in place of the chloride ligands,[32] and a bis-titanocene complex bridged by a platinum(II) center has also been reported.[33] Titanium-cyclopentadienyl units connected by oxo bridges, containing between two and eight "TiCp" fragments, linked as rings or in cage structures (Figure 5), represent another class of drug compound, although some suffer from solubility problems, and details of these compounds are provided elsewhere.[34]

Replacement of the chloride ligands in molybdenocene dichloride by thiol ligands is a facile process in aqueous solutions containing thiol ligands following their deprotonation. In this way, glutathione, 4-thiol-2,3,5,6-tetrafluorobenzoic acid, 1-thio-β-D-glucose, and 1-thio-2,3,4,5-tetraacetyl-β-D-glucose have been coordionated to the "$MoCp_2$" unit (Figure 6),[35,35a] the glutathione derivative having been proposed to form in blood plasma.

Compared to molybdenocene dichloride, the thiol derivatives are stable in water at physiological pH, and in tests on V79 Chinese hamster lung, human breast MCF7, and ovarian 2008 cell lines, they are not cycotoxic. The

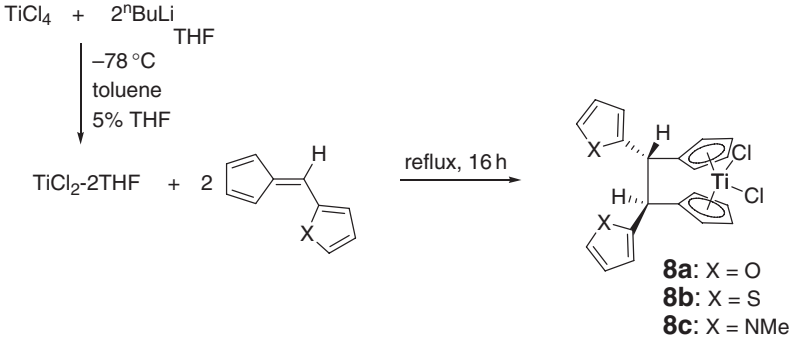

Scheme 3 Synthesis of **8a–c**.

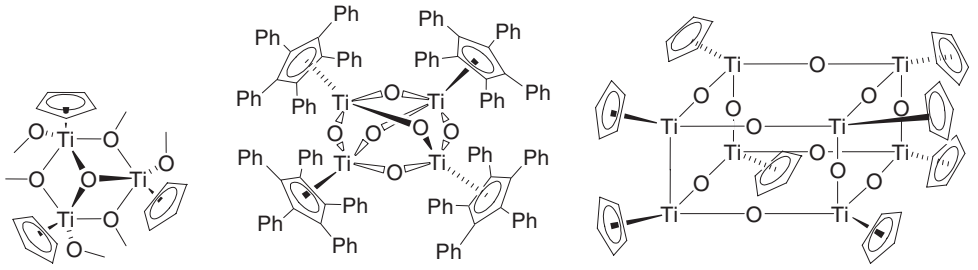

Figure 5 Examples of titanium-cyclopentadienyl oxo-bridged complexes evaluated for anticancer activity.

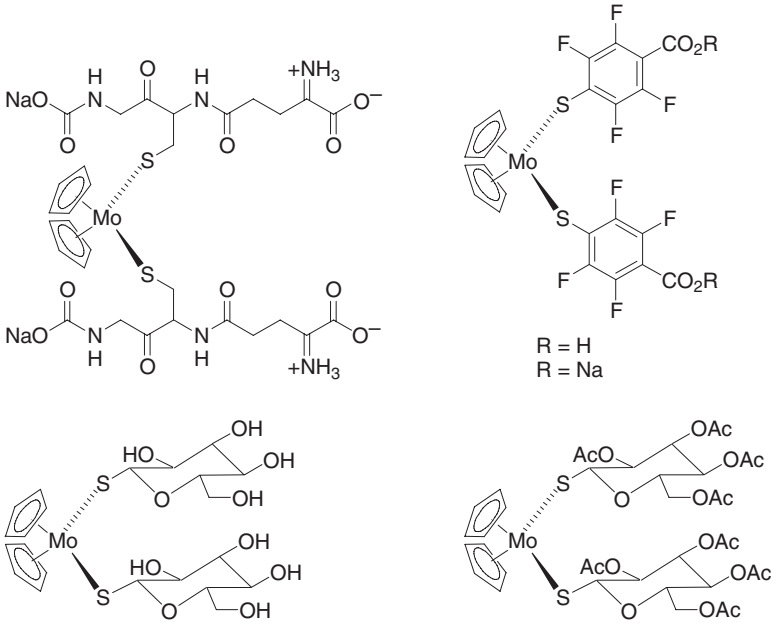

Figure 6 Examples of molybdenocene dichloride thiol derivatives of biological relevance prepared in water under facile conditions.

implication from these observations is that while rapid coordination of glutathione to molybdenocene dichloride occurs in water, the corresponding reaction in the cell must be less favored.

12.08.2.4 Ruthenium and Osmium Arene Compounds

Organoruthenium compounds have started to attract interest as potential anticancer drugs, partly motivated by the entrance of the ruthenium coordination compounds [ImH][*trans*-$RuCl_4$(DMSO)Im] (NAMI-A)[36] and [ImH][*trans*-$RuCl_4Im_2$] (KP1019)[37] into clinical trials. Although in NAMI-A and KP1019 the ruthenium is in the +III and +IV oxidation states, respectively, it has been proposed that the active species contains Ru(II), generated *in situ*, the so-called activation by reduction mechanism.[38] Consequently, a number of ruthenium(II)-arene compounds have been evaluated as anticancer agents.

The earliest examples of such compounds (summarized in Figure 7) include a 1-β-hydroxyethyl-2-methyl-5-nitroimidazole (metronidazole – a known anticancer agent) adduct of ruthenium(II)-benzene **9**, affording a compound with superior selective cytotoxicity than metronidazole itself,[39] and some ruthenium(II)-arene compounds with alanine and guanine derived co-ligands,[40] shown to be cytotoxic toward P388 leukaemia cells.[41] However, following the initial observations, further studies of these specific compounds were not reported. The ruthenium-arene DMSO compound Ru(η^6-C_6H_6)Cl_2(Me_2SO) **10** was also shown to inhibit topoisomerase II, an important target in chemotherapy.[17,17a–17c]

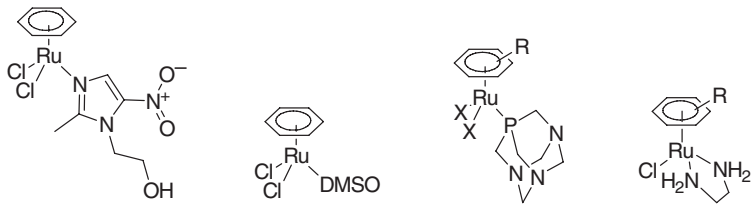

9 **10** **11** **12**

Figure 7 Ruthenium(II)-arene anticancer complexes **9**–**12**.

More recent studies, also including *in vivo* evaluations, have been undertaken on ruthenium(II)–arene complexes with the 1,3,5-triaza-7-phosphatricyclo-[3.3.1.1]decane (PTA) co-ligand, viz. [Ru(η^6-arene)Cl_2(PTA)] **11**[42] and ethylenediamine co-ligand, viz. [Ru(η^6-arene)Cl(dien)]$^+$ (dien = ethylenediamine) **12**.[43]

The compound [Ru(η^6-*p*-cymene)Cl_2(PTA)] **11a** was initially shown to exhibit pH-dependent DNA damage such that at the pH typical of hypoxic cells (characteristic of many types of cancer cells), DNA was damaged, whereas at the pH characteristic of healthy cells, little or no damage was detected. Such behavior was ascribed to the PTA ligand which can be protonated at low pH, and the protonated form was considered to be the active agent. Subsequently, it has been observed that **11a** exhibits highly selective anticancer activity in cell culture, displaying toxicity toward the TS/A mouse adenocarcinoma cancer cell line while having almost no observable effect on HBL-100 human mammary (non-tumorigenic) cells.[44] The model compound for the protonated derivative, viz. [Ru(η^6-*p*-cymene)Cl_2(PTA-Me)]$^+$, has an indistinguishable toxicity against both cancer and healthy cells. Determination of the pK_a of a series of Ru–arene PTA, (RAPTA) compounds indicates that the protonation is not accessible within the physiological range, although it is possible that once coordinated to DNA, the pK_a of PTA changes sufficiently such that it is protonated. Although drug uptake is low (and does not strongly correlate to activity), interactions with oligonucleotides have been studied and modeled. In comparison to the related dien compounds **12**, loss of the arene is observed on binding to oligonucleotides (based on mass spectrometric evidence).[45] Oligonucleotide binding of type **11** compounds was also compared to their osmium analogs, which retained the arene, due to the stronger Os–arene bond.

A detailed *in vivo* study of [Ru(η^6-*p*-cymene)Cl_2(PTA)] **11a** and [Ru(η^6-*p*-benzene)Cl_2(PTA)] **11b** has been reported, showing that these complexes are inactive toward primary tumor growth, but reduce the growth of lung metastases in CBA mice bearing the MCa mammary carcinoma as effectively as the best available known drugs. Pharmacokinetic studies of RAPTA-C following different intraperitoneal (i.p.) treatments in healthy Swiss CD-1 mice indicate that ruthenium is rapidly lost from the organs and the bloodstream overall, displaying excellent clearance rates, and no toxicological effects were detected.

The dien complexes [Ru(η^6-arene)Cl(dien)]$^+$ **12** exhibit a broad range of IC_{50} values in A2780 parental cells comparable in the best cases to carboplatin, but superior in that they did not exhibit cross-resistance.[46] *In vivo* activity was demonstrated in the A2780 and A2780cis xenografts. The mode of action of the biphenyl derivative [Ru(η^6-biphenyl)Cl(dien)]$^+$ **12a** is thought to be due to DNA binding and it was shown to exhibit selectivity toward N7 of guanine bases.[47] The reactivity of the various binding sites of nucleobases toward [Ru(η^6-biphenyl)Cl(dien)]$^+$ decreases in the order G(N7) > I(N7) > I(N1), T(N3) > C(N3) > A(N7), A(N1). The selectivity appears to be controlled by the ethylenediamine NH_2 groups, which H-bond with exocyclic oxygens, but are nonbonding and repulsive toward the exocyclic amino groups of the nucleobases. It has also been proposed that hydrophobic interactions between the arene ligand and DNA could also facilitate DNA binding, and a direct correlation between cytotoxicity and the size of the arene was observed; further details of these complexes and others prepared by the same group can be found in a recent review.[48]

Other ruthenium(II)–arene compounds have been studied *in vitro* against various cancer cell lines including those with disulfoxide ligands,[49] type **11** compounds in which the arene has been replaced with a pentamethylcyclopentadienyl ring **11′**,[50] and also those in which the arene has been replaced with a sulfur macrocycle, for example, **11″** (Figure 8); while these latter complexes are no longer organometallic, some still show selective activity toward cancer cells *in vivo*.[51] Ruthenium(II)–arene fragments have also been connected by bridging sulfoxide ligands **13** which display reasonable *in vitro* activity against a human mammary cancer cell line (MDA-MB-435s).

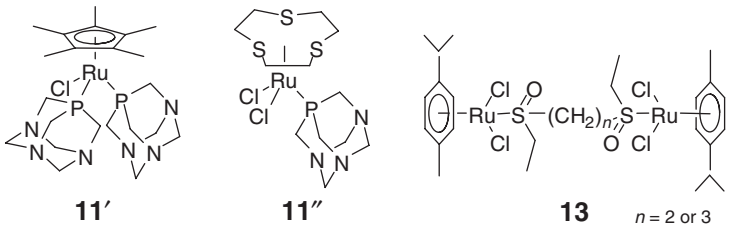

Figure 8 Further examples of piano-stool ruthenium complexes studied for anticancer activity *in vitro*.

12.08.2.5 Other Organometallic Complexes

The cobalt–methyl complex $[Co(cyclan)(H_2O)(Me)]^{2+}$ **14** has been investigated as a photosensitizer in cancer therapy.[52] The complex is stable in water and air, but is light sensitive, producing methyl radicals via homolysis of the Co–Me bond. The methyl radicals result in non-specific DNA cleavage.[53,53a] The differences in DNA replication between cancer cells and healthy cells are sufficient such that **14** has a slightly higher toxicity in diseased compared to healthy cells, but the difference is not sufficiently great to completely eliminate toxicity in healthy cells, which results in unwanted side-effects. Many compounds that strongly DNA damage are often too toxic to use in the clinic, such as organotin compounds that exhibit strong anti-proliferative activity against various cancer cell lines *in vitro*.[54,54a–54d] While DNA is believed to be the main target of organotin compounds, they appear to have a number of targets in the cell, eventually leading to the induction of apoptosis in sensitive cell lines.[55] Unfortunately, organotin compounds have limited applications clinically because of their high general toxicity.

Cells that are not provided with enough oxygen, and where waste products such as carbon dioxide accumulate, undergo changes in their physiological environment, notably a reduction in pH of the cytosol and extracellular fluid creating a reducing (hypoxic) environment. The hypoxic nature of rapidly dividing cells was also postulated to contribute to the low toxicity of ruthenium(III) drugs; when the biologically less active ruthenium(III) complex is delivered to the diseased cells, it becomes rapidly reduced to the more cytotoxic ruthenium(II) species, resulting in drug activation. Similar activation in hypoxic cells has been observed with alkylcobalt(III) complexes, such as **15** shown in Figure 9, which undergo pH-dependent degradation 3 times faster at pH 6.5 than 7.5, producing alkyl radicals that can damage tumors.[56,56a]

Nascent studies describing nucleoside analogs incorporating the iron tricarbonyl unit that represent a new class of cytostatic, apoptosis-inducing agents have been described.[57] These compounds show promising activity in cancer and leukemia therapy.[58] An organoruthenium compound with a pyridocarbazole ligand has also been shown to inhibit glycogen synthase kinase 3 which has relevance to cancer therapy.[59]

12.08.2.6 Polynuclear Complexes (with Direct Metal–Metal Bonds)

Dicobalt hexacarbonyl–alkyne compounds are easy to prepare and relatively stable.[60] Complexes have been prepared with alkynes functionalized with peptides,[61,61a] proteins,[62] therapeutic drugs,[63] steroids such as RU486, **16**,[64] corticoids and androgens,[65] mycotoxin zearalenone **17**,[66,66a] methotrexate **18**,[67] estrogens,[68,68a–68d] and pesticides [69] (see Figure 10 for some examples).

In the steroid series, the alkyne cobalt carbonyl estrogen derivatives **19** and **20**, substituted in position 17α and 11β, have proved to be the most interesting. These complexes are both well recognized by ER alpha (RBA = 12% and

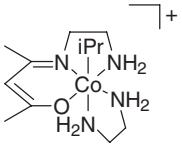

15

Figure 9 An alkylcobalt complex **15** that undergoes rapid degradation at the pH characteristic of many cancer cells producing alkyl radicals that cause cell death.

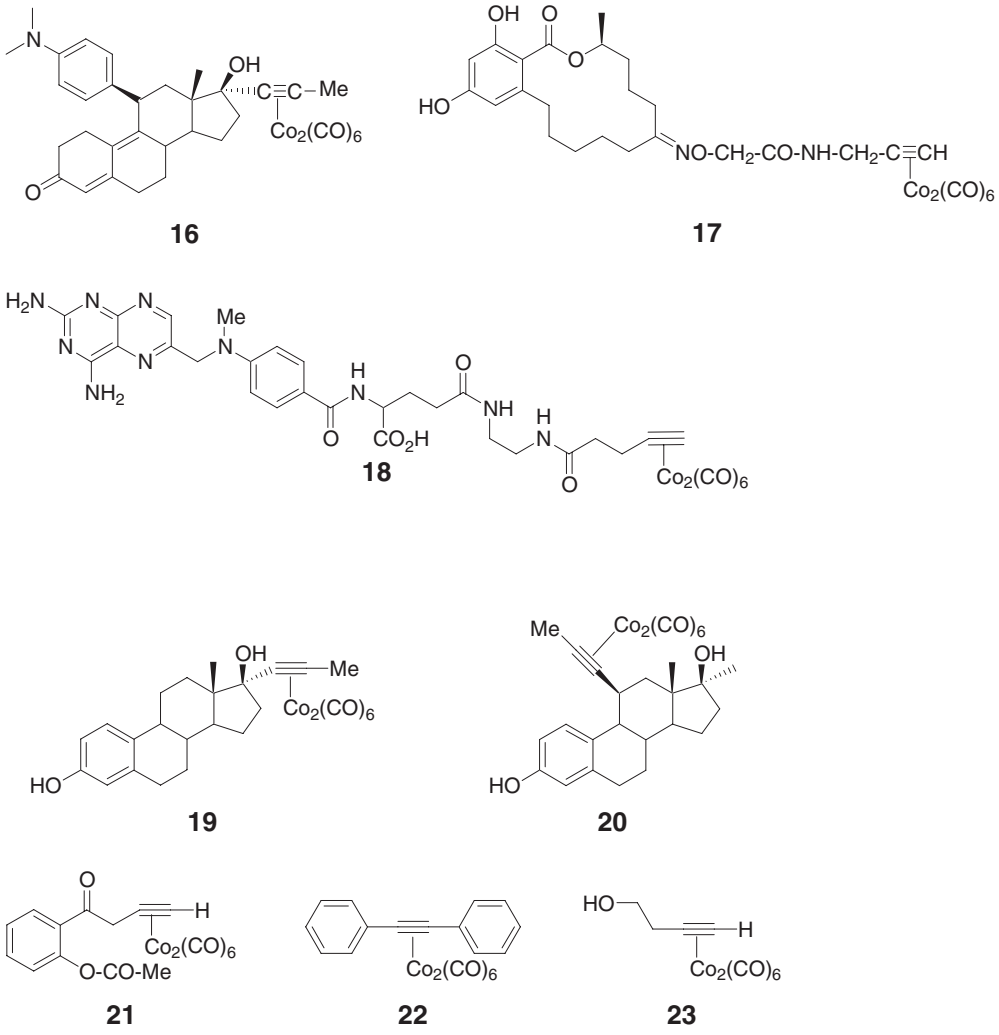

Figure 10 Alkyne cobalt carbonyl complexes of the steroid RU 486 **16**, zearalenone **17**, methotrexate **18**, 17α-propynyl ethynylestradiol **19**, 11β-ethynylestradiol **20**, aspirin **21**, diphenyl acetylene **22**, and 2-propyn-1-ol **23**.

18%, respectively) and are strongly estrogenic at molarities between 0.1 nM and 1 µM, but exhibit an anomaly with respect to their interaction with ER alpha.[70] Compound **19** bearing an alkynecobalt carbonyl group in the 17 alpha-position displays an abnormally long residence time on the active site of the receptor, resembling the behavior of an affinity marker. A possible explanation for this behavior could be the *in situ* generation of a carbenium ion stabilized by the adjacent metallic entity. The carbenium ion, easily generated by Zn^{2+} present in the receptor, could alkylate the cysteine 530, the alkylation site for affinity markers containing an aziridine function.[71] It is also possible that these compounds can interact with methionines 343 and 421, which are able to interfere with the pseudo-Co_2C_2 tetrahedral cluster at the 17alpha-position.[72] This type of mechanism, based on the particular interactions related to the structure of the cluster, could also explain the unusual behavior of **20**, which, at 25 °C, has an RBA value of 65%, much higher than the 18% observed at 0 °C, and a long residence time on the receptor.

The anti-proliferative effects of some dicobalt hexacarbonyl alkyne complexes derived from aspirin **21**, from diphenyl acetylene **22**, and from 2-propyn-1-ol **23**,[73,73a–73c] have been studied on various cell lines, including melanomas and lung cancers, leukemias and lymphomas, and also recently on hormone-dependent (MCF7) and hormone-independent (MDA-MB231) breast cancer cell lines. The most active of these compounds is still the aspirin derivative **21** with IC_{50} values between 1.4 and 10 µM. The activity of **21** is lower than that of cisplatin, except in the case of breast cancer cells, which do not to respond well to cisplatin. The cytotoxic effect of these complexes does not appear to be linked to the accumulation of cobalt in the cells, nor is it due to DNA binding. Compound **21** is a

powerful cyclooxygenase (COX-1 and COX-2) inhibitor, which could explain its mode of action, although this remains to be confirmed.

Apart from the dinuclear cobalt species, very little effort has been devoted to systematically studying the anticancer activity of polynuclear organometallic compounds with nuclearities of 3 and above. However, preliminary studies show that polynuclear compounds can bind (or damage) DNA. The water-soluble clusters $[H_4Ru_4(C_6H_6)_4]^{2+}$ (stabilized as the BF_4 salt) and $Ru_3(CO)_9(PTA)_3$ are strongly damaging toward PBR322 DNA (Figure 11). The platinum clusters $[Pt_2(dpmp)_2(XylNC)_2][PF_6]_2$, $[Pt_3(dpmp)_2(XylNC)_2][PF_6]_2$, $[Pt_3(dpmp)_2(XylNC)_2][Pt(CN)_4]_2$, and $[Pt_3(\mu_3\text{-}CO)(\mu\text{-}dppm)_3]Cl_2$ are sparingly soluble in water and are somewhat less active.

Some water-soluble triosmium carbonyl clusters have also been shown to damage DNA,[74,74a] to inhibit telomerase,[75] an enzyme crucial for cancer progression. The clusters contain a liphophilic phosphine to induce the desired water solubility. $[Os_3(CO)_9(\mu\text{-}\eta^2\text{-}(L\text{-}H))(\mu\text{-}H)L']$ (L = 3-amino quinoline, $L' = Na_3[P(C_6H_4SO_3)_3]$ **24a**; L = 3-amino quinoline, $L' = [P(OCH_2CH_2NMe_3)_3]I_3$, **24b**; L = 3-(2-phenyl acetimido) quinoline, $L' = [P(OCH_2CH_2NMe_3)_3]I_3$, **27c**; L = phenanthridine, $L' = [P(OCH_2CH_2NMe_3)_3]I_3$, **24d**) were screened, and with the exception of **27a**, which contains a negatively charged phosphine, all retarded DNA migration in an agarose gel. The relative binding affinities were in the order **24b** < **24c** ~ **24d**. The reactivity of $[Os_3(CO)_9(\mu\text{-}\eta^2\text{-}(4\text{-}CHO)\text{-}C_9H_5N)(\mu\text{-}H)(P(OCH_2CH_2N(CH_3)_3I)_3)]$ **25** with DNA has been studied and appears to involve formation of a Schiff base intermediate.

Several related clusters, viz. $[(\mu\text{-}H)Os_3(CO)_9(L)(\mu_3\text{-}\eta^2\text{-}(Q\text{-}H))]$ **26**, where $L = [P(C_6H_4SO_3Na)_3]$ or $[P(OCH_2CH_2NMe_3I)_3]$, and Q = quinoline, 3-aminoquinoline, quinoxaline, or phenanthridine (see Figure 11), were studied for telomerase inhibition.[75] Interestingly, in contrast to DNA-binding activity, only the negatively charged clusters exhibited good anti-telomerasic activity on semipurified enzyme in a cell-free assay, but were ineffective *in vitro* on *Taq*, a different DNA polymerase. The clusters were not active against the breast cancer MCF7 cell line, suggesting a low aptitude for crossing cell membranes, and exhibited non-specific, acute cytotoxicity, probably due to accumulation on cell membranes by virtue of their amphiphilic character. Despite these somewhat disappointing results, clusters warrant further study, especially very large cluster compounds. The enhanced permeability and retention (EPR) effect represents a common difference between healthy and diseased cells that results in a dramatic increase in blood vessel permeability within cancer tissues compared to normal tissues. The normal endothelial layer surrounding the blood vessels feeding healthy tissues is intact, restricting the size of molecules that can diffuse from the blood. In contrast, the endothelial layer of blood vessels in diseased tissues is more porous to large molecules providing access to the surrounding tissue, hence making cluster compounds potentially interesting anti-proliferation agents.

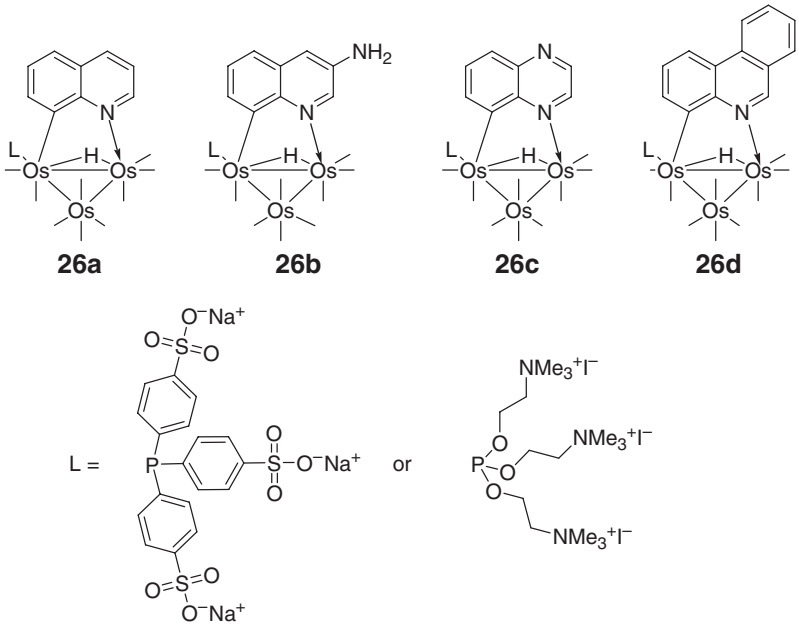

Figure 11 Structure of 26a–d: CO ligands represented by a line (–).

12.08.3 Antimicrobials

Treatments of bacterial, parasitic, fungal, or viral infections have similarities to cancer therapies in that they set out to kill the invading organism without causing harm to the host. Thus, in order to be effective, the drugs must have some selectivity for the diseased cells, exploiting differences in the biomolecules and metabolic pathway that are present in the diseased and healthy cells, thereby causing minimum damage to the healthy cells. Infections, irrespective of whether they are parasitic, bacterial, fungal, or viral, are related in that cells or, in the case of viral infections, virons proliferate in an uncontrolled fashion and in a manner that damages their "host". In addition to specific differences between healthy cells and certain types of diseased cells, there are general changes that result because of the infection or mutations, which cause the disease. Diseased cells commonly grow much more quickly than healthy cells, the exception being with diseases that go through a stage of dormancy, such as the early stages of HIV infection, but even then, when the virus revives, the proliferation rate increases. Rapid cell proliferation can cause subtle changes, for example, in nutrient requirements and cytosolic pH, giving a handle by which to target or activate drugs specifically where they are needed. Because of the similarities between all rapidly proliferating cells, nutrient transport as a targeting mechanism can be used as a tool to ensure that drugs specifically accumulate in bacterially, fungally, parasitically, and virally infected cells, as well as cancer cells. Consequently, many drugs that are active against one of these diseases may also be active against others.

12.08.3.1 Bacterial

Many of the currently available antibiotic compounds in clinical use are becoming ineffective due to drug resistance. One method of restoring activity to a drug, typically an organic compound, is to modify the structure with an organometallic fragment. For example, attachment of a ferrocenyl moiety to penicillin and cephalosporine produces compounds with altered antibacterial activity compared to the starting materials.[76]

In addition to providing an organometallic scaffold onto which organic drugs with proven activity can be grafted, some novel ferrocenyl compounds have also been shown to possess interesting clinical activity. The bis-1,1′-disubstituted ferrocenyl(carbohydrazone) complexes **27** (see Figure 12) inhibit the growth of five types of bacteria,[77] showing about half the activity of the control, imipenum. Chelation of the complexes with various metal adducts, **28**, enhances activity by up to 50%.

The antibacterial drug norfloxacin has been complexed to a tungsten tetracarbonyl unit **29** (Figure 13), which proved to exhibit excellent activity against three different strains of bacteria.[78] Rhodium, iridium, and ruthenium carbonyl complexes[79,79a,79b] show a greater selectivity toward Gram-positive bacteria compared to Gram-negative bacteria, possibly due to facilitated uptake in these organisms, inhibiting their growth at micromolar concentrations.

A number of carbene complexes have also been demonstrated to exhibit good antibacterial activity.[79,79b,79d] Notably, silver nitrate has been widely used to prevent the infection of burn wounds. The key feature of drug activity is the

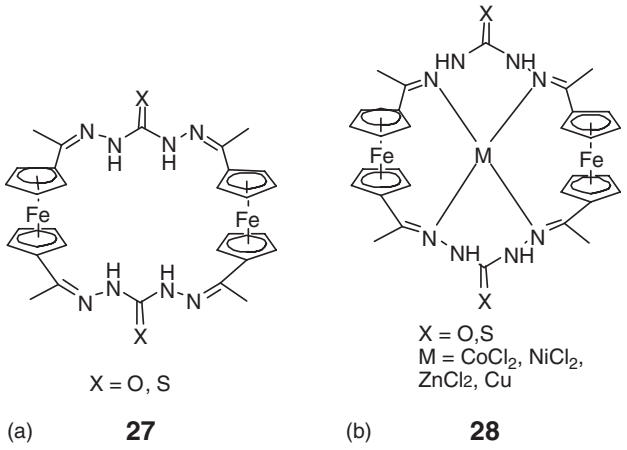

(a) **27** (b) **28**

Figure 12 Structures of (ferrocenyl)carbohydrazone complexes: (a) bis-1,1′-disubstituted (ferrocenyl)carbohydrazone complexes **27**, (b) subsequent chelation derivatives **28**.

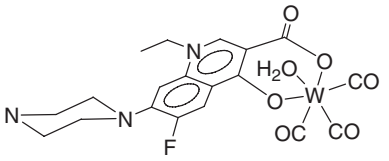

Figure 13 Structure of a tungsten tetracarbonyl unit derivatized with norfloxacin **29**.

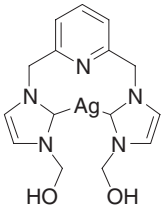

30

Figure 14 A pincer silver(I)-bis-carbene complex **30** that releases Ag^+ ions in a controlled manner to protect burn wounds from infection.

release of silver ions around the site of infection. The problem with using silver nitrate itself is that much of the drug reacts with the chloride ions that are present in the physiological environment, forming an insoluble (and inactive) precipitate, and thereby reducing the amount of therapeutic silver ions that are available to fight infection. Silver(I) *n*-pincer-type bis-carbene complexes such as **30**, shown in Figure 14, exhibit slightly improved antimicrobial activity against *Escherichia coli*, *Staphylococcus aureus*, and *Pseudomonas aeruginosa* compared to silver nitrate. The pincer ligands were shown to be inactive, and it was postulated that these ligands protected the metal center from reactions with chloride, stabilizing the compounds in biological solutions and enabling the slow release of silver ions.

12.08.3.2 Viral

Organometallic complexes that have been shown to have interesting antiviral properties include vanadocene complexes,[80,81] and a highly water-soluble tetraruthenium cluster, $[H_4Ru_4(\eta^6\text{-}C_6H_6)_4]^{2+}$ **31**.[82] The vanadocene complex **32** (Figure 15) has potential applications in preventing HIV transmission.[80,81] It is stable at physiological pH and has no detectable toxicity, but has anti-HIV and spermicidal activity, making it an interesting candidate for novel contraceptives. It is thought that **32** can intercalate with the membrane surrounding either the virus or the sperm, resulting in immobilization, without damaging the epithelial layer of the vagina. In addition to showing direct antiviral activity, metallocenes have been shown to possess interesting anti-HIV properties when used in combination with existing drugs such as 5-bromo-6-methoxy-5,6-dihydro-3′-azidiothyamine-5′-(*p*-bromophenylmethoxyalanyl)-phosphate (WHI-07).[80]

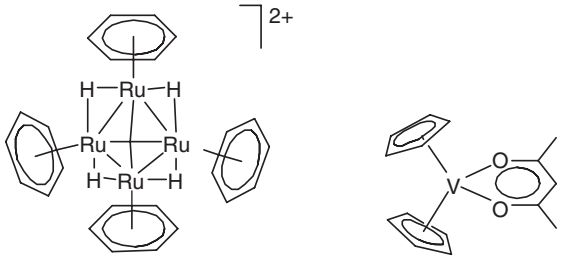

31 **32**

Figure 15 The antipolio tetraruthenium cluster $[H_4Ru_4(\eta^6\text{-}C_6H_6)_4]^{2+}$ **31** and a vanadocene spermicide/anti-HIV compound **32**.

Vanadocene dithiocarbamate was shown to be a stable and potent contraceptive.[83] Female mice were rendered reversibly infertile after intravaginal administration. During these studies, there were no observable side-effects on the mice and no long-term effects on fertility.

The ruthenium cluster **31** is active against polio virus type 1, which is still a cause of major physical disabilities, while showing little toxicity in healthy cells.

Nucleoside kinases have been shown to be important targets for antiviral and anticancer drugs. The expression of thymidine kinase is increased in proliferating cells, and, in addition to acting as a direct target, could be used as a reporter gene for diagnosis. In the case of the metal carboxamide derivatives of aminothymidine **33**, the inhibition capacity of the compound with respect to human thymidine kinase increased with spacer length, and the compounds showed only slight (if any) inhibition of the herpes simplex equivalent.[84]

12.08.3.3 Fungus and Molds

The antifungal properties of ferrocene derivatives have been studied. Compounds **27** and **28** (see above and Figure 12) have also been evaluated for their antifungal properties against six fungal strains. The antifungal activity was enhanced by up to 42% on chelation of a metal ion within the macrocyclic cavity. The activity of the chelate complexes closely approached that of the control drug miconazole.

A ferrocene–fluconazole analog **34** has been synthesized according to the method shown in Scheme 4.[85] The antifungal properties of **34** were investigated against yeast strains of medical importance, including those intrinsically resistant to fluconazole. Unfortunately, *in vitro* tests revealed a slight increase in fungal growth and a reversal of the effect of fluconazole at minimal inhibitory concentrations.

A series of bifunctional organoiron thio- and seleno-terephthalate complexes have been evaluated for their antifungal (and antibacterial and mutagenic) activity, with all the compounds tested having antifungal activity on *Candida albicans*.[86]

In the [Ru(η^6-arene)(PTA)X_2] (PTA = 1,3,5-triaza-7-phosphatricyclo[3.3.1.1]decane) series (see compound **11**, Figure 7), the anionic ligand, X, determines selectivity between fungal and yeast cells, with chloride ligands dictating selectivity for *Cladosporium resinae*, and (*S*)-norcoclaurine synthase (NCS) ligands selectivity for *Trichrophyton mentagrophytes*.[141b]

12.08.3.4 Parasites

Organometallic derivatives of organic anti-proliferation drugs have been used to overcome drug resistance of antiparasitic drugs, with antimalarials being particularly well studied. Chloroquine, primaquine, quinine, and their analogs are among the most successful drugs used to treat malaria,[87] exhibiting a rapid response, accumulating in the parasite,[88] and

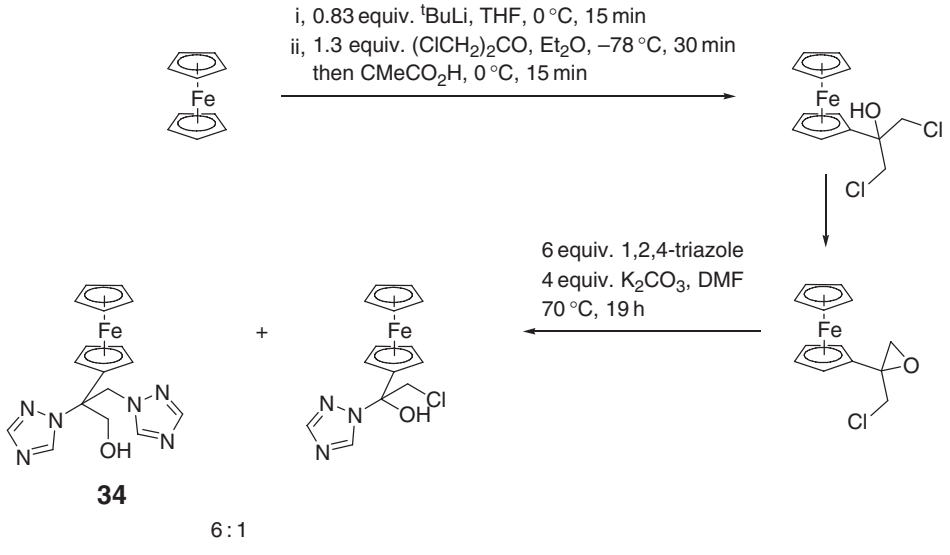

Scheme 4 Synthesis of a ferrocene–fluconazole analog **34**.

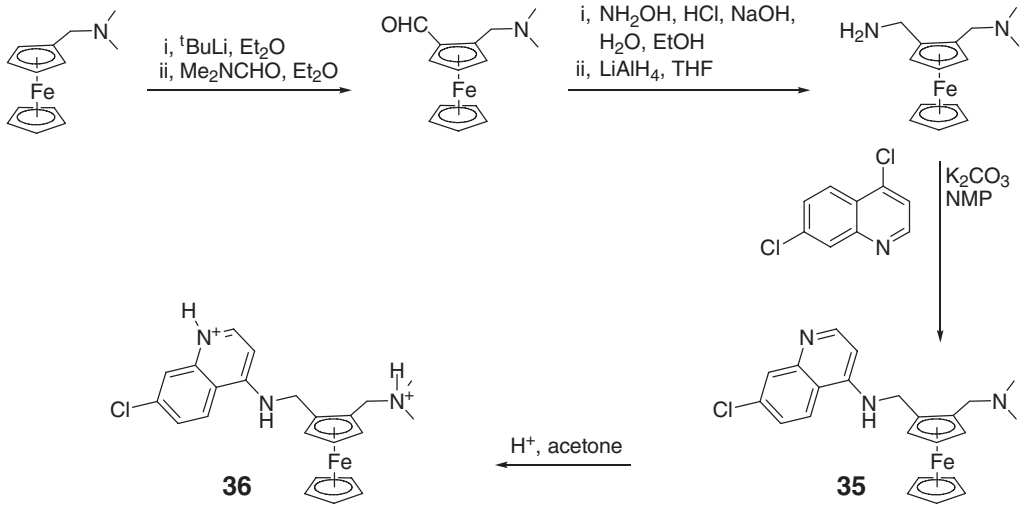

Scheme 5 Synthesis of ferroquine **35** and its salt **36**.

interfering with the way it metabolizes the host's hemoglobin, blocking the polymerization of heme into hemozin. Inhibition of this process results in the accumulation of toxic heme monomers, which are thought to poison the parasite.[89,89a–89c] These drugs may also alter the pH in the digestive vacuole disrupting enzymatic functions.[90] Organic drugs such as chloroquine are becoming increasingly ineffective, with resistance involving drug uptake[91] and efflux[92] mechanisms. The rate of chloroquine efflux is 40-fold higher in resistant parasites compared to sensitive strains.[92]

Brocard and co-workers have applied the Jaouen's "ferrocenyl" concept to the chloroquine series of drugs, to produce an analog, ferroquine **35**.[93] The synthesis of ferroquine is cheap and simple (Scheme 5), an issue of major importance if it is to be considered for development as a treatment for use in the third world countries.

The antimalarial activity of ferroquine, as compared to that of chloroquine, has been studied *in vitro* on the chloroquine-sensitive *Plasmodium falciparum* strain, HB3 5CQS, and in this case ferroquine and chloroquine were shown to have a comparable level of activity. However, a different situation is observed when the activity of the two compounds is compared on chloroquine-resistant strains such as Dd2. In this case, IC_{50} values of 22 nM for ferroquine as against 130 nM for chloroquine are obtained.[94] This interesting effect is also observed on other isolates of *Plasmodium falciparum*, originating in Gabon[95,95a] and Senegal.[96] *In vivo*, ferroquine administered to mice for 4 days at a dose of 8.4 mg kg^{-1} protects them from fatal infection.[97]

Ferroquine possesses planar chirality due to the non-symmetrical 1,2-substitution of the ferrocene entity, and the pure enantiomers (+)**35** and (−)**35** were obtained by enzymatic resolution using the *Candida rugosa* lipase as a biocatalyst. The enantiomeric purity levels exceed 98%. However, the two optical isomers display identical activity *in vitro* at the nanomolecular level. *In vivo*, however, either of the enantiomers alone is less active than the racemic mixture against both chloroquine-sensitive and chloroquine-resistant strains. In addition, (+)**35** displays better curative effects than (−)**35**, suggesting different pharmacokinetic properties. The reasons for the enhanced behavior of racemic ferroquine have not yet been elucidated. It is still not clear whether **35** is oxidized by the parasite to give the ferricinium ion, thus initiating Fenton-type reactivity. Such a hypothesis is reasonable, given that reactive oxidative species can escalate in cancer cells due to the malfunction of mitochondria.[98]

Several analogs of ferroquine have been developed,[99,99a,99b] one of which is a ferrocene triazacyclononane derivative **37** (Figure 16) active against the chloroquine-resistant *Plasmodium falciparum* strain Dd2.[100]

Drugs used to treat the parasitic diseases leishmaniasis and Chagas' disease, as well as those used to treat helminth worm infections, are also becoming increasingly ineffective due to drug resistance. *Leishmania donovani*, which causes leishmaniasis,[101] transferred via the bite of a sandfly, infects approximately 10–15 million people worldwide. The disease may be fatal if not treated, and the effectivity of traditional organic drugs such as the pentamidine, amphotericin B, aminosidine, and antimonials is declining due to drug resistance.[102] A series of iridium, platinum, rhodium, palladium, antimony, and osmium complexes of various organic drugs[103,103a] has been prepared and evaluated for activity against *L. donovani*, *T. cruzi*, the helminth worms, and other parasites. Pentamidine, one of the organic antiparasitic drugs, has been complexed to several different metal centers, and its activity has been evaluated

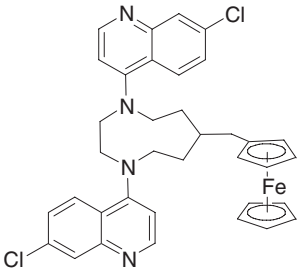

37

Figure 16 Ferrocenyl derivative of triazacyclononane **37**.

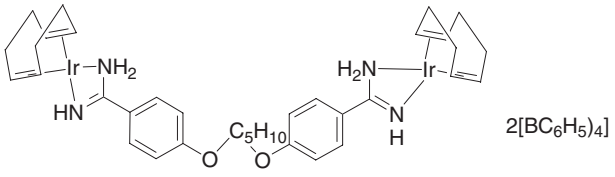

38

Figure 17 Iridium–pentamidine complex **38**.

against different parasite species. Organoplatinum[104] and organoiridium[105] derivatives were used against *T. brucei* in rodent models, curing mice infected with the parasite in a single dose. The organoiridium compound **38** (Figure 17) was also shown to have antifilarial activity with the infective larvae of human helminth parasite models of *Molinema dessetae* and *Brugia pahangi* helminth parasites.[106] Compound **38** also exhibits slight activity against leishmaniasis.[107] In this latter study, **38** was shown to found to be considerably less toxic compared to pentamidine isethionate alone, allowing administration of the drug at fatal concentrations of pentamidine isethionate in the mouse models. The organoiridium derivative of pentamidine accumulates in the *L. donovani* promastigotes, binding to ribosomal subunits *in vitro*, but not effecting macromolecular synthesis.[108] In contrast, other organometallic complexes have different mechanisms of action, for example, osmium(II) complexes incorporating amino acids and peptides as ligands inhibit *L. donovani* growth,[109] mediated through the inhibition of macromolecular (protein, RNA, and DNA) synthesis.

12.08.4 Hypertensive, Inflammation, and Vasodilation

Metal–carbonyl compounds that release carbon monoxide in a controlled manner have been shown to exert some interesting therapeutic effects.[110] Carbon monoxide-releasing molecules can induce blood vessel dilation, and act as cardio- and cytoprotectants. Carbon monoxide is naturally generated in living organisms and has been shown to induce vasodilation, and possess anti-inflammatory and antiapoptotic properties. Several carbon monoxide-releasing molecules, based on metals such as manganese, iron, cobalt, nickel, and ruthenium, have been studied. $Mn_2(CO)_{10}$ **39** and $[Ru(CO)_3Cl_2]_2$ **40** (Figure 18) release carbon monoxide under physiological conditions to cause long-lasting vasodilation, with no detectable cytotoxicity,[111] and the ruthenium glycinate compound **41** has demonstrable

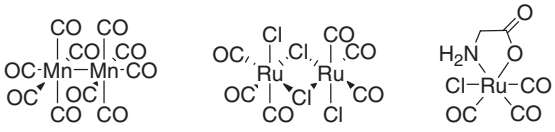

39 **40** **41**

Figure 18 Structures of CO-releasing compounds **39**, **40**, and **41**.

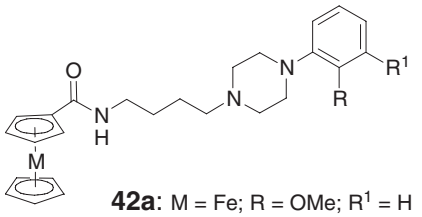

42a: M = Fe; R = OMe; R^1 = H
42b: M = Fe; R = Cl; R^1 = Cl
42c: M = Ru; R = OMe; R^1 = H
42d: M = Ru; R = Cl; R^1 = Cl
42e: M = Fe; R = OMe; R^1 = Cl

Figure 19 Bioisoesteres derivatized with metallocene units **42a–e**.

cardioprotective action and probably shows greatest promise.[112] Carbon monoxide release can be promoted by use of appropriate co-ligands[113,113a,113b] or by photodissociation.[114,114a]

Compound **41** produces a concentration-dependent relaxation in vessels precontracted with phenylephrine, exerting significant vasodilatation starting at concentrations of 25–50 μM.[115] Blockers of ATP-dependent potassium channels or guanylate cyclase activity considerably reduced **41**-dependent relaxation, confirming that potassium channels activation and cGMP partly mediate the vasoactive properties of CO. Further *in vitro* and *in vivo* studies indicate that CO liberated by **41** significantly suppresses the inflammatory response elicited by lipopolysaccharide in cultured macrophages and suggest that CO carriers can be used as an effective strategy to modulate inflammation.[116,116a]

12.08.5 Other Applications

Other areas where organometallic compounds have been evaluated are in the treatment of arthritis, for which several inorganic drugs are available,[117] and neurodegenerative diseases. For example, bioisoesteres derivatized with metallocene units **42a–e** (Figure 19) afford compounds that strongly bind the dopamine D4 receptor and therefore have potential as drugs that could be active on the central nervous system.[118]

12.08.6 Outlook

In general, organometallic compounds are considered as highly toxic, air sensitive, and incompatible with an aqueous environment. Despite these conceptions, many organometallic compounds are proving to be well suited to the physiological environment and are finding applications in medicine and diagnosis. In particular, it would appear that derivatization of known organic drugs with organometallic fragments can improve the activity of the drug and, in some cases, restore activity where resistance has developed for the organic compound.

References

1. Clarke, M. J.; Zhu, F.; Frasca, D. R. *Chem. Rev.* **1999**, *99*, 2511.
1a. Guo, M.; Sadler, P. J. *Angew. Chem., Int. Ed. Engl.* **1999**, *38*, 1513.
1b. Guo, Z.; Sadler, P. J. *Adv. Inorg. Chem.* **2000**, *49*, 183.
1c. Holm, R. H.; Solomon, E. I. *Chem. Rev.* **1996**, *96*(7) issue dedicated to Bioinorganic Enzymology.
1d. Howard-Lock, H. E.; Lock, C. J. L. In *Comprehensive Coordination Chemistry*; Wilkinson, G., Gillard, R., McCleverty, J., Eds.; Pergamon: Oxford, 1987; p 755.
1e. Keppler, B. K. In *Metal Complexes in Cancer Chemotherapy*; VCH: Weinheim, 1993.
1f. Lippert, B. In *Cisplatin: Chemistry and Biochemistry of a Leading Anticancer Drug*; Wiley: New York, 1999.
1g. Orvig, C.; Abrams, M. J. *Chem. Rev.* **1999**, *99*(5) issue dedicated to Medicinal Inorganic Chemistry.
1h. Ming, L. J. *Med. Res. Rev.* **2003**, *23*, 697.
2. Mann, J. In *The Elusive Magic Bullet: The Search for the Perfect Drug*; Oxford University Press: Oxford, 1999.
3. Lloyd, N. C.; Morgan, H. W.; Nicholson, B. K.; Ronimus, R. S. *Angew. Chem., Int. Ed.* **2005**, *44*, 941.
4. Köpf-Maier, P.; Köpf, H.; Neuse, E. W. *Angew. Chem., Int. Ed.* **1984**, *23*, 456.
4a. Toney, J. H.; Murthy, M. S.; Marks, T. J. *Chem. Biol. Interact.* **1985**, *56*, 45.
4b. Neuse, E. W.; Kanzawa, F. *Appl. Organomet. Chem.* **1990**, *4*, 19.

4c. Kopf-Maier, P.; Klapotke, T. *Cancer Chemother. Pharmacol.* **1992**, *29*, 361.
4d. Köpf-Maier, P. *Eur. J. Clin. Pharmacol.* **1994**, *47*, 1.
5. Kröger, N.; Kleeberg, U. R.; Mross, K.; Edler, L.; Hossfeld, D. K. *Onkologie* **2000**, *23*, 60.
5a. Mross, K.; Robben-Bathe, P.; Edler, L.; Baumgart, J.; Berdel, W. E.; Fiebig, H.; Unger, C. *Onkologie* **2000**, *23*, 576.
6. Alberto, R. In *Radiopharmaceutical in Bioorganometallics*; Jaouen, G., Ed.; Wiley-VCH: Weinheim, 2005; pp 97–124.
7. Reedijk, J. *Chem. Commun.* **1996**, 801.
7a. Wong, E.; Giandomenico, C. M. *Chem. Rev.* **1999**, *99*, 2451 and references cited therein.
8. Charpentier, A. H.; Bednarek, A. K.; Daniel, R. L.; Hawkins, K. A.; Gaddis, L. J. S.; MacLeod, M. C.; Aldaz, C. M. *Cancer Res.* **2000**, *60*, 5977.
8a. Osborne, C. K.; Zhao, H.; Fuqua, S. A. W. *J. Clin. Oncol.* **2000**, *18*, 3172.
9. Jordan, V. C. *J. Med. Chem.* **2003**, *46*, 883.
10. Chesne, C.; Leclercq, G.; Pointeau, P.; Patin, H. *Eur. J. Med. Chem.* **1986**, *21*, 321.
10a. Gust, R.; Schönenberger, H.; Klement, U.; Range, K. J. *Arch. Pharm.* **1993**, *326*, 967.
10b. Karl, J.; Gust, R.; Spruß, T.; Schneider, M. R.; Schönenberger, H.; Engel, J.; Wrobel, K. H.; Lux, F.; Haeberlin, S. T. *J. Med. Chem.* **1988**, *31*, 72.
10c. Gandolfi, O.; Blum, J.; Mandelbaum-Shavit, F. *Inorg. Chim. Acta* **1984**, *91*, 257.
10d. von Angerer, E. In *Metal Complexes in Cancer Chemotherapy: Platinum Complexes with Specific Activity against Hormone Dependent Tumors*; Keppler, B. K., Eds.; VCH: Weinheim, 1993; p 73.
10e. Jackson, A.; Davis, J.; Pither, R. J.; Rodger, A.; Hannon, M. J. *Inorg. Chem.* **2001**, *40*, 3964.
10f. Grenier, G.; Bérubé, G.; Gicquaud, C. *Chem. Pharm. Bull.* **1998**, *46*, 1480.
11. Top, S.; Kaloun, E. B.; Vessières, A.; Leclercq, G.; Laïos, I.; Ourevitch, M.; Deuschel, C.; McGlinchey, M. J.; Jaouen, G. *Chem BioChem.* **2003**, *4*, 754.
12. Top, S.; Kaloun, E. B.; Vessières, A.; Laïos, I.; Leclercq, G.; Jaouen, G. *J. Organomet. Chem.* **2002**, *643–644*, 350.
13. Mokdsi, G.; Harding, M. M. *J. Organomet. Chem.* **1998**, *565*, 29.
13a. Toney, J. H.; Marks, T. J. *J. Am. Chem. Soc.* **1985**, *107*, 947.
14. Guo, M.; Sun, H.; McArdle, H. J.; Gambling, L. K.; Sadler, P. J. *Biochemistry* **2000**, *39*, 10023.
15. Stoica, A.; Katzenellenbogen, B. S.; Martin, M. B. *Mol. Endo.* **2000**, *14*, 545.
15a. Johnson, M. D.; Kenney, N.; Stoica, A.; Hilakivi-Clarke, L.; Singh, B.; Chepko, G.; Clarke, R.; Sholler, P. F.; Lirio, A. A.; Foss, C., *et al. Nat. Med.* **2003**, *9*, 1081.
15b. Martin, M. B.; Reiter, R.; Pham, T.; Avellanet, Y. R.; Camara, J.; Lahm, M.; Pentecost, E.; Pratap, K.; Gilmore, B. A.; Divekar, S., *et al. Endocrinology* **2003**, *144*, 2425.
16. Top, S.; Vessières, A.; Pigeon, P.; Rager, M. N.; Huché, M.; Salomon, E.; Cabestaing, C.; Vaissermann, J.; Jaouen, G. *ChemBioChem.* **2004**, *5*, 1104.
16a. Jaouen, G.; Top, S.; Vessières, A.; Pigeon, P.; Leclercq, G.; Laïos, I. *Chem. Commun.* **2001**, 383.
17. Top, S.; Tang, J.; Vessières, A.; Carrez, D.; Provot, C.; Jaouen, G. *Chem. Commun.* **1996**, 955.
17a. Top, S.; Dauer, B.; Vaissermann, J.; Jaouen, G. *J. Organomet. Chem.* **1997**, *541*, 355.
17b. Top, S.; Vessières, A.; Cabestaing, C.; Laios, I.; Leclercq, G.; Provot, C.; Jaouen, G. *J. Organomet. Chem.* **2001**, *637*, 500.
17c. Top, S.; Vessières, A.; Leclercq, G.; Quivy, J.; Tang, J.; Vaissermann, J.; Huché, M.; Jaouen, G. *Chem. Eur. J.* **2003**, *9*, 5223.
18. Osella, D.; Ferrali, M.; Zanello, P.; Laschi, F.; Fontani, M.; Nervi, C.; Cavigiolio, G. *Inorg. Chim. Acta* **2000**, *306*, 42.
18a. Tabbi, G.; Cassino, C.; Cavigiolio, G.; Colangelo, D.; Ghiglia, A.; Viano, I.; Osella, D. *J. Med. Chem.* **2002**, *45*, 5786.
19. Montano, M. M.; Jaiswal, A. K.; Katzenellenbogen, B. S. *J. Biol. Chem.* **1998**, *273*, 25443.
19a. Yang, S. H.; Liu, R.; Perez, E. J.; Wen, Y.; Stevens, S. M.; Valencia, T.; Brun-Zinkernagel, A. M.; Prokai, L.; Will, Y.; Dykens, J., *et al. Proc. Natl. Acad. Sci.* **2004**, *101*, 4130.
20. Pigeon, P.; Top, S.; Vessières, A.; Huché, M.; Hillard, E. A.; Salomon, E.; Jaouen, G. *J. Med. Chem.* **2005**, *48*, 2814.
21. Amatore, C.; Hillard, E. A.; Jaouen, G.; Thouin, L.; Vessières, A. *Angew. Chem., Int. Ed.* (in press).
22. Köpf-Maier, P.; Köpf, H.; Neuse, E. W. *J. Cancer Res. Clin. Oncol.* **1984**, *108*, 336.
23. Neuse, E. W. *Macromol. Symp.* **2001**, *172*, 127.
23a. Johnson, M. T.; Kreft, E.; N'Da, D. D.; Neuse, E. W.; van Rensburg, C. E. J. *J. Inorg. Organomet. Polym.* **2003**, *13*, 255.
24. Neuse, E. W. *J. Inorg. Organomet. Polym.* **2005**, *15*, 3.
25. Grimes, R. N. *Coord. Chem. Rev.* **2000**, *200–202*, 773.
26. Waern, J. B.; Harris, H. H.; Lai, B.; Cai, Z.; Harding, M. M.; Dillon, C. T. *J. Biol. Inorg. Chem.* **2005**, *10*, 443.
27. Köpf-Maier, P. *Anticancer Res.* **1999**, *19*, 493.
28. Mokdsi, G.; Harding, M. M. *J. Organomet. Chem.* **1998**, *565*, 29.
28a. Meléndez, E. *Crit. Rev. Oncol. Hematol.* **2002**, *42*, 309.
29. Turel, I.; Demsar, A.; Kosmrlj, J. *J. Mol. Recognit. Macro. Chem.* **1999**, *35*, 595.
30. Braga, S. S.; Gonclaves, I. S.; Pillinger, M.; Ribeiro-Claro, P.; Teixeira-Dias, J. J. C. *J. Organomet. Chem.* **2001**, *632*, 11.
31. Rehmann, F.-J. K.; Cuffe, L. P.; Mendoza, O.; Rai, D. K.; Sweeney, N.; Strohfeldt, K.; Gallagher, W. M.; Tacke, M., *App. Organomet. Chem.* **2005**, *19*, 293.
32. Meléndez, E.; Marrero, M.; Rivera, C. *Inorg. Chim. Acta* **2000**, *298*, 178.
33. Wedgwood, J. L.; Kresinski, R. A.; Merry, S.; Platt, A. W. G. *J. Inorg. Biochem.* **2003**, *95*, 149.
34. Caruso, F.; Rossi, M. *Mini Rev. Med. Chem.* **2004**, *4*, 159.
35. Waern, J. B.; Harding, M. M. *Inorg. Chem.* **2004**, *43*, 206.
35a. Waern, J. B.; Dillon, C. T.; Harding, M. M. *J. Med. Chem.* **2005**, *48*, 2093.
36. Sava, G.; Capozzi, I.; Bergamo, A.; Gagliardi, R.; Cocchietto, M.; Masiero, L.; Onisto, M.; Alessio, E.; Mestroni, G.; Garbisa, S. *Int. J. Cancer* **1996**, *68*, 60.
37. Galanski, M.; Arion, V. B.; Jakupec, M. A.; Keppler, B. K. *Curr. Pharm. Design* **2003**, *9*, 2078.
38. Clarke, M. J. In *Metal Complexes in Cancer Chemotherapy*; Keppler, B. K., Ed.; VCH: Weinheim, 1993, p 129.
39. Dale, L. D.; Tocher, J. H.; Dyson, T. M.; Edwards, D. I.; Tocher, D. A. *Anti Cancer Drug Design* **1992**, *7*, 3.
40. Sheldrick, W. S.; Heeb, S. *Inorg. Chim. Acta* **1990**, *168*, 93.
41. Heeb S. Dissertation, Ruhr-Universität Bochum, 1990.

42. Allardyce, C. S.; Dyson, P. J.; Ellis, D. J.; Heath, S. L. *Chem. Commun.* **2001**, 1396.
43. Morris, R. E.; Aird, R. E.; Murdoch, P. D.; Chen, H. M.; Cummings, J.; Hughes, N. D.; Parsons, S.; Parkin, A.; Boyd, G.; Jodrell, D. I., *et al. J. Med. Chem.* **2001**, *44*, 3616.
44. Scolaro, C.; Bergamo, A.; Brescacin, L.; Delfino, R.; Cocchietto, M.; Laurenczy, G.; Geldbach, T. J.; Sava, G.; Dyson, P. J. *J. Med. Chem.* **2005**, *48*, 4161.
45. Dorcier, A.; Dyson, P. J.; Gossens, C.; Rothlisberger, U.; Scopelliti, R.; Tavernelli, I. *Organometallics* **2005**, *24*, 2114.
46. Aird, R. E.; Cummings, J.; Ritchie, A. A.; Muir, M.; Morris, R. E.; Chen, H.; Sadler, P. J.; Jodrell, D. I. *Brit. J. Cancer* **2002**, *86*, 1652.
47. Chen, H.; Parkinson, J. A.; Parsons, S.; Coxall, R. A.; Gould, R. O.; Sadler, P. J. *J. Am. Chem. Soc.* **2002**, *124*, 3064.
48. Yan, Y. K.; Melchart, M.; Habtemariam, A.; Sadler, P. J. *Chem. Commun.* **2005**, 4764.
49. Huxham, L. A.; Cheu, E. L. S.; Patrick, B. O.; James, B. R. *Inorg. Chim. Acta* **2003**, *352*, 238.
50. Akbayeva, D. N.; Gonsalvi, L.; Oberhauser, W.; Peruzzini, M.; Vizza, F.; Brüggeller, P.; Romerosa, A.; Sava, G.; Bergamo, A. *Chem. Comm.* **2003**, 264.
51. Serli, B.; Zangrando, E.; Gianferrara, T.; Scolaro, C.; Dyson, P. J.; Bergamo, A.; Alessio, E. *Eur. J. Inorg. Chem.* **2005**, 3423.
52. DeRosa, M. C.; Crutchley, R. J. *Coord. Chem. Rev.* **2002**, *233*, 351.
53. Bakac, A.; Espenson, J. H. *Inorg. Chem.* **1989**, *28*, 3901.
53a. Riordan, C. G.; Wei, P. *J. Am. Chem. Soc.* **1994**, *116*, 2189.
54. Crowe, A. J.; Smith, P. J.; Atassi, G. *Chem. Biol. Interact.* **1980**, *32*, 171.
54a. Crowe, A. J.; Smith, P. J.; Atassi, G. *Inorg. Chim. Acta* **1984**, *93*, 179.
54b. Han, G. Y.; Yang, P. *J. Inorg. Biochem.* **2002**, *91*, 230.
54c. Triolo, F.; Pellerito, C.; Stocco, G. C.; Fiore, T.; Aggio, F.; Pellerito, L.; Triolo, R. *Appl. Organomet. Chem.* **1999**, *13*, 733.
54d. Barbieri, R.; Silvestri, A. *J. Inorg. Biochem.* **1991**, *41*, 31.
55. Bollo, E.; Ceppa, L.; Cornaglia, E.; Nebbia, C.; Biolatti, B.; Da casto, M. *Hum. Exp. Toxicol.* **1996**, *15*, 219.
56. Pratviel, G.; Bernadou, J.; Meunier, B. *Angew. Chem., Int. Ed.* **1995**, *34*, 746.
56a. Vol'pin, M.; Levitin, I.; Osinsky, S. *Angew. Chem., Int. Ed.* **1996**, *35*, 2395.
57. Schlawe, D.; Majdalani, A.; Velcicky, J.; Heßler, E.; Wieder, T.; Prokop, A.; Schmalz, H.-G. *Angew. Chem., Int. Ed.* **2004**, *43*, 1731.
58. Prokop, A.; Wieder, T.; Schlawe, D.; Lode, H.; Henze, G.; Daniel, P. T.; Schmalz, H. G. *Blood* **2004**, *104*, 574A.
59. Bergman, H.; Williams, D. S.; Atilla, G. E.; Carroll, P. J.; Meggers, E. *J. Am. Chem. Soc.* **2004**, *126*, 13594.
60. Greenfield, H.; Sternberg, H. W.; Friedel, R. A.; Wotiz, J. H.; Markby, R.; Wender, I. *J. Am. Chem. Soc.* **1956**, *78*, 120.
61. Sasaki, N. A.; Potier, P.; Savignac, M.; Jaouen, G. *Tetrahedron Lett.* **1988**, *29*, 5759.
61a. Savignac, M.; Sasaki, N. A.; Potier, P.; Jaouen, G. *J. Chem. Soc., Chem. Commun.* **1991**, 615.
62. Varenne, A.; Salmain, M.; Brisson, C.; Jaouen, G. *Bioconjugate Chem.* **1992**, *3*, 471.
63. Vessières, A.; Salmain, M.; Brossier, P.; Jaouen, G. *J. Pharm. Biomed. Anal.* **1999**, *21*, 625.
64. Vessières, A.; Tondu, S.; Jaouen, G.; Top, S.; Ismail, A. A.; Teutsch, G.; Moguilewsky, M. *Inorg. Chem.* **1988**, *27*, 1850.
65. Philomin, V.; Vessières, A.; Gruselle, M.; Jaouen, G. *Bioconjugate Chem.* **1993**, *4*, 419.
66. Gruselle, M.; Rossignol, J. L.; Vessières, A.; Jaouen, G. *J. Organomet. Chem.* **1987**, *328*, C12.
66a. Gruselle, M.; Deprez, P.; Vessières, A.; Greenfield, S.; Jaouen, G.; Larue, J. P.; Thouvenot, D. *J. Organomet. Chem.* **1989**, *359*, C53.
67. Salmain, M.; Jaouen, G. *J. Organomet. Chem.* **1992**, *445*, 237.
68. Osella, D.; Cavigiolio, G.; Vincenti, M.; Vessières, A.; Laïos, I.; Leclercq, G.; Napolitano, E.; Fiaschi, R.; Jaouen, G. *J. Organomet. Chem.* **2000**, *596*, 242.
68a. Palyi, G.; Varadi, G.; Viziorosz, A.; Marko, L. *J. Organomet. Chem.* **1975**, *90*, 85.
68b. Vessières, A.; Jaouen, G.; Gruselle, M.; Rossignol, J. L.; Savignac, M.; Top, S.; Greenfield, S. *J. Steroid Biochem.* **1988**, *30*, 301.
68c. Vessières, A.; Top, S.; Vaillant, C.; Osella, D.; Mornon, J. P.; Jaouen, G. *Angew. Chem., Int. Ed.* **1992**, *31*, 753.
68d. Vessières, A.; Vaillant, C.; Salmain, M.; Jaouen, G. *J. Steroid Biochem.* **1989**, *34*, 301.
69. Fischer-Durand, N.; Vessières, A.; Heldt, J. M.; Le Bideau, F.; Jaouen, G. *J. Organomet. Chem.* **2003**, *668*, 59.
70. Vessières, A.; Vaillant, C.; Gruselle, M.; Vichard, D.; Jaouen, G. *J. Chem. Soc., Chem. Commun.* **1990**, 837.
71. Harlow, K. W.; Smith, D. N.; Katzenellenbogen, J. A.; Greene, G. L.; Katzenellenbogen, B. S. *J. Biol. Chem.* **1989**, *264*, 17476.
72. Top, S.; El Hafa, H.; Vessières, A.; Huché, M.; Vaissermann, J.; Jaouen, G. *Chem. Eur. J.* **2002**, *8*, 5241.
73. Jung, M.; Kerr, D. E.; Senter, P. D. *Arch. Pharm., Pharm. Med. Chem.* **1997**, *330*, 173.
73a. Gust, R.; Ott, I.; Sommer, P. D. K. *J. Med. Chem.* **2004**, *47*, 5837.
73b. Ott, I.; Kircher, B.; Gust, R. *J. Inorg. Biochem.* **2004**, *98*, 485.
73c. Ott, I.; Schmidt, K.; Kircher, B.; Schumacher, P.; Wiglenda, T.; Gust, R. *J. Med. Chem.* **2005**, *48*, 622.
74. Rosenberg, E.; Spada, F.; Sugden, K.; Martin, B.; Milone, L.; Gobetto, R.; Viale, A.; Fiedler, J. *J. Organomet. Chem.* **2003**, *668*, 51.
74a. Rosenberg, E.; Spada, F.; Sugden, K.; Martin, B.; Gobetto, R.; Milone, L.; Viale, A. *J. Organomet. Chem.* **2004**, *689*, 4729.
75. Colangelo, D.; Ghiglia, A.; Ghezzi, A.; Ravera, M.; Rosenberg, E.; Spada, F.; Osella, D. *J. Inorg. Biochem.* **2005**, *99*, 505.
76. Edwards, E. I.; Epton, R.; Marr, G. *J. Organomet. Chem.* **1975**, *85*, C23.
77. Chohan, Z. H.; Khan, K. M.; Supran, C. T. *Appl. Organomet. Chem.* **2004**, *18*, 305.
78. Chen, X.-B.; Ye, Q.; Wu, Q.; Song, Y.-M.; Xiong, R.-G.; You, X.-Z. *Inorg. Chem. Commun.* **2004**, *7*, 1302.
79. Sülü, M.; Küçükbay, H.; Durmaz, R.; Günel, S. *Arzneimittel Forsch., Drug Res.* **1998**, *48*, 291.
79a. Çetinkaya, B.; Özdemir, I.; Binbaşioğlu, B.; Durmaz, R.; Günel, S. *Arzneimittel Forsch., Drug Res.* **1999**, *49*, 538.
79b. Özdemir, I.; Denizci, A.; Öztürk, H. T.; Çetinkaya, B. *Appl. Organomet. Chem.* **2004**, *18*, 318.
80. D'Cruz, O. J.; Waurzyniak, B.; Uckum, F. M. *Antimicrob. Agents Chemother.* **2004**, *48*, 1082.
81. D'Cruz, O. J.; Waurzyniak, B.; Uckum, F. M. *Contraception* **2001**, *64*, 177.
82. Allardyce, C. S.; Dyson, P. J.; Ellis, D. J.; Salter, P. A.; Scopelliti, R. *J. Organomet. Chem.* **2003**, *668*, 35.
83. D'Cruz, O. J.; Waurzyniak, B.; Uckum, F. M. *Antiomicrob. Agents Chemother.* **2004**, *48*, 1082.
84. Schibli, R.; Netter, M.; Scapozza, L.; Birringer, M.; Schelling, P.; Dumas, C.; Schoch, J.; Schubiger, P. A. *J. Organomet. Chem.* **2003**, *668*, 67.
85. Biot, C.; Francois, N.; Maciejewski, L.; Brocard, J.; Poulain, D. *Bioorg. Med. Chem. Lett.* **2000**, *10*, 839.
86. Maslat, A. O.; Jibril, I.; Abussaud, M.; Abd-Alhadi, E. H.; Hamadah, Z. *Appl. Organomet. Chem.* **2002**, *16*, 44.
87. Muller, R.; Baker, J. R. *Medical Parasitology*; Gower Medical Publishing: London, 1990.
88. Veignie, E.; Moreau, S. *Ann. Trop. Med. Parasitol.* **1991**, *85*, 229.
89. Slater, A. F.; Swiggard, W.; Orton, B.; Flitter, W.; Goldberg, D.; Cerami, A.; Henderson, G. *Proc. Natl. Acad. Sci.* **1991**, *88*, 325.

89a. Slater, A. F.; Cerami, A. *Nature* **1992**, *355*, 167.
89b. Bendrat, K.; Berger, B.; Cerami, A. *Nature* **1995**, *378*, 138.
89c. Ridley, R.; Dorn, A.; Matile, H.; Kansy, M. *Nature* **1995**, *378*, 138.
90. Fitch, C.; Chevli, R.; Banyal, H.; Phillips, G.; Pfallar, M.; Krogstad, D. *Antimicrob. Agents Chemother.* **1982**, *21*, 819.
91. Sanchez, C.; Wunsch, S.; Lanzer, M. *J. Biol. Chem.* **1997**, *272*, 2652.
92. Krogstad, D. J.; Gluzman, I. Y.; Kyle, D. E.; Oduola, A. M.; Martin, S. K.; Milhous, W. K.; Schlesinger, P. H. *Science* **1987**, *283*, 1283.
93. Biot, C.; Glorian, G.; Maciejewski, L. A.; Brocard, J. S. *J. Med. Chem.* **1997**, *40*, 3715.
93a. Domarle, O.; Blampain, G.; Agnaniet, H.; Nzadiyabi, T.; Lebibi, J.; Brocard, J.; Maciejewski, L.; Biot, C.; Georges, A. J.; Millet, P. *Antimicrob. Agents Chemother.* **1998**, *42*, 540.
94. Delhaes, L.; Biot, C.; Berry, L.; Delcourt, P.; Maciejewski, L. A.; Camus, D.; Brocard, J. S.; Dive, D. *ChemBioChem*. **2002**, *3*, 418.
95. Atteke, C.; Ndong, J. M.; Aubouy, A.; Maciejewski, L.; Brocard, J.; Lebibi, J.; Deloron, P. *J. Antimicrob. Chemother.* **2003**, *51*, 1021.
95a. Pradines, B.; Fusai, T.; Daries, W.; Laloge, V.; Rogier, C.; Millet, P.; Panconi, E.; Kombila, M.; Parzy, D. *J. Antimicrob. Chemother.* **2001**, *48*, 179.
96. Pradines, B.; Tall, A.; Rogier, C.; Spiegel, A.; Mosnier, J.; Marrama, L.; Fusai, T.; Millet, P.; Panconi, E.; Trape, J. F.; Parzy, D. *Trop. Med. Int. Health* **2002**, *7*, 265.
97. Delhaes, L.; Abessolo, H.; Biot, C.; Berry, L.; Delcourt, P.; Maciejewski, L.; Brocard, J.; Camus, D.; Dive, D. *Parasitol. Res.* **2001**, *87*, 239.
98. Pelicano, H.; Carney, D.; Huang, P. *Drug Resist. Update.* **2004**, *7*, 97.
99. Biot, C. *Curr. Med. Chem., Anti Infective Agents* **2004**, *3*, 135.
99a. Blackie, M.; Beagley, P.; Chibale, K.; Clarkson, C.; Moss, J. R.; Smith, P. J. *J. Organomet. Chem.* **2003**, *688*, 144.
99b. Chibale, K.; Moss, J. R.; Blackie, M.; Smith, v. S. D. P. J. *Tetrahedron Lett.* **2000**, *41*, 6231.
100. Biot, C.; Dessolin, J.; Ricard, I.; Dive, D. *J. Organomet. Chem.* **2004**, *689*, 4678.
101. Ashford, R.; Desjeux, P.; de Raadt, P. *Parasitol. Today* **1992**, *8*, 104.
102. Ouellette, M.; Papadopoulou, B. *Parasitol. Today* **1993**, *9*, 150.
103. Loiseau, P. M.; Craciunescu, D. G.; Doadriovillarejo, J. C.; Certadfombona, G.; Gayral, P. *Trop. Med. Parasitol.* **1992**, *43*, 110.
103a. Mesa Valle, C. M.; Moraleda Lindez, V.; Craciunescu, D.; Alonso, M.; Osuna, A. *Arzenium Forsch. Drug Res.* **1993**, *43*, 1010.
104. Loiseau, P. M.; Dreyfuss, G.; Doadrio, L.; Parrondo, E.; Craciunescu, D. G. *J. Chemother.* **2001**, *13*, 59.
105. Loiseau, P. M.; Dreyfuss, G.; Daulouède, S.; Lachâtre, G.; Vincendaeu, P.; Craciunescu, D. G. *Trop. Med. Int. Health* **1997**, *2*, 19.
106. Loiseau, P. M.; Jaffe, J. J.; Craciunescu, D. G. *Int. J. Parasitol.* **1998**, *28*, 1279.
107. Loiseau, P. M.; Mbongo, N.; Bories, C.; Boulard, Y.; Craciunescu, D. G. *Parasite* **2000**, *7*, 103.
108. Mbongo, N.; Loiseau, P. M.; Lawerence, F.; Craciunescu, D. G.; Iglesias, E. P.; Loiseau, P. M.; Dreyfuss, G. *Trop. Med. Parasitol.* **1991**, *42*, 41.
109. Castilla, J. J.; Mesa Valle, C. M.; Sanchez Moreno, M.; Arnedo, T.; Rosales, M. J.; Mascaro, C.; Crraciunescu, D.; Osuna, A. *Arzneimittel Forsch., Drug Res.* **1996**, *46*, 990.
110. Johnson, T. R.; Mann, B. E.; Clark, J. E.; Foresti, R.; Green, C.; Motterlini, R. *Angew. Chem., Int. Ed.* **2003**, *42*, 2.
111. Motterlini, R.; Clark, J. E.; Foresti, R.; Sarathchandra, P.; Mann, B. E.; Green, C. J. *Circ. Res.* **2002**, *90*, e17.
112. Clark, J. E.; Naughton, P.; Shurey, S.; Green, C. J.; Johnson, T. R.; Mann, B. E.; Foresti, R.; Motterlini, R. *Circ. Res.* **2003**, *93*, 178.
113. Darensbourg, D. J.; Klausmeyer, K. K.; Reibenspies, J. H. *Inorg. Chem.* **1995**, *34*, 4933.
113a. Darensbourg, D. J.; Klausmeyer, K. K.; Reibenspies, J. H. *Inorg. Chem.* **1996**, *35*, 1529.
113b. Pearson, J.; Cooke, J.; Takats, J.; Jordan, R. B. *J. Am. Chem. Soc.* **1998**, *120*, 1434.
114. Wrighton, M. S.; Ginley, D. S. *J. Am. Chem. Soc.* **1975**, *97*, 2065.
114a. Hughey, J. L.; Bock, C. R.; Meyer,; Ginley, T. J. *J. Am. Chem. Soc.* **1975**, *97*, 4440.
115. Foresti, R.; Hammad, J.; Clark, J. E.; Johnson, T. R.; Mann, B. E.; Friebe, A.; Green, C. J.; Motterlini, R. *Brit. J. Pharmacol.* **2004**, *142*, 453.
116. Sawle, P.; Foresti, R.; Mann, B. E.; Johnson, T. R.; Green, C. J.; Motterlini, R. *Brit. J. Pharmacol.* **2005**, *145*, 800.
116a. Seveso, M.; Vadori, M.; Bosio, E.; Fante, F.; Besenzon, F.; Ravarotto, L.; Bedendo, S.; Johnson, T. R.; Mann, B. E.; Motterlini, R., *et al. Am. J. Transplant.* **2005**, *5*, 306.
117. Shaw, C. F. III, *Chem. Rev.* **1999**, *99*, 2589.
118. Schlotter, K.; Boeckler, F.; Hübner, H.; Gmeiner, P. *J. Med. Chem.* **2005**, *48*, 3696.

12.09 Organometallic Receptors for Charged and Neutral Guest Species

P D Beer and S R Bayly, University of Oxford, Oxford, UK

12.09.1 Introduction

The concept of molecular recognition has its origins in biochemistry and over the last 35 years has become an important and intensely studied subject in its own right.[1,2] Driven on by the objective of developing novel chemical sensor technologies, a great deal of progress has been made in the design of synthetic receptor molecules for numerous guest species, ranging from biomolecules to inorganic ions.[3] Organometallic species possess many physical and chemical properties desirable for their incorporation into host structural frameworks designed to bind cations, anions, and neutral guest species. Most commonly, the organometallic moiety is incorporated as a reporter group, whose redox or photochemical response is perturbed upon proximal binding of a target guest species. Alternatively, it can serve as a structural component, allowing (often by self-assembly) control over the topology of the binding site. Organometallic receptors, particularly where they combine these roles, show a range of functionality not available to purely organic structures.

Previous reviews have covered many aspects of molecular recognition by organometallic and other metal-based receptors,[4–7] but to our knowledge, this is the first to look exclusively at organometallic receptors as a single class. It is designed to provide an overview of the subject with particular reference to the specific properties that organometallic subunits impart to molecular receptors. The review is organized into five sections—Sections 12.09.2, 12.09.3 and 12.09.4 describe receptors for cations, anions, and neutral guest species, respectively. Section 12.09.5 deals with receptors for ion pairs. Each of these sections is subdivided according to the type of organometallic species involved.

Section 12.09.6 details recent advances toward the application of organometallic receptors as sensing devices, including their use in dendrimer, polymer, functionalized nanoparticle, and self-assembled monolayer systems.

12.09.2 Cation Receptors

Metal cations are essential in many biological processes. The functioning of the nervous system depends on the control of Na^+ and K^+ ions, while transition metal cations are present in the active site of many enzymes often playing catalytic roles. Furthermore, the selective extraction of metal salts from aqueous systems is important for both industrial and environmental reasons. Receptors that are able to extract precious metal ions from aqueous solution or detect/remove toxic and polluting cations (such as Cs^+ and Pb^{2+}) are highly desirable. In response to these diverse applications, the study of synthetic receptors for cationic guest species has become a well-established field with many organometallic examples to draw upon.

12.09.2.1 Receptors Based on Ferrocene

The well-developed and highly adaptable synthetic chemistry of ferrocene, together with its accessible ferrocene/ferrocenium (Fc/Fc^+) redox couple has led to its abundant use in redox-active receptors. The first organometallic cation receptors to be studied were the ferrocene-modified crown ethers of Saji **1** and Beer **2–4**.[8–12] The electron-rich crown ethers provide the cation-binding site—they are potent ionophores for group 1 and 2 metal cations. ^{13}C NMR (in methanol/acetone solution) and solid-state X-ray crystal structure studies demonstrated that **2–4** bind Na^+, K^+, and Cs^+. The binding stoichiometry varies depending on the receptor and cation used. Both Na^+ and K^+ form 2 : 1 cation : receptor complexes with **3**, as does Na^+ with **2**. The ability of ferrocene to swivel around the CpFeCp axis also allows the formation of a 1 : 1 intramolecular "sandwich" complex, as seen in **2** : Na^+, **2** : K^+, **2** : Cs^+ and **3** : K^+.

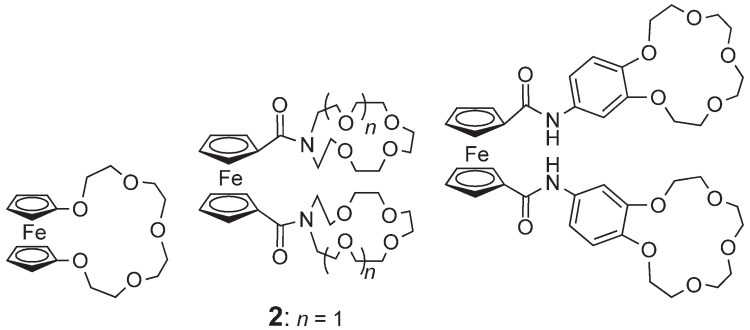

Binding of a cation at the crown ether site in receptors **1–3** causes a significant "anodic" shift in the redox potential of the Fc/Fc^+ redox couple (Table 1), due to the positive charge on the cation making the cation–receptor complex harder to oxidize than the receptor alone. No cation-induced shift in redox potential was observed with **4**, and this is attributed to the distance and lack of conjugation between the ferrocene and ionophore. It is noteworthy that due to the affinity of Li^+ for carbonyl oxygen donors, a crown ether binding site is not necessary in order to sense this cation. The simple ferrocene amide **5** actually gives a greater anodic shift in redox potential in the presence of Li^+ than **2–4**.[13]

Table 1 Cation-induced anodic shifts in the potential of the Fc/Fc^+ redox couple of **1–5**

Receptor	1[a]	*2*	3	5
ΔE (Na^+) (mV)	–	40	35	<10
ΔE (K^+) (mV)	180	20	20	<10
ΔE (Li^+) (mV)	–	70	75	390

[a]Electrochemistry carried out in CH_2Cl_2 containing 0.5 M $TBAPF_6$.
Electrochemistry carried out in acetonitrile solution containing 0.2 M $TBABF_4$ as supporting electrolyte.

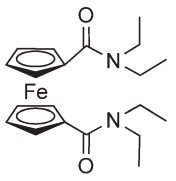

5

Oxidation of receptor **1** was found to decrease its binding affinity for alkali metal cations, due to electrostatic repulsion between $\mathbf{1}^+$ and the cation. Thus, the ferrocene unit not only enables redox sensing of alkali metal cations, but also allows the host : guest interaction to be switched on and off depending on the oxidation state of the receptor. Saji has also demonstrated that this phenomenon can be used in electrochemical ion transport across liquid membranes.[8]

Further studies on ferrocene crown ethers have demonstrated that even when the cation-binding unit is located at a distance from the metallocene redox reporter group, electrochemical sensing can take place provided there is electronic conjugation between the two. For instance, in receptor **6** an aza-crown is connected to the ferrocene via a stilbene linkage. A maximum anodic shift in the Fc/Fc^+ redox couple of 110 mV was observed for this receptor in the presence of Li^+ in CH_3CN solution. With **7**, in which the conjugation has been removed by reduction of the double bond portion of the linker, Li^+ ions produced no measurable shift in redox potential. Another example demonstrates that the effect also occurs for larger alkali metal cations—in receptor **8** two benzo-crown ethers are connected to the ferrocene Cp rings via an olefinic linkage. Anodic shifts of the Fc/Fc^+ redox couple due to complexation of Na^+ and K^+ are very similar to those observed in the directly linked systems **2** and **3** (Table 1).[14]

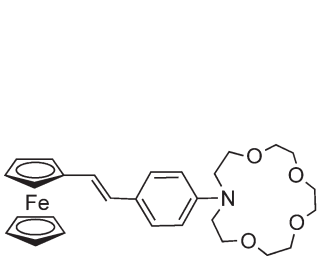

6

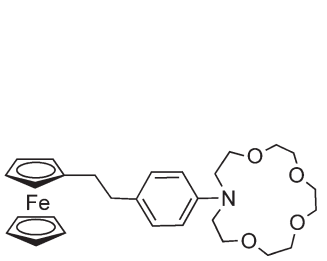

7

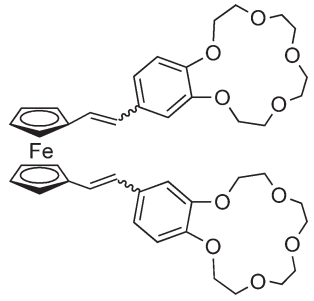

8

Extraordinary alkali metal cation-recognition behavior is exhibited by the thioether-linked receptor **9**. In CH_3CN solution, complexation of Na^+ results in a 70 mV anodic shift in the Fc/Fc^+ redox couple, whereas K^+ causes a "cathodic" shift of 60 mV. Results from ^{13}C NMR and fast atom bombardment mass spectrometry (FAB-MS) experiments show that **9** binds Na^+ with a 1 : 2 host : guest stoichiometry, but forms a 1 : 1 sandwich complex with the larger K^+ cation. Consequently, it is thought that complexation of K^+ forces the receptor to adopt a conformation in which the sulfur atoms' lone pairs of electrons are directed toward the ferrocene center, thus making it easier to oxidize and producing the observed cathodic shift in redox potential.

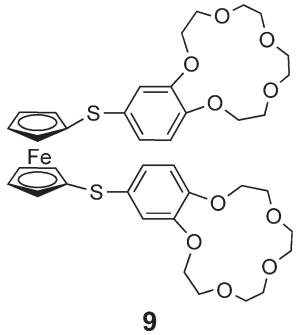

9

Beer and co-workers have devised a system that can simultaneously detect two different cations. In the presence of Mg^{2+} and Ba^{2+} in CH_3CN solution, the ditopic aza-crown receptor **10** produces three new peaks in the voltammogram. These correspond to the **10**:$2Ba^{2+}$, **10**:$2Mg^{2+}$, and **10**:$Ba^{2+}Mg^{2+}$ complexes with anodic shifts (compared to **10** alone) of 150, 395, and 275 mV, respectively.[15,16] Ferrocene receptor **11**, of Martinez-Manez and co-workers, is monofunctionalized with a smaller aza-oxa crown. In this case the binding unit is Hg^{2+} selective. Electrochemical results in CH_3CN solution show that at pH 5 the receptor is selective for Hg^{2+} over Pb^{2+}, Cu^{2+}, Cd^{2+}, or Zn^{2+}.[17]

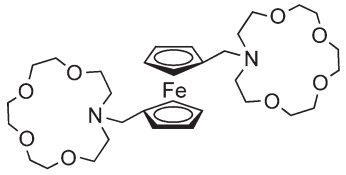

10

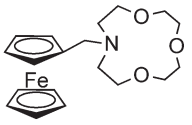

11

Apart from metal cations, ferrocene aza-crown systems have also been shown to sense the ammonium cation.[18] The bis- and tris-ferrocenyl macrocycles **12–15** display anodic shifts in redox potential in the presence of NH_4^+ and K^+. Receptor **12** gives a shift of 60 mV in response to 2 equiv. of either of these cations, whereas **13–15** are selective for NH_4^+ over K^+ (e.g., **13** gives shifts of 210 mV for NH_4^+ and 40 mV for K^+). Interestingly, the ferrocene units of **14** and **15** respond strongly to cation binding despite being separated from the aza-crown by a propyl spacer. It is thought that a hydrogen-bonding interaction between the carbonyl oxygen of the ferrocene amide and the coordinated NH_4^+ in a "lariat" fashion enables close contact of the cation and metallocene redox center.

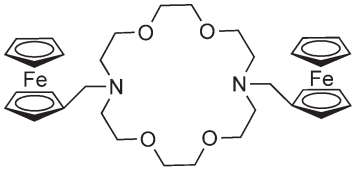

12

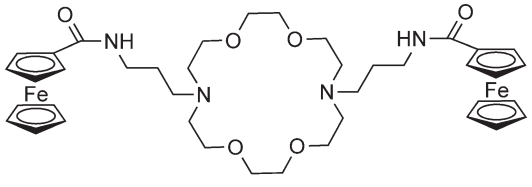

14

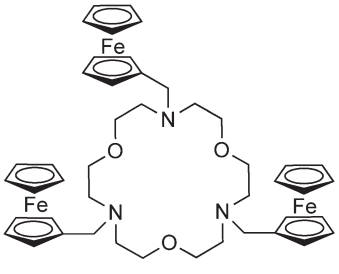

13

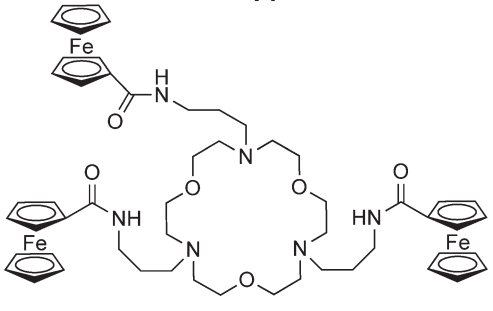

15

Ferrocene cryptands have also been studied as cation receptors. Hall *et al.* have investigated the coordination of alkaline earth and lanthanide metal cations by cryptand **16** using cyclic voltammetry in CH_3CN solution.[19] The cation-induced anodic shift of the Fc/Fc^+ redox couple was found to broadly correlate with the charge density of the cationic guest. Further electrochemical analysis revealed evidence that upon oxidation the **16**:Be^{2+} and **16**:Dy^{3+} complexes readily eject the bound cation from the cryptand cavity, presumably due to electrostatic repulsion.

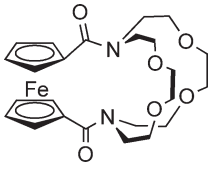

16

In examples **17–19**, Plenio and co-workers use a direct attachment of ferrocene into cryptands via oxygen donor atoms.[20] In CH_3CN solution, in the presence of group I monocations and group II dications, large anodic shifts in redox potential were measured, in the range of 80 mV for **19**:Li^+ to 380 mV for **17**:Ca^{2+}. Three general trends were observed: (i) dications generate a larger anodic shift value than monocations, (ii) the larger the binding cavity the smaller the magnitude of the perturbation, and (iii) within each group the metal ion with the best size complementarity for the cryptand cavity gives the greatest magnitude of anodic shift. These reflect (i) the greater charge density of the dications, (ii) the proportion of the charge of the cation felt by the two O donors attached to the ferrocene, and (iii) how close the cation is held to the ferrocene moiety.

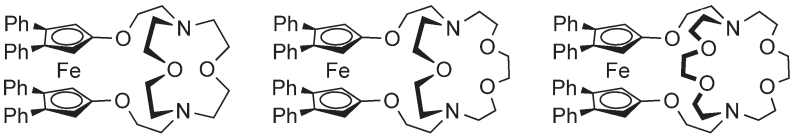

17 **18** **19**

Ferrocene has been paired with many alternative cation-binding domains. Nitrogen donors have received a great deal of attention due to their excellent transition metal cation coordination properties. Examples range from the simple amines and imines **20–22**, to polyamine chains and macrocycles such as **23–27**. The former allow the selective electrochemical sensing of Mg^{2+} and Ca^{2+} in acetonitrile solution,[21] while the latter provide pH-sensitive detection of transition metal cations in aqueous media.[22–25] Indeed, Martinez-Manez and co-workers have demonstrated quantitative sensing of Cu^{2+}, Zn^{2+}, and Cd^{2+} in THF/water (70/30) solution using **27**.[23]

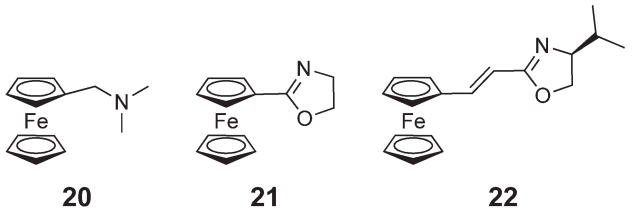

20 **21** **22**

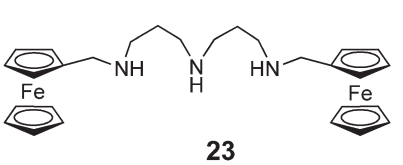

23

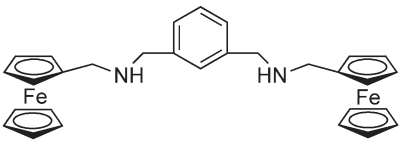

24

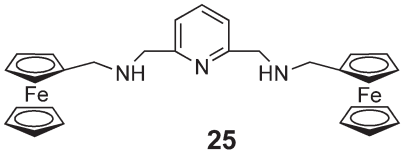

25

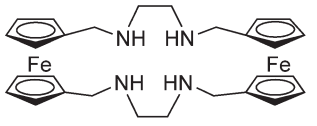

26

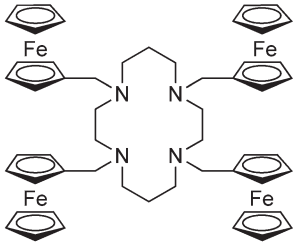

27

An interesting example from Plenio and co-workers displays perhaps the largest known anodic shifts in redox potential due to cation complexation.[26] The direct conjugation of two di(2-pyridylmethyl) arms via the amine nitrogens into ferrocene **28** results in shifts of 330 and 720 mV for **28**:Zn^{2+} and **28**:$2Zn^{2+}$, respectively. Co^{2+} complexation causes shifts of 380 and 760 mV for **28**:Co^{2+} and **28**:$2Co^{2+}$, respectively (electrochemistry carried out in CH_3CN solution).

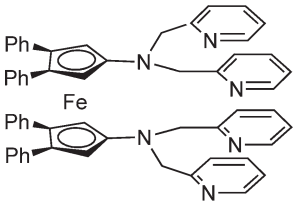

28

More recently, Molina and co-workers have devised an unusual series of azaferrocenophanes **29–37** which incorporate both a quinoline nitrogen and an alcohol oxygen for cation coordination.[27,28] Receptors **32** and **33** include an additional ferrocene unit, whereas **35–37** possess extra receptor groups: thienyl, 2-pyridyl, and 3-pyridyl groups, respectively. Anodic shifts of 300–400 mV were observed in the redox couple of the ferrocenophane in CH_3CN/CH_2Cl_2 (3/2) solution due to coordination of Mg^{2+}, Ca^{2+}, Ni^{2+}, and Zn^{2+}. The effect of cations on the redox couple of the distal ferrocenes of **32** and **33** was far less marked with shifts of 30, 10, and 0 mV for **32**:Mg^{+}, **33**:Ca^{2+}, and **33**:Mg^{2+}, respectively, reflecting both the distance from and lack of conjugation with the receptor donor atoms. In some cases, when hydrated metal salts were used, redox shifts due to protonation of the quinoline were observed. Intriguingly, the presence of secondary donor groups in **35–37** resulted in this protonation being suppressed, presumably due to the increased binding strength of these multidentate ligands for metal cations. That the increased receptor strength is not reflected in the observed anodic shifts is again due to the distance of the secondary binding site from the ferrocene. Receptor **37** was used to demonstrate that this system gives a colorimetric response to cations. In CH_2Cl_2 solution, upon chelation of Mg^{2+}, the ferrocene metal-to-ligand charge transfer (MLCT) band at $\lambda_{max} = 462$ nm disappeared and was replaced with a new band at $\lambda_{max} = 525$ nm, with an increase in absorbance. A K_a of 1.5×10^{10} M^{-1} was found for the **37**:Mg^{2+} complex in CH_2Cl_2 solution by spectrophotometric titration. This is a rare example of the use of an organometallic group as a chromophore in cation sensing.

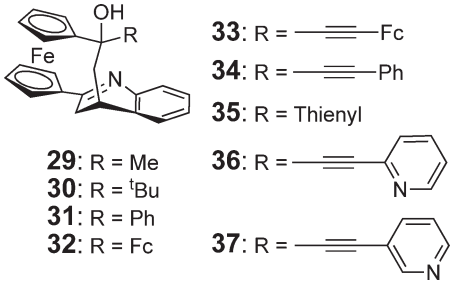

29: R = Me
30: R = ^{t}Bu
31: R = Ph
32: R = Fc

33: R = —≡—Fc
34: R = —≡—Ph
35: R = Thienyl
36: R = —≡—(2-pyridyl)
37: R = —≡—(3-pyridyl)

Fluorescence spectroscopy is a powerful technique in molecular sensing due to its sensitivity. Ferrocene derivatives are commonly efficient fluorescence quenchers, potentially precluding their use in this area. Nevertheless, Delavaux-Nicot and co-workers have developed a ferrocene-based fluorophore **38** for the detection of cations.[29] Electrochemical studies showed that the organic skeleton of the molecule undergoes irreversible oxidation before the Fc/Fc^{+} redox couple is accessed. Of the cations studied, only Ca^{2+} gave rise to any significant change in the voltammogram—causing a 120 mV "cathodic" shift in the ferrocene wave and the disappearance of the waves corresponding to the organic oxidation and reduction processes. ^{1}H and ^{13}C NMR experiments in CD_3CN indicate that Ca^{2+} interacts most strongly with the carbonyl groups, leaving the amines uncoordinated. The UV/VIS absorption properties of **35** in CH_3CN are also sensitive to Ca^{2+} coordination. At substoichiometric proportions little change is observed, but when >1 equiv. of the salt is added, the band at $\lambda_{max} = 462$ nm ascribed to amine–carbonyl charge transfer is diminished in intensity, while the absorbance around 500 nm is increased, ascribed to the Ca^{2+}–carbonyl interaction. More striking is the change in the fluorescence properties of the molecule. As Ca^{2+} was added, the intensity of the emission at 560 nm increased until 2 equiv. of cation is reached. Further addition leads to a steady decrease in emission intensity until at relatively high Ca^{2+} concentration total quenching occurred.

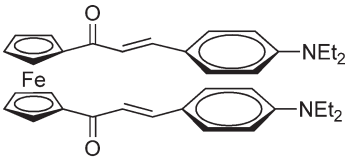

38

Molina and co-workers have created the ferrocene–anthracene dyad **39**, a fluorescent sensor for Li^+, which operates in aqueous conditions.[30] The molecule is only weakly emissive (excitation at 370 nm, $\phi = 0.042$–0.008), but in CH_3CN/H_2O (70/30) mixtures at pH = 5, the addition of 1 equiv. of Li^+ ions results in a 7.3-fold enhancement in fluorescence. At this pH, the receptor selectively responds to Li^+ over Na^+, K^+, Ca^{2+}, Cu^{2+}, and Zn^{2+}. It is noteworthy that if water is not present, no effect is seen. At lower pH some selectivity over Na^+ and K^+ is lost. A K_a of 11.76 ($\pm$0.02) M^{-1} was determined for the **39**:Li^+ complex by fluorescence titration. A colorimetric response to Li^+ was observed by UV/VIS spectroscopy, with the MLCT absorption band moving to higher energy and decreasing in intensity. ^1H NMR and density functional theory (DFT) analysis indicate that the Li^+ cation interacts directly with the ferrocene Fe atom, and is stabilized by a network of hydrogen bonds involving two water molecules and the protonated imine nitrogen of the receptor. In this case, the organometallic moiety itself is acting as the cation-binding group, albeit in concert with receptor–solvent hydrogen bonding.

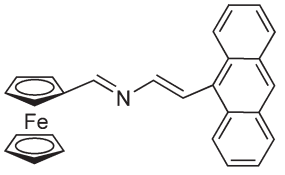

39

Using the same synthetic methodology, Molina has developed the fully conjugated macrocyclic diferrocenyl receptor **40**.[31] This functions as a redox switchable sensor, which can selectively complex and decomplex Mg^{2+}. No perturbation of the two redox waves (due to the two electronically distinct ferrocene centers) in the cyclic voltammogram (carried out in CH_2Cl_2 solution) was observed on addition of Ca^{2+}, Li^+, or Na^+, whereas Mg^{2+} caused an anodic shift in the redox couple of the ferrocene at the allylic end of the molecule, while the redox couple of the other ferrocene remained largely unchanged. The UV/VIS spectrum of **40** was also found to be sensitive to Mg^{2+}, and titration results indicated that the **40**:2Mg^{2+} complex is formed via the **40**:Mg^{2+} complex with formation constants of $K_{11} = 9.8 \times 10^5$ M^{-1} and $K_{12} = 6.3 \times 10^5$ M^{-1}. Two solutions, of **40** alone and of **40**:2Mg^{2+}, gave identical absorption spectra when oxidized electrochemically, indicating that decomplexation of Mg^{2+} occurs on oxidation of the receptor. Reduction of the solution containing Mg^{2+} regenerated the **40**:2Mg^{2+}. Utilizing this reversible complexation/decomplexation process, redox transport of Mg^{2+} across a CH_2Cl_2 membrane was also demonstrated.

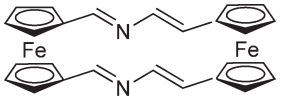

40

12.09.2.2 Pt- and Au-based Receptors

Organometallic structures based on Pt have been used as cation receptors.

Stang and co-workers have reported a series of tetranuclear Pt–Pt and Pt–Pd squares **41** and **42**, which bind Ag^+.[32] In these molecules, ethynyl Pt units form two opposite corners of a square with a bite angle of 88° between the acetylenes. The complexation of 2 equiv. of Ag^+ was observed by ^{31}P, ^{13}C, and ^1H NMR as well as by UV/VIS and IR spectroscopy. The results indicate that the cations are held in the corners of the molecule by the two acetylene units as a result of the "π-tweezer effect" giving structures **43** and **44**. Briefly, electron density from a filled acetylene π-orbital is donated into a vacant *sp*-hybridized orbital on the metal and backdonation occurs from filled metal

d-orbitals into vacant acetylene π^*-orbitals. In these receptors, the organometallic unit acts as the ionophore as well as a structural component.

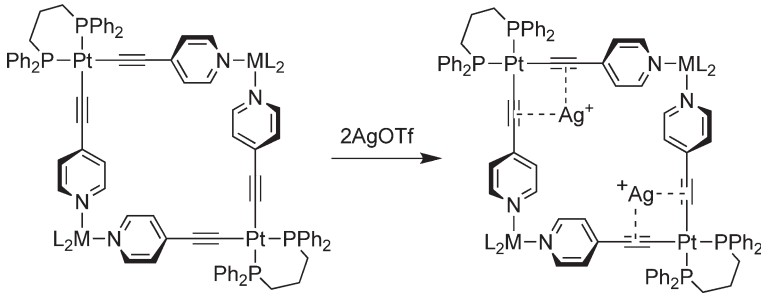

41: M = Pt; $L_2 = Ph_2P(CH_2)_3PPh_2$
42: M = Pd; $L_2 = PEt_3$

43: M = Pt; $L_2 = Ph_2P(CH_2)_3PPh_2$
44: M = Pd; $L_2 = PEt_3$

Pt acetylenes can also function as fluoresecent sensors for cations. Receptor **45** incorporates two 4-ethynylbenzo-15-crown-5 moieties with luminescent dimino Pt(II) complexes.[33] In acetonitrile solution, complex **45** is weakly emissive (excitation at 405 nm, $\lambda_{max} = 635$, $\phi = 1.1 \times 10^{-4}$). However, on addition of M^{2+}, significant increase in the emission intensity and a blue shift in λ_{max} to 555 nm were observed. At 40 equiv. of Mg^{2+} or Zn^{2+}, the measured enhancement was 1,035- and 870-fold, respectively. Other cations, namely, K^+, Na^+, and Cd^{2+}, resulted in a less than 10-fold emission enhancement. The binding stoichiometry was found to be 1 : 2 receptor : cation, and the overall stability constants calculated for Na^+, Mg^{2+}, and Zn^{2+} were $\beta = 7.9 \times 10^7$, 5.3×10^8, and 9.3×10^7 M^{-2}, respectively.

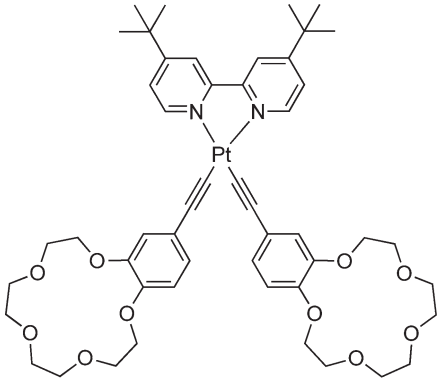

45

More recently, Stang has devised **46**, an optical sensor for Ni^{2+}, Cd^{2+}, and Cr^{3+}, based on a 1,8-Pt-functionalized anthracene, where the organometallic unit acts as a "molecular clip," enabling the self-assembly of a rectangular macrocycle.[34] Addition of Ni^{2+} to **46** in methanol solution resulted in substantial changes in the UV/VIS absorption spectrum, due to the 1 : 1 complexation of the cation. Stability constants were determined for **46** : Ni^{2+}, **46** : Cd^{2+}, and **46** : Cr^{3+} in methanol solution, $K_a = 2.01 \times 10^7$, 3.39×10^4, and 7.53×10^3 M^{-1}, respectively.

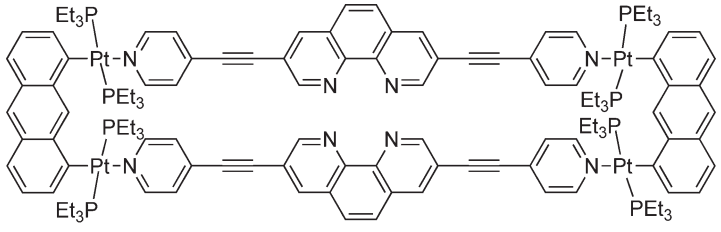

46

Yam and co-workers have investigated cation receptors based on gold–acetylide complexes.[35,36] For instance, calix[4]crown **47** functions as a colorimetric sensor for Na^+ and K^+. UV/VIS spectrophotometric titration of **47** in CH_2Cl_2/CH_3OH (1/1) solution with these cations determined a 1:1 binding stoichiometry in each case and stability constants of 1.74×10^7 and 5.62×10^2 M^{-1} for the **47**:K^+ and **47**:Na^+ species, respectively. This is a very high degree of selectivity for K^+ over Na^+ and is two orders of magnitude greater than in the parent calix[4]crown. Thus, the organometallic moieties in **47** provide improved selectivity as well as a spectroscopic probe for cation binding.

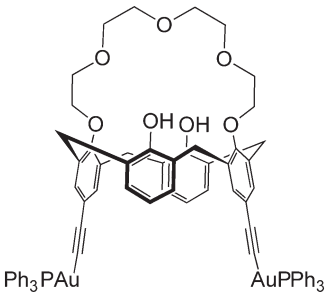

47

12.09.2.3 Other Cation Receptors

There are a few examples of organometallic cation receptors based on Ru(II), Rh(II), and Ir(III) metallocenes. Severin and co-workers have studied a series of self-assembled [12]metallacrown-3 complexes **48–53**.[37,38] The reaction of the organometallic precursor with 3-hydroxy-2-pyridinone creates a trimetallic macrocycle, in which three of the oxygen donor atoms are preorganized to bind small alkali metal ions. The π-ligands of the metal also project above the plane of the oxygen atoms to generate a solvophobic binding pocket. As a result, these ionophores have a very high affinity for Li^+ and Na^+, even in polar solvents such as CH_3OH.

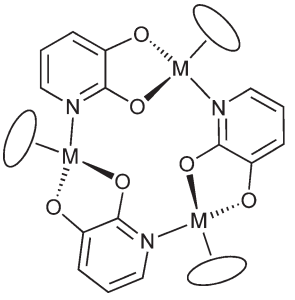

(π-ligand)M:
48: (cymene)Ru
49: (C_6H_6)Ru
50: (C_6Me_6)Ru
51: ($C_6H_3Et_3$)Ru
52: (Cp*)Rh
53: (Cp*)Ir

The binding affinity with Na^+ was found to be dependent on the halide counterion used, indicating that ion-pair binding is occurring. The following K_a values were obtained in CD_3OD solution **48**:NaCl = 3.5×10^3 M^{-1}, **48**:NaBr = 1.5×10^3 M^{-1}, **48**:NaI = 3.4×10^2 M^{-1}, **49**:NaCl = 1.1×10^2 M^{-1}. In $CDCl_3$ solution, formation of **48**:NaX and **49**:NaX (X = Cl, Br, I) is quantitative. In CD_3OD, the affinity of **48** for NaCl is comparable to that of [15]crown-5. In $CDCl_3$ it is far superior to [15]crown-5 and comparable to that of cryptands. Receptors **48–53** have such high affinity for LiCl that they bind this ion pair quantitatively even in CD_3OD. Competition experiments allowed a trend for LiCl affinity to be determined: K_a(**49**:LiCl) > K_a(**48**:LiCl) > K_a(**50**:LiCl) > K_a(**52**:LiCl) > K_a(**50**:LiCl). Electrochemical detection of cations using **48–53** in $MeCN/CH_2Cl_2$ (1/1) was also investigated. The free metallacycles exhibit three irreversible oxidation processes, presumably corresponding to the sequential oxidation of the three metal centers. On addition of LiCl or NaCl, the first of these waves undergoes an anodic shift of >300 mV, but becomes merged with the other waves; hence, exact anodic shifts could not be determined.

12.09.3 Anion Receptors

Anionic species are well known to play a fundamental role in numerous biological and chemical processes. Many biologically important species are anionic such as nucleic acids and the majority of enzyme substrates. Anions also play a role in diseases such as cystic fibrosis, which is caused by the misregulation of Cl^- ion channels. In the environment, pollutant anions such as NO_3^- and PO_4^{3-} can cause the eutrophication of waterways. In view of this, the design of receptors which can selectively bind, extract, and/or sense anions is an important goal, and has become the focus of a great deal of current research interest.

The binding of anions presents a new challenge compared to the binding of cations. Apart from possessing the opposite charge, anions are larger than their isoelectronic cations due to their reduced effective nuclear charge, that is, anions have smaller charge to radius ratios. This often means that anions are more difficult to complex because of their diffuse nature. Anions also exist in a wide variety of geometries but often lack the directionality of cations in their binding. Solvation effects and pH dependence are also important factors to take into account in the coordination of anions.

12.09.3.1 Receptors Based on Cobaltocenium

Anion receptors incorporating cobaltocenium have been studied extensively due to the combination of an accessible redox couple and potential favorable electrostatic interactions of the cationic organometallic metallocene moiety with anions. The first anion receptors utilizing the cobaltocenium motif were reported by Beer *et al.* in 1989.[39] The macrocyclic bis-cobaltocenium receptor **54** was shown to bind (via electrostatic interaction) and to electrochemically sense Br^- in CH_3CN solution.

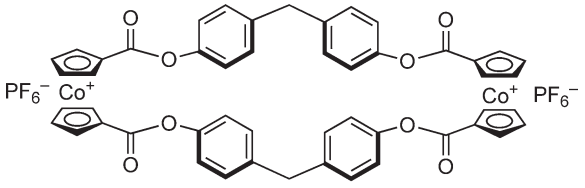

54

Augmentation of cobaltocenium receptors with hydrogen bond donor groups, such as amides in receptors **55** and **56**, generates both stronger and more selective anion binding.[40] ^{1}H NMR titration studies in CD_3CN reveal **55** and **56** to have selectivity for $H_2PO_4^-$ over Cl^- by approximately an order of magnitude.[41] This is attributed to the greater basicity of the $H_2PO_4^-$ anion. Electrochemical sensing of anions is also enhanced. For **55** and **56**, binding of Cl^- generates cathodic shifts in the $[Cp_2Co]/[Cp_2Co]^+$ redox couple of 30 and 85 mV, respectively. The more strongly bound $H_2PO_4^-$ anion causes larger cathodic shifts of 200 and 240 mV, respectively. Cathodic shifts are observed on anion binding due to the stabilization of the cationic cobaltocenium species relative to the neutral cobaltocene species by the closely bound negatively charged guest.

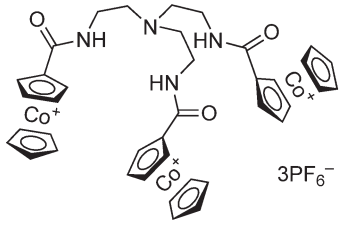

55

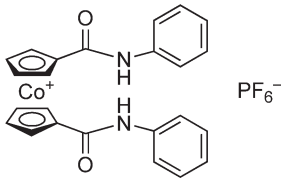

56

Parallel photo- and electrochemical sensing of anions has been accomplished using a tetracobaltocenium–porphyrin receptor **57**, which utilizes the organometallic units as redox reporter groups, while the porphryin acts as a spectroscopic probe.[42] ^{1}H NMR titrations in CD_3CN showed Cl^- and Br^- to be bound in 1 : 1 stoichiometry with $K_a = 860$ and 820 M^{-1}, respectively, whereas NO_3^- exhibited weaker binding with $K_a = 190$ M^{-1}. In the UV/VIS spectrum of **57** in CH_3CN solution the Soret band ($\lambda_{max} = 425$ nm) of the porphyrin was significantly bathochromically shifted on addition of $H_2PO_4^-$ ($\Delta\lambda_{max} = 15$ nm), hypsochromically shifted with $C1^-$ ($\Delta\lambda_{max} = 10$ nm), and split into two maxima

($\lambda = 430$, 440 nm) with HSO_4^-. Electrochemical studies displayed cathodic shifts in the $[Cp_2Co]/[Cp_2Co]^+$ redox couple of 35–75 mV on addition of Cl^- or HSO_4^-, and 225 mV for $H_2PO_4^-$. Smaller shifts were seen in the porphyrin oxidation wave. It should be noted that these anion-sensing effects are specific to the *cis*-$\alpha,\alpha,\alpha,\alpha$-atropisomer.

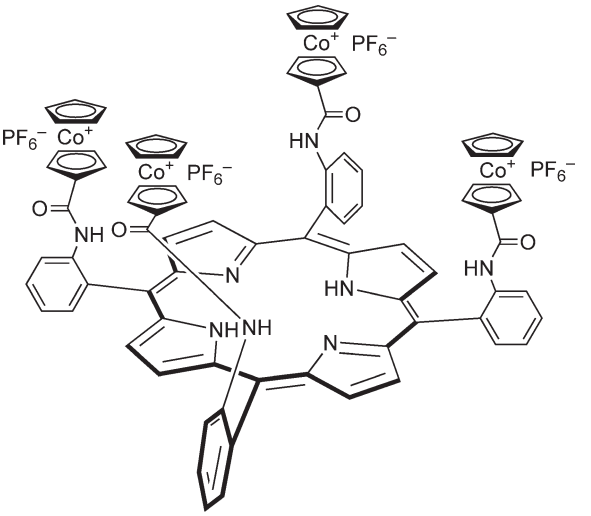

57

The anion-recognition properties of cobaltocenium calix[4]arene receptors **58–60** were found to be dependent on the structure of the upper rim of the calix[4]arene.[43] For instance, in dimethyl sulfoxide (DMSO) solution, the bis-cobaltocenium receptor **58** shows a greater affinity for $CH_3CO_2^-$ than for $H_2PO_4^-$, whereas with **59** (its isomer) the trend is reversed. Receptor **60**, in which the calix[4]arene is bridged by a single cobaltacenium moiety, displays significantly greater affinity for the above anions despite possessing only a single positive charge. This is thought to be the result of topological complementarity between the upper rim bidentate amide hydrogen bond donor cavity of **60** and bidentate anions such as carboxylates. $CH_3CO_2^-$ was found to induce a cathodic shift of 155 mV in the $[Cp_2Co]/[Cp_2Co]^+$ redox couple of this receptor. In these examples, the organometallic groups effectively control the selectivity of the anion-recognition unit to which they are attached.

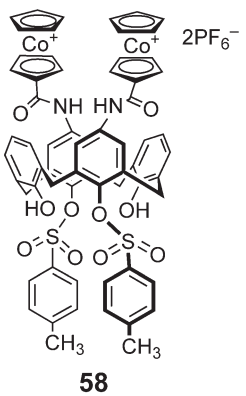

58

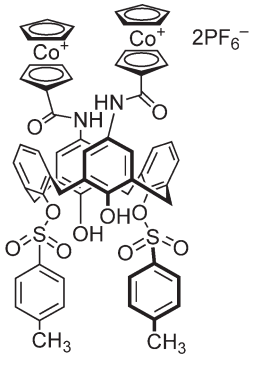

59

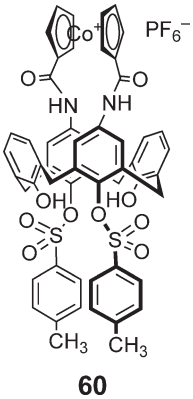

60

The incorporation of crown ether units into a cobaltocenium receptor allows switchable sensing of anions. ^1H NMR titrations of receptor **61** in CD_3CN solution gave log K values of 3.1 for chloride and 3.0 for bromide.[44] Electrochemical titrations gave cathodic shifts of the $[Cp_2Co]/[Cp_2Co]^+$ redox couple of 60 and 30 mV for the two anions, respectively. However, when carried out in the presence of K^+, the same titrations produced no significant NMR or redox response. It is postulated that the K^+ ions form a 1 : 1 intramolecular sandwich complex with the two benzo-crown ether units of the receptor. The concomitant change in conformation of the amide groups reduces their availability for anion binding.

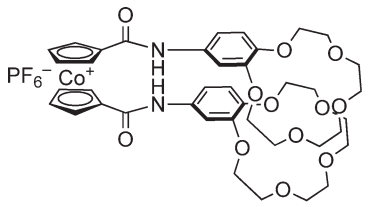

61

Macrocycle **62** combines cobaltocenium with a bridging Ru(II)trisbipyridyl unit in the form of a bimetallic macrocycle.[45] In DMSO-d_6 solution, this receptors was found by ^{1}H NMR to selectively bind Cl^- over $CH_3CO_2^-$ and $H_2PO_4^-$. In MeCN solution, the cobaltocenium unit partially quenches the {Ru(bpy)$_3$} luminescence emission. On addition of Cl^- to **62**, a 100% increase in emission intensity was observed. Restoration of the emission is thought to be due to the bound anion interrupting the intramolecular quenching process. This receptor also displays cathodic shifts in the redox potential of the $[Cp_2Co]/[Cp_2Co]^+$ couple upon addition of anions.

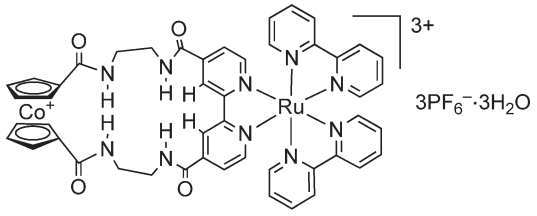

62

12.09.3.2 Receptors Based on Ferrocene

The accessible ferrocene/ferrocenium redox couple of ferrocene has led to its frequent use in electrochemical anion sensors. The chemical and structural similarity between ferrocene and cobaltocenium has meant that receptors based on these complexes often share the same design. The most relevant difference is that the ferrocene derivatives are neutral, have no inherent electrostatic interaction with anions, and hence their complexes with anions exhibit lower stability constants. However, anion recognition in these species can be "switched on" by oxidation of ferrocene to the positively charged ferrocenium ion.

Molecules **63–67** are a selection of ferrocene-based receptors, which include secondary amide groups for the hydrogen bonding of anions.[46,47] Electrochemical measurements on **63–66** in CH_3CN showed cathodic shifts in the Fc/Fc^+ oxidation wave of up to 240 mV induced by $H_2PO_4^-$. Competition experiments demonstrated the same shift even in the presence a 10-fold excess of Cl^- or HSO_4^-. A cathodic shift is expected in this class of compounds, since the coordination of an anion guest close to the ferrocene stabilizes the cationic ferrocenium redox state, facilitating the oxidation process. Therefore, it is largely the stability of the electrostatically enhanced anion–ferrocenium complex which determines the magnitude of the redox shift.

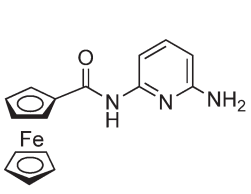

63

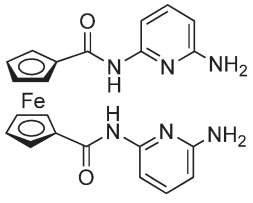

64

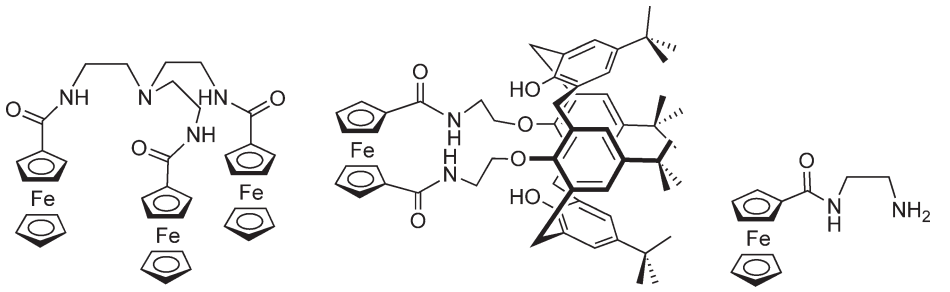

65 66 67

Receptor **67** shows opposite selectivity, providing an HSO_4^--induced shift of 220 mV, which is not affected by the presence of excess $H_2PO_4^-$. In this case, the HSO_4^- anion donates a proton to the basic amine function of the receptor, and it is the resulting cationic complex which binds the residual SO_4^{2-} anion.

A very simple cationic receptor **68** has been investigated by Moutet and co-workers. It is able to sense $H_2PO_4^-$ and ATP^{2-} in a range of solvents, displaying a cathodic shift of 470 mV in CH_2Cl_2 with $H_2PO_4^-$, solely due to a strong ion-pairing interaction. Other anion coordinating groups to which ferrocene has been attached include imidazolium, calix[4]pyrrole, pyridinium-substituted tripods, and cyclotriveratrylene, for example, **69**, **70**, **71**, and **72**, respectively.[48–51] Anion-induced cathodic shifts in redox potential were observed in each case.

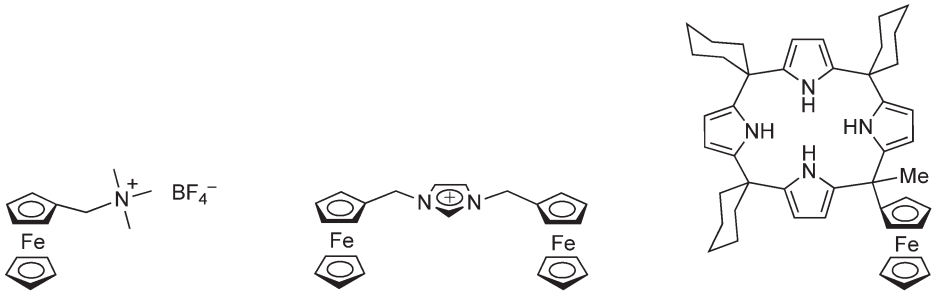

68 69 70

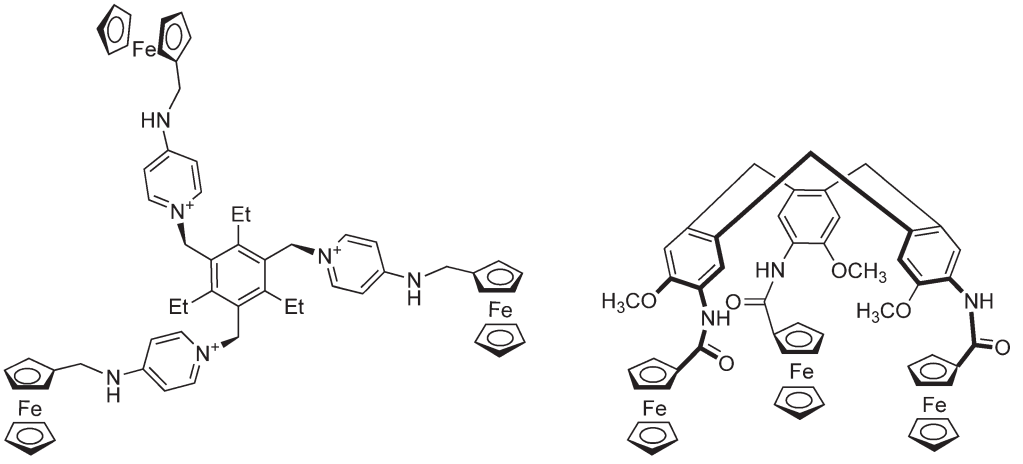

71 72

Molecules **73–75**, in which a ferrocene-1,1′-bis-amide is bridged across the upper rim of a calix[4]arene, show similar anion-sensing properties to the cobaltocenium analog **60**, described previously.[52] ^1H NMR studies in CD_3CN demonstrate that these receptors preferentially bind carboxylate anions (acetate and benzoate) over $H_2PO_4^-$ and Cl^-.

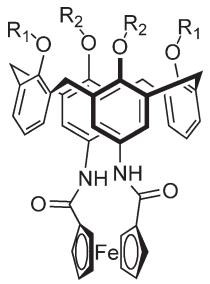

73: $R_1 = R_2 = CH_3$

74: $R_1 = CH_3$, $R_2 = CH_2COOEt$

75: $R_1 = R_2 = CH_2COOEt$

Receptor **76** incorporates a zinc–porphyrin backbone with four ferrocene amides.[53] This shares the design of the cobaltocenium receptor **57**, except that now a Lewis-acidic Zn(II) cation occupies the center of the porphyrin. The Lewis acid metal center provides an additional binding site for anion recognition. In CH_2Cl_2 solution, no significant anion-induced shifts in the ^1H NMR signals of the amide protons were seen in the free base precursor of **76**, whereas the metalloporphyrin binds Br^- ($K = 6{,}200\,M^{-1}$), NO_3^- ($K = 2{,}300\,M^{-1}$), and HSO_4^- ($K = 2{,}100\,M^{-1}$). Electrochemical studies in 3 : 2 CH_2Cl_2/CH_3CN revealed anion-induced cathodic shifts in both the porphyrin ($\Delta E = 85$–115 mV) and tetraferrocene oxidation ($\Delta E = 20$–60 mV) waves. Atropisomers of **76** (the $\alpha,\alpha,\alpha,\alpha$-atropisomer is shown) were also studied and displayed different selectivities but generally lower stability constants. This demonstrates the importance of the organometallic amide groups in the anion-recognition site and suggests that they operate cooperatively in the $\alpha,\alpha,\alpha,\alpha$-atropisomer.

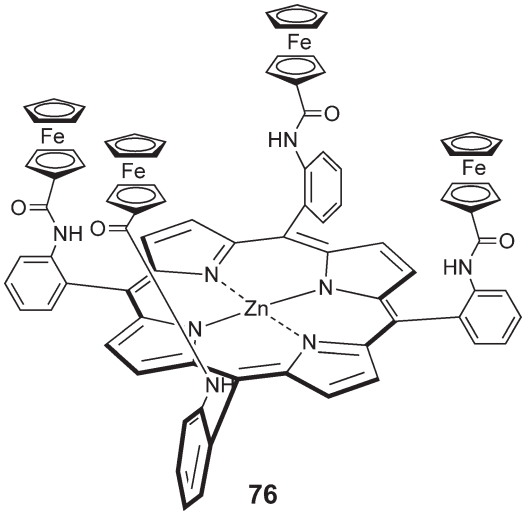

76

Organometallic receptors are also capable of operating in an aqueous environment, an important consideration in the sensing of biologically relevant anions. Anion recognition in polar solvent media requires the use of strong electrostatic interactions. Beer and co-workers have synthesized a series of ferrocene-based receptors appended with various open-chain and cyclic amine functional groups, for example, **77** and **78** bind ATP^{2-} and $H_2PO_4^-$ in water,[54–56] giving cathodic shifts of 60–80 mV in the Fc/Fc^+ couple. The selectivity of this class of receptors is pH dependent. In the 1 : 1 complexes formed at pH 6.5, at least two of the amines are protonated.

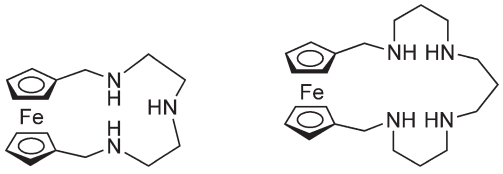

77 **78**

Metallacyclic receptors **26** and **79** were shown to be able to quantitatively determine PO_4^{3-} and SO_4^{2-} in the presence of other anions. The electrochemistry of these receptors was studied in 70 : 30 THF/H_2O over a range of pH's. A maximum selective redox shift of 54 mV for SO_4^{2-} over PO_4^{3-} was observed at pH 4 for **26**, whereas **79** gave a maximum selective redox shift of 35 mV for PO_4^{3-} over SO_4^{2-} at pH 8.

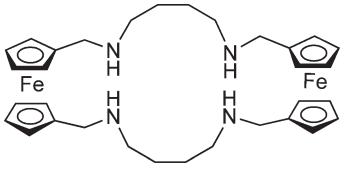

79

Recognition of fluoride in aqueous media is particularly difficult due to the strongly hydrated nature of the anion. Shinkai and co-workers have demonstrated that ferrocene–boronic acid **80** acts as a selective redox sensor for F^-, which operates in H_2O.[57] The favorable interaction between boron and F^- (a hard acid and hard base, respectively) generates a stability constant of 700 M^{-1} for the fluoride–ferrocenium complex (determined electrochemically). Stability constants for both the Br^- and Cl^- complexes are $<2\,M^{-1}$.

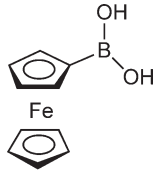

80

Aldridge *et al.* have demonstrated that a similar boryl–ferrocene **81** can be used as a selective colorimetric sensor for F^-.[58] When F^- was added to a CH_2Cl_2 solution of **81**, under aerobic conditions, a color change from orange to pale green was observed. This did not occur with any other anion tested. Spectroscopic and electrochemical measurements suggest that complexation of F^- causes the spontaneous formation of a ferrocenium species, that is, the 150 mV anodic shift in the Fc/Fc^+ redox potential caused by F^- complexation lowers the redox potential enough for the **81** : $2F^-$ complex to be aerobically oxidized.

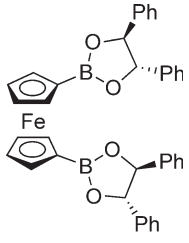

81

Combining ferrocene with another organometallic unit can lead to augmented anion sensing. For instance, the incorporation of phosphine groups into ferrocene–amide receptor **82** allowed the coordination of various transition metals to generate mixed metal complexes **83** and **84**.[59] ^1H NMR titrations were carried out, and the stability constants of these receptors with various anions in CD_2Cl_2 solution were calculated. Molecules **83** and **84** were found to bind Cl^- approximately an order of magnitude more strongly that the parent phosphine **82**. The complexes of the bimetallic molecules with Cl^-, Br^-, I^-, and $H_2PO_4^-$ were also found to be more stable, but to a lesser extent. In these examples, the addition of more Lewis-acidic metal center enhances anion binding. Significant anion-induced cathodic shifts in both the Fc/Fc^+ couple and the oxidation wave of the second metal were observed in the cyclic voltammetry.

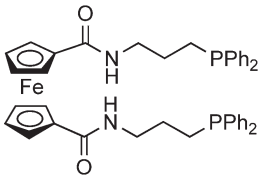

82

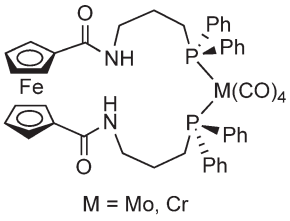

83

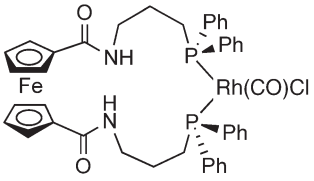

84

A unique mixed organometallic receptor has been prepared by Jurkschat and co-workers.[60] Macrocycle 85 comprises two ferrocene reporter units linked together by two Lewis-acidic organotin spacers. Electrochemical measurements in CH_2Cl_2 solution show anion-induced cathodic shifts of the Fc/Fc^+ redox couple of 130 mV for Cl^-, 210 mV for F^-, and 480 mV for $H_2PO_4^-$.

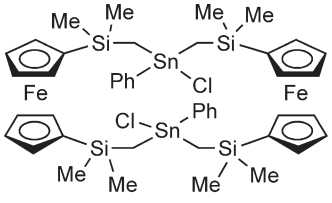

85

12.09.3.3 Other Anion Receptors Based on Metallocenes

The potential for electrostatic interaction with anions is gained if one of the cyclopentadienyl rings of ferrocene is replaced with an arene moiety to generate a cationic complex. Beer and co-workers have exploited this principle in the simple receptor 86.[61] Similarly, Atwood and co-workers have derivatized cycloytriveratrylene to generate receptor 87.[62] Qualitative ^{1}H NMR studies demonstrate that 86 binds chloride and bromide in CD_3CN, and 87 binds halides in acetone-d_6. It is proposed that the strength of the interaction in 87, which does not possess amides or other H-bonding groups, is due to the arrangement of positive charges around the upper rim of the hydrophobic cavity. No electrochemical data are reported for either receptor.

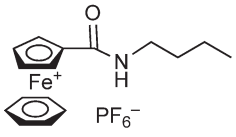

86

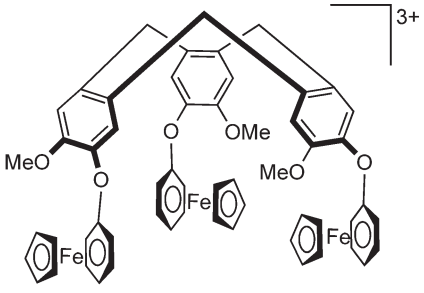

87

The anion-binding properties of a series of highly cationic metallated calix[4]arenes have also been investigated. Host 88, in which the calix[4]arene is coordinated to four Ru(η^6-*p*-cymene) units, was found by ^{1}H NMR titration to bind Cl^-, Br^- I^-, and NO_3^- in aqueous solution.[63] Stability constants were determined with $K_a = 551$, 133, 51, and 49 M^{-1}, respectively.

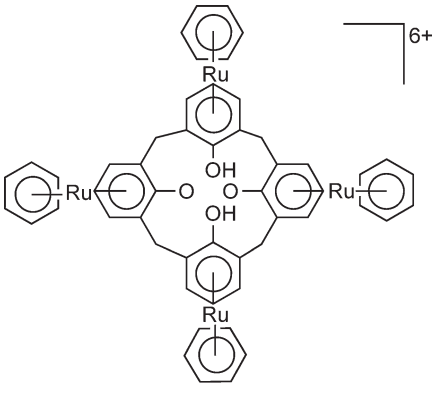

88

$Cr(CO)_3$ is an effective electron-withdrawing group.[64] The coordination of this organometallic unit to the arene substituents of the isophthalamide in **89** increases the acidity of the NH protons and hence their affinity for anions. ^{1}H NMR titrations in CD_3CN solution provided stability constants of the same order of magnitude as those for the non-metallated receptor in the far less competitive solvent CD_2Cl_2.

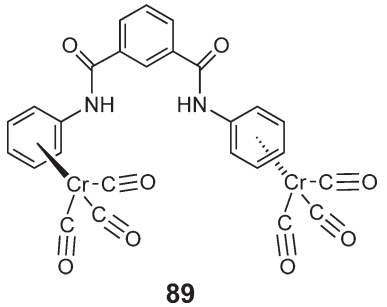

89

12.09.3.4 Rhenium(I) Tricarbonyl Chloride-based Receptors

Complexes of rhenium(I) tricarbonyl chloride with pyridyl ligands are luminophores and hence in anion sensing have principally been used as reporter groups. For instance, calix[4]diquinone receptor **90** selectively binds and senses $CH_3CO_2^-$ in DMSO solution[65] (from ^{1}H NMR titrations $K = 1790\ M^{-1}$ in DMSO-d_6 solution). The receptor exhibits relatively weak luminescence because calix[4]diquinone is an electron acceptor, quenching the Re(I) bipyridyl emission by oxidative electron transfer. Addition of anions to DMSO solutions of **90** resulted in a significant increase in luminescence intensity. It is clear that presence of the anion in the binding pocket between the {Re(bpy)} moiety and the quencher interrupts the oxidative electron-transfer process.

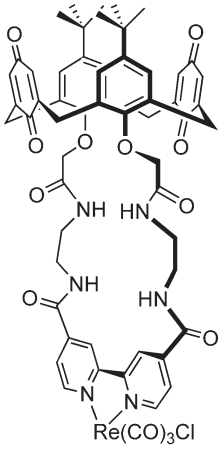

90

The mixed Re(I)/Pd(II) molecular square **91** has been found to sense ClO_4^- in acetone (giving $K = 900\,M^{-1}$) by enhancement of the Re(I) luminescent emission.[66] In this case, luminescence quenching by oxidative transfer to the Pd(II) ion is inhibited by the bound anion. Squares **92–96** are very similar, but incorporate a bis-phosphinylferrocene-supporting ligand.[67] Again the normally strong luminescence of the Re(I) component is partially quenched by the bimetallic corners. Binding studies of the squares and different inorganic anions were carried out by luminescence titrations in acetone solution. Of the anions investigated, only PF_6^- and BF_4^- induced significant changes in luminescence. As these anions were added, an initial decrease in emission intensity was followed by an increase to a plateau. This is taken to indicate presence of two competing quenching pathways which are inhibited to different extents by anion binding.

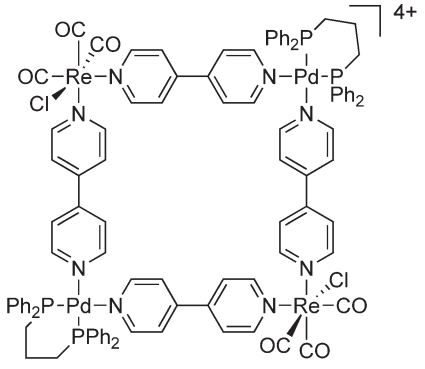

91

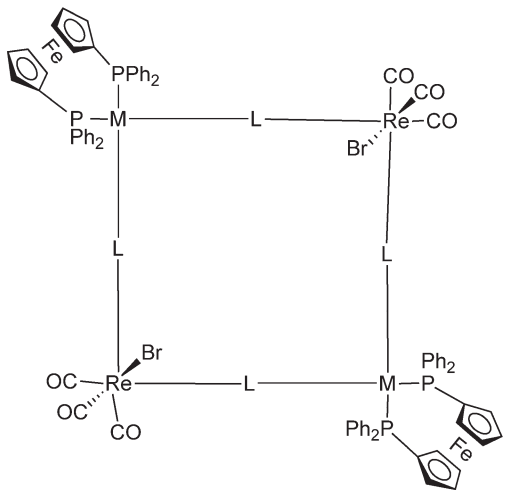

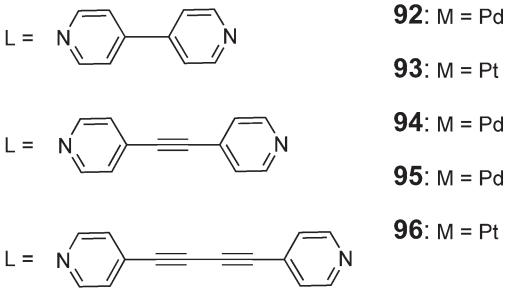

Lees and co-workers have investigated Re(I) bipyridyl anion hosts based on aryl bis-amide skeletons **97–99**.[68] Measurement of anion-induced luminescence quenching in CH_2Cl_2 showed **97** to have strong binding affinities for halides, $CH_3CO_2^-$, and CN^-, weaker affinity for $H_2PO_4^-$, and even less affinity for NO_3^- and ClO_4^-. The iso- and terephthalamide receptors **98** and **99** possess smaller stability constants for all the anions tested. It is proposed that the anion-sensing efficiency of **98** is due to intramolecular hydrogen bonding of the amido NH proton to the pyridyl nitrogen, holding the receptor in a "cleft" conformation.

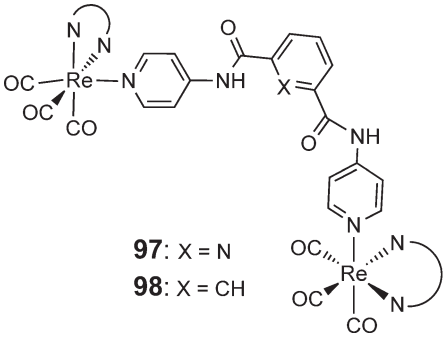

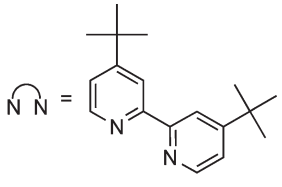

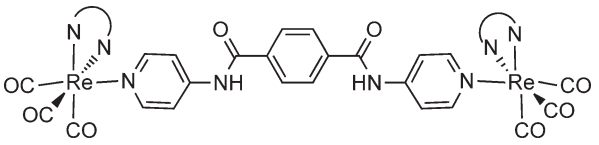

99

Interlocked supramolecular assemblies such as rotaxanes and catenanes have the potential to provide tailor-made binding cavities for guest species. An example of this is **100**, a rotaxane formed using anion-templated synthesis which incorporates the Re(I) bipyridyl fragment.[69] Addition of Cl^-, HSO_4^-, or NO_3^- to the receptor in acetone solution caused an enhancement of the fluorescence emission. Curiously, although the rotaxane was formed using Cl^- as the template, in acetone solution it was found to be selective for HSO_4^- with which a stability constant of $>10^6\,M^{-1}$ was determined.

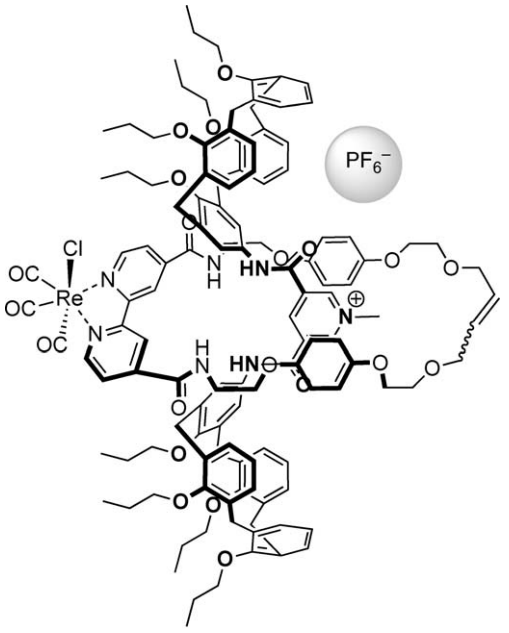

100

12.09.4 Receptors for Neutral Guest Species

Neutral guest species are perhaps the most challenging target in synthetic receptor chemistry, since their lack of electrostatic charge necessitates the use of weaker non-covalent interactions in order to bind them. The forces involved in neutral molecular recognition and complexation are principally dipole–dipole interactions, dipole–induced dipole interactions, hydrogen bonding, London dispersion forces, π-stacking interactions, charge-transfer interactions, and hydrophobic or solvophobic effects.

12.09.4.1 Receptors Based on Ferrocene

Organometallic receptors for neutral guest species were first reported in 1991 by Gokel and co-workers.[70,71] ^{1}H NMR studies revealed that bis-ferrocenyl amide **101** complexes *N*,*N*,*N*′,*N*′-tetramethyl-1,3-propanediamine, 1,4-diazabicyclo[2.2.2]octane (DABCO), and 3-propyladenine in $CDCl_3$ solution with $K_a = 341$, 604, and $1{,}270\,M^{-1}$, respectively, whereas **102** complexes 4-aminopyridine in THF-d^8 solution with $K_a = 3{,}200\,M^{-1}$. Electrochemical sensing was not reported.

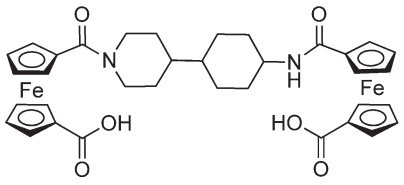

101

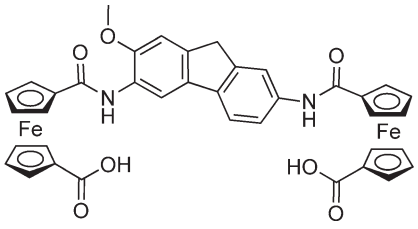

102

Tucker and co-workers have developed ferrocenyl receptors, which give an electrochemical response to neutral guest species.[72,73] The amidopyridine residues in **103** and **104** act as complementary two-point hydrogen-bonding sites for carboxylic acids, resulting in 1 : 1 and 1 : 2 receptor : guest binding in $CDCl_3$ solution for the mono- and 1,1′-ditopic receptors, respectively. Pentan-1,5-dioic acid is bound by **104** with 1 : 1 stoichiometry. In CH_2Cl_2 solution, the monoacids cause a small cathodic shift in the Fc/Fc^+ redox potential, 20–25 mV for **103** and 55–60 mV for **104**. The **104** : diacid complex shows a cathodic shift of 85 mV. That neutral guest species generate a cathodic shift indicates that the host–guest stability constant increases on oxidation, that is, the guest stabilizes the oxidized form of the receptor. This is consistent with the hydrogen bonding, increasing the electron density on the receptor.[72]

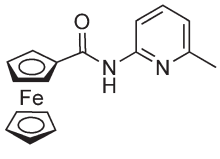

103

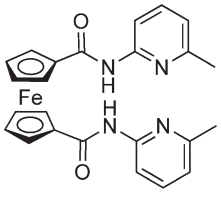

104

Molecule **104** has also been shown to bind the urea and barbiturate derivatives **105–107**. Stability constants in $CDCl_3$ and cathodic redox shifts in CH_2Cl_2 are presented in Table 2. It can be seen that the guest-induced redox shift is not directly related to the binding strength—ethyleneurea **105** gives the largest redox response, yet the **104** : **105** complex possesses the smallest stability constant. The analogous 1,3-ditopic receptor **108** provides similar selectivity to **103** for the trimethyleneurea **106**, but overall binding strength is increased. The additional hydrogen-bonding groups in **109** and **110** modify their selectivity such that they show enhanced affinity for barbital **107**. The 1,3-ditopic receptors however, where they show well-defined electrochemistry, only show small ($\leq$20 mV) cathodic shifts in redox potential with these guests. It is thought that the 1,1′ ferrocenes give a greater electrochemical response due to the guest species being bound between the two amidopyridine units close to the ferrocene center, whereas in the 1,3 systems the guest is held further away.[73]

Table 2 Cathodic shifts in potential of the Fc/Fc^+ redox couple of **104** and **108–110** induced by neutral guest species **105–107** and the stability constants of the host : guest complexes

		104	108	109	110
105	ΔE (mV)	60	–	–	–
	K_a (M^{-1})	60	250	–	–
106	ΔE (mV)	50	–	–	20
	K_a (M^{-1})	240	600	110	25
107	ΔE (mV)	35	15	–	–
	K_a (M^{-1})	200	195	3,200	2,150

Electrochemistry carried out in CH_2Cl_2 containing 0.1 M $TBAClO_4$. K_a values determined by ^1H NMR titrations in $CDCl_3$.

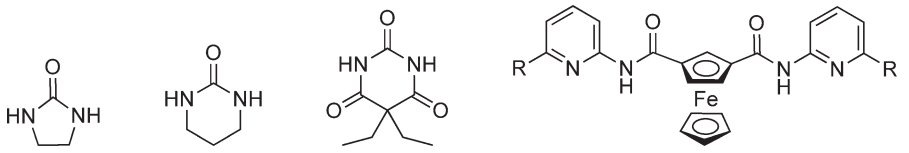

105 **106** **107**

108: R = CH_3
109: R = NH_2
110: R = HNCOEt

Inouye and co-workers have made significant progress developing organometallic receptors for sensing nucleobases.[74–78] 2,6-Diamidopyridine was selected as a complementary hydrogen-bonding site for the nucleobase 1-butylthymine and appended to one Cp ring of the ferrocenes **111–120** via an ether or ethynyl linker. The other Cp ring is functionalized with various planar aromatic groups to allow for potential π-stacking interactions to assist with guest binding. In this instance, the function of the organometallic group is to hold the hydrogen-bonding and aromatic stacking sites at the correct orientation and distance for guest binding.[73] ^{1}H NMR studies showed that the receptors bind 1-butylthymine in $CDCl_3$ solution with 1 : 1 stoichiometry and K_a values between 960 and 2,230 M^{-1} (Table 1). The series **111–115** possessing the flexible ether linkage shows increasing affinity for 1-butylthymine, whereas **116–120** exhibits a step change with **116–118**, exhibiting significantly lower stability constants than **119** and **120**. It is thought that this reflects the increased area of the aromatic group available for π-stacking (i.e., the surface area of the aromatic substituent projected beyond the diamidopyridine unit in the eclipsed conformation).

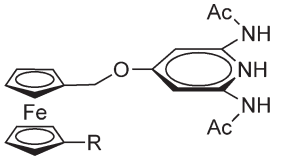

111–115

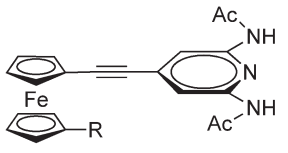

116–120

112: **117**: R =

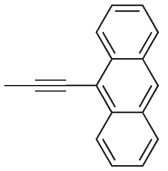

111: **116**: R = H

114: **119**: R =

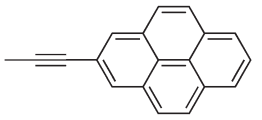

113: **118**: R =

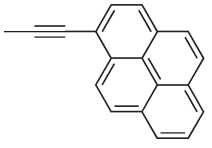

115: **120**: R =

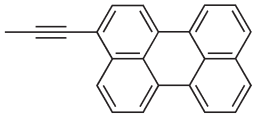

The analogous ditopic receptors **121** and **122** incorporate two ferrocenyl hydrogen bond donor units, which are attached to a pyrene ring at the 2- and 7-positions. As predicted, these bind 1-butylthymine in a 2 : 1 guest : host ratio with overall stability constants in $CDCl_3$ of 6.7×10^6 M^{-2} for **121** and 2.5×10^7 M^{-2} for **122**.[75] ^{1}H NMR evidence indicates additional π-stacking interactions compared to the monotopic receptors, and free energy calculations show a small degree of cooperativity between the two hydrogen-bonding sites.

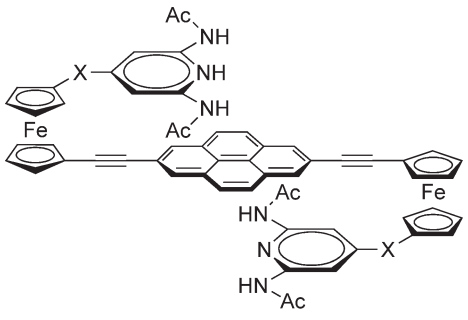

121: X = –CH_2O–
122: X = –CC–

Functionalization of ferrocene with two hydrogen-bonding groups generates receptors for dinucleosides, for instance, **123** binds thymidyl(3′-5′)thymidine in $CDCl_3$/DMSO-d_6 (85/15).[78] Incorporating the *spiro*-pryidopyran chromophore in between the ferrocene and hydrogen-bonding group provides colorimetric sensing of dinucleoside derivatives. Receptor **124** shows a dramatic increase in the absorption band at 575 nm in the presence of guanine–guanine derivative **125**, but no change was observed with analogous thymine–thymine and adenine–adenine guest species.[77]

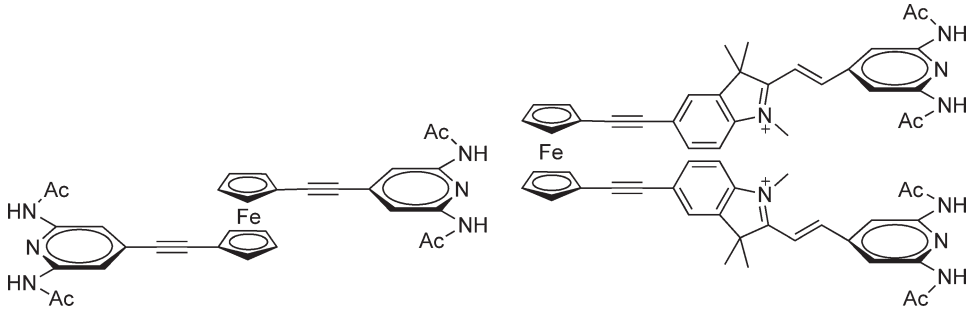

123 **124**

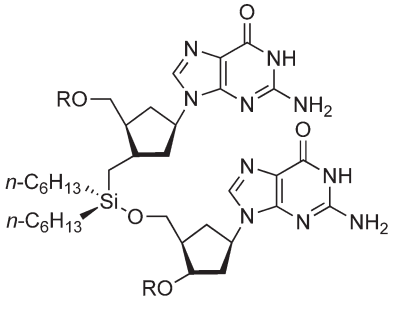

R = $OSiMe_2C(Me_2)Pr$-*i*

125

Detection of amino acids is an interesting challenge due to their multiple hydrogen-bonding sites and zwitterionic character. Ferrocene crown ether **126** is able to extract several L-amino acids into CH_2Cl_2 from acidic aqueous solution. Binding is presumed to occur ditopically via hydrogen bonding of the $–NH_3^+$ and $–CO_2H$ functions of the amino acid to the crown ether and carboxylic acid sites of the receptor, respectively.[79] The host : guest stiochiometry was found to be 1 : 1. In this example, circular dichroism (CD) spectroscopy was demonstrated as a useful probe for binding of chiral guest species. Complexation of L-amino acids by **126** resulted in the appearance of a "W-shaped" CD band around the absorption maximum of the ferrocene. Complexes of D-amino acids gave the symmetrical "M-shaped" spectra. These results indicate that the ditopic binding of the amino acids fixes the orientation of the ferrocene rings in an asymmetric fashion.

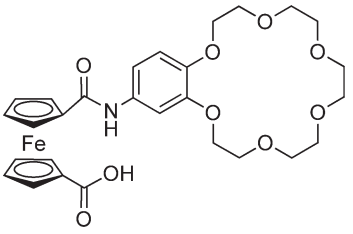

126

Roy and co-workers have recently described a ferrocene-based receptor for amino acids.[80] Strong 1 : 1 binding of **127** for amino acids in MeCN/H_2O (55/45) mixtures at pH = 7.2 was observed by UV/VIS, fluorescence, electrochemistry, isothermal calorimetry (ITC), and ^{13}C NMR. Glu and Asp, which exist in their anionic form at this pH, were found to have the greatest affinity for the receptor (K_a(**127** : Glu) = $98 \times 10^3\,M^{-1}$ and K_a(**127** : Asp) = $98 \times 10^3\,M^{-1}$, determined by UV/VIS titration). With Gln and Gly, which are zwitterionic, the stability constants are slightly lower, but within the same order of magnitude (K_a(**127** : Gln) = $68 \times 10^3\,M^{-1}$ and K_a(**127** : Gly) = $39 \times 10^3\,M^{-1}$). The highly conjugated receptor is fluorescent, and on addition of Glu, the emission maximum at 554 nm increases in intensity and shifts to 550 nm. The NMR results suggest that both the ester carbonyl groups and terminal hydroxyls are involved in guest recognition.

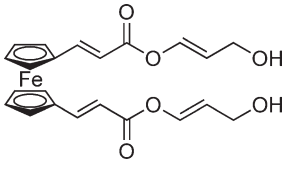

127

A ferrocenyl receptor for saccharides has also been demonstrated.[81] Electrochemical sensing of D-glucose, D-fructose, D-galactose, and D-mannose was accomplised using **128**, which teams ferrocene with a previously described diboronic acid diamine-binding unit. Anodic shifts in the Fc/Fc^+ redox couple were observed by differential pulse voltammetry on addition of saccharide. This is presumed to be due to the saccharide increasing the degree of interaction between neighboring amine and boron atoms, which in turn reduces the electron density on the amines, thereby destabilizing the oxidized form of the ferrocene.

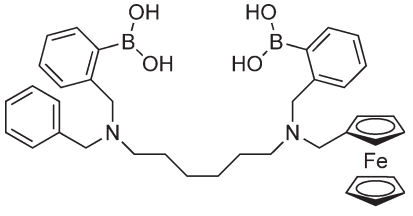

128

12.09.4.2 Other Receptors for Neutral Guest Species

Loeb and co-workers have reported a series of organometallic Pd macrocycles **129–133** capable of recognizing nucleobases.[82] Extraction experiments show that **133** is selective for cytosine in CD_3CN solution. Cytosine and adenine were bound by all the receptors in acetone-d_6 solution, whereas guanine was bound by all except **129**. None of the macrocycles possess any affinity for thymine. X-ray crystal structure analysis of the **131** : cytosine and **133** : guanine complexes shows that the nucleobases are coordinated to the receptor Pd through an aromatic nitrogen donor atom. Hydrogen bonding also occurs between the nucleobase NH_2 group and the macrocycle ether oxygen atoms. In the guanine complex π-stacking also occurs between the nucleobase and the aromatic spacer units of **133**.

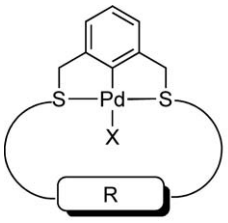

129: R = $(CH_2)_{11}$
130: R = $(CH_2)_2O(CH_2)_2$
131: R = $(CH_2)_2O(CH_2)_2O(CH_2)_2$
132: R = *p*-$CH_2(C_6H_4)O((CH_2)_2O)_3(C_6H_4)CH_2$
133: R = *m*-$CH_2(C_6H_4)O((CH_2)_2O)_3(C_6H_4)CH_2$
X = CH_3CN

Fish and co-workers have synthesized a series of trimetallic Cp^*Rh receptors supported by nucleobase, nucleoside, and nucleotide ligands.[83,84] Complexes **134–136** are not only stable in aqueous conditions, but have significant affinity for the zwitterionic form of some amino acids which occur at physiological pH. Most notable are hosts **135** and **136**, which according to ^1H NMR titration in D_2O–phosphate buffer at pH = 7 bind L-tryptophan with stability constants of 472 and 607 M^{-1}, respectively. In this example, guest recognition is driven by the hydrophobic effect. Indeed, amino acids without aromatic or long aliphatic side chains do not show appreciable binding to **134–136**. Thus, the role of the organometallic unit is to direct the self-assembly of a bowl-shaped hydrophobic cavity, which allows desolvation of one part of the guest, while the ionic amino acid group remains solvated.

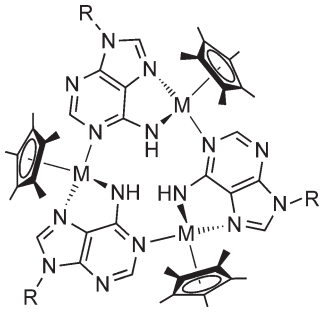

134: R = CH_3

135: R =

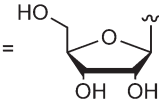

136: R =

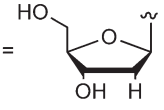

A similar dimetallic Cp^*Rh methylcytosine complex from the same research group **137** also binds aromatic amino acids in aqueous solution at pH = 7.[85] ^1H NMR studies suggest that selective hydrogen bonding occurs between the amino acid NH_3^+ and CO_2^- groups, the oxygen of the Rh(μ-OH) assemblies, and the carbonyl and amine functions of the methylcytosine ligands. No stability constants are reported.

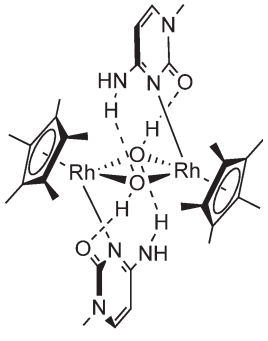

137

Lastly, Stang and co-workers have reported a series of chiral organometallic squares, **138–142**, based on the system **38–39**.[86] According to $^{31}P\{^1H\}$ NMR, IR, and CD evidence in CD_2Cl_2 or CH_2Cl_2 solution, the two precoordinated Ag^+ centers in these hexametallic supramolecular assemblies act as a binding site for linear bidentate nitrogen donor guests such as tetramethylpyrazine or phenazine. Binding is quantitative.

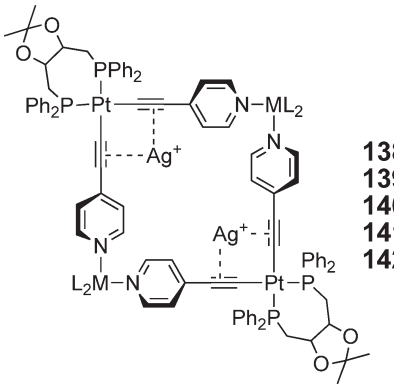

138: *R*-DIOP M = Pd; L_2 = PEt_3
139: *S*-DIOP M = Pd; L_2 = *R*-BINAP
140: *S*-DIOP M = Pd; L_2 = *S*-BINAP
141: *R*-DIOP M = Pt; L_2 = *R*-BINAP
142: *R*-DIOP M = Pt; L_2 = *S*-BINAP

12.09.5 Ion-Pair Receptors

Ditopic receptors capable of binding ion pairs are becoming the focus of considerable attention. One reason for this is that recognition of charged species by charge-neutral receptors is difficult to achieve due to ions of the opposite charge to the guest competing with the receptor in solution. Indeed, coordination of the competing counterion to the receptor, in addition to removing the competitor from solution, can lead to a considerable enhancement of the affinity of the receptor for the ion of opposite charge. Furthermore, charged species are not easily transported across biological membranes. This problem can be circumvented by a receptor that binds the cation or anion of interest as one of the partners in a charge-neutral ion pair.

Tucker and co-workers have recently reported a ferrocene ion-pair receptor which acts as a chromogenic molecular switch.[87] Appended to one cyclopentadienyl ring of the ferrocene of molecule **143** is a phenyl urea unit for anion binding and to the other a crown ether for cation binding. On addition of fluoride to a solution of **143** in CH_3CN, a significant perturbation of the UV/VIS spectrum was observed including the appearance of a new absorption at 472 nm. The stability constant for the 1 : 1 anion/receptor complex was determined as 9,340 M^{-1}. The addition of 10 equiv. of KPF_6 to the solution of **143** containing 10 equiv. of fluoride caused the complete disappearance of the 475 nm absorption. K_a of the receptor with K^+ in the presence of fluoride was calculated as 1,460 M^{-1}. It should be noted that the model receptor **144**, lacking the cation-binding site, exhibited similar switching properties. K_a of this receptor for fluoride is equivalent (9,660 M^{-1}) but the K_a for K^+ in the presence of fluoride was consequently far lower (230 M^{-1}). Inhibition by K^+ of the response of these receptors to fluoride is therefore thought to be due to the ion-pairing interaction between fluoride and K^+.

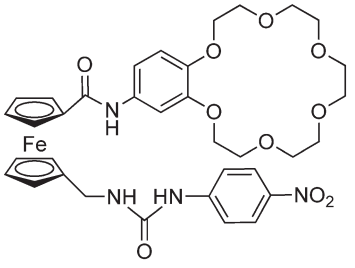

143

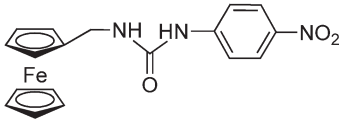

144

Recognition of ion-pair species can be achieved using a calix[4]arene tetraester functionalized with the Re(I) bipyridyl fragment.[88] The oxygen-rich lower rim of the macrocycle in **145** was designed to act as a cation-binding site. ^1H NMR titrations on **145** in CD_3CN were carried out with Br^- and I^- in the presence and absence of 1 equiv. of Li^+ or Na^+. The receptors show a preference for Br^- over I^- and significantly enhanced anion binding in the presence of the alkali metal, with up to a 60-fold enhancement in the stability constant for Br^- in the presence of Li^+. With I^-, the greatest enhancement is with co-bound Na^+, which correlates with the known selectivity preference of lower rim tetrasubstituted ethyl ester for this alkali metal.

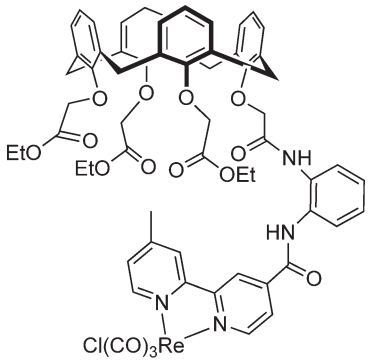

145

The Re(I) bipyridyl unit has been exploited in another series of ion-pair sensors. Molecules **146–149** incorporate crown ether components to act as cation receptors.[89,90] ^{1}H NMR titrations revealed **146–149** to be selective for $CH_3CO_2^-$ over Cl^- in CD_3CN/DMSO-d_6 (1/1) solution. This trend was also observed in fluoresence-emission titrations in CH_3CN/DMSO (95/5) solution, with anion binding, resulting in fluorescence enhancement. In all the receptors (except **147** and **149** with $CH_3CO_2^-$), stronger anion binding was observed in the presence of K^+ cations. The increase of binding strength is less in the xylyl-spaced molecules **147** and **149** (40–50%) than in **146** and **148** (80–110%). It is also relatively small compared to that seen in the calix[4]arene receptor **145**.

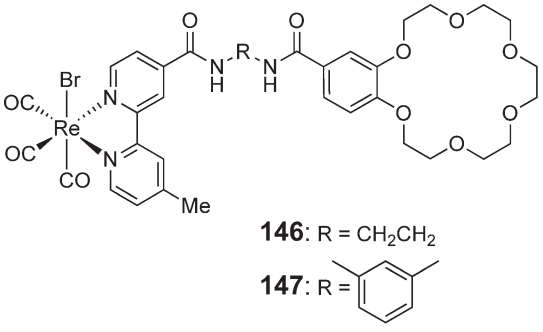

146: R = CH_2CH_2

147: R =

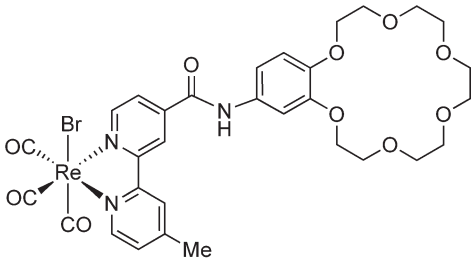

148

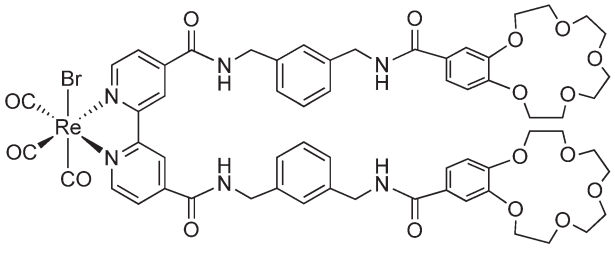

149

12.09.6 Nanoscale Receptors: Dendrimers, Organized Films, and Functionalized Nanoparticles

A recent significant advance in the development of organometallic receptors has been their incorporation onto nanostructured surfaces. Pre-organized groups of closely spaced receptors have the potential to give rise to advantageous effects such as inter-receptor cooperativity and guest desolvation, which cannot be obtained in the solution phase. Such methods of harnessing receptors in the solid state represents a potential route for the fabrication of robust sensing devices.

Ferrocene-functionalized dendrimers and gold nanoparticles, for instance, have been found to exhibit significantly enhanced binding of anions. Self-assembled monolayers of organometallic receptors on electrode surfaces similarly exhibit amplified anion binding. Organometallic dendrimers have also been used in SO_2 gas detection.

Work on thin polymer films of organometallic species has primarily been focused on anion sensing (presumably due to the positively charged nature of pyrrole electropolymers, the most commonly used type), although cation sensing by this method has also been demonstrated.

12.09.6.1 Dendrimers

Astruc and co-workers are pioneers in the field of organometallic dendrimers and have synthesized **150–152**, incorporating up to 18 amido–ferrocene units. Similarly, to simple ferrocene species, the dendrimers are able to electrochemically sense anions via a cathodic shift in the Fc/Fc^+ couple.[91] Evidence of a dendritic effect was observed in the redox response of the consecutive dendrimer generations in the presence $H_2PO_4^-$ or HSO_4^-. As the number of ferrocene units increases, so does the magnitude of the cathodic shift in the Fc/Fc^+ couple. The stability constants calculated for the HSO_4– complexes of generations **151** and **152** in CH_2Cl_2 solution are reported to be 9,390 and 216,900 M^{-1}, respectively.

Kaifer and co-workers have produced similar dendrimers (not shown) based on the DSM polyamine core with 4, 8, 16, and 32 peripheral ferrocenyl urea groups as the anion-sensing component.[92] No stability constants are reported, but cathodic shifts in the Fe^{2+}/Fe^{3+} couple with various anions in DMSO were observed. In this case, the data suggest two ferrocene urea arms bind a single $H_2PO_4^-$ anion. Changing from the first- (4 ferrocene units) to second- (8 ferrocene units) generation dendrimers resulted in an increased redox shift. No further increase in redox response was observed in the third-generation dendrimer, and the fourth-generation dendrimer showed a decreased magnitude of response, presumably due to steric crowding.

Astruc and co-workers have recently investigated five generations of pentamethyl–amidoferrocene dendrimers using the DSM polyamine core (not shown).[93] The pentamethyl-substituted ferrocene was chosen to overcome the irreversible electrochemistry and electrode adsorption occurring with **150–152**. In this series, the magnitude of the dendritic effect varied according to the anion studied. In changing from lower to higher dendrimer generations, modest increases in the anion-induced cathodic shift of the Fc/Fc^+ couple were observed with $H_2PO_4^-$ in DMF solution, whereas with ATP^{2-} anion binding progressed from weak to relatively strong. It is thought that this is a result of the anions binding with different stoichiometries, with ATP^{2-} forming a 1 : 2 anion : ferrocene complex and $H_2PO_4^-$ forming a 1 : 1 complex.

van Koten and co-workers have reported a series of aryl Pt(II) dendrimers for the colorimetric detection of $SO_{2(g)}$.[94–97] UV/VIS spectroscopic measurements on **153–155** in CH_2Cl_2 solution show the appearance of a characteristic absorption band ($\lambda_{max} = 350$ nm) on exposure to SO_2 at concentrations down to 0.1 mM. This color change is also observed in the solid material on exposure to $SO_{2(g)}$. Guest binding occurs by coordination of the SO_2 molecule to the Pt center, generating a trigonal-bipyramidal complex. ^1H NMR spectroscopy shows that each of the Pt sites in the dendrimer coordinates an SO_2 guest. In quartz crystal microbalance experiments spray-coated layers of **154** on quartz substrates were found to be sensitive to 5 ppm concentrations of SO_2 in N_2.[97]

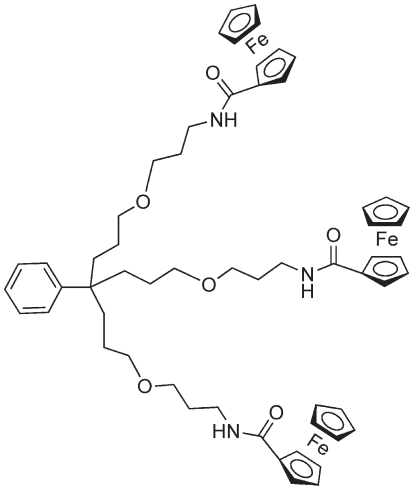

150

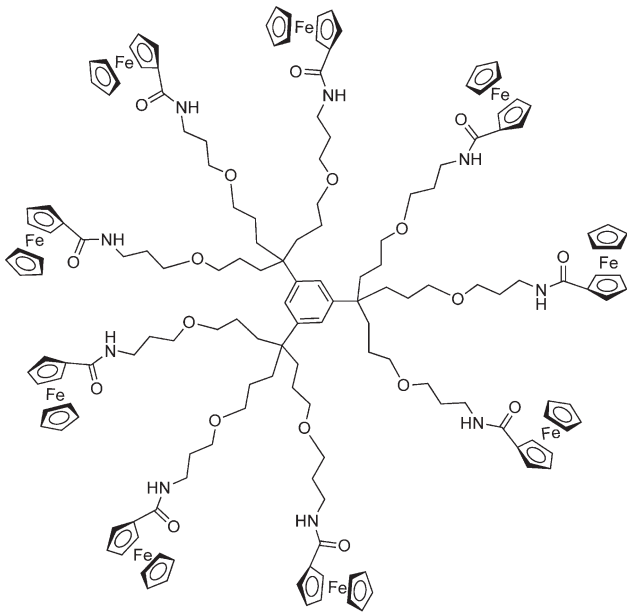

151

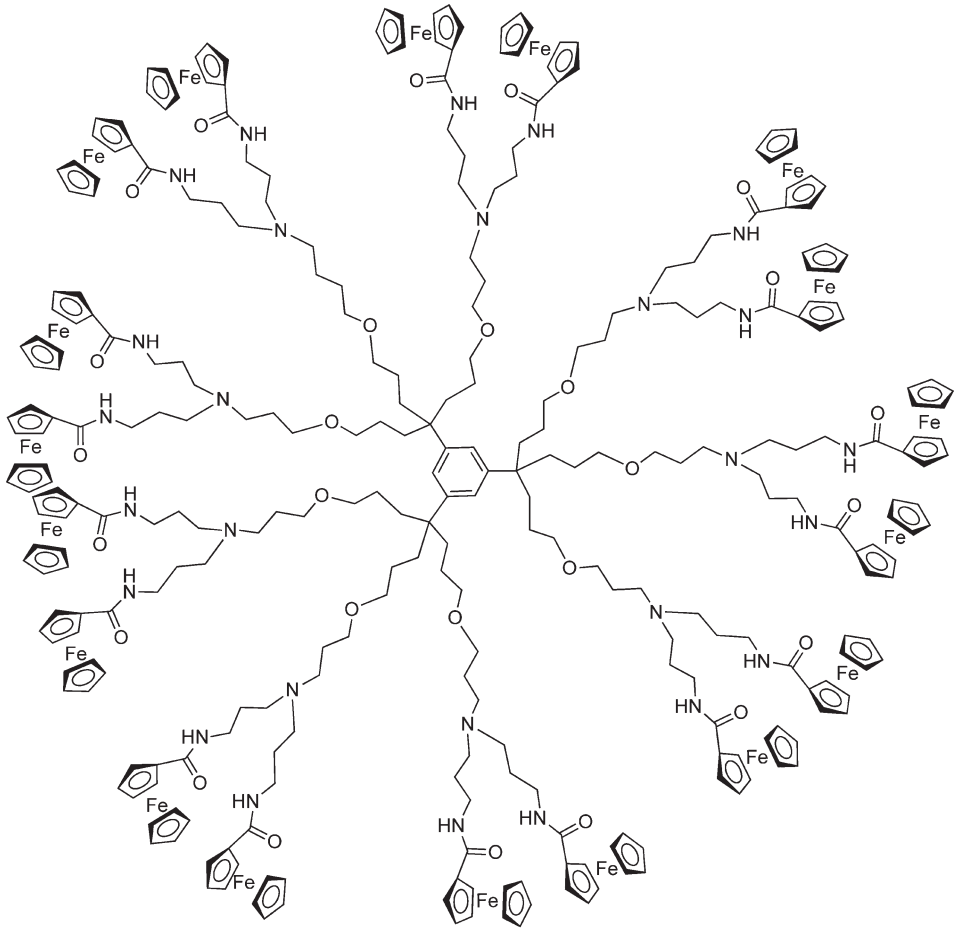

152

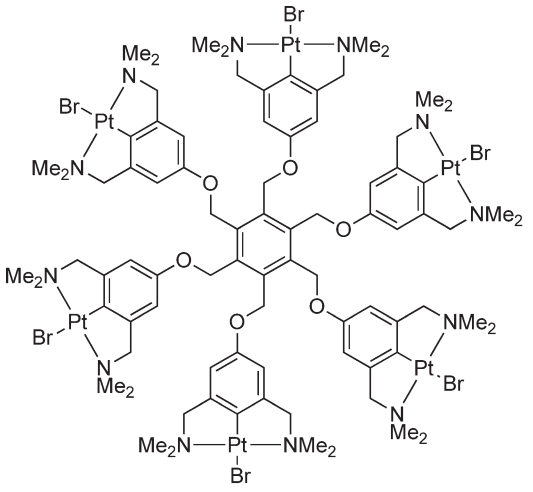

153

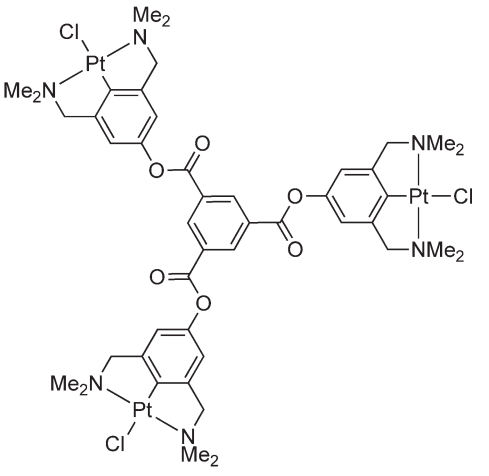

154

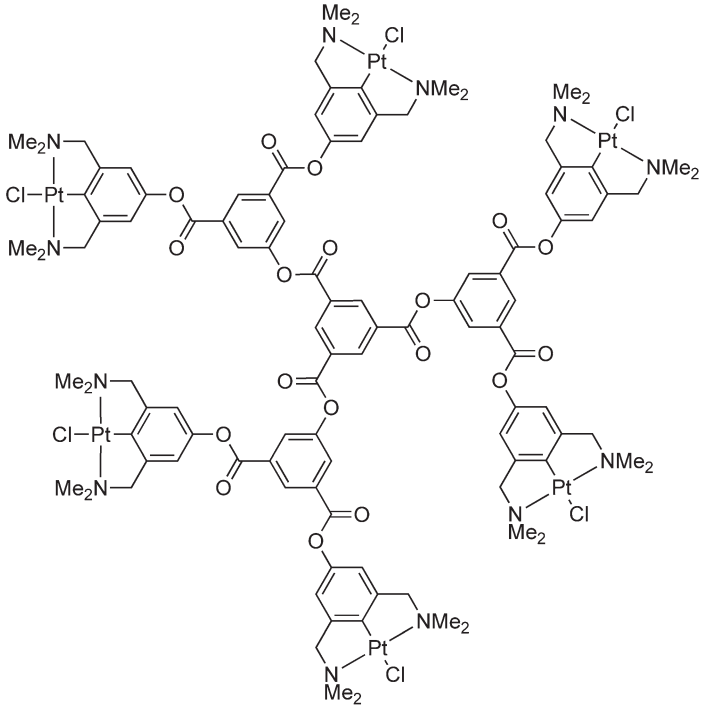

155

12.09.6.2 Thin Polymer Films and Self-assembled Monolayers

Beer and co-workers have investigated anion sensing using self-assembled monolayers (SAMs) of ferrocene amide disulfides. SAMs were formed of the 1,1′-bis(alkyl-*N*-amido)ferrocene **156** on gold electrodes.[98] The pendant disulfide groups serve to covalently anchor the receptor to the gold surface. In diffusive electrochemical experiments on **156** in CH_3CN/CH_2Cl_2 solution, anion-induced cathodic shifts of the Fc/Fc^+ redox couple were observed, with values of 40 mV for Cl^-, 20 mV for Br^-, and 210 mV for $H_2PO_4^-$. When confined to a monolayer, the anion-induced

shifts measured were 100 mV for Cl^-, 30 mV for Br^-, and 300 mV for $H_2PO_4^-$ in the same solvent system—consistently greater than for the solution-phase receptor. This represents a significant "surface-sensing amplification." The modified electrodes were also able to selectively detect $H_2PO_4^-$ in the presence of a 100-fold excess of halide. In aqueous solution, the selectivity of the system was altered, enabling the detection of the poorly hydrated anion ReO_4^- in the presence of $H_2PO_4^-$.

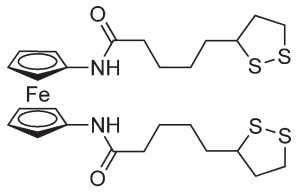

156

A number of groups have been exploring the anion sensing of thin polymer films, which incorporate organometallic receptors. Monomer **157** incorporates a cobaltocenium amide reporter with a polymerizable pyrrole unit. Thin films of the receptor were prepared by electropolymerization on a platinum or carbon electrode.[99] In CH_3CN solution, anion-induced cathodic shifts in the $[Cp_2Co]/[Cp_2Co]^+$ redox couple of the monomer were observed, with values of 45 and 20 mV for $H_2PO_4^-$ and HSO_4^-, respectively. When confined to a polymer film the anion-induced shifts measured were 210 mV for $H_2PO_4^-$ and 250 mV for HSO_4^-. Cl^- and Br^- could also be detected, both giving shifts of 20 mV. Polymerization of **157** as well as giving rise to surface-sensing amplification also results in a change in selectivity from $H_2PO_4^-$ to HSO_4^-. It was also found that film thickness influences the sensitivity of the sensor. Thin films ($\Gamma = 1.8 \times 10^{-9}$ mol cm^{-2}) exhibit higher sensitivity to $H_2PO_4^-$ at low concentrations (<50 μM), whereas thick films ($\Gamma = 2.7 \times 10^{-8}$ mol cm^{-2}) extend the measurable concentration range to higher concentrations (up to 2 mM).

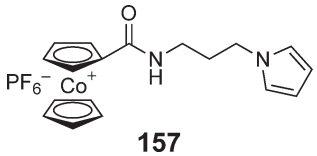

157

Films of the analogous ferrocene monomer **158** have been examined by Moutet and co-workers.[100] Anion-induced shifts of the Fc/Fc^+ couple were measured in CH_3CN for giving values of 30, 180, and 220 mV for HSO_4^-, ATP^{2-}, and $H_2PO_4^-$, respectively. Again this represents a surface-sensing amplification. The anion-sensing properties of viologen **159** in thin polymer films have also been recently explored.[101] Poly-**159** registered small anion-induced cathodic shifts of the Fe^{2+}/Fe^{3+} couple of up to 35 mV for ATP^{2-} in aqueous solution.

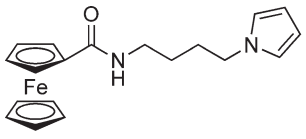

158

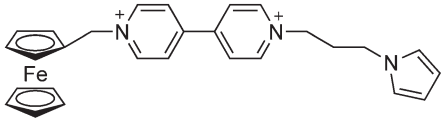

159

Cation sensing can also be accomplished using thin polymer films.[102] Moutet and co-workers have electropolymerized **160** onto Pt electrodes. The resulting films show a 120 mV cathodic shift in redox potential in the presence of Ba^{2+} ions in MeCN solution.

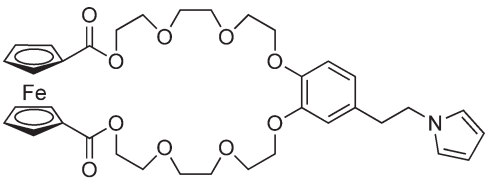

160

12.09.6.3 Functionalized Nanoparticles

Astruc and co-workers have prepared the amidoferrocenylalkylthiol (AFAT)–gold nanoparticle system depicted as **161**. The proportion of AFAT to dodecanethiol obtained by ligand substitution of dodecanethiol-stabilized nanoparticles ranged from 7% to 38%, corresponding to an average of 8–39 AFAT units per nanoparticle. In CH_2Cl_2 solution, the ferrocene-functionalized nanoparticles show a single reversible redox wave for the Fe^{2+}/Fe^{3+} couple at identical potential irrespective of surface loading. Addition of $H_2PO_4^-$ generated a cathodic shift in the redox potential of 220 mV. The magnitude of the shift was found to be the same irrespective of surface loading and is considerably larger than observed the comparable amidoferrocene monomer $FcCONHCH_2CH_2OPh$ (45 mV) or even a representative ferrocene tripod $PhC(CH_2CH_2CH_2NHCOFc)_3$ (110 mV).

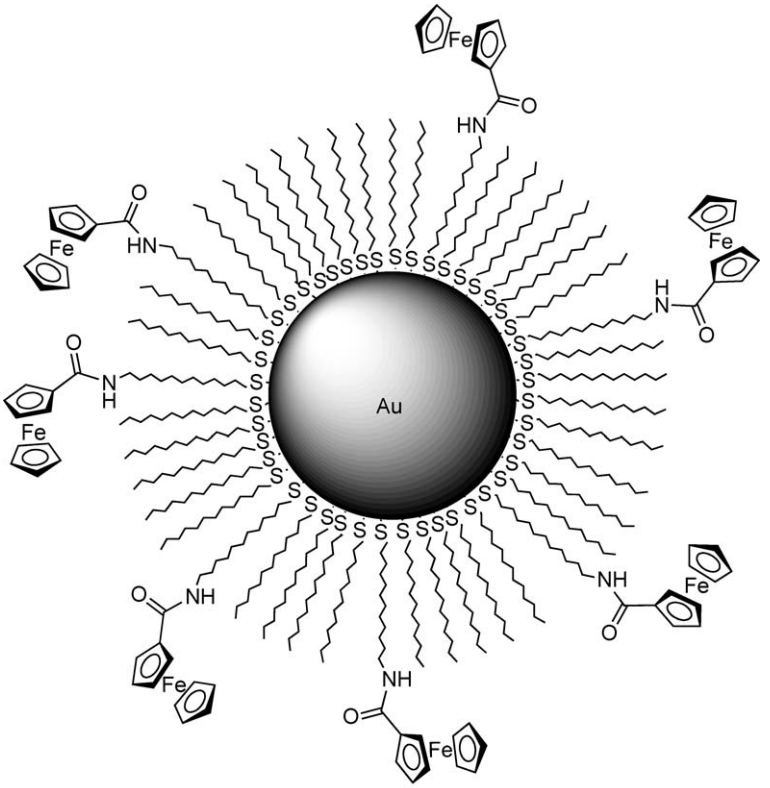

161

The same group has also investigated the anion-sensing properties of gold nanoparticles **162** and **163** substituted with dendrons comprising three amidoferrocene or silyl ferrocene branches.[103] The surface loadings of **162** and **163** were 3% and 4.8%, respectively, corresponding to an average three and five dendrons per nanoparticle. Nanoparticles of type **162** show very similar properties to the AFAT-modified nanoparticles **161**, with a $H_2PO_4^-$-induced cathodic shift of 210 mV in CH_2Cl_2 solution. Despite lacking any hydrogen-bonding groups, the nanoparticles dendronized with silyl ferrocenes, **163**, gave an $H_2PO_4^-$-induced cathodic shift of 110 mV in the same solvent.

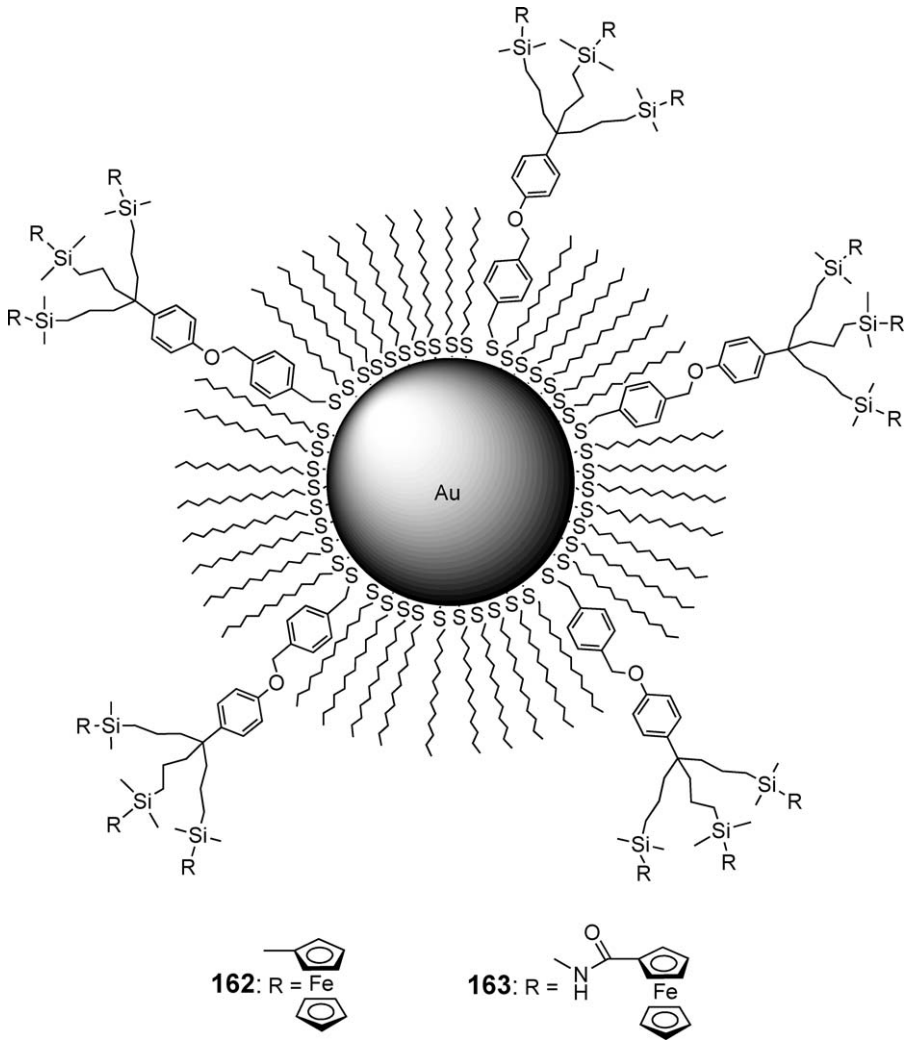

12.09.7 Conclusion

Organometallic receptors continue to play a fundamental part in molecular-sensing chemistry. The useful physicochemical properties of organometallic moieties are driving their increased use as multifunctional components in receptors for all types of guest species. They are able to combine roles such as reporter groups, binding sites, and structural components in ways which cannot be achieved solely by organic structures. Cation coordination is a well-established subject, and consequently the majority of work on organometallic receptors has been in this field. Anion recognition has been less studied, but accelerating progress in this area means that organometallic anion receptors are becoming equally advanced. Harnessing the weak non-covalent interactions required for recognition of neutral guest species is an even more difficult challenge and has relatively recently come to the attention of organometallic chemists. Ion-pair coordination has also seen comparatively little activity. Nevertheless, great strides are being made in the design of organometallic receptors for these two types of guest species, and the subject is certain to generate a great deal of interest in the future.

A significant recent advance has been the incorporation of organometallic receptors into nanostructures such as dendrimers, nanoparticles, thin polymer films, and self-assembled monolayers. The origin and development of the anion "surface-sensing amplification" observed in these preorganized systems is currently a topic receiving significant attention. The development of complex nanoscale systems such as these is already emerging as an important area of chemistry.

References

1. Atwood, J. L., Ed. *Inclusion Phenomena and Molecular Recognition*; Plenum: London, 1990.
2. Coleman, A. W., Ed. *Molecular Recognition and Inclusion, Proceedings of the Ninth International Symposium on Molecular Recognition and Inclusion*; Kluwer: London, 1998.
3. Schrader, T.; Hamilton, A. D.; Eds.; *Functional Synthetic Receptors*; Wiley-VCH: Weinheim, 2005.
4. Beer, P. D.; Cadman, J. *Coord. Chem. Rev.* **2000**, *205*, 131–155.
5. Beer, P. D.; Hayes, E. J. *Coord. Chem. Rev.* **2003**, *240*, 167–189.
6. Sun, S.-S.; Lees, A. J. *Coord. Chem. Rev.* **2002**, *230*, 171–192.
7. Bayly, S. R.; Beer, P. D. Anion Sensing by Metal-Based Receptors. In *Anion Sensing*; Stibor, I., Ed. Topics in Current Chemistry 255, Springer: Berlin, London, 2005; pp 125–162.
8. Saji, T.; Kinoshita, I. *J. Chem. Soc., Chem. Commun.* **1986**, 716–717.
9. Saji, T. *Chem. Lett.* **1986**, 275–276.
10. Beer, P. D. *J. Chem. Soc., Chem. Commun.* **1985**, 1115–1116.
11. Beer, P. D.; Crane, C. G.; Keefe, A. D.; Whyman, A. R. *J. Organomet. Chem.* **1986**, *314*, C9–C11.
12. Beer, P. D.; Sikanyika, H.; Slawin, A. M. Z.; Williams, D. J. *Polyhedron* **1989**, *8*, 879–886.
13. Beer, P. D.; Sikanyika, H.; Blackburn, C.; McAleer, J. F.; Drew, M. G. B. *J. Organomet. Chem.* **1988**, *356*, C19–C22.
14. Beer, P. D.; Sikanyika, H.; Blackburn, C.; McAleer, J. F. *J. Chem. Soc., Chem. Commun.* **1989**, 1831–1833.
15. Chen, Z.; Pilgrim, A. J.; Beer, P. D. *J. Chem. Soc., Faraday Trans.* **1995**, *91*, 4331–4333.
16. Chen, Z.; Pilgrim, A. J.; Beer, P. D. *J. Electroanal. Chem.* **1998**, *444*, 209–217.
17. Lloris, J. M.; Martinez-Manez, R.; Pardo, T.; Soto, J.; Padilla-Tosta, M. E. *Chem. Commun.* **1998**, 837–838.
18. Beer, P. D.; Crowe, D. B.; Ogden, M. I.; Drew, M. G. B.; Main, B. *J. Chem. Soc., Dalton Trans.* **1993**, 2107–2116.
19. Hall, C. D.; Sharpe, N. W.; Danks, I. P.; Sang, Y. P. *J. Chem. Soc., Chem. Commun.* **1989**, 419–421.
20. Plenio, H.; Aberle, C. *Organometallics* **1997**, *16*, 5950–5957.
21. Chesney, A.; Bryce, M. R.; Batsanov, A. S.; Howard, J. A. K.; Goldenberg, L. M. *Chem. Commun.* **1998**, 677–678.
22. Beer, P. D.; Smith, D. K. *J. Chem. Soc., Dalton Trans.* **1998**, 417–423.
23. Tendero, M. J. L.; Benito, A.; Martinez-Manez, R.; Soto, J.; Paya, J.; Edwards, A. J.; Raithby, P. R. *J. Chem. Soc., Dalton Trans.* **1996**, 343–351.
24. Benito, A.; Martinez-Manez, R.; Soto, J.; Tendero, M. J. L. *J. Chem. Soc., Faraday Trans.* **1997**, *93*, 2175–2180.
25. Padilla-Tosta, M. E.; Martinez-Manez, R.; Pardo, T.; Soto, J.; Tendero, M. J. L. *Chem. Commun.* **1997**, 887–888.
26. Plenio, H.; Burth, D. *Organometallics* **1996**, *15*, 4054–4062.
27. Lopez, J. L.; Tarraga, A.; Espinosa, A.; Velasco, M. D.; Molina, P.; Lloveras, V.; Vidal-Gancedo, J.; Rovira, C.; Veciana, J., Evans, D. J., *et al. Chem. Eur. J.* **2004**, *10*, 1815–1826.
28. Tarraga, A.; Molina, P.; Lopez, J. L.; Velasco, M. D. *Dalton Trans.* **2004**, 1159–1165.
29. Maynadie, J.; Delavaux-Nicot, B.; Fery-Forgues, S.; Lavabre, D.; Mathieu, R. *Inorg. Chem.* **2002**, *41*, 5002–5004.
30. Caballero, A.; Tormos, R.; Espinosa, A.; Velasco, M. D.; Tarraga, A.; Miranda, M. A.; Molina, P. *Org. Lett.* **2004**, *6*, 4599–4602.
31. Caballero, A.; Lloveras, V.; Tarraga, A.; Espinosa, A.; Velasco, M. D.; Vidal-Gancedo, J.; Rovira, C.; Wurst, K.; Molina, P.; Veciana, J. *Angew. Chem., Int. Ed.* **2005**, *44*, 1977–1981.
32. Whiteford, J. A.; Lu, C. V.; Stang, P. J. *J. Am. Chem. Soc.* **1997**, *119*, 2524–2533.
33. Siu, P. K. M.; Lai, S.-W.; Lu, W.; Zhu, N.; Che, C.-M. *Eur. J. Inorg. Chem.* **2003**, 2749–2752.
34. Resendiz, M. J. E.; Noveron, J. C.; Disteldorf, H.; Fischer, S.; Stang, P. J. *Org. Lett.* **2004**, *6*, 651–653.
35. Yam, V. W.-W.; Cheung, K.-L.; Yuan, L.-H.; Wong, K. M.-C.; Cheung, K.-K. *Chem. Commun.* **2000**, 1513–1514.
36. Lu, X.-X.; Li, C.-K.; Cheng, E. C.-C.; Zhu, N.; Yam, V. W.-W. *Inorg. Chem.* **2004**, *43*, 2225–2227.
37. Piotrowski, H.; Hilt, G.; Schulz, A.; Mayer, P.; Polborn, K.; Severin, K. *Chem. Eur. J.* **2001**, *7*, 3196–3208.
38. Severin, K. *Coord. Chem. Rev.* **2003**, *245*, 3–10.
39. Beer, P. D.; Keefe, A. D. *J. Organomet. Chem.* **1989**, *375*, C40–C42.
40. Beer, P. D. *Chem. Commun.* **1996**, 689–696.
41. Beer, P. D.; Hesek, D.; Kingston, J. E.; Smith, D. K.; Stokes, S. E.; Drew, M. G. B. *Organometallics* **1995**, *14*, 3288–3295.
42. Beer, P. D.; Drew, M. G. B.; Hesek, D.; Jagessar, R. *J. Chem. Soc., Chem. Commun.* **1995**, 1187–1189.
43. Beer, P. D.; Hesek, D.; Nam, K. C.; Drew, M. G. B. *Organometallics* **1999**, *18*, 3933–3943.
44. Beer, P. D.; Stokes, S. E. *Polyhedron* **1995**, *14*, 873–879.
45. Beer, P. D.; Szemes, F.; Balzani, V.; Sala, C. M.; Drew, M. G. B.; Dent, S. W.; Maestri, M. *J. Am. Chem. Soc.* **1997**, *119*, 11864–11875.
46. Beer, P. D.; Graydon, A. R.; Johnson, A. O. M.; Smith, D. K. *Inorg. Chem.* **1997**, *36*, 2112–2118.
47. Beer, P. D.; Chen, Z.; Goulden, A. J.; Graydon, A.; Stokes, S. E.; Wear, T. *J. Chem. Soc., Chem. Commun.* **1993**, 1834–1836.
48. Thomas, J.-L.; Howarth, J.; Hanlon, K.; McGuirk, D. *Tetrahedron Lett.* **2000**, *41*, 413–416.
49. Gale, P. A.; Hursthouse, M. B.; Light, M. E.; Sessler, J. L.; Warriner, C. N.; Zimmerman, R. S. *Tetrahedron Lett.* **2001**, *42*, 6759–6762.
50. Abouderbala, L. O.; Belcher, W. J.; Boutelle, M. G.; Cragg, P. J.; Dhaliwal, J.; Fabre, M.; Steed, J. W.; Turner, D. R.; Wallace, K. J. *Chem. Commun.* **2002**, 358–359.
51. Reynes, O.; Maillard, F.; Moutet, J.-C.; Royal, G.; Saint-Aman, E.; Stanciu, G.; Dutasta, J.-P.; Gosse, I.; Mulatier, J.-C. *J. Organomet. Chem.* **2001**, *637–639*, 356–363.
52. Tomapatanaget, B.; Tuntulani, T.; Chailapakul, O. *Org. Lett.* **2003**, *5*, 1539–1542.
53. Beer, P. D.; Drew, M. G. B.; Jagessar, R. *J. Chem. Soc., Dalton Trans.* **1997**, 881–886.
54. Beer, P. D.; Chen, Z.; Drew, M. G. B.; Kingston, J.; Ogden, M.; Spencer, P. *J. Chem. Soc., Chem. Commun.* **1993**, 1046–1048.
55. Beer, P. D.; Chen, Z.; Drew, M. G. B.; Johnson, A. O. M.; Smith, D. K.; Spencer, P. *Inorg. Chim. Acta* **1996**, *246*, 143–150.
56. Beer, P. D.; Cadman, J.; Lloris, J. M.; Martinez-Manez, R.; Padilla, M. E.; Pardo, T.; Smith, D. K.; Soto, J. *J. Chem. Soc., Dalton Trans.* **1999**, 127–134.
57. Dusemund, C.; Sandanayake, K. R. A. S.; Shinkai, S. *J. Chem. Soc., Chem. Commun.* **1995**, 333–334.
58. Aldridge, S.; Bresner, C.; Fallis, I. A.; Coles, S. J.; Hursthouse, M. B. *Chem. Commun.* **2002**, 740–741.
59. Kingston, J. E.; Ashford, L.; Beer, P. D.; Drew, M. G. B. *J. Chem. Soc., Dalton Trans.* **1999**, 251–258.
60. Altmann, R.; Gausset, O.; Horn, D.; Jurkschat, K.; Schuermann, M.; Fontani, M.; Zanello, P. *Organometallics* **2000**, *19*, 430–443.

61. Beer, P. D.; Dickson, C. A. P.; Fletcher, N.; Goulden, A. J.; Grieve, A.; Hodacova, J.; Wear, T. *J. Chem. Soc., Chem. Commun.* **1993**, 828–830.
62. Travis, H. K.; William, O. G.; Atwood, J. L.; Steed, J. W. *Chem. Commun.* **1998**, 2109–2110.
63. Staffilani, M.; Hancock, K. S. B.; Steed, J. W.; Holman, K. T.; Atwood, J. L.; Juneja, R. K.; Burkhalter, R. S. *J. Am. Chem. Soc.* **1997**, *119*, 6324–6335.
64. Camiolo, S.; Coles, S. J.; Gale, P. A.; Hursthouse, M. B.; Mayer, T. A.; Paver, M. A. *Chem. Commun.* **2000**, 275–276.
65. Beer, P. D.; Timoshenko, V.; Maestri, M.; Passaniti, P.; Balzani, V. *Chem. Commun.* **1999**, 1755–1756.
66. Slone, R. V.; Yoon, D. I.; Calhoun, R. M.; Hupp, J. T. *J. Am. Chem. Soc.* **1995**, *117*, 11813–11814.
67. Sun, S.-S.; Anspach, J. A.; Lees, A. J.; Zavalij, P. Y. *Organometallics* **2002**, *21*, 685–693.
68. Sun, S.-S.; Lees, A. J.; Zavalij, P. Y. *Inorg. Chem.* **2003**, *42*, 3445–3453.
69. Curiel, D.; Beer, P. D. *Chem. Commun.* **2005**, 1909–1911.
70. Medina, J. C.; Li, C.; Bott, S. G.; Atwood, J. L.; Gokel, G. W. *J. Am. Chem. Soc.* **1991**, *113*, 366–367.
71. Li, C.; Medina, J. C.; Maguire, G. E. M.; Abel, E.; Atwood, J. L.; Gokel, G. W. *J. Am. Chem. Soc.* **1997**, *119*, 1609–1618.
72. Carr, J. D.; Lambert, L.; Hibbs, D. E.; Hursthouse, M. B.; Malik, K. M. A.; Tucker, J. H. R. *Chem. Commun.* **1997**, 1649--1650.
73. Westwood, J.; Coles, S. J.; Collinson, S. R.; Gasser, G.; Green, S. J.; Hursthouse, M. B.; Light, M. E.; Tucker, J. H. R. *Organometallics* **2004**, *23*, 946–951.
74. Inouye, M.; Hyodo, Y.; Nakazumi, H. *J. Org. Chem.* **1999**, *64*, 2704–2710.
75. Inouye, M.; Itoh, M.-A. S.; Nakazumi, H. *J. Org. Chem.* **1999**, *64*, 9393–9398.
76. Inouye, M.; Takase, M. *Angew. Chem., Int. Ed.* **2001**, *40*, 1746–1748.
77. Takase, M.; Inouye, M. *Chem. Commun.* **2001**, 2432–2433.
78. Takase, M.; Inouye, M. *J. Org. Chem.* **2003**, *68*, 1134–1137.
79. Tsukube, H.; Fukui, H.; Shinoda, S. *Tetrahedron Lett.* **2001**, *42*, 7583–7585.
80. Debroy, P.; Banerjee, M.; Prasad, M.; Moulik, S. P.; Roy, S. *Org. Lett.* **2005**, *7*, 403–406.
81. Arimori, S.; Ushiroda, S.; Peter, L. M.; Jenkins, A. T. A.; James, T. D. *Chem. Commun.* **2002**, 2368–2369.
82. Kickham, J. E.; Loeb, S. J.; Murphy, S. L. *J. Am. Chem. Soc.* **1993**, *115*, 7031–7032.
83. Chen, H.; Maestre, M. F.; Fish, R. H. *J. Am. Chem. Soc.* **1995**, *117*, 3631–3632.
84. Chen, H.; Ogo, S.; Fish, R. H. *J. Am. Chem. Soc.* **1996**, *118*, 4993–5001.
85. Elduque, A.; Carmona, D.; Oro, L. A.; Eisenstein, M.; Fish, R. H. *J. Organomet. Chem.* **2003**, *668*, 123–127.
86. Mueller, C.; Whiteford, J. A.; Stang, P. J. *J. Am. Chem. Soc.* **1998**, *120*, 9827–9837.
87. Miyaji, H.; Collinson, S. R.; Prokes, I.; Tucker, J. H. R. *Chem. Commun.* **2003**, 64–65.
88. Cooper, J. B.; Drew, M. G. B.; Beer, P. D. *J. Chem. Soc., Dalton Trans.* **2001**, 392–401.
89. Redman, J. E.; Beer, P. D.; Dent, S. W.; Drew, M. G. B. *Chem. Commun.* **1998**, 231–232.
90. Uppadine, L. H.; Redman, J. E.; Dent, S. W.; Drew, M. G. B.; Beer, P. D. *Inorg. Chem.* **2001**, *40*, 2860–2869.
91. Valerio, C.; Fillaut, J.-L.; Ruiz, J.; Guittard, J.; Blais, J.-C.; Astruc, D. *J. Am. Chem. Soc.* **1997**, *119*, 2588–2589.
92. Alonso, B.; Casado, C. M.; Cuadrado, I.; Moran, M.; Kaifer, A. E. *Chem. Commun.* **2002**, 1778–1779.
93. Daniel, M.-C.; Ruiz, J.; Blais, J.-C.; Daro, N.; Astruc, D. *Chem. Eur. J.* **2003**, *9*, 4371–4379.
94. Albrecht, M.; Van Koten, G. *Adv. Mater. (Weinheim, Germany)* **1999**, *11*, 171–174.
95. Albrecht, M.; Gossage, R. A.; Lutz, M.; Spek, A. L.; van Koten, G. *Chem. Eur. J.* **2000**, *6*, 1431–1445.
96. Albrecht, M.; Hovestad, N. J.; Boersma, J.; van Koten, G. *Chem. Eur. J.* **2001**, 7, 1289–1294.
97. Albrecht, M.; Schlupp, M.; Bargon, J.; van Koten, G. *Chem. Commun.* **2001**, 1874–1875.
98. Beer, P. D.; Davis, J. J.; Drillsma-Milgrom, D. A.; Szemes, F. *Chem. Commun.* **2002**, 1716–1717.
99. del Peso, I.; Alonso, B.; Lobete, F.; Casado, C. M.; Cuadrado, I.; Losada del, B. J. *Inorg. Chem. Commun.* **2002**, *5*, 288–291.
100. Reynes, O.; Gulon, T.; Moutet, J.-C.; Royal, G.; Saint-Aman, E. *J. Organomet. Chem.* **2002**, *656*, 116–119.
101. Reynes, O.; Bucher, C.; Moutet, J.-C.; Royal, G.; Saint-Aman, E. *Chem. Commun.* **2004**, 428–429.
102. Ion, A.; Ion, I.; Moutet, J. C.; Pailleret, A.; Popescu, A.; Saint-Aman, E.; Ungureanu, E.; Siebert, E.; Ziessel, R. *Sensor. Actuator., B* **1999**, *B59*, 118–122.
103. Labande, A.; Astruc, D. *Chem. Commun.* **2000**, 1007–1008.

12.10
Surface Organometallic Chemistry

J-M Basset, J-P Candy, and C Copéret, CNRS/CPE, Villeurbanne, France

12.10.1 Introduction

Surface organometallic chemistry has the goal of understanding at a molecular level the reactions of organometallic complexes with surfaces by transferring the tools and the concepts of molecular chemistry to surface science. The aim is to bring the approach of the structure–reactivity relationship to heterogeneous catalysis in order to design and develop better catalytic systems. There are two important classes of heterogeneous catalysts based on single-atom active sites dispersed either on oxide supports or on metal particles. We have, therefore, reviewed the chemistry of organometallic reagents with the two types of surfaces, oxide supports (Section 2) and metal particles (Section 3). The catalytic properties of these systems are also discussed.

12.10.2 Surface Organometallic Chemistry on Oxide Materials

12.10.2.1 Generalities

In this section, we will examine the reactivity of organometallic and metalloorganic reagents with oxide supports.[1–8] The organometallic reagent will react with the reactive groups on the surface of oxide supports, in most cases hydroxyls (Scheme 1). In some cases, the surface also contains Lewis acid centers or nucleophilic oxygen atoms, which can be involved in the grafting process. Oxide supports are therefore briefly discussed. Metal carbonyls and clusters have not been included, because they have already been discussed extensively elsewhere.[9–11] Moreover, we have also restricted our review to amorphous oxide supports.[12–14] In some cases, the stoichiometric and catalytic properties of these supported systems will be discussed briefly to illustrate the differences and the similarities of these systems compared to their homogeneous and heterogeneous equivalents.

12.10.2.2 Oxide Supports

The main focus of this overview will be the reactivity of organometallic reagents with oxide supports, mainly silica, alumina, and silica alumina. Before discussing the reactivity, it is necessary to briefly describe these supports. An oxide support, E_xO_y, can be described as a network consisting of oxygen (O) and heteroelements (E) (Scheme 2), and the surface functionalities are, therefore, E–O–E bridges and hydroxyls groups (HO–E).[15] All these solids are usually submitted to a thermal treated under vacuum, the temperature T and surface atoms are described as $E_xO_{y-(T)}$ and E_s, respectively.

In the case of silica, the surface is therefore constituted by siloxane bridges of different sizes (12-, 10-, 8-, 6-, and 4-membered rings), and silanols of different types (isolated, vicinal, and geminal silanols).[16,17] Their proportion depends on the temperature of dehydroxylation. At low temperatures of dehydroxylation (ca. 200 °C), vicinal, geminal silanols, and large-size siloxane bridges are the main components. As the temperature of dehydroxylation rises, there is a condensation of vicinal silanols to give siloxane bridges and H_2O, gem silanols disappear, and the proportion of isolated silanols increases. Concomitantly, strained siloxane bridges appear and the surface area of silica decreases. Typically, an amorphous silica ($200\,m^2\,g^{-1}$) dehydroxylated at 200, 500, 700, and 1,000 °C contains around 0.86, 0.46, 0.26, and 0.1 mmol OH g^{-1}, respectively. At 1,000 °C, there is also about 0.04 strained siloxane bridges/g of silica. Note that in the case of mesoporous silica materials, it is important to check the stability of the network. Typically, MCM materials are much less robust (ca. 300–400 °C) than the corresponding SBA-15 materials (600 °C).

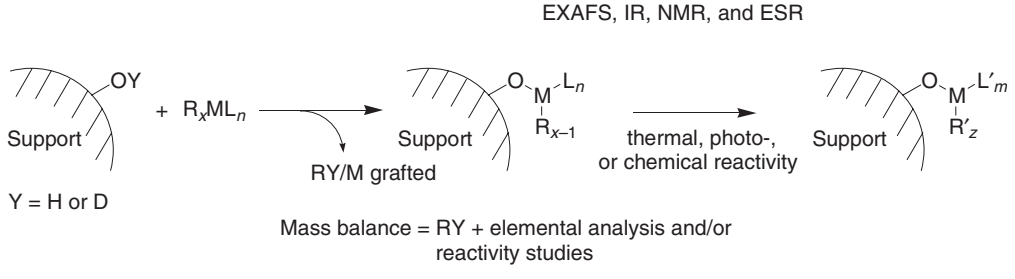

Scheme 1 General strategy to understand structures of surface complexes.

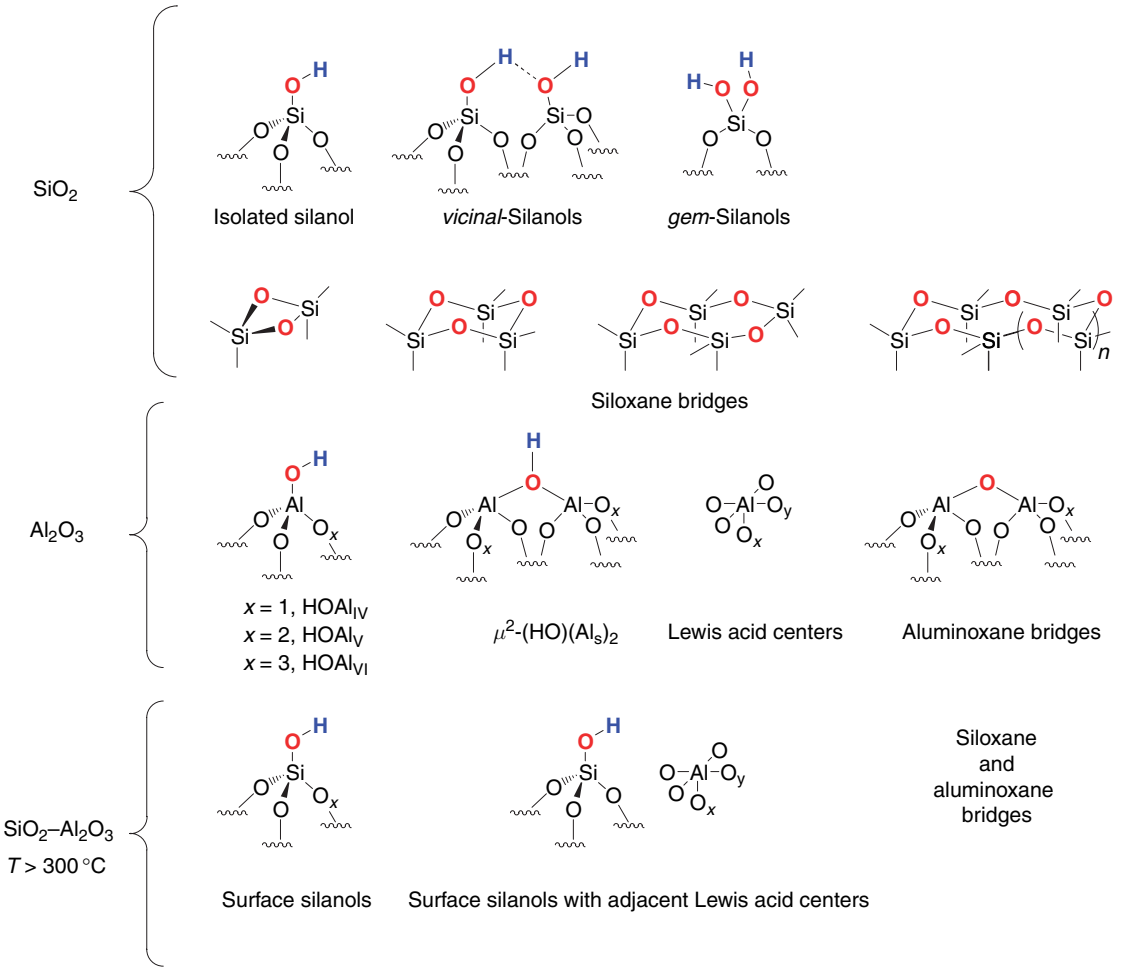

Scheme 2 Examples of surface functionalities on silica and alumina.

In the case of alumina, the surface is much more complex because Al atoms have different coordination numbers (Al(IV), Al(V), and Al(VI)), and the hydroxyl can be bridged with a different number and type of Al centers (μ^1-, μ^2-, μ^3-OH), so that their acidity and reactivity can be very different.[18] Additionally, the temperature of dehydroxylation can change the crystalline phase of this oxide, changing the proportion of each of the types of Al atoms, Al(IV) and Al(VI) atoms. Typically, a γ-alumina dehydroxylated at 500 °C contains around 4 OH nm^{-2}.[19]

In the case of silica–alumina, dehydroxylated at temperatures >300 °C, the surface is mainly composed of isolated silanols, which can be close to Al Lewis centers. Other supports such as magnesia or titanium not only contain hydroxyl groups, but also Lewis acid and basic centers.[15,20]

12.10.2.3 Main Group Complexes

12.10.2.3.1 Groups 1 and 2

There are only very few reports with detailed analysis of the reactions of group 1 and 2 organometallic reagents with oxide supports. The reaction of *t*-BuCH$_2$Li with SiO$_{2\text{-}(400)}$ or MgO$_{\text{-}(200)}$ has been reported to generate [(≡SiO)Li] and [Mg$_s$OLi], respectively, according to mass balance analysis (Scheme 3 and Table 1).[21] [(^{t}BuCH$_2$)$_2$MgL] (L = dioxane) reacts similarly to give [(≡SiO)Mg(CH$_2{}^t$Bu)L$_x$].[21] These systems have been used as models of the Lundsford methane oxidative coupling catalysts. More recently, it has been shown that Grignard reagents react with the siloxane bridges of highly dehydroxylated silica to generate Si–R fragments, and this approach has been used to graft sugar moieties onto silica.[22]

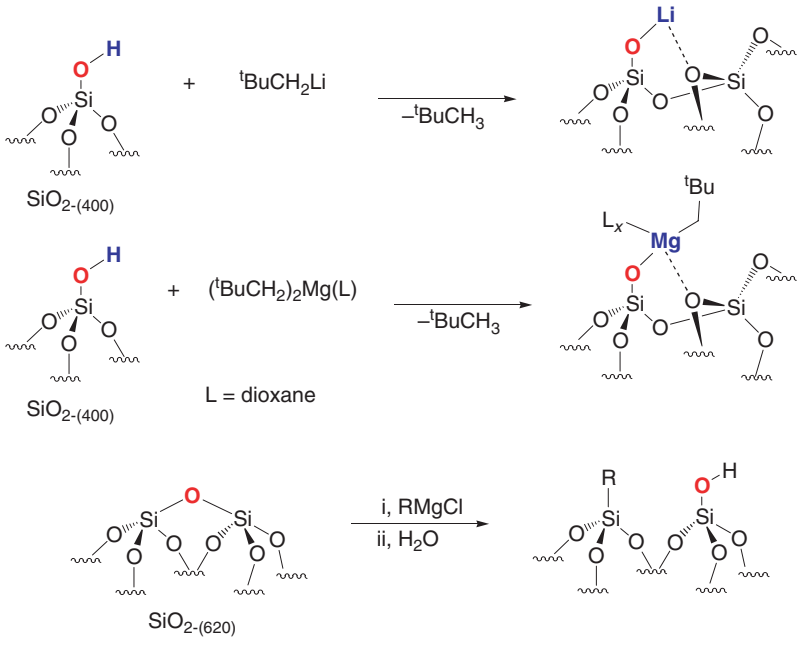

Scheme 3

Table 1 Surface species resulting from the reaction of groups 1, 2 and 13 organometallic complexes with oxide materials

Molecular complex	*Oxide support*	*Structure*	*Analytical methods*	*References*
$^{t}BuCH_2Li$	$SiO_{2\text{-}(400)}$	(≡SiO-Li)	Chem., IR	21
$^{t}BuCH_2Li$	$MgO_{\text{-}(200)}$	(Mg_sO-Li)	Chem., IR	21
$(^{t}BuCH_2)_2MgL$	$MgO_{\text{-}(200)}$	(≡SiO-$MgCH_2{}^{t}BuL_x$)	Chem., IR	21
BEt_3	$SiO_{2\text{-}(450)}$	(≡SiO)BEt_2	IR	23
$B(C_6F_5)_3 + Et_2NPh$	$SiO_{2\text{-}(800)}$	{(≡SiO)$B(C_6F_5)_3{}^{-}$} {$NEt_2PhH)^{+}$}	Chem., IR, NMR	24,25
$[Al(Me)_3]_2$	SiO_2	[a]	Chem., IR, NMR	23,26–30
$Ga(Me)_3$	$SiO_{2\text{-}(800)}$	(≡SiO)$Ga(Me)_2$	Chem., IR	32

[a]Complex reaction mixture.

12.10.2.3.2 Group 13: boron, aluminum, and gallium

As evidenced by IR spectroscopy, triethylboron, BEt_3, reacts with the surface silanols of $SiO_{2\text{-}(450)}$, and it is proposed to give the corresponding surface complex [(≡SiO)BEt_2], probably in interaction with adjacent oxygens such as those of siloxane bridges (Scheme 4 and Table 1).[23] In contrast, $B(C_6F_5)_3$ does not react with the surface hydroxyl of silica by itself, but requires the presence of Et_2NPh. In the case of $SiO_{2\text{-}(800)}$, a well-defined system, [{(≡SiO)$B(C_6F_5)_3{}^{-}$}{$NEt_2PhH)^{+}$}], can be obtained selectively as shown by exhaustive spectroscopic studies,[24,25] and it can be used to generate cationic supported complexes (*vide infra*).

The reaction of alkylaluminum reagents and oxide supports has been studied for a long time, and the surface chemistry is complex. Just as an example,[23,26–30] Me_3Al reacts with all surface sites of a silica treated under vacuum at various temperatures that are silanols and siloxane bridges, the latter yielding SiMe surface species.[28,29] Whatever the initial grafting pathways, the major surface species is [(≡SiO)$_2$AlMe] (Scheme 4 and Table 1). Note that the surface chemistry is similar on mesoporous silica.[31] The reaction of [Me_3Ga], a monomer, and $SiO_{2\text{-}(800)}$ has also been described: [(≡SiO)$GaMe_2$] is reported to be the major surface species, and it is also probably coordinated to adjacent oxygens from the surface.[32]

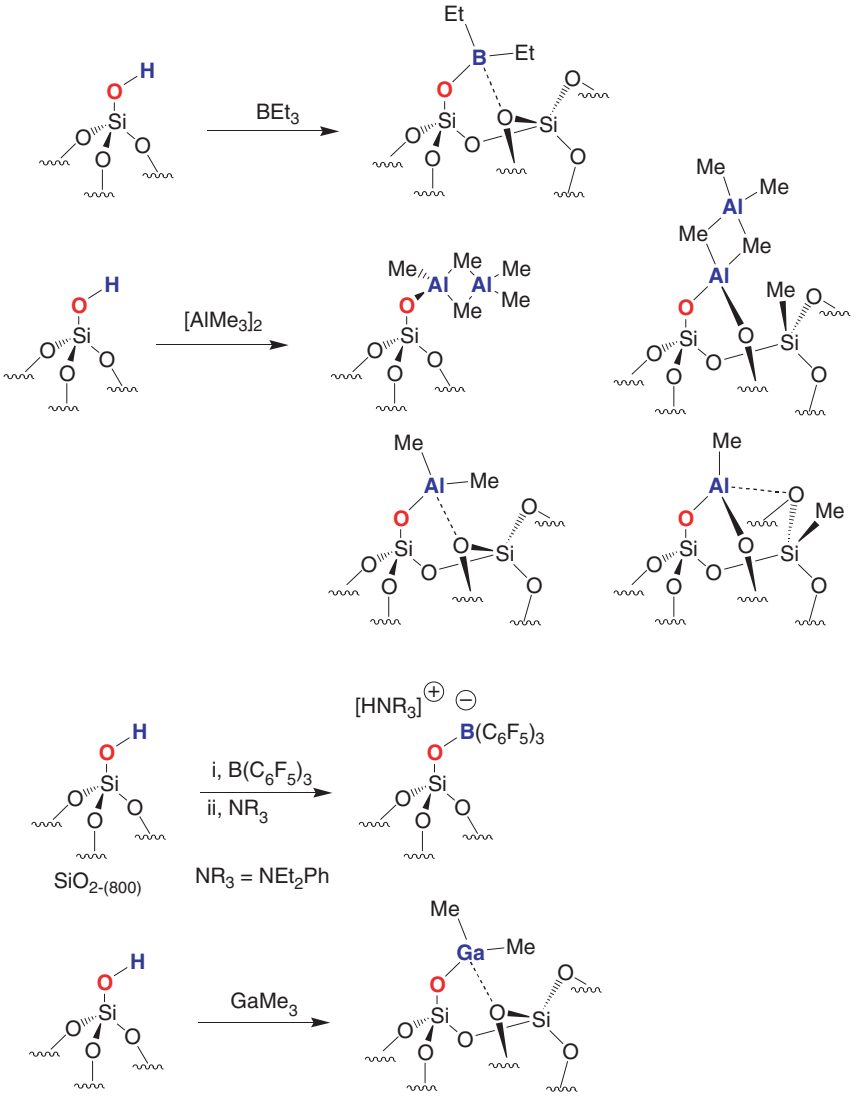

Scheme 4 Surface organometallic chemistry of group 13 elements.

12.10.2.3.3 Group 14

12.10.2.3.3.(i) Silicon

Formation of silylated silica or other supports has been carried out by using halogeno- or alkoxyalkylsilane derivatives or silazanes, $\{(R_3Si)_2NH\}$.[23,33] These methods are associated with the formation of HCl, alcohol, or ammonia. More recently, it has been shown that allylsilane [allylSi$(CH_2R^1)_2(CH_2R^2)$] can react selectively with the surface silanols of silica to give a wide range of supported alkylsilane derivatives, [(≡SiO)Si$(CH_2R^1)_2(CH_2R^2)$] (Scheme 5 and Table 2).[34,35]

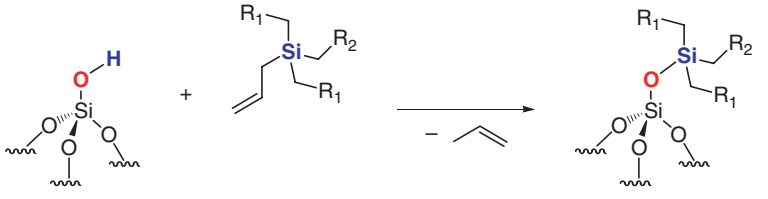

Scheme 5 Surface organometallic chemistry of organosilicon reagents.

Table 2 Surface species resulting from the reaction of group 14 organometallic complexes with oxide materials

Molecular complex	*Oxide support*	*Structure*	*Analytical methods*	*References*
$AllylSiR_2R^1$	SiO_2	$(\equiv SiO)SiR_2R^1$	Chem., IR, NMR	34,35
Bu_4Ge	SiO_2	$(\equiv SiO)GeBu_3$	Chem., IR, NMR	36
Bu_4Ge	SiO_2-Al_2O_3	$(\equiv SiO)GeBu_3$	Chem., IR, NMR	37
Bu_4Ge	Al_2O_3	$(Al_sO)GeBu_3$	Chem., IR, NMR	37
Me_4Sn	SiO_2	$(\equiv SiO)SnMe_3$[a]	Chem., IR, NMR	38,39,41
Et_4Sn	SiO_2	$(\equiv SiO)SnEt_3$	Chem., IR, NMR	38,39
$^iPr_4Sn$	SiO_2	$(\equiv SiO)Sn^iPr_3$	Chem., IR, NMR	38,39
Bu_4Sn	SiO_2	$(\equiv SiO)SnBu_3$	Chem., IR, NMR	38,39
Cy_4Sn	SiO_2	$(\equiv SiO)SnCy_3$	Chem., IR, NMR	38,39
Ph_4Sn	SiO_2	$(\equiv SiO)SnPh_3$	Chem., IR, NMR	38,39
Bu_3SnH	SiO_2	$(\equiv SiO)SnBu_3$	Chem., IR, NMR	38
$[(BuC\equiv C)_3SnR_{F14}$[b]	$SiO_{2\text{-}(200)}$	$(\equiv SiO)_3SnR_{F14}$[b]	Chem., IR, NMR	42
Bu_2SnH_2	SiO_2	$(\equiv SiO)_2SnBu_2$	Chem., IR, NMR	44
$[Bu_3SnOSnBu_3]$	$SiO_{2\text{-}(200)}$	$(\equiv SiO)SnBu_3$	Chem., IR, NMR	45
Bu_3SnH	SiO_2-Al_2O_3	$(\equiv SiO)SnBu_3$	Chem., IR, NMR	46,47
Bu_3SnH	Al_2O_3	$(Al_sO)SnBu_3$	Chem., IR, NMR	48

[a]Along with $(\equiv SiO)_2SnMe_2$ and $(\equiv SiO)_3SnMe$.
[b]$R_{F14} = \{(CH_2)_2(CF_2)_7CF_3\}$.

12.10.2.3.3.(ii) Germanium

Tetraethyl- or tetrabutylgermanium compounds $[GeR_4]$ do not react with the surface silanols of silica at room temperature and are only physisorbed. On the other hand, their reaction at higher temperatures yields $[(\equiv SiO)GeR_3]$ along with 1 equiv. of RH, independent of the temperature of partial dehydroxylation of silica, that is, 200 or 500 °C (Scheme 6 and Table 2).[36] Similarly, $[GeBu_4]$ also grafts on various supports, namely alumina[37] and silica–alumina[37] to give $[Al_sO–GeBu_3]$ and $[(\equiv SiO)–GeBu_3]_{silica–alumina}$, respectively. It is worth noting that all these surface complexes are thermally very stable, and no decomposition products are observed at temperatures up to 400 °C.

12.10.2.3.3.(iii) Tin

Tetraalkyltin, $[R_4Sn]$ {R = Me, Et, ^{i}Pr, Bu, Cy, and Ph}, compounds react between 100 and 200 °C with the surface silanols of $SiO_{2\text{-}(500)}$ to give $[(\equiv SiO)SnR_3]$ as the major surface species along with 1 equiv. of the corresponding alkane (RH), while they are reversibly physisorbed at a lower temperature (Scheme 7).[38,39] Of the various organotin reagents, $[Me_4Sn]$ is the least reactive and requires higher temperature of reaction (200 °C, *vide infra*).

The surface complex $[(\equiv SiO)SnBu_3]$ supported on $SiO_{2\text{-}(200)}$ or $SiO_{2\text{-}(500)}$ slowly decomposes above 150 °C. For instance, the thermal treatment of the surface complex $[(\equiv SiO)SnBu_3]$ supported on $SiO_{2\text{-}(200)}$ between 150 and 250 °C generates 1 equiv. of BuH, and $[(\equiv SiO)_2SnBu_2]$ is formed as a major surface species along with small amounts of $[(\equiv SiO)_3SnBu]$.[40] Above 250 °C, butene and H_2 are formed, and the surface complexes are progressively transformed into fully dealkylated species $[(\equiv SiO)_2Sn]$. Additionally, the surface complex $[(\equiv SiO)SnMe_3]$ supported on $SiO_{2\text{-}(200)}$ or $SiO_{2\text{-}(500)}$ slowly

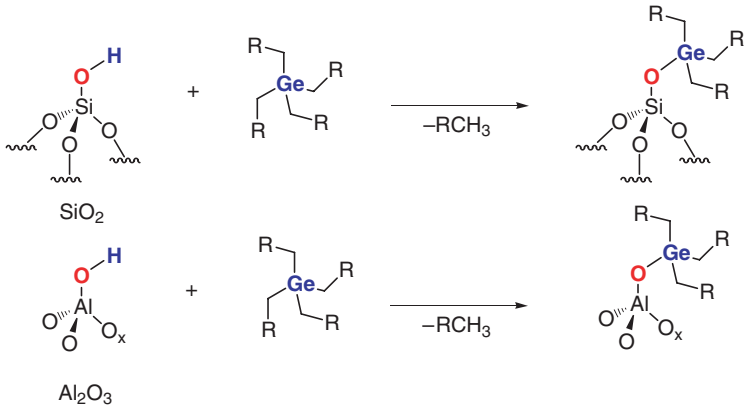

Scheme 6 Reaction of tetrabutylgermanium with silica and alumina.

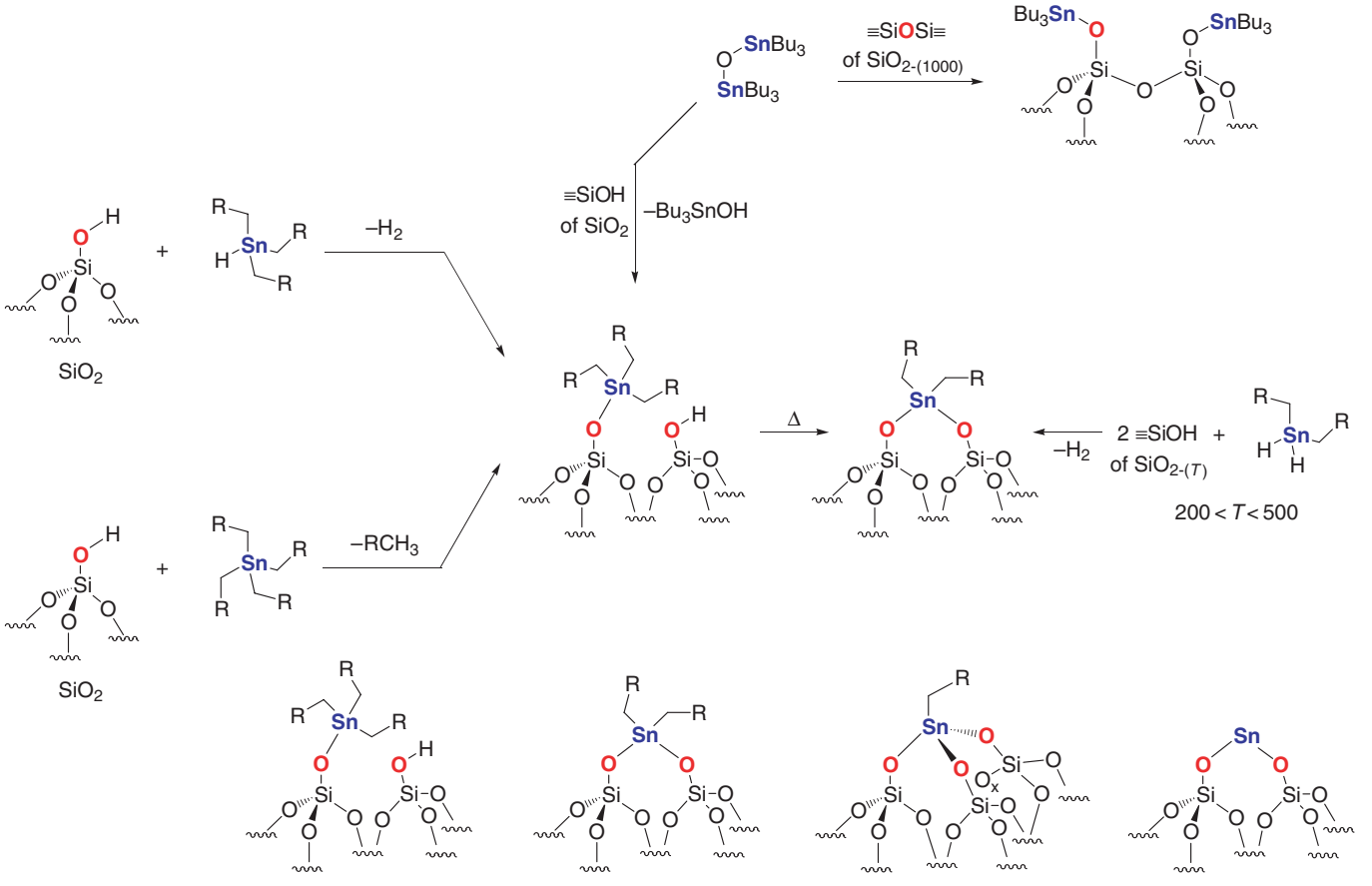

Scheme 7 Formation of tin surface species on silica.

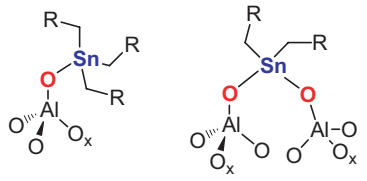

Scheme 8 Tin surface species on alumina.

decomposes above 150 °C by reaction with adjacent unreacted silanols to give a mixture of [(≡SiO)$_2$SnMe$_2$], [(≡SiO)$_3$SnMe], and fully dealkylated Sn species, [(≡SiO)$_4$Sn], the relative amounts of which change as a function of temperature to give finally at 500 °C the latter species as the sole product.[41] Note that these Sn organometallic compounds usually react at a lower temperature on $SiO_{2\text{-}(200)}$ to provide the same surface species, [(≡SiO)SnR$_3$]. It is worth noting that the reaction of [(BuC≡C)$_3$Sn{(CH$_2$)$_2$(CF$_2$)$_7$CF$_3$}] with $SiO_{2\text{-}(200)}$ gives directly 3 equiv. of 1-hexyne and [(≡SiO)$_3$Sn{(CH$_2$)$_2$(CF$_2$)$_7$CF$_3$}(≡SiOH)$_n$], which is penta- or hexacoordinated according to ^{117}Sn NMR.[42]

In contrast, tributyltin hydride, [Bu$_3$SnH], physisorbed on silica ($SiO_{2\text{-}(200)}$ or $SiO_{2\text{-}(500)}$) at room temperature as evidenced by the interaction of Sn–H with surface silanols, but then slowly reacted with these silanols to generate H_2. At 100 °C, this reaction is very fast and yields [(≡SiO)SnBu$_3$] along with 1 equiv. of H_2.[38] The reaction is general and can be applied to a wide range of substrates such as R^{1}R$_2$SnH, providing [(≡SiO)SnR^{1}R$_2$].[43] The surface species [(≡SiO)$_2$SnBu$_2$] can also be prepared using the same approach by reacting [Bu$_2$SnH$_2$] with $SiO_{2\text{-}(200)}$ or $SiO_{2\text{-}(500)}$.[44]

Similarly to [Bu$_3$SnH] or [Bu$_4$Sn], [Bu$_3$SnOSnBu$_3$] reacts with the silanols of $SiO_{2\text{-}(200)}$ to yield [(≡SiO)SnBu$_3$]. Moreover, when silica is treated at a higher temperature such as 1,000 °C ($SiO_{2\text{-}(1,000)}$), strained siloxane bridges (≡SiOSi≡) are formed, and they react with [Bu$_3$SnOSnBu$_3$] to yield [(≡SiO)SnBu$_3$] (Scheme 7).[45]

In the case of silica–alumina, [Bu$_3$SnH] reacts selectively at 25 °C with the surface silanols to give [(≡SiO)SnBu$_3$].[46,47] Grafting of [Bu$_3$SnH] on various Al_2O_3 generates [(Al$_s$O)SnBu$_3$] surface species along with 1 equiv. of H_2 (Scheme 8).[48] On α-Al_2O_3, which contains mainly octahedral Al atoms, the major species is a pentacoordinated Sn complex, [(Al$_s$O)SnBu$_3$(AlOE)] (E = H or Al$_s$). For other aluminas (γ and η), there are numerous surface species that are either tetra- or pentacoordinated, [(Al$_s$O)SnBu$_3$] and [(Al$_s$O)SnBu$_3$(AlOE)] (E = H or Al$_s$). These alumina-supported species decompose at lower temperatures than [(≡SiO)SnBu$_3$] to give first [(Al$_s$O)$_2$SnBu$_2$] and butane, and then more complex mixture of surface species.[49]

12.10.2.4 Group 3, Lanthanide and Actinide Complexes

They are only few reported attempts to prepare well-defined supported group 3, lanthanide and actinide complexes (Table 3).

Table 3 Surface species resulting from the reaction of group 3, lanthanide and actinide organometallic complexes with oxide materials

Molecular complex	*Oxide support*	*Structure*	*Analytical methods*	*References*
Cp*Ln(AlMe$_4$)$_2$	MCM-48	(≡SiO)Ln(AlMe$_4$)Cp*[a]	Chem.	50,51
Ln{N(SiMe$_3$)$_2$}$_3$	$SiO_{2\text{-}(700)}$	(≡SiO)Ln{N(SiMe$_3$)$_2$}$_2$}	Chem., IR	56
Ln{N(SiMe$_3$)$_2$}$_3$	$SiO_{2\text{-}(200)}$	(≡SiO)$_2$Ln{N(SiMe$_3$)$_2$}[b]	Chem., IR	56
Ln{N(SiHMe$_2$)$_2$}$_3$(thf)$_2$	MCM-48	(≡SiO)$_x$Ln{N(SiR$_2$H)$_2$}$_{2-x}$L$_y$}	Chem., NMR	53–55
Sm{N(SiHMe$_2$)$_2$}$_2$(thf)$_2$	MCM-48	(≡SiO)$_x$Ln{N(SiR$_2$H)$_2$}$_{2-x}$L$_y$}	Chem., ESR	61
Cp$^*_2$ThMe$_2$	$SiO_{2\text{-}(950)}$	(≡SiO)ThMeCp$^*_2$	Chem., NMR	62,63
Cp$^*_2$UMe$_2$	$SiO_{2\text{-}(950)}$	(≡SiO)UMeCp$^*_2$	Chem.	62,63
Cp$^*_2$ThMe$_2$	γ-Al_2O_3	(Al$_s$O)ThMeCp$^*_2$	Chem., NMR	63–66
Cp$^*_2$UMe$_2$	γ-Al_2O_3	(Al$_s$O)UMeCp$^*_2$	Chem., NMR	63–66
Cp*Th(CH$_2$Ar)$_3$	γ-Al_2O_3	[c]	Chem.	67–69
Th(allyl)$_4$	γ-Al_2O_3	[c]	Chem.	67–69
Cp$^*_2$ThMe$_2$	SiO_2-Al_2O_3	[c]	Chem., NMR	63,70
Cp$^*_2$ThMe$_2$	$MgCl_2$	[c]	Chem., NMR	63,70
Cp$^*_2$ThMe$_2$	$MgCl_2$	[c]	Chem., NMR	63,70

[a]Proposed.
[b]Along with 25% of (≡SiO)Ln{N(SiMe$_3$)$_2$}$_2$.
[c]Undetermined reaction mixtures.

The reaction of $[Cp^*Ln(AlMe_4)_2]$ (Ln = Y and Nd) with silica supports has been reported to give $[(\mu^2\text{-}SiO)LnCp^*(AlMe_4)(\mu^2\text{-}AlMe_3)]$ from an analogy with the reaction of $[Cp^*Ln(AlMe_4)_2]$ with molecular silanols (Scheme 9).[50,51] Another approach has been to react supported amido derivatives, namely $[(\equiv SiO)_xSc\{N(SiR_3)_2\}_{2-x}]$ (*vide infra*), with alkylating agents, Me_3Al, to generate the corresponding alkylated Sc–Me, but no well-defined species could be obtained.[52]

Alkylsilyl amido lanthanide complexes, $[Ln\{N(SiMe_3)_3]$ or $[Ln\{N(SiHMe_2)_3(thf)_2]$, react with silica to provide a mixture of surface complexes of the general formula: $[(\equiv SiO)_xLn\{N(SiR_2R^1)_2\}_{2-x}L_y]$ (Ln = Sc, Y, Nd, La; L = thf)

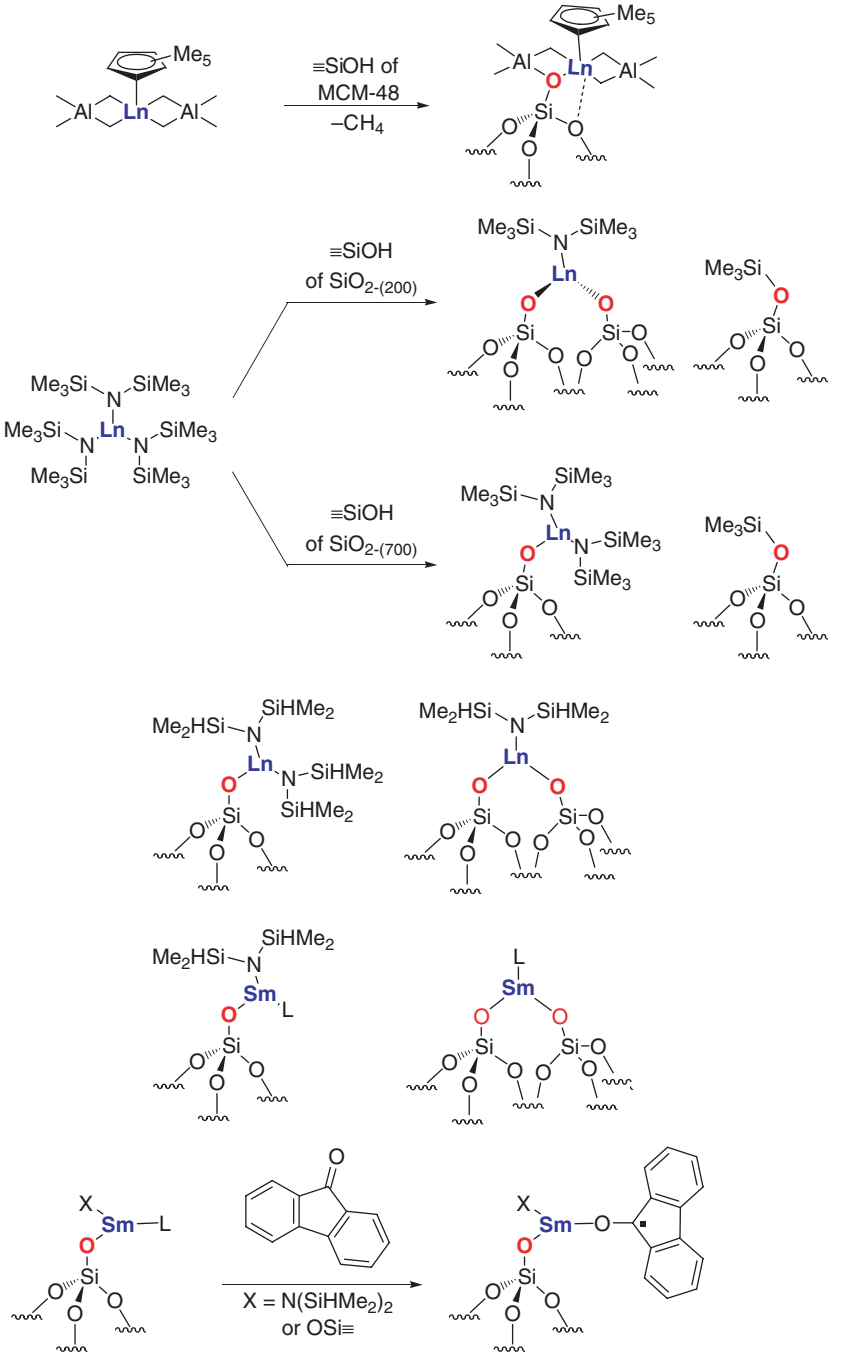

Scheme 9 Surface organometallic chemistry of group 3 and lanthanide complexes.

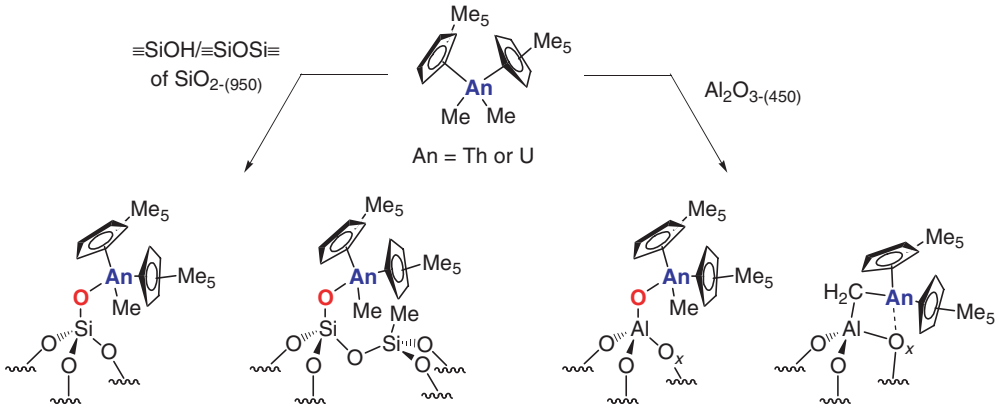

Scheme 10 Surface organometallic chemistry of actinide complexes.

along with $HN(SiR_2R^1)_2$ (R = Me; R^1 = Me or H),[53–55] which usually further react with silica to give surface $\equiv OSiR_2R_1$ groups (R = Me; R^1 = Me or H). The reaction of $Ln\{N(SiMe_3)_2\}_3$ with $SiO_{2\text{-}(700)}$ gives $[(\equiv SiO)Ln\{N(SiMe_3)_2\}_2]$ as the major surface species according to elemental analysis and IR spectroscopy, whereas a 3 : 1 mixture of $[(\equiv SiO)_2Ln\{N(SiMe_3)_2\}]$ and $[(\equiv SiO)Ln\{N(SiMe_3)_2\}_2]$ is obtained on $SiO_{2\text{-}(200)}$ (Scheme 9).[56] It is worth noting that these materials efficiently catalyze the polymerization of methyl methacrylate, and can be used as Lewis acid catalyst precursors for organic transformations, for example, the hetero-Diels–Alder reaction.[57–60] The Sm(II) derivatives react with fluorenone to generate stable ketyl radicals, as shown by ESR and ENDOR experiments.[61]

The grafting of several U and Th complexes on inorganic supports have been studied. For instance, $[Cp^*_2ThMe_2]$ reacts with a highly dehydroxylated silica $[SiO_{2\text{-}(950)}]$ to give $[(\equiv SiO)ThMeCp^*_2]$ through two pathways, the reaction with surface hydroxyls and siloxane bridges; the latter yielding surface ≡Si–Me (Scheme 10).[62,63] In the case of partially dehydroxylated γ-aluminas at 475 and 1,000 °C (γ-$Al_2O_{3\text{-}(475)}$ or $Al_2O_{3\text{-}(1,000)}$), the grafting is more complex.[63–66] On γ-$Al_2O_{3\text{-}(475)}$, the major grafting pathway for $[Cp^*_2MMe_2]$ is the reaction with surface hydroxyl groups to give $[Al_sOMMeCp^*_2]$, but other species are probably formed, such as adsorbed carbene intermediates $[Cp^*_2M(CH_2)\text{-}(OAl_s)]$ (Scheme 10). On γ-$Al_2O_{3\text{-}(1,000)}$, $[Al_sOMCp^*_2Me]$ becomes a minor species, and other grafting pathways are favored. Reaction of $[Cp^*Th(CH_2Ar)_3]$ and $[Th(allyl)_4]$ with γ-$Al_2O_{3\text{-}(1,000)}$ also provide a mixture of surface species as described for other actinide complexes.[67–69] $[Cp^*_2MMe_2]$ complexes have also been grafted on other supports, such as $MgCl_2$ and SiO_2-Al_2O_3, yielding more complex surface reactions.[63,70] All these materials have been used as catalyst precursors for either polymerization or hydrogenation.

12.10.2.5 Group 4 Complexes

12.10.2.5.1 Supported perhydrocarbyl group 4 complexes

The chemistry of group 4 perhydrocarbyl complexes on oxide supports has been studied extensively for more than three decades (see Tables 4–8). The structure of the resulting surface complex typically depends on the oxides, its morphology, and its pretreatment temperature.

Table 4 Surface species resulting from the reaction of Ti organometallic complexes with silica materials

Molecular complex	*Oxide support*	*Structure*	*Analytical methods*	*References*
$Ti(allyl)_4$	$SiO_{2\text{-}(200)}$	$(\equiv SiO)_2Ti(C_3H_5)_2$	Chem., IR	1,86
$Ti(CH_2Ph)_4$	$SiO_{2\text{-}(200)}$	$(\equiv SiO)_2Ti(CH_2Ph)_2$	Chem.	87
$Ti(CH_2Ar)_4$	$SiO_{2\text{-}(200)}$	$(\equiv SiO)_2Ti(CH_2Ar)_2$	Chem.	88,89
$Ti(CH_2{}^tBu)_4$	$SiO_{2\text{-}(200)}$	$(\equiv SiO)_2Ti(CH_2{}^tBu)_2$	Chem.	73,74
$Ti(CH_2{}^tBu)_4$	$SiO_{2\text{-}(500)}$	$(\equiv SiO)Ti(CH_2{}^tBu)_3$	Chem., IR, NMR	90,91
$Ti(CH_2{}^tBu)_4$	$SiO_{2\text{-}(700)}$	$(\equiv SiO)Ti(CH_2{}^tBu)_3$	Chem., IR, NMR	92a,b
$Cp^*Ti(Me)_3$	SiO_2	$(\equiv SiO)Ti(Me)_2Cp^*$	Chem., IR, NMR	93
$MeTi(O^iPr)_3$	SiO_2	$(\equiv SiO)Ti(O^iPr)_3$	Chem., NMR	71

Table 5 Surface species resulting from the reaction of Zr organometallic complexes with silica materials

Molecular complex	*Oxide support*	*Structure*	*Analytical methods*	*References*
$Zr(allyl)_4$	$SiO_{2\text{-}(200)}$	$(\equiv SiO)_2Zr(C_3H_5)_2$	Chem., IR	1,86,94
$Zr(allyl)_4$	$SiO_{2\text{-}(450)}$	$(\equiv SiO)Zr(C_3H_5)_3$	Chem., IR	1
$BrZr(allyl)_3$	$SiO_{2\text{-}(200)}$	$(\equiv SiO)_2Zr(C_3H_5)Br$	Chem.	1
$Zr(CH_2Ph)_4$	$SiO_{2\text{-}(200)}$	$(\equiv SiO)_2Zr(CH_2Ph)_2$	Chem., IR	1,89
$Zr(CH_2Ar)_4$	SiO_2	[a]	Chem	88,89
$Zr(CH_2SiMe_3)_4$	$SiO_{2\text{-}(200)}$	$(\equiv SiO)_2Zr(CH_2SiMe_3)_2$	Chem., IR	1
$Zr(CH_2{}^tBu)_4$	$SiO_{2\text{-}(200)}$	$(\equiv SiO)_2Zr(CH_2{}^tBu)_2$	Chem., IR,	73,74
$Zr(CH_2{}^tBu)_4$	$SiO_{2\text{-}(500)}$	$(\equiv SiO)Zr(CH_2{}^tBu)_3$	Chem., IR, NMR, EXAFS	95,96
$Zr(CH_2{}^tBu)_4$	$SiO_{2\text{-}(700)}$	$(\equiv SiO)Zr(CH_2{}^tBu)_3$	Chem., IR, NMR	92a,b
$Zr(CH_2{}^tBu)_4$	$MCM\text{-}41_{\text{-}(500)}$	$(\equiv SiO)_2Zr(CH_2{}^tBu)_2$	Chem., IR, NMR	72
Cp_2ZrMe_2	$SiO_{2\text{-}(500)}$	$(\equiv SiO)ZrMeCp_2$	Chem., IR, NMR, EXAFS	79
Cp^*ZrMe_3	$SiO_{2\text{-}(500)}$	$(\equiv SiO)ZrMe_2Cp^*$	Chem., IR,	79
Cp^*ZrMe_3	SiO_2 modified by Barf/amine	[b]	NMR, EXAFS	83,84

[a]Proposed average structure.
[b]Not characterized.

Table 6 Surface species resulting from the reaction of Hf organometallic complexes with oxide supports

Molecular complex	*Oxide support*	*Structure*	*Analytical methods*	*References*
$Hf(CH_2Ph)_4$	$SiO_{2\text{-}(200)}$	$(\equiv SiO)_2Hf(CH_2Ph)$[a]	Chem.	87
$Hf(CH_2{}^tBu)_4$	$SiO_{2\text{-}(500)}$	$(\equiv SiO)Hf(CH_2{}^tBu)_3$	Chem., IR	97
$Hf(CH_2{}^tBu)_4$	$SiO_{2\text{-}(700)}$	$(\equiv SiO)Hf(CH_2{}^tBu)_3$	Chem. IR, NMR	92a
$Hf(CH_2{}^tBu)_4$	$SiO_{2\text{-}(800)}$	$(\equiv SiO)Hf(CH_2{}^tBu)_3$	Chem., IR, NMR	92b
$Hf(CH_2R)_4$ $R = CMe_2Ph$	Al_2O_3	$(Al_sO)_2Hf(CH_2R)_2$[a]	[b]	78
$Hf(arene)_2$	Al_2O_3	$(Al_sO)Hf(H)(arene)$[a]	Chem	81,82

[a]Proposed average structure.
[b]Not characterized.

Table 7 Surface species resulting from the reaction of Ti organometallic complexes with other oxide supports

Molecular complex	*Oxide support*	*Structure*	*Analytical methods*	*References*
$Ti(allyl)_4$	$Al_2O_{3\text{-}(650)}$	[a]	Chem.	1
$Ti(CH_2Ph)_4$	$Al_2O_{3\text{-}((650)}$	[a]	Chem.	1
$Ti(CH_2R)_4$ $R = CMe_2Ph$	$Al_2O_{3\text{-}(450)}$	[a]	Chem.	78
$Ti(arene)_2$	Al_2O_3	$(Al_sO)Ti(H)(arene)$	Chem.	81
$Cp^*Ti(Me)_3$	Sulfated ZrO_2	[b]	Chem., NMR	98

[a]Proposed average structure.
[b]Not characterized.

Generally, the reaction of an organometallic complex, $[M(CH_2R)_4]$ ($R = CH{=}CH_2$, Ar, $SiMe_3$, and *t*-Bu), with a silica partially dehydroxylated at relatively low temperatures, that is 200 °C, gives the corresponding bis-siloxy complex $[(\equiv SiO)_2M(CH_2R)_2]$ as the major surface species. As the temperature of dehydroxylation increases, the concentration of silanols decreases, and for $SiO_{2\text{-}(T)}$ ($450 < T < 800$ °C), the mono-siloxy complexes $[(\equiv SiO)M(CH_2R)_3]$ are usually formed (Scheme 11). Above 800 °C, more and more strained siloxane bridges are formed, and they can become reactive.

When one, two, or three of the ligands (CH_2R, R = H, $CH{=}CH_2$, Ar, $SiMe_3$, and ^{t}Bu) are replaced by ancillary ligands like cyclopentadienyl, halide, or alkoxide ligands,[71] the organometallic complex reacts similarly via the electrophilic cleavage of the M–C by surface silanols (Scheme 11 and Tables 4–6). However, in the case of the reaction of $[Zr(CH_2{}^tBu)_4]$ on MCM-41, a mesoporous silica material, treated at 500 °C, the bis-siloxy surface complex $[(\equiv SiO)_2Zr(CH_2{}^tBu)_2]$ is obtained,[72] in contrast to what is obtained on $SiO_{2\text{-}(500)}$ for which $[(\equiv SiO)Zr(CH_2{}^tBu)_3]$ is

Table 8 Surface species resulting from the reaction of Zr organometallic complexes with other oxide supports

Molecular complex	*Oxide support*	*Structure*	*Analytical methods*	*References*
$Zr(allyl)_4$	Al_2O_3	$(Al_sO)_2Zr(C_3H_5)_2$[a]	Chem., IR	1
$Zr(CH_2Ph)_4$	Al_2O_3	$(Al_sO)_2Zr(CH_2Ph)_2$[a]	Chem., IR	1,86
$Zr(CH_2{}^tBu)_4$	Al_2O_3	$(Al_sO)_2Zr(CH_2{}^tBu)_2$[a]	Chem., IR, NMR, DFT	77,78
$Zr(CH_2R)_4$ $R = CMe_2Ph$	Al_2O_3	$(Al_sO)_2Zr(CH_2R)_2$[a]	Chem., IR	77
Cp_2ZrMe_2	$Al_2O_{3\text{-}(500)}$	$(Al_sO)ZrMeCp_2$[a]	Chem., IR, NMR, EXAFS	79,80
Cp^*ZrMe_3	$Al_2O_{3\text{-}(500)}$	$(Al_sO)ZrMe_2Cp^*$	Chem., IR, NMR, EXAFS	79,80
$Zr(arene)_2$	Al_2O_3	$(Al_sO)Zr(H)(arene)$[b]	Chem.	81,82
Cp_2ZrMe_2	$SiO_2\text{-}Al_2O_{3(500)}$	$(\equiv SiO)ZrMeCp_2$	Chem., IR, NMR, EXAFS	79
Cp^*ZrMe_3	$SiO_2\text{-}Al2O_{3\text{-}(500)}$	$(\equiv SiO)ZrMe_2Cp^*$	Chem., IR, NMR, EXAFS	79
Cp_2ZrMe_2	Sulfated Al_2O_3	[b]	Chem., NMR	99
$Zr(CH_2{}^tBu)_4$	Sulfated ZrO_2	[b]	Chem., NMR	98
Cp_2ZrMe_2	Sulfated ZrO_2	[b]	Chem., NMR	100
Cp^*ZrMe_3	Sulfated ZrO_2	[b]	Chem., NMR	101
$Zr(CH_2{}^tBu)_4$	Sulfated metal oxide	[b]	Chem., NMR	101
Cp^*ZrMe_3	Sulfated metal oxide	[b]	Chem., NMR	101
Cp^*ZrMe_3	Sulfated tin oxide	[b]	Chem., NMR	102

[a]Proposed average structure.
[b]Not characterized.

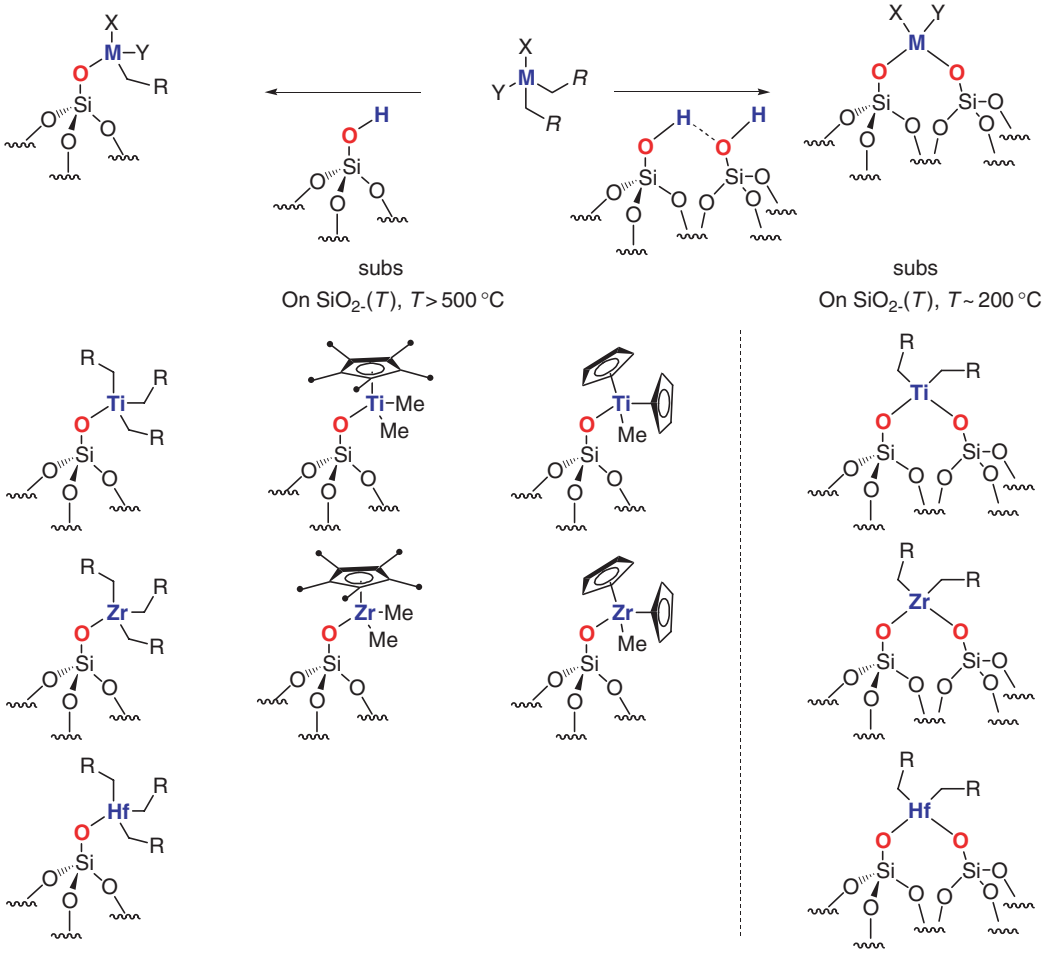

Scheme 11 Surface organometallic chemistry of group 4 organometallics.

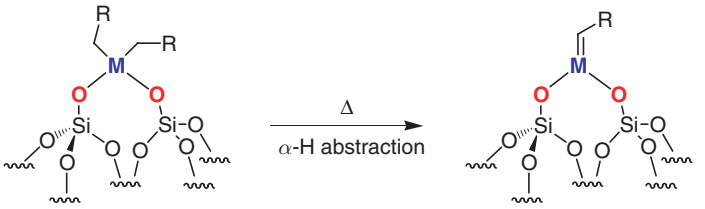

Scheme 12 Thermal decomposition of group 4 metal complexes supported on silica.

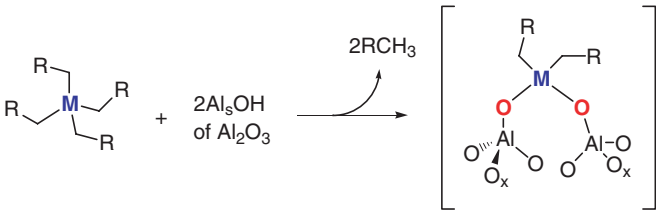

Scheme 13 Average structure of peralkyl group 4 metal complexes supported on partially dehydroxylated alumina.

selectively formed. Finally, note that $[(\equiv SiO)_2M(CH_2R)_2]$ species are thermally unstable and give 1 equiv. of *t*-$BuCH_3$ along with $[(\equiv SiO)_2M(= CHR)]$ at 80 °C according to chemical reactivity studies (Scheme 12).[73,74]

In the case of alumina, the structures of the surface species have been much less described, and usually the reaction of $[M(CH_2R)_4]$ with an alumina partially dehydroxylated at 650 °C gives species with an average structure $[(Al_sO)_2M(CH_2R)_2]$ (Scheme 13 and Tables 7 and 8).[75–77] Nonetheless, because of the complexity of the alumina surface compared to that of silica, there is most likely a population of surface species. While ill defined, these systems are efficient catalysts for the preparation of elastomeric polypropylene in contrast to the corresponding silica-supported systems, and have been associated with the presence of cationic species (*vide infra*).[77,78] In the case of cyclopentadienyl derivatives, monoaluminoxy species are obtained: the average structure based on methane evolved during grafting and methane evolved upon hydrolysis/methanolysis are consistent with the following average structures: $[(Al_sO)Zr(Me)_2Cp^*]$ and $[(Al_sO)Zr(Me)Cp_2]$ for Cp^*ZrMe_3 and Cp_2ZrMe_2, respectively.[79,80] NMR and extended X-ray absorption fine structure (EXAFS) data clearly show that these Zr species are best represented as pseudo-cationic species (Scheme 14). In contrast, on silica–alumina, the major species are well-defined neutral

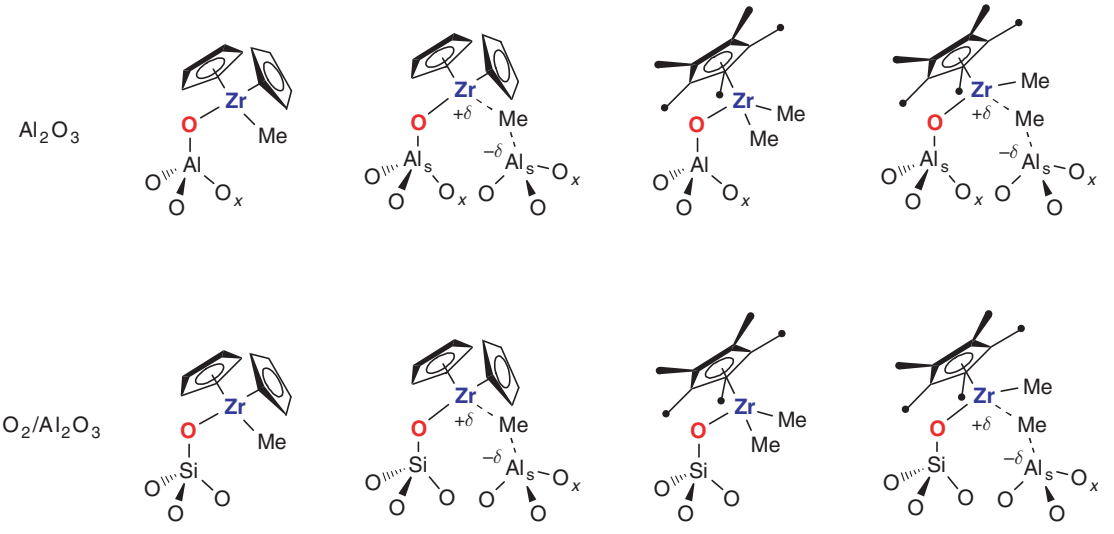

Scheme 14 Structure of cyclopentadienyl group 4 metal complexes supported on partially dehydroxylated alumina and silica–alumina.

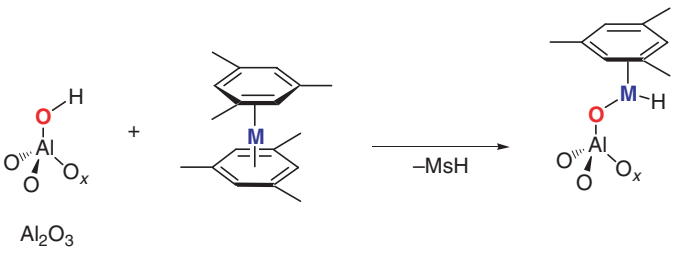

Scheme 15 Proposed reaction of d^0-bis (arene) group 4 metal complexes with alumina.

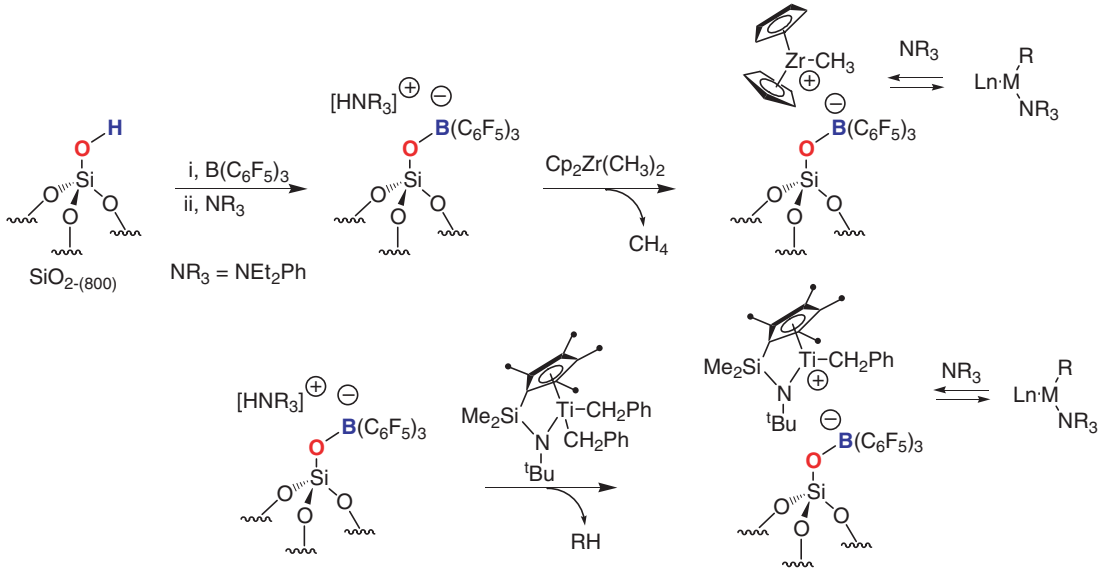

Scheme 16 Reaction of group 4 organometallic complexes with silica modified with Barf.

complexes [(≡SiO)Zr(Me)$_2$Cp*] and [(≡SiO)Zr(Me)Cp$_2$] along with minor partially cationic species, for which the methyl is probably in interaction with adjacent Al Lewis centers ($Zr^{+\delta}$-(μ-Me)-$Al^{-\delta}$ species, Scheme 14).[79] In fact, these systems are poorly active in polymerization as their silica supported analogs.

d^0-Group 4 bis(arene) complexes (arene = mesitylene) have also been used as precursors for heterogeneous polymerization catalysts. Their reaction with alumina gives 1 equiv. of mesitylene/grafted M, and it has been proposed that this reaction yields [(Al$_s$O)M(C$_6$H$_3$Me$_3$) (H)] (Scheme 15).[81,82]

More recently, Marks *et al.* have used sulfated metal oxide supports by using the acidic protons of these supports in order to generate cationic surface species (Tables 6 and 7). While NMR spectroscopy is consistent with the presence of cationic surface species, their exact nature is still unknown. However, they display very good activity in olefin hydrogenation and/or polymerization.

Another approach to generate cationic surface species is the use of [{(SiO)B(C$_6$F$_5$)$_3^-$}{NEt$_2$PhH$^+$}], prepared by the reaction of silica, B(C$_6$F$_5$)$_3$, and Et$_2$NPh (*vide supra*). The reaction of this modified silica with [Cp$_2$ZrMe$^+$] yields [{(SiO)B(C$_6$F$_5$)$_3^-$}{Cp*ZrMe$_2$)$^+$}L] along with CH$_4$ (L = Et$_2$NPh) (Scheme 16). This system becomes an active ethylene polymerization catalyst without the use of an activator like MAO.[83,84] Similarly, it is possible to prepare monocyclopentadienyl Ti complexes.[85]

12.10.2.5.2 Supported group 4 hydride complexes

Treatment of [(≡SiO)M(CH$_2$R)$_3$] with H$_2$ at 150 °C generates metal hydride surface species, and the major species has the following average structure [(≡SiO)$_3$M-H]. Their formation involves the hydrogenolysis of the M–C bond to generate putative metal hydride intermediates, which further react with the neighboring siloxane bridges of the silica

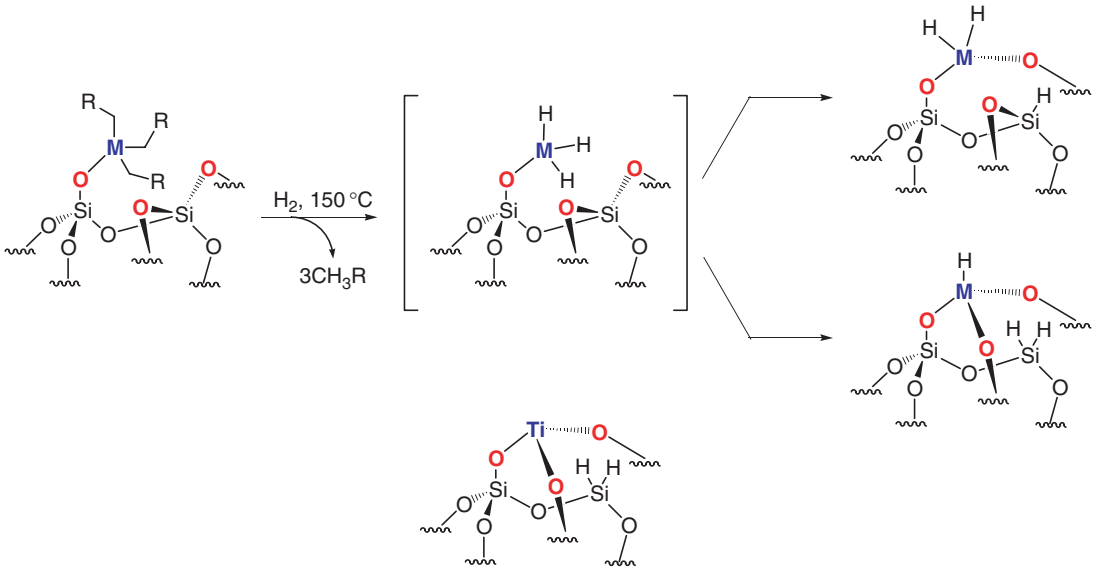

Scheme 17 Formation of supported group 4 metal hydrides.

surface, thus forming new M–O and Si–H bonds (Scheme 17). Depending on the metal, the starting surface complex, and the starting oxide materials, different ratios and types of final structures are observed.

For Ti,[88,103–106] it has been proposed that [(≡SiO)Ti(CH_2R)$_3$] (R = ^{t}Bu or Ph) gives [(≡SiO)$_3$Ti-H] along with 30% of Ti(III) formulated as [(≡SiO)$_3$Ti^{III}] based on mass balance analysis, titration of the number of M–H bonds, and ESR spectroscopy (Scheme 17).

For Zr, the most studied system,[104,105,107,108] EXAFS and chemical reactivity studies were consistent with the formation of [(≡SiO)$_3$Zr-H] as the major surface species.[109] More recent studies involving 1D and 2D solid-state NMR techniques have firmly shown that it is in fact a 65 : 35 mixture of [(≡SiO)$_3$ZrH] and [(≡SiO)$_2$ZrH_2] species.[110] The latter species is formed through the reaction of the hydride intermediates with only one siloxane bridge (Scheme 17).

In the case of Hf,[97,105] no firm assignment has been performed and the structure has been proposed to be like that of its Zr homologs (Scheme 17).

12.10.2.5.2.(i) Stoichiometric reactivity of supported group 4 hydrides

These hydrides react with proton donor molecules such as alcohol or acetylacetone to give the corresponding alkoxide and acetylacetonate (acac) derivatives with the concomitant evolution of hydrogen (Schemes 18 and 19).[111] Moreover, they also react with alkanes, for example, cycloheptane, propane, and methane, at low temperatures to give the corresponding alkylzirconium complexes.[112–115] In the case of methane, it was possible to show that the bis-hydride derivative is more reactive than the monohydride,[116] as it would be expected from a theoretical point of view.[117,118] This difference of reactivity is also observed when the zirconium hydride species react with CO_2 or N_2O (Schemes 18 and 19).[110] With N_2O, the corresponding mono- and bis-hydroxide are formed, but some of the zirconium dihydride species generate H_2. Similarly, in the case of CO_2, the mono- and the bis-formate species are formed (Schemes 18 and 19), but the monoformate hydrido intermediate is probably responsible for the formation of small amounts of methoxyzirconium complexes through the decomposition of a dioxametallacyclobutane into formaldehyde, which further reacts with an adjacent zirconium hydride moiety.

12.10.2.5.2.(ii) Catalytic activity of group 4 hydrides

All these hydrides activate alkanes at low temperatures, but also catalyze H/D exchange in D_2/alkane mixtures (Scheme 20).[119] Moreover, they also catalyze the hydrogenolysis of alkanes and polymers at low temperatures,[106,113,120–122] and the key step of carbon–carbon cleavage is the β-alkyl transfer (the microscopic reverse of an insertion, Scheme 21).

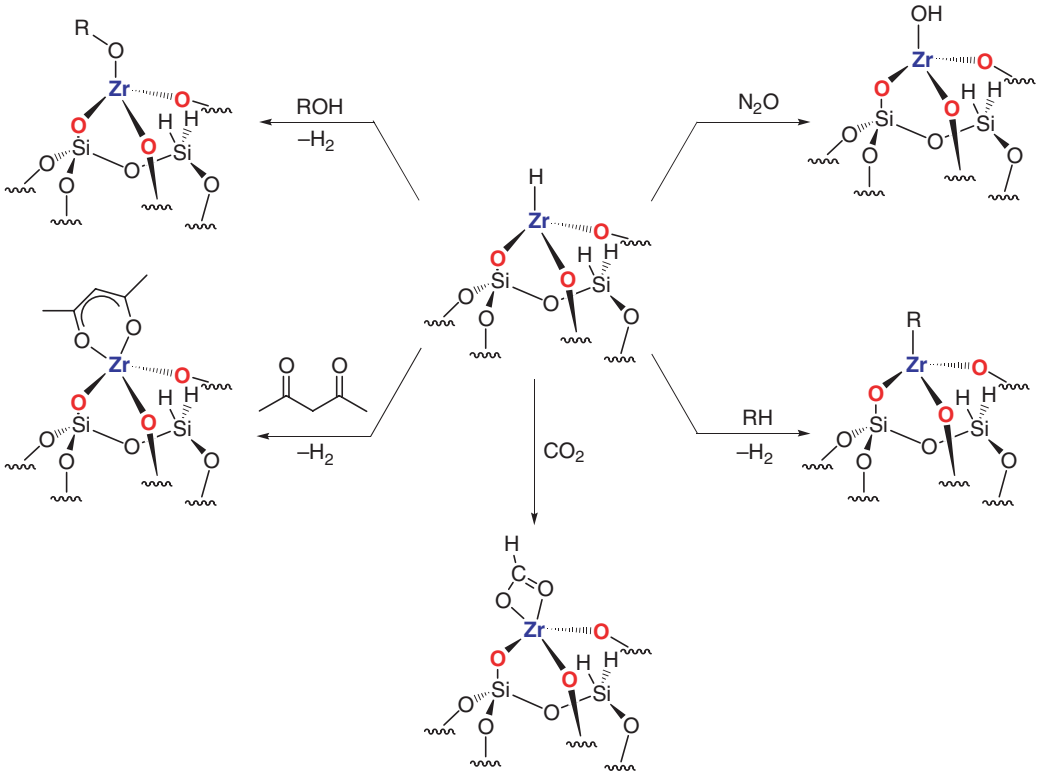

Scheme 18 Reactivity of [(≡SiO)$_3$Zr–H] with various reagents.

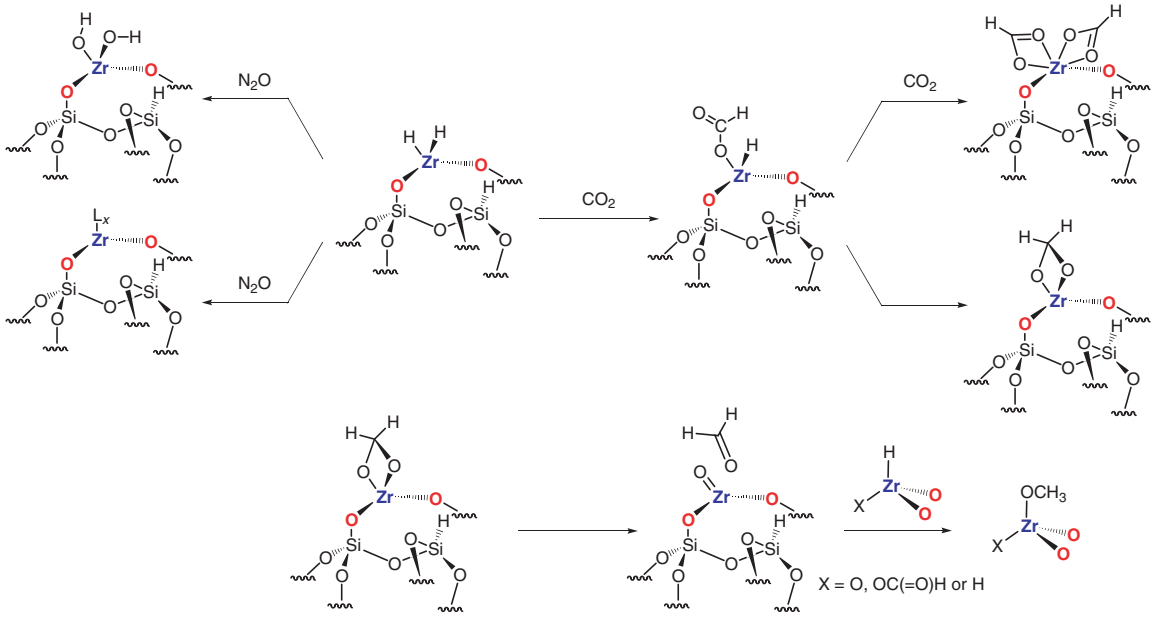

Scheme 19 Reactivity of zirconium dihydride supported on silica with CO_2 and N_2O.

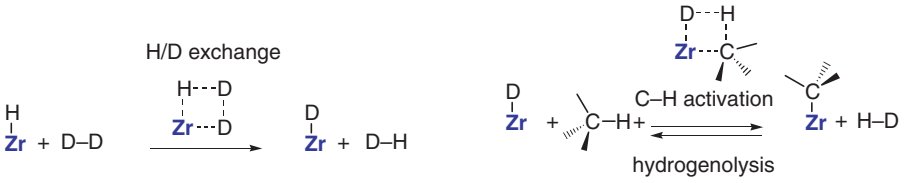

Scheme 20 Pathway for H/D exchange reactions on [(≡SiO)$_3$ZrH].

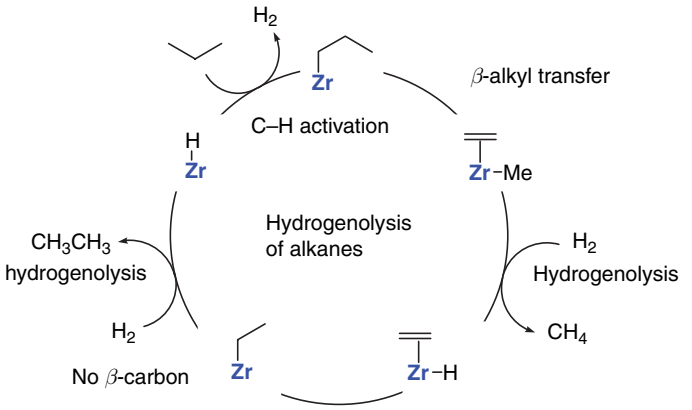

Scheme 21 Low-temperature hydrogenolysis of alkanes catalyzed by [(≡SiO)$_3$ZrH].

12.10.2.5.3 Supported alkoxide and amido group 4 complexes

One synthetic protocol is based on the alcoholysis of [(≡SiO)$_x$M(CH$_2$R)$_{4-x}$] or [(≡SiO)$_3$MH] by R^{1}OH, which provides the corresponding alkoxides [(≡SiO)$_x$M(OR^1)$_{4-x}$] (M = Ti and Zr, Scheme 22, Table 9).[90,91,96,123,124] It is worth noting that [(≡SiO)Zr(OCH$_2$^{t}Bu)$_3$] can also be prepared by the reaction of [(≡SiO)Zr(CH$_2$^{t}Bu)$_3$] with O$_2$ at room temperature even though the reaction course is still a matter of debate.[96] Additionally, the reaction of [(≡SiO)Zr(CH$_2$^{t}Bu)$_3$] with ^{t}BuCOOH gives the corresponding pivalate complex, [(≡SiO)Zr(O(O)C^{t}Bu)$_3$].[96]

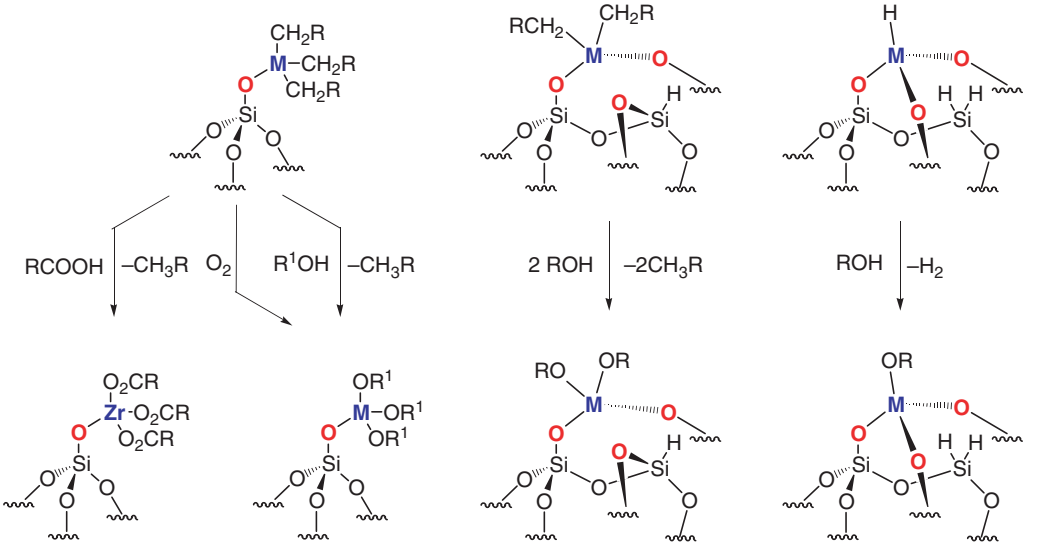

Scheme 22 Alcoholysis of group 4 supported organometallic complexes, a route for the preparation of well-defined surface alkoxides.

Table 9 Surface species resulting from the reaction of group 4 alkoxide, amido, and acetylacetonate complexes with silica materials

Molecular complex	*Oxide support*	*Structure*	*Analytical methods*	*References*
$MeTi(O^iPr)_3$	SiO_2	$(\equiv SiO)Ti(O^iPr)_3$	Chem., NMR	71
$Ti(O^iPr)_4$	$SiO_{2-(200)}$	$(\equiv SiO)Ti_2O(O^iPr)_5$	Chem., IR	125
$Ti(O^iPr)_4$	$SiO_{2-(500)}$	$(\equiv SiO)Ti(O^iPr)_2]_2O$	Chem., IR	125
$Ti(NEt_2)_4$	$SiO_{2-(200)}$	$(\equiv SiO)Ti(NEt_2)_3$	Chem., IR	125
$Ti(NEt_2)_4$	$SiO_{2-(500)}$	$(\equiv SiO)_2Ti(NEt_2)_2$	Chem., IR	125
$Ti(OSiMe_3)_4$	$SiO_{2-(500)}$	$(\equiv SiO)Ti(OSiMe_3)_3$[a]	Chem., IR	126
$Ti(OSi(O^tBu)_3)_4$	SBA-15	$(\equiv SiO)Ti(OSi(O^tBu)_3)_3$	Chem., UV	127
$(i\text{-PrO})Ti(OSi(O^tBu)_3)_3$	SBA-15	$(\equiv SiO)Ti(O^iPr)(OSi(O^tBu)_3)_2$	Chem., UV	127
$(t\text{-BuO})_3Ti(OSi(O^tBu)_3)$	SBA-15	$(\equiv SiO)Ti(O^tBu)_3$	Chem., UV	127
$[(t\text{-BuO})_2Ti\{\mu\text{-}O_2Si[OSi(O^tBu)_3]_2\}]_2$	SBA-15	[b]	Chem., UV	128
$(MeOcalixO_3)TiCl$	SiO_2	$(\equiv SiO)Ti(O_3calixOMe)$	Chem., NMR	129,130
$Zr(Oacac)_4$	$SiO_{2-(500)}$	$[(\equiv SiO)Zr(Oacac)_3]$	Chem., IR, NMR	111

[a]Along with $(\equiv SiO)SiMe_3$ and H_2O.
[b]Complex surface reaction.

These supported alkoxide derivatives can also be directly prepared from molecular alkoxide precursors (Table 9). The complex $[(\equiv SiO)Ti(O^iPr)_3]$ can be obtained by the reaction of $MeTi(O^iPr)_3$ with SiO_2.[71] It is also possible to use simple alkoxide exchange, but the reaction can be more complex (*vide infra*). $[Ti(O^iPr)_4]$ reacts with $SiO_{2-(200)}$ and $SiO_{2-(500)}$ to yield the following dimeric complexes, $[(\equiv SiO)Ti(O^iPr)_2]_2O$ and $[(\equiv SiO)Ti_2O(O^iPr)_5]$, respectively (Schemes 23 and 24).[125] The monomeric Ti system can however be prepared by reacting $[Ti(NEt_2)_4]$ with $SiO_{2-(200)}$ and $SiO_{2-(500)}$, thus giving mononuclear species $[(\equiv SiO)Ti(NEt_2)_3]$ and $[(\equiv SiO)_2Ti(NEt_2)_2]$, which can be transformed through alcoholysis to the corresponding monomeric alkoxides derivatives $[(\equiv SiO)Ti(OR)_3]$ and $[(\equiv SiO)_2Ti(OR)_2]$ (Schemes 23 and 24).[125] When the alcohol is *t*-BuOH, the titanium supported alkoxide does not contain an extra alcohol ligand, while for smaller alcohols (such as *i*-PrOH), the titanium complex cannot be obtained base-free.

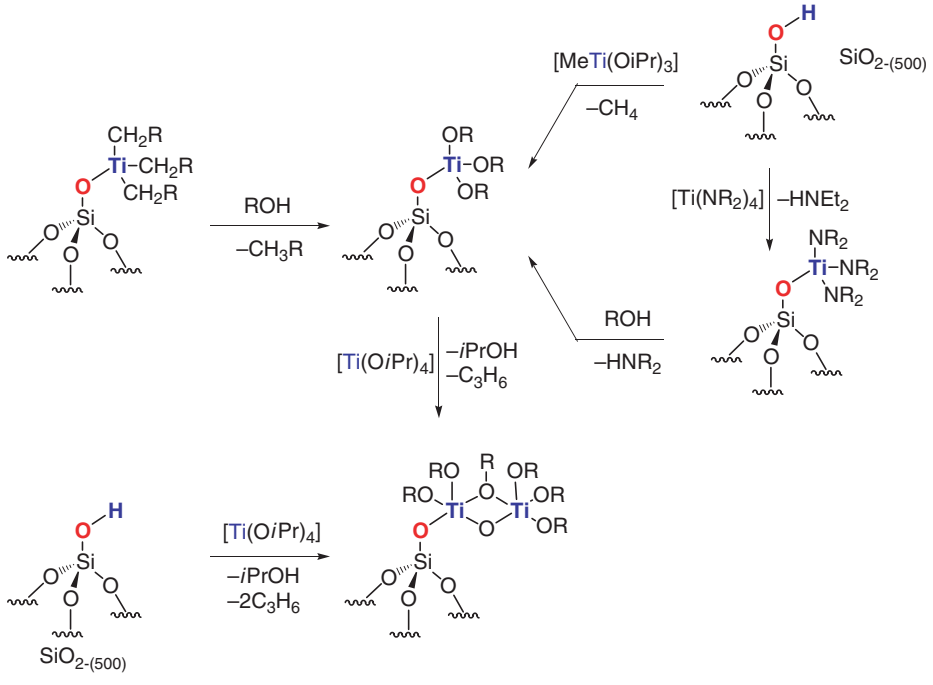

Scheme 23

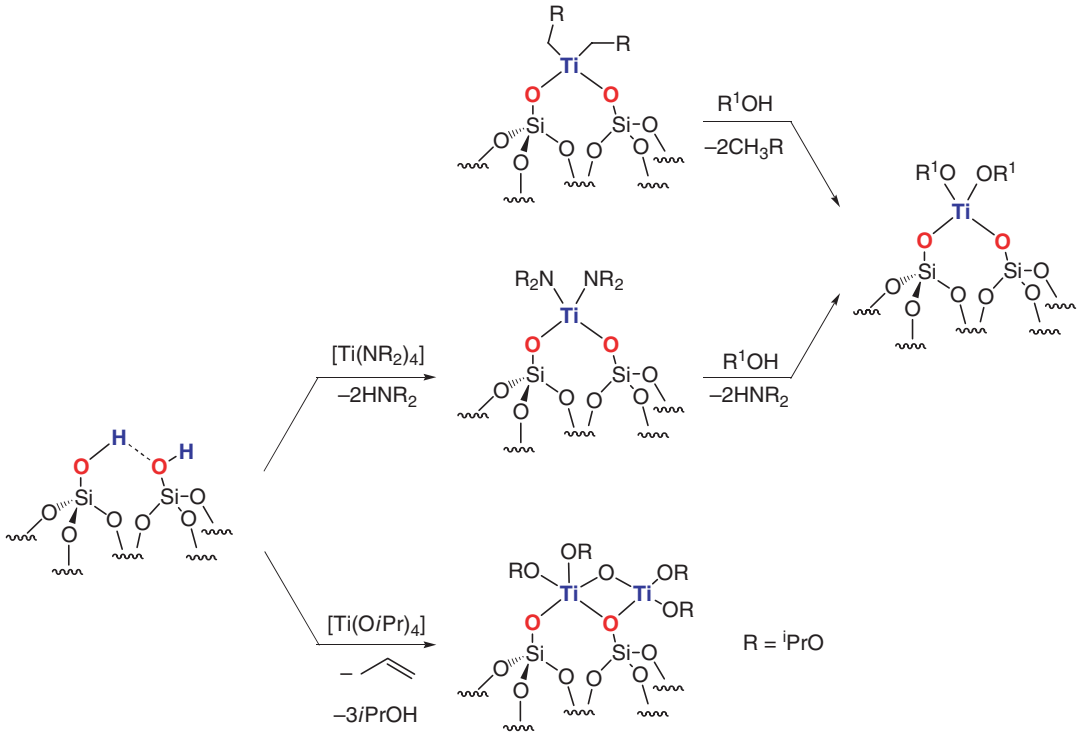

Scheme 24

When $[Ti(OSiMe_3)_4]$ is used as a precursor, it also reacts with the surface silanols of $SiO_{2\text{-}(500)}$ to give $[(\equiv SiO)Ti(OSiMe_3)_3]$ and Me_3SiOH, but this latter molecule further reacts with silica to give $[(\equiv SiO)SiMe_3]$ and H_2O (Scheme 25).[126] In contrast, grafting larger siloxide complexes, namely, $[Ti(OSi(O^tBu)_3)_4]$, $[(i\text{-PrO})Ti(OSi(O^tBu)_3)_3]$, and $[(^tBuO)_3Ti(OSi(O^tBu)_3)]$, on SBA-15 dehydroxylated at 200 °C gives mainly and respectively $[(\equiv SiO)Ti(OSi(O^tBu)_3)_3]$, $[(\equiv SiO)Ti(O^iPr)(OSi(O^tBu)_3)_2]$, and $[(\equiv SiO)Ti(O^tBu)_3]$ along with $[HOSi(O^tBu)_3)_3]$.[127] Note that the Ti–OSi bond is selectively cleaved over Ti–OR or TiO–Si bonds. Additionally, the reaction of the dimeric system $[(^tBuO)_2Ti\{\mu\text{-}O_2Si[OSi(O^tBu)_3]_2\}]_2$ is more complex and gives several surface complexes as evidenced by the formation of ^tBuOH and $[HOSi(O^tBu)_3]$ (Scheme 26).[128]

Another approach to the preparation of a well-defined Ti system is to graft $(MeOcalixO_3)TiCl$ on SiO_2, thus providing $(SiO)Ti(O_3calixOMe)$ as evidence by NMR spectroscopy (Scheme 27).[129,130]

All these systems are probably structurally close to the Shell catalysts,[131] and have been used as well-defined catalyst precursors for the epoxidation of terminal olefins by *t*-butyl hydroperoxide (TBHP).

In a similar way, acac Zr derivatives, $[(\equiv SiO)Zr(Oacac)_3]$ and $[(\equiv SiO)_3Zr(Oacac)]$ can be prepared by reacting $Zr(Oacac)_4$ with $SiO_{2\text{-}(500)}$ (Scheme 28) and by reacting $[(\equiv SiO)_3Zr\text{-}H]$ with acac (Scheme 18), respectively.[111] These systems have been used as transesterification catalyst precursors.

12.10.2.6 Group 5 Complexes

12.10.2.6.1 Supported perhydrocarbyl group 5 complexes

12.10.2.6.1.(i) Vanadium

In general, vanadium molecular organometallic complexes react with silica to give the corresponding siloxy surface complex through the cleavage of the V–C bond (Schemes 29 and 30, Table 10).

For example, $(C_5H_5)_2V\text{-}Me$ reacts with $SiO_{2\text{-}(700)}$ to give the corresponding surface complex $[(\equiv SiO)V^{III}(C_5H_5)_2]$.[132] Similarly, the molecular V(IV) complex $[V(CH_2SiMe_3)_4]$ gives $[(\equiv SiO)_2V(CH_2SiMe_3)_2]$ and $[(\equiv SiO)V(CH_2SiMe_3)_3]$, when grafted on $SiO_{2\text{-}(200)}$ and $SiO_{2\text{-}(500)}$, respectively.[74,133] Finally, grafting of $V(=NR)(CH_2{}^tBu)_3$ on $SiO_{2\text{-}(200)}$ provides $[(\equiv SiO)V((=NR)(CH_2{}^tBu))]$ as the major surface complex (Scheme 30).[134] These systems have been characterized by

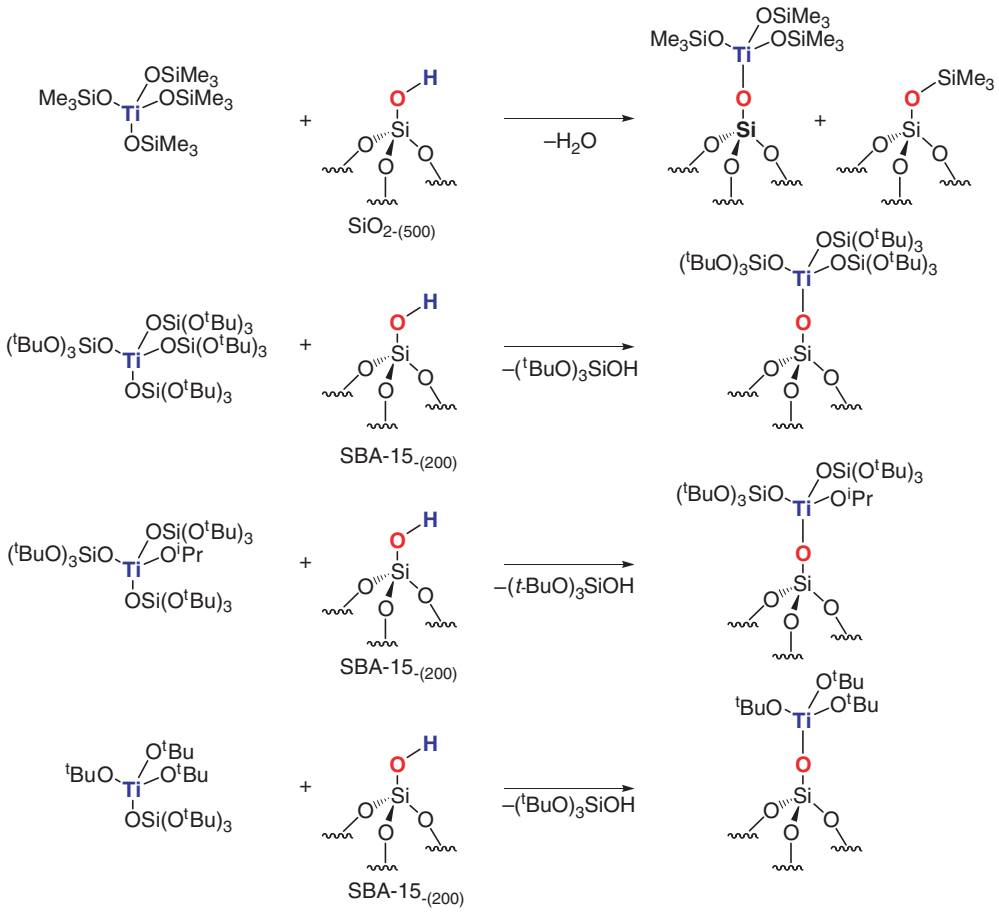

Scheme 25 Reaction of monomeric Ti siloxide complexes with silica materials.

mass balance analysis and IR spectroscopy. It is worth noting that $[(\equiv SiO)_2V(CH_2SiMe_3)_2]$ yields the corresponding carbene complexes $[(\equiv SiO)_2V(=CHSiMe_3)]$ and tetramethylsilane upon thermolysis (heated under vacuum at 70 °C).[133]

12.10.2.6.1.(ii) Niobium

The reaction of $Nb(C_3H_5)_4$ with oxide supports was studied in the early 1970s by ESR spectroscopy and showed that $[(\equiv SiO)Nb(C_3H_5)_3]$ is formed on $SiO_{2\text{-}(650)}$ (Scheme 31 and Table 10), while the corresponding reaction with $Al_2O_{3\text{-}(650)}$ gave a complex reaction mixture (at least three different species).[86]

12.10.2.6.1.(iii) Tantalum

The grafting of Ta organometallic complexes has been extensively studied (Table 10). In particular, when $[Ta(=CH^tBu)(CH_2{}^tBu)_3]$ is grafted on $SiO_{2\text{-}(500)}$, it yields a mixture of mono- and bis-siloxy surface complexes $[(\equiv SiO)Ta(=CH^tBu)(CH_2{}^tBu)_2]$ and $[(\equiv SiO)_2Ta(\equiv CH^tBu)(CH_2{}^tBu)]$.[135] Later, it was shown that the former and the latter could be obtained selectively when $SiO_{2\text{-}(700)}$ and $SiO_{2\text{-}(200)}$ are used, respectively (Scheme 32).[136] Grafting studies with deuterated silica have shown that the surface silanols react with the M–C and M=C bonds of the Ta complex. Later studies have allowed the intermediate complex $[(\equiv SiO)Ta(CH_2{}^tBu)_4]$ to be spectroscopically characterized, and this complex evolves into $[(\equiv SiO)Ta(=CH^tBu)(CH_2{}^tBu)_2]$ and 2,2-dimethylpropane through an α-H abstraction process.[137,138] It is worth noting that $[(\equiv SiO)Ta(=CH^tBu)(CH_2{}^tBu)_2]$ and $[(\equiv SiO)_2Ta(=CH^tBu)(CH_2{}^tBu)]$ are catalyst precursors for alkane metathesis (*vide infra*).[138,139] Cyclopentadienyl derivatives such as $[Cp^*TaMe_4]$ also react with the surface silanol of $SiO_{2\text{-}(450)}$ and $SiO_{2\text{-}(700)}$ to yield $[(\equiv SiO)TaMe_3Cp^*]$ (Scheme 33).[138,140] It is worth noting that $[(\equiv SiO)TaMe_2Cp_2]$ is obtained, whether starting from $[Cp_2TaMe_3]$ or $[Cp_2Ta(=CH_2)Me]$.[140]

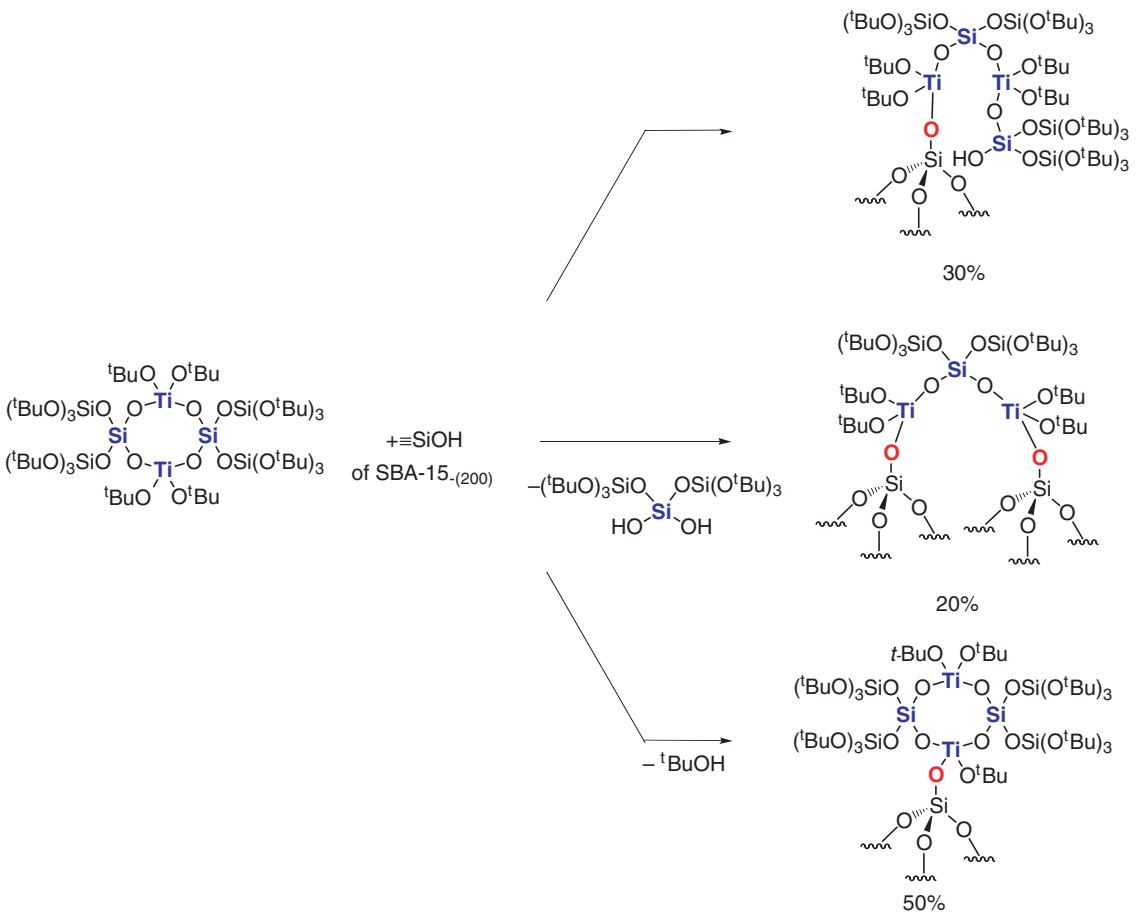

Scheme 26 Reaction of a dimeric Ti siloxide complex with SBA15.

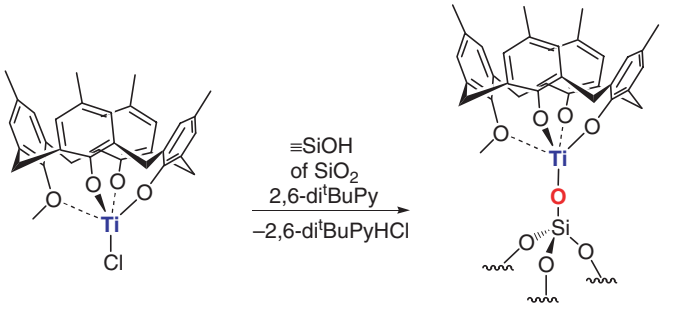

Scheme 27 Reaction of a calixarene Ti complex with silica.

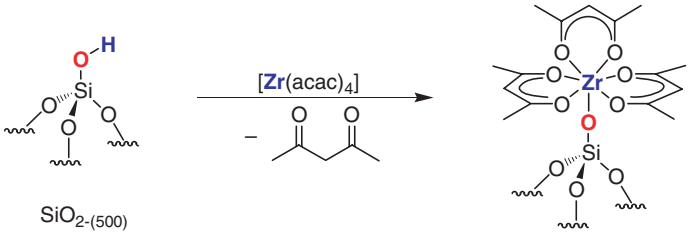

Scheme 28

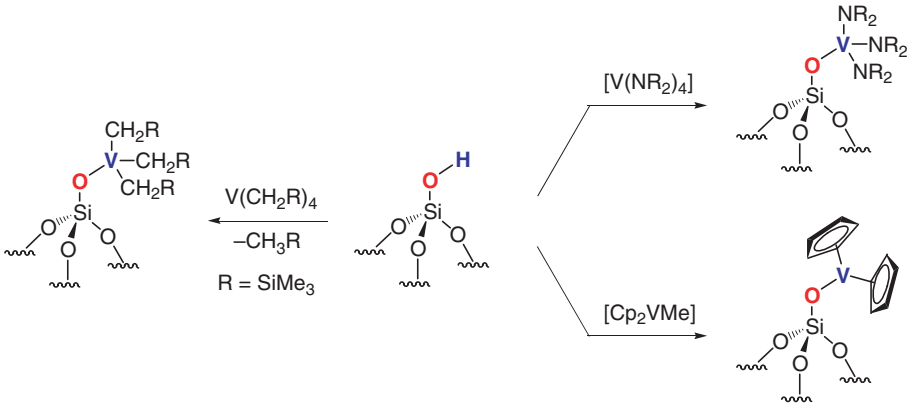

Scheme 29

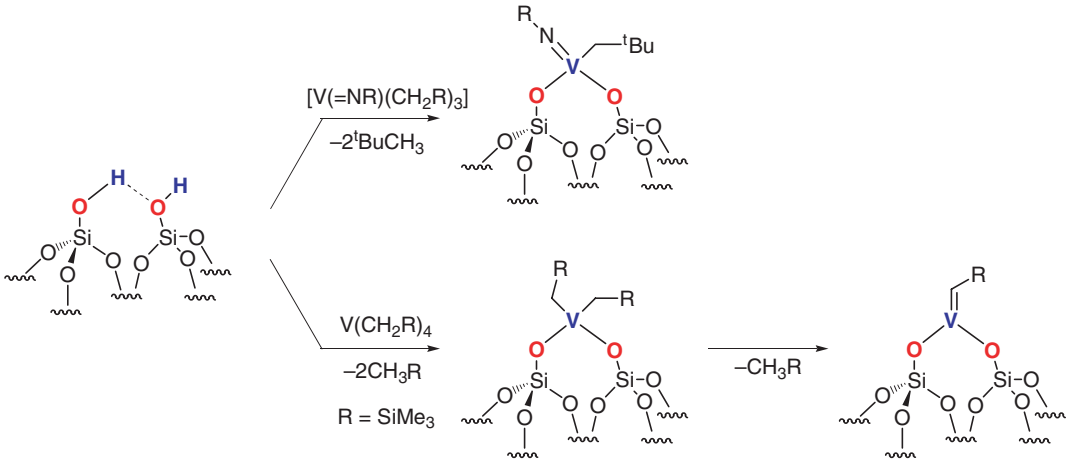

Scheme 30

Table 10 Surface species resulting from the reaction of group 5 organometallic complexes with silica materials

Molecular complex	*Oxide support*	*Structure*	*Analytical methods*	*References*
$(C_5H_5)_2$V-Me	$SiO_{2\text{-}(700)}$	$(\equiv SiO)V(C_5H_5)_2$	Chem., IR	132
$V(CH_2SiMe_3)_4$	$SiO_{2\text{-}(500)}$	$(\equiv SiO)V(CH_2SiMe_3)_3$	Chem., IR	74,133
$V(CH_2SiMe_3)_4$	$SiO_{2\text{-}(200)}$	$(\equiv SiO)_2V(CH_2SiMe_3)_2$	Chem., IR	74,133
$V(=NR)(CH_2{}^tBu)_3$	$SiO_{2\text{-}(200)}$	$(\equiv SiO)_2V(=NR)(CH_2{}^tBu)$	Chem., IR	134
$Nb(C_3H_5)_4$	$SiO_{2\text{-}(650)}$	$(\equiv SiO)Nb(C_3H_5)_3$	Chem., ESR	86
$Ta(=CH^tBu)(CH_2{}^tBu)_3$	$SiO_{2\text{-}(200)}$	$(\equiv SiO)_2Ta(=CH^tBu)(CH_2{}^tBu)$	Chem., IR	136
$Ta(=CH^tBu)(CH_2{}^tBu)_3$	$SiO_{2\text{-}(500)}$	[a]	Chem., IR	135
$Ta(=CH^tBu)(CH_2{}^tBu)_3$	$SiO_{2\text{-}(700)}$	$(\equiv SiO)Ta(=CH^tBu)(CH_2{}^tBu)_2$	Chem., IR, NMR, EXAFS	137,138
$[Cp^*TaMe_4]$	$SiO_{2\text{-}(700)}$	$(\equiv SiO)TaCp^*Me_3$	Chem., IR, NMR, EXAFS	138,139
$[Cp^*TaMe_4]$	$SiO_{2\text{-}(450)}$	$(\equiv SiO)TaCp^*Me_3$	Chem., NMR	140
$[Cp_2TaMe_3]$	$SiO_{2\text{-}(450)}$	$(\equiv SiO)TaCp_2Me_2$	Chem., NMR	140
$[Cp_2Ta(CH_2)Me]$	$SiO_{2\text{-}(450)}$	$(\equiv SiO)\ TaCp_2Me_2$	Chem., NMR	140

[a] A 35 : 65 mixture of $(\equiv SiO)_2Ta(=CH^tBu)(CH_2{}^tBu)$ and $(\equiv SiO)Ta(=CH^tBu)(CH_2{}^tBu)_2$.

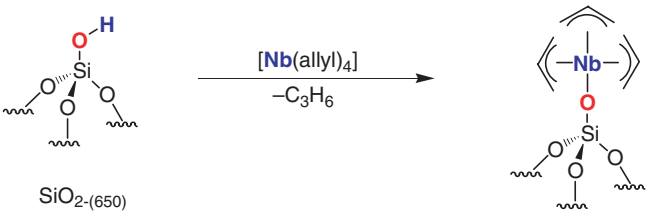

Scheme 31

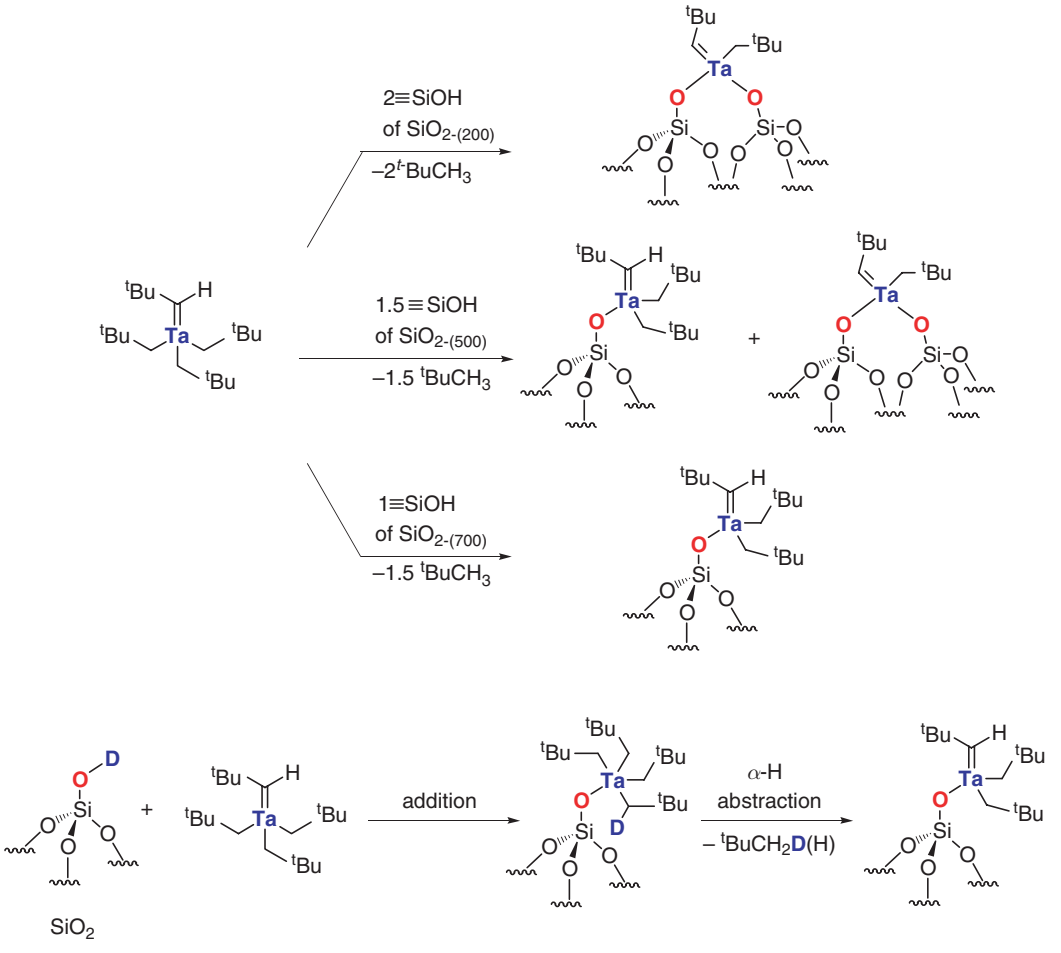

Scheme 32

12.10.2.6.2 Supported group 5 hydride complexes

The silica-supported tantalum hydride, [(≡SiO)$_2$Ta-H], is prepared by the treatment of a mixture of [(≡SiO)Ta-(=CH^{t}Bu)(CH$_2$^{t}Bu)$_2$] and [(≡SiO)$_2$Ta(=CH^{t}Bu)(CH$_2$^{t}Bu)] with H_2 at 150 °C. This method generates [(≡SiO)$_2$Ta-H] as the major species according to M–H titration, and IR and EXAFS spectroscopies (Scheme 34).[141,142] Moreover, treatment of this species with PMe_3 affords the corresponding mono-adduct [(≡SiO)$_2$Ta-H(PMe_3)] (Scheme 35),[143] whereas its treatment under H_2 at 450 °C leads to [(≡SiO)$_3$Ta].[144] Finally, cycloalkanes react with [(≡SiO)$_2$Ta-H] to give the corresponding cycloalkyl products at room temperature (Scheme 35).[141,145] These latter surface species readily dehydrogenate, and, for instance, thermolysis of the cyclopentyl derivative gives the cyclopentadienyl complex.[146]

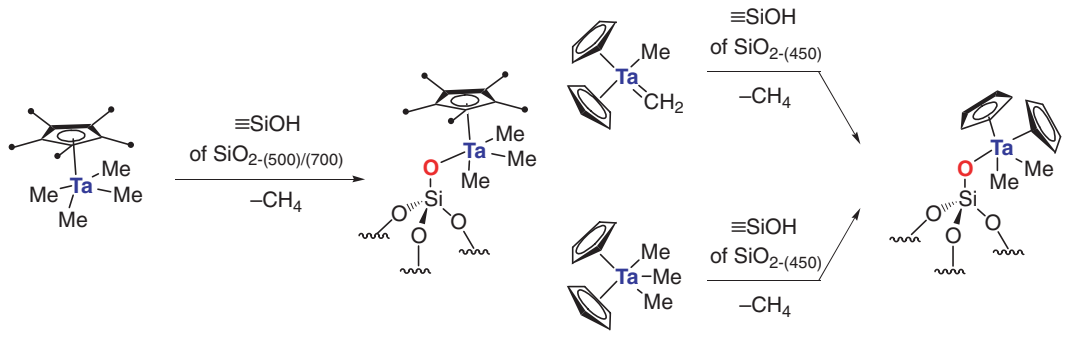

Scheme 33

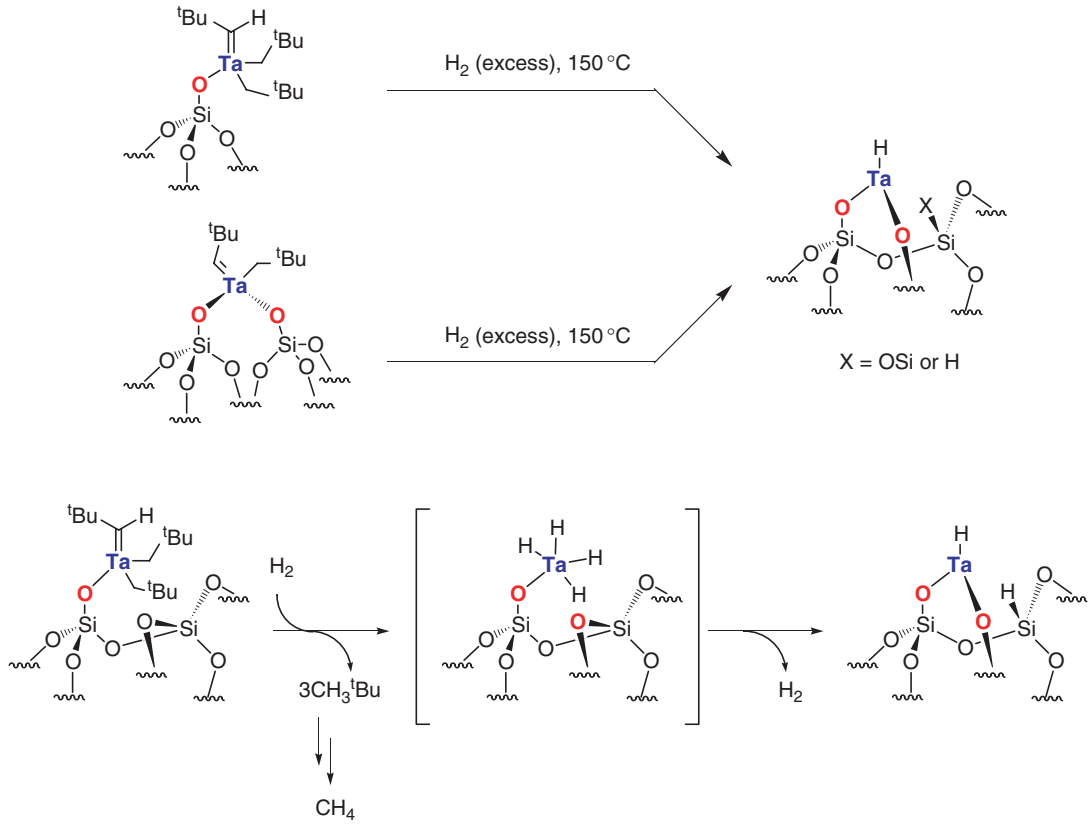

Scheme 34 Proposed mechanism of formation of the silica-supported tantalum hydride.

The catalytic properties of this silica-supported tantalum hydrides are noteworthy. First, H/D exchange in D_2/CH_4 mixture is fast (0.2 mol/mol/s at 150 °C), which shows that these systems readily cleave and reform the C–H bonds of alkanes (Scheme 36(a)).[147] Second, it also converts alkanes into its lower homologs and ultimately methane in the presence of H_2 (hydrogenolysis) at relatively low temperatures (150 °C).[148] The key step of carbon–carbon bond cleavage probably corresponds to an α-alkyl transfer on a Ta(III) intermediate followed by successive hydrogenolysis steps (Schemes 36(b) and 37). In the case of cycloalkanes, hydrogenolysis yields smaller cycloalkanes, but deactivation is very fast. This phenomenon has been associated with the rapid formation of cyclopentane and, thereby, with the formation of cyclopentadienyl derivatives (*vide supra* Scheme 35), which are inactive for the hydrogenolysis of alkanes.[146]

Third, besides hydrogenolysis properties, the silica-supported tantalum hydride catalyzes the metathesis of alkanes, which transforms a given alkane into its higher and lower homolog (Scheme 36(c)).[149,150] This reaction

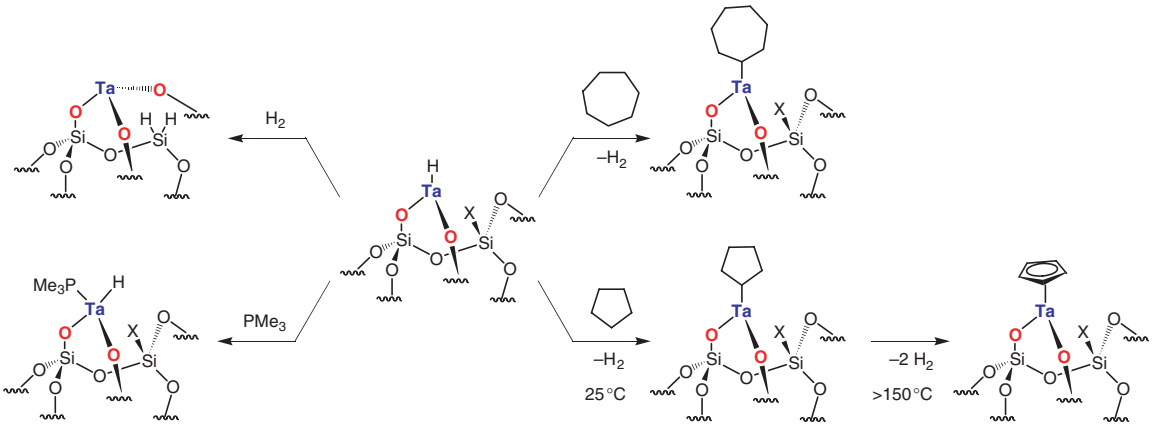

Scheme 35 Reactivity of [(≡SiO)$_2$Ta–H] with H_2, PMe_3, and cycloalkanes.

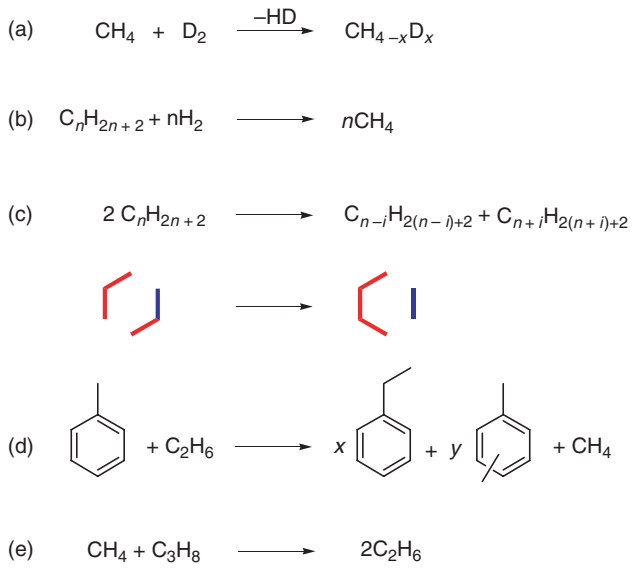

Scheme 36 (a) H/D exchange, (b) alkane hydrogenolysis, (c) alkane metathesis, (d) cross-metathesis of toluene/ethane, (e) cross-metathesis of propane/methane.

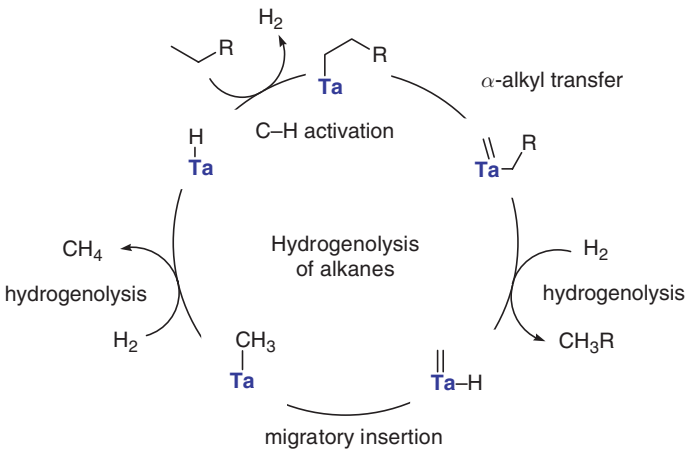

Scheme 37 Proposed mechanism for alkane hydrogenolysis.

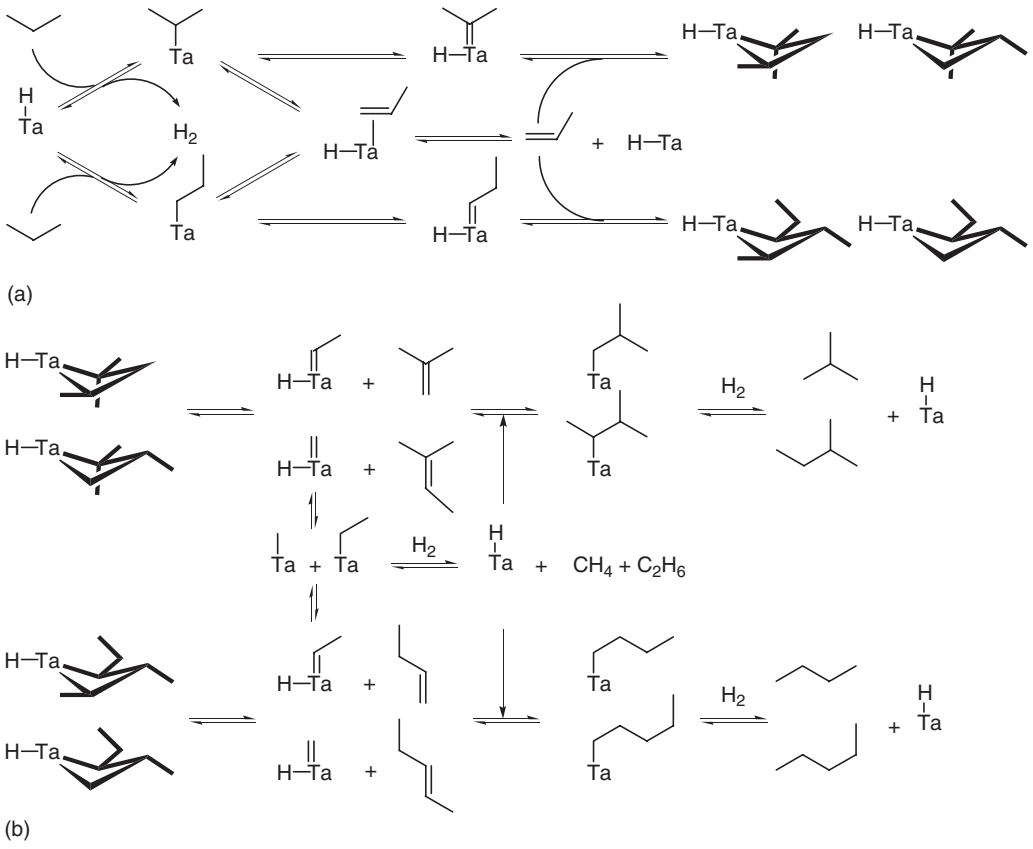

Scheme 38 Proposed mechanism for alkane metathesis.

takes place through known elementary steps of solution organometallic chemistry: C–H bond activation via σ-bond metathesis, α-H versus β-H elimination, olefin metathesis, insertion, and hydrogenolysis (Scheme 38).

This reaction can be exploited to carry out the cross-metathesis of toluene and ethane to give ethylbenzene and xylenes (Scheme 36(d))[151] or that of methane and propane to yield two ethanes (Scheme 36(e)).[152]

12.10.2.6.3 Supported group 5 alkoxide and amido complexes

12.10.2.6.3.(i) Vanadium

The vanadium complex $[V(=O)(OR)_3]$ ($R = {}^{i}Pr$) reacts with partially dehydroxylated silica to give the corresponding monosiloxy surface complexes, $[(\equiv SiO)V(=O)(OR)_2]$, independently of the temperature of pretreatment of silica (25–500 °C) according to mass balance analysis, IR spectroscopy, as well as ^{51}V MAS NMR (Scheme 39 and Table 11).[153,154] Moreover, $[(\equiv SiO)V(=O)(OR)Cl]$ can also be obtained when $[(\equiv SiO)V(=O)Cl_2]$, generated from $[V(=O)Cl_3]$,[153–155] is treated with a large excess of alcohol at room temperature. A full substitution of the chlorine ligand is observed only when the reaction is performed at higher temperatures (70 °C), thus yielding $[(\equiv SiO)V(=O)(OR)_2]$.

The reactivity of $V(NR_2)_4$ with oxides is noteworthy: it yields $[(\equiv SiO)V(NR_2)_3]$, and $[(Al_sO)_2V(NR_2)_2]$ on silica and alumina, respectively, according to mass balance analysis and ESR spectroscopy, while a mixture of species of average structure $[(Ti_sO)_3V(NR_2)]$ is obtained on titania (Scheme 40).[156]

12.10.2.6.3.(ii) Tantalum

The reaction of $(RO)_2Ta(OSiOR_3)_3$ with the surface silanols of SBA-15 gives a mixture of surface species $[(\equiv SiO)Ta(OR)_2\{OSi(OR)_3\}_2]$ and $[(\equiv SiO)_2Ta(OR)_2\{OSi(OR)_3\}]$ as 1.5 equiv. of $HOSi(OR)_3$ are formed upon grafting (Scheme 41).[157] It is worth noting that the dimer $[Ta(OMe)_5]_2$ reacts with $SiO_{2\text{-}(700)}$ to give a monomer $[(\equiv SiO)Ta(OMe)_4]$. Such types of alkoxide can also be obtained by the alcoholysis of $[(\equiv SiO)Ta(=CH^tBu)_2(CH_2{}^tBu)_2]$.[158] Ta(III) alkoxides can also be prepared from $[(\equiv SiO)_2Ta\text{-}H]$, by either its treatment with H_2 at 450 °C yielding $[(\equiv SiO)_3Ta]$[144]

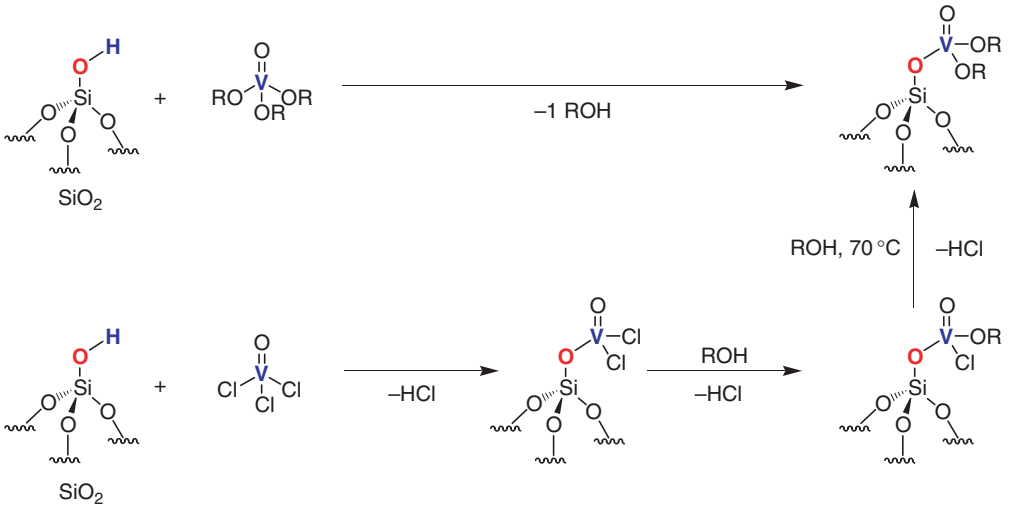

Scheme 39 Surface chemistry of molecular oxovanadium alkoxides and chlorides.

Table 11 Surface species resulting from the reaction of group 5 alkoxide complexes with silica materials

Molecular complex	*Oxide support*	*Structure*	*Analytical methods*	*References*
$[V(=O)(O^iPr)_3]$	SiO_2	$(\equiv SiO)V(=O)(O^iPr)_2$	Chem.	153,154
$V(=O)Cl_3$	SiO_2	$(\equiv SiO)V(=O)(Cl)_2$	Chem., IR, NMR	153–155
$V(NR_2)_4$	SiO_2	$(\equiv SiO)V(NR_2)_3$	Chem., IR, ESR	156
$V(NR_2)_4$	Al_2O_3	$(Al_sO)_2V(NR_2)_2$	Chem., IR, ESR	156
$V(NR_2)_4$	TiO_2	$(Ti_sO)_3V(NR_2)$	Chem., IR, ESR	156
$(RO)_2Ta(OSiOR_3)_3$	SBA-15	[a]	Chem.	157
$[Ta(OMe)_5]_2$	$SiO_{2\text{-}(700)}$	$(\equiv SiO)Ta(OMe)_4$	Chem., IR, NMR	158

[a]Mixture of $[(\equiv SiO)Ta(OR)_2\{OSi(OR)_3\}_2]$ and $[(\equiv SiO)_2Ta(OR)_2\{OSi(OR)_3\}]$.

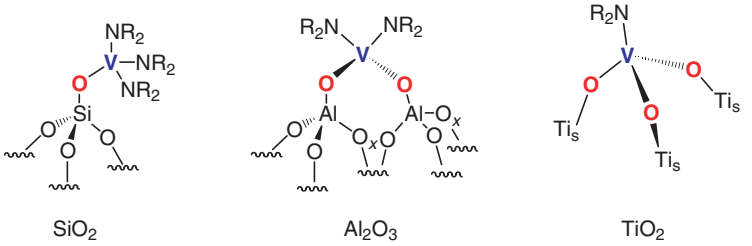

Scheme 40 Surface reaction of $[V(NR_2)_4]$ with various oxide supports.

or its reaction with *t*-Bu_2CO at room temperature giving $[(\equiv SiO)_2Ta\text{-}OCH^tBu_2]$.[141] Additionally, $[(\equiv SiO)_3Ta]$ reacts with ethanol to generate $[(\equiv SiO)_3Ta(OEt)_2]$ and 1 equiv. of H_2, and its reaction with O_2 gives $[(\equiv SiO)_3Ta{=}O]$.[144]

12.10.2.7 Group 6 Complexes

12.10.2.7.1 Chromium

A competitor of Phillips catalyst, based on chromium oxide supported on silica, is the Union Carbide catalyst, which is prepared by the reaction of chromocene with silica. When chromocene, $[Cp_2Cr^{II}]$, reacts with $SiO_{2\text{-}(800)}$, it gives $[(\equiv SiO)Cr(Cp)]$ according to mass balance analysis (Scheme 42 and Table 12), and this surface complex is highly active in ethylene polymerization.[159]

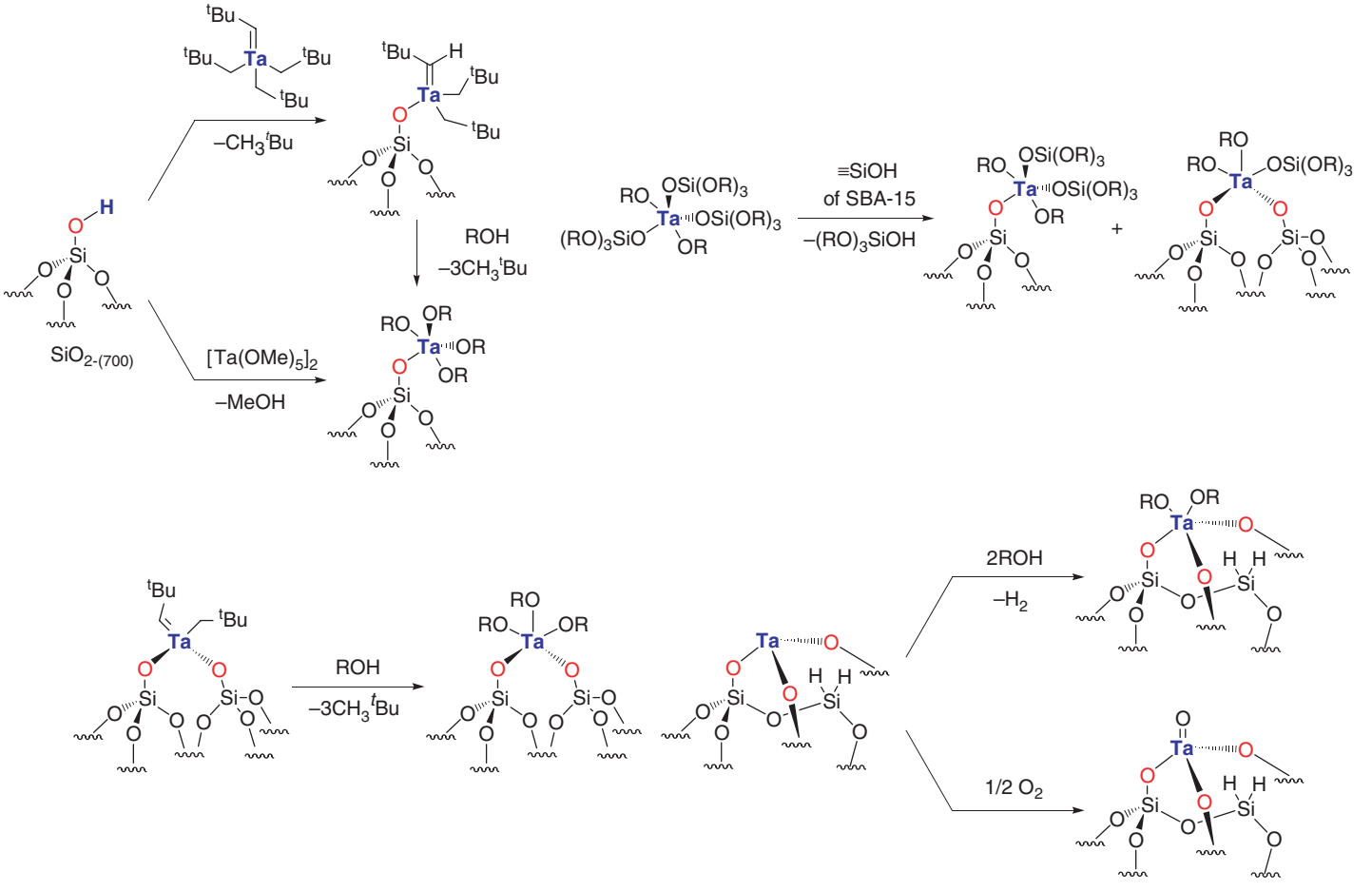

Scheme 41 Preparation of Ta alkoxide derivatives.

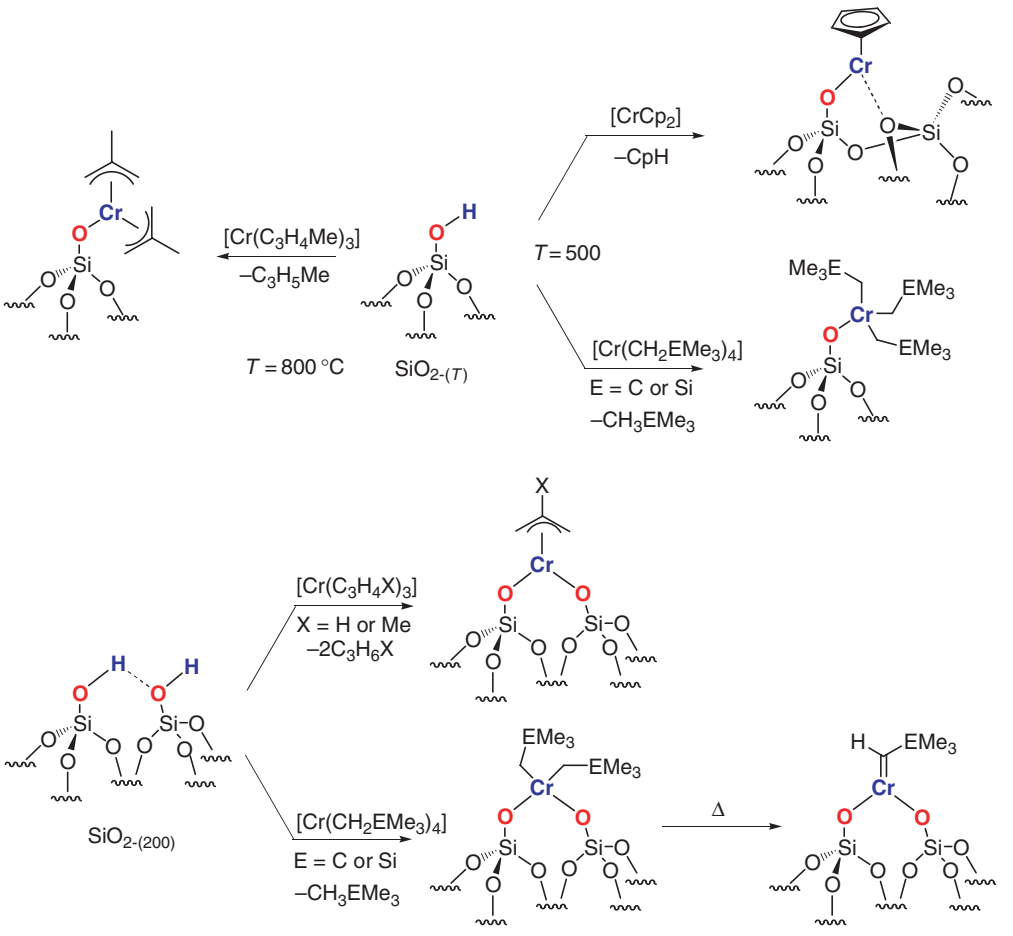

Scheme 42 Preparation of supported Cr complexes.

The grafting of other chromium alkyl derivatives has also been investigated, such as chromium(III) allyl and methallyl complexes.[86,160] The corresponding olefins (propene and 2-methylopropene) are formed upon grafting along with a small amount of dienes, thus showing that the major grafting pathway corresponds to the electrophilic cleavage of the Cr–C bond.[160] The major surface species correspond to $[(\equiv SiO)_2Cr(allyl)]$ and $[(\equiv SiO)_2Cr(methallyl)]$ on $SiO_{2\text{-}(200)}$ according to elemental analysis, while $[(\equiv SiO)Cr(methallyl)_2]$ is obtained on $SiO_{2\text{-}(800)}$ (Scheme 42).[86,160]

As its group 4 analogs, $[Cr(CH_2{}^tBu)_4]$ reacts with $SiO_{2\text{-}(200)}$ and $SiO_{2\text{-}(500)}$ to give $[(\equiv SiO)_2Cr(CH_2{}^tBu)_2]$ and $[(\equiv SiO)Cr(CH_2{}^tBu)_3]$, respectively (Table 12).[161] Similarly, the neosilyl analog also shows the same reactivity, thus providing the corresponding surface complexes, $[(\equiv SiO)_2Cr(CH_2SiMe_3)_2]$ and $[(\equiv SiO)Cr(CH_2SiMe_3)_3]$.[161] It is worth noting that when $[(\equiv SiO)_2Cr(CH_2{}^tBu)_2]$ or $[(\equiv SiO)_2Cr(CH_2SiMe_3)_2]$ is heated in a vacuum at 70 °C, they yield the corresponding carbene complexes $[(\equiv SiO)_2Cr(=CH{}^tBu)]$ and $[(\equiv SiO)_2Cr(=CHSiMe_3)]$ along with 2,2-dimethylpropane and tetramethylsilane, respectively.[74,133,162] Elimination of neopentane occurs through an α-H abstraction process, and kinetic studies further confirmed this pathway ($\Delta H^{\ddagger} = 11\ kcal\ mol^{-1}$, $\Delta S^{\ddagger} = -43\ cal\ K^{-1}\ mol^{-1}$).[163] This system is thought to be a good model of the Phillips polymerization catalysts.[164]

12.10.2.7.2 Molybdenum

12.10.2.7.2.(i) Supported molybdenum perhydrocarbyl complexes

The reaction of $Mo^{IV}(C_3H_5)_4$ and $SiO_{2\text{-}(550)}$ provides propene and 1,5-hexadiene. The complex $[(\equiv SiO)_2Mo(C_3H_5)_2]$ has been proposed as the major surface species based on the evolution of propene, but other grafting processes probably take place as evidenced by the formation of 1,5-hexadiene (Scheme 43 and Table 12).[86,165] More recently, it has been shown through IR and NMR spectroscopy that the reaction of $[Mo(\equiv C{}^tBu)(CH_2{}^tBu)_3]$ and $SiO_{2\text{-}(700)}$ gives $[(\equiv SiO)Mo(\equiv C{}^tBu)(CH_2{}^tBu)_2]$ through the replacement of one 2,2-dimethypropyl ligand by a surface siloxy ligand

Table 12 Surface species resulting from the reaction of group 6 organometallic and alkoxide complexes with oxide materials

Molecular complex	*Oxide support*	*Structure*	*Analytical methods*	*References*
Cp_2Cr	SiO_2	$(\equiv SiO)Cr(C_5H_5)$	Chem.	159
$Cr(allyl)_3$	$SiO_{2\text{-}(200)}$	$(\equiv SiO)_2Cr(allyl)$	Chem.	86,160
$Cr(methallyl)_3$	$SiO_{2\text{-}(200)}$	$(\equiv SiO)_2Cr(methallyl)$	Chem., IR	86,160
$Cr(methallyl)_3$	$SiO_{2\text{-}(800)}$	$(\equiv SiO)Cr(methallyl)_2$	Chem., IR	86,160
$Cr(CH_2{}^tBu)_4$	$SiO_{2\text{-}(200)}$	$(\equiv SiO)_2Cr(CH_2{}^tBu)_2$		161
$Cr(CH_2{}^tBu)_4$	$SiO_{2\text{-}(500)}$	$(\equiv SiO)Cr(CH_2{}^tBu)_3$	Chem., IR, ESR	161
$Cr(CH_2SiMe_3)_4$	$SiO_{2\text{-}(200)}$	$(\equiv SiO)_2Cr(CH_2SiMe_3)_2$	Chem., IR, ESR	161
$Cr(CH_2SiMe_3)_4$	$SiO_{2\text{-}(500)}$	$(\equiv SiO)Cr(CH_2SiMe_3)_3$	Chem., IR, ESR	161
$Mo(C_3H_5)_4$	$SiO_{2\text{-}(200)}$	$(\equiv SiO)_2Mo(C_3H_5)_2$[a]	Chem.	86,165
$Mo(\equiv C^tBu)(CH_2{}^tBu)_3$	$SiO_{2\text{-}(700)}$	$(\equiv SiO)Mo(\equiv C^tBu)(CH_2{}^tBu)_2$	Chem., IR, NMR	166
$Mo(\equiv N)(CH_2{}^tBu)_3$	$SiO_{2\text{-}(500)}$	$(\equiv SiO)Mo(=NH)(=CH^tBu)(CH_2{}^tBu)$	Chem., IR	167
$Mo(\equiv N)(CH_2{}^tBu)_3$	$SiO_{2\text{-}(700)}$	$(\equiv SiO)Mo(=NH)(=CH^tBu)(CH_2{}^tBu)$	Chem., IR	168
$Mo(\equiv N)(O^tBu)_3$	$SiO_{2\text{-}(700)}$	$(\equiv SiO)Mo(\equiv N)(O^tBu)_2$	Chem., IR, NMR	169
$Mo(=O)(OSiOR_3)_4$	SBA-15	$(\equiv SiO)Mo(=O)(OSiOR_3)_3$	Chem., IR, NMR, Raman, UV	170
WMe_6	SiO_2	$(\equiv SiO)_xWMe_{6-x}$[b]	Chem.	171,172
$W(allyl)_4$	SiO_2	$(\equiv SiO)_2W(allyl)_2$[a]	Chem.	86,172
$W(\equiv C^tBu)(CH_2{}^tBu)_3$	$SiO_{2\text{-}(200)}$	$(\equiv SiO)W(\equiv C^tBu)(CH_2{}^tBu)_2$	Chem, IR, NMR	173,174
$W(\equiv C^tBu)(CH_2{}^tBu)_3$	$SiO_{2\text{-}(700)}$	$(\equiv SiO)_2W(\equiv C^tBu)(CH_2{}^tBu)$	Chem., IR, NMR	173,174
$W(\equiv C^tBu)(CH_2{}^tBu)_3$	$Al_2O_{3\text{-}(500)}$	$(Al_sO)W(\equiv C^tBu)(CH_2{}^tBu)_2$	Chem., IR, NMR, EXAFS	174
$W(=O)(OSiOR_3)_4$	SBA-15	$(\equiv SiO)W(=O)(OSiOR_3)_3$	Chem., IR, NMR, Raman, UV	170

[a]Proposed average structure.
[b]Not characterized.

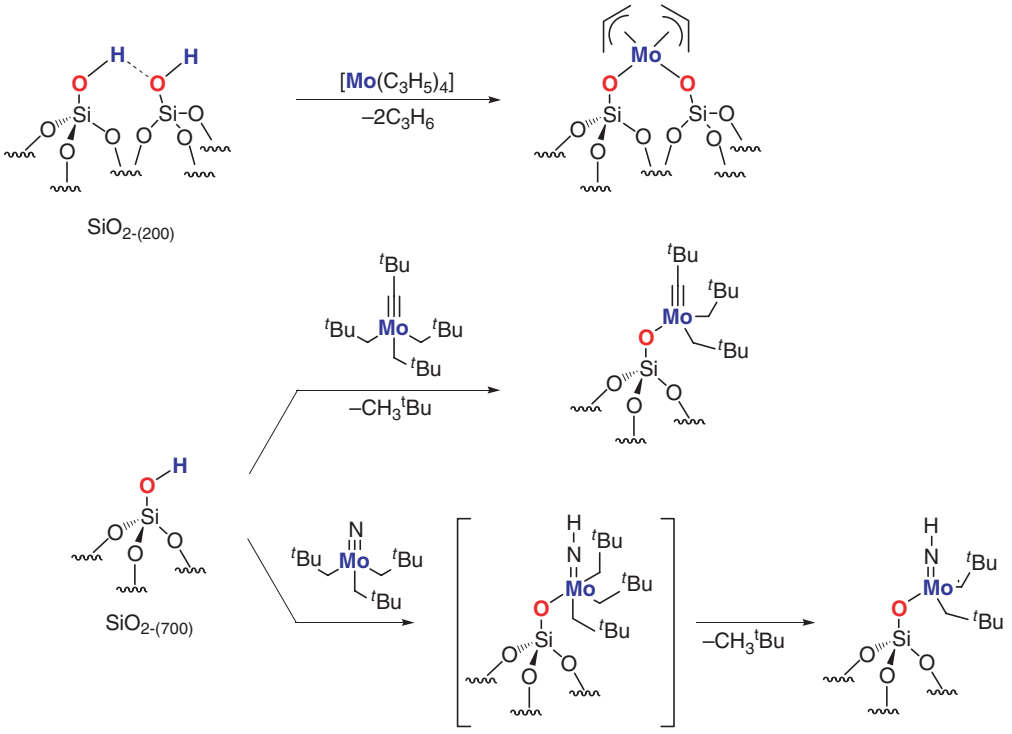

Scheme 43

through a protonolysis (Scheme 43).[166] In contrast, when the carbyne unit is replaced by a nitrido, as in [Mo(≡N)(CH$_2$^{t}Bu)$_3$], there is protonation of the nitrido ligand to give a putative surface imido intermediate [(≡SiO)Mo(=N-H)(CH$_2$^{t}Bu)$_3$], which readily decomposes to give an Mo alkylidene complex [(≡SiO)Mo(=N-H)(=CH^{t}Bu)(CH$_2$^{t}Bu)] according to mass balance analysis and chemical reactivity studies.[167] It is in fact a highly active olefin metathesis catalyst when prepared by impregnation.[168]

12.10.2.7.2.(ii) Supported molybdenum alkoxide complexes

Chemical and spectroscopic analyses of the grafting of [Mo(=N^{t}Bu)$_2$(OSiMe$_3$)$_2$] on SiO$_{2\text{-}(200)}$ are consistent with the formation of a 1 : 1 mixture of [(≡SiO)Mo(=N^{t}Bu)$_2$(OSiMe$_3$)] and [(≡SiOSiMe$_3$)] (Scheme 44).[126] The latter is due to the formation of [Me$_3$SiOH], which reacts with surface silanols, thus presumably forming water (not observed). Grafting of the corresponding alkoxide, [Mo(=N^{t}Bu)$_2$(O^{t}Bu)$_2$], is cleaner, providing [(≡SiO)$_2$Mo(=N^{t}Bu)$_2$] selectively. Similarly, [Mo(≡N)(O^{t}Bu)$_3$] grafts on SiO$_{2\text{-}(700)}$ or MCM-41$_{\text{-}(500)}$ via a direct exchange of the ^{t}BuO ligand by surface siloxy ligands to give [(≡SiO)Mo(≡N)(O^{t}Bu)$_2$] (Scheme 44 and Table 12).[169] This is in contrast to [Mo(≡N)(CH$_2$^{t}Bu)$_3$], which grafts by protonation of the nitrido ligand (*vide supra*), and this difference is probably associated with the stronger Mo–N bond in [Mo(≡N)(O^{t}Bu)$_3$] (as evidenced by its shorter Mo–N distance) and a greater polarizability of the Mo–O^{t}Bu bond. While highly active in the epoxidation of cyclohexene by TBHP, the catalyst deactivates through leaching of Mo.

Similarly, [Mo(=O)(OSiOR$_3$)$_4$] reacts with SBA-15 to generate an isolated Mo oxo species [(≡SiO)Mo(=O)(OSiOR$_3$)$_3$] (Scheme 44), which is an active olefin epoxidation catalyst.[170]

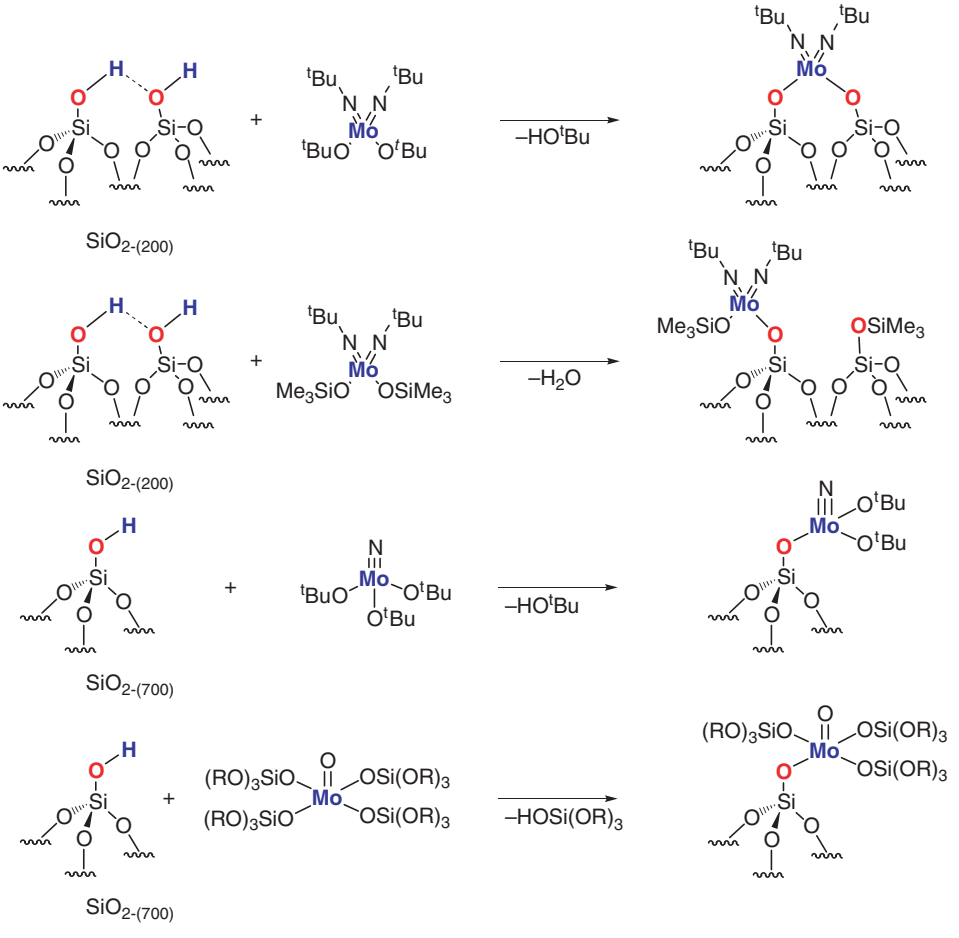

Scheme 44

12.10.2.7.3 Tungsten

12.10.2.7.3.(i) Supported tungsten perhydrocarbyl complexes

One of the first examples reported was the reaction of $[WMe_6]$ with silica (Table 12). While the structure has not been investigated in detail, it probably generates $[(\equiv SiO)_xWMe_{6-x}]$ surface species.[171,172] Similarly to Mo, the allyl W derivative $[W(allyl)_4]$ reacts with SiO_2 to give a surface complex reported as $[(\equiv SiO)_2W(allyl)_2]$ (Scheme 45).[86,172] Conversely, grafting $[W(\equiv C^tBu)(CH_2{}^tBu)_3]$ on $SiO_{2\text{-}(200)}$ and $SiO_{2\text{-}(700)}$ gives $[(\equiv SiO)W(\equiv C^tBu)(CH_2{}^tBu)_2]$ and $[(\equiv SiO)_2W(\equiv C^tBu)(CH_2{}^tBu)]$, respectively (Scheme 45).[173,174] Originally, it was proposed that grafting $[W(\equiv C^tBu)(CH_2{}^tBu)_3]$ generated a metallocarbene, because it was an highly active olefin metathesis catalyst.[175] Similar metallocarbene structures have been proposed when $[W(\equiv C^tBu)(CH_2{}^tBu)_3]$ is grafted on SiO_2-Al_2O_3,[174] Al_2O_3,[174] and Nb_2O_5 because of their very high activity in olefin metathesis.[174,176] However, a recent reinvestigation of the grafting of $[W(\equiv C^tBu)(CH_2{}^tBu)_3]$ on Al_2O_3 showed that a monoaluminoxy species $[(Al_sO)W(\equiv C^tBu)(CH_2{}^tBu)_2]$ was also formed selectively according to elemental analysis, solid-state NMR, and EXAFS spectroscopies.[174,177] Other tungstenocarbyne complexes have been grafted on silica such as $[W(\equiv C^tBu)(O^tBu)_3]$ and $[W(\equiv C^tBu)(Cl)_3]$. While the formation of carbene complexes, $[(\equiv SiO)W(=CH^tBu)(X)_3]$,[175] was proposed, they are probably metallocarbyne complexes $[(\equiv SiO)W(\equiv C^tBu)(X)_2]$, obtained by substitution of the X ligand by the surface siloxy group. More work is clearly necessary to clarify the structures of these complexes.

12.10.2.7.3.(ii) Supported tungsten hydride complexes

In contrast to groups 4 and 5 transition metal complexes supported on silica, the treatment by H_2 of W surface organometallic derivatives, namely, $[(\equiv SiO)W(\equiv C^tBu)(CH_2{}^tBu)_2]$ and $[(\equiv SiO)_2W(\equiv C^tBu)(CH_2{}^tBu)]$, mainly lead to sintering (re-formation of silanols and detection of W particles by transmission electron microscopy (TEM)) and the hydride is obtained only in minute amounts. On the other hand, $[(Al_sO)W(\equiv C^tBu)(CH_2{}^tBu)_2]$ reacts with H_2 to give tungsten hydride species $[(Al_sO)_2W(H)_x]$ with no evidence of sintering, as evidenced by the presence of W–H and Al–H bands in the IR spectrum (Scheme 46).[177]

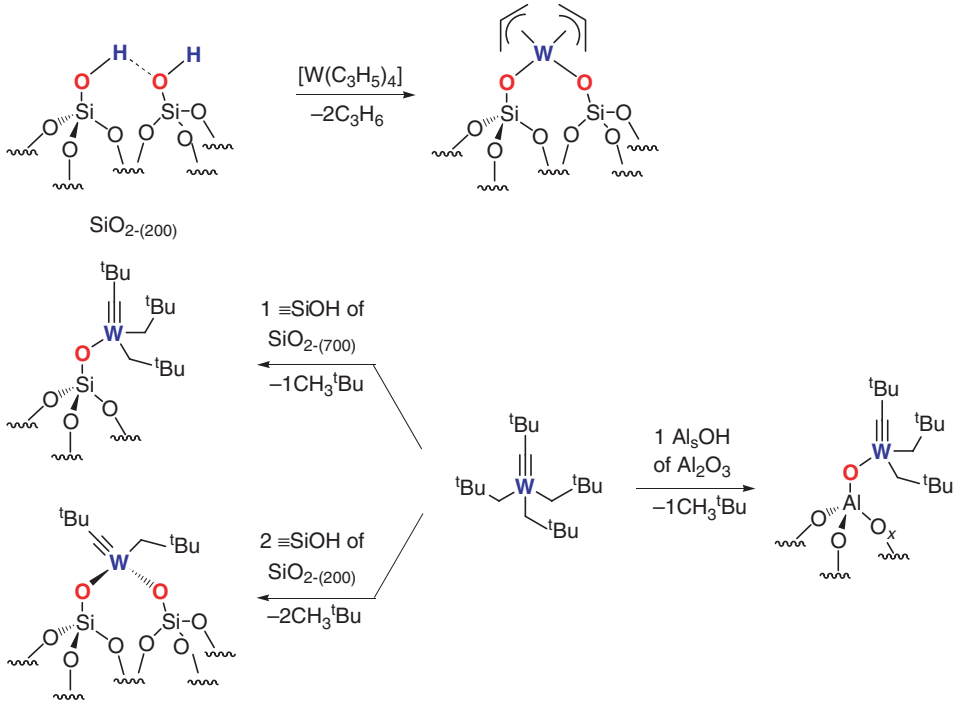

Scheme 45

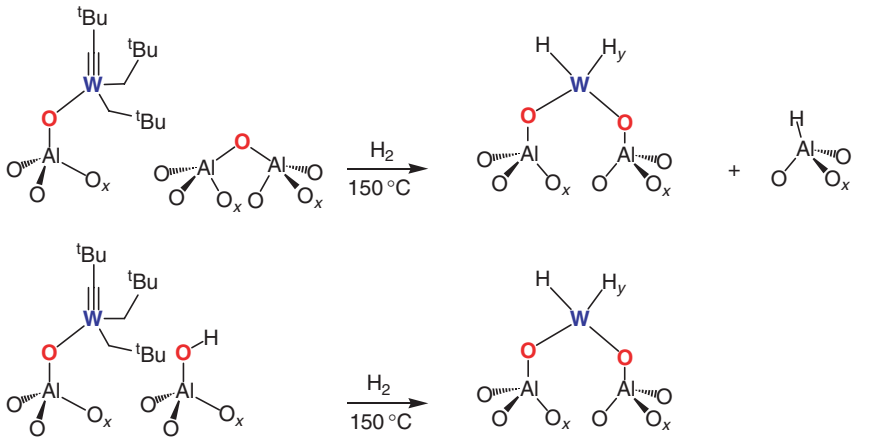

Scheme 46 Proposed formation of tungsten hydride supported on alumina.

12.10.2.7.3.(iii) Supported tungsten alkoxide complexes

As for $[Mo(=O)(OSiOR_3)_4]$, $[W(=O)(OSiOR_3)_4]$ reacts with the silanol group of an SBA-15 material to generate isolated W oxo species, $[(\equiv SiO)W(=O)(OSiOR_3)_3]$ (Scheme 47), which is an active olefin epoxidation catalyst.[170]

12.10.2.8 Group 7 Complexes

12.10.2.8.1 Manganese

Mass balance analysis and ESR spectroscopy show that a well-defined Mn(II) complex, $Mn(CH_2{}^tBu)_2(TMEDA)$, gives the $[(\equiv SiO)Mn(CH_2{}^tBu)(TMEDA)]$ on $SiO_{2\text{-}(700)}$, while a mixture of $[(\equiv SiO)Mn(CH_2{}^tBu)(TMEDA)]$ and $[(\equiv SiO)_2Mn(TMEDA)]$ are obtained on silica dehydroxylated at lower temperature (Scheme 48 and Table 13).[178] It is worth noting that these supported Mn complexes are quite unreactive; no reaction is observed with ethene and N_2O, but they react violently with O_2.

12.10.2.8.2 Rhenium

The molecular complex $[Re(\equiv C{}^tBu)(=CH{}^tBu)(CH_2{}^tBu)_2]$ reacts with the surface silanol of $SiO_{2\text{-}(700)}$ to give selectively the *syn*-rotamer of $[(\equiv SiO)Re(=C{}^tBu)(=CH{}^tBu)(CH_2{}^tBu)]$ according to elemental analysis, IR, EXAFS, and NMR spectroscopies (Scheme 49 and Table 13).[179–181] Exposure of this complex to light or heat yields a mixture of *syn*- and *anti*-rotamers. While the former displays an agostic interaction between the carbenic C–H bond and Re as evidenced by the relatively low J(C–H) coupling constant, there is no evidence of such an interaction in the latter.[180,182] This complex reacts with propene to generate 0.7 equiv. of a 3 : 1 mixture of $^tBuCH{=}CH_2$ and $^tBuCH{=}CHCH_3$ and a highly active olefin metathesis catalyst.[179,183] It catalyzes the metathesis of a wide range of olefins without activators even for functionalized olefins such as methyl oleate, for which up to TON of 900 can be achieved.[179–181,183]

The chemistry of $MeReO_3$ is very different: it is only physisorbed reversibly onto silica. Its reaction with silica–alumina[167,184a,b] or Nb_2O_5[185,186] gives nice purple solids. While the actual structure is not known, the Me–Re bond is

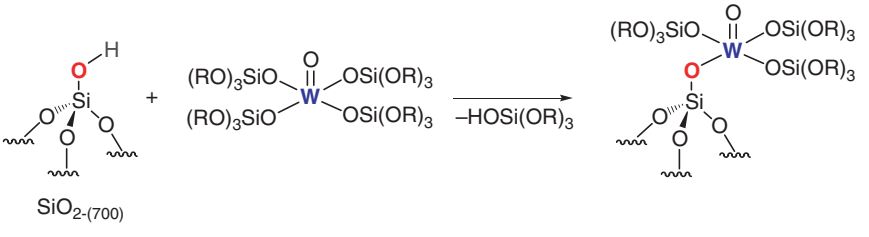

Scheme 47

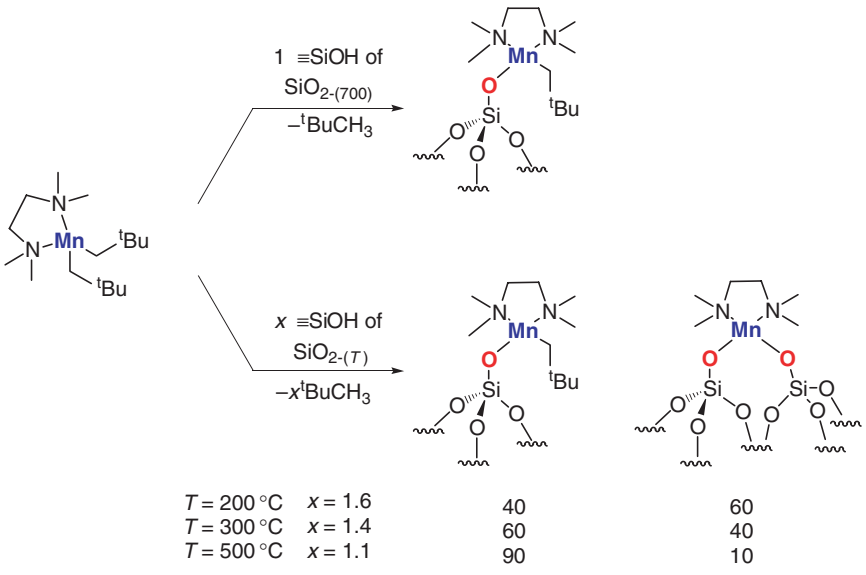

Scheme 48

Table 13 Surface species resulting from the reaction of group 7 organometallic and inorganic complexes with oxide materials

Molecular complex	*Oxide support*	*Structure*	*Analytical methods*	*References*
$Mn(CH_2{}^tBu)_2$(TMEDA)	$SiO_{2\text{-}(700)}$	(≡SiO)Mn($CH_2{}^tBu$)(TMEDA)	Chem., IR, ESR	178
$Mn(CH_2{}^tBu)_2$(TMEDA)	$SiO_{2\text{-}(200)}$	$(≡SiO)_2$Mn(TMEDA)[a]	Chem., IR, ESR	178
Re(≡C^{t}Bu)(=CH^{t}Bu)($CH_2{}^tBu)_2$	$SiO_{2\text{-}(700)}$	(≡SiO)Re(≡C^{t}Bu)(=CH^{t}Bu)($CH_2{}^tBu$)	Chem., IR, NMR, EXAFS	179–181
$MeReO_3$	SiO_2–Al_2O_3	[b]	Chem.	184a,b
$MeReO_3$	Nb_2O_5	[b]	Chem., IR, NMR	185,186
$Me_3SiOReO_3$	$SiO_{2\text{-}(1,000)}$	(≡SiO)Re(=O)$_3$	Chem., IR	187
Re_2O_7	$SiO_{2\text{-}(1,000)}$	(≡SiO)Re(=O)$_3$	Chem., IR	187

[a]Along with 40% of (≡SiO)Mn($CH_2{}^tBu$)(TMEDA).
[b]Unknown structure.

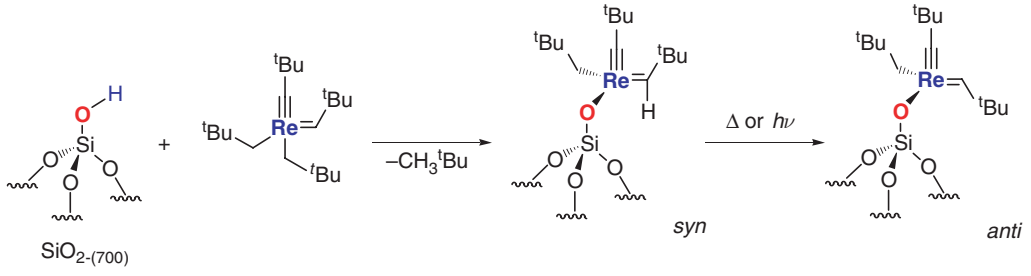

Scheme 49

not cleaved during grafting,[184a,b] and the materials thus obtained are highly active olefin metathesis catalysts. It is worth noting that the methyl does not generate the propagating carbene ligand.

Inorganic Re complexes have been used to generate well-defined oxo Re species, [(≡SiO)Re(=O)$_3$], which is formed through the reaction of $Me_3SiOReO_3$ or Re_2O_7 with the strained siloxane bridges present on a $SiO_{2\text{-}(1,000)}$ (Scheme 50 and Table 13).[187]

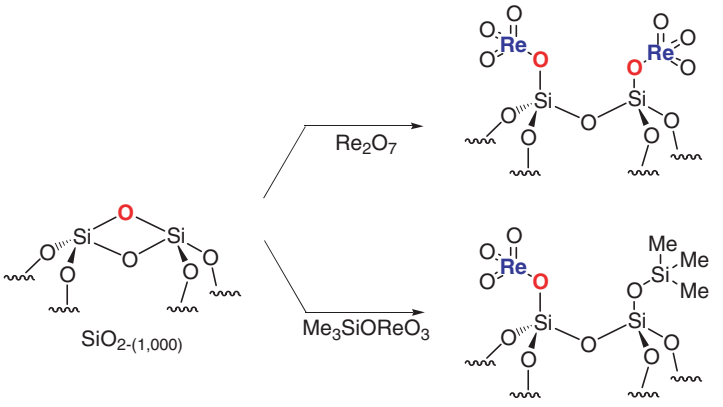

Scheme 50

12.10.2.9 Group 8–12 Complexes

There are only a few examples of the formation of well-defined species from the reactions of late transition metal complexes with oxide supports (Tables 14–17).

12.10.2.9.1 Group 8: iron, ruthenium, and osmium

12.10.2.9.1.(i) Iron

The only reported reaction of an organoiron complex is that of $[CpFeMe(CO)_2]$ with Al_2O_3, which gives mainly $[CpFe(COMe)(CO)/Al_2O_3]$ according to solid-state NMR spectroscopy.[188] In this case, there is no reaction with surface hydroxyl, but only a rearrangement of the complex, which is then chemisorbed through Lewis acid/Lewis base interaction (Scheme 51 and Table 14).

On SBA-15, $[Fe(OSi(O^tBu)_3)_3]$ reacts with the surface silanols of SBA-15 to generate 1 equiv. of $[(t\text{-}BuO)_3SiOH]$ and a well-defined complex, $[(\equiv SiO)Fe(OSi(O^tBu)_3)_2]$, according to mass balance analysis and ESR spectroscopy (Scheme 52).[189] It is worth noting that this surface complex catalyzes the epoxidation of cyclohexene in the presence of H_2O_2.

Table 14 Surface species resulting from the reaction of group 8 organometallic and alkoxide complexes with oxide materials

Molecular complex	*Oxide support*	*Structure*	*Analytical methods*	*References*
$CpFeMe(CO)_2$	Al_2O_3	$CpFe(COMe)(CO)/Al_2O_3$	Chem. NMR	188
$Fe(OSi(O^tBu)_3)_3$	SBA-15	$(\equiv SiO)Fe(OSi(O^tBu)_3)_2$	Chem., IR, ESR	189
$(dmpe)_2Ru(C_2H_4)$	SiO_2	$(\equiv SiO)Ru(dmpe)_2(H)$	Chem.	190
$(dmpe)_2Ru(H)(OH)$	SiO_2	$(\equiv SiO)Ru(dmpe)_2(H)$	Chem.	190

Table 15 Surface species resulting from the reaction of group 9 organometallic complexes with oxide materials

Molecular complex	*Oxide support*	*Structure*	*Analytical methods*	*References*
$Co(OSi(O^tBu)_3)_2Bipy_2$	SBA-15	$(\equiv SiO)Co(OSi(O^tBu)_3)Bipy_2$	Chem.	191
$Rh(allyl)_3$	SiO_2	$[(\equiv SiO)Rh(allyl)_2(L)]$[a]	Chem., IR, NMR	192–196
$Rh(allyl)_3$	Al_2O_3	$(Al_sO)Rh(allyl)_2\{O(Al_s)_2\}$	Chem., IR	195,197
$Rh(allyl)_3$	TiO_2	$(Ti_sO)Rh(allyl)_2\{O(Ti_s)_2\}$	Chem., IR	195,197
$Me\text{-}Rh(PMe_3)_3$	SiO_2	$(\equiv SiO)Rh(PMe_3)_3$	Chem., IR, NMR	200,201
$MeRh(CO)(PMe_3)_2$	SiO_2	$(\equiv SiO)Rh(CO)(PMe_3)_2$	Chem., IR, NMR	204
$CpIr(OH)Ph(PMe_3)$	SiO_2	$(\equiv SiO)CpIrPh(PMe_3)$	Chem.	205
$CpIr(OSiMe_2^tBu_2)Ph(PMe_3)$	SiO_2	$(\equiv SiO)CpIrPh(PMe_3)$	Chem.	205
$CpIr(NHTol)Ph(PMe_3)$	SiO_2	$(\equiv SiO)CpIrPh(PMe_3)$	Chem.	205

[a] L = ≡SiOH (geminal/vicinal OH) or (≡SiOSi≡).

Table 16 Surface species resulting from the reaction of group 10 organometallic complexes with oxide materials

Molecular complex	*Oxide support*	*Structure*	*Analytical methods*	*References*
$Ni(allyl)_2$	SiO_2	(≡SiO)Ni(allyl)	Chem.	206,207
$Cp^*Ni(NHTol)(PEt_3)$	SiO_2	(≡SiO)$Cp^*Ni(PEt_3)$	Chem.	211,212
$(DAD)_2Ni(CH_3)_2$	$\{(SiO)B(C_6F_5)_3^-\}\{NEt_2PhH)^+\}$	$[\{(SiO)B(C_6F_5)_3^-\}\{(DAD)_2Ni(CH_3)^+\}]$	[a]	85
$Pd(allyl)_2$	SiO_2	(≡SiO)Pd(allyl)	Chem.	208,209
$L_2Pd(Cl)(Me)$	SiO_2	*cis*-[(≡SiO)Pd(Cl)L_2]	Chem.	213,214
$L_2Pd(OTf)(Me)$	SiO_2	*cis*-[(≡SiO)Pd(OTf)L_2]	Chem.	213,214
$L_2Pd(NO_3)(Me)$	SiO_2	*cis*-[(≡SiO)Pd(NO_3)L_2]	Chem.	213,214
$Pt(allyl)_2$	SiO_2	(≡SiO)Pt(allyl)	Chem.	210

[a]Not characterized.

Table 17 Surface species resulting from the reaction of group 11 organometallic and alkoxide complexes with oxide materials

Molecular complex	*Oxide support*	*Structure*	*Analytical methods*	*References*
$[Cu(O^tBu)]_4$	SBA-15	[a]	Chem., XANES, EXAFS	215
$[Cu(OSi(O^tBu)_3]_4$	SBA-15	[a]	Chem., XANES, EXAFS	215
$Me_2Au(acac)$	Al_2O_3	$Al_SOAuMe_2\{O(Al_s)_2\}$	IR, EXAFS, XANES	216
$Me_2Au(acac)$	MgO	$Mg_SOAuMe_2\{O(Mg_s)_2\}$	IR, EXAFS, XANES	217–220
$Me_2Au(acac)$	TiO_2	$Ti_SOAuMe_2\{O(Ti_s)_2\}$	IR, EXAFS, XANES	221,222
$Me_2Au(acac)$	La_2O_3	$La_SOAuMe_2\{O(La_s)_2\}$	IR, EXAFS, XANES	223

[a]See Scheme 64.

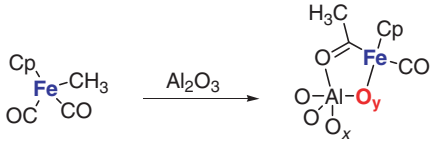

Scheme 51 Reactivity of an iron organometallic complex with alumina.

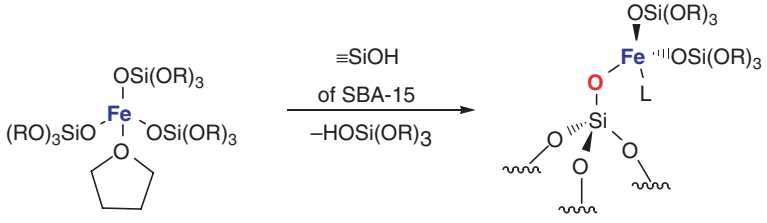

Scheme 52 Reactivity of an Fe(III) siloxide complex with a mesoporous silica.

12.10.2.9.1.(ii) Ruthenium and Osmium

The only reported examples are the reactions of $[(dmpe)_2Ru(H)(OH)]$ and $[(dmpe)_2Ru(C_2H_4)]$ with SiO_2, which is reported to give the same surface complex, [(≡SiO)Ru(dmpe)$_2$(H)], along with H_2O or ethylene, respectively (Scheme 53).[190] This surface complex readily degrafts upon treatment with a thiol. For Os, there is no study on the grafting of mononuclear Os complexes.

12.10.2.9.2 Group 9: cobalt, rhodium, and iridium

12.10.2.9.2.(i) Cobalt

Grafting of $[Co(OSi(O^tBu)_3)_2Bipy_2]$ (Bipy = 4,4′-di-^{t}Bu-bipyridine) on SBA-15 generates 1 equiv. of [(t-BuO)$_3$SiOH] and [(≡SiO)Co(OSi(O^{t}Bu)$_3$)Bipy$_2$], according to mass balance analysis, XANES, and ESR spectroscopy (Scheme 54

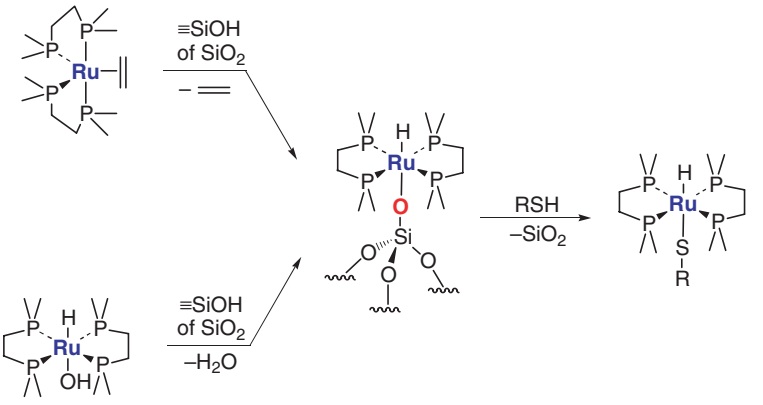

Scheme 53

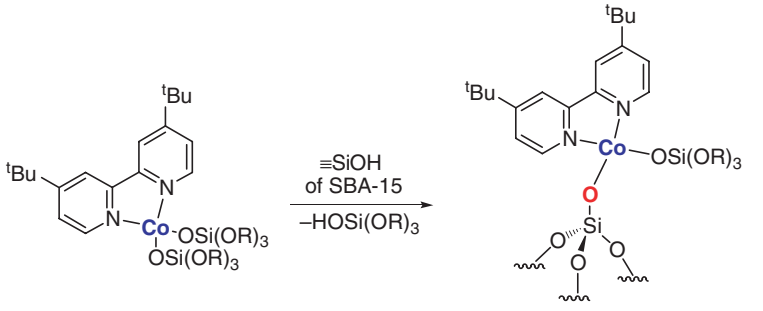

Scheme 54 Reaction of a Co alkoxide complex with SBA-15.

and Table 15), and it catalyzes the air oxidation of ethylbenzene or 2-phenylethanol into acetophenone with good selectivity (82% and 100%, respectively) and no leaching.[191]

12.10.2.9.2.(ii) Rhodium

The reaction of $[Rh(allyl)_3]$ with silica dehydroxylated at various temperatures ranging from 200 to 500 °C gives $[(\equiv SiO)Rh(allyl)_2]$ along with 1 equiv. of propene.[192–196] IR studies show that the Rh center is probably coordinated by an extra hydroxyl or a siloxane bridge of the silica surface to give species of the following general formula $[(\equiv SiO)Rh(allyl)_2(L)]$, for which L = ≡SiOH (geminal/vicinal OH) or (≡SiOSi≡) (adjacent siloxane bridge) (Scheme 55). Similar results are obtained when supporting $[Rh(allyl)_3]$ on alumina or titania providing $[(Al_sO)Rh(allyl)_2\{O(Al_s)_2\}]$ and $[(Ti_sO)Rh(allyl)_2\{O(Ti_s)_2\}]$, respectively.[195,197] These Rh species react with H_2 to give Rh particles, propane, and hexane.[195,197,198]

When $[(\equiv SiO)Rh(allyl)_2L]$ (L = adjacent oxygen from the support) is reacted with CO, it yields hexadiene and $[(\equiv SiO)Rh(CO)_2]$, which is transformed into $[(\equiv SiO)Rh(CO)_2]_2$ through a migration of Rh species on the silica surface.[195,199] It is worth noting that the reaction of $[(\equiv SiO)Rh(allyl)_2L]$ with Lewis base depends on the degree of

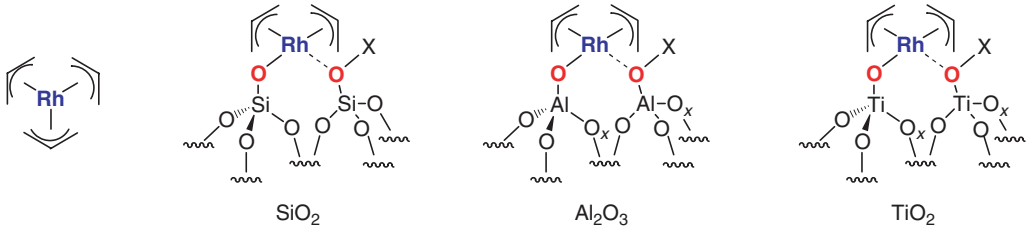

Scheme 55 Structures of surface organometallic fragments resulting from the reaction of $[Rh(allyl)_3]$ and various oxide supports (silica, alumina, and titania).

dehydroxylation of silica (Scheme 56). On the one hand, for $[Rh(allyl)_3]/SiO_{2\text{-}(550)}$, which contains mainly $[(\equiv SiO)Rh(allyl)_2\{O(Si\equiv)_2\}]$, the reaction with PMe_3 gives $[(\equiv SiO)Rh(PMe_3)_3]$ along with 1,5-hexadiene.[200–202] The compound $[(\equiv SiO)Rh(PMe_3)_3]$ was characterized by an independent synthesis via the reaction of $[Me\text{-}Rh(PMe_3)_3]$ and $SiO_{2\text{-}(400)}$.[200,201] On the other hand, for $[Rh(allyl)_3]/SiO_{2\text{-}(200)}$, which contains mainly $[(\equiv SiO)Rh(allyl)_2(HOSi\equiv)]$, the reaction with PMe_3 gives propene and $[(\equiv SiO)_2Rh(allyl)(PMe_3)_3]$. This latter species evolves into $[(\equiv SiO)Rh(PMe_3)_3]$ and [(≡SiO-allyl] as the major surface species,[202,203] but in the presence of a large concentration of SiOH, [≡SiO-allyl] yields 2-propenol, which further reacts with $[(\equiv SiO)Rh(PMe_3)_3]$ to give $[(\equiv SiO)Rh(CO)(PMe_3)_2]$ along with ethane.[202] Note that in contrast to $[(\equiv SiO)Rh(allyl)_2]$, the treatment of $[(\equiv SiO)_2Rh(allyl)(PMe_3)_3]$ under H_2 does not yield metal particles, but $[(\equiv SiO)Rh(PMe_3)_3]$, (≡SiOH), and propene, as well as $[(\equiv SiO)Rh(PMe_3)_3]$ and (≡SiOallyl).[200,201] Additionally, when $[(\equiv SiO)_2Rh(allyl)(PMe_3)_2]$ is treated under CO, it evolves into $[(\equiv SiO)_2Rh\{(C{=}O)allyl\}(PMe_3)_2]$, which decomposes into $[(\equiv SiO)Rh(CO)(PMe_3)_2]$ and [≡SiO–(C=O)allyl].[200,201]

The surface complex $[(\equiv SiO)Rh(CO)(PMe_3)_2]$ can also be prepared directly by treating $[(\equiv SiO)Rh(PMe_3)_3]$ with CO,[200,201] $[(\equiv SiO)Rh(PMe_3)_3]$ with 2-propenol,[200,201] or by reacting $[MeRh(CO)(PMe_3)_2]$ with silica (Schemes 56 and 57).[204] This species, $[(\equiv SiO)Rh(CO)(PMe_3)_2]$, reacts with PMe_3 or P^iPr_3 to give $[(\equiv SiO)^-\{Rh(CO)(PMe_3)_3\}^+]$ and $[(\equiv SiO)Rh(CO)\{P(^iPr)_3\}_2]$, respectively (Scheme 57).[204] It also reacts with electrophiles E–X such as CH_3–I or allyl chloride (C_3H_5–Cl) to give the corresponding octahedral complex, $[(\equiv SiO)Rh(X)(E)(CO)(PMe_3)_2]$.

The reaction of larger phosphines, namely $P(^iPr)_3$, with $[(\equiv SiO)Rh(allyl)_2L]$ is noteworthy (Scheme 58).[200,201,204] The reaction of $[(\equiv SiO)Rh(allyl)_2\{O(Si\equiv)_2\}]$ and $P(^iPr)_3$ gives 1,5-hexadiene and $[(\equiv SiO)Rh\{P(^iPr)_3\}_3]_2$; this latter species reacts with H_2 to give a stable monomeric dihydride complex $[(\equiv SiO)Rh\{P(^iPr)_3\}_3(H)_2]$. In the case of $[(\equiv SiO)Rh(allyl)_2(HOSi\equiv)_2]$, it evolves to $[(\equiv SiO)Rh\{P(^iPr)_3\}_2]$ and (≡SiOallyl) via the intermediate species $[(\equiv SiO)_2Rh\{P(^iPr)_3\}_2(allyl)]$.

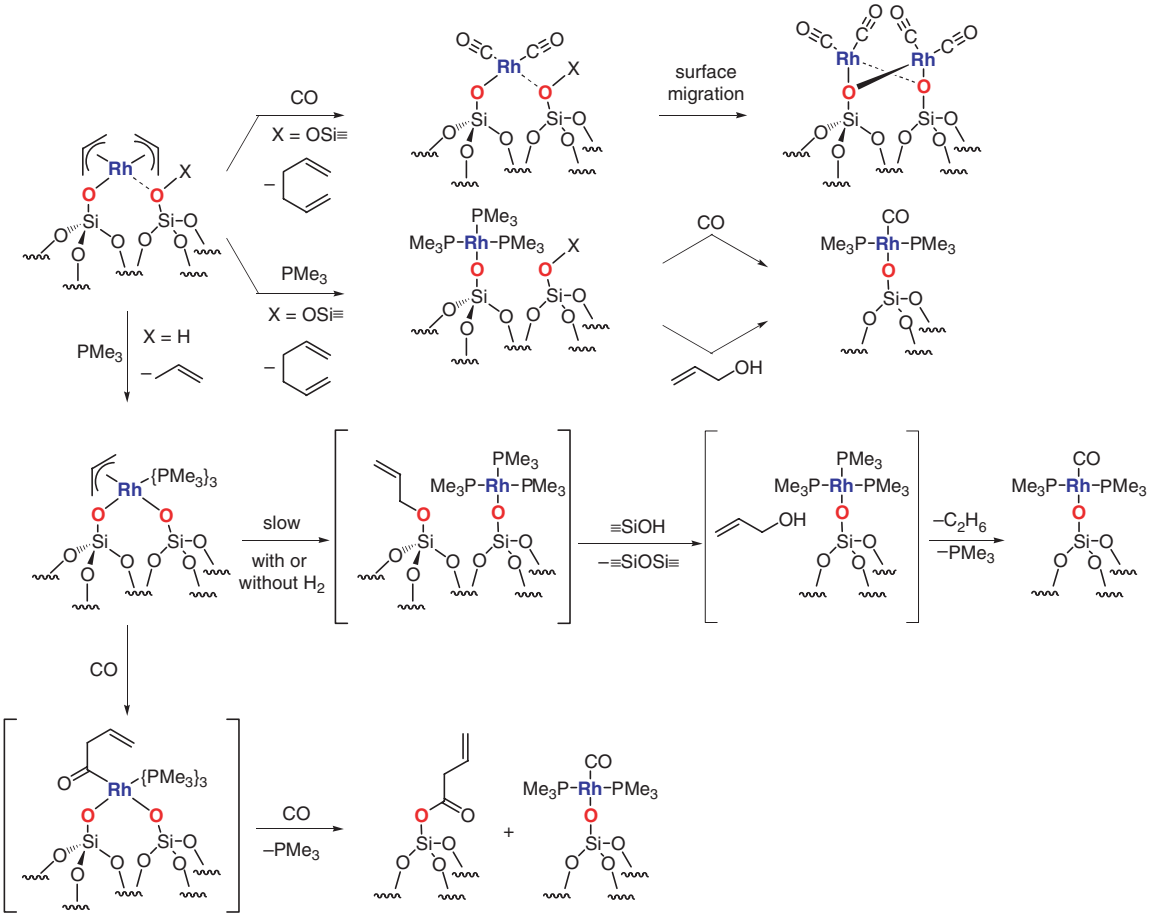

Scheme 56

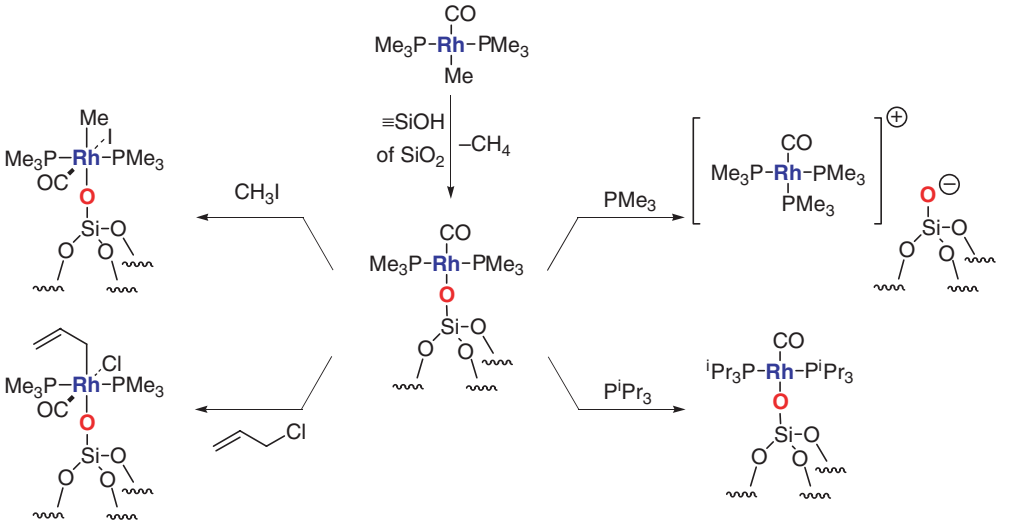

Scheme 57

12.10.2.9.2.(iii) Iridium

The only example is the reaction of [CpIr(X)Ph(PMe_3)] (X = OH, $OSiMe_2{}^tBu_2$, or NHTol) with silica, which gives [(≡SiO)CpIrPh(PMe_3)] along with XH (Scheme 59 and Table 15).[205] It is worth noting that this surface complex [(≡SiO)CpIrPh(PMe_3)] reacts with C_6D_6 to give [(≡SiO)CpIr(C_6D_5)(PMe_3)], whereas a treatment with methyl propynoate cleaves the O–Ir bond to give [($MeO_2CC{\equiv}C$)CpIrPh(PMe_3)]. The surface species can also be degrafted by treatment with phenols.

12.10.2.9.3 Group 10: nickel, palladium, and platinum

Grafting group 10 diallyl complexes, [M(allyl)$_2$] (M = N,[206,207] Pd,[208,209] Pt),[210] on silica have been reported to yield [(≡SiO)M(allyl)] as evidenced by the evolution of 1 propene per grafted metal (Scheme 60).

The reaction of [Cp^*Ni(NHTol)(PEt_3)] with silica yields [(≡SiO)Cp^*Ni(PEt_3)] (Scheme 61).[211,212] Moreover, Bochmann *et al.* have used [{(SiO)B(C_6F_5)$_3^-$}{NEt_2PhH^+}] to generate cationic alkyl Ni complexes through its reaction with [(DAD)$_2$Ni(CH_3)$_2$], thus providing [{(SiO)B(C_6F_5)$_3^-$}{(DAD)$_2$Ni(CH_3)$^+$}], as a polymerization catalyst precursor (Scheme 62 and Table 16).[85]

The only other example of formation of surface Pd complexes results from the reaction of *cis*-[L_2Pd(X)(Me)] {X = Cl^-, OTf^-, and NO_3^-} with $SiO_{2\text{-}(500)}$, which yields the corresponding surface complex *cis*-[(≡SiO)Pd(X)L_2] (Scheme 63 and Table 16). It is worth noting that the *trans*-isomers are unreactive toward the surface silanols of silica.[213,214] All these systems are used as catalysts for the ring closure of aminoalkyne.

12.10.2.9.4 Group 11: copper, silver, and gold

As observed for similar precursors, the reaction of [Cu(OR)]$_4$ (R = *t*-Bu or Si(O^tBu)$_3$) with the surface hydroxyl of an SBA-15 gives 1 equiv. of [HOR] per tetramer to give presumably a tetrameric species [(≡SiO)Cu][Cu(OSi(O^tBu)$_3$)]$_3$ (Scheme 64), which evolves into monomeric species according to XANES and EXAFS analysis.[215]

Whether using Al_2O_3,[216] MgO,[217–220] TiO_2,[221,222] or La_2O_3,[223] the reaction of [Me_2Au(acac)] generates a mononuclear Au(III) surface complex, [M_SOAuMe_2{$O(M_s)_2$}] (M = Al, Mg, and Ti) along with a chemisorbed acac ligand (Scheme 65 and Table 17).

12.10.3 Surface Organometallic Chemistry on Metals

12.10.3.1 Generalities

The reaction of organometallic compounds with the surfaces of metals are now widely used to obtain "tailor-made" bimetallic catalysts. The improvement in catalytic activity, selectivity, and stability can result from the modification

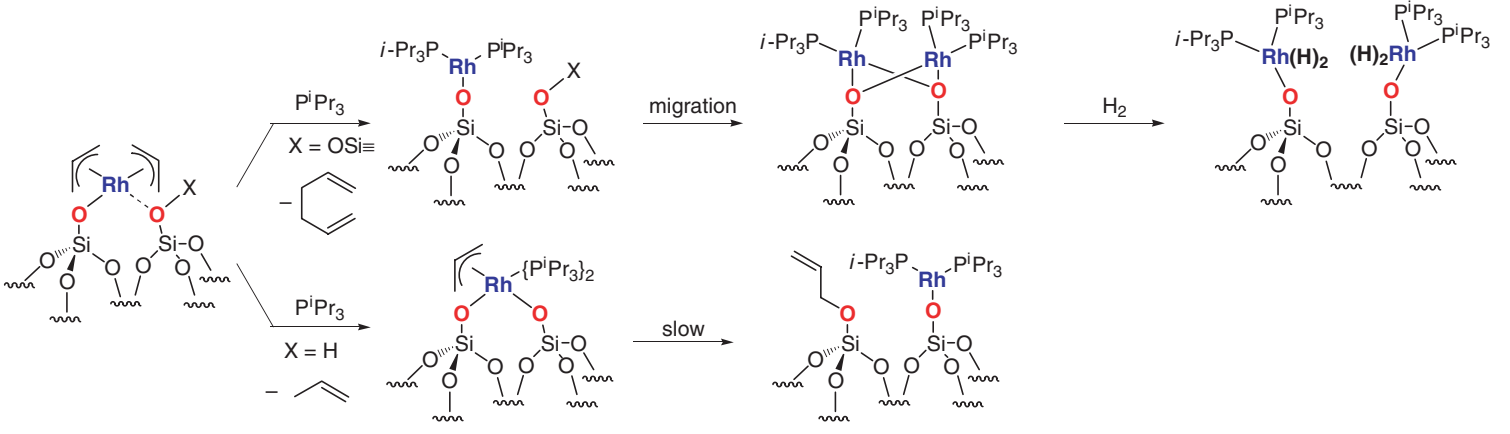
Rh
X
O
Si
Si–O
P^{i}Pr$_3$
X = OSi≡
–
X = H
{P^{i}Pr$_3$}$_2$
migration
slow
H$_2$
i-Pr$_3$P
Rh(H)$_2$
(H)$_2$Rh

Scheme 58

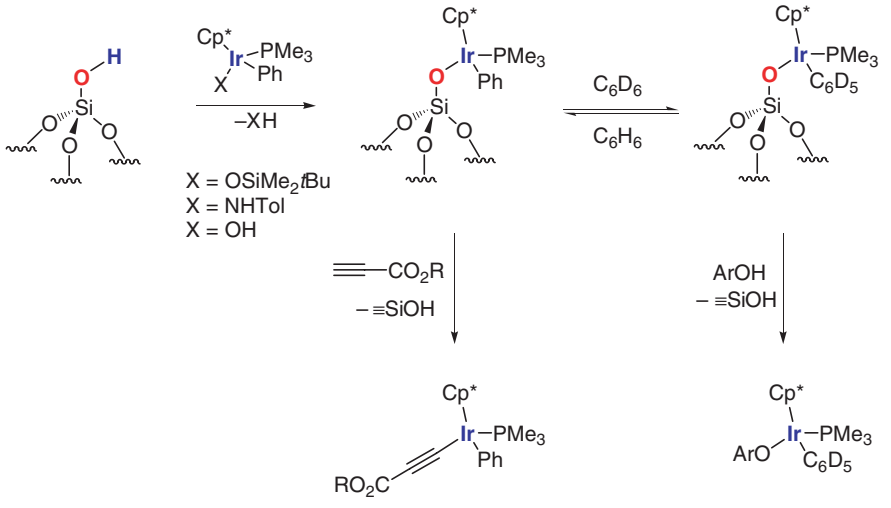

Scheme 59

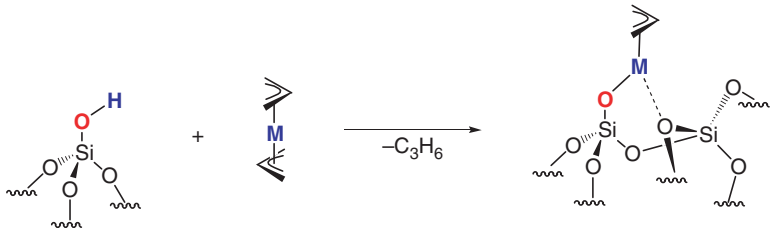

Scheme 60

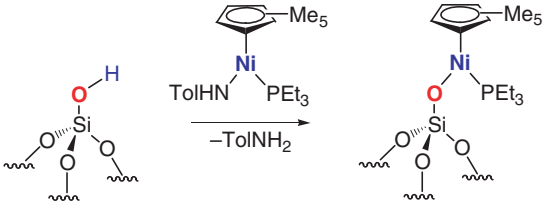

Scheme 61

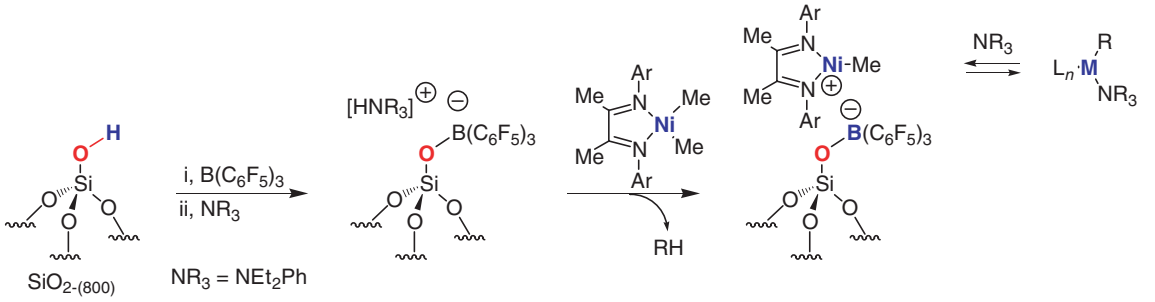

Scheme 62

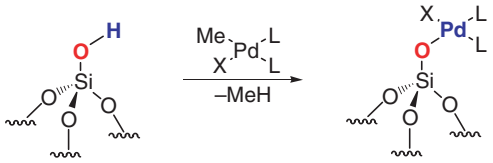

Scheme 63 Reaction of organopalladium complexes with silica.

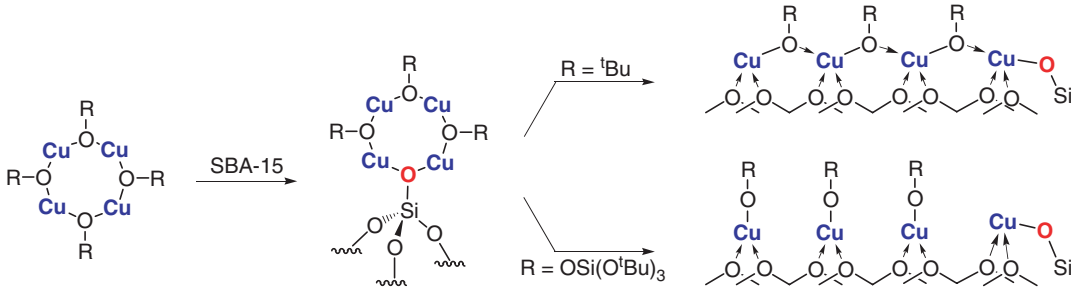

Scheme 64 Reaction of Cu alkoxides with SBA-15.

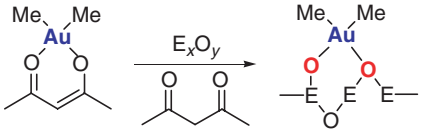

Scheme 65 Reaction of Au(III) dimethylacetylacetonate gold (III) with oxide supports (alumina, E = Al; magnesia, E = Mg; titania, E = Ti; lanthanum oxide, E = La).

of the active metal surface by the reaction with organometallic reagents through the formation of bimetallic alloys or metal particles covered with grafted organometallic fragments or adatoms. Most of the studies were conducted on catalytically active metal, generally chosen from group VIII metals, and involved two families of organometallic modifiers: (i) mainly group 14 organometallic complexes[224–226] and (ii) carbonyl clusters.[227,228] We have restricted the present survey to the reactivity of alkyl and hydride compounds with the surface of metal particles, the reaction of metal carbonyl clusters being reviewed elsewhere.[229]

12.10.3.2 Methodology and Tools

12.10.3.2.1 Characteristics of metal particles

Metal particles are defined as an ensemble of metal atoms of various sizes, and these atoms have different natures, depending on whether they are located in the core or at the surface of the particles. In general, the active centers are usually the surface metal atoms so that the properties of metal particles are related to the number of surface atoms (N_s), and characterized by the dispersion ($D = N_s/N_t$) (N_t = total number of atoms of the metal particle). Increasing the number of surface atoms (N_s) per total number of atoms (N_t) requires particles of small sizes, typically in the nanometer range (Scheme 66 and Table 18). Van Hardeveld and Hartog[230] have proposed that the shape of nanosized particles can be represented as cubooctahedrons.[231–234]

For these structures, the surface metal atoms are located on the (111) or (100) planes. Note that a cubooctahedral particle is constituted of three kinds of atoms, located on the faces (N_{face}), the edges (N_{edge}), and the corners (N_{corner}), and that the number of metal atoms on each edge is the same for a given cubooctahedron. For a particle with N_{edge} varying from 2 to 8, the number of atoms on the faces and corners, the number of surface atoms, the total number of atoms, and their dispersion are reported in Table 18. From the total number of atoms (N_t) in a given metallic particle, the diameter (d) of an equivalent sphere can be determined knowing the molecular weight (M) and the density (ρ) of the metal, by the relation: $d\,(\text{nm}) = 2[(3 \cdot M \cdot N_t)/(4 \cdot \Pi \cdot N_A \cdot \rho)]^{1/3}$, where N_A is the Avogadro number. For example, the diameters of equivalent spheres of nanoparticles of ruthenium are given in Table 18.

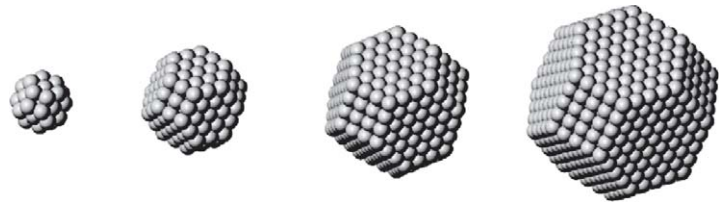

Scheme 66 Cubooctahedral particles with increasing the number of atoms on the edges.

Table 18 Number of total atoms (N_t), surface atoms (N_s), face atoms (N_{face}), edge atoms (N_{edge}) and corner atoms (N_{corner}), dispersion ($D = N_s/N_t$) and diameter (d_{Pt}) of equivalent sphere, for Pt particles for N_{edge} varying from 2 to 8

	2	3	4	5	6	7	8
N_t	38	201	586	1,289	2,406	4,033	6,266
N_s	32	122	272	482	752	1,082	1,472
N_{face}	8	62	176	350	584	878	1,232
N_{edge}	0	36	72	108	144	180	216
N_{corner}	24	24	24	24	24	24	24
D	0.84	0.61	0.46	0.37	0.31	0.27	0.23
d_{Pt}	1.03	1.80	2.57	3.34	4.11	4.88	5.66

Nanoscopic metallic particles can be prepared by various routes, and mostly by reduction of a salt or an organometallic compound of the metal, under mild conditions, but, in order to avoid coalescence of the particles (sintering), it is necessary to use organic ligands as stabilizers.[235–240] The presence of ligands coordinated at the surface prevents the particles from coalescing and allows their self-assembly onto various surfaces. Organic molecules such as amines, thiols, alcohols, or alkylsilanes were used as stabilizers for these systems.[235,236,238,241–244] Another approach is to stabilize metal particles through their dispersion on an oxide support. This approach has the advantage of providing "ligand-free" metal particles (Scheme 67). Additionally, these supports provide a large surface area, ca. 100 $m^2 \cdot g^{-1}$, and metal loadings of about 1%$_{wt}$ with particles of about 2 nm in diameter are currently used, which corresponds to having metal particles every 30 nm.

A great variety of oxides can be used as supports. These materials are chemically stable, but in some cases, interactions between the metallic particles and the support can occur. Thus, in the particular case of metal catalysts supported on some reducible oxides, the occurrence of so-called "metal–support interaction effects" has been reported.[245,246] In order to minimize the metal–support interaction, stable oxides (not reducible), such as alumina or silica, are used. Moreover, the size-dependent electronic, structural, and chemical properties of metal nanoparticles on oxide supports are an important aspect of heterogeneous catalysis.[247,248]

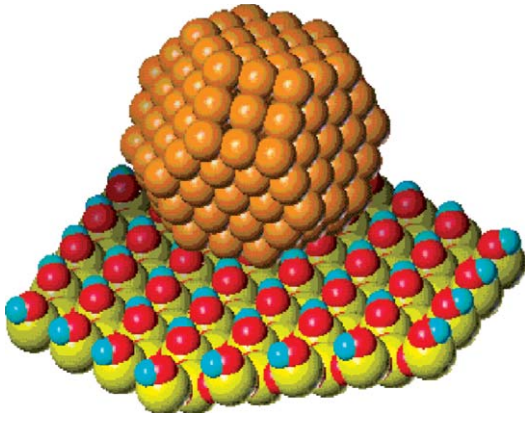

Scheme 67 Cubooctahedral particles deposited on a silica surface.

12.10.3.2.2 Characterization of metallic surfaces and metal particles

As already discussed, the size, the shape, and the dispersion are characteristic parameters of metal particles, which will determine their properties, and it is possible to characterize them as follows: (i) the size of the metal particles through TEM[249–251] and EXAFS[252,253], (ii) their structures through X-ray diffraction (XRD) and TEM, (iii) their chemical composition through TEM-EDX and elemental analysis, and (iv) the chemical state of the surface of the particles as well as their dispersion through X-ray photoelectron spectroscopy (XPS),[254] thermoprogramed reduction (TPR), and chemisorption capacity of probe molecules such as H_2, O_2, and CO (volumetric or dynamic measurements).[255–261]

In the case of metal surfaces, metallic particles can be obtained in three different states.

(i) Reduced and desorbed particles. In this case, the metal atoms are fully reduced under a flow of H_2 at high temperatures followed by a treatment under vacuum (or a flow of a neutral gas such as He/Ar at high temperature). The atoms (bulk and surface) in the particles are represented by M and M_s.

(ii) Reduced and covered by hydrogen. For these samples, the metal atoms are fully reduced under a flow of H_2 at high temperatures, then cooled down under H_2. The bulk atoms are represented by M, and the surface atoms, covered by chemisorbed hydrogen atoms, are represented by M_s–H_x. The stoichiometry of the hydrogen adsorption (value of x) depends on the nature of the metal, on the temperature of the adsorption, and on the H_2 pressure.

(iii) Oxidized particles. This state can be obtained by a treatment under O_2 (or air) of the reduced and desorbed particles (i). Depending on the nature of the metal and on the temperature of the oxidizing treatment, all the metal atoms can be oxidized, or, in some cases, only the surface atoms. The oxidized metal atoms are represented by M(x) (bulk) or M_s(x)–O_y (surface), where (x) is the oxidation state of the metal atom and y is the stoichiometry of the adsorbed oxygen.

12.10.3.3 Reactivity of Organometallic Compounds with Metallic Surfaces

12.10.3.3.1 General interaction pathway: example of the reaction of tetraalkyltin complexes on platinum particles supported onto silica

This field is devoted to the understanding of the reactivity of organometallic reagents with metal surfaces. Its development has been made possible for two main reasons: first, it is possible to prepare very small metal particles (with a nanometer size), highly dispersed on a support, with a narrow particle-size distribution; and second, when a metallic particle of a zerovalent metal is grafted on an oxide support, most organometallic compounds have a higher chemical affinity for the particle than for the oxide support. These two parameters render the field of surface organometallic chemistry on metals possible even if the surface area of the metal particles supported on SiO_2 does not exceed a few m^2 compared to the surface area of the oxide support (several $100\,m^2\,g^{-1}$). This nanoscience can then be described as the synthesis of subnanometer objects (the grafted organometallic fragments) on nanometer objects (the metal particles), which are themselves deposited on supports with a size of two orders of magnitude higher.

For example, [$SnBu_4$] reacts with metal (M = Pt, Rh, Ni...) particles at room temperature, whereas its reaction with the surface hydroxyl groups of a silica surface occurs at 150 °C.[262] The reaction proceeds as follows: [$SnBu_4$] is first physically adsorbed on the silica surface, as evidenced by the strong shift to lower wave numbers of the ν_{OH} band, from 3,760 to $3{,}700\,cm^{-1}$.[262] The tin complex migrates on the silica surface and reacts with the metal surface through the formation of a pentacoordinated surface intermediate (Scheme 68).[263,264] This pentacoordinated surface complex is unstable, and undergoes further hydrogenolysis of the Sn–R bonds. There is formation of the primary surface complex (PSC), [M_sSnR_3].[265]

Depending on the metal and the reaction conditions, [M_sSnR_3] can further lose its ligands by reaction with the surface atoms of the particle to give progressively the dibutyl, [$(M_s)_2SnR_2$], the monobutyl, [$(M_s)_3SnR$], and even the totally dealkylated tin species [$(M_s)_4Sn$]. In the latter case, the tin atom can be considered as an adatom on the metal

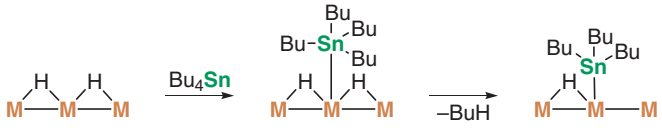

Scheme 68 Reaction of $SnBu_4$ with the surface of a metal (M = Rh, Ni, Pt, ...) particles at room temperature.

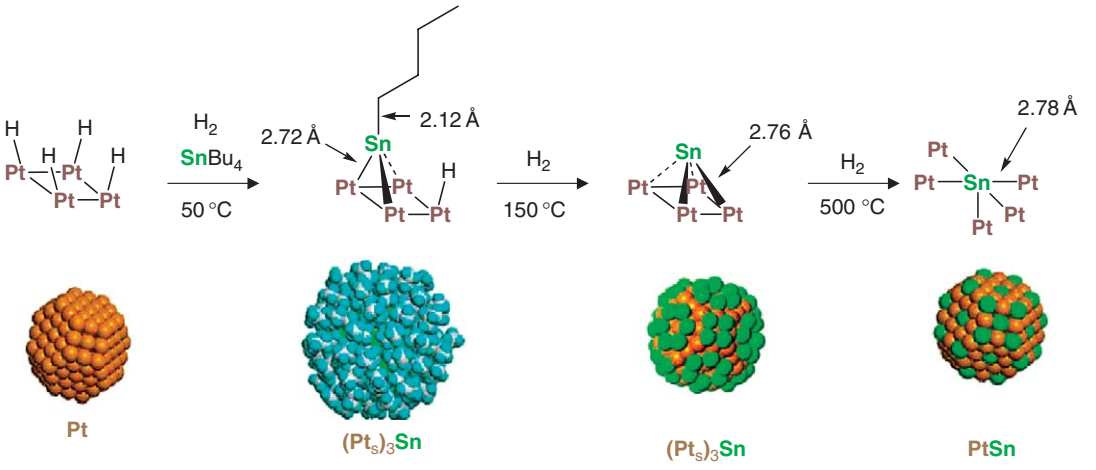

Scheme 69 Various steps observed during the hydrogenolysis of $SnBu_4$ at the surface of a Pt particle (sphere color code: orange (Pt), blue (H), white (C), green (Sn)).

surface. By thermal treatment, this adatom can migrate into the first layers of the metal particle, leading to the formation of a surface alloy (Scheme 69).

Using judicious reaction conditions, it is possible to obtain for a single and well-defined environment for tin, which can be fully characterized by physicochemical methods, including EXAFS. For instance, the tris(grafted) tin surface complex $[(M_S)_3SnBu]$ was isolated on a Pt/SiO_2 catalyst when tetrabutyltin reacts at 50 °C, under hydrogen, with the surface of reduced silica-supported platinum particles. EXAFS measurements indicate that tin is surrounded by three platinum atoms at 2.72 Å and one carbon atom at 2.12 Å (Scheme 69).[266] Naked tin adatoms can also be obtained on a Pt/SiO_2 catalyst but, in order to remove all butyl ligands, the solid needs to be further heated at 150 °C.[266,267] EXAFS data indicate that tin is only surrounded by four platinum atoms at the same distance of 2.76 Å, which clearly indicates that tin is located on the metal surface and not in the bulk.[266] Further heating the above sample under H_2 at 500 °C results in an increase in the number of platinum atoms surrounding tin, up to ca. 5, which can be explained by a migration of the tin atom into the bulk of the particle.[266,268]

This process is quite general, and we will review, hereafter, the chemistry of organometallics reagents with metal surfaces, which are limited mainly to group VIII metals.

Depending on the surface arrangements described above, it will be possible to tune the catalyst/material for a specific property.

12.10.3.3.2 Reactivity of group 12 metal complexes with group VIII metal surfaces: Hg

Diphenylmercury interacts with nickel supported on alumina, under H_2 in heptane at 373 K, to give mostly biphenyl and metallic mercury. During the reaction, Hg induces leaching of nickel (Scheme 70).[269]

12.10.3.3.3 Reactivity of group 14 metal complexes with group VIII metal surfaces

12.10.3.3.3.(i) Silicon

Triethylsilane (Et_3SiH) reacts with the surface of Ni, Rh, Pd, or Pt particles supported on silica at 573 K through the hydrogenolysis of one ethyl group at a time until a strongly adsorbed Si remains attached to the metal surface

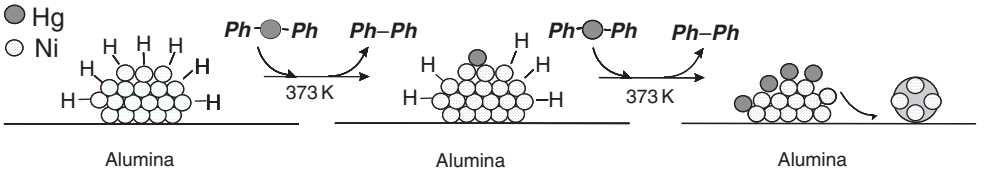

Scheme 70

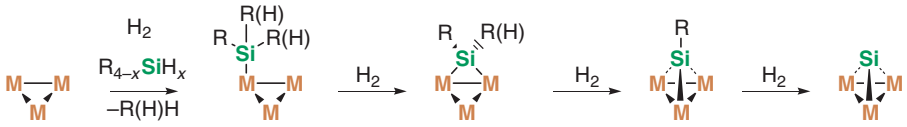

Scheme 71

(Scheme 71).[270,271] Moreover, studies on the reactivity of Pt and Rh particles supported on silica with various silanes (amylsilane, dipropylsilane, and triethylsilane) at 400, 463, and 523 K suggest a stepwise hydrogenolysis process releasing alkanes and H_2 (Scheme 71).[272] In fact, on well-defined Pt(111) surfaces,[241] *t*-$BuSiH_3$ gives [$Pt_s(Si^tBu)$] at temperatures <250 K, for which the three Si–H bonds are selectively cleaved. Similarly, [$MeSiH_3$] reacts on platinum (III), even at a temperature as low as 108 K, but the nature of the grafted fragment depends on the platinum surface coverage: [Pts(SiMe)] and [Pts{Si(Me)(H)}] are formed at low and high coverage, respectively.

Similarly, [SiH_4] generates thin alloy and intermetallic compound phases by reaction with clean Ta, Mo, W, Rh, Ni, Pt, Cu, and Au surfaces at elevated temperatures.[273]

12.10.3.3.3.(ii) Germanium

The compound [$Ge(C_4H_9)_4$] reacts at 363 K on the surface of palladium particles supported on alumina to form [$PdGe(C_4H_9)_{4-x}$]/Al_2O_3.[274] After heating at 773 K under an H_2 flow, the germanium is fully dealkylated, and a bimetallic PdGe system supported on an alumina catalyst is formed. Using the same procedure, Rh particles supported on alumina also generate a RhGe bimetallic system where the Ge atoms are randomly distributed on the rhodium surface.[275] Nonetheless, it is possible to keep the organic fragment on Ge when the reaction is carried out at room temperature: for example, adamantyl (Ad or $AdCH_2CO_2$menthyl)[276] or functionalized {(4-HOBu)GeH_3}[277] germanium derivatives react with Rh particles supported on silica under H_2 to give germylene surface complexes (Scheme 72).

12.10.3.3.3.(iii) Tin

Using various silica-supported group VIII "host" metals (Ru, Rh, Ni, Pd, Pt) in the reduced state and SnR_4 as organometallic compounds, similar grafted species were obtained by reactions at temperatures close to 300 K under hydrogen (or with the surface of the "host" metals, covered by chemisorbed hydrogen).[224,263,264,266,277–286]

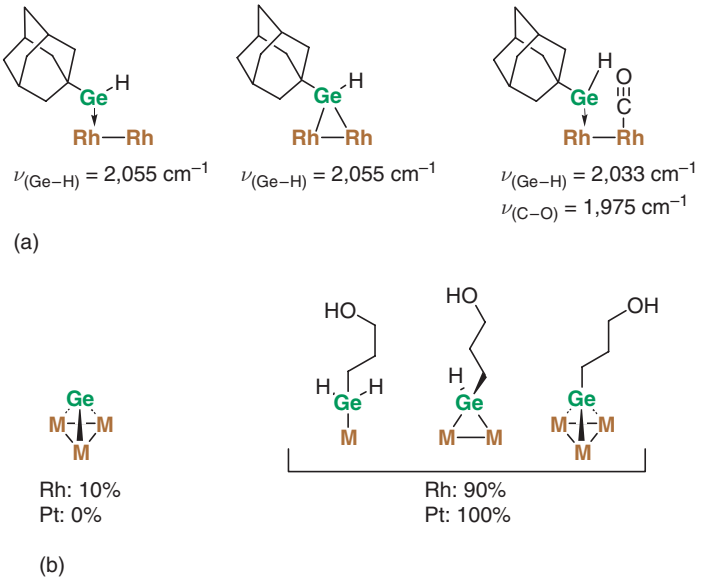

Scheme 72

The reaction proceeds selectively on the "host" metal surface by successive hydrogenolysis of the Sn–R bonds with evolution of the corresponding saturated hydrocarbons (R–H). There is a formation of partially dealkylated grafted organometallic fragments (Equation (1)).

$$M_s\text{–}H + ySnR_4 \rightarrow M_s(SnR_x)_y + y(4-x)RH \quad (1)$$

The values of x and y depend on the "host" metal, on the initial ratio between the amount of SnR_4 introduced per surface metal atoms (SnR_4/M_s), and on the reaction conditions. The various systems obtained are listed in Tables 7–9.

Of the group 8 metals, Ru has been the only one studied in detail (Table 19). When Ru particles supported on silica covered with chemisorbed hydrogen react with of 0.8 equiv. of [$SnBu_4$] at 373 K, it yields [$Ru_s(SnBu_3)_{0.8}$]. At higher temperatures, for example, 423 K, and under H_2, it provides [$Ru_s(SnBu_2)_{0.8}$] through the hydrogenolysis of another Sn–C bond (Table 19).[287]

When an Ru/SiO_2 catalyst is modified by reaction with $SnBu_4$ ($Sn/Ru = 2.4$) to give $RuSn_{2.4}/SiO_2$, the catalytic activity for hydrogenolysis of esters to aldehydes or alcohols (Scheme 73) is about the same as with unmodified catalyst, but the selectivity for the cleavage of the C–OR bond increases up to 90%.[288]

Of the group 9 metals, the chemistry of organotin agents with Rh particles supported on silica has been the only one extensively studied (Table 20). While [$SnMe_4$] is fully dealkylated on Rh particles at 300 K to give adatoms [$Rh_s(Sn)_{0.7}$], the corresponding reaction with [$SnBu_4$] gives [$Rh_s(SnBu_3)_y$], where y depends on the initial amount of [$SnBu_4$] introduced. At higher reaction temperatures and depending on the coverage, the organotin fragment is further dealkylated selectively to give [$Rh_s(SnBu_2)_y$], [$Rh_s(SnBu)_y$], and [$Rh_s(Sn)_y$].

In the case of heteroleptic organotin reagents, [Me_xSnR_{4-x}] ($x = 1$, 2, and 3; R = Bu, ^{t}Bu, Cy, and $CH_2{}^t$Bu), the smaller group, for example, Me, is preferentially cleaved, and the overall final structure is mainly [$Rh_s(SnR)_y$] (R = the larger group) when mild conditions are used (Table 20 (condition E), Scheme 74).

When Rh/SiO_2 is modified by reaction with $SnBu_4$ ($Sn/Rh_s = 0.95$) to give [$Rh_s(SnBu)_{0.95}$] as a major surface species, the catalytic hydrogenation of 3,7-dimethyl-2,6-octadienal gives 3,7-dimethyl-2,6-octadien-1-ol with a selectivity >95% with only a minor activity loss.[289] This improvement is explained by the ligand effect of [SnBu] fragments (Scheme 75).

For group 10 metals, the reactivity is similar: at low temperature, partially dealkylated surface tin species, [$M_s(SnR_{4-x})_y$], are obtained (Table 21), whereas at higher temperatures, adatoms are obtained.

While Ni/SiO_2 catalysts isomerize 3-carene into 2-carene (Scheme 76) with only a 30% yield along with >30% of byproducts, [$Ni_s(Sn)_{0.04}$], prepared by the addition of 0.04 M of Bu_4Sn/Ni_s on the Ni catalyst, increases the yield of 2-carene to 37% and decreases the amount of byproducts to <10%.[292] For this catalyst, tin is present as adatoms on the most hydrogenating sites (very likely those situated on the faces).

In the case of PtSn alloy systems, obtained by reaction of $SnBu_4$ on Pt/SiO_2, dehydrogenation of alkanes (e.g., isobutane) becomes the major pathway (vs. hydrogenolysis) and up to 98% selectivity is achieved with catalysts

Table 19 Group 8 "host" metals

M	*Organometallic reagents*	*y* (SnR_4/M_s)	*Conditions*[a]	*System obtained*	*References*
Fe	–[b]				
Ru/SiO_2	$SnBu_4$	0.8	A	$Ru_s(SnBu_3)_{0.8}$	287
Ru/SiO_2	$SnBu_4$	0.8	B	$Ru_s(SnBu_2)_{0.8}$	287
Os	–[b]				

[a]Conditions: A = 373 K, H_2 chemisorbed on Ru surface, 1 h; B = 423 K, H_2 chemisorbed on Ru surface, 1 h.
[b]No report.

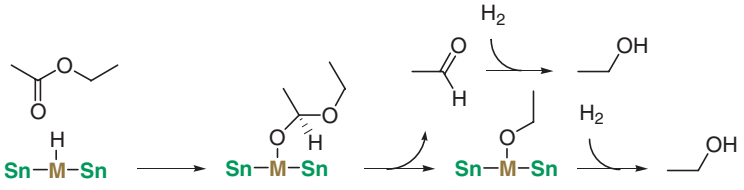

Scheme 73 Hydrogenolysis of esters to aldehydes or alcohols on $RuSn_{2.4}/SiO_2$ catalyst.

Table 20 Group 9 "host" metals

M	*Organometallic reagents*	*y* (SnR_4/M_s)	*Conditions*[a]	*System obtained*	*References*
Co	–[b]				
Rh/SiO_2	$SnMe_4$	0.8	A	$Rh_s(Sn)_{0.7}$	263
Rh/SiO_2	$SnBu_4$	0.31–0.96	A	$Rh_s(SnBu_3)_y$	266
Rh/SiO_2	$SnBu_4$	0.96	B	$Rh_s(SnBu_2)_{0.96}$	266
Rh/SiO_2	$SnBu_4$	0.31	B	$Rh_s(SnBu)_{0.31}$	266
Rh/SiO_2	$SnBu_4$	0.96	C	$Rh_s(SnBu_2)_{0.96}$	266
Rh/SiO_2	$SnBu_4$	0.31	C	$Rh_s(Sn)_{0.31}$	266
Rh/SiO_2	$SnBu_4$	0.31–0.96	D	$Rh_s(Sn)_y$	266
Rh/SiO_2	$SnBu_4$	0.5	E	$Rh_s(SnBu_{1.8})_{0.3}$	263
Rh/SiO_2	Me_3SnBu	0.7	E	$Rh_s(SnMeBu_{0.5})_{0.7}$	263
Rh/SiO_2	Me_3Sn^tBu	0.5	E	$Rh_s(SnMe_{0.4}{}^tBu_{0.4})_{0.4}$	263
Rh/SiO_2	$Me_3SnCH_2{}^tBu$	0.5	E	$Rh_s(Sn(CH_2{}^tBu)_{0.4})_{0.45}$	263
Rh/SiO_2	Me_3SnCy	0.5	E	$Rh_s(SnMe_{0.5}Cy_{0.5})_{0.5}$	263
Rh/SiO_2	Me_2SnBu_2	0.5	E	$Rh_s(SnBu)_{0.5}$	263
Rh/SiO_2	$Me_2Sn^tBu_2$	0.5	E	$Rh_s(SnMe_{0.4}{}^tBu)_{0.4}$	263
Rh/SiO_2	$Me_2Sn(CH_2{}^tBu)_2$	0.5	E	$Rh_s(Sn\{CH_2{}^tBu\})_{0.4}$	263
Rh/SiO_2	Me_2SnCy_2	0.5	E	$Rh_s(SnCy_{1.4})_{0.4}$	263
Rh/SiO_2	$MeSnBu_3$	0.5	E	$Rh_s(SnBu_{0.7})_{0.5}$	263
Ir	–[b]				

[a]Conditions: A = 300 K, 30 mbar H_2, 80 h; B = 373 K, 30 mbar H_2, 1 h; C = 423 K, 30 mbar H_2, 1 h; D = 473 K, 30 mbar H_2, 1 h; E = 300 K, 30 bar H_2 80 h.
[b]No report.

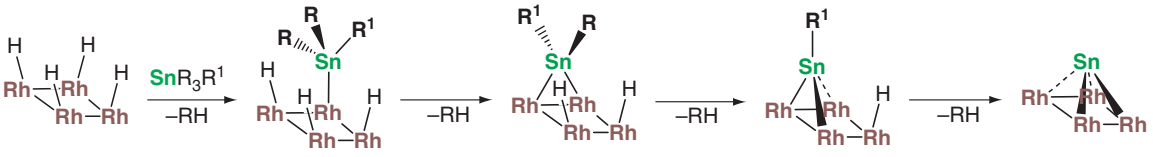

Scheme 74 Major pathway of the reaction of Me_3SnR with the surface of Pt particles under H_2 (sphere color code: orange (Pt), blue (H), white (C) and green (Sn).

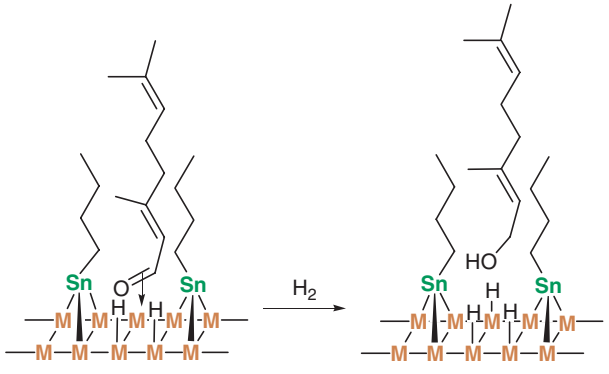

Scheme 75 Citral hydrogenation on $M_s(SnBu)_{0.95}/SiO_2$ catalyst (M = Rh).

containing Sn : Pt ratio greater than ca. 0.8.[293] This increase of selectivity has been associated with a site isolation of Pt atoms, which prevents the formation of dimetallacyclopentane intermediates, necessary for the formation of the byproducts (Scheme 77).

[$SnBu_4$] also reacts with the oxidized surface of various metal particles (M = ruthenium, rhodium, or nickel) at 323 K. In this case, butane and butenes are formed and the totality of the $SnBu_4$ introduced is fully decomposed at ca. 573 K, but the surface reactions are more complex.[287,288,294,295]

Table 21 Group 10 "host" metals

M	*Organometallic reagents*	*y* (SnR_4/M_s)	*Conditions*[a]	*System obtained*	*References*
Ni/SiO_2	Bu_4Sn	0.5	A	$Ni_s(SnBu_{2.5})_{0.5}$	290
Ni/SiO_2	Bu_4Sn	0.5	B	$Ni_s(SnBu_{1.5})_{0.5}$	290
Ni/SiO_2	Bu_4Sn		C	$Ni_s(Sn)_{0.5}$	290
Pd/Al_2O_3	Bu_4Sn		D	Pd_sSnBu_x	274
Pt/Al_2O_3	Et_4Sn		E	Pt_sSnEt_x	291

[a]Conditions: A = 298 K, 30 mbar H_2, 1 h; B = 323 K, 30 mbar H_2, 1 h; C = 373 K, 30 mbar H_2, 1 h; D = 363 K in heptane, H_2 chemisorbed on the Pd surface; E = 323 K in benzene, H_2 chemisorbed on the Pt surface.

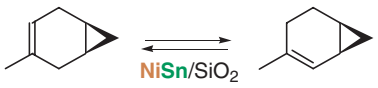

Scheme 76 Isomerization of 3-carene into 2-carene on $[Ni_s(Sn)_{0.04}]/SiO_2$ catalyst.

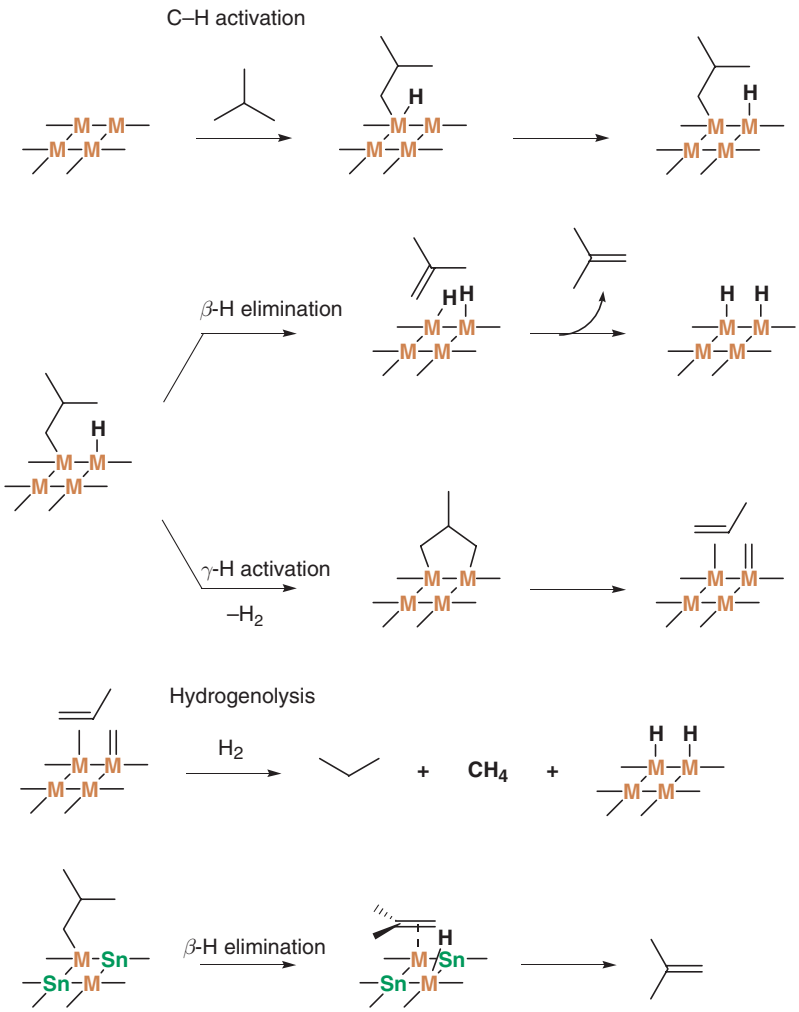

Scheme 77 Reactivity of isobutane on Pt and PtSn surfaces.

12.10.3.3.3.(iv) Lead

Reaction of [$PbEt_4$] at 300 K with Ni particles supported on alumina and covered by adsorbed H_2 leads probably to [M_sPbEt_x], as proposed in the case of [$SnEt_4$].[296] In the case of Rh particles supported on γ-alumina, the reaction of [$PbEt_4$] gives a RhPb bimetallic system after treatment under He at 673 K, and the Pb atoms are located on the rhodium surface atoms of low coordination (corners, edges).[275] Similarly, [$PbBu_4$] reacts with Pd particles supported on alumina in the presence of H_2 at room temperature to give a Pd–Pb system, which has lost all its butyl groups.[297,298] Upon reduction at 573 K, the Pd–Pb/Al_2O_3 catalysts became very selective for the hydrogenation of actetylene in the presence of ethylene[298] or for the selective hydrogenation of butadiene into butene even at high conversions.[299]

12.10.3.3.4 Group 15 complexes/group VIII metal surfaces

12.10.3.3.4.(i) Arsenic

Nickel particles supported on alumina react with triphenylarsine;[300] the reaction initially takes place selectively on the surface of the nickel particles and leads to the successive hydrogenolysis of the As–Ph bonds, releasing benzene and cyclohexane. At 303 K, the reaction stops when the Ni particles are completely covered with grafted As–Ph fragments. The quantity of triphenylarsine fixed increases with the dispersion of the metal particles, and it is proposed that more As–Ph fragments (per metallic atom) are grafted onto edge atoms than onto face atoms. When the reaction is performed at 443 K, there is a complete hydrogenolysis of the As–Ph bonds and the naked As atoms migrate inside the nickel particles easily to form intermetallic compounds such as Ni_5As_2 and NiAs (Scheme 78). The dispersion of the catalyst has no influence on the nature of the formed intermetallic species, but the rate of formation of these species increases with the dispersion of the catalysts.[300–303]

12.10.3.3.4.(ii) Antimony

The reaction of [Bu_3Sb] in heptane solution with a reduced Pd/Al_2O_3 catalyst yields a supported alloy.[274] When these final solids are reduced at 573 or 773 K, the second metal locates preferentially at the outer layer of the bimetallic aggregates. After reduction at 773 K, large metallic aggregates are obtained (particle size around 15 nm). The specific activity of the Pd surface atoms for isoprene hydrogenation is then lowered and the selectivity increased.

12.10.3.3.5 Group 16 complexes/group VIII metal surfaces: selenium

Under H_2 and at temperatures <500 K, [$(CH_3)_2Se$] reacts with Rh particles supported on ZrO_2 to give exclusively one CH_4 per reacted $(CH_3)_2Se$, and, therefore, [Rhs–SeMe] has been proposed as the major surface species (Scheme 79).[304]

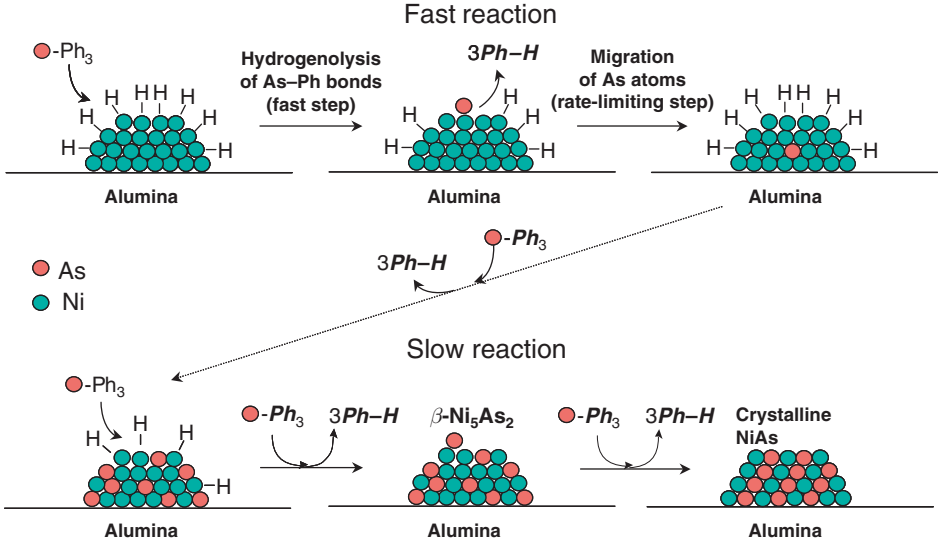

Scheme 78

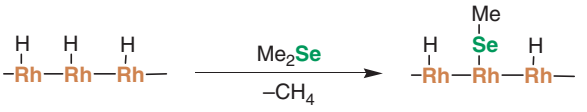

Scheme 79

References

1. Ballard, D. G. H. *Adv. Catal.* **1973**, *23*, 263.
2. Basset, J. M.; Choplin, A. *J. Mol. Catal.* **1983**, *21*, 95.
3. Burwell, R. L., Jr. *J. Catal.* **1984**, *86*, 301.
4. Burwell, R. L., Jr.; Marks, T. J. *Chemical Industries*; Dekker, 1985; Vol. 22, 207.
5. Evans, J. NATO ASI Ser., Ser. C: Math. Phys. Sci. **1988**, *231*, 47.
6. Marks, T. J. *Acc. Chem. Res.* **1992**, *25*, 57.
7. Scott, S. L.; Basset, J. M.; Niccolai, G. P.; Santini, C. C.; Candy, J. P.; Lecuyer, C.; Quignard, F.; Choplin, A. *New J. Chem.* **1994**, *18*, 115.
8. Copéret, C.; Chabanas, M.; Petroff Saint-Arroman, R.; Basset, J.-M. *Angew. Chem. Int. Ed.* **2003**, *42*, 156.
9. Canning, N.; Madix, R. J. *J. Phys. Chem.* **1984**, *88*, 2437.
10. Gates, B. C.; Lamb, H. H. *J. Mol. Catal.* **1989**, *52*, 1.
11. Guzman, J.; Gates, B. C. *Dalton Trans.* **2003**, 3303.
12. Choplin, A. *J. Mol. Catal.* **1994**, *86*, 501.
13. Theolier, A.; Choplin, A.; Basset, J. M.; Benazzi, E. *Stud. Surf. Sci. Catal.* **1994**, *84*, 1293.
14. Lefebvre, F.; De Mallmann, A.; Basset, J.-M. *Eur. J. Inorg. Chem.* **1999**, 361.
15. Zecchina, A.; Scarano, D.; Bordiga, S.; Spoto, G.; Lamberti, C. *Adv. Catal.* **2001**, *46*, 265.
16. Morrow, B. A. *Stud. Surf. Sci. Catal.* **1990**, *57*, A161.
17. Morrow, B. A.; Gay, I. D. *Surfactant Sci. Ser.* **2000**, *90*, 9.
18. Digne, M.; Sautet, P.; Raybaud, P.; Euzen, P.; Toulhoat, H. *J. Catal.* **2002**, *211*, 1.
19. Zhang, W.; Sun, M.; Prins, R. *J. Phys. Chem. B* **2002**, *106*, 11805.
20. Omegna, A.; Prins, R.; Van Bokhoven, J. A. *J. Phys. Chem. B* **2005**, *109*, 9280.
21. Chevalier, C.; Ramirez de la Piscina, P.; Ceruso, M.; Choplin, A.; Basset, J. M. *Catal.Today* **1989**, *4*, 433.
22. Lim, J. E.; Shim, C. B.; Kim, J. M.; Lee, B. Y.; Yie, J. E. *Angew. Chem., Int. Ed.* **2004**, *43*, 3839.
23. Morrow, B. A.; McFarlan, A. J. *J. Non-Cryst. Solids* **1990**, *120*, 61.
24. Millot, N.; Cox, A.; Santini, C. C.; Molard, Y.; Basset, J.-M. *Chem. Eur. J.* **2002**, *8*, 1438.
25. Millot, N.; Santini, C. C.; Lefebvre, F.; Basset, J.-M. *C. R. Chim.* **2004**, *7*, 725.
26. Yates, D. J. C.; Dembinski, G. W.; Kroll, W. R.; Elliott, J. J. *J. Phys. Chem.* **1969**, *73*, 911.
27. Morrow, B. A.; McFarlan, A. J. *Langmuir* **1991**, *7*, 1695.
28. Bartram, M. E.; Michalske, T. A.; Rogers, J. W., Jr. *J. Phys. Chem.* **1991**, *95*, 4453.
29. Bartram, M. E.; Michalske, T. A.; Rogers, J. W., Jr.; Mayer, T. M. *Chem. Mater.* **1991**, *3*, 953.
30. Blitz, J. P.; Diebel, R. E.; Deakyne, C. A.; Christensen, J. M.; Gunko, V. M. *J. Phys. Chem. B* **2005**, *109*, 5667.
31. Anwander, R.; Palm, C.; Groeger, O.; Engelhardt, G. *Organometallics* **1998**, *17*, 2027.
32. Tubis, R.; Hamlett, B.; Lester, R.; Newman, C. G.; Ring, M. A. *Inorg. Chem.* **1979**, *18*, 3275.
33. Anwander, R.; Nagl, I.; Widenmeyer, M.; Engelhardt, G.; Groeger, O.; Palm, C.; Roeser, T. *J. Phys. Chem. B* **2000**, *104*, 3532.
34. Shimada, T.; Aoki, K.; Shinoda, Y.; Nakamura, T.; Tokunaga, N.; Inagaki, S.; Hayashi, T. *J. Am. Chem. Soc.* **2003**, *125*, 4688.
35. Aoki, K.; Shimada, T.; Hayashi, T. *Tetrahedron: Asymmetry* **2004**, *15*, 1771.
36. Nedez, C.; Choplin, A.; Basset, J. M.; Benazzi, E. *Inorg. Chem.* **1994**, *33*, 1094.
37. Nedez, C.; Lefebvre, F.; Choplin, A.; Basset, J.-M. *Langmuir* **1996**, *12*, 925.
38. Nedez, C.; Theolier, A.; Lefebvre, F.; Choplin, A.; Basset, J. M.; Joly, J. F. *J. Am. Chem. Soc.* **1993**, *115*, 722.
39. Nedez, C.; Lefebvre, F.; Choplin, A.; Basset, J. M. *New J. Chem.* **1994**, *18*, 1215.
40. Nedez, C.; Lefebvre, F.; Choplin, A.; Basset, J. M.; Benazzi, E. *J. Am. Chem. Soc.* **1994**, *116*, 3039.
41. Nedez, C.; Lefebvre, F.; Basset, J.-M. *J. Chem. Soc., Faraday Trans.* **1997**, *93*, 1987.
42. Boutet, S.; Jousseaume, B.; Toupance, T.; Biesemans, M.; Willem, R.; Labrugere, C.; Delattre, L. *Chem. Mater.* **2005**, *17*, 1803.
43. de Mallmann, A.; Lot, O.; Perrier, N.; Lefebvre, F.; Santini, C.; Basset, J. M. *Organometallics* **1998**, *17*, 1031.
44. Nedez, C.; Choplin, A.; Lefebvre, F.; Basset, J. M.; Benazzi, E. *Inorg. Chem.* **1994**, *33*, 1099.
45. Adachi, M.; Lefebvre, F.; Basset, J.-M. *Chem. Lett.* **1996**, 221.
46. Nedez, C.; Choplin, A.; Lefebvre, F.; Basset, J.-M. *Inorg. Chem.* **1994**, *33*, 1575.
47. Jannini, M. J. D. M.; Buffon, R.; de Wit, A. M.; Mol, J. C. *J. Mol. Catal. A: Chem.* **1998**, *133*, 201.
48. Nedez, C.; Lefebvre, F.; Choplin, A.; Niccolai, G. P.; Basset, J.-M.; Benazzi, E. *J. Am. Chem. Soc.* **1994**, *116*, 8638.
49. Nedez, C.; Lefebvre, F.; Humblot, F.; Basset, J.-M.; Benazzi, E. *J. Chem. Soc., Faraday Trans.* **1996**, *92*, 3419.
50. Fischbach, A.; Eickerling, G.; Scherer, W.; Herdtweck, E.; Anwander, R. *Z. Naturforschung, B: Chem. Sci.* **2004**, *59*, 1353.
51. Fischbach, A.; Klimpel, M. G.; Widenmeyer, M.; Herdtweck, E.; Scherer, W.; Anwander, R. *Angew. Chem., Int. Ed.* **2004**, *43*, 2234.
52. Nagl, I.; Widenmeyer, M.; Herdtweck, E.; Raudaschl-Sieber, G.; Anwander, R. *Microporous Mesoporous Mater.* **2001**, *44–45*, 311.
53. Anwander, R.; Roesky, R. *J. Chem. Soc., Dalton Trans.: Inorg. Chem.* **1997**, 137.
54. Anwander, R.; Runte, O.; Eppinger, J.; Gerstberger, G.; Herdtweck, E.; Spiegler, M. *J. Chem. Soc., Dalton Trans.: Inorg. Chem.* **1998**, 847.
55. Anwander, R.; Nagl, I.; Zapilko, C.; Widenmeyer, M. *Tetrahedron* **2003**, *59*, 10567.
56. Gauvin, R. M.; Mortreux, A. *Chem. Commun.* **2005**, 1146.
57. Anwander, R. *Chem. Mater.* **2001**, *13*, 4419.
58. Anwander, R. *Nanostruct. Catal.* **2003**, 15.
59. Gerstberger, G.; Palm, C.; Anwander, R. *Chem. Eur. J.* **1999**, *5*, 997.

60. Gerstberger, G.; Anwander, R. *Microporous Mesoporous Mater.* **2001**, *44–45*, 303.
61. Nagl, I.; Widenmeyer, M.; Grasser, S.; Koehler, K.; Anwander, R. *J. Am. Chem. Soc.* **2000**, *122*, 1544.
62. Toscano, P. J.; Marks, T. J. *Langmuir* **1986**, *2*, 820.
63. Toscano, P. J.; Marks, T. J. *J. Am. Chem. Soc.* **1985**, *107*, 653.
64. He, M. Y.; Burwell, R. L., Jr.; Marks, T. J. *Organometallics* **1983**, *2*, 566.
65. He, M. Y.; Xiong, G.; Toscano, P. J.; Burwell, R. L., Jr.; Marks, T. J. *J. Am. Chem. Soc.* **1985**, *107*, 641.
66. Gillespie, R. D.; Burwell, R. L., Jr.; Marks, T. J. *Langmuir* **1990**, *6*, 1465.
67. Eisen, M. S.; Marks, T. J. *J. Am. Chem. Soc.* **1992**, *114*, 10358.
68. Eisen, M. S.; Marks, T. J. *Organometallics* **1992**, *11*, 3939.
69. Eisen, M. S.; Marks, T. J. *J. Mol. Catal.* **1994**, *86*, 23.
70. Finch, W. C.; Gillespie, R. D.; Hedden, D.; Marks, T. J. *J. Am. Chem. Soc.* **1990**, *112*, 6221.
71. Blandy, C.; Pellegatta, J. L.; Choukroun, R.; Gilot, B.; Guiraud, R. *Can. J. Chem.* **1993**, *71*, 34.
72. Wang, X.-X.; Veyre, L.; Lefebvre, F.; Patarin, J.; Basset, J.-M. *Microporous Mesoporous Mater.* **2003**, *66*, 169.
73. Alladin, T.; Beaudoin, M. C.; Scott, S. L. *Inorg. Chim. Acta* **2003**, *345*, 292.
74. Beaudoin, M. C.; Womiloju, O.; Fu, A.; Ajjou, J. A. N.; Rice, G. L.; Scott, S. L. *J. Mol. Catal. A: Chem.* **2002**, *190*, 159.
75. Ballard, D. G. H.; Heap, N.; Kilbourn, B. T.; Wyatt, R. J. *Makromol. Chem.* **1973**, *170*, 1.
76. Ballard, D. G. H. *J. Polym. Sci., Polym. Chem. Ed.* **1975**, *13*, 2191.
77. Ittel, S. D. *J. Macromol. Sci., Chem.* **1990**, *A27*, 1133.
78. Collette, J. W.; Tullock, C. W.; MacDonald, R. N.; Buck, W. H.; Su, A. C. L.; Harrell, J. R.; Mulhaupt, R.; Anderson, B. C. *Macromol.* **1989**, *22*, 3851.
79. Jezequel, M.; Dufaud, V.; Ruiz-Garcia, M. J.; Carrillo-Hermosilla, F.; Neugebauer, U.; Niccolai, G. P.; Lefebvre, F.; Bayard, F.; Corker, J.; Fiddy, S., *et al. J. Am. Chem. Soc.* **2001**, *123*, 3520.
80. Dahmen, K. H.; Hedden, D.; Burwell, R. L., Jr.; Marks, T. J. *Langmuir* **1988**, *4*, 1212.
81. Tullock, C. W.; Mulhaupt, R.; Ittel, S. D. *Makromol. Chem., Rapid Commun.* **1989**, *10*, 19.
82. Tullock, C. W.; Tebbe, F. N.; Mulhaupt, R.; Ovenall, D. W.; Setterquist, R. A.; Ittel, S. D. *J. Polym. Sci., Part A: Polym. Chem.* **1989**, *27*, 3063.
83. Bochmann, M.; Pindado, G. J.; Lancaster, S. J. *J. Mol. Catal. A: Chem.* **1999**, *146*, 179.
84. Millot, N.; Santini, C. C.; Baudouin, A.; Basset, J.-M. *Chem. Commun.* **2003**, 2034.
85. Lancaster, S. J.; O'Hara, S. M.; Bochmann, M. In *Metalorganic Catalysts for Synthesis and Polymerisation*; Kaminsky, W., Ed.; Springer: Berlin, 1999; p 413.
86. Candlin, J. P.; Thomas, H. *Adv. Chem. Ser.* **1974**, *132*, 212.
87. Crocker, M.; Herold, R. H. M.; Roosenbrand, B. G.; Emeis, K. A.; Wilson, A. *Coll. Surf., A: Phys. Eng. Aspects* **1998**, *139*, 351.
88. Maksimov, N. G.; Nesterov, G. A.; Zakharov, V. A.; Anufrienko, V. F.; Yermakov, Y. I. *React. Kinet. Catal. Lett.* **1978**, *8*, 81.
89. Profilet, R. D.; Rothwell, A. P.; Rothwell, I. P. *J. Chem. Soc., Chem. Commun.* **1993**, 42.
90. Holmes, S. A.; Quignard, F.; Choplin, A.; Teissier, R.; Kervennal, J. *J. Catal.* **1998**, *176*, 182.
91. Holmes, S. A.; Quignard, F.; Choplin, A.; Teissier, R.; Kervennal, J. *J. Catal.* **1998**, *176*, 173.
92a. Petroff Saint-Arroman, R.; Basset, J.-M.; Lefebvre, F.; Didillon, B. *Appl. Catal. A.* **2005**, *290*, 181.
92b. Tosin, G.; Santini, C. C.; Taoufik, M.; Mallmann, A. D.; Basset, J.-M. *Organometallics.* **2006**, *25*, 3324.
93. Scott, S. L.; Church, T. L.; Nguyen, D. H.; Mader, E. A.; Moran, J. *Top. Catal.* **2005**, *34*, 109.
94. Volodin, A. M.; Alekseev, O. S.; Bol'shov, V. A.; Ryndin, Y. A. *Kinet. Katal.* **1990**, *31*, 179.
95. Quignard, F.; Lecuyer, C.; Bougault, C.; Lefebvre, F.; Choplin, A.; Olivier, D.; Basset, J. M. *Inorg. Chem.* **1992**, *31*, 928.
96. Adachi, M.; Nedez, C.; Wang, X. X.; Bayard, F.; Dufaud, V.; Lefebvre, F.; Basset, J.-M. *J. Mol. Catal. A: Chem.* **2003**, *204–205*, 443.
97. d' Ornelas, L.; Reyes, S.; Quignard, F.; Choplin, A.; Basset, J. M. *Chem. Lett.* **1993**, 1931.
98. Ahn, H.; Nicholas, C. P.; Marks, T. J. *Organometallics* **2002**, *21*, 1788.
99. Nicholas, C. P.; Ahn, H.; Marks, T. J. *J. Am. Chem. Soc.* **2003**, *125*, 4325.
100. Ahn, H.; Marks, T. J. *J. Am. Chem. Soc.* **1998**, *120*, 13533.
101. Nicholas, C. P.; Marks, T. J. *Langmuir* **2004**, *20*, 9456.
102. Nicholas, C. P.; Marks, T. J. *Nano Lett.* **2004**, *4*, 1557.
103. Ermakov, Y. I.; Alekseev, O. S.; Shmachkov, V. A.; Sobolev, V. I.; Ryndin, Y. A. *Kinet. Katal.* **1985**, *26*, 1270.
104. Ermakov, Y. I.; Ryndin, Y. A.; Alekseev, O. S.; Kochubei, D. I.; Shmachkov, V. A.; Gergert, N. I. *J. Mol. Catal.* **1989**, *49*, 121.
105. Zakharov, V. A.; Ryndin, Y. A. *J. Mol. Catal.* **1989**, *56*, 183.
106. Rosier, C.; Niccolai, G. P.; Basset, J.-M. *J. Am. Chem. Soc.* **1997**, *119*, 12408.
107. King, S. A.; Schwartz, J. *Inorg. Chem.* **1991**, *30*, 3771.
108. Quignard, F.; Lecuyer, C.; Choplin, A.; Basset, J. M. *J. Chem. Soc., Dalton Trans.* **1994**, 1153.
109. Corker, J.; Lefebvre, F.; Lecuyer, C.; Dufaud, V.; Quignard, F.; Choplin, A.; Evans, J.; Basset, J.-M. *Science (Washington, D. C.)* **1996**, *271*, 966.
110. Rataboul, F.; Baudouin, A.; Thieuleux, C.; Veyre, L.; Copéret, C.; Thivolle-Cazat, J.; Basset, J.-M.; Lesage, A.; Emsley, L. *J. Am. Chem. Soc.* **2004**, *126*, 12541.
111. Capdevielle, V. Ph.D. Thesis, Université Lyon I, Lyon, 1996.
112. Quignard, F.; Choplin, A.; Basset, J. M. *J. Chem. Soc., Chem. Commun.* **1991**, 1589.
113. Quignard, F.; Lecuyer, C.; Choplin, A.; Olivier, D.; Basset, J. M. *J. Mol. Catal.* **1992**, *74*, 353.
114. Quignard, F.; Choplin, A.; Basset, J.-M. *J. Chem. Soc., Dalton Trans.* **1994**, 2411.
115. Niccolai, G. P.; Basset, J.-M. *Appl. Catal., A: Gen.* **1996**, *146*, 145.
116. Thieuleux, C.; Quadrelli, E. A.; Basset, J.-M.; Doebler, J.; Sauer, J. *Chem. Commun.* **2004**, 1729.
117. Besedin, D. V.; Ustynyuk, L. Y.; Ustynyuk, Y. A.; Lunin, V. V. *Mendeleev Commun.* **2002**, 173.
118. Copéret, C.; Grouiller, A.; Basset, M.; Chermette, H. *Chem. Phys. Chem.* **2003**, *4*, 608.
119. Casty, G. L.; Matturro, M. G.; Myers, G. R.; Reynolds, R. P.; Hall, R. B. *Organometallics* **2001**, *20*, 2246.
120. Lecuyer, C.; Quignard, F.; Choplin, A.; Olivier, D.; Basset, J. M. *Angew. Chem.* **1991**, *103*, 1692.
121. Dufaud, V.; Basset, J.-M. *Angew. Chem., Int. Ed.* **1998**, *37*, 806.
122. Mortensen, J. J.; Parrinello, M. *J. Phys. Chem. B* **2000**, *104*, 2901.
123. Rosier, C. Ph.D. Thesis, Université Claude Bernard, Lyon I, 1999.
124. Leyrit, P.; McGill, C.; Quignard, F.; Choplin, A. *J. Mol. Catal. A: Chem.* **1996**, *112*, 395.

125. Bouh, A. O.; Rice, G. L.; Scott, S. L. *J. Am. Chem. Soc.* **1999**, *121*, 7201.
126. Roveda, C.; Church, T. L.; Alper, H.; Scott, S. L. *Chem. Mater.* **2000**, *12*, 857.
127. Jarupatrakorn, J.; Tilley, T. D. *J. Am. Chem. Soc.* **2002**, *124*, 8380.
128. Brutchey, R. L.; Mork, B. V.; Sirbuly, D. J.; Yang, P.; Tilley, T. D. *J. Mol. Catal. A: Chem.* **2005**, *238*, 1.
129. Katz, A.; Da Costa, P.; Lam, A. C. P.; Notestein, J. M. *Chem. Mater.* **2002**, *14*, 3364.
130. Notestein, J. M.; Iglesia, E.; Katz, A. *J. Am. Chem. Soc.* **2004**, *126*, 16478.
131. Sheldon, R. A.; Van Vliet, M. C. A. In *Fine Chemicals through Heterogeneous Catalysis*; Sheldon, R. A., van Bekkum, H., Eds.; Wiley-VCH, 2001; pp 473.
132. Riollet, V. Ph.D. Thesis, Université Claude Bernard, Lyon I, 2002.
133. Ajjou, J. A. N.; Rice, G. L.; Scott, S. L. *J. Am. Chem. Soc.* **1998**, *120*, 13436.
134. Wolke, S. I.; Buffon, R.; Filho, U. P. R. *J. Organomet. Chem.* **2001**, *625*, 101.
135. Dufaud, V.; Niccolai, G. P.; Thivolle-Cazat, J.; Basset, J.-M. *J. Am. Chem. Soc.* **1995**, *117*, 4288.
136. Lefort, L.; Chabanas, M.; Maury, O.; Meunier, D.; Copéret, C.; Thivolle-Cazat, J.; Basset, J.-M. *J. Organomet. Chem.* **2000**, *593–594*, 96.
137. Chabanas, M.; Quadrelli, E. A.; Fenet, B.; Copéret, C.; Thivolle-Cazat, J.; Basset, J.-M.; Lesage, A.; Emsley, L. *Angew. Chem., Int. Ed.* **2001**, *40*, 4493.
138. Le Roux, E. L.; Chabanas, M.; Baudouin, A.; de Mallmann, A.; Copéret, C.; Quadrelli, E. A.; Thivolle-Cazat, J.; Basset, J.-M.; Lukens, W.; Lesage, A.; Emsley, L.; Sunley, G. J. *J. Am. Chem. Soc.* **2004**, *126*, 13391.
139. Copéret, C.; Maury, O.; Thivolle-Cazat, J.; Basset, J.-M. *Angew. Chem., Int. Ed.* **2001**, *40*, 2331.
140. Ahn, H.; Marks, T. J. *J. Am. Chem. Soc.* **2002**, *124*, 7103.
141. Vidal, V.; Theolier, A.; Thivolle-Cazat, J.; Basset, J.-M.; Corker, J. *J. Am. Chem. Soc.* **1996**, *118*, 4595.
142. Mikhailov, M. N.; Bagatur'yants, A. A.; Kustov, L. M. *Russ. Chem. Bull.* (translation of *Izv. Akad. Nauk, Ser. Khim.)* **2003**, *52*, 30.
143. Taoufik, M.; de Mallmann, A.; Prouzet, E.; Saggio, G.; Thivolle-Cazat, J.; Basset, J.-M. *Organometallics* **2001**, *20*, 5518.
144. Saggio, G.; de Mallmann, A.; Maunders, B.; Taoufik, M.; Thivolle-Cazat, J.; Basset, J.-M. *Organometallics* **2002**, *21*, 5167.
145. Vidal, V.; Theolier, A.; Thivolle-Cazat, J.; Basset, J.-M. *J. Chem. Soc., Chem. Commun.* **1995**, 991.
146. Rataboul, F.; Chabanas, M.; De Mallmann, A.; Copéret, C.; Thivolle-Cazat, J.; Basset, J.-M. *Eur. J. Chem.* **2003**, *9*, 1426.
147. Lefort, L.; Copéret, C.; Taoufik, M.; Thivolle-Cazat, J.; Basset, J.-M. *Chem. Commun.* **2000**, 663.
148. Chabanas, M.; Vidal, V.; Copéret, C.; Thivolle-Cazat, J.; Basset, J.-M. *Angew. Chem., Int. Ed.* **2000**, *39*, 1962.
149. Vidal, V.; Theolier, A.; Thivolle-Cazat, J.; Basset, J.-M. *Science (Washington, D. C.)* **1997**, *276*, 99.
150. Maury, O.; Lefort, L.; Vidal, V.; Thivolle-Cazat, J.; Basset, J.-M. *Angew. Chem., Int. Ed.* **1999**, *38*, 1952.
151. Taoufik, M.; Schwab, E.; Schultz, M.; Vanoppen, D.; Walter, M.; Thivolle-Cazat, J.; Basset, J.-M. *Chem. Commun.* **2004**, 1434.
152. Soulivong, D.; Copéret, C.; Thivolle-Cazat, J.; Basset, J.-M.; Maunders, B. M.; Pardy, R. B. A.; Sunley, G. J. *Angew. Chem., Int. Ed.* **2004**, *43*, 5366.
153. Rice, G. L.; Scott, S. L. *J. Mol. Catal. A: Chem.* **1997**, *125*, 73.
154. Rice, G. L.; Scott, S. L. *Langmuir* **1997**, *13*, 1545.
155. Deguns, E. W.; Taha, Z.; Meitzner, G. D.; Scott, S. L. *Journal of Physical Chemistry B* **2005**, *109*, 5005.
156. Grasser, S.; Haessner, C.; Koehler, K.; Lefebvre, F.; Basset, J.-M. *Phys. Chem. Chem. Phys.* **2003**, *5*, 1906.
157. Brutchey, R. L.; Lugmair, C. G.; Schebaum, L. O.; Tilley, T. D. *J. Catal.* **2005**, *229*, 72.
158. Petroff Saint-Arroman, R.; de Mallmann, A.; Lefebvre, F.; Basset, J.-M. Abstracts of Papers, *224th ACS National Meeting*, Boston, MA, United States, August 18–22, 2002.
159. Karol, F. J.; Wu, C.; Reichle, W. T.; Maraschin, N. J. *J. Catal.* **1979**, *60*, 68.
160. Bade, O. M.; Blom, R.; Ystenes, M. *Organometallics* **1998**, *17*, 2524.
161. Ajjou, J. A. N.; Scott, S. L. *Organometallics* **1997**, *16*, 86.
162. Ajjou, J. A. N.; Scott, S. L. *J. Am. Chem. Soc.* **2000**, *122*, 8968.
163. Ajjou, J. A. N.; Scott, S. L.; Paquet, V. *J. Am. Chem. Soc.* **1998**, *120*, 415.
164. Scott, S. L.; Amor Nait Ajjou, J. *Chem. Eng. Sci.* **2001**, *56*, 4155.
165. Iwasawa, Y.; Nakano, Y.; Ogasawara, S. *J. Chem. Soc., Faraday Trans. 1: Phys. Chem. Condens. Phases* **1978**, *74*, 2968.
166. Petroff Saint-Arroman, R.; Chabanas, M.; Baudouin, A.; Copéret, C.; Basset, J.-M.; Lesage, A.; Emsley, L. *J. Am. Chem. Soc.* **2001**, *123*, 3820.
167. Herrmann, W. A.; Stumpf, A. W.; Priermeier, T.; Bogdanovic, S.; Dufaud, V.; Basset, J.-M. *Angew. Chem., Int. Ed. Engl.* **1997**, *35*, 2803.
168. Blanc, F.; Chabanas, M.; Copéret, C.; Fenet, B.; Herdweck, E. *J. Organomet. Chem.* **2005**, *690*, 5014.
169. Yang, Q.; Copéret, C.; Li, C.; Basset, J.-M. *New J. Chem.* **2003**, *27*, 319.
170. Jarupatrakorn, J.; Coles, M. P.; Tilley, T. D. *Chem. Mater.* **2005**, *17*, 1818.
171. Mowat, W.; Smith, J.; Whan, D. A. *J. Chem. Soc., Chem. Commun.* **1974**, 34.
172. Smith, J.; Mowat, W.; Whan, D. A.; Ebsworth, E. A. V. *J. Chem. Soc., Dalton Trans.* **1974**, 1742.
173. Le Roux, E.; Taoufik, M.; Chabanas, M.; Alcor, D.; Baudouin, A.; Copéret, C.; Thivolle-Cazat, J.; Basset, J.-M.; Lesage, A.; Hediger, S., *et al. Organometallics* **2005**, *24*, 4274.
174. Buffon, R.; Leconte, M.; Choplin, A.; Basset, J.-M. *J. Chem. Soc., Dalton Trans.* **1994**, 1723.
175. Weiss, K.; Loessel, G. *Angew. Chem. Int. Ed.* **1989**, *28*, 62.
176. Buffon, R.; Leconte, M.; Choplin, A.; Basset, J. M. *J. Chem. Soc., Chem. Commun.* **1993**, 361.
177a. Le Roux, E.; Taoufik, M.; Copéret, C.; de Mallmann, A.; Thivolle-Cazat, J.; Basset, J.-M.; Maunders, B. M.; Sunley, G. J. *Angew. Chem. Int. Ed.* **2005**, *44*, 6755.
177b. Joubert, J.; Delbecq, F.; Sautet, P.; Le Roux, E.; Taoufik, M.; Thieuleux, C.; Blanc, F.; Copéret, C.; Thivolle-Cazat, J.; Basset, J.-M. *J. Am. Chem. Soc.* **2006**, *128*, 9157.
178. Riollet, V.; Quadrelli, E. A.; Copéret, C.; Basset, J.-M.; Andersen, R. A.; Köhler, K.; Boettcher, R.; Herdtweck, E. *Eur. J. Chem.* **2005**, *11*, 7539.
179. Chabanas, M.; Baudouin, A.; Copéret, C.; Basset, J.-M. *J. Am. Chem. Soc.* **2001**, *123*, 2062.
180. Lesage, A.; Emsley, L.; Chabanas, M.; Copéret, C.; Basset, J.-M. *Angew. Chem., Int. Ed.* **2002**, *41*, 4535.
181. Chabanas, M.; Baudouin, A.; Copéret, C.; Basset, J.-M.; Lukens, W.; Lesage, A.; Hediger, S.; Emsley, L. *J. Am. Chem. Soc.* **2003**, *125*, 492.
182. Solans-Monfort, X.; Clot, E.; Copéret, C.; Eisenstein, O. *Organometallics* **2005**, *24*, 1586.
183. Chabanas, M.; Copéret, C.; Basset, J.-M. *Chem. Eur. J.* **2003**, *9*, 971.
184a. Herrmann, W. A.; Wagner, W.; Flessner, U. N.; Vokhardt, U.; Komber, H. *Angew. Chem. Int. Ed.* **1991**, *30*, 1636.
184b. Moses, A. W.; Ramsahye, N. A.; Raab, C.; Leifiste, H. D.; Chattopadhyay, S.; Chmelka, B. F.; Eckert, J.; Scott, S. L. *Organometallics* **2006**, *25*, 2157.

185. Burron, R.; Auroux, A.; Lefebvre, F.; Leconte, M.; Choplin, A.; Basset, J. M.; Herrmann, W. A. *J. Mol. Catal.* **1992**, *76*, 287.
186. Buffon, R.; Jannini, M. J. D. M.; Abras, A. *J. Mol. Catal. A: Chem.* **1997**, *115*, 173.
187. Scott, S. L.; Basset, J.-M. *J. Am. Chem. Soc.* **1994**, *116*, 12069.
188. Toscano, P. J.; Marks, T. J. *Organometallics* **1986**, *5*, 400.
189. Nozaki, C.; Lugmair, C. G.; Bell, A. T.; Tilley, T. D. *J. Am. Chem. Soc.* **2002**, *124*, 13194.
190. Kaplan, A. W.; Bergman, R. G. *Organometallics* **1998**, *17*, 5072.
191. Brutchey, R. L.; Drake, I. J.; Bell, A. T.; Tilley, T. D. *Chem. Commun.* **2005**, 3736.
192. Dufour, P.; Houtman, C.; Santini, C. C.; Nedez, C.; Basset, J. M.; Hsu, L. Y.; Shore, S. G. *J. Am. Chem. Soc.* **1992**, *114*, 4248.
193. Dufour, P.; Houtman, C.; Santini, C. C.; Nedez, C.; Basset, J. M.; Hsu, L. Y.; Shore, S. G.; Shore, S. C. *J. Am. Chem. Soc.* **1992**, *114*, 9242.
194. DeCanio, S. J.; Foley, H. C.; Dybowski, C.; Gates, B. C. *J. Chem. Soc., Chem. Commun.* **1982**, 1372.
195. Foley, H. C.; DeCanio, S. J.; Tau, K. D.; Chao, K. J.; Onuferko, J. H.; Dybowski, C.; Gates, B. C. *J. Am. Chem. Soc.* **1983**, *105*, 3074.
196. Ward, M. D.; Harris, T. V.; Schwartz, J. *J. Chem. Soc., Chem. Commun.* **1980**, 357.
197. Dufour, P.; Houtman, C.; Santini, C. C.; Basset, J. M. *J. Mol. Catal.* **1992**, *77*, 257.
198. Dufour, P.; Santini, C. C.; Houtman, C.; Basset, J. M. *J. Mol. Catal.* **1991**, *66*, L23.
199. Dufour, P.; Scott, S. L.; Santini, C. C.; Lefebvre, F.; Basset, J.-M. *Inorg. Chem.* **1994**, *33*, 2509.
200. Scott, S. L.; Dufour, P.; Santini, C. C.; Basset, J.-M. *Inorg. Chem.* **1996**, *35*, 869.
201. Scott, S. L.; Mills, A.; Chao, C.; Basset, J.-M.; Millot, N.; Santini, C. C. *J. Mol. Catal. A: Chem.* **2003**, *204–205*, 457.
202. Santini, C. C.; Scott, S. L.; Basset, J.-M. *J. Mol. Catal. A: Chem.* **1996**, *107*, 263.
203. Scott, S. L.; Crippen, C.; Santini, C. C.; Basset, J.-M. *J. Chem. Soc., Chem. Commun.* **1995**, 1875.
204. Scott, S. L.; Szpakowicz, M.; Mills, A.; Santini, C. C. *J. Am. Chem. Soc.* **1998**, *120*, 1883.
205. Meyer, T. Y.; Woerpel, K. A.; Novak, B. M.; Bergman, R. G. *J. Am. Chem. Soc.* **1994**, *116*, 10290.
206. Ermakov, Y. I.; Kuznetsov, B. N.; Karakchiev, L. G.; Derbeneva, S. S. *Kinet. Katal.* **1973**, *14*, 709.
207. Ermakov, Y. I.; Kuznetsov, B. N. *React. Kinet. Catal. Lett.* **1974**, *1*, 87.
208. Ermakov, Y. I.; Kuznetsov, B. N.; Ryndin, Y. A.; Lazutkin, A. M. *Kinet. Katal.* **1973**, *14*, 1594.
209. Ryndin, Y. A.; Kuznetsov, V. L.; Kuznetsov, B. N.; Ermakov, Y. I. *Mater. Resp. Nauchno-Tekh. Konf. Molodykh Uch. Pererab. Nefti Neftekhim, 2nd*, **1974**, 113.
210. Kuznetsov, B. N.; Ermakov, Y. I.; Kuznetsov, V. L.; Ryndin, Y. A.; Karakchiev, L. G.; Shinkarenko, V. G.; Mamaeva, E. K.; Startseva, L. Y. *Kinet. Katal.* **1975**, *16*, 1356.
211. Holland, P. L.; Andersen, R. A.; Bergman, R. G.; Huang, J.; Nolan, S. P. *J. Am. Chem. Soc.* **1997**, *119*, 12800.
212. Holland, P. L.; Andersen, R. A.; Bergman, R. G.; Huang, J.; Nolan, S. P. *J. Am. Chem. Soc.* **2000**, *122*, 9352.
213. Richmond, M. K.; Scott, S. L.; Alper, H. *J. Am. Chem. Soc.* **2001**, *123*, 10521.
214. Richmond, M. K.; Scott, S. L.; Yap, G. P. A.; Alper, H. *Organometallics* **2002**, *21*, 3395.
215. Fujdala, K. L.; Drake, I. J.; Bell, A. T.; Tilley, T. D. *J. Am. Chem. Soc.* **2004**, *126*, 10864.
216. Guzman, J.; Gates, B. C. *Langmuir* **2003**, *19*, 3897.
217. Guzman, J.; Anderson, B. G.; Vinod, C. P.; Ramesh, K.; Niemantsverdriet, J. W.; Gates, B. C. *Langmuir* **2005**, *21*, 3675.
218. Guzman, J.; Gates, B. C. *Angew. Chem., Int. Ed.* **2003**, *42*, 690.
219. Guzman, J.; Gates, B. C. *J. Phys. Chem. B* **2003**, *107*, 2242.
220. Guzman, J.; Gates, B. C. *J. Catal.* **2004**, *226*, 111.
221. Fierro-Gonzalez, J. C.; Gates, B. C. *J. Phys. Chem. B* **2005**, *109*, 7275.
222. Guzman, J.; Kuba, S.; Fierro-Gonzalez, J. C.; Gates, B. C. *Catal. Lett.* **2004**, *95*, 77.
223. Fierro-Gonzalez, J. C.; Bhirud, V. A.; Gates, B. C. *Chem. Commun.* **2005**, 5275.
224. Margitfalvi, J.; Hegedüs, M.; Góbölös, S.; Kern-Tálas, E.; Szedlacsek, P.; Szabó, S.; Nagy, F. In *8th International Congress on Catalysis*; DECHEMA (Frankfurt am Main):Berlin, **1984**; Vol. IV, pp 903.
225. Travers, C.; Bournonville, J. P.; Martino, G. In *Int. Congr. Catal., [Proc.]*, 8th, 1985; Vol. 4, pp IV891.
226. Candy, J. P.; Didillon, B.; Smith, E. L.; Shay, T. B.; Basset, J. M. *J. Mol. Catal.* **1994**, *86*, 179.
227. Ryndin, Y. A.; Gordova, L. V.; Tyunina, O. V.; Davydov, A. A.; Yermakov, Y. I. *React. Kinet. Catal. Lett.* **1984**, *26*, 79.
228. Ryndin, Y. A.; Gordova, L. V.; Zaikovskii, V. I.; Yermakov, Y. I. *React. Kinet. Catal. Lett.* **1984**, *26*, 103.
229. Ryndin, Y. A.; Yermakov, Y. I. In *Surface Organometallic Chemistry: Molecular Approaches to Surface Catalysis*; Basset, J.-M., Gates, B. C., Candy, J.-P., Choplin, A., Leconte, M., Quignard, F., Santini, C., Eds.; Kluwer, 1988, pp 127.
230. Van Hardeveld, R.; Hartog, F. *Surf. Sci.* **1969**, *15*, 189.
231. Liu, J. Advanced electron microscopy in developing nanostructured heterogeneous catalysts. In *Nanotechnology in Catalysis*; Stevenson, S. A., Dumesic, J. A., Baker, R. T. K., Ruckenstein, E., Eds.; Kluwer/Plenum: New York, 2004; Vol. 2, pp 361.
232. Bernal, S.; Botana, F. J.; Calvino, J. J.; Lopez-Cartes, C.; Perez-Omil, J. A.; Rodriguez-Izquierdo, J. M. *Ultramicroscopy* **1998**, *72*, 135.
233. Neri, G.; Donato, A.; Milone, C.; Pietropaolo, R.; Schwank, J. *Mater. Chem. Phys.* **1996**, *44*, 145.
234. Arenas-Alatorre, J.; Avalos-Borja, M.; Diaz, G. *Appl. Surf. Sci.* **2002**, *189*, 7.
235. Dassenoy, F.; Philippot, K.; Amiens, C.; Casanove, M. J.; Chaudret, B. *New J. Chem.* **1998**, *22*, 703.
236. Badia, A.; Gao, W.; Singh, S.; Demers, L.; Cuccia, L.; Reven, L. *Langmuir* **1996**, *12*, 1262.
237. Sun, S.; Murray, C. B.; Weller, D.; Folks, L.; Moser, A. *Science* **2000**, *287*, 1989.
238. Pan, C.; Pelzer, K.; Philippot, K.; Chaudret, B.; Dassenoy, F.; Lecante, P. M.; Casanove, J. *J. Am. Chem. Soc.* **2001**, *123*, 7584.
239. Rodriguez, A.; Amiens, C.; Chaudret, B.; Casanove, M. J.; Lecante, P.; Bradley, J. S. *Chem. Mater.* **1996**, *8*, 1978.
240. Chaudret, B. *Top. Organomet. Chem.* **2005**, *16*, 233.
241. Hosteler, M. J.; Nuzzo, R. G.; Girolami, G. S. *J. Am. Chem. Soc.* **1994**, *116*, 11608.
242. Terrill, R. H.; Postlethwaite, T. A.; Chen, C.-H. *J. Am. Chem. Soc.* **1995**, *117*, 12537.
243. Pelzer, K.; Vidoni, O.; Philippot, K.; Chaudret, B.; Collière, V. *Adv. Funct. Mater.* **2003**, *13*, 118.
244. Pelzer, K.; Laleu, B.; Lefebvre, F.; Philippot, K.; Chaudret, B.; Candy, J. P.; Basset, J. M. *Chem. Mat.* **2004**, *16*, 4937.
245. Bernal, S.; Baker, R. T.; Burrows, A.; Calvino, J. J.; Kiely, C. J.; Lopez-Cartes, C.; Perez-Omil, J. A.; Rodriguez-Izquierdo, J. M. *Surf. Interface Anal.* **2000**, *29*, 411.
246. Stevenson, S. A.; Dumesic, J. A.; Baker, R. T. K.; Ruckenstein, E. Eds. *Metal-support Interactions in catalysis, Sintering and redispersion*; Van Nostrand Reinhold Co.: New York, 1987.
247. Santra, A. K.; Goodman, D. W. *J. Phys.: Condens. Matter* **2003**, *15*, R31.

248. Risse, T.; Freund, H. J. *Top. Organomet. Chem.* **2005**, *16*, 117.
249. Gai, P. L.; Boyes, E. D. *Electron Microscopy in Heterogeneous Catalysis*; Institute of Physics: Bristol, 2001.
250. Yacaman, M. J.; Ascencio, J. A.; Tchuacanero, S.; Marin, M. *Top. Catal.* **2002**, *18*, 167.
251. Zhou, B.; Hermans, S.; Somorjai, G. A. *Nanotechnology in Catalysis*; 2 Vols; Kluwer/Plenum: New York, Springer: 2004.
252. Koningsberger, D. C.; Prins, R. *X-Ray Absorption: Principles, Applications, Techniques of EXAFS, SEXAFS, and XANES*; Wiley: New York, 1988.
253. Bazin, D.; Dexpert, H.; Lynch, J. In *Series on Synchrotron Radiation Techniques and Applications*; World Scientific, 1996; Vol. 2, 113.
254. Briggs, D.; Grant, J. T. *Surface Analysis by Auger and X-ray Photoelectron Spectroscopy*; IM Publication: Chichester, UK, 2003.
255. Wilson, G. R.; Hall, W. K. *J. Catal.* **1972**, *24*, 306.
256. Kip, B. J.; Duivenvoorden, F. B. M.; Koningsberger, D. C.; Prins, R. *J. Catal.* **1987**, *105*, 26.
257. Ehwald, H.; Leibnitz, U. *Catal. Lett.* **1996**, *38*, 149.
258. Bond, G. C.; Hui, L. *J. Catal.* **1994**, *147*, 346.
259. Bertucco, A.; Bennett, C. *Appl. Catal.* **1987**, *35*, 329.
260. Frennet, A.; Wells, P. B. *Appl. Catal.* **1985**, *18*, 243.
261. Kip, B. J.; Duivanvoorden, F. B. M.; Koningsberger, D. C.; Prins, R. *J. Catal.* **1987**, *105*, 26.
262. Nédez, C.; Théolier, A.; Lefebvre, F.; Choplin, A.; Basset, J. M.; Joly, J. F. *J. Am. Chem. Soc.* **1993**, *115*, 722.
263. Taoufik, M.; Cordonnier, M. A.; Santini, C. C.; Basset, J. M.; Candy, J. P. *New J. Chem.* **2004**, *28*, 1531.
264. Jubert, A. H.; Michelini, M. C.; Estiu, G. L.; Ferretti, O. A. *Catal. Lett.* **1997**, *46*, 241.
265. Margitfalvi, J.; Szabó, S.; Nagy, F. *Stud. Surf. Sci. Catal.* **1986**, *27*, 373.
266. Humblot, F.; Didillon, D.; Lepeltier, F.; Candy, J. P.; Corker, J.; Clause, O.; Bayard, F.; Basset, J. M. *J. Am. Chem. Soc.* **1998**, *120*, 137.
267. Meitzner, G.; Via, G. H.; Lytle, F. W.; Fung, S. C.; Sinfelt, J. H. *J. Phys. Chem.* **1988**, *92*, 2925.
268. Meitzner, G.; Via, G. H.; Lytle, F. W.; Fung, S. C.; Sinfelt, J. H. *J. Phys. Chem.* **1988**, *92*, 2925.
269. Candy, J. P.; Ryndin, Y. A.; Bergeret, G.; Savary, L.; Uzio, D.; Basset, J. M. In *IV International Conference on Catalysis and Adsorption in Fuel Processing and Environmental Protection*, Kudowa, Poland, 1998; p 101.
270. Molnar, A.; Bucsi, I.; Bartok, M.; Notheisz, F.; Smith, G. V. *J. Catal.* **1986**, *98*, 380.
271. Tjandra, S.; Ostgard, D.; Smith, G. V.; Musoiu, M.; Wiltowski, T.; Notheisz, F.; Bartok, M.; Stoch, J. *Catalysis of Organic Reactions*; Pasoe, W. E., Ed. Dekker: New York, 1992; p 137.
272. Molnar, A.; Kiss, J. T.; Bucsi, I.; Katona, T.; Bartok, M. *J. Mol. Catal.* **1990**, *61*, 307.
273. Dubois, L. H.; Nuzzo, R. G. *J. Vac. Sci. Technol., A: Vac., Surf. Films* **1984**, *2*, 441.
274. Aduriz, H. R.; Bodnariuk, P.; Coq, B.; Figueras, F. *J. Catal.* **1989**, *119*, 97.
275. Coq, B.; Grousot, A.; Tazi, T.; Figuéras, F.; Salahub, D. *J. Am. Chem. Soc.* **1991**, *113*, 1485.
276. Taoufik, M.; Santini, C.; Basset, J. M.; Candy, J. P. J. *Chim. Phys.* **1997**, *94*, 1969.
277. Tena, E.; Candy, J. P.; Cornil, M. F.; Jousseaume, B.; Spagnol, M.; Basset, J. M. *J. Mol. Catal.* **1999**, *146*, 53.
278. Bentahar, F. Z.; Bayard, F.; Candy, J. P.; Basset, J. M. In *Fundamental and Applied Aspects of Chemically Modified Surfaces*; Blitz, J., Little, C. B., Eds.; The Royal Society of Chemistry, 1999; Vol. 235, pp 235.
279. Didillon, B.; Candy, J. P.; Le Peltier, F.; Ferretti, O. A.; Basset, J. M. *Stud. Surf. Sci. Catal.* **1993**, *78*, 147.
280. Onda, A.; Komatsu, T.; Yashima, T. *J. Catal.* **2001**, *201*, 13.
281. Lee, A. F.; Baddeley, C. J.; Hardacre, C.; Moggridge, G. D.; Ormerod, R. M.; Lambert, R. M.; Candy, J. P.; Basset, J.-M. *J. Phys. Chem. B* **1997**, *101*, 2797.
282. Tena, E.; Candy, J. P.; Cornil, M. F.; Jousseaume, B.; Spagnol, M.; Basset, J. M. *J. Mol. Catal. A: Chem.* **1999**, *146*, 53.
283. Kern-Tálas, E.; Hegedüs, M.; Gõbölös, S.; Margitfalvi, J. L. In *Preparation of Catalysts IV*; Delmon, B., Grange, P., Jacobs, P. A., Poncelet, G., Eds.; Elsevier: Amsterdam, 1987; Vol. 31, pp 145.
284. Margitfalvi, M.; Borbath, I.; Tfirst, E.; Tompos, A. *Catal. Today* **1998**, *43*, 29.
285. Margitfalvi, J. L.; Borbath, I. *J. Mol. Catal.* **2003**, *202*, 313.
286. Bentahar, F. Z.; Candy, J. P.; Basset, J. M.; Le Peltier, F.; Didillon, B. *Catal. Today* **2001**, *66*, 303.
287. Agnelli, M.; Louessard, P.; El Mansour, A.; Candy, J. P.; Bournonville, J. P.; Basset, J. M. *Catal. Today* **1989**, *6*, 63.
288. Louessard, P.; Candy, J. P.; Bournonville, J. P.; Basset, J. M. *Stud. Surf. Sci. Catal.* **1989**, *48*, 591.
289. Didillon, B.; El Mansour, A.; Candy, J. P.; Basset, J. M.; Le Peletier, F.; Boitiaux, J. P. In *Stud. Surf. Sci. Catal.* **1993**, *75*, 2371.
290. Lesage, P.; Clause, O.; Moral, P.; Didillon, B.; Candy, J. P.; Basset, J. M. *J. Catal.* **1995**, *155*, 238.
291. Margitfalvi, J. L.; Tálas, E.; Gobolos, S. *Catal. Today* **1989**, *6*, 73.
292. Lesage, P.; Candy, J. P.; Hirigoyen, C.; Humblot, F.; Leconte, M.; Basset, J. M. *J. Mol. Catal. A: Chem.* **1996**, *112*, 303.
293. Humblot, F.; Candy, J. P.; Le Peltier, F.; Didillon, B.; Basset, J. M. *J. Catal.* **1998**, *179*, 459.
294. Agnelli, M.; Candy, J. P.; Basset, J. M.; Bournonville, J. P.; Ferretti, O. A. *J. Catal.* **1990**, *121*, 236.
295. Candy, J. P.; Ferretti, O. A.; Mabilon, G.; Bournonville, J. P.; El Mansour, A.; Basset, J. M.; Martino, G. *J. Catal.* **1988**, *112*, 210.
296. Margitfalvi, J. L.; Gõbölös, S.; Tálas, E. In *Heterogeneous Catalysis and Fine Chemicals*; al, G. e., Ed.; Elsevier: Amsterdam, 1988; Vol. 41, pp 145.
297. Goetz, J.; Volpe, M. A.; Sica, A. M.; Gigola, C. E.; Touroude, R. *J. Catal.* **1997**, *167*, 314.
298. Volpe, M. A.; Rodriguez, P.; Gigola, C. E. *Catal. lett.* **1999**, *61*, 27.
299. Goetz, J.; Volpe, M. A.; Gigola, C. E.; Touroude, R. *J. Catal.* **2001**, *199*, 338.
300. Maurice, V.; Ryndin, Y. A.; Bergeret, G.; Savary, L.; Candy, J. P.; Basset, J. M. *J. Catal.* **2001**, *204*, 192.
301. Ryndin, Y. A.; Candy, J. P.; Didillon, B.; Savary, L.; Basset, J. M. *C. R. Acad. Sci. (Paris), Série IIC: Chim.* **2000**, *3*, 423.
302. Didillon, B.; Savary, L.; Ryndin, Y. A.; Candy, J. P.; Basset, J. M. *C. R. Acad. Sci. (Paris), Série IIC: Chim.* **2000**, *3*, 413.
303. Ryndin, Y. A.; Candy, J. P.; Didillon, B.; Savary, L.; Basset, J. M. *J. Catal.* **2001**, *198*, 103.
304. Izumi, Y.; Asakura, K.; Iwasawa, Y. *J. Catal.* **1991**, *127*, 631.

12.11 Organometallic Crystal Engineering

D Braga, L Maini, M Polito, and F Grepioni, Università degli Studi di Bologna, Bologna, Italy

12.11.1 Introduction

12.11.1.1 Crystal Engineering: From Molecules to Molecular Materials

"Making crystals by design" is the paradigm of crystal engineering.[1] The goal of this field of research is that of assembling functionalized molecular and ionic components into a target network of supramolecular interactions.[2,2a] This "bottom-up" process allows one to design and obtain "collective" supramolecular properties from the convolution of the physical and chemical properties of the individual building blocks with the periodicity and symmetry operators of the crystal (see Figure 1).[3]

In 1998, together with Gautam Desiraju, the authors wrote an article in *Chemical Reviews* entitled "Crystal Engineering and Organometallic Architecture."[4] The initial choice was for a title the same as that of this chapter, namely, "Organometallic Crystal Engineering." However, as the authors proceeded in searching the literature and putting together the material for the review, they felt that organometallic chemistry was still far from the "engineering stage." While in the 1990s crystal engineering of organic molecules and of coordination complexes was booming, in the organometallic chemistry field, scientists were still mainly designing "structures" rather than "functions."

How has the field evolved in these few years? This chapter intends to address this question. A turning point was the Dalton Discussion meeting on "inorganic crystal engineering" in 2000 (Bologna, Italy).[5,5a,5b] From the papers published on that occasion, it emerged in all clarity that the field was moving rapidly away from its organic cradle to begin a systematic exploration of the "realm of metals."

The very definition of crystal engineering has changed over time. Since the aim is the design, construction, and exploitation of functional materials[6] based on interactions between molecules, ions, and complexes, modern crystal engineering is essentially supramolecular solid-state chemistry. In any supramolecular chemistry approach, the first step is the choice of building blocks on the basis of their supramolecular bonding capacity and their supramolecular assembly. Clearly, this reasoning does not distinguish between a single supermolecule,[6] whose "collective" functions

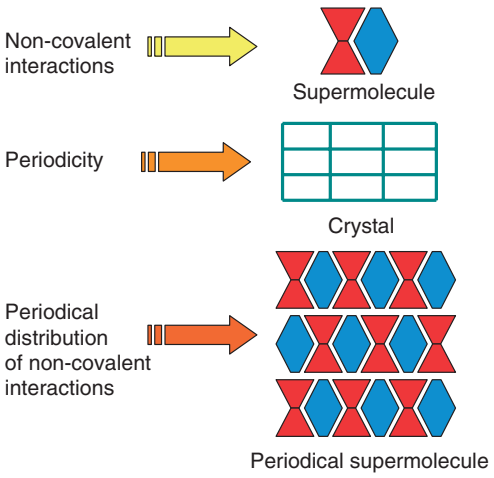

Figure 1 From molecules to periodical supermolecules: the collective properties of molecular crystals result from the convolution of the properties of the individual molecular/ionic building blocks with the periodical distribution of intermolecular non-covalent bonding of the crystal (from Ref. 3).

and properties differ from, but depend on, those of the individual components, and a crystalline material, whose collective properties result from the aggregation of a very large number of identical subunits. From this viewpoint, the construction of a molecular solid is the construction of a solid supermolecule, whose collective functions and properties depend on the aggregation via "intermolecular" bonds of two or more component units. Engineering implies application-oriented targeting of a specific property (say, chirality, conductivity, nanoporosity, etc.) or application (such as, NLO (non-linear optics), polymorphism, molecular trapping, sensing, etc.).

One can envisage two main subareas of crystal engineering, namely, those of coordination networks,[7,7a–7M] and of molecular materials,[8,8a–8l] even though all possible intermediate situations are possible. The chemistry of coordination networks (also called coordination polymers) can be appropriately described as "periodical coordination chemistry" and exploits the possibility of "divergent ligand–metal coordination," as opposed to the more traditional "convergent coordination" chemistry operated by chelating polydentate ligands[9] (see Figure 2).

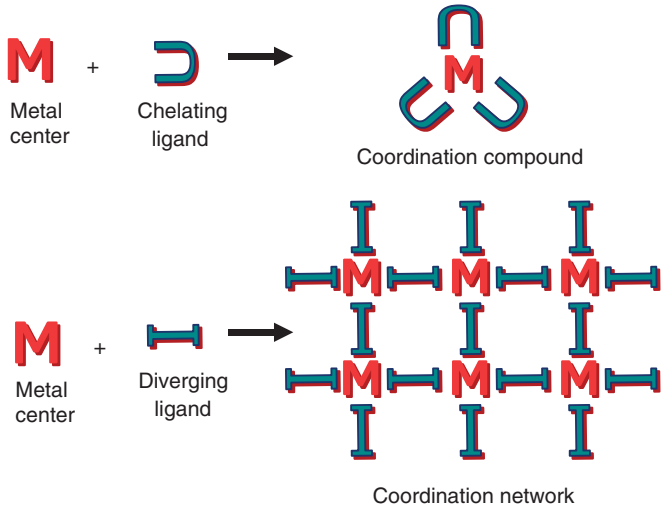

Figure 2 The relationship between molecular (left) and periodical (right) coordination chemistry: the use of bidentate ligand spacers allows construction of "periodical" coordination complexes.

The possibility of exploiting engineered coordination networks for practical applications (e.g., absorption of molecules, reactions in cavities) very much depends on whether the networks contain large empty spaces (channels, cavities, etc.),[10,10a–10f] or whether the network is close packed because of interpenetration and self-entanglement.[11,11a–11d] The possibility of a sponge-like behavior by which the network can change its shape, well, and shrink to accommodate/release guest molecules should also be taken into account.[12,12a–12g]

While in periodical coordination chemistry, it is useful to focus on the "knots" and "spacers" in order to describe the topology of the network, when dealing with molecular materials, what matters most are the characteristics of the component molecules or ions and the type of interactions holding these building blocks together. These interactions are mainly of the non-covalent type (van der Waals, hydrogen bonds, π-stacking, ionic interactions, ion pairs, etc.),[13–15k] and will lead to formation of molecular crystals. In this respect, the epithet "molecular" will be used throughout this chapter in a liberal sense, including both neutral molecules and molecular ions. The working assumption is that all those aggregates of atoms that retain their own chemical identity in gas phase or solution are "molecular" in nature. On this premise, we will call "intermolecular" all types of secondary interionic or intermolecular "non-covalent" interactions (e.g., electrostatic, hydrogen bonds, and van der Waals interactions).

Finally, we should point out that the term "organometallic" is used not only to comprise molecules and ions that contain a C–M bond,[16,16a] but also to include coordination compounds where organometallic ligands have been used in the construction of coordination netwoks. However, contrary to molecular crystals, the component "knots" and "spacers" of coordination networks cannot usually be assembled and disassembled in a reversible manner.

The use of transition metals in coordination-directed self-assembly is an extremely active area of research, especially for the synthesis of metal–organic coordination networks, whether finite (triangles, squares, etc.)[17,17a–17e] or infinite networks.[18–19b]

12.11.2 Design

12.11.2.1 Crystal Engineering with Organometallic Building Blocks

The purposed construction of molecular crystals requires "*crystal-oriented synthetic strategies*."[5] In this respect, a distinction needs to be made between crystalline solids in which the principal interactions holding crystals together are covalent, van der Waals and/or ionic, and solids where ligand–metal coordination networks are present. Molecular materials owe their stability to the network of generally weaker non-covalent interactions between molecular building blocks. Since the cohesion of covalent and coordination solids depends on interactions that require much more energy to be broken and formed than those present in molecular solids, the synthetic strategies that can be adopted to make covalent (and coordination) crystalline materials are different from those required when molecules or molecular ions are involved.[20]

Organometallic chemistry, as the name suggests, is a bridge between organic and inorganic chemistry. Organometallic networks based on hydrogen-bonding interactions are well known, and some representative cases will be discussed to some extent. The same applies to polymetallocenes and polyacetylides containing organometallic fragments.[21]

12.11.2.2 Intermolecular Interactions Involving Organometallic Molecules

The nucleation and growth of a crystalline aggregate from its component units depends crucially on the steps of recognition and self-assembly, and on the stability and persistence over time of the first crystal nuclei. Recognition is controlled mainly by the interactions between peripheral atoms, those more "exposed" on the molecular surface and hence at direct contact with neighboring molecules or ions. In coordination and organometallic chemistry, these atoms are those forming the ligands, which are mainly of "organic" nature. The metal atom is not an innocent spectator, however, and its influence on the supramolecular bonding capacity is manifold, and it can be summarized as follows.

(i) Electronic effects on the intermolecular bonding capacity of the ligands. The electronic nature of the metal centers, from electron-deficient early transition metals to electron-rich late transition metals, can be used to "tune" the intermolecular bonding capacity of the ligands. The different Lewis acid–base behavior of the metal atoms arising from the electronic configuration of the metal influences the σ–π bonding interaction between ligand and metal

centers. The polarity (acid–base behavior) of any given ligand, and in particular π-acceptor or π-donor ligands, can be tuned by changing the oxidation state of the metal(s).

(ii) Control on the geometry of the intermolecular interactions. The intermolecular bonding capacity of a molecule/ion can be controlled by placing one or more highly polar ligands (not only halides, but also $-CN^-$, $-NO^+$, $-SCN^-$, etc.) among less polar ones (*e.g.*, CO). Furthermore, ligand geometry can be combined with the metal coordination site (e.g., *cis*- and *trans*- in octahedral complexes) to preorganize complementary hydrogen-bonding acceptor and donor groups in space. Another important feature is ligand chirality, which can be exploited in the preparation of chiral complexes. Ligands can be selected to form dipolar electronic structures in the ground state (organometallic zwitterions) or in easily accessible excited states.

(iii) Direct participation of metal atoms in intermolecular interactions. It is here that organic and organometallic systems differ the most, since metal atoms may participate directly in intermolecular bonds. Electron-deficient metal atoms, for example, early transition metal complexes, may accept electron donation via intermolecular interactions into empty or partially filled low-lying orbitals. Conversely, electron-rich metals, for example, late transition metals, may utilize lone pairs to interact intermolecularly with suitable electron acceptors, including hydrogen-bonding donor systems.

(iv) Role of the ionic charge of organometallic complexes. While the chemistry of ions per se does not constitute a large portion of organic chemistry, this is not so for organometallic systems, where metal atom oxidation states and the interaction with non-neutral ligands make ions extremely abundant, as it will be made clear by a number of examples in the following.

(v) Structural flexibility versus delocalized bonding interactions: ligand fluxionality in the solid state. Most organometallic molecules are structurally non-rigid. The typical degrees of structural freedom of organic molecules are accompanied by the presence of delocalized bonding interactions (e.g., ligand–metal π-bonding) and by the possibility of different bonding modes for the same ligand (e.g., terminal and bridging carbonyls, phosphines, hydrides, etc.). This results in the presence of changeable structures with little cost in terms of energy. These factors have important consequences on the dynamic behavior of organometallic species in solution as well as in the solid state. An analysis of the different components is described by the "ligand domain model" put forward by Dance[22] and expanded by Brammer.[23]

The description of the metal–ligand and ligand–environment interactions is based on three domains (see Figure 3): the "metal domain," which consists of one or more metal atoms forming the complex core; the "ligand domain," which consists of those ligand atoms that are directly bonded to the metal core; the "periphery domain," which consists of those parts of the ligands that are far from the metal core but which are responsible for the interactions with the environment. The environment consists of all surrounding molecules, whether solvent molecules in solution or other molecules or ions packed in the solid state.

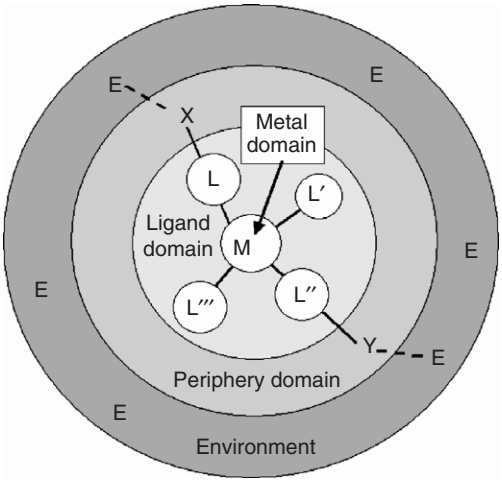

Figure 3 Schematic representation of the "ligand domain model."

12.11.2.3 Ionic Interactions and Hydrogen Bonding in Organometallic Crystals

As pointed out above, the role of ionic charge is very relevant in organometallic chemistry, because the variable oxidation states of the metal atoms combined with the charge of ligands leads to a great variety of charged species. If the ionic nature is a "bonus" in organometallic crystal engineering, because it allows the use of polar solvents (such as water), the "downside" is that crystallization "needs" counterions for electroneutrality. Counterions of course take part in intermolecular bonding. This aspect becomes particularly relevant in the case of hydrogen bonds.[24,24a–24f] This section of the chapter deals with the construction of hydrogen-bonded networks, involving organometallic complexes, where the hydrogen-bonding interactions are between "classical" donor and acceptor groups, for example, –COOH, –OH, –CONHR,[25,25a,25b] while less attention will be given to weak hydrogen-bonding interactions.[26,26a] These latter interactions, albeit important in the "fine-tuning" of the supramolecular architectures, are, generally speaking, more difficult to control than "strong" interactions with clearly defined, reproducible, and transferable directionality properties.

A high degree of control on both geometry and crystal cohesion can be attained when hydrogen bonding interactions are convoluted with Coulombic interactions.[27,27a–27e] The presence of ionic charges on the building blocks can be exploited to strengthen the interaction[28,28a,28b] because of the electrostatic nature of the hydrogen bond.[29,29a] The so-called "charge assistance" to hydrogen bond is the enhancement of donor and acceptor polarity (whether involving atoms or groups of atoms) by a combined use of cationic donors and anionic acceptors instead of neutral systems, that is, $^{(+)}$X–H—Y$^{(-)}$ versus X–H—Y.[30,30a–30f] The favorable location of ionic charges enhances proton acidity "and" acceptor basicity. It should be kept in mind, however, that "acidity" or "basicity" are "relative" concepts and cannot be transferred *tout court* to the solid state; other factors may change the polarity of the X–H bond and/or the nucleophilicity of the Y acceptor.[31] If the hydrogen bond joins ions of opposite charge, more generally $^{(+)}$X–H—Y$^{(-)}$, the bonding contribution adds to the favorable (+)—(−) Coulombic interaction between donor and acceptor systems, while if the ions carry the same charge, for example, $^{(-)}$X–H—Y$^{(-)}$ [but also $^{(+)}$X–H——Y$^{(+)}$], the contribution reduces the repulsive electrostatic terms [e.g., (−)—(−) or (+)—(+)] arising from the Coulombic interactions between like charges, electroneutrality being guaranteed in all cases by the counterions.

While the "use" of interionic hydrogen-bonding interactions in crystal engineering is well established, the interpretation of the relationship between the various energetic contributions (hydrogen-bonding and Coulombic terms) is still controversial, in particular, in the case of hydrogen bonds between ions of the same charge.[32,32a–32d]

More "exotic" interactions, such as those between a cationic hydride [MH]$^{(+)}$ as a proton donor and a metal atom or a hydride ligand as a proton acceptor, have been recently reviewed,[33,33a–33d] and will not be discussed any further here, also in view of the limited use in crystal-engineering applications. For the same reason, we shall not discuss other weaker interactions such as the CH–π hydrogen bonds.[34] A summary drawing of the hydrogen-bonding interactions involving metal-containing species is shown in Figure 4.

12.11.3 Synthesis

12.11.3.1 Strategies to Obtain Hydrogen-bonded Networks Involving Ions

The simplest way to obtain hydrogen-bonded ionic networks is that of using—or *generating in situ*—ions that can be linked together via hydrogen-bonding interactions.

There are two distinct strategies that utilize acid–base reactions to construct crystals, and they are based on charge-assisted hydrogen bonds between ions.

(i) Strategy 1. Use of a base that "cannot" form hydrogen-bonding interactions with the acid moiety. This is the case of the reaction between polycarboxylic acids and inorganic or organometallic hydroxides that do not carry strong acceptor/donor hydrogen bond groups. In fact, partial deprotonation of the –COOH groups leads to self-assembly of acid anions via O–H—O$^{(-)}$ and $^{(-)}$O–H—O$^{(-)}$ interactions. By choosing the number of carboxylic groups (hence the number of potential donor/acceptor systems) and the stoichiometric ratios in the acid–base reactions, one can control the formation of O–H—O$^{(-)}$ and/or $^{(-)}$O–H—O$^{(-)}$ interactions. In this latter circumstance, one can speak of "homoionic" self-assembly. The stability of the resulting "homoionic" network aggregate requires an adequate choice of counterions.

(ii) Strategy 2. Use of a base that "can form" charge-assisted hydrogen-bonding interactions with the acidic moiety. This is the case, for instance, of nitrogen-containing bases (amines, pyridines, pyrimidines, aminidines, etc.), which are protonated upon reaction with polycarboxylic acid molecules, for example, $RCOOH + NR_3 \rightarrow RCOO^{(-)}—^{(+)}HNR_3$, leading to the formation of strong N–H$^{(+)}$–O$^{(-)}$ interactions, hence to the formation of anion–cation pairs in the solid state.

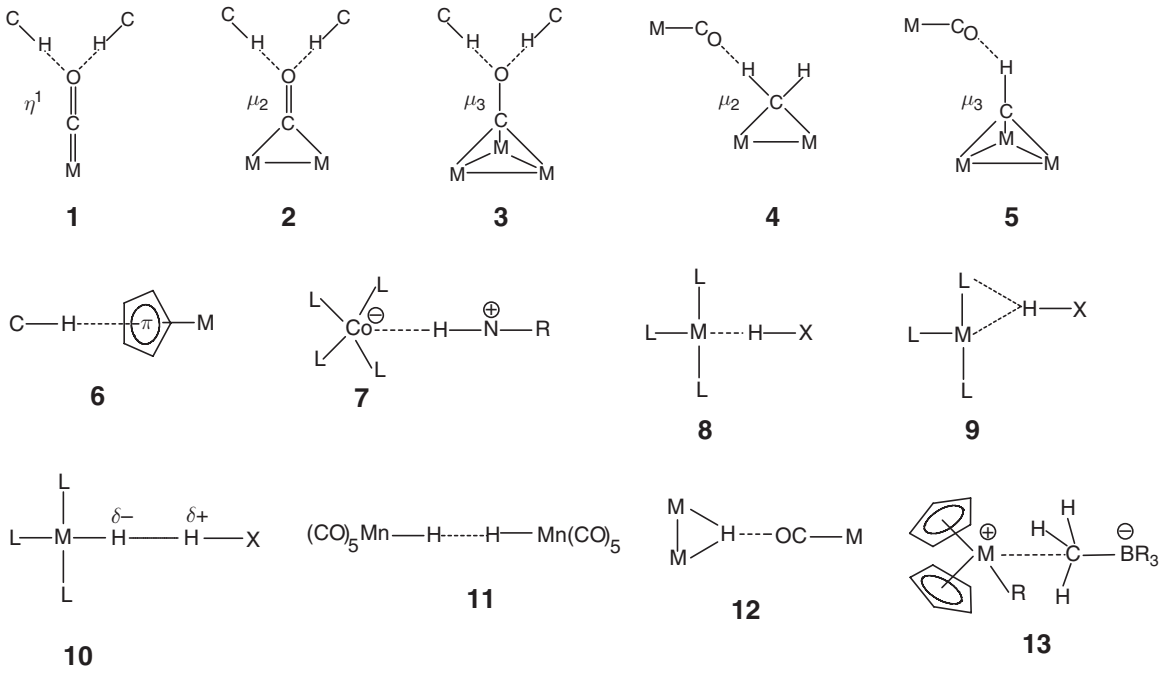

Figure 4 Non-organic hydrogen-bonding interactions involving ligands: terminal **1**, edge-bridging **2**, face-bridging **3** CO ligands, methylene μ_2-CH_2 **4**, methylidyne (μ_3-CH) **5**, and an example of –CH···π interaction involving a metal coordinate Cp ligand **6**; hydrogen-bond involving electron-rich metal atoms: charge-assisted $[Co(CO)_4^-]$–$[H–NR_3]^+$ **7**, neutral **8**, interactions involving electron-rich metal atoms and main group elements L_2(M–L)—H–X **9**, electrostatic **10** and "covalent" dihydrogen bond **11**, metal–"hydride" donation to CO ligands **12**, and pseudo-agostic interactions involving unsaturated electron-deficient metal atoms **13**. Reprinted with permission from Braga, D.; Grepioni, F. *Acc. Chem. Res.* **2000**, *33*, 601. © 2000 American Chemical Society.

It should be noted, however, that the distinction between the two strategies is only instrumental to the discussion, since intermediate situations whereby "homoionic" and "heteroionic" hydrogen-bonding interactions may co-exist, for example, $N–H^{(+)}—O^{(-)}$ and $^{(-)}O–H—O^{(-)}$, can be obtained by means of a large acid : base ratio.

12.11.3.2 Hydrogen-Bonded Networks Templated by Organometallic Sandwich Units

This section is devoted to the description of hydrogen-bonded networks obtained via strategy 1, that is, by reacting polycarboxylic acids with organometallic bases, with formation of partially deprotonated acid anions. A path of increasing building block complexity will be followed; it will be shown that size, shape, and intermolecular bonding of the building blocks can be used to control the crystal architecture. Although no hard and fast rule can be applied, the aggregation of partially deprotonated polycarboxylic acids or polyalcohols follows a sort of "aufbau" hierarchy: (i) priority goes to the maximization of the number of hydrogen-bonding interactions between strong donors and acceptors; (ii) a compromise is also required between space filling and charge equalization; and (iii) after all strong interactions have been accommodated, weaker C–H—O and similar interactions are also optimized. Even though the stability of the aggregate also depends on the topological features of the counterions, $^{(-)}O–H—O^{(-)}$ hydrogen-bonding interactions between building blocks of like charges (as it is generally the case of the compounds described in this section) contribute to crystal stability by decreasing the anion–anion (or cation–cation) repulsions.

Braga *et al.* have used an approach based on a combination of redox and acid–base processes to obtain partially deprotonated polycarboxylic acids capable of self-assembly in network structures.[35,38–42]

For instance, the oxidation by molecular oxygen of the neutral complexes $[Co(\eta^5\text{-}C_5H_5)_2]$, $[Cr(\eta^6\text{-}C_6H_6)_2]$, $[Fe(\eta^5\text{-}C_5Me_5)_2]$, and $[Co(\eta^5\text{-}C_5Me_5)_2]$ to $[Co(\eta^5\text{-}C_5H_5)_2]^+$, $[Cr(\eta^6\text{-}C_6H_6)_2]^+$, $[Fe(\eta^5\text{-}C_5Me_5)_2]^+$, and $[Co(\eta^5\text{-}C_5Me_5)_2]^+$, respectively, generates the strongly basic anion O_2^-, which is able to fully or partially deprotonate the polyprotic acid, depending on the stoichiometric ratio. Since the oxidation products are not suitable for coordination by the

–$COO^{(-)}$ groups, self-assembly of the polycarboxylic acid is forced with formation of one-, two-, or three-dimensional "homoionic" framework structures around the organometallic cations. As mentioned above, the interaction between organic framework and organometallic cations is based on a profusion of charge-assisted C–H—O bonds. Table 1 lists the compounds that have been obtained by means of this reaction strategy, together with the relevant literature entries.

When oxalic acid is used with $[Fe(\eta^5\text{-}C_5Me_5)_2]^+$ and $[Cr(\eta^6\text{-}C_6H_6)_2]^+$, the crystalline compounds $[Fe(\eta^5\text{-}C_5Me_5)_2][HC_2O_4]\cdot[H_2C_2O_4]_{0.5}$ and $[Cr(\eta^6\text{-}C_6H_6)_2][HC_2O_4]\cdot[H_2O]$ were obtained,[35] characterized by a columnar aggregation of the radical cations $[Fe(\eta^5\text{-}C_5Me_5)_2]^+$ and $[Cr(\eta^6\text{-}C_6H_6)_2]^+$. Earlier studies of crystals containing flat radical anions,[36] such as tetracyanoethylene ($TCNE^{\cdot-}$), tetracyano-*p*-quinodimethane ($TCNQ^{\cdot-}$), or other similar anions, and radical cations, such as $[Fe(\eta^5\text{-}C_5Me_5)_2]^+$, as well as other sandwich cations (e.g., $[Cr(\eta^6\text{-}C_6Me_xH_{6-x})_2]^+$), have led to the formulation of the "linear-chain paradigm," which postulates the formation of sequences of the type $A^{(-)}$–$C^{(+)}$–$A^{(-)}$–$C^{(+)}$ between radical anions and cations in crystals.[37,37a–37d] Linear arrangements of the type $C^{(+)}$–$C^{(+)}$–$C^{(+)}$–$C^{(+)}$ surrounded by chains of $A^{(-)}$–$A^{(-)}$–$A^{(-)}$–$A^{(-)}$ anions, or intercalated between layers of anions, are not easily obtained, because of the tendency of the ions of a given sign to be surrounded by ions of opposite sign.

In crystalline compound $[Fe(\eta^5\text{-}C_5Me_5)_2][HC_2O_4]\cdot[H_2C_2O_4]_{0.5}$, the hydrogen oxalate anions and the neutral oxalic acid molecules form linear chains (see Figure 5). The chains run parallel to the columns formed by the $[Fe(\eta^5\text{-}C_5Me_5)_2]^+$ and $[Co(\eta^5\text{-}C_5Me_5)_2]^+$ cations, and contain deca atomic dimers formed by two hydrogen oxalate anions joined together via $^{(-)}$O–H—$O^{(-)}$ interactions. The anions are not arranged in the usual head-to-tail chain or carboxylic ring, they rather adopt a side-to-side arrangement. The hydrogen oxalate dimers are bridged together by one molecule of oxalic acid. The hydrogen oxalate/oxalic acid chain can thus be described as a $(H_2C_2O_4)\cdots[(HC_2O_4)(HC_2O_4)]^{2-}\cdots(H_2C_2O_4)\cdots[(HC_2O_4)(HC_2O_4)]^{2-}$ sequence of ions bridged by neutral molecules. These chains form the backbone of the crystal structure and allow the cations to pile up, as shown in Figure 5(a).

A twisted conformation is adopted by the hydrogen oxalate anion in the bis-benzene chromium salt $[Cr(\eta^6\text{-}C_6H_6)_2][HC_2O_4]\cdot[H_2O]$. The twisted hydrogen oxalate anions do not interact with each other, but are linked in the chains by means of water bridges, which form complex 14-membered rings based on four hydrogen-bonding interactions.

Crystalline $[Cr(\eta^6\text{-}C_6H_6)_2]^+[HC_4O_4]^-$ has been obtained by reaction of squaric acid (3,4-dihydroxy-3-cyclobutene-1,2-dione, $H_2C_4O_4$) with $[Cr(\eta^6\text{-}C_6H_6)_2]$ in THF.[38] The flat shape and small dimensions of the squarate anion $[HC_4O_4]^-$ lead to its intercalation between the flat benzene ligands of the paramagnetic cation $[Cr(\eta^6\text{-}C_6H_6)_2]^+$, with formation of one-dimensional $C^{(+)}$–$A^{(-)}$–$C^{(+)}$–$A^{(-)}$ aggregates, comprised of alternating cation donors (C) and anion acceptors (A). The anion self-assembles into chains linked by $^{(-)}$O–H—$O^{(-)}$ interactions and intercalates between the benzene ligands (π–π-distance 3.375 Å, see Figure 6). When the reaction is carried out in water, the hydrated

Table 1 Hybrid organic–organometallic superstructures obtained with "strategy 1" and relevant literature entries

Acid	*Organometallic building block*	*Formula of the resulting system*	*References*
Oxalic	$[Fe(\eta^5\text{-}C_5Me_5)_2]$	$[Fe(\eta^5\text{-}C_5Me_5)_2][HC_2O_4]\cdot[H_2C_2O_4]_{0.5}$	35
Oxalic	$[Cr(\eta^6\text{-}C_6H_6)_2]$	$[Cr(\eta^6\text{-}C_6H_6)_2][HC_2O_4]\cdot[H_2O]$	35
Squaric	$[Cr(\eta^6\text{-}C_6H_6)_2]$	$[Cr(\eta^6\text{-}C_6H_6)_2][HC_4O_4]$	38
Squaric	$[Cr(\eta^6\text{-}C_6H_6)_2]$	$\{[Cr(\eta^6\text{-}C_6H_6)_2]\}_2[C_4O_4]\cdot 6H_2O$	38
Phthalic	$[Co(\eta^5\text{-}C_5H_5)_2]$	$\{[Co(\eta^5\text{-}C_5H_5)_2]^+\}_4\{[C_6H_4(COOH)(COO)]^-\}_2$-$[C_6H_4(COO)_2]^{2-}\cdot 4H_2O$	39
Phthalic	$[Cr(\eta^6\text{-}C_6H_6)_2]$	$[Cr(\eta^6\text{-}C_6H_6)_2]^+\{[C_6H_4(COOH)(COO)]^-[C_6H_4(COOH)_2]\}$	39
Terephthalic	$[Co(\eta^5\text{-}C_5H_5)_2]$	$\{[Co(\eta^5\text{-}C_5H_5)_2]^+\}_2[C_6H_4(COO)_2]^{2-}\cdot 6H_2O$	39
D,L-tartaric	$[Co(\eta^5\text{-}C_5H_5)_2]$	$[Co(\eta^5\text{-}C_5H_5)_2]^+$(D,L-$HO_2CCH(OH)CH(OH)CO_2$)-(D,L-$HO_2CCH(OH)CH(OH)CO_2H$)$^-$	40
L-tartaric	$[Co(\eta^5\text{-}C_5H_5)_2]$	$[Co(\eta^5\text{-}C_5H_5)_2]^+$ [(L-$HO_2CCH(OH)CH(OH)CO_2$)$]^-$	40
Trimesic	$[Co(\eta^5\text{-}C_5H_5)_2]$	$[Co(\eta^5\text{-}C_5H_5)_2]^+\{[C_6H_3(COOH)_3]$-$[C_6H_3(COOH)_2(COO)]\}^-\cdot 2H_2O$	41
(*R*)-binaphthol	$[Co(\eta^5\text{-}C_5H_5)_2]$	$(Co(\eta^5\text{-}C_5H_5)_2]((R)$-(+)-$(HOC_{10}H_6C_{10}H_6O)]\cdot[(R)$-(+)-$(HOC_{10}H_6C_{10}H_6OH)]$	42
(*R*)-binaphthol	$[Co(\eta^5\text{-}C_5H_5)_2]$	$(Co(\eta^5\text{-}C_5H_5)_2][(R)$-(+)-$(HOC_{10}H_6C_{10}H_6O)]\cdot[(R)$-(+)-$(HOC_{10}H_6C_{10}H_6OH)_{(0.5}$	42

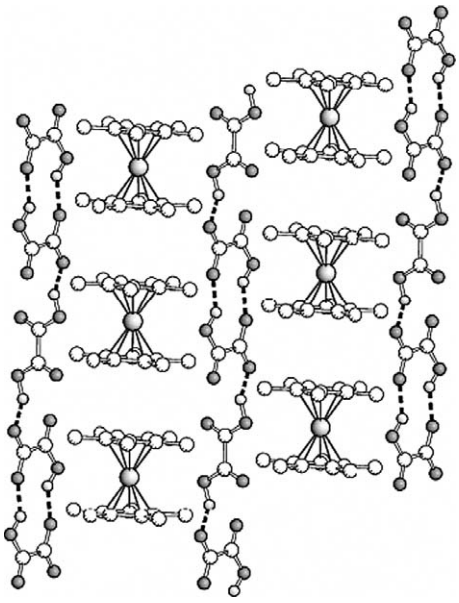

Figure 5 Chains of $[(HC_2O_4)(HC_2O_4)]^{2-}$—$(H_2C_2O_4)$—$[(HC_2O_4)(HC_2O_4)]^{2-}$ in compound $[Fe(\eta^5\text{-}C_5Me_5)_2][HC_2O_4]\cdot[H_2C_2O_4]_{0.5}$. The cations pile up at interplanar separations of 3.67 and 3.84 Å. Reprinted with permission from Braga, D.; Eckert, M.; Fraccastoro, M.; Maini, L.; Grepioni, F.; Caneschi, A.; Sessoli, I. *New J. Chem.* **2002**, *26*, 1280. © 2002, Elsevier.

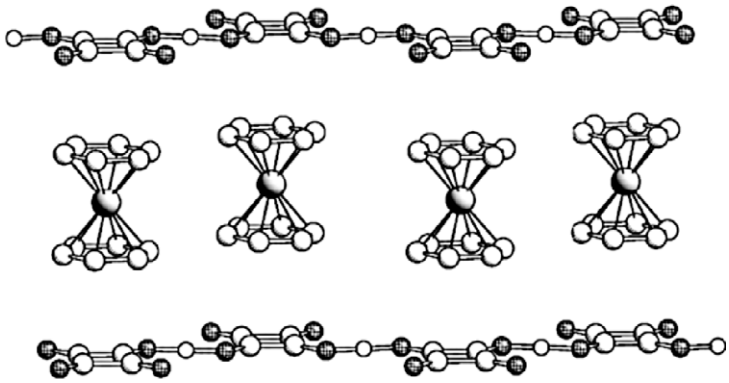

Figure 6 Crystalline $[Cr(\eta^6\text{-}C_6H_6)_2]^+[HC_4O_4]^-$; the anion self-assembles into chains linked by $^{(-)}O\text{–}H\text{–}O^{(-)}$ interactions and intercalates between the benzene ligands (π–π-distance 3.375 Å). Reprinted with permission from Braga, D.; Eckert, M.; Fraccastoro, M.; Maini, L.; Grepioni, F.; Caneschi, A.; Sessoli, I. *New J. Chem.* **2002**, *26*, 1280. © 2002, Elsevier.

crystalline material $\{[Cr(\eta^6\text{-}C_6H_6)_2]\}_2[C_4O_4]\cdot 6H_2O$ is obtained instead. $\{[Cr(\eta^6\text{-}C_6H_6)_2]\}_2[C_4O_4]\cdot 6H_2O$ contains layers of organometallic cations intercalated with layers of water molecules, hydrogen bonded to squarate dianions. Contrary to most organic salts of $[Cr(\eta^6\text{-}C_6H_6)_2]^+$ and $[Co(\eta^5\text{-}C_5H_5)_2]^+$, which are yellow, crystals of $[Cr(\eta^6\text{-}C_6H_6)_2][HC_4O_4]$ are orange in color. Reflectance spectra measured on the crystalline material $[Cr(\eta^6\text{-}C_6H_6)_2][HC_4O_4]$ show the presence of an intense tail, which was assigned to a charge-transfer transition via the $[Cr(\eta^6\text{-}C_6H_6)_2]^+/[HC_4O_4]^-$ π-stacking interactions.

When the size of hydrogen-bonding organic units exceeds that of the cationic carbocyclic ligands, intercalation is no longer possible. This is demonstrated by the use of flat and large diacids, such as phthalic acid $[C_6H_4\text{-}1,2\text{-}(COOH)_2]$, and terephthalic acid $[C_6H_4\text{-}1,4\text{-}(COOH)_2]$.[39] The architecture of crystalline $\{[Co(\eta^5\text{-}C_5H_5)_2]^+\}_4\text{-}\{[C_6H_4(COOH)(COO)]^-\}_2[C_6H_4(COO)_2]^{2-}\cdot 4H_2O$ recalls a brick wall, with large rectangular channels occupied by pairs of columns of $[Co(\eta^5\text{-}C_5H_5)_2]^+$ cations.

Honeycomb-type organic frameworks can be obtained by using the organic acids D,L- and L-tartaric acid ($HO_2CCH(OH)CH(OH)CO_2H$) (see Figure 7) forming the achiral $[Co(\eta^5\text{-}C_5H_5)_2]^+$ (D,L-$HO_2CCH(OH)CH(OH)CO_2$)-(D,L-$HO_2CCH(OH)CH(OH)CO_2H$)$^-$ and chiral crystals $[Co(\eta^5\text{-}C_5H_5)_2]^+[$(L-$HO_2CCH(OH)CH(OH)CO_2$)$]^-$.[40,40a]

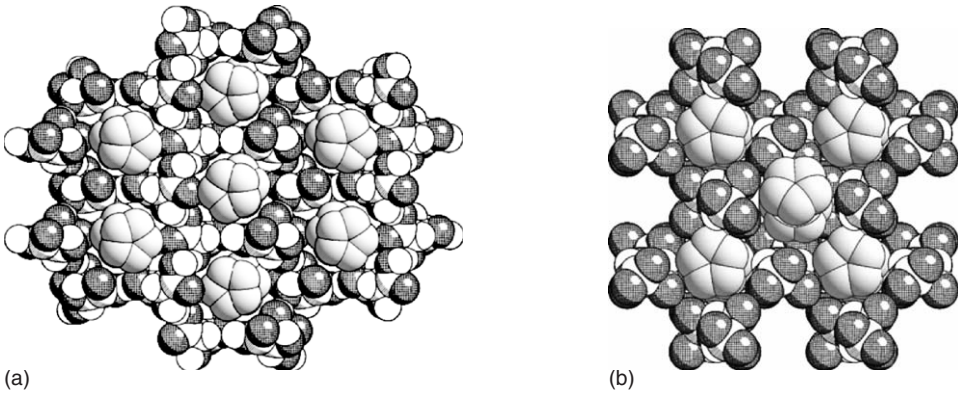

Figure 7 (a) Space-filling representation of the honeycomb framework formed by the [(D,L-$HO_2CCH(OH)CH(OH)CO_2$)(D,L-$HO_2CCH(OH)CH(OH)CO_2H$)]$^-$ units in crystalline [Co(η^5-$C_5H_5)_2$]$^+$[(D,L-$HO_2CCH(OH)CH(OH)CO_2$)(D,L-$HO_2CCH(OH)CH(OH)CO_2H$)]$^-$. (b) Space-filling representation of the L-tartaric acid framework in crystalline [Co(η^5-$C_5H_5)_2$]$^+$ [(L-$HO_2CCH(OH)CH(OH)CO_2$)]$^-$. Reprinted with permission from Braga, D.; Eckert, M.; Fraccastoro, M.; Maini, L.; Grepioni, F.; Caneschi, A.; Sessoli, I. *New J. Chem*. **2002**, *26*, 1280. © 2002, Elsevier.

Figure 8 In Co(η^5-$C_5H_5)_2$][(*R*)-(+)-($HOC_{10}H_6C_{10}H_6O$)]·[(*R*)-(+)-($HOC_{10}H_6C_{10}H_6OH$)], the neutral molecules act as bridges between monoanions, thus forming a chain system in which anions and neutral molecules alternate. Reprinted with permission from Braga, D.; Eckert, M.; Fraccastoro, M.; Maini, L.; Grepioni, F.; Caneschi, A.; Sessoli, I. *New J. Chem*. **2002**, *26*, 1280. © 2002, Elsevier.

The cobalticinium cations in both crystals are encapsulated within a hexagonal and square organic honeycomb frameworks, respectively. Similarly, trimesic acid, [C_6H_3-1,3,5-$(CO_2H)_3$], has been used to construct [Co(η^5-$C_5H_5)_2$]$^+${[$C_6H_3(COOH)_3$][$C_6H_3(COOH)_2(COO)$]}$^-$·$2H_2O$.[41]

Binaphthol, (*R*)-(+)-1,1′-bi-2-naphthol [(*R*)-(+)-($HOC_{10}H_6C_{10}H_6OH$)] has been used as a chiral building block in the construction of chiral organic–organometallic crystals.[42] The reaction of the neutral molecule with [Co(η^5-$C_5H_5)_2$] in ether yields the supramolecular salts [Co(η^5-$C_5H_5)_2$][(*R*)-(+)-($HOC_{10}H_6C_{10}H_6O$)]·[(*R*)-(+)-($HOC_{10}H_6C_{10}H_6OH$)] and (Co(η^5-$C_5H_5)_2$][(*R*)-(+)-($HOC_{10}H_6C_{10}H_6O$)]·[(*R*)-(+)-($HOC_{10}H_6C_{10}H_6OH$)]$_{0.5}$, depending on the stoichiometric ratios between the binaphthol and the organometallic sandwich compound. In [Co(η^5-$C_5H_5)_2$][(*R*)-(+)-($HOC_{10}H_6C_{10}H_6O$)]·[(*R*)-(+)-($HOC_{10}H_6C_{10}H_6OH$)], the neutral molecules act as bridges between monoanions, thus forming a chain system in which anions and neutral molecules alternate (see Figure 8), as observed before for [Fe(η^5-$C_5Me_5)_2$][HC_2O_4]·[$H_2C_2O_4$]$_{0.5}$. The O–H—O hydrogen bonds along the chain are of two types: the intermolecular O–H—$O^{(-)}$ bond between the neutral spacer and the anion (2.667(7) and 2.612(7) Å, respectively), and the intramolecular hydrogen bond between the –OH group of the anion and the deprotonated oxygen atom [2.427(7) Å]. Because of the enantiomerically pure nature of the component, the chain is chiral as in the case of L-tartaric acid.

12.11.3.3 Hydrogen-Bonded Networks Formed by Organometallic Sandwich Units

The organometallic compounds described in this section participate in the hydrogen-bonding network allowing construction of hybrid organic–organometallic and organometallic–organometallic structures. As it will be apparent in the following, a large number of hydrogen-bonded networks use ferrocenyl complexes (see Table 2).

The organometallic dicarboxylic acid [Fe(η^5-$C_5H_4COOH)_2$] has been used as a hydrogen-bonding building block in the preparation of hybrid organic–organometallic and of organometallic–organometallic crystal architectures. It

Table 2 Principal ferrocenyl complexes utilized for the construction of hydrogen-bonded networks

Organometallic complex	*Formula*	*References*
Ferrocenedicarboxylic acid	$Fe(\eta^5\text{-}C_5H_4COOH)_2$	43–47,123
1,1′-Bis(ethenyl–4–pyridyl) ferrocene	$[Fe(\eta^5\text{-}C_5H_4\text{–}CH{=}CH\text{–}C_5H_4N)_2]$	48–50
1,1′-Bis(L–Ala–L–Pro–OEt) ferrocene	$[Fe(\eta^5\text{-}C_5H_4\text{–L-Ala–L-Pro–OEt})_2]$	53
Ferrocenediboronic acid	$Fe(\eta^5\text{-}C_5H_4\text{–}B(OH)_2)_2$	54,55
Ferrocene–1-(–4 pyridyl),1′-boronic acid	$[Fe(\eta^5\text{-}C_5H_4\text{–4-}C_5H_4N)(\eta^5\text{-}C_5H_4\text{–}B(OH)_2)]$	55
Ferrocene–1,1′-diyl-bis(diphenylmethanol)	$Fe\{\eta^5\text{-}C_5H_4\text{–}C(OH)(P(C_6H_5)_2)_2\}_2$	56,57
rac-2-(Diphenylphosphino)ferrocenylmethanol	$[Fe(\eta^5\text{-}C_5H_5)(\eta^5\text{-}C_5H_3\text{–1-}(CH_2OH)\text{–2-}P(C_6H_5)_2)]$	58
N-(ferrocenylmethyl)anthracene–9-carboxamide	$[Fe(\eta^5\text{-}C_5H_5)(C_{21}H_{16}NO)]$	59

should be mentioned, on passing, that $[Fe(\eta^5\text{-}C_5H_4COOH)_2]$ is known in three polymorphic modifications (see below).[43,43a,123] A similar strategy was used to produce mixed metal crystalline materials; the organometallic cation is used to template the anionic hydrogen-bonded network formed by the organometallic acid $[Fe(\eta^5\text{-}C_5H_4COOH)_2]$. The materials $[Co(\eta^5\text{-}C_5H_5)_2]^+[Fe(\eta^5\text{-}C_5H_4COOH)(\eta^5\text{-}C_5H_4COO)]^-$, $[Co(\eta^5\text{-}C_5H_5)_2]^+[Fe(\eta^5\text{-}C_5H_4COOH)(\eta^5\text{-}C_5H_4COO)]^-\cdot H_2O$, $\{[Cr(\eta^6\text{-}C_6H_6)_2]^+\}_2\{[Fe(\eta^5\text{-}C_5H_4COOH)(\eta^5\text{-}C_5H_4COO)]_2[Fe(\eta^5\text{-}C_5H_4COOH)_2]\}^{2-}$, and $[Cr(\eta^6\text{-}C_6H_6)_2]^+[Fe(\eta^5\text{-}C_5H_4COOH)(\eta^5\text{-}C_5H_4COO)]^-\cdot H_2O$ have been prepared and structurally characterized.[44,45] The four species contain different electronic and spin metal centers: 18-electron Fe(II) and Co(III) metal atoms are present in $[Co(\eta^5\text{-}C_5H_5)_2]^+[Fe(\eta^5\text{-}C_5H_4COOH)(\eta^5\text{-}C_5H_4COO)]^-$ and $[Co(\eta^5\text{-}C_5H_5)_2]^+[Fe(\eta^5\text{-}C_5H_4COOH)(\eta^5\text{-}C_5H_4COO)]^-\cdot H_2O$, whereas 18-electron Fe(II) and paramagnetic 17-electron Cr(I) are present in $\{[Cr(\eta^6\text{-}C_6H_6)_2]^+\}_2\{[Fe(\eta^5\text{-}C_5H_4COOH)(\eta^5\text{-}C_5H_4COO)]_2[Fe(\eta^5\text{-}C_5H_4COOH)_2]\}^{2-}$ and $[Cr(\eta^6\text{-}C_6H_6)_2]^+[Fe(\eta^5\text{-}C_5H_4COOH)(\eta^5\text{-}C_5H_4COO)]^-\cdot H_2O$. The crystalline edifices are held together by the complementary contribution of neutral O–H···O and/or negatively charged $O\text{–}H\cdots O^{(-)}$ hydrogen-bonding interactions between the acid moieties and of "charge-assisted" $C\text{–}H^{\delta+}\cdots O^{\delta-}$ bonds between cations and anions. In crystalline $[Co(\eta^5\text{-}C_5H_5)_2]^+[Fe(\eta^5\text{-}C_5H_4COOH)(\eta^5\text{-}C_5H_4COO)]^-$, the $[Fe(\eta^5\text{-}C_5H_4COOH)(\eta^5\text{-}C_5H_4COO)]^-$ anions, derived from mono-deprotonation of the neutral acid, form chains via symmetric O···H···O interactions between ligands in *transoid* conformation (see Figure 9). Crystalline $\{[Cr(\eta^6\text{-}C_6H_6)_2]^+\}_2\{[Fe(\eta^5\text{-}C_5H_4COOH)(\eta^5\text{-}C_5H_4COO)]_2[Fe(\eta^5\text{-}C_5H_4COOH)_2]\}^{2-}$ shows the presence of pairs of $[Cr(\eta^6\text{-}C_6H_6)_2]^+$ cations in the packing.

$[Fe(\eta^5\text{-}C_5H_4COOH)_2]$ has been widely employed as a building block in supramolecular chemistry, because the carboxylic groups can easily react and form hydrogen bonds with bis-amidines or diamines. For example, an acid : base stoichiometric ratio of 2 : 1 allows partial deprotonation of the acid, thus affording species that show the simultaneous presence of "homoionic" $O\text{–}H^{(-)}\text{—}O^{(-)}$ and "heteroionic" $N\text{–}H^{(+)}\text{—}O^{(-)}$ interactions, as in the compounds $[C_8H_{16}N_4]^{2+}\{[Fe(\eta^5\text{-}C_5H_4COOH)(\eta^5\text{-}C_5H_4COO)]_2\}^{2-}$ and $[C_{10}H_{20}N_4]^{2+}\{[Fe(\eta^5\text{-}C_5H_4COOH)(\eta^5\text{-}C_5H_4COO)]_2\}^{2-}$, obtained by reacting $[Fe(\eta^5\text{-}C_5H_4COOH)_2]$ with the bis-amidines $[C_8H_{14}N_4]$, and $[C_{10}H_{18}N_4]$,

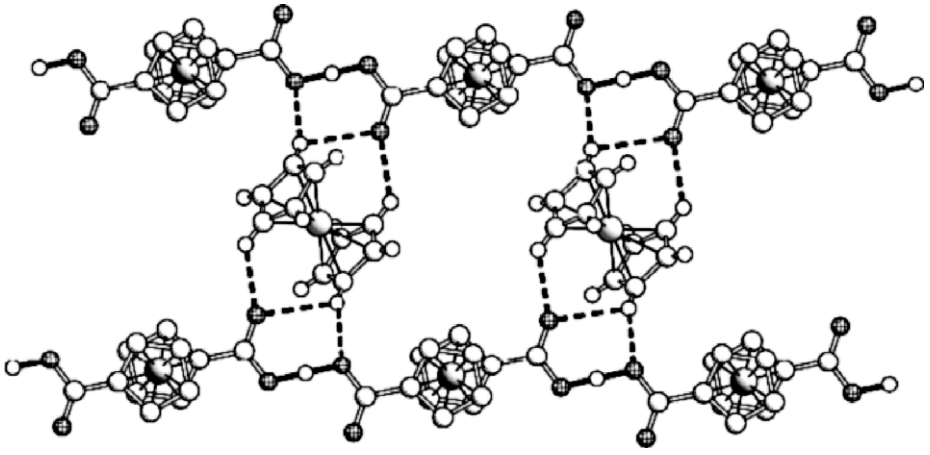

Figure 9 In crystalline $[Co(\eta^5\text{-}C_5H_5)_2]^+[Fe(\eta^5\text{-}C_5H_4COOH)(\eta^5\text{-}C_5H_4COO)]^-$, the $[Fe(\eta^5\text{-}C_5H_4COOH)(\eta^5\text{-}C_5H_4COO)]^-$ anions form parallel chains enclosing the $[Co(\eta^5\text{-}C_5H_5)_2]^+$ cations. Reprinted with permission from Braga, D.; Eckert, M.; Fraccastoro, M.; Maini, L.; Grepioni, F.; Caneschi, A.; Sessoli, I. *New J. Chem.* **2002**, *26*, 1280. © 2002, Elsevier.

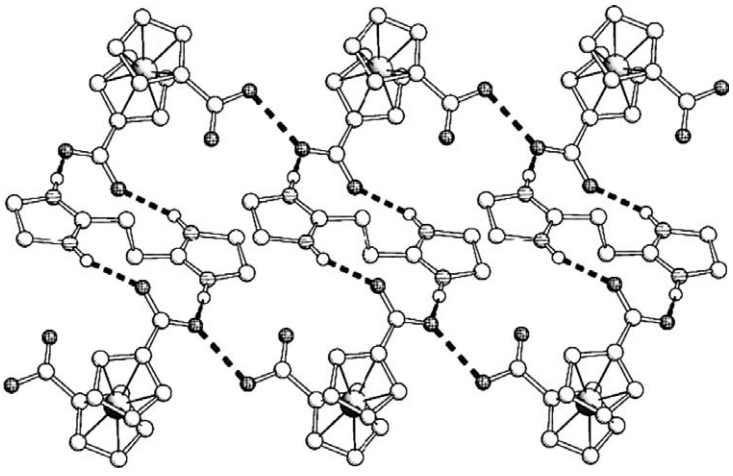

Figure 10 The two-dimensional network in $[C_8H_{16}N_4]^{2+}\{[Fe(\eta^5\text{-}C_5H_4COOH)(\eta^5\text{-}C_5H_4COO)]_2\}^{2-}$. Reprinted with permission from Braga, D.; Eckert, M.; Fraccastoro, M.; Maini, L.; Grepioni, F.; Caneschi, A.; Sessoli, I. *New J. Chem*. **2002**, *26*, 1280. © 2002, Elsevier.

respectively.[44,45] Figure 10 shows the two-dimensional network in $[C_8H_{16}N_4]^{2+}\{[Fe(\eta^5\text{-}C_5H_4COOH)(\eta^5\text{-}C_5H_4COO)]_2\}^{2-}$: the ionic arrangement can be described as composed of chains of $O\text{–}H^{(-)}\text{—}O^{(-)}$ interacting $[Fe(\eta^5\text{-}C_5H_4COOH)(\eta^5\text{-}C_5H_4COO)]^-$ anions joined by bis-amidine bridges; the crystalline structure can also be described as formed of chains of singly deprotonated acids interacting with the protonated bis-amides in dihapto mode.

In a related approach, Glidewell *et al.* have reported[46] the preparation of nine adducts formed between $[Fe(\eta^5\text{-}C_5H_4COOH)_2]$ and the organic diamines: methylamine, 1,4-diazabicyclo[2.2.2]-octane, 4,4′-bipyridyl, morpholine, octylamine, piperidine, di(cyclohexyl)amine, tris-(2-aminoethyl)amine, and 2-(4′-hydroxyphenyl)ethylamine (tyramine). All the crystal structures show strong N···(H)···O hydrogen bonds, and the proton transfer depends on the nature of the diamines. The hydrogen bonds form networks in one, two, and three dimensions. In the reactions with 1,4-diazabicyclo[2.2.2]-octane (stoichiometric ratio 2 : 1), the molecular components are linked into finite three-component aggregates by strong O–H···N hydrogen bonds.[47]

The strategy of utilizing strong N···(H)···O hydrogen bonds to construct the network has been exploited also when the organometallic moiety carries the pyridyl groups. The complex 1,1′-bis(ethenyl–4-pyridyl)ferrocene, $[Fe(\eta^5\text{-}C_5H_4\text{–}CH{=}CH\text{–}C_5H_4N)_2]$, has been used for NLO applications.[48] In the crystal structure of the complex, the two substituents on the cyclopentadienyl group of 1,1′-bis(ethenyl–4-pyridyl)ferrocene adopt a typical anti-periplanar conformation, while upon co-crystallization with 1,1′-binaphthol in methanol and ethanol, the two substituents of the ferrocene adopt a synclinal conformation.[48] The use of optically pure 1,1′-binaphthol leads to a non-centrosymmetric packing arrangement (see Figure 11), with all the molecular dipoles aligned in the same direction, that is, the crystal is polar. However, the efficiency of the second-harmonic generation was only 0.4 times that of urea (measured at 1,295 nm).

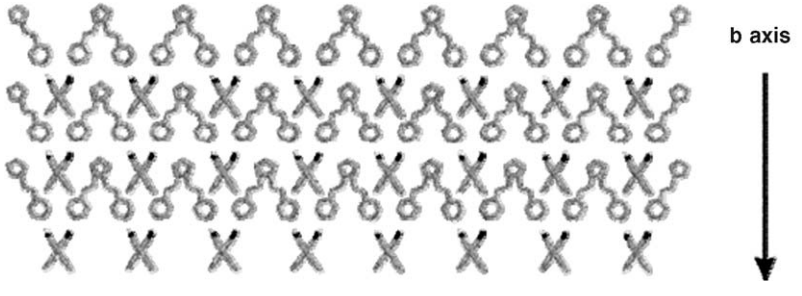

Figure 11 Two-dimensional layered structure of the co-crystal between $[Fe(\eta^5\text{-}C_5H_4\text{–}CH{=}CH\text{–}C_5H_4N)_2]$ and 1,1′-binaphthol assembled through the N–H–O and CH···π interactions (view down the *a* axis); note the perfect alignment of molecular dipole moments along the *b* axis. Reprinted with permission from Lee, I. S.; Chung, Y. K.; Mun, J.; Yoon, C. S. *Organometallics* **1999**, *18*, 5080. © 1999 American Chemical Society.

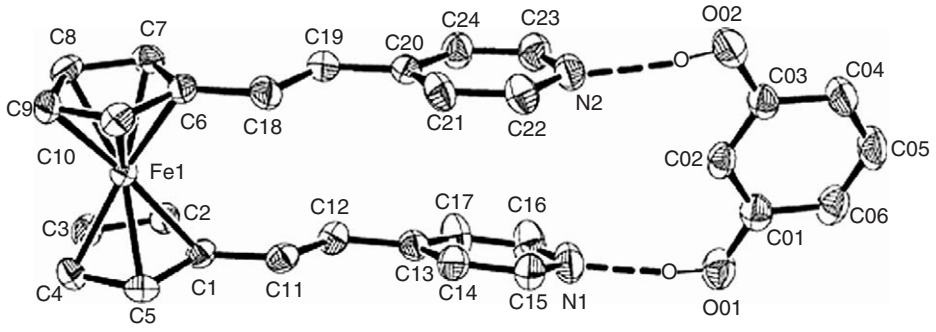

Figure 12 The molecular clip formed by [Fe(η^5-C_5H_4–CH═CH–C_5H_4N)$_2$] and resorcinol. Reproduced from Shin, D. M.; Lee, I. S.; Chung, Y. K. *Eur. J. Inorg. Chem.* **2003**, *12*, 2311, with permission from Wiley-VCH.

The complex 1,1′-bis(ethenyl–4-pyridyl)ferrocene was also co-crystallized with 1,3-dihydroxybenzene (resorcinol) and 1,3,5-trihydroxybenzene (phloroglucinol)[49] to form hydrogen-bonded molecular clips (see Figure 12), which lock the conformation of the organometallic fragment in a dipolar arrangement, a prerequisite for NLO molecules.

In yet another experiment, the same ferrocenyl complex was co-crystallized with 4-alkyloxybenzoic acids, 4-$C_nH_{2n+1}OC_6H_4COOH$ ($n = 6, 7, 8$).[50] The structures contain supramolecular arrays, in which one molecule of [Fe(η^5-C_5H_4–CH═CH–C_5H_4N)$_2$] and two molecules of alkyloxybenzoic acids are held together by strong N—H–O hydrogen bonding. Interestingly, [Fe(η^5-C_5H_4–CH═CH–C_5H_4N)$_2$][4-$C_8H_{17}OC_6H_4COOH$] shows a liquid crystalline behavior. Self-assembly with terephthalic acid, isophthalic acid, phthalic acid, and trimesic acid has also been reported.[50] When 1,1′-bis[2–(4-pyridyl)vinyl]ferrocene is co-crystallized with trimesic acid in the ratio of 2 : 3, a cage-like supramolecular array is formed (Figure 13). In the case of isophthalic acid, proton transfer from the carboxylic group to the pyridyl nitrogen takes place with formation of the cation [Fe(η^5-C_5H_4–CH═CH–C_5H_4N)(η^5-C_5H_4–CH═CH–C_5H_4NH)]$^+$. The cations are assembled via two N–H···N hydrogen bridges between protonated and neutral pyridine groups, and form a dicationic cyclic unit, in which two pyridines are stacked via π–π interaction. These supramolecular units, in turn, pile up to form a columnar structure.

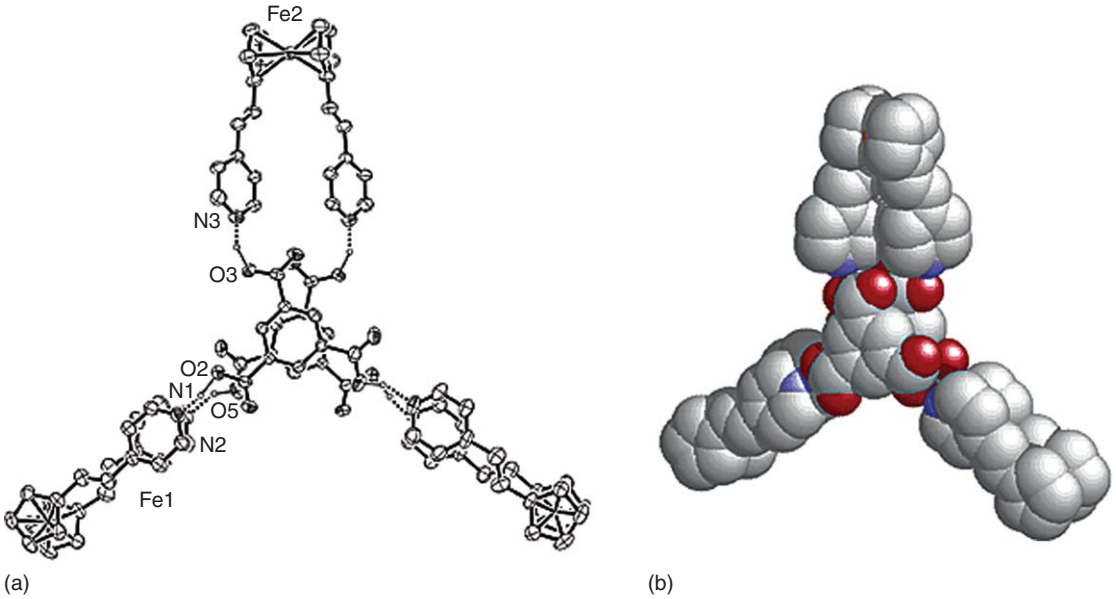

Figure 13 The cage-like supramolecular array obtained with [Fe(η^5-C_5H_4–CH═CH–C_5H_4N)$_2$] and trimesic acid. Reprinted in part with permission from Lee, I. S.; Shin, D. M.; Chung, Y. K. *Cryst. Growth. Des.* **2003**, *3*(*4*), 521. © 2003 American Chemical Society.

Ferrocene systems bearing dipeptide chains have been thoroughly investigated, since ferrocenes are recognized as organometallic scaffolds for molecular receptors and peptide mimetic models.[51,51a–51i] Conformational enantiomers based on the torsional twist about the Cp(centroid)–Fe–Cp(centroid) axis have been studied in the case of 1,1′-disubstituted ferrocenes.[52] Generally, conformational enantiomers easily interconvert because of the low energy barrier involved in the Cp-ring twisting. The introduction of peptide chains into ferrocene induces conformational enantiomerization by restriction of the torsional twist through chirality organization based on the intramolecular hydrogen bondings.[53,53a–53c]

Hirao *et al.* have been able to introduce podand dipeptide chains into the ferrocene moiety, constructing an ordered structure based on two rigid intramolecular hydrogen bonds and a helical molecular arrangement in the crystal packing.[53] The complex [Fe(η^5-C_5H_4–L-Ala–L-Pro–OEt)$_2$] shows a helical molecular arrangement in the solid state with turns of 14.91 Å. The podand dipeptide chains are considered to induce such a molecular aggregation through a hydrogen-bonding site (Ala) and a hydrophobic moiety (Pro). CD spectra suggest that the complex possesses a similar conformation also in solution.

Another interesting hydrogen-bonded system is that obtained when the boronic group is used over an organometallic ferrocenyl moiety. The diboronic acid derivative [Fe(η^5-C_5H_4-B(OH)$_2$)$_2$] has been investigated by two independent groups.[54,55] It forms chains of hydrogen-bonded ferrocenyl moieties in a *transoid* conformation (see Figure 14). The derivative [Fe(η^5-C_5H_4–4-C_5H_4N)(η^5-C_5H_4-B(OH)$_2$)], obtained from [Fe(η^5-C_5H_4-B(OH)$_2$)$_2$], carries both a B(OH)$_2$ unit and a C_5H_4N unit, and it has been isolated in three crystal forms.[55] These compounds will be described below in the section devoted to polymorphism.

Other hydrogen-bonded adducts have been obtained by reacting ferrocene–1,1′-diyl–bis(diphenylmethanol) with a wide range of amines, particularly heteroaromatic amines and diamines,[56,57,57a] while the use of the hydroxyl group as a hydrogen-bonding donor has been reported in the crystal structures of ferrocenylmethanol derivatives bearing a phosphorus substituent, such as *rac*-2-(diphenylphosphino)ferrocenylmethanol, [Fe(η^5-C_5H_5)(η^5-C_5H_3–1-(CH_2OH)–2-P(C_6H_5)$_2$], *rac*-2-(diphenylphosphinoyl)ferrocenylmethanol [Fe(η^5-C_5H_5)(η^5-C_5H_3–1-(CH_2OH)-2-PO(C_6H_5)$_2$], and *rac*-2-(diphenylthiophosphoryl)ferrocenylmethanol [Fe(η^5-C_5H_5)(η^5-C_5H_3–1-(CH_2OH)–2-PS(C_6H_5)$_2$].[58,58a] Hydrogen-bonding interactions between amido groups were observed in the crystal structure of *N*-(ferrocenylmethyl) anthracene–9-carboxamide [Fe(η^5-C_5H_5)($C_{21}H_{16}NO$)].[59]

Another important class of functionalized sandwich compounds that have been extensively used in the construction of hydrogen-bonded aggregates is that of the dicarboxylic acids of bis-benzene chromium and cobalticinium (see Table 3).

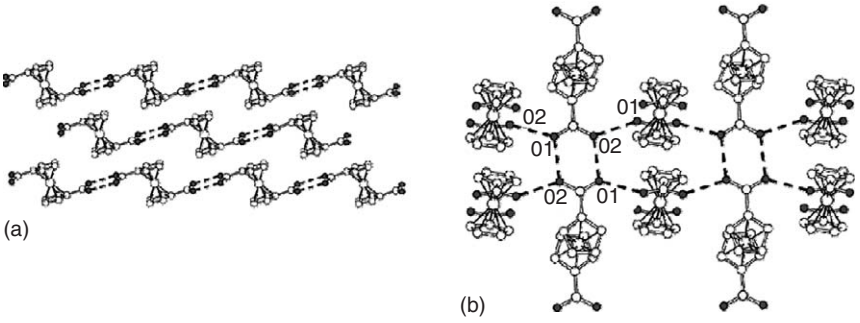

Figure 14 Two views of compound [Fe(η^5-C_5H_4–B(OH)$_2$)$_2$]: (a) chains of hydrogen-bonded ferrocenyl moieties in a *transoid* conformation; (b) crisscrossing of the chains in the crystal structure and establishment of hydrogen-bonding cross-links with lateral protons. H_{CH} atoms are not shown for clarity. Reprinted with permission from Braga, D.; Polito, M.; Bracaccini, M.; D'Addario, D.; Tagliavini, E.; Sturba, L.; Grepioni, F. *Organometallics* **2003**, *22*, 2142. © 2003 American Chemical Society.

Table 3 Bis-benzene chromium and cobalticinium sandwich units used as building blocks

Compound name	*Formula*	*References*
Bis-benzene chromium(0) dicarboxylic acid	[Cr^0(η^6-C_6H_5COOH)$_2$]	60
Bis-benzene chromium(I) dicarboxylic acid	[Cr^I(η^6-C_6H_5COOH)$_2$]$^+$	60
Cobalticinium dicarboxylic acid	[Co(η^5-C_5H_4COOH)$_2$]$^+$	61–63
Cobalticinium 1–(4-pyridyl amido),1′-carboxylic acid	[Co(η^5-$C_5H_4CONHC_5H_4N$)(η^5-C_5H_4COOH)]$^{(+)}$	65
Trovacenyl boronic acid	[V(η^7-C_7H_7)(η^5-$C_5H_4B(OH)_2$]	66
Trovacenyl carboxylic acid	[V(η^7-C_7H_7)(η^5-C_5H_4COOH)]	66

The neutral diamagnetic organometallic dicarboxylic acid $[Cr^0(\eta^6\text{-}C_6H_5COOH)_2]$ and the paramagnetic zwitterion $[Cr^I\text{-}(\eta^6\text{-}C_6H_5COOH)(\eta^6\text{-}C_6H_5COO)]$ (obtained as a co-crystal with ammonium hexafluorophosphate) both form hydrogen-bonded dimers in their solids, while the paramagnetic dicarboxylic acid cation, $[Cr^I(\eta^6\text{-}C_6H_5COOH)_2]^+$ crystallizes with formation of "homoionic" chains.[60]

The water soluble dicarboxylic cationic acid $[Co(\eta^5\text{-}C_5H_4COOH)_2]^+$[61] has proven to be an extremely versatile building block for the construction of hydrogen-bonded networks. What is more, the networks formed by the complex in cationic or zwitterionic form can be made "reactable" in solid–solid and solid–gas processes (see below). Removal of one proton from $[Co(\eta^5\text{-}C_5H_4COOH)_2]^+$ leads to formation of the neutral zwitterion $[Co(\eta^5\text{-}C_5H_4COOH)(\eta^5\text{-}C_5H_4COO)]$, while further deprotonation leads to formation of the dicarboxylate monoanion $[Co(\eta^5\text{-}C_5H_4COO)_2]^-$. The cationic form $[Co(\eta^5\text{-}C_5H_4COOH)_2]^+$ has been characterized as hexafluorophosphate or chloride salts, as well as in its co-crystals with urea and with the zwitterionic form $[Co(\eta^5\text{-}C_5H_4COOH)(\eta^5\text{-}C_5H_4COO)]$ in $\{[Co(\eta^5\text{-}C_5H_4COOH)(\eta^5\text{-}C_5H_4COO)]\ [Co(\eta^5\text{-}C_5H_4COOH)_2]\}[PF_6]$.[62]

When water solutions of $\{[Co(\eta^5\text{-}C_5H_4COOH)(\eta^5\text{-}C_5H_4COO)][Co(\eta^5\text{-}C_5H_4COOH)_2]\}[PF_6]$ are treated with alkali metal or ammonium hydroxides MOH ($M = K^+$, Rb^+, Cs^+, $[NH_4]^+$) in 1:1 stoichiometric ratio, the acid cation $[Co(\eta^5\text{-}C_5H_4COOH)_2]^+$ is partially deprotonated and the zwitterion $[Co(\eta^5\text{-}C_5H_4COOH)(\eta^5\text{-}C_5H_4COO)]$ is formed. Upon crystallization, $[Co(\eta^5\text{-}C_5H_4COOH)(\eta^5\text{-}C_5H_4COO)]$ forms a series of nearly isomorphous supramolecular aggregates with the inorganic salts MPF_6 ($M = K^+$, Rb^+, Cs^+, NH_4^+).[62] Alternatively, the same compounds can be prepared by treating water solutions of the zwitterion with a stoichiometric amount of the appropriate $[PF_6]^-$ salts, that is, MPF_6 ($M = K^+$, Rb^+, Cs^+, NH_4^+) or by mechanochemical mixing of the crystalline solids (see below).[63,63a] In all these crystalline materials the cations are encapsulated via either M^+—O interactions ($M^+ = K^+$, Rb^+, Cs^+) or N–H—O hydrogen bonds ($M^+ = NH_4^+$), within a strongly nucleophilic cage formed by four molecules of $[Co(\eta^5\text{-}C_5H_4COOH)(\eta^5\text{-}C_5H_4COO)]$. The "walls" of the cage are constituted of two "dimeric units" of $[Co(\eta^5\text{-}C_5H_4COOH)(\eta^5\text{-}C_5H_4COO)]$, held together by two O–H—O hydrogen bonds and by two C–H—O bonds, these latter involving the H-atoms of the C_5H_4-systems and the free lone pairs on the carboxylic oxygens (see Figure 15).

It is worth mentioning, on passing, that charge separation within a cationic complex is not a common situation. Another example of cationic–zwitterionic organometallic complex has been reported in the case of the zirconocene system $[Zr(C_5H_4CMe_2C_6H_4Me\text{-}p)(MeB(C_6F_5)_3]^+\ [MeB(C_6F_5)_3]$.[64]

The use of sandwich complexes as supramolecular building blocks has been recently extended to mono- and bis-amido derivatives of $[Co(\eta^5\text{-}C_5H_4COOH)_2]^+$. The prototype of this class of complexes is the carboxyl amide $[Co(\eta^5\text{-}C_5H_4CONHC_5H_4N)(\eta^5\text{-}C_5H_4COOH)]^{(+)}$.[65] The complex $[Co(\eta^5\text{-}C_5H_4CONHC_5H_4NH)(\eta^5\text{-}C_5H_4COO)][PF_6]$ possesses an eclipsed conformation of the ligands in the solid state. X-ray diffraction shows that the carboxylic group is deprotonated, while the N atom of the pyridine group is protonated. As a consequence of the formal proton transfer from the carboxylic group to the pyridine, the global ionic charge of the complex does not change, but

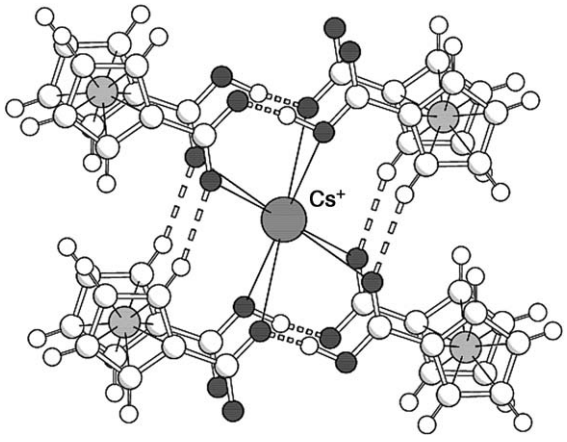

Figure 15 The cage formed by four molecules of $[Co(\eta^5\text{-}C_5H_4COOH)(\eta^5\text{-}C_5H_4COO)]$ with alkali cations K^+, Rb^+, Cs^+, and the NH_4^+ cation. Reproduced from Braga, D.; Maini, L.; Giaffreda, S. L.; Grepioni, F.; Chierotti, M. R.; Gobetto, R. *Chem. Eur. J.* **2004**, *10*, 3261, with permission from Wiley-VCH.

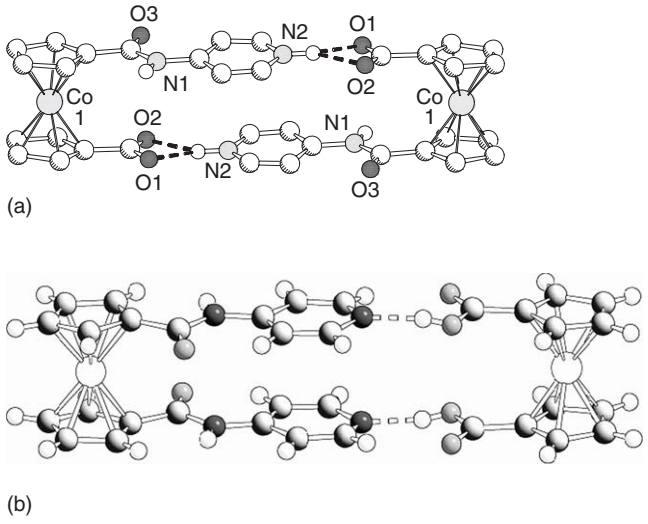

Figure 16 (a) The dimeric unit $\{[Co(\eta^5\text{-}C_5H_4CONHC_5H_4NH)(\eta^5\text{-}C_5H_4COO)]^+\}_2$ in crystalline $[Co(\eta^5\text{-}C_5H_4CONHC_5H_4NH)(\eta^5\text{-}C_5H_4COO)]\ [PF_6]$, formed via bifurcate $N\text{–}H^{(+)}\cdots O^{(-)}$ hydrogen-bonding interactions. (b) The ferrocene dicarboxylic acid molecule and the diamido molecule $[Co(\eta^5\text{-}C_5H_4CONHC_5H_4NH)_2]$ in $[Co(\eta^5\text{-}C_5H_4CONHC_5H_4N)_2][Fe(\eta^5\text{-}C_5H_4COOH)_2][PF_6]$ are linked via O–H···N hydrogen bonds. Reprinted in part with permission from Braga, D.; Palito M.; Grepioni, F. *Cryst. Growth. Des.* **2004**, *4*, 769. © 2004 American Chemical Society.

the complex acquires a "zwitterionic" nature. In the crystal, two cations $[Co(\eta^5\text{-}C_5H_4CONHC_5H_4NH)(\eta^5\text{-}C_5H_4COO)]^+$ are linked together via a bifurcate $N\text{–}H^{(+)}\cdots O^{(-)}$ hydrogen bond, forming the dimer shown in Figure 16(a).

The cationic bis-amide $[Co(\eta^5\text{-}C_5H_4CONHC_5H_4NH)_2]$ has been used in the formation of a co-crystal with $[Fe(\eta^5\text{-}C_5H_4COOH)_2]$.[65] In crystalline $[Co(\eta^5\text{-}C_5H_4CONHC_5H_4N)_2][Fe(\eta^5\text{-}C_5H_4COOH)_2][PF_6]$, the two moieties are linked by an O–H···N hydrogen bond forming a sort of dimer (see Figure 16(b)) that recalls the one observed in crystalline $[Co(\eta^5\text{-}C_5H_4CONHC_5H_4NH)(\eta^5\text{-}C_5H_4COO)]\ [PF_6]$.

Finally, on concluding the section on functionalized sandwich compounds capable of hydrogen-bond formation, the structures of trovacenyl boronic acid $[V(\eta^7\text{-}C_7H_7)(\eta^5\text{-}C_5H_4B(OH)_2)]$ and the carboxylic acid $[V(\eta^7\text{-}C_7H_7)(\eta^5\text{-}C_5H_4COOH)]$ should also be pointed out,[66,66a] which form hydrogen-bonded dimers in their crystals, as shown in Figure 17 for the carboxylic acid compound.

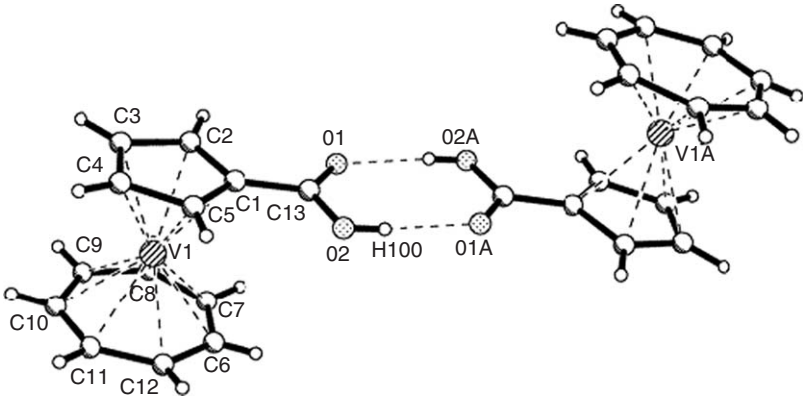

Figure 17 The hydrogen-bonded dimers present in crystalline $[V(\eta^7\text{-}C_7H_7)(\eta^5\text{-}C_5H_4COOH)]$. Reprinted with permission from Elschenbroich, C.; Schiemann, O.; Burghaus, O.; Harms, K. *J. Am. Chem. Soc.* **1997**, *119*(*32*), 7452. © 1997 American Chemical Society.

12.11.3.4 Hydrogen-bonded Networks Formed by Coordination Compounds

The use of coordination compounds with peripheral hydrogen-bonding substituents in the formation of infinite one-, two-, and three-dimensional frameworks, which can be used for host/guest chemistry, has recently been reviewed by Beatty.[67] Brammer and Rivas, on the other hand, have reviewed the hydrogen bonding in substituted ammonium salts of the tetracarbonylcobaltate(I) anion.[68] The reader is addressed to these two papers for a detailed analysis.

In the case of the salt [(*N*-methylpiperazine)$_3$H$_2$][Co(CO)$_4$]$_2$, the presence of N–H$^+$–N hydrogen-bonded trimers of *N*-methylpiperazine/piperazinium, capped at each end by Co(CO)$_4^-$ anions that interact via N–H–Co hydrogen bonds, is noteworthy. A similar type of interaction is seen in the structures where the Co(CO)$_4^-$ anion interacts with a monomeric cation based upon [N(CH$_2$CH$_2$)$_3$N] (DABCO). Crystalline [DABCO][Co(CO)$_4$]·THF contains infinite parallel cationic chains [(DABCO)$\cdots$H$^+\cdots$(DABCO)]$_n$, linked through C–H$\cdots$O hydrogen bonds to Co(CO)$_4^-$ anions that lie in the channels between these chains (see Figure 18). A hydrogen-bonded N–H$^+\cdots$N two-dimensional network is also observed in crystalline [triethylenetetraamineH$^+$] [Co(CO)$_4^-$] with formation of approximately square channels.[69]

The dinuclear complex [Re$_2$(μ-OMe)$_3$(CO)$_6$]$^-$ has been employed in a reaction with [N(CH$_2$CH$_2$)$_3$N] (DABCO), with formation of the crystalline salt [Re$_2$(μ-OMe)$_3$(CO)$_6$]$^-$[DABCO–H]$^+$.[70] The complex is arranged in a honeycomb supramolecular architecture with the protonated DABCO units forming linear hydrogen-bonded chains of [DABCO–H]$^+$ cations. Molybdenum carbonyl complexes of the type [HO-(N$\cap$N′)]Mo(CO)(3)L (L = CO, THF, PPh$_3$, CN^{t}Bu, CNCy) have been studied by Heinze.[71] Two major types of multiple intermolecular hydrogen-bonding patterns, involving the OH group and CH moieties as hydrogen donors and carbonyl groups and solvent molecules as hydrogen acceptors, have been found and interpreted in terms of hydrogen-bond strength, steric availability, and density of packing.

12.11.3.5 Coordination Networks Based on Organometallic Spacers

Sweigart's is one of the most active groups in the construction of mixed metal coordination networks where "knots" and "spacers" are constituted of organometallic moieties.[72] These are defined as metal–organometallic coordination networks (MOMNs). The organometallic ligand of choice is the anionic complex (η^4-benzoquinone)Mn(CO)$_3^-$ (*p*-QMTC hereafter). It has been shown that the attachment of a metal fragment to the π-system significantly influences the proton and electron transfers occurring in the formation of the semiquinone (η^5- *p*-semiquinone)Mn(CO)$_3$ and quinone (η^4-*p*-quinone)Mn(CO)$_3^-$ oxidation products. The cationic quinonoid complex (η^6-hydroquinone)Mn(CO)$_3^+$ can also be prepared, and a whole series of anionic, cationic, and neutral building blocks can thus be obtained.[73,73a]

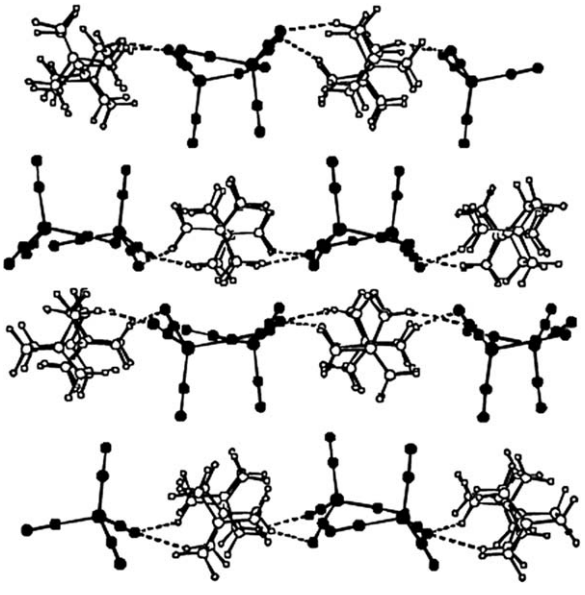

Figure 18 View down the hydrogen-bonded cationic chains in crystalline [DABCO][Co(CO)$_4$]·THF; the anions occupy the channels and are linked to the cations via C–H$\cdots$O hydrogen bonds. Reprinted with permission from Rivas, J. C. M.; Brammer, L. *Coord. Chem. Rev.* **1999**, *183*, 143. © 1999, Elsevier.

The key to the utility of (η^6-hydroquinone)$Mn(CO)_3^+$ in the construction of MOMNs is the electrophilic activation, provided by the metal fragment, which results in facile reversible deprotonation of the –OH groups to afford the η^5-semiquinoine and η^4-quinone complexes, as shown in Figure 19. An additional factor that turns out to be important is the −1 charge on the η^4-quinone complex. These features have been exploited for the preparation of many MOMNs having both backbone and pendant metal sites. The neutral η^5-semiquinone complex forms one-dimensional networks via intermolecular hydrogen bonding (with short O–O distances 2.47 Å),[74] whereas the catechol analog forms hydrogen-bonded dimers (see Figure 20). Since the anionic complex *p*-QMTC is a "divergent" bidentate ligand, it is not surprising that this molecule easily leads to formation of one-dimensional networks when reacted with metal cations.[74] The additional advantage of the anionic nature of *p*-QMTC is that it can easily interact with the electropositive metal centers forming the "knots" of the network, thus leading to formation of "neutral" coordination networks via coordination of the *p*-QMTC oxygen atoms to the added metal ions. Some results obtained in this manner are summarized in Table 4.

In the reaction of *p*-QMTC and M^{2+} (M = Cd, Mn) in the presence of 2,2′-bipyridine, both the nitrogen atoms of the organic spacer are constrained to bind to the same metal node, leading to formation of a one-dimensional "zigzag" network in crystalline $M[(\eta^6\text{-}p\text{-}(C_6H_4O_2))Mn(CO)_3]_2(C_{10}N_2H_8)$.[72] Other one-dimensional MOMNs of the type $M[(\eta^6\text{-}p\text{-}(C_6H_4O_2))Mn(CO)_3]_2$ (M = Mn, Co, Ni, Cd) are obtained if DMSO is used as solvent. DMSO functions as the axial ligands unless another ligand, for example, pyridine, is present. The structure of $[Cd(p\text{-}QMTC)_2(DMSO)_2]_\infty$ is illustrated in Figure 21 as an example.

The one-dimensional strings in $M[(\eta^6\text{-}p\text{-}(C_6H_4O_2))Mn(CO)_3]_2(DMSO)$ are linked together if 4,4′-bipyridine is present in the reaction mixture, thus leading to formation of a two-dimensional coordination network,[75] which was structurally characterized for M = Mn and Ni (see Figure 22). The rectangular grids in $M[(\eta^6\text{-}p\text{-}(C_6H_4O_2))Mn(CO)_3]_2(C_{10}N_2H_8)$ have dimensions of approximately 10 Å × 12 Å, and the DMSO co-crystallized in the structures can be replaced without loss of crystallinity by suspending $M[(\eta^6\text{-}p\text{-}(C_6H_4O_2))Mn(CO)_3]_2(C_{10}N_2H_8)$ in CD_2Cl_2 at room temperature for 2 h.

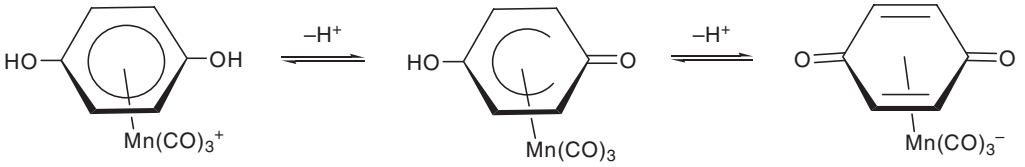

Figure 19 The cationic (η^6-hydroquinone)$Mn(CO)_3^+$, the neutral (η^5-*p*-semiquinone)$Mn(CO)_3$, and the anionic (η^4-benzoquinone)$Mn(CO)_3^-$ used in the construction of metal–organic metal–organometallic coordination networks (MOMNs). Reprinted with permission from Oh, M.; Carpenter, G. B.; Sweigart, D. A. *Acc. Chem. Res.* **2004**, *37*(*1*), 1. © 2004 American Chemical Society.

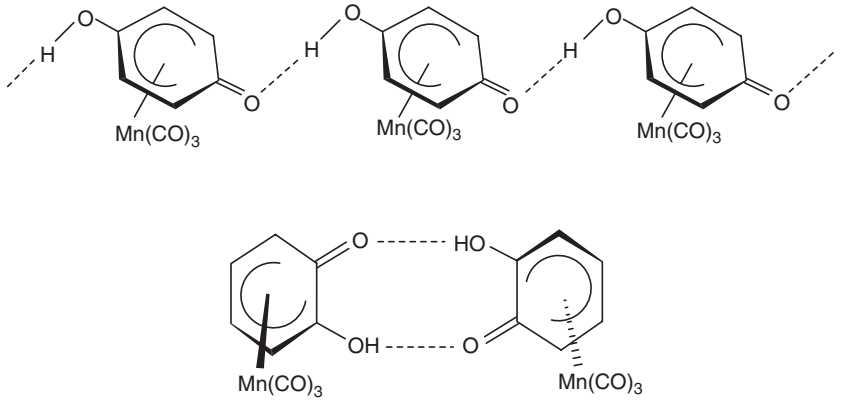

Figure 20 The neutral complex (η^5-*p*-semiquinone)$Mn(CO)_3$ forms one-dimensional networks via intermolecular hydrogen bonding (with short O–O distances 2.47 Å),[73] whereas the catechol analog forms hydrogen-bonded dimers. Reprinted with permission from Oh, M.; Carpenter, G. B.; Sweigart, D. B. *Acc. Chem. Res.* **2004**, *37*(*1*), 1. © 2004 American Chemical Society.

Table 4

Organometallic spacer	*Metal knot, M*	*Formula of the resulting system*	*References*
$(\eta^4$-*p*-quinone$)Mn(CO)_3^-$	Mn^{2+}, Cd^{2+}	$M[(\eta^6$-*p*-$(C_6H_4O_2))Mn(CO)_3]_2(C_{10}N_2H_8)$-$(C_{10}N_2H_8)_2$	72
$(\eta^4$-*p*-quinone$)Mn(CO)_3^-$	Mn^{2+}, Cd^{2+}, Co^{2+}, Ni^{2+}	$M[(\eta^6$-*p*-$(C_6H_4O_2))Mn(CO)_3]_2(DMSO)$	72
$(\eta^4$-*p*-quinone$)Mn(CO)_3^-$	Mn^{2+}, Ni^{2+}	$M[(\eta^6$-*p*-$(C_6H_4O_2))Mn(CO)_3]_2(C_{10}N_2H_8)$	75
$(\eta^4$-*p*-quinone$)Mn(CO)_3^-$	Mn^{2+}, Co^{2+}	$\{M[(\eta^6$-*p*-$(C_6H_4O_2))Mn(CO)_3]_2(C_{10}N_2H_8)\}_\infty$	74
$(\eta^4$-*p*-quinone$)Mn(CO)_3^-$	Zn^{2+}, Mn^{2+}, Co^{2+}	$\{M[(\eta^6$-*p*-$(C_6H_4O_2))Mn(CO)_3]_2\}_\infty$	74–76
$(\eta^4$-*p*-quinone$)Mn(CO)_3^-$	$(Mn^{2+})_2$	$\{M_2[(\eta^6$-*p*-$(C_6H_4O_2))Mn(CO)_3]_2(DMSO)\}_\infty$	77
$(\eta^4$-*p*-quinone$)Mn(CO)_3^-$	$Cu_2(CH_3CO_2)^{3+}$	$\{M_2[(\eta^6$-*p*-$(C_6H_4O_2))Mn(CO)_3]_2(CH_3CO_2)\}_\infty$	78
1,1′-$Fe[(\eta^5$-$C_5H_4(P(C_6H_5)_2)_2]$	Ag^+	$\{Ag_4(SO_3CF_3)_4Fe[(\eta^5$-$C_5H_4(P(C_6H_5)_2)_2]_2\}$	80
$[Fe(\eta^5$-$C_5H_4COO)_2]^{2-}$	Zn^{2+}	$NaZn_3[Fe(\eta^5$-$C_5H_4COO)_2]_2(OH)_3(H_2O)$	81
$[Fe(\eta^5$-$C_5H_4COO)_2]^{2-}$	Cd^{2+}	$Cd[Fe(\eta^5$-$C_5H_4COO)_2](DMF)_2(H_2O)$	81
$[Fe(\eta^5$-$C_5H_4COO)_2]^{2-}$	La^{3+}	$\{La_2[Fe(\eta^5$-$C_5H_4COO)_2]_3(CH_3OH)_4\}_\infty$	82
$[Fe(\eta^5$-$C_5H_4COO)_2]^{2-}$	Eu^{3+}	$[Eu_2[Fe(\eta^5$-$C_5H_4COO)_2]_3(H_2O)_5]_\infty$	82
$[Fe(\eta^5$-$C_5H_4COO)_2]^{2-}$	Gd^{3+}	$\{Gd_2[Fe(\eta^5$-$C_5H_4COO)_2]_3(CH_3OH)_2(H_2O)_3\}_\infty$	82
1,1′-$[Fe(\eta^5$-C_5H_4–S–4-$C_5H_5N)_2]$	Ag^+	$\{Ag[Fe(\eta^5$-C_5H_4–S–4-$C_5H_5N)_2]\cdot(CH_3CN)_2\}PF_6$	83
1,1′-$[Fe(\eta^5$-C_5H_4–S–4-$C_5H_5N)_2]$	Mn^{2+}, Cu^{2+}, Zn^{2+}	$\{M\ [Fe(\eta^5$-C_5H_4–S–4-$C_5H_5N)_2][CH(COCF_3)_2]_2\}$	84
1,1′-$[Fe(\eta^5$-C_5H_4–S–2-$C_5H_5N)_2]$	Cu^+	$\{Cu[Fe(\eta^5$-C_5H_4–S–2-$C_5H_5N)_2]\}PF_6$	84
$[Co(\eta^5$-$C_5H_4COO)_2]^{2-}$	Cu^{2+}	$\{Cu[Co(\eta^5$-$C_5H_4COO)_2]_2\}\cdot 2MeOH$	85
$[Fe(\eta^5$-$C_5H_4COO)_2]^{2-}$	Cd^{2+}	$\{[Cd[Fe(\eta^5$-$C_5H_4COO)_2](DMF)_2(H_2O)\}$	86

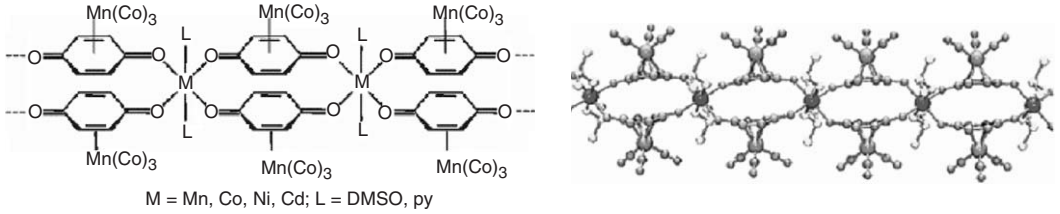

Figure 21 Structure and packing diagram for linear one-dimensional MOMN $[Cd(p\text{-QMTC})_2(DMSO)_2]_\infty$. Reprinted with permission from Oh, M.; Carpenter, G. B.; Sweigart, D. B. *Acc. Chem. Res.* **2004**, *37*(*1*), 1. © 2004 American Chemical Society.

Three-dimensional networks can also be obtained with the same MOMN 4,4′-bipyridine $[M(p\text{-QMTC})_2(4,4'\text{-bipy})]_\infty$ (M = Mn and Co) with formation of rectangular pores of dimension ca. 6 Å × 12 Å, as shown in Figure 23. The rectangular channels are filled with solvent, such that there are two DMSO molecules per molecular "box."[74]

The *p*-QMTC building block has been used also with metal knots that favor tetrahedral coordination, such as Zn(II). The resulting MOMN, $[Zn(p\text{-QMTC})_2]_\infty$, consists of two interpenetrating diamondoid networks, as shown in Figure 24.[74] The same MOMN architecture is present in the networks $[Co(p\text{-QMTC})_2]_\infty$ and $[Mn(p\text{-QMTC})_2]_\infty$.[76] The Mn^{2+} and Co^{2+} derivatives, however, require the use of MeOH instead of DMSO to form the tetrahedral diamondoid structure. In contrast, the coordination polymers $[M(2,3\text{-Me}_2\text{QMTC})_2]_\infty$ (M = Mn, Zn) grown in MeOH or EtOH solvent revealed formation of a non-interpenetrated two-dimensional rhombohedral grids.

If the reaction of *p*-QMTC with Mn^{2+} is carried out in 1:1 DMSO–MeOH, slow formation of a dinuclear dimanganese unit joined by pairs of *p*-QMTC spacers is observed in $[Mn_2(p\text{-QMTC})_4(DMSO)]_\infty$.[77] It should be mentioned on closing this section that the reaction of *p*-QMTC and $Cu(OAc)_2$ in MeOH leads instead to formation of the "three-dimensional brick wall" architecture structure $[Cu_2(p\text{-QMTC})_3(\mu\text{-}CH_3CO_2)]_\infty$, which contains bimetallic nodes of formula $Cu_2(\mu\text{-}CH_3CO_2)^{3+}$ linked via linear *p*-QMTC spacers.[77a] The use of manganese tricarbonyl transfer (MTT) reagents in the construction of novel organometallic systems has been reviewed recently.[78]

We have seen before that functionalized ferrocenyl complexes form a large family portion of the organometallic complexes investigated for their supramolecular bonding capacity. This popularity extends also to the use of ferrocenyl complexes for the preparation of coordination networks and complexes and complexes in which the ferrocenyl derivative is used as a ligand. Some recent results are summarized in Table 4.

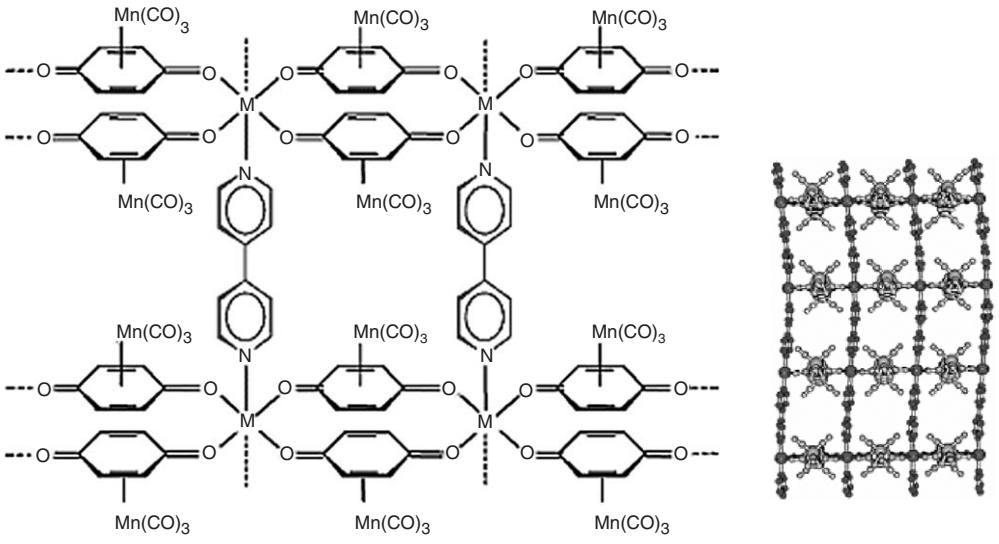

Figure 22 Structure of one layer of the two-dimensional MOMN $[M(p\text{-QMTC})_2(4,4'\text{-bipy})]_\infty$ (M = Mn, Ni). DMSO guest molecules are not shown. Reprinted with permission from Oh, M.; Carpenter, G. B.; Sweigart, D. A. *Acc. Chem. Res.* **2004**, *37*(*1*), 1. © 2004 American Chemical Society.

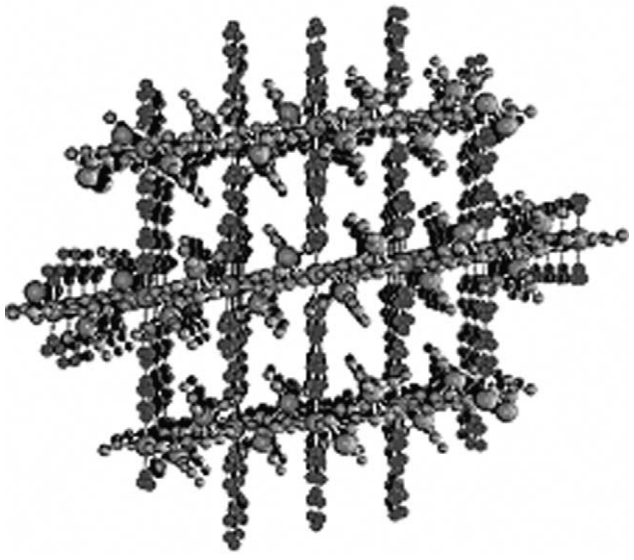

Figure 23 Structure of MOMN $[M(p\text{-QMTC})_2(4,4'\text{-bipy})]_\infty$ (M═Mn and Co), consisting of two-dimensional grid quinonoid planes linked by bipyridine spacers. Reprinted with permission from Oh, M.; Carpenter, G. B.; Sweigart D. A. *Acc. Chem. Res.* **2004**, *37*(*1*), 1. © 2004 American Chemical Society.

The ferrocenyl complex 1,1′-bis(diphenylphosphino)ferrocene has been widely used in supramolecular chemistry,[79,79a–79c] but has only recently begun to be exploited in the formation of coordination networks. For example the reaction of 1,1′-bis(diphenylphosphino)ferrocene with silver triflate has been reported to yield the two-dimensional coordination network $\{Ag_4(SO_3CF_3)_4\ Fe[(\eta^5\text{-}C_5H_4(P(C_6H_5)_2)_2]_2\}$.[80]

Heteropolynuclear organometallic coordination networks have been constructed by using $[Fe(\eta^5\text{-}C_5H_4\text{-}COOH)_2]$ as a spacer.[81] When $[Fe(\eta^5\text{-}C_5H_4COOH)_2]$ reacts with *d*-block transition metal ions, the ligand $[Fe(\eta^5\text{-}C_5H_4COO)_2]$ generally adopts a *cisoid* conformation, with formation leading to the formation of the discrete molecular architectures, but in the case of Zn and Cd, the coordination polymers $NaZn_3[Fe(\eta^5\text{-}C_5H_4COO)_2]_2(OH)_3(H_2O)$ and

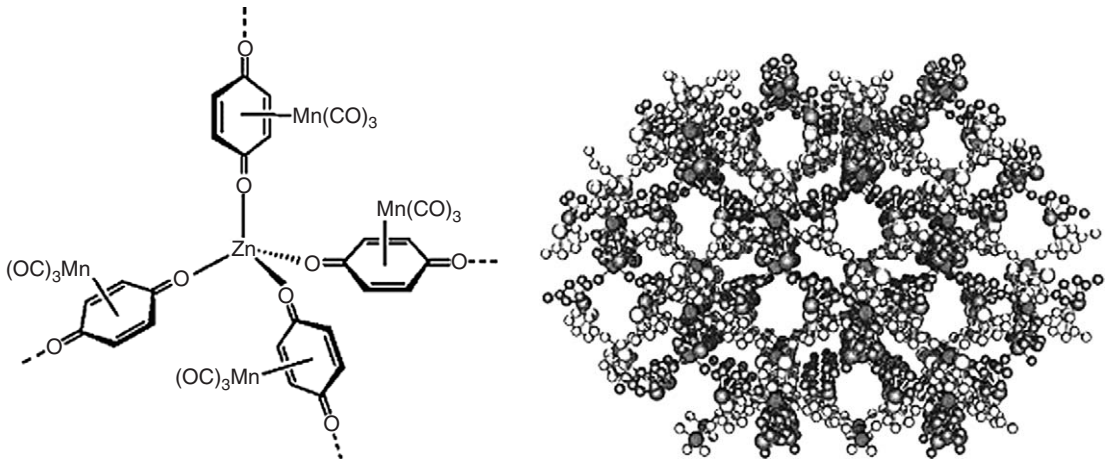

Figure 24 Structure of MOMN $[Zn(p\text{-QMTC})_2]_\infty$, consisting of tetrahedral Zn(II) nodes and two interpenetrating diamondoid quinonoid networks. Reprinted with permission from Oh, M.; Carpenter, G. B.; Sweigart D. A. *Acc. Chem. Res.* **2004**, *37*(*1*), 1. © 2004 American Chemical Society.

$Cd[Fe(\eta^5\text{-}C_5H_4COO)_2](DMF)_2(H_2O)$ have been obtained. The conformation of the cyclopentadienyl rings in $NaZn_3[Fe(\eta^5\text{-}C_5H_4COO)_2]_2(OH)_3(H_2O)$ is *syn*-periplanar, and this special conformation plays an important role in determining the unusual topological motif of $NaZn_3[Fe(\eta^5\text{-}C_5H_4COO)_2]_2(OH)_3(H_2O)$ (see Figure 25).

Heteropolynuclear organometallic compounds based on $[Fe(\eta^5\text{-}C_5H_4COOH)_2]$ have been constructed.[82] Interaction of the ligand $[Fe(\eta^5\text{-}C_5H_4COOH)_2]$ with lanthanide La^{3+}, Eu^{3+}, and Gd^{3+} ions affords the two-dimensional networks $\{La_2[Fe(\eta^5\text{-}C_5H_4COO)_2]_3(CH_3OH)_4\}$, $\{Eu_2[Fe(\eta^5\text{-}C_5H_4COO)_2]_3(H_2O)_5\}_\infty$, and $\{Gd_2[Fe(\eta^5\text{-}C_5H_4COO)_2]_3(CH_3OH)_2(H_2O)_3\}_\infty$, respectively, in which the *transoid* conformation of the ferrocene moiety provides opportunities to form infinite two-dimensional networks. In addition to this, $\pi\cdots\pi$ interactions between the ferrocene moieties were also found to stabilize the supramolecular architectures in the solid state. Complex $\{La_2[Fe(\eta^5\text{-}C_5H_4COO)_2]_3(CH_3OH)_4\}_\infty$ contains a two-dimensional network structure (see Figure 26). The two independent ferrocene dicarboxylate units adopt a different conformation: *syn*-periplanar and *anti*-periplanar. The two ligands in *syn*-periplanar conformation coordinate two lanthanum atoms forming a metallacycle. The other coordination sites of the lanthanum metals are occupied by methanol and the oxygen atoms of the $[Fe(\eta^5\text{-}C_5H_4COO)_2]$ in *anti*-periplanar conformation. The latter oxygen atoms act as bridges between the metallacycles, generating an infinite three-dimensional network.

Crystalline $\{Eu_2[Fe(\eta^5\text{-}C_5H_4COO)_2]_3(H_2O)_5\}_\infty$ and $\{Gd_2[Fe(\eta^5\text{-}C_5H_4COO)_2]_3(CH_3OH)_2(H_2O)_3\}_\infty$ are isostructural and contain a two-dimensional coordination network constructed from the lanthanide–organometallic layers. The two independent ferrocene ligands adopt a synclinal eclipsed and *anti*-periplanar conformation, and each carboxylate group coordinates to a different europium atom generating a two-dimensional brick wall structure.

Mochida and co-workers have constructed coordination networks by using ferrocene-based bidentate ligands, 1,1′-(4-dipyridinethio)ferrocene and 1,1′-(2-dipyridinethio)ferrocene.[83] In order to obtain coordination polymers, these

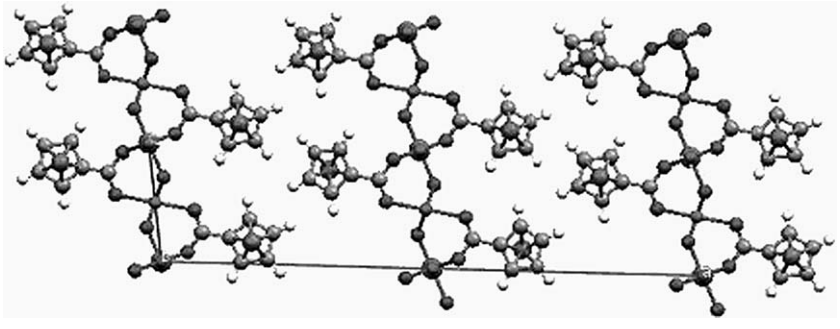

Figure 25 $NaZn_3[Fe(\eta^5\text{-}C_5H_4COO)_2]_2(OH)_3(H_2O)$ view along *b*-axis.

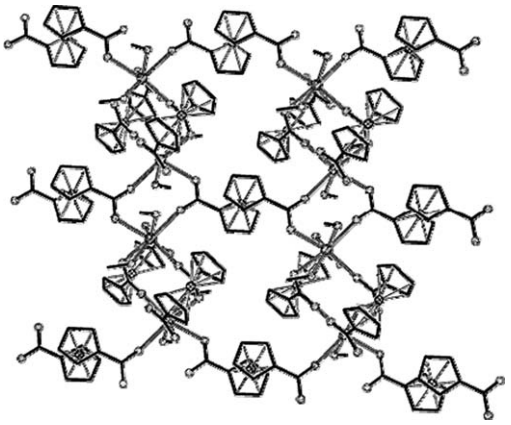

Figure 26 Two-dimensional layer of complex $\{La_2[Fe(\eta^5\text{-}C_5H_4COO)_2]_3(CH_3OH)_4\}_\infty$ showing the different conformations and coordination modes of the ligands. Reprinted in part with permission from Dong, G.; Yu-ting, L.; Chun-ying, D.; Hong, M.; Qing-jin, M. *Inorg. Chem.* **2003**, *42*(*8*), 2519. © 2003 American Chemical Society.

bidentate ligands were combined with metal ions bearing two coordination sites, Ag(I), Cu(I), and $M(hfac)_2$ (M = first row transition metal; hfac = hexafluoroacetylacetonate). $M(hfac)_2$ building blocks have been employed in the construction of coordination networks.[84,84a–84c]

The network in $\{Ag[1,1'\text{-}(4\text{-dipyridinethio})ferrocene](PF_6)\}_n$ is constituted of chains formed by Ag ions bridged by 1,1′-(4-dipyridinethio)ferrocene ligands. A relatively short Ag···Ag distance of 3.2670(8) Å is present between adjacent chains.

The reaction of 1,1′-(4-dipyridinethio)ferrocene with $M(hfac)_2$ ($M = Mn^{2+}$, Cu^{2+}, Zn^{2+}) yielded the isomorphous complexes $\{M(hfac)_2[1,1'\text{-}(4\text{-dipyridinethio})ferrocene]\}_n$ (M = Mn, Cu, Zn). The structures show a one-dimensional straight chain, which consists of the alternate linkage of $M(hfac)_2$ units and the ligand. The ligand 1,1′-(2-dipyridinethio)ferrocene also afforded a one-dimensional coordination network in the linear coordination with Cu(I) centers.

The monoanion $[Co(\eta^5\text{-}C_5H_4COO)_2]^-$ was used as a unique monoanionic dicarboxylate ligand with copper(II) to construct a new two-dimensional coordination polymer.[85] The crystal structure of $\{Cu[Co(\eta^5\text{-}C_5H_4COO)_2]_2\}\cdot 2MeOH$ is shown in Figure 27. It can be seen that four oxygen atoms of the carboxylate groups from the dianion $[Co(\eta^5\text{-}C_5H_4COO)_2]^-$ bind to the copper(II) center to form a distorted square-planar geometry. Each $[Co(\eta^5\text{-}C_5H_4COO)_2]^-$ anion adopts a conformation between anticlinal-eclipsed and *anti*-periplanar and connects two copper(II) centers to yield a two-dimensional structure with small square cavities (about 4×4 Å^2), which trap methanol molecules.

When the dianionic 1,1′-ferrocenedicarboxylate $[Fe(\eta^5\text{-}C_5H_4COO)_2]^{2-}$ is used with cadmium(II) in a 1 : 1 ligand to metal ratio, neutral coordination frameworks are obtained, such as $\{Cd[Fe(\eta^5\text{-}C_5H_4COO)_2](DMF)_2(H_2O)\}$.[86]

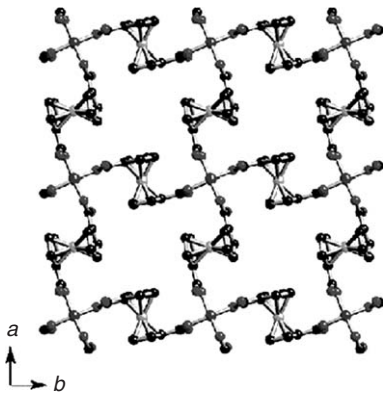

Figure 27 A view of the packing of $\{Cu\,[Co(\eta^5\text{-}C_5H_4COO)_2]_2\}\cdot 2MeOH$. Reprinted in part with permission from Kondo, M.; Hayakawa, Y.; Miyazawa, M.; Oyama, A.; Unoura, K.; Kawaguchi, H.; Naifo, T.; Maeda, K.; Uchida, F. *Inorg. Chem.* **2004**, 43(19), 5801. © 2004 American Chemical Society.

12.11.4 Reactions within and between Crystals and Solid-state Transformations

In recent years, the use of solvent-free reactions, such as those between solids and those between solids and vapors, have begun to be used as alternative ways to prepare organometallic crystals, both of the coordination network and of the molecular crystal type.[87,87a]

It is useful to remind the reader that reactions involving solid reactants or occurring between solids and gases avoid the recovery, storage, and disposal of solvents, hence they are of interest in the field of "green chemistry," where environmentally friendly processes are actively sought.[88] Furthermore, solvent-less reactions often lead to very pure products and reduce the formation of solvate species.[89,89a–89g]

In spite of these investigations, solid-state processes involving organometallic systems have only recently begun in a systematic way.[89,89a–89g]

In this section, we will discuss some relevant examples of reactions occurring within or between organometallic crystals.

The *cis*- and *trans*-complexes (η^5-C_5H_4R)M(CO)$_2$(L)I(M = W, R = Me, Bu^i, L = P[(OPr)-Pr^i]$_3$, PPh_3; M = Mo, R = Me, L = PPh_3) have been synthesized and fully characterized by elemental analysis and IR and NMR spectroscopy. These complexes undergo a thermal solid-state ligand-isomerization reaction, the favored direction of the isomerization reaction being related to the melting points of the *cis*- and *trans*- isomers, that is, to the intermolecular forces acting in the solid state. Crystal structure determinations of the *cis*- and *trans*-isomers of (η^5-C_5H_4Me)W(CO)$_2$(PPh_3)I reveal that a limited amount of isomer conversion can be accommodated in the unit cell of the *trans*-isomer, prior to crystal fragmentation. The rearrangement of the molecules within the unit cell, during isomerization, also leads to disorder in the crystal.[90]

The reaction between Mn(CO)$_4$(PPh_3)Br and solid phosphines at temperatures lower than the reactant melting points is shown to occur in the melt.[91] Analogously, it has been ascertained that the reaction between solid (η^5-C_5H_5)M(CO)$_3$$CH_3$ and solid phosphines occurs in the melt. The isomerization of *ttt*-$RuCl_2(RNC)_2(PPh_3)_2$ (R = 2,6-xylyl, Bu^t, Pr^i, benzyl, 2-OMe–4-Cl–phenyl) to *cct*-$RuCl_2(RNC)_2(PPh_3)_2$ has been carried out in the solid state. The reaction is of the first order, and kinetic measurements have yielded activation energies of 210 kJ mol^{-1} (R = Bu^t) and 221 kJ mol^{-1} (R = benzyl) for reactions performed between 160 and 180 °C. XRD analysis of the solid-state reaction of *ttt*-$RuCl_2$((BuNC)–Bu-*t*)$_2$(PPh_3)$_2$ has revealed that the *cct*-isomer produced is a polymorph of that produced by recrystallization of the pure *cct*-$RuCl_2$((BuNC)–Bu-*t*)$_2$(PPh_3)$_2$ isomer.[92,92a]

Migratory insertion reactions of organometallic complexes have been shown to occur in the absence of solvent and, more significantly, between solid reagents.[93] Reactions between (η^5-C_5H_5)M(CO)$_3$Me (M = Mo, W) or (η^5-C_5H_5)Fe(CO)$_2$Me and PPh_3, in the absence of solvent, took place at temperatures between 40 and 90 °C, and yielded the products (η^5-C_5H_5)M(CO)$_2$$PPh_3$COMe (M = Mo, W) and ($\eta^5$-$C_5H_5$)Fe(CO)($PPh_3$)COMe in moderate to good yield (60–99%). The Mo and W complexes reacted in the solid state at $T < 80$ °C. The decarbonylation of (η^5-C_5H_5)Mo(CO)$_2$$PPh_3$COMe to yield ($\eta^5$-$C_5H_5$)Mo(CO)$_2$$PPh_3$Me also occurred in the solid state at $T = 120$ °C. Reaction of (η^5-C_5H_5)Mo(CO)$_3$Me with a range of ligands L [L = PPh_3, P(*p*-$MeOC_6H_4$)$_3$, PCy_3, PEt_3, $AsPh_3$, $POPh_3$, P(OEt)$_3$; 1 : 1 reagent ratio; 90 °C; 15 min] in the absence of solvent gave (η^5-C_5H_5)Mo(CO)$_2$LCOMe (7–100% yield) and, on extended reaction, (η^5-C_5H_5)Mo(CO)$_2$LMe in varying yields. This study reveals that migratory insertion of organometallic compounds can occur, without the intervention of a solvent, between a solid organometallic complex and a ligand that exists in the "solid, liquid, or gas phase." The reactions between (η^5-C_5H_5)Mo(CO)$_3$Me or (η^5-C_5H_5)Fe(CO)$_2$Me and CO most certainly also occur in the solid phase.

The *cis*- and *trans*-{(η^5-C_5H_4Me)Mo(CO)$_2$(P[(OPr)-Pr^i]$_3$)}I complexes undergo a bidirectional thermal ligand-isomerization reaction to yield an equilibrium mixture of isomers in the solid state,[94] while the reaction between RhX(PPh_3)$_3$ (X = Cl, Br, I) and (η^5-C_5H_4Me)W(CO)$_3$Y (Y = Cl, Br, I) occurs both in solution and in the solid state, and leads to exchange of both CO/PPh_3 and X/Y between the two reactants.[95] The complex [Re(η^5-C_5H_4Me)(CO)P(OPh_3)Br_2)] also isomerizes in the solid state, while [Re(η^5-C_5H_4Bu)(CO)$_2$$Br_2$)] does not isomerize, although it has been shown to isomerize in the melt.[96] It is worth stressing that single crystal X-ray structures have been determined at intermediate stages in the single crystal to single crystal *trans*-to-*cis* thermal isomerization of [(η^5-C_5H_4Me)Re(CO)P(OPh)$_3$]Br_2 at 150 °C.[97]

12.11.4.1 Reactions Between Solids for the Preparation of Supramolecular Adducts

Direct reaction between solid reactants is an alternative way to prepare novel molecular crystals. This approach, successfully used in many organic solid-state applications, has also been used in the organometallic field.

The first class of organometallic compounds obtained in this way is that prepared by manual grinding of the ferrocenyl dicarboxylic acid complex $[Fe(\eta^5\text{-}C_5H_4COOH)_2]$ with solid nitrogen-containing bases, namely, 1,4-diazabicyclo[2.2.2]-octane, 1,4-phenylenediamine, piperazine, *trans*-1,4-cyclohexanediamine, and guanidinium carbonate, which generates quantitatively the corresponding organic–organometallic adducts (see Figure 28(a)).[98,98a] The case of the adduct $[HC_6N_2H_{12}][Fe(\eta^5\text{-}C_5H_4COOH)(\eta^5\text{-}C_5H_4COO)]$ (see Figure 28(b)) is particularly noteworthy, because the same product can be obtained in three different ways: (i) by reaction of solid $[Fe(\eta^5\text{-}C_5H_4COOH)_2]$ with vapors of 1,4-diazabicyclo[2.2.2]-octane (which possesses a small but significant vapor pressure); (ii) by reaction of solid $[Fe(\eta^5\text{-}C_5H_4COOH)_2]$ with solid 1,4-diazabicyclo[2.2.2]-octane, that is, by co-grinding of the two crystalline powders; and (iii) by reaction in MeOH solution of the two reactants. It is also interesting to note that the base can be removed by mild treatment, regenerating the structure of the starting dicarboxylic acid.

Bis-substituted pyridine/pyrimidine ferrocenyl complexes have also been obtained by mechanically induced Suzuki-coupling reaction[99] in the solid state, starting from the complex ferrocene–1,1′-diboronic acid, $[Fe(\eta^5\text{-}C_5H_4\text{–}B(OH)_2)_2]$.[100] The ligand $[Fe(\eta^5\text{-}C_5H_4\text{–}1\text{-}C_5H_4N)_2]$, obtained by both solution and solid-state methods, was then used to prepare a whole family of heterobimetallic metallamacrocycles by reaction with $AgNO_3$, $Cd(NO_3)_2$, $Cu(CH_3COO)_2$, $Zn(CH_3COO)_2$, and $ZnCl_2$; the complexes $[Fe(\eta^5\text{-}C_5H_4\text{–}1\text{-}C_5H_4N)_2]_2Ag_2(NO_3)_2\cdot 1.5H_2O$, $[Fe(\eta^5\text{-}C_5H_4\text{–}1\text{-}C_5H_4N)_2]_2Cu_2(CH_3COO)_4\cdot 3H_2O$, $[Fe(\eta^5\text{-}C_5H_4\text{–}1\text{-}C_5H_4N)_2]_2Cd_2(NO_3)_4\cdot CH_3OH\cdot 0.5C_6H_6$, $[Fe(\eta^5\text{-}C_5H_4\text{–}1\text{-}C_5H_4N)_2]_2Zn_2(CH_3COO)_4$, and $[Fe(\eta^5\text{-}C_5H_4\text{–}1\text{-}C_5H_4N)_2]_2Zn_2Cl_4$ were obtained (examples are shown in Figure 29).[101] Reaction of mechanochemically prepared $[Fe(\eta^5\text{-}C_5H_4\text{–}1\text{-}C_5H_4N)_2]$ with the ferrocenyl dicarboxylic acid complex $[Fe(\eta^5\text{-}C_5H_4COOH)_2]$ has led to formation of the supramolecular adduct $[Fe(\eta^5\text{-}C_5H_4\text{–}1\text{-}C_5H_4N)_2][Fe(\eta^5\text{-}C_5H_4COOH)_2]$.

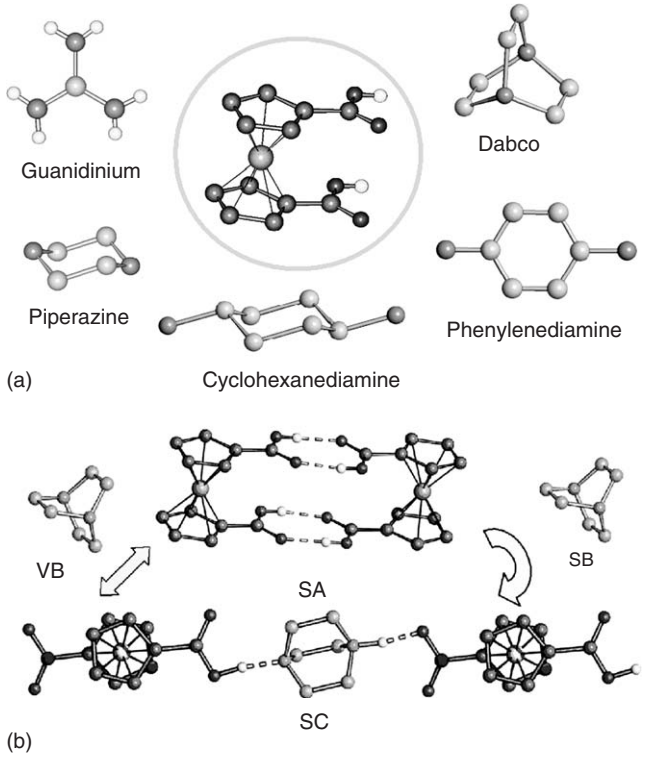

Figure 28 (a) Grinding of the organometallic complex $[Fe(\eta^5\text{-}C_5H_4COOH)_2]$ (top center) as a solid polycrystalline material with the solid bases 1,4-diazabicyclo[2.2.2]-octane, $C_6H_{12}N_2$ (top right), guanidinium cation, $[(NH_2)_3C]^+$ (top left), 1,4-phenylenediamine, $p\text{-}(NH_2)_2C_6H_4$, (bottom right), piperazine, $HN(C_2H_4)_2NH$ (bottom left), *trans*-1,4-cyclohexanediamine, $p\text{-}(NH_2)_2C_6H_{10}$ (bottom center) generates quantitatively the corresponding adducts $[HC_6H_{12}N_2][Fe(\eta^5\text{-}C_5H_4COOH)(\eta^5\text{-}C_5H_4COO)]$, $[C(NH_2)_3]_2[Fe(\eta^5\text{-}C_5H_4COO)_2]\cdot 2H_2O$, $[HC_6H_8N_2][Fe(\eta^5\text{-}C_5H_4COOH)(\eta^5\text{-}C_5H_4COO)]$, $[H_2C_4H_{10}N_2][Fe(\eta^5\text{-}C_5H_4COO)_2]$, $[H_2C_6H_{14}N_2][Fe(\eta^5\text{-}C_5H_4COO)_2]\cdot 2H_2O$. (b) The solid–gas and solid–solid reactions involving 1,4-diazabicyclo[2.2.2]-octane with formation of the linear chain.

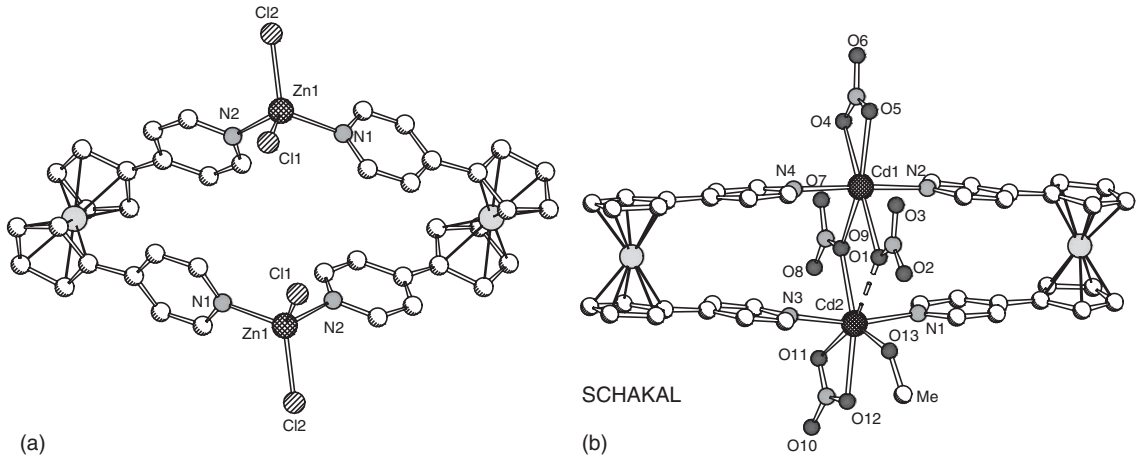

Figure 29 The metallamacrocycles produced by reaction of [Fe(η^5-C_5H_4–1-C_5H_4N)$_2$] and the salts $ZnCl_2$ (a) and $Cd(NO_3)_2$ (b). The starting material has been obtained by a Suzuki coupling reaction in the solid state starting from the complex ferrocene–1,1′-diboronic acid [Fe(η^5-C_5H_4–$B(OH)_2$)$_2$] Reprinted in part with permission from Braga, D.; D'Addario, D.; Grepioni, F.; Polito, M.; Proserpio, D.M.; Steed, J. W.; Tagliavini, E. Organometallics **2003**, *22*, 4532. © 2003 American Chemical Society.

There are not yet many examples of the utilization of mechanochemical procedures in coordination chemistry. Balema *et al.* have shown, for instance, that the *cis*-platinum complexes *cis*-$(Ph_3P)_2PtCl_2$ and *cis*-$(Ph_3P)_2PtCO_3$ can be prepared mechanochemically from solid reactants in the absence of solvent.[102] Orita *et al.*, on the other hand, have reported that the reaction of (ethylendiamine)$Pt(NO_3)_2$ with 4,4′-bipyridine, which takes as long as 4 weeks at 100 °C to form metallamacrocycle molecular squares, is brought to completion within 10 min at room temperature by mixing reactants without solvents.[103] Similar reaction acceleration has been observed also with triazine-based ligands.

Other results have been obtained by using the zwitterion sandwich complex [Co^{III}(η^5-C_5H_4COOH)(η^5-C_5H_4COO)].[62] Thanks to its amphoteric behavior, the complex undergoes reversible gas–solid reactions with the hydrated vapors of a variety of acids (e.g., HCl,[104] CF_3COOH, CCl_3COOH, CHF_2COOH, HBF_4, HCOOH)[105,105a,105b] and bases (e.g., NH_3,[104] NMe_3, NH_2Me),[106] as well as solid–solid reactions with crystalline alkali and ammonium salts of formula MX ($M = K^+$, Rb^+, Cs^+, NH_4^+; $X = Cl^-$, Br^-, I^-, PF_6^-, though not in all permutations of cations and anions).[107] These products could also be obtained by solution methods, as discussed before. Similar behavior is shown toward other volatile acids. Exposure of the zwitterion to vapors of CF_3COOH and HBF_4, for instance, quantitatively produces the corresponding salts of the cation [Co(η^5-C_5H_4COOH)$_2$]$^+$, namely, [Co(η^5-C_5H_4COOH)$_2$][CF_3COO] and [Co(η^5-C_5H_4COOH)$_2$][BF_4] (see Figure 30(a)). Exposure of the solid zwitterion to vapors of CHF_2COOH quantitatively produces the corresponding salts of the cation [Co(η^5-C_5H_4COOH)$_2$][CHF_2COO].

The zwitterion also reversibly absorbs formic acid from humid vapors forming selectively a 1 : 1 co-crystal, [Co(η^5-C_5H_4COOH)(η^5-C_5H_4COO)][HCOOH] (see Figure 30(b)), from which the starting material can be fully recovered by mild thermal treatment. Contrary to the other compounds of this class, no proton transfer from the adsorbed acid to the organometallic moiety is observed (see Figure 30(b)). Hence, the reaction between [Co(η^5-C_5H_4COOH)(η^5-C_5H_4COO)] (solid) and HCOOH(vapor) would be more appropriately described as a special kind of solvation rather than as a heterogeneous acid–base reaction, as also confirmed by ^{13}C CPMAS NMR spectroscopy.

The behavior of the zwitterion toward NH_3 and other bases is similar to that toward HCl but obviously opposite in terms of proton exchange. In the case of ammonia, the neutral system transforms into the hydrated ammonium salt [Co(η^5-C_5H_4COO)$_2$][NH_4]·3H_2O.

As mentioned above, [Co(η^5-C_5H_4COOH)(η^5-C_5H_4COO)] could also be employed in solid–solid reactions with a number of alkali salts MX ($M = K^+$, Rb^+, Cs^+, NH_4^+; $X = Cl^-$, Br^-, I^-, PF_6^-, though not in all permutations of cations and anions; see below), obtaining compounds of general formula [Co(η^5-C_5H_4COOH)(η^5-C_5H_4COO)]$_2$·M^+X^-. In some cases ($M = Rb^+$, Cs^+, $X = Cl^-$, Br^-, I^-), it was necessary to recur to "kneading" by adding a few drops of water to the solid mixture in order to obtain the desired product.[108]

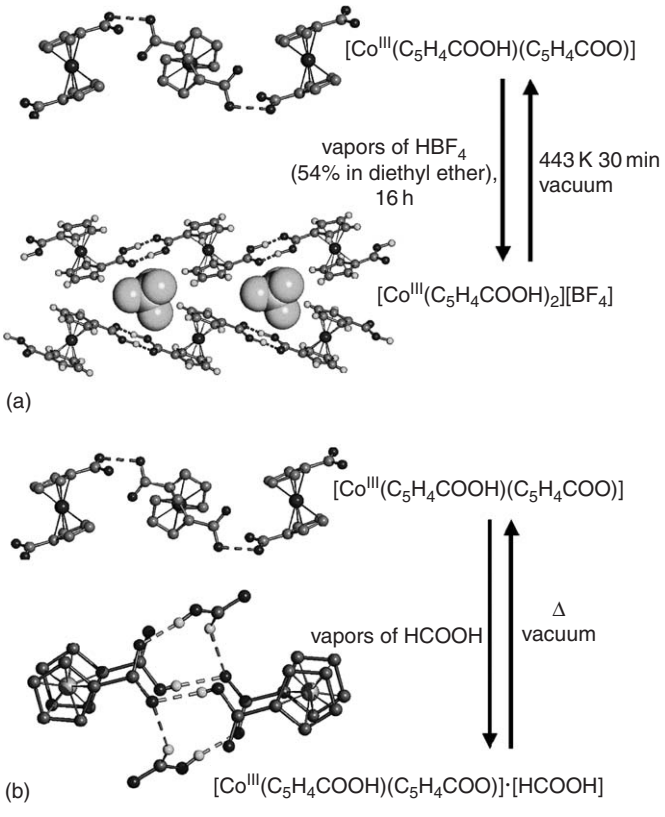

Figure 30 (a) Exposure of the solid zwitterion $[Co^{III}(\eta^5\text{-}C_5H_4COOH)(\eta^5\text{-}C_5H_4COO)]$ to vapors of HBF_4 quantitatively produces the corresponding salt $[Co(\eta^5\text{-}C_5H_4COOH)_2][BF_4]$, while (b) exposure to vapors of HCOOH yields the co-crystalline material $[Co(\eta^5\text{-}C_5H_4COOH)(\eta^5\text{-}C_5H_4COO)][HCOOH]$. Both products revert back to the solid zwitterion after mild thermal treatment. (from Ref. 105).

12.11.5 Organometallic Crystal Polymorphism, Crystal Isomerization, and Phase Transitions

Different crystalline forms containing the same molecules or ions are called polymorphs.[109,109a] Polymorphism is of major industrial importance today.[110,110a,110b] With the exception of review articles published by some of us in 1999,[111,111a] the subject of organometallic polymorphism has never been reviewed. The investigation of crystal polymorphism requires a crystal-engineering approach: the formation of different crystal forms implies that different sets of supramolecular interactions are established between the same building blocks. Under this viewpoint, therefore, polymorphs are "crystal isomers."

It should also be pointed out that structural flexibility, a key characteristic of organometallic molecules,[112] plays a particularly important role in organometallic polymorphism because structurally non-rigid organometallic molecules are likely candidates for the formation of conformational polymorphs. A classical example of "organometallic conformational polymorphism" is provided by ferrocene, for which one room-temperature-disordered and two low-temperature-ordered crystalline forms are known.[113,113a–113e] On approaching crystal polymorphism, one has to distinguish between those polymorphs that interconvert as a function of temperature via a phase transition (enantiotropic systems) and those that do not (monotropic systems). Besides, one has to take into account the existence of solvate forms, which contain the same molecule or ions but co-crystallized with a solvent molecule (these systems are often called, erroneously, "pseudo-polymorphs"[109,109a]).

Let us first focus on some example of interconverting organometallic crystals. Many crystals of globular organometallic molecules have been shown to undergo phase transitions, and for some, the formation of plastic phases characterized by short-range orientational disorder and long-range order is known. Substituted ferrocene derivatives $[Fe(\eta^5\text{-}C_5H_5)(\eta^5\text{-}C_5H_4CHO)]$[114] and $[Fe(\eta^5\text{-}C_5H_5)(\eta^5\text{-}C_5H_4CMeO)]$[114a] as well as salts of the type $[Fe(\eta^5\text{-}C_6H_5F)(\eta^5\text{-}C_5H_5)][A]$ [A = AsF_6, PF_6, SbF_6, and BF_4][114b,114c] are all known to undergo order–disorder phase

transitions. More recently, the phase transitional behaviors of the crystalline salts $[M(\eta^5\text{-}C_5H_5)_2][PF_6]$ (M = Co, Fe) have been reinvestigated.[115,115a] The room temperature-ordered monoclinic crystal (form-I) transforms, below 252 K, into another ordered monoclinic crystal (form-II) with different relative orientation of the two independent $[Co(\eta^5\text{-}C_5H_5)_2]^+$ cations, and into a "semi-plastic" system (form-III) containing ordered PF_6^- anions and orientationally disordered $[Co(\eta^5\text{-}C_5H_5)_2]^+$ cations above 314 K. From DSC thermograms, the enthalpy differences associated with the two transitions have been estimated to be 1.30 and 3.05 kJ mol^{-1}, respectively. Although isomorphous at room temperature with crystalline $[Co(\eta^5\text{-}C_5H_5)_2][PF_6]$, the ferricinium salt $[Fe(\eta^5\text{-}C_5H_5)_2][PF_6]$[116,116a,116b] shows a different phase transitional behavior with the two phase transitions taking place at 213 and 347 K, that is, 39 and 33 K below and above those of crystalline $[Co(\eta^5\text{-}C_5H_5)_2][PF_6]$.

The close structural similarity between the two complexes $[M(\eta^5\text{-}C_5H_5)_2]^+$ (M = Co, Fe) generated the idea of growing crystals from solutions containing mixtures of the two cations. It has been discovered that, in the solid state, the two cations are fully miscible in the whole range of composition, and that the composition is the same as that of the "water solutions" from which the mixed crystals are precipitated, for example, the mixed salts can be formulated as $[(\eta^5\text{-}C_5H_5)_2Co_xFe_{1-x}][PF_6]$ (with $0 < x < 1$).[117] Moreover, "the phase transition behavior depends linearly on the composition," following Vegard's rule.[118] The temperature variation of the two solid–solid transitions with composition is shown in Figure 31. This is a clear demonstration that the phase transition behavior of the crystalline material $[Co_xFe_{1-x}(\eta^5\text{-}C_5H_5)_2][PF_6]$ can be "tuned" to the varying $[Co(\eta^5\text{-}C_5H_5)_2]^+/[Fe(\eta^5\text{-}C_5H_5)_2]^+$ molar ratio, because the $[Co(\eta^5\text{-}C_5H_5)_2]^+$ and $[Fe(\eta^5\text{-}C_5H_5)_2]^+$ cations form fully miscible solid solutions. The linear response of physical properties with composition is typical of inorganic alloys. Thus, the mixed crystal $[Co_xFe_{1-x}(\eta^5\text{-}C_5H_5)_2][PF_6]$, though composed of molecular ions and soluble in water, possesses the features of a random A_xB_{1-x} alloy.

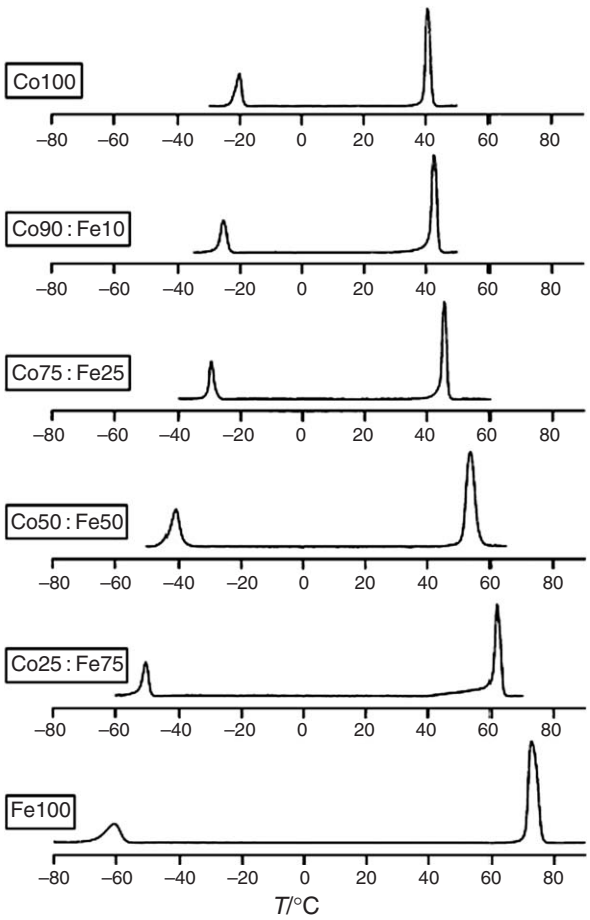

Figure 31 DSC thermograms (heating cycle) showing how the RT ⇔ LT and RT ⇔ HT transitions "diverge" from the values observed in the case of $[Co(\eta^5\text{-}C_5H_5)_2]^+$ as the percentage of $[Fe(\eta^5\text{-}C_5H_5)_2]^+$ in the mixture is increased. Reprinted with permission from Braga, D.; Cojazzi, G.; Emiliani, D.; Maini, L.; Grepioni, F. *Chem. Commun*. **2001**, *21*, 2272. © 2001 The Royal Society of Chemistry.

Structurally similar systems, however, show very different phase transitional behaviors. The compound $[Ru(\eta^5\text{-}C_5H_5)(\eta^6\text{-}C_6H_6)][PF_6]$[119] does not show a low-temperature phase transition on decreasing the temperature down to 223 K on the DSC and down to 100 K on the diffractometer, but undergoes an order–disorder phase transition on increasing the temperature to 332.5 K. The bis-benzene chromium analog, $[Cr(\eta^6\text{-}C_6H_6)_2][PF_6]$, on the other hand, even though it crystallizes in a manner that is strictly related to that of the low-temperature phases of Co and Fe, does not appear to undergo phase changes either on cooling or on heating. Table 5 collects information on the phase transitional behavior of several metallocene or metallobenzene hexafluorophosphate salts.

Hexafluoroarseniate salts show phase transition behavior. $[Fe(\eta^6\text{-}C_6H_6)(\eta^5\text{-}C_5H_5)][AsF_6]$, for instance, undergoes phase transition between three different crystal forms.[120,120a,120b]. Variable-temperature solid-state NMR measurements have shown that rotation of the entire cation takes place in a cubic phase above 310 K, while in the intermediate β-phase, the rotational motion is restricted to a 90° in-plane reorientation. Below 270 K, the crystal is in a low-symmetry phase, in which whole-body rotation does not take place though the rings execute jumping motion that persists down to 200 K. Transition from a rotational jumping state to a whole-body reorientation has also been detected from the Mössbauer spectra of the $[PF_6]^-$ salt of the same complex.[120,120a,120b]

Preformed crystals of structurally similar species (also called "heteromolecular seeding") have been used to separate the two concomitant polymorphs.[121] Precipitation of $[Fe(\eta^5\text{-}C_5H_5)_2]^+$ as its $[AsF_6]^-$ salt generates two types of crystals: a trigonal phase (Fe–T) and a monoclinic phase (Fe–M), which proved difficult to separate out. From another experiment, it was known that crystallization of the congener $[Co(\eta^5\text{-}C_5H_5)_2]^+[AsF_6]^-$ only leads to a trigonal form (Co–T), isomorphous with Fe–T. In addition, the monoclinic phase Fe–M is isomorphous with the room temperature, monoclinic phase of the pair $[Fe(\eta^5\text{-}C_5H_5)_2][PF_6]$ and $[Co(\eta^5\text{-}C_5H_5)_2][PF_6]$. The relationship between crystalline Fe–T and Fe–M is shown in Figure 32. It is worth noting that besides the differences in packing arrangements of the forms, the cyclopentadienyl ligands are eclipsed in Fe–T, while they are all staggered in Fe–M. In order to drive the crystallization process toward the formation of the separate polymorphs, "heteromolecular seeding" was used.

Crystals of trigonal $[Co(\eta^5\text{-}C_5H_5)_2][AsF_6]$ were used to grow the trigonal form of $[Fe(\eta^5\text{-}C_5H_5)_2][AsF_6]$, while crystals of monoclinic $[Fe(\eta^5\text{-}C_5H_5)_2][PF_6]$ were used to obtain the monoclinic form of $[Fe(\eta^5\text{-}C_5H_5)_2][AsF_6]$.

The preparation of the salt $[Ru(\eta^6\text{-}C_6H_6)_2][BF_4]_2$ from the solvate form $[Ru(\eta^6\text{-}C_6H_6)_2][BF_4]_2{\cdot}MeNO_2$ is instead an example of how desolvation can be exploited to prepare an elusive unsolvate crystal.[122]

As mentioned above, $[Fe(\eta^5\text{-}C_5H_4\text{-}4\text{-}C_5H_4N)(\eta^5\text{-}C_5H_4\text{-}B(OH)_2)]$ has been isolated in three forms, the two anhydrous forms **I** and **II** and the monohydrate form **III**; the three forms are compared in Figure 33.[100] In crystalline **II**, the molecules form dimers via (B)OH···N bonds, which are then linked in a secondary pattern by the (B)OH···O(B) lateral bonds. This arrangement leads to eclipsing of the $B(OH)_2$ group over the C_5H_4N group. In **II**, on the other hand, the primary motif appears to be the boronic acid ring based on (B)OH···O(B) bonds, while dimers are formed by the lateral O–H groups with the pyridyl acceptors. The conformation of the two ligands is *cisoid*. In crystalline **III**, a third, almost intermediate, topology is observed.

Another case of non-interconverting polymorph is provided by crystalline $[Fe(\eta^5\text{-}C_5H_4COOH)_2]$, which is known in three polymorphic forms, a monoclinic (form **I**) and a triclinic (form **II**) crystal form determined decades ago.[43,43a] A third polymorphic form **III** has been obtained recently.[123] All three crystal forms are based on dimers $\{[Fe(\eta^5\text{-}C_5H_4COOH)_2]\}_2$ of doubly hydrogen-bonded carboxylic rings. The simplest way to compare the three crystal

Table 5 Phase-transition behavior and thermodynamic data for the family of complexes $[M(\eta^5\text{-}C_5H_5)][PF_6]$ (M = Co, Fe), $[Cr(\eta^6\text{-}C_6H_6)_2][PF_6]$, and $[Ru(\eta^5\text{-}C_5H_5)(\eta^6\text{-}C_6H_6)][PF_6]$

Species	*Phase transition (T/K)*	ΔH kJ mol^{-1}
$[Fe(\eta^5\text{-}C_5H_5)_2][PF_6]$	LT → RT (213.1)[a]	1.95
	RT → HT (347.1)[a]	4.50
$[Co(\eta^5\text{-}C_5H_5)_2][PF_6]$	LT → RT (251.8)[a]	1.27
	RT → HT (313.9)[a]	3.06
$[Ru(\eta^5\text{-}C_5H_5)(\eta^6\text{-}C_6H_6)][PF_6]$	No RT → LT transition[b]	
	RT → HT (332.5)[a]	4.16
$[Cr(\eta^6\text{-}C_6H_6)_2][PF_6]$	No RT → LT transition[b]	

[a]DSC, heating cycle.
[b]DSC, cooling cycle down to 223 K.

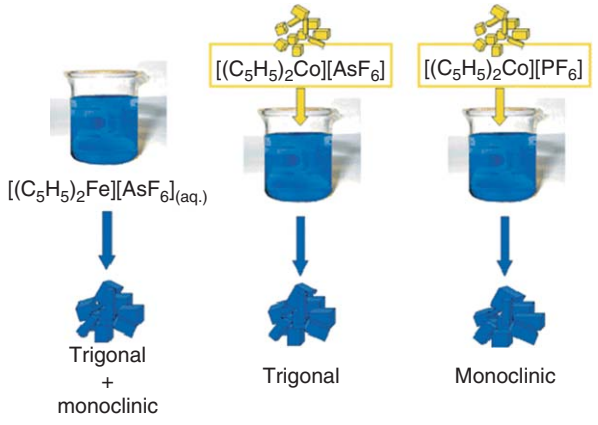

Figure 32 Precipitation of $[Fe(\eta^5\text{-}C_5H_5)_2]^+$ as its $[AsF_6]^-$ salt generates two concomitant crystals: a trigonal phase (Fe–T) and a monoclinic phase (Fe-M), which can be separated out by "heteromolecular seeding" with isomorphous crystals of trigonal $[Co(\eta^5\text{-}C_5H_5)_2][AsF_6]$ and of monoclinic $[Fe(\eta^5C_5H_5)_2][PF_6]$. The crystals are sufficiently robust to undergo a full cycle of four phase transitions directly on the diffractometer, Fe-T → Fe-M → Fe-C → Fe-M → Fe-T.

structures is by looking at molecular layers formed by these supramolecular dimers. A space-filling representation of a section of the three forms is shown in Figure 34.

Several other examples of organometallic salts that can be obtained in different forms are available. A thorough review of these cases is however beyond the scope of this section. It is worth mentioning that non-interconverting forms are known for the crystalline $[Ru(\eta^6\text{-}C_6H_6)(\eta^6\text{-}C_6H_4(1\text{-}CH_3)(2\text{-}COOCH_3)][BF_4]_2$,[124] $[(\eta^2\text{-fumaric acid})Fe(CO)_4]$,[125,125a] and $HMn(CO)_5$, one of the first carbonyl hydrides to be structurally characterized by X-ray and neutron diffraction.[126] The relationship between crystal and molecular structure of structural isomers of the coordination compound $HCo(CO)_2(PPh_3)_2$ has been discussed by Brammer.[127]

A number of solvate crystals of the same Ni and Co complexes has been prepared by Soldatov and Ripmeester by using vinylpyridine ligands. These complexes are capable of extensive inclusion properties. Out of 40 organic molecules tested as guests, 19 were shown to be encapsulated in the host, thus forming a plethora of pseudo-polymorphic modifications.[128]

Finally, it is worth mentioning that the metastable room-temperature phase of crystalline bis-formylferrocene $[Fe(\eta^5\text{-}C_5H_4CHO)_2]$ on heating undergoes a first transition at ca. 311 K. On cooling, however, the reverse process leads to a new phase.[129] Subsequent cycles of heating and cooling show that the new phase reversibly "switches" between the room-temperature and high-temperature phases, without reverting to the initial phase. This behavior suggests that the first room-temperature phase is a kinetic product of the crystallization process: on heating, the sample undergoes an order → disorder phase transition to the plastic phase, which transforms on cooling to a thermodynamically more stable form. Once this latter phase is formed, the initial phase can no longer be obtained, unless the compound is redissolved and recrystallized. The ΔH of transition ($14.0\,kJ\,mol^{-1}$) is comparable with the value ($12.1\,kJ\,mol^{-1}$) found for the mono-formyl derivative $[Fe(\eta^5\text{-}C_5H_5)(\eta^5\text{-}C_5H_4CHO)]$, which shows a mesophase between 316 K and the melting point (396 K).[130] On further heating, crystalline $[Fe(\eta^5\text{-}C_5H_4CHO)_2]$ undergoes a polymerization reaction in the solid state.

12.11.6 Conclusions

If compared with the organometallic chemistry *mare magnum* in the year 2005, this chapter admittedly deals with a somewhat limited subtopic. However, this is also an area of boiling activity. With a certain time lag with respect to its parents, organic and inorganic solid-state chemistries, organometallic solid-state chemistry is emerging as a field of extraordinary promises. Papers and results reported in this chapter are only but a small selection, arbitrary and personal, of the plethora of papers that may fall under the broad keywords "supramolecular organometallic solid-state chemistry" or "organometallic crystal engineering." Undoubtedly, organometallic chemistry has benefited from the birth of the powers of crystallography. One can hardly deny that without this powerful tool we would know very little about the structure of complex systems. This is even truer for crystal engineering, a field where traditional analytical

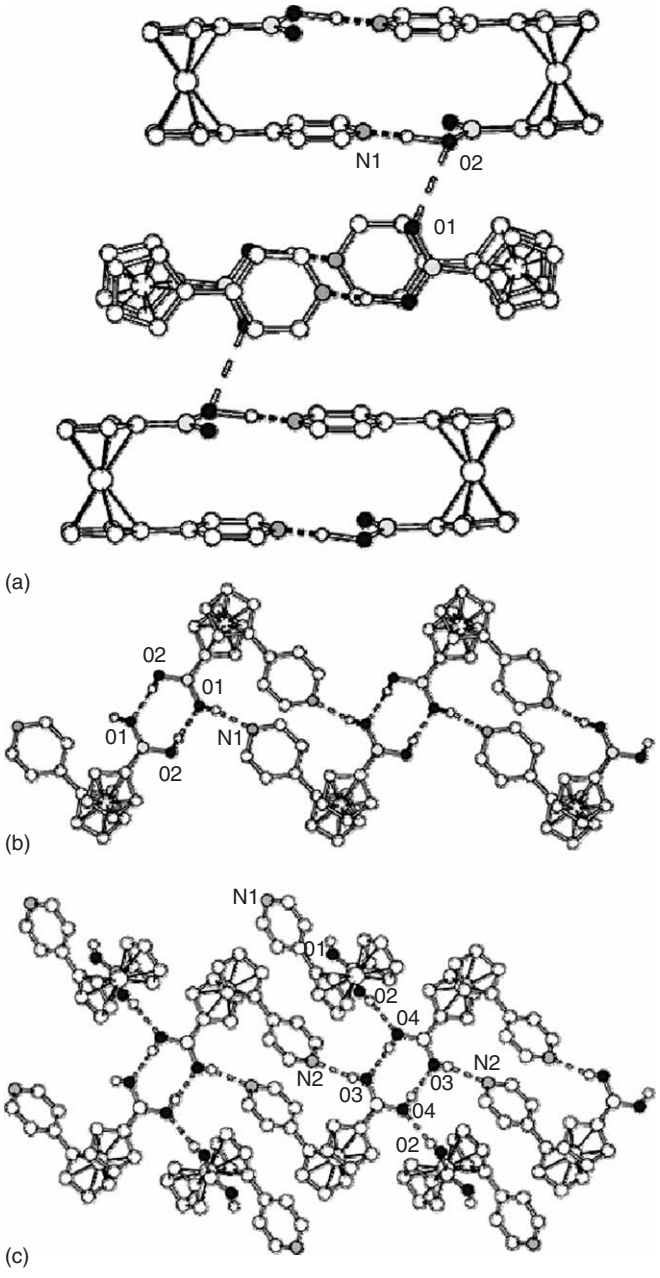

Figure 33 (a) Hydrogen-bonded dimers formed by (B)OH···N interactions in crystalline **I**. Note how the dimers are connected via (B)OH···O(B) interactions. The H atom bound to O(1) was not observed (see the Experimental Section). (b) Hydrogen-bonding pattern in crystalline **I**. Note how the ligand conformation has changed from eclipsed in **I** to *cisoid* in **II**. (c) Hydrogen-bonding pattern in crystalline **III**. Reprinted with permission from Bracaccini, M.; Braga, D.; D' Addario, D.; Gsepioni, F.; Polifo, M.; Sturba, L.; Tagliavini, E. *Organometallics* **2003**, *22*, 2142. © 2003 American Chemical Society.

tools are of limited assistance. In most cases, it is only when the product crystal structure is known that the chemist can rationalize the building up process, the sequence that brings from the selected building blocks, whether molecules or ions, to the supramolecular aggregation. Without this knowledge, the "engineering" stage, that is, the stage when properties are designed, obtained, and exploited, is rarely reached. In order to conclude the mainstream discussion of organometallic crystal architectures obtained from organometallic building blocks, we have chosen two somewhat special topics: making crystals by reacting and transforming crystals, and organometallic crystal

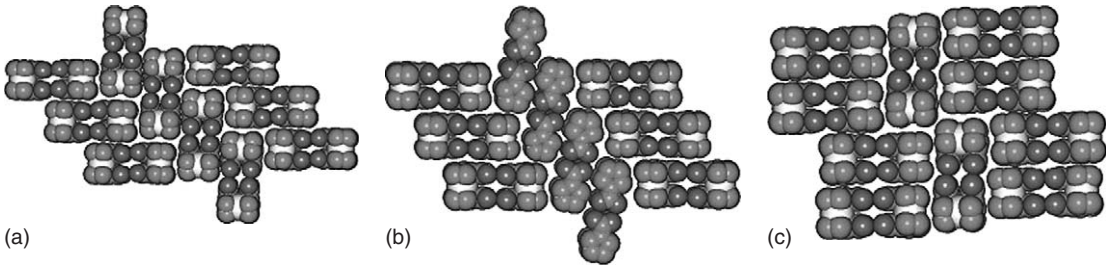

Figure 34 An in-plane, space-filling projection of the packings in (a) for I (monoclinic), (b) form II (triclinic), and (c) form III of crystalline $\{[Fe(\eta^5\text{-}C_5H_4COOH)_2]\}_2$. Reprinted with permission from Braga, D.; Polito, M.; Addorio, D.; Grepioni, F. *Crystal Growth & Design*, **2004**, *4*, 1109. © 2004 American Chemical Society.

polymorphism. We believe, in fact, that these two areas represent the new forefronts of the field, because making molecular crystals via a judicious use of supramolecular interactions (mainly hydrogen bonds) and making organometallic coordination networks by using organometallic "spacers" and "knots" are now following established routes.

Acknowledgments

We acknowledge financial support by MIUR (FIRB and PRIN) and by the University of Bologna.

References

1. Desiraju, G. R. *Crystal Engineering: The Design of Organic Solids*; Elsevier: Amsterdam, 1989.
2. Desiraju, G. R. *Angew. Chem., Int. Ed.* **1995**, *34*, 2311.
2a. Braga, D.; Grepioni, F. *Acc. Chem. Res.* **2000**, *33*, 601.
3. Braga, D., Grepioni, F., Orpen, A. G., Eds. *Crystal Engineering: from Molecules and Crystals to Materials*, Kluwer: Dordrecht, 1999.
4. Braga, D.; Grepioni, F.; Desiraju, G. R. *Chem. Rev.* **1998**, *98*, 1375.
5. Proceedings of the Dalton Discussion on Inorganic Crystal Engineering, the whole issue, *J. Chem. Soc., Dalton Trans.* **2000**, 3705.
5a. Braga, D.; Desiraju, G. R.; Miller, J.; Orpen, A. G.; Price, S. *CrystEngComm* **2002**, *4*, 500.
5b. Hollingsworth, M. D. *Science* **2002**, *295*, 2410.
6. Lehn, J. M. *Supramolecular Chemistry: Concepts and Perspectives*; VCH: Weinheim, 1995.
7. Blake, A. J.; Champness, N. R.; Hubberstey, P.; Li, W. S.; Withersby, M. A.; Schroder, M. *Coord. Chem. Rev.* **1999**, *183*, 117.
7a. Moulton, B.; Zaworotko, M. J. *Chem. Rev.* **2001**, *101*, 1629.
7b. Batten, S. R.; Hoskins, B. F.; Robson, R. *Chem. Eur. J.* **2000**, *6*, 156.
7c. Bourne, S. A.; Lu, J.; Moulton, B.; Zaworotko, M. J. *Chem. Commun.* **2001**, 861.
7d. Rather, B.; Zaworotko, M. J. *Chem. Commun.* **2003**, 830.
7e. Moulton, B.; Abourahma, H.; Bradner, M. W.; Lu, J.; McManus, G. J.; Zaworotko, M. J. *Chem. Commun.* **2003**, 1342.
7f. Fujita, M. *Chem. Soc. Rev.* **1998**, *27*, 417.
7g. Olenyuk, B.; Fechtenkötter, A.; Stang, P. J. *J. Chem. Soc., Dalton Trans.* **1998**, 1707.
7h. Pan, L.; Sander, M. B.; Huang, X.; Li, J.; Smith, M.; Bittner, E.; Bockrath, B.; Johnson, J. K. *J. Am. Chem. Soc.* **2004**, *126*, 1309.
7i. Férey, G.; Latroche, M.; Serre, C.; Millange, F.; Loiseau, T.; Percheron-Guégan, A. *Chem. Commun.* **2003**, 2976.
7j. Cotton, F. A.; Lin, C.; Murillo, C. A. *J. Chem. Soc., Dalton Trans.* **2001**, 499.
7k. Cotton, F. A.; Lin, C.; Murillo, C. A. *Chem. Commun.* **2001**, 11.
7l. Mori, W.; Takamizawa, S. *J. Solid State Chem.* **2000**, *152*, 120.
7m. Carlucci, L.; Ciani, G.; Proserpio, D. M.; Rizzato, S. *CrystEngComm* **2002**, *4*, 121.
8. See, for example Bruce, D. W.; O'Hare, D. *Inorganic Materials*; Wiley: Chichester, UK, 1992.
8a. Long, N. J. *Angew. Chem., Int. Ed. Engl.* **1995**, *34*, 21.
8b. Marks, T. J.; Ratner, M. A. *Angew. Chem., Int. Ed. Engl.* **1995**, *34*, 155.
8c. Kanis, D. R.; Ratner, M. A.; Marks, T. J. *Chem. Rev.* **1994**, *94*, 195.
8d. Khan, O. *Molecular Magnetism*; VCH: New York, 1993.
8e. Gatteschi, D. *Adv. Mater.* **1994**, *6*, 635.
8f. Ward, M. D. *Science* **2003**, *300*, 1124.
8g. Miller, J. S.; Epstein, A. J. *Chem. Eng. News* **1995**, *73*, 30.
8h. Miller, J. S. *Angew. Chem., Int. Ed.* **2003**, *42*, 27.
8i. Vos, T. E.; Liao, Y.; Shum, W. W.; Her, J. H.; Stephens, P. W.; Reiff, W. M.; Miller, J. S. *J. Amer. Chem. Soc.* **2004**, *126*, 11630.
8j. Vickers, E. B.; Giles, I. D.; Miller, J. S. *Chem. Mater.* **2005**, *17*, 1667.
8k. Toma, L.; Lescouezec, R.; Vaissermann, J.; Delgado, F. S.; Ruiz-Perez, C.; Carrasco, R.; Cano, J.; Lloret, F.; Julve, M *Chem. Eur. J.* **2004**, *10*, 6130.
8l. Pardo, E.; Bernot, K.; Juive, M.; Lloret, F.; Cano, J.; Ruiz-Garcia, R.; Pasan, J.; Ruiz-Perez, C.; Ottenwaelder, X.; Journaux, Y. *Chem. Commun.* **2004**, 920.
9. Braga, D. *Chem. Commun.* **2003**, 2751.

10. Rosi, N. L.; Eddaoudi, M.; Kim, J.; O′Keeffe, M.; Yaghi, O. M. *Angew. Chem., Int. Ed.* **2001**, *41*, 284.
10a. Yaghi, O. M.; Li, H. L.; Davis, C.; Richardson, D.; Groy, T. L. *Acc. Chem. Res.* **1998**, *31*, 474.
10b. Li, H.; Eddaoudi, M.; O′Keeffe, M.; Yaghi, O. M. *Nature* **1999**, *402*, 276.
10c. Eddaoudi, M.; Kim, J.; Rosi, N.; Vodak, D.; Wachter, J.; O′Keefe, M.; Yaghi, O. M. *Science* **2002**, *295*, 469.
10d. Rosi, N. L.; Eddaoudi, M.; Kim, J.; O′Keeffe, M.; Yaghi, O. M. *CrystEngComm* **2002**, *4*, 401.
10e. Rosi, N. L.; Eckert, J.; Eddaoudi, M.; Vodak, D. T.; Kim, J.; O'Keeffe, M.; Yaghi, O. M. *Science* **2003**, *300*, 1127.
10f. Braun, M. E.; Steffek, C. D.; Kim, J.; Rasmussen, P. G.; Yaghi, O. M. *Chem. Commun.* **2001**, 2532.
11. Batten, S. R.; Robson, R. *Angew. Chem., Int. Ed.* **1998**, *37*, 1461.
11a. Moulton, B.; Zaworotko, M. J. *Chem. Rev.* **2001**, *101*, 1629.
11b. Carlucci, L.; Ciani, G.; Proserpio, D. M. *CrystEngComm* **2003**, *5*, 269.
11c. Carlucci, L.; Ciani, G.; Proserpio, D. M. *Coord. Chem. Rev.* **2003**, *246*, 247.
11d. Barnett, S. A.; Champness, N. R. *Coord. Chem. Rev.* **2003**, *246*, 145.
12. Takamizawa, S.; Nakata, E.; Saito, T.; Akatsuka, T.; Kojima, K. *CrystEngComm* **2004**, *6*, 197.
12a. Takamizawa, S.; Nakata, E.; Saito, T. *Angew. Chem., Int. Ed.* **2004**, *43*, 1368.
12b. Takamizawa, S.; Nakata, E.; Saito, T. *CrystEngComm* **2004**, *6*, 39.
12c. Takamizawa, S.; Nakata, E.; Yokoyama, H.; Mochizuki, K.; Mori, W. *Angew. Chem., Int. Ed.* **2003**, *42*, 4331.
12d. Le Fur, E.; Demers, E.; Maris, T.; Wuest, J. D. *Chem. Commun.* **2003**, 2966.
12e. Laliberte, D.; Maris, T.; Wuest, J. D. *J. Org. Chem.* **2004**, *69*, 1776.
12f. Saied, O.; Maris, T.; Wuest, J. D. *J. Am. Chem. Soc.* **2003**, *125*, 14956.
12g. Biradha, K. *CrystEngComm.* **2003**, *5*, 374.
13. Hosseini, M. W.; De Cian, A. *Chem. Commun.* **1998**, 727.
13a. Braga, D.; Grepioni, F. *Chem. Commun.* **1996**, 571.
14. Aakeröy, C. B.; Seddon, K. R. *Chem. Soc. Rev.* **1993**, 397.
14a. Beatty, A. M. *CrystEngComm.* **2001**, 51.
14b. Biradha, K. *CrystEngComm.* **2003**, *5*, 374.
14c. Roesky, H. W.; Andruh, M. *Coord. Chem. Rev.* **2003**, *236*, 91.
14d. Beatty, A. M. *Coord. Chem. Rev.* **2003**, *246*, 131.
14e. Bruton, E. A.; Brammer, L.; Pigge, F. C.; Aakeröy, C. B.; Leinen, D. S. *New J. Chem.* **2003**, *27*, 1084.
15. Braga, D.; Grepioni, F.; Biradha, K.; Pedireddi, V. R.; Desiraju, G. R. *J. Amer. Chem. Soc.* **1995**, *117*, 3156.
15a. Zaworotko, M. J. *Chem. Soc. Rev.* **1994**, *23*, 283.
15b. Calhorda, M. J. *Chem. Commun.* **2000**, 801.
15c. Braga, D.; Maini, L.; Polito, M.; Grepioni, F. *Struc. Bond.* **2004**, *111*, 1.
15d. Janiak, C. *Angew. Chem., Int. Ed. Engl.* **1997**, *36*, 1431.
15e. Nangia, A. *CrystEngComm* **2002**, *4*(17), 93.
15f. George, S.; Nangia, A.; Bagieu-Beucher, M.; Masse, R.; Nicoud, J. F. *New J. Chem.* **2003**, *27*, 568.
15g. Nishio, M. *CrystEngComm.* **2004**, *6*, 130.
15h. Hulliger, J. *Chem. Eur. J.* **2002**, *8*, 4579.
15i. Brammer, L.; Burgard, M. D.; Eddleston, M. D.; Rodger, C. S.; Rath, N. P.; Adam, H. *CrystEngComm* **2002**, 239.
15j. Brammer, L. *Dalton Trans.* **2003**, *16*, 3145.
15k. Burrows, A. D. *Struct. Bond.* **2004**, *108*, 55.
16. Cotton, F. A.; Wilkinson, G. *Advanced Inorganic Chemistry*, 5th ed.; Wiley: New York, 1993.
16a. Elschenbroich, C.; Salzer, A. *Organometallics*; VCH: Weinheim, 1989.
17. Philp, D.; Stoddart, J. F. *Angew. Chem., Int. Ed. Engl.* **1996**, *35*, 1154.
17a. Holliday, B. J.; Mirkin, C. A. *Angew. Chem., Int. Ed. Engl.* **2001**, *40*, 2022.
17b. Fujita, M. *Struct. Bond.* **2000**, *96*, 177.
17c. Leininger, S.; Olenyuk, B.; Stang, P. J. *Chem. Rev.* **2000**, *100*, 853.
18. Robson, R. *J. Chem. Soc., Dalton Trans.* **2000**, 3735.
18a. Eddaoudi, M.; Moler, D. B.; Li, H.; Chen, B.; Reineke, T. M.; O'Keeffe, M.; Yaghi, O. M. *Acc. Chem. Res.* **2001**, *34*, 319.
18b. Evans, O. R.; Lin, W. *Acc. Chem. Res.* **2002**, *35*, 511.
18c. Moulton, B.; Zaworotko, M. J. *Chem. Rev.* **2001**, *101*, 1629.
18d. Chen, B.; Eddaoudi, M.; Hyde, S. T.; O'Keeffe, M.; Yaghi, O. M. *Science* **2001**, *291*, 1021.
19. Biradha, K.; Fujita, M. *Angew. Chem., Int. Ed.* **2002**, *41*, 3392.
19a. Desiraju, G. R. *Nature* **2001**, *412*, 397.
19b. Saalfrank, R. W.; Maid, H.; Hampel, F.; Peters, K. *Eur. J. Inorg. Chem.* **1999**, 1859.
20. Braga, D.; Grepioni, F. *Coord. Chem. Rev.* **1999**, *183*, 19.
21. Nguyen, P.; Gomez-Elipe, P.; Manners, I. *Chem. Rev.* **1999**, *99*, 1515.
22. Dance, I. D. The Crystal as Supramolecular Entity. In *Perspectives in Supramolecular Chemistry*; Desiraju, G. R., Eds.; Wiley, 1996; Vol. 2.
23. Brammer, L. Crystal Design: Structure and Function. In *Perspectives in Supramolecular Chemistry*; Desiraju, G. R., Eds.; Wiley: Chichester, 2003; Vol. 7, pp 1–75.
24. Aakeröy, C. B.; Seddon, K. R. *Chem. Soc. Rev.* **1993**, 397.
24a. Prins, L. J.; Reinhoudt, D. N.; Timmerman, P. *Angew. Chem., Int. Ed. Engl.* **2001**, *40*, 2382.
24b. Beatty, A. M. *CrystEngComm* **2001**, 51.
24c. Gilli, G.; Bellucci, F.; Ferretti, V.; Bertolasi, V. *J. Am. Chem. Soc.* **1989**, *111*, 1023.
24d. Gilli, G.; Gilli, P. *J. Mol. Struct.* **2000**, *552*, 1.
24e. Steiner, T. *Angew. Chem., Int. Ed. Engl.* **2002**, *41*, 48.
24f. Desiraju, G. R. *Acc. Chem. Res.* **2002**, *35*, 565.
25. Braga, D.; Grepioni, F.; Sabatino, P.; Desiraju, G. R. *Organometallics* **1994**, *13*, 3532.
25a. Braga, D.; Grepioni, F.; Desiraju, G. R. *Organometallics* **1998**, *17*, 2669.
25b. Braga, D.; Grepioni, F.; Desiraju, G. R. *J. Organomet. Chem.* **1997**, *548*, 33.
26. Desiraju, G. R., Steiner, T., Eds. *The Weak Hydrogen Bond in Structural Chemistry and Biology*, Oxford University Press: Oxford, 1999.

26a. Dunitz, J. D.; Gavezzotti, A. *Angew. Chem., Int. Ed.* **2005**, *44*, 1766.
27. Aullon, G.; Bellamy, D.; Brammer, L.; Bruton, E. A.; Orpen, A. G. *Chem. Commun.* **1998**, 653.
27a. Felix, O.; Hosseini, M. W.; De Cian, A.; Fischer, J. *Chem. Commun.* **2000**, 281.
27b. Hanessian, S.; Simard, M.; Roelens, S. *J. Am. Chem. Soc.* **1995**, *117*, 7630.
27c. Melendez, R. E.; Sharma, C. V. K.; Zaworotko, M. J.; Bauer, C.; Rodgers, R. D. *Angew. Chem., Int. Ed. Eng.* **1996**, *35*, 2213.
27d. Papoutsakis, D.; Kirby, J. P.; Jackson, J. E.; Nocera, D. G. *Chem. Eur. J.* **1999**, *5*, 1474.
27e. Braga, D.; Grepioni, F. *J. Chem. Soc., Dalton Trans.* **1999**, 1.
28. Braga, D.; Grepioni, F. *New J. Chem.* **1998**, 1159.
28a. Braga, D.; Grepioni, F. *J. Chem. Soc. Chem. Commun.* **1996**, 571.
28b. Braga, D.; Grepioni, F. In *Topics in Organometallic Chemistry*; Brown, J. M., Hofmann, P., Eds. Springer: Berlin, 1999; Vol. 4, 48.
29. Jeffrey, G. A., Saenger, W., Eds. *Hydrogen Bonding in Biological Structures*, Springer: Berlin, 1991.
29a. Meot-Ner(Mautner), M.; Sieck, L. W. *J. Am. Chem. Soc.* **1986**, *108*, 7525.
29b. Meot-Ner(Mautner), M. *J. Am. Chem. Soc.* **1984**, *106*, 1257.
30. Braga, D.; Maini, L.; Polito, M.; Grepioni, F. *Struct. Bond.* **2004**, *111*, 1.
30a. Mezei, G.; Raptis, R. G. *New J. Chem.* **2003**, *27*, 1399.
30b. Gilli, G.; Gilli, P. *J. Mol. Struc.* **2000**, *552*, 1.
30c. Burrows, A. D. *Struct. Bond.* **2004**, *108*, 1.
30d. Hubberstey, P.; Suksangpanya, U. *Struct. Bond.* **2004**, *111*, 33.
30e. Vilar, R. *Struct. Bond.* **2004**, *111*, 85.
30f. Hardie, M. J. *Struct. Bond.* **2004**, *111*, 139.
31. Etter, M. C. *Acc. Chem. Res.* **1990**, *23*, 120.
32. Braga, D.; Grepioni, F.; Novoa, J. J. *Chem. Commun.* **1998**, 1959.
32a. Braga, D.; Maini, L.; Grepioni, F.; Mota, F.; Rovira, C.; Novoa, J. J. *Chem. Eur. J.* **2000**, *6*, 4536.
32b. Steiner, T. *Chem. Commun.* **1999**, 2299.
32c. Mascal, M.; Marajo, C. E.; Blake, A. J. *Chem. Commun.* **2000**, 1591.
32d. Macchi, P.; Iversen, B. B.; Sironi, A.; Chokoumakas, B. C.; Larsen, F. K. *Angew. Chem., Int. Ed. Engl.* **2000**, *39*, 2719.
33. Epstein, L. M.; Shubina, E. S. *Coord. Chem. Rev.* **2002**, *231*, 165.
33a. Desmurs, P.; Kavallieratos, K.; Yao, W. B.; Crabtree, R. H. *New J. Chem.* **1999**, *23*, 1111.
33b. Klooster, W. T.; Koetzle, T. F.; Siegbahn, P. E. M.; Richardson, T. B.; Crabtree, R. H. *J. Amer. Chem. Soc.* **1999**, *121*, 6337.
33c. Braga, D.; Grepioni, F.; Tedesco, E.; Calhorda, M. J.; Lopes, P. E. M. *New J. Chem.* **1999**, *23*, 219.
33d. Braga, D.; De Leonardis, P.; Grepioni, F.; Tedesco, E.; Calhorda, M. J. *Inorg. Chem.* **1998**, *37*, 3337.
34. Nishio, M. *CrystEngComm* **2004**, *6*, 130.
35. Braga, D.; Eckert, M.; Fraccastoro, M.; Maini, L.; Grepioni, F.; Caneschi, A.; Sessoli, R. *New J. Chem.* **2002**, *26*, 1280.
36. Miller, J. S.; Epstein, A. J. *Chem. Commun.* **1998**, 1319.
37. Miller, J. S.; Epstein, A. J. *Chem. Eng. News* **1995**, *73*, 30.
37a. Miller, J. S.; Epstein, A. J.; Reiff, W. M. *Chem. Rev.* **1988**, *88*, 201.
37b. Coronado, E.; Galán-Mascarós, J.-R.; Gómez-García, C.-J.; Ensling, J.; Gütlich, P. *Chem. Eur. J.* **2000**, *6*, 552.
37c. Coronado, E.; Galán-Mascarós, J.-R.; Gómez-García, C.-J.; Laukin, V. *Nature* **2000**, *408*, 447.
37d. Zaman, M. B.; Tomura, M. T.; Yamashita, Y.; Sayaduzzaman, M.; Chowdhury, A. M. S. *CrystEngComm* **1999**, 9.
38. Braga, D.; Maini, L.; Prodi, L.; Caneschi, A.; Sessoli, R.; Grepioni, F. *Chem. Eur. J.* **2000**, *6*, 1310.
39. Braga, D.; Angeloni, A.; Maini, L.; Götz, A. W.; Grepioni, F. *New J. Chem.* **1999**, 17.
40. Braga, D.; Angeloni, A.; Grepioni, F.; Tagliavini, E. *Chem. Commun.* **1997**, 1447.
40a. Braga, D.; Angeloni, A.; Grepioni, F.; Tagliavini, E. *Organometallics* **1997**, *16*, 5478.
41. Braga, D.; Angeloni, A.; Tagliavini, E.; Grepioni, F. *J. Chem. Soc., Dalton Trans.* **1998**, 1961.
42. Grepioni, F.; Gladiali, S.; Scaccianoce, L.; Ribeiro, P.; Braga, D. *New. J. Chem.* **2001**, *25*, 690.
43. Monoclinic form: Palenik, G. J. *Inorg. Chem.* **1969**, *8*, 2744.
43a. Triclinic form: Takusagawa, F.; Koetzle, T. F. *Acta Crystallogr. Sect., B* **1979**, *35*, 2888.
44. Braga, D.; Maini, L.; Grepioni, F. *Angew. Chem.* **1998**, *37*, 2240.
44a. Braga, D.; Maini, L.; Grepioni, F. *J. Organomet. Chem.* **2000**, *594*, 101.
45. Braga, D.; Maini, L.; Grepioni, F.; De Cian, A.; Félix, O.; Fischer, J.; Hosseini, M. W. *New. J. Chem.* **2000**, *7*, 547.
46. Zakaria, C. M.; Ferguson, G.; Lough, A. J.; Glidewell, C. *Acta Crystallogr., Sect. Part 5* **2002**, *B58*, 786.
47. Zakaria, C. M.; Ferguson, G.; Lough, A. J.; Glidewell, C. *Acta Crystallogr., Sect. Part 1* **2002**, *C58*, M1.
48. Lee, I. S.; Chung, Y. K.; Mun, J.; Yoon, C. S. *Organometallics* **1999**, *18*, 5080.
49. Shin, D. M.; Lee, I. S.; Chung, Y. K. *Eur. J. Inorg. Chem.* **2003**, *12*, 2311.
50. Lee, I. S.; Shin, D. M.; Chung, Y. K. *Cryst. Growth Des.* **2003**, *3*(4), **2003**, 521.
51. Saji, T.; Kinoshita, I. *J. Chem. Soc. Chem. Commun.* **1986**, 716.
51a. Medina, J. C.; Li, C.; Bott, S. G.; Atwood, J. L.; Gokel, G. W. *J. Am. Chem. Soc.* **1991**, *113*, 366.
51b. Medina, J. C.; Goodnow, T. T.; Rojas, M. T.; Atwood, J. L.; Lynn, B. C.; Kaifer, A. E.; Gokel, G. W. *J. Am. Chem. Soc.* **1992**, *114*, 10583.
51c. Beer, P. D. *Chem. Commun.* **1996**, 689.
51d. Beer, P. D.; Graydon, A. R.; Johnson, A. O. M.; Smith, D. K. *Inorg. Chem.* **1997**, *36*, 2112.
51e. Eckert, H.; Seidel, C. *Angew. Chem., Int. Ed. Engl.* **1986**, *25*, 159.
51f. Herrick, R. S.; Jarret, R. M.; Curran, T. P.; Dragoli, D. R.; Flaherty, M. B.; Lindyberg, S. E.; Slate, R. A.; Thornton, L. C. *Tetrahedron Lett.* **1996**, *37*, 5289.
51g. Kira, M.; Matsubara, T.; Shinohara, H.; Sisido, M. *Chem. Lett.* **1997**, 89.
51h. Kraatz, H.-B.; Lusztyk, J.; Enright, G. D. *Inorg. Chem.* **1997**, *36*, 2400.
51i. Okamura, T.; Sakauye, K.; Ueyama, N.; Nakamura, A. *Inorg. Chem.* **1998**, *37*, 6731.
52. Cerichelli, G.; Floris, B.; Ortaggi, G. *J. Organomet. Chem.* **1974**, *76*, 73.
52a. Togni, A.; Hayashi, T. *Ferrocenes*; VCH: Weinheim, 1995.
53. Nomoto, A.; Moriuchi, T.; Yamazaki, S.; Ogawa, A.; Hirao, T. *Chem. Commun.* **1998**, 1963.
53a. Moriuchi, T.; Nomoto, A.; Yoshida, K.; Hirao, T. *J. Organomet. Chem.* **1999**, *589*, 50.

53b. Moriuchi, T.; Nomoto, A.; Yoshida, K.; Ogawa, A.; Hirao, T. *J. Am. Chem. Soc.* **2001**, *123*, 68.
53c. Moriuchi, T.; Yoshida, K.; Hirao, T. *J. Organomet. Chem.* **2003**, *668*(1–2), 31.
54. Bresner, C.; Aldridge, S.; Fallis, I. A.; Ooi, L. L. *Acta Crystallogr., Sect. Part 4* **2004**, *E60*, M441.
55. Braga, D.; Polito, M.; Bracaccini, M.; D'Addario, D.; Tagliavini, E.; Sturba, L.; Grepioni, F. *Organometallics* **2003**, *22*, 2142.
56. Zakaria, C. M.; Ferguson, G.; Lough, A. J.; Glidewell, C. *Acta Crystallogr. Sect. Part 1* **2002**, *C58*, M5.
56a. Zakaria, C. M.; Ferguson, G.; Lough, A. J.; Glidewell, C. *Acta Crystallogr., Sect. Part 1* **2002**, *C58*, M1.
57. Zakaria, C. M.; Ferguson, G.; Lough, A. J.; Glidewell, C. *Acta Crystallogr., Sect. Part 6* **2001**, *C57*, 687.
57a. Zakaria, C. M.; Ferguson, G.; Lough, A. J.; Glidewell, C. *Acta Crystallogr., Sect. Part 8* **2001**, *C57*, 914.
58. Stepnicka, P.; Cisarova, I. *New J. Chem.* **2002**, *26*(10), 1389.
58a. Stepnicka, P.; Cisarova, I.; Ludvik, J. *J. Organomet. Chem.* **2004**, *689*, 631.
59. J.F. Gallagher, P.N. Kelly, P.T.M. Kenny, A.J. Lough, *Acta Crystallogr. Sect. Part 12 C59*, M552.
60. Braga, D.; Maini, L.; Grepioni, F.; Elschenbroich, C.; Paganelli, F.; Schiemann, O. *Organometallics* **2001**, *20*, 1875.
61. Braga, D.; Maini, L.; Polito, M.; Grepioni, F. *Organometallics* **1999**, *18*, 2577.
62. Braga, D.; Maini, L.; Polito, M.; Rossini, M.; Grepioni, F. *Chem. Eur. J.* **2000**, *6*, 4227.
63. Braga, D.; Maini, L.; Polito, M.; Grepioni, F. *Chem. Commun.* **2002**, 2302.
63a. Braga, D.; Maini, L.; Giaffreda, S. L.; Grepioni, F.; Chierotti, M. R.; Gobetto, R. *Chem. Eur. J.* **2004**, *10*, 3261.
64. Sassmannshausen, J. *Organometallics* **2000**, *19*, 482.
65. Braga, D.; Polito, M.; Grepioni, F. *Cryst. Growth. Des.* **2004**, *4*, 769.
66. Elschenbroich, C.; Wolf, M.; Pebler, J.; Harms, K. *Organometallics* **2004**, *23*(3), 454.
66a. Elschenbroich, C.; Schiemann, O.; Burghaus, O.; Harms, K. *J. Am. Chem. Soc.* **1997**, *119*(32), 7452.
67. Beatty, A. M. *Coord. Chem. Rev.* **2003**, *246*(1–2), 131.
68. Rivas, J. C. M.; Brammer, L. *Coord. Chem. Rev.* **1999**, *183*, 43.
69. Mareque Rivas, J. C.; Brammer, L. *Acta Crystallogr.; Sect. C* **1998**, *54*, 757.
70. Kim, Y. J.; Verkade, J. G. *Inorg. Chem.* **2003**, *42*(14), 4262.
71. Heinze, K. *Dalton Trans.* **2002**, *4*, 540.
72. Oh, M.; Carpenter, G. B.; Sweigart, D. A. *Acc. Chem. Res.* **2004**, *37*(1), 1.
73. Oh, M.; Carpenter, G. B.; Sweigart, D. A. *Organometallics* **2002**, *21*, 1290.
73a. Sun, S.; Carpenter, G. B.; Sweigart, D. A. *J. Organomet. Chem.* **1996**, *512*, 257.
74. Oh, M.; Carpenter, G. B.; Sweigart, D. A. *Angew. Chem., Int. Ed.* **2001**, *40*, 3191.
75. Oh, M.; Carpenter, G. B.; Sweigart, D. A. *Angew. Chem., Int. Ed.* **2002**, *41*, 3650.
76. Oh, M.; Carpenter, G. B.; Sweigart, D. A. *Organometallics* **2003**, *22*, 2364.
77. Oh, M.; Carpenter, G. B.; Sweigart, D. A. *Chem. Commun.* **2002**, 2168.
77a. Oh, M.; Carpenter, G. B.; Sweigart, D. A. *Angew. Chem., Int. Ed.* **2003**, *42*, 2025.
78. Oh, M.; Reingold, J. A.; Carpenter, G. B.; Sweigart, D. A. *Coord. Chem. Rev.* **2004**, *248*(7–8), 561.
79. Bandoli, G.; Dolmella, A. *Coord. Chem. Rev.* **2000**, *209*, 161.
79a. Gimeno, M. C.; Jones, P. G.; Laguna, A.; Sarroca, C. *J. Chem. Soc., Dalton Trans.* **1995**, 1473.
79b. Neo, S.-P.; Hor, T. S. A.; Zhou, Z.-Y.; Mak, T. C. W. *J. Organomet. Chem.* **1994**, *464*, 113.
79c. Hor, T. S. A.; Neo, S.-P.; Tan, C. S.; Mak, T. C. W.; Leung, K. V. P.; Wang, R.-J. *Inorg. Chem.* **1992**, *31*, 4510.
80. Lu, X. L.; Leong, W. K.; Hor, T. S. A.; Goh, L. Y. *J. Organomet. Chem.* **2004**, *689*(10), 1746.
81. Dong, G.; Hong, M.; Chun-ying, D.; Feng, L.; Qing-jin, M. *J. Chem. Soc., Dalton Trans.* **2002**, *13*, 2593.
82. Dong, G.; Yu-ting, L.; Chun-ying, D.; Hong, M.; Qing-jin, M. *Inorg. Chem.* **2003**, *42*(8), **2003**, 2519.
83. Horikoshi, R.; Mochida, T.; Moriyama, H. *Inorg. Chem.* **2002**, *41*(11), 3017.
84. Horikoshi, R.; Mochida, T.; Moriyama, H. *Inorg. Chem.* **2001**, *40*, 2430.
84a. Mago, G.; Hinago, M.; Miyasaka, H.; Matsumoto, N.; Okawa, H. *Inorg. Chim. Acta* **1997**, *254*, 145.
84b. Dong, Y.-B.; Smith, M. D.; Layland, R. C.; Loye, H.-C. *Inorg. Chem.* **1999**, *38*, 5027.
84c. Shen, H.-Y.; Liao, D.-Z.; Jiang, Z.-H.; Yan, S.-P.; Sun, B.-W.; Wang, G.-L.; Yao, X.-K.; Wang, H.-G. *Polyhedron* **1998**, *17*, 1953.
85. Kondo, M.; Hayakawa, Y.; Miyazawa, M.; Oyama, A.; Unoura, K.; Kawaguchi, H.; Naito, T.; Maeda, K.; Uchida, F. *Inorg. Chem.* **2004**, *43*(19), 5801.
86. Dong, G.; Hong, M.; Chun-ying, D.; Feng, L. *J. Chem. Soc., Dalton Trans.* **2002**, 2593.
87. Braga, D.; Grepioni, F. *Angew Chem. Int Ed.* **2004**, *43*, 2.
87a. Braga, D.; Grepioni, F. In *Topics in Current Chemistry*; Toda, F. Ed., 2005, (in press)
88. Anastas, P. T.; Warner, J. C. *Green Chemistry: Theory and Practice;* Oxford University Press: New York, 1998.
89. Tanaka, K.; Toda, F. *Chem. Rev.* **2000**, *100*, 1025.
89a. Tanaka, K. *Solvent-free Organic Synthesis*; Wiley, 2003.
89b. Bradley, D. *Chem. Br.* **2002**, *9*, 42.
89c. Cave, G. W. V.; Raston, C. L.; Scott, J. L. *Chem. Commun.* **2001**, 2159.
89d. Rothenberg, G.; Downie, A. P.; Raston, C. L.; Scott, J. L. *J. Am. Chem. Soc.* **2001**, *123*, 8701.
89e. Toda, F. *CrystEngComm.* **2002**, *4*, 215.
89f. Nassimbeni, L. R. *Acc. Chem. Res.* **2003**, *36*, 631.
89g. Coville, N. J.; Levendis, D. C. *Eur. J. Inorg. Chem.* **2002**, *12*, 3067.
90. Adeyemi, A. G.; Eke, U. B.; Cheng, L.; Cook, L. M.; Billing, D. G.; Mamba, B. B.; Levendis, D. C.; Coville, N. J. *J. Organomet. Chem.* **2004**, *689*(13), 2207.
91. Mancini, S. S.; Covile, N. J. *Inorg. Chem. Commun.* **2004**, 7(5), 676.
92. Bala, M. D.; Budhai, A.; Coville, N. J. *Organometallics* **2004**, *23*(9), 2048.
92a. Nareetsile, F. M.; Horwood, O. P. M.; Billing, D. G.; Levendis, D. C.; Coville, N. J. *J. Organomet. Chem.* **2003**, *682*(1–2), 2.
93. Adeyemi, O. G.; Coville, N. J. *Organometallics* **2003**, *22*(11), 2284.
94. Adeyemi, A. G.; Fernandes, M. A.; Cheng, L.; Eke, U. B.; Levendis, D. C.; Coville, N. J. *C. R. Acad. Sci., Ser. 11 Chim.* **2002**, *5*, 387.
95. Eke, U. B.; Coville, N. J. *Inorg. Chem. Commun.* **2000**, *3*(7), 368.
96. Smith, J. M.; Cheng, L.; Coville, N. J.; Schulte, J.; Dimpe, P. S.; Adsetts, M. S.; Cook, L. M.; Boeyens, J. C. A.; Levendis, D. C. *Organometallics* **2000**, *19*(13), 2597.

97. Bogadi, R. S.; Levendis, D. C.; Coville, N. J. *J. Am. Chem. Soc.* **2002**, *124*(6), 1104.
98. Braga, D.; Maini, L.; Polito, M.; Mirolo, L.; Grepioni, F. *Chem. Commun.* **2002**, *24*, 2960.
99. Braga, D.; Maini, L.; Polito, M.; Mirolo, L.; Grepioni, F. *Chem. Eur. J.* **2003**, *9*, 4362.
100. Braga, D.; D'Addario, D.; Polito, M.; Grepioni, F. *Organometallics* **2004**, *23*, 2810.
101. Braga, D.; D'Addario, D.; Grepioni, F.; Polito, M.; Proserpio, D. M.; Steed, J. W.; Tagliavini, E. *Organometallics* **2003**, *22*, 4532.
102. Balema, V. P.; Wiench, J. W.; Pruski, M.; Pecharsky, V. K. *Chem. Commun.* **2002**, 1606.
103. Orita, A.; Jiang, L. S.; Nakano, T.; Ma, N. C.; Otera, J. *Chem. Commun.* **2002**, 1362.
104. Braga, D.; Cojazzi, G.; Emiliani, D.; Maini, L.; Grepioni, F. *Chem. Commun.* **2001**, *21*, 2272.
105. Braga, D.; Cojazzi, G.; Emiliani, D.; Maini, L.; Grepioni, F. *Organometallics* **2002**, *21*, 1315.
105a. Braga, D.; Maini, L.; Mazzotti, M.; Rubini, K.; Grepioni, F. *CrystEngComm.* **2003**, *29*, 154.
105b. Braga, D.; Maini, L.; Mazzotti, M.; Rubini, K.; Masic, A.; Gobetto, R.; Grepioni, F. *Chem. Commun.* **2002**, *20*, 2296.
106. Braga, D.; Cojazzi, G.; Emiliani, D.; Maini, L.; Grepioni, F. *Chem. Commun.* **2001**, *21*, 2272.
107. Braga, D.; Cojazzi, G.; Emiliani, D.; Maini, L.; Grepioni, F. *Organometallics* **2002**, *21*, 1315.
108. Braga, D.; Maini, L.; Polito, M.; Grepioni, F. *Chem. Commun.* **2002**, 2302.
109. McCrone, W. C. Polymorphism. In *Physics and Chemistry of the Organic Solid State*; Fox, D., Labes, M. M., Weissemberg, A., Eds. Interscience: New York, 1965; Vol. II, 726.
109a. Bernstein, J. *Polymorphism in Molecular Crystals*; Oxford University Press: Oxford, 2002.
110. Erk and other papers Byrn, S. R. In *Solid State Chemistry of Drugs*; Academic: New York, 1982, p 79.
110a. Bernstein, J.; Davey, R. J.; Henck, J.-O. *Angew. Chem., Int. Ed. Eng.* **1999**, *38*, 3440.
110b. See also: Bladgen, N.; Davey, R. J. *Chem. Br.* **1999**, *35*, 44.
111. Braga, D.; Grepioni, F. *Chem. Soc. Rev.* **2000**, *4*, 229.
111a. See also Braga, D.; Grepioni, F. In *Topics in Organometallic Chemistry*; Brown, J. M., Hofmann, P., Eds. Springer: Berlin, 1999; Vol. 4, 48.
112. Braga, D. *Chem. Rev.* **1992**, *92*, 633.
113. Seiler, P.; Dunitz, J. D. *Acta Crystallogr., Sect. B* **1979**, *B35*, 2020.
113a. Takusagawa, F.; Koetzle, T. F. *Acta Crystallogr., Sect. B* **1979**, *B35*, 1074.
113b. Seiler, P.; Dunitz, J. D. *Acta Crystallogr., Sect. B* **1979**, *B35*, 1068.
113c. Braga, D.; Grepioni, F. *Organometallics* **1992**, *11*, 711.
113d. Dunitz, J. D. *Acta Crystallogr., Sect. B* **1995**, *B51*, 619.
113e. Dunitz, J. D. *Organic Chemistry: Its Language and its State of the Art*; Kisakürek, M. V., Ed. Verlag HCA: Basel, 1993; p 9.
114. Daniel, M. F.; Leadbetter, A. J.; Meads, R. E.; Parker, W. G. *J. Chem. Soc., Faraday Trans.* **1978**, *74*, 456.
114a. Sato, K.; Katada, M.; Sano, H.; Konno, M. *Bull. Chem. Soc. Jpn.* **1984**, *57*, 2361.
114b. Fitzsimmons, B. W.; Sayer, I. *J. Chem. Soc., Dalton Trans.* **1991**, 2907.
114c. Fitzsimmons, B. W.; Marshall, W. G. *J. Chem. Soc., Dalton Trans.* **1992**, 73.
115. Braga, D.; Scaccianoce, L.; Grepioni, F.; Draper, S. M. *Organometallics* **1996**, *15*, 4675.
115a. Grepioni, F.; Cojazzi, G.; Draper, S. M.; Scully, N.; Braga, D. *Organometallics* **1998**, *17*, 296.
116. Martinez, R.; Tiripicchio, A. *Acta Crystallogr., Sect. C* **1990**, *C46*, 202.
116a. Webb, R. J.; Lowery, M. D.; Shiomi, Y.; Sorai, M.; Wittebort, R. J.; Hendrickson, D. N. *Inorg. Chem.* **1992**, *31*, 5211.
116b. Sorai, M.; Shiomi, Y. *Thermochim. Acta* **1986**, *109*, 29.
117. Braga, D.; Cojazzi, G.; Paolucci, D.; Grepioni, F. *Chem. Commun.* **2001**, 803.
118. Vegard, L.; Dale, H. *Zeits. Kristallogr.* **1928**, *67*, 148.
119. Grepioni, F.; Cojazzi, G.; Braga, D.; Marseglia, E.; Scaccianoce, L.; Johnson, B. F. G. *J. Chem. Soc., Dalton Trans.* **1999**, 553.
120. Fitzsimmons, B. W.; Hume, A. R. *J. Chem. Soc., Dalton Trans.* **1980**, 180.
120a. Fitzsimmons, B. W.; Marshall, W. G. *J. Chem. Soc., Dalton Trans.* **1992**, 73.
120b. Fitzsimmons, B. W.; Sayer, I. *J. Chem. Soc., Dalton Trans.* **1991**, 2907.
121. Braga, D.; Cojazzi, G.; Paolucci, D.; Grepioni, F. *CrystEngComm* **2001**, *38*, 1.
122. Braga, D.; Cojazzi, G.; Abati, A.; Maini, L.; Polito, M.; Scaccianoce, L.; Grepioni, F. *J. Chem. Soc. Dalton Trans.* **2000**, 3969.
123. Braga, D.; Polito, M.; D'Addario, D.; Grepioni, F. *Cryst. Growth Des.* **2004**, *4*(6), **2004**, 1109.
124. Braga, D.; Abati, A.; Scaccianoce, L.; Johnson, B. F. G.; Grepioni, F. *Solid State Sci.* **2001**, *3*, 783.
125. Pedone, C.; Sirigu, A. *Inorg. Chem.* **1968**, *7*, 2614.
125a. Hsiou, Y.; Wang, Y.; Liu, L.-K. *Acta Crystallogr., Sect. C (Cr. Str. Comm.)* **1989**, *45*, 721.
126. La Placa, S. J.; Hamilton, W. C.; Ibers, J. A.; Davison, A. *Inorg. Chem.* **1969**, *8*, 1928.
127. Zhao, D.; Brammer, L. *Inorg. Chem.* **1994**, *33*, 5897.
128. Soldatov, D. V.; Ripmeester, J. A. *Chem. Eur. J.* **2001**, *7*, 2979.
129. Braga, D.; Paganelli, F.; Tagliavini, E.; Casolari, S.; Cojazzi, G.; Grepioni, F. *Organometallics* **1999**, *18*, 4191.
130. Daniel, M. F.; Leadbetter, A. J.; Meads, R. E.; Parker, W. G. *J. Chem. Soc., Faraday Trans.* **1978**, *74*, 456.

12.12 Organometallic Compounds in Biosensing

A E G Cass, Imperial College London, London, UK

12.12.1 Introduction

A sensor is defined as "the component of an instrument that converts input signal into a quantity that is measured by another part of the instrument and changed into a useful signal for an information-gathering system."[1] Chemical sensors have as their input signal the concentration of a particular molecular species and the useful signal is typically a current or voltage. A familiar example is the pH meter that senses proton concentration and generates a voltage of 57 mV per unit change in pH.

While chemical species such as ions or gases can be sensed with inorganic materials (glasses, semiconductors, or metals), for many molecules of clinical or environmental interest a more sophisticated molecular recognition is often needed to generate the output signal. Typically, a specific molecular recognition element is coated onto the surface of the base sensor (Figure 1). Although such molecular recognition is possible through the use of synthetic molecules (giving rise to "chemosensors")[2,3] and indeed organometallic receptors are the subject of Chapter 12.09 of this volume, a common approach is to use biomolecules taking advantage of their specificity, affinity, and catalytic activity. The resulting devices are referred to as "biosensors" and have been extensively reviewed in books[4–8] and journals[9–15] over the past 25 years. Many different combinations of biomolecule and transducer have been employed in producing biosensors, but in the context of organometallic compounds the primary transduction method is electrochemistry. In electrochemical sensors, it is the redox characteristics of the organometallic compounds that are exploited through their reaction with both biomolecules and solid electrodes.

12.12.2 Principles of Biosensors

As shown in Figure 1, biosensors can be looked on as devices that convert chemical information into an electrical output, and in effecting this transduction there needs to be a link between the "soft" biological elements and the "hard" solid-state elements; organometallic compounds can act as this link and so mediate the information flow. Biosensors are heterogeneous devices and this has implications in both their design and operation, the signal

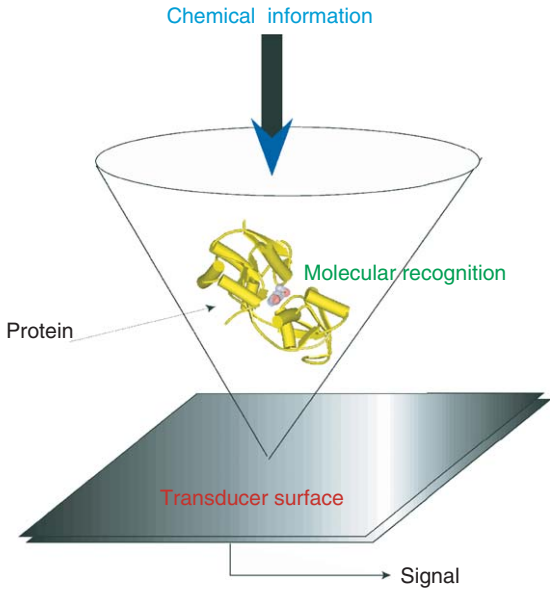

Figure 1 The conversion of chemical into electrical information by a biosensor.

transduction occurring at the sensor surface. This means that mass transport effects (diffusion and convection) are important and where the sensor is to be used in a continuous fashion both the biological recognition element as well as the organometallic element need to be immobilized on the surface. Moreover, because the signal can be determined by either a (rate-limiting) mass transport or reaction kinetics step, the performance of the device may be quite different depending upon which of the two steps is limiting.

12.12.2.1 Electrochemical Sensors

Sensors based on the oxidation (or reduction) of the analyte generate a current that is a consequence of the potential-dependent electron flow between the analyte and the electrode. If thermodynamic factors were the only determinant of the current, then there would be no need for enzymes or other components; however, the slow kinetics of many organic electrochemical reactions and the complexity of typical samples, with many interfering species, means that it is rarely possible to have an accurate analytical determination based solely on a "bare" electrode. Both kinetic and interference effects can be overcome through the use of an enzyme that specifically accelerates the redox reaction of the target analyte. Although it should then be possible for the enzyme to undergo a heterogeneous redox reaction at the electrode surface, this is often not observed to occur at a significant rate. The reasons for this are well understood and arise from the distance dependence of heterogeneous electron transfer rates, which according to Marcus theory fall as the inverse sixth power of the distance between the electrode and the redox center of the enzyme. In many enzymes, the redox center is distant from the protein surface, thus reducing electron-transfer rates and hence currents to very low values. A recent review by Armstrong discusses direct protein electrochemistry ("protein film voltammetry") in more detail and also illustrates some examples of its application.[16]

A solution to the problem of slow enzyme–electrode electron transfer is to use a small molecule as an electron shuttle or "mediator" between the enzyme active site and the electrode. The mediator needs to demonstrate both rapid homogeneous electron exchange with the enzyme and rapid heterogeneous electron exchange with the electrode. Until 1984, the few papers published on mediated enzyme electrochemistry used either metal complexes (such as hexacyanoferrate) or organic dyes; however, the paper by groups at the University of Oxford and Cranfield Institute of Technology[17] introduced the first organometallic mediator (ferrocene) and ushered in a new era in mediated enzyme electrodes. The tremendous synthetic flexibility of ferrocene and related organometallic compounds has been exploited in a wide range of electrochemical biosensor formats and these are described later.

12.12.2.2 Optical Sensors

Optical sensors based upon luminescence often offer very high limits of detection combined with versatile sensing formats. Organometallic compounds are usually employed with either fluorescence or electrogenerated chemiluminescence sensing and the typical format exploits optical fiber or planar waveguide-based sensors. Both types of luminescence sensors measure the emission of light from an electronically excited state, in the former case from photoexcitation and in the latter via an excited state generated through an electrochemical redox reaction. Fluorescence and electrogenerated chemiluminescence biosensors have recently been reviewed in Ref: 18. In this regard coordination complexes of ruthenium or lanthanides have been widely used.

12.12.3 Organometallic Electrochemical Sensors

As described above, the introduction of ferrocenes as mediators for enzyme electrodes was subsequently developed as the versatile chemistry of these molecules was exploited both in redox mediation sensors and also through the use of ferrocene derivatives as labels in affinity sensors based upon electrochemical detection.

12.12.3.1 Ferrocene-based Redox Mediation

12.12.3.1.1 Soluble ferrocenes

The use of ferrocenes as mediators is most commonly applied to redox enzymes that have a bound redox center that undergoes reaction with the analyte via a typical "ping-pong" BiBi mechanism where the redox center undergoes alternate reactions with oxidizing and reducing substrates as shown in Figure 2. The first example of the use of ferrocenes as a kinetic mediator in a biosensor was discussed in Ref: 17 although earlier papers[19,20] had described enzymatic reactions of ferrocenes. The biosensor described by Cass *et al.* was for blood glucose, a major analyte that dominates biosensor commercialization as its measurement has a central role in managing diabetes.[10] The enzyme glucose oxidase is alternately reduced by glucose and oxidized by the ferrocenium ion giving rise to a glucose-dependent current (Figure 2).

Subsequently, enzyme sensors using soluble ferrocenes were described for a number of analytes and these along with the corresponding redox enzymes are collected in Table 1. The ability of the ferrocenium ion to act as an electron acceptor and ferrocene as an electron donor results in mediation to both reducing and oxidizing enzymes. An important determinant of performance in mediated enzyme biosensors is the rate of reaction of the mediator with the enzyme, and ferrocenes have been investigated in both oxidative and reductive enzyme reactions, mainly using dynamic electrochemical methods and in particular by cyclic voltammetry. Coupling a regenerative solution reaction to the mediator's

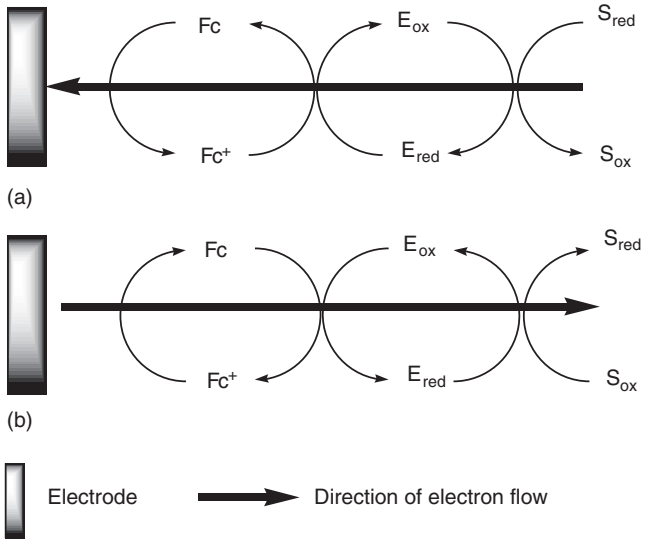

Figure 2 Ferrocene mediation to redox enzymes with (a) reducing and (b) oxidizing substrates (S).

Table 1 Electrochemical enzyme sensors that use ferrocenes

Enzyme	*Analyte*	*References*
Ferrocenes as redox co-substrates (mediators)		
Glucose oxidase	Glucose	17,74
Glucose dehydrogenase (PQQ dependent)	Glucose	75,76
NADH oxidase	NADH	77–79
Horseradish peroxidase	Hydrogen peroxide	80–82
Horseradish peroxidase	Cyanide	83
Horseradish peroxidase	Linoleic hydroperoxide	81
Cytochrome c peroxidase	Hydrogen peroxide	35,84,85
Diamine oxidase	Histamine/putrescine/cadaverine	86
Cytochrome b_2	Lactate	87
Carbon monoxide acceptor oxidoreductase	Carbon monoxide	88
Pyruvate oxidase	Pyruvate	89
Xanthine oxidase	Xanthine, hypoxanthine	89,90
Sarcosine oxidase	Sarcosine	89
Lipoamide dehydrogenase	NADH	89
Alcohol dehydrogenase (PQQ dependent)	Ethanol	89,91
Glycolate oxidase	Glycolate	92
Galactose oxidase	Galactose	92
L-amino acids oxidase	L-amino acid	92
Horseradish peroxidase	Organic peroxides	93
Horseradish peroxidase	Polyphenols	94
Theophylline oxidase	Theophylline	95
Fructose dehydrogenase (PQQ dependent)	Fructose	96,97
Bilirubin oxidase	Bilirubin	98
Trimethylamine Dehydrogenase	Trimethylamine	99
Ferrocenes as reporter substrates		
Lipase	Lipase	46
DNA ligase	DNA ligase	65
Alkaline phosphatase	Alkaline phosphatase	66

heterogeneous electron transfer results in a characteristic change in the cyclic voltammogram of the mediator as shown in Figure 3. Initial analysis of catalytic currents of the sort shown in Figure 3 assumed a simple model based on the work of Nicholson and Shain.[21] A detailed investigation of the cyclic voltammetric data by Saveant and co-workers[22,23] allowed them to extract kinetic and thermodynamic data (including the pH dependence) for both the oxidative and reductive half reactions. The kinetic parameters for the reductive half reaction were in good agreement with those previously determined using the natural oxidant (dioxygen) and the oxidative half reaction was controlled by the interaction of the mediator with the enzyme. A general method for simulating the cyclic voltammograms of a catalytically coupled mediator has been presented,[24] where the kinetics of the reaction of various ferrocenium ions with glucose oxidase was determined. Subsequent work by Ryabov and co-workers reached broadly similar conclusions in a steady-state spectrophotometric study where they concluded that the kinetics were not determined by the redox potential difference (as might be expected if the ferrocenium ions were reduced via a simple collisional electron transfer) but rather through the formation of a non-covalent complex (Michaelis complex) between reduced enzyme and ferrocenium ion.[25] In a further study of structure–function relationships[26] using the kinetic analysis of Bartlett and co-workers[27] on a series of ferrocene derivatives based upon the mediator used in commercial blood glucose sensors (viz. 1,1′-dimethyl-3-(2-amino-1-hydroxyethyl)ferrocene), the authors again concluded that although there was not a general dependence of k_m on $E_{1/2}$, within a homologous series, for example, aminoalcohol or carboxyl-substituted derivatives, a linear free energy relationship could be observed. Such behavior is consistent with different ferrocene structural series interacting at different sites on the enzyme resulting in the observed rates being dependent on a multiplicity of factors, including distance and reorganization energies that will vary from site to site. However, within a series, many of these factors will be constant and then driving force becomes the determining factor.

An obvious instance where the driving force is not a determining factor is in the reaction of chiral mediators. The inherent chirality of proteins implies that they should exhibit chiral discrimination between enantiomers and this has been widely exploited in the selective transformation of one enantiomer in a racemic mixture by enzymes,

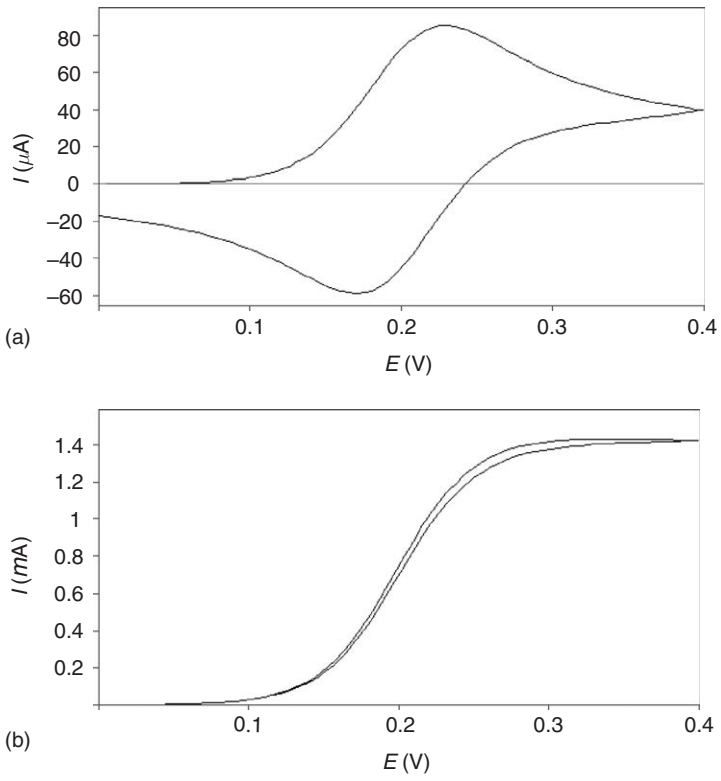

Figure 3 Simulated cyclic voltammograms for (a) a reversible redox couple and (b) a catalytically coupled reaction. The simulations were made using the program Digielch (http://www.digielch.de/).

particularly hydrolases. Ferrocenes can be chiral by having either a chiral substituent or through exhibiting planar chirality by virtue of the asymmetric arrangement of substituents on the two cyclopentadiene rings. In the latter case, the two enantiomers can be chirally discriminated by hydrolases[28] Willner and co-workers first reported chiral discrimination in the reaction of glucose oxidase with a ferrocene having a chiral substituent,[29] although subsequently Saveant and co-workers argued that this was not in fact discrimination, but rather a consequence of using too simple a kinetic model to interpret the cyclic voltammetry data.[30] In an extensive structure–function study of ferrocenium reactivity with glucose oxidase, Forrow *et al.* also found no chiral discrimination between side-chain enantiomers, but did note a weak discrimination between a pair of diastereoisomers.[26] Sadeghi *et al.* oxidized planar chiral ferrocenes with yeast cytochrome *c* peroxidase and found a twofold difference in the rate of reaction between the two enantiomers.[31] Further evidence supporting chiral discrimination in this case came from the observation of a differential acceleration in the rates of oxidation of the two enantiomers by a charge-reversal mutation (aspartate 34 to lysine, e.g., negatively charged to positively charged). The differential acceleration was sufficiently pronounced to switch the chiral selectivity of the enzyme. This use of protein engineering makes it possible to further explore mediator structure–function relationships through changing the protein as well as the mediator.

While protein engineering has been used extensively to probe physiological electron-transfer reactions of proteins,[32] relatively little has been done with mediated systems in the context of electrochemical biosensors. One example where there has been an investigation of varying both mediator structure and specific amino acid residues is yeast cytochrome *c* peroxidase. This enzyme was shown to rapidly oxidize ferrocenes[33] and has been the subject of extensive mutagenesis studies probing both the reactivity with hydrogen peroxide and cytochrome c, its physiological electron transfer donor.[34] Sadeghi *et al.* generated three charge-reversal mutants. In addition to the aspartate-to-lysine mutation at position 34, the same charge-reversal mutations were made at positions 37 and 146[35] The latter two mutations had relatively little effect on the rates of reaction with different mediators. Figure 4 shows the calculated electrostatic potentials for the wild-type protein and the three charge-reversal mutants. The two mutants where little effect was observed on oxidation rates have a similar electrostatic potential surface to the wild type while the D34K is

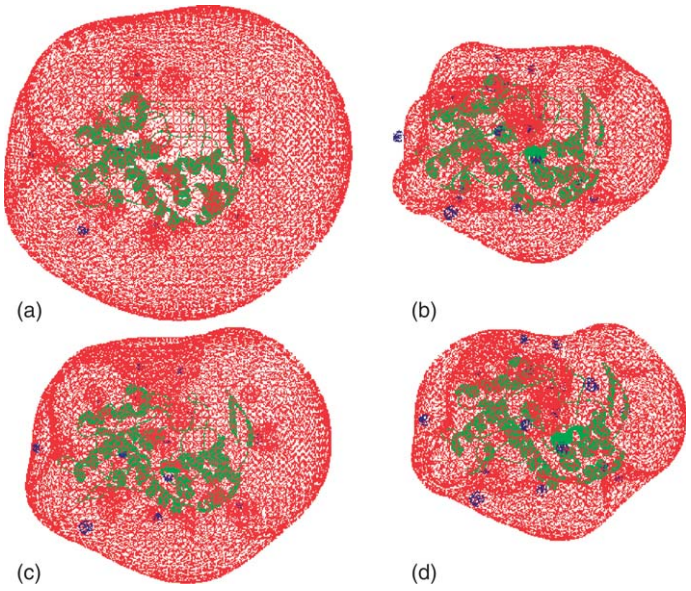

Figure 4 Calculated electrostatic potentials around (a) wild-type cytochrome *c* peroxidase and three charge reversal mutants ((b) D34K, (c) D37K, and (d) D146K). The electric potentials are generated from a simple coulombic model and are shown in red contoured at −1.8 eV. The protein backbone is shown in green.

quite distinct. The combination of the charge-reversal mutation with a suitable ferrocene yielded an overall reaction rate greater than that of the wild-type peroxidase with its physiological substrate.

12.12.3.1.2 Polymeric and surface-confined ferrocene mediators

The interest in chemically modified electrodes that developed during the 1980s resulted in the synthesis of many redox-active polymers and surface-confined redox couples, including ferrocenes. These were subsequently adapted to electrochemical biosensors, and both surface-confined and polymeric ferrocenes have been widely used. Typically, polymeric ferrocenes that have been exploited in this way include poly(vinyl) ferrocenes,[36] polysiloxanes[37], polyethylene oxide with covalently attached ferrocenes,[38] poly(allylamine) ferrocene,[39] and polacrylamide ferrocene cross-linked hydrogels.[40]

Ferrocene carboxylic acid has also been co-immobilized with glucose oxidase in a film of poly(pyrrole) electropolymerized on an electrode. In this case, the enzyme and mediator are both negatively charged and so act as counterions to the positively charged poly(pyrrole).[41] Dendritic ferrocenes based on ferrocenyl silicon dendrimers have been used as mediators to glucose oxidase in a carbon paste electrode.[42] In an affinity-sensing model, a comparison was made between direct electron transfer from a GOx label and a ferrocene mediator, both species being bound to a gold electrode through a dendrimer, the latter directly and the former through a avidin–biotin link.[43] It was found that the mediated configuration gave an improved performance. Dendrimer-attached ferrocenes have also been used as electrocatalysts in DNA[44] and immunosensing[45] based on alkaline phosphatase labeling, with the ferrocene acting as an electrocatalyst for phenol oxidation as shown in Figure 5.

Self-assembly methods have also been used to form ferrocene monolayers on electrodes, and this has been used to sense lipase activity via the enzyme-catalyzed release of surface-bound redox groups.[46]

12.12.3.1.3 Screen-printed ferrocene-based sensors

Although ferrocenes have shown themselves to be excellent mediators of enzyme electron transfer in solution, they need to be incorporated into a fabrication process to produce sensors that are suitable for clinical use. The demands of implanted sensors are quite different from those that typically use a "fingerstick" for *ex vivo* measurement.[47] The former is described later in this review; this section covers screen printed sensors. The process of screen printing lends itself well to the manufacture of disposable, single-use sensors[12,48,49] and has been widely employed for this in both the laboratory and in large-scale manufacture.

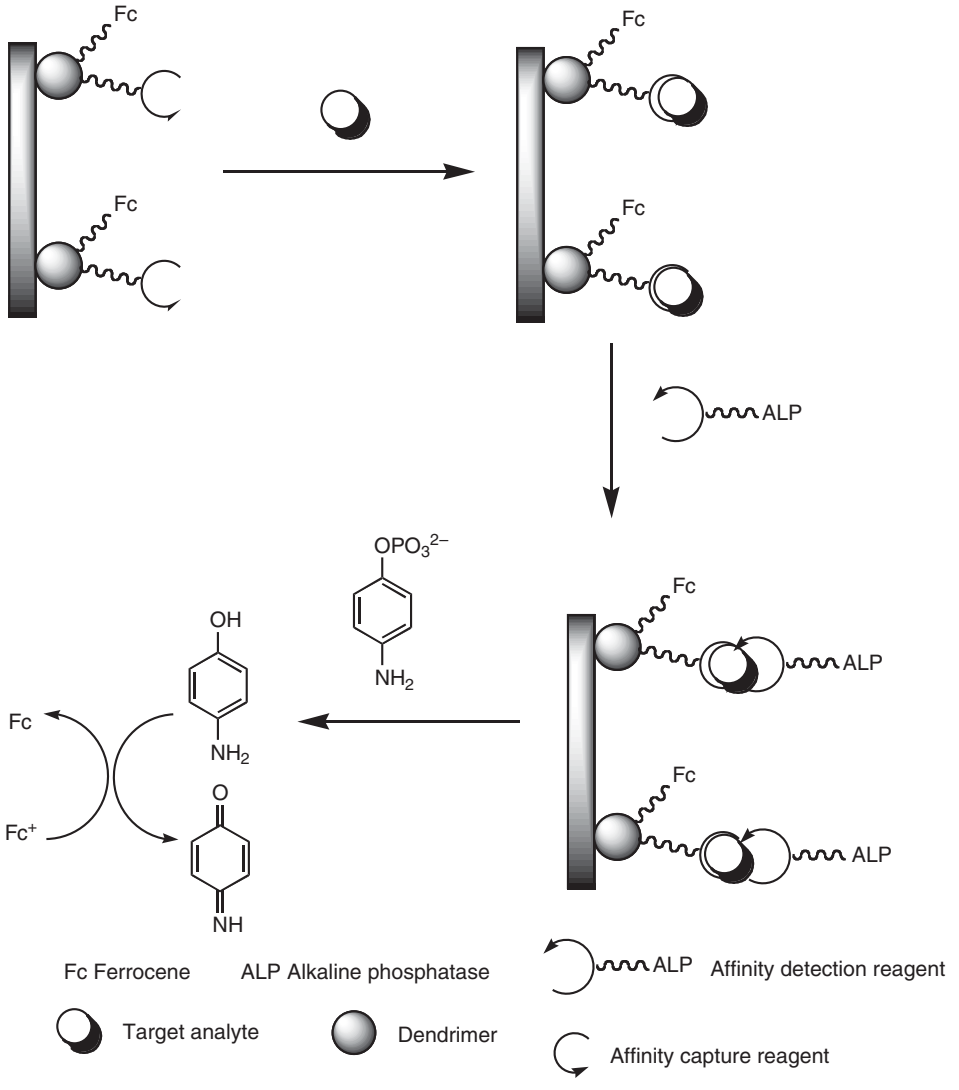

Figure 5 The use of ferrocene-modified dendrimers in affinity sensors.

12.12.3.2 Biomolecule–Ferrocene Conjugates

Covalent conjugates between ferrocenes and biomolecules have recently been extensively reviewed[50] and this section focuses only on those conjugates that have been used in sensing applications. We can divide the conjugates into two broad classes: those where the ferrocene is conjugated to macromolecules (most commonly proteins or nucleic acids) and those where the ferrocene is conjugated to small molecules (usually enzyme substrates or haptens).

12.12.3.2.1 Protein conjugates

The conjugation of ferrocenes to biomolecules has a number of potential advantages in producing biosensors, including minimal loss of the mediator from the electrode, particularly important where implanted sensors are used, and closer integration of mediator and enzyme, thereby possibly allowing more efficient electron transfer. These advantages need to be offset against the fact that the no longer freely diffusing mediator may be sterically constrained from ready access to both the enzyme's active site and the electrode, loss of enzyme activity due to the modification of key amino acid residues, and greater sensitivity to degradation of the mediator. There are relatively few amino acid residues that are suitable for modification, lysine (amine), aspartate and glutamate (carboxyl), cysteine (thiol), and histidine (imidazole). Glycoproteins can take advantage of the glycan moiety as a conjugation site.

Irrespective of the site of attachment, the chemistry is typically that which had already been employed for synthesizing many other small-molecule protein conjugates. As is usually the case, the non-specific chemistry can result in multiple conjugates being formed with a mixture of products that are not usually purified. This issue can be overcome through providing a single, unique attachment point, through protein engineering. In most cases, this is a cysteine residue as these are naturally rare and have distinctive reaction chemistry, although Zhang *et al*. described a C-terminal oligolysine tag on glucose oxidase to which ferrocene groups were coupled.[51] In this case, an added (though unexpected) benefit was that the modified protein showed better storage stability. Alternatively, a non-natural ferrocene containing amino acid can be directly incorporated during an *in vitro* transcription/translation process.[52] Site-specific labeling of proteins with ferrocene moieties has typically employed mutagenesis to introduce a cysteine residue at the desired labeling position and then reaction with an iodoacetamide derivative[53] (Figure 6). This can also be applied with non-enzyme proteins as exemplified by the maltose-binding protein labeled with a ferrocene derivative that showed a shift in midpoint potential as a function of maltose binding.[54]

Examples of ferrocene–protein conjugates are collected in Table 2.

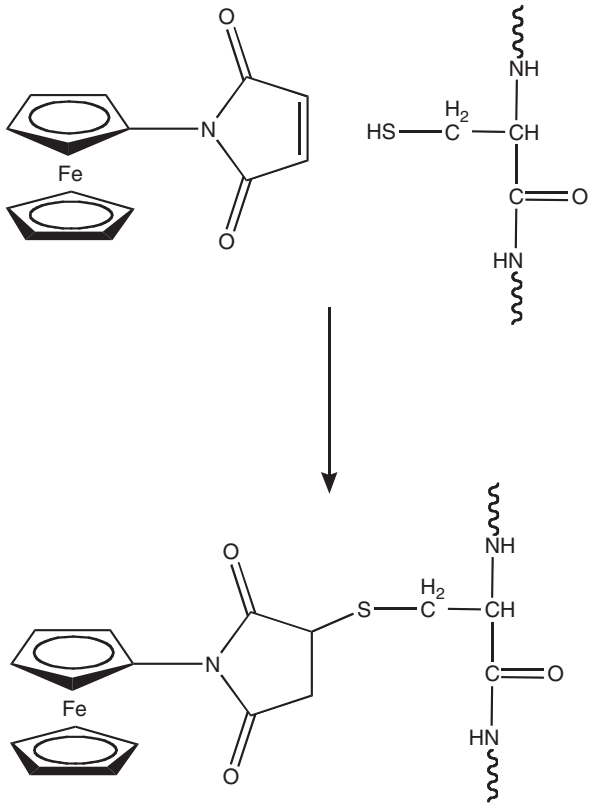

Figure 6 Modification of the thiol group of cysteine residues in proteins with ferrocene maleimide.

Table 2 Ferrocene–protein conjugates for biosensing

Protein	*Attachment residues*	*Ferrocene functional group*	*Comments*	*References*
GOx	Lysine	Carboxyl	Native	100,101
GOx	Lysine	Carboxyl	C-terminal oligolysine tag	51
HRP	Glycan	Amine	Glycan oxidized with HIO_4	102
MBP	Cysteine	Iodoacetamide	Recombinant, engineered cysteine. Maltose-dependent shift in E_0	54
β-Lactamase			Ferrocenyl alanine incorporated during synthesis	52
Cytochrome $P450_{cam}$	Cysteine	Iodoacetamide		53,103

12.12.3.2.2 Nucleic acid conjugates

The use of ferrocene labels as electrochemical probes of DNA hybridization has generated a substantial literature over the past few years. The ferrocenyl labels can be incorporated into synthetic oligonucleotides, either post-synthesis via attachment to a 5′-aminohexyl group[55] or during synthesis using ferrocenyl phosphoramidates.[56] The ferrocenyl oligonucleotides can then be used to detect their complementary sequences through changes in ferrocene electrochemistry following hybridization (Figure 7). The probes described by Ihara *et al*.[55] can form either double or triple helices depending upon whether the target DNA was single or double stranded; typically, the attached ferrocene showed a 10–30 mV shift in the midpoint potential upon hybridization. The *in situ* approach to DNA sensing was further developed by Pike *et al*., who integrated ferrocenyl DNA synthesis with semiconductor surfaces[57] Once again the ferrocene was incorporated during synthesis, but unlike the earlier work the ferrocene moiety was on a modified base rather than the phosphodiester backbone or the aminohexyl extension. These different approaches to the incorporation of ferrocene moieties into DNA are shown in Figure 8. In addition to DNA modification, ferrocenes have also been used to label peptide nucleic acid (PNA) probes[58–60] again for hybridization to target DNA.

An alternative to covalent attachment of the label is to use the intercalation between the bases of the double helix. Planar aromatic molecules are particularly good intercalators and, if modified with ferrocene, can be used to detect the duplex DNA electrochemically.[61] DNA will also bind electrostatically to polycations and this observation was used by Le Floch *et al*., who immobilized a neutral PNA probe on an electrode when the probe bound the complementary (negatively charged) DNA, the resulting PNA/DNA hybrid then being electrostatically complexed with a water-soluble polycationic poly(ferrocenylthiophene). The ferrocene groups at the electrode could then be detected by voltammetry.[62] Ferrocene-modified DNA probes have been used in a variety of applications including detecting single base changes.[63,64] An interesting application of ferrocene-modified DNA was recently described by Zauner *et al*., who attached a ferrocene moiety to a "hairpin" DNA molecule tethered to an electrode.[65] One strand of the duplex is "nicked" (hydrolyzed) but remains bound under non-denaturing conditions. When denatured, this strand dissociates and the ferrocene electrochemistry is lost. This sensor can be used to detect the activity of enzymes that repair the nick (ligases) and has potential for screening inhibitors of the ligase enzyme.

12.12.3.2.3 Small-molecule conjugates

The attachment of the ferrocene groups to small molecules has been used in two main classes of biosensor; in the first, the conjugate is an enzyme substrate such that a shift in its redox potential occurs following enzymatic modification. An example is ferrocenylethyl phosphate (Figure 9) that facilitates the electrochemical assay of alkaline phosphatase, a common enzyme label for immunoassays. The redox potential of the alcohol product is lower than the phosphate ester and hence by poising the potential, the product can be selectively measured and so the alkaline phosphatase activity measured. The sensitivity of this method was further enhanced by the use of stripping voltammetry to detect the product.[66]

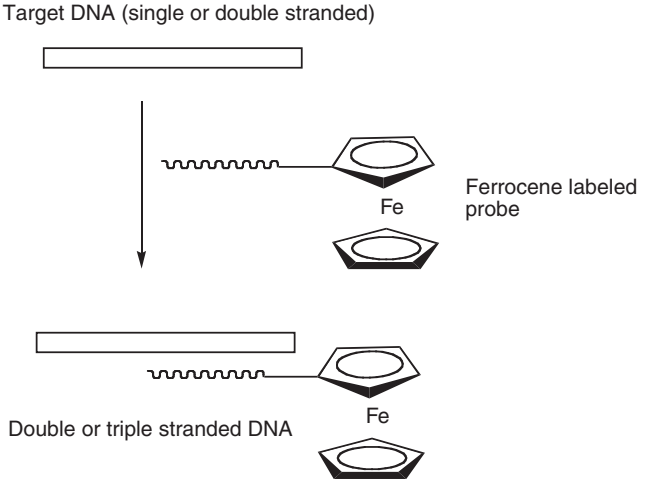

Figure 7 DNA hybridization by a ferrocene-labeled probe.

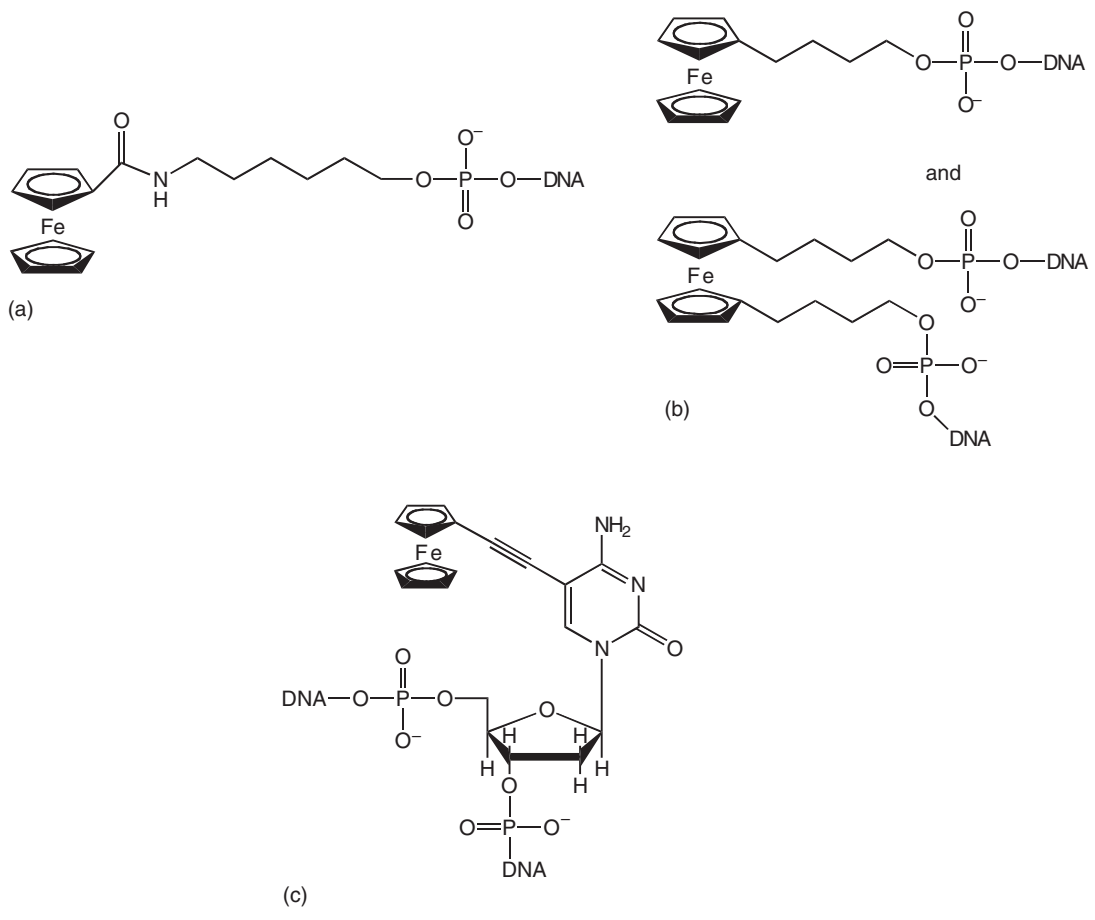

Figure 8 Different structures used to incorporate ferrocene moieties covalently into DNA.

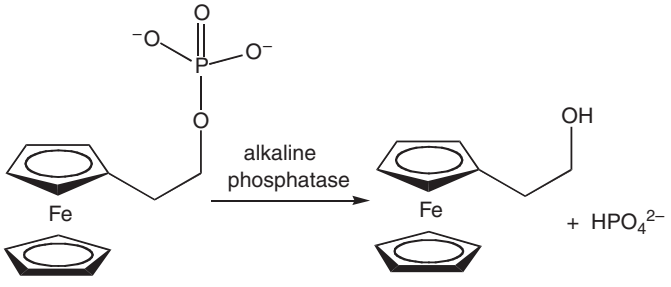

Figure 9 The enzyme-catalyzed hydrolysis of ferrocenylethyl phosphate.

Hapten-labeled ferrocene conjugates have been used in competitive immunoassays based upon the redox cycling of the ferrocene hapten by glucose oxidase as shown in Figure 10. In the original description of this approach, both the sensitivity and the dynamic range were found to be rather low[67] and a subsequent more detailed investigation showed that this was a consequence of the high affinity of the antibody for the conjugate. Subsequently, the synthesis of a quaternary amine-modified conjugate with lower affinity led to an improved performance.[68]

12.12.3.3 Composite Materials Using Ferrocenes

The discovery of new materials such as nanoparticles and nanotubes has led to their use in electrochemical sensors in combination with ferrocene mediators and redox enzymes. Davis and co-workers[69] modified single-wall carbon nanotubes (SWCNTs) by adsorbing glucose oxidase to them and then used a soluble ferrocene derivative as a

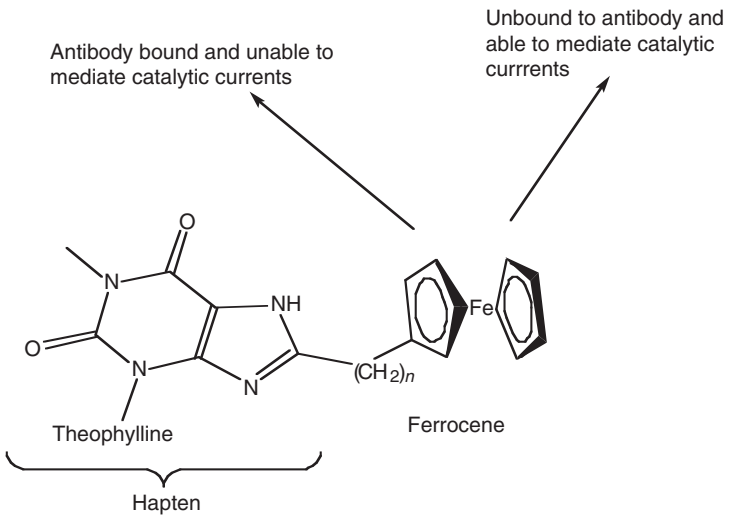

Figure 10 The principle behind using a ferrocene–hapten conjugate for electrochemical immunoassays.

mediator. The high current densities achieved were consistent with the large surface area of the CNTs and functional enzyme immobilization.[70] Functionalized SWCNTs with ferrocene in a polypyrrole matrix have used this for glucose sensing. In a similar fashion, metallic nanoparticles, combining electrical conductivity and high surface area, have also been used. Wang *et al.*[71] developed a sandwich DNA hybridization assay based on an immobilized capture probe on a gold electrode and a second soluble probe carrying a biotin group to which is attached a streptavidin molecule with a gold nanoparticle coated in ferrocenes. The formation of the sandwich brings the ferrocene into close proximity to the underlying electrode where they can undergo oxidation. The high loading of ferrocenes on the nanoparticle gives high currents and hence good detection limits for the target DNA. Baca *et al.*[72] further develops this approach. Silica nanoparticles doped with ferrocenes have been used as mediators with glucose oxidase.[73]

12.12.4 Conclusions

Introduced over 20 years as an alternative mediator to the hexacyanoferrates or organic dyes in amperometric enzyme electrodes, ferrocenes have proved to be a major enabling reagent in the design and fabrication of many different biosensors. A combination of their chemical versatility, synthetic accessibility, rapid homogeneous and heterogeneous electron-transfer kinetics, and molecular reactivity has far expanded their application beyond that of their first use. Besides their many appearances in academic publications, they were also components of the first commercial electronic blood glucose sensors and gave this field a new stimulus with devices of unprecedented convenience and accuracy.

References

1. Morris, C., Ed. *Academic Press Dictionary of Science and Technology*; Academic Press: New York, 1992.
2. Bell, T. W.; Hext, N. M. Supramolecular optical chemosensors for organic analytes. *Chem. Soc. Rev.* **2004**, *33*, 589–598.
3. Cao, H.; Heagy, M. D. Fluorescent chemosensors for carbohydrates: a decade's worth of bright spies for saccharides in review. *J. Fluoresc.* **2004**, *14*, 569.
4. Cooper, J.; Cass, T. *Biosensors: A Practical Approach*, 2nd ed.; Oxford University Press: Oxford, 2003.
5. Eggins, B. R. *Chemical Sensors and Biosensors*; Wiley: London, 2002.
6. Hall, E. A. H. *Biosensors*; Open University Press: London, 1989.
7. Kress-Rogers, E. *Handbook of Biosensors and Electronic Noses: Medicine, Food, and the Environment*; CRC Press: Boca Raton, 1997.
8. Gizeli, E. *Biomolecular Sensors*; Taylor and Francis: London, 2002.
9. Wilson, G. S.; Gifford, R. Biosensors for real-time in vivo measurements. *Biosens. Bioelectron.* **2005**, *20*, 2388–2403.
10. Newman, J. D.; Turner, A. P. F. Home blood glucose biosensors: a commercial perspective. *Biosens. Bioelectron.* **2005**, *20*, 2435–2453.
11. Andreescu, S.; Sadik, O. A. Trends and challenges in biochemical sensors for clinical and environmental monitoring. *Pure Appl. Chem.* **2004**, *76*, 861–878.

12. Hart, J. P.; Crew, A.; Crouch, E.; Honeychurch, K. C.; Pemberton, R. M. Some recent designs and developments of screen-printed carbon electrochemical sensors/biosensors for biomedical, environmental, and industrial analyses. *Anal. Lett.* **2004**, *37*, 789–830.
13. Rich, R. L.; Myszka, D. G. A survey of the year 2002 commercial optical biosensor literature. *J. Mol. Recognit.* **2003**, *16*, 351–382.
14. Leegsma-Vogt, G.; Rhemrev-Boom, M. M.; Tiessen, R. G.; Venema, K.; Korf, J. The potential of biosensor technology in clinical monitoring and experimental research. *Bio-Med. Mater. Eng.* **2004**, *14*, 455–464.
15. Castillo, J.; Gaspar, S.; Leth, S.; Niculescu, M.; Mortari, A.; Bontidean, I.; Soukharev, V.; Dorneanu, S. A.; Ryabov, A. D.; Csoregi, E. Biosensors for life quality – design, development and applications. *Sensor Actuator B-Chem.* **2004**, *102*, 179–194.
16. Armstrong, F. A. Recent developments in dynamic electrochemical studies of adsorbed enzymes and their active sites. *Curr. Opin. Chem. Biol.* **2005**, *9*, 110–117.
17. Cass, A. E. G.; Davis, G.; Francis, G. D.; Hill, H. A. O.; Aston, W. J.; Higgins, I. J.; Plotkin, E. V.; Scott, L. D. L.; Turner, A. P. F. Ferrocene-mediated enzyme electrode for amperometric determination of glucose. *Anal. Chem.* **1984**, *56*, 667–671.
18. Ligler, F. S.; Tait, C. R. *Optical Biosensors: Present and Future*; Elsevier: NewYork, 2002.
19. Epton, R.; Hobson, M. E.; Marr, G. Enzyme catalyzed oxidation of ferrocene compounds. *J. Organomet. Chem.* **1977**, *134*, C23–C26.
20. Fujihira, Y.; Kuwana, T.; Hartzell, C. R. Reversible redox titrations of cytochrome-c and cytochrome-c oxidase using detergent solubilized electrochemically generated mediator-titrants. *Biochem. Biophys. Res. Commun.* **1974**, *61*, 538–543.
21. Bard, A. J.; Faulkner, L. R. *Electrochemical Methods: Fundamentals and Applications*, 2nd ed.; Wiley: New York, 2002.
22. Bourdillon, C.; Demaille, C.; Moiroux, J.; Saveant, J. M. New insights into the enzymatic catalysis of the oxidation of glucose by native and recombinant glucose-oxidase mediated by electrochemically generated one-electron redox cosubstrates. *J. Am. Chem. Soc.* **1993**, *115*, 2–10.
23. Bourdillon, C.; Demaille, C.; Moiroux, J.; Saveant, J. M. From homogeneous electroenzymatic kinetics to antigen-antibody construction and characterization of spatially ordered catalytic enzyme assemblies on electrodes. *Acc. Chem. Res.* **1996**, *29*, 529–535.
24. Yokoyama, K.; Kayanuma, Y. Cyclic voltammetric simulation for electrochemically mediated enzyme reaction and determination of enzyme kinetic constants. *Anal Chem.* **1998**, *70*, 3368–3376.
25. Ryabov, A. D.; Firsova, Y. N.; Nelen, M. I. Ferricenium salts as true substrates of glucose oxidase – a steady-state kinetic study. *Appl. Biochem. Biotechnol.* **1996**, *61*, 25–37.
26. Forrow, N. J.; Sanghera, G. S.; Walters, S. J. The influence of structure in the reaction of electrochemically generated ferrocenium derivatives with reduced glucose oxidase. *J. Chem. Soc., Dalton. Trans.* **2002**, 3187–3194.
27. Bartlett, P.; Tebbutt, P.; Whitaker, R. *Prog. React. Kinet. Mech.* **1991**, *16*, 55.
28. Nicolosi, G.; Patti, A.; Morrone, R.; Piattelli, M. Enzyme-promoted kinetic resolution of 1-hydroxymethyl-2-dimethylaminomethyl-ferrocene. *Tetrahedron: Asymmetry* **1994**, *5*, 1275–1280.
29. Marxtibbon, S.; Katz, E.; Willner, I. Chiral recognition in mediated electron-transfer in redox proteins. *J. Am. Chem. Soc.* **1995**, *117*, 9925–9926.
30. Alzari, P.; Anicet, N.; Bourdillon, C.; Moiroux, J.; Saveant, J. M. Molecular recognition of artificial single-electron acceptor cosubstrates by glucose oxidase? *J. Am. Chem. Soc.* **1996**, *118*, 6788–6789.
31. Sadeghi, S. J.; Nicolosi, G.; Gilardi, G.; Cass, A. E. G. Chiral discrimination in the oxidation of ferrocenes by cytochrome *c* peroxidase. *Chem. Commun.* **1997**, 517–518.
32. Wong, T. S.; Schwaneberg, U. Protein engineering in bioelectrocatalysis. *Curr. Opin. Biotechnol.* **2003**, *14*, 590–596.
33. Cass, A. E. G.; Davis, G.; Hill, H. A. O.; Nancarrow, D. J. The reaction of flavocytochrome *b2* with cytochrome *c* and ferricinium carboxylate. Comparative kinetics by cyclic voltammetry and chronoamperometry. *Biochim. Biophys. Acta* **1985**, *828*, 51–57.
34. Erman, J. E.; Vitello, L. B. Yeast cytochrome *c* peroxidase: mechanistic studies via protein engineering. *Biochim. Biophys. Acta – Protein Struct. Mol. Enzym.* **2002**, *1597*, 193–220.
35. Sadeghi, S. J.; Gilardi, G.; Cass, A. E. G. Mediated electrochemistry of peroxidases – effects of variations in protein and mediator structures. *Biosens. Bioelectron.* **1997**, *12*, 1191–1198.
36. Hale, P. D.; Inagaki, T.; Lee, H. S.; Karan, H. I.; Okamoto, Y.; Skotheim, T. A. Amperometric glycolate sensors based on glycolate oxidase and polymeric electron transfer mediators. *Anal. Chim. Acta* **1990**, *228*, 31–37.
37. Hale, P. D.; Inagaki, T.; Karan, H. I.; Okamoto, Y. A new class of amperometric biosensor incorporating a polymeric electron-transfer mediator. *J. Am. Chem. Soc.* **1989**, *111*, 3482–3484.
38. Boguslavsky, L.; Hale, P. D.; Geng, L.; Skotheim, T. A.; Lee, H. S. Applications of redox polymers in biosensors. *Solid State Ionics* **1993**, *60*, 189–197.
39. Calvo, E. J.; Etchenique, R.; Danilowicz, C.; Diaz, L. Electrical communication between electrodes and enzymes mediated by redox hydrogels. *Anal. Chem.* **1996**, *68*, 4186–4193.
40. Bu, H. Z.; Mikkelsen, S. R.; English, A. M. Nad(p)h sensors based on enzyme entrapment in ferrocene-containing polyacrylamide-based redox gels. *Anal. Chem.* **1998**, *70*, 4320–4325.
41. Iwakura, C.; Kajiya, Y.; Yoneyama, H. Simultaneous immobilization of glucose oxidase and a mediator in conducting polymer films. *J. Chem. Soc., Chem. Commun.* **1988**, 1019–1020.
42. Losada, J.; Cuadrado, I.; Moran, M.; Casado, C. M.; Alonso, B.; Barranco, M. Ferrocenyl silicon-based dendrimers as mediators in amperometric biosensors. *Anal. Chim. Acta* **1997**, *338*, 191–198.
43. Yoon, H. C.; Kim, H. S. Bioelectrocatalyzed signal amplification for affinity interactions at chemically modified electrodes. *Biotechnol. Bioprocess Eng.* **2004**, *9*, 107–111.
44. Kim, E.; Kim, K.; Yang, H.; Kim, Y. T.; Kwak, J. Enzyme-amplified electrochemical detection of DNA using electrocatalysis of ferrocenyl-tethered dendrimer. *Anal. Chem.* **2003**, *75*, 5665–5672.
45. Kwon, S. J.; Kim, E.; Yang, H.; Kwak, J. An electrochemical immunosensor using ferrocenyl-tethered dendrimer. *Analyst* **2006**, *131*, 402–406.
46. Valincius, G.; Ignatjev, J.; Niaura, G.; Kazemekaite, M.; Talaikyte, Z.; Razumas, V.; Svendsen, A. Electrochemical method for the detection of lipase activity. *Anal. Chem.* **2005**, *77*, 2632–2636.
47. Newman, J. D.; Turner, A. P. F. Home blood glucose biosensors: a commercial perspective. *Biosens. Bioelectron.* **2005**, *20*, 2435.
48. Zhang, X. Screen Printed Enzyme Electrodes. In *Biosensors: A Practical Approach*; Cooper, J., Cass, T., Eds.; Oxford University Press: Oxford, 2003.
49. Albareda-Sirvent, M.; Merkoci, A.; Alegret, S. Configurations used in the design of screen-printed enzymatic biosensors. A review. *Sensor Actuator B-Chem.* **2000**, *69*, 153–163.
50. van Staveren, D. R.; Metzler-Nolte, N. Bioorganometallic chemistry of ferrocene. *Chem Rev* **2004**, *104*, 5931–5985.

51. Chen, L. Q.; Zhang, X. E.; Xie, W. H.; Zhou, Y. F.; Zhang, Z. P.; Cass, A. E. G. Genetic modification of glucose oxidase for improving performance of an amperometric glucose biosensor. *Biosens. Bioelectron.* **2002**, *17*, 851–857.
52. DiGleria, K.; Halliwell, C. M.; Jacob, C.; Hill, H. A. O. Site-specific introduction of an electroactive label into a non-electroactive enzyme (beta-lactamase i). *Febs Lett.* **1997**, *400*, 155–157.
53. Di Gleria, K.; Nickerson, D. P.; Hill, H. A. O.; Wong, L. L.; Fulop, V. Covalent attachment of an electroactive sulfydryl reagent in the active site of cytochrome p450(cam) as revealed by the crystal structure of the modified protein. *J. Am. Chem. Soc.* **1998**, *120*, 46–52.
54. Benson, D. E.; Conrad, D. W.; de Lorimier, R. M.; Trammell, S. A.; Hellinga, H. W. Design of bioelectronic interfaces by exploiting hinge-bending motions in proteins. *Science* **2001**, *293*, 1641–1644.
55. Ihara, T.; Maruo, Y.; Takenaka, S.; Takagi, M. Ferrocene–oligonucleotide conjugates for electrochemical probing of DNA. *Nucl. Acid. Res.* **1996**, *24*, 4273–4280.
56. Navarro, A. E.; Spinelli, N.; Moustrou, C.; Chaix, C.; Mandrand, B.; Brisset, H. Automated synthesis of new ferrocenyl-modified oligonucleotides: study of their properties in solution. *Nucl. Acid. Res.* **2004**, *32*, 5310–5319.
57. Pike, A. R.; Ryder, L. C.; Horrocks, B. R.; Clegg, W.; Connolly, B. A.; Houlton, A. Ferrocenyl-modified DNA: synthesis, characterization and integration with semiconductor electrodes. *Chem. Eur. J.* **2004**, *11*, 344–353.
58. Verheijen, J. C.; van der Marel, G. A.; van Boom, J. H.; Metzler-Nolte, N. Transition metal derivatives of peptide nucleic acid (pna) oligomers—synthesis, characterization, and DNA finding. *Bioconjugate Chem.* **2000**, *11*, 741–743.
59. Baldoli, C.; Falciola, L.; Licandro, E.; Maiorana, S.; Mussini, P.; Ramani, P.; Rigamonti, C.; Zinzalla, G. A new ferrocene conjugate of a tyrosine pna monomer: synthesis and electrochemical properties. *J. Organomet. Chem.* **2004**, *689*, 4791–4802.
60. Baldoli, C.; Cerea, P.; Giannini, C.; Licandro, E.; Rigamonti, C.; Maiorana, S. The metal-conjugated peptide nucleic acid challenge. *Synlett* **2005**, 1984–1994.
61. Takenaka, S. Pseudo-polyferrocene coating of double stranded DNA with ferrocenylnaphthalene diimide and its application for electrochemical gene detection. *Polym. J.* **2004**, *36*, 503–512.
62. Le Floch, F.; Ho, H. A.; Harding-Lepage, P.; Bedard, M.; Neagu-Plesu, R.; Leclerc, M. Ferrocene-functionalized cationic polythiophene for the label-free electrochemical detection of DNA. *Adv. Mater.* **2005**, *17*, 1251.
63. Yu, C. J.; Wan, Y. J.; Yowanto, H.; Li, J.; Tao, C. L.; James, M. D.; Tan, C. L.; Blackburn, G. F.; Meade, T. J. Electronic detection of single-base mismatches in DNA with ferrocene-modified probes. *J. Am. Chem. Soc.* **2001**, *123*, 11155–11161.
64. Nakayama, M.; Ihara, T.; Nakano, K.; Maeda, M. DNA sensors using a ferrocene–oligonucleotide conjugate. *Talanta* **2002**, *56*, 857–866.
65. Zauner, G.; Wang, Y. T.; Lavesa-Curto, M.; MacDonald, A.; Mayes, A. G.; Bowater, R. P.; Butt, J. N. Tethered DNA hairpins facilitate electrochemical detection of DNA ligation. *Analyst* **2005**, *130*, 345–349.
66. Limoges, B.; Degrand, C. Ferrocenylethyl phosphate: an improved substrate for the detection of alkaline phosphatase by cathodic stripping ion-exchange voltammetry. Application to the electrochemical enzyme affinity assay of avidin. *Anal. Chem.* **1996**, *68*, 4141–4148.
67. Digleria, K.; Hill, H. A. O.; McNeil, C. J.; Green, M. J. Homogeneous ferrocene-mediated amperometric immunoassay. *Anal. Chem.* **1986**, *58*, 1203–1205.
68. Forrow, N. J.; Foulds, N. C.; Frew, J. E.; Law, J. T. Synthesis, characterization, and evaluation of ferrocene–theophylline conjugates for use in electrochemical enzyme immunoassay. *Bioconjugate Chem.* **2004**, *15*, 137–144.
69. Davis, J. J.; Coleman, K. S.; Azamian, B. R.; Bagshaw, C. B.; Green, M. L. H. Chemical and biochemical sensing with modified single walled carbon nanotubes. *Chem. Eur. J.* **2003**, *9*, 3732–3739.
70. Callegari, A.; Cosnier, S.; Marcaccio, M.; Paolucci, D.; Paolucci, F.; Georgakilas, V.; Tagmatarchis, N.; Vazquez, E.; Prato, M. Functionalised single wall carbon nanotubes/polypyrrole composites for the preparation of amperometric glucose biosensors. *J. Mater. Chem.* **2004**, *14*, 807–810.
71. Wang, J.; Li, J. H.; Baca, A. J.; Hu, J. B.; Zhou, F. M.; Yan, W.; Pang, D. W. Amplified voltammetric detection of DNA hybridization via oxidation of ferrocene caps on gold nanoparticle/streptavidin conjugates. *Anal. Chem.* **2003**, *75*, 3941–3945.
72. Baca, A. J.; Zhou, F. M.; Wang, J.; Hu, J. B.; Li, J. H.; Wang, J. X.; Chikneyan, Z. S. Attachment of ferrocene-capped gold nanoparticle-streptavidin conjugates onto electrode surfaces covered with biotinylated biomolecules for enhanced voltammetric analysis. *Electroanalysis* **2004**, *16*, 73–80.
73. Zhang, F. F.; Wan, Q.; Wang, X. L.; Sun, Z. D.; Zhu, Z. Q.; Xian, Y. Z.; Jin, L. T.; Yamamoto, K. Amperometric sensor based on ferrocene-doped silica nanoparticles as an electron transfer mediator for the determination of glucose in rat brain coupled to *in vivo* microdialysis. *J. Electroanal. Chem.* **2004**, *571*, 133–138.
74. Bartlett, P. N.; Pratt, K. F. E. A study of the kinetics of the reaction between ferrocene monocarboxylic acid and glucose-oxidase using the rotating-disc electrode. *J. Electroanal. Chem.* **1995**, *397*, 53–60.
75. Razumiene, J.; Meskys, R.; Gureviciene, V.; Laurinavicius, V.; Reshetova, M. D.; Ryabov, A. D. 4-ferrocenylphenol as an electron transfer mediator in pqq-dependent alcohol and glucose dehydrogenase-catalyzed reactions. *Electrochem. Commun.* **2000**, *2*, 307–311.
76. Okuda, J.; Wakai, J.; Igarashi, S.; Sode, K. Engineered pqq glucose dehydrogenase-based enzyme sensor for continuous glucose monitoring. *Anal. Lett.* **2004**, *37*, 1847–1857.
77. Antiochia, R.; Cass, A. E. G.; Palleschi, G. Purification and sensor applications of an oxygen insensitive, thermophilic diaphorase. *Anal. Chim. Acta* **1997**, *345*, 17–28.
78. Antiochia, R.; Gallina, A.; Lavagnini, I.; Magno, F. Kinetic and thermodynamic aspects of nad-related enzyme linked mediated bioelectrocatalysis. *Electroanalysis* **2002**, *14*, 1256–1261.
79. Antiochia, R.; Lavagnini, I.; Magno, F. Electrocatalytic oxidation of dihydronicotinamide adenine dinucleotide with ferrocene carboxylic acid by diaphorase from clostridium kluveri. Remarks on the kinetic approaches usually adopted. *Electroanalysis* **1999**, *11*, 129–133.
80. Sanchez, P. D.; Ordieres, A. J. M.; Garcia, A. C.; Blanco, P. T. Peroxidase ferrocene modified carbon paste electrode as an amperometric sensor for the hydrogen-peroxide assay. *Electroanalysis* **1991**, *3*, 281–285.
81. Tsai, W. C.; Cass, A. E. G. Ferrocene-modified horseradish-peroxidase enzyme electrodes—a kinetic-study on reactions with hydrogen-peroxide and linoleic hydroperoxide. *Analyst* **1995**, *120*, 2249–2254.
82. Vidal, J. C.; Yague, M. A.; Castillo, J. R. A chronoamperometric sensor for hydrogen-peroxide based on electron-transfer between immobilized horseradish-peroxidase on a glassy-carbon electrode and a diffusing ferrocene mediator. *Sensor Actuator B-Chem.* **1994**, *21*, 135–141.
83. Smit, M. H.; Cass, A. E. G. Cyanide detection using a substrate-regenerating, peroxidase-based biosensor. *Anal. Chem.* **1990**, *62*, 2429–2436.
84. Cooper, J. M.; Bannister, J. V.; McNeil, C. J. A kinetic study of the catalysed oxidation of 1′,3-dimethylferrocene ethylamine by cytochrome *c* peroxidase. *J. Electroanal. Chem.* **1991**, *312*, 155–163.
85. Sadeghi, S. J.; Cass, A. E. G. Electron-transfer between cytochrome-*c* peroxidase and ferrocene. *Biochem. Soc. Trans.* **1995**, *23*, S153–S153.

86. Bouvrette, P.; Male, K. B.; Luong, J. H. T.; Gibbs, B. F. Amperometric biosensor for diamine using diamine oxidase purified from porcine kidney. *Enzyme Microb. Technol.* **1997**, *20*, 32–38.
87. Cass, A. E. G.; Davis, G.; Hill, H. A. O.; Nancarrow, D. J. The reaction of flavocytochrome-b2 with cytochrome-*c* and ferricinium carboxylate—comparative kinetics by cyclic voltammetry and chronoamperometry. *Biochim. Biophys. Acta* **1985**, *828*, 51–57.
88. Turner, A. P. F.; Aston, W. J.; Higgins, I. J.; Bell, J. M.; Colby, J.; Davis, G.; Hill, H. A. O. Carbon-monoxide—acceptor oxidoreductase from pseudomonas-thermocarboxydovorans strain-*c2* and its use in a carbon-monoxide sensor. *Anal. Chim. Acta* **1984**, *163*, 161–174.
89. Cass, A. E. G.; Davis, G.; Green, M. J.; Hill, H. A. O. Ferricinium ion as an electron-acceptor for oxido-reductases. *J. Electroanal. Chem.* **1985**, *190*, 117–127.
90. Okuma, H.; Takahashi, H.; Sekimukai, S.; Kawahara, K.; Akahoshi, R. Mediated amperometric biosensor for hypoxanthine based on a hydroxymethyl ferrocene-modified carbon paste electrode. *Anal. Chim Acta* **1991**, *244*, 161–164.
91. Razumiene, J.; Gureviciene, V.; Vilkanauskyte, A.; Marcinkeviciene, L.; Bachmatova, I.; Meskys, R.; Laurinavicius, V. Improvement of screen-printed carbon electrodes by modification with ferrocene derivative. *Sensor Actuator B-Chem.* **2003**, *95*, 378–383.
92. Dicks, J. M.; Aston, W. J.; Davis, G.; Turner, A. P. F. Mediated amperometric biosensors for d-galactose, glycolate and l-amino acids based on a ferrocene-modified carbon paste electrode. *Anal. Chim. Acta* **1986**, *182*, 103–112.
93. Gundogan-Paul, M.; Celebi, S. S.; Ozyoruk, H.; Yildiz, A. Amperometric enzyme electrode for organic peroxides determination prepared from horseradish peroxidase immobilized in poly(vinylferrocenium) film. *Biosens. Bioelectron.* **2002**, *17*, 875–881.
94. Horie, H.; Ujihara, T.; Kohata, K.; Uematsu, H.; Nakajima, T.; Hiromato, M.; Kakiuchi, T. Analysis of polyphenols in green tea using a polyphenol sensor. *J. Jpn. Soc. Food Sci. Technol.* **2001**, *48*, 586–590.
95. McNeil, C. J.; Cooper, J. M.; Spoors, J. A. Amperometric enzyme electrode for determination of theophylline in serum. *Biosens. Bioelectron.* **1992**, *7*, 375–380.
96. Khan, G. F.; Kobatake, E.; Ikariyama, Y.; Aizawa, M. Amperometric biosensor with pqq enzyme immobilized in a mediator-containing polypyrrole matrix. *Anal. Chim. Acta* **1993**, *281*, 527–533.
97. Tkac, J.; Vostiar, I.; Sturdik, E.; Gemeiner, P.; Mastihuba, V.; Annus, J. Fructose biosensor based on d-fructose dehydrogenase immobilised on a ferrocene-embedded cellulose acetate membrane. *Anal. Chim. Acta* **2001**, *439*, 39–46.
98. Shoham, B.; Migron, Y.; Riklin, A.; Willner, I.; Tartakovsky, B. A bilirubin biosensor based on a multilayer network enzyme electrode. *Biosens. Bioelectron.* **1995**, *10*, 341–352.
99. Loechel, C.; Basran, A.; Basran, J.; Scrutton, N. S.; Hall, E. A. H. Using trimethylamine dehydrogenase in an enzyme linked amperometric electrode—Part 1. Wild-type enzyme redox mediation. *Analyst* **2003**, *128*, 166–172.
100. Degani, Y.; Heller, A. Direct electrical communication between chemically modified enzymes and metal-electrodes.1. Electron-transfer from glucose-oxidase to metal-electrodes via electron relays, bound covalently to the enzyme. *J. Phys. Chem.* **1987**, *91*, 1285–1289.
101. Bartlett, P. N.; Whitakeer, R. G.; Green, M. J.; Frew, J. Covalent binding of electron relays to glucose oxidase. *Chem. Commun.* **1987**, 1603–1604.
102. Tsai, W. C.; Cass, A. E. G. Ferrocene-modified horseradish peroxidase enzyme elctrodes. A kinetic study of the reactions with hydrogen peroxide and linoleic hydroperoxide. *Analyst* **1995**, *120*, 2249–2254.
103. DiGleria, K.; Hill, H. A. O.; Wong, L. L. N-(2-ferrocene-ethyl)maleimide: a new electroactive sulphydryl-specific reagent for cysteine-containing peptides and proteins. *Febs Lett* **1996**, *390*, 142–144.

12.13 Environmental and Biological Aspects of Organometallic Compounds

R O Jenkins and P J Craig, De Montfort University, Leicester, UK
K A Francesconi, Karl-Franzens University Graz (Uni-Graz), Graz, Austria
C F Harrington, University of Leicester, Leicester, UK

12.13.1 Introduction

Organometallic compounds in the environment were covered in COMC (1982).[1] The present review covers the period since 1982, but with emphasis on developments since 1993. The essential principles are also summarized here. A number of detailed monograph articles exist covering the elements referred to in this chapter[2–5] and a one-volume work covering the subject was published in 2003.[6] The organometallic compounds considered here, nearly all, have conventional metal-to-carbon sigma bonds, often to the methyl group (see below).

Numerous organometallic compounds or complexes exist in the natural environment. Their importance (usually meaning their potential for transport and/or toxic impact) depends largely on their speciation (i.e., the complete molecular identity of the entity concerned). Speciation determines actual toxicity, potential for transport within organisms and the geosphere, and stability to light, heat, and water, and also to breakdown within organisms. This can be illustrated by noting the essential nontoxicity of arsenobetaine and the well-known toxic potential of the arsenic oxides, all of which are found naturally in the environment.[7] The importance of speciation to toxicity can be

Table 1 Species specificity of triorganotin compounds

Species compound	*R in most active R_3SnX*
Insects	Me
Mammals	Et
Gram-negative bacteria	*n*-Pr
Gram-positive bacteria, fish, fungi, molluscs, plants	*n*-Bu
Fish, fungi, molluscs	C_6H_5
Fish, mites	*c*-C_6H_{11}, $C_6H_5(CH_2)_2CCH_2$

demonstrated by the differential toxicities of the various alkyltin species (Table 1). The toxicity of organometallic compounds of environmental significance is given in Section 12.13.6.

Organometallic compounds may be introduced to the environment as such or they may be formed there. In the latter case, this nearly always refers to the natural formation in the environment of methylmetal species from inorganic precursors (biological methylation, biomethylation), although reports of ethylmercury and group 6 carbonyls formed in the environment exist.[8,9] Biological methylation is fundamentally important to understand environmental and biological aspects of organometallic compounds and is considered in detail in Section 12.13.3, as well as in the sections dealing individually with the different types of organometallic compounds. Organometallic compounds which are introduced to the environment may enter through deliberate use (e.g., the organotin antifouling paints) or they may enter accidentally by way of pollution.

Reference should be made to units and quantities here. Synthetic chemistry is usually carried out at the mol l^{-1} level. The organometallic compounds that occur in the natural environment usually exist at the "ppm" or "ppb" level, very roughly "grams per million grams," etc. There has been some lack of precision in the meaning and use of these environmental units, arising from the species often being present in not well-defined media (e.g., wet sediment). For the moment, it should be understood that the levels or concentrations of organometallic compounds found in the environment are much lower than those that usually exist in the laboratory. This does not mean that there is no potential for environmental impact or toxicity (see later). Indeed, the discovery of naturally occurring methylarsenic species in marine animals in 1971 has led to important developments in synthetic arsenic chemistry.[10] These very low concentrations have however stimulated great improvements in the analytical techniques necessary to identify and measure these compounds in the environment. Linked (or hyphenated) analytical techniques (e.g., gas chromatography-mass spectroscopy, liquid chromatography-mass spectroscopy, online derivatization followed by inductively coupled mass spectroscopy) are now usually used. Where the organometal is complexed or otherwise insufficiently volatile for gas chromatography, numerous derivatization techniques exist to make them so (e.g., hydride generation, Grignard reactions). In some cases, these derivatization reactions have led to new synthetic outcomes (e.g., the alkylmercury hydrides[11]). These analytical techniques are discussed in Section 12.13.5.

The organometallic compounds considered in this chapter are all from groups 12–16 of the periodic table, with particular reference to Hg, Pb, Sn, As, Sb, Si, and Se. With the exception of organosilicon and (possibly) organolead compounds, which enter the environment solely as pollutants from anthropogenic sources, organometallic forms of the other five elements are known to be formed within the environment through biological methylation (see Section 12.13.3). Some other elements from these periodic groups, such as Cd, Ti, and Bi, are also known to undergo biological methylation in the environment and are also considered briefly within Section 12.13.3. Although organometallic forms of transition metals have great importance as synthetic and catalytic intermediates, very little environmental pollution arose from their use, which is mainly because of the high cost of the metals involved. Furthermore, transition metal organometallics are not known to be formed in the environment through biological methylation. Generally, therefore, organometallic compounds of transition metals have low environmental significance. There are a few exceptions, such as environmental problems arising from use of λ-$MeC_5H_4Mn(CO)_3$ as an antiknock agent in gasoline. $Mo(CO)_6$ and $W(CO)_6$ have also been detected in the environment.

12.13.2 Environmental Stability of Organometallic Compounds

In the present context, stability is a pragmatic term, meaning stability to the many reagents encountered by the organometal in the environment, viz. light, oxygen, water, and other chemical species including free radicals and organisms. Kinetically stable organometallic species may be quite unstable in the environment. It might be

concluded that organometals will have only a very brief life in the environment but this is not always the case. In some cases, they may be chemically protected by coordinative saturation (e.g., by coordination to humic materials) and strong carbon metal bonds (e.g., arsenobetaine) or they may simply be out of reach of otherwise active reagents (e.g., buried in anoxic sediments away from light or oxygen). We now consider in a practical sense the stability of organometals in the environment to the various reagents.

12.13.2.1 Stability to Atmospheric Oxidation

All organometals are thermodynamically unstable to oxidation although many are kinetically stable. However, even compounds that in bulk might spontaneously ignite in air may not do so if they are in very dilute form in air (e.g., trimethylarsenic). This may be understood on the basis of collision theory and the matter has been discussed recently.[12] Such considerations do not always apply but they should be borne in mind. Other things being equal, stability to oxidation is of course governed by the same factors as for organometallic compounds in the laboratory, viz. bond polarity, low-lying empty valence orbitals, lack of stabilization by coordination, etc. A list of stabilities to oxygen for the compounds in bulk is given in Table 2, and this should be taken as a general guide to practical stability to oxidation.

12.13.2.2 Stability to Water

The first step in decomposition would normally be nucleophilic attack of the lone electron pair of the water oxygen atom on an empty orbital on the organometal. It is therefore connected with the existence of low-lying empty orbitals on the organometal. Such attack is related to the polarity of the metal carbon bond, strongly polarized species being

Table 2 Bulk stability of some organometallic species to oxygen

Stable	*Unstable*
Me_2Hg, $MeHg^+$	$MePb^+$
$R_nSnX_{(4-n)}$ (X not H)	Me_3As
$MeAsO(OH)_2$[a], $Me_2AsO(OH)$[a]	Me_3Sb
$Me_3AsCH_2COO^*$	Me_2AsH[a]
Me_4As^+[a]	$MeAsH_2$[a]
Me_3AsO[a]	Me_4SnH_{4-n}
$Me_nPbX_{(4-n)}$ (except for $n=1$)	Me_4PbH_{4-n}
$MeCoB_{12}$	

[a]And corresponding Sb species.
Note that unstable species, when very attenuated, may be environmentally stable for long periods.
Adapted from Craig, P. J.; Eng, G.; Jenkins, R. O. Occurrence and Pathways of Organometallic Compounds in the Environment—General Considerations. In *Organometallic Compounds in the Environment*, 2nd ed.; Craig, P. J., Ed.; Wiley: Chicester, 2003; pp 1–56.

Table 3 Bulk stability of some organometallic species to water

Organometallic	*Stability*
R_2Hg, R_4Sn, R^4Pb	Volatile, hydrophobic, diffuse to atmosphere
MeHgX	Stable, soluble depending on X
$Me_nSn_{(4-n)}^+$	Stable
$Me_nPb_{(4-n)}^+$	Stable except for $n=1$
Me_2As^+,$MeAs^{++}$	Stable
$Me_2AsO(OH)$[a]	Stable
$MeAs(OH)_2$[a]	Stable
Me_3ASO^*	Stable

[a]Also corresponding Sb species.
Table refers to stability of the metal carbon unit.
Adapted from Craig, P. J.; Eng, G.; Jenkins, R. O. Occurrence and Pathways of Organometallic Compounds in the Environment—General Considerations. In *Organometallic Compounds in the Environment*, 2nd ed.; Craig, P. J., Ed.; Wiley: Chicester, 2003; pp 1–56.

more unstable. Table 3 indicates stabilities to water and should be considered with the above guidelines in mind. Stability here refers to air-free distilled water without other complexing or reactive species being present (not usually a realistic situation) and may be taken as a general guide.

12.13.2.3 Stability to Light in the Presence of Atmospheric Reagents

Here it is essential to consider the presence not only of visible light and UV radiation, but also the presence of other atmospheric species which are normally present (usually free radicals). Organometals are much less stable in these circumstances than to radiation alone. The primary radiolytic decomposition process is electronic absorption leading to radical formation. Bearing in mind that most radiation does not penetrate to the earth's surface,[1] exceptions being light 340–700 nm (and radio waves which are insufficiently energetic for direct decomposition), specific radiolytic homolysis of metal carbon bonds alone is not the main process for decomposition of organometals in the atmosphere.

Considering direct photolysis, light stability is clearly more relevant for the saturated (RnM) type organometals that are volatile and enter the atmosphere (e.g., R_4Pb, Me_2Hg) than less volatile cationic derivatives that are found in the water and sediment zones (e.g., R_3Pb^+, $MeHg^+$). Direct photolysis of, for example, Me_2Hg produces $MeHg^0$ and Me radicals at 254 nm.[13] In general, radiation at wavelengths sufficient directly to homolyze M–C bonds tends to be absorbed by the atmosphere and does not penetrate to ground level. However, as noted, processes in the real atmosphere are more complex and lead to much reduced stability than suggested by laboratory experiments. There is the presence of oxygen, free radicals (e.g., OH, O_3P, and O_3, and in photochemically polluted areas other organic free radicals), and particle surfaces able to catalyze decomposition. Taking this into account, the lifetime of volatile organometals (e.g., Me_4P) can be estimated as hours or a few days, not decades as they might be if radiolytic fission alone was the only factor.

Processes which lead to decomposition are discussed in more detail in the appropriate sections that follow. By way of example (Equations (1)–(3)), for Me_4Pb, we can expect:[14]

$$Me_4OPb + OH = Me_3PbCH_2 + H_2O \quad (1)$$

$$Me_4Pb + O_3 = Me_3PbOOH + CH_2O \quad (2)$$

$$Me_4Pb + O(_3P) = Me_3PbCH_2 + OH \quad (3)$$

Such processes are very much more effective than radiation alone, despite gradual mixing in the higher atmosphere and consequent exposure to UV radiation at these higher levels, which would also decompose organometallic compounds into radical species and their metals. These mixing processes alone might take decades. Taking into account the radical processes above and those also mediated by other species present in polluted atmospheres (e.g., ClO_x, NO_x, etc.), the lifetimes of organometallic species in many atmospheres is, as mentioned, of the order of days or hours. Decay rates in polluted atmospheres for individual organometals are discussed in the relevant sections below.

12.13.2.4 Stability within Organisms

These aspects are intimately related to toxicity matters, which are considered in Section 12.13.6. Breakdown of organometallic compounds in organisms usually takes place by dealkylation, often to the alkane and metal (e.g., bacteria toward methylmercury). Fully saturated organometals (e.g., tetramethyllead) usually decay rapidly by loss of a methyl group to the trialkyl forms, which are more stable. These cationic forms then decay more slowly by stepwise loss of alkyl group, leading to the metal. For higher alkyls (e.g., butyltins), decay again takes place by stepwise loss of alkyl group, but not by direct metal carbon bond cleavage but, in animals, by initial hydroxylation of the alkyl group in the liver.[4] Methylarsenic species tend, by contrast, to be more stable against demethylation in animals leading to them being less toxic than the inorganic forms (because the coordinated arsenic is unavailable for biological activity). The reverse is more normal: partially decayed cationic organometallic species (e.g., methylmercury, trimethyllead) have a suitable balance of hydro- and lipophilic characteristics to be transported across membranes and to enter cells. Biological dealkylation is considered in more detail in Section 12.13.4.

12.13.3 Biological Alkylation

Biological alkylation (or bioalkylation) involves enzymatic transfer of a preformed alkyl group from a donor atom to an acceptor atom. The most common alkyl transferred is the methyl group in a process termed biomethylation, catalyzed

Table 4 Metal biomethylation

Periodic group	*Element*	*Type of organisms*	*Biological methyl donor*	*Methylated species detected in the environment*	*Key references/ reviews*
9	Co	[a–d]	Only as vitamin B_{12}		389
10	Ni	[a]	Only as Ni incorporation into organic cofactor of methanogenic bacteria		273,390
12	Cd	[a]	MC probable donor	Me_2Cd; $MeCd^{+}$[f]	391–395
	Hg	[a]	MC donor; mainly sulfur-reducing bacteria	Me_2Hg; $MeHg^{+}$; MeHgH (higher alkyl species also identified in environment)	396–398,116,124
13	Tl	[a]	Methyl donor unknown	Me_2Tl^{+}[f]	399,400
14	Ge	[a(?)]	Biomethylation not definitively established	Me_3GeH;[e] Me_2GeH_2[e]	401,402,18
	Sn	[a, b]	MC probable donor	Me_4Sn; Me_3SnH; Me_2SnH_2;[e] $MeSnH_3$ (higher alkyl species also identified in environment)	173
	Pb	[a, b(?)]	Biomethylation not definitively established[e]	Me_4Pb; Me_3PbH[e]	391–393,403
15	As	[a–d]	SAM or MC (anaerobic bacteria) donor	Me_4As_2; Me_3AsO; Me_3As; Me_2AsH; $MeAsH_2$; $MeAsO(OH)_2$; $Me_2AsO(OH)_2$ (higher alkyl species also identified in environment)	(Section 12.13.3.1)
	Sb	[a, b]	SAM donor	Me_3SbO; Me_3Sb; Me_2SbH; $MeSbH_2$	283,290,294,296
	Bi	[a]	MC probable donor	Me_3Bi; Me_2BiH; MeBiH	19,394,404
16	Se	[a–d]	SAM or selenium analog (*Se*-adenosylselenomethionine)	Me_2Se; $Me2Se_2$; Me_2SeS; MeSeH[e] (Et_2Se also found in environment)	405–407
	Te	[a, b, d]	SAM donor	Me_2Te (Et_2Te also found in environment)	294,408,409
	Po	[a, b]	Biomethylation not definitively established; MC probable donor	Me_2Po[e]	410,411

Type of organism capable of methylation:
[a]bacteria;
[b]fungi/algae;
[c]plants;
[d]animals.
[e]Identity in environment uncertain (if hydride, species identified after derivatization with $NaBH_4$).
[f]Counterion unknown.
S-adenosylmethionine, SAM; methylcobalamin, MC.

by methyltransferase enzymes. Bioalkylation not involving methyl group transfer is comparatively rare and is only associated with those metalloids (As, Se, Te) capable of being biomethylated by higher organisms. There are several recent reviews on biological methylation of metals that deal with both general and element-specific aspects.[13,15] Thayer[16] has reviewed the biological methylation of less-studied elements (i.e., excluding Hg and As). Table 4 summarizes metal biomethylation with regard to type of catalytic organism, biological mechanism, and methylated species detected in the environment.

Biomethylation of a range of metals and metalloids is known to occur in soils from disparate locations, but is particularly associated with metal-containing sediments from environmental waters such as river estuaries and harbors. Volatile methyl derivatives of metals have been found in gases released from natural and anthropogenic environments, including geothermal gases, sewage treatment plants, marine sediments, and landfill sites.[17–20] The formation of volatile compounds through biomethylation is considered to be a significant part of the biogeological cycles of some metal(loid)s such as As, Hg, Se, and Sn.

Biomethylation (enzymatic transmethylation) occurs in all living cells, and is an essential part of cellular metabolism, leading to methylation of proteins, nucleic acid bases, polysaccharides, and fatty acids. However, not all

organisms can methylate all elements. The organisms responsible for metal biomethylation are almost exclusively microorganisms (Table 4). Anaerobic bacteria are thought to be the main agents of biomethylation in sediments and other anoxic environments. Some aerobic and facultatively anaerobic bacteria, as well as certain filamentous fungi, yeasts, and lower algae, have also been shown to be capable of metal biomethylation. With the exception of their cobalt content as vitamin B_{12}, "higher organisms" do not seem to be capable of biomethylating true metals. For the metalloids arsenic, selenium, and tellurium, however, many higher organisms have been shown to form methyl derivatives of these elements, for example, methylarsenicals are formed in a wide range of organisms, including marine biota and mammals (including man).

The attachment of a methyl group to a metal changes the chemical and physical properties of that element, which in turn can substantially influence toxicity, environmental mobility, and geological cycling. Biomethylation enhances solubility of metals in lipids and usually decreases solubility in water.

12.13.3.1 Mechanisms of Biomethylation

S-Adenosylmethionine (SAM) and *N*-methylcobalamine (MC) have both been shown to be involved in the biomethylation of metals (Figure 1). Both methylating agents have an extensive chemistry and have been studied intensively in relation to methylation of organic molecules.

SAM is synthesized by the transfer of an adenosyl group from adenosine triphosphate (ATP) to the sulfur atom of the amino acid methionine. The positive charge on the sulfur atom activates the methyl group of methionine, making SAM a potent methyl carbonium ion (Me^+) donor. SAM is considered a ubiquitous methylating agent.

In biological systems, the methyl group is transferred as an intermediate radical ($Me^{\cdot}$) or as a carbonium ion. In this oxidative addition process, the atom receiving the methyl group requires an available pair of electrons in the valence shell, and alternation of M^{n+} and $M^{(n+2)+}$ oxidation states occurs. The reaction is often referred to as the Challenger mechanism, after Frederick Challenger (for historic review, see Ref: 21), who first formulated it for methylation of arsenic, involving a series of reductions and methylations; the Challenger scheme[22] is shown in Figure 2. SAM has subsequently been shown to be also the methylating agent for Sb, Se, and Te, all of which have an available lone pair of electrons (Table 4). Conversely, for MC—a derivative of vitamin B_{12}—the recipient atoms must be electrophilic, since the methyl group is transferred as a carbanion (Me^-). MC is well established as a methylating agent for mercury and is also thought to be involved in the methylation of As, Bi, Cd, Po, and Sn (Table 4).

Only one methyl group is transferred to metals in each step, irrespective of the methyl donor. Further methyl groups may then be transferred to the same receiving atom.

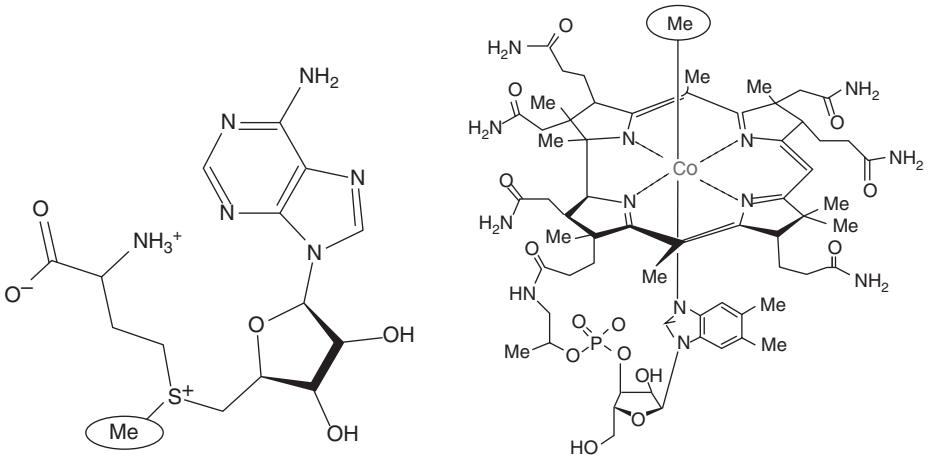

Figure 1 Biological methyl donors involved in metal biomethylation: **1** *S*-adenosylmethionine (SAM); **2** *N*-methylcobalamine (MC). The methyl group transferred to the metal is circled.

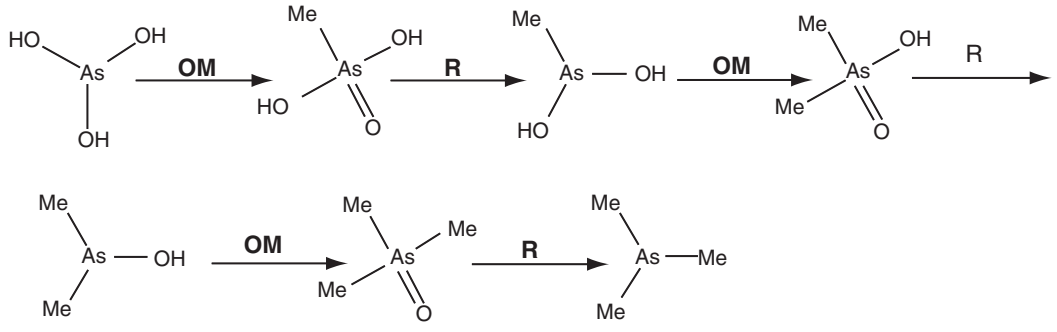

Figure 2 The Challenger[22] scheme of arsenic biomethylation involving alternate oxidative methylation (**OM**) and reduction (**R**).

12.13.4 Microbial Demethylation/Dealkylation

Microbial demethylations, or dealkylations, of organometallic forms are important reactions in detoxification mechanisms for some metals, such as mercury and tin. Bacterial detoxification of organomercurials is well established and involves the enzyme organomercurial lyase (OL)—a product of the *merB* gene—that enzymatically cleaves the Hg–C bond to form Hg^{2+}, which is then reduced by the enzyme mercuric reductase (MR) to the less toxic Hg(0) (Equations (4) and (5)). The high volatility of Hg(0) results in it being rapidly removed to the atmosphere.

$$MeHg^{+} \xrightarrow{OL} CH_4 + Hg^{2+} \xrightarrow{MR} Hg(0) \tag{4}$$

$$C_2H_5Hg^{+} \xrightarrow{OL} C_2H_6 + Hg^{2+} \xrightarrow{MR} Hg(0) \tag{5}$$

Bacterial oxidative demethylation of methylmercury, involving liberation of CO_2, is also known to occur. One mechanism is thought to involve enzymes associated with bacterial metabolism of C1 compounds and is believed to occur widely in freshwater and aqueous environments, under both aerobic and anaerobic conditions. A reaction analogous to microbial monomethylamine degradation has been proposed (Equation (6)):[23]

$$4MeHg^{+} + 2H_2O + 4H^{+} \longrightarrow 3CH_4 + CO_2 + 4Hg^{2+} + 2H_2 \tag{6}$$

Other workers[24] have proposed the involvement of an OL in cleavage of methylmercury, giving rise to Hg^{2+}.

Degradation of organotin compounds (OTCs) has been demonstrated for a wide range of microorganisms, which include bacteria, fungi, and algae.[25] Organotin degradation (Equation (7)) is thought to involve sequential cleavage of tin–carbon bonds, resulting in removal of organic groups and a general reduction in toxicity. Cleavage is initiated by hydroxo attack on a hydrogen attached to a ß-carbon atom (Equation (7)).

$$R_4Sn \longrightarrow R_3SnX \longrightarrow R_2SnX_2 \longrightarrow RSnX_3 \longrightarrow SnX_4 \tag{7}$$

Tin–carbon bonds are also cleaved abiotically, for example, by UV light, and it has proved difficult to establish the relative importance of abiotic and biotic mechanisms of organotin degradation in the natural environment.[25] In some circumstances, environmental conditions (such as pH and redox potential), established by microbial activity, greatly influence the extent of abiotic degradation of organotins.[25] These comments relating to abiotic and biotic mechanisms of organotin degradation also apply to other organometals.

Bacterial demethylation of methylarsenicals is known to occur in aerobic aqueous and terrestrial environments, giving rise to CO_2 and arsenate. Common soil bacteria, such as *Mycobacterium*, *Alcaligenes*, and *Pseudomonas*, are known to demethylate mono- and dimethylarsenic compounds.[26–28] An important part of the biogeological cycling of arsenic involves bacterial demethylation of methylarsenic acids excreted by marine algae, although the mechanism(s) of demethylation of methylated arsenic compounds is essentially unknown.

Dimethylselenide has been show to be demethylated by methanogenic and sulfate-reducing bacteria in anaerobic environments, with the liberation of CO_2 and CH_4.[29] Several bacterial isolates from aerobic soils—including members of the genera *Pseudomonas*, *Xanthomonas*, and *Corynebacterium*—are known to utilize methylselenides as sole source of carbon.

12.13.5 Analytical Methods

12.13.5.1 Introduction

Over the last decade, there has been a significant growth and diversification in the analytical methods used for the measurement of organometallic compounds in environmental and biological samples and it can now be considered a mature branch of analytical chemistry in its own right. This area of activity, termed "speciation analysis," has been defined by IUPAC[30] as the "analytical activities of identifying and/or measuring the quantities of one or more individual chemical species in a sample" and "chemical speciation" as the "distribution of an element amongst defined chemical species in a system." One of the significant features of chemical speciation analysis is the ability to measure the total metal(loid) concentration in a sample accurately, even at relatively low concentrations. These data can be used in conjunction with the concentrations of the individual organometallic compounds in the sample to determine whether there are any unidentified species and to evaluate the possibility of systematic bias at various stages in the procedure. The process used to determine an analyte in a particular sample can be characterized as having a number of inter-related steps as follows:

- Sample collection: Gather representative samples of the material under investigation and store under conditions where the analytes are stable.
- Extraction: Remove the analytes of interest from the sample matrix, so that they are in a form suitable for analysis.
- Cleanup and pre-concentration: Isolate the analytes of interest from the different compounds present in the matrix. This step is required if the matrix has the potential to affect other aspects of the protocol or the analyte concentration is low.
- Analysis: It involves several steps, including, calibration, replication, the use of quality control (QC), and quality assurance (QA) measures, and the experimental design should also address the use of suitable blanks and control samples. The measurements are obtained using specialized analytical instrumentation.

The sampling process for speciation work will not be addressed here, as it is essentially the same as for other environmental and biological applications and is described in detail elsewhere.[31] It is sufficient to say that this is the most important step, as without a representative sample, no amount of analytical wizardry will provide a representative answer. The following discussion will provide an overview of speciation analysis by dealing with each of the analytical steps identified above and highlighting important relevant publications. The regular atomic spectrometry updates (ASUs) published in the *Journal of Analytical Atomic Spectrometry* provide critical reviews of recent research in the areas of environmental analysis,[32] clinical and biological materials, foods and beverages,[33] advances in atomic emission, absorption and fluorescence spectrometry,[34] and atomic mass spectrometry.[35] Each of these particular updates has sections devoted to speciation analysis, providing a critical discussion of significant recent advances, by specialists in each of the subject areas.

12.13.5.2 Sample Preparation

The main steps in preparing samples for speciation analysis involve extraction, cleanup, and pre-concentration, although the requirement for each of these will be dependent on the analyte, the sample matrix, and the analytical method. The criteria for a successful protocol are that the analytes are quantitatively removed from the sample matrix, without loss of structural integrity, or formation of the chemical species of interest. These competing requirements are not always possible to fulfill, and decomposition, species rearrangement, and artifactual analyte formation have been reported as occurring during different parts of the determination.

In the broadest sense, the choice of preparation method will be dependent on the physical form of the sample under investigation. With air analysis, the simplest methods are to sample the gaseous analytes directly into a container, such as a polymer Tedlar bag,[36] or evacuated inert stainless steel canister,[37] and then remove subsamples for analysis. Alternatively, the volatile analytes can be isolated onto a cryogenically cooled trap containing a solid support, stored in liquid nitrogen, and then thermally desorbed into the analytical detector when required.[38] Various volatile organometal(loid) compounds including the hydrides, methylated hydrides, and permethylated species of As, Bi, Hg, Mo, Ni, Pb, Sb, Se, Sn, and Te have been detected in the environment.[39] Airborne particulate matter is usually filtered out of the air sample using a material of a specific pore size,[40] prior to extraction of the chemical species using similar methods to those used for solid samples. In the case of

particulates, the elemental oxidation states will predominate, and the presence of any metal(loid) species will be dependent on the source of the emission.

The speciation of metal(loid)s in surface waters[41,42] is principally limited to the formation of complexes with various types of ligand, including simple organic compounds, humic or fulvic acids, and larger organic colloids. The dissolved organic matter (DOM) present in surface water plays a significant role in determining the speciation, bioavailability, and fate of trace metal(loid)s, and the interaction of DOM with metal(loid)s has been intensively studied.[43] However, there are considerable problems evident when determining the elemental speciation of water samples, due to redistribution of the species during sample collection, storage, and analysis.[44] Other factors that cause more fundamental analytical problems are related to the low total metal(loid) concentration found in natural water samples, resulting in even lower levels for the species of interest.

Once a water sample has been collected, the elemental speciation of the analytes must be preserved, in particular, the oxidation states of redox sensitive elements can easily change if precautions are not taken. Many different approaches to this have been published, but the use of hydrochloric or acetic acid in combination with EDTA, is a simple, cheap, and effective method.[45,46] Sampling approaches that can be used *in situ*—without the requirement to remove the water sample—offer significant advantages for determining chemical speciation, because they eliminate the potential for post-sampling changes. However, only a small number of methods are available, and none measure the full range of metal species in solution, but they do provide data on some operationally defined species. This data can then be included in computer-generated environmental speciation models, which predict species distribution based on the measurement of parameters such as metal concentration, water temperature, pH, and dissolved organic carbon (DOC). Techniques such as diffusive gradients in thin films,[47] anodic stripping voltammetry, dialysis, and filtration[48] have been used with varying success to determine metal speciation in surface waters.

Solid samples are usually heterogeneous in nature and the analytes may be strongly bound within the matrix, or inaccessible to the extractant. The choice of the extraction method will depend on: the elemental species to be extracted, their chemical properties (polarity, volatility, stability in different solvents, and at different pH and redox potential), the sample type (soil, sediment, animal tissue, vegetation), its chemical composition (water and fat content), and the analytical method to be used. A myriad of protocols have been developed to extract organometallic species from a diverse range of solid samples, and it is not possible to summarize all of the different variations with any degree of brevity. In general, the organometallic species of interest are extracted from the samples using specific reagents, including strong and weak acids or bases, different organic solvents, or enzymatic mixtures. Often heat and/or pressure are applied to improve efficiency and speed.

Acid leaching has been widely applied to the extraction of a range of chemical species from different sample matrices. The first methods reported for the extraction of mercury species from fish[49] were based on acid leaching of the solid sample with hydrochloric acid, back extraction into benzene, followed by conversion of the extracted species to the hydroxide form to facilitate partitioning into water. This method is still the basis for studies on fish,[50] although alternative solvents such as toluene are used instead of benzene, and thiol-containing compounds (e.g., sodium diethyldithiocarbamate) are included to aid transfer into the organic solvent. In a European certification programme for methylmercury in tuna fish, the majority of extraction methods utilized this approach, or variations of it.[51] Acetic acid has been successfully applied to the extraction of antimony species from plant material.[52,53] Aqueous mixtures of acids such as trifluoroacetic and phosphoric acids have been used to extract the water-soluble arsenic species from plants and seaweed. A comprehensive review of the analytical procedures used for the determination of OTCs in sediment and biota[54] details the extraction techniques developed in the 10 years prior to 1996. The five main approaches identified include the use of non-polar solvents, non-polar solvents plus acid, polar solvents, supercritical fluid extraction (SFE), and basic and enzymatic hydrolysis. Treatment of the samples with hydrochloric acid was followed by extraction of the OTCs into a non-polar solvent such as hexane, benzene, toluene, or dichloromethane. In some instances, a complexing agent, usually tropolone (0.01–0.5%), was included to improve the solubility of the mono- and disubstituted compounds.

The use of different combinations of solvents has been used to extract a variety of metal(loid) species from a range of different sample types. The majority of As species, including the two common oxidation states, are highly polar and very water soluble. The most popular extraction methods are therefore based on using water or mixtures of methanol and water in various proportions, and these have been applied to both marine and terrestrial samples. The extraction of arsenic species from biological and environmental samples has been reviewed.[55] Research has focused mostly on the so-called "water-soluble" species, and very few methods have been developed for the other As-containing fraction termed "lipid soluble."

A method that has been widely used for tissue samples is digestion with tetramethylammonium hydroxide (TMAH) and, in some cases, further extraction into an organic solvent. The extraction efficiencies of 12 selected

methods for the analysis of butyltin and phenyltin compounds in seafood were compared using a mussel tissue CRM.[56] All of the methods used solvent extraction, some in combination with tropolone and/or an acid. The results showed a wide variation in efficiency, but a strong influence of tropolone on the extraction of the mono- and disubstituted compounds. The use of alkaline leaching with TMAH has been applied to the determination of MeHg in marine animal samples by HPLC-ICP-MS. The extraction of biomaterials has also been facilitated by the use of enzymatic digestions with lipase and protease followed by extraction of the liberated compounds with a suitable solvent.

Recent studies have concentrated on ways to increase the speed and efficiency of sample preparation and to develop fully automated analytical procedures, where extraction, cleanup, and pre-concentration are combined. Although complete automation from sample extraction to analysis has yet to be realized, the use of low-power focused microwave technology has reduced sample preparation time to less than the time taken for a GC run.[57] A number of reports on the use of SFE for a variety of OTCs from environmental matrices have been summarized.[58] The widespread use of this technology will depend to a large extent on the availability of the hardware associated with the technique. The use of accelerated solvent extraction (ASE), where the extraction media is forced through the sample at high pressure, is a technique originally designed for extraction of organic compounds from environmental samples. It is now being applied to the speciation analysis of OTCs[59] and should help with the automation and reproducibility of sample extraction.

12.13.5.3 Sample Analysis

Current state-of-the-art instrumental methods for speciation analysis employ a chromatographic separation coupled to an elemental specific detector, using an interface to facilitate transfer of the analyte between the two. A range of separation methods can be used, including GC, HPLC, SFC, and CE, which are hyphenated to detectors such as QF-AAS, AFS, ICP-AES, API-MS, EI-MS, and ICP-MS. The literature related to the analysis of chemical species using these methods has been comprehensively reviewed for the period 1985–1994[60] and 2000–2003.[61] Other reviews have covered elemental speciation using coupled techniques,[62,63] but some have focused more on biochemical species and the complementary use of different detection systems, such as ICP-MS and ESI-MS.[64] Reviews are available detailing the methods and chemical species of particular interest for a specific element, including methodologies for the determination of antimony in terrestrial environmental samples,[65] arsenic speciation analysis,[66] a critical review of the methods and applications for the determination of arsenic species reported between 2000–2003,[67] mercury, and methylmercury in environmental samples,[68–70] the selective detection and identification of selenium-containing compounds,[71] the analytical procedures for the determination of OTCs in sediment and biota,[54] and a technical report from IUPAC detailing the determination of tin species in environmental samples.[72]

The most important requirements for interfacing the separation system to the detector are that the analyte is quantitatively transferred from one to the other without loss or rearrangement. The simplest couplings are for HPLC to ICP-MS, ICP-AES, or API-MS, although ICP-AES is rarely used as the detector because of its inadequate detection limits. Coupling HPLC to AFS or AAS detection is facilitated by conversion of the analytes to a vapor such as a hydride or the elemental form, and this is introduced into the detector. Gas chromatography requires a heated transfer line when it is coupled to ICP-MS and EI-MS to maintain the chromatographic separation and reduce cold spots where the analytes could condense before reaching the detector. The initial problems with coupling CE to ESI-MS or ICP-MS have now been overcome and reliable interfaces have been developed.[73] The interface between SFC and ICP-MS involves a heated transfer line and a restrictor to maintain the high pressure required for the separation system.[74]

12.13.5.3.1 GC-based speciation methods

A requirement for GC separation is that the analyte is volatile and thermally stable. The majority of organometallic species studied require conversion to a related compound with these characteristics, and this is facilitated by reaction with a specific reagent. Different derivatization mechanisms can be used, but the three most common are: vapor generation (hydride or elemental generation), alkylation by the Grignard reaction, and aqueous phase alkylation. Table 5 shows a representative selection of methods using GC-coupled techniques for the speciation of organometallic compounds in environmental and biological samples. An important general feature of GC methods is that after derivatization, separation of the species is based on volatility, so a range of different elemental species can be quantified in a single run when using a multi-elemental detector such as ICP-MS. This is generally not possible with

Table 5 A representative selection of reports detailing elemental speciation analysis by GC-based methods

Elements	*Elemental species and sample matrix*	*Column type and packing material*	*Derivatization method*	*Detector used*	*Other comments*	*Date*	*References*
As	$MeAsO(OH)_2$, $Me_2AsO(OH)$, and Ph_3As Standards	Capillary column DB5-MS 30 m × 0.25 mm i.d. 0.25 µm film thickness	1% (v/v) PDT	MS PFPD	Thiol-derivatization of the non-volatile analytes SPME used as sample introduction method Simultaneous EI-MS/PFPD detection	2001	412
As	As, $MeAsO(OH)_2$ and $Me_2AsO(OH)$ Human urine	U-trap Polyphenylether (10%) on Chromosorb DMCS 35 cm × 3 mm i.d., 45–60 mesh	10% (m/v) SBH	QF-AAS	Batch HG to generate hydride derivatives Cryogenic pre-concentration at −196 °C on the U-trap Thermally desorbed into a QF-AAS	1998	413
Hg	$MeHg^+$ Fish tissue	Capillary column CP-SIL 8CB 30 m × 0.25 mm i.d., 0.25 µm film thickness	1% (m/v) aqueous STPB	MS	Ion trap mass spectrometer used with electron impact ionization; CRM 464, DORM-2, and DOLT-2 used to validate the method	2004	414
Hg	Hg^{2+}, $MeHg,^+$ and $EtHg^+$ Mouse tissue	Capillary column SPB-1 15 m × 0.53 mm i.d., 1.5 µm film thickness	BuMgCl	ICP-MS	Calibration by ssIDMS using isotopically enriched $Et^{199}HgCl$ and $Me^{200}HgCl$	2003	415
Pb	Me_3Pb^+ Fish tissue, shellfish, and sediment	Capillary column HP-1 21 m × 0.32 mm i.d., 0.17 µm film thickness	2% (m/v) aqueous STEB	ICP-MS	In house constructed heated transfer line; calibration by ssIDMS using isotopically enriched $Me_3{}^{206}Pb^+$ DORM-2, CRM 278, CRM 422, CRM 463, CRM 477, MURST-ISS-A2, and CRM 580 used to validate the method	2005	416
Pb	Me_3Pb^+, Me_2Pb^{2+}, Et_3Pb^+, and Et_2Pb^{2+} Rain water and peat	Capillary column HP1 25 m × 0.32 mm i.d., 0.17 µm film thickness	0.3% (m/v) methanolic TBA–TBB	MIP-AED	Butylated derivatives of the four analytes formed in aqueous solution; simultaneous sample leaching, derivatization and extraction	1998	417
Sb	Sb, $MeSb^{2+}$, Me_2Sb^+, and Me_3Sb Freshwater plants	Packed GC column Porapak-PS 50 cm × 0.4 cm i.d., 80–100 mesh	2% (m/v) SBH 1 M HCl	MS	Semicontinuous HG to generate stibine derivatives; cryogenic pre-concentration at −196 °C on a Teflon U trap; thermally desorbed into the GC-MS	1996	53
Se	Me_2Se, Et_2Se, and Me_2Se_2 Selenized yeast gastric digests	Multi-capillary column OV-17 25 cm × 0.4 µm i.d., 0.2 µm film thickness	None	MIP-AED	Volatile organoselenium compounds produced in simulated gastric digestions; SPME used as sample introduction method	2004	418

(*Continued*)

Se	Selenoamino acids Se standards	Capillary column HP-1 21 m × 0.32 mm i.d., 0.17 μm film thickness	ECF	MIP-AED	Stable volatile derivatives generated	1998	419
Si	Organosilicone compounds Landfill and sewage gas	Capillary column 2 in parallel, Rtx-1 60 m and 47 m × 0.32 mm i.d., 1.5 μm film thickness	None	EI-MS MIP-AED	Volatile analytes sampled into gas canister; cryogenic pre-concentration at −85 °C on a U trap; species simultaneously determined by EI-MS and MIP-AED	1999	37
Si	Organosilicone compounds Human blood and plasma samples	Capillary column HP-5 MS 30 m × 0.25 mm i.d., 0.25 μm film thickness	None	EI-MS	Single ion monitoring mode	2001	362
Sn	$BuSn^{3+}$ and Bu_2Sn^{2+} Marine, harbor, and river sediment	U trap SP-10 (3%) on Chromosorb DMCS 90 cm × 6 mm o.d., 60–80 mesh	1% (m/v) aqueous STEB	QF-AAS	Volatile ethylated derivatives formed; cryogenic pre-concentration at −196 °C on the U trap; thermally desorbed into the QF-AAS	1994	420
Sn	$BuSn^{3+}$, Bu_2Sn^{2+}, and Bu_3Sn^{+} Sediments & biomaterials	Capillary column DB-210 30 m × 0.32 mm i.d., 0.25 μm film thickness	1% (m/v) aqueous STEB	MIP-AED	Simultaneous sample leaching, derivatization and extraction; PACS-1, CRM 462, and NIES 11 used to validate method	1996	421
Sn	$BuSn^{3+}$, Bu_2Sn^{2+}, and Bu_3Sn^{+} Mussel tissue	Capillary column HP-5 30 m × 0.32 mm i.d., 0.25 μm film thickness	2% (m/v) aqueous STEB	ICP-MS	In house constructed heated transfer line; calibration by ssIDMS using a "triple spike" containing all three analytes enriched with different isotopes	2004	422,423
Multi	$BuSn^{3+}$, Bu_2Sn^{2+}, Bu_3Sn^{+}, $MeHg^{+}$, and Me_3Pb^{+} Marine sediment	Capillary column FSOT 30 m × 0.25 i.d., 0.50 μm film thickness	1% (m/v) aqueous STEB	ICP-MS	SPME used as sample introduction method; in house constructed heated transfer line; simultaneous analysis of organometallic Hg, Sn, and Pb species PACS-1 analyzed to validate method	1997	424
Multi	$BuSn^{3+}$, Bu_2Sn^{2+}, Bu_3Sn^{+}, and $MeHg^{+}$ Oyster tissue	Capillary column MXT Silcosteel 30 m × 0.53 mm i.d., 1.0 μm film thickness	1% (m/v) aqueous STEB	ICP-MS	ssIDMS used to determine Bu_3Sn^{+} and $MeHg^{+}$ using isotopically enriched $Me^{199}Hg^{+}$ and $Bu_3^{117}Sn^{+}$; wet and dry plasma conditions used to facilitate mass bias correction and signal optimization; CRM 710 analyzed to validate method	2003	425

(*Continued*)

Table 5 (Continued)

Elements	*Elemental species and sample matrix*	*Column type and packing material*	*Derivatization method*	*Detector used*	*Other comments*	*Date*	*References*
Multi	Me_4Sn, Et_2Me_2Sn, Me_3Sb, and Me_3Bi Landfill and sewage sludge gas	U trap SP-2100 (10%) on Chromosorb 31 cm × 6 mm o.d., 45–60 mesh	None	ICP-MS EI-MSn	Volatile analytes cryogenically pre-concentrated at −78 °C on the U trap; species identified by retention time matching, elemental isotopic fingerprints, and ion trap MSn analysis	1998	20
Multi	$MeGeH_3$, $MeAsH_2$, Me_2AsH, Me_3As, Me_2AsEt, $MeAsEt_2$, Et_3As, Me_2Se, Me_2Se_2, $MeSnH_3$, Me_2SnH_2, Me_3SnH, $BuSnH_3$, $BuSnMeH_2$, $BuSnMe_2H$, Bu_2SnH_2, $MeSbH_2$, Me_2SbH, Me_3Sb, Et_3Sb, Me_2Te, ME_2Hg & $MeBiH_2$ River and harbor sediment	U trap SP-2100 (10%) on Supelcoport size NR, 80–100 mesh	5% (m/v) alkaline SBH	ICP-MS	Batch HG to generate hydride derivatives; cryogenic pre-concentration at −196 °C on the U-trap; thermally desorbed into an ICP-MS; identification of species based on comparison with standards or calculation of boiling point	1996	276

Multi = multi-elemental method, STEB = sodium tetraethylborate, STPB = sodium tetrapropylborate, SBH = sodium borohydride, PFPD = pulsed flame photometric detection, TPA = triphenylarsine, DMCS = dimethyldichlorosilane, TBA–TBB = tetrabutylammonium tetrabutylborate, ECF = ethyl chloroformate, ssIDMS = species-specific isotope dilution mass spectrometry, PDT = 1,3-propanedithiol.

HPLC methods because of the nature of the separation mechanisms available, and most multi-elemental HPLC methods only involve the chemical species of a few different elements.

Hydride generation (HG) is a well-established method for the determination of inorganic and organometallic species[75] and its use for environmental and biological samples has been reviewed.[76] Methods involving HG can be carried out online after separation of the individual species using HPLC and offline using a batch mode approach followed by GC separation. In both configurations, sodium borohydride in an acidic environment is used to reduce the non-volatile ionic species of interest, facilitating the production of volatile hydrides. This method has been used to determine As^{3+} and As^{5+} and the inorganic species of Ge, Sb, Sn, and Hg, as well as the methylmetal and butyltin species. One particular advantage of HG is that the metal carbon bond remains unbroken during the reaction, so the original speciation in the sample is maintained. In the batch mode, the reagents are added to the sample and allowed to react; the sample is then purged with helium and the entrained hydrides are pre-concentrated onto a solid support immersed in a coolant, usually liquid nitrogen. After a sufficient purge time, the trap is heated electrothermally releasing the species according to their boiling points. The derivatized analytes are swept through a drying tube prior to detection using an element selective detector such as QF-AAS, AFS, ICP-AES, or ICP-MS. The use of a cooled U trap is a very effective pre-concentration and isolation step, often referred to as cryofocusing, and allows for the analysis of large sample volumes resulting in low LOD. The fact that it can be interfaced relatively easily to a variety of detectors means that it is a cheap and versatile speciation method.

The main drawback of HG is that some organometallic species do not react with the borohydride reagent to form a volatile hydride, in which case they have to be decomposed to one that does. This is facilitated via reaction with a suitable reagent, often with microwave heating, or the use of ultraviolet radiation. The method is also not applicable to methyl- or ethyllead, because these hydrides are difficult to form and not sufficiently stable. Difficulties can also be encountered when analyzing samples with a complex or high organic matrix content, in which case the reagent may be depleted before reacting with all of the analytes, or excess foaming can lead to a reduction in sensitivity, loss of the analytes, or unstable signals. Other problems exist when trying to simultaneously derivatize elements and their species because of the different optimum reaction conditions required for each. In some situations, this can be an advantage, for example, the different oxidation states of arsenic can be determined by carrying out the HG reaction at the pH where the reaction is specific to only one of the oxidation states. To determine the total arsenic concentration, Le *et al.*[77] overcame the problem of different As species reacting differently by adding 2% L-cysteine along with the borohydride reagent.

The Grignard reaction involves alkylation of the analyte using a derivatization reagent, leading to peralkylation of the analytes of interest. The Grignard reagent is generally both water and air sensitive, and so the analytes have to be isolated from the extract into a suitable organic solvent, which is then dried prior to derivatization. After a suitable time interval, the excess reagent is acid neutralized, and the derivatized analytes are injected onto the GC column for separation prior to detection. A number of problems have been highlighted with this approach due to the potential for introducing various errors related to the derivatization step. These include contamination of the sample extract due to poor-quality reagents, analyte loss and artifact formation, poor reaction yields, losses due to unstable derivatives, difficult-to-dry extracts, and possible formation of analyte species already present in the sample. However, under optimized conditions, it has been shown to yield quantitative results.

The second type of alkylation method can be carried out in the aqueous phase using a variety of different reagents; however, sodium tetraethylborate is used most widely and leads to the formation of ethylated derivatives. The methodology, which has been reviewed,[78] is carried out by adjusting the sample extract to pH 4–5 using a suitable buffer, prior to the addition of the reagent, which reacts with the metal(loid) species to form stable peralkyl derivatives. The limitations of this method are related to impure reagents, artifactual formation of the analyte, and the risk of incomplete derivatization due to reactions of the reagent with matrix components. However, none of these effects are insurmountable, and aqueous phase alkylation has been used to determine a variety of elemental species including organotin, organolead, and organomercury species. Once derivatized, the analytes are determined using GC-based methods, such as those detailed in Table 5.

The use of vapor-generation methods prior to ICP-MS or AAS detection improves the LOD of the method. This is because the sample introduction methods facilitated by liquid aspiration are very inefficient (1–5%), compared to methods for gaseous or vapor sample introduction (>90%).

12.13.5.3.2 HPLC-based speciation methods

The use of HPLC coupled to an element-specific detector for speciation analysis has been reviewed,[79,80] as have the HPLC methods for some specific elemental species.[81,82] A representative selection of speciation methods based on HPLC separation is given in Table 6. The main separation modes used are ion exchange (anion and cation) and

Table 6 A representative selection of reports detailing elemental speciation analysis by HPLC-based methods

Elements	*Elemental species and sample matrix*	*Separation mode*	*HPLC column and packing material*	*Detector used*	*Other comments*	*Date*	*References*
As	Water-soluble organoarsenic species Clam kidney	Anion and cation exchange	PRP X-100 25 cm × 4.6 mm, 5 µm Supelcosil SCX 25 cm × 4.6 mm, 5 µm	ICP-MS ESI-MS	Multi-dimensional column chromatography used to purify As-containing fractions; compounds identified on the basis of Q-TOF MS spectra	2002	426
As	Lipid-soluble organoarsenic species Fish oils	Normal and reversed phase	YMC-Pack Diol 120 12.5 cm × 2.1 mm, 5 µm Eclipse XDB C18 15 cm × 2.1 mm, 5 µm	ICP-MS	Low flow rate, oxygen added post-nebulization, chilled spray chamber and Pt sampler cone used; Ph_3AsO and Ph_3AsS used as calibration standards	2005	221
As	23-organoarsenicals, including $Me_2AsO(OH)$, $Me_2As(O)CH_2COOH$, $Me_3As^+CH_2COOH$, Me_2AsO, $Me_3As^+CH_2CH_2COOH$, $Me_3As^+CH_2CH_2OH$, Me_4As^+, and 16 unknown As-containing compounds Marine samples	Cation exchange	Ionospher-5C 10 cm × 3 mm, NR	ICP-MS	Gradient elution using aqueous pyridine (mM) in 3% (v/v) methanol, to pH 2.7 with formic acid; scallop kidney, krill powder, and DORM-2, BCR 626, and TORT-2 CRMs analyzed	2003	225
As	As^{3+}, As^{5+}, $MeAs(O)(OH)_2$, $MeAs(OH)_2$, $Me_2As(O)OH$, and Me_2AsOH Human urine	Ion pair	Phenomenex ODS-3 15 cm × 2.1 mm, 3 µm Column temperature 50 °C	HG-AFS	Dimercapto–1-propanesulfonate used to preserve As^{3+} oxidation states of the methylated species; tetrabutylammonium hydroxide used as ion-pair reagent at pH 5.9; continuous hydride generation	2000	427
Hg	Hg^{2+} & $MeHg^+$ Soils and sediment	Reversed phase	Supelcosil LC-18 15 cm × 2.1 mm, 5 µm.	ICP-MS	Evaluation of 5 different extraction methods to assess species interconversion using stable isotope enriched $Me^{201}Hg^+$ & $^{199}Hg^{2+}$ species	2004	101
Hg	Hg^{2+} & $MeHg^+$ Rain, sea, and process water	Reversed phase	Hypersil-ODS 8 cm × 4.6 mm, 3 µm	CV-AAS	Analytes complexed with SPDC prior to pre-concentration on C18 column; converted to CV active species post-column using UV radiation; continuous CV generation	1995	428

(*Continued*)

Hg	$MeHg^+$ Fish tissue	Reversed phase	Kromasil C18 25 cm × 4.6 mm, 5 µm	APCI-MS	Mass spectra for different mercury compounds reported; spiked DORM-1 fish tissue CRM analyzed	1998	429
Pb	Me_3Pb^+ and Et_3Pb^+ Spiked water	Reversed phase	Nucleosil C18 guard column 2 cm × 4.6 mm, 3 µm	ESI-MS	In-tube SPME to prepare samples using an open tube capillary coated on the inside with a suitable extraction polymer	2000	430
Pb	Pb^{2+}, Me_3Pb^+, and Et_3Pb^+ Rain water	Ion pair	Hypersil ODS Size NR, 5 µm	ICP-MS	Sodium pentanesulfonic acid used as ion-pair reagent at pH 5.9; gradient elution; enriched $Me_3{}^{206}Pb^+$ and $Et_3{}^{206}Pb^+$ used for calibration by ssIDMS	1994	431
Sb	Sb^{3+}, Sb^{5+}, and Me_3SbO Surface water and contaminated soil	Anion exchange	PRP X-100 15 cm × 4.1 mm, 5 µm	ICP-AES ICP-MS	Different organic acids tested as eluents; poor peak shapes for real samples	1998	432
Sb	Sb^{3+}, Sb^{5+}, and Me_3SbCl_2 Tap water	Anion exchange	IonPac AS 14 25 cm × 4.1 mm, NR	ICP-MS	Ultrasonic nebulization with membrane desolvation used as interface; plastic ware and syringes used to reduce Sb^{5+} background	2001	433
Se	23 organoselenium compounds Se-enriched plants, yeast, onion, and garlic	Ion pair	Symmetry shield RP8 15 cm × 3.9 mm, 5 µm	ESI-MS ICP-MS	Heptafluorobutanoic acid (0.1%) or trifluoroacetic acid used as ion-pair reagent	2000	434
Se	>30 Selenopeptides Selenized yeast	Reversed phase	Hypersil C18 BDS 15 cm × 300 µm, 3 µm	ICP-MS	Demonstration of a sheathless interface for capillary HPLC coupled to ICP-MS; injection volume 200 nL; at flow rates <7.5 µl min^{-1}, shown to be a total consumption nebulizer	2003	85
Si	Inorganic silicate, silanols, and poly (dimethylsiloxane) polymers environmental and industrial samples	SEC reversed phase	Phenogel 5 SEC 30 cm × 3.2 mm, 5 µm YMC-Pack C18 25 cm × 2.1 mm, NR	ICP-AES	Spray chamber temperature 32 °C; column temperature 40 °C; reversed phase used for inorganic silicate and silanols, SEC used for poly(dimethylsiloxane) polymers	1994	435

(*Continued*)

Table 6 (Continued)

Elements	*Elemental species and sample matrix*	*Separation mode*	*HPLC column and packing material*	*Detector used*	*Other comments*	*Date*	*References*
Si	Poly(dimethylsiloxane) polymers and breakdown products Spiked human plasma	SEC Reversed phase	Phenogel 5 M3 SEC 30 cm × 3.2 mm, 5 µm YMC-Pack C18 25 cm × 2.1 mm, 6 µm	SF-ICP-MS	Medium resolution mode used to resolve N_2^+ and CO^+ from $^{28}Si^+$; reversed phase used for silanols, SEC used for poly(dimethylsiloxane) polymers	2004	436
Sn	$BuSn^{3+}$, Bu_2Sn^{2+}, and Bu_3Sn^+ Marine sediment and harbor sediment	Ion pair	Hypersil ODS 15 cm × 1 mm, 5 µm	ICP-MS	Sodium 1-pentanesulfonate and tropolone used as counterions; direct injection nebulizer (DIN) used	1998	437
Sn	Bu_2Sn^{2+}, Bu_3Sn^+, Ph_2Sn^{2+}, and Ph_3Sn^+ Harbor sediment	Reversed phase	Kromasil-100 15 cm × 2.1 mm, 5 µm	APCI-MS ICP-MS	Triethylamine used to improve chromatography for Bu_3Sn^+; mass spectra for different OTCs reported; low flow rate, oxygen added post-nebulization, chilled spray chamber and Pt sampler cone used for ICP-MS	1998	438
Multi	Me_3Pb^+, Et_3Pb^+, $MeHg^+$, $EtHg^+$, and $PhHg^+$ Human urine	Ion pair	PEEK column packed with C18 phase 15 cm × 1.6 mm, NR	ICP-MS	Ammonium pentanesulfonate used as ion-pair reagent at pH 3.4; simultaneous detection of Pb and Hg compounds; direct injection nebulizer used; method validated with SRM 2670	1992	439
Multi	As^{3+}, As^{5+}, $CH_3As(OH)_2$, Hg^{2+}, and $MeHg^+$ Spiked natural freshwater	Reversed phase	Prodigy ODS3 25 cm × 4.6 mm, 5 µm	CV-AFS HG-AFS	Online oxidation via UV radiation, HG and CV generation with $NaBH_4$, detection via two AFS systems in series, Hg followed by As detection	2004	440

NR = not reported, SPDC = sodium pyrrolidinedithiocarbamate, SEC = size-exclusion chromatography, SPME = solid-phase microextraction, ssIDMS = species-specific isotope dilution mass spectrometry.

reversed phase (ion exclusion, ion pair, and micellar). Size-exclusion chromatography has also been used, but, in general, this is limited to the separation of large biomolecules or as a preliminary cleanup step in combination with the previously mentioned chromatographic methods. The majority of reversed-phase applications involve a conventional C18 analytical column with an aqueous eluent containing a proportion of organic modifier. In ion-exchange separations, the pH is critical and the buffer conditions used will be dependent on the pK_a values for the analytes.

The most versatile detector for HPLC separations is ICP-MS and one of the advantages of this approach is the simplicity of the interface between the two instruments, and the possible options available have been comprehensively reviewed.[83,84] Instruments not able to tolerate the organic component of the mobile phase without the plasma being extinguished require a cooled spray chamber (−10 to −15 °C) to reduce the organic solvent loading on the plasma. The addition of oxygen post-nebulization is necessary to eliminate carbon buildup on the sample cone, as this can lead to a loss in signal due to blockage. It is also necessary to use platinum-tipped cones because of their greater resistance to wear. Recent developmental work in this area has produced a sheathless interface using a microflow total consumption nebulizer, which allowed for the use of eluents containing 100% organic solvent, without either cooling of the spray chamber or oxygen addition.[85] This type of interface allows for the coupling of low-flow capillary HPLC separations to ICP-MS, offering significant advantages over conventional systems. Very small sample volumes (nanoliter) can be used, and the chromatographic system provides enhanced peak resolution, better signal-to-noise ratio, and ultimately a lower LOD. The second widely used detector for HPLC is AFS, and the two are interfaced via vapor generation and the use of a gas–liquid separator (GLS). As described in the previous section, some organometallic compounds have to be converted into a species that will readily form a vapor on reaction with the derivatizing agent. Multi-elemental speciation analysis using HPLC-ICP-MS is limited to species with similar elution properties because of the chromatographic separation step.

12.13.5.3.3 Other separation methods

Supercritical fluid chromatography (SFC) uses a liquefied gas as the mobile phase and programmed changes in pressure to facilitate separation, in a similar way to temperature programming in GC separations. Supercritical fluids have critical temperatures (temperature above which the fluid cannot be liquefied) below 200 °C and densities of the order 0.1–1 g l^{-1} at pressures of 1,000–6000 psi. Carbon dioxide is the most common eluent for SFC, and the majority of applications have been for the speciation of OTCs, particularly the butylated species[74,86]. SFC overcomes many of the limitations of HPLC and GC because it can be used to separate thermally labile, non-volatile, high molecular weight compounds, and affords lower detection limits associated with gaseous sample introduction, most often with ICP-MS detection. However, the analytical community has not taken up the technique to any real extent, possibly because of the high initial and ongoing costs of the instrumentation, but also because the commonly used pure CO_2 mobile phase is not compatible with some polar analytes.

Capillary electrophoresis (CE) is a family of related techniques that employ narrow bore (20–200 μm i.d.) capillaries to perform high-efficiency separations of both large and small molecules.[87] The separations are facilitated by the application of a high voltage to the capillary, which generates electroosmotic and electrophoretic flow of the species of interest. The technique has been coupled to ICP-MS[87] and ESI-MS[88] for the measurement of different elemental species in biological and environmental samples. The initial difficulties in designing a suitable interface to couple CE separations with ICP-MS were centered on the high flow rate requirements of conventional ICP nebulizers and the low flow rate nature of CE. The main problems concerned the suction generated with the conventional self-aspirating nebulizers, which caused a loss in chromatographic resolution, and the necessity to maintain effective electrical conductance to the end of the capillary. These difficulties were overcome by using a low-flow nebulizer and a small makeup buffer flow that is earthed.[89] The main advantages of CE include the high separation efficiency, low sample consumption, and the high-efficiency separation characteristics that it offers. However, because of the small sample size used, it is often difficult to detect the species present in real samples, and therefore only highly sensitive detectors, such as ICP-MS and ESI-MS, are effective.

12.13.5.3.4 Detection methods

In general, QF-AAS, AFS, AES, microwave induced plasma (MIP) and ICP-MS are used as detectors rather than the less specific FID, FPD, and ECD. The overriding reason for this is the greater sensitivity and selectivity afforded by the element-specific detectors, without which it would not be possible to determine the chemical species of interest at the low concentrations generally present in biological and environmental samples. The other main detection method that has been used is mass spectrometry in its various configurations,[90,91] but particularly electrospray ionization (ESI) and atmospheric chemical ionization (APCI), which are used with HPLC and CE separations, and

electron impact (EI), which is used with GC separations. ICP-MS offers the most versatile detection system for speciation studies because it can be coupled to all of the commonly used separation systems (GC, HPLC, SFC, HG, CE) and it offers low detection limits for the majority of elements of interest. Isotopic analysis can be carried out with ICP-MS, allowing for the use of high-accuracy methods based on isotope dilution mass spectrometry (IDMS) and also for nutritional and biogeochemical investigations using isotopically enriched materials as tracers. In most cases, the instruments used are based on quadrupole mass analyzers containing a reaction or collision cell to remove any polyatomic interferences formed in the plasma. Sector field or high-resolution instruments, and time-of-flight (TOF) mass analyzers, are also available, but not widely used except for specific applications. A summary of the main analytical characteristics of the principle detectors used in hyphenated systems for speciation analysis is given in Table 7.

When using ICP-MS as a chromatographic detector, the eluting species are identified by matching the retention time of the unknown species to that for an authentic standard. The most reliable way to do this is by spiking the sample with an appropriate amount of standard, and determining whether it co-elutes with one of the peaks. However, this approach can lead to peaks being wrongly assigned.[92] Recently, the use of ESI-MS/MS as a complementary technique to ICP-MS has been described and reviewed.[93,94] In contrast to element-selective detectors, such as ICP-MS, molecular mass spectrometry techniques provide information on the intact metal species, which can be used for the identification of the unknown species, particularly if a tandem MS/MS instrument is available. The use of mass spectrometry based on atmospheric pressure ionization, both APCI and ESI for speciation analysis have been reviewed.[93–97].

12.13.5.3.5 Calibration methods

The determination of chemical species in an environmental or biological sample can be difficult and time consuming. The accuracy and precision generally achieved for this type of work is not as good as that for total elemental analysis, even for laboratories with a proven track record in speciation analysis.[51] Only a limited number of high purity standards are available, and so calibration of the method is an important area for improvement in methodology. Standard additions and external calibration strategies have been applied and recently, the use of IDMS has been described.

Online isotope dilution analysis using chromatography coupled to inorganic mass spectrometry (ICP-MS) is a powerful analytical approach to the quantification of elemental species in different materials[98] and to highlight systematic errors in some analytical elemental speciation methods.[99–101] This analytical approach offers a high degree of precision and accuracy even at trace concentrations, and provides a means to verify speciation methods with a greater degree of confidence than methods using conventional analytical approaches.

A framework encompassing the different strategies for carrying out these measurements has been described:[102,103] species–specific spiking (ssIDMS), whereby the sample is spiked with an internal standard containing an enriched isotope of the metal at the beginning of the analytical procedure and species-unspecific spiking (suIDMS) where the enriched spike is added continuously to the eluent from the chromatographic column. In both approaches, the isotope ratios between the spike and analyte isotope are measured via ICP-MS. The former method requires that the structure of the chemical species in the sample is known and that a suitable isotopically enriched spike material is available, the latter method has been used where the elemental species of interest is unidentified or a standard containing an enriched isotope is not available.

Species-specific spiking is superior to the use of species-unspecific spiking because any chemical or physical losses of the analyte during the analytical procedure will be corrected for in the final IDMS measurement, assuming that both the spike and the analyte reach chemical equilibrium prior to extraction. The real value of the species-specific approach was highlighted during the development of a GC-ICP-MS method for the analysis of methylmercury in different environmental water samples.[99] This work identified a systematic error during the derivatization step when employing ethylation, whereby the methylmercury in the sample was converted into elemental and/or inorganic mercury prior to analysis. However, the species-specific IDMS calibration method completely corrected for these transformations, without any action being required, and demonstrates one of the major advantages of using isotopically labeled calibrants in elemental speciation analysis.

12.13.5.4 Aspects of QC/QA in Speciation Analysis

After some sustained work in this area, most notably the Standards, Measurement and Testing (SMT) Programme of the European Commission, the pitfalls that can be encountered when performing speciation analysis are better understood, and methods to evaluate and eliminate them are now reasonably well established. Publications dealing

Table 7 A summary of the main analytical characteristics of the principle detectors used in hyphenated systems for speciation analysis

Detector	*Separation mode*	*Instrumental setup*	*LOD*	*Other comments*	*References*
ICP-MS	GC	GC-heated transfer line-torch-ICP-MS	μg element l^{-1} e.g., 3–10 $\mu g\,kg^{-1}$ Hg species in mouse tissue 0.09 $\mu g\,kg^{-1}$ Me_3Pb^+ in fish tissue	Commercial systems available; non-volatile compounds require derivatization.	415,416
ICP-MS	U tube	VG-GLS-U tube-torch-ICP-MS	μg element l^{-1}	Analytes cryogenically trapped on a U tube, which can contain a solid support and thermally desorbed into detector; non-volatile compounds require derivatization, volatile analytes are trapped directly	20
ICP-MS	HPLC	HPLC-tubing-nebulizer-spray chamber-torch-ICP-MS	μg element l^{-1} e.g., 0.4 $\mu g\,l^{-1}$ butyltin in water 0.8 $\mu g\,kg^{-1}$ Se species in yeast	Commercial systems available; organic solvent introduction can require chilled spray chamber and addition of oxygen; a total consumption interface for low flow rate separations using capillary columns has been reported; non-volatile compounds determined without derivatization	85,437
ICP-MS	SFC	SFC-heated transfer line-restrictor-torch-ICP-MS	pg concentration level e.g., 0.03 pg as Sn using standard solutions	Low volume injections; volatile and non-volatile compounds determined without derivatization	74
ICP-MS	CE	CE-capillary-makeup buffer-torch-ICP-MS	fg concentration level	Commercial systems available; electrical circuit completed by using an electrically grounded makeup buffer; low volume injections; non-volatile compounds determined without derivatization	97
MIP-AED	GC	GC-heated transfer line-AED	μg element l^{-1} e.g., 2 $\mu g\,kg^{-1}$ butyltin in sediment 0.01–0.03 $\mu g\,kg^{-1}$ organolead compounds in peat	Commercial systems; detector based on atomic emission; non-volatile compounds require derivatization	417,421

(*Continued*)

Table 7 (Continued)

Detector	*Separation mode*	*Instrumental setup*	*LOD*	*Other comments*	*References*
AAS	U tube	VG-GLS-U tube-AAS	μg element l^{-1} e.g., 9–12 μg kg^{-1} butyltin in sediment	Analytes cryogenically trapped on a U-tube, which can contain a solid support and thermally desorbed into detector; non-volatile compounds require derivatization, volatile analytes are trapped directly; conversion to inorganic compounds required for chemical species that do not readily form a vapor	441
AAS	HPLC	HPLC-VG-GLS-AAS	μg element l^{-1}	Conversion to inorganic compounds required for chemical species that do not readily form a vapor; involves online derivatization	428
AFS	U tube	VG-GLS-U tube-AFS	μg element l^{-1}	Analytes cryogenically trapped on a U-tube containing a solid support and thermally purged into detector; non-volatile compounds require derivatization; conversion to inorganic compounds required for chemical species that do not readily form a vapor	70
AFS	HPLC	HPLC-VG-GLS-AFS	μg element l^{-1} e.g., 3–20 μg l^{-1} Hg and As species in water 0.5–2 μg l^{-1} As species in water	Conversion to inorganic compounds required for chemical species that do not readily form a vapor	427,440
MS	GC	GC-heated transfer line-EI ion source	Compound-specific LOD e.g., 40 μg kg^{-1} MeHg in fish	Commercial systems; non-volatile compounds require derivatization.	414
MS	HPLC	HPLC-heated nebulizer-ESI source	Compound-specific LOD e.g., 10 μg l^{-1} organolead compounds in water	Commercial systems	430
MS	HPLC	HPLC-heated nebulizer-APCI source	Compound-specific LOD	Commercial systems; corona discharge needle in APCI source	429

with the method performance studies for speciation analysis[104,105] that have been undertaken during the SMT programme are a good starting point for those workers wanting to perform speciation measurements in a controlled manner.

The errors associated with the steps identified in Section 12.13.5.1 have been discussed and the approaches used to establish and combat them will now be summarized. For the extraction step, QA considerations mean the extraction efficiency needs to be validated and this can be done either by spike recovery experiments or by using a representative CRM. The main criticism of spike recovery experiments is that the spike is not bound in the sample matrix in the same way as the naturally occurring analyte being measured. However, if a low recovery is apparent using the method chosen, it would indicate an inadequate protocol or one that requires further developmental work. The range of CRM available with values for some of the more important chemical species is increasing, and includes various sediments, fish and shellfish tissue, and human matrices such as hair and urine. However, real samples are rarely identical to the matrix CRM available, so care should be taken when validating methods to be used for real samples.

12.13.5.5 Future Prospective

Speciation analysis has come a long way in the past 10 to 15 years with improvements in the instrumental and extraction hardware leading to faster methods with better accuracy and precision even at low analyte concentrations. The wide range of CRM and the greater availability of the standards and reagents commonly used for speciation analysis have helped to improve the results. Future advances are required in the provision of methods that provide quantitation with structural characterization simultaneously, which will improve confidence in the speciation results. A recent perspective article by one of the early pioneers in chemical speciation analysis discusses the future of the area, in the context of the initial work in the subject.[106]

The early work in speciation analysis used a natural products type approach, whereby the analyte of interest was extensively purified from large quantities of sample, prior to structural characterization by NMR, MS, and X-ray crystallography.[10] With the advent of more sensitive instrumentation such as ICP-MS and ESI-MS, the current approach favors the extraction of a representative subsample of the material followed by analysis using a separation step coupled to a sensitive detector. The analytes are then identified by co-elution with an authentic standard (ICP-MS) or molecular structural analysis using mass spectrometry (ESI-MS/MS). The compounds of interest are quantified using one of the available calibration methods and comparison to identical standards. The current state-of-the-art analytical methods have provided some significant insights into the biogeochemistry, toxicology, and function of a range of elements. However, it has become apparent recently that some of the organometallic species that have been identified in this way may have been formed during the analytical procedure and that the *in vivo* forms may be different. Unfortunately, it is difficult to determine that a species has been altered during the analytical process, unless great care is taken.

To address these problems, it is necessary to use techniques which do not require the analyte to be removed from the matrix. The techniques of X-ray absorption spectroscopy (XAS), which can be divided into two components, extended X-ray absorption fine-structure spectroscopy (EXAFS) and X-ray absorption near-edge structure (XANES), have been used to establish the arrangement of atoms around a particular metal(loid) while still present in the sample, that is, without recourse to extracting the chemical species of interest. This approach has been used to determine the chemical form of mercury in fish using XAS,[107] indicating that the methylmercury in the fish tissue was coordinated to an aliphatic thiol group. On the basis of EXAFS, it was possible to identify a seleno-bis(*S*-glutathinyl) arsinium ion in rabbit bile as the complex responsible for the antagonistc behavior between arsenite and selenite,[108] and XANES has been used to investigate the *in situ* binding of different As compounds in a range of materials.[109]

There are lots of questions still to be answered in the area of chemical speciation, and these can only be addressed by using the most appropriate analytical speciation methods. In future studies, this will involve the combined use of complementary *in situ* (XAS) and *ex situ* (GC-ICP-MS, HPLC-ICP-MS, and ESI-MS/MS) methods.

12.13.6 Toxicity of Organometallic Compounds

A summary of the toxic effects of some environmentally important organometallic compounds in humans and other mammalian systems is given in Table 8. Further comments on the toxicity, including environmental toxicity, of the important classes of organometallic compounds are given in the relevant sections of this chapter. Dopp *et al.*[15] have recently reviewed the toxicity of organometallic compounds.

Table 8 Toxicity effect of some environmentally important organometallic compounds in mammalian systems

	Toxic effect	
Chemical species	*Humans*	*Other mammals/mammalian cells*
Arsenic		
Methylarsonic acid		Mammalian cells: cytotoxic;[111,112,442–444] genotoxic and clastogenic effects;[112,444–448] induction of morphological transformations[449]
Dimethylarsinic acid (V)		Mammalian cells: genotoxic and clastogenic effects;[112,444–447,450,451] affects viability and growth of human cells[452,453] Rats: reduction in brain neuron viability;[454] apotopsis;[454] cancer promoter—bladder, kidney, liver, thyroid[112,455,456] Mice: carcinogenic, co-carcinogenic or cancer promoter—skin, bladder;[112,455,456] induction of aneuploidy[457]
Dimethylarsinous acid (III)		Mammalian cells: genotoxic and chromosomal aberration effects[451,458]
Trimethylarsine oxide		Mammalian cells: affects viability and growth of human cells[452,453]
Arsenocholine		Mice: immunotoxicity[459]
Bismuth		
Triphenyl bismuth	Low level cytotoxicity[460,461]	
Mercury		
Monomethylmercury	T-cell apoptosis[462]	Mammalian cells/segments: affects metallothionein expression[463,464] Mice: cytotoxic effects;[465] immune dysfunction[465]
	Immunotoxic[466,467]	Many animals: immunotoxic[466,467]
Methylmercury	Cytogenetic effects,[468,469] destructive lesions in brain;[471] cerebral palsy in prenatally poisoned children[473]	Mammalian cells: cytotoxic effects[470] Hamster: genotoxic effects[472] Rats: cell cycle disturbance;[474] cytotoxic affects[470,475,476]
Tin		
Trimethyltin	Neurotoxic effects[114,477]	Mice: chromosome aberrations[478,479]
Trimethyltin chloride	Micronuclei and chromosomal aberrations[480,481]	
Butyltin	Inhibition of apoptosis[482]	
Dibutyltin		Rats: thymolytic and immunotoxic[483]
Tributyltin	Induction of aneuploidy[484]	Hamster: chromosome aberrations[478,479]
Tibutyltin oxide		Mice: co-clastogenic[485] Rats: thymolytic and immunotoxic[483] Mice: co-clastogenic; embryotoxic[483]
Triphenyltin		Mice: chromosome aberrations[478,479]
Triphenyltin chloride		Mice: co-clastogenic[485]
Dioctyltin		Rats: thymolytic and immunotoxic[483]

Some general comments on the toxicity of organometallic compounds can be made. Organometallic compounds are generally more toxic than their inorganic counterparts (e.g., in the case of Pb, Hg, and Sn). Such enhanced toxicity of organometals is, at least in part, accounted for by increased solubility within cellular lipid components, which allows interaction with (and diffusion across) cellular membranes. In some respects, arsenic is an exception in that organic pentavalent arsenicals have been shown to be less potent as mutagenic agents than their inorganic counterparts.[110] Sakurai *et al.*[111] have also shown that the mammalian cell cytotoxic effects of methylated arsenic compounds are lower than those of inorganic arsenicals. This suggests that mammalian methylation of inorganic arsenicals is a mechanism that reduces the immunosuppressive and elevated inflammatory response caused by inorganic arsenicals.[111] There is however accumulating evidence that trivalent methylate arsenic species, such as monomethylarsonous acid and dimethylarsinous acid, may have relatively high capability of interacting with proteins and DNA.[112]

The toxicity of organometallic compounds is usually maximal for the monopositive cation (e.g., R_3Sn^+, $MeHg^+$), and toxicity of the fully saturated organometal (e.g., R_4Sn) is usually a result of cellular biotransformation to the monopositive cation. Generally, the most toxic alkyl groups attached to common metals are methyl, ethyl, and propyl. There are however differences between organisms. In the case of organotin, trialkyltins are the most toxic of the organotin cations; methyl and ethyl groups are the most toxic to mammals, while higher alkyl groups are more toxic to invertebrates and fish.

The mechanism of toxicity is varied, but often relies on good coordination of the organometals to base atoms (e.g., O, N, S) on biological macromolecules, such as proteins (including certain enzymes), DNA, and RNA. Fundamental interferences with cell division, immune system, protein synthesis, DNA, reproductive system, and nervous system can result (Table 8). Methylmercury, for example, causes clastogenic effects in eukaryotes by binding to sulfhydryl groups in proteins. Coordination of organometallic compounds to non-enzyme sites includes thiols, histidine residues of proteins, hemoglobin, cytochrome P_{450}, and cerebral receptors. Organometallic species reacting with the active (substrate-binding) site of enzymes blocks interaction with the biological substrate, that is, enzyme inhibition. Triorganotin toxicity is caused by disruption of mitochondrial function, membrane damage, disruption of ion transport (including Ca^{2+}), and inhibition of ATP synthesis.

In vertebrates, one of the main results of organometal poisoning is damage to the central nervous system, leading to a variety of symptoms including coma, ataxia, and varied motor difficulties. Methylmercury, for example, is a neurological poison, affecting primarily brain tissue. It is lipid soluble and rapidly diffuses across biological membranes, including the blood-brain barrier and cell membranes. It is also a teratogen, causing poisoning of the fetus via the placenta, which can lead to limb deformation, mental retardation, and coordination disturbance.[113] Trimethyltin is also a potent neurotoxin, but the mechanism of action has not been established. A link between trimethyltin neurotoxicity and other degenerative conditions (e.g., Ammon's horn sclerosis) involving an imbalance between neuronal inhibition/excitation has been proposed.[114] Trialkyltin compounds are known to destroy the normal pH gradient across mitochondria membranes, thus uncoupling respiratory electron transport from oxidative phosphorylation (ATP synthesis). Inhibition of the ability of astrocytes to maintain a transmembrane K^+ gradient is thought to contribute to the neurotoxic effects of trimethyltin.[115]

12.13.7 Organomercury

Mercury in the environment has an iconic status in that it was the first organometallic compound for which an environmental (as distinct from direct toxic) importance was realized. Aspects of this matter also demonstrate the changing nature of pollution and environmental issues generally. Two early and serious mercury poisoning outbreaks were related to single-point-of-emission release of methylmercury to the environment (Minamata, 1950s) and direct consumption of methylmercury added to seed grain as a preservative (Iraq, 1975). Such large-scale point-source inputs of mercury to the environment are now very much reduced, and concern now relates to less direct forms of entry to the environment (e.g., coal burning, biomass burning, informal gold mining). Concern is also now more directed toward contamination of aquatic locations distant from the source of mercury entry to the environment (because of the volatility and relative ease of transport of mercury). For a discussion on methylmercury in the environment, see Ref: 116.

Some key features relevant to mercury in the environment were established very early on (in the late 1960s). It was shown that it is present in fish as methylmercury, that there is an explanation of the methylation route (involving methylcobalamin, see below), and that analytical methods can be developed for methylmercury in water, sediment, or organisms at the ppm level.

12.13.7.1 Mercury Methylation and Demethylation

Mercury was the first element for which it was established that there is a natural route in the environment for conversion of the inorganic form to the methyl form (biomethylation). Minamata was caused by chemical formation of methylmercury from catalytic inorganic mercury within a vinyl chloride/acetic acid factory. However, discovery of methylmercury in river or estuarine sediments adjacent to chlor-alkali plants (where metallic mercury is used as a mobile cathode) suggested subsequent methylation of the mercury outside the factory. Such methylation was detected by Jensen and Jernelov in 1969.[117] As discussed in Section 12.13.3.2, the responsible methylation agent was methylcobalamin (Table 4 and Figure 1). This reaction may be demonstrated in inorganic terms as attack of a methylcarbanion on Hg^{2+} (Equation (8)).

$$MeCoB_{12} + Hg^{2+} + H_2O = H_2OB_{12} + CH_3Hg^+ \quad (8)$$

The work of Bartha *et al.* has demonstrated the importance of sulfate-reducing bacteria, and other factors, as mercury methylators in the environment.[118–123] Addition of sulfates in experiments in freshwater and salt marsh areas shows a strong correlation between mercury methylation rates and biological sulfate reduction. The methyl intermediate in sulfate-reducing bacteria was shown by Berman *et al.* to be methylcobalamin.[124] They proposed that mercury methylation takes place by an enzymatically catalyzed reaction within cells involving methylcobalamin. This reaction takes place at much faster rates than abiotic methylation by cobalamin alone. It was suggested that methylation takes place via transfer of a methyl group from methyltetrahydrofolate to a cobalamin and then from methylcobalamin to Hg^{2+}. On this basis, mercury methylation occurs as a chemical reaction simply because the mercury is present in the vicinity of the enzymes but is not involved in a true metabolic reaction.

Decomposition of methylmercury can be achieved by numerous mercury-resistant bacteria via cleavage of the mercury carbon bond and conversion of Hg^{2+} to give methane and Hg(0), as considered in Section 12.13.4. Genetic aspects of mercury resistance have been reviewed.[125–128] Other routes to decomposition include an oxidative route producing carbon dioxide and a reductive route taking place in sediments. In the reductive case, methylmercury reacts with sulfides present (Equation (9)) as follows:[129]

$$Me_2Hg^+ + S^{2-} = (MeHg)_2S \longrightarrow Me_2Hg + HgS \qquad (9)$$

Inter alia, it should be noted that high sulfide content in anoxic sediment reduces methylation because of the presence of greater amounts of intractable mercury sulfide.

In principle, the route above can transport large quantities of non-volatile methylmercury in sediments to volatile dimethylmercury capable of entering and being transported in the atmosphere,[130] but this has only been demonstrated in quasi-environmental experiments in the laboratory.

In addition to the above factors, there is a general correlation between increasing temperature and methylation, while demethylation rates reduce with increased temperature.[131] Dissolved organic carbon may also inhibit methylation in a similar manner to sulfide again by reducing the amount of Hg^{2+} available for methylation. For inland waters, there is an inverse correlation between pH and methylation.[132,133] Finally there is a positive link between sediment[134,135] inorganic mercury concentration and methylation.

Sulfate-reducing bacteria (as noted above) are key factors for methylation, which is therefore often observed at its greatest ratio over demethylation in surface sediments where bacteriological activity is maximized.[136,137]

12.13.7.2 Cycling of Methylmercury Species in the Environment

The number of species involved here ($MeHg^+$, Me_2Hg, Hg^{2+} and Hg(0)) is small relative to those of some other elements (e.g., arsenic), with only the counterion varying. In the aquatic environment, methylmercury may be present coordinated to chloride, hydroxide, alkanethiol, or various other forms of organic material, either dissolved or in the solid phase. Coordination depends on competition between chemical, biochemical, pH or Eh (oxidation levels), and salinity. Reduction to inorganic mercury or further slow methylation to dimethylmercury may occur (this latter may lead to transport to the atmosphere). Similarly, coordinated methylmercury may enter the sediment layer. This latter may be considered as the main zone for microbial methylation of Hg^{2+} in view of the high amount of biological activity there. Similar coordination may exist as in the aquatic zone, but with more likelihood of sulfide or alkanethiol complexation.

In the aquatic region, methylmercury is usually the main methylated mercury species present, whereas in the open ocean, the proportion of the dimethyl form increases and may predominate. The proportion of methyl to inorganic mercury is usually small in well-oxygenated waters but may increase in more anoxic environments. In uncontaminated surface waters of lakes, methylmercury concentrations generally range between 0.05 to 5 pmol L^{-1} or more in anoxic or high dissolved carbon environments, reaching up to 10 pmol L^{-1} in stratified lakes.[116] The proportion of organic to inorganic mercury can increase dramatically by bioaccumulation (Section 12.13.7.3) effects in fish and marine animals.

Atmospheric methylmercury precipitated from the atmosphere is usually at less than the 1 pmol L^{-1} level and represents about 1–5% of total mercury.[116] Concentration of methylmercury in the atmospheric gas phase is estimated at 5–25 fmol m^{-3} level. Estimates for a budget of transport fluxes of methylmercury to the oceans have recently been made.[116] Despite these astoundingly small concentrations, amounts in fish and marine animal may be much higher, both absolutely and proportionately (Section 12.13.7.3) arising from transportation effects.

12.13.7.3 Bioaccumulation of Methylmercury

High amounts of methylmercury (i.e., at ppm levels) may be found in fish in lakes remote from any point source of mercury input, and this suggests that the very small amounts deposited in the lake from atmosphere and then methylated in the sediment may then be progressively concentrated.[138] The first step in the food chain, transfer from water to bacteria and phytoplankton, appears to lead to a greater bioconcentration of mercury than at any other stage.[12,139–143] Accumulation is relatively greater for methyl than inorganic mercury, so the proportion of the organic form steadily increases up the food chain, culminating in levels of methylmercury in top fish muscle as over 90% of the whole and concentrations in the 10–100s ppm level. This is the reason for the occasional warnings to limit intake of fish in the diet.[12] In sediments, the key stage is concentration in benthic invertebrates prior to accumulation at higher trophic levels. Recent overviews are given in Refs: 139,144,145. Critically important in this work are developments in analytical chemistry, including the evolution of reference materials (see for example Refs: 5,146–148).

12.13.8 Organolead

The overwhelming factor in the role of organolead compounds in the environment has been the use of tetraethyllead (TEL) and tetramethyllead (TML) (generally, tetraalkylleads (TALs)) in gasoline (petrol). Although this is largely phased out in Europe and the USA, there are many parts of the world (see Ref: 149) where it is still in use. Ironically, it was not simply lead pollution only that provoked withdrawal, but also organic pollution of city atmospheres from gasoline products (photochemical, smoke, etc.). In the attempt to reduce organic emissions from automobiles, catalytic converters were introduced in the 1970s and these were incompatible with lead in petrol. Although a very major atmospheric pollution problem when COMC (1982) appeared, air pollution from lead in Western cities is now a much less serious problem. However worldwide, in many locations, the considerations that have dominated the many reports of organolead pollution still exist (e.g., Ref: 150–153). The key factor is the overwhelming importance of lead in gasoline as the overwhelmingly dominant source of any organic lead distributed via the atmosphere to non-point sources. This still exists in proportion to the actual use of TALs in petrol. The toxic consequences of organolead pollution have been discussed and reviewed many times (e.g., see Ref: 149). Lead pollution arising from the use, loss, or distribution of inorganic lead (e.g., in old water pipes) is not discussed here.

The other concern in the 1970s and 1980s was whether or not inorganic lead could be biomethylated naturally, as in the case of mercury. In view of the bulk amounts of organoleads being used anyway at the time, this was not likely to be a key consideration in urban areas, but in pristine locations, natural lead methylation and transport might in some circumstances have led to environmental problems. In fact, there has not been any clear demonstration of such methylation, and it is unlikely to be a big environmental problem. Where organic lead compounds are detected in the remote environment, they are at very low levels, probably accountable by transport of these species. Evidence is considered in the next section.

12.13.8.1 Lead Methylation and Demethylation

Generally speaking, culture experiments with inorganic lead and bacterial cultures, water, or sediments have not been found to lead to the production of methyl leads.[154,155] Some early experiments were apparently successful, but there has been insufficient corroboration to conclude that lead methylation is a significant environmental phenomenon.[117,156–159] Sulfide-mediated dismutation of trimethyllead to TML has been demonstrated in sulfide-containing sediments, but this is a chemical, not a biological, process,[160] and generally, the sulfide factor is thought to be the explanation of some of the biological methylations previously proposed.[154–156,160,161]

Chemical model experiments have demonstrated that methylation of Pb^{2+} is possible via oxidative methyl donors such as methyl iodide (a model carbonium ion donor for SAM). Only methyl iodide has been shown to be successful with Pb^{2+} in the laboratory.[162–164] This could be environmentally relevant as it is abundant in marine compartments, such as seaweeds, and this could account for some of the methylleads found in maritime atmospheres.[117,159,165,166] Levels however are very low in such locations, and transport of the organic lead arising from losses from gasoline could still account for the effect.

In practice demethylation of organic lead is a more important environmental question, as methyl- and ethylleads can be definitely present in the atmosphere and natural waters from gasoline. It is estimated that spillage of gasoline and unconsumed TEL or TML coming out of the exhaust systems of vehicles constitutes up to 2/3% of the TALs

orginally present in gasoline, that is, about 1,500 t lost annually in 1993. It is still necessary then to consider this aspect of lead input into the environment.

As expected, TAL species are not very stable in the atmosphere and are decomposed by attack of OH radical, ozone, $O(_3P)$, oxides of nitrogen, and direct photochemical decay. In polluted atmospheres, it has been estimated that decay takes hours,[167] leading initially to trialkyl species, then more slowly to inorganic lead (but still in less than 1 week),[168] although some trialkyl species still remain present in rainwater.

TALs are also not very stable in aquatic locations, although decay may take months in pure water in darkness.[169] More realistically, in natural waters containing bacteria, organic species, metals and organisms, light and sulfide, decomposition is rapid (days). Coordinated dialkyllead on humic species, for example, may be the only long-lasting organic lead here.[149]

Decomposition of TAL in soil is also likely to be rapid in either sterile or non-sterile soils (half-life less than 1 day for TEL).[4] The products were partially alkylated lead compounds, which in turn decay or are metabolized by organisms.

Decay in organisms relates to toxicity, and half-lives and excretion rates are dealt with elsewhere in this chapter. Toxicity arises because of easy absorption in mammals, leading to the loss of one alkyl group to form the trialkyl species. It is these trialkyl species which can most easily deliver lead and so cause toxicity. Decay does therefore take place by sequential loss of alkyl groups (similar to organotin species, Section 12.13.9), and so a series of alkyl, ionic, and inorganic lead species are excreted by mammals.

12.13.8.2 Presence of Organolead Compounds in the Environment

Work in the 1980s established concentration levels to be expected in atmospheres remote from the source when TALs were routinely used in gasoline. Typically, these would be at the $ng\,m^{-3}$ level. Ionic lead would also be at similar levels.[170] Ionic leads in waters are also very low (at about the $ng\,L^{-1}$ level), with TALs being very low. There is little information about organolead species in sediments and soil. The analytical methodologies are discussed in Section 12.13.5. A recent tabular summary of organolead species detected in the various environmental compartments at the levels noted above is given in Ref: 149.

12.13.9 Organotin

12.13.9.1 Introduction

The widespread interest in the environmental chemistry of OTCs is evident in the extensive literature on the subject. This includes several books and monographs dealing with the chemistry,[171,172] environmental chemistry,[173–175] and toxicology[176] of this class of organometallic compound. This section will summarize the main OTCs of interest from a commercial perspective, their properties, uses, and industrial synthesis. The environmental aspects of the most widely used organotins will be discussed, particularly the sources, sinks, biogeochemical transformations, environmental persistence, and degradation products. The analytical methods specifically used to measure the most prevalent of these compounds in different environmental compartments will be mentioned. Finally, the toxicity of the main organotin species to organisms and humans will be highlighted.

Tin is the element with the largest number of organometallic derivatives in commercial use. Both inorganic tin and the related OTCs have a wide range of industrial applications, and of the total amount of tin currently refined, 7–10% is used to produce organometallic compounds containing this element.[177] The main industrial applications of OTC are summarized in Table 9. About 70% of the world production of OTCs are used as heat and light stabilizers in rigid polyvinyl chloride (PVC) plastics and about 20% finds use as various types of agrochemicals, such as biocides, herbicides, and wood preservatives. The worldwide use of OTCs has increased 1,000-fold over the last 50 years, from 50 t per annum in 1950 to 50,000 t per annum in early 2000. However, this level of usage may decrease to some extent due to the introduction of recent legislation on the use of antifouling paints, which will come into effect within the next few years. Notwithstanding this, pollution as a result of the use of OTCs is widespread in the environment, and the effects are particularly evident in the biosphere.

All OTCs have a central Sn atom, with sp^3-hybridization, that is covalently bonded to a maximum of four groups. These groups can be organic (R) or inorganic (X) in nature (and notation). The general formula for OTCs such as these are R_nSnX_{4-n}, in which the organic R can be alkyl or aryl and X is an inorganic counterion. It should be borne in mind that there is no direct evidence available on the form of the counterion (X), other than in the tetraorganotin compounds, the volatile hydrides, and some environmental species, where complexation with OH^-, Cl^-, and CO_3^{2-} takes place.[178] The tin–carbon bond is stable to water, atmospheric oxygen, and heat up to 200 °C.[179] Ultraviolet radiation, strong acids,

Table 9 The main industrial applications of different classes of OTCs

Compound	*Industrial application*	*Function*
R_3SnX	Total biocidal use ca. 20% of total OTC production	
R_3SnX, (R = Bu, Ph)	Antifouling paint	Biocides
R_3SnX, (R = Bu, Ph, Cy)	Agrochemicals	Different pesticides
Bu_3SnX	Wood preservative	Insecticides, fungicides
Ph_3SnX	Cloth protection	Insecticides
R_2SnX_2	Use as PVC stabilizer ca. 70% of total OTC production	
R_2SnX_2, $RSnX_3$ (R = Me, Bu, Oct)	PVC stabilizer	Heat and light stabilizers
Me_2SnX_2, $RSnX_3$ (R = Me, Bu)	Glass treatment	Precursor for SnO_2 films on glass
Bu_2SnX_2	Poultry farming	Dewormer
Bu_2SnX_2	Production of polymers	Homogeneous catalysts
$RSnX_3$	Use constitutes a minor % of total OTC production	
$RSnX_3$ (R = Me, Bu, Oct)	PVC stabilizer	Heat stabilizers
$BuSnCl_3$	Glass treatment	Precursor for SnO_2 films on glass
$BuSnCl_3$	Transesterification	Homogeneous catalysts

Adapted from Cima, F.; Craig, P. J.; Harrington, C. In *Organometallic Compounds in the Environment*, 2nd ed.; Craig, P. J., Ed.; Wiley: Chicester, 2003; pp 101–150; and from Hoch, M. Appl. Geochem. **2001**, *16*, 719–743.

and electrophilic agents can cleave this bond, and these characteristics are useful from an analytical and environmental biogeochemical point of view. The number of bonds and the length of the alkyl chains have a significant effect on the chemical, physical, and toxicological properties of the OTC. In general, the solubility of OTCs in water decreases with increasing number and length of the organic groups, but will also be affected by the nature of the X group.

The manufacture of OTC[180] involves a two-step reaction. The first step can be achieved in a number of different ways and involves reaction of tin tetrachloride ($SnCl_4$) with a suitable reagent to produce various tetraalkyltin compounds (R_4Sn). In the second step, R_4Sn reacts with $SnCl_4$ in a redistribution reaction to form less alkylated organotin chlorides such as R_3SnCl, R_2SnCl_2, or $RSnCl_3$. From these products, various other tin derivatives can be produced. A direct reaction scheme is also possible whereby the organotin halides can be synthesized by a reaction between tin metal or alloy and alkyl halides.

The most important group of OTCs from an environmental perspective is the trisubstituted compounds, which are used as biocides and have found widespread use on an international scale. Two compounds in particular have been the focus of environmental studies: tributyltin (TBT), because of its extensive use as an antifouling paint, and triphenyltin (TPhT), which is used as an agricultural fungicide. The growth and attachment of aquatic organisms on surfaces immersed in surface water, particularly the hulls of ships and boats, is a costly problem. The roughness caused by the fouling of marine craft increases fuel consumption, because of the extra energy required for powering the craft through the water. For this reason, antifouling coatings containing a biocide are applied to maintain the surface free from bioattachments, and since the early 1970s, the majority of these coatings containing TBT have been formulated. They are designed to slowly release TBT, either by diffusion or by reaction with water, reaching a constant leach rate and maintaining a thin layer of TBT near to the surface being protected. Even at low nanomolar concentrations, TBT causes chronic and acute toxicity to a range of marine organisms, which are particularly sensitive to trisubstituted OTCs.[181] It is now clear that the use of TBT-based antifouling coatings has led to a buildup of this biocide in harbors, marinas, and dockyards around the world, and this has caused wide-ranging impacts on non-target organisms. The second OTC of concern, TPhT, has been widely used as an agricultural fungicide for the control of potato blight and also in antifouling coatings, but to a much lesser degree than TBT. The agricultural use of TPhT began in the 1960s, and is an important source of pollution because of its direct application, resulting in contamination of soil and subsequently water through leaching and run-off. This compound is considered safe to use on food crops, because it is rapidly degraded by light, rain, and other environmental factors, and the remaining residues can be removed by washing and peeling before consumption.

As a result of the collapse of the oyster fishery in Archachon Bay in SW France, which was subsequently shown to be a result of the use of TBT-based antifouling coatings[182] on boats in the area, the French government regulated the use of these paints in 1982 to vessels <25 m in length. The UK government followed suit in 1985, and set an

Environmental Quality Target Concentration for TBT of 20 ng l^{-1}, which was based on the lethal concentration for some commercially important molluscs. Subsequently, a number of other countries have restricted the use of TBT-based paints, including USA (1988), Australia (1989), Canada (1989), and Japan (1990). Switzerland, Austria, and New Zealand have now banned the use of these antifouling paints completely. In October 2001, the International Maritime Organisation adopted a new convention on the use of TBT and other harmful substances as antifouling paints. The international parties to the convention agreed to a number of specific requirements relating to the reduction in use of these coatings.[174] By January 2008, the signatories to the treaty must ensure that ships bearing their flags do not have TBT-based coatings on their hulls, or if they do that, it is covered by a protective layer to prevent leaching of TBT. However, while this is a landmark undertaking in environmental protection, it should be borne in mind that a number of countries with commercial shipping operations have not signed the convention and may still be using these coatings.

12.13.9.2 The Behavior of OTCs in the Environment

Some of the most important sources of the main OTCs of environmental interest (TBT and TPhT) have been identified above. Their biological effects will be determined by how the compounds are distributed between different environmental spheres, the timescales in which they are transported within the environment, and the particular organometallic species that exist under the prevailing environmental conditions. The environmental distribution of these compounds will therefore be determined by the physical, chemical, and biological properties they exhibit, and the myriad of localized conditions they are subject to. A reasonable biogeochemical cycle for OTCs can be postulated (see Figure 3); however, there is little quantitative information about fluxes between the different compartments, despite the concentrations of the various compounds having been studied.

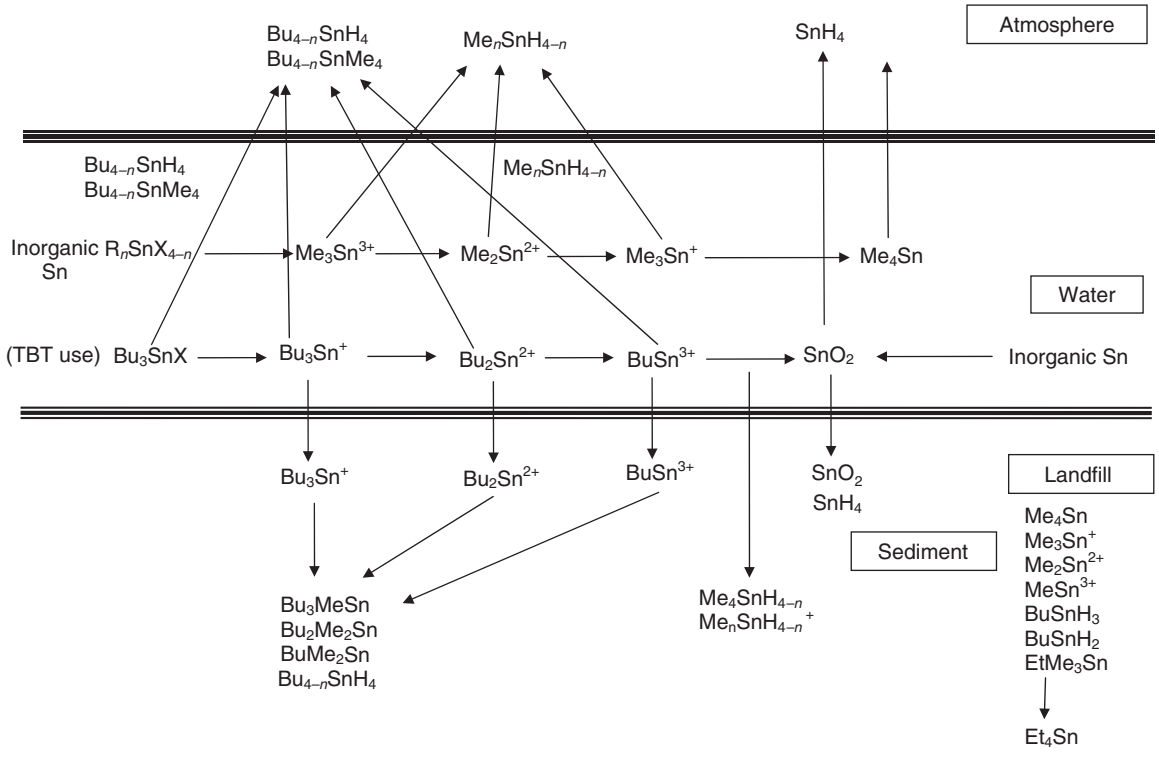

Figure 3 The biogeochemical cycle for tin. Adapted from Cima, F.; Craig, P. J.; Harrington, C. In *Organometallic Compounds in the Environment*, 2nd ed.; Craig, P. J., Ed.; John Wiley & Sons: Chicester, 2003; pp 101–150.

12.13.9.2.1 Distribution in the environment

One of the most important physical properties exhibited by OTCs from an environmental perspective is their aqueous solubility, and this is of particular interest because the majority of significant anthropogenic inputs are into water, mostly seawater, and also river water and agricultural run-off into river catchments. The trisubstituted OTCs are generally hydrophobic in nature, with aqueous solubilities highly dependent on salinity, pH, and temperature.[183] The main consequence of this is that TBT and TPhT are rapidly partitioned onto water-borne particles, and their fate will therefore be largely dependent on the hydrodynamics of the particulate phase.[184] Ultimately, the OTCs will become trapped in the sediment due to settling of the particulates when conditions allow, with the possibility of resuspension into the water column and leaching of the OTCs back into the water at a later date. Although accumulation in sediments is viewed as a significant environmental sink for OTCs, they are also a long-term source of dissolved-phase contamination.[183,184] There is evidence that as a result of their hydrophobic characteristics, OTCs accumulate in the surface microlayer located at the air–water interface. In this part of the water column, the OTCs are rapidly lost[185] due to volatilization and UV degradation, and also come into contact with the most sensitive larval stages of some marine organisms.

The formation of volatile OTCs has been recorded in a number of systems and some examples include domestic waste sites[186] and estuarine and coastal environments.[185,187] Adelman *et al.*[185] used radiolabeled (^{14}C-TBT) to determine the biogeochemistry of butyltin compounds in an enclosed marine mesocosm. In this system, TBT was lost from the water column by biodegradation to dibutyltin (DBT), which was further degraded to monobutyltin (MBT), and also directly to MBT. Some of the added TBT was lost to the sediment, and the remainder was rapidly lost from the system to the atmosphere. By using highly sensitive analytical techniques based on coupling GC to ICP-MS detection, the volatile OTCs involved in air–water transfer have been identified. Methyltin, methyltin hydride, and methylated butyltin compounds were identified, with the most ubiquitous species being dependent on the system under investigation.[186,187] The formation routes for these compounds will be discussed in more detail in the bioaccumulation and biotransformation section below.

12.13.9.2.2 Environmental stability and degradation

Environmental degradation of the OTCs[183,188] follows a common pattern for each different class of compound (Me-, Et-, Bu-, Ph-, etc.,) and involves the progressive loss of organic substituent, as shown in Equation (10), where R = alkyl or aryl group and X = a counterion (Equation (10)).

$$R_4Sn \longrightarrow R_3SnX \longrightarrow R_2SnX_2 \longrightarrow RSnX_3 \longrightarrow SnX_4 \qquad (10)$$

A number of processes have been shown to lead to the degradation of OTC in this manner, including UV photolysis, biological degradation, and chemical cleavage. Photolysis of the Sn–C bond occurs rapidly in the photic zone of surface waters, but due to the attenuation of sunlight with depth, it is less important in deeper water or sediment. This degradation process is much more rapid for TPhT than TBT. The biological degradation of OTCs due to bacteria and microalgae has also been reported,[189,190] but is limited by the prevailing conditions (light, temperature, and nutrients) and the fact that these compounds can have significant biocidal activities. Breakdown due to the interaction of OTC with specific chemicals in the environment is not considered to be significant, but is of importance when developing analytical methods for their determination.

The usual way to evaluate and compare degradation rates and to gain a greater understanding of a pollutant's persistence in the environment is by determination of its half-life[188] in a particular matrix. The half-life value for OTCs in seawater is between a few days to several months, and for sediments, it can be anywhere between a few months to 9 years. The greater range of values for sediments, compared to water, results from the wide diversity of environmental conditions found in sediments, which can influence their breakdown. Table 10 shows a number of different half-life values for TBT in different environmental compartments.

12.13.9.2.3 Bioaccumulation and biotransformation

Studies on the uptake of OTCs into a variety of organisms have been reviewed by Maguire,[176] and this documents a range of evidence, based on bioconcentration factors, that TBT is accumulated strongly by some aquatic species. Further data to support this come from measurements of the TBT concentration in the higher trophic level organisms in the marine environment. However, some species, including crustaceans and fish, were shown to contain much lower body burdens of TBT, and this was thought to be because of the possession of an efficient enzymatic mechanism for its degradation.[191]

Table 10 Estimated half-lives for TBT in a variety of different environmental compartments

Compartment	*Half-life*
Freshwater	6–26 days (light), 4 months (dark)
Estuarine water	1–2 weeks
Seawater	6–127 days
Water/sediment mixture	5 months–5 years
Estuarine sediment	3.8 years
Marine sediment	1–4, 100–800 days 1.85–8.7 years
Soil	4–5 months (TPhT)

Adapted from Cima, F.; Craig, P. J.; Harrington, C. In *Organometallic Compounds in the Environment*, 2nd ed.; Craig, P. J., Ed.; Wiley: Chicester, 2003; pp 101–150.

The most significant biotransformation of OTC in the environment is biomethylation, which has been reviewed.[192] Abiotic methylation involves chemical agents from the environment, such as: methylcobalamin, which is a co-enzyme of vitamin B_{12} and can transfer a methyl group to metals; methyl iodide, produced by macroalgae in the marine environment and which reacts with metals and metal sulfides; humic and fulvic acids, which are prevalent in fresh water as the result of the decomposition of vegetation; and other methylmetals which can transmethylate OTCs. Biotic methylation or biomethylation can involve sediment- or estuarine-containing microorganisms, which are not always fully identified, but sulfate-reducing bacteria and yeast have been shown to methylate tin and OTCs. This process of methylation is important because it changes the toxicity and biogeochemistry of the original OTC in the environment.

12.13.9.3 The Analysis of Organotin Speciation in the Environment

A number of reviews dealing with the analysis of organometallic speciation by chromatography coupled to spectroscopic detectors describe techniques for organotin compounds in environmental samples. Some of these are focused on different types of chromatography;[193,62] others deal specifically with HPLC[79,195,80] or GC.[196] A technical report from IUPAC[72] reviews the major techniques used for the determination of OTC, including all aspects of the analytical procedures developed prior to 1998. A comprehensive review of the analytical procedures used for the determination of OTC in sediment and biota pays particular attention to the extraction techniques used.[54]

12.13.9.3.1 Sample preparation methods

Most environmental studies have focused on three distinct groups of OTCs: the butyltin, phenyltin, and methyltin compounds. Differences in the chemical nature of the mono-, di-, tri-, and tetrasubstituted OTCs, particularly between the ionic and neutral forms, mean that it is difficult to find extraction methods suitable for all of the species. Extraction of the OTCs prior to their determination is required for air, water, sediment/soil, and biota samples.

The extraction step for the analysis of volatile OTCs in air or other sample matrices is considerably different to the non-volatile compounds, and involves "cryotrapping" the OTCs present in the sample on either a packed or unpacked column at low temperature.[187] The analytes are then thermally desorbed into the detector, effectively being separated by differences in boiling point. The extraction of OTC from water samples can be facilitated using a non-polar solvent, the more ionic species (mono- and di-) being complexed with tropolone, and the immiscible solvent layer is removed from the sample, dried, and the analytes determined using an analytical method with an appropriate LOD, such as GC-ICP-MS.[197] The analysis of sediment or soil requires the OTC to be leached from the sample, which is often accomplished using the combination of an acid and a polar solvent.[198] This method is preferred to the use of an organic solvent because the extract does not contain any of the large number of organic compounds usually found in these sample types. A comparison of 10 extraction methods for butyltin compounds from sediment using an organic solvent showed that only three methods produced extraction efficiencies of greater than 90% for TBT, whereas none of them gave reproducible results for MBT.[199] The analysis of sediments from harbors in southern India for butyltin and methylbutyltin compounds used acid leaching (HCl), extraction into toluene using tropolone, derivatization at pH 5 with sodium tetraethylborate, prior to analysis by GC-ICP-MS.[200] Methods for the extraction of biomaterials include the use of enzymatic

digestion with a combination of enzymes, such as lipase–protease, followed by extraction of the liberated OTC with a suitable solvent.[201] Alternatively, digestion with tetramethylammonium hydroxide and, in some cases, further extraction into an organic solvent has been applied successfully to tissue samples.[202] The application of microwave energy to the extraction step in both sediment and biota analysis has greatly improved both the extraction efficiency and reduced the sample preparation time.[57]

12.13.9.3.2 Analytical methods based on gas chromatography

The majority of studies have focused on MBT, DBT, and TBT, but there are a smaller number of methods for the methyl-, phenyl-, cyclohexyl-, and octyltin compounds. Although some OTCs, particularly the tetra species, are readily amenable to analysis by GC methods, the more environmentally important mono-, di-, and trisubstituted compounds require derivatization to a volatile and thermally stable analog.

The derivatization method established for the longest is the formation of an organotin hydride, which confers the volatility required for chromatography to take place. This can be carried out on- or offline by reducing the organotin compound with sodium borohydride, in the presence of an acid. The acid helps to produce hydrogen from $NaBH_4$, which reacts with the OTC to produce an organotin hydride. The gaseous organotin hydrides are purged from the reaction vessel using helium and trapped on a chromatographic material contained in a U-tube, immersed in liquid nitrogen. This approach is widely used for the analysis of organometallic compounds and is often referred to as cryofocusing. The organotin species are separated by slowly heating the U-tube electrothermally, which causes the analytes to elute in order of boiling point. The organotin hydrides are then detected using some form of tin-specific detector. The most widely used detectors are QF-AAS, AFS, and ICP-MS. The use of HG for the analysis of OTC in water samples works well, but for the analysis of sediment, it is less successful because of the composition of the matrix. Other metals and organic compounds interfere with the reaction between $NaBH_4$ and the OTC, either by breaking down the hydrides formed or by preferentially reacting with the borohydride reagent. Another problem that often arises is excessive foaming when the hydrides are purged into the detector, which leads to poor sensitivity when AFS is used and an excessively noisy signal with ICP-MS.

The most widely used method to prepare the OTC for GC analysis is the formation of tetrasubstituted alkyltin compounds. Two different approaches are possible; the first is carried out in a non-polar solvent by using a Grignard reagent to peralkylate the analyte. Experimental parameters such as temperature and nature of agitation differ between methods but studies have shown that only the concentration of Grignard reagent used significantly affects the derivatization efficiency.[203] The reaction requires only 5–10 min before the excess reagent is neutralized with an acid. Problems with the Grignard derivatization include losses due to the volatility of the methyl derivatives, interconversion of MPhT and TPhT, and sulfur interferences with GC-MS and GC-FPD analysis of sediment. The second method is carried out in the aqueous phase and involves alkylation using reagents based on sodium tetraalkylborate. The use of sodium tetraethylborate for derivatization of OTC in environmental samples has been extensively reviewed.[78] In summary, the protocol involves adjustment of the pH to between 4 and 5, and then the derivatization reagent dissolved in ethanol is added. In general, the Grignard derivatization gives a higher yield than aqueous-phase alkylation, but is sensitive to the presence of water, so the derivatization step is not as easy to use.

12.13.9.3.3 Analytical methods based on HPLC

Unlike GC analysis, when HPLC is used for separation, it is not possible to determine such a broad range of OTCs, differing in type and degree of alkyl substituents, in a single chromatographic run. Ion exchange, size-exclusion, reversed and normal phase separations have all been developed for organotin speciation.[195] Ion exchange chromatography is a popular separation methodology for a wide range of organotin species including methyl-, ethyl-, butyl-, propyl-, phenyl-, and cyclohexyl-substituted species and a wide range of environmental matrices have been analyzed. Reversed phase separations have been developed for separation of a wide variety of organotin species in different environmental matrices.

12.13.9.3.4 Analytical methods based on other techniques

The SFC separations that have been developed deal with a limited number of organotin compounds compared to HPLC or GC separations. The majority of SFC methods have been used to determine the tri- and tetrasubstituted butyl- and phenyltin compounds.[86] Atmospheric pressure ionization tandem mass spectrometry has been used for the quantitation of TBT. The method relied on molecular fragmentation and tandem mass spectrometry for the

specificity necessary for environmental speciation analysis.[204] A recent method for the analysis of TBT does away with the need for a separation step completely and relies on the differences in vapor pressure of the three buytltin chlorides. In this method, the greater volatility of TBTCl allows it to be sampled from the gas phase using SPME prior to desorption and analysis using ICP-MS.[205]

12.13.9.3.5 Detection methods

The main criterion for the detector is that it gives a response specifically for tin, rather than the compound. This is because of the detection limits required for environmental analysis, which are not attainable with non-specific detectors. The most popular detection methods for organotin analysis are FPD using a tin selective filter, MS, MIP-AES, and ICP-MS. Recently, HPLC-MS methods based on atmospheric ionization including electrospray, ion spray, or chemical ionization have been used to detect the organotin species.[97] These methods have the advantage that molecular information concerning the analyte is available, rather than just atomic information.

12.13.9.4 General Toxicity of OTCs

Elemental tin and its related inorganic compounds, where the tin atom is present in either of its two prominent oxidation states, Sn^{2+} or Sn^{4+}, are considered to be nontoxic. However, the organic derivatives of tin are toxic, with the target species' sensitivity and the degree of toxicity being dependent on the type of organic ligand (Me, Et, Bu, etc.) and the extent of substitution (mono-, di-, tri-, or tetra-), respectively. In general, alkyltin toxicity increases with the number of organic groups, reaching a maximum toxicity for R_3SnX, whereas $RSnX_3$ and R_4Sn species are much less toxic. This can be explained by the differences in polarity and lipophilicity between the species, which has an important role to play in uptake and accumulation of a compound by a specific organism. This also explains why an increase in the *n*-alkyl chain length leads to compounds with much lower toxicity, such as the octyltin compounds, which are essentially nontoxic to all organisms.[183] Table 11 summarizes the species-specific nature of the toxicity of triorganotin compounds of the general form R_3SnX.

12.13.9.4.1 Effects on organisms

A range of effects on non-target organisms as a result of exposure to OTC have been described,[173] but two of these in particular standout as the most important from an environmental perspective. The first effect relates to the decline in the oyster fishery in Archachon Bay due to poor larval survival rates and the formation of shell malformations, which led to the banning of TBT antifouling coatings in France. The second notable effect relates to the appearance of male sexual characteristics in female gastropods, most notably the dogwhelk, *Nucella lapillus*. This phenomenon, termed imposex, relates to the endocrine-disrupting effect of TBT. Both of these environmental impacts result from chronic, long-term exposure of the organisms involved to relatively low concentrations of TBT and, to some extent, TPhT.

The endocrine-disrupting activity of TBT to different species of gastropod can be induced in the females at TBT concentrations as low as $0.5\,ng\,Sn\,l^{-1}$,[206] a level lower than the LOD for many of the analytical methods for the measurement of TBT currently available. This gives an indication of the toxicity of TBT to marine organisms and illustrates why it has been described as the most toxic chemical ever to be deliberately introduced into the marine environment.[176] The sterilization of females occurs at concentrations from 3 to $5\,ng\,Sn\,l^{-1}$, resulting in population decline. In the most seriously affected regions near to areas of high shipping activity, the species has disappeared completely. Imposex has been observed in populations of open-water organisms spatially remote from coastal areas but close to

Table 11 The toxicity of triorganotin compounds of the general form R_3SnX

Biological species	*R in most active R_3SnX compound*
Insects	Me
Humans and other mammals	Et
Gram-negative bacteria	Pr
Gram-positive bacteria, fish, fungi, molluscs, plants	Bu
Fish, fungi, molluscs	Ph
Fish, mites	*cyclo*-C_6H_{11}

Adapted from Cima, F.; Craig, P. J.; Harrington, C. In *Organometallic Compounds in the Environment*, 2nd ed.; Craig, P. J., Ed.; Wiley: Chichester, 2003; pp 101–150.

shipping lanes, and TBT has also been detected in populations of these species.[207] Despite the OTCs being found in aquatic invertebrates, such as molluscs and gastropods, little is known about the accumulation of these compounds in higher trophic level vertebrate predators, which are exposed via food ingestion. Further studies are awaited in this area.

12.13.9.4.2 Effects on human health

The most well-documented evidence[208] for the toxic effects of OTCs on human health come from a poisoning episode involving the ingestion of stalinon, a pharmaceutical preparation for the treatment of bacterial infections, containing diethyltin diiodide as the active ingredient. The incident caused the death of 100 people from a total of 1,000 who took the drug. The acute nature of the poisoning was thought to be the result of the presence of the highly toxic compound Et_3Sn^+ as an impurity in the formulation. Triethyltin acetate is the most toxic OTC to mammals, including humans, presumably as a result of the polarity of the Et groups, and these compounds are no longer used or manufactured industrially. The symptoms of acute toxicity due to the ingestion of triethyltin include headache, nausea, vomiting, and visual disturbances. Death occurred due to cardiac or respiratory failure as a result of the formation of a cerebral edema.

At the less extreme end of intoxication, very little is known about the possible effects[209] of chronic exposure to compounds such as TBT and TPhT on humans. However, unlike some other organometallic compounds containing heavy metals, for example, Hg, degradation of the OTC of environmental concern ultimately leads to formation of the least toxic tin containing ionic compounds, such as $SnCl_2$. The degradation of the trisubstituted species will therefore result in less toxic species being formed, whereas the degradation of the tetra form will result in an increase in toxicity as a result of the formation of the trisubstituted species.

The target organs and mode of action of OTC have been discussed[173] and can be summarized as follows: the most toxic compounds tetramethyltin (TMT) and tetraethyltin (TET) are highly neurotoxic in mammals; there is evidence for the hepatotoxicity of DBT in animal models; the butyltin and TPhT compounds have been shown to be immunotoxic in mammals; TPT is classed by the US Environmental Protection Agency as a probable human carcinogen; there is some evidence that TPT exhibits endocrine-disrupting properties in rats; and the butyltin compounds exhibit teratogenic effects in mammals. However, it is very apparent from reviews in the area that the chronic effects of the widely dispersed butyltin compounds have not been studied in detail and their effects on humans are consequently not well understood.

12.13.10 Organoarsenic

Research on organoarsenic compounds up to 1993 has been previously reviewed and the following works should be consulted by readers requiring detailed information. The review of Cullen and Reimer[210] is an all-encompassing treatise of arsenic compounds (species) in the environment and includes sections on basic chemistry, biotransformations, and environmental behavior. Chemical aspects, including synthesis, are the focus of the review by Edmonds *et al.*[211] The review of arsenic in marine organisms, published in 1997,[212] adequately summarizes the relevant environmental literature up to 1993, because research on environmental organoarsenic chemistry had focused on marine systems, and terrestrial systems had remained relatively unexplored. This largely reflected the relative quantities of organoarsenicals (marine > terrestrial), and the difficulties in performing the work with low concentrations of arsenic generally found in terrestrial samples. In the following, the authors do not attempt to provide the details contained in those previous reviews. Rather, they briefly summarize that information and focus on new developments that have taken place since 1993, largely as a consequence of improved analytical techniques described elsewhere in this chapter.

12.13.10.1 A Summary of the Literature up to 1993

Although there were earlier reports of arsenic in marine samples, the widespread occurrence of high concentrations of arsenic in algae, fish, and shellfish was first established in the 1920s (an historical account of this period is provided in Ref: 213). Investigations at that time indicated that the arsenic in crustaceans comprised one major organoarsenic compound, but it was another 50 years before this compound was identified as arsenobetaine (Figure 4; **F4-7**). Shortly afterward, the structures of two major arsenicals in a brown alga were determined to be novel carbohydrate derivatives, namely, dimethylarsinoylribosides; subsequent work demonstrated that these compounds were part of a group of arsenicals collectively termed arsenosugars that predominate in marine algae. The techniques employed

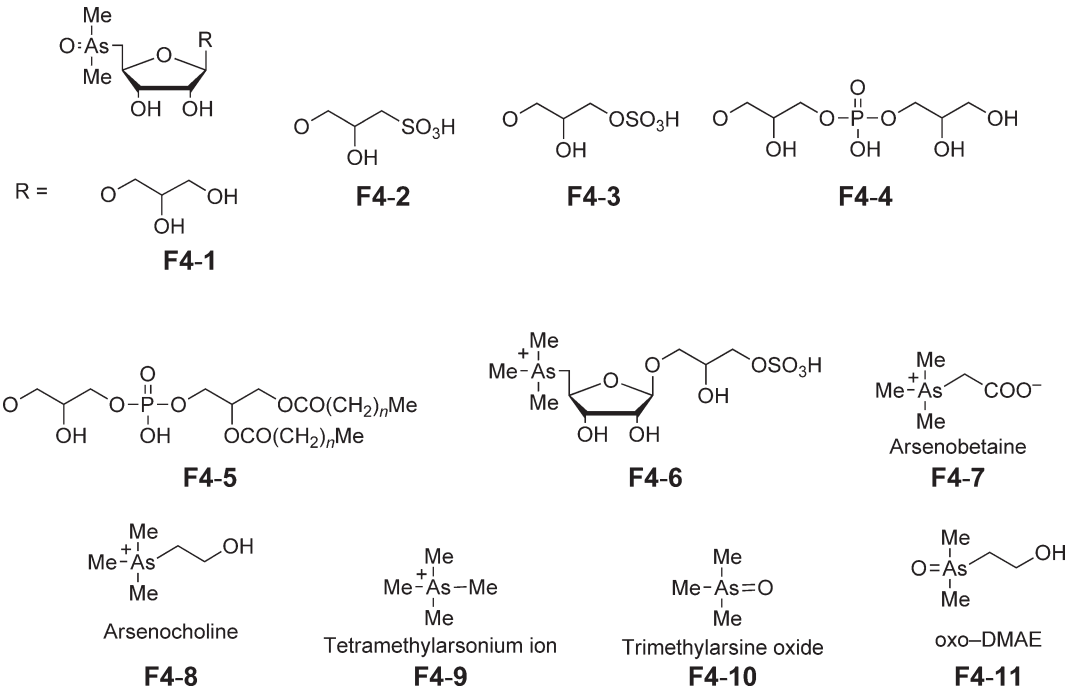

Figure 4 Significant arsenic compounds identified up to 1993.

were mainly those of the natural products chemist, and during the 1980s and early 1990s more than 20 organoarsenic compounds were isolated from marine samples and identified chiefly by NMR spectroscopy. Figure 4 provides the structures of the most significant arsenosugars and other organoarsenic compounds reported up to the end of 1993.

The state of knowledge and generally accepted views[212] of marine organoarsenic chemistry in 1993 can be summarized in the following few sentences. Arsenosugars, occurring in marine algae at concentrations of up to 100 $\mu g\,As\,g^{-1}$ dry mass or more, are produced *de novo* by the algae from arsenate, present in seawater at about 1–2 $\mu g\,As\,L^{-1}$, by sequential reduction/oxidative methylation steps involving SAM as the methyl donor. The unsubstantiated view was that this methylation process was invoked to detoxify the potentially toxic arsenate which the algae inadvertently take up as a consequence of their need for phosphate, an essential nutrient structurally similar to arsenate. About 15 arsenosugars were identified, most of which were based on a dimethylarsinoylriboside structure with the variety of compounds emanating from different aglycone groupings comprising common algal secondary metabolites. A trimethylarsonioriboside was also found which presumably resulted from further reduction/methylation of the dimethylarsinoyl compound. The situation with most marine animals was much simpler because their arsenic speciation was dominated by arsenobetaine with smaller quantities of other quaternary arsonio compounds such as arsenocholine and tetramethylarsonium ion. Trimethylarsine oxide was also reported as a minor arsenical in marine animals. These compounds commonly found in marine animals were not reported in marine algae, and hence were thought to be exclusively animal products. Arsenosugars, however, were not restricted to algae but were also found in animals that fed directly on algae, such as bivalve molluscs.

The origin of arsenobetaine formed an important topic at that time, with a popular hypothesis involving arsenosugars as precursors. The reasons for the high concentrations of arsenobetaine in marine animals were also discussed. But this was a period when environmental organoarsenic compounds were considered to be marine phenomena—a situation that was to quickly and radically change by work carried out from 1993 onward, and building on a new approach of speciation analysis with mass spectrometric detection (see Section 12.13.5). The following looks at this period of research in some detail.

12.13.10.2 Novel Organoarsenic Compounds: 1993–2005

Novel organoarsenic compounds identified since 1993 are presented in Figures 5 to 7. For convenience, we will discuss them under the following group headings.

12.13.10.2.1 Arsine oxides (oxo–dimethylarseno compounds)

Oxo–dimethylarsenoacetate (oxo–DMAA, Figure 5; **F5-12**) was first tentatively identified in extracts of marine reference materials of mussel, oyster, and lobster,[214] and was subsequently shown to be present in several other marine samples.[215,216] It has also been identified as a significant metabolic product in several studies looking at mammalian[217,218] and microbial transformations.[219,220] Homologs of oxo–DMAA, namely, oxo–dimethylarsenopropionate (oxo–DMAP; **F5-19**) and oxo–dimethylarsenobutanoate (oxo–DMAB; **F5-20**), were identified as metabolites in human urine after consuming cod liver and cod liver oil;[223] oxo–DMAP had earlier been found in several samples of marine organisms.[216] An arsine oxide derivative of sulfated ribitol (Figure 5; **F5-13**) was isolated from a red alga *Chondria crassicaulis*, and it was thought to be widely distributed in red algae.[222] A series of new arsine oxides (Figure 5; **F5-14–F5-18**) were identified in the kidney of the clam *Tridacna derasa* where their presence probably results from breakdown of arsenosugars.[215]

12.13.10.2.2 Trimethylarsonio compounds

A second arsenic betaine, trimethylarsoniopropionate (Figure 6; **F6-21**), was first found in a fish sample,[224] and has subsequently been shown to occur widely in marine animals, albeit generally at low concentrations.[225] A new trimethylarsonioriboside (Figure 6; **F6-22**) was also found as a trace constituent in several gastropod species,[226] and as a much more significant arsenic component in the intestine of fish and invertebrates.[227]

12.13.10.2.3 Arsine sulfides (thio–arsenicals)

The first (Figure 7; **F7-23**) of a most interesting group of compounds, termed thio–arsenicals, was reported by Hansen *et al.* in 2004[217] as a metabolite in sheep urine. This compound displayed unexpected chromatographic properties, which initially hindered its identification. Additionally, the thio compound readily converted to the oxo analog during sample storage. Hansen *et al.*[217] predicted that other thio–arsenicals were likely to be found, and this has certainly been shown to be true (e.g., compounds **F7-24–F7-27**; Figure 7; Hansen and Raab (2003)).[218,223] Also, in 2004, the first thio–arsenosugars were reported in mussels[228] and there have been several further.[229–231] So far the thio analogs (Figure 7; **F7-28–F7-31**) of the four major oxo–arsenosugars have been identified from natural sources. They appear to be present at higher concentrations in animal samples, although they have also been reported in algae.[232]

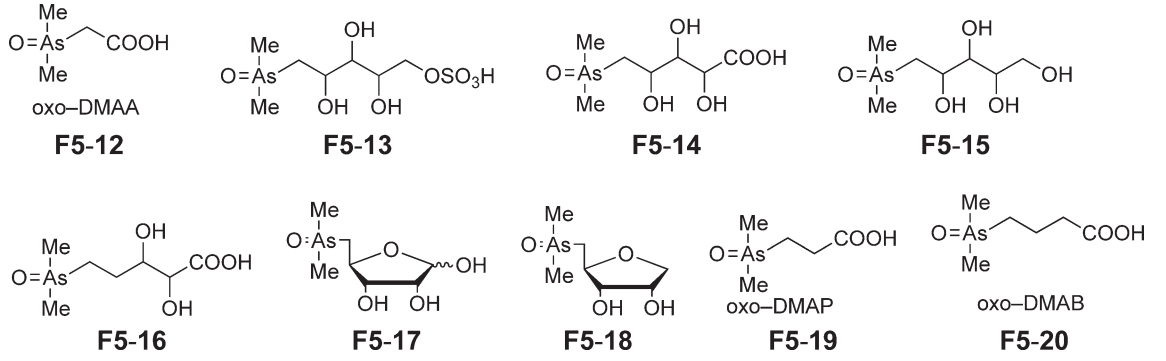

Figure 5 Arsine oxides (oxo–arsenicals) identified since 1993.

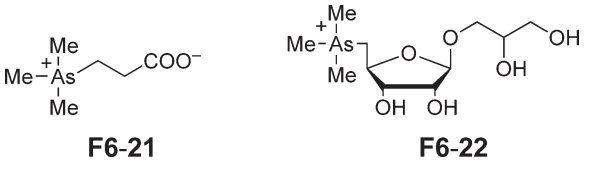

Figure 6 Trimetharsonio arsenicals identified since 1993.

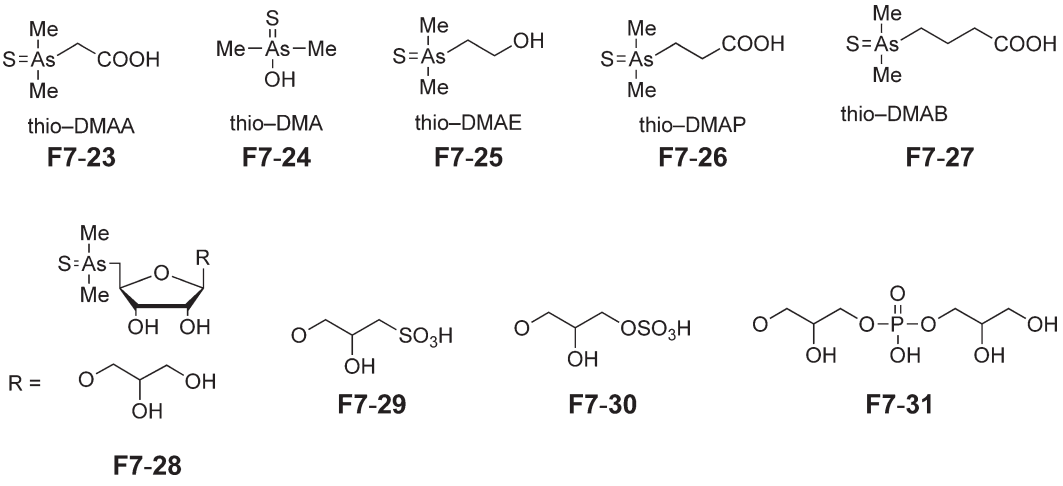

Figure 7 Arsine sulfides (thio–arsenicals) identified since 1993.

One might ask why these widespread and abundant arsenicals escaped detection for so long. The answer appears to lie in the unexpected properties of the compounds, and the widely used analytical methods for determining arsenosugars at that time. The analytical method of choice was anion-exchange HPLC (with arsenic-selective detection by atomic mass spectrometry), and the use of columns with a polymer backbone (e.g., Hamilton PRP-X100) was almost universal. The substitution of O for S on the arsenic atom leads to a considerably less polar molecule; these thio–arsenicals interact strongly with the polymer column backbone, and depending on the mobile phase conditions, may not elute from the column. The problem was initially overcome by using mobile phases at higher pH[228] and/or containing methanol,[230] and, more recently, by the use of reversed-phase columns.[218]

12.13.10.2.4 Arsenolipids

Non-polar arsenicals, loosely termed arsenolipids, constitute a significant part of many samples, and in some samples such as fatty liver tissue they contribute 70% or more of the total arsenic content.[221] So far, only a single arsenolipid has been identified, namely, the acylated arsenosugar (Figure 4; **F4-5**) isolated in 1988 from an alga.[233] The arsenolipids in fish oils,[221] of which there are at least 10, are not based on arsenosugars; their structures remain unknown. Some hints to their possible identity, however, have come from recent work on the metabolism of these compounds (see below).

12.13.10.2.5 Reduced methylated arsenic(III) species and As/Se species

The methyl- and dimethyl-reduced arsenic(III) species, methylarsinate (MA(III)) and dimethylarsinate (DMA(III)), were reported in human urine from several studies,[234–236] and a recent study[237] claimed that DMA(III) was the major arsenic metabolite in human urine. There are, however, some concerns about the rigor of the analytical methods used to determine these species,[67] and consequently, some doubt exists about their assignments.

A novel As/Se species (seleno-bis(*S*-glutathionyl) arsinium ion $[(GS)_2AsSe]^-$) was identified in the bile of rabbits administered both arsenic and selenium;[108] the long-known protective effect of selenium on arsenic toxicity seems to be well explained by this compound.

12.13.10.2.6 Organoarsenicals in novel sample types

As mentioned earlier, work up to 1993 had focused on marine systems because the concentrations of arsenic were generally much higher than those in terrestrial samples. The situation changed in the 1990s when HPLC/ICPMS, a sensitive technique for measuring arsenic species, became more widespread and the lower arsenic concentrations in terrestrial samples no longer precluded their analysis. Thus, arsenobetaine was identified as a major arsenic constituent of many species of fungi, and arsenocholine was also found to be present.[238] The simpler methylated species methylarsonate, dimethylarsinate, trimethylarsine oxide, and tetramethylarsonium ion were also reported in various fungal species.[239,240]

Arsenosugars were reported in freshwater algae,[241,242] and they are apparently also present in trace amounts in some terrestrial plants.[243] Earthworms also contain arsenosugars and traces of arsenobetaine,[244,245] and dimethylarsinate, arsenobetaine, and methylarsonate are also present in small amounts in ants.[246]

By the late 1990s, it was clear that organoarsenicals, previously thought to be exclusively marine natural products, were also present in many terrestrial samples. Continuing work[231,247–251] on freshwater organisms is supporting this observation, and, additionally, showing that for some samples, organoarsenicals can be present at concentrations comparable with those in marine samples.[231]

12.13.10.3 Biotransformations of Environmental and Biological Relevance

Although more than 30 naturally occurring arsenicals have been identified, we know surprisingly little about the biosynthesis of these compounds. It is generally accepted that methylation of inorganic arsenic occurs following the Challenger pathway, proposed by Frederick Challenger based on extensive studies in the 1930s and 1940s.[22] This pathway, originally proposed for microbial systems, involves successive reduction and oxidative methylation, leading ultimately to trimethylarsine. Several modifications and additions to this scheme are needed, however, in order to explain the arsenicals found in the environment, as discussed in the following.

12.13.10.3.1 Oxo–arsenosugars and other arsine oxides

Arsenosugars appear to be formed *de novo* from arsenate by algae, essentially following the Challenger pathway but with interesting differences. Figure 8 depicts a possible arsenic biotransformation pathway that was first proposed in 1987,[252] and has subsequently received indirect support from several studies. The pathway was originally proposed to explain the widespread occurrence of arsenosugars (ribosides) in marine algae, and the involvement of *S*-adenosylmethionine as the arsenic alkylating agent seemed to neatly explain the origin of the ribose ring. Support for the pathway has come from laboratory studies[253] with the brown alga *Fucus serratus*. When *F. serratus* was grown in arsenic-enriched water, the proposed intermediates in the pathway (As^{3+}, MA, DMA) and the final arsenosugar products increased in concentration with time. Further support has come from identification of the key intermediate, a dimethylarsenoadenosyl species (Figure 9; **F9-32**) in samples rich in arsenosugars: although compound **F9-32** had previously been isolated from a clam kidney,[254] the recent identification[255] in a crude extract of clam kidney using HPLC/tandem mass spectrometry is significant because the method appears well suited to monitor the biosynthetic processes more finely than has hitherto been possible.

Another mass spectrometric study[215] of arsenicals in the kidney of the clam *Tridacna derasa*, a rich source of arsenic, identified, in addition to many arsenosugars, several smaller arsenic oxides (Figure 5; **F5-12, F5-14–F5-18**) resulting from degradation of arsenosugars by successive oxidation and decarboxylation reactions. Some of these compounds, oxo–dimethylarsenoethanol (oxo–DMAE) and oxo–DMAA, are also found in human urine after ingestion of arsenosugars.[218] Interestingly, oxo–DMAA was also formed as an intermediate in the breakdown of arsenobetaine under microbial conditions.[219,220]

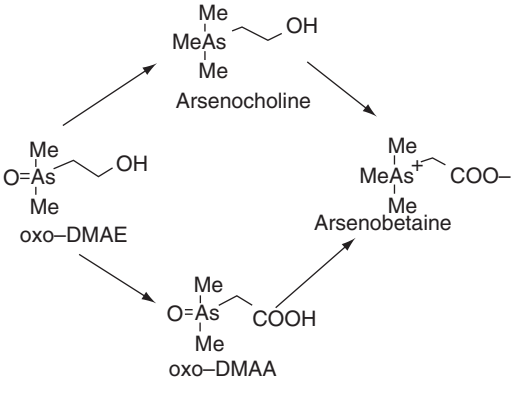

Figure 8 A possible pathway for the biosynthesis of arsenobetaine (after Ref: 261).

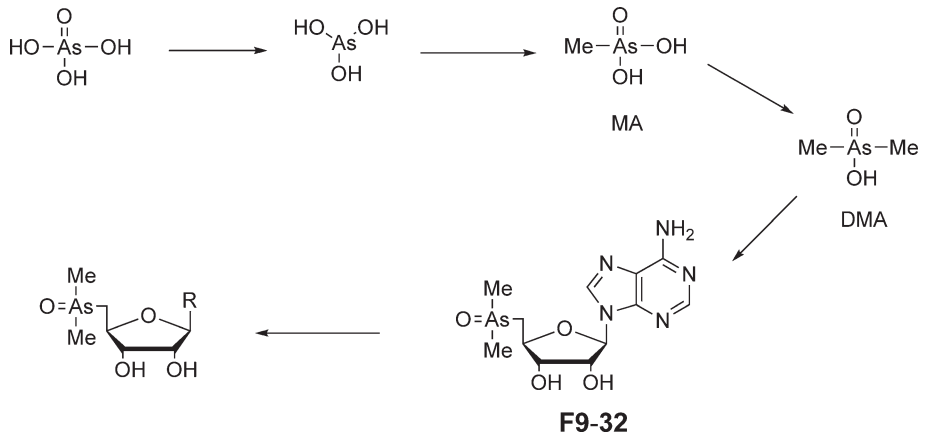

Figure 9 Proposed pathway for the biosynthesis of oxo–arsenosugars.

12.13.10.3.2 Thio–arsenosugars and other arsine sulfides

It seems likely that thio–arsenicals result from sulfuration of the oxo analogs, but how this occurs is far more speculative. The conversion occurs rapidly and quantitatively *in vitro* when the oxo–arsenical is treated with aqueous H_2S. Thus, in strongly reducing environmental conditions with concomitant production of H_2S, in anaerobic sediments, for example, one might expect to find the thio–arsenical rather than the oxo analog, as has been already observed.[256]

Many mammalian enzymes are able to catalyze the desulfuration of cysteine to H_2S (e.g., Ref: 257). Thus, the occurrence of thio–arsenicals in urine samples may be explained by *in vivo* production of H_2S and reaction with oxo–arsenicals, produced from degradation of arsenosugars ingested in the diet.[217,218] Alternatively, sulfuration may be elicited by some other active sulfur species (sulfane sulfur) in the cells.[258] The presence of thio–arsenosugars, apparently as natural products in marine animal samples, can be similarly explained. Thio–arsenosugars have also been found in algae,[232] although the concentrations are generally lower than those found in animal samples.

It is worth mentioning that before the discovery of thio–arsenicals as urinary metabolites by Hansen *et al.* in 2004,[217] several research groups reported the presence of "reduced methylated arsenic species" in urine (e.g., Ref: 236. The precise structure of these species in the samples was never firmly established, but it was considered to involve an As^{3+} species. Recent work[259] suggests that the chromatographic properties of these As^{3+} species are well accommodated by thio–arsenicals (with As^{5+}). Possibly, future work will show that thio analogs of the many oxo–arsenicals adequately explain the properties of the arsenicals found in urine without invoking the unproven presence of As^{3+} species.

12.13.10.3.3 Trimethylated arsenosugars

These compounds can easily be envisaged as the next step after the biosynthesis of oxo– and/or thio–arsenosugars shown in Figure 4. They are found in algae but surprisingly only as trace constituents. Their presence as trace constituents in gastropods[226] is consistent with their assimilation from algae. Of considerably more interest, however, is the presence of quite high concentrations of a trimethylated arsenosugar (6–41% of extractable As; Figure 6; **F6-22**) in the intestine of fish and some marine invertebrates.[227] This may just represent selective retention of the tri- over dimethylated species—laboratory experiments with shrimp showed[260] that a trimethylated arsenosugar was much more readily retained than its dimethylated analog. However, the result might also suggest that methylation was taking place within the animals. The result also has relevance to the formation of arsenobetaine as discussed below.

12.13.10.3.4 Arsenobetaine

Although arsenobetaine was first reported as the natural major arsenical in marine animals almost 30 years ago, there is still no clear biosynthetic scheme for this compound. An early proposal was that oxo–arsenosugars were the likely precursors based on several observations. First, oxo–arsenosugars are abundant in marine algae and they occur together with arsenobetaine in animals that feed on algae. Second, laboratory experiments simulating environmental conditions produced oxo–DMAE,[261] which appealed as a possible intermediate in the formation of arsenobetaine

(Figure 8). Subsequent laboratory experiments, however, were unable to elicit the final conversions necessary to produce arsenobetaine from oxo–DMAE. More recent work showed that when oxo–DMAA is used as the substrate, lysed cell extracts of a *Pseudomonas* sp. were able to produce arsenobetaine together with equivalent quantities of dimethylarsinate.[262] This work provides additional evidence for the scheme proposed in Figure 8, and suggests that in natural systems the methylation step may follow the formation of the carboxymethyl group.

Trimethylated arsenosugars (Figure 6; **F6-22**) are also found in marine algae, albeit generally at low concentrations, and when one of these compounds was ingested by shrimp in a laboratory experiment, a small proportion (2%) was converted into arsenobetaine.[260] The field study of Kirby *et al.*[227] showed the presence of considerable quantities of both arsenobetaine (28%) and trimethylated arsenosugar (41%) in the intestine of abalone (marine molluscs), which may indicate a link between them. Confirmation of this possible conversion awaits laboratory experiments under controlled conditions.

It is interesting to speculate that thio–arsenicals may be involved in the formation of arsenobetaine. Preliminary synthetic studies indicate that thio–arsenicals are much more readily reduced and methylated than their oxo analogs (Rumpler, unpublished results). Indeed, simple treatment of thio–DMAA in MeCN with methyl iodide produces a reasonable yield (70%) of arsenobetaine within 24 h, whereas similar treatment of oxo–DMAA produces no arsenobetaine. The mechanism may proceed via methylation on sulfur with concomitant formation of iodide, which then reduces the As^{5+} species to the arsine. It seems possible that thio–arsenicals *in vivo* may also be more amenable than the oxo analogs to reduction processes, leading to an arsine which can be methylated to give arsenobetaine.

All the above schemes invoke an arsenosugar as the precursor to arsenobetaine. An alternative pathway was proposed by Edmonds in 2000[263] however, which could proceed quite independently from arsenosugar biosynthesis and degradation. The scheme has analogy with amino acid biosynthesis, and involves a process of "arsenylation" as coined by Edmonds.[263] Arsenylation with dimethylarsinous acid on glyoxylate would produce oxo–DMAA, which could in turn yield arsenobetaine. Similarly, arsenylation by dimethylarsinous acid on oxaloacetate could produce oxo–DMAP en route to TMAP. Interestingly, both these compounds are natural products, and their presence cannot be explained from degradation of arsenosugars.

12.13.10.3.5 Arsenolipids

The natural arsenolipids of fish oils, currently of unknown structure, show interesting transformations in humans, producing characteristic metabolites that offer some insight into the structures of the original lipid.[223] The major metabolic products in the urine were dimethylarsinate and four fatty acids, oxo– and thio–DMAP and oxo– and thio–DMAB. It seems likely that the thio–arsenicals were formed from the oxo analogs in the body. These results suggest that the arsenic is incorporated into the lipid as a dimethylated moiety and may be present as a number of fatty acid derivatives.

12.13.11 Organoantimony

More than 3,000 organoantimony compounds have been reported in the literature. However, unlike organospecies of arsenic, lead, and tin, organoantimony compounds are generally not exposed to the natural environment during usage. Organometallic antimony compounds are commonly used as precursors in the manufacture of semiconductors and as catalysts in the polymerization of vinyl compounds. Their use, however, is restricted to controlled environments, and thus there is no obvious route for organometallic antimony compounds to enter the environment. Nevertheless, organoantimony compounds have been found in a variety of environmental matrices and are thought to arise through biological processing of inorganic antimony. Levels of inorganic antimony in the earth's crust (ca. 0.2 $\mu g\,Sb\,g^{-1}$) are around 10% of that of arsenic. However, antimony can intermingle with biological food chains at high concentrations because its widespread use in commercial products has redistributed the element.[264] Industrial use of antimony is mainly as antimony trioxide, which is added as a fire retardant to textiles, plastics, adhesives, and rubber. Elevated levels of antimony are found at antimony, arsenic, and lead mine spoils,[265] and at industrial sites where plastics containing antimony compounds as fire retardants are processed.[266]

Organoantimony in the environment [267–269] and biomethylation of inorganic antimony[162,267,270,271] have been extensively reviewed. Filella *et al.*[272] have reviewed antimony in the environment, with an emphasis of inorganic species in natural waters.

12.13.11.1 Organoantimony Compounds in the Environment

The first reports on organometallic antimony compounds in the aquatic environment were in the early 1980s, using HG-GC-AAS. More recently, the nature of the standard compounds used for the analysis has been questioned,[273,274] and the experimental conditions used for the hydride generation during analysis are now known to produce artefacts.[275] The molecular structure of the compounds with carbon–antimony linkages detected in the environment in the early reports therefore remains unresolved.

Mono-, di-, and trimethylantimony species have been detected in sediments from a river in Germany using HG-GC-ICP-MS;[276] reported concentration ranges were 0.2–9.8, 0.1–1.2, and 0.1–0.9 μg Sb kg^{-1}, respectively. All three methylantimony species have also been detected, using HG-GC-ICP-MS, in geothermal waters from New Zealand, with dimethylantimony at the highest concentration (31 ng Sb kg^{-1}). Kock *et al.* [277] detected, using HG-GC-AA, methylantimony species—including trimethylantimony—in water samples from two antimomy-rich environments in Canada.

Dodd *et al.*[53] have reported on organometallic antimony compounds in pondweed (*Potamogetan pectinatus*) from a polluted region in Canada. Trimethylantimony, dimethylantimony, and methylantimony were identified in this sample, using HG-GC-MS following extraction with 0.2 mol l^{-1} acetic acid; quantification of the methylantimony species was not reported. Methylantimony compounds have also been found in plants (liverwort and moss) associated with a disused antimony mine in Scotland, using HG-GC-AAS.[52] Levels of dimethylantimony in the 100–200 ng (g dry weight range)$^{-1}$ were present in the biota, and methylantimony was detected in some samples. In a similar study, methylantimony species were found in a variety of plant species from antimony-rich regions of Yellowstone, Canada, following extraction with methanol/water.[277] These authors also reported methylantimony species in an animal—the snail, *Stagnicola* sp. from an antimony-rich region of Yellowknife—using a headspace HG-GC-MS method.

Further reports of organoantimony compounds in the environment concerned volatile metalloid species in sewage and landfill fermentation gases,[17,18,186,278] and in hot springs.[18] Trimethylantimony was found in these emissions; reported concentration ranges for sewage and landfill fermentation gases were 0.15–0.62 and 23.9–71.6 μg Sb m^{-3}, respectively.[20] Dimethylanatimony and trimethylantimony species have been detected above, and within, algal mats growing in hot springs.[18] Condensed water samples from the landfill gas collection pipeline[186] and standing water (through which landfill gases percolate) on a landfill site [275] have been reported to contain mono-, di-, and trimethylantimony.

12.13.11.2 Biomethylation of Inorganic Antimony

Since the mid-1990s, the biomethylation of antimony has been investigated intensively in relation to sudden infant death syndrome (SIDS).[279] Involatile methylantimony species, thought to be produced through past microbial activity, have more recently been reported in polyurethane foams of some cot mattresses containing antimony trioxide as fire retardant, but a causal link with SIDS was not evident.[280]

Unequivocal evidence for *in vivo* antimony biomethylation by humans has not been found, although methylantimony species have been detected in very low abundance in human urine.[281] Administration of antimony tichloride to rats has been reported to completely inhibit the biomethylation of arsenic by rat liver cytosol, but there was no evidence of antimony biomethylation *in vivo*.[282]

Several bacteria and fungi are now known to produce one or more methylated forms of antimony from a variety of inorganic antimony substrates under aerobic and/or anaerobic growth conditions (Table 12). The structures of some antimony substrates commonly used in biomethylation studies are shown in Figure 10, along with some possible products arising from oxidation of biogenically produced trimethylstibine (Me_3Sb).

12.13.11.2.1 Aerobic microbial biomethylation of antimony

Jenkins *et al.* [283] reported the formation of trimethylstibine [$(Me)_3Sb$] by *Scopulariopsis brevicaulis*, which was the first report of antimony methylation by a characterized microorganism. A subsequent paper by these authors [284] reported that the yields of volatilized antimony in relation to fungal biomass were around twofold higher on a solid medium [ca. 6 μg antimony (g dry weight biomass)$^{-1}$], when compared to a liquid culture. The order of antimony substrates in relation to ease of biovolatilization was reported as PAT >>> Sb_2O_3 >>> Sb_2O_5 > $KSb(OH)_6$. These workers found no evidence of antimony volatilization by other fungi (*Penicillium* spp., *Aspergillus* spp., *Alternaria* sp.) or bacteria (*Bacillus* spp.) tested. The ability of *S. brevicaulis* to methylate inorganic antimony has been confirmed by other workers,[285] who detected involatile methylantimony compounds, principally trimethylantimony oxide [$(Me)_3SbO$],

Table 12 Microbial biomethylation of antimony

Organisms/enrichment	*Incubation*	*Antimony substrate*	*Phase analyzed*	*Antimony product*	*Detection*	*References*
Scopulariopsis brevicaulis	Biphasic[a]	PAT	Gas	Me_3Sb	GC-AAS/GC-MS[c]	283,284
		Sb_2O_3 or Sb_2O_5	Gas	Volatile Sb[b]	ICP-MS	283
		Sb_2O_3	Gas	Me_3Sb	GC-MS[c]	284
		Sb_2O_5 or PHHA	Gas	Volatile Sb[b]	ICP-MS	
	Aerobic	PAT	Gas	Me_3Sb	GC-AAS/GC-MS[c]	287
					GC-ICP-MS[c]	296
		Sb_2O_3	Aqueous	SbH_3, MeSb, Me_2Sb, Me_3Sb	HG-GC-ASS	285
Phaeolus schweinitzii	Aerobic	PAT or Sb_2O_3	Aqueous	Me_2Sb, Me_3Sb	HG-GC-ASS	288
Cryptococcus humicolus	Biphasic[a]	PAT	Gas	SbH_3, Me_2Sb, Me_3Sb	SPME-GC-MS	289
		PHHA	Gas	Me_3Sb	SPME-GC-MS	
	Aerobic	PAT	Aqueous	MeSb, Me_2Sb, Me_3Sb	HG-GC-AAS	298
		Sb_2O_3 or PHHA	Aqueous	Me_2Sb, Me_3Sb	HG-GC-AAS	
Flavobacterium sp.	Aerobic	PAT	Aqueous	MeSb, Me_2Sb, Me_3Sb	HG-GC-AAS	290
Clostridium acetobutylicum or *C. cochlearium*	Anaerobic	PAT	Aqueous	MeSb, Me_2Sb, Me_3Sb	HG-GC-AAS	295
C. buturicum	Anaerobic	PAT	Aqueous	MeSb, Me_3Sb	HG-GC-AAS	295
[d]*Clostridium* sp.	Anaerobic	PAT	Aqueous	MeSb, Me_2Sb	HG-GC-AAS	295
[d]*Clostridium* sp.	Anaerobic	PAT	Aqueous	MeSb	HG-GC-AAS	295
C. collogenenovorans or *Desulfovibrio vulgaris*	Anaerobi	$SbCl_3$	Gas	Me_3Sb	[c]GC-ICP-MS	294
Methanobacterium formicicum	Anaerobic	$SbCl_3$	Gas	SbH_3, MeSb, Me_2Sb, Me_3Sb	[c]GC-ICP-MS	294
Methanosarcina barkeri or *Methanobacterium thermoautotrophicum*	Anaerobic	$SbCl_3$	Gas	Me_3Sb	[c]GC-ICP-MS	294
Microbial enrichment conditions (undefined mixed cultures):						
Nitrate reducing	Anaerobic	PAT	Gas	Me_3Sb	[c]GC-AAS/GC-MS	292
		PAT or PHHA	Gas	Me_3Sb	GC-FIC/GC-MS	291
Methanogenic	Anaerobic	PAT	Gas	Me_3Sb	[c]GC-AAS/GC-MS	295,292
Fermentative	Anaerobic	PAT	Gas	Me_3Sb	[c]GC-MS	292,293

[a]Aerobic growth of fungus with trapping of headspace gases under anaerobic conditions.
[b]Volatile antimony compound not identified.
[c]Purge of headspace gases onto solid-phase trap.
[d]Isolate from fermentative enrichment culture shown to generate trimethylantimony.
PAT = potassium antimony tartrate, PHHA = potassium hexahydroxyantimonate; gas = culture headspace gases; aqueous = spent liquid culture medium.
Gas chromatography, GC; mass spectrometry, MS; hydride generation, HG; atomic absorption spectrometry, AAS; inductively coupled plasma, ICP; solid phase microextraction, SPME; fluorine-induced chemiluminescence, FIC.

at concentrations up to $7.1\,\mu g\,Sb\,l^{-1}$ in culture media containing inorganic antimony(III) compounds. Later reports[286,287] confirmed that the final biotransformation product for inorganic antimony was in fact trimethylstibine, which can be produced under entirely aerobic cultivation conditions.

The wood-rotting fungus, *Phaeolus schweinitizii*, has recently been shown to transform the Sb^{3+} compounds, PAT and antimony trioxide, to involatile dimethylantimony and trimethylantimony species.[288] The maximum yield of the

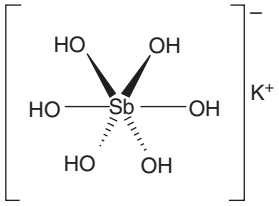

F10-1

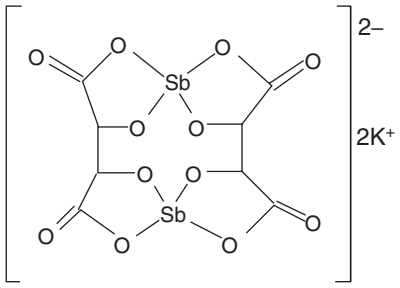

F10-2

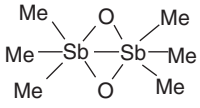

F10-3

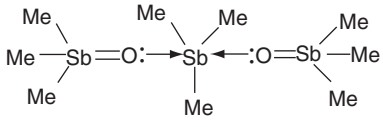

F10-4

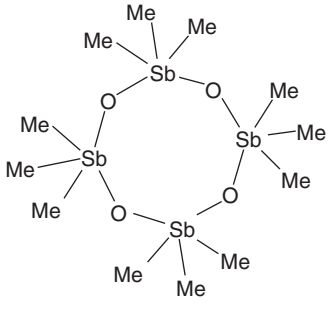

F10-5

Figure 10 Structures of selected (organo)antimony compounds: **F10-1** potassium antimonate; **F10-2** potassium antimony tartrate (PAT). Compounds **F10-1** and **F10-2** have been widely used as inorganic antimony substrates in biomethylation studies. Some possible products (**F10-3**–**F10-5**) arise from oxidation of biogenically produced trimethylstibine (Me_3Sb). Based on Craig, P. J.; Forster, S. A.; Jenkins, R. O.; Lawson, G.; Miller, D.; Ostah, N. *Appl. Organomet. Chem*. **2001**, *15*, 527–532.

trimethylantimony species was approximately 0.4%. Biomethylation of inorganic antimony has also been shown for the anamorphic basidiomycetous yeast *Cryptococcus humicolus*.[289] In this work, SPME with polydimethylsiloxane fibers and GC-MS was used to detect volatile antimony species in headspace gases.

Antimony biomethylation by an aerobic prokaryote has been reported only relatively recently.[290] Pure cultures of an aerobically grown *Flavobacterium* sp. produced methylantimony species up to 4.0 μg Sb l^{-1}; provision of inorganic As^{3+} alongside Sb^{3+} was shown to enhance formation of the involatile methylantimony species up to eightfold. The authors noted that anaerobiosis was not an obligate requirement for methylantimony formation in prokaryotes, and thus broadened the range of habitats for potential formation of methylantimony species in nature. The low yields (<0.03%) of methylantimony species produced by *Flavobacterium* sp.[290] suggests that antimony biomethylation by aerobic prokaryotes is fortuitous rather than a primary resistance mechanism for this element.

12.13.11.2.2 Anaerobic microbial biomethylation of antimony

Trimethylstibine production by anaerobic soil/sediment enrichment culture has been reported.[291–293] Gürleyük *et al*.[291] detected trimethylstibine in the culture headspace of soil bacteria enrichment cultures designed to promote bacterial growth through the use of nitrate as terminal electron acceptor in anaerobic respiration. This report represents the first characterization of a volatile antimony compound thought to arise biogenically from an inorganic antimony substrate, although the identity of microorganisms in soils responsible for the biomethylation was unknown. Different metabolic categories of prokaryotic organisms (fermentative, nitrate-reducing, methane-producing bacteria) are able to methylate antimony, which suggests that this capability is widely distributed in the natural environment.[292]

Antimony methylation by pure cultures of strictly anaerobic bacteria has also been reports.[294,295] These reported indicate that mixed community functioning is not an obligate requirement for antimony biomethylation by undefined

soil/sediment enrichment conditions. Smith *el al.* [295] found no evidence of a correlation between antimony biomethylation by characterized clostridia cultures and low-redox potential in the medium, and proposed that antimony biomethylation by mixed communities of bacteria under anaerobic cultures was determined by the presence of particular bacteria with biomethylating capability, rather than by the overall environmental conditions set up by mixed communities.

12.13.11.2.3 Biological mechanism of antimony biomethylation

Andrewes *et al.*[296] supplied $^{13}CD_3$-labeled L-methionine to cultures of *S. brevicaulis* incubated in the presence of PAT and demonstrated $^{13}CD_3$ incorporation in both trimethyl- and dimethylantimony compounds in the medium. The work suggests that SAM is the biological methyl donor for antimony biomethylation by *S. brevicaulis*. Further, the authors suggested that the mechanism of antimony biomethylation is similar to the mechanism proposed by Challenger (Figure 2) for arsenic, since the non-volatile products detected are consistent with this mechanism. Enhancement of antimony biomethylation through provision of arsenic alongside antimony substrate provides further evidence for antimony and arsenic biomethylation proceeding via the same mechanism for a variety of different microorganisms.[290,297,298] It is considered to reflect improved induction of a pathway capable of biomethylating both of these related elements.[290] Arsenic has also been shown to alter the speciation of the methylantimony biotransformation products. Since arsenic co-exists with antimony in a wide range of natural and man-made environments, the interactive influence of these metals on antimony biomethylation is likely to profoundly influence the biogeochemical cycling of antimony and its subsequent environmental and human toxicity.[290,298]

Studies on the isotope ratio of antimony in trimethylstibine indicate that isotope fractionation takes place when antimony is methylated by anaerobic bacteria.[299] Isotope ratio measurements of the different methylated species produced in anaerobic sewage cultures suggest a stepwise methylation of antimony according to the Challenger mechanism (Figure 2). These authors also showed that methylcobalamin could react as a methylating agent in an abiotic methylation, forming monomethyl- and dimethylantimony species; a role for methylcobalamin in anaerobic microbial biomethylation was proposed but not unequivocally demonstrated.

12.13.11.3 Abiotic Reactions of Relevance to Environmental Aspects of Organoantimony Compounds

Mass spectrometry studies have concluded that trimethylantimony chloride, which is commonly used as a standard for environmental studies involving organoantimony compounds, hydrolyzes in water (pH 7.0), most probably forming $[Me_3SbOH]^+$.[300,301]

Methylstibines are subject to oxidation, quaternization, and complex formation, that could enhance or inhibit their environmental mobility. Environmentally significant concentrations of halocarbons (such as MeBr, MeCl, and MeI) are known to be produced naturally, and to accumulate in various environmental compartments. Early studies (mid-1970s), using NMR, indicated that trimethylstibine oxidizes rapidly to $(Me)_3SbO$. However, detection of non-oxidized trimethylstibine produced from microbial environments that are not entirely anaerobic[287,289,298] suggests that trimethylstibine has reasonable stability in the gas phases, even in the presence of some oxygen. Stability tests on volatile forms of antimony—including trimethylstibine—suggest that these compounds have an atmospheric half-life that allows them to volatilize from landfill sites and disperse in their vicinities.[20,302]

Craig *et al.*[303] used mass spectroscopic techniques to investigate the fate of trimethylstibine when exposed to ambient oxygen. These authors showed that when trimethylstibine was allowed to oxidize, species containing one to five $(Me)_3SbO$ molecules chemically bonded together are produced in aqueous solution (Figure 10); dimethylantimony species were not detected under the experimental conditions used.

12.13.11.4 Toxicity of Organoantimony Compounds

Information on toxicity of organoantimony compounds is very limited. Early work (1930s) concluded that trimethylstibine possessed no great or pronounced toxicity to animals. The fungal toxicity of a range of di- and triphenylantimony, and trimethylantimony compounds, has been tested, and only diphenylantimony oxinate, diphenylantimony acetone, and diphenylantimony chloride have EC_{50} values $<30\,mg\,Sb\,l^{-1}$.[304] More recently, genotoxity of trimethylstibine was evaluated using an *in vitro* plasmid DNA-nicking assay and shown to be about equipotent with trimethylarsine.[305]

12.13.12 Organosilicon

Although silicon is one of the main elements in the environment, there is little evidence for naturally occurring organosilicon species. Anthropogenically produced siloxanes (organosilicones typically containing Si–O–Si bonds) are regarded to be main (or sole) source of organosilicones in the environment. Most commercial products (ca. 80%) are based on polydimethylsiloxanes (PDMS). The structures of some environmentally important organosilicones are shown in Figure 11.

Graiver *et al.*[306] have recently reviewed the fate and effects of organosilicone compounds in the environment, while Hirner *et al.*[307,308] have recently reviewed environmental, speciation, and biological aspects of organosilicones.

12.13.12.1 Volatile Methylsiloxanes (VMSs)

VMSs are siloxanes with relatively high vapor pressure and low molecular weight (<600 amu).[309] They also have very limited solubility in water ($\mu g\,l^{-1}$), have a lower density than water, and their oil–water separation coefficient is high. VMSs therefore do not accumulate in aqueous environments; they evaporate into the atmosphere from a surface oil phase.[309] Highest reported concentrations of VMSs for different environmental compartments are presented in Table 13. VMSs have been shown to have no adverse environment effects.[310,311] D4, which has a vapor pressure of 1.33 hPa and freshwater solubility $74\,\mu g\,l^{-1}$, has been estimated to have a half-life of 3 to 6 h in freshwater.[312] A bioconcentration factor of 12,400 has been estimated for this cyclic VMS.[313] In studies involving water/sediment biosystems, D4 showed no apparent biodegradation.[311]

Athough VMS fluids entering aquatic environments partition rapidly to the atmosphere, up to 46% of VMS entering a water-treatment facility will adsorb to the sludge.[314] Primary sludge removal and volatilization in the aerated sludge basin contribute equally for the removal of D4 and D5.[315] In studies on the microbial degradation of D4 in sewage sludge, Grümping *et al.*[316] reported highest rates of formation of dimethylsilanediol (DMSD) during

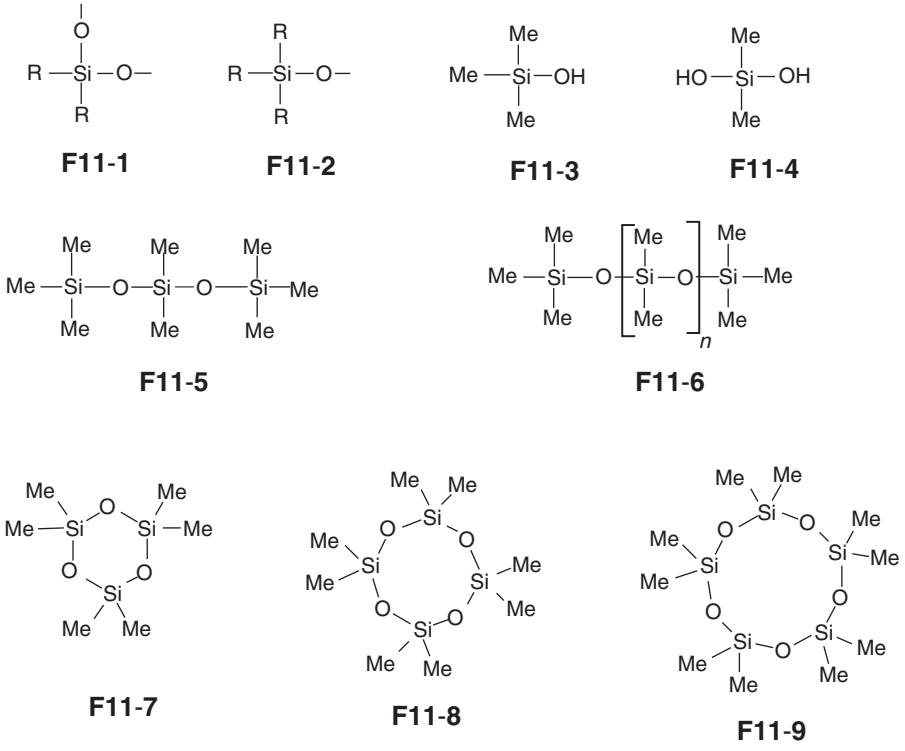

Figure 11 Structures of some environmentally important organosilicones. Both linear (L) and cyclic (D) structures are distinguished by the number of Si atoms in the structure. (**F11-1**) D; (**F11-2**) M; (**F11-3**) trimethylsilanediol (TMSD); (**F11-4**) dimethylsilanediol (DMSD); (**F11-5**) L3; (**F11-6**) MD_nM; (**F11-7**) D3; (**F11-8**) D4; (**F11-9**) D5. The basic structure of PDMS is MD*n*M (*n* = ca. 7 to >10,000).

Table 13 Concentrations of VMS and PDMS in various environmental compartments

Silicone class	*Compartment*	*Highest reported concentration*	*References*
VMS	*Gases*		
	Waste	66 mg m^{-3}	341,468
	Sewage	73 mg m^{-3}	468,486
	Diffuse sources	4 mg m^{-3}	487
	Air (industrial area)	0.03 mg m^{-3}	488
PDMS	*Water*		
	Effluent (WTP)	13 μg l^{-1}	489,322
	Rivers (Japan)	2.5 μg l^{-1}	490
	Solids		
	Sewage sludge		
	US	1,593 mg kg^{-1}	322
	Germany	701 mg kg^{-1}	491
	Sediments		
	Marine	126 mg kg^{-1}	322
	Contaminated	309 mg kg^{-1}	343
	Rivers/bays in US	96 mg kg^{-1}	492,489

WTP = wastewater-treatment plant.

100–150 days of incubation. The degradation of cyclic VMS is initiated by ring-opening hydrolysis, forming oligomeric siloxane diols, with subsequent hydrolysis of the diols to the monomer DMSD.[317]

VMSs do not persist in the atmosphere. They are removed by physical processes and transformed by several chemical reactions,[309] including photolytic and oxidative degradation.[314,318,319] Reaction rates of VMS with various atmospheric oxidants have been determined;[318,319] oxidation with the hydroxyl radical in the gas-phase was concluded to be the only significant reaction of VMS in the upper atmosphere. Under atmospheric conditions, VMS compounds are oxidatively degraded at rates comparable with that of other volatile hydrocarbons.[318] A degradation mechanism for atmospheric oxidation of Si–Me functional groups has been proposed[320] (Figure 12), first involving formation of a methylene radical (Si–CH_2·), with subsequent formation of a peroxy radical (Si–CH_2OO·). Rearrangement of the peroxy group gives an oxycarbon intermediate (Si–O–CH_2═O) that reacts with another oxygen molecule to yield an unstable oxycarbonyl silane (Si–O–CH_2═O), which is then hydrolyzed to produce a silanol (Si–OH). Ultimately, according to this scheme, reaction of VMS with atmospheric oxidants would produce silica, water, and carbonyl compounds. Degradation of VMS in the upper atmosphere is estimated to be complete within 10–30 days,[318] which suggests no accumulation of these compounds in the environment.

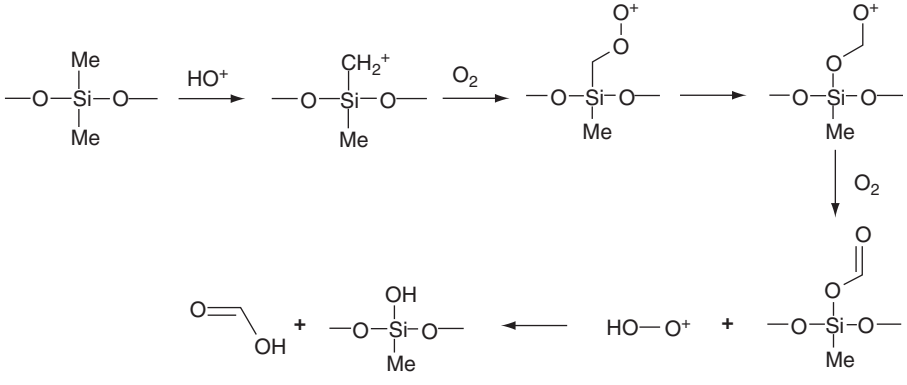

Figure 12 Scheme for atmospheric oxidation of Si–Me functional groups. Based on Atkinson, R.; Tuazon, E. C.; Kwok, E. S. C.; Asey, S.; Aschmann, S. M.; Bridier, I. *J. Chem. Soc, Faraday Trans*. **1995**, *91*, 3033–3039.

VMS does not contribute to ozone or smog formation in the lower atmosphere[321] and the US Environmental Protection Agency has not included organosilicones in its regulations concerning volatile organic compounds in the atmosphere.

12.13.12.2 High Molecular Weight Organosilicons

Organosilicons with molecular weights of between 600 and 450,000 are non-volatile and therefore do not enter the atmospheric compartment. However, the polyorganosiloxanes are flowable liquids at ambient temperature, and can potentially migrate between terrestrial and environmental compartments. Although the vast majority of organosilicon released to wastewater is as PDMS fluids, they are insoluble in water, and PDMS becomes adsorbed onto sewage sludge and is effectively removed from wastewater.[322] Subsequent disposal of solid sludge through use as agricultural fertilizer or by burial in landfill leads to PDMS entering the terrestrial environment. Table 13 compares highest reported concentrations of PDMS for various environmental compartments.

PDMS has been shown to have no significant effect on wastewater-treatment process parameters—such as biological oxygen demand, pH, and suspended solids—or on sludge digestion.[323] PDMS does not degrade during wastewater treatment or adversely influence the process, but is transferred almost quantitatively to the solid sludge.[323,324]

Various studies have shown that PDMS in aqueous environments has no significant effect on fish, invertebrates, amphibians, and microorganisms. Furthermore, PDMS is only transiently present in the aqueous environment, mainly during transport to wastewater-treatment plants. The high molecular weight of PDMS prevents its bioaccumulation,[312,325,326] which is confirmed by low levels of PDMS in fish tissues.[327]

Sludge-adsorbed PDMS incorporated into soil is expected to be mineralized aerobically through soil-catalyzed degradation.[328–334] The small amounts of sludge-associated PDMS that enter the receiving waters for wastewater-treatment facilities end up in the sediment, where PDMS will eventually mineralize to silica, water, and carbon dioxide. In the soil, degradation of PDMS by abiotic hydrolytic cleavage of the siloxane bond is random, which rapidly decrease the molecular weight of the polymer in early stages of degradation. Eventually, the hydrolysis produces mainly dimethylsilanediol (DMSD; $Me_2Si(OH)_2$); small amounts of trimethylsilanediol (TMSD; Me_3SiOH) and methylsilanetriol ($MeSi(OH)_3$) are produced from the end groups and branches of PDMS, respectively.[335,336] The low molecular weight silanols evaporate slowly to the upper atmosphere and are degraded mainly by the OH radical mechanism already described (Section 12.13.12.1); the fate of the monomeric methylsilanols is considered in more detail in Section 12.13.12.3. In aluminum–montmorillonite clays, depolymerization of radioactive PDMS by hydrolysis of the siloxane bonds has been shown to be 95% complete within 30 min and complete within 21 days. Soil factors, such as clay content and moisture content, influence the rate of PDMS degradation;[335,337] surprisingly the rate of depolymerization is inversely related to relative humidity. The half-life of PDMS in different soils (type, geographical location, composition, moisture content, pH) varies from 4 to 28 days.[338]

Ecotoxicological studies have shown that in soils neither PDMS nor its degradation products influence plant development, microorganisms, or reproduction of earthworms.[333,339]

Sludge-adsorbed PDMS is expected to be hydrolyzed anaerobically during sludge composting[335] or following addition to landfill.[340,341] Evidence for PDMS hydrolysis during sludge composting comes from detection of the main intermediate (DMSD) in the pathway of hydrolyis of PDMS.[335] Products of PDMS hydrolysis have also been detected in waste deposit gases and in leachates.[340,341]

In sedimentary environments, PDMS is generally regarded as being immobile.[342] However, around 10% of PDMS was converted to DMSD during 1 year incubation in an aerobic sedimentary environment.[329] Powell *et al.*[343] measured PDMS levels in the surface sediment of marine and freshwater areas heavily impacted by municipal wastewater discharge. Generally, concentrations of PDMS were greatest in sediments near effluent outfalls, ranging from 0.6 to 78 $\mu g\,g^{-1}$, and were lowest in areas having an advanced wastewater-treatment facility.

PDMS can also be degraded by enzyme-catalyzed hydrolysis of the siloxane bond.[344] Various bacteria, including some *Pseudomonas* spp. and *Proteus* spp., can grow on silicone oils or in silicon-containing medium.[330,344]

Silicone rubber is widely used as a high-voltage insulator. In the outdoor environment, the hydrophobic surface of the silicone rubber can become covered by a hydrophilic biofilm, which can alter the electrical properties of the insulator.[345,346] Wallstrom *et al.*[345,347,348] have studied biofilm formation on silicone rubber voltage insulators using a variety of techniques, including image analysis and laser-induced fluorescence spectroscopy. They found no evidence of biodegradation of the PDMS molecule from the silicone rubber insulaors.

Kovac *et al.*[349] recently reported that organosilicon compounds prevailed in the water-insoluble fraction of macroaggregates in the Adriatic, which are associated with phytoplankton blooms.

12.13.12.3 Organosilanols

The fundamental building blocks of the silicone industry are the monomeric methylsilanols, $Me_xSe(OH)_{4-x}$ ($x = 1$–3).[336] Compared to the siloxanes, they have higher aqueous solubility and lower volatilization rates.[350] The principal source of organosilanols in the environment is PDMS.[336] As indicated in Section 12.13.12.2, PDMS undergoes hydrolyis to DMSD, with formation of small amounts of TMSD and methylsilanetriol. In the atmosphere, methylsilanols undergo oxidative degradation involving hydroxyl radicals to silica and carbon dioxide, as described for VMS (Section 12.13.12.2); the atmospheric lifetime of DMSD is expected to be 2–9 days.[351] However, because of their relatively high solubility and low volatility, methylsilanols are expected to be found in both aqueous and atmospheric environmental compartments. Although methylsilanols can bind to soil and sediment, they are readily released from the solid phase by aqueous hydrolysis of the chemical bonds.[331,332,338]

Photooxidative degradation of methylsilanols also occurs in aqueous environments.[352–354] When exposed to light in an aqueous solution containing nitrate or nitrite, DMSD has also been shown to undergo oxidative demethylation to silicate, with methylsilanediol as intermediate.[353] Levels of nitrates and nitrites in natural waters are considered high enough for such oxidative degradation of DMSD to occur.[307]

Biodegradation of DMSD has been established by using ^{14}C-labeled substrate.[355] The biodegradative mechanism for DMSD involves initial oxidation of a methyl group (Equation (11)), with the formation of methylsilanetriol as intermediate, in a pathway leading to silica.[355,356]

$$HO–Si(Me)_2–OH \longrightarrow Me–Si(OH)_3 \tag{11}$$

Cultures of bacteria (*Arthrobacter* sp.) and fungi (*Fusarium oxysporus*) have been shown to aerobically degrade ^{14}C-DMSD with release of $^{14}CO_2$.[355] Lehmann *et al.*[357] studied the fate of DMSD in a grass and soil system and concluded that only small proportions (<0.03%) of DMSD enter grass but are not biochemically incorporated. This was considered to be of negligible importance in the overall environmental fate of organosiloxane polymers.

12.13.12.4 Silicones in Medicine

Silicones are widely used as inert materials in medicine. In particular, their use in silicon breast implants and catheters has raised questions regarding the interaction of silicones with human cells and tissues. The mobility, toxicology, and immunology of silicones in higher animal systems have been investigated extensively over the last decade. It is not possible to adequately cover the relevant literature in this chapter and readers are directed to a recent review dealing with these aspects.[307]

Abiotic hydrolysis of the siloxane bond in aqueous solution is accelerated under acidic conditions. In the acid environment of the stomach therefore, injected siloxanes and silanes are degraded to silanols. Methylsiloxanes are known to undergo hydroxylation *in vivo* and various diols—such as $MeSi(OH)_3$, $Me_2Si(OH)_2$, $HOMe_2Si–O–SiMe_2OH$—have been detected as urinary metabolites in rats.[358] In humans, the major routes of excretion of cyclic siloxane D4, which is commonly found in personal care products, have been shown to be urine and expired air.[359]

Studies with mice have shown that injection of mixtures of cyclic siloxanes (primarily D3 and D7) or PDMS oil lead to accumulation of low molecular mass silicones in major organs, including brain, heart, lungs, and lymph nodes.[359] Linear siloxanes accumulated preferentially in brain, as well as in lung and lymph nodes, indicating that these species could pass the blood-brain barrier.

Organosilicones are generally considered to have very low toxicity and to be non-carcinogenic and non-mutagenic; the rodenticide silatranes and the herbicide mival are exceptions. A mixture of cyclosiloxanes (D3 to D6) injected into mice produced liver cell necrosis and inflammatory lesions of the lung.[360] Flassbeck *et al.*[361] found siloxanes (D4–D6) in the capsular, muscle, and fat tissues of women with silicone breast implants, at levels in the range 10–1,400 ng g^{-1}; no siloxanes were detected in control breast tissues from non-augmented women. D3 and D4 have also been found in the plasma and blood of women with silicone implants.[362] Highest concentrations were for blood, ranging from 20–28 μg l^{-1} for D3 and 79–92 μg l^{-1} for D4. The toxicology and immune interaction of siloxanes have been extensively reviewed (e.g., see Ref: 363). However, the breast cancer risk among women with silicone implants remains an unresolved dispute. Brinton *et al.*[364] have recently reported an increased risk of cervical and vulvar cancers for women with silicone breast implants.

12.13.13 Organoselenium

The environmental chemistry of selenium reflects to some extent that of the non-metal sulfur (not covered here). Many analogous selenium compounds are found in water, sediment, atmosphere, biota, and food. Food issues are not covered here but can be consulted in Ref: 6. Selenium is an essential trace element and these aspects are also covered in the above reference. Similarly, agricultural aspects are covered in Ref: 365. The environmental chemistry of selenium was reviewed in 2003.[366]

In a similar manner to the biomethylation processes discussed elsewhere in this chapter, methylation of selenium to a number of derivatives may occur: Me_2Se, Me_2Se_2, mixed Se–S, MeSeH, and Me_3Se^+ derivatives are found in water, sediment, and atmosphere (see Figures 10.1 and 10.2 in Ref: 366; Figure 10.2 shows a useful biogeochemical cycle). More complicated organoselenium species are found in food, plants, and other organisms (Table 14).

Since the early 1990s, there have been few major developments in the selenium environmental area, and research has dealt mainly with the human health relevance of selenium and its compounds. The multifaceted role of selenium in human health, selenium deficiency, and selenium as a possible anticancer agent, has been well covered in several dedicated books (e.g., Ref: 367). However, a relevant aspect of selenium metabolism, namely, the biotransformation of ingested selenium and urinary excretion, has been largely neglected. Significant results in this area were first reported almost 40 years ago, but there then followed a long period of essentially no new data. Results in the last few years, however, are changing the way we view the biotransformation and excretion of excess selenium. Accordingly, the following will focus on the recently reported results identifying novel chemical forms of selenium excreted in urine.

Since the first reports of trimethylselenonium ion (TMSe) as the major selenium metabolite in rat urine,[367–370] there have been many reports of its presence in rat and human urine.[371] The early work also reported the presence of a significant unidentified selenium urinary species, and the identification of this compound was seen as a worthwhile research goal pursued by several research groups. After many years, success finally appeared to come in 1995 with the identification of methylselenol (MeSeH) by Suzuki and co-workers in several reports.[372–374] The data presented for this assignment, however, were not convincing, and not unexpectedly, the work was retracted in 1997.[375] Subsequently, the Suzuki group in 2002[376] conclusively identified the unknown selenium metabolite in rat urine as a galactopyranoside, namely, methyl 2-acetamido–2-deoxy–1-seleno–β-D-galactopyranoside (Figure 13, selenosugar **F13-1**). On this occasion, the structure was confirmed by chemical synthesis. This metabolite appears to be the unknown compound in urine reported by many researchers during the previous 30 years.

Table 14 Organoselenium compounds in food, plants, and other organisms

$HSeCH_2CH(NH_2)COOH$
$HOOC(NH_2)CHCH_2SeSeCH_2CH(NH_2)COOH$
$MeSeCH_2CH(NH_2)COOH$
$(C_6H_5)_3Se^+$
$(C_6H_5)_2Se$
C_6H_5MeSe
$Me_2SeCH_2CH_2(NH_2)COOH$
$Se(CH_2CH(NH_2)COOH)CH_2CH(NH_2)COOH$
$MeSeCH_2CH(NH_2)COOH$
$MeSe(O)CH_2CH(NH_2)COOH$
$HOOSeCH_2CH(NH_2)COOH$
$PrSe(O)CH_2CH(NH_2)COOH$
$HSeCH_2CH(NH_2)COOH$
Gl–$SeMeCH_2CH(NH_2)COOH$ (Gl = gamma-L-Glutamyl)
Me_2Se
Me_2Se_2
$MeSe(Aden)CH_2CH_2CH(NH_2)COOH$ (Aden = Adenosyl)
Aden–$SeCH_2CH(NH_2)COOH$
$Me_2SeCH_2COO^-$
Al-$SeCH_2CH(NH_2)COO^-$ (Al = allyl)

Based on Craig, P. J.; Maher, W. A. Organoselenium Compounds in the Environment. In *Organometallic Compounds in the Environment*, 2nd ed.; Craig, P. J., Ed.; Wiley: Chichester, 2003; pp 391–398.

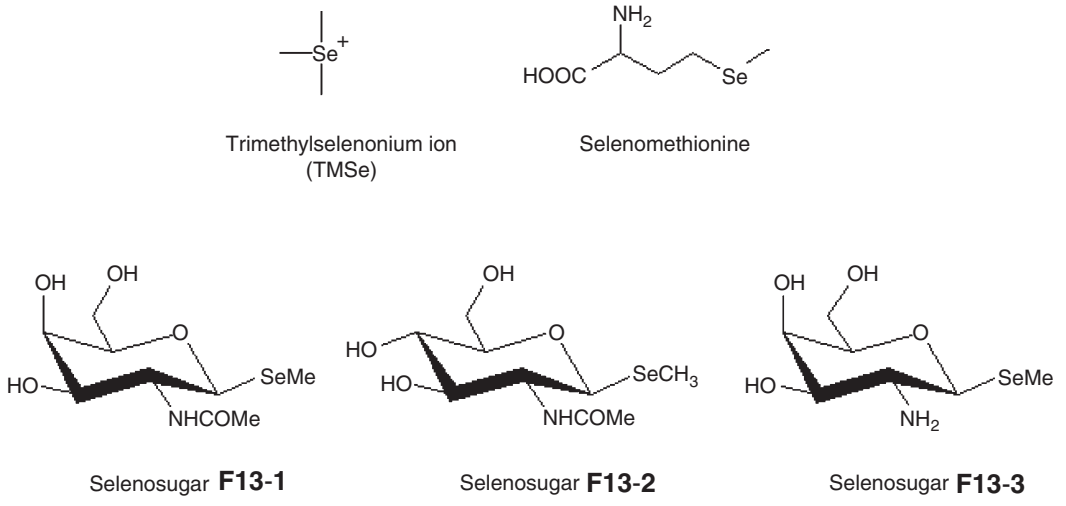

Figure 13 Organic selenium species reported to be present in urine.

The work of the Suzuki group generated renewed interest and activity in the field, and a report quickly followed on the presence of selenosugar **F13-1** in human urine.[377] Subsequently, two other selenosugars, namely methyl 2-acetamido–2-deoxy–1-seleno–β-D-glucopyranoside (selenosugar **F13-2**) and methyl 2-amino–2-deoxy–1-seleno–β-D-galactopyranoside (selenosugar **F13-3**) were identified in human urine by Gammelgaard and co-workers,[378,379] and those results have been confirmed by other groups.[380,381]

The work of Kuehnelt *et al.*[381] provided the first quantitative data on excretion rate and relative quantities of the various selenium metabolites, and showed that selenosugar **F13-1** was by far the major metabolite (70%) with smaller quantities of selenosugars **F13-2** and **F13-3**. Differences in excretion rate were also noted depending on the form of selenium ingested, but the metabolic pattern of compounds remained the same.[381] These data support an accepted metabolic pathway for selenium that describes various selenium sources converting to selenide, which is then transformed into selenocysteine and incorporated into selenoproteins.[382]

Interestingly, TMSe, which is said to be the major metabolite in rats, was not detected in the single human subject of the Kuehnelt study[381] nor in the seven human subjects in the study of Gammelgaard *et al.*[383] Traces of TMSe, however, were found in two of 11 subjects in the earlier study of Gammelgaard *et al.*[384] Thus, there may be interesting qualitative and quantitative differences in the selenium metabolites in rats and humans. Rats appear to have TMSe as the major metabolite and also produce selenosugar **F13-1**, whereas humans have mainly selenosugar **F13-1** and formation of TMSe is minor and less common. We note that the generally held view that TMSe is dose dependent[385] and is only produced at high selenium exposure does not seem to hold in all cases, as shown by recent work with rats.[386]

In addition to selenosugars, there are smaller quantities of other currently unknown selenium species in urine. The presence of selenomethionine has also been reported in some urine samples,[381,387] but its likely origin is D-selenomethionine, deliberately ingested in those experiments and shown[381] to be poorly metabolized in comparison with L-selenomethionine. The inorganic selenium species, selenite and selenate, which are also likely to be ingested in significant quantities in food and water, are not usually detected in urine.[371]

The presence of these novel selenosugars has also raised the issue of their possible toxicity. It is generally thought that TMSe is the product of a detoxification process designed to remove excess, potentially toxic inorganic selenium. Toxicity studies showing that TMSe is considerably less toxic than selenite have supported this view.[388] This appears to also apply to the selenosugars which were shown in cytotoxicity studies to be 1,000-fold less toxic than selenite.[381]

Work reported on selenium urinary metabolites has provided a firm basis for further research in the area. The biosynthetic pathway for these metabolites remains a challenging and interesting problem. Other interesting aspects include the effect of dose and type of ingested selenium on the formation of selenosugars and other, currently unknown, selenium species, and the individual variability in the way humans handle exposure to selenium.

References

1. Craig, P. J. Environmental Aspects of Organometallic Chemistry. In *Comprehensive Organometallic Chemistry 1*; Wilkinson, G., Gordon, F., Stone, A., Abel, E. W., Eds.; 1982; *2*, 979–1020.
2. Hirner, A. V.; Emons, H. *Organic Metal and Metalloid Species in the Environment*; Springer: Heidelberg, 2004.
3. Ebdon, L.; Pitts, R.; Cornelis, R.; Crews, H.; Donard, O. F. X.; Quevauviller, P. H. *Trace Element Speciation for Environment, Food and Health*; Royal Society of Chemistry: London, 2001.
4. Sigel, H.; Sigel, A. *Metal Ions in Biological Systems*; Dekker: New York, 1993; Vol. 29.
5. Bozke, L. *Chem. Anal.* **2005**, 489–505.
6. Craig, P. J. *Organometallic Compounds in the Environment*, 2nd ed.; Wiley: Chichester, 2003.
7. Edmonds, J. S.; Francesconi, K. A. Organoarsenic Compounds in the Marine Environment. In *Organometallic Compounds in the Environment*, 2nd ed.; Craig, P. J., Ed.; Wiley: Chichester, 2003; pp 195–222.
8. Hippler, J.; Kresimon, J.; Hirner, A. V. In *Organic Metal and Metalloid Species in the Environment*; Hirner, A. V., Emons, H., Eds.; Springer: Heidelberg, 2004; pp 113–135.
9. Feldmann, J. *J. Environ. Monit.* **1999**, *1*, 33–37.
10. Edmonds, J. S.; Francesconi, K. A.; Cannon, J. R.; Raston, C. L.; Skelton, B. W.; White, A. H. *Tetrahedron Lett.* **1977**, *18*, 1543–1546.
11. Craig, P. J.; Mennie, D.; Needham, M.; Ostah, N.; Donard, O. F. X.; Martin, F. J. *J. Organomet. Chem.* **1993**, *447*, 5–8.
12. Zahir, F.; Rizini, S. J.; Haq, S. K.; Khan, R. H., *Environ. Toxicol. Pharmacol.* 205, 351–360
13. Craig, P. J.; Eng, G.; Jenkins, R. O. Occurrence and Pathways of Organometallic Compounds in the Environment - General Considerations. In *Organometallic Compounds in the Environment*, 2nd ed.; Craig, P. J., Ed.; Wiley: Chichester, 2003; pp 1–56.
14. Harrison, R. M.; Laxen, D. P. *Environ. Sci. Technol.* **1978**, *12*, 1384-.
15. Dopp, E.; Hartmann, L. M.; Florea, A.-M.; Rettenmeier, A. W.; Hirner, A. V. *Crit. Rev. Toxicol.* **2004**, *34*, 301–333.
16. Thayer, J. S. *Appl. Organomet. Chem.* **2002**, *16*, 677–691.
17. Hirner, A. V.; Feldmann, J.; Goguel, R.; Rapsomanikis, S.; Fischer, R.; Andreae, M. O. *Appl. Organomet. Chem.* **1994**, *8*, 65–69.
18. Hirner, A. V.; Feldmann, J.; Krupp, E.; Grumping, R.; Goguel, R.; Cullen, W. R. *Org. Geochem.* **1998**, *29*, 1765–1778.
19. Feldmann, J.; Hirner, A. V. *Int. J. Environ. Anal. Chem.* **1995**, *60*, 339–359.
20. Feldmann, J.; Koch, I.; Cullen, W. R. *Analyst* **1998**, *123*, 815–820.
21. Chasteen, T. G.; Bentley, R. *Appl. Organomet. Chem* **2003**, *17*, 201–211.
22. Challenger, F. *Chem. Rev.* **1945**, *36*, 315–361.
23. Marvin-Dipasquale, M. C.; Oremland, R. S. *Environ. Sci. Technol.* **1998**, *32*, 2556–2563.
24. Pak, K. R.; Bartha, R. *Appl. Environ. Microbiol.* **1998**, *64*, 1013–1017.
25. Gadd, G. M. *Sci. Total Environ.* **2000**, *258*, 119–127.
26. El Ali, B.; Okuro, K.; Vasapollo, G.; Alper, H. J. *J. Am. Chem. Soc.* **1996**, *118*, 4264–4270.
27. Vasapollo, G.; Scarpa, A.; Mele, G.; Ronzini, L.; El Ali, B. *Appl. Organomet. Chem.* **2000**, *14*, 739–743.
28. Lehr, C. R.; Polishchuk, E.; Radoja, U.; Cullen, W. R. *Appl. Organomet. Chem.* **2003**, *17*, 831–834.
29. Newman, D. K.; Beveridge, T. J.; Morel, F. M. M. *Appl. Environ. Microbiol.* **1997**, *63*, 2022–2028.
30. Templeton, D. M.; Ariese, F.; Cornelis, R.; Danielsson, L.-G.; Muntau, H.; Van Leeuwen, H. P.; Lobinski, R. *Pure Appl. Chem.* **2000**, *72*, 1453–1470.
31. Keith, L. H. *Principles of Environmental Sampling*; Oxford University Press: New York, 1996.
32. Butler, O. T.; Cook, J. M.; Harrington, C. F.; Hill, S. J.; Rieuwerts, J.; Miles, D. L. *J. Anal. At. Spectrom.* **2005**, *20*, 130–157.
33. Taylor, A.; Branch, S.; Halls, D.; Patriarca, M.; White, M. *J. Anal. At. Spectrom.* **2005**, *20*, 323–369.
34. Evans, E. H.; Day, J. A.; Palmer, C. D.; Price, W. J.; Smith, C. M. M.; Tyson, J. F. *J. Anal. At. Spectrom.* **2005**, *20*, 562–590.
35. Bacon, J. R.; Linge, K. L.; Van Vaeck, L. *J. Anal. At. Spectrom.* **2005**, *20*, 763–802.
36. Haas, K.; Feldmann, J. *Anal. Chem.* **2000**, *72*, 4205–4211.
37. Schweigkofler, M.; Niessner, R. *Environ. Sci. Technol.* **1999**, *33*, 3680–3685.
38. Grumping, R.; Mikolajczak, D.; Hirner, A. V. *Fresenius J. Anal. Chem.* **1998**, *361*, 133–139.
39. Feldmann, J. Volatile Metal Compounds of Biogenic Origin. In *Handbook of Elemental Speciation II: Species in the Environment, Food, Medicine and Occupational Health*; Cornelis, R., Crews, J., Caruso, J., Heumann, K. G., Eds.; Wiley: Chichester, 2005.
40. Samanta, G.; Boring, C. B.; Dasgupta, P. K. *Anal. Chem.* **2001**, *73*, 2034–2040.
41. Byrne, R. H. *Pure Appl. Chem.* **1996**, *68*, 1639–1656.
42. Batley, G. E.; Apte, S. C.; Stauber, J. L. *Aust. J. Chem.* **2004**, *57*, 903–919.
43. Donat, J. R.; Bruland, K. W. In *Trace Metals in Natural Waters*; Salbu, B., Steinnes, E., Eds.; CRC Press: Boca Raton, 1995; p 302.
44. Buffle, J.; Leppard, G. G. *Environ. Sci. Technol.* **1995**, *29*, 2169–2175.
45. Gallagher, P. A.; Schwegel, C. A.; Parks, A.; Gamble, B. M.; Wymer, L.; Creed, J. T. *Environ. Sci. Technol.* **2004**, *38*, 2919–2927.
46. Gault, A. G.; Jana, J.; Chakraborty, S.; Mukherjee, P.; Sarkar, M.; Nath, B.; Polya, D. A.; Chatterjee, D. *Anal. Bioanal. Chem.* **2005**, *381*, 347–353.
47. Warnken, K. W.; Zhang, H.; Davison, W. *Anal. Chem.* **2005**, *77*, 5440–5446.
48. Gimpel, J.; Zhang, H.; Davison, W.; Edwards, A. C. *Environ. Sci. Technol.* **2003**, *37*, 138–146.
49. Westoo, G. *Acta Chem. Scand.* **1966**, *20*, 2131–2137.
50. Snell, J. P.; Quetel, C. R. *J. Anal. At. Spectrom.* **2005**, *20*, 447–454.
51. Quevauviller, P.; Drabaek, I.; Muntau, H.; Griepink, B. BCR Information EUR 15902 EN, Final Report: 1994.
52. Craig, P. J.; Forster, S. N.; Jenkins, R. O.; Miller, D. *Analyst* **1999**, *124*, 1243–1248.
53. Dodd, M.; Pergantis, S. A.; Cullen, W. R.; Li, H.; Eigendorf, G. K.; Reimer, K. J. *Analyst* **1996**, *121*, 223–228.
54. Abalos, M.; Bayona, J.-P.; Campano, R.; Granados, M.; Leal, C.; Prat, M. D. *J. Chromatogr. A* **1997**, *788*, 1–49.
55. Hudson-Edwards, K. A.; Houghton, S. L.; Osborn, A. *Trends Anal. Chem.* **2004**, *23*, 745–752.
56. Pellegrino, C.; Massanisso, P.; Morabito, R., *Trends Anal. Chem.* **2000**, *19*, 97–106.
57. Szpunar, J.; Schmitt, V. O.; Donard, O. F. X.; Lobinski, R. *Trends Anal. Chem.* **1996**, *15*, 181–187.
58. Bayona, J. M.; Cai, Y. *Trends Anal. Chem.* **1994**, *13*, 327–332.
59. Arnold, C. G.; Berg, M.; Muller, S. R.; Dommann, U.; Schwarzenbach, R. P. *Anal. Chem.* **1998**, *70*, 3094–3101.

60. Lobinski, R.; Marczenko, Z. *Spectrochemical Trace Analysis for Metals and Metalloids*; Elsevier: New York, 1996.
61. Waddell, R.; Lewis, C.; Hang, W.; Hassell, C.; Majidi, V. *Appl. Spectrosc. Rev.* **2005**, *40*, 33–69.
62. Lobinski, R. *Appl. Spectrosc.* **1997**, *51*, 260A–278A.
63. Lobinski, R. S.; Pereiro, I. R.; Chassaigne, H.; Wasik, A.; Szpunar, J. *J. Anal. At. Spectrom.* **1998**, *13*, 859–867.
64. Szpunar, J.; Lobinski, R.; Prange, A. *Appl. Spectrosc.* **2003**, *57*, 102A–112A.
65. Nash, M. J.; Maskall, J. E.; Hill, S. J. *J. Environ. Monit.* **2000**, *2*, 97–109.
66. Gong, Z. L.; Lu, X. F.; Ma, M. S.; Watt, C.; Le, X. C. *Talanta* **2002**, *58*, 77–96.
67. Francesconi, K. A.; Kuehnelt, D. *Analyst* **2004**, *129*, 373–395.
68. Horvat, M. Mercury Analysis and Speciation in Environmental Samples. In *Global and Regional Mercury Cycles: Sources, Fluxes and Mass Balances*; Baeyens, W., Ebinghaus, R., Vasiliev, O., Eds.; Kluwer: Dordrecht, 1996; pp 1–31.
69. Weber, J. H. Analytical Methods for the Determination of Mercury(II) and Methylmercury Compounds: The Problem of Speciation. In *Metal Ions in Biological Systems*; Sigel, A., Siegel, F., Eds.; Dekker: New York, 1997; Vol. 34, pp 1–20.
70. Leermakers, M.; Baeyens, W.; Quevauviller, P.; Horvat, M. *Trends Anal. Chem.* **2005**, *24*, 383–393.
71. Uden, P. C.; Boakye, H. T.; Kahakachchi, C.; Tyson, J. F. *J. Chromatogr. A* **2004**, *1050*, 85–93.
72. Leroy, M. J. F.; Quevauviller, P.; Donard, O. F. X.; Astruc, M. *Pure Appl. Chem.* **1998**, *70*, 2051–2064.
73. Prange, A.; Schaumloffel, D. *J. Anal. At. Spectrom.* **1999**, *14*, 1329–1332.
74. Blake, E.; Raynor, M. W.; Cornell, D. *J. Chromatogr. A* **1994**, *683*, 223–231.
75. Howard, A. G. *J. Anal. At. Spectrom.* **1997**, *12*, 267–272.
76. Weber, J. H. *Trends Anal. Chem.* **1997**, *16*, 73–78.
77. Le, X. C.; Cullen, W. R.; Reimer, K. J. *Anal. Chim. Acta* **1994**, *285*, 277–285.
78. Rapsomanikis, S. *Analyst* **1994**, *119*, 1429–1439.
79. Sarzanini, C.; Mentasti, E. *J. Chromatogr. A* **1997**, *789*, 301–321.
80. Sutton, K. L.; Caruso, J. A. *J. Chromatogr.* **1999**, *856*, 243–258.
81. Harrington, C. F.; Eigendorf, G. K.; Cullen, W. R. *App. Organomet. Chem.* **1996**, *10*, 339–362.
82. Harrington, C. F. *Trends Anal. Chem.* **2000**, *19*, 167–179.
83. Michalke, B. *Trends Anal. Chem.* **2002**, *21*, 154–165.
84. Michalke, B. *Trends Anal. Chem.* **2002**, *21*, 142–153.
85. Schaumloffel, D.; Encinar, J. R.; Lobinski, R. *Anal. Chem.* **2003**, *75*, 6837–6842.
86. Vela, N. P.; Caruso, J. A. *J. Anal. At. Spectrom.* **1992**, *7*, 971–978.
87. Majidi, V. *Microchem. J.* **2000**, *66*, 3–16.
88. Olesik, J. W.; Kinzer, J. A.; Grunwald, E. J.; Thaxton, K. K.; Olesik, S. V. *Spectrochim. Acta Part B: At. Spectrosc.* **1998**, *53*, 239–251.
89. Olesik, J. W.; Kinzer, J. A.; Olesik, S. V. *Anal. Chem.* **1995**, *67*, 1–12.
90. Ray, S. J.; Andrade, F.; Gamez, G.; McClenathan, D.; Rogers, D.; Schilling, G.; Wetzel, W.; Hieftje, G. M. *J. Chromatogr. A* **2004**, *1050*, 3–34.
91. Moldovan, M.; Krupp, E. M.; Holliday, A. E.; Donard, O. F. X. *J. Anal. At. Spectrom.* **2004**, *19*, 815–822.
92. Quevauviller, P.; Ritsema, R.; Morabito, R.; Dirkx, W. M. R.; Chiavarini, S.; Bayona, J. M.; Donard, O. F. X. *Appl. Organomet. Chem.* **1994**, *8*, 541–549.
93. Houk, R. S. *Spectrochim. Acta Part B: At. Spectrosc.* **1998**, *53*, 267–271.
94. Rosen, A. L.; Hieftje, G. M. *Spectrochim. Acta Part B: At. Spectrosc.* **2004**, *59*, 135–146.
95. McSheehy, S.; Mester, Z. *Trends Anal. Chem.* **2003**, *22*, 210–224.
96. McSheehy, S.; Mester, Z. *Trends Anal. Chem.* **2003**, *22*, 311–326.
97. Rosenberg, E. *J. Chromatogr.* **2003**, *1000*, 841–889.
98. Clough, R.; Truscatt, J.; Belt, S. T.; Evans, E. H.; Faitman, B.; Catterick, T. *Appl. Spectrosc. Rev.* **2003**, *38*, 101–132.
99. Demuth, N.; Heumann, K. G. *Anal. Chem.* **2001**, *73*, 4020–4027.
100. Monperrus, M.; Krupp, E.; Amouroux, D.; Donard, O. F. X.; Martin-Doimeadios, R. C. *Trends Anal. Chem.* **2004**, *23*, 261–272.
101. Rahman, G. M. M.; Kingston, H. M. *Anal. Chem.* **2004**, *76*, 3548–3555.
102. Heumann, K. G.; Rottmann, L.; Vogl, J. *J. Anal. At. Spectrom.* **1994**, *9*, 1351–1355.
103. Rottmann, L.; Heumann, K. G. *Fresenius J. Anal. Chem.* **1994**, *350*, 221–227.
104. Quevauviller, P. *J. Anal. At. Spectrom.* **1996**, *11*, 1225–1231.
105. Quevauviller, P. *Method Performance Studies for Speciation Analysis*; Royal Society of Chemistry: Cambridge, 1998.
106. Adams, F. C. *J. Anal. At. Spectrom.* **2004**, *19*, 1090–1097.
107. Harris, H. H.; Pickering, I. J.; George, G. N. *Science* **2003**, *301*, 1203–1203.
108. Gailer, J.; George, G. N.; Pickering, I. J.; Prince, R. C.; Ringwald, S. C.; Pemberton, J. E.; Glass, R. S.; Younis, H. S.; DeYoung, D. W.; Aposhian, H. V. *J. Am. Chem. Soc.* **2000**, *122*, 4637–4639.
109. Smith, P. G.; Koch, I.; Gordon, R. A.; Mandoli, D. F.; Chapman, B. D.; Reimer, K. J. *Environ. Sci. Technol.* **2005**, *39*, 248–254.
110. Moore, M. M.; Harrington Brock, K.; Doerr, C. L. *Mutat. Res. Rev. Mutat. Res.* **1997**, *386*, 279–290.
111. Sakurai, T.; Kaise, T.; Matsubara, C. *Chem. Res. Toxicol.* **1998**, *11*, 273–283.
112. Kitchin, K. T. *Toxicol. Appl. Pharmacol.* **2001**, *172*, 249–261.
113. Clarkson, T. W. *Environ. Health Perspect.* **2002**, *110*, 11–23.
114. Koczyk, D. *Acta Neurobiol. Exp.* **1996**, *56*, 587–596.
115. Aschner, M.; Gannon, M.; Kimelberg, H. K. *Brain Res.* **1992**, *582*, 181–185.
116. Mason, R. P.; Benoit, J. M. Organomercury Compounds in the Environment. In *Organometallic Compounds in the Environment*, 2nd ed.; Craig, P. J., Ed.; Wiley: Chichester, 2003; pp 57–99.
117. Jarvie, A. W. P. *Sci. Total Environ.* **1988**, *73*, 121–126.
118. Compeau, G. C.; Bartha, R. *Appl. Environ. Microbiol.* **1985**, *50*, 498–502.
119. Compeau, G. C.; Bartha, R. *Appl. Environ. Microbiol.* **1987**, *53*, 261–265.
120. Gilmour, C. C.; Henry, E. A.; Mitchell, R. *Environ. Sci. Technol.* **1992**, *26*, 2281–2287.
121. Gilmour, C. C.; Riedel, G. S. *Water Air Soil Pollut.* **1995**, *80*, 747–756.
122. Gray, J. E.; Hines, M. E.; Higueras, P. L.; Adatto, I.; Lasorsa, B. K. *Environ. Sci. Technol.* **2004**, *38*, 4285–4292.
123. Wang, W. X.; Wong, R. S. K.; Wang, J. F.; Yan, Y. F. *Aquat. Toxicol.* **2004**, 39–55.

124. Berman, M.; Chase, T.; Bartha, R. *Appl. Environ. Microbiol.* **1990**, *56*, 298–300.
125. Foster, T. J. *Crit. Rev. Microbiol.* **1987**, *15*, 117–140.
126. Summers, A. O. *Ann. Rev. Microbiol.* **1986**, *40*, 607–634.
127. Silver, S.; Misra, T. K. *Ann. Rev. Microbiol.* **1988**, *42*, 717–743.
128. Moore, M. J.; Distefano, M. D.; Zydowsky, L. D.; Cummings, R. T.; Walsh, C. T. *Acc. Chem. Res.* **1990**, *23*, 301–308.
129. Craig, P. J.; Bartlett, P. D. *Nature* **1978**, *275*, 635–637.
130. Craig, P. J.; Moreton, P. A. *Mar. Pollut. Bull.* **1984**, *15*, 406–408.
131. Bodaly, R. A.; Rudd, J. W. M.; Fudge, R. J. P.; Kelly, C. A. *Can. J. Fish. Aqua. Sci.* **1993**, *50*, 980–987.
132. Wren, C. D.; Maccrimmon, H. R. *Can. J. Fish. Aqua. Sci.* **1983**, *40*, 1737–1744.
133. Suns, K.; Hitchin, G. *Water Air Soil Pollut.* **1990**, *50*, 255–265.
134. Cope, W. G.; Wiener, J. G.; Rada, R. G. *Environ. Toxicol. Chem.* **1990**, *9*, 931–940.
135. Johnson, M. G. *Can. J. Fish. Aqua. Sci.* **1987**, *44*, 3–13.
136. Korthals, E. T.; Winfrey, M. R. *Appl. Environ. Microbiol.* **1987**, *53*, 2397–2404.
137. Callister, S. M.; Winfrey, M. R. *Water Air Soil Pollut.* **1986**, *29*, 453–465.
138. Jitaru, P.; Adams, F. *J. de Physique* **2004**, *121*, 185–193.
139. Bisinoti, M. C.; Jardin, W. F. *Quim. Nova* **2004**, *27*, 593–600.
140. Mason, R. P.; Reinfelder, J. R.; Morel, F. M. M. *Environ. Sci. Technol.* **1996**, *30*, 1835–1845.
141. Back, R. C.; Watras, C. J. *Water Air Soil Pollut.* **1995**, *80*, 931–938.
142. Harrison, R. M.; Laxon, D. P. In *Pollution; Causes Effects and Controls*; 1990; Royal Society of Chemistry: Cambridge, 1990; pp 1–20.
143. Ranchandren, M. *Chemosphere* **2004**, *55*, 319–331.
144. Hines, N. A.; Brezonik, P. L.; Engstrom, D. R. *Environ. Sci. Technol.* **2004**, *38*, 6610–6617.
145. Booth, S.; Zeller, D. *Environ. Health Perspect.* **2005**, *113*, 521–526.
146. Morabito, R.; Massanisso, P.; Camara, C.; Larsson, T.; Frech, W.; Kramar, K. J. M.; Bianchi, M.; Muntau, H.; Donard, O. F. X., Lobinski, R., *et al. Trac. Trends. Anal. Chem.* **2004**, *23*, 664–676.
147. Bramanti, E.; Lomonte, C.; Onov, M.; Zamboni, D.; D'Ulivo, G. R. *Talanta* **2005**, 762–768.
148. Huang, J. H. *Anal. Chim. Acta* **2005**, *532*, 113–120.
149. Yoshinaga, J. Organolead Compounds in the Environment. In *Organometallic Compounds in the Environment*, 2nd ed.; Craig, P. J., Ed.; Wiley: Chichester, 2003; pp 151–194.
150. Huang, J. H.; Klemm, O. *Atmosp. Environ.* **2004**, *38*, 5013–5023.
151. Gallert, C.; Winter, J. *Water Res.* **2004**, *38*, 4204–4212.
152. Huang, J. H.; Marzner, E. *Biogeochemisty* **2004**, *71*, 125–139.
153. Boutron, C.; Rosman, K.; Barbante, C.; Bolshov Madams, F.; Hong, S. M.; Ferrari, C. *C. R. Geoscience* **2005**, *21*, 847–867.
154. Reisinger, K.; Stoeppler, M.; Nurnberg, H. W. *Nature* **1981**, *291*, 228–230.
155. Jarvie, A. W. P.; Whitmore, A. P.; Markall, R. N.; Potter, H. R. *Environ. Pollut. Ser. B: Chem. Phys.* **1983**, *6*, 81–94.
156. Wong, P. T. S.; Chau, Y. K.; Luxon, P. L. *Nature* **1975**, *253*, 263–264.
157. Thompson, J. A. J.; Crerar, J. A. *Mar. Pollut. Bull.* **1980**, *11*, 251–253.
158. Walton, A. P.; Ebdon, L.; Millward, G. E. *Appl. Organomet. Chem.* **1988**, *2*, 87–90.
159. Hewitt, C. N.; Harrison, R. M. *Environ. Sci. Technol.* **1987**, *21*, 260–266.
160. Jarvie, A. W. P.; Markall, R. N.; Potter, H. R. *Nature* **1975**, *255*, 217–218.
161. Craig, P. J. *Environ. Technol. Lett.* **1980**, *1*, 17–20.
162. Ahmad, I.; Chau, Y. K.; Wong, P. T. S.; Carty, A. J.; Taylor, L. *Nature* **1980**, *287*, 716–717.
163. Craig, P. J.; Rapsomanikis, S. *Environ. Sci. Technol.* **1985**, *19*, 726–730.
164. Jarvie, A. W. P.; Whitmore, A. P. *Environ. Technol. Lett.* **1981**, *2*, 197–204.
165. Harrison, R. M.; Laxen, D. P. H. *Nature* **1978**, *275*, 738–740.
166. Hewitt, C. N.; Harrison, R. M.; Demora, S. J. *Mar. Chem.* **1984**, *15*, 189–190.
167. Harrison, R. M.; Laxen, D. P. H. *Environ. Sci. Technol.* **1978**, *12*, 1384–1392.
168. Hewitt, C. N.; Harrison, R. M. *Environ. Sci. Technol.* **1986**, *20*, 797–802.
169. Jarvie, A. W. P.; Markall, R. N.; Potter, H. R. *Environ. Res.* **1981**, *25*, 241–249.
170. Hewitt, C. N.; Harrison, R. M.; Radojevic, M. *Anal. Chim. Acta.* **1986**, *188*, 229–247.
171. Davies, A. G. *Organotin Chemistry*; Wiley: Weinheim, 1997.
172. Patai, S. *The Chemistry of Organic Germanium, Tin and Lead Compounds*; Wiley: Chichester, 1995.
173. Cima, F.; Craig, P. J.; Harrington, C. In *Organometallic Compounds in the Environment*, 2nd ed.; Craig, P. J., Ed.; Wiley: Chichester, 2003; pp 101–150.
174. Champ, M. A. *Environ. Sci. Technol.* **2000**, *258*, 21–27.
175. De Mora, S. J. *Tributyltin: Case Study of an Environmental Contaminant*; Cambridge University Press: Cambridge, 1996.
176. Maguire, R. J. *Water Qual. Res. J. Can.* **2000**, *35*, 633–679.
177. Rosenberg, E. Speciation of Tin. In *Handbook of Elemental Speciation II: Species in the Environment, Food, Medicine and Occupational Health*; Cornelis, R., Caruso, J., Crews, H., Heumann, K., Eds.; Wiley: Chichester, 2005; pp 422–463.
178. Laughlin, R. B.; Guard, H. E.; Coleman, W. M. *Environ. Sci. Technol.* **1986**, *20*, 201–204.
179. Zuckerman, J. J.; Reisdorf, R. P.; Ellis, H. V.; Wilkinson, R. R. Organotins in Biology and the Environment. In *Organometals and Organometalloids Occurrence and Fate in the Environment*; Brinckman, F. E., Bellama, J. M., Eds.; American Chemical Society: Washington, DC, 1978; Vol. 82, pp 388–422.
180. Blunden, S. J.; Evans, C. J. Organotin Compounds. *The Handbook of Environmental Chemistry: Anthropogenic Compounds*; Hutzinger, O., Ed.; Springer: Berlin, 1990; Vol. 3, pp 1–44.
181. Gibbs, P. E.; Bryan, G. W. Reproductive Failure in the Gastropod *Nucella Lapillus* Associated with Imposex Caused by Tributyltin Pollution: A Review. In *Organotin: Environmental Fate and Effects*; Champ, M., Seligman, P. F., Eds.; Chapman and Hall: London, 1996; pp 259–281.
182. Alzieu, C.; Sanjuan, J.; Deltreil, J. P.; Borel, M. *Mar. Pollut. Bull.* **1986**, *17*, 494–498.
183. Hoch, M. *Appl. Geochem.* **2001**, *16*, 719–743.

184. Donard, O. F. X.; Lespes, G.; Amouroux, D.; Morabito, R. Organotin Compounds in the Environment: Still a Critical Issue. In *Trace Element Speciation for Environment, Food and Health*; Ebdon, L., Cornelius, R., Crews, H., Pitts, R., Quevauviller, P., Eds.; Royal Society of Chemistry: Cambridge, 2001; pp 142–177.
185. Adelman, D.; Hinga, K. R.; Pilson, M. E. Q. *Environ. Sci. Technol.* **1990**, *24*, 1027–1032.
186. Feldmann, J.; Grumping, R.; Hirner, A. V. *Fresenius J. Anal. Chem.* **1994**, *350*, 228–234.
187. Amouroux, D.; Tessier, E.; Donard, O. F. X. *Environ. Sci. Technol.* **2000**, *34*, 988–995.
188. De Mora, S. J.; Stewart, C.; Phillips, D. *Mar. Pollut. Bull.* **1995**, *30*, 50–57.
189. Shizhong, T.; Chau, Y. K.; Liu, D. *App. Organomet. Chem.* **1989**, *3*, 249–255.
190. Landmeyer,; Tanner, J. E. T. L.; Watt, B. E. *Environ. Sci. Technol.* **2004**, *38*, 4106–4112.
191. Laughlin, R. B. Bioaccumulation of TBT by Aquatic Organisms. In *Organotin: Environmental Fate and Effects*; Champ, M., Seligman, P. F., Eds.; Chapman and Hall: London, 1996; pp 331–355.
192. Hamasaki, T.; Nagase, H.; Yoshioka, Y.; Sato, T. *Crit. Rev. Environ. Sci. Technol.* **1995**, *25*, 45–91.
193. Hill, S. J.; Bloxham, M. J.; Worsfold, P. J. *J. Anal. At. Spectrom.* **1993**, *8*, 499–515.
194. Byrdy, F. A.; Caruso, J. A. *Environ. Sci. Technol.* **1994**, *28*, 528A–534A.
195. Harrington, C. F.; Eigendorf, G. K.; Cullen, W. R. *Appl. Organomet. Chem.* **1996**, *10*, 339–362.
196. Ebdon, L.; Hill, S.; Ward, R. W. *Analyst* **1986**, *111*, 1113–1138.
197. Tao, H.; Babu Rajendran, R. B.; Quetal, C. R.; Nakazato, T.; Tominaga, M.; Miyazaki, A. *Anal. Chem.* **1991**, *71*, 4208–4215.
198. Gomez-Ariza, J. L.; Beltran, R.; Morales, E.; Giraldez, I.; Ruiz-Benitez, M. *Appl. Organomet. Chem.* **1995**, *9*, 51–64.
199. Zhang, S.; Chau, Y. K.; Chau, A. S. Y. *Appl. Organomet. Chem.* **1991**, *5*, 431–435.
200. Babu Rajendran, R. B.; Tao, H.; Miyazaki, A.; Ramesh, R.; Ramachandran, S. *J. Environ. Monit.* **2001**, *3*, 627–634.
201. Ceulemans, M.; Witte, C.; Lobinski, R.; Adams, F. C. *Appl. Organomet. Chem.* **1994**, *8*, 451–461.
202. Wong, P. T. S.; Chau, Y. K.; Brown, M.; Whittle, D. M. *Appl. Organomet. Chem.* **1994**, *8*, 385–391.
203. de la Calle-Guntinas, M. B.; Scerbo, R.; Chiavarini, S.; Quevauviller, P.; Morabito, R. *Appl. Organomet. Chem.* **1997**, *5*, 431–435.
204. Corr, J. J. *J. Anal. At. Spectrom.* **1997**, *12*, 537–546.
205. Mester, Z.; Sturgeon, R. E.; Lam, J. W.; Maxwell, P. S.; Peter, L. *J. Anal. At. Spectrom.* **2001**, *16*, 1313.
206. Bryan, G. W.; Gibbs, P. E.; Burt, G. R. *J. Mar. Biol. Assoc. U.K.* **1988**, *68*, 733–744.
207. Ten Hallers-Tjabbes, C. C.; Kemp, J. F.; Boon, J. P. *Mar. Pollut. Bull.* **1994**, *28*, 311–313.
208. Saxena, A. K. *Appl. Organomet. Chem.* **1987**, *1*, 39–56.
209. Agency for Toxic Substances and Disease Registry (ATSDR) *Toxicological Profile for Tin*; Department of Health and Human Services, Public Health Services, Atlanta, 2003.
210. Cullen, W. R.; Reimer, K. J. *Chem. Rev.* **1989**, *89*, 713–764.
211. Edmonds, J. S.; Francesconi, K. A.; Stick, R. V. *Nat. Prod. Rep.* **1993**, *10*, 421–428.
212. Francesconi, K.; Edmonds, J. S. *Adv. Inorg. Chem.* **1997**, *44*, 147–189.
213. Francesconi, K. A.; Edmonds, J. S. Arsenic in the Sea. In *Oceanography and Marine Biology: An Annual Review*; Ansell, A. D., Gibson, R. N., Barnes, M., Eds.; UCL Press: London, 1993; Vol. 31, pp 111–151.
214. Larsen, E. H. *Fresenius J. Anal. Chem.* **1995**, *352*, 582–588.
215. McSheehy, S.; Szpunar, J.; Lobinski, R.; Haldys, V.; Tortajada, J.; Edmonds, J. S. *Anal. Chem.* **2002**, *74*, 2370–2378.
216. Sloth, J. J.; Larsen, E. H.; Julshamn, K. *Rapid Commun. Mass Spectrom.* **2005**, *19*, 227–235.
217. Hansen, H. R.; Pickford, R.; Thomas-Oates, J.; Jaspars, M.; Feldmann, J. *Angew. Chem., Int. Ed.* **2004**, *43*, 337–340.
218. Raml, R.; Goessler, T.; Traar, P.; Ochi, T.; Francesconi, K. A. *Chem. Res. Toxicol.* **2005**, *18*, 1444–1450.
219. Khokiattiwong, S.; Goessler, W.; Pedersen, S. N.; Cox, R.; Francesconi, K. A. *Appl. Organomet. Chem.* **2001**, *15*, 481–489.
220. Jenkins, R. O.; Ritchie, A. W.; Edmonds, J. S.; Goessler, W.; Molenat, N.; Kuehnelt, D.; Harrington, C. F.; Sutton, P. G. *Arch. Microbiol.* **2003**, *180*, 142–150.
221. Schmeisser, E.; Goessler, W.; Kienzl, N.; Francesconi, K. A. *Analyst* **2005**, *130*, 948–955.
222. Edmonds, J. S.; Shibata, Y.; Yang, F. Q.; Morita, M. *Tetrahedron Lett.* **1997**, *38*, 5819–5820.
223. Schmeisser, E.; Rumpler, A.; Kollroser, M.; Rechberger, G.; Goessler, W.; Francesconi, K. A. *Angew. Chem. Int. Ed.* **2006**, *45*, 150–154.
224. Francesconi, K. A.; Khokiattiwong, S.; Goessler, W.; Pedersen, S. N.; Pavkov, M. *Chem. Commun.* **2000**, *12*, 1083–1084.
225. Sloth, J. J.; Larsen, E. H.; Julshamn, K. *J. Anal. At. Spectrom.* **2003**, *18*, 452–459.
226. Francesconi, K. A.; Goessler, W.; Panutrakul, S.; Irgolic, K. J. *Sci. Total Environ.* **1998**, *221*, 139–148.
227. Kirby, J.; Maher, W.; Spooner, D. *Environ. Sci. Technol.* **2005**, *39*, 5999–6005.
228. Schmeisser, E.; Raml, R.; Francesconi, K. A.; Kuehnelt, D.; Lindberg, A. L.; Soros, C.; Goessler, W. *Chem. Commun.* **2004**, *16*, 1824–1825.
229. Fricke, M. W.; Creed, P. A.; Parks, A. N.; Shoemaker, J. A.; Schwegel, C. A.; Creed, J. T. *J. Anal. At. Spectrom.* **2004**, *19*, 1454–1459.
230. Kahn, M.; Raml, R.; Schmeisser, E.; Vallant, B.; Francesconi, K. A.; Goessler, W. *Environ. Chem.* **2005**, *2*, 171–176.
231. Soeroes, C.; Goessler, W.; Francesconi, K. A.; Schmeisser, E.; Raml, R.; Kienzl, N.; Kahn, M.; Fodor, P.; Kuehnelt, D. *J. Environ. Monit.* **2005**, *7*, 688–692.
232. Meier, J.; Kienzl, N.; Goessler, W.; Francesconi, K. A. *Environ. Chem.* **2005**, *2*, 304–307.
233. Morita, M.; Shibata, Y. *Chemosphere* **1988**, *17*, 1147–1152.
234. Aposhian, H. V.; Zheng, B. S.; Aposhian, M. M.; Le, X. C.; Cebrian, M. E.; Cullen, W.; Zakharyan, R. A.; Ma, H. S.; Dart, R. C., Cheng, Z., *et al. Toxicol. Appl. Pharmacol.* **2000**, *165*, 74–83.
235. Le, X. C.; Ma, M. S.; Lu, X. F.; Cullen, W. R.; Aposhian, H. V.; Zheng, B. S. *Environ. Health Perspect.* **2000**, *108*, 1015–1018.
236. Mandal, B. K.; Ogra, Y.; Suzuki, K. T. *Chem. Res. Toxicol.* **2001**, *14*, 371–378.
237. Valenzuela, O. L.; Borja-Aburto, V. H.; Garcia-Vargas, G. G.; Cruz-Gonzalez, M. B.; Garcia-Montalvo, E. A.; Calderon-Aranda, E. S.; Del Razo, L. M. *Environ. Health Perspect.* **2005**, *113*, 250–254.
238. Slejkovec, Z.; Byrne, A. R.; Stive, T.; Goessler, W. E.; KJ, I. *Appl. Organomet. Chem.* **1997**, 673–682.
239. Byrne, A. R.; Slejkovec, Z.; Stijve, T.; Fay, L.; Gossler, W.; Gailer, J.; Irgolic, K. J. *Appl. Organomet. Chem.* **1995**, *9*, 305–313.
240. Larsen, E. H.; Hansen, M.; Gossler, W. *Appl. Organomet. Chem.* **1998**, *12*, 285–291.
241. Koch, I.; Feldmann, J.; Wang, L. X.; Andrewes, P.; Reimer, K. J.; Cullen, W. R. *Sci. Total Environ.* **1999**, *236*, 101–117.
242. Lai, V. W. M.; Cullen, W. R.; Harrington, C. F.; Reimer, K. J. *Appl. Organomet. Chem.* **1997**, *11*, 797–803.
243. Koch, I.; Wang, L. X.; Ollson, C. A.; Cullen, W. R.; Reimer, K. J. *Environ. Sci. Technol.* **2000**, *34*, 22–26.

244. Geiszinger, A.; Goessler, W.; Kuehnelt, D.; Francesconi, K.; Kosmus, W. *Environ. Sci. Technol.* **1998**, *32*, 2238–2243.
245. Geiszinger, A. E.; Goessler, W.; Kosmus, W. *Appl. Organomet. Chem.* **2002**, *16*, 473–476.
246. Kuehnelt, D.; Goessler, W.; Schlagenhaufen, C.; Irgolic, K. J. *Appl. Organomet. Chem.* **1997**, *11*, 859–867.
247. Huang, Y. K.; Lin, K. H.; Chen, H. W.; Chang, C. C.; Liu, C. W.; Yang, M. H.; Hsueh, Y. M. *Food Chem. Toxicol.* **2003**, *41*, 1491–1500.
248. Shiomi, K.; Sugiyama, Y.; Shimakura, K.; Nagashima, Y. *Appl. Organomet. Chem.* **1995**, *9*, 105–109.
249. Slejkovec, Z.; Bajc, Z.; Doganoc, D. Z. *Talanta* **2004**, *62*, 931–936.
250. Slejkovec, Z.; Byrne, A. R.; Smodis, B.; Rossbach, M. *Fresenius J. Anal. Chem.* **1996**, *354*, 592–595.
251. Zheng, J.; Hintelmann, H. *J. Anal. At. Spectrom.* **2004**, *19*, 191–195.
252. Edmonds, J. S.; Francesconi, K. A. *Experientia* **1987**, *43*, 553–557.
253. Geiszinger, A.; Goessler, W.; Pedersen, S. N.; Francesconi, K. A. *Environ. Toxicol. and Chem.* **2001**, *20*, 2255–2262.
254. Francesconi, K. A.; Edmonds, J. S.; Stick, R. V. *J. Chem. Soc., Perkin Trans. 1* **1992**, 1349–1357.
255. Francesconi, K. A.; Pergantis, S. A. *Analyst* **2004**, *129*, 398–399.
256. Francesconi, K. A. PhD Thesis at The University of Western Australia, Perth 1991.
257. Eto, K.; Kimura, H. *J. Biol. Chem.* **2002**, *277*, 42680–42685.
258. Toohey, J. I. *Biochem. J.* **1989**, *264*, 625–632.
259. Hansen, H. R.; Raab, A.; Jaspars, M.; Milne, B. F.; Feldmann, J. *Chem. Res. Toxicol.* **2004**, *17*, 1086–1091.
260. Francesconi, K. A.; Hunter, D. A.; Bachmann, B.; Raber, G.; Goessler, W. *Appl. Organomet. Chem.* **1999**, *13*, 669–679.
261. Edmonds, J. S.; Francesconi, K. A.; Hansen, J. A. *Experientia* **1982**, 38.
262. Ritchie, A. W.; Edmonds, J. S.; Goessler, W.; Jenkins, R. O. *FEMS Microbiol. Lett.* **2004**, *235*, 95–99.
263. Edmonds, J. S. *Bioorg. Med. Chem. Lett.* **2000**, *10*, 1105–1108.
264. Maeda, S. In *The Chemistry of Organic Arsenic Antimony and Bismuth Compounds*; Patai, S., Ed.; Wiley: Chichester, 1994; pp 725–759.
265. Hamilton, E. I. *Sci. Total Environ.* **2000**, *249*, 171–221.
266. Meharg, A. A.; French, M. C. *Chemosphere* **1995**, *30*, 1987–1994.
267. Andrewes, P.; Cullen, W. R. In *Organometallic Compounds in the Environment*, 2nd ed.; Craig, P. J., Ed.; Wiley: Chichester, 2003; pp 277–304.
268. Craig, P. J.; Jenkins, R. O. *Organic Metal and Metalloid Species in the Environment*; Hirner, A. V., Emons, H., Eds.; Springer: Heidelberg, 2004; pp 1–11.
269. Craig, P. J.; Forster, S. N.; Jenkins, R. O.; Miller, D. P.; Ostah, N.; Smith, L. M.; Morris, T.-A. In *Chemical Processes in Marine Environments*; Gianguzza, A., Pelizzetti, E., Sammartano, S., Eds.; Springer: New York, 2000; pp 265–280.
270. Bentley, R.; Chasteen, T. G. *Microbiol. Mol. Biol. Rev.* **2002**, *66*, 250–271.
271. Jenkins, R. O. *Trends Oraganomet. Chem.* **2002**, *4*, 109–121.
272. Filella, M.; Belzile, N.; Chen, Y.-W. *Earth Sci. Rev.* **2002**, *57*, 125–176.
273. Thayer, J. S. *Environmental Chemistry of the Heavy Elements: Hydrido and Organo Compounds*; VCH: New York, 1995.
274. Dodd, M.; Grundy, S. L.; Reimer, K. J.; Cullen, W. R. *Appl. Organomet. Chem.* **1992**, *6*, 207–211.
275. Koch, I.; Feldmann, J.; Lintschinger, J.; Serves, S. V.; Cullen, W. R.; Reimer, K. J. *Appl. Organomet. Chem.* **1998**, *12*, 129–136.
276. Krupp, E. M.; Grumping, R.; Furchbar, U. R. R.; Hirner, A. V. *Fresenius J. Anal. Chem.* **1996**, *354*, 546–549.
277. Koch, I.; Wang, L. X.; Feldmann, J.; Andrewes, P.; Reimer, K. J.; Cullen, W. R. *Int. J. Environ. Anal. Chem.* **2000**, *77*, 111–131.
278. Maillefer, S.; Lehr, L. R.; Cullen, W. R. *Appl. Organomet. Chem.* **2003**, *17*, 154–160.
279. Limerick, S. *Expert Group to Investigate Cot Death Theories*; HMSO: London, 1998.
280. Jenkins, R. O.; Morris, T.-A.; Craig, P. J.; Goessler, W.; Ostah, N.; Wills, K. M. *Human Exp. Toxicol.* **2000**, *19*, 693–702.
281. Kresimon, J.; Gruter, U. M.; Hirner, A. V. *Fresenius J. Anal. Chem.* **2001**, *371*, 586–590.
282. Buchet, J. P.; Lauwerys, R. *Arch. Toxicol.* **1985**, *57*, 125–129.
283. Jenkins, R. O.; Craig, P. J.; Goessler, W.; Miller, D.; Ostah, N.; Irgolic, K. J. *Environ. Sci. Technol.* **1998**, *32*, 882–885.
284. Jenkins, R. O.; Craig, P. J.; Goessler, W.; Irgolic, K. J. *Human Exp. Toxicol.* **1998**, *17*, 231–238.
285. Andrewes, P.; Cullen, W. R.; Feldmann, J.; Koch, I.; Polishchuk, E.; Reimer, E. *Appl. Organomet. Chem.* **1998**, *12*, 827–842.
286. Andrewes, P.; Cullen, W. R.; Polishchuk, E. *Appl. Organomet. Chem.* **1999**, *13*, 659–664.
287. Craig, P. J.; Jenkins, R. O.; Dewick, R.; Miller, D. P. *Sci. Total Environ.* **1999**, *229*, 83–88.
288. Andrewes, P.; Cullen, W. R.; Polishchuk, E.; Reimer, K. J. *Appl. Organomet. Chem.* **2001**, *15*, 473–480.
289. Smith, L. M.; Maher, W. A.; Craig, P. J.; Jenkins, R. O. *Appl. Organomet. Chem.* **2002**, *16*, 287–293.
290. Jenkins, R. O.; Forster, S. N.; Craig, P. J. *Arch. Microbiol.* **2002**, *178*, 274–278.
291. Gürleyük, H.; Van Fleet-Stalder, V.; Chasteen, T. G. *Appl. Organomet. Chem.* **1997**, *11*, 471–483.
292. Jenkins, R. O.; Craig, P. J.; Miller, D. P.; Stoop, L.; Ostah, N.; Morris, T. A. *Appl. Organomet. Chem.* **1998**, *12*, 449–455.
293. Gates, P. N.; Harrop, H. A.; Pridham, J. B.; Smethurst, B. *Sci. Total Environ.* **1997**, *205*, 215–221.
294. Michalke, K.; Wickenheiser, M.; Mehring, A.; Hirner, A. V.; Hensel, R. *Appl. Environ. Microbiol.* **2000**, *66*, 2791–2796.
295. Smith, L. M.; Craig, P. J.; Jenkins, R. O. *Chemosphere* **2002**, *47*, 401–407.
296. Andrewes, P.; Cullen, W. R.; Feldmann, J.; Koch, I.; Polishchuk, E. *Appl. Organomet. Chem.* **1999**, *13*, 681–687.
297. Andrewes, P.; Cullen, W. R.; Polishchuk, E. *Environ. Sci.Technol.* **2000**, *34*, 2249–2253.
298. Hartmann, L. M.; Craig, P. J.; Jenkins, R. O. *Arch. Microbiol.* **2003**, *180*, 347–352.
299. Wehmeier, S.; Raab, A.; Feldmann, J. *Appl. Organomet. Chem.* **2004**, *18*, 631–639.
300. Lintschinger, J.; Scramel, O.; Kettrup, A. *Fresenins J. Anal. Chem.* **1998**, *361*, 96–102.
301. Zheng, J.; Takeda, A.; Furuta, N. *J. Anal. At. Spectrom.* **2001**, *16*, 62–67.
302. Feldmann, J. In *Biogeochemistry of Environmentally Important Trace Elements*; Cai, Y., Braids, O. C., Eds.; *ACS Symposium Series*; American Chemical Society: Washington, DC, 2002; pp 128–140.
303. Craig, P. J.; Forster, S. A.; Jenkins, R. O.; Lawson, G.; Miller, D.; Ostah, N. *Appl. Organomet. Chem.* **2001**, *15*, 527–532.
304. Burrell, R. E.; Corke, C. T.; Goel, R. G. *J. Agric. Food Chem.* **1983**, *31*, 85–88.
305. Andrewes, P.; Kitchin, K. T.; Wallace, K. *Toxicol. Appl. Pharmacol.* **2004**, *194*, 41–48.
306. Graiver, D.; Farminer, K. W.; Narayan, R. *J. Polymer. Environ.* **2003**, *11*, 129–136.
307. Hirner, A. V.; Flassbeck, D.; Gruemping, R. In *Organometallic Compounds in the Environment*, 2nd ed.; Craig, P. J., Ed.; Wiley: Chichester, 2003; pp 305–351.
308. Hirner, A. V.; Flassbeck, D. Speciation of Silicon. In *Handbook of Elemental Speciation II: Species in the Environment, Food, Medicine & Occupational Health*; Cornelis, R., Caruso, J., Crews, H., Heumann, K., Eds.; Wiley: Chichester, 2005; pp 366–377.

309. Hobson, J. F.; Atkinson, R.; Carter, W. P. L. In *Organosilicon Materials: Handbook of Environmental Chemistry*; Hutzinger, O., Ed.; Springer: Berlin, 1997; pp 137–179.
310. Hamelink, J.; Simon, P.; Silberhorn, E. M. *Environ. Sci. Technol.* **1996**, *30*, 1946–1952.
311. Kent, D.; Fackler, P.; Hartley, D.; Hobson, J. *Environ. Toxicol. Water Qual.* **1996**, *11*, 145–149.
312. Hobson, J.; Silberhorn, E. M. *Environ. Toxicol. Chem.* **1995**, *14*, 1667–1673.
313. Fackler, P. H.; Dionne, E.; Hartley, D. A.; Hamelink, J. L. *Environ. Toxicol. Chem.* **1995**, *14*, 1649–1656.
314. Mueller, J. A.; DiToro, D. M.; Maiello, J. A. *Environ. Toxicol. Chem.* **1995**, *14*, 1657–1666.
315. Parker, W. J.; Shi, J. C.; Fendinger, N. J.; Monteith, H. D.; Chandra, G. *Environ. Toxicol. Chem.* **1999**, *18*, 172–181.
316. Grumping, R.; Michalke, K.; Hirner, A. V.; Hensel, R. *Appl. Environ. Microbiol.* **1999**, *65*, 2276–2278.
317. Xu, S. *Environ. Sci. Technol.* **1999**, *33*, 603–605.
318. Sommerdale, R.; Parlar, H.; Wrobel, D.; Kochs, P. *Environ. Sci. Technol.* **1993**, *27*, 2435–2440.
319. Atkinson, R. *Environ. Sci. Technol.* **1991**, *25*, 863–866.
320. Atkinson, R.; Tuazon, E. C.; Kwok, E. S. C.; Arey, S.; Aschmann, S. M.; Bridier, I. *Chem. Soc., Faraday Trans.* **1995**, *91*, 3033–3039.
321. Carter, W. P. L. *J. Air Waste Manage. Assoc.* **1994**, *44*, 881–899.
322. Fendinger, N. J.; McAvoy, D. C.; Eckhoff, W. S. *Environ. Sci. Technol.* **1997**, *31*, 1555–1563.
323. Watts, R. J.; Kong, S.; Haling, C. S.; Gearhart, L.; Frye, C. L.; Vigon, B. W. *Water Res.* **1995**, *29*, 2405–2411.
324. Matsui, S.; Murakami, T.; Sasaki, T.; Hirose, Y.; Iguana, Y. *Prog. Wat. Tech.* **1975**, *7*, 645–650.
325. Bruggemann, W. A.; Weber-Fung, D.; Opperhuizen, A.; Van der Steen, J.; Wijbenga, A.; Hutzinger, O. *Toxicol. Environ. Chem.* **1984**, *7*, 287–293.
326. Opperhuizen, A.; Damen, H. W. J.; Asyee, G. M.; Van der Stehen, J. M. D. *Toxicol. Environ. Chem.* **1987**, *13*, 265–285.
327. Annelin, R. B.; Frye, C. L. *Sci. Total Environ.* **1989**, *83*, 1–11.
328. Stevens, C. *Inorg. Biochem.* **1998**, *69*, 203–207.
329. Lehmann, R. G.; Varaprath, S.; Frye, C. L. *Environ. Toxicol. Chem.* **1994**, *13*, 1061–1064.
330. Lehmann, R. G.; Varaprath, S.; Frye, C. L. *Environ. Toxicol. Chem.* **1994**, *13*, 1753–1759.
331. Carpenter, J. C.; Cella, J. A.; Dorn, S. B. *Environ. Sci. Technol.* **1995**, *29*, 864–868.
332. Lehmann, R. G.; Miller, J. R.; Xu, S.; Singh, U. B.; Reece, C. F. *Environ. Sci. Technol.* **1998**, *32*, 1260–1264.
333. Lehmann, R. G.; Frye, C. L.; Tolle, D. A.; Zwick, T. C. *Water Air Soil Pollut.* **1996**, *87*, 231–243.
334. Grissbach, E. F. C.; Lehmann, R. G. *Chemosphere* **1999**, *38*, 1461–1468.
335. Spivack, J.; Dorn, S. B., *Environ. Sci. Technol.* **1994**, *28*, 2345–2352.
336. Spivack, J. L.; Pohl, E. R.; Kochs, P. In *Organosilicon Materials: Handbook of Environmental Chemistry*; Hutzinger, O., Ed.; Springer: Berlin, 1997; pp 105–135.
337. Xu, S.; Lehmann, R. G.; Miller, J. R.; Chandra, G. *Environ. Sci. Technol.* **1998**, *32*, 1199–1206.
338. Lehmann, R. G.; Varaprath, S.; Annelin, R. B.; Arndt, J. L. *Environ. Toxicol. Chem.* **1995**, *14*, 1299–1305.
339. Garvey, N.; Collins, M. K.; Mihaich, E. M. *SETAC 17th Annual Meeting*. Abstract no. 256: Washington DC, 1996.
340. Gast, C. H.; Kraak, J. C.; Poppe, H.; Haessen, F. J. M. J. *J. Chromatrogr.* **1979**, *185*, 549.
341. Grumping, R.; Mikolajczak, D.; Hirner, A. V. *Fresenius J. Anal. Chem.* **1998**, *361*, 133–139.
342. Fendinger, N. J.; Lehmann, R. G.; Mihaich, E. M. In *Organosilicon Materials: Handbook of Environmental Chemistry*; Hutzinger, O., Ed.; Springer: Berin, 1997; pp 181–223.
343. Powell, D. E.; Annelin, R. B.; Gallavan, R. H. *Environ. Sci. Technol.* **1999**, *33*, 3706–3710.
344. Heinen, W. In *Biochemisty of Silicon and Related Problems*; Plenum: New York, 1978; Vol. 40, pp 129–146.
345. Wallstrom, S.; Dernfalk, A. D.; Bengtsson, M.; Kroll, S.; Gubanski, S. M.; Karlsson, S. *Polym. Degrad. Stab.* **2005**, *88*, 394–400.
346. Gorur, R. S.; Bernstein, B. S. *IEEE Trans. Power Delivery* **1998**, *13*, 316–322.
347. Bengtsson, M.; Gronlund, R.; Sjoholm, M.; Abrahamsson, C.; Dernfalk, A. D.; Wallstrom, S.; Larsson, A.; Weibring, P.; Karlsson, S., Gubanski, S. M., *et al. Optics Lasers Eng.* **2005**, *43*, 624–632.
348. Wallstrom, S.; Karlsson, S. *Polym. Degrad. Stab.* **2004**, *2004*, 841–846.
349. Kovac, N.; Faganeli, J.; Bajt, O.; Sket, B.; Orel, B.; Penna, N. *Org. Geochem.* **2004**, *35*, 1095–1104.
350. Massoni, S. M.; Roy, S.; Grigoras, S. In *Organosilicon Materials: Handbook of Environmental Chemistry*; Hutzinger, O., Ed.; Springer: Berlin, 1997; pp 53–81.
351. Lehmann, R. G.; Miller, J. R. *Environ. Toxicol. Chem.* **1996**, *15*, 1455–1460.
352. Anderson, C.; Hochgeschwender, K.; Weidemann, H.; Wilmes, R. *Chemosphere* **1987**, *16*, 2567–2577.
353. Buch, R. R.; Lane, T. H.; Annelin, R. B.; Frye, C. L. *Environ. Toxicol. Chem.* **1984**, *3*, 215–222.
354. Chandra, G.; Maxim, L. D.; Sawano, T. In *Organosilicon Materials: Handbook of Environmental Chemistry*; Springer: Berlin, 1997; pp 295–319.
355. Sabourin, C. L.; Carpenter, J. C.; Leib, K.; Spivack, J. L. *Appl. Environ. Microbiol.* **1996**, *62*, 4352–4360.
356. Sabourin, C. L.; Carpenter, J. C.; Leib, K.; Spivack, J. L. *Environ. Toxicol. Chem.* **1999**, *18*, 1913–1919.
357. Lehmann, R. G.; Miller, J. R.; Kozerski, G. E. *Appl. Soil Ecol.* **2002**, *19*, 103–111.
358. Varaprath, S.; Salyers, K. L.; Plotzke, K. P.; Nanavati, S. *Anal. Biochem.* **1998**, *256*, 14–22.
359. Kala, S. V.; Lykissa, E. D.; Neely, M. W.; Lieberman, M. W. *Am. J. Pathol.* **1998**, *152*, 645–649.
360. Lieberman, M. W.; Lykissa, E. D.; Barrios, R.; Ou, C. N.; Kala, G.; Kala, S. V. *Environ. Health Perspect.* **1999**, *107*, 161–165.
361. Flassbeck, D.; Pfleiderer, B.; Klemens, P.; Heumann, K. G.; Eltze, E.; Hirner, A. V. *Anal. Bioanal. Chem.* **2003**, *375*, 356–362.
362. Flassbeck, D.; Pfleiderer, B.; Gruemping, R.; Hirner, A. V. *Anal. Chem.* **2001**, *73*, 606–611.
363. Bar-Meir, E.; Eherenfeld, M.; Shoenfeld, Y. *Autoimmunity* **2003**, *36*, 193–197.
364. Brinton, L. A.; Lubin, J. H.; Burich, M. C.; Colton, T.; Brown, S. L.; Hoover, R. N. *Ann. Epidemiol.* **2001**, *11*, 248–256.
365. Anon, *Trace Elements in Human Nutrition and Human Health*; World Health Organisation: Geneva, 1996.
366. Craig, P. J.; Maher, W. A. Organoselenium Compounds in the Environment. In *Organometallic Compounds in the Environment*, 2nd ed.; Craig, P. J., Ed.; Wiley: Chichester, 2003; pp 391–398.
367. Hatfield, D. L. *Selenium: Its Molecular Biology and Role in Human Health*; Kluwer Academic Publishers: Boston, 2001.
368. Byard, J. L. *Arch. Biochem. and Biophys.* **1969**, *130*, 556–560.
369. Palmer, I. S.; Fischer, D. D.; Halverson, A. W.; Olson, O. E. *Biochem. Biophys. Acta* **1969**, *177*, 336–342.
370. Palmer, I. S.; Gunalus, R. P.; Halverson, A. W.; Olson, O. E. *Biochem. Biophys. Acta* **1970**, *208*, 260–266.
371. Francesconi, K. A.; Pannier, F. *Clin. Chem.* **2004**, *50*, 2240–2253.

372. Itoh, M.; Suzuki, K. T. *Arch. Toxicol.* **1997**, *71*, 461–466.
373. Suzuki, K. T. *Tohoku J. Exp. Med.* **1996**, *178*, 27–35.
374. Suzuki, K. T.; Itoh, M.; Ohmichi, M. *Toxicology* **1995**, *103*, 157–165.
375. Shiobara, Y.; Ogra, Y.; Suzuki, K. T. *Analyst* **1999**, *124*, 1237–1241.
376. Kobayashi, Y.; Ogra, Y.; Ishiwata, K.; Takayama, H.; Aimi, N.; Suzuki, K. T. *Proc. Natl. Acad. Sci. USA* **2002**, *99*, 15932–15936.
377. Gammelgaard, B.; Madsen, K. G.; Bjerrum, J.; Bendahl, L.; Jons, O.; Olsen, J.; Sidenius, U. *J. Anal. At. Spectrom.* **2003**, *18*, 65–70.
378. Bendahl, L.; Gammelgaard, B. *J. Anal. At. Spectrom.* **2004**, *19*, 950–957.
379. Gammelgaard, B.; Bendahl, L. *J. Anal. At. Spectrom.* **2004**, *19*, 135–142.
380. Diaz Huerta, V.; Szpunar, J.; Lobinski, R.; Fernandez Sanchez, M. L.; Sanz Medel, A. *J. Anal. At. Spectrom.* **2003**, *18*, 1471–1476.
381. Kuehnelt, D.; Kienzl, N.; Traar, P.; Hoang Le, N.; Francesconi, K. A.; Ochi, T. *Anal. Bioanal. Chem.* **2005**, *383*, 235–246.
382. Rayman, M. P. *Br. J. Nutr.* **2004**, *92*, 557–573.
383. Gammelgaard, B.; Bendahl, L.; Jacobsen, N. W.; Sturup, S. *J. Anal. At. Spectrom.* **2005**, *20*, 889–893.
384. Gammelgaard, B.; Jessen, K. D.; Kristensen, F. H.; Jons, O. *Anal. Chim. Acta* **2000**, *404*, 47–54.
385. Zeisel, S. H.; Ellis, A. L.; Sun, X. F.; Pomfret, E. A.; Ting, B. T. G.; Janghorbani, M. *Am. Inst. Nutr.* **1987**, *117*, 1609–1614.
386. Suzuki, K. T.; Kurasaki, K.; Okazaki, N.; Ogra, Y. *Toxicol. Appl. Pharmacol.* **2005**, *206*, 1–8.
387. Cao, T. H.; Cooney, R. A.; Woznichak, M. M.; May, S. W.; Browner, R. F. *Anal. Chem.* **2001**, *73*, 2898–2902.
388. Olson, O. E. *J. Am. Coll. Toxicol.* **1986**, *5*, 45–70.
389. Ragsdale, S. W.; Kumar, M.; Zhao, S.; Menon, S.; Seravalli, J.; Doukov, T. In *Vitamin B_{12} and B_{12}-Proteins*; Kraeuteer, B., Arigoni, A., Golding, B. T., Eds.; Wiley-VCH: Weinheim, 1999; pp 167–177.
390. Berkessel, A. In *Bioinorganic Chemistry*; Trautwein, A. X., Ed.; Wiley-VCH: Weinheim, 1997; pp 431–445.
391. Pongratz, R.; Heumann, K. G. *Chemosphere* **1998**, *36*, 1935–1946.
392. Pongratz, R.; Heumann, K. G. *Chemosphere* **1999**, *39*, 89–102.
393. Pongratz, R.; Heumann, K. G. *Anal. Chem.* **1996**, *68*, 1262–1266.
394. Feldmann, J.; Krupp, E. M.; Glingemann, D.; Hirner, A. V.; Cullen, W. R. *Appl. Organomet. Chem.* **1999**, *13*, 739–748.
395. Panichev, N. A.; Diakov, A. O.; Kvitko, K. V. *Can. J. Anal. Sci. Spectrosc.* **1997**, *42*, 116–120.
396. Fatoki, O. S. *S. Afr. J. Sci.* **1997**, *93*, 366–370.
397. Weber, J. H. *Mar. Chem.* **1999**, *65*, 67–75.
398. Kim, J. P. *Sci. Total. Environ.* **1995**, *164*, 209–219.
399. Schedlbauer, O. F.; Heumann, K. G. *Anal. Chem.* **1999**, *71*, 5459–5464.
400. Schedlbauer, O. F.; Heumann, K. G. *Appl. Organomet. Chem.* **2000**, *14*, 330–340.
401. Craig, P. J.; Van Eltern, J. T. In *The Chemistry of Organic Germanium, Tin and Lead Compounds*; Patai, S., Ed.; Wiley: Chichester, 1995; pp 843–855.
402. Santosa, S. J.; Wada, S.; Mokudai, H.; Tanaka, S. *Appl. Organomet. Chem.* **1997**, *11*, 403–414.
403. Feldmann, J.; Cullen, W. R. *Environ. Sci. Technol.* **1997**, *31*, 2125–2129.
404. Michalke, K.; Meyer, J.; Hirner, A. V. *Appl. Organomet. Chem.* **2002**, *16*, 221–227.
405. Whanger, P. D. *J. Trace Elem. Exp. Med.* **1998**, *11*, 227–240.
406. Edmonds, J. S.; Morita, M. *Appl. Organomet. Chem.* **2000**, *14*, 133–145.
407. Wrobel, K.; Wrobel, K.; Caruso, J. A. *J. Anal. At. Spectrom.* **2002**, *17*, 1048–1054.
408. Basnayake, R. S. T.; Bius, J. H.; Akpolat, O. M.; Chasteen, T. G. *Appl. Organomet. Chem.* **2001**, *15*, 499–510.
409. Razak, A. A.; Ramadan, S. E.; Ragab, A. M.; Elmeleigy, M. A. *Afr. J. Mycol. Biotechnol.* **1994**, *2*, 17–24.
410. Hussain, N.; Ferdelman, T. G.; Church, T. M.; Luther, G. W., III. *Aquat. Geochem.* **1995**, *1*, 175–188.
411. Momoshima, N.; Song, L. X.; Osaki, S.; Maeda, S. *Environ. Sci. Technol.* **2001**, *35*, 2956–2960.
412. Killelea, D. R.; Aldstadt, J. H. *J. Chromatogr. A* **2001**, *918*, 169–175.
413. Ng, J. C.; Johnson, D.; Imray, P.; Chiswell, B.; Moore, M. R. *Analyst* **1998**, *123*, 929–933.
414. Chen, S.-S.; Chou, S.-S.; Hwang, D.-F. *J. Chromatogr. A* **2004**, *1024*, 209–215.
415. Qvarnstrom, J.; Lambertsson, L.; Havarinasab, S.; Hultman, P.; Frech, W. *Anal. Chem.* **2003**, *75*, 4120–4124.
416. Poperechna, N.; Heumann, K. G. *Anal. Chem.* **2005**, *77*, 511–516.
417. Heisterkamp, M.; Adams, F. C. *Fresenius J. Anal. Chem.* **1998**, *362*, 489–493.
418. Sanz-Landaluze, J.; Dietz, C.; Madrid, Y.; Camara, C. *Appl. Organomet. Chem.* **2004**, *18*, 606–613.
419. Uden, P. C.; Bird, S. M.; Kotrebai, M.; Nolibos, P.; Tyson, J. F.; Block, E.; Denoyer, E. *Fresenius J. Anal. Chem.* **1998**, *362*, 447–456.
420. Cai, Y.; Rapsomanikis, S.; Andreae, M. O. *Talanta* **1994**, *41*, 589–594.
421. Szpunar, J.; Schmitt, V. O.; Lobinski, R.; Monod, J. L. *J. Anal. At. Spectrom.* **1996**, *11*, 193–199.
422. Rodriguez-Gonzalez, P.; Encinar, J. R.; Alonso, J. I. G.; Sanz-Medel, A. *J. Anal. At. Spectrom.* **2004**, *19*, 685–691.
423. Rodriguez-Gonzalez, P.; Alonso, J. I. G.; Sanz-Medel, A. *J. Anal. At. Spectrom.* **2004**, *19*, 767–772.
424. Moens, L.; DeSmaele, T.; Dams, R.; VandenBroeck, P.; Sandra, P. *Anal. Chem.* **1997**, *69*, 1604–1611.
425. Monperrus, M.; Martin-Doimeadios, R. C. R.; Scancar, J.; Amouroux, D.; Donard, O. F. X. *Anal. Chem.* **2003**, *75*, 4095–4102.
426. McSheehy, S.; Szpunar, J.; Lobinski, R.; Haldys, V.; Tortajada, J.; Edmonds, J. S. *Anal. Chem.* **2002**, *74*, 2370–2378.
427. Le, X. C.; Lu, X. F.; Ma, M. S.; Cullen, W. R.; Aposhian, H. V.; Zheng, B. S. *Anal. Chem.* **2000**, *72*, 5172–5177.
428. Falter, R.; Scholer, H. F. *Fresenius J. Anal. Chem.* **1995**, *353*, 34–38.
429. Harrington, C. F.; Romeril, J.; Catterick, T. *Rapid Commun. Mass Spectrom.* **1998**, *12*, 911–916.
430. Mester, Z.; Lord, H.; Pawliszyn, J. *J. Anal. At. Spectrom.* **2000**, *15*, 595–600.
431. Brown, A. A.; Ebdon, L.; Hill, S. J. *Anal. Chim. Acta* **1994**, *286*, 391–399.
432. Ulrich, N. *Anal. Chim. Acta* **1998**, *359*, 245–253.
433. Krachler, M.; Emons, H. *Anal. Chim. Acta* **2001**, *429*, 125–133.
434. Kotrebai, M.; Tyson, J. F.; Block, E.; Uden, P. C. *J. Chromatogr. A* **2000**, *866*, 51–63.
435. Dorn, S. B.; Frame, E. M. S. *Analyst* **1994**, *119*, 1687–1694.
436. Carter, J.; Ebdon, L.; Evans, E. H. *Microchem. J.* **2004**, *76*, 35–41.
437. Chao, W.-S.; Jiang, S.-J. *J. Anal. At. Spectrom.* **1998**, *13*, 1337–1341.
438. White, S.; Catterick, T.; Fairman, B.; Webb, K. *J. Chromatogr. A* **1998**, *794*, 211–218.
439. Shum, S. C. K.; Pang, H. M.; Houk, R. S. *Anal. Chem.* **1992**, *64*, 2444–2450.

440. Gomez-Ariza, J. L.; Lorenzo, F.; Garcia-Barrera, T. *J. Chromatogr. A* **2004**, *1056*, 139–144.
441. Cai, Y.; Rapsomanikis, S.; Andreae, M. O. *J. Anal. At. Spectrom.* **1993**, *8*, 119–125.
442. Petrick, J. S.; Ayala-Fierro, F.; Cullen, W. R.; Carter, D. E.; Aposhian, H. V. *Toxicol. Appl. Pharmacol.* **2000**, *163*, 203–207.
443. Styblo, M.; Del Razo, L. M.; Vega, L.; Germolec, D. R.; LeCluyse, E. L.; Hamilton, G. A.; Reed, W.; Wang, C.; Cullen, W. R.; Thomas, D. J. *Arch. Toxicol.* **2000**, *74*, 289–299.
444. Sordo, M.; Herrera, L. A.; Ostrosky-Wegman, P.; Rojas, E. *Teratogenesis Carcinog. Mutagen.* **2001**, *21*, 249–260.
445. Mass, M. J.; Tennant, A.; Roop, B. C.; Cullen, W. R.; Styblo, M.; Thomas, D. J.; Kligerman, A. D., *Chem. Res. Toxicol.* **2001**, *14*, 355–361.
446. Moore, M. M.; HarringtonBrock, K.; Doerr, C. L. *Mutat. Res. Rev. Mutat. Res.* **1997**, *386*, 279–290.
447. OyaOhta, Y.; Kaise, T.; Ochi, T. *Mutat. Res. Fundam. Mol. Mech. Mutagen.* **1996**, *357*, 123–129.
448. Schwerdtle, T.; Walter, I.; Mackiw, I.; Hartwig, A. *Carcinogenesis* **2003**, *24*, 967–974.
449. Landolph, J. R. *Biol. Trace Elem. Res.* **1989**, *21*, 459–467.
450. Yamanaka, K.; Hayashi, H.; Tachikawa, M.; Kato, K.; Hasegawa, A.; Oku, N.; Okada, S. *Mutat. Res. Genet. Toxicol. Environ. Mutagen.* **1997**, *394*, 95–101.
451. Dopp, E.; Hartmann, L. M.; von Recklinghausen, U.; Florea, A. M.; Rabieh, S.; Zimmermann, U.; Shokouhi, B.; Yadav, S.; Hirner, A. V.; Rettenmeier, A. W. *Toxicol. Sci.* **2005**, *87*, 46–56.
452. Vega, L.; Styblo, M.; Patterson, R.; Cullen, W.; Wang, C. Q.; Germolec, D. *Toxicol. Appl. Pharmacol.* **2001**, *172*, 225–232.
453. Ochi, T.; Nakajima, F.; Sakurai, T.; Kaise, T.; OyaOhta, Y. *Arch. Toxicol.* **1996**, *70*, 815–821.
454. Namgung, U.; Xia, Z. G. *Toxicol. Appl. Pharmacol.* **2001**, *174*, 130–138.
455. Yamamoto, S.; Konishi, Y.; Matsuda, T.; Murai, T.; Shibata, M. A.; Matsuiyuasa, I.; Otani, S.; Kuroda, K.; Endo, G.; Fukushima, S. *Cancer Res.* **1995**, *55*, 1271–1276.
456. Huff, J.; Chan, P.; Nyska, A. *Toxicol. Sci.* **2000**, *55*, 17–23.
457. Kashiwada, E.; Kuroda, K.; Endo, G. *Mutat. Res. Genet. Toxicol. Environ. Mutagen.* **1998**, *413*, 33–38.
458. Kuroda, K.; Yoshida, K.; Yoshimura, M.; Endo, Y.; Wanibuchi, H.; Fukushima, S.; Endo, G. *Appl. Organomet. Chem.* **2005**, *19*, 221–225.
459. Sakurai, T.; Ochiai, M.; Kojima, C.; Ohta, T.; Fujiwara, K. *Appl. Organomet. Chem.* **2005**, *19*, 226–230.
460. Rawls, H. R.; Marshall, M. V.; Cardenas, H. L.; Bhagat, H. R.; Cabasso, I. *Dent. Mater.* **1992**, *8*, 54–59.
461. Arata, T.; Oyama, Y.; Tabaru, K.; Satoh, M.; Hayashi, H.; Ishida, S.; Okano, Y. *Environ. Toxicol.* **2002**, *17*, 472–477.
462. Shenker, B. J.; Guo, T. L.; Shapiro, I. M. *Environ. Res.* **1998**, *77*, 149–159.
463. Dufresne, J.; Cyr, D. G. *J. Androl.* **1999**, *20*, 769–778.
464. Yao, C. P.; Allen, J. W.; Aschner, M. Metallothioneins Attenuate Methylmercury-induced Neurotoxicity in Cultured Astrocytes and Astrocytoma Cells. In *Neuroprotective Agents: Fourth International Conference*; Trembly, B., Slikker, W., Jr., Eds.; New York, 1999; Vol. 890, pp 223–226.
465. Thompson, S. A.; Roellich, K. L.; Grossmann, A.; Gilbert, S. G.; Kavanagh, T. J. *Immunopharmacol. Immunotoxicol.* **1998**, *20*, 299–314.
466. Moszczynski, P.; Rutowski, J.; Slowinski, S.; Bem, S.; JakusStoga, D. *Arch. Med. Res.* **1996**, *27*, 503–507.
467. Moszczynski, P.; Rutowski, J.; Slowinski, S.; Bem, S. *Analyst* **1998**, *123*, 99–103.
468. Ahrendt, G.; Kohl, E. G. In *Trierer Berichte zur Abfallwirtschaft*; Rettenberger, G., Ed.; Economica Verlag: Bonn, 1996; Vol. 9, pp 9–20.
469. Ogura, H.; Takeuchi, T.; Morimoto, K. *Mutat. Res. Rev. Genet. Toxicol.* **1996**, *340*, 175–182.
470. Nishioku, T.; Takai, N.; Miyamoto, K.; Murao, K.; Hara, C.; Yamamoto, K.; Nakanishi, H. *Brain Res.* **2000**, *871*, 160–164.
471. Eto, K. *Neuropathology* **2000**, *20*, S14–S19.
472. Ehrenstein, C.; Shu, P.; Wickenheiser, E. B.; Hirner, A. V.; Dolfen, M.; Emons, H.; Obe, G. *Chem.-Biol. Interact.* **2002**, *141*, 259–274.
473. Castoldi, A. F.; Coccini, T.; Ceccatelli, S.; Manzo, L. *Brain Res. Bull.* **2001**, *55*, 197–203.
474. Ponce, R. A.; Kavanagh, T. J.; Mottet, N. K.; Whittaker, S. G.; Faustman, E. M. *Toxicol. Appl. Pharmacol.* **1994**, *127*, 83–90.
475. Ochi, T. *Toxicology* **2002**, *175*, 111–121.
476. Betti, C.; Barale, R.; Poolzobel, B. L. *Environ. Mol. Mutagen.* **1993**, *22*, 172–180.
477. Eskes, C.; Juillerat-Jeanneret, L.; Leuba, G.; Honegger, P.; Monnet-Tschudi, F. *J. Neurosci. Res.* **2003**, *71*, 583–590.
478. Sasaki, Y. F.; Yamada, H.; Sugiyama, C.; Kinae, N. *Mutat. Res.* **1993**, *300*, 5–14.
479. Ganguly, B. B. *Mutat. Res.* **1994**, *312*, 9–15.
480. Ghosh, B. B.; Talukder, G.; Sharma, A. *Mutat. Res.* **1990**, *245*, 33–39.
481. Ghosh, B. B.; Talukder, G.; Sharma, A. *Mech. Ageing. Dev.* **1991**, *57*, 125–137.
482. Whalen, M. M.; Loganathan, B. G.; Kannan, K. *Environ. Res.* **1999**, *81*, 108–116.
483. Boyer, I. J. *Toxicology* **1989**, *55*, 253–298.
484. Jensen, K. G.; Andersen, O.; Ronne, M. *Mutat. Res.* **1991**, *246*, 109–112.
485. Yamada, H.; Sasaki, Y. F. *Mutat. Res.* **1993**, *301*, 195–200.
486. Martin, P.; Ellersdorfer, E.; Zeman, A. *Korrespondenz Adwasser* **1996**, *43*, 1574–1580.
487. Schroder, H. F. Habilitation Thesis, Technische Hochschule, Aachen, 1997.
488. Wang, X. M.; Lee, S. C.; Sheng, G. Y.; Chan, L. Y.; Fu, J. M.; Li, X. D.; Min, Y. S.; Chan, C. Y. *Appl. Geochem.* **2001**, *16*, 1447–1454.
489. Pellenbarg, R. E. *Environ. Sci. Technol.* **1979**, *13*, 565–569.
490. Watanabe, N.; Nagase, H.; Ose, Y. *Sci. Total Environ.* **1988**, *73*, 1–9.
491. Siebert, F. PhD Dissertation, University of Heidelberg, 1988.
492. Pellenbarg, R. E. *Mar. Pollut. Bull.* **1982**, *13*, 427–429.

12.14
Polymer-supported Organometallic Catalysts

N E Leadbeater, University of Connecticut, Storrs, CT, USA

12.14.1 Introduction

Organometallic complexes find several uses in organic synthesis, affecting transformations that are otherwise not possible and offering highly selective ways to perform functional group interconversions. This is evidenced by the fact that three volumes of this edition have been dedicated to the applications of organometallics in organic synthesis. Metal-catalyzed reactions are performed daily on both small and large scales. Two particular issues facing organic chemists using organometallic complexes in their chemistry are the cost of preparation or purchase of the catalyst and

the removal of the metal from the product at the end of the reaction. This, coupled with recent interest in the development of environmentally benign synthesis, has evoked a renewed interest in developing immobilized metal catalysts and reagents for organic synthesis that maintain the high activity and selectivity of homogeneous analogs. The immobilization of transition metals on polystyrene (PS) supports offers a number of advantages over traditional solution-phase chemistry. In an ideal case, the supported complexes can be recovered from reaction mixtures by simple filtration, they do not contaminate the product solution, they can be recycled, and they can help increase selectivity. Immobilization on a support thereby enabling simple extraction and recyclability makes for commercial advantage as well as ease of manipulation. There are however a number of disadvantages including the fact that often there is metal leaching during the course of a reaction and they are often not recyclable. In addition, when considering asymmetric synthesis, the enantioselectivity of polymer-supported complexes can be less than that of the homogeneous analog. As a result, much recent work has been focused on developing and screening new ligand-derivitized supports for attachment of metals and on developing methods for increasing activity and selectivity.

The area of polymer-supported catalysis was reviewed in COMC (1982) by Pittman.[1] The field has expanded greatly since 1981 and it would take a whole volume of this new edition to cover all the material that has appeared in the literature since then. Therefore, in putting this chapter together the aim has been to discuss from an organometallic viewpoint the preparation of immobilized metal complexes with the objective of giving an insight into how chemists have gone about the task of attaching ligands and metal complexes that have shown great promise in homogeneous catalysis to supports. As shown, this is often a far from trivial exercise and the full synthetic tool kit is required. As well as grafting ligands onto prefabricated supports, the co-polymerization of suitably derivitized ligand precursors as a route to immobilized organometallics is also discussed. The scope of the chapter will be limited on the whole to ligands and their metal complexes attached to derivitized organic supports, as inorganic supports are discussed in Chapter 4 of this volume. Following a general introduction to the organic supports and methods used for immobilization of organometallic complexes, this chapter will focus on the preparation and use of supported phosphine, *N*-heterocyclic carbene, and metallocene-containing organometallics as these constitute the majority of the work published since the review by Pittman. Selected other examples of supported catalysts will be discussed in order to illustrate particular techniques that are used by chemists for immobilization of organometallic complexes.

There have been a range of books published on polymer-supported chemistry,[2–7] including many focused purely on supported catalysts and their applications.[8–10] For supported complexes reported before 1981, the reader is directed to the chapter by Pittman in COMC (1982)[1] as well as that by Bailey and Langer.[11] There are numerous reviews on the general area of supported catalysis and reagent chemistry[12–19] including a major review by Ley and co-workers[20] and a series of review articles published in 2002 on recoverable catalysts and reagents.[21] However, the majority of these have been focused particularly on the use of supported complexes rather than their preparation. Supported catalysts have also been used for rapid production of compound libraries.[22,23] Also, there has been an increase in reports presenting the use of combinatorial methods to discover new catalysts, as discussed in the reviews by Senkan,[24] Reetz,[25] and Bräse and Dahmen.[26]

Throughout this chapter, the convention of representing a polymer support by a shaded sphere is used when referring to a simple polystyrene backbone. For grafted supports derived from polystyrene, the same shaded sphere is used but the grafted fragment will be shown. For dendrimer-derived supports, a shaded star is used and the (n^{th}) generation of the dendrimer represented by the suffix G_n.

12.14.2 Polymer Supports for the Immobilization of Metal Complexes

12.14.2.1 Introduction

The concept of solid-phase synthesis has its roots in the peptide synthesis field with the work of Merrifield.[27] Since then, the wide adoption of combinatorial and parallel strategies for compound synthesis in the drug discovery process has led to the development of a wide range of solid supports.[28–31] In essence, there are two options a chemist can consider when contemplating immobilizing a chemical entity on a polymer support; namely to use a cross-linked (insoluble) or non-cross-linked (soluble) polymer. Both strategies have their advantages and disadvantages.[32–35] The general strategy when immobilizing a transition metal complex on a polymer support is to append it to a ligand which in turn is attached to the polymer backbone. Incorporation of a spacer group between the polymer and the ligand linker functionality is often performed in order to increase activity. The general structure is shown in Figure 1.

Figure 1

12.14.2.2 Insoluble Polymer Supports

The advantage of using an insoluble polymer support is the ease of extraction at the end of a reaction, a simple filtration being all that is needed. In addition, much of the literature so far has been focused around the use of insoluble supports. Indeed, insoluble resins functionalized with transition metal reagents and catalysts are also now appearing in chemical suppliers' catalogs. Disadvantages of using these types of material are that often access to functionalized sites can be limited and thus larger amounts of catalyst are required to effect the transformation. Also, leaching of the catalyst from the support can become a significant problem, especially when the metal is attached to the polymer via a monodentate ligand.

12.14.2.2.1 Polystyrene supports

The most used polymer support (resin) both for organic synthesis and for immobilization of catalysts is cross-linked polystyrene. Numerous types of polystyrene resin are commercially available and can be obtained in different sizes, loading capacities (level of functionalization), and degrees of cross-linking. This makes immobilization of organometallic complexes a reasonably simple operation since the metal complex bearing a suitably functionalized ligand can be attached directly to a commercially available polymer backbone or, if necessary, built up on the support.

Polystyrene (PS) resins are generally prepared by suspension polymerization of a mixture consisting of monomers, a radical initiator, and a cross-linking agent in water. The mixture is agitated by vigorous stirring in the presence of a polymeric surfactant, which governs the final size distribution of the polymer beads. For applications in catalysis, spherical particles, typically in the range of 50–500 μm, are ideal. In order to generate insoluble resins, a cross-linking agent has to be added. This is generally a bi- or multifunctional molecule that can be incorporated in two or more growing chains during the polymerization process, leading to interconnections in the polymer backbone. The most popular cross-linking agent is divinylbenzene (DVB) but more recently cross-linkers such as ethyleneglycol dimethylacrylate (EGDMA) have been used to give different solvation properties in the final polymer. It is important to have a good understanding of the internal structure and morphology of the final polymer support, since this strongly influences the physical properties and as a consequence the reactivity of the functional sites. If, for example, active sites are located in highly cross-linked microdomains, they will remain inaccessible for further chemistry.

Microporous resins contain a relatively small proportion of cross-linker and have an essentially homogeneous internal structure. This class of support is the most widely used for supporting metal complexes and is typically prepared from styrene co-polymerized with 1–2% DVB. The polystyrene prepared in this manner is functionalized by electrophilic aromatic substitution and the number of sites generated for further chemistry, called the loading value, is controlled by the yield of the initial substitution reaction. Typical loading values range between 0.2–4 mmol g^{-1}. A loading of 1.5 mmol g^{-1} corresponds to 20% of the aromatic groups on the polymer backbone being functionalized. For generation of higher-loading resins, chloromethylstyrene or bromomethylstyrene are often used as monomers in the polymerization process. This also has the advantage of generating an even distribution of functionalized sites on the final polymer matrix. When placed in an organic solvent, microporous polystyrene resins swell considerably. The extent of the swelling is controlled by the solvent used as well as the level of cross-linking in the polymer backbone. Clearly, since polystyrene is hydrophobic, the resins will not swell in polar protic solvents such as water or low molecular weight alcohols, or apolar aprotic solvents such as alkanes; solvents such as dioxane, dichloromethane, dmf, thf, or toluene must be used, thus limiting the chemistry. Also, care has to be taken when working with microporous resins. They are prone to osmotic shock—the rapid shrinking of a bead when it is placed from a good swelling solvent into a poor swelling solvent causing mechanical stress. Also, the beads can break if agitation is too vigorous and thus can only be stirred gently during the course of the reaction. The consequence of this is clogging of filters used during extraction of the beads at the end of a reaction. Generally, it is better to shake rather than stir reaction mixtures.

Macroporous polystyrene resins contain greater than 5% of a cross-linker and, as their name suggests, have a permanent porous structure even when dry. They are prepared by the suspension polymerization method but with the addition of a porogen, which is generally a low-boling solvent. They have a high surface area, typically ranging from 50–1000 $m^2 g^{-1}$. Macroporous resins show very little swelling in organic solvents due to the high level of cross-linking. While this does mean that they can be used in polar solvents such as water or alcohols, a drawback of the

highly heterogeneous structures is the low accessebility of solvents and reagents to the very highly cross-linked areas within the resin with the consequence that loading capacities are generally in the range of 0.8–1.0 mmol g^{-1}.

12.14.2.2.2 Polystyrene hybrid supports

One of the limitations of polystyrene supports is their poor swelling in polar solvents such as water. To overcome this, 1 or 2% cross-linked polystyrene resins can be modified by grafting poly(ethyleneglycol) (PEG) chains onto the polystyrene backbone. The incorporation of the PEG chains dramatically increases resin compatibility with polar solvents. Typically, their composition is 70 wt.% PEG grafts and 30 wt.%polystyrene. Therefore, the loading of these amphiphilic PEGylated resins (PS-PEG) is relatively low, ranging from 0.15–0.6 mmol g^{-1}. TentaGel and ArgoGel are two commercially available examples of these resins (Figure 2). PS-PEG hybrid resins also allow for on-bead screening of reactions but one drawback is their hygroscopic nature, originating from the PEG structure. This can be a problem if a moisture sensitive catalyst is immobilized.

12.14.2.3 Soluble Polymer Supports

Solid supports have a number of disadvantages associated with them, in particular, the effective heterogeneous reaction conditions, low loading capacities, low reactivity, and difficulty of analysis. These problems can be overcome using polymers that are soluble in the reaction medium or else form a biphasic mixture.[36–40] A wide range of functionalized organic polymers have been used successfully for this including poly(ethylene), poly(ethyleneglycol), poly(acrylate), poly(acrylamide) and block co-polymers of different organic materials. Representative examples of some soluble supports are shown in Figure 3.

Soluble supports feature homogeneous reaction conditions and enable the application of standard analytical techniques as well as the orthogonal use of insoluble reagents. They can either be linear polymers with functionalized end groups or else contain reactive groups along the polymer chain. However, in the case of the latter, their characteristics such as solubility and chemical stability, as well as their material properties can be problematic in some cases.[41] With the use of soluble polymers, however, comes another issue, namely efficient removal of the supported material at the end of the reaction. This has been overcome using techniques such as ultrafiltration, dialysis, precipitation, or liquid-phase separation. Of all these, perhaps the most used is precipitation and it works particularly well when the glass transition temperature of the polymer is above room temperature. The precipitation can be induced by adding a poor solvent to a solution of the support (e.g., ether or hexane to a PEG-based support or methanol to a poly(ethylene)-based support), by using polymers with temperature-dependent solubility (e.g., poly(ethylene) or poly(*N*-alkylacrylamides)), or by using polymers which precipitate upon change of the ionic strength of the solution.

A separation technique receiving increasing interest for use in polymer-supported chemistry is ultrafiltration, sometimes called nanofiltration.[42–44] To perform a separation by size, the polymer support needs to have a molecular weight between 5000 and 1000 and a narrow molecular weight distribution. Both ultrafiltration and dialysis involve using a membrane with a molecular weight cutoff, smaller-sized molecules passing through while larger ones remain behind. The same principle has been used in the so-called continuous membrane reactors. In this case, the membrane is used to retain a soluble polymer-bound catalytic species. Low molecular weight substrates are transformed continuously in the reactor and pure product can be collected beyond the membrane. These systems are very demanding on support and membrane, since, for efficient use, a retention of more than 99.9% has to be guaranteed.[33] In addition, even the best membranes cannot prevent metal leaching.

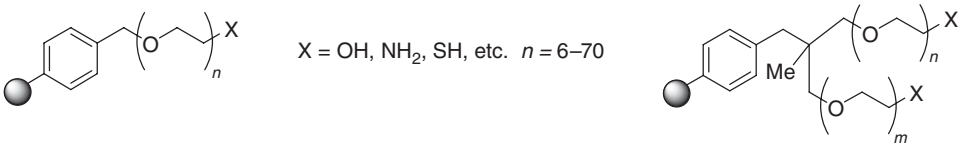

TentaGel ArgoGel

Figure 2

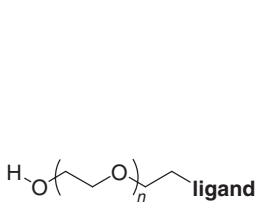

PEG-derived support

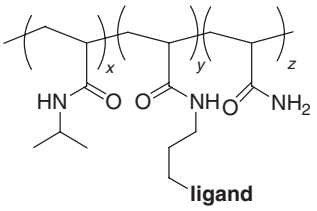

Poly(acrylate)-derived support

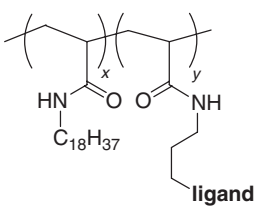

Poly(N-alkylacrylamide)-derived support

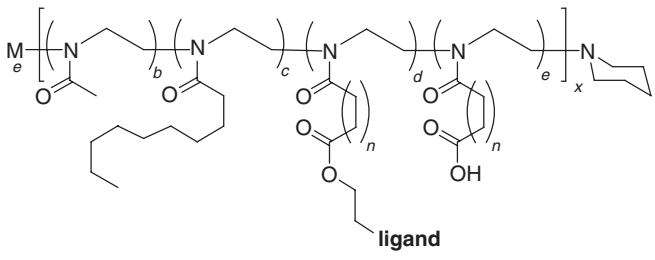

Poly(2-oxazoline)-derived block co-polymer

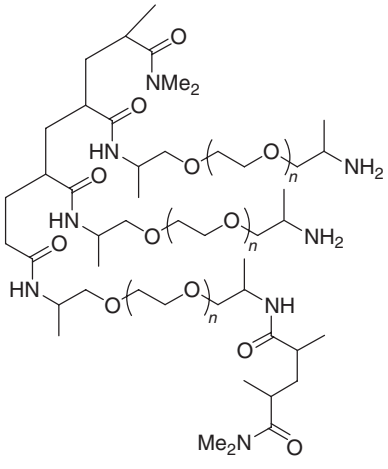

Commercially available amine-functionalized PEG-based support (PEGA-NH_2)

Figure 3

12.14.2.4 Dendrimers as Supports

Dendrimers are oligomeric, ordered, modularly built, tree-like structures and have been found to have a wide range of applications, one of which is as supports for metal catalysts.[42,45–51] Dendrimeric metal complexes can combine the advantages of both homogeneous and heterogeneous catalysts, namely a number of well-defined active sites as well as simple separation and reuse. The relative proximity of metal sites can be controlled by the nature and generation number of the dendrimer. Catalytically active metal complexes can be introduced into the core or the branches of dendrimer (Figure 4).

Dendrimers can be prepared using either a divergent or convergent approach. The former is more suited to the synthesis of supported metal complexes and is the most frequently used (Scheme 1). For higher-generation dendrimers however, incomplete conversion can be a problem as can purification of the materials. This can be partially overcome by building the dendrimer on an insoluble polymer support. In this case, it is possible to use an excess of reagents to drive the reaction to completion and also separation and purification is facilitated.

In core-functionalized dendrimers, metal loading is obviously very low. In higher-generation branched dendrimers, a high local concentration of the catalyst exists and the framework may be used to enforce and control cooperative interactions between individual metal sites and therefore increase activity and/or selectivity. This so-called positive dendritic effect has been observed by several groups.[52–56] But there are also examples where site–site interactions or steric crowding are believed to be responsible for catalyst deactivation.[57,58] In these cases, where a negative dendritic effect is observed, it would be better to use lower-loading polymers with isolated sites. An increasing number of dendrimer-based supported metal complexes are being reported that are heterogeneous by design.[59] Most have been prepared on dendritic templates grown stepwise on insoluble organic or inorganic supports and frequently demonstrate positive dendritic effects in reactions such as hydroformylation, Pd-catalyzed C–C bond formations, oxidation, and enantioselective addition to aldehydes.

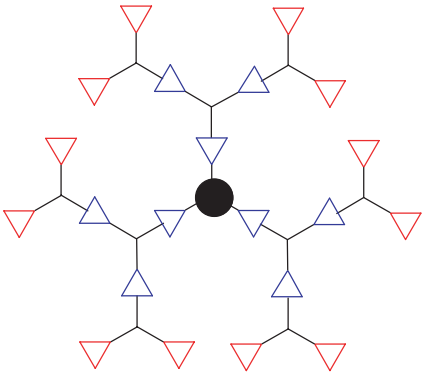

Core-functionalized dendrimer

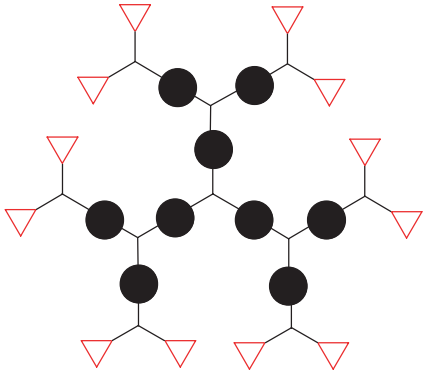

Interior branch-functionalized dendrimer

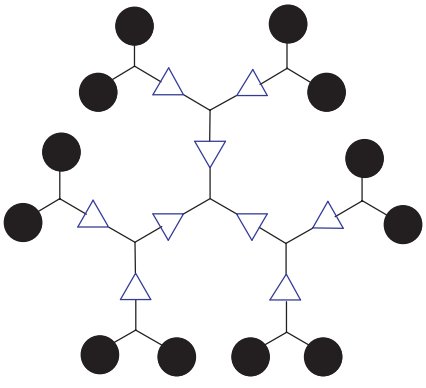

Periphery branch-functionalized dendrimer

Figure 4

12.14.2.5 Ring-opening Metathesis (ROM) Polymerization-derived Supports

ROM polymerization can be used in two distinct ways to prepare functionalized supports for catalysis.[60] Surface-grafted ROM polymers can be prepared on polystyrene or silica supports by polymerization of suitably functionalized norbornene monomers. There are two approaches for the elaboration of such grafted ROM polymers. It is possible first to grow living polymers by adding catalyst to the monomer in solution and then immobilizing them onto the support. Alternatively, the ROM catalyst is first immobilized onto the support and then monomer added, this starting the grafting process and building up the polymer. In a typical procedure, the solid support is reacted with 1% catalyst by weight and 10% monomer by weight. ROM can be used for the preparation of supports without a polystyrene or silica backbone simply by polymerizing functionalized monomers. The final materials can be made with or without cross-linking depending on the nature of the monomer. Using this method, it is possible to prepare materials with a high loading capacity that are either soluble, gel-like or insoluble in organic solvents.

An extension of this method has been to prepare monolithic systems.[61,62] Monoliths are single-body structures containing interconnected repeating cells or channels. Standard monolithic supports have been used mainly in liquid chromatography but, using ROM-based polymerization techniques, it is possible to prepare suitably functionalized materials for applications in catalysis. Monoliths have been prepared within the confines of columns by co-polymerization of norbornene and other monomers using ROM in the presence of a porogen (Scheme 2). Due to the living nature of the polymerization process, ligand-functionalized monomers can then be added thereby grafting onto the surface of the monolith. These are then treated with metal to give the desired monolithic catalysts with solely surface-bound catalytic sites. These materials are amenable to continuous-flow applications.

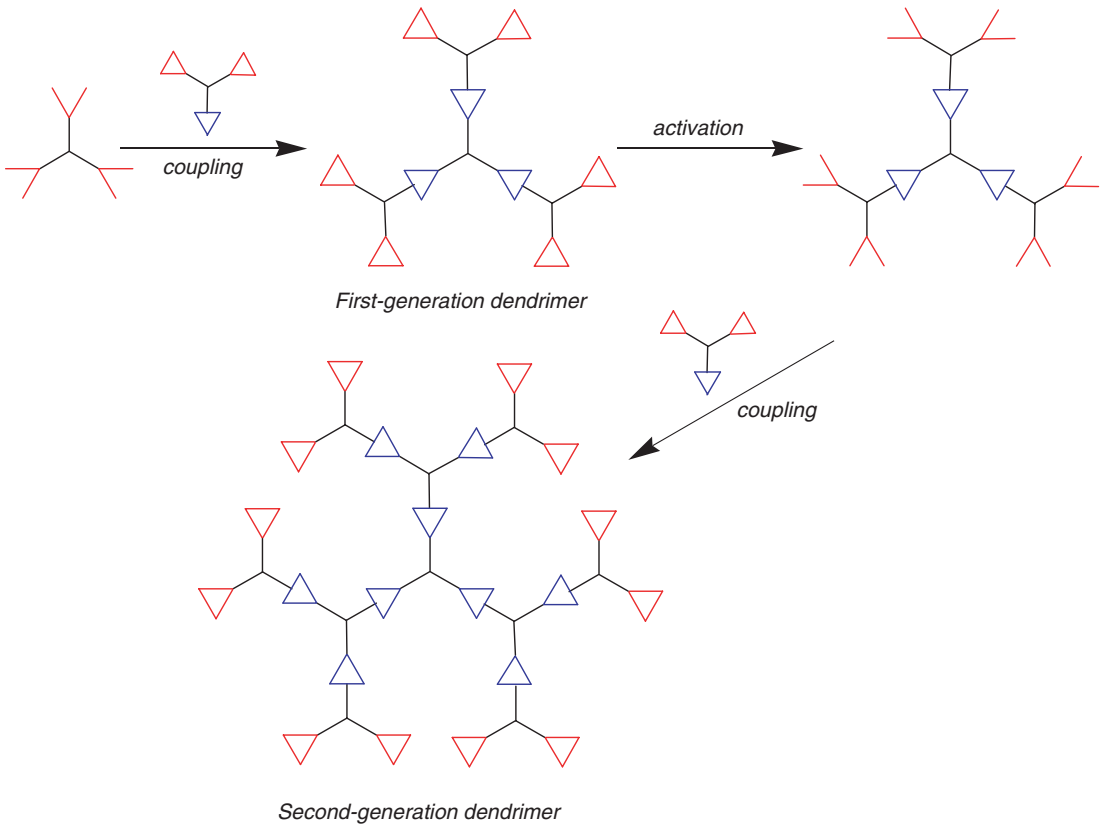

Scheme 1

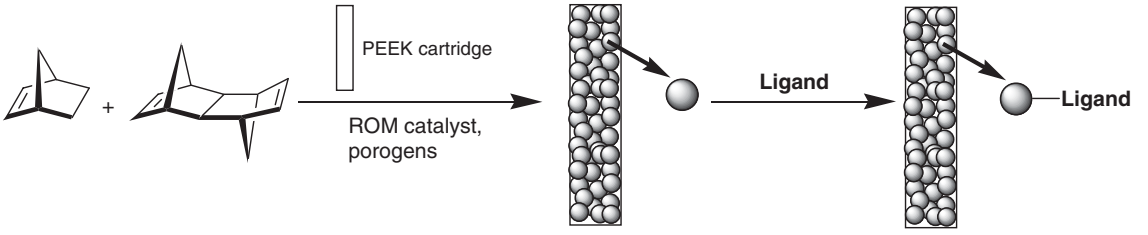

Scheme 2

12.14.2.6 Microencapsulation of Metal Complexes

Encapsulating or entrapping materials in a polymeric coating offers an alternative to covalently linked supported metal complexes.[63] A number of metal-containing microcapsules have been made using polystyrene as the encapsulating polymer and the procedure is operationally simple. The metal complex is added to a solution of polystyrene in cyclohexane. This mixture is then cooled to 0 °C while being stirred vigorously during which time microcapsules form. These are soft–walled, so a solvent such as hexane or methanol is added to harden them. Washing then leaves the microencapsulated metal complex ready for use. The procedure is shown in Scheme 3. Other encapsulation protocols have been developed including the use of interfacial polymerization[64] or a self-assembly process between non-cross-linked amphiphilic polymer ligands and a metal complex.[65]

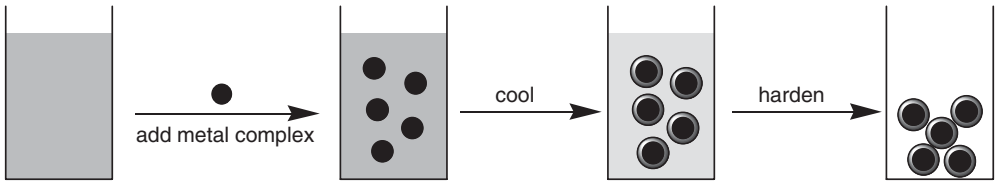

Scheme 3

12.14.3 Polymer-supported Metal Phosphine Complexes

12.14.3.1 Introduction

The number and diversity of transition metal phosphine complexes is vast and a wide range have been used as catalysts for synthetic organic transformations for many years. It therefore comes as little surprise that the preparation of polymer-supported metal phosphine complexes and assessment of their catalytic activity has attracted much attention. Supported phosphine ligands and their metal complexes prepared from 1981 to 2001 can be found in a review published in 2002.[66] Discussed here are examples in the literature from 1996 to the present together with a selected number of those from 1981 to 1996 where particularly notable synthetic methods have been used or where key points should be raised.

One of the simplest ways to prepare an insoluble supported phosphine ligand is the direct reaction of a simple functionalized polymer such as bromopolystyrene or Merrifield's resin with a derivative of the desired ligand.[67] This route has been used many times and is often still the preparative method of choice. The ready availability of polystyrene resins in a variety of cross-link densities, particle sizes and types permits investigation of these variables on catalytic performance. Simple ligands such as **1** are relatively easily prepared from bromopolystyrene by initial lithiation of the support to form lithiated polystyrene and then reaction with PPh_2Cl. There are however disadvantages with the lithiation approach. Treatment of cross-linked polystyrene or bromopolystyrene with butyllithium can often lead to unwanted side-reactions such as attack on the C═C bonds of the DVB cross-linking. As a result, often the product resin formed becomes contaminated and has poor swelling properties. An alternative way to introduce phosphines is by reacting brominated or chloromethylated resins with $LiPR_2$ or KPR_2. This offers a useful route for the preparation of a wide range of polymer-supported phosphines and is the more common method for attachment of simple monodentate phosphines to polymer supports. Attachment of metals to a phosphine derivitized polymer support is often achieved by one of the two methods, namely via a phosphine substitution reaction or by the direct formation of the phosphine complex by reaction with an organometallic precursor. These synthetic approaches are shown in Scheme 4.

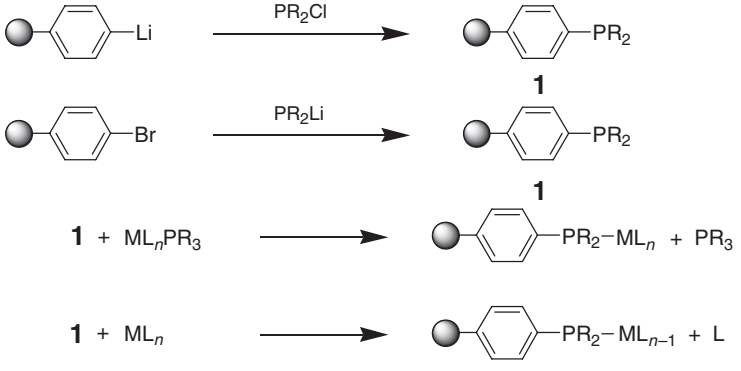

Scheme 4

12.14.3.2 Polymer-supported Triphenylphosphine

Polymer-supported triphenylphosphine (Ps-PPh_2) has attracted much attention as a ligand for immobilization of metal complexes, as it is the supported analog of the ubiquitous simple tertiary phosphine ligand PPh_3. Also, it is commercially available from a range of suppliers.

12.14.3.2.1 Complexes of palladium

The attachment of palladium complexes to organic polymer supports and their subsequent use in catalysis has been a topic of a considerable number of publications.[68] Two of the first reports of the preparation and use of the supported analog **2** of the well-known palladium complex $Pd(PPh_3)_4$ were presented in the 1970s by Pittman and co-workers[69] and Keinan and Trost.[70] They reported that heating a solution of the parent metal complex with PS-PPh_2 leads to **2** containing between 1.5% and 2% Pd (Scheme 5). Since then, **2** has found numerous applications in catalysis, in many cases with differing selectivity to the homogeneous analog. Although a number of uses of "polymer-supported $Pd(PPh_3)_4$" have been reported, care should be taken when considering them, due to the widely differing methods of preparation and lack of definitive characterization. For example, it has been used as a catalyst for the reaction of allylic acetate **3** with diethylamine to give the substitution product **4a** with net retention of stereochemistry (Scheme 6).[70] When using non-supported $Pd(PPh_3)_4$, a mixture of **4a** and its diastereomer **4b** is produced. The difference in selectivity has been attributed to the inability of the amine nucleophile to coordinate to the supported palladium complex, thus stopping a pathway that is known to lead to inversion of configuration.

Hallberg and co-workers[71] have prepared supported analogs of $PdCl_2(PPh_3)_2$ from PS-PPh_2 and $PdCl_2(PhCN)_2$ again by simple mixing of the two components (Scheme 7). They prepared supported complexes with Pd : P ratios of 1 : 1, 1 : 2, 1 : 3, and 1 : 4 and found that the bonding of the metal to the support changes with metal loading complex **5** being formed at low metal loading and **6** at higher metal loading. These complexes have been used in the Heck arylation with interesting results. When using aryl iodide substrates, the supported complexes with low PS-PPh_2 : Pd ratios were found to be most active whereas with the bromo analogs, the complexes with high PS-PPh_2 : Pd ratios were the best. In the case of the aryl bromides, the rate of reaction is significantly slower than when using homogeneous analogs, reaction times being days rather than hours.

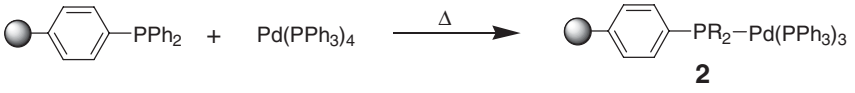

Scheme 5

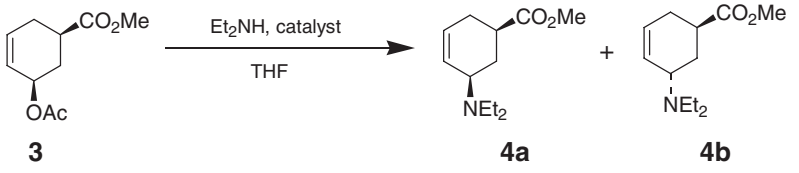

	Yield	
Catalyst	**4a**	**4b**
$Pd(PPh_3)_4$	67	33
2	100	0

Scheme 6

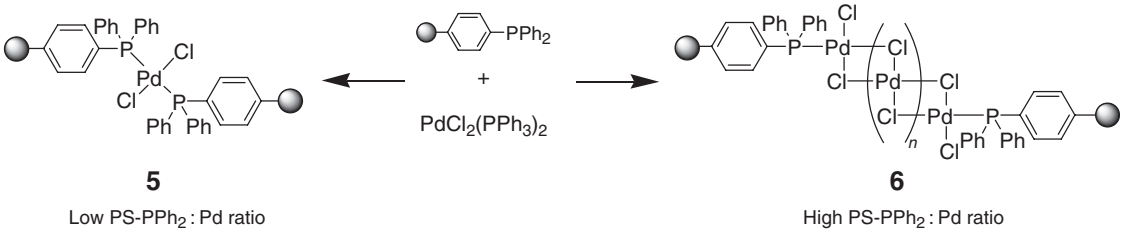

Scheme 7

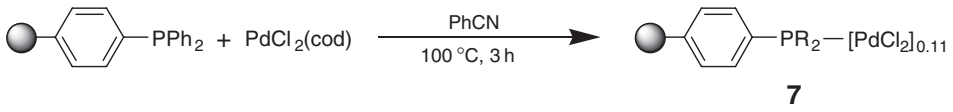

7

Scheme 8

A similar methodology was used in the preparation of **7**,[72] this complex being shown to be highly active in cross-coupling reactions involving chloropyridines and activated aryl chlorides (Scheme 8). The supported complex was prepared by stirring a mixture of PS-PPh_2 and $PdCl_2$(cod) [cod = 1,5-cyclooctadiene] in benzonitrile at 100 °C for 3 h. Elemental analysis showed a P : Pd ratio of 11 : 1.

Other workers[73,74] have used mixtures of PS-PPh_2 and palladium salts to prepare supported Pd phosphine complexes for use in cross-coupling reactions but these have been used directly as cross-coupling catalysts and the supported palladium complex not characterized. None of these show the activity of **7**, the reports only showing couplings with aryl bromides and iodides. One recent report was by Jang,[75,76] who prepared a polymer-supported palladium phosphine complex by modification of previous procedures. By treating **5** with PPh_3 and hydrazine hydrate a green polymer-supported complex was formed but not characterized. It proved active as a catalyst in Suzuki reactions and also in the coupling of allylic alcohols with hypervalent iodonium salts. The supported complex has a P : Pd ratio of 3.9 to 1 and some later reports suggest that it is in fact **2** but this should not be assumed, particularly as **2** is deep red in colour. This highlights the fact that it is very important to determine the nature of a supported complex as this is essential to understanding its use in catalysis and for developing further synthetic applications. Pitter and co-workers[77] have studied the co-oligomerization of 1,3-butadiene and CO_2 using a supported palladium complex prepared *in situ* from PS-PPh_2 and Pd(η^5-C_5H_5)(η^3-C_3H_5) by reaction in acetonitrile.

One of the problems with preparing polymer-supported phosphines from simple polystyrene precursors such as bromopolystyrene or lithiated polystyrene is that often only modest levels of phosphine loadings are possible. Building on a methodology for the preparation of resins containing poly amino acid chains,[78] a method has been developed for the multiplication of the level of phosphine functionalizstion on a solid support through the use of *N*-carboxyanhydride (NCA) derivatives of amino acids (Scheme 9).[79] With an amine initiator, NCA derivatives of amino acids oligomerize in a stepwise manner. Using leucine-NCA, ε-^{t}Boc-protected lysine-NCA, and TentaGel®-NH_2, an amine derivitized PEG/PS graft co-polymer, peptide derivative **8**, was formed. Although the exact degree of polymerization could not be determined, the authors suggest an approximate fourfold increase in the number of amine functionalities. Deprotection of the ^{t}Boc-protected amine functionalities in **8** with TFA to form **9** followed by functionalization of all the amine groups with *p*-diphenylphosphinobenzoic acid (DPPBA) using EDCl and HOBt

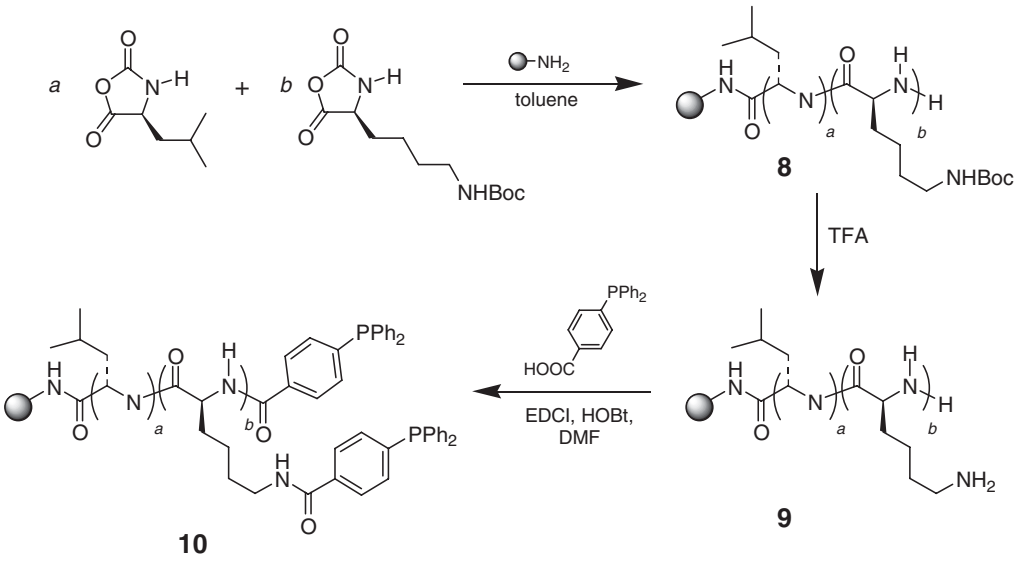

Scheme 9

gives supported phosphine **10**. A combination of IR spectroscopic data on **8** and ^{31}P NMR data on **10** suggests that the composition of the co-polymer is statistically distributed in a ratio corresponding to that of the NCAs used and that phosphine derivitization is almost quantitative. When only the leucine-NCA is used in the polymerization step, the phosphorus content of the resin after treatment with DPPBA is low due to the fact that only the terminal nitrogen is available for amide formation. The phosphine loading then increases with inclusion of lysine-NCA in the polymerization step but when only lysine-NCA is used not all the amine groups of the resultant polymer are functionalized on treatment with DPPBA, this being attributed to steric hindrance around the active sites. The potential use of the phosphines as ligands for catalysis was assessed by screening palladium allyl complexes, prepared *in situ* by treatment of the supported ligand with $[PdCl(CH_2CHCH_2)]_2$, for the addition of dimethyl malonate to an allylic acetate. The homolysine polymer gave the best result in terms of reaction time and product yield but this, and all the other polymers screened, did not show any notable asymmetric induction. This is at first surprising considering that the incorporation of metals into an enantiomerically pure peptide chain is known to be capable of generating a reagent with the capacity to control absolute stereochemistry in certain reactions. However, the authors suggest that the phosphine-functionalized side chains in the polymers prepared are somewhat distant from the chiral centers in the chain and perhaps too far for any chiral induction to be possible.

Another way of increasing loading on an insoluble support is to generate a functionalized dendrimer on a solid matrix. This strategy has been used in the preparation of dendronized polymer resins $\mathbf{15G_1}$, $\mathbf{15G_2}$, and $\mathbf{15G_3}$ (Scheme 10).[3] Starting from a hydroxymethyl-derivatized polystyrene support, the functionalization took the format of treatment with dimethyl 5-hydroxyisophthalate in a Mitsunobu reaction followed by reduction to form the corresponding bis(benzyl)-alcohol. Each repetition of these two steps builds a further generation of the dendrimer. For the etherification steps, product purity problems arose when the standard diethylazodicarboxylate (DEAD) was used as a coupling agent. Much better results were obtained using a triphenylphosphine-sulfonamide betaine. Once prepared, the supported dendrimer was treated with 4-(diphenylphosphino)benzoic acid to form the phosphine-functionalized analog, $\mathbf{16G_1}$. Reaction of this with $Pd_2(dba)_3$ yielded the immobilized palladium complex, $\mathbf{17G_1}$, analysis of which suggests that two phosphine moieties bind to one palladium center and one dba molecule remains coordinated to the metal.

Four supported complexes were then screened in the Heck reaction of bromobenzene with methyl acrylate: $\mathbf{17G_1}$, $\mathbf{17G_2}$, $\mathbf{17G_3}$, and one derived from the starting hydroxymethyl polystyrene support.[83] Two coupling products can be formed during the course of the reaction, namely the Heck product (methyl cinnamate) or biphenyl formed by homocoupling of bromobenzene. The authors found that the selectivity of the reaction improved significantly with increasing dendron generation with a 38 : 1 ratio of methyl cinnamate to biphenyl being observed with the **G3**-derived catalyst as compared to a 4.3 : 1 ratio with the **G1** analog. When analogous dendrimers based on a polythioether framework were screened in the Heck reaction, notably lower yields were obtained. This observation is, however, not surprising given the literature precident for inhibition of catalytic activity of metal complexes by low-valent sulphur compounds. (For examples, see Refs: 82,82a) What it does emphasize is the important impact of the dendritic architecture on catalytic activity of supported metal complexes.

A wide range of amphiphilic derivatives of PS-PPh_2 have been prepared by Uozumi and co-workers (Scheme 11).[83–86] Starting from an amine-functionalized poly(ethylene glycol)–polystyrene resin, supported phosphines (PS-PEG-PPh_2) **18** have been prepared with total conversion using 2- or 4-(diphenylphosphino) benzoic acid under standard conditions for solid-phase amide synthesis. Allylpalladium complexes of the PS-PEG-PPh_2 supports have been prepared by treatment of the supported phosphine with 0.5 equiv. of $[PdCl(\mu^3\text{-}C_3H_5)]_2$ in dichloromethane at room temperature for 10 min. Gel-phase ^{31}P NMR spectroscopy suggests the formation of the bis-phosphine complex **19**. By varying the stoichiometry, it is also possible to prepare the monophosphine complex **20**. The amphiphilic supported metal complexes have been screened for activity as catalysts in allylic substitution reactions using water as a solvent with considerable success.[83] Indeed, the yields of product were far greater than those obtained using homogeneous palladium complexes bearing water-soluble ligands. The supported complexes have also been used in water for the hydroxycarbonylation of aryl halides[86] as well as a range of Suzuki couplings.[85] Not surprisingly, on steric grounds, the supported complexes prepared from 2-(diphenylphosphino) benzoic acid were much less active than those prepared from the 4-substituted analog. The supported complexes have been shown to be recyclable without loss of activity.

Although soluble PEG-supported triarylphosphines have been developed for some time and used in organic transformations, such as the Mitsunobu esterification and the Staudinger reduction of azides,[87] it is only recently that they have been used as supported ligands for palladium complexes. A monomethyl polyethyleneglycol (MeOPEG) analog of triphenylphosphine has been prepared starting from iodophenol (Scheme 12).[88] The palladium-catalyzed treatment of this with PPh_2H followed by reaction with mesylated MeOPEG gives the desired product in good yield. For use in biphasic catalysis and efficient removal at the end of the reaction, the supported phosphine needs to be

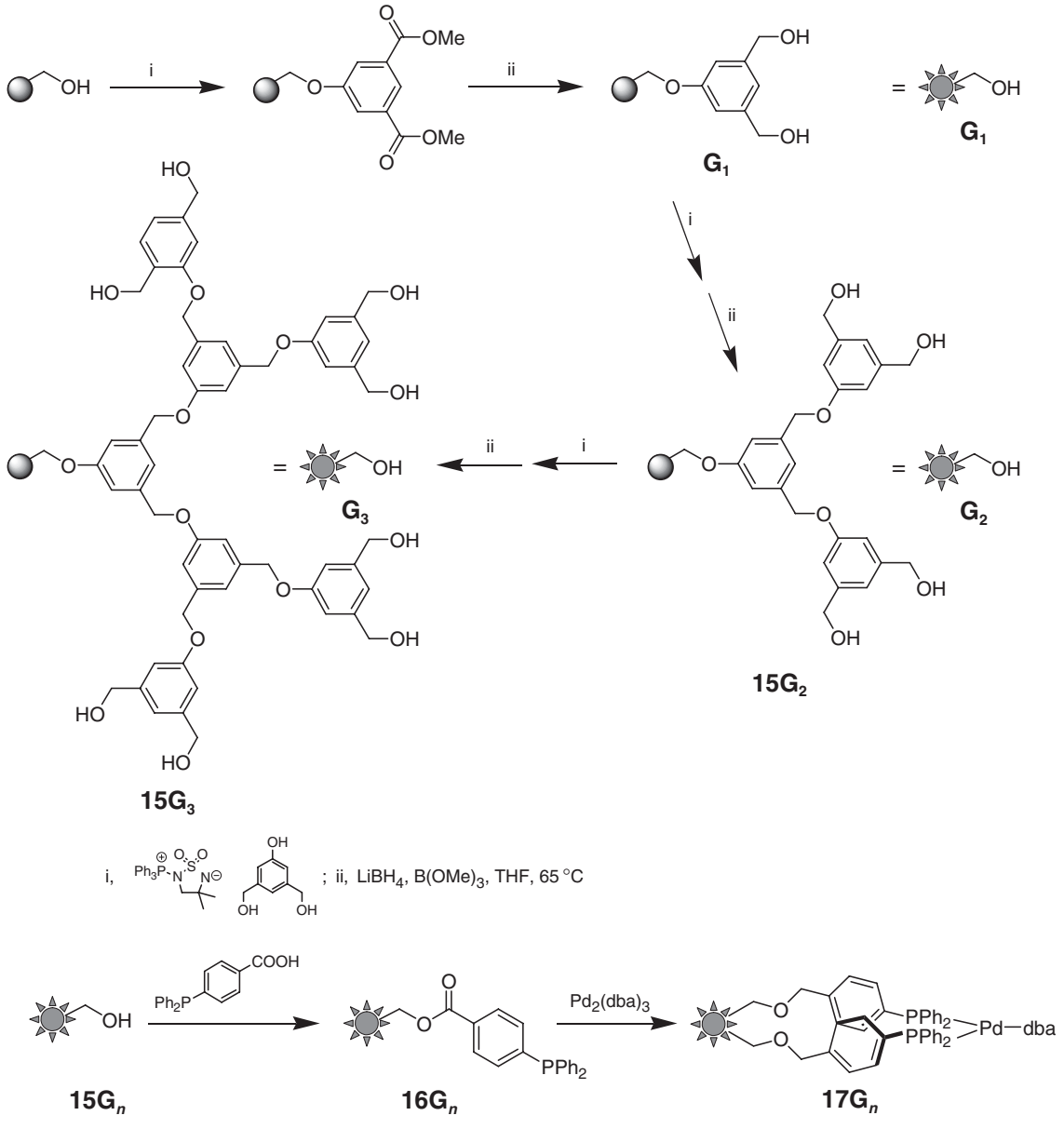

Scheme 10

soluble in binary and ternary solvent mixtures above the critical mixing temperature but insoluble in a component at room temperature. To this end, an MeOPEG starting material of molecular mass 2000 was found to be the best for use as the support since the phosphine formed from this was insoluble in heptane and thus organic products could be separated from the phosphine by using this hydrocarbon solvent as a component of the biphasic mixture. The supported phosphine was used as a ligand for biphasic Sonogashira couplings of aryl halides with acetylenes. The catalyst was formed *in situ* by the reaction of $(MeCN)_2PdCl_2$ with 2 equiv. of the MeOPEG-PPh_2 and the reactions run in a ternary solvent mixture of MeCN, heptane and triethylamine, the latter acting not only as a solvent but also as the base for the reaction. The reaction mixture was initially biphasic but once heated above 80 °C, becomes monophasic. At the end of the reaction, cooling to room temperature causes phase separation, the heptane layer containing the product while the ligated palladium complex remained in the acetonitrile/NEt_3 layer. Using this phosphine, the Sonogashira reaction works well for aryl iodides but not for the corresponding bromides.

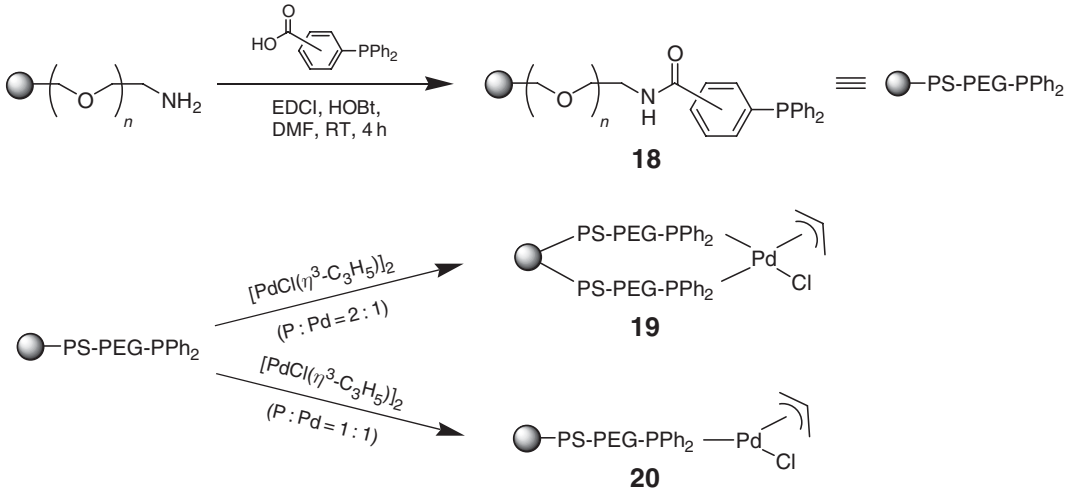

Scheme 11

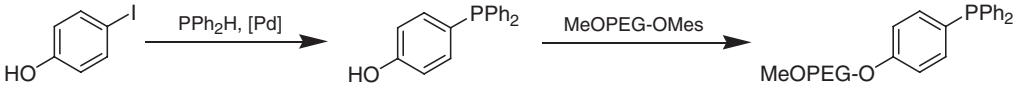

Scheme 12

A plug-shaped polymer support bearing a palladium phosphine complex has been prepared (Scheme 13).[89] The basic concept of the plug methodology is to sinter polymer supports such as functionalized polystyrene or PEG-PS with an inert polymer matrix, in this case, ultra-high-molecular weight polyethylene.[90] A 1 : 1 mixture of Merrifield's resin and the polyethylene were loaded into PTFE-lined cylindrical moulds and then passed through a sintering oven, the temperature being raised to a point where the polyolefin matrix begins to soften. Cooling and removal from the moulds leaves the plugs. The size chosen was 9 mm long and 7.5 mm diameter. Starting with Merrifield's resin of loading 0.96 mmol g^{-1}, the plugs have a loading of 81.6 μmol g^{-1}. The plugs are porous to solvent and, in essence, can act as microreactors. To prepare the plug-bound palladium complex, the Merrifield-derived plug was treated with $LiPPh_2$ followed by 24 h reflux with $Pd(PPh_3)_4$ in benzene. Neither the metal loading nor the exact nature of the palladium complex is reported, except that the plug is black at the end of the preparation step. The plugs were used for the preparation of a Suzuki reaction-based library and for the removal of allyl protecting groups. They could be easily recycled with reportedly minimal loss of activity.

Palladium complexes such as $Pd(OAc)_2$, $Pd_2(dba)_3$, $Pd(MeCN)_2Cl_2$, and $Pd(PhCN)_2Cl_2$ have been immobilized on to phosphine-derivatized polyethylene-based supports, the products being named FibreCat catalysts (Figure 5). For general information on FibreCats, see Refs: 91,91a,92. The complexes, with the exception of FC-Pd(dba), have a 1 : 1 Pd/supported ligand ratio as evidenced by the 0.5–0.6 mmol Pd g^{-1} FibreCat loading observed. For FC-Pd(dba), a loading of only 0.25–0.3 mmol Pd g^{-1} FibreCat is found, this indicating a 1 : 2 Pd/supported ligand ratio. By using high-throughput screening methods, optimum conditions for Suzuki couplings using the FibreCat materials were developed. Also during the course of the screening, second-generation FibreCats were prepared and tested to show the ease by which they can be modified.

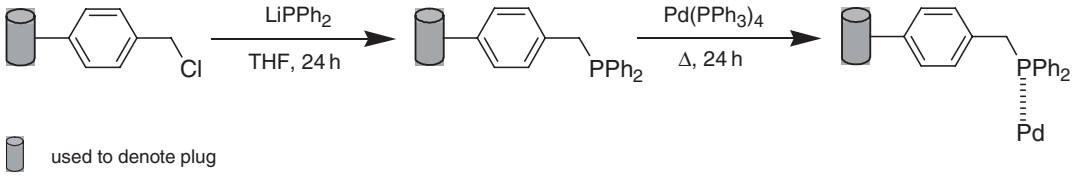

Scheme 13

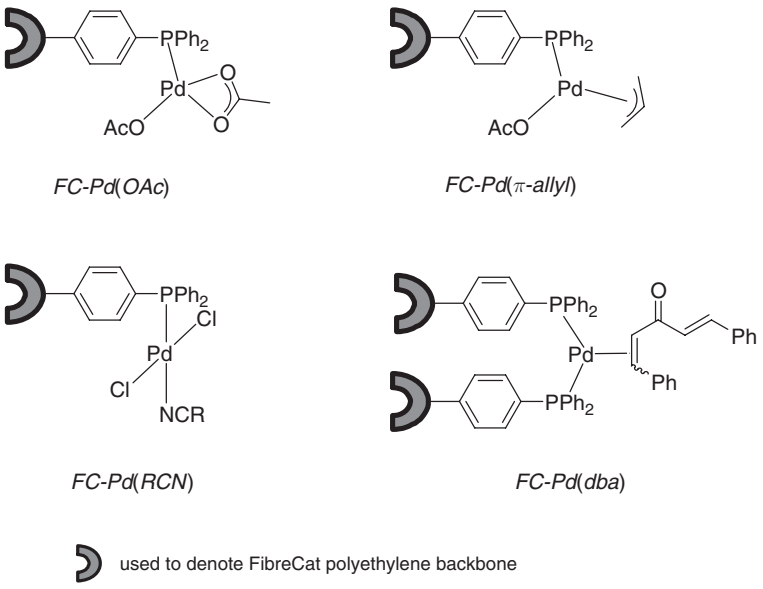

Figure 5

Functionalized hyperbranched polyethylene supports can be used as insoluble materials for applications in organic synthesis and catalysis by a grafting methodology.[93,94] High density polyethylene was firstly etched with chromic acid to oxidize the surface and hence functionalize the otherwise hydrocarbon material. This oxidation process yields approximately 0.01 mmol of acid groups per gram of polyethylene. The acid groups were next activated using $ClCO_2Et$ before treatment with a pre-prepared poly(*tert*-butylacrylate) oligomer (PTBA). The resultant *tert*-butyl esters were then converted to acids under non-aqueous conditions with methanesulfonic acid to give the polyacrylic acid (PAA) analog. The PTBA/hydrolysis procedure was then repeated a further four times to generate a polyethylene powder rich in surface functionalization ($\sim$0.3 mmol—$CO_2H\,g^{-1}$). To make an immobilized palladium complex on this support,[95] the derivatized polyethylene powder was once again treated with $ClCO_2Et$ and the resultant mixed anhydride then allowed to react with 3-diphenylphosphinopropylamine to produce a hyperbranched graft containing diphenylphosphinopropyl amides. Treatment of the resultant phosphinated powder with $Pd_2(dba)_3$ gave a material containing $\sim$0.04 mmol Pd g^{-1} polyethylene powder. The synthetic route to this material is shown in Scheme 14. The immobilized palladium complex was screened for catalytic activity in the Heck coupling but was inactive. However, it could be used in allylic substitution chemistry and was reusable. Less than 0.1% Pd leached off the support during the reaction.

A method has been developed that combines the advantages of solid-supported catalyst extraction and solution-phase reactivity.[96] By preparing a palladium complex bearing an anthracene tag, this can then be attached to a solid support via a chemoselective Diels–Alder cycloaddition to sequester the palladium catalyst along with any dissociated phosphine or phosphine oxide at the end of the reaction, leaving the desired catalysis product in the solution. The basis of the methodology is shown in Scheme 15.

A range of soluble phosphine-derivitized polyethylene supports have been prepared and used for the immobilization of palladium complexes.[97] The supports were prepared by anionic living polymerization of ethene with BuLi–TMEDA (tetramethylethylenediamine) followed by quenching of the resulting long-chained alkyllithiums with PPh_2Cl. Treatment with $Pd(PPh_3)_4$ at 100 °C in toluene produced the supported palladium complexes which, upon cooling, precipitate out of solution as yellow powders (Scheme 16). Interestingly, even when a 1 : 1 ratio of the polyethylenediphenylphosphine and $Pd(PPh_3)_4$ is used, all the palladium complex ends up on the support. This could be due to the greater σ-basisity of the polyethylenediphenylphosphine as compared to triphenylphosphine. Alternatively, interactions of the ethylene monomers or the precipitation process may favor the generation of polyethylene-bound complex. The materials have been used as catalysts for a range of synthetic transformations such as π-allylic substitution of allyl esters and was found to have almost identical activity to $Pd(PPh_3)_4$.

Poly(acrylamide) and poly(acrylate) supports have been prepared and used in organic synthesis and catalysis.[36] Water-soluble poly(*N*-isopropyl)acrylamide (PNIPAM) has been derivitized to prepare a supported phosphine onto

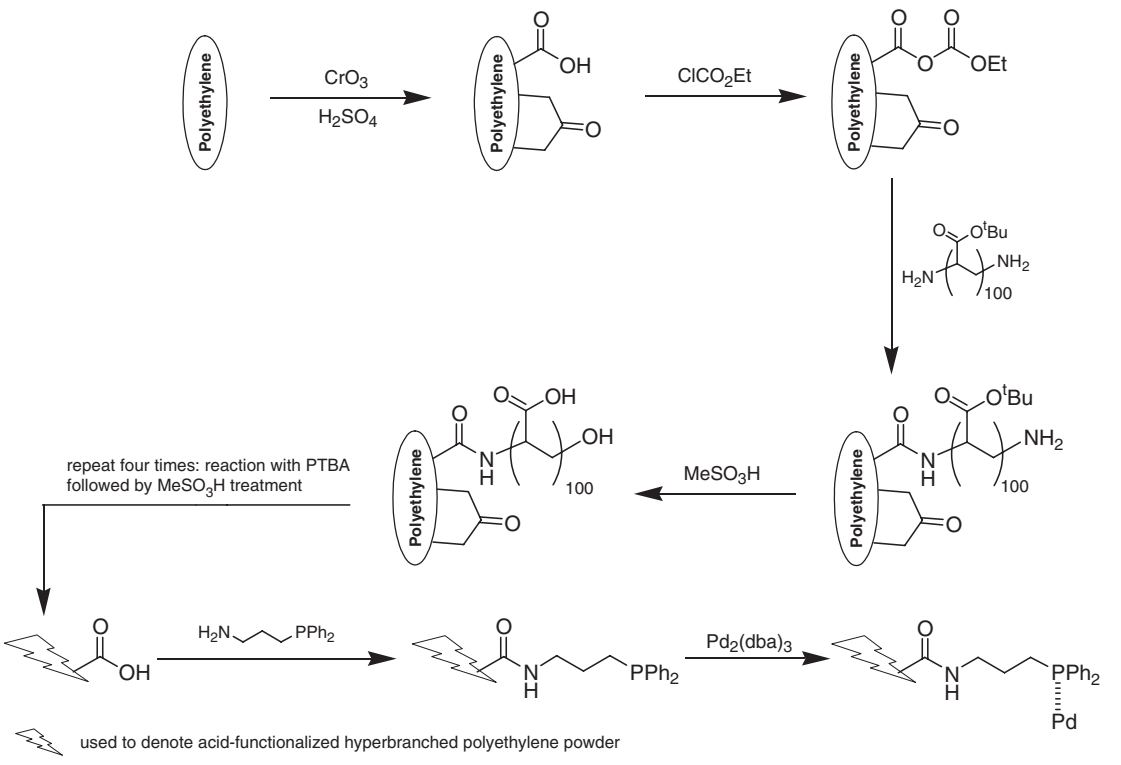

Scheme 14

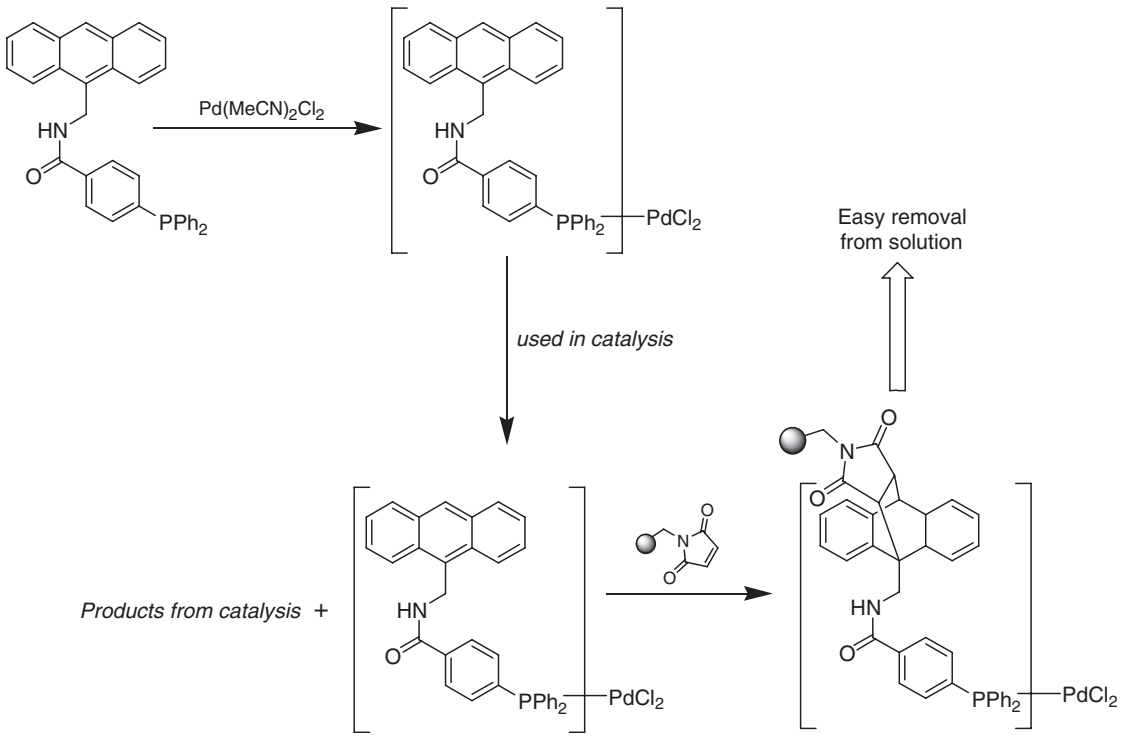

Scheme 15

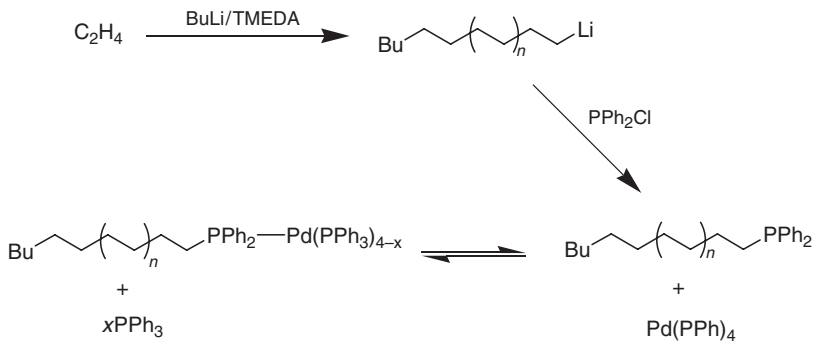

Scheme 16

which palladium can be attached (Scheme 17).[98,99] PNIPAM is prepared by the radical polymerization of *N*-isopropylacrylamide and *N*-(acryloyloxy)succinamide.[100] This can be easily phosphine functionalized by reaction with 3-diphenylphosphinopropylamine at room temperature. The polymer was palladated by treatment with $Pd_2(dba)_3$ to give a supported Pd(0) complex. This has been used as a catalyst for C–C bond-forming reactions both in aqueous and organic media. When using ethanol/heptane or dimethylacetamide/heptane biphasic mixtures as the solvent system, whereas a monophase is formed at elevated temperatures, the supported catalyst remains in the more polar organic solvent at the end of the reaction when the mixture is cooled back to room temperature.

Analogs of the phosphine-derivatized PNIPAM range of supports have been prepared bearing long alkyl[101] or fluoroalkyl[102–104] chains for use in non-polar organic or fluorous solvents, respectively, as shown in Figure 6.

Rather than introduce the phosphine functionality into a polymer by a chemical transformation, an alternative strategy is to polymerize phosphine-containing monomers with suitable co-monomers. Interestingly, some of the earliest reports of the preparation of polymer-bound phosphine reagents involved the radical co-polymerization[105] and homopolymerization[106] of 4-styryldiphenylphosphine **21**. Despite the apparent simplicity of these routes, they never became widely used. However, this and other direct strategies have received renewed attention recently. One reason for the early work not becoming popular may have been the issue of preparing useful quantities of **21**. More recently, a simple synthesis of **21** has been reported, based on the simple Grignard reaction of 4-bromostyrene using magnesium followed by treatment with PPh_2Cl.[107] With this in hand, they have prepared triphenylphosphine-containing polystyrene polymers with P loadings ranging from 0.1–3.2 mmol g^{-1} by radical polymerization of **21** and styrene either with or without addition of 1,4-bis(4-vinylphenoxy)-butane as a cross-linker, giving soluble and

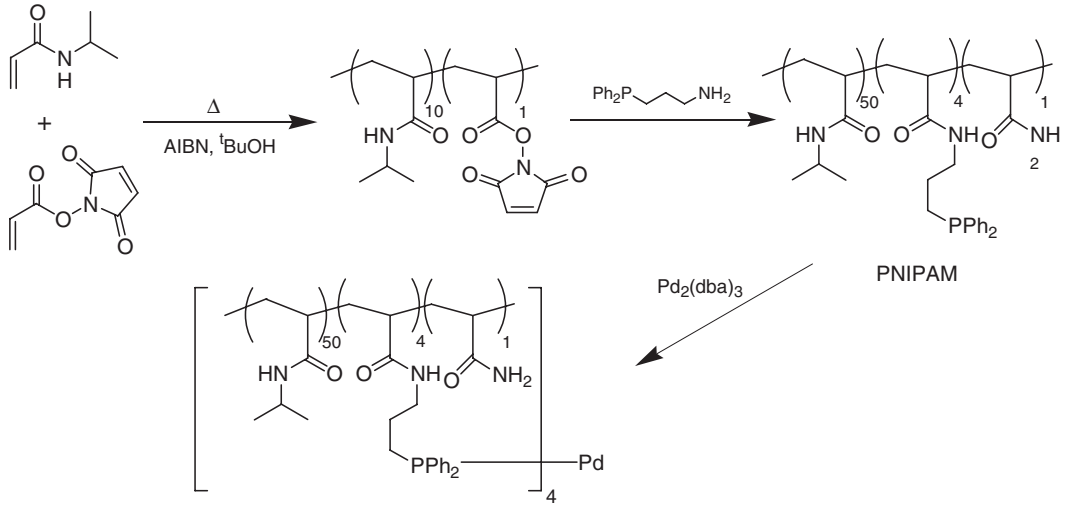

Scheme 17

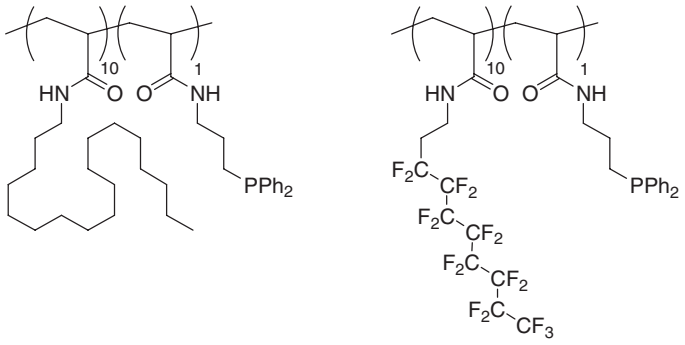

Figure 6

insoluble materials, respectively (Scheme 18). Using the same methodology, the corresponding arsine-derivatized supports have also been prepared.[108] This is noteworthy given that reports of supported triphenylarsine materials are few. For other examples, see Refs: 109,109a.

Phosphine-derivatised poly(4-*tert*-butylstyrene) has been prepared for use as a soluble support in homogeneous catalysis.[110] It was used in a monophasic medium and separation of the catalysts after reaction was effected either by cooling- or water-induced phase separation. The support was prepared by co-polymerisation of *tert*-butylstyrene with a phosphine oxide-containing styrene monomer (Scheme 19) A small quantity of a methyl red-labelled comonomer was also added to act as a colorometric tag to facilitate studies of the extent of separation and recycling of the polymeric material. The phosphine oxide was reduced to the free phosphine after the polymerisation step was complete.

ROM has been used to prepare phosphine-containing polymer supports (Scheme 20). Norbornyl-substituted monomer **22** was prepared in two steps from 4-bromo-iodobenzene.[111] This was then polymerized with diene **23**. It was initially envisioned that it would be necessary to convert the phosphine to the borane adduct in order not to poison the metathesis catalyst. Although protection was needed when using the Grubb's type 1 complex as a catalyst, when employing the more active second-generation complex **24**, the free phosphine monomer could be used. This has been attributed to the lower affinity of the active form of the catalyst toward coordination of phosphines due to the presence of the electron-rich heterocyclic carbene ligand.

Yang and Luh used ROM to prepare a further example of a norbornene-derived phosphine-substituted polymer.[112] Starting from 1,4-benzoquinone, monomer **25** was prepared in three steps. This was then polymerized at room

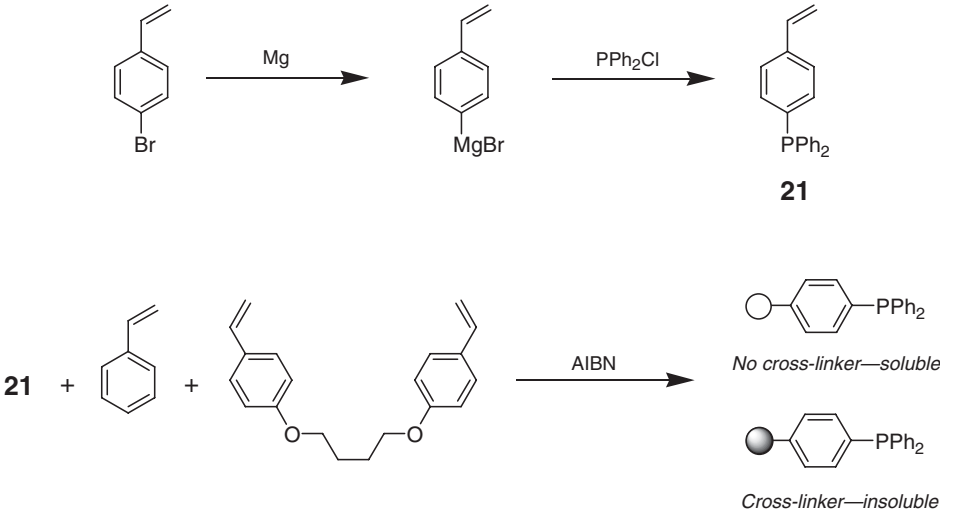

Scheme 18

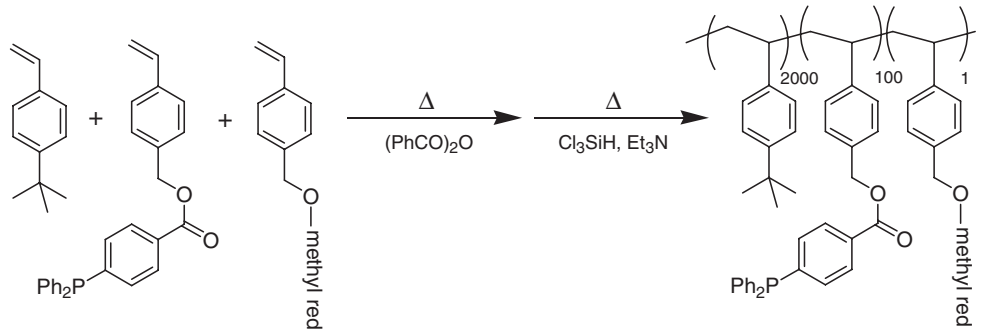

Scheme 19

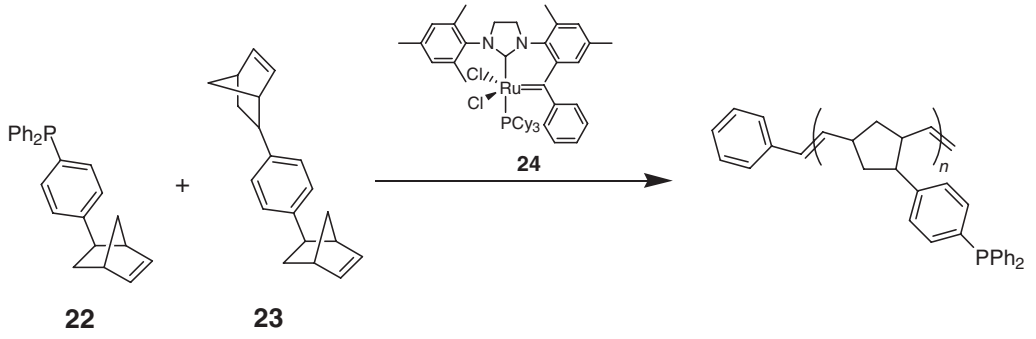

Scheme 20

temperature using **24** to give a material containing 4–6 repeating units and with a phosphine loading of ~2.8 mmol g^{-1} (Scheme 21). The polymer is soluble in moderately polar organic solvents such as thf, toluene, and dichloromethane but insoluble in hydrocarbons. In dmf, a thermomorphic behavior was observed, the polymer being soluble at elevated temperatures but insoluble at room temperature. This behavior was exploited in Heck and Sonogashira couplings using an *in situ* prepared palladium complex of the supported phosphine.

New hybrid inorganic–organic polymers bearing palladated phosphine groups have been prepared by radical polymerization of a functionalized cyclophosphazene monomer **27** with DVB (Scheme 22).[113,114] Monomer **27**, bearing multiple phosphine functionalities and a styryl group, was made from the reaction of $N_3P_3Cl_6$ **26** in three steps. Polymerization of **27** with DVB produced a cross-linked polymeric material which, when treated with $Pd(PhCN)_2Cl_2$, gave a material with a palladium loading of 1.8 mmol g^{-1}. The polymer was tested in the Heck reaction and found to be less active than the corresponding palladium complex made from monomer **27**. It was however recyclable and no significant palladium leaching was observed.

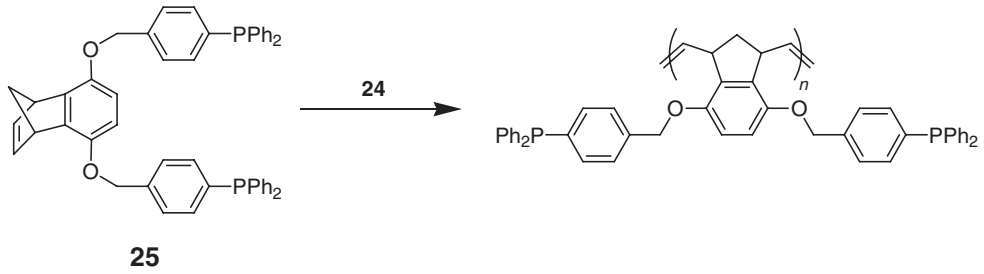

25

Scheme 21

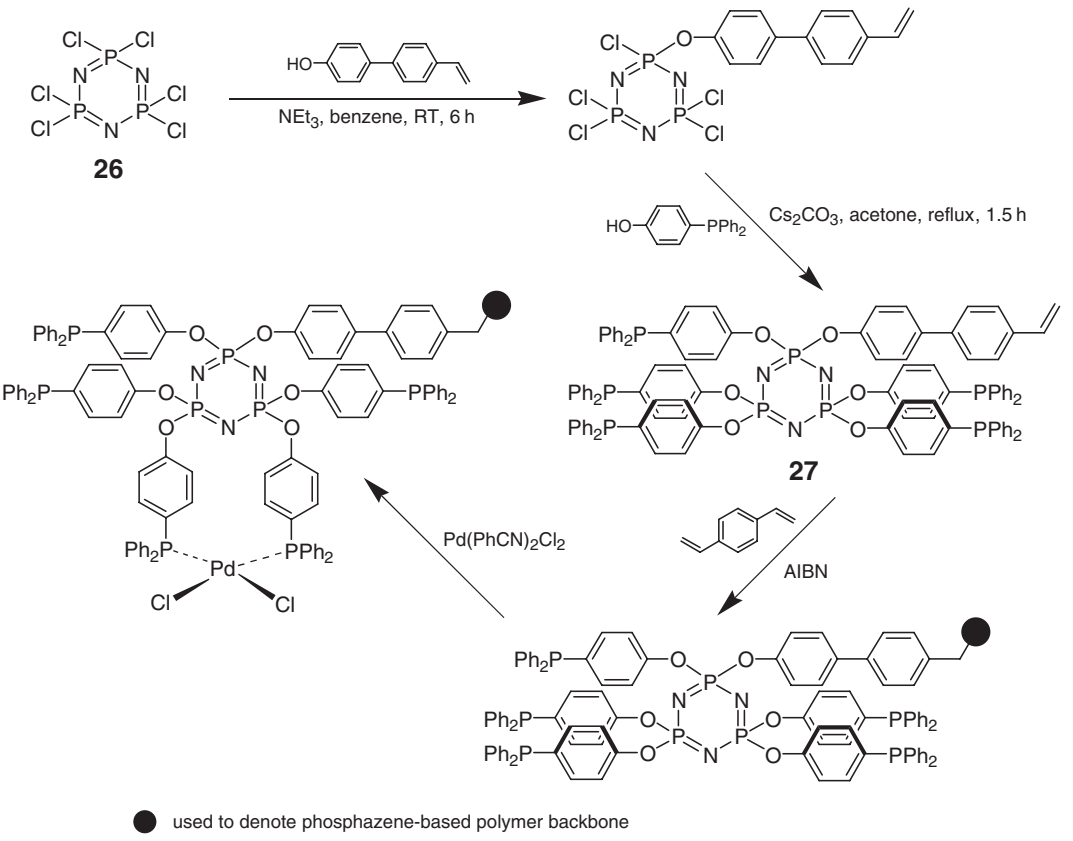

Scheme 22

12.14.3.2.2 Complexes of cobalt

The immobilized cobalt carbonyl complex $Co_2(CO)_6(PS\text{-}PPh_2)_2$ **30** has been prepared by Gibson and co-workers using $Co_2(CO)_8$ as a starting material and has been used as a catalyst for the Pauson–Khand reaction[115] and as a "traceless" alkyne linker[116] (Scheme 23).[117] Reaction of PS-PPh_2 (loading 1.6 mmol g^{-1}) with $Co_2(CO)_8$ in thf at room temperature generates a mixture of phosphine-substituted cobalt carbonyl complexes **28** and **29** with a metal loading of ~0.96 mmol [Co_2] g^{-1}. Heating this mixture to 75 °C in dioxane leads cleanly to the formation of **30** with a resultant metal loading of ~0.22 mmol [$Co_2(CO)_6$] g^{-1}. This can be prepared directly from PS-PPh_2 and $Co_2(CO)_8$ without isolation of **28** and **29** by performing the whole reaction in dioxane with a much higher resultant metal loading of ~0.42 mmol [$Co_2(CO)_6$] g^{-1}. Reaction of **28**, **29**, or **30** with an alkyne leads readily to the formation of polymer-supported alkyne complexes. These can alternatively be prepared indirectly by the reaction of the alkyne with $Co_2(CO)_8$ followed by coordination of the alkyne complex formed to PS-PPh_2. Chemistry can then be performed at a remote site on the alkyne unit before cleavage from the support in a traceless manner. When used as a catalyst for the intramolecular Pauson–Khand reaction, a reaction useful to medicinal chemists,[118] **30** shows better activity than the mixture of **28** and **29**.

Functionalized dendron polystyrene materials have been used as supports for a cobalt complex analogous to **30** and have been used in the Pauson–Khand reaction (Scheme 24).[119] Phosphine-derivatized supports were prepared by the reaction of **15G**$_1$, **15G**$_2$, and **15G**$_3$ with 2- or 4-(diphenylphosphino)benzoic acid giving two sets of ligands. Cobalt complexes were then prepared by incubation of the supports (one derived from Wang resin and one from each of the **G**$_1$, **G**$_2$, and **G**$_3$ dendrimers) with $Co_2(CO)_8$ in dioxane at 75 °C giving **31**. In the Pauson–Khand reaction studied, moving from **31G**$_1$ to **31G**$_3$ leads to an increase in conversion, product yield, and selectivity, particularly in the case of the supports derived from the 4-(diphenylphosphino)benzoic acid. This positive dendritic effect is attributed to two factors, namely the nature of the supported cobalt complex (bidentate vs. monodentate coordination) and the degree of cross-linking in the support. For non-dendronized materials, each cobalt dimer coordinated to two phosphines in essence provides an extra cross-linking connection whereas in the dendrimers, such coordination can be obtained

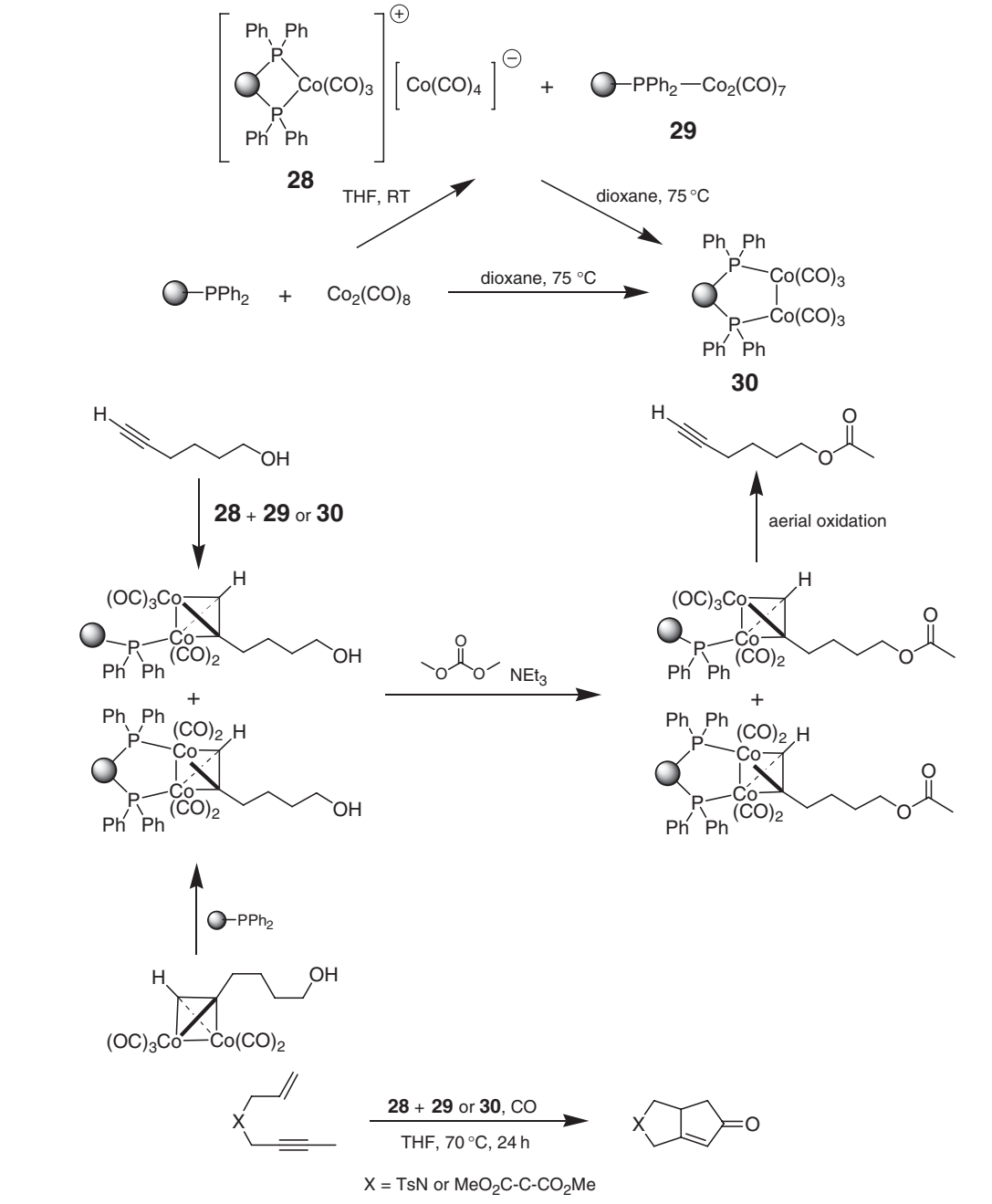

Scheme 23

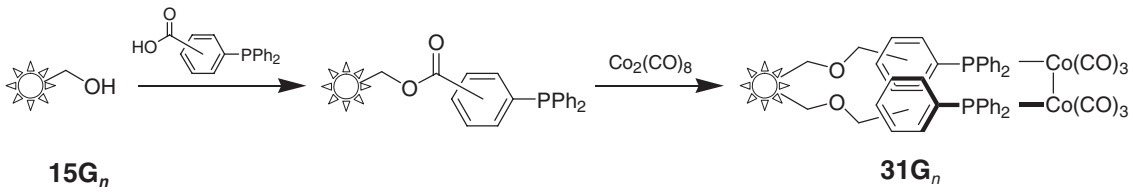

Scheme 24

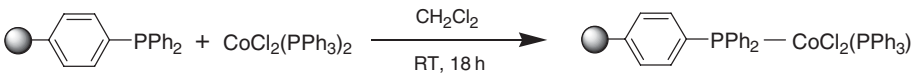

32

Scheme 25

without extra cross-linking. Since a higher level of cross-linking in a support limits the swelling of a resin, transport inside the pores of a non-dendronized support is going to be less than in the dendrimers. While the increased distance of the active site from the polymer matrix in the second- and third-generation dendritic complexes could contribute to the improved catalytic activity, the authors state that, when using resins where a non-branched spacer was used to imitate the distance between the phosphine moieties and the polystyrene core, the activity of their corresponding cobalt complexes was inferior to that of the dendronized materials.

Starting from PS-PPh_2, a supported cobalt phosphine complex has been prepared for use in alcohol oxidation.[120] The immobilized complex **32** was made by stirring a dichloromethane solution of $CoCl_2(PPh_3)_2$ with the functionalized support (Scheme 25). The polymer-bound complex formed is stable in air, no decomposition being noted over a period of 4 months at room temperature. In the presence of a catalytic amount of **32**, the efficient oxidation of benzylic alcohols using *t*-butyl hydroperoxide as oxidant can be performed. A point of interest is that, in the case of primary alcohol oxidation, whereas with $CoCl_2(PPh_3)_2$ equal yields of aldehyde and acid are observed, using the supported catalyst the acid formation is greatly reduced although not fully inhibited. This shows that the selectivity of a polymer-supported complex can be very different to that of its homogeneous analog.

12.14.3.2.3 Polymer-supported chromium–phosphine complexes

A number of reports of the synthesis of polymer-supported phosphine-linked chromium arene complexes have been prepared and their use both as linkers and as catalysts explored. Although not actually attaching the metal complex to a solid support, Semmelhack and co-workers[121] have undertaken an interesting study on the effects on the rate of nucleophilic substitution in fluoroarene–$Cr(CO)_2L$ complexes **34** of changing the ligand, L, with the specific aim of finding the best linker for the formation of polymer-supported chromium arene complexes. In evaluating candidates for the linker, their attention focused on phosphorus-based ligands. They prepared substituted chromium–fluorobenzene complexes shown in Scheme 26. The series of complexes were prepared by initial formation of the arene–$Cr(CO)_2(\eta^2$-cyclooctene) derivative, **33**, by photolysis of the parent tricarbonyl complex with cyclooctene followed by thermal replacement of the highly labile cyclooctene with the ligand of choice. The relative rates of nucleophilic substitution of the complexes with pyrrolidine have been determined by ^{19}F NMR studies. The results show that with triphenylphosphine as a ligand the substitution reaction is strongly inhibited. Even when using the amine as solvent, no reaction was observed at 50 °C. Triphenylphosphite is a more suitable ligand with the substitution reaction occurring at room temperature but still being some 3600 times slower than with $Cr(CO)_3(C_6H_5F)$. The best results are reported with tris(pyrrolyl)phosphine, the substitution occurring only 1.4 times slower than with $Cr(CO)_3(C_6H_5F)$. As an extension to the work, an amino phosphine bearing a benzylmethylamino substituent on phosphorus was prepared as this best represents the sort of ligand that could be easily immobilized on polystyrene starting from Merrifield's resin or an analog. Using this ligand the rate of the substitution reaction was not as close to the parent as tris(pyrrolyl)phosphine but still gave good results. These studies highlight

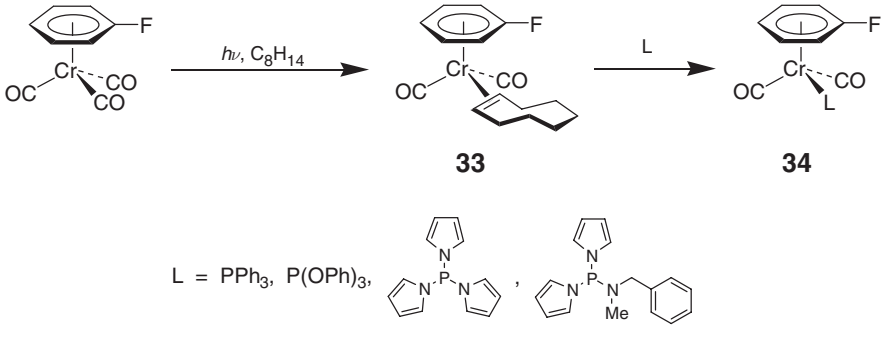

Scheme 26

how important it is to consider the effects of substituting groups on metal complexes in order to facilitate attachment to a polymer support. Clearly, for S_NAr reactions, attachment of the chromium arene complexes to a support such as PS-PPh_2 would be of no use due to the impeding reaction.

Polymer-supported arene complex **34** was prepared by direct photolysis of a solution of PS-PPh_2 and $Cr(CO)_3$(arene) [arene = 4-(4-methoxyphenyl)-butan-2-one] in THF.[122] The ^{31}P NMR analysis of the support after photolysis suggests that coverage with the $Cr(CO)_2$(arene) complex is ~40% with the remainder being PS-PPh_2-$Cr(CO)_5$ (20%), PS-PPh_2=O (10%) and unreacted PS-PPh_2 (30%). Also prepared was **35**, the 4-(4-methoxyphenyl)propan-1-ol analog of **34**, using the same methods and a similar coverage of $Cr(CO)_2$(arene) complex obtained. The ketone and alcohol moieties of the supported complexes were chemically manipulated and then the arene released from the polymer showing the use of arene–chromium complexes as traceless linkers. This has been demonstrated further by immobilizing the phenylalanine derivative Fmoc-Phe-O^{t}Bu via its aromatic ring and the resulting supported complex **36** successfully subjected to standard amino acid deprotection and coupling procedures before cleavage of the linker to yield the derivitized amino acid product.[123] The chemistry is summarized in Scheme 27.

Rigby and co-workers[124] have reported a higher yielding route to phosphine-supported chromium arenes using the same methodology as applied by the Semmelhack group[121] for their synthesis of homogeneous phosphine-substituted complexes (Scheme 28), namely by photolysis of the parent arene–tricarbonyl complex with cyclooctene to form **37** followed by thermal replacement of the cyclooctene with the ligand of choice, in this case, polymer-supported benzyldiphenylphosphine (PS-*p*-CH_2-PPh_2) **38** to form **39**. With simple arenes such as benzene and toluene, the PS-*p*-CH_2-PPh_2 supported chromium arene is formed easily and the resulting complexes have been used as catalysts for effecting $[6\pi + 2\pi]$-cyclooaddition reactions. To probe whether the chromium complex dissociates from the support during the course of the catalysis, they prepared supported phosphine complex **40** containing a much longer linker chain. Their reasoning was that if the chromium complex does not dissociate from the support during the catalysis, then the yields of product should be greater using **40** than with the PS-*p*-CH_2-PPh_2 supported analog. This interestingly is the case providing some circumstantial evidence for the notion that the metal is retained on the support during the course of the reaction.

They have extended the studies to the immobilization of arenes bearing oxygen atoms in the side chain.[125] However, partial decomposition of the organometallic complex is observed on photolysis with cyclooctene. This has been attributed to interaction of the chromium center with the oxygen substituent on the arene in the

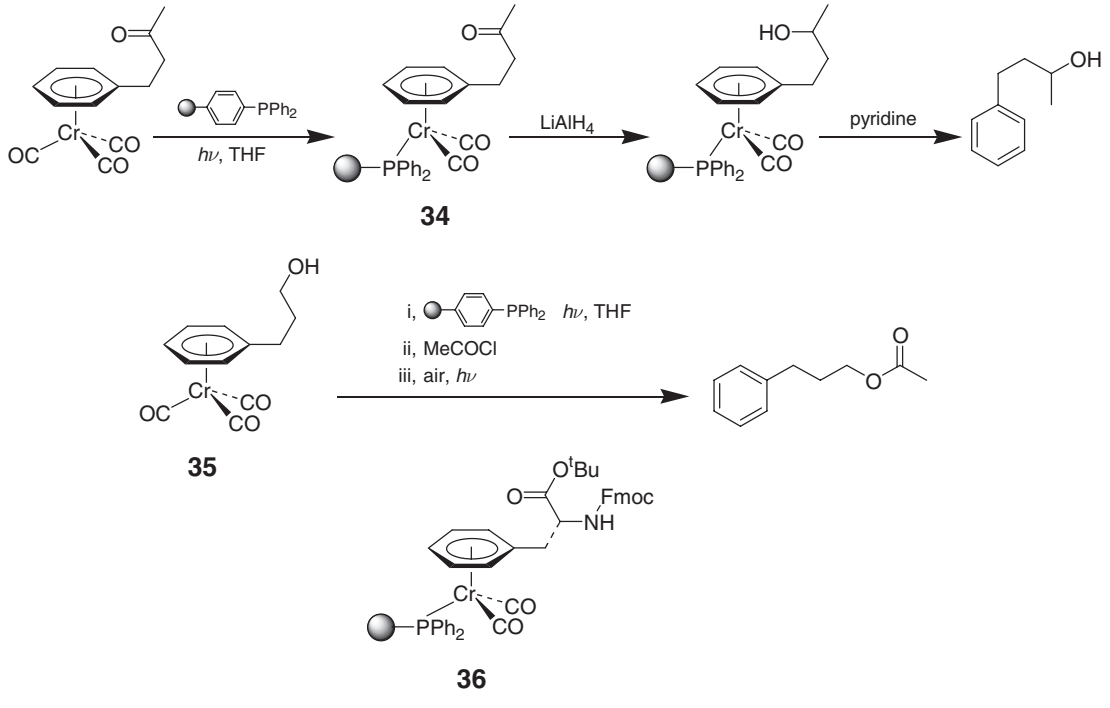

Scheme 27

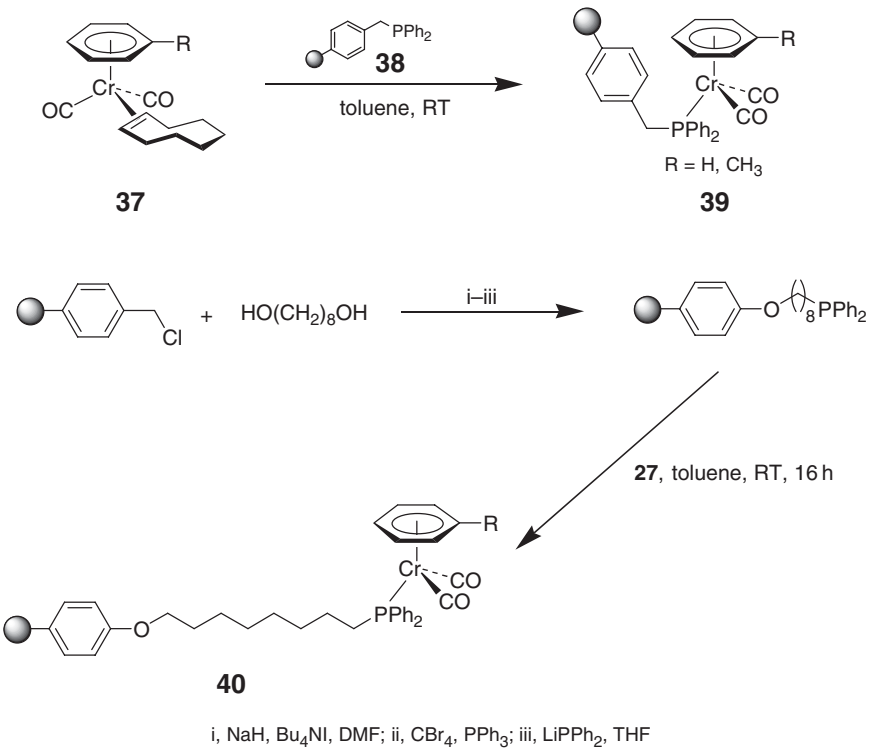

Scheme 28

photogenerated fragment [$Cr(CO)_2$(arene)]. This is avoided by use of a large excess (70 to 80 equiv.) of cyclooctene to trap out the [$Cr(CO)_2$(arene)] complex as its cyclooctene adduct, which can then be loaded onto PS-*p*-CH_2-PPh_2 as before. The loading methodology was used for the preparation of a range of homoarene supported complexes as well as for simultaneous incorporation of a variety of starting materials onto the solid support (Scheme 29). Irradiation of equimolar quantities of four different arenes with excess cyclooctene followed by treatment with PS-*p*-CH_2-PPh_2 gave **41**, which contains all four substrates. The range of supported arene complexes were subsequently used for the solid-phase synthesis of tertiary alcohols **42**. There is particular interest in this methodology because of the potential use in combinatorial or parallel synthesis, considerable time being saved in preparing and testing diverse libraries.

The authors have also performed a C–C and a C–O bond-forming reaction on supported chromium complexes (Scheme 30).[126] Starting from supported ester **43**, the enolate anion **44** was prepared using lithium diisopropylamide (LDA), quenching of which with a range of electrophiles gave the corresponding α-substituted esters **45** in almost quantitative yield. Supported alcohol **46** was prepared from the corresponding arene complex in three steps. Interestingly, significant decomposition occurred during the immobilization step. This seemed to be general for substrates bearing a secondary alcohol functionality. It was possible to perform Mitsunobu esterifications on **36** with good yields; this is significant since PPh_3 is used as a reagent and it may have been predicted that competitive cleavage of the arene–chromium bond could have posed a problem.

Polymer-bound Fischer chromium alkoxy and aminocarbene complexes **47a–c** have also been reported (Scheme 31).[127] The supported alkoxycarbenes were prepared by heating the appropriate pentacarbonylchromium carbene complex with PS-PPh_2, variable loadings being reported. They were converted to their aminocarbene analogs by reaction at room temperature in THF with a range of simple amines. Aminocarbenes were also prepared by the reaction of alkoxycarbenes with leucine and phenylalanine grafted on to polystyrene and polystyrene/polyethyleneglycol (PS-PEG) supports. After removal of the Fmoc group, a THF solution of the alkoxycarbene was added and the mixture stirred for 3 h at room temperature to give the supported aminocarbenes which were characterized by IR spectroscopy but the loadings not determined.

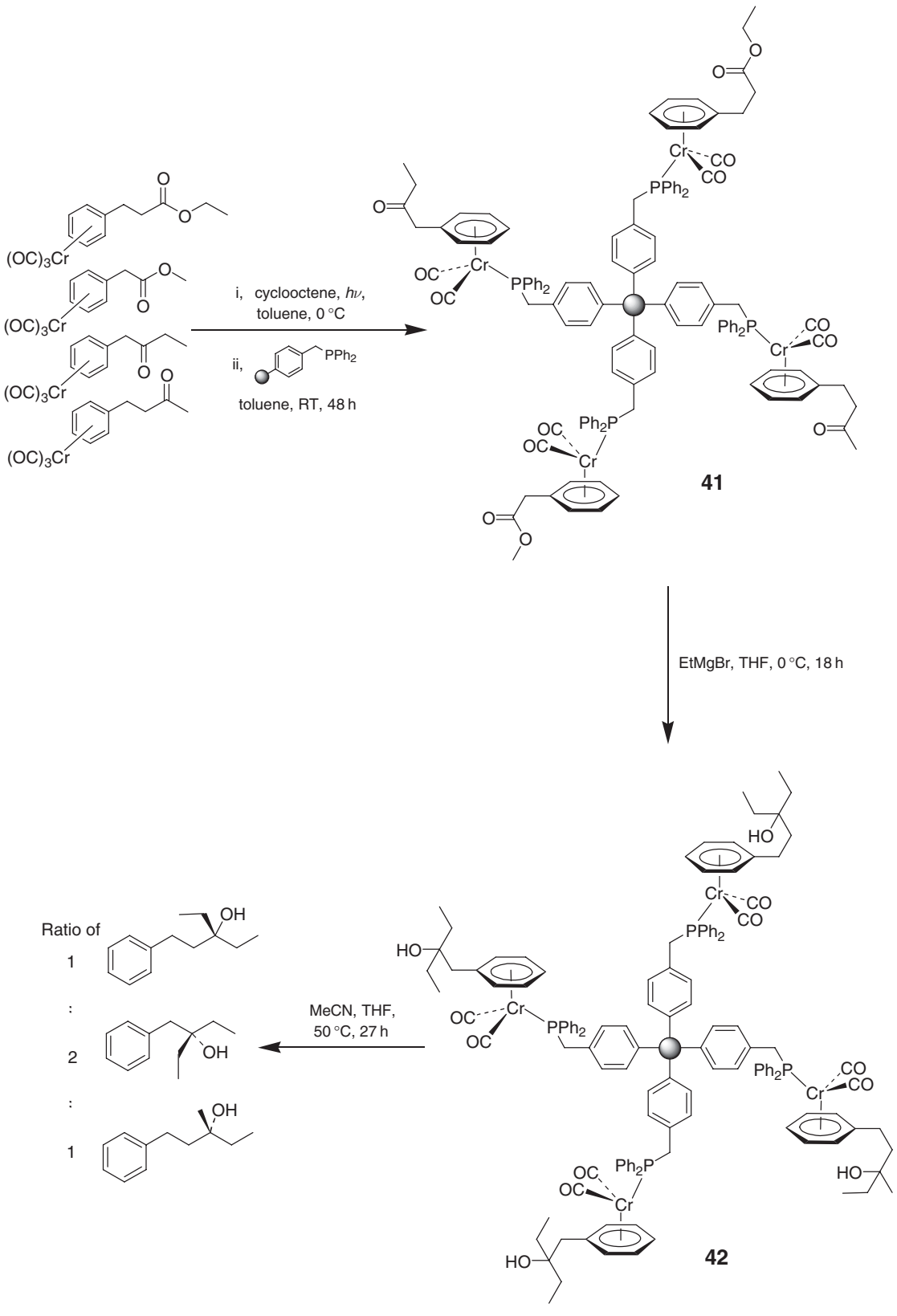
(OC)3Cr
i, cyclooctene, hν, toluene, 0 °C
ii,
PPh2
toluene, RT, 48 h
41
EtMgBr, THF, 0 °C, 18 h
42
MeCN, THF, 50 °C, 27 h
Ratio of
1
:
2
:
1
OH
HO

Scheme 29

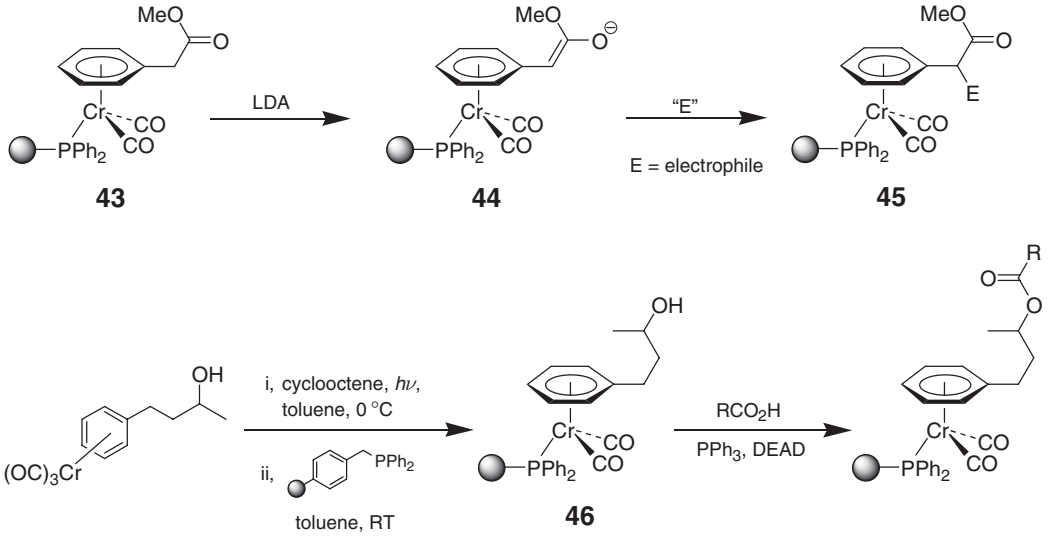

Scheme 30

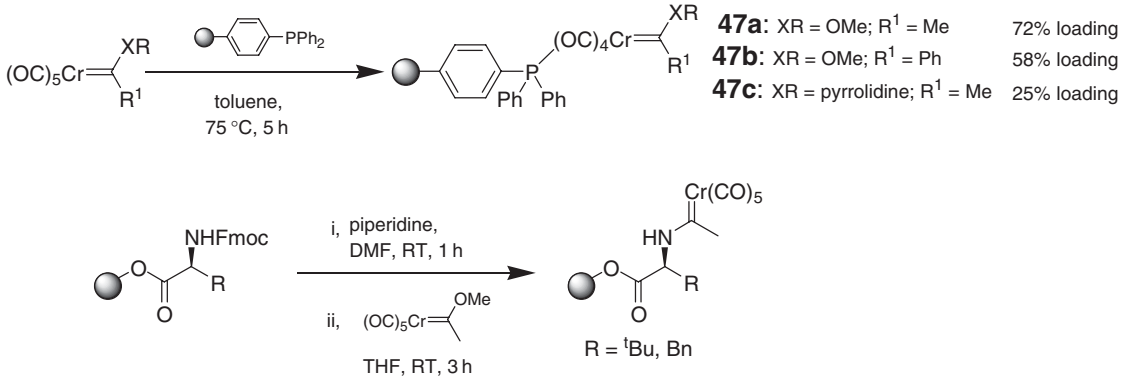

Scheme 31

12.14.3.2.4 Complexes of ruthenium

A supported ruthenium arene complex was made and used as a catalyst for enol formate synthesis and olefin cyclopropanation.[128] The immobilized complex **48** was prepared by thermolysis of the dimer $[Ru(p\text{-cymene})Cl_2]_2$ with PS-PPh_2, a metal loading of 0.25 mmol g^{-1} being obtained (Scheme 32). The homogeneous analog $Ru(p\text{-cymene})Cl_2PPh_3$ is prepared in toluene but the problem with this when using PS-PPh_2 is that the support does not swell well in toluene and so a modified solvent mixture of a 1 : 1 mix of dichloromethane/toluene was used. Unlike the homogeneous analog, **48** is stable in air, no decomposition being noted over a period of 3 months at room temperature. This shows one of the advantages of immobilization of organometallic complexes—namely increased stability.

Using a similar methodology, **49** was prepared and used as a catalyst for oxidation of a range of alcohols and hydrocarbons (Scheme 33).[129] Of interest is that studies suggest that the metal comes off the support during the course of the reaction, returning at the end—very much like the "boomerang" catalysts reported by Barrett and co-workers for olefin metathesis[130,131] and discussed later in this chapter.

The hexanuclear ruthenium cluster $Ru_6C(CO)_{17}$ has been immobilized on a PS-PEG-PPh_2 support.[132] The supported phosphine was prepared by treatment of chloride-functionalized PS-PEG with $KPPh_2$, the metal cluster then being attached by agitating the support with an excess of $Ru_6C(CO)_{17}$ for 5 days (Scheme 34). Starting with a phosphine loading of 0.4 mmol g^{-1}, a metal loading of 0.24 mmol g^{-1} was obtained.

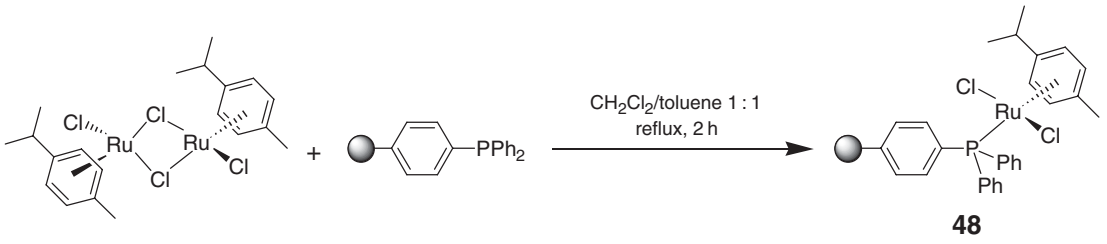

48

Scheme 32

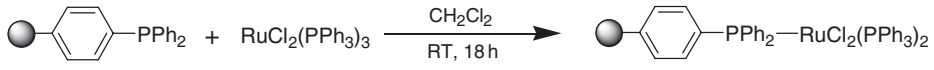

49

Scheme 33

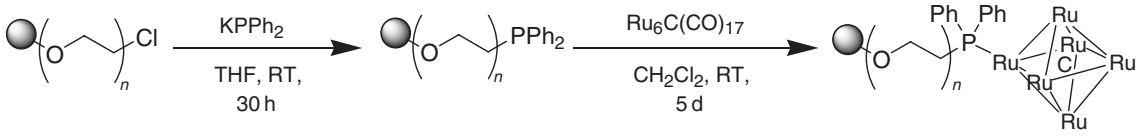

Scheme 34

12.14.3.3 Other Supported Monodentate Phosphines

Immobilized dialkylphosphinobiphenyl ligands **52a** and **52b** have been prepared, the homogeneous analogs of which[133] show high activity when used in palladium-catalyzed C–C and C–N bond-forming reactions (Scheme 35).[134] The immobilized ligand **52a** is prepared starting from 2-methoxyphenylmagnesium bromide and benzyne (formed *in situ* from 2-bromochlorobenzene), these reacting to form **50**. This is then treated with $ClPR_2$ before deprotection of the methyl ether forming **51a**. Deprotonation of **51a** using NaH in DMF followed by addition of Merrifield's resin leads to **52a** with ~80% of the chloromethylated sites being occupied by phosphine ligand. The di-^{t}butylphosphinobiphenyl analog **52b** is more difficult to prepare. The starting phosphine **51b** is prepared from dibenzofuran and then attached to the support in the same method as for **52a** but by using a dilute solution of **51b**. Due to the easier preparation, chemistry using **52a** has received most attention. Although not isolated, palladium complexes of **52a** have been prepared using $Pd(OAc)_2$ and $Pd_2(dba)_3$. These complexes have then been used as catalysts for amination and Suzuki coupling reactions. Under standard conditions, using ~1.0 mol% Pd, primary amines, secondary cyclic and acyclic amines, and anilines were all coupled successfully with unactivated or deactivated aryl halides. However, pre-mixing of the catalyst system was essential for high activity. In the Suzuki reaction, aryl bromides and iodides were coupled with aryl boronic acids with great success. With aryl chlorides, competitive hydrolytic deboronation of the aryl boronic acid was observed and in order to drive the reaction to completion increased quantities of the boronic acid (1.5–3 equiv.) were needed but, with this modification, good yields of product were obtained. The supported complexes were recycled with similar activity without the need for further addition of palladium.

Soluble MeOPEG-supported analogs of **52a** and **52b** have also been reported.[135] This was achieved by reacting the HBF_4 salts of **51a** and **51b** with MeOPEG-OTs (molecular weight 2000) to give **53a** and **53b**, respectively. The materials are stored as the HBF_4 salts since these are much more air and moisture stable compared to the free phosphines. An MeOPEG-supported diadamantylphosphine **54** has also been prepared from diadamantylphosphine and a bromomethyl-functionalized MeOPEG support. Again the polymer is stored as the HBF_4 salt. A range of

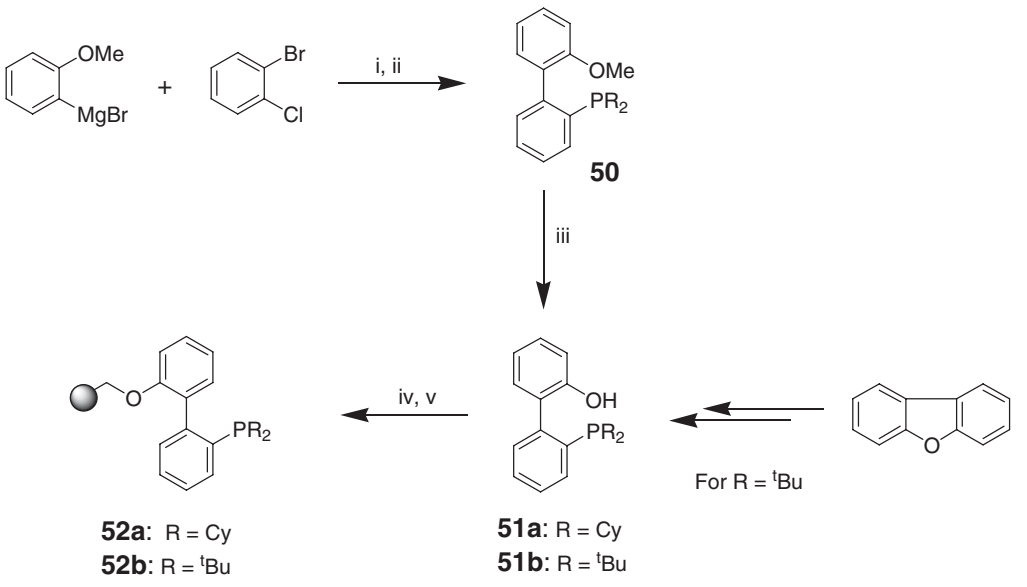

i, Mg, THF, 60 °C, 2.5 h; ii, CuCl, $ClPR_2$, THF, RT, 16 h; iii, BBr_3, CH_2Cl_2, –78 °C → RT, 16 h; iv, NaH, DMF, RT, 15 min; v, Merrifield's resin (1.23 mmol Cl g^{-1}), DMF, RT, 23 h

Scheme 35

palladium complexes have been formed from these supported ligands and a detailed study of their catalytic activity, efficiency of removal, and recyclability undertaken.

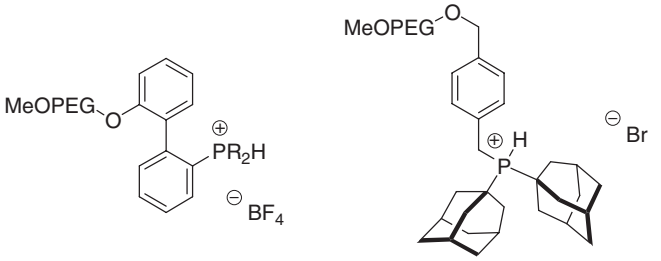

A procedure for the synthesis of **55**, a soluble polystyrene-supported analog of **54** has also been published (Scheme 36).[136] Starting from 4-methylstyrene, anionic polymerization gives a linear poly(4-methylstyrene), the substoichiometric bromination of which converts 5–18% of the CH_3 units to CH_2Br which were then reacted with diadamantylphosphine to give **55**. The molecular weight of the resultant phosphine materials ranged from 5000–36000. The ligands have been used in Heck, Suzuki, and Sonogashira couplings, the catalyst being separated at the end of the reaction using nanofiltration over a solvent-resistant membrane composed of a dense poly(dimethylsiloxane) layer cast on a porous sublayer of poly(acrylonitrile). The membrane displays almost quantitative retention of the soluble catalyst.

Soluble phosphine support **57** was prepared starting from mesityl-substituted phosphaalkene **56** (Scheme 37). This was co-polymerized with various equivalents of styrene to give a series of materials, soluble in dichloromethane, thf, and toluene, with phosphine loadings ranging from 5–39 mol%. This methodology in essence shows that P═C bonds can mimic C═C bonds in their polymerization chemistry and opens avenues for the synthesis of other phosphine-substituted supports since a wide range of phosphaalkenes are known.

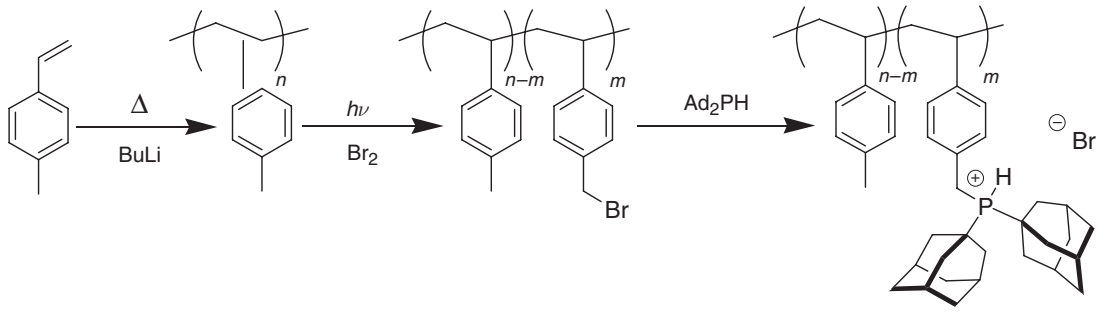

55

Scheme 36

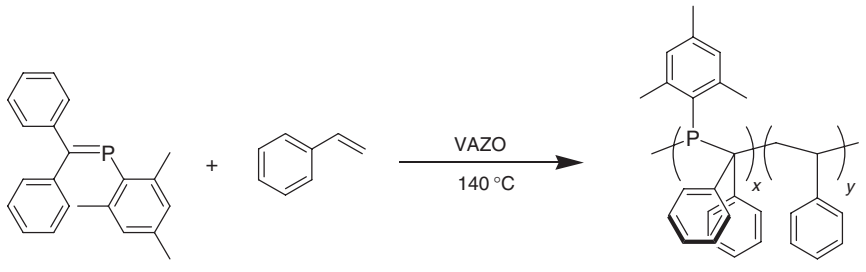

56 57

Scheme 37

12.14.3.4 Polymer-supported Polydentate Phosphines and Their Metal Complexes

A number of polymer-supported polydentate phosphine ligands have been prepared as have their corresponding metal complexes. As polydentate phosphines show superior ligating properties over their monodentate analogs, attaching them to supports has a number of advantages such as possibly limiting leaching of the metal off the support during the course of a reaction when used as a catalyst.

Polymer-supported bis(diphenylphosphino)methane (DPPM) has been prepared by treatment of Merrifield's resin with lithiated DPPM and subsequent reduction of the phosphine oxide.[137] A palladium complex of this was screened in a range of catalytic transformations including the selective hydrogenation of cinnamaldehyde to hydrocinnamaldehyde.[138,139]

Polymer-immobilized bis(diphenylphosphino)ferrocene (DPPF) **58** and palladium complexes of this have been reported.[140] The immobilized ligand was prepared by AIBN-initiated suspension polymerization of vinyl DPPF, styrene, and DVB (Scheme 38). This procedure gave macromolecular beads having a ligand loading of 0.22 mmol g^{-1}. The ratio of vinyl DPPF : styrene : divinylbenzene of 0.02 : 0.48 : 0.50 used leads to a highly cross-linked polymer and ensures site isolation of the ligand moieties. The Pd(0) complex of **58** was prepared by refluxing a 1 : 1 mixture of immobilized ligand and $Pd(PPh_3)_4$ in toluene for 2 h with almost quantitative palladium attachment being observed. This palladium complex was subsequently used for the synthesis of large-ring keto lactones by intramolecular carbonylative coupling reactions.

Polymer-supported bidentate **60**[141] and tridentate **63**[142] ligands were made by co-polymerization of styrene and DVB with styrene-derivitized monomeric phosphines (Scheme 39). Using NaH, 2,2-bis(diphenylphosphinomethyl)propanol was coupled to 4-vinylbenzylchloride to yield the desired styrene-substituted phosphine **59** which was co-polymerized (0.5 equiv. phosphine) with styrene (1 equiv.) and DVB (36 equiv.) using AIBN as an initiator to give **60**. The tridentate analog **63** is prepared in an analogous method but using 3,3-bis(diphenylphosphinomethyl)oxacyclobutane as a starting material. Nucleophilic attack with $LiPPh_2$ followed by coupling with 4-vinylbenzylchloride gives **62**; polymerization of **62** with either DVB on its own or styrene and DVB yields **63**. Rhodium complexes **61** and **64** have been prepared by stirring $[RhCl(COD)]_2$, Bu_4NPF_6, and the respective supported phosphine in dichloromethane. The key advantage of preparing

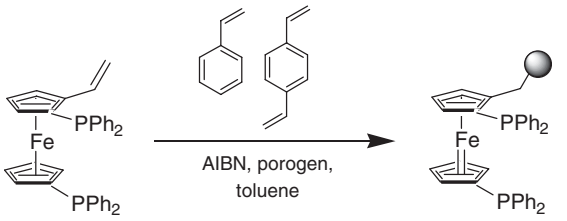

58

Scheme 38

the chelating phosphines by co-polymerization rather than by grafting is that the synthesis is easier; it not being necessary to reduce the phosphine oxide back to the phosphine as is the case when treating chlorinated supports with metallated phosphines. Also, there is no problem of removing trapped metal salts (such as LiCl) from the pores of the support.

In the synthesis of polymer-supported *o*-phenylenediphenylphosphine, PS-PP **66**, 3,4-difluorobenzyl alcohol was used as the starting material, the diphosphine **65** being generated by the reaction of this with $NaPPh_2$ (Scheme 40).[143] The point of attachment of the diphosphine to the support is through an ether linkage, **65** being deprotonated using NaH and treatment with Merrifield's resin gave **66** with replacement of approximately one-third of the chlorines by diphosphine units. This offers significant advantages over previous routes involving the preparation of mixed chloroalkyl substituted bidentate phosphines and subsequent lithiation and reaction with a suitable support in that such phosphines are difficult to prepare in good yield and are very air and moisture sensitive.[144] A number of metal complexes were prepared using **66** as a ligand, treating this with a THF solution of metal salts and using a range of techniques to characterize the supported species, including EXAFS and diffuse reflectance UV–VIS spectroscopy, comparing data recorded for the supported complexes with that for homogeneous model compounds containing the *o*-phenylenediphenylphosphine ligand.

An alternative approach to the synthesis of polymer-supported bidentate phosphorus-containing ligands has been reported (Scheme 41).[145] The polymer-supported phosphine complexes are prepared from polymer-supported secondary amine **66** by reaction with 1,2-bis(dichlorophosphino)ethane in the presence of NEt_3 to give intermediate **67**. This can then be reacted with a variety of organomagnesium or organolithium reagents to give supported phosphines **68** or with the sodium salts of alcohols to yield supported phosphites **69**. Of interest is that only one phosphorus atom of the bis(dichlorophosphino)ethane is linked to the resin. This has been attributed to the steric constraints of the *t*-butyl groups on the resin and the excess of diphosphine used. Although the work was directed at the generation of libraries of C_1-symmetric ligands for use in homogeneous catalysis, the polymer-supported phosphines and phosphites being cleaved from the support using PCl_3, the immobilized ligands themselves show significant scope for use in supported catalysis.

A range of polymer-supported β-aminophosphines have been prepared by a similar method. (Scheme 42).[146] The point of attachment chosen was the nitrogen as this offered the most synthetic simplicity together with the greatest diversity of possible building blocks that can be used. Starting from Merrifield's resin, the polymer-supported amino alcohol **70** was formed by reaction with ethanolamine. Chlorodehydroxylation with $SOCl_2$ followed by deprotonation of the chloroethylammonium salt formed gave chloroamine **71**. Reaction of this with $LiPR_2$ (R = Ph, *o*-Tol) gave the desired supported β-aminophosphine **72**. A number of derivatives have been prepared varying the substituents at nitrogen, the α-carbon, and phosphorus. Each step of the reactions was thoroughly monitored spectroscopically by a combination of gel-phase ^{13}C- and ^{31}P-NMR techniques. Of particular interest is that a number of the steps in the preparation of **72** and its analogs proceed much better than their solution counterparts. The chlorodehydroxylation of **70** occurs almost quantitatively compared to 35% for its solution analog, similar observations being made in the deprotonation step to give **71**. These differences have been attributed to the site isolation on the solid–support, thus preventing oligomerization of intermediates or products formed in the reactions, this being known to be a problem in solution.

Other similar phosphorus ligands on solid supports and screened them in the Heck reaction.[147] Starting from supported amino alcohols, representative members of five different families of phosphine and phosphinite ligands were synthesised: β-aminophosphines **73**, *N*,β-diphosphinoamines **74**, α,β-diphosphinoamines **75**, β-aminophosphinites **76**, and *N*-phosphino-β-aminophosphinites **77**. Following their complexation with $Pd(OAc)_2$, the ligands were screened in the Heck reaction and led to the identification of two lead ligands for future studies.

As a continuation of their studies into the immobilization of $Ru_6C(CO)_{17}$ for use in hydrogenation, Johnson and co-workers[132] have prepared a bidentate phosphine ligand based on a PS-PEG support and immobilized the hexanuclear ruthenium cluster on it. The supported bidentate phosphine **78** was prepared by treatment of

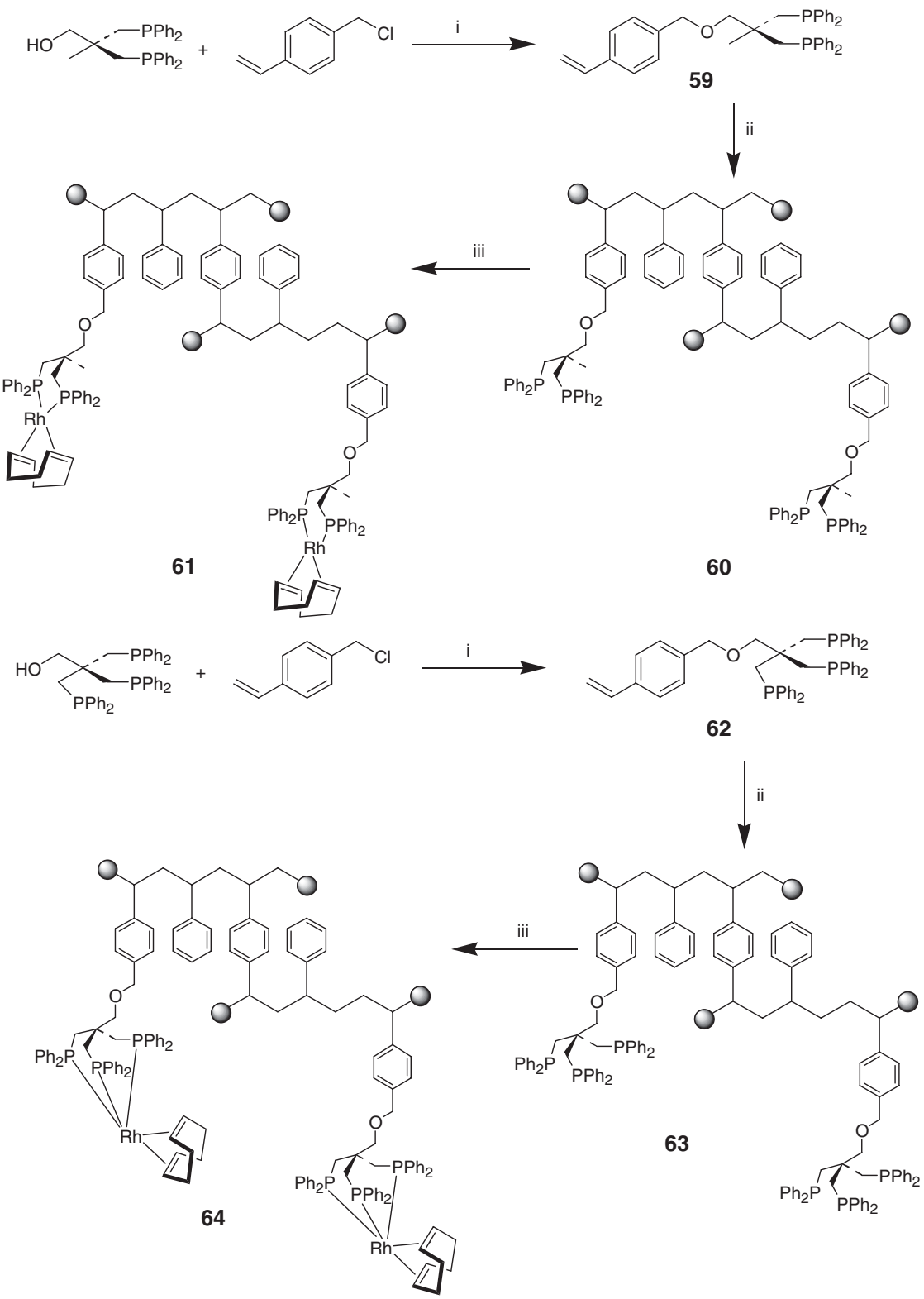

i, NaH, DMF; ii, styrene, DVB, AIBN, THF/MeOH (1 : 2), 85 °C; iii, $[RhCl(cod)]_2$, Bu_4NPF_6, CH_2Cl_2

Scheme 39

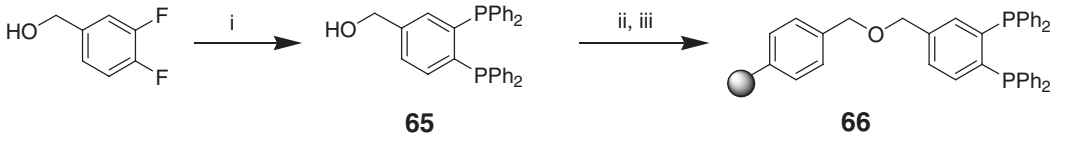

i, 3 equiv. $NaPPh_2$, dioxane, reflux, 3 h then 1 M HCl; ii, NaH, THF; iii, Merrifield's resin (1.7 mmol Cl/g), RT, overnight

Scheme 40

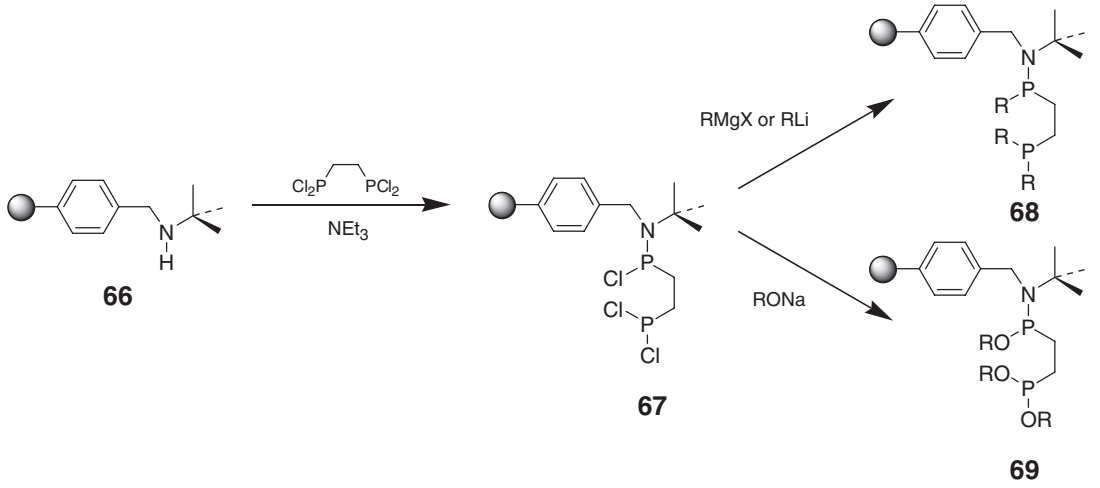

Scheme 41

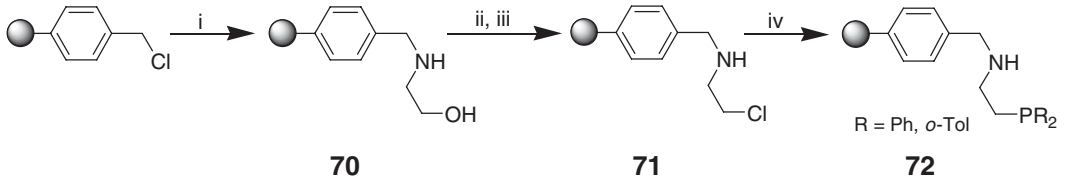

i, ethanolamine, DMF, 50 °C, 17 h; ii, $SOCl_2$, $CHCl_3$, 60 °C, 2 h; iii, N^iPr_2Et, THF, RT, 2 h; iv, $LiPR_2$, THF, RT, 24 h

Scheme 42

amine-functionalized PS-PEG with diphenylphosphinomethanol, the metal cluster then being attached by agitating the support with an excess of $Ru_6C(CO)_{17}$ for 5 days giving **79** (Scheme 43). Starting with a phosphine loading of 0.68 mmol g^{-1}, a metal loading of 0.12 mmol g^{-1} was obtained indicating that only 18% of the phosphine sites were metallated. A simple palladium complex of the analogous ligand to **78** but derived from aminomethylated polystyrene has been prepared and used in the Sonogashira coupling.[148] The same ligand has also been employed as an efficient scavenger for the Grubbs type 1 olefin-metathesis catalyst.[149]

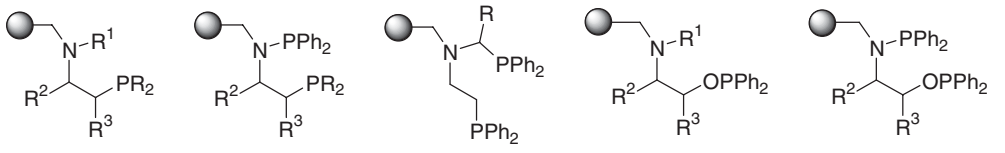

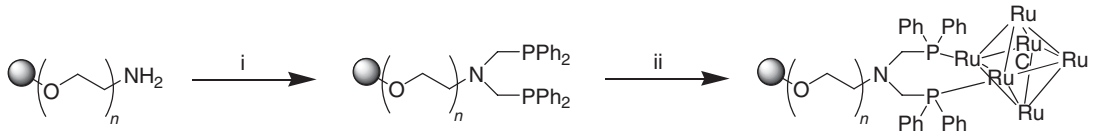

78 **79**

i, $HPPh_2$/HCHO, MeOH/toluene, 60 °C, 3 h, then RT, 15 h; ii, $Ru_6C(CO)_{17}$, CH_2Cl_2, RT, 5 d

Scheme 43

A similar support was used to prepare a bidentate analog of **20**.[150] The support was treated with $[PdCl(\eta^3\text{-}C_3H_5)]_2$ to give **80** which was used as a catalyst for high-throughput cross-coupling in water. A ruthenium complex has also been attached to this support and the diethylphosphine-functionalized analog by a ligand exchange reaction with $RuCl_2(PPh)_3$ forming **81a** and **81b**, respectively.[151] These have been used as catalysts for the hydrogenation of supercritical carbon dioxide.

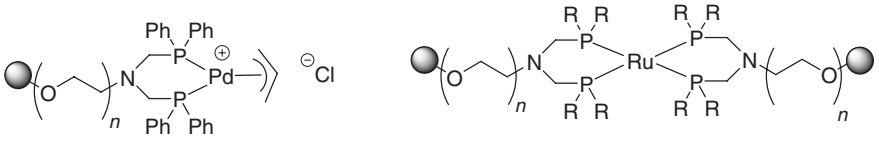

80

81a: R = Ph
81b: R = Et

A route to bidentate phosphine-functionalized dendrimeric support has been reported (Scheme 44).[152] Starting from commercially available third-, fourth-, and fifth-generation poly(propylene imine) dendrimers, the primary amine groups at the periphery were converted into bidentate phosphines with diphenylphosphinomethanol to give **82**. The resultant material was reacted with $PdCl_2(PhCN)_2$ to form a supported Pd(II) complex which was then reduced, using hydrazine, in the presence of PPh_3 to **83**. This was used as a catalyst in allylic amination reactions. Solvent precipitation, membrane filtration, and thermomorphic liquid/liquid separation were all used to recycle the complex. The latter procedure proved to be the simplest with the best recovery of active catalyst.

The same ligand motif has been used in the preparation of dendronized polymer resins to which rhodium carbonyl complexes have been attached and then screened for catalytic activity in hydroformylation of alkenes. Although attached to inorganic supports and thus outside the direct remit of this chapter, the dendrimers prepared using silica or carbosilane supports should be mentioned here.[153–155] A number of polyaminoamide (PAMAM) dendrimers have been prepared and then reacted with diphenylphosphinomethanol (prepared *in situ* from paraformaldehyde and diphenylphosphine) to give phosphine-functionalized supports onto which a range of metal complexes have been attached, including rhodium.[156] The general structure of the dendrimers is shown in Figure 7. At first, only the ligands and complexes of G_0, G_1, and G_2 could be prepared efficiently. Due to steric hindrance, the functionalization and complexation of G_3 and G_4 was possible only with extremely low efficiency. The catalysts prepared showed good

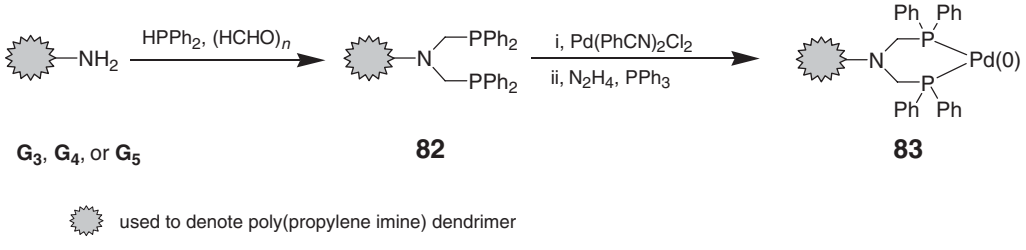

G_3, G_4, or G_5 **82** **83**

Scheme 44

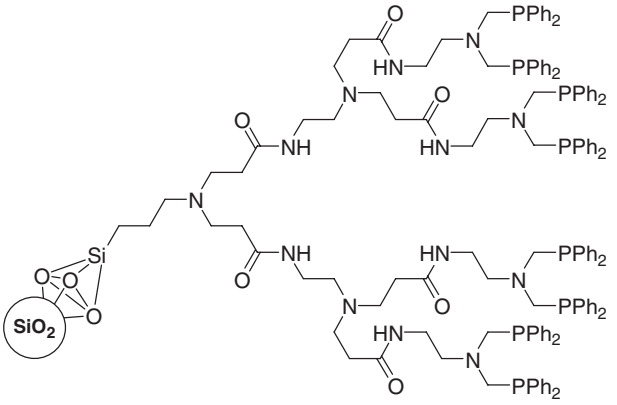

Figure 7

activity in hydroformylation reactions and, from the reported turnover rate measurements, it seemed that the activity of the catalyst increased as a function of the generation. However, as Dahan and Portnoy stress in their review of dendrimer chemistry,[58] this point cannot be unequivocally proved since in this study and in subsequent reports from these groups, the catalysts were compared with an equal amount of silica rather than metal. The apparent turnover frequency is often affected by the initial amount of the catalyst. The synthesis of the third- and fourth-generation dendrimers was improved through the elongation of the diamine fragment of the branching module of the PAMAM dendrons.[157] Substitution of the 1,2-diaminoethane moiety by 1,4-diaminobutane, 1,6-diaminohexane, or 1,12-diaminododecane reduced steric crowding and increased metal catalyst loadings. In addition, these new dendrimers were more active in the hydroformylation reactions than their predecessors. Best results were found for the fourth-generation catalyst based on 1,12-diaminododecane.

Polyamino dendrons have also been attached to polystyrene supports.[158]Key to the success of the methodology was the synthesis of building block **84**, built from 3,5-diaminobenzoic acid by the coupling with strategically protected amino acids. Coupling this with an amine-functionalized polystyrene support gave **85**, deprotection of which, followed by reaction with diphenylphosphinomethanol, gave first-generation phosphine dendrimer **86**-G_1. The subsequent generations of supported ligand were prepared by repeating the required steps. The dendrimers were metallated by stirring with $[RhCl(CO)_2]_2$ in dichloromethane. The second- and third-generation complexes were more active in hydroformylation than the first-generation one and could be recycled a number of times without a loss of activity.

The influence of the isolation of the catalyst environment on the polystyrene-supported dendrimers has been investigated.[159] First- and second-generation polyamino dendrons very similar to those used for making the **86**-G_n family were constructed on polystyrene. The first-generation module was phosphinated and metallated but in the second-generation dendrons, **87**-G_2, the outer layer modules were not phosphinated and did not carry metal. Instead, they were used to isolate the catalytic site from the environment. Despite the fact that the metal loading of the second-generation catalyst was lower than that of the first (since the number of metal atoms per dendron was equivalent for both), the reactivity and recyclability of the second-generation-derived catalyst were notably better with some substrates.

First- and second-generation dendrimers bearing lysine-containing peptide-like modules have been assembled on a polystyrene support (Scheme 45).[160] Again, a building block **88** generated from 3,5-diaminobenzoic acid by the coupling with strategically protected amino acids was used. Coupling this with an amine-functionalized polystyrene support gave **89**, deprotection of which, followed by reaction with diphenylphosphinomethanol, gave **90**-G_1. The second-generation supported ligand **90**-G_2 was prepared by reaction of **89** with **88** followed by the same deprotection and phosphination steps used for **90**-G_1. The dendrimers were again metallated by stirring with $[RhCl(CO)_2]_2$. Loadings of 0.74 and 0.83 mmol g^{-1} were obtained for the complexes prepared from **90**-G_1 and **90**-G_2, respectively. The dendrimers were very efficient catalysts in the hydroformylation of a range of alkenes, affording excellent selectivity for branched aldehydes. The reactions work well even at room temperature. This catalytic system has also been successfully applied to the carbonylative ring expansion of aziridines.[161]

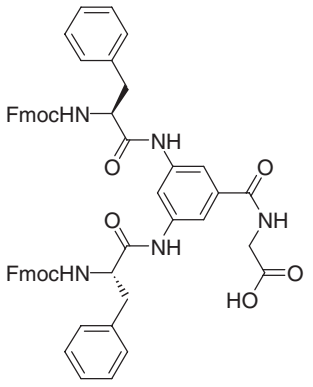

84

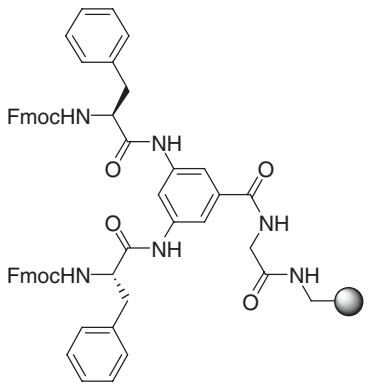

85

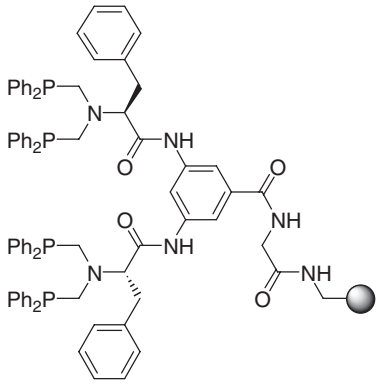

86-G_1

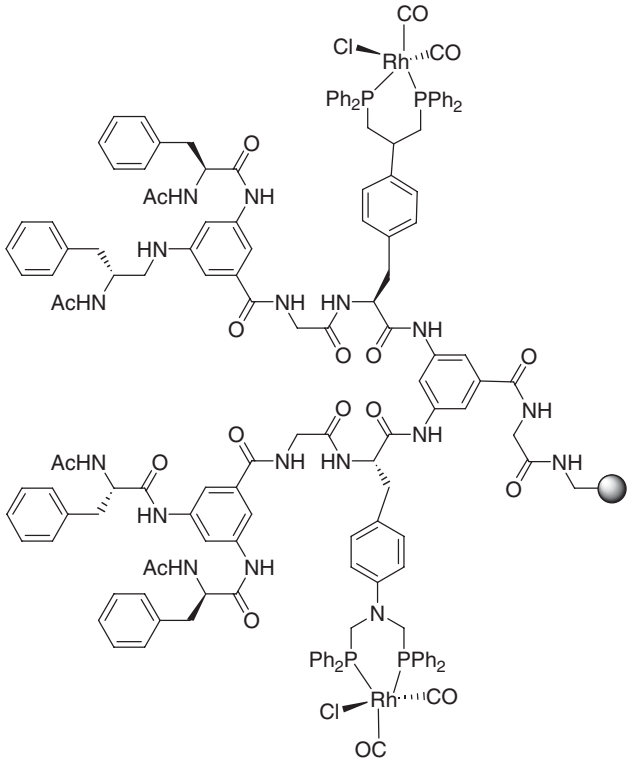

87-G_2

An amphoteric, water-soluble polymer support functionalized with a bidentate phosphine has been reported (Scheme 46).[162] Starting from poly(maleic anhydride)-*c*-poly(methylvinylether), **91** was prepared by reaction with a bis(diphenylphosphino)ethylamine. Polymers with different phosphine loadings were made and soluble Rh complexes formed by reaction with [Rh(COD)] + OTf. These supported metal complexes were then screened for activity in hydrogenation reactions. Recovery of the catalyst was effected by changing the pH of the reaction mixture to <7.5.

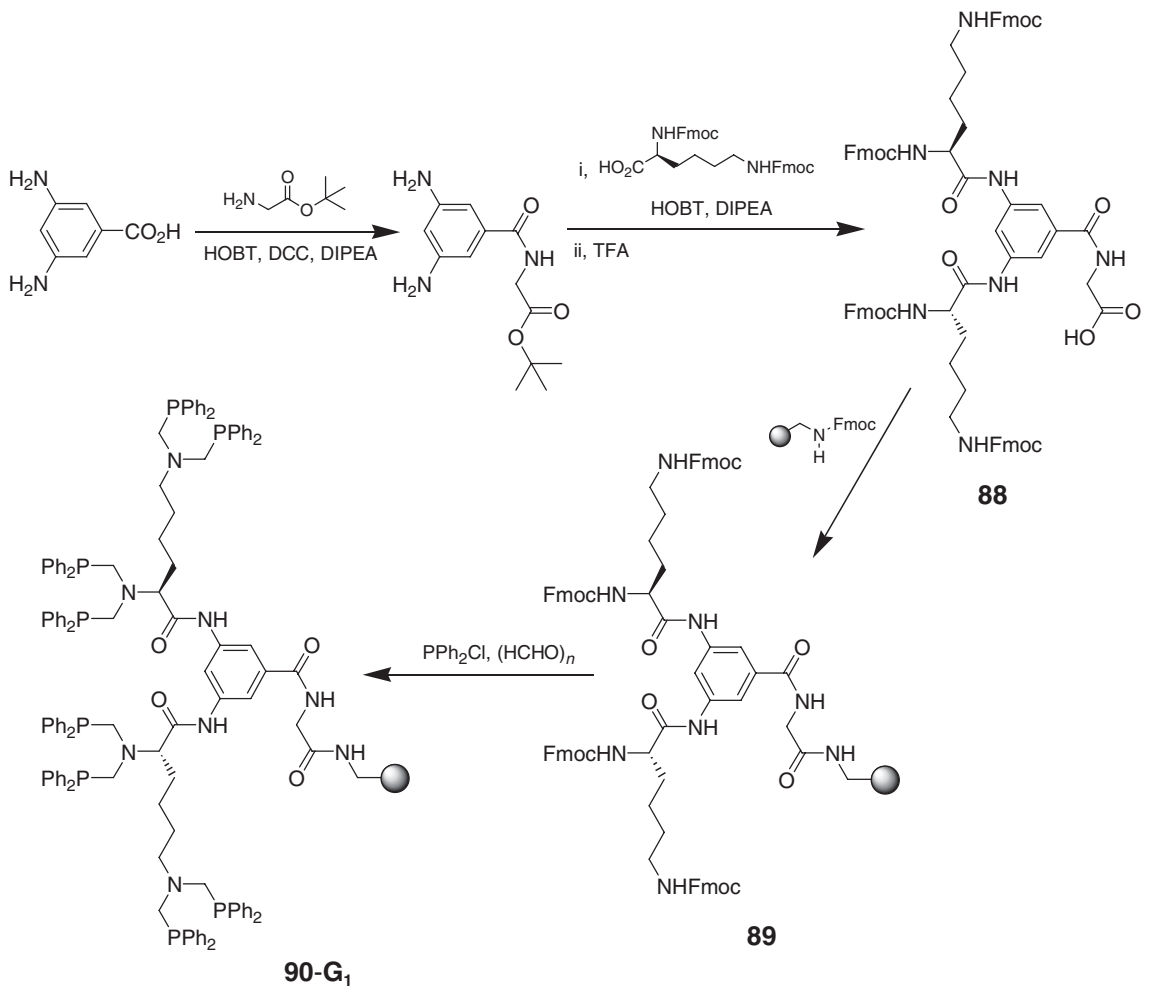

Scheme 45

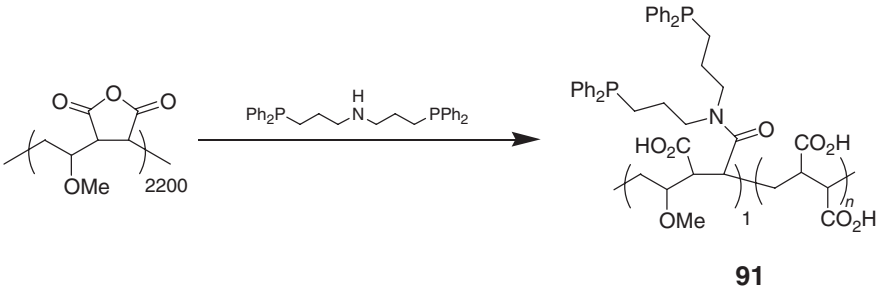

Scheme 46

To complement this work, **92**, a rhodium complex attached to a monophosphine PNIPAM polymer support, has also been prepared and screened[163]

A polypyrrole-supported diphosphine borane complex has been prepared by electrochemical polymerization of a diphosphine-substituted monomer and used as a supported ligand for Rh and Pd catalysis.[164,165]

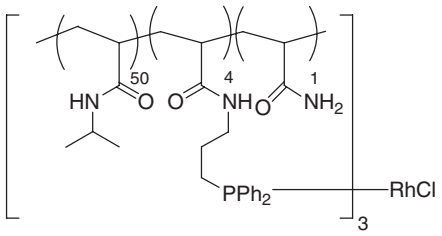

92

12.14.3.5 Achiral Phosphines Attached to Polymer-supported Peptides

A range of variants of supported phosphines have been reported based on standard peptide synthesis resins. Gibertson and co-workers first reported solution-phase routes to incorporation of phosphines into peptides in 1994.[166] They achieved this initial protection of the phosphine of choice by using its sulfide to stop oxidation to its phosphine oxide during subsequent peptide synthesis steps. The phosphine sulfide is then incorporated into an amino acid building block such as serine[166,167] or proline[168] to give the thiophosphine-substituted analog (Scheme 47). This can then be incorporated into polypeptides using traditional peptide synthesis methods and the sulfur-protecting group is then removed from the phosphine groups using Raney nickel to give the free phosphine-substituted peptide. This method has been used to prepare the 12-residue peptide Ac-Ala-Aib-Ala-Pps-Ala-Aib-Cps-Ala-Ala-Aib-Ala-OH **93** (Pps = diphenylphosphinylserine, Cps = dicyclohexylphosphinylserine). Assuming the peptide has an α-helical secondary structure, the phosphine-containing amino acids were placed in positions such that they are on the same side of the helix. Rhodium complex **94** was prepared by treatment of **93** with [Rh(nbd)][ClO_4], prepared from [Rh(nbd)Cl]$_2$ and $AgClO_4$. Less than 1 equiv.of metal complex was used in the preparation to prevent coordination to other functional groups in the peptide.

This methodology has been developed for the synthesis of phosphine-substituted peptides immobilized on polystyrene supports, **96**, the immobilized analog of **93**, being prepared (Scheme 48).[169] The synthesis is analogous to the solution-phase case with one notable change. Although suitable for solution-phase synthesis, the use of Raney nickel as a reagent for reducing supported thiophospine-substituted polypeptides to their corresponding free phosphines is not a viable option. Instead, the phosphine sulfide **95** is methylated with methyl trifluoromethanesulfonate to give a phosphonium salt, treatment of which with tris(dimethylamino)phosphine gives the free substituted phosphine-substituted peptide **96**. The metallated supported peptide **97** has been screened for catalytic activity in hydrogenation reactions and found to be very efficient, 100% conversion being obtained in the hydrogenation of a prochiral enamide with an enantiomeric excess (ee) of 4–9% being observed. This is perhaps rather surprising on two counts. First, the peptide backbone puts the metal in **97** in close proximity to amide and carbonyl functionalities either of which could potentially coordinate and stop catalysis but this does not seem to occur. Second, the peptide backbone in **97** contains nine chiral centers and so the degree of asymmetric induction in the hydrogenation is remarkably low. The low ee observed is not as a result of the immobilization of the peptide since the same result is obtained with **94**.[167]

Libraries of peptide-based phosphine ligands have been reported by the same group using a Chiron Multipin Multiple Peptide Synthesis system, and they formed metal complexes from these and screened them for catalytic activity.[170,171] The synthesis of peptides on pins allows the identity of each peptide attached to a given pin to be monitored and kept separate, so screening of individual ligand–metal complexes can be performed. In their first-generation library, supported peptides of general form Ac–Ala–Aib–Ala–[variable peptide sequence]–Ala–Aib–Ala–support were prepared where, in the variable sequence, two phosphine-containing peptides are placed in either i and $i+1$ or i and $i+4$ positions. The two phosphine-containing peptides were either both Pps, both Cps, or one of each. Rhodium complexes of each of the library members were prepared and screened in the hydrogenation of methyl 2-acetamidoacrylate. Only 10 of the 63 library members gave the product in greater than 10% ee. Building on the results from the first library, a second series of peptides were designed where the positioning of the phosphines was such that they would be on the same side of the α-helix. Both 12 and 13 residue peptides containing a *d*-phosphine-containing peptide in the i-position and a phosphine-containing peptide in either the $i+3$ or $i+4$ position were prepared as they were thought to fulfill this criterion. These were metallated and screened in the hydrogenation reaction but again only a few of the library members led to the product in greater than 10% ee (8 out of 48 members), the highest being 38% ee.

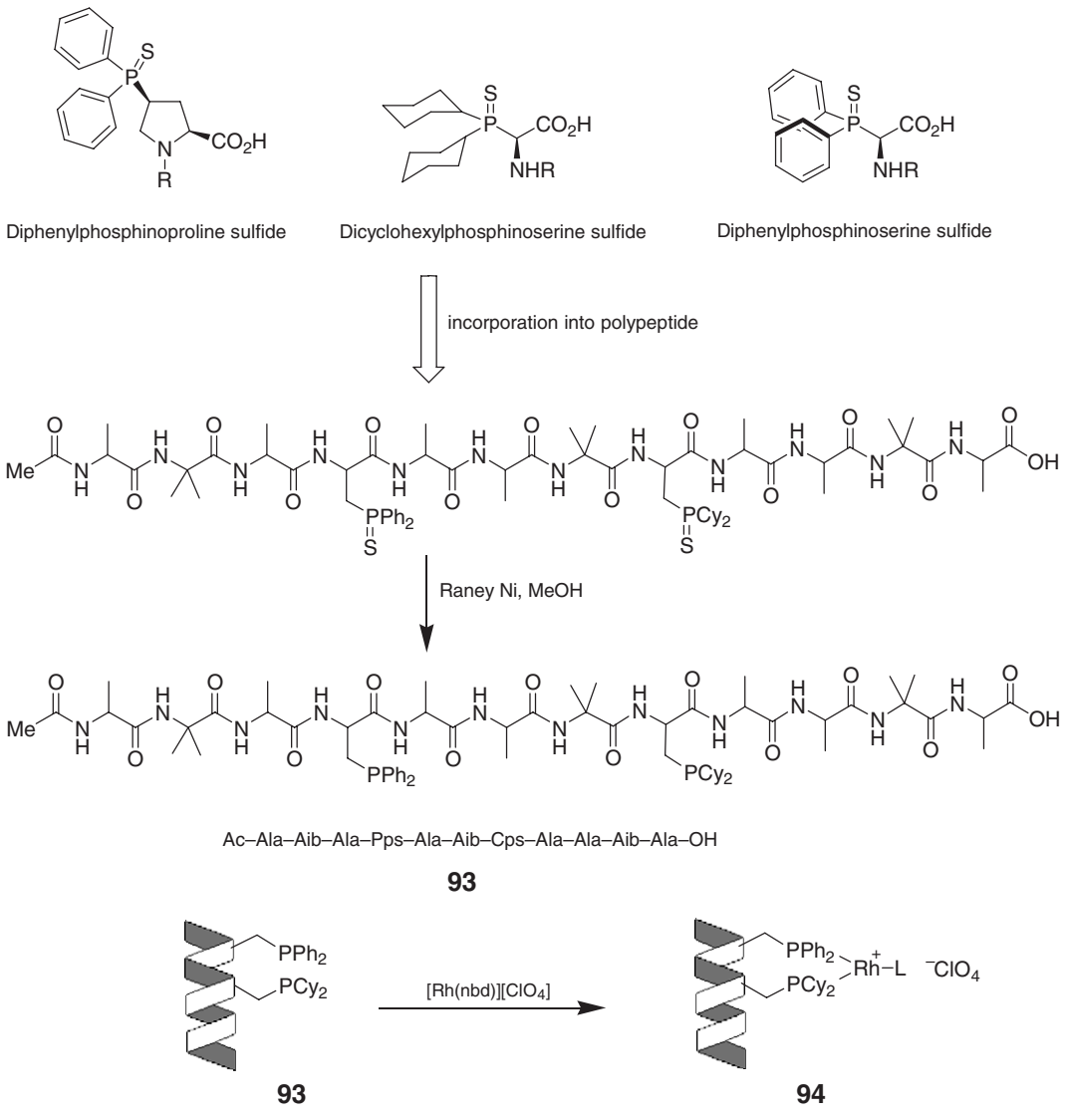

Scheme 47

When test reactions were performed on solution analogs of three of the best peptides found in the screen of the supported complexes, the selectivities in a range of solvents were found to be very different to those found on the pins. Indeed, the catalysis of the soluble peptides in thf gave results that not only did not correlate with those obtained when using the pins, but also in some cases yielded product of the opposite topicity (handedness). Similar results were obtained in dichloromethane but results similar to those on the pins were obtained in water. Bearing in mind that the peptides studied are highly hydrophobic they may well have some tertiary structure when aggregated in water. It has therefore been suggested that these aggregates are similar to the structures formed when the peptides are attached to the pins.

They have presented a further library synthesis of phosphines which show very different properties in catalysis to those above. A library of phosphines **98** was prepared based on the well-known β-turn forming motif –Pro–D–Yyy– (where Yyy is a D-amino acid) with the phosphine-containing amino acids flanking this element.[172] The structural features that were varied in the initial library prepared were the amino acids at the N- and C-termini and substitutions of D-amino acids next to the proline of the –Pro–D–Yyy– fragment. Palladium complexes of the library members were formed on the pins from $[PdCl(\eta^3\text{-}C_3H_5)]_2$ and these screened for catalytic activity in the asymmetric addition of dimethyl malonate to cyclopentenyl acetate (Scheme 49). The selectivities obtained ranged from 34% ee for the

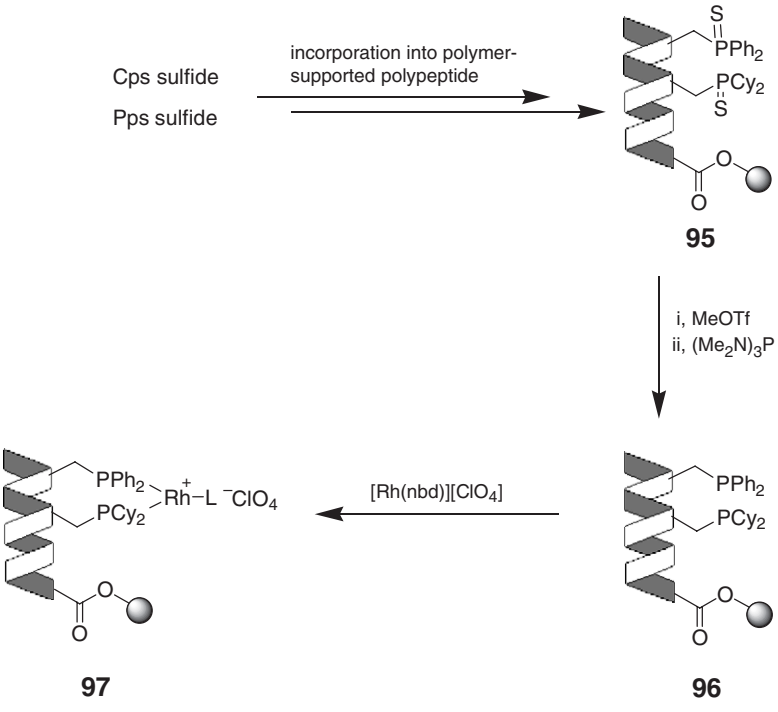

Scheme 48

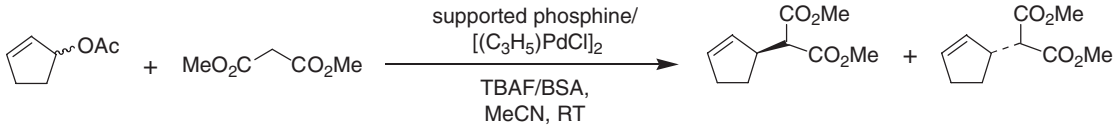

Scheme 49

lowest to 80% ee for the highest. To probe whether it was possible in this case to screen the library members accurately without having to remove them from the pins, one of the best ligands found from the investigations was prepared and then removed from the support before treating with the palladium source and screening in the test reaction. The selectivity obtained was identical to that of the supported complex showing that, in this case, it is possible to undertake screening of libraries while they are attached to the supports they are synthesized on.

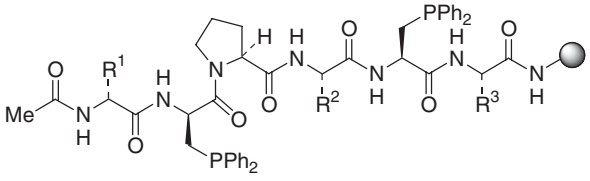

Ac–Xxx–Pps–Pro–D–Yyy–PPs–Zzz–Support

98

The methodology has been honed in a parallel approach employing phosphine-containing amino acids in conjunction with natural amino acids to develop a sensitive ligand system. Ligand candidates were screened both attached to a polymer support and also in solution. Selectivities in the addition of dimethyl malonate to cyclopentenyl acetate of up to 95% ee are reported.[173–175] Through a series of experiments, they have subsequently been able to determine

that in the peptide-derived systems either the catalyst or catalyst precursor for the reaction is a bisphosphine complex and that a phosphine–amide complex is probably not involved in the catalytic cycle.[176] It appears that the selectivity in the reaction is principally due to the phosphine amino acid in the *i*-position. Since the stereochemistry of the Pps in the $i+3$ position is not critical for selective catalysis, it is possible that the peptide region near that is not structurally well organized.

For the same reaction, the effects on catalytic activity and selectivity of varying the support upon which the peptide is immobilized have been studied.[177] The conversion and ee were determined for the addition of dimethyl malonate to cyclopentenyl acetate in six solvents using the same catalyst immobilized to six supports and data for homogeneous catalysis were obtained. From the results, Gilbertson and Yamada conclude that, if the proper match between solvent and support is possible, polymer-supported catalysts can be used to screen for selectivity with the corresponding ligand in homogeneous reaction conditions. In cases other than when there is extreme incompatibility between the solvent and support, selectivities that correlate with the results in solution are observed. While some supports appear to be relatively insensitive to different solvent systems, ultimately to obtain maximum selectivity, it is necessary to optimize the reaction conditions for a catalyst in a homogeneous environment.

It is clear that, in addition to providing a useful and simple approach for the synthesis of interesting new ligands, a peptide-based approach to ligand synthesis provides an opportunity to use peptide secondary structure to control catalyst selectivity. This is an area where real progress has already been made but where more work is needed for a more thorough understanding of how catalyst activity can be predicted.

12.14.3.6 Polymer-supported Asymmetric Phosphines and Their Metal Complexes

Many thousands of chiral ligands and their metal complexes have been reported for asymmetric C–C, C–O, and C–N bond-forming reactions but remarkably few are used on an industrial scale. One of the reasons for this is the difficulty of separating them from reaction mixtures and recycling them. Immobilization on polymer supports offers a useful solution to these problems.[178] For recent general reviews of polymer-supported asymmetric catalysis, see Refs: 12,179. The number of organometallic complexes immobilized on chiral phosphine-derived polymeric supports is quite small compared to the corresponding number of supported coordination compounds. It is the aim of this section to give an overview of the classes of supported chiral phosphine ligands found in the literature with attention focused on those where one or more organometallic case has been reported but, for completeness, selected coordination chemistry examples are also highlighted.

One of the key contributions to early polymer-supported asymmetric phosphine development was made by Kagan and co-workers with their report in 1973 of polymer-supported DIOP **101** [DIOP = 2,3-*O*-isopropylidene-2,3-dihydroxy-1,4-bis(diphenylphosphino)butane] (Scheme 50).[180] Diol **99**, prepared by ethanolysis of the corresponding acetonide, was attached to polymer-supported benzaldehyde to give the ditosylate **100** with the acetalization taking place in ~70% yield. This was then treated with $LiPPh_2$ to give **101**. This was treated with $[RhCl(C_2H_4)_2]_2$ at room temperature in benzene to give a supported Rh–DIOP complex with a metal loading of 0.12 mmol g^{-1}. Although not fully characterized, this complex was shown to contain **101**, Rh, Cl, and C_6H_6, and was used successfully as a catalyst in asymmetric hydrogenation and hydrosilylation reactions.

For completeness, it should be mentioned here that Stille and co-workers[181–183] have presented two routes to immobilized DIOP ligands **104a** and **104b** by polymerization of suitably derivitized DIOP monomers with styrene and DVB (Scheme 51). In the first approach, the optically active styryl monomer **103**, prepared from **102** and 4-styrylbenzaldehyde, was suspension polymerized with styrene and DVB using AIBN as initiator. The resulting

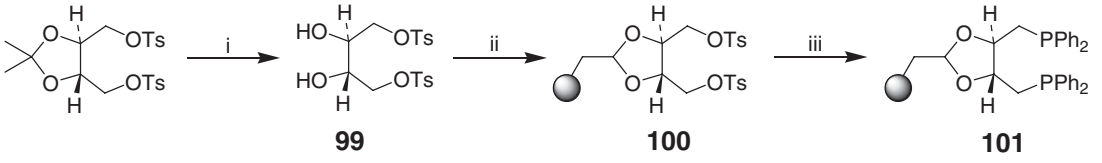

i, *p*-toluenesulfonic acid, ethanol, reflux, 24 h; ii, benzaldehyde-derivatized polystyrene, *p*-toluenesulfonic acid, benzene, reflux using Dean–Stark apparatus, 24 h; iii, PPh_2Li, THF, 20 °C, 20 h

Scheme 50

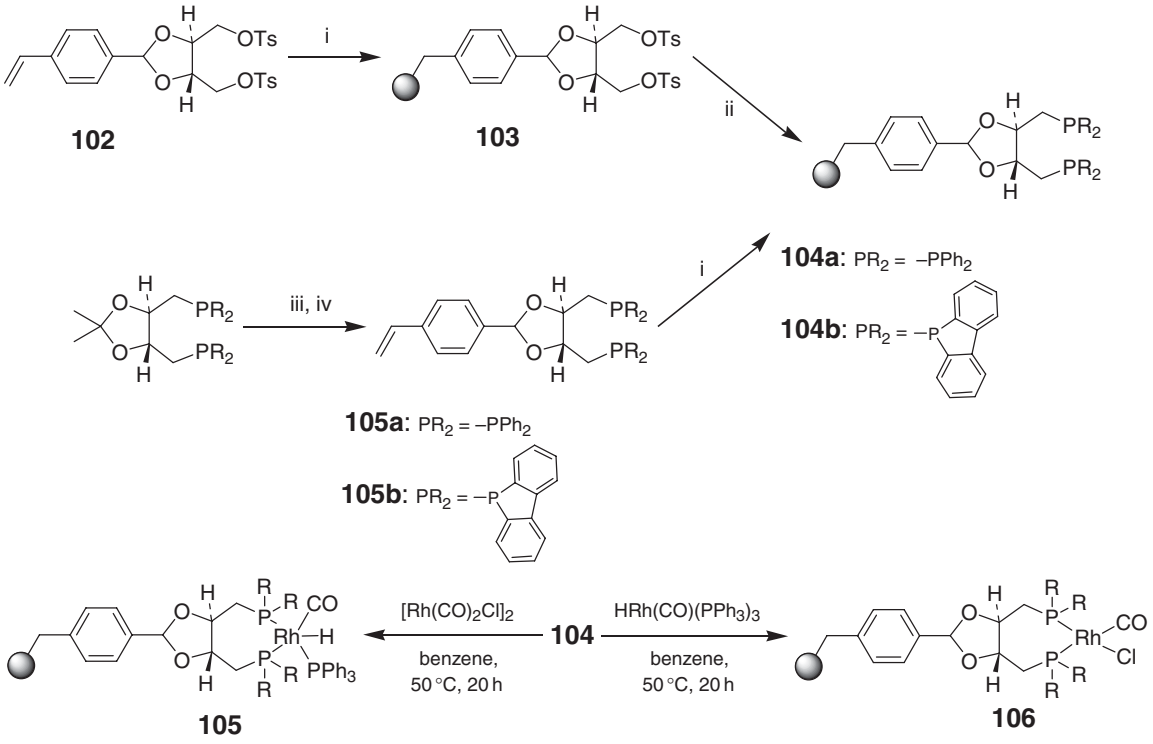

i, Styrene, DVB, AIBN, benzene, 60 °C, 10 h; ii, PR_2Li, THF, RT, 5 d; iii, conc. HCl, ethanol, reflux, 2 h; iv, *p*-toluenesulfonic acid, 4-vinylbenzaldehyde, benzene, reflux, 13 h

Scheme 51

polymer **103** was then treated with $LiPR_2$ to give **104a** or **104b**. In the other method, diphenylphosphine styryl monomer **105a** or diphenylphosphole styryl monomer (**105b**) was prepared from the corresponding enantiomerically pure DIOP by ethanolysis followed by treatment with 4-styrylbenzaldehyde. These were then suspension polymerized with styrene and DVB giving **104a** or **104b**, respectively. Using both methods, an inclusion of ~10 mol.% DIOP ligand was obtained. Rhodium complexes **105** and **106**, prepared by ligand exchange reactions with $[Rh(CO)_2Cl]_2$ and $HRh(CO)(PPh_3)_3$, respectively, were used in asymmetric hydroformylation reactions. Comparable chemical and optical yields were obtained with the supported complexes and the homogenous analogs.

Polymer-supported BINAP **110** was first prepared by Bayston and co-workers (Scheme 52).[184] Their methodology involves the preparation of a suitably functionalized BINAP monomer derivative in solution and attachment of this to a commercially available polymer support. Starting from enantiomerically pure (*R*)-BINOL, the enantiomerically pure acylated compound **107** was formed in two steps, building in an ester moiety offering the link between the ligand and a support. Reduction of the ketone functionality followed by deprotection of the phenol moieties yielded **108**, formed in good yield and left the ethyl ester intact. The phosphine groups were attached to the ligand by formation of the ditriflate and then nickel-mediated double phosphination with $HPPh_2$ giving **109**. The ligand was then attached to aminopolystyrene (0.21 mmol NH_2g^{-1}) under standard conditions for solid-phase amide synthesis to give **110** (ligand loading of 0.18 mmol g^{-1}). Aminopolystyrene was chosen as the support of choice since the amide functionality of **110** was considered to be robust to any hydrogenation conditions employed when using the supported ligand.

Two PEG-PS supported BINAP ligands have been prepared by reaction of a suitably derivitized support and dihydroxy BINAP **112** (Scheme 53).[185] Starting from acid-functionalized support **111**, **112** was attached to form **113**. A ligand loading of 0.1 mmol g^{-1} was obtained. Starting from bromo-functionalized support **114**, supported BINAP **115** was made by first treating **112** with BuLi before adding the resin.

An alternative approach to a PS-PEG amphiphilic BINAP has been reported involving reaction of BINAP-carboxylic acid **116** with an amine-functionalized PEG-PS support to give **117** (Scheme 54).[186]

An insoluble polymer containing BINAP **119** was synthesized by polymerization of 6,6′-di(aminomethyl)BINAP **118** with 2,6-toluene diisocyanate (Scheme 55).[187] Ruthenium complexes of this were then screened for activity in

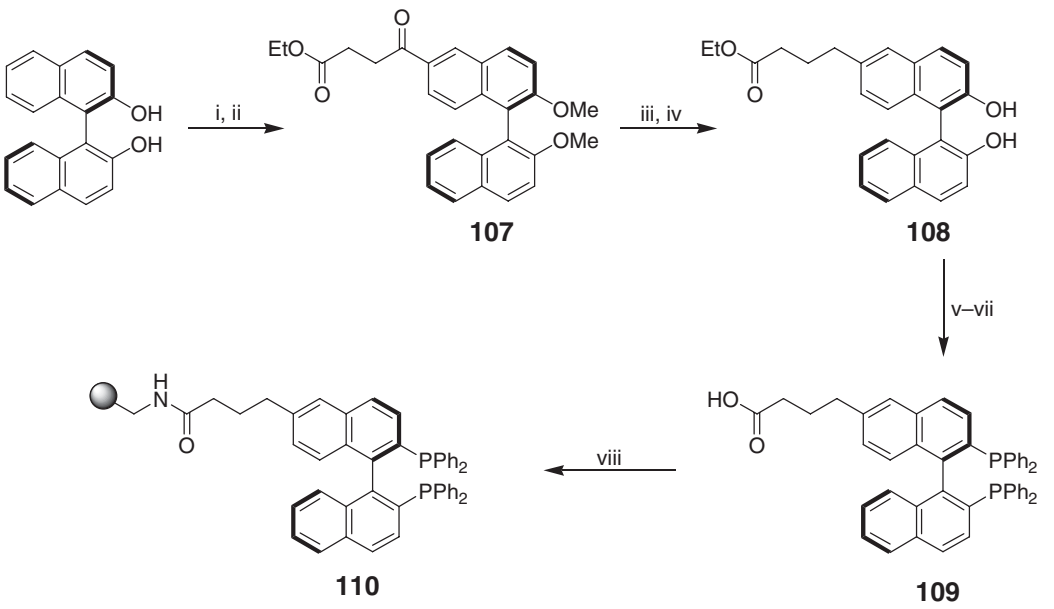

i, MeI, K_2CO_3, acetone, reflux, 18 h; ii, ethylsuccinyl chloride, $AlCl_3$, CH_2Cl_2, 0 °C → RT, 18 h;
iii, Pd on C, H_2, AcOH/EtOH/EtOAc, RT, 18 h; iv, BBr_4, CH_2Cl_2, –78 °C → RT, 3.5 h;
v, Tf_2O, 2,6-lutidine, CH_2Cl_2, 0 °C → RT, 20 h; vi, 2 equiv. + 2 equiv. $HPPh_2$, 1.2 equiv. $NiCl_2$(dppe),
DABCO, DMF, 100 °C, 24 h; vii, LiOH, THF, reflux, 20 h; viii, polystyrene-NH_2 (loading 0.21 mmol NH_2 g^{-1}),
DIC, HOBt, NEt^iPr_2, DMF, RT, 24 h

Scheme 52

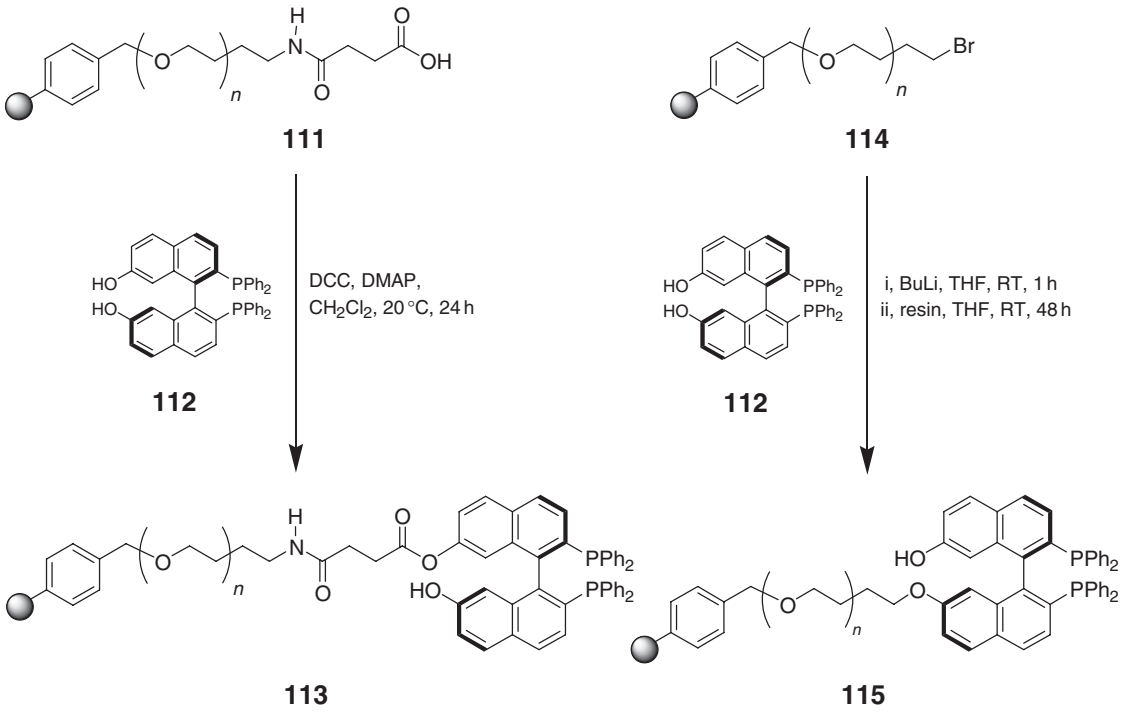

Scheme 53

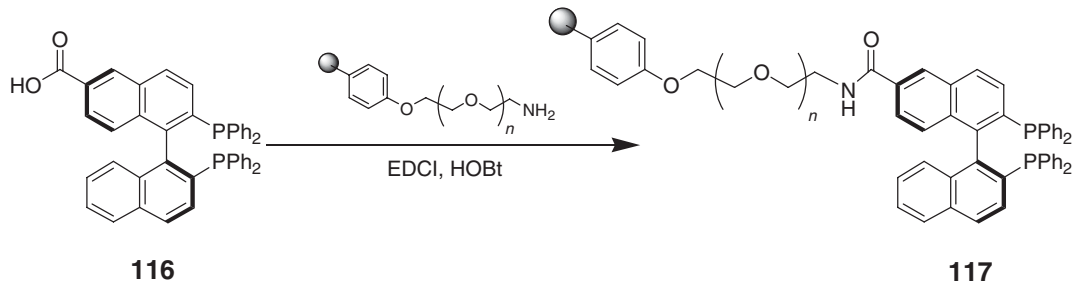

116 **117**

Scheme 54

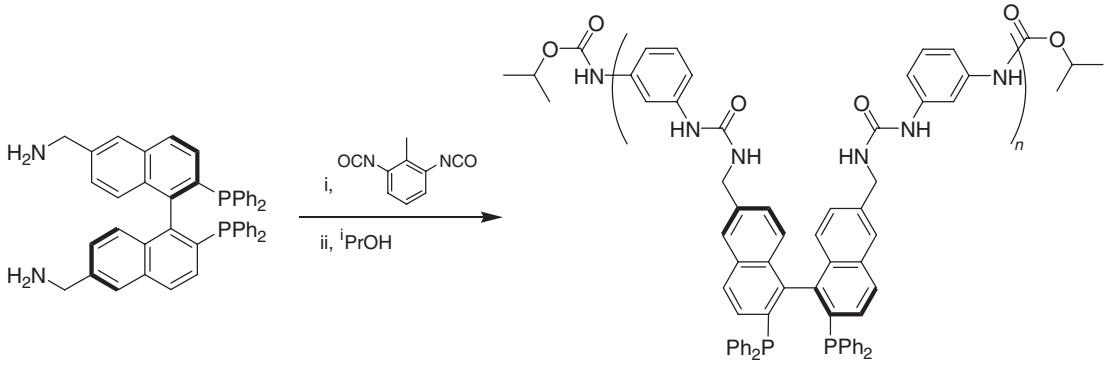

118 **119**

Scheme 55

the catalytic hydrogenation of β-keto esters[188] and aryl ketones[189] and found to compare favorably with analogs prepared from homogeneous BINAP.

Attempts to form organometallic complexes of **110** and screen them in catalysis have been somewhat limited to date, but show the usefulness and versatility of the ligand which is now commercially available. Polymer-supported BINAP′ is commercially available from Evotec-OAI. Although the ligand described in the literature has an amide linkage, the commercially available one has an ether linkage. Bayston and co-workers[184] have formed what they propose to be **121**, a ruthenium diallyl complex of **110**, by mixing **120**, HBr, and supported ligand and have found it to be an efficient and enantioselective hydrogenation catalyst (Scheme 56). The results show that the perturbation of the ligand from C_2 symmetry to *pseudo*-C_2-symmetry and the act of immobilization is not detrimental to enantioselectivity or chemical yield, a drop of only 2% in ee being observed in going from a heterogeneous catalyst from the homogeneous analog (97% vs. 99% ee). The catalyst is recyclable with only slight decreases in chemical and optical yields although reaction times need to be extended.

Two palladium coordination complexes of **68** have been reported and used in asymmetric aldol and Mannich-type reactions.[190] Both the catalysts are recyclable although longer reaction times are needed on subsequent uses. Diamine ruthenium complexes bound to **68** have also been made and used in the asymmetric hydrogenation of ketones.[191]

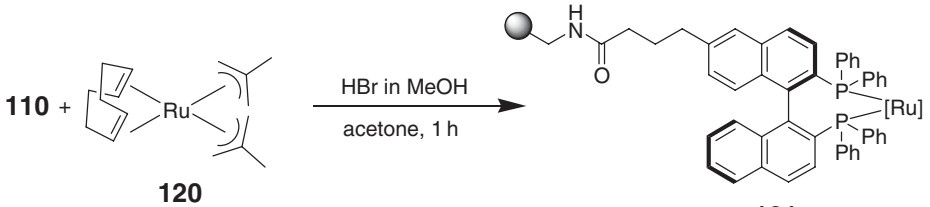

120 **121**

Scheme 56

The PEG-PS supported BINAPs **113** and **115** were used as ligands for Rh-catalyzed asymmetric isomerizations, the metal complexes being formed *in situ* by reaction of the supported ligands with $[Rh(cod)_2]^+[CF_3SO_3]^-$. Both these and their silica-immobilized counterparts were found to be less reactive than their homogenous analogs although the selectivity was found to be the same.

Several approaches to BINAP-functionalized soluble polymers have been reported. PEG-supported ligand **122** was prepared from **116** and ruthenium complexes of this screened for activity in asymmetric hydrogenation.[192] Polymer-bound BINAP ligand **123** has also been made in which the backbone is rigid and does not modify the steric or electronic environment around the active center.[193] Another approach to a PEG-supported BINAP analog was reported by Chan and co-workers.[194] In their initial work, they had prepared an insoluble polymer by direct polymerization of a BINAP precursor and terephtaloyl chloride to incorporate BINAP into a polyamide.[195] They found that ruthenium complexes formed from this material, although more active than monomeric Ru–BINAP complexes in hydrogenation reactions, did not significantly influence asymmetric catalysis. They attributed this to the fact that a stable catalyst conformation was not achieved. To overcome this, they synthesized an MeO-PEG supported polyamide material functionalized with BINAP. Starting from 5,5′diamino (*R*)-BINAP **124**, they formed a polyamide by polymerization with terephtaloyl chloride. This was then attached to a 5000 MW MeO-PEG support giving **125**. Reaction of this with $[Ru(\eta^6\text{-cymene})Cl_2]_2$ gave the η^6-aryl ruthenium complex **126**, which showed high catalytic activity and enantioselectivity in hydrogenation reactions (Scheme 57).

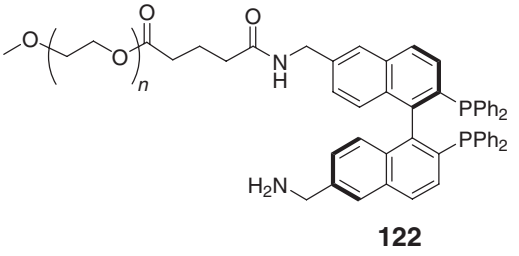

122

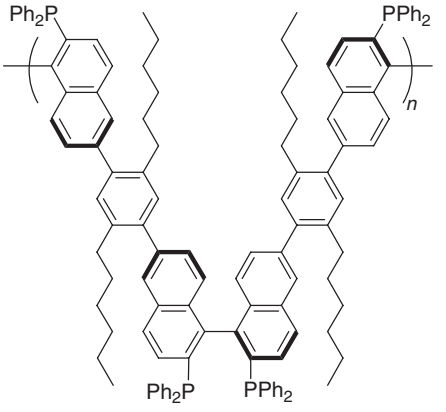

123

Dendrimer based-BINAP polymers have been prepared from **124**. A series of soluble dendritic mono-BINAP ligands with Fréchet-type polyether wedges like **127**[196] and dendritic poly-BINAP ligands like **128** have been reported[197] Ruthenium complexes of both classes of dendrimer were prepared and found to be comparable both in catalytic activity and enatioselectivity as homogeneous BINAP analogs in asymmetric hydrogenation reactions.

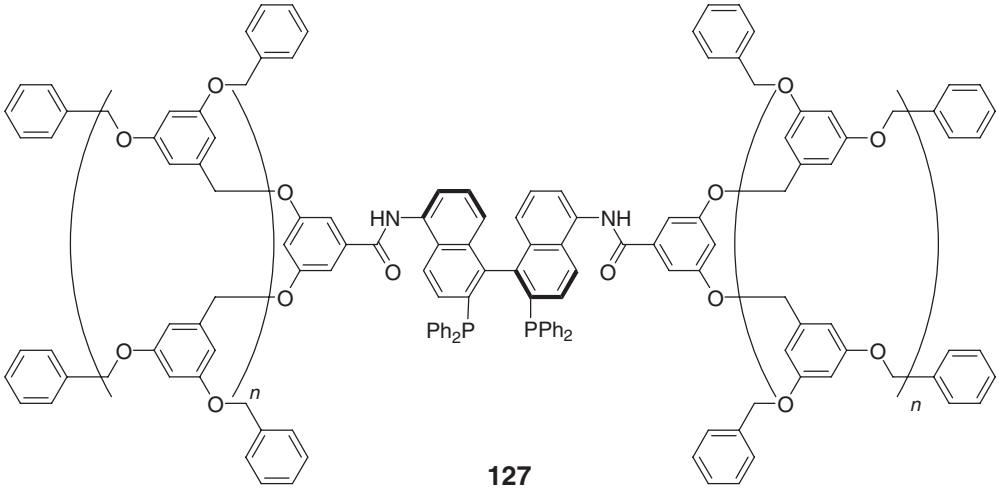

127

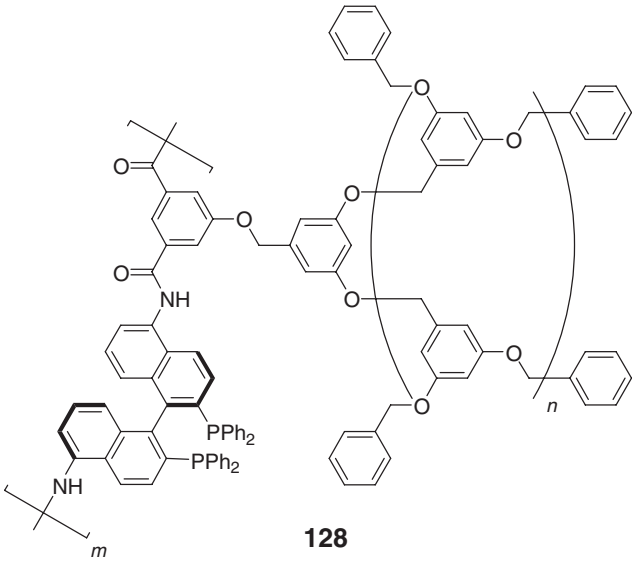

128

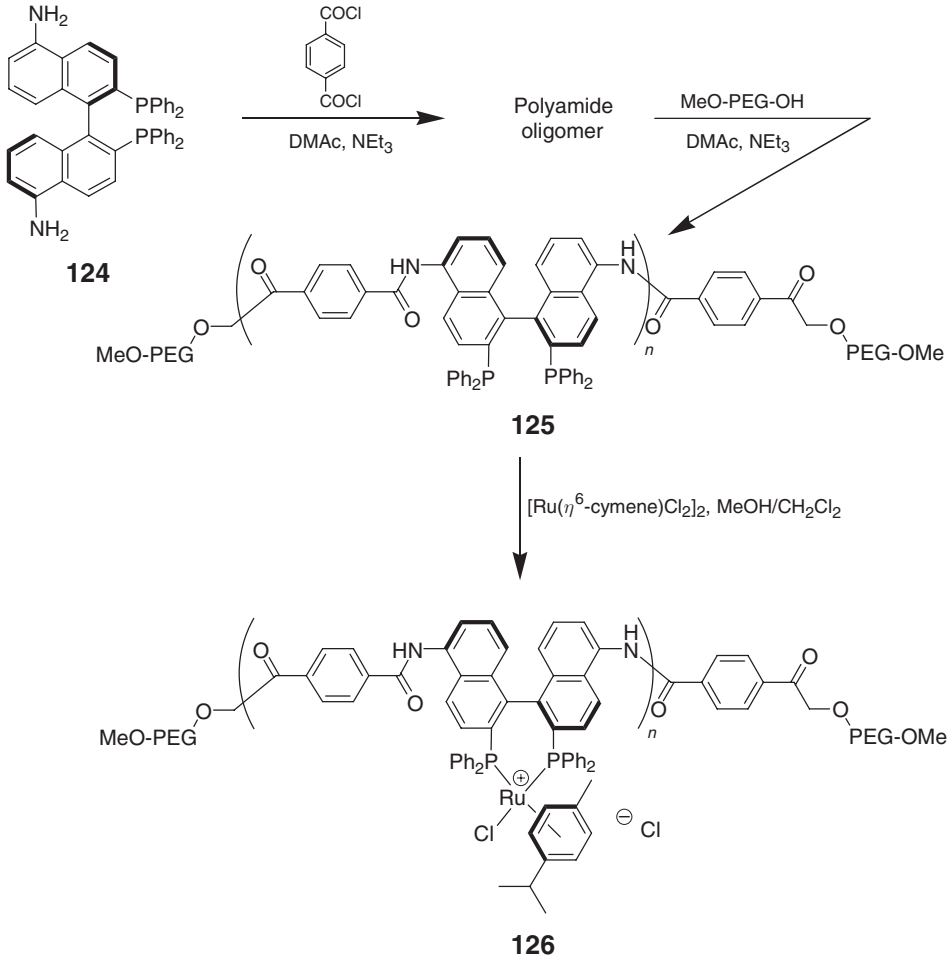

Scheme 57

Two interesting bifunctional polymeric ligands have been reported. Incorporating BINAP and BINOL functionalities, **129**[198,199] and **130**[200] have been used in ruthenium-catalyzed transformations with considerable success.

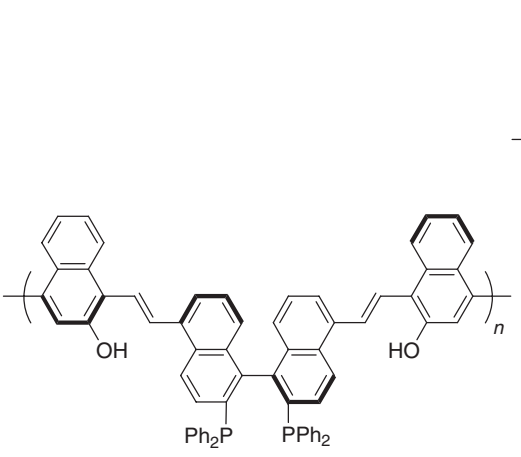

129

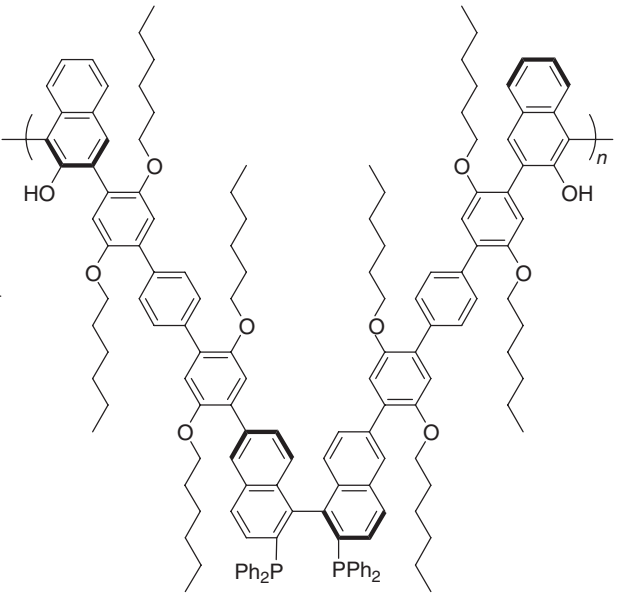

130

Nozaki and co-workers[201,202] have prepared an immobilized analog of BINAPHOS, **134** (Scheme 58). The synthesis starts with **130**, bromination of which gives **131** with the bromo substituent in the 6-position of the napthol ring. Reduction to the corresponding phosphine and Suzuki coupling with a vinyl boronic ester then gives monovinylphosphine **132**. This is coupled with either an unsubstituted or divinyl-substituted chlorophosphite to give derivitized BINAPHOS's **133** which were co-polymerized with DVB and ethylstyrene using 2,2′azobis(2,4-dimethylpentanenitrile), V-65, as the initiator to give the corresponding immobilized BINAPHOS analogs **134**. The resulting polymers contained a high degree of cross-linking. The supported Rh–BINAPHOS complexes **135** were prepared by reacting **134** with $Rh(acac)(CO)_2$ and these complexes used in asymmetric hydroformylation reactions. An alternative synthesis of **135** from **133** is also reported. First, **133** was treated with $Rh(acac)(CO)_2$ to form the metal-coordinated BINAPHOS complex which was the co-polymerized with DVB and ethylstyrene again using V-65 as initiator. Structure **135** prepared this way showed higher catalytic activity and enantioselectivity than that prepared by immobilization of the ligand followed by metal attachment. This is not that unexpected because this second route leads to a polymer with higher metal loadings as all the BINAPHOS ligand centers are coordinated to Rh and also the environment around the metal centers will be more accessible. In the route where the ligand is first incorporated in the polymer **134** and then loaded with metal **135**, the ligand is frozen as a matrix of different conformations only some of which are accessible to Rh. The authors report no difference in activity or selectivity on variation of the degree of cross-linking. Also, they find that any remaining vinyl groups in the supported catalysts, left from the polymerization step, are hydroformylated under the reaction conditions but report that this does not cause any change in the activity of the catalyst as evidenced by the reusability of the supported complex a number of times with similar activity. They have subsequently developed a solvent-free methodology using their supported Rh complexes, the reaction taking place in the gaseous phase either in a bath- or flow-type reactor.[203]

Palladium complex **136** has also been prepared.[204] This was achieved by treatment of **134** with PdMeCl(cod). A cationic derivative of this, **137**, was prepared by treatment of **136** with $NaBAr_4$ ($Ar = 3,5\text{-}(CF_3)_2\text{-}C_6H_3$) and used as a catalyst in alternating co-polymerization of ω-perfluoroalkyl-1-alkenes with CO.

With a similar methodology to that for the preparation of **18**, amphiphilic supported 2-diarylphosphino-1,1′-binapthyls **138** (MOP ligands) and corresponding coordinated palladium complexes have been prepared (Scheme 59).[205] Starting from an amine-functionalized PS-PEG support, ligands have been prepared with total conversion using acid-functionalized 2-diarylphosphino-1,1′-binapthyls under standard conditions for solid-phase amide synthesis. Using an analogous methodology, a library of supported MOP ligands **139** bearing an α-amino acid unit between the resin and the phosphine have also been prepared. Allylpalladium complexes of the PEG-PS-MOP supports have been prepared by treatment of the supported phosphine with $[PdCl(\mu^3\text{-}C_3H_5)]_2$ in dichloromethane at room temperature for 10 min. Analysis of the Pd-bound phosphines showed that all P sites are occupied, the ratio of P : Pd being 1 : 1.

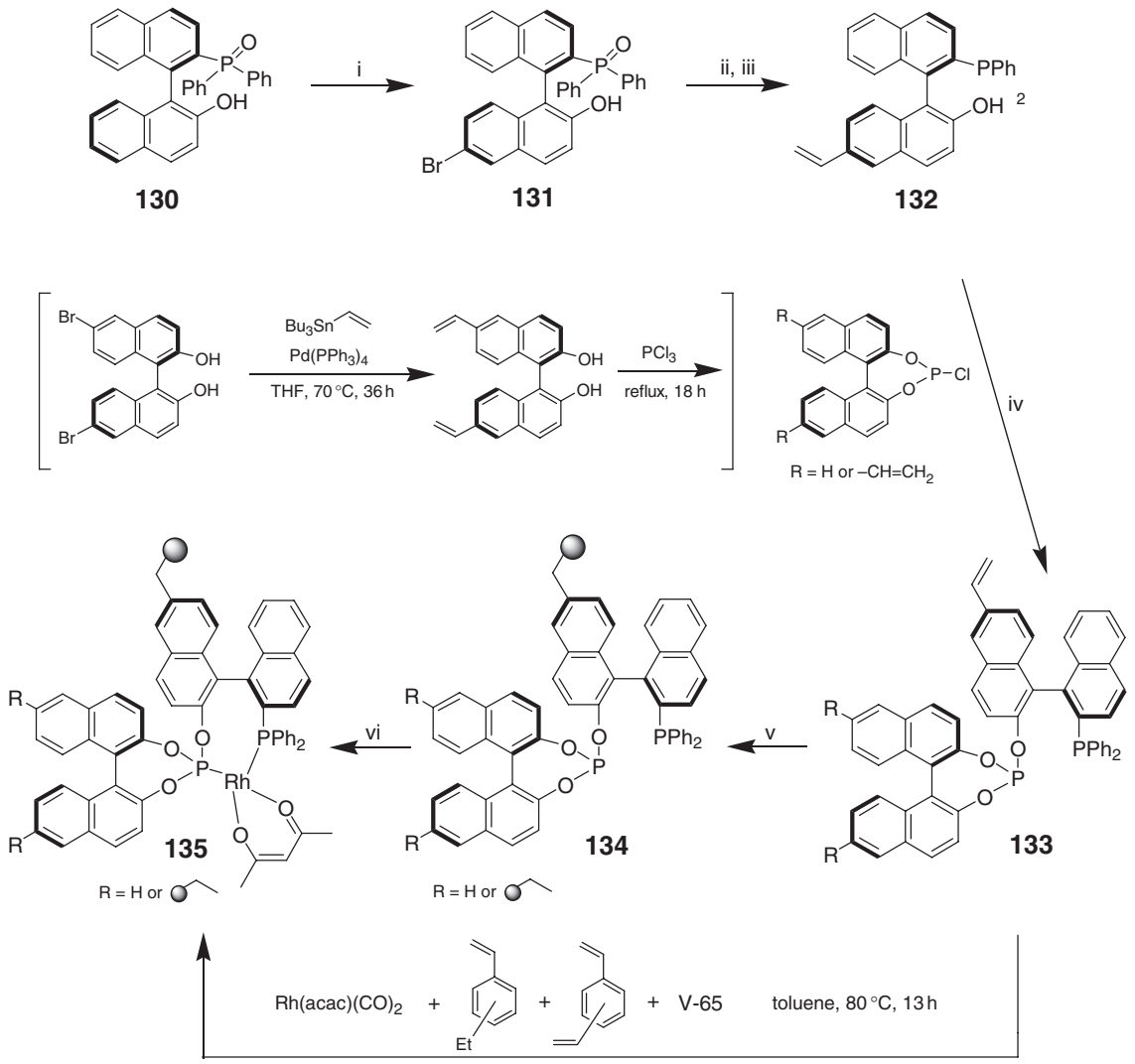

i, Br_2, dioxane, 5 °C, 2 h; ii, $HSiCl_3$, NEt_3, xylene, 0 °C → 110 °C, 22 h;
iii, 2-vinyl-5,5-dimethyl-1,3,2-dioxaborane, $Pd(PPh_3)_4$, DMF, 80 °C, 16 h; iv, NEt_3, Et_2O, 0 °C → RT, 24 h;
v, DVB, ethylstyrene, V-65, toluene, 70 °C, 5 h; vi, $Rh(acac)(CO)_2$, benzene, 60 °C, 1 d

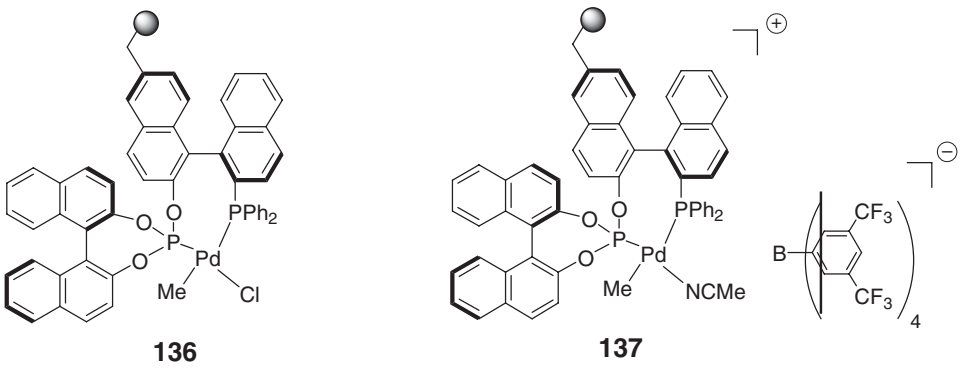

Scheme 58

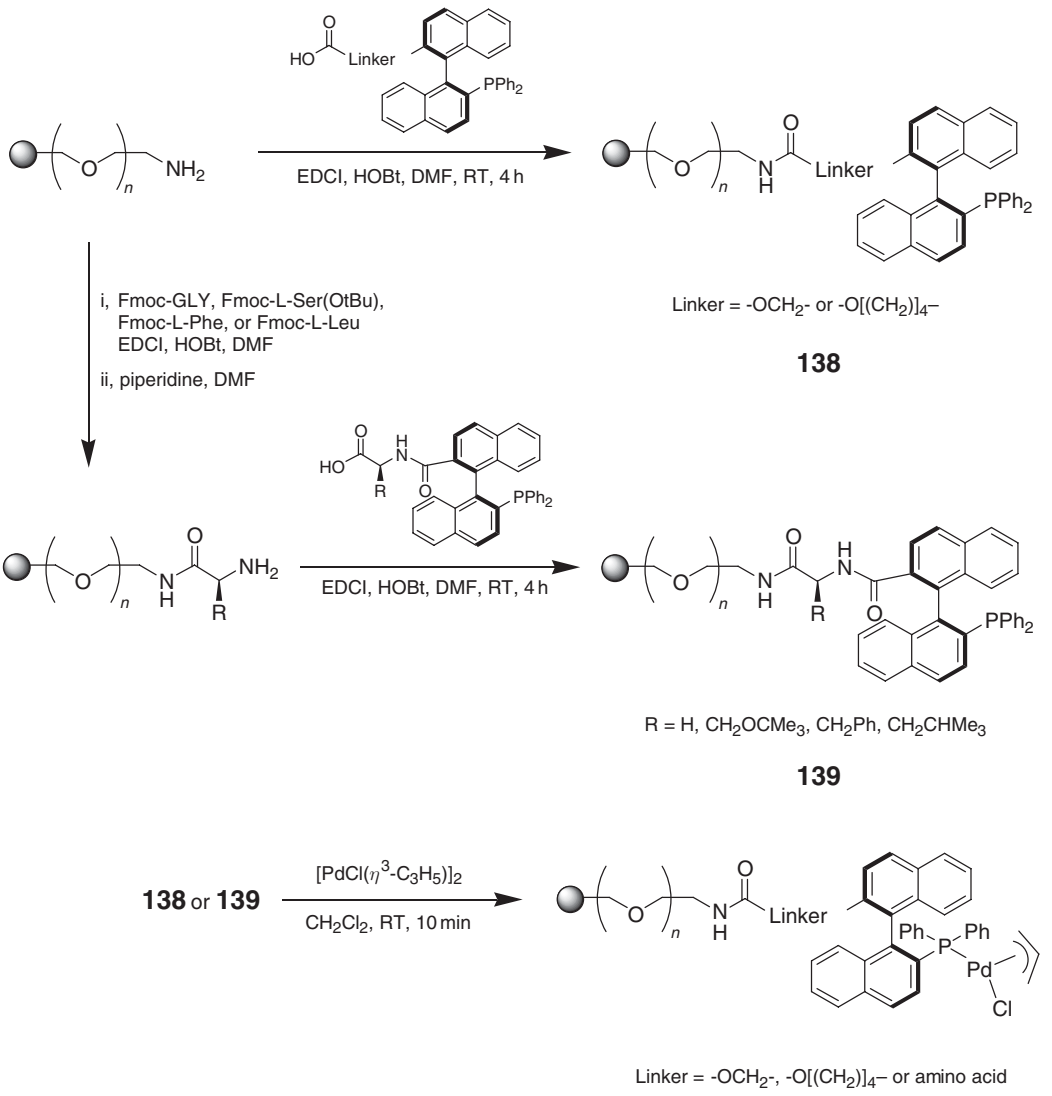

Scheme 59

Subsequent to this, the 6- and 6′-anchored PS-PEG MOP ligands **140** and **141** have been prepared and the catalytic activity in asymmetric π-allylic reduction of their corresponding allylpalladium complexes compared and contrasted.[206] The 6-anchored ligand was found to be the best and the 6′-analog the worst. This has been attributed to the fact that the 6′-position on a MOP ligand is in close proximity with the substrate moiety and thus the effect of attaching a sterically demanding tether at this position may well be to reduce catalytic activity.

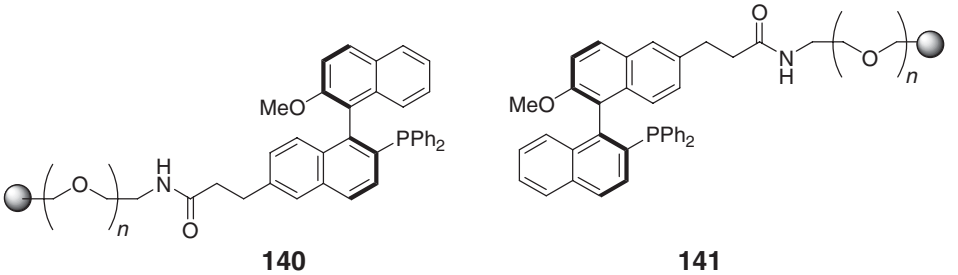

140 **141**

Also based on PS-PEG supports, ligands **142**,[207] **143**,[207] and **144**[209] have been prepared and palladium complexes formed from them screened for activity in asymmetric transformations on π-allylic functionalities.

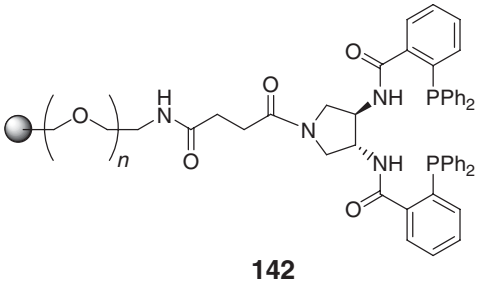

142

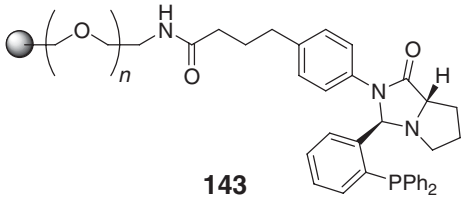

143

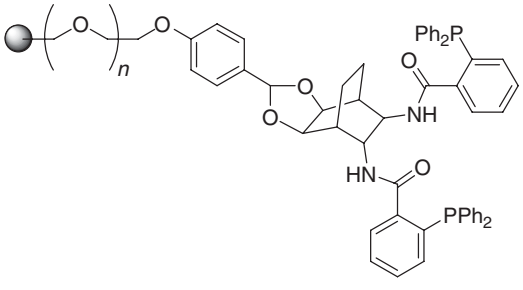

144

Built on a cyclophosphazene core, Togni and co-workers have prepared dendritic analogs **145** of the well-known ferrocene-based JOSIPHOS ligand with 6, 8, 12, and 16 functionalities.[210,211] They were used in Rh-catalyzed hydrogenation reactions and separated by nanofiltration.

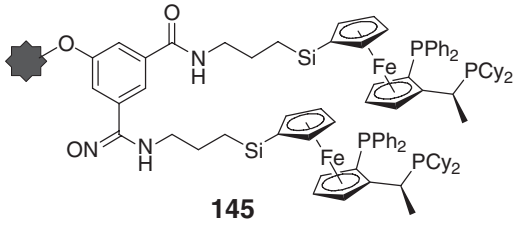

145

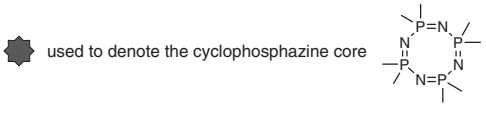

Four generations of dendrimers bearing C_2-symmetrical diphosphine rhodium complexes have been prepared and used in asymmetric hydrogenation (Scheme 60).[212,213] Acid-functionalized analog **146** of the easily immobilized phosphine pyrphos was attached to poly(propylyene)imine backbones first developed by Reetz[214] and these were treated with $[Rh(cod)_2]BF_4$.

Another pyrrolidone-based phosphine has been incorporated into amphiphilic, water-soluble diblock co-polymers based on 2-oxazalone derivatives (Scheme 61).[215] The synthesis involved the initial preparation of a diblock co-polymer precursor with ester functionalities in the side chain. This was achieved by sequential polymerization of 2-methyl-2-oxazoline to form the hydrophilic block that provides water solubility, and subsequently a mixture of ester-functionalized oxazoline **147** and 2-nonyl-2-oxazoline, the latter increasing the hydrophobicity of the second polymer block. Having made the backbone, the ester functionalities were converted into carboxylic acids giving polymer **148**, which was then reacted with the phosphine ligand to give the desired supported material, **149**. This was used in asymmetric hydrogenation reactions with success.

A polymeric ruthenium–phosphine complex using ring-opening olefin metathesis polymerization has been prepared starting from monomer **150**, which is obtained by reaction of *trans*-$RuCl_2(NBD)Py_2$ and (*R*,*R*)-Norphos **151**.[216] Attempts to affect ROMP of **150** were unsuccessful regardless of the catalyst used. This was attributed to the steric crowding of the alkylidene formed by reaction of **150** with the metathesis catalysts, making it too bulky to react again with another molecule of **150**. However, using cyclooctene as a spacing monomer, a range of polymeric complexes

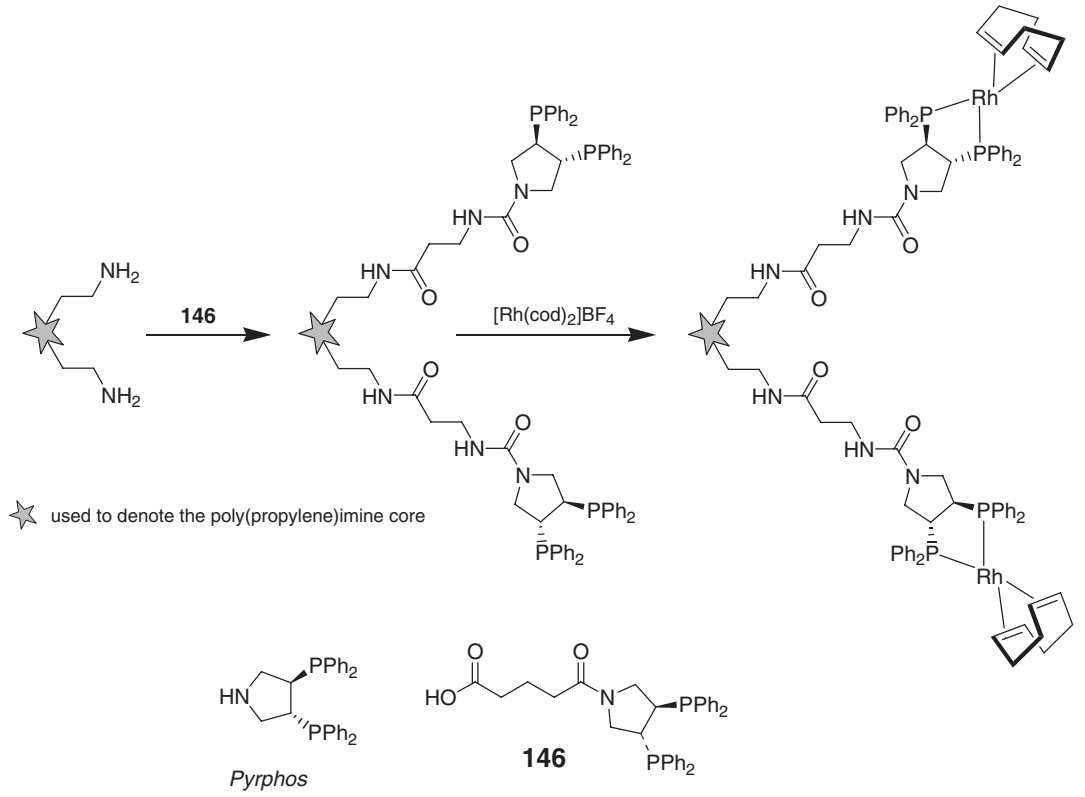

Scheme 60

could be prepared. The ends of the long-chain polymers **152** prepared this way were cross-linked with dicyclopentadiene, again using a ROMP methodology, and then the material coated as a thin film over barium sulfate., $BaSO_4$ acts as a filtration aid and also improves mechanical stability of the polymer apart from having other advantages. The polymer material was tested for activity in asymmetric hydrogenation of 1′-acetonapthone. Although the rate of reaction was much lower than that with monomer **150**, the ee was significantly higher (48% with **150**, 88% with **152**). The exact reason for this effect is currently not fully understood.

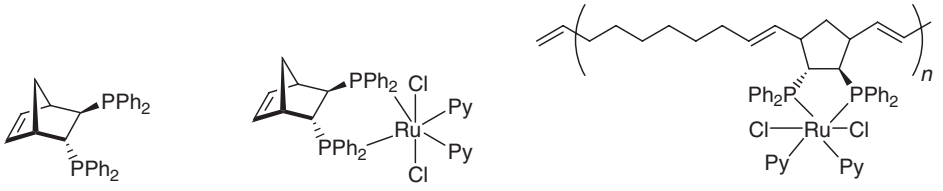

150 **151** **152**

12.14.3.7 Encapsulation and Other Entrapment Procedures

Encapsulating or entrapping materials in a polymeric coating offers an alternative to covalently linked supported metal complexes.[63] The first report of an encapsulated palladium phosphine complex was by Akiyama and Kobayashi (Scheme 62).[217] Polystyrene of 280,000 MW was dissolved in cyclohexane at 40 °C and to this was added to $Pd(PPh_3)_4$. Allowing this mixture to stir for 1 h and then cooling slowly to 0 °C leads to the formation of black capsules. The capsule walls were hardened by addition of hexane to the mixture. Analysis of the microcapsules suggested that the palladium was encapsulated as [$Pd(PPh_3)$]. The microencapsulated palladium complex (MC[$Pd(PPh_3)$]) was used in allylation and Suzuki coupling reactions, the reactions proceeding in high yields upon

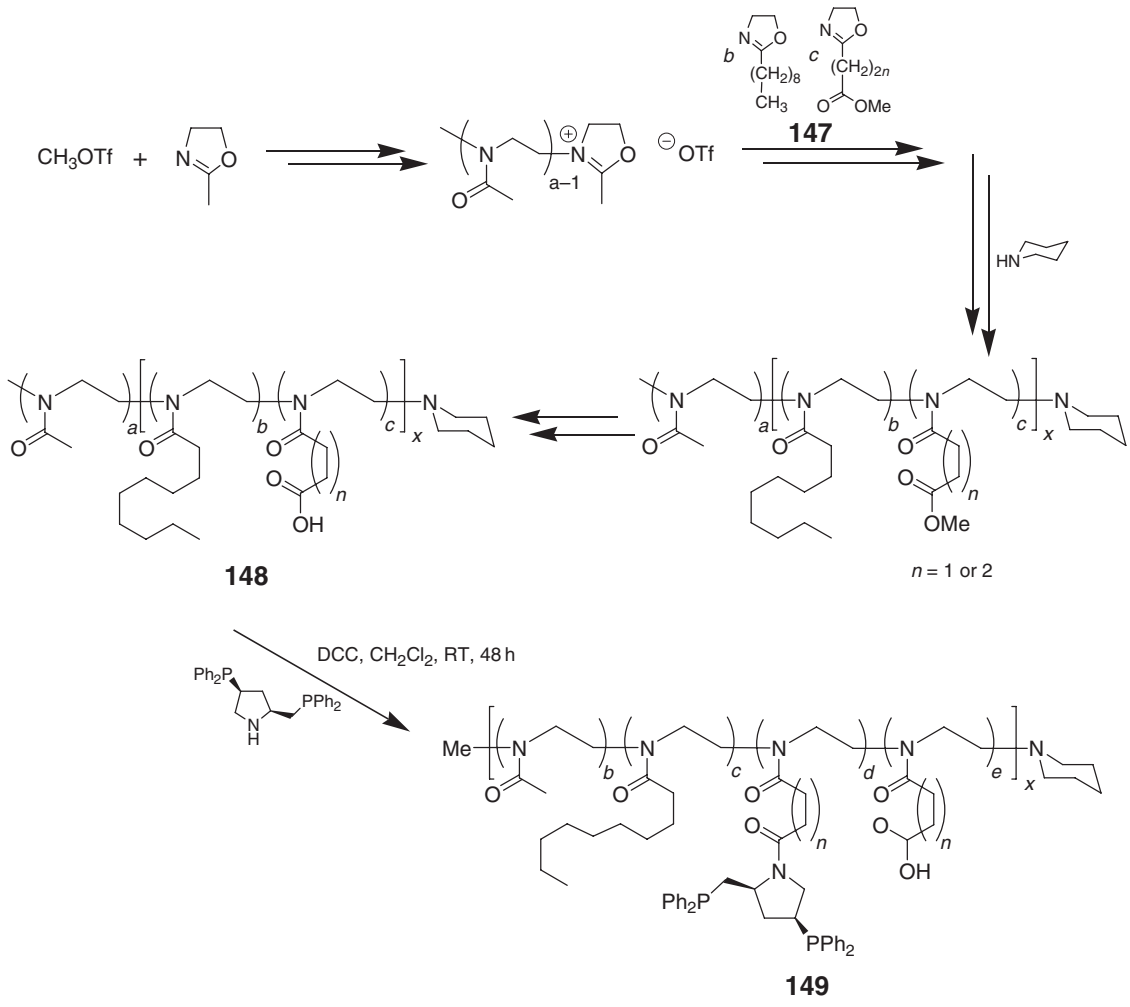

Scheme 61

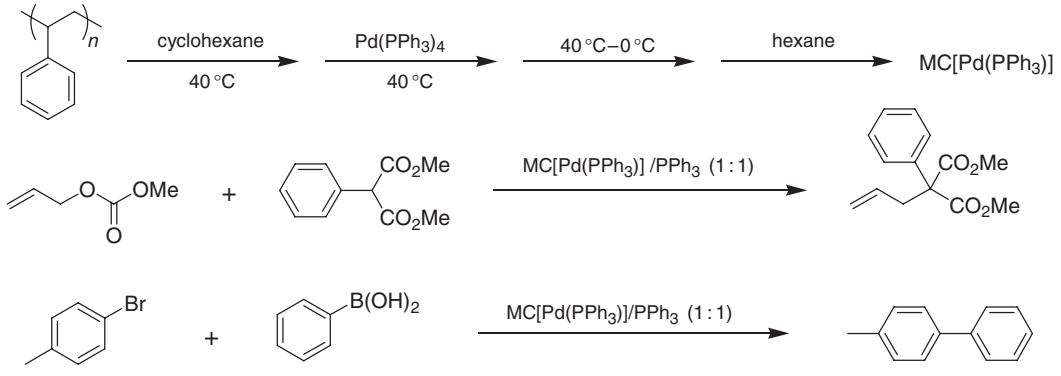

Scheme 62

addition of an additional equivalent of a phosphine ligand. For the structure and mode of operation of MC[Pd(PPh_3)], the authors suggest an 18-electron metal center that is coordinated by the one PPh_3 ligand and by aromatic rings of the polystyrene matrix. On the addition of an additional equivalent of phosphine ligand, an encapsulated 14- or 16-electron Pd(0) complex is formed, this being the catalytically active species.

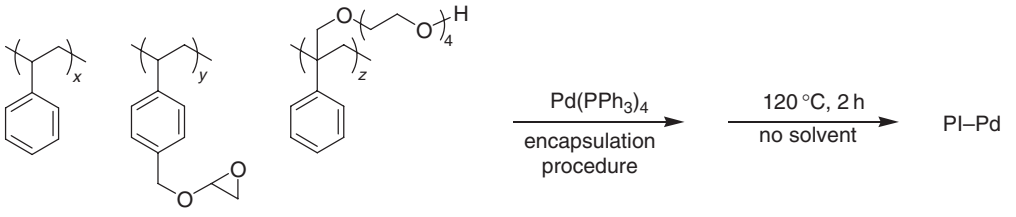

Scheme 63

A problem with the microencapsulation methodology is that the capsules formed are soluble in many organic solvents. In addition, there can be issues associated with leaching of the metal complex out of the capsules during the course of a reaction. In their second-generation encapsulated palladium complexes, Akaiyama and Kobayashi added epoxide-containing co-monomers as constituents of the matrix instead of just polystyrene and added a cross-linking step at the end of the microencapsulation process (Scheme 63).[218] This forms an insoluble polymeric material termed polymer-incarcerated palladium (PI-Pd). Again, $Pd(PPh_3)_4$ was used as the initial palladium source for encapsulation but at the end of the procedure the PI-Pd was found to contain no PPh_3. PI-Pd has been used in hydrogenation[219] and Suzuki coupling reactions.[220]

Ikegami and co-workers have prepared assembled complexes of palladium and a non-cross-linked amphiphilic polymer (Scheme 64).[221] The material, denoted as PdAS, was prepared by reaction of $(NH_4)_2PdCl_4$ with poly-[*N*-isopropylacrylamide)-*co*-(4-diphenylstyrylphosphine)], itself made by random co-polymerization of 4-diphenylstyrylphosphine and *N*-isopropylacrylamide in the presence of AIBN. The material can be used in very low loadings and with remarkably high turnover numbers.[222,223] For example, the Suzuki coupling of iodobenzene with phenylboronic acid at 100 °C in neat water using sodium carbonate as a base can be achieved using a catalyst loading of 0.00008 mol.% of PdAS.[224] The reaction did however take 96 h to reach completion and required an excess of the boronic acid. If the catalyst loading is increased to 0.005 mol.%, it is possible to perform the same reaction in 24 h using the same conditions.

For completeness, it should be noted that other groups have also developed encapsulated palladium materials but starting from palladium salts.[225] Palladium-containing polyurea microcapsules have been synthesized and used in

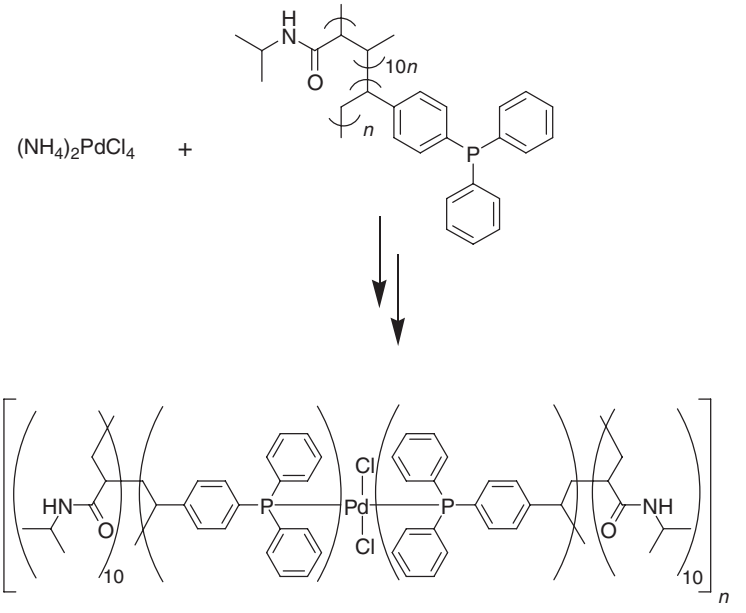

PdAS

Scheme 64

catalysis.[226] Palladium nanoparticles stabilized by poly(*N*-vinyl-2-pyrrolidone) (PVP) have been prepared from H_2PdCl_4[227] and the effects on catalytic activity of varying the size of the PVP-stabilized nanoparticles have been studied.[228] The effect of different stabilizers on the catalytic activity and stability of palladium colloidal nanoparticles has subsequently been studied.[229–231] Attention was focused on three stabilizers, namely PVP, hydroxyl-terminated poly(amido-amine) (PAMAM) dendrimers, and polystyrene-*b*-poly-(sodium acrylate). Of all the nanoparticles prepared, those with the PAMAM stabilizers were amongst the most robust but were the least catalytically active because the palladium particles are effectively encapsulated, thus limiting the access of reaction substrates. A further report of the use of PAMAM-stabilized nanoparticles has been published.[232] Cyclodextrin-capped palladium nanoparticles (CD-Pd) have been prepared and screened for catalytic activity in the Suzuki coupling reaction.[233] A difference between the palladium nanoparticles prepared here as compared to those prepared using a PVP stabilizer is that, in CD-Pd, the cyclodextrin molecules are covalently attached to the palladium particles thus rendering ~ 50% of the surface inaccessible by substrates. This, not surprisingly, impacts on the turnover frequency observed when using CD-Pd. Another problem is the solubility mismatch between the hydrophilic CD-Pd particles and the hydrophobic reaction substrates. If water-rich solvent mixtures are used, then substrate solubility becomes a real issue but the formation constants of cyclodextrin inclusion complexes are adversely effected by the presence of non-aqueous solvents. Microgel-stabilized palladium nanoclusters have been prepared and screened in the coupling reaction of aryl bromides and chlorides with phenylboronic acid.[234] The microgels were prepared from *N*,*N*-dimethylamino ethyl methacrylate (DMAM) or 4-vinyl pyridine (VP), as the functional, metal-binding co-monomer, ethylene dimethylacrylate as the cross-linker and methyl methacrylate as the non-functional co-monomer. They were loaded with palladium by reaction with $Pd(OAc)_2$. Reduction of the resultant solution gave the microgel-stabilized nanoclusters. Both the non-reduced Pd(II) material and the reduced Pd(0) nanoclusters were screened for activity in the Suzuki coupling. The Pd(0) materials are more active than their corresponding Pd(II) precursors, presumably because the latter need to be reduced *in situ* before they can enter the catalytic cycle. The nanoclusters generated from VP-functionalized microgels are less active than those from DMAM due to nanocluster aggregation.

12.14.4 Supported Catalysts for use in Olefin Metathesis

In the last 10–15 years, interest in olefin metathesis catalysis using transition metal alkylidene complexes has rapidly increased and it is now seen as one of the most important chemical reactions in organic, organometallic, polymer, and medicinal chemistry arenas.[235,236] For recent reviews on olefin metathesis and its applications, see Refs: 237,237a–237e. As research effort has increased in the area, a number of approaches for the immobilization of olefin metathesis catalysts on organic supports have appeared in the literature.[238] The first, in 1995, was by Grubbs and Nguyen using PS-PPh_2, treating it with a solution of carbene $Cl_2(PPh_3)_2Ru{=}CH{-}CH{=}CPh_2$ **153** giving **154** (Scheme 65).[239] They have also prepared the PS-PCy_2 and PS-*p*-CH_2-PCy_2 (Cy = cyclohexyl) analogs of **154**. Loadings of metal of between 0.1 and 0.56 mmol g^{-1} resin were obtained.

A polymer-supported version, **156**, of Grubbs' first-generation catalyst, $RuCl_2(PCy_3)_2Ru{=}CHPh$ **155**, has been prepared by attachment through the alkene functionality (Scheme 65).[130] Simply shaking vinyl polystyrene with **155** (~10 mol.% based on calculated vinyl resin sites) leads to the formation of **156** with complete incorporation of the metal. Complex **156** was termed a boomerang catalyst since the active alkylidene is released from the support into solution during the course of the reaction and then, in theory, recaptured on completion. However, the inherent instability of the ruthenium methylidene intermediates formed during the course of the reaction means that not only catalyst decomposition but also the recapturing at the end of the reaction by the vinyl polystyrene support is a problem. Although the longevity of intermediates can be enhanced by using regenerating agents such as styrene or

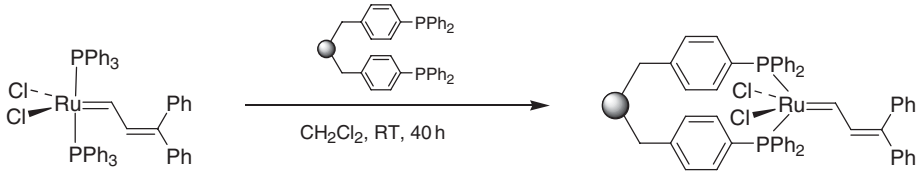

153 **154**

Scheme 65

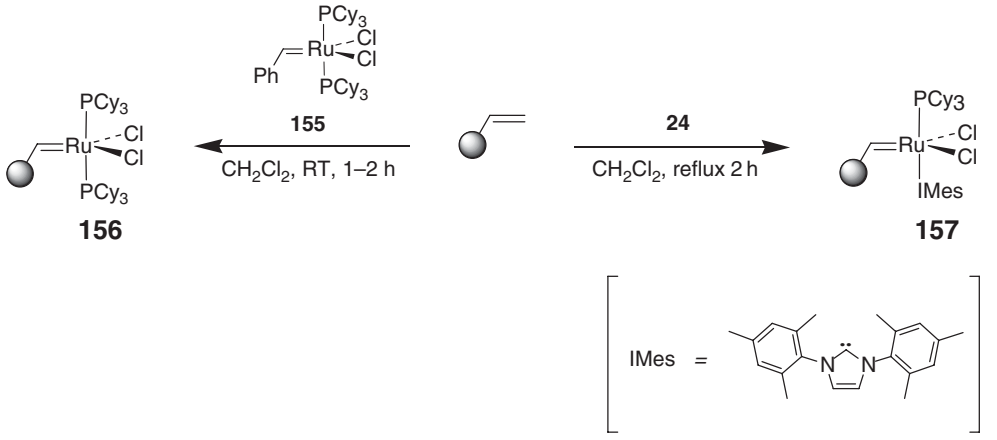

Scheme 66

bis(acetoxy)but-2-ene-1,4-diol,[240] ruthenium contamination of the products can be high and reuse of the supported complexes is not trivial. An analogous supported complex **157**, containing an *N*-heterocyclic carbene (NHC) ligand in the place of a phosphine, has also been reported (Scheme 66).[131] Ruthenium NHC complexes like **24** have increased metathesis activity and air and moisture stability over their phosphine analogs. Using **157**, ruthenium contamination levels were reported to be significantly lower than in the case of **156**.

An alternative approach to the preparation of boomerang-type supported catalysts for use in metathesis has been reported.[241,242] The metal complex was immobilized on a macroporous polymer rather than lightly cross-linked supports such as those derived from Merrifield's resin, the advantages being that swelling is not necessary to ensure accessibility of pore sites. The resin used was prepared from DVB using toluene as a porogen, the bulk polymer having a high degree of cross-linking (55%) (Figure 8). Metal complexes **24**, **155**, **158**, **159**, and **160** were immobilized on the support using a simple impregnation protocol involving heating the metal complex with the support in toluene for 1 h followed by filtration, washing, and then drying to give the supported complexes with metal loadings of 0.5, 0.35, 1.2, 0.12, and 0.46 mmol g^{-1} for **24**, **155**, **158**, **159**, and **160** respectively. The increased loading of **158** onto the support has been attributed to the increased cross-metathesis activity of the parent metal complex. Similarly, the low loading of **159** has been attributed to the low activity of the parent complex. In ring-closing metathesis reactions, they find that in many cases the supported complexes containing **24**, **155**, **158** show similar

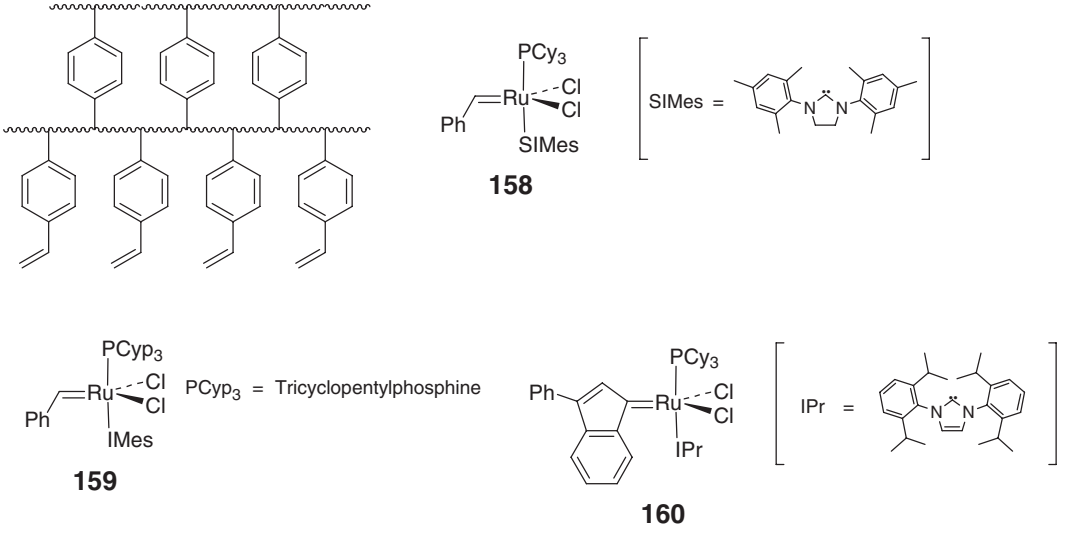

Figure 8

activity to their homogeneous analogs. In the case of **159** and **160**, the activity of the metal complex is often increased by immobilization. Although all the immobilized complexes can be recycled, that incorporating **158** exhibits particular effective recyclability, whereas that incorporating **160** displays significant loss of activity after initial use. The supported complexes however perform poorly with substrates such as oxygen-containing dienes, where a stable oxygen-ligated ruthenium carbene complex can be formed. This complex proves to be more stable and less reactive than the supported ruthenium carbene complex and, as a result, the metal stays in solution rather than attach back onto the polymer support. Consequently, the active sites on the polymer support are depleted leading to a loss of activity in subsequent cycles.

By using a carboxylate linker, **155** has been immobilized on a polystyrene support, the ruthenium complex being bound permanently to the support rather than as a boomerang catalyst (Scheme 67).[243] The support chosen for this application was fluoro-derivatized silver carboxylate **161**, prepared from hydroxyethyl-derivatized polystyrene and hexafluoroglutaric anhydride. Treatment of this with **155** gave **162** where 3% of the functional groups in the starting polystyrene resin had been metallated. The supported complex was active in olefin metathesis reactions but significant loss of activity was noted on reuse.

Blechert and co-workers used a different strategy to immobilize a metathesis catalyst bearing an NHC ligand (Scheme 68).[244] Their methodology employed for the preparation of **167** revolves around construction of the NHC ligand on the support and then appending the metal. Attachment of amine **163**, prepared from 2,3-dibromo-1-propanol and 2,4,6-trimethylaniline, to Merrifield's resin gives **164**, cyclization of which followed by anion exchange yields the supported dihydridoimidazolium chloride **165**. This is then converted to the corresponding dihydroimidazoline **166**, which is, in essence, a protected carbene. Treatment of this with **155** yields **167**. Loadings of metal complex between 0.14 and 0.40 mmol g^{-1} are reported based on a loading of Cl on the parent Merrifield's resin of 0.50 to 0.90 mmol g^{-1}.

A polymer supported version **171** of Hoveyda's robust olefin metathesis catalyst **168** has been developed (Scheme 69).[245] This was achieved starting from δ-hexanolactone, opening the ring with NaOMe followed by Mitsunobu reaction with 2-vinylphenol and saponification to give derivitized styrene **169**, which was attached to aminomethyl polystyrene to give the supported ligand **170**. Attachment of the metal occurred through the olefin metathesis reaction of **170** with **155** to give **171** with maximum loadings of 0.2 mmol Ru g^{-1} resin being obtained after five successive treatments of ligand with metal complex. The low loading and need for the arduous synthesis is attributed to the accumulation of free phosphine during the course of the reaction, something that is known to inhibit olefin metathesis.[246]

There have been other reports of immobilization of Hoveyda-type complexes on polystyrene supports. Blechert and co-workers have extended their methodology for immobilization of NHC complexes to the preparation of **172** (Scheme 70).[247] The supported NHC ligand was prepared in the same manner as for **166**, the metal complex then being attached to the support via a ligand exchange reaction. Metal loadings of 0.7 mmol g^{-1} resin were obtained. The authors also report a metal complex **174** bound to the support via

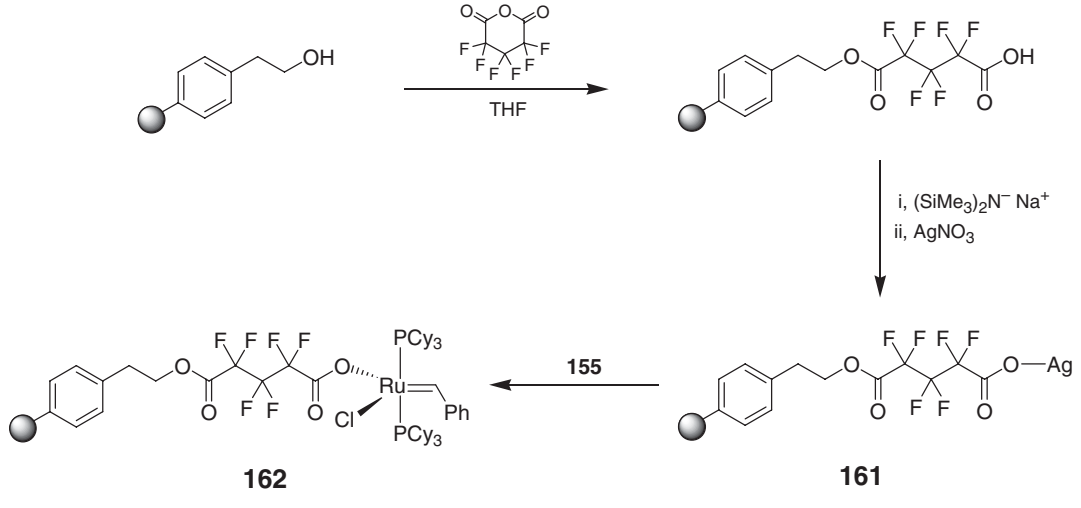

Scheme 67

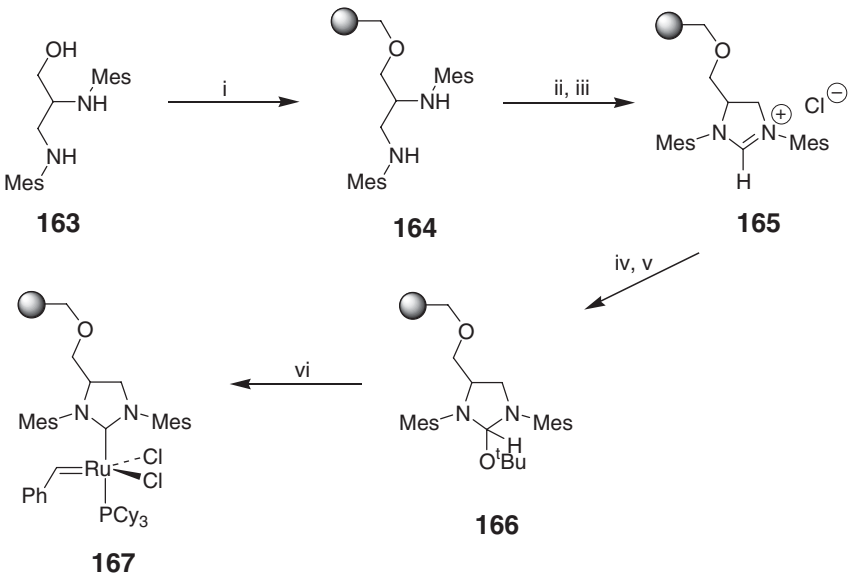

163 **164** **165** **166** **167**

i, 1.0 equiv. KO^{t}Bu, DMF, RT, 20 min, then 0.5 equiv. Merrifield's resin (1% DVB), ^{t}Bu$_4$NI, DMF, 60 °C, 12 h); ii, NC(OMe)$_3$, HCOOH, toluene, 100 °C, 100 mbar, 15 h; iii, 0.1 M HCl in THF, RT, 5 min; iv, TMSOTf, 2,6-lutidine, CH_2Cl_2, RT, 30 min; v, KO^{t}Bu, THF, RT, 1 h; vi, 1.5 equiv. **155**, toluene, 70–80 °C, 1 h

Scheme 68

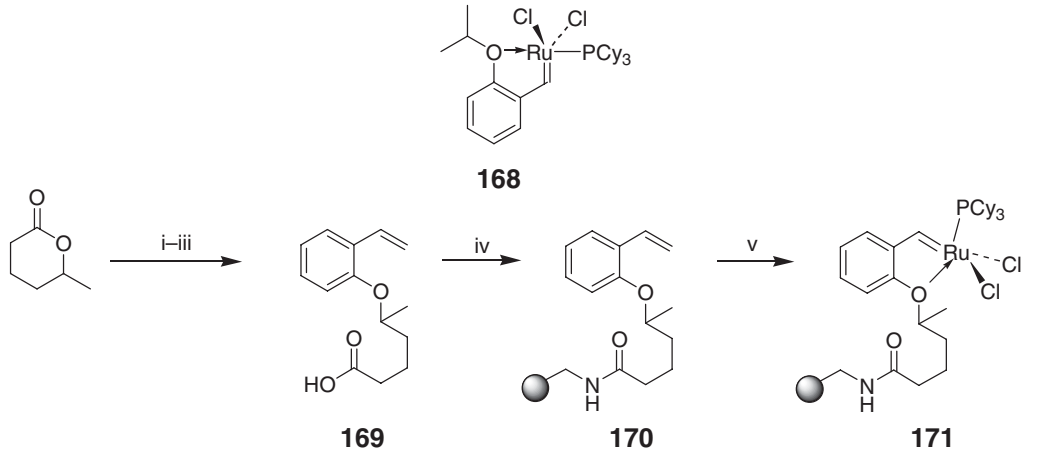

168 **169** **170** **171**

i, NaOMe, MeOH, 0 °C → RT, 6 h; ii, 2-vinylphenol, *d*-isopropyl azodicarboxylate, PPh_3, THF, 0 °C → RT, 14 h; iii, 1 M NaOH in dioxane, RT, 12 h; iv, polystyrene-NH_2, DIC, HOBt, CH_2Cl_2-DMF (1 : 1), RT, 12 h; v, **155**, dichloroethane, RT, 12 h

Scheme 69

styrene-functionalized ligand **173**. The supported ligand was prepared by coupling of 2-isopropoxy-5-hydroxystyrene to Wang resin (loading 0.72 mmol g^{-1}), used in place of Merrifield's resin in order to maximize accessibility of the metal sites. Attachment of the metal to form **174** was again by ligand exchange but using CuCl as a phosphine scavenger. By using this method, it was possible to obtain a metal loading of 0.35 mmol g^{-1} in one treatment of ligand with the metal complex.

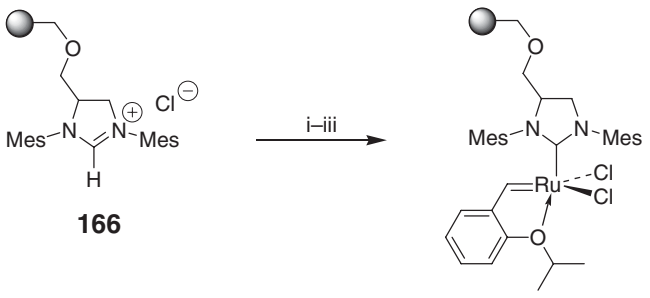

166 172

i, TMSOTf, 2,6-lutidine, CH_2Cl_2, RT, 30 min; ii, KO^{t}Bu, THF, RT, 1 h; iii, 2 equiv. **168**, toluene, 70–80 °C, 1 h

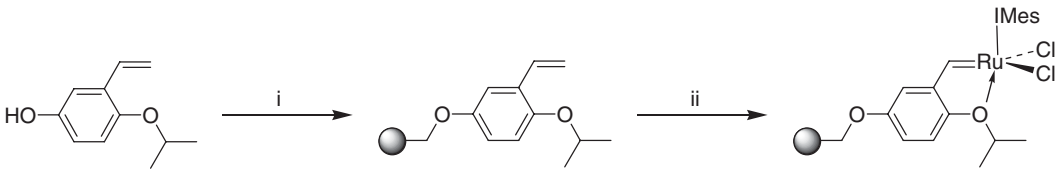

173 174

i, Wang resin, Mitsunobu coupling; ii, 1.1 equiv. **94**, 1.1 equiv. CuCl, CH_2Cl_2, reflux, 3 h

Scheme 70

Starting from butyldiethylsilylpolystyrene (PS-DES), immobilized complex **176** has been prepared using a method similar to that used for **174** (Scheme 71).[248,249] The supported ligand was made by coupling of 2-isopropoxy-5-bromostyrene to PS-DES which had been activated to form the silyl chloride **175**. Attachment of the metal to form **175** was again by ligand exchange but four successive loadings were performed since no phosphine scavenger was used. The immobilized complex could be recycled 5 to 6 times in metathesis reactions directed toward the synthesis of cyclic structures based on trisubstituted double bonds.

Starting from hydroxmethylpolystyrene and using a similar methodology to functionalize and metallate the support as used for **162**, immobilized complex **177** has been prepared.[250] Treating this with trifluoroacetic acid also gave supported complex **178**. A catalyst loading 5 times higher than that reported for **162** was achieved. Part of this can be attributed to the way that the supported silver salt is generated. Mol and co-workers use sodium bis(trimethylsilyl)-azide to deprotonate the acid moiety on the support in their synthesis of **162** whereas, for **177**, sodium hydroxide is used. The amide agent is reported also to lead to significant cleavage of the ester linkage, thus reducing the loading on the support at this early stage. In ring-closing metathesis, both **177** and **178** were found to be highly active, the latter more so than the former, and ruthenium leaching very low.

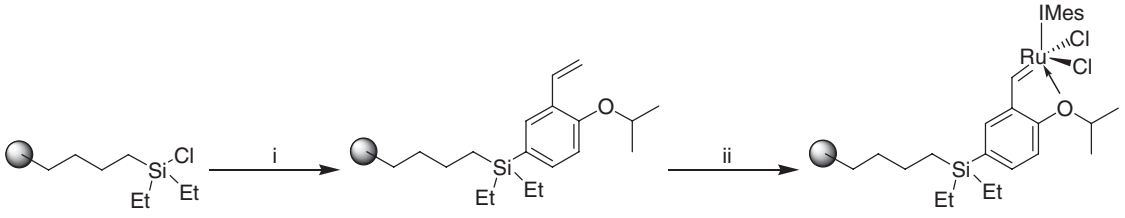

175 176

i, ^{t}BuLi, Et_2O, –78 °C then 2-isopropoxy-5-bromostyrene, –78 °C to RT, 24 h; ii, 0.25 equiv. **24**, RT 24 h—four times

Scheme 71

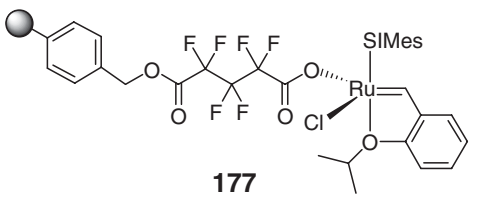

177

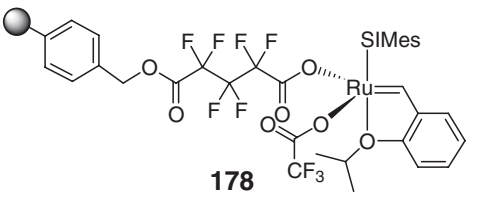

178

The tetrahydropyrimidin-2-ylidene anlogs of **177** and **178** have also been reported[251] The supported complexes **179** and **180** were prepared by an analogous route. Again, they showed excellent activity in ring-closing metathesis and leaching levels were sub-ppm.

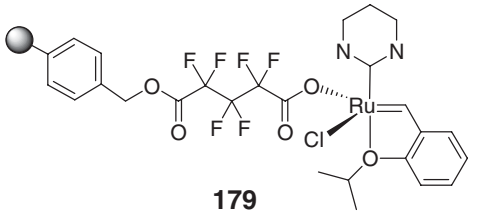

179

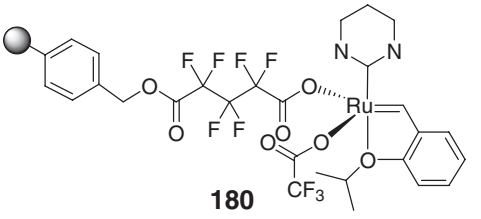

180

Solid-supported SIMes functionalized complex **181** has been prepared for use as a recoverable olefin metathesis catalyst for use in methanol and water.[252] Using a commercially available amine-functionalized PEG-based support (PEGA-NH_2), **181** was prepared in three steps (Scheme 72). It was found to promote relatively efficient ring-closing and cross-metathesis reactions.

Several routes to soluble supported metathesis catalysts have been reported. MeO-PEG based complex **182** was prepared by first attaching 2-isopropoxy-5-hydroxystyrene to the support and then treating this immobilized ligand

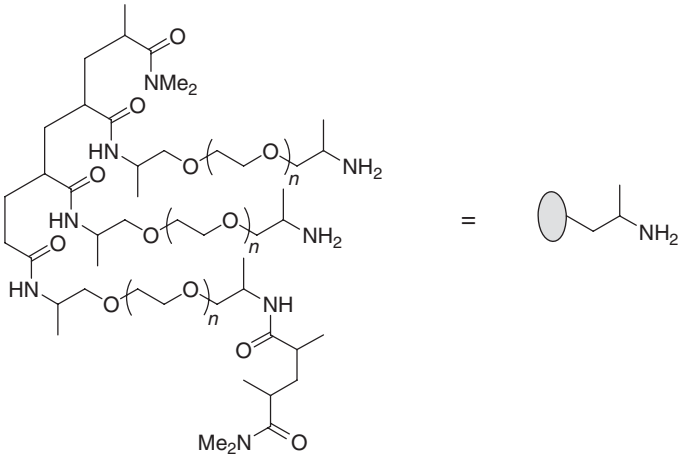

PEGA-NH_2

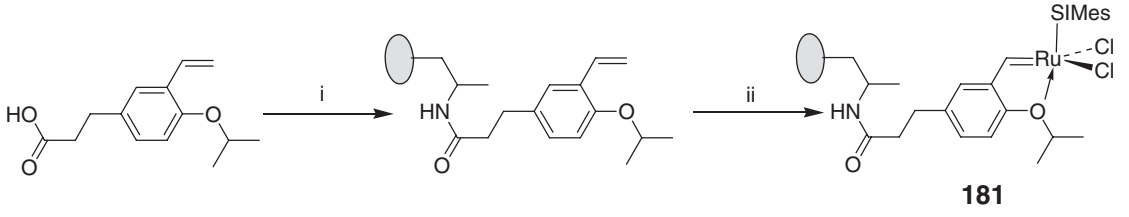

181

i, two-step standard coupling protocol; ii, 1.3 equiv. **158**, 1.3 equiv. CuCl, CH_2Cl_2, 45 °C, 4 h

Scheme 72

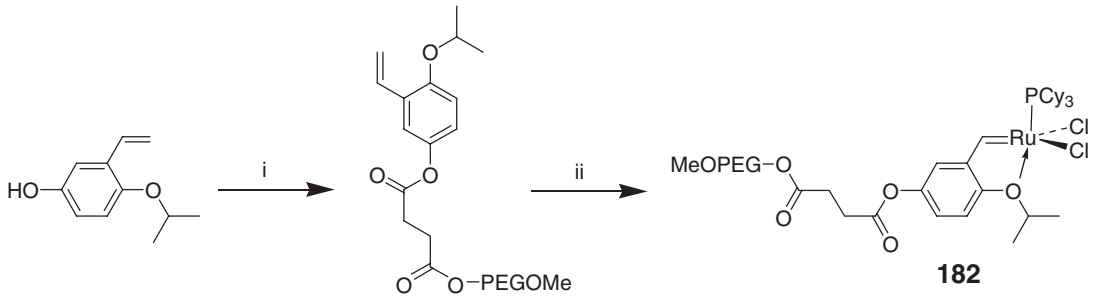

i, DCC, DMAP, CH_2Cl_2, reflux, 12 h; 0 °C Et_2O; ii, **155**, CH_2Cl_2, reflux, 2 h; 0 °C Et_2O

Scheme 73

with **155** (Scheme 73).[253] A similar strategy to prepare **184** is shown in Scheme 74.[254] Using well-defined block co-polymer **183**, reaction with 2-isopropoxy-5-hydroxystyrene followed by metallation with **158** gave **184**. A PEG-based analog of **184** was made by reaction of **158** with supported ligand **186**, itself prepared from known isopropoxy-styrene derivative **185** (Scheme 75).[255] The three supported complexes **182**, **184**, and **187** all proved active and recyclable in ring-closing metathesis reactions.

The synthesis of three soluble PEG-supported ruthenium complexes **188**, **189**, and **190** have been reported.[256] Their activity in olefin metathesis reactions as well as the ease of recovering and recycling has been compared and contrasted. Boomerang-type complex **188**, although being catalytically active, could not be recovered or recycled.

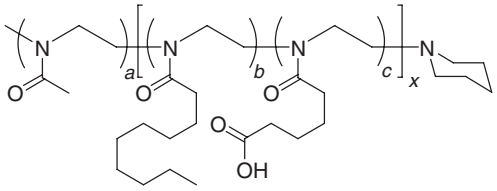

183

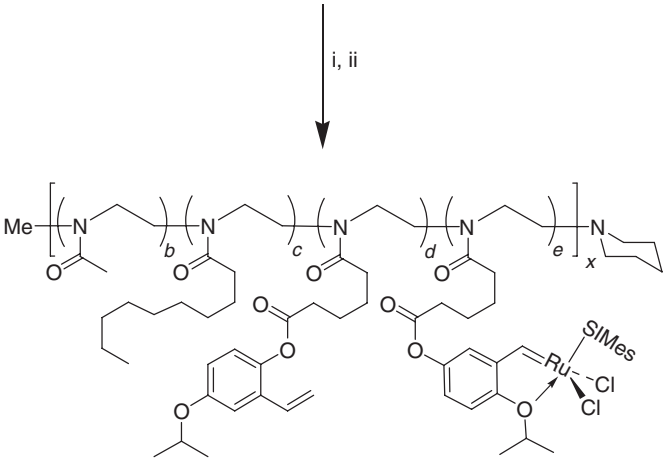

184

i, DCC, DMAP, CH_2Cl_2, RT, 48 h ii, **158**, CuCl, CH_2Cl_2, 45 °C, 1 h

Scheme 74

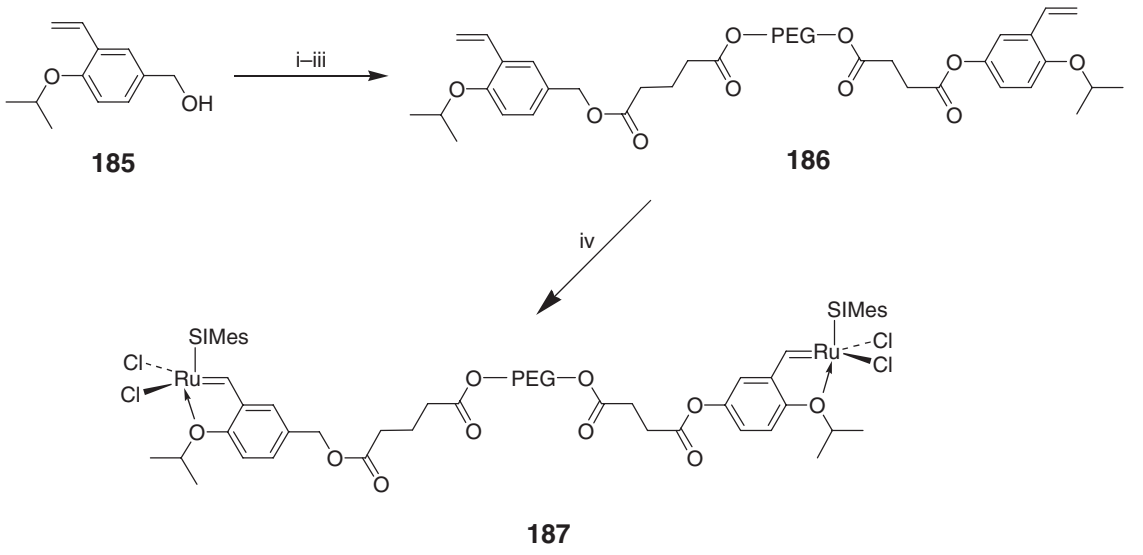

i, glutaric anhydride, Et_3N, DMAP, THF, reflux, 16 h; ii, PivCl, Et_3N, Et_2O, 0 °C, 2 h; iii, PEG, Et_3N, DMAP, CH_2Cl_2, RT, 16 h iv, **158**, CH_2Cl_2, CuCl, 40 °C

Scheme 75

Both **189** and **190** were catalytically active and also could be recovered and recycled, the carbene complex **190** being better in all three regards than the phosphine-substituted analog **188**.

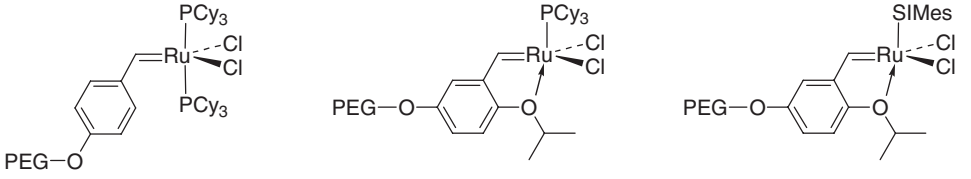

Hoveyda and co-workers have reported the preparation of **198**, the first polymer-supported chiral catalyst for enantioselective olefin metathesis.[257] Complex **198** is based on **191**, an enantioselective catalyst prepared and screened by the same workers. The route to the preparation of **198** is shown in Scheme 76. The strategy taken was to prepare a system where the chiral ligand was attached to the polymer by a non-labile tether that imposes little or no steric influence on the metal center. Treatment of biphenol **192** with bromine and sodium acetate in acetic acid yields the non-aromatic bromide **193** which, after 5 days in the solid state, rearranges to give **194**. Reaction of this with 4 equiv. of *p*-vinylbenzyl magnesium chloride and subsequent protection of the phenol groups as the MOM ethers leads to the formation of **195**. This was then co-polymerized with styrene before removing the MOM-protecting groups to give the supported chiral ligand **196**. The supported metal complex **198** was prepared by deprotonation of **196** with $KN(TMS)_2$ followed by treatment with **197**. A metal loading of 0.23 mmol g^{-1} was obtained. The supported complex proves active in asymmetric ring-closing metathesis reactions, showing lower activity than the homogeneous analog but as good an enantioselectivity. Structure **198** can be recycled but increasing degrees of leaching occur on each use.

Metathesis polymerization has been used to prepare supported complexes for use in olefin metathesis. Blechert and co-workers have made what they term as self-generating recyclable olefin metathesis catalysts (Scheme 77).[258] Oxanorbornene monomer **201** was prepared by the reaction of the potassium salt of **199** with bromide **200** followed by a Wittig olefination. Treatment of **201** with **158** in the presence of CuCl as a phosphine scavenger gave polymer **202** with a metal loading of 1%. Although this was itself an active olefin metathesis catalyst, the rate of reaction was very slow, reaction times of 7–12 h being required for quantitative conversion. The poor reactivity of **202** was attributed to the difficulty in forming the catalytically active 14-electron species in the presence of 99 equiv. of

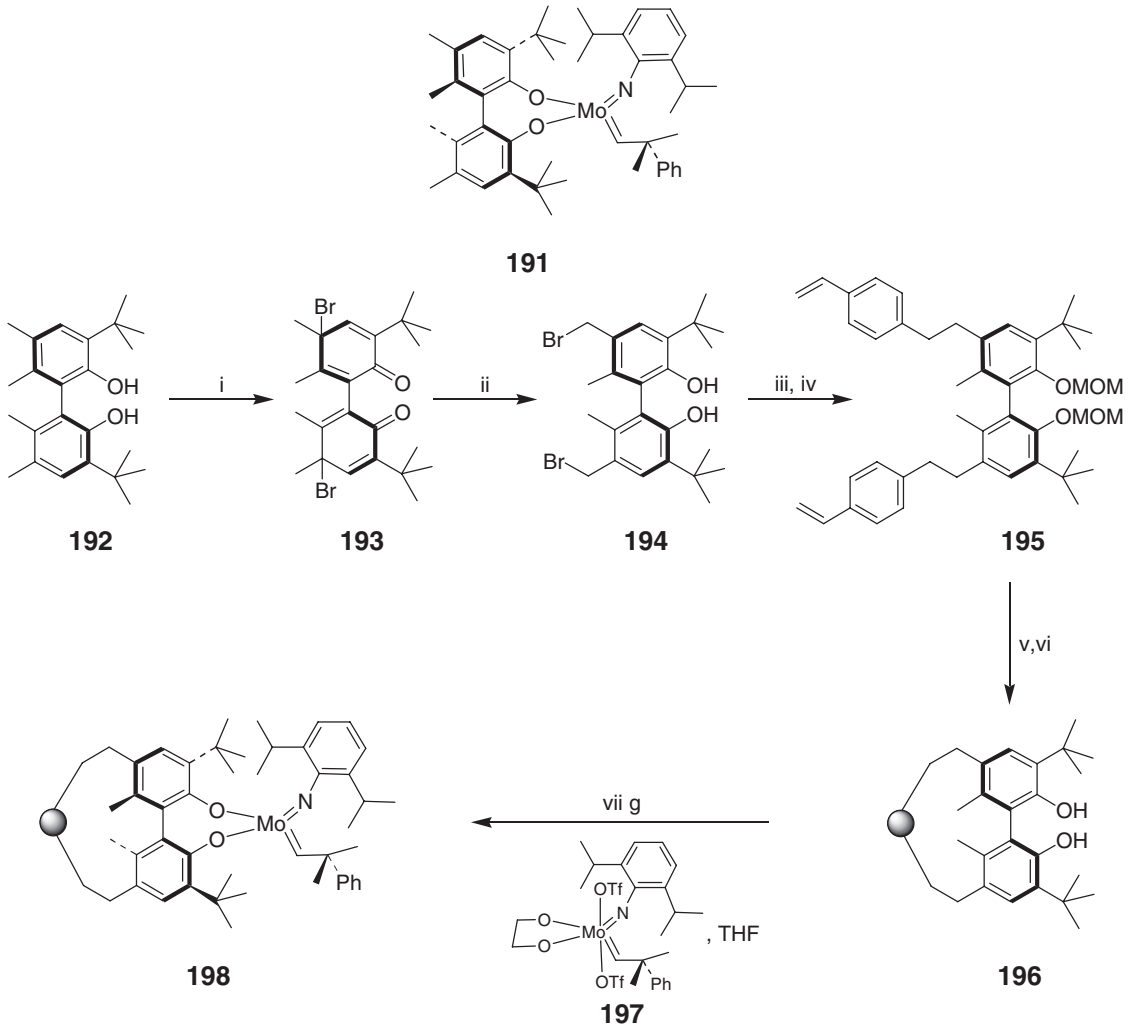

i, Br_2, 2 equiv., NaOAc, AcOH, RT, 30 min; ii, 5 days in solid state; iii, *p*-vinylphenyl magnesium chloride, THF, –20 °C, MeOH, 1 h; iv, KH, MOMCl; v, benzoylperoxide, styrene, poly(vinyl alcohol), H_2O, toluene, 90 °C, 24 h; vi, MeOH, HCl, THF, RT, 48 h; vii, $KN(TMS)_2$, THF, RT, 24 h

Scheme 76

ligand. Therefore, **203**, a polymer with a higher metal loading, was prepared. Rather than generate this by simply increasing quantity of **158** added to monomer **201**, it was decided to add oxanorbornene **204** as a co-monomer, thus minimizing the chances of two catalyst groups ending up next to each other in the final polymer. Using **203**, it was possible to perform a wide range of ring-closing metathesis reactions under mild conditions and to recycle and reuse the supported catalyst by precipitation with diethyl ether.

A ROM-derived version of chiral Schrock catalyst **191** has been prepared (Scheme 78).[259] Reaction of **205** with sodium norborn-5-ene-2-methanolate yielded polymerizable phenol **206**. Treatment of this with catalyst **207** produced the desired ROM polymer **208** which could be treated with **197** to yield **209** with loadings up to 0.552 mmol g^{-1}. High yields as well as good enatioselectivities were obtained when using **209** in test reactions.

Hoveyda, Shrock and co-workers also invoked **206** in their synthesis of chiral Mo complexes bound to polynorbornene supports.[260] Reacting this with equal amounts of **210** and norbornene and 1 equiv. of **197** gave polymer **211**, via an Mo alkylidene (Scheme 79). Polymers with different levels of cross-linking were prepared by varying the ratio of **206** to **210** used. In the same study, analogs **212** and **213** were also prepared by use of the appropriately substituted derivative of **197**. In addition, the corresponding polystyrene-bound complexes **214** and **215** were synthesized by the

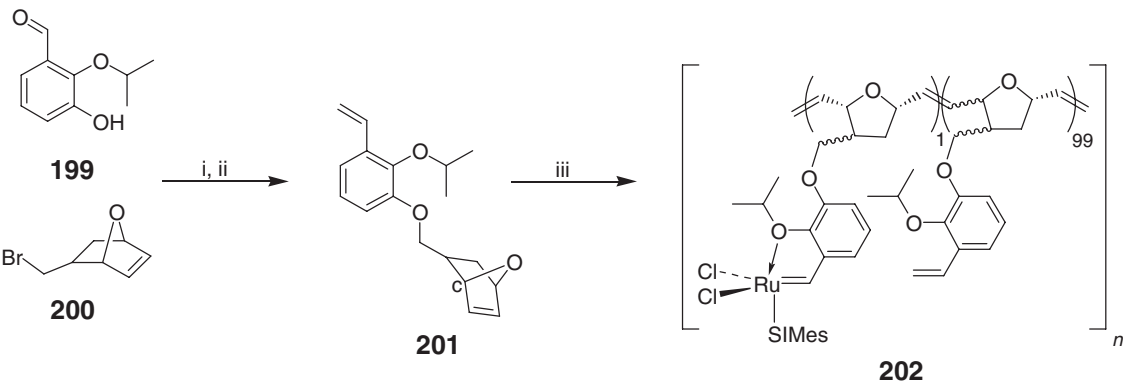

i, K_2CO_3, DMF, 60 °C; ii, $Ph_3P{=}CH_3Br$, Et_2O; iii, **96** (1 mol%), CH_2Cl_2, CuCl, 20 °C

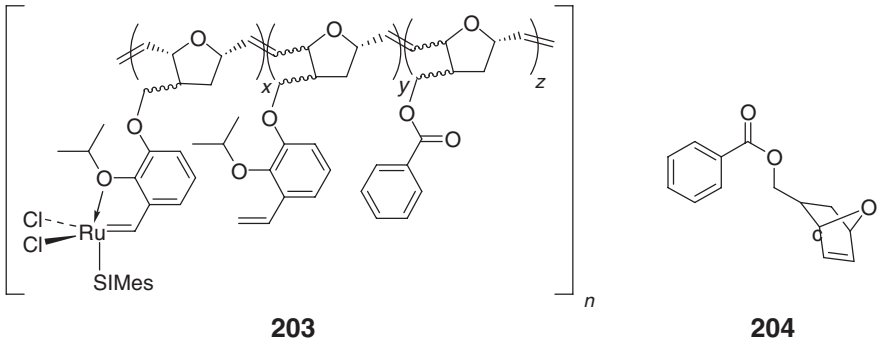

Scheme 77

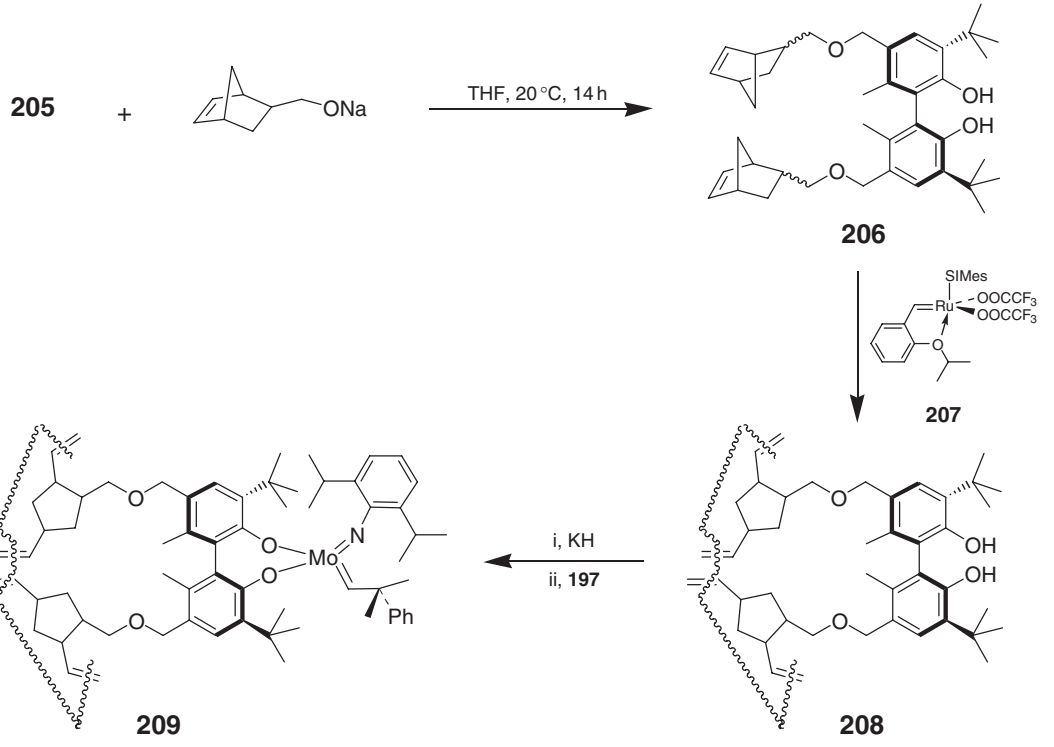

Scheme 78

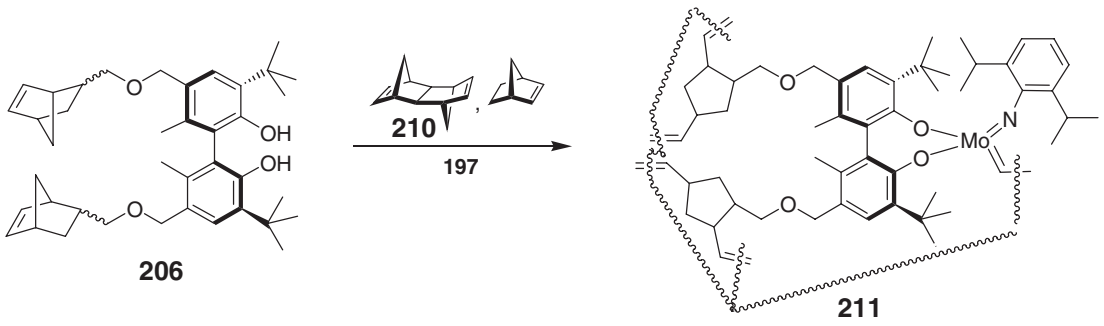

Scheme 79

method used for **198**. All these were then screened in enantioselective olefin metathesis reactions. When using **211**, as the degree of cross-linking was reduced, the reaction efficiency increased such that when using an 8% cross-linked polymer, levels of reactivity were nearly identical to those of the homogeneous analog. At this level of cross-linking, the polynorbornene-based complexes were more active than their polystyrene analogs, this being attributed to a higher degree of swelling and flexibility in the former. A major problem with olefin metathesis catalysts is decomposition of the metal complex. It was observed that the supported complexes had the same lifespan as their homogeneous analogs. There could be sufficient structural mobility within the polymers such that bimolecular decomposition is possible, particularly because the concentration of metal centers within the polymer is significantly higher than in the related homogeneous systems. If site isolation was possible even then decomposition could occur via metallacyclobutane intermediates. Interestingly, while olefins in the polymer backbone of **209** are not attacked during catalytic metathesis reactions, the opposite is true when using the more reactive, less sterically crowded **212** and **213**.

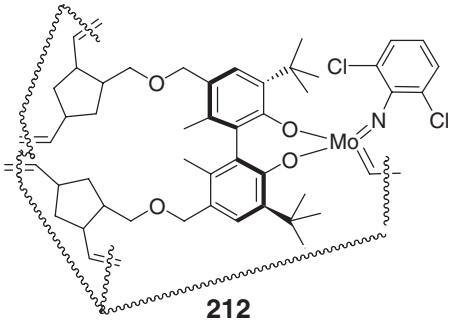

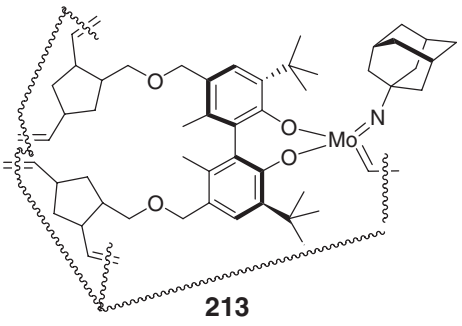

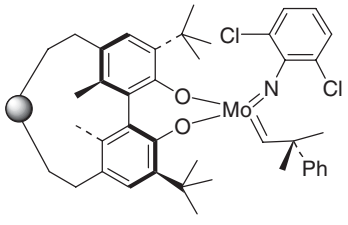

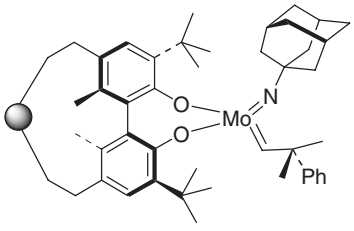

A wide range of metathesis catalysts immobilized on monolithic supports have been reported by Buchmeiser and co-workers. These non-porous supports are amenable to continuous-flow applications or can be prepared in a disk-shaped format applicable to high-throughput screening.[261] Using a ring-opening metathesis based protocol, a number of functionalized monoliths have been prepared in a one-step procedure within the confines of a poly ether ether ketone (PEEK) column from norborn-2-ene and **210** or **216**, toluene and 2-propanol, using **155** as the polymerization catalyst.[61,262] The "living" ruthenium termini located at the surface of the resultant

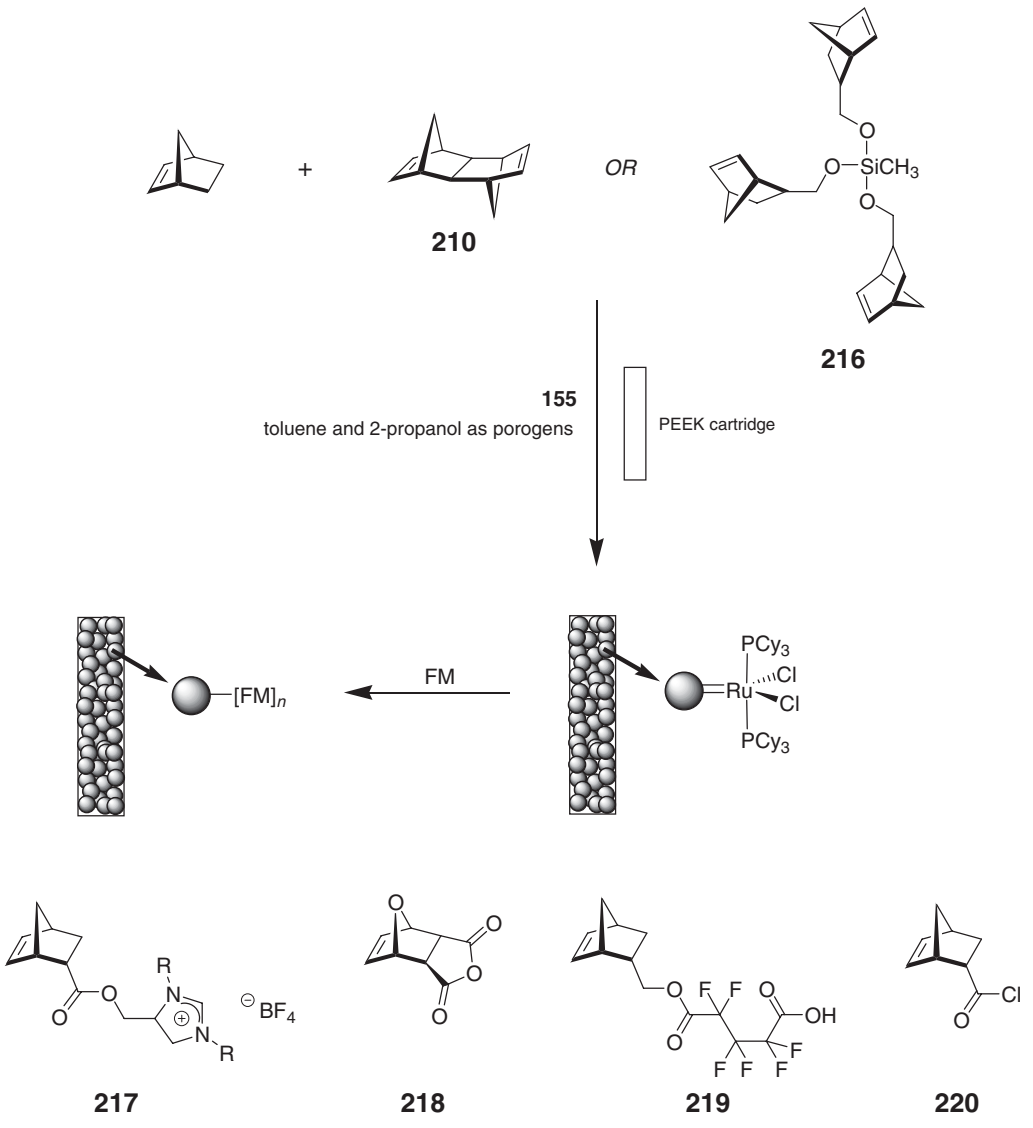

Scheme 80

polymer microglobules were then used for the graft polymerization of functionalized monomers (FM) such as **217**, **218**, **219**, **220**, or **206**.[263] This gives monoliths to which metal complexes can be attached as shown diagrammatically in Scheme 80.

Using a monolith suitably grafted by polymerization with **217**, it was possible to prepare **221**, an immobilized version of **24**, by simply passing a solution of **155** over the rigid rod.[264] Monolith-bound acetate-ligated complex **222** was prepared by reaction of the **218**-grafted monolith firstly with silver nitrate in ammonia to form the corresponding bis-silver dicarboxylate which was then treated with **158**.[265] Monolith **224**, bearing a Hoveyda-type ligand, was prepared by reaction of the **219**-grafted monolith with silver nitrate, then with **223** and finally with silver trifuoroacetate.[266] Monolith **226** was prepared in one step from **220**-grafted monolith by reaction with **225**.[267] Chiral–catalyst-containing monolith **227** was prepared by metallation of **206**-grafted monolith.[267] The synthesis of all the monoliths is summarized in Scheme 81. The monolith-immobilized metal complexes all proved active in olefin metathesis reactions, detailed discussion of this being presented in two reviews of the area.[2,238] Of particular note is that, with many substrates, **227** shows enantioselectivity that is at least comparable with the other supported chiral catalysts discussed here.[267]

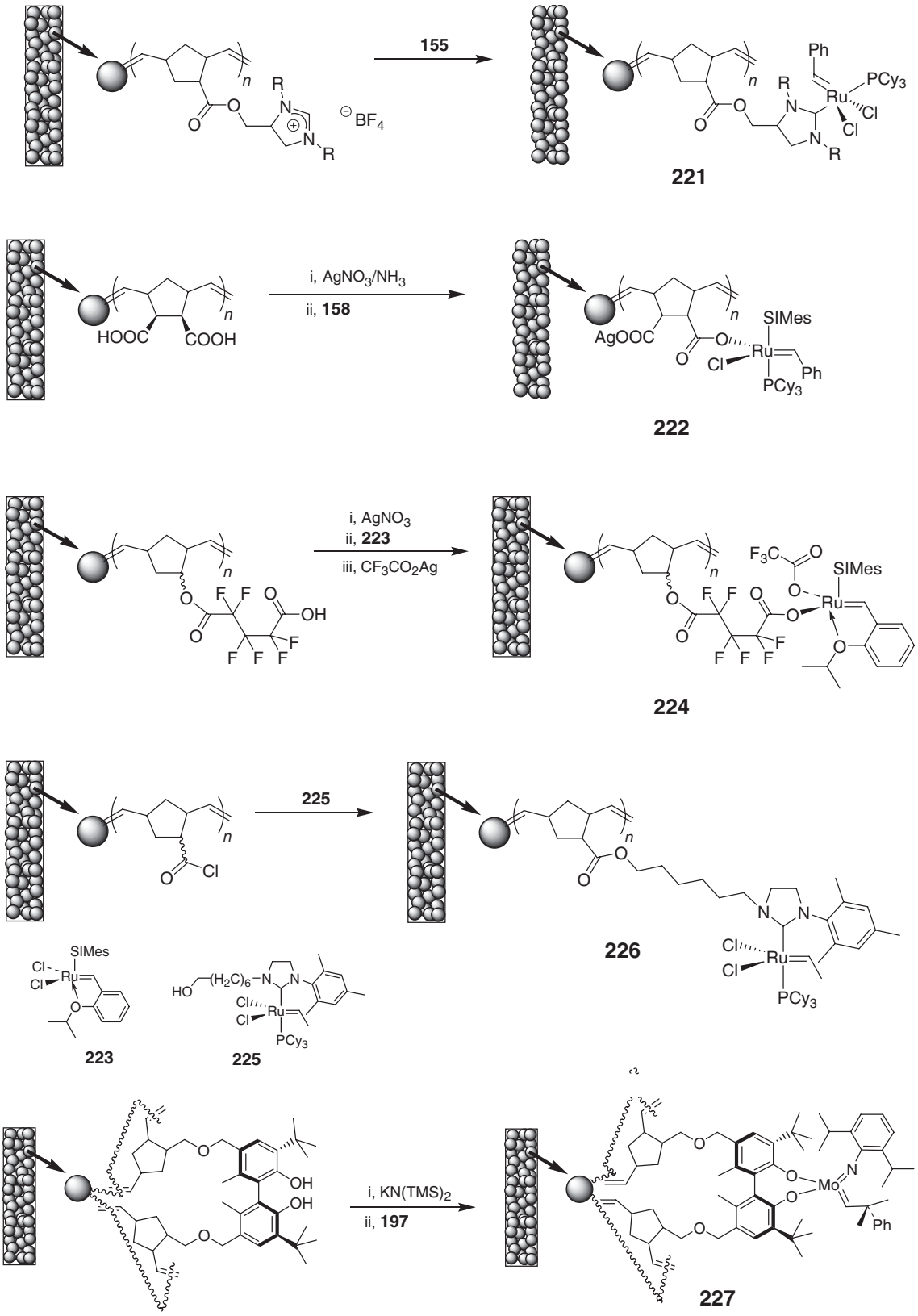
155
221
i, $AgNO_3/NH_3$
ii, **158**
222
i, $AgNO_3$
ii, **223**
iii, CF_3CO_2Ag
224
225
226
223
225
i, $KN(TMS)_2$
ii, **197**
227

Scheme 81

Two routes to microencapsulated olefin metathesis catalysts have been reported. Complex **24** was encapsulated in polystyrene[268] by the same method as that employed by Akiyama and Kobayashi[217] for $Pd(PPh_3)_4$ and found to be active in ring-closing metathesis, although not as efficiently as the optimized Nolan[238,239] macroporous polystyrene system. Akiyama and Kobayashi have themselves prepared an encapsulated ruthenium complex **228** using polystyrene in which the benzene rings of the polymer coordinate in an η^6-manner to the metal center.[269] Starting from polystyrene dissolved in cyclohexane, $Ru(\eta^6\text{-}C_6H_5CO_2Et)(PR_3)Cl_2$ (R = Ph, Cy) was added and then the mixture allowed to cool thereby generating the beads of encapsulated metal complex. The coordination mode of the ruthenium was ascertained by magic-angle spinning NMR spectroscopy. An immobilized ruthenium–allenylidiene complex **229** was prepared from **228** (R = Ph), PCy_3, 1,1-diphenyl-2-propynol, and $NaPF_6$ and this tested in ring-closing metathesis reactions as well as other Ru(II)-catalyzed reactions.

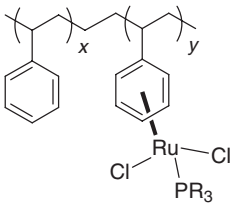

228

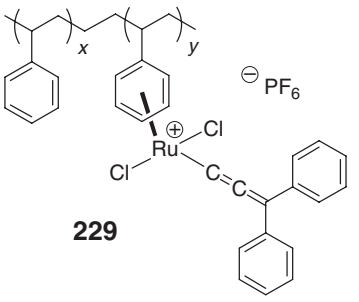

229

Dendritic ruthenium-based metathesis catalysts **230** and **231** have been prepared by Hoveyda and co-workers.[270] They were found to be as active as their corresponding monomers but have the advantage of ease of separation from the product mixture.[271]

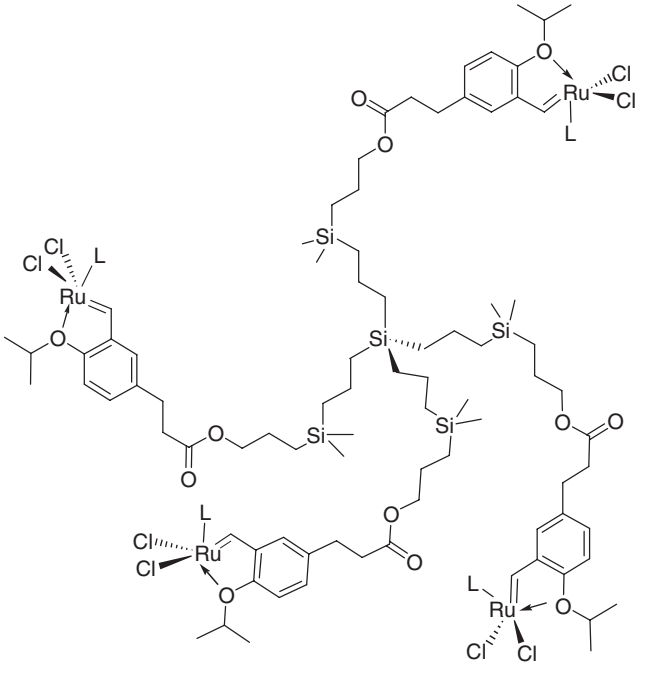

230: L = PCy_3
231: L = IMes

A ruthenium benzylidene complex has been incorporated into G_1–G_4 phosphine-substituted dendrimers by Astruc and co-workers (Scheme 82).[272–275] Starting from the commercially available poly(propylyene)imine dendrimer backbone first reported by Reetz,[214] they immobilized **232** by a ligand substitution. The ruthenium carbene dendrimers generated contained 4, 8, 16, and 32 Ru=C bonds for G_1, G_2, G_3, and G_4, respectively. Having made

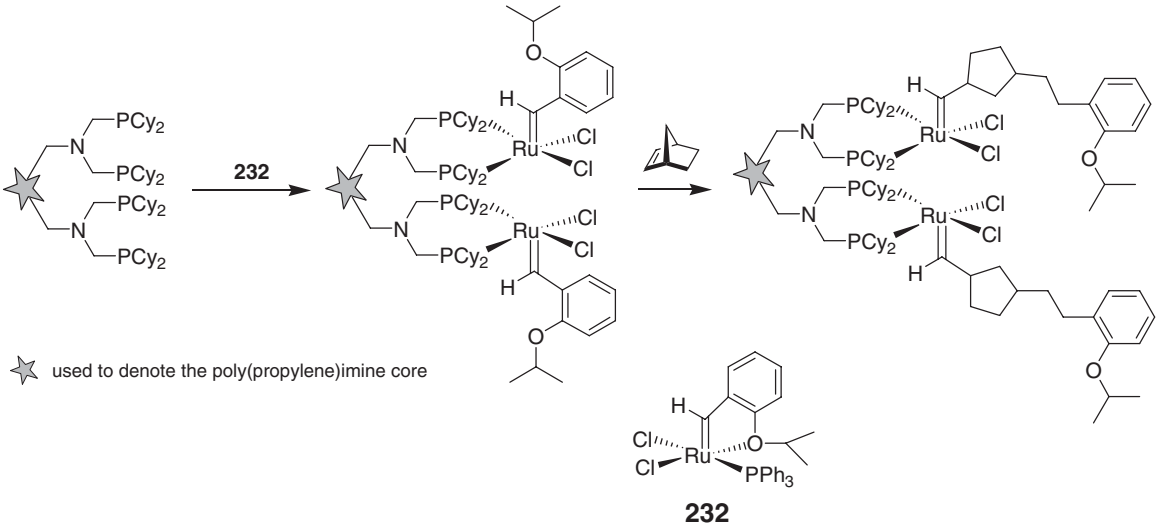

Scheme 82

the metallodendrimers, they were screened as catalysts for ring-opening metathesis polymerization of norbornene under ambient conditions. The first three generations of metallodendrimers were active whereas the fourth was not, this being attributed to the poor solvation of the material in common organic solvents. The polymerization produced dendritic-cored stars with an average of about 100 norbornene units on each dendritic branch.

12.14.5 Polymer-supported Metallocenes

The synthesis and reactivity of transition metal metallocene complexes has attracted much research interest particularly with their wide catalytic applications in processes such as hydrogenation, hydroformylation, and olefin polymerization.[276] The chemistry of metallocenes is discussed in depth in Chapter 8 of this volume. Like their homogeneous analogs, polymer-bound metallocenes have found many applications in catalysis, much of the initial work being carried out in the 1970s and discussed in the review by Pittman in COMC (1982).[1] Supported cyclopentadiene (Cp) ligands have traditionally been prepared by treating a suitably functionalized polymer support with an alkali metal cyclopentadienide (Scheme 83). Merrifield's resin proved the support of choice for a number of the early experiments giving the simple supported complex **233**. A range of metals have been attached to **233**.[1]

A new route to polymer-supported cyclopentadienes that circumvents the use of alkali metal cyclopentadienides has been reported (Scheme 84).[277] Using nickelocene ($NiCp_2$), it is possible to transfer the Cp rings from the metallocene to polymer-supported trityl chloride to give **234**, both cyclopentadiene moieties on the nickelocene being transferred to the polymer support. A ratio of $NiCp_2$: supported trityl chloride of 0.55 : 1 is used with a total reaction time of 30 min. Simple chloromethylated polystyrene does not react directly with $NiCp_2$ but in the presence of 1 equiv. of NaI and one of PPh_3, Cp transfer occurs forming **235**. The NaI is used for an *in situ* Finkelstein reaction turning Merrifield's resin to the corresponding iodo derivative. PPh_3 promotes the reaction between the supported iodide and nickelocene. Using a similar methodology, a cyclopentadiene-derivitized PS-PEG based support **236** was also prepared.

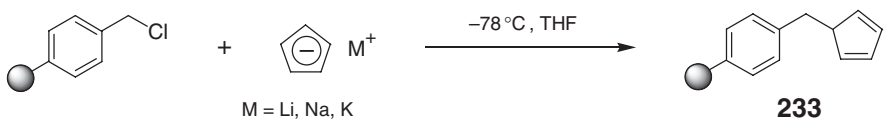

Scheme 83

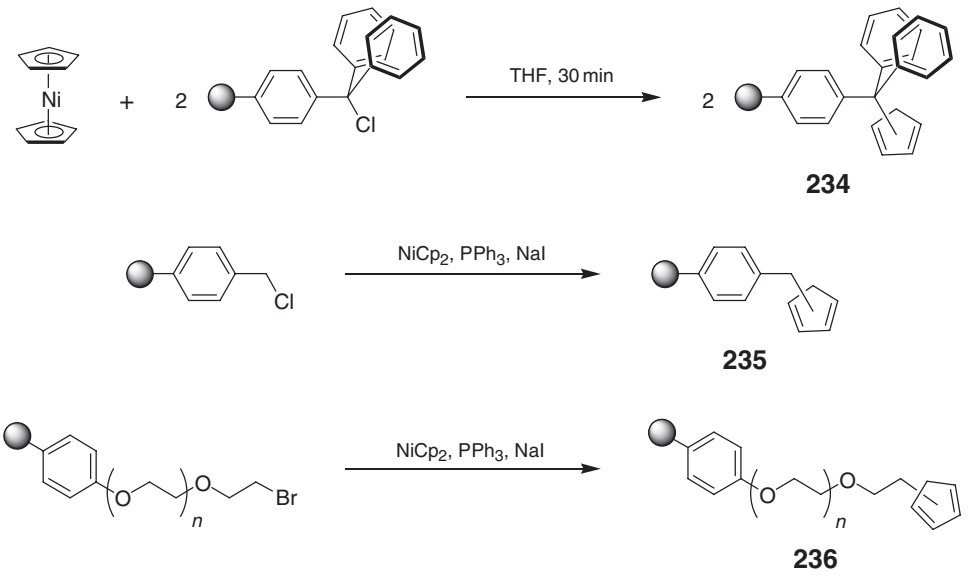

Scheme 84

There have been a number of reports of polystyrene-supported Cp–metal complexes, the majority being used as heterogeneous single-site catalysts for olefin polymerization. For reviews of the use of supports other than polystyrene, see Refs: 278,278a–278c. A polymer-supported cyclooctadiene nickel complex CpNi(cod) **237** has been prepared by treating **233** with $Ni(cod)_2$ at 0 °C in toluene (Scheme 85).[279] Care was taken in the preparation of **233** for use in the immobilization of the $Ni(cod)_2$, any remaining chloro functionalities left after treatment of Merrifield's resin with NaCp being removed by reaction of the support with excess methyllithium followed by reprotonation with ethanol. This was necessary because of the propensity of $Ni(cod)_2$ toward oxidative addition to alkyl and aryl halides. Structure **237** was found to be an active catalyst for olefin polymerization, the selectivity of the process being dramatically different to that of the homogeneous analog, the former giving high-density polyethylene, the latter giving lower oligomers (majority being C_4–C_6).

An immobilized Cp–$TiCpCl_2$ complex **241** has been reported and used for ethylene polymerization (Scheme 86).[280,281] The polymer-supported Cp ligand was prepared by initial attachment of a glycol spacer unit to lithiated polystyrene to give **238**. After elaboration, the corresponding supported nosyl complex, **239**, was treated with $NaCpMe_3Et$ to form the supported Cp ligand **240**. The metal complex **241** was then prepared by lithiation of the supported Cp ligand followed by addition of $CpTiCl_3$. The loading of the Cp on the support was estimated to be 0.28 mmol g^{-1} by derivitization with 4-phenyl-1,2,4-triazoline-3,5-dione (Cookson's reagent) and subsequent analysis of the Diels–Alder product **242**. The metal loading of **241** was estimated at 0.07 mmol g^{-1} and it was used as a catalyst for ethane polymerization but activity was not as high as expected. This may be due to poor swelling of the supported catalyst and therefore limited accessibility of the metal centers. A word of caution should be said regarding the use of Cookson's reagent as a method for determining the Cp loading on polymer supports. Values obtained from this

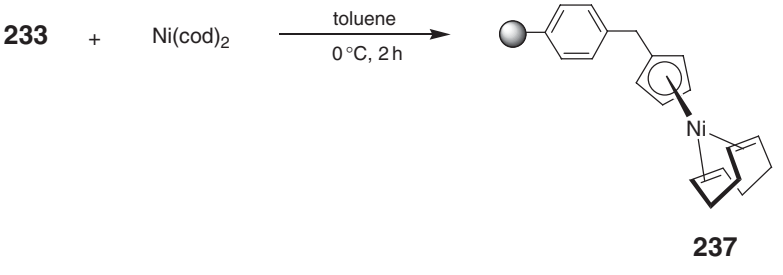

Scheme 85

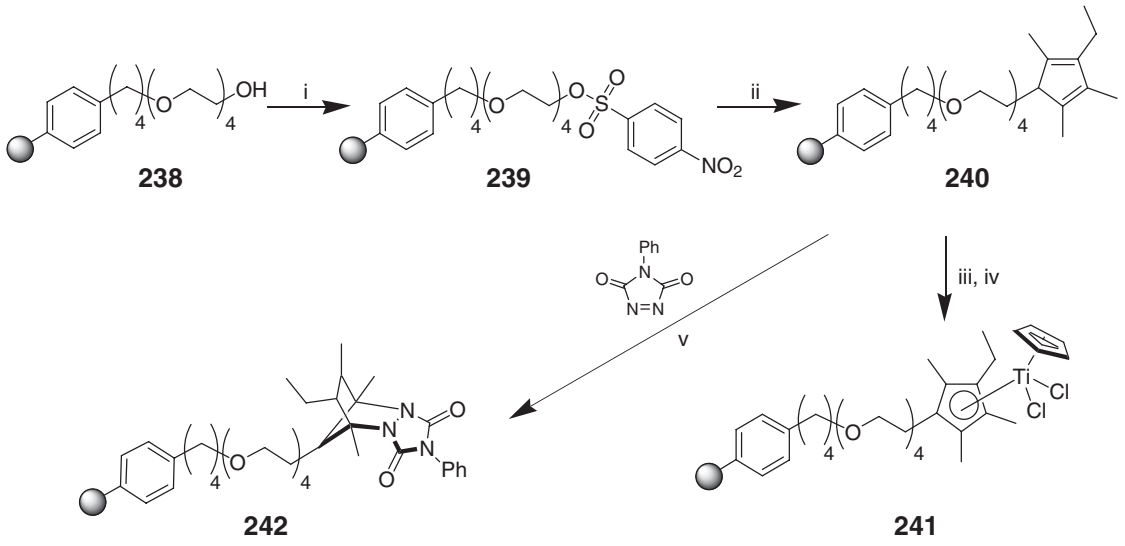

i, 2 × *p*-O_2NPhSO_2Cl, pyridine, CH_2Cl_2; ii, $NaCpMe_3Et$, THF; iii, MeLi, THF; iv, $CPTiCl_3$, toluene; v, –78 °C, CH_2Cl_2

Scheme 86

method are often significantly higher than those obtained independently from microanalysis on the resins. The anomalously high values obtained could be as a result of the Cookson's reagent not only undergoing a Diels–Alder reaction with the supported Cp but also a competitive ene reaction with the cross-links of the support.

A strategy for the immobilization of a cationic pentamethylcyclopentadienyl zirconium amidinate complex on lightly cross-linked polystyrene has been reported.[282] This represents the first report of an immobilised Ziegler–Natta initiator on a solid support for use in the living polymerization of olefins. The synthesis (Scheme 87) starts from dichloride **243** which is deprotonated using the highly hindered base $Ph_3SiLi(thf)_3$ followed by reaction with chloromethylated polystyrene to form supported complex **244**. This is then methylated using MeLi and then monodemethylated using the borate $[PhNMe_2H][B(C_6F_5)_4]$ to give the desired supported cationic complex **245**. Approximately half of the chloride functionalities on the starting support are metallated. The supported complex was found to be a good Ziegler–Natta initiator for use in the living polymerization of 1-hexene. Also, it has a much longer shelf life than its homogeneous analog.

Soga and co-workers[283] have prepared four supported zirconocenes **245–248** bearing indenyl (C_9H_7, Ind) groups either by treating lithiated polystyrene with Ind-derivitized chlorosilanes or by treating Merrifield's resin with Li-Ind and then treating lithiated supported ligand with $ZrCl_4$ (Scheme 88). Metal loadings ranging from of 0.017 mmol g^{-1} down to 0.0017 mmol g^{-1} were obtained. The supported complexes have been used in polymerization of ethene and propene.

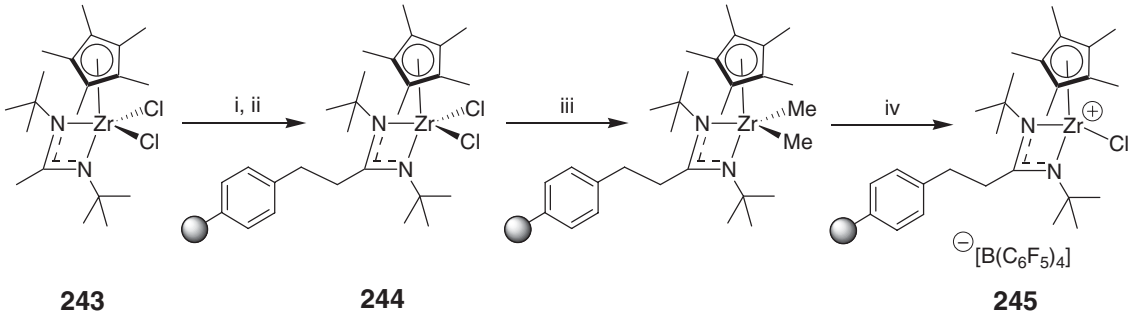

i, $Ph_3SiLi(THF)_3$, THF, 25 °C, 2 h; ii, chloromethylated polystyrene, toluene, 2 h; iii, MeLi, Et_2O, –78 °C to RT, 3 h; iv, $[PhNMe_2H]^+[B(C_6F_5)_4]^-$, PhCl, –10 °C, 5 min

Scheme 87

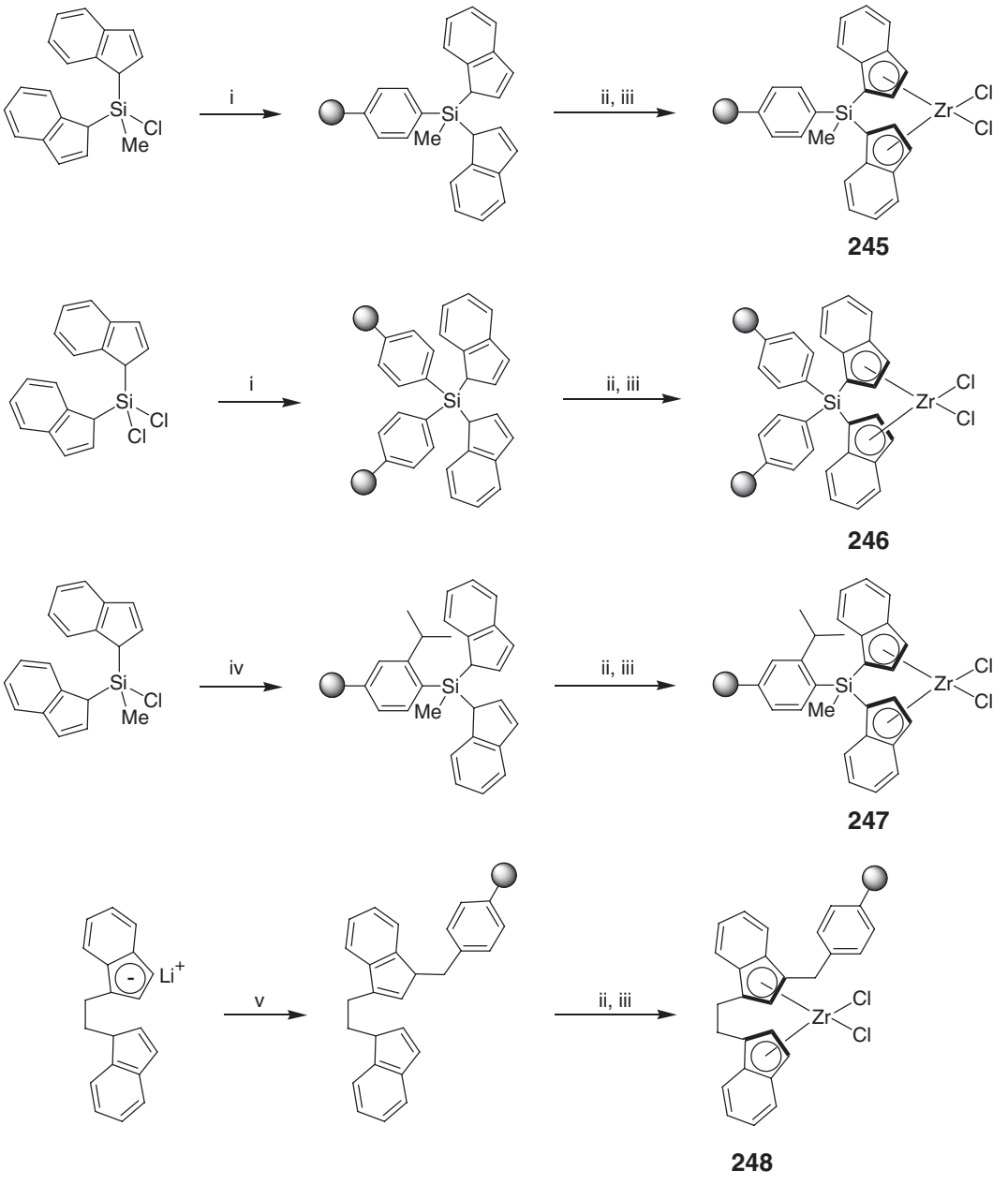

i, lithiated polystyrene, toluene, 40 °C, 8 h; ii, BuLi, THF, 0 °C → RT, 6 h; iii, $ZrCl_4$, THF, 0 °C → RT, 12 h; iv, lithiated polymer-supported cumene, toluene, 40 °C, 8 h; v, Merrifield's resin, toluene, 40 °C, 8 h

Scheme 88

As an extension to their work, the same group[284] have prepared polymer-supported Zr di-Ind complex **251** from polystyrene (Scheme 89). Lithiation of the polystyrene, treatment with 1,4-dibromobenzene, and further lithiation gave **249** which was treated with $PhSi(Ind)_2Cl$ to give the supported ligand **250**. The metal complex **251** was formed by treatment of this with $ZrCl_4$. The use of **251** for ethane polymerization was assessed and subsequently[285] the mechanism of polyethylene growth on the surface of the supported catalyst beads has been studied.

A supported Cp/fluorene ligand has been prepared by AIBN-initiated polymerization of styrene-derivitized monomer **254** with styrene (Scheme 90).[286] The monomer was prepared in three steps from bromoacetophenone. First, the ketone was treated with CpLi to generate methylfulvene **252**. Lithiated fluorene (FluLi) was then added to

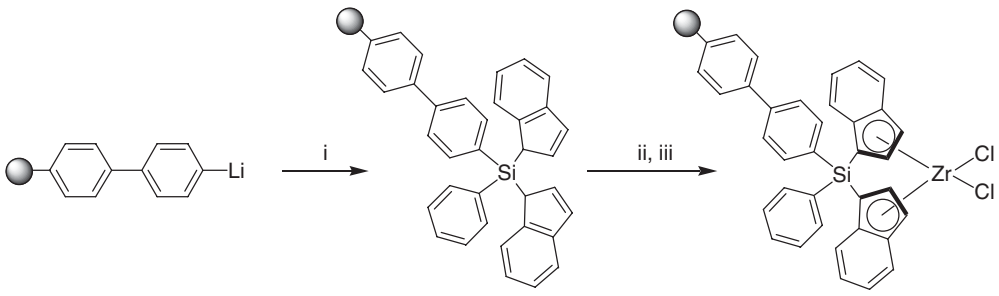

249 **250** **251**

i, $PhSi(Ind)_2Cl$, toluene, 40 °C, 8 h; ii, BuLi, THF, 0 °C → RT, 6 h; iii, $ZrCl_4$, THF, 0 °C → RT, 12 h

Scheme 89

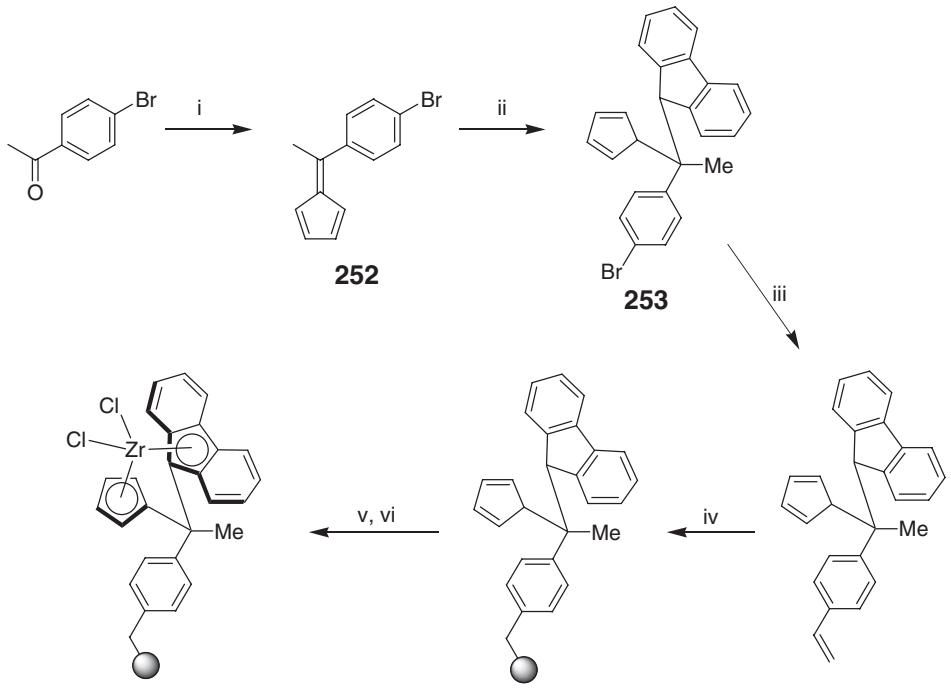

252 **253** **256** **255** **254**

i, CpLi, THF, 0 °C → reflux, 3 h; ii, FluLi, Et_2O, 0 °C → RT, 8 h; iii, vinyltributyltin, $Pd(PPh_3)_4$, toluene, reflux, 8 h; iv, styrene, AIBN, toluene, 60 °C,12 h; v, BuLi, THF, 0 °C → RT, 6 h; vi, $ZrCl_4$, THF, 0 °C → RT, 12 h

Scheme 90

form a Cp/Flu functionalized compound, **253**, which was converted to **254** by a $Pd(PPh_3)_4$-mediated Stille coupling with vinyltributyltin. Once polymerized with styrene to form **255**, a Zr complex **256** was generated by treatment of the supported ligand with $ZrCl_4$. Analysis of **256** showed that less than 25% of the ligand sites were metallated. In addition to the problems of accessibility of ligand sites, a competing side-reaction occurred forming a supported cyclobutane which rendered a significant proportion of the ligand sites to be of no use. Three supported complexes were prepared with Zr loadings ranging from 0.04 mmol g^{-1} to 0.31 mmol g^{-1} and, although all were found to be active for the polymerization of propene, the activity is very low compared to the homogeneous analog.

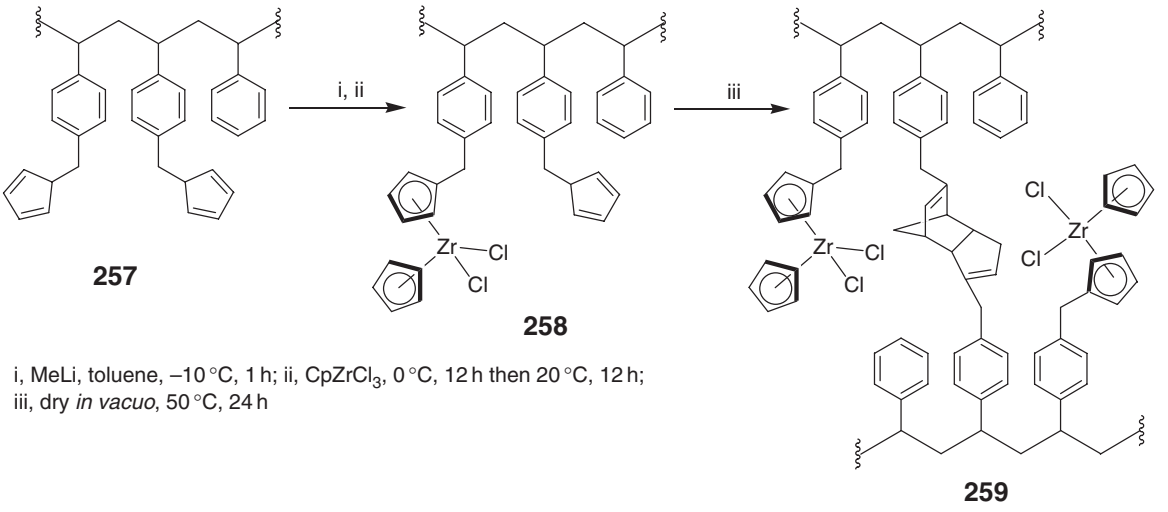

Scheme 91

Müllen and co-workers[287] have prepared a supported Zr complex **259** starting from **257**, a soluble polystyrene support bearing Cp functionalities, and found it to be very active in ethene polymerization (Scheme 91). $CpZrCl_3$ was added to lithiated **257** leading to the supported zirconocene **258**. This was then dried and heated at 50 °C for 24 h during which time Diels–Alder reactions occurred between unmetallated cyclopentadiene functionalities thereby forming reversibly cross-linked polymer-supported metallocene **259**. This method of preparation has the advantage that the metal sites can be more uniformly distributed across the particles as there are no steric constraints in the metal-loading step since at that stage the polymer is soluble. In addition, as the Diels–Alder reaction forming the cross-linking is reversible, this allows for fragmentation of the catalyst support during polyethylene processing.

Co-polymerization of a vinyl-functionalized zirconocene and styrene in a test tube followed by extraction of the bulk polymer and slicing into disks gives a simple supported material that exhibits both stoichiometric and catalytic activity.[288] To prepare the desired functionalized monomer, **260**, the synthesis started from *p*-vinylbenzyl chloride (Scheme 92). Treating this with a NaCp containing a catalytic quantity of tetrabutylammonium iodide gives *p*-vinylbenzylcyclopentadiene as a mixture of double-bond isomers. Immediate deprotonation followed by reaction with $ZrCl_4$ yields **260**. Under air- and water-free conditions, various concentrations of **260**, styrene, and DVB were mixed with dichlorobenzene until homogeneous. The solution was then transferred to a pyrex test tube and charged

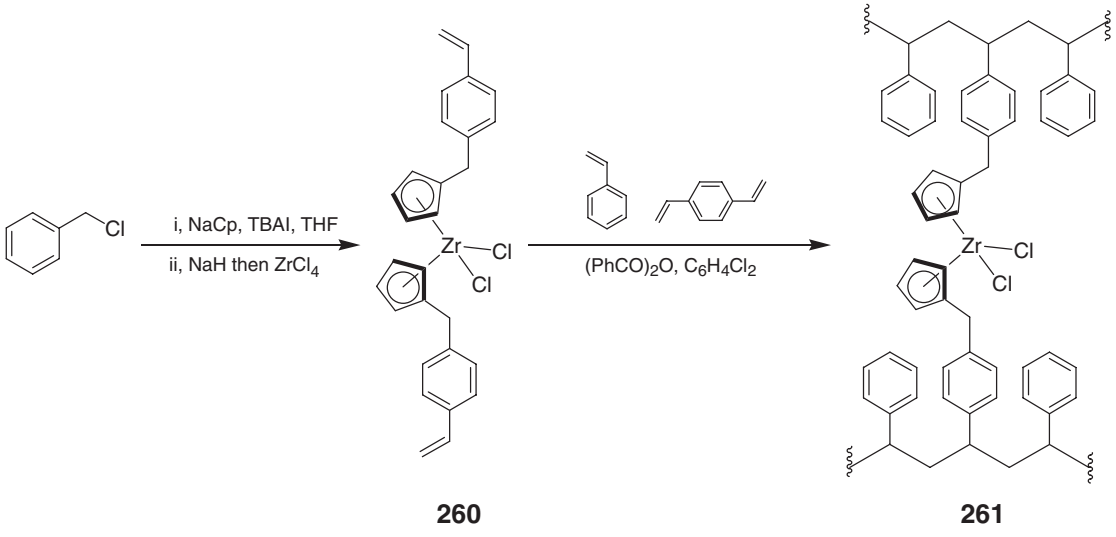

Scheme 92

with benzoyl peroxide, heated and agitated, polymerization being allowed to continue for 2–3 days. Upon cooling, the tube was broken and the polymer rod sliced into disks and extracted using Soxhlet apparatus for several days to give the desired pure polymer **261**. This was used successfully for stoichiometric hydrozircanation of styrene and catalytic carbometallation of phenylacetylene.

A polymer containing an *ansa*-bridged zirconacene **262** was prepared by co-polymerization of monomer **263** with styrene.[289] This was then used as a catalyst for ethane polymerization but found not to give good results due to the non-uniform distribution of the metal sites on the polymer backbone. Questions were also raised regarding the accessibility of the metal sites.

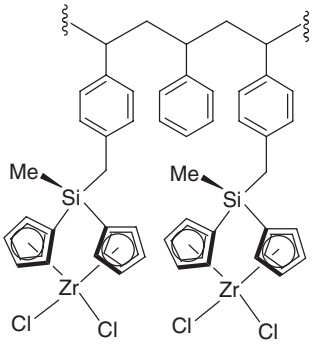

262

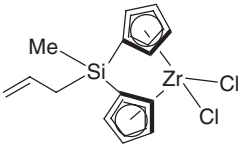

263

Apart from immobilizing metallocenes via supported Cp or Ind functionalities, there have been reports of other methods of attachment (Scheme 93). Fréchet and co-workers[290] have immobilized metal cyclopentadienyl complexes on a non-interacting polystyrene support. The aim of the work was to prepare a supported catalyst that allowed a nominally heterogeneous polymerization to proceed in a microscopically homogeneous solution-like environment. The supported catalysts were prepared by first treating lightly-cross-linked Merrifield's resin with dimethylamine to form the corresponding supported amine **264**. This was then treated with $[PhNMe_2H]^+[B(C_6F_5)_4]^-$, which protonates the basic support and binds the perfluorinated borate anion to the support by ion pairing, giving **265**. The active catalyst **266** is formed by reacting the borated support with the neutral dialkylmetallocene, $(C_5HMe_4)_2HfMe_2$, generating the free supported amine, the metallocenium cation $[(C_5HMe_4)_2HfMe]^+$, and methane. Metal loadings of 0.14–0.77 mmol g^{-1} are reported depending on the initial loading of the Merrifield's resin. The metal complex is bound to the support through a weakly coordinating interaction between the Zr and the N of the supported amine. The catalyst proves very active in ethene/1-hexene co-polymerization, the weak coordination between metallocene and this support being strong enough to retain the metal complex on the support during the course of the reaction. The appealing feature of this polymer-supported catalyst is that the modular synthesis allows for simple variation of each of the components (amine, ammonium salt, and metallocene) thereby opening avenues to parallel and combinatorial catalyst preparation and screening. The only requirements are that the amine component must be nucleophilic enough to displace a benzylic halide, the ammonium salt must be more acidic than the supported amine, and the metallocene must be capable of reacting with a tertiary ammonium cation to generate a free amine, methane, and a metallocenium cation. Indeed, the authors have since prepared a range of other supported metallocenes using this methodology[291] and have screened them for activity in olefin polymerization, looking at both the polymer

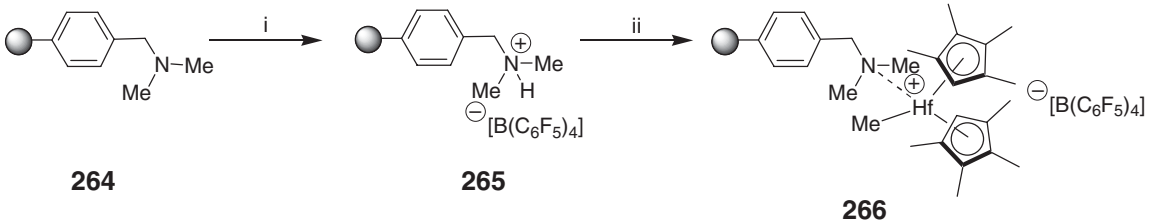

264 **265** **266**

i, $[PhNMe_2H]^+[B(C_6F_5)_4]^-$, CH_2Cl_2, RT, 1.5 h; ii, $(Me_4C_5H)_2HfMe_2$, toluene, RT, 1 h

Scheme 93

composition and morphology. They have investigated the effects of varying the amine, metallocene, and also the degree of cross-linking (and hence swelling ability) of the polymer support.

A similar methodology was used to prepare supported Zr metallocene catalyst **267**.[292] Using a pyridine-derivitized support they have attached the cationic Zr complex $[Cp_2ZrMe]^+[B(C_6F_5)_4]^-$ by treating the support with a mixture of Cp_2ZrMe and $[PhNMe_2H]^+[B(C_6F_5)_4]^-$ with B and Zr loadings of 0.083 mmol g^{-1} and 0.069 mmol g^{-1}, respectively, being obtained. The supported catalyst shows high activity in ethene polymerization. An analog of **267**, supported on pyridine or polyethyleneoxide/pyridine-functionalized latex nanoparticles, has also been reported.[293]

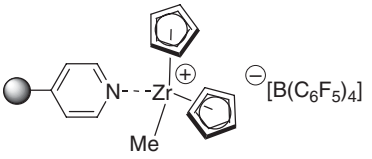

267

Hong, Kristen, and Reif have immobilized metallocenes inside polystyrene, taking advantage of the swelling–shrinking characteristics of poly(styrene-co-DVB) beads (Scheme 94).[294] The method used was however somewhat different to the Kobayashi microencapsulation method.[63] They prepared the immobilized metallocenes by swelling the polystyrene in toluene, then by adding a slurry of the beads to a solution of metallocene. They added triisobutylaluminum or methylaluminoxane (MAO) and then removed the solvent from the mixture to leave dry beads with the metal encapsulated within them. These were then washed with heptane, a non-swelling solvent, to remove traces of metal from the surface of the beads to obtain a free-flowing consistency. Among other techniques, electron probe microanalysis was used to study the composition of the beads. This technique essentially allows for the spacial distribution of various components across the beads to be established. In this case, the distribution of Zr, Al, and F was determined and found to be homogeneous over the polystyrene bead particles. The beads were then used for ethene co-polymerization. They showed a slow initiation toward polymerization but then activity increases with time. Clearly, with this method of immobilization, the main concern is leaching of the metal out of the support during the course of the reaction but the authors report that they have investigated this and found no evidence for metal leaching. This method of immobilization has the advantages of being simple to prepare and, because the metal is encapsulated within the support and not on the surface, the metallocenes are more air and moisture stable; exposure to air for a few seconds or prolonged storage under nitrogen for months does not affect the catalytic activity. It should be noted at this stage that usually these catalysts have to be used in thoroughly dried and argon-degassed solvents.

Müllen and co-workers[295] have extended their work using reversibly cross-linked polystyrene supports to immobilize metallocenes through non-covalent bonding (Scheme 95). This is achieved by functionalizing the support with nucleophilic groups which, like the amine examples discussed previously, can then bind to the metallocene complex in a non-covalent manner. Heterogeneous support **268** was prepared from the soluble terpolymer of 4-bromostyrene, 4-chloromethylstyrene, and styrene. After complete etherification of the chloromethyl groups using NaOMe to form **269**, the Cp functionalities are introduced via the 4-bromophenyl substituents by reaction of the polymer with dimethylfulvene yielding **270**. The cross-linking to give **271** is then achieved by heating **270** to 85 °C overnight. The metal complex is supported by treating **271** with a solution of metallocene **272** and MAO. MAO plays a key role in the immobilization process and it is not possible in its absence. This is believed to be due to the fact that the methoxy groups on the support coordinate to the MAO to form a cage-like structure around the metallocene complex. An optimum MAO : Zr ratio of 730 : 1 was found at which catalytic activity was greatest and no leaching was observed. At lower MAO : Zr ratios, that is, with more metallocene, activity decreases and leaching is observed. The group has developed polyether-functionalized analogs of **271** and used them for supporting metallocenes.[294] Using similar methodologies, metallocenes have been immobilized on functional polypropylene granules[296] as well as porous polystyrene beads[297,298] by other research groups.

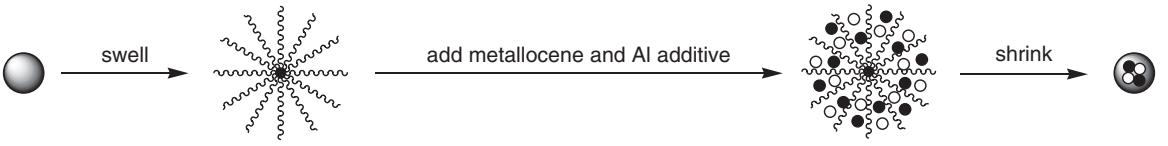

Scheme 94

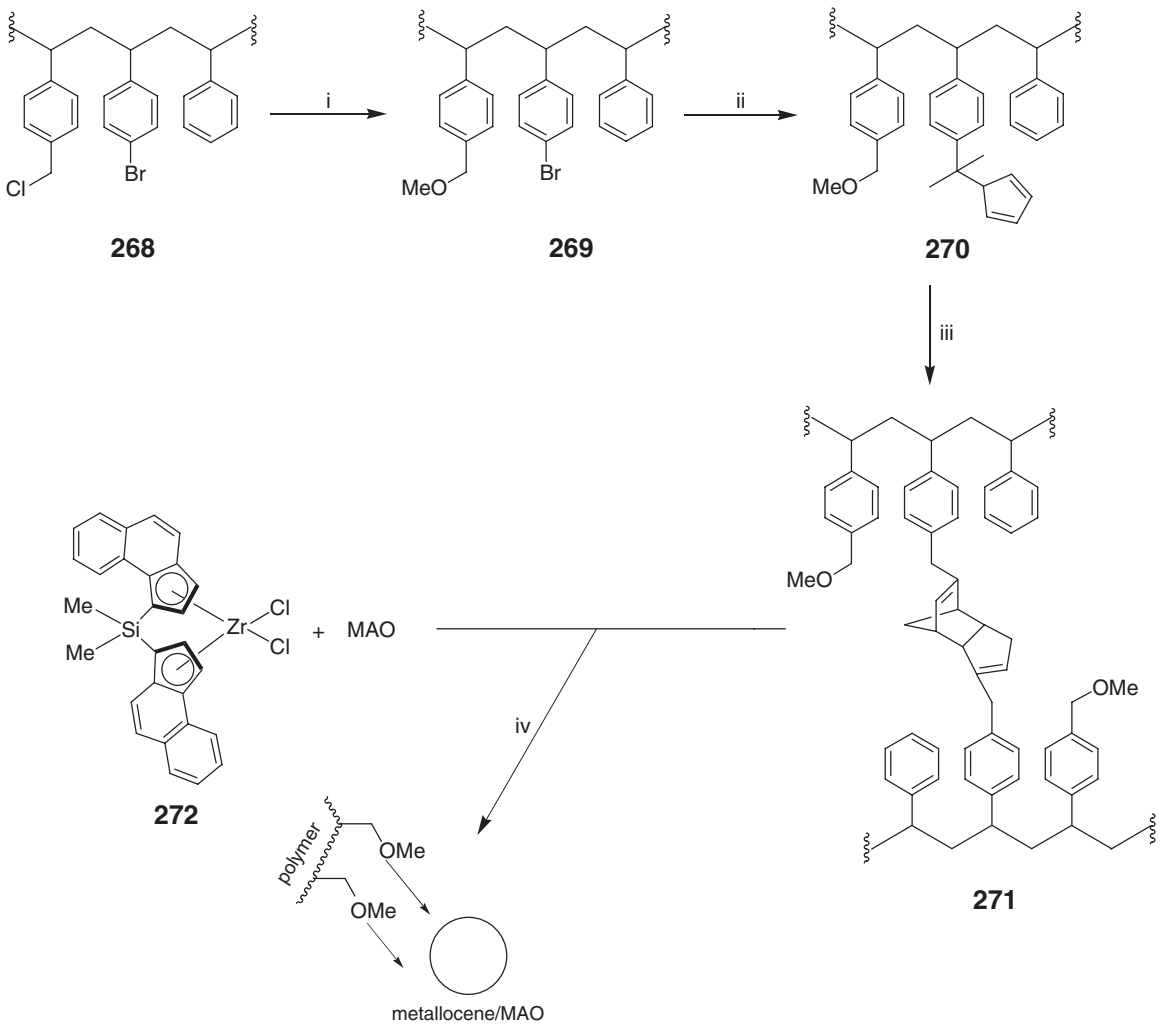

i, NaOMe, THF/MeOH (2 : 1), 60 °C, 18 h; ii, BuLi, dimethylfulvene, THF, $CpZrCl_3$, –78 °C → RT, 1 h; iii, toluene, 85 °C, 18 h; iv, **272** and MAO in toluene, RT,10 min then add **271**, RT, 30 min

Scheme 95

Although not falling within the direct remit of a discussion of polymer-supported complexes, it is worthwhile at this point to mention briefly that a number of dendrimers containing metal–cyclopentadienyl functionalities on their periphery have been reported.[48–50] A diverse range of ferrocenyl-substituted dendrimers have been prepared and studied, particularly due to their interesting properties. Most of the uses for these ferrocenyl systems exploit their well-studied redox properties and some speciality devices have been fashioned in which electrodes with dendrimer coatings have been built for alalyte sensing. Other applications include electrochemical sensing of biorelevant molecules, such as biotin, DNA, nucleic acids, and carbohydrates.[299] Astruc and co-workers employed non-covalent hydrogen bonding as a way to construct dendrimers bearing ferrocene groups.[300] Using commercially available polyamine dendrimers of generations 1–4 and dendrons containing three ferrocenyl groups, and a single phenolic functionality, N–H–O bonding interactions were used to generate the dendrimer assembly **273**. These have been used in the recognition of $H_2PO_4^-$ anions. Using similar polyamine core structural units, other groups have published routes to ferrocene-containing dendrimers where the metal functionalities are joined to the core by covalent bonds, and have studied their electrochemical[301,302] and non-linear optical properties.[303] A mixed ferrocene/cobaltacene dendrimer family **274** has also been prepared using the polyamine core.[304] A cyclophospazene core has also been employed for the assembly of ferrocene-derivatized dendrimers.[305,306] Whereas most cores allow for introduction of

three or four dendrimer arms, as already shown in the synthesis of **27** and **145**, the phosphazene core allows for incorporation of six arms.

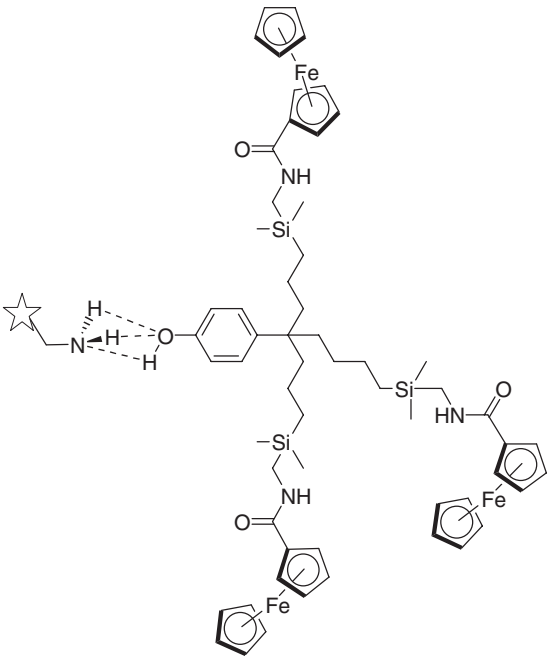

273

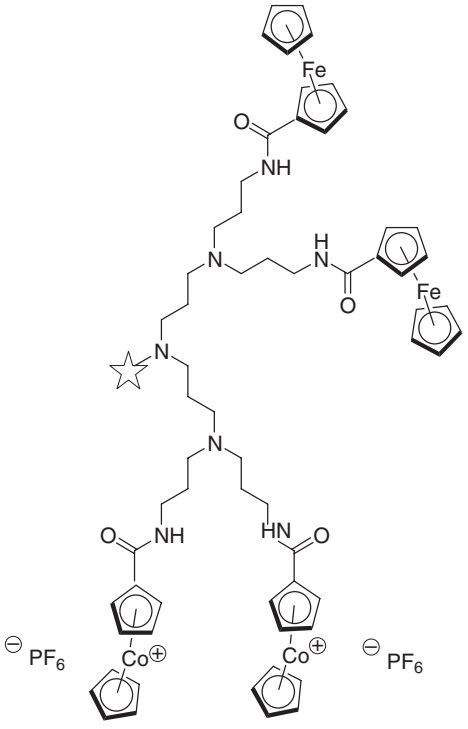

274

Majoral and co-workers have prepared phosphorus-containing dendrimers in which ferrocene units were sequentially buried within two further organic dendrimer generations and the effects of the position of a chiral ferrocene within the dendrimer structure on both chiroptical and electrochemical properties were studied.[307–309] To prepare these materials **275**, firstly an aldehyde-functionalized ferrocene unit was attached to varying generations of prefabricated phosphorus-containing backbones. The additional organic dendrimer layers were added via repetitive condensation of a phosphorhydrazide $H_2NNMeP(S)Cl_2$ and subsequent reaction of the PCl_2 moiety with 2 equiv. of the sodium salt of 4-hydroxybenzaldehyde.

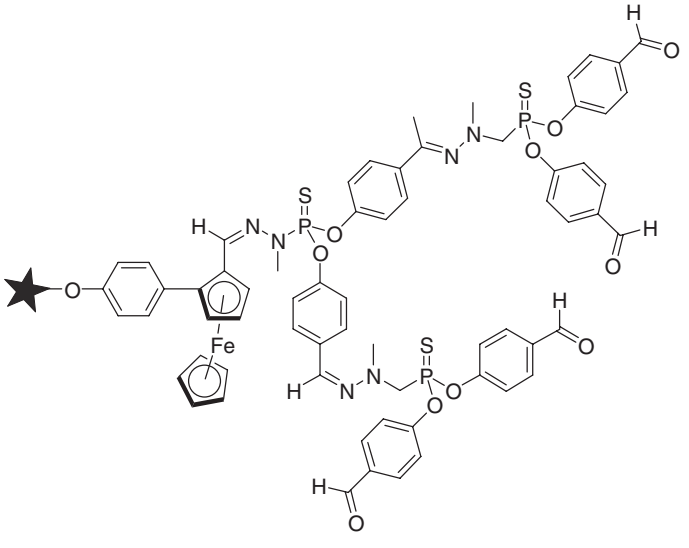

275

Carbosilane dendrimers containing titanium and zirconium complexes on their periphery have been prepared and used in olefin polymerization reactions.[153,310–313] Generally, the best synthetic route to these materials involves the synthesis of generations of suitably functionalized dendrimers to which the metal is added in the final step giving products such as **276**. Routes involving the incorporation of pre-metallated building blocks gave only low yields of the desired dendrimers.

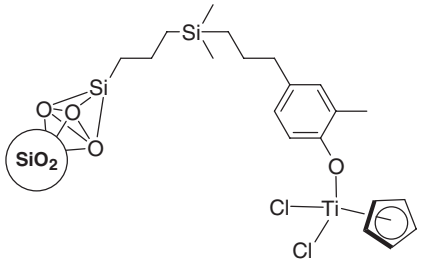

276

12.14.6 Solid-supported Organometallic Synthesis

As this review has shown, the driving force behind majority of the work in the area of polymer-supported metal complexes is the use of these complexes in catalysis. However, despite the great potential, there are only a few examples to date where preparative inorganic and organometallic chemists have taken advantage of using solid-supported synthesis in their chemistry. Heinze has attached a molybdenum carbonyl complex to a diimine-functionalized support, performed a ligand substitution reaction on the support, and then cleaved the final complex off the support (Scheme 96).[314] The polymer support contains a silyl ether linkage The tris-acetonitrile substituted complex $Mo(CO)_3(MeCN)_3$ was attached to the diimine support to give an immobilized metal complex bearing a labile acetonitrile ligand. The MeCN group could be substituted for CO, PPh_3, or *t*-butyl isocyanide by adding the ligand to a suspension of the supported complex. The complexes can then be cleaved off the support using tetrabutylammonium fluoride (TBAF) which, interestingly, has no deleterious effect on the metal complexes. Homogeneous analogs of the supported complexes were prepared and the kinetics of ligand substitution compared. Not surpisingly, the reactions proceed somewhat slower on the support as compared to in solution.

Peptide-tethered platinum(II) complexes have been prepared using solid-supported techniques[315,316] and gel-phase Pt-195 NMR spectroscopy used as a non-destructive analytical method for on-support analysis.[317] This

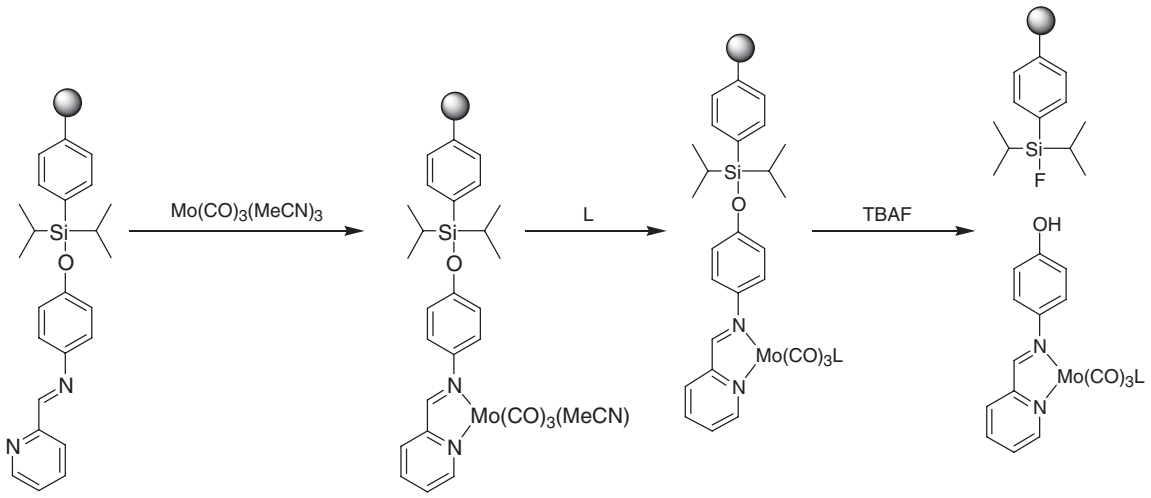

Scheme 96

chemistry was used for the preparation of potentially anti-tumor active dinuclear platinum coordination compounds.[318] Grinstaff and co-workers have used solid-phase chemistry to incorporate an $[Ru(diimine)_3]^{2+}$ complex at the nucleobase in an oligonucleotide.[319,320] They have incorporated $[Ru(bpy)_3]^{2+}$ into an oligonucleotide by first preparing an $[Ru(bpy)_3]^{2+}$ phosphoramidite complex and then attaching this to the 5′terminus of DNA using a standard protocol on an automated DNA solid-phase synthesizer with the metallo-phosphoramidite introduced at the last step in the reaction sequence.

Polymer-supported ruthenium and molybdenum carbonyl fragments have been immobilized and their use demonstrated in ligand exchange reactions.[321] Metal carbonyl olefin complexes such as $Ru(CO)_4(\eta^2\text{-}C_2H_4)$ and $Mo(CO)_5(\eta^2\text{-}C_2H_4)$ prove to be valuable synthetic intermediates for the preparation of a wide range of organometallic complexes since they are in essence sources of $[RuCO)_4]$ and $[Mo(CO)_5]$ fragments, the olefin ligands being very labile. One of the problems with the olefin complexes is that they have to be made just prior to use and many are sensitive to air, moisture, and decompose on removal of solvents. In solid-phase chemistry, the support can give increased stability to reactive intermediates by blocking bimolecular reaction steps. We have prepared storable sources of $[Ru(CO)_4]$ and $[Mo(CO)_5]$ by immobilizing these fragments on olefin-functionalized polymer supports. This showed that these sources were stable and that it was possible to remove the metal fragments from the support in a simple ligand exchange reaction to a phosphine. Taking a solution of triphenylphosphine and the supported complex and stirring it overnight, the metal came off the support, the metal phosphine complex was formed, and the olefin-functionalized polymer support regenerated. The whole process is shown in Scheme 97.

Butenyl polystyrene **277** and acryloyl polystyrene **278** were chosen as supports. The former is analogous to ethene and the latter to methyl acrylate, both of which have been used to prepare $Ru(CO)_4(\eta^2\text{-olefin})$ complexes previously. Any complex formed with **277** would be expected to be less stable than that formed with **278** but, at the same time, less reactive in ligand-transfer reactions. The supported compounds were prepared by irradiating a dichloromethane solution containing the swollen support and the parent metal carbonyl ($Ru_3(CO)_{12}$ or $Mo(CO)_6$). The ruthenium complexes were found to be more stable than their molybdenum congeners and are stable in air at room temperature, no loss of activity being observed over a period of 2 days. Ligand substitution reactions were performed at 40 °C, the quantity of metal coming off the support being between 45% and 85% depending on the metal.

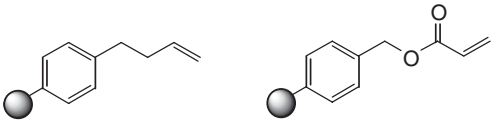

277 **278**

Cyclopentadienylmanganese tricarbonyl units have been immobilized on polystyrene and then ligand substitutions studied (Scheme 98).[322] The point of attachment to the support was chosen to be the cyclopentadiene moiety and two different methods were used for preparing the supported complex. In the first approach, acid chloride-functionalized carbonyl **279** was reacted with **280** to yield the supported complex **281**. This was suitable for small-scale production of **281** but problems in the synthesis of **280** limited the scope of this approach. Instead, a better route was found to be treatment of lithiated complex **282** with an isocyanate-functionalized polystyrene support, itself prepared from aminomethylated polystyrene, to give **283**. The photoinduced ligand substitution chemistry of **283** was studied. Photolysis in thf solution gave intermediate **284**, which, in the presence of an alkene ligand, reacted to form the corresponding η^2-alkene complex **285**. Attempts to recover the alkene from the supported complex were made using a variety of oxidative conditions to demonstrate that the cyclopentadienylmanganese tricarbonyl resin could be a potential traceless support for olefins. The treatment of **285** with trimethylamine-*N*-oxide proved to be the most satisfactory method for this but only gave a modest recovery of the alkene.

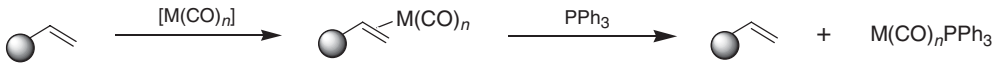

Scheme 97

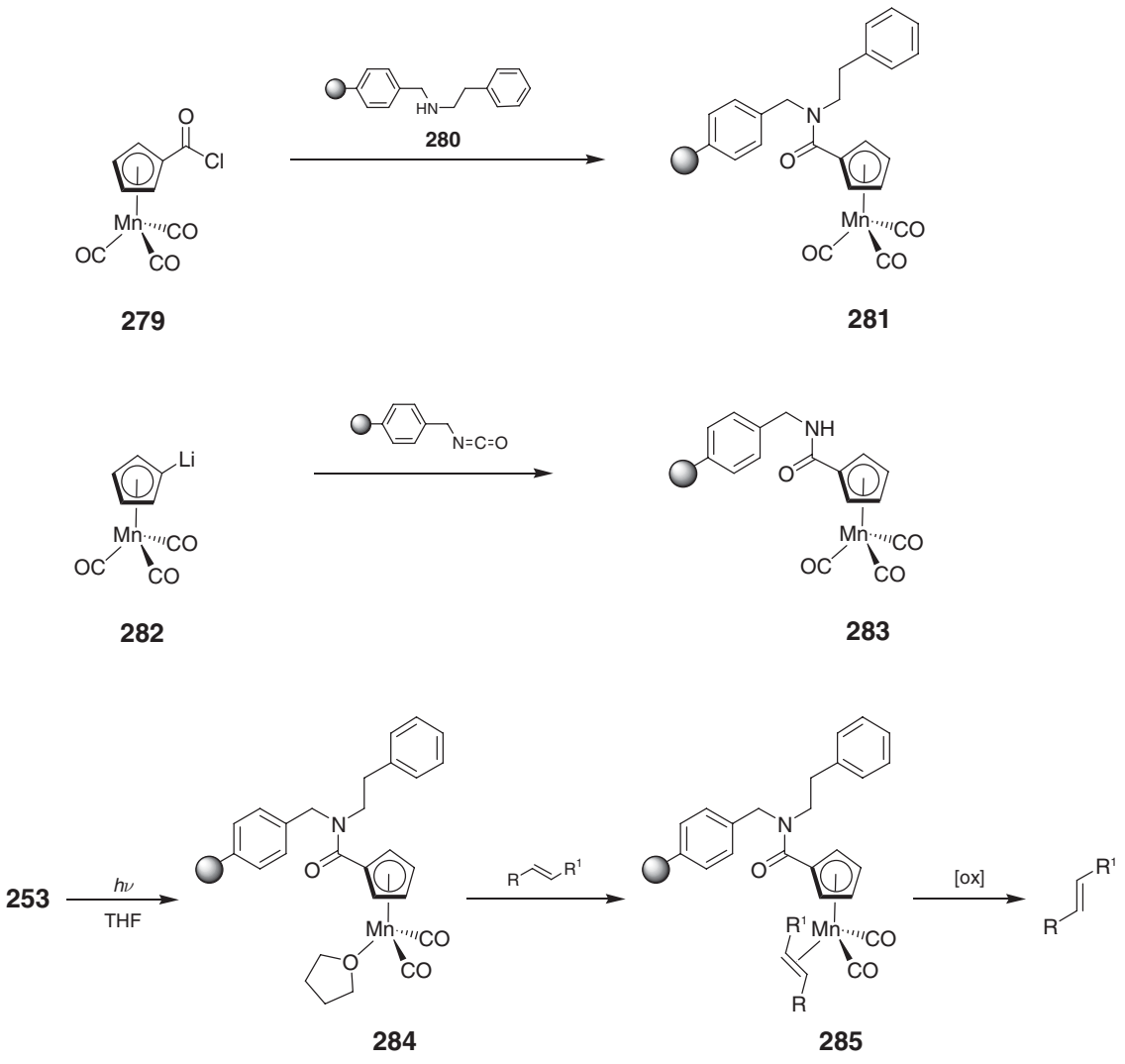

Scheme 98

12.14.7 Preparation of Selected Other Supported Ligands and Metal Complexes

12.14.7.1 Polymer-supported NHC Ligands and Immobilized Palladium and Rhodium Complexes

NHCs represent a class of ligands that form air and moisture stable complexes with a range of transition metals.[323–325] As already discussed, compounds of ruthenium can show remarkable catalytic activity in olefin metathesis reactions. Many NHC-containing metal complexes of palladium have also been reported and these are found to catalyze other C–C bond-forming reactions such as the Suzuki and Heck couplings. For selected examples, see Refs: 326,32a–32d. It is therefore not surprising that supported analogs have begun to appear in the literature. The first polymer-supported NHC palladium complex **287** was reported by Herrmann and co-workers.[327] This has been achieved by the direct reaction of readily prepared alcohol-functionalized palladium carbene complexes **286** with a bromomethyl-functionalized polystyrene support using Scheme 99. The loading of the metal complex on the support was found to be substantially lower than that estimated for one molecule of carbene complex being bound to each bromomethylphenyl functional group of the support, indicating that only a small proportion of the functionalized sites on the support are accessible for attaching the complex. Screening in the Heck reaction of aryl bromides showed that **287** was an active catalyst. Recycling was possible although activity dropped considerably in cases using non-activated aryl bromides.

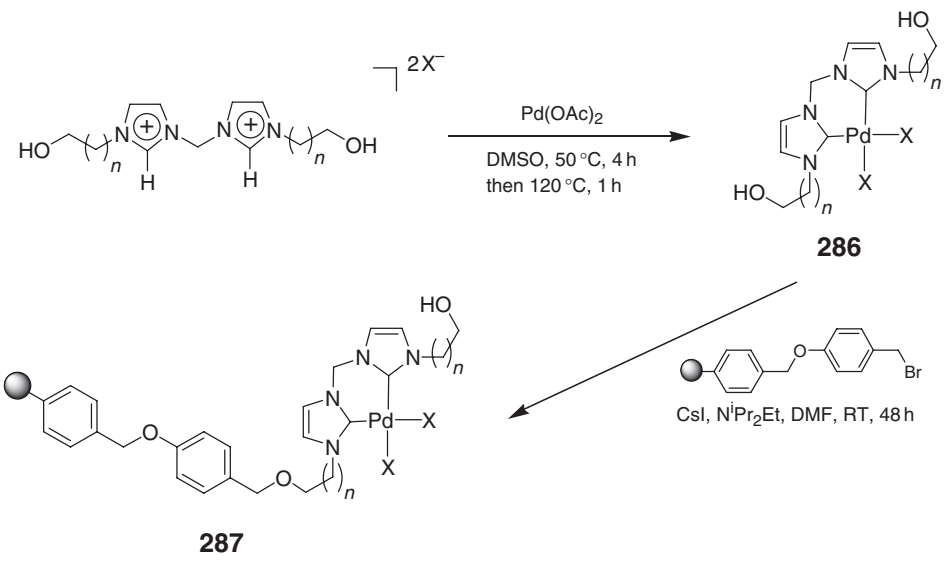

Scheme 99

Byun and Lee have prepared a supported NHC complex, starting from Merrifield's resin.[328] Treating this with 1-methylimidazole gave supported imidazolium salt **288**. A small survey on the effects on swelling of different loadings of the imidazolium functionality was performed. As the loading increased, the swelling in polar solvents such as water and methanol also increased to such an extent that, with a loading of 1.91 mmol g^{-1} of the imidazolium functionalities, the polystyrene resin had a swelling volume of 4.2 ml g^{-1}. Using this high-loading support, a palladium complex was prepared by reaction with $Pd(OAc)_2$ with a resultant metal loading of 0.29 mmol g^{-1}. This was screened in Suzuki reactions in aqueous conditions and found to be catalytically active. Some loss of activity was noted on reuse, this being attributed to partial Pd leaching.

The same group have subsequently prepared a supported NHC ligand by co-polymerizing vinyl-functionalized imidazolium salt **289** with styrene and DVB.[329] The loading varied from 0.23 to 1.12 mmol g^{-1} depending on the quantity of **289** used in the polymerization. Again, the swelling properties of the supported imidazolium salts were studied. With **289** however, the difference in swelling volume between hydrophobic and hydrophilic solvents was quite low, thus indicating that these supports are amphiphilic as compared to **288**. The supported ligand resultant materials were metallated in an identical manner to **289** and screened in the Suzuki reaction and found to be more active than the palladium complexes formed from **289** but again some loss of activity was noted on reuse.

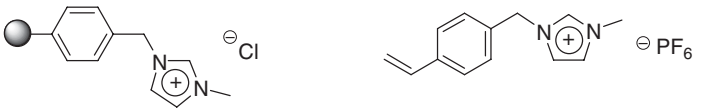

288 **289**

The CNC pyridyl bis-carbene–palladium pincer complex **290** has been immobilized on polystyrene by way of an amide linkage.[330] Initially assessed were the effects of incorporation of an amide linkage in the ligand backbone on catalytic activity in Heck- and Suzuki-coupling reactions. A range of homogeneous amide-containing CNC complexes like **291** were prepared and screened in the coupling reactions. The reaction rate was only marginally slower than that using **290**. The synthesis of palladium complexes bearing the amide-derivatized ligands by coupling the corresponding free acids to amine-functionalized polystyrene supports was unsuccessful. The alternative approach of immobilizing the ligand and then metallating was also ineffective and resulted in precipitated palladium being formed which stuck to the polymer support and was difficult to remove. Ultimately, a reliable and reproducible loading method was found, this involving coupling pre-formed complex **292** with a polymer-supported caproate produced from an amine-functionalized polystyrene support (Scheme 100). A palladium loading of 0.22 mmol g^{-1} was obtained. The supported complex **293** was found to be highly active in both Suzuki and Heck couplings and leaching

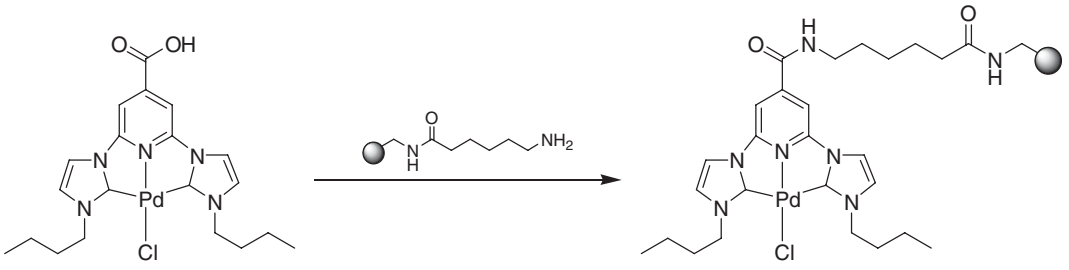

292 293

Scheme 100

levels were very low. Although the complex could be used in air, higher reaction rates and more recycles were achieved using anerobic conditions.

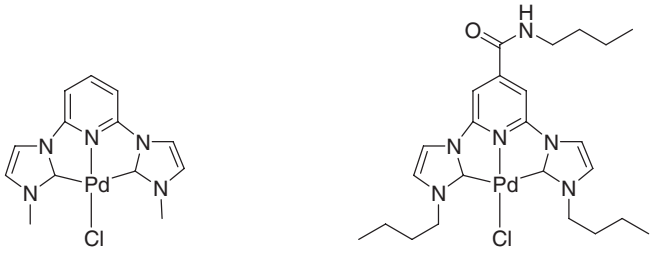

290 291

Using amphiphilic poly(2-oxazoline) derived block co-polymer backbones, immobilized palladium and rhodium carbene NHC complexes have been prepared for use in C–C couplings and hydroformylation, respectively. For the synthesis of the supported rhodium complex, the NHC ligand was attached to prefabricated support **148**.[331] This was achieved by preparing **294** and using standard esterification conditions to attach this to the support giving **295**. Both **294** and **295** were screened for activity in the hydroformylation of 1-octene. Using **294**, very high rates of reaction were observed but with moderate selectivity. With **295**, reaction rates around half of those for **294** were found and studies showed that the supported catalyst needed around 4 h to become fully active. After the reaction was stopped, instantaneous phase separation occurred, thus making catalyst extraction easy. Interestingly, the selectivity of the reaction was greatly improved by immobilization, this indicating that a pronounced change in the microenvironment of the catalytically active Rh center occurs when covalently bound to the amphiphilic block co-polymer.

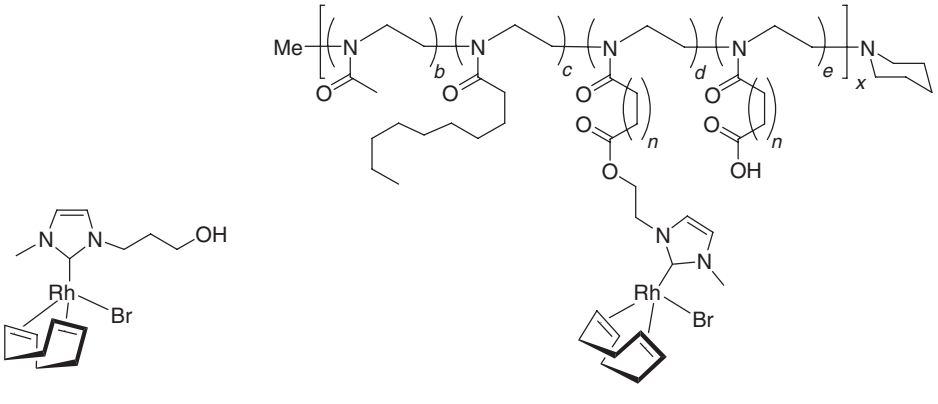

294 295

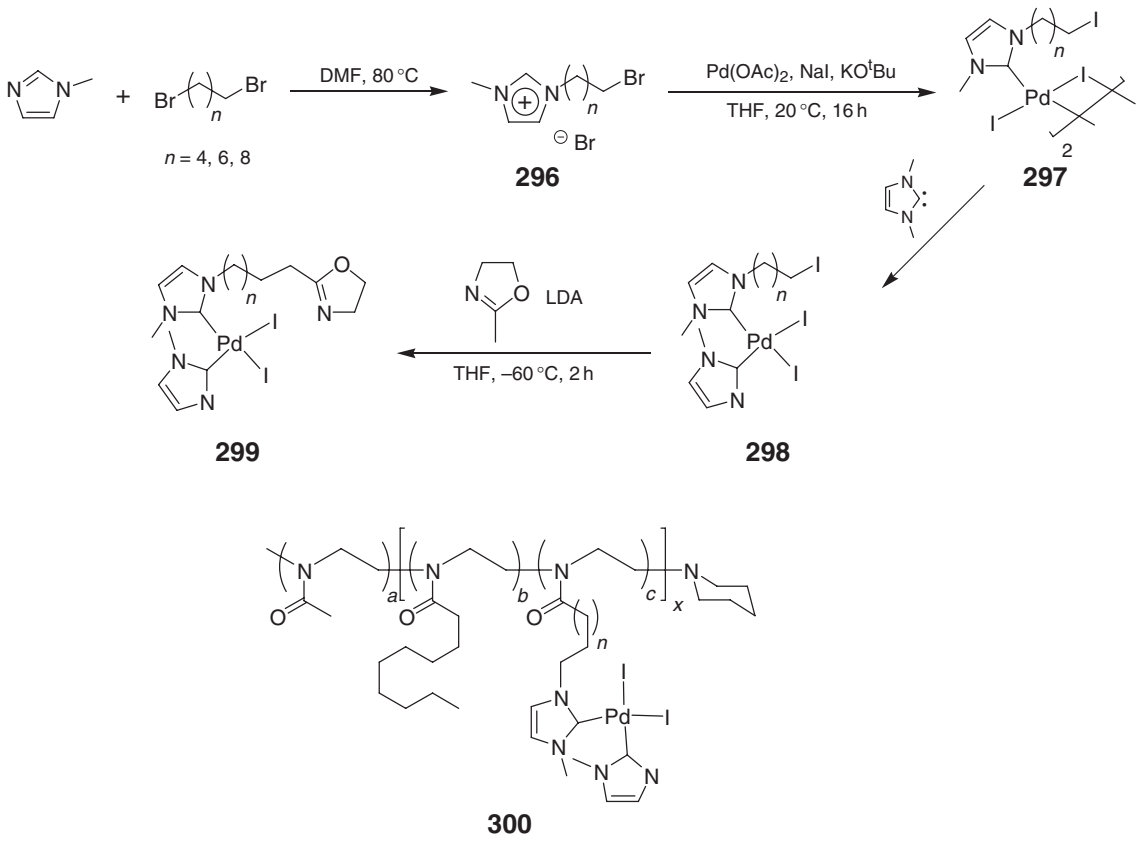

Scheme 101

For the synthesis of the supported palladium complex, rather than using a post-polymerization modification method, metallated NHC-functionalized monomer **299** was used in the polymerization process itself (Scheme 101)[332] The monomer was prepared in four steps. Alkylation of *N*-methylimidazole with a 1,ω-dibromoalkane gave immidazolium salt **296**, which was then treated with palladium acetate at room temperature in the presence of sodium iodide and KO^{t}Bu to generate dimeric complex **297**. Reaction of this with 1,3-dimethylimidazoline-2-ylidene gave dicarbene complex **298**. Due to the quantity of sodium iodide in the reaction mixture during the metallation step, Br → I halogen exchange on the ligand also occurred; this was an advantage in the final step of the synthesis of **299** which was coupling with 2-methyl-2-oxazoline which had been deprotonated with lithium diisopropylamide (LDA). The monomer was then incorporated into a block co-polymer using a methodology analogous to that for the preparation of **149** but using **299** in the place of **147**, thus yielding **300**. This was active as a catalyst for the Heck reaction of iodobenzene and styrene in water but some loss of activity was noted on reuse.

12.14.7.2 Polymer-supported Chromium Isocyanides

Building on the results of Semmelhack and co-workers[121] for studying the effects on the rate of nucleophilic substitution in fluoroarene–$Cr(CO)_2L$ complexes of changing the ligand L, Maiorana and co-workers[333] have prepared polymer-supported fluorobenzene–chromium complex **302** using an isocyanide moiety as linker. The isocyanide-derivatized polymer support **301** was prepared from hydroxymethyl polystyrene in four steps giving ligand loadings of ~0.85 to 0.9 mmol g^{-1} (Scheme 102). After studying the synthesis and reactivity of homogeneous analogs, $Cr(CO)_3(C_6H_5F)$ was attached to the support by direct photolysis with **301** giving **302** with a metal loading of 0.3 mmol g^{-1}. The supported complex was subsequently used successfully in S_NAr reactions.

The *o*- and *m*-dichlorobenzene analogs of **302** have subsequently been prepared and their reactivity toward different nucleophiles investigated.[334] They were found to behave similarly to the corresponding solution-phase

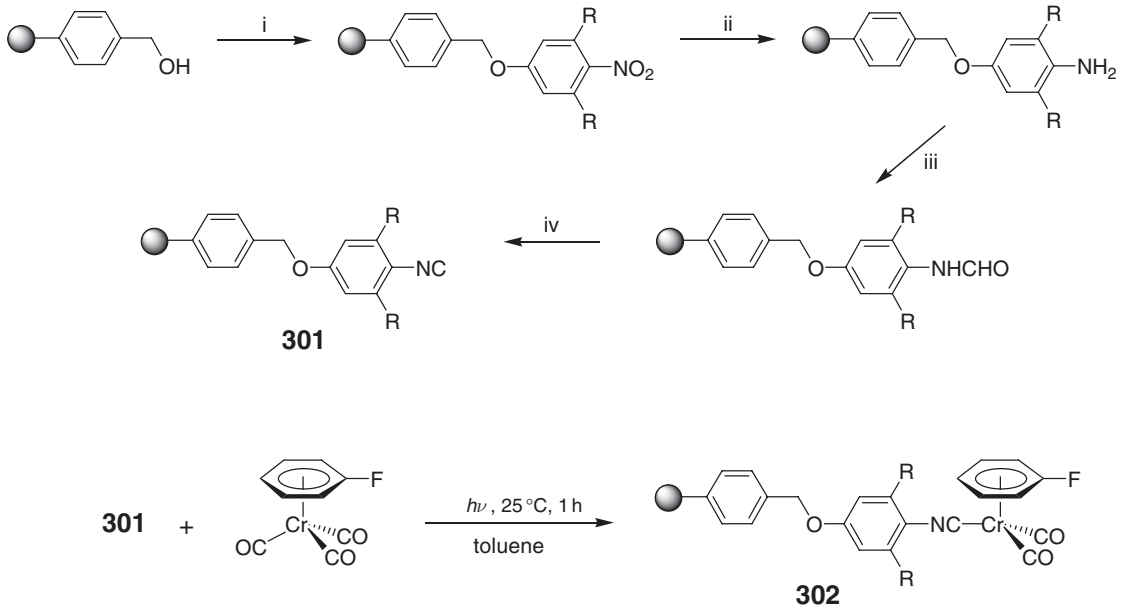

i, 3 equiv. PPh_3, 3 equiv. DEAD, 3 equiv. *p*-NO_2ArOH, THF, RT, 24 h; ii, 9 equiv. $SnCl_2$, DMF, RT, 24 h; iii, 30 equiv. Ac_2O/HCOOH,THF, 60 °C, 2 h; iv, 5.5 equiv. PPh_3, 11 equiv. NEt_3, 5.5 equiv. CCl_4, CH_2Cl_2, RT, 36 h

Scheme 102

(arene)$Cr(CO)_3$ complexes. The *meta*-supported complex **303** was the most reactive, substitution occurring at room temperature whereas the *ortho*-supported complex **304** required slight heating (35 °C) and a higher stoichiometric excess of nucleophile.

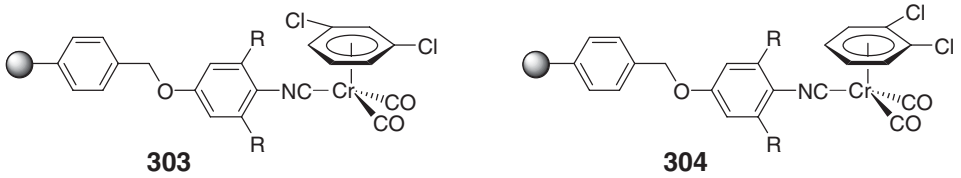

12.14.7.3 Polymer-supported Palladacyclic Complexes

Palladacyclic complexes have attracted significant attention due to their high activity as catalysts for C–C bond-forming reactions. For reviews, see Refs: 335,335a,335b. One of the first palladacyclic complexes used in catalysis was **305**, developed by Herrmann and co-workers, this forming one of a category classed as half-pincer ligands.[336] Other palladacylic complexes have been developed that bind to the metal through three points like **306**,[337] these being classed as pincer ligands. The development of stable palladacycle complexes has spurred a debate about a possible new mechanism in Heck catalysis. Since these complexes are so catalytically active and have highly stable Pd–C bonds, it was surmised that perhaps they could potentially operate by a Pd(II)–Pd(IV) catalytic process instead of the generally accepted Pd(0)–Pd(II) cycle.[338,339] However, more in-depth investigations have shown that it is likely that these complexes are reduced to form soluble or insoluble Pd(0) catalytic species.[340,341] For the pincer complexes, there is substantially less data available on the nature of the catalytic cycle but recent reports suggest that the catalysis is again via the formation of Pd(0) species.[342,343]

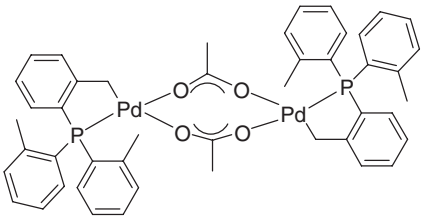

305

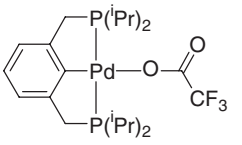

306

With this in mind, it is not surprising that the few examples of polymer-supported palladacyclic complexes that have been reported have not shown much activity after the first use. However, it is worth mentioning briefly some of the immobilized complexes prepared and highlighting the approaches taken in their preparation. Lin and Luo have prepared a polystyrene-immobilized analog of **305**.[344] They first prepared styrene-functionalized palladacyclic monomer **307** in five steps which they then co-polymerized with different equivalents of styrene to give a range of soluble-supported complexes **308** (Scheme 103). They were all active in Heck, Suzuki, and Sonogashira coupling reactions and could be precipitated out of solution at the end of the reaction using ether or acetonitrile. Problems were found with recyclability but the authors do say that if they use an organic base such as triethylamine in the catalysis rather than the traditional mineral bases such as NaOAc, the lifetime of the supported complex can be extended.

Nowotny and co-workers prepared polystyrene-immobilized complex **309**.[345] The supported complex is labile under typical Heck conditions, the active catalyst being transferred to solution. When the reaction is run at 140 °C, the kinetics are sigmoidal, showing that the active species slowly builds up in solution, and then decomposes. In addition, on the second recycle, all activity is in solution, probably as colloidal Pd(0) and no activity is left within the polymer support. This is consistent with **308** and other supported palladacycles being simply a slow source of active colloidal palladium particles.

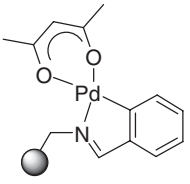

309

Immobilized dicyclohexylphosphine ligand, **310**, has been used as the starting point for the preparation of supported palladacycles **313** and **314**.[346] Simply stirring **310** and dimeric palladium complexes **311** and **312** for 1 h in dichloromethane gave **313** and **314**, respectively (Scheme 104). They are active Suzuki coupling catalysts on the first use but cannot be recycled.

The immobilization of SCS pincer ligands has attracted considerable attention. An SCS ligand was attached to an MeO-PEG backbone via an aryl ether linkage to give **315** which was then metallated by treatment with $Pd(PhCN)_2Cl_2$ yielding **316**.[347] Although active in the Heck reaction, **316** slowly decomposed during the course of the reaction

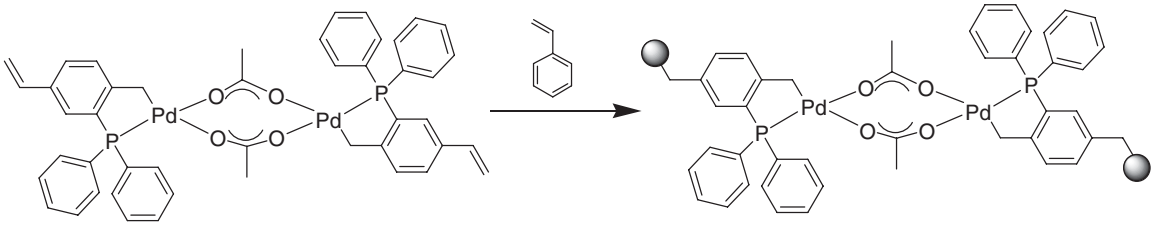

307 **308**

Scheme 103

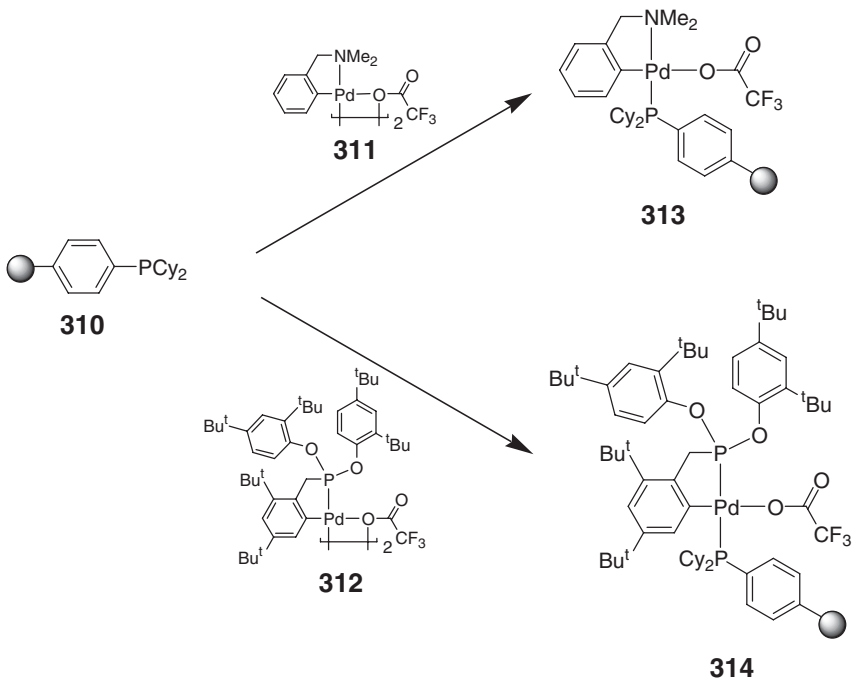

Scheme 104

giving a black precipitate of Pd(0). Changing the aryl ether linkage to the more robust acetamide linker proved successful, and the new catalyst **317** was stable and recyclable with no apparent loss of activity reported.[99] The same SCS pincer complex has been immobilized on poly(acrylate) and poly(*N*-alkylacrylamide) supports giving **318**[348] and **319**,[163] respectively. A dendritic equivalent of the complex has also been attached to polystyrene.[349]

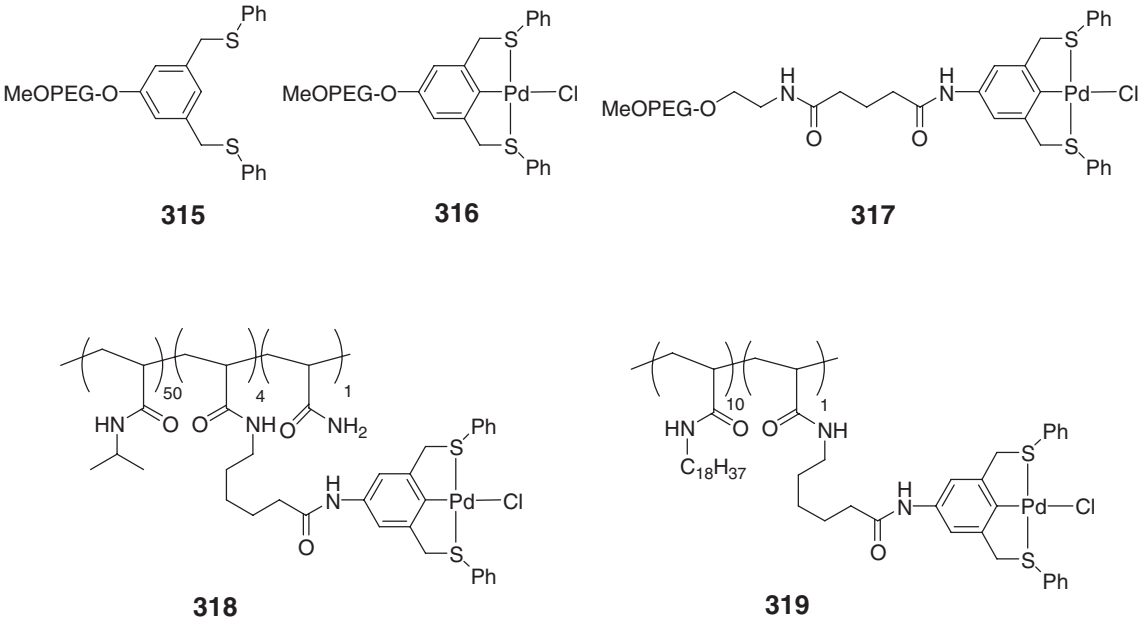

Also worth mentioning here are studies based around the preparation and use of silica-supported palladacyclic complexes. It was the use of these that gave valuable evidence for the decomposition of half-pincer[350] and SCS pincer[342] complexes during Heck reactions, generating soluble Pd(0) species that are the true catalysts.

12.14.7.4 A Polymer-supported $Fe(CO)_3$ Transfer Agent

Tricarbonyliron diene complexes have found many uses in synthetic chemistry but their synthesis is often not easy. Knölker has developed a range of tricarbonyl(η^4-1-aza-1,3-butadiene) iron complexes that are excellent transfer agents for the $Fe(CO)_3$ complexation of 1,3-dienes, and showed their versatility.[351,352] As an extension to this work, Knölker and Gonser[353] have prepared a polymer-supported 1-aza-1,3-butadiene **321** by reaction of Merrifield's resin with phenolic 1-aza-1,3-butadiene **320**, formed from cinnamaldehyde and *para*-hydroxyaniline (Scheme 105). The corresponding tricarbonyl iron complex **322** was formed by treatment of **321** with an excess of $Fe_2(CO)_9$ in THF using ultrasound. The iron complex was subsequently used efficiently as a transfer agent for the tricarbonyliron complexation of 1,3-dienes.

12.14.8 Concluding Remarks

As this chapter shows, a large number of supported ligands and corresponding metal complexes have been prepared and used as catalysts for synthetic organic transformations; this trend is growing at a fast rate. A wide and diverse range of ligands have been attached to polystyrene by reaction of simple derivitized polystyrenes with suitable derivatives of the ligands. Supported ligands have also been prepared by co-polymerization of styryl derivatives with styrene and DVB. Soluble polymer backbones have been prepared and functionalized with metal complexes. These can either be used for synthesis by themselves or else grafted on to solid supports to give amphiphilic materials. The use of dendritic architectures has led to a new avenue for supporting metal complexes and is an area of growing interest. Encapsulation offers a totally different method for immobilizing metal complexes. Each strategy has its inherent advantages and disadvantages but, with the range of immobilized complexes that have been prepared, there is a great deal of choice when it comes to using supported metal catalysts in metal-mediated organic synthesis. The use of polymer-supported techniques is not limited to organic chemistry. Although there have been surprisingly few reports of the preparation of organometallics using solid-supported chemistry, this offers an exciting avenue for further research for organometallic and inorganic chemists.

There are several key areas that need to be developed in order to be able to prepare supported metal complexes more reliably and better understand their activity. Polymer supports are still expensive to purchase and in order for them to have more widespread use it will be necessary to develop more cost effective routes for their preparation.[354] It is important to understand the role of the polymeric backbone in the catalytic activity of immobilized metal complexes and to realize that very different reactivities and selectivities can be found if, for example, the linker or the degree of cross-linking is altered.[355,356] When using dendrimer-derived materials, particular attention needs to be focused on dendritic effects.

The development of new analytical tools that can be applied to the characterization of polymer-supported metal complexes is proving ever more important.[357] There are already a wide range of techniques that have been used. These include colorimetry,[358] gel-phase and solid-state NMR,[359] Mössbauer,[360] IR, and FT-Raman[361] spectrocopies, together with elemental analysis, chemical titration, cyclic and rotating-disk voltammetry,[362] and a range of X-ray techniques. It is important that more than one technique is used to characterize supported catalysts since one technique in isolation may give erroneous results, and so confirmation from another method is invaluable. A number of the supported complexes discussed in this chapter have not been fully characterized. This is of particular concern if the metal complexes are going to be used in catalysis and especially if comparisons are going to be made with "homogeneous analogs."

As shown by Semmelhack and co-workers in their preparation of chromium phosphine complexes and supported rhodium acetate, it is important to think about how best to immobilize a metal complex on a polymer support before

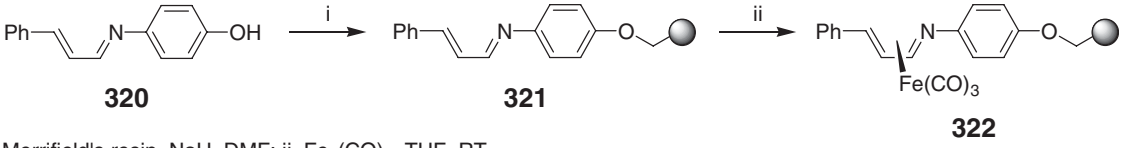

320 **321** **322**

i, Merrifield's resin, NaH, DMF; ii, $Fe_2(CO)_9$, THF, RT

Scheme 105

embarking on the project. By preparing homogeneous analogs, they showed that certain phosphine ligands were unsuitable for use as linkers for chromium arene complexes if they were to be used in S_NAr reactions.

Another point for attention is eradication or at least minimization of leaching of the metal complex off the support during the course of a reaction. This is a particular problem when they are being used in applications such as synthesis of fine chemicals, where contamination of the product with heavy metals is highly undesirable. Leaching still proves to be a weakness of supported metal catalysis and the development of new ligands that hold the metal complex firmly during the course of a reaction proves an area for future research. If only a small amount of leaching is observed, then one option would be to use polymer-supported scavengers to remove the small quantities of metal from the product solution.[363,364]

In conclusion, the area of polymer-supported organometallic chemistry is exciting and growing rapidly. The objective of this chapter is to give a flavor of this and to show the range of immobilization techniques available and briefly outline the use of the supported complexes in organic synthesis. The work covered here has been limited to ligands and their metal complexes attached to derivitized organic supports. There are other areas based on the immobilization of organometallics on inorganic supports on surfaces and the incorporation of organometallics into functional polymers. For these, readers are directed to Chapters 4, 8, and 12 of this volume.

References

1. Pittmann, C. U., Jr. In *Comprehensive Organometallic Chemistry I*; Wilkinson, G., Stone, F. G. A., Abel, E. W., Eds.; Pergamon: Oxford, 1982: Vol. 8.
2. Buchmeiser, M. R., Ed. *Polymeric Materials in Organic Synthesis and Catalysis*; Wiley-VCH: Weinheim, 2003.
3. Seneci, P. *Solid-Phase Synthesis and Combinatorial Techniques*; Wiley: New York, 2001.
4. Burgess, K. *Solid-phase Organic Synthesis*; Wiley: New York, 2000.
5. Lazlo, P. *Preparative Chemistry Using Supported Reagents*; Academic Press, 1987.
6. Hodnett, K.; Kybett, A. P.; Clark, J. H.; Smith, K., Eds. *Supported Reagents and Catalysts in Chemistry*; Royal Society of Chemistry: Cambridge, 1998.
7. Wöhrle, D.; Pomogailo, A. D. *Metal Complexes and Metals in Macromolecules: Synthesis, Structure and Properties*; Wiley-VCH: Weinheim, 2003.
8. Kirschning, A., Ed. In *Immobilized Catalysts: Solid Phases, Immobilization and Applications*; Topics in Current Chemistry; Springer: Berlin, 2004: Vol. 242.
9. Sherrington, D. C.; Kybett, A. P., Eds. *Supported Catalysts and their Applications*; Royal Society of Chemistry: Cambridge, 2000.
10. Pomogailo, A. D. *Catalysis by Polymer-Immobilized Metal Complexes*; Gordon and Breach: Amsterdam, 1998.
11. Bailey, D. C.; Langer, S. H. *Chem. Rev.* **1981**, *81*, 109–148.
12. Bräse, S.; Lauterwasser, F.; Ziegert, R. E. *Adv. Synth. Catal.* **2003**, *345*, 869–929.
13. Clapham, B.; Reger, T. S.; Janda, K. D. *Tetrahedron* **2001**, *57*, 4637–4662.
14. de Miguel, Y. R. *J. Chem. Soc., Perkin Trans. 1* **2000**, 4213–4221.
15. de Miguel, Y. R.; Brulé, E.; Margue, R. G. *J. Chem. Soc., Perkin Trans. 1* **2001**, 3085–3094.
16. Saluzzo, C.; ter Halle, R.; Touchard, F.; Fache, F.; Schulz, E.; Lemaire, M. *J. Organomet. Chem.* **2000**, *603*, 30–39.
17. Shuttleworth, S. J.; Allin, S. M.; Sharma, P. K. *Synthesis* **1997**, *11*, 1217–1239.
18. Shuttleworth, S. J.; Allin, S. M.; Wilson, R. D.; Nasturica, D. *Synthesis* **2000**, *8*, 1035–1074.
19. Eames, J.; Watkinson, M. *Eur. J. Org. Chem.* **2001**, 7, 1213–1224.
20. Ley, S. V.; Baxendale, I. R.; Bream, R. N.; Jackson, P. S.; Leach, A. G.; Longbottom, D. A.; Nesi, M.; Scott, J. S.; Storer, I.; Taylor, S. J. *J. Chem. Soc., Perkin Trans. 1* **2000**, 3815–4195.
21. *Chem Rev.* **2002**, *102*, 3215–3892.
22. Kobayashi, S. *Chem. Soc. Rev.* **1999**, *28*, 1–15.
23. Kobayashi, S. *Curr. Opin. Chem. Biol.* **2000**, *4*, 338–345.
24. Senkan, S. *Angew. Chem., Int. Ed.* **2001**, *40*, 312–329.
25. Reetz, M. T. *Angew. Chem., Int. Ed.* **2001**, *40*, 284–310.
26. Dahmen, S.; Bräse, S. *Synthesis* **2001**, *10*, 1431–1449.
27. Merrifield, R. B. *J. Am. Chem. Soc.* **1963**, *85*, 2149–2154.
28. Burgess, K. L., Ed. *Solid-Phase Organic Synthesis*; Wiley: New York, 2000.
29. Dörwald, F. Z. *Organic Synthesis on Soild Phase: Supports, Linkers, Reactions*; VCH: Weinheim, 2000.
30. Wilson, S. R.; Czarnik, A. W. *Combinatorial Chemistry*; Wiley: New York, 1997.
31. Guillier, F.; Orain, D.; Bradley, M. *Chem. Rev.* **2000**, *100*, 2091–2157.
32. Haag, R.; Roller, S. *Top. Curr. Chem.* **2004**, *242*, 1–42.
33. de Miguel, Y. R.; Rohr, T.; Sherrington, D. C. In *Polymeric Materials in organic Synthesis and Catalysis*; Buchmeiser, M. R., Ed.; Wiley-VCH: Weinheim, 2003.
34. Tzschucke, C. C.; Markert, C.; Bannwarth, W.; Roller, S.; Hebel, A.; Haag, R. *Angew. Chem., Int. Ed.* **2002**, *41*, 3964–4000.
35. Labadie, J. W. *Curr. Opin. Chem. Biol.* **1998**, *2*, 346–352.
36. Bergbreiter, D. E. *Top. Curr. Chem.* **2004**, *42*, 113–176.
37. van Klink, G. P. M.; Dijkstra, H. P.; van Koten, G. *C. R. Chim.* **2003**, *6*, 1079–1085.
38. Dickerson, T. J.; Reed, N. N.; Janda, K. D. *Chem. Rev.* **2002**, *102*, 3325–3344.
39. Bergbreiter, D. E. *Chem. Rev.* **2002**, *102*, 3345–3383.
40. Toy, P.; Janda, K. D. *Acc. Chem. Res.* **2000**, *33*, 546–554.
41. Haag, R. *Chem. Eur. J.* **2001**, *7*, 327–335.
42. Schäfer, A., Ed. *Nanofiltration-principles and Applications*; Elsevier: Amsterdam, 2004.
43. Dijkstra, H. P.; van Klink, G. P. M.; van Koten, G. *Acc. Chem. Res.* **2002**, *35*, 798–810.
44. Vankelcom, I. F. J. *Chem. Rev.* **2002**, *102*, 3779–3810.

45. Newkome, G. R.; Moorfield, C. N.; Vogtle, F. *Dendrimer and Dendrons: Concept, Synthesis and Application*; VCH: Weinheim, 2001.
46. Bosman, A. W.; Jansen, E. W.; Meijer, E. W. *Chem. Rev.* **1999**, *99*, 1665–1688.
47. Mayoral, J.-P.; Caminade, A.-M. *Chem. Rev.* **1999**, *99*, 845–880.
48. Astruc, D.; Chardac, F. *Chem. Rev.* **2001**, *101*, 2991–3023.
49. van Heerbeek, R.; Kamer, P. C. L.; van Leeuwen, P. W. N. M.; Reek, J. N. H. *Chem. Rev.* **2002**, *102*, 3717–3756.
50. Chase, P. A.; Klein, G. J. M.; van Koten, G. *J. Organomet. Chem.* **2004**, *689*, 4016–4054.
51. Twyman, L. J.; King, A. S. H.; Martin, I. K. *Chem. Soc. Rev.* **2002**, *31*, 69–82.
52. Breinbauer, R.; Jacobsen, E. N. *Angew. Chem., Int. Ed.* **2000**, *39*, 3604–3607.
53. Maraval, V.; Laurent, R.; Caminade, A.-M.; Majoral, J.-P. *Organometallics* **2000**, *19*, 4025–4029.
54. Ropartz, L.; Haxton, K. J.; Foster, D. F.; Morris, R. E.; Slawin, A. M. Z.; Cole-Hamilton, D. J. *J. Chem. Soc., Dalton Trans.* **2002**, 4323–4334.
55. Dijkstra, H. P.; Slagt, M. Q.; McDonald, A.; Kruithof, C. A.; Kreiter, R.; Mills, A. M.; Lutz, M.; Spek, A. L.; Klopper, W.; van Klink, G. P. M., *et al. Eur. J. Inorg. Chem.* **2003**, 830–838.
56. Rodríguez, G.; Lutz, M.; Spek, A. L.; van Koten, G. *Chem. Eur. J.* **2002**, *8*, 45–57.
57. Kleij, A. W.; Gossage, R. A.; Klein, G. R. J. M.; Brinkmann, N.; Reijerse, E. J.; Kragl, U.; Lutz, M.; Spek, A. L.; van Koten, G. *J. Am. Chem. Soc.* **2000**, *122*, 12112–12124.
58. Kleij, A. W.; Gossage, R. A.; Jastrzebski, J. T. B. H.; Boersma, J.; van Koten, G. *Angew. Chem., Int. Ed.* **2000**, *39*, 176–178.
59. Dahan, A.; Portnoy, M. *J. Polym. Sci., A: Polym. Chem.* **2005**, *43*, 235–262.
60. Barrett, A. G. M.; Hopkins, B. T.; Köbberling, J. *Chem. Rev.* **2002**, *102*, 3301–3324.
61. Lubbad, S.; Mayr, B.; Mayr, M.; Buchmeiser, M. A. *Macromol. Symp.* **2004**, *210*, 1–9.
62. Sinner, F. M.; Buchmeiser, M. R. *Macromolecules* **2000**, *33*, 5777–5786.
63. Kobayashi, S.; Akiyama, R. *Chem. Commun.* **2003**, 449–460.
64. Pears, D. A.; Smith, S. C. *Aldrichim. Acta* **2005**, *38*, 23–33.
65. Yamada, Y. M. A.; Takeda, K.; Takahashi, H.; Ikegami, S. *Org. Lett.* **2001**, *3*, 1837–1840.
66. Leadbeater, N. E.; Marco, M. *Chem. Rev.* **2002**, *102*, 3217–3274.
67. Farrall, M. J.; Fréchet, J. M. J. *J. Org. Chem.* **1976**, *41*, 3877–3882.
68. For a recent review see: Uozumi, Y. In *Immobilized Catalysts: Solid Phases, Immobilization and Applications*; Kirschning, A., Ed., Topics in Current Chemistry; Springer: Berlin, 2004; Vol. 242, pp 77–112.
69. Pittman, C. U., Jr.; Wuu, S. K.; Jacobson, S. E. *J. Catal.* **1976**, *44*, 87–100.
70. Trost, B. M.; Keinan, E. *J. Am. Chem. Soc.* **1978**, *100*, 7779–7781.
71. Andersson, C. M.; Karabelas, K.; Hallberg, A. *J. Org. Chem.* **1985**, *50*, 3891–3895.
72. Inada, K.; Miyaura, N. *Tetrahedron* **2000**, *56*, 8661–8664.
73. Fenger, I.; Le Drian, C. *Tetrahedron Lett.* **1998**, *39*, 4287–4290.
74. Zhang, T. Y.; Allen, M. J. *Tetrahedron Lett.* **1999**, *40*, 5813–5816.
75. Jang, S-B. *Tetrahedron Lett.* **1997**, *38*, 1793–1796.
76. Jang, S-B. *Tetrahedron Lett.* **1997**, *38*, 4421–4424.
77. Holzhey, N.; Pitter, S.; Dinjus, E. *J. Organomet. Chem.* **1997**, *541*, 243–248.
78. Itsuno, S.; Sakakura, M.; Ito, K. *J. Org. Chem.* **1990**, *55*, 6047–6049.
79. Edwards, C. W.; Shipton, M. R.; Wills, M. *Tetrahedron Lett.* **2000**, *41*, 8615–8619.
80. Dahan, A.; Portnoy, M. *Macromolecules* **2003**, *36*, 1034–1038.
81. Dahan, A.; Portnoy, M. *Org. Lett.* **2003**, *5*, 1197–1200.
82. Luo, T.; Vohs, J. M.; Gorte, R. J. *J. Catal.* **2002**, *210*, 397–404.

82a. Pinna, F.; Menegazzo, F.; Pernicone, N. *Appl. Catal. A* **2001**, *219*, 195–200.

83. For an overview see: Uozumi, Y. *J. Synth. Org. Chem.* **2002**, *60*, 1063–1068.
84. Danjo, H.; Tanaka, D.; Hayashi, T.; Uozumi, Y. *Tetrahedron* **1999**, *55*, 14341–14352.
85. Uozumi, Y.; Danjo, H.; Hayashi, T. *J. Org. Chem.* **1999**, *64*, 3384–3388.
86. Uozumi, Y.; Wanatabe, T. *J. Org. Chem.* **1999**, *64*, 6921–6923.
87. Wentworth, P.; Vandersteen, A. M.; Janda, K. D. *Chem. Comm.* **1997**, 759–760.
88. Köllhofer, A.; Plenio, H. *Chem. Eur. J.* **2003**, *9*, 1416–1425.
89. Atrash, B.; Reader, J.; Bradley, M. *Tetrahedron Lett.* **2003**, *44*, 4779–4782.
90. Atrash, B.; Bradley, M.; Kobylecki, R.; Cowell, D.; Reader, J. *Angew. Chem., Int. Ed.* **2001**, *40*, 938–941.
91. For general information on FibreCats see: www.johnsonmatthey.com

91a. Buckley, S. *Manuf. Chem.* **2002**, *January, 26–27*.

92. Colacot, T. J.; Gore, E. W.; Kuber, A. *Organometallics* **2002**, *21*, 3301–3304.
93. Bergbreiter, D. E.; Tao, G.; Kippenberger, A. M. *Org. Lett.* **2000**, *2*, 2853–2855.
94. Bergbreiter, D. E.; Boren, D.; Kippenberger, A. M. *Macromolecules* **2004**, *37*, 8686–8691.
95. Bergbreiter, D. E.; Kippenberger, A. M.; Tao, G. *Chem. Comm.* **2002**, 2158–2159.
96. Lan, P.; Berta, D.; Porco, J. A.; South, M. S.; Parlow, J. J. *J. Org. Chem.* **2003**, *68*, 9678–9686.
97. Bergbreiter, D. E.; Weatherford, D. A. *J. Org. Chem.* **1989**, *54*, 2726–2730.
98. Bergbreiter, D. E.; Liu, Y.-S. *Tetrahedron Lett.* **1997**, *38*, 7843–7846.
99. Bergbreiter, D. E.; Osburn, P. L.; Wilson, A.; Sink, E. M. *J. Am. Chem. Soc.* **2000**, *122*, 9058–9064.
100. Bergbreiter, D. E.; Weatherford, D. A. *J. Org. Chem.* **1989**, *54*, 2726–2730.
101. Bergbreiter, D. E.; Osburn, P. L.; Friels, J. D. *J. Am. Chem. Soc.* **2001**, *123*, 11105–11106.
102. Bergbreiter, D. E.; Franchina, J. G. *Chem. Commun.* **1997**, 1531–1532.
103. Bergbreiter, D. E.; Franchina, J. G. *Org. Lett.* **2000**, *3*, 393–395.
104. Bergbreiter, D. E.; Franchina, J. G.; Case, B. L.; Williams, L.; Frels, J. D.; Koshti, N. *J. Comb. Chem.* **2000**, *3*, 153–164.
105. For a report (but without any experimental detail) see: McKinley, S. V.; Rakshys, J. W. *J. Chem. Soc., Chem. Commun.* **1972**, 134–135.
106. Naaktgeboren, A. J.; Nolte, R. J. M.; Drenth, W. *J. Am. Chem. Soc.* **1980**, *102*, 3350–3354.
107. Choi, M. K. W.; He, H. S.; Toy, P. H. *J. Org. Chem.* **2003**, *68*, 9831–9834.
108. Yun, K. C.; He, H. S.; Chiu, P.; Toy, P. H. *J. Comb. Chem.* **2004**, *6*, 955–960.
109. Smith, C. P.; Temme, G. H. *J. Org. Chem.* **1983**, *48*, 4681–4685.

109a. Steiner, U. B.; Caseri, W. R.; Suter, U. W. *Langmuir* **1998**, *14*, 347–351.
110. Bergbreiter, D. E.; Li, C. *Org. Lett.* **2003**, *5*, 2445–2447.
110. Årstad, E.; Barrett, A. G. M.; Hopkins, B. T.; Köbberling, J. *Org. Lett.* **2002**, *4*, 1975–1977.
112. Yang, Y.-C.; Luh, T.-Y. *J. Org. Chem.* **2003**, *68*, 9870–9873.
113. Chandrasekhar, V.; Athimoolam, A. *Org. Lett.* **2002**, *4*, 2113–2116.
114. For a review on hybrid polymeric ligands and polymer-supported catalysts containing cyclophosphazenes see: Chandrasekhar, V.; Krishnan, V.; Thilagar, P. *C. R. Chim.* **2004**, *7*, 915–925.
115. Comely, A. C.; Gibson, S. E.; Hales, N. J. *Chem. Commun.* **1999**, 2075–2076.
116. Comely, A. C.; Gibson, S. E.; Hales, N. J. *Chem. Commun.* **2000**, 305–306.
117. Comely, A. C.; Gibson, S. E.; Hales, N. J.; Johnson, C.; Stevenazzi, A. *Org. Biomol. Chem.* **2003**, 1959–1968.
118. Welker, M. E. Organocobalt complexes in organic synthesis. *Curr. Org. Chem.* **2001**, *5*, 785–807.
119. Dahan, A.; Portnoy, M. *Chem. Commun.* **2002**, 2700–2701.
120. Leadbeater, N. E.; Scott, K. A.; Scott, L. J. *J. Org. Chem.* **2000**, *65*, 4770–4772.
121. Semmelhack, M. F.; Hilt, G.; Colley, J. H. *Tetrahedron Lett.* **1998**, *39*, 7683–7686.
122. Gibson, S. E.; Hales, N. J.; Peplow, M. A. *Tetrahedron Lett.* **1999**, *40*, 1417–1418.
123. Comely, A. C.; Gibson, S. E.; Hales, N. J.; Peplow, M. A. *J. Chem. Soc., Perkin Trans. 1* **2001**, 2526–2531.
124. Rigby, J. H.; Kondratenko, M. A.; Fiedler, C. *Org. Lett.* **2000**, *2*, 3917–3919.
125. Rigby, J. H.; Kondratenko, M. A. *Org. Lett.* **2001**, *3*, 3683–3686.
126. Rigby, J. H.; Kondratenko, M. A. *Bioorg. Med. Chem. Lett.* **2002**, *12*, 1829–1831.
127. Maiorana, S.; Seneci, P.; Rossi, T.; Baldoli, C.; Ciraco, M.; de Magistris, E.; Licandro, E.; Papagni, A.; Provera, S. *Tetrahedron Lett.* **1999**, *40*, 3635–3638.
128. Leadbeater, N. E.; Scott, K. A.; Scott, L. J. *J. Org. Chem.* **2000**, *65*, 3231–3232.
129. Leadbeater, N. E. *J. Org. Chem.* **2001**, *66*, 2168–2170.
130. Ahmed, M.; Barrett, A. G. M.; Braddock, D. C.; Cramp, S. M.; Procopiou, P. A. *Tetrahedron Lett.* **1999**, *40*, 8657–8662.
131. Ahmed, M.; Arnauld, T.; Barrett, A. G. M.; Braddock, D. C.; Procopiou, P. A. *Synlett* **2000**, 1007–1009.
132. Judkins, C. M. G.; Knights, K. A.; Johnson, B. F. G.; de Miguel, Y. R.; Raja, R.; Thomas, J. M. *Chem. Commun.* **2001**, 2624–2625.
133. Muci, A. R.; Buchwald, S. L. *Top. Curr. Chem.* **2002**, *219*, 131–209.
134. Parrish, C. A.; Buchwald, S. L. *J. Org. Chem.* **2001**, *66*, 3820–3827.
135. van der Heiden, M.; Plenio, H. *Chem. Eur. J.* **2004**, *10*, 1789–1797.
136. Datta, A.; Ebert, K.; Plenio, H. *Organometallics* **2003**, *22*, 4685–4691.
137. Benvenuti, F.; Carlini, C.; Marchionna, M.; Patrini, R.; Raspolli, G. A. M.; Sbrana, G. *J. Inorg. Organomet. Polym.* **1997**, *7*, 183–201.
138. Benvenuti, F.; Carlini, C.; Marchionna, M.; Raspolli, G. A. M.; Sbrana, G. *J. Mol. Catal. A: Chem.* **1999**, *145*, 221–228.
139. Benvenuti, F.; Carlini, C.; Marchionna, M.; Patrini, R.; Raspolli, G. A. M.; Sbrana, G. *J. Mol. Catal. A: Chem.* **1999**, *139*, 177–187.
140. Stille, J. K.; Su, H.; Hill, D. H.; Schneider, P.; Tanaka, M.; Morrison, D. L.; Hegedus, L. S. *Organometallics* **1991**, *10*, 1993–2000.
141. Bianchini, C.; Frediani, M.; Mantovani, G.; Vizza, F. *Organometallics* **2001**, *20*, 2660–2662.
142. Bianchini, C.; Frediani, M.; Vizza, F. *Chem. Commun.* **2001**, 479–480.
143. Champness, N. R.; Levason, W.; Oldroyd, R. D.; Gulliver, D. J. *J. Organomet. Chem.* **1994**, *465*, 275–281.
144. Wang, P-W.; Fox, A. M. *J. Org. Chem.* **1994**, *59*, 5358–5364.
145. Li, G. Y.; Fagan, P. J.; Watson, P. L. *Angew. Chem., Int. Ed.* **2001**, *40*, 1106–1109.
146. Mansour, A.; Portnoy, M. *J. Chem. Soc., Perkin Trans. 1* **2001**, 952–954.
147. Mansour, A.; Portnoy, M. *Tetrahedron Lett.* **2003**, *44*, 2195–2198.
148. Gonthier, E.; Breinbauer, R. *Synlett* **2003**, 1049–1051.
149. Westhus, M.; Gonthier, E.; Breinbauer, R. *Tetrahedron Lett.* **2004**, *45*, 4131–3142.
150. Uozumi, Y.; Nakai, Y. *Org. Lett.* **2002**, *4*, 2997–3000.
151. Kayaki, Y.; Shimokawatoko, Y.; Ikariya, T. *Adv. Synth. Catal.* **2003**, *345*, 175–179.
152. Mizugaki, T.; Murata, M.; Ooe, M.; Ebitani, K.; Kaneda, K. *Chem. Comm.* **2002**, 52–53.
153. For a review on metal-containing carbosilane dendrimers see: Rossell, O.; Seco, M.; Angurell, I. *C. R. Chim.* **2003**, *6*, 803–817.
154. Alper, H.; Arya, P.; Bourque, S. C.; Manzer, L. E. *Can. J. Chem.* **2000**, *78*, 920–924.
155. Eggeling, E. B.; Hovestad, N. J.; Jastrzebski, J. T. B. H.; Vogt, D.; Van Koten, G. *J. Org. Chem.* **2000**, *65*, 8857–8865.
156. Bourque, S. C.; Maltais, F.; Xiao, W.-J.; Tardiff, O.; Alper, H.; Arya, P.; Manzer, L. E. *J. Am. Chem. Soc.* **1999**, *121*, 3035–3038.
157. Bourque, S. C.; Alper, H.; Manzer, L. E.; Arya, P. *J. Am. Chem. Soc.* **2000**, *122*, 956–957.
158. Arya, P.; Rao, N. R.; Singkhonrat, J.; Alper, H.; Bourque, S. C.; Manzer, L. E. *J. Org. Chem.* **2000**, *65*, 1881–1886.
159. Arya, P.; Panda, G.; Rao, N. V.; Alper, H.; Bourque, S. C.; Manzer, L. E. *J. Am. Chem. Soc.* **2001**, *123*, 2889–2890.
160. Lu, S.-M.; Alper, H. *J. Am. Chem. Soc.* **2003**, *125*, 13126–13131.
161. Lu, S.-M.; Alper, H. *J. Org. Chem.* **2004**, *69*, 3558–3561.
162. Bergbrieter, D. E.; Liu, Y.-S. *Tetrahedron Lett.* **1997**, *38*, 3703–3706.
163. Bergbrieter, D. E.; Liu, Y.-S.; Osburn, P. L. *J. Am. Chem. Soc.* **1998**, *120*, 4250–4251.
164. Stéphan, O.; Riegel, S.; Jugé, S. *J. Electroanal. Chem.* **1997**, *421*, 5–8.
165. Riegel, N.; Darcel, C.; Stéphan, O.; Jugé, S. *J. Organomet. Chem.* **1998**, *567*, 219–233.
166. Gilbertson, S. R.; Chen, G.; McLoughlin, M. *J. Am. Chem. Soc.* **1994**, *116*, 4481–4482.
167. Gilbertson, S. R.; Wang, X. *J. Org. Chem.* **1996**, *61*, 434–435.
168. Gilbertson, S. R.; Pawlick, R. V. *Angew. Chem., Int. Ed.* **1996**, *35*, 902–904.
169. Gilbertson, S. R.; Wang, X.; Hoge, G. S.; Klug, C. A.; Schaefer, J. *Organometallics* **1996**, *15*, 4678–4680.
170. Gilbertson, S. R.; Wang, X. *Tetrahedron Lett.* **1996**, *37*, 6475–6478.
171. Gilbertson, S. R.; Wang, X. *Tetrahedron* **1999**, *55*, 11609–11618.
172. Gilbertson, S. R.; Collibee, S. E.; Agarkov, A. *J. Am. Chem. Soc.* **2000**, *122*, 6522–6523.
173. Greenfield, S. J.; Agarkov, A.; Gilbertson, S. R. *Org. Lett.* **2003**, *5*, 3069–3072.
174. Agarkov, A.; Greenfield, S. J.; Ohishi, T.; Collibee, S. E.; Gilbertson, S. R. *J. Org. Chem.* **2004**, *69*, 8077–8085.
175. The palladium-catalysed desymmetrization of 2,4-cyclopentenediol has also been studied using a similar approach. See: Greenfield, S. J.; Agarkov, A.; Gilbertson, S. R. *Org. Lett.* **2003**, *5*, 3069–3072.

176. Agarkov, A.; Gilbertson, S. R. *Tetrahedron Lett.* **2005**, *46*, 181–183.
177. Gilbertson, S. R.; Yamada, S. *Tetrahedron Lett.* **2004**, *45*, 3917–3920.
178. De Vos, D. E.; Vankelcom, I. F. I.; Jacobs, P. A. *Chiral Catalyst Immobilisation and Recycling*; VCH: Weinheim, 2000.
179. Fan, Q. H.; Li, Y. M.; Chan, A. S. C. *Chem. Rev.* **2002**, *102*, 3385–3465.
180. Dumont, W.; Poulin, J-C.; Dang, T-P.; Kagan, H. B. *J. Am. Chem. Soc.* **1973**, *95*, 8295–8299.
181. Parrinello, G.; Deschenaux, R.; Stille, J. K. *J. Org. Chem.* **1986**, *51*, 4189–4195.
182. Deschenaux, R.; Stille, J. K. *J. Org. Chem.* **1985**, *50*, 2299–2302.
183. Fritschel, S. J.; Ackerman, J. J. H.; Keyser, T.; Stille, J. K. *J. Org. Chem.* **1979**, *44*, 3152–3157.
184. Bayston, D. J.; Fraser, J. L.; Ashton, M. R.; Baxter, A. D.; Polywka, M. E. C.; Moses, E. *J. Org. Chem.* **1998**, *63*, 3137–3140.
185. Chapuis, C.; Barthe, M.; de Saint, L. J.-Y. *Helv. Chim. Acta* **2001**, *84*, 230–242.
186. Otamaru, Y.; Senda, T.; Hayashi, T. *Org. Lett* **2004**, *6*, 3357–3359.
187. ter Halle, R.; Colasson, B.; Schulz, E.; Spagnol, M.; Lamaire, M. *Tetrahedron Lett.* **2000**, *41*, 643–656.
188. Lamouille, T.; Saluzzo, C.; ter Halle, R.; Le Guyader, F.; Lamaire, M. *Tetrahedron Lett.* **2001**, *42*, 663–664.
189. ter Halle, R.; Schulz, E.; Spagnol, M.; Lamaire, M. *Synlett* **2000**, 680–682.
190. Fujii, A.; Sodeoka, M. *Tetrahedron Lett.* **1999**, *40*, 8011–8014.
191. Ohkuma, T.; Takeno, H.; Honda, Y.; Noyori, R. *Adv. Synth. Catal.* **2001**, *343*, 369–375.
192. Guerreiro, P.; Ratovelomanana-Vidal, V.; Genêt, J. P.; Dellis, P. *Tetrahedron Lett.* **2001**, *42*, 3423–3426.
193. Yu, H.-B.; Hu, Q.-S.; Pu, L. *Tetrahedron Lett.* **2000**, *41*, 1681–1685.
194. Fan, Q.-H.; Deng, G.-J.; Lin, C.-C.; Chan, A. S. C. *Tetrahedron: Asymmetry* **2001**, *12*, 1241–1247.
195. Fan, Q.-H.; Ren, C.-Y.; Yeung, C.-H.; Hu, W.-H.; Chan, A. S. C. *J. Am. Chem. Soc.* **1999**, *121*, 7407–7408.
196. Deng, G.-J.; Fan, Q.-H.; Chen, X.-M.; Chan, A. S. C. *J. Mol. Catal. A: Chem* **2003**, *193*, 21–25.
197. Deng, G.-J.; Yi, B.; Huang, Y.-Y.; Tang, W.-J.; He, Y.-M.; Fan, Q.-H. *Adv. Synth. Catal.* **2004**, *346*, 1440–1444.
198. Fan, Q. H.; Liu, G. H.; Deng, G. J.; Chen, X. M.; Chan, A. S. C. *Tetrahedron Lett.* **2001**, *42*, 9047–9050.
199. Fan, Q. H.; Wng. R.; Chan, A. S. C. *Bioorg. Med. Chem. Lett.* **2002**, *12*, 1867–1871.
200. Yu, H. B.; Hu, Q. S.; Pu, L. *J. Am. Chem. Soc.* **2000**, *122*, 6500–6501.
201. Nozaki, K.; Itoi, Y.; Shibahara, F.; Shirakawa, E.; Ohta, T.; Takaya, H.; Hiyama, T. *J. Am. Chem. Soc.* **1998**, *120*, 4051–4052.
202. Nozaki, K.; Shibahara, F.; Itoi, Y.; Shirakawa, E.; Ohta, T.; Takaya, H.; Hiyama, T. *Bull. Chem. Soc. Jpn.* **1999**, *72*, 1911–1918.
203. Shibahara, F.; Nozaki, K.; Hiyama, T. *J. Am. Chem. Soc.* **2003**, *125*, 8555–8560.
204. Nozaki, K.; Shibahara, F.; Elzner, S.; Hiyama, T. *Can. J. Chem.* **2001**, *79*, 593–597.
205. Uozumi, Y.; Danjo, H.; Hayashi, T. *Tetrahedron Lett.* **1998**, *39*, 8303–8306.
206. Uozumi, Y.; Hocke, H. *Tetrahedron* **2004**, *60*, 9297–9306.
207. Song, C. E.; Yang, J. W.; Roh, E. J.; Lee, S.-G.; Ahn, J. H.; Han, H. *Angew. Chem., Int. Ed.* **2002**, *41*, 3852–3854.
208. Uozumi, Y.; Shibatomi, K. *J. Am. Chem. Soc.* **2001**, *123*, 2919–2920.
209. Trost, B. M.; Pan, Z.; Zambrano, J.; Kujat, C. *Angew. Chem., Int. Ed.* **2002**, *41*, 4691–4693.
210. Köllner, C.; Pugin, B.; Togni, A. *J. Am. Chem. Soc.* **1998**, *120*, 10274–10275.
211. Schneider, R.; Köllner, C.; Weber, I.; Togni, A. *Chem. Commun.* **1999**, 2415–2416.
212. Gade, L. H.; Engel, G. D. *Chem. Eur. J.* **2002**, *8*, 4319–4329.
213. Ribourdouille, Y.; Gade, L. H.; Engel, G. D. *C. R. Chim.* **2003**, *6*, 1087–1096.
214. Reetz, M. T.; Lohmer, G.; Schwickardi, R. *Angew. Chem., Int. Ed.* **1997**, *36*, 1526–1529.
215. Zarka, M. T.; Nuyken, O.; Weberskirch, R. *Chem. Eur. J.* **2003**, *9*, 3228–3234.
216. Ralph, C. K.; Akotsi, O. M.; Bergens, S. H. *Organometallics* **2004**, *23*, 1484–1486.
217. Akiyama, R.; Kobayashi, S. *Angew. Chem., Int. Ed.* **2001**, *40*, 3469–3471.
218. Akiyama, R.; Kobayashi, S. *J. Am. Chem. Soc.* **2003**, *125*, 3412–3413.
219. Akiyama, R.; Kobayashi, S. *J. Org. Chem.* **2004**, *69*, 2871–2873.
220. Akiyama, R.; Kobayashi, S. *Org. Lett.* **2004**, *6*, 1987–1990.
221. Yamada, Y. M. A.; Takeda, K.; Takahashi, H.; Ikegami, S. *Org. Lett.* **2002**, *4*, 3371–3374.
222. Yamada, Y. M. A.; Takeda, K.; Takahashi, H.; Ikegami, S. *Tetrahedron Lett.* **2004**, *44*, 2379–2382.
223. Yamada, Y. M. A.; Takeda, K.; Takahashi, H.; Ikegami, S. *Tetrahedron* **2004**, *60*, 4097–4105.
224. Yamada, Y. M. A.; Takeda, K.; Takahashi, H.; Ikegami, S. *J. Org. Chem.* **2003**, *68*, 7733–7741.
225. Pears, D. A.; Smith, S. C. *Aldrichim. Acta* **2005**, *38*, 23–33.
226. Ramarao, C.; Ley, S. V.; Smith, S. C.; Shirley, I. M.; DeAlmeida, N. *Chem Commun.* **2002**, 134–1135.
227. Li, Y.; Hong, X. M.; Collard, D. M.; El-Sayed, M. A. *Org. Lett.* **2000**, *2*, 2385–2388.
228. Li, Y.; Boone, E.; El-Sayed, M. A. *Langmuir* **2002**, *18*, 4921–4925.
229. Li, Y.; El-Sayed, M. A. *J. Phys. Chem. B* **2001**, *105*, 8938–8943.
230. Narayanan, R.; El-Sayed, M. A. *J. Am. Chem. Soc.* **2003**, *125*, 8340–8327.
231. Narayanan, R.; El-Sayed, M. A. *J. Phys. Chem. B* **2004**, *108*, 8572–8580.
232. Pittelkow, M.; Moth-Poulsen, K.; Boas, U.; Christensen, J. B. *Langmuir* **2003**, *19*, 7682–7684.
233. Strimbu, L.; Liu, J.; Kaifer, A. E. *Langmuir* **2003**, *19*, 483–485.
234. Biffis, A.; Sperotto, E. *Langmiur* **2003**, *19*, 9548–9550.
235. Grubbs, R. H., Ed. *Handbook of Metathesis*; Wiley-VCH: Weinheim, 2003.
236. Furstner, A., Ed. *Olefin Metathesis and Metathesis Polymerization*; Springer: Berlin, 1998.
237. Astruc, D. *New J. Chem.* **2005**, *29*, 42–56.
237a. Schrock, R. R. *J. Mol. Catal. A: Chem.* **2004**, *213*, 21–30.
237b. Hoveyda, A. H.; Gillingham, D. G.; van Veldhuizen, J. J.; Kataoka, O.; Garber, S. B.; Kingsbury, J. S.; Harrity, J. P. A. *Org. Biol. Chem.* **2004**, *2*, 8–24.
237c. Connon, S. J.; Blechert, S. *Angew. Chem., Int. Ed.* **2003**, *42*, 1900–1923.
237d. Furstner, A. *Angew. Chem., Int. Ed.* **2000**, *39*, 3012–3043.
237e. Buchmeiser, M. R. *Chem. Rev.* **2000**, *100*, 1565–1604.
238. For a review on supported metathesis catalysts, see: Buchmeiser, M. R. *New J. Chem.* **2004**, *28*, 549–557.
239. Nguyen, S. B. T.; Grubbs, R. H. *J. Organomet. Chem.* **1995**, *497*, 195–200.
240. Mayr, M.; Mayr, B.; Buchmeiser, M. R. *Angew. Chem., Int. Ed.* **2001**, *40*, 3839–3842.

241. Jafarpour, L.; Nolan, S. P. *Org. Lett.* **2000**, *2*, 4075–4078.
242. Jafarpour, L.; Heck, M.-P.; Baylon, C.; Lee, H. M.; Mioskowski, C.; Nolan, S. P. *Organometallics* **2002**, *21*, 671–679.
243. Nieczpor, P.; Buchowicz, W.; Meester, W. J. N.; Rutjes, P. J. T.; Mol, J. C. *Tetrahedron Lett.* **2001**, *42*, 7103–7105.
244. Schürer, S. C.; Gessler, S.; Buschmann, N.; Blechert, S. *Angew. Chem., Int. Ed.* **2000**, *39*, 3898–3901.
245. Dowden, J.; Savović, J. *Chem. Commun.* **2001**, 37–38.
246. Dias, E. L.; Nguyen, S. T.; Grubbs, R. H. *J. Am. Chem. Soc.* **1997**, *119*, 3887–3897.
247. Randl, S.; Buschmann, N.; Connon, S. J.; Blechert, S. *Synlett* **2001**, 1547–1550.
248. Grela, K.; Tryznowski, M.; Bieniek, M. *Tetrahedron Lett.* **2002**, *43*, 9055–9059.
249. Bujok, R.; Bieniek, M.; Masnyk, M.; Michrowska, A.; Sarosiek, A.; Stepowska, H.; Arit, D.; Grela, K. *J. Org. Chem.* **2004**, *69*, 6894–6896.
250. Krause, J. O.; Nuyken, O.; Wurst, K.; Buchmeiser, M. R. *Chem. Eur. J.* **2004**, *10*, 777–784.
251. Yang, L.; Mayr, M.; Wurst, K.; Buchmeiser, M. R. *Chem. Eur. J.* **2004**, *10*, 5761–5770.
252. Connon, S. J.; Blechert, S. *Bioorg. Med. Chem. Lett.* **2002**, *12*, 1873–1876.
253. Yao, Q. *Angew. Chem., Int. Ed.* **2000**, *39*, 3896–3898.
254. Zarka, M. T.; Nuyken, O.; Webesrskirch, R. *Macromol. Rapid Commun.* **2004**, *25*, 858–862.
255. Yao, Q.; Rodriguez, M. A. *Tetrahedron Lett.* **2004**, *45*, 2447–2451.
256. Varray, S.; Lazaro, R.; Martinez, J.; Lamaty, F. *Organometallics* **2003**, *22*, 2426–2435.
257. Hultzsch, K. C.; Jernelius, J. A.; Hoveyda, A. H.; Schrock, R. R. *Angew. Chem., Int. Ed.* **2002**, *41*, 589–593.
258. Connon, S. R.; Dunne, A. M.; Blechert, S. *Angew. Chem., Int. Ed.* **2002**, *41*, 3835–3838.
259. Kroll, R. W.; Schuler, N.; Lubbad, S.; Buchmeiser, M. R. *Chem. Commun.* **2003**, 2742–2743.
260. Dolman, S. J.; Hultzsch, K. C.; Pezet, F.; Teng, X.; Hoveyda, A. H.; Schrock, R. R. *J. Am. Chem. Soc.* **2004**, *126*, 10945–10953.
261. Mayr, M.; Mayr, B.; Buchmeiser, M. R. *Des. Monomers Polym.* **2002**, *5*, 325–337.
262. Sinner, F. M.; Buchmeiser, M. R. *Angew. Chem., Int. Ed.* **2000**, *39*, 1433–1436.
263. Lubbad, S.; Buchmeiser, M. R. *Macromol. Rapid Commun.* **2003**, *24*, 580–584.
264. Mayr, M.; Mayr, B.; Buchmeiser, M. R. *Angew. Chem., Int. Ed.* **2001**, *40*, 3839–3842.
265. Krause, J. O.; Lubbad, S.; Nuyken, O.; Buchmeiser, M. R. *Adv. Synth. Catal.* **2003**, *345*, 996–1004.
266. Krause, J. O.; Lubbad, S.; Nuyken, O.; Buchmeiser, M. R. *Macromol. Rapid Commun.* **2003**, *24*, 875–878.
267. Krause, J. O.; Lubbad, S.; Nuyken, O.; Buchmeiser, M. R. *Adv. Synth. Catal.* **2005**, *347*, 484–492.
268. Gibson, S. E.; Swamy, V. M. *Adv. Synth. Catal.* **2002**, *344*, 619–621.
269. Akiyama, R.; Kobayashi, S. *Angew. Chem., Int. Ed.* **2002**, *41*, 2602–2604.
270. Garber, S. B.; Kingsbury, J. S.; Gray, B. L.; Hoveyda, A. H. *J. Am. Chem. Soc.* **2000**, *122*, 8168–8179.
271. Similar complexes have been immobilized on monolithic sol-gels: Kingsbury, J. S.; Garber, S. B.; Giftos, J. M.; Gray, B. L.; Okamoto, M. M.; Farrer, R. A.; Fourkas, J. T.; Hoveyda, A. H. *Angew. Chem., Int. Ed.* **2001**, *40*, 4251–4256.
272. Astruc, D.; Heuzé, K.; Gatard, S.; Méry, D.; Nlate, S. *Adv. Synth. Catal.* **2005**, *347*, 329–338.
273. Méry, D.; Astruc, D. *J. Mol. Catal. A: Chem.* **2005**, *227*, 1–5.
274. Gatard, S.; Nlate, S.; Cloutet, E.; Bravic, G.; Blais, J.-C.; Astruc, D. *Angew. Chem., Int. Ed.* **2003**, *42*, 452–456.
275. Gatard, S.; Kahlal, S.; Méry, D.; Nlate, S.; Cloutet, E.; Saillard, J.-Y.; Astruc, D. *J. Org. Chem.* **2004**, *23*, 1313–1324.
276. Hlatky, G. C. *Chem. Rev.* **2000**, *100*, 1347–1376.
277. Leadbeater, N. E. *Tetrahedron Lett.* **2002**, *43*, 691–693.
278. Wang, W. Q.; Wang, L. *J. Polymer Mat.* **2003**, *20*, 1–8.
278a. Duchateau, R. *Chem. Rev.* **2002**, *102*, 3525–3542.
278b. Imanishi, Y.; Naga, N. *Prog. Polym. Sci.* **2001**, *26*, 1147–1198.
278c. Alt, H. G. *J. Chem. Soc., Daton Trans.* **1999**, 1703–1710.
279. Raspolli, G. A. M.; Geri, G.; Sbrana, G.; Marchionna, M.; Ferrarini, P. *J. Mol. Catal. A: Chem.* **1996**, *111*, 273–280.
280. Barrett, A. G. M.; de Miguel, Y. R. *Chem. Commun.* **1998**, 2079–2080.
281. Barrett, A. G. M.; de Miguel, Y. R. *Tetrahedron Lett.* **2002**, *58*, 3785.
282. Zhang, Y.; Sita, L. R. *Chem. Commun.* **2003**, 2358–2359.
283. Nishida, H.; Uozumi, T.; Arai, T.; Soga, K. *Macromol. Rapid Commun.* **1995**, *16*, 821–830.
284. Hong, S. C.; Ban, H. T.; Kishi, N.; Jin, J. Z.; Uozumi, T.; Soga, K. *Macromol. Chem. Phys.* **1998**, *199*, 1393–1397.
285. Hong, S. C.; Teranishi, T.; Soga, K. *Polymer* **1998**, *39*, 7153–7157.
286. Kitagawa, T.; Uozumi, T.; Soga, K.; Takata, T. *Polymer* **1997**, *38*, 615–620.
287. Stork, M.; Koch, M.; Klapper, M.; Müllen, K.; Gregorius, H.; Rief, U. *Macromol. Rapid Commun.* **1999**, *20*, 210–213.
288. Hok, S.; Vassilian, J.; Schore, N. E. *Org. Lett.* **2002**, *4*, 2365–2368.
289. Zhu, H.; Jin, G.-X.; Hu, N. *J. Organomet. Chem.* **2002**, *655*, 167–171.
290. Roscoe, S. B.; Fréchet, J. M. J.; Walzer, J. F.; Dias, A. J. *Science* **1998**, *280*, 270–273.
291. Roscoe, S. B.; Gong, C.; Fréchet, J. M. J.; Walzer, J. F. *J. Polym. Sci. A: Polym. Chem.* **2000**, *38*, 2979–2992.
292. Musikabhumma, K.; Uozumi, T.; Sano, T.; Soga, K. *Macromol. Rapid Commun.* **2000**, *21*, 675–679.
293. Klapper, M.; Jang, Y.-J.; Bieber, K.; Nemnich, T.; Nenov, N.; Müllen, K. *Macromol. Symp.* **2004**, *213*, 131–145.
294. Hong, S. C.; Rief, U.; Kristen, M. O. *Macromol. Rapid Commun.* **2001**, *22*, 1447–1454.
295. Koch, M.; Stork, M.; Klapper, M.; Müllen, K.; Gregorius, H. *Macromolecules* **2000**, *33*, 7713–7717.
296. Liu, J.; Dong, J.-Y.; Cui, N.; Hu, Y. *Macromolecules* **2004**, *37*, 6275–6282.
297. Qin, Y.; Tang, T.; Zhao, Z. *Chem. Commun.* **2004**, 222–223.
298. Qin, Y.; Tang, T.; Zhao, Z.; Huang, B. *J. Polymer. Sci. A: Chem.* **2003**, *41*, 3313–3319.
299. Kim, E.; Kim, K.; Yang, H.; Kim, Y. T.; Kwak, J. *Anal. Chem.* **2003**, *75*, 5665–5672.
300. Daniel, M.-C.; Ruiz, J.; Astruc, D. *J. Am. Chem. Soc.* **2003**, *125*, 1150–1151.
301. Alvarez, J.; Ren, T.; Kaifer, A. E. *Organometallics* **2001**, *20*, 3543–3549.
302. Salmon, A.; Jutzi, P. *J. Organomet. Chem.* **2001**, *637–639*, 595–608.
303. Chuard, T.; Bèguin, M.-T.; Deschenaux, R. *C. R. Chim.* **2003**, *6*, 959–962.
304. Casado, C. M.; Gonzales, B.; Cuadrado, I.; Alonso, B.; Moran, M.; Losada, J. *Angew. Chem., Int. Ed.* **2000**, *39*, 2135–2138.
305. Sengupta, S. *Tetrahedron Lett.* **2003**, *44*, 7281–7284.
306. Chandrasekhar, V.; Andavan, G. T. S.; Nagendran, S.; Krishnan, V.; Azhakar, R.; Butcher, R. J. *Organometallics* **2003**, *22*, 976–986.

307. Turrin, C.-O.; Chiffre, J.; Daran, J. C.; de Montauzon, D.; Caminade, A.-M.; Manoury. E.; Balavoine, G.; Majoral, J.-P. *Tetrahedron* **2001**, *57*, 2521–2536.
308. Turrin, C.-O.; Chiffre, J.; de Montauzon, D.; Balavoine, G.; Manoury, E.; Caminade, A.-M.; Majoral, J.-P. *Organometallics* **2002**, *21*, 1891–1897.
309. Caminade, A.-M.; Maraval, V.; Laurent, R.; Turrin, C.-O.; Sutra, P.; Leclaire, J.; Griffe, L.; Marchand, P.; Baudoin-Dehoux, C.; Rebout, C., *et al. C. R. Chim.* **2003**, *6*, 791–801.
310. Andrés, R.; de Jesús, E.; de la Mata, J.; Flores, J. C.; Gómes, R. *J. Organomet. Chem.* **2005**, *690*, 939–943.
311. Andrés, R.; de Jesús, E.; de la Mata, J.; Flores, J. C.; Gómes, R. *Eur. J. Inorg. Chem.* **2002**, 2281–2286.
312. Arévalo, S.; de Jesús, E.; de la Mata, J.; Flores, J. C.; Gómes, R. *Organometallics* **2001**, *20*, 2583–2592.
313. Arévalo, S.; Benito, J. M.; de Jesús, E.; de la Mata, J.; Flores, J. C.; Gómes, R. *J. Organomet. Chem.* **2000**, *602*, 208–210.
314. Heinze, K. *Chem. Eur. J.* **2001**, 7, 2922–2932.
315. Robillard, M. S.; Valentijn, A. R. P. M.; Meeuwenoord, N. J.; van der Marel, G. A.; van Boom, J. H.; Reedijk, J. *Angew. Chem., Int. Ed.* **2000**, *39*, 3096–3099.
316. Robillard, M. S.; Bacac, M.; van den Elst, H.; Flamigni, A.; van der Marel, G. A.; van Boom, J. H.; Reedijk, J. *J. Comb. Chem.* **2003**, *5*, 821–825.
317. Robillard, M. S.; Lieth, J. S.; van der Marel, G. A.; van Boom, J. H.; Reedijk, J. *Eur. J. Inorg. Chem.* **2003**, 1529–1532.
318. Van Zutphhen, S.; Robillard, M. S.; van der Marel, G. A.; Overkleeft, H.; den Culk, H.; Brouwer, J.; Reedijk, J. *Chem. Comm.* **2003**, 634–635.
319. Khan, S. I.; Beilstein, A. E.; Tierney, M. T.; Sykora, M.; Grinstaff, M. W. *Inorg. Chem.* **1999**, *38*, 5999–6002.
320. Grinstaff, M. W.; Beilstein, A. E.; Hu, X.; Tierney, M. T.; Smith, G. D.; Sykora, M.; Khan, S. I. *J. Inorg. Biochem.* **1999**, *38*, 3922–3925.
321. Leadbeater, N. E.; Sharp, E. L. *Organometallics* **2003**, *22*, 4167–4169.
322. Zhang, Z.; Lepore, S. D. *Tetrahedron Lett.* **2002**, *43*, 7357–7360.
323. Crudden, C. M.; Allen, D. P. *Coord. Chem. Rev.* **2004**, *248*, 2247–2273.
324. Peris, E.; Crabtree, R. H. *Coord. Chem. Rev.* **2004**, *248*, 2239–2246.
325. Herrmann, W. A. *Angew. Chem., Int. Ed.* **2002**, *41*, 1290–1309.
326. Herrmann, W. A.; Elison, M.; Fischer, J.; Kocher, C.; Artus, C. R. J. *Angew. Chem., Int. Ed.* **1995**, *34*, 2371–2374.
326a. Herrmann, W. A.; Elison, M.; Fischer, J.; Kocher, C.; Artus, C. R. J. *Chem. Eur. J.* **1996**, *2*, 772–780.
326b. Herrmann, W. A.; Kocher, C. *Angew. Chem., Int. Ed.* **1997**, *36*, 2163–2187.
326c. Herrmann, W. A. *Angew. Chem., Int. Ed.* **2002**, *41*, 1290–1309.
326d. Herrmann, W. A.; Ofele, K.; Von Preysing, D.; Schneider, S. K. *J. Organomet. Chem.* **2003**, *687*, 229–248.
327. Schwarz, J.; Böhm, V. P. W.; Gardiner, M. G.; Grosche, M.; Herrmann, W. A.; Hieringer, W.; Raudaschl-Sieber, G. *Chem. Eur. J.* **2000**, *6*, 1773–1780.
328. Byun, J.-W.; Lee, Y.-S. *Tetrahedron Lett.* **2004**, *45*, 1837–1840.
329. Kim, J.-H.; Jun, B.-H.; Byun, J.-W.; Lee, Y.-S. *Tetrahedron Lett.* **2004**, *45*, 5827–5831.
330. Steel, P. G.; Teasdale, C. W. T. *Tetrahedron Lett.* **2004**, *45*, 8977–8980.
331. Schönfelder, D.; Fischer, K.; Schmidt, M.; Nuyken, O.; Weberskirch, R. *Macromolecules* **2004**, *38*, 254–262.
332. Zarka, M. T.; Bortenschlager, M.; Wurst, K.; Nuyken, O.; Weberskirch, R. *Organometallics* **2004**, *23*, 4817–4820.
333. Maiorana, S.; Baldoli, C.; Licandro, E.; Casiraghi, L.; de Magistris, E.; Paio, A.; Provera, S.; Seneci, P. *Tetrahedron Lett.* **2000**, *41*, 7271–7275.
334. Baldoli, C.; Maiorana, S.; Licandro, E.; Casiraghi, L.; Zinzalla, G.; Seneci, P.; de Magistris, E.; Paio, A.; Marchioro, C. *J. Comb. Chem.* **2003**, *5*, 809–813.
335. Beford, R. B. *Chem. Commun.* **2003**, 1787–1796.
335a. Dupont, J.; Pfeffer, M.; Osborn, J. *Eur. J. Inorg. Chem.* **2001**, 1917–1927.
335b. Herrmann, W. A.; Böhm, V. P. W.; Reisinger, C.-P. *J. Organomet. Chem.* **1999**, *576*, 23–41.
336. Herrmann, W. A.; Brossmer, C.; Öfele, K.; Reisinger, C.-P.; Priermeier, T.; Beller, M.; Fischer, H. *Angew. Chem., Int. Ed.* **1995**, *34*, 1844–1848.
337. Ohff, M.; Ohff, A.; van der Boom, M. E.; Milstein, D. *J. Am. Chem. Soc.* **1997**, *119*, 11687–11688.
338. Shaw, B. L. *New J. Chem.* **1998**, *22*, 77–79.
339. Shaw, B. L.; Perera, S. D.; Staley, E. A. *Chem. Commun.* **2001**, 1361–1362.
340. For a review, see: Farina, V. *Adv. Synth. Catal.* **2004**, *346*, 1553–1582.
341. deVries, A. H. M.; Mulders, J. M. C. A.; Mommers, J. H. M.; Henderickx, H. J. W.; de Vries, J. G. *Org. Lett.* **2003**, *5*, 3285–3288.
342. Yu, K.; Sommer, W.; Weck, M.; Jones, C. W. *J. Catal.* **2004**, *226*, 101–110.
343. Eberhard, M. R.; Wang, Z. *Org. Lett.* **2004**, *6*, 2125–2128.
344. Knölker, H.-J. *Chem. Soc. Rev.* **1999**, *28*, 151–157.
345. Nowotny, M.; Hanefeld, U.; van Koningsveld, H.; Maschmeyer, T. *Chem. Commun.* **2000**, 1877–1878.
346. Bedford, R. B.; Coles, S. J.; Hursthouse, M. B.; Scordia, V. J. M. *Dalton Trans.* **2005**, 991–995.
347. Bergbreiter, D. E.; Osburn, P. L.; Liu, Y-.S. *J. Am. Chem. Soc.* **1999**, *121*, 9531–9538.
348. Bergbreiter; Osburn, P. L.; Frels, D. J. *J. Am. Chem. Soc.* **2001**, *123*, 11105–11106.
349. Dahan, A.; Weissberg, A.; Portnoy, M. *Chem. Commun.* **2003**, 1206–1207.
350. Bedford, R. B.; Cazin, C. S. J.; Hursthouse, M. B.; Light, M. E.; Pike, K. J.; Wimperis, S. *J. Organomet. Chem.* **2001**, *633*, 173–181.
351. Knölker, H.-J. *Chem. Rev.* **2000**, *100*, 2941–2962.
352. Knölker, H.-J. *Chem. Soc. Rev.* **1999**, *28*, 151–157.
353. Knölker, H.-J.; Gonser, P. *Synlett* **1992**, 517–520.
354. Le Carre, E.; Lewis, N.; Ribas, C.; Wells, A. *Org. Process Res. Dev.* **2000**, *4*, 606–610.
355. Alexandratos, S. D.; Miller, D. H. J. *Macromolecules* **2000**, *33*, 2011–2015.
356. Santora, B. P.; Gagne, M. R.; Moloy, K. G.; Radu, N. S. *Macromolecules* **2001**, *34*, 658–661.
357. Scicinski, J. J.; Congreve, M. S.; Kay, C.; Ley, S. V. *Curr. Med. Chem.* **2002**, *9*, 2103–2127.
358. Galindo, F.; Altava, B.; Burguete, M. I.; Gavara, R.; Luis, S. V. *J. Comb. Chem.* **2004**, *6*, 859–861.
359. Fruchart, J.-S.; Lippens, G.; Kuhn, C.; Gras-Masse, H.; Melnyk, O. *J. Org. Chem.* **2002**, *67*, 526–532.
360. Gressier, J. C.; Levesque, G.; Patin, H.; Varret, F. *Macromolecules* **1983**, *16*, 1577–1581.
361. Altava, B.; Burguete, M. I.; Garcia-Verdugo, E.; Luis, S. V.; Vicent, M. J. *Tetrahedron* **2001**, *57*, 8675–8683.
362. Shan, J.; Pickup, P. G. *Electrochim. Acta* **2000**, *46*, 119–125.
363. Eames, J.; Watkinson, M. *Eur. J. Org. Chem.* **2001**, 1213–1224.
364. Hodges, J. C. *Synlett* **2000**, 152–158.

12.15 Organometallic Clusters

J B Keister, University at Buffalo, Buffalo, NY, USA

12.15.1 Overview

The coverage of this chapter concerns applications of "organometallic clusters" in the period 1993 to mid-2005. One definition of a metal cluster is "a molecular compound containing three or more metals in a closed array, and held together by metal–metal bonds."[1] This definition focused on the importance of the metal–metal interactions and the unique structural features presented by closed metal arrays. However, this definition has been considerably broadened by common usage. Compounds containing only two metal atoms, compounds containing several metal atoms held together by bridging ligands and without metal–metal bonds, or even small metal particles are commonly referred to as "metal clusters." The term "organometallic" defined refers to complexes containing at least one metal–carbon bond, including metal carbonyls. This chapter adopts the broader definition of molecular clusters, and includes clusters which do not contain metal–carbon bonds if they appear in applications for which organometallic clusters are used.

Many monographs and review articles of organometallic cluster chemistry have appeared in the preceding two decades.[1–3] In COMC (1995), chapters relating specifically to metal clusters are to be found in Volumes 7, 8, and 10, which cover the metals which are present in the largest number of known molecular metal clusters; in other volumes, metal clusters are intermixed with mononuclear metal complexes. No previous chapter has been concerned with applications of organometallic clusters.

Through the years 1970–1990, most applications of organometallic clusters concerned catalysis, either as homogeneous catalysts or as precursors for heterogeneous catalysts. Since these two applications have been extensively reviewed and since homogeneous catalysis is treated elsewhere, the stricter definition of a metal cluster was used: a

metal cluster is a molecular compound of three or more metal atoms in a closed array and having a substantial metal–metal interaction. Since the syntheses and structures of the clusters included in this chapter would have been presented in earlier chapters associated with the metals themselves, only limited coverage is included here; the focus is on the application of the clusters rather than on the clusters themselves.

Recently, clusters have been examined as precursors for nanoscale materials, as biomedical imaging agents, and as optical materials. For these newer applications, the broadest definition of a metal cluster has been used, including compounds containing several metal atoms held together by bridging ligands and without metal–metal bonds, or even small metal particles if the particles are stabilized by a ligand shell rather than a heterogeneous support.

12.15.2 Metal Clusters in Homogeneous Catalysis

One of the justifications for research in metal cluster chemistry was the hope that clusters would be improved catalysts for known reactions or novel catalysts for new reactions. Limited success has been achieved. A number of reviews have appeared.[4–8] While there are well-established examples of clusters as homogeneous catalysts, none are superior to well-known and widely used monometallic catalysts. In many cases of clusters used as catalyst precursors, the catalytically active species is a lower-nuclearity product of fragmentation of the cluster precursor or heterogeneous metal particles formed by decomposition.

One important class of "cluster catalysts" are dimetallic catalysts such as $Rh_2(carboxylate)_4$, which effect additions and insertions of carbenoids derived from diazoalkanes. This class is not included below because the strict definition of a cluster as containing three or more metal atoms has been adopted. This area of homogeneous catalysis has been reviewed recently[9,10] and is treated in the current edition concerning transition metals in organic synthesis.

12.15.2.1 Clusters of Metals in Groups 6 and 7

Relatively few clusters of the groups other than 8–10 have been investigated for catalytic activity, mainly because there are many fewer examples of clusters in these groups. Early transition metals have relatively weak metal–metal bonds, and polymetallic complexes typically are held together by bridging ligands and without substantial metal–metal bonding, thus excluding them from this chapter.

Trinuclear or tetranuclear phosphido-bridged rhenium carbonyl clusters were catalysts for hydrogenation and isomerization behavior of 1-hexene. The clusters were prepared by hydrogenolysis of $Re_2(\mu\text{-}P(C_6H_4\text{-}4\text{-}X)_2)_2(CO)_8$ (X = H, F) at 493 K, which gave $Re_3(\mu_3\text{-}H)_2(\mu\text{-}P(C_6H_4\text{-}4\text{-}X)_2)_3(CO)_6$, $Re_4(\mu\text{-}H)_2(\mu\text{-}P(C_6H_4\text{-}4\text{-}X)_2)_4(\mu_4\text{-}P(C_6H_4\text{-}4\text{-}X))(CO)_8$, and $Re_4(\mu\text{-}H)(\mu\text{-}P(C_6H_4\text{-}4\text{-}X)_2)_3(\mu_4\text{-}P(C_6H_4\text{-}4\text{-}X))_2(CO)_8$. These clusters catalyzed 1-hexene hydrogenation and isomerization in dioxane solution and 443–453 K and a hydrogen pressure of 30 atm, without apparent fragmentation. $Re_3(\mu_3\text{-}H)_2(\mu\text{-}P(C_6H_4\text{-}4\text{-}F)_2)_3(CO)_6$ and $Re_4(\mu\text{-}H)_2(\mu\text{-}P(C_6H_4\text{-}4\text{-}F)_2)_4(\mu_4\text{-}P(C_6H_4\text{-}4\text{-}F))(CO)_8$ (the most active of the catalysts) were more selective for hydrogenation, whereas the others gave predominantly isomerization.[11]

Catalytic hydrogenation of ethylene was achieved using $W_6(\mu\text{-}H)_4H(\mu\text{-}C\text{-}i\text{-}Pr)(\mu\text{-}O\text{-}i\text{-}Pr)_7(O\text{-}i\text{-}Pr)_5$ as the catalyst.[12]

12.15.2.2 Fe, Ru, and Os Clusters

Since $Ru_3(CO)_{12}$ and substituted derivatives are among the most readily available clusters, they have served as the starting point for many investigations of cluster catalysis. A key question is when the observed catalytic activity is due to the cluster precursor and when it is due to a fragmentation product or metallic Ru.

Careful studies showed that benzene hydrogenation in the presence of $[Ru_3(\mu\text{-}H)_3(\eta^6\text{-}C_6H_6)(\eta^6\text{-}C_6Me_6)_2(\mu_3\text{-}O)]^{1+}$, a possible example of "supramolecular catalysis,"[13] is actually catalyzed by metallic ruthenium.[14] In a series of papers, $[Ru_3(\mu\text{-}H)_3(\eta^6\text{-}C_6H_6)(\eta^6\text{-}C_6Me_6)_2(\mu_3\text{-}O)]^{1+}$, and related derivatives, were studied as catalysts for hydrogenation of benzene and other arenes to cyclohexanes under mild conditions in aqueous biphasic conditions.[15–20] The oxo-bridged clusters could be formed from a variety of precursors, including $[(\eta^6\text{-}C_6H_6)_4Ru_4H_4]^{2+}$, or by reaction of dinuclear $[H_3Ru_2(\eta^6\text{-}C_6H_2Me_4)_2]^{+}$ with mononuclear complexes such as $[Ru(\eta^6\text{-}C_6H_6)(H_2O)_3]^{2+}$.[21] The mechanism which was originally proposed invoked the substrate arene hosted inside the hydrophobic pocket formed by the three arene ligands of the cluster, giving rise to the term "supramolecular catalysis." To distinguish between homogeneous and heterogeneous catalysis, a combination of kinetic studies, poisoning experiments, H/D exchange rates,

transmission electron microscopy (TEM) studies was used. Kinetics established that at least 99.7% of the reactions could be attributed to metallic Ru.

Based upon these results, other reports of arene hydrogenation catalyzed by other ruthenium clusters should be viewed with caution. The use of ionic liquids as solvents for the catalytic hydrogenation of arenes and for the carbon–carbon coupling reactions of haloarenes with arylboronic acids was discussed. The cluster $[H_6Ru_4(\eta^6\text{-}C_6H_6)_4]^{2+}$ was claimed to be an effective catalyst for hydrogenation of arenes in ionic liquids.[22] The catalytic hydrogenation of benzene and other arenes under biphasic conditions was also claimed for $Ru(\eta^6\text{-}C_{10}H_{14})(pta)Cl_2$ (pta = 1,3,5-triaza-7-phosphaadamantane), $Ru(\eta^6\text{-}C_{10}H_{14})(tppts)Cl_2$ (tppts = tris-3-sulfonatophenylphosphine trisodium salt), and $[Ru(\eta^6\text{-}C_{10}H_{14})(pta)_2Cl]^{1+}$. The active catalysts formed during the hydrogenations were attributed to be a trinuclear cluster, a colloid, and a mononuclear complex, respectively.[23] A review has delineated various experiments which may be used to determine whether the active catalyst is a cluster, colloidal, or a nanoparticle, including the role of solvent.[24]

A number of studies have examined alkene hydrogenation catalyzed by $Ru_3(CO)_{12}$ and substituted derivatives, many reported prior to 1993. One study reported that $Ru_3(CO)_{12}$ and $Ru_3(CO)_9(PPh_3)_3$ were catalyst precursors for hydrogenation and isomerization of 1-hexene at 303–363 K. After the hydrogenations, the IR spectra of the solutions showed $H_4Ru_4(CO)_{12}$ and $H_4Ru_4(CO)_{12-n}(PPh_3)_n$ ($n = 1$–4), respectively. In addition to hexane, the isomerization products were *trans*-2-hexene (up to 61%), *cis*-2-hexene (up to 23%), and *trans*-3-hexene (up to 20%).[25]

One tool to identify hydride-containing intermediates present at low concentration is the amplification of ^1H NMR resonances by using parahydrogen-induced polarization (PHIP). PHIP was used to identify pathways in the hydrogenation of alkenes and alkynes with $Ru_3(CO)_{12-n}(L)_n$ (L = PMe_3, PMe_2Ph, PPh_3, and PCy_3; $n = 1$–3) as the catalyst precursor. Solvent was found to play an important role. When $n = 2$, three isomers of $Ru_3(H)(\mu\text{-}H)(CO)_9(L)_2$ are formed, which differ in the arrangement of their equatorial phosphines. Kinetic studies reveal the presence of intra- and interisomer exchange processes, with activation parameters and solvent effects indicating the involvement of ruthenium–ruthenium bond heterolysis and CO loss, respectively. When $n = 3$, reaction with hydrogen forms the same products, but hydrogenation of the monosubstituted clusters gives only one isomer of $Ru_3(H)(\mu\text{-}H)(CO)_{10}(L)$. $Ru_3(H)(\mu\text{-}H)(CO)_9(L)_2$ is kinetically significant in the alkyne hydrogenation. Fragmentation to mononuclear $Ru(H)_2(CO)_2(L)$(alkyne) is also observed and is favored in non-polar solvents.[26,27] Parahydrogen was used to identify intermediates in catalytic hydrogenation of diphenylacetylene by $Ru_3(CO)_{10}$(dppe) and $Ru_3(CO)_8(dppe)_2$ (dppe = 1,2-bis(diphenylphosphino)ethane). Fragmentation dominates in low-polarity solvents. In solvents of higher polarity, the clusters are active hydrogenation catalysts, and the bidentate phosphine complexes are less active than monodentate analogs $Ru_3(CO)_{10}(L)_2$ (L = PPh_3, PMe_2Ph, PMe_3, PCy_3).[28]

The clusters $Ru_3(CO)_{12-n}(L)_n$ (L = PPh_3, NCMe, or $(EtO)_3Si(CH_2)_3NH_2$, $n = 0$–3) have been employed as catalyst precursors for hydrogenation and isomerization of 1-octene at 1 atm at 343 K or below. The highest activity for hydrogenation was found for $Ru_3(CO)_{12}$ combined with 15 equiv. of acetonitrile, with turnover numbers (TONs) up to 1,000. However, the kinetics indicated that fragmentation of the cluster gave rise to the active species. Isomerization displays a 10–20 min induction period, and the catalytically active species is proposed to be a higher-nuclearity cluster. The isomerization gave *trans*-2-octene only. The effects of other factors on the rates of hydrogenation and isomerization reactions were described.[29]

The catalytic precursor $Ru_3(CO)_{10}$(dppm) (dppm = $Ph_2PCH_2PPh_2$) isomerizes 1-hexene, mainly to the kinetic product *cis*-2-hexene, at low hydrogen pressure, and causes hydrogenation to hexane at higher pressures.[30] Other unsaturated functional groups can also be reduced. Turnover frequency (TOF) studies were interpreted to indicate cluster catalysis.[31] The bis(chelate) $Ru_3(CO)_8(dppm)_2$ also isomerizes 1-hexene, mainly to the kinetic product *cis*-2-hexene, at low hydrogen pressure, and causes hydrogenation to *n*-hexane at higher pressures. The reaction is first order on substrate, and turnover studies suggest that the cluster is the active catalyst.

The water-soluble cluster $Ru_3(CO)_9(tppms)_3$ (tppms = sodium diphenylphosphinobenzene-*m*-sulfonate) was used as the catalyst precursor for hydrogenation of acrylic acid and styrene.[32] The cluster also catalyzed the hydroformylation of propylene with syngas in water, forming mainly butanal, along with smaller amounts of 2-methylpropanal, butanol, and 2-methylpropanol. Typical conditions were 393 K and 40 atm of 1 : 1 CO : H_2. TOFs of 61 mol products (mol cluster h)$^{-1}$ and product *n* : *iso* ratio of 15.9 were obtained. Ethylene hydroformylation was also examined.

The chiral Ru cluster-based catalyst systems generated *in situ* from $Ru_3(CO)_{12}$ and chiral diiminodiphosphine tetradentate ligands effected asymmetric transfer hydrogenation of propiophenone in 2-propanol, forming 1-phenyl-1-propanol in 94% yield and with 96% ee.[33] Other chiral diamine ligands were also investigated. Although in most examples the active catalyst was not isolated and characterized, the complex $[NEt_4][HRu_3(CO)_{10}\{S,S\text{-}C_6P_2N_2\}]$ was fully characterized and effected hydrogen-transfer reduction of acetophenone to 1-phenylethanol in 96% yield and 47% ee. The fact that the reaction rate was first order in this cluster and that the mononuclear complex $Ru(CO)_3(PPh_3)_2$ was inactive when combined with the chiral diphosphine suggested that the cluster was the active catalyst.

Asymmetric hydrogenation was catalyzed by ruthenium clusters containing atropoisomeric diphosphines.[34] Catalyst precursors were $Ru_4(\mu\text{-}H)_4(CO)_{10}$\{(S)-(–)-BINAP\} (BINAP = 2,2′-bis(diphenylphosphino)-1,1′-binaphthyl) and $Ru_4(\mu\text{-}H)_4(CO)_{10}$\{(S)-(–)-MOBIPH\} (MOBIPH = 2,2′-bis(diphenylphosphino)-6,6′-dimethoxy-1,1′-diphenyl). Substrates included prochiral alkenes such as tiglic acid, (*Z*)- and (*E*)-2-methylbutendioic acids, (*E*)-2-methylbutenoic acid, and acetophenone. Optical purities up to 38% were obtained, but most results were low ee's.

Hydrogenation of 1-hexene is catalyzed in the presence of $(\mu\text{-}H)_2Ru_3(CO)_9(\mu_3\text{-}\eta^2\text{-}C_8H_{12})$.[35] However, the cluster reacts with hydrogen to form $H_4Ru_4(CO)_{12}$ and, under more severe conditions, a black solid.

The cluster $Ru_3(\mu_3\text{-ampy})(\mu,\eta^1{:}\eta^2\text{-PhCCHPh})(CO)_8$ (Hampy = 2-amino-6-methylpyridine) is a catalyst for hydrogenation of diphenylacetylene selectively to *cis*- and *trans*-stilbene under mild conditions (353 K and less than 1atm hydrogen).[36] Only this complex was observed by IR spectroscopy under catalytic conditions. Hydrogenation in the absence of diphenylacetylene gives $Ru_3(\mu\text{-}H)(\mu_3\text{-ampy})(CO)_9$ and $Ru_6(\mu\text{-}H)_6(\mu_3\text{-}\eta^2\text{-ampy})_2(CO)_{14}$. Reaction of $Ru_3(\mu_3\text{-ampy})(\mu,\eta^1{:}\eta^2\text{-PhCCHPh})(CO)_8$ with CO displaces the alkenyl bridge to form $Ru_3(\mu_3\text{-ampy})(\eta^1\text{-PhCCHPh})(CO)_9$. The rate law is of the form $-d[Ph_2C_2]/dt = \{k_a + k_b[Ph_2C_2]^{-1}\}[Ru_3(\mu_3\text{-ampy})(\mu,\eta^1{:}\eta^2\text{-PhCCHPh})(CO)_8]\,[P(H_2)]$. The proposed mechanism is thought to involve two coupled catalytic cycles, both containing trinuclear cluster species. Phosphine-substituted derivatives, for example, $Ru_3(\mu\text{-}H)(\mu_3\text{-ampy})(CO)_8(PPh_3)$, also catalyze hydrogenations.[37] It was possible to isolate intermediates containing bridging vinyl groups, $Ru_3(\mu_3\text{-ampy})(\mu,\eta^1{:}\eta^2\text{-}Ph_2C_2H)(CO)_7(PPh_3)$ and $Ru_3(\mu\text{-}H)_2(\mu_3\text{-ampy})(\mu,\eta^1{:}\eta^2\text{-}Ph_2C_2H)(CO)_6(PPh_3)$, by reaction of the starting cluster sequentially with diphenylacetylene and hydrogen. The disubstituted derivative $Ru_3(\mu_3,\eta^2\text{-ampy})(\mu,\eta^1{:}\eta^2\text{-PhC:CHPh})(CO)_6(PPh_3)_2$ is also a catalyst precursor for hydrogenation of diphenylacetylene, but the catalyst gradually deactivates. Thermolysis of $Ru_3(\mu_3,\eta^2\text{-ampy})(\mu,\eta^1{:}\eta^2\text{-PhC:CHPh})(CO)_6(PPh_3)_2$ at higher temperatures (383 K) causes oxidative addition of a P–Ph bond, forming $Ru_3(\mu_3,\eta^2\text{-ampy})(\mu,\eta^1{:}\eta^2\text{-PhC:CHPh})(\mu\text{-}PPh_2)(Ph)(CO)_5(PPh_3)$ in quantitative yield. The dihydride $Ru_3(\mu\text{-}H)_2(\mu_3,\eta^2\text{-ampy})(\mu,\eta^1{:}\eta^2\text{-PhC:CHPh})(CO)_5(PPh_3)_2$ is observed spectroscopically and is a proposed intermediate in the catalytic cycle.[38] The PCy_3 analogs are less active catalysts.[39] A review of this chemistry has appeared.[40]

A related cationic cluster $[Ru_3(\mu\text{-}H)(\mu_3\text{-ampy})(\mu,\eta^1{:}\eta^2\text{-PhC:CHPh})(CO)_8][BF_4]$ is a catalyst precursor for homogeneous hydrogenation of diphenylacetylene to *cis*- and *trans*-stilbene under very mild conditions, 333 K and less than 1 atm hydrogen. Reactivity, spectroscopic, and kinetic studies suggest that the active catalyst is a cationic trimetallic cluster.[41]

The 48-electron $Ru_3(\mu\text{-}H)(\mu_3\text{-ampy})(CO)_9$ reacts directly with hydrogen (1 atm) at 383 K to give the 92-electron hexanuclear $Ru_6(\mu\text{-}H)_6(\mu_3\text{-}\eta^2\text{-ampy})_2(CO)_{14}$, which regenerates $Ru_3(\mu\text{-}H)(\mu_3\text{-ampy})(CO)_9$ under CO.[42] Ligand substitution by PR_3 gives $Ru_6(\mu\text{-}H)_6(\mu_3,\eta^2\text{-ampy})_2(PR_3)_2(CO)_{12}$ (R = 4-tolyl or Ph). The X-ray crystal structure of the PPh_3 derivative shows that it consists of two trinuclear fragments connected to each other through two bridging hydrides, and two weak metal–metal bonds. The phosphine-substituted derivative was characterized by X-ray crystallography. $Ru_6(\mu\text{-}H)_6(\mu_3\text{-}\eta^2\text{-ampy})_2(CO)_{14}$ is a catalyst precursor for hydrogenation of alkynes.[43] The rate law for reduction of diphenylacetylene is first order in cluster concentration and hydrogen pressure and zero order in acetylene concentration; the rate law suggests that the active catalyst is hexanuclear.

Hydrogenation of alkynes is catalyzed by alkyne cluster complexes $Fe_3(CO)_9(RC_2R^1)$. In addition to hydrogenation, formation of metallacyclic byproducts such as $Fe_3(CO)_8\{(RC_2R^1)(RC_2R^1)\}$ was observed, resulting in decreased catalytic activity.[44]

Homogeneous hydrogenation of 1-hexene to hexane was catalyzed using $HRu_3(CO)_9(\mu_3\text{-}\eta^3\text{-}1,3\text{-dithiacyclohexane})$ as a catalyst precursor. The optimum rate (0.085 mol h^{-1}) was at 414 K and 60 atm of hydrogen. The rate was first order in catalyst precursor and at lower hydrogen pressure, leveling off above 50 atm. At higher temperatures, cluster fragmentation was noted, but the decomposition product, while active for hexene isomerization, was inactive for reduction of 1-hexene.[45]

Homogeneous catalytic hydrogenation of acetylenes and isomerization of *cis*-stilbene was catalyzed by $(C_5H_5)_2Ru_3(CO)_3(\mu\text{-}CO)(\mu_3\text{-}CO)(C_2Ph_2)$ as catalyst precursor. The cluster was reported to be a good catalyst for reduction of diphenylacetylene. The authors attribute the catalytic activity to a cluster even though fragmentation to lower-nuclearity species does occur under the reaction conditions.[46]

One approach to combining the advantages of homogeneous catalysts (higher activity and selectivity, the ability to readily modify catalyst activity) and heterogeneous catalysis (ease of separation of catalyst from products) is to anchor the catalyst to a heterogeneous substrate. This approach has been used for clusters as well as monometallic catalysts.

Various ruthenium clusters were evaluated as catalysts for solid–gas phase hydrogenations of alkynes and cyclic dienes. The clusters $H_4Ru_4(CO)_{12}$, $Ru_3(CO)_{12}$, and $(C_5H_5)_2Ru_3(CO)_3(\mu\text{-}CO)(\mu_3\text{-}CO)(C_2Ph_2)$, all previously shown to be precursors for homogeneous hydrogenation catalysts, were deposited on porous glass disks and reacted with gas-phase 1,4-cyclohexadiene or hex-3-yne and dihydrogen. Reduction occurred selectively to monoenes, but low

turnovers were obtained. The behavior of the clusters under solid–gas conditions is similar to that under homogeneous conditions and metal products isolated after the reaction were the same as in solution.[47]

The clusters $Ru_3(CO)_{12}$, $H_4Ru_4(CO)_{12}$, $H_2Ru_4(CO)_{13}$, and $H_2FeRu_3(CO)_{13}$ supported on pyrex borosilicate glass were examined as catalysts for heterogeneous hydrogenation of hex-3-yne and 1,4-cyclohexadiene. $Ru_3(CO)_{12}$ was also supported on aluminas and silica of different acidities, surface areas, and water content, all of which had some influence on activity. In particular, the surface organometallic reactions of $Ru_3(CO)_{12}$ and $H_4Ru_4(CO)_{12}$ supported on silica were monitored by IR spectroscopy, and the supported catalysts were also characterized by HRTEM microscopy. The results are consistent with the behavior of the clusters for similar reactions in solution.[48]

The clusters $Ru_3(CO)_9(\mu\text{-H})(\mu\text{-PPh}_2)$, $Ru_3(CO)_{10}(\mu\text{-H})(\mu\text{-PPh}_2)$, $Ru_3(CO)_7(\mu\text{-PPh}_2)_2(\mu_3\text{-}C_6H_4)$, and $Ru_4(CO)_{11}(\mu_4\text{-PPh})(\mu_4\text{-}C_6H_4)$ deposited on pyrex glass, silica, and alumina were tested in the hydrogenation of 3-hexyne, 1,3-cyclohexadiene, and 1,4-cyclohexadiene under solid–gas conditions. All supported clusters were active hydrogenation catalyst precursors, but were relatively unselective for hydrogenation of dienes to monoenes, and disproportionation of 1,3- and 1,4-cyclohexadiene to hydrogenated products and benzene also occurred. Clusters supported on silica and pyrex glass were more active than those supported on alumina. Attempts were made to detect organometallic intermediates or byproducts.[49]

Ru clusters which had been heterogenized in silica matrices by the sol–gel method were tested as catalysts for 1-hexene hydrogenation and isomerization. Gels prepared with $Ru_3(CO)_9(PPh_2CH_2CH_2Si(OMe)_3)_3$ effected 1-hexene hydrogenation at 1 atm and 363 K with turnovers of 380–460 over 15 h. Isomerization to *trans*-2-hexene, *cis*-2-hexene, and *trans*-3-hexene was also observed. Leaching of ca. 0.05% ruthenium in each run was determined. UV–VIS and FT-IR spectra of the gels before and after the catalytic reactions showed that during the gel preparation the clusters remain intact, but are decomposed when the gel is heated under vacuum or used in catalytic hydrogenation reactions.[50]

One study looked at the use of a supported triruthenium ketenylidene cluster in catalysis. The precursor $[PPN]_2[Ru_3(CO)_6(\mu\text{-CO})_3(\mu_3\text{-CCO})]$ was deposited on MgO, silica, and SiO_2-Al_2O_3. The supported material was characterized by vibrational spectroscopy. The cluster observed on the surface depended upon the water content of the support. With MgO, which had been dehydrated below 573 K, the spectrum of supported cluster was characteristic of $[Ru_3(CO)_6(\mu\text{-CO})_3(\mu_3\text{-CCO})]^{2-}$. With MgO, which had been dehydrated at 673 K, the spectrum was assigned to a new species, $[HRu_3(CO)_9(\mu_3\text{-CCO})]^{1-}$. On silica or SiO_2-Al_2O_3, the spectra suggested stoichiometric protonation by surface hydroxyl groups to form species such as $[HRu_3(CO)_9(\mu_3\text{-CCO})]^-\{SiO^-\}$. The clusters could be extracted from the supports at this stage. The MgO-supported triruthenium ketenylidene was active for hydroformylation of ethylene, but the SiO_2-Al_2O_3-supported cluster caused reduction to ethane.[51]

Catalytic homogeneous hydrogenation of phenylacetylene to styrene was achieved with $Ru_5(CO)_{13}(\mu_5\text{-C})(PhC_2H)(PtP(t\text{-Bu})_3)$ as catalyst precursor. Also formed was the hydride-containing cluster $Ru_5(CO)_{12}(\mu_5\text{-C})(PtP(t\text{-Bu})_3)(PhC_2H)(\mu\text{-H})_2$. The Pt atom promoted catalytic activity.[52]

The clusters $Ru_3(CO)_7(\mu\text{-PPh}_2)_2(C_6H_4)$, $Ru_4(CO)_{11}(\mu_4\text{-PPh})(C_6H_4)$, $Ru_3(CO)_7(\mu\text{-PPh}_2)_2(HC_2Ph)$, and $Ru_4(CO)_{11}(\mu_4\text{-PPh})(C_2Ph_2)$ catalyze the hydrogenation of alkynes and of 1,4-cyclohexadiene. The benzyne-substituted clusters, $Ru_3(CO)_7(PPh_2)_2(C_6H_4)$ and $Ru_4(CO)_{11}(PPh)(C_6H_4)$, showed the highest hydrogenation activity for substituted metal carbonyl clusters toward alkynes at that time.[53]

The high sensitivity afforded by using parahydrogen was exploited to identify intermediates in alkyne hydrogenation catalyzed by $Ru_3(CO)_9(\mu\text{-H})(\mu\text{-PPh}_2)$. This cluster adds molecular hydrogen, forming $Ru_3(CO)_9(H)(\mu\text{-H})_2(\mu\text{-PPh}_2)$ and a number of other phosphido-bridged clusters. This mixture catalyzes hydrogenation of alkynes. For diphenylacetylene, the resting state is believed to be $Ru_3(\eta^2\text{-PhC}{=}{=}\text{CHPh})(CO)_8(\mu\text{-H})(PHPh_2)$. The phosphido bridge was proposed to prevent fragmentation during catalysis.[54]

Hydrogenation of alkynes and of 1,4-cyclohexadiene is also reported to be catalyzed by the acetylide-containing cluster $HRu_3(CO)_9(C_2\text{-}t\text{-Bu})$. The active catalyst was believed to be a cluster, but some fragmentation occurs under catalytic conditions.[55]

$(Cp'Ru)_3(\mu_3\text{-H})(\mu\text{-H})_3$ catalyzes hydrogenation of azobenzene, forming aniline and 1,2-diphenyl hydrazine. At 373 K and 100 atm, 68% conversion was obtained. Stoichiometric reactions allowed the characterization of a μ_3-imido cluster, which may be an intermediate.[56]

Hydroformylation of ethylene was catalyzed by the cluster anion $[Ru_6C(CO)_{16}Me]^-$, supported on a highly dehydrated silica (823 K). The catalysis was nearly 100% selective at 398 K. The retention of the cluster framework under the reaction conditions was shown by extended X-ray adsorption fine-structure curve fitting. The cluster anion does not catalyze this reaction in homogeneous solution, and a heterogeneous Ru–SiO_2 catalyst prepared by conventional methods gave ethane rather than propanal.[57]

The cluster $[PPN][Ru_6C(CO)_{16}(CH_3)]$, which contains an interstitial carbide within an octahedral metal core, was found to be a catalyst precursor for hydrogenation of olefins at 333 K, but after an induction period. Reaction of the

cluster with hydrogen at 403 K gives an unsaturated cluster [PPN][$Ru_6C(CO)_{15}H$], which behaves as the catalyst at room temperature.[58]

Homogeneous hydrogenation of carbon dioxide to methanol is catalyzed by ruthenium cluster anions in the presence of halide anions. The catalyst system was $Ru_3(CO)_{12}$ and alkyl iodides in *N*-methylpyrrolidone (NMP) solution at 513 K. Some methane was also formed. FT-IR spectra of the reactions allowed identification of several ruthenium carbonyl anions.[59]

One of the most extensively studied clusters is the unsaturated cluster $(\mu\text{-H})_2Os_3(CO)_{10}$, which because of its unsaturation undergoes a wide variety of reactions under mild conditions. Stoichiometric reactions with alkenes and alkynes give products arising from insertion of the C–C multiple bond into an Os–H bond, sometimes followed by reductive elimination. The cluster also catalyzes hydrogenations of alkenes and alkynes. Reactions with terminal alkynes typically give four products: vinyl complexes $(\mu\text{-H})Os_3(\mu\text{-}\eta^2\text{-CH=CHR})(CO)_{10}$, acetylide complexes $(\mu\text{-H})Os_3(\mu\text{-}\eta^2\text{-CCR})(CO)_{10}$, $Os_3(\mu_3\text{-}\eta^2\text{-HCCR})(\mu\text{-CO})(CO)_9$, and metallacyclohexadienones $Os_3(CO)_9(\mu_3\text{-}\eta^4\text{-(RC=CH)}_2C(O))$. The high sensitivity afforded by the use of parahydrogen was exploited to probe the nature of the intermediates in catalytic hydrogenation of 1-pentyne and acetylene with $(\mu\text{-H})_2Os_3(CO)_{10}$ at 3–4 atm and 323–333 K. It was found that of the four products usually formed, only the vinyl complex $(\mu\text{-H})Os_3(\mu\text{-}\eta^2\text{-CH=CHR})(CO)_{10}$ (R = H or *n*-Pr) goes on to yield alkene and the starting $(\mu\text{-H})_2Os_3(CO)_{10}$. The acetylido complex $(\mu\text{-H})Os_3(\mu\text{-}\eta^2\text{-CCR})(CO)_{10}$ was not formed. The alkyne complex $Os_3(\mu_3\text{-}\eta^2\text{-HCCR})(\mu\text{-CO})(CO)_9$ is formed when $Os_3(CO)_{10}(CH_3CN)_2$ reacts with alkynes, but this complex does not react with parahydrogen. An unstable aldehyde complex $(\mu\text{-H})Os_3(\mu_3\text{-}\eta^4\text{-RC=CC(O)H})(CO)_9$ was detected; this intermediate was proposed to lose hydrogen and insert a second alkyne, forming the metallacyclohexadienone cluster $Os_3(CO)_9(\mu_3\text{-}\eta^4\text{-(RC=CH)}_2C(O))$. $(\mu\text{-H})Os_3(CO)_9(\mu_3\text{-}\eta^4\text{-RC=CC(O)H})$ was also detected when $Os_3(CO)_{10}(CH_3CN)_2$ was reacted with 1-pentyne or acetylene in the presence of parahydrogen.[60]

Ruthenium clusters were evaluated for catalytic activity for hydrodesulfurization (HDS) of benzo[b]thiophene. At 423–443 K and 100 atm, hydrogen benzo[b]thiophene was converted to 2,3-dihydrobenzo[b]thiophene and 2-ethylthiophenol. The best catalyst precursor was $H_4Ru_4(CO)_8(PPh_3)_4$, which gave 81% conversion to 2,3-dihydrobenzo[b]thiophene after 384 h at 443 K; about 5% ethylbenzene was also formed, showing some HDS activity. The clusters were more active than the monometallic precursor $Ru(CO)_3(PPh_3)_2$. However, the reaction conditions are rather severe and the involvement of decomposition products is very possible.[61]

12.15.2.3 Co, Rh, and Ir Clusters

The iridium clusters $Ir_4(CO)_{11}PPh_2H$, $Ir_4(CO)_8(\mu_3\text{-}\eta^2\text{-HCCPh})(\mu\text{-PPh}_2)_2$, $Ir_4(CO)_9(\mu_3\text{-}\eta^3\text{-Ph}_2PC(H)CPh)(\mu\text{-PPh}_2)$, and $Ir_4(CO)_{12}$ were investigated as catalyst precursors for the hydrogenation of 1,5-cyclooctadiene (1,5-COD) to cyclooctene. The clusters showed high activity (average TON was 2,816) and selectivity for cyclooctene and the isomerization products 1,3-COD and 1,4-COD, with very little cyclooctane. Monometallic precursors or Ir metal gave complete hydrogenation to cyclooctane. Other experiments were performed, including light scattering measurements to exclude metal particles and addition of mercury to poison any heterogeneous metal catalysts. By comparison with the structures of known Ir_4 complexes with cyclooctadiene-based ligands, it was proposed that the high selectivity for the cluster catalysts was due to an "anchor-type" interaction with an $\eta^2\text{-}\eta^2$-1,5-COD ligand, which activates one of the double bonds for reduction.[62]

Photo-assisted catalytic hydrogenation of norbornadiene and quadricyclane was achieved with $Rh_6(CO)_{16}$. Using 2-propanol in acetone as a source of hydrogen in the photo-assisted hydrogen transfer, norbornane and nortricyclene are formed by reduction of quadricyclane. During the reduction of norbornadiene, at higher substrate concentrations, the acetone-sensitized isomerization to quadricyclane occurs before hydrogenation. At a lower norbornadiene concentration, sequential hydrogenation gives norbornene and then norbornane. Catalytic hydrogenation of norbornadiene, rather than photo-assisted hydrogen transfer, gave a larger yield of norbornene, with <1% nortricyclene and no quadricyclane being formed.[63]

Polymer-bound rhodium clusters were used for catalytic hydrogenations of α,β-unsaturated aldehydes to allylic alcohols. Amination of chloromethylated polystyrene with 2-(2-(dimethylamino)ethoxy)ethanol gave an amine-functionalized polymer. Using the aminated polystyrene and $Rh_6(CO)_{16}$ in the presence of H_2 and CO or CO and water, various α,β-unsaturated aldehydes were chemoselectively hydrogenated to give allylic alcohols in high yields, generally >95% conversion and 80–100% selectivity, at 303 K. Under the reaction conditions, a number of anionic clusters form, which can be recovered as ions paired to the ammonium cations of the polymer. Clusters identified by

IR include $[Rh_6(CO)_{15}]^{2-}$ and $[Rh_{12}(CO)_{30}]^{2-}$. The polymer-bound Rh cluster complexes were reusable catalysts for the hydrogenation.[64,65]

One of the first clusters to be examined for catalytic hydroformylation was the alkylidyne cluster series $Co_3(CO)_9(\mu_3\text{-CR})$. One such study looked at hydroformylation of oct-1-ene in the presence of $Co_3(CO)_9(\mu_3\text{-CR})$ (R = H, Me, Ph, CO_2(alkyl), Cl, Br, OMe) and PPh_3-substituted derivatives, and heteronuclear Co_2Ni complexes.[66] Careful studies using *in situ* spectroscopic techniques have revealed that these alkylidyne clusters, while exceptionally stable, undergo fragmentation under catalytic conditions, and the active catalyst is the same as that would be generated from $Co_2(CO)_8$. Cylindrical internal reflectance (CIR) spectroscopy was used to monitor the hydroformylation of 1-pentene using the benzylidyne-capped cluster $Co_3(CO)_9(\mu_3\text{-CPh})$ as the catalyst precursor. At 130°, cluster fragmentation was observed. Product aldehydes form coincident with fragmentation.[67] Chelating ligands can sometimes retard or prevent cluster fragmentation. However, CIR evidence showed facile fragmentation of $PhCCo_3(CO)_7$(*cis*-$Ph_2PCH{=}CHPPh_2$) during the hydroformylation of 1-pentene at 403 K and 40 atm H_2/CO (1 : 1). The intact cluster could only be isolated in <10% yield at the end of the reaction. Cluster fragmentation to $[Co(CO)_4]^{1-}$ occurs early in the reaction, prior to alkene hydroformylation, followed by the formation of the phosphine-substituted complexes $[Co(CO)_3(Ph_2PCH{=}CHPPh_2)]^{1+}$ and $[Co(CO)_2(Ph_2PCH{=}CHPPh_2)]^{1-}$.[68]

The high-nuclearity carbonyl cluster $Na_2[Rh_{12}(CO)_{30}]$ is a catalyst precursor for hydroformylation of 2,4,4-trimethyl-1-pentene in THF at 300–400 K and 20–120 atm of CO–H_2. The reaction is highly chemoselective, approaching 100% selectivity for 3,4,4-trimethylhexanal, and only traces of the reduction products 2,4,4-trimethyl-1-pentane and 3,4,4-trimethyl-1-hexanol are formed. Typical TONs were 100–1000. During the reaction, clusters of lower nuclearity, $[(Me_3CCH_2CHMeCH_2CO)Rh_6(CO)_{15}]^{1-}$ or $[Rh_5(CO)_{15}]^{1-}$, were observed by IR spectroscopy. The dependencies of the rates on CO and catalyst concentrations were interpreted to indicate that CO-driven cluster fragmentation was occurring.[69]

$Rh_4(\mu\text{-bpnap})(CO)_{10}$ (bpnap = 2,2′-bis[(1,1′-biphenyl-2,2′-diyl)phosphite]-1,1′-binaphthyl) is a catalyst precursor for the isomerization and hydroformylation of 1-octene. The cluster was synthesized by reaction of $Rh_2(CO)_4Cl_2$ with bpnap under CO. Two isomers were identified. The hydroformylation of α-methylstyrene with mononuclear Rh(acac)$(CO)_2$ and R-(+)-bpnap gave essentially no ee of 3-phenylbutanal. The crystal structure established that the bpnap ligand bridged two rhodium atoms of a tetrahedral metal framework. The same isomers were formed from Rh(acac)$(CO)_2$ and bpnap under 1 : 1 CO/H_2.[70]

12.15.2.4 Pd and Pt Clusters

The catalytic properties of $[Pd_4(dppm)_4(H)_2]^{2+}$ toward the homogeneous hydrogenation of phenylacetylene, diphenylethyne, and phenyl-1-propyne were evaluated under a variety of conditions. The cluster is a pre-catalyst that exhibits a good catalytic activity under mild conditions (1 atm of H_2 at 293 K) for the hydrogenation of alkynes and alkenes. For the alkyne substrates, the TOFs range between 200 and 500 h^{-1}, and predominantly *cis*-alkenes are obtained (75–90% of *cis*-selectivity). The rate of hydrogenation is half-order in $[Pd_4]$, indicating cluster dissociation into two dimeric species. The rate is also first order in unsaturated substrate and first order at hydrogen pressure. At 110 atm of H_2, the TOF can reach 2,500–3,000 h^{-1} in THF. The TOF also increases with temperature up to ca. 308 K (1,000–1,300 h^{-1}), but at higher temperatures catalyst decomposition occurs.[71]

12.15.2.5 Heterometallic Clusters

The mixed metal cluster $HIrRu_3(CO)_{13}$ is reported to be an effective catalyst for the hydrogenation of diphenylacetylene to stilbene. Direct reaction of alkyne with this cluster forms $HIrRu_3(CO)_{11}(\mu_3\text{-}\eta^2\text{-RCCR}^1)$ and $IrRu_3(CO)_{10}(\mu_4\text{-}\eta^2\text{-RCCR}^1)(\mu\text{-}\eta^2\text{-RCCHR}^1)$, but these clusters are not believed to be directly involved in the catalytic cycle.[72]

The tetrahedral clusters $H_4Ru_4(CO)_{12}$, $H_2Ru_4(CO)_{13}$, and $H_2FeRu_3(CO)_{13}$, and also $Fe_2Ru(CO)_{12}$, were examined as homogeneous catalysts for the hydrogenation of 1,3- and 1,4-cyclohexadiene. Although catalytic activity was observed, some cluster decomposition occurred and clusters were not believed to be the active catalysts. After the hydrogenation, a number of organometallic products were identified.[73]

The clusters $M_3(CO)_{12}$ (M = Ru, Fe), $Fe_2Ru(CO)_{12}$, $FeRu_2(CO)_{12}$, $H_4Ru_4(CO)_{12}$, and $H_2M'M_3(CO)_{13}$ (M = Ru; M′ = Fe, Ru) were tested as homogeneous catalysts for the hydrogenation of diphenylacetylene and isomerization of *cis*-stilbene. Reaction of the clusters with PhCCPh gives fragmentation and aggregation to alkyne-substituted clusters, which, except for $H_2Ru_3(CO)_9(C_2Ph_2)$, are not good catalysts as they react slowly with hydrogen.[74]

Hydrogenation of diphenylacetylene to (*Z*)-stilbene is catalyzed by $Pt_3Ru_6(CO)_{20}(\mu_3\text{-}PhC_2Ph)(\mu_3\text{-}H)(\mu\text{-}H)$ at 323 K and 1 atm. The TOF was 47 h^{-1} at a cluster concentration of 10^{-4} and 10^{-2} M alkyne. The rate law for the hydrogenation has the form: rate $= k[\text{cluster}][PhC_2Ph]P(H_2)/\{P(CO)(1 + k'([PhC_2Ph]\}$. Activation parameters were determined. At high alkyne/cluster ratios (1,000/1), side-reactions form species of low catalytic activity. Four of these complexes have been isolated and characterized as $Ru_6Pt_3(CO)_{18}(\mu_3\text{-}\eta^6\text{-}PhC_2H_4Ph)(\mu_3\text{-}H)_4$, $Ru_6Pt_3(CO)_{18}(\eta^6\text{-}PhCH_2CH_2Ph)(\mu_3\text{-}H)_4$, $Ru_6Pt_3(CO)_{15}(\mu_3\text{-}PhC_2Ph)_3(\mu\text{-}H)_6$, and $Ru_6Pt_3(CO)_{14}(\mu_3\text{-}Ph_2C_2)_3$. The hydrogenation of $TolC_2Tol$ to *cis*-Tol(H)C:C(H)Tol by $Pt_3Ru_6(CO)_{20}(\mu_3\text{-}TolC_2Tol)(\mu_3\text{-}H)(\mu\text{-}H)$ was also examined. The catalytic activity of a variety of related platinum and ruthenium complexes toward hydrogenation of PhC_2Ph was tested under identical conditions, but all were less active than the mixed metal clusters; this suggests that the high activity of the mixed metal cluster is due to synergism of molecular activation at the Pt and Ru layers. The proposed mechanism involves CO dissociation, followed by oxidative addition of hydrogen and then alkyne addition, which induces the transfer of hydrogen to the coordinated alkyne.[75]

A study of catalysis by metal cluster anions in ionic liquids found that activity for hydrogenation of alkenes can be greater than three times higher than that observed in organic solvents. The clusters $[HFe_3(CO)_{11}]^-$, $[HWOs_3(CO)_{14}]^-$, $[H_3Os_4(CO)_{12}]^-$, and $[Ru_6C(CO)_{16}]^{2-}$ were evaluated as catalysts/pre-catalysts for the hydrogenation of styrene in [bmim][BF_4] ionic liquid (bmim = 1-butyl-3-methylimidazolium), octane, and methanol. The activities for $[HFe_3(CO)_{11}]^-$ (low activity) and $[Ru_6C(CO)_{16}]^{2-}$ (the most active) were essentially the same in all solvents, but $[HWOs_3(CO)_{14}]^-$ and $[H_3Os_4(CO)_{12}]^-$ were more active in the ionic liquids compared to octane and methanol. A variety of experiments, including high-pressure NMR and tests for the presence of colloids, were performed to determine the nature of the active catalysts. Using high-pressure NMR, it was possible to trace the improvements in activity to the increased stability of the cluster species in the ionic liquid. The ionic liquid solvent also gave higher regioselectivity for hydrogenation of cyclic dienes to monoenes.[76]

The mixed metal clusters $[(CO)_4Fe(\mu\text{-}PPh_2)Pd(\mu\text{-}Cl)_2]_2$, $[Et_4N][FeCo_3(CO)_{12}]$, and $Rh_2Co_2(CO)_{12}$ were entrapped in SiO_2 sol–gel matrices. These materials were then tested as recyclable catalysts for several different reactions, including isomerization of 1-octene, dimerization of norbornadiene to "binor-S," and hydrogenation and hydrogenolysis of styrene, nitrobenzene, and 1-chloronaphthalene. During the reduction of nitrobenzene and chloronaphthalene, decomposition of $Rh_2Co_2(CO)_{12}$ formed metal nanoparticles which were active for arene reduction.[77]

12.15.3 Metal Clusters as Precursors for or Models of Heterogeneous Metal Catalysts

12.15.3.1 Metal Clusters as Models for Metal Surfaces

One of the seminal reviews which launched metal cluster chemistry was entitled, "*Clusters and Surfaces*," in which Muetterties *et al.* made a case for an analogy between metal surfaces and molecular metal clusters.[78] Since then, numerous reviews and research articles have focused on aspects of this analogy, but activity in the past decade has slowed. Some reviews addressing various aspects of the analogy have appeared.[79–86]

High-nuclearity clusters display metal atom packings that resemble bulk metal. Reduction of $PdCl_2(PPh_3)_2$ with $[Ni_6(CO)_{12}]^{2-}$ was used to prepare the very large cluster anions $[Pd_{16}Ni_4(CO)_{22}(PPh_3)_4]^{2-}$ and $[Pd_{33}Ni_9(CO)_{41}(PPh_3)_6]^{4-}$. The structures of both were determined by X-ray crystallography of the $[PPh_4]^+$ salts. The $Pd_{16}Ni_4$ core of $[Pd_{16}Ni_4(CO)_{22}(PPh_3)_4]^{2-}$ may be viewed as a four-layer stacking of 20 metal atoms in a ccp [a(Ni1) b(Pd3) c(Pd6) a(Pd7Ni3)] sequence. Comparison of the ligand arrangements about the metal core geometries of $[Pd_{16}Ni_4(CO)_{22}(PPh_3)_4]^{2-}$ and the previously reported $[Os_{20}(CO)_{40}]^{2-}$ was discussed in terms of possible modes of CO attachment to ccp metal(111) surfaces. The geometry of the $Pd_{33}Ni_9$ core of $[Pd_{33}Ni_9(CO)_{41}(PPh_3)_6]^{4-}$ consists of five equilateral triangular layers that are stacked in an hcp [a(Pd7Ni3) b(Pd6) a(Pd7Ni3) b(Pd6) a(Pd7Ni3)] sequence. Reactions of these cluster anions with acetic acid allowed isolation of $Pd_{12}(CO)_{12}(PPh_3)_6$ and $[PPh_4]_2[Pd_{29}(CO)_{28}(PPh_3)_7]$ as minor decomposition products. The structure of $Pd_{12}(CO)_{12}(PPh_3)_6$ shows that it is a highly deformed hexacapped octahedral member of the previously established homopalladium family of clusters containing uncapped, monocapped, bicapped, and tetracapped Pd_6 octahedra. The unprecedented centered 28-atom polyhedron for the Pd_{29} core of $[Pd_{29}(CO)_{28}(PPh_3)_7]^{2-}$ is described as a four-layer stacking of 29 metal atoms in a mixed hcp/ccp [a(Pd1) b(Pd3) a(Pd10) c(Pd15)] sequence.[87]

The binding of norbornene to a triosmium cluster may model the coordination of this molecule to metal surface sites. Reactions of the "lightly stabilized" cluster $Os_3(CO)_{10}(NCMe)_2$ with norbornene (bicyclo[2.2.1]hept-2-ene) led

to two isomeric triosmium clusters $Os_3(\mu\text{-H})(CO)_{10}(\mu\text{-}\eta^1\text{:}\eta^2\text{-}C_7H_9)$, which differ in the orientation of the C_7H_8 with respect to the metal triangle, and also the dihydride species $Os_3(\mu\text{-H})_2(CO)_9(\mu_3\text{-}\eta^1\text{:}\eta^2\text{-}C_7H_8)$. The crystal structure of $Os_3(\mu\text{-H})_2(CO)_9(\mu_3\text{-}\eta^1\text{:}\eta^2\text{-}C_7H_8)$ shows norbornene–metal binding similar to the proposed adsorption mode of norbornene found on the Pt(111) surface. The two isomers $Os_3(\mu\text{-H})(CO)_{10}(\mu\text{-}\eta^1\text{:}\eta^2\text{-}C_7H_9)$ exhibit an intermediate bonding mode between the solely π-bound ligand and the di-σ,π-bonding mode of $Os_3(\mu\text{-H})_2(CO)_9(\mu_3\text{-}\eta^1\text{:}\eta^2\text{-}C_7H_8)$. Thermal interconversion between the isomeric $Os_3(\mu\text{-H})(CO)_{10}(\mu\text{-}\eta^1\text{: }\eta^2\text{-}C_7H_9)$ clusters was reported, and thermolysis ultimately generates $Os_3(\mu\text{-H})_2(CO)_9(\mu_3\text{-}\eta^1\text{: }\eta^2\text{-}C_7H_8)$ by C–H bond activation.[88]

The alkylidyde fragment was among the first to be identified on a metal surface by comparison of spectroscopic features to cluster models. The μ_3-CR unit has been identified on numerous metal surfaces, including the Pt(111), Ru(001), Rh(111), and Pd surfaces. Chemisorption of ethylene, acetylene, propene, and other small hydrocarbons can give rise to alkylidyne fragments through C–H cleavage and hydrogen migration, common reactions for molecular metal clusters. Reactions of the fragment with other small molecules have been suggested to mimic reactions on metal surfaces. One example is the alkylidyne–alkyne coupling. Reaction of the alkylidyne cluster $Os_3(\mu\text{-H})_2(CO)_9(\mu_3\text{-}CNC_5H_4CH{=}CH_2)$ with phenylacetylene gives two pairs of geometrical isomers involving methylidyne–alkyne coupling. $Os_3(\mu\text{-H})(CO)_9\{\mu_3\text{-}\eta^3\text{-PhCCHC(CH}{=}\text{CHPh)}\}$ (30%) has a structure derived from coupling of the methylidyne with two phenylacetylene molecules to form a C_5 hydrocarbyl coordinated in an allyllic fashion to the Os_3 unit; $Os_3(CO)_9(\mu_3\text{-}\eta^1,\eta^2,\eta^2,\eta^1\text{-PhCHCH}{=}\text{CHCH}{=}\text{CPh})$ (24%) is an isomer which contains a *cis*,*cis*-1,5-diphenylpenta-1,3-diene ligand on a triangular array of Os atoms, which, together with one of the Os atoms, forms an osmacyclohexa-2,4-diene ring with two localized double bonds. $Os_3(CO)_7\{\mu\text{-}\eta^2,\eta^3\text{-CH}_2{=}\text{CHC(Ph)CHCPh}\}\{\mu_3\text{-}\eta^2\text{-C(O)C(Ph)}{=}\text{CH}\}$ (8%) and $Os_3(CO)_7\{\mu\text{-}\eta^2,\eta^3\text{-PhCH}{=}\text{CHC(Ph)CHCH}\}\{\mu_3\text{-}\eta^2\text{-C(O)C(Ph)}{=}\text{CH}\}$ (6%) differ only in the spatial positions of the Ph substituents in the C_5 hydrocarbyl fragments; these clusters arise from the coupling of three alkynes with the methylidyne in different ways, along with the coupling of one carbonyl ligand and a phenylacetylene to form a keto ligand with a $\mu_3\text{-}\eta^2$-coordination mode. The same reaction, carried out in acetone, yielded another new cluster $Os_3(CO)_8(\mu\text{-}\eta^2\text{-PhCCH}_2)(\mu_3\text{-}\eta^3\text{-CHCPhCH})$ as a major product (34%); this is yet another example of the carbon–carbon bond formation from a bridging carbon fragment which is similar to metal surface-bound species. The proposed mechanism involves the cleavage of the N–C(alkylidyne) bond in $Os_3(\mu\text{-H})_2(CO)_9(\mu_3\text{-}CNC_5H_4CH{=}CH_2)$, giving a carbido species "$[Os_3(\mu\text{-H})_2(CO)_9(\mu_3\text{-C})]$" or a alkylidyne fragment "$[Os_3(\mu\text{-H})(CO)_9(\mu_3\text{-CH})]$" as the intermediate.[89]

A model system for the reductive C–O bond cleavage in the Fischer–Tropsch reaction was proposed, based upon hydrosilane reduction of the CO ligand of $Mo_2(\eta^5\text{-}C_5H_4R^1)_2(CO)_4$. Photolysis of the dimolybdenum complex $(\eta^5\text{-}C_5H_4R^1)_2Mo_2(CO)_4$ ($R^1 = H$, Me) in the presence of excess $HSiMe_2Ph$ produced the μ_3-methylidyne complex $(\mu_3\text{-CH})\{Mo(\eta^5\text{-}C_5H_4R^1)(CO)_2\}_3$ and the μ_3-ethylidyne complex $(\mu_3\text{-CMe})\{Mo(\eta^5\text{-}C_5H_4R^1)(CO)_2\}_3$. The silane product was the siloxane $O(SiMe_2Ph)_2$. Isotopic labeling was used to show that the H and C atoms of the μ_3-alkylidynes originate from $HSiMe_2Ph$ and the CO ligands. This reaction was viewed as analogous to the crucial step in Fischer–Tropsch mechanism: deoxygenative reduction of CO by adsorbed hydrogen, giving CH and CMe species. The model reaction is facilitated by use of the oxophilic silane replacing hydrogen.[90]

Some oxide-containing organometallic clusters have been proposed as model compounds for intermediates in catalysis on metal oxide surfaces. The hydrolysis of $(\eta^5\text{-}C_5Me_5)WMe_4$ gives $(\eta^5\text{-}C_5Me_5)_2W_2O_2(\mu\text{-CH}_2)_2$ and $(\eta^5\text{-}C_5Me_5)_2W_2O_2(\mu\text{-CH}_2)(\mu\text{-O})$, containing both methylidene and oxo ligands. Reaction of $(\eta^5\text{-}C_5Me_5)MoMe_4$ with water leads instead to the trinuclear cluster $(\eta^5\text{-}C_5Me_5)_3Mo_3(\mu\text{-O})_2(\mu\text{-CH}_2)(\mu_3\text{-CH})$ with oxo, methylidene, and methylidyne groups.[91]

Arene ligands bond to monometallic complexes as η^6-, η^4-, and η^2-C_6R_6 species. Unique to trimetallic or larger clusters is the $\mu_3\text{-}\eta^2\text{:}\eta^2\text{:}\eta^2\text{-}C_6R_6$ ligand.[92] This coordination mode is believed to model the geometry of benzene, non-dissociatively chemisorbed on the surface of a close-packed metal lattice. One prototypical example of such a cluster is $Os_3(CO)_9(\mu_3\text{:}\eta^2\text{:}\eta^2\text{:}\eta^2\text{-}C_6H_6)$. The crystal structure shows that the benzene ring symmetrically caps the triangular cluster, with bond distances distorting toward cyclohexa-1,3,5-triene description. A number of related derivatives, including $Os_3(CO)_9(\mu_3\text{:}\eta^2\text{:}\eta^2\text{:}\eta^2\text{-}C_6H_5Me)$, $Os_3(CO)_8(NCMe)(\mu_3\text{:}\eta^2\text{:}\eta^2\text{:}\eta^2\text{-}C_6H_6)$, $Os_3(CO)_8(PPh_3)(\mu_3\text{:}\eta^2\text{:}\eta^2\text{:}\eta^2\text{-}C_6H_6)$, and $Os_3(CO)_8(C_2H_4)(\mu_3\text{:}\eta^2\text{:}\eta^2\text{:}\eta^2\text{-}C_6H_6)$, have been prepared by substitution reactions. All retain the face-capping benzene moiety. Semi-empirical MO calculations reveal that primary contributions to metal–arene bonding come from overlap of the benzene HOMO with the LUMO of the cluster fragment and through π-backdonation to the benzene LUMO from a high-lying cluster-based MO. The ring distortion was explained by an internal mixing of the benzene π-system that leads to increased overlap in the C–C bonds eclipsing the metal atoms, at the expense of the alternate non-eclipsing bonds which consequently become elongated.[93]

The cluster–surface analogy has been mainly used for adsorbates on heterogeneous metal surfaces in catalysis. Electrode metal surfaces also offer an opportunity to learn from the cluster–surface analogy.

IR spectroelectrochemistry was used to compare the carbonyl stretching frequencies of CO ligands on large Pt clusters with those of CO adsorbed on Pt electrodes. The charge n on the clusters $[Pt_{24}(CO)_{30}]^n$, $[Pt_{26}(CO)_{32}]^n$, and $[Pt_{38}(CO)_{44}]^n$ was varied by electrochemically reducing/oxidizing in a variety of solvents. The clusters displayed reversible electrochemical and spectroscopic behavior, with a sequence of redox steps spanning $n = 0$ to (in one case) -10, at potentials between ca. 0.5 and -2.5 V versus ferrocenium ferrocene. For $[Pt_{26}(CO)_{32}]^n$, redox processes were mainly two-electron, with $n = -2$, -4, -6, -8, and -10. On the other hand, $[Pt_{24}(CO)_{30}]^n$ and $[Pt_{38}(CO)_{44}]^n$ underwent sequential one-electron steps, with the odd-electron states ($n = -1$, -3, -5, -7) of lower stability. The C–O stretching frequencies for the bridging CO ligands(ν_{bCO}) and the terminal (ν_{tCO}) CO ligands decrease systematically as n becomes more negative, as expected because of greater backbonding with greater negative charge. The charge-dependent spectral properties were compared with the potential-dependent properties of CO adsorbed on platinum electrode surfaces, which also display decrease in ν_{tCO} and ν_{bCO} as the electrode potential is made more negative, which is associated with more negative surface charge. The ν_{tCO}–potential slopes for CO adsorbed at both single crystal and polycrystalline Pt–solution interfaces are smaller than for the solvated Pt clusters (about 15–20 cm^{-1} per added electron). The smaller slope was attributed to larger "'effective surface' capacitances" for the clusters than those measured for the electrode–solution interfaces. When the ν_{tCO} values are plotted versus the electronic charge per surface Pt atom ("surface charge density"), the same slope is obtained for all the clusters and the behavior is similar to that of Pt electrodes. These results suggest that the analogy between clusters and electrode surfaces bears further investigation.[94]

12.15.3.2 Metal Clusters as Precursors for Heterogeneous Metal Catalysts

One well-known application of molecular metal clusters is as precursors for dispersed, heterogeneous metal catalysts. Typically, the cluster is deposited on a high surface area support and then decomposed to metal particles, usually under a steam of hydrogen or an inert gas. Clusters will only be the precursor of choice if (i) the metal particles thus produced are unique from those derived from monometallic precursors, and (ii) they are stable for extended reaction times under catalytic conditions. Numerous reviews have appeared. [95–106]

12.15.3.2.1 Clusters of group 8 metals

Mild heating was used to decarbonylate $Fe_3(CO)_{12}$, which had been precipitated on alumina without pretreatment. The supported Fe particles thus produced showed good catalytic selectivity for the hydrogenation of carbon monoxide to lower olefins. K-edge EXAFS (extended X-ray absorption fine structure) analyses of the fresh catalyst and the used catalyst suggest that the active site on the surface is an ensemble of three iron atoms with one short Fe–Fe bond of 2.52 Å and two longer Fe–Fe bonds of 2.74 Å. However, over time, aggregation of the Fe_3 clusters generates particles of over 10 Å in size, resulting in a short lifetime and poor selectivity for the catalyst. The aggregated particles are still two-dimensional, consisting of at least three iron trimers in which the interatomic distance for each trimer is of ca. 2.48 Å.[107]

Cesium nitrate was found to be a promoter for an ammonia synthesis catalyst based on the cluster $K_2[Ru_4(CO)_{13}]$. The catalyst was prepared by depositing the cluster on carbonized magnesium oxide or on original graphite-like active carbon "Sibunit," and then introducing cesium nitrate into the samples and reducing with hydrogen. The optimum effect was at a Cs : Ru molar ratio of 1.51 : 1 for the magnesium oxide-supported catalyst. The cesium-promoted catalyst on carbonized MgO is noticeably more active in ammonia synthesis than that on "Sibunit" carbon.[108]

Heterogeneous Ru catalysts were prepared by thermolysis of $Ru_3(\mu\text{-H})(\mu_3,\eta^2\text{-ampy})(CO)_9$ supported on silica and alumina. The face-bridging ampy ligand does not prevent cluster fragmentation on the support surface, and mononuclear Ru surface species are formed. The heterogeneous catalysts are poorer for hydrogenation of phenylacetylene than the cluster is in homogeneous solution.[109]

Silica-supported Ru catalysts were prepared by sol–gel methods. The procedure involved combining $Ru_3(CO)_{12}$ or $[Ru_3H(CO)_{11}]^{1-}$ as the metal source, $Si(OMe)_4$ and water to generate sol–gel-entrapped clusters, followed by thermal activation in helium up to 573 K and reduction with hydrogen. TEM investigations showed metal particles (1–4 nm) embedded in the silica matrix. These catalysts were compared with an analogous catalyst derived from $RuCl_3$ and the sol–gel. The cluster precursors gave heterogeneous catalysts with higher metal dispersions than $RuCl_3$. The catalytic activities of the cluster-derived catalysts were higher for the hydrogenation of CO.[110]

The supported ruthenium clusters $[Ru_6N]$ were prepared from $[Ru_6N(CO)_{16}]^{1-}$ salts deposited on MgO, K^+/MgO, and Cs^+/MgO. The supported materials were characterized by EXAFS. The decarbonylated $[Ru_6N]$ cluster unit was

found to remain intact on MgO even after heating in vacuum at 813 K and in hydrogen at 588 K; the alumina-supported cluster, on the other hand, degraded to $[Ru_3]$ units after heating in vacuum at 813 K. The decarbonylated $[Ru_6N]$ framework also remained on K^+/MgO and Cs^+/MgO without aggregation or fragmentation after heating in hydrogen at 588 K. The Ru–O distance was shorter for $[Ru_6N]$ on K^+/MgO and Cs^+/MgO (2.00–2.03 Å) than on MgO (2.13 Å); this was interpreted to imply that the $[Ru_6N]$ interacted with O atoms bonded to K^+ or Cs^+ ions, which may give rise to a direct support effect on catalysis.[111] These catalysts were investigated for the reduction of nitrogen to ammonia. The activities of these catalysts were higher than catalysts prepared from non-nitrido $[Ru_6(CO)_{18}]^{2-}$, degraded $[Ru_3]$ clusters, or conventional Ru catalysts. Also, the H_2–D_2 exchange reactions proceeded faster on supported $[Ru_6N]$ clusters than the other catalysts. The dependence of Ru loading on catalytic activities of $[Ru_6N]$/MgO suggested the importance of the Ru_6 ensemble and the cluster/support interface.[112]

12.15.3.2.2 Clusters of group 9 metals

The effect of pretreatment of the catalysts prepared from $Rh_4(CO)_{12}$ and $Co_4(CO)_{12}$ deposited on silica on the activity and selectivity in CO hydrogenation was examined. The catalysts prepared by thermolysis under hydrogen exhibited a higher degree of decomposition of the cluster framework, greater hydrogen uptake, and lower carbon content than those decomposed under CO, which gave rise to lower activity, because some of the active sites of the catalysts were encapsulated by carbon. The activity of the hydrogen-treated $Rh_4(CO)_{12}/SiO_2$ was similar to that of the CO-treated catalyst, but significantly fewer oxygenates were formed. [113]

Hexarhodium clusters supported on zeolites were prepared and examined as catalysts for toluene hydrogenation. At 396 K, carbonylation of $Rh(CO)_2$(acac) adsorbed in the cages of zeolite NaX formed $[Rh_6(CO)_{15}]^{2-}$ in ca. 80% yield (termed as "ship-in-a-bottle synthesis"). The cluster was identified by ^{13}C NMR, IR, and EXAFS spectra. Decarbonylation in hydrogen at 473 K gave partially decarbonylated clusters with the metal frame nearly intact; decarbonylation at higher temperatures gave aggregated rhodium. The partially decarbonylated clusters could be recarbonylated to give $[Rh_6(CO)_{15}]^{2-}$. Thermolysis in He at 473–573 K gave fully decarbonylated clusters with an Rh–Rh first-shell coordination number of ca. 2.6, suggesting that the cluster frames were intact but slightly flattened or fragmented. These materials catalyze toluene hydrogenation at 353–393 K.[114,115]

Hexarhodium clusters supported by the surface of La_2O_3 powder were prepared and examined as catalysts for ethene hydrogenation. The rhodium carbonyl clusters were prepared by carbonylation (1 atm, 373 K) of La_2O_3 (calcined at 673 K)-supported $Rh(CO)_2$(acac). Thermolysis in He at 573 K removed the carbonyl ligands, giving site-isolated La_2O_3-supported clusters, characterized by EXAFS as Rh_6 octahedra. The supported clusters were examined for catalytic hydrogenation of ethene to ethane. The EXAFS analysis showed that the Rh_6 octahedra remained intact and were inferred to be the catalytically active species. IR spectra identified species believed to be π-bonded ethene, ethyl, ethylidyne, and di-σ-bonded ethene on the working catalyst. The concentration of hydride on Rh_6 increased during an induction period in a flow reactor as the catalytic activity increased almost proportionately, implying that the hydrides are reactive intermediates. The mechanism was proposed to involve insertion of π-bonded ethene into an Rh–H bond to form ethyl, which is subsequently hydrogenated to give ethane. Rh_6/La_2O_3 is 50 times more active for ethene hydrogenation catalysis than Rh_6/γ-Al_2O_3.[116]

MgO-supported Rh_6 and Ir_6 clusters were also investigated as catalysts for ethene hydrogenation. Decarbonylation of hexanuclear metal carbonyl cluster precursors on MgO was used to prepare the catalysts. EXAFS data support octahedral clusters as the catalytically active species. Rh_6/MgO is 1–2 orders of magnitude more active than Ir_6/MgO, as is the activity ratio for the conventionally prepared supported metals on silica.[117]

A large body of work has focused on heterogeneous catalysts prepared from Ir_4 or Ir_6 clusters deposited on a variety of supports and with different pretreatments. A review of some of this work has appeared. [118] Many reactions, such as the hydrocarbon hydrogenations, are structure insensitive, proceeding at approximately the same rate on metal particles of various size, provided that they are larger than about 1 nm and show bulk-like metallic behavior. However, it was not known whether the catalytic properties of metal particles become size dependent as the particles become so small that they are no longer metallic in character. This work explored the effect of cluster size on several reactions, including toluene hydrogenation, alkene hydrogenation, and CO reduction to hydrocarbons. The Ir_4 and Ir_6 clusters differ in catalytic activity both from each other and from metallic Ir particles. This raises the possibility of tailoring the catalytic behavior of metal clusters by controlling the cluster size.[119]

Tetrairidium clusters supported on γ-Al_2O_3 were examined for catalytic activity for toluene hydrogenation. Partial decarbonylation of $Ir_4(CO)_{12}$ on γ-Al_2O_3 (previously dehydroxylated *in vacuo* at 673 K) was achieved by heating in helium at 373 K and occurred without cluster fragmentation. Chemisorption of hydrogen showed an H/Ir of 0.13, less than what is observed with larger Ir particles. The $Ir_4(CO)_{12}$ clusters could be partially reconstructed from Ir_4/γ-Al_2O_3

by treatment in CO at 423–473 K. The supported Ir_4 clusters were catalytically active for toluene hydrogenation at 333 K and 1 atm pressure. The activity increased with increasing decarbonylation, until the degree of decarbonylation reached about 70%, whereupon the catalytic reaction rate became almost independent of the degree of decarbonylation.[120] The decarbonylated $Ir_4/\gamma\text{-}Al_2O_3$ was treated in hydrogen under various conditions to give samples with aggregated iridium having average cluster or particle diameters up to about 70 Å. The samples were used as catalysts for toluene hydrogenation at 1 atm and 333 K. The data show that the catalytic activity per exposed Ir atom increased by more than an order of magnitude as the iridium cluster or particle size increased from that of Ir_4 to about 20 Å.[121–123]

Hexairidium clusters supported on $\gamma\text{-}Al_2O_3$ were also examined for catalytic activity for toluene hydrogenation. $[Ir_6(CO)_{15}]^{2-}$ was formed by surface-mediated synthesis on $\gamma\text{-}Al_2O_3$ powder by treatment of adsorbed $Ir(CO)_2(acac)$ in CO at 373 K and 1 atm. Treatment in He at 573 K caused decarbonylation without fragmentation of the cluster frame, giving $Ir_6/\gamma\text{-}Al_2O_3$, as indicated by EXAFS analysis. The supported Ir_6 clusters were catalytically active for toluene hydrogenation at 333–373 K with a TOF of $1.7 \times 10^{-3}\ s^{-1}$ at 333 K and 0.93 atm of hydrogen in a flow reactor. EXAFS results for the used catalyst indicated that the nuclearity of the supported Ir_6 clusters was essentially unchanged during the catalysis. The $Ir_6/\gamma\text{-}Al_2O_3$ catalyst was an order of magnitude less active (per Ir atom) for toluene hydrogenation than a catalyst consisting of small aggregates of iridium (ca. 50 atoms each) supported on $\gamma\text{-}Al_2O_3$. Because toluene hydrogenation is known to be a structure-insensitive catalytic reaction, the data suggested that the concept of structure insensitivity in catalysis does not extend to clusters as small as Ir_6, but the relatively low activity of the clusters may be also be due to the effect of the support as a ligand, changing the electronic properties of the iridium.[124]

Other supports have been used for tetrairidium clusters. Catalysts were prepared by heating, under He, $Ir_4(CO)_{12}$ deposited on MgO that had been calcined at different temperatures to obtain various degrees of hydroxylation. These were then evaluated for toluene hydrogenation. EXAFS was used to show that the catalysts retained the Ir_4 tetrahedral cluster core even after extended operation. The catalyst with the most highly hydroxylated support eventually aggregated, giving $Ir_{6\pm2}$ clusters. Adsorption of $Ir_4(CO)_{12}$ onto MgO that had been partially dehydroxylated in vacuum at 673 K formed $[HIr_4(CO)_{11}]^{1-}$ on the surface, as identified by IR and EXAFS spectroscopies. Decarbonylation was achieved by treatment in He or H_2. Decarbonylation in H_2 caused metal aggregation, with CO reduction to water and hydrocarbons. Decarbonylation in He left the tetrahedral Ir_4 cluster frame intact. The partially decarbonylated tetrairidium clusters chemisorbed hydrogen, and temperature-programmed desorption (TPD) showed that the strength of hydrogen adsorption increased with increasing cluster decarbonylation. The completely decarbonylated clusters were characterized by low chemisorption capacities (H/Ir 0.27 and CO/Ir 0.39). Chemisorption and EXAFS data show that the amount of hydrogen or CO chemisorbed increases with increasing size of the iridium clusters and aggregates, consistent with a support effect that is maximized for the smallest clusters, Ir_4. Catalytic hydrogenation of toluene shows that the rate depends on the amount of hydrogen on the clusters, rather than the degree of decarbonylation. This was interpreted to support the suggestion that bare iridium atoms are not sufficient for catalysis.[125,126]

Catalysis of toluene hydrogenation and *n*-hexane dehydrocyclization over zeolite-supported iridium clusters was reported. Iridium carbonyl clusters were formed by treatment of $Ir(CO)_2(acac)$, adsorbed on KLTL zeolite, in CO at 1 atm and 448 K. Then, decarbonylation of the clusters was achieved by heating at 673 K in H_2. The supported metal clusters were characterized by IR and EXAFS spectroscopies as mainly Ir_6. The Ir_6/KLTL zeolite is catalytically active for toluene hydrogenation at 333–373 K, with the activity about the same as those of Ir_4 and Ir_6 clusters supported on alumina or MgO, but an order of magnitude less than that of a conventional supported iridium catalyst consisting of aggregates of about 50 atoms each. The catalyst is also active for hexane dehydrocyclization at 613–693 K, but the selectivity for aromatization is low and that for hydrogenolysis is high, consistent with earlier results for conventionally prepared iridium catalysts supported in KLTL zeolite.[127]

Alkene hydrogenation catalyzed by supported Ir clusters has also been examined.[128] Supported metal clusters, $Ir_4(CO)_{12}]/\gamma\text{-}Al_2O_3$, $[Ir_6(CO)_{15}]^{2-}/\gamma\text{-}Al_2O_3$, and $[HIr_4(CO)_{11}]^{1-}$/MgO, were thermally decarbonylated in He to prepare supported metal clusters modeled as $Ir_4/\gamma\text{-}Al_2O_3$, $Ir_6/\gamma\text{-}Al_2O_3$, and Ir_4/MgO. The samples were characterized by IR and EXAFS spectroscopy. Treatment of the catalysts with propene/hydrogen at 298 K gave propane, with retention of the cluster frameworks.[129] IR spectra of $Ir_4/\gamma\text{-}Al_2O_3$ during catalysis indicate propylidyne and highly dehydrogenated C_3 fragments (suggested to be C_3H_2 and C_2H) bonded to the clusters, but these species are not reactive intermediates. The formation of these fragments is much less for Ir_4/MgO. This was attributed to the more basic MgO support being a better electron donor to the clusters than $\gamma\text{-}Al_2O_3$, causing the strength of the interaction between the clusters and propene to be less for the former.[130] Ethene hydrogenation was catalyzed by $Ir_4/\gamma\text{-}Al_2O_3$ and $Ir_6/\gamma\text{-}Al_2O_3$ at 1 atm and 273–300 K. EXAFS spectroscopy shows that the cluster frames remain intact during catalysis. Di-σ-bonded ethene

(dominant below 0.26 atm) and π-bonded ethene (dominant at higher ethene pressure), were identified as intermediates by IR spectroscopy and compete as the principal reaction intermediates. The rate of ethene hydrogenation on Ir_4 is several times greater than that on Ir_6.[131] Zeolite-supported Rh and Ir clusters catalyze alkene hydrogenations. Decarbonylation of zeolite-supported $Rh_6(CO)_{16}$ or $Ir_4(CO)_{12}$, supported in the cages of the Na form of the faujasite zeolite Y, was carried out in H_2 at 473 or 573 K, respectively. Larger aggregates consisting of about 10–20 atoms of Rh or Ir each were formed when zeolite-supported $Rh_6(CO)_{16}$ or $Ir_6(CO)_{16}$ were heated in H_2 at 523 or 573 K. All samples were characterized by EXAFS spectroscopy under vacuum and in pure hydrogen, pure propene, and H_2/propene mixtures. Catalytic hydrogenation of propene was achieved with the metal frames unchanged in all conditions at temperatures up to 413 K.[132]

Catalysis of CO hydrogenation by iridium clusters supported on zeolites was studied. Treatment of $Ir(CO)_2(acac)$ in the pores of NaX zeolite with CO gave $[HIr_4(CO)_{11}]^{1-}$ at 343 K, but predominantly $[Ir_6(CO)_{15}]^{2-}$ at 448 K. The materials were characterized by IR and EXAFS. The zeolite-supported samples catalyzed CO hydrogenation at 20 atm and 523 K, but the activities were low compared to typical Fischer–Tropsch catalysts. A non-Schulz–Flory distribution of hydrocarbon products was obtained, with a maximum at C_1 and a relative maximum at C_4. The predominant species after catalysis was $[Ir_6(CO)_{15}]^{2-}$.[133] When NaY zeolite was used as the support, reductive carbonylation of $Ir(CO)_2(acac)$ in CO at 1 atm and 323 K gave $Ir_4(CO)_{12}$, which was converted in CO at 398 K and 1 atm to the isomer of $Ir_6(CO)_{16}$ with edge-bridging CO ligands and in CO/H_2 at 523 K and 20 atm to another isomer of $Ir_6(CO)_{16}$ with face-bridging ligands. The zeolite-supported cluster catalyzed CO hydrogenation at 20 atm and 523 K, giving a high selectivity to propane. Either isomer of $Ir_6(CO)_{16}$ in the zeolite could be decarbonylated in H_2 at 523 K and 1 atm and recarbonylated. The decarbonylated cluster was characterized by EXAFS spectra to be predominantly Ir_6 with an octahedral structure.[134]

12.15.3.2.3 Clusters of group 10 metals

Heterogeneous Pt catalysts were prepared by controlled thermolysis of salts of $[Pt_3(CO)_6]_5^{2-}$, which had been deposited in the hexagonal channel of the mesoporous zeolite FSM-16. The catalysts were active for hydrogenation of ethylene at 300 K. With a partially decarbonylated catalyst, 1,3-butadiene was selectively hydrogenated to 1-butene; complete decarbonylation above 463 K gave a Pt catalyst which completely hydrogenated butadiene to butane.[135]

A modified zeolite was used to support Pt particles derived from the cluster anions $[Pt_3(CO)_6]_n^{2-}$ ($n = 4$–6). Mesoporous channels (2.7 and 4.7 nm pore size) of FSM-16 were modified with TiO_2 or zirconia by the impregnation and hydrolysis of Ti or Zr alkoxides with subsequent calcination. The Pt carbonyl cluster anions were synthesized within the modified FSM-16 by the reaction of H_2PtCl_6 with CO and water, and then characterized by IR and UV–VIS spectroscopies. Pyrolysis under vacuum at 573 K gave supported nanoparticles, which were more active for CO hydrogenation and more selective for C_2–C_3 alkanes than the unmodified Pt/FSM-16 catalyst.[136]

Support effects were studied for hydrogenation catalysts derived from Pt clusters. The cluster anion $[Pt_{12}(CO)_{24}]^{2-}$ was anchored by ion pairing with fumed silica, silica gel, silica–alumina, and cross-linked polystyrene, all of which had been functionalized with quaternary ammonium groups; a catalyst was also prepared by the adsorption of the sodium salt of the cluster on unfunctionalized fumed silica. The catalytic activities of catalysts derived from these supported clusters and also commercially available 5% platinum on alumina have been studied for the hydrogenation of a variety of substrates: α-acetamidocinnamic acid, cyclohexanone, acetophenone, methyl pyruvate, ethyl acetoacetate, nitrobenzene, and benzonitrile. The oxide-supported catalysts had higher surface areas and higher activities than the polystyrene-supported catalysts. The functionalized fumed silica-based catalyst gives higher conversions than either the catalyst on functionalized silica gel or the silica–alumina-based catalysts, and higher activity than either the commercial platinum catalyst or the catalyst derived from adsorption of the cluster on an unfunctionalized fumed silica. All the cluster-derived catalysts caused reduction of benzonitrile to *N*,*N*′-diphenylhydrazine, whereas the commercial Pt catalysts gave benzylamine as the main product.[137–139]

12.15.3.2.4 Heterometallic clusters

Heterogeneous catalysts for hydrogenation of alkenes and arenes were prepared by thermolysis, under a flow of hydrogen, of the tetrahedral clusters $H_2Ru_4(CO)_{13}$, $H_2FeRu_3(CO)_{13}$, and $HRuCo_3(CO)_{12}$ supported on Chromosorb P. The catalysts were active for the hydrogenation of pentenes, cyclic monoenes and dienes, benzene, and toluene. Experiments under nitrogen showed that complex hydrogenation–dehydrogenation processes occur, as already observed for the same clusters during the homogeneous hydrogenation of cyclohexadienes. After the catalytic runs with $H_2Ru_4(CO)_{13}$ as precursor, TEM microscopy showed the presence of very small supported metal particles (mean size 7.5 nm). The decomposition of $H_2Ru_4(CO)_{13}$ to metal particles on Aerosil upon thermolysis under vacuum or

under hydrogen was followed by means of IR spectroscopy; this catalyst rapidly hydrogenates benzene at 298 K with 100% conversion.[140]

Bimetallic nanoparticle catalysts were prepared by thermolysis of $[PPN]_2[Ru_6C(CO)_{16}Cu_2Cl]_2$ anchored inside the mesoporous channels of silica. A variety of physical methods, including *in situ* X-ray absorption and FT-IR spectroscopies and high resolution scanning TEM, were used to monitor the conversion of the precursors to bare bimetallic nanoparticles. The particles thus obtained were ca. 15 Å in diameter with 12 exposed Ru atoms connected to a square base composed of relatively concealed Cu atoms, which in turn are anchored by four oxygen bridges to four Si atoms. The particles were resistant to sintering or fragmentation. These bimetallic particles were catalysts for hydrogenation of 1-hexene at 373 K and 20 atm hydrogen with a TOF of 5×10^4 mol substrate (mol cluster h)$^{-1}$.[141]

Bimetallic Ag/Ru nanoparticles were prepared by thermal decomposition of $[AsPh_4]_2[Ag_3Ru_{10}C_2(CO)_{28}Cl]$ adsorbed on mesoporous silica (MCM-41). The nanoparticles were characterized as electron microscopy and EXAFS. This material was examined as a catalyst for the hydrogenation of 1-hexene.[142]

A bimetallic Ru/Sn nanoparticle was catalytically active for hydrogenation of 1,5,9-cyclododecatriene. The catalytic performance of a supported Ru_6Sn nanoparticle was studied and compared with that of finely dispersed bimetallic catalysts, that is, Ag–Ru, Cu–Ru, and Pd–Ru. The nanoparticles were prepared by loading mesoporous silica MCM-41 with $[PPN][Ru_6C(CO)_{16}SnCl_3]$ (PPN = bis(triphenylphosphine)iminium) or with $Ru_6C(CO)_{16}SnCl_2$ via a slurry process; IR and EXAFS analysis showed that the cluster core remained intact and firmly attached to the siliceous surface after decarbonylation at 353 K. At 80°, hydrogenation of 1,5,9-cyclododecatriene was 70% selective to cyclododecene, and was >90% selective at 373 K.[143]

The mixed metal carbonylate cluster $[Pd_6Ru_6(CO)_{24}]^{2-}$ was used as a precursor in the synthesis of a highly active hydrogenation catalyst. A salt of the anionic cluster was deposited on the interior surface of mesoporous silica and was heated for 1 h at 453 K under vacuum to generate the supported PdRu catalyst, which was characterized by electron microscopy and X-ray absorption spectroscopy. The PdRu catalyst hydrogenates alkenes and naphthalene (the latter predominantly to *cis*-decalin) under mild conditions. The PdRu catalyst was more active and selective than Pd or Ru catalysts alone. Analysis of the particles after catalysis showed that segregation of Pd and Ru had not occurred and there was no evidence of sintering.[144]

Mixed Co/Ru catalysts have been prepared from mixtures of the homometallic clusters and from mixed metal clusters supported on silica. Their catalytic activities and product distributions in hydrogenation of CO were evaluated.[145,146] FT-IR studies suggested that $Ru_4H_4(CO)_{12}$, $CoRu_3H_3(CO)_{12}$, and $Co_3RuH(CO)_{12}$ on silica were more stable at room temperature than $Co_4(CO)_{12}$, $Co_2Ru_2H_2(CO)_{12}$, and $Co_2Ru_2(CO)_{13}$. TPD found that the CO desorption peak maxima for the precursors were 396 K for $[Co_4(CO)_{12} + Ru_4H_4(CO)_{12}]$, 400 K for $CoRu_3H_3(CO)_{12}$, 406 K for $Co_2Ru_2(CO)_{13}$, 410 K for $Co_4(CO)_{12}$, 417 K for $Co_2Ru_2H_2(CO)_{12}$, 412 K for $Co_3RuH(CO)_{12}$, and 458 K for $Ru_4H_4(CO)_{12}$. The catalysts thus prepared have activity in Fischer–Tropsch synthesis. The activities were highest for the catalysts derived from homometallic clusters, and lowest for catalysts with 1 : 1 metal ratios. The highly active homometallic Co catalyst was the most resistant to deactivation. The selectivities for oxygenated compounds were promoted by the bimetallic sites of Co–Rh catalysts.[147] The CO hydrogenation activities of these cluster-derived silica-supported bimetallic catalysts prepared by reflux method were compared with activity of the corresponding catalysts prepared by impregnation. The activity and selectivity of these catalysts in CO hydrogenation were different from those obtained with catalysts prepared by impregnation. In general, catalysts derived from clusters showed a higher activity per g metal than did impregnated catalysts, although minimum activity was approached at a 1 : 1 Co–Ru molar ratio. The cluster-derived catalysts also showed some activity for water gas shift catalysis and hydroformylation.[148]

Mixed iron–rhodium catalysts were prepared from silica-supported salts of $[Fe_5RhC(CO)_{16}]^{1-}$ and $[Fe_4RhC(CO)_{14}]^{1-}$ clusters. At 323 K, $[Fe_5RhC(CO)_{16}]^{1-}$ was completely converted to $[Fe_4RhC(CO)_{14}]^{1-}$, and the latter cluster was converted to $Fe_2Rh_4C(CO)_{16}$ and $[Fe_3Rh_3C(CO)_{15}]^{1-}$ at 373–423 K, in addition to Fe^{2+} ions. At temperatures of 523–623 K, highly dispersed FeRh particles were located on the silica surface, and the Fe atoms existed mainly in the oxidized state, even after H_2 reduction. The catalysts showed increased activity and selectivity for CO hydrogenation to oxygenated products and for propene hydroformylation compared to catalysts similarly prepared from homometallic clusters.[149]

The clusters $M_4O[(CO)_9Co_3CCO_2]_6$ (M = Zn, Co) were used as single-source precursors for porous, high surface area materials, referred to as ZnCo and CoCo, respectively. These materials were catalysts for hydrogenation of 1,3-butadiene at 50–573 K. At <423 K, both catalysts maintained activity for up to 4 days on stream. CoCo has both higher activity and different selectivity than conventionally prepared Co on silica. It was suggest that both the composition and microstructure derived from the precursor contribute to the catalytic behavior. At 573 K, the activity of these catalysts decrease due to the formation of carbon on the surface and the partial collapse of the porous structure.[150,151]

Catalysts for the selective hydrogenation of crotonaldehyde were obtained by controlled pyrolysis of $M_4O[(CO)_9Co_3CCO_2]_6$ (M = Co and Zn) or $M'_2\{(CO)_9Co_3CCOO\}_4$ (M′ = Co, Mo, and Cu). The pyrolyses yield high surface area, amorphous solids. These catalysts are active for the hydrogenation of crotonaldehyde to crotyl alcohol. This differs from conventional metal catalysts, which are selective for the double bond hydrogenation.[152]

Mixed metal heterogeneous catalysts were prepared by thermolysis of metal complexes $M_2\{\mu\text{-}[(CO)_9Co_3(\mu_3\text{-}CCO_2)]\}_4$ (M = Mo, Cu) with the cobalt carbonyl cluster ligand derived from $(CO)_9Co_3(\mu_3\text{-}CCOOH)$. Two different solids were obtained from each complex, depending on the temperature of thermolysis. At 400 K, the solid, designated LT-MCo (M = Mo, Cu), is only partially decarbonylated and retains the metal carboxylate linkages. Thermolysis at 500 K gives a solid, designated HT-MCo, which is fully decarbonylated and also decarboxylated when heated under hydrogen. These materials were evaluated as catalysts for the hydrogenation of 1,3-butadiene to butane and 1- and 2-butenes. No significant differences were found between the two LT-MCo materials with regard to selectivities. The HT-CuCo catalyst is more selective for 1-butene, whereas the HT-MoCo catalyst is more selective for butane.[153] The reaction of lead acetate with $(CO)_9Co_3(\mu_3\text{-}CCOOH)$ gives $[Pb\{(CO)_9Co_3(\mu_3\text{-}CCO_2)\}_2]_n$. The pyrolysis of $[Pb\{(CO)_9Co_3(\mu_3\text{-}CCO_2)\}_2]_n$ gives two metastable forms of solid materials, designated LT (formed at lower temperatures, 373–453 K) and HT (formed at higher temperatures, 474–523 K). Both forms were characterized spectroscopically. The LT form acted as a catalyst for hydrogenation of 2-butenal to butanol (19%), butanal (42%), and 2-butenol (35%) at 10% conversion, selectivities similar to those of LT materials derived from other Co cluster metal carboxylates. The HT material was totally inactive due to the release of Pb, which totally inactivates the catalyst.[154]

Mixed metal Pt/W catalysts derived for organometallic clusters supported on MgO were examined for toluene hydrogenation. Samples were prepared by adsorption on MgO of either the cluster $Pt[W(CO)_3(C_5H_5)]_2(PhCN)_2$ or from monometallic precursors $PtCl_2(PhCN)_2$ and $W(CO)_6$. The materials thus prepared were heated at 400 °C under hydrogen. The catalysts were characterized by IR spectroscopy, EXAFS spectroscopy, TEM, and chemisorption of H_2, CO, and O_2. Incorporation of W reduced the chemisorption of CO and of H_2, with the reduction being greater for the cluster-derived catalyst than for the catalyst prepared from the monometallic precursors. EXAFS spectra showed substantial Pt–W contributions only for the cluster-derived catalyst, with a Pt–W coordination number of about 2 and an average Pt–W distance of 2.71 Å. TEM and EXAFS results indicate that the interactions between Pt and W cations in the sample made from $\{Pt[W(CO)_3(C_5H_5)]_2(PhCN)_2\}$ maintained the Pt in a highly dispersed form, with supported Pt clusters being smaller than about 10 Å. The cluster-derived catalyst was more than an order of magnitude less active for toluene hydrogenation at 1 atm and 60 °C than the catalyst derived from the two monometallic precursors.[155]

A mixed metal Au/Pt catalyst was prepared by deposition of $[(AuPPh_3)_6Pt(PPh_3)](NO_3)_2$ on silica. The catalyst was characterized by a variety of physical methods. The cluster framework was reported to remain intact up to 400 K under vacuum. The supported Au/Pt catalyst was very active in H_2/D_2 isotope scrambling (TOF of 29.8 s^{-1}), while it showed low activity for ethene hydrogenation and CO oxidation at 303 K. Silica-supported particles prepared from either $Pt(PPh_3)_4$ or $[Au_9(PPh_3)_8](NO_3)_3$ were inactive, suggesting a synergistic interaction between the metals in the mixed metal catalyst.[156,157]

12.15.4 Metal Clusters as Precursors for Nanoscale Materials

Metal clusters have been considered as models for monodispersed nanoscale metal particles in a dielectric matrix or as precursors for nanoscale particles (see Chapter 12.03 for organometallic-derived metals, colloids, and nanoparticles). The number of metal atoms in well-defined molecular compounds can be varied from 2 to 3 up to hundreds, and the physical properties change from localized molecular to nearly bulk metal. They offer the advantage that clusters can be studied by a wide variety of experimental techniques.[158–162]

Large gold clusters have been the object of study. Clusters, like $Au_{55}(PPh_3)_{12}Cl_6$, which fall in the size of 1–2 nm, can be thought of as colloidal nanoparticles with quantum properties in the transitional range between metals and semiconductors. The organic ligand shell surrounding the metal cluster acts like a dielectric "spacer" generating capacitances between neighboring clusters down to 10–18 F. Therefore, charging effects superposed by level spacing effects can be observed. The ligand-stabilized colloidal quantum dots in a condensed state can be described as a novel kind of artificial solid with extremely narrow mini- or hopping bands, depending on the thickness of the ligand shell and its properties.[163,164]

The current–voltage characteristics of small structures made from the large gold cluster $Au_{55}[P(C_6H_5)_3]_{12}Cl_6$ were reported. Electron-beam lithography was used to define structures with highly non-linear characteristics. The current–voltage behavior was said to be consistent with Coulomb charging of the gold clusters in a disordered array.[165]

One example of a very large molecular cluster which is in itself "nanoscale" is $Pd_{59}(CO)_{32}(PMe_3)_{21}$. This cluster, reported to be the largest discrete cluster with metal–metal bonding, has an ellipsoidal core with 11 interior Pd atoms.[166]

12.15.5 Applications in Biomedical Imaging and Pharmaceuticals

The high heavy atom content of metal clusters makes them attractive candidates for imaging in electron microscopy, for X-ray contrast agents, or for determining the phasing in the crystallography of biological molecules.

The use of Au_{11} clusters in electron microscopy has been reviewed.[167] By attachment of ligands capable of covalently bonding to specific functional groups of proteins, structural information can be obtained. Heavy metal clusters derivatized to bind to designated chemical groups on proteins have potential as labels for cryo-electron microscopy. A tetrairidium cluster was attached to the *C*-terminus of the hepatitis B virus (HBV) capsid protein through a maleimide link. Although the clusters were not visible in unprocessed cryo-electron micrographs, they could be visualized in three-dimensional density maps calculated from them, even at only partial occupancy. The Ir_4 label was visualized in maps at 11–14 Å resolution of both size variants of the HBV capsid. It was found that the clusters penetrated to the interior of intact capsids to label this site on their inner surface, unlike undecagold for which an earlier study found that labeling was achieved only with dissociated dimers that were then reassembled into capsids.[168] The Ir_4 clusters could be seen at resolutions as low as 25 Å.[169]

Well-defined ligand-stabilized transition metal colloids can be regarded as very large clusters. Methods for preparing these clusters have been developed.[170] These materials have potential applications as TEM labels. "Greengold" is a large metallic cluster thought to contain 75 gold atoms in a compact 1.4 nm core surrounded by an organic ligand shell. Scanning TEM imaging shows uniform mass and size distributions with an apparent mass of 24 kDa, unaffected by radiation damage. The signal-to-noise ratio is adequate for visualization at low dose and in the presence of a relatively thick biological matrix. Under some conditions, these clusters can form linear chains and hexagonal arrays with a spacing of 2.6 nm. The feasibility of using these in labeling was explored.[171] A new class of covalently linkable platinum cluster reagents with core diameters close to 2 nm was prepared by reduction of platinum(II) acetate in the presence of 1,10-phenanthroline ligands which had been synthetically modified to include solubilizing and reactive cross-linkable functional groups. These were then conjugated site-specifically to antibody IgG molecules and to Fab′ fragments and visualized by scanning TEM. The resulting conjugates show sensitivity similar to that of Nanogold conjugates in immunoblotting experiments and exhibited labeling of tissue antigens and penetrate to access nuclear targets. The new label offers the performance advantages and versatility of the 1.4 nm Nanogold in a larger label, which is more clearly visualized against electron-dense regions of a specimen.[172]

Metal clusters have also been considered as heavy metal labels for determining the phasing in crystallography of large biological molecules.[173] Heavy atom labeling by a tetrairidium cluster was used to determine the X-ray crystal structure of the small subunit from *Thermus thermophilus*. Attachment of the cluster was made to the surface-exposed SH groups prior to crystallization. The positions of these sulfhydryls were localized in difference Fourier maps that were constructed with the multiple isomorphous replacement (MIR).[174]

X-ray attenuation coefficients for several metal clusters were determined with the goal of evaluating the potential of metal clusters as radiographic contrast agents.[175] At higher X-ray energies (80 keV), the clusters Ta_6Br_{14}, $K_8Ta_6O_{19}$, and $(H_3O)_2W_6Cl_{14}$ showed a 3–5 times greater attenuation relative to iodinated contrast agents at the same molar concentrations.[176]

Some tungsten cluster complexes were evaluated as X-ray contrast agents for medical diagnostic imaging in both *in vitro* and *in vivo* animal studies. The 2 : 3 cluster–ligand complexes, $[(W_3SO_3)_2L_3]^{4-}$ (L = linear polyaminopolycarboxylate ligands), were isolated from the reaction of $[W_3SO_3(H_2O)_9]^{4-}$ with the appropriate ligand in refluxing DMF. The salts of $[(W_3SO_3)_2L_3]^{4-}$ were fully characterized by a variety of methods, including single crystal X-ray diffraction. Attachment of the polyaminopolycarboxylate ligands gives the clusters stability, high water solubility, and biological compatibility.[177] Analogous complexes of ethylene glycol bis(2-aminoethyl ether)-*N*,*N*,*N*′,*N*′-tetraacetic acid (EGTA) with the trinuclear tungsten sulfur cluster W_3S_4 were prepared by reaction of $[W_3S_4(H_2O)_9]^{4+}$ with EGTA in refluxing DMF, yielding a mixture of clusters $(W_3S_4)_x(EGTA)_y$ (x, $y \geq 1$). One of these, $[(W_3S_4)_2(EGTA)_3]^{4-}$, was isolated after size-exclusion chromatography in 25–40% yield, and was fully characterized by X-ray crystallography. The cluster is water soluble and stable in the pH range 2–10. Animal studies of $[(W_3S_4)_2(EGTA)_3]^{4-}$ indicated a low acute toxicity and a pharmacokinetic profile similar to that of an existing heavy metal cluster complex with a known extracellular biodistribution.[178]

DNA binding was observed for $[H_4Ru_4(C_6H_6)_4]^{2+}$ and $Ru_3(CO)_9$(1,3,5-triaza-7-phosphatricyclo[3.3.1.1]decane)$_3$ in methanol–water and water. The clusters have good water solubilities, and their ability to bind DNA suggests that they may have applications as anticancer drugs.[179]

12.15.6 Optical Properties of Metal Clusters

12.15.6.1 Non-linear Optical (NLO) Properties of Clusters

Among other inorganic and organic materials, metal clusters have attracted recent interest as optical limiters to protect personnel and equipment from high power laser radiation. An ideal optical limiter exhibits a high, linear transmittance below a certain "limiting" threshold, but transmittance intensity is greatly attenuated (opaque with constant, low, and non-linear transmittance) above the threshold. Compared to organic optical limiting materials, these compounds have the advantage of multiple electronic transitions such as metal–ligand charge transfers, but frequently suffer from chemical instability, photochemical degradation, and inefficient optical limiting. For more information on optical properties of organometallic compounds, see Chapter 12.04. Reviews are available.[180–182]

The 38-metal-atom cluster $(Ph_3P)_{12}Au_{18}Ag_{20}Cl_{14}$ is reported to be a highly efficient optical limiter in a polymer matrix or in solution. It was proposed that the optical limiting behavior is related to the third-order non-linear optical effect.[183]

The two new clusters $(\mu\text{-H})Os_3(\mu\text{-NHInTTP})(CO)_{10}$ and $(\mu\text{-H})_2Os_3(\mu_3\text{-NInTTP})(CO)_9$ (InTTP = (tetra-*p*-tolylporphyrinato)indium(III)) exhibit large non-linear optical absorptions at 532 nm with an ns pulse laser and are potential optical limiting materials for sensor protection in the visible region. These clusters were prepared by reaction of azido(tetra-*p*-tolylporphyrinato)indium(III) [TTPInN$_3$] and $Os_3(\mu\text{-H})_2(CO)_{10}$ in toluene at 353 K overnight. Decarbonylation of $(\mu\text{-H})Os_3(\mu\text{-NHInTTP})(CO)_{10}$ in refluxing toluene gives $(\mu\text{-H})_2Os_3(\mu_3\text{-NInTTP})(CO)_9$. These complexes were the first axially linked porphyrin–metal cluster complexes.[184]

Mixed metal group 6 (Mo, W)/Ir clusters were incorporated into oligourethanes, and their optical limiting properties were assessed by open-aperture *Z*-scan (ns pulses, 523 nm) and time-resolved pump-probe studies (ps pulses, 527 nm). The tetrahedral [M_2Ir_2] cluster cores (M = Mo, W) displayed a greater effective non-linear absorption coefficient β^2 than the [$MoIr_3$] cores. $W_2Ir_2(CO)_{10}(\eta^5\text{-Cp})_2$ displayed the highest response. Substitution at the cyclopentadienyl group and incorporation into the polymer backbone had little effect on the response measured. A time-resolved study of $Mo_2Ir_2(\mu_4\text{-}\eta^2\text{-MeC}_2\text{Ph})(CO)_8(\eta^5\text{-}C_5H_4Me)_2$ using picosecond pulses at 527 nm showed that optical-power-limiting behavior results from a fast non-linear absorption process followed by reverse saturable absorption involving long-lived (>1,000 ps) metastable excited states.[185]

The real and imaginary parts of third-order non-linear optical susceptibilities of 10^{-4} M solutions of $\{Fe_2(CO)_6\}(\mu_3\text{-}E_3P)\{CpCr(CO)_2\}$ (E = S or Se) and the well-known precursor clusters $Fe_3(CO)_9(\mu_3\text{-E})_2$ in toluene were measured using *Z*-scan and ARINS techniques, respectively. The mixed metal clusters display nearly three times the second molar hyperpolarizability values of the corresponding Fe_3 precursors. The results suggest a rich potential of mixed metal, mixed non-metal class of clusters as materials exhibiting large non-linearity.[186]

The third-order optical non-linearity properties of the mixed metal, mixed chalcogen clusters $Cp_2Mo_2Fe_2STe(CO)_7$ and $Cp_2Mo_2Fe_2(\mu_3\text{-S})(\mu_3\text{-Te})(\mu\text{-SPh})(\mu_3\text{-H})(CO)_5$ were measured. The effective non-linear absorption coefficients and non-linear index intensity coefficients of these compounds were measured by the *Z*-scan technique, using 532 nm, 6 ns laser pulses. The cubic hyperpolarizabilities indicate a high non-linearity comparable to some of the best values reported previously for clusters. Both clusters are strong optical limiters with superior photostabilities.[187] High non-linearity, strong optical limiting, and good photostability were also found for $Fe_2(CO)_6\{\mu\text{-SeC(Ph):C(Se)}\}\{(OEt)C:Cr(CO)_5\}$ and $Fe_2(CO)_6Se_2\{\mu\text{-}(CO)_3Cr(\eta^5\text{-}C_5H(CH_2Ph)(Ph)(OEt))\}$.[188]

The non-linear optical properties of the new clusters $Cp_2Mo_2M(\mu_3\text{-E})(CO)_7$ (M = Fe, Ru, Os; E = S, Se) were determined through the *Z*-scan technique, using 35 ps laser pulses at 532 nm. Large refractive third-order non-linearities for these clusters were measured, suggesting that these materials may have applications as optical limiters.[189] Non-linear optical properties of $Fe_4Se_2(\mu\text{-}Se_2PCBut)(CO)_{11}$ also indicate significant magnitudes for the third-order susceptibility.[190] The third-order non-linear optical susceptibilities for $[(\mu\text{-SPh})_2Fe_2(CO)_6]_2(\mu_4\text{-S})$ and $[PPN][(\mu_3\text{-}S)_2Mn_3(CO)_9]$ were measured as 5.4×10^{-13} and 1.2×10^{-13} esu, respectively, in dichloromethane solution.[191]

The new mixed metal Co–Fe–S cluster $[Et_4N][Fe_2Co(CO)_8S(PPh_3)]$ was prepared by reaction of $Co(CNS)_2$ with $Fe_2S_2(CO)_6$, $LiBEt_3H$, and PPh_3 in THF–MeCN. Characterization included the X-ray crystal structure, which allowed calculation of the non-linear optical first-molecular hyperpolarizability component of 28.5×10^{-30} esu.[192]

A large number of group 6/group 10 metal clusters with bridging group 16 or 17 anions have been examined for NLO behavior. Theoretical studies have been applied to suggest that the polarizabilities and hyperpolarizabilities compounds of the Mo(W)/Cu(Ag, Au)S are such that they are promising second harmonic generation (SHG) crystals that may be applied in the IR region.[193] Although most of these would not be classified as "organometallic," they are listed in Table 1 to display the range of "clusters" which is being investigated for this application.

Table 1 Other clusters for which NLO properties have been measured

CompoundReferences	
$Ag_3MoSe_4(PPh_3)_3Cl$	194,213
$Ag_3MoS_4(PPh_3)_3\{S_2P(OR)_2\}$ (R = Et, *i*-Pr, Bu)	195,196
$Ag_3WSe_4(PPh_3)_3Cl$	197,198
$Ag_3WOS_3(PPh_3)_3\{S_2P(O\text{-}i\text{-}Pr)_2\}$	195,218
$Ag_3WS_4(PPh_3)_3\{S_2P(OR)_2\}$ (R = Et, *i*-Pr)	195
$\{[La(Me_2SO)_8][Ag_3W_3Se_{12}]\}_n$	199
$Ag_4Mo_2S_8(PPh_3)_4$	200
$[Me_4N]_2[Ag_6(SPh)_8]$	222
$Au_2MoS_4(PPh_2Py)_2$	201
$Au_2W_2(\eta^5\text{-}C_5Me_5)_2S_6$	202
$Au_2WS_4(PPh_2Py)_2$	201
$Cu_2MoS_4(Ph_2PPy)_4$	203
$Cu_2MoS_4(dppf)\cdot 2DMFMeCN$	203
$Cu_2MoOS_3(Ph_2PPy)_3$	205
$Cu_2WS_4(dppf)_2\cdot 4DMF$ (dppf = 1,1′-bis(diphenylphosphino)ferrocene)	204
$Cu_2WOS_3(PPh_3)_4$	205
$[Bu_4N]_2[Cu_3MoOS_3(NCS)_3]$	206
$Cu_4MoS_4Br_2(py)_6$	207
$Cu_3MoSe_4(PPh_3)_3Cl$	194
$Cu_3MoOS_3(CN)(py)_3$	208
$[Cu_3MoOS_3(4\text{-picoline})_6]Br$	209
$Cu_3MoS_4(PyPPh_2)_3Cl$	210
$[Cu_3MoOS_3IL_2]$ (L = Phen, bpy, 4,4′-dimethyl-2,2′-bipyridyl)	212
$Cu_3MoOS_3(PPh_3)_3$(acetate)	211
$[MoI(bpy)2][Cu_3MoOS_3I_2(bpy)_2]$	212
$Cu_3MoSe_4(PPh_3)_3Cl$	213
$[Cu_3MoS_4(dppm)_3][BF_4]$	214
$Cu_3MoO_{0.75}S_{3.25}Cl(bpy)_2$	215
$[Bu_4N]_2[Cu_3MoOS_3BrCl_2]$	216
$Cu_3MoOS_3(PPh_3)_3\{S_2P(OBu)_2\}$	198
$Cu_3WOS_3(CN)(py)_4$	208
$Cu_3WOS_3(PPh_3)_3\{S_2P(OPri_2)_2\}$	217
$[WI(bpy)_2][Cu_3WOS_3I_2(bpy)_2]$	212
$Cu_3WS_4(PPh_3)_3\{S_2P(OCH_2Ph)_2\}$	218
$[Cu_3WOS_3(4\text{-picoline})_6]Br$	209
$Cu_3WOS_3I(2\text{-picoline})_3$	219
$Cu_3W(\eta^5\text{-}C_5Me_5)S_3Br_2(EPh_3)_2$ (E = As, P)	220
$[NEt_4]_3[Cu_3WOS_3Br_3(\mu\text{-Br})]2H_2O$	221
$[Me_4N]_2[Cu_4(SPh)_6]$	222
$[Et_4N]_2[Cu_4MoS_4(SCN)_4(2\text{-picoline})_4]$	223
$[Et_4N]_2[Cu_4MoS_4(CN)_4]$	224
$[Et_4N]_2[Cu_4WS_4(CN)_4]$	224
$Cu_4MoS_4(SCN)_2(py)_6$	225
$Cu_4MoS_4(2\text{-picoline})_5Br_2$	226
$\{[Cu_4MoS_4(2\text{-picoline})_3Br](\mu\text{-Br})\}_n$	226
$[Et_4N]_2[Cu_4WS_4(SCN)_4(2\text{-picoline})_4]$	223
$Cu_4WS_4(SCN)_2(py)_6$	225
$Cu_4WS_4I_2(py)_6$	227
$\{[Et_4N]_2[Cu_4WSe_4(CN)_4]\}_n$	199
$[Cu_4W_2O_2S_6(NCMe)_4]_n$	228
$[Et_4N]_4[Cu_6Mo_2O_2S_6I_6]$	229
$[Et_4N]_4[Cu_8Mo_4O_4S_{12}\{(Ph_2PS)_2N\}_4]$	230
$[Mo_2Pd_4S_8(dppm)_2]\cdot 4DMF$	231
$[Pd_4W_2S_8(dppm)_2]\cdot 4DMF$	231

Coordination of a metal cluster to a ligand can be used to tune the electronic properties to enhance a higher second-order NLO response. Complexes of styrylpyridines with the $Os_3(CO)_{11}$ cluster core were studied to determine the coordination-induced enhancement of quadratic hyperpolarizability (β_{EFISH}) of the ligands and solvatochromic effects. The complexes were prepared by reaction of $Os_3(CO)_{11}(MeCN)$ with *trans*-4-(4-$RC_6H_4CH{:}CH)C_5H_4N$ (R = NMe_2, *t*-Bu, or CF_3) or *trans*,*trans*-4-[(4-dimethylaminophenyl)-1,3-butadienyl]pyridine afforded complexes $Os_3(CO)_{11}$(styrylpyridine). An enhancement of the quadratic hyperpolarizability of pyridine ligands of these complexes was measured by the solution-phase d.c. electric-field-induced second harmonic (EFISH) generation method. This effect is due either to a red shift of the intraligand charge-transfer (ILCT) transition upon coordination when the *para*-substituent is a strong electron donor or to a metal-to-ligand charge-transfer (MLCT) transition when the *para*-substituent is a strong electron acceptor. In the latter case, the quadratic hyperpolarizability has a negative sign, due to the negative of value of $\Delta\mu_{eg}$, the variation of the dipole moment upon excitation. Therefore the "$Os_3(CO)_{11}$" cluster core displays an ambivalent acceptor or donor role. The clusters were stable to laser excitation. Some of the complexes investigated in this study show significant values (between 500×10^{-48} and 900×10^{-48} esu) of the product $\mu\beta_0$, values comparable to that of Disperse Red 1, which is currently used in electro-optic polymers.[232]

12.15.6.2 Luminescent Clusters

Luminescent metal clusters have been studied for possible applications in OLED display technology as dopant emitters, in solar photoconversion chemistry as chromophores, and in sensor development for luminescence detection (for more information on optical properties of organometallic compounds, see Chapter 12.04). Some reviews of various classes of luminescent clusters are available.[233–236] Most of these are clusters of group 10 or 11 metals. A representative set of results is summarized below, with other luminescent clusters listed in Table 2.

A series of tetrametallic luminescent clusters were prepared by condensation reactions involving $Pt_2(dba)_3$ (dba = dibenzylideneacetone). The homometallic Pt_4 clusters $[Pt_4(dmb)_4(PPh_3)_2]Cl_2$ (dmb = 1,8-diisocyano-*p*-menthane) and $\{[Pt_4(dmb)_4(diphos)]Cl_2\}_n$ (diphos = dppb, dppp, dpph) were prepared in good yields from the reaction of $Pt_2(dba)_3$ with dmb and the appropriate phosphine ligand. The structure for $[Pt_4(dmb)_4(PPh_3)_2]Cl_2$ consists of a quasi-linear $Pt_4L_2^{2+}$ species with the dmb ligands bridging the Pt atoms to form a catenate. For the other three clusters, the diphos ligands result in the formation of amorphous polymeric materials with molecular weights ranging from 84,000 to 307,000. Theoretical calculations indicate that the HOMO and LUMO are the two $d\sigma^*$-orbitals arising from four interacting Pt atoms. A low-energy UV–VIS band at $\lambda_{max} = 405$ nm (ε 35,800 M^{-1} cm^{-1}; EtOH) for $[Pt_4(dmb)_4(PPh_3)_2]Cl_2$ is assigned to the $d\sigma^*$- → $d\sigma^*$-transition. All four clusters are luminescent at 77 K in ethanol, with emissions at ca. 750nm and lifetimes of 2.7–5.2 ns. From the Stokes shifts (10,000–12,000 cm^{-1}) and the long emission lifetimes, the emissions are assigned to a phosphorescence $d\sigma^*$- → $d\sigma^*$-transition.[237] Analogously, the mixed metal Pt/Au cluster $[Pt_2Au_2(dmb)_2(PPh_3)_4][PF_6]_2$ is luminescent at low temperatures in the solid state or as frozen glasses, and in the solid state at room temperature. The compound displays an emission band at 875 nm with an emission lifetime of 4.4 ns in butyronitrile at 77 K. The cluster was synthesized by reaction of $Pt_2(dba)_3$ and $[Au(PPh_3)_2][PF_6]$ in the presence of dmb. The crystal structure shows a quasi-linear PPh_3Au–$AuPPh_3$ fragment encapsulated inside a $Pt_2(dmb)_2^{2+}$ ring. The absorption spectra were characterized by strong bands at λ_{max} (ε, M^{-1} cm^{-1}) 316 (32,300), 366 (37,800), and 418 nm (21,500) and lower intensity features at 516 (2,860) and 655 nm (834).[238]

Mixed Pt/Cd clusters are luminescent at room temperature. The reaction of $[NBu_4]_2[Pt(CCPh)_4]$ with $Cd[ClO_4]_2$ yielded a white, insoluble solid $[PtCd(CCPh)_4]_n$ (75% yield). Reaction of this solid with 1 equiv. of $[NBu_4]X$ (X = Cl, Br, CN) gave soluble complexes $[NBu_4]_2[\{Pt(CCPh)_4\}_2(CdX)_2]$; these complexes contain two platinate fragments connected by two CdX units through Pt–Cd and mainly Cd–C interactions. All complexes are strongly emissive in the solid state at room temperature.[239]

An unusual "chain polymeric co-crystallization" adduct, $[\{Pt_2Ag_4(CC\text{-}t\text{-}Bu)_8(bpy)\}]_\infty$, was obtained from the reaction of the hexanuclear cluster $[Pt_2Ag_4(CC\text{-}t\text{-}Bu)_8]$ with 2,2′-bpy. The crystal structure shows an extended polymeric chain constructed by long-range, secondary misdirected Ag–N interactions between the cluster units and the 2,2′-bpy ligand. This compound is highly emissive in the solid state and in frozen solution. A considerable enhancement of the luminescence and a notable red shift in the emission maximum of $[\{Pt_2Ag_4(CC\text{-}t\text{-}Bu)_8(bpy)\}]_\infty$ ($\lambda_{max} = 513$ nm) relative to $[Pt_2Ag_4(CC\text{-}t\text{-}Bu)_8]$ ($\lambda_{max} = 476$ nm) was noted.[240]

The brilliantly luminescent Au–Ag complexes $[Au_3(\mu_3\text{-}E)Ag(PPh_2py)_3][BF_4]_2$, where E = O, S, Se, and Ph_2Ppy = 2-diphenylphosphinopyridine, were synthesized and characterized. The structural core of these complexes

Table 2 Other luminescent clusters

Cluster	*References*
$\{[Ag_3(Tab)_4](PF_6)_3 \cdot 2DMF\}_n$	250
$[Ag_3(CCPh)_2(dppm)_3]Cl$	251
$[Ag_4(\mu\text{-dppm})_4(\mu_4\text{-E})][OTf]_2$ (E = S , Se, and Te)	252,253
$[Ag_8Pt_2(CCBut)_8(OClO_3)_2(acetone)_2][O_2ClO_2)_2]_n$	254
$[Ag_{14}(\mu_6\text{-S})(Tab)_{12}(PPh_3)_8][PF_6]_{12}$ (TabH = 4-(trimethylammonio)benzenethiol)	250
$Au_2Tl_2(C_6Cl_5)_4$	255
$[Au_3(\mu\text{-dppm})_2(CCPh)_2][Au(CCPh)_2]$	256
$[Au_4(dppm)_2(3,5\text{-}Ph_2Pz)_2][NO_3]_2$	257
$Au_4\{(PPh_2)_2C_2B_9H_{10}\}_2(PR_3)_2$ (R = Ph, 4-MeC_6H_4, 4-$OMeC_6H_4$)	258
$[Au_9(\mu\text{-dppm})_4(\mu\text{-}p\text{-tc})_6][PF_6]_3$ (*p*-tc = *p*-thiocresolate)	259,260
$Co_2\{\mu\text{-}HC_2CC[Re(CO)_3(N\text{–}N)]\}(CO)_6$ (N–N = $^tBu_2$bpy, bpy)	261
$[Cu_3(dppm)_3OH][BF_4]_2$	262
$[Cu_3(\mu\text{-LL})_3\{\mu_3\text{-}\eta^1\text{-}CCC_6H_4CCRe(NN)(CO)_3\}_2][PF_6]$ (LL = dppm, $(Ph_2P)_2NPr$; NN = bpy, 4,4′-t-Bu_2bpy; R = H, Me)	263
$[Cu_4I_4(bpp)_2]_n$ (bpp = 1,3-bis(4-pyridyl)propane)	264
$Cu_4I_4(py)_4$	265,266
$Cu_4(CCPh)_4L_2$ (L = $Ph_2PCH_2(CH_2OCH_2)_2CH_2PPh_2$)	267
Cu_4I_4(1,3-bis(4-pyridyl)propane)$_n$	268
$[Cu_4(\mu\text{-dtpm})_4(\mu_4\text{-S})][PF_6]_2$ (dtpm = bis(bis(4-methylphenyl)phosphino)methane)	269
$Cu_4X_4(dpmp)_4$ (dpmp = 2-(diphenylmethyl)pyridine; X = I, Br, Cl)	270
$Cu_4(\mu\text{-dppm})_3(\mu\text{-}\mu\text{-}NS_2)(\ \mu\text{-}\mu_4\text{-}NS_2)$ (NS_2 = 1,8-naphthalenedithiolate)	271
$[Cu_5(\mu\text{-dppm})_4(\mu_3\text{-}\mu_3\text{-}NS_2)_2]PF_6$	271
Cu_6(methylpyridinethiolate)$_6$	272,273
$Cu_{16}(hfac)_8(CC\text{-}t\text{-}Bu)_8$	274
$Cu_{20}(hfac)_8(CCCH_2Ph)_{12}$	274
$Cu_{18}(hfac)_{10}(CBu)_8$	274
$Cu_{26}(hfac)_{11}(CCPr)_{15}$	274
$Cu_{26}(hfac)_{12}(CCR)_{14}$ (R = Bu, *n*-C_5H_{11}, *n*-C_6H_{13})	275
$[Ag([Au(\mu\text{-C2,N3-bzim})]_3)_2][BF_4]$ (bzim = 1-benzylimidazolate)	276
$[Tl([Au(\mu\text{-C2,N3-bzim})]_3)_2][PF_6]$	276
$[Tl([Au(\mu\text{-C(OEt):}NC_6H_4CH_3)]_3)_2][PF_6]$	276
$[NBu_4][Pb\{Pt(\mu\text{-Cl})(C_6F_5)_2\}_3]$	277
$Pt_2(AuCl)(\mu\text{-dppm})_2Cl_2$	278
$Pt_2(HgCl_2)(\mu\text{-dppm})_2Cl_2$	278
$[NBu_4]_2[(C_6F_5)_6(\mu\text{-OH})_3Pt_3HgCl]$	279
$[Bu_4N]_2[Re_6Se_8I_4(\mu\text{-dpph})]$ (dpph = 1,6-bis(diphenylphosphino)hexane)	280
cis- and *trans*-$Re_6Se_8I_2(\mu\text{-dpph})_2$	280
$[Re_6Se_8(\mu\text{-dpph})_3][SbF_6]_2$	280
$[Re_6E_7O(3,5\text{-}Me_2PzH)_6]Br_2$ (E = S, Se; $3,5\text{-}Me_2PzH$ = 3,5-dimethylpyrazole)	281

is an Au_3Ag tetrahedron with a μ_3-group 16 atom capping the three Au atoms. The emission energy depends strongly on the group 16 atom, changing from O (blue) to S (yellow) and Se (orange). The luminescent 4-methylpyridyl analog with E = S was also reported. For E = S, Se, the change in emission energy with μ_3-bridging atom allows assignment of the excited state as LMMCT, and lifetime measurements support its spin-forbidden nature. Frozen glass measurements indicate a higher-energy emitting state for these systems, and for the E = O system, either LMMCT or metal-centered cluster-based emission can be proposed. [241]

The photoluminescent properties of several polynuclear gold(I) selenide complexes were investigated. $[Au_{18}Se_8(dppe)_6]Br_2$ displays bright red long-lived photoluminescence (quantum yield, φ_{PL}, 7.5×10^{-2} at 293 K and ca. 0.8 at 77 K) in the solid state, with high photostability. $[Au_{10}Se_4(dpppe)_4]Br_2$ (dpppe = bis(diphenyl-phosphino)pentane) shows a broad near-IR photoluminescence at 880 nm in dichloromethane ($\varphi_{PL} = 4 \times 10^{-3}$), which is shifted up to 1,020 nm in the solid state at 77 K (φ_{PL} 3×10^{-3}). Although the quantum efficiency of this compound as a luminophor is only moderate, it is comparable to that of organic IR laser dyes such as Styryl-20 and IR26. A particular configuration of the $Au_{10}Se_4$ core appears to be crucial for the near-IR photoluminescence, as the related complexes $[Au_{10}Se_4(dppm)_4]Br_2$ and $[Au_{10}Se_4(depe)_4]Cl_2$ (depe = bis(diethylphosphino)ethane) are not photoluminescent.[242]

The luminescent cluster $[Ag_4(P_2\text{-bpy})_2][BF_4]_4$ (P_2-bpy = 6,6-bis(diphenylphosphinyl)-2,2′-bipyridyl) was synthesized by reaction of $AgBF_4$ with the P_2-bpy ligand. Addition of bromide or iodide caps the Ag_4 faces, forming $[Ag_4(P_2\text{-bpy})_2(X)_2]$ (X = Br or I). In coordination solvents, adducts $[Ag_4(P_2\text{-bpy})_2(X)_2(L)_2]$ (X = Br, L = MeCN; X = I, L = DMSO) are formed. The luminescence of $[Ag_4(P_2\text{-bpy})_2][BF_4]_4$ is quenched by exposure to air, CO_2, or coordinating solvents, but it can be restored by purging with nitrogen. It was suggested that the cluster may act as a solution-state sensor.[243]

Polynuclear copper(I) complexes with bridging bis(dicyclohexylphosphino)methane (dcpm) and iodide ligands, $[Cu_2(dcpm)_2(MeCN)_2][BF_4]_2$, $(CuI)_3(dcpm)_2$, $(CuI)_4(dcpm)_2$, $(CuI)_2(dcpm)_2$, and $[Cu_2(dcpm)_2][BF_4]_2$, were prepared and characterized by X-ray crystallography. Powder samples of the first four display intense, long-lived phosphorescence with λ_{max} at 460, 626, 590, and 456 nm, and emission quantum yields of 0.26, 0.11, 0.12, and 0.56, respectively, at room temperature. In the solid state, $[Cu_2(dcpm)_2][BF_4]_2$ displays both a weak emission at 377 nm and an intense one at 474 nm with an overall emission yield of 0.42; in acetone, the complex gives a bright emission at 625 nm at room temperature. The difference in emission properties among these complexes suggests that both Cu–Cu interaction and coordination around the Cu center affect the excited-state properties.[244]

The luminescence of the 28-atom Au nanoclusters, stabilized by a glutathione (GSH) adsorbate layer, was determined. These clusters show a distinct absorption onset at 1.3 eV, corresponding to the opening of an electronic gap within the conduction band (HOMO–LUMO gap). The clusters luminesce over a broad spectral region extending from the visible to the IR (2.0–0.8 eV). The luminescence could be separated into two bands with maxima around 1.5 and 1.15 eV, indicating that radiative recombination between the ground state and two distinctively different excited states takes place. The total quantum yield of the luminescence is 3.5×10^{-3} at room temperature.[245]

The ligand-exchanged nanoparticle $Au_{38}(PEG135S)_{13}(SC_2H_4Ph)_{11}$, where PEG135S is $-SCH_2CH_2OCH_2CH_2OMe$, exhibits a broad (1.77–0.89 eV) near-IR luminescence band, resolvable into maxima at 902 nm (1.38 eV) and 1025 nm (1.2 eV). Much of the luminescence occurs at energies less than the HOMO–LUMO gap energy. The HOMO–LUMO energy gap was estimated to be 1.33 eV, on the basis of voltammetry. At low energies, the optical absorbance spectrum contains bands at 675 nm (1.84 eV) and 770 nm (1.61 eV) and an absorbance edge at 1.33 eV consistent with the estimated HOMO–LUMO energy gap. These nanoparticles were prepared by ligand exchange with the well-characterized, 1.1 nm diameter Au nanoparticle, $Au_{38}(SC_2H_4Ph)_{24}$. Properties of other Au_{38} nanoparticles made by exchanging the monolayer ligands with different thiolate ligands are also described. [246]

A series of luminescent AgI–CuI heteropolynuclear acetylide complexes were synthesized. Reaction of $(AgCCC_6H_4\text{-}4\text{-}R)_n$ with $[Cu_2(\mu\text{-}Ph_2PNHPPh_2)_2(MeCN)_2][ClO_4]_2$ gave hexanuclear $[Ag_4Cu_2(\mu\text{-}Ph_2PNHPPh_2)_4(CCC_6H_4\text{-}4\text{-}R)_4][ClO_4]_2$ (R = H, Me); these clusters have bicapped cubic metal framework consisting of four AgI and two CuI units and four acetylide *C*-donors. Reaction of $(AgCCC_6H_4\text{-}4\text{-}R)_n$ with $[Cu_2(\mu\text{-dppm})_2(MeCN)_2][ClO_4]_2$ afforded octanuclear species $[Ag_6Cu_2(\mu\text{-dppm})_3(CCC_6H_4\text{-}4\text{-}R)_6(MeCN)][ClO_4]_2$ (R = H, Me, OMe, NO_2); the structures of these clusters involve a "waterwheel-like" structure of two $Ag_3Cu(CCC_6H_4\text{-}4\text{-}R)_3$ units held together by three bridging dppm ligands. When the reaction was attempted with the acetyl-substituted acetylide–silver complex, the product was $[Ag_6Cu_2(\mu\text{-dppm})_3(CCC_6H_4\text{-}4\text{-}Ac)_6]_2[ClO_4]_4$, a dimer of heterooctanuclear "waterwheel-like" Ag_6Cu_2 units connected by acetyl–silver bonds. All of the complexes show intense, long-lived luminescence in the solid states and in acetonitrile and dichloromethane solutions. The microsecond scale of lifetimes in the solid state at 298 K indicates phosphorescent emission. The emissive state in $[Ag_4Cu_2(\mu\text{-}Ph_2PNHPPh_2)_4(CCC_6H_4\text{-}4\text{-}R)_4][ClO_4]_2$ and $[Ag_6Cu_2(\mu\text{-dppm})_3(CCC_6H_4\text{-}4\text{-}R)_6(MeCN)][ClO_4]_2$ (R = H, Me, OMe) was thought to be derived from a 3LMCT (acetylide $\rightarrow Ag_4Cu_2$ or Ag_6Cu_2) transition, mixed with a metal cluster-centered ($d \rightarrow s$) excited state. For the clusters with electron-deficient 4-nitrophenylacetylide and 4-acetylphenylacetylides, the lowest-lying excited state was thought to be an intraligand $3[\pi \rightarrow \pi^*]$ transition.[247]

The hexarhenium(III) clusters $[Re_6Se_8I_{6-n}(\eta^1\text{-diphosO})_n]^{2+}$, $n = 1$–6, are highly luminescent, with microsecond-scale emissive lifetimes at room temperature. The complexes were obtained by the substitution of the diphosphines $Ph_2P(CH_2)_xPPh_2$ ($x = 1$–5) for the iodide ions in the parent octahedral hexarhenium cluster $[Re_6Se_8I_6]^{3+}$. The diphosphine ligands are η^1-bonded, and the non-coordinated *P*-donor atom is oxygenated in most cases. The strongest luminescence with the longest emission lifetimes are found for the hexaphosphine complexes.[248]

Metal clusters containing fluorescent 5-(dimethylamino)naphthalene-1-sulfonyl (R1) and acridone (R2) frameworks were synthesized, and their photophysical properties were explored. Reactions of the fluorescent-labeled alkynes R1CH_2CCH and R2CH_2CCH with various metal carbonyl clusters $Co_2(CO)_8$, $[Et_3NH][Fe_2(CO)_6(\mu\text{-CO})(\mu\text{-S-}t\text{-Bu})]$, and $M_3(CO)_{10}(NCMe)_2$ (M = Ru, Os) afforded the fluorescent cluster complexes $Co_2(CO)_6(\mu\text{-}\eta^2\text{-RCH}_2CCH)$, $Fe_2(CO)_6(\mu\text{-S-}t\text{-Bu})(\mu\text{-}\eta^2\text{-RCH}_2C{:}CH_2)$, $Ru_3(CO)_9(\mu\text{-CO})(\mu_3\text{-}\eta^2\text{-RCH}_2CCH)$, and $Os_3(CO)_9(\mu\text{-CO})(\mu_3\text{-}\eta^2\text{-RCH}_2CCH)$ (R = R1, R2), respectively, in moderate to good yields. All were fluorescent in solution at room temperature with the luminescence fluorophore, but strong quenching of the fluorescence intensity resulted from the presence of the metal cluster units.[249]

12.15.7 Other Applications

The bimetallic cluster $H_{12}Pd_{28}(PtPMe_3)(PtPPh_3)_{12}(CO)_{27}$ was synthesized and fully characterized, including by X-ray crystallography. The cluster core consists of a four-layer hcp $Pd_{28}Pt$ unit which has 12 square-pyramidal Pd_5 cavities, each capped by a $PtPh_3$ fragment on the surface. The hydrides were found to undergo H/D exchange under deuterium gas. It was suggested that the cluster might be viewed as a molecular model for hydrogen storage in Pd metal.[282]

Polymers containing pendant metal clusters or clusters as part on the polymer backbone have been prepared. Polymerization of the monomer $Co_3(CO)_9\{C(CO)O(CH_2)_2O(CO)CH{:}CH_2\}$ was used to prepare a polyacrylate resin with pendant $CCo_3(CO)_9$ fragments.[283]Soluble carbosilane dendrimers terminated with $AuFe_2$ and $AuFe_3$ carbonyl cluster units were prepared. $Si(CH_2CH_2SiMe(CH_2PPh_2AuCl)_2)_4$ reacts with $[Fe_2(CO)_6(\mu\text{-}CO)(\mu\text{-}PPh_2)]^{1-}$ and $[Fe_3(CO)_{11}]^{2-}$ to give the mixed metal cluster dendrimers $Si(CH_2CH_2SiMe(CH_2PPh_2AuFe_2(CO)_6(\mu\text{-}CO)(\mu\text{-}PPh_2))_2)_4$ and $[PPh_4]_8[Si(CH_2CH_2SiMe(CH_2PPh_2AuFe_3(CO)_{11})_2)_4]$, respectively. Both compounds are soluble in acetone, THF, and dichloromethane.[284]

References

1. King, R. B. *Prog. Inorg. Chem.* **1972**, *15*, 287–473.
2. Johnson, B. F. G.; Lewis, J. *Adv. Inorg. Chem. Radiochem.* **1981**, *24*, 225–335.
3. Shriver, D. F.; Kaesz, H. D.; Adams, R. D. *The Chemistry of Metal Clusters*; VCH: New York, 1990.
4. Suess-Fink, G.; Meister, G. *Adv. Organomet. Chem.* **1993**, *35*, 41–134.
5. Suss-Fink, G.; Jahncke, M. In *Catalysis by Di- and Polynuclear Metal Cluster Complexes*; Adams, R. D., Cotton, F. A., Eds.; Wiley-VCH: New York, 1998; pp 167–248.
6. Adams, R. D. *J. Organomet. Chem.* **2000**, *600*, 1–6.
7. Cabeza, J. A. Homogeneous catalysis with ruthenium carbonyl cluster complexes: hydrogenation of alkynes. In *Metal Clusters in Chemistry*; Braunstein, P., Oro, L. A., Raithby, P. R., Eds.; Wiley-VCH Verlag GmbH: Weinheim, 1999; Vol. 2, pp 715–740.
8. Braunstein, P.; Rose, J. Heterometallic Clusters in Catalysis. In *Metal Clusters in Chemistry*; Braunstein, P., Oro, L. A., Raithby, P. R., Eds.; Wiley-VCH Verlag GmbH: Weinheim, 1999; Vol. 2, pp 616–677.
9. Davies, H. M. L.; Beckwith, R. E. J. *Chem. Rev.* **2003**, *103*, 2861–2903.
10. Davies, H. M. L.; Loe, O. *Synthesis* **2004**, 2595–2608.
11. Haupt, H.-J.; Wittbecker, R.; Floerke, U. *J. Organomet. Chem.* **1996**, *518*(1–2), 213–219.
12. Chisholm, M. H.; Kramer, K. S. *J. Chem. Soc., Chem. Commun.* **1996**, 1331–1332.
13. Therrien, B.; Vieille-Petit, L.; Tschan, M.; Romakh, V. B.; Suess-Fink, G. *Chimia* **2003**, *57*, 593–596.
14. Hagen, C. M.; Vielle-Petit, L.; Laurenczy, G.; Suss-Fink, G.; Finke, R. G. *Organometallics* **2005**, *24*, 1819.
15. Plasseraud, L.; Suss-Fink, G. *J. Organomet. Chem.* **1997**, *539*, 163–170.
16. Vieille-Petit, L.; Therrien, B.; Suss-Fink, G.; Ward, T. R. *J. Organomet. Chem.* **2003**, *684*, 117–123.
17. Matthieu, J. M.; Neels, A.; Stoeckli-Evans, H.; Suss-Fink, G. *Polyhedron* **1999**, *18*, 2679–2685.
18. Suss-Fink, G.; Faure, M.; Ward, T. R. *Angew. Chem., Int. Ed.* **2002**, *41*, 99–101.
19. Faure, M.; Tesouro Vallina, A.; Stoeckli-Evans, H.; Suss-Fink, G. *J. Organomet. Chem.* **2001**, *621*, 103–108.
20. Meister, G.; Rheinwald, G.; Stoeckli-Evans, H.; Suess-Fink, G. *J. Chem. Soc., Dalton Trans.* **1994**, 3215–3223.
21. Vieille-Petit, Ludovic; Therrien, Bruno; Suss-Fink, G *Inorg. Chim. Acta* **2003**, *355*, 394–398.
22. Dyson, P. J.; Ellis, D. J.; Lincoln, R.; Russell, K.; Smith, P. J.; Welton, T. *Proceedings - Electrochemical Society* **2000**, 99–41(Molten Salts XII), 161–168.
23. Dyson, P. J.; Ellis, D. J.; Laurenczy, G. *Adv. Synth. Catal.* **2003**, *345*(1–2), 211–215.
24. Dyson, P. J. *J. Chem. Soc., Dalton Trans.* **2003**, 2964–2974.
25. Dallmann, K.; Buffon, R. *J. Mol. Catal. A: Chemical* **2001**, *172*, 81–87.
26. Blazina, D.; Duckett, S. B.; Dyson, P. J; Lohman, J. A. B. *Chemistry* **2003**, *9*, 1045–1061.
27. Blazina, D.; Duckett, S. B.; Dyson, P. J.; Lohman, J. A. B. *Angew. Chem., Int. Ed.* **2001**, *40*, 3874–3877.
28. Prestwich, T. G.; Blazina, D.; Duckett, S. B.; Dyson, P. J. *Eur. J. Inorg. Chem.* **2004**, 4381–4387.
29. Hilal, H. S.; Jondi, W.; Khalaf, S.; Abu-Halawa, R. *J. Organomet. Chem.* **1993**, *452*, 161–165.
30. Fontal, B.; Reyes, M.; Suarez, T.; Bellandi, F.; Ruiz, N. *J. Mol. Catal. A: Chemical* **1999**, *149*, 87–97.
31. Fontal, B.; Reyes, M.; Suarez, T.; Bellandi, F.; Diaz, J. C. *J. Mol. Catal. A: Chemical* **1999**, *149*, 75–85.
32. Gao, J.; Xu, P.; Yi, X.; Wan, H.; Tsai, K. *J. Mol. Catal. A: Chemical* **1999**, *147*, 99–104.
33. Zhang, H.; Yang, C.; Li, Y.; Donga, Z.; Gao, J.; Nakamura, H.; Murata, K.; Ikariya, T. *J. Chem. Soc., Chem. Commun.* **2003**, 142–143.
34. Matteoli, U.; Beghetto, V.; Scrivanti, A. *J. Mol. Catal. A: Chemical* **1996**, *109*, 45–50.
35. Kallinen, K. O.; Pakkanen, T. T.; Pakkanen, T. A. *J. Mol. Catal. A* **1998**, *135*, 233–239.
36. Cabeza, J. A.; Fernandez-Colinas, J. M.; Llamazares, A.; Riera, V.; Garcia-Granda, S.; Van der Maelen, J. F. *Organometallics* **1994**, *13*, 4352–4369.
37. Cabeza, J. A.; Fernandez-Colinas, J. M.; Llamazares, A.; Riera, V. *Organometallics* **1993**, *12*, 4141–4144.
38. Cabeza, J. A.; Llamazares, A.; Riera, V.; Briard, P.; Ouahab, L. *J. Organomet. Chem.* **1994**, *480*, 205–212.
39. Alvarez, S.; Briard, P.; Cabeza, J. A.; del Rio, I.; Fernandez-Colinas, J. M.; Mulla, F.; Ouahab, L.; Riera, V. *Organometallics* **1994**, *13*, 4360–4366.
40. Cabeza, J. A.; Fernandez-Colinas, J. M.; Llamazares, A. *Synlett* **1995**, 579–586.
41. Cabeza, J. A.; del Rio, I.; Fernandez-Colinas, J. M.; Riera, V. *Organometallics* **1996**, *15*, 449–451.

42. Cabeza, J. A.; Fernandez-Colinas, J. M.; Garcia-Granda, S.; Llamazares, A.; Lopez-Ortiz, F.; Riera, V.; Van der Maelen, J. F. *Organometallics* **1994**, *13*, 426–428.
43. Cabeza, J. A.; del Rio, I.; Fernandez-Colinas, J. M.; Llamazares, A.; Riera, V. *J. Organomet. Chem.* **1995**, *494*, 169–177.
44. Campagnola, D.; Giordano, R.; Sappa, E. *J. Cluster Sci.* **1998**, *9*, 487–504.
45. Kallinen, K. O.; Pakkanen, T. T.; Pakkanen, T. A. *J. Mol. Catal. A: Chemical* **1995**, *99*, 29–33.
46. Giordano, R.; Sappa, E.; Knox, S. A. R. *J. Cluster Sci.* **1996**, *7*, 179–190.
47. Campagnola, D.; Castiglioni, M.; Dastru, W.; Deabate, S.; Giordano, R.; King, P. J.; Sappa, E. *Inorg. Chim. Acta* **1997**, *262*, 157–165.
48. Bonelli, B.; Brait, S.; Deabate, S.; Garrone, E.; Giordano, R.; Sappa, E.; Verre, F. *J. Cluster Sci.* **2000**, *11*, 307–326.
49. Allasia, C.; Castiglioni, M.; Giordano, R.; Sappa, E.; Verre, F. *J. Cluster Sci.* **2000**, *11*, 493–509.
50. Dallmann, K.; Buffon, R. *J. Mol. Catal. A: Chemical* **2002**, *185*, 187–194.
51. Xiao, F.-S.; Ichikawa, M. *J. Mol. Catal. A: Chemical* **1996**, *113*, 427–444.
52. Adams, R. D.; Captain, B.; Zhu, L. *J. Amer. Chem. Soc.* **2004**, *126*, 3042–3043.
53. Castiglioni, M.; Deabate, S.; Giordano, R.; King, P. J.; Knox, S. A. R.; Sappa, E. *J. Organomet. Chem.* **1998**, *571*, 251–260.
54. Blazina, D.; Duckett, S. B.; Dyson, P. J.; Lohman, J. A. B. *J. Chem. Soc., Dalton Trans.* **2004**, 2108–2114.
55. Campagnola, D.; Deabate, S.; Giordano, R.; Sappa, E. *J. Cluster Sci.* **1998**, *9*, 205–222.
56. Nakajima, Y.; Suzuki, H. *Organometallics* **2005**, *24*, 1860–1866.
57. Izumi, Y.; Chihara, T.; Yamazaki, H.; Iwasawa, Y. *J. Chem. Soc., Dalton Tran.* **1993**, 3667–3673.
58. Chihara, T.; Yamazaki, H. *J. Organomet. Chem.* **1994**, *473*, 273–284.
59. Tominaga, K.; Sasaki, Y.; Watanabe, T.; Saito, M. *Bull. Chem. Soc. Jpn* **1995**, *68*, 2837–2842.
60. Gobetto, R.; Milone, L.; Reineri, F.; Salassa, L.; Viale, A.; Rosenberg, E. *Organometallics* **2002**, *21*, 1919–1924.
61. Frediani, P.; Salvini, A.; Finocchiaro, S. *J. Organomet. Chem.* **1999**, *584*, 265–273.
62. Moura, F. C. C.; dos Santos, E. N.; Lago, R. M.; Vargas, M. D.; Araujo, M. H. *J. Mol. Catal. A: Chemical* **2005**, *226*, 243–251.
63. Akioka, T.; Inoue, Y.; Yanagawa, A.; Hiyamizu, M.; Takagi, Y.; Sugimori, A. *J. Mol. Catal. A: Chemical* **2003**, *202*, 31–39.
64. Kaneda, K.; Mizugaki, T. *Organometallics* **1996**, *15*, 3247–3249.
65. Mizugaki, T.; Ebitani, K.; Kaneda, K. *Appl. Surf. Sci.* **1997**, *121/122*, 360–365.
66. Tsoy, A. A.; Korneeva, G. A.; Kayumov, F. F.; Grudtsyn, Yu. D.; Slivinskii, E. V.; Yur'ev, V. P.; Kaverin, V. V. *Izv. Akad. Nauk Ser. Khim.* **1993**, 1388–1393.
67. Don, M.; Chien, H.; Richmond, M. G. *J. Mol. Catal.* **1994**, *88*, 133–139.
68. Yang, K.; Chien, H.; Richmond, M. G. *J. Mol. Catal.* **1994**, *88*, 159–166.
69. Della Pergola, R.; Garlaschelli, L.; Martinengo, S.; Repossi, A. *J. Mol. Catal. A: Chemical* **1997**, *115*, 265–271.
70. Moasser, B.; Gladfelter, W. L. *Inorg. Chim. Acta* **1996**, *242*, 125–136.
71. Evrard, D.; Groison, K.; Mugnier, Y.; Harvey, P. D. *Inorg. Chem* **2004**, *43*, 790–796.
72. Ferrand, V.; Suss-Fink, G.; Neels, A.; Stoeckli-Evans, H. *J. Chem. Soc., Dalton Trans.* **1998**, 3825–3832.
73. Castiglioni, M.; Giordano, R.; Sappa, E. *J. Organomet. Chem.* **1995**, *491*, 111–120.
74. Giordano, R.; Sappa, E. *J. Organomet. Chem.* **1993**, *448*, 157–166.
75. Adams, R. D.; Barnard, T. S.; Li, Z.; Wu, W.; Yamamoto, J. *J. Amer. Chem. Soc.* **1994**, *116*, 9103–9113.
76. Zhao, D.; Dyson, P. J.; Laurenczy, G.; McIndoe, J. S. *J. Mol. Catal. A: Chemical* **2004**, *214*, 19–25.
77. Blum, J.; Gelman, F.; Abu-Reziq, R.; Miloslavski, I.; Schumann, H.; Avnir, D. *Polyhedron* **2000**, *19*, 509–512.
78. Muetterties, E. L.; Rhodin, T. N.; Band, E.; Brucker, C. F.; Pretzer, W. R. *Chem Rev.* **1979**, *79*, 91–137.
79. Moskovits, M. *J. Mol. Catal.* **1993**, *82*, 195–209.
80. Gates, B. C. *Angew. Chem.* **1993**, *105*, 240–241.
81. Bradshaw, A. M. NATO ASI Series, Series C: Mathematical and Physical Sciences, 465 (*Synergy between Dynamics and Reactivity at Clusters and Surfaces*); Kluwer: Dordrecht, Holland, 1995; pp 1–20.
82. Mingos, D. M. P. *J. Cluster Sci.* **1992**, *3*, 397–409.
83. Brait, S.; Deabate, S.; Knox, S. A. R.; Sappa, E. *J. Cluster Sci.* **2001**, *12*, 139–174.
84. Shriver, D. F. *J. Cluster Sci.* **1992**, *3*, 459–467.
85. Wang, N.; Xu, X.; Zhang, Q. *THEOCHEM* **1992**, *94*, 105–116.
86. Diana, E.; Rossetti, R.; Stanghellini, P. L. *J. Cluster Sci.* **1993**, *4*, 19–32.
87. Kawano, M.; Bacon, J. W.; Campana, C. F.; Winger, B. E.; Dudek, J. D.; Sirchio, S. A.; Scruggs, S. L.; Geiser, U.; Dahl, L. F. *Inorg. Chem* **2001**, *40*, 2554–2569.
88. Brown, D. B.; Johnson, B. F. G.; Martin, C. M.; Wheatley, A. E. H. *J. Chem. Soc., Dalton Trans.* **2000**, 2055–2060.
89. Wong, W.; Chan, S.; Wong, W. *J. Chem. Soc., Dalton Trans.* **1995**, 1497–1509.
90. Akita, M.; Noda, K.; Takahashi, Y.; Moro-oka, Y. *Organometallics* **1995**, *14*, 5209–5220.
91. Guzyr, O. I.; Prust, J.; Roesky, H. W.; Lehmann, C.; Teichert, M.; Cimpoesu, F. *Organometallics* **2000**, *19*, 1549–1555.
92. Johnson, B. F. G.; Lewis, J.; Gallup, M.; Martinelli, M. *Faraday Discussions* **1991**, *92*(Chem. Phys. Small Met. Part.), 241–254.
93. Gallop, M. A.; Gomez-Sal, M. P.; Housecroft, C. E.; Johnson, B. F. G.; Lewis, J.; Owen, S. M.; Raithby, P. R.; Wright, A. H. *J. Am. Chem. Soc.* **1992**, *114*, 2502–2509.
94. Roth, J. D.; Lewis, G. J.; Safford, L. K.; Jiang, X.; Dahl, L. F.; Weaver, M. J. *J. Am. Chem. Soc.* **1992**, *114*, 6159–6169.
95. Gates, B. C. In *Catalysis by Di- and Polynuclear Metal Cluster Complexes*; Adams, R. D., Cotton, F. A., Eds.; Wiley-VCH: New York, 1998; pp 509–538.
96. Braunstein, Pierre; Rose, Jacky In *Catalysis by Di- and Polynuclear Metal Cluster Complexes*; Adams, R. D., Cotton, F. A., Eds.; Wiley-VCH: New York, 1998; pp 443–508.
97. Gates, B. C. In *Preparation of Solid Catalysts*; Ertl, G., Knoezinger, H., Weitkamp, J., Eds.; Wiley-VCH Verlag GmbH: Weinheim, 1999; pp 371–388.
98. Gates, B. C. *Chem. Rev.* **1995**, *95*, 511–522.
99. Sachtler, W. M. H. *Acc. Chem. Res.* **1993**, *26*, 383–387.
100. Hermans, S.; Khimyak, T.; Raja, R.; Sankar, G.; Thomas, J. M.; Johnson, B. F. G. In *Nanotechnology in Catalysis*; Zhou, B., Hermans, S., Somorjai, G. A., Eds.; Kluwer /Plenum: New York, 2004; Vol. 1, pp 33–49.
101. Johnson, B. F. G. *Top. Catal.* **2003**, *24*, 147–159.
102. Alexeev, O. S.; Gates, B. C. *Ind. Eng. Chem. Res.* **2003**, *42*, 1571–1587.

103. Gates, B. C. *J. Mol. Catal. A: Chemical* **2000**, *163*, 55–65.
104. Alexeev, O.; Gates, B. C. *Top. Catal.* **2000**, *10*, 273–293.
105. Gates, B. C. Supported Metal Cluster Catalysts. In *Preparation of Solid Catalysts*; Ertl, G., Knoezinger, H., Weitkamp, J., Eds.; Wiley-VCH Verlag GmbH: Weinheim, 1999; pp 371–388.
106. Lewis, L. N *Chem. Rev.* **1993**, *93*, 2693–2730.
107. Kou, Y.; Wang, H.; Te, M.; Tanaka, T.; Nomura, M. *J. Catal.* **1993**, *141*, 660–670.
108. Yunusov, S. M.; Likholobov, V. A.; Shur, V. B. *Appl. Catal., A: General* **1997**, *158*, L35–L39.
109. Cabeza, J. A.; Fernandez-Colinas, J. M.; Choplin, A.; Theolier, A. *Inorg. Chim. Acta* **1995**, *237*, 103–109.
110. Moggi, P.; Predieri, G.; Di Silvestri, F.; Ferretti, A. *Appl. Catal., A: General* **1999**, *182*, 257–265.
111. Izumi, Y.; Aika, K. *J. Phys. Chem.* **1995**, *99*, 10336–10345.
112. Izumi, Y.; Aika, K. *J. Phys. Chem.* **1995**, *99*, 10346–10353.
113. Kiviaho, J.; Niemelae, M. K.; Reinikainen, M.; Vaara, T.; Pakkanen, T. A. *J. Mol. Catal. A: Chemical* **1997**, *121*, 1–8.
114. Weber, W. A.; Phillips, B. L.; Gates, B. C. *Chem. Eur. J* **1999**, *5*, 2899–2913.
115. Weber, W. A.; Gates, B. C. *Precious Metals* **1997**, Proceedings of the 21st Conference in San Francisco, 187–201.
116. Bhirud, V.; Goellner, J. F.; Argo, A. M.; Gates, B. C. *J. Phys. Chem. B* **2004**, *108*, 9752–9763.
117. Argo, A. M.; Gates, B. C. *J. Phys. Chem. B* **2003**, *107*, 5519–5528.
118. Gates, B. C. *J. Mol. Catal. A: Chemical* **2000**, *163*, 55–65.
119. Xu, Z.; Xiao, F.-S.; Purnell, S. K.; Alexeev, O.; Kawi, S.; Deutsch, S. E.; Gates, B. C. *Nature* **1994**, *372*, 346–348.
120. Alexeev, O.; Panjabi, G.; Gates, B. C. *J. Catal.* **1998**, *173*, 196–209.
121. Zhao, A.; Gates, B. C. *J. Catal.* **1997**, *168*, 60–69.
122. Xiao, F.-S.; Weber, W. A.; Alexeev, O.; Gates, B. C. *Stud. Surf. Sci. Catal.* **1996**, *101*, (Pt. B, 11th International Congress on Catalysis–40th Anniversary, 1996, Pt. B), 1135–1144.
123. Alexeev, O.; Gates, B. C. *J. Catal.* **1998**, *176*, 310–320.
124. Zhao, A.; Gates, B. C. *J. Am. Chem. Soc.* **1996**, *118*, 2458–2469.
125. Alexeev, O. S.; Kim, D.-W.; Gates, B. C. *J. Mol. Catal. A: Chemical* **2000**, *162*, 67–82.
126. Deutsch, S. E.; Xiao, F.-S.; Gates, B. C. *J. Catal.* **1997**, *170*, 161–167.
127. Zhao, A.; Jentoft, R. E.; Gates, B. C. *J. Catal.* **1997**, *169*, 263–274.
128. Argo, A. M.; Odzak, J. F.; Lai, F. S.; Gates, B. C. *Nature* **2002**, *415*, 623–626.
129. Panjabi, G.; Argo, A. M.; Gates, B. C. *Chem. Eur. J.* **1999**, *5*, 2417–2423.
130. Argo, A. M.; Gates, B. C. *Langmuir* **2002**, *18*, 2152–2157.
131. Argo, A. M.; Odzak, J. F.; Gates, B. C. *J. Am. Chem. Soc.* **2003**, *125*, 7107–7115.
132. Weber, W. A.; Zhao, A.; Gates, B. C. *J. Catal.* **1999**, *182*, 13–29.
133. Kawi, S.; Chang, J.-R.; Gates, B. C. *J. Catal.* **1993**, *142*, 585–601.
134. Kawi, S.; Chang, J. R.; Gates, B. C. *J. Am. Chem. Soc.* **1993**, *115*, 4830–4843.
135. Yamamoto, T.; Shido, T.; Inagaki, S.; Fukushima, Y.; Ichikawa, M. *J. Phys. Chem. B* **1998**, *102*, 3866–3875.
136. Fukuoka, A.; Osada, M.; Shido, T.; Inagaki, S.; Fukushima, Y.; Ichikawa, M. *Inorg. Chim. Acta* **1999**, *294*, 281–284.
137. Paul, H.; Basu, S.; Bhaduri, S.; Lahiri, G. K. *J. Organomet. Chem.* **2004**, *689*, 309–316.
138. Paul, H.; Bhaduri, S.; Lahiri, G. K. *Organometallics* **2003**, *22*, 3019–3021.
139. Paul, H.; Bhaduri, S.; Lahiri, G. K. *Indian J. Chem., Sect. A* **2003**, *42A*, 2392–2397.
140. Castiglioni, M.; Deabate, S.; Garrone, E.; Giordano, R.; Onida, B.; Predieri, G.; Sappa, E. *J. Cluster Sci.* **1997**, *8*, 381–405.
141. Shephard, D. S.; Maschmeyer, T.; Sankar, G.; Thomas, J. M.; Ozkaya, D.; Johnson, B. F. G.; Raja, R.; Oldroyd, R. D.; Bell, R. G. *Chem. Eur. J.* **1998**, *4*, 1214–1224.
142. Shephard, D. S.; Maschmeyer, T.; Johnson, B. F. G.; Thomas, J. M.; Sankar, G.; Ozkaya, D.; Zhou, W.; Oldroyd, R. D.; Bell, R. G. *Angew. Chem., Int. Ed.* **1997**, *36*, 2242–2245.
143. Hermans, S.; Raja, R.; Thomas, J. M.; Johnson, B. F. G.; Sankar, G.; Gleeson, D. *Angew. Chem., Int. Ed.* **2001**, *40*, 1211–1215.
144. Raja, R.; Sankar, G.; Hermans, S.; Shephard, D. S.; Bromley, S.; Thomas, J. M.; Johnson, B. F. G. *J. Chem. Soc., Chem. Commun.* **1999**, 1571–1572.
145. Kiviaho, J.; Niemela, M. K.; Reinikainen, M.; Pakkanen, T. A. *Appl. Catal., A: General* **1997**, *149*, 353–372.
146. Kiviaho, J.; Niemelae, M. K.; Morioka, Y.; Kataja, K. *Appl. Catal., A: General* **1996**, *144*, 93–109.
147. Kiviaho, J.; Reinikainen, M.; Niemelae, M. K.; Kataja, K.; Jaeaeskelaeinen, S. *J. Mol. Catal. A: Chemical* **1996**, *106*, 187–195.
148. Reinikainen, M.; Kiviaho, J.; Kroeger, M.; Niemelae, M.; Jaeaeskelaeinen, S. *J. Mol. Catal. A: Chemical* **1997**, *118*, 137–144.
149. Kovalchuk, V. I.; Mikova, N. M.; Chesnokov, N. V.; Naimushina, L. V.; Kuznetsov, B. N. *J. Mol. Catal. A: Chemical* **1996**, *107*, 329–337.
150. Kalenik, Z.; Ladna, B.; Wolf, E. E.; Fehlner, T. P. *Chem. Mater.* **1993**, *5*, 1247–1252.
151. Banares, M. A.; Laurent, D.; Calvo-Perez, V.; Fehlner, T. P.; Wolf, E. E *J. Catal.* **1995**, *152*, 396–409.
152. Banares, M.; Patil, A. N.; Fehlner, T. P.; Wolf, E. E. *Catal. Lett.* **1995**, *34*, 251–258.
153. Banares, M. A.; Dauphin, L.; Lei, X.; Cen, W.; Shang, M.; Wolf, E. E.; Fehlner, T. P. *Chem. Mater.* **1995**, 7, 553–561.
154. Lei, X.; Shang, M.; Patil, A.; Wolf, E. E.; Fehlner, T. P. *Inorg. Chem* **1996**, *35*, 3217–3222.
155. Alexeev, O.; Shelef, M.; Gates, B. C. *J. Catal.* **1996**, *164*, 1–15.
156. Yuan, Y.; Asakura, K.; Wan, H.; Tsai, K.; Iwasawa, Y. *J. Mol. Catal. A: Chemical* **1997**, *122*, 7147–7157.
157. Yuan, Y.; Asakura, K.; Wan, H.; Tsai, K.; Iwasawa, Y. *Chem. Lett.* **1996**, 129–130.
158. de Jongh, L. J. *Appl. Organomet. Chem.* **1998**, *12*, 393–399.
159. Schmid, G. *J. Chem. Soc., Dalton Trans.* **1998**, 1077–1082.
160. Ichikawa, M. In *Metal Clusters in Chemistry*; Braunstein, P., Oro, L. A., Raithby, P. R., Eds.; Wiley-VCH Verlag GmbH: Weinheim, Germany, 1999; Vol. 3, pp 1273–1301.
161. Schmid, G.; Hornyak, G. L. *Curr. Opin. Solid State Mater. Sci.* **1997**, *2*, 204–212.
162. Johnson, B. F. G. *Coord. Chem. Revs.* **1999**, *190–192*, 1269–1285.
163. Schoen, G.; Simon, U. *Colloid Polym. Sci.* **1995**, *273*, 101–117.
164. Schoen, G.; Simon, U. *Colloid Polym. Sci.* **1995**, *273*, 202–218.
165. Clarke, L.; Wybourne, M. N.; Yan, Mingdi; Cai, S. X.; Keana, J. F. W. *Appl. Phys. Lett.* **1997**, *71*, 617–619.
166. Tran, N. T.; Kawano, M.; Powell, D. R.; Dahl, L. F. *J. Amer. Chem. Soc.* **1998**, *120*, 10986–10987.

167. Frey, P. A.; Frey, T. G. *J. Struct. Biol.* **1999**, *127*, 94–100.
168. Zlotnick, A.; Cheng, N.; Stahl, S. J.; Conway, J. F.; Steven, A. C.; Wingfield, P. T. *Proc. Natl. Acad. Sci.* **1997**, *94*, 9556–9561.
169. Cheng, N.; Conway, J. F.; Watts, N. R.; Hainfeld, J. F.; Joshi, V.; Powell, R. D.; Stahl, S. J.; Wingfield, P. E.; Steven, A. C. *J. Struct. Biol.* **1999**, *127*, 169–176.
170. Schmid, G. In *Physics and Chemistry of Metal Cluster Compounds (Springer Series in Physics and Chemistry of Materials with Low-Dimensional Structures 18)*; de Jongh, L. J., Ed.; Springer: Berlin, Germany, 1994; pp 107–134.
171. Wall, J. S. *J.Struct. Biol.* **1999**, *127*, 161–168.
172. Powell, R. D.; Halsey, C. M. R.; Liu, W.; Joshi, V. N.; Hainfeld, J. F. *J. Struct. Biol.* **1999**, *127*, 177–184.
173. Thygesen, J.; Weinstein, S.; Franceschi, F.; Yonath, A. *Struct.* **1996**, *4*, 513–518.
174. Weinstein, S.; Jahn, W.; Glotz, C.; Schlunzen, F.; Levin, I.; Janell, D.; Harms, J.; Kolln, I.; Hansen, H. A. S.; Gluhmann, M., *et al. J. Struct. Biol.* **1999**, *127*, 41–151.
175. Yu, S.; Watson, A. D. *Chem. Rev.* **1999**, *99*, 2353–2377.
176. Mullan, B. F.; Madsen, M. T.; Messerle, L.; Kolesnichenko, V.; Kruger, J. *Acad. Radiol.* **2000**, *7*, 254–259.
177. Yu, S.; Droege, M.; Downey, S.; Segal, B.; Newcomb, W.; Sanderson, T.; Crofts, S.; Suravajjala, S.; Bacon, E.; Earley, W., *et al. Inorg. Chem.* **2001**, *40*, 1576–1581.
178. Yu, S.-B.; Droege, M.; Segal, B.; Downey, S.; Sanderson, T.; Fellmann, J.; Watson, A. *Inorg. Chim. Acta* **1997**, *263*, 61–67.
179. Allardyce, C. S.; Dyson, P. J. *J. Cluster Sci.* **2001**, *12*, 563–569.
180. Perry, J. W. In *Nonlinear Optics of Organic Molecules and Polymers*; Nalwa, H. S., Miyata, S., Eds.; CRC: Boca Raton, 1997; pp 813–840.
181. Kreibig, U.; Vollmer, M. *Optical Properties of Metal Clusters*; (Springer Series in Materials Science); Springer; Berlin, 1995; Vol. 25.
182. Coe, B. J. In *Comprehensive Coordination Chemistry II*; McCleverty, J. A., Meyer, T. J., Eds.; Elsevier: Oxford, 2004; Vol. 9, pp 621–687.
183. Zhang, H.; Zelmon, D. E.; Deng, L.; Liu, H.; Teo, B. K. *J. Am. Chem. Soc.* **2001**, *123*, 11300–11301.
184. Yang, G. Y.; Ang, S. G.; Chng, L. L.; Lee, Y. W.; Lau, E. W.-P.; Lai, K. S.; Ang, H. G. *Chem. Eur. J.* **2003**, *9*, 900–904.
185. Lucas, N. T.; Notaras, E. G. A.; Humphrey, M. G.; Samoc, M.; Luther-Davies, B. *Proc. SPIE-The International Society for Optical Engineering* **2000**, *5212*, 318–325.
186. Mathur, P.; Chatterjee, S.; Singh, B. P.; Kundu, T.; Trivedi, R.; Umbarkar, S. B.; Scheer, M. *J. Cluster Sci.* **2004**, *15*, 13–18.
187. Philip, R.; Kumar, G. R.; Mathur, P.; Ghose, S. *Opt. Commun.* **2000**, *178*, 469–475.
188. Philip, R.; Kumar, G. R.; Mathur, P.; Ghosh, S. *Chem. Phys. Lett.* **1999**, *313*, 719–724.
189. Mathur, P.; Ghose, S.; Hossain, M. M.; Satyanarayana, C. V. V.; Chadha, R. K.; Banerjee, S.; Kumar, G. R. *J. Organomet. Chem.* **1998**, *568*, 197–204.
190. Mathur, P.; Ghose, S.; Hossain, M. M.; Satyanarayana, C. V. V.; Banerjee, S.; Kumar, G. R.; Hitchcock, P. B.; Nixon, J. F. *Organometallics* **1997**, *16*, 3815–3818.
191. Yao, W.-R.; Guo, D.-S.; Liu, Z.-H.; Zhang, Q.-F. *J. Mol. Struct.* **2003**, *657*, 165–175.
192. Zhuang, B.; Sun, H.; He, L.; Zhou, Z.; Lin, C.; Wu, K.; Huang, Z. *J. Organomet. Chem.* **2002**, *655*, 233–238.
193. Wu, K.; Chen, X.; Snijders, J. G.; Sa, R.; Lin, C.; Zhuang, B. *J. Cryst. Growth* **2002**, *237–239* (Pt. 1), 663–667.
194. Xiong, Y.; Zhang, Q.; Xin, X.; Ji, W. *Proc. SPIE-The International Society for Optical Engineering* **1999**, *3899*, 483–488.
195. Wu, X.; Wang, Q.; Shi, S. *Polyhedron* **1997**, *16*, 945–948.
196. Wang, Y.; Song, Y.-L.; Lappert, M. F.; Xin, X.-Q.; Usman, A.; Fun, H.-K.; Zheng, H.-G. *Inorg. Chim. Acta* **2005**, *358*, 2217–2223.
197. Song, Y.; Qu, S.; Wang, Y.; Zhang, Q.; Xin, X. *Chem. Phys. Lett.* **2001**, *338*, 108–112.
198. Long, D.-L.; Shi, S.; Xin, X.-Q.; Luo, B.-S.; Chen, L-R.; Huang, X.-Y.; Kang, B.-S. *J. Chem. Soc., Dalton Trans.* **1996**, 2617–2622.
199. Zhang, Q-F.; Leung, W.-H.; Xin, X.-Q.; Fun, H.-K. *Inorg. Chem* **2000**, *39*, 417–426.
200. Ji, W.; Shi, S.; Du, H. J.; Ge, P.; Tang, S. H.; Xin, X. Q. *J. Phys. Chem.* **1995**, *99*, 17297–17301.
201. Zhou, J.-L.; Song, Y.-L.; Mo, H.-B.; Li, Y.-Z.; Zheng, H.-G.; Xin, X.-Q. *Z. Anorg. Allg. Chem.* **2005**, *631*, 182–186.
202. Lang, J.-P.; Yu, H.; Ji, S.-J.; Sun, Z.-R. *Phys. Chem. Chem. Phys.* **2003**, *5*, 5127–5132.
203. Niu, Y.-Y.; Chen, T.-N.; Liu, S.-X.; Song, Y.-L.; Wang, Y.-X.; Xue, Z.-L.; Xin, X.-Q. *J. Chem. Soc., Dalton Tran.* **2002**, 1980–1984.
204. Cai, Y.; Song, Y.; Zheng, H.; Niu, Y.; Du, C.; Xin, X. *Chem. Lett.* **2002**, 508–509.
205. Shi, S.; Hou, H. W.; Xin, X. Q. *J. Phys. Chem.* **1995**, *99*, 4050–4053.
206. Shi, S.; Ji, W.; Xie, W.; Chong, T. C.; Zeng, H. C.; Lang, J. P.; Xin, X. Q. *Mater. Chem. Phys.* **1995**, *39*, 298–303.
207. Song, Y.; Zhang, C.; Wang, Y.; Fang, G.; Jin, G.; Liu, S.; Chen, L.; Xin, X. *Opt. Mater.* **2000**, *15*, 187–190.
208. Hou, H.; Zheng, H.; Ang, H. G.; Fan, Y.; Low, M. K. M.; Zhu, Y.; Wang, W.; Xin, X.; Ji, W.; Wong, W.-T. *J. Chem. Soc., Dalton Trans.* **1999**, 2953–2957.
209. Zhang, C.; Song, Y.; Xu, Y.; Jin, G.; Fang, G.; Wang, Y.; Fun, H.; Xin, X. *Inorg. Chim. Acta* **2000**, *311*, 25–32.
210. Cai, Y.; Zheng, H.; Li, Y.; Zhou, J.; Song, Y.; Xin, X. *J. Coord. Chem.* **2003**, *56*, 595–601.
211. Zeng, D.; Ji, W.; Wong, W.-T.; Wong, W.-Y.; Xin, X.-Q. *Inorg. Chim. Acta* **1998**, *279*, 172–177.
212. Hou, H.; Ang, H. G.; Ang, S. G.; Fan, Y.; Low, M. K. M.; Ji, W.; Lee, Y. W. *Inorg. Chim. Acta* **2000**, *299*, 147–154.
213. Zhang, Q.-F.; Xiong, Y.-N.; Lai, T.-S.; Ji, W.; Xin, X.-Q. *J. Phys. Chem. B* **2000**, *104*, 3446–3449.
214. Tan, W.; Zheng, H.; Jin, Q.; Jin, G.; Ji, W.; Long, D.; Xin, X. *Polyhedron* **2000**, *19*, 1545–1549.
215. Zhou, J.-L.; Li, Y.-Z.; Zheng, H.-G.; Xin, X.-Q.; Yin, T.; Wang, Y.-X.; Song, Y.-L. *Transition Met. Chem.* **2004**, *29*, 185–188.
216. Hou, H.; Ye, X.; Xin, X.; Liu, J.; Chen, M.; Shi, S. *Chem. Mater.* **1995**, *7*, 472–476.
217. Cai, Y.; Ma, M.-H.; Zheng, H.-G.; Xin, X.-Q.; Usman, A.; Fun, H.-K.; Song, Y.-L. *Transition Met. Chem.* **2003**, *28*, 137–141.
218. Zheng, H.-G.; Tan, W.-L.; Low, M. K. L.; Ji, W.; Long, D.-L.; Wong, W.-T.; Yu, K.-B.; Xin, X.-Q. *Polyhedron* **1999**, *18*, 3115–3121.
219. Zhang, C.; Song, Y.-L.; Jin, G.-C.; Wang, Y.-X.; Pan, T.; Xin, X.-Q. *J. Coord. Chem.* **2002**, *55*, 33–42.
220. Lang, J.-P.; Sun, Z.-R.; Xu, Q.-F.; Yu, H.; Tatsumi, K. *Mater. Chem. Phys.* **2003**, *82*, 493–498.
221. Chen, Z. R.; Hou, H. W.; Xin, X. Q.; Yu, K. B.; Shi, S. *J. Phys. Chem.* **1995**, *99*, 8717–8721.
222. Shi, S.; Zhang, X.; Shi, X. F. *J. Phys. Chem.* **1995**, *99*, 14911–14914.
223. Zhang, C.; Song, Y.; Jin, G.; Fang, G.; Wang, Y.; Raj, S. S. S.; Fun, H.-K.; Xin, X. *J. Chem. Soc., Dalton Trans.* **2000**, 1317–1323.
224. Zhang, C.; Song, Y.; Xu, Y.; Fun, H.; Fang, G.; Wang, Y.; Xin, X. *J. Chem. Soc., Dalton Trans.* **2000**, 2823–2829.
225. Zheng, H.-G.; Tan, W.-L.; Ji, W.; Leung, W.-H.; Williams, I. D.; Long, D.-L.; Huang, J.-S.; Xin, X.-Q. *Inorg. Chim. Acta* **1999**, *294*, 73–78.
226. Zhang, W.-H.; Chen, J.-X.; Li, H.-X.; Wu, B.; Tang, X.-Y.; Ren, Z.-G.; Zhang, Y.; Lang, J.-P.; Sun, Z.-R. *J. Organomet. Chem.* **2005**, *690*, 394–402.
227. Song, Y.; Zhang, C.; Wang, Y.; Fang, G.; Jin, G.; Chang, C.; Liu, S.; Xin, X.; Ye, H. *Chem. Phys. Lett.* **2000**, *326*, 341–343.

228. Zheng, H.; Zhou, J.; Lappert, M. F.; Song, Y.; Li, Y.; Xin, X. *Eur. J. Inorg. Chem.* **2004**, 2754–2758.
229. Hou, H.; Long, D.; Xin, X.; Huang, X.; Kang, B.; Ge, P.; Ji, W.; Shi, S. *Inorg. Chem* **1996**, *35*, 5363–5367.
230. Niu, Y.-Y.; Song, Y.-L.; Zheng, H.-G.; Long, D.-L.; Fun, H.-K.; Xin, X.-Q. *New J. Chem.* **2001**, *25*, 945–948.
231. Zheng, H.; Leung, W.-H.; Tan, W.; Long, D.; Ji, W.; Chen, J.; Xin, F.; Xin, X. *J. Chem. Soc., Dalton Trans.* **2000**, 2145–2149.
232. Lucenti, E.; Cariati, E.; Dragonetti, C.; Manassero, L.; Tessore, F. *Organometallics* **2004**, *23*, 687–692.
233. Harvey, P. D. *Macromol. Symp.* **2004**, *209*, 81–95.
234. Vitale, M.; Ford, P. C. *Coord. Chem. Rev.* **2001**, *219–221*, 3–16.
235. Ford, P. C.; Cariati, E.; Bourassa, J. *Chem. Rev.* **1999**, *99*, 3625–3647.
236. Yam, V. W.-W.; Lo, K. K.-W.; Fung, W. K.-M.; Wang, C.-R. *Coord. Chem. Rev.* **1998**, *171*, 17–41.
237. Zhang, T.; Drouin, M.; Harvey, P. D. *Inorg. Chem* **1999**, *38*, 957–963.
238. Zhang, T.; Drouin, M.; Harvey, P. D. *Inorg. Chem* **1999**, *38*, 4928–4936.
239. Fornies, J.; Gomez, J.; Lalinde, E.; Moreno, M. T. *Inorg. Chem* **2001**, *40*, 5415–5419.
240. Ara, I.; Fornies, J.; Gomez, J.; Lalinde, E.; Moreno, M. T. *Organometallics* **2000**, *19*, 3137–3144.
241. Wang, Q.-M.; Lee, Y.-A.; Crespo, O.; Deaton, J.; Tang, C.; Gysling, H. J.; Gimeno, M. C.; Larraz, C.; Villacampa, M. D.; Laguna, A.; Eisenberg, R. *J. Am. Chem. Soc.* **2004**, *126*, 9488–9489.
242. Lebedkin, S.; Langetepe, T.; Sevillano, P.; Fenske, D.; Kappes, M. M. *J. Phys. Chem. B* **2002**, *106*, 9019–9026.
243. Catalano, V. J.; Kar, H. M.; Garnas, J. *Angew. Chem., Int. Ed.* **1999**, *38*, 1979–1982.
244. Fu, W.-F.; Gan, X.; Che, C.-M.; Cao, Q.-Y.; Zhou, Z.-Y.; Zhu, N. N.-Y. *Chem. Eur. J.* **2004**, *10*, 2228–2236.
245. Link, S.; Beeby, A.; FitzGerald, S.; El-Sayed, M. A.; Schaaff, T. G.; Whetten, R. L. *J. Phys. Chem. B* **2002**, *106*, 3410–3415.
246. Lee, D.; Donkers, R. L.; Wang, G.; Harper, A. S.; Murray, R. W. *J. Am. Chem. Soc.* **2004**, *126*, 6193–6199.
247. Wei, Q.-H.; Yin, G.-Q.; Zhang, L.-Y.; Shi, L.-X.; Mao, Z.-W.; Chen, Z.-N. *Inorg. Chem* **2004**, *43*, 3484–3491.
248. Chen, Z.-N.; Yoshimura, T.; Abe, M.; Tsuge, K.; Sasaki, Y.; Ishizaka, S.; Kim, H.-B.; Kitamura, N. *Chem. Eur. J.* **2001**, *7*, 4447–4455.
249. Wong, W.-Y.; Choi, K.-H.; Lin, Z. *Eur. J. Inorg. Chem.* **2002**, 2112–2120.
250. Chen, J.-X.; Xu, Q.-F.; Zhang, Y.; Chen, Z.-N.; Lang, J.-P. *J. Organomet. Chem.* **2004**, *689*, 1071–1077.
251. Wang, C.-F.; Peng, S.-M.; Chan, C.-K.; Che, C.-M. *Polyhedron* **1996**, *15*, 1853–1858.
252. Yam, V. W.-W.; Lo, K. K.-W.; Wang, C.-R.; Cheung, K.-K. *Inorg. Chem* **1996**, *35*, 5116–5117.
253. Wang, C.-R.; Lo, K. K.-W.; Yam, V. W.-W. *Chem. Phys. Lett.* **1996**, *262(1,2)*, 91–96.
254. Ara, I.; Fornies, J.; Gomez, J.; Lalinde, E.; Merino, R. I.; Moreno, M. T. *Inorg. Chem. Commun.* **1999**, *2*, 62–65.
255. Fernandez, E. J.; Lopez-de-Luzuriaga, J. M.; Monge, M.; Olmos, M. E.; Perez, J.; Laguna, A. *J. Am. Chem. Soc.* **2002**, *124*, 5942–5943.
256. Che, C. M.; Yip, H. K.; Lo, W. C.; Peng, S. M. *Polyhedron* **1994**, *13*, 887–890.
257. Mohamed, A. A.; Lopez-de-Luzuriaga, J. M.; Fackler, J. P., Jr. *J. Cluster Sci.* **2003**, *14*, 61–70.
258. Calhorda, M. J.; Crespo, O.; Gimeno, M. C.; Jones, P. G.; Laguna, A.; Lopez-de-Luzuriaga, J. M.; Perez, J. L.; Ramon, M. A.; Veiros, L. F. *Inorg. Chem* **2000**, *39*, 4280–4285.
259. Chen, J.; Mohamed, A. A.; Abdou, H. E.; Bauer, J. A. K.; Fackler, J. P., Jr.; Bruce, A. E.; Bruce, M. R. M. *J. Chem. Soc., Chem. Commun.* **2005**, 1575–1577.
260. Chen, J.; Mohamed, A. A; Abdou, H. E; Bauer, J. A. K.; Fackler, J. P., Jr.; Bruce, A. E.; Bruce, M. R. M. *J. Chem. Soc.,Chem. Commun.* **2005**, 1575–1577.
261. Hung-Fai Chong, S.; Chan-Fung Lam, S.; Ko, C.-C.; Wing-Wah Yam, V. *J. Cluster Sci.* **2004**, *15*, 301–314.
262. Provencher, R.; Harvey, P. D. *Inorg. Chem* **1996**, *35*, 2235–2241.
263. Yam, V. W.-W.; Fung, W. K.-M.; Wong, K. M.-C.; Lau, V. C.-Y.; Cheung, K.-K. *J. Chem. Soc., Chem. Commun.* **1998**, 777–778.
264. Hu, S.; Tong, M.-L. *J. Chem. Soc., Dalton Trans.* **2005**, 1165–1167.
265. Tran, D.; Bourassa, J. L.; Ford, P. C. *Inorg. Chem* **1997**, *36*, 439–442.
266. Lindsay, E.; Ford, P. C. *Inorg. Chim. Acta* **1996**, *242*, 51–56.
267. Chan, W.-H.; Zhang, Z.-Z.; Mak, T. C. W.; Che, C.-M. *J. Organomet. Chem.* **1998**, *556*, 169–172.
268. Hu, S.; Tong, M.-L. *J. Chem. Soc., Dalton Trans.* **2005**, 1165–1167.
269. Yam, V. W.-W.; Lo, K. K.-W.; Wang, C.-R.; Cheung, K.-K. *J. Phys. Chem. A* **1997**, *101*, 4666–4672.
270. Ryu, C. K.; Vitale, M.; Ford, P. C. *Inorg. Chem* **1993**, *32*, 869–874.
271. Xu, H.; Yip, J. H. K. *Inorg. Chem* **2003**, *42*, 4492–4494.
272. Xie, H.; Tougezaka, M.; Oishi, S.; Kinoshita, I.; Kanemoto, K.; Akai, I.; Karasawa, T. *J. Lumin.* **2004**, *108*, 91–95.
273. Xie, H.; Kinoshita, I.; Karasawa, T.; Kimura, K.; Nishioka, T.; Akai, I.; Kanemoto, K. *J. Phys. Chem. B* **2005**, *109*, 9339–9345.
274. Baxter, C. W.; Higgs, T. C.; Jones, A. C.; Parsons, S.; Bailey, P. J.; Tasker, P. A. *J. Chem. Soc., Dalton Trans.* **2002**, 4395–4401.
275. Higgs, T. C.; Parsons, S.; Bailey, P. J.; Jones, A. C.; McLachlan, F.; Parkin, A.; Dawson, A.; Tasker, P. A. *Organometallics* **2002**, *21*, 5692–5702.
276. Burini, A.; Bravi, R.; Fackler, J. P., Jr.; Galassi, R.; Grant, T. A.; Omary, M. A.; Pietroni, B. R.; Staples, R. J. *Inorg. Chem* **2000**, *39*, 3158–3165.
277. Ara, I.; Falvello, L. R.; Fornies, J.; Gomez-Cordon, J.; Lalinde, E.; Merino, R. I.; Uson, I. *J. Organomet. Chem.* **2002**, *663*, 284–288.
278. Toronto, D. V.; Balch, A. L.; Tinti, D. S. *Inorg. Chem* **1994**, *33*, 2507–2508.
279. Casas, J. M.; Falvello, L. R.; Fornies, J.; Gomez, J.; Rueda, A. *J. Organomet. Chem.* **2000**, *593–594*, 421--426.
280. Chen, Z.-N.; Yoshimura, T.; Abe, M.; Sasaki, Y.; Ishizaka, S.; Kim, H.-B.; Kitamura, N. *Angew. Chem., Int. Ed.* **2001**, *40*, 239–242.
281. Mironov, Y. V.; Shestopalov, M. A.; Brylev, K. A.; Yarovoi, S. S.; Romanenko, G. V.; Fedorov, V. E.; Spies, H.; Pietzsch, H.-J.; Stephan, H.; Geipel, G., *et al. Eur. J. Inorg. Chem.* **2005**, 657–661.
282. Bemis, J. M.; Dahl, L. F. *J. Am. Chem. Soc.* **1997**, *119*, 4545–4546.
283. Johnson, B. F. G.; Blake, A. J.; Brown, A. J.; Parsons, S.; Taylor, P. *J. Chem. Soc., Chem. Commun.* **1995**, 2117–2118.
284. Benito, M.; Rossell, O.; Seco, M.; Segales, G. *Organometallics* **1999**, *18*, 5191–5193.

12.16 Organometallic Inclusion and Intercalation Chemistry

E Monflier and F Hapiot, Université d'Artois, Lens, France
D O'Hare, University of Oxford, Oxford, UK

12.16.1 Organometallic Inclusion Chemistry

12.16.1.1 Introduction to Organometallic Inclusion Chemistry

Organometallic inclusion is defined by the formation of at least one direct metal–carbon bond in an organometallic supramolecular system consisting of a cavity-shaped host and a guest which is partially or deeply included inside the host. This area has experienced accelerated activity during the last 10 years, particularly in catalytic complexes construction. Both the syntheses and the applications of organometallic host/guest complexes have had significant impact on the understanding of the structure and reactivity of these supramolecular materials. The aim of the present review of the organometallic inclusion systems is to extensively cover the literature period between 1993 and the beginning of 2005. For convenience, relevant references prior to 1993 have been included. We shall restrict ourselves to studies in which organometallic inclusions have been well identified or are strongly suspected of existing. We will not discuss situations where the receptor was used more as a scaffold than as a true host. Owing to space limitations only representative examples of these organometallic inclusions will be presented. We discuss here supramolecular edifices constituted of an organic or organometallic guest included inside an organic, inorganic, or organometallic host, the guest being covalently bound or not to the host. This chapter is subdivided into several divisions and subdivisions. To bring up the richness of the organometallic inclusion processes, we decided to classify the supramolecular complexes according to the nature of the host molecules. Cyclodextrins are discussed first, followed by calixarenes and resorcinarenes, bioorganometallic hosts, clusters, polymers, and finally less common structures. For each supramolecular host, references to recent key papers are given to provide an entry to the literature.

12.16.1.2 Cyclodextrins

12.16.1.2.1 Introduction to cyclodextrins as supramolecular hosts

Native cyclodextrins are oligosaccharides composed of six or more D-glucopyranose residues attached by α-1,4-linkages in a cyclic array. The most current cyclodextrins contain six, seven, or eight glucose residues and are named α-cyclodextrin (α-CD), β-cyclodextrin (β-CD) and γ-cyclodextrin (γ-CD), respectively (Figure 1).[1]

The specific coupling of the glucose monomers gives a rigid conical molecular structure with a hollow interior of a specific volume (Table 1).

This internal cavity which is highly hydrophobic can accommodate a wide range of guest molecules, ranging from polar compounds such as alcohols, acids, amines, and small inorganic anions to apolar compounds such as aliphatic and aromatic hydrocarbons.[2] In all cases, the guest is bound at least partially, within the cavity of the CD. The driving forces for the inclusion complexation of CD with substrates are attributed to several factors such as van der Waals forces, hydrophobic interactions, electronic effects, and steric factors.[3]

The ability of CDs to include a part of organometallic complex into its internal hydrophobic has also been demonstrated by numerous researchers.[4–8] The inclusion modifies generally the chemical, electrochemical, and photochemical properties of organometallic compounds. Although the inclusion leads in most cases to stable compounds, it must be kept in mind that the CD can also destabilize organometallic compounds. Thus, it has been clearly demonstrated that the stability of water-soluble organometallic compounds bearing phosphine ligands strongly depends on the structure of the phosphine. While water-soluble organometallic complexes containing bis-(3-sodium sulfonatophenyl)-(4-(4-*tert*-butylphenyl)phenyl)phosphine formed stable adducts with β-CD, a ligand dissociation leading to the formation of phosphine low-coordinated species was observed with common water-soluble phosphines such as triphenylphosphine trisulfonated.[9–11] This phenomenon was attributed to the strong affinity of CD for water-soluble phosphine ligand.[12–15] In particular, it was assumed that the phosphorus donor atom located near the CD cavity is not available for coordination to a metal center due to steric crowding.

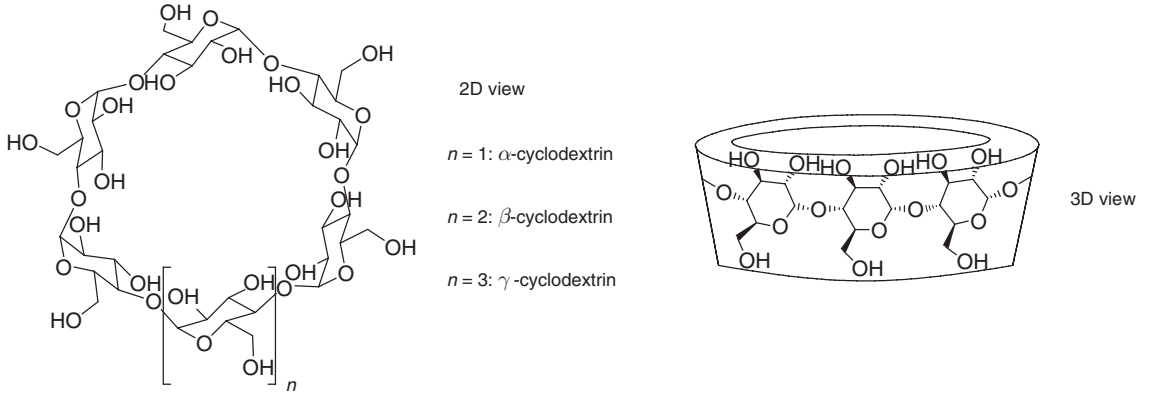

Figure 1

Table 1 Important molecular parameters of α-, β-, and γ-cyclodextrins (CDs)

Parameter	*α-CD*	*β-CD*	*γ-CD*
Glucose residues	6	7	8
Molecular weight	973	1135	1297
Cavity diameter (Å)	4.7–5.3	6–6.6	7.5–8.3
Cavity height (Å)	7.9	7.9	7.9
Cavity volume (ml mol^{-1})	174	262	472

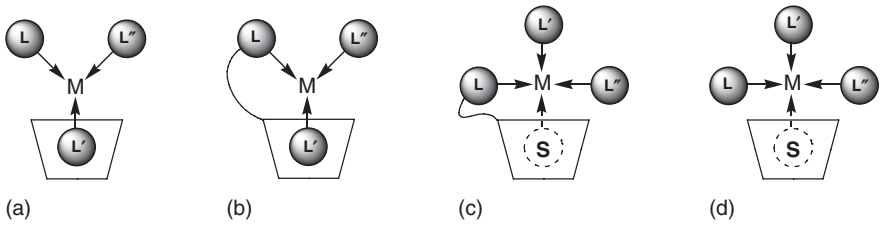

Figure 2

When the organometallic complex is not destabilized by the CD and interacts with the CD, four types of adduct can be observed:

(i) the CD behaves as a second-sphere ligand, binding non-covalently the first-sphere ligands of the metal center as schematically represented in Figure 2(a).
(ii) the CD acts simultaneously as a first- and second-sphere ligand. In fact, the CD is attached covalently to a ligand of the organometallic complex and includes another ligand of the complex into its cavity as depicted in Figure 2(b).
(iii) the CD acts simultaneously as a first-sphere ligand and as a transient second-sphere ligand. In this case, the CD is covalently connected to a ligand of the organometallic complex and temporarily includes in its cavity a substrate that reacts with the organometallic complex (Figure 2c). This type of adduct is observed in catalytic processes conducted in one-phase or two-phase systems.
(iv) the CD can be considered as a transient second-sphere ligand when a hydrophobic substrate included into the CD cavity binds temporarily to a water-soluble organometallic catalyst (Figure 2d). Contrary to the above case, these adducts form only in catalytic processes conducted in an aqueous organic two-phase medium. Indeed, the presence of water is required to force inclusion of the substrate into the CD cavity.

The characteristics and the properties of these four types of adducts will be separately discussed.

12.16.1.2.2 Cyclodextrins as second-sphere ligands

12.16.1.2.2.(i) Organometallic complexes bearing cyclopentadienyl and/or η^6-arene ligands

12.16.1.2.2.(i).(a) Adducts with sandwich complexes

First examples of second-sphere coordination adduct between a CD and such organometallic complexes were observed with the ferrocene and its derivatives. Thus, Breslow was the first to report in 1975 that ferrocene forms a 1 : 1 adduct with the β-CD in both *N*,*N*-dimethylformamide and dimethyl sulfoxide.[16] Nevertheless, the first crystalline inclusion complexes of ferrocene and its derivatives were prepared by Harada and Takahashi in 1984.[17] The inclusion complexes were obtained by direct addition of crystals of ferrocene or its derivatives into aqueous solutions of CD. The stoichiometry of the inclusion complexes was found to be dependent on the sizes of the CD. The β-CD and γ-CD formed 1 : 1 stoichiometric inclusion complexes whereas α-CD formed a 2 : 1 (CD : guest) complex with ferrocene. From induced circular dichroism experiments, three structures were proposed for these adducts as shown in Figure 3.[18–20]

The crystal structure of the α-CD/ferrocene inclusion compound has been determined by an X-ray analysis which shows that the ferrocene molecule is encapsulated by the dimer of the α-CD in a tail-to-tail orientation and inclined

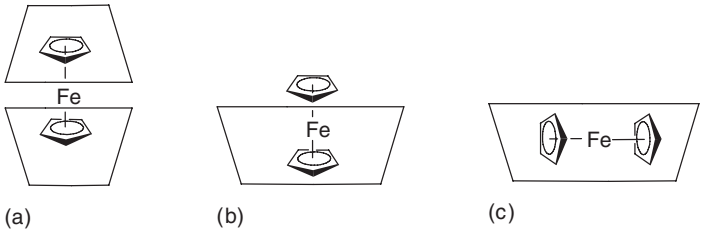

Figure 3

by 42° relative to the six-fold axes of the α-CD of the dimer.[21] The orientation of the ferrocene in the CD cavity was also confirmed by solid state ^{2}H NMR spectroscopy experiments[22] and by comparing the induced circular dichroism spectrum of 1,4,7,10,13-pentaoxa[13]ferroceneophane in the presence of β-CD with that of ferrocene in β-CD or γ-CD.[23] However, it should be noticed that calculations on the β-CD/ferrocene adduct indicate that the ferrocene can adopt both axial and equatorial orientation in the β-CD cavity.[24] Reports on the inclusion compound formed between ferrocene and β-CD also indicated that inclusion into the cavity altered the dynamics in the solid state of the guest molecule compared to that observed for pure compound.[25–28] The association constant of ferrocene with β-CD was determined in various solvents and was found to be 60 M^{-1} in DMSO by cyclic voltammetry,[29] 320 M^{-1} in 20% aqueous DMSO by the same technique,[29] and 1.65×10^4 M^{-1} in water by the solubility measurements.[30] The second-sphere coordination adducts between native or chemically modified CD and ferrocene or its derivatives have been the subject of numerous studies using a range of techniques such as cyclic voltammetry,[31–37] induced circular dichroism,[31,38–41] Mössbauer spectroscopy,[42] dynamic force microscopy,[43,44] mass spectroscopy,[45] NMR spectroscopy,[46] and thermogravimetry.[47] The above studies[29–47] and others[48–65] show that the affinity of ferrocene or its derivatives for the CD strongly depends on numerous factors such as the solvent, the presence of oxidants, the substituent on the cyclopentadienyl ring of ferrocene and the type of CDs. Although adducts between the CD and ferrocene or its derivatives are generally stable, a reaction between the encapsulated guest and the β-CD can occur. Thus, a β-CD covalently grafted with a ferrocenyl moiety has been obtained after formation of a 2 : 1 (host to guest) complex between β-CD and (1,1′-ferrocenediyl)dimethylsilane as shown in Figure 4.[66]

The formation of the β-CD bearing a ferrocenyl group was explained by a nucleophilic attack of one of the β-CD hydroxyl groups on the strained C—Si—C bridge of the organometallic complex. Interestingly, ferrocene derivatives interact with highly ordered monolayers of β-CD modified with seven thioether moieties. Measurements of the thermodynamics of the complexation of ferrocenemethanol in such monolayers yielded a complexation constant of 9.9×10^3 M^{-1} and a $\Delta G°$ of −5.4 kcal mol^{-1}.[67] A monolayer composed of cationic ferrocene was found to bind with β- and γ-CD.[68] The CD hosts are believed to interact with the monolayer assembly in two ways: by inclusion of the ferrocene moiety within the CD cavity and, surprisingly, by interactions between the counterions and hydrophilic CD.

The ability of ferrocene to bind strongly to β-CD has been exploited to investigate the suitability of β-CD as a model for the chymotrypsin enzyme. Rate accelerations and enantiomeric selectivity were observed in the presence of β-CD during the hydrolysis of *p*-nitrophenyl acetates of some ferrocene derivatives.[69–71] For instance, one of enantiomer of the *p*-nitrophenyl ester of (*E*)-3-(carboxymethylene)1,2-ferrocenecyclopentene is hydrolyzed 5 900 000 times faster in the presence of β-CD.[69] The strong affinity of ferrocene derivatives for the β-CD was also used to modify the surface of CD-capped nanoparticles. So, Kaifer *et al*. showed that hydrophilic β-CD-capped nanoparticles can be solubilized in chloroform by adding cationic ferrocenes that have long aliphatic chains as schematically represented in Figure 5.[72]

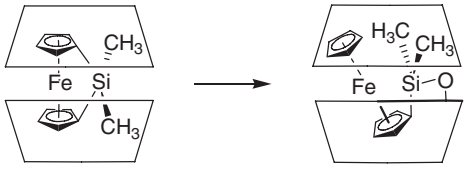

Figure 4

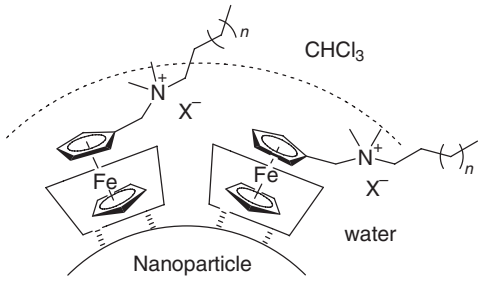

Figure 5

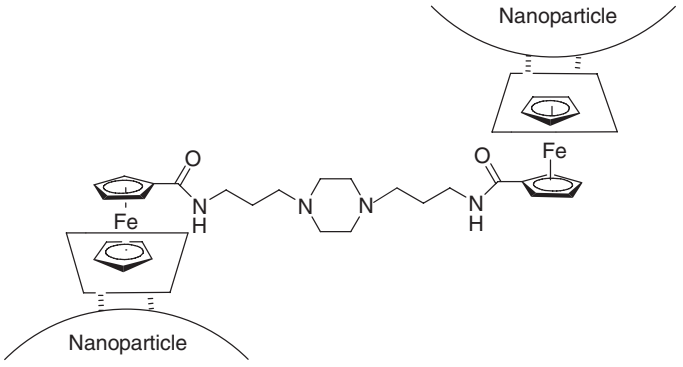

Figure 6

Through a series of solubility experiments, it has been proved that the presence of a water thin layer surrounding the surface particles was required to stabilize the CD/ferrocene inclusion complexes. Flocculation of gold nanoparticles has also been achieved by the same author using dimeric ferrocene guest (Figure 6).[73]

Flocculation properties in this system were controlled through host–guest interactions. For instance, competitive binding of a monomeric ferrocene guest resulted in partial redissolution of the precipitated aggregates. Dendrimers with 4, 8, and 16 ferrocene peripheral residues and their interactions with β-CD have been investigated by Kaifer *et al.*[74] Compound with 16 ferrocene peripheral residues showed the lowest solubility in β-CD-containing aqueous solution, suggesting that steric hindrance due to the increased proximity of ferrocene subunits prevents full complexation by the 16 β-CD hosts. Unsymmetric dendrimers containing only one ferrocene unit have been synthesized to investigate the effect of dendrimer growth and shape on the β-CD complexation.[75,76] Results showed that increasing dendrimer growth inhibits binding of β-CD to the ferrocenyl dendrimer. Similar results were reported with ferrocenyl glycodendrimer.[77] Finally, it is worth mentioning that the interaction between ferrocene and CD has also been used to elaborate mediators and molecular sensors[78–81] or to perform asymmetric inductions.[82] Recently, catalytically active second-sphere coordination adducts have been prepared by Gonçalves *et al.* Thus, a dioxomolybdenum(VI) complex bearing the diimine ligand *N*,*N*′-bis(ferrocenylmethylene)ethylenediamine encapsulated within the cavity of permethylated β-CD catalyzes with high selectivity the liquid-phase epoxidation of cyclooctene using *tert*-butyl hydroperoxide as the oxidant (Figure 7).[83]

The same authors also reported that the methyltrioxorhenium(VII) complexed by a 4-ferrocenylpyridine/β-CD adduct was not effective as a catalyst for the epoxidation of cyclooctene by hydrogen peroxide due to its poor solubility in reaction medium.[84] As observed with the ferrocene, the complex $[Rh(\eta^5\text{-}C_5H_5)_2]PF_6$[85] forms 2 : 1 inclusion complexes with the α-CD. The α-CD molecules are arranged head-to-head to form a dimer. The cation is encapsulated within the cavity of the dimer, while the PF_6^- anion is located outside the cavities. The complex cation is titled against the mean planes of oxygen atoms of the 12 secondary hydroxyl groups of the α-CD molecules by angles of 42/43°. The thermodynamics parameters for association of ruthenocene and osmocene in ethylene glycol at 25 °C were determined by Sokolov *et al.* The association constants were found to be 790 M^{-1} and 510 M^{-1} for the ruthenium and osmium compounds, respectively.[51,86] The same author reported that $[Ru(\eta^5\text{-}C_5H_5)_2]$ has high

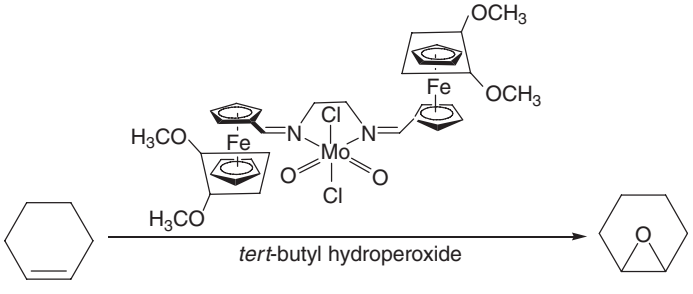

Figure 7

mobility within the β-CD cavity, undergoing rapid isotropic rotation (E_a: 43.2 kJ mol^{-1}). At low temperatures, reorientation of the cyclopentadienyl rings was also observed.[25] It was found that inclusion of [Ru(η^5-C_5H_5)$_2$] in β-CD cavity slows down the oxidation of ruthenocene by iodine.[25,87] Nevertheless, ^{13}C NMR MAS spectrum revealed that longer keeping to iodine vapor induces the formation of [Ru(η^5-C_5H_5)$_2$I]$^+$. Matsue *et al.* reported that the retention of radionuclides formed by irradiation of β-CD/metallocenes inclusion compounds decreases in the order Fe > Ru > Os. After the reaction, the metals are found as metallocenes.[88–90] Separation of racemates of planar-chiral cyclopentadienyl rhodium complexes into enantiomers can be achieved by liquid chromatography using aqueous β-CD as a mobile phase.[91] The origin of this separation was attributed to the formation of an inclusion compound between the CD and the rhodium complex. Although the positively charged cobaltocenium [Co(η^5-C_5H_5)$_2$]$^+$ does not interact appreciably with the β-CD, it has been found that its reduced form, that is, the cobaltocene forms stable 1 : 1 inclusion complex with the β-CD.[92] This "electrochemical activation" has been used by Kaifer *et al.* to bind β-CD to a series of poly(propyleneimine) dendrimers containing 4, 8, and 16 cobaltocenium units.[93] The same author has also shown that a 1 : 1 inclusion complex between cobaltocene and β-CD can be obtained when the reduction of a strong 1 : 2 complex between cobaltocenium and the octaanionic form of calix[6]-arene hexasulfonate is performed in the presence of β-CD.[94] Recently, Turel *et al.* have reported that titanocene dihalides of formula: [(η^5-C_5H_5)$_2$TiX$_2$] (X: F, Cl) can form second-sphere coordination adducts with the β-CD and γ-CD. Changes in the NMR spectra suggested a shallow penetration of the titanocene into the β-CD cavity and a deeper penetration in the case of the γ-CD.[95] From the NMR data, the authors assume that [(η^5-C_5H_5)$_2$Ti(H$_2$O)(Cl)]$^+$ and [(η^5-C_5H_5)$_2$Ti(H$_2$O)$_2$]$^{2+}$ are the species incorporated in the CD cavity when the starting material is [(η^5-C_5H_5)$_2$TiCl$_2$], and that cleavage of the cyclopentadienyl–titane bond occurs partially in the case of [(η^5-C_5H_5)$_2$TiF$_2$]. Contrary to [(η^5-C_5H_5)$_2$TiCl$_2$], Gonçalves *et al.* have reported that the analogous molybdenum complex [(η^5-C_5H_5)$_2$MoCl$_2$] is the species incorporated in the β-CD cavity rather than the hydrolysis products [(η^5-C_5H_5)$_2$Mo(H$_2$O)(Cl)]$^+$ and [(η^5-C_5H_5)$_2$Mo(H$_2$O)$_2$]$^{2+}$.[96] The existence of a true 1 : 1 inclusion complex was proved by using a combination of solid-state physical methods and *ab initio* calculations. The potential antiproliferative and cytotoxic activity of inclusion complexes between [(η^5-C_5H_5)$_2$MoCl$_2$] and the permethylated β-CD or the 2-hydroxypropyl β-CD were also evaluated.[97] The inclusion complex with the permethylated β-CD was the most effective antiproliferative and cytotoxic agent, exhibiting a 60%, hardly reversible, viability decrease in adenocarcinoma and low toxicity toward healthy cells.

12.16.2.2.2.(i).(b) Adducts with mixed-sandwich complexes

Contrary to the sandwich complexes, the formation of second-sphere coordination adducts between CD and mixed-sandwich complexes has been scarcely studied. The first example of a structurally characterized adduct of CD and such complexes was reported by Klingert and Rihs in 1990.[98] As shown by elemental analysis and ^{1}H NMR spectroscopy, the mixed-sandwich complex [(η^5-C_5H_5)Fe(η^6-C_6H_6)]PF$_6$ formed crystalline 2 : 1 (host : guest) inclusion complexes with the α-CD and the β-CD. It should be noticed that this stoichiometry is in contrast to the structurally related neutral ferrocene molecule, which forms a 2 : 1 adduct with α-CD but a 1 : 1 adduct with the β-CD. The crystal structure of the α-CD adduct has been determined by single-crystal X-ray diffraction. In the crystal, two α-CDs form a head-to-head dimer by means of intermolecular hydrogen bonding across the secondary hydroxyl faces of adjacent α-CD monomers. The [(η^5-C_5H_5)Fe(η^6-C_6H_6)]$^+$ cation is encapsulated within the cavity and is tilted by an angle of 39° (C_5H_5)/40° (C_6H_6) against the mean planes of the α-CD molecules. The complex [Ru(η^5-C_5H_5)(η^6-C_6H_6)]PF$_6$[99] forms 2 : 1 inclusion complex with the α-CD as observed with the complex [(η^5-C_5H_5)Fe(η^6-C_6H_6)]PF$_6$. The α-CD molecules are arranged head-to-head to form a dimer. The cation is encapsulated within the cavity of the dimer and titled against the mean planes of oxygen atoms of the 12 secondary hydroxyl groups of the α-CD molecules by angles of 36°. Finally, the formation of inclusion complexes between CDs and a range of cyclopentadienyl(arene)iron(II) sandwich and (tetramethylcyclobutadiene)cobalt complexes have also been reported by Klingert and Rihs.[100]

12.16.2.2.2.(i).(c) Adducts with half-sandwich complexes

The first example of half-sandwich complexes interacting with CD was reported by Harada in 1985.[101,102] A range of (η^6-arene) chromium tricarbonyl complexes has been shown to form crystalline adducts with the β-CD and γ-CD, the aromatic ring of the complex being bound within the cavity of the CD (Figure 8).

The formation of the inclusion compounds was selective. β-CD formed 1 : 1 inclusion compounds with benzene, toluene, and *o*-xylene chromium tricarbonyl complexes, and not with *m*-xylene, *p*-xylene, guaiacol, methyl anthranilate mesitylene, or hexamethylbenzene chromium tricarbonyl complexes.[101,103] Whereas α-CD did not form inclusion complexes with any arene chromium complexes, γ-CD formed 1 : 1 inclusion complexes with all arene chromium

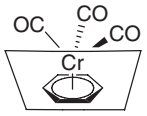

Figure 8

complexes tested. Interestingly, the ^{13}C CP/MAS NMR spectrum of a crystalline sample of the $[(\eta^6\text{-}C_6H_6)_2Cr(CO)_3]$/$\beta$-CD inclusion compound is strictly analogous to the spectrum obtained in solution, indicating that the carbonyl moiety rotates freely along its principal coordination axis.[104]

The first example of half-sandwich iron complexes encapsulated by CD was reported by Harada *et al.* in 1991.[105] The authors communicated the preparation of inclusion compounds between native CDs and $[(\eta^5\text{-}C_5H_5)\text{-}Fe(CO)_2(CH_3)]$ complex and reported that the included complexes insert carbon monoxide and sulfur dioxide into the Fe—R bond in solid state. The trend observed for insertion activity was γ-CD > β-CD $\gg$ α-CD, showing that CD is capable of controlling the activity of the alkyl iron complex. The reactivity of the included iron complex was also observed by Welker *et al.*[106] Whereas complexes $[(\eta^5\text{-}C_5H_5)Fe(CO)_2(CH_3)]$ and $[(\eta^5\text{-}(CH_3)C_5H_4)Fe(CO)_2(CH_3)]$ normally participate in CO insertion/alkyl migration reactions when they are heated in the presence of phosphines, the inclusion compounds of these complexes participated in ligand substitution reactions with no CO insertion/alkyl migration products when heated with phosphines as shown in Figure 9.

This result was attributed to a slowing down of the alkyl migration rate due to ligand/cyclodextrin steric interactions. Unfortunately, it was found that this ligand substitution reaction was not enantioselective. Under electrochemical conditions, the reactivity of the $[(\eta^5\text{-}C_5H_5)Fe(CO)_2(CH_3)]$/$\beta$-CD inclusion complex was different. Thus, Pospisil *et al.* have reported that the $[(\eta^5\text{-}C_5H_5)Fe(CO)_2(CH_3)]$/$\beta$-CD inclusion complex undergoes a CO insertion into the methyl–metal bond.[107] In the presence of free CO, an enhanced rate of acyl migration from the metal center to the cyclopentadienyl ligand was even observed. Qualitative ^1H NMR experiments have revealed that $[(\eta^5\text{-}C_5H_5)Fe(CO)_2NH_3]PF_6$ formed adduct with α-CD and β-CD.[8,108] The formation of inclusion compounds between CD and various mononuclear half-sandwich complexes of iron, that is, $[(\eta^5\text{-}C_5H_5)Fe(L)_2X]$ (X: Cl, I; L: CO, dppe) and $[(\eta^5\text{-}C_5H_5)Fe(L)_2L']PF_6$ (L′: neutral donor ligand) and one binuclear complex $[((\eta^5\text{-}C_5H_5)(dppe)Fe)_2\text{-}\mu\text{-}CN]PF_6$, was investigated by Diaz and Arancibia[109,110] A 1 : 1 stoichiometry for the inclusion compounds containing mononuclear organometallic complexes and a 2 : 1 stoichiometry for the inclusion compound containing the binuclear organometallic complex have been found. Interestingly, the inclusion compounds $[(\eta^5\text{-}C_5H_5)\text{-}(dppe)Fe—NCCH_3]PF_6$/$\gamma$-CD and $[(\eta^5\text{-}C_5H_5)(dppe)Fe—(\eta^5\text{-}dppm)]PF_6$/$\gamma$-CD exhibited an unusual laminar structure. The synthesis of 1 : 1 adduct between the β-CD and various cationic iron complexes of formula $[(\eta^5\text{-}C_5H_5)Fe(CO)_2L]BF_4$ (L: aromatic nitriles, triphenylphosphine, triphenylphosphite) has been achieved by Sokolov *et al.* to obtain potential nonlinear optics material.[111] The formation of inclusion complexes was strongly hindered by the presence of the bulky aromatic nitrile or phosphines.

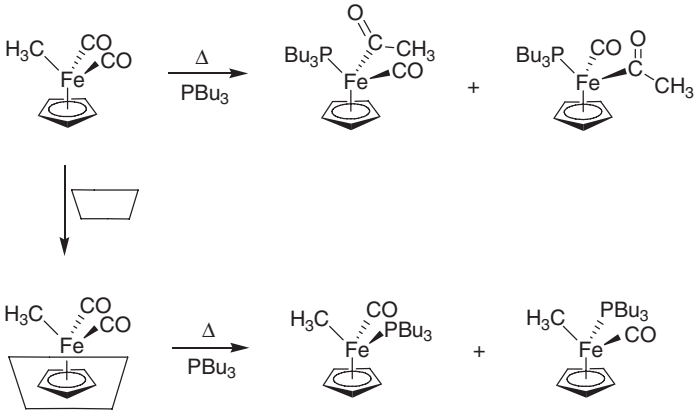

Figure 9

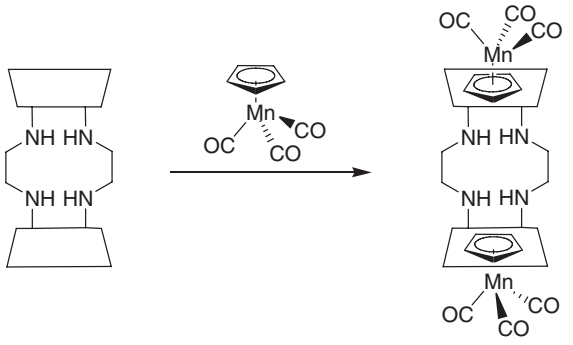

Figure 10

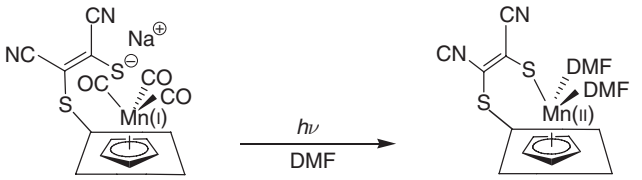

Figure 11

The formation of adducts between CD and η^5-pyrrolyl[112] or cyclopentadienyl[113] manganese tricarbonyl complexes has been investigated using various techniques. As in the case of (η^6-arene) chromium tricarbonyl complexes, these manganese complexes formed 1 : 1 inclusion complexes with the organic ligand included within the cavity. In 1995, the inclusion compound of [(η^5-C_5H_5)Mn(CO)$_3$] with a β-CD dimer bridged with two 1,2-diaminoethanes was prepared as the first example of CD dimer inclusion compounds with organotransition metal complex (Figure 10).[114]

The spectroscopic studies and elemental analysis revealed that stoichiometry of the inclusion compound in water is identical to its stoichiometry in solid state. The mono[6-deoxy-6-(2-butenedinitrile-2,3-dimercapto sodium salt)]-β-CD can also be encapsulated [(η^5-C_5H_5)Mn(CO)$_3$].[115] Upon irradiation of the inclusion compound in DMF solution, an interesting intramolecular photosubstitution resulting in the formation of a very stable self-included compound was observed (Figure 11).

A similar phenomenon has been reported by the same authors when the complex [(η^5-C_5H_5)Mn(CO)$_3$] is included in the host cavity of the mono[6-deoxy-6-(2-aminoethylthio-1,2-dicyane ethylenylthio)]-β-CD and irradiated in DMF solution at 20 °C.[116]

The inclusion compounds formed between β-CD and the dicarbonylmolybdenum complexes [(L)Mo(η^4-C_6H_8)(CO)$_2$]BF_4 and the neutral derivatives [(L)Mo(η^3-C_6H_7)(CO)$_2$] (L: (η^5-C_5H_5) or (η^5-C_9H_7)) were investigated by Lima *et al.*[117] The cationic and neutral cyclopentadienyl analogs formed stable 2 : 1 (host : guest) channel-type inclusion compound in a crystalline state. By contrast, the η^5-indenyl analogs formed only weak complexes with the β-CD. The *ab initio* calculations revealed that the steric hindrance arising from the presence of the indenyl ligand is a possible explanation for the experimentally observed lower stability of these compounds. Half-sandwich complexes of molybdenum of the type [(L)Mo(η^3-C_3H_5)(CO)$_2$] (L: (η^5-C_5H_5), $C_5H_4SiMe_3$, C_9H_7) formed stable, crystalline 1 : 1 inclusion complexes with the β-CD.[118] Channel-type structures were observed with ligands (η^5-C_5H_5) and C_9H_7, suggesting that the organometallic complexes are fully enclosed within the CD cavity. A completely different result was obtained with the ligand $C_5H_4SiMe_3$ as the arrangement of the CD molecules was more similar to that of the free β-CD hydrate.

12.16.1.2.2.(ii) Organometallic complexes bearing alkyl, diene, π-allyl, or carbonyl ligand

Contrary to organometallic complexes bearing cyclopentadienyl and arene ligand, there are few reports concerning this class of second-sphere coordination adducts. In 1986, Harada and Takahashi reported that β-CD and γ-CD can

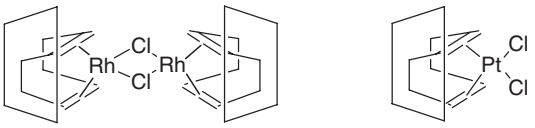

Figure 12

form adducts with metal complexes bearing cod or nbd ligand.[119–121] 1 : 1 and 2 : 1 inclusion complexes were obtained in high yields by the treatment of β-CD with monomeric complexes [(cod)PtX_2] (X: Cl, Br, and I) and with dimeric complexes [Rh(μ-Cl)L]$_2$ (L: cod, nbd), respectively. On the basis of spectroscopic and analytical measurements, it was proposed that the cod or nbd ligand was included within the cavity as schematically shown in Figure 12.

The thermal stability of the organometallic compounds was found to be increased when they were included in the cavity. For instance, the decomposition temperature of the complex [Rh(μ-Cl)(cod)]$_2$ and [Rh(μ-Cl)(cod)]$_2$/β-CD adduct was ca. 200 °C and 275 °C, respectively.[120] The β-CD was also enable to encapsulate the complex [Rh(η^5-C_5H_5)(nbd′)] (nbd′: 2-formylnorbornadiene) in its cavity.[122] Interestingly, the [$PdCl_2$(cod)]/β-CD or [$PtCl_2$(cod)]/β-CD inclusion complexes were evaluated as command-cure catalyst in the hydrosilylation reactions.[123–125] The [$PdCl_2$(cod)]/β-CD adduct was a good catalyst whereas the complex [$PdCl_2$(cod)] was not active. The [$PtCl_2$(cod)]/β-CD adduct was also an effective catalyst contrary to the complex [$PtCl_2$(cod)] which was too active at low temperature for the hydrosilylation reaction. Although Harada has reported that α-CD cannot bind to transition metal complexes containing cod ligand, a 1 : 1 adduct between the α-CD and complex [Rh(cod)$(NH_3)_2$]PF_6 has been isolated by Stoddart *et al.*[126,127] The X-ray structure of the 1 : 1 adduct revealed that the cyclooctadiene ligand adopts a boat conformation with one of the two —CH_2—CH_2— units in the CD cavity. Intramolecular hydrogen bonds between the NH_3 ligand and the hydroxyl group of the CD could be the driving force for the formation of the 1 : 1 adduct. The analogous complex [Rh(cod)(H_2N—NH_2)]PF_6 was found to be more stable than [Rh(cod)$(NH_3)_2$]PF_6. The association constant for the [Rh(cod)(H_2N—NH_2)]PF_6/α-CD inclusion complex was determined by ^{1}H NMR spectroscopy and was equal to 520 mol^{-1} kg.[126]

The formation of adduct between CD and various π-allylpalladium complexes was investigated by Harada *et al.* in 1986.[128,129] The dimeric complexes [{Pd(η^3-C_3H_5)(μ-X)$_2$}] (X: Cl, Br, I) and the analogous crotyl and 2-methylallyl complexes (X: Cl) do not interact with the α-CD but form 1 : 1 inclusion compounds with β-CD and/or γ-CD. From the examination of CPK models, it was concluded that the π-allylpalladium complexes are too large to fit in the α-CD cavity.

A 1 : 1 inclusion complex between allyl-di-*n*-butyl tin chloride and β-CD was prepared by Marton *et al.* in good yield by a coprecipitation method.[130] A Mössbauer spectroscopy study indicates that the metal center displays a pentacoordination, probably due to Sn—O long range contacts with the hydroxyl groups of secondary face of the β-CD. Although no definitive evidence has been obtained, the authors suggest that inclusion occurred via one of the butyl group.

CDs form inclusion compounds with some mononuclear and binuclear metal carbonyl complexes. While $Fe(CO)_5$ and Co(NO)$(CO)_3$ form 1 : 1 inclusion complexes with the β-CD and the γ-CD, these metal carbonyl complexes form 2 : 1 inclusion complexes with the α-CD.[6,131] Napolitano *et al.* have studied by ^{13}C CP/MAS NMR spectroscopy the $Fe(CO)_5$/β-CD inclusion compound.[132]It was found that the metal carbonyl complex $Fe(CO)_5$ reorients isotropically within the β-CD cavity and shows rapid axial–equatorial exchange. The formation of a 1 : 1 inclusion complex between $Cr(CO)_6$ and γ-CD was proved by the same authors.[132] As in the case of $Fe(CO)_5$/β-CD inclusion compound, a rapid and isotropic reorientation of $Cr(CO)_6$ within the γ-CD cavity was observed. Note that a different behavior was observed with the (η^6-C_6H_6)$Cr(CO)_3$/β-CD inclusion complex. Indeed, (η^6-C_6H_6)$Cr(CO)_3$ reorients only about its principal axis in the β-CD cavity.[104] CD can also bind to dinuclear metal complexes such as $Mn_2(CO)_{10}$, $Co_2(CO)_8$, and $Co_2(CO)_6L_2$ (L: PMe_3, PEt_3, $P(OMe)_3$).[6,131,132] While $Co_2(CO)_8$ forms inclusion complex with the β-CD and γ-CD, the other binuclear metal carbonyl complexes only form inclusion complexes with the γ-CD. A series of 1 : 1 inclusion complexes between cobalt cluster complexes and γ-CD was prepared by Shimada *et al.* by adding the cobalt cluster to a twofold molar excess of saturated aqueous γ-CD solution at 40 °C.[133] The structures of cobalt clusters interacting with the γ-CD are displayed in Figure 13.

The metal cluster complexes included in the γ-CD were found to be thermally more stable than the free complexes.

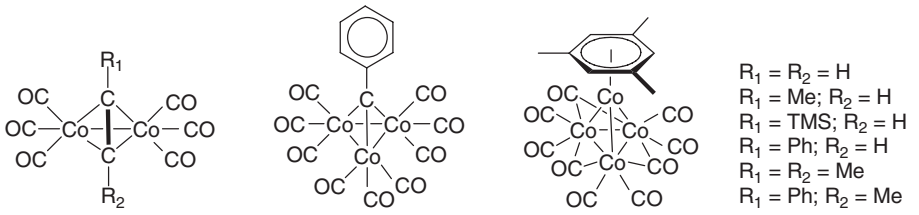

Figure 13

12.16.1.2.3 Cyclodextrins acting simultaneously as first- and second-sphere ligands

The formation of adducts between CDs and organometallic complexes exhibiting simultaneous first- and second-sphere coordination was reported for the first time by Osa in 1985.[134–137] Data obtained from induced circular dichroism studies on CDs bearing a ferrocene derivative suggest that one of cyclopentadienyl rings of the ferrocene is included within the CD cavity as shown in Figure 14.

In this complex, the first-sphere cyclodextrinylcyclopentadiene carboxylate ligand is acting as a second-sphere ligand for the unsubstituted first-sphere cyclopentadienyl ligand. The lability of the NH_3 ligands of $[Rh(cod)(NH_3)_2][PF_6]$ in the presence of α-CD or methylated α-CD has been attributed to a displacement of the NH_3 ligands by the hydroxyl groups of the CD.[126,127] If this suggestion is true and the cod ligand of the complex still enters into the cavity, the resulting adduct is another example of simultaneous first- and second-sphere coordination. The reaction products obtained after irradiation of inclusion complexes: $(\eta^5\text{-}C_5H_5)Mn(CO)_3$/mono[6-deoxy-6-(2-butenedinitrile-2,3-dimercapto sodium salt)]-β-CD and $(\eta^5\text{-}C_5H_5)Mn(CO)_3$/mono[6-deoxy-6-(2-aminoethyl thio-1,2-dicyane ethylenylthio)]-β-CD belong undoubtedly also to this type of adduct (see Figure 11, for example).[115,116]

The possibility to obtained first- and second-sphere coordination adducts with α-CDs containing phosphine or phosphite units has been extensively investigated by Matt *et al.*[138–145] Both modified α-CDs readily formed transition metal chelate complexes in which the metal centers were immobilized at the entrance or outside the cavity. The structure of these adducts will not be discussed here as most of them do not possess a metal–carbon bond. Surprisingly, it was found that the organic fragment of the organometallic complexes was not included within the α-CD cavity. For instance, reaction of [PdClMe(cod)] with α-CDs containing two C(5)-linked CH_2PPh_2 units afforded organometallic complexes with the Pd–methyl moiety outside the cavity and Pd–chloride moiety inside the cavity as schematically represented in Figure 15.[143,144]

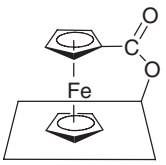

Figure 14

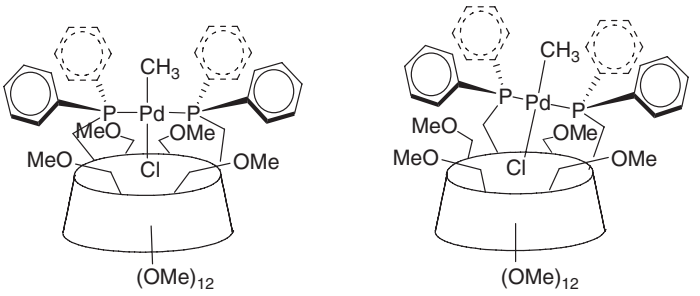

Figure 15

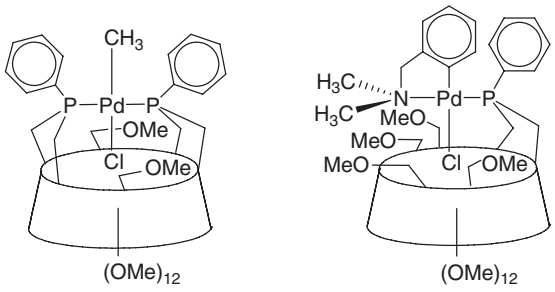

Figure 16

The preference of the cavity for the polarized Pd—Cl moiety rather than for the less-polar Pd–organic fragments was also observed with other modified α-CDs. Indeed, reaction of [PdClMe(cod)] with phosphinidene-capped α-CDs gave rise to organometallic complexes, where the metal—chloride bond points toward the center of the cavity as shown in Figure 16.[145]

The ability of α-CD cavity to recognize a metal—chloride bond rather than organic groups in non-aqueous media is likely a consequence of the absence of stronger competing supramolecular forces such as the hydrophobic effect which usually plays a prevailing role in the formation of CD inclusion complexes.

Note that the reaction product between β-CD and the (1,1′-ferrocenediyl)dimethylsilane can be considered as a first- and second-sphere coordination adduct (Figure 4).[66] Indeed, the β-CD is covalently bound to the cyclopentadienyl ring (first-sphere ligand) but also partially includes the ferrocenyl moiety (second-sphere ligand).

12.16.1.2.4 Cyclodextrins acting simultaneously as first- and transient second-sphere ligands

When a CD covalently connected to a ligand of the organometallic complex temporarily includes in its cavity a substrate that reacts with the organometallic complex, the CD can be considered as transient second-sphere ligand. This phenomenon is observed when the organometallic complex is involved in catalytic processes. Such a type of coordination occurs likely during the ethylene polymerization catalyzed by an iron complex-containing tridentate nitrogen ligands based on 2,6-bis(imino)–pyridine-capped β-CD.[146] As shown in Figure 17, the *endo*-oriented 1,3-diiminopyridine–$FeCl_2$ unit bridges the entrance of the β-CD derivative and compels the substrate to enter into the cavity by the secondary face to interact with the catalytic site.

After activation with a large excess of methylaluminoxane (Al/Fe $>$ 2000 equiv.), the iron complex depicted in Figure 17 polymerizes ethylene in toluene with a maximum turnover frequency of 125 h^{-1}. This catalytic activity remains 1000 times lower than that of conventional Brookhart/Gibson iron catalysts, possibly because the catalytic center is surrounded by five coordinating methoxy groups. Note that the iron complex based on the α-CD is not active at all in ethylene polymerization, suggesting that the cavity of the α-CD is not sufficiently large to allow the chain growing process.

The substrate selectivity observed during the hydrogenation of a 1 : 1 mixture of olefins and the increase in the linear to branched aldehyde ratio during the hydroformylation of 1-octene were attributed to the formation of transient adducts between the substrate and a water-soluble rhodium complexes bearing β-CD-modified diphosphines (Figure 18).[147–150]

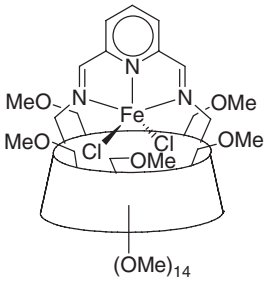

Figure 17

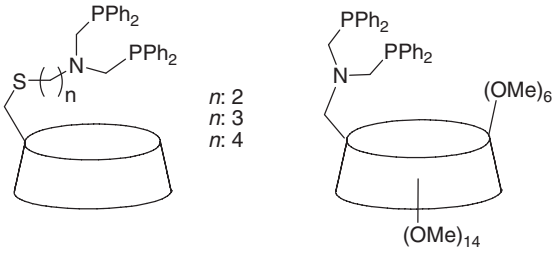

Figure 18

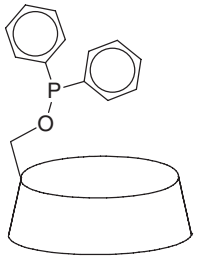

Figure 19

Indeed, no substrate selectivity or increase in aldehydes ratio was observed when the reactions were conducted in the presence of a free β-CD analogous catalyst $[PhN(CH_2PPh_2)_2Rh(cod)]BF_4$. It must be pointed out that the reactions were performed in an aqueous organic two-phase system with an aqueous phase containing 30% DMF. The presence of an aqueous phase is supposed to force inclusion of the substrate in the cavity during the catalysis. In one-phase medium composed of DMF, the formation of transient adducts between substrate and a rhodium complex modified by a phosphinite β-CD ligand also seems possible (Figure 19).[151]

Indeed, Ichikawa *et al*. have explained the reactivity difference between 1-decene and 4-phenyl-1-butene in the hydroformylation reaction by assuming that the 4-phenyl-1-butene fits better into the cavity of the β-CD/Rh complex than the 1-decene.

12.16.1.2.5 Cyclodextrins as transient second-sphere ligands

The CD can be considered as a transient second-sphere ligand when it is used as inverse phase-transfer agent in aqueous organometallic catalysis. Indeed, when the CD transfers the water-insoluble substrate into the aqueous phase via an inclusion complex, it is postulated that the included substrate binds to the water-soluble organometallic catalyst to form transient second-sphere coordination adducts (Figure 20).

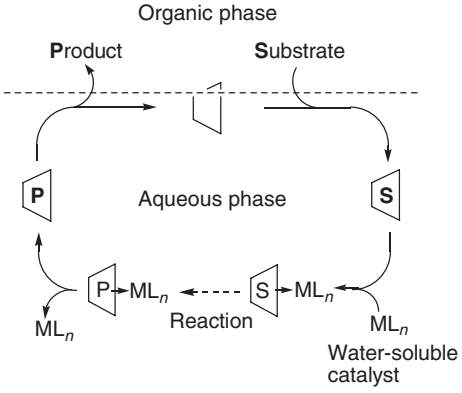

Figure 20

Nevertheless, it must be pointed out that the formation of such transient species has never been spectroscopically observed. Native CDs are effective inverse phase-transfer catalysts for the deoxygenation of allylic alcohols,[152] epoxydation,[153] or oxidation[154–157] of olefins, reduction of α,β-unsaturated acids,[158] α-keto ester,[159] conjugated dienes,[160] or aryl alkyl ketones.[161] Interestingly, chemically modified CDs like the partially *O*-methylated CDs show a better catalytic activity than native CDs in numerous reactions such as the Wacker oxidation,[162,163] hydrogenation of aldehydes,[164,165] Suzuki cross-coupling reaction,[166] hydroformylation,[167–174] or hydrocarboxylation[175,176] of olefins. Methylated β-CDs were also used successfully to perform substrate-selective reactions in a two-phase system.[177–180]

12.16.1.3 Calixarenes and Resorcinarenes

12.16.1.3.1 Introduction to calixarenes as supramolecular hosts

As previously described for cyclodextrins, calixarenes have widely been used as first- and/or second-sphere ligands and have been the subject of numerous studies involving structural determination and catalytic applications.[181–184] Calix[*n*]arenes ($n = 4-20$)[185,186] are macrocycles comprising phenolic units and methylenes groups, most readily obtained from the base-induced condensation of *p*-Bu^t—phenol and formaldehyde. Many of them are known for their rigid, well-defined three-dimensional structure, and they have become popular substrates for the selective sequestration of inorganic ions.[187] In the past decade, an appreciable amount of phosphorus-containing calix[4]- and calix[6]arenes has been studied to put forward the complexating properties of calixarenes toward transition metal.[188,189] We recall here the main examples of the last 10 years concerning supramolecular assemblies made of calixarenes and organic or organometallic guests. Some of these architectures possess the capability to promote metal-centered reactions that are sterically constrained, thereby allowing combined shape control and regioselectivity. The supramolecular calixarenes/guest complexes are classified according to the organometallic character of the host or the guest and according to the coordination type of the ligands (first- and/or second-sphere) as well.

12.16.1.3.2 Calixarenes as second-sphere ligands

This section is devoted to calixarenes which are not engaged in coordination with metallic species. They act as hosts for first-sphere coordination ligands and modify their properties. Some of them are considered as transient second-sphere ligands for catalytic organometallic species. As an example, the behavior of modified calixarenes (Figure 21; $n = 4$; $R^1 = H$; $R^2 = SO_3Na$ or CH_2NMe_2) as inverse phase-transfer catalysts has first been evaluated in a Suzuki–Miyaura coupling reaction of iodobenzene and phenyl boronic acid but the initial activities were 1.5, higher at most compared with the reaction in the absence of any calixarene.[190]

By contrast, calixarenes possessing extended hydrophobic host cavities and surface-active properties were found to be very efficient as mass-transfer promoters for the palladium-mediated Suzuki cross-coupling reaction of 1-iodo-4-phenylbenzene and phenyl boronic acid in aqueous medium.[166] Actually, Monflier *et al.* showed that, using sulfonatoalkyloxycalix[6]arene substituted in *para*-position by alkyl or aryl groups (Figure 21; $n = 6$; $R^1 = H$, $(CH_2)_xSO_3Na$ ($x = 3$ or 4); $R^2 = H$, Me, Ph), the cross-coupling rates were up to 92 times higher than those obtained without addition of any compound which could be rationalized by invoking π/π- or CH/π-interactions between the calixarene and the aromatic rings of the substrate. Under the same catalytic conditions, modified cyclodextrins gave lower enhancements of the initial activity.

Modified calixarenes also constitute stable, and not transient, second-sphere ligands. For instance, the binding affinity of calix[6]arene hexasulfonate hosts for ferrocene or cobaltocenium guests is highly dependent on the extent of intramolecular hydrogen bonding in the lower rim of the calixarene. Voltammetric measurements have shown that the binding affinity of calix[6]arene hexasulfonate hosts for ferrocene or cobaltocenium guests is a consequence of the preorganized and rigid character of the octaanionic calixarene, which is determined by the network of hydrogen bonds

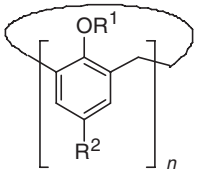

Figure 21

in its lower rim (Figure 21; $n = 6$; $R^1 = H$ or Me; $R^2 = SO_3^-$).[191] Due to its deprotonated structure, the host bound more strongly to the oxidation states of the guests bearing a higher positive charge.

12.16.1.3.3 Calixarenes acting simultaneously as first- and second-sphere ligands

In this category, we deal with calixarenes that are directly connected to a transition metal atom (Zn, Pd, etc.) and whose cavity can wrap around other first-sphere ligands. In that case, the calixarenes behave as second-sphere ligands that partly protect the metal center.

Reaction of *p*-Bu^t-calix[4]arene (H_4L) with excess $Zn(Et_2)$ in toluene affords the *exo*-bimetallic dicalixarene complex $[Zn_5L_2Et_2(tmeda)_2]$.[192] In the solid state, the two calixarenes are fused by three of the five zinc centers. The other two metals' centers are coordinated by the ethyl groups which are located inside the cavities of the calixarenes (Figure 22).

Astonishingly, an unusual bimetallic zinc complex was formed upon treatment of the similar 1,3-dimethoxycalixarene with 2 equiv. of diethylzinc.[193] The solid-state structure of this complex revealed the distorted flattened-cone conformation of the calixarene moiety with two phenolate units lying nearly in the same plane (Figure 23). Each of the Zn atoms is bound to three oxygen atoms and the ethyl group, and the organometallic fragments are equivalent both in solution and in the solid state.

Starting from these observations, Vigalok *et al.* proved the substituent-dependent formation of bimetallic calixarene inclusion complexes with spontaneous discrimination between the organometallic fragments.[194] Reaction of 1,3-di-*O*-substituted calixarene ligands with Et_2Zn gives organo-transition metal bimetallic calix[4]arene inclusion complexes when the substituent is larger than methyl. The resulting complexes showed strong interactions between the incorporated organometallic fragment and the hydrophobic cavity of the calixarene group. The X-ray structure showed coordination of two ethylzinc groups to a single calixarene unit in the pinched-cone conformation. Interestingly, the two ethylzinc fragments demonstrate different binding modes, with one of the zinc atoms capping

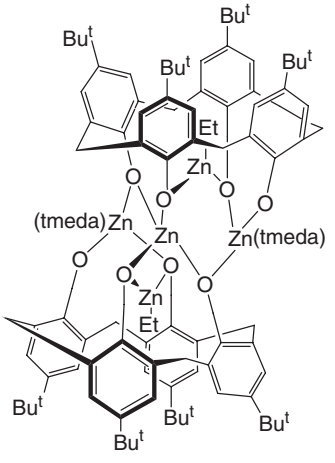

Figure 22

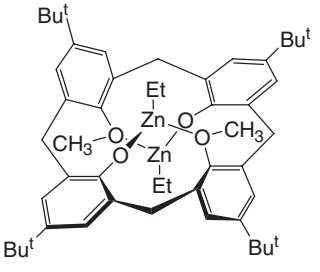

Figure 23

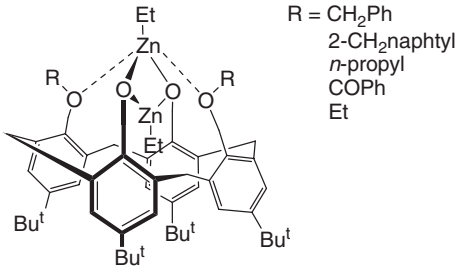

Figure 24

the calixarene cone in the five-coordinate arrangement, while the other is fully immersed in the calixarene cavity in the formal three-coordinate environment. Due to the steric bulk of the substituents, the second diethylzinc molecule must approach the remaining phenolic group by penetrating the hydrophobic calixarene cavity (Figure 24).

Loeb *et al.* synthesized organopalladium calix[4]arenes that demonstrated simultaneous first- and second-sphere coordination of substrates such as acetonitrile[195] or 4-phenylpyridine.[196] ^{1}H NMR spectral data were consistent with binding the substrate to the palladium center via σ-donation and interaction of the substrate with the calix[4]arene unit (Figure 25).

Mononuclear rhenium *p*-Bu^t-calix[4]arene complexes and their use in the stepwise construction of a phenoxo-bridged Re–Pd heterodinuclear core inside the cavity of the calix[4]arene have also been described.[197] Taking advantage of the anionic nature of the dioxorhenium species, complexation of a second transition metal fragment with the Re(VII) complex [Ph_4P][ReO_2{*p*-Bu^t-calix[4]arene-$(O)_4$}] was examined. When an EtOH solution of this rhenium complex was treated with the solvated allylpalladium complex [Pd(η^3-C_3H_5) $(Me_2CO)_x$](OTf), the Re–Pd complex [ReO_2{*p*-Bu^t-calix[4]arene-$(O)_4$}Pd(η^3-C_3H_5)] was obtained. X-ray crystallography clearly confirms that the {Pd(η^3-C_3H_5)$^+$} fragment is encapsulated in the calixarene pocket, surrounded by the aromatic rings and coordinated by the two phenoxy oxygen atoms situated *trans* to the oxo ligands (Figure 26).

Matt *et al.* reported the first calix[4]arene diphosphines (in which the P donor atoms are *trans*) with organometallic fragments positioned inside the larger opening of the cavity.[198] By forming such complexes the geometry of the

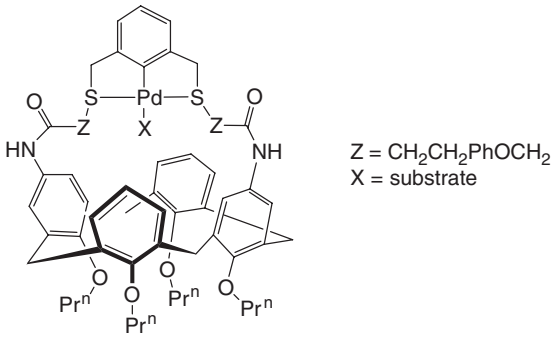

Figure 25

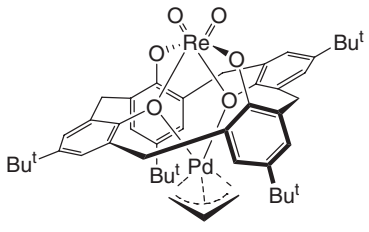

Figure 26

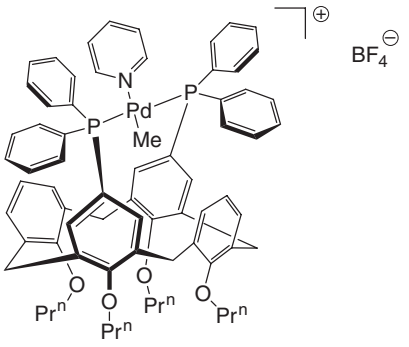

Figure 27

calixarene core flattens and becomes rigid. Small ligands such as a methyl group could then be encapsuled in the space (5.5 Å) between the two phenol rings bearing the phosphine units. Reaction of the calixarene ligand with the cationic alkylpalladium complex [PdMe(cyclooctadiene)(THF)]BF_4 and subsequent addition of pyridine resulted in the quantitative formation of the complex depicted in Figure 27.

The use of cavities equipped with non-chelating ligands may also lead to complexes having a partially included ligand sphere. Thus, reaction of a tribromo-monophosphine calix[4]arene with [$RuCl_2$(*p*-cymene)]$_2$ gave a quantitative yield of an organometallic complex where the *p*-cymene unit fills the calixarene basket (Figure 28).[199] Owing to the presence of bulky bromine atoms that increase the cavity depth and hence maintain the metal fragment inside the calixarene core, rotation about the P–C(phenol) is restricted. A coordination of a bromide atom to an $RuCl_2$(*p*-cymene) fragment is believed to be responsible for the organometallic inclusion due to a possible Ru–Br bond, which might guide the $RuCl_2$(*p*-cymene) unit to the neighboring phosphorus atom. However, steric effects that orientate the phosphorus lone pair toward the calixarene axis prior to coordination could also account for the observed phenomenon.

A dirhodium tetracarboxylate complex coordinated by two bromocalix[4]arene macrocycles exhibited two toluene molecules coordinated to the rhodium centers and inserted in the clefts, which are formed by the vicinal *p*-bromophenyl rings of the two calixarene units (Figure 29).[200] This complex has been found to be an efficient catalyst for two carbene transfer reactions, alkene cyclopropanation, and intramolecular C–H insertion, in terms of stereo- and regioselectivity.

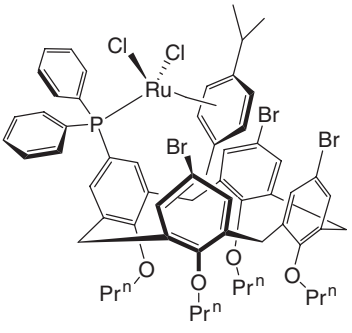

Figure 28

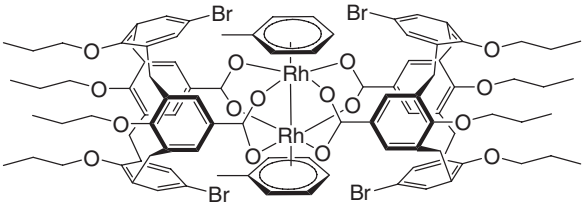

Figure 29

12.16.1.3.4 Calixarenes acting simultaneously as first- and transient second-sphere ligands

This section is dedicated to first-sphere coordination calixarenes connected to a metal for which another ligand might temporarily penetrate in the host cavity. For that purpose, the idea of rational catalyst design could be taken a step further by using sterically hindered chelated bisphosphines or bisphosphites with a calix[4]arene backbone.

The first bisphosphine calixarenes that have been used in catalysis are di(amide)–phosphine hybrids calix[4]arene.[201] Reaction of $[RhCl(norbornadiene)]_2$ with these calixarene derivatives gave an organometallic complex whose norbornadiene–rhodium moiety lies above the cavity defined by the four substituents of the calixarene and between the two amide functionalities. This complex was applied in the hydroformylation reaction of styrene. The rather low reaction rate observed (7.5 turnovers per Rh per hour) has been attributed to a partial encapsulation of the metal center preventing the approach of the substrate. Indeed, the metal center may be viewed as located in a hemispherical ligand environment.

A calix[4]arene phosphine ligand has been developed to coordinate palladium and platinium in a polymeric form whereas reaction with $[(cod)RhCl]_2$ afforded a dirhodium derivative (Figure 30) that was an active catalyst for the hydroformylation of oct-1-ene and styrene.[202] This complex catalyzed the hydroformylation of 1-octene (CO/H_2 (1/1), 800 psi, 70 °C, 5 h) to give mostly nonanal and branched octanals in approximately 90% yield. The ratio of linear to branched aldehyde products is only 2.21 probably because of interactions of reaction intermediates with the calixarene cavity. An increase in the phosphacalix[4]arene ligand (4 equiv.) gave a slightly higher *l*/*b* ratio (2.48) and aldehyde yield is approximately 93%. In the case of styrene hydroformylation, styrene conversion is 98.6% and aldehyde yield is approximately 98%. The selectivity toward branched aldehyde (*l*/*b* = 1/6.2) is lower than that of the Bu^t-substituted analog (*l*/*b* = 9/91) which might be due to the fact that the intermediate to the linear aldehyde can better fit into the calixarene cavity and thus is favored.

More hindered bisphosphites catalysts have also been studied and were less active but far more regioselective in the hydroformylation of *n*-oct-1-ene (more than 90% of *n*-nonanal) than their monophosphites equivalents (Figure 31).[203] Here again, the coordination of the organic substrate to the included metallic center constitutes the determining step to control both the activity and the regioselectivity of the hydroformylation reaction.

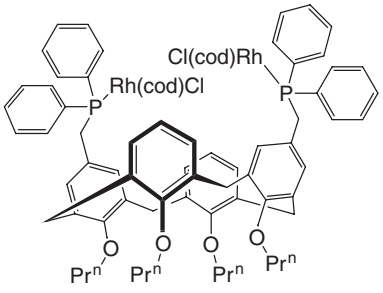

Figure 30

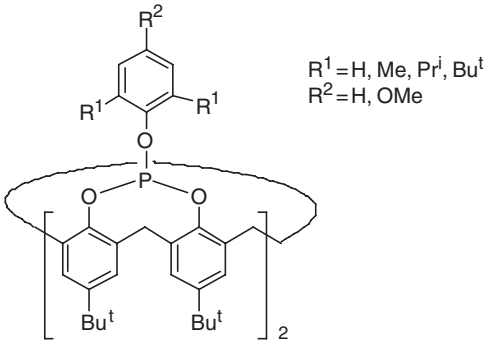

Figure 31

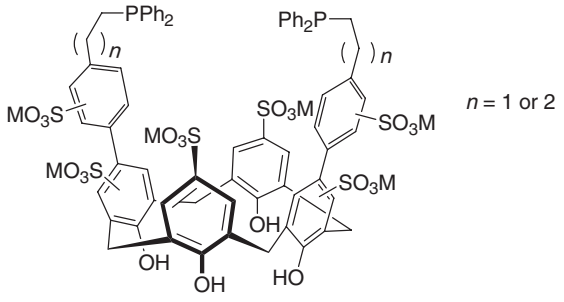

Figure 32

Enhanced catalytic activity has also been observed for the hydroformylation of oct-1-ene and dec-1-ene with water-soluble phosphine–calix[4]arene—rhodium complexes (Figure 32).[204] These organometallic compounds behave, not only as homogeneous metal catalysts but also as inverse phase-transfer catalysts, that is, they perform a dual functional catalysis. The olefin is believed to be included in the hydrophobic cavity and to simultaneously interact with a catalytic transition metal center coordinated to the phosphine moieties.

The biphasic hydroformylation of water-insoluble internal olefins was also achieved using the above temporarily supramolecular host which appeared to be more efficient than the second-sphere ligand RAME-β-CD.[205] The initial activities obtained with the above calixarene derivative were improved by a factor of 3.5 compared to RAME-β-CD for the case of trans-4-octene but the selectivities were similar for both systems.[167,171]

12.16.1.3.5 Calixarenes as organometallic hosts for organic molecules

Capsule-shaped Ir(I) and Rh(I) cationic complexes with a triphosphinocalix[6]arene as a multidentate ligand were recently synthesized (Figure 33).[206] These organometallic bis-calixarene complexes showed dynamic behavior with size-selective molecular encapsulation, which was confirmed by variable-temperature $^{31}P\{^{1}H\}$ NMR measurements in the presence of various molecules. X-ray crystal analysis showed that the calix[6]arene moiety adopted the same pinched-cone conformation as the non-coordinated calixarene. Molecules such as CH_xCl_y or $ClCH_2CH_2Cl$ are too small to fit the cavity of the iridium and rhodium bis-calixarene complexes and cannot restrict the dynamic behavior at 25 °C. On the contrary, molecules such as X_2CHCHX_2 (X = Cl or Br), benzene, toluene, *o*- or *m*-xylene just fit in the cavity and show the dynamic behavior. Finally, large molecules (*p*-xylene, cumene, mesitylene, etc.) could not enter the cavity.

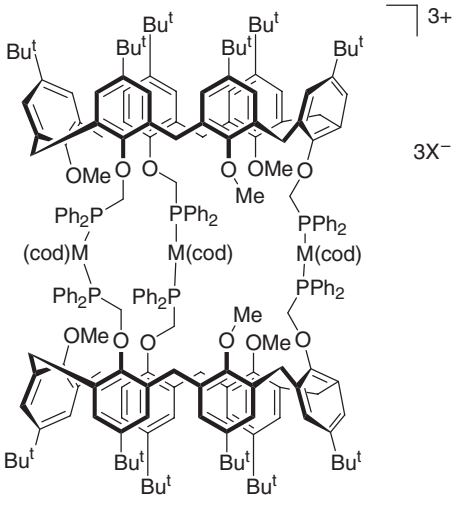

Figure 33

12.16.1.3.6 Resorcinarenes as second-sphere of ferrocene and its derivatives

Högberg's resorcin[4]arenes[207,208] with a cavity deepened supramolecularly have also been used as second-sphere ligands. Co-crystallization of *C*-methylcalix[4]resorcinarene with 4,4′-bipyridine typically yields a host cavity able to recognize ferrocene and its acetylated derivatives in the solid state.[209] Owing to the ability of supramolecular host to interact with the complex in an equatorial fashion, it is possible to affect the conformation of a ferrocene guest such that, for $Fc(Ac)_2$, the substituents of the complex lie eclipsed. As a matter of fact, the cavity of the host is polar and, therefore, may be used to control the orientation, and possibly the conformation, of a ferrocene guest in which the structure of the guest is dictated by the electron-rich, bowl-shaped cavity of *C*-methylcalix[4]resorcinarene.

12.16.1.4 Dendrimers

12.16.1.4.1 Introduction to dendrimers as supramolecular hosts

Research interest on functionalized dendrimers has exploded during recent years and several comprehensive reviews have documented the large amount of research work in this area.[210–214] Dendrimers are well-defined hyperbranched macromolecules obtained by an iterative sequence of reaction steps. Each shell is called a generation (G0, G1, G2, etc.). Large dendrimers are characterized by globular structures possessing cavities that can be used to accommodate guest molecules.[215] Consequently, they constitute supramolecular hosts for organometallic guests or organometallic hosts for organic molecules. Major developments in the use of dendrimers for organometallic catalysis included the development of an extensive control of their sizes and shapes and significant advances in the stereochemical control in the dendrimeric core.

Dendrimers could be modified by organometallic entities at their periphery or their core. Periphery-functionalized dendrimers have their organometallic moiety at the surface of the dendrimer, whereas, in core-functionalized or focal-point-functionalized systems, the transition metal complex is located at the center of the molecule, thereby being shielded from the exterior environment by the dendritic architecture. The difference between core-functionalized and focal-point-functionalized dendrimers relies on the greater efficiency of the former in shielding the organometallic complex than the latter. In this section core- and focal-point-functionalized dendrimers and their applications will be discussed. In particular, their use in organometallic catalysis will be extensively developed. Indeed, one of the main challenges of the last decade was to find the optimum size of dendrimers that would lead to recyclable catalysts but do not suffer from a low activity.

12.16.1.4.2 Dendrimers as organometallic hosts

The benefits of an organometallic inclusion process have been widely demonstrated for core-functionalized dendrimers.[216] Actually, they may benefit from the local catalyst environment created by the dendrimer which may be viewed as a molecular enzyme-like structure. Dendrimers that contain bis(diarylphosphine) ligands have been especially targeted because they can increase the stability of the catalyst situated at the core.

One of the first applications of dendrimers as organometallic hosts was their use as enantioselective catalysts.[217–220] Indeed, dendrimers that are functionalized with transition metals in the core potentially can mimic the properties of enzymes. Brunner introduced the term "dendrizymes" for core-functionalized transition metal catalysts which might be used in enantioselective catalysis.[221] The dendrimeric organometallic complex shown in Figure 34 is an example of such a dendrizyme inside which the chiral dendritic branches create a chiral pocket around the transition metal.

The ion pairs formed by the Rh(I) cation and the PF_6^- anion are encapsulated into the long arms of the expanded phosphine which looks like a cell membrane (Figure 35). Thanks to the methyl groups on the outside, these ionic complexes could be soluble in aliphatic hydrocarbons. Dendrizymes were tested in various reactions such as hydrogenation, hydrosilylation, allylation, and Grignard cross-coupling but only poor enantioselectivities (from <2% enantiomeric excess (ee) to about 10% ee) were measured.[222] A lack of rigidity in the outer layer of chiral groups was held responsible for these low enantioselectivities. Remarkably, a high-generation dendrimer based on 1,2-bis(diphenylphosphinyl)ethane (dppe) resulted in a faster hydrogenation catalyst of acetamidocinnamic acid than the parent ligand.[223]

Van Leeuwen *et al.* have elaborated numerous diphosphine-core-functionalized dendrimers, among which are the carbosilane dendritic analogs of [1,1′-bis(diphenylphosphino)ferrocene] (Figure 36, **A**).[224] Experiments showed that palladium complexes of these dendrimers are active catalysts in the allylic alkylation reaction of 3-phenylallyl acetate with diethyl 2-sodio-2-methylmalonate. A significant change in the product selectivity is observed for the largest dendrimer. This change in selectivity might be due to the increasing steric bulk of the dendrimer hindering the attack of the nucleophile on the Pd–allyl. The apolar microenvironment created by the carbosilane wedges could also be the reason for this observed selectivity effect. The 1,1′-bis(diphenylphosphino)ferrocene rhodium complexes

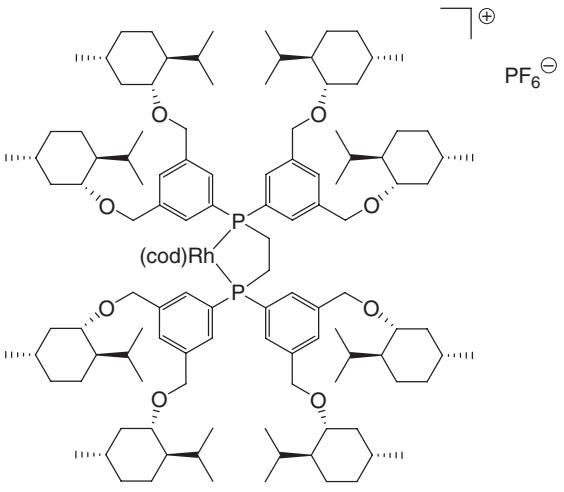

Figure 34

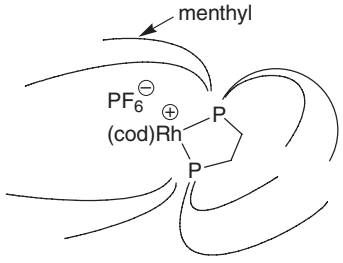

Figure 35

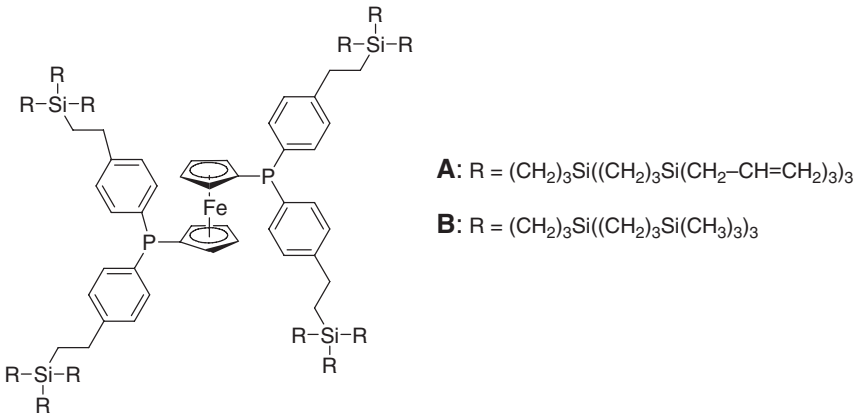

Figure 36

at the carbosilane dendrimer core such as that depicted in Figure 36 (compound **B**) are also active catalysts in the hydroformylation of oct-1-ene and the hydrogenation of dimethyl itaconate in a continuous-flow membrane reactor.[225] The palladium- and rhodium-dendrimeric catalysts could be recycled several times without significant loss of activity, suggesting that the stability of core-functionalized systems is larger than that of their periphery-functionalized analogs. These experiments clearly demonstrate that dendrimeric catalysts can indeed combine facile catalyst–product separation with high activity.

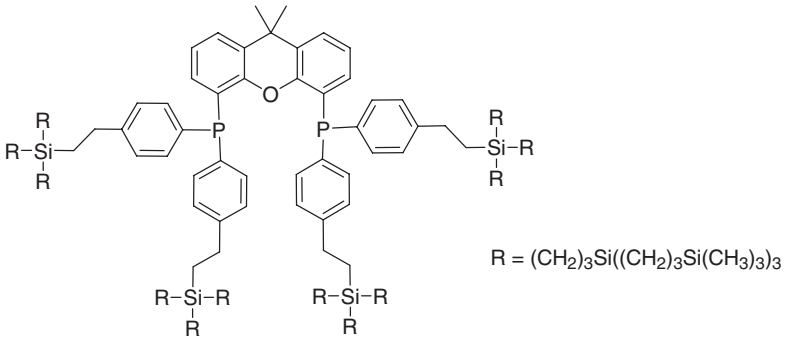

Figure 37

In the hydroformylation of oct-1-ene, the dendrimeric ligands based on the rigid xanthene backbone (Figure 37), all show a high preference for the formation of the linear aldehyde (95%). A high linear to branched (*l*/*b*) ratio of around 55, which is similar to that induced by the parent xantphos ligand, is found for all generations of dendrimeric ligands. The regioselectivity in the hydroformylation of oct-1-ene is determined by the rigid ligand in the core and is not affected by the size of the dendrimeric encapsulation. Interestingly, this dendrimeric catalyst is sufficiently large to allow separation by nanofiltration techniques. This shows the potential advantage of dendrimeric catalysis compared to other immobilization techniques, which generally result in somewhat lower activities upon immobilization. Moreover, a decrease in the activity for the bulky substrate 4,4,4-triphenylbut-1-ene using large dendrimeric ligands is observed, suggesting that these larger dendrimers can be used for substrate-selective catalysis.[225]

Chiral diphosphine ligands bearing dendritic wedges for asymmetric hydrogenation have also been reported. Asymmetric hydrogenation of 2-[*p*-(2-methylpropyl)phenyl] acrylic acid was used as the model reaction for the investigation of the catalytic activity and enantioselectivity of these dendritic Ru(BINAP) catalysts.[226] Hydrogenated product (ibuprofen) was obtained with 92.6% ee and 100% conversion in 20 h. These catalysts showed higher ee values than Ru(BINAP), although the highest-generation catalyst gave slightly lower enantioselectivity. Most interestingly, the size of the dendritic wedges influenced the reactivity of these catalysts. Unlike common dendritic catalysts, the rate of the reaction increased using higher generation catalysts. This effect is most pronounced when going from generation 1 to 2. The profound size effect is probably due to the steric bulk of the dendritic wedges which affects the dihedral angle of the two naphthalene rings in the Ru(BINAP) complex (BINAP = 2,2-bis(diphenyl–phosphanyl)-1,1-binaphthyl), and thus leads to a faster rate and/or better enantioselectivity of reaction.

Palladium diphosphine complexes located at the core have also been found to be efficient, recoverable catalysts in a Stille coupling involving iodobenzene ant tributylvinyltin.[227] This palladium complex, composed of a dendrimer of generation 3 bearing only one metallic center located at the core, was prepared *in situ* by reacting the dendrimer (Figure 38) with $Pd(OAc)_2$. The obtained complex (1 or 5 mol.%) appeared to be a very efficient catalyst under mild conditions. Steric hindrance around the metallic center due to the dendrimer shell allowed the system to be recycled several times without loss of activity.

Dendrimers having phosphines as branching points (Figure 39; Rh = [Rh(cod)Cl]) were synthesized by acid–base hydrolysis of aminosilanes with alcohols.[228] This organometallic compound could be considered as a periphery- and core-functionalized dendrimer. Interestingly, the complexes can be formed before or after the acid–base reaction that forms the dendrimer. The Rh(I) metallodendrimer of Figure 39 was catalytically active in the hydrogenation of

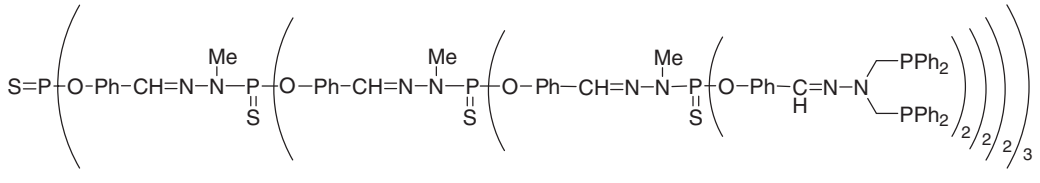

Figure 38

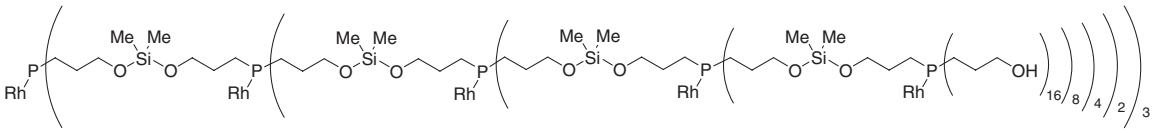

Figure 39

decene and showed only a small decrease in activity compared to the monomeric rhodium complex. Rates around 400 mol (mol rhodium)$^{-1}$ h^{-1} were obtained in THF at 25 °C and 20 bar of hydrogen. After extraction and recrystallization the catalysts were reused showing 95% of the original activity in the second run.

12.16.1.4.3 Dendrimers as hosts for organometallic catalysts

Core-functionalized dendrimers containing inorganic catalysts have also proved to be very useful as enantiomeric catalysts. In this case, the dendrimer is viewed as an inorganic host able to include an organometallic complex. Here again, the dendritic cavities provide a confined environment around the catalytic core where regio- and shape selectivity could be improved. The Ti-catalyzed enantioselective nucleophilic addition of diethylzinc to aldehydes, yielding optically active secondary alcohols,[229] has often been used as model reaction to evaluate the catalytic performances of these inorganic dendrimers. Indeed, if a reaction proceeds by a bimetallic mechanism, the dendritic catalysts might show better performances than the monomeric species due to the higher proximity of the metallic species.[230,231] Seebach *et al.* described the synthesis of dendrimers with TADDOLs ((*R*,*R*)-$\alpha,\alpha,\alpha',\alpha'$-tetraaryl-1,3-dioxolane-4,5-dimethanol) as asymmetric active sites in the core (Figure 40).[232,233] These dendrimers were converted into Ti–TADDOLates, which were employed as catalysts for the enantioselective nucleophilic addition of Et_2Zn to PhCHO. When compared with the simple Ti–TADDOLates, no decrease of selectivity (98 : 2) was detected up to the second generation, and the rates hardly decreased up to the third generation. A small decrease in enantioselectivity with increasing generation number (G0 to G3) was observed. On going from G3 to G4, the structure changes from roughly planar to globular and densely packed. In that case, the branches become sterically too demanding and access of substrates is therefore hindered, which provides an explanation for the drop in catalytic activity.

The above TADDOL-cored dendrimers were immobilized by co-polymerization of styryl-substituted TADDOLs in cross-linked polystyrene using divinylbenzene and TADDOL-centered dendrimers with peripheral styryl groups as cross-linkers.[232] These ligands were coordinated to Ti by exchange with $Ti(OCHMe_2)_4$. As shown before, the branches of the dendritic catalyst have only a minor influence on the selectivity of the enantioselective nucleophilic addition of Et_2Zn to PhCHO (98% vs. 96%ee). However, using polymers with a high TADDOLate content (thus

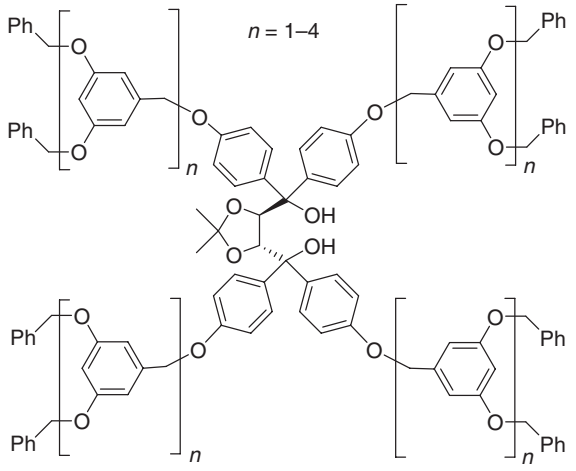

Figure 40

higher cross-linking) resulted in much lower enantioselectivities due to "frozen-in" conformations of the ligand. Introduction of spacers between the Ti–TADDOLates and the styryl-functionalities results in a drop of selectivity, which might be caused by a lesser control of the active site and the swelling properties of the polystyrene beads.[234] All the polymeric systems were recycled with high enantioselectivity in 20 consecutive reactions by decanting/filtration and subsequent washing with toluene.

Rigid and optically active dendrimers containing cross-conjugated units were synthesized from the coupling of phenylacetylene-based dendrons with an optically pure diacetate of 4,4′,6,6′-tetrabromo-1,1′-bi-2-naphthol (Figure 41).[235] In the asymmetric reaction of diethylzinc with aldehydes, the generation 2 dendrimer behaves very differently from the small parent 1,1′-bi-2-naphthol (BINOL) molecule. The (*S*)-dendrimer shows much higher catalytic activity than (*S*)-BINOL which indicates that the zinc complex generated from the reaction of this dendrimeric ligand with diethylzinc may have much higher Lewis acidity than the zinc complex generated from BINOL. Moreover, this dendrimer also generates the opposite enantiomeric product which also indicates that the *in situ* generated catalytically active species when these ligands are used are very different. These bulky and rigid dendritic arms prevent the dendrimer from forming oligomers through Zn–O–Zn bonds, yet still allow small molecules such as benzaldehyde and diethylzinc to approach the chiral core for the catalytic reaction. In these catalytic reactions, the dendrimer can be easily recovered from the reaction mixture by precipitation with methanol due to the large size differences between this dendritic molecule and the products and reagents.

Similarly, Yoshida *et al.* prepared chiral dendritic 1,1′-binaphthol derivatives having poly(benzyl ether) wedges at the 6,6′-positions (Figure 42).[236] The molecular optical rotation was identical for all generations, which is in agreement with the presence of a single chiral group. From circular dichroism spectroscopy, it was concluded that the chiral environment of the binaphthol remained unchanged for all systems. Here again, as previously observed for the Seebach's system, the enantioselectivity decreased only slightly for the larger dendritic catalysts in titanium-catalyzed asymmetric allylation of aldehydes by allyl stanane (92–88% ee compared to 87% ee for the parent (*R*)-binaphthol).

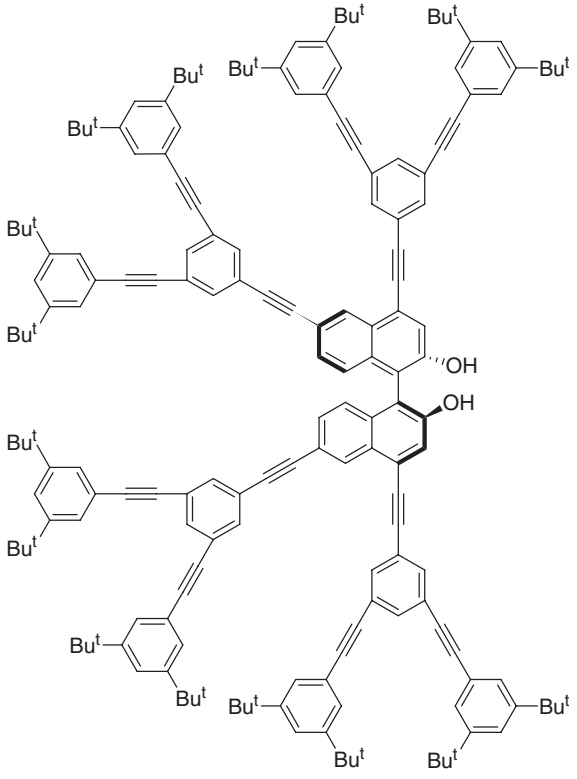

Figure 41

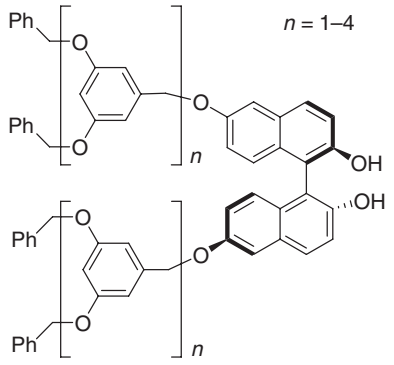

Figure 42

12.16.1.4.4 Dendrimers as third-sphere ligands of ferrocene

Based on Newkome-type dendrimers, ferrocenyl structures such as that depicted in Figure 43 have been prepared by Kaifer *et al.*[237] These dendrimers show hydrophilic properties resulting from their terminal carboxylic acid residues. Their interactions with β-cyclodextrin were investigated in aqueous solution by voltammetric techniques. The degree of binding affinity between the ferrocenyl compound and β-CD is typically evidenced by both a positive shift in the half-wave potential ($E1/2$) and a decrease in the voltammetric current due to the slower diffusion of the β-CD complex compared to that of the free ferrocenyl derivative. In that case, the CD/ferrocenyl complex is included inside the dendrimer's cavity. The dendrimer may then be considered as a third-sphere ligand of ferrocene. Results showed that increasing dendrimer growth inhibits binding of β-CD to the ferrocenyl dendrimer. This finding suggested that growth of the dendrimer interferes with the approach of the CD host and its inclusion of the ferrocene moiety, likely due to steric crowding.

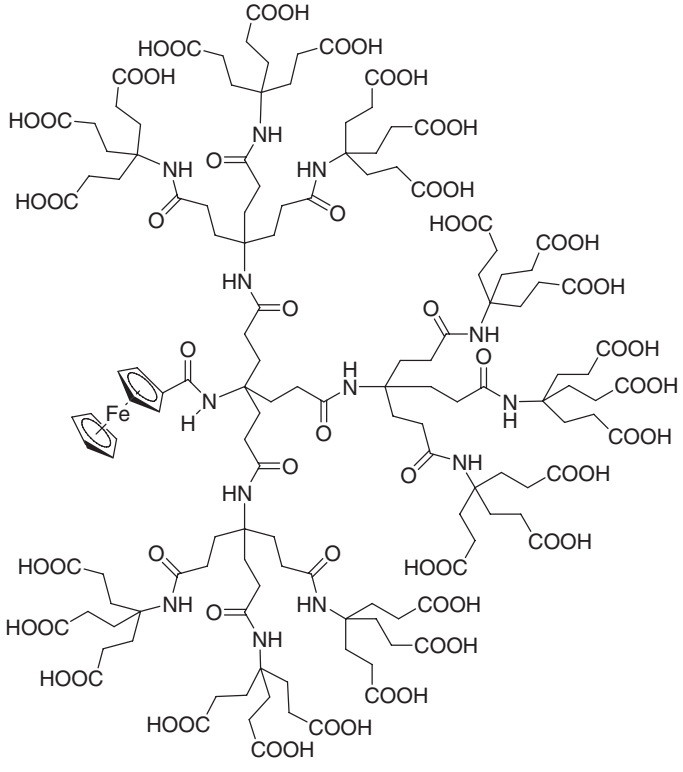

Figure 43

12.16.1.5 Bioorganometallic Hosts and Guests

12.16.1.5.1 Introduction to bioorganometallic inclusion

Apart from the exception of the coenzyme of vitamin B12 and its derivatives, in which a direct cobalt—carbon bond is one of the features of the system,[238] only a few examples of natural organometallic metal enzymes have been reported in the literature.[239,240] Thanks to the enormous amount of synthetic work that has been done in the field of organometallic compounds, bioorganometallic chemistry has now become an important subtopic in organometallic chemistry. This section is devoted to bioorganometallic inclusions for which a bioorganic molecule or organometallic complex is included inside an organometallic host or a natural supramolecular receptor, respectively.

12.16.1.5.2 Bioorganometallic hosts for polypeptides

A molecular recognition process using guests that encompass aromatic and aliphatic amino acids, substituted aromatic and aliphatic carboxylic acids with supramolecular, bioorganometallic hosts, (η^5-pentamethylcyclopentadienyl)rhodium (Cp^*Rh)-nucleobase, nucleoside, and nucleotide (L) cyclic trimer complexes of general formula $[Cp^*RhL]_3(OTf)_3$, has been studied in aqueous solution at pH 7 (Figure 44).[241] The non-covalent π–π, hydrophobic, and possible subtle H-bonding interactions were found to be fully operational in aqueous solution by solvophobic forces that enhanced host–guest complexation, with steric, electronic, and molecular conformational parameters as important criteria. For example, the molecular recognition of L-tryptophan with $[Cp^*Rh\text{-}(2'\text{-deoxyadenosine})]_3(OTf)_3$ occurred via the inclusion of the amino acid aromatic rings inside of the host cavity. Moreover, both the π–π and hydrophobic interactions seem to be equally important when competing aromatic and aliphatic carboxylic acid guests.[242]

A host–guest molecular recognition process of L-tryptophan, with the above various triangular, bowl-shaped Cp^*Rh–nucleobase/nucleoside/nucleotide cyclic trimer molecular receptors, was also detected in a gas phase by electrospray ionization mass spectrometry.[243] In this case, the supramolecular complex formation was found to occur predominately via non-covalent π–π interactions; non-covalent hydrophobic forces apparently being weak or non-existent. Trp–Met–Asp–Phe tetrapeptide with the trimeric-rhodium host $[Cp^*Rh(2'\text{-deoxyadenosine})]_3[OTf]_3$ also formed a host–guest complex in water that is detected in the gas phase.

12.16.1.5.3 Proteins as hosts for bioorganometallic complexes

Experiments of organometallic pharmaceuticals at estrogen receptor-binding sites have been carried out to examine the consequences of the attachment of an organometallic moiety to a modified drug structure, with respect to the receptor-binding site.[245] Jaouen *et al.* prepared and studied hydroxyferrocifen derivatives (Figure 45) which have been evaluated on human cells derived from breast cancer and possessing estradiol receptor sites.

These molecules whose anti-estrogenic properties (i.e., the ability to block the estrogen receptor) are preserved or even improved also show increased cytotoxicity. The ferrocene (Fc) moiety does indeed have some toxicity *in vivo*

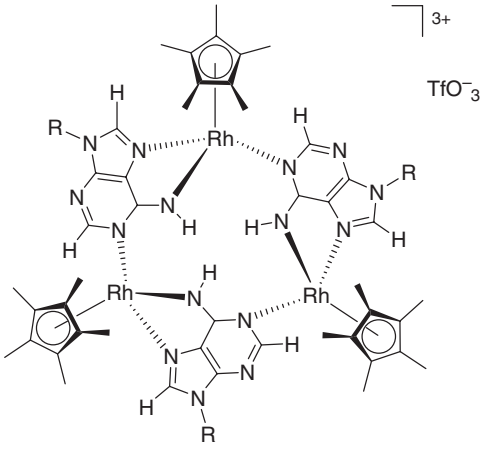

Figure 44

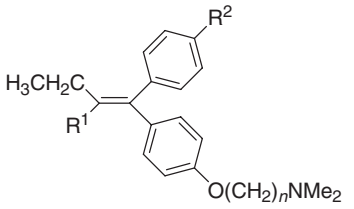

R^1 = Ph, R^2 = H, tamoxifen

R^1 = Fc, R^2 = OH, hydroxyferrocifene derivatives (n = 2, 3, 4, or 5)

Figure 45

owing to its oxidation to a radical ferricinium cation which interacts with DNA. It has been shown that the hydroxyferrocifen bioligands/protein-binding site couple constitutes a supramolecular complex for which the length of the dimethylaminoalkyl chain in the bioligand determines their antiproliferative effects. Thanks to the ferrocenyl group which is bulkier than the phenyl in the β-position present in tamoxifen (Figure 46), the ferrocifen series with $n = 3$, 4 or 5 appeared to have a higher level of efficacy than tamoxifen, both *in vivo* and *in vitro*. By contrast, the basic chain with a two C arm might not bind firmly to one of the amino acids of the protein-binding site (Asp 351), resulting in a lower anti-estrogenic effect.

It was also demonstrated that dramatic conformational and non-covalent bonding differences, with the estrogen protein-binding site between the two organometallic modified drugs such as ferrocifen derivatives and estradiol ruthenocene complex, is possibly the reason why the organometallic pharmaceutical as ferrocifen derivative is a potential anticancer agent, while the organometallic estradiol ruthenocene complex is not.[246,247] The relative binding affinity values for estradiol receptor alpha showed that recognition was good (between 20% and 13.5%) when the organometallic moiety was attached at the end of a rigid alkyne spacer. However, the affinity of the modified hormone for the receptor was severely reduced (1%) for a substituent such as $-CH_2-(\eta < \rho\chi >^5\text{-}C_5H_4)-RuCp$, in which the spacer is reduced to a single flexible sp^3 carbon atom, allowing the organometallic moiety greater freedom of movement around the attachment point. The relative binding affinity values found were in agreement with results obtained from a molecular-modeling study. This molecular-level explanation may prove useful in the future in evaluating factors that influence recognition when designing customized estrogen vectors for well-defined targets, for example, organometallic radiopharmaceutical products attached to bioligands of this type.

Another application of bioorganometallic ligands is relative to enzymatic catalysis which has emerged as an important alternative tool for the synthesis of enantiopure compounds in recent years. Here again, the strategy relies on the use of non-covalent incorporation of the organometallic precursor into the protein (Figure 47). Attention has been focused on the use of semi-synthetic enzymes to produce efficient enantioselective hybrid catalysts for a given reaction.

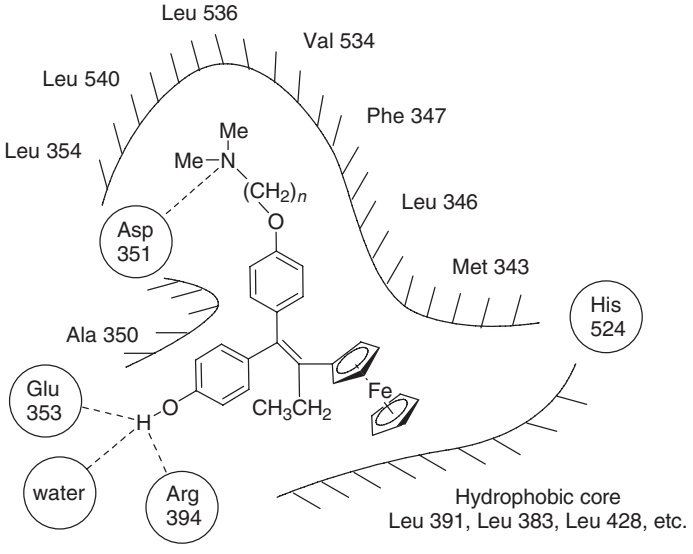

Figure 46

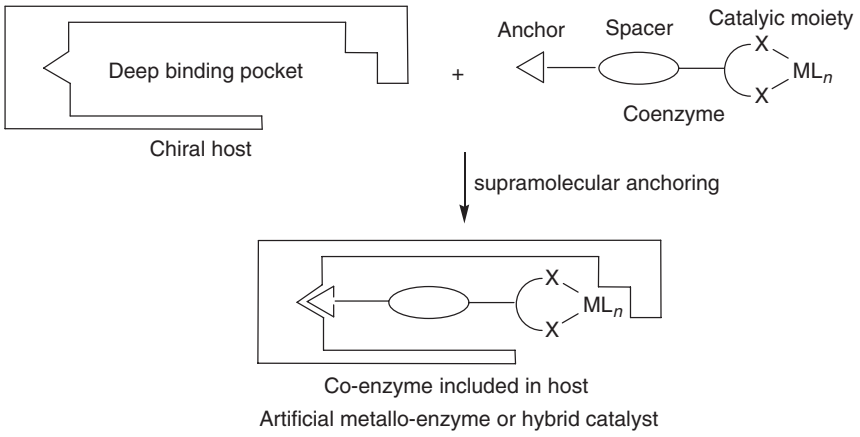

Figure 47

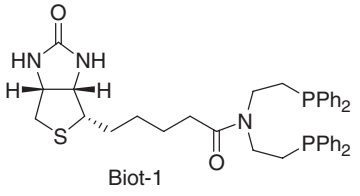

Figure 48

Recently, Ward *et al.* described the incorporation of achiral biotinylated rhodium–diphosphine complexes into (strept)avidin.[248–250] Compared with avidin, streptavidin possesses a similar affinity for biotin ($Ka \approx 10^{14}$ M^{-1}) but is endowed with a deeper binding pocket. Catalyst precursor $[Rh(cod)(Biot\text{-}1)]^+$ displayed good enantioselectivity, in favor of the (*R*)-enantiomer (92% ee) (Figure 48). Substitution of serine 112 by a glycine residue in the loop of streptavidin (S112G) yields an improved host protein for the reduction of acetamidoacrylic acid with $[Rh(cod)(Biot\text{-}1)]^+$-streptavidin 112G (96% ee (*R*)). The artificial metallo-enzymes offer an attractive way to exploit the second-coordination sphere provided by a host protein to produce versatile enantioselective catalysts with features reminiscent both of enzymatic and of organometallic catalysts. Moreover, the enantioselectivity may be optimized either chemically and/or genetically (i.e., chemogenetic), thus offering an ideal scaffold for high-throughput optimization of enantioselective catalysts. These results suggest that semi-synthetic approaches will play a key role in the development of future biocatalysts.

12.16.1.6 Polymers

12.16.1.6.1 Introduction to polymers as supramolecular hosts

In nature, reactive metal centers are located within enzymes in well-defined sites, attenuating their otherwise unselective chemistry. To direct the selectivity of substrate–catalyst interactions, highly cross-linked molecular imprinting polymers (MIPs) should provide ideal matrices for transition metal catalysts as the access of substrates is constrained by the polymer backbone and site geometry.[251] The MIP binding environment could be designed to generate a highly defined outer coordination sphere around the transition metal catalyst.

12.16.1.6.2 Organometallic complexes in polymer matrix

The first strategy consists in attaching a non-polymerizable imprinting ligand (which acts as a pseudo-substrate) to the metal center as a template. The metal is then incorporated into the cross-linked backbone by one or more polymerizable ligands (most frequently containing a styrene side chain to allow its incorporation into organic

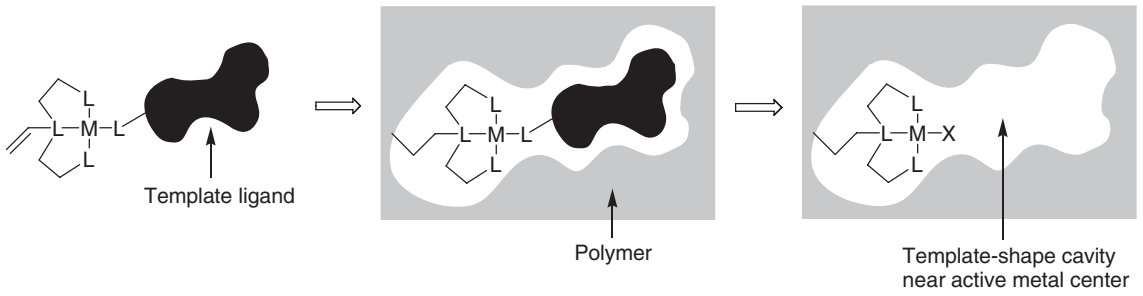

Figure 49

polymers). Stripping off the ancillary ligands is expected to provide catalytic materials with improved control of both activity and stereoselectivity of the organometallic catalyst (Figure 49).

Polymerization of the coordinated species and subsequent cleavage of the transition state analog should yield a macroporous polymer possessing specific cavities in close proximity to the active sites in the form of the immobilized catalyst. Polborn and Severin developed this technique to produce an MIP catalyst for the reduction of benzophenone, employing an immobilized ruthenium catalyst coordinated with phosphinato ligand with similar shape to transition state-mimicking intermediate of the reaction as the catalytic precursor.[252] Thus, chloro-(η^6-arene) complexes of Ru(II) derivatives were co-polymerized with ethylene glycol dimethacrylate in the presence of a porogen. After polymerization, the polymers were ground and sieved to obtain uniform particule sizes (25–100 μm). The polymers were then treated with a solution of ($BnNEt_3$)Cl in methanol. During this process, the phosphinato ligands are removed and replaced by chloro ligands, thereby generating a form-selective cavity in close proximity to the catalytically active metal center. In the asymmetric reduction of benzophenone, the MIP systems displayed high activities with rate enhancements threefold in comparison with the uncatalyzed process.

The same methodology was used to generate an immobilized chiral rhodium(III) complex, which catalyzes the asymmetric reduction of benzophenone with significantly higher activity than a control polymer without a cavity.[253] Excellent enantioselectivities were obtained (up to 95% ee vs. 2–9% ee for the control polymer). Competitive experiments with acetophenone and a second co-substrate have revealed that the cavity generated with the phosphinato ligand is specific for acetophenone.

Both the activity and the selectivity of the imprinted catalyst are dependent on how the ruthenium complexes are attached to the polymer backbone. Actually, the work was extended to include ruthenium species locked in the polymeric matrix by two ligands to avoid conformational "flipping" during and after polymerization (Figure 50).[254] This double connection proved to give superior results because the digrafted material is considered to have more rigid matrix and reduce its flexibility by connection to the polymer backbone at two points. Indeed, the ruthenium complex-containing MIP led to a significantly higher activity than control polymers without cavities (up to a factor of 7), high selectivity for benzophenone against other ketonic substrates and also regioselectivity.

An $[(arene)RuCl_2]_2$ complex with a methacrylate side chain has also been prepared in two steps using commercially available starting materials.[255] This complex reacts with PPh_3, pyridine, or toluidine to give the corresponding mononuclear adducts which were immobilized by co-polymerization with divinylbenzene (DVB) or ethyleneglycol

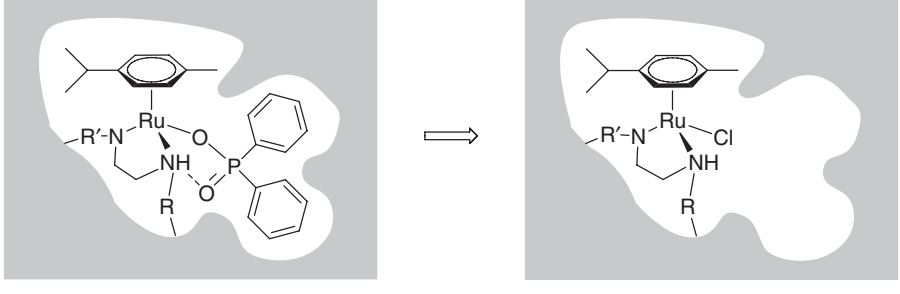

Figure 50

dimethacrylate (EGDMA). The resulting EGDMA co-polymer containing the PPh_3-ruthenium complex was tested as a catalyst in asymmetric-transfer hydrogenations. Using (1*R*,2*R*)-(−)-*N*-*p*-tosyl-1,2-diphenylethylenediamine as the chiral ligand and azeotropic NEt_3/HCO_2H as the reducing agent, aromatic ketones were converted into the corresponding alcohols with selectivities between 87 and 97% ee.

A similar approach was adopted by Cammidge *et al*., who used polymerizable triphenylphosphine ligands to fix otherwise labile palladium species in a *cis*-geometry for catalysis of Suzuki and Stille coupling reactions.[256] Imprinted polymer palladium catalysts were found to be as active and selective, or more so, than homogeneous systems, which was attributed to their semi-rigid ligand geometry retained by the imprinting process.

Gagné *et al*. developed polymer active sites that additionally contained a receptor (recognition sites) displayed in the outer sphere of the metal center (reactive site).[257] The Suzuki reaction of *p*-bromoanisole with phenyl boronic acid and the allylation of dimethyl malonate with allyl acetate were both chosen to assess the presence and/or effect of the crown-ether in crown-ether-molecular imprinting polymer–palladium complex. The results showed that molecular imprinting can be used to functionalize the second-coordination sphere of a transition metal complex and subsequently affect its catalytic behavior.

12.16.1.6.3 Imprinted organometallic complexes on oxide surface

Another strategy using the molecular imprinting of metal–monomer complex on oxide surface has been developed by Iwasawa *et al*.[258] SiO_2-attached Rh–monomer catalyst, which has two $P(OCH_3)_3$ ligands per Rh, was prepared by impregnating $RhCl(P(OCH_3)_3)_3$ precursor on oxide surface. Imprinted catalysts with template cavity were created by polymerization of $Si(OCH_3)_4$ and by using one of the two $P(OCH_3)_3$ ligands as template for molecular imprinting. The phosphite ligand was used as a template molecule for a half-hydrogenated alkyl intermediate of hydrogenation of 3-ethyl-2-pentene. Stacking of SiO_2 matrix overlayers on the surface changed catalytic activity of the rhodium complex for hydrogenation of 2-pentene. The selectivity of the surface-attached Rh monomers was also subjected to regulation by the surface which was regarded as a unique and large ligand in addition to the electronic and geometric effects of the ligands.

Similarly, starting from the bridged Rh-dimer precursor $Rh_2Cl_2(CO)_4$, Rh-dimer molecular imprinting catalyst was attached at SiO_2 surface for hydrogenation of alkenes, and exposed to $P(OCH_3)_3$ to make rhodium–phosphite complex at the surface.[259,260] Hydrogenation of linear alkenes such as 2-pentene, 2-octene, and 1-phenylpropene was faster than non-imprinting catalysts (TOF ratios up to 51). The reader can consult Chapter 12.10 for more details on "surface organometallic chemistry."

12.16.1.7 Organometallic Clusters

The chemistry and catalytic applications of organopolymetallic ruthenium complexes have been extensively described in COMC (1982) (volume 4, Chapter 32.5 to 32.8) and COMC (1995) (volume 7, Chapter 12–14) and continue to attract considerable interest. Actually, ruthenium-specific electronic and steric interactions are expected to lead to increased selectivity in the overall chemical transformation.

To take benefits of the synergistic changes in activity and/or selectivity generated by the proximity of an organic guest included in a ruthenium-cluster pocket, Süss-Fink *et al*. have been interested in trinuclear clusters of ruthenium. The trinuclear arene–ruthenium cluster cations $[H_3Ru_3\{C_6H_5(CH_2)_nOH\}(C_6Me_6)_2(O)]^+$ ($n = 2$ or 3) have been synthesized from the dinuclear precursor $[H_3Ru_2(C_6Me_6)_2]^+$ and the mononuclear complexes $[\{C_6H_5(CH_2)_nOH\}Ru(H_2O)_3]^{2+}$ in aqueous solution (Figure 51).[261]

In all cases, the metal core consists of three ruthenium atoms, the three Ru–Ru distances being in accordance with a metal–metal single bond. The three ruthenium atoms are capped by a μ^3-oxo ligand which is almost symmetrically coordinated. The three hydrido ligands bridging the three ruthenium–ruthenium bonds could be localized and fully refined. The single-crystal X-ray structure analyses of $[C_6H_6\subset[H_3Ru_3\{C_6H_5(CH_2)_2OH\}(C_6Me_6)_2(O)]][PF_6]$ and $[C_6H_6\subset[H_3Ru_3\{C_6H_5(CH_2)_3OH\}(C_6Me_6)_2(O)]][BF_4]$ show that benzene is held inside the hydrophobic pocket of the clusters, the angle between the metal (Ru3) plane and the aromatic plane being 67.8 and 89.8, respectively. Contrary to what was classically observed with benzene molecules, no π-stacking were detected for the above host–guest complexes. The guest molecule interacts in both cases weakly with the host only by hydrophobic and van der Waals contacts.

The closed-structural complex $[H_3Ru_3(C_6H_6)(C_6Me_6)_2(O)]^+$ was first thought to efficiently catalyze the hydrogenation of benzene to cyclohexane under biphasic conditions, but it has been proved that this complex was not the true catalyst.[262] Nevertheless, supramolecular, host–guest complexation of benzene by this complex was

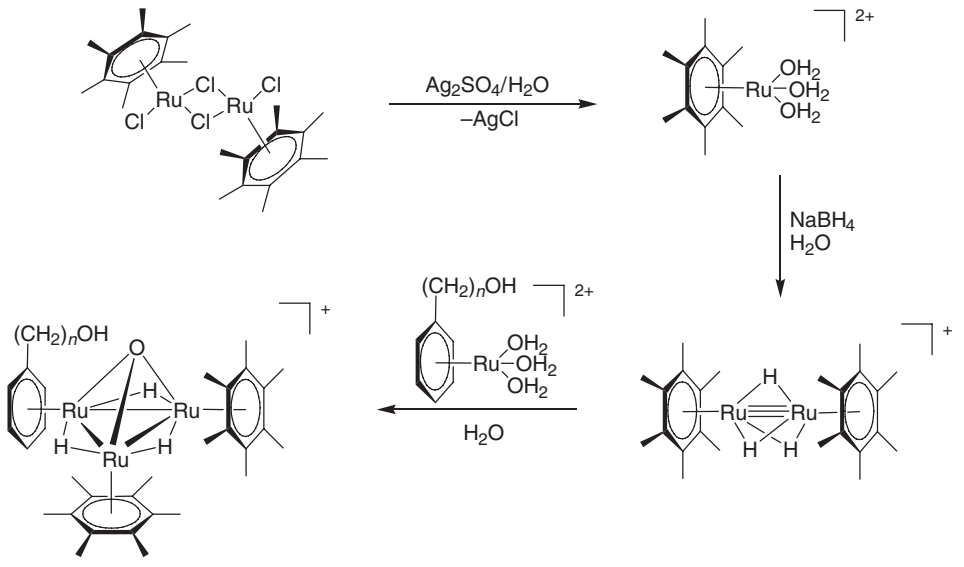

Figure 51

unequivocally demonstrated by X-ray crystallography, electrospray mass spectroscopy (ES-MS) and molecular mechanics data.

The hydrogen-bonded systems formed between monocarboxylic acid derivatives and the trinuclear arene–ruthenium cluster cation $[H_3Ru_3(C_6H_6)(C_6Me_6)_2(O)]^+$ have also been studied in solution by cold-spray ionization mass spectroscopy (CSI-MS) and in the solid state by single-crystal X-ray structure analysis of the tetrafluoroborate salts.[263] The presence of 1 : 1 (acid : cluster) adducts in acetone solution has been clearly demonstrated. Single-crystal X-ray structure analyses show that the μ^3-oxo ligand is a strong acceptor to form hydrogen bonds, and that the hydrophobic pocket spanned by the three arene ligands acts as a bowl to host different molecules in the solid state. For example, in the presence of benzoic acid, the phenyl group is incorporated in the hydrophobic pocket of the cluster, whereas the hydroxyl group of the acid function is hydrogen-bonded to the μ^3-oxo ligand of a neighboring molecule (Figure 52).

12.16.1.8 Inorganic Hosts for Organometallic Complexes

Raymond *et al.* have reported the formation and host–guest properties of supramolecular tetrahedral assemblies of $[M_4L_6]^{12-}$ stoichiometry ($M = Ga^{3+}$, Al^{3+}, Fe^{3+}; L = bis(bidentate) catecholamide).[264,265] The M_4L_6 assemblies contain four metal centers, each of which can adapt either a Δ or Λ configuration. Only homochiral isomers of the assemblies form, that is, each assembly is either $\Delta,\Delta,\Delta,\Delta$- or $\Lambda,\Lambda,\Lambda,\Lambda$-configured and does not racemize. In these assemblies the metal atoms are located at the vertices of the tetrahedron and six bis-bidentate naphthalene-based catechol amide ligands span the edges (Figure 53).

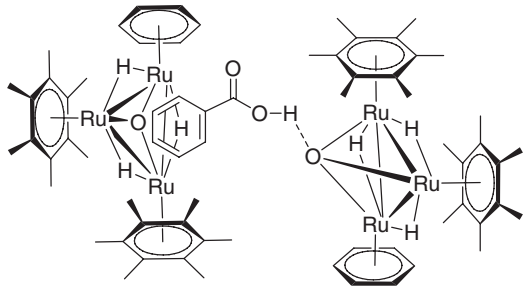

Figure 52

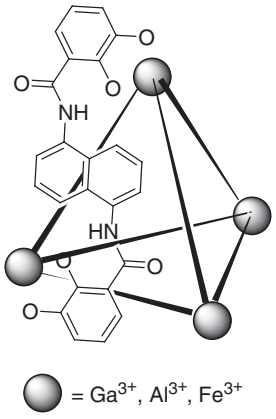

Figure 53

The assemblies are water soluble, yet they contain a flexible hydrophobic cavity of 350–500 $Å^3$ into which they can bind a broad range of monocationic guest molecules, from alkyl ammonium cations to half-sandwich complexes such as $[Cp_2Fe]^+$, $[Cp_2Co]^+$, and $[CpRu(C_6H_6)]^+$ ($Cp = \eta^5$-C_5H_5). These findings highlight the ability of container-like molecules to provide size- and shape-defined nanospaces, highly capable of catalysis of unimolecular organic reactions. By binding the substrates in a reactive conformation, the host assembly accelerates the rates of rearrangement by up to three orders of magnitude. As an example, the iridium methyl ethene adduct $[Cp^*(PMe_3)Ir(Me)(C_2H_4)][OTf]$ was added to the formally "empty" $Na_{12}[Ga_4L_6]$ assembly to form $Na_{11}[Cp^*(PMe_3)Ir(Me)(C_2H_4)\subset Ga_4L_6]$.[266] This supramolecular iridium host–guest assembly led to the C–H bond activation of aldehydes with highly specific size and shape selectivity, as well as modest diastereoselectivity (Figure 54).

The encapsulation of the organometallic complexes $[CpRu(\eta^6\text{-}C_6H_6)]^+$ and $[CpRu(p\text{-cymene})]^+$ into the chiral tetrahedral host M_4L_6 has also been investigated. The host–guest complexes $K_{11}[CpRu(\eta^6\text{-}C_6H_6)\subset Ga_4L_6]$ and $K_{11}[CpRu(p\text{-cymene})\subset Ga_4L_6]$ were characterized by one- and two-dimensional NMR techniques as well as by ES-MS.[267] Encapsulation of the prochiral complex [CpRu(*p*-cymene)] by the chiral host renders the enantiotopic methyl protons diastereotopic as evidenced by ^1H NMR spectroscopy.

Upon combination and vigorous stirring of an aqueous solution of $[NMe_4\subset Ga_4L_6]_{11}^-$ and an ethereal layer of CpRu(2,3-dimethylbutadiene)Cl, guest exchange took place, and the host–guest complex $[CpRu(2,3\text{-dimethylbutadiene})(H_2O)\subset Ga_4L_6]_{11}^-$ was isolated from the aqueous layer in almost quantitative yield.[268] Formation of the two diastereomeric host–guest complexes of $[Cp^*Ru(isoprene)(H_2O)\subset Ga_4L_6]_{11}^-$ was observed by ^1H NMR spectroscopy, with one of the diasteromers present in slight excess (4% diastereomeric excess (de)). The encapsulation of Cp^*Ru(2-ethylbutadiene)Cl proceeded similarly to yield two diastereomers of $[Cp^*Ru(2\text{-ethylbutadiene})(H_2O)\subset Ga_4L_6]_{11}^-$. Here, a de of 70% is observed. The host assembly recognizes one enantiomer of the chiral ruthenium complex relative to the other with high selectivity, reflecting the guest molecule's close fit into the cavity. The chiral metal–ligand assemblies have a high potential for asymmetric recognition processes, illustrating the assemblies' large influence on the bound substrate. Moreover, a dynamic resolution of the reactive catalyst precursor was accomplished by utilizing the resolved supramolecular assembly.

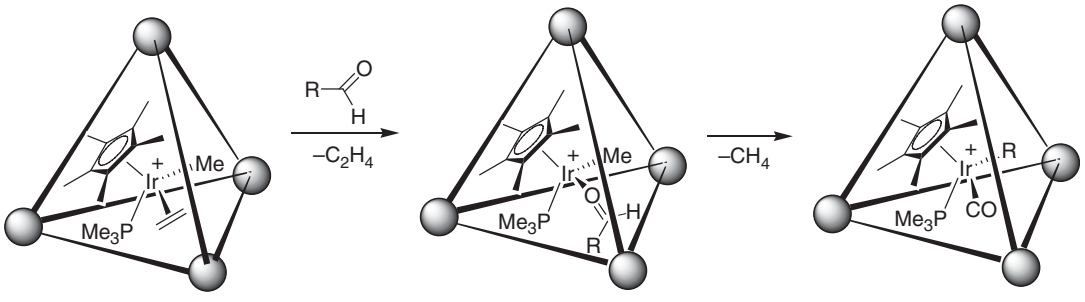

Figure 54

12.16.1.9 Other Organometallic Inclusion Systems

12.16.1.9.1 Crown-ethers as organometallic hosts

The use of crown-ethers as first- and second-sphere ligands has been widely documented.[269] Nonetheless, examples of organometallic inclusion are very few. Loeb *et al.* described the synthesis of organopalladium crown-ether complexes $[Pd(L^3)(MeCN)]^+$ and $[Pd(L^4)(MeCN)]^+$ able to bind the hydrazinium ion, $[NH_2NH_3^+]$, via simultaneous first- and second-sphere coordination featuring σ-donation to Pd and hydrogen bonding to aliphatic ether oxygen atoms (Figure 55).[270] The degree of second-sphere coordination depends on the ability of the $NH_2NH_3^+$ ion to penetrate the different sized crown-ether rings and the number of ether oxygen atoms that can potentially act as hydrogen bond acceptors. For $[Pd(L^4)(MeCN)]^+$, the fit of receptor and substrate is quite remarkable. The $NH_2NH_3^+$ ion is nested in the larger crown-ether ring and six hydrogen-bonding interactions accompany the Pd–N σ-bond. This study demonstrated that this type of multiple interaction mode can be designed into a receptor and tuned to fit a particular molecule ion.

These organopalladium complexes have also been shown to be efficient metalloreceptors for nucleobases.[271] This was accomplished by σ-donation to the palladium and non-covalent bonding (hydrogen bonds, π–π stacking) to peripheral receptor sites on the ligand. Although the combination of metal coordination, hydrogen bonding, and π–π stacking interactions was common to each nucleobase, the relative placement of these binding sites was different for each and acts as a source of discrimination.

12.16.1.9.2 Carceplexes

Carcerands are defined as closed-surface, globe-shaped molecules with an enforced internal cavity within which small molecules, ions, or both can be incarcerated. Carceplexes are carcerands that contain permanently entrapped guest molecules or ions within their confines.[272] Guest escape from a carceplex is thus only possible through breaking of the covalent bonds that link the atoms which form the walls of the molecular shell. Hemicarcerands can recognize ferrocene,[273] but also other organometallic compounds. For instance, the octaimine hemicarcerand depicted in Figure 56 was prepared by a fourfold shell closure of a tetraformyl bowl with 1,3-phenylenediamine. This

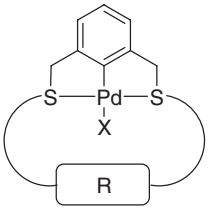

L^1: R = $(CH_2)_{11}$
L^2: R = $(CH_2)_2O(CH_2)_2$
L^3: R = $(CH_2)_2O[(CH_2)_2O]_2(CH_2)_2$
L^4: R = $(CH_2)_2O[(CH_2)_2O]_4(CH_2)_2$
L^5: R = *p*-$CH_2(C_6H_4)O[(CH_2)_2O]_3(C_6H_4)CH_2$
L^6: R = *m*-$CH_2(C_6H_4)O[(CH_2)_2O]_3(C_6H_4)CH_2$

Figure 55

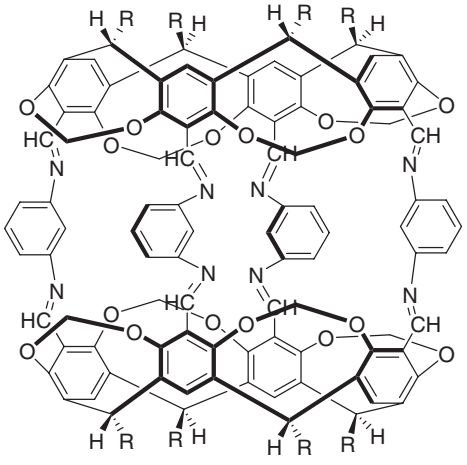

Figure 56

hemicarcerand possesses a substantial internal cavity. Thus, fairly large guest molecules such as ferrocene and ruthenocene sterically inhibit dissociation and permit the isolation and characterization of stable complexes.[274,275]

12.16.1.9.3 Porphyrin-pyridylphosphine complexes

Catalyst hemispherical assemblies using simple building blocks such as porphyrins and pyridylphosphines show enhanced activity in the palladium-catalyzed Heck reaction of iodobenzene and styrene and rhodium-catalyzed hydroformylation of 1-octene.[276] The self-assembled structures are based on selective coordination of pyridyl groups to zinc porphyrins with a transition metal pyridylphosphine complex as the template (Figure 57). These supramolecular ligands can encapsulate well-defined transition metal catalysts such as palladium or rhodium complexes. The performances of the catalytic processes can be regulated by the assembly of porphyrin building blocks with the pyridylphosphine rhodium complex.

Using a similar strategy, monomeric pyridine phosphorus compounds and bis-zinc porphyrin template were used to prepare monodentate and bidentate ligands which were tested in the rhodium-catalyzed hydroformylation of 1-octene.[277] The bidentate assembled ligand resulted in a rhodium catalyst with a slightly lower activity than that of the monodentate but the selectivity increased in favor of the linear product (94% compared with the 83%). Complexes displayed enhanced selectivity compared to the non-template analog. The templated ligand assemblies also resulted in significantly higher enantioselectivity (33% vs. 7% for the monodentate ligand), along with an increase in activity in the rhodium-catalyzed hydroformylation of styrene.

12.16.1.9.4 Glycoluril derivatives

Nolte *et al*. described the synthesis and properties of a redox-active metallo-host based on a basket-shaped rigid molecule diphenylglycoluril {3a,6a-diphenyltetrahydroimidazo[4,5-*d*]imidazole-2,5-(1*H*,3*H*)-dione} (Figure 58), to which a ferrocene unit has been connected.[278] Hydrogen bonds between the urea carbonyl groups of the host molecule and π–π stacking interactions between the aromatic walls of the host and the aromatic ring of the guest molecule contribute to the process of binding. A new coordination mode assisted by these Na^+ ions was discerned, which can explain the relatively large association constant found for this multicomponent host–guest complex.

It can also be noticed that the supramolecular metallo-host consisting of a diphenylglycoluril to which a catalytically active Rh(I) complex is attached has been found to preferentially hydrogenate and isomerize dihydroxy-substituted allylarenes.[279] The rhodium metallocage selectively bound catechol and resorcinol by π–π stacking and hydrogen bonds interactions so that the phenyl moiety of the guest molecule was included in the cavity of the host and the allyl part was coordinated to the rhodium. Hydrogenation reaction preferentially takes place inside the cavity,

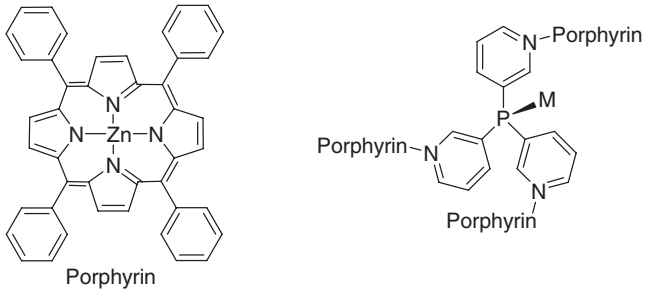

Figure 57

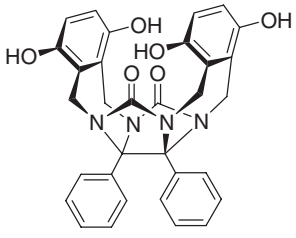

Figure 58

whereas the faster isomerization reaction occurs on the outside. Moreover, discrimination between different added substrates was possible by the process of molecular recognition. An enzyme-like behavior was displayed through Michaelis–Menten kinetics and rate-enhancement measurements. On binding a substrate the conformational behavior of the diphenylglycoluril host was affected considerably, suggesting that the substrate forces the system to adopt a more symmetrical geometry.[280]

12.16.1.9.5 Cucurbiturils

Cucurbit[*n*]urils ($n = 5$–11) are oligomeric macrocyclic compound self-assembled from an acid-catalyzed condensation reaction of glycoluril and formaldehyde.[281] The pumpkin-shaped molecule has a highly symmetrical structure with two identical openings that distinguishes it from cyclodextrins or calixarenes. Neutral molecules such as ferrocene get easily encapsulated in cucurbit[7]uril (CB7) in aqueous solution. In particular, Kaifer *et al.* have shown that ferrocenium and cobaltocenium form highly stable 1 : 1 inclusion complexes with the host CB7 (Figure 59).[282] From electronic absorption spectroscopic data the association equilibrium constants for both complexes were found to be larger than $10^6\,l\,mol^{-1}$. The electrochemical reduction of either guest leads to a modest loss in binding affinity. Mapping of the electrostatic potential surface of CB hosts revealed an electron-rich center, suggesting that Fc^+ and Cob^+ may fit very well in the inner cavity of CB7 both from steric and electrostatic standpoints. Thus, their tight binding is most likely a simultaneous combination of hydrophobic interactions with the inner cavity of CB7 as well as ion–dipole interactions with the two oligourea rims and its inner cavity. Subsequent reduction of both guests probably removes some of the electrostatic components in the stabilization of these complexes.

12.16.2 Organometallic Intercalation Chemistry

12.16.2.1 Introduction to Organometallic Intercalation Chemistry

It appears that the first scientific description of the insertion of a mobile guest species (atom, molecule, or ion) into a crystalline host lattice (i.e., intercalation) dates from 1926 when Karl Fredenhagen and Gustav Cadenbach described the uptake of potassium vapor into graphite.[283] Today we would write the generalized intercalation reaction using the equation below (1).

$$x_{Guest} + \square_x\,[Host] \rightleftharpoons \{Guest\}_x[Host] \qquad (1)$$

As indicated by Equation (1), intercalation reactions are usually reversible, and they may also be characterized as topochemical processes, since the structural integrity of the host lattice is formally conserved in the course of the forward and reverse reactions. Typically, these reactions occur near room temperature, but this is in sharp contrast with most conventional solid-state synthetic procedures which often require temperatures in excess of 600 °C, the term "Chemie Douce" has been coined to describe this type of low-temperature reaction. Remarkably, a wide range of host lattices has been found to undergo these low-temperature reactions, including framework (3D), layer (2D), and linear chain (1D) lattices.

To date, organometallic guests have been intercalated almost exclusively into layered host lattices. The structural flexibility of the layer structures, with their ability to adapt to the geometry of the inserted guest species by free adjustment of the interlayer separation, is presumably responsible for this observation. It is remarkable that in spite of the differences in composition and detail of the sheet unit structures, the basic chemical reactivity of these phases

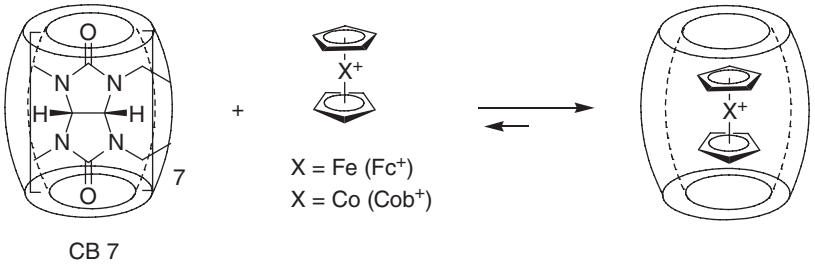

Figure 59

Table 2 Examples of layered host structures that exhibit intercalation of organometallic guests

Lattice type with examples	*Layer charge*	*References*
Elemental		
Graphite	Neutral	284,284a
Metal chalcogenides		
MX_2 (M = Ti, Zr, Hf, V, Nb, Ta, Mo, X = S, Se)	Neutral	285
MPX_3 (M = Mg, V, Mn, Fe, Co, Ni, Zn, Cd, In; X = S, Se)	Neutral	286
$(MX)_{1+y}(TX_2)_2$ (M = Sn, Pb; T = Ti, Nb; X = S, Se)	Neutral	287
Metal oxides		
M_xO_y (MoO_3, V_2O_5)	Neutral	288,288a
$MOXO_4$ (M = Ti, V, Cr, Fe; X = P, As)	Neutral	289
Metal oxy-halides		
MOX (M = Ti, V, Cr, Fe; X = Cl, Br)	Neutral	290
Metal halides		
β-ZrNCl	Neutral	291
Hydrous metal oxides		
Uranium Micas $\{(A^{z+})_{1/z}(H_2O)_y[UO_2XO_4]^{z-}$; X = P, As, V$\}$	Negative	292
Double hydroxides $\{X^-\ (H_2O)_n[Zn_2Cr(OH)_6]^+\}$	Negative	293
$M(HPO_4)_2$ (M = Ti, Zr, Hf, Ce, Sn)	Negative	294
Metal phosphates and phosphonates		
$Zr(RPO_3)_2$, $Zr(ROPO_3)_2$ (R = Ph, Me, Et, CH_2COOH)	Negative	295
Smectite clays		
Hectorite $\{Na_{0.6}[Li_{0.6}Mg_{5.4}](Si_{8.0})O_{20}(OH,F)_4\}$	Negative	296
Montmorillonite $\{Ca_{0.35}[Mg_{0.7}Al_{3.3}](Si_8)O_{20}(OH)_4\}$	Negative	297
Hydrotalcites		
$LiAl_2(OH)_6OH{\cdot}2H_2O$, $Zn_2Cr(OH)_6Cl{\cdot}2H_2O$	Positive	298

turns out to be closely related. However, all these layer phases are characterized by strong intralayer covalent bonding and weak interlayer interactions. The layers may be electrically neutral, or possess an overall charge which may be either positive or negative: examples of each category can be found in Table 2. In compounds with neutral layers, the interlayer bonding is often described as van der Waals', and the interlayer space is a connected network of empty lattice sites. In the charged layered systems, the layers are held together by weak electrostatic forces and the interlayer sites are partially or completely filled by ions or by a combination of ions and solvent molecules. As a class of materials, layered host lattices and their intercalates span the entire spectrum of electronic behavior from insulators (such as clays) through semiconductors and semimetals (dichalcogenides) to superconducting metals (some dichalcogenides). The range of organometallic molecules that may act as guests is expanding all the time; some illustrative examples are tabulated in Table 3.

The remainder of this chapter will review the reactions involving the intercalation of organometallic molecules and ions into host lattices.

12.16.2.2 Intercalation in Metal Dichalcogenide Hosts

12.16.2.2.1 Host structures

Many of the transition metal dichalcogenides possess layered structures as shown in Figure 60a. These lattices consist of two hexagonally close-packed chalcogen layers between which reside the metal ions. The metal ions can be found in sites of either octahedral or trigonal prismatic symmetry (Figure 60b, c).[285,285a–285c] These six-coordinate building blocks are then stacked together to form the overall structure. The bonding within the layers is strong and largely ionic in character, whereas the interaction between the layers is much weaker and is often described as van der Waals' in origin.

More recently, a new family of composite-layered chalcogenides with $(MX)_{1+y}(TX_2)_2$ stoichiometry (M = Sn, Pb, Bi; T = Ti, Nb, Ta,; X = S, Se) has been prepared and characterized.[287] A common feature of these compounds is a misfit layer structure consisting of a double layer of MX and TX_2 sandwiches along the *c*-axis. From the point of view of intercalation reactions, these hosts have the potential to separate the two adjacent TX_2 slabs in order to accommodate new guest molecules.

Table 3 Examples of organometallic compounds that exhibit intercalation reactions

Guest type with examples[a]	*Host lattices*	*References*
Molecular ions		
$[M(Cp)_2]^+$ (M = Co, Cr)	MS_2,MPS_3	299
$[Fe(Cp)(diphos)(CO)]^+$, $[Fe(Cp)(Bz)]^+$	MPS_3	300
$[Co(PMe_3)_3(C_2H_4)]^-$	Graphite	301
$[Ir(COD)(PPh_3)_2]^+$	Montmorillonite	302
Neutral molecules		
$[M(Cp)_2]$ (M = Co, Cr, Fe, Ni), $[Fe(Cp^*)_2]$	FeOCl, MS_2	303
$[Fe(Cp^*)_2]$	FeOCl,	303
$[Mo(Cp)_2H_2]$	ZrS_2, FeOCl	303,304
$[M(Bz)_2]$ (M = Cr, Mo)	ZrS_2, MPS_3	305
[Ti(COT)(Cp)], [Cr(CHT)(Cp)], [Cr(Cp)(Bz)]	ZrS_2, TaS_2	304
$[Ir(PMe_3)_3H]$	ZrS_2	303
$[Fe_4(\eta\text{-}C_5H_4Me)_4(\mu^3\text{-}S)_4]$	MoO_3	303
$[Fe(Cp)(\eta\text{-}C_5H_4CH_2CH_2NH_2)]$	α-$Zr(HPO_4)_2$	375
$[Fe(Cp)(\eta\text{-}C_5H_4CH_2NMe_2)]$	$HUO_2PO_4{\cdot}4H_2O$	307,307a
$[SnMe_3(NMe_3)]$, $[Sn(NMe_2)_4]$	FeOCl	308

[a]Cp = η-C_5H_5, Cp* = η-C_5Me_5, Bz = η-C_6H_6, COT = η-C_8H_8, CHT = η-C_7H_7, diphos = $Ph_2P(CH_2)_2PPh_2$, Bz = η-C_6H_6, COD = η^4-C_8H_{12}.

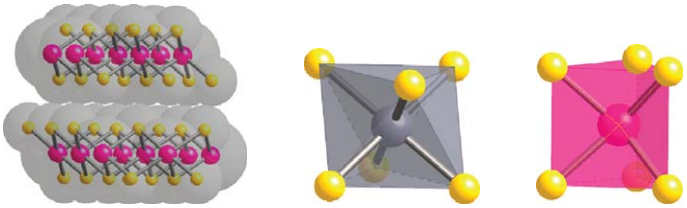

Figure 60 (a) Hexagonal closed packed metal dichalcogenide layers showing van der Waals surface of the atoms. The local metal coordination within each layer can be either (b) octahedral coordination or (c) trigonal prismatic.

12.16.2.2.2 Synthesis and structural aspects

Redox active organometallic compounds can be intercalated into the metal dichalcogenides by either direct reaction, ion exchange, or by electrochemical routes. This observation was initially reported in 1975 when Dines described the intercalation of $[Co(Cp)_2]$ and $[Cr(Cp)_2]$ into a range of metal disulfides (MS_2: M = Ti, Zr, Nb, Ta, and Sn).[310] Today, the range of organometallic guests which can be intercalated into these hosts is now quite extensive (Table 4), including metal π-complexes,[311] metal clusters,[312] and metal phosphine complexes.[313]

The electron-transfer mechanism from guest to host is the dominant process for these reactions. As a result there is the correlation between the reducing power of the organometallic guest and its ability to intercalate into a given host lattice. For example, ferrocene does not appear to intercalate into MS_2 (M = Ti, Nb, Sn) compounds whereas cobaltocene readily intercalates into a wide range of the dichalcogenides. The magnetic susceptibilities of $TaS_2\{Co(Cp)_2\}_{0.25}$ and $TaS_2\{Cr(Cp)_2\}_{0.25}$ are consistent with complete electron transfer from the metallocenes to the hosts. However, X-ray photoelectron studies on $SnS_2\{Co(Cp)_2\}_{0.3}$ indicate that this may not always occur and complex mixed-valence behavior may result.[314] The orientation of the unsubstituted metallocenes with respect to the host layers has been subject to much debate since Dines' initial report.[310] The complication arises from the fact that the lattice expansion of ca. 5.31 Å observed for all simple metallocene intercalates does not immediately reveal the orientation of the guest. These molecules have almost a spherical van der Waals' surface of approx. 6.5 Å diameter. For $SnS_2\{Co(Cp)_2\}_{0.3}$ the debate has been resolved by a combined X-ray and neutron diffraction study, which shows that the cobaltocene molecules are ordered within the van der Waals' gap with their principal axes parallel to the layer planes (Table 4).[315] In addition, variable-temperature solid-state ^2H NMR can be used to great effect to study the metallocene orientations within these layers.[316,316a] More recently, a study of a series of π-bonded

Table 4 Selected examples of intercalation compounds formed by layered metal dichalcogenides with different organometallic guests

Host	*Guest*[a]	*Guest occupancy/x host [G]x*	*Interlayer spacing* (c) (Å)	*Lattice expansion* (Δc) (Å)	*References*
ZrS_2			5.83	None	
	$Cr(Cp)_2$	0.25	11.64	5.81	309
	$Co(CpMe)_2$	0.25	11.17	5.34	310
	$Co(CpPr^i)_2$	0.15	11.57	5.74	310
	$Co(CpBu^n)_2$	0.13	11.17	5.34	310
	$Cr(Bz)_2$	0.16	11.73	5.90	309
	$Mo(Bz)_2$	0.16	11.64	5.81	309
	$Mo(Tol)_2$	0.13	11.63	5.80	309
	$Mo(Mes)_2$	0.08, 0.20	11.61, 13.6	5.78, 7.78	309
	Ti(Cp)(COT)	0.23	12.23	6.4	309
	Cr(Cp)(CHT)	0.25	12.0	6.17	309
	Cr(Cp)(Bz)	0.24	11.9	6.07	309
1T TaS_2			6.04	None	
	$[Co(Cp)_2]$	0.25	11.45	5.41	310
	$Co(CpMe)_2$	0.21	11.59	5.68	310
	$Co(CpPr^i)_2$	0.17	12.05	6.18	310
	$Co(CpBu^n)_2$	0.13	11.44	5.53	310
	$[Fe_6S_8(PEt_3)]$	0.05	17.49	11.45	312
$SnSe_2$					
	$Co(Cp)_2$	0.33	11.51	5.38	315
$NbSe_2$			6.00	None	
	$Co(Cp)_2$	0.31		5.53	310
	$Cr(Cp)_2$	0.20		5.56	310
MoS_2			6.14	None	
	$Co(Cp)_2$	0.31	11.68	5.53	318
$(PbS)_{1.18}(TiS_2)_2$	$Co(Cp)_2$	0.15	11.21	5.52	287
$(PbSe)_{1.12}(NbSe_2)_2$	$Co(Cp)_2$	0.15	11.58	5.59	287

[a]Bz = η-C_6H_6, CHT = η-C_7H_7, COT = η-C_8H_8.

sandwich complexes $[M(\eta^n\text{-}C_nH_n)(\eta^m\text{-}C_mH_m)]$ intercalated in ZrS_2 shows that for any ring size (C_5–C_8) the principal axis of the complex lies parallel to the host layers (Figure 61).[317]

The development of significant intercalation chemistry of MoS_2 is relatively recent. The material is chemically more inert and this can be traced back to the coordination of the molybdenum as well as the ligand field properties of the d^2 ion defined in the interlaminar region. MoS_2 avoids direct intercalation, except for lithium. However, syntheses of single-layer suspensions of MoS_2 in water have been developed by rapid hydrolysis of Li_xMoS_2 producing molecular H_2 causing the exfoliation of the sulfide.[318]

Ferrocene and a number of other non-electron donor ferrocenes have been intercalated into MoS_2 by treating a saturated CCl_4 solution of the guest with a suspension of exfoliated MoS_2. The interlayer spacings for the substituted

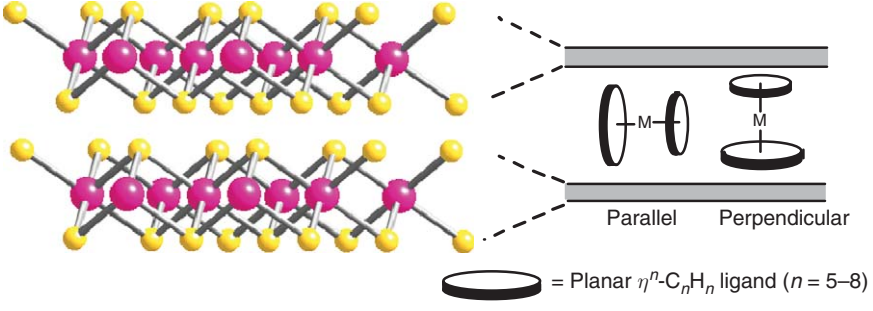

Figure 61 Schematic representation of a sandwich molecule intercalated in a metal dichalcogenide host. Two orientations of the sandwich molecule are illustrated; C_n molecular axis either parallel or perpendicular to the host layers.

ferrocene intercalates indicate the formation of a bilayer of guest molecules.[319] Direct reaction of metallocene cations $[M(Cp)_2]^+Cl^-$ (M = Fe, Co) with exfoliated MoS_2 yields a material with alternating layers of metallocenium guest and partially negatively charged MoS_2 layers. Intercalation of $[(\eta\text{-arene})Ru(H_2O)_2]^{2+}$ (arene = C_6H_6, 1,2,4,5-$C_6H_2Me_4$) gives two phases, depending on the pH of the reaction. At pH 3.2, the ruthenium complex is inserted as a monomer, while at pH 8.5, the ruthenium species is binuclear.[320]

12.16.2.2.3 Electronic properties

Changes in the electronic properties of the layered metal dichalcogenides after intercalation may be investigated by measurements, for example, of the optical absorption spectra, electrical conductivity, Hall constant, magnetic susceptibility, and solid-state NMR spectra. In general, these measurements provide evidence for our premise of charge transfer from the intercalant to the host lattice.

Over the last few decades, there was great excitement when some of the intercalation compounds of the metal dichalcogenides were found to have significantly higher superconducting critical temperatures (T_c) than the parent host lattices.[321] Today, superconductivity has been widely observed in the intercalation complexes of the group 4, 5, and 6 metal dichalcogenides. Of the unintercalated transition metal dichalcogenides, only the group 5 dichalcogenides are metallic and only the trigonal prismatic coordination polytypes are superconductors. In a very few cases, layered semiconductor dichalcogenide hosts have been transformed into superconductors on intercalation of the appropriate guest. For example, the semiconductor $SnSe_2$ becomes superconducting ($T_c = 8.1$ K) when intercalated by $[Co(Cp)_2]$.[322,322a]

A number of fundamental questions has arisen regarding the physical description of the dimensionality of superconductivity in view of the highly anisotropic character of these materials. For example, the increased transition temperatures of some of these intercalates suggest a novel mechanism for the superconductivity?

It is now generally agreed, however, that the observed increase in T_c results from suppression of charge density wave formation rather than some exotic quasi-two-dimensional mechanism.[323] However, the effect of the two-dimensional anisotropy of the material is of considerable interest. It has been found that the critical field behavior is in broad agreement with theoretical predictions based on a model of a layered compound containing two-dimensional superconducting layers weakly coupled via Josephson tunneling.[324]

12.16.2.2.4 Kinetic and mechanistic studies

The reaction of a potential guest molecule with a prospective inorganic host lattice is a heterogeneous reaction; as a result both mechanistic and kinetic data are very hard to obtain. New *in situ* methods still need to be developed that can probe all aspects of the reaction non-invasively. However, O'Hare and co-workers have developed a time-resolved, *in-situ* energy dispersive X-ray diffraction (EDXRD) experiment to probe intercalation reactions.[325] The kinetic studies of the intercalation of cobaltocene, $Co(\eta\text{-}C_5H_5)_2$, into a range of layered dichalcogenides ZrS_2, 2H–SnS_2, 2H–$SnSe_2$, 2H–TaS_2, 2H–NbS_2, 1T–TaS_2, and TiS_2 have been performed. They used the integrated intensities of the Bragg reflections to determine the extent of reaction, (α), versus time for each of these reactions. The half-lives ($t_{1/2}$) for reaction of an excess of cobaltocene with ZrS_2, 2H–SnS_2, 2H–$SnSe_2$, 2H–TaS_2, 2H–$NbSe_2$, and TiS_2 at 120 °C in dimethoxyethane were found to be <5, 31, 410, 16 000, 2 960, and >60 000 s respectively.[326] The activation energy for the intercalation of $Co(\eta\text{-}C_5H_5)_2$ in 2H–SnS_2 has been shown to be 41 kJ mol^{-1}. The guest concentration and solvent dependence of the rate of $Co(\eta\text{-}C_5H_5)_2$ intercalation into 2H–SnS_2 has also been determined. Surprisingly, the rate of intercalation is invariant to the initial $Co(\eta\text{-}C_5H_5)_2$ concentration over a wide concentration range. The kinetic data are consistent with a mechanism in which nucleation is a random statistical phenomenon which involves separation of the host layers: guest molecules then fill the layer in a diffusion-controlled process before a new layer is nucleated.

12.16.2.3 Intercalation in Metal Oxyhalides

12.16.2.3.1 Host structures

Of the small number of metal oxyhalides that form layered structures, only the FeOCl structure type (e.g., FeOCl, TiOCl, and VOCl) is known to undergo topotactic redox intercalation reactions. The FeOCl structure consists of a stack of double sheets of *cis*-$FeCl_2O_4$-distorted octahedra linked together by shared edges within the crystallographic *ac*-plane. The neutral layers of FeOCl are orientated perpendicular to the *b*-direction, with chlorine forming the outermost atoms of each layer (Figure 62). The easy cleavage plane is perpendicular to the *b*-direction and it is this cell parameter which is most affected on intercalation. Other compounds which adopt the FeOCl structure are MOCl (M = Ti, V, and Cr) and InOX (X = Cl, Br, and I).

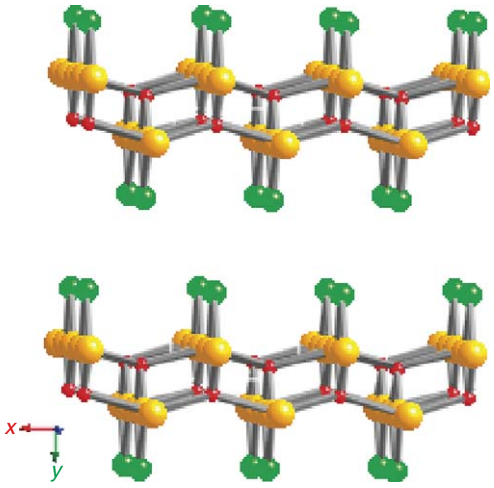

Figure 62 Structure of FeOCl viewed along the crystallographic *z*-axis.

12.16.2.3.2 Synthesis and structural aspects

FeOCl is the most reactive host toward the intercalation of molecular guest due to its stronger oxidizing power. Consequently, a much wider range of organometallic guest compounds, including metallocenes, has been intercalated into this host lattice (Table 5). FeOCl is one of the very few host lattices that will directly intercalate ferrocenes. Even the peralkylated derivatives $[Fe(\eta\text{-}C_5Me_5)_2]$ and $[Fe(\eta\text{-}C_5Me_4Et)_2]$ have been intercalated by direct reaction with FeOCl.[327]

Intercalation of organometallic guests in FeOCl is generally carried out by direct reaction in sealed glass ampoules at temperatures up to ca. 120 °C. Two structural consequences result from intercalation: (i) the unit cell expansion along the *b*-axis, depending on the size of the intercalated molecule and (ii) a change in the stacking of successive layer planes. The lattice expansion (Δb) is always smaller than the shortest dimension of the guest molecule which implies that there is a significant interpenetration of the guest molecule into the van der Waals' layers defined by the chlorine atoms (Table 5).

For example, the lattice expansion ($\Delta b = 5.13$ Å) observed when ferrocene is intercalated into FeOCl suggests that the metallocenes are accommodated with the η-cyclopentadienyl rings perpendicular to the layers.[328] The stoichiometry $FeOCl\{Fe(Cp)_2\}_{0.16}$ is close to that calculated for close-packed metallocene cations in this model. In addition, the powder X-ray diffraction patterns from the intercalates indicate a change in lattice symmetry from primitive to body centered showing that the intercalation produces a relative translation of adjacent layers (Figure 63).

12.16.2.3.3 Electronic structure

Mössbauer spectroscopy has proved to be a very useful technique for studying electron transfer and mixed valency in the FeOCl intercalates. The nature of the electron-transfer process which occurs on formation of $FeOCl\{Fe(Cp)_2\}_{0.16}$ has been studied in detail by ^{57}Fe Mössbauer spectroscopy. At temperatures in the range 77–100 K, the Mössbauer spectrum exhibits resonance characteristic of the ferrocenium cation and two chemically distinct Fe^{3+} sites. The two Fe^{3+} sites are different in the number of nearest-neighbor Fe^{2+} ions. Quantitative measurements confirm that all the ferrocene guest molecules are oxidized and complete electron transfer to the host has occurred. At 300 K, only one

Table 5 Comparison of the superconducting metal dihalcogenides hosts and other organometallic intercalates

Host	T_c (K)	*Intercalate*	T_c (K)	*References*
2H–TaS_2	0.6	$TaS_2\{Co(Cp)_2\}_{0.25}$	3.2	324
2H–NbS_2	6.1	$TaS_2Mn_{0.16}(H_2O)_2$	2.6	380
2H–$NbSe_2$	7.1	$NbS_2(py)_{1.2}$	4.1	380
$SnSe_2$	None	$SnSe_2\{Co(Cp)_2\}_{0.3}$	8.1	325

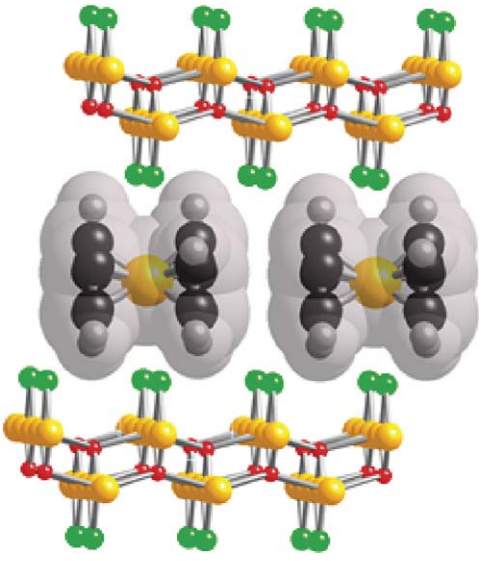

Figure 63 Schematic view of the structure of FeOCl{Fe(η-C_5Me_5)$_2$}$_{0.16}$ showing the van der Waals surface of the guest.

^{57}Fe resonance is observed as a consequence of rapid electron hopping between iron ions, both within layers and between layers, presumably via the guest molecules.[329]

These metal oxyhalides are paramagnetic semiconductors. The room temperature conductivity (σ_{rt}) of single crystals of FeOCl is ca. 10^{-7} Ω^{-1} cm^{-1}. Intercalation of organometallic guest molecules substantially increases the electrical conductivity; for example, FeOCl{Fe(Cp_2)$_2$}$_{0.16}$ has a σ_{rt} ca. 10^{-1} Ω^{-1} cm^{-1}.[330] These phases all show a temperature dependence of the conductivity indicative of semiconducting behavior. In all cases where it has been measured, the thermoelectric power is negative, suggesting that the charge carriers are electrons.

Pristine FeOCl exhibits a paramagnetic to antiferromagnetic phase transition with a Néel temperature of 91 K, which can be conveniently studied by Mössbauer spectroscopy. The major effect of the magnetic properties of FeOCl on intercalation of organometallic guests is the depression of the Néel temperature.[331] The lower temperatures required for the onset of three-dimensional magnetic ordering have been attributed to a decrease in the interlayer magnetic-exchange interactions and site-disorder effects.[329]

12.16.2.4 Intercalation in Metal Phosphorus Trisulfides

12.16.2.4.1 Host structures

Klingen[332] was the first to describe a series of lamellar semiconductors of the formula MPS_3, where M is a wide range of divalent metal ions (M = Mg, V, Mn, Fe, Co, Zn, Ni, Pd, and Cd). The selenides ($MPSe_3$) also form similar structures with M = Mg, Mn, Fe, Ni, and Cd. These materials can be prepared by standard solid-state procedures, that is, by heating the elements in sealed evacuated quartz ampoules at ca. 700 °C.[333]

The first-row transition metal phosphorus trisulfides all form a common monoclinic structure (C2/m) based on the $CdCl_2$ type (Figure 64). This consists of a cubic close-packed anion array with alternate layers of cation sites vacant. Within a layer, two-thirds of the cation sites are occupied by M^{2+} cations and one-third by P_2 pairs. The structure is related to the $CdCl_2$ lattice, since the M^{2+} ions and the center of the P–P pairs occupy the Cd positions and the sulfur ions occupy the chloride positions.

12.16.2.4.2 Synthesis and structural aspects

The metal phosphorus trisulfides exhibit two types of intercalation reactions. Redox intercalation involves electron-donating guests using chemical or electrochemical routes and with low bandgap MPS_3 host lattices. The second reaction type is unique to the MPS_3 compounds and involves intercalation of cation species with concomitant loss of the M^{2+} cations from the MPS_3 layers into the solution to maintain charge balance. This produces cation vacancies in

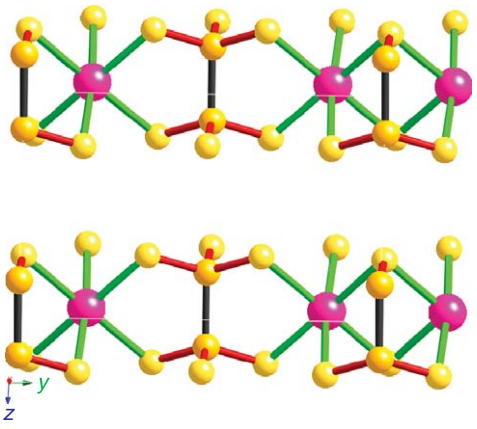

Figure 64 Structure of $MnPS_3$ viewed along the crystallographic *x*-axis.

the MPS_3 layers and, as we shall see, is responsible for some of the unique reactivity and potentially important properties of these materials.

MPS_3 hosts (M = Fe, Ni, Mn, and Cd) react directly with cobaltocene in toluene solution to give $MPS_3\{Co(Cp)_2\}_{0.3}$; $CdPS_3\{Co(Cp)_2\}_{0.40}$ has been extensively studied using EPR spectroscopy by Cleary and Francis.[299,334] Quantitative EPR measurements concluded that complete electron transfer from the $Co(Cp)_2$ to the $CdPS_3$ layers does not occur and both $[Co(Cp)_2]$ molecules and $[Co(Cp)_2]^+$ cations coexist between the layers. Higher bandgap materials, for example, $MnPS_3$, $CdPS_3$, and $ZnPS_3$, can be intercalated using stable metallocenium salts such as $[Co(Cp)_2]^+Cl^-$ by treatment with an aqueous solution of the appropriate cation salt. These reactions are believed to occur by an ion-exchange mechanism forming an intercalate phase with general stoichiometry $M_{1-x}PS_3(G)_{2x}(H_2O)_y$ (Table 6). The positive charge of the guest cation (G^+) is counterbalanced by the removal of an equivalent amount of interlayer M^{2+} ions.

This is a unique type of intercalation reaction, and implies that the M^{2+} cations are able to leave their intralamellar site and go into solution. This direct ion-exchange reaction fails if the guest ion is above a critical size, for example, $[Ru(2,2'\text{-bipy})_3]^{2+}$; however, this cation can be intercalated into $MnPS_3$ by pre-intercalation with K^+ cations giving $M_{1-x}PS_3(K)_{2x}(H_2O)_y$ and then ion exchanging the K^+ cations for the larger $[Ru(2,2'\text{-bipy})_3]^{2+}$.[335]

Among the MPS_3 series, $MnPS_3$ is by far the most reactive with regard to this ion-exchange reaction and consequently has been studied most extensively. Other members of the series M = Cd, Zn, and Fe undergo this "ion-transfer" reaction, but the reaction requires assistance usually achieved by complexing the leaving M^{2+} ions (typically 0.1 M EDTA, pH ≈ 9–10) (Table 7).[336]

Table 6 Examples of organometallic intercalation compounds of MOCl (M = Fe, V, and Ti)

Host	*Guest*	*Guest occupancy/x host* $\{G\}_x$	*Interlayer spacing* (b) (Å)	*Lattice expansion* (Δb) (Å)	*References*
FeOCl			7.91	None	
	$[SnMe_3(C_5H_4N)]$	0.13	14.11	6.20	373
	$[Fe_4(\eta\text{-}C_5H_4Me)_4(\mu^3\text{-}S)_4]$	0.08	17.02	9.11	306
	$[Fe(Cp)_2]$	0.16	13.03	5.11	367
	$[Cr(Cp)_2]$	0.14	13.10	5.19	367
	$[Fe(\eta\text{-}Cp^*)_2]$	0.06	15.00	7.09	327
	$[Fe(\eta\text{-}C_5Me_4Et)_2]$	0.16	15.46	7.54	368
VOCl			7.91	None	
	$[Co(Cp)_2]$	0.16	12.77	4.86	369
TiOCl			8.03	None	
	$[Co(Cp)_2]$	0.16	13.16	5.13	369

Table 7 Examples of intercalates obtained by cation exchange with alkali metal pre-intercalated MPS_3

Host	*Guest*	*Interlayer spacing* (c) (Å)	*Lattice expansion* (Δc) (Å)	*Formulation*	*References*
$MnPS_3$		6.5	None		
	$[Co(Cp)_2]^+I^-$	11.82	5.32	$Mn_{0.83}PS_3[Co(Cp)_2]_{0.33}(H_2O)_{0.3}$	299
	$[Cr(Bz)_2]^+I^-$	12.26	5.76	$Mn_{0.83}PS_3[Co(Cp)_2]_{0.33}(H_2O)_{0.3}$	299
	$[Fe(Cp)(Bz)]^+[PF_6]^-$	12.05	5.55	$Mn_{0.85}PS_3[Fe(Cp)(Bz)]_{0.20}(H_2O)y$	371
	$[Fe(Cp)(C_6Me_6)]^+$	13.5	7.0	$Cd_{0.62}PS_3[Fe(Cp)(C_6Me_6)]_{0.28}Na_{0.18}(H_2O)$	370
	$[Ru(Cp)(p\text{-cymene})]^+$	12.2	5.7	$Mn_{0.71}PS_3[Ru(Cp)(p\text{-cymene})]_{0.21}Na_{0.37}(H_2O)_{0.65}$	370
	$[Fe(Cp)(o\text{-}C_6H_4Cl_2)]^+$	12.6	6.1	$Mn_{0.8}PS_3[Fe(Cp)(o\text{-}C_6H_4Cl_2)]_{0.4}(H_2O)$	370
	$[Ru(Cp^*)(C_6H_6)]^+$	13.6	7.1	$Mn_{0.87}PS_3[Ru(Cp^*)(C_6H_6)]_{0.25}(H_2O)_{0.25}$	370
$CdPS_3$		6.55	None		
	$[Co(Cp)_2]^+I^-$	11.84	5.32	$Cd_{0.84}PS_3[Co(Cp)_2]_{0.32}(solv)_{0.3}$	372
	$[Fe(Cp)(C_6Me_6)]^+$	13.5	6.95	$Cd_{0.62}PS_3[Fe(Cp)(C_6Me_6)]_{0.28}Na_{0.18}(H_2O)$	370
$ZnPS_3$		6.34	None		
	$[Co(Cp)_2]^+I^-$	11.72	5.29	$Zn_{0.86}PS_3[Co(Cp)_2]_{0.28}(H_2O)_y$	371
	$[Cr(Bz)_2]^+I^-$	12.25	5.82	$Zn_{0.9}PS_3[Co(Cp)_2]_{0.21}(H_2O)_y$	371
	$[Fe(Cp)(Bz)]^+[PF_6]^-$	12.08	5.65	$Zn_{0.9}PS_3[Fe(Cp)(Bz)]_{0.20}(H_2O)_y$	371

12.16.2.4.3 Electronic and magnetic properties

The electronic structure and properties of MPS_3 hosts and their intercalates has been reviewed by Brec.[337] The hosts are all described as broadband semiconductors; a more detailed picture of the electronic structure is given in a recent tight-binding band structure calculation.[338] Depending on the particular metal ion, the energy values for the bandgaps of these semiconducting MPS_3 lattices lie in the range 3.5–1.6 eV. For example, $CdPS_3$ is colorless and transparent (bandgap 3.5 eV), $MnPS_3$ appears transparent with bright green coloration (bandgap 3.0 eV), whereas $FePS_3$ and $NiPS_3$ are dark with bandgaps close to 1.6 eV. The metal ions are octahedrally coordinated and have high-spin electronic configurations where applicable. The MPS_3 phases containing paramagnetic M^{2+} ions (Mn^{2+}, S = 5/2; Fe^{2+}, S = 2; Ni^{2+}, S = 1) are antiferromagnets with Néel temperatures of 110, 126, and 253 K, respectively. However, the susceptibility maxima are broad, indicative of the strong two dimensionality of these materials.

The electronic conductivity of the intercalates formed via the ion-transfer route does not appear to be significantly altered relative to the pristine host lattice. For example, the room-temperature single-crystal electronic conductivity of pristine $MnPS_3$ is $3 \times 10^{-9}\ \Omega^{-1}\ cm^{-1}$ compared with $1 \times 10^{-8}\ \Omega^{-1}\ cm^{-1}$ for $Mn_{0.8}PS_3(K)_{0.4}(H_2O)_y$. All the MPS_3 hosts and their known organometallic intercalates are semiconductors.

In contrast, the magnetic properties of the strongly coupled two-dimensional Heisenberg antiferromagnet $MnPS_3$ are dramatically changed. Intercalation via the ion-transfer route yields intercalation compounds with reduced antiferromagnetic interactions, and the susceptibility of many of these intercalates increases dramatically below 40 K. In fact, the magnetic susceptibility of $Mn_{0.84}PS_3\{Co(Cp)_2\}_{0.32}(H_2O)_{0.3}$ exhibits a spontaneous magnetization in zero applied magnetic field, which is indicative of weak ferromagnetism.[339] In addition, the low-temperature powder neutron diffraction data show coherent magnetic scattering indicative of long-range magnetic order.[340,340a] Refinement of the neutron data suggests that the origin of the spontaneous magnetization arises from an Mn^{2+}-ordered vacancy model, which results in an uncompensated antiferromagnet or a ferrimagnet.[340,340a]

12.16.2.5 Intercalation in Metal Oxides

12.16.2.5.1 Host structures

Simple-layered metal oxide structures with true van der Waals' gaps are found only for the oxides of the transition metals in high formal oxidation states. In these metal oxides the layer structure is stabilized by the formation of strong multiple covalent bonds to oxygen, for example, MoO_3 and V_2O_5 (Table 8).

12.16.2.5.2 Intercalation into molybdenum trioxide

Molybdenum trioxide possesses a unique-layered structure.[341] It may be thought of as being formed from ReO_3-like chains, with edge- and vertex-sharing MoO_3 octahedra which form a puckered-layered unit. These layers are

Table 8 Examples of organometallic intercalation compounds formed by the layered metal oxides

Host	*Intercalates*[a]	*Interlayer spacing* (b) (Å)	*Lattice expansion* (Δb) (Å)	*References*
MoO_3		6.93	None	
	$MoO_3\{Co(Cp)_2\}_{0.66}$	12.73	5.80	380
	$MoO_3\{Fe(Cp)(Cp'')\}_{0.6}$	21.43	14.5	313,375
	$MoO_3\{Fe_4(Cp')_4(\mu^3\text{-}S)_4\}_{0.15}$	17.23	10.3	380
V_2O_5		4.37	None	
	$V_2O_5\{Co(Cp)_2\}_{0.4}\cdot H_2O$	13.2	4.6	374

[a]$Cp' = \eta\text{-}C_5H_4CH_3$; $Cp'' = \eta\text{-}C_5H_4CH_2CH_2NH_2$.

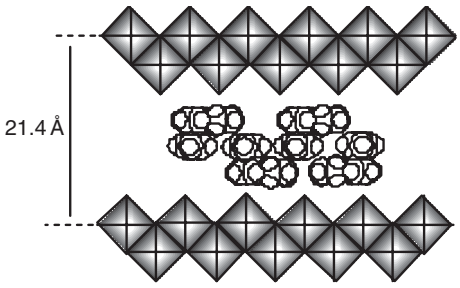

Figure 65 Schematic view of the structure of $MoO_3\{Fe(\eta\text{-}C_5H_5)(\eta\text{-}C_5H_4CH_2CH_2NH_2)\}_{0.6}$ showing the proposed bilayer arrangement of the guest molecules.

separated by a true van der Waals' gap and the oxide undergoes a full range of topotactic redox chemistry similar to that outlined for the metal dichalcogenides.

MoO_3 will also accommodate quite large organometallic guests. For example, the cubane cluster $[Fe_4(\eta\text{-}C_5H_4Pr^i)_4(\mu^3\text{-}Se)_4]$ has been intercalated into MoO_3, producing an observed lattice expansion $\Delta b = 15.2$ Å.[313] Although ferrocene does not directly intercalate into MoO_3 the ring functionalized amino-ferrocene derivative, $[Fe(Cp)(\eta\text{-}C_5H_4CH_2CH_2NH_2)]$ readily intercalates into MoO_3 forming $MoO_3\{Fe(Cp)(\eta\text{-}C_5H_4CH_2CH_2NH_2)\}_{0.6}$. The success of this reaction appears to result from the affinity of MoO_3 to intercalate amine guests. The amino-ferrocene is proposed to adopt a bilayer structure as shown in Figure 65 in common with many other amine intercalates of MoO_3.[313]

12.16.2.5.3 Intercalation into vanadium pentoxide

V_2O_5 gels prepared by polycondensation of decavanadic acid have an average molecular weight of ca. 10^6 and approximate composition $V_2O_5\cdot 1.6H_2O$. X-ray diffraction studies of orientated films indicate that the structure is layered with an interlayer spacing of 11.55 Å. Intercalation compounds of these gels with cobaltocenium and ferrocenium cations have been reported.[342]

12.16.2.6 Intercalation in Metal Phosphates, Hydrogen Phosphates, and Phosphonates

12.16.2.6.1 Host structures

The group 4 elements and group 14 elements (except carbon) form a series of isostructural hydrogen phosphates $\{M^{(IV)}(HPO_4)_2\}$.[343] The structure and intercalation chemistry of zirconium hydrogen phosphate $\{\alpha\text{-}Zr(HPO_4)_2\cdot H_2O\}$ is used here as an illustrative example of this class of lamellar host lattice. The structure of $\alpha\text{-}Zr(HPO_4)_2\cdot H_2O$ has been elucidated by Clearfield and Smith.[344] It crystallizes in the monoclinic system with each layer consisting of zirconium atoms lying in a plane and linked by bridging phosphate groups. Three oxygens of each tetrahedral phosphate are linked to three zirconium atoms so that each zirconium is octahedrally coordinated with six oxygens from six different phosphate groups as shown in Figure 66.

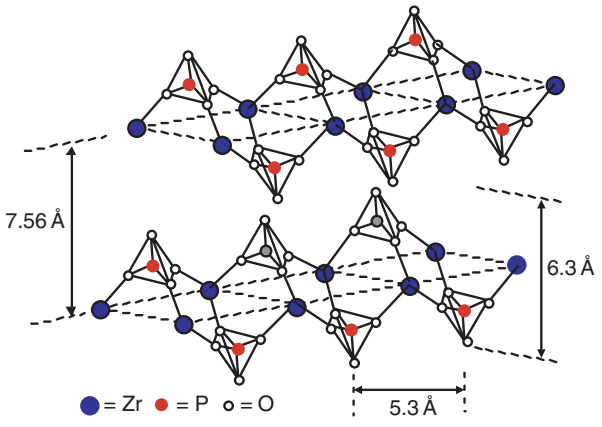

Figure 66 Structure of α-$Zr(HPO_4)_2{\cdot}H_2O$.

Another series of layered complex metal oxides have general formula $MOXO_4$ (M = V, Nb, Ta, and Mo; X = P, As, and S). The α-form of $VOPO_4$ is a member of this series; it has the richest intercalation chemistry of any member of this series, and so has been chosen as an illustrative example. The tetragonal layer structure of these compounds is made up of distorted VO_6 octahedra and PO_4 tetrahedra linked by corner-sharing oxygen atoms. The oxygen atoms in each VO_6 unit form a near regular octahedron, with the V atoms displaced along the c-axis.[345] The vanadium coordination is similar to that observed for V_2O_5. However, the interlayer interactions in α-$VOPO_4$ are much weaker due to the fact that the number of V═O···V interactions is reduced by the presence of PO_4 groups.

The related uranium mica compounds with general formula $M(UO_2PO_4)_2{\cdot}nH_2O$, where M is a monovalent or divalent cation, possess layer structures. They contain negatively charged layers of $(UO_2PO_4)_n^{n-}$ separated by staggered layers of water molecules and compensating cations.[346] The proton exchanged form $HUO_2PO_4{\cdot}4H_2O$ crystallizes in the tetragonal system with an interlaminar spacing of 8.8 Å and has proved to be the most common starting material for preparing intercalation complexes of this lattice type.

12.16.2.6.2 Organometallic intercalates of metal phosphates

The majority of investigations on the intercalation chemistry of layered acid salts have been performed with α-zirconium hydrogen phosphate. This phase exhibits a rich and varied intercalation chemistry.[347] Its reactivity arises from the high acidity in the protonic form and the weak forces between the layers. Organometallic guests such as cobaltocene[348] and $[FcCH_2CH_2NH_2]$ {Fc = Fe(Cp)(η-C_5H_4)} have been intercalated.[349]

α-$Zr(HPO_4)_2{\cdot}H_2O$ is optically transparent into the ultraviolet; several studies have been performed on the photochemical reactivity of inorganic complexes intercalated into this host lattice.[350] For example, photolysis of the dimeric manganese tricarbonyl complex $[Mn(CO)_3(\eta\text{-}C_5H_3(CH_3)CH_2]_2NH$ intercalated in α-$Zr(HPO_4)_2{\cdot}H_2O$ leads to a steady decrease of the intensity of ν_{CO} bands of the guest and the growth of absorptions assigned to a phosphinol-bound manganese dicarbonyl complex (Table 9).[351]

$VOPO_4{\cdot}2H_2O$ readily undergoes redox intercalation reactions with organometallic guests. Matsubayahi and co-workers have successfully intercalated both $Fe(Cp)_2$ and $Co(Cp)_2$. A combination of electron spin resonance (ESR) and X-ray photoelectron spectroscopy (XPS) measurements confirmed that intercalation was accompanied by an oxidation of the guests and reduction of the host. Interesting trends in the lattice expansion were observed with ferrocene and the methyl, methoxy, and ethoxy derivatives, each giving an initial increase in interlamellar separation of ca. 6.0 Å, whereas the Et and Bu^n ferrocene derivatives gave an expansion of 4.7 Å. The methylferrocene intercalate exhibited a decrease to 4.7 Å after 30 days suggesting that the guest molecules dynamically reorient over time.[352,352a] An important difference between $VOPO_4{\cdot}2H_2O$ and other oxide lattices is that redox intercalation of the type discussed above gives materials with low electrical conductivity (Table 9).

Hydrogen uranyl phosphate ($HUO_2PO_4{\cdot}4H_2O$) intercalates (dimethylaminomethyl)ferrocene by direct reaction in methanol or aqueous solutions (Table 9).[307,307a]

Table 9 Examples of organometallic intercalation compounds formed by the layered phosphates

Host	*Intercalate*	*Interlayer spacing* (b) (Å)	*Lattice expansion* (Δb) (Å)	*References*
α-$VOPO_4{\cdot}H_2O{\cdot}EtOH$		6.93	None	
	$VOPO_4\{Fe(Cp)_2\}_{0.35}$	9.9	5.8	352,376
	$VOPO_4\{Fe(CpMe)_2\}_{0.21}$	10.3	6.2	352
	$VOPO_4\{Fe(Cp)(CpEt)\}_{0.19}$	8.8	4.7	352
	$VOPO_4\{Fe(Cp)(CpBu^n)\}_{0.08}$	8.8	4.7	352
	$VOPO_4\{Fe(Cp)(CpCH_2OH)\}_{0.23}$	10.0	5.9	352
	$VOPO_4\{Fe(Cp)(CpCH_2CH_2OH)\}_{0.31}$	10.0	5.9	352
	$VOPO_4\{Co(Cp)_2\}_{0.52}$	10.1	6.0	352
α-$ZrHPO_4{\cdot}2H_2O$		7.54	None	
	$ZrHPO_4\{Co(Cp)_2\}_{0.5}$	12.0	4.4	378
	$ZrHPO_4\{Fe(Cp)(CpCH_2CH_2NH_2)\}$	22.08	14.54	379
α-$Sn(HPO_4){\cdot}H_2O$		7.8	None	
	$SnHPO_4\{Fe(Cp)(CpCH_2NMe_2)\}_{0.81}$	20.7	12.9	376
$HUO_2PO_4{\cdot}4H_2O$		8.69	None	
	$HUO_2PO_4\{Co(Cp)_2\}_{0.5}$	12.59	3.9	378
	$HUO_2PO_4\{Fe(Cp)(CpCH_2CH_2NMe_2)\}_{0.8}$	18.80	10.11	307a

12.16.2.7 Intercalation in Layered Clay Minerals

12.16.2.7.1 Host structures

Clay minerals are typically layered oxides or silicates and are the products of the weathering of primary oxides.[353] Many members of this group are able to undergo intercalation reactions and they can be divided into two subgroups, the kandite minerals and the smectites and vermicalites.

The smectite clays, for example, montmorillonite, hectorite, beidellite, and the mica minerals, for example, talc and pyrophillite possess a structure which is exemplified in Figure 67. The host lattice is formally composed of three sublayers: two tetrahedral Si/O and one octahedral M/O, OH (M = Al, Mg) central layer. These layers bear an excess negative charge and compensation of these charges is achieved by the presence of interlayer cations.

12.16.2.7.2 Organometallic intercalates of layered clay minerals

The majority of organometallic intercalation reactions involving clay mineral hosts employ the host lattice montmorillonite $\{Ca_{0.35}[Mg_{0.70}Al_{3.3}](Si_{8.0})O_{20}(OH)_4\}$. Montmorillonite contains exchangeable metal cations sandwiched between silicate layers. Intercalation reactions are ion-exchange process involving displacement of the intergallery alkali metal cations by a suitable organometallic cation.

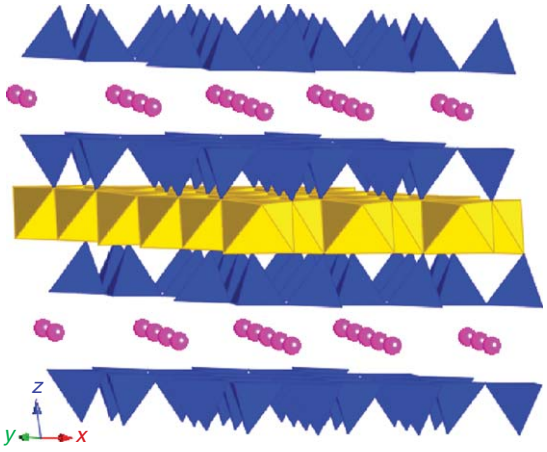

Figure 67 Structure of an idealized talc mineral, $Mg_3Si_4O_{10}(OH)_2$.

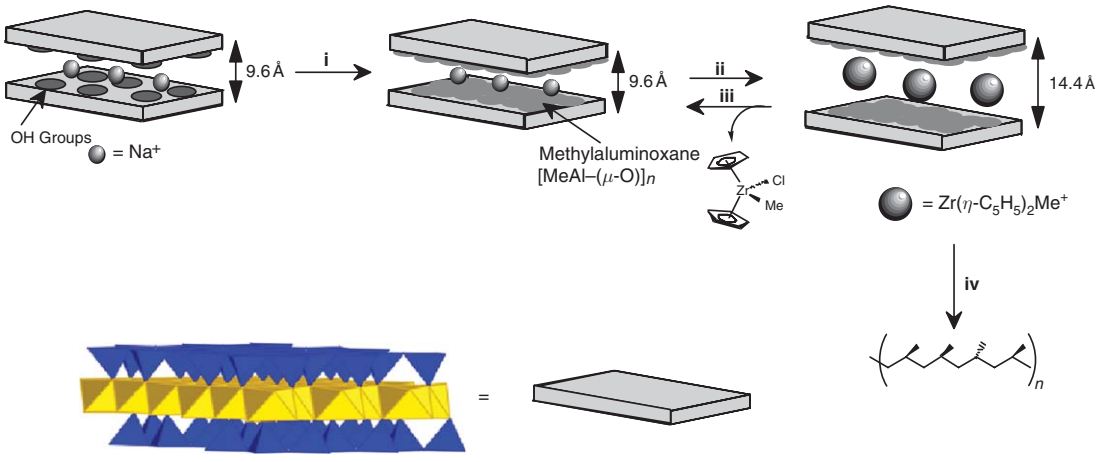

Figure 68 Schematic representation of the modification of mica-type silicate mineral to allow the intercalation of a Ziegler–Natta olefin polymerization catalyst precursor.

Dimethylaminomethylferrocene (DMAMF) has been intercalated in Westone-L, a low iron content montmorillonite, as the ammonium salt. ^{57}Fe Mossbauer spectroscopy revealed that the iron experiences a very similar environment within the host compared to a pure hydrochloride salt.[354] The cationic hydrogenation catalyst precursor $[Rh(PPh_3)_3]^+$ can be intercalated in the smectite clays montmorillonite and hectorite.[355] These materials are hydrogenation catalysts which reduce terminal olefins without isomerization, whereas with the analogous homogeneous system isomerization to an internal olefin occurs. Reactions of cationic iridium(I) complexes $[Ir(COD)(PPh_3)_2]ClO_4$ and $\{Ir(COD)(PPh_3)(PhCN)\}ClO_4$ with water-swelled sodium montmorillonite produce iridium complex intercalated clays.[356] These materials react with H_2 to release cyclooctane and leave uncharacterized iridium complexes remaining between the layers. The iridium-clay complexes have slightly lower catalytic activity for both hydrogenation and isomerization of double bonds, but selectivity for hydrogenation of the vinyl groups of 4-vinylcyclohexene was somewhat higher with the iridium-clay complex compared to the homogeneous system.[357]

The cationic Ziegler–Natta polymerization catalyst, $[ZrCp_2Me(THF)]^+$, has been intercalated in a synthetic fluorinated mica-type silicate (FTSM, $NaMg_{2.5}Si_4O_{10}F_2$) and also the modified, swelling synthetic hectorite (LaponiteRD, $Na_{0.46}Mg_{5.42}Li_{0.46}Si_8(OH)_4O_{20}$), by ion exchange of $[ZrCp_2Me(THF)]^+$ ions in CH_3CN with the interlamellar cations of the layered silicates.[358] Powder X-ray diffraction indicates an increase in the basal spacing of the host lattice from $c = 9.8$ to 14.3 Å. Elemental microanalysis shows that this material contains 0.55 mmol Zr/g silicate. Laponite has a cation-exchange capacity (CEC) of 0.60 meq g^{-1} and essentially all the available Na^+ ions can be replaced by $[ZrCp_2Me]^+$, which accounts for almost all the zirconium found by elemental microanalysis. For the FTSM (CEC = 0.94 meq g^{-1}) exchanged material, 68% of the exchangeable cations are replaced by the zirconocenium ions. The intercalated cations can be exchanged out of the mica by reaction with THF solutions of NaCl giving $Cp_2ZrMeCl$. In the presence of methylalumoxane (MAO, $[\{MeAlO\}_n]$), these organometallic intercalation compounds are active catalysts for the polymerization of propene giving low molecular weight atactic polypropylene with a narrow molecular weight distribution (Figure 68).[358]

12.16.2.8 Intercalation in Other Layered Hosts

12.16.2.8.1 Intercalation in β-ZrNCl

β-ZrNCl has a layer structure consisting of zirconium nitride double layers sandwiched between two close-packed chloride ion layers. These ZrNCl (Cl–Zr–N–N–Zr–Cl) layers are then stacked on each other giving the overall structure.[359]

Intercalation of cobaltocene, 1,1′-dimethylcobaltocene and decamethylcobaltocene into ZrNCl can be achieved by stirring the host with an excess of the metallocene in THF at 60 °C.[360] The interlayer separations of the cobaltocene and 1,1′-dimethylcobaltocene intercalates are the same, and less than that observed for the decamethylcobaltocene intercalate. Thus, it can be deduced that the guest molecules are orientated with their principal axes parallel to the host layers. The β-ZrNCl structure contains two types of van der Waals' gaps, between Cl···Cl layers and in between

N···N layers. The one-dimensional electron density synthesis clearly shows that the guest molecules are intercalated between the Cl···Cl layers.

$ZrNCl\{Co(Cp)_2\}_{0.10}$ has been shown to be a Type II superconductor with a superconducting transition at 14 K. This is the highest T_c for any metallocene intercalation compound. The superconducting transition temperatures for all three metallocene intercalation compounds are the same as those in the alkali metals intercalates with the same doping level reported by Yamanaka *et al.*[361] The transition temperature appears not to be dependent on the interlayer separation and on the doping level which suggests that the superconductivity is largely confined to the thin two-dimensional ZrN layers of the host lattice.

12.16.2.8.2 Intercalation in layered double hydroxides

Layered double hydroxides (LDHs), also commonly referred to as anionic clays or hydrotalcite-like materials, are an extremely widely studied class of lamellar solids. The structure consists of positively charged mixed-metal hydroxide layers separated by charge-balancing anions. The structure type spans a very broad range of composition $[M_2^{2+}M^{3+}(OH)_6]^+X_{1/n}^{n-}\cdot mH_2O$ ($M^{2+} = Mg^{2+}$, Zn^{2+}, Ni^{2+}..; $M^{3+} = Al^{3+}$, Ga^{3+}, Cr^{3+}..; $X^- =$ organic, inorganic, organometallic anion).[362]

Apart from the metal cyano complexes, for example, $Fe(CN)_6^{3-}$ and $Fe(CN)_6^{4-}$, there are relatively few examples of ion exchange of organometallic anions into LDHs. The exceptions are ferrocenes containing sulfonate,[363] and carboxylate functional groups. For example, the Zn/Al–LDH can be intercalated by ferrocenecarboxylate and 1,1′-ferrocenedicarboxylate anions by co-precipitation from aqueous solution. The powder X-ray diffraction data indicate that Zn_2Al-$Fe(COO)_2$ contains a monolayer of organometallic guest anions resulting in a basal spacing of 15.5 Å. Dehydration of this phase prompts reorientation of the ferrocene guest anions, resulting in a collapsed phase with an interlayer separation of 12.3 Å.[364]

The limitation that guest molecules must be anionic to undergo ion-exchange intercalation in LDHs has been overcome by functionalization for the internal surfaces of the LDH with carboxymethyl β-cyclodextrin cavities (Figure 69). The parent Mg/Al LDH was prepared by conventional co-precipitation. Functionalization was then accomplished by ion exchanging the interlayer nitrate ions with carboxymethyl β-cyclodextrin anions. With an average degree of carboxmethyl, substitution of 3.8 per cyclodextrin gives complete ion exchange in $Mg_{0.7}Al_{0.4}(OH)_2(NO_3)_{0.3}$ and an increase in interlayer spacing form 8.9Å to 24.6Å. Ferrocene was included within this functionalized LDH by adsorption from a 3 : 2 methanol/water solution. The adsorption isotherms indicate a partitioning process with a maximum uptake of ferrocene of 0.95 molecules per grafted β-cyclodextrin.[365]

12.16.2.9 Intercalation in Other Hosts

12.16.2.9.1 Zeolites

When dehydrated nay zeolite ($Na_{55}(AlO_2)_{55}(SiO_2)_{137}$) is exposed to ferrocene vapor, the metallocene is intercalated into the supercages of the host structure. The material has been studied by both X-ray and neutron diffraction. The ferrocenes order within the structure and were located above a line joining the two neighbouring Na ions at the sii

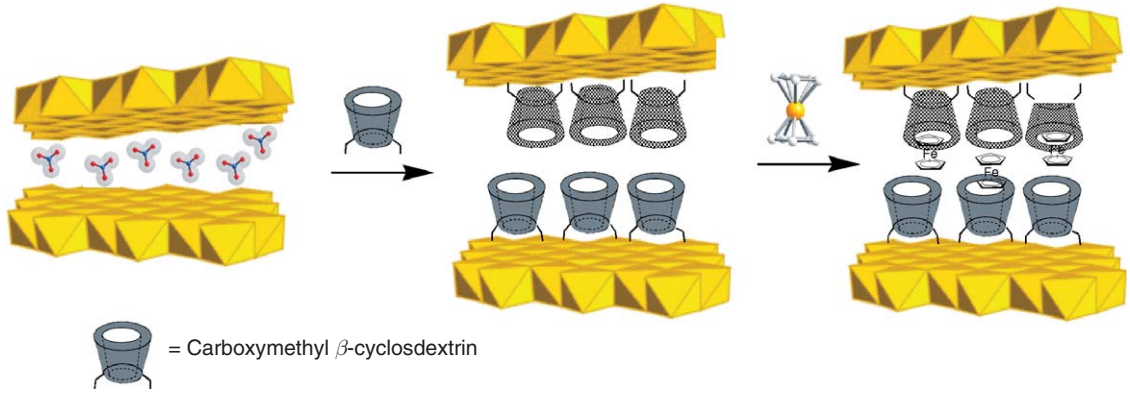

Figure 69 Schematic representation of the intercalation of ferrocene in a β-cyclodextrin functionalized layered double hydroxide.

positions in the zeolite supercages. The η-C_5H_5 rings are oriented toward the Na cations. Structural refinement of the intercalated zeolite shows very little change of the geometry of the guest molecules. Quantum calculations indicate that the main interactions between the host and guests are coulombic and hydrogen bonding.[366]

12.16.2.10 Conclusions

Inclusion and intercalation chemistry are now well established as important disciplines interconnecting with solid-state chemistry, material science, analytical, organic, inorganic, physical and supramolecular chemistry. In particular, most of the studies that have been carried out to date in that field have been directed at defining the potential of supramolecular hosts (inclusion) or crystalline host lattice (intercalation) for altering the behavior of an organometallic guest when included in the host structure. This ability greatly depends on the nature of the host in closed relation to that of the guest.

Above and beyond the chemistry of covalent bonds, the knowledge is now at hand to design organometallic included or intercalated edifices offering electrochemical, sensor, mediator, catalytic, electronic, or magnetic properties. With the above applications already published in the literature, it is possible to speculate that, in the near future, the degree of complexity of these organometallic systems will increase. While the potential of organic molecules or crystalline lattices as hosts for organometallic guests has not been fully exploited, it is hoped that this review has clearly pointed out the very substantial progress that has already been made to this end and that the advances made so far will stimulate more chemists to prepare novel included or intercalated materials which exhibit new phenomenon for many more potential applications.

References

1. Wenz, G. *Angew. Chem., Int. Ed.* **1994**, *33*, 803.
2. Szejtli, J. *Chem. Rev.* **1998**, *98*, 1743.
3. Rekharsky, M. V.; Inoue, Y. *Chem. Rev.* **1998**, *98*, 1875.
4. Joh, T.; Harada, A.; Takahashi, S. *Mem. Inst. Sci. Ind. Res., Osaka Univ.* **1989**, *46*, 37.
5. Stoddart, J. F.; Zarzycki, R. *Recl. Trav. Chim. Pays-Bas* **1988**, *107*, 515.
6. Harada, A. Preparation, Properties and Stereochemical Aspects of Inclusion Compounds of Organometallic Complexes with Cyclodextrins. In *Chain, Clusters, Inclusion Compounds, Paramagnetic Labels and Organic Rings*; Zanello, P., Ed.; Stereochemistry of organometallic and inorganic compounds; Elsevier: Amsterdam, 1994; Vol. 5, pp 411–455.
7. Fenyvesi, E.; Szente, L.; Russell, N.; McNamara, M. Specific Guest Types In *Cyclodextrins*; Atwood, J. L.; Davies, J. E. D.; MacNicol, D. D.; Vögtle F., Eds.; Comprehensive Supramolecular Chemistry; Pergamon: Oxford, 1996; Vol. 3, pp 305–366.
8. Colquhoun, H. M.; Stoddart, J. F.; Williams, D. J. *Angew. Chem., Int. Ed. Engl.* **1986**, *25*, 487.
9. Caron, L.; Canipelle, M.; Tilloy, S.; Bricout, H.; Monflier, E. *Eur. J. Inorg. Chem.* **2003**, 595.
10. Monflier, E.; Bricout, H.; Hapiot, F.; Tilloy, S.; Aghmiz, A.; Masdeu-Bultó, A. M. *Adv. Synth. Catal.* **2004**, *346*, 425.
11. Caron, L.; Bricout, H.; Tilloy, S.; Landy, D.; Fourmentin, S.; Monflier, E. *Adv. Synth. Catal.* **2004**, *346*, 1449.
12. Monflier, E.; Tilloy, S.; Méliet, C.; Mortreux, A.; Fourmentin, S.; Landy, D.; Surpateanu, G. *New. J. Chem.* **1999**, *23*, 469.
13. Monflier, E.; Tilloy, S.; Caron, L.; Wieruszeski, J. M.; Lippens, G.; Fourmentin, S.; Landy, D.; Surpateanu, G. *J. Inclusion Phenom.* **2000**, *38*, 6111.
14. Caron, L.; Christine, C.; Tilloy, S.; Monflier, E.; Landy, D.; Fourmentin, S.; Surpateanu, G. *Supramol. Chem.* **2002**, *14*, 11.
15. Canipelle, M.; Caron, L.; Caline, C.; Tilloy, S.; Monflier, E. *Carbohyd. Res.* **2002**, *337*, 281.
16. Siegel, B.; Breslow, R. *J. Am. Chem. Soc.* **1975**, *97*, 6869.
17. Harada, A.; Takahashi, S. *J. Chem. Soc., Chem. Commun.* **1984**, 645.
18. Harada, A.; Takahashi, S. *J. Inclusion Phenom.* **1984**, *2*, 791.
19. Harada, A.; Takahashi, S. *Chem. Lett.* **1984**, 2089.
20. Harada, A.; Hu, Y.; Yamamoto, S.; Takahashi, S. *J. Chem. Soc., Dalton Trans.* **1988**, 729.
21. Odagaki, Y.; Hirotsu, K.; Higuchi, T.; Harada, A.; Takahashi, S. *J. Chem. Soc., Perkin Trans. 1* **1990**, 1230.
22. Clayden, N. J.; Dobson, C. M.; Heyes, S. J.; Wiseman, P. J. *J. Inclusion Phenom.* **1987**, *5*, 65.
23. Kobayashi, N.; Opallo, M. *J. Chem. Soc., Chem. Commun.* **1990**, 477.
24. Menger, F. M.; Sherrod, S. J. *J. Am. Chem. Soc.* **1988**, *110*, 8606.
25. Narankiewicz, Z.; Alexander, A. L.; Bondareva, L.; Mamedyarova, I. A.; Nefedova, M. N.; Sokolov, V. I. *J. Inclusion Phenom.* **1991**, *11*, 233.
26. Schneider, H. J.; Hacket, F.; Rudiger, V. *Chem. Rev.* **1998**, *98*, 1755.
27. Imashiro, F.; Kuwahara, D.; Kitazaki, N.; Terao, T. *Magn. Reson. Chem.* **1992**, *30*, 796.
28. Kuwahara, D.; Imashiro, F.; Terao, T. *Chem. Phys. Lett.* **1993**, *204*, 533.
29. Matsue, T.; Akiba, U.; Suzufuji, K.; Osa, T. *Denki Kagaku* **1985**, *53*, 508 (*Chem. Abtr.* **1985**, *103*, 130 044).
30. Wu, J. S.; Toda, K.; Tanaka, A.; Sanemasa, I. *Bull. Chem. Soc. Jpn.* **1998**, *71*, 1615.
31. Matsue, T.; Evans, D. H.; Osa, T.; Kobayashi, N. *J. Am. Chem. Soc.* **1985**, *107*, 3411.
32. Ryabov, A. D.; Tyapochkin, E. M.; Varfolomeev, E. D.; Karyakin, A. A. *J. Electroanal. Chem., Bioelectrochem. Bioenerg.* **1990**, *24*, 257.
33. McCormack, S.; Russel, N. R.; Cassidy, J. F. *Electrochim. Acta* **1992**, *37*, 1939.
34. Strelets, V. V.; Mamedjarova, I. A.; Nefedova, M. N.; Pysnograeva, N. I.; Sokolov, V. I.; Pospisil, L.; Hanzlik, J. *J. Electroanal. Chem.* **1991**, *310*, 179.

35. Komura, T.; Yamaguchi, T.; Noda, K.; Hayashi, S. *Electrochim. Acta* **2002**, *47*, 3315.
36. Cassidy, J.; O'Gorman, J.; Ronane, M.; Howard, E. *Electrochem. Commun.* **1999**, *1*, 69.
37. Kutner, W.; Doblhofer, K. *J. Electroanal. Chem.* **1992**, *326*, 139.
38. Ueno, A.; Moriwaki, F.; Osa, T.; Hamada, F.; Murai, K. *Tetrahedron Lett.* **1985**, *26*, 899.
39. Kobayashi, N.; Osa, T. *Chem. Lett.* **1986**, 421.
40. Sokolov, V. I.; Bondareva, V. L.; Golovaneva, I. F. *Metalloorg. Khim.* **1988**, *1*, 716 (*Chem. Abstr.* **1989**, *110*, 135 446).
41. Sokolov, V. I.; Bondareva, V. L.; Golovaneva, I. F. *J. Organomet. Chem.* **1988**, *358*, 401.
42. Maeda, Y.; Ogawa, N.; Tahashima, Y. *J. Chem. Soc., Dalton Trans.* **1987**, 627.
43. Schönherr, H.; Beulen, M. W.; van Veggel, F. C. J. M.; Bügler, J.; Huskens, J.; Reinhoudt, D. N.; Vancso, G. J. *J. Am. Chem. Soc.* **2000**, *122*, 4963.
44. Zapotoczny, S.; Auletta, T.; de Jong, M. R.; Schönherr, H.; Huskens, J.; van Veggel, F. C. J. M.; Reinhoudt, D. N.; Vancso, G. J. *Langmuir* **2002**, *18*, 6988.
45. Bakhtiar, R.; Kaifer, A. E. *Rapid Commun. Mass Spectrom.* **1998**, *12*, 111.
46. Roberts, R. M. G.; Warmsley, J. F. *J. Organomet. Chem.* **1991**, *405*, 357.
47. Yilmaz, V. T.; Karadag, A.; Içbudak, H. *Thermochim. Acta* **1995**, *261*, 107.
48. Godinez, L. A.; Schwartz, L.; Criss, C. M.; Kaifer, A. E. *J. Phys. Chem. B* **1997**, *101*, 3376.
49. Lu, C.; Ren, X.; Liu, L.; Zhang, Y.; Hu, C.; Zhu, H.; Meng, Q *J. Inclusion Phenom.* **2002**, *43*, 19.
50. Sokolov, V. I. *Metalloorg. Khim.* **1988**, *1*, 25 (*Chem. Abstr.* **1989**, *110*, 173 273).
51. Sokolov, V. I.; Bondareva, V. L.; Shustov, G. V. *Metalloorg. Khim.* **1991**, *4*, 697 (*Chem. Abstr.* **1992**, *116*, 21 369).
52. Isnin, R.; Salam, C.; Kaifer, A. *J. Org. Chem.* **1991**, *56*, 35.
53. Sherrod, M. J. *Carbohydr. Res.* **1989**, *192*, 17.
54. Thiem, H. J.; Brandl, M.; Breslow, R. *J. Am. Chem. Soc.* **1988**, *110*, 8612.
55. Matsue, T.; Kato, T.; Akida, U.; Osa, T. *Chem. Lett.* **1986**, 843.
56. Ueno, A.; Hamada, F.; Tomokazu, T.; Osa, T. *Macromol. Chem., Rapid Commun.* **1985**, *6*, 231.
57. Ueno, A.; Moriwaki, F.; Osa, T.; Hamada, F.; Murai, K. *Chem. Pharm. Bull.* **1986**, *34*, 438.
58. Imonigie, J. A.; Macartney, D. H. *Inorg. Chem. Acta* **1994**, *225*, 51.
59. Imonigie, J. A.; Macartney, D. H. *J. Inclusion Phenom.* **1993**, *15*, 195.
60. Macartney, D. H.; Roszak, A. W.; Smith, K. C. *Inorg. Chim. Acta* **1999**, *291*, 365.
61. Nielson, R. M.; Lyon, L. A.; Hupp, J. T. *Inorg. Chem.* **1996**, *35*, 970.
62. Kobayashi, N.; Osa, T. *Bull. Chem. Soc. Jpn.* **1991**, *64*, 1878.
63. Godinez, L. A.; Patel, S.; Criss, C. M.; Kaifer, A. E. J. *Phys. Chem.* **1995**, *99*, 17449.
64. Lu, C. S.; Ren, X. M.; Hu, C. J.; Zhu, H. Z.; Meng, Q. *J. Chem. Pharm. Bull.* **2001**, *49*, 818.
65. Osella, D.; Carretta, A.; Nervi, C.; Ravera, M.; Gobetto, R. *Organometallics* **2000**, *19*, 2791.
66. Ferreira, P.; Gonçalves, I. S.; Pillinger, M.; Rocha, J.; Santos, P.; Teixeira-Dias, J. J. C. *Organometallics* **2000**, *19*, 1455.
67. de Jong, M. R.; Huskens, J.; Reinhoudt, D. N. *Chem. Eur. J.* **2001**, *7*, 4164.
68. Sabapathy, R. C.; Bhattacharyya, S.; Cleland, W. E.; Hussey, C. L. *Langmuir* **1998**, *14*, 3797.
69. Trainor, G. L.; Breslow, R. *J. Am. Chem. Soc.* **1981**, *103*, 154.
70. Breslow, R.; Trainor, G. L.; Ueno, A. *J. Am. Chem. Soc.* **1983**, *105*, 2739.
71. le Noble, W. J.; Srivastava, S.; Breslow, R.; Trainor, G. L. *J. Am. Chem. Soc.* **1983**, *105*, 2745.
72. Liu, J.; Alvarez, J.; Ong, W.; Roman, E.; Kaifer, A. E. *J. Am. Chem. Soc.* **2001**, *123*, 11148.
73. Liu, J.; Mendoza, S.; Roman, E.; Lynn, M. J.; Xu, R.; Kaifer, A. E. *J. Am. Chem. Soc.* **1999**, *121*, 4304.
74. Castro, R.; Cuadrado, B.; Alonso, B.; Casado, C. M.; Moran, M.; Kaifer, A. E. *J. Am. Chem. Soc.* **1997**, *117*, 5760.
75. Cardona, C. M.; Alvarez, J.; Kaifer, A. E.; McCarley, T. D.; Pandey, S.; Baker, G. A.; Bonzagni, N. J.; Bright, F. V. *J. Am. Chem. Soc.* **2000**, *122*, 6139.
76. Cardona, C. M.; McCarley, T. D.; Kaifer, A. E. *J. Org. Chem.* **2000**, *65*, 1857.
77. Ashton, P. R.; Balzani, V.; Clemente-leon, M.; Colonna, B.; Credi, A.; Jayaraman, N.; Raymo, F.; Stoddart, J. F.; Venturi, M. *Chem. Eur. J.* **2002**, *8*, 673.
78. Tian, M.; Dong, S. *Electroanalysis* **1995**, *7*, 1063.
79. He, P.; Ye, J.; Fang, Y.; Suzuki, I.; Osa, T. *Anal. Chim. Acta* **1997**, *337*, 217.
80. Liu, H.; Li, H.; Wing, T.; Sun, K.; Qin, Y.; Qi, D. *Anal. Chim. Acta* **1998**, *358*, 137.
81. Ju, H.; Leech, D. *Langmuir* **1998**, *14*, 300.
82. Kawajiri, Y.; Motohashi, N. *J. Chem. Soc., Chem. Commun.* **1989**, 1336.
83. Petrovski, Z.; Braga, S. S.; Santos, A. M.; Rodrigues, S. S.; Gonçalves, I. S.; Pillinger, M.; Kühn, F. E.; Romao, C. C. *Inorg. Chim. Acta* **2005**, *358*, 981.
84. Cunha-Silva, L.; Gonçalves, I. S.; Pillinger, M.; Xue, W. M.; Rocha, J.; Teixeira-Dias, J. J. C.; Kühn, F. E. *J. Organomet. Chem.* **2002**, *656*, 281.
85. Klingert, B.; Rihs, G. *J. Inclusion Phenom.* **1991**, *10*, 255.
86. Sokolov, V. I.; Bondareva, V. L.; Golovaneva, I. F. *Metalloorg. Khim.* **1989**, *2*, 1252 (*Chem. Abstr.* **1990**, *112*, 235 546).
87. Sokolov, V. I.; Blyumenfel'd, A. L.; Narankiewicz, Z.; Nefedova, M. N.; Mamedyarova, I. A. *Izv. Akad. Nauk SSSR, Ser. Khim.* **1991**, 2165 (*Chem. Abstr.* **1992**, *116*, 21 233).
88. Matsue, H.; Sekine, T.; Yoshihara, K. *Kakuriken Kenkyu Hokoku (Tohoku Daigaku)* **1991**, *24*, 77 (*Chem. Abstr.* **1991**, *115*, 264 815).
89. Matsue, H.; Sekine, T.; Yoshihara, K. *Kakuriken Kenkyu Hokoku (Tohoku Daigaku)* **1992**, *25*, 165 (*Chem. Abstr.* **1993**, *118*, 242 521).
90. Matsue, H.; Sekine, T.; Yoshihara, K. *J. Radioanal. Nucl. Chem.* **1992**, *166*, 123.
91. Morimoto, Y.; Ando, K.; Uno, M.; Takahashi, S. *Chem. Lett.* **1996**, 887.
92. Wang, Y.; Mendoza, S.; Kaifer, A. E. *Inorg. Chem.* **1998**, *37*, 317.
93. González, B.; Cuadrado, I.; Alonso, B.; Casado, C. M.; Morán, M.; Wang, Y.; Kaifer, A. E. *Chem. Commun.* **1998**, 2569.
94. Wang, Y.; Alvarez, J.; Kaifer, A. E. *Chem. Commun.* **1998**, 1457.
95. Turel, I.; Demsar, A.; Kosmrlj, J. *J. Inclusion Phenom.* **1999**, *35*, 595.
96. Braga, S. S.; Gonçalves, I. S.; Pillinger, M.; Ribeiro-Claro, P.; Teixeira-Dias, J. J. C. *J. Organomet. Chem.* **2001**, *632*, 11.
97. Braga, S. S.; Marques, M. M.; Sousa, J. B.; Pillinger, M.; Teixeira-Dias, J. J. C.; Gonçalves, I. S. *J. Organomet. Chem.* **2005**, *690*, 2905.
98. Klingert, B.; Rihs, G. *Organometallics* **1990**, *9*, 1135.

99. Meister, G.; Stoeckli-Evans, H.; Süss-Fink, G. *J. Organomet. Chem.* **1993**, *453*, 249.
100. Klingert, B.; Rihs, G. *J. Chem. Soc., Dalton Trans.* **1991**, 2749.
101. Harada, A.; Saeki, K.; Takahashi, S. *Chem. Lett.* **1985**, 1157.
102. Harada, A.; Saeki, K.; Takahashi, S. *Organometallics* **1989**, *8*, 730.
103. Chang, C. A.; Abdel-Aziz, H.; Melchor, N.; Wu, Q.; Pannell, K. H.; Armstrong, D. W. *J. Chromatogr.* **1985**, *347*, 51.
104. Aime, S.; Canuto, H. C.; Gobetto, R.; Napolitano, F. *Chem. Commun.* **1999**, 281.
105. Shimada, M.; Harada, A.; Takahashi, S. *J. Chem. Soc., Chem. Commun.* **1991**, 263.
106. Patel, P. P.; Welker, M. E. *J. Organomet. Chem.* **1997**, *547*, 103.
107. Pospisil, L.; Hromadova, M.; Fiedler, J.; Amatore, C.; Verpeaux, J. N. *J. Organomet. Chem.* **2003**, *668*, 9.
108. Alston, D. R. Ph.D. Thesis, Sheffield University, Sheffield, UK, 1985.
109. Diaz, C.; Arancibia, A. *Bol. Soc. Chil. Quim.* **1996**, *41*, 291 (*Chem. Abstr.* **1996**, *125*, *276 127).*
110. Diaz, C.; Arancibia, A. *J. Inclusion Phenom.* **1998**, *30*, 127.
111. Dias, A. R.; Garcia, M. H.; Robalo, M. P.; Tekheira, A. P. S.; Bulygina, L. A.; Sokolov, V. I. *Russ. J. Org. Chem.* **2001**, *37*, 620.
112. Song, L. X.; Meng, Q. J.; You, X. Z. *Chinese Chem. Lett.* **1994**, 1047 (*Chem. Abstr.* **1995**, *122*, 187 937).
113. Song, L. X.; Meng, Q. J.; You, X. Z. *Synth. React. Inorg. Met. Org. Chem.* **1995**, *25*(5), 671 (*Chem. Abstr.* **1995**, *123*, 199 032).
114. Song, L. X.; Meng, Q. J.; You, X. Z. *J. Organomet. Chem.* **1995**, *498*, C1.
115. Lu, C. S.; Zhang, W. W.; Ren, X. M.; Hu, C. J.; Zhu, H. Z.; Meng, Q. J. *J. Chem. Soc., Dalton Trans.* **2001**, 3052.
116. Lu, C. S.; Ni, Z.; Liu, W.; Zou, Y.; Xie, J.; Ni, C.; Zhu, H.; Meng, Q.; Yao, Y. *J. Organomet. Chem.* **2003**, *681*, 269.
117. Lima, S.; Gonçalves, I. S.; Ribeiro-Claro, P.; Pillinger, M.; Lpoes, A. D.; Ferreira, P.; Teixeira-Dias, J. J. C.; Rocha, J.; Romao, C. C. *Organometallics* **2001**, *20*, 2191.
118. Braga, S. S.; Gonçalves, I. S.; Lopes, A. D.; Pillinger, M.; Roch, J.; Romao, C. C.; Teixeira-Dias, J. J. C. *J. Chem. Soc., Dalton Trans.* **2000**, 2964.
119. Harada, A.; Takahashi, S. *J. Chem. Soc., Chem. Commun.* **1986**, 1229.
120. Harada, A; Yamamoto, S.; Takahashi, S. *Organometallics* **1989**, *8*, 2560.
121. Harada, A.; Takahashi, S. *J. Macromol. Sci. Chem. A* **1989**, *26*, 373.
122. Sokolov, V. I.; Bondareva, V. L.; Chizhevskii, I. T.; Reutov, O. A. *Izv. Akad. Nauk SSSR, Ser. Khim.* **1987**, *7*, 1689 (*Chem. Abstr.* **1988**, *109*, 23 110).
123. Lewis, L. N.; Sumpter, C. A. *J. Mol. Catal. A: Chem.* **1996**, *104*, 293.
124. Lewis, L. N.; Sumpter, C. A.; Stein, J. *J. Inorg. Organomet. Polymers* **1996**, *6*, 123.
125. Lewis, L. N.; Sumpter, C. A.; Davies, M. *J. Inorg. Organomet. Polymers* **1995**, *5*, 377.
126. Alston, D. R.; Slawin, A. M. Z.; Stoddart, J. F.; Williams, D. J. *Angew. Chem., Int. Ed. Engl.* **1985**, *24*, 786.
127. Alston, D. R.; Ashton, P. R.; Lilley, T. H.; Stoddart, J. F.; Zarzycki, R. *Carbohydr. Res.* **1989**, *192*, 259.
128. Harada, A.; Takeuchi, M.; Takahashi, S. *Chem. Lett.* **1986**, 1893.
129. Harada, A.; Takeuchi, M.; Takahashi, S *Bull. Chem. Soc. Jpn.* **1988**, *61*, 4367.
130. Fornasier, R.; Marcuzzi, F.; Marton, D.; Favero, G.; Russo, U. *J. Organomet. Chem.* **2000**, *605*, 127.
131. Shimada, M.; Morimoto, Y.; Takahashi, S. *J. Organomet. Chem.* **1993**, *443*, C8.
132. Canuto, H. C.; Heyes, S. J.; Aime, S.; Gobetto, R.; Napolinato, F. *J. Chem. Soc., Dalton Trans.* **2000**, 4075.
133. Shimada, M.; Harada, A.; Takahashi, S. *J. Organomet. Chem.* **1992**, *428*, 199.
134. Ueno, A.; Moriwaki, F.; Matsue, T.; Osa, T. *Makromol. Chem., Rapid Commun.* **1985**, *6*, 231.
135. Ueno, A.; Suzuki, I.; Osa, T. *Makromol. Chem., Rapid Commun.* **1987**, *8*, 131.
136. Ueno, A.; Moriwaki, F.; Osa, T.; Hamada, F.; Murai, K. *Chem. Pharm. Bull.* **1986**, *34*, 438.
137. Chen, Q.; Suzuki, I.; Osa, T. *Anal. Chem.* **1992**, *64*, 1650.
138. Armspach, D.; Bagatin, I.; Engelddinger, E.; Jeunesse, C.; Harrowfield, J.; Lejeune, M.; Matt, D. *J. Iran. Chem. Soc.* **2004**, *1*, 10.
139. Engeldinger, E.; Armspach, D.; Matt, D. *Chem. Rev.* **2003**, *103*, 4147.
140. Armspach, D.; Matt, D. *Chem. Commun.* **1999**, 1073.
141. Engeldinger, E.; Armspach, D.; Matt, D.; Toupet, L.; Wesolek, M. *C. R. Chimie* **2002**, *5*, 359.
142. Engeldinger, E.; Armspach, D.; Matt, D. *Angew. Chem., Int. Ed.* **2001**, *40*, 2526.
143. Engeldinger, E.; Armspach, D.; Matt, D.; Jones, P. G.; Welter, R. *Angew. Chem., Int. Ed.* **2002**, *41*, 2593.
144. Engeldinger, E.; Armspach, D.; Matt, D.; Jones, P. G. *Chem. Eur. J.* **2003**, *9*, 3091.
145. Engeldinger, E.; Poorters, L.; Armspach, D.; Matt, D.; Toupet, L. *Chem. Commun.* **2004**, 634.
146. Armspach, D.; Matt, D.; Peruch, F.; Lutz, P. *Eur. J. Inorg. Chem.* **2003**, 805.
147. Reetz, M. T.; Waldvogel, S. R. *Angew. Chem., Int. Ed. Engl.* **1997**, *36*, 865.
148. Reetz, M. T. *J. Heterocyclic Chem.* **1998**, *35*, 1065.
149. Reetz, M. T. *Top. Catal.* **1997**, *4*, 187.
150. Reetz, M. T. *Catal. Today* **1998**, *42*, 399.
151. Deshpande, R. M.; Fukuoka, A.; Ichikawa, M. *Chem. Lett.* **1999**, 13.
152. Lee, J. T.; Alper, H. *Tetrahedron Lett.* **1990**, *31*, 4101.
153. Ganeshpure, P. A.; Satish, S. *J. Chem. Soc., Chem. Commun.* **1988**, 981.
154. Zahalka, H. A.; Januszkiewicz, K.; Alper, H. *J. Mol. Catal.* **1986**, *35*, 249.
155. Harada, A.; Hu, Y.; Takahashi, S. *Chem. Lett.* **1986**, 2083.
156. Karakhanov, E. A.; Filippova, T. Y.; Martynova, S. A.; Maximov, A. L.; Predeina, V. V.; Topchieva, I. N. *Cat. Today* **1998**, *44*, 189.
157. Karakhanov, E.; Maximov, A.; Kirillov, A. *J. Mol. Catal. A: Chem.* **2000**, *157*, 25.
158. Lee, J. T.; Alper, H. *Tetrahedron Lett.* **1990**, *31*, 1941.
159. Pinel, C.; Gendreau-Diaz, N.; Bréhéret, A.; Lemaire, M. *J. Mol. Catal. A: Chem.* **1996**, *112*, L157.
160. Lee, J. T.; Alper, H. *J. Org. Chem.* **1990**, *55*, 1854.
161. Zahalka, H.; Alper, H. *Organometallics* **1986**, *5*, 1909.
162. Monflier, E.; Blouet, E.; Barbaux, Y.; Mortreux, A. *Angew. Chem., Int. Ed. Engl.* **1994**, *33*, 2100.
163. Monflier, E.; Tilloy, S.; Blouet, E.; Barbaux, Y.; Mortreux, A. *J. Mol. Catal. A: Chem.* **1996**, *109*, 27.
164. Tilloy, S.; Bricout, H.; Monflier, E. *Green Chem.* **2002**, *4*, 188.
165. Monflier, E.; Tilloy, S.; Castanet, Y.; Mortreux, A. *Tetrahedron Lett.* **1998**, *39*, 2959.
166. Hapiot, F.; Lyskawa, J.; Tilloy, S.; Bricout, H.; Monflier, E. *Adv. Synth. Catal.* **2004**, *346*, 83.
167. Monflier, E.; Fremy, G.; Castanet, Y.; Mortreux, A. *Angew. Chem., Int. Ed. Engl.* **1995**, *34*, 2269.

168. Monflier, E.; Tilloy, S.; Fremy, G.; Castanet, Y.; Mortreux, A. *Tetrahedron Lett.* **1995**, *52*, 9481.
169. Kalck, P.; Moquel, L.; Dessoudeix, M. *Catal. Today* **1998**, *42*, 431.
170. Dessoudeix, M.; Urrutigoïty, M.; Kalck, P. *Eur. J. Inorg. Chem.* **2001**, 1797.
171. Mathivet, T.; Méliet, C.; Castanet, Y.; Mortreux, A.; Caron, L.; Tilloy, S.; Monflier, E. *J. Mol. Catal. A: Chem.* **2001**, *176*, 105.
172. Leclercq, L.; Sauthier, M.; Castanet, Y.; Mortreux, A.; Bricout, H.; Monflier, E. *Adv. Synth. Catal.* **2005**, *347*, 55.
173. Leclercq, L.; Hapiot, F.; Tilloy, S.; Ramkisoensing, K.; Reek, J. N. H.; van Leeuwen, P. W. N. M.; Monflier, E. *Organometallics* **2005**, *24*, 2070.
174. Anderson, J. R.; Campi, E. M.; Jackson, W. R. *Catal. Lett.* **1991**, *9*, 55.
175. Monflier, E.; Tilloy, S.; Bertoux, F.; Castanet, Y.; Mortreux, A. *New J. Chem.* **1997**, *21*, 857.
176. Tilloy, S.; Bertoux, F.; Mortreux, A.; Monflier, E. *Catal. Today* **1999**, *48*, 245.
177. Lacroix, T.; Bricout, H.; Tilloy, S.; Monflier, E. *Eur. J. Org. Chem.* **1999**, 3127.
178. Bricout, H.; Caron, C.; Bormann, D.; Monflier, E. *Catal. Today* **2001**, *66*, 355.
179. Torque, C.; Bricout, H.; Hapiot, F.; Monflier, E. *Tetrahedron* **2004**, *60*, 6487.
180. Torque, C.; Sueur, B.; Cabou, J.; Bricout, H.; Hapiot, F.; Monflier, E. *Tetrahedron* **2005**, *61*, 4811.
181. Gutsche, C. D. *Calixarenes Revisited: Monographs in Supramolecular Chemistry*; Stoddart, J. F., Ed.; The Royal Society of Chemistry: Cambridge, 1998.
182. Mandolini, L., Ungaro, R., Eds.; *Calixarenes in Action*, Imperial College Press: London, 2000.
183. Asfari, Z., Böhmer, V., Harrowfield, J., Vicens, J., Eds.; *Calixarenes*; Kluwer Academic Publishers: Dordrecht, 2001.
184. Ikeda, A.; Shinkai, S. *Chem. Rev.* **1997**, *97*, 1713.
185. Stewart, D. R.; Gutsche, D. *J. Am. Chem. Soc.* **1999**, *121*, 4136.
186. Redshaw, C. *Coord. Chem. Rev.* **2003**, *244*, 45.
187. Arnaud-Neu, F.; Collins, E. M.; Deasy, M.; Ferguson, G.; Harris, S. J.; Kaitner, B.; Lough, A. J.; McKervey, M. A.; Marques, E. B.; Ruhl, B. L., *et al. J. Am. Chem. Soc.* **1989**, *111*, 8681.
188. Wieser, C.; Dieleman, C.; Matt, D. *Coord. Chem. Rev.* **1997**, *165*, 93.
189. Antipin, I. S.; Kazakova, E. K.; Habicher, W. D.; Konovalov, A. I. *Russ. Chem. Rev.* **1998**, *67*, 905.
190. Baur, M.; Frank, M.; Schatz, J.; Schildbach, F. *Tetrahedron* **2001**, *57*, 6985.
191. Alvarez, J.; Wang, Y.; Gómez-Kaifer, M.; Kaifer, A. *Chem. Commun.* **1998**, 1455.
192. Atwood, J. L.; Junk, P. C.; Lawrence, S. M.; Raston, C. L. *Supramol. Chem.* **1996**, 7, 15.
193. Gardiner, M. G.; Lawrence, S. M.; Raston, C. L.; Skelton, B. W.; White, A. H. *Chem. Commun.* **1996**, 2491.
194. Bukhaltsev, E.; Goldberg, I.; Vigalok, A. *Organometallics* **2004**, *23*, 4540.
195. Cameron, B. R.; Loeb, S. J. *Chem. Commun.* **1996**, 2003.
196. Cameron, B. R.; Loeb, S. J.; Yap, G. P. A. *Inorg. Chem.* **1997**, *36*, 5498.
197. Iwasa, K.; Kochi, T.; Ishii, Y. *Angew. Chem., Int. Ed. Engl.* **2003**, *42*, 3658.
198. Wieser-Jeunesse, C.; Matt, D.; De Cian, A. *Angew. Chem., Int. Ed. Engl.* **1998**, *37*, 2861.
199. Lejeune, M.; Jeunesse, C.; Matt, D.; Kyritsakas, N.; Welter, R.; Kintzinger, J.-P. *J. Chem. Soc., Dalton Trans.* **2002**, 1642.
200. Seitz, J.; Maas, G. *Chem. Commun.* **2002**, 338.
201. Loeber, C.; Wieser, C.; Matt, D.; De Cian, A.; Fischer, J.; Toupet, L. *Bull. Soc. Chim. Fr.* **1995**, *132*, 166.
202. Fang, X.; Scott, B. L.; Watkin, J. G.; Carter, C. A. G.; Kubas, G. J. *Inorg. Chim. Acta* **2001**, *317*, 276.
203. Paciello, R.; Siggel, L.; Röper, M. *Angew. Chem,. Int. Ed. Engl.* **1999**, *38*, 1920.
204. Shimizu, S.; Shirakawa, S.; Sasaki, Y.; Hirai, C. *Angew. Chem., Int. Ed. Engl.* **2000**, *39*, 1256.
205. Shirakawa, S.; Shimizu, S.; Sasaki, Y. *New J. Chem.* **2001**, *25*, 777.
206. Obora, Y.; Liu, Y. K.; Jiang, L. H.; Takenaka, K.; Tokunaga, M.; Tsuji, Y. *Organometallics* **2005**, *24*, 4.
207. Timmerman, P.; Berboom, W.; Reinhoudt, D. N. *Tetrahedron* **1996**, *52*, 2663.
208. Schneider, H.-J.; Schneider, U. *J. Inclusion Phenom.* **1994**, *19*, 67.
209. MacGillivray, L. R.; Spinney, H. A.; Reid, J. L.; Ripmeester, J. A. *Chem. Commun.* **2000**, 517.
210. Gittins, P. J.; Twyman, L. J. *Supramol. Chem.* **2003**, *15*, 5.
211. Fréchet, J. *Proc. Natl. Acad. Sci. USA* **2002**, *99*, 4782.
212. Bosman, A. H.; Janssen, H. M.; Meijer, E. W. *Chem. Rev.* **1999**, *99*, 1665.
213. Newkome, G. R.; He, E.; Moorefield, C. N. *Chem. Rev.* **1999**, *99*, 1689.
214. Fischer, M.; Vögtle, F. *Angew. Chem., Int. Ed. Engl.* **1999**, *38*, 884.
215. Jansen, J. F. G. A.; den Brabander-van der Berg, E. M. M.; Meijer, E. W. *Science* **1994**, *266*, 1226.
216. Oosterom, G. E.; Reek, J. N. H.; Kamer, P. C. J.; van Leeuwen, P. W. N. M. *Angew. Chem., Int. Ed. Engl.* **2001**, *40*, 1828.
217. Seebach, D.; Lapierre, J.-M.; Greiveldinger, G.; Skobridis, K. *Helv. Chim. Acta* **1994**, *77*, 1673.
218. Seebach, D.; Lapierre, J.-M.; Skobridis, K.; Greiveldinger, G. *Angew. Chem., Int. Ed. Engl.* **1994**, *33*, 440.
219. Seebach, D.; Herrmann, G. F.; Lengweiler, U. D.; Bachmann, B. M.; Amrein, W. *Angew. Chem., Int. Ed. Engl.* **1996**, *35*, 2795.
220. Murer, P.; Seebach, D. *Angew. Chem., Int. Ed. Engl.* **1995**, *34*, 2116.
221. Brunner, H. *J. Organomet. Chem.* **1995**, *500*, 39.
222. Brunner, H.; Altmann, S. *Chem. Ber.* **1994**, *127*, 2285.
223. Brunner, H.; Fürst, J.; Nagel, U.; Fischer, A. *Z. Naturforsch. B* **1994**, *49*, 1305.
224. Oosterom, G. E.; van Haaren, R. J.; Reek, J. N. H.; Kamer, P. C. J.; van Leeuwen, P. W. N. M. *Chem. Commun.* **1999**, 1119.
225. Oosterom, G. E.; Steffens, S.; Reek, J. N. H.; Kamer, P. C. J.; van Leeuwen, P. W. N. M. *Top. Catal.* **2002**, *19*, 61.
226. Fan, Q.-H.; Chen, Y.-M.; Chen, X.-M.; Jiang, D.-Z; Xi, F.; Chan, A. S. C. *Chem. Commun.* **2000**, 789.
227. Maraval, V.; Laurent, R.; Caminade, A.-M.; Majoral, J.-P. *Organometallics* **2000**, *19*, 4025.
228. Petrucci-Samija, M.; Guillemette, V.; Dasgupta, M.; Kakkar, A. K. *J. Am. Chem. Soc.* **1999**, *121*, 1968.
229. O'Brien, P. In *Comprehensive Oorganometallic Metallic Chemistry-II*; Abel, E. W., Stone, F. G. A., Wilkinson, G., Eds.; Elsevier: Oxford, 1995; vol. 4, p. 175.
230. Adams, R. D., Cotton, F. A., Eds.; *Catalysis by Di- and Polynuclear Metal Cluster Complexes*; Wiley-VCH: New York, 1998.
231. Broussard, M. E.; Juma, B.; Train, S. G.; Peng, W.-J.; Laneman, S. A.; Stanley, G. G. *Science* **1993**, *260*, 1784.
232. Rheiner, P. B.; Sellner, H.; Seebach, D. *Helv. Chim. Acta* **1997**, *80*, 2027.
233. Rheiner, P. B.; Seebach, D. *Chem. Eur. J.* **1999**, *5*, 3221.
234. Sellner, H.; Seebach, D. *Angew. Chem., Int. Ed. Engl.* **1999**, *38*, 1918.
235. Hu, Q.-S.; Pugh, V.; Sabat, M.; Pu, L. *J. Org. Chem.* **1999**, *64*, 7528.

236. Yamago, S.; Furukawa, M.; Azuma, A.; Yoshida, J.-I. *Tetrahedron Lett.* **1998**, *39*, 3783.
237. Ong, W.; Gómez-Kaifer, M.; Kaifer, A. E. *Chem. Commun.* **2004**, 1677.
238. Kaim, W.; Schwederski, B. *Bioinorganic Chemistry: Inorganic Elements in the Chemistry of Life*; Wiley: New York, 1994.
239. Crabtree, R. H. *The Organometallic Chemistry of the Transition Elements*; Wiley: New York, 1994.
240. Fontecilla-Camps, J. C.; Ragsdale, S. W. *Adv. Inorg. Chem.* **1999**, *47*, 283.
241. Chen, H.; Maestre, M. F.; Fish, R. H. *J. Am. Chem. Soc.* **1995**, *117*, 3631.
242. Chen, H.; Ogo, S.; Fish, R. H. *J. Am. Chem. Soc.* **1996**, *118*, 4993.
243. Bakhtiar, R.; Chen, H.; Ogo, S.; Fish, R. H. *Chem. Commun.* **1997**, 2135.
245. Jaouen, G.; Top, S.; Vessikes, A.; Alberto, R. *J. Organomet. Chem.* **2000**, *600*, 23.
246. Top, S.; El Hafa, H.; Vessières, A.; Huché, M.; Vaissermann, J.; Jaouen, G. *Chem. Eur. J.* **2002**, *8*, 5241.
247. Top, S.; Vessières, A.; Cabestaing, C.; Laios, I.; Leclercq, G.; Provot, C.; Jaouen, G. *J. Organomet. Chem.* **2001**, *639*, 500.
248. Collot, J.; Gradinaru, J.; Skander, M.; Humbert, N.; Zocchi, A.; Ward, T. R. *J. Am. Chem. Soc.* **2003**, *125*, 9030.
249. Skander, M.; Humbert, N.; Collot, J.; Gradinaru, J.; Klein, G.; Loosli, A.; Sauser, J.; Zocchi, A.; Gilardoni, F.; Ward, T. R. *J. Am. Chem. Soc.* **2004**, *126*, 14411.
250. Thomas, C. M.; Ward, T. R. *Appl. Organometal. Chem.* **2005**, *19*, 35.
251. Severin, K. *Curr. Opin. Chem. Biol.* **2000**, *4*, 710.
252. Polborn, K.; Severin, K. *Chem. Commun.* **1999**, 2481.
253. Polborn, K.; Severin, K. *Eur. J. Inorg. Chem.* **2000**, 1687.
254. Polborn, K.; Severin, K. *Chem. Eur. J.* **2000**, *6*, 4604.
255. Wendicke, S. B.; Burri, E.; Scopelliti, R.; Severin, K. *Organometallics* **2003**, *22*, 1894.
256. Cammidge, A. N.; Baines, N. J.; Bellingham, R. K. *Chem. Commun.* **2001**, 2588.
257. Viton, F.; White, P. S.; Gagné, M. R. *Chem. Commun.* **2003**, 3040.
258. Tada, M.; Sasaki, T.; Iwasawa, Y. *Phys. Chem. Chem. Phys.* **2002**, *4*, 4561.
259. Tada, M.; Sasaki, T.; Iwasawa, Y. *J. Catal.* **2002**, *211*, 496.
260. Tada, M.; Sasaki, T.; Shido, T.; Iwasawa, Y. *Phys. Chem. Chem. Phys.* **2002**, *4*, 5899.
261. Vieille-Petit, L.; Therrien, B.; Süss-Fink, G.; Ward, T. R. *J. Organomet. Chem.* **2003**, *684*, 117.
262. Süss-Fink, G.; Therrien, B.; Vieille-Petit, L.; Tschan, M.; Romakh, V. B.; Ward, T. R.; Dadras, M.; Laurenczy, G. *J. Organomet. Chem.* **2004**, *689*, 1362.
263. Therrien, B.; Vieille-Petit, L.; Süss-Fink, G.; Sei, Y.; Yamaguchi, K. *J. Organomet. Chem.* **2004**, *689*, 2820.
264. Caulder, D. L.; Powers, R. E.; Parac, T. N.; Raymond, K. N. *Angew. Chem., Int. Ed.* **1998**, *37*, 1840.
265. Caulder, D. L.; Brueckner, C.; Powers, R. E.; Koenig, S.; Parac, T. N.; Leary, J. A.; Raymond, K. N. *J. Am. Chem. Soc.* **2001**, *123*, 8923.
266. Leung, D. H.; Fiedler, D.; Bergman, R. G.; Raymond, K. N. *Angew. Chem., Int. Ed. Engl.* **2004**, *43*, 963.
267. Fiedler, D.; Pagliero, D.; Brumaghim, J. L.; Bergman, R. G.; Raymond, K. N. *Inorg. Chem.* **2004**, *43*, 846.
268. Fiedler, D.; Leung, D. H.; Bergman, R. G.; Raymond, K. N. *J. Am. Chem. Soc.* **2004**, *126*, 3674.
269. Colquhoun, H. M.; Stoddart, J. F.; Williams, D. J. *Angew. Chem., Int. Ed. Engl.* **1986**, *25*, 487.
270. Kickham, J. E.; Loeb, S. J. *J. Chem. Soc., Chem. Commun.* **1993**, 1848.
271. Kickham, J. E.; Loeb, S. J.; Murphy, S. L. *J. Am. Chem. Soc.* **1993**, *115*, 7031.
272. Jasat, A.; Sherman, J. C. *Chem. Rev.* **1999**, *99*, 931.
273. Cram, D. J.; Cram, J. M. In *Container Molecules and Their Guests*; Stoddart, J. F., Ed.; Royal Society of Chemistry: Cambridge, 1994.
274. Quan, M. L. C.; Cram, D. J. *J. Am. Chem. Soc.* **1991**, *113*, 2754.
275. Parola, A. J.; Pina, A. J. P. F.; Maestri, M.; Armaroli, N.; Balzani, V. *New J. Chem.* **1994**, *18*, 659.
276. Slagt, V. F.; Reek, J. N. H.; Kamer, P. C. J.; van Leeuwen, P. W. N. M. *Angew. Chem., Int. Ed. Engl.* **2001**, *40*, 4271.
277. Slagt, V. F.; van Leeuwen, P. W. N. M.; Reek, J. N. H. *Chem. Commun.* **2003**, 2474.
278. Dol, G. C.; Kamer, P. C. J.; Hartl, F.; van Leeuwen, P. W. N. M.; Nolte, R. J. M. *J. Chem. Soc., Dalton Trans.* **1998**, 2083.
279. Coolen, H. K. A. C.; Meeuwis, J. A. M.; van Leeuwen, P. W. N. M.; Nolte, R. J. M. *J. Am. Chem. Soc.* **1995**, *117*, 11906.
280. Coolen, H. K. A. C.; van Leeuwen, P. W. N. M.; Nolte, R. J. M. *J. Org. Chem.* **1996**, *61*, 4739.
281. Lee, J. W.; Samal, S.; Selvapalam, N.; Kim, H.-J.; Kim, K. *Acc. Chem. Res.* **2003**, *36*, 621.
282. Ong, W.; Kaifer, A. E. *Organometallics* **2003**, *22*, 4181.
283. Fredenhagen, K.; Cadenbach, G. *Z Anorg. Allg. Chem.* **1926**, *158*, 249.
284. Csuk, R.; Glanzer, B. I.; Furstner, A. *Adv. Organomet. Chem.* **1990**, *28*, 85.
284a. Selig, H.; Ebert, L. B. *Adv. Inorg. Chem. Radiochem.* **1980**, *23*, 281.
285. Jacobson, A. J. Intercalation Reactions of Layered Compounds. In *Solid State Chemistry: Compounds*; Cheetham, A. K., Day, P., Eds.; Oxford University Press: Oxford, 1992.
285a. Riekel, C.; Reznik, H. G.; Schöllhorn, R. *J. Solid State Chem.* **1980**, *34*, 253.
285b. Lerf, A.; Schöllhorn, R. *Inorg. Chem.* **1977**, *16*, 2950.
285c. Whittingham, M. S. *Prog. Solid State Chem.* **1978**, *12*, 41.
286. Brec, R. *Solid State Ionics* **1986**, *22*, 3.
287. Hernan, L.; Morales, J.; Sanchez, L.; Tirado, J. L.; Espinos, J. P.; Gonzalez Elipe, A. R. *Chem. Mater.* **1995**, *7*, 1576.
288. Schöllhorn, R.; Kuhlmann, R.; Besenhard, J. C. *Mat. Res. Bull.* **1976**, *11*, 83.
288a. Dickens, P.; French, S. J.; Hight, A. T.; Pye, M. F. *Mat. Res. Bull.* **1979**, *14*, 1259.
288b. Murphy, D. W.; Christian, P. A.; Disalvo, F. J.; Waszczak, J. V. *Inorg. Chem.* **1979**, *18*, 2800.
289. Jacobson, A. F.; Johnson, J. W.; Brody, J. F.; Scanlon, J. C.; Lewandowski, J. T. *Inorg. Chem.* **1985**, *24*, 1782.
290. Rouxel, J.; Palvadeau, P. *Rev. Chimie. Miner.* **1982**, *19*, 317.
291. Ohashi, M.; Uyeoka, K.; Yamanoka, S.; Hattori, M. *Chem. Lett.* **1990**, 93.
292. Rosenthal, G. L.; Ellis, A. B. *J. Am. Chem. Soc.* **1987**, *87*, 3157.
293. Lal, M.; Lowe, A. T. *J. Chem. Soc., Chem. Commun.* **1980**, 737.
294. Clearfield, A. *Inorganic Ion Exchange Materials*; CRC Press: Boca Raton, Florida, 1982.
295. Clearfield, A. *Comments Inorg. Chem.* **1990**, *10*, 89.
295a. Dines, M. B.; Digiacomo, P. M.; Callahan, K. P.; Griffith, P. C.; Lane, R. H.; Cooksey, R. E. *ACS Symp. Ser.* **1982**, *192*, 223.
296. Pinnavaia, T. J. *NATO ASI SER, Ser. B* **1987**, *172*, 233.

297. Adams, J. M. *J. Chem. Soc., Dalton Trans.* **1974**, 2286.
298. Drezdzon, M. A. *Inorg. Chem.* **1988**, *27*, 4628.
299. Clement, R. *J. Chem. Soc., Chem. Commun.* **1980**, 647.
300. Clement, R. *J. Am. Chem. Soc.* **1981**, *103*, 6998.
301. Besenhard, J. O.; Kain, I.; Klein, H. F.; Witty, H. *Mater. Res. Soc. Symp. Proc.* **1983**, *20*, 221.
302. Chin, C. S.; Lee, B.; Yoo, I.; Kwon, T.-H. *Dalton Trans.* **1993**, *4*, 581.
303. Halbert, T. R.; Johnston, D. C.; McCandlish, L. E.; Thompson, A. H.; Scanlon, J. C.; Dumesic, J. A. *Physica. B* **1980**, *99*, 128.
304. Clement, R. P.; Davies, W. B.; Ford, K. A.; Green, M. L. H.; Jacobson, A. J. *Inorg. Chem.* **1978**, *17*, 2754.
305. Mathey, Y.; Clement, R.; Sourisseau, C.; Lucazeau, G. *Inorg. Chem.* **1980**, *19*, 2773.
306. Chatakondu, K.; Green, M. L. H.; Qin, J.; Thompson, M. E.; Wiseman, P. J. *J. Chem. Soc., Chem. Commun.* **1988**, 223.
307. Pozas-Tormo, R.; Moreno-Real, L.; Martinez-Lara, M.; Rodriguez-Castellon, E. *Can. J. Chem.* **1986**, *64*, 30.
307a. Moreno-Real, L.; Pozas-Tormo, R.; Martinez-Lara, M.; Bruque, S. *Mat. Res. Bull.* **1987**, *22*, 19.
308. Phillips, J. E.; Herber, R. H. *Inorg. Chem.* **1986**, *25*, 3081.
309. Davies, W. B.; Green, M. L. H.; Jacobson, A. J. *J. Chem. Soc., Chem. Commun.* **1976**, 781.
310. Dines, M. B. *Science* **1975**, *188*, 1210.
311. Clement, R. P.; Davies, W. B.; Ford, K. A.; Green, M. L. H.; Jacobson, A. J. *Inorg. Chem.* **1979**, *17*, 2754.
312. Nazar, L. F.; Jacobson, A. J. *J. Chem. Soc., Chem. Commun.* **1986**, 570.
313. Chatakondu, K.; Green, M. L. H.; Qin, J.; Thompson, M. E.; Wiseman, P. J. *J. Chem. Soc., Chem. Commun.* **1988**, 223.
314. O'Hare, D.; Jaegermann, W.; Williamson, D. L.; Ohuchi, F. S.; Parkinson, B. A. *Inorg. Chem.* **1988**, *27*, 1537.
315. O'Hare, D.; Evans, J. S. O.; Prout, C. K.; Wiseman, P. J. *Angew. Chem., Int. Ed. Eng.* **1991**, *30*, 1156.
316. Heyes, S. J.; Clayden, N. J.; Dobson, C. M.; Green, M. L. H.; Wiseman, P. J. *J. Chem. Soc., Chem. Commun.* **1987**, 1560.
316a. Mason, S. J.; Heyes, S. J.; Wong, H.-V.; O'Hare, D. *Inorg. Chem.* **1995**, *34*, 4287–4289.
317. Wong, H.-V.; Evans, J. S. O.; Barlow, S.; Mason, S. J.; O'Hare, D. *Inorg. Chem.* **1994**, *33*, 5515–5521.
318. Benavente, E.; Santa Ana, M. A.; Mendizabal, F.; Gonzalez, G. *Coord. Chem. Rev.* **2002**, *224*, 87.
319. Tagaya, H.; Hashimoto, T.; Karasu, M.; Izumi, T.; Chiba, K. *Chem. Lett.* **1991**, *12*, 2113.
320. Golub, A. S.; Shumilova, I. B.; Zubavichus, Y. Y.; Jahncke, M.; Suss-Fink, G.; Danot, M.; Novikov, Y. Y. *J. Mater. Chem.* **1997**, *7*, 163.
321. Gamble, F. R; Thompson, A. H. *Solid State Commun.* **1978**, *27*, 379.
322. O'Hare, D.; Formstone, C.; Hodby, J.; Kermoo, M.; FitzGerald, E.; Cox, P. A. *J. Chem. Soc., Chem. Commun.* **1990**, 11.
322a. O'Hare, D. *Chem. Rev.* **1992**, *21*, 121–126.
323. Prober, D. E.; Schwall, R. E.; Beasly, M. R. *Phys. Rev. B* **1980**, *21*, 2717.
324. Morris, R. C.; Coleman, R. V. *Phys. Rev. B* **1973**, *7*, 991.
325. Clark, S. M.; Evans, J. S. O.; O'Hare, D.; Nuttall, C. J.; Wong, H.-V. *J. Chem. Soc., Chem. Commun.* **1994**, 809–810.
326. Evans, J. S. O.; Price, S. J.; Wong, H.-V.; O'Hare, D. *J. Am. Chem. Soc.* **1998**, *120*, 10837–10846.
327. Stahl, H. *Inorg. Nucl. Chem. Lett.* **1980**, *16*, 271.
328. Rouxel, J.; Palvadeau, P. *Rev. Chimie. Miner.* **1982**, *19*, 317.
329. Herber, R. H. *Z Phys. Chim. Neu. Fol. B* **1987**, *151*, 69.
330. Bringley, J. F.; Fabre, J. M.; Averill, B. A. *J. Am. Chem. Soc.* **1990**, *112*, 4577.
331. Herber, R. H.; Maeda, Y. *Inorg. Chem.* **1981**, *20*, 1409.
332. Klingen, W.; Ott, R.; Hahn, H. *Z Anorg. Allg. Chem.* **1973**, *396*, 271.
333. Taylor, B. E.; Steger, J.; Wold, A. *J. Solid State Chem.* **1973**, *7*, 461.
334. Cleary, D. A.; Francis, A. H. *J. Phys. Chem.* **1985**, *89*, 97.
335. Clement, R. *J. Am. Chem. Soc.* **1981**, *103*, 6998.
336. Clement, R.; Doeuff, M.; Gledel, C. *J. Chimie. Phy.* **1998**, *85*, 1053.
337. Brec, R. *Solid State Ionics.* **1986**, *22*, 3.
338. Mercier, H.; Mathey, Y.; Canadell, E. *Inorg. Chem.* **1987**, *26*, 963.
339. Clement, R.; Girerd, J. J.; Morgenstern-Badarau, I. *Inorg. Chem.* **1980**, *19*, 2852.
340. Evans, J. S. O.; O'Hare, D.; Clement, R. *J. Am. Chem. Soc.* **1995**, *117*, 4595.
340a. Evans, J. S. O.; O'Hare, D.; Clement, R.; Leaustic, A.; Thuéry, P. *Adv. Matter.* **1995**, *7*, 735–739.
341. Kihlborg, L. *Ark Kemi.* **1963**, *21*, 357.
342. Aldebert, P.; Baffier, N.; Legendre, J. J.; Livage, J. *Rev. Chim. Miner.* **1982**, *19*, 485.
343. Clearfield, A. *Inorganic Ion Exchange Materials*; CRC Press: Boca Raton, 1982.
344. Clearfield, A.; Smith, G. D. *Inorg. Chem.* **1969**, *8*, 431.
345. Jordan, B; Calvo, C. *Can. J. Chem.* **1973**, *51*, 2621.
346. Morosin, B. *Acta Crystallogr., Sect. B* **1978**, *34*, 3733.
347. Clearfield, A. *Comments Inorg. Chem.* **1990**, *10*, 89.
348. Johnson, J. W. *J. Chem. Soc., Chem. Commun.* **1980**, 263.
349. O'Hare, D.; Kermoo, M.; Formstone, C.; FitzGerald, E.; Cox, P. A. *J. Mater. Chem.* **1991**, *1*, 51.
350. Rosenthal, G. L.; Caruso, J. *J. Solid State Chem.* **1991**, *93*, 128.
351. Lee, C. F.; Thompson, M. E. *Inorg. Chem.* **1991**, *30*, 4.
352. Matsubayashi, G. E.; Ohta, S.; Okuno, S. *Inorg. Chemica. Acta* **1991**, *184*, 47.
352a. Matsubayashi, G. E.; Ohta, S. *Chem. Lett.* **1990**, 787.
353. Pinnavaia, T. J. *NATO ASI SER., Ser. B* **1987**, *172*, 233.
354. Breen, C.; Brooks, J. S.; Forder, S.; Hamer, J. C. E. *J. Mater. Chem.* **1996**, *6*, 849.
355. Pinnavaia, T. J.; Raythatha, R.; Lee, J. G. S.; Halloran, L. J.; Hoffman, J. F. *J. Am. Chem. Soc.* **1979**, *101*, 6891.
356. Claver, C.; Fernandez, E.; Margalef-Catala, R.; Medina, F.; Salagre, P.; Sueiras, J. E. *J. Catal.* **2001**, *201*, 70.
357. Chin, C. S.; Lee, B.; Yoo, I.; Kwon, T.-H. *Dalton Trans.* **1993**, *4*, 581.
358. Tudor, J.; Willington, L.; O'Hare, D.; Royan, B. *Chem. Commun.* **1996**, 2031–2032.
359. Juza, R.; Friedrichsen, H. *Z Anorg. Allg. Chem.* **1964**, *332*, 173.
360. Fogg, A. M.; Green, V. M.; O'Hare, D. *Chem. Mater.* **1999**, *11*, 216.
361. Yamanaka, S.; Kawaji, H.; Hotchama, K.; Ohashi, M. *Adv. Mater.* **1996**, *8*, 771.

362. Khan, A. I.; O'Hare, D. *J. Mater. Chem.* **2002**, *12*, 3191.
363. Wang, P.; Zhu, G. *Electrochem. Commun.* **2002**, *4*, 36.
364. Gago, S.; Pillinger, M.; Santos, T. M; Rocha, J.; Goncalves, I. S. *Eur. J. Inorg. Chem.* **2004**, 1389.
365. Mohanambe, L.; Vasudevan, S. *Inorg. Chem.* **2005**, *44*, 2128.
366. Kemmer, E.; Overweg, A. R.; van Eijck, L.; Fitch, A. N.; Suard, E.; de Schepper, I. M.; Kearley, G. J. *J. Chem. Phys.* **2002**, *116*, 10838.
367. Schafer-Stahl, H.; Abele, R. *Angew. Chem., Int. Ed. Engl.* **1980**, *19*, 477.
368. Schafer-Stahl, H. *Synth. Met.* **1981**, *4*, 65.
369. Halbert, T. R.; Johnston, D. C.; McCandlish, L. E.; Thompson, A. H.; Scanlon, J. C.; Dumesic, J. A. *Physica B* **1980**, *99*, 128.
370. Glueck, D. S.; Brough, A. R.; Mountford, P.; Green, M. L. H. *Inorg. Chem.* **1993**, *32*, 1893.
371. Clement, R.; Green, M. L. H. *J. Chem. Soc., Dalton Trans.* **1979**, 1566.
372. Clement, R.; Garnier, O.; Jegoudez, J. *Inorg. Chem.* **1986**, *125*, 1404.
373. Phillips, J. E.; Herber, R. H. *Inorg. Chem.* **1986**, *25*, 3081.
374. O'Hare, D; Evans, J. S. O.; Turner, P. A.; Mason, S.; Heyes, S. J.; Greenwood, J. *J. Mater. Chem.* **1995**, *5*, 1383.
375. Mason, S. J.; Bull, L. M.; Grey, C. P.; Heyes, S. J.; O'Hare, D. *J. Mater. Chem.* **1992**, *2*, 1189.
376. Rodriguez-Castellon, E.; Jimenez-Lopez, A.; Martinez-Lara, M.; Morene-Real, L. *J. Inclusion Phenom.* **1987**, *5*, 335.
377. Davidson, A.; Villeneuve, G.; Fournes, L.; Smith, H. *Mat. Res. Bull.* **1992**, *27*, 357.
378. Johnson, J. W. *J. Chem. Soc., Chem. Commun.* **1980**, 263.
379. Chatakondu, K.; Formstone, C.; Green, M. L. H.; O'Hare, D.; Twyman, J. M.; Wiseman, P. *J. Mater. Chem.* **1991**, *1*, 205.
380. O'Hare, D. Inorganic intercolation compounds. In *Inorganic Materials*; Bruce, D. W., O'Hare, D., Eds.; Wiley: Chichester, 1996; vol. 4, pp 171–254.

12.17
Green Organometallic Chemistry

E G Hope, A P Abbott, D L Davies, G A Solan, and A M Stuart, University of Leicester, Leicester, UK

12.17.1 Introduction

Green chemistry, a term only coined in the past decade, is not a new or alternative branch of science, rather an approach, philosophical or conceptual, that can be applied throughout chemistry and chemical engineering. By its very nature, it is extremely broad in that it can be applied to processes or procedures that may involve one or more of a number of issues: (i) reduce or eliminate the use and generation of hazardous substances, (ii) reduce waste, (iii) reduce energy consumption, and (iv) utilize renewable resources; these ideals are elegantly delineated in Paul Anastas' 12 principles of green chemistry.[1] These concepts have not just been invented; indeed, the synthetic chemist and chemical engineer have always sought better selectivities, higher activities, better catalysts, and improved process conditions. Rather societal, political, and economic pressures for sustainable development have focused the chemist's attention (in both industry and academia) on providing products, valued and needed by society, without damaging the environment. The green chemistry–organometallic chemistry interface is, therefore, very large, and it might be argued that most, if not all, of organometallic chemistry seeks to deliver against one or more of Anastas' principles. Throughout this collection, specialist authors have highlighted, in context, developments in green chemistry, whether it involves improved syntheses, catalysis, neoteric solvents, alternative energy sources, renewable resources, or new technologies. In this contribution, we highlight the two principal aspects of organometallic chemistry: synthesis of organometallic compounds and the application of organometallic compounds in synthesis, as viewed from a green chemistry perspective, using hydroformylation and olefin polymerization as in-depth illustrations. For further information, the reader is directed to the specialist contributions in this compilation, special topics elsewhere in this compilation (Chapter 12.12), green chemistry websites,[2–5] and textbooks.[6–23]

The comparison of the relative merits of alternative processes is probably the most fundamental problem facing the development of green organometallic chemistry. Full life cycle assessment (LCA) is the only complete tool to quantitatively evaluate the environmental impact of a particular process, but here the absence of data introduces assumptions and approximations, which make it difficult to draw firm conclusions.[24] In a direct comparison of the asymmetric hydrogenation of ketoesters using enzymatic yeast, heterogeneous (Pt on alumina + chinchinodine) and homogeneous (Ru–BINAP) processes, the homogeneous processes offer the lowest cumulated environmental impact.[25] However, the authors here deduce that the environmental impact of a synthetic reaction depends more on the process parameters than the individual technology, where volume of solvent, number of distillations, and catalyst losses have the greatest impact on the LCA. Alternative approaches include the application of a variety of metrics (Figure 1),[26–30] which often focus on individual components of green chemistry (waste generation, reaction stoichiometry, amount of solvent or auxiliaries), but only seldom offer insight into the integration of technology and chemistry to deliver overall environmental benefits.[31]

Atom economy is a simple metric for the initial comparison between different reactions that is receiving considerable attention.[28] In an ideal scenario, all the atoms in the starting materials are incorporated into the product with anything else needed in only catalytic amounts, and from this viewpoint, addition reactions are ideal green reactions. Many types of addition reactions are known, catalytic hydrogenation and hydroformylation are examples that are

$$\text{Effective mass yield} = \frac{\text{Mass of products} \times 100}{\text{Mass of non-benign reagents}}$$

$$\text{Sheldon E-factor} = \frac{\text{Total waste (kg)}}{\text{kg product}}$$

$$\text{Atom economy} = \frac{\text{Mol wt. of product} \times 100}{\text{Sum of mol wt. of reactants}}$$

$$\text{Mass intensity} = \frac{\text{Total mass used in a process (kg)}}{\text{Mass of product (kg)}}$$

$$\text{Reaction mass intensity} = \frac{\text{Mass of products} \times 100}{\text{Mass of reagents}}$$

Figure 1 Commonly used green chemistry metrics.

performed on very large scales, and even in complex organic synthesis, addition reactions (e.g., Diels–Alder reactions) are well established. Over the last 10 to 15 years, the use of ruthenium complexes in atom-economic transformations has been greatly expanded from two-component to three- and even four-component coupling reactions, and the area has been reviewed.[32–34] Similarly, impressive strides have been made in rhodium-catalyzed reactions, for example, [4 + 2]-, [5 + 2]-, and [4 + 4]-cycloaddition reactions,[35,36] redox isomerizations, for example, the conversion of allylalcohols into ketones,[32–34] where aqueous techniques allow the catalyst to be recycled,[37] and C–H activation and functionalization.[38–40] In 1993, Murai and co-workers reported the first example[38] of a highly efficient, selective ruthenium-catalyzed C–H/alkene coupling reaction, which may in certain cases replace the palladium-catalyzed processes that require stoichiometric base and halogenated or similarly functionalized aromatic starting materials, and the process has since been reviewed.[39] Catalytic methods of C–H functionalization have also been reviewed recently.[39,40]

12.17.2 Alternative Solvents

The replacement of relatively harmful volatile organic solvents with, alternative, less environmentally damaging solvent systems/approaches is generating interest from a green perspective for synthetic chemistry and catalysis. A number of these are reviewed elsewhere in this compilation. Here, we highlight some notable developments in green applications of water, supercritical (sc) fluids, ionic liquids, and fluorous solvents in organometallic chemistry.

12.17.2.1 Water

Organometallic chemistry in water is covered elsewhere (Volume 1) and has been reviewed on several occasions.[16–18,41–44] A wide variety of reactions have been catalyzed in water including hydrogenation of alkenes and ketones and imines,[45] conjugate addition,[46] isomerization of allylic alcohols,[37] and many Pd-catalyzed C–C bond-forming reactions[47,48] (see also Section 12.17.3.1). Various transition metal-catalyzed polymerizations have also been effected in water, including CO/alkene polymerization,[49] alkene polymerization,[50] and ring-opening metathesis polymerization.[51] Selected examples of organometallic catalysis in water are discussed below to illustrate the use of aqueous phase reactions in green chemistry. These will be considered in two sections on aqueous biphasic hydrogenation catalysis, which may be done on a larger scale where recycling of the catalyst is an important issue, and C–C bond-forming reactions, which are generally carried out on a smaller scale for which the use of water provides practical benefits in terms of reduced hazard of the reagents involved.

The green credentials of water as a solvent are that it is nonflammable, not combustible, and nontoxic. In addition, its polarity and density make it easy to separate from most organic compounds, and it has favorable thermal properties. Hydrophobic effects and hydrogen bonding can each contribute to the rate enhancement of some reactions in water.[52,53] In addition, the low solubility of oxygen in water can facilitate the use of air sensitive transition metal catalysts in air. The use of water as a solvent implies that there is no need for protection–deprotection processes for acidic hydrogen-containing functional groups, thereby increasing synthetic efficiency. Similarly, laborious derivatization processes are not necessary for water-soluble compounds such as carbohydrates. Potential drawbacks include the low solubility of organic substrates and reactions involving water sensitive compounds, though it is noteworthy that larger rate increases are sometimes found for insoluble substrates.[54]

12.17.2.1.1 Biphasic hydrogenation

The need to retain catalysts in the aqueous phase has led to the development of specifically designed ligands. The design principles are well illustrated by phosphine ligands.[55] These fall into three groups: (i) those with anionic substituents such as sulfonate, carboxylate, or phosphate groups, for example, **1a**; (ii) those with cationic substituents such as ammonium or guanidinium groups, for example, **2**; and (iii) those with neutral hydrophilic groups such as alcohol, phenol, or carbohydrate groups, for example, **3** (Figure 2). Water-soluble bidentate and chiral ligands have also been synthesized based on the same substituents. Triphenylphosphine trisulfonate (TPPTS; **1a**),[56] used in the industrial hydroformylation of propene, has a solubility of 1.1 kg l^{-1}.[57]

In a slight variation using an amine-substituted ligand, the reaction may be carried out homogeneously in an organic solvent with addition of acid after the reaction to enable extraction of the ammonium-substituted catalyst into an aqueous phase.[58,59]

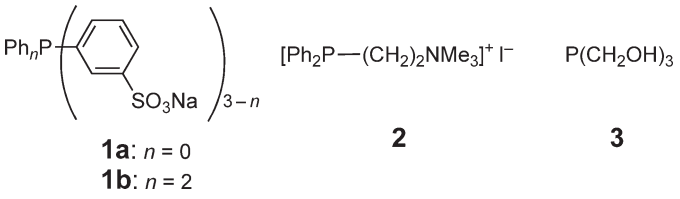

Figure 2 Water-soluble monodentate phosphine ligands.

In many cases, a co-solvent or surfactants are added to increase the solubility of the substrate in the aqueous phase. In hydrogenation, the activity and selectivity is often decreased in water, but addition of a micelle forming amphiphile leads to a significant increase in reaction rate and enantioselectivity. Using a rhodium complex of a neutral bisphosphine, these effects were found with charged and non-ionic surfactants, with the biggest change in activity and selectivity occurring near the critical micelle concentration.[60] Indeed, enantioselectivity could be observed using an achiral rhodium catalyst in the presence of carbohydrate amphiphiles.[61] Chen *et al.* carried out a systematic study of the use of surfactants on hydroformylation of higher alkenes with Rh–TPPTS complexes; in this case, only cationic amphiphiles had a significant effect on yield and regioselectivity.[62] The effect of amphiphiles has led to the development of amphiphilic ligands.[63] However, the use of amphiphiles leads to problems with separation of the products, amphiphile, and catalyst after the reaction. Attempts to overcome this problem have included the use of amphiphilic polymers.[64] An alternative approach to catalysis in water that is experiencing a revival is coupling organometallic catalysts with proteins. The huge advance in protein engineering in recent years means that such catalysts are amenable to combinatorial optimization through genetic modification of the protein.[65] Examples of this approach applied to hydroformylation[66] and asymmetric hydrogenation[67] have been reported recently.

12.17.2.1.2 C–C bond-forming reactions in water

Conventionally, organometallic reagents require dry solvents and inert atmosphere techniques, particularly for organomagnesium and organolithium reagents that often also require low temperatures. Recently, alternatives have been developed based on late transition and main group metals, for example, Pd, Rh, In, Sn, Zn.[46,68,69] Examples include Barbier–Grignard-type reactions of allyl halides with carbonyl compounds and imines,[70] rhodium-catalyzed addition of aryl or alkenylboronic acids to enones[71] or aldehydes,[72] and palladium catalyzed C–C[47,48] and C–N[73] bond-forming reactions, some of which are also performed with microwave irradiation.[74] However, a drawback of all these reactions is the need for a halide starting material and the generation of stoichiometric quantities of halide waste, and stoichiometric metal waste in several cases. Thus, direct C–H activation in water would provide a more green solution. Such processes have been demonstrated in the synthesis of propargyl alcohols from catalytic C–H activation of an alkyne and *in situ* reaction with an aldehyde.[75] This methodology has been extended to a three-component coupling of aldehyde, amine, and alkyne with a gold catalyst in water.[76] The importance of water is evidenced by low yields in organic solvents but almost quantitative conversions in water.

It is clear that apart from the green benefits in terms of reduced hazards and toxicity, the special properties of water as a solvent can have dramatic effects on reactions. Further research in this area is very likely to produce new reactions of general applicability.

12.17.2.2 Supercritical Fluids

Substances in the sc state have a unique set of physical properties that make them attractive alternatives as reaction solvents. They have high miscibility with gases, liquid-like solvating power, and better-than-liquid transport properties, which invariably provide improved reaction rates. By far, the most commonly used fluid is CO_2 because it is inexpensive, nontoxic, nonflammable, environmentally benign, and has low critical constants ($T_c = 304.2$ K; $P_c = 72.8$ bar). Accordingly, it has been lauded as a replacement for volatile organic solvents. The sc fluids also offer the potential to tune the solvent properties and affect yield, rate, and selectivity with pressure. In addition, the morphology of the product can be controlled by rapid expansion of sc solutions, and selective extraction of products from complex mixtures can be achieved by careful choice of solution density.

The sc solvents have already found significant application for the extraction of natural products,[77] purification of lubricating oils,[77] pharmaceutical processing, spray painting,[78] and dry cleaning. The key advantage that has been exploited with these processes is the lack of solvent residues following processing which is particularly important for consumer products. The decreased emission of organic solvents associated particularly with the last two applications could have a significant environmental impact. Multi-tonne processes such as the decaffeination of coffee or the extraction of hops[77] have led to industrial confidence in the application of sc fluids. Reactor systems capable of operating up to 300 bar are readily available; hence, these solvents need not be considered as exotic media. While the application of sc fluids is not advantageous for all reactions, there are specific applications where their use is clearly desirable.

Examples of the industrial use of sc fluids for synthesis are less extensive with only fluorinated polymer production[79] and heterogeneous hydrogenation that have been commercialized.[80] Academic studies have, however, covered the vast majority of reaction types. By far, the most comprehensive review is that by Leitner and Jessop,[12] which details not only all of the reaction types studied up to that point (1999) but also explains the underlying physical principles of the fluids. The book includes stoichiometric organic reactions, photochemical processes, polymerization reactions, heterogeneous catalysis, as well as metal complex-catalyzed reactions. A special issue of *Chemical Reviews* in 1999 (issue 2) covered a wide range of organometallic reactions in sc fluids.[81] A condensed overview of CO_2 as a green reaction medium is presented by Leitner.[82] Numerous other reviews detail specific reaction types and compare CO_2 with other solvents.[83–87]

One of the main difficulties experienced with the design of catalysts for sc fluids is the low polarity, particularly, of CO_2 (the dielectric constant ranges from 1.5 to 1.7 depending on pressure).[12] This means that most organometallic complexes traditionally used in conventional liquid solvents are insoluble in $scCO_2$. This has led to most studies being carried out using heterogeneous catalysts. Comprehensive reviews of heterogeneous hydrogenations in sc fluids have been published.[12,88]

The design of catalysts for use in $scCO_2$ involves the same principles as those required for fluorous biphase catalysis (*vide infra*), that is, fluorous- or trialkyl-phosphine groups are used as ligands.[89,90] An alternative approach is to use conventional catalysts and change the sc fluid. Hope and co-workers have used $scCF_2H_2$ and $scCF_3CFH_2$ for a variety of reaction types and showed that hydrogenation catalysts, such as Wilkinson's catalyst, are soluble without modification.[91] A few detailed cases are given below using hydrogenation as a specific reaction. The solubility of substrates and catalysts has been studied for most reactions and the majority of the data is brought together in two studies. Depressurization of the solution at the end of the reaction leads to a complex mixture of product and catalyst, and a number of methodologies have been devised to circumvent this. The solvent polarity can be tuned using changes in temperature or pressure, and this has been shown to be effective at separating the catalyst from the substrate.[90] Work by Leitner and co-workers also showed that facile solute separation could be achieved when the substrate acted as a co-solvent, but the product was a catalyst antisolvent.[92] A membrane reactor was used by Broeke and co-workers to carry out the continuous, homogeneous hydrogenation of 1-butene using a fluorous derivative of Wilkinson's catalyst in $scCO_2$.[93] The silica membrane in the reactor had a pore size of 0.5–0.8 nm, whereas the catalyst was 2–4 nm in size. The substrate and product were able to diffuse through the membrane and, therefore, efficient catalyst recovery was facilitated. The catalyst was prepared *in situ* and conversions of around 40% were obtained during the investigation. The sc fluids have also been used in biphasic catalysis, and the use of sc fluids in conjunction with ionic liquids is seen as being particularly desirable, as CO_2 can act as both a medium to extract the product and also as an expansion medium to decrease solvent viscosity.[94–96] An overview of catalyst immobilization is given in a recent review.[97]

12.17.2.2.1 Homogeneous hydrogenation

The rates of many hydrogenation reactions in liquids are proportional to hydrogen concentration and are sometimes limited by the rate of diffusion of hydrogen from the gas to the liquid phase.[98] These problems are overcome by the use of sc fluids as reaction media which offer a significant potential rate advantage for hydrogenation reactions over more conventional processes. It should be noted that in $scCO_2$, the insertion of CO_2 into the metal–hydride bond of catalytic species to produce formate complexes is also possible.[99,100] This has the potential to inhibit hydrogenation reactions in $scCO_2$, depending on the ability of the formate to revert back to the hydride and CO_2. One of the first examples of hydrogenation in $scCO_2$ (Equation (1)) was the hydrogenation of 3,3-dimethyl–1,2-diphenylcyclopropene **4** by $[MnH(CO)_5]$ via a radical mechanism.[101] Depending on the alkene and the solvent, either hydrogenation or hydroformylation products were observed.[101,102]

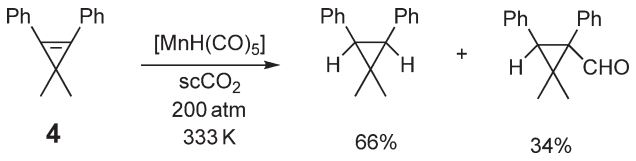

(1)

The selectivity for hydrogenation over hydroformylation has been used as a measure of the strength of the solvent cage, with stronger cages favoring hydroformylation where the selectivities obtained from radical hydrogenations in $scCO_2$ were similar to those obtained in liquid organic solvents.[101,103]

The use of CO_2 as a starting material for the synthesis of organic compounds has been of great interest to synthetic chemists. The hydrogenation of CO_2 has been particularly attractive but remains difficult under conventional gas-phase conditions. In 1994, Noyori and co-workers reported the use of ruthenium(II) phosphine catalysts **5** or **6** (Figure 3) for the hydrogenation of CO_2 to formic acid **7** (Scheme 1) employing $scCO_2$ as both solvent and substrate.[99] The catalysts were chosen for their known solubility in non-polar solvents such as hexane and were shown to be more active than $[RuH_2\{P(C_6H_5)_3\}_4]$, which was considered to be the most active catalyst in benzene solution. Other reactions include the one-pot synthesis of dimethylformamide (DMF) and methyl formate from $scCO_2$.[100] Catalyst **5** showed a catalytic activity which was two orders of magnitude greater than any reported in liquid solvents, giving 99% selectivity to DMF production and a conversion of 99% for the dimethylamine.[104]

It is only over the last few years that the mechanistic aspects of homogeneous hydrogenation in sc fluids have been investigated. One of the first such investigations, Equation (2), was carried out by Leitner and co-workers using dimethyl itaconate **8** and a rhodium catalyst **9** as a model reaction in both hexane and $scCO_2$.[105] They concluded that the mechanism was the same in both solvents and that CO_2 did not interfere with the activation and transfer of the hydrogen molecule at the catalyst.

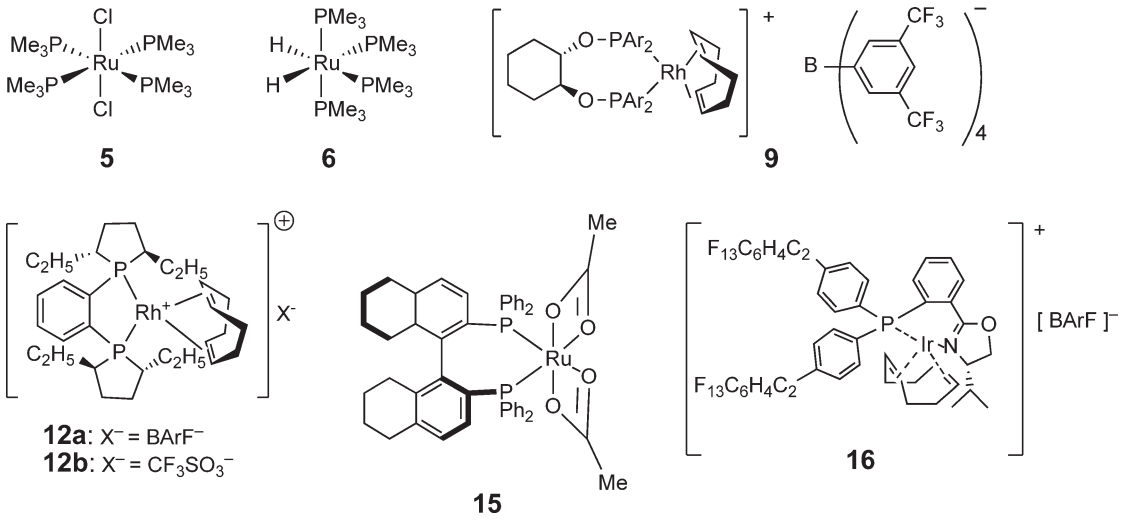

Figure 3 Representative examples of catalysts used for hydrogenation in sc CO_2.

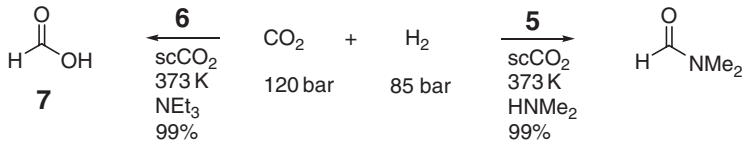

Scheme 1

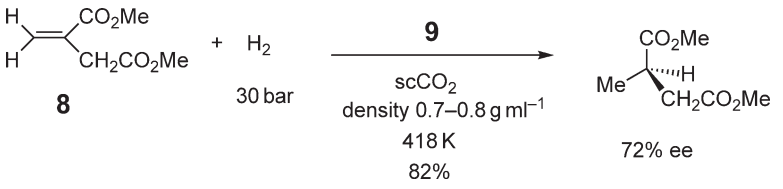

(2)

12.17.2.2.2 Asymmetric hydrogenation

The enantioselectivity of asymmetric hydrogenation of a prochiral olefin depends strongly on the hydrogen concentration, and higher concentrations can lead to higher, lower, or reversed enantioselectivity.[12] It has been suggested by Burk *et al.* that the miscibility of hydrogen gas in sc fluids may lead to better enantioselectivity.[106] They studied the asymmetric hydrogenation of β-disubstituted enamide **10** in $scCO_2$, which gave the valine derivative (*R*)-**11** in 85% ee (Equation (3)).[106] The previous highest reported enantioselectivity for this substrate was 55% ee.[107] The same reaction was carried out in hexane pressurized to 345 bar with nitrogen. This additional experiment indicated that this enhancement of enantioselectivity was not a pressure effect but was associated with the use of $scCO_2$. In the asymmetric hydrogenation of several α-enamides in $scCO_2$ using the cationic Rh complexes **12a** or **12b** (Equation (4)), the ee's obtained were comparable to those obtained in methanol and hexane.[106]

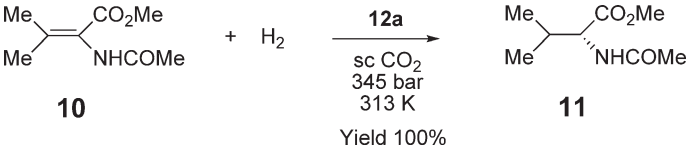

(3)

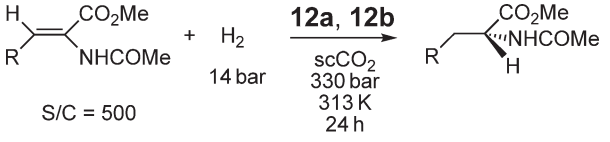

Catalyst	*R*	*Yield* (%)	*ee* (%)
12a	H	100	99.5
12b	C_2H_5	100	98.8
12a	C_6H_5	100	99.5
12a	3,5-$(CF_3)_2C_6H_3$	100	99.5
12b	H	100	99.1
12b	C_2H_5	100	98.8
12b	C_6H_5	100	99.1
12b	3,5-$(CF_3)_2C_6H_3$	100	99.1

(4)

While fluoroalkylated monodentate phosphite, phosphonite, and phosphoramidite ligands offer good selectivity and enantioselectivity in the Rh-catalyzed asymmetric hydrogenation of dimethylitaconate in CH_2Cl_2, the levels of reactivity and selectivity are not retained in $scCO_2$.[108] In contrast, Xiao *et al.* found that α,β-unsaturated carboxylic acids, such as tiglic acid **13**, could be hydrogenated in $scCO_2$ by [Ru$(OCOCH_3)_2${(*S*)-H_8-BINAP}] **15** to give (*S*)-2-methylbutanoic acid **14** (Equation (5)).[109] The product was obtained with an 81% ee, which is comparable to that in methanol (82%) and greater than that in hexane (73%). The partially hydrogenated BINAP catalyst **15** (which gave 99% yield) showed increased solubility in $scCO_2$ over the fully aromatic derivative, which gave poorer yield (50%) and selectivity (37% ee). Addition of the perfluorinated alcohol $CF_3(CF_2)_6CH_2OH$ to **15** offered solubility enhancement and produced an increase in enantioselectivity (89% ee). However, Xiao and co-workers add a note of caution regarding the apparent enhancements observed when polar co-solvents are introduced into sc catalytic systems. In a series of experiments on the Ru–BINAP-catalyzed asymmetric hydrogenation of dimethyl itaconate in $scCO_2$, the high reaction rates and enantioselectivities obtained in the presence of MeOH could arise from pre-reaction in a CO_2-saturated liquid solvent.[110]

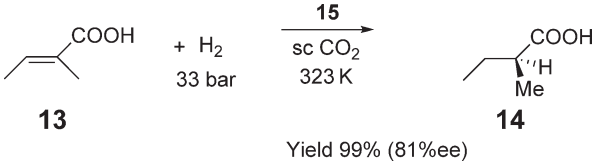

(5)

Leitner and co-workers have used $scCO_2$ for the homogeneous iridium-catalyzed hydrogenation of prochiral imines.[92] Cationic iridium(I) complexes **16**, modified with perfluoroalkyl groups for increased CO_2-philicity, were synthesized and used in the hydrogenation of *N*-(1-phenylethylidene)aniline **17** to give (*R*)-*N*-phenyl–1-phenyl–ethylamine **18** (Equation (6)). In 6 h with 0.078 mol% catalyst, 81% ee was obtained in $scCO_2$, while, in dichloromethane, more than 22 h and 5 times the amount of catalyst were required to give comparable results.

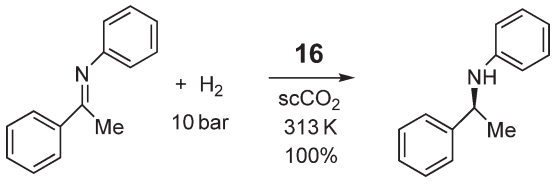

17 **18**
81% ee

(6)

In conclusion, it can be seen that organometallic catalysis in sc fluids has moved on significantly during the last decade. Many of the issues associated with catalyst solubility and separation have been addressed. Also, since many of the technical difficulties concerning high-pressure chemistry have been solved, it should be anticipated that over the next 10 years, some processes could be commercialized and new ligand chemistry could provide opportunities to extend the types of reactions studied in these solvents.

12.17.2.3 Fluorous Media

In 1994, Horváth and Rábai introduced a new approach to the heterogenization of homogeneous catalysts called fluorous biphase catalysis.[111] In essence, the approach is very similar to that in the aqueous biphase system, but the aqueous phase is replaced by perfluorocarbon solvents that are immiscible with most common organic solvents at ambient temperature. By modifying ligands with long perfluoroalkyl groups, often nicknamed fluorous ponytails, the catalyst can be anchored in the fluorous solvent while the substrate(s) and product(s) are preferentially soluble in the upper organic phase. Upon heating or under pressure, the fluorous biphase system (FBS) becomes monophasic, allowing genuine homogeneous catalysis to occur, and on cooling, the transition is reversed so that the two discrete phases are observed again, enabling straightforward separation and recycling by simple decantation. For example, Schneider and Bannwarth synthesized four different perfluoroalkylated analogs of triphenylphosphine and investigated their applications in palladium-catalyzed Suzuki couplings (Scheme 2).[112] The FBS was nearly homogeneous at 75 °C enabling the catalysis to occur, while at room temperature, the fluorous catalysts partitioned into the fluorous phase and were recycled 6 times without significant decrease in the yield. Although a quantitative conversion could be achieved when the catalyst loading was reduced from 1.5 mol% to 0.1 mol%, the yields dropped dramatically on recycling (89%, 78%, 50% for **19a**).

This approach has now been applied to a broad range of catalytic reactions, such as hydrogenation, hydroformylation, hydroboration, and many palladium-catalyzed cross-coupling reactions, and excellent catalyst recovery and reuse have been reported.[113–119] Although there are many comprehensive reviews of fluorous biphase catalysis,[113–119] the *Handbook of Fluorous Chemistry* provides the most detailed accounts of all aspects of fluorous chemistry and includes an excellent experimental section on optimized procedures from the literature.[13] As it stands, fluorous biphase

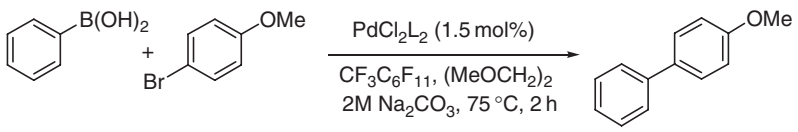

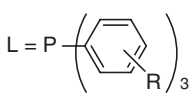

19a: R = 4-$C_2H_4C_8F_{17}$ 87, 90, 92, 89, 86, 90%
19b: R = 3-$C_2H_4C_8F_{17}$ 95, 95, 93, 92, 94, 89%
19c: R = 4-C_8F_{17} 95, 93, 91, 90, 91, 88%
19d: R = 3-C_8F_{17} 99, 96, 90, 86, 83, 88%

Scheme 2

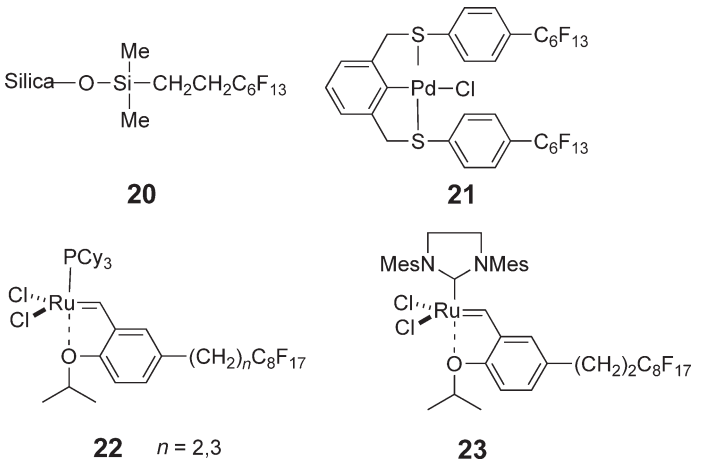

Figure 4 Representative examples of perfluoroalkyl supports and catalysts.

catalysis is not a viable option for industry because of the prohibitive expense and the environmental persistence of the perfluorocarbon solvents. Fluorous reverse-phase (FRP) silica gel **20** (Figure 4) was developed originally by Curran for high-throughput organic synthesis because it can be used to separate fluorous-labelled compounds from conventional organic molecules on a preparative scale.[120] Recently, it has been used to develop two new methods for recycling fluorous catalysts without using perfluorocarbon solvents: (i) fluorous solid-phase extraction, (ii) solid-supported catalysis.

In the first approach, a fluorous SCS pincer palladium complex **21** was used to promote the Heck reaction (Equation (7)) under microwave or thermal heating.[121] At the end of the reaction, the crude reaction mixture was charged directly onto a short column of fluorous silica and was eluted with 90% MeOH–H_2O to give the organic fraction which was then filtered through conventional silica gel to give the pure product. By changing the solvent to diethyl ether, the fluorous catalyst was recovered quantitatively from the fluorous silica gel and was reused twice without loss of activity. The major advantages of this approach are that: (i) fewer and shorter fluorous ponytails are required (<40% fluorine content by molecular weight) compared to fluorous biphase catalysis (>60% fluorine content by molecular weight) and (ii) fluorous solvents are no longer required for either the reaction or separation step. The only other successful organometallic example of this technique is the recycling of light fluorous Grubbs–Hoveyda catalysts **22** and **23** after alkene metathesis.[122]

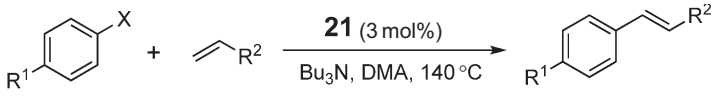

R^1 = OMe, H, COMe, CN, NO_2
R^2 = Ph, CO_2Me
X = I, Br, OTf

R^1	R^2	X	*Yield* (%)
OMe	Ph	I	76
CN	Ph	Br	78
COMe	Ph	I	89
COMe	Ph	Br	92

(7)

In the second approach, Bannwarth and co-workers[123] immobilized fluorous-tagged bis(triphenylphosphine) palladium catalysts **19a–19d**, on FRP silica gel for Suzuki and Sonogashira reactions in conventional organic solvents. Although the supported catalysts showed activities comparable to those found in the FBS, the recycling results were only good for highly active substrates. Recent detailed studies have demonstrated that the activity of the solid-supported catalysts does actually decrease in organic solvents, and this was attributed to catalyst decomposition rather than catalyst leaching.[124] On the other hand, their behavior in water is completely different and the activity remains high upon recycling.[124,125] In related work, Hope and Stuart have been investigating the applications of alternative fluorinated solid supports, such as perfluoroalkylated polystyrene beads and amorphous perfluoroalkylated zirconium phosphonates, in the Heck reaction, hydrogenation, and cyclopropanation.[126]

Besides rising to the challenge of developing new methods for recycling fluorous catalysts, there are also many reports on the synthesis and applications of new perfluoroalkylated chiral catalysts.[127–129] It is difficult to envisage the successful application of the FBS for asymmetric catalysis, but these new lightly fluorinated approaches offer significant potential.

12.17.2.4 Ionic Liquids

Ionic liquids offer a number of potential advantages over organic solvents from a green perspective. Loss of solvent by evaporation is effectively zero. Reactions may be more selective in an ionic liquid, thereby reducing separation costs both from an economic and environmental perspective. For catalytic reactions as well as increasing selectivity, an ionic liquid may stabilize a catalyst and so increase lifetime and turnover number. The use of ionic liquids in catalysis has been the subject of several reviews in recent years,[130–135] and organometallic chemistry in ionic liquids is reviewed in Volume 1.

Most studies of catalysis in ionic liquids have focused on issues of increased selectivity and particularly the easy separation of product from the catalyst and catalyst recycling via use of a biphase. In some cases, the reaction may occur in a biphase; in others, the biphase is only used for product separation. In some special cases, the second phase is exclusively product, due to insolubility of the organic products in the ionic liquid, and is easily separated by decantation, allowing the recovered ionic catalytic solution to be reused. Of course, use of an organic solvent for extraction does reduce some of the potential green benefits of the ionic liquid approach. More recently, $scCO_2$ has been used to extract the products. Alternatively, volatile products can be separated from the ionic liquid and catalyst by distillation.

An advantage of ionic liquids compared to other catalyst immobilization strategies is that many catalytically active transition metal complexes can be immobilized in ionic liquid solvents without the need for specially modified ligands. However, leaching to an organic phase may occur; hence, charged ligands may be preferable to minimize leaching. Hence, many ligands, such as sulfonated phosphines, developed for aqueous biphase reactions, work well in ionic liquids. In the early 1990s, Chauvin *et al.* demonstrated the oligomerization of alkenes catalyzed by a nickel complex in an organoaluminate ionic liquid in the presence of $AlEtCl_2$.[136] In this case, the liquid products formed are immiscible with the ionic liquid, and the reaction could be run in a batch or semicontinuous process. The discovery of air and moisture stable ambient-temperature ionic liquids,[137,138] such as 1-*n*-butyl–3-methylimidazolium [BMIM] salts with $[PF_6]$, $[BF_4]$, $[NTf_2]$, [OTf], or Br as anion, has led to a huge increase in the use of ionic liquids, and a wide range of reactions have now been catalyzed in ionic liquids including hydrodimerizations,[139] alkoxycarbonylations,[140] hydroformylation,[138,141] epoxidations,[142,143] alkene metathesis,[144,145] hydrogenations, and a wide variety of palladium coupling reactions. For further details of these and other reactions, readers are directed to the reviews mentioned above. Hydrogenation and palladium-catalyzed cross-coupling reactions are discussed here as illustrations of the potential beneficial effects and complications arising from the use of ionic liquids as green solvents.

12.17.2.4.1 Hydrogenation

Hydrogenations which occur by oxidative addition,[137,138] heterolytic activation,[146] and homolytic cleavage[146] of hydrogen can all occur in ionic liquids. Alkane products are easily recovered by decantation and the recovered catalyst solution can be reused several times. It is noteworthy that isomerization products were not observed in ruthenium-catalyzed hydrogenation of 1-hexene performed in $[BMIM][BF_4]$[146] though they are formed in aqueous biphase reactions. However, Chauvin and co-workers reported that isomerization did occur for rhodium-catalyzed hydrogenation of 1-pentene; when the ionic liquids contained trace amounts of chloride ions, the rate of hydrogenation dropped while the selectivity to the isomerization product pent-2-ene increased.[138]

The catalytic hydrogenation of arenes with an arene ruthenium catalyst precursor has also been performed in ionic liquids and the products separated from the ionic solution by distillation under high vacuum, allowing the same batch of ionic liquid to be used repeatedly for the catalytic hydrogenation of several different arenes.[147] Interestingly, colloidal rhodium catalysts can hydrogenate arenes in aqueous/sc fluid biphasic media whereas the reactions do not work in $[BMIM][BF_4]$.[148]

Hydrogenation has also been extended to asymmetric versions using an Ru–BINAP complex dissolved in $[BMIM][BF_4]$ with isopropanol as a co-solvent to solubilize the substrates.[149] The enantioselectivity is comparable to those obtained in conventional organic solvents though the ionic liquid did increase the catalyst stability. Similarly, an Rh–DUPHOS catalyst was found to be much more air stable in $[BMIM][PF_6]$ than in an organic solvent and could be reused five times with very little drop in enantioselectivity.[150] The effect of hydrogen pressure on enantioselectivity is not simple, and apparently conflicting results have been found using $[BMIM][BF_4]$ and $[BMIM][PF_6]$. These results were explained on the basis of differing concentrations of molecular hydrogen in the ionic liquids;[151] however, a more recent study suggests that there is little difference in the solubility of H_2 in the pure ionic liquids.[152] More recently, asymmetric hydrogenation of tiglic acid has been performed in $[BMIM][PF_6]$ with some added water, with extraction of the products by $scCO_2$.[153]

12.17.2.4.2 Palladium-catalyzed cross-coupling reactions

The first reported example of palladium-catalyzed C–C bond-forming reactions in an ionic liquid was the Heck reaction in ammonium and phosphonium halide ionic liquids using simple catalyst precursors such as $[PdCl_2]$ or $[Pd(OAc)_2]_3$ without phosphine ligands.[154] The products could be distilled from the ionic liquid and the remaining catalyst solution still showed catalytic activity. Seddon and co-workers reported that Heck reactions proceed better in hexylpyridinium rather than dialkylimidazolium-based ionic liquids. Addition of phosphine inhibited the reaction in $[C_6py]Cl$ but increased the reactivity in imidazolium-based ionic liquids.[155] Herrmann and co-workers also noted poorer reactivity in imidazolium-based ionic liquids compared to tetraalkylammonium salts.[156,157] The first evidence that palladium *N*-heterocyclic carbene (NHC) complexes were being formed came from the observation that the Heck reaction proceeds more efficiently in [BMIM]Br than $[BMIM][BF_4]$ and that palladium black precipitated in the latter solvent but not the former.[158] In addition, NHC complexes, **24** and **25**, (Figure 5) could be isolated from the reaction in [BMIM]Br. While NHC complexes are implicated in some cases, catalysis by palladium nanoparticles is an alternative proposition, particularly where the formation of NHC complexes is not possible.[159]

The Suzuki coupling[160] of 4-bromotoluene with phenylboronic acid catalyzed by $[Pd(PPh_3)_4]$ has been carried out in $[BMIM][BF_4]$.[161] The best results were achieved by preheating the aryl halide in the ionic liquid with the Pd complex before adding the arylboronic acid and Na_2CO_3. The use of $[BMIM][BF_4]$ has several advantages over toluene as a solvent; a significant increase in reactivity (turnover frequency (TOF) = $455\,h^{-1}$ in $[BMIM][BF_4]$, in comparison to $5\,h^{-1}$ in toluene); the formation of homocoupling aryl byproducts is eliminated; the reaction can be performed in air; and the catalyst can be reused 3 times without loss of its activity.[161] In these cases, the products were extracted with diethyl ether, and the inorganic byproducts, which modify the miscibility of water with $[BMIM][BF_4]$ such that two phases are formed at ambient temperature, were removed by washing with water, leaving the clean ionic liquid catalyst solution. Alternatively, the product could be isolated from the $[BMIM][BF_4]$ reaction mixture by sublimation or precipitation by addition of water, all without any apparent leaching of palladium species into the product. Welton and co-workers have now shown that for Suzuki reactions, in imidazolium-based ionic liquids, NHC complexes are always found when the reaction is successful and not when the reaction is unsuccessful.[162]

In conclusion, it was initially assumed in many reactions that ionic liquids were acting as entirely innocent non-coordinating solvents; this is now known not to be the case.[163] In several examples of palladium-catalyzed reactions, formation of NHC complexes is established;[162] however, even in these cases, the precise nature of the active catalyst is not known since palladium nanoparticles are known to be stabilized in ionic liquids.[159] Other problems may arise through the presence of halide impurities from the initial preparation of the ionic liquids which can poison many metal catalysts, particularly cationic complexes.[138,164] Although ionic liquids might be thought to be ideal to stabilize ionic species, Daguenet and Dyson have suggested that dissociation of a halide from a transition metal complex can be thermodynamically disfavored in an ionic liquid.[165] Also, particularly in $[BMIM][PF_6]$, traces of water can lead to hydrolysis of the anion, generating HF and phosphate and subsequently metal fluorides.[166] On a more general note, as solvents, imidazolium-based ionic liquids are rather expensive, certainly when compared to traditional organic solvents, let alone water. In this regard, the use of a supported ionic liquid phase, analogous to the well-established supported aqueous phase catalysis,[167] has been reported in a hydroformylation reaction[168] (Section 12.17.4.4.2). In addition, the toxicity of ionic liquids has not yet been extensively investigated.[169,170] Notwithstanding these issues, the enhanced stability and selectivity of many catalysts in ionic liquids mean that further exploration of the biphase applications of ionic liquids is likely in the next few years.

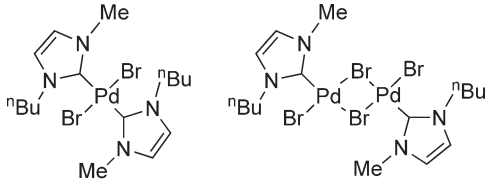

24 **25**

Figure 5 NHC–palladium complexes identified in [BMIM]Br/Pd(II) systems.

12.17.3 Enhanced Technologies

A variety of new and old technologies are generating interest from a green perspective for synthetic chemistry and catalysis, including alternative energy sources, process intensification, and catalyst handling. A number of these have found relatively few applications in organometallic chemistry and others are reviewed elsewhere in this compilation. Here, we highlight some notable developments in green applications of microwaves, sonochemistry, microreactors, membranes, thermoregulated and supported catalysts in organometallic chemistry.

12.17.3.1 Microwave Chemistry

Microwaves can provide a rapid and efficient method of heating, and as such microwave chemistry is attracting interest from the point of view of green chemistry; microwave heating, microwave-assisted synthesis and scale-up have been reviewed.[171–175] Microwave heating is not only rapid but also occurs directly in the solution rather than via the walls; hence, side-reactions, particularly catalyst decomposition, may be slower, giving longer catalyst lifetimes and/or lower catalyst loadings.

The recent advent of microwave reactors specifically designed for chemistry has led to an increase in reproducibility in conditions and, hence, reaction outcomes, leading to a much wider use of microwave chemistry. However, most reactions have been investigated on rather small scales and, therefore, the greatest impact of microwave chemistry to date has been in drug discovery programs in the pharmaceutical industry.[171,176,177] Here, the increased speed and yield of reactions, particularly on polymeric supports, have led to a rapid acceptance of this methodology.

In terms of organometallic chemistry, microwave chemistry has been used in the preparation of several simple organometallic complexes, for example, $[ML(CO)_4]$ (M = Cr, Mo, W; L = en, bipy, dppm, dppe),[178,179] which might be routinely prepared in undergraduate laboratories. Other examples include the preparation of cyclometallated iridium complexes that may have application as OLEDs.[180] Recently, microwave acceleration of homogeneous catalysis has been investigated and the topic has been reviewed.[181] Perhaps, the greatest impact of microwaves on organometallic catalysis has been in the area of palladium-catalyzed reactions such as the Heck, Sonogashira, Suzuki, and Stille cross-couplings. Many such reactions have the additional green benefit of being performed in water,[182] since this is reasonably effective at absorbing microwaves, or sometimes with no solvent at all. Moreover, there have been reports that Suzuki and Sonogashira-type coupling reactions can be performed in water with microwave irradiation with no transition metal catalyst.[183–185] Leadbetter has subsequently shown that small impurities (50 ppb) of palladium in the Na_2CO_3 used as base were actually responsible for the catalysis effectively at very low loading.[186] The same group has since published similar methodology for performing the Heck reaction using ultralow metal catalyst concentrations.[187] The microwave-assisted Suzuki reaction has been scaled up in a continuous flow capillary reactor using a supported palladium catalyst,[188] and in an automated batch process.[189]

Other examples of microwave-assisted catalysis include allylic alkylation, both palladium catalyzed[190] and molybdenum catalyzed.[191] In the latter case, air stable precursor complexes could be used under non-inert conditions. Microwave-enhanced Pauson–Khand reactions have also been reported,[192] as have hydroamination of alkynes,[193] and metathesis of functionalized alkynes.[194] Recently, microwave enhancement has been applied to C–H activation reactions, for example, for the formation of functionalized heterocycles,[195] allowing the reaction to be performed with no solvent purification and minimal precautions to exclude air. A solvent-free chelation-assisted hydroacylation reaction has also been reported.[196]

12.17.3.2 Sonochemistry

Volume 1 includes a thorough review of the applications of sonochemistry in organometallic chemistry, and here we present selected examples to illustrate the green advantages arising from the extreme localized conditions generated by cavitational collapse under acoustic radiation; rate enhancements, catalyst regeneration, non-classical reagents, unusual selectivities.[197] In heterogeneous hydrogenation over Pd black or Raney-Ni, up to 20-fold improvements in reaction rates under ultrasound conditions are reported, with better recycle of the catalyst, which appear to be ascribed not only to the extreme reaction conditions but also to decontamination of the surface active sites and creation of fresh active sites as a direct consequence of the mechanical stress in the catalyst induced by the ultrasonic field.[198,199] The extension to the enantioselective hydrogenation of 1-phenyl-1,2-propanedione over 5% Pt/silica fibers modified with cinchonidine afforded increases in initial reaction rate and enantioselectivity of 4 and 2 times, respectively, under sonication.[200] In Suzuki coupling reactions, up to fourfold improvements in the reaction rate are reported with ultrasound.[201,202] Issues of scale-up of sonochemical reactors are now being contemplated.[203]

12.17.3.3 Microreactors

Traditional chemical manufacturing, which is heavily dependent on large batch processes and associated transport and storage of raw materials, brings with it risk, in terms of health and safety considerations, for both the operators and the local communities. The miniaturization of chemical reactors offers some fundamental and practical advantages, including the minimization of chemical storage and inventory, improved *in situ* reaction monitoring and control, solvent-free mixing, *in situ* reagent formation and integrated separation, often alongside increased reaction rates, improved reaction yields and selectivity. Furthermore, advocates of this new technology identify scale-out as opposed to scale-up (i.e., increasing the number of parallel reaction channels as opposed to building larger reactors) as an intrinsically safer philosophy when converting laboratory-based reactions into full-scale plant operation.[204–207] Essentially, microreactors consist of a series of channels (10–300 μm) etched, by substrate-dependent techniques, for example, photolithography, laser microforming, injection molding, or hot embossing,[208] into a solid substrate (silicon, quartz, glass, metals, polymers).[209,210] For typical organometallic chemistry or catalytic processes, the channel networks are linked to a series of reservoirs, containing reagents, catalysts, or products, to form the complete device, which is typically no more than a few cm^3 in volume.[211] Under process conditions, reagents are brought together, in specific sequences, mixed, and allowed to react in a carefully controlled region of the device using electrokinetic (electroosmotic or electrophoretic) or hydrodynamic pumping. In this way, reaction profiling (temperature, pressure, small reaction inventories, flow rate, reagent concentrations, real time product separation) provides a level of reaction control that is unimaginable in classical bulk stirred-tank reactors. Although this technology is still in its infancy, organic synthesis research has shown that microreactor methodology is compatible with both gas-phase and liquid-phase chemistry, offering considerable potential for safer and more efficient processes. The range of organometallic synthesis and catalysis is currently limited and, here, representative illustrations of the application of microreactors in these areas are highlighted.

12.17.3.3.1 Heterogeneous catalysis in microreactors

The microreactor technology is particularly suited to heterogeneous catalysis, where either the walls of the reaction channels can be used as the catalyst support or a supported catalyst can be placed in the reaction channels. Impregnation of a solution of $[Pd(acac)_2]$ into an aluminum wafer microreactor with mechanical and anodical etching generated microchannels with 0.18% palladium metal in layers 18 μm thick.[212] This device was used in the gas-phase hydrogenation of benzene, cyclodienes, and cyclotrienes, with controlled selectivity to the partially or fully reduced products. Similarly, palladium-coated silica channels, deposited from $[Pd(PPh_3)_4]$, have been used for the rapid room-temperature hydrogenation of a variety of alkenes and alkynes under triphasic conditions, with no detectable metal leaching to the organic product.[213] Yields comparable to those reported under homogenous conditions, together with negligible metal leaching and the absence of an external base, were obtained in palladium-catalyzed Suzuki reactions using 1.8% palladium on silica sandwiched between microporous silica frits within microreactor reaction channels.[214]

12.17.3.3.2 Homogeneous catalysis in microreactors

Increased reaction rates, over those in conventional reactors, were reported for the Kumada–Corriu cross-coupling reaction using an Ni–salen catalyst anchored onto a Merrifield resin as a catalytic plug in a polytetrafluoroethylene (PTFE) microreactor.[215] Issues of channel blocking caused by the polymer swelling under process conditions were overcome using the same Ni–salen catalyst, tethered, with a $C_{11}H_{22}$ linker, to a functionalized silica support.[216] Although reaction rates remained high in the microreactor, a gradual reduction in performance was apparent over extended reaction runs (>5 h). This was ascribed to blocking of active sites on the supported catalyst by reaction byproducts ($MgBr_2$, MgBrCl). Increased reaction rates (20×) are also reported for a Pd–salen catalyst supported on a Merrifield resin in the Suzuki–Miyaura reaction in a microreactor.[217] Here, the supported catalyst is solvent expanded to completely fill the reaction channel such that the liquid path is through the microchannels of the macroporous resin structure. In the asymmetric hydrogenation of a series of substrates with Rh–Josiphos/Diop catalysts, enantioselectivities obtained in a single channel falling-film microreactor were comparable to those obtained in conventional batch reactors.[218] However, the key advantage is the extremely low catalyst loading, typically 0.1 μg, allowing catalyst screening to be accomplished on substantially reduced catalyst inventories. In a combination of microreactor and aqueous biphase technologies, the Ru–TPPTS-catalyzed hydrogenation of α,β-unsaturated aldehydes under plug flow, alternating organic and aqueous slugs, has been reported.[219]

12.17.3.4 Membranes for Integrated Catalysis and Separation

Membranes are either permeable or semi-permeable thin films, which offer advantages, such as lower energy requirements and reductions in capital investment, over conventional separation processes, and are finding increasing applications in the petrochemical and pharmaceutical industries. Essentially, membranes function by controlling, either by sieving or by influencing relative rates of transport, the exchange of materials between two adjacent fluids, and current membrane processes include microfiltration, ultrafiltration, nanofiltration, and gas/vapor separation. Membrane materials include porous inorganic solids (silica, alumina, zeolites, zirconia), organic polymers (polypropylene, fluoropolymers, polyamides, polysulfones, silicones), and microporous carbons. However, the major step forward in green chemical technology is the combination of the separation step with the synthetic step using membranes in the "membrane reactor" concept, which has been made possible with the development of organic solvent-resistant membranes. This coupling of the two key processes results in the continuous separation/feed of reactants/products, which can result in enhancements in selectivity and/or yield.[220,221] The application of this technology in organometallic chemistry can be illustrated by hydrogenation and C–C bond-coupling processes. In the reduction of acetophenone in isopropanol, a polysiloxane-bound ruthenium(II)-transfer hydrogenation catalyst afforded excellent enantioselectivity (97%) with slightly reduced activity (as compared to the homogeneous catalyst) in a continuous flow system equipped with an MPF-50 membrane (Koch Membrane Systems, Germany).[222] Membrane technology can also be combined with catalysis in $scCO_2$.[93] Using a perfluoroalkylated Wilkinson's catalyst analog, van Koten and co-workers have reported the continuous hydrogenation of 1-butene with a tubular microporous silica membrane (ECN Petten, the Netherlands), where high reaction rates were coupled with low (<0.1%) rhodium leaching levels.[93] Metal leaching levels were poorer in a palladium-mediated cross-coupling synthesis of *trans*-stilbene following post-reaction nanofiltration with a polyimide Starmem 122 membrane (W.R. Grace & Co., USA), but this was ascribed to catalyst decomposition rather than difficulties with the membrane technology.[223]

12.17.3.5 Thermoregulated Catalysis

Bergbreiter[224] synthesized smart phosphine ligands **26** and **27** (Figure 6) from an ethylene oxide–propylene oxide–ethylene oxide triblock co-polymer that possesses a property termed inverse temperature-dependent solubility.[225] This means that at low temperature, the phosphines and their rhodium complexes are soluble in water through the formation of hydrogen bonds between oxygen atoms and water molecules, but, on heating above the critical-temperature cloud

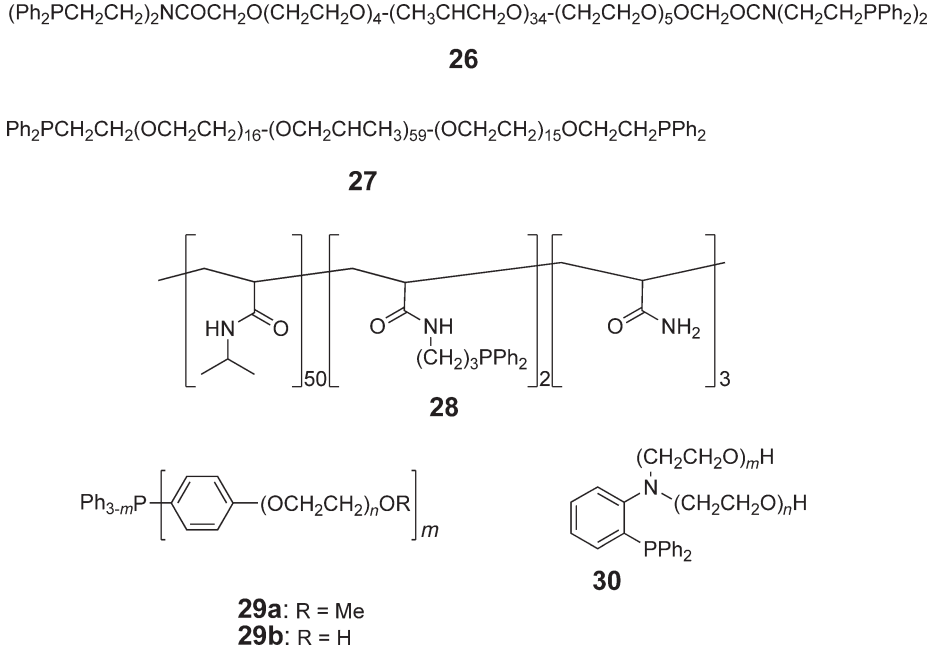

Figure 6 Representative examples of ligands used in thermomorphic catalysis.

point (Cp), they phase separate from the aqueous systems on account of the disruption of the hydrogen bonds. Bergbreiter elegantly illustrated this concept by demonstrating that the cationic rhodium complex of **27** catalyzed the hydrogenation of allyl alcohol in an aqueous system at 0 °C, but on heating to 40–50 °C, the reaction stops. What is most striking is the reversibility of this process, and by cooling the reaction mixture back down to 0 °C, the catalyst is rehydrated and the hydrogenation of allyl alcohol continues.

The inverse temperature-dependent solubility in aqueous media of polymer-bound palladium(0)–phosphine catalysts, based on the water-soluble polymer poly(*N*-isopropyl)acrylamide (PNIPAM) **28**, was also used to recycle and reuse these catalysts in nucleophilic allylic substitutions (Equation (8)) and cross-coupling reactions between aryl iodides and terminal alkynes (Equation (9)). The catalyst was highly active in both reactions, and it was recycled 10 times with an average yield of 93% in the allylic nucleophilic substitution by precipitation with hexane.[226]

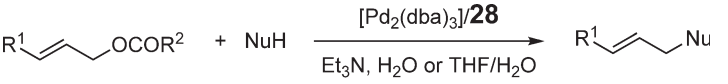

R^1 = H, Ph
R^2 = Me, Et, $C_2H_4CO_2Na$

NuH = Et_2NH, 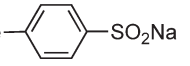

(8)

R^1	R^2	NuH	Temp (°C)	Time (h)	Yield (%)
H	Me	4-$MeC_6H_4SO_2Na$	50	6	89
Ph	Me	4-$MeC_6H_4SO_2Na$	50	6	82
Ph	OEt	4-$MeC_6H_4SO_2Na$	25	8	74

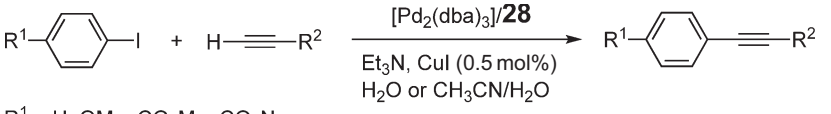

R^1 = H, OMe, CO_2Me, CO_2Na
R^2 = Ph, Bu, $C(CH_3)_2OH$

(9)

R^1	R^2	Yield (%)
H	$C(CH_3)_2OH$	92
OMe	$C(CH_3)_2OH$	96
CO_2Me	$C(CH_3)_2OH$	95

Jin and co-workers introduced the strategy of thermoregulated phase-transfer catalysis in order to solve the mass-transfer limitations associated with aqueous biphase catalysis.[227,228] They initially investigated the inverse temperature-dependent solubility of poly(ethylene oxide)-substituted triphenylphosphines (PETPPs) **29b** (Figure 6) in the hydroformylation of long-chain alkenes in the aqueous biphase system.[229] Before the reaction, the catalyst resides in the aqueous phase while the substrate is in the organic phase, but at high temperatures above the critical-temperature Cp (52–95 °C), the catalyst is transferred into the organic phase enabling homogeneous catalysis to occur. On cooling the reaction mixture, the catalyst becomes water-soluble again, and the aqueous catalyst solution can be readily separated from the products, recycled, and reused. The catalyst activity, however, was only retained for the first four recycles, because the solubility of the catalyst in the organic phase was increased by the presence of the polar aldehyde product. More recently, the group introduced the water-soluble phosphine, *N*,*N*-dipolyoxyethylene-substituted–2-(diphenylphosphino)phenylamine (PEO–DPPPA) **30**, and demonstrated that the high reactivity of the Rh–PEO–DPPPA complex in the aqueous-organic biphasic hydroformylation of 1-decene can be maintained over 20 catalyst recycles.[230]

In order to broaden the scope of the thermoregulated phase-transfer catalysis principle, the hydrogenation of styrene using an $[Ru_3(CO)_{12}]$/PETPP complex in toluene was investigated (Equation (10)).[231] In this system, the catalyst is insoluble in toluene at room temperature and the organic phase remains colorless. On heating above the critical-temperature Cp, the catalyst became soluble, enabling the reaction to proceed homogeneously, and, on cooling to room temperature, the catalyst precipitated back out of solution as a viscous membrane at the bottom of the reactor. The products were conveniently removed by syringe and the catalyst was recycled 10 times without loss of activity.

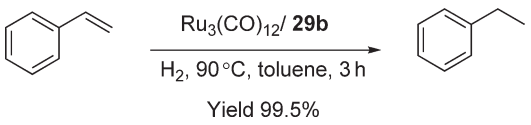

(10)

12.17.3.6 Solid-supported Organometallic Systems

Any review on green organometallic chemistry would not be complete without reference to the heterogenization of homogeneous catalysts on solid supports for recycle, recovery, and reuse, particularly since, despite the wealth of research on homogeneously catalyzed reactions that occur in high yields and selectivities under mild conditions, the industrial use of homogeneously catalyzed processes is relatively limited.[232] However, it would require a whole volume of this compilation to do justice to the exponential expansion of work in this area in the last 10 years: Organometallic complexes from across the periodic table interacting via covalent bonds, adsorption, ion-pair formation, encapsulation or entrapment with support materials such as soluble and insoluble organic and inorganic polymers, dendrimers, mesoporous and microporous inorganic solids, including glasses, ceramics, zeolites, and clays, possibly with a thin film of a solvent (water, organic, fluorous, ionic liquid), and sol–gels. This area has been extensively reviewed, and the reader is directed to these authoritative articles.[18,233–252]

12.17.4 Hydroformylation: A Green Case Study I

Metal-catalyzed, homogeneous hydroformylation of alkenes, an archetypal atom-economic addition reaction, has been extensively investigated and can be used as an exemplar of green organometallic chemistry in practice. Originally exploited commercially in the 1950s using cobalt carbonyl catalysts,[253] enhanced hydrogenation to alcohols coupled with improved hydroformylation selectivity have been achieved following the incorporation of phosphine ligands,[254] and both of these technologies are still in use for the hydroformylation of long-chain alkenes. More selective, rhodium–triphenylphosphine catalysts, operating at lower temperatures and pressures, have replaced the cobalt-based catalysts in the hydroformylation of propene in continuous processes operating at 3.5 million tonnes per annum.[255] Here, commercialization of these homogeneous processes relies upon the straightforward isolation of either the volatile organic product (*n*-butanal) or the catalyst with thermally stable co-ligands, (cobalt carbonyls). Further commercialization of the homogeneous hydroformylation reaction for product/catalyst combinations that do not satisfy these limited criteria hinges upon new technologies, and four major green strategies have been developed and investigated toward this goal.

12.17.4.1 Hydroformylation of Olefins on Supported Catalysts

Many systems using rhodium hydroformylation catalysts chemically bound to either insoluble (e.g., inorganic oxides or polymers)[20] or soluble (e.g., dendrimers[250] or polymers[224,244]) supports have been reported. The high physical strength and chemical inertness of inorganic materials make them particularly suited to act as heterogeneous catalyst support materials. The principal problems are their non-uniform and partly unknown structures, mass-transport limitations due to slow diffusion, and metal leaching. However, acceptable catalyst leaching (<100 ppb rhodium) coupled with reasonable activity and excellent regioselectivity have been demonstrated for a sol–gel solution incorporating a triethoxysilyl-functionalized Xantphos-type ligand **31**[256] (Figure 7). The mass-transport limitations of insoluble supported catalysts can be overcome by using soluble supports, which lead to recyclable catalyst systems with activities similar to their monomeric analogs. Dendrimers, as solid supports, have recently received considerable attention since their well-defined macromolecular structures enable catalyst structures to be accurately and precisely controlled. Tulchinsky and Miller have patented rhodium hydroformylation catalysts on phosphite-functionalized polyamidoamine (PAMAM) dendrimers **32**.[257] Following application in the hydroformylation of propene (good reactivities and poor regioselectivities), nanofiltration afforded excellent rhodium and dendrimer retention, and the catalyst could be recycled with virtually no drop in activity.

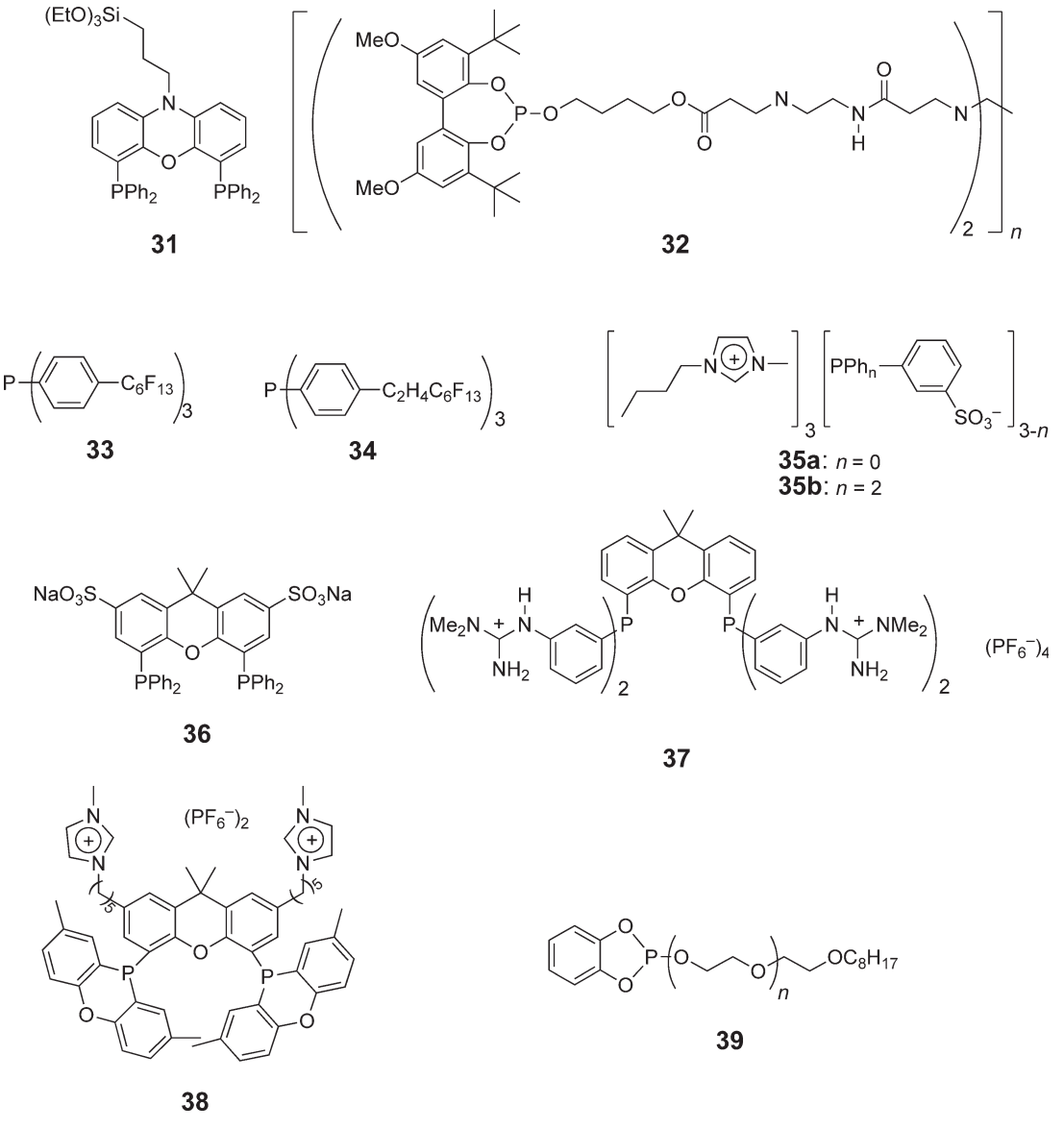

Figure 7 Representative ligand systems used in hydroformylation catalysis.

12.17.4.2 Hydroformylation of Olefins in $scCO_2$

Although organometallic complexes, particularly rhodium-based hydroformylation catalysts incorporating phosphine ligands, are virtually insoluble in apolar $scCO_2$, solubility can be enhanced by the incorporation of long perfluoroalkyl groups in the ligands **33** and **34**. Using these derivatized catalysts in the hydroformylation of 1-octene, reaction rates and regioselectivities in $scCO_2$ comparable to those observed in conventional media have been reported,[90,258] while significantly enhanced reaction rates have been reported for the rhodium-catalyzed hydroformylation of acrylic esters in $scCO_2$.[259,260] However, although removal of the solvent by decompression back to the gaseous state is attractive, this does not *per se* deal with the issue of product/catalyst separation. The combination of $scCO_2$ with an ionic liquid, **35a** and **35b**,[93] or a supported catalyst,[261] are potentially powerful alternative approaches to catalyst/product separation, but in both cases, the reported hydroformylation reaction rates are relatively low.

An alternative twist exemplified in a recent report uses $scCO_2$ not as the solvent for the reaction, but rather the antisolvent for post-reaction catalyst precipitation.[262] The rhodium catalyst, which incorporates a

poly(ethyleneglycol) (PEG)-modified phosphine ligand **29a** for hydroformylation in neat 1-octene, precipitates on pressurization with CO_2, allowing the product to be removed by sc extraction and the catalyst to remain *in situ* for subsequent catalytic cycles.

12.17.4.3 Hydroformylation of Olefins in Biphase Systems

Alkene hydroformylation has been evaluated in three types of biphasic system where the catalyst is designed to be soluble in a solvent that, under some conditions, is immiscible with that containing the product.

12.17.4.3.1 Hydroformylation of olefins in aqueous media

The thermal instability of rhodium-based hydroformylation catalysts has already been overcome commercially in the Ruhrchemie/Rhône–Poulenc process for propene hydroformylation in which the sodium salt of a sulfonated triphenylphosphine ligand (TPPTS, **1a**) is used to solubilize the catalyst in the aqueous phase. In this process, the second phase is toluene and the reaction is carried out as a batch process with rapid stirring to intimately mix the two immiscible phases. After reaction, the system is allowed to separate and the organic phase is simply decanted from the aqueous catalyst phase.[263] Both water-soluble polymers[264,265] and PAMAM dendrimers[32,266] have been reported as supports for rhodium-catalyzed hydroformylation under aqueous biphase conditions, but reactivities and regioselectivities were only comparable to or worse than those obtained with the reference TPPTS ligand. The aqueous biphase approach has found limited application for the hydroformylation of longer-chain alkenes, because of their very low solubility in water leading to prohibitively slow reaction rates, but there have been a variety of approaches directed at the solution of this problem.

(i) Amphiphilic phosphines,[63] particularly those based on the Xantphos ligand **36**,[267] offer high activities and regioselectivities for hydroformylation under aqueous biphase conditions. Alternatively, cationic surfactants dramatically increase the rate and regioselectivity for hydroformylation of 1-octene by the Rh–TPPTS catalyst system as a result of micelle formation.[62]

(ii) Catalytic amounts of water-soluble receptors, such as cyclodextrins or calixarenes, can be used to promote the solubilization of water-insoluble substrates in the aqueous phase in the presence of the water-soluble organometallic catalyst. Partially methylated β-cyclodextrins with rhodium complexes of TPPTS or TPPMS **1b** have given good reactivities and modest regioselectivities in the hydroformylation of 1-decene under aqueous biphase conditions, with <0.5 ppm rhodium leaching to the product phase.[268] Alternatively, bonding a bidentate phosphine unit to the cyclodextrin via a spacer unit seeks to combine aqueous biphase organometallic catalysis, phase-transfer catalysis, and molecular recognition. Unfortunately, although activities and regioselectivities are high, the catalytic systems offered modest recycle (50% activity on the second run) due to some loss of the catalyst to the product phase.[269] In contrast, catalyst recycle following hydroformylation was excellent for phosphine-modified, sulfonated calixarenes, but the chemoselectivity was poor with yields of the aldehyde product ranging from 52% to 86%.[270] Most recently, it has been reported that a functionalized cationic α-cyclodextrin is an efficient mass-transfer promoter affording both enhanced reactivity and regioselectivity in the rhodium-catalyzed hydroformylation of 1-decene, possibly via the *in situ* formation of a new catalytic supramolecular species by ion exchange between the ligand and the α-cyclodextrin.[271]

(iii) In thermoregulated phase-transfer catalysis, replacement of the sulfonated ligand with phosphines incorporating PEG or other polyoxyethylene ponytails **30** generates rhodium–phosphine catalysts that are exclusively soluble in water at room temperature, but when the ponytail undergoes a phase transition on heating, the catalysts become preferentially soluble in the organic phase: that is, at process temperature, the catalyst acts homogeneously, while on cooling, reversal of the phase transition returns the catalyst to the aqueous phase for separation by decantation. The results are promising, with systems recycled up to 20 times, excellent chemoselectivity but poor regioselectivity ("linear : branched" ca. 0.6).[228,229,272–274]

12.17.4.3.2 Hydroformylation of olefins in fluorous media

Hydroformylation of long-chain alkenes under fluorous biphasic conditions, in which perfluoroalkylated phosphine/phosphite ligands are used to solubilize the catalyst in the fluorous phase, have been extensively investigated by a number of groups.[275–278] Good reaction rates, regioselectivity, catalyst stability, and rhodium leaching levels have all been reported, but the latter can be improved substantially by omitting the organic phase. While 1-octene is fully miscible with the fluorous phase, the hydroformylation product, 1-nonanal, is completely immiscible, forming a

second product phase as the reaction proceeds; rhodium-leaching levels were reported as 80 ppb alongside good regioselectivity ("linear : branched" 6.3). This concept has been incorporated into a continuous reactor using **33** where the fluorous catalyst underwent 15,500 turnovers at an average rate of 750 h^{-1}.[279]

12.17.4.3.3 Hydroformylation of olefins in ionic liquids

Chauvin *et al.* investigated the biphasic hydroformylation of pent-1-ene with the neutral $[Rh(CO)_2(acac)]$/triarylphosphine as the catalyst precursor in $[BMIM][PF_6]$.[138] Although high activities were observed, slight leaching of the catalyst into the organic phase occurred. Although the use of **1b** was able to suppress this completely by making the catalyst more soluble in the ionic liquid, the activity of the system was significantly reduced. Four groups, using different approaches, have delivered substantial improvements over this early work. Salzer and Brasse have developed and synthesized a cobaltocenium ligand[280] and showed the benefits of using ligand systems that are specifically designed for this application. Not only did they observe high activity for longer chain α-olefins such as 1-octene and good regioselectivity for the linear aldehyde, but also the rhodium leaching into the organic layer was less than 0.5%. Dupont *et al.*, Wasserscheid and co-workers, and van Leeuwen and co-workers have independently reported highly active and regioselective hydroformylation of 1-octene with different Xantphos ligands **36–38** in ionic liquids, with excellent regioselectivities, very low rhodium leaching levels, and facile product separation by straightforward decantation.[281–283] Jin and co-workers have reported the synthesis and application of a novel PEG-functionalized tetraalkylammonium tosylate room-temperature ionic liquid in combination with either **1a** or their octylpolyethyleneglycol–phenylene–phosphite **39** for the hydroformylation of 1-tetradecene.[284] Following an induction period (20 h), good conversions, but with poor regioselectivities, over three recycles in an ionic liquid : *n*-heptane biphase were obtained with as little as 0.5% rhodium leaching.

12.17.4.4 Hydroformylation of Olefins in Supported Liquid-phase Catalysis

Supported liquid-phase catalysis,[167,265] in which the catalyst is dissolved in a small volume of solvent, adsorbed on, usually, a hydrophilic solid, seeks to resolve issues associated with substrate solubility in multi-phase catalysis and performance/catalyst leaching in supported catalysis; reports on the hydroformylation of long-chain alkenes under both supported aqueous phase and supported ionic liquid-phase regimes have been reported.

12.17.4.4.1 Hydroformylation of olefins in supported aqueous phase catalysis

In the hydroformylation of alkenes using Rh–TPPTS catalysts in a thin layer of water adsorbed on silica, TOFs are independent of alkene chain length as a direct consequence of the large interfacial surface, indicating a major advance over hydroformylation under aqueous biphase conditions.[285] However, catalyst-support stability, regioselectivity, and levels of rhodium leaching are still unacceptable. These issues have been overcome by van Leeuwen *et al.* using their water-soluble sulfonated Xantphos ligand **36**, where excellent regioselectivities combined with multiple recycles without loss of activity and <1 ppm rhodium leaching levels have been reported, but reaction rates are disappointing.[286] Alternatively, Naughton and Drago describe the hydroformylation of 1-hexene and 1-octene using the Rh–TPPTS catalyst dissolved in a hydrophilic, PEG film.[287] Activities and regioselectivities comparable to those in a homogeneous system are obtained, although the amount of rhodium leaching was not measured.

12.17.4.4.2 Hydroformylation of olefins in supported ionic liquid-phase catalysis

Rhodium–**35a** and rhodium–**35b** catalysts in $[BMIM][PF_6]$ supported on a silylimidazolium-modified silica have been shown to have activities and regioselectivities comparable to those under ionic liquid-biphase conditions in the hydroformylation of 1-hexene. Unfortunately, rhodium leaching levels were quite high, possibly as a consequence of the solubility of the ionic liquid in the organic phase at high aldehyde concentrations.[288,289] In contrast, negligible amounts of rhodium were detected in the organic phase following the hydroformylation of either propene or 1-octene using either the sulfonated Xantphos **36** or bis(*m*-phenylguanidinium)phenylphosphine **37** in $[BMIM][PF_6]$ in a continuous fixed-bed reactor.[290,291]

12.17.4.5 Overview

In many cases, it is not possible to make direct comparisons between catalytic results from different research groups as a result of differences in approach and reporting. However, Table 1 summarizes key catalytic data from some of

Table 1 Rhodium-catalyzed hydroformylation of alkenes[a]

System	*Substrate*	*Ligand*	*Pressure* (bar)	*Temp.* (°C)	*TOF* (h^{-1})	*Rate* (mol $dm^{-3} h^{-1}$)	*n* : *i*	*Rh loss* (mg per mol product)	*References*
Homogeneous	1-Octene	PPh_3	15	95	770	2.0	8.8 : 1	n.a.	255
Supported	1-Octene	**31**	50	80	287	0.19	40 : 1	<0.1	256
Supported	Propene	**32**	7	70	n.r.	1.8	1.4 : 1	<0.1%[b]	257
$scCO_2$	1-Octene	**34**	200	65	430	12.2	5.5 : 1	<0.17	90
$scCO_2$/ionic liquid	1-Octene	**35b**	200	100	8	0.12	3.1 : 1	<0.06%[b]	93
$scCO_2$/supported	1-Octene	**31**	170	90	160	n.r.	33 : 1	<1.2	261
Aqueous biphase	Propene	**1a**	50	120	400	1.1	19 : 1	<0.005	263
Aqueous biphase	1-Decene	**1a**	50	80	n.r.	n.r.	1.9 : 1	<0.5 ppm	268
Aqueous/supported	1-Octene	**36**	50	80	15	n.r.	46 : 1	<1 ppm	286
Thermoregulated	1-Octene	**29b**	50	100	182	n.r.	n.r.	n.r.[b]	229
Fluorous biphase	1-Octene	**33**	20	70	4400	8.8	6.3 : 1	0.08	277
Ionic liquid	1-Octene	**37**	30	100	50	n.r.	21 : 1	<0.07%[b]	282
Ionic liquid	1-Octene	**38**	46	100	318	1.2	49 : 1	<0.005	283
Ionic liquid	1-Tetradecene	**1a**	5	105	94	n.r.	0.4 : 1	<0.5%[b]	284
Ionic liquid/supported	Propene	**37**	5	120	21	n.r.	1 : 1	<0.7%	291

[a]n.a. = not applicable; n.r. = not reported.
[b]Reported as % of catalyst loading.

these methodologies, offering an insight into their relative values from a green chemistry perspective. The results from the bidentate Xantphos-type ligands in SAPC generally offer the most promising results; excellent regioselectivity to the desired linear aldehydes with very low rhodium leaching levels. However, even at elevated temperatures, the reaction rates and TOFs for these systems offer some room for improvement.

12.17.5 Olefin Polymerization: A Green Case Study II

Over the last two decades, organometallic complexes have been at the heart of many of the key advances in metal-mediated alkene polymerization technology, with many examples now reaching the early stages of commercialization. While early transition metal complexes (e.g., metallocenes, constrained-geometry catalysts) have led the way, the advent of late transition metal catalysts has presented a rich library of highly active systems that can be employed to polymerize a variety of olefins. Comprehensive reviews covering the chronological development of both early[292–295] and late transition metal systems can be found elsewhere.[296–299] In this section, we highlight some of the key advances that have occurred with regard to their application in alternative reaction media, aqueous, $scCO_2$, fluorous, and ionic liquids, for ethylene or propylene polymerization.

12.17.5.1 Metal-mediated Polymerizations of Olefins in Aqueous Media

Despite the industrial importance of free-radical-initiated emulsion polymerization,[300] the use of water as a medium for transition metal-mediated coordination polymerization of olefinic monomers has received relatively little attention.[50,301–310] This can be mainly attributed to the water sensitivity of commercially important early transition metal catalysts in which hydrolysis of a metal alkyl bond can readily occur.[292–295] Otherwise, the water molecule can act as a good ligand and fill the vacant site, or the water can attack coordinated monomers or other ligands. With the advent of late transition metal catalysts and their expected tolerance for polar groups, the likelihood for aqueous polymerizations has started to show great potential. The following section highlights reports of transition metal catalysts that have been employed either as aqueous soluble or as suspensions. General reviews on the use of organometallic complexes as catalysts in aqueous media have been presented elsewhere,[16–18] while two reviews specific to aqueous alkene polymerizations have appeared recently.[300,301]

In 1993, Flood and co-workers reported that the well-defined water-soluble monocationic rhodium complex $[(N^{\wedge}N^{\wedge}N)RhMe(OH_2)(OH)]^+$ **40** ($N^{\wedge}N^{\wedge}N$ = trimethyl–1,4,7-triazacyclononane) produced low molecular weight polyethylene at room temperature and 60 bar ethylene after extended reaction times (ca. 90 days).[302] Increasing

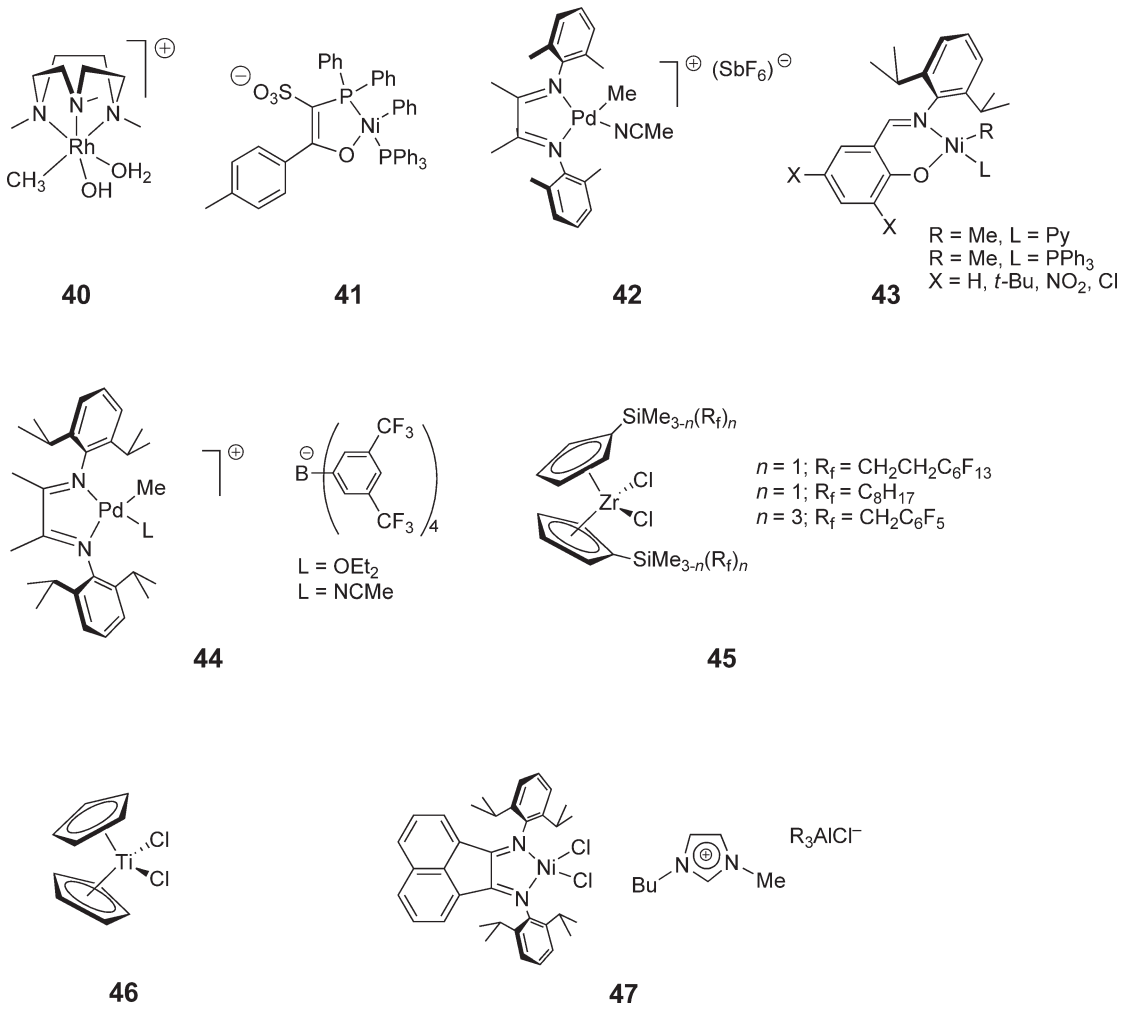

Figure 8 Representative catalyst or precatalyst systems for olefin polymerization.

the temperature only led to hydrolysis of the Rh–C bond. Despite the low activity of this system, it signposted the possibilities for polymerization catalysis in aqueous media (Figure 8).

More recently, the sodium salt of **41** has been reported and found to be soluble in water (stable for several hours), and can promote the aqueous polymerization of ethylene producing low molecular weight linear polyethylene with 10^3 turnovers h^{-1} under moderate conditions (70 °C, 50 bar ethylene pressure).[303–305] A variety of other nickel catalysts containing variations of the P^O ligand in **41** have been reported,[306] including the fluorinated derivative [$Ph_2PC(COOEt)C(R_F)ONiPh$] ($R_F = CF_3$, C_6F_5; generated *in situ*), which produces low molecular weight linear polyethylene with much higher activities in aqueous emulsion.[307] In general, the catalyst activities and polymer molecular weight are reduced in the aqueous polymerizations when compared with polymerizations in organic media such as toluene. This observation has been attributed to insufficient local concentrations at the active centers leading to a lower rate of chain growth.

As an alternative strategy, Mecking and co-workers reported the use of an α-diimine Pd(II) complex of type **42** in a suspension-type process where the catalyst is not solubilized since no organic solvent is added to the aqueous phase.[50,303] Amazingly, the activities observed at pressures above 20 bar are similar to the highest ones obtained for polymerization in a soluble organic medium [900 vs. 1,100 (in CH_2Cl_2) mol mol_{Pd}^{-1} h^{-1}]. Notably, solubilization of **42** by introducing sulfonate groups results in an inactive ethylene polymerization catalyst,[308] and it has been concluded that the suspension-type system operates by encapsulation of the water-insoluble catalyst in the

hydrophobic polymer. Suspension-type polymerization also occurs using the neutral salicylaldiminate–nickel systems **43**, and, in contrast to the P∧O systems discussed above, much higher molecular weight polymers are afforded with moderate amounts of methyl branches evident.

12.17.5.2 Metal-mediated Polymerizations of Olefins in $scCO_2$

In spite of the numerous reports of metallocene-mediated polymerizations in sc media such as ethylene and propylene,[311–313] the use of carbon dioxide as the sc medium is considerably more scarce. The unique properties of $scCO_2$ as the reaction phase, such as its nontoxic and nonflammable nature along with it being inexpensive, make it an attractive medium to carry out metal-mediated polymerizations.[314–316] With regard to olefin polymerization, the paucity of examples can be attributed, in some measure, to the oxophilicity (and hence reactivity) of traditional early transition metal catalysts. However, late transition metal catalysts for olefin polymerization are less oxophilic[295–298] and can, therefore, be used in $scCO_2$. Using the α-diimine Pd(II) catalysts **44**,[296] ethylene can be polymerized in $scCO_2$, affording high molecular weight polyethylene; use of 1-hexene as the monomer also forms high molecular weight polymer.[317–319] The polyethylene generated is highly branched and similar to that generated in an organic solvent (e.g., CH_2Cl_2) even though the polymerization in $scCO_2$ is a precipitation polymerization. In addition, some evidence for a new branch-on-branch structure is apparent for the polyethylene generated during this $scCO_2$ polymerization.[319]

12.17.5.3 Metal-mediated Polymerizations of Olefins in Fluorous Media

Despite the interesting solvent properties exhibited by perfluorocarbon (PFC) solvents and their close relationship to $scCO_2$,[113,319,320] examples of coordination polymerization in PFC solvents are relatively scarce.[321–328] The very low catalyst loadings that can be employed in some of the more active polymerization catalysts mean that catalyst recovery issues are not of major importance in coordination polymerization. Nevertheless, inspired by what the potential effects a fluorous reaction medium (pure PFC solvent or FBS conditions) and, in some cases, a highly fluorinated catalyst would have on the physical properties of the polymer, some work has started to appear in both the academic and industrial literature.[324–328]

For example, the zirconocene complexes **45** are hydrocarbon soluble and moderately soluble in PFC solvents. All three complexes form active ethylene polymerization catalysts when reacted with an excess of methylaluminoxane (MAO; Al/Zr = 500/1) either in pure toluene or in fluorous biphasic solvent systems (e.g., toluene/perfluorohexanes).[324,325] Increased robustness and productivity over prolonged polymerization times in comparison to the non-fluorous reference system $[Zr(\eta^5\text{-}C_5H_4SiMe_3)_2Cl_2]$ are observed in each case. This phenomenon has been ascribed to phase segregation of the fluorous metallocene moiety from the polyethylene matrix. Remarkably, fluorous biphasic conditions during the polymerization reaction, in general, result in higher molecular weight polymer. This phenomenon was even observed for non-fluorous $[Zr(\eta^5\text{-}C_5H_4SiMe_3)_2Cl_2]$ and is most likely caused by a suppression of the rate of β-H transfer to the metal center in these relatively non-polar solvent combinations.

12.17.5.4 Metal-mediated Polymerizations of Olefins in Ionic Liquids

Ambient-temperature ionic liquids have received much attention in both academia and industry due to their potential as replacements for volatile organic compounds (VOCs).[134,329] Recent years have witnessed an increased amount of interest in using an ionic liquid as the medium for alkene oligomerization and polymerization.[330–342] The first example of a polymerization system in an ionic liquid was reported by Carlin and Wilkes.[330] Titanocene **46** in an ionic liquid composed of acidic 1-ethyl–3-methylimidazolium chloride/$AlCl_3$ (EMIC), using $AlCl_{3-x}R_x$ (R = Me, Et) as co-catalyst, was used to polymerize ethylene with a catalytic activity up to 0.023 g of ethylene per min. Interestingly, neither $[Zr(\eta^5\text{-}Cp)_2Cl_2]$ nor $[Hf(\eta^5\text{-}Cp)_2Cl_2]$ were catalytically active in the ionic liquids employed. No recycling experiments using **46** were, however, reported.

Late transition metals have a lower oxophilicity relative to early transition metals and, therefore, a higher tolerance for a wide range of functional groups (e.g., –COOR and –COOH groups).[295–298] Consequently, the use of late transition metal systems for alkene polymerization in ionic liquids has been disclosed in both the academic and patent literature.[331–334] For example, de Souza and co-workers disclosed the use of the nickel complex **47** for the homopolymerization of ethylene in an ambient-temperature ionic liquid [BMIM][Cl–$AlCl_3$–$EtAlCl_2$] and toluene.[331] The polyethylene formed was easily isolated from the reaction mixture by decanting the upper toluene layer allowing the

ionic liquid and 47 to be recycled for use in further polymerizations. Nevertheless, to allow reuse, trimethylaluminum was added to overcome the loss of free alkylaluminum species into the separated organic phase. Notably, the performance of the catalyst changes on reuse with subsequent reactions, giving a progressive shift from crystalline to amorphous polymer, with a period that gives rise to bimodal product distributions. This change in performance has been attributed to the changing composition of the ionic liquid with different active species being generated on addition of trimethylaluminum.

12.17.6 Future Perspectives

The increasing legislative drivers to phase out chlorinated and carcinogenic solvents means the use of alternative reaction media is bound to see considerable advances over the next decade. This review shows that organometallic catalysts have now been developed for a wide range of reactions in solvents from non-polar $scCO_2$ through to the highly polar water and ionic liquids. Similarly, organometallic catalysis has been used as a test bed for new enhanced reaction technologies. Over the next decade, organometallic chemistry will continue to play an increasing crucial role in the development of more atom-efficient and selective reactions and, hence, green chemistry.

References

1. Anastas, P. C.; Warner, J. C. *Green Chemistry Theory and Practice*; Oxford University Press: New York, 1998.
2. Crystal www.crystalfaraday.org.
3. US Environmental Protection Agency www.epa.gov.
4. Chemistry.org www.chemistry.org.
5. Chemsoc www.chemsoc.org.
6. Nelson, W. M. *Green Solvents for Chemistry*; Oxford University Press: Oxford, 2003.
7. Lancaster, M. *Green Chemistry: An Introductory Text*; RSC: Cambridge, 2002.
8. Clark, J. H.; MacQuarrie, D. J. *Handbook of Green Chemistry and Technology*; Blackwell: Oxford, 2002.
9. Ahluwalia, V. K.; Kidwai, M. *New Trends in Green Chemistry*; Kluwer: Dordrecht, 2004.
10. Matlack, A. S. *Introduction to Green Chemistry*; Dekker: New York, 2001.
11. Adams, D. J.; Dyson, P. J.; Tavener, S. J. *Chemistry in Alternative Reaction Media*; Wiley: Chichester, 2004.
12. Jessop, P. G.; Leitner, W. *Chemical Synthesis using Supercritical Fluids*; Wiley-VCH: Weinheim, Germany, 1999.
13. Gladysz, J. A., Curran, D. P., Horváth, I. T., Eds. *Handbook of Fluorous Chemistry*; Wiley-VCH: Weinheim, Germany, 2004.
14. Wasserscheid, P., Welton, T., Eds. *Ionic Liquids in Synthesis*; Wiley-VCH: Weinheim, Germany, 2003.
15. Cornils, B., Herrmann, W. A., Eds. *Applied Homogeneous Catalysis with Organometallic Compounds*, 2nd ed.; Wiley-CH: Weinheim, Germany, 2002.
16. Grieco, P. A. *Organic Synthesis in Water*; Thomson Science: London, 1998.
17. Joo, F. *Aqueous Organometallic Catalysis*; Kluwer: Dordrecht, 2001.
18. Cornils, B.; Herrmann, W. E. *Aqueous-Phase Organometallic Catalysis*, 2nd ed.; Wiley-VCH: Weinheim, Germany, 2004.
19. Cornils, B., Herrmann, W. E., Horváth, I. T., Leitner, W., Mecking, S., Olivier-Bourbigou, H., Vogt, D., Eds. *Multiphase Homogeneous Catalysis*; Wiley-VCH: Weinheim, Germany, 2005.
20. Hartley, R. R. *Supported Metal Complexes*; Reidel: Dordrecht, 1985.
21. Tooze, B.; Cole-Hamilton, D. J. *Recovery and Recycling in Homogeneous Catalysis*; Kluwer: Dordrecht, 2005.
22. Wang, Y.; Holladay, J. *Microreactor Technology and Process Intensification*; American Chemical Society: Washington, DC, 2005.
23. DeSimone, J. M.; Tumas, W. *Green Chemistry using Liquid and Supercritical Carbon Dioxide*; Oxford University Press: New York, 2003.
24. Udo de Haes, H. A. *J. Clean. Prod.* **1993**, *1*, 131–137.
25. Jödicke, G.; Zenklusen, O.; Weidenhaupt, A.; Hungerbühler, K. *J. Clean. Prod.* **1999**, *7*, 159–166.
26. Hudlicky, T.; Frey, D. A.; Koroniak, L.; Claeboe, C. D.; Brammer, L. E. *Green Chem.* **1999**, *1*, 57–59.
27. Sheldon, R. A. *Chem. Ind. (London)* **1992**, 903–906.
28. Trost, B. M. *Science* **1991**, *254*, 1471–1477.
29. Curzons, A. D.; Constable, D. J. C.; Mortimer, D. N.; Cunningham, V. L. *Green Chem.* **2001**, *3*, 1–6.
30. Constable, D. J. C.; Curzons, A. D.; Cunningham, V. L. *Green Chem.* **2002**, *4*, 521–527.
31. Lapkin, A.; Joyce, L.; Crittenden, B. *Environ. Sci. Technol.* **2004**, *38*, 5815–5823.
32. Trost, B. M.; Frederiksen, M. U.; Rudd, M. T. *Angew. Chem., Int. Ed.* **2005**, *44*, 6630–6666.
33. Trost, B. M. *Acc. Chem. Res.* **2002**, *35*, 695–705.
34. Trost, B. M.; Toste, F. D.; Pinkerton, A. B. *Chem. Rev.* **2001**, *101*, 2067–2096.
35. Wender, P. A.; Bi, F. C.; Gamber, G. G.; Gosselin, F.; Hubbard, R. D.; Scanio, M. J. C.; Sun, R.; Williams, T. J.; Zhang, L. *Pure Appl. Chem.* **2002**, *74*, 25–31.
36. Wender, P. A.; Baryza, J. L.; Brenner, S. E.; Clarke, M. O.; Gamber, C. G.; Horan, J. C.; Jessop, T. C.; Kan, C.; Pattabiraman, K.; Williams, T. J. *Pure Appl. Chem.* **2003**, *75*, 143–155.
37. Crochet, P.; Díez, J.; Fernández-Zúmel, M. A.; Gimeno, J. *Adv. Synth. Catal.* **2006**, *348*, 93–100.
38. Murai, S.; Kakiuchi, F.; Sekine, S.; Tanaka, Y.; Kamatani, A.; Sonoda, M.; Chatani, N. *Nature* **1993**, *366*, 529–531.
39. Kakiuchi, F.; Murai, S. *Acc. Chem. Res.* **2002**, *35*, 826–834.
40. Kakiuchi, F.; Chatani, N. *Adv. Synth. Catal.* **2003**, *345*, 1077–1101.
41. Herrmann, W. A.; Kohlpaintner, C. W. *Angew. Chem., Int. Ed.* **1993**, *32*, 1524–1544.
42. Papadogianakis, G.; Sheldon, R. A. *New J. Chem.* **1996**, *20*, 175–185.

43. Lindstrom, U. M. *Chem. Rev.* **2002**, *102*, 2751–2772.
44. Joo, F.; Katho, A. *J. Mol. Catal. A: Chem.* **1997**, *116*, 3–26.
45. Dwars, T.; Oehme, G. *Adv. Synth. Catal.* **2002**, *344*, 239–260.
46. Li, C. J. *Acc. Chem. Res.* **2002**, *35*, 533–538.
47. Amengual, R.; Genin, E.; Michelet, V.; Savignac, M.; Genet, J.-P. *Adv. Synth. Catal.* **2002**, *344*, 393–398.
48. Venkatraman, S.; Huang, T.; Li, C. J. *Adv. Synth. Catal.* **2002**, *344*, 399–405.
49. Verspui, G.; Feiken, J.; Papadogianakis, G.; Sheldon, R. A. *J. Mol. Catal. A: Chem.* **1999**, *146*, 299–307.
50. Held, A.; Mecking, S. *Chem. Eur. J.* **2000**, *6*, 4623–4629.
51. Lynn, D. M.; Mohr, B.; Grubbs, R. H. *J. Am. Chem. Soc.* **1998**, *120*, 1627–1628.
52. Breslow, R. *Acc. Chem. Res.* **1991**, *24*, 159–164.
53. Furlani, T. R.; Gao, J. *J. Org. Chem.* **1996**, *61*, 5492–5497.
54. Narayan, S.; Muldoon, J.; Finn, M. G.; Fokin, V. V.; Kolb, H. C.; Sharpless, K. B. *Angew. Chem., Int. Ed.* **2005**, *44*, 3275–3279.
55. Pinault, N.; Bruce, D. W. *Coord. Chem. Rev.* **2003**, *241*, 1–25.
56. Kuntz, E., Fr. Pat. 2.314.910, 1975.
57. Kuntz, E. G. *Chem. Tech.* **1987**, *17*, 570–575.
58. Buhling, A.; Kamer, P. C. J.; van Leeuwen, P. W. N. M. *J. Mol. Catal. A: Chem.* **1995**, *98*, 69–80.
59. Buhling, A.; Kamer, P. C. J.; van Leeuwen, P. W. N. M.; Elgersma, J. W. *J. Mol. Catal. A: Chem.* **1997**, *116*, 297–308.
60. Grassert, I.; Vill, V.; Oehme, G. *J. Mol. Catal. A: Chem.* **1997**, *116*, 231–236.
61. Grassert, I.; Schmidt, U.; Ziegler, S.; Fischer, C.; Oehme, G. *Tetrahedron: Asymmetry* **1998**, *9*, 4193–4202.
62. Chen, H.; Li, Y.; Chen, J.; Cheng, P.; He, Y.-E.; Li, X. *J. Mol. Catal. A: Chem.* **1999**, *149*, 1–6.
63. Hanson, B. E. *Coord. Chem. Rev.* **1999**, *185–186*, 795–807.
64. Uozumi, Y.; Nakazono, M. *Adv. Synth. Catal.* **2002**, *344*, 274–277.
65. Thomas, C. M.; Ward, T. R. *Chem. Soc. Rev.* **2005**, *34*, 337–346.
66. Bertucci, C.; Botteghi, C.; Giunta, D.; Marchetti, M.; Paganelli, S. *Adv. Synth. Catal.* **2002**, *344*, 556–562.
67. Ward, T. R. *Chem. Eur. J.* **2005**, *11*, 3798–3804.
68. Li, C. J.; Chen, L. *Chem. Soc. Rev.* **2006**, *35*, 68–82.
69. Li, C. J. *Green Chem.* **2002**, *4*, 1–4.
70. Li, C.-J. *Tetrahedron* **1996**, *52*, 5643–5668.
71. Sakai, M.; Hayashi, H.; Miyaura, N. *Organometallics* **1997**, *16*, 4229–4231.
72. Sakai, M.; Ueda, M.; Miyaura, N. *Angew. Chem., Int. Ed.* **1998**, *37*, 3279–3281.
73. Huang, X.; Anderson, K. W.; Zim, D.; Jiang, L.; Klapars, A.; Buchwald, S. L. *J. Am. Chem. Soc.* **2003**, *125*, 6653–6655.
74. Leadbeater, N. E. *Chem. Commun.* **2005**, 2881–2902.
75. Wei, C. M.; Li, C. J. *Green Chem.* **2002**, *4*, 39–41.
76. Wei, C.; Li, C.-J. *J. Am. Chem. Soc.* **2003**, *125*, 9584–9585.
77. McHugh, M. A.; Krukonis, V. J. *Supercritical Fluid Extraction*; Butterworth Heinemann: Boston, 1994.
78. Reverchon, E. *J. Supercrit. Fluid* **1999**, *15*, 1–21.
79. DeSimone, J. M.; Maury, E. E.; Menceloglu, Y. Z.; Combes, J. R.; McClain, J. B.; Romack, T. *Science* **1994**, *265*, 356–359.
80. Licence, P; Ke, J.; Sokolova, M.; Ross, S. K.; Poliakoff, M. *Green Chem.* **2003**, *5*, 99–104.
81. Jessop, P. G.; Ikariya, T.; Noyori, R. *Chem. Rev.* **1999**, *99*, 475–493.
82. Leitner, W. *Acc. Chem. Res.* **2002**, *35*, 746–756.
83. Campestrini, S.; Tonellato, U. *Curr. Org. Chem.* **2005**, *9*, 31–47.
84. Prajapati, D.; Gohain, M. *Tetrahedron* **2004**, *60*, 815–833.
85. Francio, G.; Leitner, W. *Transition Metals for Organic Synthesis*, 2nd ed.; Wiley-VCH: Weinheim, 2004; pp 545–558.
86. Jessop, P. G. In *Supercritical Fluid Technology for Drug Development*: Vol. 138; York, R., Kompella, U. B., Shekunov, B. Y., Eds.; Marcel Dekker, Inc: New York, 2003, pp 461–495.
87. Alonso, F.; Beletskaya, I. P.; Yus, M. *Tetrahedron* **2005**, *61*, 11771–11835.
88. Jessop, P. G. *Top. Catal.* **1998**, *5*, 95–103.
89. Sellin, M. F.; Bach, I.; Webster, J. M. *J. Chem. Soc., Dalton Trans.* **2002**, 4569–4576.
90. Koch, D.; Leitner, W. *J. Am. Chem. Soc.* **1998**, *120*, 13398–13404.
91. Abbott, A. P.; Eltringham, W.; Hope, E. G.; Nicola, M. *Green Chem.* **2005**, *7*, 721–725.
92. Kainz, S.; Brinkmann, A.; Leitner, W.; Pfaltz, A. *J. Am. Chem. Soc.* **1999**, *121*, 6421–6429.
93. Goetheer, E. L. V.; Verkerk, A. W.; van den Broeke, L. J. P.; de Wolf, E.; Deelman, B-J.; van Koten, G.; Keurentjes, J. T. F. *J. Catal.* **2003**, *219*, 126–133.
94. Sellin, M. F.; Webb, P. B.; Cole-Hamilton, D. J. *Chem. Commun.* **2001**, 781–782.
95. Blanchard, L. A.; Hancu, D.; Beckman, E. J.; Brennecke, J. F. *Nature* **1999**, *399*, 28–29.
96. Blanchard, L. A.; Brennecke, J. F. *Ind. Eng. Chem. Res.* **2001**, *40*, 287–292.
97. Leitner, W. *Pure Appl. Chem.* **2004**, *76*, 635–644.
98. Sun, Y.; LeBlond, C.; Wang, J.; Blackmond, D. G. *J. Am. Chem. Soc.* **1995**, *117*, 12647–12648.
99. Jessop, P. G.; Ikariya, T.; Noyori, R. *Nature* **1994**, *368*, 231–233.
100. Jessop, P. G.; Hsiao, Y.; Ikariya, T.; Noyori, R. *J. Am. Chem. Soc.* **1996**, *118*, 344–355.
101. Jessop, P. G.; Ikariya, T.; Noyori, R. *Organometallics* **1995**, *14*, 1510–1513.
102. Naesnik, T. E.; Freudenberger, J. H.; Orchin, M. *J. Organomet. Chem.* **1982**, *236*, 95–100.
103. Matsui, Y.; Orchin, M. *J. Organomet. Chem.* **1983**, *244*, 369–373.
104. Jessop, P. G.; Hsiao, Y.; Ikariya, T.; Noyori, R. *J. Am. Chem. Soc.* **1994**, *116*, 8851–8852.
105. Lange, S.; Brinkmann, A.; Trautner, P.; Woelk, K.; Bargon, J.; Leitner, W. *Chirality* **2000**, *12*, 450–457.
106. Burk, M. J.; Feng, S.; Gross, M. F.; Tumas, W. *J. Am. Chem Soc.* **1995**, *117*, 8277–8278.
107. Oakes, R. S.; Clifford, A. A.; Rayner, C. M. *J. Chem. Soc., Perkin Trans. 1* **2001**, 917–941.
108. Adams, D. J.; Chen, W.; Hope, E. G.; Lange, S.; Stuart, A. M.; West, A.; Xiao, J. *Green Chem.* **2003**, *5*, 118–122.
109. Xiao, J.; Nefkens, S. C. A.; Jessop, P. G.; Ikariya, T.; Noyori, R. *Tetrahedron Lett.* **1996**, *37*, 2813–2826.
110. Hu, Y.; Birdsall, D. J.; Stuart, A. M.; Hope, E. G.; Xiao, J. *J. Mol. Cat. A: Chem.* **2004**, *219*, 57–60.

111. Horváth, I. T.; Rábai, J. *Science* **1994**, *266*, 72–75.
112. Schneider, S.; Bannwarth, W. *Helv. Chim. Acta* **2001**, *84*, 735–742.
113. Horváth, I. T. *Acc. Chem. Res.* **1998**, *31*, 641–650.
114. Hope, E. G.; Stuart, A. M. *J. Fluorine Chem.* **1999**, *100*, 75–83.
115. De Wolf, E.; Van Koten, G.; Deelman, B.-J. *Chem. Soc. Rev.* **1999**, *28*, 37–41.
116. Cavazzini, M.; Montanari, F.; Pozzi, G.; Quici, S. *J. Fluorine Chem.* **1999**, *94*, 183–193.
117. Fish, R. H. *Chem. Eur. J.* **1999**, *5*, 1677–1680.
118. Barthel-Rosa, L. P.; Gladysz, J. A. *Coord. Chem. Rev.* **1999**, *190–192*, 587–605.
119. Dobbs, A. P.; Kimberley, M. R. *J. Fluorine Chem.* **2002**, *118*, 3–17.
120. Curran, D. P. *Synlett* **2001**, *9*, 1488–1496.
121. Curran, D. P.; Fischer, K.; Moura-Letts, G. *Synlett* **2004**, 1379–1382.
122. Matsugi, M.; Curran, D. P. *J. Org. Chem.* **2005**, *70*, 1636–1642.
123. Tzschucke, C. C.; Markert, C.; Glatz, H.; Bannwarth, W. *Angew. Chem., Int. Ed.* **2002**, *41*, 4500–4503.
124. Tzschucke, C. C.; Andrushko, V.; Bannwarth, W. *Eur. J. Org. Chem.* **2005**, 5248–5261.
125. Tzschucke, C. C.; Bannwarth, W. *Helv. Chim. Acta* **2004**, *87*, 2882–2889.
126. Audic, N. A.; Bennett, J. A.; Dyer, P. W.; Hope, E. G.; Stuart, A. M.; Suhard, S. *1st International Symposium on Fluorous Technologies*; Bordeaux: France, 2005.
127. Pozzi, G.; Cavazzini, M.; Quici, S.; Maillard, D.; Sinou, D. *J. Mol. Catal. A: Chem.* **2002**, *182–183*, 455–461.
128. Pozzi, G.; Shepperson, I. *Coord. Chem. Rev.* **2003**, *242*, 115–124.
129. Fache, F. *New J. Chem.* **2004**, *28*, 1277–1283.
130. Wasserscheid, P.; Keim, W. *Angew. Chem., Int. Ed.* **2000**, *39*, 3773–3789.
131. Sheldon, R. *Chem. Commun.* **2001**, 2399–2407.
132. Olivier-Bourbigou, H.; Magna, L. *J. Mol. Catal. A: Chem.* **2002**, *182*, 419–437.
133. Gordon, C. M. *Appl. Catal. A: Gen.* **2001**, *222*, 101–117.
134. Dupont, J.; de Souza, R. F.; Suarez, P. A. Z. *Chem. Rev.* **2002**, *102*, 3667–3691.
135. Welton, T. *Coord. Chem. Rev.* **2004**, *248*, 2459–2477.
136. Chauvin, Y.; Gilbert, B.; Guibard, I. *J. Chem. Soc., Chem. Commun.* **1990**, 1715–1716.
137. Suarez, P. A. Z.; Dullius, J. E. L.; Einloft, S.; de Souza, R. F.; Dupont, J. *Polyhedron* **1996**, *15*, 1217–1219.
138. Chauvin, Y.; Mussmann, L.; Olivier, H. *Angew. Chem., Int. Ed. Engl.* **1995**, *34*, 2698–2700.
139. Dullius, J. E. L.; Suarez, P. A. Z.; Einloft, S.; de Souza, R. F.; Dupont, J.; Fischer, J.; de Cian, A. *Organometallics* **1998**, *17*, 815–819.
140. Zim, D.; de Souza, R. F.; Dupont, J.; Monteiro, A. L. *Tetrahedron Lett.* **1998**, *39*, 7071–7074.
141. Knifton, J. F. *J. Mol. Catal.* **1987**, *43*, 65–77.
142. Song, C. E.; Roh, E. J. *Chem. Commun.* **2000**, 837–838.
143. Owens, G. S.; Abu-Omar, M. M. *Chem. Commun.* **2000**, 1165–1166.
144. Buijsman, R. C.; van Vuuren, E.; Sterrenburg, J. G. *Org. Lett.* **2001**, *3*, 3785–3787.
145. Semeril, D.; Olivier-Bourbigou, H.; Bruneau, C.; Dixneuf, P. H. *Chem. Commun.* **2002**, 146–147.
146. Suarez, P. A. Z.; Dullius, J. E. L.; Einloft, S.; de Souza, R. F.; Dupont, J. *Inorg. Chim. Acta* **1997**, *255*, 207–209.
147. Dyson, P. J.; Ellis, D. J.; Parker, D. G.; Welton, T. *Chem. Commun.* **1999**, 25–26.
148. Bonilla, R. J.; James, B. R.; Jessop, P. G. *Chem. Commun.* **2000**, 941–942.
149. Monteiro, A. L.; Zinn, F. K.; de Souza, R. F.; Dupont, J. *Tetrahedron: Asymmetry* **1997**, *8*, 177–179.
150. Guernik, S.; Wolfson, A.; Herskowitz, M.; Greenspoon, N.; Geresh, S. *Chem. Commun.* **2001**, 2314–2315.
151. Berger, A.; de Souza, R. F.; Delgado, M. R.; Dupont, J. *Tetrahedron: Asymmetry* **2001**, *12*, 1825–1828.
152. Dyson, P. J.; Laurenczy, G.; Ohlin, C. A.; Vallance, J.; Welton, T. *Chem. Commun.* **2003**, 2418–2419.
153. Brown, R. A.; Pollet, P.; McKoon, E.; Eckert, C. A.; Liotta, C. L.; Jessop, P. G. *J. Am. Chem. Soc.* **2001**, *123*, 1254–1255.
154. Kaufmann, D. E.; Nouroozian, M.; Henze, H. *Synlett* **1996**, 1091–1092.
155. Carmichael, A. J.; Earle, M. J.; Holbrey, J. D.; McCormac, P. B.; Seddon, K. R. *Org. Lett.* **1999**, *1*, 997–1000.
156. Böhm, V. P. W.; Herrmann, W. A. *Chem. Eur. J.* **2000**, *6*, 1017–1025.
157. Herrmann, W. A.; Böhm, V. P. W. *J. Organomet. Chem.* **1999**, *572*, 141–145.
158. Xu, L.; Chen, W.; Xiao, J. *Organometallics* **2000**, *19*, 1123–1127.
159. Moreno-Mañas, M.; Pleixats, R. *Acc. Chem. Res.* **2003**, *36*, 638–643.
160. Suzuki, A. *J. Organomet. Chem.* **1999**, *576*, 147–168.
161. Mathews, C. J.; Smith, P. J.; Welton, T. *Chem. Commun.* **2000**, 1249–1250.
162. McLachlan, F.; Mathews, C. J.; Smith, P. J.; Welton, T. *Organometallics* **2003**, *22*, 5350–5357.
163. Dupont, J.; Spencer, J. *Angew. Chem., Int. Ed.* **2004**, *43*, 5296–5297.
164. Seddon, K. R.; Stark, A.; Torres, M.-J. *Pure Appl. Chem.* **2000**, *72*, 2275–2287.
165. Daguenet, C.; Dyson, P. J. *Organometallics* **2004**, *23*, 6080–6083.
166. Swatloski, R. P.; Holbrey, J. D.; Rogers, R. D. *Green Chem.* **2003**, *5*, 361–363.
167. Arhancet, J. P.; Davis, M. E.; Merola, J. S.; Hanson, B. E. *Nature* **1989**, *339*, 454–455.
168. Mehnert, C. P.; Cook, R. A.; Dispenziere, N. C.; Afeworki, M. *J. Am. Chem. Soc.* **2002**, *124*, 12932–12933.
169. Stock, F.; Hoffmann, J.; Ranke, J.; Störmann, R.; Ondruschka, B.; Jastorff, B. *Green Chem.* **2004**, *6*, 286–90.
170. Pernak, J.; Goc, I.; Mirska, I. *Green Chem.* **2004**, *6*, 323–329.
171. Loupy, A., Ed. *Microwaves in Organic Synthesis*; Wiley-VCH: Weinheim, 2002.
172. Hayes, B. L. *Aldrichim. Acta* **2004**, *37*, 66–76.
173. Perreux, L.; Loupy, A. *Tetrahedron* **2001**, *57*, 9199–9223.
174. Lidstrom, P.; Tierney, J.; Wathey, B.; Westman, J. *Tetrahedron* **2001**, *57*, 9225–9283.
175. Nüchter, M.; Ondruschka, B.; Bonrath, W.; Gum, A. *Green Chem.* **2003**, *6*, 128–141.
176. Blackwell, H. E. *Org. Biomol. Chem.* **2003**, *1*, 1251–1255.
177. Kappe, C. O. *Curr. Opin. Chem. Biol.* **2002**, *6*, 314–320.
178. VanAtta, S. L.; Duclos, B. A.; Green, D. B. *Organometallics* **2000**, *19*, 2397–2399.
179. Ardon, M.; Hogarth, G.; Oscroft, D. T. W. *J. Organomet. Chem.* **2004**, *689*, 2429–2435.

180. Konno, H.; Sasaki, Y. *Chem. Lett.* **2003**, *32*, 252–253.
181. Larhed, M.; Moberg, C.; Hallberg, A. *Acc. Chem. Res.* **2002**, *35*, 717–727.
182. Leadbeater, N. E. *Chem. Commun.* **2005**, 2881–2902.
183. Leadbeater, N. E.; Marco, M. *Angew. Chem., Int. Ed.* **2003**, *42*, 1407–1409.
184. Leadbeater, N. E.; Marco, M. *J. Org. Chem.* **2003**, *68*, 5660–5667.
185. Appukkuttan, P.; Dehaen, W.; Van der Eycken, E. *Eur. J. Org. Chem.* **2003**, 4713–4716.
186. Arvela, R. K.; Leadbeater, N. E.; Songi, M. S.; Williams, V. A.; Grenados, P.; Singer, J. D. *J. Org. Chem.* **2005**, *70*, 161–168.
187. Arvela, R. K.; Leadbeater, N. E. *J. Org. Chem.* **2005**, *70*, 1786–1790.
188. He, P.; Haswell, S. J.; Fletcher, P. D. I. *Appl. Cat. A: Gen.* **2004**, *274*, 111–114.
189. Arvela, R. K.; Leadbeater, N. E.; Collins, J.; Michael, J. *Tetrahedron* **2005**, *61*, 9349–9355.
190. Kaiser, N. F. K.; Bremberg, U.; Larhed, M.; Moberg, C.; Hallberg, A. *J. Organomet. Chem.* **2000**, *603*, 2–5.
191. Kaiser, N. F. K.; Bremberg, U.; Larhed, M.; Moberg, C.; Hallberg, A. *Angew. Chem., Int. Ed.* **2000**, *39*, 3596–3598.
192. Fischer, S.; Groth, U.; Jung, M.; Schneider, A. *Synlett* **2002**, 2023–2026.
193. Bytschkov, I.; Doye, S. *Eur. J. Org. Chem.* **2001**, 4411–4418.
194. Villemin, D.; Heroux, M.; Blot, V. *Tetrahedron Lett.* **2001**, *42*, 3701–3703.
195. Tan, K. L.; Vasudevan, A.; Bergman, R. G.; Ellman, J. A.; Souers, A. J. *Org. Lett.* **2003**, *5*, 2131–2134.
196. Loupy, A.; Chatti, S.; Delamare, S.; Lee, D.-Y.; Chung, J.-H.; Jun, C.-H. *J. Chem. Soc., Perkin Trans. 1* **2002**, 1280–1285.
197. Cintas, P.; Luche, J.-L. *Green Chem.* **1999**, *1*, 115–125.
198. Disselkamp, R. S.; Hart, T. R.; Williams, A. M.; White, J. F.; Peden, C. H. F. *Ultrason. Sonochem.* **2005**, *12*, 319–324.
199. Mikkola, J.-P.; Kubicka, D.; Kuusisto, J.; Granholm, N.; Salmi, T.; Holmborn, B. *J. Chem. Technol. Biotechnol.* **2003**, *78*, 203–207.
200. Toukoniitty, B.; Toukoniiitty, E.; Mäki-Arvela, P.; Mikkola, J.-P.; Salmi, T.; Murzin, D. Yu.; Kooyman, P. J. *Ultrason. Sonochem.* **2006**, *13*, 68–75.
201. Poláčková, V.; Hut'ka, M.; Toma, Š. *Ultrason. Sonochem.* **2005**, *12*, 99–102.
202. Cravotto, G.; Palmisano, G.; Tollari, S.; Nano, G. M.; Penoni, A. *Ultrason. Sonochem.* **2005**, *12*, 91–94.
203. Gogate, P. R.; Pandit, A. B. *Ultrason. Sonochem.* **2004**, *11*, 105–117.
204. Ehrfeld, W.; Hessel, V.; Löwe, H. *Microreactors: New Technology for Modern Chemistry*; Wiely-VCH: Weinheim, 2000.
205. Fletcher, P. D. I.; Haswell, S. J.; Pombo-Villar, E.; Warrington, B. H.; Watts, P.; Wong, S. Y. F.; Zhang, X. L. *Tetrahedron* **2002**, *58*, 4735–4757.
206. Haswell, S. J.; Watts, P. *Green Chem.* **2003**, *5*, 240–249.
207. Watts, P.; Haswell, S. J. *Chem. Soc. Rev.* **2005**, *34*, 235–246.
208. Madou, M. *Fundamentals of Microfabrication*; CRC Press: Boca Raton, FL, 1997.
209. Manz, A.; Harrison, D. J.; Verpoorte, E.; Fettinger, J. C.; Ludi, H.; Widmer, H. M. *Chimia* **1991**, *45*, 103–105.
210. Jensen, K. F. In *Microreactor Technology and Process Intensification*; Wang, Y., Halladay, J. D., Eds.; ACS Symposium Series 914; American Chemical Society: Washington, DC, 2005; pp 2–22.
211. Kiwi-Minsker, L.; Renken, A. *Catal. Today* **2005**, *110*, 2–14.
212. Dietzsch, E.; Hönicke, D.; Fichtner, M.; Schubert, K.; Weißmeier, G. *IMRET 4: 4th International Conference of Micro Reaction Technology Topical Conference Proceedings, AIChE, Spring National Meeting*, Atlanta, GA, USA, March 5–9, 2000, American Institute of Chemical Engineers, Indianapolis, IN, USA, p 89.
213. Kobayashi, J.; Mori, Y.; Okamoto, K.; Akiyama, R.; Ueno, J.; Kitamori, T.; Kobayashi, S. *Science* **2004**, *304*, 1305–1308.
214. Greenway, G. M.; Haswell, S. J.; Morgan, D. O.; Skelton, V.; Styring, P. *Sens. Actuators B* **2000**, *63*, 153–158.
215. Haswell, S. J.; O'Sullivan, B.; Styring, P. *Lab Chip* **2001**, *1*, 164–166.
216. Phan, N. T. S.; Brown, D. H.; Styring, P. *Green Chem.* **2004**, *6*, 526–532.
217. Phan, N. T. S.; Kan, J.; Styring, P. *Tetrahedron* **2005**, *61*, 12065–12073.
218. de Bellefon, C.; Lamouille, T.; Pestre, N.; Bornette, F.; Pennemann, H.; Neumann, F.; Hessel, V. *Catal. Today* **2005**, *110*, 179–187.
219. Önal, Y; Lucas, M.; Claus, P. *Chem.-Ing.-Tech.* **2005**, 77, 101–105.
220. Sanchez Marcano, J.; Tsotsis, T. T. *Catalytic Membranes and Membrane Reactors*; Wiley-VCH: Weinheim, 2002.
221. Sanchez Marcano, J. In *Aqueous-Phase Organometallic Catalysis*, 2nd ed.; Cornils, B., Herrmann, W. E., Eds.; Wiley-VCH: Weinheim, 2004; pp 122–131.
222. Laue, S.; Greiner, L.; Wöltinger, J.; Liese, A. *Adv. Synth. Catal.* **2001**, *343*, 711–720.
223. Nair, D.; Luthra, S. S.; Scarpello, J. T.; White, L. S.; Freitas dos Santos, L. M.; Livingston, A. G. *Desalination* **2002**, *147*, 301–306.
224. Bergbreiter, D. E. *Catal. Today* **1998**, *42*, 389–397.
225. Bergbreiter, D. E.; Zhan, L.; Mariagnanam, V. M. *J. Am. Chem. Soc.* **1993**, *115*, 9295–9296.
226. Bergbreiter, D. E.; Liu, Y. S. *Tetrahedron Lett.* **1997**, *38*, 7843–7846.
227. Wang, Y.; Jin, Z. *Trends in Organometallic Chemistry* **2002**, *4*, 71–79. CA141: 190824
228. Jin, Z.; Wang, Y.; Jiang, J.; Wen, F. *Current Topics in Catalysis* **2002**, *3*, 15–32. CA141: 206536
229. Wang, Y.; Jiang, J.; Miao, Q.; Wu, X.; Jin, Z. *Catal. Today* **2002**, *74*, 85–90.
230. Liu, C.; Jiang, J.; Wang, Y.; Cheng, F.; Jin, Z. *J. Mol. Catal. A: Chem.* **2003**, *198*, 23–27.
231. Wang, Y.; Wu, X.; Cheng, F.; Jin, Z. *J. Mol. Catal. A: Chem.* **2003**, *195*, 133–137.
232. Diressen-Höllscher, B. *Adv. Catal.* **1998**, *42*, 473–505.
233. Burgess, K. *Solid-Phase Organic Synthesis*; Wiley: New York, 2000.
234. De Vos, D. E., Vankelecom, I. F. J., Jacobs, P. A., Eds. *Chiral Catalyst Immobilization and Recycling*; Wiley-VCH: Weinheim, 2000.
235. Seneci, P. *Solid-phase Synthesis and Combinatorial Techniques*; Wiley: New York, 2001.
236. Shuttleworth, S. J.; Allin, S. M.; Sharma, P. K. *Synthesis* **1997**, 1217–1239.
237. Ley, S. V.; Baxendale, I. R.; Bream, R. N.; Jackson, P. S.; Leach, A. G.; Longbottom, D. A.; Nesi, M.; Scott, J. S.; Storer, I.; Taylor, R. S. *J. Chem. Soc., Perkin Trans. 1* **2000**, 3815–4195.
238. Montheard, P.; Jegat, C.; Camps, C. J. M. *J. Macromol. Sci., Rev. Macromol. Chem. Phys.* **1999**, *C39*, 135–174.
239. Astruc, D.; Chardac, F. *Chem. Rev.* **2001**, *101*, 2991–3023.
240. Leadbeater, N. E.; Marco, M. *Chem. Rev.* **2002**, *102*, 3217–3274.
241. McNamara, C. A.; Dixon, M. J.; Bradley, M. *Chem. Rev.* **2002**, *102*, 3275–3300.
242. Barrett, A. G. M.; Hopkins, B. T.; Köbberling, J. *Chem. Rev.* **2002**, *102*, 3301–3324.

243. Dickerson, T. J.; Reed, N. N.; Janda, K. D. *Chem. Rev.* **2002**, *102*, 3325–3344.
244. Bergbreiter, D. E. *Chem. Rev.* **2002**, *102*, 3345–3384.
245. Fan, Q.-H.; Li, Y.-M.; Chan, A. S. C. *Chem. Rev.* **2002**, *102*, 3385–3466.
246. Clark, J. H.; MacQuarrie, D. J. *Org. Process Rev. Dev.* **1997**, *1*, 149–162.
247. Song, C. E.; Lee, S. *Chem. Rev.* **2002**, *102*, 3495–3524.
248. Duchateau, R. *Chem. Rev.* **2002**, *102*, 3525–3542.
249. De Vos, D. D.; Dams, M.; Sels, B. F.; Jacobs, P. A. *Chem. Rev.* **2002**, *102*, 3615–3640.
250. van Heerbeek, R.; Kamer, P. C. J.; van Leeuwen, P. W. N. M.; Reek, J. N. H. *Chem. Rev.* **2002**, *102*, 3717–3756.
251. Wight, A. P.; Davis, M. E. *Chem. Rev.* **2002**, *102*, 3589–3624.
252. Lu, Z.-L.; Lindner, E.; Mayer, H. A. *Chem. Rev.* **2002**, *102*, 3579–3588.
253. Cornils, B. In *New Syntheses with Carbon Monoxide*; Falbe, J., Ed.; Springer: Berlin, 1980; Chapter 1.
254. Johnson, T. H. U.S. Patent 4,584,411, 1985.
255. Frohning, C. D.; Kohlpainter, C. W. In *Applied Homogeneous Catalysis with Organometallic Compounds*; Cornils, B., Herrmann, W. E., Eds.; Wiley-VCH: Weinheim, 1996; pp 61–65.
256. Sandee, A. J.; Reek, J. N. H.; Kamer, P. C. J.; van Leeuwen, P. W. N. M. *J. Am. Chem. Soc.*, **2001**, *128*, 8468–8476.
257. Tulchinsky, M. L.; Miller, D. J. U.S. Patent 6,350,819, 2002.
258. Banet Osuna, A. M.; Chen, W.; Hope, E. G.; Kemmitt, R. D. W.; Paige, D. R; Stuart, A. M.; Xiao, J.; Xu, L *J. Chem. Soc., Dalton Trans.* **2000**, 4052–4055.
259. Hu, Y.; Chen, W.; Banet Osuna, A. M.; Stuart, A. M.; Hope, E. G.; Xiao, J. *Chem. Commun.* **2001**, 725–726.
260. Hu, Y.; Chen, W.; Banet Osuna, A. M.; Iggo, J. A.; Xiao, J. *Chem. Commun.* **2002**, 788–789.
261. Meehan, N. J.; Sandee, A. J.; Reek, J. N. H.; Kamer, P. C. J.; van Leeuwen, P. W. N. M.; Poliakoff, M. *Chem. Commun.* **2000**, 1497–1498.
262. Solinas, M.; Jiang, J.; Stelzer, O.; Leitner, W. *Angew Chem., Int. Ed.* **2005**, *44*, 2291–2295.
263. Frohning, C. D.; Kohlpainter, C. W. In *Applied Homogeneous Catalysis with Organometallic Compounds*; Cornils, B., Herrmann, W. E., Eds.; Wiley-VCH: Weinheim, 1996; pp 80–82.
264. Chen, J.; Alper, H. *J. Am. Chem. Soc.* **1997**, *119*, 893–895.
265. Ajjou, A. N.; Alper, H. *J. Am. Chem. Soc.* **1998**, *120*, 1466–1468.
266. Gong, A.; Fan, Q.; Chen, Y.; Liu, H.; Chen, C.; Xi, F. *J. Mol. Catal. A: Chem.* **2000**, *159*, 225–232.
267. Reek, J. N. H.; Kamer, P. C. J.; van Leeuwen, P. W. N. M. In *Rhodium Catalyzed Hydroformylation*; van Leeuwen, P. W. N. M., Claver, C., Eds.; Kluwer: Dordrecht, 2000; pp 253–279.
268. Monflier, E.; Fremy, G.; Castanet, Y.; Mortreux, A. *Angew Chem., Int. Ed. Engl.* **1995**, *34*, 2269–2271.
269. Reetz, M. T.; Waldvogel, S. R. *Angew. Chem., Int. Ed. Engl.* **1997**, *36*, 865–867.
270. Shimizu, S.; Shirakawa, S.; Sasaki, Y.; Hirai, C. *Angew. Chem., Int. Ed.* **2000**, *39*, 1256–1258.
271. Sueur, B.; Leclercq, L.; Sauthier, M.; Castanet, Y.; Mortreux, A.; Bricout, H.; Tilloy, S.; Monflier, E. *Chem. Eur. J.* **2005**, *11*, 6228–6236.
272. Zheng, X.; Jiang, J.; Liu, X.; Jin, Z. *Catal. Today* **1998**, *44*, 175–182.
273. Jin, Z.; Zheng, X.; Fell, B. *J. Mol. Catal. A: Chem.* **1997**, *116*, 55–58.
274. Jiang, J.; Wang, Y.; Liu, C.; Xiao, Q.; Jin, Z. *J. Mol. Catal. A: Chem.* **2001**, *171*, 85–89.
275. Horváth, I. T.; Kiss, G.; Cook, R. A.; Bond, J. E.; Stevens, P. A.; Rábai, J.; Mozeleski, E. J. *J. Am. Chem. Soc.* **1998**, *120*, 3133–3143.
276. Foster, D. F.; Adams, D. J.; Gudmunsen, D.; Stuart, A. M.; Hope, E. G.; Cole-Hamilton, D. J. *Chem. Commun.* **2002**, 722–723.
277. Foster, D. F.; Gudmunsen, D.; Adams, D. J.; Stuart, A. M.; Hope, E. G.; Cole-Hamilton, D. J.; Schwarz, G. P.; Pogorzelec, P. *Tetrahedron* **2002**, *58*, 3901–3910.
278. Mathivet, T.; Monflier, E.; Castanet, Y.; Mortreux, A.; Couturier, J. L. *Tetrahedron* **2002**, *58*, 3877–3888.
279. Perperi, E.; Huang, Y.; Angeli, P.; Manos, G.; Mathison, C. R.; Cole-Hamilton, D. J.; Adams, D. J.; Hope, E. G. *Dalton Trans.* **2004**, 2062–2064.
280. Brasse, C. C.; Englert, U.; Salzer, A.; Waffenschmidt, H.; Wasserscheid, P. *Organometallics* **2000**, *19*, 3818–3823.
281. Dupont, J.; Silva, S. M.; de Souza, R. F. *Catal. Lett.* **2001**, *77*, 131–133.
282. Wasserscheid, P.; Waffenschmidt, H.; Machnitzki, P.; Kottsieper, K. W.; Stelzer, O. *Chem. Commun.* **2001**, 451–452.
283. Bronger, R. P. J.; Silva, S. M.; Kamer, P. C. J.; van Leeuwen, P. W. N. M. *Chem. Commun.* **2002**, 3044–3045.
284. Kong, F.; Jiang, J.; Jin, Z. *Catal. Lett.* **2004**, *96*, 63–65.
285. Horváth, I. T. *Catal. Lett.* **1990**, *6*, 43–48.
286. van Leeuwen, P. W. N. M.; Sandee, A. J.; Reek, J. N. H.; Kamer, P. C. J. *J. Mol. Catal. A: Chem.* **2002**, *182–183*, 107–123.
287. Naughton, M. J.; Drago, R. S. *J. Catal.* **1995**, *155*, 383–389.
288. Mehnert, C. P.; Cook, R. A.; Dispenziere, N. C.; Afeworki, M. *J. Am. Chem. Soc.* **2002**, *124*, 12932–12933.
289. Mehnert, C. P. *Chem. Eur. J.* **2005**, *11*, 50–56.
290. Riisager, A.; Wasserscheid, P.; van Hal, R.; Fehrmann, R. *J. Catal.* **2003**, *219*, 452–455.
291. Riisager, A.; Eriksen, K. M.; Wasserscheid, P.; Fehrmann, R. *Catal. Lett.* **2003**, *90*, 149–153.
292. Brintzinger, H. H.; Fischer, D.; Mülhaupt, R.; Rieger, B.; Waymouth, R. *Angew Chem., Int. Ed. Engl.* **1995**, *34*, 1143--1170.
293. Bochmann, M. *J. Chem. Soc., Dalton Trans.* **1996**, 255–270.
294. Kaminsky, W.; Arndt, M. *Adv. Polym. Sci.* **1997**, *127*, 143–187.
295. Britovsek, G. J. P.; Gibson, V. C.; Wass, D. F. *Angew. Chem., Int. Ed.* **1999**, *38*, 419–447.
296. Ittel, S. D.; Johnson, L. K.; Brookhart, M. *Chem. Rev.* **2000**, *100*, 1169–1203.
297. Mecking, S. *Angew. Chem., Int. Ed.* **2001**, *40*, 534–540.
298. Gibson, V. C.; Spitzmesser, S. *Chem. Rev.* **2003**, *103*, 283–315.
299. Lovell, P. A., El-Aasser, M. S., Eds. *Emulsion Polymerisation and Emulsion Polymers*; Wiley: Chichester, 1997.
300. Mecking, S.; Held, A.; Bauers, F. M. *Angew. Chem., Int. Ed. Engl.* **2002**, *144*, 544–561.
301. Claveriea, J. P.; Soula, R. *Prog. Polym. Sci.* **2003**, *28*, 619–662.
302. Wang, L.; Lu, R. S.; Bau, R.; Flood, T. C. *J. Am. Chem. Soc.* **1993**, *115*, 6999–7000.
303. Held, A.; Bauers, F. M.; Mecking, S. *Chem. Commun.* **2000**, 301–302.
304. Bauers, F. M.; Mecking, S. *Macromolecules* **2001**, *34*, 1165–1171.
305. Mecking, S.; Bauers, F. M.; Thomann, R. *Polym. Mater. Sci. Eng.* **2001**, *84*, 1049–1050.
306. Tomov, A.; Broyer, J.-P.; Spitz, R. *Macromol. Symp.* **2000**, *150*, 53–58.

307. Soula, R.; Novat, C.; Tomov, A.; Spitz, R.; Claverie, J.; Drujon, X.; Maligne, J.; Saudemont, T. *Macromolecules* **2001**, *34*, 2022–2026.
308. Held, A.; Weiss, F.; Mecking, S. *Polym. Prepr.* **2001**, *42*, 466–467.
309. Brookhart, M. S.; Johnson, L. K.; Killian, C. M.; Arthur, S. D.; Feldman, J.; McCord, E. F.; Mclain, S. J.; Kreutzer, K. A.; Bennett, A. M. A.; Coughlin, E. B., *et al.* (E.I. Du Pont De Nemours and Co.). WO 96/23010, 1996.
310. Brown, K. A.; Lamana, W. M.; Siedle, A. R.; Stewart, E. G.; Swanson, P. J. (3M). WO 97/17380, 1997.
311. Rau, A.; Schmitz, S.; Luft, G. *Chem. Eng. Technol.* **2002**, *25*, 494–498 and references therein.
312. Brant, P.; Rix, F. C.; Kiss, G.; Reynolds, R. (ExxonMobil Chemical Co.). WO-A 06/025545, 2006.
313. Brant, P.; Luft, G. F.; Shutt, J. R.; Smith, L. C.; McLain, D. J.; Burkhardt, T. J. (ExxonMobil Chemical Co.). WO 04/026921, 2004.
314. Super, M. S.; Berluche, E.; Costello, C. A.; Beckman, E. *Macromolecules* **1997**, *30*, 368–372.
315. Hori, H.; Six, C.; Leitner, W. *Macromolecules* **1999**, *32*, 3178–3182.
316. Kendall, J. L.; Canelas, D. A.; Young, J. L.; DeSimone, J. M. *Chem. Rev.* **1999**, *99*, 543–563.
317. de Vries, T. J.; Duchateau, R.; Vorstman, M. A. G.; Keurentjes, J. T. F. *Chem. Commun.* **2000**, 263–264.
318. de Vries, T. J.; Kemmere, M. F.; Keurentjes, J. T. F. *Macromolecules* **2004**, *11*, 4241–4246.
319. Kemmere, M. F.; de Vries, T. J.; Vorstman, M.; Keurentjes, J. T. F. *Chem. Eng. Sci.* **2001**, *56*, 4197–4204.
320. Smart, B. E. In *Organofluorine Chemistry, Principles and Commercial Applications*; Banks, R. E., Smart, B. E., Tatlow, J. C., Eds.; Chapter 3 Plenum: New York, 1994; pp 57–67.
321. Malanga, M. T.; Newman, T. H. Eur. Pat. Appl. EP 361309A2, 1990.
322. Jones, E.; Walker, J. Ger. Offen. DE 2501239, 1975.
323. Mitani, M.; Furuyama, R.; Mohri, J.-I.; Saito, J.; Ishii, S.; Terao, H.; Nakano, T.; Tanaka, H.; Fujita, T. *J. Am. Chem. Soc.* **2003**, *125*, 4293–4305.
324. Merle, P. G.; Cheron, V.; Hagen, H.; Lutz, M. L.; Spek, A. L.; Deelman, B.-J.; van Koten, G. *Organometallics* **2005**, *24*, 1620–1630.
325. Merle, P. G.; Deelman, B.-J.; van Koten, G. *Second European Catalysis Symposium: Organic Catalysis for a Sustainable Development*; Pisa, Italy, September 23–26, 2001; Book of Abstracts, Poster 48.
326. Hagerty, R. O.; Laird, R. B.; Risch, M. A.; Shirodkar, P. P.; Jiang, P. (ExxonMobil Chemical Co.). WO 06/009979, 2006.
327. Jiang, P.; Shutt, J. R.; Speed, C. S.; Hagerty, R. O.; Shirodkar, P. P. (ExxonMobil Chemical Co.). WO 06/002132, 2006.
328. Cheron, V.; Couturier, J.-L.; Hagen, H.; van Koten, G.; Deelman, B.-J. (to ATOFINA). Int. Pat. Appl. WO/0214337, 2002.
329. Welton, T. *Chem. Rev.* **1999**, *99*, 2071–2083.
330. Carlin, R. T.; Wilkes, J. S. *J. Mol. Catal.* **1990**, *63*, 125–129.
331. Pinheiro, M. F.; Mauler, R. S.; de Souza, R. F. *Macromol. Rapid Commun.* **2001**, *22*, 425–428.
332. Lavastre, O.; Bonnette, F.; Razavi, A. (Atofina res.). WO 05/047350, 2005.
333. Lavastre, O.; Bonnette, F.; Razavi, A. (Atofina res.). WO 05/030392, 2005.
334. Hlatky, G.G. (Equistar Chem.). WO 01/81436, 2001.
335. Carlin, R. T.; Osteryoung, R. A.; Wilkes, J. S.; Rovang, J. *Inorg. Chem.* **1990**, *29*, 3003–3009.
336. Shaughnessy, K. H.; Klingshirn, M. A.; P'Pool, S. J.; Holbrey, J. D.; Rogers, R. D. In *Ionic Liquids As Green Solvents: Progress and Prospects; ACS symposium series 856*; Rogers, R. D., Seddon, K. R., Eds.; American Chemical Society: Washington, DC, 2003; pp 300–313.
337. Wasserscheid, P.; Gordon, C. M.; Hilgers, C.; Muldoon, M. J.; Dunkin, I. R. *Chem. Commun.* **2001**, 1186–1187.
338. Wasserscheid, P.; Gordon, C. M.; Hilgers, C.; Muldoon, M. J.; Dunkin, I. R. *Chem. Commun.* **2001**, 1700.
339. Wasserscheid, P.; Hilgers, C.; Keim, W. *J. Mol. Catal. A: Chem.* **2004**, *214*, 83–90.
340. Gu, Y. L.; Shi, F.; Deng, Y. Q. *Catal. Commun.* **2003**, *4*, 597–601.
341. Shaughnessy, K. H.; P'Pool, S. J.; Klingshirn, M. A.; Rogers, R. D. *Polym. Prepr.* **2004**, *44*, 317–318.
342. Bernardo-Gusmao, K.; Queiroz, L. F. T.; de Souza, R. F.; Leca, F.; Loup, C.; Reau, R. *J. Catal.* **2003**, *219*, 59–62.

Index

The index is in letter-by-letter order, whereby hyphens and spaces within index headings are ignored in the alphabetization, and it is arranged in set-out style, with a maximum of three levels of heading. Location references refer to the volume number (in bold) and page number (separated by a comma). Major discussion of a subject is indicated by a bold page range. Page numbers suffixed by *F* or *T* refer to figures or tables.

B

C

D

E

F

G

H

I

K

L

M

N

O

P

Q

R

S

T

U

V

W

X

Z